

**FINAL PROGRAM**



# **TMS** 2011

**140th Annual Meeting & Exhibition**

February 27 - March 3, 2011 • San Diego Convention Center  
San Diego, California USA

***“Linking Science and Technology  
for Global Solutions”***

LEARN • NETWORK • ADVANCE

# Thanks!

## to our Corporate Sponsors





# Welcome to the TMS 2011 Annual Meeting & Exhibition!



Dear Colleagues and Friends:

As president of TMS, I welcome our members, exhibitors, and society guests here to sunny San Diego for our 140th annual gathering!

This year, the heart of our annual meeting—technical programming—has grown to four full days! This is an unprecedented opportunity to reap the ultimate in professional development through a robust menu of high quality, engaging presentations. We are also focusing on inspiring a renewed sense of volunteerism as a key to building a bigger and better TMS.

I invite you to visit the Volunteer Concierge booth here at the San Diego Convention Center to learn how to get involved in society activities. Get further engaged by attending the Annual Meeting of Membership on Monday.

Here is a brief synopsis of the other invaluable offerings here at TMS 2011:

**Technical & Poster Sessions** – Over 70 symposia will spotlight the efforts of some of the world's greatest materials science and engineering minds. Technical areas include Aluminum and Magnesium; Advanced Characterization, Modeling & Materials Performance; High Performance Materials; Materials & Society: Energy & Sustainable Production; Materials Processing & Production; Nanoscale & Amorphous Materials; Professional Development.

**Continuing Education** – Knowledge is the power that fuels developments in research and builds careers. TMS 2011 features five compelling courses and workshops designed to enhance your conference experience through education.

**Networking** – Your presence at TMS 2011 contributes to one of the greatest benefits: connecting with colleagues from around the world! Gather with professionals in your field at one of our 12 symposia-related welcome receptions on Sunday evening. Then, join all attendees at the President's Welcoming Reception on Monday and Happy Hour on Tuesday. All receptions will be at the San Diego Convention Center.

**Special Lectures** – One of the hallmarks of our annual meeting are the special lectures presented by prestigious professionals in the materials field. Whether you attend a luncheon lecture, plenary talk, or awards presentation, you will learn from the accomplishments of your colleagues. See page 15 for speakers.

**Awards Presentation** – Celebrating the accomplishments of fellow colleagues builds our society. The TMS and AIME Awards Dinner is a must-attend event on Tuesday evening. See page 16 for a preview.

**Student Events** –The future of TMS is fulfilled by its student members. Visit the Student Poster Contest and see what students are working on, and enjoy their competitive spirit at the Materials Bowl sponsored by Alcoa. Details are on page 18.

Welcome to TMS 2011. Let's make the most of all this conference has to offer.

Sincerely,

George T. "Rusty" Gray III

## Table of Contents

|                            |    |                         |    |
|----------------------------|----|-------------------------|----|
| Registration .....         | 2  | Awards .....            | 16 |
| Meeting Policies .....     | 2  | Student Activities..... | 18 |
| Schedule of Events.....    | 3  | Proceedings .....       | 19 |
| Maps.....                  | 12 | TMS Leadership .....    | 20 |
| Lectures & Luncheons ..... | 14 | Exhibit Directory ..... | 21 |
| Speakers .....             | 15 | Technical Program.....  | 37 |

# TMS 2011

## 140th Annual Meeting & Exhibition

### Full Conference Registration

Your full conference badge provides you admission to each of these premier events!

- Technical & Poster Sessions
- Exhibition
- President's Welcoming Reception in the Exhibit Hall
- Symposia-Related Welcome Receptions/Poster Sessions
- Hosted Exhibit Hall Reception
- Young Leaders Tutorial Lecture
- Women in Science Breakfast (pre-registration required)
- Student Poster Contest
- Student Materials Bowl
- Lunch & Learn Sessions

### Internet Options

Free wireless access will be available on the upper level of the San Diego Convention Center in the Sails Pavilion (Authors' Coffee area) Sunday - Thursday, and in the Exhibit Hall concession area Monday - Wednesday. Username: TMS2011, Password: MATERIALS

Cyber Center Internet work stations sponsored by Stellar Materials Inc. will be available in the exhibit hall at the San Diego Convention Center during regular show hours.

### Policies


#### Badges

All attendees must wear registration badges at all times during the conference to ensure free admission to events included in the paid fee such as technical sessions, exhibition and receptions. "Exhibit Only" badges provide exclusive admittance to the show floor for events in the exhibit hall. "Guest" badges are for spouses or companions of registered attendees and used as identification only. "Guest" and "Exhibit Only" may not attend technical sessions.

#### Refunds

The deadline for all refunds was February 2, 2011. No refunds will be issued at the conference. Fees and tickets are nonrefundable.

#### Americans with Disabilities Act

 TMS strongly supports the federal Americans with Disabilities Act (ADA) which prohibits discrimination against, and promotes public accessibility for those with disabilities. In support of, and in compliance with, ADA, we ask those requiring specific equipment or services to contact TMS Meeting Services in advance.

#### Audio/Video Recording Policy

TMS reserves the right to all audio and video reproduction of presentations at TMS sponsored meetings. Recording of sessions (audio, video, still photography, etc.) intended for personal use, distribution, publication, or copyright without the express written consent of TMS and the individual authors is strictly prohibited. Contact TMS Technical Programming at (724) 776-9000, ext 212, to obtain a copy of the waiver release form.

#### Photography Notice

By registering for the meeting, all attendees acknowledge that they may be photographed by TMS personnel while at events. Photos may be used for promotional purposes in print and online.

#### Cell Phone Use

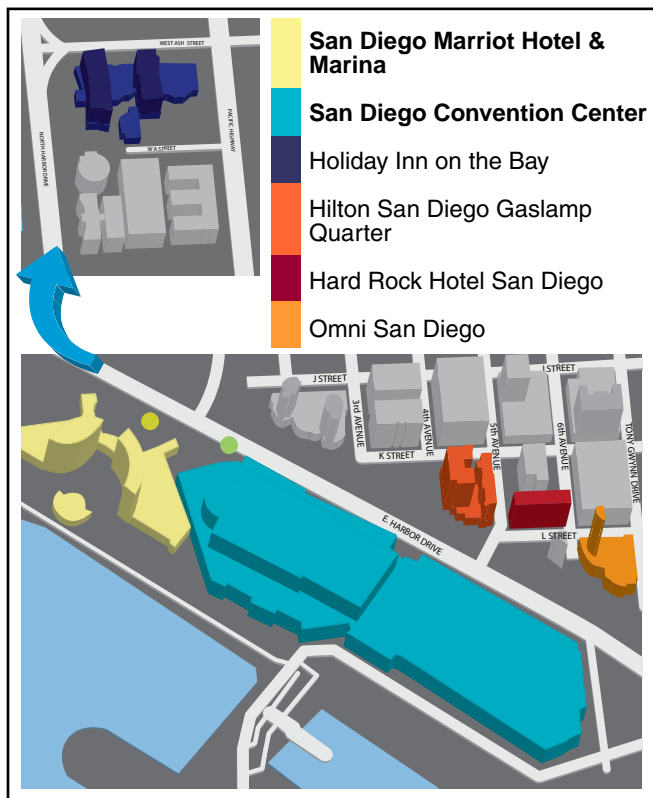
In consideration of attendees and presenters, TMS kindly requests that you minimize disturbances by setting all cell phones or PDA's on "silent" while in meeting rooms.

#### Recycling

##### Be Materials Minded!

Join TMS in reusing and recycling. Deposit discarded badges and programs in the bins located in the lobby of the San Diego Convention Center.

MEETING INFORMATION





## Schedule of Events

as of January 18, 2011

TMS Meetings & Events are scheduled on the following days, times and locations:

Key: **C** San Diego Convention Center

**M** San Diego Marriott Hotel & Marina

### SATURDAY, FEBRUARY 26

#### COMMITTEE MEETINGS

|  |                  |   |            |
|--|------------------|---|------------|
| Professional Registration Workshop and Committee Meeting | 9 a.m. to 5 p.m. | M | Point Loma |
|--|------------------|---|------------|

#### SOCIAL FUNCTIONS

|  |              |   |          |
|--|--------------|---|----------|
| Cal Poly Materials Engineering Alumni and Friends Get-Together | 7 to 10 p.m. | - | Off-Site |
|--|--------------|---|----------|

### SUNDAY, FEBRUARY 27

|                           |                      |   |                              |
|---------------------------|----------------------|---|------------------------------|
| REGISTRATION              | 11 a.m. to 7:30 p.m. | C | Exhibit Hall AB1             |
| TMS MEMBER WELCOME CENTER | 11 a.m. to 7:30 p.m. | C | Ground Level, Outside Hall A |

#### WORKSHOPS, SHORT COURSES, FORUMS & TUTORIALS

|  |                        |   |          |
|--|------------------------|---|----------|
| Lead-Free Solder Technology 2011                 | 8:30 a.m. to 5:30 p.m. | C | Room 31C |
| Proper Anode Baking Furnace Operations-How & Why | 8:30 a.m. to 4 p.m.    | C | Room 33B |
| Casting & Solidification of Metals               | 8:30 a.m. to 4 p.m.    | C | Room 33C |

#### STUDENT EVENTS

|                          |                |   |                     |
|--------------------------|----------------|---|---------------------|
| Materials Bowl           |                |   |                     |
| Elimination Rounds       | noon to 3 p.m. | M | Marina Ballroom G   |
| Championship Round       | 8:30 p.m.      | M | Marina Ballroom G   |
| Student Networking Mixer | 9 to 11 p.m.   | M | Marina Ballroom E&F |

#### SOCIAL FUNCTIONS

|   |                   |   |             |
|---|-------------------|---|-------------|
| Fellows and Invited Guests Reception                                | 4:30 to 6:30 p.m. | M | Torrance    |
| Young Leader/New Member Reception                                   | 5 to 6 p.m.       | M | Solana      |
| Microstructural Processes in Irradiated Materials Poster Reception  | 6 to 8 p.m.       | C | Room 3      |
| Polycrystal Modeling with Experimental Integration Poster Reception | 6 to 8 p.m.       | C | Ballroom 6C |
| Frontiers in Solidification Science Poster Session                  | 6 to 8 p.m.       | C | Ballroom 6E |
| Computational Thermodynamics & Kinetics Reception                   | 6 to 8 p.m.       | C | Room 9      |
| 2011 Functional and Structural Nanomaterials Reception              | 6 to 8 p.m.       | C | Room 8      |

MEETING INFORMATION



# TMS 2011

## 140th Annual Meeting & Exhibition



### Schedule of Events

as of January 18, 2011

Key: **C** San Diego Convention Center

**M** San Diego Marriott Hotel & Marina

MEETING INFORMATION

|   |             |          |             |
|---|-------------|----------|-------------|
| Neutron and X-Ray Studies of Advanced Materials IV Poster Session   | 6 to 8 p.m. | <b>C</b> | Room 10     |
| Light Metals Reception  | 6 to 8 p.m. | <b>C</b> | Room 17A    |
| Magnesium Technology 2011 Reception   | 6 to 8 p.m. | <b>C</b> | Ballroom 6F |
| Pb-Free Solders and other Materials for Emerging Interconnect and Packaging Technologies Reception                          | 6 to 8 p.m. | <b>C</b> | Room 7B     |
| Physical and Mechanical Metallurgy of Shape Memory Alloys for Actuator Applications Reception                               | 6 to 8 p.m. | <b>C</b> | Room 11B    |
| Materials Processing Fundamentals Poster Session  | 6 to 8 p.m. | <b>C</b> | Room 12     |
| Silicon Production, Purification and Recycling for Photovoltaic Cells Poster Session  | 6 to 8 p.m. | <b>C</b> | Room 14A    |
| Characterization of Minerals, Metals and Materials Reception  | 6 to 8 p.m. | <b>C</b> | Room 14B    |
| Biological Materials Science Reception  | 6 to 8 p.m. | <b>C</b> | Room 15A    |
| The Second Symposium on the Recycling of Electronic Wastes Poster Session   | 6 to 8 p.m. | <b>C</b> | Room 15B    |
| Chloride 2011 Poster Session  | 6 to 8 p.m. | <b>C</b> | Room 19     |
| Surfaces and Heterostructures at Nano or Micro Scale and Their Characterization, Properties and Applications Poster Session | 6 to 8 p.m. | <b>C</b> | Room 31B    |
| Approaches for Investigating Phase Transformations At the Atomic Scale Poster Session                                       | 6 to 8 p.m. | <b>C</b> | Room 32B    |
| Processing and Properties of Powder-Based Materials Poster Session  | 6 to 8 p.m. | <b>C</b> | Room 33A    |

#### COMMITTEE MEETINGS

|  |                      |          |                   |
|--|----------------------|----------|-------------------|
| Financial Planning Committee                     | 7 to 9 a.m.          | <b>M</b> | Leucadia          |
| Professional Registration Leadership Committee   | 8 to 10 a.m.         | <b>M</b> | Business Suite 3  |
| TMS Board of Directors Orientation               | 9 to 10 a.m.         | <b>M</b> | Point Loma        |
| TMS Board of Directors Meeting                   | 10 a.m. to 1:30 p.m. | <b>M</b> | Point Loma        |
| Recycling & Environmental Technologies Committee | noon to 1:30 p.m.    | <b>M</b> | Del Mar           |
| Young Leader Committee Business Meeting          | 12:30 to 2 p.m.      | <b>M</b> | Balboa            |
| Accreditation Committee                          | 12:30 to 2:30 p.m.   | <b>M</b> | Solana            |
| Magnesium Committee                              | 1:30 to 3:15 p.m.    | <b>M</b> | Rancho Las Palmas |
| Pyrometallurgy Committee                         | 1:30 to 3 p.m.       | <b>M</b> | Carlsbad          |

#### Programming Booth

The programming booth will be located in the Ballroom 6 Lobby on the Upper Level of the San Diego Convention Center. TMS staff will be available to answer programming questions or provide participation certificates.

## Schedule of Events

as of January 18, 2011

Key: **C** San Diego Convention Center

**M** San Diego Marriott Hotel & Marina

|   |                   |   |                   |
|---|-------------------|---|-------------------|
| Nominating Committee                            | 2 to 3 p.m.       | M | Boardroom         |
| Aluminum Committee                              | 3 to 4:30 p.m.    | M | Pacific           |
| Materials Characterization Committee            | 3 to 5 p.m.       | M | Del Mar           |
| Program Committee                               | 3 to 5 p.m.       | M | Oceanside         |
| ABET Training Session                           | 3 to 5 p.m.       | M | Cardiff           |
| Public & Governmental Affairs Committee         | 3:30 to 5 p.m.    | M | Boardroom         |
| ICME Committee                                  | 4 to 5:30 p.m.    | M | Rancho Las Palmas |
| Nanomaterials Committee                         | 4 to 5 p.m.       | M | Balboa            |
| Thin Films & Interfaces Committee               | 4 to 5 p.m.       | M | Carlsbad          |
| LMD Council Meeting                             | 4:30 to 6 p.m.    | M | Leucadia          |
| Global Innovations Committee                    | 5 to 5:45 p.m.    | M | Green Room        |
| Content Development and Dissemination Committee | 5 to 7 p.m.       | M | Newport Beach     |
| Nanomechanical Materials Behavior Committee     | 5:45 to 6:45 p.m. | M | Point Loma        |
| Mechanical Behavior of Materials Committee      | 7 to 8:30 p.m.    | M | Point Loma        |
| Alloy Phases Committee                          | 7:30 to 9:30 p.m. | M | Rancho Las Palmas |
| Phase Transformation Committee                  | 7:30 to 9:30 p.m. | M | Mission Hills     |

## Networking Receptions

Join your colleagues for some informal discussions at these networking events:

### Sunday

Symposia-related Welcome Receptions and Poster Sessions  
(All receptions are held at the San Diego Convention Center from 6 to 8 p.m.)

- 2011 Functional and Structural Nanomaterials: Fabrication, Properties, Applications & Implications ..... Room 8
- Light Metals: Alumina and Bauxite; Aluminum Reduction Technology; Electrode Technology for Aluminium Production ..... Room 17A
- Biological Materials Science ..... Room 15A
- Characterization of Minerals, Metals and Materials ..... Room 14B
- Computational Thermodynamics and Kinetics ..... Room 9
- Magnesium Technology 2011 ..... Room 6F
- Microstructural Processes in Irradiated Materials ..... Room 3
- Pb-Free Solders and Other Materials for Emerging Interconnect and Packaging Technologies ..... Room 7B
- Physical and Mechanical Metallurgy of Shape Memory Alloys for Actuator Applications ..... Room 11B
- Polycrystal Modelling with Experimental Integration: A Symposium Honoring Carlos Tomé ..... Room 6C

### Monday

- President's Welcoming Reception ..... 5 to 6:30 p.m. .... Exhibit Hall

### Tuesday

- Happy Hour Reception ..... 5 to 6 p.m. .... Exhibit Hall



# TMS 2011

## 140th Annual Meeting & Exhibition

### Schedule of Events

as of January 18, 2011

Key: **C** San Diego Convention Center      **M** San Diego Marriott Hotel & Marina

#### MONDAY, FEBRUARY 28

|                           |                   |          |                              |
|---------------------------|-------------------|----------|------------------------------|
| AUTHORS' COFFEE           | 7:30 to 8:30 a.m. | <b>C</b> | Upper Level, Sails Pavilion  |
| REGISTRATION              | 7 a.m. to 6 p.m.  | <b>C</b> | Exhibit Hall AB1             |
| TMS MEMBER WELCOME CENTER | 7 a.m. to 6 p.m.  | <b>C</b> | Ground Level, Outside Hall A |
| GENERAL POSTER SESSION    | noon to 6:30 p.m. | <b>C</b> | Exhibit Hall AB1             |

#### 2011 TMS EXHIBITION

|                                 |                   |          |                  |
|---------------------------------|-------------------|----------|------------------|
| Exhibit Hours                   | noon to 6:30 p.m. | <b>C</b> | Exhibit Hall AB1 |
| President's Welcoming Reception | 5 to 6:30 p.m.    | <b>C</b> | Exhibit Hall AB1 |

#### WORKSHOPS, SHORT COURSES, FORUMS & TUTORIALS

|   |                         |          |                  |
|---|-------------------------|----------|------------------|
| Lunch & Learn: TMS Annual Meeting of the Membership | 12:30 p.m. to 1:30 p.m. | <b>C</b> | Exhibit Hall AB1 |
|---|-------------------------|----------|------------------|

#### POSTER CONTESTS

|   |                |          |                  |
|---|----------------|----------|------------------|
| Technical Division Student Poster Contest And Biological Materials Science Poster Contest | 5 to 6:30 p.m. | <b>C</b> | Exhibit Hall AB1 |
|---|----------------|----------|------------------|

#### SOCIAL FUNCTIONS

|   |                |          |                   |
|---|----------------|----------|-------------------|
| Guest Hospitality                       | 7 to 10 a.m.   | <b>M</b> | Laguna            |
| Women in Science Breakfast              | 7 to 8 a.m.    | <b>M</b> | Marina Ballroom E |
| UBC Alumni Reception                    | 6 to 7:30 p.m. | <b>M</b> | Newport Beach     |
| Carlos Tome Honorary Symposium Dinner   | 6 to 9 p.m.    | <b>M</b> | Point Loma        |
| Hume-Rothery Symposium Dinner           | 6 to 9 p.m.    | <b>M</b> | Rancho Las Palmas |
| John T. Berry Honorary Symposium Dinner | 6 to 9 p.m.    | <b>M</b> | Torrance          |

#### **Visit the Volunteer Concierge Booth!**

Located on the Upper Level of the Convention Center (near the Sails Pavilion)

Learn how to get involved, grow professionally & personally, and give back to your industry through a myriad of TMS activities. Great opportunities include participating on a technical committee, authoring a paper, writing an article for *JOM*, and more!

**Stop by to find the right opportunity for you!**

# TMS

Your Professional Partner for Career Advancement.

## Schedule of Events

as of January 18, 2011

Key: **C** San Diego Convention Center

**M** San Diego Marriott Hotel & Marina

### COMMITTEE MEETINGS

|   |                   |   |                   |
|---|-------------------|---|-------------------|
| Met Trans "A" Board of Review   | 7 to 8 a.m.       | M | Oceanside         |
| Process Technology & Modeling Committee                                     | 7 to 8 a.m.       | M | Del Mar           |
| Pyrometallurgy Committee / Smelting Technology Symposium Organizing Meeting | 8 to 9:30 a.m.    | M | Solana            |
| Membership & Student Development Committee                                  | 8:30 to 9:45 a.m. | M | Pacific           |
| Graduate Student Advisory Council   | 9 to 10 a.m.      | M | Leucadia          |
| EPD Council Meeting   | noon to 2 p.m.    | M | Leucadia          |
| Superalloys 2012 Program Committee  | noon to 2 p.m.    | M | Carlsbad          |
| EMPMD Council Meeting   | 12:30 to 2 p.m.   | M | Solana            |
| Past Presidents' Meeting  | 2 to 3 p.m.       | M | President's Suite |
| Energy Conversion & Storage Committee                                       | 5 to 6 p.m.       | C | Room 12           |
| Superalloys 2012 Organizing Committee                                       | 5 to 7 p.m.       | M | Carlsbad          |
| Advanced Characterization, Testing & Simulation Committee                   | 5:30 to 6:30 p.m. | C | Room 17A          |
| Chemistry & Physics of Materials Committee                                  | 5:30 to 6:30 p.m. | C | Room 33A          |
| Nuclear Materials Committee   | 5:30 to 7 p.m.    | C | Room 32B          |
| Surface Engineering Committee   | 5:30 to 6:30 p.m. | C | Room 17B          |
| Composite Materials Committee   | 5:45 to 6:45 p.m. | C | Room 4            |
| Biomaterials Committee  | 6 to 7 p.m.       | C | Room 7B           |
| Solidification Committee  | 6 to 7 p.m.       | C | Room 16A          |
| Technical Division Council  | 6 to 8 p.m.       | M | Business Suite 3  |
| Materials & Society Committee   | 7 to 9 p.m.       | M | Pacific           |
| Computational Materials Science & Engineering Committee                     | 8 to 9 p.m.       | M | Del Mar           |
| Magnetic Materials Committee  | 8 to 9 p.m.       | M | Cardiff           |

MEETING INFORMATION

### MONDAY LUNCH & LEARN

#### **TMS Annual Meeting of the Membership**

**Time: 12:30 to 1:30 p.m.**

#### **Speakers:**

Garry Warren ..... 2011 TMS President  
George T. "Rusty" Gray III .. 2010 TMS President  
Warren Hunt, Jr. .... TMS Executive Director  
Stanley M. Howard..... TMS Board of Directors,  
Financial Planning Officer

**Lunch & Learn Area, Exhibit Hall  
San Diego Convention Center**

**Get engaged in your Society!** Attend this inaugural meeting to participate in discussions and learn about:

- Recent accomplishments of the society
- Recent and expected financial performance
- Preview of 2011 initiatives
- Strategic projects

# TMS 2011

## 140th Annual Meeting & Exhibition

### Schedule of Events

as of January 18, 2011

Key: **C** San Diego Convention Center

**M** San Diego Marriott Hotel & Marina

#### TUESDAY, MARCH 1

|                           |                      |   |                              |
|---------------------------|----------------------|---|------------------------------|
| AUTHORS' COFFEE           | 7:30 to 8:30 a.m.    | C | Upper Level, Sails Pavilion  |
| REGISTRATION              | 7 a.m. to 6 p.m.     | C | Exhibit Hall AB1             |
| TMS MEMBER WELCOME CENTER | 7 a.m. to 6 p.m.     | C | Ground Level, Outside Hall A |
| GENERAL POSTER SESSION    | 10:30 a.m. to 6 p.m. | C | Exhibit Hall AB1             |

#### 2011 TMS EXHIBITION

|                      |                      |   |                  |
|----------------------|----------------------|---|------------------|
| Exhibit Hours        | 10:30 a.m. to 6 p.m. | C | Exhibit Hall AB1 |
| Happy Hour Reception | 5 to 6 p.m.          | C | Exhibit Hall AB1 |

#### POSTER CONTESTS

|   |                      |   |                  |
|---|----------------------|---|------------------|
| Technical Division Student Poster Contest And Biological Materials Science Poster Contest | 10:30 a.m. to 6 p.m. | C | Exhibit Hall AB1 |
|---|----------------------|---|------------------|

#### STUDENT EVENTS

|  |                     |   |                  |
|--|---------------------|---|------------------|
| Technical Division Student Poster Contest Awards | 12:15 to 12:45 p.m. | C | Exhibit Hall AB1 |
| Student Career Forum                             | 3 to 5 p.m.         | C | Exhibit Hall AB1 |

#### WORKSHOPS, SHORT COURSES, FORUMS & TUTORIALS

|   |                |   |                   |
|---|----------------|---|-------------------|
| Young Leaders Tutorial Lecture/Luncheon | noon to 2 p.m. | M | Marina Ballroom E |
| Lunch & Learn: Energy with Cindy Belt   | noon to 2 p.m. | C | Exhibit Hall AB1  |

#### TMS-AIME ANNUAL AWARDS BANQUET

|                   |                   |   |                       |
|-------------------|-------------------|---|-----------------------|
| Reception         | 6:30 to 7:15 p.m. | M | Marina Ballroom Foyer |
| Dinner and Awards | 7:15 to 10 p.m.   | M | Marina Ballroom F&G   |

#### SOCIAL FUNCTIONS

|   |                  |   |               |
|---|------------------|---|---------------|
| Guest Hospitality                                 | 7 to 10 a.m.     | M | Laguna        |
| Acta Materialia, Inc. Board of Governors Luncheon | 8 a.m. to 5 p.m. | M | Warner Center |

#### TECHNICAL DIVISION LUNCHEON

|                   |                   |   |         |
|-------------------|-------------------|---|---------|
| EPD/MPMD Luncheon | noon to 2:15 p.m. | C | Room 6B |
|-------------------|-------------------|---|---------|



## Schedule of Events

as of January 18, 2011

Key: **C** San Diego Convention Center

**M** San Diego Marriott Hotel & Marina

| COMMITTEE MEETINGS   |                    |   |                   |
|--|--------------------|---|-------------------|
| Electronic Packaging & Interconnection Committee           | 7 to 8 a.m.        | M | Solana            |
| Met Trans "B" Board of Review                              | 7 to 8 a.m.        | M | Oceanside         |
| MPMD Council Meeting                                       | 7 to 9 a.m.        | M | Leucadia          |
| Fellows Award Committee                                    | 7:30 to 9 a.m.     | M | Rancho Las Palmas |
| Mathewson, Hume-Rothery & IOM/Mehl Awards Subcommittee     | 7:30 to 9 a.m.     | M | Rancho Las Palmas |
| Chalmers, Smith & Cohen Awards Subcommittee                | 7:30 to 9 a.m.     | M | Rancho Las Palmas |
| Leadership, Scott, Educator & Practice Awards Subcommittee | 7:30 to 9 a.m.     | M | Rancho Las Palmas |
| Acta Materialia, Inc. Board of Governors Meeting           | 8 a.m. to 5 p.m.   | M | Torrance          |
| Honors & Professional Recognition Award Committee          | 9 to 10 a.m.       | M | Rancho Las Palmas |
| TMS Executive Committee                                    | 11:00 a.m. to noon | M | President's Suite |
| SMD Council Meeting  | noon to 2 p.m.     | M | Solana            |
| Powder Materials Committee                                 | 12:30 to 2 p.m.    | C | Room 12           |
| MetSoc/TMS Leadership Meeting                              | 2:30 to 3:30 p.m.  | M | Presidents Suite  |
| Women in Materials Science & Engineering Committee         | 3 to 4:30 p.m.     | M | Point Loma        |
| IOMMMS Leadership Meeting                                  | 4 to 5 p.m.        | M | Leucadia          |
| Energy Committee   | 5 to 6 p.m.        | C | Room 16A          |
| High Temperature Alloys Committee                          | 5:30 to 7 p.m.     | M | Carlsbad          |
| Refractory Metals & Materials Committee                    | 5:30 to 6:30 p.m.  | M | Del Mar           |
| Shaping & Forming Committee                                | 6 to 8 p.m.        | M | Leucadia          |
| Titanium Committee   | 6 to 7 p.m.        | C | Room 17B          |
| Corrosion & Environmental Effects Committee                | 6:30 to 7:30 p.m.  | C | Room 11B          |

MEETING INFORMATION

### TUESDAY LUNCH & LEARN

#### **Energy Management: Things Your Mother Didn't Teach You**

**Time: Noon to 2 p.m.**

**Lunch & Learn Area, Exhibit Hall  
San Diego Convention Center**

#### **Speakers:**

Cindy Belt, consulting energy engineer, previously with Superior Industries and Aleris International

Brajendra Mishra, professor and associate director, Kroll Institute for Extractive Metallurgy and Advanced Coatings & Surface Engineering Laboratory, Colorado School of Mines

Steve Coppinger, director, energy services, CalPortland Company



# TMS 2011

## 140th Annual Meeting & Exhibition



### Schedule of Events

as of January 18, 2011

Key: **C** San Diego Convention Center      **M** San Diego Marriott Hotel & Marina

#### WEDNESDAY, MARCH 2

|                           |                         |   |                              |
|---------------------------|-------------------------|---|------------------------------|
| AUTHORS' COFFEE           | 7:30 to 8:30 a.m.       | C | Upper Level, Sails Pavilion  |
| REGISTRATION              | 7 a.m. to 5 p.m.        | C | Exhibit Hall AB1             |
| TMS MEMBER WELCOME CENTER | 7 a.m. to 5 p.m.        | C | Ground Level, Outside Hall A |
| GENERAL POSTER SESSION    | 10:30 a.m. to 2:30 p.m. | C | Exhibit Hall AB1             |

#### 2011 TMS EXHIBITION

|               |                      |   |                  |
|---------------|----------------------|---|------------------|
| Exhibit Hours | 10:30 a.m. to 3 p.m. | C | Exhibit Hall AB1 |
|---------------|----------------------|---|------------------|

#### TECHNICAL DIVISION LUNCHEON

|              |                   |   |         |
|--------------|-------------------|---|---------|
| LMD Luncheon | noon to 2:00 p.m. | C | Room 6B |
|--------------|-------------------|---|---------|

#### WORKSHOPS, SHORT COURSES, FORUMS & TUTORIALS

|  |                |   |                  |
|--|----------------|---|------------------|
| Lunch & Learn: Materials Cyberinfrastructure | noon to 2 p.m. | C | Exhibit Hall AB1 |
|--|----------------|---|------------------|

#### SOCIAL FUNCTIONS

|                   |              |   |        |
|-------------------|--------------|---|--------|
| Guest Hospitality | 7 to 10 a.m. | M | Laguna |
|-------------------|--------------|---|--------|

#### COMMITTEE MEETINGS

|  |                    |   |            |
|--|--------------------|---|------------|
| TMS Board of Directors Meeting             | 7:30 to 11:30 a.m. | M | Point Loma |
| TMS Advocacy Strategy Session              | noon to 4 p.m.     | M | Pacific    |
| PRICM-8 International Organizing Committee | 1 to 3 p.m.        | M | Solana     |
| Medalist, Hardy & ECFE Awards Subcommittee | 3:30 to 5:00 p.m.  | M | Oceanside  |
| Aluminum Processing Committee              | 6:30 to 8 p.m.     | M | Leucadia   |

MEETING INFORMATION

### WEDNESDAY LUNCH & LEARN

#### Materials Cyberinfrastructure

**Time: Noon to 1:50 PM**

**Lunch & Learn Area, Exhibit Hall  
San Diego Convention Center**

#### Speakers:

John Allison, *University of Michigan*..... Noon

The following speakers will provide live demonstrations of computer platforms:

Paul Mason, *ThermoCalc, Inc., Thermocalc*..... 12:30 p.m.

Andy Geltmacher, *Naval Research Laboratory, 3D Materials Atlas* ..... 1:10 p.m.

Alejandro Strachan, *Purdue University, NanoHub*..... 1:30 p.m.

Laura Bartolo, *Kent State University, MatDL/MatForge*..... 1:50 p.m.

## Schedule of Events

as of January 18, 2011

Key: **C** San Diego Convention Center

**M** San Diego Marriott Hotel & Marina

### THURSDAY, MARCH 3

|                           |                     |          |                              |
|---------------------------|---------------------|----------|------------------------------|
| AUTHORS' COFFEE           | 7:30 to 8:30 a.m.   | <b>C</b> | Upper Level, Sails Pavilion  |
| REGISTRATION              | 7 a.m. to 2:30 p.m. | <b>C</b> | Exhibit Hall AB1             |
| TMS MEMBER WELCOME CENTER | 7 a.m. to 2:30 p.m. | <b>C</b> | Ground Level, Outside Hall A |

### WORKSHOPS, SHORT COURSES, FORUMS & TUTORIALS

|   |                  |          |             |
|---|------------------|----------|-------------|
| Workshop on the Development of a Reference Self-Diffusion Mobility Database for the Pure Elements | 9 a.m. to 3 p.m. | <b>C</b> | Ballroom 6B |
|---|------------------|----------|-------------|

### SOCIAL FUNCTIONS

|                   |              |          |        |
|-------------------|--------------|----------|--------|
| Guest Hospitality | 7 to 10 a.m. | <b>M</b> | Lagana |
|-------------------|--------------|----------|--------|

### TECHNICAL DIVISION LECTURE

|  |                   |          |          |
|--|-------------------|----------|----------|
| Extraction & Processing Division Distinguished Lecture | 8:30 to 9:10 a.m. | <b>C</b> | Room 16A |
|--|-------------------|----------|----------|

### COMMITTEE MEETINGS

|   |                   |          |          |
|---|-------------------|----------|----------|
| Hydrometallurgy & Electrometallurgy Committee | 4:45 to 6:15 p.m. | <b>C</b> | Room 16A |
|---|-------------------|----------|----------|

## TMS 2011 Fun Facts

|                 |  |
|-----------------|--|
| <b>4</b>        | Full Days of Technical Programming                           |
| <b>4</b>        | The Total Number of Gaslamps in San Diego's Gaslamp District |
| <b>7</b>        | Technical Themes   |
| <b>12</b>       | Welcoming Receptions   |
| <b>25</b>       | Years Since the First TMS Exhibition                         |
| <b>54</b>       | Number of U.S. Navy Ships Docked in San Diego Harbor         |
| <b>Over 68</b>  | Countries Represented  |
| <b>70</b>       | In Degrees Fahrenheit, the Average Temperature in San Diego  |
| <b>Over 70</b>  | Unique Symposia  |
| <b>Over 700</b> | Formal lectures, keynotes, invited and plenary talks         |
| <b>450</b>      | Posters  |
| <b>3,397</b>    | Presentations  |
| <b>4,000</b>    | Population of 'Residents' at the San Diego Zoo               |



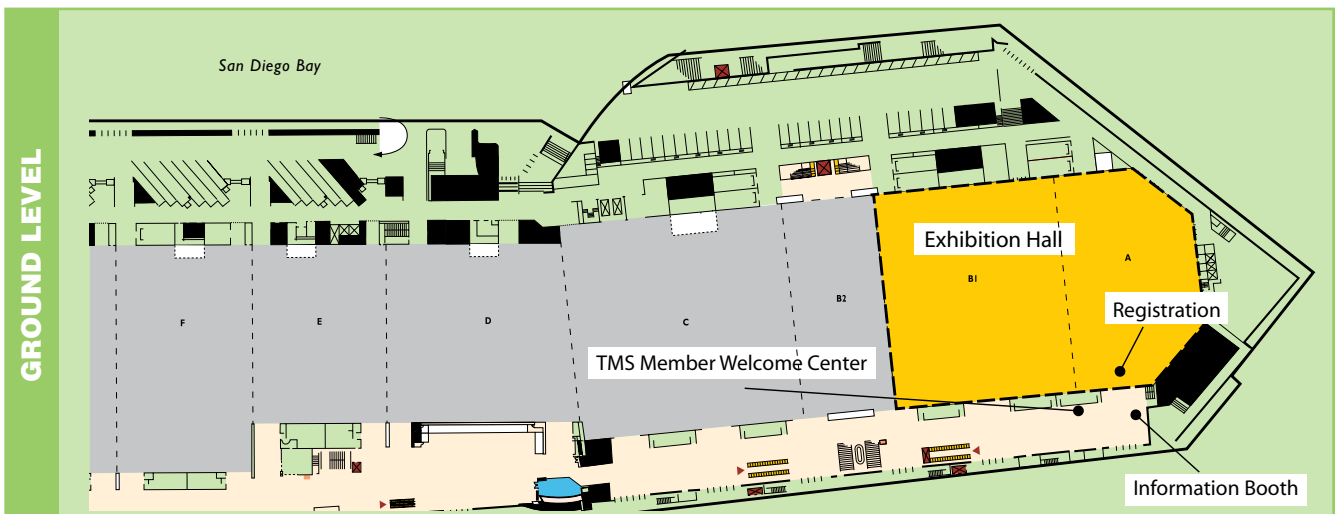
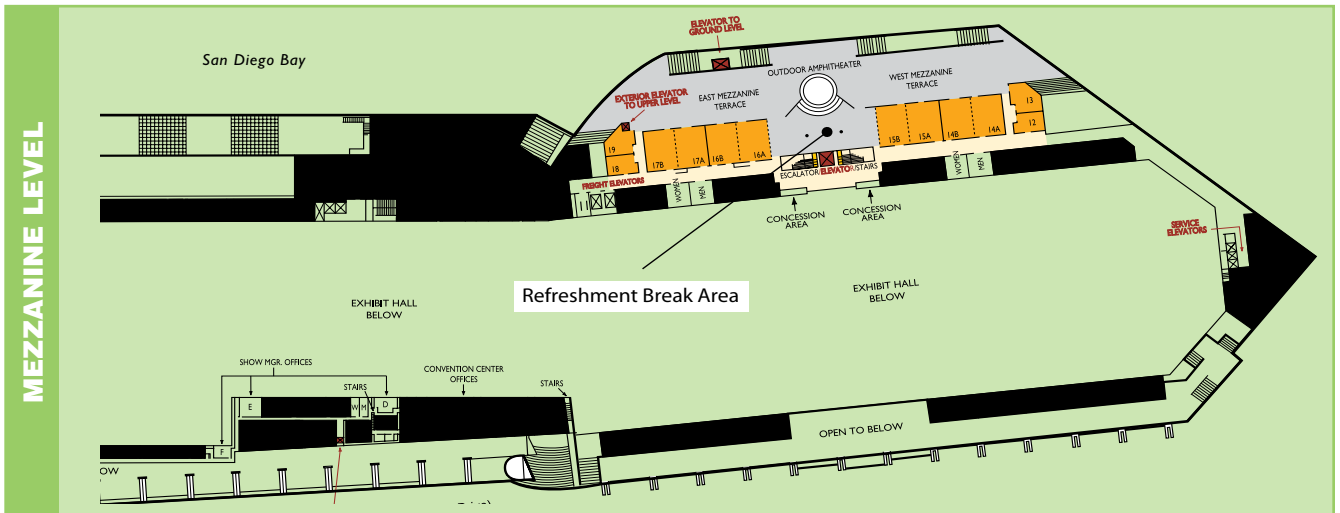
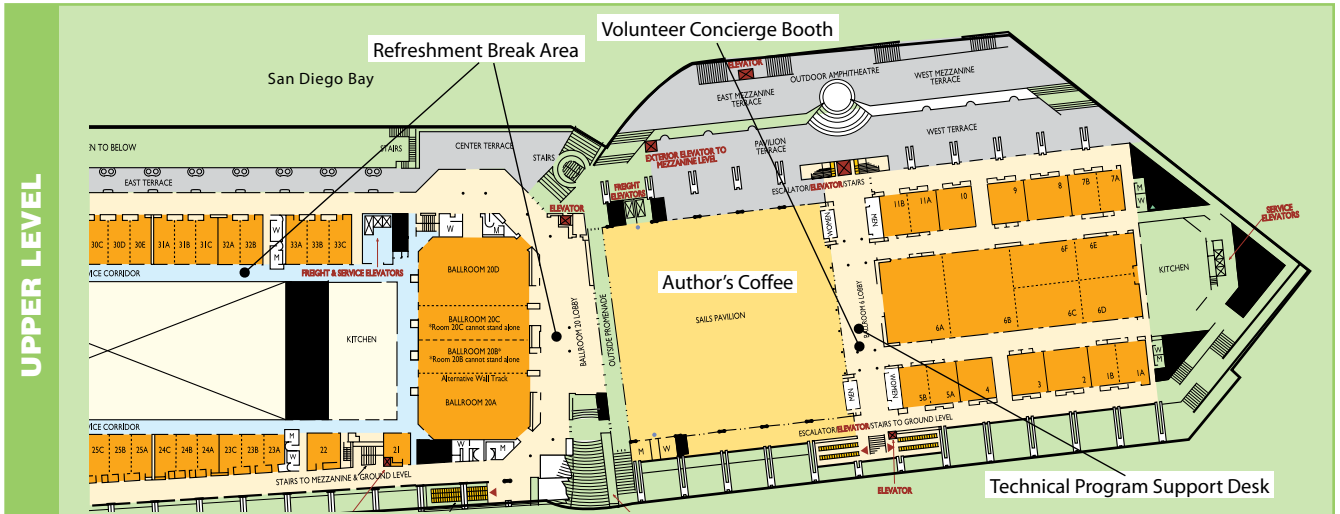


# TMS 2011

140th Annual Meeting & Exhibition

## San Diego Convention Center Maps

MEETING INFORMATION



# San Diego Marriot Hotel & Marina Maps

## SOUTH TOWER LEVEL 1



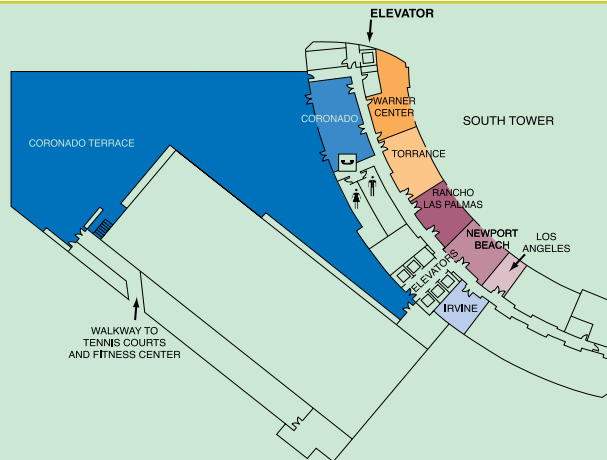
## SOUTH TOWER LEVEL 3

- MARINA BALLROOM
- BOARD ROOM
- GREEN ROOM
- MISSION HILLS
- BALBOA
- CARDIFF
- CARLSBAD
- DEL MAR
- ENCINITAS
- BUSINESS SUITES 1, 2 & 3



## SOUTH TOWER LEVEL 4

- CORONADO TERRACE
- CORONADO
- IRVINE
- WARNER CENTER
- TORRANCE
- RANCHO LAS PALMAS
- NEWPORT BEACH
- LOS ANGELES



## MEETING INFORMATION

## Lectures & Luncheons

### Young Leaders Tutorial Luncheon Lecture

*"Integrative Materials-Process-Component Design: A Prospective View"*

**Tuesday • Noon • Marriott, Marina Ballroom E**



Speaker: **Diana Lados**,  
Assistant Professor, Worcester  
Polytechnic Institute, USA

About the Topic: The challenges in modern materials process component design revolve around the successful integration of several important and sometimes competing concepts such as high performance & reliability, societal impact, and economics. This generates a fertile future of opportunities for the clever materials engineer to develop a holistic approach based on a fundamental understanding in tandem with suitable and sustainable application driven design and manufacturing strategies. These ideas will be systematically reviewed and discussed in the context of needs and developments, and exciting materials research opportunities will be presented.

### Light Metals Division Luncheon Lecture

*"The Intersection of Materials, Design and Manufacturing with Lightweight Materials"*

**Wednesday • Noon**  
**Convention Center, Room 6B**



Speaker: **Anil K. Sachdev**,  
Inventor, General Motors Global  
Research & Development Center,  
USA

About the Topic: There is an increasing need for lightweight materials in automotive applications due to their large impact on fuel economy, emissions, and performance. This need also extends to other industries like aerospace and consumer electronics. Sachdev will describe opportunities for lightweight materials from a perspective that includes their properties, product design, and manufacturing, all aimed at driving the total sub-system cost to minimize cost penalty for their pervasive use. Sachdev will also discuss the many challenges that need to be addressed, including improved computational methods to develop higher performance materials including corrosion mitigation; robust materials processing that provides properties with narrow distributions; and manufacturing methods that can produce the designs optimized for minimum mass.

### Extraction & Processing/ Materials Processing & Manufacturing Joint Division Luncheon

*"Advances in Sulfide Smelting-A Practical Overview"*

**Tuesday • Noon**  
**Convention Center, Room 6B**



Speaker: **David George**,  
Principal Advisor of Processing,  
Technology and Innovation,  
Rio Tinto, USA

About the Topic: Over the last 40 years, environmental and cost pressures fostered technology advances that have redefined the copper smelting industry. In the United States, Japan and Europe, the small, primitive and polluting mine site-based smelters have nearly all been shut down. Clean, high capacity, and energy efficient smelting technology is now the standard for new smelters and this technology is rapidly being adopted in China. A review of the last 40 years of technology advances may give some hints about the opportunities for improvement in the coming decades.

### Extraction & Processing Division Distinguished Lecture

*"The Removal of Arsenic, Selenium and Metals from Aqueous Solution by Iron Precipitation and Reduction Techniques"*

**Thursday • 8:30 a.m.**  
**Convention Center, Room 16A**



Speaker: **Larry Twidwell**,  
Professor Emeritus, Montana Tech  
of the University of Montana, USA

About the Topic: The removal of arsenic, selenium, and metal species from hydrometallurgical solutions and waste water continues to be an important research topic. This presentation includes a discussion of the research conducted at Montana Tech of the University of Montana over the past 20 years along with current literature studies. The discussion will focus on removal of arsenic by co-precipitation with Fe(III) and Fe(II), co-precipitation with Fe(III) and Al(III), reduction using elemental iron; the removal of selenium by elemental iron and catalysed iron; and the removal of cadmium, copper, nickel, zinc by co-precipitation with Fe(III) and Al(III).



## Award-Winning Speakers

### William Hume-Rothery Award Lecture

*"Thermodynamics and Diffusion Coupling in Alloys - Application Driven Science"*

**Monday • 8:40 to 9:20 a.m.**  
**Convention Center, Room 31A**



Speaker: **John Agren**,  
*Professor, Royal Institute of Technology, Sweden*

About the Topic: As emphasized by Stokes in 1997, the common assumption of a linear progression from basic research (science) via applied research, to technological innovations (engineering),

should be questioned. This presentation will address some of them, as well as the effect of various ordering phenomena on activation barriers, the strength and practical importance of correlation effects, etc.

### Institute of Metals/Robert Franklin Mehl Lecture

*"The Ubiquitous Interfacial Free Energy in Phase Transformations"*

**Monday • 10:15 a.m.**  
**Convention Center, Room 32B**



Speaker: **David Seidman**,  
*Walter P. Murphy Professor of Materials Science & Engineering, Northwestern University, USA*

About the Topic: In this talk, the focus is on the diverse roles played by interfacial free energy in phase transformations in multi-component metallic alloys, which are studied experimentally by atom-probe tomography and transmission electron microscopy. The results of simulations employing lattice kinetic Monte Carlo, where the phase transformation is mediated by a vacancy mechanism, will be presented and compared in detail with experimental observations. First-principles calculations of interfacial energies in the same metallic alloys will be discussed in terms of their relevance to the aforementioned.

### SPOTLIGHT EVENT

#### Technical Division Student Poster Contest Awards

**Tuesday 12:15 to 12:45 p.m.**  
 Exhibit Hall, San Diego Convention Center

### Vittorio de Nora Prize Lecture

*"Recycling of Contaminated Aluminum Scrap"*

**Wednesday • 2:05 p.m.**  
**Convention Center, Room 12**



Speaker: **Anne Kvithyld**,  
*SINTEF, Norway*

Kvithyld holds a doctorate in aluminum recycling and has worked extensively with the decoating of aluminum and other light metals. She is a member of the society's Recycling and Environmental Technologies Committee, and recently organized an aluminum recycling workshop. Through her dedication to aluminum recycling, she has emerged as a respected leader in the light metals professional community.

The Vittorio de Nora Prize was established last year by the TMS Foundation to honor its namesake, who was both a pioneer in the materials processing field and one of the great Italian technologists of the 20th century. Kvithyld will receive a \$20,000 cash prize as the recipient of this prestigious award.

About the Topic: Recycling is important in the aluminum industry. Removal of contaminants such as the coat and organic materials—applied for protection and appearance—are the tail that wags the recycling dog. Successful removal of contaminants from scrap would ensure that more aluminum be recycled, minimize losses and prevent downgrading of the resource.

### JIM International Scholar Award Winners

*"Fracture Mechanism and Toughness in Fine- and Coarse-Grained Magnesium Alloys"*

**Monday • 12:10 to 12:30 p.m.**  
**Convention Center, Room 6F**

*(During the Magnesium Technology 2011 Opening Session)*

Speaker: **Hidetoshi Somekawa**,  
*National Institute for Materials Science*

*"Crack Tip Dislocations and the Sequential Multiplication Process of Dislocation Sources along the Crack Front Revealed by HVEM-Tomography"*

**Wednesday • 10 to 10:30 a.m.**  
**Convention Center, Room 32 A**

*(During the David Pope Honorary Symposium)*

Speaker: **Masaki Tanaka**, *Kyushu University*

# 140th TMS and AIME Dinner, Awards Presentation, and Installation of the 2011 President

## Garry Warren, 2011 TMS President

### About 2011 TMS President Garry Warren



Garry Warren is a professor in the Department of Metallurgical and Materials Engineering at the University of Alabama, Tuscaloosa. He joined the university in 1986 after spending

eight years as a faculty member at Carnegie Mellon University in Pittsburgh, Pennsylvania. Warren received both a B.S. and M.S. in metallurgical engineering from the University of Texas – El Paso and his Ph.D. in metallurgy from the University of Utah.

He has also served in various capacities within the Extraction & Processing Division (EPD), chairing the following committees: Programming, Continuing Education, and Publications, which included editorship of the EPD Congress proceedings for 1994–1996. He is also on the editorial review board for Metallurgical Transactions B, and was the faculty advisor for the University of Alabama Material Advantage Student Chapter. The chapter was named a “Chapter of Excellence” for four consecutive years 1994–1997, and again in 2000.

Warren’s research efforts have focused on the electrochemistry and leaching behavior of various sulfide minerals, corrosion behavior of NdFeB permanent magnets, degradation of metal particle recording media, use of electrochemical techniques to evaluate the protective ability of polymers and polymer coatings, and the corrosion of Ti-Al intermetallics.

The TMS-AIME Awards Banquet will be held **Tuesday, March 1, at 7 p.m.** at the **San Diego Marriott Hotel & Marina in Marina Ballrooms F&G**. The event will begin with a reception from 6:30 to 7:15 p.m., followed by dinner and the awards presentation through 10 p.m. After the awards ceremony, 2010 President George T. “Rusty” Gray III will present the annual address to the society. Gray will then introduce 2011 TMS President Garry Warren.

## Society Awards

### Presented by George T. “Rusty” Gray III



George T. “Rusty” Gray III Gray, the 2010 TMS President, is a laboratory fellow at Los Alamos National Laboratory in Los Alamos, New Mexico. He is a member of the TMS Titanium and Mechanical Metallurgy committees and has served as the Structural Materials Division representative to the TMS Program Committee.

### TMS Fellows Class of 2011

- David Bourell *University of Texas, USA*
- Kazuhiro Hono *National Institute for Materials Science, Japan*
- Marc A. Meyers *University of California – La Jolla, USA*
- Anthony Rollett *Carnegie Mellon University, USA*
- Steven Zinkle *Oak Ridge National Laboratory, USA*

- Application to Practice Award *Brian Thomas, University of Illinois, USA*
- Bruce Chalmers Award *Peter Voorhees, Northwestern University, USA*
- Champion H. Mathewson Award *Christopher Szczepanski, University Technology Corp / AFRL, USA*  
*Sushant K. Jha, Universal Technology Corp., USA*  
*James M. Larsen, U.S. Air Force, USA*  
*J. Wayne Jones, University of Michigan, USA*
- Early Career Faculty Fellow Award *Diana Lados, Worcester Polytechnic Institute, USA*
- Educator Award *Krishan Chawla, University of Alabama, USA*
- Institute of Metals/Robert Franklin Mehl Award *David Seidman, Northwestern University, USA*
- John Bardeen Award *Stephen Pearton, University of Florida, USA*
- Leadership Award *Y. Austin Chang, University of Wisconsin, USA*
- Robert Lansing Hardy Award *Shriram Ramanathan, Harvard University, USA*
- William Hume-Rothery Award *John Agren, Royal Institute of Technology, Sweden*
- Shri Ram Arora Award *Vivek Verma, Indian Institute of Technology, India*
- Vittorio de Nora Prize for Environmental Improvements in Metallurgical Industries *Anne Kvithyld, SINTEF, Norway*

## AIME Awards



### Presented by Brajendra Mishra

Brajendra Mishra is president-elect designate of The American Institute of Mining, Metallurgical, and Petroleum Engineers. A member of TMS since 1992, Mishra served as president in 2006. He is a professor of metallurgical and materials engineering and the associate director of the Kroll Institute for Extractive Metallurgy and the Advanced Coatings and Surface Engineering Laboratory, Colorado School of Mines. He is also the associate director of the National Science Foundation Industry-University Cooperative Research Center for Resource, Recovery and Recycling.

**AIME Distinguished Service Award** Dan Thoma, *Los Alamos National Laboratory, USA*  
**AIME Rossiter W. Raymond Memorial Award** Markus Buehler, *Massachusetts Institute of Technology, USA*

## TMS Division Awards

These awards are presented at special technical division events.

### Electronic, Magnetic & Photonic Materials Division

#### Distinguished Scientist/Engineer Award

Long-Qing Chen, *Pennsylvania State University, USA*

#### Distinguished Service Award

Sinn-wen Chen, *National Tsing Hua University, Taiwan*

#### EMPMD/JEM Best Paper

Christopher Kinney, *University of California – Berkeley, USA*

### Extraction & Processing Division

#### Distinguished Lecturer Award

Larry Twidwell, *Montana Tech of the University of Montana, USA*

#### Distinguished Service Award

William Imrie, *Bechtel Mining & Metals, Australia*

#### Science Award

Dimitrios Filippou  
Guillaume Hudon  
*Rio Tinto Iron & Titanium, Canada*

#### Technology Award

Min Zhou  
Aidong Wan  
Guang Li  
*Jinchuan Non-Ferrous Metals Corporation, China*  
Ross Baldock, *Outotec, Australia*  
Harry Li, *Ausmelt, Australia*

### Light Metals Division

#### Distinguished Service Award

Halvor Kvande, *Hydro Aluminium AS, Norway*

#### Technology Award

Adam Gesing, *Gesing Consultants Inc, Canada*

#### Light Metals Award

Bodil Monsen  
Arne Petter Ratvik  
*SINTEF Materials and Chemistry, Norway*  
Lorentz Petter Lossius, *Hydro Aluminium – PMT, Norway*

#### Aluminum Reduction Technology Award

Tian Yingfu, *Chongqing Tiantai Aluminum Industry Co. Ltd, China*  
Feng Naixiang  
Peng Jianping  
Wang Yaowu  
Qi Xiquan  
Tu Ganfeng  
*Northeastern University, China*

#### Bauxite & Alumina Award

Joanne Loh  
Greta Bodie  
Fatima Naim  
*CSIRO Light Metals Flagship (CSIRO Minerals), Australia*

#### Warren Peterson Cast Shop for Aluminum Production Award

Don Doutre, *Novelis Global Technology Center, Canada*

#### Energy Best Paper –

**Professional Award**  
James E. Miller, *Sandia National Laboratories, USA*

#### JOM Best Paper Award

Subodh K. Das  
*Phinix, LLC*  
John A.S. Green  
*JASG Consulting USA*

#### Magnesium Best Paper – Application Award

John Grandfield, *Grandfield Technology Pty Ltd, Australia*

Mark Turski  
Tim Wilks  
*Magnesium Elektron, UK*  
Bruce Davis  
Rick DeLorme  
*Magnesium Elektron North America, USA*  
Kyu Cho, *U.S. Army Research Laboratory, USA*

#### Magnesium Best Paper – Fundamental Research Award

Young B. Chun  
Christopher Davies  
*Monash University, Australia*

#### Magnesium Best Paper – Student Award

Jin-kyu Lee  
Shae K. Kim  
*Korea Institute of Industrial Technology, Korea*

### Material Processing & Manufacturing Division

#### Distinguished Scientist/Engineer Award

Amit Misra, *Los Alamos National Laboratory, USA*

### Structural Materials Division

#### Distinguished Scientist/Engineer Award

Tresa Pollock, *University of California Santa Barbara, USA*

#### Distinguished Service Award

Tresa Pollock, *University of California Santa Barbara, USA*

#### JOM Best Paper Award

Rebecca A. MacKay  
Timothy P. Gabb  
James L. Smialek  
Michael V. Nathal  
*NASA Glenn Research Center, USA*



## Student Activities

TMS 2011 features a number of events designed to captivate and educate young materials science minds. Registered student attendees are invited to:

### Sunday

#### 2011 Materials Bowl

(Sponsored by Alcoa)



Elimination Rounds Noon to 3 p.m.  
Championship Round 8:30 p.m.  
Marriott, Marina Ballroom G

#### Student Networking Mixer

(GE Global Research sponsor)



imagination at work

9 to 11 p.m. • Marriott, Marina Ballroom E&F

The TMS Graduate Student Advisory Council (GSAC) invites TMS members to attend the student mixer. The student mixer has a welcoming atmosphere that is ideal for informally meeting new people and engaging in casual conversations.

### Monday

#### Poster Contest

5 to 6:30 p.m. • Exhibit Hall

Undergraduate and graduate students will vie for cash prizes at the annual TMS Technical Division Student Poster Contest sponsored by the five technical divisions of TMS – Electronic, Magnetic & Photonic Materials; Extraction & Processing; Light Metals; Materials Processing & Manufacturing, and Structural Materials. Participants in this dynamic and interactive event compete for a \$500 prize in each division for the best undergraduate and best graduate poster. A top prize of \$500 will be awarded for the “Best of Show” poster in undergraduate and graduate.

### Tuesday

#### Graduate Student Advisory Council

9 to 10 a.m. • Marriott, Leucadia Room

All graduate students are invited to attend the Graduate Student Advisory Council meeting. The council focuses on meeting the unique needs of graduate students within the Material Advantage program and offers graduate students a forum to share their ideas and concerns. Because the meeting is scheduled between sessions, you can participate in the advisory council without missing a technical presentation.

#### Poster Contest Judging, Best of Show

Exhibit Hall  
12:15 p.m.

#### Student Career Forum

3 to 5 p.m. • Exhibit Hall AB1

Organized by the TMS Young Leader Committee, this session will feature a panel of speakers from a variety of materials science backgrounds and career stages who discuss how to navigate a career path to ultimate goals.

#### Early Career Panel

Brad Boyce, *Sandia National Laboratories, USA*  
Eric Brown, *Los Alamos National Laboratory, USA*  
Amy Clark, *Los Alamos National Laboratory, USA*  
Rachel DeLucas, *H.C. Starck, USA*  
Paul Edwards, *Boeing Research and Technology, USA*  
Julia Greer, *California Institute of Technology, USA*  
Subu Nayak, *Science Tomorrow, LLC, USA*  
Greg Thompson, *University of Alabama, USA*  
Dallas Trinkle, *University of Illinois Urbana-Champaign, USA*  
Ben Poquette, *GE Healthcare, USA*

#### A Note to Student Monitors:

Report to the Programming Desk at 7:15 a.m. each day you are scheduled to monitor session(s) to receive your assignments. There will be a training session each day at 7:50 a.m. After receiving your assignments, you should go to authors' coffee to meet with your session chair(s).



# The Valuable Resource that Keeps on Giving...

## TMS 2011 Annual Meeting Proceedings

The following proceedings volumes are available from the TMS 2011 Annual Meeting:

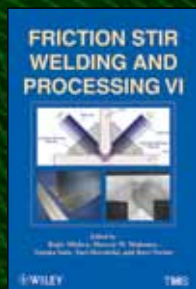
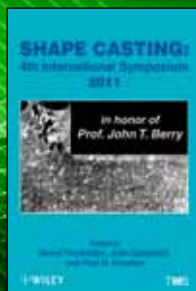
- 2nd International Symposium on High-Temperature Metallurgical Processing
- Energy Technology 2011: Carbon Dioxide and Other Greenhouse Gas Reduction Metallurgy and Waste Heat Recovery
- EPD Congress 2011
- Friction Stir Welding and Processing VI
- Light Metals 2011
- Magnesium Technology 2011
- Recycling of Electronic Waste II, Proceedings of the Second Symposium
- Sensors, Sampling and Simulation for Process Control
- Shape Casting: Fourth International Symposium 2011
- Supplemental Proceedings: Volume 1: Materials Processing and Energy Materials
- Supplemental Proceedings: Volume 2: Materials Fabrication, Properties, Characterization, and Modeling
- Supplemental Proceedings: Volume 3: General Paper Selections

Attendees may purchase books at the Wiley Bookstore, located in the ground level lobby of the San Diego Convention Center. After the conference, orders can be placed at [www.wiley.com](http://www.wiley.com).

### Collected Proceedings CD-ROM

A collected proceedings CD-ROM containing select TMS 2011 presentations is available free of charge for all full conference registrants including TMS members, senior members, recent graduates, nonmember authors, nonmembers and exhibitors. This valuable resource offers endless use for future research and educational purposes.

Additional copies of the Collected Proceedings CD-ROM may be purchased on the Registration Form and will not be available after the meeting. The cost is \$150, with a special student rate of \$75 plus 8.25% California sales tax. All CD-ROMS must be picked up at the meeting. Shipping is not available.



## TMS 2010-2011 Leadership Executive Committee

### President:

George T. "Rusty" Gray III,  
Los Alamos National Laboratory, USA

### Past President:

Ray D. Peterson,  
Aleris International Inc., USA

### Vice President:

Garry Warren,  
University of Alabama – Tuscaloosa, USA  
Wolfgang Schneider,  
Hydro Aluminum GMBH (incoming), Norway

### Financial Planning Officer:

Stanley Howard,  
South Dakota School of Mines and Technology, USA

## FUNCTIONAL AREA DIRECTORS

### Professional Development

David Shifler, Office of Naval Research, USA

### Membership and Student Development

Ellen K. Cerreta, Los Alamos National Laboratory, USA

### Programming

Hani Henein, University of Alberta, Canada

### Information Technology

Nikhilesh Chawla, Arizona State University, USA  
Jud Ready, Georgia Institute of Technology, USA  
(incoming)

### Public and Governmental Affairs

Kevin J. Hemker, Johns Hopkins University, USA

### Publications

Elizabeth Holm, Sandia National Laboratories, USA  
Carl Cady, Los Alamos National Laboratory, USA  
(incoming)

## TECHNICAL DIVISION DIRECTORS

### Electronic, Magnetic & Photonic Materials

Zi-Kui Liu, The Pennsylvania State University, USA  
Srinivas Chada, Henkel of America (incoming), USA

### Extraction & Processing

Thomas P. Battle, Midrex Technologies, USA  
Adrian C. Deneys, Praxair, Inc, USA (incoming)

### Light Metals

John N. Hryn, Argonne National Laboratory, USA

### Materials Processing & Manufacturing

James W. Sears, South Dakota School of Mines & Technology, USA

### Structural Materials

Dennis M. Dimiduk, U.S. Air Force Research Laboratory

## TMS 2010 ANNUAL MEETING TECHNICAL PROGRAM COMMITTEE

### Director/Chairperson:

Hani Henein, University of Alberta, Canada  
Electronic, Magnetic & Photonic Materials Division

### Electronic, Magnetic & Photonic Materials Division Representatives:

Long Qing Chen, The Pennsylvania State University, USA  
Sung K. Kang, IBM, USA  
Mark A. Palmer, Kettering University, USA

### Extraction & Processing Division Representatives:

Boyd R. Davis, Kingston Process Metallurgy, Canada  
Jian Li, Natural Resources Canada

### Light Metals Division Representatives:

Alan A. Luo, General Motors Corp., USA  
Eric A. Nyberg, Pacific Northwest National Laboratory, USA

### Materials Processing & Manufacturing Division Representatives:

Corbett C. Battaile, Sandia National Laboratories, USA  
Thomas R. Bieler, Michigan State University, USA  
Amit Misra, Los Alamos National Laboratory, USA

### Structural Materials Division Representatives:

Robert J. Hanrahan, Jr., National Nuclear Security Administration, USA  
Eric Allen Ott, GE Aviation, USA  
Judy Schneider, Mississippi State University, USA



25th Exhibition Anniversary



# TMS 2011

## 25th EXHIBITION

February 27 - March 3, 2011 • San Diego Convention Center  
San Diego, California USA

### **Exhibit Hours**

Monday, February 28 ..... Noon to 6:30 p.m.  
Tuesday, March 1 ..... 10:30 a.m. to 6 p.m.  
Wednesday, March 2 ..... 10:30 a.m. to 3 p.m.

### **Table of Contents**

Exhibiting Companies ..... 22  
Exhibit Floor Plan ..... 23  
Products & Services Index ..... 24  
Company Descriptions ..... 25  
Sponsors ..... Inside Front Cover

# TMS2011

## 140th Annual Meeting & Exhibition

### Exhibiting Companies

(as of January 18, 2011)

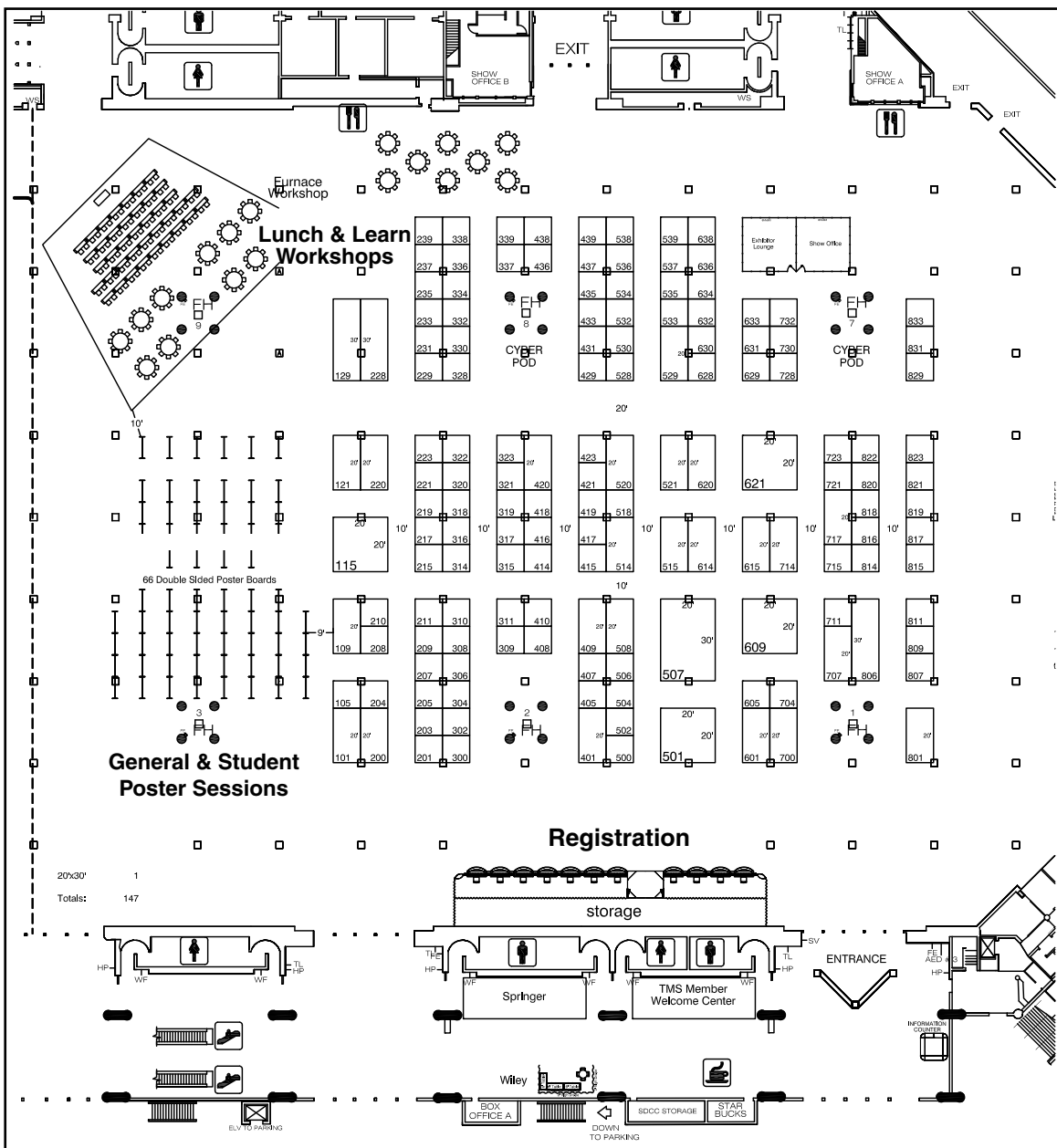
| Company   | Booth number | Company  | Booth number |
|---|--------------|--|--------------|
| ABB Bomem   | 700          | Hertwich Engineering                             | 506          |
| Advanced Dynamics   | 807          | Hysitron   | 614          |
| Agilent   | 420          | Innovatherm                                      | 429          |
| Almeq Norway AS   | 515          | IPI (Initiatives et Projets Industriels)         | 817          |
| Almex USA   | 321          | Jervis B. Webb Company                           | 508          |
| Alstom  | 529          | John Wiley & Sons, Inc.                          | Lobby        |
| Aluminium International Journal                           | 308          | Kempe Engineering                                | 514          |
| Aluminium International Today                             | 721          | L.P. Royer, Inc.                                 | 414          |
| Aluminium Network   | 304          | Light Metal Age                                  | 417          |
| Aluminum Times  | 518          | Major  | 811          |
| ATR National Scientific User Facility                     | 405          | Maney Publishing                                 | 304          |
| AUMUMD Holding BV   | 504          | Metal 7  | 306          |
| B&P Process Equipment                                     | 801          | Metallurgy and Materials Society of CIM (MetSoc) | 723          |
| Beijing General Research Institute of Mining & Metallurgy | 728          | Micro Materials                                  | 818          |
| Big C   | 823          | Microtrac  | 630          |
| Bloom Engineering   | 821          | Momentum Press                                   | 416          |
| Boreal Laser  | 629          | MTI Corporation                                  | 528          |
| BUSS ChemTech   | 520          | MTS Systems, Inc.                                | 819          |
| C A Picard Intl   | 221          | NFC  | 521          |
| CANMET Natural Resources Canada                           | 711          | NIST   | 322          |
| Center for Advanced Energy Studies                        | 336          | NIST Technology Innovation Program               | 320          |
| Chongqing Runji Alloy Co., Ltd                            | 809          | NKM Noell Special Cranes GmbH                    | 707          |
| CIMM Group  | 815          | Olympus Innov - X                                | 201          |
| Claudius Peters Projects GmbH                             | 419          | Opsis  | 715          |
| Colt  | 302          | Outotec  | 507          |
| Computherm  | 309          | Parker Hannifin                                  | 409          |
| Conductix-Wampfler  | 204          | Proto Manufacturing Inc.                         | 215          |
| CSM Instruments   | 310          | RHI AG   | 816          |
| Cytec Industries Inc                                      | 620          | Riedhammer GmbH                                  | 605          |
| Dantherm Filtration                                       | 314          | Rio Tinto Alcan                                  | 501          |
| Dubai Aluminium   | 717          | Romidot LTD                                      | 401          |
| EBSD Analytical   | 217          | Sente Software                                   | 810          |
| ECE Fast  | 219          | Shanghai Electric Import & Export                | 210          |
| ECL   | 500          | Shanghai Zhengyu Special Alloys Co., Ltd         | 829          |
| EDAX  | 223          | SIMULIA  | 408          |
| Eirich Machines, Inc.                                     | 315          | SLM Co., LTD                                     | 229          |
| Energoprom  | 530          | Sohar Aluminum                                   | 211          |
| Evans Analytical Group                                    | 311          | Springer Science + Business Media                | Lobby        |
| Fives Solios  | 609          | STAS   | 601          |
| FLSmidth Minerals   | 714          | Stratonics Inc & Optomec Inc                     | 407          |
| Friggi  | 316          | Sunstone   | 822          |
| Gautschi Engineering GmbH                                 | 317          | Techmo Car S.p.A                                 | 502          |
| Gillespie & Powers, Inc.                                  | 806          | Thermo Scientific                                | 423          |
| GLAMA   | 615          | Thermo Scientific Niton Analyzers                | 421          |
| Gouda Refractories  | 415          | Thermo-Calc Software, Inc.                       | 814          |
| Hebei Sitong  | 109          | UES, Inc.  | 628          |
| Hencon  | 300          | Viek Thermal Textiles Coating Industrial         | 328          |
| Hereaus   | 621          | Xiamen C&D                                       | 208          |
|   |              | York Linings                                     | 115          |



0.000

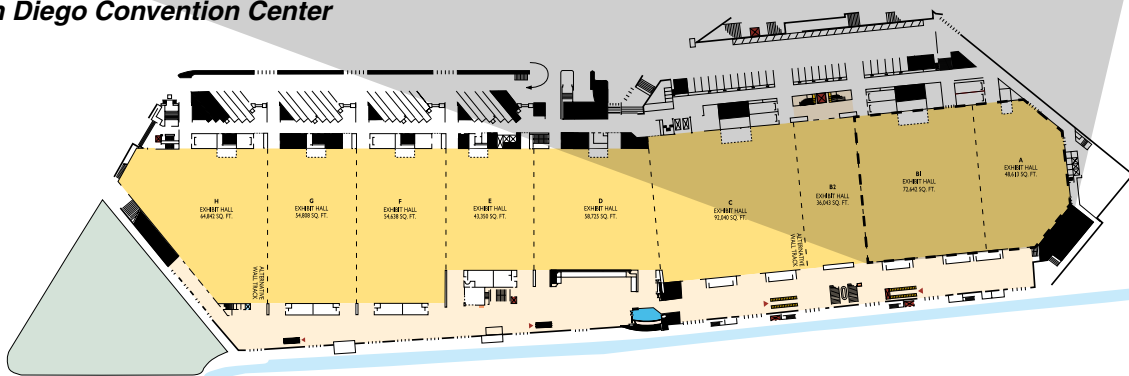
$$KT_0 = \frac{2 \cdot V \cdot (K_0)}{K_0}$$

0.000  
0.25



San Diego Convention Center

GROUND LEVEL



## Products & Services Index

### Aluminum & Magnesium

ABB Bomem  
 Advanced Dynamics Corporation Ltd.  
 Aluminum International Journal  
 B&P Process Equipment  
 Beijing General Research Institute of Mining & Metallurgy  
 Boreal Laser  
 CIMM Group Co., LTD  
 Colt  
 Dubal Aluminum Company Ltd.  
 ECL  
 EDAX  
 Fives Solios  
 FLSmidth Minerals  
 Hencon  
 Light Metal Age  
 Metallurgy and Materials Society of CIM  
 Outotec  
 Rio Tinto Alcan  
 RHI AG  
 Shanghai Zhengyu Special Alloys Co., Ltd  
 SLM Co., LTD  
 Sohar Aluminium  
 Stratronics, Inc. & Optomec Inc.  
 Techmo Car S.p.A  
 Thermo-Calc Software, Inc.

### Advanced Characterization, Modeling & Materials Performance

ABB Bomem  
 Agilent Technologies  
 ATR National Scientific User Facility  
 EDAX  
 FLSmidth Minerals  
 Metal 7  
 Micro Materials Ltd.  
 Microtrac  
 MTS Systems Corporation  
 Olympus Innov – X  
 Stratronics, Inc. & Optomec Inc.  
 Thermo Scientific Niton Analyzers  
 Thermo-Calc Software, Inc.

### High Performance Materials

Agilent Technologies  
 ATR National Scientific User Facility  
 Beijing General Research Institute of Mining & Metallurgy  
 Chongqing Runji Alloy Co., LTD. / Okaya (U.S.A.), Inc.  
 CIMM Group Co., LTD  
 ENERGOPROM Group  
 Gouda Refractories B.V.  
 Metal 7  
 Micro Materials Ltd.  
 National Institute of Standards and Technology (NIST)  
 NIST Technology Innovation Program  
 Parker Hannifin  
 RHI AG  
 Veik Thermal Textiles Coating Industrial

### Materials & Society: Energy & Sustainable Production

ATR National Scientific User Facility  
 Boreal Laser  
 Chongqing Runji Alloy Co., LTD. / Okaya (U.S.A.), Inc.  
 EDAX  
 FLSmidth Minerals  
 Light Metal Age  
 Metallurgy and Materials Society of CIM  
 NIST Technology Innovation Program  
 Olympus Innov – X  
 Outotec  
 Rio Tinto Alcan  
 Sohar Aluminium  
 Veik Thermal Textiles Coating Industrial

### Materials Processing and Production

Advanced Dynamics Corporation Ltd.  
 Beijing General Research Institute of Mining & Metallurgy  
 Big C  
 Boreal Laser  
 C A Picard International  
 Chongqing Runji Alloy Co., LTD. / Okaya (U.S.A.), Inc.  
 CIMM Group Co., LTD  
 Colt  
 Cytec Industries Inc.  
 EDAX  
 ENERGOPROM Group  
 Hencon  
 Light Metal Age  
 Metal 7  
 Metallurgy and Materials Society of CIM  
 Micro Materials Ltd.  
 National Institute of Standards and Technology (NIST)  
 NIST Technology Innovation Program  
 Olympus Innov – X  
 Outotec  
 Parker Hannifin  
 RHI AG  
 Rio Tinto Alcan  
 Shanghai Zhengyu Special Alloys Co., Ltd  
 SLM Co., LTD  
 Techmo Car S.p.A  
 Thermo-Calc Software, Inc.  
 Veik Thermal Textiles Coating Industrial

### Nanoscale & Amorphous Materials

ABB Bomem  
 Agilent Technologies  
 National Institute of Standards and Technology (NIST)

### Professional Development

Hencon  
 Momentum Press  
 Sohar Aluminium  
 Stratronics, Inc. & Optomec Inc.

## Company Descriptions

### ABB

ABB Analytical Business Unit designs, manufactures and markets high-performance analytical system solutions and spectroradiometers for petroleum, chemical, life science, semiconductor, metallurgy and remote sensing/aerospace markets. Building on its 37 years of experience in analytical instrumentation, the company's dedicated team of engineers offers the best solutions with its complete range of reliable analytical instruments for inclusions and dissolved hydrogen measurement: AISCAN, LIMCA II, LIMCA CM, Prefil®-Footprinter, PoDFA and Metallographic Analysis Service.

### Advanced Dynamics

For over four decades, Advanced Dynamics (ADCL) has supplied our global customer base with state-of-the-art material handling systems for carbon plants and cast houses. Our handling technology includes fully automated or semi-automated equipment for anode handling and cleaning, aluminum ingot and T-Bar handling, sawing and packaging systems. We also have experience in specialty systems for the magnesium, copper, zinc, steel and lead industries.

ADCL is a one-stop shop for your material handling needs including mechanical and controls engineering, fabrication, assembly, test and commissioning. Whether you need a new system or upgrades to existing systems or simply individual pieces of equipment, we can help improve your company's productivity. Remember "Our ingenuity delivers productivity" when you think of ADCL for your next project.

### Agilent Technologies

Agilent Technologies, the premier measurement company, offers a wide range of high precision measurement and imaging systems to meet your unique research needs. Agilent's industry-leading nanomechanical testing systems are the world's most accurate flexible and user friendly for nanoscale mechanical testing. Electromagnetic actuation technology allows the systems to achieve unparalleled dynamic range in force and displacement.

Agilent is introducing the compact 8500FE-SEM that has been optimized for low-voltage imaging, extremely high surface contrast, and resolution typically found only in much larger and more expensive field emission microscopes. About the size of a laser printer, the easy-to-install 8500 provides convenient plug-and-play performance. No dedicated facilities are required, only an AC power outlet. The novel scientific-grade system offers several imaging techniques for enhancing surface contrast allowing nanoscale features to be observed. Please stop by the booth for a demonstration.

### Almeq Norway AS

### Booth #700

### Almex USA

### Booth #321

### Alstom

Alstom is a global leader in the world of power generation, power transmission and rail infrastructure and sets the benchmark for innovative and environmentally friendly technologies.

Alstom builds the fastest train and the highest capacity automated metro in the world. It provides turnkey integrated power plant solutions and associated services for a wide variety of energy sources, including hydro, nuclear, gas, coal and wind, and it offers a wide range of solutions for power transmission, with a focus on smart grids. The Group employs 96,500 people in more than 70 countries, and had sales of over 23 billion\* in 2009-10. (\*Pro forma figures)

### ALUMINIUM International Journal

(Giesel Verlag GmbH)

ALUMINIUM International, journal for industry, research and applications, is the leading international journal (bilingual: German/English) for more than 80 years.

It deals with everything that concerns the material—its extraction, processing, recycling and applications. Matters of economics and the ecological consequences of using aluminium are also considered. The scope of the month-by-month reporting includes scientific contributions and condensed information about new technologies and applications. The journal addresses aluminium producers, semis manufacturers, foundries, processors, metal and semis traders and, not least, research institutes concerned with aluminium. ALUMINIUM is circulated in over 40 countries worldwide – made in Germany, distributed to the world. [www.giesel-verlag.de](http://www.giesel-verlag.de)

### Aluminium International Today

Aluminium International Today is the aluminum industry's leading international publication reporting on aluminum production and processing. Founded in 1989, it provides a wealth of technical features aimed at equipping producers and processors with information on latest developments. Added to this is a digest of industry news, contracts, events, new technology, and conference reports.

Supported by the Aluminium Federation in the UK, Aluminium International Today publishes six times a year in English plus two Chinese issues and two Russian issues. It is the main sponsoring publication for the ALUMINIUM series of exhibitions and conferences in Essen, Shanghai, Mumbai and Chicago. [aluminium@quartzltd.com](mailto:aluminium@quartzltd.com), web [www.aluminiumtoday.com](http://www.aluminiumtoday.com).

### Booth #807

### Booth #420

### Booth #515

### Booth #529

### Booth #308

### Booth #721

## Company Descriptions

### Aluminium Network

**Booth #304**

A Global Network for the Primary Aluminium Industry aluminiumNetwork.com is your internet based portal to supply and support you with a wide range of services; your meeting place with like-minded partners who can assist in improving your business and accelerate your project.

The main focus of aluminiumnetwork.com is the primary aluminum industry and it is aimed particularly at:

- Primary producers
- Suppliers of raw materials or intermediates
- Equipment suppliers
- Providers of services, including consulting services and project support.

The AluminiumNetwork.com Consultants / Freelancers data base is the perfect source for independent expertise in all of the engineering disciplines, from alumina through to primary aluminum production, including all the support functions of the process. By providing a global platform, AluminiumNetwork.com is THE place to meet with Consultants and Freelancers within the primary aluminum industry. The clients of AluminiumNetwork.com will have access to the Consultants and Freelancers database and will be able to select their required need by qualification and skills.

Please visit [www.AluminiumNetwork.com](http://www.AluminiumNetwork.com) for detailed information

### Aluminum Times

**Booth #518**

### ATR National Scientific User Facility

**Booth #405**

The ATR National Scientific User Facility offers materials science engineers and scientists the opportunity to test materials in an irradiation environment and perform analyses on the irradiated specimens. Capabilities available include three test reactors and a host of post irradiation examination facilities across the United States. Non-proprietary research is cost free to U.S. university led teams.

Access to facilities is through a solicitation and review process. The kinds of research solicited include, but are not limited to, advanced materials for high performance reactor systems, understanding light water reactor core materials including austenitic steels and nickel alloys, determining properties of material joints after exposure to a neutron irradiation environment and the applicability of nanostructured materials to radiation resistant applications. To learn more about ATR NSUF, please visit our website at: <http://atrnsl.inl.gov>.

### AUMUMD Holding BV

**Booth #504**

### B&P Process Equipment

**Booth #801**

At B&P Process Equipment, we take our traditional strengths in engineering high-precision, high-reliability machines and add a customized dimension of innovation. We are manufacturers of Continuous anode paste mixers used in Primary aluminum production.

Our new generation mixers have become more nimble, more agile and versatile. Increased efficiency, improved wear life and greater anode density are the benefits of a B&P system. Instead of trying to keep up as your needs change, we're becoming the driving force of change itself. Our products are customer-driven. Each machine is engineered to solve specific problems, meet unique challenges and seize opportunities!

We made the first batch mixer used in anode Paste mixing in 1897. For over 120 years, customer satisfaction has remained the hallmark of the B&P name. Today, when it comes to anode paste mixers, No other supplier brings the longevity, performance and experience that B&P offers the world over.

### Beijing General Research Institute of Mining & Metallurgy

**Booth #728**

BGRIMM is a premier Chinese technology corporate delivering innovative technologies, diverse products, quality engineering and project management in mineral and material industries. Established as a research institute in 1956, BGRIMM quickly built a reputation for providing technical support in the mining and metallurgy industry. Since 1999, BGRIMM became a large state technology corporation directly under SASAC (State-owned Assets Supervision and Administration Commission of the State Council). Today, BGRIMM has grown into a multi-disciplined technology corporate primarily engaged in providing integrate solutions, advanced material technology and products, and effective engineering service to clients in mineral and material industries.

For the aluminum industry, BGRIMM developed aluminum alloy tablets in 1988, which were then protected by two patents. Ever since then BGRIMM has been delivering the high quality and environmentally-friendly products and most conscientious service. BGRIMM will continue to invest on research and development, manufacturing technology and capacity to support our customers around the world.

### Big C

**Booth #823**

Big C offers the Dino-Lite Portable Digital Microscope, which provides high-quality microscopy video interfacing to PC and MAC with clear and steady imaging and 10X-200X magnification. The included software "DinoCapture" makes it easy and convenient to take snapshots, record videos, manipulate images, and save and e-mail discoveries. It is a single lens device with diverse applications.



## Company Descriptions

### Bloom Engineering

Booth #821

### Boreal Laser

Booth #629

Boreal Laser makes GasFinder laser based toxic and hazardous gas detectors that are used in a variety of open path (ambient, environmental and safety), stack, vent and process monitoring applications. Portable GasFinders are light, battery operated and easy to set up and use. Multiple path/point GasFinder MC systems can monitor up to eight paths or points with a single analyzer. Both portable and fixed GasFinders are self-calibrating, robust, reliable and maintenance free. GasFinders benefits also include fast one second response, lack of interference from other gases and low cost of ownership. GasFinders are currently available for hydrogen fluoride (HF), hydrogen chloride (HCl), hydrogen sulfide (H<sub>2</sub>S), ammonia (NH<sub>3</sub>), methane (CH<sub>4</sub>), carbon dioxide (CO<sub>2</sub>), hydrogen cyanide (HCN), ethylene (C<sub>2</sub>H<sub>4</sub>) and acetylene (C<sub>2</sub>H<sub>2</sub>). Typical applications include Aluminum smelting, Refineries (esp. HF Alkylation), Petrochemical and Chemical Plants, Gas Production and Processing, Green House Gas applications, plus Bricks and Ceramics.

### BUSS ChemTech

Booth#520

### CANMET Natural Resources Canada Booth #530

In collaboration with industry, CANMET-MTL a Federal laboratory of Natural Resources Canada, develops and deploys technologies to improve all aspects of producing and using value-added products from minerals and metals. Specifically, CANMET-MTL focuses on research related to metal processing (casting, forming, joining, advanced materials and prototype development) and maintains in-depth competencies for materials assessment (microstructural characterization, corrosion, physical and mechanical testing) to:

- Achieve higher performance from metal alloys and metal- or mineral-based materials for a wide range of end-use applications
- Develop advanced materials for next-generation vehicles
- Improve the reliability of the energy infrastructure, such as oil and gas pipelines and nuclear power generation systems
- Develop specialized materials for current and future industrial systems to help companies use energy efficiently and reduce air emissions and waste
- Provide sound technical input to standards and codes development
- Promote innovation and enhance the competitiveness of Canada's value-added and related product industries
- Assist firms to use more efficient production techniques, resulting in energy and cost savings.

### C.A. PICARD International

Booth #711

C.A. PICARD is specialized in manufacturing of high quality wear parts for continuous kneaders for the manufacture of green anodes for the primary aluminum industry.

PICARD manufactures kneading teeth, wearing plates / liners and screw flights out of high wear resistant qualities.

### Center for Advanced Energy Studies

Booth #336

The Center for Advanced Energy Studies is a research partnership between Boise State University, Idaho National Laboratory, Idaho State University and University of Idaho.

### Chongqing Runji Alloys/OKAYA

Booth #809

We specialize in producing all kinds of alloying tablets. We are continuing to improve, modernize and expand our company's production capacity in order to increase productivity and efficiency. This includes the acquisition last year of the biggest Mn ore mines in Jingxi County, Guangxi province of China. The capacity of this Mn ore mine is more than 3 million tons and our new production line of Mn flakes has also been completed. The new capacity is 30,000 tons per year. With the development of these programs along with our state-of-the-art production management, technologies and facilities, we can guarantee enough raw material supply at very competitive price levels while maintaining our high level of quality.

Information about our partners: Okaya (U.S.A.), Inc. is an international trading house that provides representation in North America for Chongqing Runji Alloy Company, LTD. This partnership is an example of Okaya's expansion of our business domain from its core area of iron and steel to various related fields of business. We can also perform marketing, logistics and processing functions to fulfill our role as the "Best Global Sourcing Partner". As an independent trading company with a high level of flexibility, Okaya will continue to propose insightful and creative business opportunities by looking at various areas with a broad perspective.

Also visit us online at [www.okaya.co.jp/en](http://www.okaya.co.jp/en)

## Company Descriptions

### CIMM Group

**Booth #815**

As the company certified by ISO 9001:2008 and the International Projects Contractor accredited by P.R.China, CIMM GROUP is a healthy and fast growing integrated multinational corporation professionally engaged in providing technology, engineering, manufacturing, trade and EPC service in fields of aluminum and Steel, Mineral, Metals and Metallurgy, cement and construction, refinery and petrochemical, ports and shipyards, oil and gas, power generation and transmission, green resource, and energy, etc.

Our main products for aluminum smelting is Anode blocks, Cathode blocks, Aluminum fluoride, cryolite, silicon nitride bonded silicon carbide blocks, refractory bricks, insulations bricks, CPC, silicon metal, aluminium tablets, etc. which have been supplied to overseas market to establish good and steady relationships with Greece, Brazil, Australia, Egypt, India, Kazakhstan, Turkey, Dubai, etc. The supplied products have a great reputation among our customers. CIMM GROUP is always committed to be a trustworthy business partner.

### Claudius Peters Projects GmbH

**Booth#419**

### Colt

**Booth #302**

Colt is a global supplier and manufacturer of natural and mechanical ventilation systems.

The principal activity of Colt is the supply of specialist products and systems in the field of building services with particular emphasis on gravity ventilation and the environmental control of industrial and commercial buildings. Especially for the aluminum industries, Colt is supplier of Static roof Ventilators and air intake louvers for potroom buildings, anode bake buildings and cast houses. The product folio also includes perforated, reinforced fiber walls.

#### MISSION STATEMENT:

Our vision is to make the world a better place in which to live and work by helping to make the environment associated with buildings healthy, safe, productive and comfortable.

### Computherm

**Booth #309**

### Conductix-Wampfler

**Booth#204**

Conductix-Wampfler is the world's leading designer and manufacturer of energy and data transmission products. We have specific expertise in "mill-duty" conductor bar, cable festoon systems, cable reeling equipment, and cable chain systems. Our rugged products have been field-tested in the most demanding environments. We also design and build custom slip rings for pot line cranes, rotary casters, and similar equipment. Lastly, we offer a series of push button

pendants and radio controls designed for mill use. And we can service what we sell, too, to keep you operations running 24/7/365. If you want the right solution for the applications, contact Conductix-Wampfler. We Move Your Business!

### CSM Instruments

**Booth#310**

### Cytec Industries

**Booth #620**

Cytec collaborates with mining companies to optimize their operations through the delivery of innovative chemical technologies. We utilize our superior application expertise to develop solutions based on our customer's specific needs.

We offer technologies that:

- Decrease the cost of operations
- Provide better recovery and selectivity
- Process difficult ores
- Prevent or limit employee's exposure to hazards
- Optimize the use of natural resources
- Minimize waste and re-tooling
- Do not require on-staff scientists or engineers

Cytec is committed to partnering with our customers to meet their needs. Our network of technical staff provides on-site technical assistance worldwide. We are dedicated to on-time delivery, even to the worlds harder to reach areas. Our unique approach to servicing our customers has made Cytec the leading provider of reagents to the mining industry.

### Dantherm Filtration

**Booth #314**

Dantherm Filtration / Nederman is a leading supplier of Dust Control and Air Pollution Control solutions for a wide range of industries all over the world. Dantherm Filtration focuses on individual solutions for individual customer needs. Since May 2010 Dantherm Filtration is part of the Swedish Nederman Group. We combine the experience and expertise of the internationally recognized suppliers to provide the customers with high efficiency, unbeatable reliability, low energy consumption, and full compliance with all mandatory requirements. Our focuses are: Foundry industry, non iron-industry, quarry industry, asphalt industry, primary and secondary aluminum industry, waste incineration and waste to energy industry and Cement industry. Our reference list reflects more than 40 years of experience and broad application expertise.

### Dubai Aluminium Company

**Booth #717**

Dubai Aluminium Company Limited ("DUBAL") owns and operates one of the world's largest primary aluminium smelters. The DUBAL complex comprises a 990,000 mtpa smelter, a 2,350 MW power station (at 30°C), a large carbon plant, casthouse operations, a water desalination plant, and other facilities.

High quality aluminum products are made in three main

## Company Descriptions

forms: foundry alloy for automotive applications; extrusion billet for construction, industrial, transportation and forging purposes in automotive industries; and high purity aluminum for electronics and aerospace. More than 250 customers are served in at least 45 countries predominantly in the Far East, Europe, the ASEAN region, the MENA region, and North America. The company holds ISO 9001, ISO/TS 16949, ISO/IEC 27001, ISO/IEC 20000, ISO 14001 and OHSAS 18001 certification. Over 4,000 people are employed, 22% of whom are UAE Nationals. DUBAL also owns 50% of Emirates Aluminium Company Limited ("EMAL"), a green-field smelter development at Al Taweelah, Abu Dhabi.

### EBSD Analytical

**Booth #217**

EBSD Analytical offers micro structural analysis services specializing in EBSD and EDS. With over 15 years experience in EBSD, we guarantee the highest quality results with a quick turnaround.

We also specialize in preparation of difficult materials for EBSD analysis. Call us today to see how we can help with your specific needs, whether it is grain size, texture, misorientation, phase ID, local deformation, or any number of additional applications.

### ECEFast

**Booth # 219**

Temperature sensor manufacturer making "Excalibur" fully swaged sensor for Carbon Bake Furnace Flue application. Featuring long life with zero maintenance, unbreakable and not prone to distortion, the Excalibur offers the lowest cost of ownership of any sensor used in this application to 1190C. Supplied normally in N to provide minimum drift over the operating life, but K is available. Cost is somewhat higher than Inconel 601 tube + wire & bead, but life is more than double with no insert replacement. [www.ecefast.com.au](http://www.ecefast.com.au)

### ECL

**Booth #500**

With over 60 years experience, ECL is the world leading smelter equipment manufacturer with a long time dedication to the aluminum industry. ECL offers complete solutions for the smelter's reduction, carbon and metal sectors.

From design and manufacturing to erection, through training, maintenance, audit and refurbishment, ECL provides products and services adapted to the needs and demands of its customers, whatever the reduction technology. A high level of innovation and an unmatched expertise allow ECL to offer solutions, from single machines to complete turnkey projects that help aluminum smelters in their productivity and HSE efforts.

### EDAX

**Booth #223**

EDAX is the technical innovator and the world's largest supplier of EDS, EBSD, WDS and Micro-XRF systems. Smart Features are at the core of our new TEAM EDS system providing analytical intelligence to easily obtain exceptional results. EDAX's EBSD Data Collection provides a powerful and easy to use environment for acquiring EBSD data in the SEM. The EBSD Analysis has virtually unlimited potential for interrogating the wealth of information contained in EBSD data. EDAX offers detector solutions to meet all your EBSD needs. Combined with the power of WDS to enhance qualitative and quantitative analysis, EDAX provide today's scientist with the ultimate materials characterization solution, offering vastly improved speed and accuracy. Orbis provides analytical flexibility for MicroXRF applications. EDAX products provide a powerful and unique combination of elemental and structural information providing a complete solution.

Trident Image Caption: Trident is the ultimate materials characterization tool integrating the latest technologies of EDS, EBSD and WDS. [www.edax.com](http://www.edax.com)

### Eirich Machines, Inc.

**Booth #315**

### ENERGOPROM Group

**Booth #530**

ENERGOPROM MANAGEMENT (EPM) is one of the most efficient companies in non-raw material sector of the Russian economy. We are doing business all over the world, supplying more than 50% of our carbon and graphite products to the world market. EPM's Novochoerkassk, Novosibirsk and Chelyabinsk electrode plants manufacture graphite and carbon products for the steel, aluminum, silicon, ferroalloy and other industries. All enterprises of the Company are furnished with up-to-date and highly productive equipment. Our products and applied technologies have no comparison in the world. Our products satisfy the requirements of world standards. In order to boost our competitive capacity, our plants have been comprehensively modernized and rebuilt. We have built new facilities to meet the requirements of the most advanced metallurgical producers, as well as to satisfy the growing global demand for carbon and graphite products.

## Company Descriptions

### Evans Analytical Group

Booth #311

Evans Analytical Group (EAG) is the leading provider of surface analysis and materials characterization services to the materials supply chain and to high technology industries. We specialize in providing the widest range of characterization techniques available, such as GDMS, ICPMS, SIMS, SEM, (S) TEM (including EELS and EDS), Auger, XPS and XRD, via our network of laboratories in North America, Asia and Europe.

Our aim is to provide our customers with the most reliable, highest quality data as quickly as possible, to enable them to meet their goals regarding materials development and process optimization. EAG is certified to ISO17025 and ISO9001.

### Fives Solios

Booth #609

FIVES SOLIOS is one of the companies of Fives, a major International Group, with considerable experience in industrial engineering and management of large projects all over the world. Fives Solios is specifically dedicated to the Aluminium Industry and develops innovative solutions in order to comply with more and more stringent environmental standards while increasing safety and reliability. Fives Solios most particularly works on reducing energy consumption in its process technologies.

- Reduction: Gas Treatment Centers on electrolysis pots and Bath Processing Units.
- Carbon: High Capacity Green Anode Plants, Pitch storage and processing, Liquid Pitch Marine Terminal, Firing & Control Systems for anode baking furnaces, and Fume Treatment Centers on anode baking furnaces.
- Casthouse Area: Melting and Holding furnaces including water cooling systems as well as integration of downstream casting machines, Heat Treatment furnaces for rolling mills and associated control systems.

[www.fivesgroup.com](http://www.fivesgroup.com)

### FLSmidth

Booth #714

FLSmidth is your major equipment supplier from Bauxite Mining and Refining through Calcination and Smelting. Every day, worldwide, our equipment crushes, conveys, grinds, digests, clarifies, precipitates, stores, and calcinates bauxite to produce alumina. Combining the respected brand names of MÖLLER, KOCH-MVT, FULLER-TRAYLOR, WEMCO, EIMCO, DORR-OLIVER, PNEUMAPRESS, KREBS, ABON, RAHCO, CEntry, Conveyor Engineering and Raptor, FLSmidth offers a broad range of equipment and processes while increasing recoveries, lowering energy consumption, and providing proven reliability. We also offer metallurgical testing utilizing the expertise of FLSmidth Dawson's metallurgical laboratories. FLSmidth is your One Source, One Partner providing integrated solutions that will save you valuable time on your project schedule!

### Friggi

Booth #316

Friggi is a manufacturer of high quality band saws, waterjets and plasma machines. Specialized high-speed machines for rapid cutting of aluminum with tight tolerances.

### Gautschi Engineering GmbH

Booth#317

Gautschi Engineering GmbH is a leading supplier of equipment for primary aluminum casthouses and recycling plants. The product range of Gautschi™ includes:

- Melting – and holding furnaces
- Pusher-type furnaces for rolling slab
- Homogenizing furnaces for extrusion billet and rolling slab
- Multiple chamber furnaces for coil and foil annealing
- Single coil annealing furnaces
- Horizontal D.C. casting plants
- Open mould ingot casting and stacking plants
- Vertical D.C. Casters for extrusion billet and rolling slab
- AIR GLIDE® and AIRSOL VEIL® mould technology

### Gillespie & Powers, Inc.

Booth #806

### GLAMA

Booth #615

### Gouda Refractories

Booth #415

Gouda Refractories is an innovative refractory producer (refractory bricks, castables, mortar, self-flowing castables, complex pre-cast shapes) with global experience and a long track record of supplying superior quality refractories all over the world, combined with innovative installation technology for more than 100 years.

Gouda Refractories develops, manufactures, sells and installs top quality refractory linings. Gouda's solutions play an important role in, non-ferrous metal (mainly aluminium), petrochemical, environmental and energy industries. Based on an industry-oriented structure and highly competent employees, Gouda Refractories guarantees an optimal support which results in efficiency and reduction of refractory cost. Gouda Refractories supplies total solutions to customers which are cost effective, state of the art, and reliable. Gouda's R&D department is conducted in close co-operation with its customers and renowned research institutes. Gouda's quality assurance is based on the international ISO 9001 standard.



## Company Descriptions

### Hebei Sitong New Metal Material Co., Ltd

**Booth #109**

As the leading excellent manufacturer of master alloy in China, we mainly produce the followed items:

- Aluminum master alloy: AlTi5B1 AlTi10,AlSr10,AlZr10,AlMn20,AlB4,AlV5
- Shape:Coil, Cut Rod, Waffle, Ingot
- Application: Widely applied in manufacture of Aluminum Profile,Strip, Foil, Castings Electricity, Automobile, Aerospace etc.

This booth is presented in cooperation with Leway International Fairs, one of the leading international exhibition agencies in China. Located in Beijing, Leway has served in over 500 important overseas exhibitions in its eight-year history and has served nearly 2,000 Chinese companies. Leway provides comprehensive one-stop solution services for Chinese companies.

### Hencon

**Booth #300**

A profound knowledge of special vehicles, over 50 years of experience, creativity, robustness, stamina and entrepreneurship makes Hencon a world leader in the design, manufacturing and service of special vehicles in the aluminium industry.

### Hereaus Electro-Nite

**Booth #621**

### Hertwich Engineering

**Booth #506**

### Hysitron

**Booth #614**

As world leader in nanomechanical testing, Hysitron is dedicated to providing testing solutions for nanoscale mechanical characterization. Hysitron's nanomechanical test instruments provide high-speed in-situ SPM imaging in addition to the quantitative measurement of many mechanical properties, including hardness, modulus, fracture toughness, and wear resistance. Our instruments feature advanced techniques such as nanoDMA™ for time dependent and viscoelastic materials, Modulus Mapping for quantitative large area property mapping, and nanoECR™ enabling simultaneous electrical and mechanical property measurements. We are excited to demonstrate the TI 950 Tribolndenter™ nanomechanical test system featuring 25x faster feedback, a nanoNewton to Newton force range, and an unprecedented <30nN noise floor. Stop by our booth to see how the TI 950 redefines the world of nanomechanical testing. Hysitron will also be showcasing the PI 95 and PI 85 PicoIndenter™, the truly quantitative depth-sensing indenters capable of direct-observation testing inside a TEM and SEM.

### Innovatherm

**Booth#429**

### IPI (Initiatives et Projets Industriels)

**Booth#817**

### Jervis B. Webb Company

**Booth#508**

### Kempe Engineering

**Booth#514**

### Light Metal Age

**Booth #417**

Light Metal Age is the pre-eminent magazine of the light metal world. For over 69 years, Light Metal Age has covered primary production and semi fabrication of the light metals aluminum, titanium, and magnesium. Circulation is international and goes to primary and secondary smelters; casthouses; extrusion operations; rolling mills; sheet, rod, and wire mills; and foundries. Coverage of associated metal processes and equipment includes DC casting, anodizing, furnaces and melting, degassing and filtration, automation and instrumentation, and handling. Recipients are executives, general managers, plant managers, technicians, metallurgists, chemists, and engineers responsible for fabrication, production, and operations.

Light Metal Age also produces select article archive content on CDs, including the Titanium Article Archives (Nov. 1945 – Aug. 2009) and the Magnesium Article Archive (May 1943 – April 2009). For more information, visit Light Metal Age on the web at [www.lightmetalage.com](http://www.lightmetalage.com).

### L.P. Royer, Inc.

**Booth #414**

### Major

**Booth #811**

### Maney Publishing

**Booth #304**

Maney delivers a personalized service to authors, societies, readers and libraries for the publishing and international dissemination of high quality, peer-reviewed scholarship and research.

Specializing in print and electronic journal publishing, Maney is committed to technical and editorial innovation combined with traditional values of quality and collaboration. Maney publishes an impressive collection of highly regarded, peer-reviewed journals covering both niche and general topics in materials science and engineering. Coverage ranges from fundamental research to engineering application and from the extraction and refining of minerals to the characterization, processing and fabrication of materials and their performance in service.

## Company Descriptions

### Metal 7

Metal 7 has been providing services to the primary industry since February 1974, specializing in the design and production of high performance equipment for the primary sector. Metal 7 has a very sound knowledge of the iron ore, aluminum smelter and pulp and paper industries. It distinguishes itself from its competitors due to its expertise in surface engineering. Thanks to its leading expertise, the company stands out from its competitors by proposing extremely sophisticated, high-performance solutions. This competitive edge allows the company to thrive on the international market with numerous important companies in the metallurgical sector, like Aluminerie Alouette, Rio Tinto, ArcelorMittal, Outotec, etc.

Each year, Metal 7 invests important sums in research and development (R&D). These investments are targeted towards developing new coatings and new applications for those coatings, as well as improving the manufacturing processes and the products made by Metal 7.

### Metallurgy and Materials Society of CIM

### Booth #306

### Booth #723

We are a world class Canadian organization that serves society and the needs of professionals in the global metallurgy and materials community. The purpose of MetSoc is to serve our members, society and others involved in the research, development and application of the science and technologies for the environmentally responsible extraction, fabrication, utilization and recycling of metals and materials.

### Micro Materials

### Booth #718

The NanoTest system from MML offers a range of methods of materials characterization, including nanoindentation, nano-impact and nano-scratch and wear measurements.

In recent years, MML have pioneered nanomechanical testing in real-world conditions. The NanoTest offers unique testing modules, among them the high temperature testing module, which allows testing of a sample heated up to temperatures of 750°C.

### Microtrac

### Booth #630

Our focus is rapid particle size analysis utilizing advanced solid state tri-laser technology. The S3500 line of particle size analyzers provide the broadest size range with compact design from .02 to 3000 microns. Features include rapid wet to dry conversion, advanced Flex software, small footprint, and TurboTrac dry feeder. The NanoTrac Dynamic Light Scatter units are available for nanometer sizing, while the Ultra is for low concentration < 20nm applications. New Blue Laser Technology "Bluewave" next generation is here. Zeta potential, surface area and imaging systems will also be shown.

### Momentum Press

### Booth #416

Momentum Press provides the very best information and knowledge on today's advancements in science, engineering, and applied technology. We publish books in traditional print, as well as electronically, for practitioners, researchers, educational faculty, and students. Some of our bestselling titles include: Alarm Management for Process Control by Doug Rothenberg; Protecting Industrial Control Systems from Electronic Threats by Joe Weiss; and Characterization in Silicon Processing by Yale E. Strausser. We are happy to publish individual authors as well as to work with schools and institutions in publishing such collective works as proceedings, seminar materials, and various types of instructional tools. We have sales offices throughout the world, with a particularly strong presence in Asia, North America, and Latin America, as well as Europe and the Middle East.

### MTI Corporation

### Booth #528

### MTS Systems Corporation

### Booth #819

Engineers and researchers worldwide rely on MTS for the testing technology and expertise required to support the research and development of advanced metals, composites and ceramics. Reliable, high-performance MTS solutions are deployed across a diversity of industries such as aerospace, power generation, civil engineering and automotive, accurately and efficiently meeting the most demanding materials testing requirements.

The MTS portfolio is engineered to address a full spectrum of materials testing requirements - from tension/compression to fracture mechanics to complex multi-axial fatigue studies at elevated temperatures. This portfolio features: high-performance servohydraulic and electromechanical testing systems; versatile, high-resolution controls; proven application software; precision accessories; robust environmental simulation systems; and unmatched service and support.

Explore the MTS booth and discover how innovative MTS test solutions and decades of industry expertise can optimize the effectiveness and efficiency of your specific materials research and advanced development program.

### NFC

### Booth #521

### National Institute of Standards and Technology (NIST)

### Booth #322

NIST Standard Reference Materials supports accurate and compatible measurements by certifying and providing over 1100 Standard Reference Materials with well-characterized composition or properties, or both. SRMs are used to perform instrument calibrations as part of overall quality assurance programs, verify the accuracy of specific measurements and

## Company Descriptions

support the development of new measurement methods. The Standard Reference Data Group has provided well-documented numeric data to scientists and engineers for use in technical problem-solving, research, and development. The Calibration Services are designed to help the makers and users of precision instruments achieve high levels of measurement quality and productivity.

### **NIST Technology Innovation Program Booth #320**

The Technology Innovation Program (TIP) at the National Institute of Standards and Technology is a cost-shared, federal funding program to support, promote, and accelerate innovation in the U.S. through high-risk, high-reward research in areas of critical national need. TIP funds innovation research that is expected to transform the Nation's capacity to deal with major societal challenges that are not being addressed. Participants in TIP include U.S. businesses and institutions of higher education or other organizations, such as national laboratories and nonprofit research institutions.

### **NKM Noell Special Cranes GmbH Booth #707**

### **Olympus Innov – X Booth #811**

Olympus Innov-X provides portable handheld X-Ray Fluorescence (HHXRF) analyzers for simple, non-destructive sorting of challenging grade separations, alloy chemistry and grade ID in seconds. They provide highly specific material chemistry to rapidly and accurately identify pure metals and alloy grades. HHXRFs allow for testing of literally thousands of types of materials anywhere, anytime. For scrap recycling applications, our HHXRFs provide reliable ID in 1-2 seconds for most grades. They are designed for durability – to withstand the tough processing environment. Our HHXRFs are used for fast, reliable alloy sorting and analysis for a wide variety of ferrous and non-ferrous material. We provide optimized HHXRF configurations for cost-effective analysis when time is of the essence and when materials cannot be transported, damaged, or altered. Our X-5000 Mobile XRF analyzers offer maximum portable power with a closed beam configuration and large touch screen interface.

### **Opsis Booth #715**

### **Outotec Booth #507**

Outotec develops and provides technology solutions for the sustainable use of Earth's natural resources. As the global leader in minerals and metals processing technology, Outotec has developed several breakthrough technologies. Outotec serves the light metals industries including the provision of cutting-edge alumina refineries and aluminum smelters. The company has over 50 years experience helping customers worldwide in both segments of the aluminum process to reach their goals. What sets Outotec apart from its competition? They are there to help their customers from start to finish in terms of plant design, and they customize solutions to fit a client's specific needs. Outotec's processes and equipment have become industry standards and their references stretch back decades – a track record that has led to their current reputation as a leading innovative technology partner. The company also offers innovative solutions for the chemical industry, industrial water treatment and the utilization of alternative energy sources.

### **Parker Hannifin Booth #409**

Parker is the world's leading diversified manufacturer of motion and control technologies and systems. Parker provides precision engineered solutions for a variety of commercial mobile, industrial and aerospace markets. We design and manufacture optimal systems using fluid connectors, hydraulics, pneumatics, instrumentation, refrigeration, filters, electromechanical components, and seals required in motion-control systems.

Parker's experience in the aluminum industry spans more than 40 years. Parker has equipped machinery in all phases of aluminum production including smelters, casters and extruders through grinders, rolling mills and strip processing lines, etc.

### **Proto Manufacturing Inc. Booth #215**

## Company Descriptions

### RHI AG

**Booth #816**

Refractory competence for the non ferrous metals industry: RHI is the world's leading supplier of high-grade ceramic refractory products and services. As a reliable and competent partner it is our constant aim to add value to the process of our customers by achieving the best price/performance ratio with our refractory system solutions.

The comprehensive program of products and services ranges from basic and non-basic mixes and bricks to prefabricated products, slide gate plates, purging plugs, as well as computer simulations like CFD or FEM. We also offer special machines, repair systems and technical equipment used to install refractory products into the various production units of the non ferrous metals industry. Our metallurgists are active around the globe and cooperate with renowned research facilities and universities to support the improvement of metallurgical processes and furnace integrity.

### Riedhammer GmbH

**Booth #605**

Since 1924 dedicated to the design and construction of furnace plants for carbon products (OPEN as well as CLOSED type), RIEDHAMMER is presently the only independent supplier worldwide being able to deliver complete solutions and technology for baking of anodes, cathodes, electrodes and special carbon products. More than 85 years of experience and know-how guarantee a high economic efficiency and reliability of the plants. In total RIEDHAMMER has executed more than 300 bake furnace projects in 25 countries. Our reference list includes major global players in the production of primary aluminum with pre-baked technology as well as top suppliers of cathodes and electrodes respectively for the aluminum and steel industry.

### Rio Tinto Alcan

**Booth #501**

Global leader in the aluminium industry Building on more than a century of experience and expertise, Rio Tinto Alcan is a global leader in the aluminium industry. We supply high quality bauxite, alumina and aluminium worldwide and our AP smelting technology is the industry benchmark. Our enviable hydroelectric power position delivers significant competitive advantages in today's carbon constrained world. Rio Tinto Alcan is the aluminium product group of Rio Tinto, a leading international business involved in each stage of metal and mineral production. The Group is listed on the London Stock Exchange and Australian Securities Exchange under the symbol RIO. Rio Tinto's major products are aluminium, copper, diamonds, coal, iron ore, uranium, gold and industrial minerals.

### Romidot Ltd

**Booth #401**

### Sente Software

**Booth #810**

### Shanghai Electric Import And Export Co.,Ltd

**Booth #210**

Main products include: alloy welding material, coils, aluminum alloy slabs, hot rolled plate, tubes, ground bar, electric steel.

This booth is presented in cooperation with Leway International Fairs, one of the leading international

exhibition agencies in China. Located in Beijing, Leway has served in over 500 important overseas exhibitions in its eight-year history and has served nearly 2,000 Chinese companies. Leway provides comprehensive one-stop solution services for Chinese companies.

### Shanghai Zhengyu Special Alloys Co., Ltd

**Booth #829**

Shanghai Zhengyu Special Alloy Co., Ltd. is one of the Chinese major and professional manufacturers in China. Our main products AlSi, AlTiB, AlTi & aluminum alloy additives etc, are reviewed favorably and accepted widely in world market.

### SIMULIA

**Booth #408**

SIMULIA is the Dassault Systems brand that delivers a scalable portfolio of Realistic Simulation solutions including the Abaqus product suite for Unified Finite Element Analysis, multiphysics solutions for insight into challenging engineering problems, and lifecycle management solutions for managing simulation data, processes, and intellectual property. By building on established technology, respected quality, and superior customer service, SIMULIA makes realistic simulation an integral business practice that improves product performance, reduces physical prototypes, and drives innovation. Headquartered in Providence, RI, USA, with R&D centers in Providence and in Velizy, France, SIMULIA provides sales, services, and support through a global network of over 30 regional offices and distributors. [www.simulia.com](http://www.simulia.com)

### SLM Co., Ltd

**Booth #229**

We are an Aluminium Master Alloys Manufacturer located in Korea. Our company is specialized in Grain Refiners(AlTiB Alloys), Modifiers(AlSi Alloys) and Other Aluminium Alloys such as AlTi, AlB, AlV, AlMg, AlMn etc. We produce aluminium alloys in various form such as Rod in coil, Cut Rod, Bar and Plate.

We have been producing high quality of Aluminium Master Alloys for 19 years and we export to over 20 countries. We supply high quality materials at competitive price.

We are looking for distributors now. Please visit our stand!



## Company Descriptions

### Sohar Aluminium

**Booth #211**

One of the newest additions to the Middle East's metals circuit and Oman's first foray into the Aluminium industry Sohar Aluminium Company was formed in September 2004. Jointly owned by Oman Oil Company, TAQA and Rio Tinto Alcan, Sohar Aluminium has already won global acclaim for its superior, environmentally-friendly and energy-efficient technology. By implementing decades of industry insight in its design, specification and construction Sohar Aluminium has been created to ensure efficiency, environmental protection and the utmost safety of its workforce. Noteworthy examples include the world's highest known capacity ingot casters and innovative elevated walkways traversing the entire site to keep man and machine separate except when absolutely necessary. In addition, Sohar Aluminium has since inception achieved 70% Omanisation of its workforce; invested 53% of its total spend in the local market and established a growing network of local downstream companies. In many ways, Sohar Aluminium's development mirrors the Sultanate of Oman's own emergence onto the world stage - driving forward at a formidable pace, but all the while mindful and respectful of its cultural heritage and values.

### STAS

**Booth #601**

### Stratronics, Inc. & Optomec Inc.

**Booth #407**

Stratronics, Inc. will exhibit the ThermaViz® Sensor, an innovative two-wavelength imaging pyrometer that provides accurate, high resolution temperature maps for intelligent metals processing in real time. This online imaging pyrometer has been developed to monitor the temperature distribution of the melt pool in laser additive manufacturing processes. ThermaViz, with Windows based analysis software, is now an integrated option to Optomec's LENS technology.

Optomec® is the world-leading provider of additive manufacturing solutions for high performance applications in the Electronics, Solar, Medical, and Aerospace & Defense markets. These systems utilize Optomec's patented Aerosol Jet Printed Electronics technology and LENS powder-metal fabrication technology. The company has a global customer base of more than 100 users that includes many industry-leading manufacturers and Universities.

Stratronics and Optomec will present "On-Line Imaging Pyrometer for Laser Deposition Processing" in the Sensors, Sampling, and Simulation for Process Control Symposium.

### Sunstone

**Booth #822**

### Techmo Car S.p.A

**Booth #502**

Techmo is an Italian independent company focused in the engineering and production of special mobile and stationary equipment for the aluminium and non ferrous metals industry. The full range of purpose designed machines covers different types of equipment performing a large number of operations in pot-rooms, rodding shops and cast-houses. The Company's aim is to provide the most innovative, rational, cost effective and user friendly technical solutions. Among the most significant families of mobile equipment are the Tapping Vehicles, Anode Transporters, Crucible Transporters and Tilters, Alumina/ AIF3 Feeding Vehicles, Furnace Charging Vehicles and Furnace Tending Vehicles, Multipurpose Anode Changers and Crust Breakers. Beside its line of purposed designed vehicles, Techmo provides a number of stationary equipment such as Crucible Cleaning Machines, the Crucible Tilting stations and the Anode Butts Cleaning Stations.

### Thermo Scientific

**Booth #423**

### Thermo Scientific Niton Analyzers

**Booth #421**

When it comes to accurate analysis of metal alloys, Thermo Scientific Niton XRF analyzers set the industry standard. With a unique library of 400+ alloy grades, our handheld instruments provide immediate, nondestructive chemical analysis of aluminum, titanium, and nickel alloys; superalloys; stainless steel; and more. They deliver superior performance through faster analysis, lower detection limits, and unparalleled analytical precision, meaning decreased potential for material mix-ups and instant recovery of lost traceability.

Using the Niton® XL3t with GOLDD technology, you not only gain rapid grade identification and lab-quality composition, but also improvements in light element detection, overall sensitivity, and measurement times.

### Thermo-Calc Software

**Booth #814**

Thermo-Calc Software is a leading developer of software and databases for calculations involving computational thermodynamics and diffusion controlled simulations. Thermo-Calc is a powerful tool for performing thermodynamic calculations for multicomponent systems. Calculations are based on thermodynamic databases produced by expert evaluation of experimental data. Databases are available for steels, Ti, Al, Ni-superalloys and other materials. Programming interfaces are available which enable Thermo-Calc to be called directly from in-house developed software or MatLab. DICTRA is used for accurate simulations of diffusion in multicomponent alloys. Applications include: homogenization of alloys, microsegregation during solidification, coarsening of precipitates, and welding.

## Company Descriptions

### UES, Inc.

**Booth #628**

UES, Inc. is an innovative science and technology company that provides its industry and government customers with superior research and development expertise. We create products and services from our technology breakthroughs and successfully commercialize them.

RoboMet.3D™ is a fully automated, serial sectioning system that generates two-dimensional data for three-dimensional reconstruction.

Robo-Met.3D™ enables more time for data analysis and characterization and ensures repeatable and accurate data is collected in an efficient and cost-effective manner.

Additional areas of expertise for UES include materials science, metallurgy, ceramics, processing science, modeling and simulation, surface engineering, materials characterization, biotechnology, sensor development and nanomaterials.

### Veik Thermal Textiles Coating Industrial

**Booth #328**

Veik Thermal Textiles Coating Industrial, Our Manufacturing facility is located in China. Here we skillfully produce various styles of PTFE & Silicone coated fiberglass fabric and other products to the highest of professional standards. With advanced technology, strict quality control and unbeatable after-sales service, we can ensure our customers will receive high-quality products.

### XIAMEN C&D ALUMINIUM CO., LTD Booth #208

Wholly invested by Xiamen C&D INC. (Stock: C&D INC. Code: 600153), Xiamen C&D Aluminium Co., Ltd., is a trade company specializing in aluminum industry. We mostly engage in aluminum products' domestic trading, and importing and exporting for more than ten years. The company has strong overall operational capabilities, rich experience in international trade, and the stable procurement channels and is in the markets of aluminum sheet, coil, profiles, aluminum circle, aluminum foil etc.

This booth is presented in cooperation with Leway International Fairs, one of the leading international exhibition agencies in China. Located in Beijing, Leway has served in over 500 important overseas exhibitions in its eight-year history and has served nearly 2,000 Chinese companies. Leway provides comprehensive one-stop solution services for Chinese companies.

### York Linings

**Booth #115**

# Thanks!

## TMS Thanks the Following for their Symposia Support:

### Magnetic Materials for Energy Applications

Lake Shore Cryonics, Inc.  
AMT&C  
Mitsuyo Shimizu JSPS

### David Pope Honorary Symposium

JEOL Co., Ltd.  
Shimadzu Co., Ltd.  
Euro System  
Tokyo University  
Hong Kong Polytechnic University

### Functional & Structural Nanomaterials

Qualcomm  
Lead-Free Solder Materials Workshop  
Nihon Superior



# TMS 2011

## 140th Annual Meeting & Exhibition

February 27 - March 3, 2011 • San Diego Convention Center  
San Diego, California USA

### **Table of Contents**

|                          |     |
|--------------------------|-----|
| Program At a Glance..... | 2   |
| Sunday Posters .....     | 12  |
| Monday.....              | 58  |
| Tuesday .....            | 173 |
| Wednesday .....          | 292 |
| Thursday.....            | 415 |
| General Posters.....     | 505 |
| Index.....               | 524 |



| Page  | Room | Sun. |    | Mon. |    | Tue. |    | Wed. |    | Thur. |    |
|---|------|------|----|------|----|------|----|------|----|-------|----|
|   |      | AM   | PM | AM   | PM | AM   | PM | AM   | PM | AM    | PM |
| <b>2011 Aluminum Plenary Symposium</b>  |      |      |    |      |    |      |    |      |    |       |    |
| 58  | 6B   |      | X  |      |    |      |    |      |    |       |    |
| The 125th Anniversary of the Hall-Héroult Process   |      |      |    |      |    |      |    |      |    |       |    |
| <b>2011 Functional and Structural Nanomaterials: Fabrication, Properties, Applications and Implications</b> |      |      |    |      |    |      |    |      |    |       |    |
| Characterizations of Nanomaterials and Session in Honor of Prof. T. Kang                                    |      |      |    |      |    |      |    |      |    |       |    |
| 352   | 8    |      |    |      |    |      |    | X    |    |       |    |
| 173   | 8    |      |    | X    |    |      |    |      |    |       |    |
| 415   | 8    |      |    |      | X  |      |    |      |    |       |    |
| 115   | 8    |      |    |      |    |      |    |      |    |       |    |
| 59  | 8    |      | X  |      |    |      |    |      |    |       |    |
| 463   | 8    |      | X  |      |    |      |    |      |    |       | X  |
| 12  | 8    |      | X  | X    | X  | X    | X  | X    | X  | X     | X  |
| 232   | 8    |      |    |      |    | X    |    |      |    |       |    |
| 292   | 8    |      |    |      |    |      |    | X    |    |       |    |
| <b>2nd International Symposium on High-Temperature Metallurgical Processing</b>                             |      |      |    |      |    |      |    |      |    |       |    |
| Energy Efficient New Metal Production Technology  |      |      |    |      |    |      |    |      |    |       |    |
| 60  | 18   |      | X  |      |    |      |    |      |    |       |    |
| 233   | 18   |      |    |      | X  |      |    |      |    |       |    |
| 116   | 18   |      |    |      |    |      |    |      |    |       |    |
| 354   | 18   |      |    |      | X  |      |    |      | X  |       |    |
| 174   | 18   |      |    |      | X  |      |    |      |    |       |    |
| 417   | 18   |      |    |      |    |      |    |      |    | X     |    |
| 293   | 18   |      |    |      |    |      |    | X    |    |       |    |
| <b>Advances in Mechanics of One-Dimensional Micro/Nano Materials</b>  |      |      |    |      |    |      |    |      |    |       |    |
| Nanomechanics: In-Situ Techniques   |      |      |    |      |    |      |    |      |    |       |    |
| 418   | 1B   |      |    |      |    |      |    |      |    |       | X  |
| 464   | 1B   |      |    |      |    |      |    |      |    |       | X  |
| 295   | 1B   |      |    |      |    |      |    | X    |    |       |    |
| 355   | 1B   |      |    |      |    |      |    |      | X  |       |    |
| Nanomechanics: Size Scale and Theory  |      |      |    |      |    |      |    |      |    |       |    |
| <b>Advances in Science-Based Processing of Superalloys for Cost and Sustainment</b>                         |      |      |    |      |    |      |    |      |    |       |    |
| Application of Modeling and Simulation to Component Design and Life Prediction                              |      |      |    |      |    |      |    |      |    |       |    |
| 118   | 33B  |      |    |      | X  |      |    |      |    |       |    |
| 62  | 33B  |      | X  |      |    |      |    |      |    |       |    |
| 176   | 33B  |      |    |      | X  |      |    |      |    |       |    |
| Processing Advancements via Modeling and Simulation   |      |      |    |      |    |      |    |      |    |       |    |
| Residual Stress and NDE Technologies for Components   |      |      |    |      |    |      |    |      |    |       |    |
| <b>Alumina and Bauxite</b>  |      |      |    |      |    |      |    |      |    |       |    |
| Alternative Alumina Sources - Poster Session  |      |      |    |      |    |      |    |      |    |       |    |
| 21  | 17B  |      | X  |      |    |      |    |      |    |       |    |
| 120   | 17A  |      |    |      | X  |      |    |      |    |       |    |
| 177   | 17A  |      |    |      | X  |      |    |      |    |       |    |
| 357   | 17A  |      |    |      |    |      |    |      | X  |       |    |
| 297   | 17A  |      |    |      |    |      |    | X    |    |       |    |
| 235   | 17A  |      |    |      |    |      | X  |      |    |       |    |
| Red Mud   |      |      |    |      |    |      |    |      |    |       |    |
| <b>Aluminum Alloys: Fabrication, Characterization and Applications</b>                                      |      |      |    |      |    |      |    |      |    |       |    |
| Development and Application   |      |      |    |      |    |      |    |      |    |       |    |
| 64  | 14A  |      |    | X    |    |      |    |      |    |       |    |
| 358   | 14A  |      |    |      |    |      |    |      |    | X     |    |
| 298   | 14A  |      |    |      |    |      |    | X    |    |       |    |
| 121   | 14A  |      |    |      | X  |      |    |      |    |       |    |
| 178   | 14A  |      |    |      | X  |      |    |      |    |       |    |
| 236   | 14A  |      |    |      |    |      | X  |      |    |       |    |
| Thermal Mechanical Processing   |      |      |    |      |    |      |    |      |    |       |    |



| Page  | Room | Sun. |    | Mon. |    | Tue. |    | Wed. |    | Thur. |    |
|---|------|------|----|------|----|------|----|------|----|-------|----|
|   |      | AM   | PM | AM   | PM | AM   | PM | AM   | PM | AM    | PM |
| <b>Aluminum Reduction Technology</b>  |      |      |    |      |    |      |    |      |    |       |    |
| 419   | 17B  |      |    |      |    |      |    |      | X  |       |    |
| 299   | 17B  |      |    |      |    | X    |    |      |    |       |    |
|   | 238  |      |    |      |    | X    |    |      |    |       |    |
| 466   | 17B  |      |    |      | X  |      |    |      |    |       | X  |
| 122   | 17B  |      |    |      |    |      |    |      |    |       |    |
| 179   | 17B  |      |    |      | X  |      |    |      |    |       |    |
| 360   | 17B  |      |    | X    | X  | X    | X  | X    | X  | X     | X  |
| 22  | 17B  |      |    | X    | X  | X    | X  | X    | X  | X     | X  |
| <b>Aluminum Rolling</b>   |      |      |    |      |    |      |    |      |    |       |    |
| 65  | 16A  |      |    | X    |    |      |    |      |    |       |    |
| <b>Approaches for Investigating Phase Transformations at the Atomic Scale</b>                 |      |      |    |      |    |      |    |      |    |       |    |
| Other Systems and Transformations   |      |      |    |      |    |      |    |      |    |       |    |
| 239   | 32B  |      |    |      |    | X    |    |      |    |       |    |
| 23  | 32B  |      | X  | X    | X  | X    |    |      |    |       |    |
| 66  | 32B  |      |    | X    |    |      |    |      |    |       |    |
| 124   | 32B  |      |    | X    |    |      |    |      |    |       |    |
| 181   | 32B  |      |    |      | X  |      |    |      |    |       |    |
| <b>Battery Recycling</b>  |      |      |    |      |    |      |    |      |    |       |    |
| Session I   |      |      |    |      |    |      |    |      |    |       |    |
| 301   | 12   |      |    |      |    |      |    |      | X  |       |    |
| <b>Biological Materials Science</b>   |      |      |    |      |    |      |    |      |    |       |    |
| Bio-Inspiration and Bio-Inspired Materials I: Hard Biomaterials                               |      |      |    |      |    |      |    |      |    |       |    |
| 67  | 15A  |      |    | X    |    |      |    |      |    |       |    |
| 125   | 15A  |      |    | X    |    |      |    |      |    |       |    |
| 240   | 15A  |      |    |      | X  |      |    |      |    |       |    |
| 302   | 15A  |      |    |      |    |      | X  |      |    |       |    |
| 361   | 15A  |      |    |      |    |      |    | X    |    |       |    |
| 420   | 15A  |      |    |      |    |      |    |      | X  | X     | X  |
| 23  | 15A  |      | X  | X    | X  | X    | X  | X    | X  | X     | X  |
| 183   | 15A  |      |    |      |    | X    |    |      |    |       |    |
| Surface Engineering and Biological Interactions   |      |      |    |      |    |      |    |      |    |       |    |
| <b>Bridging Microstructure, Properties and Processing of Polymer Based Advanced Materials</b> |      |      |    |      |    |      |    |      |    |       |    |
| Session I   |      |      |    |      |    |      |    |      |    |       |    |
| 304   | 32B  |      |    |      |    |      |    | X    |    |       |    |
| Session II  |      |      |    |      |    |      |    |      |    |       |    |
| 362   | 32B  |      |    |      |    |      |    |      | X  |       |    |
| <b>Bulk Metallic Glasses VIII</b>   |      |      |    |      |    |      |    |      |    |       |    |
| Alloy Development and Application I   |      |      |    |      |    |      |    |      |    |       |    |
| 69  | 6D   |      |    | X    |    |      |    |      |    |       |    |
| 127   | 6D   |      |    | X    |    |      |    |      |    |       |    |
| 305   | 6D   |      |    |      | X  |      |    |      |    |       |    |
| 422   | 6D   |      |    |      |    |      |    |      | X  |       | X  |
| 467   | 6D   |      |    |      |    |      |    |      |    | X     |    |
| 364   | 6D   |      |    |      |    |      |    |      | X  |       |    |
| 184   | 6D   |      |    |      |    | X    |    |      |    |       |    |
| 242   | 6D   |      |    |      |    |      | X  |      |    |       |    |
| <b>Carbon Dioxide and Other Greenhouse Gas Reduction Metallurgy - 2011</b>                    |      |      |    |      |    |      |    |      |    |       |    |
| CO2 and GHG Reduction in Metal Industries   |      |      |    |      |    |      |    |      |    |       |    |
| 469   | 15B  |      |    |      |    |      |    |      |    |       | X  |
| 424   | 15B  |      |    |      |    |      |    |      |    |       | X  |
| Electrochemical Reduction Methods - CO2 Use and Other Metal Production                        |      |      |    |      |    |      |    |      |    |       |    |

# PROGRAM AT-A-GLANCE

| Page   | Room | Sun. |    | Mon. |    | Tue. |    | Wed. |    | Thur. |    |
|--|------|------|----|------|----|------|----|------|----|-------|----|
|  |      | AM   | PM | AM   | PM | AM   | PM | AM   | PM | AM    | PM |
| <b>Cast Shop for Aluminum Production</b>   |      |      |    |      |    |      |    |      |    |       |    |
| 129  | 16A  |      |    | X    |    |      |    |      |    |       |    |
| 186  | 16A  |      |    |      | X  |      |    |      |    |       |    |
| 244  | 16A  |      |    |      |    | X    |    |      |    |       |    |
| 366  | 16A  |      |    |      |    |      |    | X    |    |       |    |
| 307  | 16A  |      |    |      |    |      |    |      | X  |       |    |
| <b>Challenges in Mechanical Performances of Materials in Next Generation Nuclear Power Plants</b>          |      |      |    |      |    |      |    |      |    |       |    |
| 426  | 5A   |      |    |      |    |      |    |      |    | X     |    |
| 470  | 5A   |      |    |      |    |      |    |      |    |       | X  |
| <b>Characterization of Minerals, Metals and Materials</b>  |      |      |    |      |    |      |    |      |    |       |    |
| 71   | 14B  |      |    | X    |    |      |    |      |    |       |    |
| 245  | 14B  |      |    |      |    | X    |    |      |    |       |    |
| 427  | 14B  |      |    |      |    |      | X  |      |    |       |    |
| 187  | 14B  |      |    |      | X  |      |    |      |    |       |    |
| 130  | 14B  |      |    | X    |    |      |    |      |    |       |    |
| 368  | 14B  |      |    | X    | X  | X    | X  | X    | X  | X     | X  |
| 25   | 14B  |      | X  | X    | X  | X    | X  | X    | X  | X     | X  |
| 309  | 14B  |      |    |      |    |      |    | X    |    |       |    |
| <b>Characterization of Nuclear Reactor Materials and Components with Neutron and Synchrotron Radiation</b> |      |      |    |      |    |      |    |      |    |       |    |
| 370  | 4    |      |    |      |    |      |    |      | X  |       |    |
| 472  | 4    |      |    |      |    |      |    |      |    |       | X  |
| 430  | 4    |      |    |      |    |      |    |      |    | X     |    |
| <b>Chloride 2011: Practice and Theory of Chloride-Based Metallurgy</b>                                     |      |      |    |      |    |      |    |      |    |       |    |
| 73   | 19   |      |    | X    |    |      |    |      |    |       |    |
| 189  | 19   |      |    |      | X  |      |    |      |    |       |    |
| 26   | 19   |      | X  | X    | X  | X    |    |      |    |       |    |
| 132  | 19   |      |    |      | X  |      |    |      |    |       |    |
| <b>Coatings for Structural, Biological, and Electronic Applications II</b>                                 |      |      |    |      |    |      |    |      |    |       |    |
| 431  | 6E   |      |    |      |    |      |    |      |    | X     |    |
| 311  | 6E   |      |    |      |    |      |    | X    |    |       |    |
| 371  | 6E   |      |    |      |    |      |    |      | X  |       |    |
| <b>Commonality of Phenomena in Composite Materials II</b>  |      |      |    |      |    |      |    |      |    |       |    |
| 433  | 6A   |      |    |      |    |      |    |      |    | X     |    |
| 312  | 6A   |      |    |      |    |      |    |      | X  |       |    |
| 373  | 6A   |      |    |      |    |      |    |      |    | X     |    |
| <b>Computational Plasticity</b>  |      |      |    |      |    |      |    |      |    |       |    |
| 247  | 1A   |      |    |      |    |      | X  |      |    |       |    |
| 314  | 1A   |      |    |      |    |      |    | X    |    |       |    |
| 374  | 1A   |      |    |      |    |      |    |      | X  |       |    |
| 434  | 1A   |      |    |      |    |      |    |      |    | X     |    |
| 473  | 1A   |      |    |      |    |      |    |      |    |       | X  |

| Page  | Room | Sun. |    | Mon. |    | Tue. |    | Wed. |    | Thur. |    |
|---|------|------|----|------|----|------|----|------|----|-------|----|
|   |      | AM   | PM | AM   | PM | AM   | PM | AM   | PM | AM    | PM |
| <b>Computational Thermodynamics and Kinetics</b>  |      |      |    |      |    |      |    |      |    |       |    |
| 133   | 9    |      |    | X    |    |      |    |      |    |       |    |
| 191   | 9    |      |    |      | X  |      |    |      |    |       |    |
| 74  | 9    |      |    | X    |    |      |    |      |    |       |    |
| 249   | 9    |      |    |      |    | X    |    |      |    |       |    |
| 315   | 9    |      |    |      |    |      |    | X    |    |       |    |
| 27  | 9    | X    |    | X    | X  | X    | X  | X    | X  | X     | X  |
| 435   | 9    |      |    |      |    |      |    |      |    |       | X  |
| 376   | 9    |      |    |      |    |      |    |      | X  |       |    |
| <b>David Pope Honorary Symposium on Fundamentals of Deformation and Fracture of Advanced Metallic Materials</b> |      |      |    |      |    |      |    |      |    |       |    |
| 317   | 32A  |      |    |      |    |      |    | X    |    |       |    |
| 250   | 32A  |      |    |      |    | X    |    |      |    |       |    |
| 377   | 32A  |      |    |      |    |      |    |      | X  |       |    |
| 76  | 32A  |      |    | X    |    |      |    |      |    |       |    |
| 134   | 32A  |      |    |      |    |      | X  |      |    |       |    |
| 192   | 32A  |      |    |      |    |      |    |      |    |       |    |
| <b>Deformation, Damage, and Fracture of Light Metals and Alloys</b>   |      |      |    |      |    |      |    |      |    |       |    |
| 193   | 13   |      |    |      |    | X    |    |      |    |       |    |
| 252   | 13   |      |    |      |    |      | X  |      |    |       |    |
| 318   | 13   |      |    |      |    |      |    | X    |    |       |    |
| <b>Dynamic Behavior of Materials V</b>  |      |      |    |      |    |      |    |      |    |       |    |
| 136   | 5A   |      |    |      | X  |      |    |      |    |       |    |
| 320   | 5A   |      |    |      |    |      |    | X    |    |       |    |
| 379   | 5A   |      |    |      |    |      |    |      | X  |       |    |
| 78  | 5A   |      |    | X    |    |      |    |      |    |       |    |
| 253   | 5A   |      |    |      |    |      |    | X    |    |       |    |
| 195   | 5A   |      |    |      |    |      | X  |      |    |       |    |
| <b>Electrode Technology for Aluminium Production</b>  |      |      |    |      |    |      |    |      |    |       |    |
| 137   | 16B  |      |    |      | X  |      |    |      |    |       |    |
| 322   | 16B  |      |    |      |    |      |    | X    |    |       |    |
| 197   | 16B  |      |    |      |    | X    |    |      |    |       |    |
| 381   | 16B  |      |    |      |    |      |    |      | X  |       |    |
| 436   | 16B  |      |    |      |    |      |    |      |    | X     |    |
| 475   | 16B  |      |    |      |    |      |    |      |    |       | X  |
| 255   | 16B  |      |    |      |    |      |    | X    |    |       |    |
| 30  | 17B  | X    |    | X    | X  | X    | X  | X    | X  | X     | X  |
| <b>Electrometallurgy Fundamentals and Applications</b>  |      |      |    |      |    |      |    |      |    |       |    |
| 476   | 18   |      |    |      |    |      |    |      |    |       | X  |
| <b>Fatigue and Corrosion Damage in Metallic Materials: Fundamentals, Modeling and Prevention</b>                |      |      |    |      |    |      |    |      |    |       |    |
| 256   | 31C  |      |    |      |    |      |    |      | X  |       |    |
| 198   | 31C  |      |    |      |    |      | X  |      |    |       |    |
| 139   | 31C  |      |    |      |    | X    |    |      |    |       |    |
| 79  | 31C  |      |    | X    |    |      |    |      |    |       |    |
| 323   | 31C  |      |    |      |    |      |    |      | X  |       |    |

# PROGRAM AT-A-GLANCE

| Page   | Room         | Sun. |    | Mon. |    | Tue. |    | Wed. |    | Thur. |    |
|--|--------------|------|----|------|----|------|----|------|----|-------|----|
|  |              | AM   | PM | AM   | PM | AM   | PM | AM   | PM | AM    | PM |
| <b>Federal Funding Workshop</b>  |              |      |    |      |    |      |    |      |    |       |    |
| 140  | 6E           |      |    | X    |    |      |    |      |    |       |    |
| <b>Friction Stir Welding and Processing VI</b>                                 |              |      |    |      |    |      |    |      |    |       |    |
| 199  | 5B           |      |    |      | X  |      |    |      |    |       |    |
| 258  | 5B           |      |    |      |    | X    |    |      |    |       |    |
| 325  | 5B           |      |    |      |    |      | X  |      |    |       |    |
| 437  | 5B           |      |    |      |    |      |    |      |    | X     |    |
| 81   | 5B           |      |    | X    |    |      |    |      |    |       |    |
| 141  | 5B           |      |    | X    |    |      |    |      |    |       |    |
| 382  | 5B           |      |    |      |    |      |    |      | X  |       |    |
| <b>Frontiers in Solidification Science</b>                                     |              |      |    |      |    |      |    |      |    |       |    |
| 82   | 6E           |      |    | X    |    |      |    |      |    |       |    |
| 201  | 6E           |      |    |      | X  |      |    |      |    |       |    |
| 142  | 6E           |      |    | X    |    |      |    |      |    |       |    |
| 260  | 6E           |      |    |      | X  |      |    |      |    |       |    |
| 30   | 6E           | X    |    | X    | X  | X    |    |      |    |       |    |
| <b>Furnace Efficiency - Energy and Throughput</b>                              |              |      |    |      |    |      |    |      |    |       |    |
| 326  | 4            |      |    |      |    |      |    | X    |    |       |    |
| <b>Geek Speak on the Hill</b>  |              |      |    |      |    |      |    |      |    |       |    |
| 83   | 17B          |      |    | X    |    |      |    |      |    |       |    |
| <b>General Abstracts: Electronic, Magnetic and Photonic Materials Division</b> |              |      |    |      |    |      |    |      |    |       |    |
| 84   | 16B          |      |    | X    |    |      |    |      |    |       |    |
| 477  | 9            |      |    |      |    |      |    |      |    |       | X  |
| <b>General Abstracts: Light Metals Division</b>                                |              |      |    |      |    |      |    |      |    |       |    |
| 478  | 14B          |      |    |      |    |      |    |      |    |       | X  |
| 439  | 17A          |      |    |      |    |      |    |      |    | X     |    |
| 85   | 17A          |      |    | X    |    |      |    |      |    |       |    |
| <b>General Abstracts: Materials Processing and Manufacturing Division</b>      |              |      |    |      |    |      |    |      |    |       |    |
| 480  | 2            |      |    |      |    |      |    |      |    |       | X  |
| 482  | 5B           |      |    |      |    |      |    |      |    |       | X  |
| 484  | 7B           |      |    |      |    |      |    |      |    |       | X  |
| <b>General Abstracts: Structural Materials Division</b>                        |              |      |    |      |    |      |    |      |    |       |    |
| 384  | 31C          |      |    |      |    |      |    | X    |    |       |    |
| 486  | 11B          |      |    |      |    |      |    |      |    |       | X  |
| 489  | 6A           |      |    |      |    |      |    |      |    |       | X  |
| <b>General Poster Session</b>  |              |      |    |      |    |      |    |      |    |       |    |
| 505  | Exhibit Hall |      |    | X    | X  | X    | X  | X    | X  | X     | X  |



| Page   | Room | Sun. |    | Mon. |    | Tue. |    | Wed. |    | Thur. |    |
|--|------|------|----|------|----|------|----|------|----|-------|----|
|  |      | AM   | PM | AM   | PM | AM   | PM | AM   | PM | AM    | PM |
| <b>Hume-Rothery Symposium Thermodynamics and Diffusion Coupling in Alloys - Application Driven Science</b>   |      |      |    |      |    |      |    |      |    |       |    |
| 328  | 31A  |      |    |      |    |      |    |      | X  |       |    |
| 202  | 31A  |      |    |      |    | X    |    |      |    |       |    |
| 261  | 31A  |      |    |      |    |      | X  |      |    |       |    |
| 386  | 31A  |      |    |      |    |      |    | X    |    |       |    |
| 143  | 31A  |      |    |      | X  |      |    |      |    |       |    |
| 87   | 31A  |      |    | X    |    |      |    |      |    |       |    |
| <b>Hydrogen Storage in Materials: Theory and Experiment</b>  |      |      |    |      |    |      |    |      |    |       |    |
| 88   | 13   |      |    | X    |    |      |    |      |    |       |    |
| 144  | 13   |      |    |      | X  |      |    |      |    |       |    |
| <b>Hydrometallurgy Fundamentals and Applications</b>   |      |      |    |      |    |      |    |      |    |       |    |
| 440  | 16A  |      |    |      |    |      |    |      |    | X     |    |
| 491  | 16A  |      |    |      |    |      |    |      |    |       | X  |
| <b>ICME: Overcoming Barriers and Streamlining the Transition of Advanced Technologies to Engineering Practice - The 12th MPMD Global Innovations Symposium</b> |      |      |    |      |    |      |    |      |    |       |    |
| 203  | 7A   |      |    |      |    |      | X  |      |    |       |    |
| 146  | 7A   |      |    |      | X  |      |    |      |    |       |    |
| 89   | 7A   |      |    | X    |    |      |    |      |    |       |    |
| <b>Intelligent Materials and Structural Health Monitoring</b>  |      |      |    |      |    |      |    |      |    |       |    |
| 91   | 33C  |      |    | X    |    |      |    |      |    |       |    |
| <b>Magnesium Technology 2011</b>   |      |      |    |      |    |      |    |      |    |       |    |
| 492  | 6F   |      |    |      |    |      |    |      |    |       | X  |
| 205  | 6F   |      |    |      |    | X    |    |      |    |       |    |
| 147  | 10   |      |    |      | X  |      |    |      |    |       |    |
| 493  | 10   |      |    |      |    |      |    |      |    |       | X  |
| 387  | 6F   |      |    |      |    |      | X  |      |    |       |    |
| 329  | 6F   |      |    |      |    |      |    | X    |    |       |    |
| 262  | 6F   |      |    |      |    |      | X  |      |    |       |    |
| 441  | 6F   |      |    |      |    |      |    |      |    | X     |    |
| 92   | 6F   |      |    | X    |    |      |    |      |    |       | X  |
| 32   | 6F   | X    |    | X    | X  | X    | X  | X    | X  | X     | X  |
| 149  | 6F   |      |    |      | X  |      |    |      |    |       |    |
| <b>Magnetic Materials for Energy Applications</b>  |      |      |    |      |    |      |    |      |    |       |    |
| 331  | 11A  |      |    |      |    |      |    |      | X  |       |    |
| 495  | 11A  |      |    |      |    |      |    |      |    |       | X  |
| 150  | 11A  |      |    |      |    | X    |    |      |    |       |    |
| 208  | 11A  |      |    |      |    |      | X  |      |    |       |    |
| 389  | 11A  |      |    |      |    |      |    | X    |    |       |    |
| 207  | 11A  |      |    |      |    |      | X  |      |    |       | X  |
| 443  | 11A  |      |    |      |    |      |    |      |    | X     |    |
| 444  | 11A  |      |    |      |    |      |    |      |    | X     |    |
| 263  | 11A  |      |    |      |    | X    |    |      |    |       |    |

# PROGRAM AT-A-GLANCE

| Page   | Room | Sun. |    | Mon. |    | Tue. |    | Wed. |    | Thur. |    |
|--|------|------|----|------|----|------|----|------|----|-------|----|
|  |      | AM   | PM | AM   | PM | AM   | PM | AM   | PM | AM    | PM |
|  |      |      |    |      |    |      |    |      |    |       |    |
| <b>Massively Parallel Simulations of Materials Response</b>  |      |      |    |      |    |      |    |      |    |       |    |
| 93   | 1A   |      |    | X    |    |      |    |      |    |       |    |
| 152  | 1A   |      |    |      | X  |      |    |      |    |       |    |
| 208  | 1A   |      |    |      |    | X    |    |      |    |       |    |
| <b>Material Science Advances Using Test Reactor Facilities</b>                                       |      |      |    |      |    |      |    |      |    |       |    |
| 332  | 3    |      |    |      |    |      |    |      | X  |       |    |
| <b>Materials and Society: Linking Science and Technology for Global Energy Solutions</b>             |      |      |    |      |    |      |    |      |    |       |    |
| 94   | 11A  |      |    | X    |    |      |    |      |    |       |    |
| <b>Materials for the Nuclear Renaissance II</b>  |      |      |    |      |    |      |    |      |    |       |    |
| 154  | 4    |      |    |      | X  |      |    |      |    |       |    |
| 95   | 4    |      |    | X    |    |      |    |      |    |       |    |
| 210  | 4    |      |    |      | X  |      |    |      |    |       |    |
| 265  | 4    |      |    |      |    | X    |    |      |    |       |    |
| <b>Materials in Clean Power Systems VI: Clean Coal-, Hydrogen Based-Technologies, and Fuel Cells</b> |      |      |    |      |    |      |    |      |    |       |    |
| 155  | 33C  |      |    |      | X  |      |    |      |    |       |    |
| 212  | 33C  |      |    |      |    | X    |    |      |    |       |    |
| 391  | 33C  |      |    |      |    |      |    | X    |    |       |    |
| 267  | 33C  |      |    |      |    |      | X  |      |    |       |    |
| 334  | 33C  |      |    |      |    |      |    |      | X  |       |    |
| <b>Materials Processing Fundamentals</b>   |      |      |    |      |    |      |    |      |    |       |    |
| 39   | 12   | X    |    | X    | X  | X    | X  |      |    |       |    |
| 213  | 12   |      |    |      | X  |      |    |      |    |       |    |
| 156  | 12   |      |    |      | X  |      |    |      |    |       |    |
| 268  | 12   |      |    |      |    | X    |    |      |    |       |    |
| 97   | 12   |      |    | X    |    |      |    |      |    |       |    |
| <b>Microstructural Processes in Irradiated Materials</b>   |      |      |    |      |    |      |    |      |    |       |    |
| 99   | 3    |      |    | X    |    |      |    |      |    |       |    |
| 157  | 3    |      |    |      | X  |      |    |      |    |       |    |
| 215  | 3    |      |    |      |    | X    |    |      |    |       |    |
| 393  | 3    |      |    |      |    |      |    | X    |    |       |    |
| 496  | 3    |      |    |      |    |      |    |      |    | X     |    |
| 445  | 3    |      |    |      |    |      |    |      |    | X     |    |
| 270  | 3    |      |    |      |    |      | X  |      |    |       |    |
| 40   | 3    | X    |    | X    | X  | X    | X  | X    | X  | X     | X  |
| <b>Neutron and X-Ray Studies of Advanced Materials IV</b>  |      |      |    |      |    |      |    |      |    |       |    |
| 133  | 9    |      |    |      | X  |      |    |      |    |       |    |
| 217  | 10   |      |    |      |    | X    |    |      |    |       |    |
| 271  | 10   |      |    |      |    |      | X  |      |    |       |    |
| 394  | 10   |      |    |      |    |      |    | X    |    |       |    |
| 446  | 10   |      |    |      |    |      |    |      | X  |       |    |
| 100  | 10   |      |    | X    |    |      |    |      |    | X     |    |
| 44   | 10   | X    |    | X    | X  | X    | X  | X    | X  | X     | X  |
| 335  | 10   |      |    |      |    |      |    |      |    | X     |    |

| Page  | Room | Sun. |    | Mon. |    | Tue. |    | Wed. |    | Thur. |    |
|---|------|------|----|------|----|------|----|------|----|-------|----|
|   |      | AM   | PM | AM   | PM | AM   | PM | AM   | PM | AM    | PM |
| <b>Pb-Free Solders and Other Materials for Emerging Interconnect and Packaging Technologies</b>       |      |      |    |      |    |      |    |      |    |       |    |
| 219   | 7B   |      |    |      |    | X    |    |      |    |       |    |
| 397   | 7B   |      |    |      |    |      |    |      | X  |       |    |
| 102   | 7B   |      |    | X    |    |      |    |      |    |       |    |
| 45  | 7B   |      |    | X    |    | X    |    | X    |    |       |    |
| 449   | 7B   |      |    |      |    |      |    |      | X  |       |    |
| 274   | 7B   |      |    |      |    |      |    |      |    |       |    |
| 337   | 7B   |      |    |      |    |      |    |      | X  |       |    |
| 159   | 7B   |      |    |      | X  |      |    |      |    |       |    |
| <b>Phase Stability, Phase Transformations, and Reactive Phase Formation in Electronic Materials X</b> |      |      |    |      |    |      |    |      |    |       |    |
| 398   | 7A   |      |    |      |    |      |    |      | X  |       |    |
| 497   | 7A   |      |    |      |    |      |    |      |    |       | X  |
| 339   | 7A   |      |    |      |    |      |    | X    |    |       |    |
| 451   | 7A   |      |    |      |    |      |    |      |    |       | X  |
| 275   | 7A   |      |    |      |    |      | X  |      |    |       |    |
| <b>Physical and Mechanical Metallurgy of Shape Memory Alloys for Actuator Applications</b>            |      |      |    |      |    |      |    |      |    |       |    |
| 340   | 11B  |      |    |      |    |      |    |      | X  |       |    |
| 452   | 11B  |      |    |      |    |      |    |      |    |       | X  |
| 104   | 11B  |      |    | X    |    |      |    |      |    |       |    |
| 220   | 11B  |      |    |      |    | X    |    |      |    |       |    |
| 161   | 11B  |      |    |      | X  |      |    |      |    |       |    |
| 400   | 11B  |      |    |      |    |      |    |      |    | X     |    |
| 277   | 11B  |      |    |      |    |      | X  |      |    |       |    |
| 50  | 11B  |      |    | X    |    | X    |    | X    |    | X     |    |
| <b>Polycrystal Modelling with Experimental Integration: A Symposium Honoring Carlos Tome</b>          |      |      |    |      |    |      |    |      |    |       |    |
| 342   | 6C   |      |    |      |    |      |    |      | X  |       |    |
| 105   | 6C   |      |    | X    |    |      |    |      |    |       |    |
| 454   | 6C   |      |    |      |    |      |    |      |    |       | X  |
| 222   | 6C   |      |    |      |    | X    |    |      |    |       |    |
| 163   | 6C   |      |    |      |    |      |    | X    |    |       |    |
| 278   | 6C   |      |    |      |    |      |    | X    |    |       |    |
| 52  | 6C   |      |    | X    |    | X    |    | X    |    | X     |    |
| 401   | 6C   |      |    |      |    |      |    |      | X  |       |    |
| <b>Processing and Properties of Powder-Based Materials</b>  |      |      |    |      |    |      |    |      |    |       |    |
| 223   | 33A  |      |    |      |    |      |    | X    |    |       |    |
| 403   | 33A  |      |    |      |    |      |    |      |    |       |    |
| 54  | 33A  |      |    | X    |    | X    |    | X    |    | X     |    |
| 343   | 33A  |      |    |      |    |      |    |      |    | X     |    |
| 280   | 33A  |      |    |      |    |      |    |      |    |       | X  |
| 164   | 33A  |      |    |      |    |      | X  |      |    |       |    |

**PROGRAM AT-A-GLANCE**

| Page  | Room | Sun. |    | Mon. |    | Tue. |    | Wed. |    | Thur. |    |
|---|------|------|----|------|----|------|----|------|----|-------|----|
|   |      | AM   | PM | AM   | PM | AM   | PM | AM   | PM | AM    | PM |
| <b>Properties, Processing, and Performance of Steels and Ni-Based Alloys for Advanced Steam Conditions</b>            |      |      |    |      |    |      |    |      |    |       |    |
| 281   | 33B  |      |    |      |    | X    |    |      |    |       |    |
| 404   | 33B  |      |    |      |    |      | X  |      |    |       |    |
| 345   | 33B  |      |    |      |    |      |    | X    |    |       |    |
| <b>Recent Developments in the Processing, Characterization, Properties and Performance of Metal Matrix Composites</b> |      |      |    |      |    |      |    |      |    |       |    |
| 107   | 6A   |      |    | X    |    |      |    |      |    |       |    |
| 166   | 6A   |      |    |      | X  |      |    |      |    |       |    |
| 225   | 6A   |      |    |      |    | X    |    |      |    |       |    |
| 283   | 6A   |      |    |      |    |      | X  |      |    |       |    |
| <b>Recycling General Session</b>  |      |      |    |      |    |      |    |      |    |       |    |
| 499   | 12   |      |    |      |    |      |    |      |    |       | X  |
| 406   | 12   |      |    |      |    |      |    |      | X  |       |    |
| 456   | 12   |      |    |      |    |      |    |      |    | X     |    |
| <b>Refractory Metals 2011</b>   |      |      |    |      |    |      |    |      |    |       |    |
| 500   | 19   |      |    |      |    |      |    |      |    |       | X  |
| 284   | 19   |      |    |      |    | X    |    |      |    |       |    |
| 407   | 19   |      |    |      |    |      |    | X    |    |       |    |
| 457   | 19   |      |    |      |    |      |    |      | X  |       |    |
| 346   | 19   |      |    |      |    |      | X  |      |    |       |    |
| <b>Sensors, Sampling, and Simulation for Process Control</b>  |      |      |    |      |    |      |    |      |    |       |    |
| 409   | 13   |      |    |      |    |      |    |      | X  |       |    |
| 502   | 13   |      |    |      |    |      |    |      |    | X     |    |
| 459   | 13   |      |    |      |    |      |    |      |    | X     |    |
| <b>Shape Casting IV: Light Metals Division Symposium in Honor of Prof. John T. Berry</b>                              |      |      |    |      |    |      |    |      |    |       |    |
| 410   | 15B  |      |    |      |    |      |    |      | X  |       |    |
| 226   | 15B  |      |    |      |    | X    |    |      |    |       |    |
| 348   | 15B  |      |    |      |    |      |    | X    |    |       |    |
| 285   | 15B  |      |    |      |    |      | X  |      |    |       |    |
| 55  | 14A  |      | X  | X    | X  | X    | X  | X    | X  | X     | X  |
| 460   | 14A  |      |    |      |    |      |    |      |    | X     |    |
| 503   | 14A  |      |    |      |    |      |    |      |    |       | X  |
| <b>Silicon Production, Purification and Recycling for Photovoltaic Cells</b>  |      |      |    |      |    |      |    |      |    |       |    |
| Poster Session  |      |      |    |      |    |      |    |      |    |       |    |
| Session I   |      |      |    |      |    |      |    |      |    |       |    |
| Session II  |      |      |    |      |    |      |    |      |    |       |    |
| <b>Size Effects in Mechanical Behavior</b>  |      |      |    |      |    |      |    |      |    |       |    |
| 286   | 2    |      |    |      |    | X    |    |      |    |       |    |
| 461   | 2    |      |    |      |    |      |    |      |    | X     |    |
| 227   | 2    |      |    |      | X  |      |    |      |    |       |    |
| 349   | 2    |      |    |      |    |      | X  |      |    |       |    |
| 411   | 2    |      |    |      |    |      |    |      | X  |       |    |
| 108   | 2    |      |    | X    |    |      |    |      |    |       |    |
| 167   | 2    |      |    |      |    |      |    |      |    | X     |    |



| Page   | Room | Sun. |    | Mon. |    | Tue. |    | Wed. |    | Thur. |    |
|--|------|------|----|------|----|------|----|------|----|-------|----|
|  |      | AM   | PM | AM   | PM | AM   | PM | AM   | PM | AM    | PM |
| <b>Surfaces and Heterostructures at Nano- or Micro-Scale and Their Characterization, Properties, and Application</b> |      |      |    |      |    |      |    |      |    |       |    |
| 229  | 31B  |      |    |      |    | X    |    |      |    |       |    |
| 350  | 31B  |      |    |      |    |      | X  |      |    |       |    |
| 110  | 31B  |      |    | X    |    |      |    |      |    |       |    |
| 169  | 31B  |      |    |      | X  |      |    |      |    |       |    |
| 288  | 31B  |      |    |      |    |      |    | X    |    |       |    |
| 55   | 31B  |      | X  |      |    |      |    |      |    |       |    |
| <b>The Second Symposium on the Recycling of Electronic Wastes</b>  |      |      |    |      |    |      |    |      |    |       |    |
| 111  | 15B  |      |    |      | X  |      |    |      |    |       |    |
| 56   | 15B  |      |    |      | X  |      |    |      |    |       |    |
| 170  | 15B  |      |    | X    |    |      |    |      |    |       |    |
| <b>Thermally Activated Processes in Plastic Deformation</b>  |      |      |    |      |    |      |    |      |    |       |    |
| 289  | 1B   |      |    |      |    |      | X  |      |    |       |    |
| 230  | 1B   |      |    |      |    |      | X  |      |    |       |    |
| 171  | 1B   |      |    |      | X  |      |    |      |    |       |    |
| 112  | 1B   |      |    | X    |    |      |    |      |    |       |    |
| <b>Ultrasonic Welding for Lightweight Components</b>   |      |      |    |      |    |      |    |      |    |       |    |
| 114  | 33A  |      |    |      | X  |      |    |      |    |       |    |
| <b>Waste Heat Recovery</b>   |      |      |    |      |    |      |    |      |    |       |    |
| 413  | 31B  |      |    |      |    |      |    |      | X  |       |    |

# PROGRAM AT-A-GLANCE

## 2011 Functional and Structural Nanomaterials: Fabrication, Properties, Applications and Implications: Poster Session

*Sponsored by:* The Minerals, Metals and Materials Society, TMS Electronic, Magnetic, and Photonic Materials Division, TMS: Nanomaterials Committee

*Program Organizers:* Jiyoung Kim, Univ of Texas; David Stollberg, Georgia Tech Research Institute; Seong Jin Koh, University of Texas at Arlington; Nitin Chopra, The University of Alabama; Suveen Mathaudhu, U.S. Army Research Office

Sun PM-Thurs PM Room: 8  
Feb 27-Mar 3, 2011 Location: San Diego Conv. Ctr

*Session Chairs:* Jiyoung Kim, University of Texas at Dallas; Seong Jin Koh, University of Texas at Arlington; David Stollberg, GTRI

### A Novel Type of Carbon Coated Sulfur Nanoparticles for Li/S Batteries:

*Yan Yuan*<sup>1</sup>; Elton Cairns<sup>1</sup>; <sup>1</sup>LBNL

This kind of carbon coated sulfur nanoparticles have been synthesized via a novel liquid-synthesis technique, this reaction in the presence of a surfactant (polyethylene glycol-400) has been developed to get S-C nanoparticles by using sublimed sulfur powders, sodium sulfide, formic acid and carbon black (battery grade) under room temperature. It has been physically characterized by scanning electron microscopy, EDS, and thermogravimetric analysis instrument. The SEM image shows that the size of carbon coated sulfur nanoparticles is around 30nm. The TGA result shows that the S-C sample is quite pure, and the ratio of sulfur and carbon is equal to what we set initially. Besides, it can be used as cathode in Li/S batteries, it improved the electrochemical performance of Li/S batteries.

**Chemical Deposited CdS Nanoparticles on TiO<sub>2</sub> Nanotube Arrays:** *Amin Azizi*<sup>1</sup>; *Mojtaba Hamed*<sup>2</sup>; *Seyyed Khatiboleslam Sadmezhaad*<sup>2</sup>; <sup>1</sup>Tulane University; <sup>2</sup>Sharif Univesity of Technology

In this research, chemically deposition of CdS nanoparticles on the surface of TiO<sub>2</sub> nanotube-arrays is report. Highly-ordered TiO<sub>2</sub> nanotube arrays with the diameter of ~100nm were synthesized by anodization of a titanium foil. According to the results, the surface of nanotube arrays was homogenously covered by a thin layer of the CdS nanoparticulates consist of spherical nanoparticles with ~50 nm diameter.

**Chemical Synthesis and Characterization of Manganese Nanoparticles:** *Lei Zhang*<sup>1</sup>; *David Nikles*<sup>1</sup>; *Gregory Thompson*<sup>1</sup>; <sup>1</sup>University of Alabama

Metallic phase manganese nanoparticles have drawn attention because of its unique structure and magnetic properties. The stable phase of manganese has an A12 structure with 58 atoms in a cubic cell, and is paramagnetic with a Neel temperature of TN=95K. Manganese nanoparticles were prepared by an n-butyl lithium reduction of manganese chloride in phenyl ether at elevated temperature with oleic acid. The particles had a thin oxide layer and oleic acid coating, which stabilized them in air. The particle sizes were altered by varying the oleic acid concentration and the reaction temperature. X-ray diffraction and transmission electron microscopy, including convergent electron beam diffraction, were done to determine the crystal structure as a function of particle size.

**Effect of Mn on AOT Capped CdS Nanoparticles and Thin Films:** *Dhanasekaran Venkatesan*<sup>1</sup>; *Dorairaj Deepan*<sup>2</sup>; *Ram Kumar*<sup>3</sup>; *S. Moorthy Babu*<sup>3</sup>; *Prabhu Megharaj*<sup>4</sup>; *Gokula Krishna Muralidharan*<sup>2</sup>; *Guruhariharan Rajendran*<sup>2</sup>; <sup>1</sup>KTH, Royal Institute of Technology, Sweden; <sup>2</sup>KU Leuven; <sup>3</sup>Anna University Chennai; <sup>4</sup>University of Cincinnati

Diocetyl sodium sulfosuccinate (AOT) capped CdS nanoparticles are prepared using CdCl<sub>2</sub> and Na<sub>2</sub>S as precursors. Concentration of AOT is optimized and it is found that 0.04M AOT, the particle is found to have smaller size, the absorption peak is at 422 nm. Varying mol % of Mn is added to CdS system. The UV-Vis absorption peak is found at 459 nm is observed for the Mn doped CdS nanoparticles. In PL, the emission at 488nm

is due to the surface defect in CdS system and 575 nm is due to the 4T<sub>1</sub> → 6A<sub>1</sub> transition of Mn<sup>2+</sup> ion. FT-IR spectra shows the C=O band at 1643 cm<sup>-1</sup> and C-H band at 2800-2900cm<sup>-1</sup>. Thin films are casted on the glass substrate. XRD patterns confirm the hexagonal crystal structure of CdS, shifts are observed in doped sample. SEM images reveal the agglomerated nanoparticles, found to be 50 to 100 nm. EDX shows varying percentage of Mn content and Cd:S were found to be in ratio 1:2.2. The low temperature Electro Paramagnetic Spectrometer spectrum line width of samples is due magnetic interactions between manganese ions.

**Preparation and Characterization of ZnS Thin Films Using Chemical Bath Deposition Method: Effects of Deposition Time and Thermal Treatment:** *Way-Ming Hsieh*<sup>1</sup>; *Kong-Wei Cheng*<sup>1</sup>; *Shing-jiang Jessie Lue*<sup>1</sup>; <sup>1</sup>Chang Gung University

This research focuses on zinc sulphide thin film preparation using the chemical bath deposition (CBD) method. The obtained product is to be used as the Cd-free buffer layer for CIGS solar cells. The zinc sulfate, thiourea, hydrazine, and ammonia parameters were carefully selected to obtain ZnS thin films. The deposition time and annealing effects on the optical properties and electrical properties were studied. Scanning electron microscope images show that the film surface consists of small uniform grains (about 40 nm in size), free of pin-hole defects. Hall Effect measurements show the synthesized ZnS was an n-type semiconductor with a resistivity of 1 × 10<sup>3</sup> Ω cm. The UV-visible spectrometry analysis showed the high transmittance film thickness increased from 50 to 120 nm. The transmittance values decreased after annealing. The resulting chemical composition of the ZnS thin films are discussed in terms of the CBD process parameters.

**Enhanced Photocatalytic Activity of Modified TiO<sub>2</sub> for Degradation of CH<sub>2</sub>O in Aqueous Suspension:** *Tong Haixia*<sup>1</sup>; *Yang Daowu*<sup>1</sup>; <sup>1</sup>Changsha University of Science and Technology

Butyltitanate, ethanol and glacial acetic acid were chosen as titanium source, solvent and chelating agent respectively via a sol - gel method combined impregnation method to prepare N, Fe co-doped and WO<sub>3</sub> compounded photocatalyst TiO<sub>2</sub> powder. The synthesized products were characterized by X-ray diffraction (XRD), Diffuse reflectance UV-Vis spectra (UV-DRS), and scanning electron microscopy(SEM). The catalytic activity investigated employing photocatalytic degradation of formaldehyde. The results show that when the concentration of N is fixed on, the optimum proportioning ratio of n (Fe): n (W): n (Ti) is 0.5:2:100, and the degradation rate is 77.61% in 180min under UV light irradiation.

**Fabrication of ITO Nano-Powder:** *Mingyu Zhang*<sup>1</sup>; *Liping Wang*<sup>1</sup>; <sup>1</sup>Central South University

At present, the products of ITO nanopowder mainly comes from China. The precursor of ITO nanopowder is fabricated by chemical coprecipitation method and dispersed in the ethanol. Then, ITO nanopowder was achieved after 600 centigrade degree. The ITO nanopowder was characterized by SEM, TEM, BET, XRD,small-angle X-ray scattering(SAXS), ZETA potential analysis. The diameters of ITO nanopowder were among 10nm and 50nm, spherical particles. The formation mechanism was investigated and proposed on the basis of previous study.

**Selective Area ALD Deposition with Nanolithography:** *Jie Huang*<sup>1</sup>; *Mingun Lee*<sup>1</sup>; *Jiyoung Kim*<sup>1</sup>; <sup>1</sup>University of Texas at Dallas

In this presentation, self-assembled monolayers (SAMs) have been investigated as a soft mask materials for future nano-lithography. While a conventional photo-resist (or hard mask) acts as a local protection layer during etching process, a novel SAMs can modify characteristics of surface, e.g. from hydrophilic to hydrophobic, so thin film growth occurs selectively where surface conditions are appropriate. We have evaluated selective ALD of dielectrics in conjunction with patterned OTS as a surface modifier on top of SiO<sub>2</sub>/Si substrate. We also explored the limitation of scaling down of selective ALD with EBL as well as a modified nano-imprint methodology. Well-defined nano-patterned surfaces after metal-oxide deposition will be introduced in our presentation. Acknowledgement: CNMT

(code#2010K000351, '21st Century Frontier R&D Programs' of the MEST, Korea) and FUSION (COSAR/MKE, Korea).

**Steel Mesh Coated with Carbon Nanotubes: Its Superhydrophobicity and W/O Emulsion Dewatering Capability:** Chee Huei Lee<sup>1</sup>; Nick Johnson<sup>1</sup>; Jaroslav Drellich<sup>1</sup>; Yoke Khin Yap<sup>1</sup>; <sup>1</sup>Michigan Technological University

Dense structures of multi-walled carbon nanotubes (CNTs) having a diameter of 10 to 50 nm and length > 5 μm were grown on a stainless steel (SS) mesh using thermal vapor chemical deposition. This 3-dimensional and porous SS-CNTs substrate was found to be superhydrophobic and superoleophilic, and could serve as phase separation membrane. Water advancing contact angles were 145-150 degrees for water drops suspended on the SS-CNTs mesh in air and oil (gasoline, isooctane). Oil, on the other hand, completely wet the SS-CNTs mesh. Simple filtration tests demonstrate the potential application of the SS-CNTs mesh as a filtration screen in dewatering of the water-in-oil emulsions.

**Synthesis of CuO-NiO Nanopowders via Alkalinization Precipitation Process:** R. Roohibakhsh<sup>1</sup>; H.R. Rezaei<sup>1</sup>; H. Razavizadeh<sup>1</sup>; <sup>1</sup>Iran University of Science and Technology

The aim of this study is to achieve a new method to synthesize CuO-NiO nanopowders via hydrometallurgical method. Influence of nickel content on characteristics of the synthesized nanopowders was investigated. Copper and nickel sulfate and sodium hydroxide were used as raw materials. Copper sulfate/nickel sulfate solution was precipitated by addition of sodium hydroxide. Considering the information obtained from STA result, calcination was done on precipitates. Eventually to study the formed phases and microstructure in each stage, X-ray diffraction (XRD) and scanning electron microscopy (SEM) were performed on the precipitates and obtained nanopowders after calcination. The final particle size of nanopowders was in the range of 29-31 nanometers.

**Application of Biomass Waste Materials in the Nano Mineral Synthesis:** Abram Bishay<sup>1</sup>; <sup>1</sup>NMA

Voluminous biowaste materials are produced every year which represent occasional hazardous problem through uncontrolled disposal. Some of the biomass waste material were effectively applied to the nano-sized minerals synthesis under controlled boundary experimental conditions. The produced nano minerals have a characteristic photocatalytic behaviour that could be applied in many environmental applications and safe treatment of many industrial and mine waste effluents. The advantage of such treatment can be summarized in the recycling of the biomass waste, enhancing mineral processing conditions (economically and environmentally) as well as cheap production of different nano particle forms for environmental and industrial applications.

**Characterization of Hybrid Carbon-Nanotube Composite Interfaces as a Function of Length Scale:** Harry Malecki<sup>1</sup>; Michael Duffy<sup>1</sup>; Sam Markkula<sup>1</sup>; Marc Zupan<sup>1</sup>; <sup>1</sup>University of Maryland Baltimore County

The use of carbon nanotubes (CNTs) in composite materials is studied to improve overall performance and provide multi-functionality. More specifically, because the elements of these nano-materials are engineered and span across multiple length scales, the incorporation of CNTs is expected to improve interfacial properties by affecting the small scale mechanisms which govern various interactions in the material structure. In the research presented, CNT-based hybrid filaments produced via a continuous in situ growth process are used to understand the effect of well aligned and dispersed CNTs on the strength of the filament reinforcement and the interfacial properties of the resulting bulk structure. Because of the multiple processing steps used to produce hybrid fibers, the effect of CNT incorporation on filament tensile properties is demonstrated using single filament and dry tow tests. Understanding the fiber properties, interfacial properties of the nano-scale structure are evaluated through nano-indentation of the multiple engineered interfaces.

**Development of Polymer-Based Position-Sensitive Photodetectors:** Dmitri Nassyrov<sup>1</sup>; Malte Schmidt<sup>1</sup>; Ovidio Peña<sup>1</sup>; Alejandro R. Goñi<sup>1</sup>; M. Isabel Alonso<sup>1</sup>; Miquel Garriga<sup>1</sup>; Mariano Campoy-Quiles<sup>1</sup>; <sup>1</sup>Institute of Materials Science of Barcelona (ICMAB-CSIC)

Organic photodetectors provide a cost-effective alternative to conventional inorganic devices due to the possibility of fabricating them via solution-based deposition methods such as coating and printing. Recently, postdeposition treatments such as vapour annealing have been shown to promote crystallisation of the materials, which proportionally improves the optoelectronic properties of the organic devices by enhancing light absorption and charge transport. Here, we first show that the degree of crystallisation of the active layer depends on the vapour annealing time. Then, we use this method to locally enhance light absorption in polythiophene:fullerene blends in order to create films exhibiting lateral gradients of the degree of crystallisation that could be used in applications such as position-sensitive photodetectors. The procedure developed permits us to produce devices with reproducible performance. Ellipsometry and photometry measurements allowed us to elucidate the local nanostructure of the thin films with a resolution at a level of tens of microns.

**Electrochemical Performances of Nanoporous Carbon Anode for Super Lithium Ion Capacitor:** Zhou Xiangyang<sup>1</sup>; Lou Shiju<sup>1</sup>; Yang Juan<sup>1</sup>; <sup>1</sup>Central South University

Hierarchical nanoporous carbon (HNC) anode material with average pore size of 4.7nm and Brunauer Emmett Teller (BET) surface area of 248.66 m<sup>2</sup>/g was prepared for super lithium ion capacitor by using phenolic resin as raw materials and Ni(OH)<sub>2</sub> / NaNO<sub>3</sub> / NaOH composites as templates. The electrochemical performance of the carbon electrode was tested in both electric double-layer capacitor (EDLC) and lithium ion battery (LIB). Voltage-current profiles for the carbon electrode in EDLC exhibit non-ideal rectangular response to different scan rates from 10 mV/s to 100 mV/s, confirming the double-layer behavior and high reversibility of the carbon studied. When acting as LIB anode, it exhibits a good cyclability after the initial irreversibility, associated with a stable capacity of 234 mAh/g during the first 50 cycles at a reasonable current density (0.2C).

**Integration of Surface Treatment Techniques for Uniform and Conformal ALD High-k Dielectric on Graphene:** Greg Mordt<sup>1</sup>; Srikar Jandhyala<sup>1</sup>; Bongki Lee<sup>1</sup>; Jiyoung Kim<sup>1</sup>; <sup>1</sup>University of Texas at Dallas

Graphene, a purely two-dimensional (2D) hexagonal carbon lattice is considered to be a potential candidate for future nanoelectronics because of its exceptional electronics properties. The need to integrate graphene with high quality insulating films that act as gate dielectrics for graphene field effect transistors is essential. Atomic layer deposition (ALD) provides a means to deposit high quality and uniform dielectric films on graphene while avoiding damages to the graphene layer. However, to ensure uniform, continuous films on graphene, a nucleation layer is required due to the chemical inertness of a pristine graphene layer. We investigate various surface treatment techniques prior to the ALD deposition process as a means to functionalize graphene surface to achieve a uniformly deposited high-k dielectric. We employ atomic force microscopy and Raman spectroscopy to characterize the samples and we extract electrical properties such as leakage current and dielectric capacitance. Acknowledgement: SWAN (SRC-NRI)

**Microfluidic Synthesis of Nickel Nanoparticles:** Ravindranadh Eluri<sup>1</sup>; Brian Paul<sup>1</sup>; <sup>1</sup>Oregon State University

Nickel nanoparticles has many applications varying from industrial (brazing filler) to bio medical (MRI contrasting agent). Conventional chemical synthesis of these nanoparticles in a flask results in wide size ranges and not always repeatable. Properties of nanoparticles are very sensitive to their sized due to their significant effect on surface-to-volume ratio. In the current investigation, we aim at synthesizing nickel nanoparticles of nearly monosize particles using microfluidic devices. These devices consist of microchannels of high surface-to-volume ratio leading to short diffusional distances and high diffusion rates. Effect of salt (NiCl<sub>2</sub>.6H<sub>2</sub>O) to reducing agent ratio (N<sub>2</sub>H<sub>4</sub>, NaBH<sub>4</sub>), surface capping agent, flow rate and concentration on particle size are analyzed using SEM, TEM and dynamic



light scattering (DLS) particle size analyzer. Keywords: Nickel nanoparticles, microfluidics, SEM and DLS

**Nanowire Rearrangement by the Pick-and-Place Nano-Manipulation Technique:** *Mingun Lee*<sup>1</sup>; Jie Huang<sup>1</sup>; Kook-Nyung Lee<sup>2</sup>; Moon Kim<sup>1</sup>; Jiyoung Kim<sup>1</sup>; <sup>1</sup>University of Texas at Dallas; <sup>2</sup>Korea Electronics Technology Institute (KETI)

Constructing a nano-device of minimum footprint from nano-components such as nanotubes and nanowires requires precise movement of the constituents. This can be achieved by locating the building blocks with an SEM and rearranging them via pick-and-place with a nano-manipulator inside the chamber. Our research presents every step of pick-and-place by nano-manipulation with Si nanowire, including preparation, and evaluates feasibility of nanowire rearrangement. For the sake of advancing our related study on nanotube-based sensors, we have coated the nanowires with TiO<sub>2</sub> for appropriate electrical conductance. Also discussed in the text are potential implementations of this technology in arranged nanowire devices of the future. Acknowledgement: CNMT(code #:2010K000351, MEST, Korea), and FUSION (COSAR/MKE, Korea).

**Reactive Nanoparticles for Bacteria Decontamination:** *David Stollberg*<sup>1</sup>; <sup>1</sup>Georgia Tech Research Institute

A significant challenge today is protection and decontamination of personnel in environments contaminated with chemicals and/or biological substances which pose acute or chronic health risks through exposure routes of skin, mucus membranes, and/or respiratory tracts. To increase maneuverability, low-weight, low-restriction garments capable of protecting against chemical and biological contaminants are needed. The development of uniquely functionalized nanoparticles and nanomaterials could address needs for enhanced reactive chemical and biological barrier materials and neutralization technologies for contaminated environments. The current work has focused on increased reactivity of nanomaterials, specifically silver and titania nanoparticles, for direct neutralization and/or decontamination of *Staphylococcus aureus*.

**Size Tunable Synthesis of Monodispersed Hexadecylamine -Capped ZnSe Nanoparticles:** *Oluwafemi Oluwatobi*<sup>1</sup>; *Vuyelwa Ncapayi*<sup>1</sup>; *Sandile Songca*<sup>1</sup>; <sup>1</sup>Walter Sisulu University

We herein report the synthesis of hexadecylamine-capped ZnSe nanoparticles via an environmentally benign method. By varying the reduction time we systematically studied the size, optical and structural properties of the as-synthesized nanoparticles. All the particles show quantum confinement with band edge luminescence in their optical spectra and were stable upon aging for several months. The sharpness of the absorption edges and excitonic shoulder increases as the reduction times increases while the emission width decreases as the reduction time decreases. The TEM images show well defined, monodispersed, small spherical particles with increase in particle sizes as the reduction time decreases. The XRD pattern of the particles show that they are of sphalerite cubic phase with increase in crystallinity as the reduction time decreases while the FTIR spectra confirmed the capping of the as-synthesized

**Sonochemistry as a Tool for Synthesis of Ion-Substituted Calcium Phosphate Nanoparticles:** *Ali Shokuhfar*<sup>1</sup>; *Milad Mohebbali*<sup>1</sup>; <sup>1</sup>K.N.Toosi Univ. of Technology

Calcium phosphates are of special interest for biomedical applications in hard tissue engineering. Indeed, the mineral phase of hard tissues in body is not a calcium phosphate, but rather a complex structure of ion-substituted calcium phosphate in form of nanoparticles with low crystallinity. Sonochemistry is known to alter chemical reactions in a number of ways such as changing the kinetics of reactions or activating some, which don't take place in normal conditions. In this study, a particular attention is given to these effects of sonochemistry for fabrication of ion-substituted calcium-phosphates like fluoroapatite and Mg-whitlockite. It's been tried to use calcium, phosphorous and ion precursors which do not contain foreign elements, in order to avoid subsequent treatments for their removal, which might have adverse effects on the structure of the as-synthesized nanoparticles.

**Structure and Mechanical Stability Studies of Tethered Lipid Bilayer Membranes Assembled on Template-Stripped Gold:** *Xi Wang*<sup>1</sup>; *Regina Ragan*<sup>1</sup>; <sup>1</sup>University of California, Irvine

Tethered phospholipid bilayer membrane (tLBM), an artificial membrane system, attracts considerable interest due to its potential application as biosensing platforms for studying transmembrane protein functions and membrane-protein interactions. TLBMs have a polymer spacer between LBM and substrate, preventing transmembrane proteins denaturation. AFM topography and force measurements acquired in fluid confirmed tLBM formation for vesicles composed of 2.5%DSPE-PEG-PDP/97.5%POPC, indicating the sulfur-containing PDP group promotes tLBM formation on template-stripped gold (TSG) via gold-thiolate bonds. Breakthrough distances relating to membrane thickness are analyzed from force-distance curves. The yielded breakthrough distance of tLBM on TSG (4.8±0.4nm) is 1.7nm thicker than that of POPC LBM on mica, demonstrating the presence of a PEG spacer layer between tLBM and TSG. Fluorescence microscopy results indicate tLBMs have greater mechanical stability than LBMs on mica. Our work yields robust tLBM on TSG without need of functionalizing TSG, providing potential for membrane microarray fabrication used for protein analysis.

**The Versatility of Catalytic LCVD Technique to Grow Carbon Nanotubes:** *Iuliana Soare*<sup>1</sup>; *Ion Morjan*<sup>2</sup>; *Rodica Alexandrescu*<sup>2</sup>; *Catalin Luculescu*<sup>2</sup>; *Eugeniu Vasile*<sup>3</sup>; *Monica Scarisoreanu*<sup>2</sup>; *Ernest Popovici*<sup>2</sup>; *Elena Dutu*<sup>2</sup>; *Lavinia Gavrilă Florescu*<sup>2</sup>; *Ion Voicu*<sup>2</sup>; <sup>1</sup>IMT-Bucharest; <sup>2</sup>National Institute for Lasers, Plasma and Radiation Physics; <sup>3</sup>METAV-R&D

The catalytic LCVD offers the advantage of high versatility and control since it separates the catalyst preparation from the catalytic growth of nanotubes. The method is characterized by the CO<sub>2</sub> laser thermal dissociation of volatile carbon-containing precursors over silicon substrates. Different iron based core-shell nanocomposites (iron-based core surrounded by carbon, iron oxide) were employed as catalysts. Gas mixtures containing ethylene, acetylene and ammonia were used. Other main experimental parameters such as laser power and total gas pressure were also varied. It cannot be excluded that impurities like nitrogen may promote formation of coiled carbon nanotubes. Structural characterization of the samples by SEM, TEM, Raman spectroscopy and X-ray diffraction was performed.

**Towards Integrated Systems of Nanopillar Devices:** *Liang-Chieh Ma*<sup>1</sup>; *Seong Jin Koh*<sup>1</sup>; <sup>1</sup>University of Texas at Arlington

One-dimensional nanoscale building blocks such as nanowires, nanotubes, and nanopillars have been investigated as functional elements for future nanoscale devices and sensors. For their practical implementations, however, these one-dimensional entities need to be placed on desired locations as well as connected to the outside macroscopic world. We present an integrated approach where bottom-up and CMOS-compatible top-down techniques are systematically combined to produce nanopillar devices that are individually addressable and probed. The fabrication was carried out in complete parallel processing over a large area. The nanopillars were created through two-step reactive ion etching (RIE); ~50nm Au nanoparticles were used as RIE hardmasks to produce silicon oxide nanopillars, which in turn served as hardmasks to produce desired Cr nanopillars with diameter of ~30nm and height of ~200nm. These nanopillars were selectively created only between the source and drain contacts. Application of this integrated fabrication scheme to single-electron transistor fabrication will be discussed.

**Zn-Ni Ferrite Spinels via Salt-matrix Heat Treatment:** *Amin Azizi*<sup>1</sup>; *Seyyed Mohammad Mostafavi*<sup>2</sup>; *Seyyed Khatiboleslam Sadrnezhad*<sup>2</sup>; *Ziarat Ali Nemati*<sup>2</sup>; <sup>1</sup>Department of Chemical and Biomolecular Engineering, Tulane University; <sup>2</sup>Department of Materials Science and Engineering, Sharif University of Technology

The capability of a salt-matrix (NaCl as a dispersion medium) for prevention of particle growth and agglomeration during annealing of mechanically alloyed Zn-Ni ferrite powders was examined via microstructure observation and magnetic measurements. Using the solid salt-matrix resulted in excellent avoidance of the sintering and growth of the particles as well as significant magnetic properties improvements. TEM observation showed that cube



shape nanoparticles with the average size of ~30 nm were formed by salt-matrix annealing of the milled powders at 700°C for 1 h. The magnetization saturation of the as-milled particles considerably increased and the coercivity also reduced after the salt-matrix heat treatment.

**Development of Hafnia Based Thermal Barrier Coating and Its Microstructural Analysis:** *Mohammed Noor-A-Alam*<sup>1</sup>; Chandan Roy<sup>1</sup>; Christopher Bradley<sup>1</sup>; Ahsan Choudhuri<sup>1</sup>; Chintalapalle Ramana<sup>1</sup>; <sup>1</sup>University of Texas at El Paso

The development of nano-structured hafnia based thermal barrier coatings (TBC) which have very high temperature tolerance are investigated in the present work. Ytria stabilized hafnia (YSH) coatings have been fabricated by magnetron sputtering onto the nickel-based super alloy (Inconel-738) and 403-stainless steel substrates. The coatings have been grown at various temperatures. Characterization of the coatings has been performed by studying their micro-structural and mechanical properties. The thickness of the coatings evaluated using the cross sectional imaging is about 500 nm. The structural characterization performed by X-ray diffraction (XRD) indicates the cubic crystal structure of YSH. The microstructure evaluated by scanning electron microscopy (SEM) shows the columnar structure of all the coatings. The microhardness investigated by using a diamond tip microhardness testing machine indicates the hardness of the coatings is ~3 GPa. The temperature stability of the coatings examined by thermal cycling at various temperatures indicates the stability of the coatings.

**Effect of Temperature Schedule on the Particle Size of NiFe2O4 Spinel Nanopowder during Solid-State Reactions:** *Zhigang Zhang*<sup>1</sup>; Guangchun Yao<sup>1</sup>; Yihan Liu<sup>1</sup>; Jinjing Du<sup>1</sup>; <sup>1</sup>Northeastern University

NiFe2O4 spinel nanopowder was synthesized by solid-state reactions in air using a two-step heat treatment process. The dependence of the particle size and morphology of nanopowder on the temperature schedule was investigated emphatically. The temperature was held for 5h at an intermediate temperature before heating to the target temperature of 800 °C for 1.5h. Although more heat was consumed and the technological process was more complicated, the powders synthesized by the two-step heat treatment method showed a smaller particle size with better dispersity than those produced by direct heating. Scanning electron microscopy (SEM) and laser particle analyzer indicated that the powder prepared at the intermediate temperature of 500 °C for 5h was spherical and well-dispersed with the average particle size of 50 nm, while it was more than 80 nm with particle agglomeration for direct heating to the same target temperature of 800 °C.

**Femtosecond Laser-Induced Synthesis of Colloidal AuAg Nanoalloys from Aqueous Mixture of Metallic Ions:** *Yuliati Herbani*<sup>1</sup>; Takahiro Nakamura<sup>1</sup>; Shunichi Sato<sup>1</sup>; <sup>1</sup>Institute of Multidisciplinary Research for Advanced Materials/Tohoku University

The synthesis of colloidal AuAg nanoalloys of various compositions has been performed by femtosecond laser irradiation of the aqueous mixture of metallic ions. The mixture of silver-ammonia complex and chloroaurate ions was simply introduced into a glass vial and exposed for several minutes to tightly focused femtosecond laser pulses which induced a strong optical breakdown in the solution and promoted the formation of reactive species to reduce the metallic ions. Homogeneous AuAg nanoalloys have been produced as indicated by the presence of surface plasmon bands that were linearly shifted from 400 to 528 nm with the increase of gold molar fraction in the solution. The result suggested that the atomic gold fraction in the nanoparticles were the same as the gold molar fractions in the solution. Oxidation of Ag nanoparticles possibly caused by oxygen species produced upon the irradiation was not observed.

**Interfacial Properties of Cu-Nb Multilayers as a Function of Dislocation/Disconnection Content:** *Niaz Abdulrahim*<sup>1</sup>; Ioannis Mastorakos<sup>1</sup>; Hussein Zbib<sup>1</sup>; David Bahr<sup>1</sup>; <sup>1</sup>washington state university

Nanoscale metallic multilayers (NMM) exhibit very high strength compared to bulk materials. For layer thickness less than 50 nm, the role of the interface in defining the whole behavior of the structure becomes very significant. The interface properties evolve continuously during deformation

because of dislocations passing through it or being absorbed by it, leaving disconnections at the interface. The disconnections which basically can be defined as the composition of a dislocation and a step, act as extra barriers for slip transmission. The effect of such disconnections, with different heights, on the strengthening mechanisms of nanolayers is explored using MD simulations. The interfacial strain energy and shear stresses are computed for a various dislocation configurations. Particularly, we develop energy maps for sheared interface as a function of dislocation content and disconnection density. Such measurements can be used in the development of a hardening law for NMM with incoherent interfaces.

**Investigation of Effect on BET Specific Surface Area of ACF/CNT Composites:** *Liping Wang*<sup>1</sup>; Zhucheng Huang<sup>1</sup>; Mingyu Zhang<sup>1</sup>; <sup>1</sup>Central South University

ACF/CNT composites were fabricated by chemical vapor deposition (CVD) method. The properties of ACF/CNT composites were characterized by SEM and BET specific surface area measurements. Three major variables effects on BET specific surface area of ACF/CNT composites were evaluated. The results show that BET specific surface area decreases with pyrolysis temperature increasing in the range of 550□-850□, while increases as the concentration of catalyst precursor from 0.02 mol/L to 0.1 mol/L. BET specific surface area reaches to minimum with pyrolysis time 40 min, while augments with more longer or shorter pyrolysis time.

**Synthesis and Characterization of Mullite:** *Kasturi Paithankar*<sup>1</sup>; Dipika Barbadikar<sup>1</sup>; Dilip Peshwe<sup>1</sup>; Ashutosh Gandhi<sup>2</sup>; <sup>1</sup>Visvesvaraya National Institute of Technology; <sup>2</sup>Indian Institute of Technology - Madras

In the current paper, an attempt is made to synthesize a mullite EBCs using sol-gel synthesis. Two general procedures were practiced for preparing mullite gel. First, by ageing the Aluminium Nitrate Nona Hydrate and Tetra Ethyl Ortho Silicate (TEOS) in solution of Ethyl Alcohol at various temperatures and Second, by preparing Aluminium Isopropoxide from continuous stirring of Aluminium Chloride (AlCl3) with 2-Propanol in different amounts in Refluxing vessel for 24 hrs and then mixing it with TEOS at various pH values. Characterization of the synthesized mullite has been performed by X-Ray Diffraction (XRD), Fourier Transformation Infra-Red Spectroscopy (FTIR) as well as Scanning Electron Microscopy (SEM). The effects of variations in the processing parameters such as pH, ageing temperatures, amount of propan-2-ol and calcinations temperatures have been discussed. Keywords: Environmental barrier coatings, sol-gel technique, Mullite.

**Synthesis and Characterization of Nanostructure Forsterite Bioceramic for Tissue Engineering Applications:** *Fariborz Tavangarian*<sup>1</sup>; Rahmatollah Emadi<sup>1</sup>; *Mohammad Hossein Enayati*<sup>1</sup>; <sup>1</sup>Isfahan University of Technology

Modern technologies require new biomaterials to match better with natural bone in terms of mechanical properties. Recently, forsterite (Mg2SiO4) has been introduced as a possible bioceramics due to its good biocompatibility. It has a better bending strength and fracture toughness than those of commercially available hydroxyapatite ceramics. The aim of the present work was synthesis, characterization, and bioactivity evaluation of nanostructure forsterite powder. Furthermore, the influence of crystallinity on apatite formation ability and degradation rate was investigated. Nanostructure forsterite powder unlike micron sized forsterite showed apatite formation ability. The bioactivity, biocompatibility, and good mechanical properties of nanostructure forsterite ceramic make it a suitable candidate for tissue engineering.

**Synthesis and Microstructure of Bulk Nanostructured Cu by Spark Plasma Sintering of Cryomilled Powders:** *Haiming Wen*<sup>1</sup>; Yonghao Zhao<sup>1</sup>; Zhihui Zhang<sup>1</sup>; Ying Li<sup>1</sup>; Osman Ertorer<sup>1</sup>; Enrique Lavernia<sup>1</sup>; <sup>1</sup>University of California, Davis

Powder metallurgy is widely used to synthesize bulk nanostructured metals. Cryomilling is one of the commonly used approaches to producing nanostructured metal powders. Spark plasma sintering (SPS) is an efficient consolidation technique. However, it has been found that it is difficult to fully densify cryomilled powders of some pure metals such as Al, Ni and Cu

by SPS. In this study, densification of cryomilled Cu powders by SPS, and microstructure of consolidated bulk nanostructured Cu were related to the change of microstructure and chemistry of cryomilled Cu powders during SPS. It was revealed that although with very low contents, O and N in the cryomilled Cu powders, which were introduced by oxidation and cryomilling respectively, significantly influenced the SPS process. In addition, how O and N exist in the cryomilled Cu powders was ascertained through the combined study of electron microscopy and thermal analysis.

**Synthesis and Sintering of W-Cu-Ag Composite Powders Produced by Co-Precipitation Method:** G. Taghavi<sup>1</sup>; H.R. Rezaie<sup>1</sup>; H. Razavizadeh<sup>1</sup>; <sup>1</sup>Iran University of Science and Technology

W-10wtCu-10wtAg powders were prepared by a precipitation process. In order to synthesis W-Cu-Ag composite powders, the dried precipitates were calcined in air at 600°C for 2h. Then calcined precipitates, reduced at 850°C for 2h in hydrogen atmosphere in a tube type electrical furnace to obtain W,Cu and Ag powders. The reduced powders consisted of metallic phases after mixing with PVA were uni-axially compacted at a pressure of 200 MPa. The effect of sintering temperature was investigated on densification of the synthesized powders. The powders were characterized by X-ray diffraction (XRD) technique. The morphologies of the powders were investigated by scanning electron microscopy (SEM).

**Fe-Based Amorphous-Nanocrystalline Thermal Spray Coatings:** B. Movahedi<sup>1</sup>; M.H. Enayati<sup>2</sup>; <sup>1</sup>Isfahan University; <sup>2</sup>Isfahan University of Technology

In this work, a new composition of Fe-15Cr-4Mo-5P-4B-1C-1Si (wt.%) amorphous powder was produced by mechanical alloying of elemental powder mixture. Thermal spraying of amorphous powder was done by high velocity oxy fuel spraying technique at various spraying conditions to obtain the desirable amorphous and nanocrystalline coatings. It was found that a-Fe based supersaturated solid solution is first formed during mechanical alloying which transforms to amorphous structure at longer milling times. The crystallization kinetic parameters suggest that the crystallization mechanism is dominantly governed by a three-dimensional diffusion-controlled growth. The crystallization of amorphous structure occurs in one single stage. By carefully controlling the spraying parameters and proper selection of powder composition, the desired microstructure with different fraction of amorphous and nanocrystalline phases and therefore with different properties could be obtained.

**High Performance Dye Sensitized Solar Cells Based on Surfactant Templated Mesoporous Titania Coatings:** Saquib Ahmed<sup>1</sup>; Dunbar Birnie<sup>1</sup>; Teddy Asefa<sup>1</sup>; <sup>1</sup>Rutgers University

We have prepared crystalline, high surface area mesoporous titania using surfactant-based supramolecular self-assembly of Titanium Oxy-Sulfate precursor. XRD of the synthesized titania (denoted S1 from hereon) revealed a fully anatase phase, which is corroborated by characteristic diffraction rings in SAED from TEM studies. BET studies showed a specific surface area of S1 over three times that of P25. DSSC films were fabricated using both S1 as well as P25 as a standard. Dye loading capacity using Beer-Lambert analysis and UV-spectroscopy revealed a much better performance of S1 over P25. Actual I-V data giving cell performance showed more than a 1% improvement by using S1 over P25 at optimal film thickness. EIS was conducted to study and compare electron motion and recombination kinetics at the titania/dye/electrolyte interface between S1 with respect to P25 at various film thicknesses. Mercury Porosimetry corroborated pore size and structure seen by SEM imaging of samples.

**Magnetic Properties of Chemically-Synthesized FeRh/FePt Nanocomposites:** Zhiyong Jia<sup>1</sup>; R.D.K Misra<sup>1</sup>; <sup>1</sup>University of Louisiana at Lafayette

We report here the synthesis and magnetization behavior of FeRh/FePt nanocomposites. FeRh and FePt nanoparticles were fabricated individually using a polyol co-reduction process. Subsequently, FeRh and FePt nanoparticles were mixed in the ratio of 4:1 (by volume). Magnetic measurements were made for the nanocomposites films on silicon

wafers both before and after the annealing at different temperatures. The temperature dependent magnetization measurement of Fe51Rh49/Fe52Pt48 nanocomposite annealed at 500°C for 30 minutes indicated antiferromagnetic-ferromagnetic transition consistent with x-ray diffraction measurements. However, Fe51Rh49/Fe52Pt48 nanocomposite annealed at 700°C for 30 minutes, the magnetization behavior was typical of a ferromagnetic material. High-resolution transmission electron microscopy (HRTEM) suggested that ferromagnetic L10 FePtRh ternary alloy was partially formed during the annealing process at 700°C for 30 minutes.

**Optical Gas Sensors for Advanced Coal-Fired Power Plants:** Paul Ohodnicki<sup>1</sup>; Congjun Wang<sup>1</sup>; Douglas Kauffman<sup>1</sup>; Kristi Kauffman<sup>1</sup>; Christopher Matrangola<sup>1</sup>; <sup>1</sup>National Energy Technology Laboratory

The National Energy Technology Laboratory is developing technologies for the next generation of higher-efficiency, lower emission fossil plants including more efficient oxy-fuel combustion processes and coal gasification to produce H<sub>2</sub>-rich synthetic gas which can be converted to electrical power using solid-oxide fuel cells or gas turbines. Advanced remote sensor technologies that can operate under extreme conditions (high temperature, high pressure, corrosive gases) are needed for process control. Commercially available metal oxide-based conductometric gas sensors are not adequate and advanced materials / novel gas sensing techniques are required. Optical sensors based on metal oxides are important candidates and an improved understanding of the fundamental link between optical properties and the presence of various gas species under relevant conditions is needed to aid in sensor development efforts. Early results on synthesis and characterization of metal oxide-based films will be presented and plans for future work will be outlined.

**Managing High Strength and High Ductility in UFG IF-Steel by ECAE plus Post-ECAE Annealing:** Gencaga Purcek<sup>1</sup>; Onur Saray<sup>1</sup>; Ibrahim Karaman<sup>2</sup>; Hans Maier<sup>3</sup>; <sup>1</sup>Karadeniz Technical University; <sup>2</sup>Texas A&M University; <sup>3</sup>University of Paderborn

The UFG IF-steel produced by equal-channel angular extrusion/pressing (ECAE/P) following different routes and number of passes have been annealed for different annealing time intervals and temperatures in order to obtain an IF-steel having both high strength and high ductility. Firstly, the recrystallization curves showing thermal stability were obtained for all conditions. After that, stress-strain curves of the samples that were annealed at a specific temperature for different time intervals were determined to get a good strain hardening rate (high uniform elongation). A bimodal grain size distribution inside the previously deformed microstructure was formed at 600°C for different annealing times. In this microstructure, while the larger grains facilitate the motion and accumulation of dislocations and caused to enhance the ductility, the finer grains contribute to strength increase.

**Texture, Dislocation Structure, and Interface Structure of Nanolamellar Metallic Composites Fabricated via Rolling and Accumulated Roll Bonding:** John Carpenter<sup>1</sup>; Sven Vogel<sup>1</sup>; Thomas Wynn<sup>1</sup>; Robert Dickerson<sup>1</sup>; Rod McCabe<sup>1</sup>; Irene Beyerlein<sup>1</sup>; Nate Mara<sup>1</sup>; <sup>1</sup>Los Alamos National Laboratory

The use of rolling and accumulated roll bonding (ARB) as alternate techniques to physical vapor deposition (PVD) in the fabrication of metallic multilayer composites with nanoscale layer thicknesses is explored. 200 nm/200 nm Cu/Ag multilayers that were initially fabricated via PVD to a total thickness of 40  $\mu$ m are rolled to nominal reductions of 10%, 20%, 30%, and 50% and compared to cast and rolled Cu/Ag lamellar eutectic material. In addition, Cu/Nb multilayers are fabricated via ARB after initially starting with single layers of polycrystalline Cu and Nb. Cu/Nb multilayers with individual layer thicknesses ranging from tens of microns to tens of nanometers are fabricated. Neutron diffraction is performed on the samples in order to ascertain texture and transmission electron microscopy (TEM) is performed in order to look at local dislocation and interface structures. Deformation behavior and microstructure of the ARB composites is compared with as-deposited multilayers produced via PVD.

## Structural and Dielectric Properties of Polar Polymer Nanocomposites:

Mulayam Gaur<sup>1</sup>; <sup>1</sup>Hindustan College of Science and Technology

The polar materials exhibit a high dielectric constant and are therefore also investigated as high-k polymers in semiconductor sensor industry. The present paper demonstrate the factors such as preparation mechanism, size of nanoparticles, amorphous and crystalline nature of polymer, precondition of samples affecting the dielectric and structural properties of polar polymers. We have chosen the polymethylmethacrylate (PMMA), polysulfone, polyvinylidene fluoride (PVDF) as polymer and TiO<sub>2</sub>, ZnO, SiO<sub>2</sub> as a nanoparticle. We have observed that TiO<sub>2</sub> strongly affected the structural and dielectric properties of PVDF by drastic increase of dielectric constant and formation of nanocluster. The XRD spectra of nanocomposite shows the crystallinity of nanocomposite increases upto certain ratio of nanoparticles and then decreases, however glass transition temperature increases significantly. The dielectric relaxation could be studied using thermally stimulated depolarization technique. It is found that the Maxwell Wagner and dipolar polarization are dominating factor.

## A Detailed Study of Ozone Process on Graphene for Ozone-Based

Atomic Layer Deposition: Bongki Lee<sup>1</sup>; Geunsiik Lee<sup>2</sup>; Greg Mordis<sup>1</sup>; Srikanth Jandhyala<sup>1</sup>; Robert Wallace<sup>1</sup>; Jiyoung Kim<sup>1</sup>; <sup>1</sup>University of Texas at Dallas; <sup>2</sup>POSTECH

Dielectric deposition on graphene has been an object of great interest because the chemically inert nature of the graphene surface inhibits the deposition of conformal dielectric films. We have reported an O<sub>3</sub>-based atomic layer deposition method for depositing a high quality of ALD dielectric on graphene. Here, we study that the O<sub>3</sub> reaction with single-layer graphene using in-situ electrical characterization. We find that O<sub>3</sub> exposure on graphene at 25°C results in the positive shift in the Dirac voltage, indicating that O<sub>3</sub> adsorption on graphene is likely governed by physisorption. This observation is consistent with the density of state calculation of the graphene-adsorbate system. We also explore the effects of dielectric deposition using O<sub>3</sub> process on graphene at different temperatures. Finally, we will demonstrate that the O<sub>3</sub> process can be successfully applied for dielectric deposition on graphene. Acknowledgement: MSD (FCRP-SRC) & NBIT Fusion Technology R&D program of MKE (Korea)

## Graphene-CNT Hybrid Structure Based Transparent and Flexible Field Emission Device:

Indranil Lahiri<sup>1</sup>; Ved Prakash Verma<sup>1</sup>; Wonbong Choi<sup>1</sup>;

<sup>1</sup>Florida International University

In recent years, graphene has been promoted as a very important material for future electronics. One of such future applications is transparent, flexible electronic devices. We present here our recent research efforts in developing all-graphene based cathode and anode structures as flexible and transparent field emission device. Graphene film was grown on Cu foil by thermal chemical vapor deposition process and transferred to polymer substrate through hot press lamination. Cathode of the field emission device was prepared by spin-coating multiwall carbon nanotubes (MWCNT) onto graphene film on the transparent, flexible substrate. A green-phosphor coated graphene-PET film was used as the anode. The device offered appreciable emission current and showed good transparency and flexibility. Processing techniques followed in this study can easily be up-scaled and be modified for any transparent and flexible substrate. Our results offer exciting applications of graphene in foldable electronics.

## Development of Al-TiB<sub>2</sub> Nanocomposite:

Z. Sadeghian<sup>1</sup>; M.H. Enayati<sup>2</sup>;

B. Lotfi<sup>1</sup>; P. Beiss<sup>3</sup>; <sup>1</sup>Shahid Chamran University; <sup>2</sup>Isfahan University of

Technology; <sup>3</sup>RWTH Aachen University

Al-20 wt.% TiB<sub>2</sub> nanocomposite was prepared by mechanical alloying (MA) of elemental Ti, B and Al powder mixture. A double step process was used to prevent the formation of undesirable phases. The resulting powder was consolidated by spark plasma sintering (SPS) followed by hot extrusion. The structural characteristics of powder particles and consolidated samples were studied by X-ray diffractometry (XRD), scanning electron microscopy (SEM) and transmission electron microscopy (TEM). The hardness and the tensile behavior of samples were evaluated. The results showed that the prepared Al-20wt.%TiB<sub>2</sub> nanocomposite has good thermal stability against

grain growth and particle coarsening. Extruded Al-20wt. %TiB<sub>2</sub> showed a hardness value of 180 VHN and yield and tensile strength of 480 and 540 MPa, respectively which are much higher than those reported for similar composites made by other processes.

## Polymer-Graphene-Polymer Composite Structured Flexible Nonvolatile Bistable Organic Memory Devices:

Won Kook Choi<sup>1</sup>; Dong-Ick Son<sup>1</sup>;

<sup>1</sup>Korea Institute of Science and Technology

The I-V curves at 300 K for the Al/PMMA/graphene(ultra thin graphite)/PMMA/ITO/PET devices exhibited electrical bistable behaviors before and after bending. Current-time, and current-cycle measurements in flat and bent conditions demonstrated the memory stabilities of the bistable organic memory (BOM) devices. Flexible organic memory device showed the maximum  $I_{on}/I_{off}$  ratio of the I-V curves of  $5 \times 10^6$ , a retention stability of  $4.8 \times 10^4$ s and the endurance to electrical stress above  $1 \times 10^5$  cycles. The memory characteristics of the BOM devices after bending maintained almost the same values as those of the devices before bending and were stable during repetitive bendings of the BOM devices. From the results, we discuss carrier transport mechanism of a bistable behavior for the fabricated bistable organic memory devices structures

## Hydrogen Production by Reacting Water with Mechanically Milled Composite Aluminum-Metal Oxide Powders:

Paul Dupiano<sup>1</sup>; Demitrios

Stamatis<sup>1</sup>; Edward Dreizin<sup>1</sup>;

<sup>1</sup>New Jersey Institute of Technology

Composite aluminum-metal oxide powders were prepared by mechanical milling and considered for hydrogen production in the Al-water split reaction. The powders included compositions capable of independent, highly exothermic thermite reaction between components: Al•MoO<sub>3</sub>, Al•Bi<sub>2</sub>O<sub>3</sub>, and Al•CuO, as well as chemically inert compositions, Al•MgO and Al•Al<sub>2</sub>O<sub>3</sub>. Experiments used a water displacement method to quantify hydrogen production. The hydrogen yield was close to 100 % for all compositions. Reaction rates and rate variations were affected by the specific composition, temperature, and thermal cycling of samples. Al-water split reaction initiated at 80 °C completely stopped when flask was cooled to room temperature. The reaction could be resumed at its original rate by heating the flask back to 80 °C. Redox reactions interfered with the Al-water split reaction so that metallic Bi and Cu were produced when respectively Al•Bi<sub>2</sub>O<sub>3</sub> and Al•CuO composites were used.

## Atomic Scale Investigation of Nano Structures in Ni-Based Superalloy through Advanced Characterization:

Gopal Viswanathan<sup>1</sup>; Rajarshi

Banerjee<sup>2</sup>; R Srinivasan<sup>3</sup>; S Nag<sup>2</sup>; A Shiveley<sup>4</sup>; J Tiley<sup>1</sup>; Hamish Fraser<sup>5</sup>;

<sup>1</sup>Air Force Research Laboratory; <sup>2</sup>University of North Texas; <sup>3</sup>ExxonMobil

Research and Engineering; <sup>4</sup>UTC, Dayton; <sup>5</sup>The Ohio State University

The atomic-scale investigation in complex multi-phase multicomponent systems is a challenging but important undertaking. This study highlights the coupling of recently developed advanced characterization techniques such as high resolution scanning transmission electron microscopy, carried out in an aberration-corrected microscope, and atom probe tomography, to study two vital issues related to nickel-base superalloys, namely (i) to study the complexity of the structural and compositional transition at the atomic scale across  $\gamma$ (FCC Ni)/ $\gamma'$ (ordered Ni<sub>3</sub>Al) solid-solid interface and (ii) to capture the early formation of  $\gamma'$  the ordered Ni<sub>3</sub>Al phase within  $\gamma$  disordered matrix. Possible implications of such investigations on the understanding of physical and mechanical properties will be discussed.

## Thermal Stability and Mechanical Behavior of Cu-Nb and Cu-Nb-Ag Super-Saturated Metastable Solid Solutions Prepared by Mechanical Alloying:

Suhrit Mula<sup>1</sup>; K. Youssef<sup>2</sup>; M. Atwater<sup>2</sup>; H. Bahmanpour<sup>2</sup>; Ron

Scattergood<sup>2</sup>; Carl Koch<sup>2</sup>; <sup>1</sup>North Carolina State University, Raleigh, USA

and National Institute of Technology, Rourkela, India; <sup>2</sup>North Carolina State

University, Raleigh

Blend compositions of Cu<sub>92.5</sub>Nb<sub>7.5</sub>, Cu<sub>92.5</sub>Nb<sub>2.5</sub>Ag<sub>5</sub> and Cu<sub>87.5</sub>Nb<sub>7.5</sub>Ag<sub>5</sub> were

subjected to high-energy ball-milling at room temperature(RT) to study metastable solid solubility extension of Nb/Ag in Cu. XRD and TEM studies revealed that 7.5%Nb, or 7.5%(Nb+Ag) was metastably dissolved in Cu at RT, and the solid solutions are stable up to 500°C. This is in contrast to the



equilibrium solid solubility of either element in Cu, whereas, complete solid solubility was not detected when Ag+Nb content exceeds 7.5%. Enhancement of lattice parameter is more effective for  $\text{Cu}_{92.5}\text{Nb}_{2.5}\text{Ag}_5$  and this is possibly due to dissolution of larger Ag atoms. Hardness decreased from 5.5GPa for  $\text{Cu}_{92.5}\text{Nb}_{7.5}$  to 4.35GPa for  $\text{Cu}_{92.5}\text{Nb}_{2.5}\text{Ag}_5$ , although crystallite size was almost same (10nm). But, higher electrical conductivity was achieved in  $\text{Cu}_{92.5}\text{Nb}_{2.5}\text{Ag}_5$ . Stabilization of matrix grains by formation of solid solution and possible segregation of Nb and/or Ag along grain boundaries may play pivotal role for the high strength.

**Scaling Theory of Continuum Dislocation Dynamics in Two and Three Dimensions:** *Yong Chen*<sup>1</sup>; *Woosong Choi*<sup>1</sup>; *Stefanos Papanikolaou*<sup>1</sup>; *James Sethna*<sup>1</sup>; <sup>1</sup>Cornell University

When crystalline materials deform plastically, complex dislocation structures have been observed experimentally<sup>1</sup>. We provide a continuum plasticity theory to study the emergent self-similar morphologies<sup>2</sup>. We analyze the self-similarity in terms of critical exponents for correlation functions of dislocation density, crystalline orientation and plastic distortion, and explore the connection to the power spectrum of the total free energy. In two and three dimensions, we apply anisotropic loadings, and observe little anisotropy in the critical properties. We explore the addition of quenched disorders to our continuum theory, to investigate the relation between dynamics (plasticity avalanches) and static dislocation morphologies. <sup>1</sup>P. Hahner et al., Phys. Rev. Lett. 81, 2470, 1998. <sup>2</sup>Y.S.Chen et al., Phys. Rev. Lett. 105, 105501, 2010.

**Synthesis and Characterization of Vertically Oriented Sr-doped TiO<sub>2</sub> Nanotubes Using Electrochemical Anodization Process:** *Hoda Amani Hamedani*<sup>1</sup>; *Nageh Khalaf Allam*<sup>1</sup>; *Hamid Garmestani*<sup>1</sup>; <sup>1</sup>Georgia Institute of Technology

The present work reports on fabrication of self-organized strontium-doped titania nanotubes arrays as a potential material for photocatalysis applications. Doping process was performed in two ways: during electrochemical anodization process and using spray pyrolysis technique. The microstructure and morphology of as-prepared and heat treated doped-nanotubes were characterized by field emission scanning electron microscopy (FESEM) and high resolution transmission electron microscopy (HRTEM). Also, composition of the synthesized materials was analyzed by energy dispersive X-ray diffraction (EDX) and x-ray photoelectron spectroscopy (XPS). Results showed that the length, morphology and diameter of the nanotubes can be controlled by adjusting the anodization parameters such as the PH of the electrolyte, applied voltage and processing time. Photocatalytic activity of the fabricated materials was also investigated to evaluate the proper doping level as well as the quality of doped nanotubes for use in photoelectrochemical applications.

**Synthesis of W-25 Wt%Cu Composite Powders Using Ammonium Paratungstate and Copper Nitrate as Precursors:** *Mojtaba Babapour Naseri*<sup>1</sup>; <sup>1</sup>Cabok

An investigation has been made to prepare homogeneous powders of  $\text{CuWO}_4$  and  $\text{WO}_3$  from ammonium paratungstate and copper nitrate to prepare nanosized W-Cu powder. Hence, a mixture of ammonium paratungstate and copper nitrate with predetermined weight proportion was made in distilled water; while the content of the beaker was being stirred at a certain speed to reach the desired composition of W-25wt %Cu. Mixture was heated to 80-100C for 6 h. Also, pH range was adjusted at about 3-4. The mixture was then evaporated and dried in the air. To reach W-Cu composite powder, the precursor powders burned out at 520C for 2 h in the air to form W-Cu oxide powder and then were ball milled and reduced in H<sub>2</sub> atmosphere to convert it into W-Cu composite powder. The resulting powders were evaluated using scanning electron microscopy, X-ray diffraction, thermogravimetric analysis and differential thermal analysis techniques. The results showed that homogeneous powders of W-Cu with particle size of about 100 nm and a nearly spherical shape could be obtained by this process.

**Effect of Welding on the Fatigue Strength of Welded Joints Using the GMAW Process in Transformation Induced Plasticity Steels (TRIP) Used in the Automotive Industry:** *Victor Lopez*<sup>1</sup>; *Arturo Reyes*<sup>1</sup>; *Patricia Zambrano*<sup>2</sup>; *Joaquin Del prado*<sup>3</sup>; <sup>1</sup>Corporacion Mexicana de Investigacion en Materiales; <sup>2</sup>universidad autonoma de nuevo leon; <sup>3</sup>METALSA

GMAW is the welding process used in the automotive industry, for joining mild steels. TRIP steel, however don't offer the same ease of welding, and control welding parameters is critical. The effects of the heat input variations is important and TRIP steel has a narrower parameters window in which acceptable welds can be made. Mechanical and Metallurgical properties of the lap joints of TRIP 780 steel 2.8 mm thickness is analyzed fusion welds were evaluated using optical and SEM microscopy. Static and fatigue tests were conducted on these joints for different heat inputs. Fatigue testing was conducted under a different number of stress ranges to obtain the S/N curves of the weld joints. It was found that welding process parameters, especially travel speed, have significant impact on static and fatigue performance of the lap joints. Failure location of static and fatigue tested lap joints will also be analyzed.

**Effect of Initial Microstructure on the Processing of Titanium Using Equal Channel Angular Pressing:** *Shehreen Dheda*<sup>1</sup>; *Nima Farhi*<sup>1</sup>; *Farghalli Mohamed*<sup>1</sup>; <sup>1</sup>University of California, Irvine

Equal channel angular pressing (ECAP) is a metal processing technique that is used to produce materials with ultrafine (< 1 μm) grain sizes. In this work, the effect of the initial microstructure on ECAP of commercially pure titanium (CP Ti), a material used in many industrial applications, was investigated. To produce different initial microstructures, samples of CP Ti were exposed to several different annealing treatments. Samples associated with each treatment were subjected to one pass of ECAP and the resulting microstructures were analyzed using SEM and TEM, and compared to the microstructures before ECAP. Microhardness and tensile tests were also performed on the samples. The results are discussed in terms of the microstructures associated with each treatment before and after one pass of ECAP and the effect of these microstructures on mechanical properties.

**Production and Mechanical Properties of Nanostructured Copper and Copper Zinc Alloys:** *Mohsen Samadi Khoshkoo*<sup>1</sup>; *Hamed Bahmanpour*<sup>2</sup>; *Sergio Scudino*<sup>1</sup>; *Jens Freudenberger*<sup>1</sup>; *Michael Zehetbauer*<sup>3</sup>; *Carl Koch*<sup>2</sup>; *Jürgen Eckert*<sup>1</sup>; <sup>1</sup>Leibniz Institute for Solid State and Materials Research (IFW); <sup>2</sup>Department of Materials Science and Engineering, North Carolina State University; <sup>3</sup>University of Vienna

In this work, bulk nanocrystalline (NC) and ultrafine-grained (UFG) Cu-based samples have been produced by in-situ consolidation during mechanical alloying as well as by conventional ex-situ consolidation of the milled powders through hot extrusion. The effect of the milling parameters (e.g. milling temperature and intensity) on the structure of the milled materials was studied in detail and particular attention was paid to reach the optimal conditions for successful in-situ consolidation during milling. Extrusion experiments were carried out at the lowest possible temperature in order to limit grain growth. Room temperature compression tests of the samples produced by the different processing routes reveal very encouraging mechanical properties regarding the combination of high strength (600 - 1100 MPa) and good plastic deformation (> 50 %) and indicate that NC/UFG materials with specific combination of properties can be produced by the optimization of the processing parameters.

**Experimental Investigation of Deformation Mechanisms Present in Ultra-Fine-Grained Metals:** *Adam Kammer*<sup>1</sup>; *Samantha Daly*<sup>1</sup>; <sup>1</sup>The University of Michigan

This talk presents an experimental investigation into UFG metals in order to determine the active deformation mechanisms and the relative contributions of different deformation modes that result in their remarkable capacity for high strength and ductility. UFG pure aluminum and an AZ-61 magnesium alloy produced by equal-channel angular pressing (ECAP) are investigated. A new experimental methodology is used, in which an optical metrology known as Digital Image Correlation (DIC) is combined with scanning electron microscopy to track the quantitative development of full-



field strains on the length scale of the microstructure. The results obtained through the combined SEM and DIC approach, and corresponding electron backscatter diffraction (EBSD) analysis, enable the investigators to track the real-time, micro-scale evolution of Lagrangian strain and to determine the deformation inside the grains and across grain boundaries as the material is heated and strained.

**Thermal Stability of Electrodeposited Nanocrystalline Copper:** *Ming-Je Sung*<sup>1</sup>; Farghalli Mohammed<sup>1</sup>; <sup>1</sup>University of California, Irvine

Electrodeposition is a process in which metal films are obtained by electroplating from a suspension of small particles that are deposited with the plated metal. In this work, nanocrystalline copper was fabricated by *Pulsed Current Electrodeposition* (PED). Samples were heat treated for several different temperatures. The results showed the presence of highly thermal stable copper nano-twinning. Also, results on preferred orientations and microstructures are presented.

**Ultrahigh Strength and Good Ductility in Bulk Nanostructured TWIP Steel:** *Hongning Kou*<sup>1</sup>; Jian Lu<sup>2</sup>; <sup>1</sup>The Hongkong Polytechnic University; <sup>2</sup>City University of HongKong

Different from varieties of nanocrystalline metals and alloys that usually achieve their ultrahigh strength at the expense of ductility, we present nanostructured TWIP (twinning induced plasticity) steel samples subjected to surface mechanical attrition treatment (SMAT) with simultaneous ultrahigh strength and good ductility. Their yield strength is increased by fold, while still accompanied by acceptable elongation. The excellent mechanical properties primarily result from the twin structure evolution caused by plastic deformation. This new type of nanostructured TWIP steel with good combination of strength and ductility shows great potential in energy saving and lightweight engineering in automobile industry.

**Shear-Induced Nanostructured Zirconium with Unique Mechanical Properties:** *Srinivasa Rao Bonta*<sup>1</sup>; Alexander Zhyliaev<sup>2</sup>; María Teresa Pérez Prado<sup>1</sup>; <sup>1</sup>IMDEA Materials; <sup>2</sup>National Center for Metals Research

Pure Zr undergoes a wide range of phase transformations when subjected to high temperatures or high pressures. Under ambient conditions, the stable phase (alpha) has a hexagonal close packed structure. At temperatures higher than 1135 K it transforms into a bcc phase (beta). When the alpha phase is subjected to hydrostatic pressure it transforms into a simple hexagonal structure (omega) at applied pressures ranging from 2 to 6 GPa and, finally, to the bcc (beta) phase when the applied pressure exceeds 30 GPa. It has recently been discovered that pure omega plus beta nanostructured Zirconium can be stabilized at room temperature and atmospheric pressure by the application of shear under pressure. The properties of omega plus beta Zirconium have not been investigated yet, as these two phases could previously only be stabilized under very extreme conditions. Here the mechanical behavior of these novel nanostructured Zr phases will be investigated.

**Industrial Potential of Bulk Nanostructured Metals:** *Malgorzata Lewandowska*<sup>1</sup>; Halina Garbac<sup>1</sup>; Krzysztof Kurzydowski<sup>1</sup>; <sup>1</sup>Warsaw University of Technology

Nano-metals have been a subject of extensive research which resulted in the development of a number of fabrication routes, among others utilizing methods of severe plastic deformation. One of such methods is hydrostatic extrusion, which can be used to produce relatively long products, in the form of rods and wires. Such rods and wires allow for better characterization of the mechanical properties of SPD nano-metals and alloys. They also lead to new applications, in particular as components of the more complex structures. In this paper, three possible fields of application, namely Al-based lightweight structures for transport related industry, biomedical applications of nano-Ti and nano-steels for advanced energy power systems, will be described in more detail. These three examples address the major global challenges - reduction in CO2 emission, life quality of ageing society, efficient and clear energy production - indicating that nanometals may contribute to solving world's problems.

**Progress and Potential of Free Pressure-less Spark Plasma Sintering (FPSPS) Processing:** *William Bradbury*<sup>1</sup>; Ridvan Yamanoglu<sup>2</sup>; Wei Li<sup>1</sup>; Randall German<sup>1</sup>; Eugene Olevsky<sup>1</sup>; <sup>1</sup>San Diego State University; <sup>2</sup>Kocaeli University

Experimental aspects of recently developed free pressure-less spark plasma sintering (FPSPS) processing of powder based materials provides encouraging potential for nano-scale structural integration of porous components, nano-wire thin film production and rapid consolidation. Current development has encompassed SiC nanowire network synthesis as well as ZnO consolidation, activated carbon production and nanowire thin film deposition. Complete removal of external load applied to the sample during spark plasma sintering allows simple introduction of this rapid sintering technology to 1-D nanostructure development. Partial retention of contact pressure allows utilization of current flow without destruction or distortion of delicate macrostructure under high loading. The FPSPS process can be utilized independently, or as a sample pretreatment for microstructural development, followed by conventional SPS consolidation.

**Microstructure and Mechanical Behavior of Wet-Processed Cu-Zr-Based BMG Composites:** *Jonathan Nguyen*<sup>1</sup>; Sangmin Lee<sup>2</sup>; Zhihui Zhang<sup>1</sup>; Ying Li<sup>1</sup>; Troy Topping<sup>1</sup>; Yizhang Zhou<sup>1</sup>; Akihisa Inoue<sup>2</sup>; Enrique Lavernia<sup>1</sup>; <sup>1</sup>University of California, Davis; <sup>2</sup>Tohoku University

Cu-Zr (CZ) based bulk metallic glasses (BMG) have become a subject of recent interest due to their high strength and enhanced ductility. In this study, wet process dispersion of multi-wall carbon nanotube (CNT) using a zwitterionic surfactant has been used to synthesize CNT reinforced BMG. A fundamental criterion is that the surfactant used must functionalize the CNTs thereby enabling it to attach to metallic powder surfaces. Spark plasma sintering was used to consolidate CZ-CNT composite powders with varying amounts of CNT (0.1 to 1.5 wt%). The microstructural evolution and the interface between the CNT and the BMG matrix was characterized using electron microscopy, DSC, and Zeta potential measurement. Compression tests were carried out to evaluate the mechanical behavior of consolidated bulk samples. Particular emphasis has been placed on establishing the structural and mechanical interaction at the interface between CNT and the BMG matrix.

**Heterogeneity of Microstructure Evolution in NiTi (50 at% Ni) Alloy Severely Deformed by High Pressure Torsion:** *Reeti Singh*<sup>1</sup>; Jochen Fiebig<sup>1</sup>; Stefan Ostendorf<sup>1</sup>; Harald Rösner<sup>1</sup>; E.A. Prokofyev<sup>2</sup>; Ruslan Valiev<sup>2</sup>; Sergiy Divinski<sup>1</sup>; Gerhard Wilde<sup>1</sup>; <sup>1</sup>Institute of Material Physics, Westfälische Wilhelms-University Münster, Germany; <sup>2</sup>Institute of Physics of Advanced Materials, Ufa State Aviation University, Ufa, Russian Federation

A comparative study on slightly Ni-rich NiTi, deformed by high-pressure torsion (HPT) and repeated cold rolling (RCR) was investigated. The development of the microstructure in dependence of deformation was investigated by differential scanning calorimetry (DSC), X-ray diffraction analysis and transmission electron microscopy. The DSC signals observed during continuous heating experiments indicate that RCR is the more efficient deformation route with respect to grain refinement in comparison to HPT. Unusually large separation between crystallization and growth stages of NiTi is observed. A detailed analysis of the evolution of enthalpy release reveals reproducibly non-monotonous trends with annealing temperature that cannot be explained solely with nucleation and growth of crystalline volume fractions. Instead, these results as well as detailed kinetics analyses indicate that a reverse amorphization process occurs during annealing around 523 K. This behavior is discussed with respect to the nanoscale microstructural heterogeneity after initial deformation processing by HPT and RCR.

**Effect of Repetitive Corrugation and Straightening Rolling on Microstructure and Mechanical Behavior of Metallic Materials:** *Arya Mirsepassi*<sup>1</sup>; *Mahmoud Nili-ahmadabadi*<sup>2</sup>; Mohammad Habibi-parsa<sup>1</sup>; <sup>1</sup>University of Tehran

Severe plastic deformation (SPD) is a promising procedure to achieve ultrafine grained (UFG) microstructures in metallic materials. The homogeneity of microstructure, large applied strains, minimum dimensional changes and industrial applicability are the significant issues that should

be taken into consideration in SPD methods. The mostly applied SPD methods despite their widespread use, don't provide all the mentioned issues simultaneously. A new SPD process called repetitive corrugation and straightening rolling (RCSR), has been developed for fabrication of UFG metallic materials to induce high strains after repetitive cycles, more homogenous microstructure with minor dimensional changes and proper potential industrial application. RCSR consists of corrugated rollers and has the capability of changing the position of the specimens during different routes. Fe-Ni-Mn martensitic steel sheets were subjected to RCSR process. Optical and scanning electron microscopy with mechanical testing were used to study the microstructure and mechanical properties of the specimens.

**Deformation Behavior of Bulk Nanostructured Copper and Copper Alloys Processed by Ball Milling and High Pressure Torsion:** *Hamed Bahmanpour*<sup>1</sup>; Jelena Horky<sup>2</sup>; Sladjana Kahofer<sup>2</sup>; Ronald O. Scattergood<sup>1</sup>; Carl C. Koch<sup>1</sup>; Michael Zehetbauer<sup>2</sup>; <sup>1</sup>North Carolina State University; <sup>2</sup>Research Group Physics of Nanostructured Materials, University of Vienna

Nanostructured copper and copper alloys were produced by high energy ball milling. Powders were consolidated by applying high-pressure torsion (HPT) on cold compacted samples. With HPT pressures < 6 GPa and cyclically applied shear strains > 50 fully dense samples were achieved which showed microhardness values up to 2.8 GPa. These values markedly exceed any strength data reported in literature from in-situ consolidated ball milled or SPD processed Cu. The results are related to the very small crystallite size, as well as high densities of deformation induced defects like dislocations and vacancy agglomerates as being determined by X-ray profile analysis and DSC. Additional investigations of the mechanical behavior of nanostructured copper and copper alloys were done by means of stress relaxation tests in order to clarify the basic deformation mechanisms in the regime of very small grain size.

**Synthesis of High Strength Nano-Structured Alpha and Beta Tantalum:** *Anahita Navid*<sup>1</sup>; Andrea Hodge<sup>1</sup>; <sup>1</sup>University of southern california

High strength nano-structured (d = 50 nm) alpha and beta tantalum films (H=10-17 GPa) were synthesized at room temperature using DC magnetron sputtering. The variations in hardness values are related to phase formation, texture and residual stresses of the film. Several studies combining XRD, surface morphology evaluation and resistivity tests are utilized to verify the formation of alpha tantalum. The role of the substrate/film interface, underlayer materials, grain size and film texture were also investigated. In addition, the phase formation as a function of sputtering pressure is correlated to the effect of impurities and ion energy applied to the film during deposition.

**Ultra-high-Strength Nano-Grained Composites Produced by High-Pressure Torsion:** *Kaveh Edalati*<sup>1</sup>; Zenji Horita<sup>1</sup>; <sup>1</sup>Kyushu University

Processing of pure aluminum, titanium and nickel through the application of high-pressure torsion (HPT) results in a grain refinement at the sub-micrometer level (> 100 nm). In this paper, different fractions of Al, Ti and Ni powders are mixed and subjected to HPT. A significant grain refinement at the nanometer level (<30 nm) and high hardness (>500 Hv) are achieved following the HPT. The hardness values are much higher than 32, 265 and 308 Hv of the bulk form of the HPT-processed Al, Ti and Ni, respectively. High resolution electron microscopy is conducted to analyze the microstructures.

**Dry Sliding Wear and Corrosion Behavior of Ultrafine-Grained HSLA Steel Processed Using Multi Axial Forging:** *Aditya Padap*<sup>1</sup>; G Chaudhari<sup>1</sup>; S. Nath<sup>1</sup>; <sup>1</sup>Indian Institute of Technology Roorkee

A number of studies have been carried out in recent past years to optimize the relationship between mechanical properties and microstructure of steels processed by severe plastic deformation (SPD) techniques. Very few studies are available that correlate the microstructural changes and the mechanical properties of ultrafine grained (UFG) steels obtained by SPD, to the degradation phenomena such as wear and corrosion. In present study HSLA steel was severely deformed by warm (500°C) multiaxial forging (MAF) technique using up to nine strain steps. Submicron sized grain size was obtained after warm MAF. The hardness and strength properties

improved significantly, with adequate ductility. UFG steel obtained from warm MAF processing did not show any improvement in wear resistance. Low pull-off-work and fragmented nano sized pearlitic cementite particles were the two factors found responsible for lower wear resistance of UFG steel. The corrosion resistance of HSLA steel after warm MAF remained largely unaffected.

**Effects of Boron Carbide Additions on Kinetics of Grain Refinement in Cryomilled Al Powders:** *Yuzheng Zhang*<sup>1</sup>; Byungmin Ahn<sup>1</sup>; Rustin Vogt<sup>2</sup>; Zhihui Zhang<sup>2</sup>; Julie Schoenung<sup>2</sup>; Enrique Lavernia<sup>2</sup>; Steven Nutt<sup>1</sup>; <sup>1</sup>University of Southern California; <sup>2</sup>University of California, Davis

Al powders were blended with B4C particles and cryomilled in liquid nitrogen. Microstructural evolution as a function of milling time was investigated via transmission and scanning electron microscopy, and X-ray diffractometry. Al grain size distributions and grain refinement kinetics were determined by analysis of SEM images, and the effects of B4C addition (14.3 wt. %) were revealed by comparisons with unblended powders. The morphology and size of the milled powders and the size distribution of B4C particles were also determined. The grain refinement was achieved by repeated fracture and cold-welded processes. The grain size decreased with the increasing milling time, as did the variance in grain size. The addition of B4C particles facilitated the grain refinement process, and smaller grain sizes were observed in regions with high concentrations of B4C particles.

**Effect of Precipitation on the Mechanical Properties of Hot Extruded Nanostructured Aluminum Powder Alloys:** *Claudemiro Bolfini*<sup>1</sup>; Mauricio Peres<sup>1</sup>; Joao Fogagnolo<sup>2</sup>; Claudio Kiminami<sup>1</sup>; Walter Botta<sup>1</sup>; Alberto MoreiraJorge<sup>1</sup>; <sup>1</sup>Universidade Federal de São Carlos; <sup>2</sup>Universidade Estadual de Campinas

The effect of the extrusion temperature and ram speed during consolidation by hot extrusion of mechanical-alloyed Al-4.5%Cu alloy and Al6061 matrix reinforced with Si3N4 particle composite is discussed. Pre-existent precipitates in Al-Si3N4 alloy were very effective to control grain growth and to promote good mechanical properties on the consolidated alloys. Precipitation of Al2Cu was observed when extruding the mechanical-alloyed Al-4.5%Cu alloy at 375°C and 400°C, but no precipitation was observed in the material extruded at 425°C. The mechanical properties of the consolidated alloys were found to be strongly dependent on the extrusion conditions and this behavior is discussed in association with the original and modified microstructures, which increased with decreasing temperature and increasing ram speed.

**Mechanical Behavior of Cryomilled Al-B<sub>2</sub>C Ultrafine-Grained Metal Matrix Composite Extrusions Attributed to Stress Assisted Grain Growth and Particulate Reinforcement:** *Troy Topping*<sup>1</sup>; Cory Smith<sup>2</sup>; Ying Li<sup>1</sup>; Zhihui Zhang<sup>1</sup>; Bhaskar Majumdar<sup>3</sup>; Kyu Cho<sup>4</sup>; Mark van den Bergh<sup>2</sup>; Julie Schoenung<sup>1</sup>; Enrique Lavernia<sup>1</sup>; <sup>1</sup>University of California, Davis; <sup>2</sup>DWA Aluminum Composites; <sup>3</sup>New Mexico Tech University; <sup>4</sup>U.S. Army Research Laboratory

Aluminum based cryomilled ultrafine-grained metal matrix composites (UFG-MMCs) are of interest for their high specific strength when compared to conventional Al alloys – sometimes in excess of three times the strength on an unreinforced conventional alloy. These MMCs present unique challenges to understanding the effect of thermomechanical processing on microstructure, which is essential to maintaining desirable mechanical properties in the UFG-MMC. Trimodal UFG-MMCs, consisting of cryomilled Al 5083, B<sub>2</sub>C, and unmilled Al 5083, were vacuum hot pressed and extruded for this investigation. Extrusions at various temperatures and ratios were studied, with powders cryomilled at different times to change the contribution of nitrogen to strength. Microstructural evidence reveals a change in grain size scaled with extrusion ratio attributed to stress assisted grain growth, and wet chemical analysis shows variations in the nitrogen content that scale directly with strength. Zener-Holloman and Hall-Petch parameters of the UFG-MMCs are discussed.

**Basal-Plane Stacking-Fault Energies of Mg: A First-Principles Study of Li- And Al-Alloying Effects:** Zhao-Hui Jin<sup>1</sup>; Jian Han<sup>1</sup>; X.-M. Su<sup>1</sup>; Y.T. Zhu<sup>2</sup>; <sup>1</sup>Shanghai Jiao Tong University; <sup>2</sup>North Carolina State University

The understanding of physical mechanisms associated with particular deformation modes helps to develop materials with improved strength and ductility. For design purpose, it is necessary to understand various possible slip pathways associated with basal planes in hcp metals and how alloying effects may influence such pathways. With prototypical hcp metal Mg, we aimed to calculate the generalized stacking fault energies (GSFEs) associated with basal-plane slip pathways. In particular, we focused on to reveal the so-called sequential faulting mechanism in hcp metals, a deformation process quite similar to mechanical twinning in fcc metals. The GSFE profiles were obtained using first-principles technique in combination with climbing-image nudged elastic band methods. Our results show that Li-alloying can facilitate dislocation-mediated process, while with Al-alloying the sequential faulting across basal planes becomes favorable. Such difference is attributed to that the two alloying elements tend to form different types of bond critical points in Mg.

**Effect of Reinforcement Volume Fraction on the Properties of Nanocrystalline Mg Matrix Composite Reinforced with Ti<sub>2</sub>AlC:** Babak Anasori<sup>1</sup>; Shahram Amini<sup>1</sup>; Volker Presser<sup>1</sup>; Michel Barsoum<sup>1</sup>; <sup>1</sup>Drexel University

Herein we report on the effect of the reinforcement volume fraction on the mechanical properties of a novel nanocrystalline magnesium, Mg, matrix composite reinforced with Ti<sub>2</sub>AlC. Increasing the volume fraction of the reinforcement reduced the average size of Mg nanograins. Both Mg and Ti<sub>2</sub>AlC have been classified as kinking nonlinear elastic (KNE) solids. KNE solids trace fully reversible, reproducible, hysteretic stress-strain loops that can be characterized by three independent parameters: stress,  $\sigma$ , nonlinear strain,  $\epsilon_{NL}$ , and energy dissipated per cycle per unit volume,  $W_d$ , all of which can be obtained from the stress-strain loops. The results are in excellent agreement with our incipient kink band (IKB) based model. The Mg nanograins are also extraordinarily thermally stable; heating the composite three times to temperatures 50 °C above the melting point of Mg did not lead to coarsening of the nanograins.

**Effect of the Second Phase Particles on the Grain Refinement of an Al-Si-Mg Alloy Processed by ECAP:** Edgar Garcia-Sanchez<sup>1</sup>; Edgar Lopez-Chipres<sup>2</sup>; Rafael Colás-Ortiz<sup>1</sup>; <sup>1</sup>FIME-UANL; <sup>2</sup>UJED

Three initial microstructural conditions were considered with the aim to study the second phase particles effect on the grain refinement and mechanical properties in an aluminum alloy. In this work a commercial Al-Mg-Si alloy under various initial microstructural conditions has been deformed at room temperature by multi-pass 90° equal channel angular pressing (ECAP). The alloy after ECAP was aging under different conditions. The post ECAP annealing heat treatments in some cases promote high strengths and relatively high ductility; these were evaluated by means of tensile tests carried out at room temperature. The grain refinement was promoted by the presence of particles as observed by SEM and TEM. With this work was possible to obtain the optimal conditions for processing an Aluminum alloy under SPD and post aging heat treatments improving the mechanical properties and obtaining an ultrafine grained microstructure.

**Alumina and Bauxite: Alternative Alumina Sources**  
**Light Metals Poster Session**

*Sponsored by:* The Minerals, Metals and Materials Society, TMS Light Metals Division, TMS: Aluminum Committee, TMS: Aluminum Processing Committee

*Program Organizers:* James Metson, University of Auckland; Carlos Suarez, Hatch Associates Consultants Inc

Sun PM-Thurs PM  
Feb 27-Mar 3, 2011

Room: 17A  
Location: San Diego Conv. Ctr

**Adsorption of Polyethylene Glycol at the Interface of Dicalcium Silicate – Sodium Aluminate Solution:** Yu Haiyan<sup>1</sup>; Xiaolin Pan<sup>1</sup>; Zhongke Lu<sup>2</sup>; Tingting Ding<sup>1</sup>; <sup>1</sup>Northeastern University; <sup>2</sup>Shandong Branch, Chalco

Surfactants, such as polyethylene glycol (PEG), are widely used to inhibit the secondary reaction of dicalcium silicate ( $\beta$ -CaO•SiO<sub>2</sub>) in sodium aluminate solution. The adsorption isotherm of PEG on  $\beta$ -CaO•SiO<sub>2</sub> in sodium aluminate solution at 80°C was researched in this paper. It was found that the type of surface adsorption of PEG is saturated adsorption, and the adsorption behavior belongs to “S”-type, according with the multi-molecular layer adsorption model of the Freundlich Equation. The surface coverage of PEG close to saturated adsorption derived from the specific surface area of  $\beta$ -CaO•SiO<sub>2</sub> is 0.723 mol/μm<sup>2</sup>. The relation curves between the surface pressure and the molecular area of adsorption film were obtained according to the adsorption results at the solid-liquid interface by Gibbs formula. The variation of interfacial energy caused by adsorption, as well as the relationship between the relation curves and the type of adsorption was also discussed.

**The Effect of Cooling Rate on the Leachability of Calcium Aluminate Slags:** Wang Bo<sup>1</sup>; Sun Huilan<sup>1</sup>; Zhang Xuezheng<sup>1</sup>; Bi Shiwen<sup>2</sup>; <sup>1</sup>Hebei University of Science and Technology; <sup>2</sup>Northeastern University

The calcium aluminate slag was synthesized by CaCO<sub>3</sub>, SiO<sub>2</sub> and Al<sub>2</sub>O<sub>3</sub> under the conditions of 1500°C for 1h. The effect of cooling rate on alumina leaching property and self-disintegrating property of calcium aluminate slag were studied, and the effect mechanism was discussed by the method of XRD, SEM, and laser particle size analyzer. The results indicated that the phase components, alumina leaching property and self-disintegrating property of calcium aluminate slag were better when cooling rate was lower than 20°C•min<sup>-1</sup>. The formation of 2CaO•Al<sub>2</sub>O<sub>3</sub>•SiO<sub>2</sub> and 3CaO•Al<sub>2</sub>O<sub>3</sub> would decrease alumina leaching rate and self-disintegrating rate obviously when cooling rate was higher than 20°C•min<sup>-1</sup>. The crystal conversion rate from  $\beta$ -2CaO•SiO<sub>2</sub> to  $\gamma$ -2CaO•SiO<sub>2</sub> was still high when cooling rate was between 20°C•min<sup>-1</sup> and 50°C•min<sup>-1</sup>. Therefore, the main reason of the decrease of self-disintegrating rate was the formation of 2CaO•Al<sub>2</sub>O<sub>3</sub>•SiO<sub>2</sub>.

**The Effect of Ultrasonic Treatment on Alumina Leaching from Calcium Aluminate Slag:** Sun Huilan<sup>1</sup>; Wang Bo<sup>1</sup>; Guo Dong<sup>1</sup>; Zhang Xuezheng<sup>1</sup>; Bi Shiwen<sup>2</sup>; <sup>1</sup>Hebei University of Science and Technology; <sup>2</sup>Northeastern University

The effect of ultrasonic on alumina leaching property of calcium aluminate slag was investigated. The effects of the main leaching parameters such as ultrasonic power, leaching time, leaching temperature, and the concentration of sodium carbonate on alumina leaching rate were determined. The effect mechanism of ultrasonic was also discussed. It was found that the increase of leaching rate was slight, but leaching conditions were improved obviously when ultrasonic was used in leaching process. Leaching temperature and sodium carbonate concentration decreased by 30°C and 60g•L<sup>-1</sup> when there was ultrasonic wave. Ultrasonic would not promote the decomposition of  $\gamma$ -2CaO•SiO<sub>2</sub>. The agglomeration of leaching residue was prevented by the cavitation and mechanical effect of ultrasonic.



**Preparing Polymerized Aluminum-Ferrum Chloride with Red Mud:** *Lu Guilin*<sup>1</sup>; Yu Haiyan<sup>1</sup>; Bi Shiwen<sup>1</sup>; <sup>1</sup>School of Sciences; Shenyang University of Technology

Put forward a new method to prepare polyaluminium ferric chloride(PAFC) with red mud. Discuss the effect of pH of PAFC on basicity, study the difference of products in the process of red mud hydrolyzing from products in the process of sodium hydroxide hydrolyzing. The results show that basicity increases with the increases of pH, the prefer pH value is 3.5, and basicity is up to 85.55%. Comparing appearance of PAFC with that of crystal aluminium chloride, polyaluminium chloride by SEM can indicate that distribution of materials is not uniform on the surface of PAFC. Energy chromatogram analysis indicate that content of aluminum, iron, oxygen elements accounts for 60.73% in the white areas, 43.95% in the black areas in process of red mud hydrolyzing; the content of aluminum, iron, oxygen elements in white areas is 49.74% , 23.45% in black areas in process of sodium hydroxide hydrolyzing.

**Production of Hematite Ore from Red Mud:** *Puliyur Krishnaswamy Narasimha Raghavan*<sup>1</sup>; Nand Kumar Kshatriya<sup>1</sup>; <sup>1</sup>Bharat Aluminium Co. Ltd., (A Unit of Vedanta Resources Plc.), BALCO Nagar, Korba

Red Mud generated as a waste material in the Bayer process is a potential source of metal values. Disposal and storage problems will prevail due to the leachable soda content and the bulk to be handled. Jarosite is a waste of Zinc refinery and is both difficult and costly to manage and to dispose safely. Jarosite is normally associated with sulphuric acid and Ferric iron which produce additional acid on hydrolysis. Reaction between red mud and jarosite is expected to produce a liquid phase containing and a solid phase dominated by iron hydroxide. A precipitated Solid (Sodium Sulphate) is obtained from the Liquid Phase and the solid phase was calcined to produce ferruginous solid that could be used as an iron ore. In this paper an attempt is made to evaluate procedure for the preparation of iron ore and marketable salts by reacting the Red Mud and Jarosite.

**Extraction of Alumina from Red Mud by Divalent Alkaline Earth Metal Soda Ash Sinter Process:** *Shib Narayan Meher*<sup>1</sup>; Ashok Kumar Rout<sup>1</sup>; Balakrushna Padhi<sup>2</sup>; <sup>1</sup>Kiit University; <sup>2</sup>National Aluminum Company Limited

A novel method for extraction of alumina from red mud using divalent alkaline earth metal oxide soda ash sinter process followed by thermo chemical leaching in suitable caustic concentration at 105°C for different time is presented in this paper. During sintering Sodalite / Cancrinite , Gibbsite and Boehmite in red mud is converted to sodium aluminate as well as stable phases of divalent alkaline earth metal ferrite, titanate and silicate. In the above novel economic process the extraction of alumina from red mud is achieved 97.64% , 98.7% and 99.5 % by using CaO, MgO and BaO respectively. The morphological study of sinter product as well as leached residue was studied by SEM and XRD . Key Word-Red Mud, Sintering, Leaching and Divalent alkaline earth metal oxide.

**Study on the Strength of Powders Seed-Precipitated from Sodium Aluminate Solutions:** *Gang Xie*<sup>1</sup>; Yu Xiaohua<sup>1</sup>; <sup>1</sup>Technology Center of Yunnan Metallurgy Group Co.Ltd.

The mechanical strength of alumina powders from sintering and precipitation of sodium aluminate solutions were investigated in bench scale studies. The experimental results show that the mechanical strength of the alumina powders increases with increased precipitating temperature and appropriate times of seeds. A higher strength of alumina powders can be obtained as the strength of Al(OH)<sub>3</sub> powders brings to higher.

**The Role of Quasi Web Structure of Nano SiC Whiskers on Strengthen and Density in Bauxite Based Composite Materials:** *Ebrahim Karamian*<sup>1</sup>; Ehsan Mohammadi Zahrani<sup>2</sup>; <sup>1</sup>Isfahan University of Technology; <sup>2</sup>Department of Materials Engineering, University of British Columbia

This study describes the role of quasi web structure of nano β-SiC whiskers on cold crushing strength (CCS) and bulk density in Bauxite based composite materials. SiC whisker is excellent in characteristics (specific strength, specific modulus) and its usefulness as a composite reinforcing

material. Nano β-SiC whiskers can synthesize by the VLS mechanism and using of Fe catalyst at different temperatures. Specimens were composed of a blend of 65 wt.% Chinese bauxite aggregate, 15 wt.% SiC containing material, 10 wt.% coke, 10 wt.% resole and different quantities of silicon compounds carbonized at 800 °C (2 h). The process is consist of a heating at 200 °C (2 h) followed by firing at 1100 °C or 1400 °C (2 h). The web structure formed at 1400 °C and CCS values improved by almost 3-4 times. But they did not fully form at 1100 °C, so that CCS decreased.

**Theory and Experiment on Cooling Strategy during Seeded Precipitation:** *Zhanwei Liu*<sup>1</sup>; Wenmi Chen<sup>1</sup>; Wangxing Li<sup>2</sup>; <sup>1</sup>Central South University; <sup>2</sup>Zhengzhou Research Institute of Chalco

The η-t curve is derived from the dynamical equation of seeded precipitation. The curve has the characteristic of hyperbolic function and the experimental results conform to the characteristic of the curve. The η-t curve indicates that the precipitation ratio rise rapidly at the preliminary stage of precipitation, the precipitation ratio ascend slowly at middle stage of precipitation and the precipitation ratio increase slower and slower at final stage of precipitation. On the basis of this character of the η-t curve and the technology feature of seeded precipitation of producing sandy alumina in Chinese alumina plant, various parameters are determined in precipitation process with intermediate lowering temperature.

**Dissolution Kinetics of Silicon from Sintering Red Mud in Pure Water:** *Xiaohui Li*<sup>1</sup>; Kai Huang<sup>1</sup>; *Hongmin Zhu*<sup>1</sup>; <sup>1</sup>University of Science & Technology Beijing

In the present study, the dissolution kinetics of silicon from sintering red mud in pure water was studied. The different experimental conditions such as liquid-solid ratio (0.3g/L, 0.5g/L, 1.0g/L), particle size (74~185μm, 39~46μm), stirring speed (80r/min, 160r/min, 300r/min), temperature (20°, 40°, 60°) were evaluated. It was found that the silicon extraction increases with temperature, liquid-solid ratio, stirring speed and decreasing in the particle size of red mud. A simple dissolution model, i.e., external film diffusion was determined to be the main step to control the whole dissolution process. The expression of the diffusion model is as follows:  $\ln(C_s/(C_s-C)) = (DA/d) \times t$  The apparent activation energy was correspondingly determined to be 8.67 kJ/mol.

## Aluminum Reduction Technology: Light Metals Poster Session

*Sponsored by:* The Minerals, Metals and Materials Society, TMS Light Metals Division, TMS: Aluminum Committee, TMS: Aluminum Processing Committee

*Program Organizers:* Mohd Mahmood, Aluminium Bahrain; Abdulla Ahmed, Aluminium Bahrain (Alba); Charles Mark Read, Bechtel Corporation; Stephen Lindsay, Alcoa, Inc.

Sun PM-Thurs PM  
Feb 27-Mar 3, 2011

Room: 17A  
Location: San Diego Conv. Ctr

**Human Factors in Operational and Control Decision Making in Aluminium Smelters:** *Yashuang Gao*<sup>1</sup>; Mark Taylor<sup>1</sup>; John Chen<sup>1</sup>; Michael Hautaus<sup>1</sup>; <sup>1</sup>University of Auckland

The aluminium smelting process involves highly complex mechanisms, has rich information but low observability. To operate such a process at maximum current efficiency while striving for continual improvement requires a set of scientific and systematic approaches to problem solving and decision making along with constant human intervention and interaction with the process. Understanding the influence of human factors on the process is important to the improvement of the performance of the operational staff and enhancement of positive impact while minimising negative effects on the process. This poster explains the human factors and decision making involved in the smelting reduction operations and control process, which includes sensing and monitoring signals, identifying abnormalities and implementing appropriate response to not only correct the immediate causes



of the identified problems but also to reduce the variation and continuous improvement of the process over time.

### Approaches for Investigating Phase Transformations at the Atomic Scale: Posters

*Sponsored by:* The Minerals, Metals and Materials Society, ASM International, TMS Materials Processing and Manufacturing Division, TMS/ASM: Computational Materials Science and Engineering Committee, TMS/ASM: Phase Transformations Committee  
*Program Organizers:* Neal Evans, Oak Ridge National Laboratory; Francisca Caballero, Spanish National Research Center for Metallurgy (CENIM-CSIC); Chris Wolverton, Northwestern University; David Seidman, Northwestern University; Rajarshi Banerjee, University of North Texas

Sun PM-Tues PM  
Feb 27-Mar 1, 2011

Room: 32B  
Location: San Diego Conv. Ctr

### An Identification Scheme of Grain Boundaries and Construction of Grain Boundary Energy Database: *Byeong-Joo Lee*<sup>1</sup>; <sup>1</sup>Pohang University of Science and Technology

As there exists no systematic way to identify grain boundaries between two grains with arbitrary misorientation relationships, we have developed a systematic scheme to uniquely define individual grain boundaries in polycrystalline materials. This allows us to construct a grain boundary energy database for body-centered-cubic (bcc) Fe in a suitable form for implementation on grain growth simulations. The scheme can be equally applied to identify grain boundaries for different structures and/or individual interfaces between two different phase grains, and enables realistic simulations of phase transformations as well as grain growth assigning real crystallographic orientations to individual grains.

### Computing Thermodynamic Properties of FeCr Alloys by Path Sampling Simulations: *Gilles Adjanor*<sup>1</sup>; Manuel Athènes<sup>2</sup>; <sup>1</sup>EDF R&D; <sup>2</sup>CEA-Saclay

For the prediction of thermal ageing of austeno-ferritic elbows of nuclear reactors primary circuit, as well as to propose candidate chromium ferritic/martensitic steels for Generation IV reactors, the phase diagram of the FeCr system is of primary importance. As ab initio results predict that the mixing enthalpy changes its sign at low temperature due to magnetism, this phase diagram has been recently revised. We report on the application to this system of a path-sampling method, which can be seen as a combination of thermodynamic integration and semi-grand canonical ensemble methods, allowing to alleviate their respective limitations by tuning paths length. As it consists in sampling multiple thermodynamic integrations, the method naturally takes into account both configurational and vibrational contributions to the chemical potential, which can be evaluated separately. In addition, the analysis of path histograms yields a built-in criterion for diagnosing the convergence of chemical potential estimates.

### Identification of Phase Transformation Using Optical Emission Spectroscopy for Direct Metal Deposition Process: *Lijun Song*<sup>1</sup>; Jyoti Mazumder<sup>1</sup>; <sup>1</sup>University of Michigan

The microstructure of an alloy, which is related to the characteristics of its phase diagram, is strongly correlated to its mechanical properties. However, the analysis of microstructure of an alloy has been limited to the postmortem analysis such as optical or scanning electron microscopes. Real time microstructure diagnosis during processing is still not possible. Here we report an in-situ identification of phase transformation by diagnosing the laser induced plasma during direct metal deposition process. Within the same microstructure range, the spectral line intensity ratio is proportional to the composition ratio; however, when there is a phase change, the linear relationship is broken and another linear relationship within the range of the new phase is formed. This phase related plasma change reflects the initial nucleation of the crystallography of the alloy in early stage and will be applicable for in-situ phase transformation identification during any process where plasma is generated.

### Study of the Interaction of Solutes with Interfaces in Iron Using Density-Functional Theory: *Hao Jin*<sup>1</sup>; Ilya Elfimov<sup>1</sup>; Matthias Militzer<sup>1</sup>; <sup>1</sup>The University of British Columbia

Substitutional alloying elements significantly affect the austenite-ferrite phase transformation rates in steels. However, the detailed mechanisms of their interaction with the moving interfaces are not fully understood. To gain insight into the solute-interface interaction density functional studies have been carried using VASP. Simulations have been performed for a Sigma 5 tilt grain boundary in bcc-Fe containing commonly used alloying elements, e.g. Mn, Mo, Nb and V, to determine the binding energies of these solutes to the grain boundary and their activation energies for diffusion along and across the boundary. Further, the interactions of different solutes at the grain boundary have been investigated. This study confirms the strong interaction of Nb with interfaces that is consistent with experimental observations of the effects of Nb in solution in delaying the austenite-to-ferrite transformation.

### Biological Materials Science: Poster Session

*Sponsored by:* The Minerals, Metals and Materials Society, TMS Electronic, Magnetic, and Photonic Materials Division, TMS Structural Materials Division, TMS: Biomaterials Committee  
*Program Organizers:* Jamie Kruzic, Oregon State University; Nima Rahbar, University of Massachusetts, Dartmouth; Po-Yu Chen, University of California, San Diego; Candan Tamerler, University of Washington

Sun PM-Thurs AM  
Feb 27-Mar 3, 2011

Room: 15A  
Location: San Diego Conv. Ctr

### A Crystallographic and Textural Perspective of Aging and Diagenetic Degradation of Mechanical Properties on Hard Malacological Paleo-Tissues: *Raúl Bolmaro*<sup>1</sup>; María Bayer<sup>2</sup>; Gonzalo Duarte<sup>1</sup>; Natalia De Vincentis<sup>1</sup>; Sandra Gordillo<sup>2</sup>; <sup>1</sup>IFIR; <sup>2</sup>Universidad Nacional de Córdoba

Sea shells of different species are characterized by X-ray diffraction, micro-indentation tests and electron scanning microscopy. A few samples of Amiantis and Prototaca collected on holocene and pleistocene deposits on the Argentine sea coasts were tested in search of crystallographic modifications and mechanical strength degradation in comparison with identical species modern individuals. X ray diffraction was used to look for aragonite replacement by its more stable calcite structure and possible variations on the known highly oriented orientation distribution. On the same samples the strength was evaluated by micro-indentation and the results were correlated with the microscopic observations.

### Antibacterial Microporous Coating Formation on Ti6Al4V Alloy via Micro Arc Oxidation Process: *Faiz Muhaffel*<sup>1</sup>; Eyüp Kayali<sup>1</sup>; Hüseyin Çimenoglu<sup>1</sup>; <sup>1</sup>Istanbul Technical University

Titanium and its alloys have high mechanical properties, superior corrosion resistance, low elasticity module, low density and high biocompatibility. In order to provide the bio-active surface in medical titanium alloys, a hydroxyapatite layer can be developed over the titanium oxide layer by micro-arc oxidation method in recent days. In micro-arc oxidation, an electrolytic solution containing calcium and phosphorus ions, the oxide layer is formed on the anode material. In the micro-arc oxidation of titanium and its alloys, microporous and rough titanium oxide layer containing hydroxyapatite precipitates formed on the surface and it is bonded firmly to the implant surface. The aim of this study is to develop a microporous, rough and antibacterial surface over Ti6Al4V alloy via micro arc oxidation process. Different amount of silver added to micro arc oxidation solution and examined the antibacterial effect of silver concentration.

### Bactericidal Effect of Silver Reinforced Hydroxyapatite and Carbon Nanotubes: *Atif Faiz Mohammed*<sup>1</sup>; Pallavi Kesarwani<sup>2</sup>; Kantesh Balani<sup>1</sup>; <sup>1</sup>Indian Institute of Technology; <sup>2</sup>Visvesvaraya National Institute of Technology

Bacterial infection remains an important risk factor in orthopedic surgery. Present work aims at the synthesis of silver reinforced hydroxyapatite

(HAp-Ag) and carbon nanotube (CNT-Ag) via spark plasma sintering (SPS) processing route. Phase analysis from X-ray diffraction and Raman spectroscopy confirmed the retention of initial phases even after SPS. Energy dispersive spectroscopy of the spark plasma sintered samples elicited the uniform distribution of silver. Antibacterial test with *Escherichia coli* showed significant difference in number of bacterial colonies in HA-Ag and CNT-Ag w.r.t. HA and CNT. Silver reinforcement depicted an increase in hardness (from 7.754 to 8.966 GPa) and elastic modulus (from 119.98 to 125.31 GPa) for HA sintered sample, whereas a decrease in the hardness (from 0.370 to 0.238 GPa) and modulus (from 5.06 to 3.65 GPa) was observed for CNT sintered sample. Silver reinforcement has shown to influence mechanical properties while rendering bactericidal effect in HA and CNT biocomposites.

**Characteristics and Wear Performance of Nitrided Ti6Al7Nb:** *Farid Siyahjani*<sup>1</sup>; Huseyin Cimenoglu<sup>1</sup>; <sup>1</sup>Istanbul Technical University

Samples of a Ti6Al7Nb were treated by thermochemical gas nitriding for 5 h at 1120 °C. X-ray diffraction analysis of the samples was carried out to identify new phases of chemical compounds in the Ti6Al7Nb. Microstructures were analysed using scanning electron microscopy. The hardness of the nitride layer was over 1800 HV. Cross-sectional microhardness profiles of the samples were obtained using a mikro hardness. The titanium nitride layer exhibited excellent wear resistance along with a lower coefficient of friction against sapphire ball under dry lubricated sliding conditions when compared to the as-received state and measured average friction coefficient of nitride layer.

**Development of Hydroxyapatite and Silicon Carbide Composites via Thermal Plasma Route:** *Atif Faiz Mohammed*<sup>1</sup>; Saroj K Singh<sup>2</sup>; <sup>1</sup>Indian Institute of Technology Kanpur; <sup>2</sup>Institute of Materials and Minerals Technology

Hydroxyapatite (HA) and Silicon Carbide are known to be excellent biocompatible materials. In this study composites of Hydroxyapatite and Silicon carbide have been prepared to enhance mechanical properties. The composites were processed via thermal plasma sintering route. In this technique sintering time is the most important parameter. An optimized sintering time was tried to achieve where no HA phase dissociation and no reaction between HA and SiC is observed. Samples were sintered for four different time durations of 15, 30, 45 and 60 seconds. Also no Silicon dioxide formation took place, which could be attributed to the rapid sintering. In 60 seconds, formation of other phases was observed. Phase analysis was studied using Raman spectroscopy and X-ray diffractometry. Microstructural analysis was done by FESEM and EDX. The results for 45 seconds show homogenous distribution of SiC, no reaction between HA and SiC or any formation of Tricalcium phosphates were observed.

**Fatigue and Mechanical Properties of Co-Cr Alloy Tube for Stents after Ultrasonic Nanocrystal Surface Modification:** *Young Sik Pyun*<sup>1</sup>; Auezhan Amanov<sup>1</sup>; Jun Hyong Kim<sup>1</sup>; Sang Ho Kim<sup>2</sup>; Chae Jong Park<sup>2</sup>; <sup>1</sup>Sun Moon University; <sup>2</sup>M.I.Tech Co., Ltd.

The stent made of Co-Cr alloy tube is widely using for treating peripheral artery disease, including the superficial femoral, carotid, and renal arteries. However, fracture occurrences of up to 50% have been reported in some stents after one year. These stent fractures are likely due to in vivo cyclic displacements. Since Ultrasonic Nanocrystal Surface Modification (UNSM) treatment improves surface integrity, surface hardness, and induces compressive residual stress in surface layers, it was applied to stent tube which was made of Co-Cr alloy in order to prevent these stent fractures and to improve its fatigue life and mechanical properties. In this study, the effects of the UNSM treatment on mechanical characteristics and fatigue life of Co-Cr alloy tube are investigated and compared to untreated one. The experiment results show that UNSM-treated specimen has provided good long-term fatigue life than untreated one.

**Improvement of Mechanical Properties of Ti-6Al-4V after EDM Surface Treatment for Biomedical Applications:** Josef Stráský<sup>1</sup>; Miloš Janeček<sup>1</sup>; Petr Harcuba<sup>1</sup>; Jitka Vrátná<sup>1</sup>; Lothar Wagner<sup>2</sup>; Lucie Bacakova<sup>3</sup>; <sup>1</sup>Charles University; <sup>2</sup>Clausthal University of Technology; <sup>3</sup>Institute of Physiology, Academy of Sciences

EDM (electric discharge machining, spark erosion, electro-erosion) was performed to prepare the surface of the Ti-6Al-4V alloy for biomedical application, namely for optimum bone cell ingrowth into orthopaedic implant. Positive bone cells reaction to surface treated by EDM has been analyzed. However, mechanical properties were found to markedly suffer from this treatment making the implant material unacceptable for biomedical applications. Poor properties are not sufficiently improved by simple annealing or variations in original structure (globular, bimodal etc.). This is due to persisting cracks and voids in the surface and subsurface layers. Therefore subsequent shot peening was performed to reduce the detrimental effect of EDM surface treatment. Mechanical properties were finally evaluated and correlated with modifications in microstructure as observed by SEM.

**Investigation of Incorporating Zirconia Particles into Titanium Oxide Coated by Plasma Electrolytic Oxidation:** *Ki Ryong Shin*<sup>1</sup>; Kang Min Lee<sup>1</sup>; Young Gun Ko<sup>2</sup>; Dong H. Shin<sup>1</sup>; <sup>1</sup>Hanyang University; <sup>2</sup>Yeungnam University

The present study investigated the incorporation of zirconia particles into titanium oxide via plasma electrolytic oxidation (PEO) coating with an AC current density of 200 mA/cm<sup>2</sup>. After PEO coating, a number of fine zirconia particles were uniformly distributed throughout the oxide layer. Based on microstructural observation, it was suggested that mechanisms for the incorporation of zirconia particles were electrophoresis, sintering, and melting in series during coating. In addition, zirconia particles incorporated into the oxide layer played an important role in accelerating the occurrence of biomimetic apatite in a simulated body fluid solution.

**Laser Hardening of Beta Titanium Alloy (Ti-23Nb-0.7Ta-2Zr-1O) for Biomedical Applications:** *Velayutham Nainar*<sup>1</sup>; Geetha Manivasagam<sup>1</sup>; Nandy<sup>2</sup>; Asokamani<sup>1</sup>; <sup>1</sup>VIT University; <sup>2</sup>Defence Metallurgical Research Laboratory

Gum metal (Ti-23Nb-0.7Ta-2Zr-1O) is a new beta titanium alloy possessing ultra- low elastic modulus and high strength to weight ratio. As titanium alloys generally suffer from poor tribological properties an attempt is being made to modify the surface of the samples using Nd-YAG pulsed laser by varying its processing parameters. The phases formed and the microstructures of the laser hardened samples were characterized using X-ray diffraction and scanning electron microscopy. The change in the hardness due to laser hardening treatment was also measured using Vicker hardness tester. Apart from the above, corrosion and the sliding wear behavior of the laser hardened and un-modified gum metal were investigated in simulated body fluid (Hank's solution). The results of the above studies will be discussed in detail.

**Microwave Augmented Fabrication and Evaluation of CNT-Reinforced Nanohydroxyapatite:** M Bilal Khan<sup>1</sup>; Rafaqat Hussain<sup>2</sup>; *Muhammad Aftab Akram*<sup>1</sup>; <sup>1</sup>National University of Sciences and Technology (NUST), SCME; <sup>2</sup>COMSATS

Bioactive CNT reinforced hydroxyapatite nano-composite is synthesized by in-situ precipitation for use in load bearing orthopedic applications. Microwaves augment the synthesis, enhance the reaction rate, and institute energy savings. Heat and acid treated purified CNTs in microwaves are functionalized and dispersed in calcium nitrate tetrahydrate. Diammonium hydrogen phosphate is incorporated in calcium ion solution to furnish the required Ca:P ratio. Refluxing of the precursor solution is accomplished under microwaves. XRD shows the phase purity and crystallinity, FTIR spectroscopy indicates the functionalization of CNTs and SEM analysis depicts the nanoporous nanomorphology of synthesized powder. TGA measures the thermal endurance of product, showing good CNTs retention at high temperatures (1100°C) in nitrogen ambient, otherwise they get oxidized in air in that temperature range. CNT reinforced sintered biomaterial exhibits

excellent consolidation and a Vicker hardness increment of 30%. The relation of between mechanical properties and sintering time is correlated by SEM.

**Multifunctional Nanowire Systems for Drug Delivery:** *Karla Brammer*<sup>1</sup>; Chulmin Choi<sup>1</sup>; Sungho Jin<sup>1</sup>; <sup>1</sup>UC San Diego

Nanostructured materials as drug delivery devices can play a key role in localization and controlled/sustained release of therapeutic drugs within the body. We have prepared vertically aligned silicon nanowire (SiNW) arrays, with a 10-40 nm diameter, by chemical etching and utilized them as novel nanostructures for mediating drug delivery. Here we report antibiotic drug release kinetics from SiNW array "motherships", which are desirably anti-biofouling, as well as capable of storing a relatively large amount of drug which allows for a sustained, therapeutic drug release level and longevity for 42 days. Such antibiotic release from this nanostructured surface can provide more reliable antibiotic protection at a targeted implantation or biosensor site with a low probability of biofouling or clogged pores due to the foreign body response. Furthermore, the bio-degradable nature of these nanowires can eventually allow natural disintegration and removal of the drug delivery vehicles.

**Surface Modification of Bio-implantable Ti-alloy by Hybrid Laser-Arc Processes:** *Soundarapandian Santhanakrishnan*<sup>1</sup>; Mehdi Asgharifar<sup>1</sup>; Radovan Kovacevic<sup>1</sup>; <sup>1</sup>Southern Methodist University

In this study, a new hybrid laser-arc process is proposed to modify the surface texture and mechanical properties of the bio-implantable Ti-alloy. A 2-kW high power diode laser (HPDDL) of 808 nm in wavelength with uniform distribution (top-hat) of laser power coupled with an atmospheric DC arc discharge is used to carry out the experiments. The effect of process parameters such as laser power, scanning speeds, and the current on the variation of surface texture and mechanical properties are studied. The study of microstructure, energy dispersive X-ray spectroscopy (EDX), and hardness measurements are performed to quantify the effect of process parameters on the variation of surface texture and the change of mechanical properties.

**Enhanced Functions of Osteoblasts on Nanophase Titania-Coated Nanostructured Austenitic Stainless Steel:** *Pavan Challa*<sup>1</sup>; Devesh Misra<sup>1</sup>; <sup>1</sup>University of Louisiana at Lafayette

We describe here the significance of electrocrystallized nanonodular titania-coated nanogained/ultrafine grained (NG/UFG) austenitic stainless steel in comparison to bare NG/UFG substrate. The study demonstrates that nanophase titania-coated substrate exhibited higher degree of cell attachment and proliferation which are regulated via cellular and molecular interactions with proteins, actin and vinculin. An accompanying objective is to study the antimicrobial activity. The antimicrobial activity associated with the photocatalytic property of titania was assessed in terms of degradation of methyl orange and effectiveness in killing E Coli.

**Design Considerations for Developing Biodegradable Magnesium Implants:** *Harpreet Brar*<sup>1</sup>; Benjamin Keselowsky<sup>1</sup>; Malisa Sarntinoranont<sup>1</sup>; Michele Manuel<sup>1</sup>; <sup>1</sup>University of Florida

The integration of biodegradable and bioabsorbable magnesium implants into the human body is a complex undertaking that faces major challenges. Developing causal relationships between alloy chemistry and microstructure, and its effect on cellular behavior can be a difficult and time intensive process. A systems design approach driven by thermodynamics has the power to provide significant contributions in developing the next generation of magnesium alloy implants with controlled degradability, biocompatibility, and optimized mechanical properties, at reduced time and cost. This approach couples experimental research with theory and mechanistic modeling for the accelerated development of materials. The aim of this article is to enumerate this strategy, design considerations, and hurdles for developing new magnesium alloys for use as biodegradable implant materials [1]. Reference[1] H.S. Brar, B.G. Keselowsky, M. Sarntinoranont, M.V. Manuel, "Design Considerations for Developing Biodegradable Magnesium Implants." JOM 63/4 (2011), to be published.

## Characterization of Minerals, Metals and Materials: Poster Session

*Sponsored by:* The Minerals, Metals and Materials Society, TMS Extraction and Processing Division, TMS/ASM: Composite Materials Committee, TMS: Materials Characterization Committee  
*Program Organizer:* Sergio Monteiro, State University of the Northern Rio de Janeiro - UENF

Sun PM-Thurs AM  
Feb 27-Mar 3, 2011

Room: 14B  
Location: San Diego Conv. Ctr

*Session Chairs:* Sergio Monteiro, UENF; Felipe Perisse Lopes, UENF

**A Method for Measuring the Critical Fracture Strain at Any Temperature during the Quenching of Tool Steels:** *Chao Zheng*<sup>1</sup>; *Daniel Watt*<sup>1</sup>; <sup>1</sup>University of Windsor

A new type of resistance heated tensile specimen allows the measurement of the critical fracture strain at any temperature during the heat treatment of tool steels in a vacuum. It is unique because it controls the temperature variation along the gage length within +/- 8C over a 0-1200C range. The specimen maintains this throughout heating, soaking, and quenching. During quenching, the cooling rate can be varied over a wide range by controlling the heater current decline, combined with an optional nitrogen gas manifold spray. The process can be interrupted at any stage, and held at constant temperature to measure the critical fracture strain. This includes the period when there are austenite-martensite mixtures; the range where quench cracks commonly form. The lack of having these critical fracture strain measurements in this range has hindered existing, but otherwise powerful, FEA simulations to reliably predict quench fractures.

**Effects of Arc Welding Process on Microstructure and Morphology of Flake Graphite in Grey Cast Iron:** *Arash Elhami Khorasani*<sup>1</sup>; Alireza Kiani-Rashid<sup>2</sup>; <sup>1</sup>Ferdowsi University of Mashhad; <sup>2</sup>Associated Professor at Material Science and Engineering Dept., Ferdowsi University of Mashhad

According to the role of factors such as cooling rate, alloying elements and thickness of specimen, in micro-structure of a welded grey cast iron; the effect of these parameters on graphite structure during arc welding process was studied. Results have shown great influence on localized segregation, dendritical structures and the variation of graphite's morphology, even after annealing. It has also been observed that the presence of temperature gradient within the specimen, especially among the welded metal zone, has resulted in a noticeable change of graphite's essence and cast iron's micro-structure in those areas.

**Preparation SCR Catalyst Carrier by Using APCVD and Sol-Gel Technology to Load TiO<sub>2</sub> on Cordierite Ceramic:** *Jian Yang*<sup>1</sup>; Qingcai Liu<sup>1</sup>; Mei Yang<sup>2</sup>; Wei Gao<sup>1</sup>; Wenchang Xi<sup>1</sup>; <sup>1</sup>university of Chongqing; <sup>2</sup>Southwest Petroleum University

TiO<sub>2</sub> has been loaded on cordierite porous ceramic to prepare the SCR catalyst carrier by using both APCVD and sol-gel technology. In APCVD method, TiCl<sub>4</sub> and O<sub>2</sub> were used as reaction precursor. TiCl<sub>4</sub> was gasified by using N<sub>2</sub> as carrier gas which was controlled to 500scm. Its reaction temperature and reaction time were limited to 773K and 30min respectively. The tests showed that TiO<sub>2</sub> loaded by APCVD method were of graininess shape and even accumulation. The loading rate of TiO<sub>2</sub> and the specific area of carrier sample were increased 114% and 21% respectively comparing with sol-gel technology. In the result of sol-gel method, the maximal difference of Ti content was 66.92%, while the result of APCVD method was 18.89%. It demonstrated that TiO<sub>2</sub> was uniformly attached with the cordierite ceramic by using APCVD method, which would ensure the active ingredients well loaded on the cordierite-TiO<sub>2</sub> carrier in the next procedure.



**Pretreatment of Sulfur and Arsenic Containing Gold Concentrate by Double-Layered Ball Solidification Roast:** Jiang Tao<sup>1</sup>; Li Shan<sup>1</sup>; Ge Jie<sup>1</sup>; Qian Li<sup>1</sup>; Yang Bin<sup>1</sup>; <sup>1</sup>Central South University

Sulfur and arsenic containing gold ore is a typical refractory gold ore. In this paper, double-layered ball solidification roast was proposed, which made gold concentrate pellets in the form of small balls and coated the balls with a layer of solidifying reagent in a certain thickness before roasting. As a result, volatilized  $\text{SO}_2$ ,  $\text{As}_2\text{O}_3$  from inner balls were absorbed by the coats and solidified. The results showed that, double-layer ball roast realized not only effective removal of sulfur and arsenic from gold concentrate, but also complete solidification of volatilized  $\text{SO}_2$ ,  $\text{As}_2\text{O}_3$  from inner balls without any emission pollution, showing superiority compared with conventional solidification roast which inevitably has slight amount of emission that failed to be absorbed. In addition, Solidification products were effectively separated from gold ore calcine. The calcine product showed favorable performance in following cyanide leaching and the obtained gold leaching recovery is more than 95%.

**Pullout Tests of Sisal Fibers in Epoxy Matrix for Characterization of Interfacial Shear Stress:** Wellington Inacio<sup>1</sup>; Artur Pereira<sup>1</sup>; Sergio Monteiro<sup>1</sup>; Fernando Wypych<sup>2</sup>; Rafael Marangoni<sup>2</sup>; <sup>1</sup>State University of the Northern Rio de Janeiro - UENF; <sup>2</sup>UFPR

The efficiency by which an applied load is transmitted from the matrix to reinforcing fibers in a composite depends on the fiber/matrix adhesion strength. This is determined as the interfacial shear stress, IFSS, by means of pullout tests that measure the force needed to pull a single fiber out of a block of material simulating the composite matrix. Different techniques are used to perform pullout tests. The objective of this work was to characterize the IFSS of sisal fibers embedded in epoxy matrix through the determination of the critical length pullout curves. As the main results, a relatively small critical length was found for the sisal fiber/epoxy pullout specimens, corresponding to a lower IFSS. This result was compared to others applying different pullout techniques. Scanning electron microscopy observation identified the mechanism responsible for the weak sisal fiber adhesion to the epoxy matrix.

**Shape-Controlled Synthesis of a Novel Precursor for Preparing Rod Silver Powders:** Jing Zhan<sup>1</sup>; Chuanfu Zhang<sup>1</sup>; Weiyan Jiang<sup>1</sup>; <sup>1</sup>Central South University

A novel precursor of rod silver particles have been synthesized by coordination-precipitation process using ammonia as complex agent, silver nitrate and oxalate or ammonia oxalate as starting material. The phase, composition and morphology of the precursor were characterized by XRD and SEM analysis. The influences of various parameters including the pH value, precipitation temperature, reactant concentration, surfactant on the morphology and size of the precursor particles were investigated in detailed. The results show that the precursors obtained in reaction system  $\text{Ag(I)-C}_2\text{O}_4^{2-}\text{-NH}_3\text{-NH}_4\text{+H}_2\text{O}$  is oxalate silver ammonia complex salt, the morphology is rod and the optimum reaction conditions were 3.8~4.8 for pH value, 0.3 mol/L~0.5 mol/L for silver ions concentration, 50~60°C for precipitation temperature and 0.1~0.5% (wt) PVP for surfactant. The rod silver particles with 1.054 m<sup>2</sup>/g for specific surface area can be produced by thermal decomposition of the precursor with rod morphology in mixed atmosphere of nitrogen and carbon dioxide.

**Tensile Behavior of Epoxy Composites Reinforced with Continuous and Thinner Ramie Fibers:** Frederico Margem<sup>1</sup>; Jarbas Bravo<sup>1</sup>; Sergio Monteiro<sup>1</sup>; <sup>1</sup>State University of the Northern Rio de Janeiro - UENF

The mechanical behavior and the fracture characteristics of composites with DGEBA/TETA epoxy matrix reinforced with up to 40% in volume of continuous and thinner ramie fibers were evaluated by tensile tests. Specimens with selected thin fibers aligned along the tensile axis were room temperature tested to rupture. The fracture surface was analyzed by scanning electron microscopy. The results showed significant increase in both the ultimate tensile strength and the elastic modulus. The fracture analysis indicated the possible mechanism for the fiber/matrix interaction, which could be responsible for the composite performance.

**Thermo-Mechanical Properties of Epoxy Diamond Abrasive Composites:** Ruben Jesus Rodriguez<sup>1</sup>; Camila Amaral<sup>1</sup>; <sup>1</sup>Universidade Estadual do Norte Fluminense

Diglycidyl ether of bisphenol A (DGEBA) epoxy resins cured with aliphatic amines present mechanical properties that depend on the amine functionality. In this work an investigation on the thermomechanical behaviour and microstructure of composites with dispersed diamond microparticles in DGEBA resin cured with different functionalities, Tetraethylenetetramine, Tetraethylenepentamine and Jeffamine D230 aliphatic amines was carried out by dynamical mechanical analysis (DMA) and scanning electron microscopy (SEM). The DMA results of the epoxy formulation showed that the storage modulus increases with the amount of diamond particles incorporated into the composite. The composites with epoxy matrix cured with TEPA and D230 aliphatic amines showed distinct mechanical behaviors, mainly as consequence of microstructure difference due to microparticles distribution in epoxy phase. Composites with up to 40 wt. % of diamond microparticles dispersed in epoxy thermosetting matrix DGEBA/TEPA shown better abrasive properties than DGEBA/D230 and DGEBA/TETA formulations.

**Thermodynamic Study on Complex System for Structure-Directed Synthesis of Fibrous Cobalt Powder Precursor:** Jing Zhan<sup>1</sup>; Jianfeng Yue<sup>1</sup>; Chuanfu Zhang<sup>1</sup>; <sup>1</sup>Central South University

Based on the principles of simultaneous equilibrium and mass balance, a series of thermodynamic equilibrium equations of  $\text{Co(II)-C}_2\text{O}_4^{2-}\text{-NH}_3\text{-NH}_4\text{+H}_2\text{O}$  system at ambient temperature are deduced theoretically and the logarithm concentration versus pH (logc-pH) diagrams at different solution compositions are drawn. The results show that when pH is above 8.0, cobalt ions coordinate with ammonia and the precipitation proceeds slowly accompanying with the release of cobalt ions from the multicoordinated  $\text{Co(NH}_3)_n^{2+}$  (n=1, 2, ..., 6), the morphology of cobalt powder precursor is fibrous; when pH is below 8.0, cobalt ions directly react with  $\text{C}_2\text{O}_4^{2-}$ , the morphology of cobalt powder precursor is cubic-shape. According to thermodynamics analysis and calculation, some experiments were done to validate the relation between the total concentration of cobalt ions and pH in this study.

**Chloride 2011: Practice and Theory of Chloride-Based Metallurgy: Poster Session**

*Sponsored by:* The Minerals, Metals and Materials Society, Canadian Institute of Metals, TMS Extraction and Processing Division, TMS: Magnesium Committee, TMS: Energy Committee  
*Program Organizers:* Dirk Verhulst, Consultant, Extractive Metallurgy; V.I. (Lucky) Lakshmanan, Process Research Ortech, Inc.

Sun PM-Tues AM  
Feb 27-Mar 1, 2011

Room: 19  
Location: San Diego Conv. Ctr

*Session Chair:* To Be Announced

**Plutonium Removal from Fluoride Spent Salts:** Jerome Serp<sup>1</sup>; Nathalie Loppinet<sup>1</sup>; Gilles Bourges<sup>1</sup>; <sup>1</sup>CEA

A pyroprocess is developed to remove plutonium from  $\text{CaF}_2$  spent salt in the frame of legacy residues treatment programs. Due to the high melting point of  $\text{CaF}_2$  (mp > 1400°C), the process requires  $\text{CaCl}_2$  addition to the salt residue (60% molar  $\text{CaCl}_2$  – 40%  $\text{CaF}_2$ ) in order to obtain a liquid melt below 700°C. Metallic calcium is used to reduce plutonium species ( $\text{PuO}_2$ ,  $\text{PuF}_4$ ...) into plutonium metal. The obtained metal is recovered after cooling at the bottom of the ceramic crucible used as reaction vessel. In this work, key parameters have been identified in order to optimise the plutonium recovery yield. The shape of the salt to treat (powder or chunks) plays a determining role since  $\text{CaF}_2$  dissolution rate is rather slow. The initial plutonium mass in the spent salt is also important to obtain plutonium metal coalescence as a massive button. Plutonium recovery yield greater than 90% is obtained.



## Computational Thermodynamics and Kinetics: Poster Session

*Sponsored by:* The Minerals, Metals and Materials Society, ASM International, TMS Electronic, Magnetic, and Photonic Materials Division, TMS Materials Processing and Manufacturing Division, TMS: Alloy Phases Committee, TMS: Chemistry and Physics of Materials Committee, TMS/ASM: Computational Materials Science and Engineering Committee, ASM: Alloy Phase Diagrams Committee  
*Program Organizers:* Raymundo Arroyave, Texas A & M University; James Morris, Oak Ridge National Laboratory; Mikko Haataja, Princeton University; Jeff Hoyt, McMaster University; Vidvuds Ozolins, University of California, Los Angeles; Xun-Li Wang, Oak Ridge National Laboratory

Sun PM-Thurs AM Room: 9  
Feb 27-Mar 3, 2011 Location: San Diego Conv. Ctr

*Session Chair:* Raymundo Arroyave, Texas A&M University

### A Heat Management Model for Hardness Uniformity of Multi-Pass Laser Heat Treatment Using Direct Diode Laser: *Soundarapandian Santhanakrishnan*<sup>1</sup>; Radovan Kovacevic<sup>1</sup>; <sup>1</sup>Southern Methodist University

In this study, a cooling rate model coupled the finite element (FE) technique and the thermo-kinetic (TK) equations are developed to predict the temperature history, rates of heating and cooling, phase transformations, and the hardness. As-used boundary conditions, temperature dependent materials properties, and phase change kinetics are adopted in this model. A 2-kW HPDDL of 808 nm in wavelength with the uniform distribution (top-hat) of laser power is used to heat treat the material of tool steel AISI S7. A heat balance between the heat input of HPDDL and the cooling by a cold air jet is established. A number of experiments are carried out by changing the laser power, scanning speeds, and the rate of cooling. Microstructural characterization and hardness measurement are performed to evaluate the effect of cooling by the cold air during heat treatment on the variation of microstructure, and the hardness.

### Critical Temperature for Grain Boundary Unpinning and Subsequent Grain Growth: *Corentin Guebels*<sup>1</sup>; Phi Thanh<sup>1</sup>; Joanna Groza<sup>1</sup>; Elizabeth Holm<sup>2</sup>; Jean-Pierre Delplanque<sup>1</sup>; <sup>1</sup>University of California, Davis; <sup>2</sup>Sandia National Laboratories

The mechanisms of grain boundary pinning and grain growth inhibition by second-phase particles are well known. This investigation extends work done by Holm and co-workers on this topic and focuses on conditions in which some grain boundaries may become unpinning in an otherwise stable, pinned microstructure. The influence of temperature on grain boundary unpinning was investigated numerically using a 3D Monte-Carlo Potts approach. The probability of grain boundaries becoming unpinning as a result of thermally activated microstructural fluctuations increases with temperature while the characteristic time for unpinning decreases. If the probability of grain boundary unpinning is relatively low and the characteristic time for unpinning is not too large, it is possible for a single grain to become unpinning and grow to overtake the microstructure; this is particle assisted abnormal grain growth (PAAGG). The critical values of temperature for the occurrence of PAAGG at prescribed particle volume fractions are characterized.

### Development of Accurate Models for The Microstructure and Properties of Mixed-Oxide Slags: *Angus Gray-Weale*<sup>1</sup>; Patrick Masset<sup>2</sup>; Aurelie Jacob<sup>1</sup>; <sup>1</sup>Monash University; <sup>2</sup>TU Bergakademie Freiberg

Molten oxide slags present in important industrial processes usually have at least three components, for example CaO-SiO<sub>2</sub>-Al<sub>2</sub>O<sub>3</sub>. Useful simulation requires an accurate description of all interactions, at many different compositions. The oxide's high polarisability, and the importance of its higher order deformations, complicates matters further. Any useful model needs a reasonably realistic model of the melt's network structure, and the effect of calcium and aluminium ions on this structure. We report comparisons of the results of simulations and integral-equation calculations

on a selection of molten salts. We show that for all of these, the structures from these two methods of calculation are in good agreement. We also describe the first integral-equation calculation of a molten salt with intermediate-range order based on a realistic interaction potential that includes polarisable ions, and find a structure in good agreement with experiment. This work opens up the possibility that we may use integral-equation methods to predict the structures and thermodynamic properties of complex and ordered molten salt mixtures over a wide range of conditions.

### Domain Structures of Nanoparticles in Magnetic Films: *Jiayang Li*<sup>1</sup>; Yan Yang<sup>1</sup>; Yongmei Jin<sup>1</sup>; <sup>1</sup>Michigan Technological University

Domain structures of nanoparticles in soft magnetic yttrium iron garnet (YIG) and hard magnetic FePt films are studied by using micromagnetic modeling. The two types of magnetic films find important applications in Farady rotator and magnetic storage, respectively, where stable domain structures with high remanent magnetization and large reversal field are required. Computer simulations show details of domain structures and magnetic switching processes in these nanoparticles, and reveal important roles of particle size, shape, and spatial arrangement acting through magnetostatic interactions. It is found that magnetic domain structure largely depends on the particle shape in the soft magnetic YIG, while strongly depends on the particle crystallographic orientation in the hard magnetic FePt. Based on the simulation results and analysis of various energy contributions to domain phenomena, domain mechanisms in YIG and FePt nanoparticle films are explained, which provide insights for nanostructure optimization of magnetic films.

### Engineering Microstructures via General Two-stage Anneals: *Siu Sin Quek*<sup>1</sup>; Marcelo Ciappina<sup>1</sup>; David Wu<sup>1</sup>; <sup>1</sup>Institute of High Performance Computing Singapore

We consider the crystallization of a thin film via interface-/diffusion-limited growth and a nucleation process controlled by general two-stage isothermal anneals. We show that this schedule leads to a two-parameter family of microstructures. The two parameters can be directly related to the annealing temperatures at the two stages and the annealing time for the first stage (we anneal the second stage to a fully transformed microstructure). We use the time-cone method to generate the microstructures, which is subsequently used to compute statistics of various geometrical properties of the crystals. We find that the statistics vary strongly with different combinations of the two parameters. Our results suggest a possible way to easily engineer certain types of microstructures via isothermal annealing stages.

### Entropic Stabilization and Retrograde Solubility in $\beta$ -Zn<sub>4</sub>Sb<sub>3</sub>: *Gregory Pomrehn*<sup>1</sup>; G. Jeffrey Snyder<sup>1</sup>; Axel van de Walle<sup>1</sup>; <sup>1</sup>California Institute of Technology

$\beta$ -Zn<sub>4</sub>Sb<sub>3</sub>, a phase of interest for thermoelectric application, is shown to be entropically stabilized with respect to Zn and ZnSb with significant entropic contributions from both configurational disorder and lattice vibrations. Zn<sub>4</sub>Sb<sub>3</sub> is shown to have retrograde Zn solubility from the ground state stoichiometry of Zn<sub>13</sub>Sb<sub>10</sub> resulting in a p-doped semiconductor. A new phase of interest,  $\beta$ -Zn<sub>3</sub>Sb<sub>3</sub>, is shown to be a potential competing phase on the Zn-deficient side of  $\beta$ -Zn<sub>4</sub>Sb<sub>3</sub>.

### Integrating Finite Temperature Magnetism Into Ab Initio Free Energy Calculations: *Fritz Körmann*<sup>1</sup>; Alexey Dick<sup>1</sup>; Tilmann Hickel<sup>1</sup>; Jörg Neugebauer<sup>1</sup>; <sup>1</sup>Max-Planck-Institut für Eisenforschung

The free energy of a system is a fundamental quantity for predicting phase diagrams, finite temperature materials parameters, or kinetic barriers. An ab initio derivation of it makes a highly accurate evaluation of all excitation processes mandatory. One of the most challenging - but for many engineering materials crucial - contribution is coming from the magnetic degrees of freedom. We have developed an approach that eliminates shortcomings of conventional approaches and that is firmly based on an exact solution of an effective Heisenberg model employing the quantum Monte Carlo approach. We demonstrate the high accuracy achievable by the new approach by computing magnetic heat capacities and free energies for the magnetic pure elements Fe, Co, and Ni, and by extending it to magnetic compounds such

as Cementite (Fe<sub>3</sub>C). Generally, an excellent agreement with experimental data is found.

**Phase Equilibria of the La-Ni-Cu Ternary System at 673 K: Thermodynamic Modeling and Experimental Validation:** *Xuehui An*<sup>1</sup>; Qian Li<sup>1</sup>; Jieyu Zhang<sup>1</sup>; Shuanglin Chen<sup>2</sup>; Ying Yang<sup>2</sup>; <sup>1</sup>Shanghai Key Laboratory of Modern Metallurgy and Materials Processing, Shanghai University; <sup>2</sup>CompuTherm, LLC

Phase equilibria and thermodynamic properties in the La-Ni-Cu ternary system were studied by coupling thermodynamic modeling and experimental validation. A set of self-consistent thermodynamic descriptions for phases in the La-Ni-Cu system were obtained on the basis of those of three constituent binaries and ternary experimental data in literature. The isothermal section at 673 K and the enthalpy of mixing of liquid calculated from the currently established ternary thermodynamic description were compared favorably with available experimental data. Three alloy samples in the La-Ni-Cu system were then selected, synthesized and annealed at 673 K in order to further validate the calculated phase equilibria. These alloys were analyzed with ICP, XRD, OM, SEM/BSE and EDS, and the experimental results agreed well with the calculated phase equilibrium relationships.

**Phase Field Modeling of Static Recrystallization for Deformed Alloys:** *Gao Yingjun*<sup>1</sup>; <sup>1</sup>Guangxi University

Considering characteristics of different deformation region and non-uniform distribution of storage energy in alloy, a multi-state free energy function is proposed to simulate microstructure evolution of static recrystallization for deformation alloy in phase field modeling. The transformation kinetics curve of recrystallization and the time index for Avrami curve are systematic analyzed. The simulation results are well in agreement to other theoretical results and experimental results

**Solubility Modeling of Methanol Aqueous Solutions in Nafion Membrane at 30-60°C:** Hsin-Yi Chen<sup>1</sup>; Shingjiang Jessie Lue<sup>1</sup>; <sup>1</sup>Chang Gung University

The adjective of this study was to establish a mathematical model for predicting liquid sorption levels from binary component systems in Nafion-117 membrane as a function of solvent activities. Flory-Huggins thermodynamic equations were adopted for the solubility modeling. The Flory-Huggins interaction parameters ( $\chi_{im}$ ) between the solvents and membrane were calculated based on the pure solvent solubility results in the membranes. The water-methanol interaction parameter ( $\chi_{12}$ ) was taken from the vapor-liquid equilibrium data and expressed as a function of binary liquid composition. In this modeling procedure, only the interaction parameters between any two components were needed to estimate the sorption levels of water and methanol in the Nafion in a ternary systems. The sorption results of methanol aqueous solutions in Nafion were predicted at temperatures ranging from 30-60 °C. These data are valuable for predicting the methanol permeability in direct methanol fuel cell performance employing Nafion.

**Statistical Model of Precipitation Kinetics for Recycled Commercial Aluminum Alloys:** *Zhenshan Liu*<sup>1</sup>; Volker Mohles<sup>1</sup>; Olaf Engler<sup>2</sup>; Guenter Gottstein<sup>1</sup>; <sup>1</sup>Institut fuer metallkunde und metallphysik; <sup>2</sup>Hydro Aluminium Deutschland GmbH

A thermodynamics based precipitation model for aluminum alloys is presented. The model is capable of describing the simultaneous nucleation, growth and coarsening of all important precipitates in multi-component systems for arbitrary heat treatments. The thermodynamic data required to calculate the nucleation driving force and the equilibrium phase compositions is taken from a database (provided by GTT Technologies, Herzogenrath, Germany) that contains 15 elements (Al, B, C, Cr, Cu, Fe, Mg, Mn, Ni, Si, Sr, Ti, V, Zn, Zr). As a result, the model can be applied on most of commercial aluminum alloys. The model was validated by comparing the simulation with the experiment results of various alloys, such as the precipitate volume fractions and the matrix composition. This validated model was utilized to predict the precipitation kinetics of recycled commercial alloys. In particular, the sensitivity of precipitation on composition fluctuations, which are inherent with recycled materials, is evaluated.

**Surface Prefreezing and Its Effect on Surface Tension of AuSi Nanoparticles:** *Moneesh Upmanyu*<sup>1</sup>; Hailong Wang<sup>1</sup>; <sup>1</sup>Northeastern University

AuSi nanoparticles have emerged as the catalysts of choice for growth of high density silicon nanowire (SiNW) arrays. The surface tension is a critical parameter which is implicated in both direction selection and morphological evolution, yet quantitative understanding remains elusive. In this talk, we use atomistic simulations based on angular EAM classical potential to investigate the interplay between surface structure and surface tension in near-eutectic AuSi liquid alloys. Semi-grancanonical Monte-Carlo simulations reveal a pre-frozen surface structure, consistent with experiments. A combination of surface capillary fluctuation method and surface virial calculations allows us to map the effect of temperature and composition in thin films, while Laplace pressure is exploited to extract the size effect down to 10 nm diameter particles. The implications for morphological and composition growth are discussed.

**The Application of Thermodynamic Analysis In Preparing the MnZn Ferrites Precursor:** *Xue Ping*<sup>1</sup>; Yuan Yaohua<sup>1</sup>; Zhao Peiyu<sup>1</sup>; Chen Xiaofang<sup>1</sup>; <sup>1</sup>Jiangnan University

The thermodynamic analysis on the system of Me(II)-NH<sub>3</sub>-C<sub>2</sub>O<sub>4</sub>-2-(HCO<sub>3</sub>)<sub>2</sub>-H<sub>2</sub>O (Me represents Fe, Mn, Zn) is carried out. The relationship between pH and the total concentration of Me(II) is determined, and the field of coprecipitation is included in the preparing MnZn Ferrites, it shows the thermodynamic analysis coincides with experimental results. The mean diameter of the powder is 2.0 μm after calcination, the sintering temperature is about 40°C lower than that by ordinary dry method. The initial permeability of thermoresponsive MnZn Ferrites is around 4550, the Sensitivity-temperature is less than 1.5°C, and there is good application in the Temperature-Sensitive Sensor.

**The Effect of Nb on the Amount of Retained Austenite and Strengthening in Cold-Rolled TRIP Steels:** *Jong Min Choi*<sup>1</sup>; Bong June Park<sup>1</sup>; Chang Yeon Lee<sup>1</sup>; Seong Ho Han<sup>2</sup>; Kyung Jong Lee<sup>1</sup>; <sup>1</sup>Hanyang University; <sup>2</sup>Automotive Steel Products Research Group, POSCO

The microalloyed TRIP (transformation induced plasticity) steels has been widely studied with the demand of the weight reduction and the safety requirement of vehicle in automotive industry in order to develop high strength and good formability steels. TRIP steels with Nb addition had a potential for 1 GPa grade by grain refinement and precipitation strengthening. However, with increasing Nb contents, the fraction of retained austenite and carbon contents were decreased. In this study, the cold-rolled process was simulated and the predicted microstructures were compared with the measured. The model was mainly focused on the role of Nb on the retained austenite by the carbon redistribution and the bainite and martensite formation. The optimum Nb contents based on strength and formability was also suggested.

**Thermodynamic Modeling of LiNO<sub>3</sub>-NaNO<sub>3</sub>-KNO<sub>3</sub> Ternary Salt for Solar Energy Storage:** *Divakar Mantha*<sup>1</sup>; Ramana Reddy<sup>1</sup>; <sup>1</sup>The University of Alabama

Thermodynamic modeling of the LiNO<sub>3</sub>-NaNO<sub>3</sub>-KNO<sub>3</sub> ternary salt was carried out to predict the eutectic composition and melting point. The predicted salt composition was synthesized and its melting point and heat capacity were experimentally determined using DSC technique. The experimental melting point showed an excellent agreement with the calculated melting point data and was also comparable with the existing literature data. New specific heat capacity of the ternary salt was determined as a function of temperature. Application of these ternary salts for solar energy storage was discussed.

**Thermodynamic Modeling of S-M (M=Al, Zr, Ti and La) Systems Supported by First-Principles Calculations:** *Rongxiang Hu*<sup>1</sup>; Michael Gao<sup>1</sup>; Ömer Dogan<sup>2</sup>; <sup>1</sup>URS at National Energy Technology Laboratory; <sup>2</sup>National Energy Technology Laboratory

CuPd alloys have been widely investigated as promising hydrogen separation membranes and membrane reactors due to their high hydrogen selectivity and permeability. In order to reduce the cost and enhance

hydrogen permeability, NETL has developed CuPd-based ternary alloys using first-principles calculations and CALPHAD modeling. However, sulfur poisoning seriously affects hydrogen permeability of Pd alloys and is a major hurdle for their commercial applications. Although the mechanisms for sulfur poisoning are not well understood, it is worth studying the bulk thermodynamics of these alloys in presence of sulfur. In this study, a series of S-M (M=Al, Zr, Ti and La) binary systems are thermodynamically assessed using CALPHAD method based on available experimental phase equilibria and thermochemistry data. First-principles calculations are used to provide enthalpy formation data when experimental data are not available. Alloying elements that reduce the propensity of sulfur poisoning will be assessed and discussed.

**Thermodynamics Calculation of CuO-NH<sub>3</sub>+NH<sub>4</sub>Cl Solution System:** Weilian Zheng<sup>1</sup>; Dan Li<sup>2</sup>; *Zhongliang Xiao*<sup>1</sup>; Qiyuan Chen<sup>2</sup>; Haixia Tong<sup>1</sup>; <sup>1</sup>Changsha University of Science and Technology; <sup>2</sup>Central South University

A thermodynamic model of dissolution equilibrium process of CuO in NH<sub>3</sub>-NH<sub>4</sub>Cl solution is built according to thermodynamic data, mass action law and the mass conservation principle. Using couple-solving results, a equilibrium surface figure between CuO solid phase and solution-phase, and a overlay figure of the curve of CuO and the leaching solution at simultaneous equilibrium and the curve of Cu(OH)<sub>2</sub>·5Cu<sub>2</sub>O and the solution at precipitation reaction equilibrium attained in this paper.

**A Phase-Field Model with a Novel Way of Coupling to Multi Component Thermodynamic Data:** *Nils Warnken*<sup>1</sup>; <sup>1</sup>University of Birmingham

Phase-field models are remarkable. They are nowadays widely used in materials science and engineering to simulate microstructure evolution in two and three dimensions. Some models are capable to perform simulations for multi component alloys, which is of special interest for alloy development and other engineering applications. However, the coupling of phase-field models with multi component thermodynamics is still quite complicated and not straight forward. In this work a phase-field model for binary and higher order systems is presented, which uses a novel and simple way of incorporating thermodynamic alloy data. This allows for straight forward coupling to CALPHAD type software packages. Alternatively ideal or regular solution descriptions can be used. The model does not assume local equilibrium assumption at the moving interface. Simulations of diffusion controlled phase transformation in binary and multi component systems are shown.

**A Hybrid MD-kMC Algorithm to Study Diffusion in the Presence of Fields: Effect of Coherent Interfaces:** *Enrique Martinez Saez*<sup>1</sup>; Alfredo Caro<sup>1</sup>; <sup>1</sup>LANL

A new hybrid Molecular Dynamics-kinetic Monte Carlo algorithm has been developed in order to study the basic mechanisms taking place in diffusion in concentrated alloys under the action of chemical and stress fields. Parallel implementation of the k-MC part based on a recently developed synchronous algorithm [J. Comp. Phys. 227 (2008) 3804-3823] resorting on the introduction of a set of null events aiming at synchronizing the time for the different subdomains, added to the parallel efficiency of MD, provides the computer power required to evaluate jump rates 'on the flight', incorporating in this way the actual driving force emerging from chemical potential gradients, and the actual environment-dependent jump rates. The time gain has been analyzed and the parallel performance reported. The algorithm is tested on a simple coherent interface sink strength calculation analyzing the bias between vacancies and self-interstitial atoms depending on the character of the interface.

**A Phenomenological Model for Prediction of the Martensite Start Temperature in Steels:** *Albin Stormvinter*<sup>1</sup>; Annika Borgenstam<sup>1</sup>; <sup>1</sup>KTH Royal Inst. of Technology

A phenomenological model for prediction of the martensite start temperature (Ms) in steels has been developed. The model was based on experimental data on Ms from rapid cooling experiments together with a new thermodynamic description. The effects of important alloying elements in steels, such as C, Mn, Cr and Ni on Ms were taken into account. An important

aspect was to describe the different Ms for the formation of lath and plate martensite respectively, based on the experimental results. The modeling work has been assisted by experimental characterization to strengthen the metallographic evidence on how the transition from lath to plate martensite takes place.

**New Approach in Simulating Anisotropy in Thin Film Growth:** *Solmaz Torabi*<sup>1</sup>; John Lowengrub<sup>1</sup>; <sup>1</sup>University of California Irvine

We study the influence of surface and strain energies on heteroepitaxial thin-film growth. We propose an alternate way of simulating anisotropy for the surface energy by using the higher order terms in the free energy. To the second order, the system only has isotropic properties. We can produce different equilibrium shapes by adding higher order terms to the energy. By choosing diamond-cubic-symmetry, we can study the behavior of SiGe/Si thin-films. For this case, we need to add 4th and 6th order terms in the extended-Cahn-Hilliard model. One advantage of this method is its intrinsic regularized behavior. As a result we are able to utilize the energy-stable-scheme in order to have large time steps without losing accuracy. We present numerical results using an adaptive, nonlinear, multigrid finite-difference method. Finally, we add the elastic energy to our diffuse model to predict different Qdot shapes, such as pyramids and domes.

**First Principles Calculation of the  $\alpha$ -ZrO<sub>2</sub>-X, 0 < X < 1 Phase Diagram:** *Benjamin Burton*<sup>1</sup>; A. Van De Walle<sup>2</sup>; <sup>1</sup>NIST; <sup>2</sup>Caltech

Octahedral-interstitial order-disorder in hcp-based ZrO<sub>2</sub>-X suboxides, 0 < X < 1, promotes stress corrosion cracking in Zircalloy cladding on UO<sub>2</sub> fuel rods. A first principles based phase diagram calculation was performed for the  $\alpha$ -ZrO<sub>2</sub>-X solid solution. Planewave pseudopotential calculations of formation energies were used as a basis for fitting a cluster expansion Hamiltonian. As expected near neighbor O-O pairwise interactions are strongly repulsive, but further neighbor interactions are small. The calculated phase diagram has four ordered ground-states, three of which are predicted to be ground-states of the Zr-O binary system.

**Phase Field Crystal Study of Alloys under Irradiation:** *Nana Ofori-Opoku*<sup>1</sup>; Jeffrey Hoyt<sup>1</sup>; Nikolas Provatas<sup>1</sup>; <sup>1</sup>McMaster University

This paper outlines an extension of the Phase Field Crystal (PFC) method in examining the evolution of materials under irradiation. Bombarding highly energetic particles often have deleterious effects on alloys due to this type of athermal ballistic mixing. We incorporate a mesoscopic model of radiation into the atomistic level phase field crystal model. To demonstrate the equilibrium properties, the model is examined in the long wavelength limit, where the equilibrium contributions to the free energy are attained. Radiation effects are determined on an equilibrium basis by considering changes arising in the phase diagrams. The evolution of defect microstructure and the composition field are then modeled and discussed under the application of: grain growth and coarsening kinetics, radiation induced segregation and effects on phase transformations in a eutectic alloy.

**A Novel Approach to Modeling Phase Transformations Free of Numerical Anisotropy:** *Klemens Reuther*<sup>1</sup>; Markus Rettenmayr<sup>1</sup>; <sup>1</sup>Friedrich-Schiller-University Jena

An approach to model phase transformations without any grid anisotropy is presented. The advantageous combination of three main elements allows for a distinct reduction of artificial anisotropy: (1) The governing partial differential equation is solved using the meshless Diffuse Approximation Method with a variety of boundary conditions. (2) The meshless method is applied on a fully amorphous grid which is isotropic on both a mesoscopic and macroscopic scale. (3) The migrating phase interface is tracked precisely by a Moving Particle Method where the tracking particles are directly connected to the grid. The method is at present applied on two-dimensional problems. It combines the precision of regular grids with the isotropy of the moving particle method on an amorphous grid. The opportunities of this method are demonstrated using simulation results on solidification processes that correspond to different practical cases. The further prospects of the method are discussed in detail.



## Electrode Technology for Aluminium Production: Light Metals Poster Session

*Sponsored by:* The Minerals, Metals and Materials Society, TMS Light Metals Division, TMS: Aluminum Committee  
*Program Organizers:* Alan Tomsett, Rio Tinto Alcan; Ketil Rye, Alcoa Mosjøen; Barry Sadler, Net Carbon Consulting Pty Ltd

Sun PM-Thurs PM  
Feb 27-Mar 3, 2011

Room: 17A  
Location: San Diego Conv. Ctr

### Cold Water Model Simulation of Aluminum Liquid Fluctuations Induced by Anodic Gas in New Tape of Cathode Structure Aluminum Electrolytic Cell: Yan Liu<sup>1</sup>; Ting'an Zhang<sup>1</sup>; Zhihe Dou<sup>1</sup>; Hongxing Wang<sup>1</sup>; Guozhi Lv<sup>1</sup>; Qiuyue Zhao<sup>1</sup>; Naixiang Feng<sup>1</sup>; Jicheng He<sup>1</sup>; <sup>1</sup>Key Laboratory of Ecological Utilization of Multi-metal Intergrown Ores of Ministry of Education & School of Materials and Metallurgy, Northeastern University

Compared to conventional cathode structure electrolytic cell, the new tape of cathode structure electrolytic cell can effectively inhibit the fluctuation of liquid aluminum, which can reduce the polar distance, decrease cell voltage, save energy. Cold water model was designed according to scale of 1:3 with 160KA industrial electrolytic cell to examine aluminum liquid fluctuation induced by anodic gas in new tape of cathode structure electrolytic cell. By means of high-speed photography, shooting liquid interface wave in different anode-cathode distance, electrolyte level, aluminum liquid level, and gas flow rate under different factors such as the cathode structure model of the aluminum electrolytic cells water interface wave image. Study shows that in the new tape of cathode structure electrolytic cell, the largest interface wave height will be reduced significantly along with the increase of the anode cathode distance.

Compared to conventional cathode structure electrolytic cell, the new tape of cathode structure electrolytic cell can effectively inhibit the fluctuation of liquid aluminum, which can reduce the polar distance, decrease cell voltage, save energy. Cold water model was designed according to scale of 1:3 with 160KA industrial electrolytic cell to examine aluminum liquid fluctuation induced by anodic gas in new tape of cathode structure electrolytic cell. By means of high-speed photography, shooting liquid interface wave in different anode-cathode distance, electrolyte level, aluminum liquid level, and gas flow rate under different factors such as the cathode structure model of the aluminum electrolytic cells water interface wave image. Study shows that in the new tape of cathode structure electrolytic cell, the largest interface wave height will be reduced significantly along with the increase of the anode cathode distance.

### Influence of Ultrafine Powder on the Properties of Carbon Anode Used in Aluminum Electrolysis: Xiao Jin<sup>1</sup>; Deng Songyun<sup>1</sup>; Li Jie<sup>1</sup>; Lai Yanqing<sup>1</sup>; Liu Yexiang<sup>1</sup>; <sup>1</sup>Central South University

The ultrafine powder (<400 mesh) content of ball milling powder has a great influence on the carbon anode quality. Experiment was set on the base of the formula and raw material of an aluminum carbon anode plant in China. The ultrafine powder was separated from ball milling powder by screening method. On the premise of unchanged powder purity and content, anode samples with different ultrafine powder content were prepared and analyzed on their properties. Powder material was characterized by Blaine Number and BET specific area. Results showed that good electrical conductivity, thermal conductivity and air/CO<sub>2</sub> reactivity behavior could be obtained with low ultrafine powder content (3100~4000 Blaine, 2.510~3.734 m<sup>2</sup>/g specific area). Anode properties such as baked density and air permeability were closely related with the ultrafine powder content and Blaine value of powder material. The results have positive meaning on optimizing the properties of carbon anode.

### Preparation NiFe<sub>2</sub>O<sub>4</sub> Matrix Inert Anode Used in Aluminum Electrolysis by Adding Nanopowder: Zhigang Zhang<sup>1</sup>; Guangchun Yao<sup>1</sup>; Yihan Liu<sup>1</sup>; Xiao Zhang<sup>1</sup>; <sup>1</sup>Northeastern University

Two-step sintering process was adopted to prepare NiFe<sub>2</sub>O<sub>4</sub> matrix inert anode in this research. In the process of synthesizing NiFe<sub>2</sub>O<sub>4</sub> spinel, Fe<sub>2</sub>O<sub>3</sub> and NiO powders as raw materials added additives were synthesized at 1000°C. Through crushing and screening, adding NiFe<sub>2</sub>O<sub>4</sub> nanopowder, particle gradation and compression molding, the nickel ferrite matrix ceramic inert anode was sintered secondarily at 1250°C for 6h. The effect of addition level of nanopowder on the density and porosity, bending strength and impact toughness was investigated emphatically. The results showed the addition of NiFe<sub>2</sub>O<sub>4</sub> nanopowder had significantly increased the bending strength and impact toughness of NiFe<sub>2</sub>O<sub>4</sub> matrix ceramic inert anode. Inert anodes had the best comprehensive properties while adding 60wt% nanopowder. The values of density and porosity were 4.62g/cm<sup>3</sup> and 5.2% respectively, the value of bending strength was 53.39MPa and the value of impact toughness was 3.19J/cm<sup>2</sup>.

### Effects of Physical Properties of Anode Raw Materials on the Paste Compaction Behavior: Kamran Azari Dorcheh<sup>1</sup>; Hany Ammar<sup>1</sup>; Houshang Alamdari<sup>1</sup>; Donald Picard<sup>1</sup>; Mario Fafard<sup>1</sup>; Donald Ziegler<sup>2</sup>; <sup>1</sup>Université Laval; <sup>2</sup>Alcoa

The current study investigates the effects of coke particle characteristics and paste formulation on the flowability and the compression behavior of anode pastes. Shape factor and texture of different fractions of cokes were characterized using an image analysis system where the characteristics of each coke were correlated to its vibrated bulk density (VBD). A compression test was designed to study the effects of particle characteristics and paste recipe on the compactability of pastes. The test was applied on four anode pastes, prepared from different coke types, particle size distributions and pitch contents. It was observed that the compression test is significantly sensitive to any changes in raw materials characteristics and formulations. Consequently, the compression test may be used as a tool for evaluating anode quality in relation with material variations.

### Frontiers in Solidification Science: Poster Session

*Sponsored by:* The Minerals, Metals and Materials Society, TMS Electronic, Magnetic, and Photonic Materials Division, TMS: Chemistry and Physics of Materials Committee, TMS: Solidification Committee

*Program Organizers:* Jeffrey Hoyt, McMaster University; Daniel Lewis, Rensselaer Polytechnic Institute

Sun PM-Tues PM  
Feb 27-Mar 1, 2011

Room: 6E  
Location: San Diego Conv. Ctr

### A Numerical Benchmark on the Prediction of Macroregregation in Binary Alloys: Hervé Combeau<sup>1</sup>; Michel Bellet<sup>2</sup>; Yves Fautrelle<sup>3</sup>; Dominique Gobin<sup>4</sup>; Eric Arquis<sup>5</sup>; Olga Budenkova<sup>3</sup>; Bernard Dussoubs<sup>1</sup>; Yves Duterrail<sup>3</sup>; Arvind Kumar<sup>1</sup>; Benoît Goyeau<sup>6</sup>; Salem Mosbah<sup>2</sup>; Thibault Quatravaux<sup>1</sup>; Mohamed Rady<sup>5</sup>; Charles-André Gandin<sup>2</sup>; Miha Založnik<sup>1</sup>; <sup>1</sup>Institut Jean Lamour, CNRS – Nancy-Université – UPV-Metz; <sup>2</sup>CEMEF, CNRS – Mines-ParisTech; <sup>3</sup>SIMAP, CNRS – INPG – Université Joseph Fourier; <sup>4</sup>FAST, CNRS – Université Pierre et Marie Curie; <sup>5</sup>TREFLE, CNRS – Université de Bordeaux – ENSAM-ParisTech – ENSCPB; <sup>6</sup>EM2C, CNRS – Ecole Centrale Paris

During the solidification of metal alloys, chemical heterogeneities at the product scale (macroregregation) develop. Numerical simulation tools are beginning to appear in the industry, however their predictive capabilities are still limited. We present a numerical benchmark exercise treating the performance of models in the prediction of macroregregation. In a first stage we defined a “minimal” (i.e. maximally simplified) solidification model describing the coupling of the solidification of a binary alloy and of the transport phenomena (heat, solute transport and fluid flow) that lead to macroregregation in a fully columnar ingot with a fixed solid phase. This model is solved by six different numerical codes, employing different numerical methods (FV and FE) and various solution schemes. We compare the predictions of the evolution of macroregregation in small (10x6 cm) ingots of Pb-18wt%Sn and Sn-10wt%Pb alloys. Further, we present the sensitivities concerning the prediction of instabilities leading to banded channel mesosegregations.

### Binary Alloy Solidification at 35 Tesla: Jason Cooley<sup>1</sup>; Thomas Ott<sup>1</sup>; Sally Tracy<sup>2</sup>; Tim Tucker<sup>1</sup>; Kristen Collar<sup>3</sup>; Scott Lillard<sup>1</sup>; James Foley<sup>1</sup>; Tyler Wheeler<sup>1</sup>; John Balog<sup>1</sup>; Andrew Duffield<sup>1</sup>; Bobby Pullum<sup>3</sup>; <sup>1</sup>Los Alamos National Laboratory; <sup>2</sup>California Institute of Technology; <sup>3</sup>National High Magnetic Field Laboratory

S. Chandrasekar showed in 1954 that the viscosity of a metallic liquid increases quadratically perpendicular to an applied magnetic field. At tens of tesla, this increase in viscosity can be by orders of magnitude, resulting in very anisotropic diffusion constants. Also, the field can orient paramagnetic crystallites in the liquid. Our work is focused on identifying alloys in which an applied field has an effect on the solidification microstructure,



determining its magnitude, and understanding why it occurs. Because the field is an external parameter independent of temperature, composition, and pressure, its ability to effect solidification microstructures has profound implications for the development of engineered microstructures. We report on the solidification microstructures of binary alloys at and near eutectic compositions in 0 and 35 Tesla fields. In Al-Ni and Mg-Sb alloys the microstructures are layered perpendicular to the applied field, while those in the Al-Cu and Ag-Ge systems are parallel.

**Dendritic Growth: Phase Field Crystal Vs. Phase Field Simulations:** *Tamás Pusztai*<sup>1</sup>; Gyula Tóth<sup>1</sup>; György Tegze<sup>1</sup>; László Gránásy<sup>1</sup>; <sup>1</sup>Research Institute for Solid State Physics and Optics

In colloidal systems the particle density relaxes diffusively. As in other systems, the associated Mullins-Sekerka type diffusional instability leads to the formation of dendritic crystals. A simple dynamical density functional theory termed as the phase field crystal (PFC) model has recently been successfully applied to model solidification and pattern formation in colloidal systems. Herein, we demonstrate that large-scale PFC simulations that inherently incorporate elasticity, the anisotropies of the interfacial free energy and kinetic coefficient, surface reconstruction, and surface roughening predict complex dendritic forms of BCC structure in 3D, which vary from faceted dendrites to compact growth forms of rounded shape as the thermodynamic driving force increases. Next, we investigate how far these predictions can be recovered within the framework of a conventional phase-field (PF) model that relies on a Ginzburg-Landau free energy with model parameters (driving force, interface free energy, and kinetic anisotropy) deduced from the PFC model.

**High Speed Synchrotron Tomography for the *In Situ* Quantification of Pore Evolution during the Solidification of Al-Si-Cu-Fe Alloys:** *Chedha Puncreobutr*<sup>1</sup>; Junsheng Wang<sup>2</sup>; Thomas Connolley<sup>3</sup>; Robert Atwood<sup>3</sup>; Peter Lee<sup>1</sup>; <sup>1</sup>Imperial College London; <sup>2</sup>Ford Research and Advanced Engineering Lab; <sup>3</sup>Diamond Light Source Ltd

The presence of pores in aluminum alloy cast components can often limit final fatigue life. In this study we use high speed synchrotron tomography (one scan every 6 s) to quantify the three dimensional evolution of porosity. The alloy studied was W319, Al-7.5Si-3.5Cu-1.2Fe (wt.%). Three different cooling rates were used, comparing the temperature at which the pores formed, as well as quantifying their change in morphology and growth rate. The interaction of the pores with the developing iron intermetallics is also examined. The results are compared to predictions using the  $\mu$ matIC microstructural model.

**In Situ Observations of Rapid Solidification of Metal Thin Films:** *Andreas Kulovits*<sup>1</sup>; Jorg Wiezorek<sup>1</sup>; Thomas LaGrange<sup>2</sup>; Bryan Reed<sup>2</sup>; Geoffrey Campbell<sup>2</sup>; <sup>1</sup>University of Pittsburgh; <sup>2</sup>Lawrence Livermore National Laboratory

We study rapid solidification of metal alloy thin films using the Dynamic Transmission Electron Microscope at Lawrence Livermore National Laboratory. The DTEM combines a conventional TEM with two lasers and provides unprecedented spatio-temporal resolution of about 10 nanometers and 12 nanoseconds facilitating in-situ study of rapid solidification. We used electron diffraction to establish complete melting of the thin films in the illuminated area and imaging mode to monitor the morphology of the liquid-solid interface with nanometer resolution. We determined the interfacial velocity and document morphological evolution during solidification, providing experimental data for validation and verification of theoretical models and computer simulations. The Work was performed under the auspices of the U.S. Department of Energy by the Lawrence Livermore National Laboratory and supported by the Office of Science, Office of Basic Energy Sciences, Division of Materials Sciences and Engineering, of the U.S. Department of Energy under contract No. DE-AC52-07NA27344.

**Measurement of the Minimum-Undercooling Spacing of In-In<sub>2</sub>Bi Eutectic Alloys Using Real-Time Videomicroscopy in Thin-Sample Directional Solidification:** *Sabine Bottin-Rousseau*<sup>1</sup>; Silvère Akamatsu<sup>2</sup>; Gabriel Faivre<sup>2</sup>; <sup>1</sup>UPMC / CNRS; <sup>2</sup>INSP

We present an experimental study of the dynamics of lamellar eutectic patterns in directional solidification of In-In<sub>2</sub>Bi alloys in 12- $\mu$ m thick glass-wall samples. The solidification front is observed in real time using reflected-light videomicroscopy. We checked the 1D character of the pattern post-mortem using transverse metallographic sectioning. We focus on the time evolution of patterns that initially contained a smooth spatial modulation of the interlamellar spacing  $\lambda$  about an average value  $\langle \lambda \rangle$ . The spacing distributions obeyed a diffusion-like equation with a  $\lambda$ -dependent coefficient. We determined a threshold spacing value  $\lambda_E$  (where the subscript E stands for « Eckhaus instability »), above which  $\lambda$  modulations relax towards uniformity, and below which they amplify, eventually leading to lamella elimination. Using the semi-empirical corrections to Langer's approximate formula for  $\lambda_E$  [Akamatsu et al. Metall. Mater. Trans. 35A 1815 (2004)], we estimated the material constant  $\lambda_{min}^2 V$  for In-In<sub>2</sub>Bi alloys ( $\lambda_{min}$ : minimum-undercooling spacing).

**Morphology of Graphite Formation from Melt:** *Shaahin Amini*<sup>1</sup>; Haamun Kalaantari<sup>1</sup>; Reza Abbaschian<sup>1</sup>; <sup>1</sup>University of California Riverside

The morphology of graphite and/or graphene layers grown from molten hypereutectic Ni-, Cu- and Fe-c alloys has been investigated. The process involved dissolving carbon in the melt using induction and arc melting processes, followed by cooling to allow the saturated carbon to nucleate and grow as graphite. Experiments showed graphite morphology would depend on the type of metal, nucleation sites, amount of carbon and cooling rate. The optical and scanning electron microscopy as well as Raman spectroscopy showed the thickness of graphite formed on the surface ranged from nanometer to bulk graphite, and were bounded by triangular cross section ridges. The ridge formation is believed to be due to the accommodation of thermal expansion coefficient mismatch between the metal substrate and graphite layer. The morphology of surface graphite was compared with those grown inside the melt and graphite formed as secondary phase on surface of metal dendrite in hypoeutectic alloys.

**Multicomponent Segregation Path with Solid and Liquid Diffusion Coupled with Thermodynamic Equilibrium Calculations:** *Charles-Andre Gandin*<sup>1</sup>; Haithem Ben Hamouda<sup>1</sup>; Hongwei Zhang<sup>2</sup>; Damien Tournet<sup>1</sup>; <sup>1</sup>MINES-ParisTech; <sup>2</sup>Northeastern University

A microsegregation model for the solidification of multicomponent alloys is presented. It couples the volume-averaged conservation equations for total mass, solute mass and energy assuming a uniform temperature. The model includes the effect of diffusion in the liquid and solid phases, the growth kinetics of the solidifying microstructure and the velocity of the solid/liquid interface. Equilibrium between phases is taken into account and computed using a thermodynamic software. Illustration is provided by the solidification of a Fe-1wt%Cr-10wt%Ni alloy. Predictions include the occurrence of a recalescence due to the growth of the microstructure and the progress of solidification. Results are compared with previous works, including Rappaz and Boettinger (Acta materialia 47 (1999) 3205) and Chen and Sundman (Materials Transactions 43 (2002) 551).

**Solidification Processing via Contactless Electromagnetic Acoustic Transmission (EMAT) Driven by High Magnetic Fields:** *Orlando Rios*<sup>1</sup>; John Wilgen<sup>1</sup>; Roger Kisner<sup>1</sup>; Gerard Ludtka<sup>1</sup>; Gail Mackiewicz Ludtka<sup>1</sup>; <sup>1</sup>Oak Ridge National Laboratory

When induction heating is applied in a high magnetic field environment, the induction heating coil is typically configured in such a way that a high intensity ultrasonic signal is superimposed. The resulting non-contact electromagnetic acoustical transducer (EMAT) dramatically impacts nucleation and growth by fundamentally altering the solid/liquid interfaces. The current study examines the microstructure of three materials consisting of pure Mg, a commercial Mg alloy and a commercial cast iron. Solidification experiments were conducted at the NHMFL using a custom sample environment and instrumentation developed by the magnetic processing

team at ORNL. Each material was induction melted by conventional means and parallel samples solidified under EMAT near 10 kHz driven by magnetic fields up to 20 Tesla under a controlled atmosphere in custom cylindrical crucibles. A comparison to the conventionally solidified material reveals that the high intensity acoustic frequency EMAT promotes a finer scale microstructure and uniquely interesting morphological features.

**Three-Dimensional Characterization and Modeling of Solidified Microstructures of Magnesium-Based Alloys:** *Mingyue Wang*<sup>1</sup>; Tao Jing<sup>1</sup>; Nikhilesh Chawla<sup>2</sup>; <sup>1</sup>Tsinghua University; <sup>2</sup>Arizona State University

Microstructural features of most of engineering materials involved solidification processes are typically three-dimensional and polycrystalline network structure geometrically. The importance of the full three-dimensional characterization including morphologies selection, microstructures evolution, and growth mechanism, and modeling of microstructures and how to bridge that is being realized. Here we demonstrate the use of dual-beam focused ion beam-scanning electron microscopy (DB FIB-SEM) to make a complete three-dimensional reconstruction of the solidified microstructures of magnesium-based alloys, further, on the basis of that, the three-dimensional phase field model derived directly from thermodynamic theory is improved and modified by experimental observations and correlated simulations were conducted. The combined description of three-dimensional microstructural characterization and modeling has important potential applications to the understanding of interaction relationship model of processing-microstructures-properties which is the foundation of modern materials science.

**Theoretical and Computational Study of Lamellar Three-Phase Patterns in a Model Ternary Eutectic System:** *Abhik Choudhury*<sup>1</sup>; Mathis Plapp<sup>2</sup>; Britta Nestler<sup>1</sup>; <sup>1</sup>Institute of Materials and Processes; <sup>2</sup>Ecole Polytechnique

We investigate lamellar three-phase patterns that form during the directional solidification of ternary eutectic alloys in thin samples. A distinctive feature of this system is that many different geometric arrangements of the three phases are possible, contrary to the widely studied two-phase patterns in binary eutectics. Here, we first analyse the case of stable lamellar coupled growth of a symmetric model ternary eutectic alloy, using a Jackson-Hunt type calculation in thin film morphology, for arbitrary configurations, and derive expressions for the front undercooling as a function of velocity and spacing. Next, we carry out phase-field simulations to study the instabilities of the simplest periodic lamellar arrays. For large spacings, we observe different oscillatory modes that are similar to those found previously for binary eutectics and that can be classified using the symmetry elements of the steady pattern. For small spacings, we observe a new instability that leads to a change in the sequence of the phases. Its onset can be well predicted by our analytic calculations. Finally, some preliminary phase-field simulations of three-dimensional patterns are presented.

## Magnesium Technology 2011: Poster Session

Sponsored by: The Minerals, Metals and Materials Society, TMS Light Metals Division, TMS: Magnesium Committee

Program Organizers: Wim Sillekens, TNO Science and Industry; Sean Agnew, University of Virginia; Suveen Mathaudhu, US Army Research Laboratory; Neale Neelameggham, US Magnesium LLC

Sun PM-Thurs PM  
Feb 27-Mar 3, 2011

Room: 6F  
Location: San Diego Conv. Ctr

Session Chair: Eric Nyberg, Pacific Northwest National Laboratory

## Interdiffusion in the Mg-Al System and Intrinsic Diffusion in $\beta$ (Al<sub>3</sub>Mg<sub>2</sub>)

**Phase:** *Sarah Brennan*<sup>1</sup>; Katrina Bermudez<sup>1</sup>; Nagraj Kulkarni<sup>2</sup>; Yongho Sohn<sup>1</sup>; <sup>1</sup>University of Central Florida; <sup>2</sup>Oak Ridge National Laboratory

Intrinsic and interdiffusion between pure Mg (99.9%) and pure Al (99.999%) was examined using three solid-to-solid diffusion couples. The couples were annealed at 300°, 350° and 400°C for 30, 15 and 10 days,

respectively. The interaction layers that developed were examined by optical and scanning electron microscopy. Concentration profiles were determined by energy dispersive spectroscopy and electron microprobe analysis. A thick layer of  $\beta$  (Al<sub>3</sub>Mg<sub>2</sub>) and a thin layer of  $\beta$  (Al<sub>12</sub>Mg<sub>17</sub>), both with measurable concentration gradients, formed in all three couples. However, the  $\epsilon$ -phase was not observed at any temperature studied. The marker plane was identified within the  $\beta$ -phase, close to the Al/ $\beta$  interface. Interdiffusion coefficients in Mg- and Al-solid solution,  $\beta$ -phase,  $\gamma$ -phase, and intrinsic diffusion coefficients within  $\beta$  (Al<sub>3</sub>Mg<sub>2</sub>) are reported and discussed.

**High Strain-Rate Behaviour of Die Casting Magnesium-Aluminium Alloys:** N.V. Dudamell<sup>1</sup>; F. Gálvez<sup>2</sup>; M.T. Pérez-Prado<sup>1</sup>; <sup>1</sup>Madrid Institute for Advanced Studies in Materials (IMDEA Materials); <sup>2</sup>ETS Ingenieros de Caminos

Magnesium alloys, due to their relative low density, are considered as very attractive candidates to be used in the transportation industry where weight saving entails a drop of fuel consumption and, therefore, a reduction of CO<sub>2</sub> emissions. Die casting is the most extended technique used in the fabrication of magnesium components because it allows high productivity and good mechanical properties, being the automotive industry one of the main customers. To increase the application of magnesium components in the automotive industry it is extremely necessary to understand the deformation mechanisms that take place during dynamic straining of die casting magnesium alloys, which are nowadays widely unknown. This investigation is focused on the analysis of the high-strain-rate mechanical behavior of Mg-Al die casting alloys. With this purpose, tests have been performed in a Hopkinson bar, in tension and in compression, at temperatures between 25°C and 400°C.

**High-Temperature Elastic Properties of Two Wrought Magnesium Alloys:** *Matt Freels*<sup>1</sup>; Elena Garlea<sup>2</sup>; Jonathan Morrell<sup>2</sup>; Miladin Radovic<sup>3</sup>; Peter Liaw<sup>1</sup>; <sup>1</sup>Department of Materials Science and Engineering, University of Tennessee; <sup>2</sup>Applied Technologies Division, Y-12 National Security Complex; <sup>3</sup>Department of Mechanical Engineering, Texas A&M University

The elastic constants of the hexagonal close-packed (hcp) wrought magnesium alloys, ZK60A and AZ31B, were measured by dynamic and static methods from room temperature to 450°C. The ZK60A and AZ31B alloys exhibit two different crystallographic textures, respectively, typical for extrusion and rolling. The dynamic resonant ultrasound spectroscopy (RUS) method was selected to investigate the effects of crystallographic texture on the elastic mechanical properties in three directions (extruded or rolled, transverse, and normal). The results from RUS were compared to those from static mechanical testing. From RUS measurements, the Young's, shear, and bulk moduli were found to decrease with temperature, while the Poisson's ratio increased with temperature. At lower temperatures the Young's moduli obtained from mechanical testing agreed well with the RUS measurements. However, at higher temperatures, the Young's moduli from mechanical testing were significantly lower when compared to those from RUS.

## Development and Characterization of New AZ41 and AZ51 Magnesium

**Alloys:** *Md Ershadul Alam*<sup>1</sup>; Han Samson<sup>2</sup>; Abdelmagid Hamouda<sup>1</sup>; Quy Nguyen<sup>2</sup>; Manoj Gupta<sup>2</sup>; <sup>1</sup>Qatar University; <sup>2</sup>National University of Singapore

In the present study, new AZ41 and AZ51 magnesium alloys were successfully synthesized by adding 1 wt. % and 2 wt. % aluminum into AZ31B matrix, respectively, using an innovative disintegrated melt deposition technique followed by hot extrusion. Microstructural characterization studies revealed equiaxed grain morphology, reasonably uniform distribution of intermetallics in the matrix and minimal porosity. Physical properties characterization revealed that addition of Al reduced the coefficient of thermal expansion (CTE) of monolithic AZ31B. The presence of higher percentage of aluminum also assisted in improving overall mechanical properties including microhardness, modulus of elasticity, 0.2% yield strength, ultimate tensile strength, and work of fracture of AZ31. The results suggest that these newly developed AZ magnesium alloys have significant potential in diverse engineering applications when compared to AZ31 alloy.

**Edge-Wise Determination of Compression Strength in Magnesium Alloy Sheet:** *Eric Nyberg*<sup>1</sup>; Curt Lavender<sup>1</sup>; Elizabeth Stephens<sup>1</sup>; Richard Davies<sup>1</sup>; Robert Klingensmith<sup>2</sup>; <sup>1</sup>Pacific Northwest National Laboratory; <sup>2</sup>DOE Academies Creating Teacher Scientists

Quantifying the anisotropic properties in bulk HCP metals is common; however, determining the inhomogeneous properties is inherently more difficult with sheet products. To compare the edge-wise compressive strength of magnesium sheet to standard tensile tests, the compression samples were oriented in the rolling direction, accounting for their tendency to buckle. The edge-wise compressive strength is compared to the tensile yield strength of AZ31 sheet. The compressive strength is determined using a test fixture to prevent buckling, identified for use in ASTM D-695, Standard Test Method for Compressive Properties of Rigid Plastics. The testing was followed according to ASTM E9-09, Standard Test Methods of Compression Testing of Metallic Materials at Room Temperature. The in-situ strain evolution is captured optically using speckle pattern strain imaging. Comparison is made of the anisotropy in fine grained, friction stir processed material versus coarse grained sheet. The compressive strength is compared to bulk compression properties.

**The Grain-Size Dependence of Fatigue Failure Mechanism in Tension Cycles in AZ31 Mg Alloys:** *Daisuke Ando*<sup>1</sup>; Junichi Koike<sup>1</sup>; Yuji Sutou<sup>1</sup>; <sup>1</sup>Tohoku University

The mechanisms of fatigue deformation and failure were studied in rolled AZ31 sheets having a grain size of 5 and 220  $\mu\text{m}$ . Tensile cycle tests were carried out at room temperature to investigate the effects of {10-12} twinning and dislocation slip on cyclic deformation behavior. Fatigue tests were also performed in tension cycle at 10 Hz and  $R = 0.1$ . Deformation twinning of {10-12} type was observed both below and above the fatigue limit. Prismatic slip was observed only above the fatigue limit. They indicated the fatigue limit coincides with the stress required to activate cross-slipping of prismatic slip. In the coarse grain, {10-11}-{10-12} double twinning gave rise to the formation of surface steps and subsequent fatigue cracks. In contrast, the fine grain sample showed neither surface steps nor deformation twinning. Fatigue failure occurred in an intra-granular manner. The failure was probably caused by work hardening with cross-slipping.

**Effect of 15kHz Ultrasonic Treatment on Purification of Magnesium Alloy Melts:** *Qichi Le*<sup>1</sup>; <sup>1</sup>Northeastern University

The effective substitution methods of fluxing processing for magnesium melt purification are paid more attention recent years in order to avoid the risk of flux inclusions and alleviate environmental pressure. The former research in our group had showed the 20kHz ultrasonic treatment could promote and accelerate the separation of oxidation inclusions from magnesium melt by its conglomeration effect. In this research, 15kHz ultrasonic treatments on AZ80 and GW103K magnesium melts were also investigated and the similar results were achieved. The results show that the metal temperature, the ultrasonic power, treating time, and holding time all influent the purification degree, and the over 80% and over 70% of inclusions in AZ80 and GW103K melts could settle into the bottom layer at the optimum treating condition, respectively. In addition, the electrical conductivity study of ingot showed that the electrical conductivity of ingot could characteristic its purification degree commendably.

**The Effect of Different Physical Fields on the Process of Direct Chill Casting for AZ80 Magnesium Alloy Billets:** *Zhiqiang Zhang*<sup>1</sup>; Qichi Le<sup>1</sup>; Jianzhong Cui<sup>1</sup>; <sup>1</sup>Northeastern University

On the basis of conventional direct chill (DC) casting, different physical fields are applied during DC casting of F165mm AZ80 magnesium alloy billets. The effects of low frequency electromagnetic field (LFEC) and ultrasonic field (US) on microstructures, macrosegregation of alloying elements and mechanical properties of AZ80 billets was investigated. The results show that microstructures of DC casting AZ80 billets under different physical fields are significantly refined. Mechanical properties are increased and alloying element distribution are also very uniform. The effective refinement takes place in the edge of AZ80 billets cast by LFEC. However, the effective refinement takes place in the center of AZ80 billets cast by US.

A new process for DC casting of magnesium alloy billets was developed by application of combining LFEC with US which can significantly refine the microstructures in the entire cross section of the billets, and the mechanical properties of the billets were improved.

**Extrusion-Processed Mg-Zn-Al-(Y) Base Alloys with Dispersion of Quasicrystal Phase:** *Guangyin Yuan*<sup>1</sup>; Jian Tong<sup>1</sup>; Hua Huang<sup>1</sup>; Wenjiang Ding<sup>1</sup>; <sup>1</sup>Shanghai Jiao Tong University

The structure and mechanical properties of extrusion-processed Mg-Zn-Al-(Y) base alloys containing an icosahedral quasicrystal phase (i-phase) as a main strengthening phase were investigated. Mg-8Zn-4Al-xY ( $x=0,1$ ) base alloys containing the i-phase were prepared by casting into a permanent mold at moderate cooling rates and then extruding at 598K with the extrusion ratio of 9. The Y addition was effective for decreasing the size of the i-phase and the increasing the homogeneity of its dispersed state. This Mg-Zn-Al-(Y) alloys reinforced with quasicrystal and related phase particles showed high strength and ductility balance, which was superior to that of the well-known quasicrystal phase dispersed in Mg-Zn-RE alloys.

**Engineering a More Efficient Zirconium Grain Refiner For Magnesium:** *Srinath Viswanathan*<sup>1</sup>; Partha Saha<sup>1</sup>; David Foley<sup>2</sup>; K. Ted Hartwig<sup>2</sup>; <sup>1</sup>University of Alabama; <sup>2</sup>Texas A&M University

A systematic study of the grain refinement of magnesium by zirconium was conducted: variables included the amount of zirconium, the pouring temperature, and the settling time prior to casting. Optical microscopy was utilized to measure the grain size. Sample dissolution followed by SEM was used to characterize particle size and morphology both in the master alloy and grain refined samples. It was apparent that only 1 to 3% of the total particles serve as nucleation sites, but a comparison of the grain density vs. faceted particle density showed close agreement, suggesting that only faceted particles were likely nucleation sites. ECAE processing of the magnesium-15wt% zirconium master alloy to increase the number of faceted particles resulted in improved grain refinement efficacy.

**Severe Plastic Deformation Temperature Influences on Texture Development in AZ31B Magnesium:** *David Foley*<sup>1</sup>; Sonia Modarres Razavi<sup>1</sup>; K.T. Hartwig<sup>1</sup>; Laszlo Kecskes<sup>2</sup>; Ibrahim Karaman<sup>1</sup>; Suveen Mathaudhu<sup>2</sup>; <sup>1</sup>Texas A&M University; <sup>2</sup>U.S. Army Research Lab

Depending on the route and "class" of alloy, Equal Channel Angular Extrusion of Mg alloys produces several archetypal textures. However, these textures are the result of "warm" deformation, on the order of 200C. In an effort to obtain high strength through grain refinement, several groups have explored lower temperature deformation where dynamic recrystallization does not limit grain refinement. The authors have found that when AZ31 is deformed at sufficiently low temperature in a preferentially basal slip route, non-basal slip seems to be completely inactive. This generates a closely oriented texture and ultra-fine grain size. The typical ECAE textures for AZ31 have either a split or spread peak character, making it difficult to isolate grain size effects on specific deformation modes. In this case, comparison with coarse-grain material is straightforward. The effect of grain size on the yield strength under various deformation modes will be discussed.

**Microstructure and Mechanical Properties of Mg-1.7Y-1.2Zn Sheet Processed by Hot Rolling and Friction Stir Processing:** *V. Jain*<sup>1</sup>; J.Q. Su<sup>2</sup>; R.S. Mishra<sup>2</sup>; R. Verma<sup>3</sup>; A. Javaid<sup>4</sup>; M. Aljarrah<sup>4</sup>; E. Essadiqi<sup>1</sup>; <sup>1</sup>Division of Engineering Materials, National Physical Laboratory, CSIR; Center for Friction Stir Processing and Department of Materials Science and Engineering, Missouri University of Science and Technology, Rolla; <sup>2</sup>Center for Friction Stir Processing and Department of Materials Science and Engineering, Missouri University of Science and Technology, Rolla; <sup>3</sup>General Motors R&D Center; <sup>4</sup>Materials Technology Laboratory-CANMET, Ottawa

The use of lightweight structural materials is an integral part of mass reduction strategy in transportation applications. Magnesium based sheet products have gained significant interest in the automobile industry. Newer magnesium alloys such as Mg-Y-Zn have potential to develop sheet products with superior mechanical properties owing to improved precipitation hardening response. In the present work, rolled sheet of an Mg-1.7Y-1.2Zn



alloy containing small amounts of Al and Ce was investigated. Microstructure and mechanical properties were examined in as-rolled, rolled+aged, friction stir processed (FSP) and FSP+aged conditions. Mechanical properties (YS, UTS and %El) of the sheet showed certain anisotropy in rolling and transverse directions, which was marginally reduced upon ageing. However, FSP led to a significant range of mechanical properties depending on the test direction. Ageing of FSPed sheet showed improvement in mechanical properties and reduced anisotropy in the two directions. The static recrystallization due to ageing caused reduced anisotropy in FSP treated sheet. The overall strength-ductility variation is discussed in terms of relative contributions of grain boundary strengthening, texture and precipitation strengthening.

**Texture Evolution in Large Strain Extrusion Machining of Magnesium Alloy AZ31B:** *Dinakar Sagapuram*<sup>1</sup>; Mert Efe<sup>1</sup>; Wilfredo Moscoso<sup>1</sup>; Kevin Trumble<sup>1</sup>; Srinivasan Chandrasekar<sup>1</sup>; <sup>1</sup>Purdue University

Large Strain Extrusion Machining, a single-cut, constrained machining process efficient in introducing large shear strains (1-10) is used to produce magnesium alloy AZ31B strip. By exploiting the heat that is inherently generated, this process proves to be capable of producing high quality thin strip (~200 \956m thick) from a workpiece starting at ambient temperature. The texture analysis using two-dimensional XRD on the strips produced from unheated workpiece showed strong non-basal textures, with the c-axes of the grains inclined towards the cutting direction. In contrast, strips produced from a preheated workpiece (200°C) showed splitting of the basal pole in the transverse direction, consistent with the increased prismatic slip activity. The process also yields a fine equiaxed grain structure (~2-6 \956m). The influence of the resulted texture and microstructure on the mechanical properties, and the implications of scaling up the process to produce wider and thicker sheets will be addressed.

**The Microstructure and Mechanical Properties of Cast Mg-5Sn Based Alloys:** Mahsa Keyvani<sup>1</sup>; Reza Mahmudi<sup>1</sup>; *Ghazal Nayyeri*<sup>1</sup>; <sup>1</sup>University of Tehran

The effects of 1 wt.% Ce-rich misch-metal, 3 wt.% Bi, 0.4 wt.% Sb, and 2 wt.% Ca additions on the microstructure, mechanical properties, and creep resistance of a cast Mg-5Sn alloy were studied. Impression creep tests were carried out at 150 and 225 oC under constant stresses of 300 and 175 MPa. The results showed that creep resistance, hardness, and shear strength of the base alloy were significantly enhanced with the addition of ternary alloying elements. This was attributed to the concurrent formation of Mg<sub>2</sub>Sn particles with the more thermally stable CaMgSn, Mg<sub>3</sub>Sb<sub>2</sub>, Mg<sub>3</sub>Bi<sub>2</sub> and MgSnRE phases which strengthen both matrix and grain boundaries during deformation in the investigated system. Among all tested materials, the Mg-5Sn-2Ca alloy indicated the highest mechanical properties and creep resistance due to the refined microstructure as well as the type and volume fraction of the intermetallic phases present in this alloy.

**Effects of Misch Metal on Microstructure and Mechanical Properties of Mg-Nd Alloys:** *Bo Keon Kwon*<sup>1</sup>; Il Hwan Choi<sup>1</sup>; Kwang Seon Shin<sup>1</sup>; <sup>1</sup>Magnesium Technology Innovation Center / Seoul National University

In recent years, there have been efforts to develop gravity casting magnesium alloys for automobile engine applications. In order to achieve high temperature mechanical properties required for engine blocks, precipitation hardenable Mg-Nd-Y alloys have been developed. For elevated temperature strength, it is necessary to add considerable amounts of rare earth (RE) elements such as Nd, Y, etc. to magnesium alloys, because these RE elements form thermally stable precipitates which are essential for high temperature strength. However, the amounts of RE elements should be minimized to reduce the cost of alloy ingots. In the present study, it was attempted to utilize misch metal in order to reduce the amounts of expensive alloying elements in Mg-Nd alloys. All specimens were produced by the gravity casting process. The microstructures of the as-cast and the heat-treated specimens were examined by optical and scanning electron microscopy. Mechanical properties were examined both at room and elevated temperatures.

**A Study on Combined Effect of Forging and Ageing in Mg-Y-RE Magnesium Alloy:** *S. K. Panigrahi*<sup>1</sup>; R.S. Mishra<sup>1</sup>; K. Kumar<sup>1</sup>; R. DeLorme<sup>2</sup>; B. Davies<sup>2</sup>; R. A. Howell<sup>3</sup>; K. Cho<sup>3</sup>; <sup>1</sup>Centre for Friction Stir Welding and Material science and Engineering; <sup>2</sup>Magnesium Elektron North America Inc.; <sup>3</sup>Manufacturing and Materials Technology Branch, Army Research Laboratory

The recent thrust for weight reduction in aircraft, automobiles and other transportation vehicles have made magnesium-rare earth (Mg-RE) alloys very attractive as structural materials. Among various Mg-RE alloys, WE43 is one of the most promising candidates due to the remarkable age hardening response, good thermal stability, corrosion resistance, and creep resistance up to relatively high temperatures. The increased usage of these alloys depends on enhancing their mechanical properties by implementing a combination of strain hardening, grain refinement and age hardening. The present work explores forging of F temper plate and subsequent ageing to maximize the strength-ductility combination of a WE43 alloy. The forged samples with peak ageing treatment (64 hours at 180 oC) showed a significant enhancement of both strength and ductility as compared to previous reported values. These results are discussed in the framework of grain boundary and precipitate strengthening mechanisms.

**Effect of Cooling Rate and Chemical Modification on the Tensile Properties of Mg-5wt. % Si Alloy:** F. Mirshahi<sup>1</sup>; M. Meratian<sup>1</sup>; *M. Mohammadi Zahrani*<sup>1</sup>; E. Zahrani<sup>1</sup>; <sup>1</sup>Isfahan University of Technology

Hypereutectic Mg-Si alloys are suitable candidates to replace Al-Si alloys used in aerospace and engine applications. In this study the effects of both cooling rate and bismuth addition on the microstructure and tensile properties of Mg-5wt% Si alloy were investigated. It was found that the addition of 0.5%Bi, altered the morphology of primary Mg<sub>2</sub>Si precipitate from dendritic to polygonal shape and reduced their size from ~20 to ~8 μm. The tensile strength and elongation of the modified alloy increased at ambient and elevated temperatures, which should ascribed to the modification of Mg<sub>2</sub>Si morphology and more uniform distribution of the particles. Adding Bi also reduced the number of decohered particles observed in fracture surfaces thereby increasing the alloy ductility. Increase in both tensile strength and elongation values with increase in cooling rate were observed witch is attributed to polygonal morphology of Mg<sub>2</sub>Si precipitates in higher cooling rates.

**On Predicting the Channel Die Compression Behavior of HCP Magnesium AM30 using Crystal Plasticity FEM:** *Q. Ma*<sup>1</sup>; E.B. Marin<sup>1</sup>; A. Antonyraj<sup>1</sup>; Y. Hammi<sup>1</sup>; H. El Kadiri<sup>1</sup>; P.T. Wang<sup>1</sup>; M.F. Horstemeyer<sup>1</sup>; <sup>1</sup>Mississippi State University

Deformation of polycrystalline aggregates of HCP crystals was investigated by employing crystal plasticity and finite element simulations. Results were validated using channel die compression tests. The three dimensional polycrystal, represented by Voronoi techniques, was assigned an initial distribution of crystallographic orientations determined from X-Ray Diffraction. The mechanical properties from the channel die compression tests were used to correlate the material parameters of the crystal plasticity model. Simulations predicted grain-to-grain interactions and the resulting texture evolution under channel die compression. The inhomogeneous deformation among grains was mapped by a stress and a strain distribution and grain orientation spread. The simulation results were compared with experimental observations of an HCP polycrystal subjected to channel die compression.

**Hardening of Pure Magnesium Due to Higher Order Deformation Twins:** *Fumiaki Hiura*<sup>1</sup>; Marek Niewczas<sup>1</sup>; <sup>1</sup>McMaster University

Hardening effect due to {10-12} deformation twins was studied in magnesium single crystals, by means of a latent hardening experiments. Large parent single crystals oriented for tensile twinning were deformed up to 10% of strain. Subsequently, the secondary samples with the tensile axis oriented 90o to the tensile axis of the parent samples were cut and deformed to evaluate the work-hardening behavior of secondary samples. The microstructure and micro-texture observations of secondary samples by SEM/EBSD technique revealed formation of higher order {10-12} twins



inside the primary twin regions. The secondary samples showed enhanced work hardening, influenced by the density of higher order {10-12} twins. The mechanical properties and the work hardening behavior of secondary samples are interpreted in terms of a dynamical Hall-Petch effect arising from the grain refinement and the reduction of the dislocation mean free path due to formation of higher order twins.

**Slip and Twin Behavior in Magnesium Single Crystals:** *Ming Zhe Bian*<sup>1</sup>; Kwang Seon Shin<sup>1</sup>; <sup>1</sup>Seoul National University

Deformation behavior of magnesium single crystals was investigated by compression tests parallel or perpendicular to the c-axis between room temperature and 623K. {10-12} tensile twin and {10-11} compression twin, as well as {10-11}-{10-12} double twins, were observed during compression tests as reported earlier. In addition, {10-13} twins and {10-13}-{10-12} double twins were also observed at low temperatures. Electron backscattered diffraction (EBSD) data revealed that shear bands developed from compression twins and localized recrystallization in twins took place at 473K. Twin induced dynamic recrystallization (DRX) during compression tests was systematically investigated by optical microscopy (OM) and EBSD technique.

**Investigation of Microhardness and Microstructure of AZ31 Alloy after High-Pressure Torsion (HPT):** *Jitka Vrátná*<sup>1</sup>; Miloš Janeček<sup>1</sup>; Petr Hrcubá<sup>1</sup>; Robert Král<sup>1</sup>; Hyoung Seop Kim<sup>2</sup>; <sup>1</sup>Charles University; <sup>2</sup>Chungnam National University

Cast commercial magnesium alloy AZ31 was processed by high pressure torsion (HPT) at room temperature for 1, 3, 5 and 15 rotations. Texture and microstructure evolutions were observed using electron backscatter diffraction (EBSD). Lattice defects formed during HPT straining were determined by positron annihilation spectroscopy (PAS). Mechanical properties were revealed by detailed 2-D microhardness measurements. The variations of microstructure, defects structure and microhardness were observed along the diameter of particular specimen since deformation energy differs between the centre and the periphery of the disc. The differences between specimens strained by different number of rotations were also analyzed.

**Plastic Deformation of Magnesium Alloy Subjected to Compression-First Cyclic Loading:** *Soo Yeol Lee*<sup>1</sup>; Michael A. Gharghour<sup>2</sup>; John H. Root<sup>2</sup>; <sup>1</sup>The University of British Columbia; <sup>2</sup>National Research Council Canada

In-situ neutron diffraction has been employed to study the deformation mechanisms in a precipitation-hardened and extruded Mg-8.5wt.% Al alloy subjected to compression followed by reverse tension. The starting texture is such that the basal poles of most grains are oriented normal to the extrusion axis and a small portion of grains are oriented with the basal pole parallel to the extrusion axis. Diffraction peak intensities for several grain orientations monitored in-situ during deformation show that deformation twinning plays an important role in the elastic-plastic transition and subsequent plastic deformation behavior. Significant non-linear behavior is observed during unloading after compression and appears to be due to detwinning. This effect is much stronger after compressive loading than after tensile loading.

**Dislocation Slip and Stacking Fault Formation during Cold Deformation of Mg and Mg-Y Alloys:** *Stefanie Sandlöbes*<sup>1</sup>; Stefan Zaeferrer<sup>1</sup>; Igor Schestakow<sup>1</sup>; Sangbong Yi<sup>2</sup>; <sup>1</sup>Max-Planck-Institut für Eisenforschung GmbH; <sup>2</sup>GKSS-Forschungszentrum Geesthacht GmbH

Solid solution Mg-Y alloys show a significantly increased room temperature ductility compared to pure Mg and commercial wrought Mg alloys. It was shown before that this ductility improvement is caused by enhanced activity of deformation mechanisms on pyramidal planes, as {10-11}<10-12> compression and {10-11}{10-12} secondary twinning and pyramidal dislocation slip. It is assumed that the higher activation of these deformation modes is caused by a change in the stacking fault energies by solid solution of Y. The present study focuses on identification of the Burgers vectors of activated perfect and partial dislocations in Mg-Y alloys and determination of the kind of stacking faults and their frequency by transmission electron

microscopy (TEM). Complementary ab initio calculations on Mg and Mg-Y alloys are performed. Based on these results assumptions about the magnitude of the corresponding stacking fault energies are given and their relevance for the activation of different deformation modes is discussed.

**Investigation of Dynamic Recrystallization Mechanisms during Hot Deformation of a Mg Alloy:** *Zhenzhen Yu*<sup>1</sup>; Hahn Choo<sup>1</sup>; Tamás Ungár<sup>2</sup>; Levente Balogh<sup>2</sup>; Edward Kenik<sup>3</sup>; <sup>1</sup>University of Tennessee; <sup>2</sup>Eötvös University; <sup>3</sup>Oak Ridge National Laboratory

The deformation and recrystallization mechanisms of AZ31B Mg wrought plate were investigated using x-ray line profile analysis (XLP) and electron back-scatter diffraction (EBSD) techniques. First, a series of through-thickness (TT) compression tests were performed at a wide range of temperatures and strain rates for various strain levels. A relationship was established between the final recrystallized grain size and deformation conditions represented by Zener-Hollomon parameter (Z). The results show a transition of dynamic recrystallization (DRX) mechanism as Z was increased. At high Z values, twinning preceded the DRX and resulted in dramatic changes in the texture as well as the grain refinement process. The XLP and EBSD results provide further insights to the evolution of deformation microstructure including the dominant deformation mechanisms, and the influence of twinning on DRX and micro-texture distribution. Finally, compression tests were also performed along in-plane direction to compare the DRX processes observed along the TT direction.

**High Strain-Rate Behaviour in a Weakly Textured Extruded Mg-Mn-Nd (MN11) Alloy:** *N.V. Dudamell*<sup>1</sup>; F. Gálvez<sup>2</sup>; S. Yi<sup>3</sup>; J. Bohlen<sup>3</sup>; D. Letzig<sup>3</sup>; M.T. Pérez-Prado<sup>1</sup>; <sup>1</sup>Madrid Institute for Advanced Studies in Materials (IMDEA Materials); <sup>2</sup>Universidad Politécnica de Madrid; <sup>3</sup>GKSS Research Center

Magnesium alloys, due to their relative low density (1.74 g cm<sup>-3</sup>), are considered as potential materials to be used in components in which weight reduction is desired. Manganese and Neodymium have received special attention as alloying elements. Manganese, due to its effect in the enhancement of corrosion resistance and in the prevention of hot-cracking at high extrusion speeds and neodymium, due to its effect on the dynamic recrystallization during hot extrusion, leading to the formation of a weak texture. The mechanical behaviour of Mg-Mn-Nd alloys at high strain-rate has not been investigated yet. The main purpose of this contribution is to characterize the mechanical behaviour of an Mg-Mn-Nd alloy tested in tension and in compression at high strain-rate and to establish the deformation mechanisms activated under the dynamic straining. Tests will be carried out in tension and in compression in a Hopkinson bar at temperatures between 25°C and 400°C.

**The Effect of Strain Rate on Flow Behavior and Microstructure Evolution of AZ31 Mg Alloys:** *Mehdi Sanjari*<sup>1</sup>; S.A. Farzadfar<sup>1</sup>; S. Yue<sup>1</sup>; E. Essadiqi<sup>2</sup>; <sup>1</sup>McGill University, Department of Materials Engineering; <sup>2</sup>CANMET - Materials Technology Laboratory

In this work, the effects of strain rate on the flow behaviour and microstructure evolution on AZ31 Mg alloy were studied by compression testing over a wide range of strain rates (0.01-1000 s<sup>-1</sup>). The results showed that the recrystallization mechanism changed with increasing strain rate at a constant temperature. Also, the recrystallized volume fraction increased significantly with strain rate. Two types of constitutive equations were used to analyze the flow behaviour. Average activation energies of 162 kJ/mol and 135 kJ/mol were obtained for the peak and steady-state strain, respectively.

**Microstructure and Texture Effects on the Deformation Behaviors of the Statically Recrystallized Mg-Zn-MM Alloy Sheets:** *Heon Kang*<sup>1</sup>; Beomsoo Shin<sup>1</sup>; Donghyun Bae<sup>1</sup>; <sup>1</sup>yonsei university

The Mg-Zn-MM alloy sheets were annealed at two different temperatures and mechanical properties and texture effect were evaluated. Few grains were observed in as-rolled sheets and the different grains size and orientations were analyzed in annealed sheets at 220 °C, 380°C for 5min by using Electron back scattering diffraction (EBSD). Tensile tests were performed at a strain rate of 10<sup>-4</sup>s<sup>-1</sup> at room temperature in three directions ; RD, 45°, TD.

The sheets annealed at 220°C exhibited superior elongations (higher than 30%) and similar elongations in three tensile directions at room temperature. 10~50nm sizes of the nano twins were observed in the deformed region. The alloy sheets were deformed by not only the activation of non-basal slips which caused by the presence of refined grains, but also formation of the nano twins. The details of texture effect of the alloy will be also presented.

**The Mechanical Response of a Magnesium Alloy under a Range of Biaxial Loading Conditions:** *Philip Tomlinson*<sup>1</sup>; Warren Poole<sup>1</sup>; Chad Sinclair<sup>1</sup>; <sup>1</sup>University of British Columbia

Owing to the strong mechanical anisotropy of magnesium alloys, simple uniaxial testing is insufficient for complete mechanical performance characterization. The fact that deformation mechanisms in magnesium alloys are very sensitive to external testing conditions as well as microstructural and compositional modifications means that one expects strong variations in the anisotropy as indicated, for example, by the yield surface and its expansion. Despite the practical and theoretical importance of understanding the stress state/strain path dependence of the yielding, work hardening and fracture, few studies have been reported in the literature for magnesium alloys. A testing solution that allows for experiments where a range of biaxial stress states can be accessed has been developed. In this talk this facility will be described and experimental results from testing of an AM30 alloy will be presented. These results will be discussed in relation to the expected path dependence of various deformation modes.

**Microstructural Investigations into Novel Alloys Based on The Mg-Y-Nd System:** *Andy Williams*<sup>1</sup>; Mark Rainforth<sup>1</sup>; Brad Wynne<sup>1</sup>; Bruce Davis<sup>2</sup>; <sup>1</sup>University of Sheffield; <sup>2</sup>Magnesium Elektron USA

Three novel Mg-Y-Nd based alloys have been produced, containing reduced levels of Y as compared to the current Mg-RE systems, and are intended, in particular, as potential cost effective option for the automotive industry. Hot axisymmetric compression tests are employed on these alloys to investigate their deformation behaviour at raised temperatures, with the resulting data used to develop constitutive equations to describe flow behaviour as a function of temperature, strain and strain rate. A complimentary TEM and EBSD study is conducted to examine the active deformation mechanisms during hot working. The relationship between the slip, twinning, dynamic recrystallisation and flow behaviour will be considered with the aim being to isolate a viable processing window for the hot rolling of these new alloys, potentially widening their applications range.

**Deformation Behavior and Microstructure Evolution during the Hot Compression of AM50 Mg Alloy by Cooling Slope:** *Dae-Hwan Kim*<sup>1</sup>; Seung-Hwa Choi<sup>1</sup>; Hee-Kyeong Kim<sup>1</sup>; Su-Gun Lim<sup>1</sup>; <sup>1</sup>i-Cube Center, Engineering Research Institute, Gyeongsang National University

For the hot forming of Mg alloy such as hot extrusion and forging, it is important to have knowledge on the deformation behavior of the material with the variation of temperature. Therefore, the deformation behavior and microstructure variation of Mg alloy by cooling slope during the hot compression with different deformation temperature in this study was investigated. The material used for this experiment was AM50A Mg alloy used for production of automotive wheels and other parts. And the experiments for deformation behavior of the alloy were conducted at deformation temperatures of 300°C, 350°C and 400°C under Ar gas atmosphere. AM50A alloy by cooling slope was composed with equiaxed grains. The microstructure of the alloy during the hot compression test varied more finely than that of as-cast. Also, with increasing deformation temperature, the compression stress of AM50A alloy decreased.

**Deformation Characteristics of Thixo-processed Mg Sheet Alloy:** *Muammer Koc*<sup>1</sup>; Ryan Snell<sup>1</sup>; Omer Cora<sup>1</sup>; John Cheng<sup>2</sup>; <sup>1</sup>Virginia Commonwealth University; <sup>2</sup>Thixomat

This study was conducted to understand the material behavior and formability limits of thixo-cast Mg alloy sheets at elevated temperature as well as room temperature conditions. Uniaxial tensile and hydraulic bulge tests were conducted to investigate the material behavior at different temperatures (25°C -300°C) and strain rates (0.0013, 0.013, and 0.13 s<sup>-1</sup>).

Based on the test results, flow stress and the maximum plastic strain were found to increase with increasing temperature and decreasing strain rate. Effect of test technique (tensile or bulge tests) on the results (strain, strength levels). Apart from tensile and bulge tests, closed die hydroforming tests were conducted to evaluate the formability of the alloy. Die filling and thinning of the sheet blanks were measured with non-contact optical photogrammetry. Results showed that slower strain rates and higher temperatures increase formability, with benefits from lower strain rates being more dominant at temperatures over 200°C.

**Texture Evolution in As-Cast AZ31 Magnesium Alloy Sheet under Various Rolling and Annealing Conditions:** *Jun-ho Park*<sup>1</sup>; Hyun-Sik Choi<sup>1</sup>; Ju-Heon Kim<sup>2</sup>; Dong-Ik Kim<sup>2</sup>; Kyu Hwan Oh<sup>1</sup>; Heung Nam Han<sup>1</sup>; <sup>1</sup>Seoul National University; <sup>2</sup>Korea Institute of Science and Technology

Wrought magnesium alloys show poor formability at room temperature due to the shortage of independent slip systems. Thus hot rolling method is generally used for manufacturing the magnesium alloy sheets. In this study, in order to observe the deformation and annealing texture of the rolled Mg alloy sheet, the multi-pass cold and 1-pass hot rolling was adopted in as-cast AZ31 magnesium alloys. Subsequently, some of the cold-rolled sheets were annealed under various time period and temperature conditions to observe the recrystallization texture. Then, the analysis of microstructure and texture evolution with depth of the rolled sheet was performed with Optical Microscope (OM), X-Ray Diffractometer (XRD) and Electron Back-Scattered Diffraction (EBSD). As a result, the rolled Mg sheets revealed the texture with basal poles tilted about ±15° up to ±25° from the normal direction towards the rolling direction. After the recrystallization, it was observed that the basal texture became strong.

**Texture Development in Rolled Mg Alloy Sheets:** *Hyun-Sik Choi*<sup>1</sup>; Jun-Ho Park<sup>1</sup>; Se-Jong Kim<sup>1</sup>; Dong Nyung Lee<sup>1</sup>; Heung Nam Han<sup>1</sup>; <sup>1</sup>Seoul National University

In this study, in order to observe experimentally the texture development after rolling and annealing of the Mg alloy sheet, an AZ31 magnesium alloy was used. Microstructure and texture evolution in the rolled Mg sheets was observed with optical microscope, X-ray diffractometer and electron back-scattered diffraction. It was found that the rolled Mg sheets revealed the texture with basal poles tilted about ±20° from the normal direction towards the rolling direction. After the recrystallization, it was observed that the basal texture became strong. To analyze the deformation texture during rolling, a visco-plastic self-consistent polycrystal model was employed. As for the calculation of annealing texture, the concept of Strain-Energy-Release-Maximization proposed by D.N. Lee [Philos. Mag. 85 (2005), pp. 297–322], in which the texture evolves to maximize the mechanical internal energy release during recrystallization, was generalized. The calculated results were compared with the experiments.

**Effect of Differential Speed Rolling on Texture Evolution of Mg-4Zn-1Gd Alloy:** *Myeong-shik Shim*<sup>1</sup>; Jun ho Bae<sup>1</sup>; Dong-wook Kim<sup>1</sup>; Byeong-chan Suh<sup>1</sup>; Sunghak Lee<sup>1</sup>; Nack Joon Kim<sup>1</sup>; <sup>1</sup>POSTECH

Mg alloys generally have low ductility and formability at room temperature because of the strong basal texture developed during conventional symmetric rolling. It has been recently shown that the differential speed rolling (DSR) utilizing the different rotation speeds for upper and lower rolls introduces intense shear deformation, which might lead to the development of weaker basal texture than the conventional rolling process. In the present study, twin-roll cast Mg-4Zn-1Gd alloy sheet was subjected to high speed-ratio DSR to modify its texture and microstructure. It shows that there is a development of deformation bands by DSR and dynamic recrystallization occurs along the deformation bands. In addition to such microstructural changes, the DSR sheet has a texture characterized by the basal pole tilted from the normal direction (ND) towards the rolling direction (RD). However, the maximum intensity of basal texture is quite similar between the DSR sheet and the conventionally rolled sheet.

**Texture and Microstructure Control of AZ91 Mg Alloy Sheet by High Speed Rolling:** Akinori Hashimoto<sup>1</sup>; Tetsuo Sakai<sup>1</sup>; Hiroshi Utsunomiya<sup>1</sup>; <sup>1</sup>Osaka University

The present authors succeeded in single pass large draught rolling of AZ31 magnesium alloy sheets below 473K without heating rolls by rolling at the speed higher than 250m/min. The rolled and quenched sheets had fine recrystallized microstructure and exhibited excellent mechanical properties. It remains uncertain whether the high limiting reduction by high speed rolling can be attained in other magnesium alloys. In this study, we tried to roll the sheet of AZ91 magnesium alloy at 1000m/min below 473K. Rollability of AZ91 sheet is improved, and the maximum reduction in thickness of 50% is obtained. However, rollability of AZ91 is lower than that of AZ31. The sheets rolled show fine recrystallized grains with the average diameter of 3 $\mu$ m. Basal texture with double peaks is formed. The best result shows the tensile strength of 350MPa and the elongation of 29%, which is an excellent strength-ductility balance.

**Cavitation Behavior of AZ31 Sheet during Gas Blow Forming:** Yong-Nam Kwon<sup>1</sup>; Wonkyu Bang<sup>2</sup>; <sup>1</sup>Korea Institute of Materials Science; <sup>2</sup>RIST

Superplastic behavior of fine grained AZ31 sheet has been reported to occur in the temperature over 400°C and the strain rate of 10-4/s order. Cavitations usually bring out as result of poor accommodation of grain boundary sliding in the AZ31 sheet. As well known in superplastic Al alloys, it was reasonable to assume that back pressure could prohibit cavitations effectively in AZ31 sheet. In the present study, blow forming behavior was measured with the variation of back pressure. Especially, cavitation behavior was characterized in terms of strain, strain rate and temperature. Particles sitting along rolling direction would be the preferable sites for cavity opening in microstructure observation. However, results showed that back pressure did not influence the overall blow forming characteristics in AZ31 system as much as in superplastic Al alloys. This tendency might be originated from a limited accommodation system for grain boundary sliding of AZ31.

**Mechanical and Terminal Ballistic Properties of Magnesium Yttrium Rare Earth WE43 Alloy Rolled Plate:** Richard DeLorme<sup>1</sup>; Bruce Davis<sup>1</sup>; Jonathan Montgomery<sup>2</sup>; Tyrone Jones<sup>2</sup>; Kyu Cho<sup>2</sup>; <sup>1</sup>Magnesium Elektron North America; <sup>2</sup>U.S. Army Research Laboratory

The publication of MIL-DTL-32333(MR) in July 2009 represents the first magnesium alloy armor plate specification published. While the current scope of MIL-DTL-32333(MR) is limited to AZ31B (H24) rolled plate, higher performance nonflammable magnesium alloy classes are being considered as potential inclusion candidates to this specification. Magnesium Elektron North America (MENA) and U.S. Army Research Laboratory have collaborated in the research, development, manufacturing, testing, and evaluation of one such candidate magnesium alloy WE43. The present work summarizes the mechanical and terminal ballistic properties of the WE43 rolled plate. The results are also compared with those reported from other nonferrous light alloy armor plates.

**A Development of Mg Alloy Reinforced by Quasicrystalline Phase:** J.S. Kyeong<sup>1</sup>; Won Tae Kim<sup>2</sup>; D.H. Kim<sup>1</sup>; <sup>1</sup>Yonsei University; <sup>2</sup>Cheongju University

Mg-Zn-Y based alloys, reinforced by icosahedral quasicrystalline phase (I-phase) have been developed by ingot casting, followed by thermomechanical treatment and post heat treatment. Microstructure and mechanical properties of the resulting specimens were characterized by using optical microscopy, scanning electron microscopy, transmission electron microscopy, electron backscatter diffraction, X-ray diffractometry and tensile test. The alloys show relatively homogeneous distribution of I-phase particle in an alpha Mg matrix. The alloys exhibited high strength and good formability, due to high thermal stability and symmetry of I phase and stable interface formation with matrix. With increasing the volume fraction of the I-phase, tensile strength of the specimens increased. Also the small addition of Ca was very effective to weakening the basal texture in statically recrystallized specimen as well as hot-rolled specimen. The effect of Ca on texture evolution will be discussed in terms of enhanced particle stimulated nucleation during the process of recrystallization.

**Nano-Structured Mg-Al-Zn Alloy via Cryomilling and Spark Plasma Sintering:** Baolong Zheng<sup>1</sup>; Osman Ertoer<sup>1</sup>; Ying Li<sup>1</sup>; Troy Topping<sup>1</sup>; Yizhang Zhou<sup>1</sup>; Chi Tsao<sup>2</sup>; Enrique Lavernia<sup>1</sup>; <sup>1</sup>University of California, Davis; <sup>2</sup>National Cheng Kung University

Nanostructured Mg alloys have become of interest in various engineering applications due to their high specific strength. The mechanical behavior and microstructure of nanocrystalline (nc) Mg AZ80 alloy, synthesized via a cryomilling (mechanical milling under cryogenic temperature) and spark plasma sintering (SPS) approach are herein reported. First, Mg-based AZ80 powders, with an average grain size of 40 nm were synthesized via cryomilling for 8 hours. Second, the cryomilled AZ80 powder was subsequently consolidated using SPS at 300, 350, 400 and 450°C. SEM and TEM analysis shows that the SPS'ed Mg AZ80 consists of a bimodal microstructure with nc grains and coarse grains. The underlying mechanisms for the formation of bimodal microstructure during SPS sintering and the effect of bimodal microstructure to properties are discussed. A microhardness of 140 HV and a compressive strength of 546 MPa are achieved in the SPS'ed Mg AZ80.

**Microstructure Evolution in AZ61L During TTMP and Subsequent Annealing Treatments:** Tracy Berman<sup>1</sup>; William Donlon<sup>1</sup>; Raymond Decker<sup>2</sup>; Jack Huang<sup>2</sup>; Tresa Pollock<sup>3</sup>; J. Wayne Jones<sup>1</sup>; <sup>1</sup>University of Michigan; <sup>2</sup>nanoMAG, LLC.; <sup>3</sup>University of California, Santa Barbara

Microstructure evolution is studied in Thixomolded Thermomechanical Processed (TTMP) AZ61L sheet at various stages of processing. Transmission electron microscopy (TEM) is utilized to examine (1) grain refinement and recrystallization and (2) refinement and re-distribution of the  $\beta$ -Mg<sub>17</sub>Al<sub>12</sub> phase in the as-Thixomolded, as-TTMP, and annealed conditions. Electron backscatter diffraction (EBSD) is used to study texture evolution through the TTMP and annealing process. The influence of microstructure by the TTMP and annealing on the mechanical properties will be presented.

**Fine Scale Microstructure and Deformation Behavior of AZ61L:** Ramasis Goswami<sup>1</sup>; Khershed Cooper<sup>2</sup>; Ray Decker<sup>3</sup>; Steve LeBeau<sup>3</sup>; <sup>1</sup>SAIC/Naval Research Laboratory; <sup>2</sup>Naval Research Laboratory; <sup>3</sup>nanoMAG LLC

The effect of size and distribution of Al<sub>12</sub>Mg<sub>17</sub> precipitate in hcp  $\alpha$ -Mg matrix on deformation behavior was studied in Mg alloys produced by the thixomolded thermomechanical processing (TTMP) route. Precipitate size and distribution were controlled by varying process parameters at a given Al content. The strength and ductility were enhanced by TTMP as a result of grain and particle size refinement, and an increase in dislocation density. The Al<sub>12</sub>Mg<sub>17</sub> particles were divided by this process into smaller particles. Also, some particles were found to have dissolved and reprecipitated as nano-scale precipitates during thermomechanical processing. The nucleation and growth of the Al<sub>12</sub>Mg<sub>17</sub> particles within the grain will be discussed.

**Role of Secondary phases for Improved Plasticity in Mg-based Bulk Metallic Glass Composites:** Je-In Lee<sup>1</sup>; Eun Soo Park<sup>1</sup>; <sup>1</sup>Seoul National University

Considerable demands for new low-cost and light-weight structural materials have prompted a wide variety of research on Mg-based bulk metallic glasses (BMGs). Despite their high strength and large elastic limit, Mg-based BMGs confront a serious problem that they exhibit brittle fracture by the formation of localized shear bands. In the present study, we reported a series of in-situ composites with different scales and fractions of secondary phases in Mg-Cu-Zn-Gd BMG-forming alloy systems. When the Mg contents increased, the density of the alloys decreased and a fully amorphous phase of the alloys was transformed into a combination of a partial amorphous phase and relatively small secondary phases. In comparison with monolithic Mg-based BMGs, the in-situ composites definitely exhibited enhanced plasticity, which was obtained by preventing propagation of localized shear bands during deformation. The effect of both scales and fractions of secondary phases by controlling alloy composition will be systematically reported.



**Microstructural Characteristics and Charge-Discharge Behavior of Mg-Li-C System Materials:** *Hung Fei-Yi*<sup>1</sup>; <sup>1</sup>Institute of Nanotechnology and Microsystems Engineering, Center for Micro/Nano Science and Technology, National Cheng Kung University

Magnesium-carbon powders and Magnesium-lithium powders were used as the anode materials for lithium ion batteries to investigate the structure and electrochemical behavior in room temperature. The composition of Mg-C powders contained 1:1 and 9:1. The powders and the thermal coated films of Mg-10Li were compared with the Mg-C systems. In addition, the Mg-10Li thermal evaporated film was used as the experimental materials to process the post-treatment. The results show that Mg-C powders system had an interface effect of Cu foil to reduce the electrochemical reaction. With increasing the carbon content, the charge-discharge characteristics of Mg-C powders had raised. Notably, the Mg-10Li specimen had better cycling properties than that of Mg-50C. After annealing at 200 °C, it was found that the Mg-10Li film not only increased the capacity, but also improved the charge-discharge cyclability.

**Modeling the Corrosive Effects of Various Magnesium Alloys Exposed to Two Saltwater Environments:** *Holly Martin*<sup>1</sup>; M. Horstemeyer<sup>1</sup>; Paul Wang<sup>1</sup>; <sup>1</sup>Center for Advanced Vehicular Systems, Mississippi State University

The use of magnesium within the automotive industry is limited by its corrosion rate in the presence of saltwater. By adding various elements, the magnesium microstructure and corrosion rate can be altered. In the Center for Advanced Vehicular Systems at Mississippi State University, a model is being developed to elucidate the total corrosion of magnesium alloys and is comprised of general corrosion and pitting corrosion, respectively:

$\phi = \phi_{GC} + \phi_{IC}$  where pitting corrosion is based on the pit number density, pit surface area, and a nearest neighbor distance function, respectively:  
 $\phi_{IC} = \eta_p v_p c^p$  The exposure environment resulted in differences in the amount of pit nucleation, in the size of the pits formed, and in the rate of coalescence. Time also affected the surface characteristics, as general corrosion began to degrade the number and size of the pits. The research presented here will cover the model development, calibration, and validation.

**Corrosion Performance of Mg-Ti Alloys Synthesized By Magnetron Sputtering:** *Zhenqing Xu*<sup>1</sup>; *Guang-Ling Song*<sup>2</sup>; *Daad Haddad*<sup>1</sup>; <sup>1</sup>MEDA engineering and technical services; <sup>2</sup>GM Global Research & Development

Mg if alloyed with Ti may become corrosion resistant. This hypothesis is verified in this study. Mg<sub>1-x</sub>Ti<sub>x</sub> alloy thin films (with x=0, 0.2, 0.4, 0.6, 0.8 and 1) were deposited by dc magnetron sputtering onto glass substrate. Film compositions were identified by electron probe micro-analyzer (EPMA). The corrosion properties of these alloys were characterized in saturated Mg(OH)<sub>2</sub> solutions with and without 0.1 M NaCl. The morphology of the thin film alloys was compared before and after polarization and immersion test. Polarization results showed that the corrosion resistance of the alloy was improved with increasing Ti content. No material loss and corrosion damage was observed for alloys with 80% or more Ti content in both solutions.

**Structure and Mechanical Properties of Magnesium-Titanium Solid Solution Thin Film Alloys Prepared by Magnetron-Sputter Deposition:** *Daad Haddad*<sup>1</sup>; *Guang-Ling Song*<sup>2</sup>; *Yang-Tse Cheng*<sup>3</sup>; <sup>1</sup>MEDA Engineering and Technical Services LLC; <sup>2</sup>GM Global Research & Development; <sup>3</sup>Chemical and Materials Engineering, University of Kentucky

The mechanical properties of Mg<sub>1-x</sub>Ti<sub>x</sub> thin film alloys, with x=0, 0.2, 0.4, 0.6, 0.8 and 1, were obtained using nanoindentation. The Mg-Ti alloys were deposited by dc magnetron sputtering on Si substrates. EPMA was used to determine the film compositions. XRD measurements showed that single phase magnesium-titanium solid solutions were obtained across the full range of magnesium and titanium mixtures. The topography and the rms roughness of the different alloys were studied using AFM. The mechanical properties of the Mg<sub>1-x</sub>Ti<sub>x</sub> thin films were determined by analyzing the load-displacement traces based on the Oliver-Pharr method. The nanoindentation results show that both the elastic modulus and hardness of the Mg<sub>1-x</sub>Ti<sub>x</sub> alloy thin films are higher than those of conventional Mg alloys.

**The Influence of Sol-Gel Coatings on the Corrosion Resistance of Magnesium and AZ91D:** *Daniela Zander*<sup>1</sup>; *Anna Pipetz*<sup>1</sup>; <sup>1</sup>TU Dortmund

The low corrosion resistance of magnesium alloys is known to limit significantly the application area. Among others the sol-gel process is a promising coating method to improve the corrosion of magnesium alloys. The aim of the present study is to investigate the influence of surface pre-treatments and subsequent sol-gel processing on the corrosion resistance of magnesium and die-cast AZ91D. The sol-gel coating was prepared by an acid catalyzed sol-gel process using Methyltriethoxysilan as a major compound. Various etching procedures were used to improve the adhesion between material and coating. The corrosion resistance was investigated by immersion tests and electrochemical methods in pH7 without and with NaCl. The etching and coating procedure was characterized by SEM and TEM. A strong influence of the microstructure on the etching procedure and on the adhesion of the coating was observed. A significant decrease of the corrosion rate was obtained by applying the sol-gel coating.

**Effect of Adding SiO<sub>2</sub>-Al<sub>2</sub>O<sub>3</sub> Sol into Anodizing Bath on Corrosion Resistance of Oxidation Film on Magnesium Alloy:** *Huicong Liu*<sup>1</sup>; *Liqun Zhu*<sup>1</sup>; *Weiping Li*<sup>1</sup>; <sup>1</sup>Beihang University, Key Laboratory of Aerospace Materials and Performance (Ministry of Education), School of Materials Science and Engineering

In order to extend the application area of magnesium alloy, many methods such as sol-gel, anodic oxidation, plating, micro-arc oxidation have been researched, each method has its own specialties and disadvantages. In this paper, three kinds of films were made on magnesium alloy by anodic oxidation together with sol-gel method. The first one named as anodic oxidation film was prepared by anodic oxidation in the usual alkaline solution, the second one named as multiple film was prepared by coating SiO<sub>2</sub>-Al<sub>2</sub>O<sub>3</sub> sol on the samples and heat-treating before anodic oxidation, the third one named as modified oxidation film was prepared by anodic oxidation in the usual alkaline solution added by 5%(vol) SiO<sub>2</sub>-Al<sub>2</sub>O<sub>3</sub> sol. Corrosion resistance, thickness, surface morphologies of the films were studied. The results showed that, compared with anodic oxidation film and multiple film, the modified oxidation film has the biggest thickness, has the most even and compact configuration, and thus it owns best corrosion resistance. Silicon and aluminum in the sol acted in the process of forming the modified oxidation film, and resulted in improving of comprehensive abilities of magnesium alloy samples.

**Effect of Zirconium Oxide on Corrosion Properties of Mg Alloy Subjected to Plasma Electrolytic Oxidation:** *In Jun Hwang*<sup>1</sup>; *Byung Uk Lee*<sup>1</sup>; *Young Gun Ko*<sup>2</sup>; *Dong H. Shin*<sup>1</sup>; <sup>1</sup>Hanyang University; <sup>2</sup>Yeungnam University

In current automobile and electronic industries, the use of magnesium alloys where energy and weight saving are attainable is increasing. Despite their light weight, there has been an inherent drawback arising from the surface vulnerable to be oxidized with ease, specifically under corrosive environments. To protect magnesium alloys from corrosion, the present work deals with the electrochemical response of the oxide layer on magnesium alloy specimen prepared by plasma electrolytic oxidation (PEO) method in an electrolyte containing zirconia powder. Surface observation evidences that a number of zirconia particles are effectively incorporated into oxide layer, resulting in higher oxidation resistance. This is a result of micro-arc during PEO treatment in spite of no polarization of zirconia. From the results of potentiodynamic tests in 3.5% NaCl solution whose pH is 7.8, corrosion behavior of the PEO-treated magnesium alloy is also discussed in relation to Stern-Geary equation.

**Weight Function and Stress Intensity Factors of Friction Stir Spot Welds of Magnesium AZ31 Alloy:** *Tian Tang*<sup>1</sup>; *Mark F. Horstemeyer*<sup>2</sup>; *Brian Jordan*<sup>2</sup>; *Paul Wang*<sup>2</sup>; <sup>1</sup>Mississippi State University; <sup>2</sup>National Chung Hsing University

Weight functions were derived for the critical points of friction stir spot welds. Both cases, namely, infinitesimal kinked crack and finite kinked crack were considered. These weight functions were developed based on the general format proposed by Fett et al. (2004). The unknown constants in these



equations were determined from reference stress intensity factors obtained from the three dimensional finite element computations. The accuracy and validity of these equations were verified using finite element results.

**Friction Stir Welding of Magnesium Alloy AZ31B-H24 Rolled Plate:** Richard DeLorme<sup>1</sup>; Jonathan Perrett<sup>2</sup>; Bruce Davis<sup>1</sup>; Kyu Cho<sup>3</sup>; <sup>1</sup>Magnesium Elektron North America; <sup>2</sup>TWI; <sup>3</sup>Army Research Laboratory

Magnesium Elektron North America (MENA) produces AZ31B-H24 rolled plate for many different applications. Although alloy AZ31B is weldable by traditional fusion welding methods, optimal friction stir welding (FSW) parameters for the required thickness of some applications have not been previously published. As such, MENA enlisted TWI to develop tooling and optimal FSW parameters for producing single-pass butt joints on MENA's 1.5 inch thick AZ31B-H24 plate. TWI also produced and delivered butt-jointed panels representing the optimal process; and, MENA and US Army Research Laboratory (ARL) have tested and evaluated the plate for strength and terminal ballistic performance. The present work describes the process and resulting optimal parameters developed by TWI and the MENA/ARL testing and evaluation results.

**Monotonic and Fatigue Behavior of Mg AZ31 in Friction Stir Spot Welds: An International Benchmark Test in the "Magnesium Front End Research and Development" Project:** B Badarinarayan<sup>1</sup>; S Behraves<sup>2</sup>; S Bhole<sup>3</sup>; D Chen<sup>3</sup>; H Patel<sup>3</sup>; M Horstemeyer<sup>4</sup>; H Jahed<sup>2</sup>; J Jordan<sup>5</sup>; S Lambert<sup>2</sup>; X Su<sup>6</sup>; Y Yang<sup>7</sup>; <sup>1</sup>Hitachi America Limited; <sup>2</sup>University of Waterloo; <sup>3</sup>Ryerson University; <sup>4</sup>Mississippi State University; <sup>5</sup>The University of Alabama; <sup>6</sup>Ford Motor Co; <sup>7</sup>Institute for Metals Research

This paper presents the experimental results of benchmark coupon testing of monotonic and cyclic conditions on friction stir spot welded coupons of Mg AZ31 alloy. The results presented here are a product of a collaborative multinational research effort involving research teams from Canada, China, and the United States. Fatigue tests were conducted in load control at R=0.1 at two different maximum loads: 1kN and 3kN. Good agreement was found between the participating labs regarding the number of cycles to failure. Differences in the failure modes were observed for the two different loading conditions tested. At the higher load, fatigue failure was caused by interfacial fracture. However, at the lower load, fatigue cracks formed perpendicular to the loading direction, which led to full width separation. For additional comparison, the monotonic and cyclic results of the friction stir spot welds are compared to resistance spot welded coupons of similar nugget size.

## Materials Processing Fundamentals: Poster Session

*Sponsored by:* The Minerals, Metals and Materials Society, TMS Extraction and Processing Division, TMS: Process Technology and Modeling Committee

*Program Organizers:* Prince Anyalebechi, Grand Valley State University; Srikanth Bontha, Temple University

Sun PM-Tues PM  
Feb 27-Mar 1, 2011

Room: 12  
Location: San Diego Conv. Ctr

*Session Chair:* Prince Anyalebechi, Grand Valley State University

**Change of Iron Content in Metal Pad and Potling Failure during Start-up Period of Aluminum Reduction Cells:** Yongliang Wang<sup>1</sup>; Jilai Xue<sup>1</sup>; Jun TIE<sup>1</sup>; <sup>1</sup>University of Science and Technology Beijing

Iron content in metal pad in aluminum reduction cell is very important indication for pot lining failure during cell start-up period. Usually, higher iron content may indicate a leakage occurring in the potlining. If the lining failure could be detected in its early time, it might be possible to take action to limit further damage. In this paper, the change of the iron content in metal pad in aluminum reduction cell has been investigated to develop a method for possible early detection of potlining failure. It is found that the dispersed

degree of the iron content' fluctuation in the cell start-up of period can reflect potlining leakage in the future to some extent. For instance, when seven consecutive measurements of iron content above the center line(CL), or six consecutive measurements showing a rise trend, or the measurements beyond the upper center line(UCL), the cell is going to break down.

**Preparation and Characterization of Porous Ni-Ti Alloys:** Luxing Feng<sup>1</sup>; Jilai Xue<sup>1</sup>; Jun Zhu<sup>1</sup>; Yuanling Gao<sup>1</sup>; Chen Dong<sup>1</sup>; <sup>1</sup>University of Science and Technology Beijing

Porous Ni-Ti alloy has many applications in a wide range of engineering areas. The porous NiTi alloys were prepared from Al and Ni powders in sintering process under argon atmosphere. The major chemical compositions of the sintered Ni-Ti body were NiTi, Ni<sub>2</sub>Ti<sub>4</sub>O and Ni<sub>2</sub>Ti, respectively. The internal pore structures were characterized by image analysis technique, which were dependent on various processing parameters such as sintering temperature, amount of pore-forming agent, forming pressure, etc. The results show that the porous alloy samples had the characteristics of uniform pore and high open porosity; pore-forming agent and sintering temperature are important factors in porous; pressure affected the sintered products' pore, by affecting the combination of alloy powder with pore-forming agent.

**Production Technology of Cored Wire Used For Liquid Metal Treatment in Steel Plants (Part-I):** Pradeep Kumar Maitra<sup>1</sup>; <sup>1</sup>Dipaly Consultants

Structurally the CW is made up of two components only i.e. a steel jacket and an additive core. CW is produced by roll forming the steel strip into a tube (9 to 13mm diameter) which is simultaneously filled with additives and sealed longitudinally and wound on a cable drum, CW is used for metal cleaning, alloying, inoculating, nodularizing etc. The performance of the CW depends on its quality and method of its application. For quality assessments the CW users have to get familiarized with CW metallurgy, chemistry of additive-metal inter-action, etc to develop their internal standards. In this context following matter has been discussed in this presentation. Liquid metal chemistry, genesis of CW, morphology of CW, quality of steel strip and additives, mill configuration, CW manufacturing process, quality of CW and recommendations. Hope the article will be useful for both users and producers of CW.

**Recent Improvements at Mount Isa Copper Smelter:** Pengfu Tan<sup>1</sup>; <sup>1</sup>Xstrata Copper

Xstrata Copper Smelter at Mount Isa in Australia has operated one copper Isasmelt furnace, two Rotary Holding Furnaces (RHF), four Peirce-Smith P-S converters, two anode furnaces, one casting wheel, slag crushing and screening plant, and ESP dust recovery plant. Some recent technical improvements have been presented in this paper: 1) Development of smelting and converting process models, slag chemistry models and slag viscosity model 2) Reduction of copper loss in RHF slag 3) Reduction of converter foamover frequency 4) Improvements of smelter reporting system 5) Development of throughput model 6) Improvement of yields and throughput 7) Lab test works for ESP dust recovery process 8) ESP dust recovery plant trials, commissioning and operations 9) Slag slow cooling trial and improvement of slag milling recovery 10) Improvement of Isasmelt brick campaign life 11) Improvement of separation efficiency of Slag Crushing and Screening Plant

**Surface Treatment of Aluminum Alloys by Atmospheric Plasma Arc Discharge:** Mehdi Asgharifar<sup>1</sup>; Rouzbeh Sarrafi<sup>1</sup>; Radovan Kovacevic<sup>1</sup>; <sup>1</sup>Research Center for Advanced Manufacturing, Southern Methodist University

The surface treatment of aluminum alloys using atmospheric-pressure low intensity DC plasma arc discharge is investigated in terms of surface properties. Despite the conventional surface treatment process for aluminum alloys based on chemical process, this process is very environmental-friendly and economic. The effect of two processing parameters, the current and the plasma torch scanning speed, on the surface morphology was studied by using scanning electron microscope. The effects of cathode spots within the tested range of process parameters were determined, and the limiting factors of the process (such as surface cracking) were discussed. The topographical

studies of the treated surfaces have suggested potential enhancement of surface properties in different applications.

**Ultrasound-Assisted Electrolysis in NaOH Solution for Hydrogen Generation:** Jigang Li<sup>1</sup>; Jilai Xue<sup>1</sup>; Zhenjun Chen<sup>1</sup>; Lei Zhang<sup>1</sup>; Yifang Zheng<sup>1</sup>; Jun Zhu<sup>1</sup>; <sup>1</sup>University of Science and Technology Beijing

Water electrolysis in 0.4 M NaOH solution for hydrogen generation was carried out with ultrasound introduced through the anode. It was found that the cell voltage reduced by 150-250 mV in the current range of 20 mA to 40 mA with ultrasound frequency at 25.3 Hz. The cell operation became unstable when the cell current was larger than 75 mA with ultrasound. This reduction in cell voltage was due to removal of the gas bubbles on the electrode surface, which can be directly observed in the see-through cell of water electrolysis. Ultrasound with frequency of 33.3 Hz was also tried, but no better effect was obtained. The results suggest that ultrasound assisted water electrolysis can have potential in energy savings for hydrogen production.

## Microstructural Processes in Irradiated Materials: Poster Session

*Sponsored by:* The Minerals, Metals and Materials Society, TMS Structural Materials Division, TMS/ASM: Nuclear Materials Committee

*Program Organizers:* Gary Was, University of Michigan; Thak Sang Byun, Oak Ridge National Laboratory; Shenyang Hu, Pacific Northwest National Laboratory; Dane Morgan, UW Madison; Yasuyoshi Nagai, Tohoku University

Sun PM-Thurs PM  
Feb 27-Mar 3, 2011

Room: 3  
Location: San Diego Conv. Ctr

*Session Chairs:* Dane Morgan, University of Wisconsin; Yasuyoshi Nagai, Tohoku University; Shenyang Hu, Pacific Northwest National Laboratory

**Characterization of Swift Heavy Ion and Proton Damage in CeO<sub>2</sub>:** Peng Xu<sup>1</sup>; Tony Schulte<sup>1</sup>; Todd Allen<sup>1</sup>; <sup>1</sup>University of Wisconsin

The material response to irradiation is of prime importance for fuel property prediction. The focus in this study is to investigate radiation damage in CeO<sub>2</sub>, a fluorite type material which serves as a surrogate for UO<sub>2</sub>. Due to the similarities in their structures and physical properties, the knowledge learned in CeO<sub>2</sub> is of value for understanding the radiation damage mechanisms in fluorite type compounds such as UO<sub>2</sub>. To simulate fission fragments damage, 300 and 1000 MeV Au ions were used to irradiate CeO<sub>2</sub> to fluences from 1010 to 5x10<sup>12</sup> /cm<sup>2</sup> as well as 2.6 MeV protons to doses up to 1 dpa. The structure and microstructure evolution of the irradiated CeO<sub>2</sub> as a function of ion fluences was characterized using Raman spectroscopy, glancing angle XRD and HRTEM. The chemistry of the tracks was studied using local electrode atom probe. Structure recovery under thermal annealing will be discussed.

**Growth Behavior of Dislocation Loops in CeO<sub>2</sub> Irradiated with Krypton:** Bei Ye<sup>1</sup>; Jeffrey Rest<sup>2</sup>; Jerome Jonnet<sup>3</sup>; Wei-Ying Chen<sup>1</sup>; Mark Kirk<sup>2</sup>; Abdellatif Yacout<sup>2</sup>; James F. Stubbins<sup>1</sup>; <sup>1</sup>University of Illinois at Urbana-Champaign; <sup>2</sup>Argonne National Laboratory; <sup>3</sup>Delft University of Technology

Irradiation damage processes in UO<sub>2</sub> are studied by simulation of ion irradiation of CeO<sub>2</sub>, which shares the same fluorite structure. *In-situ* transmission electron microscopy is performed on a single crystal CeO<sub>2</sub> thin foil bombarded with 1MeV Kr at 800°C to an accumulated dose of 5x10<sup>15</sup> ions/cm<sup>2</sup>. Sequential change of defect microstructure is recorded as a function of dose. Qualitative assessment of dislocation loop growth is achieved by measuring loop diameter and density at varied dose levels. In order to interpret the combined effects of irradiation-induced re-resolution and coalescence on the kinetics of loop growth, a chemical rate theory based model is employed to calculate the evolution of the dislocation loop size distribution. In addition, the contribution of the evolving interstitial loop population to the change in CeO<sub>2</sub> lattice parameter is assessed, and estimates

of loop coalescence and re-resolution rates based on *in-situ* observation are discussed.

**Stoichiometric Dependence of Oxygen Diffusivity in La<sub>x</sub>Ce<sub>1-x</sub>O<sub>2-x/2</sub>:** Aaron Oaks<sup>1</sup>; Di Yun<sup>1</sup>; Bei Ye<sup>1</sup>; Wei-Ying Chen<sup>1</sup>; James Stubbins<sup>1</sup>; <sup>1</sup>University of Illinois, Urbana-Champaign

To study the stoichiometric dependence of oxygen diffusivity in fluorite-type mixed oxide nuclear fuels (UPuO<sub>2</sub>), a generalized Kinetic Monte Carlo code was developed and demonstrated on the surrogate material La<sub>x</sub>Ce<sub>1-x</sub>O<sub>2-x/2</sub>. Molecular Statics simulations were performed using interatomic potentials for cerium oxide provided by Gotte et al., Minervini et al. and Sayle et al. to calculate local configuration-dependent oxygen vacancy migration energies. Kinetic Monte Carlo simulations of oxygen vacancy diffusion were performed at varying lanthanum dopant concentrations (x=0 to x=0.33) using the developed generalized Kinetic Monte Carlo code and the calculated configuration-dependent migration energies. All three interatomic potentials were found to confirm the lanthanum trapping effect. The results of the simulations were compared with experimental data and the Gotte potential was concluded to yield the most realistic diffusivity curve.

**Irradiation Behavior of the Interaction Product of U-Mo Fuel Particle Dispersion in an Al Matrix:** Yeon Soo Kim<sup>1</sup>; Gerard Hofman<sup>1</sup>; <sup>1</sup>Argonne National Laboratory

The irradiation behavior of the interaction product in U-Mo fuel particle dispersion in an Al matrix is that of a typical amorphous material. At high burnup, large-scale pores form in the interaction layer, which can lead to a potential fuel failure. Addition of a small amount of Si in the matrix Al was shown to be effective to suppress the interaction layer growth and pore formation in the interaction layer. Analyses of microstructures of the irradiated samples with and without a Si addition are presented. A comparison with other dispersion fuel systems such as U-Si intermetallic particles in an Al matrix and U-Al intermetallic particles in an Al matrix, the interaction layers of which are also amorphous, is provided.

**Atomistic Validation of Kinetic Methodology via Multiscale Simulation of Nuclear Fuels:** Z. Insepov<sup>1</sup>; J. Rest<sup>1</sup>; G. Hofman<sup>1</sup>; A. Yacout<sup>1</sup>; A.Yu. Kuskun<sup>2</sup>; G.E. Norman<sup>2</sup>; S.V. Starikov<sup>2</sup>; V.V. Stegailov<sup>2</sup>; A.V. Yanilkin<sup>2</sup>; <sup>1</sup>Argonne National Laboratory; <sup>2</sup>Joint Institute for High Temperatures

A new approach for gas-driven swelling of fuels is under development based on the kinetic theory of defect accumulation, interaction, and growth of cavities during irradiation. This multiscale formulation will be used to assess the impact of elemental defect kinetics on important nuclear fuel performance parameters. Our new concept introduces an Ab-initio force matching method combined with atomistic molecular dynamics (MD) simulation for calculation of the defect energies, atomistic configurations, interatomic potentials, the elemental processes and reactions, and the kinetic coefficients that are applicable to high burn-up nuclear materials. The models include the interaction of the fission gas and gas filled bubbles with irradiation-induced dislocation loops. The equations describing the evolution of the vacancy, interstitial, interstitial loop and, fission gas concentrations contain materials dependent parameters such as the rate coefficients for radiation defects and gas atoms. This approach allows direct comparison of the analysis to in-reactor experimental data.

**Application of Phase-Field Method in Predicting the Kinetics of Microstructure Evolution in Irradiated Materials:** Yulan Li<sup>1</sup>; Shenyang Hu<sup>1</sup>; Chuck H. Henager Jr<sup>1</sup>; Fei Gao<sup>1</sup>; Xin Sun<sup>1</sup>; Mohammad A. Khaleel<sup>1</sup>; <sup>1</sup>Pacific Northwest National Laboratory

There are multiple microstructural processes taking place in fuel and cladding materials including generation/migration of defects and fission products, defect recombination/annihilation and emission/resolution, nucleation/growth/coalescence of gas bubbles and voids, precipitation of second-phase particles, and grain growth. These processes lead to structural instability such as swelling and cracking as well as mass/heat transport and thermo-mechanical property changes. A fundamental understanding of these processes and developing the capability to predict microstructure evolution in three-dimensions (3D) and property evolution are critical to the design of

nuclear reactor components as well as the optimization of nuclear reactor operation. The phase-field method based on the fundamental thermodynamic and kinetic information is a powerfully computational approach at the meso-scale for predicting phase stability and microstructural evolution kinetics. This talk will discuss the application of the phase-field approach coupling atomic mechanisms in predicting the microstructure evolution in irradiated materials that are far from equilibrium. Some results on volume swelling, void migration, void lattice formation, gas bubble nucleation and evolution will be presented to demonstrate the successful applications.

**Atomic-Scale Modeling of the Sliding Behavior of {110} Twist Grain Boundaries in Alpha-Iron:** *Jinbo Yang*<sup>1</sup>; Yuri Osetsyki<sup>1</sup>; Roger Stoller<sup>1</sup>; <sup>1</sup>ORNL

Grain boundary sliding (GBS) plays an important role in the plastic deformation and fracture of polycrystalline materials used in nuclear applications. Great attention is therefore paid to understanding factors affecting GB sliding such as segregation, modification under irradiation etc. In this paper we present first results on atomic-scale properties of twist grain boundaries (TGB) in iron. Molecular statics was applied to study structure and sliding TGB of different twist angles  $T$  at zero temperature. The structure of TGB in {110} plane with  $T < 120^\circ$  presents a network of intersecting screw dislocations segments with Burgers vectors  $\frac{1}{2}\langle 111 \rangle$  and  $\langle 100 \rangle$ . The resolved stress for sliding depends on the twist angle and can drop down to the value below the Peierls stress for an edge dislocation. The results are compared with available experimental observations. This work will be continued to investigate the effect of radiation induced defects and impurity segregation on sliding process.

**Helium Sequestration in Oxide Dispersion Strengthened Steels from First-Principles:** *Paul Erhart*<sup>1</sup>; Jaime Marian<sup>1</sup>; <sup>1</sup>Lawrence Livermore National Laboratory

Oxide dispersion strengthened steels have been proposed for structural components in next generation nuclear reactors in part thanks to their larger tolerance to He induced swelling than their oxide-free counterparts. Here, we explore this behavior by means of quantum-mechanical calculations. To this end, we have studied the properties of He-related point defects in several characteristic oxides within density functional theory using both conventional and hybrid exchange-correlation functionals. We find that He interstitials have very low formation energies compared to Fe, and He does not bind to intrinsic vacancies. Our results indicate that there is a strong thermodynamic driving force for storing He inside the oxide particles that should thus serve as volumetric sinks. We discuss the effect of the formation of a metal-oxide interface on the thermodynamic properties of the oxide particles and their ability to store helium.

**Small Scale Mechanical Testing and Atom Probe Analysis on New Materials for Nuclear Applications:** *E. Stergar*<sup>1</sup>; P. Hosemann<sup>1</sup>; A.T. Nelson<sup>2</sup>; Y.Q. Wang<sup>2</sup>; S.A. Maloy<sup>2</sup>; <sup>1</sup>UC Berkeley; <sup>2</sup>Los Alamos National Laboratory

Nanostructured alloys like ODS steels contain a high density of (oxide) precipitates providing outstanding high temperature properties and remarkable radiation tolerance. It has been shown that proper heat treatment of specialized tool steels (maraging steels) lead to the formation of coherent nm sized fine dispersed intermetallic precipitates with a number density of  $10^{23}$ - $10^{24}$  m<sup>-3</sup>. These precipitates are formed by solution annealing and a subsequent heat treatment. Therefore the formation of nm sized precipitates does not require a mechanical alloying step. In this work the concept of utilizing intermetallic precipitates and their effectiveness as defect sinks or He traps is explored. In this study Ion beam irradiations were performed to cause significant radiation damage and He implantation. High resolution post irradiation examination (nano indentation, TEM, atom probe) was used to assess the materials properties and micro structural changes on two commercially available maraging steels.

**TEM Characterization of the Structure and Composition of Nanofeatures and Oxides in Nanostructured Ferritic Alloys:** *Yuan Wu*<sup>1</sup>; Nicholas Cunningham<sup>1</sup>; George Odette<sup>1</sup>; Erich Stergar<sup>1</sup>; Auriane Etienne<sup>1</sup>; Erin Haney<sup>1</sup>; <sup>1</sup>UCSB

The structure and composition of the complex Ti-Y oxides in the nanostructure ferrite alloys (NFA) MA957 and model NFA 14YWT were characterized by high-resolution transmission electron/scanning electron microscopy (HRTEM/STEM) and energy dispersive X-ray (EDX). HRTEM fast Fourier transform diffraction show that some of the intermediate sized precipitates (5 to 15 nm) are consistent with orthorhombic Y<sub>2</sub>TiO<sub>5</sub>, while other vary from any known Y-Ti oxides. The EDX compositions of these features range from about 0.4 to 2, and differ slightly between French and US heats of MA957. About 20% of oxides in the 14YWT alloy show Y/Ti greater than 2, while about 80% show Y/Ti less than 2.0. FFT and powder diffraction measurements show that the smaller precipitates are generally consistent with cubic Y<sub>2</sub>Ti<sub>2</sub>O<sub>7</sub>, with EDX Y/Ti ~ 1.0. Results of high angle annular dark field (HAADF) TEM measurements of the size distribution and morphology of phases in NFA are also described.

**Effect of Grain Size and Grain Boundaries on the Proton Irradiation Response of Nanostructured Austenitic Model Alloy:** *Yong Yang*<sup>1</sup>; Cheng Sun<sup>2</sup>; Xinghang Zhang<sup>2</sup>; Allen Todd<sup>1</sup>; <sup>1</sup>University of Wisconsin-Madison; <sup>2</sup>Texas A&M University

A steel with nanometer-sized grain structure has the possibility to provide radiation resistance by increasing the grain boundary length and subsequently providing a greater amount sinks for absorbing mobile defect. Optimizing the type of boundary to include a greater number of sinks might further improve the radiation resistance. A model austenitic alloy was processed using the equal channel angular pressing (ECAP) method for eight passes at 500 °C to obtain an average grain size of ~360 nm. Grain boundary engineering (GBE) was then applied to optimize the grain boundary character distribution (GBCD) by promoting a higher population of low  $S$  grain boundaries. The effect of grain refinement and GBE on the radiation response was studied using a 2 MeV proton irradiation at 400 °C to dose up to 3 dpa. The irradiated microstructures was examined using transmission electron microscopy (TEM), and irradiation induced hardening was studied using Vickers hardness test.

**Friction Stir Welding and Irradiation Effects of Oxide Dispersion Strengthened Alloys:** *Chun-Liang Chen*<sup>1</sup>; Asta Richter<sup>2</sup>; R. Kögler<sup>3</sup>; L.T. Wu<sup>4</sup>; <sup>1</sup>Department of Materials Science and Engineering, I-Shou University, Kaohsiung 840, Taiwan; <sup>2</sup>Department of Engineering, Technical University of Applied Sciences Wildau, Bahnhofstrasse 1, 15745 Wildau, Germany; <sup>3</sup>Institute of Ion Beam Physics and Materials Research, Research Center Dresden-Rossendorf (FZD), Bautzner Landstraße 400, 01328 Dresden, Germany; <sup>4</sup>Met Ind Res & Dev Ctr, Kaohsiung 811, Taiwan

Nanostructured oxide dispersion strengthened (ODS) Fe-based alloys have potential for application in fission/fusion power plant materials, particularly in the use of a first-wall and blanket structure of a next generation reactor. These steels usually contain a high density of Y-Al-O nanoparticles. Structural analysis including HRTEM shows the chemical composition of the Y-Al-O oxides. Friction stir welding (FSW) is a very promising technique for the joining of ODS materials without oxide particle agglomeration and loss in mechanical properties in the weld zone. In this study, irradiation of these alloys was performed with a Fe+/He+ dual beam irradiation. Irradiation causes atomic displacements resulting in vacancy and self-interstitial lattice defects and dislocation loops. SRIM calculations for ODS steel indicate a clear separation between the vacancy distribution close to the surface and the interstitials in deeper layers of the material surface. The helium atoms will mainly accumulate in the vacancies.

**Stress Relaxation Behavior of Ferritic ODS Alloys:** *Jeoung Han Kim*<sup>1</sup>; Thak Sang Byun<sup>1</sup>; David T. Hoelzer<sup>1</sup>; <sup>1</sup>Oak Ridge National Lab

Stress relaxation (SR) has been investigated for the particle-strengthened steels including nanostructured ferritic alloy 14YWT(SM10), ODS Eurofer97, and commercial PM2000. The SR tests were carried out at temperatures ranging from 600 to 1000°C. The relaxation rates of 14YWT



and ODS Eurofer97 were lower than that of PM2000. Up to 700°C the activation energies of the three alloys were in a narrow range of 35 ~ 40 b<sup>3</sup>. Above 700°C, however, the activation energy of PM2000 and ODS Eurofer97 increased abruptly with test temperature while that of 14YWT showed relatively lower temperature dependence. To analyze the strain rate sensitivity of the alloys, the load drop-time curves were converted to the stress-strain rate curves. In the log-log plots of these curves no significant change in slope was observed in the strain rate range of 2×10<sup>-5</sup> ~ 10<sup>-3</sup>/sec. Rate-controlling mechanism for the three alloys was dislocation glide and climb process.

**Role of Microstructural Defect on Radiation Hardening of Ion Irradiated Fe-Cr Binary Alloys:** *Hyung-Ha Jin*<sup>1</sup>; Chansun Shin<sup>1</sup>; Junhyun Kwon<sup>1</sup>; <sup>1</sup>Korea Atomic Energy Research Institute

The role of microstructural defects on radiation hardening of Fe-Cr binary alloys was investigated using transmission electron microscopy. The experimental specimens were irradiated with 8MeV Fe ions at room temperature up to 5.8E14 ion/cm<sup>2</sup> (~1dpa at peak damage depth). Nano indentation result showed that radiation hardening of Fe-15Cr alloy was significantly larger than that of Fe-5Cr alloy. TEM observation showed that nanometer sized black dots were observed in both Fe-5Cr and Fe-15Cr alloy. On the other hands, some coffee bean contrasts were observed under the 020 reflection in only Fe-15Cr alloy, which were identified with <100> dislocation loops. By means of in-situ strain TEM technique, we will analyze the change of defects in ion irradiated Fe-Cr alloys during interaction with moving dislocation to understand radiation hardening behavior in Fe-Cr binary alloys.

**Nanoindentation at Elevated Temperature on Ion Beam Irradiated Advanced Structural Alloys for Nuclear Applications:** *Peter Hosemann*<sup>1</sup>; Adrian Harris<sup>2</sup>; Yongqiang Wang<sup>3</sup>; Stuart Maloy<sup>3</sup>; <sup>1</sup>UC Berkeley; <sup>2</sup>Micro Materials; <sup>3</sup>Los Alamos National Laboratory

In the past several years small scale material testing methodologies have been developed to investigate mechanical property changes as a result of ion irradiation. Specifically, micro hardness, nano indentation, micro and nano compression measurements were performed to investigate the basic processes of materials deformation and the effects of ion irradiation upon these processes. In this work we applied nano indentation experiments on ion beam irradiated samples at room temperature and elevated temperatures. Besides simple indentation also indentation creep experiments were performed. We learned that the irradiation significantly increased near-surface indentation creep rates and hardness of the selected oxide dispersion strengthened alloys studied here. While long term high temperature behavior was not measured, this study gives us an important insight into how defect mobility supports dislocation movement in the alloy of interest.

**Ab Initio Calculations on FeNiCr Model Austenitic Alloys: Chemical and Magnetic Disorder Treatment:** *Jean-Baptiste Piochaud*<sup>1</sup>; Charlotte Becquart<sup>1</sup>; Christophe Domain<sup>2</sup>; <sup>1</sup>CNRS; <sup>2</sup>EDF-R&D

Under irradiation, in austenitic steels, the microstructure and microchemistry evolution due to radiation induced segregation (RIS) can lead to a degradation of the mechanical properties. In order to better predict this evolution, a multiscale modelling approach is developed within the PERFORM60 project. The objective of our work is to simulate RIS at the atomic level in model FeNiCr alloys by an Atomic Kinetic Monte Carlo (AKMC) approach. For this purpose a suitable set of data is needed to build a cohesive model in the AKMC for both configurational and migration energies. We use Density Functional Theory which allows to determine accurate input interaction and migration energies. The FeNiCr paramagnetic alloys are modelled by considering both structural and magnetic disorder based on quasi-random structures. Their stability and magnetic ground state will be analysed and discussed. Some elementary properties (defect formation energies) will also be presented.

**Response of 321 Analog Austenitic Stainless Steel Microstructure of Reactor Core Internals to Neutron Irradiation in VVER-440:** *Jan Michalicka*<sup>1</sup>; <sup>1</sup>Nuclear Research Institute Rez plc.

This paper surveys analysis of radiation-induced microstructure defects in reactor core internals of VVER-440 Greifswald's reactor, decommissioned after 15 years of service. Studied material was irradiated to 2.4, 5.2 and 11.4 dpa and irradiation temperatures was between 270-400°C, and depended on the location of the particular component, namely the core barrel, core shroud basket, baffle and baffle bolts. Each of the components was made of Ti-stabilized austenitic stainless steel 08Ch18N10T. The irradiated microstructure revealed characteristic radiation defects: Frank loops, cavities and precipitates. Frank loops were saturated in all cases, excepting the core barrel. Cavities density and size distribution revealed strong dependence on temperature. Nano-cavities appeared at 270°C already and relatively significant cavities formation revealed at higher temperatures. Precipitates were minor, in form of G-phase. A baffle bolt was investigated along its longitudinal axis to assess the dependence of temperature gradient on radiation defects. Microhardness was measured in the same direction.

**Evolution of Radiation-induced Precipitates in Proton-irradiated HCM12A:** *Zhijie Jiao*<sup>1</sup>; Gary Was<sup>1</sup>; <sup>1</sup>University of Michigan

Ferritic-martensitic (F-M) alloy HCM12A is one of the candidates for cladding and structural materials in fast fission and fusion reactors. However, radiation-induced precipitates may cause serious hardening and embrittlement in this alloy. In this study, HCM12A was irradiated to 3, 7 and 10 dpa at 400 and 500/176C using 2 MeV protons. Radiation-induced precipitates were characterized using atom probe tomography. Preliminary results have showed that Ni/Si/Mn-rich, Cu-rich and Cr-rich precipitates form under irradiation and they are temperature dependent. The evolution of radiation-induced precipitates with irradiation dose and temperature in HCM12A will be presented and discussed.

**Examination of Precipitates in T91 and HCM12A Alloy by the Replica Extraction Technique:** *Liang Chen*<sup>1</sup>; Vani Shankar<sup>1</sup>; Zhijie Jiao<sup>1</sup>; Lumin Wang<sup>1</sup>; Gary Was<sup>1</sup>; <sup>1</sup>University of Michigan

Replica extraction of precipitates has been done on T91 and HCM12A alloys for analytical TEM examination. Precipitates are found to be of several different morphologies, ranging from rectangle to sphere. Three different types of precipitates have been observed in the replica obtained from the T91 alloy. The larger and most abundant of these precipitates are the M<sub>23</sub>C<sub>6</sub> type, accompanied by a small fraction of V-rich and Nb-rich precipitates in smaller size (<100 nm). Only M<sub>23</sub>C<sub>6</sub> precipitates are found in the HCM12A replica. The compositions of different precipitates are analyzed in detail using energy dispersive x-ray spectroscopy (EDS). Results from proton irradiated T91 samples with irradiation doses up to 100 dpa will be presented and compared with that from the unirradiated samples. The radiation effects on the evolution of precipitate size and composition will be discussed.

**Effects of Irradiation Dose on Microstructural Evolution and Hardening of High- and Low-Cu Reactor Pressure Vessel Steels:** *Akira Kuramoto*<sup>1</sup>; Tomoaki Takeuchi<sup>2</sup>; Takeshi Toyama<sup>1</sup>; Yasuyoshi Nagai<sup>1</sup>; Masayuki Hasegawa<sup>3</sup>; Toshimasa Yoshiie<sup>4</sup>; Nishiyama Yutaka<sup>2</sup>; <sup>1</sup>International Research Center for Nuclear Materials Science, Institute for Materials Research, Tohoku University; <sup>2</sup>Japan Atomic Energy Agency; <sup>3</sup>Institute for Materials Research, Tohoku University; <sup>4</sup>Research Reactor Institute, Kyoto University

Microstructural evolution and mechanical property change of A533B-1 steel with high and low Cu impurity subjected to well-controlled neutron irradiation (temperature: 563±2 K; flux: 1.7×10<sup>13</sup> n/cm<sup>2</sup>/s) in a wide range of dose from 0.32 to 9.9×10<sup>19</sup> n/cm<sup>2</sup> using JMTR have been investigated using atom probe tomography (APT), positron annihilation technique and Vickers micro-hardness test. The hardening rate of the steels was steep up to 0.59×10<sup>19</sup> n/cm<sup>2</sup> and gradual with further doses regardless of Cu composition. These hardness changes were consistent with the dose dependence of positron lifetime and coincidence Doppler broadening spectra, implying that the hardening in the lower doses was mainly caused by irradiation-induced defects for both high and low Cu steels. On the other hand, the contribution of the solute clusters to irradiation hardening, estimated using APT data

based on the Russell and Brown model, was consistent with the gradual hardening in the higher doses.

**Mechanical Properties and Radiation Response of Ultra-Fine Grained Stainless Steels:** *J. Gonzalez<sup>1</sup>; C. Sun<sup>1</sup>; K.T. Hartwig<sup>1</sup>; Y. Yang<sup>2</sup>; T. R. Allen<sup>2</sup>; S. A. Maloy<sup>3</sup>; X. Zhang<sup>1</sup>;* <sup>1</sup>Texas A&M University; <sup>2</sup>University of Wisconsin-Madison; <sup>3</sup>Los Alamos National Laboratory

We present microstructure and mechanical properties of 304L and 316L austenitic stainless steels and a model Fe-Cr-Ni alloy, processed by equal channel angular pressing (ECAP). The average grain size of ECAPed alloy is on the order of a few hundred nm. Helium ion irradiations to a dose of a few dpa are performed on these alloys with ultra-fine grains. The evolution of microstructure, defect density, and mechanical properties of alloys are investigated.

**Microstructural Evolution of Cu based Complex Alloys Under Prolonged Particle Irradiation:** *Rannesh Lokesh<sup>1</sup>;* Pascal Bellon<sup>1</sup>; Robert Averback<sup>1</sup>; <sup>1</sup>University of Illinois Urbana Champaign

Nanostructured materials are believed to be resistant to radiation damage due to the presence of large concentration of defect sinks which prevent large super-saturations of point defects. However, such far-from-equilibrium microstructures coarsen when exposed to high temperature and particle irradiation. A stabilized microstructure having radiation resistance can be obtained by exploiting the concepts of self organization. This paper investigates the effect of borides in copper based alloys under the conditions of ion irradiation and elevated temperature. Borides are extremely hard compounds with high melting point making it an interesting system. Various analytical techniques such as X-ray diffraction, Transmission electron microscopy were employed to characterize the microstructure. It was found that macroscopic coarsening was suppressed at high temperatures and irradiation doses due to the formation of precipitates which pin the grain boundaries. The Copper grain size remained stabilized at around 28 nm even at 0.65 of the melting temperature of Copper.

**Evolution of Microstructures in Helium Ion Irradiated MgO/W Multilayers:** *Engang Fu<sup>1</sup>;* Yongqiang Wang<sup>1</sup>; Amit Misra<sup>1</sup>; Michael Nastasi<sup>1</sup>; <sup>1</sup>LANL

MgO/W multilayer films were deposited on Si (100) substrates by magnetron sputtering technique with individual layer thickness (h) of 2 to 100 nm. Helium (He) ion irradiations on MgO/W multilayers were performed to study the effect of interfaces as defects sinks on reducing radiation induced defects. The influence of size dependence (different individual layer thickness) of MgO/W multilayers on ion irradiation tolerance is investigated. X-ray diffraction (XRD) and transmission electron microscopy (TEM) were used to characterize the microstructure change of the MgO/W multilayers before and after ion irradiation. The interfacial stability of the MgO/W multilayers upon ion irradiation was examined by scanning transmission electron microscopy (STEM). The potential mechanisms of interface-defect (induced by radiations) interactions under the context of length scale and growth of He bubbles will be discussed.

**The Response of Polycrystalline Tungsten to 30keV Helium Ion Implantation at High Temperatures and Its Dependence on the Angle of Incidence:** *Samuel Zenobia<sup>1</sup>;* *Lauren Garrison<sup>1</sup>;* Gerald Kulcinski<sup>1</sup>; <sup>1</sup>University of Wisconsin-Madison

Twelve polycrystalline tungsten samples were irradiated with 30keV helium ions in the Materials Irradiation Experiment (MITE-E). Samples were held at temperatures between 500–900 °C while irradiated to fluences of  $\sim 6 \times 10^{16}$ – $\sim 4 \times 10^{19}$  He/cm<sup>2</sup>. Severe changes to the surface morphology were observed at implant doses exceeding  $\sim 1 \times 10^{18}$  He/cm<sup>2</sup> and classified as blisters, pitting, or a highly directional surface structure dubbed “grass.” Morphological details of the grass structure depended on the crystal orientation of the grains to the sample surface. A sub-surface semi-porous layer was formed during irradiation, and post-implantation analysis revealed that this layer extended up to  $\sim 1000$  nm below the surface in the highest fluence cases. Specimens irradiated to fluences of  $\sim 1 \times 10^{18}$  He/cm<sup>2</sup> and greater experienced statistically significant mass loss which increased with higher implant dose. Implications

of this mass loss are discussed for the plasma facing components of both magnetic and inertial fusion reactors.

**Precipitation in Irradiated W Alloys:** *Emmanuelle Marquis<sup>1</sup>;* Colin English<sup>2</sup>; Samuel Humphry-Baker<sup>3</sup>; <sup>1</sup>University of Michigan; <sup>2</sup>University of Oxford; <sup>3</sup>Massachusetts Institute of Technology

Tungsten is being considered for plasma facing and diverter components in future fusion reactors. A major issue for the use of tungsten is the transmutation of W into Re and Os under neutron irradiation, and current neutronic calculations (Cottrell, J. Nucl. Mater. 2004) predict that pure tungsten would transform into W-13%Re-12%Os after just five years of service. As demonstrated in past studies by Seidman et al. (acta Metall. 1984) and Williams et al. (Metall. Trans. A 1983), irradiated W-Re alloys exhibit precipitation of Re-rich phases even in undersaturated solid-solutions. The precipitation mechanisms are unclear and understanding the kinetics of precipitation is a necessary step towards establishing predictive tools for the structural and mechanical integrity of the reactor components during service, thereby ensuring reactor safety and optimizing reactor efficiency. We report on a systematic series of atomic scale investigations on W alloys implanted using 2MeV W<sup>+</sup> ions. The formation of solute-rich clusters and the kinetics of precipitation will be discussed.

**In-Situ Transmission Electron Microscopic Study of the E-Beam Damage Process in the Next Generation Nuclear Graphites:** *Karthik Chinnathambi<sup>1</sup>;* Josh Kane<sup>1</sup>; Darryl Butt<sup>1</sup>; Rick Ubic<sup>1</sup>; <sup>1</sup>Boise State University

Under irradiation, graphite is known to undergo changes in its thermo-mechanical properties, especially via irradiation-induced creep. Developing an understanding of these life-limiting phenomena is very important for the development of new grades of nuclear graphite. We have in-situ observed the atomic level processes involved in the swelling of the nuclear graphites (IG-110, NBG-18, PCEA and PGX) under e-beam irradiation using high resolution electron microscopy (HREM) and electron energy loss spectroscopy (EELS). Under e-beam irradiation, the structural ordering parallel to the basal plane gradually deteriorated because of the appearance of dislocation loops, bending and fragmentation of the basal planes in addition to a dilation in the lattice parameter along the c-axis causing the swelling and closing of the micro cracks. EELS studies showed that the p bonding in the basal plane was retained. Preliminary results on the structural changes associated with thermal creep using HREM and EELS will also be discussed.

**Experimental Study of <c> Component Loops Nucleation and Growth under Charged Particles Irradiation in Recrystallized Zircaloy-4:** *Lea Tournadre<sup>1</sup>;* F. Onimus<sup>1</sup>; D. Gilbon<sup>1</sup>; J.-M. Cloue<sup>2</sup>; J.-P. Mardon<sup>2</sup>; X. Feaugas<sup>3</sup>; O. Toader<sup>4</sup>; C. Bachelet<sup>5</sup>; <sup>1</sup>Commissariat à l’Energie Atomique (CEA); <sup>2</sup>AREVA AREVA NP Fuel BusinessUnit10; <sup>3</sup>Laboratoire d’Etude des Matériaux en Milieux Agressifs (LEMMA), Université de La Rochelle; <sup>4</sup>Michigan Ion Beam Laboratory (MIBL), University of Michigan; <sup>5</sup>Centre de Spectrométrie Nucléaire et de Spectroscopie de Masse (CSNSM), Université Paris-sud 11

Recrystallized zirconium alloys, used as structure materials for the Pressurised Water Reactor fuel assembly, undergo under neutron irradiation stress free growth which accelerates for high irradiation doses. This acceleration is correlated to the formation of <c> component vacancy dislocation loops in the basal plane. In the present work, two types of charged particle irradiations have been conducted on recrystallized Zircaloy-4. A 2MeV proton irradiation was performed on the Tandatron in the MIBL up to  $1.2 \times 10^{19}$  protons/cm<sup>2</sup> at 350°C, and 600keV Zr ion irradiations were carried out on the ARAMIS facility (CSNSM/IN2P3) at 300°C up to  $9.5 \times 10^{14}$  ions/cm<sup>2</sup>. For the first time after such irradiations, <c> loops have been observed by Transmission Electron Microscopy. It has been shown that using ions, they start to nucleate and grow beyond a threshold dose. Irradiated microstructures – loop diameter and density – will be discussed for both proton and ion irradiations and compared to the neutron irradiated one.

**FIM of Defects in Pt Induced by Neutron Irradiation:** *Elena Medvedeva<sup>1</sup>; Elena Kalinina; Mihail Ivchenko<sup>1</sup>; <sup>1</sup>Institute of Electrophysics, Urals Division of Russian Academy of Sciences*

The aim of report is to analyze, using FIM, the structure of radiation-induced defects in the platinum bulk, which were formed by radiation effects of low-temperature bombardment by fast neutrons ( $E > 0.1$  MeV). The neutron bombardment of platinum up to a fluency of  $6.7 \times 10^{17} \text{ cm}^{-2}$  led to the formation of a defect structure in platinum, which is characterized by the high concentration of single point defects and their complexes whose dimensions are comparable with the inter atomic distance. As the fluency is increased up to  $3.5 \times 10^{18} \text{ cm}^{-2}$ , radiation-induced clusters whose average size was 3.2 nm, were observed in the irradiated plate. The experimental concentration of radiation-induced clusters in platinum was  $9 \times 10^{22} \text{ m}^{-3}$ . Work is executed with support of the federal target program «Scientific and scientific and pedagogical cadres of innovative Russia» for 2009-2013 (N 831).

**Evolution of the Residual Stresses in Zirconium Nitride Films Irradiated by High-Energy Xe Ions:** *Vladimir Uglov<sup>1</sup>; Sergey Zlotski<sup>1</sup>; Vladimir Skuratov<sup>2</sup>; Aleksandr Sohatsky<sup>2</sup>; Alina Shashok<sup>1</sup>; <sup>1</sup>Belorussian State University; <sup>2</sup>Joint institute for nuclear research*

Ceramics (different transition metals nitrides) due to their high radiation stability under neutron and alpha-particle irradiation and additional thermal and corrosion stability are the best candidates as the inert matrix for nuclear fuel. The radiation effects of zirconium nitride films with different thickness (0.1 and 3  $\mu\text{m}$ ) are investigated. The films were deposited by vacuum arc evaporation in nanocrystalline state (average size of crystallites in order to 4 nm). Irradiation was carried out at the cyclotron by Xe ions with energy 167 MeV and dose from  $3 \cdot 10^{12}$  to  $5 \cdot 10^{14} \text{ cm}^{-2}$ . Post-irradiated TEM and XRD investigations revealed that microstructure and phase composition of nanocrystalline films are stable. It is established that change of the macrostresses type occurs for the thick coatings with an increase in the radiation dose: from tensile to compressive. The mechanisms of the evolution of residual stresses in ZrN films during the high-energy ion irradiation are discussed.

**Chemically Bonded Phosphate Ceramics Composites Response to Irradiation:** *H. A. Colorado<sup>1</sup>; C. Hiel<sup>2</sup>; J. M. Yang<sup>1</sup>; H. T. Hahn<sup>1</sup>; J. Pleitt<sup>3</sup>; C. H. Castano<sup>3</sup>; <sup>1</sup>University of California, Los Angeles; <sup>2</sup>Composites Support and Solutions Inc.; <sup>3</sup>Missouri University of Science and Technology, Nuclear Engineering Department*

The effect of gamma rays and neutron radiation on chemically bonded phosphate ceramics (CBPC) composites have been investigated. The effect of lead concentration incorporated into the CBPC is presented. CBPC has been proved to be good structural material [1] and some research already showed their potential for radiation shielding applications [2]. CBPC is a composite material itself, with several crystalline and amorphous phases [1]. In addition, irradiation experiments were also conducted on different CBPCs with reinforcements as well as wollastonite powders (raw material). CBPC samples were irradiated at room temperature up to 6.5 MRad in the Missouri S&T nuclear reactor (MSTR). Preliminary simulation study of the materials effects as well as radiation shielding potential and attenuation coefficients in a broad range of energies pertinent to engineering applications are also included. Microstructure was identified by using optical and scanning electron microscopes, X-ray diffraction and Raman Spectroscopy.

**Defect Structures before Steady Void Growth in Austenitic Stainless Steels:** *Toshimsa Yoshie<sup>1</sup>; Koichi Sato<sup>1</sup>; Xingzhong Cao<sup>1</sup>; Qiu Xu<sup>1</sup>; Troyo Troev<sup>2</sup>; <sup>1</sup>Kyoto University; <sup>2</sup>Bulgarian Academy of Sciences*

The existence of a transient stage before steady void growth in austenitic stainless steels is well known. The incubation period depends on alloy compositions remarkably. As most of experimental studies have been performed by transmission electron microscopy, point defects and their clusters under the resolution limits are impossible to detect. In this study, defect structures during the incubation period in austenitic stainless steels, both practical alloys such as SUS316 and their model alloys such as Fe-Cr-Ni were studied by using positron annihilation lifetime measurement. Large

vacancy clusters were formed in model alloys, while only life times smaller than 150 ps, which is smaller than that of single vacancies of 180 ps were detected in practical alloys with neutron irradiation to 0.2dpa at 573 K. The defect evolution in the incubation period will be discussed based on results of electron irradiation and neutron irradiation.

**Ab Initio Calculations of Point Defects in Tungsten:** *Lisa Ventelon<sup>1</sup>; François Willaime<sup>1</sup>; Mihai-Cosmin Marinica<sup>1</sup>; Chu Chun Fu<sup>1</sup>; <sup>1</sup>CEA*

The development of plasma facing components is one of the critical issues to realize next generation fusion devices. Tungsten has the highest melting point of all the non-alloyed metals and is the only material, with carbon composites, that can resist to high heat fluxes, which the divertor is subject to from the plasma. Ab initio calculations have revealed unexpected behaviors of radiation point defects in tungsten. The vacancy-vacancy interaction is not attractive and an intermediate configuration between the  $\langle 111 \rangle$  and  $\langle 110 \rangle$  dumbbells has been proposed for the self-interstitial. We have confirmed these results and investigated the effects of electronic entropy and cell geometry. Empirical potentials for tungsten have been developed, including in their fitted properties, besides the experimental values of the bulk properties, the ab initio formation energies of several self-interstitial configurations. They have been tested on gamma-surfaces and properties of screw dislocations: core structure, Peierls barrier and glide plane.

**Benchmarking of Structural Materials Pre-Selected for Advanced Nuclear Reactors:** *P. Salame<sup>1</sup>; A Zeman<sup>1</sup>; V. Inozemtsev<sup>1</sup>; A. Stanculescu<sup>1</sup>; <sup>1</sup>International Atomic Energy Agency*

Advanced materials capable of operation over a wide range of elevated temperatures to high radiation damage levels are highly required for the innovative nuclear reactor concepts. Newly developed ferritic/martensitic steels with oxide dispersion strengthened (ODS) features is a very unique and promising candidate material qualified for both fission and fusion applications. Nevertheless, there are several issues to be addressed, specifically (1) Microstructure optimisation (size and distribution of oxide particles, etc.), (2) Larger scale fabrication process and (3) technological aspects. New IAEA coordinated research project will help to optimise the recent class of ODS steels, as well as detailed mechanical and microstructural characterisation. It is expected, this initiative will speed up R&D activities and pre-normative research of such materials through comprehensive Round Robin testing.

## Neutron and X-Ray Studies of Advanced Materials IV: Poster Session

*Sponsored by: The Minerals, Metals and Materials Society, TMS Structural Materials Division, TMS/ASM: Mechanical Behavior of Materials Committee, TMS: Chemistry and Physics of Materials Committee*

*Program Organizers: Rozaliya Barabash, Oak Ridge National Laboratory; Xun-Li Wang, Oak Ridge National Laboratory; Jaimie Tiley, Air Force Research Laboratory; Peter Liaw, The University of Tennessee; Erica Lilleodden, GKSS Research Center; Brent Fultz, California Institute of Technology; Y-D Wang, Northeastern University*

Sun PM-Thurs AM  
Feb 27-Mar 3, 2011

Room: 10  
Location: San Diego Conv. Ctr

**Probing Li-Ni Cation Disorder in  $\text{Li}_{1-x}\text{Ni}_{1-x-y}\text{Al}_y\text{O}_2$  Cathode Materials by Neutron Diffraction:** *Lu Cai<sup>1</sup>; Zengcai Liu<sup>1</sup>; Ke An<sup>1</sup>; Chengdu Liang<sup>1</sup>; Xun-Li Wang<sup>1</sup>; <sup>1</sup>Oak Ridge National Laboratory*

Neutron diffraction is unique in the studies of Li-ion batteries: its power to detect lithium ions provides ways to accurately determine the positions of lithium ions; and its ability of differentiating cations via coherent scattering lengths of metal ions enables the probing of cation disorder. The rich structure information provided by neutron diffraction is essential for understanding the subtle structure/property relationships of metal oxides and phosphates, which are the active cathode materials in lithium-ion batteries. In this study, we will present the research on probing the cation mixing of



LiNiO<sub>2</sub> with and without Al<sup>3+</sup> substitution. LiNi<sup>3+</sup>O<sub>2</sub> is an attractive cathode material for lithium-ion batteries, but the cycling properties has been greatly depressed by the Ni<sup>2+</sup> ions entering into Li<sup>+</sup> sites. The appearance of Ni<sup>2+</sup> in the Li<sup>+</sup> sites obstructs Li<sup>+</sup> diffusion and causes irreversible capacity loss. Al<sup>3+</sup> substitution of Ni<sup>3+</sup> stabilizes the structure of lithium nickelate (LiNi<sub>1-y</sub>Al<sub>y</sub>O<sub>2</sub>) and reduces the formation of Ni<sup>2+</sup>, therefore mitigating the migration of Ni<sup>2+</sup> into the Li<sup>+</sup> sites. The Rietveld refinement of the powder neutron diffraction patterns will be used to determine the cation disorder of Li and Ni in samples synthesized at different conditions. The correlation of structure with synthesis conditions will be discussed in details. We expect the results will provide guidance on the development of new materials to meet the needs of lithium-ion batteries.

**Pb-Free Solders and Other Materials for Emerging Interconnect and Packaging Technologies: Poster Session**

*Sponsored by:* The Minerals, Metals and Materials Society, TMS Electronic, Magnetic, and Photonic Materials Division, TMS; Electronic Packaging and Interconnection Materials Committee  
*Program Organizers:* Indranath Dutta, Washington State University; Darrel Frear, Freescale Semiconductor; Sung Kang, IBM; Eric Cotts, SUNY Binghamton; Laura Turbini, Research in Motion; Rajen Sidhu, Intel Corporation; John Osenbach, LSI Corporation; Albert Wu, National Central Univ, Taiwan; Tae-Kyu Lee, Cisco Systems

Sun PM-Thurs AM Room: 7B  
 Feb 27-Mar 3, 2011 Location: San Diego Conv. Ctr

**Oxidation Behavior of ENIG and ENEPIG Surface Finish:** C. Li<sup>1</sup>; H. Chuang<sup>1</sup>; C. Chung<sup>1</sup>; C. Kao<sup>1</sup>; <sup>1</sup>National Taiwan University

In this study, two commonly used surface finishes, electroless Ni immersion Au (ENIG) and electroless Ni electroless Pd immersion Au (ENEPIG) were investigated on their resistance to oxidation. AES and SIMS analysis were carried out to reveal oxide species and estimate their relative thickness after an isothermal aging at 150°C for 200 hours. Elemental mapping revealed that the oxide formed as a continuous layer on the surface of ENIG and ENEPIG. NiO and NiO<sub>2</sub> were detected on the surface of ENIG, but the oxide thickness of ENEPIG is much thinner than that of ENIG according to the depth profiling examination. This result that ENEPIG exhibits better oxidation resistance and Pd suppresses the growth of Ni oxides on surface.

**Bond Strengths of Au Stud Bumps Joined with Pb-Free Solders:** Young-Kyu Lee<sup>1</sup>; Chang-Woo Lee<sup>2</sup>; Sehoon Yoo<sup>2</sup>; <sup>1</sup>University of Science & Technology; <sup>2</sup>Korea Institute of Industrial Technology

Joining properties of Au stud bumps joined with Pb-free solders were investigated in this study. A conventional wire bonding process was used to form the Au studs. The Au stud bumps were bonded on the solder bumps on the substrate with flip chip bonder. After bonding, intermetallic compound (IMC), AuSn and AuSn<sub>2</sub> was formed at the interface of Au and Sn. An aging test was performed, and the IMC thickness increased as the aging time increased. The joint strength and microstructure of stud bumps were evaluated by scanning electron microscope (SEM), energy dispersive spectroscopy (EDS), and shear tester as well.

**Joule Heating Effect in Microbumps for 3D IC Packaging:** Yu-Chun Liang<sup>1</sup>; Chih Chen<sup>1</sup>; <sup>1</sup>National Chiao Tung University

For high-capability packaging, the flip-chip bump is a well-known technology. To accommodate the performance requirement of portable devices, the size of bumps continuously shrinks. This trend accounts for increasing chip temperature and current density in each solder bump called Joule-heating effect and current-crowding effect. Recently, the dimensions of flip-chip bumps reduce to 20-30 micrometers known as "microbumps" sandwiched between two Si chips. In this study, the temperature distribution during current-stressing in microbumps is directly examined by using infrared microscopy. The Joule-heating effect in microbumps is less serious

than those in flip-chip bumps on polymer substrates. The temperature increase is only few degrees when the current density is 1.06x10<sup>5</sup> A/cm<sup>2</sup>. In addition, the temperature in the aluminum trace of top die is lower than that in the aluminum trace of bottom die. That is, the direction of thermal gradient in microbumps is opposite from that in the traditional solder bumps.

**Distribution of Pd within Solder Joints in the Reaction between SAC305 and ENEPIG Surface Finish:** H. Chuang<sup>1</sup>; J. Ke<sup>1</sup>; C. Chung<sup>1</sup>; C. Li<sup>1</sup>; C. Kao<sup>1</sup>; <sup>1</sup>National Taiwan University

The interfacial reaction between electroless Ni, electroless Pd, immersion Au (ENEPIG) surface finish and the SAC305 lead-free solder is investigated. The microstructure analysis reveals no detectable Pd content in either IMCs or in the solder region after multiple reflows. However, after high temperature storage at 150°C for 500 h, a Sn-Ni-Au-Pd-Cu compound is observed both within the solder region and in the vicinity of the interface. The composition of this compound is 80.2Sn-11Ni-4.4Au-3.8Pd-0.6Cu (at.%), which likely corresponds to (Au<sub>0.22</sub>Pd<sub>0.2</sub>Ni<sub>0.55</sub>Cu<sub>0.03</sub>)Sn<sub>4</sub>. This stoichiometry suggests that this compound is related to AuSn<sub>4</sub>, which tends to induce the well-known Au embrittlement phenomenon if its amount is large enough. This result suggests that the amount of Au and Pd should be considered together when establishing the safe upper limit for these two elements.

**Effect of SnAg Solder Height on Metallurgical Reaction in Microbumps for 3D IC Packaging:** Wei-Chi Sung<sup>1</sup>; Chih Chen<sup>1</sup>; <sup>1</sup>National Chiao Tung University

The shrinkage of bump size for better performance has become a trend on the electronic packaging industry. Microbumps have been adopted as interconnects between chips in 3D IC packaging. So far the bumps size decreases dramatically to 20 microns and thus the bump height may range from 10 microns to 20 microns. As the bump size decrease, the volume of solder decreases. Thus, the formation of intermetallic compounds (IMCs) play crucial role on the joint performance. In this study, we use different heights of SnAg<sub>2.6</sub> solders, including 5µm, 10µm, and 20µm to analyze microstructure evolution in the microbumps during reflowing at 260°C and solid state aging at 150°C on both Cu and Ni metallization. Cross-sectional and plan-view SEM images are employed to observe the morphology of Ag<sub>3</sub>Sn, Cu<sub>6</sub>Sn<sub>5</sub>, and Ni<sub>3</sub>Sn<sub>4</sub> IMCs. The effect of solder volume on IMC formation will be presented.

**Preferred Crystal Orientations of Cu<sub>6</sub>Sn<sub>5</sub> Formed on Ni Substrate:** W. M. Chen<sup>1</sup>; C. R. Kao<sup>1</sup>; <sup>1</sup>National Taiwan University

Texture as well as epitaxial growth of intermetallic compounds (IMCs) has become an important issue due to the increasing IMCs to solder ratio in micro-bumps under development today. The existence of preferred orientations of Cu<sub>6</sub>Sn<sub>5</sub> formed over Cu substrates had been reported by several research groups and was a well-established fact. In this study, we show for the first time that Cu<sub>6</sub>Sn<sub>5</sub> formed over Ni substrate also exhibits preferred crystal orientations. In this study, solders doped with Cu are reacted with large grain, annealed Ni substrate to induce the formation of Cu<sub>6</sub>Sn<sub>5</sub>. It is demonstrate that Cu<sub>6</sub>Sn<sub>5</sub> has the following orientation relationship with Ni: (1-20)Cu<sub>6</sub>Sn<sub>5</sub>II(1-11)Ni and [001]Cu<sub>6</sub>Sn<sub>5</sub>II[110]Ni.

**Correlation between Elemental Distribution and Shear Impact Resistance in Sn-3.0Ag-0.5Cu Solder Alloy Joints before and after Board Assembly:** Chi-Yang Yu<sup>1</sup>; Jenq-Gong Duh<sup>1</sup>; Tae-Kyu Lee<sup>2</sup>; Michael Tsai<sup>2</sup>; Kuo-Chuan Liu<sup>2</sup>; <sup>1</sup>National Tsing Hua University; <sup>2</sup>Cisco Systems, Inc.

Elemental distribution in the solder joints affects the reliability of the device with ball grid array package, and the distribution is continuously changing based on the assembly process. The mechanical stability change is identified based on these elemental distribution changes. The shear impact performances for each process steps are observed. During first step reflow process, components with Ni/Au surface finish are attached with Sn-3.0Ag-0.5Cu solder balls. An additional second step reflow process connects the component solder joints with Cu pads on the printed circuit board. Each reflow process produced a different compound layer structure and elemental re-distribution. The quantitative analysis reveals the Cu and Ni distribution near the Ni/Au substrate for each step and the impact resistance is measured

using a high speed shear tester. The results show the correlation between elemental distribution and impact resistance in stand alone solder joints right after ball attached components and after board assembled.

**Investigation of Stress Evolution Induced by High Current Density in Lead-Free Solder Joints Based on X-Ray Diffraction Technique:** *Guangchen Xu<sup>1</sup>; Fu Guo<sup>1</sup>; Hongwen He<sup>2</sup>; Haiyan Zhao<sup>2</sup>; <sup>1</sup>Beijing University of Technology; <sup>2</sup>Tsinghua University*

The lifetime of solder joints under high current density is associated with the interactions among electrical field, thermal field, and stress field. Effects of electrical field and thermal field on microstructural evolution of various solder alloys have been investigated by many researchers. Accordingly, critical current density and endured temperature at solder joints are identified as the most important two parameters to determine the occurrence of EM. However, the directional movement of metal atoms/ions during current stressing can induce obvious stress concentration at the anode and cathode interfaces. In order to evaluate the stress evolution of lead-free solder joints during the current stressing, nondestructive X-ray diffraction technique was employed, in which the strain in the crystal lattice was measured, and residual stress producing the strain was calculated. Moreover, different lead-free solder alloys, i.e. eutectic SnAgCu, SnBi, are used to demonstrate their distinct stress evolution under high current density.

**Electromigration Reliability of Sn-Ag-Cu Solder Joints Containing Various Ag Contents:** *Bo-Zung Chen<sup>1</sup>; Chih-Nan Chen<sup>1</sup>; Cheng-En Ho<sup>1</sup>; <sup>1</sup>Yuan Ze University*

The influence of Ag content on the electromigration reliability of Sn-Ag-Cu solder joints was systematically investigated in this study. The joints had a typical line-to-bump geometry with the Cu/Sn-Ag-Cu/Cu configuration, and the Ag contents of the Sn-Ag-Cu were 0, 1, 2, 3, 3.5, 4 wt.%, respectively. Electromigration tests were carried out at an ambient temperature (25 degree Celsius) with a fixed 9600 A/cm<sup>2</sup> at the contact of the Cu/Sn-Ag-Cu. After the tests, a SEM, FIB (focused ion beam), and CLSM (confocal laser scanning microscopy) were employed to observe the microstructure evolution with current stressing time. Research showed doping an adequate Ag to the Sn-Cu alloy significantly increased resistance to electromigration. This diminished the electromigration-induced Sn-Cu alloy deformations and Cu metallization consumption, extending the lifetime of solder joints. More details about the Ag effect on the electromigration reliability of solder joints will be presented in this talk.

**Solder Thickness Effect on Mechanical and Electrical Reliabilities of Cu Pillar/ Sn-3.5Ag Bump:** *Byung-Hyun Kwak<sup>1</sup>; Myeong-Hyeok Jeong<sup>1</sup>; Byoung-Joon Kim<sup>2</sup>; Kiwook Lee<sup>2</sup>; Jaedong Kim<sup>3</sup>; Young-Chang Joo<sup>2</sup>; Young-Bae Park<sup>1</sup>; <sup>1</sup>Andong National University; <sup>2</sup>Seoul National University; <sup>3</sup>Amkor Technology Korea, Inc.*

Cu pillar/Sn-3.5Ag bump is widely adopted as chip-to-substrate interconnect in TSV stack as well as flip chip package because it provides the finer pitch and uniform current distribution. However, Cu pillar bump makes large amount of IMC and Kirkendall void at Cu/solder interface under current stressing conditions, which can degrade electrical and mechanical reliability. In this work, solder thickness effects on the IMC growth kinetics in Cu pillar/solder bump with pure Sn or Sn-3.5Ag were quantitatively evaluated by using in-situ annealing and electromigration test in a SEM chamber during pure annealing or current stressing conditions with current density of 3.5 x 10<sup>4</sup> A/cm<sup>2</sup> at 120 ~ 175°C. IMC growth was significantly enhanced by current stressing where the growth rate follows a linear relationship with stressing time. Also, their effect on the mechanical and electrical reliability of Cu pillar/Sn-3.5Ag bump will be discussed in detail.

**Supersaturation and Recrystallization in Solder Alloys Induced by Current Stressing:** *Kwang-Lung Lin<sup>1</sup>; Ying-Ta Chiu<sup>1</sup>; Shi-Min Kuo<sup>1</sup>; Chia-Hao Liu<sup>1</sup>; Yi-Shao Lai<sup>2</sup>; <sup>1</sup>National Cheng Kung University; <sup>2</sup>Advanced Semiconductor Engineering, Inc.*

Current stressing is known to induce electromigration in solder joints. This present study reports that current stressing will also induce supersaturation and the subsequent recrystallization in solder alloys. An in-situ SEM-EDS

investigation shows that the Sn rich phase of the 95Pb-5Sn solder disappears upon current stressing. The Sn concentration in the Pb matrix increases and reaches a maximum value after long time current stressing. The maximum Sn concentration achievable exceeds the thermal equilibrium magnitude as described by phase diagram. The maximum supersaturation concentration of Sn increases with current density increase in 5 x 10<sup>3</sup> ~ 1 x 10<sup>4</sup> A/cm<sup>2</sup>. The Zn rich phase of Sn-9Zn solder and the Sn rich phase in 95Pb-5Sn show recrystallization behavior after current stressing. The recrystallization forms one dimensional nano crystals of Sn in the Pb matrix while forms nano sheet Zn crystal in the Sn-9Zn solder. The nano crystals will appear only after the current stops.

**The Control Tin Whisker Growth by Lithography Process:** *Chien-Hao Su<sup>1</sup>; Li-Wei Zou<sup>1</sup>; Hao Chen<sup>1</sup>; Albert T. Wu<sup>1</sup>; <sup>1</sup>National Central University*

The growth of tin whiskers on lead-free finishes coated on the leadframes is spontaneous and contributed by stress generation and relaxation. A protective layer of tin oxide that grown on the surfaces is required for the formation of tin whiskers. Cracks on the oxide served as weak spots that are essential for the protrusion of whiskers to release the stresses. This paper presents a new approach to control the grown positions of tin whiskers. The original tin oxide was removed by etchant and polishing. The lithography process was used immediately after surface treatments to define the pattern on tin oxide thin film that was deposited by sputter. The purpose of the pattern is to intentionally form weak oxide spots for stress relaxation. The results suggested that hillocks or whiskers would grow in these pre-defined areas. The location of tin whiskers can thus be well predicted by this approach.

**Simulation on Current Density Distribution in Micro-Bumps with Various UBM and Solder Structures:** *Chung Kuang Lin<sup>1</sup>; Chih Chen<sup>1</sup>; <sup>1</sup>National Chiao Tung University*

Three-dimensional simulations on current-density distribution in solder joints of micro-bumps under 30 mA current stressing were carried out by finite element method. The current density in solder joints will reach to 10<sup>4</sup> A/cm<sup>2</sup> which will induce electromigration damage in SnAg solder joints. The different UBM structures could change the maximum current density in solder joints. Six micro-bump structures were simulated, including different thickness SnAg solder joints and Cu / Ni UBM in chip side and board side. The maximum current density occurred at the entrance of Cu trace into UBM and current crowding effect took place within 3 μm of current entrance, while there was the uniform current density distribution in the solder joints. The thickness of UBM layer played important role in current density distribution. Therefore, the micro-bumps with 10 μm Cu UBM on both sides had the lowest maximum current density in solder layer.

**Phase-Field Simulations of Microstructure and Crystal Orientation Evolution of Intermetallic Compound (Cu<sub>6</sub>Sn<sub>5</sub>) during Early Stages of Lead-Free Soldering:** *Min Soo Park<sup>1</sup>; Colton Shannon<sup>1</sup>; Raymundo Arroyave<sup>1</sup>; <sup>1</sup>Texas A&M University*

We present phase-field simulations of the evolution of crystallographic orientation and morphology (including precipitation) of intermetallic compound (IMC) during early stages of soldering. We focus on the interactions between liquid Sn-based solder (L) and copper substrate (α) in a Cu/Sn system. It is assumed that IMC (Cu<sub>6</sub>Sn<sub>5</sub>, η) grains precipitate at the L/α interface with its own crystallographic orientation. Classical nucleation theory is used to model the precipitation of IMC grains. A crystalline-field model considering grain's misorientation is included in the formulation. CALPHAD models are used to define the bulk thermodynamics of the phases. The simulations will show the evolution of the morphology and kinetics of IMC growth with different grain boundary diffusion and L/η interface energies. The effects of considering nucleation and crystal orientation on the resulting morphology of the IMC layer will be explored. Experimental investigations will be used to validate the models developed in this work.

**Mechanisms of Deformation in Cerium (Ce)-Containing Pb-Free Solders:** *Huxiao Xie*<sup>1</sup>; Nikhilesh Chawla<sup>1</sup>; Kabir Mirpuri<sup>2</sup>; Aleks Aleksov<sup>2</sup>; <sup>1</sup>Arizona State University; <sup>2</sup>Intel Corp

Traditional Pb-free solders such as Sn-Ag-Cu (SAC) show relatively low ductility and poor damage tolerance. Our research has shown that SAC-alloy doped with trace amounts of Ce exhibits a substantial improvement in ductility, with a relatively small decrease in strength. These alloys also have better oxidation resistance than other rare earth-containing solders such as Lanthanum and Yttrium. In addition to the beneficial bulk and surface properties, it is imperative to understand the mechanisms for enhanced mechanical properties in Ce-containing SAC solders. Using interrupted experiments in a scanning electron microscope, we have been able to elucidate the relevant deformation mechanisms in these materials. We will discuss the influence of CeSn<sub>3</sub> particle fracture and interfacial debonding on enhanced macroscopic ductility.

**Electromigration Failure in Micro-Bumps for 3D IC Packaging:** *Hsiang-Yao Hsiao*<sup>1</sup>; Chih Chen<sup>1</sup>; <sup>1</sup>National Chiao Tung University

The three-dimensional chip stacking technology with fine-pitch and high input/output interconnects has emerged due to the requirements of multi-function and high performance in electronic devices. When the electronic packaging technology develops toward the miniaturization trend, the reliability of the fine-pitch-solder bump interconnections will become a critical issue in advanced 3D chip stacking technology. With the joint size becoming small and the increasing current in each solder bump, the current density flowing in each individual bump continues to increase. Therefore, electromigration has become a major reliability issue in microelectronic devices. In this study, electromigration in SnAg solder micro-bump with a pitch of 20- $\mu$ m was investigated under current stressing at hot stage. Ni/Cu under-bump-metallurgy layer was selected on both top and bottom chips. Kelvin-probes are employed to monitor the bump resistance during current stressing. Electromigration characteristics of fine pitch micro-bump will be discussed with the microstructure evolution of micro-bump during current stressing.

**Interfacial Reactions at Pogo Probe Pins/Sn-Ag-Cu Solder Interfaces:** *Mao Gao*<sup>1</sup>; Eric Cotts<sup>1</sup>; <sup>1</sup>Binghamton University

Au and PdCo plated, 0.32mm diameter pogo probe pins were used for the repeated functional testing of printed circuit boards. For repeated test insertions into PbSn solder, these pins were found to be highly reliable. However, very early failures, due to increased contact resistance, were experienced when these pins were used with Pb free, Sn-Ag-Cu solder alloys. This study focused on an examination of contamination of the surfaces of probe pins, including failed probe pins. These devices were cold mounted in epoxy and careful cross sections were produced. Optical microscopy, and field-emission scanning electron microscopy equipped with energy dispersive X-ray spectroscopy, were used to investigate the Sn contamination and intermetallic compounds at the surface of pins. Correlations with failures are reported.

**Electro-Migration Behavior of 3-D Flip Chip Packaging by Thermal Compression Bonding with Pb-Free Solder:** *Jong-Gun Lee*<sup>1</sup>; Jong-Bum Lee<sup>1</sup>; Jae-Hyun Yoon<sup>1</sup>; Sang-Su Ha<sup>1</sup>; Seung-Boo Jung<sup>1</sup>; <sup>1</sup>Sungkyunkwan University

The electro-migration of solder joints under high current stressing is an important concern for the solder joint system's reliability, especially with the increase in the required device density and power of 3-D flip chip packages. In this study, the electro-migration phenomena in Sn-3.0Ag-0.5Cu (in wt.%) solder bumps was investigated for application in the flip chip structure. Flip chip samples were cross-sectioned and polished to observe the electro-migration behavior under high current stressing. The electro-migration behavior was characterized by measuring the failure time at high current density and temperature. Current stressing was carried out in an ambient temperature of 120°C. A current was passed through the six solder joints, producing a nominal current density of  $2.0 \times 10^4$  A/cm<sup>2</sup>. The microstructure of the solder bumps at the cathode and anode sides were compared before

and after current stressing. Cross-sectional studies were conducted with scanning electron microscopy (SEM).

**Interfacial Reaction Comparison between Sn-3.0Ag-0.5Cu Solder Joint Attached to ENIG and ENEPIG Surface Finishes:** *Chien-Fu Tseng*<sup>1</sup>; Jenq-Gong Duh<sup>1</sup>; Tae-Kyu Lee<sup>2</sup>; Kuo-Chuan Liu<sup>2</sup>; <sup>1</sup>National Tsing Hua University; <sup>2</sup>Cisco Systems, Inc.

Solid-state interfacial reactions of Sn-3.0Ag-0.5Cu solder joint with ENIG and ENEPIG surface finish are investigated in this study. For the ENIG solder joint, two kinds of voids are observed at the interface, i.e. columnar voids in the P-rich layer and nano-voids among IMC. These two kinds of voids are believed to deteriorate the reliability of lead free solder joint. Therefore, retarding the formation of these two kinds of voids is a critical issue in the microelectronic packaging. Interestingly, only columnar voids were observed in the ENEPIG solder joint. Also, the grow rate of (Cu, Ni)<sub>6</sub>Sn<sub>5</sub> was found to be slower in the ENEPIG solder joint. Thus, the insertion of Pd layer seemed to improve the interfacial reaction which might improve the mechanical reliability. The detailed mechanism of microstructure variation for solder joint with different surface finish will be addressed with a discussion about the mechanism in this alloy system.

**High Bump Resistance of Ultra-Fine-Pitch Microbumps for Three-Dimensional Integrate Circuits Packaging:** *Yuan-wei Chang*<sup>1</sup>; Chih Chen<sup>1</sup>; <sup>1</sup>National Chiao Tung University

In decades, the technological improvement follows the Moore's law; the size of devices shrinks and the I/O number increases dramatically. In order to continually increase the I/O number, the three-dimensional integrate circuits (3D-IC) package is needed. In 3D-IC packaging, ultra-fine-pitch microbumps have been adopted to achieve the goal. Ultra-fine-pitch microbumps of 30  $\mu$ m were fabricated in this study. The bump resistance of the microbumps is obtained with the Kelvin-bump-structures. The bump resistance is approximate a hundred milliohms, much higher than that of a flip-chip bump. The unexpected high bump resistance causes high circuit inductance and RC delay. A finite-element-model (FEM) was also built to analyze the high bump resistance. The FEM shows the high resistance is caused by the current crowding. Increasing the trace thickness is an effective way to reduce the bump resistance. When the trace thickness increases from 0.8 to 3.0  $\mu$ m, the resistance reduces to a third.

**Joint Properties of Cu-Solder-Cu for Fine Pitch 3D Packaging:** *Min-Kyu Han*<sup>1</sup>; Se-Min Park<sup>2</sup>; Sehoon Yoo<sup>1</sup>; Chang-Woo Lee<sup>1</sup>; <sup>1</sup>Korea Institute of Industrial Technology; <sup>2</sup>Chosun University

Cu pillar has been received great attention in ultra fine pitch 3D packaging. In this study, Sn-Bi capped Cu pillars were bonded to Cu pads at 150~200°C. After bonding, the specimens were aged at 150°C up to 400 hrs to study on the microstructure of intermetallic compounds. Before aging, Cu<sub>6</sub>Sn<sub>5</sub> intermetallic compounds (IMCs) were observed at the Cu-SnBi interface. As aging time increased, the Cu<sub>6</sub>Sn<sub>5</sub> IMC thickness increased and Cu<sub>3</sub>Sn was formed below the Cu<sub>6</sub>Sn<sub>5</sub>. After 400hrs of aging, Bi was separated from the IMC interface. Continuous Kirkendall voids were also observed at the Cu<sub>6</sub>Sn<sub>5</sub>/Cu<sub>3</sub>Sn interfaces after 400 hr aging. Such void formation decreased the shear strength of the Cu pillar bumps.

**In-Situ Synchrotron Characterization of Melting, Dissolution and Resolidification in Lead-Free Solder Joints:** *Bite Zhou*<sup>1</sup>; Thomas Bieler<sup>1</sup>; Tae-Kyu Lee<sup>2</sup>; Kuo-Chuan Liu<sup>2</sup>; <sup>1</sup>Michigan State University; <sup>2</sup>Cisco Systems, Inc.

Melting and solidification of SAC 305 and 405 lead-free solders in a Wafer-Level-Chip-Scale package were examined in-situ with synchrotron x-ray diffraction. The chips with balls attached (but not assembled to a board) were reflowed 1-3 times. The temperature and time history was similar to an industrial reflow process. Laue patterns were collected every half second during the melting and solidification process. The melting and solidification of the Sn in the solder joint occurred in about 0.5-1 second, whereas it takes several 10's of seconds for some diffraction peaks from Cu<sub>6</sub>Sn<sub>5</sub> and Ni<sub>3</sub>Sn<sub>4</sub> precipitates to disappear as they dissolve in molten Sn. Some intermetallic peaks were persistent and did not change throughout



the melting and solidification process. The crystal orientation of tin and thermal strains were analyzed after each reflow. Different orientations of Sn always developed upon resolidification. Supported by NSF GOALI research contract DMR-1006656 with Cisco Systems.

**Joint Properties of Pb-Free Solder Bumps on Flexible Board:** *Won-Myoung Ki*<sup>1</sup>; *Sehoon Yoo*<sup>1</sup>; *Chang-Woo Lee*<sup>1</sup>; <sup>1</sup>Korea Institute of Industrial Technology

The aim of this study is to investigate mechanical properties and reliability according to changing process variables on mounting components by a roll-to-roll (R2R) process. The R2R process is an important method to improve productivity, especially for the packaging of flexible electronic modules. The R2R process was composed of underfill dispensing, chip mounting and thermal compression. Si chip with Pb-free solder bumps were joined on polyimide substrate by R2R process. Solder bumps to interconnect between chips and flexible substrates were made by electroplating. The microstructure and mechanical properties of the solder bump were evaluated by SEM, EDS and shear tester. Also the bumps were aged up to 400 hours at 100°C for estimation of its reliability.

**Effect of Zn Content on the Electrification-Fusion and Failure Behaviors of Sn-xZn Alloys:** *Gong-An Lan*<sup>1</sup>; *Chung-Wei Yang*<sup>2</sup>; *Truan-Sheng Lui*<sup>1</sup>; *Li-Hui Chen*<sup>1</sup>; <sup>1</sup>National Cheng Kung University; <sup>2</sup>National Formosa University

Microstructural features of Sn-xZn alloys with varying Zn content of 7, 9, 20, 30 wt.% on the electrification-fusion phenomenon was investigated in this study. Experimental results showed that the critical fusion current density (CFCD) of Sn-xZn alloys increased with increasing Zn content. The enrichment of Zn-rich phase was the main factor in the improvement of electrical conductivity and the required electrical current density for triggering microstructural evolution for the hypereutectic Sn-30Zn alloy was much higher than the hypoeutectic Sn-7Zn alloy. The increasing rate of CFCD has an obvious variation at the transition from the hypoeutectic composition (Sn-7Zn) to the eutectic composition (Sn-9Zn) due to the microstructural change caused by Zn content. The in-situ examination of microstructural evolution provided a constructive method for ascertaining the relationship between each individual phase, the CFCD and the fusion-induced failure mechanism of Sn-xZn alloys.

**High Temperature Gold Based Lead Free Solder:** *Heiner Lichtenberger*<sup>1</sup>; <sup>1</sup>Williams Advanced Materials

With the conversion to lead free solders, and their higher processing temperatures, a need has arisen for a Gold Tin solder with a higher melting point than the conventional 278C, 80Au 20Sn eutectic electronic solder. In this work we examine the effects of minor Germanium or Indium additions to the 80Au20Sn composition in an effort to raise its Liquidus and Solidus to 300C. In order to study the AuGeSn and AuInSn ternary phase diagrams, we made a series of ternary alloys to map out the Au20Sn area, with up to 6% Ge or 6% Sn, compositions of the diagrams. We found that additions of Germanium increased the Liquidus, but decreased the Solidus, leaving these ternary alloys vulnerable to reflow during subsequent lead free SAC alloy soldering. Successful alloys were created by adding Indium to the Au Sn binary system, generating a ternary eutectic solder with a melting point of 300C.

**Study of Interfacial Morphology in Flip Chip Solder Joints under Extra-High Current Density with Local Temperature Control:** *Ting-Li Yang*<sup>1</sup>; *Jia-Hong Ke*<sup>1</sup>; *C. Robert Kao*<sup>1</sup>; <sup>1</sup>National Taiwan University

Temperature and current density are two key factors in electromigration behaviors. A temperature control device, employing forced fluid convection, was used to de-couple the chip temperature from the applied current density. With this temperature control, the electromigration effect on UBM consumption and interfacial reactions in Cu/Sn2.6Ag/Cu flip chip solder joints was investigated under varied extra-high current densities of  $3.5 \times 10^4$  A/cm<sup>2</sup> and  $4.5 \times 10^4$  A/cm<sup>2</sup> at the chip temperature of 50 °C. A unique sawtooth-type Cu UBM morphology was observed at the cathode/chip and cathode/substrate side under extra-high current stressing. In this study, the possible mechanism for this sawtooth-type morphology resulting from the

particular condition of low temperature and extra-high current density will be discussed.

**Study of PCB Dynamics and Reliability Assessment of BGA's under Shock and Vibration Loading:** *Pradosh Guruprasad*<sup>1</sup>; *Brian Roggeman*<sup>2</sup>; *James Pitarresi*<sup>1</sup>; <sup>1</sup>Binghamton University; <sup>2</sup>Universal Instruments

Traditional electronics reliability testing centers around thermal cycling lifetimes, however with the transition to Pb-free soldering and the popularity prevalence of portable and handheld devices, mechanical loading is many times of much greater concern. Even those high reliability industries that are exempt from RoHS and still using SnPb soldering, shock and vibration loading is many times a greater risk for failure than thermal cycling. Unlike thermal cycling, test parameters in shock and vibration are not general but very specific to the test vehicle. The shock and vibration responses of a PCB are highly sensitive to the geometry, construction boundary conditions, and test inputs, which all need to be considered to run a relevant reliability test. This paper intends to discuss the dynamic factors of the printed circuit board under shock and vibration loading, the use of these as reliability tools, and the consequences in terms of failures modes and lifetimes.

**Shear Strength and the Weibull Failure Analysis of Sn-Ag-Cu Solder Ball Joints with Different Reflow Processes:** *Chung-Wei Yang*<sup>1</sup>; *Truan-Sheng Lui*<sup>2</sup>; *Li-Hui Chen*<sup>2</sup>; <sup>1</sup>National Formosa University; <sup>2</sup>National Cheng Kung University

This study evaluated the shear strength of Sn-3Ag-0.5Cu (SAC305) and Sn-4Ag-0.5Cu (SAC405) solder balls on Cu/Ni/Au substrate after reflow soldering. The failures of joints were evaluated by the Weibull model. Experimental results show the shear strength increased with increasing ball sizes after 245°C reflow. However, shear strength was decreased for applying reflow at 235 and 255°C. Fracture morphologies displayed the failure of joints was occurred within solder balls. It represented the solder/substrate interface was bonded for 245°C reflow. The strength of joints was not related to the thickness of interfacial intermetallic compounds (IMCs). The minimum shear strength of joints was increased and data fluctuation was decreased with applying an aging at 105°C for 8 h after 245°C reflow. The Weibull analysis showed SAC305 and SAC405 were reliable joints with a wear-out failure model. The knowledge of minimum shear strength is helpful for understanding the joint reliability of electronic packaging applications.

**Interfacial Reaction and Elemental Redistribution in Sn3.0Ag0.5Cu-xPd/ENIG Solder Joints after Aging:** *I-Tai Wang*<sup>1</sup>; *Jenq-Gong Duh*<sup>1</sup>; *Chin-Yuan Cheng*<sup>2</sup>; *Jim Wang*<sup>2</sup>; <sup>1</sup>National Tsing Hua University; <sup>2</sup>Shenmao Technology Inc.

Electroless Nickel/Electroless Palladium/Immersion Gold (ENEPIG) surface finish has been developed to overcome the "black pad" issue of Electroless Nickel/Immersion Gold (ENIG). After reflow, the electroless Pd layer of ENEPIG would dissolve in Cu6Sn5, which might reduce the growth of IMC and P-rich layer. Moreover, the solderability and reliability of ENEPIG are superior to those of ENIG. However, the Pd distribution in solder joint is not yet clear. In this study, the Sn3.0Ag0.5Cu solder was doped with 100~500ppm Pd, and then was reflowed with ENIG. Afterward, the Sn3.0Ag0.5Cu-xPd/ENIG solder joints were aged at 150 deg-C for various periods of time. The Pd distribution in solder and IMCs was systematically analyzed by a field emission electron probe microanalyzer. The correlation between Pd distribution and interfacial reaction of Sn3.0Ag0.5Cu-xPd/ENIG solder joints was probed and discussed. In addition, the role of Pd in the solder joint reliability was also addressed.

**Microstructure and Brazing Performance of Spray-Formed Si-40Al Alloy Used for Electronic Packaging:** *Bin Yang*<sup>1</sup>; <sup>1</sup>University of Science and Technology Beijing

The experimental results have shown that the wettability between spray-formed Si-40Al alloy and Sn-3.0Ag-0.5Cu solder was very poor. The high frequency impulse electro-deposition technique is beneficial to form a fine and sound nano-nickel coating on the surface of Si-40Al sample, which can effectively improve the brazing performance of the alloy. A new galvanized method to prepare nano-nickel coating on the surface of Si-Al alloys was

proposed. The brazing performance of spray-deposited Si-Al alloys with Ni coating was improved effectively. It is found that the galvanized surface of spray-formed Si-40Al alloy was activated for succeeding impulse electro-deposition nano-nickel coating. The brazing performance of plated Si-40Al alloy with Ni coating was tested again. It is found that certain element diffusion was carried out between the coating and weld layer, the weld layer and bond Cu, showing that the interface strength was fairly good.

**Interfacial Reactions and Physical Properties of the Sn-Cu-Based Lead-Free Solder Joints:** Petr Harcuba<sup>1</sup>; Miloš Janeček<sup>1</sup>; <sup>1</sup>Charles University in Prague

In this study the influence of Cu content and minor Ni addition on the growth kinetic and morphology of the layers of intermetallic compound was study during the reaction of liquid solder and Cu substrate and subsequent ageing. The strength and electric resistance of simulated solder joints were also investigated. The reaction of a Sn-0.7Cu alloy with the substrate leads to the formation of a thin layer of Cu<sub>6</sub>Sn<sub>5</sub> ( $\eta$ -phase) of typical scallop morphology, which does not grow with longer reaction time. Higher Cu content in Sn-1.4Cu alloy leads to the extensive growth with reaction time and at long reaction times, a Cu<sub>3</sub>Sn ( $\epsilon$ -phase) was observed at the interface between the Cu substrate and the Cu<sub>6</sub>Sn<sub>5</sub> layer. A small nickel addition to a Sn-0.7Cu alloy significantly changes the IMC morphology, accelerates its growth kinetics, prevents the formation of the Cu<sub>3</sub>Sn layer and reduces the rate of substrate dissolution.

**Effect of Multiple Reflow Processes on the Reliability and Microstructure of Sn-Ag-Cu-In Solder Joint:** A-Mi Yu<sup>1</sup>; Jae-Won Jang<sup>1</sup>; Mok-Soon Kim<sup>1</sup>; Jong-Hyun Lee<sup>2</sup>; Jun-Ki Kim<sup>3</sup>; <sup>1</sup>Inha University; <sup>2</sup>Seoul National University of Technology; <sup>3</sup>Korea Institute of Industrial Technology

The authors have previously reported that the quaternary Sn-1.2Ag-0.7Cu-0.4In(wt%) alloy showed excellent wettability and mechanical reliability. Moreover, the addition of small amount of Pd or Mn was considered to improve its reliability to a greater extent especially in drop impact condition. In this study, the effect of multiple reflow processes on the drop impact reliability and microstructure of Sn-1.2Ag-0.7Cu-0.4In-X solder joints was investigated. The test package was prepared with OSP (organic solderability preservative)/Cu finished FR-4 PCB and ENIG finished BGA package. After the first reflow, the samples were repeated reflow of 3 and 5 cycles. The drop impact reliability tests were performed in a various ways and the results were compared with those of Sn-1.0Ag-0.5Cu and Sn-3.0Ag-0.5Cu alloys. The microstructure and partitioning of alloying elements in the solder joint were analyzed using SEM, EDS, XRD, EPMA and XPS.

**In Situ Stress Measurement by Synchrotron Radiation X-Ray in Pure Tin Stripes and Flip Chip with Microbumps on Silicon Substrates:** Hsueh-Hsien Hsu<sup>1</sup>; Chun-Yang Tsai<sup>1</sup>; Hsin-Yi Lee<sup>2</sup>; Ching-Shun Ku<sup>2</sup>; Albert T. Wu<sup>1</sup>; <sup>1</sup>National Central University; <sup>2</sup>National Synchrotron Research Center

The first part of the talk emphasizes the electromigration induced stress in pure tin stripes measured by Synchrotron radiation X-ray. Tin stripes were current stressed by  $5 \times 10^3$  A/cm<sup>2</sup> at 100°C while in situ detecting the diffraction signals. Both  $\theta$  and  $\Psi$  angles varied to measure the stresses at the cathode and the anode by  $\sin^2\Psi$  method. The transient changes in stress gradient provide the kinetics information of tin atoms under current. The  $DZ^*$  was calculated to be about  $2.6 \times 10^{-12}$  m<sup>2</sup>/s under electromigration. The second part focuses on in situ analyze the stress in silicon of flip chips with microbumps that were assembled on Si substrates. Each microbump was stressed with an average current density of  $1 \times 10^4$  A/cm<sup>2</sup>. Comparing to the conventional FR-4 substrates, the chips with silicon substrates showed less deformation. However, the results suggested that the deformation of the chips were greatly affected by underfill.

**Microstructure and Native Oxide Scale Characteristics of a Cu-9at.%La Alloy:** Bilge Senturk<sup>1</sup>; Yong Liu<sup>1</sup>; Joseph Mantese<sup>2</sup>; Pamir Alpay<sup>1</sup>; Mark Aindow<sup>1</sup>; <sup>1</sup>University of Connecticut; <sup>2</sup>United Technologies Research Center

Copper is used widely for electrical contacts due to its high electrical conductivity, ease of fabrication and low cost. The main drawback is

that copper forms a low-conductivity native oxide scale resulting in the development of high contact resistance. To overcome this, copper-based alloys that form inherently conductive native oxide scales are being developed. Here we present a study of the microstructure and electrical contact resistance behavior of a Cu-9 at.%La alloy to demonstrate the viability of this approach. The alloy has a uniform eutectic microstructure with rods of Cu in a Cu<sub>6</sub>La matrix. The oxide scale formed in air on the rods comprises a thin layer of pure Cu<sub>2</sub>O on the Cu rods and a thicker La-doped Cu<sub>2</sub>O layer on the Cu<sub>6</sub>La matrix. Although the scale is thicker than that formed on pure Cu, the contact resistance is lower and the mechanisms for this effect will be discussed.

**Electromigration Behavior of Sn-In Lead-Free Solder Alloy Under High Current Stress:** Kiju Lee<sup>1</sup>; Keun-Soo Kim<sup>1</sup>; Katsuaki Sukanuma<sup>1</sup>; <sup>1</sup>Osaka University

The electromigration behaviors of Cu/Sn-In/Cu solder strip models were examined under high electrical current density (10 kA/cm<sup>2</sup>) at high temperature (140 °C). The composition of Indium was 0, 4, 8 and 16 in wt%. The Sn-In solder interconnection with bare Cu substrate was prepared by reflow soldering up to 250°C. As a result of microstructural analysis, primary intermetallic compounds formed at the interface of Cu/Sn-In was confirmed as Cu<sub>6</sub>(In, Sn)<sub>5</sub> with various indium composition. After current stressing, voids and cracks formed at the cathode side and intermetallic compounds formed at the anode side. The addition of indium effectively reduces the grain size and forms an intermetallic compound network along grain boundaries of Sn. In the case of the Sn-8-16wt%In solder, migration of Cu and Sn atoms can be effectively suppressed.

**Multiscale Simulation of Fracture in Lead-Free Solder Joints:** Huiyang Fei<sup>1</sup>; Kyle Yazzie<sup>1</sup>; Nikhilesh Chawla<sup>1</sup>; Hanqing Jiang<sup>1</sup>; <sup>1</sup>Arizona State University

The structural reliability of lead-free solder joint is of great interest in both academic and industrial societies. In this talk, a combination of fracture models has been used to study the fracture mechanism of lead-free solder joint with a Cu-Sn-Cu bar structure. In our analysis, Copper is considered as isotropic elastic-plastic and the intermetallic compound (IMC) fails by brittle fracture. The key contribution of our work is that we developed a stochastic enhancement for the Modified Gursion Model, and have applied it to lead-free solder alloys. This stochastic enhancement method better characterizes the real distribution of microvoids in porous metals, and better predicts the failure than non-randomized Modified Gursion Model. The simulation was conducted in the FEA package ABAQUS with our enhancement. This work gives a reasonable explanation for the fracture mechanism of lead-free solder joint, and furthermore points out a way to improve the structural reliability of the joint.

**Thermomigration of Al in Flip-Chip Solder Joints:** Hsiao-Yun Chen<sup>1</sup>; Chih Chen<sup>1</sup>; <sup>1</sup>National Chiao Tung University

The electromigration and thermomigration behaviors of lead-free solders have been investigated under a current density of  $9 \times 10^3$  A/cm<sup>2</sup> at 150°C. It is found that voids not only formed inside solder bumps with and without current stressing, but also formed inside the upper Al trace, which was without current passing through. Theoretical calculation indicates that the thermomigration force under this condition is large enough to push Al atoms migrate from upper chip side to the cold end on substrate side. Moreover, the original Ti layer between Al trace and Cu UBM was vanished and Cu-Al intermetallic compounds (IMCs) can also be found. The results here inferred that thermomigration of Al itself can induce deterioration of Al trace and therefore followed by resistance increase and greater Joule heating effect. This study can provide us a new insight in understanding the deterioration of Al trace under a thermal gradient during the electromigration test.

**Calculation of Ni/Cu<sub>6</sub>Sn<sub>5</sub> Inter-Diffusion Coefficient and Activation Energy by Using Bulk Cu<sub>6</sub>Sn<sub>5</sub> Substrate:** *Kuan Chih Huang*<sup>1</sup>; Yu Hsiang Hsiao<sup>2</sup>; Cheng Yi Liu<sup>2</sup>; Fuh Sheng Shieue<sup>1</sup>; <sup>1</sup>National Chung Hsing University; <sup>2</sup>National Central University

Ni layer is usually introduced as a diffusion barrier layer at Cu/Sn interface for Flip-Chip and ball-grid array (BGA) solder bumps. The diffusion of Ni atoms in Cu/Sn intermetallic compound (IMC) and activation energy of compound growth is studied. Ni thin film was deposited on bulk Cu<sub>6</sub>Sn<sub>5</sub> and annealed for 2 hours in vacuum. The Ni atomic depth profiles would be detected by electron spectroscopy for chemical analysis (ESCA). We can calculate the Ni inter-diffusion coefficient "D" by Matano method. In our study, the annealing temperatures are 120°C, 160°C, 200°C, 255°C, 290°C, and 320°C. From six Ni atomic depth profiles, the activation energy Q (based on Cu<sub>6</sub>Sn<sub>5</sub> and Ni<sub>3</sub>Sn<sub>4</sub> crystal structure) for different atomic percentage of Ni atoms were determined by using Arrhenius plot based upon the equation:  $\ln D = -Q/kT + \ln D_0$ .

**Effects of the Substrate Topography on the Black Pad Formation after Electroless Nickel Immersion Gold (ENIG) Process:** *Ji Hee Kim*<sup>1</sup>; Jin Yu<sup>1</sup>; <sup>1</sup>Korea Advanced Institute of Science and Technology

Black Pad phenomenon reported to occur in the ENIG UBM (under bump metallurgy) seriously damages the wetting property of the solder and thereby degrades the solder joint reliability. Black pad is known to be caused by the hypercorrosion of Ni in the IG solution, however a thorough understanding on the phenomenon has not been procured yet due to the difficulty of the sample reproducibility. At EPL (electronics packaging laboratory) of KAIST, black pad was reproduced using standard chemicals, and a systematic work has been carried out. Most recently, a corrosion couple made of two electroless nickel films with different P content demonstrated the occurrence of black pad on the low P side (Scripta Materialia 2010). Here, three specimens with different substrate topography; Cu block, rolled Cu foil and sputter deposited Cu film underwent the same ENIG process; thereby the same P content in the EN film, and characteristics of the black pad formation were analyzed. Using AFM, SEM, XRD and TEM. All the specimens showed preferential corrosion along the nodule boundaries after the IG process, however, there were large variations in the corrosion susceptibility, which was ascribed to surface roughness, texture and others.

## Physical and Mechanical Metallurgy of Shape Memory Alloys for Actuator Applications: Poster Session

*Sponsored by:* The Minerals, Metals and Materials Society  
*Program Organizers:* S. Raj, NASA Glenn Research Center; Raj Vaidyanathan, University of Central Florida; Ibrahim Karaman, Texas A&M University; Ronald Noebe, NASA Glenn Research Center; Frederick Calkins, The Boeing Company; Shuichi Miyazaki, Institute of Materials Science, University of Tsukuba

Sun PM-Thurs AM  
Feb 27-Mar 3, 2011

Room: 11B  
Location: San Diego Conv. Ctr

**Adaptive Shape Memory Actuator Systems for Applications at Varying Boundary Conditions:** Horst Meier<sup>1</sup>; Alexander Czechowicz<sup>1</sup>; Sven Langbein<sup>1</sup>; <sup>1</sup>Ruhr-University Bochum

Due to their possibility to recover an imprinted shape by thermal or electrical activation, shape memory alloys (SMA) are suitable for actuator applications. Their dynamical behavior depends inter alia on the boundary conditions, exemplary the thermally field. Therefore the wide range of possible applications is today reduced to systems with slight thermal variations, and to temperatures which are less than the retransformation temperature (Mf). In order to design systems which adapt automatically to these changes, various experiments with SMA-alloys have been made, which are presented in this paper. The solutions to the boundary condition problem can be subdivided into active and passive approaches, which are presented as automotive applications in this elaboration.

**Effect of H in Metals and Alloys: An Application to bcc W and NiTi Alloy:** *Amitava Moitra*<sup>1</sup>; Kiran Solanki<sup>1</sup>; <sup>1</sup>Center for Advanced Vehicular Systems

Strengthening and embrittlement are controlled by the interactions between lattice defects and hydrogen induced defect structures that can inversely affect the deformation mechanisms in materials. These interactions depend on the character of the defects, the nature of the material, and the impurity. To understand environmental effects on the damage of materials, we performed first principles density functional theory based study in a pure bcc W, and NiTi shape memory alloy. Local distortions due to interstitial H are examined along with the diffusion barrier for an H atom from one interstitial to another. Finally H adsorption and penetration through the surface to the bulk has been analyzed.

**Growth of Oriented Nickel Manganese Gallium Single Crystals via the Bridgman Method:** *Douglas Kellis*<sup>1</sup>; K. Ullakko<sup>1</sup>; P. Müllner<sup>1</sup>; <sup>1</sup>Boise State University

Magnetic shape memory alloys such as nickel manganese gallium show great promise as actuating and sensing applications due a strong coupling between magnetic and crystallographic domains (twins) leading to magnetic-field-induced strains of up to 10%. Fabrication of Ni-Mn-Ga single crystals is hampered by strong chemical segregation during crystal growth and material losses resulting from the off-axis orientation of crystals grown by the Bridgman method. We built a single crystal growth furnace with a temperature gradient of 20 K/mm capable of growing crystals from an oriented seed. Systematic crystal growth experiments were performed by varying the growth velocity and the seed temperature. At a growth velocity of 0.08 mm/min, oriented single crystals were obtained with a constant composition over 60% of the crystal. With increasing growth velocity, the tendency for nucleation increases, resulting in off-axis oriented crystals and elongated grains. This technique provides a method for the rapid and efficient production of Ni-Mn-Ga single crystals.

**Mechanism of Artifact Formation on NiTi Alloy during Metallographic Preparation:** *Andreas Undisz*<sup>1</sup>; Klemens Reuther<sup>2</sup>; Helfried Reuther<sup>2</sup>; Markus Rettenmayr<sup>2</sup>; <sup>1</sup>University of Jena; <sup>2</sup>Friedrich-Schiller-University; <sup>3</sup>Research Center Dresden-Rossendorf

Statements on the structure/property relationship of NiTi via structure characterization based on metallographic preparation have been shown to be ambiguous. In the literature, acicular structures on NiTi after metallographic preparation are often interpreted as martensite or martensitic surface relief. The composition of the acicular structures cannot be distinguished from the bulk material by standard analysis, e.g. EDX or AES. However, these structures were recently identified as artifacts. NiTi samples were observed at different stages of preparation using SEM, EDX and AES. Rod-like crystals were detected on the NiTi surface. The crystals form during etching with solutions containing hydrofluoric acid and were identified as NiTiF<sub>6</sub>·6H<sub>2</sub>O by XRD. During etching, the crystals locally prevent contact of etching solution and NiTi. Further etching solely removes NiTi at adjacent uncovered areas. During cleaning with water the crystals dissolve and the surface relief with a shape according to that of the dissolved crystals remains.

**Microstructure and Martensitic Transformation Characteristics of CoNiGa High Temperature Shape Memory Alloys:** *Ebubekir Dogan*<sup>1</sup>; Ibrahim Karaman<sup>1</sup>; Zhiping Luo<sup>1</sup>; Yuriy Chumlyakov<sup>2</sup>; <sup>1</sup>Texas A&M University; <sup>2</sup>Siberian Physical Technical Institute

Microstructure and martensitic transformation characteristics of Co<sub>46</sub>Ni<sub>27</sub>Ga<sub>27</sub> and Co<sub>44</sub>Ni<sub>26</sub>Ga<sub>30</sub> high temperature shape memory alloys were investigated as a function of heat treatment. Heat treatments were selected to introduce single, two, and three phase structures, where the precipitate phases don't martensitically transform. The effects of these precipitates, and associated compositional changes, on transformation temperatures and microstructural evolution during thermal cycling were revealed. The most cyclically stable compositions with narrow hysteresis (<40 °C) were identified. It was also found that Ms temperature linearly depends on the valence electron concentration (e/a) of the matrix, if the Ga content is constant. For a given e/a, the higher the Ga content is, the higher



the transformation temperatures become. The samples with narrow hysteresis demonstrate reversible martensitic transformation in constant-stress thermal cycling experiments. However, their crystallographic texture should be engineered to increase the transformation strain, and ductile  $\gamma$ -phase content should be reduced to improve cyclic reversibility.

**Microstructure and Shape Memory Characteristics of Powder Metallurgical Processed TiNiCu Alloys:** *Yeon-wook Kim*<sup>1</sup>; Young-soo Chung<sup>2</sup>; Eunsoo Choi Choi<sup>3</sup>; Tae-hyun Nam Nam<sup>4</sup>; <sup>1</sup>Keimyung University; <sup>2</sup>Chungang University; <sup>3</sup>Hongik University; <sup>4</sup>Gyeongsang National University

Although Ti-Ni-Cu alloys have attracted a lot of attention due to their high performance of shape memory effect and decrease of thermal and stress hysteresis in comparison with Ti-Ni binary alloys, their poor workability restrains the practical applications of Ti-Ni-Cu shape memory alloys. Consolidation of TiNiCu alloy powders is very useful for the fabrication of bulk near-net-shape shape memory alloy. Ti50Ni30Cu20 shape memory alloy powders were prepared by gas atomization, and the dense cylindrical bulk was prepared from the powders by spark plasma sintering. Single step martensitic transformation of B2-B19' was observed for both powders and bulk. Ms of the 10-20  $\mu\text{m}$  powders was 30°C and continued to decrease inconsiderably with increasing powder size. The difference of Ms between 10-20  $\mu\text{m}$  powders and 150-200  $\mu\text{m}$  powders is only 2°C. However, Ms of bulk samples was lower than those of as-atomized powders because of microstructural changes during SPS sintering.

**Origin of Non Recoverable Strain in NiTi and NiTiFe Shape Memory Alloys on Thermal Cycling:** *Ritwik Basu*<sup>1</sup>; Bikas Maji<sup>2</sup>; Prita Pant<sup>1</sup>; Indradev Samajdar<sup>1</sup>; Madangopal Krishnan<sup>2</sup>; <sup>1</sup>Indian Institute of Technology Bombay; <sup>2</sup>Bhabha Atomic Research Centre, Mumbai

The aim of this work is to study the effect of thermal cycling on the non-recoverable strain for alloys of two different compositions, NiTi and NiTiFe. We started with three different microstructures for each of these alloy composition. The major results of this work concern the microstructure of these alloys and distribution of fine grains. We have shown that the microstructure which shows largest clustering of fine grains exhibits the largest non recoverable strains after a few thermal cycles. Finally we have shown that the main condition for the martensite to revert back to austenite is to obey an orientation relationship which in successive thermal cycle is violated and therefore the fraction of retained martensite increases after every cycle which is the key factor for the non recoverable strain. The micro texture and microstructure have been studied using electron backscattering diffraction and orientation imaging mapping (EBSD-OIM).

**Oxidation Behavior of Sputter-Deposited TiNiPd Sharp Memory Films:** *Shiqiang Qian*<sup>1</sup>; <sup>1</sup>School of Materials Engineering, Shanghai University of Engineering Science

Using TGA and AES the oxidation dynamics of sputter-deposited TiNiPd films and the contents of oxygen and other elements in surface layer of the films were investigated. It was found that TiNiPd films are oxidizable more than TiNi films and their short time oxidation character accords with linearity-parabola law. The results showed oxygenizing activation energy of amorphous films is almost equal to that of titanium dioxide (TiO<sub>2</sub>) but that of crystal films is less than the half of titanium dioxide. This is one reason that TiNiPd films are oxidizable easily. The research attested that the Pd atom promoted the combine of O atom and Ti atom and excluded Ti atom of oxide at interface, therefore, led the Ti atom in the film to diffuse out through oxide interface, which is the principal reason that TiNiPd films is more oxidizable than that of TiNi films.

**Phase Transformations in Sputtered NiMnGa Thin Films:** Nishitha Jetta<sup>1</sup>; Steven Rios<sup>1</sup>; Nevin Ozdemir<sup>1</sup>; Ibrahim Karaman<sup>1</sup>; *Xinghang Zhang*<sup>1</sup>; <sup>1</sup>Texas A&M University

NiMnGa films have been prepared by the DC magnetron sputtering technique on partially oxidized Si (100) substrates. As-deposited films show a quasi-amorphous structure that crystallize on heating to ~ 230°C. Crystallization study using Kissinger's analysis reveals a relatively low activation energy indicating partial crystallinity in the films. Phase transformations studied

using in-situ and ex-situ XRD and TEM techniques show reversible transitions between martensite and austenite phases, and phase segregation to non-transforming L12 precipitates at higher temperatures. It was observed that phase segregation can be suppressed by proper heat treatment.

**Powder Metallurgy Processing of Replicated Ni-Mn-Ga Foams:** *Peiqi Zheng*<sup>1</sup>; Bing Ye<sup>1</sup>; Cassie Witherspoon<sup>2</sup>; Peter Müllner<sup>2</sup>; David Dunand<sup>1</sup>; <sup>1</sup>Northwestern University; <sup>2</sup>Boise State University

Previously, we demonstrated very large magnetic-field induced strain (MFIS) of up to ~8.7% in replication-cast Ni-Mn-Ga foams, where the molten alloy infiltrates a bed of space-holder which is subsequently dissolved to create porosity. This casting process requires a space-holder with very high melting point (NaAlO<sub>2</sub>) which is difficult to remove. Here, we apply the powder metallurgy replication method to produce a Ni-Mn-Ga foam by densifying Ni-Mn-Ga and BaCl<sub>2</sub> (melting point of 965 °C) blend powders and then dissolving BaCl<sub>2</sub>. Vacuum hot pressing at 930 °C under a 30 MPa pressure results in densified Ni-Mn-Ga/BaCl<sub>2</sub> composites. The high solubility of BaCl<sub>2</sub> in water permits a rapid removal while the powder metallurgy route opens the door to easy manipulation of pore size, shape and connectivity. We compare architecture, microstructure, magnetic properties, and MFIS of the present hot-pressed Ni-Mn-Ga foams with those of the previous cast foams.

**Relationship between Orientation and Strain of Polycrystalline Ni<sub>50</sub>Mn<sub>20</sub>Ga<sub>21</sub> Samples:** *Claudia Hürrieh*<sup>1</sup>; Martin Pötschke<sup>1</sup>; Stefan Roth<sup>1</sup>; Bernd Rellinghaus<sup>1</sup>; Ludwig Schultz<sup>1</sup>; <sup>1</sup>IFW Dresden

The Ni-Mn-Ga magnetic shape memory alloy provokes plenty of interest for application because of the effect that twin variants reorient by the action of an external magnetic field. Most of the experiments were concentrated on single crystals. But, this effect can also be realized in polycrystals which can be prepared much more efficiently. Here, polycrystalline samples were prepared by directional solidification with a <100> fibre texture of the high temperature cubic phase parallel to the heat flow. A heat treatment was applied for chemical homogenisation and stress relaxation. Samples were heated up to the austenitic state and cooled down under load. The microstructure was analyzed by EBSD before and after that treatment. Stress-strain curves were measured at room temperature and at 40°C. As a result of such treatment the twinning stress is reduced and the twinning strain is maximized. This work is supported by DFG within SPP 1239.

**Standardized Shape Memory Actuators for Axis Drives in Modular Machine Tools:** Horst Meier<sup>1</sup>; *Alexander Czechowicz*<sup>1</sup>; Sven Langbein<sup>1</sup>; <sup>1</sup>Ruhr-University Bochum

Shape memory alloys (SMA) are materials which are able to generate high forces and adaptive strokes in actuator applications. It is remarkable that available systems using shape memory drives are commonly individual designs done by system developers. The SMA-development process is complicated due to underestimation of the complex material behavior and there is no wide field of SMA-development experience in medium-sized enterprises. Therefore standardized systems are essential to invent new products with SMA. As an example, an axis drive for a modular machine tool is presented, using standardized shape memory actuators. Because of the unique properties of SMA, this machine can move a slide precisely and with a minimum of effort. This paper contains the approaches towards the development of standardized systems and the experimental results of their combination to positioning modules.

**Study of Magnetic Domain Structures in a Ni-Mn-Ga Alloy by Aberration Corrected Lorentz Transmission Electron Microscopy:** *Abhijeet Budruk*<sup>1</sup>; Marc De Graef<sup>1</sup>; <sup>1</sup>Carnegie Mellon University

Magnetic shape memory alloys (MSMAs) have a large magnetic field induced strain (up to 9.5% in non-stoichiometric Ni-Mn-Ga alloys). These large strains are thought to result from a rearrangement of martensite twin variants under the influence of a magnetic field. The Lorentz TEM observation mode is used regularly to study the magnetic domain structure in thin foils of ferromagnetic materials. Until recently, the spatial resolution for such magnetic imaging was limited by objective lens aberrations. In

this study, we have employed an aberration corrected Lorentz TEM to image the magnetic domain structures associated with lattice defects in a  $\text{Ni}_{49.9}\text{Mn}_{28.3}\text{Ga}_{21.8}$  alloy. Anti-phase boundaries and twin boundaries were found to interact strongly with magnetic domain walls, whereas dislocations do not show significant interactions. Depending on the orientation of the magnetic easy axis, the twin variants displayed either a maze like domain structure or a 180 degree domain wall pattern.

**The Effect of Composition on the Shape Memory and Super Elasticity Effect of Nano-Structured Ni-Ti Thin Films:** Maryam Mohri<sup>1</sup>; *Mahmoud Nili-Ahmadabadi*<sup>1</sup>; Hamidreza Rezaeean<sup>1</sup>; <sup>1</sup>university of Tehran

Shape memory thin films formed by sputtering are attractive candidates for micro actuators owing to their large deformation and strong recovery force. In this study three types of Ni-Ti thin films have been deposited on polyimide substrates by dc magnetron sputtering source fitted with an alloy target. Ti and Ni-rich thin films were separately deposited on polyimide substrate. And also a composite layer of Ti and Ni-rich. In order to obtain a variety of film compositions, several discs of alloy target were used. The as deposited Ni-Ti thin films were crystallized at different temperatures and times to change the amorphous structure to a nano-structured material. The effect of composition on film structure, transformation temperature and mechanical behavior was studied by using energy dispersive X-ray spectroscopy, X-ray diffraction (XRD), atomic force microscope (AFM), electrical resistivity and nanoindentation. Superelasticity effect and transformation temperatures of thin films have been compared to each other.

**Thermomechanical Treatment Effects on Two-Way Shape Memory in Ti-49.2%Ni Alloy:** Fatemeh Daei<sup>1</sup>; *Mahmoud Nili-Ahmadabadi*<sup>1</sup>; <sup>1</sup>University of Tehran

In this research, the effect of thermomechanical treatment (cold working + annealing) and number of training cycles was investigated on two-way shape memory effect (TWSME) in a Ti-49.2at.%Ni alloy. The ingot was prepared in a vacuum arc remelting furnace with non-consumable electrode followed by forging, homogenization at 1000°C and water quenching. The samples prepared from the homogenized ingot were cold rolled to induce different cold workings. Annealing treatment was performed at 450°C for 30 and 60 min after 10, 20 and 25% cold working. The samples were trained in martensitic state in order to investigate the two-way shape memory effect by bending deformation. Results indicate that the optimum recovery was obtained after 25% cold working followed by annealing at 450°C for 60 min. Also, the TWSME recovery increases by increasing the training cycles and finally reaches to steady state.

**Turning of NiTi Based Shape Memory Alloy Using Ultrasonic Vibration:** Amir Chegini<sup>1</sup>; *Saeed Tamimi*<sup>2</sup>; Zahra Chegini<sup>1</sup>; Hang Baharuddin<sup>1</sup>; Mehdi Sanjari<sup>3</sup>; <sup>1</sup>Department of Mechanical Engineering; <sup>2</sup>TEMA; <sup>3</sup>Department of Material Science

In this study, vibration cutting has been applied to machining of NiTi based shape memory alloy (SMA), using a commercial ultrasonic piezoelectric transducer to vibrate a standard insert geometry cutting tool. The effect of vibration in turning process was characterized by investigating the surface roughness of work piece and surface quality assessment of machined surface using Light microscopy. Turning was conducted by ultrasonic cutting vibration applied in the direction of feed using auto-resonant control software. The surface roughness of the conventionally and ultrasonically machined work pieces are measured. The intend of the current research is to make a facility of ultrasonic-assisted turning (UAT) to machining NiTi based SMA and to guess the potential improvements in surface quality, using commercial transducers and standard insert cutting tool. The results indicate that the use of ultrasonic vibration can significantly get better the surface quality of NiTi based alloy up to 30%.

## Polycrystal Modelling with Experimental Integration: A Symposium Honoring Carlos Tome: Poster Session

*Sponsored by:* The Minerals, Metals and Materials Society, TMS Structural Materials Division, TMS Materials Processing and Manufacturing Division, ASM-MSCTS: Texture and Anisotropy Committee, TMS/ASM: Mechanical Behavior of Materials Committee, TMS/ASM: Computational Materials Science and Engineering Committee

*Program Organizers:* Ricardo Lebensohn, Los Alamos National Laboratory; Sean Agnew, University of Virginia; Mark Daymond, Queens's University

Sun PM-Thurs AM  
Feb 27-Mar 3, 2011

Room: 6C  
Location: San Diego Conv. Ctr

*Session Chairs:* Carlos Tome, Los Alamos National Laboratory; Ricardo Lebensohn, Los Alamos National Laboratory

**An Electron Microscopy Study of the Intermetallic Phases in a Hot Dip Galvanize Coating on IF Steel:** *Md Zakaria Quadir*<sup>1</sup>; Syahbuddin Syahbuddin<sup>1</sup>; Karen Privat<sup>1</sup>; Charlie Kong<sup>1</sup>; Paul Munroe<sup>1</sup>; <sup>1</sup>University of New South Wales

The quantitative distribution of structural morphology and crystallography of a hot dipped galvanized zinc coating on an interstitial free steel has been investigated. After 5 to 60 seconds dipping the gamma, delta, zeta and eata-Zn phases were found to be organized sequentially in the coating on the steel surface. The interfaces between the phases are irregular and the interface between zeta and eata-Zn phases was much diffused. The eata-Zn phase was also found to be trapped in the zeta phase and the spatial distribution of the eata-Zn in the zeta (FeZn13) is correlated to the interface profile between the zeta and delta (FeZn10) phases. The presence of compositional variation within zeta phases indicates the occurrence of spinodal decomposition along <110> monoclinic direction as proved by TEM diffraction analysis. The growth of the zeta phase is highly textured along [100] and [001] crystallographic directions of their monoclinic lattice.

**Deformation Behavior of Steel Alloys under Combined Axial-Torsional Loading:** *Dayakar Penumadu*<sup>1</sup>; Akawat Siriruk<sup>1</sup>; Elena Garlea<sup>2</sup>; <sup>1</sup>University of Tennessee; <sup>2</sup>B&W Y-12, L.L.C.

Using hollow cylinder samples with suitable geometry obtained from round bar stock and flat dog-bone samples from sheets, the deformation behavior of bcc alloys is evaluated under multi-axial conditions. A strain gage rosette mounted at the mid height of the specimen provided strain tensor as a function of applied stress for pure tensile and torsion tests prior to yielding. Flat specimens are not ideal for use in experiments which involves varying rotation of principal stress, but are quite practical to study the behavior in the limit (pure tension versus torsion) for sheet metals. To study the elastic and yield behavior as a function of microstructure, hollow cylinder shape (tubes) with small wall thickness and relatively (to its thickness) large inner diameter was used. The variation of observed yield surface in deviatoric plane and the effect on mode of deformation (tension versus torsion and their combination) on texture is discussed.

**Deformation Localization in Two-Dimensional Single Crystals:** *M. Arulkumar*<sup>1</sup>; Sivasambu Mahesh<sup>1</sup>; P. Venkitanarayanan<sup>1</sup>; <sup>1</sup>Indian Institute of Technology, Kanpur

A novel methodology to predict localization of deformation in single crystals is developed. This approach regards the single crystal as a stack of sub-granular rate-independent rigid-plastic domains separated by parallel dislocation walls. Traction and velocity continuity are enforced across the dislocation walls. If dislocation wall mobility and dynamic recrystallization induced reduction in the hardening rate are suitably incorporated, small initial lattice perturbation across the walls can develop into large intragranular misorientations for suitably oriented single crystals. The present methodology is used to map out regions of deformation localization

in the lattice orientation and slip system hardening spaces of ideal two dimensional single crystals endowed with two slip systems (Asaro 1979). It also successfully predicts deformation localization in several experimentally well studied fcc single crystal orientations.

**Development of an In-Situ Experimental Technique for Characterizing Strain Localization in Polycrystalline Ni-Base Superalloys:** *Jennifer Walley*<sup>1</sup>; Robert Wheeler<sup>2</sup>; Michael Uchic<sup>3</sup>; Michael Mills<sup>1</sup>; <sup>1</sup>The Ohio State University; <sup>2</sup>UES; <sup>3</sup>Air Force Research Laboratory

An in-situ experimental methodology is being developed to characterize local strain heterogeneities in polycrystalline nickel-based superalloys. The data collected is directly applicable towards validating crystal plasticity models. Initial work was conducted on Rene 104 that was heat treated to produce two sets of samples with similar grain size distributions but different  $\square$ ' distributions and grain boundary morphologies. This talk will focus on the technical issues associated with performing quasi-isostatic tensile tests at elevated temperature in a scanning electron microscope (SEM). Electron beam lithography techniques were developed to produce a suitable speckle pattern on the surface to facilitate full field strain analysis. The speckle pattern and microscope magnification were optimized to obtain the resolution necessary to discern strain localizations within grain interiors and along grain boundaries using Correlated Solutions VIC-2D strain mapping software. Limitations due to SEM image distortions and the in-situ tensile stage and heating element will be discussed.

**Evolution of Dislocation Density and Burgers Vector Types with Annealing Temperature in Compressed Texture-Free and Compressed Rolled Beryllium Samples Determined by Diffraction Line Profile Analysis:** *Levente Balogh*<sup>1</sup>; Donald Brown<sup>1</sup>; Bjorn Clausen<sup>2</sup>; Diana Donati<sup>2</sup>; Thomas Sisneros<sup>1</sup>; <sup>1</sup>Materials Science and Technology Division, Los Alamos National Laboratory; <sup>2</sup>Los Alamos Neutron Science Center, Los Alamos National Laboratory

Texture-free and rolling induced textured pure beryllium samples were deformed to 20% by compression and then annealed on temperatures between 100 and 550 degrees Celsius with steps of 50 degrees. In situ neutron diffraction measurements have been conducted during the annealing process using the Neutron Powder Diffractometer (NPDF) instrument located at the Lujan Neutron Scattering Center (LANSCE), Los Alamos National Laboratory. The powder diffraction patterns were evaluated by the Diffraction Line Profile Analysis method (DLPA). The DLPA procedure is able to provide the sub-grain size distribution and the characteristic parameters of the dislocation structure for a variety of crystal structures. When used on hexagonal powder diffraction patterns, besides the sub-grain size distribution and total dislocation density, DLPA is able to determine the ratio of the partial densities consisting of dislocations with  $\langle a \rangle$ ,  $\langle c+a \rangle$  and  $\langle c \rangle$  Burgers vector types. Results show, that the recovery rate of the dislocation density depends on the relative orientation of the compression axis to the rolling induced texture. The evolution of the partial dislocation densities consisting of the different Burgers vector types show, that dislocations with  $\langle a \rangle$  type Burgers vectors recover faster, than  $\langle c+a \rangle$  type dislocations.

**EBSD Measurement of Deformation Behavior and Orientation Change in Dual Phase Steel Sheet during Equi-Biaxial Tension:** *Do Hyun Kim*<sup>1</sup>; Se-Jong Kim<sup>1</sup>; Anthony Rollett<sup>2</sup>; Heung Nam Han<sup>1</sup>; Kyu Hwan Oh<sup>1</sup>; <sup>1</sup>Seoul National University; <sup>2</sup>Carnegie-Mellon University

Modern steels rely on a two-phase microstructure with soft ferrite and hard martensite. This dual phase microstructure leads to an excellent combination of tensile strength and elongation. A novel experimental setting for electron backscattering diffraction was developed to characterize equi-biaxial tensile tests. To measure the orientation change in the same area on the specimen during equi-biaxial deformation, four micro-indentation marks were placed on the center top of the surface before loading. The distribution and amount of martensite before loading were derived from the band contrast map. The local misorientation change in each ferrite grain was measured as a function of strain. The effect of the hard martensite on local misorientation change in soft ferrite grains was analyzed, as well as interactions between adjacent ferrite grains. Surface topography was also measured before and after

the equi-biaxial deformation by Atomic Force Microscope to investigate 3-dimensional strain character.

**Experimental and Simulation Studies on the Texture Evolution during Deformation of ARB Processed Cu-Cu Multilayer:** *Suresh Santharam*<sup>1</sup>; Satyam Suwas<sup>1</sup>; Anthony Rollett<sup>2</sup>; <sup>1</sup>Indian Institute of Science; <sup>2</sup>Carnegie Mellon University

Texture evolution during large strain deformation of a Cu-Cu multilayer is investigated. The Cu-Cu multilayer was produced by the Accumulative Roll Bonding (ARB) technique and then further rolled to 93% reduction at room temperature. The 8-pass ARB processed material was, in effect, the initial material for deformation, which consisted of grains with an average aspect ratio of 1:10. After 93% rolling reduction the aspect ratio decreased to 1:2.5. The bulk X-ray texture measurement showed a stronger Brass  $\{011\}\langle 211 \rangle$  component evolution compared to that of the Copper  $\{112\}\langle 111 \rangle$  component. The texture strength stabilizes after 87% reduction. Texture evolution was simulated using the ViscoPlastic Self-Consistent (VPSC) code. The slip systems, work hardening behavior, grain aspect ratio, initial texture and shear strain arising from surface friction were considered for texture simulation. The addition of shear strain leads to reduced texture sharpening. The simulated texture is in good agreement with the experimental measurements.

**Full Field Study of Local Interactions between Twin and Its Parent Grain:** *Anand Kanjarla*<sup>1</sup>; Irene Beyerlein<sup>1</sup>; Carlos Tomé<sup>1</sup>; Ricardo Lebensohn<sup>1</sup>; <sup>1</sup>Los Alamos National Laboratory

In the present study, we use a full field method, namely the Fast Fourier Transform Technique (FFT), to study the interaction of an existing twin with its parent grain in Zirconium. Both compressive and tensile twins are considered. By allowing the development of spatially resolved heterogeneous micromechanical fields inside a parent and a twin, accurate estimates of the interaction between them can be obtained. By altering the twin volume fraction and the surrounding local neighborhood grains, one can obtain realistic trends about local fields and localization criteria that can, in turn, be used to improve the assumptions made about these interactions in Homogenized Effective Media (HEM) models, such as the Visco-plastic and Elasto-plastic self consistent models.

**Investigation of Texturing and Bending during Asymmetric Rolling of AZ31B:** *Jaehyung Cho*<sup>1</sup>; SukBong Kang<sup>1</sup>; <sup>1</sup>Korea Institute of Materials Science

Asymmetric deformation generated by differential speed rolling produced bending of AZ31 magnesium alloy sheets. Bending curvature and texture and microstructure evolution of the AZ31 magnesium alloys were investigated and compared with model predictions. Modeling asymmetric rolling process was carried out using finite element approaches and obtained deformation gradients were used to predict texture evolution. Texturing was predicted based on a visco-plastic self consistent (VPSC) model. Asymmetric rolling was carried out with various roll speed ratios and reduction area. Bending curvatures were predicted to dynamically depend on ratio of the roll speeds, reduction area and friction. AZ31B alloy sheets initially had some texture gradient along the thickness direction. Top and bottom surface showed the similar basal texture and the center had elongated basal fiber along the transverse direction. The overall feature of the texture gradient remained after 10% and 20% reduction area.

**Modelling the Mechanical Behavior of Dual-Phase Steels under Strain Reversal:** *Smritikana Dutta*<sup>1</sup>; <sup>1</sup>University of Aveiro

In this work we analyze the mechanical behavior of dual-phase steels under strain reversal with the previous proposed Phi-Model. In this model the proposed interaction law is based on a new non-linear intermediate approach. In the formulation, it is proposed to minimize an error function which combines the deviations of the local fields from the corresponding macroscopic ones. A scalar weight parameter was introduced to span the entire solution domain between the upper and lower bound approaches. The model takes into account the texture evolution and micro structural features



related with changes in strain path. A comparison between the self-consistent model (VPSC code) and the Phi-model is also considered.

**Phase Field Simulation of Static Recrystallization for AZ31 Mg Alloy:** Gao Yingjun<sup>1</sup>; <sup>1</sup>Guangxi University

In order to obtain the deformation grain structure for static recrystallization, an initial grain structure for deformation grain structure are produced by lattice deformation model; aiming at characteristics of different deformation regions and non-uniform distribution of the stored energy in deformed alloy, a multi-state free energy (MSFE) function are proposed by introducing a weight factor for the stored energy and a characteristics state factor for different deformation regions. Based on these models, the microstructure evolutions of static recrystallization for deformation Mg alloys are simulated by phase field model. The transformation dynamic curve of recrystallization and the time index for Avrami curve, and the stored energy released regularity and distribution of grain size in recrystallization process are systematic analyzed. Based on our established MSFE model, the simulation results here are well in accordance with the other theoretical results and experimental results.

**Physical Parameters Determination from 3D Phase Field Simulations of Martensitic Transformations in Steels:** Hemantha Yeddu<sup>1</sup>; John Ågren<sup>1</sup>; Annika Borgenstam<sup>1</sup>; <sup>1</sup>Royal Institute of Technology (KTH)

Typically Phase Field Modeling (PFM) is applied to simulate microstructure evolution in order to understand the physical phenomena involved in the phase transformations, viz. solidification, martensitic transformations, spinodal decomposition etc. In the present work the limits of applicability of PFM are extended to determine various process as well as material parameters that control the martensitic transformation in steels apart from the above mentioned typical application. Plastic relaxation rate, i.e. the rapidity of the response by the material to accommodate the elastic stresses by means of plastic deformation, and the driving forces needed for nucleation as well as growth of martensite are calculated from the simulations. Usage of anisotropic physical parameters, acquired from experimental works performed on different Fe-C alloys, as the simulation parameters has yielded the simulation results as close to reality as possible.

**Residual Stress Concentration and Distribution in Polycrystalline Ceramic Materials Using a 3D Fast Fourier Transform Thermoelastic Method:** Benjamin Anglin<sup>1</sup>; R Hay<sup>2</sup>; T. A. Parthasarathy<sup>3</sup>; R.A. Lebensohn<sup>4</sup>; A.D. Rollett<sup>1</sup>; <sup>1</sup>Carnegie Mellon University; <sup>2</sup>Air Force Research Laboratory; <sup>3</sup>UES, Inc.; <sup>4</sup>Los Alamos National Laboratory

Residual stresses develop in non-cubic polycrystalline materials with anisotropic thermal expansivity. These can lead to microcracking and/or can reduce the mechanical properties of the bulk solid. These stresses are difficult to experimentally measure in 3D and numerical methods have attempted to model them. A common numerical method for modeling residual stresses is finite element; previous studies have used 2D models to show that residual stresses in ceramic polycrystals are distributed over tens of grains. Extending this to 3D is complicated since this method requires a mesh for the microstructure and requires large computation time for realistic polygrain arrangements. A computationally more efficient method is the FFT thermoelastic method which uses a periodic mesh independent of grain geometry. In this work, the thermoelastic FFT method is used to determine the residual stress concentration and distribution within a polycrystalline ceramic material in 3D; the results will be presented and their implications discussed.

**The Texture Evolution of Interstitial-Free Steel Processed by Different Speed Rolling:** Jordan Suharto<sup>1</sup>; Jae Sik Lee<sup>1</sup>; Yeon Jin Gil<sup>1</sup>; Young Gun Ko<sup>1</sup>; <sup>1</sup>Yeungnam University

The texture evolution of the interstitial free steel sheets severely deformed at room temperature using differential speed rolling (DSR) method was investigated in which the variation of roll speed ratio from 1:2 to 1:4. The effects of speed ratio in texture evolution and grain boundary orientation of IF steel were analyzed by electron back scattered diffraction and TEM interpretation. With the increasing of rolls speed ratio, the textures were

transformed which were affected by misorientations on grain boundary during deformation. As compared to initial stage, the presence of fine ferrite grain has increased and microstructure homogeneity increased. The stress-strain curve of rolled specimen will be discussed in relation to the degree of formability in this study.

**Processing and Properties of Powder-Based Materials: Poster Session**

*Sponsored by:* The Minerals, Metals and Materials Society, TMS Materials Processing and Manufacturing Division, TMS: Powder Materials Committee

*Program Organizers:* K. Morsi, San Diego State University; Ahmed El-Desouky, San Diego State University

Sun PM-Wed PM  
Feb 27-Mar 2, 2011

Room: 33A  
Location: San Diego Conv. Ctr

*Session Chair:* K Morsi, San Diego State University

**High Temperature Oxidation Behaviors of Fe-Cr-Al Bulk and Powder Sintered Materials:** Kee-Ahn Lee<sup>1</sup>; Song-Yi Kim<sup>1</sup>; Sung-Hwan Choi<sup>1</sup>; Jung-Yeol Yun<sup>2</sup>; Hye-Moon Lee<sup>2</sup>; Byung-Kee Kim; <sup>1</sup>Andong National University; <sup>2</sup>Korea Institute of Machinery and Materials

Bulk specimens and powder sintered specimens were each produced from Fe-22%Cr-5.8% Al alloy and the high-temperature oxidation behaviors of the specimens were compared and analyzed. Temperatures of 900°, 1000°, and 1100° (24 hours) and gas atmosphere of 79%N<sub>2</sub>+ 21%O<sub>2</sub> were set as testing conditions. The results of the oxidation testing showed that both bulk and powder sintered specimens gained weight as the temperature increased, with the powder sintered specimens exhibiting far more weight gain than the bulk specimens. In the powder sintered specimens, the internal diffusion of O<sub>2</sub> toward the powder interfaces easily took place due to weak binding between powder particles constituting the microstructure. The Fe-Cr-Al alloy bulk and powder sintered specimens' oxidation behaviors and mechanism of microstructures were further discussed in relation to temperature rise. [supported by the Fundamental R&D program for Core technology of Materials funded by the Ministry of Knowledge Economy, Republic of Korea]

**Investigation of Engineered Pore Structures in Powdered Metals by Means of Freeze Tape Casting:** David Driscoll<sup>1</sup>; Adam Weisenstein<sup>1</sup>; Stephen Sofie<sup>1</sup>; <sup>1</sup>Montana State University

Engineered metal foams have strong potential in applications such as fuel cell electrodes, sensors, differential springs, filtering media, and composite structures. In this study the variation in mechanical and electrical properties were characterized in engineered porous metal foams with aligned porosity. Utilizing freeze tape casting, aqueous 440SS metal powder suspensions were drawn onto a freeze bed. After directional solidification, the solvent was sublimed from the ~1mm thick tapes, yielding porous green metal compacts which were sintered in a vacuum furnace from 900 – 1100C. Densification was shown to begin at 1000C yielding shrinkage variations relative to pore alignment. The resulting disks exhibit highly ordered acicular pores with substantial anisotropy in the mechanical and electrical properties. DC conductivity revealed up to 62% variation depending on direction of measurement relative to the alignment of pores. The affects of rigidity and tensile strength in relation to pore orientation will also be reported.

## Silicon Production, Purification and Recycling for Photovoltaic Cells: Poster Session

*Sponsored by:* The Minerals, Metals and Materials Society, TMS Extraction and Processing Division, TMS Light Metals Division, TMS: Energy Conversion and Storage Committee, TMS: Recycling and Environmental Technologies Committee

*Program Organizers:* Anne Kvithyld, SINTEF; Gregory Hildeman, Consultant; Gabriella Tranell, Norwegian University of Science and Technology (NTNU); Arjan Ciftja, SINTEF; Shadia Ikhmayies, Al Isra University

Sun PM-Thurs PM  
Feb 27-Mar 3, 2011

Room: 14A  
Location: San Diego Conv. Ctr

## Parallel Developments of a Cellular Automaton - Finite Element Model for the Prediction of Grain Structure in Casting: *Tommy Carozzani*<sup>1</sup>; Charles-André Gandin<sup>2</sup>; Hugues Dignonnet<sup>2</sup>; <sup>1</sup>MINES - Paristech; <sup>2</sup>MINES ParisTech

A coupled Cellular Automaton (CA) - Finite Element (FE) model is developed to predict grain structure in casting. The model tracks the nucleation and growth of each grain. The outputs are the final grain structure and texture. Macroscopic equations are solved on the FE mesh, while grain structure is described on the CA grid. Coupling of heat and mass transfers are set up between the two modeling scales. Grains are typically represented with a 100 microns resolution (cell size), in a 15x15x100 cm quarter of ingot. The huge amount of data involved (22.5 10<sup>9</sup> cells) cannot be processed on a single computer. The present implementation uses massive parallel computation to solve the industrial scale problem. Developments have been done to balance the load between processors, the only limitation of the domain size being the computing resources available.

## Study of Pellets and Lumps as Raw Material for Silicon Production: *Elena Dal Martello*<sup>1</sup>; Gabriella Tranell<sup>1</sup>; Sean Gaal<sup>2</sup>; Ola Raanes<sup>2</sup>; Merete Tangstad<sup>1</sup>; Lars Arnborg<sup>1</sup>; Rune Larsen<sup>1</sup>; <sup>1</sup>Norwegian University of Science and Technology; <sup>2</sup>SINTEF

The aim of this paper is twofold: to compare the behaviour of pellets and lumps and to compare the properties of two hydrothermal quartzes during carbothermic reduction. Small scale carbothermic reduction experiments have been carried out in an induction furnace. High purity silicon carbide and two different high purity hydrothermal quartzes were charged as raw materials at different molar ratios, either in the form of lumps (size 2-5 mm), or as powder, mixed and agglomerated as pellets (size 1-3 mm) and reacted at 2000°C. The high temperature properties of the two quartzes were also investigated in a sessile drop experimental set-up. A quantitative XRD-based method has been tested in order to estimate the reaction products between quartz and silicon carbide at 2000°C.

## Surfaces and Heterostructures at Nano- or Micro-Scale and Their Characterization, Properties, and Applications: Poster Session

*Sponsored by:* TMS Electronic, Magnetic, and Photonic Materials Division, TMS Materials Processing and Manufacturing Division, TMS: Nanomaterials Committee, TMS: Surface Engineering Committee

*Program Organizers:* Nitin Chopra, The University of Alabama; Ramana Reddy, The University of Alabama; Jiyoung Kim, Univ of Texas; Arvind Agarwal, Florida International Univ; Sandip Harimkar, Oklahoma State University

Sun PM-Wed AM  
Feb 27-Mar 2, 2011

Room: 31B  
Location: San Diego Conv. Ctr

## Novel Carbon Nanotubes-Nanoparticle Heterostructures and Their Utilization in Soft Nanocomposite Fabrication: Adrika Venkatanarayan<sup>1</sup>; Wenwu Shi<sup>1</sup>; *Nitin Chopra*<sup>1</sup>; <sup>1</sup>The University of Alabama

Development of multi-functional and multi-component carbon nanotube-nanoparticle heterostructures is critical for future analytical platforms and biosensors. In this, we demonstrate here a unique approach to fabricate carbon nanotube-multiple nanoparticle heterostructures in a single step facile synthetic approach. These heterostructures were understood by SEM, TEM, UV-vis, and EDS studies. It was observed that uniform coating of nanoparticles on carbon nanotubes could be formed and there was no free nanoparticle formation in the solution, thus indicating the importance to carbon nanotube surface characteristics and dimensionality. These heterostructures are further incorporated into a stimuli-responsive hydrogels to result in a smart, hybrid, and soft nanocomposites. These nanocomposites will be useful for developing novel chemical and biological sensors.

## Effect of Pulsed Electrodeposition Conditions and Reinforcement Content on Microstructure and Tribological Properties of Nickel Composite Coatings: *Tushar Borkar*<sup>1</sup>; Sandip Harimkar<sup>1</sup>; <sup>1</sup>Oklahoma State University

Pure nickel and nickel composite coatings (Ni-Al<sub>2</sub>O<sub>3</sub>, Ni-SiC, and Ni-ZrO<sub>2</sub>) were deposited from Watts bath using direct current (DC), pulsed current (PC), and pulsed reverse current (PRC) deposition conditions. Detailed investigations on the effect of deposition conditions on the evolution of surface microstructure, crystallographic micro-texture, microhardness, and sliding wear behavior of pure nickel and nickel composite coatings are presented. Coatings deposited by PC and PRC techniques resulted in more random crystallographic texture. The composite coatings deposited using PC and PRC deposition also exhibited significant improvement in microhardness and wear resistance. Also, the effect of nanoparticle content of the electrolyte bath on the surface microstructure, tribological properties, and level of reinforcement in the Ni-Al<sub>2</sub>O<sub>3</sub> composite coating is investigated. The reinforcement of nanoparticles as well as microhardness and wear resistance of Ni-Al<sub>2</sub>O<sub>3</sub> composite coatings increased linearly with the amount of nanoparticle loading in the electrolyte bath.

## Spark Plasma Sintering of Amorphous-Crystalline Laminated Composites: *Tushar Borkar*<sup>1</sup>; *Ashish Singh*<sup>1</sup>; Sandip Harimkar<sup>1</sup>; <sup>1</sup>Oklahoma State University

In this paper, a novel approach involving pulsed electrodeposition (PED) and spark plasma sintering (SPS) of Fe-B-Si amorphous ribbons is presented for the processing of amorphous-crystalline laminated composites. The PED allowed the deposition of nanocrystalline Ni or Cu layers (thickness: <3 μm) on the Fe-B-Si amorphous ribbons (thickness: <25 μm). The coated ribbons were subsequently stacked and SPS sintered under the influence of pulsed direct current and uniaxial pressure. The SPS sintered amorphous ribbons (uncoated) and amorphous-Ni laminates exhibited partial crystallization of the ribbons and poor lamellar bonding in the composites. With the similar SPS sintering parameters (temperature: 450°C; pressure: 350 MPa; sintering

time: 20 min), the amorphous-Ni-Cu laminates were sintered to full densification without undesirable crystallization of the amorphous ribbons.

**Mechanical Properties of Grain Boundary-Containing Al Nano-Pillars:** Allison Kunz<sup>1</sup>; Siddhartha Pathak<sup>1</sup>; Andrew Jennings<sup>1</sup>; Julia Greer<sup>1</sup>; <sup>1</sup>Caltech

Mechanical behavior of bi-crystalline aluminum nano-pillars under uniaxial compression reveals size effects, stochastic stress-strain signature, and strain-hardening. Pillar diameters range from 400nm to 2 microns and contain a single high-angle grain boundary oriented parallel to pillar axes. Loading-unloading cycles reveal no Bauschinger effect, suggesting that the native oxide does not trap mobile dislocations. Our results indicate that these bi-crystalline pillars are characterized by intermittent strain bursts and exhibit an identical size effect to their single crystalline counterparts. Further, we find that the presence of the grain boundary generally decreased the degree of work hardening relative to the single-crystalline micro-pillars. These findings suggest that micro-pillar plasticity in the presence of a grain boundary is also dislocation nucleation-controlled and that the grain boundary likely serves as a dislocation sink rather than a dislocation source. Transmission electron microscopy (TEM) analysis provides further insight into dislocation density evolution in these bicrystalline pillars.

**Silicon Nanorod Formation for Solar Absorbers Using Nanosphere Lithography:** Blake Whitley<sup>1</sup>; Faisal Salman<sup>1</sup>; Chris Redden<sup>1</sup>; Anusha Natarajathinam<sup>1</sup>; Alton Highsmith<sup>1</sup>; Subhadra Gupta<sup>1</sup>; <sup>1</sup>The University of Alabama

Solar absorption has been realized through strategically located geometries, including closely spaced nanorods. For this research, polystyrene nanospheres have been used as masking agents in the top-down formation of nanorods through nanosphere lithography (NSL). NSL requires a uniform monolayer of polystyrene spheres on a substrate as the initial step in the formation of nanorods. Monolayers were successfully created over select areas of the wafer through spin-coating. The effects of ashing on polystyrene spheres were then studied in detail. The Bosch process was carried out in an inductively coupled plasma deep reactive ion etcher (ICP-DRIE) to etch several microns into the silicon substrate, producing nanorods of aspect ratios exceeding 50. A statistical design of experiments was carried out to optimize the absorption of the etched silicon as a function of nanorod aspect ratio and spacing, which was optimized as a function of the etch parameters.

**Development and Mechanical Characterization of Novel Alumina Based Composites for Reduced Friction and Wear Applications:** Rajeshwari Paluri<sup>1</sup>; Sudeep Ingole<sup>1</sup>; <sup>1</sup>Texas A&M University

Self-lubricating materials with superior surface properties for reduced friction and wear application are always a point of attention for surface scientists, tribologists and lubrication engineers. Alumina is one such material which is a merit choice for wear resistance applications like pump bearings, piston components, etc. We attempt to develop a novel alumina based ceramic composite to further enhance its surface properties. This presentation will focus on mechanical and surface characterization of alumina under influence of varying percentages of boron as friction modifier. The results of XRD, optical microscopy and ESEM will be presented along with hardness and fracture toughness. Effect of sintering temperature and percentage of boron on mechanical properties, density, porosity and grain size will be presented. Preliminary results show that increasing percent of boron resulted in grain boundary diffusion and high sintering temperatures resulted in low porosity. X-ray diffractograms confirm formation of aluminum diboride and aluminum borate.

**Data Transmission Performance of Graphene Interconnects:** Cengiz Ozkan<sup>1</sup>; <sup>1</sup>University of California

This poster describes our recent work on emerging interconnect technologies based on graphene layers and on the materials processing challenges for large scale applications. Interconnects fabricated from graphene layers could serve as a future replacement for metal interconnects. An attractive aspect of using graphene interconnects is the potential dual-functionality where they could also serve as thermal spreaders given their excellent thermal conductivity characteristics. We present results on digital data transmission performance

of graphene interconnects grown by chemical vapor deposition, and the initial studies demonstrated that they can sustain data rates up to 90 megabits per second. Graphene interconnects behave as RLC lines and the bandwidth is inversely proportional to resistance caused by defects in the synthesized graphene layers and the inductance and capacitance of the interconnect lines. We are continuously improving the quality of CVD grown graphene layers to improve the bandwidth of transmission beyond the gigabits per second level.

## The Second Symposium on the Recycling of Electronic Wastes: Poster Session

*Sponsored by:* The Minerals, Metals and Materials Society, TMS Electronic, Magnetic, and Photonic Materials Division, TMS Extraction and Processing Division, TMS Light Metals Division, TMS: Electronic Packaging and Interconnection Materials Committee, TMS: Recycling and Environmental Technologies Committee  
*Program Organizers:* Lifeng Zhang, Missouri University of Science and Technology; Gregory Krumdick, Argonne National Laboratory; Jaan Kers, Tallinn University of Technology; Thomas P. Schuman, Missouri University of Science and Technology (Missouri S&T); Markus Reuter, Ausmelt Limited

Sun PM-Mon PM  
Feb 27-28, 2011

Room: 15B  
Location: San Diego Conv. Ctr

**A Novel Process for Foam Glass Preparation from Waste CRT Panel Glass:** Mengjun Chen<sup>1</sup>; Fu-shen Zhang<sup>2</sup>; Jianxin Zhu<sup>2</sup>; <sup>1</sup>Southwest University of Science and Technology (SWUST); <sup>2</sup>Chinese Academy of Sciences

A novel approach for foam glass preparation, namely vacuum-aided powder sintering technique, was preliminarily investigated in the present study. The key point of this approach was to prepare foam glass at a negative pressure. Compared to normal powder sintering process, the new approach could benefit the foaming process by shorting the holding time, reducing the amount of foaming agent and especially decreasing relative density of the product. Optimum conditions were 750 °C, 1000 Pa, 5 min and 1 wt.% foaming agent, respectively.

**Development of Reproduction of Glass Substrate from Old TFT-LCD Panel:** Sung-Jei Hong<sup>1</sup>; Jong-Woong Kim<sup>1</sup>; Min-Sun Kim<sup>1</sup>; Tae-Whan Hong<sup>2</sup>; Young-Sung Kim<sup>3</sup>; Nam-Ki Kang<sup>1</sup>; <sup>1</sup>Korea Electronics Technology Institute; <sup>2</sup>Chungju National University; <sup>3</sup>Seoul National University of Science and Technology

The glass substrate is one of important parts of TFT-LCD panel. In general, most of the glass substrates included in old TFT-LCD panel is crashed and melt into the furnace with high temperature to recycle it. However, the complex recycling process uses lots of harmful chemicals and high electrical power, and waste water and CO<sub>2</sub> gas are generated during the process. Therefore, in this work, the new reproduction of glass substrate from old TFT-LCD panel was attempted without any crashing and melting process. The front-plane panel was used for the reproduction of glass substrate. As a result, ITO layer on the glass substrate were clearly separated using the newly attempted process. No damage was given to the glass during the process, and surface roughness was less than 1 nm. Also, the good optical transmittance more than 90% was achieved from the reproduced glass because the reproduced state was clear.

**Environmental Leaching Characteristics and Bioavailabilities of Waste Cathode Ray Tube Glass:** Mengjun Chen<sup>1</sup>; Fu-Shen Zhang<sup>2</sup>; Jianxin Zhu<sup>2</sup>; <sup>1</sup>Southwest University of Science and Technology (SWUST); <sup>2</sup>Chinese Academy of Sciences

In China hazardous e-waste, cathode ray tube (CRT) glass, is usually left around and it is likely to contact with water resources directly. To identify the real leaching characteristics and bioavailabilities of heavy metals Pb and Ba contained in CRT glass in the nature environment, experiments were carried out by simulating the nature environment. The results indicated that Pb and Ba contained in CRT glass were stable in most conditions, which only showed obvious leaching toxicities in strong acidic/alkali conditions. EDTA



and DTPA extractable Pb and Ba amounts were extremely high, e.g., EDTA extractable Pb of color funnel glass was up to 1960.07  $\mu\text{g}/\text{kg}$ , indicating that the potential bioavailability of waste CRT glass is very high.

**Leaching Toxicity of Pb and Ba Containing in Cathode Ray Tube Glasses by SEP-TCLP:** Mengjun Chen<sup>1</sup>; Fu-Shen Zhang<sup>2</sup>; Jianxin Zhu<sup>2</sup>; <sup>1</sup>Southwest University of Science and Technology (SWUST); <sup>2</sup>Chinese Academy of Sciences

In the present study, different types of cathode ray tube (CRT) glasses were examined by sequential extraction, combined with TCLP, to provide possible explanations for how Pb and Ba leach out from the waste CRT glasses. Sequential extraction results showed that Pb and Ba in the CRT glasses dominantly presented as the residual fraction. The exchangeable fractions of Pb and Ba were extremely low, less than 0.01 % of the total content, but they were higher than those required by the regulation limits, 5 and 100 mg/L for Pb and Ba, respectively. TCLP tests of the original CRT glasses, and their residue after each step of sequential extraction, demonstrated that the extremely high leaching toxicity of CRT glasses was mainly caused by its exchangeable and carbonate fractions of Pb and Ba.

**Recovery of Copper from Printed Circuit Boards Waste by Bioleaching:** Luciana Yamane<sup>1</sup>; Denise Espinosa<sup>1</sup>; Jorge Tenório<sup>1</sup>; <sup>1</sup>Polytechnic School of São Paulo University

The present work investigated the influence of Fe+2 initial concentrations in the bioleaching of copper from printed circuit board using *Acidithiobacillus ferrooxidans*-LR. Printed circuit boards were collected from obsolete computers and mechanically processed through size reduction followed by magnetic separation. The bacteria *Acidithiobacillus ferrooxidans*-LR were grown and adapted in presence of printed circuit boards. A shake flask study was carried out on the printed circuit boards samples (non-magnetic fraction) using a rotary shaker under the following fixed conditions (185 rpm, 30°C). The bioleaching efficiency was evaluated by comparison between the concentration in the initial sample and in the leached liquor, pH of the medium and concentration of ferrous iron produced. Inductively coupled plasma optical emission spectrometry (ICP-OES) was used to determine the metals concentration. The results showed that *Acidithiobacillus ferrooxidans*-LR leached 63% copper from printed circuit boards using supplemented medium with Fe+2.

**Recovery of Nickel from Leaching Liquor of Printed Circuit Board by Solvent Extraction:** Adriana Santanilla<sup>1</sup>; Beatriz Campos<sup>1</sup>; Jorge Tenório<sup>1</sup>; Denise Espinosa<sup>1</sup>; <sup>1</sup>Polytechnic School of University of São Paulo

The aim of the present work is to investigate the recovery of nickel from obsolete cell phones. Printed circuit boards from cell phone scrap was submitted prior to a grinding process and then leached in sulfuric acid. Nickel was extracted from aqueous solution using Cyanex 272. Aqueous/organic ratio was set equal to 1. The effect of both pH and temperature on selectivity was investigated.

# NOTES

## 2011 Aluminum Plenary Symposium: The 125th Anniversary of the Hall-Héroult Process

Sponsored by: The Minerals, Metals and Materials Society, TMS Light Metals Division, TMS: Aluminum Committee  
Program Organizer: John Johnson, JCG

Monday AM Room: 6B  
February 28, 2011 Location: San Diego Conv. Ctr

Session Chair: John Johnson, Johnson's Consulting Group

### 8:30 AM Plenary

**Paul Héroult: The Early Days of the European Aluminium Industry:** Claude Vanvoren<sup>1</sup>; <sup>1</sup>Rio Tinto Alcan

Paul Héroult story is indistinguishable from the early days of the European aluminium industry in France and Switzerland. The personal engagement of the co-inventor of the electrolytic process, a true entrepreneur, tells a lot about his conviction on the bright future of the light metal. The lecture will come back on those adventurous early days and illustrate how they gave birth to an industry which since, relentlessly, devoted effort to innovate and facilitate access to a material which developed from semi-precious to commodity status in less than 125 years.

### 9:05 AM Plenary

**Charles Martin Hall and Warren Haupin: Over 100 Years of Technical Innovation:** Gary Tarcy<sup>1</sup>; <sup>1</sup>Alcoa

Two scientists at Alcoa stand above all others. The first, of course is Charles Martin Hall, one of the co-inventors of the electrolysis process that is still used today. C. M. Hall was also one of the co-founders of what was originally the Pittsburgh Reduction Company that later became the Aluminum Company of America (ALCOA). Looking back on some of his early work and in particular his invention one only wonders what he would think of what became a worldwide metals industry that in volume is only surpassed by steel. Although the process is essentially the same as it was invented 125 years ago. A second Alcoa scientist, Warren Haupin, was one of the essential people to increase the understanding of the process that has led to a multitude of incremental improvements over the last 60 years. The lecture will discuss the contributions and some antidotal information about both of these scientists.

### 9:40 AM Plenary

**The Rise and Fall of the Knowledge Base for Aluminium Smelting – The Last 50 Years:** Barry Welch<sup>1</sup>; <sup>1</sup>University of New South Wales- Australia, and Welbank Consulting Ltd - New Zealand

In the second half of the 1950's the space race was with us. Cheaper more efficient production of light metals (such as titanium, magnesium and aluminium) as well as the refractory metals and materials - including zirconium and titanium diborides for example - that would withstand extremely high temperatures became a major research thrust. As a flow-on from the European and Russian research eminence in these areas during the 1930's and 1940's, a few academic Western-world research "cells" (to pinch a George Bush phrase) specialising in the structure, properties and electro chemistry of molten salts were being established and active. The activities were heavily biased to molten fluorides included research aiming at developing more efficient nuclear reactors (ORNL) and a better understanding of aluminum smelting electrolyte. "Young-bloods" trained in academic institutions (especially the University of Toronto, the Technical University of Norway and Imperial College -London Penn State Univ., and MIT) spearheaded and intense research that developed an excellent understanding of the fundamentals of the properties of molten electrolytes and the electrochemistry. The glowing example was Kai Grjotheim's thesis in 1956. The Symposium on Aluminium organised by TMS in 1962 was the first one that brought together some of the academic understanding and industrial issues associated with aluminium smelting. Inspiring papers by Eric Ransley on titanium diboride (with concepts quite different to those

that are being considered in the decades since), the reactivity and properties of carbon anodes and cathodes, and the options for maximising current efficiency stood alongside one on Bus-bar designs which initiated magnetic modelling of the cells - then computing was in its infancy. From these and other papers presented the growth in design features that enabled an increase in amperage took off. The impact of some of the "characters" who became leaders in the early 1960s, together with their contributions will be traced and highlighted. As also will be the decline that started following the change in emphasis introduced by aluminium industry leaders in the second half of the 1980s, to the point to day where it is harming performance and displaying a greater lack of understanding of core fundamentals than existed 50 years ago!

### 10:20 AM Break

### 10:30 AM Plenary

**The Early Years of Light Metals, TMS:** Nolan Richards<sup>1</sup>; <sup>1</sup>Richards & Associates

The symposium held in New York, 1962, "Extractive Metallurgy of Aluminum", under the auspices of the Metallurgical Society of AIME, was a ground breaking event in the U. S.A. for the entire aluminum industry. As a result of two-years of organizing, fifty five contributors, thirty one embracing the production of aluminum, freely shared results of research done within their companies or universities with this tentative opening up of communication and sharing that had occurred previously only in a few conferences in Europe. The amicable interactions and success of this meeting led to the beginning of annual meetings organized by the Light Metals Committee, the Metallurgical Society (TMS) of the American Institute of Mining Metallurgical and Petroleum Engineers Inc. (AIME). Before this conference, technologists involved in improving the operation, design and safety of alumina reduction cells, apart from their in-house, guarded data, had recourse to the monographs of J.W. Richards (1896), T.G. Pearson 1955), Kai Grjotheim (1956) and excepting the Russian literature, a few papers in The Journal of the Electrochemical and Faraday Societies. While it took a while, the consensus was that sharing non-competitive technical and discovering some of the trends in the strategies of competitors was that these aspects were all conducive to advancing the competitiveness of the whole aluminum industry, raising the awareness of the effectiveness of in-house R&D and enhancing the innovations and creativity of all technologists. Therefore, in 1971, again in New York, now the TMS Light Metal, began its series of annual meetings involving the international aluminum industry and academia. There participation increased to ninety-seven contributors with sixty four concerned with the reduction process. This presentation explores the first eight or nine TMS Light metals symposia with the objective of categorizing the topic fields, the extent to which they were "cutting edge", comments on how they influenced the electrolytic production of aluminum and inspired competitive research with improved funding, the attraction of future technologists into the industry and nurturing of "centers of excellence" for research in the Hall Héroult Process, novel processes and advanced materials.

### 10:55 AM Plenary

**Russian Aluminium Industry:** Peter Polyakov<sup>1</sup>; Victor Mann<sup>2</sup>; <sup>1</sup>Siberian Federal University; <sup>2</sup>Russian Aluminum Industry

1. Prehistory: Professor Fedotyeff's, Professor Pushin's investigations. 2. Soviet Union Early stage: 1932 – Volkov Smelter (PB); 1933 – Zaporozhye Smelter (PB); 1939 – Ural Smelter (HSS). 3. Scientific research: Professor M. Rappoport – Sodium intercalation; Professor A. Belyaev – bath for Al-cells; Professor M. Vetyukov – carbon technology; Professor Korobov – heat transfer; Candidate Science Forsblom A. Tsyplakov – magnetic fields; Professor Kaluzhsky – from VSS to PB; Professor P. Polyakov – Al-cell as a living creature. 4. After WW II. Huge Smelters: 1964 – Krasnoyarsk (VSS); 1966 – Bratsk (VSS); 1985 – Sayanogorsk (PB); 2007 – Khakas (PB). 5. Current scientific investigations: Soderberg technology improvement; PB-cells development; Al laboratory studies.

### 11:35 AM Plenary

#### **Brief Overview of Environmental Control within the Primary Aluminium Industry:** Erik Keul<sup>1</sup>; <sup>1</sup>ALSTOM Environmental Norway

The Aluminium Industry has come a long way with respect to Environmental Control during the 125 years with the Hall-Heroult process. The initial smelters were small and any adverse effects were either of no concern or were not detected. As the smelters grew in size improved potroom ventilation was the major method for reducing exposure of the workers to fumes as well as for protection of equipment. The first noticeable damage to vegetation was detected in St. Jean de Maurienne in 1909. Environmental Control within the industry was basically a voluntary effort and evolved due to concern about worker's health and obvious damage to the local environment, but has been helped along due to legislations. Various types of roof scrubbers were introduced in the 1930's and were applied by some smelters as the only treatment systems until the 1970's. None of these had reached the expected removal efficiencies due to inadequate sampling methods. Hooded cells were also introduced in the 1930's and in the following decades the concentrated fumes were either dispersed by tall stacks or cleaned by cyclones, electrostatic precipitators, wet scrubbers or a combination of these. Since the late 1960s dry scrubbers operating with alumina for removal of gaseous fluorides and particulates have been the state of the art emission control technology. Mega-smelters may introduce local environmental impact from SO<sub>2</sub> which would need to be treated in additional downstream scrubbers such as seawater scrubbers for coastal smelters. As per IAI the reduction in fluoride emission can be divided into three generations: 1st generation plants 1940 – 1955 12 – 15 kg per tonne; 2nd generation plants 1955 – 1975 2 – 6 kg per tonne; 3rd generation plants 1975 – today 0.3 – 1 kg per tonne. Today fluoride emission is not a major concern and due to legislation as well as to potential loss of costly raw materials all new smelters employ efficient pot hooding combined with dry scrubbers at +99% collection efficiencies. The focus today is on SO<sub>2</sub> removal, on greenhouse gases like CF<sub>4</sub>/C<sub>2</sub>F<sub>6</sub> and on PAHs from the green-mills and baking kilns. Future legislation (in EU) will likely enforce reductions in particulate emissions in addition to CO<sub>2</sub> limitations.

### 12:00 PM Plenary

#### **The Future for Aluminium Smelting:** Mark Taylor<sup>1</sup>; J.J.J. Chen<sup>1</sup>; <sup>1</sup>University of Auckland

The future of aluminium smelting is not assured. A primary driver of this situation is that the reasons for continuously reducing real margin for primary aluminium are not openly acknowledged, or even agreed. Is it the total cash cost of production? Or is it the community perception first, which causes a loss of public support for investment in infrastructure and resources to support heavy industries like aluminium smelting? Of course this is not a new question and many countries including USA and Europe have been confronted with the competing requirements of energy or resource intensive industries. In this competition, the wider community must prevail eventually. And as these competitive situations play out in the customary adversarial manner between business and Government, the new question is becoming: Is there another way for the business community to think about the place of energy intensive industries in our interconnected, interdependent societies where energy and other natural resources are apparently in short supply? In this paper we discuss specific energy consumption across the industry, the perceived barrier in reducing it, and enabling factors. Lastly we explore the possibility that aluminium smelters could become an integral part of the network for power supply in the community, and across communities and countries.

### 2011 Functional and Structural Nanomaterials: Fabrication, Properties, Applications and Implications: Nanomaterials: General

*Sponsored by:* The Minerals, Metals and Materials Society, TMS Electronic, Magnetic, and Photonic Materials Division, TMS: Nanomaterials Committee

*Program Organizers:* Jiyoung Kim, Univ of Texas; David Stollberg, Georgia Tech Research Institute; Seong Jin Koh, University of Texas at Arlington; Nitin Chopra, The University of Alabama; Suveen Mathaudhu, U.S. Army Research Office

Monday AM  
February 28, 2011

Room: 8  
Location: San Diego Conv. Ctr

*Session Chairs:* Jiyoung Kim, University of Texas at Dallas; Suveen Mathaudhu, US Army Research Lab

### 8:30 AM Introductory Comments

#### 8:35 AM Keynote

#### **Materials Research Support at the National Science Foundation:** Alan Ardell<sup>1</sup>; <sup>1</sup>National Science Foundation

The NSF/DMR perspective on materials research and education will be presented. DMR invested ~\$303M in FY10, supporting people, ideas, and instrumentation primarily through awards to the nation's colleges and universities. Apart from DMR, there is also substantial support for materials and materials-related research and education from other programs in NSF. Specific new opportunities – including the 4+ year-old program in biomaterials and the SOLAR and EFRI initiatives – will be discussed. There are also avenues for collaborative research, nationally and internationally, via different types of special funding programs such as the new CEMRI and MIRT, which have replaced the MRSEC program, and the established MWN program. Other The projects supported by the MMN program in FY10 and the budgetary outlook for FY11 will be described. General information on all the programs in DMR can be found on the DMR Web page: <<http://www.nsf.gov/mps/divisions/dmr/>>.

#### 9:05 AM Keynote

#### **Nanostructured Materials Development by the Center for Nanostructured Materials Technology:** Sang-Hee Suh<sup>1</sup>; <sup>1</sup>KIST, Center for Nanostructured Materials Technology

Over the last 10 years Korea has put large effort on nanotechnology development. Since Korean government started Korea Nanotechnology Initiative, we have seen tremendous increase in nanotechnology related publications, patents filed, new venture companies, and commercial products. Sponsored by the Ministry of Education, Science and Technology of Korea, the Center for Nanostructured Materials Technology has been managing one of the biggest programs for developing nanotechnologies in Korea. This Program aims to develop various nanostructured materials with superior properties by creating new materials or by applying nanotechnology to the already existing materials. The R&D areas covered by the Program include nanostructured materials for structural applications, environment and energy applications, and information technology applications. By the program, more than 30 original nanotechnologies have been developed, including 11 platform technologies. 22 technologies have been transferred to industry with many of them commercialized. Commercialized products include cutting tools with nano-layered coating; carbon nanotube/metal nanocomposites; amorphous structured thermal sprayed ceramic coating; nano-membrane with dual functionalities of catalytic reaction; and separation and nano-cathode materials for Li rechargeable batteries. The author will introduce some of the platform and commercialized technologies developed by the program.



**9:35 AM Invited**

**Nanomaterials: Research, Development and Technology (R&D&T) Roadmaps - 2020:** *Marcel Van De Voorde*<sup>1</sup>; <sup>1</sup>TU Delft

An overview will be given of nanomaterials Science and Technology in the world. Fundamental research will be the backbone for future industrial success including new theories, design of third generation nanoMaterials, macro, and micro-nano computer modelling. Potential nanoMaterials will be highlighted. Research-development-technology “nanoMaterials” roadmaps: 2010 - 2025 for: Breakthroughs in communication and information; Grand challenges in life science and medical applications; NanoMaterials with tailored functionalities for new generation energy sources; Role of nanoMaterials in transportation: aeronautics and car industry; Potentials for the chemical industry; NanoConsumer products. Roadmaps 2010 – 2020 for nanoscience environment and climate change and safety; Man-Made environment; Climate Change; Nanopotentials in Safety; (Toxicology) and Security. Guidelines for a prosperous modern university - industry and welfare for the society: Initiate “university – science/technology institutes -industry” partnerships; Create International NanoMaterials R&D&T Centres; Promote Nanoindustrialisation: Technology Parks, nanometrology and standardisation. Initiate International Infrastructures for nanoMaterials R&D&T; and Familiarise the Society with the new Culture of NanoMaterials Technology. Countries and Industries investing in NanoMaterials Science and Technology: Model for a global nanoMaterials landscape: NanoMaterials - science, technology and nanoindustrialisation are complex topics and cannot be subject anymore for one institute or industry, or nation. The success rate will depend on joining brilliancies. Models for research and industrial collaboration will be elaborated and mechanisms for execution proposed.

**10:05 AM Break**

**10:20 AM Invited**

**Nanomaterials Control for Biotech Applications:** *Sungho Jin*<sup>1</sup>; <sup>1</sup>UC San Diego

There has been a strong trend in recent years toward convergence of nanotechnology and biotechnology for advanced biomedical applications. For example, biomagnetics is potentially a huge field for science and applications of magnetism and magnetic materials. Magnetic nanoparticles (e.g., superparamagnetic Fe-oxide) are one of the most versatile nanotech/biotech materials actively investigated for targeted cancer treatment, cell sorting and manipulations, guided drug delivery, bio-imaging and medical diagnosis. Nanowires and nanopore arrays are also useful for a variety of biotech applications. These are all very rapidly advancing fields. For practical applications for biomedical devices, proper engineering of these nanomaterials is essential. In addition, some aspects of nanotoxicity need to be understood for safe bio applications. This talk describes materials science aspects of these nano-biomaterials, their control, and implications for safe, therapeutic applications.

**10:50 AM Invited**

**Can Single-Atom Change Affect Electron Transport Properties of Molecular Nanostructures such as C60 Fullerene?:** *Xiaoliang Zhong*<sup>1</sup>; *Ravindra Pandey*<sup>1</sup>; *Alexandre Rocha*<sup>2</sup>; *Shashi Karna*<sup>3</sup>; <sup>1</sup>Michigan Tech; <sup>2</sup>Universidade Federal do ABC; <sup>3</sup>Army Research Lab

At the nanoscale, even a single atom change in the structure can noticeably alter the properties, and therefore, the application space of materials. We examine this critical behavior of nanomaterials using fullerene as a model structure in (i) endohedral (B@C60 and N@C60), in which the doping atom is encapsulated inside the fullerene cage, and (ii) substitutional (BC59 and NC59), in which the doping atom replaces a C atom on the fullerene cage, configurations. The calculated results reveal that the conductivity for the doped fullerene is higher than that of the pristine fullerene. In the low-bias regime, the current-voltage characteristic of the endohedral as well as the substitutional configurations are very similar. However, as the external bias increases beyond 1.0 V, the substitutional BC59 fullerene exhibits a considerably higher magnitude of current than all other species considered, thus suggesting that it can be an ineffective semiconductor in p-type devices.

**11:20 AM Invited**

**Atomic Layer Deposition - A Modern Tool for Nanoscience:** *Mato Knez*<sup>1</sup>; <sup>1</sup>Max-Planck-Institute MSP

Atomic layer deposition (ALD) is a thin film deposition technique which was developed in the 1970s to meet the needs for processing thin film electroluminescent displays (TFEL). Technically and chemically it is similar to chemical vapor deposition (CVD). However, in contrast to CVD, ALD incorporates as a specific feature the separation of the chemical reaction into two half-reactions. Being a non-line-of-sight deposition technique, ALD allows for good coating conformality even with 3D nanostructured substrates or structures with a high aspect ratio. Our mission is to make use of the precision of ALD for fabrication or functionalization of a variety of nanostructures, optical coatings, encapsulation, replication or even infiltration of soft materials with metals. This talk will step through a selection of strategies on how to modify existing nanostructures or even change some physical properties of the structures making use of ALD for coating and infiltration, respectively.

**11:50 AM**

**Advancing The Science of Nanomanufacturing:** *Khershed Cooper*<sup>1</sup>; <sup>1</sup>Naval Research Laboratory

Nanomanufacturing is the fabrication of materials, components and devices with nano-scale features and their integration into viable engineering systems. A key ingredient is the enhancement or creation of new properties and functions by nano-scale physical phenomena. Nanomaterial building blocks, such as, quantum dots, nanotubes, nanowires, nanopillars and nanoparticles can be manipulated by top-down (e.g., atomic layer deposition) and bottom-up (e.g., self-assembly) processes to build novel nanodevice structures and useful nanosystems. The challenges for nanomanufacturing are achieving functionality, quality, repeatability, scalability and affordability. To address some of these challenges, basic research in areas such as nanoDDM (direct digital manufacturing), massively parallel processing, high-throughput (e.g., roll-to-roll) processing and system-level integration is needed. These concepts will be described in this paper and illustrated with research examples.

**12:20 PM Concluding Comments**

---

**2nd International Symposium on High-Temperature Metallurgical Processing: Energy Efficient New Metal Production Technology**

*Sponsored by:* The Minerals, Metals and Materials Society, TMS Extraction and Processing Division, TMS: Pyrometallurgy Committee, TMS: Energy Committee

*Program Organizers:* Jiann-Yang Hwang, Michigan Technological University; Jerome Downey, Montana Tech; Jaroslaw Drelich, Michigan Technological University; Tao Jiang, Central South University; Mark Cooksey, CSIRO

Monday AM  
February 28, 2011

Room: 18  
Location: San Diego Conv. Ctr

*Session Chairs:* Jiann-Yang Hwang, Michigan Technological University; Anton Vernigora, Baikal Mining Company LLC

---

**8:30 AM**

**A Breakthrough Application of Electricity at High Temperature for Steel Production: Molten Oxide Electrolysis:** *Antoine Allanore*<sup>1</sup>; *Luis Ortiz*<sup>1</sup>; *Donald Sadoway*<sup>1</sup>; <sup>1</sup>MIT

In the search for more energy efficient processes together with a mitigation of GHG emissions, the use of a high-temperature electrolytic process to produce iron from its molten oxide is of interest as an alternative to traditional iron making. The intensive use of electricity for a steelmaking process is not new, but its application in electrochemical reactors can lead to a drastic reduction of its emission of pollutants together with the production of a new product: pure liquid iron. A description of the thermodynamics of the iron

oxide conversion to metal will be presented. This approach shows that at high temperature, electricity is a suitable energy vector for both the heat and work required for the reaction. The key physico-chemical parameters that govern the corresponding energy balance of the electrolysis process will then be discussed, to depict the process design conditions for best energetic efficiency.

**8:50 AM**

**Intrinsic Hydrogen Reduction Kinetics of Magnetite Concentrate Particles Relevant to a Novel Green Ironmaking Technology:** Haitao Wang<sup>1</sup>; Moo Eob Choi<sup>1</sup>; Hong Yong Sohn<sup>1</sup>; <sup>1</sup>University of Utah

A novel ironmaking technology is under development at the University of Utah. This technology produces iron directly from iron ore concentrate by gas-solid suspension reduction. Hydrogen is the main reducing agent for high reactivity and for the elimination of carbon dioxide release in this ironmaking process. The direct use of concentrates allowing bypassing the problematic pelletization/sintering and cokemaking steps in the steel industry. Intrinsic kinetics of the suspension reduction of magnetite concentrate particles by hydrogen have been measured. Experiments were carried out in the temperature range of 1423 - 1673 K, other experimental variable being hydrogen partial pressure, the amount of excess hydrogen and particle size. Under most experimental conditions, 95% reduction was attained within several seconds, which presents sufficiently rapid kinetics for a suspension reduction process. The reaction kinetics followed the nucleation-and-growth equation, and a rate equation that contains all the effects of the experimental parameters has been obtained.

**9:10 AM**

**A Laboratory Investigation of the Reduction of the Iron Carbonate Bearing Ore to Iron Nugget by Means of the ITmk3 Technology:** Nikolay Panishev<sup>1</sup>; Rafkat Tahautdinov<sup>1</sup>; Anton Posazhennikov<sup>1</sup>; Vasily Bastrygin<sup>1</sup>; <sup>1</sup>Magnitogorsk Iron & Steel Works

The Bakal (South Ural, Russia) deposit of iron ore bearing iron carbonate with the capacity of more than 1 billion tones belongs to the MMK. This ore cannot be fully processed via blast furnace technology because of high content of MgO. According to the investigations carried out in the USA and Japan in 1999-2004 the ITmk3 RHF technology is a breakthrough in ironmaking technology. Four iron ore types (hematite, magnetite, high and low Al<sub>2</sub>O<sub>3</sub>/SiO<sub>2</sub>) were tested. The main objective of the investigation is to establish optimum operation conditions for the production of iron nuggets from iron carbonate bearing ore via the ITmk3 by means of the lab scale testing. Green pellets were processed via a lab tube furnace to simulate RHF conditions. This preliminary test work provides valuable information which may be used for large-scale testing in a commercially sized RHF.

**9:30 AM**

**Prospects of Making Directed Reduction Iron by Microwave Heating:** Linqing Dai<sup>1</sup>; <sup>1</sup>Kunming University of Science and Technology

Based on selectively summarized the characteristics of microwave heating and the research advances on making directed reduction iron by microwave heating. It was pointed out that microwave heating on making directed reduction iron has a good future by analyzing the development direction of directed reduction iron technology

**9:50 AM**

**Behavior of Coal-Based Direct Reduction Reaction of Iron Oxide Pellets by Microwave Heating:** Zhu-cheng Huang<sup>1</sup>; Hua Wang<sup>1</sup>; Bing Hu<sup>1</sup>; Hu Peng<sup>2</sup>; Guang-bin Xia<sup>2</sup>; <sup>1</sup>Central South University; <sup>2</sup>Changsha SYNO-THERM Co., Ltd

The temperature rising characteristics and reaction of the reduction of iron oxide pellets with anthracite fines were studied using a MW-L0316V microwave oven and Leica-DM-RXP polarizing microscope. The results show that iron oxide pellets and anthracite fines have good microwave absorbing properties, and high temperature and reducing atmosphere in a relatively short time for reduction of iron oxide pellets can be achieved. The reduction reaction, which follows the unreacted core model, is rapid and the metallization increases from 13.41% to 56.57% as the reduction end

point temperature increases from 850° to 950°. The iron is formed, fine grain crystals of iron are transferred and the contraction of metal phase occurs firstly at the surface of pellets, which hinders the reduction reaction at the center of pellets. The rate of reduction reaction increases slowly as the reduction end point temperature increases from 950° to 1050°.

**10:10 AM**

**Sustainable Developments in High Temperature Mineral and Metals Extraction and Processing:** Florian Kongoli<sup>1</sup>; Edward O'Brien<sup>1</sup>; S. Llubani<sup>1</sup>; Ian McBow<sup>1</sup>; <sup>1</sup>FLOGEN Technologies Inc

Sustainability has become a more frequent prerequisite for any project in any field of life. Any major development project has started to include sustainability as a criteria in evaluating its objectives and outcome. However for heavy multibillion dollar industries such as high temperature mineral processing and metals extraction, sustainability is a major criteria since the impact this industry has in the world and its sustainable future is much more pronounced than in many other fields. Environment, energy, residues, efficiency, etc are all important factors related to sustainability of high temperature mineral and metals extraction and processes. Improving or updating these characteristics make these industries more sustainable. However high temperature minerals and metal extraction and processing industries face the competition of low temperature minerals extraction and processing such as hydrometallurgical, electrochemical routes. Low temperature processes sometimes look more popular than high temperature ones. The real question is: Which one of these 2 different routes is more sustainable for the future? Are low temperature processes capable of replacing high temperature ones and if yes are they more sustainable? This paper will give an overview of aspects of sustainability of various high and low temperature mineral and metal processing routes in terms of environmental protection and residues, productivity, energy etc. and will offer a glimpse of the future that waits us.

**10:30 AM**

**Carbothermal Reduction of Titanium Concentrate at High Temperature:** Rin Huang<sup>1</sup>; Chenguang Bai<sup>1</sup>; Xuewei Lv<sup>1</sup>; Guibao Qiu<sup>1</sup>; Lei Lei<sup>1</sup>; <sup>1</sup>College of Materials Science and Engineering, Chongqing University

The TiO<sub>2</sub>-rich slag and pig iron can be produced from ilmenite concentrate by the electric furnace process. In this study, ilmenite concentrate was reduced in a vertical furnace equipped with a weighting data acquisition system. The effects of reducing agent (carbon) amount on the iron reduction were studied. The phase transformation, morphology and chemical compositions of reduced samples were investigated by X-ray diffractometry (XRD), scanning electron microscopy (SEM) and energy dispersive spectroscopy (EDS), respectively. It was found that the reductive degree of ilmenite concentrate increased with the increase of reducing time. The phases of reduced samples were mostly iron, rutile, Ti<sub>3</sub>O<sub>5</sub> and Fe<sub>2</sub>TiO<sub>5</sub>. The mass loss percentage increased with increasing the carbon amount from 8% to 12%. When the carbon amount exceeded 12%, the mass loss percentage decreased with the increasing of carbon amount.

**10:50 AM**

**A Simulation Study on Flue Gas Circulating Sintering (FGCS) for Iron Ores:** Tao Jiang<sup>1</sup>; Zhenyu Fan<sup>1</sup>; Yuanbo Zhang<sup>1</sup>; Bin Xu<sup>1</sup>; Guanghui Li<sup>1</sup>; Xiaohui Fan<sup>1</sup>; <sup>1</sup>Central South University

Iron ore sintering process is the main source of SO<sub>2</sub> generated in the steel industry, of which the discharge amount of SO<sub>2</sub> emission accounts for about 60% of the total. Aiming at the features of sintering flue gases and existing problems during the flue gas desulphurization, a technical route of flue gas circulation sintering (FGCS) for iron ores has been put forward. Under the simulated experimental conditions, effects of FGCS process on the main output and quality indexes and SO<sub>2</sub> emission rule are researched using simulating flue gases. Compared the novel FGCS with conventional sintering process, SO<sub>2</sub> in the final sintering flue gas is obviously enriched and the total exhaust gases can be reduced evidently. The decreasing of oxygen content in circulating gases has bad effect on the sintering indexes. Increasing the oxygen potential is beneficial to obtain high quality sinters. This investigation shows that the FGCS process is promising.

11:10 AM

**Energy And Exergy Analysis of Different Technologies of Copper, Zinc and Lead Production – Entropy Generation and Thermoecological Cost:** *Bozena Boryczko*<sup>1</sup>; Adam Holda<sup>1</sup>; Zygmunt Kolenda<sup>1</sup>; <sup>1</sup>AGH University of Science and Technology

Copper, zinc and lead can be produced with different technologies. Most popular copper technologies are shaft furnace and flash smelting. Zinc and lead are produced by shaft furnace or by hydrometallurgical method. Main problem of all metallurgical technologies is the consumption of exergy connected with inevitable depletion of nonrenewable natural resources. One of the most important (from thermodynamic point of view) measure of their depletion is Cumulative Exergy Consumption as the basis of calculation of thermoecological cost (defined as the cumulative exergy consumption of non-renewable natural resources). Difference in exergy consumption is the result of different kinds of driving energy. In shaft furnace technologies, driving energy is the chemical exergy of coke and for flash smelting or hydrometallurgical processes, electric energy plays principal rule. Because of those different exergy sources, the CexC values can differ significantly. The concept of thermoecological cost allows to choose technology with the lowest value of CexC.

11:30 AM

**Optimizations of Preparation for U3O8 by Calcination from Ammonium Durante Using Response Surface Methodology:** *Bingguo Liu*<sup>1</sup>; Jinhui Peng<sup>1</sup>; Daifu Huang<sup>1</sup>; <sup>1</sup>Kunming University of Science and Technology

The conditions of technique to prepare U3O8 by calcinations from ammonium diuranate were optimized, and the response surface design was applied to analyze the influence on the total uranium and of calcination temperature, calcination time mass of sample. A quadratic equation model for the total uranium and of U3O8 was built and effects of main factors and their corresponding relationships were obtained. The analysis of variance shows that calcination temperature and calcination time significantly affected the value of total uranium and of U3O8. The optimal calcination conditions were as follows: calcination temperature 931.83 K, calcination time 24.32min and 43.89 g. Under these conditions the value of total uranium and of U3O8 was 84.78% and 28.02%, respectively. The validity of the model was confirmed experimentally and the results were satisfactory.

11:50 AM

**Microwave Field Attenuation Length and Half-power Depth in Magnetic Materials:** *Zhiwei Peng*<sup>1</sup>; Jiann-Yang Hwang<sup>1</sup>; Xiaodi Huang<sup>1</sup>; Matthew Andriese<sup>1</sup>; Wayne Bell<sup>1</sup>; <sup>1</sup>Michigan Technological University

The equations for determining microwave field attenuation length and half-power depth in magnetic materials were derived from Maxwell's equations. The microwave field attenuation length and the half-power depth for a magnetite concentrate were calculated and the temperature dependence of them was determined. It is demonstrated the microwave field attenuation length and the half-power depth highly depend on temperature and decrease with increasing temperature up to 900 °C. The variations of field attenuation length and the half-power depth with temperature indicate the microwave power attenuates much faster than the field strength in materials. The evaluations of field attenuation length and microwave half-power depth can be used to characterize the microwave dissipation behaviors in the sample and optimize the dimensions of the material in microwave heating.

12:10 PM

**Vanukov Furnace Technology: Application Experience for Processing Different Types of Raw Materials and General Development Trends:** *Valentin Bystrov*<sup>1</sup>; Valery Paretsky<sup>2</sup>; Anton Vernigora<sup>1</sup>; Rostislav Kamkin<sup>1</sup>; *Alexander Mamaev*<sup>1</sup>; Alexander Kuznetsov<sup>1</sup>; <sup>1</sup>National University of Science and Technology (MISIS); <sup>2</sup>State Research Center of Russian Federation "Gintsvetmet" Institute

Vanukov Furnace Technology is an efficient, proven pyrometallurgical injection technology, extensively used in Russia and Kazakhstan for a number of different applications. Technology was most widely adopted for processing copper sulfide concentrates for matte in smelters of Norilsk, Revda (Russia) and Balkhash (Kazakhstan). Also the following applications

were developed and tested in industrial scale: treatment of sulfide lead and lead-zinc concentrates, laterite nickel ore, production of cast iron, treatment of antimony gold-containing ores and municipal solid waste. In this paper, current experience of Vanukov Furnace application to these technologies is described with a number of general development trends and new ways of applications.

## Advances in Science-Based Processing of Superalloys for Cost and Sustainment: Processing Advancements via Modeling and Simulation

*Sponsored by:* The Minerals, Metals and Materials Society, TMS Materials Processing and Manufacturing Division, TMS Structural Materials Division, TMS/ASM: Computational Materials Science and Engineering Committee, TMS: High Temperature Alloys Committee, TMS: Advanced Characterization, Testing, and Simulation Committee

*Program Organizers:* Donna Ballard, US Air Force; David Furrer, Pratt & Whitney; Paul Jablonski, US Department of Energy; Christopher Woodward, Air Force Research Laboratory; Jeff Simmons, AFRL; Mark Blodgett, Wright-Patterson AFB

Monday AM

February 28, 2011

Room: 33B

Location: San Diego Conv. Ctr

*Session Chairs:* Paul Jablonski, US Department of Energy; Lee Semiatin, US Air Force Research Laboratory

## 8:30 AM Introductory Comments

### 8:35 AM Keynote

**Nickel-Based Superalloys: Construction, Use and Validation of Numerical Models:** *Roger Reed*<sup>1</sup>; <sup>1</sup>University of Birmingham

In recent years, the use of numerical modelling in the field of high temperature materials – particularly for the superalloys – has increased markedly. There are now very tangible advantages to be gained from modelling work, e.g. for (i) the invention of new grades of alloy, (ii) the analysis and optimisation of manufacturing processes (casting, welding, heat treatment etc) and (iii) the design of high-integrity components such as turbine blades and discs. In this presentation, examples of successful modelling work in each of these areas will be given. The advantages, limitations and future expectations are given. The overarching observation is that the field has grown from one of mere academic curiosity to one which is of great importance to the viability of businesses operating in the high temperature world.

### 9:15 AM Invited

**Air Force Research Laboratory R&D in Science-Based Superalloy Processing:** *Lee Semiatin*<sup>1</sup>; Donna Ballard<sup>1</sup>; David Mahaffey<sup>1</sup>; Jonathan Miller<sup>1</sup>; Jaimie Tiley<sup>1</sup>; Todd Turner<sup>1</sup>; Donald Weaver<sup>1</sup>; Adam Pilchak<sup>2</sup>; JP Thomas<sup>3</sup>; Kyle McClary<sup>4</sup>; Peter Lee<sup>5</sup>; <sup>1</sup>US Air Force Research Laboratory; <sup>2</sup>UTC, Inc; <sup>3</sup>ATI Allvac; <sup>4</sup>Wright State University; <sup>5</sup>Imperial College London

Basic research at AFRL to develop science-based understanding and predictive models for microstructure evolution during the thermomechanical and solidification processing of superalloys will be summarized. For cast-and-wrought superalloys, the physics of homogenization heat treatment and recrystallization during hot working have been established. These observations have been interpreted using 2D diffusion analysis, crystal-plasticity FEM to quantify deformation nonuniformity, and a mesoscale modeling technique that treats the effects of dislocation generation/annihilation and boundary migration on the kinetics of recrystallization. With respect to powder-metallurgy superalloys, the evolution of grain structure during TMP will be described. Specifically, the effect of hot working/heat treatment conditions and second phases on the final grain size and the status of associated models will be presented. Last, the effect of solidification conditions on the propensity for lateral dendrite growth during directional solidification will be described. Phenomenological (processing-map) and



mesoscale (cellular-automaton) models to describe such phenomena will be briefly reviewed.

**9:45 AM**

**Recrystallization and Grain Growth of a Hot Pack Rolled Nickel-Base Superalloy:** *Adam Pilchak*<sup>1</sup>; *S. Semiatin*<sup>1</sup>; *Donna Ballard*<sup>1</sup>; *Donald Weaver*<sup>1</sup>; <sup>1</sup>Air Force Research Laboratory

Microstructure and texture evolution of a hot pack rolled and annealed Ni-Al-Cr-base superalloy were investigated with electron backscatter diffraction. In the as-rolled condition, the microstructure consisted of elongated, unrecrystallized grains that were in orientations consistent with typical rolling deformation texture components. Subsequent heat treatment recrystallized the microstructure which resulted in an overall decrease in the intensity of the various deformation texture components, but not the development of new orientations. Grain growth kinetics during subsolvus heat treatment were quantified and analyzed on the basis of existing models for grain growth in the presence of second phase pinning particles and texture controlled grain growth. Grain growth behavior during supersolvus heat treatment was also investigated. The results were compared to simulations performed using 3D Monte-Carlo methods incorporating misorientation dependent grain boundary energy and mobility.

**10:05 AM Break**

**10:20 AM**

**HIP of Ni-Base PM Superalloys- Back to the Future:** *Charles Barre*<sup>1</sup>; *Viktor Samarov*<sup>1</sup>; *Dmitry Seliverstov*<sup>1</sup>; <sup>1</sup>Synertech PM Inc.

HIP of complex shape parts from PM superalloys is coming back for critical applications. This comeback is based on a suit of the advanced technologies related to this consolidation process. These technologies include: - Advanced computer process modeling that enables to provide very complex shapes and a significant reduction of development and manufacturing cost. - Enhancement of mechanical properties due to the control of the powder size and inclusions during manufacturing of powder and filling of the HIP capsules - Shape control during HIP due to the adequate design of the HIP tooling and filling procedures - Control of the quality for the net shape surfaces and their enhancement for the environmental compatibility - New technologies of non-destructive testing for the complex shape components. The paper analyses the developed technological tools and numerous applications.

**10:40 AM Invited**

**Microstructural Level Modelling of Freckle Initiation during Directional Solidification:** *Peter D. Lee*<sup>1</sup>; *Lang Yuan*<sup>1</sup>; <sup>1</sup>Imperial College London

Freckles are severe channel-like segregations commonly observed in directionally solidified and single-crystal Ni-base superalloy turbine blade castings, causing part rejection. Freckles arise from the segregation of solute from the solidifying dendrites, altering the density of the interdendritic liquid, causing a Rayleigh instability initiated flow. To predict the on-set of flow the interaction of thermal gradients, microstructure, and permeability all need to be modelled. However, prior work has focused on macrosegregation, with the onset of flow initiated due to numeric noise. In this study, a microstructural model is coupled with a flow solver to provide direct simulation of freckle simulation. The predictions are compared to the extensive prior experimental results in the model binary alloy system, Pb-Sn. Solute channel formation was predicted under different solidification conditions (based on temperature gradient and cooling rate). Using the Rayleigh number, a good correlation between the numerical simulations and experimental was found.

**11:10 AM Invited**

**Heat Extraction and Structure Evolution in LMC Single-Crystal Growth:** *Jonathan Miller*<sup>1</sup>; *Lang Yuan*<sup>2</sup>; *Michael Eisman*<sup>3</sup>; *Peter Lee*<sup>2</sup>; *Tresa Pollock*<sup>4</sup>; <sup>1</sup>AFRL/RXLM; <sup>2</sup>Imperial College; <sup>3</sup>Wright State University; <sup>4</sup>University of California, Santa Barbara

The liquid-metal-cooling (LMC) process for growth of single-crystal superalloys provides enhanced heat extraction, higher cooling rates and refinement of dendritic structure. However, some processing conditions cause substantial lateral heat extraction that promotes lateral growth of

dendrites – the formation of long secondary dendrite arms overgrowing favorably aligned primary dendrites. The conditions under which lateral growth occurs during solidification of alloys CMSX-486 and René N4 have been studied experimentally and with solidification modeling at the macro- and meso-scales. Solidification experiments have been conducted in a LMC furnace that utilizes liquid tin as the cooling medium and a floating ceramic baffle. A mold geometry was designed to evaluate a range of thermal conditions and assess the tendency for lateral growth. Correlations between dendritic structure, solidification-front curvature, solidification rate and thermal gradient will be presented. The presence of lateral growth is strongly dependent on the solidification-front curvature at the casting surface.

**11:40 AM**

**Residual Strain Measurements in a Single-Crystal Nickel-Based Superalloys Turbine Blade using Neutron Diffraction:** *Stephane Pierret*<sup>1</sup>; *Alexander Evans*<sup>1</sup>; *Ania Paradowska*<sup>2</sup>; *Thomas Etter*<sup>3</sup>; *Helena Van Swygenhoven*<sup>1</sup>; <sup>1</sup>Paul Scherrer Institute; <sup>2</sup>ISIS; <sup>3</sup>Alstom

Rafting in nickel-based superalloys describes the directional coarsening of the gamma prime precipitates when subjecting the alloy to high temperature creep deformation. But rafting has also been observed at very localised areas in a non-crept fully heat-treated single-crystal (SX) Ni-based superalloy turbine blade. The influence of macro residual stresses and the associated inhomogeneous plastic strain fields on the rafting of the precipitates has been investigated using neutron diffraction in a 2nd generation SX Ni-based superalloy turbine blade following cooling from the solution heat treatment. A novel approach was used to localise the measurements in the partially hollow blade, by combining a 3D digitisation with a 3D reconstructed image obtained by neutron tomography. Complementary hard energy synchrotron diffraction followed on a cross-section of the blade at the position where the maximum residual strains were determined with neutrons. This revealed the variation of the diffraction peak width and the lattice parameter misfit.

**12:00 PM**

**Numerical Simulation of Directional Solidification of Turbine Blade by LMC Process:** *Ning Tang*<sup>1</sup>; *Qingyan Xu*<sup>1</sup>; *Baicheng Liu*<sup>1</sup>; <sup>1</sup>Tsinghua University

Directionally solidified blade castings are widely used in turbines, because the directional solidified microstructure leads to outstanding high temperature properties. A very strict process control is needed to avoid stray grains. In recent years, liquid metal cooling (LMC) is used as a new process in manufacturing of the blade casting, and it still needs to be improved. Numerical simulation of the LMC process is helpful to optimize the technical parameters and reduce the development cycle and cost. In this paper, a model of a LMC process considering the convection between the shell and the cooling metal was established, which was validated by the experimental results. Different processes of LMC solidification were simulated. The results indicated that higher withdrawal rate or lower cooling liquid metal temperature can obtain higher temperature gradient and lead to thinner mushy zone. However, if the withdrawal rate is too high, the mushy zone becomes more concave.

## Aluminum Alloys: Fabrication, Characterization and Applications: Development and Application

Sponsored by: The Minerals, Metals and Materials Society, TMS Light Metals Division, TMS: Aluminum Processing Committee  
Program Organizers: Subodh Das, Phinix LLC; Zhengdong Long, Kaiser Aluminum; Tongguang Zhai, University of Kentucky

Monday AM Room: 14A  
February 28, 2011 Location: San Diego Conv. Ctr

Session Chair: Zhengdong Long, Kaiser Aluminum

### 8:30 AM

#### Scandium/Zirconium Modified Aluminum Alloys for Improved Mechanical Properties: *Jennifer Gaines*<sup>1</sup>; <sup>1</sup>NSWC Carderock Division

Due to the need for high speed lightweight ships there is an increased use of aluminum alloys in ship construction. These applications require materials with the following combination of properties: high welded strength, ductility and elongation, corrosion resistance, and fatigue and corrosion fatigue resistance. The most commonly used aluminum alloy families in marine applications are the Al-Mg (5XXX series) alloys which derive their strength from work hardening and are not heat-treatable. Reduced as-welded strengths limit their practical structural applications. The high temperatures introduced during the welding process reverse some of the effects of the strengthening mechanisms so aluminum alloys which can retain the greatest amount of post-welded strength are, therefore, greatly desired. Small additions of Sc and Zr have been shown to improve mechanical and corrosion properties of aluminum alloys and their effect as additions to commercial 5XXX alloys are investigated.

### 8:50 AM

#### Continuous Cast Superplastic Grade Aluminum Sheet: *Ravi Verma*<sup>1</sup>; <sup>1</sup>General Motors

Thermo-mechanical processing of a twin-belt continuous cast (CC) Al 5083 slab is investigated with the objective of developing superplastic (SP) grade aluminum sheet. The effect of small variations in the Mn content of the alloy on its SP formability is also investigated. The optimized process is capable of breaking down the as-cast structure of the CC slab to a fine equiaxed microstructure (grain size 7  $\mu\text{m}$ ) suitable for superplastic forming. Compared to the conventional Direct-Chill (DC) process, which uses massive rolling to achieve the necessary grain refinement, the developed process achieves similar level of grain refinement in much less rolling reduction. The SP grade sheet produced with the developed process exhibit tensile ductility of 302% at 500°C and  $10^{-3} \text{ s}^{-1}$  strain rate, which is impressive for this initial material. This work demonstrates the technical feasibility of producing high quality SP grade aluminum sheet based on low-cost, twin-belt continuous cast technology.

### 9:10 AM

#### Study of Aluminum Sensitization at Moderately Elevated Temperatures: *William Golumbskie*<sup>1</sup>; Catherine Wong<sup>2</sup>; <sup>1</sup>Naval Surface Warfare Center, Carderock Division; <sup>2</sup>NAVSEA

Structural aluminum alloys are seeing increased use in marine applications, with the shipbuilding industry looking to reduce weight. The 5xxx series is an ideal candidate, combining high specific strength, corrosion resistance, and weldability. A particular concern is sensitization. Aluminum becomes sensitized when beta phase (Al<sub>3</sub>Mg<sub>2</sub>) is precipitated at grain boundaries, which may lead to stress corrosion cracking. Sensitization is believed to occur when aluminum is exposed to temperatures greater than 50°C. This study will investigate the effects of exposure at lower temperatures (>30°C) on sensitization. Such "moderately" elevated temperatures are of great importance as ship decking and superstructures experience such temperatures while in service. The ASTM G67 mass loss test is being used to quantify the extent of sensitization. The new data will aid in determining the degree

of sensitization for in-service 5xxx alloys and estimate the lifetime until the material has fully sensitized.

### 9:30 AM

#### Forming Limit Diagrams for AA5182 after Preform Annealing: *Jingjing Li*<sup>1</sup>; *John Carsley*<sup>2</sup>; Theresa Lee<sup>2</sup>; S. Jack Hu<sup>1</sup>; <sup>1</sup>University of Michigan; <sup>2</sup>General Motors

Preform Annealing is a process of forming aluminum sheet panels in which a blank is partially stamped, heat treated and then stamped to the final desired shape. Because strain from the first deformation event is recovered by annealing, the process significantly improves product formability. The effects of prestraining along different strain paths and subsequent annealing on the ultimate forming limits of aluminum alloy 5182-O were investigated by determining forming limit diagrams (FLDs) using digital image correlation (DIC) and circle grid analysis (CGA). Aluminum panels were prestrained in uniaxial, equibiaxial and plane strain tension at 15 and 20% equivalent strains, perpendicular to the rolling direction; and annealed at 350°C for short (10 seconds) and long (20 minutes) durations. Calculations of total effective forming limit curves (FLC) were compared to experimental CGA and DIC results. The improvement in FLCs shows the advantage of annealing that can extend the formability of strained materials.

### 9:50 AM

#### A Positron Annihilation Study of Hot Band of a Continuous Cast AA 2037 Al Alloy after Annealing: *Yichu Wu*<sup>1</sup>; *Tongguang Zhai*<sup>2</sup>; <sup>1</sup>University of Wuhan; <sup>2</sup>University of Kentucky

Continuous cast AA 2037 Al alloy hotband was annealed at temperatures ranging from 25 to 500°C for 3h. Vacancy-solute interactions and precipitates in the samples during annealing were investigated using positron annihilation techniques (coincidence Doppler broadening (CDB) and lifetime, respectively) and TEM. It was found that there were vacancy-Cu and vacancy-Cu-Mg complexes at room temperature. Positron mean lifetime peaked at 200°C because of the formation of semicoherent precipitates. The measured CDB ratio curve, characteristic to Mn in shape, indicated the formation of vacancy-Mg-Mn complexes or Mn clusters in these precipitates. Above 250°C, coarsening and dissolution of semicoherent precipitates resulted in decrease in mean lifetime and disappearance of Mn signal, but Cu signal increased clearly with annealing temperature. Over 350°C, Cu signal started to saturate, indicating that Cu dissolved might agglomerate and cluster with vacancies, while new increase in mean lifetime might be attributed to the formation of incoherent phase.

### 10:10 AM Break

### 10:25 AM

#### Aluminium-Titanium Alloys for Thermal Spraying: *Christopher Wheatley*<sup>1</sup>; <sup>1</sup>CJ Wiretech Limited

Arc-spraying using pure aluminium wire (TSA) has been accepted for many years in the oil industry for barrier protection of steel structures in aggressive marine environments. Aluminium-titanium alloys provide an even better physical barrier which exhibits extremely good resistance to erosion and this is achieved with no detrimental affect on corrosion properties. The combination of wear resistance and the macroscopic surface roughness from thermal spraying provides a surface of extremely low slip potential which can remain 'non-slip' for over 20 years at 1000 footfalls per day. Data of slip testing for pedestrians and vehicles is presented and this is supported by case studies in real life situations. Data from corrosion testing in laboratory conditions demonstrates that in some cases the aluminium-titanium alloys sprayed onto steel structures can give improved protection against corrosion in very severe conditions.

### 10:45 AM

#### Hot Tensile Behaviour and Constitutive Analysis of Al-5.5Zn-1.2Mg/Zr Alloys: *Paola Leo*<sup>1</sup>; Emanuela Cerri<sup>1</sup>; Hugh McQueen<sup>2</sup>; <sup>1</sup>Università del Salento; <sup>2</sup>Concordia University

In this study hot tensile behaviour of Al-5.5Zn-1.2Mg and Al-5.5Zn-1.2Mg-0.16Zr alloys deformed in the as-cast state has been analyzed. Tensile tests have been performed in the range 250°C-350°C and 10<sup>-5</sup>s<sup>-1</sup> to 10<sup>-3</sup>s<sup>-1</sup>

1. At the lowest test temperature the stress-strain curves shows a gradual softening after a stress maximum or peak while at the other temperatures a plateau is attained which is lower as temperature T rises and strain rates decrease. For each fixed temperature T, the ductility is almost independent of strain rate for Al-5.5Zn-1.2Mg whereas, for the Zr modified alloy, it decrease slightly with  $\epsilon$ . The constitutive analysis by the sinh equation give  $Q_{HW}=218\text{kJ/mol}$  and  $Q_{HW}=271\text{kJ/mol}$  for unmodified and Zr modified alloys respectively. These values of activation energy are quite high and similar to that of other 7000 alloy containing Cu. The microstructure of all tensioned samples is characterized by cavitation phenomena.

11:05 AM

**Production of Continuous Cast 3105 Coil-Stock for Thin Gauge Roller Shutters:** *Dionisios Spathis*<sup>1</sup>; John Tsiros<sup>1</sup>; <sup>1</sup>Hellenic Aluminium industry (ELVAL SA)

An optimum industrial process was established through trials of continuous cast 3105 alloy for roller shutters. Several thermomechanical processes were investigated regarding final gauge mechanical properties, bendability and surface quality. Softening curves were determined through laboratory annealing trials at intermediate and final gauge in order to choose the proper coil anneal temperature regime.

11:25 AM

**Microstructure Evolution of the Modified AA 5083 Alloy: From the As-Cast State to the Final Product:** *Endre Romhanji*<sup>1</sup>; Miljana Popovic<sup>1</sup>; Tamara Radetic<sup>1</sup>; <sup>1</sup>University of Belgrade

In this work, we characterized the microstructure evolution of industrially processed, commercial AA 5083 with a small Zr addition throughout complete processing route: from the as-cast state to the final hot rolled product. We investigated the effect of multiple stage thermal soaking of the cast alloy and homogenization of the industrially hot-rolled alloy on recrystallization and recovery during the final hot rolling. Microstructural changes during the thermo-mechanical treatments were followed by electrical resistivity measurements, optical and TEM. Two populations of the Mn-based secondary phases were identified in as-cast state. Coarse, eutectic particles containing Fe precipitated at grain boundaries, while finer Mn particles alloyed with Cr formed within grains. Although further processing affected the particle morphology and distribution, both types of precipitates remained distinct and had significant, but different effect on recrystallization process. This work is supported by Ministry of Science and Technological Development, Republic of Serbia under contract number E!4569.

## Aluminum Rolling: Session I

*Sponsored by:* The Minerals, Metals and Materials Society, TMS Light Metals Division, TMS: Aluminum Committee, TMS: Aluminum Processing Committee

*Program Organizer:* Kai Karhausen, Hydro Aluminium Rolled Products GmbH

Monday AM  
February 28, 2011

Room: 16A  
Location: San Diego Conv. Ctr

*Session Chair:* Kai Karhausen, Hydro Aluminium

### 8:30 AM Introductory Comments

### 8:35 AM Keynote

**Simulation of Particle Effects on Recrystallization in Commercial Al Alloys:** *Günter Gottstein*<sup>1</sup>; Volker Mohles<sup>1</sup>; Carmen Schaefer<sup>1</sup>; <sup>1</sup>RWTH Aachen University

Depending on particle size and precipitation kinetics, second phase particles can affect recrystallization in various ways. Large particles which exist prior to recrystallization can cause particle stimulated nucleation which makes itself felt by an acceleration of recrystallization and a change of the recrystallization texture. A complex case arises when recrystallization and precipitation occur concurrently. This will have a significant influence on

the recrystallization kinetics as well as grain size and texture. By means of finite element modeling and recrystallization simulation with the adaptive cellular automata code CORE the various cases were studied. The results will be discussed with respect the predictive power of recrystallization modeling in such cases.

9:05 AM

**Texture Evolution during Symmetric and Asymmetric Rolling of Al-Si-Mg Alloys Fabricated by Twin Roll Casting:** *Jaehyung Cho*<sup>1</sup>; Hyung Wook Kim<sup>1</sup>; <sup>1</sup>Korea Institute of Materials Science

6K21 aluminum alloys (1%Si-0.6Mg) fabricated by twin roll casting were cold-rolled using differential speed rolls. Effect of speed ratio and reduction in area on texture evolution was examined using XRD. Overall reduction in area was 75%. Loads measured in the rolls were decreased with speed ratio. As-casted alloys had texture gradient from the surface to the center. {111}//ND textures were found in the surface and weak rolling textures were located in the center. The initial textures changed into rotated cube, {100}<011> and rolling textures, a (Goss-Brass) and b (Brass-S-Copper). Shear texture, rotated cube, was found in both symmetric and asymmetric rolling processes. Various rolling parameters were investigated to generate shear texture. Roll speed ratios greater than 1.4 produced shear texture throughout the whole thickness direction.

9:30 AM

**An Investigation of Deformation Behavior of Bimetal Clad Sheets by Asymmetrical Rolling at Room Temperature:** *Li Xiaobing*<sup>1</sup>; Zu Guoyin<sup>1</sup>; Deng Qiang<sup>2</sup>; <sup>1</sup>School of Materials and Metallurgy, Northeastern University; <sup>2</sup>Cold rolling company, Pangang group company LTD.

The different thickness metals mild steel, aluminum and copper were bonded with each other by means of asymmetrical rolling at room temperature. The deformation behaviors, bonding conditions and interfacial layer thickness of the clad sheets were discussed. According to the slab stress in the plastic deformation region at the roll gap, the relations of bonding condition and metal flow were analyzed. The influence of cross shear on the bonding due to the roll speed mismatch is obvious. The large speed mismatch makes a good bonding and drops the critical reduction. The improvement of bonding is achieved with the increase of the total rolling reduction. The reduction of both layers increases in direct proportion with the total reduction, and the difference between hard and soft metals gradually diminishes. The large initial thickness ratio of hard and soft metal is unhelpful for the bonding due to the inconsistent deformation of bimetal.

9:55 AM Break

10:15 AM

**Parameter Study within the Through-Process-Modeling Chain of AA8xxx-Alloys and Its Validation:** *Thiemo Brüggemann*<sup>1</sup>; Volker Mohles<sup>1</sup>; Carmen Schäfer<sup>1</sup>; Günter Gottstein<sup>1</sup>; Kai Karhausen<sup>2</sup>; <sup>1</sup>Institute; <sup>2</sup>Hydro Aluminium Deutschland GmbH

Optimization of alloys and whole process chains for aluminum sheets and foils is a major goal of the aluminum industry. Since experimental methods are cost- and time-intensive, simulation tools are to be used to predict effects of material and process parameter changes on the product. Within this work the behavior of a through-process-modeling-chain is tested for its reaction on various parameter changes within the group of 8xxx-Aluminum alloys. The modeling chain consists of a thermally coupled roll gap model with subsequent simulation of rolling- and recrystallization-texture by grain-interaction and cellular automata models, respectively. Parameter studies will include microchemistry changes such as solute contents and particle sizes and radii. Data from industrial trials and experiments will be used for validation.

10:40 AM

**Coil Build up Compensation during Cold Rolling to Improve Off-Line Flatness:** *Lourival Almeida Neto*<sup>1</sup>; Tuggan Ayhan<sup>2</sup>; <sup>1</sup>Achenbach Buschhütten GmbH; <sup>2</sup>Assan Alüminyum

During rolling, overlaps of material with a convex profile at recoiler cause greater tension in strip center fibers than in fibers of the edges, which is



known as coil build up. The high tension on central area is understood by the automation system as zones tighter than reference commanding its actuators to put back such zones on target, loosening the correspondent strip fibers. The difficulty is that the buckles created by the flatness controller are not seen at operator's screen. A coil build up compensation based on material profile was developed in order to have the cause of center buckles after unwinding reduced to the coiling process. From 24 coils with thickness ranging between 0.7 and 2.0mm, 100% presented better offline flatness. Flatness carpets related to profile suggested a paradigm breaking: perhaps we have to accept rolling with not so good flatness in order to have the desired offline flatness.

#### 11:05 AM

**Through Process Effects on Final Al-Sheet Flatness:** *Stefan Neumann*<sup>1</sup>; Kai Karhausen<sup>1</sup>; <sup>1</sup>Hydro Aluminium Dts. GmbH

In the process of rolled products to achieve a defined flatness of the strip in ever decreasing tolerances becomes more and more a key challenge. The typical process chain of strip material consists of hot rolling, cold rolling, annealing as well as coil winding and unwinding at various stages. Some Aluminium alloys exhibit the strong tendency to reduce internal stresses by creep and relaxation. This transformation of elastic into plastic strains frequently leads to considerable changes of shape and flatness of the product over the different steps of the process chain. This contribution introduces a model based through process analysis with emphasis to the evolution of strip flatness via the most decisive production stages. Case studies from aluminium strip production will be used to illustrate the impact of different process parameters.

#### 11:30 AM Concluding Comments

### Approaches for Investigating Phase Transformations at the Atomic Scale: Transformation Kinetics and Mechanisms

*Sponsored by:* The Minerals, Metals and Materials Society, ASM International, TMS Materials Processing and Manufacturing Division, TMS/ASM: Computational Materials Science and Engineering Committee, TMS/ASM: Phase Transformations Committee  
*Program Organizers:* Neal Evans, Oak Ridge National Laboratory; Francisca Caballero, Spanish National Research Center for Metallurgy (CENIM-CSIC); Chris Wolverton, Northwestern University; David Seidman, Northwestern University; Rajarshi Banerjee, University of North Texas

Monday AM  
February 28, 2011

Room: 32B  
Location: San Diego Conv. Ctr

*Session Chairs:* S. Babu, Ohio State University; Neal Evans, ORNL & Univ. Tennessee, Knoxville

#### 8:30 AM Keynote

**Solid-State Diffusion and Transformation Kinetics:** *Georges Martin*<sup>1</sup>; <sup>1</sup>Retired

The recent dramatic increase in efficiency of atomic scale observation and modeling techniques opens new routes to the understanding of diffusion controlled phase transformations. The kinetic pathway for phase separation in ternary Ni(Cr, Al) supersaturated solid solutions is discussed\*. First principle calculations and empirical fits to simple experiments give the parameters for kinetic Monte Carlo simulations of long sequences of vacancy jumps in the solution. The latter result in the precipitation of the  $\square^{\prime}$  Ni<sub>3</sub>(Al<sub>1-x</sub>, Cr<sub>x</sub>) phase (L12), and perfectly reproduce quantitative and qualitative features revealed in real alloys by 3DAP. The same parameters are also used to measure the Onsager and diffusion matrices in the model solid solutions; several intriguing features of the observed pathways are shown to result from kinetic couplings between the diffusion fluxes of the alloy components, a coupling ignored by existing models. \*Collaboration with David Seidman et al. NWU.

#### 9:10 AM Invited

**Atomistic Modeling of Diffusive Phase Transformations Kinetics by Monte Carlo Simulations:** *Frederic Soisson*<sup>1</sup>; <sup>1</sup>CEA Saclay

The kinetics of diffusive phase transformations are essentially controlled by the concentrations, jump mechanisms and jump frequencies of point defects, and by the way they depend on the local atomic configurations. Atomistic Kinetic Monte Carlo (AKMC) simulations are nowadays one of the most efficient tools for taking into account such details and therefore for predicting the kinetic pathways, especially when associated with ab initio calculations, which provide a reliable way to compute the key physical properties and the corresponding Monte Carlo parameters. We present a few recent AKMC simulations of phase transformations in model systems of industrial interest, especially in iron-based alloys. Comparison with experimental kinetics using 3D atom probe and neutron scattering techniques is emphasized.

#### 9:35 AM Invited

**Chemical Mixing at Hetero-Interfaces Forced by Severe Plastic Deformation:** *Pascal Bellon*<sup>1</sup>; Robert Averback<sup>1</sup>; Nhon Vo<sup>1</sup>; Xuan Zhang<sup>1</sup>; Elvan Ekiz<sup>2</sup>; Yinon Ashkenazy<sup>1</sup>; Daniel Schwen<sup>1</sup>; Mohsen Pouryazdan<sup>2</sup>; Horst Hahn<sup>2</sup>; <sup>1</sup>University of Illinois; <sup>2</sup>Karlsruhe Institute of Technology

Severe plastic deformation (SPD) can lead to the stabilization of supersaturated solid solutions in the case of moderately immiscible elements such as Cu and Ag, and to self-organization into lamellar structures in the case of highly immiscible elements, such as Cu and Nb. In this work, we contrast the different mechanisms operating in Cu-Ag and Cu-Nb alloys subjected to SPD, including high pressure torsion testing and ball milling. Combining experiments and molecular dynamics simulations, we show that the atomic mixing in Cu-Ag, surprisingly, increases linearly with strain as the elements are brought into solution. In contrast, Cu-Nb alloys can either remain phase separated or they can mix, depending on the initial crystallographic orientation of the Cu-Nb interfaces. Special orientations such as Kurdjumov-Sachs, for example, are remarkable stability against mixing, whereas others are not. In these latter cases, local amorphization is often observed at the interfaces.

#### 10:00 AM Break

#### 10:15 AM Keynote

**THE INSTITUTE OF METALS LECTURE AND ROBERT FRANKLIN MEHL AWARD WINNER: The Ubiquitous Interfacial Free Energy in Phase Transformations:** *David Seidman*<sup>1</sup>; <sup>1</sup>Northwestern University

The interfacial free-energy of a grain boundary or a heterophase interface is a ubiquitous and important quantity in all microstructures, and its short and long-term stability or lack of stability is intimately related to this fundamental quantity. Interfacial free energy affects important physical phenomena such as nucleation, growth and coarsening of different phases in multicomponent alloys, which are integral to the decomposition of a single-phase solid-solution. In this talk I focus on the diverse roles played by interfacial free energy in phase transformations in multicomponent metallic alloys, which are studied experimentally by atom-probe tomography and transmission electron microscopy. The results of simulations employing lattice kinetic Monte Carlo, where the phase transformation is mediated by a vacancy mechanism, will be presented and compared in detail with experimental observations. First-principles calculations of interfacial energies in the same metallic alloys will be discussed in terms of their relevance to all of the above.

#### 10:55 AM Invited

**Atomic Scale Investigation of Alpha Nucleation in the Beta Matrix of Titanium Alloys:** Soumya Nag<sup>1</sup>; Robert Williams<sup>2</sup>; Arun Devaraj<sup>1</sup>; Peter Collins<sup>1</sup>; Gopal Viswanathan<sup>3</sup>; Rajarshi Banerjee<sup>1</sup>; *Hamish Fraser*<sup>2</sup>; <sup>1</sup>University of North Texas; <sup>2</sup>The Ohio State University; <sup>3</sup>Air Force Research Laboratory

The solid-state decomposition of the beta phase of titanium alloys, leading to the precipitation of the equilibrium alpha phase, is a rather complex phenomenon involving multiple competing compositional and structural instabilities. The generally accepted mechanism of alpha precipitation

in these alloys is via classical nucleation and growth. Coupling advanced characterization techniques such as synchrotron-based in situ x-ray diffraction, aberration-corrected high-resolution (S)TEM, and atom probe tomography, the early stages of alpha precipitation at the atomic to near-atomic scale have been investigated in two titanium alloys, a commercial beta alloy, Ti-5Al-5Mo-5V-3Cr-0.5Fe (TIMETAL-5553 or Ti-5553), and a model ternary Ti-Mo-Al system. These experimental observations indicate that depending on temperature the decomposition can take place via a novel pseudospinodal mechanism that involves homogeneous alpha precipitation at a composition far-from equilibrium, followed by a continuous change in the compositions of both the parent beta and the product alpha phases towards equilibrium.

**11:20 AM**

**In Situ Studies and Simulations of Rapid, Self-Propagating Phase Transformations in Nanolayer Foils:** *Timothy Weihs*<sup>1</sup>; *Sara Barron*<sup>1</sup>; *Todd Hufnagel*<sup>1</sup>; *Steve Kelly*<sup>1</sup>; *Michael Falk*<sup>1</sup>; *Rong Xu*<sup>1</sup>; *Omar Knio*<sup>1</sup>; *Francesco Rizzi*<sup>1</sup>; *Geoffrey Campbell*<sup>2</sup>; *Judy Kim*<sup>3</sup>; <sup>1</sup>Johns Hopkins University; <sup>2</sup>Lawrence Livermore National Lab; <sup>3</sup>Oxford University

Exothermic formation reactions are known to self-propagate in multilayer foils with nanoscale layers and large, negative heats of mixing, such as Ni/Al, Nb/Si and Ti/B multilayers. The exothermic reactions can travel at velocities greater than 10 m/s and they reach temperatures as high as 3000 K. The combination of rapid propagation and high temperatures produces extremely fast heating rates ( $\sim 10^7$  K/sec) within the reaction front, while the nanoscale layers provide steep chemical gradients. Here we investigate the impact of both extremes (heating rate and chemical gradient) on reaction paths and phase morphologies using in situ X-ray diffraction, Dynamic TEM, Molecular Dynamic Simulations, and numerical modeling. The sequence of phase transformations and the phase morphologies that appear under fast and slow ( $\sim 1$  K/sec) heat rates are shown to be different and the impact of steep chemical gradients is assessed. Work performed under auspices of USDOE OBES by JHU under contract DE-SC0002509 and by LLNL under contract DE-AC52-07NA27344.

**11:35 AM**

**Molecular Dynamics Studies of Phase Transformations during Rapid Heating of Nanolayer Foils:** *Rongguang Xu*<sup>1</sup>; *Michael Falk*<sup>1</sup>; <sup>1</sup>Johns Hopkins University

A series of molecular dynamics studies of multilayer metallic foils undergoing rapid heating due to exothermic reaction reveal a number of salient details regarding the sequence of reaction. In simulations of Ni-Al foils melting is followed by the sequential precipitation of a number of intermetallic phases. The sequence of phase formation is observed to be sensitive to the interlayer mixing prior to the onset of the reaction. In simulations of Ni-Zr foils spontaneous amorphization precedes the formation of an ordered intermetallic. Atomic scale diagnostics are used to quantify the fraction of the material that has undergone phase transformation, identifying both atoms in ordered alloy and solid solution phases. This work was performed under DOE contract DE-FG02-09ER46648.

**11:50 AM**

**Interplay between Interfacial Segregation and Diffusion Shapes the Growth of Gold-Catalyzed Silicon Nanowires:** *Moneesh Upmanyu*<sup>1</sup>; *Hailong Wang*<sup>1</sup>; *Luis Zepeda-Ruiz*<sup>1</sup>; <sup>1</sup>Northeastern University

The vapor-liquid-solid for nanowire synthesis route has gained relevance of late as it in principle allows direct control over nanowire morphology and composition during synthesis. Here, we present classical computations on a small diameter, gold-catalyzed  $\langle 111 \rangle$  silicon nanowire that for the first time allow access to the atomistics underlying the growth process. We find a direct effect of the interfacial segregation, at the catalytic particle surface and at the faceted particle-nanowire interphase, on the diffusive kinetics that builds up the supersaturation necessary for interphase nucleation. The silicon-rich surface layer suppresses diffusion to an extent that the supersaturation is carried by the bulk of the particle. Their key structural aspect is the Au segregation at the interphase. The enhanced undercooling is kinetically offset by Au metastability around nucleated steps that arrests lateral flow

such that the growth is no longer layer-by-layer. We discuss the implications controlled growth of nanowire arrays.

**12:05 PM**

**Ta Clustering and Microstructural Evolution in the A1 to L10 Fe52PtX(Ta1-X) Phase Transformation:** *Diondra Means*<sup>1</sup>; *Billie Wang*<sup>1</sup>; *Gregory Thompson*<sup>1</sup>; <sup>1</sup>University of Alabama

FePt magnetic films have application in ultrahigh magnetic storage media. Their chemical ordering phase transformation and microstructure can be controlled by the addition of ternary elements. Controversy has existed on whether Ta additions promote or hinder the A1 to L10 ordering transformation. A series of Fe52Pt48, Fe52.3Pt46.3Ta1.4 and Fe52Pt40.7Ta7.3 thin films were sputter deposited and subsequently annealed. The as-deposited films had a change from a {111} fiber texture to {002} with the Ta additions. Annealing at 550°C facilitated the L10 order in Fe52Pt48 and Fe52.3Pt46.3Ta1.4 films. Upon annealing at 750°C, all three compositions L10 phase transformed. Atom probe tomography revealed nano-scale clustering in the annealed Ta containing films. The formation of these clusters appeared to be a necessary initial step to allow the L10 ordering reaction to occur. Additionally, clustering at grain boundaries provided a Zener-based pinning mechanism for grain growth measured by TEM.

## Biological Materials Science: Bio-Inspiration and Bio-Inspired Materials I: Hard Biomaterials

*Sponsored by:* The Minerals, Metals and Materials Society, TMS Electronic, Magnetic, and Photonic Materials Division, TMS Structural Materials Division, TMS: Biomaterials Committee  
*Program Organizers:* *Jamie Kruzic*, Oregon State University; *Nima Rahbar*, University of Massachusetts, Dartmouth; *Po-Yu Chen*, University of California, San Diego; *Candan Tamerler*, University of Washington

Monday AM  
February 28, 2011

Room: 15A  
Location: San Diego Conv. Ctr

*Session Chairs:* *Jamie Kruzic*, Oregon State University; *Candan Tamerler*, University of Washington

**8:30 AM Introductory Comments**

**8:35 AM Keynote**

**Nature-Inspired Hybrid Structural Materials for Bone Repair:** *Antoni Tomsia*<sup>1</sup>; <sup>1</sup>Lawrence Berkeley Lab

While the need for organ repair is being partly addressed by transplantation, the development of a systematic method to generate new organs would transform medicine. So far we have made little progress in engineering bone and cartilage even at relatively small scales. A critical component of this engineering approach is the development of porous 3D structures — scaffolds — that will provide cell support and guide tissue regeneration. Ceramics will play an important role in the development of new scaffolds but this will require materials and structures able to combine the optimum environment for bone formation with the optimized mechanical response. We will describe how new processing techniques can be combined with novel design principles taken, in part, from natural material such as nacre or bone to fabricate ceramic-based scaffolds and composites for bone repair. The critical design and material parameters as well as future research directions will be discussed.

**9:15 AM**

**Bone Regeneration in CaP Scaffolds: The Complementary Roles of BMP-2 and Microporosity:** *Amy Wagoner Johnson*<sup>1</sup>; *Samantha Polak*<sup>1</sup>; *Sheeny Lan Levensgood*<sup>2</sup>; *Aaron Maki*<sup>1</sup>; *Matthew Wheeler*<sup>1</sup>; *Sherrie Clark*<sup>1</sup>; <sup>1</sup>University of Illinois at Urbana-Champaign; <sup>2</sup>University of Wisconsin, Madison

BMP-2 is a well-known stimulant for bone regeneration. Microporosity ( $< 20\mu\text{m}$ ), has also been shown to influence regeneration in CaP scaffolds

MONDAY AM

that contain both macro (>100µm) and microporosity. This study shows that BMP-2 and microporosity have different, yet complementary, roles in bone regeneration in biphasic calcium phosphate (BCP) scaffolds. Microporosity increases the volume of bone (BV), but does not influence the specific surface area (SSA), in a study using a pig mandible model. In contrast, BMP-2 influences SSA, but not BV. Both make regeneration more uniform throughout scaffolds. Bone concentrates at the defect margin in scaffolds without microporosity or BMP-2. Additionally, BMP-2 and microporosity accelerate healing up to four-fold. Thus, microporosity may be as influential in healing large defects as BMP-2, as demonstrated by rapid and uniform regeneration. Mechanisms controlling regeneration for these two variables will be discussed.

**9:35 AM**

**Enhanced Functions of Osteoblasts on Biomimetic Nanohydroxyapatite-Grafted Chitosan Scaffolds for Bone Tissue Engineering:** *Dilip Depan*<sup>1</sup>; Bhupinder Girase<sup>1</sup>; Pavan Challa<sup>1</sup>; Devesh Misra<sup>1</sup>; <sup>1</sup>University of Louisiana at Lafayette

We describe here three dimensional biodegradable chitosan-nanohydroxyapatite (nHA) composite scaffolds with improved mechanical, physico-chemical, and biological properties compared to pure chitosan scaffolds for bone tissue engineering. High and medium molecular weight chitosan scaffolds with 0.5, 1, and 2 wt % fraction of nHA were fabricated by freezing and lyophilization. The nanocomposite scaffolds were characterized by a highly porous structure with interconnected pores and the pore size was similar for the scaffolds with varying content of nHA. The nanocomposite scaffolds exhibited greater compression modulus, slower biodegradation rate and reduced water uptake, but the water retention ability was similar to pure chitosan scaffolds. Favorable biological response of pre-osteoblast (MC 3T3-E1) on nanocomposite scaffolds includes improved cell adhesion, higher proliferation, and well spreading morphology in relation to pure chitosan scaffold. The study underscores chitosan-nHA composite as a potential scaffold material for bone regeneration.

**9:55 AM**

**Structure and Mechanical Properties of Bioinspired Inorganic/Polymer Multi-Layer Composites:** *Gustavo Hirata*<sup>1</sup>; Sandra Payán<sup>1</sup>; Yu-Chen Chan<sup>2</sup>; Po-Yu Chen<sup>3</sup>; Jenq-Gong Duh<sup>2</sup>; Joanna McKittrick<sup>2</sup>; <sup>1</sup>Centro de Nanociencias y Nanotecnología-UNAM; <sup>2</sup>National Tsing Hua University; <sup>3</sup>University of California, San Diego

Abalone nacre has mechanical properties that are far beyond its constituents, CaCO<sub>3</sub> and biopolymer, due to the well-defined structure at varying hierarchical levels. Abalone-inspired ZrN/PMMA multi-layer composites are synthesized by combining DC-magnetron sputtering and pulsed laser deposition on silicon substrates in a single chamber. SEM and high resolution TEM images show uniform polymeric layers (10-50 nm) sandwiched between nanocrystalline ZrN layers (0.3-0.5 µm). The thickness ratio of the inorganic/polymer layers is the same as that in abalone. Multi-layered ZrN/PMMA thin films with increasing interfacial roughness were also made to mimic the nano-sized asperities and bridges observed in abalone. Nanoindentation and nanoscratch tests are conducted on the synthetic thin films and abalone nacre followed by SEM and AFM characterization. Failure mechanisms are discussed and comparisons are made. This research is supported by the NSF Grant DMR 1006931.

**10:15 AM Break**

**10:25 AM Invited**

**Mimicking Bone Formation Using Anionic Polymeric Process-Directing Agents:** *Taili Thula*<sup>1</sup>; *Laurie Gower*<sup>1</sup>; <sup>1</sup>University of Florida

Bone is a hierarchically-structured composite which imparts it with unique mechanical properties and bioresorptive potential. These properties are primarily influenced by the underlying nanostructure of bone, which consists of nanocrystals of hydroxyapatite embedded and uniaxially aligned within collagen fibrils. There is also a small fraction of non-collagenous proteins in bone, and these are thought to contribute both to bone's formation as well as its mechanical properties. In our in vitro model system of bone

formation, polyanionic peptides and proteins are used to mimic the role of the non-collagenous proteins. Intrafibrillar mineralization of collagen can be achieved using a polymer-induced liquid-precursor (PILP) mineralization process, which yields a nanostructured composite closely mimicking the nanostructure of bone. This talk will focus on our studies comparing the effectiveness of different polymeric process-directing agents, as measured by the kinetics of mineralization, degree of mineral content, and depth of penetration of mineral into dense-packed collagen matrices.

**10:55 AM**

**Bionanomineralization through Genetically Engineered Peptides and Fusion Proteins:** *Candan Tamerler*<sup>1</sup>; <sup>1</sup>University of Washington & Istanbul Technical University

Biomimetic synthesis of nanoinorganics have been a major focus in hard tissue engineering as well as developing a new generation of hybrid materials through environmentally-benign processing. Bio-based molecular building blocks are, therefore, developed for practical water-based pathways to novel biologically compatible structures. Here we use recombinant DNA technologies and biochemical conjugation to produce single or multifunctional peptides and fusion proteins and enzymes that can controllably bind to a given solid material including variety of materials, and in particular to those relevant for medical applications. Examples of the use of solid-binding peptides are given with specific implementations in self-mineralization and in forming hybrid molecular scaffolds in tissue restoration and regeneration, surface biofunctionalization of implants with antibacterial bifunctional peptide coatings, and conjugated linkers towards directed enzyme immobilization. Research is supported the NSF-MRSEC at UW, NSF-BIOMAT, TUBITAK-NSF IRES Joint Projects, and TR-SPO.

**11:15 AM**

**Engineered Mineral-Directing Peptides for Hard Tissue Engineering:** *Mustafa Gungormus*<sup>1</sup>; Hanson Fong<sup>1</sup>; Joel Schneider<sup>2</sup>; Candan Tamerler<sup>1</sup>; Mehmet Sarikaya<sup>1</sup>; <sup>1</sup>University of Washington; <sup>2</sup>National Cancer Institute-Frederick

During normal development of hard tissues, mineral morphogenesis is heavily influenced by soluble extracellular matrix (ECM) proteins. Polymer scaffolds, while providing architectural support, lack the molecular control over mineralization. We demonstrate use of engineered peptides to functionalize scaffolds or defect sites to exert control on mineral formation at molecular level. Mineralization-directing peptides can be engineered to interact with the mineral surfaces or precursor ions to regulate the mineral formation mimicking the ECM proteins synthesized during tissue development. In vitro solution based or cell mediated mineralization assays have shown that a precise control can be achieved over the mineral morphology and the formation kinetics. Moreover, these peptides do not require any hostile chemistry for functionalization and show no cytotoxic effects. The results presented here indicate that these peptides may find substantial use in tissue engineering for successful restoration and regeneration of hard tissues. Research is supported by the NSF-MRSEC at UW.

**11:35 AM**

**Structural Characterization of the Mineral Phase in Bony Tissues: A Comparative Study:** *Po-Yu Chen*<sup>1</sup>; Maria Lopez<sup>2</sup>; Ekaterina Novitskaya<sup>1</sup>; Marc Meyers<sup>1</sup>; Joanna McKittrick<sup>1</sup>; <sup>1</sup>University of California, San Diego

Bone is a hierarchically structured composite of type-I collagen fibrils and mineral crystallites. We examined structural features of the mineral phase in some unique bony tissues, including antlers, turtle shells, armadillo carapaces and fish scales. A chemical method to completely remove the protein constituents without altering the original structure has been developed and verified. TEM observations of carbonated apatite crystallites derived from various bony tissues showed similar platelet-like geometry. The hierarchical structure of untreated and deproteinized samples was characterized by micro-computed tomography, optical microscopy, SEM, and AFM. The most significant finding was that the minerals retain structural integrity after completely removing protein constituents. High resolution SEM images showed minerals formed sheet-like structure, aligned in a coherent manner



along the orientation of collagen fibrils. Organized porous structure (vascular channels, lacunae, canaliculi) was observed. Comparisons between bony tissues were made. This research is supported by NSF Grant (Ceramics and Biomaterials Program) 1006931.

11:55 AM

**Bone Demineralization and Deproteinization Studies: A Biochemical-Kinetic Focus:** Ana Castro<sup>1</sup>; Ekaterina Novitskaya<sup>2</sup>; Po-Yu Chen<sup>2</sup>; M. del Pilar Sánchez-Saavedra<sup>1</sup>; Gustavo Hirata<sup>3</sup>; Joanna McKittrick<sup>2</sup>; <sup>1</sup>CICESE; <sup>2</sup>UC San Diego; <sup>3</sup>CNyN-UNAM

There is an increasing interest on the study of bone demineralization and deproteinization due to their different clinical applications and, the Material Science, also. In the present work, cortical and cancellous bovine femur bones were demineralized and deproteinized. Demineralization was performed at different temperatures and concentrations of hydrochloric acid. Deproteinization was carried out using 6% NaOCl at distinct temperatures. The goal of this work was to calculate the kinetic parameters of the demineralization and deproteinization reactions. Demineralization and deproteinization were found to follow first-order kinetics. The rate of demineralization increased with both HCl concentration and temperature. Three different stages were clearly identified during the demineralization reactions. The activation energy for demineralization increased with increasing HCl concentration. Concerning on deproteinization, the activation energy calculated was different between cortical and cancellous bovine femur bones. This work provides a better understanding of the details of bone demineralization and deproteinization reactions.

## Bulk Metallic Glasses VIII: Alloy Development and Application I

*Sponsored by:* The Minerals, Metals and Materials Society, TMS Structural Materials Division, TMS/ASM: Mechanical Behavior of Materials Committee

*Program Organizers:* Gongyao Wang, University of Tennessee; Peter Liaw, Univ of Tennessee; Hahn Choo, Univ of Tennessee; Yanfei Gao, Univ of Tennessee

Monday AM  
February 28, 2011

Room: 6D  
Location: San Diego Conv. Ctr

*Session Chairs:* Jan Schroers, Yale University; Marios Demetriou, California Institute of Technology

8:30 AM Keynote

**Millisecond Thermoplastic Processing of Bulk Metallic Glasses:** William Johnson<sup>1</sup>; Georg Kaltenboeck<sup>1</sup>; Marios Demetriou<sup>1</sup>; Joe Schramm<sup>1</sup>; <sup>1</sup>California Institute of Technology

A novel method is introduced for millisecond time scale experiments and processing of bulk metallic glass forming liquids. Electrical energy is used to uniformly heat BMG cylinders, plates, and sheets to a predefined temperature in the undercooled (or equilibrium) liquid at rates of order  $10^6$  K/s. Excellent temperature uniformity is achieved throughout the sample. The sample can be deformed under mechanical loading or injected into mold cavities to form net shapes. Measurements are carried out in millisecond time scales under "near adiabatic" conditions. The platform can be used to measure liquid specific enthalpy  $h(T)$ , heat capacity  $c(T)$ , viscosity, crystallization kinetics, etc.. High speed video and infrared thermal imaging are used to collect data. The new "Rapid Discharge Heating and Forming" (RDHF) method overcomes limitations created by intervention of crystallization in glass forming liquids enabling measurements and processing of both marginal and superior glass forming alloys.

9:00 AM

**Bulk Metallic Glass: The Smaller the Better:** Golden Kumar<sup>1</sup>; Jan Schroers<sup>1</sup>; <sup>1</sup>Yale University

Despite their superb properties, bulk metallic glasses (BMGs) find limited utility due to their macroscopic brittle nature, high costs, and difficulty of

processing, particularly when complex shapes are desired. As a consequence of strong size-dependent mechanical properties of BMGs, abovementioned drawbacks can be mitigated when BMGs are used in miniature parts ( $< 1$  cm), an application which takes advantage of BMGs' enhanced plasticity at small length scales as well the insignificant material cost associated with such parts. As an alternative to traditional metal processing techniques, thermoplastic forming (TPF)-based microfabrication methods have been developed which can process some BMGs like plastics. We will discuss the properties and fabrication of BMGs for application in small-scale devices including miniature parts, nano-imprinting, and self-assembly substrates.

9:10 AM Invited

**The Production of Iron Based BMGs by Spray Forming:** Claudemiro Bolfarini<sup>1</sup>; Walter Botta<sup>1</sup>; Claudio Kiminami<sup>1</sup>; <sup>1</sup>Universidade Federal de São Carlos

This paper describes results obtained by spray forming of iron-based alloys, whose compositions derived from rapid solidification studies aiming to obtain amorphous structures. Atomization with high gas to metal flow ratio is necessary for amorphous phase formation, and most important for keeping it by avoiding excessive reheating and consequent crystallization during deposit build-up. The amorphous regions of the deposit were formed by the participation of a great numbers of amorphous particles that were kept in the supercooled liquid region for a sufficient time in order to allow bonding of one to each other and viscous flow under the influence of the gas pressure and impacting droplets. The [(Fe0.6Co0.4)0.75B0.2Si0.05]96 Nb4 al alloy presented the highest glass forming ability among the Fe-based alloys investigated, showing a high volume percent of amorphous phase formation up to 4mm thickness of the deposit, a similar value obtained for this alloy when processed by copper mould casting.

9:30 AM

**Development of Mass Production System for Zr-Based Bulk Glassy Alloys:** A. Inoue<sup>1</sup>; Y. Yokoyama<sup>1</sup>; <sup>1</sup>Institute for Materials Research

For the implementation of high-reproducibility and high-quality of bulk metallic glasses (BMGs), mass production system of Zr-based BMGs was newly developed. This mass production system is composed of three machines; weighing-, master alloying- and casting-machines. The automatic weighing is composed of three processes, materials feeding, cutting, and weighing, and these three processes are automatically controlled by LabVIEW in PC. The weight deviation of automatically measure system is about 1 % in this process, we are trying much higher accuracy of this value to be less than 0.5 %. Recently, full-automatic arc furnace was commercialized by DIAVAC Ltd. [<http://www.diavac.co.jp/>] using a patent developed by YKK co. Ltd. and Tohoku university. The usage of full-automatic arc furnace suppresses the human error and dependence human's skill. By using this machine, we can control the homogeneity of alloying as a relative evaluation. This developed mass production system will accelerate the standardization of BMGs.

9:40 AM Invited

**Ductility Enhancement and Size Enlargement of Bulk Glassy Alloys:** H. Tokunaga<sup>1</sup>; K. Fujita<sup>1</sup>; T. Yamasaki<sup>2</sup>; A. Yavari<sup>3</sup>; P. Liaw<sup>4</sup>; A. Inoue<sup>5</sup>; Y. Yokoyama<sup>5</sup>; <sup>1</sup>Department of Machine Engineering; <sup>2</sup>Department of Material Science and Engineering; <sup>3</sup>SIMAP-CNRS; <sup>4</sup>University of Tennessee; <sup>5</sup>Institute for Materials Research

We examined hypoeutectic Zr-Cu-Al bulk glassy alloys exhibit high-fracture toughness and almost no degradation in mechanical properties due to structural relaxation. Furthermore, in the quaternary Zr-Ni-Cu-Al alloys, the hypoeutectic Zr70Ni16Cu6Al8 bulk glassy alloy with extremely low Young's modulus (70 GPa) and high Poisson's ratio (0.39) enables to show the distinct tensile plastic elongation at room temperature. We also examined tensile plasticity of the hypoeutectic BMG at low temperature with various strain rate. Size enlargement of metallic glass has been performed by combination of compositional optimization and production process optimization. The former focused on the glass forming ability, and the later focused on the homogenizing and purification of master alloy to achieve vitrification. The quantity of master alloy should be limited for

homogenizing. Homogenized small master alloys promote easy handling of the melting and casting processes, whereas we have to fabricate the large number of master alloys.

#### 10:00 AM Break

#### 10:10 AM Invited

**Bulk Metallic Glasses Form Like Plastics:** *Jan Schroers*<sup>1</sup>; <sup>1</sup>Yale University

The sluggish crystallization kinetic of bulk metallic glass results in two fundamentally different processing opportunities. BMG can be directly cast. But even for BMGs with low critical cooling rates geometries with high aspect ratio are particularly challenging since during casting cooling and filling of the mold must occur simultaneously. This limits the complexity of the geometries that can be cast even when processing parameters are carefully balanced. Alternatively, BMG can be thermo plastically formed in the supercooled liquid region. In this case the required fast cooling and forming are decoupled. The BMG is formed in a high viscous state where it behaves very similar to plastics when compared by processing temperature and forming pressure. A measure for the formability of BMGs will be introduced. Processing potentials and challenges will be discussed and various examples will be given including blow-molding, miniature fabrication, and nano-patterning.

#### 10:30 AM

**A Novel Preparation Method for Mg-based BMG Matrix Composite with the In-Situ Ti Dispersoids:** *Hideki Oka*<sup>1</sup>; *Takeshi Wada*<sup>1</sup>; *Kunio Yubuta*<sup>1</sup>; *Hidemi Kato*<sup>1</sup>; *Akihisa Inoue*<sup>1</sup>; <sup>1</sup>Tohoku University

The Mg-Cu-RE (rare earth) bulk metallic glass (BMG) is known for its high specific strength ( $\sim 2.2 \times 10^5$  Nm/kg), which is higher than the conventional AZ91 alloy ( $\sim 1.4 \times 10^5$  Nm/kg). However, the fracture toughness of the alloy is comparable to the ceramics, which is a serious disadvantage for the practical use. For improving the fracture toughness of the alloy, Mg-Cu-RE BMG matrix composites have been developed by dispersing the ex-situ particles such as Fe, TiB<sub>2</sub>, SiC, Ti and so on. Although the plastic elongation of the Mg-based BMG is highly enhanced by these particles, the composite effect is achieved only in the compressive mode. In this work, we intend to introduce a novel method of dispersing in-situ  $\alpha$ - &  $\beta$ -Ti particles in a Mg-Cu-Gd BMG based on an earlier work by Li et al. (Mater. Trans. 48(2007)3193) to improve the fracture toughness of the brittle Mg-based BMG.

#### 10:40 AM Invited

**Novel Net-Shape Processing of Metallic Glass by Rapid Joule Heating:** *Marios Demetriou*<sup>1</sup>; *Georg Kaltenboeck*<sup>1</sup>; *Joseph Schramm*<sup>1</sup>; *William Johnson*<sup>1</sup>; <sup>1</sup>California Institute of Technology

In an effort to process metallic glass into net shape, thermoplastic methods that take advantage of the vitreous state of the undercooled liquid have been explored. These methods are limited by the relatively low stability of the liquid against crystallization, which prohibits processing within the optimum viscosity range of 10-1000 Pa-s utilized in conventional thermoplastic processes. Consequently, thermoplastic forming of metallic glass typically requires very high pressures, often approaching the flow stresses of tools. Recently, a joule heating method for processing metallic glass has been developed. The method takes advantage of the unique electrical properties of the metallic glass to heat rapidly and uniformly across the entire undercooled liquid region bypassing crystallization. Processing in the viscosity range of 10-1000 Pa-s is achievable by this method, which promotes low-cost fabrication of high-precision net-shape metallic glass parts. The rapid joule heating and forming method constitutes a powerful platform for processing metallic glass.

#### 11:00 AM Invited

**The Effect of Purification on the Glass-Forming Ability of Pd-Cu-Si Alloys:** *Ke-Fu Yao*<sup>1</sup>; *Sheng-Bao Qiu*<sup>1</sup>; *Hong-Yu Ding*<sup>1</sup>; *Yang Li*<sup>1</sup>; <sup>1</sup>Tsinghua University

In present work, the Pd-Cu-Si alloy melt has been purified by fluxing with B<sub>2</sub>O<sub>3</sub> at high temperature and effect of melt purification on the glass-forming ability has been studied. It has been found that with the purified Pd-Cu-Si ingots glassy bars with a diameter of 8 mm have been successively

prepared by water quenching method and the glassy bars with a diameter of 4 mm have been prepared by copper mould casting. But without purification even for 2mm glassy bar it could not be prepared. It has also been found that the glassy alloy prepared with purified ingots exhibits much higher thermal stability than that prepared with the ingots without purification. The present results indicate that melt purification can effectively enhance the glass-forming ability of Pd-Cu-Si alloys through removing the inhomogeneous nucleus by fluxing method.

#### 11:20 AM Invited

**Processing and Tensile Tests of Amorphous Wires:** *Yong Zhang*<sup>1</sup>; <sup>1</sup>University of Science and Technology Beijing

The amorphous wires of Cu<sub>50</sub>Zr<sub>46</sub>Al<sub>4</sub> and Co<sub>36</sub>Fe<sub>36</sub>Nb<sub>4</sub>Si<sub>4.8</sub>B<sub>19.2</sub> alloys were prepared by the In-rotation water melting spinning and Taylor-Ulitovsky technique, respectively. The amorphous wires of Cu<sub>50</sub>Zr<sub>46</sub>Al<sub>4</sub> alloy can be in diameter of 50-120  $\mu$ m and length of 1 m, while the amorphous wires of Co<sub>36</sub>Fe<sub>36</sub>Nb<sub>4</sub>Si<sub>4.8</sub>B<sub>19.2</sub> alloy by Taylor-Ulitovsky method can be in diameter of 10-50  $\mu$ m and length of 5 m or more, and with glass coated. The tensile strength of the Cu<sub>50</sub>Zr<sub>46</sub>Al<sub>4</sub> amorphous alloy wires is about 1800 MPa, that of Co<sub>36</sub>Fe<sub>36</sub>Nb<sub>4</sub>Si<sub>4.8</sub>B<sub>19.2</sub> alloy is about 2400 MPa. The tensile strength of the glass coated amorphous wire of Co<sub>36</sub>Fe<sub>36</sub>Nb<sub>4</sub>Si<sub>4.8</sub>B<sub>19.2</sub> alloy linearly increases from 800 MPa to 2400 MPa with the ratio of the diameter of the inner amorphous wire to the outer diameter with the glass coating from 0.3 to 0.9. The wire forming parameters were compared with the glass forming ability of the alloys.

#### 11:40 AM Invited

**Formation and Properties of New Zr-Based Bulk Glassy Alloys with High Glass-Forming Ability:** *Wei Zhang*<sup>1</sup>; *Yanhui Li*<sup>2</sup>; *Chuang Dong*<sup>2</sup>; *Akihisa Inoue*<sup>1</sup>; <sup>1</sup>Institute for Materials Research, Tohoku University; <sup>2</sup>School of Materials Science and Engineering, Dalian University of Technology

Although Zr-Al-Ni alloy system is the first Zr-based glassy alloys reported in 1990 [1], the glass-forming ability (GFA) and mechanical properties have not been investigated yet systematically. Here we report on the thermal stability, GFA and mechanical properties of Zr-Al-Ni glassy alloys with high Zr concentrations. The glassy rods with critical diameter (dc) above 10 mm were obtained in a wide composition range. The maximum dc of  $\sim 15$  mm was formed for an off-eutectic Zr<sub>60</sub>Ni<sub>25</sub>Al<sub>15</sub> alloy, which has the largest supercooled liquid region and  $\Delta T_c$  value. Compression tests revealed that the bulk glassy alloys exhibit high yield strength of over 1.65 GPa and a distinct plastic strain [2]. The effects of additional alloying elements on the thermal stability, GFA, mechanical properties, and corrosion resistance of Zr-Al-Ni glassy alloys are also investigated. [1] A. Inoue et al., Mater. Trans. JIM. 31, 177 (1990). [2] Y.H. Li et al., Intermetallics. (2010), on line.

#### 12:00 PM Invited

**High Strength Amorphous and Nanocrystalline Ni-W Electrodeposits:** *Tohru Yamasaki*<sup>1</sup>; *Masako Sonobe*<sup>1</sup>; *Kazutaka Fujita*<sup>2</sup>; *Takeyuki Kikuchi*<sup>1</sup>; *Hye Jung Chang*<sup>3</sup>; *Do Hyang Kim*<sup>3</sup>; <sup>1</sup>University of Hyogo; <sup>2</sup>Ube National College of Technology; <sup>3</sup>Yonsei University

Structure and tensile plastic deformation behaviors of amorphous and nanocrystalline Ni-W electrodeposited alloys have been examined. By controlling the surface roughness of the Cu-substrate, a high strength nanocrystalline Ni-16.9 at % W alloy with mesoscale Ni-segregated network structure has been prepared by electrodeposition. When the W-content was increased to 22 at. %, the alloy has consisted of amorphous phase in general. Nominal tensile strength of the Ni-16.9 at % W alloy was attained to about 2,900 MPa with the total strain before fracture was about 3 % containing the large plastic strain of about 1.0 %. A large necking phenomenon of about 30% at the fracture surface was observed, resulting the high true tensile strength at fracture of about 4,100 MPa. These results have suggested that the Ni-segregated mesoscale structure is effective for improvement of the tensile plasticity of high strength nanocrystalline alloys.

12:20 PM

**Synthesis of Plastic Mg-Based Bulk Metallic Glass Matrix Composites by the Bridgman Solidification:** *Liang Zhang*<sup>1</sup>; <sup>1</sup>Nanjing University of Science and Technology

The microstructures of the in situ Mg-based bulk-metallic-glass-matrix composites synthesized by the copper-mold suction casting are inhomogeneous, and the optimized mechanical properties were usually realized through alloy composition design. In this paper, Mg-based bulk-metallic-glass-matrix composites containing uniform flake-shaped precipitates with a fixed composition of Mg<sub>70</sub>Cu<sub>8.33</sub>Y<sub>8.33</sub>Gd<sub>8.33</sub>Zn<sub>5</sub> are synthesized by the Bridgman solidification. The sizes and volume fractions of precipitates in the composites are controlled by adjusting the withdrawal velocities. Large plasticity can be obtained by only controlling the cooling condition. The Bridgman solidification is an effective way not only to fabricate the homogeneous BMG-matrix composites but also to tailor and optimize its mechanical properties.

### **Characterization of Minerals, Metals and Materials: Characterization Methods and Synthesis Techniques**

*Sponsored by:* The Minerals, Metals and Materials Society, TMS Extraction and Processing Division, TMS/ASM: Composite Materials Committee, TMS: Materials Characterization Committee  
*Program Organizer:* Sergio Monteiro, State University of the Northern Rio de Janeiro - UENF

Monday AM  
February 28, 2011

Room: 14B  
Location: San Diego Conv. Ctr

*Session Chairs:* Jian Li, CANMET-MTL; Sergio Monteiro, UENF

8:30 AM

**Materials with Controlled Microstructural Architecture (MCMA) Fabricated by Electron Beam Melting (EBM):** *Sara Gaytan*<sup>1</sup>; *Diana Ramirez*<sup>2</sup>; *Lawrence Murr*<sup>1</sup>; *Edwin Martinez*<sup>1</sup>; *Jose Martinez*<sup>1</sup>; *Daniel Hernandez*<sup>1</sup>; *Brenda Machado*<sup>1</sup>; *Frank Medina*<sup>1</sup>; *Ryan Wicker*<sup>1</sup>; <sup>1</sup>UTEP

While traditional or contemporary materials science and engineering utilizes various processing technologies including thermo-mechanical or mechanical processing to create and manipulate microstructures to control properties and establish performance features, there are currently no processing routes for the selective or systematic organization of microstructures to create architectures. In this paper we demonstrate the novel development of carbide (M<sub>23</sub>C<sub>6</sub>) precipitate architecture in the EBM fabrication of Co-base alloy components, and an oxide (Cu<sub>2</sub>O) precipitate-dislocation architecture in the EBM fabrication of Cu components. These architectures are characterized by special arrays of precipitate columns extending (generally) in the EBM build direction for the additive (powder layer) manufacturing process. Microstructures and associated architectures have been examined by optical metallography, and scanning and transmission electron microscopy.

8:45 AM

**Quantifying Damage Accumulation during Ductile Plastic Deformation Using Synchrotron Radiation:** *Reeju Pokharel*<sup>1</sup>; *Jonathan Lind*<sup>1</sup>; *Xi Tan*<sup>1</sup>; *Robert Suter*<sup>1</sup>; *Anthony Rollett*<sup>1</sup>; <sup>1</sup>CMU

High Energy X-ray Diffraction and absorption tomography were used to study void nucleation process in polycrystalline materials, during ductile fracture. The experimental techniques were developed at the Advanced Photon Source beam line 1-ID. Preliminary tests were performed on the tabletop microtomography system at Carnegie Mellon University. 1mm diameter Cu wire was selectively electropolished to form a neck of ~200um in the middle, to localize the strain. Synchrotron diffraction and tomography data were collected while performing in-situ uniaxial tensile test. These non-destructive techniques were able to more accurately confirm the position of the void nucleation sites in relation to the crystallographic orientation and microstructural features, such as, grain boundaries, triple points, and

quadruple points. This study will aid in quantifying anisotropic microstructural distribution of strain and understanding damage accumulation, which are the main sources of failure in polycrystalline materials.

9:00 AM

**Design and Implementation of Low Cost Measurement System for Determination of Thermal Conductivity Coefficient:** *Juan Calderón*<sup>1</sup>; *Nora Ramírez*<sup>1</sup>; *Leobardo López*<sup>1</sup>; <sup>1</sup>ITESM Campus Toluca

One of the most important parameters to characterize the thermal behavior of any material is the coefficient of thermal conductivity. The present work proposes a design of a low cost measurement system in order to determine this coefficient with the lower possible error. The system is based on ASTM C 518 – 04 and integrated by two plates. A control system checks in real time plates temperatures in order to determine the effective power applied to the system. The contact faces of the plates contain a group of temperature sensors connected to a data acquisition system that process and records the temperature in each measurement point. With the power applied to the system, the measurement of temperatures and a process of calibration it is possible to determine the coefficient of thermal conductivity.

9:15 AM

**Material Performance of TBCs at High Temperature in Moisture-Containing Environments Using a Load-Based Micro-Indentation Technique:** *Jared Tannenbaum*<sup>1</sup>; *Bruce Kang*<sup>1</sup>; *Mary Anne Alvin*<sup>2</sup>; <sup>1</sup>West Virginia University; <sup>2</sup>National Energy Technology Laboratory

A load-based micro-indentation technique has been developed for damage assessment and non-destructive spallation detection of TBCs at room temperature. This micro-indentation technology has been further extended to the development of a high temperature (HT) test methodology. Elastic modulus calibration tests performed on H13 Tool Steel to 500°C and Haynes 230 at 1000°C displayed excellent agreement with reported values. Moreover, indentation creep tests of Haynes 230 at 1200°C were found to be in agreement with known creep exponents as well. Finally, a HT thermal flux indentation apparatus was assembled for conducting TBC turbine component testing under high temperature moisture-containing environments (e.g. =50% steam with controlled gas content temperatures up to 1250°C). Description and design considerations of this test apparatus are discussed. Preliminary tests of RenéN5/MCrAlY/APS TBC coupons in =50% steam/air environments with in-situ HT micro-indentation testing are conducted. Furthermore, the coupon is removed and examined for damage assessment at periodical intervals.

9:30 AM

**Raman Spectroscopy of C-A Domain Switching in (001) BaTiO<sub>3</sub> Single Crystals under Uniaxial Loading:** *Carolina Diliegros Godines*<sup>1</sup>; *Juan Muñoz - Saldaña*<sup>1</sup>; *Molly Gentleman*<sup>2</sup>; *Amy Bolon*<sup>2</sup>; *Luis Gutierrez Ladron de Guevara*<sup>1</sup>; <sup>1</sup>Cinvestav-Queretaro; <sup>2</sup>Texas A&M University

Ferroelastic domain switching occurs progressively as a function of applied stress in ferroelectric-ferroelastic materials such as BaTiO<sub>3</sub>. The first steps of switching were characterized using 325 nm polarized confocal Raman spectroscopy on a (001) oriented BaTiO<sub>3</sub> single crystal with 90°-aa and cc domain arrangements under compressive loading. Direction of the polarization vectors for a-domains from the unloaded crystal were unambiguously identified by Raman mapping, through observation of orientation intensity gradients due to contribution from subsurface a and c domains. A similar gradient was observed by measuring the elastic modulus across 90°-ac domains by nanoindentation. A set of mappings was recorded from the loaded surface as a function of applied stress that shows the switching sequence. Under this mechanical configuration out-of-plane domains from the surface become unstable and switch to in-plane domains. Raman spectroscopy also allowed identification of the preferential switching sites and A+x, A-x, A+y or A-y domains.

MONDAY AM



9:45 AM

**Synthetic Generation of Annealing Twins in Three-Dimensional Microstructures:** *Lisa Chan*<sup>1</sup>; Michael Groeber<sup>2</sup>; Gregory Rohrer<sup>3</sup>; Anthony Rollett<sup>3</sup>; <sup>1</sup>EDAX-TSL; <sup>2</sup>Air Force Research Laboratory; <sup>3</sup>Carnegie Mellon University

In face-centered cubic metals, the density of high symmetry boundaries is often maximized in order to improve grain boundary dependent properties. Twinning events have been found to be very effective in increasing the density of these high symmetry boundaries that are denoted by low sigma values for Coincident Site Lattice relationships. In this study, annealing twins are generated in synthetic microstructures by using the  $\Sigma 3$  cluster distribution as the target. To illustrate the capabilities of the method, a 3D dataset for a nickel alloy was collected using serial sectioning in a dual-beam FIB with OIM™. Twin-related grains were synthetically removed from the structure and subsequently regenerated. The statistics used to quantify the differences between the twin-regenerated and experimentally observed microstructures are texture, five-parameter grain boundary character distribution, and the number and area fractions of  $\Sigma 3$  boundaries.

10:00 AM Break

10:15 AM Invited

**Experimental Characterization of Negative Thermal Expansion in Oxides:** *Fernando Rizzo*<sup>1</sup>; Monica Ari<sup>1</sup>; Bojan Marinkovic<sup>1</sup>; Paula Jardim<sup>1</sup>; Roberto de Avillez<sup>1</sup>; Fabio Furlan Ferreira<sup>2</sup>; <sup>1</sup>PUC Rio de Janeiro; <sup>2</sup>ABC Federal University

For several technological applications such as Fiber Bragg gratings sensors, illumination system, integrated circuits, electronic components, optical devices, shock thermal resistance, etc, controllable thermal expansion materials, pure or composites are required. It has been the driving force in the search for crystal phases with unusually low, zero, or even negative thermal expansion (NTE). Some open-framework classes of known ceramics, such as AO<sub>2</sub>, AMO<sub>5</sub>, AM<sub>2</sub>O<sub>7</sub>, A<sub>2</sub>O<sub>5</sub> and A<sub>2</sub>M<sub>3</sub>O<sub>12</sub> have emerged as potential sources of crystal phases with low or NTE. The A<sub>2</sub>M<sub>3</sub>O<sub>12</sub> family is especially attractive due to the chemical flexibility that results in a large range of variation of linear coefficients of thermal expansion ( $\alpha$ ) after phase transition from monoclinic to orthorhombic structure. Both structures consist of corner-sharing AO<sub>6</sub> octahedra and MO<sub>4</sub> tetrahedra. It is assumed that the low-energy transverse thermal vibration of the oxygen in the A–O–M linkage within lower-density orthorhombic structure produces NTE.

10:45 AM

**Digital Construction and Characterization of Reticulated Porous Microstructures from Sacrificial Templates:** *Jason Kulp*<sup>1</sup>; Stephanie Lin<sup>2</sup>; Jason Nadler<sup>2</sup>; <sup>1</sup>Georgia Institute of Technology; <sup>2</sup>Georgia Tech Research Institute

A numerical method has been developed to predict the microstructural characteristics of reticulated metal foam. The porosity of this foam is derived from sacrificial template particles of known particle size distribution, which are incorporated with other precursor components. In this approach, a porous structure is numerically generated starting with Powell's sphere packing algorithm. The resulting stochastic structure has characteristics similar to those of corresponding metal foam. Deterministic inter-sphere connections are calculated to more accurately model the pore morphology that evolves during thermochemical synthesis. Estimations of pore morphology and specific surface area of the simulated material are compared to lab-synthesized materials composed of equivalent constituent compositions. In addition, the effect of template particle size, inter-sphere connections, and the geometric constraints on pore morphology and permeability are investigated to refine microstructural evolution and design.

11:00 AM

**Thermodynamic Measurement of CaO-P<sub>2</sub>O<sub>5</sub>-SiO<sub>2</sub> System:** *Takashi Nagai*<sup>1</sup>; Hisao Kimura<sup>1</sup>; Masafumi Maeda<sup>1</sup>; <sup>1</sup>The University of Tokyo

Hot metal pretreatment for de-phosphorization is a common practice in the iron and steel industry, and has been developed as an effective refining process. Although a molten flux was used traditionally in this process, a

multi-phase flux, which contained liquids and solidus phases, is used today in order to avoid use of harmful element for environment such as fluorine. In addition, it is possible to reduce wasted flux by use of this flux because P<sub>2</sub>O<sub>5</sub> is increased to solidus phase in the flux. Since the solidus phase is based on CaO-P<sub>2</sub>O<sub>5</sub>-SiO<sub>2</sub> system, thermodynamic properties of this system are necessary to improve this process optimally. However, the available thermodynamic information on this system is limited. In this study, activity of P<sub>2</sub>O<sub>5</sub> in CaO-P<sub>2</sub>O<sub>5</sub>-SiO<sub>2</sub> system was measured by double Knudsen cell mass spectrometry. And the optimal condition of this process was considered.

11:15 AM

**Applying Modular DOE to Improve Material Characterization and Performance:** *Paul Funkenbusch*<sup>1</sup>; <sup>1</sup>University of Rochester

Design Of Experiments (DOE) methods are routinely applied in many engineering applications. However, they have not been as extensively used for material characterization and, when applied, they have often been in the form of standard product/process optimization methodologies (e.g. "Taguchi methods") that may not be well adapted to material engineering applications. The modular approach to DOE seeks to build experimental designs tailored to specific applications, by allowing the designer to make appropriate choices for each of four design element (array design, choice of the characteristic response, incorporation of variability, and data analysis). In this presentation, the use of a modular approach to build experimental designs suitable for characterizing material performance is illustrated using a variety of examples. These include development of an erosion testing protocol, identification of tool material property effects on precision grinding performance, and characterization of diamond bur performance degradation in dental burrs.

11:30 AM

**Selective Removal of Thiophene from Liquid Fuels over Nickel-Based Nanocrystalline Zinc Oxide:** *Mohammad Islam*<sup>1</sup>; Jewel Gomes<sup>1</sup>; Hylton McWhinney<sup>2</sup>; Doanh Tran<sup>1</sup>; Sameer Pallavkar<sup>1</sup>; Md Islam<sup>1</sup>; George Irwin<sup>1</sup>; David Cocke<sup>1</sup>; <sup>1</sup>Lamar University; <sup>2</sup>Prairie View A&M University

Low temperature deep desulfurization of fuels via selective adsorption of sulfur compound is receiving increasing attention worldwide in order to satisfy the upcoming environmental regulations and fuel specifications. The Ni/ZnO adsorbents were prepared by thermal decomposition and incipient impregnation method from their nitrate precursors. A model fuel (20 mL) consisting of pentane (C<sub>5</sub>H<sub>12</sub>), heptane (C<sub>7</sub>H<sub>16</sub>) and thiophene was prepared and adsorption experiments were performed by a batch method under ambient conditions. The physicochemical behaviors of the adsorbents were obtained using BET, XRD, XRF, TG-DSC, SEM/EDAX, and XPS. The sulfur concentration in the mixture was monitored by UV-vis spectrophotometry. The adsorption reaction confirmed that ZnO played a crucial role in taking up S element to convert it into ZnS. The deposition of nickel on ZnO is an innovative approach which takes advantage of the selectivity of Ni towards S species and the high adsorptive capacity of ZnO support.

11:45 AM

**Extending the Effective Range of Wilkinson's Method Via a Geometry-Based Pattern Center Correction Algorithm:** *Calvin Gardner*<sup>1</sup>; Brent Adams<sup>1</sup>; David Fullwood<sup>1</sup>; <sup>1</sup>Brigham Young University

Electron Backscatter Diffraction based Orientation Imaging Microscopy has generated worldwide interest in the localized recovery of the elastic displacement gradient tensor in diverse crystalline materials. Wilkinson's cross-correlation based method, with angular resolution of  $\pm 0.006^\circ$ , is sufficiently precise to determine the sought-after tensor. However, the method is limited by reliance on the comparison of two like oriented patterns that must be of similar pattern center, collected within  $\sim 75$  micrometers of one another. Moreover, if the absolute pattern center is not known, the method's accuracy decreases correspondingly. Both a single crystal germanium scan and a series of simulations are presented to demonstrate the problems of pattern center variation and imprecise absolute pattern center. An analytic algorithm based in system geometry is employed to correct for pattern center variations and the effective range of Wilkinson's method is extended to  $\sim 500$

micrometers. Additionally, an analysis of the necessary absolute pattern center precision is presented.

#### 12:00 PM

**Thermodynamical Studies on the Carbothermal Reduction and Nitride Preparing for Vanadium Nitride:** *SS Yu<sup>1</sup>; WX Li<sup>1</sup>; ZL Ji<sup>1</sup>; NX Fu<sup>2</sup>; ZT Sui<sup>2</sup>*; <sup>1</sup>Shenyang University of Chemical Technology; <sup>2</sup>Northeastern University

In this paper, the producing process of using V<sub>2</sub>O<sub>3</sub> as raw material to obtain vanadium nitride was analyzed through the predominance area diagrams. The analysis shows that VN-phase can be accessed in the conversion process of V<sub>2</sub>O<sub>3</sub> by controlling gas phase composition and temperature of the reaction system and the one-step method preparing for vanadium nitride is feasible. Thermalgravimetric analysis and X-ray diffraction were used to determine the reaction pathways of vanadium carbide, namely the following sequential reaction: V<sub>2</sub>O<sub>3</sub>  $\square$  V<sub>8</sub>C<sub>7</sub> in higher temperature stage, the rule of vanadium nitride synthesized was established, and defined conditions of temperature for the production of the carbides and nitrides were determined. The nitridation process is simultaneous with the carbothermal reduction. A one-step mechanism of the carbothermal reduction with simultaneous nitridation led to a lower terminal temperature in nitridation process for vanadium nitride produced, compared with that of carbothermal reduction process without nitridation.

### Chloride 2011: Practice and Theory of Chloride-Based Metallurgy: Hydrometallurgy

*Sponsored by:* The Minerals, Metals and Materials Society, Canadian Institute of Metals, TMS Extraction and Processing Division, TMS: Magnesium Committee, TMS: Energy Committee  
*Program Organizers:* Dirk Verhulst, Consultant, Extractive Metallurgy; V.I. (Lucky) Lakshmanan, Process Research Ortech, Inc.

Monday AM  
February 28, 2011

Room: 19  
Location: San Diego Conv. Ctr

*Session Chairs:* V. Ram Ramachandran, Consultant; George Demopoulos, McGill University

#### 8:30 AM

**Hydrometallurgy of Chlorides: A Review of Recent Developments:** *Dirk Verhulst<sup>1</sup>; Vaikuntam Lakshmanan<sup>2</sup>*; <sup>1</sup>Consultant, Extractive Metallurgy; <sup>2</sup>Process Research ORTECH Inc

Past, existing and developing processes are reviewed, with emphasis on base and precious metals as well as titanium dioxide.

#### 8:55 AM

**Development of a Novel High-Chloride Circuit for the Starfield Resources' Ferguson Lake Project:** *Mike Dry<sup>1</sup>; Niels Verbaan<sup>2</sup>; Ernesto Bourricaudy<sup>2</sup>; Michael Moran<sup>3</sup>*; <sup>1</sup>Arithmetek Inc.; <sup>2</sup>SGS Canada Lakefield; <sup>3</sup>Starfield Resources Inc.

Starfield Resources is developing a novel circuit for the recovery of nickel, copper, cobalt, iron oxide and possibly also precious metals from the Ferguson Lake deposit in Nunavut, Canada. This deposit contains massive sulphides in which pentlandite is too finely disseminated in pyrrhotite for the production of a smelter-grade nickel concentrate at anywhere near an acceptable nickel recovery, meaning that commercial exploitation of this orebody is not possible via established technology. The circuit under development contains leaching, oxidation of ferrous chloride, hydrolysis of ferric chloride to saleable hematite and gaseous hydrochloric acid that is recycled and conventional steps for separating and recovering the valuable metals from the solution after hydrolysis. This paper presents a process model of the circuit and the results of experimental work on the main enabling steps, viz. the leaching, the oxidation of ferrous chloride and the hydrolysis of ferric chloride to hematite and gaseous hydrochloric acid.

#### 9:20 AM

**Synthesis of TiO<sub>2</sub> by an Innovative Atmospheric Mixed Chloride Leach Process:** *V.I. Lakshmanan<sup>1</sup>; Ram Sridhar<sup>1</sup>; Raja Roy<sup>1</sup>*; <sup>1</sup>Process Research Ortech Inc.

TiO<sub>2</sub> is used in paints, plastics, rubber, paper, inks, textiles and other miscellaneous applications. The demand for the pigment grade TiO<sub>2</sub> is growing at 3.0% on average and this invites for the development of innovative and cost effective processes. The current processes are not designed to recycle the reagents and thereby discharge the effluents into the environment causing an environmental concern.

During this study, synthesis of TiO<sub>2</sub> from an ilmenite concentrate was investigated using an innovative atmospheric mixed chloride leach process. The solution purification was carried out using solvent extraction in two stages. In the first stage iron removal was carried out and in the second stage titanium was extracted. The strip solution obtained from the second stage solvent extraction contained the purified titanium and from this stream pigment grade TiO<sub>2</sub> was recovered. The barren solution was used for reagent recovery and the regenerated leach liquor was recycled.

#### 9:45 AM

**Solvent Extraction for the Separation into Nickel and Cobalt with Anionic Extractant:** *Tomohiko Yokogawa<sup>1</sup>; Satoshi Matsumoto<sup>1</sup>; Nobuhiro Matsumoto<sup>1</sup>*; <sup>1</sup>Sumitomo Metal Mining Co., Ltd.

At Niihama Nickel Refinery (NNR), the plant capacity of electrolytic nickel expanded from 36kt/A to 41kt/A as nickel/cobalt mixed sulfide (MS) feed increased. At the same time, cobalt input from MS also increased. For the separation into nickel and cobalt, NNR has installed a solvent extraction process by using tri-n-octylamine (TNOA) as anionic extractant to change into the effective purification. As a result, NNR has achieved cost reduction, more stable operation and products of better quality, comparing new process with conventional ones of oxidation and neutralization. This paper describes improvements of the operation conditions such as continuous phase control.

#### 10:10 AM Break

#### 10:25 AM

**Integrated Plant to Recover Zinc, Lead and Silver from Crude Zinc Oxides Applying ZINCEX and PLINT Technologies:** *Carlos Frias Gomez<sup>1</sup>; Gustavo Diaz<sup>1</sup>; Daniel Martin<sup>1</sup>; Francisco Sanchez<sup>1</sup>; Ana Mejias<sup>1</sup>*; <sup>1</sup>Tecnicas Reunidas

Crude zinc oxides are the major source of secondary zinc and are produced from fuming processes like Waelz kilns. The impurities of crude zinc oxides make difficult their processing in primary zinc refineries due to mainly high chloride tenor. Washing with sodium carbonate is a costly operation and chloride removal efficiency is not good enough, so further purification steps are required. The crude zinc oxides are easily treated using ZINCEXTM technology based on leaching, solvent extraction, and electrowinning. The ZINCEXTM process is commercially available and is designed to be a perfect barrier for impurities and halogens, allowing selective zinc extraction in mixed chloride and sulphate leaching solutions. Other valuable components like lead and silver can be efficiently recovered from the leaching residue using PLINT technology in chloride media. Silver is recovered as silver cement and lead is precipitated as pure lead oxide or carbonate able for smelting at low temperature.

#### 10:45 AM

**N,N'-Tetrasubstituted Malonamide Derivatives and Hydrochloric Acid Solutions: An Interfacial Study:** *Maria Soledade Santos<sup>1</sup>; Marc Font Cornella<sup>1</sup>; João Nuno Reis<sup>1</sup>; Sandra Santos Reis<sup>1</sup>; Ana Paiva<sup>1</sup>*; <sup>1</sup>FCUL

N,N'-tetrasubstituted malonamides have increasingly been used as extractants for various metal ions, such as Fe(III) and platinum-group metals, from HCl media, hence it is important to understand the involved interfacial phenomena. In this work, the influence of the malonamide structure, acidity of the aqueous phase and diluent on the equilibrium interfacial tension (IT) of N,N'-dimethyl-N,N'-diphenylmalonamide and N,N'-dimethyl-N,N'-dicyclohexylmalonamide in 1,2-dichloroethane, and N,N'-dimethyl-N,N'-dicyclohexylmalonamide in toluene, with aqueous HCl, were investigated.

ITs were determined using the Du Nouy ring method. Densities of the organic phases were also determined, and used to screen solute-diluent interactions. Formation of third phases was never observed; furthermore, ITs increase with the phase separation period, constant values being obtained for separation periods larger than 1000 seconds. Each malonamide interfacial efficiency at the oil/water interface is interpreted in terms of malonamide basicity, diluent polarity and malonamide - hydrochloric acid- diluent interfacial interactions.

#### 11:10 AM

**Recovery of Precious Metals from Base Metal Sulfide Ores by a Hydrometallurgical Process:** *V.I. Lakshmanan*<sup>1</sup>; Ram Sridhar<sup>1</sup>; Raja Roy<sup>1</sup>; <sup>1</sup>Process Research Ortech Inc.

Base metals and PGMs are currently recovered from sulfide concentrates using pyrometallurgical processes. These processes suffer from several limitations such as being capital intensive, scaling problems, SO<sub>2</sub> emissions and long delay in value recognition. Alternative hydrometallurgical technologies have so far not been successful and currently total pressure oxidation and partial pressure oxidation hydrometallurgical technologies are being evaluated. Process Research ORTECH has developed a unique hydrometallurgical process to recover base metals and precious metals using mixed chloride technology. In a first stage leach, base metals are recovered and elemental sulfur is liberated from hydrogen sulfide formed during this leaching stage. During second stage leach, precious metals are recovered using proven separation technologies. Some of the advantages of the process are the recovery of elemental sulfur from sulfide sulfur, recycle of the chloride lixiviant thereby eliminating effluent treatment steps and use of excess energy from the Claus reactor for the pyrohydrolysis step.

#### 11:35 AM

**Recovery of Precious Metals from Chloride Media Using Microalgae Waste from Biofuel Extraction:** *Katsutoshi Inoue*<sup>1</sup>; Kanjana Khunathai<sup>1</sup>; Keisuke Ohto<sup>1</sup>; Hidetaka Kawakita<sup>1</sup>; Kinya Atsumi<sup>2</sup>; Hisaya Kato<sup>2</sup>; <sup>1</sup>Saga University; <sup>2</sup>Denso Corporation

Crosslinked microalgae were prepared from the residue generated in the production of biofuel, by crosslinking-condensation in concentrated sulfuric acid. These microalgae were tested for adsorption of various metal ions in hydrochloric acid medium. The crosslinked microalgae exhibited high selectivity for Au(III) over other precious and base metal ions. From an isotherm experiment, the maximum adsorption capacity was evaluated to be 3.25 mol/kg of dry gel for Au(III) which was many times higher than that of the original microalgae residue. SEM and X-ray diffraction confirmed the formation of metallic gold particles, suggesting the occurrence of a redox reaction between surface functional groups on the gel surface and trivalent gold ion.

## Computational Thermodynamics and Kinetics: Defects: Thermodynamics and Kinetics of Grain Boundaries, Interfaces, Surfaces and Dislocations

*Sponsored by:* The Minerals, Metals and Materials Society, ASM International, TMS Electronic, Magnetic, and Photonic Materials Division, TMS Materials Processing and Manufacturing Division, TMS: Alloy Phases Committee, TMS: Chemistry and Physics of Materials Committee, TMS/ASM: Computational Materials Science and Engineering Committee, ASM: Alloy Phase Diagrams Committee  
*Program Organizers:* Raymundo Arroyave, Texas A & M University; James Morris, Oak Ridge National Laboratory; Mikko Haataja, Princeton University; Jeff Hoyt, McMaster University; Vidvuds Ozolins, University of California, Los Angeles; Xun-Li Wang, Oak Ridge National Laboratory

Monday AM  
February 28, 2011

Room: 9  
Location: San Diego Conv. Ctr

*Session Chairs:* Kedarnath Kolluri, MIT; Alexey Dick, Max-Planck-Institut für Eisenforschung GmbH

#### 8:30 AM

**Grain Boundary Energy in Binary Alloys:** *Jonathan Stolle*<sup>1</sup>; Nikolas Provatas<sup>1</sup>; <sup>1</sup>McMaster University

The microstructure of a metal -- and hence grain boundaries -- determines its macroscopic properties. The structural component of grain boundary energy is analytically described by the Read-Shockley (RS) Law (1951). The RS law can be applied rigorously for the low angle grain boundaries, where it is related to elastic coefficients, and empirically for large angles. Recently, Elder and Grant (2004) and Mellenthin et al (2008) have used a phase field crystal method (PFC) to demonstrate that the Read Shockley law can be used to describe grain boundary energy in pure materials. This work extends those investigations by using a binary alloy PFC model in conjunction with the Gibbs absorption theorem to systematically investigate the role of alloying impurities on grain boundary energy, wetting, and pre-melting.

#### 8:45 AM

**A First Principles Investigation into Hydrogen-Grain Boundary Binding in bcc Fe:** *William Counts*<sup>1</sup>; Ron Gibala<sup>2</sup>; Chris Wolverton<sup>1</sup>; <sup>1</sup>Northwestern University; <sup>2</sup>University of Michigan

Hydrogen embrittlement of iron and steels is a classic but still unresolved problem in metallurgy. While hydrogen can freely move through the Fe lattice, its diffusion is hindered by lattice imperfections. Experimentally quantifying the binding energy of hydrogen to these defects has proven to be difficult. Fortunately, computational tools are ideally suited to study defect trapping because it is possible to isolate individual traps. Density function theory was used to quantify the binding energy of hydrogen to a number of Sigma boundaries in bcc Fe. We find that the H-Sigma boundary binding energies range from 0.1 to 0.5 eV. We observe that the H binding energy to Sigma boundaries with mirror symmetry across the grain boundary plane correlates with grain boundary energy, while the H binding energy for boundaries without the mirror symmetry is related to the grain boundary volume.

#### 9:00 AM

**Interaction of Grain Boundaries with Voids:** *Stephen Foiles*<sup>1</sup>; <sup>1</sup>Sandia National Laboratories

The Zener-Smith model for the pinning of microstructures by precipitates assumes that the interaction energy between the precipitate and boundary is given by the product of the grain boundary energy times the area of the intersection of the precipitate with the boundary. Here we perform atomic-scale simulations of the interaction energy between a grain boundary and a void in Ni in order to test this assumption. It is found that the interaction energy is close to the Zener-Smith approximation, but that a better estimate is obtained if one includes an additional energy term that dimensionally is equivalent to a line energy associated with the boundary-void junction. Sandia



is a multi-program laboratory operated by Sandia Corporation, a Lockheed Martin Company, for the United States Department of Energy's National Nuclear Security Administration under Contract DE-AC0494AL85000.

#### 9:15 AM

**On the Interaction of Point Defects with Semicoherent Heterophase Interfaces:** *Kedarnath Kolluri*<sup>1</sup>; Michael Demkowicz<sup>1</sup>; <sup>1</sup>Massachusetts Institute of Technology

We use atomistic modeling to investigate the relation between atomic structure of semicoherent heterophase interfaces and their interaction with point defects. Using Cu-Nb Kurdjumov-Sachs interfaces as a model system, we show that misfit dislocations present at such interfaces play a governing role in point defect absorption and migration. Interactions between point defects and the interface misfit networks can be described quantitatively within dislocation theory. Implications of these insights for predicting point defect interactions with interfaces in other orientations like Nishiyama-Wasserman and in other semicoherent heterophase systems like Cu-V are discussed. This material is based upon work supported as part of the Center for Materials at Irradiation and Mechanical Extremes, an Energy Frontier Research Center funded by the U.S. Department of Energy, Office of Science, Office of Basic Energy Sciences under Award Number 2008LANL1026.

#### 9:30 AM

**First Principles Modeling of Dislocation/Twin Boundary and Oxygen Solute Interactions in Ti:** *Maryam Ghazisaeidi*<sup>1</sup>; Dallas Trinkle<sup>1</sup>; <sup>1</sup>university of Illinois at Urbana-Champaign

Interaction of gliding dislocations and twin boundaries influences the plastic deformation of titanium. In addition, oxygen greatly affects both strength and twinning in Ti. Predictive models of strength and twinning rely on understanding the underlying atomic-scale deformation mechanisms. We model a [1-210] screw dislocation interacting with a Ti (10-12) twin boundary using density functional theory that provides more accurate results for dislocation/twin boundary interactions compared to previous classical potential approaches and allows for considering the effects of oxygen. Flexible boundary conditions are used to calculate the accurate geometry. We compute the dislocation core structure and transmission stresses through the boundary and repeat these calculations with an oxygen solute. This is a computationally tractable approach that marks the first ab initio study of isolated line defects in interfaces. The results show the effect of oxygen on core structure and transmission mechanisms of a screw dislocation interacting with a twin boundary.

#### 9:45 AM

**Stacking Fault Energies in Fe-Mn-C: Ab Initio Determination of Thermodynamic and Chemical Trends:** *Alexey Dick*<sup>1</sup>; Tilmann Hickel<sup>1</sup>; Afshin Abbasi<sup>1</sup>; Joerg Neugebauer<sup>1</sup>; <sup>1</sup>Max-Planck-Institut fuer Eisenforschung GmbH

High-Mn steels are promising candidates for light-weight high-strength materials. Their excellent mechanical properties are caused by sophisticated deformation mechanisms: the transition induced and the twinning induced plasticity. The preference of a certain mechanism is directly related to the stacking fault energy (SFE) of the material. The latter can be determined using CALPHAD based Gibbs free energies in relations that typically contain empirical, experimentally not accessible parameters. Extending the concept of density functional theory to finite temperatures by taking the effect of lattice vibrations, chemical and magnetic disorder into account, we were able to determine the chemical trends for both, the empirical parameters and the stacking fault energy. A combination of this knowledge with CALPHAD bulk data allows to predict mechanism maps over the entire composition range of Fe-Mn-C alloys.

#### 10:00 AM Break

#### 10:15 AM

**Topological Characteristics and Events in 3D Grain Growth:** *Burton Patterson*<sup>1</sup>; Robert DeHoff<sup>1</sup>; Alan Sprague<sup>2</sup>; Zhiwei Sun<sup>2</sup>; Veena Tikare<sup>3</sup>; <sup>1</sup>University of Florida; <sup>2</sup>University of Alabama at Birmingham; <sup>3</sup>Sandia National Laboratory

Topological description of the 3D grain structure throughout grain growth provides a novel insight into the process. Characteristics investigated include stability of the grain volume and face class distributions and the tendencies for different grain classes to have preferred contact and interaction among themselves and with different topological events, such as contacting a disappearing grain or making or breaking contact, respectively, to form and lose faces. Characterization of grain shape enables following the path of topological decay of grains to final disappearance. The balance of the different topological rates of the different face classes leads to the eventual stability of the face and volume distributions. Determination of these parameters is available from 3D computer simulation and serial sectioning.

#### 10:30 AM

**An Inverse Problem in Nucleation and Growth:** *Mark Jhon*<sup>1</sup>; Siu Sin Quek<sup>1</sup>; David Wu<sup>1</sup>; <sup>1</sup>Institute of High Performance Computing

There has been recent interest in constructing realistic, polycrystalline microstructures based on a given grain size distribution. Such configurations may be analyzed using various simulation techniques to help develop property-structure relationships. Methods based on the reverse Monte Carlo algorithm have been shown to be very successful in reproducing size distributions. However, such methods have not yet been related to a physically meaningful growth process. In the present study, reverse Monte Carlo algorithms are developed that are consistent with diffusion-limited and interface-limited growth. These techniques are compared using characteristics of the grain distribution that are not explicitly fitted.

#### 10:45 AM

**Application of a Monte Carlo Grain Growth Simulation to Test the Growth Path Envelope Analysis Formalism:** *Robert DeHoff*<sup>1</sup>; Burton Patterson<sup>1</sup>; Alan Sprague<sup>2</sup>; Zhiwei Sun<sup>2</sup>; Veena Tikare<sup>3</sup>; <sup>1</sup>University of Florida; <sup>2</sup>University of Alabama at Birmingham; <sup>3</sup>Sandia National Laboratory

During grain growth the volume of a grain varies with time along some path,  $V = V(V_0, t)$ , called its growth path. The collection of growth paths for all the grains in the structure is defined to be the growth path envelope for the process. Analysis of a Monte Carlo simulation of grain growth developed at Sandia National Laboratories permits the full determination of the growth path envelope. This envelope is not directly experimentally accessible for grain growth in real physical grain structures. However, an analysis exists that permits its determination from the time dependence of the grain volume distribution, which is experimentally accessible. At the base of this analysis are two critical assumptions. The simulation provides both the growth path envelope and the time dependence of the grain volume distribution, and therefore an assessment of the applicability of these assumptions in modeling real grain growth.

#### 11:00 AM

**Phase Field Simulation of Grain Growth in a System with Dissolving Precipitates:** *Sina Shahandeh*<sup>1</sup>; Matthias Militzer<sup>1</sup>; <sup>1</sup>University of British Columbia

Controlling grain boundaries migration with addition of second phase particles has important technological applications. Conventional theories assume inert particles. However, in many processes particles are not stable at high temperature. Dissolution of precipitates changes particles size and volume fraction thus decreasing particle pinning force on the interface. On the other hand, particle dissolution injects solutes to the matrix therefore increasing solute drag effect. Phase field method has been used to simulate grain growth combined with an effective formulation for the interface drag using a friction force. The approach includes interface drag caused by both particles and solutes. Kinetics of grain growth and grain size distributions have been predicted in 3D simulations. Based on these studies conditions can

MONDAY AM

be quantified where the variable interface drag due to gradual dissolution of particles can trigger abnormal grain growth.

**11:15 AM**

**A Phase-Field Model for Recrystallization Grain Growth: Effects of Grain Boundary Energy Anisotropy and Second-Phase Particles:**

*Mohsen Asle Zaeem*<sup>1</sup>; *Haitham El Kadiri*<sup>1</sup>; *Paul Wang*<sup>1</sup>; *Mark Horstemeyer*<sup>1</sup>;  
<sup>1</sup>Mississippi State University

We use a phase-field model to investigate the effects of grain boundary (GB) energy anisotropy and the presence of second-phase inert particles on grain growth (GG) in polycrystalline materials. Different conditions are studied. System of grains with anisotropic GB energies is considered by including models of low and high misorientation angles between adjacent grains. Systems without particles reach a steady state grain growth rate and this rate decreases by including GB anisotropy. The presence of particles significantly alters the microstructures during grain growth. It was shown that for systems with particles the critical average grain size to stop grain growth depends not only on volume fraction and size of particles but also on GB anisotropy.

**11:30 AM**

**Phase-Field Simulation of Segregation to Stacking Fault (Suzuki Effect) in Co-Ni Based Superalloy:**

*Yuichiro Koizumi*<sup>1</sup>; *Sho Suzuki*<sup>1</sup>; *Takuma Otomo*<sup>1</sup>; *Shingo Kurosu*<sup>1</sup>; *Yunping Li*<sup>1</sup>; *Hiroaki Matsumoto*<sup>1</sup>; *Akihiko Chiba*<sup>1</sup>;  
<sup>1</sup>Tohoku University

Co-Ni based superalloy exhibits excellent high-temperature mechanical properties[1,2] and peculiar microstructural development such as: good creep resistance with dynamic strain aging, ultra-grain refinement by conventional rolling-and-annealing process and very wide extension of stacking faults (SFs). These behaviors have been attributed to the chemical interaction between SFs and solute atoms, i.e. Suzuki effect. However, Suzuki effect has not been verified either experimentally or theoretically. In this study, a phase-field simulation for evaluating Suzuki effect has been developed and applied to Co-33Ni-20Cr-10Mo (wt%) alloy which exhibits the peculiar behaviors remarkably. The simulation suggested that Co-segregation and Ni-depletion can be very significant, and the deviation in concentration can exceed 10wt% at 973 K, for instance. Thus, Suzuki effect has been verified computationally. This approach may be applicable to many alloys for optimizing material properties. [1] Takahashi, Sugawara, Chiba: US Patents 2005/0016645 A1, [2] Chiba et al. Philos Mag A 1999;79:1533.

**11:45 AM**

**Simulating Triple Junction Drag Using a 2D Phase Field Model:**

*Anthony Johnson*<sup>1</sup>; *Peter Voorhees*<sup>1</sup>; <sup>1</sup>Northwestern University

Two-dimensional grain growth kinetics have been shown to deviate from the classical Von Neumann-Mullins relation at low temperatures or for small grains due to limited triple junction mobility. A multiorder parameter phase field model was developed to account for triple junction mobility. In a tri-crystal system, decreasing the triple junction mobility causes the triple junction velocity to decrease and the angle to decrease well below its isotropic equilibrium value of  $120\sqrt{176}$ . For a range of triple junction mobilities, this simple geometry remains consistent with the analytical theory developed by Gottstein and Shvindlerman, et al. Triple junction energies have also been measured as a function of the parameters in the phase field model. For larger 2D polycrystalline systems, preliminary simulations using this model show that the triple junction mobility significantly alters (quantitatively and qualitatively) the grain growth kinetics: triple junction angles deviate significantly from  $120\sqrt{176}$  and the growth rate is slowed.

**12:00 PM**

**Thermal-Activated Buckling Swapping of Topological Defects in Graphene:**

*Chun-Wei Pao*<sup>1</sup>; *Te-Huan Liu*<sup>2</sup>; *Chien-Cheng Chang*<sup>2</sup>; <sup>1</sup>Research Center for Applied Sciences, Academia Sinica; <sup>2</sup>Institute of Applied Mechanics, National Taiwan University

Topological defects in graphene, such as dislocations and grain boundaries, often introduce out-of-plane bucklings. For example, symmetrical tilt grain boundaries in graphene are consisted of regular arrays of dislocations,

and some of them can introduce bucklings. In this paper, we present our recent long-time-scale accelerated molecular dynamics simulation results on the swapping dynamics of these out-of-plane bucklings at symmetrical tilt graphene grain boundaries. We demonstrate that these even-distributed out-of-plane bucklings along grain boundaries can have thermal-activated deflections swapping: they can swap from deflecting upward to downward with rates up to thousands of times per second at room temperature. Our discovery will shed new lights on the mechanisms of defects migration in graphene, and the potential possibilities of fabricating extremely durable nanoscale actuators.

**12:15 PM**

**Defects in Ferrite: An Ab Initio Based Description of Long-Range Elastic Effects:**

*Alexander Udyansky*<sup>1</sup>; *Johann von Pezold*<sup>1</sup>; *Alexey Dick*<sup>1</sup>; *Vladimir Bugaev*<sup>2</sup>; *Jörg Neugebauer*<sup>1</sup>; <sup>1</sup>Max-Planck-Institut für Eisenforschung GmbH; <sup>2</sup>Max-Planck-Institut für Metallforschung

We study interstitial Fe-based solid solutions containing C, N, O, B, C+N and H impurities by combining first principles simulations with the reciprocal space microscopic elasticity theory (MET), which allows us to account for long-ranged elastic interactions. The short-range chemical interactions, as well as the parameters entering the MET are obtained by density functional theory (DFT) in the generalized gradient approximation, using rather modest supercell sizes. This approach provides a direct insight into the formation mechanism of martensite and its stability limits: in particular, tetragonal states are predicted to be preferred even at low impurity concentrations due to a thermodynamically driven orientational ordering of impurities. The temperature of the martensitic cubic-tetragonal transition is found to be in agreement with available experimental data and sensitively depends on the external pressure. Furthermore, the impurity content strongly affects the vacancy concentration within the host matrix.

**David Pope Honorary Symposium on Fundamentals of Deformation and Fracture of Advanced Metallic Materials: Intermetallics I**

*Sponsored by:* The Minerals, Metals and Materials Society, TMS Materials Processing and Manufacturing Division, TMS Structural Materials Division, TMS: High Temperature Alloys Committee, TMS/ASM: Mechanical Behavior of Materials Committee, TMS: Nanomechanical Materials Behavior Committee

*Program Organizers:* E. P. George, Oak Ridge National Laboratory; Haruyuki Inui, Kyoto University; C. T. Liu, The Hong Kong Polytechnic University

Monday AM  
February 28, 2011

Room: 32A  
Location: San Diego Conv. Ctr

*Session Chairs:* John Bassani, University of Pennsylvania; Sharvan Kumar, Brown University

**8:30 AM Introductory Comments**

**8:35 AM Invited**

**What Controls the Choice of the Slip Systems in Different Compounds with B2 Structure:** *Vasek Vitek*<sup>1</sup>; *Yi-Shen Lin*<sup>1</sup>; *Miroslav Cak*<sup>1</sup>; *Vaclav Paidar*<sup>2</sup>; <sup>1</sup>University of Pennsylvania; <sup>2</sup>Academy of Sciences of the Czech Republic

Usual slip systems in B2 compounds are  $\langle 111 \rangle \{101\}$  and  $\langle 010 \rangle \{101\}$  but different slip systems dominate in different alloys. The dislocation property that often controls the choice of the slip system is dislocation dissociation and thus available stacking fault-like defects. A common wisdom has been that such fault is the  $\frac{1}{2}\langle 111 \rangle$  APB but, as shown in 1981 by Pope and co-workers, it may but need not exist. The existence of stacking faults was studied by calculating  $\{101\}$  \{111\}-surfaces in nine B2 compounds using a density functional theory based method. The displacement vectors of stacking fault-like defects differ from  $\frac{1}{2}\langle 111 \rangle$ . Using this information and anisotropic elasticity theory we analyzed dislocation dissociations and

concluded that in order to decide which slip system dominates it is necessary to consider elastic anisotropy, vectors of stacking faults and their energies. The corresponding analysis is in full agreement with observations.

#### 9:05 AM Invited

**Recent Development of Porous Materials Based on Aluminide Intermetallics:** *C. T. Liu*<sup>1</sup>; Yuehui He<sup>2</sup>; Baiyun Huang<sup>2</sup>; <sup>1</sup>Hong Kong Polytechnic University; <sup>2</sup>Central South University

Porous metals are of great interest as a potential engineering material in various industrial fields. Aluminide intermetallics based on TiAl, NiAl and FeAl are particularly suitable for use as porous materials for gas and liquid permeation applications because of their good oxidation resistance at elevated temperatures, high corrosion resistance in acid and alkali solutions, good high and room temperature strength, and excellent thermal shock resistance. This paper summarizes the recent work on low-cost manufacturing of aluminide porous materials by self-propagation high-temperature synthesis, where the size, shape and their distribution can be well controlled by exothermal reactions and preheating conditions. The near-net-shape porous tubes have been verified to possess excellent corrosion & oxidation resistance, microstructure stability, and mechanical strength for filtering industrial applications. \*This research was supported by Natural Science Foundation and National High-Tech R&D Program of China, and internal funding from Honk Kong Polytechnic University

#### 9:35 AM Invited

**Size-Affected Flow and Intermittency in Small Ni3Al Crystals:** *Dennis Dimiduk*<sup>1</sup>; Michael Uchic<sup>1</sup>; Ed Nadgorny<sup>2</sup>; Satish Rao<sup>3</sup>; Jaafar El-Adawy<sup>4</sup>; Paul Shade<sup>4</sup>; Chris Woodward<sup>1</sup>; <sup>1</sup>Air Force Research Laboratory; <sup>2</sup>Michigan Technological University; <sup>3</sup>UES, Inc.; <sup>4</sup>UTC, Inc.

Experimental studies reveal that nano- and micrometer-scale crystals show strengthening effects, irrespective of the material type. Their flow behavior is characterized by four clear attributes: (i) a rising flow stress with decreasing sample size; (ii) stochastic variation in flow stress that exhibits wider scatter at smaller sample sizes; (iii) intermittent flow as revealed by either repeated load drops or constant-stress flow avalanches; and (iv) an extended elastic-plastic transition. These attributes are known for FCC, BCC and HCP metals, LiF and other metallic alloys. However, studies show that Ni3Al exhibits selected unique characteristics at small scales. The present work examines the microcrystal phenomenology of Ni3Al and, evaluates behavior mechanisms relative to samples size or conditions for this material. The evaluation suggests that limitations exist for understanding Ni3Al behavior from current data and, that some of these limitations pertain for microcrystal deformation behavior more generally.

#### 10:05 AM

**Plasticity of L1<sub>2</sub> Intermetallics: A New Insight Using AFM Observations:** *Joël Bonneville*<sup>1</sup>; Christophe Coupeau<sup>1</sup>; <sup>1</sup>University of Poitiers

Atomic force microscopy (AFM) is an experimental technique that allows for the investigation of surface structures at the atomic scale, which is particularly sensitive to surface relief. When dislocations move on crystallographic planes, they produce steps at the intersection of these planes and the crystal surfaces. The steps appear as lines at the sample surface, whose tracking gives information on dislocation movements. Slip lines are therefore intimately associated with both the crystal structure and plastic deformation, and give useful information concerning the elementary dislocation processes. We intend to present a study of L1<sub>2</sub> intermetallic plasticity using AFM by investigating the number, height and length of slip lines that reflect dislocation source activity and dislocation mean free path, which are key parameters for the understanding of crystal plasticity. The contribution of D. Pope to the understanding of the plastic behaviour of L1<sub>2</sub> intermetallics will be highlighted.

#### 10:20 AM Break

#### 10:30 AM Invited

**Properties of New Cobalt Alloys with High Volume Fractions of Ordered Precipitates:** *Tresa Pollock*<sup>1</sup>; Akane Suzuki<sup>2</sup>; <sup>1</sup>University of California Santa Barbara; <sup>2</sup>GE Global Research

New cobalt-base alloys containing ordered L12 precipitates have been investigated. Two phase  $\gamma-\gamma'$  microstructures are maintained with additions of Cr, Mo, Ni, Re, Ta and V to the ternary Co-Al-W system. Solidus and liquidus temperatures are 100 – 150°C higher than advanced nickel-base single crystal alloys strengthened with the L12 phase. An anomalous rise in flow stress with temperature is observed. The temperature dependence of deformation mechanisms has been studied. Single crystals have been solidified and partitioning during solidification is limited in the ternary system, suggesting a high resistance to convective instabilities. Directions for alloy design will be discussed.

#### 11:00 AM Invited

**Temperature Dependence of Yield Stress and Dislocation Dissociation in L12-Ordered Intermetallic Compounds:** *Haruyuki Inui*<sup>1</sup>; <sup>1</sup>Kyoto University

L12 compounds are usually classified into three groups depending on their yield stress versus temperature curves. All these temperature dependences of yield stress have been explained in terms of the planarity of dislocation cores. While the core of 1/2[110] dislocations separated by APB on {111} is planar, those of 1/2[110] dislocations separated by APB on {001} and 1/3[121] dislocations separated by SISF on {111} are believed to be non-planar, giving rise to the rapidly decreasing yield stress at low temperatures for some types of L12 compounds such as Pt3Al and Co3Ti. However, our recent study indicates that the rapidly decreasing yield stress at low temperatures can also be observed for many L12 compounds with dislocations being dissociated into two 1/2[110] partials separated by APB on {111}. The classification of L12 compounds in terms of the temperature dependence of yield stress is discussed in relation to the observed dislocation dissociation modes.

#### 11:30 AM Invited

**Microstructure and Mechanical Properties of Dual Two-Phase Intermetallic Alloys Composed of Geometrically Close Packed Ni<sub>3</sub>Al and Ni<sub>3</sub>V Structures:** *Takayuki Takasugi*<sup>1</sup>; Yasuyuki Kaneno<sup>1</sup>; <sup>1</sup>Osaka Prefecture University

The so-called dual two-phase intermetallic alloy, which is composed of Ni<sub>3</sub>Al(L1<sub>2</sub>) and Ni solid solution (A1) phases at high temperature and is additionally refined by a eutectoid reaction at low temperature aging, according to which the Al phase is decomposed into the Ni<sub>3</sub>Al(L1<sub>2</sub>)+Ni<sub>3</sub>V(DO<sub>22</sub>) phases, was recently developed. The dual two-phase intermetallic alloys showed high tensile strength, accompanied with high tensile elongation and fracture toughness over a broad temperature range, and also superior oxidation/corrosion resistance. Also, wear resistance at high temperature was very excellent and therefore attractive as high temperature tool. The obtained results are thus promising for the development of the dual two-phase intermetallic alloy as a new-type of high-temperature structural material. In the presentation, microstructure, various properties and applications of dual two-phase intermetallic alloys will be presented.



## Dynamic Behavior of Materials V: Fundamentals of Dynamic Behavior

Sponsored by: The Minerals, Metals and Materials Society, TMS Structural Materials Division, TMS/ASM: Mechanical Behavior of Materials Committee

Program Organizers: Marc Meyers, UCSD; Naresh Thadhani, Georgia Institute of Technology; George Gray, Los Alamos National Laboratory

Monday AM

Room: 5A

February 28, 2011

Location: San Diego Conv. Ctr

Session Chair: Marc Meyers, UCSD

### 8:30 AM Introductory Comments

#### 8:40 AM Keynote

**Impact Testing and Dynamic Behavior of Materials:** *Lothar Meyer*<sup>1</sup>; Norman Herzig<sup>1</sup>; Frank Pursche<sup>1</sup>; Shawkly Abdel-Malek<sup>1</sup>; <sup>1</sup>Nordmetall GmbH

An overview about different testing facilities and the mechanical material behavior including monoaxial and multi axial testing under high rate loading is given. Special emphasis is laid on difficult loading conditions and loading states like high temperature and high strain loading ( $T > 1200^{\circ}\text{C}$ ,  $\dot{\gamma} > 1$ ) and multiaxial impact tests. Thereby, the impact behavior of selected materials is presented and compared under different loading conditions. A distinction is made between virgin and manufactured material behavior (e.g. welding) or pre-damaged materials. Especially, if the influence of the manufacturing history is investigated, under certain loading states the impact material properties show a dramatic difference compared to virgin material state. This paper shows some examples of different material behavior under the conditions described before.

#### 9:20 AM

**Atomistically-Informed Dislocation Dynamics Simulations of High Rate Deformation of Single fcc Crystals:** *Zhiqiang Wang*<sup>1</sup>; <sup>1</sup>University of North Texas

Predicting dynamic deformation of single fcc crystals with dislocation dynamics (DD) has been a new computational approach to connecting fundamental dislocation mechanisms and microstructure evolutions to macroscopic behavior of materials. In DD method, some physical parameters are essential in controlling the behavior of individual dislocations, and thereafter macroscopic properties. Dislocation mobility is one of the most important among them, which are hard to be measured with experimental techniques while critical to the fidelity of DD methods. This talk will present some results of determining dislocation mobility under complex loading conditions with atomistic simulations. Large scale DD simulations, integrating atomistic results, are applied to predict stress-strain curves of single crystal materials in high rate deformation. It is shown that accurate dislocation mobility information is of paramount importance to develop a reliable mesoscale DD method.

#### 9:40 AM

**Plastic Response of Low- and High-Energy Grain Boundaries in Copper under Shock Loading:** *Christian Brandl*<sup>1</sup>; Timothy Germann<sup>1</sup>; <sup>1</sup>Los Alamos National Laboratory

Previous molecular dynamics (MD) simulations have revealed that the preferred nucleation sites for partial dislocations at grain boundaries are related to the local atomic interface structure. Moreover, shock experiments discovered different post-mortem defect structures for low-energy and high-energy grain boundaries. In the present study, MD simulations are conducted to understand the structural origin of the differences in dislocation activity under shock compression, and failure upon unloading. We present MD simulations of shock/spallation loading conditions in copper bicrystals corresponding to grain boundaries studied in recent shock experiments. The defect structures produced in the MD studies are compared with the

experimental post-mortem defect analysis, and the differences in the dynamic response are discussed in terms of the local grain boundary structures.

#### 10:00 AM

**Void Initiation, Growth and Collapse in BCC Tantalum: Molecular Dynamics Simulations:** *Yizhe Tang*<sup>1</sup>; Eduardo Bringa<sup>2</sup>; Bruce Remington<sup>3</sup>; Marc Meyers<sup>1</sup>; <sup>1</sup>University of California, San Diego; <sup>2</sup>Univ. Nac.Cuyo; <sup>3</sup>Lawrence Livermore National Laboratory

The growth and collapse of nanoscale voids in BCC tantalum is investigated under different stress states and strain rates. Three principal mechanisms of deformation were identified and quantitatively evaluated: (a) shear loop emission and subsequent expansion from the surface of the void; (b) cooperative shear loop emission from slip planes that parallel to the same  $\langle 111 \rangle$  slip direction and their combination, forming prismatic loops; (c) twinning starting at the void surface. The generation and evolution of these defects is found to be a function of stress state and strain rate. Void initiation in Nanocrystalline tantalum was also discussed

#### 10:20 AM Break

#### 10:30 AM Invited

**Atomistic Simulations of Shock-Induced Plasticity in Tantalum:** *Eduardo Bringa*<sup>1</sup>; J. Hawreliak<sup>2</sup>; N. Park<sup>3</sup>; A. Higginbotham<sup>4</sup>; <sup>1</sup>CONICET-Universidad Nacional de Cuyo; <sup>2</sup>Lawrence Livermore National Laboratory; <sup>3</sup>AWE; <sup>4</sup>University of Oxford

We have carried non-equilibrium atomistic simulations of shocks in tantalum, using 0.5-100 million atoms, with samples nearly 1 micron long and shock rise times of up to 200 ps. Our samples include perfect single crystals, single crystals with dislocation sources, and polycrystals. We find agreement with the experimental Hugoniot of polycrystalline Ta up to ~20% compression. We present an analysis of the resulting plastic behavior as a function of strain rate and shock pressure. There is no homogeneous nucleation of dislocations as in simulations of fcc metals. Dislocations originate only from pre-existing dislocations sources. Twinning dominates plastic deformation at high stress and strain rate, as suggested by high pressure recovery experiments from gas-guns. X-ray diffraction simulations are used to mimic future experiments that will take advantage of dynamic diffraction capabilities.

#### 11:00 AM

**The Viscosity of Liquid Tantalum\*:** *James Belak*<sup>1</sup>; <sup>1</sup>Lawrence Livermore National Laboratory

Tantalum is used as a prototype material for multi-scale modeling. Despite this attention, the interatomic force models have been validated with static experimental information only. Dynamic information, e.g. dislocation mobility, has proven a difficult experiment. Here we focus on a different kinetic experiment, the shear viscosity of the liquid. Because of tantalum's high melting point, limited viscosity data is available. In a tour de force experiment, Paradis et al. used electrostatic levitation to measure the relaxation of liquid droplets and extracted viscosity data. Use non-equilibrium molecular dynamics, our simulated the shear viscosity (validated on copper) agrees with the experiment at the melting point. However, the temperature dependence (activation energy) is significantly softer in the simulation, suggesting a possible reinterpretation of the experiment. Results will be presented for both the MGPT and Finnis-Sinclear models for tantalum. \*Work performed under the auspices of the U.S. DOE by LLNL under Contract DE-AC52-07NA27344.

#### 11:20 AM

**"Driving Forces" for Moving Inclusion and Inhomogeneity Boundaries with Transformation Strains:** *Xanthippi Markenscoff*<sup>1</sup>; Luqun Ni<sup>1</sup>; <sup>1</sup>University of California, San Diego

A half-space constrained Eshelby inclusion (in an infinite elastic matrix) with general uniform eigenstrain (or transformation strain) is analyzed when the plane boundary is moving from rest in general subsonic motion. The radiated fields are calculated based on the Willis expression for constrained time dependent inclusions, which involves the three-dimensional dynamic Green's function in an infinite traction-free body, and they constitute the

unique elastodynamic solution, with initial condition the Eshelby static fields obtained as the unique minimum energy solution by a limiting process from the spherical inclusion. The mechanical energy-release rate and associated "driving force" to create dynamically an incremental region of eigenstrain (due to any physical process) is calculated for general eigenstrain. By extending the Eshelby equivalent inclusion method to dynamics, the solution for a moving inhomogeneity (different elastic constants) is also obtained. In the absence of dissipation, Noether's theorem requires that the total (with external loading) "driving force", or total dynamic J integral (equal to the energy-release rate) vanishes, which yields the "kinetic relation", comprising a Peach-Koehler type force and a self-force. This, in turn, results in an evolution equation for a moving plane phase boundary.

#### 11:40 AM

**Dynamic-Tensile-Extrusion Response of Polymers:** *Eric Brown*<sup>1</sup>; George Gray<sup>1</sup>; <sup>1</sup>Los Alamos National Laboratory

Dynamic-Tensile-Extrusion (Dyn-Ten-Ext) experiments have been utilized to probe the dynamic tensile responses of polytetrafluoroethylene (PTFE) and polychlorotrifluoroethylene (PCTFE). These fluoropolymers exhibit more irregular deformation and stochastic-based damage and failure mechanisms than the stable plastic elongation and shear instabilities observed in metals. Similar to the observed ductile-to-brittle transition for Taylor Impact loading, PCTFE failure occurs at a peak velocity greater than for PTFE. However, for the Dyn-Ten-Ext PCTFE exhibits even greater resistance to failure due to the tensile stress-state. While PTFE generates a large number of small fragments when extruded through the die, PCTFE draws out a smaller number of larger particles that dynamically evolve during the extrusion process through a combination of local necking mechanisms and bulk relaxation.

#### 12:00 PM

**The Dynamic Constitutive Response of Four Light Metals: Al 7039, Al 5083, Al 5059, and AZ31B:** *Sara Perez-Bergquist*<sup>1</sup>; George Gray III<sup>1</sup>; Ellen Cerreta<sup>1</sup>; Carl Trujillo<sup>1</sup>; Mike Lopez<sup>1</sup>; <sup>1</sup>Los Alamos National Laboratory

While a great number of studies have examined the uni-axial stress behavior of a wide range of light metals and their alloys under quasi-static loading conditions, less is known about the dynamic response of these same metals as a function of stress state. For this reason, the dynamic constitutive response of four light metals has been examined as a function of stress state, temperature, texture, and dynamic strain rate. Specimens of Al 7039, Al 5083, Al 5059, and AZ31B, a magnesium alloy, have been characterized prior to deformation and then dynamically loaded in compression, tension, shear, and torsion. Post mortem characterization of these specimens, using optical microscopy, scanning electron microscopy, and electron back scattered diffraction has been utilized to correlate the observed mechanical response to the microstructural evolution during loading and leading to damage and failure of these materials.

#### 12:20 PM

**Structure and Shear Resistance of an Asymmetric Tilt Grain Boundary as Function of Temperature:** *Saryu Fensin*<sup>1</sup>; Mark Asta<sup>2</sup>; Richard Hoagland<sup>1</sup>; <sup>1</sup>Los Alamos National Laboratory; <sup>2</sup>University of California, Berkeley

Grain boundaries play an important role in governing the microstructure and deformation evolution in a material. Hence, it is important to understand the structure of grain boundaries that are subjected to high homologous temperatures. Boundaries that are susceptible to extreme structural disorder as the temperature is increased might drastically change the dynamic damage in a material under shock loading conditions. In this talk we will present the results of molecular dynamics simulations studying the temperature dependence of the structure of an asymmetric tilt grain boundary in copper. At high homologous temperatures a grain boundary can either form a disordered structure or can completely premelt. The change in grain boundary structure can be drastic enough to alter its response to an applied external force. The nature of the structural disorder in the grain boundary will be investigated by using the grain boundary width and its resistance to an applied shear strain.

## Fatigue and Corrosion Damage in Metallic Materials: Fundamentals, Modeling and Prevention: Fundamentals of Fatigue Damage and Modeling

*Sponsored by:* The Minerals, Metals and Materials Society, TMS Structural Materials Division

*Program Organizers:* Tongguang Zhai, University of Kentucky; Zhengdong Long, Kaiser Aluminum; Peter Liaw, University of Tennessee

Monday AM  
February 28, 2011

Room: 31C  
Location: San Diego Conv. Ctr

*Session Chairs:* Angus Wilkinson, University of Oxford; Mark Hardy, Rolls Royce

### 8:30 AM Introductory Comments

#### 8:35 AM Invited

**High Resolution EBSD Studies of Fatigued Metals:** *Angus Wilkinson*<sup>1</sup>; Philip Littlewood<sup>1</sup>; Benjamin Britton<sup>1</sup>; Phani Karamched<sup>1</sup>; <sup>1</sup>University of Oxford

We have used the relatively new cross-correlation-based analysis of EBSD patterns to map variations of elastic strain and lattice rotation tensors within selected grains of cyclically deformed metals. This method gives improved sensitivity of  $\sim 10^{-4}$  (rads) compared to  $\sim 10^{-2}$  rads for conventional Hough-transform-based analysis. The measured rotation (and elastic strain) gradients have been used within the Nye geometrically necessary dislocation (GND) framework to generate maps of the GND density distribution. Examples will be given for cyclically loaded OFHC Cu and Ti-6Al-4V polycrystal. The method allows the GND density distributions to be correlated with the orientation of a particular grain and those in its neighbourhood. We have also applied the technique to examine the plastic zones associated with fatigue crack tips. Examples will be given for cracks grown in single crystal Ni-based superalloy at elevated temperature and mid-Paris regime loading conditions.

#### 8:55 AM

**A Quantitative Crystallographic Model for Fatigue Crack Propagation through Grain Boundaries:** *Wei Wen*<sup>1</sup>; Tongguang Zhai<sup>1</sup>; <sup>1</sup>University of Kentucky

A crystallographic model for short fatigue crack propagation through grain boundaries was developed to quantify the resistance of grain boundaries to crack growth. The model was based on the early discovery that the twist and tilt components of crack plane deflection across a grain boundary were the key factors controlling the crack growth in high strength Al alloys. The model developed in this work was a function of twist angle at each grain boundary that interacted with a short crack, and allowed calculation of variation in growth rate at different grain boundaries and prediction of the crack front. Further work needs to be done to incorporate other factors, such as tilt angle and Schmidt factor, into the model to simulate the growth behavior of a short fatigue crack in 3-D.

#### 9:15 AM Invited

**Cyclic Deformation and Fatigue Cracking Mechanisms of F.C.C. Crystalline Materials:** *Zhefeng Zhang*<sup>1</sup>; Peng Li<sup>1</sup>; Peng Zhang<sup>1</sup>; Shen Qu<sup>1</sup>; Zhenjun Zhang<sup>1</sup>; <sup>1</sup>Institute of Metal Research, Chinese Academy of Sciences

The cyclic dislocation evolution and fatigue cracking behaviors in various f.c.c. metal and alloys, including various single crystals, Cu bicrystals and polycrystals, Cu-Al and Cu-Zn polycrystalline alloys, ultrafine-grained Cu-Al and Cu-Zn alloys, were systematically investigated and reviewed. It is confirmed that the effect of stacking fault energy (SFE) on cyclic deformation behaviors of f.c.c. single crystals is decisive and a new criterion is proposed to judge the formation of regular saturation dislocation patterns or not in various f.c.c. single crystals. In Cu, Cu-Al, Cu-Zn single crystals, fatigue cracking always nucleates along slip bands (SBs) and strain localization becomes weak gradually with decreasing SFE. The large-angle

grain boundaries (GBs) also become preferential sites for crack nucleation in Cu bicrystals and polycrystals. Fatigue cracking can also nucleate along SBs and twin boundaries (TBs) in pure Cu, Cu-Al and Cu-Zn alloys. The fatigue cracking mechanisms along SBs, GBs, TBs were compared and discussed.

**9:35 AM Invited**

**The Effect of Pore Position in Depth on Stress Field around the Pore on Sample Surface:** Zhiqiang Xu<sup>1</sup>; Wei Wen<sup>2</sup>; *Tongguang Zhai*<sup>2</sup>; <sup>1</sup>Yanshan University; <sup>2</sup>University of Kentucky

Stress field around a pore was analyzed as a function of the pore position in depth in the surface of a linear elastic solid using FEM. It was found that the pore depth dominated the stress field around the pore on surface and that the maximum stress was increased sharply when the pore intercepted with the surface at its top. Given the applied nominal stress, the magnitude of the maximum main stress only depended on the relative depth of the pore, while the pore size affected the stress distribution in surface. An elastic-plastic model was also used to account for the yielding effect in the region where stress was over the yield strength. The results still indicated a significant maximum stress concentration when the pore was just buried underneath the surface, but with a lowered value than that of the linear elastic model. These results were consistent with experimental observations.

**9:55 AM Invited**

**Fatigue Weak-Link Density and Strength Distribution in High Strength Al Wrought and Cast Alloys:** *Tongguang Zhai*<sup>1</sup>; Yuanbin Zhang<sup>2</sup>; <sup>1</sup>University of Kentucky; <sup>2</sup>Shandong Jianzhu University

An experimental methodology was developed to measure fatigue weak-link density and strength distribution by measuring surface crack population as a function of the maximum applied stress. The method was applied to wrought and cast Al alloys such as AA8090 Al-Li, AA2026, AA2524, AA2024 and A713 alloys where fatigue cracks were initiated at either coarse particles or pores on surface. It was found that the surface crack populations were a Weibull function of the applied maximum stress. By fitting this measured curves, fatigue weak-link density could be quantified in these alloys. The derivative of the measured Weibull function was the strength distribution of the fatigue weak-links. Fatigue weak-link density and strength distribution are materials fatigue properties and useful for alloy development and applications.

**10:15 AM Break**

**10:25 AM**

**Effect of Cooling Rate on the Fatigue Life of a Nickel-Base Superalloy Used for Disc Rotor Applications:** *Mark Hardy*<sup>1</sup>; Robert Mitchell<sup>1</sup>; Hang-Yue Li<sup>2</sup>; <sup>1</sup>Rolls-Royce plc; <sup>2</sup>University of Birmingham

It is understood that the strain hardening behaviour of precipitation strengthened nickel alloys is produced from the interactions of dislocations with gamma prime particles. Furthermore, the degree of resistance to inelastic deformation is determined by the volume fraction and size of these particles. Since the particles that are precipitated from quenching after solution heat treatment offer the most effective resistance to inelastic deformation, this study has evaluated the effect of cooling rate on the fatigue endurance of alloy RR1000. It was found from testing at 300°C that fatigue life at this temperature is sensitive to cooling rate under conditions that produce limited plasticity. Under conditions that give rise to either significant inelastic strain or lives beyond 105 cycles, in which the deformation is predominantly elastic, endurance was found to be relatively insensitive to cooling rates. A rationale for the observed behaviour is proposed.

**10:45 AM**

**An Energy-Based Microstructure Model to Account for Fatigue Scatter in Polycrystals:** *Michael Sangid*<sup>1</sup>; Huseyin Sehitoglu<sup>1</sup>; <sup>1</sup>University of Illinois, Urbana-Champaign

Excessive scatter is observed in the fatigue response of a nickel-based superalloy, U720, which is partly attributed to the variability in the microstructure. There is great interest in linking the microstructure to fatigue properties using a multi-scale approach that focuses on integrating the results of atomic simulations to the continuum level. Our approach is to model

the energy of a persistent slip band (PSB) structure and use its stability with respect to dislocation motion as our failure criterion for fatigue crack initiation. Through this methodology, the fatigue life is predicted based on the energy of the PSB, which inherently accounts for the microstructure of the material. From this framework, we construct simulated microstructures based on the measured distributions of grain size, orientation, neighbor information, and grain boundary character, which allows us to calculate fatigue scatter using a deterministic approach. Good agreement is shown between the model predictions and experimental data.

**11:05 AM**

**Tail Departure of Log-Normal Grain Size Distribution in 3D Synthetic Microstructures:** *Joseph Tucker*<sup>1</sup>; <sup>1</sup>Carnegie Mellon University

Techniques are discussed that have been used to produce statistical volume elements using geometric shape distributions to simulate single-phase polycrystals. Current methods assume log-normal distributions of grain size; this gives rise to an issue with nonphysical large grains that cannot be accommodated in finite simulation volumes. Other distributions which have better control of the upper tails, e.g. truncated distributions, resolves the problem and allows more realistic distributions to be generated. These points are illustrated with an example of generation of a synthetic 3D microstructure to represent a 7075-T651 aluminum alloy.

**11:25 AM**

**Fatigue Crack Initiation Processes in a Polycrystalline Ni-Base Superalloy:** *Jiashi Miao*<sup>1</sup>; Tresa M. Pollock<sup>2</sup>; J. Wayne Jones<sup>1</sup>; <sup>1</sup>University of Michigan; <sup>2</sup>University of California, Santa Barbara

The very high cycle fatigue behavior of a polycrystalline nickel-based superalloy René 88 DT was investigated under fully reversed loading at a frequency of 20 KHz at room temperature using an ultrasonic fatigue system. Microstructural features associated with microcrack initiation and failure were identified by orientation imaging microscopy. Focused ion beam sectioning was used to examine selected microcrack initiation sites. Deformation substructures were characterized using transmission electron microscopy. The early stages of fatigue were dominated by localized slip adjacent to twin boundaries in grains at the high end of the grain size distribution. A fatigue crack initiation model is proposed that incorporates local microstructure features in the initiation process as well as the interaction between local microstructure and small crack growth. A novel approach to quantify crack initiation life using in situ nonlinear ultrasonic analysis is described.

**11:45 AM**

**3D Short Fatigue Crack Investigation Using Diffraction and Phase Contrast Tomography:** *Michael Herbig*<sup>1</sup>; *Wolfgang Ludwig*<sup>1</sup>; Henry Proudhon<sup>2</sup>; Peter Reischig<sup>3</sup>; Andrew King<sup>4</sup>; Jean-Yves Buffière<sup>5</sup>; <sup>1</sup>ESRF / INSA Lyon; <sup>2</sup>MINES ParisTech; <sup>3</sup>ESRF / KIT; <sup>4</sup>GKSS-Research Center; <sup>5</sup>INSA Lyon

In order to investigate the influence of the microstructure on the propagation of short fatigue cracks, a combination of two synchrotron imaging techniques has been used. Grain shape and orientation are measured non-destructively in 3D by means of X-ray diffraction contrast tomography. The crack propagation is monitored at regular intervals using high resolution phase contrast tomography, a technique capable of revealing cracks of sub-micrometer thickness. A technique enabling visualization of the fracture surface orientation and, for the first time, quantification of the local crack growth rate in the bulk of the material has been developed. Its application on two beta titanium alloys gives new insight into several aspects of crack - microstructure interactions during the growth of microstructurally short fatigue cracks.



## Friction Stir Welding and Processing VI: High Temperature Materials I

Sponsored by: The Minerals, Metals and Materials Society, TMS Materials Processing and Manufacturing Division, TMS: Shaping and Forming Committee

Program Organizers: Rajiv Mishra, Missouri University of Science and Technology; Murray Mahoney, Retired from Rockwell Scientific; Yutaka Sato, Tohoku University; Yuri Hovanski, Pacific Northwest National Laboratory; Ravi Verma, General Motors

Monday AM Room: 5B  
February 28, 2011 Location: San Diego Conv. Ctr

Session Chair: Rajiv Mishra, Missouri University of Science and Technology

### 8:30 AM Introductory Comments

#### 8:50 AM Keynote

##### A Decade of Progress in Friction Stirring of High-Temperature Materials: Carl Sorensen<sup>1</sup>; <sup>1</sup>Brigham Young University

Friction stir welding and processing of high-temperature materials, such as ferrous alloys, has been reported in the literature for a little more than a decade. The past decade has seen significant improvements in tool materials, changes in tool features, new understanding of recommended parameters, and an increased number of high-temperature materials being welded. This presentation surveys the state of the art in welding of steel, stainless steel, nickel-base alloys, copper alloys, and titanium alloys. Tool materials, tool features, control parameters, tool performance, and material properties are covered. Based on the history of the past decade, prospects for the future are considered. New applications in tool steels and pipeline steels for the oil and gas industry are presented, along with demonstrations for naval applications. The most significant obstacles to commercial implementation are discussed. With continued development, friction stir processing of high temperature materials shows promise for a bright future.

#### 9:20 AM

##### Development of Co-Based Alloy FSW Tool for High-Softening-Temperature Materials: Yutaka Sato<sup>1</sup>; Masahiro Miyake<sup>1</sup>; Hiroyuki Kokawa<sup>1</sup>; Toshihiro Omori<sup>1</sup>; Kiyohito Ishida<sup>1</sup>; Shinya Imano<sup>2</sup>; Seung Hwan Park<sup>2</sup>; Satoshi Hirano<sup>2</sup>; <sup>1</sup>Tohoku University; <sup>2</sup>Hitachi, Ltd.

The authors have developed new friction stir welding (FSW) tool that enables to weld high-softening-temperature materials, such as steels and titanium alloys. The new tool is made of Co-based alloys which are strengthened by dispersing intermetallics, Co<sub>3</sub>(Al,W), with L12 structure at high temperatures. The Co-based alloy tool can be manufactured at a low cost through a simple production method consisting of casting, heat-treatment and then cutting. They exhibit yield strengths higher than 500 MPa at 1000 degC, so that they might have great potential as FSW tool for high-softening-temperature materials. In this study, feasibility of the Co-based alloy tool to various high-softening-temperature materials, such as carbon steels, Ti-6Al-4V and so on, was examined. Change in tool shape during FSW, and the weld appearances and microstructure produced with the Co-based alloy tool will be briefly shown.

#### 9:40 AM

##### Friction Stir Welding and Processing of Advanced Materials for Coal and Nuclear Power Applications: Glenn Grant<sup>1</sup>; Scott Weil<sup>1</sup>; Yuri Hovanski<sup>1</sup>; Jens Darsell<sup>1</sup>; <sup>1</sup>Pacific Northwest National Laboratory

A wide range of materials are anticipated in the next generation of power plant designs. To increase efficiency and reduce carbon emissions, boilers, heat exchangers, and turbines all will be asked to perform at higher temperature and pressure. New alloys including precipitation hardenable Ni alloys, Ferritic ODS, and high-chrome steels will be employed. A significant barrier to implementing many of these is that joining technologies are either immature or unknown. This is especially true for ODS alloys where

conventional fusion welding produces a weld nugget that does not have the creep performance of the parent material. Friction Stir Welding has an opportunity to provide a joining solution to these difficult to weld materials. This presentation will outline efforts to develop the FSW weld process on several materials including Ni-alloys, ferritic ODS, and 9Cr2Mo steels. Data will be presented on high-temperature strength, creep performance, and joint microstructure.

#### 10:00 AM

##### Friction Stir Welding of Alloy 22: Bharat Jasthi<sup>1</sup>; Willaim Arbegast<sup>1</sup>; Stanley Howard<sup>1</sup>; <sup>1</sup>South Dakota School of Mines and Technology

The main objective of this work is to characterize and compare Alloy 22 weld microstructures formed in friction stir (FS), gas tungsten arc (GTA), and electron beam (EB) welding. Topologically closed packed (TCP) phases were identified in all the as-welded condition. TCP phases that precipitated in the FS weld nugget were extremely small (~50 to 300 nm) compared to those in the EB and GTA welds. Compared to the parent material the FS weld nugget microhardness increased from (~206 HV) to (~327 HV). Only a slight increase in microhardness was observed for the EB and GTA welds. The area fraction of the TCP phases in FS weld nugget increased with aging temperature and time. The activation energy calculated for the TCP phase growth in friction stir welds was determined to be ~252.5 kJ/mol.

#### 10:20 AM

##### Effect of Processing Parameters and Post-Weld Microstructure on Friction Stir Welded HSLA-65 Charpy V-Notch Impact Toughness: Sam Sanderson<sup>1</sup>; Tracy Nelson<sup>1</sup>; <sup>1</sup>Brigham Young University

Correlations between post-weld mechanical properties, post-weld microstructure and processing parameters in FSW HSLA-65 were investigated. FSW was conducted at combinations of spindle speed and welding speed to cover a range of heat inputs, from about 1 kJ/mm to 4 kJ/mm. Longitudinal, all-weld tensile tests, and Charpy V-notch (CVN) impact tests of weld centerline and heat-affected zone (HAZ) were evaluated. CVN results of weld centerline showed increased transition temperature over base metal transition temperature, with a large spread in absorbed energies near the transition temperature. Results from CVN testing of weld HAZ showed the transition temperature to be at or below base metal transition temperature. Longitudinal, all-weld tensile tests exhibited ultimate tensile strengths above ASTM A945 requirements for HSLA-65, while yield strengths were slightly below ASTM specification. The results show strong correlations between post-weld microstructure, tensile properties and weld heat input, while CVN results show only weak correlations.

#### 10:40 AM

##### Friction Stir Processing of Cast Inconel 718: Bharat Jasthi<sup>1</sup>; Edward Chen<sup>2</sup>; William Arbegast<sup>1</sup>; Matthew Heringer<sup>1</sup>; Douglas Bice<sup>2</sup>; Stanley Howard<sup>1</sup>; <sup>1</sup>South Dakota School of Mines and Technology; <sup>2</sup>Transition45 Technologies, Inc

The objective of this work was to investigate the effects of friction stir processing (FSP) on the microstructure and mechanical properties of Inconel 718 castings. Polycrystalline cubic BN pin tools were used to process 0.35-in. thick cast Inconel 718 plates. Successful bead-on-plate welds were produced at a rotational speed of 225 RPM and travel speed of 0.5 IPM. FSP created a homogeneous microstructure and produced extremely fine grains (< 10 μm) in the weld nugget while eliminating casting defects. Post-FSP heat treatment cycles increased the strength of the FSP nugget over that of the parent material. Fracture toughness and microhardness of the welds were superior to that of parent material. This paper describes the microstructure and the mechanical properties of friction stir processed Inconel 718 castings.

## 11:00 AM Break

## 11:10 AM Invited

**Fabrication of Nanostructured Tool Steel Layer by Combination of Laser Cladding and Friction Stir Processing:** *Yoshiaki Morisada*<sup>1</sup>; Hidetoshi Fujii<sup>2</sup>; Tadashi Mizuno<sup>3</sup>; Genryu Abe<sup>3</sup>; Toru Nagaoka<sup>1</sup>; Masao Fukusumi<sup>1</sup>; <sup>1</sup>Osaka Municipal Technical Research Institute; <sup>2</sup>Joining and Welding Research Institute, Osaka University; <sup>3</sup>AMC Corporation

A fabrication process of the nanostructured tool steel layer with various carbides by the combination of laser cladding and friction stir processing (FSP) was proposed. The segregated carbide particles on the grain boundary of the matrix formed by the laser cladding with a coaxial cladding head were crushed into the carbide nanoparticles during the FSP, and were uniformly dispersed in the matrix. The carbide nanoparticles assisted in forming the fine recrystallized grains of the matrix by the FSP due to the increment in the induced stress and a pinning effect for the static grain growth. The nanostructured tool steel layer showed a higher hardness than conventional tool steel.

## 11:30 AM Invited

**Friction Stir Welding of Oxide Dispersion Strengthened Alloy MA956:** *Michael West*<sup>1</sup>; *bharat jasthi*<sup>1</sup>; Peter Hosemann<sup>2</sup>; Viswanath Sodesetti<sup>1</sup>; <sup>1</sup>South Dakota School of Mines and Technology; <sup>2</sup>University of California at Berkeley

Ferritic oxide dispersion strengthened MA956 alloys (ODS) were joined using friction stir welding (FSW) as a means of joining these alloys without disturbing the dispersion characteristics. Two MA956 plates of thickness 12.7 mm and 6.4 mm were successfully plasticized by friction stir welding (FSW). Fully consolidated welds were made at 400 RPM (50 mm/min) with Q60 composite pin tools and 600 RPM (13 mm/min) with W-Re pin tool. Post weld heat treatment was performed at 1000°C and 1300°C to observe the effects of heat treatment on the weld properties. Microstructural characterization, grain size analysis, and mechanical property measurements were performed as a function of weld processing parameters. Microhardness in the weld region showed a modest reduction in the strength compared to the as-processed MA956. The oxide dispersion between the bulk and the weld was analyzed by small angle neutron scattering (SANS) and scanning electron microscope (SEM).

## 11:55 AM

**Friction Stir Processing of Ti-6Al-4V for Grain Size Reduction in Fusion Welds:** *Jason Livingston*<sup>1</sup>; Jeff Rodelas<sup>1</sup>; John Lippold<sup>1</sup>; <sup>1</sup>The Ohio State University

Friction Stir Processing (FSP) is a solid-state process that produces microstructure modification in a wide range of materials (Al, Ti, Cu, Ni, and steels). In Ti alloys, such as Ti-6Al-4V, fusion welding results in coarse-grained microstructure with reduced mechanical properties (toughness and ductility). In this study, FSP was used to both modify the as-welded and base metal microstructure. FSP was conducted on beta-processed Ti-6Al-4V plate using a tungsten-rhenium tool. The as-received base material exhibited a prior beta grain size in the range from 1.2 to 1.5mm, while FSP produced a fine, equiaxed alpha microstructure with grain diameters from 1 to 5 microns. Thermal data collected in situ confirmed processing temperatures were below the beta transus. Single pass GTAW welding on FSP-conditioned base metal resulted in reduced weld metal grain size, based on epitaxial nucleation and growth from the refined microstructure. Optical metallography and EBSD were used to characterize these microstructures.

## 12:15 PM

**Microstructure and Mechanical Properties of Friction Stir Processed Grade 40 Grey Cast Iron:** *Michael West*<sup>1</sup>; Bharat Jasthi<sup>1</sup>; Nicholas Smith<sup>1</sup>; Josiah Oduor<sup>2</sup>; Yong-Ching Chen<sup>3</sup>; <sup>1</sup>South Dakota School of Mines and Technology; <sup>2</sup>University of Tennessee, Knoxville; <sup>3</sup>Cummins Technical Center

Friction stir processing (FSP) of Grade 40 grey cast iron was performed using bead-on-plate friction stir welds with a PCBN pin tool. Approaches for FSP focused on the use of induction preheating and the use of a mild steel

cover plate. Successful welds were made using the cover plate approach in forge force mode. Microhardness tests show high hardness (~600 HV) in regions of mixed cast iron and steel above the weld nugget. Significant refinement in the graphite structure and increase in microhardness is observed in the nugget region compared to the base material. Results of tensile testing are also presented. Transverse tensile specimens show low strength because of alignment of graphite flakes in the thermo-mechanically affected regions adjacent to the weld nugget region.

## Frontiers in Solidification Science: Atomistic Simulations

*Sponsored by:* The Minerals, Metals and Materials Society, TMS Electronic, Magnetic, and Photonic Materials Division, TMS: Chemistry and Physics of Materials Committee, TMS: Solidification Committee

*Program Organizers:* Jeffrey Hoyt, McMaster University; Daniel Lewis, Rensselaer Polytechnic Institute

Monday AM  
February 28, 2011

Room: 6E  
Location: San Diego Conv. Ctr

*Session Chair:* To Be Announced

## 8:30 AM Invited

**Characterization of the Structure, Thermodynamics and Transport at the Chemically Heterogeneous Cu/Pb Interface by Atomistic Simulation:** *Brian Laird*<sup>1</sup>; J. Pablo Palafox-Hernandez<sup>1</sup>; Mark Asta<sup>2</sup>; <sup>1</sup>University of Kansas; <sup>2</sup>University of California-Berkeley

Using MD simulation, we examine the equilibrium interface between crystalline Cu and liquid Pb, modeled. This interface is characterized by the calculation of density, energy, stress and diffusion profiles, and by Fourier analysis of the interfacial layers for two crystal orientations: (100) and (111). At 625 K, we observe significant surface alloying in the first layer of the (100) interface, consistent with earlier investigations. No surface alloying is seen in the (111) orientation; however, a "prefreezing" layer of crystalline Pb, approximately 2-3 lattice layers in thickness, is observed to form at the (111) Cu surface. These layers are hexagonal with a lattice spacing that is 33% larger than the underlying Cu (111) planes and rotated by an angle of ~6.176 relative to the Cu lattice. Further simulations show that the prefreezing layers significantly enhance heterogeneous nucleation in the (111) orientation relative to (100).

## 9:00 AM Invited

**Finite Size Effects in Molecular Dynamics Simulations of Nucleation and Growth:** *James Morris*<sup>1</sup>; Trevor Pate<sup>2</sup>; Lujian Peng<sup>2</sup>; <sup>1</sup>Oak Ridge National Laboratory; <sup>2</sup>University of Tennessee

Molecular dynamics provides a direct, unbiased approach for simulating the processes associated with phase transformations. However, the small size and time scales can limit the applicability of these methods. In this talk, recently observed finite-size effects in simulations of both crystal nucleation times and growth are reviewed: both nucleation dynamics and initial grain structures have been shown to have important size effects, sometimes requiring millions of atoms to converge. Both size effects are statistical in nature. We examine the connection between these two effects, and demonstrate that simple arguments can provide estimates of the relevant size scale and how this depends on undercooling conditions. Moreover, the nucleation times are well predicted by nucleation theory, without fitting parameters, in contrast to experimental work in both colloids and glasses. This research was sponsored by the Division of Materials Sciences and Engineering, U.S. Department of Energy, Office of Basic Energy Sciences.

### 9:30 AM Invited

**Heterogeneous Nucleation of Solid Al from the Melt: Molecular Dynamics Studies:** Junsheng Wang<sup>1</sup>; Peter D. Lee<sup>1</sup>; Andrew Horsfield<sup>1</sup>; Peter Brommer<sup>2</sup>; Udo Schwingenschloegl<sup>3</sup>; <sup>1</sup>Imperial College London; <sup>2</sup>Universität Stuttgart; <sup>3</sup>King Abdullah University of Science and Technology

Nucleation of solid Al from the melt by TiB<sub>2</sub> is well established, but the atomic scale mechanisms are not fully understood. It is believed to be a two step process: Al<sub>3</sub>Ti is formed which then nucleates solid Al. Using molecular dynamics (MD) simulations with embedded atom method potentials we simulated the nucleation and early stages of growth of Al on Al<sub>3</sub>Ti. A strong anisotropy in the growth depending on the crystal orientation was found and explained in terms of interfacial energies. Using Density Functional Theory MD the early stages of Al nucleation on TiB<sub>2</sub> were simulated. We find no signs of incipient growth of solid Al at the B-terminated surface, but see fcc-like ordering at the Ti-terminated surface. For the Al<sub>3</sub>Ti substrate, fcc-like structures are observed which extend rapidly into the melt.

### 10:00 AM Break

### 10:15 AM Invited

**Molecular Dynamics Simulations of Alloy Rapid Solidification:** Mark Asta<sup>1</sup>; Hariith Humadi<sup>2</sup>; Yang Yang<sup>3</sup>; Brian Laird<sup>4</sup>; Deyan Sun<sup>3</sup>; Jeff Hoyt<sup>2</sup>; <sup>1</sup>University of California, Berkeley; <sup>2</sup>McMaster University; <sup>3</sup>East China Normal University; <sup>4</sup>University of Kansas

Molecular dynamics (MD) simulations are employed to investigate the kinetic properties of alloy crystal-melt interfaces under rapid-solidification conditions. The MD simulations yield results for velocity dependent partition coefficients, and the relationship between interface velocity and thermodynamic driving force. Both sets of results are compared to available sharp-interface models for solute trapping and solute drag. The MD results for fcc-based alloy systems can be characterized as follows. For interface mobilities, the MD results are best described by models that account for some degree of solute drag. Results for solute trapping are best described by models that account for an abrupt transition to partitionless growth at a critical velocity. A key finding in the MD simulations is the presence of a significant degree of crystalline anisotropy and composition dependence of interface mobility. Preliminary results for bcc alloys will also be described.

### 10:45 AM Invited

**Heterogeneous Nucleation of Liquid at Grain Boundaries:** T. Frolov<sup>1</sup>; Y. Mishin<sup>1</sup>; <sup>1</sup>George Mason University

At temperatures approaching the bulk melting point, many grain boundaries exhibit premelting by developing liquid-like layers. Some boundaries can be overheated above the melting point until the material suddenly melts. Both premelting and melting processes can involve nucleation of liquid droplets existing in unstable equilibrium with the boundary. We report on atomistic simulations of grain boundary premelting, melting and formation of critical liquid nuclei at grain boundaries in copper. We show, in particular, that nuclei can be effectively stabilized using the NVE ensemble of molecular dynamics, allowing systematic studies of the nucleus size and shape depending on temperature. By varying the system size, different morphologies of the nuclei are observed, including the cylindrical (quasi-2D) and the lens (3D) shapes. We demonstrate how a cylindrical nucleus can break up into several lens-shape nuclei when the system size is increased. The results are compared with homogeneous liquid nucleation inside the crystal.

### 11:15 AM Invited

**Molecular Dynamics Study of Solid-Liquid Interface Migration in FCC Metals:** Mikhail Mendeleev<sup>1</sup>; <sup>1</sup>Ames Laboratory

The recent MD simulation results for the solid-liquid interface (SLI) migration in fcc metals will be discussed. First, it will be shown that the generation of latent heat at the moving SLI during MD simulations can lead to significant underestimations of the interface mobility. Second, the kinetic coefficient for all systems will be compared to theoretical predictions. It will be shown that near the melting temperature the magnitude of the kinetic coefficient correlates well with the value of the diffusion coefficient in the liquid. Finally, the results of the MD simulation of the SLI migration at very

low temperatures will be presented. It will be shown that the results of such simulations are extremely sensitive to the way how the liquid part of the simulation cell was created. Work at the Ames Laboratory was supported by the Department of Energy, Office of Basic Energy Sciences, under Contract No. DE-AC02-07CH1135.

## Geek Speak on the Hill: Communicating Science to Policy Makers

*Sponsored by:* The Minerals, Metals and Materials Society, TMS: Public and Governmental Affairs Committee

*Program Organizers:* Jud Ready, Georgia Tech; Marlit Hayslett, Georgia Tech

Monday AM  
February 28, 2011

Room: 17B  
Location: San Diego Conv. Ctr

*Session Chair:* Marlit Hayslett, Georgia Tech

### 8:30 AM Introductory Comments by Kevin Hemker, Chair, Public & Governmental Affairs Committee

### 8:35 AM Invited

**Recap of Congressional Visit Days:** Iver Anderson<sup>1</sup>; <sup>1</sup>Iowa State University  
TMS, MRS, ASM, FMS, IEEE, and numerous other societies visit congressional leaders each year to provide them with scientific information (typically in the spring: Next for TMS is April 6-7, 2011). This talk will include an overview of that "CVD" program as well as details for upcoming events.

### 8:55 AM Invited

**Legislative Process 101:** Arnie Thomas<sup>1</sup>; <sup>1</sup>Senior Vice President, Client Relationships, CQ Rollcall Group

The many stakeholders, nuances and steps involved in legislative public policy will be covered. The role of committees, special interests, lobbyists and other aspects of the legislative process are included.

### 9:15 AM Break

### 9:30 AM Invited

**Case Studies in Reality Colliding with Science-Policy:** Jim Treglio<sup>1</sup>; <sup>1</sup>Consultant, Technology and Marketing, Molecular Metallurgy

The speaker will share real-world examples where scientific interchange with policy makers could have resulted in a different outcome.

### 9:50 AM Invited

**Communicating Science to Policy Makers:** Marlit Hayslett<sup>1</sup>; <sup>1</sup>Director, Office of Policy Analysis and Research

This talk will encompass how to translate technical jargon into a language understandable by federal, state and local public policy makers.

### 10:10 AM Invited

**Tools and Techniques for Being an Effective Communicator:** Gina Schatteman<sup>1</sup>; <sup>1</sup>University of Iowa

This session will review tactics and approaches for effective delivery of scientific information to public policy makers. Oral and written testimony, letters to representatives, constituent visits and other types of interactions will be discussed.

### 10:30 AM Break

### 10:45 AM Panel Discussion

**"The Congress shall promote the progress of science..." US Constitution; Article 1, Section 8**

Each speaker will participate in a strategic discussion of how members of the materials community can effectively interact with federal, state and local legislatures to influence public policy for the betterment of society.

### 11:45 AM Concluding Comments



## General Abstracts: Electronic, Magnetic and Photonic Materials Division: Session I

Sponsored by: The Minerals, Metals and Materials Society, TMS Electronic, Magnetic, and Photonic Materials Division, TMS: Alloy Phases Committee, TMS: Biomaterials Committee, TMS: Chemistry and Physics of Materials Committee, TMS: Electronic Materials Committee, TMS: Electronic Packaging and Interconnection Materials Committee, TMS: Energy Conversion and Storage Committee, TMS: Magnetic Materials Committee, TMS: Nanomaterials Committee, TMS: Thin Films and Interfaces Committee

Program Organizers: Long Qing Chen, Pennsylvania State University; Sung Kang, IBM Corporation; Mark Palmer, Kettering University

Monday AM  
February 28, 2011

Room: 16B  
Location: San Diego Conv. Ctr

Session Chair: To Be Announced

8:30 AM

### Charged Point Defect Configurations, Domain Stabilization Effects, and Ferroelectric Aging: Tianle Cheng<sup>1</sup>; Yu Wang<sup>1</sup>; <sup>1</sup>Michigan Technological University

Configurations of charged point defects and resultant internal electric field are investigated based on point ion model to understand ferroelectric aging phenomenon. Analysis of the energetics of various defect configurations reveals that the interactions among point defect dipoles play a most important role, which leads to a formation of asymmetric L-shaped defect configuration, generating internal electric field sufficient to stabilize ferroelectric domains. Such short-range ordering of charged point defects is believed to be the origin of ferroelectric aging. To study domain stabilization effect in aged ferroelectrics, domain-dependent internal electric field associated with the short-range ordering of charged point defects is incorporated into phase field ferroelectric model. Computer simulation is performed to estimate the internal electric field strength. Clausius-Clapeyron-type thermodynamic analysis of field-induced ferroelectric phase transition is used to evaluate aging-associated internal electric field magnitude from available experimental data, which is in agreement with the theoretical analysis and computer simulation.

8:50 AM

### Correlated Nucleation and Self-Accommodating Kinetic Pathway of Ferroelectric Phase Transformation: Jie Zhou<sup>1</sup>; Tian-Le Cheng<sup>1</sup>; Yu Wang<sup>1</sup>; <sup>1</sup>Michigan Technological University

Mechanisms of nucleation and growth of domains during ferroelectric phase transformation are investigated by using theoretical and computational approaches. It is shown that ferroelectric phase transformation exhibits some interesting behaviors due to strong long-range dipole-dipole-like interactions involved in the system. Incorporation of electrostatic and elastostatic energies into the classical Landau-Ginzburg-Devonshire theory effectively modifies the coefficients of the polynomial free energy function and introduces extra energy barrier for ferroelectric phase transformation. It is found that independent nucleation of ferroelectric phase in the context of classical nucleation theory is impossible, because electrostatic interaction generates an insurmountable energy barrier to isolated nucleus. Phase field simulation reveals that, in order to circumvent such an energy barrier, nucleation exhibits strong spatial correlation and self-organization behaviors from the very beginning, and ferroelectric phase transformation proceeds via spatial and temporal evolution of self-accommodating domains that provide a low-energy kinetic pathway throughout the entire phase transformation process.

9:10 AM

### Bipolar Resistive Switching Behavior in Ti/MnO<sub>2</sub>/Pt Structure for Nonvolatile Memory Devices: Min Kyu Yang<sup>1</sup>; Sun Young Choi<sup>1</sup>; Jeon Kook Lee<sup>1</sup>; <sup>1</sup>Korea Institute of Science and Technology

We examined the electrical properties of Ti/MnO<sub>2</sub>/Pt devices with stable and reproducible bipolar resistive switching behavior. The dependency of the memory behavior on the cell area and operating temperature suggest that the conducting mechanism in the low resistance states is due to the locally conducting filaments formed. X-ray photoelectron spectroscopy showed that non-lattice oxygen ions form at the MnO<sub>2</sub> surface. The mechanism of resistance switching in the system examined involves the generation and recovery of oxygen vacancies with the non-lattice oxygen ions. The Ti/MnO<sub>2</sub>/Pt device has potential applications in nonvolatile resistive switching memory devices due to the reasonable switching endurance over the course of 10<sup>5</sup> cycles, long term retention at 85 °C and a uniform distribution of both resistance states and operation voltage. A high content of non-lattice oxygen ions exists on the MnO<sub>2</sub> film surface. The switching behavior can be explained by the generation and recovery of oxygen vacancies with non-lattice oxygen ions.

9:30 AM

### Preparation and Characterization of Oxide Thin Films for the Resistance Random Access Memory (RRAM) Application: W. Z. Chang<sup>1</sup>; J. Chu<sup>1</sup>; S. F. Wang<sup>2</sup>; <sup>1</sup>National Taiwan University of Science and Technology; <sup>2</sup>National Taipei University of Technology

RRAM is considered as a promising candidate for next-generation memory application because of high-density, fast write/read access, low energy operation, and high performance of endurance and retention. Many oxide systems such as NiO, TiO<sub>2</sub>, and SrZrO<sub>3</sub> have been proposed for this application. In this study, sputtered HoScO<sub>3</sub> (HSO) and TiO<sub>x</sub> thin films with working atmospheres of different Ar/O<sub>2</sub> flow ratios have been characterized for the RRAM resistance switching (RS) behavior. After deposition, HSO and TiO<sub>x</sub> thin films with a thickness of approximately 50 nm are post-annealed in O<sub>2</sub> and N<sub>2</sub> atmospheres at various temperatures. As-deposited HSO films exhibit RS behavior, except at an Ar/O<sub>2</sub> ratio of 10/10, while as-deposited TiO<sub>x</sub> films exhibit RS behavior only with high O<sub>2</sub> pressures. HSO samples annealed in N<sub>2</sub> atmosphere exhibit a better RS behavior than those annealed in O<sub>2</sub>. However, an opposite trend is observed in the case of TiO<sub>x</sub> films.

9:50 AM

### Investigation of Electronic Properties for Nano-Titania/Metal-Ion-Doped Titania Semiconductor Prepared by Sol-Gel Methods: Leo Chau-Kuang Liao<sup>1</sup>; <sup>1</sup>Yuan Ze University

Semiconductor homojunction devices were designed and fabricated by coating a metal-ion-doped TiO<sub>2</sub> film on top of a TiO<sub>2</sub> nanoparticle film. The sample films were prepared with synthesized sol-gel TiO<sub>2</sub>, verified to be nano-size particles with anatase structure. The semiconductor characteristics of the ion-doped and undoped films were analyzed by current-voltage (I-V). Results showed that the semiconductor properties of TiO<sub>2</sub> were greatly influenced by doping with different types and amounts of metal ions, i.e. Fe<sup>2+</sup>, Cr<sup>3+</sup>, Zn<sup>2+</sup>, and Ag<sup>+</sup>. The semiconductor characteristics of the TiO<sub>2</sub>/metal-ion-doped TiO<sub>2</sub> devices, such as onset voltage and rectifying curves, were affected by the fabrication of the ion-doped layer. The fabricating conditions of the ion-doped layer, i.e. thickness, and types and amounts of metal ions, can change the electronic properties of the device.

10:10 AM Break

10:30 AM

### Effects of Structural Heterogeneities on Magnetization Processes in FePt Crystals: Yan Yang<sup>1</sup>; Jianyang Li<sup>1</sup>; Yongmei Jin<sup>1</sup>; <sup>1</sup>Michigan Technological University

Magnetic domain evolutions in FePt crystals of different structural heterogeneities are studied by micromagnetic modeling. In particular, {110} transformation twins and {111} annealing twins in L<sub>1</sub><sub>0</sub> phase, and A1+L<sub>1</sub><sub>0</sub> two phase systems are considered. Computer simulations reveal detailed

magnetization processes through domain wall motion and magnetization rotation, and show strong interactions of magnetic domain walls with twin boundaries and inter-phase interfaces. It is found that magnetostatic interaction between magnetic domains across interfaces generates local magnetic charges, which produce heterogeneous internal magnetic field. The competition between the internal and external magnetic fields under the constraint of high magnetocrystalline anisotropy of  $L1_0$  phase determines magnetic domain structures and their evolution paths, which explains the different characteristics of magnetic properties of FePt crystals with different structural heterogeneities. The influences of size and morphology of heterogeneities on magnetic processes are discussed.

#### 10:50 AM

**Phase Formation, Microstructure and Magnetic Properties of Rapidly Solidified SmCo Alloys Modified with Hf and C:** *Shampa Aich*<sup>1</sup>; Jeffrey Shield<sup>2</sup>; <sup>1</sup>Indian Institute of Technology; <sup>2</sup>University of Nebraska-Lincoln

A series of  $(\text{Sm}_{0.12}\text{Co}_{0.88/95}\text{Hf}_{3-x}\text{C}_x)$  ( $x = 0, 1, 2, 3, 4$  and  $5$ ) alloys were arc-melted in a TIG arc melting furnace and then melt-spun on a copper wheel surface at a wheel speed of 30 m/s. X-ray diffraction indicated that the primary phase was  $\text{SmCo}_5$ , with the metastable  $\text{TbCu}_5$ -type structure. While rapid solidification of binary Sm-Co alloys results in coarse grains (grain size  $\sim 1 \mu\text{m}$ ) and a coercivity of 0.8 kOe, combined additions of Hf and C resulted in effective grain refinement (grain size  $\sim 100$ -200 nm). The reduction in grain size resulted in dramatic increase in magnetic properties dependent on the Hf/C ratios. The coercivity ( $H_c$ ) increased systematically from approximately 6 kOe to 17 kOe and the magnetization ( $M_s$ ) decreased from 92 emu/g to 55.3 emu/g with a maximum reduced remanence ( $M_r/M_s$ ) value of 0.78 as the Hf/C ratio varied from 1/4, 2/3, 3/2, 4/1 to 5/0.

#### 11:10 AM

**Structure and Magnetic Properties Characterization of Electro-Deposited Co37Fe63 Containing Oxygen for Magnetic Recording Applications:** *Shereen Elhalawaty*<sup>1</sup>; Ray Carpenter<sup>1</sup>; Jinnie George<sup>2</sup>; Stanko Brankovic<sup>2</sup>; <sup>1</sup>Arizona State University; <sup>2</sup>University of Houston

Soft and high magnetic moment Co37Fe63 alloys have been electro-deposited with variable additives on Cu/Ti/Si substrate. The correlation between structure and magnetic properties has been investigated. TEM showed that the crystal structure of the deposits was BCC with a  $\langle 111 \rangle$  texture, and 10 to 20 nm grain size. Oxygen in the deposited film has been identified by High Annular Dark Field STEM combined with EDS and EELS. The oxygen content in the deposits has also been analyzed using RBS. SIMS showed that both oxygen and hydrogen are present in the deposited CoFe films. The magnetic properties of the deposits have been measured by magnetometer quantifying the impact of oxygen and hydrogen on the saturation magnetic flux density BS. Analytical results showed that the oxygen was mainly distributed along the grain boundaries in the CoFe film. Where oxygen was present in the film, the Fe content was enhanced relative to Co.

#### 11:30 AM

**High Permeability Co-Hf-Ta Thin Films:** *Shu-Wen Huang*<sup>1</sup>; Yuan-Tai Lai<sup>1</sup>; Jenq-Gong Duh<sup>1</sup>; <sup>1</sup>National Tsing Hua University

High permeability Co-Hf-Ta thin films were fabricated by adjusting the Hf content from 1 at.% to 8 at.%. It was revealed that appropriate Hf addition can effectively reduce the Co grain size and improve magnetic properties. Magnetic properties were shown to strongly depend on the microstructure of Co-Hf-Ta films. X-ray diffraction and transmission electron microscope diffraction patterns revealed that appropriate Hf addition would promote the formation of nanocrystalline structure. Such microstructure could be beneficial to obtain soft magnetic properties and a superior permeability ( $\mu'$ ). In this study, by optimizing the Hf content, the film with Hf concentration of 2.81 at.% exhibits excellent soft magnetic properties: high saturation magnetization (4pMS  $\sim 13.6$  kG), and low coercivity (HC  $\sim 0.6$  Oe). The effective permeability of the film reaches 800 and remains nearly unchanged up to 1 GHz.

#### 11:50 AM

**Tungsten Doping Effect on Thermoelectric Properties of Heusler Fe<sub>2</sub>VAl Alloy:** *Haruka Morishita*<sup>1</sup>; Masashi Mikami<sup>1</sup>; Kimihiro Ozaki<sup>1</sup>; Keizo Kobayashi<sup>1</sup>; <sup>1</sup>National Institute of Advanced Industrial Science and Technology

A Heusler alloy,  $\text{Fe}_2\text{VAl}$ , is a promising candidate for thermoelectric power generation near room temperature because of its high thermoelectric power factor  $PF (=S^2/\rho 63)$ , where  $S$  is the Seebeck coefficient,  $\rho 63$  is the electrical conductivity). However, the thermoelectric figure of merit  $Z (=S^2\sigma/\kappa)$  where  $\kappa$  is the thermal conductivity) of this alloy is poor by reason of its high thermal conductivity ( $\kappa = 28$  W/mK). We had reported that microstructural refinement using powder metallurgy technique enhances phonon scattering at grain boundaries, resulting in the reduction of  $\kappa = 16$  W/mK. In this study, we investigated the effect of substitution of W, which has the larger atomic mass, for V to achieve thermal conductivity reduction within grains by the mass-difference scattering. The  $\kappa$  of 6 W/mK was then obtained at 300 K for  $\text{Fe}_2\text{V}_{0.9}\text{W}_{0.1}\text{Al}$ . W doping effect on electric properties will also be presented.

#### 12:10 PM

**The Introduction of Nano-Scale Inclusions in to Bulk MgB<sub>2</sub> via Infiltration and Growth Process:** *Hari babu Nadendla*<sup>1</sup>; Anthony Dennis<sup>2</sup>; Yunhua Shi<sup>2</sup>; David Cardwell<sup>2</sup>; <sup>1</sup>Brunel University; <sup>2</sup>University of Cambridge

It is well established that magnetic flux pinning in MgB<sub>2</sub> bulk samples can be enhanced significantly by the introduction of nano-sized, non-superconducting second phase particles into the MgB<sub>2</sub> phase matrix, and this has been achieved primarily by co-sintering a mixture of MgB<sub>2</sub> and nano-scale second phases. The density of material fabricated by this technique, however, is low and bulk samples are typically porous, with a relatively low critical current density ( $J_c$ ). In this paper, we report an extension of the infiltration and growth process to the fabrication of high density (90-95% of theoretical), bulk MgB<sub>2</sub> that contains nano-scale inclusions (SiC, Y<sub>2</sub>O<sub>3</sub>, and ZrO<sub>2</sub>). This process also allows to fabricate complex shaped bulk MgB<sub>2</sub> superconductor. The influence of the presence of these inclusions on  $J_c$  as a function of external field in the temperature range of 5 K - 38 K is investigated in detail for various nano composites.

### General Abstracts: Light Metals Division: Primary Production and General Issues

*Sponsored by:* The Minerals, Metals and Materials Society, TMS Light Metals Division, TMS: Aluminum Committee, TMS: Aluminum Processing Committee, TMS: Energy Committee, TMS: Magnesium Committee, TMS: Recycling and Environmental Technologies Committee  
*Program Organizers:* Alan Luo, General Motors Corporation; Eric Nyberg, Pacific Northwest National Laboratory

Monday AM

February 28, 2011

Room: 17A

Location: San Diego Conv. Ctr

*Session Chair:* Eric Nyberg, Pacific Northwest National Laboratory

#### 8:30 AM

**A Model for the Collapse of the World Trade Center:** *Christian Simensen*<sup>1</sup>; <sup>1</sup>SINTEF

Two airplanes of Boeing 767 flew into the Twin Towers in the morning of September 11th 2001. The crashes caused petrol to come on fire, and the airplanes to be fragmented. They were subsequently heated to a high temperature. Aluminium alloys in the airplanes were melted at 660°C while the surrounding building was only heated to a much lower temperature due to suitable insulation. When the temperature reached 750-800°C, the approximately 30 ton melt managed to stream down to the lower floors. There it came in contact with water from the sprinkler devices and other sources. The encounter resulted in a series of fierce explosions by generation of hydrogen gas and local heating to high temperatures well above 1000°C. A section of the buildings was torn apart, and the upper part fell on the bottom part so the whole building collapsed.

9:00 AM

**Analysis on the Market Developing Conditions of Prebaked Carbon Anodes for the Aluminium Industries:** Guanghui Lang<sup>1</sup>; Chunyu Fu<sup>1</sup>; Ronald Logan<sup>1</sup>; Yan Li<sup>1</sup>; <sup>1</sup>Sunstone

In recent years, with the sustained and rapid development of the aluminium electrolytic industries worldwide, an unprecedented growth of Chinese prebaked carbon anode production has been achieved. The high-quality and abundant sources of raw materials for anode production, unique production technologies, experienced operators, governmental support of research, and efficient logistics have made the further development of large-scale and integrated anode production facilities possible. China is positioned to become the production base of prebaked carbon anodes for the electrolytic business all over the world in the future.

9:20 AM

**Qatalum – Organizational Challenges in Starting up a Modern Smelter:** Roald Holten<sup>1</sup>; Lene Solli<sup>1</sup>; Jan Arve Haugan<sup>2</sup>; <sup>1</sup>Norsk Hydro; <sup>2</sup>Qatalum

The Qatalum smelter in Qatar started its operation in December 2009, with target production of 585 kt by the end of 2010. Two experienced industrial partners teamed up to create this modern aluminium smelter: Hydro with its strong position in reduction technology and Qatalum Petroleum as a key provider of industrial infrastructure in Qatar. Bringing this new large plant up to speed demands an efficient organization with competent and well-trained employees as well as well-functioning organizational structures and processes. The diversity in having thousand employees of 32 nationalities and from 35 company cultures represents a challenge, as does serving demanding customers with customized, high-quality casthouse products. The Qatalum Production System, a local adaptation of Hydro's own production system, has been devised as the main mechanism to align the organization and ensure quality in all processes. This presentation summarizes experiences and main learning points from the first year of operation.

9:40 AM

**Building Qatalum – A Large, Modern Smelter:** Tom Rotjer<sup>1</sup>; Erik Smith<sup>1</sup>; Anton Husøy<sup>1</sup>; <sup>1</sup>Norsk Hydro

On December 19 2009 production started at the Qatalum aluminium smelter, a joint venture between Hydro and Qatar Petroleum. With this the main milestone of the USD 5.7 billion project was successfully achieved, and a modern smelter based on the HAL300 reduction technology was ready for ramp-up of production within cost, on time and according to specifications. A construction village was built to accommodate the huge number of workers, providing welfare standards that Hydro are proud of. Likewise, environmental considerations, safety precautions and working conditions were all along on top of the priority list of the project team. The project was managed by Hydro Projects and was divided into 21 main contracts based on an EPC procurement strategy. This presentation provides detailed insights into how the project team handled the technical and organizational complexities during its work to construct one of the largest aluminium smelter ever built in one step.

10:00 AM

**Removal of Fluoride from Waste Water of Aluminium Smelter by Aluminium Ion Loaded Ion Exchange Resin Method:** Balakrushna Padhi<sup>1</sup>; Arun Kumar Sharma<sup>1</sup>; <sup>1</sup>National Aluminum Company Limited

Strong Acid Cation resin has sulphonic acid functional group (H<sup>+</sup> form) possesses appreciable defluoridation capacity and it has been enhanced by chemical modification into Al<sup>3+</sup> form by loading of Aluminium ions in H<sup>+</sup> form of resin. The defluoridation Al<sup>3+</sup> forms was found to be 480 mg F-/kg, at 15 mg/L initial fluoride concentration. The nature and morphology of sorbents are characterized using XRD, FTIR and SEM analysis. The fluoride sorption was explained using the Freundlich, Langmuir and Redlich-Peterson isotherms and kinetic models. The calculated thermodynamic parameters such as  $\Delta G^\circ$ ,  $\Delta H^\circ$ ,  $\Delta S^\circ$  and sticking probability ( $S^*$ ) explains the nature of sorption. A Defluoridation Plant is in service at aluminium smelter of National Aluminium Company to treatment the waste water for removing Fluoride and reutilise the water to minimise the water loss.

10:20 AM Break

10:40 AM

**Theoretical Study of Light Weight Materials on Replacement of Traditional Materials:** Pradeep Raja<sup>1</sup>; <sup>1</sup>Government College of Technology

Materials innovation and application are increasingly vital to sustain advanced manufacturing and modern methods of construction. The demand for lighter designs is growing for a broad spectrum of products. In this juncture, the paper aims at the study in development of cost-effective, high-strength, lightweight materials that reduces the weight of a product without compromising cost, performance or safety that is necessary to compete in today's global market. As a result of more stringent requirements for improved fuel economy and emissions, there is a growing trend to substitute Al and Carbon-fiber for conventional steel and cast irons in vehicles. However, because of their different tribology, strength, and ductility, light-metal castings require improved foundry procedures and more sophisticated design rules before product engineers will use them in larger quantities. A major challenge for lightweight materials is the ability to produce a functional component at an acceptable price.

11:00 AM

**Corrosion Behavior of Cermet Anodes in Na<sub>3</sub>AlF<sub>6</sub>-K<sub>3</sub>AlF<sub>6</sub>-based Baths for Low-Temperature Aluminium Electrolysis Cells:** Guihua Wang<sup>1</sup>; Xiaofei Sun<sup>1</sup>; Wenshan Wang<sup>1</sup>; Deren Wang<sup>1</sup>; Yedong He<sup>1</sup>; <sup>1</sup>University of Science and Technology Beijing

5Cu/ (10NiO-90NiFe<sub>2</sub>O<sub>4</sub>) cermet anodes were tested in different Na<sub>3</sub>AlF<sub>6</sub>-K<sub>3</sub>AlF<sub>6</sub>-based electrolytes at three temperature regimes: 740-780, 820-840, 940-960 °C. Post-electrolysis microscopic examination was carried out with SEM-EDS and XRD. The Fe, Ni and Cu contents in the bath and aluminum were measured with ICP-AES, according to which the corrosion rate was calculated. The results indicate that low temperature electrolysis can reduce the corrosion rate effectively. However, as temperature decreases too near the liquidus line, solid cryolite can form on the cathode, and high current density can be caused locally, which is detrimental to the anodes. The cermet anodes show best anti-corrosion properties when electrolysis temperature is controlled at 830-840 °C, and the corrosion resistance can be further enhanced by increasing superheat degree.

11:20 AM

**Quantifying Casting Processing Variability Due to Ingot Source: Primary vs. Secondary:** Darius Singh<sup>1</sup>; Ian Paine<sup>2</sup>; <sup>1</sup>AUT University; <sup>2</sup>Glucina Alloys Ltd

A fundamental issue of processing variability still exists in industry in terms of casting products using ingots that have been produced from either primary, secondary, or directly internally recycled. Downstream problems of oxide and other non-metallic inclusion borne defects are usually attributed to a myriad of visible and directly controllable processing parameters, however the alloy source, its manufacturing technique, quality rating and testing is often overlooked or taken for granted as a "workable" baseline to operate from. This work investigates the quality of CC601/A356 ingots produced from a primary smelter vs. a secondary producer. Best practices in manufacturing each ingot are described from each plant and measurements of melt cleanliness are made using the following foundry techniques: Prefil Footprinter, Spiral mold, Tensile, K mold, plus a modified K+ mold technique. The sensitivities of each testing method are discussed and differences between the ingot quality are revealed.

11:40 AM

**Grain Refiner Characteristics of a Novel Chemical Grain Refiner for Al Alloys:** Hari babu Nadendla<sup>1</sup>; M Nowak<sup>1</sup>; <sup>1</sup>Brunel University

We have recently developed an effective chemical grain refiner for Al alloys. Addition of this grain refiner to commercial pure Al and Al-Si alloy is observed to decrease the undercooling of the melt. As a result, fine grain structure is obtained for Al alloys cast at various cooling rates. Microstructural investigations of newly developed master alloy reveals presence of fine sized second phases. Their chemical composition has been investigated using high



resolution electron microscopy. It is found that there is a good lattice match between the second phase and Al, suggesting that these particles enhance heterogeneous nucleation sites in the Al melt. The paper also discusses optimization of chemical composition of newly grain refiner, microstructures of various casting alloys and their mechanical properties.

12:00 PM

**Modern Trends and Methods for Debottlenecking Primary Aluminum Smelters:** *Joe Petrolito*<sup>1</sup>; <sup>1</sup>Hatch

At the advent of the global financial crisis, aluminum smelters around the world are faced with similar challenges: generate more revenue with minimum capital investments. Accordingly, smelters are paying close attention to their existing operations in order to increase production via amperage creep to improve the bottom line. However, this cannot be accomplished solely by operations, finance or engineering working in isolation. Determining the best practical approach which delivers the highest returns with the least technical risk requires the continuous collaboration of all three parties. This paper will examine the interface between these parties: what are the recent trends in terms of debottlenecking projects and what methods are being used to ensure that both capex and opex are properly analyzed to ensure the operational, financial and technical success of the project.

12:20 PM

**Preparation of Al-Mg Alloys from MgO in KCl-MgF<sub>2</sub>-LiF Electrolyte by Molten Salt Electrolysis Method:** Fengli Yang<sup>1</sup>; Sh Yang<sup>1</sup>; Xianwei Hu<sup>2</sup>; Zhaowei Wang<sup>2</sup>; Zhongning Shi<sup>2</sup>; Bingliang Gao<sup>2</sup>; <sup>1</sup>Jiangxi University of Science and Technology; <sup>2</sup>School of Materials and Metallurgy117#, Northeastern University

Aluminum-magnesium alloys were prepared from magnesium oxide by molten salt electrolysis method. 30w% KCl-40w% MgF<sub>2</sub>-30w% LiF was taken as electrolysis. Effect of temperature on electrolysis was great. Back electromotor force (BEMF) was reduced 0.2-0.4V with electrolytic temperature from 800° to 840°. The process of electrolysis was controlled together by electrochemical polarization and concentration polarization. Content of magnesium in alloys was 6-8w%, and to be controlled by electrolytic time. Prepared aluminum-magnesium alloys were even. The results showed it was feasible to prepare aluminum-magnesium alloys from magnesium oxide in KCl-MgF<sub>2</sub>-LiF electrolyte by molten salt electrolysis method.

**Hume-Rothery Symposium Thermodynamics and Diffusion Coupling in Alloys - Application Driven Science: Thermodynamics and Diffusion**

*Sponsored by:* The Minerals, Metals and Materials Society, TMS Electronic, Magnetic, and Photonic Materials Division, TMS: Alloy Phases Committee

*Program Organizers:* Zi-Kui Liu, The Pennsylvania State University; Larry Kaufman, CALPHAD, Inc.; Annika Borgenstam, Royal Institute of Technology; Carelyn Campbell, NIST

Monday AM  
February 28, 2011

Room: 31A  
Location: San Diego Conv. Ctr

*Session Chairs:* Gary Purdy, McMaster University; Staffan Hertzman, Outokumpu Stainless Research Foundation

8:30 AM Introductory Comments

8:40 AM Keynote

**WILLIAM HUME-ROTHERY AWARD LECTURE: Thermodynamics and Diffusion Coupling in Alloys - Application Driven Science:** *John Agren*<sup>1</sup>; <sup>1</sup>Royal Institute of Technology

As emphasized by Stokes (1997) the common assumption of a linear progression from basic research (science), via applied research, to technological innovations (engineering), should be questioned. In fact society would gain much by supporting long-term research that stems from practical problems and has usefulness as a key word. Such research may be quite

fundamental and often it cannot be distinguished from "basic" research if it were not for its different motivation. The development of the Calphad method and the more recent development of accompanying kinetic approaches for diffusion, serve as excellent examples and are the themes of this symposium. The drivers are, e.g., development of new materials, processes, and life-time predictions. Many challenges of utmost practical importance require long-term fundamental research. This presentation will address some of them, e.g. effect of various ordering phenomena on activation barriers, the strength and practical importance of correlation effects, etc.

9:20 AM Invited

**Application of Thermodynamic Equilibria and Kinetic Calculations to Phase Transformations in High Performance Stainless Steels:** *Staffan Hertzman*<sup>1</sup>; <sup>1</sup>Outokumpu Stainless Research Foundation

In the development and processing of modern stainless steels the phase evolution during thermal cycles plays a crucial role since the microstructure strongly influences the material performance. In order to facilitate the understanding and control of the transformations, computational thermodynamics is a prerequisite. Alloy development, weldability, processability and service performance require however different approaches and examples are given to illustrate the importance of relevant thermodynamic and kinetic modelling tools.

9:50 AM Invited

**The Implications of Thermodynamic Models on Diffusion Simulations:** *Ursula Kattner*<sup>1</sup>; Carelyn Campbell<sup>1</sup>; <sup>1</sup>National Institute of Standards and Technology

The importance of appropriate models for phase descriptions in thermodynamic modeling of systems employing the Calphad method is well known. Models should take into account crystal structure and preferred site occupancies on deviation from stoichiometry in multicomponent systems and reflect whether an order/disorder transformation is present. Models must also use a minimum number of independent parameters to describe the thermochemistry of phases. These requirements necessitate that compromises be made in the description of many phases, resulting in so-called simplified model descriptions. Improper simplification of a phase may not necessarily manifest itself during the thermodynamic calculations, but may become present during diffusion simulations. For instance, describing order/disorder phases with an order/disorder model or different sublattice models may not result in noticeable differences in the calculated phase diagram but may produce unreliable results if thermodynamic and diffusion mobility descriptions do not agree. Examples from calculations of superalloys and photovoltaics will be presented.

10:20 AM Break

10:40 AM Invited

**Modeling of Diffusion-Controlled Phase Transformations in Steel:** *Joakim Odqvist*<sup>1</sup>; <sup>1</sup>Royal Institute of Technology (KTH)

The local equilibrium hypothesis is usually adopted when modeling diffusion-controlled phase transformations. However, for finite interface velocities there will be a deviation from local equilibrium at the moving phase interface. Different approaches to model this deviation for the austenite-ferrite transformation are reviewed and compared with recent experimental findings. Furthermore, Larsson's model for modeling diffusion in the lattice-fixed frame of reference is modified to account for a cooperative mechanism for the interface migration.

11:10 AM Invited

**A Computationally Based Approach to Homogenizing Advanced Alloys:** *Paul Jablonski*<sup>1</sup>; Christopher Cowen<sup>1</sup>; <sup>1</sup>US Department of Energy

We have developed a computationally based approach to optimizing the homogenization heat treatment of complex alloys. The Scheil module within the Thermo-Calc software is used to predict the as-cast segregation present within alloys, and DICTRA (Diffusion Controlled TRAnsformations) is used to model the homogenization kinetics as a function of time, temperature and microstructural scale. We will discuss this approach as it is applied to both Ni based superalloys as well as the more complex (computationally)

case of alloys that solidify with more than one matrix phase as a result of segregation. Such is the case typically observed in martensitic steels. With these alloys it is doubly important to homogenize them correctly, especially at the laboratory scale, since they are austenitic at high temperature and thus constituent elements will diffuse slowly. The computationally designed heat treatment and the subsequent verification real castings are presented.

### 11:40 AM Invited

**Kinetic Transitions in the Growth of Ferrite during the Decarburization of Alloyed Austenite:** Gary Purdy<sup>1</sup>; Hatem Zurob<sup>1</sup>; Damon Panahi<sup>1</sup>; Christopher Hutchinson<sup>2</sup>; Yves Brechet<sup>3</sup>; <sup>1</sup>McMaster University; <sup>2</sup>Monash University; <sup>3</sup>Institut National Polytechnique de Grenoble

The growth of ferrite from alloyed austenite under conditions of controlled decarburization has proven a rich area for study, permitting the inference of the contact conditions for carbon at a migrating planar interface. In this contribution, we summarize recent findings with emphasis on transitions between full local equilibrium in the absence of alloying element partitioning (LE-NP) and the constrained local equilibrium state, paraequilibrium (PE). We have utilized Agren's evaluations of the diffusion coefficients of carbon in ferrite and austenite, first to validate the binary (Fe-C) results, then for the evaluation of the interfacial carbon concentrations for several cases of ternary iron alloys (Fe-C-X, where X is a substitutional solute). The implications of these observations are discussed in terms of new models for the migrating interfaces.

### Hydrogen Storage in Materials: Theory and Experiment: Session I

*Sponsored by:* The Minerals, Metals and Materials Society, ASM Materials Science Critical Technology Sector, TMS: Energy Conversion and Storage Committee

*Program Organizer:* Louis Hector Jr, GM R&D Center

Monday AM

Room: 13

February 28, 2011

Location: San Diego Conv. Ctr

*Session Chair:* Eric Majzoub, University of Missouri - St. Louis

### 8:30 AM

**A Consistent Thermodynamic Description of Hydrogen Diffusion and Defect Interaction in a Material Containing Dislocations, Voids and Micro-cracks:** Kiran Solanki<sup>1</sup>; Douglas Bammann<sup>1</sup>; <sup>1</sup>Mississippi State University

A finite deformation, rate and temperature dependent model of inelasticity is developed within the thermodynamic framework of Gurtin to describe the hydrogen effect on material deformation and material deformation on hydrogen transport. Internal state variables associated with statistically stored dislocations, the concentration of hydrogen and associated gradients and a consistent damage-elastic strain metric are introduced into the Helmholtz free energy, in addition to the standard variable of temperature. The theory is developed for large strains, whereby the total deformation gradient is multiplicatively decomposed into contributions from elasticity, damage, plasticity and hydrogen effects. Thermodynamic restrictions from the dissipation inequality result in the restriction that the stress and microforces are defined as derivatives of the free energy with respect to elastic-damage metric, and H concentration and its gradient, respectively. Furthermore, a general form for the chemical potential is constructed, based upon thermodynamic restrictions. Simplified models are examined and compared with experimental examples.

### 8:50 AM Invited

**Formation of Hydrogen Cottrell Atmosphere in Palladium: Theory and Measurement from Inelastic Neutron Scattering:** Dallas Trinkle<sup>1</sup>; Hyunsu Ju<sup>1</sup>; Brent Heuser<sup>1</sup>; <sup>1</sup>University of Illinois, Urbana-Champaign

Palladium has a high hydrogen solubility and diffusivity. H can be stored both in octahedral sites and in dislocation cores, which act as nanoscale

H traps--forming Cottrell atmospheres that are metal-hydride-like at low temperatures. The formation of a Cottrell atmosphere can be measured in situ with inelastic neutron scattering. Ab initio density-functional theory computes the potential energy for a hydrogen in the core of a partial dislocation and with volumetric strains. We model changes in the hydrogen potential from neighboring Pd vibrations to predict the vibrational density of states for hydrogen from 0K to room temperature. The predicted inelastic neutron scattering intensity compare with new measurements, which show a shoulder at 0K from the core and hydride formation, widening of the peak at 200K from spreading of the Cottrell atmosphere, and a shift in the peak at 300K as the atmosphere dissolves

### 9:30 AM

**Effects of Gaseous Impurities in Hydrogen on the Long Term Cycling Stability and Storage Capacity of Li3N:** Joshua Lamb<sup>1</sup>; Dhanesh Chandra<sup>1</sup>; Wen-Ming Chien<sup>1</sup>; Delphine Phanon<sup>2</sup>; Nicolas Penin<sup>2</sup>; Radovan Cerny<sup>2</sup>; Klaus Yvon<sup>2</sup>; <sup>1</sup>University of Nevada, Reno; <sup>2</sup>University of Geneva

We have studied the effect of gaseous impurities in hydrogen on Li-N-H. The gaseous contamination effects were studied using 100 ppm levels of impurity gases such as O<sub>2</sub>, H<sub>2</sub>O, CH<sub>4</sub>, CO and NH<sub>3</sub> mixed with UHP hydrogen. In addition, commercial-grade industrial hydrogen was also used. In the case of industrial hydrogen we found a ~50% loss (~2.6wt% out of ~5.6wt%H<sub>2</sub>) after 1100 pressure cycles. X-ray diffraction studies revealed formation of Li<sub>2</sub>O. The addition of H<sub>2</sub>O, CH<sub>4</sub>, NH<sub>3</sub>, and CO showed varying degrees capacity loss. We observed significant improvement in the reversible capacity up to ~10wt.%H after 516 cycles with 80/20 H<sub>2</sub>/N<sub>2</sub> mixtures, an improvement of ~7.1wt.H as compared to using hydrogen without nitrogen additives. We attribute this enhancement to the reaction of nitrogen with liquid lithium during cycling as the Gibbs energies of formation of Li<sub>3</sub>N ( $\Delta G_o = -100.16$  kJ/mol) are more negative than that of LiH phase ( $\Delta G_o = -50.74$  kJ/mol).

### 9:50 AM

**Analysis of Deformation Twins and the Partially Dehydrogenated Microstructure in Nanocrystalline Magnesium Hydride (MgH<sub>2</sub>):** David Mitlin<sup>1</sup>; Mohsen Danaie<sup>1</sup>; Shu Xia Tao<sup>2</sup>; Peter Kalisvaart<sup>1</sup>; <sup>1</sup>University of Alberta and NINT NRC; <sup>2</sup>Eindhoven University of Technology

We employed cryo-stage transmission electron microscopy (TEM), supported by density functional theory (DFT), to explore the microstructure of magnesium hydride (MgH<sub>2</sub>) powders. Mechanical milling results in deformation twinning of the hydride. The crystallography of the twins is established. DFT analysis shows that the twin unit cell is just as thermodynamically stable as the un-deformed a-MgH<sub>2</sub> matrix. We hypothesize that the twins contribute significantly to the observed milling-induced kinetic enhancement, by acting as high diffusivity paths for hydrogen. Energy-Filtered TEM (EFTEM) analysis on partially desorbed MgH<sub>2</sub> demonstrates that nucleation and growth of metallic magnesium occurs non-uniformly. Larger powder particles are a composite of isolated magnesium grains heterogeneously nucleated on the remaining hydride. Smaller particles are either fully transformed to magnesium or remain entirely a hydride. There is little evidence for any "core-shell" structure. We also show that in-situ hydrogen desorption in the TEM is not representative of the elevated-temperature ex-situ sequence.

### 10:10 AM Break

### 10:30 AM

**Mechanical Properties and Hydrogen Sorption in Mg/Nb Multilayer Films:** Byoungsoo Ham<sup>1</sup>; Xinghang Zhang<sup>1</sup>; <sup>1</sup>Texas A&M University

Mg/Nb multilayers with layer thickness varying from a few to 200 nm were prepared by the magnetron sputtering technique. The as-deposited films have Mg (0002) and Nb (110) textures. The hardness of films is greater at smaller individual layer thickness, and approaches a maximum when h is a few nm. The strengthening mechanisms in the multilayer are discussed. Hydrogen sorption studies were performed in some of the sputtered Mg/Nb multilayers. Sputtered multilayer films were loaded in hydrogen for 24 hr

at elevated temperature. The hydrogen desorption characteristic of textured Mg/Nb multilayer films will be reported.

**10:50 AM**

**Mg-Based Nanocomposites for Room Temperature Hydrogen Storage:** *Mieczyslaw Jurczyk*<sup>1</sup>; Marek Nowak<sup>1</sup>; Leslaw Smardz<sup>2</sup>; Andrzej Szajek<sup>2</sup>; <sup>1</sup>Poznan University of Technology; <sup>2</sup>Polish Academy of Sciences

In the last decade a great interest has been observed in the field of nanoscale materials. In this work, we study experimentally the electrochemical and electronic properties of Mg<sub>2</sub>M/A (M = Ni, Cu; A = C, Pd) and Mg<sub>2</sub>Ni/LaNi<sub>5</sub>/A nanocomposite hydrides. The nanocomposites were prepared by mechanical alloying followed by annealing. Results showed that the XPS valence bands measured for MA nanocrystalline alloys and composites showed a significant broadening compared to those obtained for microcrystalline materials. Furthermore, the surface segregation process of La (Mg) atoms in LaNi<sub>5</sub>/A (Mg<sub>2</sub>M/A) nanocomposites is stronger compared to that observed for the MA nanocrystalline LaNi<sub>5</sub> (Mg<sub>2</sub>M) alloys. Additionally, the nanocomposite structure reduced hydriding temperature and enhanced hydrogen storage capacity of Mg-based materials. The nanocomposite Mg<sub>2</sub>Ni (50 wt%)-LaNi<sub>5</sub> (50 wt%) material releases 1.6 wt% hydrogen at 250C. The strong modifications of the electronic structure and surface segregation effect in the nanocomposites could significantly influence their hydrogenation properties.

**11:10 AM**

**Desorption Kinetics of the Alkali Hexahydride Alanates (M<sub>2</sub>M'AlH<sub>6</sub>) at Constant Pressure Thermodynamic Driving Forces:** *Hongwei Yang*<sup>1</sup>; Andrew Goudy<sup>1</sup>; <sup>1</sup>Delaware State University

A study was done to compare the desorption kinetics of the first decomposition step in a series of the hexahydride alanates (Na<sub>3</sub>AlH<sub>6</sub>, Na<sub>2</sub>LiAlH<sub>6</sub> and K<sub>2</sub>NaAlH<sub>6</sub>). This comparison was made using a novel procedure in which the ratio of the equilibrium plateau pressure (Pm) to the opposing pressure (Pop), or the N-value, was the same. This represents the first time that such a comparison has been made in a complex hydride displaying two decomposition steps. Since the Gibbs free energy change is proportional to Ln(Pm/Pop), it was concluded that these experiments were carried out under constant thermodynamic driving forces. The results demonstrate that appropriate cation substitutions can be adopted to stabilize or destabilize the complex hydride. Modeling studies reveal the mechanisms controlling the kinetics for each alanate.

**11:30 AM**

**Ammonia Borane at High Pressures:** *Jiuhua Chen*<sup>1</sup>; Helene Couvy<sup>1</sup>; Vadym Drozd<sup>1</sup>; Haozhe Liu<sup>2</sup>; Yongzhou Sun<sup>1</sup>; Shah Najiba<sup>1</sup>; <sup>1</sup>Florida International University; <sup>2</sup>Harbin Institute of Technology

In situ synchrotron x-ray diffraction and Raman spectroscopy experiments of ammonia borane were performed at high pressures up to 23 GPa and elevated temperatures (300K – 505K). At ambient temperature, one first-order phase transition (I4mm to Cmc21) was observed at 1.3 GPa and one second-order phase transition were observed at about 5 GPa. The experiments reveal a bulk modulus of  $K = 9.3 \pm 0.4$  GPa ( $K' = 4.8$ ) for the I4mm phase,  $K = 11.9 \pm 0.5$  GPa ( $K' = 4.6$ ) for the Cmc21 phase below 5 GPa, and  $K = 37 \pm 4$  GPa ( $K' = 4.6$ ) for pressure above 5 GPa. There is a 6% volume drop at the first order phase transition. Transition pressures from I4mm to Cmc21 phases were determined at elevated temperatures. The phase boundary has a negative claperon slope of -1.67MPa/K. Rehydrogenation of decomposed ammonia borane was observed above 6 GPa.

**11:50 AM**

**Hydrogen Interactions with Li<sub>3</sub>N and Formation of Intermediate Complex Hydride Phases:** *Joshua Lamb*<sup>1</sup>; Anjali Talekar<sup>1</sup>; Wen-Ming Chien<sup>1</sup>; Dhanesh Chandra<sup>1</sup>; Delphine Phanon<sup>2</sup>; Nicolas Penin<sup>2</sup>; Radovan Cerny<sup>2</sup>; Klaus Yvon<sup>2</sup>; <sup>1</sup>University of Nevada, Reno; <sup>2</sup>University of Geneva

Complex of Lithium nitride are important for hydrogen storage. In this study we found evidence of solid solution phases Li<sub>2-x</sub>NH<sub>1+x</sub>, particularly at  $x=1/2$  (Li<sub>1.5</sub>NH<sub>1.5</sub>) during the progression of hydrogenation of Li<sub>2</sub>NH. In-situ x-ray diffraction data shows the progression of Li<sub>2</sub>NH to Li<sub>1.5</sub>NH<sub>1.5</sub> to LiNH<sub>2</sub> transitioning through single and two phase regions as the concentration of

hydrogen increases. In-situ x-ray diffraction, thermodynamic data, such as heat capacities of Li<sub>3</sub>N and Li-N-H complex hydrides, differential scanning calorimetric and thermogravimetric data will be presented.

**12:10 PM**

**Aluminoboranes and Boron Compounds for Hydrogen Storage:** *Ji-Cheng Zhao*<sup>1</sup>; Xuenian Chen<sup>1</sup>; Zhenguo Huang<sup>1</sup>; Teshome Yisgedu<sup>1</sup>; Hima Lingman<sup>1</sup>; Beau Billet<sup>1</sup>; Sheldon Shore<sup>1</sup>; <sup>1</sup>The Ohio State University

Boron-containing compounds have been studied extensively around the world in recent years for hydrogen storage due to their high gravimetric hydrogen density. We are investigating many boron hydrides including aluminoboranes and boron-cage compounds in addition to borohydrides. The materials we are synthesizing and studying include AlB<sub>4</sub>H<sub>11</sub>, (NH<sub>4</sub>)<sub>2</sub>B<sub>10</sub>H<sub>10</sub>, and (NH<sub>4</sub>)<sub>2</sub>B<sub>12</sub>H<sub>12</sub>. Results we obtained on their syntheses, structures and desorption processes will be presented.

## **ICME: Overcoming Barriers and Streamlining the Transition of Advanced Technologies to Engineering Practice -- The 12th MPMD Global Innovations Symposium: Plenary Session and the Integration of ICME**

*Sponsored by:* The Minerals, Metals and Materials Society, TMS Materials Processing and Manufacturing Division  
*Program Organizers:* Paul Mason, Thermo-Calc Software Inc; Mei Li, Ford Motor Company; James Warren, National Institute of Standards and Technology; Jeff Simmons, AFRL

Monday AM  
February 28, 2011

Room: 7A  
Location: San Diego Conv. Ctr

*Session Chair:* Paul Mason, Thermo-Calc Software

**8:30 AM Plenary**

**Integrated Computational Materials Engineering: Current Status and Future Challenges and Opportunities:** *John Allison*<sup>1</sup>; <sup>1</sup>Department of Materials Science and Engineering, The University of Michigan

ICME is now a recognized field of study within some sectors of the materials community and industry. ICME has lead to substantial increases in the efficiency with which new components are developed and promises to improve the efficiency and robustness of the development of new materials. When it is fully embraced as a discipline within the materials profession, ICME has the potential to revolutionize the way the materials community provides input to the engineering and scientific communities. This talk will attempt to define the current status of the field by drawing from a National Academies report on ICME and reflecting on what has transpired since that report. It will also draw from the presenter's prior experience at Ford Motor Company in development and implementation of a successful ICME tools. The author will attempt to identify future challenges and opportunities for realization of the full potential offered by ICME.

**9:05 AM Plenary**

**Recent Progress of Multi-Scale Modeling of Solidification Process of Shape Casting:** *Baicheng Liu*<sup>1</sup>; Tao Jing<sup>1</sup>; Qinyan Xu<sup>1</sup>; Zhiqiang Han<sup>1</sup>; <sup>1</sup>Tsinghua University

The development of manufacturing industries requires an advanced and comprehensive system which integrates and optimizes the product design and manufacturing process and makes the product development efficient, economic and environment friendly. Integrated computational materials engineering (ICME) could be considered as a promising approach to fulfill this requirement. This paper presents recent progress of ICME, especially multi-scale modeling of solidification process of shape casting in China, including mathematical models and engineering application as well. Some case studies, including microstructure simulation of unidirectionally solidified turbine blade castings for aviation industry, microstructure simulation of aluminum and magnesium alloy castings based on cellular

MONDAY AM



automaton and phase field methods for automobile industry and simulation of casting and heat-treatment processes of turbine blade casting of water-turbine are discussed.

#### 9:40 AM Plenary

**Microstructure-Based Descriptions of the Deformation of Metals:** *Peter Gumbsch*<sup>1</sup>; Daniel Weygand<sup>2</sup>; Stefan Sandfeld<sup>2</sup>; Dirk Helm<sup>1</sup>; Alexander Butz<sup>1</sup>; <sup>1</sup>Fraunhofer IWM; <sup>2</sup>izbs, KIT

Metal forming simulations today are based on classical constitutive descriptions of yield behavior and hardening. Microstructural materials characteristics like texture, grain size or dislocation microstructure are rarely considered and never systematically evolved. This is due to a lack of available methodology. There is therefore a need for mechanistic and physically-consistent descriptions of plastic deformation on all levels of structural complexity. I will address three levels. First, single crystalline microcomponents are assessed using discrete dislocation dynamics simulations, which are inherently able to represent size effects. Second, progress in the development of a dislocation density based continuum theory of plasticity is demonstrated. Third, advanced homogenization techniques are used to bridge from single crystal plasticity to the deformation behavior of polycrystals. In a "virtual lab" one thereby computes texture evolution and associated changes in the yield locus. Such computed data can then be used to adjust the parameters of classical plasticity models.

#### 10:15 AM Break

#### 10:30 AM Invited

**The Development of the ICME Supply-Chain: Route to ICME Implementation and Sustainment:** *David Furrer*<sup>1</sup>; <sup>1</sup>Rolls-Royce

Integrated computational materials engineering (ICME) has been an evolving field for many years. Models which simulate materials-related phenomena have been developed and are being validated for industrial application. The integrating computational methods into material, process and component design has been a challenge, however, in part due to the development of a supply-chain that supports this emerging technology area. ICME touches many disciplines, which results in a requirement for many levels of computational-based technology organizations to be involved to provide tools that can be rapidly developed, validated, deployed and maintained for industrial applications. This talk will assess the need and current state of ICME supply-chain development and future requirements for the continued pace of introduction of ICME into industrial design practices.

#### 10:55 AM Invited

**On the Competitive and Pre-Competitive Aspects of ICME in New Technology Insertion - A Material Supplier Perspective:** *Robert Bucci*<sup>1</sup>; Mark James<sup>1</sup>; Markus Heinimann<sup>1</sup>; Michael Kulak<sup>1</sup>; <sup>1</sup>Alcoa Technical Center

Analytical consensus between supplier and OEM is key to new product acceptance - particularly so when design/certification path changes are needed to capture full advantage of promising approaches. The underpinnings of ICME facilitate new technology insertion with benefits to all. This in turn enables competitive advantage via product differentiation and knowledge transfer. This presentation describes how Alcoa is deploying ICME and related best practices to accelerate new product development. Past examples of material solutions that did and did not transition are reviewed with key lessons learned. The presentation main focus is on Alcoa's current application of ICME to: a) Bulk residual stress management in large single-piece airframe components machined from Alcoa Signature Stress Relief™ aluminum die-forgings; b) Mature advanced hybrid structural concepts utilizing optimized combinations of aluminum alloys and fiber metal laminates. Finally, pre-competitive and competitive aspects of ICME are discussed in context of the preceding.

#### 11:20 AM Invited

**Air Force Adoption of ICME for Materials and Manufacturing R&D:** *Katherine Stevens*<sup>1</sup>; Chuck Ward<sup>2</sup>; <sup>1</sup>Air Force Research Laboratory; <sup>2</sup>US Air Force

Numerous challenges and opportunities face the Air Force with regard to materials and manufacturing R&D. An aging Air Force aircraft fleet, a smaller defense industrial base, fewer major weapon systems produced, and a need for a more rapid and agile development cycle are all current challenges. Advances in physical understanding of materials and computational capability, when combined with a holistic systems engineering approach toward design of and with materials, provide a compelling case for adopting ICME as the necessary path to take for conducting materials and manufacturing R&D. The emerging ICME paradigm for materials engineering holds promise for reducing development time, cost, and risk. The transition to that paradigm presents needs for improved data structures, model verification and validation standards, and growth in quantitative descriptions of material behavior and manufacturing methods. Efforts by the Materials and Manufacturing Directorate to adopt ICME throughout its research and development program will be described.

#### 11:45 AM

**Cyberinfrastructure Support for Integrated Computational Material Engineering:** *Tomasz Haupt*<sup>1</sup>; <sup>1</sup>Mississippi State University

The goal of this effort is to develop a cyberinfrastructure to exploit the recent transformative research in material science involving multiscale physics-based predictive modeling, multiscale experiments and design. The cyberinfrastructure comprises a collection of materials databases as well as model, model calibration, and simulation tools at multiple size scales. It streamlines the process of gathering experimental results and deriving material properties and linking processes and properties at different length scales enabling one to design and develop the next generation materials and structural components exploiting the integrative nature of ICME. Moreover, through an Open Source process, it serves as a platform for collaborative research and transitioning research tools and codes to more robust tools ready for industrial use. The cyberinfrastructure is implemented using the Web 2.0 technologies including Wiki, AJAX-based rich user interfaces, Service Oriented Architectures (SOA), Web Services and Grid computing.

#### 12:05 PM Invited

**Building Knowledge Systems for the Design and Processing of Materials with Improved Performance Characteristics:** *Surya Kalidindi*<sup>1</sup>; Stephen Niezgoda<sup>1</sup>; Tony Fast<sup>1</sup>; Giacomo Landi<sup>1</sup>; <sup>1</sup>Drexel University

There exists a critical need to couple simulations over several length scales to predict macroscale performance characteristics, which tantamounts to executing complex numerical models within other sophisticated numerical models in a hierarchical manner. High performance data-mining tools are critically needed for harvesting efficiently the essential knowledge contained in the very large experimental and modeling datasets being produced by experts in the materials related fields. We have developed a novel framework called Materials Knowledge Systems that aims to establish highly accurate local interaction laws at each length scale by data-mining results from numerical models. Once established these local influence laws can be exercised with minimal computational effort as part of a scale-bridging framework for multi-scale materials modeling and design problems.

---

## Intelligent Materials and Structural Health Monitoring: Session I

*Sponsored by:* The Minerals, Metals and Materials Society, TMS Electronic, Magnetic, and Photonic Materials Division, TMS Structural Materials Division, ASM Materials Science Critical Technology Sector, TMS/ASM: Composite Materials Committee, TMS/ASM: Computational Materials Science and Engineering Committee, TMS/ASM: Corrosion and Environmental Effects Committee, METSOC-CIM: Metal Processing and Fabrication Committee

*Program Organizer:* Subu Nayak, ScienceTomorrow

Monday AM  
February 28, 2011

Room: 33C  
Location: San Diego Conv. Ctr

*Session Chair:* To Be Announced

---

### 8:30 AM

**Robustness of Ultrasonic Nonlinearity Measurements:** *Aurora Zinck*<sup>1</sup>; Krishnan Balasubramanian<sup>2</sup>; Sridhar Krishnaswamy<sup>1</sup>; <sup>1</sup>Northwestern University; <sup>2</sup>IIT Madras

Ultrasonic nonlinearity has been shown to be highly sensitive to microstructural changes compared to conventional ultrasonic techniques for structural health monitoring. Changes in the ultrasonic nonlinearity parameter,  $\backslash 946$ , have been qualitatively linked to changes in dislocation structures of mechanically loaded metals. In this work the limitations of current experimental techniques for measuring the ultrasonic nonlinearity by second harmonic generation are studied. Polycrystalline copper samples are monotonically loaded and the varied nonlinearities are measured by longitudinal waves traversing through the samples. The effect of experimental variables is explored through the use of multiple laboratory setups and procedures are outlined for optimized experimentation. Finally, the non-destructive measurements are compared to corresponding destructive measurements for an evaluation of the change in  $\backslash 946$  with respect to plastic deformation. These results suggest a comparison of ultrasonic nonlinearity testing methods that could be applicable for future use of ultrasonic nonlinearity as a structural health monitoring tool.

### 8:55 AM

**Impact Monitoring for Composite and Ceramic:** *Jyoti Agrawal*<sup>1</sup>; Subu Nayak<sup>1</sup>; <sup>1</sup>ScienceTomorrow

A structural health monitoring technology for composite and ceramic structures based on differential sensors is developed. While vibration-based frequency response function (FRF) used for structural health monitoring, the threshold of damage detection is too high and in case of an externally imposed vibration (such as that of an engine in an aircraft). The differential sensor in ScienceTomorrow's technology eliminates the effect of temperature and external vibration. Differential strain gauges amplify signal and reduce noise, for example, by subtracting a compressive strain signal from a tensile signal. A neural network algorithm calibrates the signal against temperature, external signal and noise. Tunable amplitude modulation uses the externally imposed vibration as the carrier vibration and detects any transient change in vibration such as an impact loading. The SHM system records impact loading (the composite and ceramics are most susceptible to) and correlates any damages as indicated by shift in natural frequency.

### 9:20 AM

**Nanocomposite Sensing Skins for Damage Identification and Localization:** *Kenneth Loh*<sup>1</sup>; *Bryan Loyola*<sup>1</sup>; <sup>1</sup>University of California, Davis

Structural systems are susceptible to damage resulting from yielding, cracking, impact, and corrosion during operation or service. In this study, structural damage identification and localization is performed via layer-by-layer assembled carbon nanotube-polyelectrolyte "sensing skins." Previous studies have verified that these conformable films exhibit highly sensitive electromechanical and electrochemical responses to applied strain

and corrosion processes, respectively. Instead of using these thin films as point sensors, they are coupled with an electrical impedance tomographic (EIT) spatial conductivity mapping technique. EIT relies on boundary electrical measurements to reconstruct the spatial conductivity map of the nanocomposite. Since electrical conductivity is calibrated to applied external stimuli, the conductivity maps directly correspond to spatial damage maps; one can then use the maps to precisely identify damage location and severity. A series of experiments are conducted to characterize the damage identification and localization performance of the sensing skins, namely non-uniform strains, impact, and corrosion.

### 9:45 AM

**Recent Progress on Processing of Amorphous Coatings:** *Sandip Harimkar*<sup>1</sup>; <sup>1</sup>Oklahoma State University

Amorphous materials or bulk metallic glasses represent a new class of advanced materials exhibiting attractive combinations of properties such as high strength/hardness and excellent wear/corrosion resistance. Even though the rapid solidification (casting) methods for processing amorphous alloys are well established, the need for simultaneous mold filling and rapid cooling rate limits the range of geometries that can be formed. These processing difficulties in combination with low tensile ductility and toughness are likely to limit the applications of amorphous materials as bulk structural materials. However, the amorphous materials can be good candidates for wear/corrosion resistant coatings on the crystalline substrates. In this presentation, an overview of the newest processing approaches, including thermal spraying, cold spraying, electrodeposition, and laser surface treatments (surface amorphization and cladding) for the fabrication of amorphous coatings will be highlighted. Also, the results of our recent research on spark plasma sintering of iron-based amorphous coatings will be presented.

### 10:10 AM

**Thermography Detection of Both Crystalline and Amorphous Materials during Cyclic Loading:** *P. Liaw*<sup>1</sup>; *Gongyao Wang*<sup>1</sup>; *B. Yang*<sup>2</sup>; *L. Jiang*<sup>3</sup>; *Y. Yokoyama*<sup>4</sup>; *A. Inoue*<sup>4</sup>; <sup>1</sup>University of Tennessee; <sup>2</sup>Shell Company; <sup>3</sup>General Electric Global Research Center; <sup>4</sup>Institute for Materials Research

It is of critical importance to find new ways to in-situ monitor the structural material fatigue damage so that in-time repairs will be possible, and failures or losses can be controlled. Usually temperature patterns serve as fingerprints during loading. In our lab, a state-of-art infrared (IR) thermography camera is employed to monitor the temperature evolutions of both crystalline and amorphous materials during fatigue experiments. With the understanding of the temperature evolutions during fatigue, thermography could provide the direct information and evidence of the stress-strain distribution, crack initiation and propagation, shear-band formation and growth, and plastic-zone evolution, which will open up wide applications in studying the structural integrity of engineering components in service. In-situ visualizations as well as qualitative and quantitative analyses of fatigue-damage processes have been performed using thermography results. Theoretical models combining thermodynamics and heat-conduction theory are developed to understand the fatigue behavior of both crystalline and amorphous alloys.

### 10:35 AM

**Differential Signal vs. Differential Sensor in Structural Health Monitoring:** *Subu Nayak*<sup>1</sup>; <sup>1</sup>ScienceTomorrow

Structural health monitoring circuit design are typically based on differential signaling. While noise and distortion are reduced in differential signal, the resolution is limited by the sensitivity of the sensor. Also, temporal and spatial information is not captured or processed. In this work, a novel differential sensor approach is being proposed. In lieu of or in addition to differential signal circuit, differential pair of sensors is being used to improve structural health monitoring. For example, in a mechanical system sensors strategically located to capture tensile as well as compressive stress are most effective in determining stress and health of structures. In corrosion, sensors monitoring local anodes and cathodes work as differential sensor. In dynamic systems, additional information in form of time stamping can provide temporal resolution for more accurate monitoring such as an impact

# TMS2011

## 140th Annual Meeting & Exhibition

loading. This new approach is also fault tolerant when used in a distributed sensor network.

### Magnesium Technology 2011: Opening Session

*Sponsored by:* The Minerals, Metals and Materials Society, TMS Light Metals Division, TMS: Magnesium Committee

*Program Organizers:* Wim Sillekens, TNO Science and Industry; Sean Agnew, University of Virginia; Suveen Mathaudhu, US Army Research Laboratory; Neale Neelameggham, US Magnesium LLC

Monday AM                      Room: 6F  
February 28, 2011              Location: San Diego Conv. Ctr

*Session Chairs:* Wim Sillekens, TNO Science and Industry; Suveen Mathaudhu, US Army Research Office

### 8:30 AM Opening of the Symposium and Presentation of the Best Paper Awards 2010

#### 8:50 AM Keynote

**Magnesium in North America: A Changing Landscape:** *Susan Slade*<sup>1</sup>; <sup>1</sup>US Magnesium LLC

The changing landscape of North American manufacturing in the context of global competition is impacting the market of all raw materials, including magnesium. Current automotive fuel economy legislation and pending legislation on the emissions of greenhouse gases are impacting magnesium's largest consuming industries, such as aluminum, automotive components, steel and transition metals. These industries are all considering innovative ways to efficiently incorporate the needed raw materials into their processes. The North American magnesium market differs from other regions based on maturity, supply streams, changing manufacturing capabilities and trade cases, combined with the transformation of North American manufacturing. The impact of these factors on the supply/demand dynamics of the North American magnesium market in both the short and long-term will be reviewed. The influence of new applications, products, and legislative changes are considered in the equation.

#### 9:20 AM Keynote

**Global Magnesium Research: State-of-the-Art and What's Next?:** *Karl Kainer*<sup>1</sup>; <sup>1</sup>GKSS Research Centre Geesthacht

In recent years magnesium and its alloys have been successfully introduced into weight-saving applications in the transportation industries in order to reduce fuel consumption and greenhouse gas emissions as well as to increase the performance of modern cars. Besides advantages, e.g. superior specific strength and excellent processability, applications of magnesium alloys are limited due to their inferior properties at elevated temperatures, e.g. low creep resistance and reduced corrosion behavior, especially when in galvanic contact with other metallic materials. Current developments are revealing possibilities to improve these properties by using modern alloys and processing routes. While the majority of industrial applications utilize cast products, the use of wrought magnesium alloys is still at an early stage. Within the framework of ongoing research and development, the corrosion behavior of both cast and wrought magnesium materials in standalone uses or in galvanic couples with other metallic materials is gaining increasing attention. New coating systems tailored to selected applications will have to be developed in order to increase the usage of magnesium alloys in the transportation industries in the future. This work also needs to be coordinated with new processes for joining magnesium alloys with similar and dissimilar metals and alloys, to achieve a broad spectrum of materials that fulfill the requirements given by the applications. This presentation will first address these issues and challenges, then discuss new developments and finally show some examples of new applications. In the conclusions, gaps and challenges will be analyzed and recommendations for sustainable research and development will be given.

#### 9:50 AM Keynote

**Environmental Challenges for the Magnesium Industry:** *Robert E. Brown*<sup>1</sup>; <sup>1</sup>Magnesium Assistance Group Inc.

The subject of environmental concerns with magnesium production and magnesium processing first started showing up in technical analysis of problems about the time of Life Cycle Analysis articles. Magnesium is produced and processed in relatively small quantities throughout the world. Annual magnesium production has been around 500-700,000 metric tons per year. This compares to aluminum which is produced in annual amounts up to 35 million metric tons. There have been some excellent review papers done, but a great amount of work related to electrolytic magnesium production which was the predominant method of production. That situation has changed totally in the past 10 years and now 85% of the world's magnesium is produced by thermal processes and most of that is in China. Comparison papers have been written comparing the environmental impacts of the two main magnesium production processes. As the measurement technology improves and as the total information references are better understood the environmental challenges can be more clearly identified. This paper reviews the situation and suggests some forward looking steps that might need to be taken.

#### 10:20 AM Break

#### 10:40 AM Keynote

**Predicting Mg Strength from First-Principles: Solid-Solution Strengthening, Softening, and Cross-Slip:** *Dallas Trinkle*<sup>1</sup>; *Joseph Yasi*<sup>1</sup>; *Louis Hector*<sup>2</sup>; <sup>1</sup>University of Illinois, Urbana-Champaign; <sup>2</sup>General Motors R&D Center

Predictive modeling of strength from first-principles electronic structure methods offers great promise to inform Mg alloy design. Simulating the mechanical behavior for new alloys requires an understanding of mechanisms for deformation at atomic-length scales, with accurate chemistry, extended to larger length- and time-scales. To design ductile Mg alloys, we identify solutes that strengthen basal slip and increase cross-slip. We use first-principles modeling of dislocations to predict dislocation motion under stress through a field of solutes at a finite temperature. First-principles flexible boundary conditions compute accurate core structures of basal and prismatic dislocations, and dislocation/solute interactions. We develop new models to predict the solute-strengthening for basal dislocations; cross-slip from basal- to prismatic-slip for a-type screw dislocations; and cross-slip stress with solutes. The first-principles data provides insight into the response of dislocations to solutes and the quantitative data to build new predictive models.

#### 11:10 AM Keynote

**Biodegradable Magnesium Implants - How do They Corrode In-Vivo?:** *Frank Witte*<sup>1</sup>; *Norbert Hort*<sup>2</sup>; *Frank Feyerabend*<sup>2</sup>; <sup>1</sup>Hannover Medical School; <sup>2</sup>GKSS Research Centre

Biodegradable magnesium implants are currently breaking the paradigm of designing and producing only corrosion resistant metallic biomaterials. The academic and industrial interest in this novel class of biomaterials is increasing dramatically in the recent years. First biodegradable metal implants have been realized as vascular stents and bone screws. However, the knowledge of the underlying degradation mechanism of these metal implants remains mainly undiscovered. This lecture will summarize the current published knowledge and recent advances in elucidating the in-vivo corrosion processes of these novel biodegradable magnesium implants.

#### 11:40 AM Keynote

**The Next Generation of Magnesium Based Material to Sustain the Intergovernmental Panel on Climate Change Policy:** *Fabrizio D'Errico*<sup>1</sup>; *Gerardo Garces*<sup>2</sup>; *Stefano Fare*<sup>1</sup>; <sup>1</sup>Politecnico di Milano; <sup>2</sup>Consejo Superior de Investigaciones Científicas (CSIC)

Current Mg alloys have several drawbacks that limit wide and profitable utilization in the industrial sector. From an environmental point of view, lighter metals like magnesium are currently considered unclean products as they are energy-intensive. But they have been proven to be "clean" in



the transport sector, as they can reduce fuel consumption. Here the potential of magnesium based materials is addressed through double-tasking: a) establish innovative lean-manufacturing processes, avoid the classic melting step to substantially reduce carbon footprint of the magnesium products; b) encourage the using of no-melt processes, realizing high-resistant ultra-fine microstructures. In September the European Union started the "Green Metallurgy 2020" project through the LIFE+ 2009 Programme. The program, which is coordinated by the Politecnico di Milano (ITA), was started in September 2010. And by using the no-melting route CENIM (SPA) has achieved up to 400 MPa UTS and an elongation capability of about 13% for some ultrafine bi-phase Mg-Zn-Y.

#### 12:10 PM Keynote

**JIM INTERNATIONAL SCHOLAR AWARD WINNER: Fracture Mechanism and Toughness in Fine- and Coarse-Grained Magnesium Alloys:** *Hidetoshi Somekawa*<sup>1</sup>; *Alok Singh*<sup>1</sup>; *Toshiji Mukai*<sup>1</sup>; <sup>1</sup>National Institute for Materials Science

The fracture mechanisms in the extruded magnesium alloys with two different grain sizes, 2 and 50  $\mu\text{m}$ , were investigated by SEM, TEM and EBSD microstructural observations. The coarse-grained alloy showed that the {10-12} type deformation twins formed at the beginning of test, and the crack was propagated into the boundaries between twins and matrix. On the other hand, the fine-grained alloy showed that the sub-grain boundaries formed instead of the deformation twins. No formation of twins at the early deformation stage causes a crack-tip blunting, and thus, the fracture toughness is a high value.

### Massively Parallel Simulations of Materials Response: Session I

*Sponsored by:* The Minerals, Metals and Materials Society, TMS Materials Processing and Manufacturing Division, TMS Structural Materials Division, TMS/ASM: Computational Materials Science and Engineering Committee, TMS: High Temperature Alloys Committee  
*Program Organizers:* Diana Farkas, Virginia Tech; Susan Sinnott, University of Florida

Monday AM Room: 1A  
February 28, 2011 Location: San Diego Conv. Ctr

*Session Chair:* To Be Announced

#### 8:30 AM Introductory Comments

#### 8:40 AM Keynote

**Mesoscale Molecular Dynamics with LAMMPS:** *Steve Plimpton*<sup>1</sup>; <sup>1</sup>Sandia National Labs

I'll briefly describe our LAMMPS molecular dynamics (MD) code and highlight some of its design features that have made it easy for users to modify and extend. One area of recent development in the code has been for modeling solvated nanoparticle or colloidal systems. In an MD code this requires coarse-graining to achieve meaningful simulation times for the study of rheological and other manufacturing properties. This involves treating the nanoparticles as single point particles, moving from explicit to coarse-grained to implicit solvent, and capturing hydrodynamic effects. I'll describe efficient techniques we've developed for several models. The first is nanoparticles in a Lennard-Jones solvent, which involves multiple length scales. The second is the stochastic rotation dynamics (SRD) formalism, where solvent particles interact with nanoparticles via collisions but not with each other. Together these algorithms can enable speed-ups of several orders of magnitude, making solvated nanoparticle systems more accessible to modeling.

#### 9:20 AM Invited

**Implementation of Multi-level Parallelism in LAMMPS for Improved Scaling on PetaFLOP Supercomputers:** *Axel Kohlmeyer*<sup>1</sup>; <sup>1</sup>Temple University

Understanding the properties of vesicles with diameters between a few tens and hundreds of nanometers has many applications from transport mechanism in cells to the formulation of consumer products. Mechanism that guide fusion of vesicles or stabilize them are to specific for continuum level theory and too costly for all-atom molecular dynamics simulations. Coarse grain potentials for MD can help to overcome this dilemma. Still, petaflop range supercomputers are required and scaling and throughput of LAMMPS need to be improved to make those kind of studies possible. This has motivated the implementation of a hybrid OpenMP/MPI parallelization strategy into many modules of LAMMPS that span nearly the full range of applications. We will discuss the results of benchmark calculations using a variety of test systems and supercomputers and demonstrate how to scale inputs with long-range electrostatic and tens of millions of particles to over 100,000 processor cores.

#### 9:45 AM Invited

**Atoms-to-Continuum (AtC): A User Package for LAMMPS:** *Jonathan Zimmerman*<sup>1</sup>; *Reese Jones*<sup>1</sup>; *Jeremy Templeton*<sup>1</sup>; *Gregory Wagner*<sup>1</sup>; <sup>1</sup>Sandia National Laboratories

To enhance the capabilities of LAMMPS and expand its usefulness in the modeling and simulation of nanostructures, we have developed the user package and associated "fix", atc (atoms-to-continuum). This multi-purpose toolset can perform coupled finite element-molecular dynamics simulations, as well as calculate on-the-fly estimates of continuum mechanical fields (e.g. stress, temperature, displacement gradient) based on atomistic simulation results. In this talk, we discuss objectives, capabilities, and use-details for this user package. We also present several examples of how it's been used to perform multi-scale analysis of phenomena in physics, materials science and applied mechanics. Sandia is a multiprogram laboratory operated by Sandia Corporation, a Lockheed-Martin Company, for the United States Department of Energy's National Nuclear Security Administration under contract DE-AC04-94AL85000.

#### 10:10 AM Break

#### 10:25 AM Invited

**Large-scale Excited Electron Molecular Mechanics/Dynamics:** *Andres Jaramillo-Botero*<sup>1</sup>; *Julius Su*<sup>1</sup>; *William Goddard*<sup>1</sup>; <sup>1</sup>Caltech

To simulate large electronically excited systems, we have developed [at the Materials and Process Simulation Center at Caltech] a molecular dynamics (MD) method that considers electrons explicitly - called the Electron Force Field (eFF). In eFF, the electrons interact with the nuclei and each other via pairwise effective potentials, and their motions are propagated independently, making it possible to go beyond adiabatic dynamics. Unlike other fermionic MD methods, our approach achieves a balanced description of both ground-state condensed systems and highly excited systems containing ionized electrons. eFF is thus uniquely suited to simulate materials in extreme conditions, where many electronically excited states of matter can occur and coexist, and overcomes salient limitations of quantum mechanics methods, restricted to tens of atoms and sub-picosecond time scales. I will summarize recent progress in developing the method, as well as results using the extended capabilities of our parallel implementation under LAMMPS, code-named pEFF.

#### 10:50 AM Invited

**Interface Free Energy of CuNb Multilayers Using Massively Parallel Metropolis Monte Carlo Simulations:** *Alfredo Caro*<sup>1</sup>; *Enrique Martinez*<sup>1</sup>; <sup>1</sup>LANL

Recent experimental discoveries and computational modeling of CuNb multilayers under irradiation suggest a particularly high resistance of these nanostructures to extreme environments. In this work we investigate the connection between interface stability under extremes and interface free energy. We use a recently developed algorithm (B. Sadigh et al. to be

published) called variance constrained semi-grand canonical Metropolis Monte Carlo, implemented into Lammmps, to predict microstructure and free energy of several CuNb nanostructures.

**11:15 AM Invited**

**Simulation of Nanofoams under Irradiation:** *Eduardo Bringa*<sup>1</sup>; J. Rodriguez-Nieva<sup>2</sup>; J. Monk<sup>3</sup>; D. Farkas<sup>3</sup>; A. Caro<sup>4</sup>; R. Johnson<sup>5</sup>; <sup>1</sup>CONICET-Universidad Nacional de Cuyo; <sup>2</sup>Instituto Balseiro; <sup>3</sup>Virginia Polytechnic Institute and State University; <sup>4</sup>Los Alamos National Laboratory; <sup>5</sup>University of Virginia

High-porosity materials can be found in a number of situations, from reactor materials to grains in space. Using LAMMPS for molecular dynamics (MD) simulations, we analyze the case of high porosity nano-scale foams, where experimental techniques are difficult to use and interpret. We consider two irradiation scenarios: (a) irradiation with ions with energies in the range 1-25 keV, of interest for fusion and fission energy applications; (b) swift heavy ion irradiation, with energies up to 5 GeV, relevant for track formation and interstellar grain evolution. Irradiation effects have larger spatial extent than for compact, full-density solids, and include the production of point-defects and twins which change the foam mechanical properties. In addition, we analyze the swift-heavy ion induced sputtering of these nanofoams.

**11:40 AM**

**A Two Temperature Model of Radiation Damage in  $\alpha$ -Quartz:** *Carolyn Phillips*<sup>1</sup>; Rudolph Magyar<sup>2</sup>; Paul Crozier<sup>2</sup>; <sup>1</sup>University of Michigan; <sup>2</sup>Sandia National Laboratories

Two temperature models are used to model the interaction between the electronic subsystem and the atomic subsystem during thermal transients such as radiation damage, laser heating, and cascade simulations. By coarse-graining the electronic subsystem, its impact on thermal transients can be modeled in longer and larger classical molecular dynamics simulations. Building on the LAMMPS code, we introduce a new version of an inhomogeneous finite reservoir two-temperature model applied to an insulator,  $\alpha$ -quartz, to model heat deposition in a SiO<sub>2</sub> lattice. Our model of the SiO<sub>2</sub> electronic subsystem is based on quantum simulations of the electronic response in a SiO<sub>2</sub> repeat cell. The parameterization of the electronic subsystem has a significant impact on the degree of permanent amorphization of the lattice. We argue that the inclusion of a simple electronic subsystem substantially improves the realism of such radiation damage simulations.

**12:00 PM**

**Parallel Molecular Dynamics for Radiation Damage Modeling in Structural Materials:** *Christophe Domain*<sup>1</sup>; Charlotte Becquart<sup>2</sup>; Ghiath Monnet<sup>1</sup>; Dmitry Terentyev<sup>3</sup>; <sup>1</sup>EDF R&D; <sup>2</sup>UMET, UMR 8207; <sup>3</sup>SCK-CEN

To understand the microstructure evolution under irradiation, the defect formation mechanisms and interaction with the microstructure have to be investigated. Neutron or ion irradiation leads to displacement cascades, phenomena occurring at nanometer scale for few tens of picoseconds. The cascades are simulated using millions of atoms simulation boxes. The study of the dislocation interaction with irradiation defects requires also very large simulation boxes and long simulations to achieve the level of dislocation velocity comparable with the experimental one. Large parallel MD simulations are thus also required. Parallel MD simulations done using the DYMOKA code in Fe will be discussed for the modeling of pressure vessel steels. The importance of ab initio calculations will be underlined to assess the validity of the interatomic potentials used [Phil. Mag. 89 (2009) 3215]. The use of these results in multiscale modeling will be presented emphasizing their integration in upper scale models.

## Materials and Society: Linking Science and Technology for Global Energy Solutions: Plenary Session

*Sponsored by:* The Minerals, Metals and Materials Society, TMS: Materials and Society Committee

*Program Organizer:* Christina Meskers, Umicore

Monday AM  
February 28, 2011

Room: 11A  
Location: San Diego Conv. Ctr

*Session Chairs:* Iver Anderson, Ames Laboratory; James Foley, Los Alamos National Laboratory

**8:30 AM Plenary**

**A Plan for a Sustainable Future Using Wind, Water, and Sun:** *Mark Z. Jacobson*<sup>1</sup>; <sup>1</sup>Stanford University

In this talk, I will lay out a plan for the world to supply 100% of its energy for all purposes from wind, water, and sunlight (WWS) within the next 20-40 years and how materials will play a role in this plan. The study starts by reviewing and ranking major proposed energy-related solutions to global warming, air pollution mortality, and energy security while considering other impacts of the proposed solutions, such as on water supply, land use, resource availability, reliability, wildlife, and catastrophic risk. It then evaluates a scenario for powering the world on the energy options determined to be the best while considering materials, transmission infrastructure, costs, and politics. The study concludes that powering the world with wind, water, and solar technologies, which are found to be the best when all factors are considered, is technically feasible but politically challenging.

**8:55 AM Plenary**

**Metallurgical Considerations in the Photovoltaic Module:** *Funsho Ojebuoboh*<sup>1</sup>; <sup>1</sup>First Solar, Inc.

The incipience of thin film photovoltaic as a commercial power generator has occurred even as the device continues to be developed. At the same time, the commercial deployment of photovoltaic module manufacturing and the deployment of photovoltaic power plants have together emerged as a business sector on its own. In particular, since its incipience, CdTe PV has been on the cutting edge of a drive to achieve grid parity. Materials are invariably critical to all aspects of power generation and photovoltaic power generation is no exception. In fact, photovoltaic power generation is an increasingly active research and development thrust in Materials Engineering. One aspect of the thrust is investigating the sources, synthesis and characterization of input materials (raw materials) and the management of output materials, including spent process materials. In this presentation, we consider materials important to the production of the photovoltaic module; invariably, our focus is on thin film modules and particularly CdTe PV. In accord with the theme of the session, "Linking science and technology for global energy solutions," the presentation includes a discussion of a world powered by clean, affordable solar electricity and the materials challenges.

**9:20 AM Plenary**

**Electrical Energy Storage for Renewable Integration and Grid Applications: Status, Challenges and Opportunities:** *Zhenguo "Gary" Yang*<sup>1</sup>; <sup>1</sup>Pacific Northwest National Laboratory

Growing concerns over the environmental consequences of burning fossil fuels and their resource constrains, along with the increasing world energy consumption, have spurred great interests in renewable energy from sources such as wind and solar. However, the power from these intermittent sources is constantly varied, making quite challenging for its use and dispatch through the aging electrical grid. One effective way to smooth out the intermittency is to employ electrical energy storage. There are potential technologies for the applications, including batteries, super-capacitors, fly-wheels, compress air, pump hydro, etc. But these technologies either cannot meet the performance and cost matrices for broad market penetration or are simply limited by site selection or environmental constrains. As such there have been growing

interests and R&D activities in advancing the storage technologies. This paper offers an overview on varied technologies, in particular batteries, and discusses the status, challenges and research needs.

#### 9:45 AM Plenary

**The Rare Earth Contributions to Global Energy Solutions:** *Karl Gschneidner*<sup>1</sup>; <sup>1</sup>Iowa State University

The rare earths have many unique physical and chemical properties which make them important, if not critical, components in a variety of energy technologies. In the transportation sector: La is used in batteries; Ce in gasoline cracking catalysts and in three-way catalytic converters; Nd in the electric motors; Y as an oxygen sensor to control lean/rich fuel mixtures and as an oxidation resistant coating in aircraft turbine engines; and Y, Gd, Lu as the hosts and Eu, Tb, Dy and Er as the activators in phosphors for display units. In the energy generating and transmission sectors: Nd in NdFeB permanent magnets for wind generators; and Y in YBa<sub>2</sub>Cu<sub>3</sub>O<sub>7</sub> superconductors in both wind generators and electrical transmission lines. While in the energy efficiency sector: phosphors (as noted above) in lighting – compact fluorescent lamps (CFL) and LED devices; La, Nd and Gd in magnetic refrigeration.

#### 10:10 AM Break

#### 10:25 AM Plenary

**Materials R&D to Enable a Nuclear Energy Renaissance:** *Steven Zinkle*<sup>1</sup>; <sup>1</sup>Nuclear Science and Engineering Directorate Oak Ridge National Laboratory

As part of a balanced portfolio of sustainable energy options, nuclear energy offers significant promise as a proven, cost-effective, and reliable baseline power option. In order to explore the potential to enhance the nuclear power contribution beyond its current level of 20% of US electricity production, three key initiatives are under investigation. The first initiative is examining the potential to safely and reliably extend the operational lifetime of existing nuclear power plants by quantifying the key materials degradation mechanisms and identifying materials replacement or damage mitigation solutions. The second initiative is exploring a broad range of new fission reactor concepts, encompassing Small (<300 MW) Modular Reactor designs that may be attractive for replacement of aging fossil energy plants as well as so-called “Generation IV” reactor concepts that offer further improvements in fuel sustainability, economics and safety. Finally, materials challenges for realizing practical fusion energy systems will be briefly reviewed.

#### 10:50 AM Plenary

**Energy Efficiency Studies:** *Ken Somers*<sup>1</sup>; <sup>1</sup>McKinsey

Abstract not available.

#### 11:15 AM Plenary

**Materials Challenges for Solid Oxide Fuel Cells: Application of Metallic Materials and Analysis of Oxide Ionic Diffusion at the Component Interfaces:** *Teruhisa Horita*<sup>1</sup>; <sup>1</sup>AIST

Solid Oxide Fuel Cells (SOFCs) can convert the chemical energy to the electricity directly with high efficiency. Because of their high operation temperatures around 873-1273 K, the component materials should be high temperature resistance materials such as alloy and ceramics. In this presentation, technological issues and challenges will be shown for improving the SOFC performance. Our recent activities related to the SOFC materials will be presented: 1) high temperature oxidation of alloy and compositional modification of alloy, 2) oxygen ionization and oxide ionic diffusion of cell components, and 3) degradation and durability of SOFC component materials with small amount of impurities. A short technological review will be made on the SOFC demonstration project in Japan as well as PEFC commercialized system.

#### 11:40 AM Plenary

**The Pivotal Role of Materials Science and Engineering for an Energy Efficient and Low Carbon Economy:** *Diran Apelian*<sup>1</sup>; <sup>1</sup>Worcester Polytechnic Institute

The most critical issue we face as a global society for a sustainable 21st century on the planet earth is energy. During the last 10 years, world population increased by 1 billion - from 6 billion to 7 billion in one decade. Annual projections for population growth hover a bit over 1.4% whereas energy consumption is growing at a faster rate ~1.7%; certainly not a sustainable scenario. Innovation in materials and material processing technologies is critical to achieving the longer term objectives of an energy-efficient and low-carbon world. While significant efforts have been made to identify breakthrough materials and their benefits, less attention has been given to the integration with materials manufacturing, including synthesis science, needed to propel promising materials candidates across the “valley of death” into cost-effective application at scale. This presentation will provide an overview of a study commissioned by the U.S. Department of Energy focused on identifying those areas where materials science and engineering can have the most significant impacts on energy efficiency and carbon reduction.

#### Materials for the Nuclear Renaissance II: Materials and Welding

*Sponsored by:* The Minerals, Metals and Materials Society, TMS Structural Materials Division, TMS/ASM: Corrosion and Environmental Effects Committee, TMS/ASM: Nuclear Materials Committee

*Program Organizers:* Raul Rebak, GE Global Research; Brian Cockeram, Bechtel-Bettis; Peter Chou, Electric Power Research Institute; Micah Hackett, TerraPower, LLC

Monday AM  
February 28, 2011

Room: 4  
Location: San Diego Conv. Ctr

*Session Chair:* Raul Rebak, GE Global Research

#### 8:30 AM Introductory Comments

#### 8:35 AM Invited

**Nickel Alloys Used in Nuclear Power Systems:** *Julie Tucker*<sup>1</sup>; *George Young*<sup>1</sup>; *Micah Hackett*<sup>1</sup>; <sup>1</sup>Knolls Atomic Power Laboratory

Nickel based alloys are used extensively in nuclear power systems due to their excellent combination of corrosion resistance, strength, and toughness. However, primary water stress corrosion cracking (PWSCC) of Alloy 600-type materials has been a significant issue in the commercial nuclear industry. Attempts to mitigate PWSCC via weld repair using high chromium filler metals is hindered by their susceptibility to both subsolidus (e.g. ductility dip cracking) and supersolidus (e.g. solidification cracking) defects. New construction utilizing PWSCC resistant alloys (e.g. A690) face similar challenges; high chromium nickel based alloys are susceptible to welding-induced cracking. This talk presents an overview of weldability and environmentally assisted cracking in nuclear power systems; presents work to quantify and predict primary water stress corrosion crack growth rates; and summarizes alloy 690 weld metal development research. This research has resulted in a new nickel alloy filler metal with a desirable combination of PWSCC resistance and weldability.

#### 9:15 AM

**Effect of Residual Stresses on SCC Crack Growth Specimens Fabricated from Weld Metal:** *Matthew Kerr*<sup>1</sup>; *Mike Hill*<sup>2</sup>; *Alexandrea Bogdan*<sup>3</sup>; *Darrell Dunn*<sup>1</sup>; <sup>1</sup>US Nuclear Regulatory Commission; <sup>2</sup>Hill Engineering, LLC; <sup>3</sup>Argonne National Laboratory

Pressurized water reactor piping system dissimilar metal welds are susceptible to primary water stress corrosion cracking (PWSCC) as an active degradation mechanism. PWSCC is highly influenced by the state of stress within susceptible material with tensile residual stresses in welds an



established driving force for PWSCC. Proper predictions or measurements of these residual stresses are essential to accurate crack growth assessment. The US Nuclear Regulatory Commission Office of Research is currently undertaking several programs aimed PWSCC mitigation and weld residual stress characterization. This talk focuses on the effect of residual stresses on welded SCC crack growth specimens fabricated from weld metal typical of nuclear reactor piping systems.

9:35 AM

**Enhancement of Intergranular Corrosion Resistance of TIG Welded and Laser-surface Melted SUS 304 for Nuclear Power Plants:** *Joung Soo Kim*<sup>1</sup>; Chin-Man Chung<sup>1</sup>; Sung-Hoon Baik<sup>1</sup>; Sang-Bae Lee<sup>2</sup>; <sup>1</sup>Korea Atomic Energy Research Institute; <sup>2</sup>Korea Institute of Science and Technology

In order to improve intergranular corrosion including intergranular stress corrosion cracking resistance of Type 304 stainless steel weld, its surface was melted using an pulse Nd:YAG laser beam. The thickness of surface melted by the laser beam was obtained to be around 390  $\mu\text{m}$  at a scan speed of 600 mm/min. and a laser power density of 20 J/mm<sup>2</sup>. The microstructures of the TIG welded region and the region laser-surface melted on the TIG weld were observed and analyzed using OM, SEM, and TEM attaching EDS. Then intergranular corrosion resistance of the two different specimens were characterized using a double loop electrochemical potentiodynamic reactivation(DL-EPR) polarization method at the same test condition. Intergranular corrosion resistance of the laser-surface melted SUS 304 weld was observed to be much higher than that of only TIG welded SUS 304. In this presentation, the mechanism of intergranular corrosion improvement by laser-surface melting will be discussed.

9:55 AM

**Mechanical Properties and Microstructural Evolution of ODS Alloys Joined by Solid State Welding:** *Evan Young*<sup>1</sup>; James Carillo<sup>1</sup>; Brian Jaques<sup>1</sup>; Jatu Burns<sup>1</sup>; Larry Zirker<sup>2</sup>; Indrajit Charit<sup>3</sup>; Darryl Butt<sup>1</sup>; Megan Frary<sup>1</sup>; <sup>1</sup>Boise State University; <sup>2</sup>Idaho National Laboratory; <sup>3</sup>University of Idaho

Oxide dispersion strengthened (ODS) alloys are used in nuclear reactors for their excellent high temperature strength, corrosion resistance and radiation damage resistance. Although the properties of ODS alloys make them ideal for nuclear reactor applications, conventional joining techniques degrade material properties. This study evaluates the mechanical properties and microstructural evolution that result from joining a ferritic alloy (HT-9) to an ODS alloy (Fe-based MA956 or Ni-based MA754) using either friction stir welding or pressure resistance welding. The mechanical properties of the welds are determined using both hardness mapping across the weld interface and crack growth experiments. Microstructural evolution is evaluated using electron backscatter diffraction and energy dispersive spectroscopy. Results show discrete regions with differing grain size and orientation across the weld affected zone. The goal of the work is to develop better welding procedures for ODS alloys such that these materials could be used more widely in nuclear applications.

10:15 AM Break

10:25 AM

**Laser Welding for Nuclear Power Systems:** *Julie Tucker*<sup>1</sup>; Terrance Nolan<sup>1</sup>; George Young<sup>1</sup>; <sup>1</sup>Knolls Atomic Power Laboratory

Advances in laser welding technology are increasing the applicability of this joining technique to nuclear system welds. Advantages of laser welding include fiber optic delivery, high power density, small heat affected zones, minimal distortion and limited susceptibility to solidification or liquation cracking. These advantages are of special interest to next generation nuclear power systems where dissimilar metal welds are likely. Laser welds can be prone to defects, especially porosity and oxide inclusions. This work uses the corrosion resistant, nuclear structural material Alloy 690 to illustrate the effects of shielding, travel speed, focal point, and joint type on the penetration, defect type, and defect density in autogenous welds. The test welds were characterized by light optical microscopy, scanning electron microscopy, and x-ray computed tomography to quantify welding defects. Results show that

defect density decreases with increasing defocus. Additionally shielding gas can have a large effect on defect type and weld penetration.

10:45 AM

**Pressure Resistance Welding for Advanced Reactor Applications:** *Nathan Jerred*<sup>1</sup>; Larry Zirker<sup>2</sup>; Indrajit Charit<sup>1</sup>; Jim Cole<sup>2</sup>; Brian Jaques<sup>3</sup>; Troy Bradshaw<sup>4</sup>; James Carrillo<sup>3</sup>; Evan Young<sup>3</sup>; Megan Frary<sup>3</sup>; Darryl Butt<sup>3</sup>; Mitch Meyer<sup>2</sup>; K. Murty<sup>4</sup>; <sup>1</sup>University of Idaho; <sup>2</sup>Idaho National Laboratory; <sup>3</sup>Boise State University; <sup>4</sup>North Carolina State University

Pressure resistance welding (PRW) has been used to produce solid-state joints of high temperature materials, such as oxide dispersion strengthened (ODS) alloys, ferritic/martensitic steels and tungsten. The key emphasis of this study is to optimize the PRW parameters and characterize the welds of these alloys joined in similar and dissimilar fashions, and establish appropriate processing-microstructure-property relationships to facilitate their use in various nuclear applications. Initial studies have suggested that high quality welds can be made between MA957 cladding tubes and HT9 end-plugs. Initial bend and burst tests have shown encouraging results. Current efforts also include joining similar ODS alloys (MA956 and MA754) and tungsten coupons. A multi-physics program (COMSOL) has been employed to model the PRW process and predict initial input parameters prior to welding. Weld characterization experiments include micro-hardness, three-point bend, burst and tensile tests for mechanical integrity, and optical microscopy and scanning electron microscopy for microstructural characteristics.

11:05 AM

**Surface Modification of 316L Stainless Steel by a Low Temperature Severe Plastic Deformation Linear Raking Process:** *Giovanni Facco*<sup>1</sup>; Shashank Shekhar<sup>1</sup>; Andreas Kulovits<sup>1</sup>; Ravi Shankar<sup>1</sup>; Jorg Wiecek<sup>1</sup>; <sup>1</sup>University of Pittsburgh

The plane-strain machining process, linear raking, is a novel technique to modify microstructures of complex multi component alloy systems, which can be easily up-scaled. Linear raking offers access to severe plastic straining at high rate, modifies heat treatment alloy responses, often improving properties. Here we apply linear raking to 316L stainless steel to produce nano-structured and grain-boundary-engineered sub-surface layers, which could provide for enhanced mechanical and corrosion performance and improve irradiation tolerance. We use electron backscatter diffraction in the scanning electron microscope and automated acquisition and indexing of transmission electron microscope diffraction patterns to monitor the microstructure changes imposed by linear raking and annealing based processing. We correlate them with mechanical properties and stress corrosion susceptibility studies. We acknowledge using facilities of the Materials Micro-Characterization Laboratory, Department of Mechanical Engineering and Materials Science, University of Pittsburgh, and support by a grant from the Nuclear Regulatory Commission, NRC-38-09-935.

11:25 AM

**Serrations in Austenitic Fe-Cr-Ni Alloys:** *Young Suk Kim*<sup>1</sup>; Sung Soo Kim<sup>1</sup>; Dae Whan Kim<sup>1</sup>; <sup>1</sup>Korea Atomic Energy Research Institute

Tensile tests were conducted on 316L stainless steel with nitrogen over a temperature range of RT to 750oC at different strain rates of 1x10<sup>-2</sup>/s to 2x10<sup>-4</sup>/s. The 316L stainless steel showed serrated flow, a linear increase of strain hardening from 400 to 600oC and a negative strain rate sensitivity of strain hardening due to dynamic strain aging (DSA). Using neutron diffraction, the lattice contraction due to short range ordering (SRO) was seen to occur in the 40% cold-worked 316 stainless steel on aging at 400oC corresponding to a minimum of the tensile elongations. We first suggest that SRO is the cause of shear localization and serrated flow in austenitic Fe-Cr-Ni alloys. Using TEM, planar dislocations were confirmed in the 316L stainless steel after tensile deformation at 400oC where SRO was operating. This study definitively demonstrates that SRO is the cause of serrations and DSA in austenitic Fe-Cr-Ni alloys.

11:45 AM

**Precipitation and Spinodal Decomposition in a Lean Grade of Duplex Stainless Steel:** *Julie Tucker*<sup>1</sup>; *George Young*<sup>1</sup>; *Daniel Eno*<sup>1</sup>; <sup>1</sup>Knolls Atomic Power Laboratory

Duplex stainless steels are desirable for use in power generation systems due to their attractive combination of strength, corrosion resistance, and cost. However, thermal embrittlement at high temperature (~750°C), due to the precipitation of undesirable phases, can complicate fabrication. Similar embrittlement at low temperatures (~475°C), via spinodal decomposition, limits upper service temperatures for many applications. The recent development of lean grade alloys may improve the manufacturing margin and potentially increase the upper service temperature of these alloys. The present work assesses the thermal stability of lean grade of duplex stainless steel, AL2003 through a series of isothermal agings between 280°C and 815°C for times between 1 and 10,000 hours. Aged samples were characterized by changes in microhardness and Charpy-impact toughness. Microstructural characterization of the aged samples via transmission electron microscopy was also performed. This analysis has determined the rates and the temperatures at which these phase transformations occur.

12:05 PM

**High Temperature Fracture Toughness of Thermally Aged Inconel 617:** *Mikhail A. Sokolov*<sup>1</sup>; *Randy Nanstad*<sup>1</sup>; <sup>1</sup>Oak Ridge National Laboratory

Nickel-base alloy Inconel 617 is being considered as a structural material for application in the secondary heat exchanger of the New Generation Nuclear Plant, a very high temperature gas-cooled reactor. Inconel 617 has previously been shown to exhibit degraded toughness following thermal aging at elevated temperatures. Thermal aging of Inconel 617 plate and welds is being performed with tensile, Charpy impact, and fracture toughness tests conducted at temperatures to 950°C. Results of testing for thermal aging to 2,000 h have been obtained and are presented; varying effects of thermal aging temperature and time on fracture toughness are observed.

## Materials Processing Fundamentals: Solidification, Deformation, and Heat Treatment

*Sponsored by:* The Minerals, Metals and Materials Society, TMS Extraction and Processing Division, TMS: Process Technology and Modeling Committee

*Program Organizers:* Prince Anyalebechi, Grand Valley State University; Srikanth Bontha, Temple University

Monday AM  
February 28, 2011

Room: 12  
Location: San Diego Conv. Ctr

*Session Chair:* Prince Anyalebechi, Grand Valley State University

8:30 AM

**The Influence of Solidification Rates on Hot Workability and Mechanical Properties of AM60 Magnesium Alloy:** *Goran Kugler*<sup>1</sup>; *Milan Tercej*<sup>1</sup>; <sup>1</sup>University of Ljubljana, NTF-OMM

The use of the up-to date light alloys and their development are in the sharp ascent especially in transportation industry. In the last years the use of the magnesium alloys for the various purposes was strongly increased. The aim of present research was to study the influence of solidification rate on hot workability and on obtained mechanical properties of AM60 magnesium alloy. The study was also focused on possibility to omit prior homogenisation process which would result in cost reduction. The solidification of gravity cast alloy has been investigated with various methods of the thermal analysis: "in situ" simple thermal analysis and simultaneous thermal analysis. In order to reveal optimal hot working conditions the deformation behavior was studied in the temperature range 200-450 °C and strain rates between 0.001-10 s<sup>-1</sup>. Mechanical properties have been studied with tensile and impact toughness testing.

8:45 AM

**Interplay of Flow and Solidification in a Horizontal Centrifugal Casting:** *Autumn Fjeld*<sup>1</sup>; <sup>1</sup>University of Leoben

A large-scale industrial centrifugal casting is simulated to investigate the interplay of flow and solidification during filling. In the casting under study the behavior of the flow is not fully understood; the relative motion of molten metal in the axial and circumferential directions is examined as well as the existence of a layered structure as the liquid contacts the mold and begins to solidify. Pick-up speed of the incoming metal is determined and influences of casting temperature, heat extraction, pouring rate, and rotation are considered. A single alloy and dual-alloy casting are simulated. In the case of a dual-alloy casting the mixing of the two alloys as the second alloy is poured onto the existing first alloy layer is characterized.

9:00 AM

**On the Homogenization of Cobalt Modified 17-4 PH Stainless Steel:** *Arpana Murthy*<sup>1</sup>; *Simon Lekakh*<sup>1</sup>; *Von Richards*<sup>1</sup>; *David Van Aken*<sup>1</sup>; <sup>1</sup>Missouri S&T

Three heats of 17-4PH stainless steel: with zero, three percent, and seven percent cobalt addition were melted in a 45kg (100lb) induction furnace under argon; and cast into no-bake molds and investment shell molds. Specimens were sealed into quartz tubes under vacuum, and homogenized at 1200°C from 2h to 72h. Computational thermodynamics and optical microscopy were used to predict and characterize the microstructures. A compromise between decrease in segregation and increase in lath martensite packet size was chosen for homogenization time. The specimens were austenitized, quenched, and characterized for retained austenite using X-Ray diffraction. Age hardening kinetics were studied at 454°C(850°F), 468°C(875°F) 482°C(900°F), and the activation energies for precipitation of copper were calculated. Tensile properties and Charpy V-notch toughness were measured in the peak aged condition. Fracture surfaces were observed using Scanning Electron Microscope. The addition of cobalt was found beneficial for the improvement of strength and Charpy V-notch toughness.

9:15 AM

**Investigation of the Effects of Solidification Rate and Melt Hydrogen Concentration on Porosity Formation in Aluminum Alloy 2024:** *Prince Anyalebechi*<sup>1</sup>; <sup>1</sup>Grand Valley State University

The effects of solidification rate, melt hydrogen concentration, and grain refining on porosity formation in aluminum alloy 2024 have been investigated with unidirectionally cooled laboratory-size ingots. The ingots were prepared from melts containing hydrogen concentration of 0.067, 0.19 cm<sup>3</sup>/100 g, and 0.27 cm<sup>3</sup>/100 g and solidified at 0.2-10 K/s. As expected, the amount of porosity and average pore size increased with increase in melt hydrogen concentration and decrease in solidification rate. However, the effect of solidification rate was greater at the relatively very low melt hydrogen concentration (0.067 cm<sup>3</sup>/100 g). Interestingly, addition of grain refiner decreased the amount of porosity and the average pore size. These results are consistent with reported effects of solidification rate, melt hydrogen content, and grain refining on porosity formation in other aluminum alloys.

9:30 AM

**Characterization of the Microstructure of Commercial-Size Ingots of Aluminum Alloy 3004:** *Prince Anyalebechi*<sup>1</sup>; <sup>1</sup>Grand Valley State University

The as-cast microstructure of two commercial-size electromagnetic cast ingots of aluminum alloy 3004 was quantitatively characterized. This involved the quantitative determination of across-width and through-thickness variations in dendrite cell size, grain size, macrosegregation of alloying elements, interparticle spacing, and the types, volume fractions, and sizes of the constituent or second phase particles. A significant microstructural heterogeneity across the width and through the thickness of both ingots was observed. For example, macrosegregation, and the sizes of the constituent phase particles, dendrite cells, and grains increased concomitantly from edge to mid-width and from surface to center of the ingots. There was a -20% depletion of Mg and a +54-87% enrichment of Ti in the center of the ingots. With the exception of grain size, there was no significant microstructural difference between the two ingots examined. The causes and practical

MONDAY AM

implications of the observed microstructural heterogeneity in the ingots are discussed.

**9:45 AM**

**Expansion and Collapse of Liquid Aluminum Foams:** *Zhuokun Cao*<sup>1</sup>; Chuan Li<sup>1</sup>; Hongjie Luo<sup>1</sup>; Guangchun Yao<sup>1</sup>; <sup>1</sup>Northeastern University, China

The expansion rate and collapse time of liquid aluminum foams are essential for the determination of operating time and quality of the resulting foam. In the present paper, liquid aluminum foams was fabricated by adding in TiH<sub>2</sub> as blowing agent, and the variation of expansion rate with foaming time was non-contact detected by a laser distance measurer. The influence of different stabilizing agent and alloying elements was studied. The results show the fact that the fraction of stabilizing agent only perform little effects on the maximum expansion rate of liquid aluminum foams, while the influence of alloy elements are remarkable. The maximum expansion rate would increase much when Mg is added, and the liquid foam also collapse at a shorter time. Comparison was made between experimental results and mathematic cancelations, which reveal the fact that it is the change of TiH<sub>2</sub> decomposition responsible for the change.

**10:00 AM Break**

**10:15 AM**

**Review of Classical Design Methods as Applied to Aluminium Billet Heating with Induction Coils:** *Mark Kennedy*<sup>1</sup>; Shahid Akhtar<sup>1</sup>; Jon Bakken<sup>1</sup>; Ragnhild Aune<sup>1</sup>; <sup>1</sup>Norwegian University of Science and Technology

In the present study classical induction design tools are applied to the problem of heating non-magnetic metal billets, using 50 Hz AC. As an example of great practical industrial interest, the induction heating of aluminum billets is addressed specifically. The predicted work piece power is compared with the measured work piece power for a long and a short coil, using well established methods, such as those of Burch and Davis, introduced in 1926/28, Dwight and Bagai in 1935, Baker in 1944/57, Vaughan and Williamson in 1945, and by Tudbury in 1960. A calculation methodology based on a combination of the available tools is also introduced and discussed. The method has proven to give an error of <10% of the actual work piece power. An equation for Tudbury's work piece shortness correction factor is disclosed for the first time.

**10:30 AM**

**Interactions of Non-metallic Inclusions with Steel and Slag: Thermodynamic Modeling, Experiments and Metallographic Analyses:** *Susanne Michelic*<sup>1</sup>; Mario Hartl<sup>1</sup>; Christian Bernhard<sup>1</sup>; <sup>1</sup>University of Leoben

One aspect of an efficient process and product optimization of the liquid steelmaking process is the understanding of reactions and interactions between the components steel, slag and non-metallic inclusions. The present paper focuses on a fundamental study of this topic by combining the powerful methods of thermodynamic modeling with systematic experiments on a laboratory scale and subsequent SEM/EDS analyses. The modeling aspect is addressed by the commercial software FactSage 6.1; laboratory experiments are performed for a low-alloyed, Ca-treated carbon steel combined with varying slag compositions. The consequent SEM/EDS analyses provide a detailed insight into the inclusion landscape which offers a strong tool for characterizing the modification of inclusions. In the present study the combination of these methods is mainly applied to oxides, due to their crucial influence on the final product quality, thus giving important indications for further optimizing the secondary metallurgy processes.

**10:45 AM**

**Liquid Metal Flows under Non-Homogeneous Magnetic Field: Lorentz Force Flowmeters in Metallurgy:** *Jurijs Kolesnikov*<sup>1</sup>; Christian Karcher<sup>1</sup>; André Thess<sup>1</sup>; <sup>1</sup>Ilmenau University of Technology

During the motion of molten metal under external non-homogeneous magnetic field the induced electric currents produce Lorentz body forces in the opposite direction to the flow, causing deformation of velocity profile, vortical structures, and adding a pressure drop across the magnetic field. The same Lorentz force acts on the magnet system. We analyse these phenomena in metallurgy, namely, at molten metal pumping, stirring, continuous casting,

and in contactless Lorentz force flowmeter (LFF). Experiments with liquid metal alloy, including direct measurements of Lorentz forces, velocities, electrical potentials, and flow structure visualization were conducted. Based on this study the industrial prototypes of LFF systems were designed, built, and tested in non-ferrous metallurgy and secondary aluminium production. A molten metal flow at high temperature (700°C–1200°C) can be effectively measured. The LFF technique method allows measuring precisely the volumetric and mass flow rates linearly linked with Lorentz force, and the mass accumulated within production process.

**11:00 AM**

**Study of Bake Hardening Effect on Laser Welded Hot Rolled Bainitic Steel:** *Mehdi Asadi*<sup>1</sup>; Heinz Palkowski<sup>1</sup>; Nicole Schlosser<sup>1</sup>; <sup>1</sup>TU Clausthal

The influence of bake hardening (BH) effect on laser welded hot rolled bainitic steel (BS) with respect to the process condition was investigated. Two process conditions were developed for this study. At the first one the samples were pre-strained and then laser welded. At the second one the samples were firstly laser welded and then pre-strained. Pre-straining the samples with defined degrees of deformation and a subsequent aging treatment leads to enhanced hardness and strengthening for the both conditions. The microstructure of the laser track zone (LTZ) and heat affected zone (HAZ) was studied. A high volume fraction of martensite could be observed in the LTZ as well as HAZ. The BS steel exhibited a clear BH effect in both, the as-received and the laser welded conditions. The BH effect is more pronounced in the pre-strained laser welded condition.

**11:15 AM**

**Research on the Combination of Microwave and Heat Pump Drying of Silica Sand:** *Hao Niu*<sup>1</sup>; Yu Li<sup>1</sup>; Ying Lei<sup>1</sup>; Libo Zhang<sup>1</sup>; *Jinhui Peng*<sup>1</sup>; Huilong Luo<sup>1</sup>; Shenghui Guo<sup>1</sup>; <sup>1</sup>Key Laboratory of Unconventional metallurgy, Ministry of Education

In this work, the combination of microwave drying (MWD) and heat pump drying (HPD) drying experiments were designed by response surface methodology (RSM) based on central composite design (CCD) using design expert software (Version 7.15), and the process parameters were optimized. The conditions given by software are: the MWD time is 4.6 or 4.4 min; the HPD time is 9.0 or 8.6 min; and the sample mass is 620 or 600 g. Under those conditions the moisture content is 1.0 10-2kg water/kg wet basis, and the effectiveness ratio is 0.70 kg water/kwh. The results of confirmatory experiments conducted under the optimized conditions show the combined drying have superiority of decrease of energy consumption and increase of handling capacity over the single MWD or HPD.

**11:30 AM**

**Surface Modification by Burnishing and Shot Peening Processes:** *Syed Hasan*<sup>1</sup>; M.A. Sadiq<sup>1</sup>; G. Rangajanardhan<sup>2</sup>; V Murti<sup>3</sup>; <sup>1</sup>Deccan College of Engg & Tech; <sup>2</sup>J N T U Vijayanagaram; <sup>3</sup>S V I T S

Burnishing and shot peening are surface modification processes involving cold working of the cutaneous layer of the part surface. Their commonality extends to the generation of compressive residual stresses and improvement of fatigue strength. Burnishing employs a spherical ball to press and shot peening employs spherical shots to impinge on the target surface. Their relative characteristics form the subject of this study. Burnishing reduces surface roughness and produces highly improved surface texture. Whereas peening produces a coarse surface texture with increased surface roughness thus clearly demarcating their suitable applications for surface modification. Burnished surfaces showed furrows from penetration and feed of the ball along the surface. Shot peening produces a matty surface with overlapping dents from impinging shots. The residual stresses and microhardness were more in shot peening compared to burnishing. Stainless steel with higher yield strength had higher induced stresses as well as microhardness compared to aluminium.



## Microstructural Processes in Irradiated Materials: Defects and Defect Processes

Sponsored by: The Minerals, Metals and Materials Society, TMS Structural Materials Division, TMS/ASM: Nuclear Materials Committee

Program Organizers: Gary Was, University of Michigan; Thak Sang Byun, Oak Ridge National Laboratory; Shenyang Hu, Pacific Northwest National Laboratory; Dane Morgan, UW Madison; Yasuyoshi Nagai, Tohoku University

Monday AM Room: 3  
February 28, 2011 Location: San Diego Conv. Ctr

Session Chairs: Gary Was, University of Michigan; Roger Stoller, Oak Ridge National Laboratory

### 8:30 AM Introductory Comments

#### 8:40 AM Invited

#### Modeling Point Defect Cluster Behavior and Their Impact on RPV Embrittlement: Roger Stoller<sup>1</sup>; <sup>1</sup>Oak Ridge National Laboratory

Almost all radiation damage accumulation is the result of incomplete recombination of the vacancies and interstitials produced by the primary damage events. Thus, understanding the behavior of these point defects is essential to any predictive radiation damage model. The role of point defect clusters is particularly important in the case of cascade-producing neutron irradiation. A previously developed kinetic embrittlement model has been revised to account for recent advances in cluster dynamics modeling and insights obtained from molecular dynamics simulations. The impact of these revisions will be presented and assessed in terms of available experimental data, including data from commercial reactor surveillance programs. The new model will provide an improved basis for evaluating the effects of neutron flux (displacement rate) which is critical for determining how high flux data is being used to obtain high fluence data for reactor life extension.

#### 9:20 AM

#### Evolution Kinetics and Sink Strength of Interstitial Loops in Irradiated Materials: A Phase-field Model: Shenyang Hu<sup>1</sup>; Chuck Henager Jr.<sup>1</sup>; Yulan Li<sup>1</sup>; Fei Gao<sup>1</sup>; Xin Sun<sup>1</sup>; Mohammad Khaleel<sup>1</sup>; <sup>1</sup>Pacific Northwest National Laboratory

Interstitial loops are one of evolving defects in irradiated alloys. Their evolution, including spatial and size distributions, affects both vacancy and interstitial accumulation in the matrix, hence, the void formation and volume swelling. In this talk, we present a phase-field model to simulate the growth kinetics of interstitial loops under irradiation. The model takes into account the generation and reaction of vacancies and interstitials, and elastic interaction between interstitial loops and point defects. The local defect flux around the interstitial loop, the effect of defect generation rate, defect mobility and elastic interaction on growth kinetics and the sink strength, and the stability of interstitial loops are investigated. We will compare and discuss the results obtained from simulations and calculated by an empirical formula that is derived with a number of assumptions.

#### 9:40 AM

#### Void Ordering and Swelling Saturation as a "Chicken and Egg Problem": Stanislav Golubov<sup>1</sup>; Alexander Barashev<sup>2</sup>; Roger Stoller<sup>1</sup>; <sup>1</sup>ORNL; <sup>2</sup>The University of Liverpool

Formation of void lattices in metallic crystals exposed to irradiation with energetic particles is a most intriguing phenomenon, which has drawn the attention of both experimentalists and theoreticians for about 40 years. Two striking features of the void lattices are: (1) coincidence of their type and orientation with the crystal lattice and (2) the saturation of swelling. It is commonly believed that (1) is due to one-dimensional migration of self-interstitial clusters produced in displacement cascades, while (2) is due to the resistance of voids to growth when arranged in a lattice. However, there is a

contradiction between these two explanations since the swelling rate would increase due to free channel formation. In this paper the situation is critically analyzed, so as to determine whether either phenomenon can be implicated as the cause of the other, or whether an underlying mechanism is responsible for both the void lattice and swelling saturation.

#### 10:00 AM

#### Non-Saturable Sinks at Grain Boundaries in Nanostructured Molecular Dynamics Simulations: Yongfeng Zhang<sup>1</sup>; Hanchen Huang<sup>2</sup>; Paul Millett<sup>1</sup>; Michael Tonks<sup>1</sup>; Dieter Wolf<sup>1</sup>; Simon Phillpot<sup>3</sup>; <sup>1</sup>Idaho National Lab; <sup>2</sup>University of Connecticut; <sup>3</sup>University of Florida

The defect accumulation in nanocrystalline Mo under electron irradiation is studied using molecular dynamics (MD) simulations. The nanostructured Mo is simulated using a bi-crystal model with  $<100>$   $\square$   $29$  twist boundaries as representation of high angle/energy grain boundaries. By assigning a kinetic energy of 40 eV to randomly selected Primary Knock-on Atoms (PKA), electron irradiation is simulated under 2000K until the defect concentration reaches steady state (in  $< 100$  ns). The development of defect concentration obtained from MD simulations agrees well with the prediction of rate theory with parameters derived from MD simulations. With regard to the constant sink strength used in rate theory, this result suggests that high angle/energy grain boundaries are non-saturable sinks for point defects under electron irradiation. In supporting, structural analysis of both short range order by pair correlation function and long range order by planar structure factor shows no change in the grain boundary structure.

#### 10:20 AM Break

#### 10:40 AM

#### Modelling of Displacement Cascades in Thin Foils of Iron: Andy Calder<sup>1</sup>; Yuri Osetsky<sup>2</sup>; David Bacon<sup>1</sup>; Alexander Barashev<sup>1</sup>; <sup>1</sup>University of Liverpool; <sup>2</sup>ORNL

Recent MD simulations of cascades in bulk iron have revealed a sub-picosecond shock-front mechanism for the creation of large interstitial clusters and that the nature of this damage is determined before the thermal spike phase of the cascade. A decelerating supersonic front from the primary recoil event produces an expanding volume of destroyed lattice. Large self-interstitial clusters form on the transonic boundary of this zone if a peripheral hypersonic recoil had created a secondary zone just ahead of this boundary. Where the two zones meet, one injects atoms into the low-density core of the other and they become interstitial clusters. Modelling has now been extended to study free-surface effects in thin samples of iron, allowing direct comparison with experimental results on ion-irradiated films from earlier TEM studies and current picosecond-to-microsecond time-resolved x-ray scattering measurements of displacement cascade dynamics.

#### 11:00 AM

#### Stoichiometry Dependence of the Evolution of Irradiation-Induced Defect Clusters in $Ce_xLa_{1-x}O_2$ : Wei-Ying Chen<sup>1</sup>; Di Yun<sup>2</sup>; Aaron Oaks<sup>1</sup>; Bei Ye<sup>1</sup>; Mark Kirk<sup>2</sup>; James Stubbins<sup>1</sup>; Yinbin Miao<sup>1</sup>; <sup>1</sup>U of Illinois at Champaign-Urbana; <sup>2</sup>Argonne National Lab

To study the stoichiometry dependence of irradiation effects in fluorite-type mixed oxide nuclear fuel ( $UPuO_2$ ), the technique of ion implantation in La doped ceria ( $Ce_xLa_{1-x}O_2$ ) is used. Xe ions were implanted into cerium dioxide single crystals with 0%, 5% and 25% La concentration at 600°C. In-situ transmission electron microscope (TEM) was utilized to observe the damage process and defects created by the ion beam irradiation. A substantial difference in dislocation loop density for 5% and 25% cases was observed at the same dose. For example, loop density is  $2 \times 10^{11} \text{ cm}^{-2}$  on  $CeO_2$  doped with 5% La and  $2 \times 10^{10} \text{ cm}^{-2}$  with 25% La when the dose reaches  $1 \times 10^{14} \text{ ions/cm}^2$ . Kinetic Monte Carlo calculations were also performed to study the oxygen diffusivity in  $Ce_xLa_{1-x}O_2$  at different stoichiometric conditions. Calculation results show the oxygen diffusivity dependence on La concentration, which compliments the experiment results.

11:20 AM

**Relevance of fcc-bcc Interface Structure to Defect Properties at Interfaces in Irradiation Environment:** *Xiang-Yang Liu*<sup>1</sup>; Richard Hoagland<sup>1</sup>; Michael Demkowicz<sup>2</sup>; Xiang-Ming Bai<sup>1</sup>; Blas Uberuaga<sup>1</sup>; Michael Nastasi<sup>1</sup>; Amit Misra<sup>1</sup>; John Hirth<sup>1</sup>; <sup>1</sup>Los Alamos National Lab; <sup>2</sup>Massachusetts Institute of Technology

Nanolayered Cu-Nb composites exhibit high strength and enhanced radiation damage tolerance. To understand the relevance of interface structure to interface properties in fcc-bcc systems, tunable potentials offer a fairly simple way to selectively vary parameters independently. In this work, the parameterization of the EAM interatomic potential in fcc-bcc system is modified to understand the interface properties. We first change the dilute heats of mixing between Cu and Nb and investigate the effect on interface structure and defect formation energies near interface. To understand the interface behavior in different lattice misfit environment, the relative lattice constants between Cu and the bcc crystal are varied. Interface dislocation analysis based on Frank-Bilby formulation is to be presented, together with atomistic simulation result. Defect-interface interactions are studied with molecular dynamics (MD) and accelerated MD method, to predict the radiation damage tolerance of these interface systems.

11:40 AM

**Towards a Unified Framework for Interatomic Potential Development: Application to the Fe-He System:** *Mark Tschopp*<sup>1</sup>; Kiran Solanki<sup>1</sup>; Mike Baskes<sup>2</sup>; Mark Horstemeyer<sup>1</sup>; Fei Gao<sup>3</sup>; Xin Sun<sup>3</sup>; Moe Khaleel<sup>3</sup>; <sup>1</sup>Mississippi State University; <sup>2</sup>LANL; <sup>3</sup>PNNL

Atomistic simulations require interatomic potentials that are able to reproduce electronic structures information while predicting properties outside of the values they were fit to. However, the design cycle for new interatomic potential development is often a lengthy process. The objective of this research is to outline a methodology for efficiently probing potential parameter space to locate optimal interatomic potentials. Here, we use a combination of random sampling techniques, response surface methodology, and optimization methods to develop an Fe-He modified embedded atom method (MEAM) interatomic potential. This methodology will be used to develop multiple Fe-He potentials, which will then be used to calculate the variability in atomistic properties based on the interatomic potential. Moreover, this methodology will be applied to other interatomic potentials to show the robustness of the methodology. Atomistic simulations rely upon good interatomic potentials and shortening this design cycle can encourage tailoring interatomic potentials for specific applications.

12:00 PM

**A New Directional Model for the Electronic Frictional Forces in Molecular Dynamics Simulations of Radiation Damage in Metals:** *Christopher Race*<sup>1</sup>; Daniel Mason<sup>2</sup>; Adrian Sutton<sup>2</sup>; <sup>1</sup>Max-Planck-Institute for Iron Research; <sup>2</sup>Department of Physics, Imperial College London

The damage caused by collision cascades in irradiated materials forms the initial conditions for longer term microstructural evolution. The exchange of energy between electrons and ions during cascades can significantly affect this damage. Models for incorporating this exchange within classical molecular dynamics (MD) simulations exist, but all approximate the ion-electron energy transfer via a damping force, opposed to ionic motion. Although such forces predict the total energy transfer over the duration of cascades, they do not capture the complex dependence of the electronic friction force on the speed, direction and atomic environment of individual ions. Here we present a new model for the electronic friction force, derived from quantum-classical Ehrenfest dynamics, which captures this complexity and is suitable for inclusion in existing MD codes at near zero computational cost. We show that our model reproduces the atomic level detail of the electronic friction force in time-dependent tight-binding simulations of cascades.

## Neutron and X-Ray Studies of Advanced Materials IV: Interfaces, Surfaces, Nanostructures

*Sponsored by:* The Minerals, Metals and Materials Society, TMS Structural Materials Division, TMS/ASM: Mechanical Behavior of Materials Committee, TMS: Chemistry and Physics of Materials Committee

*Program Organizers:* Rozaliya Barabash, Oak Ridge National Laboratory; Xun-Li Wang, Oak Ridge National Laboratory; Jaimie Tiley, Air Force Research Laboratory; Peter Liaw, The University of Tennessee; Erica Lilleodden, GKSS Research Center; Brent Fultz, California Institute of Technology; Y-D Wang, Northeastern University

Monday AM  
February 28, 2011

Room: 10  
Location: San Diego Conv. Ctr

*Session Chairs:* Dean Haefner, Argonne National Laboratory; Rozaliya Barabash, Oak Ridge National Laboratory

8:30 AM Keynote

**Study of Advanced Materials and Devices Using High-Resolution Hard X-Ray Microscopy:** *Jörg Maser*<sup>1</sup>; Martin Holt<sup>1</sup>; Robert Winarski<sup>1</sup>; Volker Rose<sup>1</sup>; Peter Fuesz<sup>1</sup>; Brian Stephenson<sup>1</sup>; <sup>1</sup>Argonne National Laboratory

The Center for Nanoscale Materials' Hard X-ray Nanoprobe (HXN) provides characterization of composition and structure of nanoscale materials and devices with high spatial resolution. A major contrast mode is nanodiffraction, which allows mapping of local phase and strain with a spatial resolution of 40 nm. This provides a powerful tool for investigation of advanced thin film materials and devices, where strain can play an important role in materials properties such as phase transition temperature and electrical conductivity. Our high spatial resolution allows us to study materials systems at technologically relevant length scales. We will present studies of structural changes in resistive RAM structures, strained nanoscale silicon-on-insulator channels, and ferroelectric domains in nanocapacitors, as well as discuss a coherence-based techniques for the high resolution study of crystalline thin films.

8:55 AM

**Depth-Dependent Strain Gradients and Interface Strength of Submicron Single Crystalline Mo in Brittle or Ductile Environment from 3D Micro-Laue Diffraction:** *Rozaliya Barabash*<sup>1</sup>; Hongbin Bei<sup>1</sup>; Yanfei Gao<sup>1</sup>; Oleg Barabash<sup>1</sup>; Gene Ice<sup>1</sup>; <sup>1</sup>Oak Ridge National Laboratory

Advanced composites with metal or ceramic constituents offer high strength and have a number of advantages with respect to individual phases. As the size of reinforcing fibers/whiskers/lamellae decreases, the importance of defects, boundaries and interfaces increase. Using 3D X-ray microdiffraction we nondestructively probe the depth-dependent strain gradients and interface strength in model systems of submicron single crystalline Mo in NiAl or Ni matrix (JMR 25, 2, 2010). Coupled with micromechanical analysis, our study shows that the relaxation of the residual thermal strains in the NiAl/Mo or Ni/Mo composites results in the formation of the near-surface "slip zone" with large strain gradients in both the reinforcing Mo fibers and the matrix. Based on these results we suggest a new approach to determine the fiber/matrix interface strength for nano- and micro-composites. Research was supported by the Materials Sciences and Engineering Division, Office of Basic Energy Science, U.S. Department of Energy.

9:10 AM Invited

**Strain Screening by Oxygen Vacancies in SrTiO<sub>3</sub>:** *Joel Brock*<sup>1</sup>; <sup>1</sup>Cornell University

Recently, Freedman et al. [Phys. Rev. B80, 064108, 2009] calculated the elastic dipole tensor for several types of point defects in SrTiO<sub>3</sub> and showed that it is nearly traceless for oxygen vacancies. Thus, oxygen vacancies are able to screen elastic strain fields. Here, we report detailed diffuse x-ray scattering measurements of bulk SrTiO<sub>3</sub> crystals prepared with controlled oxygen vacancy distributions. We verify the traceless nature of the elastic

dipole tensor of an oxygen vacancy and demonstrate both correlations between oxygen vacancies and elastic strain screening by oxygen vacancies.

#### 9:30 AM Invited

**Structure and Thermal Evolution of a Metallic Glass That Grows from the Melt through a First-Order Transition:** *Gabrielle Long*<sup>1</sup>; *Karena Chapman*<sup>1</sup>; *Peter Chupas*<sup>1</sup>; *Leonid Bendersky*<sup>2</sup>; *Lyle Levine*<sup>2</sup>; *Judith Stalick*<sup>2</sup>; *Frederic Mompiou*<sup>3</sup>; *John Cahn*<sup>4</sup>; <sup>1</sup>Argonne National Laboratory; <sup>2</sup>NIST; <sup>3</sup>CNRS; <sup>4</sup>University of Washington

In recent decades, metallic glass structures have been documented with increasing precision, but our understanding is still at best incomplete. One direct proof of this is the proliferation of partially successful models attempting to classify the underlying generalized structure. To approach a fundamental understanding of metallic glasses, it can be illuminating to investigate extreme examples. We investigated an unusual metallic glass that grows from the melt by a first order phase transition in the manner of a crystal, but scatters as a metallic glass. Well-defined nano-domains that closely resemble atomic arrangements within alpha-AlFeSi were identified. Under an isothermal anneal, the glass rejects aluminum and relaxes into a more stable and persistent configuration. As the anneal continues, there is a peritectic reaction in which the rejected aluminum-plus-glass undergoes a first order phase transition to a crystalline phase unrelated to the nano-ordered domains in the original glass, as if no nano-ordering existed.

#### 9:50 AM Invited

**Nanosecond Piezoresponse Measurements on Thin Epitaxial Ferroelectric Films at the Hard X-Ray Nanoprobe Beamline:** *Matthew Highland*<sup>1</sup>; *Martin Holt*<sup>1</sup>; *Robert Winarksi*<sup>1</sup>; *John Pearson*<sup>1</sup>; *G. Brian Stephenson*<sup>1</sup>; *Jorg Maser*<sup>1</sup>; *Stephen Streiffer*<sup>1</sup>; *Ralu Divan*<sup>1</sup>; *Carol Thompson*<sup>2</sup>; <sup>1</sup>Argonne National Laboratory; <sup>2</sup>Northern Illinois University

Our goal is to study polarization dynamics in nanoscale ferroelectric heterostructures as the size of the structure approaches the domain size, and in ultrathin films where interfacial effects dominate. In this talk, we describe the development of stroboscopic scattering techniques using the Hard X-ray Nanoprobe at the Advanced Photon Source by implementing a chopper to isolate individual 100 ps x-ray pulses and synchronize them to electrical stimulation of the sample. We also describe our progress in developing protocols to pattern and integrate working devices from ultrathin epitaxial PbTiO<sub>3</sub> films on SrRuO<sub>3</sub>/SrTiO<sub>3</sub> substrates. These devices retain the ferroelectric properties and crystalline quality of the virgin film, and allow electrical access within the constraints imposed by nanoprobe focusing optics. Results are presented showing nanosecond piezoelectric response of thin ferroelectric films using these devices. Work supported by US-DOE under Contract No. DE-AC02-06CH11357.

#### 10:10 AM Invited

**Kinetic Studies of Microstructure Evolution in Nanostructured Materials:** *Matteo Leoni*<sup>1</sup>; *Paolo Scardi*<sup>1</sup>; *Mirco D'Incau*<sup>1</sup>; <sup>1</sup>University of Trento

The knowledge of the evolution in temperature of a nanocrystalline material is the key to its optimization for industrial applications. Synchrotron radiation X-ray diffraction and modern line profile analysis (e.g. the Whole Powder Pattern Modeling) are ideal tools to follow in situ kinetics on the nanoscale. The microstructure evolution data obtained from the analysis of diffraction patterns collected in ramp at several heating rates, show how X-ray diffraction can be the ideal complementary tool to thermal analysis. Basics and examples will be discussed.

#### 10:30 AM Keynote

**Advances in Neutron and X-ray Micro/Nano Diffraction:** *Gene Ice*<sup>1</sup>; <sup>1</sup>Oak Ridge National Laboratory

Both X-ray and neutron microdiffraction methods are rapidly evolving due to the availability of powerful new sources and advanced focusing optics and detectors. Achromatic optics and methods are particularly interesting for studies of materials with unknown crystallographic orientation, and are essential to efficiently use spallation neutron sources. We describe recent spatially-resolved studies with X-ray and neutron probes that illustrate the

future of these methods. We also describe how these techniques can be optimized to exploit a coming generation of new ultra-high-brilliance third generation X-ray sources and the new spallation neutron sources. Work sponsored by the U.S. Department of Energy (DOE), Office of Basic Energy Sciences, Division of Materials Sciences and Engineering. Experiments performed on Beamline 34-ID at the Advanced Photon Source Argonne II, and the SNAP beamline at the SNS. Both 34-ID and SNAP are supported by the DOE Office of Basic Energy Science, Division of User Facilities.

#### 10:55 AM Break

#### 11:05 AM Invited

**Adhesion, Cohesion and Plasticity of Thin Metal Films:** *Ralph Spolenak*<sup>1</sup>; <sup>1</sup>ETH Zurich

Thin metal films as conductor materials for wearable microelectronics are usually deposited on polymeric substrates. Thus in addition to their electrical resistivity, the adhesion to the substrate, their plastic deformation modes and their resistance against fracture are of relevance for the application. In the current paper comprehensive studies of fracture patterns by direct observation (optical and scanning electron microscopy) as well as synchrotron based X-ray diffraction are presented. The materials range from brittle Ta and Ti films, where the effects of phase and patterning on fracture are discussed, to the precursors of plastic failure in the Au-Cu, Al-Mg and Al-Li systems. X-ray peak shifts as well as peak broadening is related to microstructural changes in the thin film materials and pathways for optimal ductility are elucidated.

#### 11:25 AM Invited

**X-Ray Diffraction Studies of Structural Transitions in Some Pnictide Superconductors:** *Zahirul Islam*<sup>1</sup>; *Jiun-Haw Chu*<sup>2</sup>; *Ian Fisher*<sup>2</sup>; <sup>1</sup>Argonne National Laboratory; <sup>2</sup>Stanford University

In FeAs-based superconductors a structural transition coincides with or precede the antiferromagnetic transition for compositions in the underdoped regime. This transition lowers the rotational symmetry (e.g. from 4-fold to 2-fold in the case of tetragonal to orthorhombic transition) of the lattice. In these materials a strong anisotropy in electronic resistivity is observed, which increases as the superconducting phase is approached with compositional variation. Although a resistivity anisotropy is expected to arise from electronic order of some kind, its origin is made difficult to determine by the onset of a structural transition. In order to clarify the role of the lattice symmetry in this anisotropy a set of single-crystal diffraction studies of structural transitions was carried out. Results of these studies reveal that the degree of structural anisotropy is inadequate to account for resistivity anisotropy indicating an electronic origin.

#### 11:45 AM Invited

**X-Ray Diffraction in Short-Period Superlattices:** *Emil Zolotoyabko*<sup>1</sup>; <sup>1</sup>Technion

Short-period superlattices, based on semiconductor or oxide layers, have wide range of applications ranging from infrared imaging to giant magneto-resistance. Some applications require deposition of sub-layers with thicknesses one monolayer and below. Under such conditions, the interface quality becomes crucial for device functioning. Most common imperfections are related to atomic intermixing during growth, which on this scale is difficult to characterize by electron microscopy methods. In this paper, we show how atomic intermixing levels can be extracted from high-resolution X-ray diffraction (HRXRD) data. For this purpose, we develop fast algorithm, which is based on analyzing the positions of diffraction peaks originated from the substrate and superlattice layers. High-resolution transmission electron microscopy (HRTEM) and scanning tunneling microscopy (STM) are applied as complementary characterization methods in order to estimate the number of atomic planes constituting different sub-layers. HRTEM and STM data are then used as an input for HRXRD analysis.



**12:05 PM Invited**

**Wafer Curvature and Stress Measured in-situ for Sputtered WSi<sub>2</sub>/Si Multilayer Thin Films on Silicon Wafers:** K. MacArthur<sup>1</sup>; B. Shi<sup>1</sup>; R. Conley<sup>1</sup>; *Albert Macrander*<sup>1</sup>; A. Genis<sup>2</sup>; L. Zhou<sup>3</sup>; Y-P. Wang<sup>3</sup>; H. Zhou<sup>3</sup>; M. Li<sup>3</sup>; R. Headrick<sup>3</sup>; <sup>1</sup>Argonne National Laboratory; <sup>2</sup>Northern Illinois University; <sup>3</sup>University of Vermont

Wafer curvature was measured in-situ in a magnetron sputtering chamber at Argonne National Laboratory as a function of the pressure of the Ar plasma. Pressures between 2.3 mTorr and 18 mTorr were studied to investigate the trade-off between interface roughness [Y-P Wang et al., J. Appl. Phys. 101, 023503 (2007)] and stress in choosing the optimal pressure for growing thick multilayer stacks. The results support conclusions of in-situ x-ray diffuse scattering experiments at beamline X21 at NSLS at Brookhaven National Lab. The x-ray diffuse scattering measurements lead to the conclusion that there is a transition from deposition of atoms at low pressure to deposition of nanoparticles at high pressure [L. Zhou et al., Phys. Rev. B 82, 075408 (2010)]. Work supported by U.S. Department of Energy, Office of Science, Office of Basic Energy Sciences under contracts DE-AC02-06CH11357 and DE-AC02-98CH10886, and under Department of Energy Grant DE-FG02-07ER46380.

**12:25 PM Invited**

**Understanding Structural Effects upon Macroscopic Phenomena in Strained Ordered Oxide Films:** *Philip Ryan*<sup>1</sup>; Jong Woo Kim<sup>1</sup>; Steve May<sup>2</sup>; Evguenia Karapetrova<sup>1</sup>; <sup>1</sup>Argonne National Laboratory; <sup>2</sup>Drexel University

The plethora of rapidly emerging high quality epitaxial, strained complex ordered oxide films have demonstrated several macroscopic phenomena including magnetism, metal-insulator transitions and multiferroicity whereby strain induces or changes the respective phenomenon. Understanding the coupling between the structure, including spin and charge, and the macro-characteristic is examined using synchrotron based resonant x-ray diffraction. In this talk I will present examples of recent measurements on strained nickelate(M-I transition), manganate (Enhanced TN) and titanate (Multiferroicity) films. The results will demonstrate the invaluable information that standardized albeit advanced x-ray scattering techniques provide for emerging novel ordered oxide film systems.

**12:45 PM Invited**

**Correlation Phenomena in Wurtzite-type GaN-based and ZnO Epilayers:** *Alois Krost*<sup>1</sup>; Juergen Blaesing<sup>1</sup>; <sup>1</sup>Otto-von-Guericke University Magdeburg

In this contribution we report on extremely sharp x-ray peaks which very often appear in transverse omega scans of, e.g. InAlN, AlGaIn, or ZnO thin films. Such correlation peaks are still visible in (0002) omega scans of 500 nm GaN which might mislead an observer to conclude incorrectly that there exists an extremely high structural quality. As one source of correlation peaks a high density of spatially correlated edge-type dislocations with in-plane Burgers vector and associated stacking faults could be identified. Another source might be surface steps on the sapphire substrate.

**Pb-Free Solders and Other Materials for Emerging Interconnect and Packaging Technologies: Next Generation Packaging**

*Sponsored by:* The Minerals, Metals and Materials Society, TMS Electronic, Magnetic, and Photonic Materials Division, TMS: Electronic Packaging and Interconnection Materials Committee  
*Program Organizers:* Indranath Dutta, Washington State University; Darrel Frear, Freescale Semiconductor; Sung Kang, IBM; Eric Cotts, SUNY Binghamton; Laura Turbini, Research in Motion; Rajen Sidhu, Intel Corporation; John Osenbach, LSI Corporation; Albert Wu, National Central Univ, Taiwan; Tae-Kyu Lee, Cisco Systems

Monday AM  
February 28, 2011

Room: 7B  
Location: San Diego Conv. Ctr

*Session Chairs:* Indranath Dutta, Washington State University; Darrel Frear, Freescale Semiconductor

**8:30 AM Introductory Comments**

**8:35 AM Keynote**

**Creation and Manipulation of Aligned Nanowires for Packaging and Circuit Integration:** *Sungho Jin*<sup>1</sup>; <sup>1</sup>University of California San Diego

Control of the nanowire structure is essential for their successful electronics applications including advanced solder connections and other packaging. Some electronic consumer products require protection against water-related damages through packaged structures, for which a superhydrophobic surface can be useful. Ceramic or metallic superhydrophobic coatings are more desirable than polymer coatings for long term, wear-resistant performances. In this talk, novel fabrication approaches to create vertically aligned nanowire configurations will be discussed, some of which exhibit superhydrophobic, non-wetting surface properties. Well controlled and processed vertically aligned semiconductor nanowire arrays can also be useful for solar cells and vertical nanotransistor arrays. Planarization of such periodically-arranged nanowire structures will be discussed in relation to circuit interconnection and routing of hundreds of millions of vertical nanodevices as well as for construction of three-dimensional multilayer device configurations.

**9:15 AM Keynote**

**All Copper Flip-Chip Interconnect:** *Paul Kohl*<sup>1</sup>; Hyo-Chol Koo<sup>1</sup>; Ping Nicole An<sup>1</sup>; Rajarshi Saha<sup>1</sup>; <sup>1</sup>Georgia Institute of Technology

A novel flip-chip technology using electroless copper deposition has been used to produce all-copper, chip-to-substrate interconnect. This process replaces solder in flip-chip connections by electrolessly joining copper pillars or pads between the chip and substrate. Solder has many weaknesses such as the formation of brittle intermetallics and poor electromigration resistance. The electroless copper joints formed in this project are annealed after plating to improve the copper bond strength. The process parameters and bond strength were investigated as a function of pillar diameter, and offset distance between the chip and its substrate. The composition of the plating bath determines the bond strength of the copper joints. Plating bath additives, such as surfactants, accelerators, and suppressors influence the quality of electroless joint. A finite element model was developed to understand the stress distribution within the copper pillar and joined components.

### 9:55 AM Invited

#### **Plasticity and Reliability: From Unexpected Plasticity-Induced Damages in Advanced Cu Interconnects to Novel Reliability Phenomena in 3-D Interconnect Schemes Using Through-Silicon Vias (TSV) Technology:**

*Arief Budiman*<sup>1</sup>; Rao Morusupalli<sup>2</sup>; Tae-Kyu Lee<sup>2</sup>; Yu-Lin Shen<sup>3</sup>; Sung-Hwan Hwang<sup>4</sup>; Byoung-Joon Kim<sup>4</sup>; Ho-Young Son<sup>5</sup>; Min-Suk Suh<sup>5</sup>; Qwan-Ho Chung<sup>5</sup>; Kwang-Yoo Byun<sup>6</sup>; Martin Kunz<sup>6</sup>; Nobumichi Tamura<sup>6</sup>; Young-Chang Joo<sup>4</sup>; <sup>1</sup>Los Alamos National Laboratory; <sup>2</sup>Cisco Systems, Inc.; <sup>3</sup>University of New Mexico; <sup>4</sup>Seoul National University; <sup>5</sup>Hynix Semiconductor Inc.; <sup>6</sup>Lawrence Berkeley National Laboratory

Plastic deformation plays an important role in the control of mechanical properties and reliability of advanced microelectronics devices. Studying how materials evolve during the service of the devices will be crucial in understanding the degradation mechanisms leading to the eventual failures of the devices. In an effort to shed light on these topics, experiments using in situ synchrotron-based white-beam (Laue) x-ray microdiffraction technique to measure plasticity and mechanical stresses in the devices during their real and/or accelerated service conditions were conducted. In this talk, I will highlight two cases – advanced Cu interconnects and a 3-D interconnect scheme using TSV technology, in which this technique has been utilized to reveal degradation mechanisms that could lead to eventual failures. Our findings in these two cases further underline the importance of both measuring and controlling plasticity and stresses in the technology development as well as reliability improvement of advanced interconnect schemes.

### 10:20 AM Invited

#### **Residual Stress of Si near Through-Silicon-Via Structure for 3-Dimensional Packaging:**

*Young-Chang Joo*<sup>1</sup>; Arief Budiman<sup>2</sup>; Sung-Hwan Hwang<sup>1</sup>; Byoung-Joon Kim<sup>1</sup>; Ho-Young Son<sup>3</sup>; Min-Suk Suh<sup>3</sup>; Kwang-Yoo Byun<sup>3</sup>; Nobumichi Tamura<sup>4</sup>; Martin Kunz<sup>4</sup>; <sup>1</sup>Seoul National University; <sup>2</sup>Los Alamos National Laboratory; <sup>3</sup>Hynix Semiconductor Inc.; <sup>4</sup>Lawrence Berkeley National Laboratory

Through-silicon via technology is widely used for 3-dimensional integration. However, stress arise in Si near TSV due to the difference in the coefficient of thermal expansion of Si and Cu. Devices cannot be located in the strained Si region (keep-away zone) due to mobility change. The plastic deformation of Cu during thermal load is the cause of the residual stress of Si, so comparing the stresses of Si and Cu is important in understanding the origin and size of keep-away zone. We used the synchrotron white beam X-ray to measure stresses of Cu and Si in TSV. Finite element method simulation was also conducted to analyze the keep-away zone. Keep-away zone was about 30  $\mu\text{m}$  away from edge of TSV. By the comparison of the evolution of Cu and Si stresses and Cu grain structure during annealing, the cause of Si residual stress is discussed.

### 10:45 AM Break

### 10:55 AM Invited

#### **The Effect of Filler-Network Heterogeneity on the Thermal Resistance of Polymeric Thermal Bondlines:**

*David Rae*<sup>1</sup>; Peter Borgesen<sup>2</sup>; Eric Cotts<sup>2</sup>;

<sup>1</sup>Universal Instruments; <sup>2</sup>Binghamton University

The influence of processing on filled-polymeric bondline thermal performance was examined, with a focus on factors that promote local filler entrapment and compaction. The materials studied were viscously applied, adhesive thermal interface materials with dispersed filler particles. All stages of bondline assembly were controlled in an attempt to create high density regions of compacted filler particles. These included material deposition (initial material location and thickness), bondline formation (normal forces, assembly speeds, assembly temperatures), and post-formation bondline stabilization (force during cure). Following cure, bondline thermal resistances and microstructures were characterized. For one high-performing, commercial thermal interface material, a four-fold decrease in thermal resistance was achieved. The general response of filled-polymeric thermal interface materials to such processing is under investigation.

### 11:20 AM Invited

#### **Recent Development of Lead-Free Nano-Solders for Nanowire and Nanoelectronics Assembly:**

*Zhiyong Gu*<sup>1</sup>; <sup>1</sup>University of Massachusetts Lowell

Many new nanomaterials and nanostructures have been fabricated in the past twenty years. With the dramatic development of nanotechnology in the past decade, promise has been shown in many potential applications of nanomaterials, including nanoelectronics, nanosensors, nanophotonics, and nanomedicine. However, in order to realize the manufacturing of nanoelectronic devices and systems, efficient and effective integration strategies have to be developed. In this talk, I will present our recent effort in the synthesis of lead-free nano-solders and the development of “nano-soldering” techniques. We have used the electrodeposition method in nanoporous templates to synthesize multisegmented nanowires with nano-solders, with diameter of 15-200 nm and length up to 20  $\mu\text{m}$ . Self-assembly method, such as magnetic assembly or dielectrophoretic (DEP) assembly, has been utilized to integrate nanowires into large-scale 2D or 3D network structures with conductive solder joints. These nanowires and nano-soldering techniques have great potential in the assembly and integration of functional nanoelectronics devices.

### 11:45 AM

#### **Deformation and Interfacial Effects during Thermal Cycling of Cu Filled Through-Silicon Vias (TSV):**

*Praveen Kumar*<sup>1</sup>; Indranath Dutta<sup>1</sup>; Muhannad Bakir<sup>2</sup>; <sup>1</sup>Washington State University; <sup>2</sup>Georgia Institute of Technology

Large shear stresses develop at interfaces between dissimilar materials during thermal excursions when there is a significant difference in the coefficient of thermal expansion between them. In TSVs, these interfacial shear stresses prevail over a larger fraction of via-length as the chip thickness becomes smaller. Under thermal cycling conditions, the interface may slide via diffusional process, thereby accommodating relative dimensional changes between via-fill(Cu) and Si. This phenomenon can become a significant reliability issue in 3-D interconnect architectures involving TSVs. Here we present experimental evidence of interfacial sliding between Cu and Si in Cu filled TSV. TSV samples were thermally cycled under different conditions (temperature ranges and heating/cooling rates). Under rapid cycling conditions, evidence of interfacial fracture was found, whereas significant diffusional sliding was found to occur at the Cu-Si interface during slow cycling. A simple 1-D analytical model and associated numerical simulations will be presented to rationalize the experimental observations.

### 12:05 PM

#### **Adhesive Selection and Bonding Parameter Optimization for Hybrid Bonding in 3D Integration:**

*Kuan-Neng Chen*<sup>1</sup>; Chuan-An Cheng<sup>1</sup>; Wen-Chun Huang<sup>1</sup>; Cheng-Ta Ko<sup>1</sup>; <sup>1</sup>National Chiao Tung University

Bonding technology is one of the key technologies for 3D integration in future packaging and semiconductor applications. Bonding temperature optimization of several polymer materials for metal/adhesive hybrid bonding was investigated. In general, the strong bond quality can be achieved with the increase of bonding temperature. However, when the bonding temperature reaches to certain point, bond failure of adhesive wafers were observed. In this research, several analysis techniques were used to evaluate the evolution of adhesive properties during the bonding process. Mechanisms are proposed to explain the failure of each adhesive. This study further conducts the criteria of adhesive selection for hybrid bonding in different 3D-IC applications.

## Physical and Mechanical Metallurgy of Shape Memory Alloys for Actuator Applications: Characterization of Shape Memory Alloys: Deformation Behavior

*Sponsored by:* The Minerals, Metals and Materials Society  
*Program Organizers:* S. Raj, NASA Glenn Research Center; Raj Vaidyanathan, University of Central Florida; Ibrahim Karaman, Texas A&M University; Ronald Noebe, NASA Glenn Research Center; Frederick Calkins, The Boeing Company; Shuichi Miyazaki, Institute of Materials Science, University of Tsukuba

Monday AM                      Room: 11B  
February 28, 2011              Location: San Diego Conv. Ctr

*Session Chairs:* Ronald Noebe, NASA Glenn Research Center; Raj Vaidyanathan, University of Central Florida

### 8:30 AM Welcome and Introductory Remarks

#### 8:35 AM Plenary

**Recent Development of High Temperature Shape Memory Alloys for Actuator Applications:** *Shuichi Miyazaki*<sup>1</sup>; *Hee Young Kim*<sup>1</sup>; <sup>1</sup>University of Tsukuba

Ti-Ni alloys have been extensively developed to expand their application fields by adding new characteristics, shapes and dimensions, e.g., small transformation temperature or stress hysteresis, high transformation temperatures, porous structures, tubes, fine wires and thin films. Among them, some high temperature shape memory alloys have been developed: e.g., Ti-Ni-X (X=Au, Pd, Pt, Hf, Zr). The transformation temperatures of these alloys reach up to 1273K. However, it is not easy to make fine wires or thin plates with these alloys because of their lack of ductility. Recently, deformable high temperature shape memory alloys such as Ti-Ni-Zr(Hf)-Nb, Ti-Ta-Al have been developed, and they can reveal SME at temperatures between 373K and 473K, where commercial Ti-Ni alloys can not reveal SME. They can be cold-rolled with reductions higher than 60% and 90%, respectively, without revealing final fracture. In this lecture, the development of the Ti-Ni-Zr(Hf)-Nb and Ti-Ta-Al alloys is to be presented.

#### 9:05 AM Invited

**Energetics of Plastic Deformation and Transformation in NiTi:** *Huseyin Sehitoglu*<sup>1</sup>; *Tawhid Ezaz*<sup>1</sup>; <sup>1</sup>University of Illinois at Urbana-Champaign

The shape memory alloys are an important class of materials that undergo reversible transformations. We provide an overview of the plastic deformation and its consequences in NiTi class shape memory alloys. Initially, we are concerned with determining the energy barriers associated with twinning and slip in the B2 phase. The NiTi alloys are considerably more ductile compared to their B2 counterparts, which points to the occurrence of twinning in the B2 phase. We study the energetics of twinning via atomistic simulations and continuum theory. Then, we study twinning in the martensitic phase. The results should shed light into several issues. What are the approximate magnitudes of the energy barriers for different shears for twinning and slip? What new information can be obtained from simulations to design new shape memory alloys with higher levels of recoverable strains?

#### 9:25 AM Invited

**Deformation of the U-14at% Nb Shape Memory Alloy: Experiments and Modeling:** *Robert Field*<sup>1</sup>; *Carlos Tomé*<sup>1</sup>; *Rodney McCabe*<sup>1</sup>; *Amy Clarke*<sup>1</sup>; *Donald Brown*<sup>1</sup>; *Catherine Tupper*<sup>1</sup>; <sup>1</sup>Los Alamos National Laboratory

U-14at%Nb is a shape memory effect (SME) alloy that undergoes deformation by the motion of complex twins and twin related lath boundaries up to the limit of SME deformation (~7%). In the SME regime a simple Bain strain model qualitatively predicts variant selection, texture development in polycrystalline samples, and stress-strain behavior as a function of parent phase orientation in single crystal micropillars. In the post-SME regime, unrecoverable deformation occurs by a combination of slip and twinning, with the first few percent of strain in tension apparently governed by a

twin species specifically associated with the monoclinic distortion in the martensite phase. A review of the Bain strain model for SME deformation will be presented in conjunction with experimental data. In addition, results from modeling of post-SME behavior using the Visco-Plastic Self-Consistent (VPSC) model will be compared to experimental texture measurements.

#### 9:45 AM Invited

**Observations on the Deformation Characteristics of NiTi:** *Santo Padula*<sup>1</sup>; <sup>1</sup>NASA Glenn Research Center

Transformation-induced plasticity (TRIP) and slip are among the more common explanations provided for the dimensional instability observed in shape memory actuators, but alternate mechanisms have been shown to be responsible for the evolution in macroscopic strain. Many conditions including altering the upper-cycle temperature (UCT), performing multiple thermal cycles under load or mechanically cycling the material have all been shown to create dimensional instability. Through in situ neutron diffraction experimentation, it has been shown that martensite texture evolution and retained martensite are the dominant mechanisms responsible for the observed evolutionary response. It has also been shown that the isothermal, cyclic deformation response of NiTi (in combined tension and compression) is different than that observed for traditional elastic-plastic materials. The aforementioned experimental observations will be discussed in relation to the limited role of plasticity in shape memory behavior.

#### 10:05 AM Break

#### 10:15 AM Invited

**Modeling and Experimental Study of Simultaneous Creep, Plasticity and Transformation of High Temperature Shape Memory Alloys during Cyclic Actuation:** *Yves Chemisky*<sup>1</sup>; *Parikshith Kumar*<sup>2</sup>; *George Chatzigeorgiou*<sup>1</sup>; *Ibrahim Karaman*<sup>3</sup>; *Dimitris C. Lagoudas*<sup>1</sup>; *Glen Bigelow*<sup>4</sup>; *Ron Noebe*<sup>4</sup>; <sup>1</sup>Texas A & M University, Aerospace Engineering; <sup>2</sup>Texas A & M University; <sup>3</sup>Texas A & M University, Mechanical Engineering; <sup>4</sup>NASA Glenn Research Center

High Temperature Shape Memory Alloys (HTSMAs) represent a class of Shape Memory Alloys (SMAs) with transformation temperatures greater than 100°C. As a consequence of their high transformation temperatures, the HTSMAs can be exposed to a temperature regime where creep behavior can occur simultaneously during the transformation. This effect has a critical impact on the actuation response, due to the generation of irrecoverable strains. The creep behavior of ternary NiTiPd and the interaction between transformation and creep occurring simultaneously has been recently studied and a thermodynamic model was developed to capture this interaction. However the experimental and modeling effort were limited to one actuation cycle. An extensive experimental effort on a NiTi30Pd was conducted in order to determine the cyclic actuation response of such HTSMAs. In addition to plastic strains during martensitic transformation, retained martensite due to thermomechanical cycling and irrecoverable strains due to primary and secondary creep

#### 10:35 AM

**Low Temperature Creep Behavior of Extruded Near-Stoichiometric NiTi Alloy:** *S. Raj*<sup>1</sup>; *Ronald Noebe*<sup>1</sup>; <sup>1</sup>NASA Glenn Research Center

It is expected that NiTi shape memory alloys (SMA) actuators would provide simple and light weight replacements for controlling chevron-shaped nozzles in aircraft engines to reduce jet engine noise. An understanding of the low temperature creep properties of NiTi is important in determining the design life of these SMA actuators. Long term constant load tensile creep tests lasting several months to about a year were conducted on hot-extruded NiTi specimens at room temperature, 373 and 473 K under initial applied stresses varying between 250 and 350 MPa. These temperatures correspond to the martensitic, two-phase and the austenitic phase fields, respectively. The range of stresses corresponded to the region of the stress-strain curves for the alloy, where detwinning of the martensitic structure occurs. The low temperature creep behavior of NiTi are discussed. The results of stress and temperature change experiments conducted between room temperature and 473 K are reported.



10:50 AM

**In Situ Observations of Deformation and Fracture in Single Crystal NiTi:** *Adam Creuziger*<sup>1</sup>; *Laura Bartol*<sup>2</sup>; *Ken Gall*<sup>3</sup>; *Wendy Crone*<sup>2</sup>; <sup>1</sup>National Institute of Standards and Technology; <sup>2</sup>University of Wisconsin-Madison; <sup>3</sup>Georgia Institute of Technology

The pseudoelastic transformation and fracture behavior of two crystallographic orientations of a single crystal NiTi shape memory alloy (SMA) were investigated. Uniaxial tension and notched tension samples are considered with the tensile axes along the [100] and [111] directions. The phase transformation was observed using optical techniques in situ. For the uniaxial tension samples, martensite plates and Luders-band structures are observed. For the notched samples, transformation structures in the [100] sample appeared predominantly on the sides of the notch and crack tip with stable crack propagation. In the [111] notched samples transformation occurred directly ahead of the notch and unstable crack propagation is observed. An available work criterion is used to predict the location of the transformation, with good agreement to the experimental observations. The different fracture behavior of the two notched sample orientations is explained utilizing the available work calculations.

11:05 AM

**NiTiHf High-Temperature Shape-Memory Alloys for near Term Applications:** *Glen Bigelow*<sup>1</sup>; *Sayed Saghaian*<sup>2</sup>; *Haluk Karaca*<sup>2</sup>; *Santo Padula*<sup>1</sup>; *Anita Garg*<sup>3</sup>; *Darrell Gaydosh*<sup>4</sup>; *Ronald Noebe*<sup>1</sup>; *Yuriy Chumlyakov*<sup>5</sup>; <sup>1</sup>NASA Glenn Research Center; <sup>2</sup>University of Kentucky; <sup>3</sup>University of Toledo; <sup>4</sup>Ohio Aerospace Institute; <sup>5</sup>Siberian Physical Technical Institute

Although high-temperature shape-memory alloys (HTSMA) with useful transformation temperatures above 150°C are highly desirable, there is a near-term need for alloys with transformation temperatures even slightly above what conventional binary NiTi alloys can provide. Such materials would find immediate on-wing and in-cabin applications in the aeronautics sector, and would be equally utilized in the automotive and other commercial sectors. Polycrystalline and single crystal ([001], [-340], and [678] orientations) Ni<sub>50.3</sub>Ti<sub>29.7</sub>Hf<sub>20</sub> with an MF ~130°C was investigated using isothermal compression tests in the martensite and austenite states and load-biased thermal cycling to determine its viability in the aforementioned applications. Unlike conventional SMA actuator materials, the NiTiHf alloy investigated here exhibited high work output, good dimensional stability, and varying amounts of superelasticity, without the need for complicated thermomechanical processing. Results of the polycrystalline and single crystal tests will be compared and reasons discussed for the inherent dimensional stability of the polycrystalline material.

11:20 AM

**Thermo-Mechanical Behavior of Cu-Al-Ni SMA for High Temperature Actuators:** *Jose San Juan*<sup>1</sup>; *Iñaki Lopez-Ferreño*<sup>1</sup>; *Tomasz Breczewski*<sup>1</sup>; *Isabel Ruiz-Larrea*<sup>1</sup>; *Angel López-Echarri*<sup>1</sup>; *María N6*<sup>1</sup>; <sup>1</sup>Universidad del Pais Vasco

Among the different families of shape memory alloys, Cu-Al-Ni alloys are firm candidates to be used in the temperature range between 100°C to 200°C as SMA actuators. In the present work we have studied the thermo-mechanical properties of several alloys exhibiting the martensitic transformation in such temperature range 100°C-200°C. Both, superelastic and shape memory effects have been characterized, as well as the evolution of the transformation behavior with thermal treatments and transformation cycling. The thermal transformation behavior under stress has been also studied in order to obtain a precise determination of the Clausius-Clapeyron stress line, and the shape recovery under stress. Finally we discuss the microstructural design of Cu-Al-Ni SMA and the different measured properties, in terms of their capability to be used in real high temperature actuators.

11:35 AM

**Microstructure Analysis and Thermomechanical Behaviour during Superelastic Cycling in Cu-Al-Ni Single Crystals:** *Maria N6*<sup>1</sup>; *A. Ibarra*<sup>1</sup>; *A. López-Echarri*<sup>1</sup>; *I. Ruiz-Larrea*<sup>1</sup>; *D. Caillard*<sup>2</sup>; *J. San Juan*<sup>2</sup>; <sup>1</sup>Universidad del Pais Vasco; <sup>2</sup>CEMES-CNRS

The aim of this work is to establish the relationship between the macroscopic behaviour during tensile superelastic cycling in Cu-Al-Ni shape memory alloy single crystals and the evolution of the microstructure. The analysis has been carried out as a function of the temperature, the maximum reached deformation and the number of cycles. Tensile superelastic cycles were performed in two samples with different compositions, which themally transform to different kinds of martensite. A calorimetric study and a TEM (post mortem and in situ) analysis were carried out on these superelastic cycled samples in order to determine the evolution of thermal transformation. Finally the results obtained by tensile superelastic cycling are discussed and compared with the previously obtained results on the same single crystal alloys by compression superelastic tests.

11:50 AM

**Superelastic Phenomena and Martensite Destabilization in Ni-Mn-Ga Alloys:** *Volodymyr Chernenko*<sup>1</sup>; *E. Villa*<sup>2</sup>; *S. Besseghini*<sup>3</sup>; *J.M. Barandiaran*<sup>4</sup>; *V. A. L'vov*<sup>5</sup>; <sup>1</sup>Universidad del Pais Vasco UPV/EHU - and - Ikerbasque, Basque Foundation for Science; <sup>2</sup>CNR-IENI, C.Promessi Sposi; <sup>3</sup>CNR-IENI, C. Promessi Sposi; <sup>4</sup>Universidad del Pais Vasco; <sup>5</sup>Institute of Magnetism

Thermomechanical properties of two Ni-Mn-Ga single crystalline alloys with MT temperatures of 310 K (A1) and 620 K (A2) are studied. DMA Q800 analyzer made it possible to register, from the same sample, temperature dependencies of elastic modulus in the dynamic tensile mode, stress versus strain curves at constant temperatures, and strain versus temperature curves at zero stress in static tensile mode. A multistep superelasticity of about 10% and one-step superelasticity of about 7% have been found in alloys A1 and A2, respectively. The stress - temperature phase diagrams of MTs are constructed. The stress-strain curves for alloy A2 demonstrate the gradual elevation of plateau as a result of mechanical cycling through MT. Theoretical estimations showed that this effect may be due to a decrease of MT temperature caused by the mechanical cycling. In correspondence to the commonly used terminology this effect should be referred to as martensite destabilization.

## Polycrystal Modelling with Experimental Integration: A Symposium Honoring Carlos Tome: Emerging Polycrystal Models with Experimental Integration I

*Sponsored by:* The Minerals, Metals and Materials Society, TMS Structural Materials Division, TMS Materials Processing and Manufacturing Division, ASM-MSCTS: Texture and Anisotropy Committee, TMS/ASM: Mechanical Behavior of Materials Committee, TMS/ASM: Computational Materials Science and Engineering Committee  
*Program Organizers:* Ricardo Lebensohn, Los Alamos National Laboratory; Sean Agnew, University of Virginia; Mark Daymond, Queens's University

Monday AM  
February 28, 2011

Room: 6C  
Location: San Diego Conv. Ctr

*Session Chairs:* Ricardo Lebensohn, Los Alamos National Laboratory; Alain Molinari, Universite Paul Verlaine - Metz; Grethe Winther, RISOE National Laboratory

8:30 AM Introductory Comments

8:40 AM Keynote

**Modeling of Polycrystal Plasticity: A Personal Overview of Past, Present and Future:** *Carlos Tome*<sup>1</sup>; <sup>1</sup>Los Alamos National Laboratory

In this talk I review, from my personal experience, the advances made in the last 25 years in the areas of crystal and polycrystal plasticity. I will

MONDAY AM

emphasize how advances in experimental methods and in computational capabilities have motivated and accompanied the development of increasingly sophisticated models and increasingly physically-based constitutive descriptions. The temporal line of research spans from simple Taylor models of aggregates in the past, to sophisticated polycrystal models that account for microstructural evolution (dislocations, twins, grain size, grain boundaries) in the present, and ambitious, but at the moment incipient, scale-linking approaches in the future. The theoretical developments have been aided by phenomenal advances on material characterization techniques, such as automated EBSD, FIB sectioning, X-ray and neutron diffraction, in-situ TEM.

#### 9:25 AM Invited

**First Evaluation of ALAMEL - Predictions of Texture-Induced Plastic Anisotropy:** *Paul Van Houtte*<sup>1</sup>; *Jurij Sidor*<sup>2</sup>; *Xie Qingge*<sup>1</sup>; *Laurent Delannay*<sup>3</sup>; *Bert Van Bael*<sup>1</sup>; *Leo Kestens*<sup>2</sup>; <sup>1</sup>Katholieke Universiteit Leuven; <sup>2</sup>Ghent University; <sup>3</sup>Université Catholique de Louvain

Texture-induced plastic anisotropy is usually assessed by means of mechanical testing, for example by measuring  $r$ -values. It can also be predicted by a multi-scale model for the plastic deformation of polycrystalline materials. Before using such virtual test data to identify an anisotropic constitutive law to be implemented in FE simulations of metal forming processes, it is recommended to make a serious assessment of the multi-scale model used. Best known model for this application is the Taylor model, experimental validation having been published. However, several other, more advanced models exist which could also be used. One of these is the ALAMEL model, known to be successful in the prediction of deformation textures. So far, no systematic experimental validations of plastic anisotropy modeling using ALAMEL have been published. In this paper, a first series of such results will be given, as well as comparisons with the results of some other models.

#### 9:50 AM

**Microstructural Influences on the Local and Global Deformation of TiAl Polycrystal Investigated by Experiments and Numerical Multi-Scale Approach Incorporating Crystal Plasticity FE Model:** *Mohammad Rizviul Kabir*<sup>1</sup>; *Liudmila Chernova*<sup>1</sup>; *Marion Bartsch*<sup>1</sup>; <sup>1</sup>German Aerospace Center (DLR)

The influences of the microstructural heterogeneity on the local and global mechanical behavior of a TiAl polycrystal have been investigated with experiments and numerical modeling. Two types of microstructure, duplex and near-lamellar, which are classified according to the presence of globular grains (consists of  $\gamma$ 947-phases) and lamellar colonies (consists of  $\gamma$ 945<sub>2</sub>+ $\gamma$ 947-phases), have been studied. The representative microstructures were calculated from SEM and TEM analysis and were incorporated in a two-scale FE model. The micromechanics of deformation of the phases are described in a crystal plasticity FE model. With this polycrystal modeling approach microstructure dependent alloy properties were reliably predicted, with focus on the influence of the microstructural heterogeneity on the elastic properties at grain scale, anisotropic dependency of the material yield and contribution of dislocation-slip of the phases to the plastic deformation at local and global scale.

#### 10:10 AM Break

#### 10:20 AM Invited

**Elastic Viscoplastic Heterogeneous Materials: From the Inclusion Problem to Homogenization Schemes:** *Alain Molinari*<sup>1</sup>; *Sébastien Mercier*<sup>1</sup>; <sup>1</sup>Université Paul Verlaine-Metz

Micro-macro transition schemes contain two important steps. First, the localization process must link the fields inside the inclusion to those applied at the remote boundary. Secondly, an averaging process is used to derive the macroscopic behaviour. Molinari et al. (1987) have developed the tangent model where the non-linear viscoplastic behavior of the material is approximated by a first order Taylor expansion at the overall strain rate. This model is dedicated to rigid viscoplastic material. To account for elasticity, a simple interaction law has been proposed based on the tangent approximation

of the non-linear Eshelby problem. This interaction law has been validated using Finite Element calculations and is used to develop Mori-Tanaka and self consistent schemes, Mercier and Molinari, (2009). Applications are shown for cyclic loading of composite materials.

#### 10:45 AM Invited

**On New Intermediate Modeling for the Large Viscoplastic and Elastic-Viscoplastic Deformation Behavior of Polycrystals: The Intermediate Phi-Model:** *Said Ahzi*<sup>1</sup>; *Siham M'Guil*<sup>1</sup>; <sup>1</sup>University of Strasbourg

In a first part of the presentation, we discuss the problem of homogenization of polycrystalline metals. Then, we present the new homogenization technique leading the formulation of the viscoplastic intermediate phi-model for crystal plasticity. With the phi-model, as in the self-consistent approach, a non-linear interactions law is derived but without the call for the Eshelby tensor. Thus, the phi-model takes into account the grain interactions with the homogeneous equivalent medium but without explicit shape effects. In a second part of the presentation, we present the extension of the phi-model to large elastic-viscoplastic deformation. Finally, we compare the results predicted from our new modeling, in terms of stress-strain response, textures, slip activity, ..., to those of the viscoplastic self-consistent model as well as to the experimental results.

#### 11:10 AM Invited

**Insights into Microstructure Evolution Using Crystal Plasticity Modelling:** *Matthew Barnett*<sup>1</sup>; <sup>1</sup>Deakin University

Crystal plasticity ignores certain mechanisms of microstructure evolution. However, it can shed important light on the operation of these very mechanisms. The present talk examines four attempts to use crystal plasticity models in this manner. Taylor type modelling is employed to examine the generation of high angle boundaries in shear. Self consistent type modelling is employed to reveal the abnormal formation of secondary twins, the possible role of grain boundary sliding and the formation of dynamically recrystallized grains. Although these uses of the models push the limits of what they were designed to achieve, important insight can be gained into how new structures are generated during plastic deformation.

#### 11:35 AM Invited

**Effects of Crystallographic Orientation vs. Grain Interaction on Slip Systems:** *Grethe Winther*<sup>1</sup>; <sup>1</sup>Risø DTU

When studying the deformation behaviour of individual grains both the overall rotation of the crystallographic grain orientation and the subdivision of grains are of interest. Often grains of similar orientations are compared to study the effect of grain orientation vs. grain interaction. Such investigations reveal both similarities and differences. The present contribution gives an overview of a series of investigations, including transmission electron microscopy as well as three-dimensional x-ray diffraction on polycrystalline aluminium deformed to strains of 5-50%. The data are analysed focusing on the set of activated slip systems, more precisely whether the observed differences can be attributed to fluctuations in the relative activities of the same set of systems or whether activation of truly different systems is the origin of the variations between and within grains.

#### 12:00 PM

**VPSC Modelling in the Development of a Commercial Product:** *Dincer Bozkaya*<sup>1</sup>; *Peter Jepson*<sup>1</sup>; <sup>1</sup>H.C. Starck Inc.

Texture Control is very important for planar sputtering targets, since the sputtering rate of a grain depends on its orientation. When tantalum is rolled to plate using conventional methods, the texture developed at mid-thickness is different from that developed near the surface because of differences in shear strain. At H.C. Starck, we used an FEM code and VPSC together to create models and thereby speed up the development of a product with no through-thickness texture gradient. The development of the new rolling process will be described, with emphasis on how VPSC was used and its usefulness.

12:20 PM

**Modelling of Texture and Microstructure Evolution during Dynamic Recrystallization:** *Denis Solas*<sup>1</sup>; Julien Thebault<sup>2</sup>; Julien de Jaeger<sup>2</sup>; Colette Rey<sup>2</sup>; Thierry Baudin<sup>1</sup>; <sup>1</sup>Univ Paris Sud; <sup>2</sup>Ecole Centrale Paris

The changes in texture and microstructure during thermomechanical process are related to crystal plasticity and annealing phenomena. Numerical studies has been carried out in which a crystalline plasticity modelling implemented in the finite element code Abaqus® coupled to a recrystallization Cellular automaton code. A sequential approach is used to simulate hot forging of a nickel based superalloy. Modelling is performed on aggregates built up from EBSD maps. Each grain is decomposed into smaller domains. In particular, the deformation model predicts intragranular deformation in terms of misorientations between elements and local variations in stored energy. A cellular Automaton algorithm is used for simulating nucleation and grain boundary migration. The parameters used for the sequential modelling were identified using an inverse method from experimental results. This numerical and experimental approach is used to understand the experimental observations and it improves our knowledge of the recrystallization process.

12:40 PM

**A Physically-Based Fatigue Model for Prediction of Crack Initiation from Persistent Slip Bands in Polycrystals:** *Huseyin Sehitoglu*<sup>1</sup>; Michael Sangid<sup>1</sup>; <sup>1</sup>University of Illinois

A model is constructed for prediction of fatigue crack initiation based on the material's microstructure. Our approach is to model the energy of a persistent slip band (PSB) structure and use its stability with respect to dislocation motion as our failure criterion for fatigue crack initiation. The components that contribute to the energy of the PSB are identified, namely, the stress field resulting from the applied external forces, dislocation pile-ups, and work-hardening of the material is calculated at the continuum scale. Further, energies for dislocations creating slip in the matrix/precipitates, interacting with the GBs, and nucleating/agglomerating within the PSB are computed via atomistics. The predicted fatigue life is driven by the microstructure such as grain orientations, widely distributed grain sizes, precipitates, PSB-GB interactions, as well as the effect of neighboring grains. Good agreement is shown between the model predictions and experimental data.

**Recent Developments in the Processing, Characterization, Properties and Performance of Metal Matrix Composites: General and Nano-Composites**

*Sponsored by:* The Minerals, Metals and Materials Society  
*Program Organizers:* Martin Pech-Canul, Centro de Investigacion y de Estudios Avanzados del Instituto Politecnico Nacional; Zariff Chaudhury, Arkansas State University; Golam Newaz, Wayne State University

Monday AM  
February 28, 2011

Room: 6A  
Location: San Diego Conv. Ctr

*Session Chair:* Zariff Chaudhury, Arkansas State University

8:30 AM

**Al/Al-Cu-Fe Metal Matrix Composites:** *Guillaume Laplanche*<sup>1</sup>; Joël Bonneville<sup>1</sup>; Anne Joulain<sup>1</sup>; Véronique Brunet-Gauthier<sup>1</sup>; Sylvain Dubois<sup>1</sup>; <sup>1</sup>University of Poitiers

The mechanical properties of icosahedral quasicrystalline (i-QC) Al-Cu-Fe alloys make them very attractive as reinforcement particles for metallic matrix composites (MMC). Al-base composites reinforced by i-QC Al-Cu-Fe particles have been synthesised since nearly two decades, but their mechanical properties are still poorly known. In this work, Al/Al-Cu-Fe MMCs were produced at two temperatures, i.e. T=673K and T=873K, by hot isostatic pressing. Crystallographic and chemical composition investigations were performed on the as-synthesised MMCs for identifying the resulting phases.

At T=673K, the reinforcement particles are still of the original i-QC phase, whereas at T=873K a phase transformation occurs for the reinforcement particles, which have the ω-Al-Cu-Fe tetragonal crystalline structure. The flow stress of both composites is strongly temperature dependent, suggesting that thermally activated processes control plastic flow. Transmission electron microscopy observations suggest that micro- and nano-particles play different roles in the strengthening of the two composites.

8:50 AM

**Copper Matrix Composites Reinforced with a High Fraction of Alumina Particles:** *Carmen Krueger*<sup>1</sup>; Andreas Mortensen<sup>1</sup>; <sup>1</sup>EPFL STI IMX LMM

The aim of this project is to explore the production of copper-based composites containing a high volume fraction of ceramic particles. Alumina is chosen as ceramic reinforcement phase due to its high Young's modulus, low density, chemical compatibility with copper and high availability, in combination with matrices of aluminum bronze. Two processing routes are explored, namely (i) pressure infiltration, and (ii) in-situ reaction, the latter being based on the thermic reduction of copper-oxides by aluminum. Success in the former method is shown to hinge on control of the structure and evolution of the metal/ceramic interface, while the latter is tributary to the rates of competing interdiffusion phenomena, as often found with in-situ composite production methods.

9:10 AM

**Low Density Magnesium Matrix Syntactic Foams:** *John DeFouw*<sup>1</sup>; Pradeep Rohatgi<sup>1</sup>; <sup>1</sup>University of Wisconsin Milwaukee

Low density magnesium matrix syntactic foams were synthesized through pressure infiltration of a packed bed of hollow carbon spheres with liquid magnesium of both pure and alloy (AZ91) compositions. Through varying the applied gas pressure for infiltration, the resulting composites varied in density as low pressures resulted in incomplete infiltration of regions between spheres and higher pressures resulted in infiltration into sphere interiors through cracks or small pores producing higher densities, ranging from 0.7 to 1.1 g cm<sup>-3</sup> (40-60% relative density). The foams were studied under mechanical compression with modulus, strength, and energy absorption described in relation to foam density and heat treatment as well as microstructural observations of metal matrix fraction, hollow sphere porosity, incomplete infiltration porosity, and carbide formation.

9:30 AM

**Metal Matrix Composites: History, Status, and Future:** *Ajith Cyriac*<sup>1</sup>; Jay Hanan<sup>1</sup>; <sup>1</sup>Oklahoma State University

A study of the history, status, and opportunities of Metal Matrix Composites is presented by evaluating the progression of available literature. The trends that existed and issues that still prevail are discussed and a prediction of the future for MMCs is presented. In many developed countries and in several developing countries there exists continued interest in MMCs. Researchers tried numerous combinations of matrices and reinforcements since work on MMCs began in the 1950s. This led to developments for aerospace, but resultant commercial applications were limited. The introduction of ceramic whiskers as reinforcement and the development of in-situ eutectics in the 1960s aided high temperature applications in aircraft engines. In the late 1970s the automobile industries started to take MMCs seriously. In the last 20 years, MMCs evolved from laboratories to a class of materials with numerous applications and commercial markets. A summary histogram depicting the progression is presented.

9:50 AM

**Processing, Characterization and Thermal Properties of Diamond-Containing Metal Matrix Composites:** *Vikas Sinha*<sup>1</sup>; Sabyasachi Ganguli<sup>1</sup>; Robert Wheeler<sup>1</sup>; Jonathan Spowart<sup>1</sup>; <sup>1</sup>Air Force Research Laboratory

An ideal substrate/ packaging material for high power density electronic component should have a very high thermal conductivity and a coefficient of thermal expansion (CTE) comparable to the electronic component. Diamond-containing Ag-matrix and Cu-matrix composites potentially can be excellent solutions for thermal management. In the current research, diamond-containing Ag-matrix and Cu-matrix composites were fabricated

MONDAY AM



via spark-plasma-sintering or liquid-metal-infiltration techniques. Cu was pre-alloyed with Cr or B, whereas Ag was pre-alloyed with Si. The effects of different micro-alloying elements on thermal properties were compared. Thermal conductivity of composites was modeled to estimate thermal conductance for metal/diamond interfaces for different material and processing conditions. The CTE of composites were compared with model predictions. Prior studies indicate that the interface chemistry has a strong influence on thermal properties. The chemistry changes near the metal/diamond interfaces were examined via High-Resolution Transmission Electron Microscopy (HRTEM), using energy dispersive spectroscopy and energy-filtering techniques.

#### 10:10 AM Break

#### 10:30 AM

**Use of Cenosphere for Making Functionally Graded Aluminum Cenosphere Syntactic Foam through Liquid Metallurgy Route:** *Dehi Mondal*<sup>1</sup>; Satyabrata Das<sup>1</sup>; <sup>1</sup>Advanced Materials and Processes Research Institute

Attempts have been made to make functionally graded aluminum cenosphere syntactic foam wherein volume fraction of cenosphere varies along the thickness of the casting. Cenosphere has been used to make such microporous materials. The sample from different depths were examined for cenosphere volume fraction, density, hardness and compressive stress-strain curves and these properties are varying along the depth. The thickness of the layer corresponding to particular average cenosphere content and the average volume fraction of cenosphere in each layer was found to be strong function of processing parameters like melt temperature, cooling rate, number of heating and cooling cycles. As the frequency of heating and cooling cycles increases, the volume fraction of cenosphere at top most surface increases. Through this process, thus a bulk dense material with functionally graded microporous syntactic foam on one side could be made where a strong bonding between the foam and bulk material will exist.

#### 10:50 AM

**Micro-Tomography Based Characterization and Geometrical Parameter Evaluation of Advanced Woven Ceramic-Matrix Composites:** *Hrishikesh Bale*<sup>1</sup>; David Marshall<sup>2</sup>; Brian Cox<sup>2</sup>; Robert Ritchie<sup>1</sup>; <sup>1</sup>University of California Berkeley; <sup>2</sup>Teledyne Scientific LLC

Structural components operating under extreme environments (>1200°C) demand the use of a new class of advanced materials. Environments typically experienced in rocket engines, hypersonic flow paths and thermal protection systems are beyond the realm of current structural materials. However, woven ceramic-matrix composites (CMC's) incorporating textile manufacturing techniques utilizing 3-D architectures makes the development of such structures feasible. Lifetime prediction within CMC's is non-trivial though; microscopic flaws within fibres and matrix can be governing factors controlling the ultimate performance of these materials in service. Synchrotron micro-tomography was utilized to evaluate CMC's in 3-D with ~1-µm resolution. The use of micro-tomography in evaluating the otherwise difficult-to-measure structural parameters such as 3-D tow spacing, orientation, cross section and matrix porosity in SiC/SiC CMC's is demonstrated which facilitates the understanding of damage and failure. This would further lead in developing comprehensive and accurate constitutive laws for computational models.

#### 11:10 AM

**Synthesis and Characterization of Hot Extruded Al-15wt%Mg2Si In-Situ Composite:** *Ashkan Zolriasatein*<sup>1</sup>; *Masoud Emamy*<sup>2</sup>; *Amin Bahrami*<sup>3</sup>; *Hamid Reza Jafari Nodooshan*<sup>4</sup>; *Ali Shokuhfar*<sup>4</sup>; <sup>1</sup>K. N. Toosi University of Technology; <sup>2</sup>Tehran University; <sup>3</sup>Imam Khomeini International University; <sup>4</sup>Islamic Azad University

This study investigates the hot extrusion of Al-15wt%Mg2Si in-situ composite at various extrusion ratios (6:1, 12:1, and 18:1) to determine the relationship between the process parameters, microstructure and the properties of the extruded composite. Microstructure of the composite after this type of extrusion was studied by optical microscopy. Mechanical

properties of the composite after various extrusions were tested by hardness and tensile tests. These results indicate that extrusion leads to reduction of porosity and particle fracture. With the increase of the extrusion ratio at a relatively low temperature, the microstructure of the extruded samples becomes finer and more uniform, and higher mechanical properties can be brought for the as-extruded samples in comparison with as-cast samples.

#### 11:30 AM

**Thermal Conductivity and Interfacial Nanostructure in Diamond Based Composites:** *F. Khalid*<sup>1</sup>; <sup>1</sup>GIK Institute of Engineering Sciences and Technology

Processing parameters is critical in achieving the interfacial nanostructure of Al/diamond and Cu/diamond composite materials. These composites are produced by sintering and pressurised liquid metal infiltration have the potential for thermal management Applications. Attempts have been made to develop new composites to improve thermal conductivity. In this work it is demonstrated that thermal conductivity of diamond based composites can be achieved up to 700 Wm/K. It is illustrated that the liquid metal infiltration is better production route for Al-diamond and Cu/diamond composites. The examination of the interfacial nanostructure of the composite samples by using advanced analytical techniques is carried out. Emphasis is also placed on the understanding of preferential interfacial bonding between matrix and diamond (100) and (111) surfaces. The formation of Al<sub>4</sub>C<sub>3</sub> particles at the interface between Al and diamond particles was found that indicated a greater level of stability and bond strength between the diamond particles and matrix.

---

### Size Effects in Mechanical Behavior: Size Dependent Mechanical Behavior of Nanotwinned and Nanocrystalline Metals

*Sponsored by:* The Minerals, Metals and Materials Society, Not Applicable, TMS: Nanomechanical Materials Behavior Committee  
*Program Organizers:* Erica Lilleodden, GKSS Research Center; Amit Misra, Los Alamos National Laboratory; Thomas Buchheit, Sandia National Laboratories; Andrew Minor, UC Berkeley & LBL

Monday AM  
February 28, 2011

Room: 2  
Location: San Diego Conv. Ctr

*Session Chairs:* Erica Lilleodden, GKSS Research Center; Dominique Schryvers, University of Antwerp

---

#### 8:30 AM

**Study of Twins in Nanoscale Pd Films with High Strain Hardening Capacity:** *Dominique Schryvers*<sup>1</sup>; *Hosni Idrissi*<sup>1</sup>; *Binjie Wang*<sup>1</sup>; *Marie-Stéphane Colla*<sup>2</sup>; *Jean-Pierre Raskin*<sup>2</sup>; *Thomas Pardoen*<sup>2</sup>; <sup>1</sup>University of Antwerp; <sup>2</sup>Université Catholique de Louvain

Nanocrystalline metallic films often suffer from a lack of ductility due to poor strain hardening capacity. Nanograin Pd thin films (80 - 310 nm film thickness) with very large strain hardening when deformed by on-chip nanomechanical tensile testing have been produced by low pressure chemical vapour deposition and photolithography. TEM and HRTEM reveal the presence of a few coherent growth twins in more than 20% of the grains, offering additional barriers to dislocation motion, as well as sources for dislocation storage and multiplication. The twin boundaries become incoherent after a few percent of plastic deformation. The related dislocation/twin boundary reactions explain part of the high strain hardening capacity, the remaining resulting from microstructure heterogeneities with softer and harder grains, leading to a long elastoplastic transition. These two aspects constitute the main ingredients of a multigrain homogenization model which provides a rationale for the evolution of the strain hardening capacity.

### 8:50 AM

**Effects of Differently Oriented Twin Boundaries on Mechanical Properties in Nanotwinned Ag Films:** Daniel Bufford<sup>1</sup>; Xinghang Zhang<sup>1</sup>; Haiyan Wang<sup>1</sup>; <sup>1</sup>Texas A&M University

Epitaxial nanotwinned Ag (111) and Ag (110) films were deposited by magnetron sputtering. Although both films were deposited with similar deposition parameters, the twin boundary spacing is 9 nm in Ag (111) and 42 nm in Ag (110). Twin boundaries in the Ag (111) films are oriented normal to the growth direction and at an angle in the Ag (110) films. The fine twins greatly enhance the indentation hardness of both films, and there is a factor of two differences in hardness between the (111) and (110) Ag films. The mechanisms for twin formation and the influences of twin boundary orientation on mechanical deformation will be discussed.

### 9:10 AM Invited

**Inverse Grain-Size Effect on Twinning in Nanocrystalline FCC Metals:** Yuntian Zhu<sup>1</sup>; Xiaolei Wu<sup>2</sup>; <sup>1</sup>North Carolina State University; <sup>2</sup>Chinese Academy of Sciences

A long-standing controversy exists between molecular dynamics (MD) simulations and experiments on the twinning propensity of nanocrystalline (nc) face-centered-cubic metals. For example, three-dimensional MD simulations rarely observed twins in nc Ni, whereas experiments readily observed them. Here this discrepancy is resolved by experimental observation of an inverse grain-size effect on twinning. Specifically, decreasing the grain size first promotes twinning in nc Ni and then hinders twinning due to the inverse grain-size effect. Interestingly, no inverse grain-size effect exists on stacking fault formation. These observations are explained by generalized planar fault energies and grain-size effect on partial emissions.

### 9:40 AM

**A Twist of the Eshelby Twist: Unraveling the Mystery of Twinning:** Ting Zhu<sup>1</sup>; Ju Li<sup>2</sup>; Sankar Narayanan<sup>1</sup>; <sup>1</sup>Georgia Institute of Technology; <sup>2</sup>University of Pennsylvania

The principal difficulty in understanding the deformation mechanisms of small-volume crystals has been to explain how the plastic deformation carriers such as dislocations and twins are generated and multiplied. The sources of such carriers and associated triggering processes have not been well established. In 1953 Eshelby showed that the central region of a rod can act as a trap to stabilize the screw dislocation that, in turn, induces the torsional deformation of the rod. While studying this so-called Eshelby twist effect, we incidentally discovered a twinning mechanism in fcc Cu. We found that the axial screw can initiate the regenerative twinning through a 3D process of dislocation intersection followed by spiral gliding of a sweeping dislocation around the pole. Our work is the first atomistic realization of 3D twinning, and it opens up the possibilities of studying the experimentally relevant twinning mechanisms for a wide range of materials and applications.

### 10:00 AM Break

### 10:30 AM

**Detwinning Mechanisms for Growth Twins in Epitaxial Nanotwinned Cu:** Nan Li<sup>1</sup>; Jian Wang<sup>1</sup>; Xinghang Zhang<sup>2</sup>; Jianyu Huang<sup>3</sup>; Amit Misra<sup>1</sup>; <sup>1</sup>Los Alamos National Laboratory; <sup>2</sup>Texas A&M University; <sup>3</sup>Sandia National Laboratory

Using in situ nanoindentation in a transmission electron microscope (TEM), we have studied the migration mechanisms of S3 {112} incoherent twin boundary (ITB) in epitaxial nanotwinned Cu films. ITB's migrate via the collective glide of multiple twinning dislocations that form an ITB and the propagation steps or disconnections are with heights of three or multiples of three {111} interplanar distances. The migration may lead to de-twinning process of nanotwins in face-centered cubic metals. The transmission of a glide dislocation across an ITB is shown to form a sessile dislocation in the ITB and locally pin the boundary at the site of the slip transmission.

### 10:50 AM Invited

**Deformation Effects in Cu with Highly Aligned Nanotwins:** Julia Weertman<sup>1</sup>; Carla Shute<sup>1</sup>; <sup>1</sup>Northwestern University

Nanotwinned metals have been found, by the work of K. Lu, S. Suresh, and others, to be very strong, with stable microstructures and possessed of moderate ductility. The present research examines the effect of various forms of deformation on the internal structure, damage and crack nucleation in Cu with highly aligned columns of nanotwins. It is found that surface fatigue cracks form at the intersection of regions where there is incompatibility in the deformation process, e.g. between a nanotwinned and de-nanotwinned region. High densities of dislocations form in such places. The median spacing of nanotwin boundaries in the samples is unchanged by fatigue, except in the close vicinity of cracks, where there is a substantial increase. TB spacing under extreme compression decreases in the amount expected from the negative strain. HPT experiments indicate the limit of stability of the nanotwins under shear strain.

### 11:20 AM

**Fatigue Properties of Nano Structured Copper:** Aparna Singh<sup>1</sup>; Lei Lu<sup>2</sup>; Ming Dao<sup>1</sup>; <sup>1</sup>MIT; <sup>2</sup>Chinese Academy of Sciences

Nano twinned materials exhibit a combination of both high strength and ductility unlike nano grained materials. However, their properties under cyclic loading have not been explored as yet. In this presentation, we outline our results of fatigue studies done on nano twinned materials, and the observations are compared with those for nano grained materials in order to get conclusions on the role of micro structural size scale in influencing the damage tolerance characteristics of metals. General strategies for improving strength, ductility, damage resistance and tolerance will be presented.

### 11:40 AM

**Tensile Plastic Deformation of Gradient Nano-Grained Copper:** W. L. Li<sup>1</sup>; N. R. Tao<sup>1</sup>; K. Lu<sup>1</sup>; <sup>1</sup>Chinese Academy of Sciences

Nanocrystalline or nano-grained metals are strong, but brittle. Experimental identification of plastic deformation mechanisms of nano-grained structures is challenging, indeed, because tensile plastic strain cannot be sustained in nano-grained samples which has basically no work-hardening. In this work, we prepared a unique sample for experimental study on the plastic deformation of nano-grained metals: a gradient nano-micro-grained (GN) surface layer on a bulk Cu specimen. The GN layer is produced by means of surface mechanical grinding treatment (SMGT) at cryogenic temperature. The GN samples exhibit a considerable plastic strain above 30% in tension, indicating that the nano-grained structure can be plastically deformed with a substantial tensile strain. Systematic structure characterization revealed that plastic deformation of the nano-grained structure is localized and accompanied with stress-induced grain growth. Discussions will be made on accommodation capability of plastic deformation in the GN structure in comparison with that of the polycrystalline coarse-grained structure.

## Surfaces and Heterostructures at Nano- or Micro-Scale and Their Characterization, Properties, and Applications: Growth, Characterization, and Devices I

*Sponsored by:* TMS Electronic, Magnetic, and Photonic Materials Division, TMS Materials Processing and Manufacturing Division, TMS: Nanomaterials Committee, TMS: Surface Engineering Committee

*Program Organizers:* Nitin Chopra, The University of Alabama; Ramana Reddy, The University of Alabama; Jiyoung Kim, Univ of Texas; Arvind Agarwal, Florida International Univ; Sandip Harimkar, Oklahoma State University

Monday AM                      Room: 31B  
February 28, 2011              Location: San Diego Conv. Ctr

*Session Chairs:* Nitin Chopra, The University of Alabama; Ritesh Agarwal, University of Pennsylvania

### 8:30 AM Introductory Comments

#### 8:35 AM Invited

#### Transforming Semiconductor Nanowires into Heterostructures and Superlattices by Size-Dependent Cation Exchange Reactions: *Ritesh Agarwal*<sup>1</sup>; <sup>1</sup>University of Pennsylvania

The unique properties of nanostructured materials enable their transformation into complex, kinetically-controlled morphologies which cannot be obtained otherwise. Solution-phase cation-exchange reactions can transform sub-10 nm nanocrystals/nanorods into varying compositions and superlattices; however, due to their small size, cation-exchange reaction rates are extremely fast which limits control over the transformed products. Nanowires are routinely synthesized via gas-phase reactions with 5-200 nm diameters and to realize their full potential, it is desirable to develop techniques which can transform nanowires into tunable morphologies. We report transformation of single-crystalline cadmium-sulfide nanowires into composition-controlled  $Zn_xCd_{(1-x)}S$  nanowires, core-shell heterostructures, metal-semiconductor superlattices, ZnS nanotubes, and metallic Zn nanowires by utilizing size-dependent cation-exchange reactions. Simulations that account for elastic interactions and diffusional kinetics reveal the conditions for forming these structures and the peculiarities of 1D systems. This versatile ability to transform nanowires offers new opportunities to study size-dependent phenomena and tune their chemical/physical properties to design reconfigurable circuits.

#### 9:05 AM Invited

#### Does Function Follow Form? Coiled Carbon Nanotube and Nanowire Structures- Thermodynamic Model, Experiment, and Applications: *Prabhakar Bandaru*<sup>1</sup>; Apparao Rao<sup>2</sup>; <sup>1</sup>University of California San Diego; <sup>2</sup>Clemson University

New paradigms in materials and devices lead to new technologies, which are necessary for continued scientific progress. We have determined, in foundational studies, that nonlinear nanostructures, such as carbon nanotube based helices and coils, may be synthesized through the use of specific catalysts in chemical vapor deposition and could open up new vistas in electrical, mechanical, and optical engineering, e.g. as electrical inductors, nanoscale mechanical springs, and metamaterials. First, a thermodynamic model based on exclusion volume principles common in chemical and biological systems that could potentially explain coiling in nanostructures, will be introduced. The crucial role of the interactions between specific catalyst particles, e.g. indium and tin, and the growing nanostructure for coil growth, which has been verified through experiment, will be elucidated. The talk will be concluded with a brief exposition on the unique applications of these structures, say in localized energy absorption and electromagnetic radiation coupling.

#### 9:35 AM Invited

#### Atom-by-Atom Characterization of Low-Dimensional Materials: *Stephen Pennycook*<sup>1</sup>; Matthew Chisholm<sup>1</sup>; Gerd Duscher<sup>2</sup>; Timothy Pennycook<sup>3</sup>; James McBride<sup>3</sup>; Sandra Rosenthal<sup>3</sup>; <sup>1</sup>Oak Ridge National Laboratory; <sup>2</sup>University of Tennessee; <sup>3</sup>Vanderbilt University

The aberration-corrected scanning transmission electron microscope offers a new level of sensitivity for revealing the origin of nanomaterials functionality through its ability to image and identify individual substitutional dopants and adatoms. Examples will be shown of O and C dopants in monolayer BN and of defects and adatoms in monolayer graphene. In the case of semiconducting nanocrystals, their size, shape and crystal termination can be identified with no lower size limit. Such images reveal the mechanisms behind the growth and luminescent properties of core/shell quantum dots and ultrasmall white light-emitting nanocrystals.

#### 10:05 AM Invited

#### Micro and Nanostructured Porous Heterostructures by Electrodeposition: *Martin Bakker*<sup>1</sup>; Nikolas Cordes<sup>1</sup>; Franchesca Saylor Maddox<sup>1</sup>; Jan-Henrik Smatt<sup>2</sup>; Mika Linden<sup>2</sup>; <sup>1</sup>The University of Alabama; <sup>2</sup>Ako Akademi University

Electrodeposition into insulating templates is an extremely powerful method of making metal/insulator heterostructures. With careful selection of the electrochemistry, electrodeposition can also be used to deposit the insulating templates. We will present recent work on 1) electrodeposition of mesoporous silica thin films, and electrodeposition of micrometer structured mesoporous silica on planar and three dimensional substrates, 2) electrodeposition of metal into electrodeposited mesoporous silica templates 3) the use of humidity to control the electrodeposition of metals into the mesoporous of hierarchically meso-microstructured porous silica monoliths.

#### 10:35 AM Break

#### 10:45 AM Invited

#### Synthesis and Characterization of Silicon Oxide Nanowires Using Nickel Nanoparticles: *Seonhee Jang*<sup>1</sup>; Youngil Lee<sup>1</sup>; Suhwan Cho<sup>1</sup>; Jungwook Seo<sup>1</sup>; Donghoon Kim<sup>1</sup>; <sup>1</sup>Samsung Electro-Mechanics

We attempt to produce silicon oxide nanowires (SiOxNWs) in a simple way without complicated deposition processes, gaseous Si containing precursors, or starting material of SiO<sub>2</sub>. Nickel (Ni) nanoparticles (NPs) were applied on Si wafer and thermally treated in a furnace. The temperature in the furnace was kept in the ranges between 900 and 1100 °C and a forming gas, i.e. mixture of nitrogen (N<sub>2</sub>) and hydrogen (H<sub>2</sub>) flowed through the furnace. The growth of SiOxNWs was obtained via carbothermal reduction of NiO. The SiOxNWs had widths ranging from 100 to 200 nm with length extending up to ~ 10 μm and their structure was amorphous. Ni NPs were acted as catalysts. Photoluminescence (PL) showed that blue emission spectrum was centered at the wavelength of 450 nm (2.76 eV). The details of growth mechanism of SiOxNWs and the effect of Ni NPs on the formation of SiOxNWs will be presented.

#### 11:15 AM

#### Novel Architectures of Hierarchical Heterostructures: Non-Catalytic Growth of ZnO Nanowires and Their Multifunctional Heterostructures with Gold Nanoparticles: *Wenwu Shi*<sup>1</sup>; Austin Starnes<sup>1</sup>; Nitin Chopra<sup>1</sup>; <sup>1</sup>The University of Alabama

Multi-functional heterostructures comprised of semiconducting nanowires and metal nanoparticles are of significance for optoelectronics and energy applications. Herein, for the first time, we report a simple and non-catalytic CVD process that produced branched ZnO nanowires (BZN). As a next step, gold nanoparticles were nucleated on the surface of BZN in a surfactant-free approach resulting in novel nanowire-nanoparticle heterostructures. Fundamental understanding of the heterostructures and their crystal structures, phases, interfaces, chemical functionality, composition, and thermal stability was developed using SEM, HR-TEM, XRD, DTA-TGA, FT-IR. The kinetics of heterostructure formation and their unique optical properties were studied in real-time. The growth mechanisms of BZN and their unique branched configuration have also been discussed here.



11:30 AM

**Induced Chemical Changes in Ni/NiO Core Shell-Carbon Nanotube Heterostructures in a High Temperature Post-Fabrication Treatment:** *Hylton McWhinney*<sup>1</sup>; *Wenwu Shi*<sup>2</sup>; *Nitin Chopra*<sup>2</sup>; <sup>1</sup>Texas A & M University; <sup>2</sup>The University of Alabama

High temperature surface migration of Ni/NiO core-shell nanoparticles (~5-10 nm) on the surface of carbon nanotubes (CNC Heterostructures, Shi, Krews, and Chopra, *Materials Technology*, 2010) was thoroughly studied. Heat treatments were carried out in a nitrogen-enriched furnace and the CNC heterostructures were carefully dispersed on a substrate. The samples were treated between 125 – 750 °C for 1 h. It was observed in SEM, TEM, and EDS analysis that nanoparticles significantly migrate on the CNT surfaces and their morphology was changed. In addition, massive agglomeration of nanoparticles was observed at higher annealing temperatures. XPS analysis of the heterostructures, as a function of their heat treatments, suggested that nanoparticle precursor solution, CNT surface, and annealing temperature played an important role in the morphological evolution of nanoparticles on CNTs. Shifts in the XPS elemental peaks revealed new critical information about the bonding characteristics of such heterostructures.

11:45 AM

**Nanoparticle Cluster Size Control using Chemically Modified Self-Assembly on Copolymer Surfaces:** *Sarah Adams*<sup>1</sup>; *Regina Ragan*<sup>1</sup>; <sup>1</sup>University of California Irvine

Organized clustering of metallic nanoparticles was examined for the development of field-enhanced chemical and biological detection devices, with the capacity to achieve single-molecule level detection resulting from surface enhanced Raman scattering, associated with closely-spaced noble metal nanostructures. Using chemical self-assembly techniques, we attached monodisperse, colloidal gold nanoparticles on self-organized polymer templates, patterning arrays of nanoparticle clusters with sub-10 nanometer interparticle spacing, to engineer enhanced optical fields. Poly(methyl methacrylate) domains in phase-separated polystyrene-*b*-poly(methyl methacrylate) diblock copolymer thin films were chemically modified with surface amination for controlled arrangements. Chemically synthesized sub-20 nanometer diameter gold nanoparticles were attached to the amine-functionalized surfaces using EDC crosslinking chemistry with thioctic acid ligand-bound to the nanoparticle surface, preferentially immobilizing the Au nanoparticles on PMMA domains of the copolymer template. By controlling particle size relative to PMMA domain size, nanoparticle clustering was controlled.

12:00 PM

**Thermodynamics and Processing of Nanomaterials:** *Ramana Reddy*<sup>1</sup>; <sup>1</sup>The University of Alabama

This presentation includes nanoscale materials thermodynamics and processing. Thermodynamic properties of nano-particles are different as compared to that of bulk material due to the surface energy changes. Melting temperature of nano-particles varies with the size (radius) of particles. This variation in melting temperature was calculated for different nanoscale materials. In-situ processing of nanomaterials has immense potential over the conventional nanoscale materials due to several advantages such as inherent chemical stability, lack of impurities, and fine dispersion. The results of thermal plasma production of nanoscale metal, ceramic and composite powders and the various process parameters that influence the final product were discussed.

12:15 PM

**Magnetron Sputtering of Thin Film MIM Capacitors with Al and Pt Electrodes:** *Jack Murray*<sup>1</sup>; *Wayne Huebner*<sup>1</sup>; *Matthew O'Keefe*<sup>1</sup>; <sup>1</sup>Missouri University of Science and Technology

The deposition of thin film metal-insulator-metal (MIM) capacitors for high frequency applications by magnetron sputtering was investigated. Pt-Al<sub>2</sub>O<sub>3</sub>-Pt and Al-Al<sub>2</sub>O<sub>3</sub>-Al with symmetric electrode areas were the material combinations tested in this study. All devices were deposited through a shadow mask under the same sputtering conditions resulting in a metal electrode thickness of ~160 nm and dielectric thickness of ~450 nm.

DC current-voltage measurements ( $E = 5 \text{ MV/cm}$ ) coupled with impedance analysis ( $\approx 15 \text{ MHz}$ ) was used to characterize the resulting devices. MIM structures with Pt electrodes exhibited a significantly lower resistivity and higher permittivity than devices with Al electrodes. These results indicate the formation of a space charge layer near the metal/insulator interface that depends on the electrode material.

---

## The Second Symposium on the Recycling of Electronic Wastes: Technologies for the Recycling of Electronic Wastes

*Sponsored by:* The Minerals, Metals and Materials Society, TMS Electronic, Magnetic, and Photonic Materials Division, TMS Extraction and Processing Division, TMS Light Metals Division, TMS: Electronic Packaging and Interconnection Materials Committee, TMS: Recycling and Environmental Technologies Committee  
*Program Organizers:* Lifeng Zhang, Missouri University of Science and Technology; Gregory Krumdick, Argonne National Laboratory; Jaan Kers, Tallinn University of Technology; Thomas P. Schuman, Missouri University of Science and Technology (Missouri S&T); Markus Reuter, Ausmelt Limited

Monday AM

February 28, 2011

Room: 15B

Location: San Diego Conv. Ctr

*Session Chairs:* Lifeng Zhang, Missouri S&T; Gregory Krumdick, Argonne National Lab.

---

8:30 AM **Introductory Comments**

8:35 AM

**Mechanical Recycling of Electronic Wastes for Materials Recovery:** *Viktor Laurmaa*<sup>1</sup>; *Jaan Kers*<sup>1</sup>; *Kaspar Tall*<sup>1</sup>; *Valdek Mikli*<sup>1</sup>; *Dmitri Goljandin*<sup>1</sup>; *Kristiina Vilsaar*<sup>1</sup>; *Priidu Peetsalu*<sup>1</sup>; *Mart Saarna*<sup>1</sup>; *Riho Tarbe*<sup>1</sup>; <sup>1</sup>Tallinn University of Technology

In this paper, the mechanical milling of the Printed Circuit Boards (PCB) was carried out. First goal of the work was to examine the management of the WEEE, in particular the re-use of PCB. Firstly, recycling methods of PCBs were summarized. During the study, mechanical separation methods (magnetic-, density- and air separation), electrical, and chemical methods were examined. Secondly, the optimal particle size for air-classification was determined. Several tests were carried out to find the most effective separation method for separation of different material groups from PCB scrap. The new air classification stand was developed for testing the separation of lightweight particles such as tin foil stripes and plastics. The test results showed sufficiently good separation of heavier Al and Cu. For milled materials characterization, the SA, IA, laser diffraction analysis and SEM were used. The chemical composition of the PCB powders was studied by means of energy dispersive X-ray microanalysis (EDS).

9:05 AM

**Processing of Discarded Liquid Crystal Display for Recovering Indium:** *Gjergj Dodbiba*<sup>1</sup>; *Kunihiko Takahashi*<sup>1</sup>; *Toyohisa Fujita*<sup>1</sup>; *N. Sato*<sup>2</sup>; *Seiji Matsuo*<sup>1</sup>; *Katsunori Okaya*<sup>1</sup>; <sup>1</sup>The University of Tokyo; <sup>2</sup>Tohoku University

Different materials are used for manufacturing various parts of a cellular phone. Considering that a great number of mobile phones are being discarded every year, it is important to recover these materials and then recycle them in order to save resources. The primary objective of this work is, therefore, to find and suggest ways on how to recover various materials from discarded cellular phones for recycling. Much effort, for example, has been put into recovering and recycling tin oxide (ITO), a mixture of indium(III) oxide, (In<sub>2</sub>O<sub>3</sub>) and tin(IV) oxide from the discarded LCDs. Here we report a simple and cost-effective process, which includes a HCl treatment process for altering the structure of the indium(III) compound into a chloride-induced indium compound, in order to facilitate the vaporization of indium at a relatively low temperature. The chloride-induced indium compound is then vaporized, condensed and recovered.

MONDAY AM

9:35 AM

**Green Pyrolysis of Used Printed Wiring Board Powders:** *Lucas Damoah*<sup>1</sup>; Xiangjun Zuo<sup>1</sup>; Lifeng Zhang<sup>1</sup>; Thomas Schuman<sup>1</sup>; <sup>1</sup>Missouri University of Science and Technology

Rapid technological innovation has propelled the use of electronic equipment leading to the generation of more and more waste electrical and electronic equipments (WEEE). Printed wire board (PWB) is a component made of one or more layers of insulating material with electrical conductors. Current technology for recycling PWBs uses pyrometallurgical or hydrometallurgical methods, which generate atmospheric pollution releasing dioxins and furans or high effluent volumes. To investigate an environmentally friendly process to recycle PWBs, 50g each of PWB samples with and without 10g of CaCO<sub>3</sub> additives were pyrolyzed in a tube furnace. Liquid, gas and solid products were realized with a PWB conversion fraction of 52.65 %. Analysis of the exhaust gases from the experiments using GCMS and MS showed that without CaCO<sub>3</sub> additives poisonous gases such as C<sub>6</sub>H<sub>6</sub> and HBr are produced which are adequately controlled when CaCO<sub>3</sub> is added. The exhaust gas was treated using concentrated NaOH solution.

10:05 AM

**Leaching of Lead from Solder Material Used in Electrical and Electronic Equipment:** *Manis Kumar Jha*<sup>1</sup>; Pankaj Choubey<sup>1</sup>; Archana Kumari<sup>1</sup>; Rakesh Kumar<sup>1</sup>; Vinay Kumar<sup>1</sup>; Jae-chun Lee<sup>2</sup>; <sup>1</sup>National Metallurgical Laboratory (CSIR); <sup>2</sup>Korea Institute of Geosciences & Mineral Resources

Present work is a part of developing novel recycling technique for waste printed circuit boards (PCBs), i.e. the liberation of metals from PCBs by organic swelling followed by the treatment of resin to remove/ recover hazardous soldering materials. In order to recover the hazardous metallic constituent lead from the liberated resin, initially the leaching studies were made using fresh solder containing 63.9% Pb and remaining tin. Experimental results obtained in different conditions viz. time, temperature and acidity showed ~97.20% of lead dissolution with 6M HNO<sub>3</sub> at solid to liquid (S:L) ratio 1:10 (g/mL) and temperature 90°C in 75 minutes. The result of the studies validated with crushed PCBs shows that almost total lead and tin was leached out with 6M HNO<sub>3</sub> and 6M HCl respectively at S:L ratio 1:10 (g/mL) and temperature 90°C within 50 minutes. The results will be useful for the treatment and safe disposal of PCBs resin.

10:35 AM Break

10:45 AM

**Copper Recovery from Printed Circuit Board of E-Waste:** *Toyohisa Fujita*<sup>1</sup>; Hiroyuki Ono<sup>1</sup>; Gjergj Dodbiba<sup>1</sup>; Seiji Matsuo<sup>1</sup>; Katsunori Okaya<sup>1</sup>; <sup>1</sup>The University of Tokyo

Here, we discuss the copper recovery from circuit boards. In an attempt to raise the copper grade of printed circuit boards (PCB), carbonization treatment was investigated. The crushed PCB without surface-mounted parts was carbonized under nitrogen atmosphere. After screening, the char was classified by size into oversized pieces, undersized pieces and powder. The copper foil and glass fiber pieces were liberated and collected in undersized fraction. The copper foil was liberated easily from glass fiber by a "stamping" treatment. Liberation rate of copper foil was high at high carbonized temperature. The experimental results indicated that 90% of oversized char was liberated and the copper foil recovery from PCB carbonized at 1073 K was 110 kg/t. The copper recovery from char powder by flotation was also investigated. Of the copper grade 15% and of the copper recovery 80% were obtained.

11:15 AM

**Recovery of Silver from Spent Plasma TV Monitors:** *Katsutoshi Inoue*<sup>1</sup>; Biplob Biswas<sup>2</sup>; Hidetaka Kawakita<sup>1</sup>; Keisuke Ohto<sup>1</sup>; Atsushi Hoshino<sup>2</sup>; <sup>1</sup>Saga University; <sup>2</sup>Nishinohon Kaden Recycle Corporation

The method of extraction of silver from scrap of plasma TV monitors using noncyanide reagents – sodium thiosulfate and acidothiourea – was investigated, which was followed by silver recovery from acidothiourea leach solutions. It was found that acidothiourea solution gave almost

complete extraction of silver while thiosulfate provided only 40% extraction. The rate of silver extraction using acidothiourea solution was found to be extremely fast. An increased dissolution rate was also found at elevated temperature. The recovery of silver through coagulation-precipitation from acidothiourea leach solutions was carried out with a natural biodegradable material, persimmon tannin extract. It was proved to be a promising material for complete silver recovery. Besides, precipitative recovery of silver by means of cementation with zinc powder was conducted. It was found that simple cementation with zinc powder exhibits a very good precipitative property for which it could be used in hydrometallurgical processing.

11:45 AM

**A Process for Efficient Material Recovery from Scrap Electronics:** *Jeffrey S. Spangenberg*<sup>1</sup>; Joseph Pomykala<sup>1</sup>; John Hryn<sup>1</sup>; Bassam Jody<sup>1</sup>; Edward Daniels<sup>1</sup>; <sup>1</sup>Argonne National Laboratory

End-of-life electronic devices continue to grow rapidly. With only about 20% of these devices entering the existing recycling infrastructure valuable resources are ending up in our landfills limiting the supply of raw material feed for the electronics industry. We evaluated the recovery rate of various materials in electronic scrap using our versatile material recovery pilot plant. The process uses a 2-stage approach; the first stage is a bulk separation which classifies materials into specific types while the second stage refines these materials further. The scrap processed for this study included electronics of various types including computers, copiers, and musical keyboards but not video monitors. The study focused on the segregation of circuit board material from commingled shred. A novel method was evaluated to concentrate this material so that platinum group metals could be recovered. Ferrous and non-ferrous metals, along with polymers were separated for recovery and subsequent re-use as well.

## Thermally Activated Processes in Plastic Deformation: Nucleation and Diffusive Processes

*Sponsored by:* The Minerals, Metals and Materials Society, TMS Materials Processing and Manufacturing Division, TMS/ASM; Computational Materials Science and Engineering Committee  
*Program Organizer:* Christopher Woodward, Air Force Research Laboratory

Monday AM

February 28, 2011

Room: 1B

Location: San Diego Conv. Ctr

*Session Chairs:* Jeffery Rickman, Lehigh University; Carelyn Campbell, NIST

8:30 AM Invited

**Challenges in the Modeling of Nucleation and Growth Processes:** *Jeffrey Rickman*<sup>1</sup>; <sup>1</sup>Lehigh University

In this talk I will review several methodologies for modeling nucleation and growth processes in different contexts. In particular, I will first outline the calculation of nucleation rates using both atomic-level and coarse-grained descriptions of transforming systems and highlight the computational challenges that must be overcome to perform these calculations. In addition, I will explore the use of stochastic geometry to characterize the kinetics of a first-order phase transition and suggest several microstructural descriptors that can be employed to distinguish among different nucleation scenarios. Finally, as an application of the methods described here, I will examine the problem of deducing nucleation conditions from a coalesced microstructure and the tailoring of microstructures in transforming, misfitting thin films.

9:00 AM Invited

**Analysis and Modeling of Nucleation Controlled Reactions:** *John Perepezko*<sup>1</sup>; Seth Imhoff<sup>1</sup>; <sup>1</sup>University of Wisconsin Madison

Nucleation reactions control the initial stage of microstructure development. The product phase number density, size distribution and morphology are nucleation reaction signatures that are directly related to the nucleation

pathway. An effective experimental study of nucleation reactions requires the documentation of the nucleation reaction signatures and the associated stochastic behavior. Kinetic models based upon the classical nucleation theory can provide valuable mechanistic insight on the rate controlling steps. An inherent characteristic of nucleation reactions is the initial metastable state of the parent phase that is often treated as a uniformly undercooled or supersaturated condition, but recent developments in local atomic structure analysis indicate that nanoscale heterogeneities can be important at high driving free energies. Several aspects of the experimental modeling and analysis approaches are illustrated from recent progress in the examination of nanoscale microstructures and nucleation statistics measurements.

#### 9:30 AM Invited

**Diffusive Molecular Dynamics:** *Ju Li*<sup>1</sup>; Sanket Sarkar<sup>2</sup>; William Cox<sup>2</sup>; Thomas Lenosky<sup>2</sup>; Erik Bitzek<sup>1</sup>; Yunzhi Wang<sup>2</sup>; <sup>1</sup>University of Pennsylvania; <sup>2</sup>The Ohio State University

The interplay between diffusional and displacive atomic movements is a key to understanding deformation mechanisms and microstructure evolution in solids. The ability to handle the diffusional time scale and the structural complexity in these problems poses a general challenge to atomistic modeling. We present here an approximate approach, called Diffusive Molecular Dynamics (DMD), which can capture diffusional time scale while maintaining atomic resolution, by coarse-graining over atomic vibrations. DMD combines long-range elastic and short-range atomic coordinate interactions simultaneously with gradient chemical thermodynamics. The model is applied to nanoindentation, void growth under tension and sintering. Intimate coupling between diffusional mechanisms such as diffusional creep and displacive mechanisms such as dislocation nucleation, are observed in these processes.

#### 10:00 AM Invited

**Predicting Diffusion Coefficients of Multi-Component Solids from First Principles:** *Anton Van der Ven*<sup>1</sup>; <sup>1</sup>University of Michigan

Diffusion in technologically important materials often involves non-dilute atomic transport that depends on the nature of intrinsic defects, the energetically most favorable hop mechanisms and the degree of short- and long-range order among the constituents of the solid. In this talk, I will describe how these factors can be rigorously accounted for in a first-principles prediction of diffusion coefficients in non-dilute alloys. The approach relies on the evaluation of Kubo-Green expressions, which provide the link between macroscopic diffusion coefficients and atomic trajectories sampled in kinetic Monte Carlo simulations. A first-principles description of the thermodynamics of short- and long-range order in multi-component solids is achieved with the cluster expansion formalism. I will describe recent work on the prediction of diffusion coefficients in intermetallic compounds and Li ion battery electrode materials.

#### 10:30 AM Break

#### 10:45 AM Invited

**Predicting Volume-Based Diffusion in Multicomponent Multiphase Alloys:** *Carelyn Campbell*<sup>1</sup>; <sup>1</sup>National Institute of Standards and Technology

Modeling of many thermally activated processes requires accurate prediction of the volume-based (bulk) diffusion in a multicomponent multiphase alloy. CALPHAD-based multicomponent diffusion mobility databases, in combination with multicomponent thermodynamic databases, provide a powerful tool for predicting multicomponent diffusion behavior. The development of these multicomponent diffusion databases requires assessment of diffusion mobilities based on the optimization of individual diffusion coefficient measurements, measured multicomponent diffusion couple profiles, and available first principle data. These assessment methods are applied to both disordered and ordered phases in a variety of alloy systems, including Ni-based superalloys, steels, and Cu-In-Se based photovoltaic absorber materials. The quality of the assessment is determined by comparing the assessment predictions to available experimental data not included in the assessment process and various published diffusion correlations. The inclusion of additional diffusion mechanisms, such as

grain boundary and stress-induced mechanisms, to the bulk diffusion will be discussed.

#### 11:15 AM Invited

**Advanced Methods for Modeling Thermally Activated Processes:** *Arthur Voter*<sup>1</sup>; <sup>1</sup>Los Alamos National Laboratory

A significant issue in accurately modeling diffusion in materials is that the dominant mechanisms are not always the simple unit processes we might think they are. Thus, even if barriers and prefactors are calculated accurately using a high-quality potential or electronic structure method, the predicted evolution may be wrong because key reaction paths are missing from the kinetic model. I will present an introduction to methods such as adaptive kinetic Monte Carlo and accelerated molecular dynamics, developed beginning in the late 1990's, for simulating the long-time dynamics of diffusive systems with no prior assumptions about the reaction mechanisms. I will discuss the strengths and weaknesses of the different methods and give some examples of recent results. I will also discuss prospects for the future and the main issues standing in the way of making these methods into general tools that can reach relevant time scales for real engineering materials.

#### 11:45 AM Invited

**Equilibrium and Time-Dependent Solute Segregation at Grain Boundaries: Systematic Monte Carlo Studies:** *Irina Belova*<sup>1</sup>; *Graeme Murch*<sup>1</sup>; Thomas Fiedler<sup>1</sup>; <sup>1</sup>The University of Newcastle

Solute segregation to grain boundaries has long been quantified by segregation factors. Segregation factors are generally obtained in a grain boundary diffusion experiment in the Harrison Type-B and C kinetics regimes. The location of the limits and even the existence of the Harrison kinetics regimes are poorly known in the presence of segregation and this has important consequences on the experimental values of segregation factors. Another important aspect is that the segregation is assumed to be at equilibrium at all times. This requirement may not always be fulfilled in a transient diffusion experiment. In this talk, we provide an overview of solute segregation, the Harrison kinetics regimes and the recent progress that has been made using the Lattice Monte Carlo method for delineating these regimes in the presence of segregation for various grain boundary diffusion models. The time dependence of the segregation factor and associated effects will also be discussed.

#### 12:15 PM

**Atomistic Modeling of Interactions of Dislocation Pile-Up with Grain Boundaries:** *Jian Wang*<sup>1</sup>; Steven Valone<sup>1</sup>; Richard Hoagland<sup>1</sup>; Timothy Germann<sup>1</sup>; <sup>1</sup>Los Alamos National Laboratory

Interfaces are a common planar defect in materials and can act as Sources, Sinks and Barriers for point defects and line defects. Interfaces possess many metastable states for a given set of macroscopic degrees-of-freedom. These various states may differ in energy, but by relatively small amounts, and may be separated by small energy barriers. Consequently, they may easily change state and configuration in response to changes in stress, temperature, and composition. These easy configurational changes enable such multi-state interfaces to actively participate in and influence a broad array of reactions and processes. Using atomic scale models (topological model and atomistic simulation), interface structures and properties and the interaction of interface with dislocations are studied. The results show that interfaces play a crucial role in determining material strength due to the dislocations-interfaces interactions and in nucleating lattice dislocations in associated with the reconstruction of interface structures.



## Ultrasonic Welding for Lightweight Components: Session I

*Sponsored by:* The Minerals, Metals and Materials Society, American Welding Society, TMS Light Metals Division, TMS Structural Materials Division, TMS: Young Leaders Committee, ASM-MSCTS: Materials and Processing Committee, METSOC-CIM: Metal Processing and Fabrication Committee

*Program Organizer:* Frank Balle, University of Kaiserslautern

Monday AM Room: 33A  
February 28, 2011 Location: San Diego Conv. Ctr

*Session Chair:* Frank Balle, Institute of Materials Science and Engineering, University of Kaiserslautern (Germany)

### 8:30 AM Introductory Comments, Frank Balle, Organizer

#### 8:35 AM

**Mechanisms of Joint Formation in Ultrasonic Spot Welding Aluminium Automotive Sheet:** *Phil Prangnell*<sup>1</sup>; Dimitrios Bakavos<sup>1</sup>; Yingchun Chen<sup>1</sup>; <sup>1</sup>The University of Manchester

High power ultrasonic spot welding (HP-USW) is an extremely efficient new method for welding Al alloys using ~ 2% of the energy of RSW. The overall objective of this work was to improve our current poor understanding of the mechanisms of weld formation when HP-USW is applied to aluminium automotive sheet. To this end, we report on the results of a detailed investigation, where we have studied the material flow, combined with x-ray tomography, FEG-SEM and EBSD, to characterise the weld defects, stages of weld formation, and microstructure evolution, as a function of welding energy, for a standard automotive material AA6111-T4 in 0.92 mm thick sheet. Results include a discussion of the origin of the complex flow features, noted by other researchers, which were found to occur on three length scales, the observation of a HAZ, and the grain structure developed in a typical weld.

#### 8:55 AM

**Ultrasonic Welding of Cables and Wires:** *Stefan Heinz*<sup>1</sup>; Dietmar Eifler<sup>1</sup>; Guntram Wagner<sup>1</sup>; <sup>1</sup>University of Kaiserslautern

In the automotive industry the ultrasonic metal welding technology is an established method to join aluminium or copper wires. At the WKK systematic investigations with ultrasonic welded Al-wires and flat flexible cables (FFCs) made of copper were carried out. In the case of Al-wires, joints with a cross sectional area of up to 120 mm<sup>2</sup> and a maximum tensile shear load of about 3500 N were realized. In addition, methods to reduce the unintentional adherence between the sonotrode coupling face and the Al-wires were developed. For FFCs, ultrasonic spot welding systems as well as ultrasonic torsion welding systems were used to weld wire to wire and wire to connector joints. With these joints maximum tensile shear loads comparable to the base material were achieved. Furthermore, a system was developed, which enables the welding of FFCs through the insulation of the cables.

#### 9:15 AM Invited

**Ultrasonic Metal Welding of Hybrid Joints:** *Guntram Wagner*<sup>1</sup>; Frank Balle<sup>1</sup>; Dietmar Eifler<sup>1</sup>; <sup>1</sup>University of Kaiserslautern

A central research field of the WKK is the realization of innovative hybrid joints by ultrasonic metal welding. The presentation gives an overview about suitable ultrasonic welding systems and essential machine and material parameters which influence the quality of the welds. Besides the ultrasonic welding of dissimilar metals such as Al to Cu or Al to steels, also welds between nonstandard materials like aluminum foam sandwiches or Al-wires can be realized. Moreover, the joining of glass and ceramic with metals is a point of interest at the WKK. By using the ultrasonic metal welding process, it is possible to realize glass/metal welds with tensile shear strengths of 50 MPa. Even, for ceramic/metal-joints actually shear strengths values up to 120 MPa were measured. Finally, selected results about the effects of

thermally induced residual stresses on the hybrid joints and questions of the bonding mechanisms will be discussed.

#### 9:45 AM

**Optimization of Aluminium to Magnesium Ultrasonic Spot Welding:** *Lexi Pantelli*<sup>1</sup>; Yingchun Chen<sup>1</sup>; David Strong<sup>1</sup>; Xiaoyun Zhang<sup>2</sup>; Phil Prangnell<sup>1</sup>; <sup>1</sup>The University of Manchester; <sup>2</sup>Beijing Institute of Aeronautical Materials

Dissimilar joining of aluminium and magnesium alloys is problematic due to the formation of brittle intermetallic phases at the interface. Successful joining will afford significant weight savings in the automotive industry as dissimilar materials combinations could be used to create lighter, more fuel efficient multi-material structures. Ultrasonic welding may offer a joining solution, but the process of joining aluminium to magnesium is not well understood. Here, we have investigated the effect of energy input and welding time on joint formation between aluminium 6111 and magnesium AZ31, and report on the optimum welding conditions, interfacial heat generation and the formation of a significant intermetallic layer. Further, the effect of pre-coating the magnesium with aluminium is discussed and the resulting reduction in intermetallic formation is shown.

#### 10:05 AM Break

#### 10:15 AM

**Fatigue Failure Behavior and Life Estimation of Ultrasonic Spot Welds in Lap-Shear Specimens of Magnesium and Steel Sheets:** *Teresa Franklin*<sup>1</sup>; Jwo Pan<sup>1</sup>; Michael Santella<sup>2</sup>; Tsung-Yu Pan<sup>2</sup>; <sup>1</sup>University of Michigan; <sup>2</sup>Oak Ridge National Laboratory

Fatigue behavior of ultrasonic spot welds in lap-shear specimens of magnesium AZ31B-H24 and hot-dipped-galvanized mild steel sheets is investigated based on experimental observations and a fatigue life estimation method. Optical micrographs of the welds before and after fatigue tests are examined to understand the failure mechanism of the welds. The optical micrographs indicate that the magnitude of the load range has significant influence on the location of kinked fatigue crack initiation. The location of the kinked fatigue crack initiation affects the failure mode of the welds. The failure mode changes from a partial nugget pullout mode through the magnesium sheet at high load ranges to an eyebrow crack growth mode through the magnesium sheet at lower load ranges. A structural stress model based on the closed-form structural solution is adopted to predict the fatigue lives of spot welds. The predicted fatigue lives are compared with the experimental results.

#### 10:35 AM

**Effect of Zinc Coatings on Joint Properties and Interface Reactions in Aluminum to Steel Ultrasonic Spot Welding:** *Farid Haddadi*<sup>1</sup>; Phil Prangnell<sup>1</sup>; <sup>1</sup>The University of Manchester

Dissimilar joining of aluminium to steel sheet is an important potential application of USW for multi-material automotive structures. Here, the weldability of un-coated and zinc coated steel with aluminium is discussed, using a 2.5 kW USW welder. Results show that zinc steel results in a higher weld performance than uncoated steel. The effect of parameters such as energy and clamping force have been investigated. For Al6111-T4 to DC04 joints it has been found that the tensile strength reaches a maximum after ~1.5 second welding time before decreasing, which is about 90% of the strength of an Al-Al joint. In comparison welds between Al6111-T4 and zinc coated steel took longer to achieve the same weld energy and maximum strength, because of melting of the Zinc coat, but matched the Al-Al joint properties. The reasons for these different behaviours are discussed in terms of the interfacial reactions, that take place.

#### 10:55 AM

**Ultrasonic Spot Welding of AZ31B to Galvanized Mild Steel:** *Michael Santella*<sup>1</sup>; Teresa Franklin<sup>2</sup>; Tsung-Yu Pan<sup>1</sup>; Elliot Brown<sup>3</sup>; Jwo Pan<sup>2</sup>; <sup>1</sup>Oak Ridge National Laboratory; <sup>2</sup>University of Michigan; <sup>3</sup>EB Scientific Enterprises

Ultrasonic spot welds were made between sheets of 0.8-mm-thick hot-dip-galvanized mild steel and 1.6-mm-thick AZ31B-H24. Lap-shear strengths of 3.0-4.2 kN were achieved with weld times of 0.3-1.2 s. Failure to achieve

strong bonding of joints where the Zn coating was removed from the steel surface indicate that Zn is essential to the bonding mechanism. Microstructure characterization and microchemical analysis indicated temperatures at the AZ31-steel interfaces reached at least 344°C in less than 0.3 s. The elevated temperature conditions promoted annealing of the AZ31-H24 metal and chemical reactions between it and the Zn coating.

**11:15 AM**

**Ultrasonic Welding of Hybrid Aluminum/CFRP-Joints: Microstructure, Monotonic Properties and Fatigue Behavior:** Stefan Huxhold<sup>1</sup>; Frank Balle<sup>1</sup>; Guntram Wagner<sup>1</sup>; Dietmar Eiffler<sup>1</sup>; <sup>1</sup>University of Kaiserslautern

Ultrasonic metal welding is well suited to realize aluminum alloy/carbon fiber reinforced polymer (CFRP) – joints. Important advantages of the ultrasonic welding process are: welding times less than three seconds and welding temperatures below 450°C. The joints are realized by softening and displacing of the polymer out of the welding zone as a result of the ultrasonic shear oscillation. In contrast to conventional joining processes this is the pre-condition that a direct contact between the aluminum and the carbon fibers takes place. In investigations with rolled blank sheets shear strengths of about 30 MPa were realized for AA5754/CF-PA66 – joints. By special surface pre-treatments of the metal, like shot peening or etching, the joint strength was increased up to 60% and the aging behavior of the joints was enhanced. Furthermore, bonding mechanisms and the fatigue behavior of the ultrasonic welded hybrid joints were examined in detail.

**11:35 AM Concluding Comments**

---

## 2011 Functional and Structural Nanomaterials: Fabrication, Properties, Applications and Implications: Nanomaterials: Energy

*Sponsored by:* The Minerals, Metals and Materials Society, TMS Electronic, Magnetic, and Photonic Materials Division, TMS: Nanomaterials Committee

*Program Organizers:* Jiyoung Kim, Univ of Texas; David Stollberg, Georgia Tech Research Institute; Seong Jin Koh, University of Texas at Arlington; Nitin Chopra, The University of Alabama; Suveen Mathaudhu, U.S. Army Research Office

Monday PM                      Room: 8  
February 28, 2011              Location: San Diego Conv. Ctr

*Session Chairs:* Seong Jin Koh, University of Texas at Arlington; Seung Kang, Qualcomm

---

**2:00 PM Introductory Comments**

**2:05 PM Invited**

**Titanium Oxides Thin Film Anodes for All-Solid-State Lithium Ion Batteries:** Ming-Che Yang<sup>1</sup>; Danijel Gostovic<sup>2</sup>; Shirley Meng<sup>2</sup>; <sup>1</sup>University of Florida; <sup>2</sup>U.C. San Diego

The requirements of low power and small size energy source in CMOSRAM and Micromechanics (MEMS) have brought up the use of all-solid state thin film batteries. Metallic lithium is not a suitable anode material for all-solid-state thin film batteries because of the large irreversible capacity and high reactivity with air. Spinel lithium titanate Li<sub>4</sub>Ti<sub>5</sub>O<sub>12</sub> and anatase TiO<sub>2</sub> have attracted great attention as potential anode materials because of the following attributes: stable in the air atmosphere, good Li-storage capacity, safety against overcharging and stable voltage plateau. Pulsed laser deposition was used for the electrode deposition. Film depositions were carried out at different temperature, different oxygen partial pressure and different substrate. In order to understand the relationship between crystal structure and electrochemical properties of thin films, the thin films were studied by X-ray diffraction, scanning electron microscopy (SEM), and TEM. Electrochemical performances were investigated by galvanostatic techniques in lithium cells.

**2:35 PM**

**Synthesis of Titania Nanotubes for Lithium Ion Batteries:** Hyukjae Lee<sup>1</sup>; Sang-Jun Park<sup>1</sup>; <sup>1</sup>Andong National University

Titania nanotubes are synthesized via hydrothermal and anodization techniques for an alternative anode material of lithium ion battery and their properties are measured via X-ray diffraction, electron microscopy, potentiostat, etc. Different synthetic conditions and post synthesis treatments cause various crystallographic phases and structural morphologies in the synthesized titania nanotubes. The lithium electrochemical behavior of the synthesized titania nanotubes is studied by the use of coin cells, and the results show that final crystallographic phase and morphology are the most important factors for lithium intercalation behavior in both synthetic methods. However, there are distinct differences in lithium intercalation behavior between titania nanotubes synthesized from hydrothermal and anodization methods as well. The lithium intercalation performance of titania nanotubes are further enhanced by the introduction of the carbon sources during synthesis which, in turn, results in carbon coating or doping at titania nanotubes.

**2:50 PM**

**Nanogenerators from Piezoelectric-Coated Carbon Nanotubes:** David Stollberg<sup>1</sup>; <sup>1</sup>Georgia Tech Research Institute

This research creates an energy harvesting device that harnesses ambient and extraneous motion of a vehicle or wind, etc. and converts it to electrical energy: a “nanogenerator” using carbon nanotubes (CNTs) and piezoelectrics. The CNTs serve as an efficient, lightweight, robust electrical conduit and structural support for nanothickness piezoelectrics, zinc oxide (ZnO). Arrays of ZnO-coated CNTs are built on rigid silicon substrates or flexible carbon fiber substrates. Disturbances, vibrations and other inertial motions cause the ZnO-coated CNTs to bend and stress, producing a current. A simple ZnO-coated CNT structure can generate an electric current density of ~0.3 μA/cm<sup>2</sup> to 4 mA/cm<sup>2</sup> with a power density of 0.1pW/cm<sup>2</sup> to 0.01μW/cm<sup>2</sup> under a small applied load. With optimization of the pattern and dimensions, there is promise for significantly increasing the current density to over 40 mA/cm<sup>2</sup> and the power density to over 10μW/cm<sup>2</sup>, enough to power small sensors and/or MEMS/NEMS devices.

**3:05 PM**

**Structural and Electrochemical Characterization of Individual Nanowires for Li-ion Batteries:** John Sullivan<sup>1</sup>; Arunkumar Subramanian<sup>1</sup>; Jianyu Huang<sup>1</sup>; Michael Shaw<sup>1</sup>; Nicholas Hudak<sup>1</sup>; Yongjie Zhan<sup>2</sup>; Jun Lou<sup>2</sup>; <sup>1</sup>Sandia National Labs; <sup>2</sup>Rice University

Nanowire (NW) anode and cathode materials offer the possibility of increased capacity and/or rate performance in Li-ion batteries through better accommodation of the large stresses incurred during lithiation/delithiation and through reduction in the path length for Li-ion or electron transport. One challenge with NW materials development is their electrochemical characterization, particularly diagnostics at the individual NW level. To meet this need, we have developed chip-based platforms that allow the isolation and electrochemical, structural, and electrical characterization of individual NWs. We have demonstrated this approach by isolating single MnO<sub>2</sub> NW cathodes and measuring their structural changes by transmission electron microscopy following increasing levels of electrochemical lithiation. We observe a rapid disordering of the MnO<sub>2</sub> lattice and a monotonic decrease in electrical conductance with increasing Li content. Sandia is operated by Sandia Corp., a wholly owned subsidiary of Lockheed Martin Co., for the U.S. DOE's NNSA under contract DE-AC04-94AL85000.

**3:20 PM**

**Phase Field Simulations of Morphological Evolution during Lithium Intercalation/Extraction in Li-ion Batteries:** Saswata Bhattacharya<sup>1</sup>; Linyun Liang<sup>1</sup>; Long-Qing Chen<sup>1</sup>; <sup>1</sup>Pennsylvania State University

We present a three-dimensional phase field model to study the morphological evolution during the intercalation/extraction of Li-ions into a host electrode in Li-ion batteries. The effects of anisotropic diffusional mobility of Li-ions in the electrode host lattice, flux of Li-ions across the electrode/electrolyte interface, and coherency strains arising from the lattice parameter mismatch

MONDAY PM

between the lithiated and unlithiated phases are studied using  $\text{LiFePO}_4$  as an example. We use spectral smoothed boundary method to solve the governing equations. Our simulations show the formation of plate-like crystallites of the lithiated phase when anisotropic bulk transport of Li-ions is assumed to be the rate limiting mechanism. We compare the microstructural features obtained from our simulations with available experimental observations.

### 3:35 PM Break

### 3:50 PM Invited

**Dye Sensitized Solar Cells with 3-Dimensional Anodes, and Prospects for Incorporating Unusual Photophysical Processes:** *Michael Tauber*<sup>1</sup>; <sup>1</sup>University of California, San Diego

Dye sensitized solar cells (DSSCs) are an emerging class of photovoltaics that are potentially much less expensive than traditional silicon solar cells. Presently the record-holding 11% efficient DSSC is only half as efficient as the best commercial silicon solar cells. Furthermore, the challenge of large-area scaling of DSSCs has slowed their commercialization and utilization. We have designed and constructed new DSSCs that incorporate titanium dioxide nanotubes anodically grown in a 3-D array from titanium metal substrate. The cells have >5% efficiency, and are free of transparent conductive oxide. The highly conductive all-metal substrates will make cells of this kind easy to scale to large areas, and at low cost. The 3-D cells are an optimal platform for testing new dyes and dye mixtures in DSSCs. Prospects for exploiting unusual photophysical processes in DSSCs, including triplet excited states and singlet fission, will be described.

### 4:20 PM

**Formation of Silver Nanocube Array via Silica-Polymer Nanocomposites:** *Chi-Kai Chiu*<sup>1</sup>; *Yong-Jae Choi*<sup>1</sup>; *Tzy-Jiun Luo*<sup>1</sup>; <sup>1</sup>North Carolina State University

Silver nanocubes are spontaneously formed at room temperature on the surface of sol-gel silica nanocomposite film that consists of polyethyleneglycol (PEG) and silver ions. The formation of silver nanocubes can be achieved without the presence of poly(vinylpyrrolidone), which was found to enhance the sharpness of nanocube edges. The geometry (e.g., spherical or cubic shape) nanocubes are critically dependent on the thickness of nanocomposite film while the dimension of nanocubes are the function of film thickness. The spontaneous reduction of silver occurs inside the nanoporous structures of silica where PEG serves as both mobile phase and reducing agent. This phenomenon is driven by the shrinkage of the sol-gel silica layer during aging process and is controllable through surface functional groups. The ability to create silver nanocubes on a solid substrate at room temperature suggests that it is possible to control both position and size of silver nanocubes using imprint technique.

### 4:35 PM

**Self-Assembled Epitaxial Quantum Dot Multilayers: A Stochastic Continuum Modeling Approach:** *Lawrence Friedman*<sup>1</sup>; <sup>1</sup>National Institute of Standards and Technology

Some strained semiconductor heterostructures such as  $\text{Ge}_x\text{Si}_{1-x}/\text{Si}$  and  $\text{In}_y\text{Ga}_{1-y}\text{As}/\text{GaAs}$  spontaneously form into zero-dimensional nanoelectronic structures known as self-assembled quantum dots (SAQDs). These structures are simple in composition, yet they exhibit rich behavior such as strain-induced zero- and finite-temperature phase transitions, nanoscale stochastic behavior and the ability to form multilayer superlattices that are ordered by strain-coupling. Thus, modeling their formation addresses many interesting aspects of nanoscale science and nanomechanics, while at the same time aiding in the design and manufacture of functional materials. To investigate the ordering (quality improving) and disordering (quality degrading) influences, a previously developed continuum stochastic model is refined and adapted to SAQD multilayers. The continuum stochastic approach enables large volume and long-time scale modeling that is necessary to collect statistics that characterize the order and quality of self-assembled quantum dots.

### 4:50 PM

**Three Dimensional Carbon Nanotube Photovoltaics:** *Jack Flicker*<sup>1</sup>; *Jud Ready*<sup>2</sup>; <sup>1</sup>Georgia Institute of Technology; <sup>2</sup>Georgia Tech Research Institute

The use of a nanostructured, three dimensional morphology in photovoltaics devices has occurred only relatively recently. We introduce a three dimensional photovoltaic device with carbon nanotube pillars coated with photoactive materials to create a solar cell. The extra dimensionality of this cell added by the nanotubes has been theorized to increase the relative energy generated over planar cells by up to four times. The energy increase is due to an increase in the interactions between photons and the photoactive material as the sun is at an off normal angle to the cell substrate. Prototypes of these cells have been made and, although suffering from a low overall efficiency, do show an increased energy production in the same manner that theory predicts when the light source is at an off normal angle. Increases in device efficiency by evolution of processes and structures will also be discussed.

### 5:05 PM

**New Silicon Alloy Nano-Particulate Materials for Lithium Ion Battery Anodes:** *Emma White*<sup>1</sup>; *Lisa Rueschhoff*<sup>1</sup>; *Iver Anderson*<sup>2</sup>; *Steve Martin*<sup>3</sup>; <sup>1</sup>Iowa State University & Ames Laboratory; <sup>2</sup>Ames Laboratory & Iowa State University; <sup>3</sup>Iowa State University

Lithium ion batteries currently offer the highest energy density, ~400 mAh/g, combined with high voltage, but the theoretical energy density of metallic lithium, ~4,000 mAh/g, has been difficult to achieve so far in a secondary cell. Poor cycle life has limited the use of higher charge capacity materials, such as silicon. A novel composite material made of alloyed silicon nano-particles has been produced which may circumvent the previous issues in using pure silicon as an anode material. The spark discharge method of particle production, the characterization of the resulting particles, and their initial performance in a lithium battery cell will be described. Funding provided by Ames Lab Seed Fund through Ames lab Contract DE-AC02-07CH11358.

### 5:20 PM Concluding Comments

## 2nd International Symposium on High-Temperature Metallurgical Processing: Microwave Heating and Iron and Steel Production

*Sponsored by:* The Minerals, Metals and Materials Society, TMS Extraction and Processing Division, TMS: Pyrometallurgy Committee, TMS: Energy Committee

*Program Organizers:* Jiann-Yang Hwang, Michigan Technological University; Jerome Downey, Montana Tech; Jaroslaw Drelich, Michigan Technological University; Tao Jiang, Central South University; Mark Cooksey, CSIRO

Monday PM  
February 28, 2011

Room: 18  
Location: San Diego Conv. Ctr

*Session Chairs:* Chenguang Bai, Chongqing University; Jerome Downey, Montana Tech of the Univ of Montana

### 2:00 PM

**A Study of Coal-Based Direct Reduction of Composite Binder Magnetite Preheated Pellets:** *Deqing Zhu*<sup>1</sup>; *Tiejun Chun*<sup>1</sup>; *Vinicius Mendes*<sup>1</sup>; *Jian Pan*<sup>1</sup>; *Jian Li*<sup>2</sup>; <sup>1</sup>Central South University; <sup>2</sup>Research Institute of Baosteel

A study of the coal-based direct reduction behaviors of composite binder magnetite pellets was carried out in a simulating coal-based grate-rotary kiln process. It is shown that preheated pellets possess much better reducibility than fired oxide pellets: 40 min are required for preheated pellets to reach over 90% metallization degree compared to 100 min for fired oxide pellets. The compressive strength of preheated pellets decreases dramatically at the earlier stage of reduction, climbs quickly after reducing for 30min and achieves a high value at the end of reduction. However, the compressive strength of metallized pellets from reducing of fired pellets is much lower,



more cracks and fractures being formed. In the preheated pellets, crystallite of metal iron is coarse. In the oxide pellet, a large number of interconnected crystals of metal iron are formed inside pellets, and pellet structure is very compact.

**2:20 PM**

**A Model of Decarburization of Iron/Carbon Droplets:** *Mark Schwarz*<sup>1</sup>; <sup>1</sup>CSIRO

A computer model which follows decarburization of Fe/C/S droplets and predicts the onset of "carbon boil" has been developed based on the mechanism of El-Kaddah and Robertson. According to this mechanism, boil occurs when the supersaturation pressure of CO within the droplet reaches a critical value. Predicted times to boil have been compared with measurements made at CSIRO under various operating conditions. The model results generally agree well with measured times to boil, thereby validating the boil mechanism. The critical supersaturation pressure for boil determined by comparing predicted and measured boil times is similar to that determined by El Kaddah and Robertson (48-240 atm) and depends on the kinetics of the surface decarburization reaction. The computer model predicts that the time to boil decreases as the gas-droplet velocity increases, as the drop temperatures decreases and as the droplet diameter decreases.

**2:40 PM**

**Non-Isothermal Kinetics of Reduction Reaction of Oxidized Pellet under Microwave Irradiation:** *Wu Kai*<sup>1</sup>; *Huang Zhu-Cheng*<sup>1</sup>; *Peng Hu*<sup>2</sup>; <sup>1</sup>CSU; <sup>2</sup>Syno-Therm Co. Ltd

The microwave heating characteristics of the mixture of acid pellet and coal was researched, and the non-isothermal reductive dynamics was discussed in the paper. The results show that, the slow-heating stage of the temperature rising process can be segmented into two heating temperature curve that have good linear relationship. It can be seen temperature programming. In the first stage, i.e., between 827K and 1073K, the reaction mechanism obeys three-dimensional diffusion model. In the second stage, i.e., between 1093K and 1323K, the reaction mechanism obeys chemical reaction model. The apparent activation energies are found respectively to be 63.96kJ/mol for the first stage and 61.27kJ/mol for the second stage. That is lower than the apparent activation energy under conventional heating. The research of the microstructure shows microwave can improve the kinetics of the reduction. Microwave has anxo-action to the reaction obviously.

**3:00 PM**

**Microwave Dielectric Properties of Pyrolyzed Carbon:** *Zhiwei Peng*<sup>1</sup>; *Jiann-Yang Hwang*<sup>1</sup>; *Wayne Bell*<sup>1</sup>; *Matthew Andriese*<sup>1</sup>; *Shuqian Xie*<sup>2</sup>; <sup>1</sup>Michigan Technological University; <sup>2</sup>Northeastern University

Pyrolyzed carbons are generally known as good microwave absorbers and their dielectric properties still remain to be fully explored. In the present study the dielectric properties and dielectric polarization-relaxation phenomenon of a typical activated carbon was investigated. The experimental results indicate the complex permittivity is highly dependent on temperature and frequency. The decrease of permittivity with increasing temperature from room temperature to ~100 °C is probably ascribed to the release of the water vapor adsorbed on the surface of activated carbon, and the variations of permittivity with temperatures between 100 °C and 450 °C in the frequency range of 300 MHz to 3000 MHz are mainly attributed to the decreased relaxation time of dielectric polarization.

**3:20 PM**

**Fugitive Emissions Related to Oxidation of Liquid Silicon During Ladle Refining:** *Mari Ness*<sup>1</sup>; *Gabriella Tranell*<sup>1</sup>; *Nils Eivind Kamfjord*<sup>1</sup>; <sup>1</sup>Norwegian University of Science and Technology

In oxidative ladle refining (OLR) of silicon, the metal surface is oxidized resulting in the formation of a condensed silica fume (SiO<sub>2</sub>). In the current work, industrial measurement campaigns were performed aiming to measure the fume generation during OLR. A thorough discussion of the possible mechanisms has been included in order to get a better understanding of the system. The measurement campaigns were done at the Elkem Salten plant in Norway. In addition to fume generation from OLR, the metal temperatures

and ladle purge gas amount were recorded. Other mechanisms of SiO<sub>2</sub> formation were considered, however found insignificant. The results of this work suggest that the dominant source of SiO<sub>2</sub> fume generation during OLR is the oxidation of the metal surface, with oxygen transport to the metal surface being the limiting factor.

**3:40 PM**

**Reduction Kinetics of Iron Oxide in CaO-SiO<sub>2</sub>-Al<sub>2</sub>O<sub>3</sub>-Fe<sub>x</sub>O-C Mixtures:** *Yuanyuan Zhang*<sup>1</sup>; *Patrick Masset*<sup>1</sup>; <sup>1</sup>TU Bergakademie Freiberg

In iron and steelmaking technologies, the determination of the interfacial reaction kinetics between CO/CO<sub>2</sub> based mixtures and iron ores represents a challenging and valuable input for the modelling of such high temperature conversion processes. In this work, experiments on the reduction of iron oxides were carried out using high pressure thermogravimetric analysis (HP-TGA) under CO/CO<sub>2</sub> mixtures at temperatures and pressures up to 1000°C and 5 bars, respectively. Through analyzing the TGA curves recorded at different heating rates, the reduction rate of the iron oxides by CO/CO<sub>2</sub> mixtures and the activation energies of the reduction reactions have been determined. For well defined transformation rate, the iron oxide particles were observed by SEM/EDX analysis to understand the reaction mechanism occurring at the oxide/gas interface. In addition, Mössbauer spectroscopy was used to estimate Fe<sup>3+</sup>/Fe<sup>2+</sup> ratio.

**4:00 PM Break**

**4:10 PM**

**Optimization of the Process Variables for Making Direct Reduced Iron by Microwave Heating using Response Surface Methodology:** *Linqing Dai*<sup>1</sup>; *Jinhui Peng*<sup>1</sup>; *Hongbo Zhu*<sup>1</sup>; <sup>1</sup>Kunming University of Science and Technology

To optimize the process variables for making direct reduced iron (DRI) by microwave heating, the reduction temperature, reduction time and the ratio of coal to material were studied with the central composite design (CCD) and their interactions on the Metallization rate were also investigated. The predictive polynomial quadratic equations model was analyzed by ANOVA. Optimal conditions of making DRI can be concluded as follows: 28 min at 1139°, the ratio of coal to material is 20.95%. Under these conditions, the metallization rate is up to 97.06%.

**4:30 PM**

**Study on Nucleation and Growth Mechanism of Iron Crystal Grain in Coal-Based Shaft Furnace Direct Reduction Iron Pellets by Microwave Heating:** *Zhucheng Huang*<sup>1</sup>; *Zhenyuan Liao*<sup>1</sup>; *Bing Hu*<sup>1</sup>; *Lingyun Yi*<sup>1</sup>; *Yuanbo Zhang*<sup>1</sup>; <sup>1</sup>Central South University

Nucleation and growth mechanism of iron crystal grain in coal-based shaft furnace direct reduction process by microwave heating were investigated by optical microscope, scanning electron microscope and EDX. The results indicate that microwave has selectivity on various minerals which absorb microwaves. The high temperature in certain area of pellets and thermal stress on the interface of minerals are formed, results in the wustite grain smashed along the joints, and iron crystal grains turned out a spherical shape obviously. The iron crystal nucleus is formed firstly at the edge of wustite, on the interface between grains and in the holes in pellets, and grows gradually while reduction carries on from surface layer to inner core. Microwave heating promotes the rate of transportation and accumulation of the iron crystal grain, increases growth rate of iron crystal grain and contributes to formation of dense iron-jointed crystal texture eventually.

**4:50 PM**

**In-Situ Mass, Temperature, and Resistance Measurements during Microwave Metallization of Iron Ore and Zink Dust for On-Line Optimization:** *Wayne Bell*<sup>1</sup>; <sup>1</sup>Michigan Technological University

Microwave reduction furnaces have a great potential to eliminate traditional electric arc and blast furnaces that are inefficient and environmentally unfriendly. A rotary microwave/electric arc reduction furnace was developed at Michigan Technological University to be marketed commercially in the United States with the hope of rapidly becoming the first green alternative to existing reduction-metallization technologies. Materials are fed onto a 6'

refractory disc in a waveguide attached to 3 100kW microwave applicators. Upon formation of a conductive metallic network from microwaving, an electric arc is used to melt the network into a nugget for extraction. To effectively and continuously run a microwave/EAF furnace, several working parameters must be controlled by the user before operation: Microwave and EAF power, processing speed, mixing ratios of input materials. Using a simple household microwave, several materials properties (resistance, mass, and temperature) can be easily measured and correlated to expose the unknown on-line working parameters.

#### 5:10 PM

**Research on the Reduction Mechanism of Vanadium Oxides in Lumpy Zone in Blast Furnace:** *YongHong Wang*<sup>1</sup>; Bing Xie<sup>1</sup>; QingYun Huang<sup>1</sup>; JiaRong Yang<sup>1</sup>; <sup>1</sup>ChongQing university

Vanadium-bearing titanomagnetite is used as one of raw materials in blast furnace in Panzhihua Iron and Steel Group Corp. Thermodynamic calculation on reduction of vanadium oxides from ore in lumpy zone of blast furnace showed that with the occurrence of iron the pressure of PCO<sub>2</sub>/PCO of the vanadium oxides reduction could evidently increased because vanadium could unlimitedly dissolve in liquid iron. Also, the process of iron and vanadium reduction from magnetite ore is simulated in reduction furnace. Chemical analysis method is used to analysis the composition of reduction samples. It is concluded that the reduced degree of iron oxide can be higher than 80% after three hours. And when the reduced degree of iron oxide is between 85% and 90%, vanadium oxides begin to be reduced and the content could reach 0.083% when the reduced degree is 97.4%.

#### 5:30 PM

**Investigation on a Microwave High-Temperature Air Heat Exchanger:** Jianhua Liu<sup>1</sup>; Yingwei Li<sup>1</sup>; Lijun Liu<sup>1</sup>; Jinhui Peng<sup>1</sup>; Libo Zhang<sup>1</sup>; *Shenghui Guo*<sup>1</sup>; Huilong Luo<sup>1</sup>; Hongpo Wang<sup>1</sup>; Guo Chen<sup>1</sup>; <sup>1</sup>Kunming University of Science and Technology

As essential equipment in the metallurgical industry, current air heat exchanger can not meet the requirements of high temperature heat transfer. In present paper, an energy efficient air heat exchanger, based on accumulation of the heat generated by microwave absorbing materials is presented according to heat transfer theory and principle of the microwave field. A tubular shape structure of heat exchanger was designed and built up through temperature-rising curve, heat transfer performance of different materials heat exchanger. And it was indicated from experiments that tubular shape heat exchanger fabricated by using material B could be used for high temperature heat transfer system, and equilibrium temperature could reach up to 457—485°C.

## Advances in Science-Based Processing of Superalloys for Cost and Sustainment: Application of Modeling and Simulation to Component Design and Life Prediction

*Sponsored by:* The Minerals, Metals and Materials Society, TMS Materials Processing and Manufacturing Division, TMS Structural Materials Division, TMS/ASM: Computational Materials Science and Engineering Committee, TMS: High Temperature Alloys Committee, TMS: Advanced Characterization, Testing, and Simulation Committee

*Program Organizers:* Donna Ballard, US Air Force; David Furrer, Pratt & Whitney; Paul Jablonski, US Department of Energy; Christopher Woodward, Air Force Research Laboratory; Jeff Simmons, AFRL; Mark Blodgett, Wright-Patterson AFB

Monday PM  
February 28, 2011

Room: 33B  
Location: San Diego Conv. Ctr

*Session Chairs:* David Furrer, Pratt & Whitney; Jeff Simmons, AFRL

#### 2:00 PM Invited

**Extreme Values in Materials Microstructure:** *Anthony Rollett*<sup>1</sup>; Seth Wilson<sup>1</sup>; Jeff Simmons<sup>2</sup>; Katayun Barmak<sup>1</sup>; Michael Groeber<sup>2</sup>; David Rowenhorst<sup>3</sup>; <sup>1</sup>Carnegie Mellon University; <sup>2</sup>Air Force Research Lab.; <sup>3</sup>Naval Research Lab.

Materials scientists and engineers commonly report a single value for a property or microstructural feature. Some properties, however, probe the weakest link in a system. Thus there are references to the use of extreme value statistics to link particle sizes to fatigue life, for example, going back to the 1940s. Grain size is an example where the community has been content to argue over the applicability of, say, the log-normal distribution versus other candidate distributions. Yet, the impact of grain size may be through the presence of large grains in the system, rather than the average. Thus determining the extreme values for grain size is also important for understanding microstructure-property relationships. Several experimental data sets and some derived from computer simulation of microstructure evolution are analyzed to characterize the upper tails of the grain size distribution.

#### 2:30 PM Invited

**Uncertainty in Process-Structure-Property Relations: Robust Materials Design:** *David McDowell*<sup>1</sup>; <sup>1</sup>Georgia Institute of Technology

Designing materials for targeted performance requirements demands a combined strategy of bottom-up and top-down modeling, simulation, experiments, and systems engineering. In materials design applications, uncertainty can be both stochastic and epistemic. Stochastic (i.e., aleatory) uncertainty stems from stochastic variability and inherent randomness of material processing and morphology, as manifested in heterogeneous, randomly distributed microstructure attributes and defects. Epistemic (i.e., model) uncertainty stems from limits to the knowledge captured in models (model idealization and approximation of reality) and databases. This manifests itself in the limited fidelity and accuracy of predictions, inevitable lack of information, and modeling errors due to interpolations, approximations, convergence, assumptions, and other factors related to methods of obtaining approximate solutions. Characterizing and managing both types of uncertainty are essential in pursuing materials design applications. Components of a practical approach for robust design of materials to achieve specified functionality are presented, addressing uncertainty.

### 3:00 PM Invited

#### **Rolls-Royce Perspective on Advances in Science-Based Processing of Superalloy Materials and Components:** *Mary Lee Gambone*<sup>1</sup>; <sup>1</sup>Rolls-Royce

Recent advances in superalloy material and component capabilities have been attributed to the refinement of processing methods and controls. These refinements have been supported and driven by further understanding of the metallurgical phenomena that subsequently result in enhanced mechanical performance. Physics-based understanding of microstructure evolution and deformation processes has led to unique combinations of processes and processing control methods. Efforts to develop and apply fundamental understanding of physical and mechanical metallurgy of superalloy materials is not new, however recent discoveries in mechanical behavior and material characterization methods have provided renewed emphasis and insight into the importance of processing. This talk will provide an industrial perspective on how recent advances in focused technical areas are leading to further superalloy capabilities through advances in science-based processing.

### 3:30 PM Break

### 3:45 PM Invited

#### **Modeling and Simulation in Fossil Energy Systems – Current Prospectus:** *Jeffrey Hawk*<sup>1</sup>; Liang Jiang<sup>2</sup>; <sup>1</sup>U.S. Department of Energy; <sup>2</sup>GE Global Research

Within the realm of energy research, there are many opportunities for modeling and simulation, from large scale power plant systems to the interaction between atoms in an alloy. Specifically in the materials science focus area at NETL, materials modeling and simulation has been used to expedite the development of new materials as well as improve upon, and/or optimize, existing alloys for new fossil energy applications. At GE modeling and simulation research is directed at accelerating the introduction of a component into an existing energy platform through Materials Design Acceleration (MDA). Superalloys remain near the forefront of these activities due to their widespread use in current generations of gas turbines and their potential incorporation into A-USC power plants. Modeling activities at NETL and GE specific to superalloy development and product incorporation will be discussed with emphasis on the computational materials modeling approaches in each instance.

### 4:15 PM

#### **Modeling Deformation Mechanisms and Grain Structure Evolution during Forging of Powder-Metallurgy Nickel-Base Turbine Disk Alloy:** *Wen Tu*<sup>1</sup>; Tresa Pollock<sup>2</sup>; <sup>1</sup>University of Michigan; <sup>2</sup>University of California - Santa Barbara

The properties of superalloy disk materials are sensitive to the microstructure at the end of a series of thermomechanical processing. In this study, high temperature compression testing combined with high resolution Electron Backscatter Diffraction (EBSD) analysis has been used to analyze microstructural-scale straining processes that occur during high temperature forging of a nickel-base superalloy, René 88DT. Orientation imaging has been employed to study grain-level straining and strain storage. Using experimental evidence, constitutive models of deformation mechanisms and microstructure evolution during high temperature compression are proposed. The models predict: 1.) boundaries of superplastic deformation as a function of temperature, strain rate, and grain size, 2.) rate of superplasticity-enhanced grain growth as a function of strain, strain rate, and temperature and 3.) the saturation recrystallized grain size as a function of strain rate and temperature. The sum of the models predicts grain structure evolution during high temperature forging of Ni-base superalloys.

### 4:35 PM

#### **The Progression of Oxidation Damage for an Advanced Powder Metallurgy Disk Superalloy:** *Chantal Sudbrack*<sup>1</sup>; James Smialek<sup>1</sup>; Tim Gabb<sup>1</sup>; David Hull<sup>1</sup>; Timothy Gorman<sup>2</sup>; Doug Wei<sup>3</sup>; Jeff Marshman<sup>3</sup>; <sup>1</sup>NASA Glenn Research Center; <sup>2</sup>University of Dayton; <sup>3</sup>Carl Zeiss SMT Inc.

With the drive towards higher operating temperatures in newly developed gas turbine engines, oxidation resistance and protection of advanced nickel-

based turbine disk components are becoming increasingly important. Oxidizing environments are known to impair disk fatigue life at temperatures above 500°C, yet development of protective disk coatings is still in its infancy. Microstructural response of an ME3 disk superalloy is evaluated for moderate (704°C) and aggressive (760-816°C) isothermal exposures up to 2,020 hours. Slow growing Cr-rich scales form superficially and deviate from classic parabolic growth, possibly due to Cr<sub>2</sub>O<sub>3</sub> grain boundary (GB) diffusion or shifts in Cr<sub>2</sub>O<sub>3</sub>-TiO<sub>2</sub>-CrTaO<sub>4</sub>-Al<sub>2</sub>O<sub>3</sub> complex scale phase make-up. Cross section analysis reveals sub-surface damage (significant for aggressive exposures) that consists of Al<sub>2</sub>O<sub>3</sub> “fingers”, interfacial voids, a recrystallized precipitate-free layer and GB carbide dissolution. The effects of a Nichrome coating on this response are also assessed. Detailed spatial and chemical quantification of these microstructures are presented.

### 4:55 PM

#### **Diffusion Simulation and Oxidation Life Prediction of Turbine Metallic Coatings:** *Fan Zhang*<sup>1</sup>; Shuanglin Chen<sup>1</sup>; Weisheng Cao<sup>1</sup>; Y. Austin Chang<sup>2</sup>; Kang Lee<sup>3</sup>; Donna Ballard<sup>4</sup>; Jeff Simmons<sup>4</sup>; <sup>1</sup>CompuTherm, LLC; <sup>2</sup>University of Wisconsin-Madison; <sup>3</sup>Rolls-Royce Corporation; <sup>4</sup>Air Force Research Laboratory

Oxidation protection coatings have become an integral part of advanced gas turbine engine hot section components. These coatings rely on the formation of a slow-growing and adherent Al<sub>2</sub>O<sub>3</sub> scale. Due to the scale formation/spallation at the coating/gas interface and Al diffusion into the superalloy at the coating/substrate interface during service, aluminum is depleted from coating materials. The oxidation life of a coating ends when aluminum is depleted below the critical concentration. In this study, we have developed a modeling tool which integrates thermodynamic calculation, 1-D diffusion model, and an empirical oxidation model (COSIP) to understand the oxidation life of coatings. With this modeling tool, the aluminum depletion due to diffusion and Al<sub>2</sub>O<sub>3</sub> scale formation/spallation can be simulated. The oxidation life of a coating, therefore, can be predicted as a function of coating and alloy type and service condition, which is critical for intelligent coating selection, component design, and component maintenance.

### 5:15 PM

#### **Nitridation of HAYNES® NS-163® Alloy: Thermodynamics and Kinetics:** *Michael Fahrman*<sup>1</sup>; Krishna Srivastava<sup>1</sup>; <sup>1</sup>Haynes International Inc.

Nitride dispersion-strengthened HAYNES® NS-163® alloy is a new unique cobalt-base sheet alloy that offers significantly enhanced creep strength over HAYNES® 617, 230®, and even 188 alloys at temperatures exceeding 1650°F (900°C). This new alloy approaches the performance of oxide dispersion-strengthened alloys while being fabricable and less costly to process since it employs conventional mill technologies. Nitride dispersion strengthening is accomplished via a post-fabrication heat treatment. A thorough understanding and control of the nitridation process will be key to the alloy's commercial viability. In this context, microstructures of partially and fully nitrided sheet samples have been examined. The nitride reaction front advanced following a parabolic growth law. The nature and sequence of formation of the various nitride compounds formed is rationalized by comparing their respective Gibbs free energies of formation. Dispersoid nucleation densities and morphologies are discussed in terms of the locally varying speed of the reaction front.



## Alumina and Bauxite: Bauxite Resources and Utilisation

*Sponsored by:* The Minerals, Metals and Materials Society, TMS Light Metals Division, TMS: Aluminum Committee, TMS: Aluminum Processing Committee

*Program Organizers:* James Metson, University of Auckland; Carlos Suarez, Hatch Associates Consultants Inc

Monday PM                                      Room: 17A  
February 28, 2011                                Location: San Diego Conv. Ctr

*Session Chair:* To Be Announced

### 2:00 PM Introductory Comments

#### 2:05 PM

**New Development Model for Bauxite Deposits:** *Peter-Hans ter Weer*<sup>1</sup>; <sup>1</sup>TWS Services and Advice

Developing a greenfield bauxite deposit generally includes constructing an alumina refinery. Economics have resulted in ever-increasing production capacities for recently-built and future planned greenfield refineries. Rationale: economy of scale. As a result the complexity of a greenfield project has significantly increased and its capital cost has grown to several billion USD. Important consequences: 1. Project owners aim at risk reduction through project financing and formation of joint ventures, further complicating project implementation; 2. Globally only a limited number of (large) companies have the resources to develop greenfield bauxite & alumina projects; 3. Only a limited number of engineering firms have the required skills and experience to successfully implement these mega projects; 4. Only large bauxite deposits get developed. This paper proposes an alternative development model for bauxite deposits resulting in a more efficient use of resources and a lower threshold to develop bauxite & alumina projects.

#### 2:30 PM

**Study on the Characterization of Marginal Bauxite from Pará/Brazil:** *Fernanda Silva*<sup>1</sup>; João Sampaio<sup>2</sup>; Marta Medeiros<sup>1</sup>; Francisco Garrido<sup>1</sup>; <sup>1</sup>IQ/UFRJ - CETEM; <sup>2</sup>Centro de Tecnologia Mineral

Bauxite from Pará is divided into five different layers. However, only one is processed. The crystallized-amorphous (BCBA) phase is considered a marginal bauxite because it presents a high quantity of SiO<sub>2</sub> reactive and its use depends on special technologies. BCBA was characterized and results were compared to the bauxite used, nowadays, in the alumina plant. Characterization was performed by XRD, XRF, chemical analysis, TGA and SEM. XRD determined the mineral content: such bauxite is gibbsitic and has been associated with kaolinite and hematite. XRF determined the sample's chemical composition. The chemical content of Al<sub>2</sub>O<sub>3</sub> available and SiO<sub>2</sub> reactiva was determined by potentiometric titration and FAAS. The results found for the Bayer process sample were 41.7% and 7.1%, respectively. TGA observed the bauxite decomposition and SEM supplied chemical and thermal analysis. Thus, based on stoichiometric relations of the bauxite components decomposition, it was possible to confirm the following phases: gibbsite and kaolinite.

#### 2:55 PM

**Resource Utilization of High-Sulfur Bauxite of Low-Median Grade in Chongqing China:** *Jianguo Yin*<sup>1</sup>; Wentang Xia<sup>1</sup>; Mingrong Han<sup>1</sup>; <sup>1</sup>Chongqing University of Science and Technology

Resource utilization of high-sulfur bauxite is one of technical problems for alumina refineries in China. There are a lot high-sulfur bauxite of low-median grade in Chongqing China, which are not been utilized until now. Sulfur in bauxite will cause many negative effects on the alumina production. There exist some disadvantages for current desulfurization technologies. It is difficult to attain breakthrough progress from the view of desulfurization technologies. So it is necessary to have fundamental theoretical studies on the occurrence of sulfur in high-sulfur bauxite, occurrence, reaction behavior and changing rule for sulfur in the production process and its effect. Combined

theoretical research with experiments, it is possible to develop a feasible desulfurization process. It will be technical support and theory guidance for utilization of high-sulfur bauxite in Chongqing, and also advantageous for prolonging bauxite resource guarantee for Chinese alumina industry.

#### 3:20 PM Break

#### 3:30 PM

**Development of Bauxite and Alumina Resources in the Kingdom of Saudi Arabia:** *AbdulGhafoor Al-Dubaisi*<sup>1</sup>; <sup>1</sup>Saudi Arabian Mining Co. (Maden)

Driven by desire to diversify its economy in an oil rich country and by the need to create jobs for the increasing number of Saudi youth, the Kingdom of Saudi Arabia established the Saudi Arabian Mining Company (MA'ADEN) to develop its mineral resources. Local bauxite will be developed into an integrated mine-to-metal aluminum industry. Numerous challenges have to be overcome. Major Infrastructure has to be built; construction and operating costs have to be contained to ensure the economic viability of the project. The lack of expertise in the kingdom to run such an operation created the need to involve an international joint venture partner. The human development is no less challenging and early plans have to be in place to recruit and train a large number of Saudis to be the core of the operating organization.

#### 3:55 PM

**Digestion Studies on Central Indian Bauxite:** *Puliyur Krishnaswamy Narasimha Raghavan*<sup>1</sup>; Nand Kumar Kshatriya<sup>1</sup>; <sup>1</sup>Bharat Aluminium Co. Ltd., (A Unit of Vedanta Resources Plc.), BALCO Nagar, Korba

Indian bauxite deposits are grouped into five namely, Eastern Ghats, Central Indian, West Coast, Gujrat and Jammu & Kashmir. Each of the Bauxite has its own typical digestion and settling conditions due to variation in mineralogy. Bauxite digestion depends much on the temperature-pressure conditions, the recycled liquor concentration bauxite mineralogy and charge quantity. The productivity of the entire Bayer process depends to a large extent on the digestion process. In an attempt to optimize the digestion conditions for the central Indian Bauxites, in order to achieve low caustic soda loss coupled with minimum bauxite consumption a series of experiments were conducted to find out the best parameter for conducting digestion at laboratory scale. The effect of deslucation and digestion temperature, bauxite charge, lime quantity and digestion liquor MR is discussed in this paper. Attempt shall be made to compare the conditions with Bauxite from other locations.

#### 4:20 PM

**Effects of Roasting Pretreatment in Intense Magnetic Field on Digestion Performance of Diasporic Bauxite:** *Zhang Ting-an*<sup>1</sup>; Dou Zhihe<sup>1</sup>; Lv Guozhi<sup>1</sup>; Liu Yan<sup>1</sup>; Du Juan<sup>1</sup>; Wang Xiaoxiao<sup>1</sup>; Li Yan<sup>1</sup>; <sup>1</sup>Northeastern University

This paper investigated the changes of phase and apparent morphology under the combined effects of intense magnetic field and temperature field and the effect law of different roasting conditions on the digestion performance of roasted diasporic. The results indicated that the roasting pretreatment under high magnetic field can change the microstructure and improve the digestion properties of bauxite. The reasonable roasting conditions of intense magnetic field follow as that the roasting temperature is 550°, roasting time is 60min and the magnetic field intensity is 6T. The digesting rate of alumina of roasted ore is 84.17% and the digesting liquid ratio is 1.39 while the digesting temperature is 190° with the digestion time of 60mins. The digesting rate of alumina of roasted ore increases higher 52.85% than this of the raw ore. The digesting temperature of roasted ore decreases lower 30° than this of the raw ore.

---

## Aluminum Alloys: Fabrication, Characterization and Applications: Numerical Modeling

Sponsored by: The Minerals, Metals and Materials Society, TMS Light Metals Division, TMS: Aluminum Processing Committee  
Program Organizers: Subodh Das, Phinix LLC; Zhengdong Long, Kaiser Aluminum; Tongguang Zhai, University of Kentucky

Monday PM Room: 14A  
February 28, 2011 Location: San Diego Conv. Ctr

Session Chair: John Chinella, U.S. Army Research Laboratory

---

### 2:00 PM

#### Modeling Performance of Protection Materials Aluminum 7020-T651 and Steel: John Chinella<sup>1</sup>; <sup>1</sup>U.S. Army Research Laboratory

This presentation compares protection and characteristics of aluminum 7020-T651 and a modern rolled homogeneous armor steel (RHA) and compares performance to historical protection levels of RHA. Comparisons are shown with RHA plots of protection level mean response, confidence intervals, and cumulative probability distributions over the range of performance. The protection levels and the failure modes of 7020-T651 aluminum suggest that weight savings will be achieved through: (1) excellent protection, multiple hit or projectile damage tolerance, and minimal need for spall liners; and (2) equal structural stiffness at half the weight of steel. Results of ballistic test characterization in this study, literature of Al-Zn-Mg alloys, Thermo-Calc phase diagrams, and JMatPro temperature step calculations reveals alloy 7020 has unique metallurgical characteristics and capabilities to meet improvements in structural, monolithic or advanced armor designs, and the needs of processing, fabricability or field repair, durability, weight and cost efficiency, and extreme climate.

### 2:20 PM

#### The Influence of Temperature on the Tensile Anisotropy of a Forged 7XXX Aluminum Alloy: Agouti Siham<sup>1</sup>; Bozzolo Nathalie<sup>1</sup>; Bouchard Pierre-Olivier<sup>1</sup>; Le Brun Pierre<sup>2</sup>; Piellard Mickael<sup>3</sup>; <sup>1</sup>Centre of materials forming; <sup>2</sup>Voreppe Research Center; <sup>3</sup>Aubert et Duval Isoire

Aluminum ingots are usually submitted to hot forging processes to increase their ductility before the final stamping process. The subject of this work is to investigate the effect of temperature on the mechanical anisotropy of a forged 7XXX Aluminium alloy. At the as forged state, this material contains iron-intermetallics observed as large heaps of particles. At room temperature, the longitudinal direction is more ductile than the forging direction as the iron-intermetallics are oriented along the longitudinal direction. On the contrary, tensile tests at high temperatures (300-430°C) showed that the forging direction is more ductile than the longitudinal direction. Microstructure investigations along the strain gradient produced on tensile test specimens allowed to understand deformation and damage mechanisms occurring at high temperature and the resulting mechanical anisotropy.

### 2:40 PM

#### Modeling the Strain Path Change Effect in 5754-O Aluminum Alloy Sheet: Lin Hu<sup>1</sup>; Anthony Rollett<sup>1</sup>; Mark Iadicola<sup>2</sup>; Tim Foecke<sup>2</sup>; Steve Banovic<sup>2</sup>; <sup>1</sup>Carnegie Mellon University; <sup>2</sup>National Institute of Standards and Technology

Strain-path change tests were performed on 5754-O aluminum alloy sheet sample by using equibiaxial stretch followed by uniaxial tension. A self-consistent viscoplastic polycrystal model was used to simulate the material response under non-linear strain paths and fit the experimental data. Recovery that occurred during the first and second loading steps was also assessed. Anisotropic strain hardening behaviors were incorporated in the model, which accounted for the transient behaviors upon the strain path change.

### 3:00 PM

#### Micromechanical Simulations for Fatigue Damage Incubation at Debonded Particles Using Cohesive Zone Model: Tong Li<sup>1</sup>; Yibin Xue<sup>1</sup>; <sup>1</sup>Utah State University

Fatigue damage initiates at debonded micrometer-sized intermetallic particles for some high strength Al alloys in the high cycle fatigue regime. Cohesive zone model is implemented to investigate the interfacial debonding and propagation under cyclic loads. Representative Volume Elements (RVE) are set to position the intermetallic particle at different spatial locations regarding the boundary of the RVEs to account for the random distribution of the particle in the alloys. Maximum plastic shear strain range (MPSS) and Fatemi-Socie (FS) parameter for multiaxial fatigue are introduced as nonlocal damage parameters to evaluate the severity of the damage level of RVEs and loading sets. This set of the simulations will be compared with simulation results on fatigue damage incubated at the fractured particles. This effort completes the fatigue damage incubation evaluation for wrought Al alloys.

### 3:20 PM

#### Comprehensive Thermo-Mechanical Validation of Extrusion Simulation Cycle for Al 1100 Using HyperXtrude: Abdulafoo Parker<sup>1</sup>; Clemence Bouvard<sup>1</sup>; Stephen Horstemeyer<sup>1</sup>; Esteban Marin<sup>1</sup>; Paul Wang<sup>1</sup>; Mark Horstemeyer<sup>1</sup>; <sup>1</sup>Center for Advanced Vehicular Systems, Mississippi State University

A laboratory-scale extrusion capability facilitates parametric study of metal extrusion processes. Commercial simulation code, HyperXtrude, was used to simulate laboratory experiments performed using a flat-die. In the experiments, ram velocity and billet temperature were the process parameters that were controlled. Simulation model was validated by comparing the results with experimentally obtained load and temperature histories on tooling. The results of simulation and experiments were found to be in good agreement. 'Optimized' values for friction and convection film-coefficient were used to reach the best fit. The breakthrough load is predicted with good accuracy; however, the accuracy in load correlation is not sustained throughout the process duration as the predicted load trend deviates from experimental data towards the end of the ram stroke. The aim of this work is to benchmark a commercial extrusion simulation code for a range of profiles.

### 3:40 PM Break

### 3:55 PM

#### Deformation and Rupture Modeling of an Aluminum Metal Matrix Composite: James DeMarco<sup>1</sup>; Justin Karl<sup>1</sup>; Ali Gordon<sup>1</sup>; <sup>1</sup>UCF MMAE Dept.

While aluminum metal-matrix composites (MMCs) have come into broader use for high-tech applications where their combined light weights and large elastic moduli are sufficiently advantageous, widespread application is limited by high processing costs. In the case of hot-rolled aluminum MMC sheets, material lost to edge cracking is a major contributor to decreased production yield and high cost. Determining the optimal thermo-mechanical processing parameters which minimize losses due to edge cracking can be achieved through numerical modeling of the temperature-dependent mechanical response of the material. An elastic-viscoplastic constitutive model incorporating strain rate and temperature dependence is presented for A359-SiC -30%. Perzyna viscoplasticity and Cockroft-Latham ductility are assumed. Modeling parameters for the as-cast material are optimized to fit tensile and torsion data obtained at a variety of temperature and strain rate combinations.

### 4:15 PM

#### Mechanical Properties and Casting Characteristics of the Secondary Aluminum Alloy AlSi9Cu3(Fe) (A226): Philip Pucher<sup>1</sup>; Holm Bötcher<sup>2</sup>; Helmut Kaufmann<sup>3</sup>; Helmut Antrekowitsch<sup>1</sup>; Peter J. Uggowitzer<sup>4</sup>; <sup>1</sup>University of Leoben; <sup>2</sup>AMAG Casting GmbH; <sup>3</sup>Austria Metall AG (AMAG); <sup>4</sup>ETH Zurich

Due to its excellent castability, good mechanical properties and cost-effectiveness the secondary alloy AlSi9Cu3 (A226) finds wide application for

the production of permanent mould castings and high pressure die castings (HPDC). Variations of the chemical composition within the tolerance limits cause pronounced changes in the mechanical properties and castability. For example the yield strength of permanent mold cast samples ranges from 100 MPa to 200 MPa, while the elongation varies between 0.3 % and 4 %. The present study was performed to investigate the mechanical properties and casting characteristics depending on the combined effect of the main alloying elements in the whole composition range. The results – based on 48 industry-oriented permanent mold casting experiments – are discussed on a systematic basis of thermodynamic calculations and metallographic investigations. These results were implemented in the software tool AMAG Top Cast® Alloy Designer (TCAD) for the prediction of mechanical properties and casting characteristics.

4:35 PM

#### Comparison of Different FEM Codes Approach for Extrusion Process

**Analysis:** *Lorenzo Donati*<sup>1</sup>; Luca Tomesani<sup>1</sup>; Noman Ben Khalifa<sup>2</sup>; A. Erman Tekkaya<sup>2</sup>; <sup>1</sup>University of Bologna; <sup>2</sup>Technische Universität Dortmund

The simulation of the extrusion process by means of FE codes has been applied in a great number of papers available in literature but its application in everyday production was limited due to several factors like computational times, user's skills as well as prediction accuracy. Indeed, the inner complexity of the process, characterized by extremely high deformations, strain rates and heat exchange phenomena, has led only in the last few years commercial FE codes to gain sufficient accurate solving capabilities. In the paper, five FEM codes based on different approaches were applied in the simulation of the same experiment: the results were compared in terms of set-up times, computational time as well as process prediction accuracy. Process load, profile speeds, die and profile temperatures were accurately monitored during the experiment in order to realize an effective comparison of the different FEM codes approaches.

4:55 PM

#### Numerical Prediction of Grain Shape Evolution during Extrusion of AA6082 Alloy

**Analysis:** *Antonio Segatori*<sup>1</sup>; Lorenzo Donati<sup>1</sup>; Luca Tomesani<sup>1</sup>; <sup>1</sup>University of Bologna

Extruded profiles applications require a strict control of the mechanical properties of the extrudates, in particular when undergoing severe loading conditions like in the transportation sector. Profile mechanical properties directly depend from its microstructure and texture, which are the result of multiple mechanisms based on precipitation mechanism or on grain shape evolution (grain refinement, recrystallizations, recovery and grain growth). In this direction the opportunity to predict the final profile microstructure under specific process parameters directly in the die design stage is of great relevance. The study involved experimental activity on grain size measurements during interrupted direct extrusion of an AA6082 round profile. The grain size measurements were coupled with the results of the simulation in order to regress analytical models based on effective strain, strain rate and temperature. Finally, the developed model was implemented in the numerical code through user subroutine so as to be used as microstructure prediction tool.

5:15 PM

#### Analysis of Charge Weld Evolution for a Multi-Hole Extrusion Die

**Analysis:** *Antonio Segatori*<sup>1</sup>; Lorenzo Donati<sup>1</sup>; Barbara Reggiani<sup>1</sup>; Luca Tomesani<sup>1</sup>; <sup>1</sup>University of Bologna

Extrusion process presents two types of welding mechanism inside the die: seam and charge weld. The first type is unavoidable in the production of hollow profiles while the second is generated during billet to billet transition. Differently from seam weld, charge weld represent an unacceptable defect that require profile discard. Nevertheless charge weld extent and location on extrudates is not evident, thus requiring scrap definition by means of time-consuming trials or to repetitive tests on each batch. In the paper an industrial four holes porthole die for hollow profile production was investigated during billet to billet transition. Extrusion of four billet was performed under strict parameter control. The profiles were microscopically analyzed in order to determine weld evolution: in particular start and end points of weld for

each profile were determined. Finally, weld evolution was studied through HyperXtrude code so as to evaluate weld prediction capabilities and accuracy.

### Aluminum Reduction Technology: Environment-Emissions/ Anode Effect I

**Sponsored by:** The Minerals, Metals and Materials Society, TMS Light Metals Division, TMS: Aluminum Committee, TMS: Aluminum Processing Committee

**Program Organizers:** Mohd Mahmood, Aluminium Bahrain; Abdulla Ahmed, Aluminium Bahrain (Alba); Charles Mark Read, Bechtel Corporation; Stephen Lindsay, Alcoa, Inc.

Monday PM

February 28, 2011

Room: 17B

Location: San Diego Conv. Ctr

**Session Chair:** Robert Baxter, Bechtel Corp

2:00 PM

#### HF Measurements Inside an Aluminium Electrolysis Cell

**Analysis:** *Karen Osen*<sup>1</sup>; Thor Aarhaug<sup>1</sup>; Asbjørn Solheim<sup>1</sup>; Egil Skybakmoen<sup>1</sup>; Camilla Sommerseth<sup>2</sup>; <sup>1</sup>SINTEF Materials and Chemistry; <sup>2</sup>Norwegian Institute of Science and Technology, NTNU

HF emissions to the working atmosphere may still be a problem for the aluminium industry. The objective in the present work was to study how the HF evolution is distributed between feeder holes, other openings in the crust, gases diffusing through the crust, fumes from the secondary alumina residing on top of the crust etc. A movable "gas sniffer" connected to a Tunable Diode Laser was used to measure the HF concentrations at the above mentioned locations. The stationary HF level in an open flaming feeder hole was approximately 9000 ppm, when measured a few cm above the bath surface. In comparison, when the probe was positioned 5-10 cm above a crust area with good integrity, the HF concentration was in the range 5-10 ppm. The results support the notion that most of the HF evolves at the open flaming feeder holes and tap hole.

2:20 PM

#### LasIRTM -R – The New Generation RoHS-Compliant Gas Analyzers Based on Tunable Diode Lasers

**Analysis:** *Jean-Pierre Gagne*<sup>1</sup>; John Pisano<sup>2</sup>; Alak Chanda<sup>3</sup>; Gervase Mackay<sup>3</sup>; Keith Mackay<sup>3</sup>; Pierre Bouchard<sup>1</sup>; <sup>1</sup>STAS; <sup>2</sup>University of California at Riverside; <sup>3</sup>Unisearch Associates Inc.

The laser-based optical gas sensor using Tunable Diode Laser Absorption Spectroscopy (TDLAS) is rapidly gaining favor wherever high sensitivity, real time measurement and freedom from interferences are required, specifically for the measurement of HF in primary aluminium smelters. It eliminates the problems associated with extractive gas sampling techniques. A first generation of equipment designed by Unisearch Associates and based on the TDLAS appeared on the market in the mid 90s. It has since been improved significantly by employing fast scan measurement techniques. Now, the system is more robust, easier to operate and calibrate, and it can be simply audited. The utilization of fast scan measurement techniques not only provides enhanced stability and sensitivity but expands the dynamic range of the measurements. This new generation instrument is also very inexpensive compared to other TDLAS instruments. This paper describes the evolution of the new generation gas sensor.

2:40 PM

#### Use of Spent Potlining (SPL) in Ferro Silicomanganese Smelting

**Analysis:** *Paulo von Krüger*<sup>1</sup>; <sup>1</sup>Universidade Federal de Ouro Preto

In this work an evaluation on the possibilities of the employ of Spent Potlining (SPL), as a component of the burden of a Submerged Arc Furnace, producing Ferro Silicomanganese Alloy, is investigated. On this subject, a characterization of the SPL's most probable components as well as their interaction with the existing species in the ferroalloy furnace were carried out. Additionally relevant features of the ferroalloy smelting were identified and characterized. Those figures were introduced in a thermochemical



program where the SAF operational conditions were simulated in order to check the technical feasibility of that use. The simulation results showed that, on the technical point of view, the SPL carbonaceous fraction is a suitable component of the SAF burden, producing Ferro Silicomanganese alloys. Although some of the figures generated by simulation were confirmed in a couple of industrial exploratory tests, a more detailed test program is advisable.

### 3:00 PM

#### **Reduction of PFC Emissions at Pot Line 70 kA of Companhia Brasileira De Alumínio:** *Henrique Santos*<sup>1</sup>; Danilo Melo<sup>1</sup>; Jocimar Calixto<sup>1</sup>; Jefferson Santos<sup>1</sup>; João Miranda<sup>1</sup>; <sup>1</sup>Companhia Brasileira de Alumínio

Following world tendency Primary Aluminum Industry has been committed in the reduction of PFC's emissions in order to reduce the greenhouse effect. Anode Effect is the source for such emission. The CBA Pot Room 70kA VSS Montecatini technology from the end of 60's with side feed pots, has been making efforts and developing actions to improve process with the aim of reducing both the duration and frequency of anode effect. Projects were developed and implemented as follow: Liquids control, Resistance control, Feed control, Anode/Cathode control and mainly the team qualify through an operating training. In this paper, are shown achievements for projects cited, that caused significant impacts in reducing the duration and frequency of anode effect at the level of world reference. A reduction of 66 % of PFC's emissions was achieved from 1,2 to 0,4 t CO<sub>2</sub> eq./t Al.

### 3:20 PM Break

### 3:30 PM

#### **Towards Redefining the Alumina Specifications Sheet – The Case of HF Emissions:** *Linus Perander*<sup>1</sup>; Marco Stam<sup>2</sup>; Margaret Hyland<sup>1</sup>; James Metson<sup>1</sup>; <sup>1</sup>Light Metals Research Centre; <sup>2</sup>Aluminium Delfzijl B.V.

For smelting applications, alumina quality is typically defined in terms of chemical and physical properties, with emphasis on impurity elements, surface area, moisture content, particle size distribution and attrition index. However, these properties fail in prediction of the true HF generation potential, as well as the real capacity for HF removal in the dry scrubbers. Using plant measurements and additional laboratory characterization of a number of alumina samples a broadening of how alumina quality is specified is argued for. Measurements of the residual gibbsite/boehmite content and the pore size distribution, coupled with characterization of the alumina microstructure, can be used to predict and understand the generation of HF during feeding and dissolution as well as the ability to capture HF in the dry scrubbers.

### 3:50 PM

#### **Design of Experiment to Minimize Fluoride and Particulate Emissions at Alumar:** *Eliezer Batista*<sup>1</sup>; Paulo Miotto<sup>1</sup>; Edson Montoro<sup>1</sup>; Luciano Souza<sup>1</sup>; <sup>1</sup>Alcoa

Most of Aluminum plants have been struggling to minimize the fluoride and particulate emissions to reduce the environmental impacts. Nowadays, this challenge has been more difficult to be reached because of amperage increase, alumina quality deterioration and pot room expansions. Alumar, one of Alcoa's units, following a corporate vision, is continuously searching for alternatives to the environmental impact caused by its operations. This full factorial experiment 2k identified the main factors and their impacts on fluoride and particulate emissions. The statistical model indicates that the fluoride emission has been affected mainly by Pot Draft, Pot Dressing, and the Usage of Compressed air for Housekeeping with R2 at 82%, and for particulate at 58%. Based on the models, certain actions were recommended to minimize both of these emissions. In addition, this paper describes, step by step, how this kind of experiment can be applied to the Aluminum industry.

### 4:10 PM

#### **Innovative Distributed Multi-Pollutant Pot Gas Treatment System:** *Geir Wedde*<sup>1</sup>; Odd Bjarno<sup>1</sup>; Anders Sorhuus<sup>1</sup>; <sup>1</sup>Alstom

Gas Treatment Centers (GTC) are traditionally arranged in courtyard between pot rooms and handle vast quantities of pot gas (3- 4mill. m<sup>3</sup>/h) in large number of filter compartments (15-30) with demanding space

requirement and challenging control of operation. Arranging the gas treatment in decentralized installations as Distributed Decentralised Scrubbers (DDS) will obviously save on duct work, alumina handling, storage and civil work. In addition Alstom's DS integrates silos, heat exchangers, scrubbers, fans and stack into an extremely compact and efficient multi-pollutant control and recovery technology with incomparable footprint. The close integration with pots improves pot gas collection and simplifies the alumina distribution to pots. Module based design allows for short delivery time and early start-up. This paper discusses and reviews the new technologies, benefits and mitigation of the technical challenges of the DS solution.

### 4:30 PM

#### **Fluoride Emissions Management Guide (FEMG) for Aluminium Smelters:** *Nursiani Tjahyono*<sup>1</sup>; Yashuang Gao<sup>1</sup>; David Wong<sup>1</sup>; Wei Zhang<sup>1</sup>; Mark Taylor<sup>1</sup>; <sup>1</sup>Light Metals Research Centre

All smelters worldwide operate under strict fluoride emission limits and the reduction of fluoride emissions is further driven by health considerations. A Fluoride Emissions Management Guide (FEMG) has been written by the Light Metals Research Centre, on invitation of the Australian Aluminum Council, under the Asia-Pacific Partnership on Clean Development and Climate. The FEMG aims to provide better understanding of factors affecting fluoride evolution and emission in smelters, and further, to provide smelters with an operational guide for reducing and managing fluoride emissions. The guide uses practical examples with pictures of improvements that are applicable to operational, control and maintenance practices in potrooms, GTCs and other smelter systems. It is customizable to meet the need of any specific smelter. Along with incorporated audit guidelines and training packages, implementation of this guide can, in a short time, lead to significant reduction in fluoride emissions and improvement of operational standards in smelters.

### 4:50 PM

#### **Considerations Regarding High Draft Ventilation as an Air Emission Reduction Tool:** *Stephan Broek*<sup>1</sup>; Neal Dando<sup>2</sup>; Stephen Lindsay<sup>2</sup>; Alain Moras<sup>2</sup>; <sup>1</sup>Hatch Ltd; <sup>2</sup>Alcoa

High draft ventilation is an effective technique for reducing emissions from electrolysis cells while panel covers are removed to perform maintenance. In recent years, many new smelters have implemented high draft ventilation as one of the tools to further reduce air emissions from potrooms. In this paper the principles of high draft ventilation are discussed followed by a presentation on its impact on smelter performance. Comments are provided that concern implementation of high draft ventilation in greenfield and brownfield smelters.

## Approaches for Investigating Phase Transformations at the Atomic Scale: Transformations in Fe, Ni and Al based Systems I

*Sponsored by:* The Minerals, Metals and Materials Society, ASM International, TMS Materials Processing and Manufacturing Division, TMS/ASM: Computational Materials Science and Engineering Committee, TMS/ASM: Phase Transformations Committee  
*Program Organizers:* Neal Evans, Oak Ridge National Laboratory; Francisca Caballero, Spanish National Research Center for Metallurgy (CENIM-CSIC); Chris Wolverton, Northwestern University; David Seidman, Northwestern University; Rajarshi Banerjee, University of North Texas

Monday PM Room: 32B  
February 28, 2011 Location: San Diego Conv. Ctr

*Session Chairs:* Francisca Caballero, Spanish National Research Center for Metallurgy (CENIM-CSIC); Michael Miller, Oak Ridge National Laboratory

### 2:00 PM Invited

**Nano-scale Analysis of Precipitation in Nitrided Steels:** *Tadashi Furuhashi*<sup>1</sup>; Goro Miyamoto<sup>1</sup>; <sup>1</sup>Institute for Materials Research, Tohoku University

Microstructure formed during nitriding of steels is a quite complex phenomena because precipitation of fine alloy nitrides occurs in a chemically inhomogeneous matrix under continuous supply of nitrogen from the surface. In this presentation, the precipitation behaviors of nano-sized nitrides in various ferritic alloys are discussed based on the results of advanced analysis in atomic scale utilizing HREM and 3DAP. In the alloys containing strong nitride forming elements, precipitation of metastable nitrides occurs. Particularly, phase separation in ferrite is enhanced by strong interaction between the element such as Ti or V and nitrogen, resulting in uniform and fine dispersion of G.P zone like metastable clusters. Transition of those metastable phases to stable nitrides takes place gradually during further nitriding. Presence of excess nitrogen in ferrite is also recognized which might contribute to hardening by nitriding partly. A numerical approach to simulate the precipitation of alloy nitrides will be also presented.

### 2:25 PM Invited

**Atomic Structure of NbN GP Like Zones in a Model Fe-Nb-(C)-N Alloy:** *Frederic Danoux*<sup>1</sup>; Thierry Epicier<sup>2</sup>; David Tingaud<sup>3</sup>; Philippe Maugis<sup>4</sup>; <sup>1</sup>CNRS - Université de Rouen; <sup>2</sup>INSA de Lyon; <sup>3</sup>Université Paris 13; <sup>4</sup>Université Paul Cezanne - Marseille

The precipitation of GP like zones in a model Fe-Nb-(C)-N alloy is evidenced on the basis of atomic scale investigations using field ion microscopy (FIM), atom probe tomography (APT) and high resolution electron microscopy (HREM). These techniques support the existence of Nb and N rich monolayers, fully coherent, and lying in the {001} planes of the bcc ferrite ( $\alpha$ -Fe). HREM image simulations strongly suggest that Nb substitutes Fe in these monolayers. However, the position of N atoms, and therefore the elementary unit cell of these platelets, is still not fully understood. First-principle calculations, using the VASP software, were used to investigate the stability of possible unit cells, on the basis of the various NbX (X=C, N) bulk phases under strains similar to the coherency strains. The role of structural vacancies in the stabilisation of the NbN platelets is also investigated.

### 2:50 PM Invited

**Nanometric Scale Investigation of Phase Transformations in Advanced Steels for Automotive Applications:** *Josée Drillet*<sup>1</sup>; Thierry Lung<sup>1</sup>; Nathalie Valle<sup>1</sup>; <sup>1</sup>ArcelorMittal

The current trend towards vehicle lightening in the automotive industry is driven by the need to conform to the new exhaust emission control regulations. This objective presents a challenge to steel manufacturers. The difficulty lies in designing new alloys with the optimum strength/formability/

cost balance for the various components. Here, the key to success lies in controlling the steel microstructure and especially phase transformations at the finest possible scale. Among the different alloying elements, light elements as carbon and boron are of prime importance due to their major effects on the kinetics for phase transformations. Characterization tools combining high spatial and analytical resolution as NanoSIMS and FEG-TEM, have been used. In the paper, examples are presented concerning: • Local carbon distribution in advanced high strength steels, with a specific emphasis on martensite tempering, austenite stabilisation or low density Fe-Mn-Al-C steels. • Boron segregation and precipitation effects to control hardenability.

### 3:15 PM

**Precipitation Strengthening of a Nano-Cluster-Strengthened Ferritic Steel:** *Z. W. Zhang*<sup>1</sup>; Ai Serizawa<sup>2</sup>; C. T. Liu<sup>1</sup>; Xun-Li Wang<sup>2</sup>; M. K. Miller<sup>2</sup>; Bryan Chin<sup>1</sup>; <sup>1</sup>Auburn University; <sup>2</sup>Oak Ridge National Laboratory

The strength of Cu-rich nanocluster strengthened ferritic steels is derived mainly from nanocluster precipitation. This gives the ability to control the alloy's strength and ductility through the control of the precipitation process of nanocluster. The studies on the effects of composition and processing routes on the nature and development of these nanoclusters will enhance our understanding of the underlying mechanisms and to enhance the mechanical properties further. In this study, atom probe tomography (APT), small angle neutron scattering (SANS) have been used to study the nanocluster precipitation in FeCuNiAlMn and FeCuNiAlMnMoVTi steels thermally aged up to 500 h at 500°C. The microhardness results show a typical dependence on Cu-rich precipitate aging time. APT results show no precipitates in as-quenched specimens while Cu-rich clusters appeared and grew during aging for both steels. The results on cluster composition, number density, size distribution obtained by using APT and SANS were compared.

### 3:30 PM Break

### 3:45 PM Invited

**Atom Probe Tomography as a Tool to Advance Steels Design and Performance:** *Elena Pereloma*<sup>1</sup>; Ilana Timokhina<sup>2</sup>; <sup>1</sup>University of Wollongong; <sup>2</sup>Deakin University

Development of modern steels consisting of complex or nano-scale microstructures with advanced properties requires in-depth understanding of the mechanisms responsible for their microstructure/property relationships. The evolution of microstructure during processing is often associated with various changes taking place at atomic level. These include solute distribution between phases as a result of phase transformations, formation of atmospheres at dislocations, clustering and precipitation phenomena due to various thermo-mechanical processing schedules and/or heat treatments. Atom probe tomography (APT) is invaluable tool for gaining insight into events at atomic scale determining the steel properties. This technique also contributes to the fundamental understanding of phase transformations, which is essential for nano-scale engineering of modern steels and optimization of their performance. In this work application of APT to study solute segregation, clustering and precipitation in TRIP steels and nano-structured bainitic steels after isothermal heat-treatment and after thermo-mechanical processing will be discussed.

### 4:10 PM Invited

**Transformation of Martensite to Austenite During Aging in Steel Studied by Atom Probe Tomography and Simulation:** *Dirk Ponge*<sup>1</sup>; Olga Dmitrieva<sup>1</sup>; Gerhard Inden<sup>1</sup>; Julio Millán<sup>1</sup>; Pyuck-Pa Choi<sup>1</sup>; Jilt Sietsma<sup>2</sup>; Dierk Raabe<sup>1</sup>; <sup>1</sup>Max-Planck-Institut für Eisenforschung GmbH; <sup>2</sup>Delft University of Technology

We present atom probe tomography results on phase boundaries between martensite and retained austenite in steel after aging at 450°C. Due to partitioning of Mn and very different diffusibilities of Mn in martensite and austenite a strong accumulation of Mn at the interface is developed. The Mn profile can be explained in terms of the successive motion of the phase boundary into the martensite during aging owing to the formation of new austenite driven by diffusion of Mn into the austenite. This interpretation

is supported by dynamic diffusion calculations where we use the modeling method DICTRA to solve this coupled initial and boundary value problem, as well as the mixed-mode approach involving also the interface mobility. Good agreement between experiment and simulation is obtained by taking into account an increased mobility of Mn in martensite which is attributed to the high defect density of martensite.

**4:35 PM**

**Complementary Use of Transmission Electron Microscopy and Atom Probe Tomography for the Examination of Plastic Accommodation in Nanocrystalline Bainitic Steels:** *Francisca Caballero*<sup>1</sup>; Hung-Wei Yen<sup>2</sup>; Michael Miller<sup>3</sup>; Jer-Ren Yang<sup>2</sup>; Juan Cornide<sup>1</sup>; Carlos Garcia-Mateo<sup>1</sup>; <sup>1</sup>CENIM-CSIC; <sup>2</sup>National Taiwan University; <sup>3</sup>Oak Ridge National Laboratory

A displacive transformation involves the motion of a glissile interface. As in work-hardening, its motion can be halted by defects, such as dislocations, stacking faults or twins in the austenite. The defects are created when the shape deformation accompanying bainite growth is accommodated by plastic relaxation of the surrounding austenite. The growing plate stops before it collides with the austenite grain boundary. Because transformation from strong austenite leads to fine plates, alloys can be designed such that the bainite transformation is suppressed to low temperatures (200-350°C) leading to a nano-scale bainitic microstructure. Complementary high resolution transmission electron microscopy and atom tomography has provided new experimental evidence on the accommodation of transformation strain, subjects critically relevant to understand the atomic mechanism controlling bainitic ferrite growth. Research at the SHaRE User Facility was sponsored by the Scientific User Facilities Division, Office of Basic Energy Sciences, U.S. Department of Energy.

**4:50 PM Invited**

**Effect of Solute Atoms Distribution on the Phase Transformation in Steel:** *Genichi Shigesato*<sup>1</sup>; Shunsuke Taniguchi<sup>1</sup>; Taishi Fujishiro<sup>1</sup>; Masaaki Sugiyama<sup>1</sup>; <sup>1</sup>Nippon Steel Corporation

The phase transformation in steel is strongly affected by the distribution of solute elements. Boron is one of the most effective elements to hinder the diffusional transformation from austenite to ferrite. It has been considered that boron atoms segregate on grain boundaries in austenite phase and lower the grain boundary energy resulting in delaying the ferrite transformation. Manganese also impedes the phase transformation. The segregation of Mn atoms on the grain boundaries of austenite disturbs the nucleation of ferrite while the depletion of Mn around Ti oxide inclusions dispersed in austenite phase promotes the nucleation of ferrite transformation. The behavior of distribution of B and Mn atoms in the vicinity of the grain boundaries and the oxide-matrix interface examined with conventional and aberration corrected STEM will be presented and the influence on the phase transformation will be discussed.

**5:15 PM**

**Influence of Forging Conditions on Mechanical Properties of Ti and V-Bearing High Strength Forging Steels and Associated Precipitation Microstructure Characterized by TEM and 3D-Atom-Probe:** *Naoyuki Sano*<sup>1</sup>; Tatsuya Hasegawa<sup>2</sup>; <sup>1</sup>Sumitomo Metal Industries, Ltd.; <sup>2</sup>Sumitomo Metals (Kokura), Ltd.

Non-heat treated V-bearing high strength low alloy (HSLA) forging steels have been widely used for machine structural use. To improve mechanical properties further, other alloying elements are added in association with vanadium. It has been found that the addition of 0.15wt.% Ti to a V-bearing HSLA steel with the chemical composition of Fe-0.28C-0.55Si-0.75Mn-0.17V leads to lower the Charpy impact toughness and to increase tensile strength, however this effect is quite sensitive to processing conditions, i.e., hot forging temperatures and subsequent cooling rates. Precipitation microstructure evolved during forging process pronouncedly varied depending on the forging temperature range. At high finishing temperature, aligned fine coherent precipitates of (V, Ti)C carbides originated from interphase interface precipitation developed. However, lower finishing temperature induced coarsened and randomly-distributed precipitate

particles, which resulted in the increased impact energy and lower tensile strength.

---

## Biological Materials Science: Bio-Inspiration and Bio-Inspired Materials II: Soft Biomaterials

*Sponsored by:* The Minerals, Metals and Materials Society, TMS Electronic, Magnetic, and Photonic Materials Division, TMS Structural Materials Division, TMS: Biomaterials Committee  
*Program Organizers:* Jamie Kruzic, Oregon State University; Nima Rahbar, University of Massachusetts, Dartmouth; Po-Yu Chen, University of California, San Diego; Candan Tamerler, University of Washington

Monday PM  
February 28, 2011

Room: 15A  
Location: San Diego Conv. Ctr

*Session Chairs:* Paul Calvert, University of Massachusetts; Nima Rahbar, University of Massachusetts Dartmouth

---

**2:00 PM Invited**

**Gelation of Mucin Glycoproteins:** *Rama Bansil*<sup>1</sup>; <sup>1</sup>Boston University

In this talk, I will describe the unusual properties of mucin, a high molecular weight glycoprotein found in mucus, which prevents the stomach from being digested by the acidic gastric juices. Light scattering and rheological techniques show that purified pig gastric mucin solutions form a gel under acidic pH. Atomic Force Microscopy (AFM) of mucin solutions and gels as a function of pH provide direct visual evidence of aggregation. A model of gelation based on the interplay of hydrophobic and electrostatic interactions will be discussed. Molecular Dynamics simulation studies of folding and aggregation of mucin domains provide further support for this model. As an application I will describe how the motility of *H. Pylori*, the bacterium that causes ulcers, is influenced by the pH-dependent gelation of mucin, and conversely how the bacterium affects the gelation of mucin.

**2:30 PM**

**Synthesis of Vitrified Collagen Gels with Optimized Transparency and Mechanical Strength for Repair of Ocular Injuries:** Jennifer Breidenich<sup>1</sup>;

Daniel Mulreany<sup>2</sup>; Freddy Espinoza<sup>2</sup>; Yo-Rhin Rhim<sup>1</sup>; Xiomara Calderon-Colon<sup>1</sup>; Qiongyu Guo<sup>2</sup>; R.L. McCally<sup>1</sup>; *Morgan Trexler*<sup>1</sup>; Oliver Schein<sup>3</sup>; Jennifer Elisseff<sup>2</sup>; <sup>1</sup>Johns Hopkins University Applied Physics Laboratory; <sup>2</sup>Johns Hopkins University; <sup>3</sup>Wilmer Eye Institute

The frequency of ocular injuries on the battlefield has been steadily increasing during recent conflicts. Combat-related eye injuries are difficult to treat and solutions requiring donor tissue are not ideal. Vitrified collagen gels have been developed for repair of ocular injuries, but increased transparency and mechanical strength are desirable for improved vision and ease of handling, respectively. Synthesis of collagen vitrigels was optimized to yield the best combination of high transparency and high mechanical strength. Vitrification parameters that were investigated included temperature, humidity, and vitrification time. Transparency as well as tensile and tear strengths were characterized for each combination of synthesis conditions to evaluate the effects of the vitrification parameters on material properties. Changes in denaturing temperature and collagen fiber organization were also evaluated to correlate properties with structure. Preliminary results of ocular injury repair studies utilizing vitrigels with optimized properties will also be reported.

**2:50 PM Invited**

**Progress Towards Cartilage Engineering Using Peptide Hydrogels:** *Joel Schneider*<sup>1</sup>; <sup>1</sup>National Cancer Institute

Hydrogel materials are finding use for the encapsulation and delivery of mammalian cells for tissue regenerative therapy and cytomedical applications. We have designed a class of small peptides that undergo a triggered intramolecular folding event to form an amphiphilic beta-hairpin conformation that is prone to self-assembly. Self-assembly leads to the formation of a physically crosslinked network of beta-sheet rich fibrils that

MONDAY PM



constitute a mechanically rigid hydrogel. When peptide folding and self-assembly is triggered in the presence of cells, they are directly encapsulated in a uniform and cytocompatible manner. Peptide hydrogels, with or without cells, are shear thinning but have the capacity to quickly re-heal after the cessation of shear. This attribute allows hydrogel loaded with cells to be easily delivered from a syringe/catheter. Primary chondrocyte encapsulation and delivery is demonstrated and phenotype response studied, highlighting our efforts towards cartilage engineering.

### 3:20 PM

#### **Molecular Biomimetics Enables Biological Materials Science and Engineering:** *Mehmet Sarikaya*<sup>1</sup>; <sup>1</sup>University of Washington

Proteins enable biology to be viable through molecular interactions. Using biology as a guide, we biocombinatorially select, bioinformatically enhance and genetically tailor solid binding peptides and utilize them as molecular building blocks in carrying out molecular and nanomaterials science and engineering through biology. In this emerging field of molecular biomimetics, genetically engineered peptides for inorganic materials (GEPI) are used as bionanosynthesizers in biomaterialization, heterofunctional linkers to create thermodynamically stable interfaces between dissimilar materials, and as molecular assemblers for the targeted and directed assembly of nanomaterials towards addressable ordered architectures with genetically designed functions. Here, we will give an update of the utility of various kinds of GEPIs in nanoparticle formation for hybrid probe design and for bionanosensors; biomineral formation for tissue regeneration, and graphite-binding peptides for nano-electronics to demonstrate the power of the approach enabling nanotechnology and nanomedicine through materials science. Funded by NSF-MRSEC and NSF-BioMat programs.

### 3:40 PM Break

### 3:50 PM Invited

#### **Hydrogels Formed by Inkjet Printing through Ionic Self-Assembly for Tissue Engineering and Drug Delivery:** Skander Limem<sup>1</sup>; Donald McCallum<sup>2</sup>; David Kaplan<sup>3</sup>; Marc in het Panhuis<sup>2</sup>; Gordon Wallace<sup>2</sup>; *Paul Calvert*<sup>1</sup>; <sup>1</sup>University of Massachusetts; <sup>2</sup>University of Wollongong; <sup>3</sup>Tufts University

Self-assembled ionic hydrogels are familiar when formed by the layer-by-layer method, which adds a monolayer of each polymer on every dipping cycle. We have been using inkjet printing to form similar gels at a rate 100x faster by printing anionic (polystyrenesulfonate) and cationic (polydimethylallylamine hydrochloride) polymers sequentially from a two-color printer. Gels of this type are not well understood because they have not previously been formed in bulk. We have characterized the swelling and dye-release properties and find that these change depending on the relative proportions of the two polymers and the extent of annealing of the structure. Similar gels can be formed from carboxylate polymers such as alginate and hyaluronic acid with chitosan and from polyglutamic acid with polylysine. Growth of cells on and in these gels is also being studied as a model for intercellular matrix.

### 4:20 PM

#### **Fabrication of 3D Hydrogel Matrices Containing Yeast and Human Cells:** *Paul Calvert*<sup>1</sup>; Swati Mishra<sup>1</sup>; Dapeng Li<sup>1</sup>; <sup>1</sup>University of Massachusetts Dartmouth

Acrylate hydrogels containing yeast and mammalian cells are formed by a blue-light activated polymerization that does not damage the cells. The viability and metabolic rate of the cells entrapped in the gel are determined and related to the thickness of the gel layers. Using a monomer paste thickened with nanoparticulate silica, 3D porous structures can be built. This is viewed as a route to tissue mimics and bioreactors but methods must be developed to control cell multiplication in order to avoid disruption of the gel layers.

### 4:40 PM

#### **Synthesis of Cellulose Hydrogels with High Strength and Transparency for Use as an Ocular Bandage:** *Morgan Trexler*<sup>1</sup>; Jenna Graham<sup>1</sup>; Jeffrey Maranchi<sup>1</sup>; Jennifer Breidenich<sup>1</sup>; Russell McCally<sup>1</sup>; Marcia Patchan<sup>1</sup>; Freddy Espinoza<sup>2</sup>; Jeremy Chae<sup>2</sup>; Iossif Strehin<sup>2</sup>; Oliver Schein<sup>3</sup>; Jennifer Elisseeff<sup>2</sup>; <sup>1</sup>Johns Hopkins University Applied Physics Laboratory; <sup>2</sup>Johns Hopkins University; <sup>3</sup>Wilmer Eye Institute

Cellulose is a biologically-derived material with excellent wound healing properties. The high strength of cellulose fibers and the ability to synthesize gels with high optical transparency makes these materials amenable for ocular bandage applications, which are becoming increasingly important in combat. Hydrogels were synthesized from cellulose derived from plant and bacterial sources. Material properties including mechanical strength, optical transparency, oxygen permeability, water content, and contact angle were evaluated, as these parameters are all critical for ocular applications, and compared with the natural cornea. Based on these materials characterization results and biocompatibility tests, cellulose types were down-selected for use in a temporary ocular bandage. The resulting cellulose gels were then functionalized with amine groups to achieve compatibility with a previously developed ocular adhesive. Results from preliminary in vivo tests will also be presented.

### 5:00 PM

#### **Fabrication of a Cellulosic Nanocomposite Scaffold with Improved Supermolecular Structure as a Potential Cardiovascular Tissue-Engineered Graft:** *Parisa Pooyan*<sup>1</sup>; Hamid Garmestani<sup>1</sup>; Rina Tannenbaum<sup>1</sup>; <sup>1</sup>Georgia Institute of Technology

Cellulose nanowhiskers (CNWs) with its renewable and environmentally benign nature, and its abundance and excellent biocompatibility could potentially open a new avenue in cardiovascular tissue engineering for small caliber grafts. Inspired by this bioapplication, we have designed a fully bio-based nanocomposite of aligned CNWs embedded in a matrix of cellulose acetate possessing a controlled biodegradability, 3D porosity, and non-acidic byproducts as opposed to degradable PLA/PGA. To ensure uniform distribution, CNW were delicately extracted from a multi-stage process and dissolved in a solvent of choice prior to mixing with the matrix to inhibit whiskers flocculation. Comparable to Carbon Nanotubes and Kevlar, CNWs imparts significant strength and directional rigidity to the composite even at 0.2 wt% yet intensifies to about 40% within a controlled magnetic field of 0.3T. We believe our novel aligned nanocomposite could have groundbreaking features withstanding the physiological pressure and mimicking the topographical texture of the native extracellular graft.

### 5:20 PM

#### **Lessons from Nature: Biomimicry of Leaf Surfaces:** *John Nychka*<sup>1</sup>; <sup>1</sup>University of Alberta

The biological environment is vast yet the common denominator for life is water. While water is a requisite for most life on Earth too much water can be deleterious; for example plant leaf surfaces must remain dry to maintain gas exchange and prevent rotting. Various plant surfaces showing different wetting behavior will be described in this presentation; analysis of the structure of the epicuticular wax morphology on leaf surfaces will be discussed in the context of its effect on wetting behavior. Biomimicry of certain leaf surfaces using engineering materials will be described along with potential biomaterials applications of such technology.

## Bulk Metallic Glasses VIII: Alloy Development and Application II

Sponsored by: The Minerals, Metals and Materials Society, TMS Structural Materials Division, TMS/ASM: Mechanical Behavior of Materials Committee

Program Organizers: Gongyao Wang, University of Tennessee; Peter Liaw, Univ of Tennessee; Hahn Choo, Univ of Tennessee; Yanfei Gao, Univ of Tennessee

Monday PM Room: 6D  
February 28, 2011 Location: San Diego Conv. Ctr

Session Chairs: J. Eckert, IFW Dresden; Jinn Chu, National Taiwan University of Science and Technology

### 2:00 PM Invited

#### Ti-Based Bulk Metallic Glasses and Composites for Structural and Functional Applications: J. Eckert<sup>1</sup>; <sup>1</sup>IFW Dresden

Ti-based bulk glassy alloys and composites have potential for use in various fields due to the low density of the main constituent element Ti and high corrosion resistance. Their ultimate strength exceeds the values achievable for conventional microcrystalline alloys significantly. However, the strong monolithic amorphous/nanostructured alloys usually lack ductility, and an additional toughening phase is often needed to improve plasticity and to promote local shear events to be distributed more homogeneously. Recent results obtained for the structural and compositional analysis of the microstructures of Ti-based bulk metallic glasses and composites will be presented. The deformation behaviour and possible phase transitions during deformation and upon heating to elevated temperatures will be related to the structure of the glass in order to derive guidelines for the design of macroscopically ductile high-strength materials. The role of mechanically induced phase transitions and twinning of crystals for improving the ductility will be critically discussed.

### 2:20 PM

#### Evaluation of Physical and Mechanical Properties of Metallic Glasses in Micro/nano Scales: Jinn Chu<sup>1</sup>; Yen-Chen Chen<sup>1</sup>; Jason Jang<sup>2</sup>; Tsong-Ru Tsai<sup>3</sup>; Hidemi Kato<sup>4</sup>; <sup>1</sup>National Taiwan University of Science and Technology; <sup>2</sup>National Central University; <sup>3</sup>National Taiwan Ocean University; <sup>4</sup>Tohoku University

Recently, the process development of metallic glasses and the improvement of their mechanical properties have attracted considerable attention from the view point of potential applications. However, for industrial applications, the important issues that need to be overcome are their size limitation and room-temperature ductility. From this point of view, metallic glasses (MGs) exhibit viscous flow at high temperatures in the supercooled liquid region; thus they can be used to produce micro-devices via micro-/nano-imprinting. In this study, we demonstrate that various micro-/nano-patterns of Pd-based BMG can be imprinted from a mold in air. In addition, the physical and mechanical properties of the BMGs are evaluated. The obtained results suggest that the BMG is a suitable material for micro-/nano- imprinting, and is also a good mold material for imprinting.

### 2:30 PM Invited

#### Alloying Effects on Glass-Forming Ability and Soft Magnetic Properties of Fe-Based Bulk Metallic Glasses with a High Fe Concentration: H. X. Li<sup>1</sup>; J. E. Gao<sup>1</sup>; Z. B. Jiao<sup>1</sup>; Z. P. Lu<sup>1</sup>; <sup>1</sup>University of Science and Technology Beijing

Compared to the commercial silicon steels, Fe-based amorphous and nanocrystalline alloys which usually exhibit lower coercive force and core loss are attracting more and more attention as the transformer cores for high energy efficiency. However, the low glass-forming ability makes them available only as ribbons, powders or wires, as demonstrated by commercial products of FINEMET and NANOPERM alloys. In this talk, effects of metallic elements on the ferromagnetic system Fe-(P,C,Si,B) will be summarized and a group of newly developed soft magnetic Fe-C-Si-B-P-TM

(TM-transition metals) bulk amorphous alloys with a unique combination of super-high saturation magnetization (>1.5T), high glass-forming ability (=1mm) and high compressive fracture strength (= 3GPa) will be reported. Alloying effects on glass-forming ability and soft magnetic properties will also be discussed in detail.

### 2:50 PM Invited

#### Superplastic Deformation at Nanoscale in Metallic Glass: Scott Mao<sup>1</sup>; J. Luo<sup>1</sup>; Jianyu Huang<sup>2</sup>; <sup>1</sup>University of Pittsburgh; <sup>2</sup>Sandia National Lab

Metallic glasses are regarded as potential engineering materials for their high strength, hardness and large elastic strain. However, due to their high plastic instability, metallic glasses fail catastrophically once the shear band propagates throughout the specimen body, leading to near zero global plastic strain at room temperature. However, if the "brittle" metallic glass has extremely small dimensions at tens of nanometres, the shear bands will no longer operate, the flow and fracture mechanisms may change. Here we show that Al90Fe5Ce5 metallic glass with nanoscale size can undergo superplastic deformation with tensile elongation of ~200%. Finally necking occurred without shear bands in the nanoscale sample with the area reduction nearly 100%. Remarkably, even an atomic chain can be formed in the necking area approaching fracture, which is never found in metallic glass systems. Our discovery is fundamentally important for understanding the physics nature of metallic glasses in small scale.

### 3:10 PM

#### Atomic Mobility Inside Shear Bands and the Impact on Tracer Diffusion, Nucleation and Growth: Gerhard Wilde<sup>1</sup>; Joachim Bokeloh<sup>1</sup>; Gerrit Reglitz<sup>1</sup>; Harald Rösner<sup>1</sup>; Sergiy Divinski<sup>1</sup>; <sup>1</sup>University of Muenster

Although the occurrence of shear bands during plastic deformation of metallic glasses is well known, their actual physical properties remain fairly unknown. Here, experimental data on the rate of atomic diffusion within shear bands has been obtained using the radiotracer method on post-deformed specimens. The experimental results indicate unambiguously that the diffusivity is largely enhanced as compared to volume diffusion in metallic glasses. Moreover, nanocrystal formation has been observed in metallic glasses during different deformation processes. This finding has generated great interest as well as controversial discussions concerning the underlying mechanism. Here, different deformation methods with largely different strain and pressure levels have been applied on metallic glasses to investigate the deformation-induced nanocrystallization reaction with the strain as a metric for the transformation. The experimental results are discussed with respect to the underlying mechanism, utilizing also the first experimentally determined values of the diffusivity within a shear band.

### 3:20 PM Break

### 3:30 PM Invited

#### Bending-Ductility Improvements of Bulk Metallic Glass by Surface Coatings: Jinn Chu<sup>1</sup>; Bo-Shian Houn<sup>1</sup>; Jason S. C. Jang<sup>2</sup>; Yin-Yu Chang<sup>3</sup>; Peter K. Liaw<sup>4</sup>; Yoshihiko Yokoyama<sup>5</sup>; Akihisa Inoue<sup>5</sup>; <sup>1</sup>National Taiwan University of Science and Technology; <sup>2</sup>National Central University; <sup>3</sup>Mingdao University; <sup>4</sup>The University of Tennessee; <sup>5</sup>Tohoku University

Room-temperature mechanical properties of bulk metallic glasses (BMGs) are characterized by excellent strength and elasticity with a lack of plasticity. Many attempts have been made to improve the ductility of BMGs, including surface modifications by shot peening. Our present study reports the use of Zr-based metallic-glass thin films as a promising coating to enhance the BMG bending ductility. The Zr-based BMG substrate is sputtered and coated with a 200 nm-thick Zr-based film and thin Ti adhesive layer. The coated sample has a maximum four-point bending loading of ~ 7 KN, a rise of ~ 75% from the uncoated one, with the 10-fold increased toughness to ~ 1,432 J and surface elongation reaching ~ 10%. Fractographic studies reveal that shear bands become highly populated for the coated BMG, suggesting that the ductility is closely related to the multiplication of the shear bands in the BMG substrate.

3:50 PM

**Characterization and Mechanical Response of Amorphous Fe<sub>45</sub>Ni<sub>45</sub>Mo<sub>7</sub>B<sub>3</sub> Honeycombs:** *Balaji Jayakumar*<sup>1</sup>; Jay Hanan<sup>1</sup>; <sup>1</sup>Oklahoma State University

The high yield strength and elastic modulus of metallic glasses implies that they could perform an important role in structural applications. In order to produce materials with a high strength-to-weight ratio and excellent energy absorption capabilities, it is advantageous to form amorphous alloys as cellular solids. Using the elastic property of slip cast amorphous Fe<sub>45</sub>Ni<sub>45</sub>Mo<sub>7</sub>B<sub>3</sub> ribbons, a metallic glass honeycomb was manufactured with a unique manufacturing approach. First prototypes were manufactured with a porosity of 96%, cell wall thickness of 0.028 mm and a cell size of 3 mm. We report ongoing studies of the mechanical properties of Fe<sub>45</sub>Ni<sub>45</sub>Mo<sub>7</sub>B<sub>3</sub> honeycombs. Experimentally measured mechanical properties are comparable to that of existing analytical models. Also, suggesting that potentially a 3X improvement in the strength properties in the out-of-plane direction are achievable when compared to that of crystalline Aluminum and Nomex honeycombs.

4:00 PM *Invited*

**Air-Oxidation of a [(Co<sub>50</sub>Cr<sub>15</sub>C<sub>15</sub>Mo<sub>14</sub>B<sub>6</sub>)<sub>97.5</sub>Er<sub>2.5</sub>]<sub>93</sub>Fe<sub>7</sub> Bulk Metallic Glass at 600 - 725 °C:** *Wu Kai*<sup>1</sup>; P.C. Lin<sup>1</sup>; Y.H. Wu<sup>1</sup>; W.S. Chen<sup>1</sup>; Z.Z. Liang<sup>1</sup>; H.L. Jia<sup>2</sup>; P.K. Liaw<sup>2</sup>; <sup>1</sup>Institute of Materials Engineering, National Taiwan Ocean University; <sup>2</sup>Department of Materials Science and Engineering, The University of Tennessee

The oxidation behavior of a [(Co<sub>50</sub>Cr<sub>15</sub>C<sub>15</sub>Mo<sub>14</sub>B<sub>6</sub>)<sub>97.5</sub>Er<sub>2.5</sub>]<sub>93</sub>Fe<sub>7</sub> bulk metallic glass (Co7-BMG) was studied over the temperature range of 600 – 725 °C in dry air. Nearly no oxidation was observed after oxidation at 625 °C for 36 h, indicative of an excellent oxidation resistance of the amorphous alloy. In addition, the oxidation kinetics of the Co7-BMG followed a two- to three-stage parabolic-rate law at T > 650 °C, having its steady-state parabolic-rate constants (kp values) increased with temperature. The scales formed on the Co7-BMG were very thin, consisting of an intermixed layer-structure mostly of CoMoO<sub>4</sub>, minor amounts of Cr<sub>2</sub>O<sub>3</sub>, CoCr<sub>2</sub>O<sub>4</sub>, and uncorroded Co<sub>3</sub>B at T > 650 °C. The formation of Co<sub>3</sub>B implied that a phase transformation of the amorphous substrate was occurred during oxidation at the temperature of interest.

4:20 PM

**Deformation Behaviour of Metallic Glasses:** *B Vishwanadh*<sup>1</sup>; R Tewari<sup>1</sup>; S Sharma<sup>1</sup>; R Kishore<sup>1</sup>; G K Dey<sup>1</sup>; <sup>1</sup>Bhabha Atomic Research Centre

The present paper reports on the influence of deformation on the structure and on mechanical properties of rapidly solidified ribbon (RSR) and bulk metallic glass (BMG) of the Zr<sub>52</sub>Ti<sub>6</sub>Al<sub>10</sub>Cu<sub>18</sub>Ni<sub>14</sub>(at%) alloy. The structure of as-solidified as well as deformed glasses has been probed by X-ray diffraction, transmission electron microscopy, positron annihilation, differential scanning calorimetry and nano indentation. Through these studies it has been established that the as-solidified structure is different at the different regions of BMG. For example, the peripheral region had lower medium range order (MRO) and higher free volume in comparison to the central region leading to higher hardness at periphery than in the central region. Through nano-indentation experiments, it has been demonstrated that subsequent to deformation BMG undergoes work softening whereas RSR undergoes work hardening. These behaviors have been explained in the present paper on the basis of change in free volume and MRO.

4:30 PM *Invited*

**Deformation Behavior and Deformation-Induced Nanocrystallization of Bulk Metallic Glasses:** *Tao Zhang*<sup>1</sup>; <sup>1</sup>Beihang University

For extensive applications of bulk metallic glasses (BMGs) with high strength as structural materials, development of BMGs with good plasticity and understanding the mechanism of their plastic deformation are of great importance, which have been widely studied in the last decade. We will review our recent work on the syntheses and deformation behavior of Cu-, Ti- and Zr-based BMGs with good plasticity. Especially, the Zr-based BMG exhibited remarkable work hardening besides plastic strain of ~20% in compression. For understanding the underlying mechanism of the deformation behavior of the present BMGs, the structural changes induced

by deformation as well as thermal stability of the BMGs were studied. It was found that deformation-induced nanocrystallites in glassy matrix as well as their crystalline defects could be responsible for the improved deformation behavior.

4:50 PM

**Dependence of Fracture Toughness on the Configurational State of a Metallic Glass:** *Glenn Garrett*<sup>1</sup>; Jin-Yoo Suh<sup>1</sup>; Michael Floyd<sup>2</sup>; Angeliki Kapoglou<sup>3</sup>; Marios Demetriou<sup>1</sup>; William Johnson<sup>1</sup>; <sup>1</sup>CalTech; <sup>2</sup>UC Berkeley; <sup>3</sup>European Space Agency

The fracture toughness of a metallic glass is thought to be determined by the ability of the glass to undergo extensive plastic shearing by hopping across a potential energy landscape while simultaneously resisting crack formation. Here, the fracture toughness of Zr<sub>35</sub>Ti<sub>30</sub>Cu<sub>8.25</sub>Be<sub>26.75</sub> relaxed at different configurational states in the potential energy landscape was measured using single-edge-notch bending specimens. Key potential energy landscape variables such as the elastic constants and stored enthalpy were measured at each configurational state, and correlated to fracture toughness. The fracture toughness is found to correlate more strongly with the shear elastic constant, thereby revealing that toughness is limited predominantly by the resistance of the glass to undergo plastic shearing.

5:00 PM *Invited*

**Dynamic Mechanical Behavior of Bulk Metallic Glass and Its Composite:** *Morgana Trexler*<sup>1</sup>; *Naresh Thadhani*<sup>2</sup>; <sup>1</sup>The Johns Hopkins University Applied Physics Laboratory; <sup>2</sup>Georgia Institute of Technology

The mechanical behavior of bulk metallic glass and its composite with tungsten particles is investigated as a function of dynamic uniaxial-stress and uniaxial-strain conditions. Anvil-on-rod impact tests instrumented with high-speed digital photography and velocity interferometry, were performed to determine the localized deformation and failure response, and elastic-plastic wave propagation characteristics. Imaging of transient deformation states and sample back surface velocity profiles obtained from the experiments were correlated with predictions from numerical simulations to validate the applicability of the Stassi-Drukker-Prager constitutive model used for describing the behavior of the BMG and the composite. Uniaxial-strain shock loading experiments were also performed to obtain evidence of shock-induced polymorphism which was observed to result in increase in strength and failure stresses. The state of the understanding of high-strain-rate deformation and shock compression response of bulk metallic glasses and their composites will be discussed in this presentation. [Research funding provided by U.S. Army Research Office].

5:20 PM

**Dynamic Compressive Behavior of Fe Based Amorphous Metal Honeycomb Cellular Structures:** *Advait Bhat*<sup>1</sup>; Jay Hanan<sup>1</sup>; Ganapathi Mahadevan<sup>1</sup>; <sup>1</sup>Oklahoma State University

Cellular solids like honeycombs have potential applications as energy absorbers. The typical applications are in dynamic stress environments. Quasistatic compression behaviors of honeycombs have been widely explored, however, their dynamic compression properties remain largely unknown. Also, no prior testing has been carried out on amorphous metal based honeycombs. The dynamic compressive behavior of a Fe<sub>45</sub>Ni<sub>45</sub>Mo<sub>7</sub>B<sub>3</sub> amorphous metal based honeycomb was investigated and mechanical properties were compared to those at quasistatic strain rates. The results indicate significant strain rate sensitivity. The observations can be compared to those seen in amorphous metal foams tested under similar conditions. The energy absorption capacity of this honeycomb is found to exceed that of aluminum counterparts of similar relative density.

5:30 PM *Invited*

**Atomic-Scale Structural Heterogeneity, Percolation and Unified Yielding Behavior in Metallic Glasses:** *Yong Yang*<sup>1</sup>; Jianchao Ye<sup>1</sup>; C.T. Liu<sup>1</sup>; Jian Lu<sup>1</sup>; <sup>1</sup>the Hong Kong Polytechnic University

Recent studies indicate that metallic glasses (MGs) can be viewed as atomic-scale composites containing soft free-volume zones and hard atomic clusters. In this study, the dynamic microcompression method developed recently was



utilized to characterize the atomic-scale structural heterogeneity of MGs and further to understand their yielding mechanisms. Based on the experimental findings, a percolation model was constructed to quantify the observed deformation-controlled yielding phenomenon in MGs. The experimental and theoretical results clearly show that the apparent universal yielding strain of ~2%, as measured from a wide range of MG alloys, originates from a percolation process that involves the destabilization of the sharing zones among solute-centered atomic clusters. The deformation mechanism proposed here is basically consistent with the spirit of the potential energy landscape (PEL) concept and provides an insight into the structure-property relationship in MGs, which has been remaining as a longstanding unresolved scientific problem for many years.

#### 5:50 PM

**The Oxidation Behavior of an FeCo-Based Bulk Metallic Glass at 600 - 700°C:** *Wu Kai*<sup>1</sup>; Pin-Chen Lin<sup>1</sup>; Yan-Hao Wu<sup>1</sup>; Z.Z. Liang<sup>1</sup>; P.K. Liaw<sup>2</sup>; <sup>1</sup>Taiwan Ocean University; <sup>2</sup>University of Tennessee

The oxidation behavior of an [(Fe<sub>50</sub>Co<sub>50-75</sub>B<sub>20-30</sub>Si<sub>3-96</sub>)<sub>100-x</sub>Nb<sub>x</sub> bulk metallic glass (FeCo5-BMG) was studied over the temperature range of 600 – 700 °C in dry air. The results showed that nearly no oxidation was observed for the FeCo5-BMG after oxidized at 600 °C for 36 h, indicative of a better oxidation resistance. In addition, the oxidation kinetics of this glassy alloy followed a two- to three-stage parabolic-rate law at higher temperatures, having its parabolic-rate constants ( $k_p$  values) increased with temperature. The scales formed on the FeCo5-BMG were very thin, consisting of an intermixed layer-structure of Fe<sub>3</sub>O<sub>4</sub>, Co<sub>3</sub>O<sub>4</sub>, B<sub>2</sub>O<sub>3</sub>, and uncorroded Fe<sub>3</sub>B. The formation of Fe<sub>3</sub>B further indicated that a phase transformation of the amorphous substrate was taken place during oxidation at the temperature of interest.

### Cast Shop for Aluminum Production: Casthouse Productivity and Safety

*Sponsored by:* The Minerals, Metals and Materials Society, TMS Light Metals Division, TMS: Aluminum Committee, TMS: Aluminum Processing Committee

*Program Organizers:* Geoffrey Brooks, Swinburne University of Technology; John Grandfield, Grandfield Technology Pty Ltd

Monday PM  
February 28, 2011

Room: 16A  
Location: San Diego Conv. Ctr

*Session Chairs:* Leonard Aubery, SELEE Corporation; David De Young, Alcoa

#### 2:00 PM Introductory Comments

#### 2:10 PM

**New Casthouse Smelter Layout for the Production of Small Non-Alloyed Ingots: Three Furnaces/Two Lines:** Jacques Berlioux<sup>1</sup>; Arnaud Bourcier<sup>1</sup>; Jean-Louis Baudrenghien<sup>1</sup>; Christian Jonville<sup>1</sup>; Nicolas Tardy<sup>1</sup>; <sup>1</sup>Rio Tinto Alcan

This paper deals with a layout for a smelter casthouse producing small non-alloyed ingots. The layout of aluminium casthouses has important consequences with respect to safety, investment and operating cost. Traditional solution for casthouse producing non-alloyed ingots is two furnaces per one ingot line. In order to improve the economics and logistics the casthouse a detailed study was done, which required: detailed performance analysis, in particular relating to furnace/ingot line connections, impact on maintenance, operations, etc, hazard study, modeling of metal flow from tapping in the potline through to the end-product, including breakdowns and downgraded operation, thermal and flow modeling in the launder, in steady state and temporary operation and detailed determination of the launder. It was demonstrated that a layout based on such a configuration is superior in terms of full economic cost. This design is now part of our casthouse basic engineering package.

#### 2:35 PM

**Use of Process Simulation to Design a Billet Casthouse:** *Gwenola Jaouen*<sup>1</sup>; <sup>1</sup>Rio Tinto - Aluval

Designing a casthouse for billet is a complex activity. The billet casthouse must be properly sized to optimize the metal flow, and continuously feed the homogenization shop, while bearing in mind that oversizing adds no value and is costly. To solve this problem, it is necessary to accurately analyze the operations of the casthouse in real time and this requires a discrete simulation model. A model has been developed with a library that includes all the necessary equipment: conveyors, continuous and batch furnaces, finishing stations. The model was used to design an expended casthouse which requests the management of complex product mixes and which challenges the robustness and flexibility of the installation. By combining this model with the metal flow sizing model, it was possible to validate the performance of the design and its impact on casthouse operation. This resulted in a shop designed for customer needs, at optimal cost.

#### 3:00 PM

**Optimizing Scrap Reuse as a Key Element in Efficient Aluminium Cast Houses:** *Tom Schmidt*<sup>1</sup>; Jan Migchielsen<sup>1</sup>; <sup>1</sup>Otto Junker

In the last decades, the market share of secondary aluminium is slowly replacing primary aluminium. However, as the demand for aluminium is still considerable larger than the collection of used aluminium, primary aluminium will also be needed for the coming decades. This paper will address the current position of this development and the possibility to further increase the part of used aluminium scrap as the source for production of new aluminium to come to a durable production. The second part of the paper will concern the melting facilities for recycling used scrap.

#### 3:25 PM

**Implementation of an Effective Energy Management Program Supported by a Case Study:** *Roger Courchee*<sup>1</sup>; <sup>1</sup>K B Alloys, LLC

Effective energy management programs require commitment and leadership from Upper Management supported by an experienced Energy Manager. The vehicle for change is the Energy Management Working Party. The Working Party will be led by a Senior Manager and include other line managers under the technical guidance the Energy Manager. The first step is to use historical data to calculate an energy management performance indicator called Specific Energy Consumption [SEC] and then continue the calculations using real time data. The Working Party will initiate programs to achieve a continuous improvement in the SEC and in conjunction with Upper Management agree long term targets. Techniques will include evaluating base load data (energy consumed when not in production), projects targeted at energy inefficient equipment and a review of the various manufacturing processes to develop low energy solutions. This presentation is supported by a case study of the KB Alloys facility at Wenatchee WA.

#### 3:50 PM Break

#### 4:00 PM

**Molten Metal Safety Approach through a Network:** *Christian Pluchon*<sup>1</sup>; Bruno Hannart<sup>1</sup>; Laurent Jouet-Pastré<sup>1</sup>; <sup>1</sup>Alcan Engineered Product

Molten Metal explosion or splash is a major risk encountered in the aluminium casthouses. Alcan EP has had to face an accident in 2006, in one explosion in its casthouse. Unfortunately an employee had 2nd degree burns on the face. After expertise of the accident and implementation of corrective action in the plant, it appeared that we had a potential of improvement in management of Molten Metal risk by sharing experience coming from the merged companies, Alcan, Pechiney and Algroup. The EP management decided to create a network constituted of experienced managers of most of the casthouses. It was key to look deeply in the details and to think to the practical aspects of every decision. A novel approach of the management of Molten Metal risk was born in the company. The system was very powerful to align the whole organization on the objective to minimize risks.

4:25 PM

**Improved Monolithic Materials for Lining Aluminum Holding and Melting Furnaces:** *Andy Wynn*<sup>1</sup>; *John Coppack*<sup>1</sup>; *Tom Steele*<sup>1</sup>; *Ken Moody*<sup>1</sup>; <sup>1</sup>Thermal Ceramics

To remain competitive, aluminum producers continue to increase productivity through their Melt-Hold furnaces. Increasing heat input to the furnace using more powerful burners is common practice. But faster melting leads to increased metal losses from surface oxidation and to segregation from large heat gradients. These effects are countered by increased use of fluxes and increased stirring. Given the increasingly challenging environment within which the refractory lining has to work, traditional lining solutions can no longer be relied upon to provide the service lives that were previously achieved. Therefore, a new generation of furnace lining materials is required to cope with today's aluminum furnace. This work reports on a new monolithic material with improved performance, compared to existing materials, suitable for use in the critical metal contact areas of aluminum furnaces. Improved corundum growth resistance, salt resistance and thermal shock resistance are demonstrated in the laboratory using industry standard test methods.

4:50 PM

**Cost of Poor Quality in Aluminium Cast House Processes:** *Puliyur Krishnaswamy Narasimha Raghavan*<sup>1</sup>; <sup>1</sup>Bharat Aluminium Co. Ltd., (A Unit of Vedanta Resources Plc.), BALCO Nagar, Korba

Over 30 years aluminium casthouse technology has been driven by a number of factors such as, Competition from alternative materials, Lightweighting, Market requirements for enhanced properties affecting gas levels, impurities, inclusions, physical and chemical properties, ease of downstream processing, reduced cost and improved delivery, Reduction in conversion cost by various means including capacity increase, maximising asset utilization, minimizing scrap, reducing melt loss, labour, reduction in inspection with improved processes control activity, energy costs and need for improved safety performance. This paper will explore how these, and related considerations have provided the stimulus for improved casthouse technology by reducing Cost Of Poor Quality (COPQ). An attempt has been made to monitoring the COPQ and there by brining in improvement in the quality of the Aluminium Cast House products with a competitive reduction in Cost of production COP).

## Characterization of Minerals, Metals and Materials: Mineral Processing and Analysis

*Sponsored by:* The Minerals, Metals and Materials Society, TMS Extraction and Processing Division, TMS/ASM: Composite Materials Committee, TMS: Materials Characterization Committee  
*Program Organizer:* Sergio Monteiro, State University of the Northern Rio de Janeiro - UENF

Monday PM  
February 28, 2011

Room: 14B  
Location: San Diego Conv. Ctr

*Session Chairs:* Donato Firrao, Politecnico di Torino; Joner Alves, University of Sao Paulo

2:00 PM

**A Study on a Greensand Slate from Abaeté as a Source of Potassium: Thermal Treatment on Different Temperatures and Extraction on Acidic Media:** *Adriana da Silva*<sup>1</sup>; *Francisco Garrido*<sup>1</sup>; *Marta Medeiros*<sup>1</sup>; *João Sampaio*<sup>2</sup>; <sup>1</sup>UFRJ; <sup>2</sup>CETEM

Brazil is a great agricultural potential and its crop success is related to the soil's chemical and physical characteristics. The production of potassium fertilizers is a major concern because in 2009 Brazil produced only 10% of its needs and spent almost US\$ 2 billion on the purchase of this fertilizer. In this context, a potassium rock has been studied in order to evaluate its use as an alternative source of potassium to the Brazilian agriculture. This rock has been thermal treated with CaO (from 10 to 30%) at different temperatures

(from 800 to 1200°C) and its structural modifications have been supervised using x-ray diffraction and infrared spectroscopy. At the temperature of 1200°C and 10% of CaO, it was possible to observe the formation of new phases, such as spinel, that could improve the potassium availability that was quantified on acidic extractions using citric acid.

2:15 PM

**Application of High-Power Nanosecond Pulses to Flotation Separation of Sulfide Minerals:** *Igor Bunin*<sup>1</sup>; *Valentine Chanturiya*<sup>1</sup>; *Alexey Kovalev*<sup>1</sup>; *Irina Khabarova*<sup>1</sup>; *Elizaveta Kopolulina*<sup>1</sup>; <sup>1</sup>Research Institute of Comprehensive Exploitation of Mineral Resources RAS

The paper presents new theoretical and experimental results about mechanisms of disintegration of mineral complexes and structural transformations of the sulfide surface under high-power nanosecond electromagnetic pulses (HPEMP). The heated gas outflow from nanosecond breakdown channels of sulfide minerals under HPEMP is considered. It is shown that the gas outflow from channels can be an additional destructive factor in the processes of the electric pulse discharge disintegration of mineral complexes. It is shown that the effect of HPEMP changes chemical surface composition and, respectively, technological properties of pyrrhotite and pentlandite. Morphology and elementary composition of new micro- and nanoformations on mineral surface of pentlandite and pyrrhotite have been investigated using up-to-date methods of SEM/EDX and Scanning Probe Microscopy. Preliminary electropulse effect on mineral products before flotation allows producing optimal conditions for flotation separation of pentlandite and pyrrhotite owing to forming the new nanophases and defects on the surface of sulfides.

2:30 PM

**Sulfur Deposition Impact on Surface Morphology of Fly Ash-Based Adsorbent for Mercury Removal:** *Yaohua Chen*<sup>1</sup>; *Wei Gao*<sup>1</sup>; *Qingcai Liu*<sup>1</sup>; *Cunfang Lu*<sup>1</sup>; *Jian Yang*<sup>1</sup>; <sup>1</sup>University of Chongqing

Mercury is a toxic air pollution, and coal-fired utility plants are the largest anthropogenic emission source in China. Due to rapidly decreasing the cost and increasing the efficiency, it is becoming necessary to develop alternative technologies/materials for mercury removal. The adsorbents made from fly ash of coal-fired, and became spherical after sintering at temperature 500°C. Finally, it has been treated by thermal precipitation sulfur, to remove mercury in fuel gas. High temperature deposition furnace was applied to increase sulfur content in fly ash based adsorbents produced in lab. The experiments can increase its sulfur content of adsorbent, and found that sulfur attached to the surface, mesopore structure, microporous structure of fly ash-based adsorbents. So these treatments can increase their surface area and enhanced their adsorption capacity, while the sulfur was filled in interspace as small molecule S2 and S5. And the specific surface area increased by sulfur-loading and increasing temperature.

2:45 PM

**Sulfur Contents on the Distribution Characteristics of Mercury in Coals:** *Wei Gao*<sup>1</sup>; *Qingcai Liu*<sup>1</sup>; *Cunfang Lu*<sup>1</sup>; *Jian Yang*<sup>1</sup>; *Huimin Zheng*<sup>1</sup>; *Juan Wen*<sup>1</sup>; *Chunling Yao*<sup>1</sup>; <sup>1</sup>university of Chongqing

The coal samples were collected from coal fields in 12 provinces. There were studied on concentration, distribution, mode of occurrences and impact factors of mercury in Chinese coals. Sulfur and mercury in bituminous coals have been examined using X-ray fluorescence spectrometry, X-ray diffraction, and mercury spectrometer. Mercury levels in coal are related to the geographic location of the coals and types of the coals. A synthesis of result indicated that most likely occurrence modes of mercury in high-sulfur and high-mercury coals are in solid solution in pyrite. Coal samples showed that most values of mercury concentration in coal varied from 100 to 1000 ng/g with an average of approximately 500ng/g, and mathematical model about correlation between mercury and sulfur was gained by mathematical statistics. This is apparent that mercury and sulfur vary concomitantly from coal data, the high correlation between them at confidence of 95%( $\alpha=0.05$ ).

### 3:00 PM

**Characterization of Burrows from Mining District of Pachuca - Real Del Monte, in Hidalgo State and Viability Study to Use These Residues as Alternate Industrial Material:** Juan Hernández<sup>1</sup>; Eleazar Salinas<sup>1</sup>; Francisco Patiño<sup>1</sup>; Isauro Rivera<sup>1</sup>; Martín Reyes<sup>1</sup>; Miguel Pérez<sup>1</sup>; Eduardo Cerecedo<sup>1</sup>; <sup>1</sup>Universidad Autónoma del Estado de Hidalgo

A complete characterization of burrows from mining district of Pachuca - Real del Monte was done. These kind of residues had not been seriously characterized, and the results found lead to an average chemical composition of 79.43 % wt SiO<sub>2</sub>, 7.032 % wt Al<sub>2</sub>O<sub>3</sub>, 2.69 % wt Fe<sub>2</sub>O<sub>3</sub>, 0.70 % wt Mn, 3.98 % wt K<sub>2</sub>O, 3.34 % wt CaO, 2.50 % wt Na<sub>2</sub>O, 1.01 % wt MgO, 0.26 % wt TiO<sub>2</sub>, 0.04 % wt Zn, 0.026 % wt Pb, 56 g/t Ag and 0.6 g/t Au; showing as principal mineralogical phases: Quartz, Berlinite, Orthoclase, Feldspar, Anorthoclase and Calcite. By the other hand, joint with the big volume of these deposits and its chemical and mineralogical characteristics, this material can be used to the fabrication of ceramics, mixing it with agglutinants to produce, refractory bricks, in the industry of cement and to recover metallic values such as gold and silver.

### 3:15 PM

**Structural Characterization of Apatite Type Rare Earth Silicates:** Lii-Cherng Leu<sup>1</sup>; Sherin Thomas<sup>2</sup>; Mailadil Sebastian<sup>2</sup>; Rick Ubic<sup>1</sup>; Scott Mixture<sup>3</sup>; <sup>1</sup>Boise State University; <sup>2</sup>National Institute for Interdisciplinary Science and Technology; <sup>3</sup>Alfred University

Apatite-type rare-earth silicates have received much attention recently owing to their wide range of applications in microelectronics, solid-oxide fuel cells, solid-state lasers and phosphors. The crystal structure of Rare-earth apatite type Sr<sub>2</sub>RE<sub>8</sub>(SiO<sub>4</sub>)<sub>6</sub>O<sub>2</sub> (RE=La, Pr, Tb, Tm and Y) ceramics which were synthesized in a phase-pure form are characterized crystallographically via both electron and X-ray diffraction. The results show evidence of hexagonal crystal structure with space group P6<sub>3</sub>/m (No.176) for Sr<sub>2</sub>RE<sub>8</sub>(SiO<sub>4</sub>)<sub>6</sub>O<sub>2</sub> (RE=La, Pr, Tb and Y). The Rietveld structure refinement on X-ray diffraction data indicated a decrease in metaprimism twist angle for Sr<sub>2</sub>Tm<sub>8</sub>(SiO<sub>4</sub>)<sub>6</sub>O<sub>2</sub> and suggested that the hexagonal metric of apatite might not be sustained and the symmetry is reduced to monoclinic space group P2<sub>1</sub>/m (No.11) in order to compensate shorter bond length of the Tm ions.

### 3:30 PM Break

### 3:45 PM Keynote

**Materials Characterization is the Key to Effective and Efficient Processing: Case Studies in Extractive Cu Leaching and Mineral Processing Post-Evaluation of Drywall:** Ann Hagni<sup>1</sup>; <sup>1</sup>Geoscience Consultant

Obtaining efficient and effective processing is a main component to profitability in materials processing and production environments. Materials characterization, in turn, is the key to understanding pre-processing and post-processed materials, which enables improvements in processing and increasing profits. Two case studies will be examined showing how the same materials characterization skills and abilities can be applied to very different real world scenarios in resolving processing dilemmas. Case 1 is an extractive copper leaching project at Johnson Camp Mine in Cochise County, Arizona, in which economic copper-bearing phases and deleterious clay phases are identified, quantified, and phase relationships imaged. Case 2 is a characterization study of one of the largest building construction materials problems ever to occur in the US of problematic drywall installed primarily during 2006 and 2007. Examining American-made versus Chinese-made drywall reveals clear distinctions between the two as post-mortem (after installation) evaluations.

### 4:25 PM

**The Influence of Ca on (Sr<sub>2-x</sub>Ca<sub>x</sub>)(MgTe)O<sub>6</sub> Double Perovskites:** Steven Letourneau<sup>1</sup>; Rick Ubic<sup>1</sup>; Sherin Thomas<sup>2</sup>; G. Subodh<sup>3</sup>; M. Sebastian<sup>2</sup>; <sup>1</sup>Boise State University; <sup>2</sup>National Institute for Interdisciplinary Science and Technology; <sup>3</sup>Physikalisches Institut

Complex perovskite oxides (A<sub>2-x</sub>A'<sub>x</sub>)(B<sub>2-y</sub>B'<sub>y</sub>)O<sub>6</sub> are ubiquitous in electronic applications, and a complete understanding of such structures

and the mechanisms which affect them is essential in predicting and controlling properties. Oxygen octahedral tilting and chemical ordering, in particular, are known to lower symmetry and influence dielectric properties. By investigating the appearance of superlattice reflections in electron and X-ray diffractograms, a summary of the octahedral tilting (tilt system) of the structure can be identified, cation ordering inferred, and space group symmetry established. In the case of the (Sr<sub>2-x</sub>Ca<sub>x</sub>)(MgTe)O<sub>6</sub> system, a phase transformation occurs from a tetragonal *I4/m* symmetry at *x* = 0 (Sr<sub>2</sub>MgTeO<sub>6</sub>) to monoclinic *P2<sub>1</sub>/n* symmetry for *x* = 0.5; however, B-site cation ordering causes ½{odd,odd,odd} type reflections in all compositions, complicating crystallographic characterization. The temperature coefficient of resonant frequency is negative throughout the series; permittivities were in the range 13.2-14.3, and quality factors varied from 27,500 to 81,000 (5-6GHz).

### 4:40 PM

**Technological Characterization of Phonolite Rock to Be Applied as Source of Nutrients to the Brazilian Agriculture:** Aline Maria Teixeira<sup>1</sup>; João Sampaio<sup>2</sup>; Francisco Garrido<sup>3</sup>; Marta Medeiros<sup>3</sup>; <sup>1</sup>IQ/UFRJ - CETEM; <sup>2</sup>CETEM-MCT; <sup>3</sup>IQ-UFRJ

The rocks for crops is a natural practice for soils fertilization and consists on adding rocks to the soil while the water by chemical weathering decomposes the rock and release the nutrients gradually to the soil solution. This practice can be considered an alternative to the low production of potassium fertilizers in Brazil. In this context, the phonolite rock will be characterized in order to evaluate its application as an alternative source of nutrients to the Brazilian agriculture. The phonolite that will be studied is an igneous, volcanic rock as alkaline character that chemically is composed by a high grade of potassium due to the presence of feldspar minerals. In order to quantify the minerals present in the sample the characterization will be carried out using several techniques such as X-ray diffraction, X-ray fluorescence and scanning electron microscopy.

### 4:55 PM

**Study on Thermal Stabilities of 2- Substituted Benzimidazoles Copper and Zinc Complex:** Yan Shi<sup>1</sup>; Dan Li<sup>1</sup>; Qingqiao Liu<sup>2</sup>; Zhongliang Xiao<sup>1</sup>; <sup>1</sup>Changsha University of Science and Technology; <sup>2</sup>Hunan Hualing Xiantan Steel Co. Ltd.

2-substituted benzimidazole-zinc and 2-substituted benzimidazole-copper complex were main components of organic solderability preservative (OSP) in PCB producing process and affect the thermal stability of OSP film. So these two complexes were prepared by 2-substituted-benzimidazole reacting with zinc ion and copper ion, the complex crystals were determined by IR, its thermal stabilities were studied by TG method. The results indicated that the thermal stability of 2-substituted benzimidazole-zinc is higher than the 2-substituted benzimidazole-copper, and the thermal decomposition mechanism was presented.

### 5:10 PM

**Investigation on Extracting Boric Acid from Saline Brine by Boron Specific Chelating Resin:** Xiang Xiao<sup>1</sup>; Baizhen Chen<sup>1</sup>; Xichang Shi<sup>1</sup>; Yunfeng Fu<sup>1</sup>; Hui Xu<sup>1</sup>; Xiyun Yang<sup>1</sup>; <sup>1</sup>Central South University School

Extracting boric acid from saline brine by boron specific ion-exchange resin was investigated. Effects of resin amount, temperature, time and stirring speed on boron adsorption rate were studied in the experiments. The results indicated that the XSC-700 resin showed excellent boron adsorbability and it performed better property for elution. The maximum boron adsorption capacity was 6.16 mg.ml<sup>-1</sup> in the optimum conditions: the resin concentration of 5ml/100ml (brine), the temperature of 60°C, the time of 5-6h and the stirring speed of 100r/min. Boron was eluted from the resin with HCl and boric acid was crystallized by evaporating the eluate. The product of boric acid was in pure form as confirmed by XRD and other analysis techniques.



5:25 PM

**Low Temperature Carbothermic Reduction of Panzhihua Low Grade Ilmenite after Ball Milling:** Ying Lei<sup>1</sup>; Yu Li<sup>1</sup>; Jinhui Peng<sup>1</sup>; Libo Zhang<sup>1</sup>; Shenghui Guo<sup>1</sup>; Wei Li<sup>1</sup>; <sup>1</sup>Key Laboratory of Unconventional Metallurgy, Ministry of Education

In this work, low temperature carbothermic reduction of Panzhihua low grade ilmenite after ball milling were investigated. The ball milling of ilmenite and graphite were processed in a ball mill. The milling process can attenuate the particle of ilmenite, and the ilmenite characteristic peak were broadened and weakened. The reduction temperature and behaviors are studied on the thermo gravimetric apparatus; lower temperature and higher reaction rate were obtained for the reduction of ilmenite with graphite after milled. The reduction temperature and times of ilmenite decreased to 1000~1025°C and 40~60min via milled for 4 or 8h; Low down the reduction temperature can eliminate the solution of Mg<sup>2+</sup> and FeTiO<sub>3</sub> in a certain degree; the reduced ilmenite has an obvious loose structure, can favored the subsequent procedure such as leaching.

## Chloride 2011: Practice and Theory of Chloride-Based Metallurgy: Pyrometallurgy and Acid Regeneration

*Sponsored by:* The Minerals, Metals and Materials Society, Canadian Institute of Metals, TMS Extraction and Processing Division, TMS: Magnesium Committee, TMS: Energy Committee  
*Program Organizers:* Dirk Verhulst, Consultant, Extractive Metallurgy; V.I. (Lucky) Lakshmanan, Process Research Ortech, Inc.

Monday PM  
February 28, 2011

Room: 19  
Location: San Diego Conv. Ctr

*Session Chairs:* Khamal Adham, Hatch Ltd.; Lisa Helberg, E.I. DuPont de Nemours

2:00 PM

**Chloride Metallurgy: Process Technology Development:** Edgar Peek<sup>1</sup>; <sup>1</sup>Xstrata Process Support

The two dominant metallurgical problems in treating most base metal (sulphide) concentrates in both the chloride and sulphate system are iron removal and sulphur elimination, respectively. In this paper the opportunities, limitations and fundamentals of the chloride metallurgy system are described against this background. Only the treatment of oxide and sulphide ores is considered. Both hydrometallurgical and pyrometallurgical unit process operations are highlighted, since most successful base metal processes are based on a combination of the two. Hence, an overview of the technical and also some economical aspects of chloride metallurgy are presented. This overview summarizes the successful applications of chloride metallurgy, but it will not give exhaustive process and plant descriptions. It predominantly focuses on the essential technical features of the metallurgical unit process operations, while providing numerous references separately.

2:25 PM

**Purification of Titanium Tetrachloride: A History:** Lisa Helberg<sup>1</sup>; <sup>1</sup>E.I. DuPont de Nemours

Titanium tetrachloride is produced through the chlorination of a variety of titanium bearing ores, some occurring in nature, and others enriched in titanium content by a variety of "beneficiation" processes. The chlorination step can produce a variety of metal chloride impurities, such as iron chlorides and vanadium chlorides, which must be removed from the TiCl<sub>4</sub> before it can be used to produce pigmentary TiO<sub>2</sub>, titanium metal or for any other commercial use. The requisite manipulations involve both physical and chemical separations in a multi-step process. The history of various purification strategies will be discussed.

2:50 PM

**Zirconium Chlorination Behavior: A Literature Review:** Donald Voir<sup>1</sup>; <sup>1</sup>Westinghouse

The reaction rate between zircon or zirconia, carbon, and chlorine is controlled by temperature, and the degree of contact intimacy between the carbon and the zirconium. Chlorination behavior observed in static beds (and pellets) is characterized by a thin reacting front that advances through the bed or pellet. Excess and unreacted material becomes an "ash layer" that limits chlorine access to the reacting front. The reaction rate for stoichiometric, well mixed, pelletized, sub-sieve zirconia is about 100 mmoles/cm<sup>2</sup>/hr at 800°C. The reaction rate for loosely packed, ~100μ carbon and zirconia is about 1 mmole/cm<sup>2</sup>/hr. Plug flow and fluid bed reactors, using much coarser zircon or zirconia and carbon particles, have a reaction rate of about 1 μmole/cm<sup>3</sup>/hr. The reaction rate is controlled by a slow reaction between carbon and zirconium species that results in an essentially zero order reaction rate dependency for the chlorine concentration.

3:15 PM

**HCl Leaching and Acid Regeneration Using MgCl<sub>2</sub> Brines and Molten Salt Hydrates:** Jan deBakker<sup>1</sup>; Joshua LaMarre<sup>1</sup>; Vladimiro Papangelakis<sup>2</sup>; Boyd Davis<sup>1</sup>; <sup>1</sup>Queen's University; <sup>2</sup>University of Toronto

HCl leaching using molten salt hydrates has the potential to improve the extraction of nickel from laterite ores. However, as in other HCl leaching applications, recovery of HCl is problematic. Spray pyrohydrolysis, which is used in current chloride-based flowsheets, represents a high energy cost. The authors have developed a proposed molten salt hydrate laterite leach circuit using an alternative HCl recovery route. The leach circuit envisions a leach by HCl gas in a MgCl<sub>2</sub> MSH medium, followed by Ni/Co recovery, iron hydrolysis, precipitation of magnesium from solution as magnesium hydroxychloride, and thermal decomposition of the hydroxychloride to produce HCl gas. The flowsheet will allow a chloride leach circuit to take place with simpler equipment requirements and lower energy cost than is currently available. The laboratory work investigates key aspects of the flowsheet, including precipitation of magnesium hydroxychlorides and their composition; magnesium hydroxychloride thermal decomposition; and iron control by selective pyrohydrolysis.

3:40 PM

**Precipitation of Hematite and Recovery of Hydrochloric Acid from Concentrated Iron Chloride Solutions by a Novel Hydrolytic Decomposition Process:** Levente Becze<sup>1</sup>; Sebastian Hock<sup>1</sup>; George Demopoulos<sup>1</sup>; <sup>1</sup>McGill University

Regeneration of HCl from chloride solutions is commercially practiced by high temperature (800-900°C) pyrohydrolysis associated with high energy consumption and capital cost. As an alternative to pyrohydrolysis a novel low temperature (<200°C) non-autoclave hydrolytic process has been studied in this research work, which comprises two steps. In the first step, ferrous chloride is oxidized by oxygen at T=150 °C, followed by hydrolytic decomposition of ferric chloride to coarse hematite particles and superazeotropic hydrochloric acid (8-9M) operated at approximately 180°C. This paper provides a summary of the laboratory results related to both oxidation and hydrolysis and presents a newly designed conceptual process flowsheet.

4:05 PM Break

4:20 PM

**Application of Oxygen Enrichment for the Pyrohydrolysis of Metal Chlorides:** Kamal Adham<sup>1</sup>; Cassandra Lee<sup>1</sup>; <sup>1</sup>Hatch Ltd.

Metal chlorides (e.g. iron and nickel) can be pyrohydrolysed at elevated temperatures to yield a HCl rich off-gas and an oxide product. Typically, the high energy requirement for pyrohydrolysis is provided by the combustion of a hydrocarbon fuel with air. Here, it is demonstrated that the use of oxygen-enriched air can result in lower fuel consumption and better HCl concentration. In addition, the oxygen enrichment can result in smaller quantity of off-gas and less expensive process equipment. This new concept can be applied to both the spray roaster and the fluidized bed reactor. Similar

to the air-combustion case, the O<sub>2</sub> enriched process can use a direct contact venturi scrubber, to recover energy from the roaster off gas, but at a higher efficiency. The new process also uses an absorption tower for capturing HCl from the roaster off-gas, but generates a stronger HCl solution, than is currently possible with air roasting.

4:45 PM

**Chlorine, Copper and “De Novo” Synthesis of Dioxins:** Alfons Buekens<sup>1</sup>; Shao Ke<sup>1</sup>; <sup>1</sup>Zhejiang University, Institute for Thermal Power Engineering (ITPE)

The de novo synthesis of dioxins involves a low temperature catalytic conversion of carbonaceous substrates in a flow of air. The theory as developed by Dr. Stieglitz (FZ Karlsruhe) involves copper as most potent catalyst. Tests on various sources of carbon (activated carbon, three types of soot, and graphite) conducted at 300°C allowed comparing native samples (without) with cupric chloride doped ones. Steam addition to the combustion air raises the rate of oxidation, which in turn is severely suppressed by sulphur dioxide. This paper presents thermodynamic calculations on the system Cu-Cl-O-S at the temperature of the experiments (300°C), as well as in a wider range of potential copper catalysed dioxin generation. For the sake of comparison, the results are compared with those obtained while using other transition metals as a catalyst. Some preliminary computations are presented.

5:10 PM

**Segregation Roasting of a Saprolitic Laterite Ore: An Experimental Investigation:** Munyaradzi Kwatara<sup>1</sup>; Juzer Tayabally<sup>1</sup>; Edgar Peek<sup>1</sup>; Ron Schonewille<sup>2</sup>; <sup>1</sup>Xstrata Process Support; <sup>2</sup>Xstrata Nickel

The potential recovery of nickel from a South-American saprolitic laterite ore using the segregation roasting technique was investigated. The ore was heated to temperatures that ranged between 900 and 1000°C in a rotary kiln. In all the tests, the laterite ore was first mixed with a predetermined amount of calcium chloride and either coal or coke. By varying the temperature, calcium chloride and reductant in the different tests, a preliminary set of optimal conditions was established for the specific laterite ore that was tested. A combination of chemical analysis and electron-probe-micro-analysis (EPMA) were used to determine and evaluate the effectiveness of segregation roasting on the recovery of nickel. The present paper describes the test procedure and the results that were obtained.

5:35 PM

**Mechanism of Selective Chlorination of Reduced Limonitic Nickel Laterite Using a Solid Chloride Agent:** Chuanlin Fan<sup>1</sup>; Xiujing Zhai<sup>1</sup>; Yan Fu<sup>1</sup>; Yongfeng Chang<sup>1</sup>; Binchuan Li<sup>1</sup>; Ting-an Zhang<sup>1</sup>; <sup>1</sup>Northeastern University

The mechanism of the selective chlorination of nickel and cobalt in reduced limonitic laterite was investigated. Reduced ores were obtained from the reduction roasting of a limonitic nickel laterite. The thermal decomposition of related chlorides and the selective chlorination of the reduced ore were carefully studied using Differential Thermal analysis – Thermogravimetry (DTA-TG), X-Ray Diffraction and chemical leaching methods. In the temperature range of 300 - 500 °C, aluminum chloride hexahydrate was chosen as chloride agent. During the selective chlorination, reduced ore was partly chlorinated by hydrogen chloride generated from the thermal decomposition of chloride agent. Then the oxydrolisis of ferrous chloride re-generated hydrogen chloride used to further the chlorination. Finally, iron was mostly rejected as hematite, while nickel and cobalt were selectively chlorinated. More than 91%Ni,90%Co and about 4%Fe in the chlorinated ore was extracted using a water leaching method.

---

## Computational Thermodynamics and Kinetics: Brent Fultz Honorary Session I: Joint Session with Neutron and X-Ray Studies of Advanced Materials IV Symposium

*Sponsored by:* The Minerals, Metals and Materials Society, ASM International, TMS Electronic, Magnetic, and Photonic Materials Division, TMS Materials Processing and Manufacturing Division, TMS: Alloy Phases Committee, TMS: Chemistry and Physics of Materials Committee, TMS/ASM: Computational Materials Science and Engineering Committee, ASM: Alloy Phase Diagrams Committee  
*Program Organizers:* Raymundo Arroyave, Texas A & M University; James Morris, Oak Ridge National Laboratory; Mikko Haataja, Princeton University; Jeff Hoyt, McMaster University; Vidvuds Ozolins, University of California, Los Angeles; Xun-Li Wang, Oak Ridge National Laboratory

Monday PM  
February 28, 2011

Room: 9  
Location: San Diego Conv. Ctr

*Session Chairs:* Xun-Li Wang, Oak Ridge National Laboratory; Michael Manley, Lawrence Livermore National Laboratory

---

2:00 PM Introductory Comments

2:05 PM Invited

**Megawatts and Petaflops:** Ian S. Anderson<sup>1</sup>; <sup>1</sup>Oak Ridge National Laboratory

A new generation of MW spallation neutron sources is providing unprecedented measurements of the dynamics of systems in, and away from, equilibrium. This ever-increasing experimental sophistication in synthesizing and interrogating matter at all levels is now taking place under the guidance of elaborate predictive models whose solution and simulation has been enabled by powerful cyber-capabilities and sophisticated mathematical and computational algorithms. Combining computational and experimental methods is increasingly important in materials science and engineering to extract critical information from data (e.g., intrinsic correlations between structure, processing, and properties/behavior), as well as being increasingly necessary for breakthroughs. Although numerous examples exist of successful combinations of modeling and experiment the question arises: how to make the most impact from the new capabilities?

2:35 PM Keynote

**High Temperature Thermodynamics and Atom Vibrations:** Brent Fultz<sup>1</sup>; <sup>1</sup>California Institute of Technology

The harmonic model often gives a good starting point for the vibrational thermodynamics of materials. The vibrational entropy is big, however, and at high temperatures relatively small non-harmonic effects can alter substantially the thermodynamics of alloy phases. One effect can be understood as standard “quasi-harmonic” behavior, where vibrational frequencies are lowered as a crystal expands against its bulk modulus. Most materials show a second effect from phonon-phonon interactions (PPI), and sometimes a third from how electronic excitations interact with vibrations (electron-phonon interaction, EPI). New results are presented from a study on the phonon lifetimes in aluminum, where we show with perturbation theory that the PPI from cubic anharmonicity accounts well for the lifetimes of the individual phonons. In other metals, the EPI can be important thermodynamically to temperatures approaching 1000 K. Rules of thumb for these effects are emerging from chemical and structural trends of electronic and phonon dispersions.

3:05 PM Invited

**Collective Behavior of Intrinsic Localized Modes Observed in the Vibrational Spectrum Of NaI:** Michael Manley<sup>1</sup>; <sup>1</sup>Lawrence Livermore National Laboratory

Intrinsic localized modes (ILMs) form in the lattice vibrations of both metallic uranium and ionic sodium iodide. These dynamic nonlinear hot

MONDAY PM

spots have been found to impact a variety of technologically important properties including thermal expansion, diffusion, mechanical behavior, phase transformations, and thermal conductivity. In this talk I will present recent discoveries on the ILMs in NaI that are challenging the independent local mode picture. First, the polarization of the ILMs collectively switch between  $\langle 111 \rangle$  and  $\langle 011 \rangle$  with very small temperature changes. Second, once an ILM polarization locks in the parent mode fragments into several distinct dispersive modes of different symmetry. This suggests that the ILMs are organizing into arrays or patterns that modulate the parent mode. Pattern formation by ILMs in anharmonic crystals was predicted more than a decade ago but never observed. Invited talk for symposium in honor of Brent Fultz

#### 3:35 PM Break

#### 4:00 PM Invited

**Ab Initio above Zero: Alloy Thermodynamics from First Principles:** Axel van de Walle<sup>1</sup>; <sup>1</sup>Caltech

Although ab initio methods excel at calculating physical properties for any given atomic arrangements, proper modeling of the thermodynamic properties of solid-state alloys demands a sampling of the large number of states visited in thermal equilibrium, a task that is computationally intractable via a brute-force approach. This talk describes how this impasse can be resolved through a combination of automated computational techniques that are able to efficiently model electronic excitations, lattice vibrations and configurational disorder within a unified framework: the cluster expansion formalism in conjunction with a suitable coarse-graining of the partition function.

#### 4:30 PM Invited

**Studies on Vibrational Entropy in Alloys Using Inelastic Neutron Scattering at ORNL:** Jack Robertson<sup>1</sup>; <sup>1</sup>Oak Ridge National Laboratory

Inelastic neutron scattering spectra and neutron diffraction patterns were measured for a verity of binary alloys using the triple-axis spectrometers at the High Flux Isotope Reactor (HFIR) at Oak Ridge National Laboratory. Phonon density-of-states curves were calculated from the inelastic scattering spectra, allowing estimates of the vibrational entropy in the harmonic and quasiharmonic approximations. A survey of studies done in collaboration with Professor Fultz and his students will be presented.

#### 5:00 PM Invited

**Time-of-Flight Inelastic Neutron Scattering Studies of Phonons and Magnetism in Polycrystalline Samples:** Robert McQueeney<sup>1</sup>; <sup>1</sup>Iowa State University

Neutron time-of-flight inelastic spectrometers with large area detectors provide complex data sets containing the wavevector and energy dependences of vibrational and magnetic excitations in solids. Extracting detailed information about the excitations continues to spur the development of more and more powerful calculations of the dynamics of solids. Over the last several years, our efforts have focused on the ability to analyze and interpret data from polycrystalline samples. In this talk, I summarize how the simultaneous development of new time-of-flight spectrometers and computation has furthered our understanding of the phonons and magnetism in several materials, most notably, our studies of cerium and plutonium metals and orthoferrite-based oxides. Although these materials appear quite dissimilar, in each case electronic valence fluctuations have profound effects on the structural phase diagrams and magnetic properties.

## David Pope Honorary Symposium on Fundamentals of Deformation and Fracture of Advanced Metallic Materials: Intermetallics II and Ti Alloys

*Sponsored by:* The Minerals, Metals and Materials Society, TMS Materials Processing and Manufacturing Division, TMS Structural Materials Division, TMS: High Temperature Alloys Committee, TMS/ASM: Mechanical Behavior of Materials Committee, TMS: Nanomechanical Materials Behavior Committee  
*Program Organizers:* E. P. George, Oak Ridge National Laboratory; Haruyuki Inui, Kyoto University; C. T. Liu, The Hong Kong Polytechnic University

Monday PM  
February 28, 2011

Room: 32A  
Location: San Diego Conv. Ctr

*Session Chairs:* Kevin Hemker, Johns Hopkins University; Michael Smith, Federal Bureau of Investigation

#### 2:00 PM Invited

**Transformation-Induced Plasticity during Pseudo-Elastic Deformation in Ni-Ti Microcrystals:** Michael Mills<sup>1</sup>; Peter Anderson<sup>1</sup>; Matthew Bowers<sup>1</sup>; Sivom Manchiraju<sup>1</sup>; Peter Sarosi<sup>2</sup>; Michael Uchic<sup>3</sup>; <sup>1</sup>The Ohio State University; <sup>2</sup>General Motors R & D Tech Center; <sup>3</sup>Air Force Research Labs RXLM

Micromechanical testing of single crystal Ni-Ti based shape memory alloys is being performed in an effort to understand the effects of specimen size and crystal orientation on martensite-induced pseudoelastic and shape memory response. The primary goal in this investigation is to determine the means by which the matrix accommodates the large strain associated with the martensitic transformation. This information is critical in extending the working life of components under cyclic loading and/or heating. Micron-scale pillars of several crystallographic orientations have been prepared by FIB and tested in compression. Post-mortem TEM analysis has revealed the plasticity induced by the transformation. We demonstrate through this method that it is possible to directly study the mechanical response and defect generation associated with individual, isolated martensitic transformations. The experimental results are correlated with the predicted transformations and local stresses due to the crystallographic theory of martensite.

#### 2:30 PM Invited

**Some Unusual Aspects of the Deformation of FeAl and Fe<sub>2</sub>MnAl:** I. Baker<sup>1</sup>; <sup>1</sup>Dartmouth College

An overview of three unusual aspects of the behavior of the B2 compound FeAl and the L21 derivative Fe<sub>2</sub>MnAl is presented. First, both compounds show a yield anomaly. A model for the anomaly in FeAl, based on vacancy hardening (E.P. George and I. Baker, Phil. Mag. A, 77 (1998) 737), is outlined along with both data supporting and predictions of the model. The applicability of the model to describe the yield anomaly in Fe<sub>2</sub>MnAl is discussed. Second, both the room-temperature ductility and yield strength of these compounds are affected by water vapor. The phenomenology associated with this behavior is discussed along with a possible fracture mechanism. Finally, both compounds show a paramagnetic to ferromagnetic transition upon room-temperature deformation, which is reversed upon annealing. A model for this behavior (Y. Yang, I. Baker, and P. Martin, Phil. Mag. B, 79 (1999) 449), based on the formation of anti-phase boundary tubes, is presented.

#### 3:00 PM Invited

**Recent Progress in High Temperature TiAl Alloys:** Guoliang Chen<sup>1</sup>; Junpin Lin<sup>2</sup>; <sup>1</sup>Univ. of Science and Technology Beijing; <sup>2</sup>univ. of Science and Technology Beijing

Conventional cast TiAl alloys have been used for the engine GENx. However, the conventional TiAl alloys are not strong enough for applications at higher temperatures. TiAl alloy have been developed into two categories: conventional TiAl and high temperature TiAl (high niobium containing)



alloys. These state-of-the-art alloys have great advantage that the service temperature is 60-100 oC higher than that of conventional TiAl alloys. The presentation discuss the relationships among composition, microstructure and properties for high temperature TiAl alloys, including the phase relationship with high Nb contents, the high temperature strengthening mechanisms of Nb, Al and other elements, excellent oxidation resistance at high temperature, especially focusing the new technology for the fabrication and processing of pilot ingots.

### 3:30 PM

**Atomistic Simulations of Cross-Slip Nucleation in L12 Ni3Al:** *Satish Rao*<sup>1</sup>; Dennis Dimiduk<sup>2</sup>; Jaafar El-Awady<sup>3</sup>; Triplicane Parthasarathy<sup>1</sup>; Michael Uchic<sup>2</sup>; Christopher Woodward<sup>2</sup>; <sup>1</sup>UES Inc.; <sup>2</sup>Air Force Research laboratory; <sup>3</sup>Johns Hopkins University

Using atomistic (molecular statics) simulations with embedded atom potentials, we evaluate the configurations for a dislocation to form the PPV lock by intersecting a forest dislocation in L12 Ni3Al. The activation energies were estimated by determining equilibrium configurations (energies) when variable pure tensile or compressive stresses are applied along the [111] direction on the intersection configurations. We show that the activation energy at the forest dislocation intersection is significantly lower than that for cross slip in bulk. These results suggest that cross-slip should be preferentially observed at selected screw dislocation intersections in L12 Ni3Al.

### 3:45 PM

**Effect of Lamellar Microstructure on Impact Toughness and Fracture Behavior in Wrought Gamma TiAl Alloy:** *Hirotoyo Nakashima*<sup>1</sup>; Toshikazu Kikugawa<sup>1</sup>; Shun Oinuma<sup>2</sup>; Masao Takeyama<sup>1</sup>; <sup>1</sup>Tokyo Institute of Technology; <sup>2</sup>Former graduate student (Currently Toshiba Corporation Power Systems Company)

Impact properties and fracture behavior of wrought  $\gamma$ -TiAl based alloys with various microstructures have been evaluated by means of an instrumented Charpy impact test and a specially designed three-point bend machine installed in SEM chamber, respectively. The alloy studied is Ti-42Al-8V (at.%) with a unique transformation pathway of  $\gamma$ -Ti  $\rightarrow$   $\gamma$ -Ti  $\rightarrow$   $\gamma$ -Ti  $\rightarrow$   $\gamma$ -Ti  $\rightarrow$   $\gamma$ -Ti. The alloy can easily be hot free-forged by 70% reduction in height by one stroke in the  $\gamma$ -Ti  $\rightarrow$   $\gamma$ -Ti two-phase region. The load-displacement curves of the impact test clearly detect the microstructure change, and the impact toughness increases with increasing the volume fraction of the lamellar grains. Further improvement was obtained in the specimens with fine  $\gamma$ -Ti particles within lamellae. *In-situ* observation and the corresponding load-displacement curves of the bend test revealed that the higher the lamellar angle with respect to the loading axis the larger the crack propagation resistance, thereby increasing the fracture toughness.

### 4:00 PM Break

### 4:10 PM

**The Role of Microtexture on Fatigue Lifetime Variability and Crack Initiation Mechanisms in Ti-6Al-4V:** *Christopher Szczepanski*<sup>1</sup>; James Larsen<sup>2</sup>; S. Lee Semiatin<sup>2</sup>; <sup>1</sup>UTC/AFRL; <sup>2</sup>AFRL/RX

To quantify the effect of microtexture on the fatigue behavior of  $\alpha$ + $\beta$  titanium alloys, Ti-6Al-4V material, initially containing bands of microtexture with a strong transverse texture was hot rolled to produce materials with varying levels of microtexture. These materials were heat treated to produce a range of microstructures: an equiaxed microstructure containing microtexture, a beta annealed structure containing microtexture and an equiaxed microstructure free of microtexture. The effect of test orientation on fatigue behavior for each of these microstructural variants was investigated by replicate testing of specimens along three different orientations; RD, TD, and 45° from the RD. Initial fatigue results indicate that specimens with their loading axis along the original plate TD tend to have the longest lifetimes. Orientation imaging microscopy and fractographic analysis were used to identify the mechanisms of fatigue crack initiation in these samples and to elucidate the role of microtexture.

### 4:25 PM

**Understanding of the Fracture Behavior of Titanium Alloy Ti-6Al-4V:** *Santhosh Koduri*<sup>1</sup>; Vikas Dixit<sup>1</sup>; Peter Collins<sup>2</sup>; Babu Viswanathan<sup>1</sup>; Hamish Fraser<sup>1</sup>; <sup>1</sup>The Ohio State University; <sup>2</sup>University of North Texas

A rigorous approach based upon integrated characterization and neural network modeling has resulted in the differentiation of the roles that microstructure, composition, and continuum variables (e.g., tensile properties, stress state at the crack tip) have on the fracture toughness for  $\alpha$ + $\beta$  processed Ti-6Al-4V. This approach has been applied to a high-fidelity database containing composition, microstructure and the resulting tensile and fracture toughness properties. The modeling tools have been used to isolate a key microstructural variable, which have been subsequently characterized in great depth using a suite of advanced characterization techniques. The details of one particular type of interface associated with crack initiation ahead of the moving crack tip will be discussed.

### 4:40 PM

**Extended Zonal Dislocations Mediating {11-22}<11-2-3> Twinning in Titanium:** *Bin Li*<sup>1</sup>; <sup>1</sup>Center for Advanced Vehicular Systems

We present atomistic simulation results on the mechanism for the {11-22}<11-2-3> twin growth in titanium (Ti) by analyzing the interfacial structure at the twin boundary (TB). The simulation results reveal interesting twin growth controlled by interfacial dislocations at the TB. The elementary twinning dislocations (bt) nucleate and glide in pairs but separately and sequentially on two neighboring twinning planes, distinctly different from that of conventional zonal dislocations with the core spreading over two or more twinning planes and each plane comprising one Burgers vector of an elementary twinning dislocation. These two separate elementary twinning dislocations add up to a net Burgers vector  $2bt \sim 0.2$  nm along the twinning vector, with the components in the in-plane direction perpendicular to the twinning vector canceled out. A reason for such an extended zonal dislocation will be discussed.

### 4:55 PM

**Characterization of {11-21} Twinning in  $\gamma$ -Ti:** *Leyun Wang*<sup>1</sup>; Rozaliya Barabash<sup>2</sup>; Yiyi Yang<sup>1</sup>; Thomas Bieler<sup>1</sup>; Martin Crimp<sup>1</sup>; Philip Eisenlohr<sup>3</sup>; Wenjun Liu<sup>4</sup>; Gene Ice<sup>2</sup>; <sup>1</sup>Michigan State University; <sup>2</sup>Oak Ridge National Laboratory; <sup>3</sup>Max-Planck-Institut für Eisenforschung GmbH; <sup>4</sup>Argonne National Laboratory

Activity of two tensile twinning systems, {10-12}<-1011>(T1) and {11-21}<-1-126>(T2), is observed in textured polycrystalline  $\gamma$ -Ti deformed by four-point bending. This work focuses on the relatively rare and less studied T2 twins. Owing to its large shear strain, T2 twins are often accompanied by accommodating T1 twins, surface ledges and in some cases, microcracks at grain boundaries. Using high resolution electron backscattering diffraction (EBSD), significant orientation gradients were observed in some T2 twins that were only several microns thick. The subsurface geometry of one T2 twin was examined by 3D X-ray diffraction. Streaking of Laue peaks indicates the presence of geometrically necessary dislocations (GNDs) in both the twin and the parent grain. Analysis of GND presence is used to identify a possible twin nucleation and propagation mechanism. This work is supported by NSF grant DMR-0710570 and DFG grant EI681/2-1.

## Dynamic Behavior of Materials V: Dynamic Behavior of Reactive Materials

Sponsored by: The Minerals, Metals and Materials Society, TMS Structural Materials Division, TMS/ASM: Mechanical Behavior of Materials Committee

Program Organizers: Marc Meyers, UCSD; Naresh Thadhani, Georgia Institute of Technology; George Gray, Los Alamos National Laboratory

Monday PM Room: 5A  
February 28, 2011 Location: San Diego Conv. Ctr

Session Chair: Naresh Thadhani, Georgia Institute of Technology

### 2:00 PM Invited

**Behavior of Laminate Reactive Materials under Dynamic Loading**  
Conditions: Timothy Weihs<sup>1</sup>; Adam Stover<sup>1</sup>; David Lunking<sup>1</sup>; Jason Jouet<sup>2</sup>; Naresh Thadhani<sup>3</sup>; S Wu<sup>3</sup>; Kenneth Vecchio<sup>4</sup>; F Jiang<sup>4</sup>; Richard Lee<sup>2</sup>; <sup>1</sup>Johns Hopkins University; <sup>2</sup>Naval Surface Warfare Center; <sup>3</sup>Georgia Institute of Technology; <sup>4</sup>UC San Diego

Reactive materials are typically designed to produce rapid bursts of heat and light upon initiation of an exothermic reaction such as the formation of an intermetallic compound. The development of layered reactive materials offers the exciting opportunity to control the ignition threshold and propagation rates for these reactions. It also provides an ideal geometry, with uniform and consistent reactant spacing, for modeling material behavior. This presentation reviews results of dynamic studies of exothermic formation reactions in dense compacts of reactive laminate particles and it focuses on 3 separate dynamic impact studies performed using the same materials. This combination of studies provides information on ignition thresholds, pressure rises, degree of reaction and oxidation, and sample fragmentation following impact. Rapid thermal studies will also be reviewed to help explain the results of the dynamic impact experiments.

### 2:30 PM

**Dynamic Pressure Sensing during Rapid Combustion of Metal Powders in Bomb Calorimetry:** Adam Stover<sup>1</sup>; Nicholas Krywopusk<sup>1</sup>; David Lunking<sup>1</sup>; Timothy Weihs<sup>1</sup>; <sup>1</sup>The Johns Hopkins University

Reactive materials show promise for increasing the energy content of future weapon systems and many of these new materials rely on rapid and complete combustion of metal particles. However, many desirable metallic fuels such as aluminum, zirconium or titanium have potential drawbacks such as a high ignition temperatures or low stabilities. Bomb calorimetry coupled with dynamic pressure sensing is utilized to compare these metallic fuels to each other in various oxygen rich atmospheres to determine which produces the largest energy release and hence the largest pressure rise upon ignition. We will present results describing the ignition thresholds for each metallic fuel, the effects of average particle size and alloying on oxidation rates, and the use of reactive laminate particles to drive oxidation of the fuel particles in loose and dense compacts. In future applications the reactive laminate particles may serve as ignition sources for these fuels under dynamic loading conditions.

### 2:45 PM

**Fabrication and Properties of Hot Explosive Consolidation of Ni-Al Composites:** Laszlo Kecskes<sup>1</sup>; Akaki Peikrishvili<sup>2</sup>; Elguja Chagelishvili<sup>2</sup>; Zhiliang Pan<sup>3</sup>; Weihua Lin<sup>3</sup>; Qiuming Wei<sup>3</sup>; <sup>1</sup>US Army Research Laboratory; <sup>2</sup>Tsulukidze Institute of Mining and Technology; <sup>3</sup>University of North Carolina Charlotte

Clad and mechanical blends of Ni-Al powders were formed into cylindrical rods using a hot explosive consolidation process (HEC). A multi-stage loading of explosive consolidation was applied to fabricate highly dense billets having correct cylindrical geometry to form mostly Ni and Al with some intermetallic phases. The consolidation temperature was varied from ambient temperature up to 900°C; the shock loading intensity was as high as

10 GPa. The combination of high temperatures and explosive compression was beneficial to the consolidation of the both type of Ni-Al compositions, resulting in near theoretical densities and high hardness values. Right circular cylinders were cut from the HEC billets and were compressed at quasi-static and dynamic strain rates. Results show that there is a significant difference in the mechanical response of the Ni-Al specimens that were made from powder blends and those made from the Ni-coated Al particles. The results will be discussed.

### 3:00 PM

**Investigating Reaction Mechanisms in Ni+Al Configurations Using Laser-Accelerated Thin Foil Impact:** Sean Kelly<sup>1</sup>; Naresh Thadhani<sup>1</sup>; <sup>1</sup>Georgia Institute of Technology

The reaction mechanisms in various Ni+Al binary metal configurations are being investigated using laser-accelerated thin foil set-up. Dynamic deformation (such as in an impact event) can allow rapid mixing of the components and lead to chemical reaction and release of energy in the form of heat, even with little or no porosity. Reaction mechanisms in these material systems must be characterized as a function of reactant configuration in order to control the initiation and the extent of reaction at various temporal and spatial scales. Experiments conducted using laser-accelerated thin foil impact of various Ni+Al configurations have been performed at a range of loading conditions to determine the process of deformation, flow, and mixing occurring up to the point of complete reaction. The results based on time-resolved interferometry measurements and microstructural characterization of recovered materials are used to isolate the reaction mechanisms for the various Ni+Al configurations.

### 3:15 PM

**Mesoscale Modeling of the Deconsolidative Burning in Polymer-Bonded Explosives:** H.Keo Springer<sup>1</sup>; <sup>1</sup>Lawrence Livermore National Lab

Polymer-bonded explosives (PBXs) can transition from conductive burning to more violent deconsolidative burning and subsequently detonate under heavy confinement. Previous studies have demonstrated that relatively more brittle PBXs with lower binder content have an increased propensity for deconsolidative burning. The initial stage of deconsolidative burning is characterized by the pressure-dependent infiltration of cracks and pores by product gases at the burn-front. However, the mechanism underlying the formation of this damage in (initially) intact PBX is poorly understood. The objective of this study is to use mesoscale simulations to investigate the role of energetic volume fraction and burn rate characteristics, as well as damage and fracture properties, on deconsolidative burning. The key metric of deconsolidative burning in these studies is the formation of damage at the burn-front. These modeling studies are important because they can enable the design of PBXs that do not escalate to violent burning modes.

### 3:30 PM Break

### 3:50 PM Invited

**Wave Propagation and Instabilities in "Soft" Heterogeneous Materials:** Vitali Nesterenko<sup>1</sup>; <sup>1</sup>University of California, San Diego

The wave propagation and dynamic behavior of "soft" heterogeneous materials (granular, granular composites, laminates composed from granular layers, forest of carbon nanotubes) in a broad range of impact conditions and types of deformation (shock, shear) will be discussed. The current interest on these materials is due to their efficiency as mitigators of blast/impact loading. These materials also combine high compressive strength with the ability to bulk distribute fracture resulting in a small size reactive fragments and even possible reaction on later stages of dynamic deformation. The behavior of granular metamaterials (with specially assembled mesostructure, e.g., random and periodic one or two mass low dimensional structures) under plane shock loading will be analyzed. Energy absorption and inertia based dispersive properties of these materials, crucial for intense stress wave mitigation, will be addressed. The support for this project provided by ONR MURI N00014-07-1-0740 (Program Officer Dr. Clifford Bedford).

4:20 PM

**Quasi-Static and Dynamic Response of Explosively Consolidated Reactive Mixtures:** *Chung-Ting Wei*<sup>1</sup>; Vitali Efrem<sup>2</sup>; Fengchun Jiang<sup>1</sup>; David Benson<sup>1</sup>; Kenneth Vecchio<sup>1</sup>; Naresh Thadhani<sup>3</sup>; Marc Meyers<sup>1</sup>; <sup>1</sup>University of California, San Diego; <sup>2</sup>Lawrence Livermore National Lab; <sup>3</sup>Georgia Institute of Technology

Five different nearly fully dense (> 95% TMD) reactive mixtures, Nb+Al, Ni+Al, Mo+Al, W+Al, Ta+Al, were produced by using double tube explosive shock consolidation. It is found that the elastic modulus of the compacts are not fully consistent with the theoretical predictions due to the soft matrix material (aluminum), imperfections of the compacts, and the different morphologies of the inclusions. The quasi-static behaviors are interpreted using Orowan and force chain mechanism and found that the differences of mechanical properties of the inclusions are not determinants. The dynamically mechanical and fracture behaviors are investigated using the split Hopkinson pressure bar, the high-speed camera (Phantom v12), and the simulation tool "RAVEN". It is found that the geometric properties of inclusions significantly influence the dynamic properties of the compacts. By conducting experimental and computational studies, it helps us understand the utmost importance of material factors to the explosively consolidated reactive mixtures.

4:35 PM

**The Role of Plastic Deformation in Initiating Intermetallic Formation Reactions:** *Brady Aydelotte*<sup>1</sup>; Naresh Thadhani<sup>1</sup>; <sup>1</sup>Georgia Tech

Rod-on-anvil experiments are conducted on uniaxially pressed and explosively compacted nickel+aluminum and tantalum+aluminum systems. The reactivity of these systems is compared and contrasted. Mesoscale simulations are conducted on real material microstructures to explore the role of plastic deformation in reaction initiation.

4:50 PM

**Numerical Modeling of Dynamic Deformation of Al/W Granular Composites:** *Karl Olney*<sup>1</sup>; Sophia Wang<sup>1</sup>; David Benson<sup>1</sup>; Vitali Nesterenko<sup>1</sup>; <sup>1</sup>UCSD

Aluminum/Tungsten granular composites are materials which combine high density and strength with bulk distributed fracture under impact or shock loading. They are processed using cold and hot isostatic pressing of W particles/rods in the matrix of Al powder. The presentation will describe modeling of these materials on the stage of cold isostatic pressing and under quasistatic and dynamic conditions. It will be demonstrated that morphology of W component and bonding between Al particles dramatically affects their strength and mode of fracture of Al matrix similar to observed in experiments. Funding was provided from the Grant: ONR MURI N00014-07-1-0740.

5:05 PM

**Investigation of Al-Metal Reactions Induced by High-Rate Mechanical Loading:** *Eric Herbold*<sup>1</sup>; Jennifer Jordan<sup>2</sup>; Naresh Thadhani<sup>1</sup>; <sup>1</sup>Georgia Tech; <sup>2</sup>AFRL

The reaction/combustion characteristics of compressed Al-metal powder combinations are presented in a modified rod-on-anvil Taylor impact-test set-up. The reaction threshold conditions for initiation of chemical reaction of these materials are discussed in terms of a critical energy and dynamic deformation requirement. These requirements depend on the pellet density, ratio and material properties of constituents, and level of pre-conditioning of the powders by ball-milling, which are shown to affect the sensitivity of the powders.

5:20 PM

**Processing and Dynamic Testing of Al/W Granular Composites:** *Po-Hsun Chiu*<sup>1</sup>; Vitali Nesterenko<sup>1</sup>; <sup>1</sup>UCSD

High density Al-W granular composites with an identical weight ratio between Al and W and with different porosities, size, shape and orientation of W component were investigated at strain rate 1000 1/s. Samples were fabricated by Cold Isostatic Pressing and also with subsequent Hot Isostatic Pressing. Size of particles and morphology of W inclusions had a strong effect on dynamic strength. Samples with W wires arranged in axial direction

(diameter 100 microns) had a highest dynamic strength and exhibited bulk distributed fragmentation of Al matrix. The support for this project provided by the Office of Naval Research Multidisciplinary University Research Initiative Award N00014-07-1-0740 (Program Officer Dr. Clifford Bedford).

5:35 PM

**Meso-Scale Simulations of Epoxy-Based Reactive Materials at High Strain-Rates:** *Bradley White*<sup>1</sup>; H. Keo Springer<sup>2</sup>; Jonathan Spowart<sup>3</sup>; Jennifer Jordan<sup>4</sup>; Naresh Thadhani<sup>1</sup>; <sup>1</sup>Georgia Institute of Technology; <sup>2</sup>Lawrence Livermore National Laboratory; <sup>3</sup>AFRL/RXLMD; <sup>4</sup>AFRL/RWME

Particle reinforced polymer composites are increasingly being studied for use as structural energetic materials. This requires a greater understanding of the mechanisms of high strain-rate particle deformation and mixing, which influences chemical reactions occurring in reactive materials. To determine the effect that each composite constituent has on the bulk and particle level mechanical behavior at high strain-rates, meso-scale simulations were conducted on epoxy reinforced with nickel and aluminum particles. The composite was subjected to compressive strain-rates of  $10^3$ – $10^4$  /s. The constituent phases were then examined to determine the effects that highly contrasting material properties have on the stress transfer and deformation response of the particles. Preliminary results show that the stress-strain response of epoxy is highly influenced by the presence of particles and consequently its effect on the mechanical behavior of the particles. In this presentation results from simulations and experiments will be presented, including representative microstructures from each.

---

## Electrode Technology for Aluminium Production: Anode Baking

*Sponsored by:* The Minerals, Metals and Materials Society, TMS Light Metals Division, TMS: Aluminum Committee

*Program Organizers:* Alan Tomsett, Rio Tinto Alcan; Ketil Rye, Alcoa Mosjøen; Barry Sadler, Net Carbon Consulting Pty Ltd

Monday PM

February 28, 2011

Room: 16B

Location: San Diego Conv. Ctr

*Session Chair:* Said Al Maawali, Sohar Aluminium

---

2:00 PM **Introductory Comments**

2:05 PM

**Determination of Coke Calcination Level and Anode Baking Level – Application and Reproducibility of  $L_c$  Based Methods:** *Stein Rørvik*<sup>1</sup>; Lorentz Petter Lossius<sup>2</sup>; Arne Petter Ratvik<sup>3</sup>; <sup>1</sup>SINTEF Materials & Chemistry; <sup>2</sup>Hydro Primary Metal Technology; <sup>3</sup>Norwegian University of Science and Technology (NTNU)

The average crystallite size ( $L_c$ ) is an important property of carbon materials for aluminium electrolysis;  $L_c$  is used for characterizing the petroleum coke calcination level, and sometimes also to estimate the baking level of anodes. The paper discusses problems when comparing  $L_c$  results from different laboratories with examples from round robins. The main cause are peak broadening errors introduced by the XRD instrument and sample preparation. The  $L_c$  standards ISO 20203 and ASTM 5197 neglect these errors, and two ways are demonstrated to minimize the effect and improve the standards, 1) by using thin sample thickness and 2) by embedding the coke in a high absorptive medium. Additionally ISO 17499, the equivalent baking level method for anodes is discussed and compared to  $L_c$  measurement for anode baking level. The equivalent baking level method completely bypass the peak broadening problem and is suited for baking level comparisons between anode plants.



2:30 PM

**Operation of an Open Type Anode Baking Furnace with a Temporary Crossover:** *Esteban Cobo*<sup>1</sup>; Luis Beltramino<sup>1</sup>; Juan Artola<sup>1</sup>; Jorge Rey Boero<sup>1</sup>; Pierre-Jean Roy<sup>2</sup>; Jean Bigot<sup>2</sup>; <sup>1</sup>Aluar Aluminio Argentino; <sup>2</sup>Rio Tinto Alcan

As part of the Puerto Madryn smelter expansion project, Aluar Aluminio Argentino has built and now operates an open type furnace designed with Rio Tinto Alcan AP Technology™. The furnace was built and started in two stages, each of them with 34 sections and 2 fires. In order to allow the construction of the second stage and the connection between both halves of the furnace, a method was used that had prior success on other projects with a temporary crossover to connect two sections at the extremity of the first stage. This paper describes the experience gained while operating in this mode and the procedural and process control modifications that were necessary to maintain quality anode baking. Footnote: AP Technology™ is a trademark of Aluminium Pechiney.

2:55 PM

**Recent Developments in Anode Baking Furnace Design:** Dagoberto Severo<sup>1</sup>; Vanderlei Gusberti<sup>1</sup>; Peter Sulger<sup>2</sup>; Felix Keller<sup>2</sup>; *Markus Meier*<sup>2</sup>; <sup>1</sup>CAETE Engenharia Ltda.; <sup>2</sup>R&D Carbon Ltd.

Today, furnace design still proceeds mainly by extrapolation from existing furnaces. Investigating existing furnaces shows the dangers of underestimating the impact of apparently small modifications: e.g., larger pits to accommodate higher anodes can result in furnaces with substandard performance. Side effects such as soot creation have then to be accepted. This paper presents an approach to bake furnace design which completely eliminates extrapolation from existing furnaces. The same approach can be used to estimate the optimization potential for existing furnaces.

3:20 PM

**Sohar Aluminium's Anode Baking Furnace Operation:** *Said Al Hosni*<sup>1</sup>; Jim Chandler<sup>1</sup>; Olivier Forato<sup>1</sup>; François Morales<sup>2</sup>; Christian Jonville<sup>2</sup>; Jean Bigot<sup>2</sup>; <sup>1</sup>Sohar Aluminium; <sup>2</sup>Rio Tinto Alcan

The Sohar Aluminium anode baking furnace was commissioned in 2008 and the furnace performance since has excellent in terms of gas consumption, baking level, fire productivity and firing cycle range. With 10 fluewalls per section, the furnace has productivity levels of 70 kt per fire. Gas consumption of less 1.9 GJ/t for a baking level (Lc) of greater than 33 angstrom has been maintained. Operation has been demonstrated across a fire cycle range from 24 to 36 hours. Refractory condition is excellent and first generation refractory life is likely to be > 175 fire cycles due to a thorough maintenance program and a very low anode sodium concentration of less than 150 ppm. These results have been achieved through a combination of design, process control and operation which places it amongst the benchmark operations of its type today. Some of the challenges in achieving these results are discussed.

3:45 PM Break

3:55 PM

**Meeting the Challenge of Increasing Anode Baking Furnace Productivity:** *François Ordronneau*<sup>1</sup>; Magali Gendre<sup>1</sup>; Luc Pomerleau<sup>1</sup>; Nigel Backhouse<sup>1</sup>; Adam Berkovich<sup>1</sup>; Xin Huang<sup>1</sup>; <sup>1</sup>Rio Tinto Alcan

The need to support amperage creep in smelters requires an increase in anode baking furnace productivity. The furnace operation must be adapted to provide more anodes while maintaining adequate baking performance, minimizing energy consumption and assuring anode quality. To do so, the essential factors to optimize include the firing strategy to ensure the appropriate baking level for a given fire cycle, fuel combustion efficiency and adequate cooling capability even at accelerated fire cycles and high ambient temperatures. Through the operation of 28 baking furnaces of differing technologies, tools have been developed to support this process. Simulations of firing and baking as a function of the fire cycle and key furnace design parameters such as anode size, pit width and flue design; injector combustion efficiency and cooling capability are now routinely

used. Industrial examples are shown from a number of sites using varying technology that demonstrate the gains achieved.

4:20 PM

**Wireless Communication for Secured Firing and Control Systems of Anode Baking Furnaces:** *Nicolas Fiot*<sup>1</sup>; Christian Coulaud<sup>1</sup>; <sup>1</sup>SOLIOS CARBONE

Anode baking requires firing and control systems which move every day as the fire progresses around the furnace. Wired connections between the moving equipment and the central control unit have always been an operation and maintenance concern. Wireless networks have become the modern solution with standard PLCs. However, modern furnace control requires new safety loops between the firing equipment. Wireless communication has encountered numerous drawbacks when used for secured control of the furnace via a safe communication between safety PLC's due to the nature of the safety communication protocol and interference with other wifi systems in the baking furnace area. Extensive development work has been completed with major PLC suppliers to find the right combination of modems and antenna and to fine tune the PLC's and wifi systems so that operational performance and safety requirements are fully met. Wifi is now available for the secured baking of anodes.

4:45 PM

**Full Control of Pitch Burn during Baking: It's Impact on Anode Quality, Operational Safety, Maintenance and Operational Costs:** *Detlef Maiwald*<sup>1</sup>; Domenico Di Lisa<sup>1</sup>; Peter Mnikoleiski<sup>1</sup>; <sup>1</sup>Innovatherm

Due to the physical design of the open top ring furnace the pitch burn development is not homogeneous in the individual flues of a section. As a primary result, the consistency of the anode quality will be affected. Secondary, other disadvantages will occur as well as there are unburned pitch fractions which are condensing downstream in the furnace and filter ducts, increase of emissions, higher operational costs, negatively impact on operational safety and a higher fuel consumption. The physics of the occurrence of the pitch burn is quite complex. Once the pitch burn process is started it behaves exothermal and is hard to control. This paper will describe the different control strategies which have been developed to gain full control of the pitch burn, and will show the results as remarkable improvements on anode quality, emissions, fuel consumption and running costs.

5:10 PM

**High Performance Sealing for Anode Baking Furnaces:** Pierre Mahieu<sup>1</sup>; Sébastien Neple<sup>1</sup>; Nicolas Fiot<sup>1</sup>; Ismael Ofico<sup>2</sup>; Manuel Eufrazio<sup>2</sup>; <sup>1</sup>Solios Carbone; <sup>2</sup>Mozaal

Anode baking requires important volumes of air and fumes for combustion and thermal exchange. Efficient refractory port sealing is an important condition required to reach rated flows inside flue walls. This function, apparently simple, has been facing many problems with conventional sealing techniques which can lead to process inefficiency and degraded operating conditions. A reliable and proven technology has been developed to enhance this sealing function: it is based on the use of advanced materials that combine flexibility, resistance to the extreme conditions in the furnace and offers a new potential of process improvement in anode baking furnaces. This patented system held between two rigid plates and surrounding the inner refractory port reduces drastically the incursion of cold air into the fume exhaust ramp. The most favorable outcomes of this technology are the limited condensation of exhausted fumes and increased furnace thermal efficiency.

---

## Fatigue and Corrosion Damage in Metallic Materials: Fundamentals, Modeling and Prevention: Fatigue Property-Microstructure Relationships and Crack Growth

Sponsored by: The Minerals, Metals and Materials Society, TMS Structural Materials Division

Program Organizers: Tongguang Zhai, University of Kentucky; Zhengdong Long, Kaiser Aluminum; Peter Liaw, University of Tennessee

Monday PM  
February 28, 2011

Room: 31C  
Location: San Diego Conv. Ctr

Session Chairs: Tongguang Zhai, University of Kentucky; Antonios Kontsos, Drexel University

---

### 2:00 PM

#### Effects of Materials Strength on Very-High-Cycle Fatigue Behavior for Low Alloy Steels: *Youshi Hong*<sup>1</sup>; Aiguo Zhao<sup>1</sup>; <sup>1</sup>Institute of Mechanics, Chinese Academy of Sciences

The researches on the behavior of very-high-cycle fatigue (VHCF) for low alloy steels have become a new branch in the field of metal fatigue since 1980s. The behavior of VHCF for low alloy steels is evidently dominated by the strength level (yield strength and ultimate strength), which is dependent on the composition and the microstructure of the steel. The first part of this paper is a short review, summarizing a large number of experimental data from literature, and the second part is our experimental investigation on the VHCF behavior of a low alloy steel with four kinds of strength levels. All of these attempt to show the effects of materials strength on VHCF behavior for low alloy steels, including the effects on fatigue limit, on the difference of fatigue strength, on crack origination and on S-N curve characteristics.

### 2:20 PM

#### Effect of Porosity on the Mechanical and High Cycle Fatigue Behavior of Casting AM60B Magnesium Alloy: *Kee-Ahn Lee*<sup>1</sup>; Kyu-Sik Kim<sup>2</sup>; Jung-Cheol Park<sup>3</sup>; Chang-Dong Im<sup>4</sup>; <sup>1</sup>Andong National University; <sup>2</sup>Hanyang University; <sup>3</sup>RIST; <sup>4</sup>KIMM

The effect of casting defects on the high cycle fatigue behavior of magnesium alloy was investigated. Two AM60B magnesium alloys were manufactured by high pressure die casting with different processing parameters such as die morphology, melt and die temperature. One of AM60B alloys with relatively high porosity was called Alloy A(4.06%) and the other was called Alloy B(0.07%). Microstructures of both Alloy A and B were composed of primary dendrite a-Mg, Al rich a-Mg and Mg<sub>17</sub>Al<sub>12</sub> phases. Tensile properties of both alloys were showed that Alloy B had superior tensile, yield strength and elongation. Alloy A had significantly lower fatigue life than that of Alloy B. From the observation of the differences in porosities and fractography of two AM60B magnesium alloys, an attempt to explain the high cycle fatigue fracture behavior of casted magnesium alloys was made by using stress concentration factor  $K_{max}$ . [supported by "the program for Materials Bank", Korea]

### 2:40 PM

#### The Effect of Precipitate State on the Cyclic Deformation Behaviour of Al Alloys: Experiments and Modelling: Weizhong Han<sup>1</sup>; Alexei Vinogradov<sup>2</sup>; Christopher Hutchinson<sup>1</sup>; <sup>1</sup>Monash University; <sup>2</sup>Osaka City University

Fatigue deformation involves the repeated moving backwards and forwards of dislocations. A degree of irreversibility is inherent in the dislocation motion and it is generally thought that the greater the degree of reversibility, the better the fatigue properties of the material. A measure of the reversibility of deformation can be calculated from the shape change of the hysteresis loop during cyclic loading. In this work, the evolution of the hysteresis loop shape as a function of precipitate state and plastic strain amplitude has been studied at room temperature in a model Al-4Cu alloy containing shear-resistant theta prime precipitates only. An expression for

the slip reversibility is derived that explicitly includes the characteristics of the precipitate distribution. Coupling the expression for the slip reversibility to an expression for the strengthening response is shown to describe well the evolution of hysteresis loop shape with both microstructural changes and plastic strain amplitude.

### 3:00 PM Invited

#### Effect of Microstructure on Fatigue Behavior of Two Pipeline Steels: *Gongyao Wang*<sup>1</sup>; Muralidharan Govindarajan<sup>2</sup>; Douglas Stalheim<sup>3</sup>; Peter Liaw<sup>1</sup>; <sup>1</sup>University of Tennessee; <sup>2</sup>Oak Ridge National Laboratory; <sup>3</sup>DGS Metallurgical Solutions, Inc

In recent years, significant advances have been made in the microstructural design and inclusion control of advanced pipeline steels. A range of microstructures containing various amounts of polygonal ferrite, pearlite, bainite, and acicular ferrite can be achieved in pipeline steels with comparable tensile properties. Thus, there is a need to understand the effect of the presence/absence of these microstructural constituents on the fatigue and fracture behavior of these pipeline steels. In the current investigation, fatigue crack growth behavior in air and inert atmosphere of two X70/X80 grade pipeline steels with a mixture of polygonal ferrite/acicular ferrite microstructures has been evaluated. The effect of microstructures on the fatigue properties are compared and discussed. This work was funded by the US Department of Transportation Federal Aviation, under Grant No. USDOT-DTPH56-10-T-000001, with Dr. J. Merritt as contract monitor and by the Department of Energy, Office of Hydrogen, Fuel Cells and Infrastructure Technologies

### 3:20 PM

#### Fatigue and Fracture Performance of 500MPa Grade High Strength Bridge Steel: *Huaxin Hou*<sup>1</sup>; *Chengjia Shang*<sup>2</sup>; *Yuling Zhang*<sup>3</sup>; <sup>1</sup>Ansteel Company; <sup>2</sup>University of Science and Technology Beijing; <sup>3</sup>Institute of Railway Science and Technology

High strength bridge steel has a lot of advantages, not only with high strength, good toughness and weldability, but also with anti-weather resistance property. These years, a kind of low carbon low alloy steel is developing for bridge building. With the development of rail road and highway, tow long span bridges were built over Yangtze river with 420MPa grade low carbon bainitic steels. The thickness of plate has reached 80mm. Meanwhile, much higher strength bridge steel (yield strength 500MPa) is developing. In this paper, the performance such as fatigue, fracture, wide plate tensile properties of 500MPa grade plate steel and welding conjunction were invested. Moreover, a full size girder was also tested to invest the mechanical parameters of plastic deformation during loading.

### 3:40 PM Break

### 3:50 PM

#### Study the High-Cycle-Fatigue Behavior of a Nano-Precipitate Strengthened Alloy by In-Situ Neutron-Diffraction Experiments: *E-Wen Huang*<sup>1</sup>; Michael Hofmann<sup>2</sup>; Saurabh Kabra<sup>3</sup>; Sven Vogel<sup>4</sup>; Peter Liaw<sup>5</sup>; <sup>1</sup>National Central University; <sup>2</sup>Forschungsneutronenquelle Heinz Maier-Leibnitz (FRM II); <sup>3</sup>Australian Nuclear Science and Technology Organisation; <sup>4</sup>Los Alamos National Laboratory; <sup>5</sup>University of Tennessee

A tension-tension high-cycle-fatigue experiment was investigated to resolve the structural evolution of a nano-precipitate-strengthened alloy. A tension loading-unloading test was studied for comparison. Applying the in-situ neutron-diffraction experiments, the ensemble-averaged-diffraction results incorporating with the macroscopic stress-strain curves yield the deformation mechanisms of the alloy. In comparison with the fracture surfaces, the different deformation mechanisms of the alloy subjected to two types of loadings have been characterized by the evolution of the lattice-strain and peak-profile evolution. A complementary texture investigation was used to gauge its validity.

### 4:10 PM Invited

**Fatigue Crack Tip Mechanics Following a Tensile Overload:** *Soo Yeol Lee*<sup>1</sup>; Peter K. Liaw<sup>2</sup>; Hahn Choo<sup>2</sup>; Ronald B. Rogge<sup>3</sup>; Ke An<sup>4</sup>; Camden R. Hubbard<sup>4</sup>; <sup>1</sup>The University of British Columbia; <sup>2</sup>The University of Tennessee; <sup>3</sup>National Research Council Canada; <sup>4</sup>Oak Ridge National Laboratory

The improvement in lifetime of numerous engineering components exposed to fatigue is highly dependent on the accurate understanding of fundamental principles of the failure mechanism. One aspect that is still not completely understood is the overload-retardation micromechanism and crack-closure behavior in structural materials subjected to fatigue. Here we report in-situ neutron diffraction and electric potential investigations that allow us to observe the crack opening/closing processes and associated internal-stress distributions around the crack tip during real-time fatigue crack propagation following a tensile overload. The results provide insights into (i) the crack-tip deformation and fracture behaviors under applied loads, (ii) the overload-induced transient crack growth micromechanism, (iii) the applicability of the effective stress intensity factor range as the fatigue crack tip driving force, and (iv) the quantitative relationship between the crack tip driving force and crack growth behavior.

### 4:30 PM

**A Modified LEFM Approach for the Prediction of the Notch Effect in Fatigue:** *Masahiro Endo*<sup>1</sup>; Keiji Yanase<sup>1</sup>; Satoshi Ikeda<sup>2</sup>; Arthur McEvily<sup>3</sup>; <sup>1</sup>Fukuoka University; <sup>2</sup>Kawasaki Heavy industries, Ltd.; <sup>3</sup>University of Connecticut

Engineered designs usually contain stress-raising details such as holes, fillet, grooves and keyways which are known to have a deleterious effect on the fatigue limit and fatigue lifetimes because of the growth of fatigue cracks emanating from these details. A recent paper has dealt with the behavior of small cracks emanating from one type of stress-raiser, namely holes. In that paper, a modified LEFM approach was used and it involved consideration of elastic-plastic behavior, the Kitagawa effect, and the development of crack closure in the wake of a newly formed crack. The present paper extends this approach to deal with notches of elliptical shape. The proposed approach is validated by comparing predicted and experimental results.

### 4:50 PM

**Resistivity Based Evaluation of the Fatigue Behaviour of Cast Iron:** *Holger Germann*<sup>1</sup>; Peter Starke<sup>1</sup>; *Dietmar Eifler*<sup>1</sup>; <sup>1</sup>University of Kaiserslautern

Cast irons are used in particular for highly stressed components in the automotive and commercial vehicle industry, e.g. for crankcases and in the wind power industry, e.g. for rotor hubs. The microstructure of cast irons and consequently their mechanical properties are strongly influenced by graphite shape, micro-shrinkage cavities, micro-pinholes, micro-cracks etc. The measurement of the electrical resistance in the virgin state and its change during fatigue loading offers the possibility to get detailed information about the actual defect density and the cyclic deformation behaviour. In the scope of the present research work stress-controlled load increase tests and constant amplitude tests were carried out at ambient temperature with specimens of the perlitic cast irons EN-GJL-250 (ASTM A48 35B), EN-GJS-600 (ASTM 80-55-06) and EN-GJV-400. Beside electrical measurements scanning electron microscopy (SEM) was used to characterize the microstructure and to correlate microstructural details with cyclic properties.

### 5:10 PM

**Microstructure-Sensitive Probabilistic Fatigue Modeling of Notched Components:** *William Musinski*<sup>1</sup>; David McDowell<sup>1</sup>; <sup>1</sup>Georgia Institute of Technology

Microstructure-sensitive, simulation-based strategies for modeling fatigue life reduction in cyclically loaded notched components offer a means to augment costly experiments and facilitate consideration of microstructures not yet processed. Using computational polycrystal plasticity and probabilistic arguments, a strategy is presented that links notch root microstructure heterogeneity to scatter in fatigue response and notch size effects. The notch root stress gradient field, grain size distribution, and

defect distribution (pores, nonmetallic inclusions) effects are considered for a polycrystalline PM processed Ni-base superalloy IN100. The probability of forming and propagating a crack from the grain scale to a transition crack length (LEFM applicable) is approximated using shear-based fatigue indicator parameters computed within the uncracked notched specimen. This model for crack formation and early growth is calibrated to existing smooth specimen experiments. Cumulative distribution functions and probabilistic strain life functions are constructed for various notch root radii and remote strain amplitudes.

### 5:30 PM

**Metallurgical Aspects of Stress Corrosion Cracking of X100 High-Strength Pipeline Steel:** *Frank Cheng*<sup>1</sup>; <sup>1</sup>University of Calgary

It is generally acknowledged that an elevated strength level of steels tends to decrease their resistance to stress corrosion cracking (SCC), particularly, hydrogen-induced SCC (HISCC). This work summarized the author's recent research in high-strength pipeline steel SCC phenomenon. The microstructure of X100 steel was characterized by scanning electron microscopy and energy-dispersive x-ray analysis, and various metallographic phases and inclusions were identified. Furthermore, micro-electrochemical measurement techniques and photo-electrochemical technique were combined to characterize the local activity of micro-defects, such as inclusions and grain boundaries, and the galvanic effect between the defect and the steel matrix. Micro-electrochemical measurements were also conducted on the X100 steel weld, where the typical microstructures and mechanical properties were introduced during welding. It is attempted to develop an essential insight into the effect of the welding metallurgy on local dissolution rate and the SCC susceptibility of X100 line pipe steel.

### Federal Funding Workshop: Panel Discussion

*Sponsored by:* The Minerals, Metals and Materials Society, TMS: Public and Governmental Affairs Committee

*Program Organizers:* Robert Shull, National Institute of Standards and Technology; Jud Ready, Georgia Tech

Monday, 4:00-6:00 PM

February 28, 2011

Room: 6E

Location: San Diego Conv. Ctr

*Session Chairs:* Robert Shull, NIST; Jud Ready, Georgia Tech

### 4:00 PM Introductory Comments by Robert Shull

#### Panel Discussion with Panelists:

*Zakya Kafafi*, National Science Foundation (NSF), Director, Division of Materials Research

*Michael Kassner*, Office of Naval Research (ONR), Director of Research

*Harriet Kung*, Department of Energy (DOE), Director, Basic Energy Sciences

*Jon Mogford*, Defense Advanced Research Projects Agency (DARPA), Deputy Director, Defense Sciences Office

*Thomas Russell*, U.S. Air Force Office of Scientific Research (AFOSR), Director, Aerospace Chemical and Materials Division

*David Stepp*, U.S. Army Research Office (ARO), Chief, Materials Science Division

#### Summary Comments by Jud Ready

#### Networking Reception



## Friction Stir Welding and Processing VI: High Temperature Materials II

Sponsored by: The Minerals, Metals and Materials Society, TMS Materials Processing and Manufacturing Division, TMS: Shaping and Forming Committee

Program Organizers: Rajiv Mishra, Missouri University of Science and Technology; Murray Mahoney, Retired from Rockwell Scientific; Yutaka Sato, Tohoku University; Yuri Hovanski, Pacific Northwest National Laboratory; Ravi Verma, General Motors

Monday PM Room: 5B  
February 28, 2011 Location: San Diego Conv. Ctr

Session Chair: Yuri Hovanski, Pacific Northwest National Laboratory

### 2:00 PM Invited

**Reliable Sealing of Copper Canisters through Cascaded Control of Power Input and Tool Temperature:** Lars Cederqvist<sup>1</sup>; Olof Garpinger<sup>2</sup>; Tore Haggglund<sup>3</sup>; Anders Robertsson<sup>3</sup>; <sup>1</sup>SKB/Lund University; <sup>2</sup>XDIN; <sup>3</sup>Lund University

The Swedish Nuclear Fuel and Waste Management Company (SKB) will join at least 12,000 lids and bottoms to the copper tubes containing Sweden's nuclear waste using friction stir welding (FSW). The paper shows how the 45 minute long weld cycle, with variable thermal boundary conditions, can be reliably controlled by an inner regulator loop controlling the power input and a slower outer regulator loop controlling the tool temperature. The results from recent, automatically controlled, welds are compared to those of early, manually controlled, welds. It is also shown how relatively small changes in the control strategy, depending on sequence in the weld cycle, can improve the overall performance and repeatability of the process. In addition to this, the controller is also compared to manual control when it comes to suppressing torque disturbances. The authors most definitely believe that the chosen, cascaded, controller structure can be successfully used in other applications in which the temperature signal reacts relatively slow to fast and distinct torque disturbances.

### 2:25 PM Invited

**Friction Stir Welding (FSW) of a Hardenable Alloy Steel in 'Dry' and 'Wet' Environments:** Norman Overfield<sup>1</sup>; Murray Mahoney<sup>2</sup>; Russell Steel<sup>3</sup>; Jon Babb<sup>3</sup>; Sarath Menon<sup>1</sup>; Terry McNelley<sup>1</sup>; <sup>1</sup>Naval Postgraduate School; <sup>2</sup>Consultant, Brigham Young University; <sup>3</sup>MegaStir Technologies

Recent advances in FSW tool material and design will facilitate numerous applications of this solid-state joining technology to steels. A single W-Re-CBN tool was used to conduct a series of bead-on-plate FSW traverses, approximately 1.5m in total length, on 6.3mm thick plates of a hardenable alloy steel. The first series of traverses involved various RPM/IPM combinations and a dry plate. A second series was carried out while a plate was immersed in water in order to assess potential for inducing hydrogen assisted cracking (HAC) during FSW of susceptible alloys. All traverses were defect-free. The FSW nuggets exhibited refined microstructures and increased hardness relative to the base plate. The influence of FSW parameters on nugget microstructure and mechanical properties will be summarized.

### 2:50 PM Invited

**Friction Stir Welding of Industrial Steels:** Jonathan Perrett<sup>1</sup>; Jonathan Martin<sup>1</sup>; Jeremy Peterson<sup>2</sup>; Russell Steel<sup>2</sup>; Scott Packer<sup>3</sup>; <sup>1</sup>TWI; <sup>2</sup>MegaStir Technologies; <sup>3</sup>Advanced Metal Products

Friction Stir Welding of steel has been in development for over a decade, but only in recent years have the strength and wear characteristics of tool materials improved extensively. Tool materials have been developed that have excellent high-temperature wear resistance, and consistently achieve weld lengths in excess of 50 meters in steel. These newly developed material characteristics comprise of a fine balance of high-temperature strength, hardness and ductility. Shipbuilding, bridge decking, pipe seam welding, or applications which require long uninterrupted steel welds, are now attractive

target markets for the friction stir process. It is the process's ability to create high-strength, low-distortion welds that make it potentially attractive to industry. This paper shows the results from welding and testing of five common industrial steels, as well tool wear profiles and demonstrative 6m length welds.

### 3:15 PM Invited

**Localized Mechanical Behavior Of Ti-5111 Friction Stir Welds:** Jennifer Wolk<sup>1</sup>; Marc Zupan<sup>2</sup>; Christopher Cheng<sup>2</sup>; <sup>1</sup>Naval Surface Warfare Center; <sup>2</sup>University of Maryland Baltimore County

Titanium (Ti) and titanium alloys have shown excellent mechanical, physical, and corrosion properties for marine applications. Friction stir welding (FSW) is being investigated as a possible joining alternative due to difficulties in conventional welding of Ti alloys. Due to the natural asymmetry of the FSW process, bulk mechanical properties may not be representative of the localized properties. This work focuses on direct measurement of the base metal, heat affected zone (HAZ), thermomechanically affected zone (TMAZ), and stir zone mechanical properties in friction stir welded Ti-5111. The localized mechanical properties are measured using micro scale tensile tests (~3 mm long by 1 mm wide with a cross-sectional gage section ~250  $\mu$ m square) extracted directly from the transverse cross-section of the weld. After testing, the mechanical response is correlated to the underlying material microstructure and texture for the different regions of the Ti-5111 friction stir weld.

### 3:40 PM

**Mechanical Properties of Thick Section Titanium 6Al-4V Friction Stir and Electron Beam Welds:** Paul Edwards<sup>1</sup>; Gary Coleman<sup>1</sup>; Marc Petersen<sup>1</sup>; <sup>1</sup>The Boeing Company

In this study, Friction Stir Welding of Ti-6Al-4V was developed in 1.0 inch thickness material. The microstructure and mechanical properties such as static, fatigue, fracture toughness and crack growth of these thick section Friction Stir Welds were evaluated and compared to Electron Beam Welds produced in the same thickness material. It was found that the Friction Stir Welds did possess a more wrought type structure than the Electron Beam Welds, leading to better ductility, fatigue life and fracture toughness. The solidified structure of the Electron Beam Welds resulted in higher strengths and showed slower crack growth rates. This screening data will allow design engineers to down select these processes, considering both cost and performance, for advanced aircraft structures.

### 4:00 PM

**Transformation and Deformation Texture Study in Friction Stir Processed API X80 Steel:** Majid Abbasi<sup>1</sup>; Tracy Nelson<sup>1</sup>; Carl Sorensen<sup>1</sup>; <sup>1</sup>Brigham Young University

The nature of deformation in FSW is very complex. This complexity becomes even more challenging when allotropic phase transformations are present. In this research, Electron Backscattered Diffraction is used as a means to reconstruct the prior austenite texture and grain structure. Considering the fact that the room temperature microstructure contains very little or no residual PA, the prior austenite microstructure was reconstructed from the room temperature ferrite utilizing transformation orientation relationships. Analysis shows that there is little evidence of shear deformation texture in the reconstructed PA, however; room temperature ferrite exhibits strong shear deformation texture components. This implies that extended plasticity mechanisms are occurring in prior austenite which weaken the shear deformation texture. The observed shear deformation texture in the room temperature microstructure implies that FSW imposes deformation during and after the phase transformation. The evolution of both elevated and room temperature textures in FSW HSLA steel will be presented.

#### 4:20 PM Break

#### 4:30 PM Invited

##### **The Mechanisms of Microstructure Control and Homogenization in Multi-Pass Friction Stir Processing (FSP) of NiAl Bronze:** *Terry McNelley*<sup>1</sup>; *Sarath Menon*<sup>1</sup>; *Carolyn England*<sup>1</sup>; <sup>1</sup>Naval Postgraduate School

Multi-pass FSP of cast NiAl bronze provides a refined, homogeneous and isotropic surface layer in which both strength and ductility are doubled, relative to the as-cast condition. For large marine components this technology improves performance and reduces costs. The as-cast microstructure comprises primary and eutectoid constituents. The stir zone (SZ) microstructures reflect rapid transients and steep gradients in strain, strain rate and temperature. Field-emission scanning electron microscopy (FE-SEM) methods, including orientation imaging microscopy (OIM) have been applied to the evolution of thermomechanically affected zone (TMAZ) and SZ microstructures during single- and multi-pass FSP. A duplex  $\alpha$ (fcc)/ $\beta$ (bcc) microstructure develops in the TMAZ ahead of the tool and compatible deformation of these two phases enables estimation of strains and temperatures in this region. The development of the refined SZ microstructure in association with fragmentation of the duplex structure will be described.

#### 4:55 PM

##### **Wear Testing of Friction Stir Spot Welding Tools and Evaluation of Weld Performance as a Function of Tool Condition:** *Chris Ridges*<sup>1</sup>; *Michael Miles*<sup>1</sup>; *Yuri Hovanski*<sup>2</sup>; *Russell Steel*<sup>1</sup>; <sup>1</sup>BYU; <sup>2</sup>Pacific Northwest National Lab; <sup>3</sup>Megastir Technologies

Friction stir spot welding has been shown to be a viable method of joining ultra high strength steel, both in terms of joint strength and process cycle time. However, the cost of tooling must be reasonable in order for this method to be adopted as an industrial process. Several tooling materials have been evaluated in prior studies, including silicon nitride and polycrystalline cubic boron nitride (PCBN). Recently a new tool alloy has been evaluated, where a blend of PCBN and tungsten rhenium (W-Re) was used in order to improve toughness while maintaining an acceptable level of hardness and wear resistance. Wear testing and weld strength results will be presented for a PCBN tool as well as for tools that contain a blend of PCBN and W-Re, in the proportions of 60% PCBN, 70% PCBN, and 80% PCBN, where the balance in each case is W-Re.

#### 5:15 PM

##### **Tungsten Based Tool Material Development for the Friction Stir Welding of Hard Metals:** *Brian Thompson*<sup>1</sup>; <sup>1</sup>EWI

The Friction Stir Welding (FSW) of hard metals such as steel and titanium requires unique tool materials capable of achieving long linear lengths while minimizing tool degradation. W-based materials have demonstrated success as a FSW tool in resisting degradation while maximizing tool life. This presentation will review the development of current and future W-based tool materials for the FSW of hard metals. Results from the characterization of tool material microstructures identifying tool degradation mechanisms will be presented along with the evaluation of cutting edge tool materials for their performance in X-70 High Strength Steel and Titanium 6-4. In addition, resulting weld mechanical properties from these welds with corresponding stir zone microstructural characterization will be presented. This on-going work has resulted in a greater understanding of W-based tool materials and the development of improved W-based tool material compositions capable of achieving tool life in the hundreds of feet.

#### 5:35 PM

##### **Improving Heat-Affected Zone Liquefaction Cracking Resistance of Nickel-Base Alloys by Friction Stir Processing:** *James Rule*<sup>1</sup>; *Jeffrey Rodelas*<sup>1</sup>; *John Lippold*<sup>1</sup>; <sup>1</sup>Welding and Joining Metallurgy Group, The Ohio State University

Friction stir processing (FSP) was evaluated as a means to reduce the susceptibility of two solid-solution strengthened Ni-Base alloys, Alloy 625 and Hastelloy X, and a Ni-Base superalloy, Inconel 718, to heat-affected zone (HAZ) liquefaction cracking. FSP of the base metal resulted in

severe reduction in grain size (average grain diameter of less than 10 $\mu$ m). These grains contained highly tortuous grain boundaries with a very fine distribution of second phases. Cracking resistance was evaluated using the spot-varestraint test. Testing showed a reduction in cracking susceptibility relative to the baseline due to the reduction in HAZ grain size. Optical microscopy evaluation revealed that HAZ liquefaction cracking resistance is enhanced due to a higher density of grain boundaries resulting in finer, more discontinuous networks of low melting eutectic and second phases.

#### 5:55 PM

##### **Using Electron Backscatter Diffraction to Characterize the Texture and Microstructure of Friction Stir Welded AISI 304L Stainless Steel:** *Benjamin Nelson*<sup>1</sup>; *Carl Sorensen*<sup>1</sup>; <sup>1</sup>Brigham Young University

The crystallographic texture of friction stir welded (FSW) metals has been shown to resemble the torsional simple shear deformation (TSSD) texture of metals. In this study, electron backscatter diffraction (EBSD) was used to analyze the texture and microstructure of FSW AISI 304L stainless steel (304L). Locations at the retreating side, weld center, advancing side, and TMAZ were scanned and analyzed. For texture analysis, EBSD data was rotated to match the sample coordinate system of TSSD. Quantitative analysis of the texture showed that over 90% of the non-random textures correspond to TSSD; the remainder corresponds to a discontinuous dynamic recrystallization texture. EBSD microstructure analysis shows that dislocation cells are formed in the final microstructure of FSW 304L. Texture and microstructure analysis results suggest that dynamic recovery and continuous dynamic recrystallization (recovery phenomena) are active in the final microstructure of FSW 304L, while discontinuous dynamic recrystallization (nucleation phenomenon) is not.

### **Frontiers in Solidification Science: Nucleation and Related Phenomena**

*Sponsored by:* The Minerals, Metals and Materials Society, TMS Electronic, Magnetic, and Photonic Materials Division, TMS: Chemistry and Physics of Materials Committee, TMS: Solidification Committee

*Program Organizers:* Jeffrey Hoyt, McMaster University; Daniel Lewis, Rensselaer Polytechnic Institute

Monday PM

February 28, 2011

Room: 6E

Location: San Diego Conv. Ctr

*Session Chair:* To Be Announced

#### 2:00 PM Invited

##### **Heterogeneous Nucleation of Anisotropic Solids:** *Aurèle Mariaux*<sup>1</sup>; *Michel Rappaz*<sup>1</sup>; <sup>1</sup>EPFL

Surprisingly, the well-known theory of heterogeneous nucleation of a solid from a liquid phase on a foreign substrate did not consider anisotropic situations. Taking the case of zinc grains forming in thin coatings deposited by hot-dipping on steel sheets as a motivation to this study, the xsi-vector formalism of Cahn and Hoffman was first used to handle anisotropic nucleation situations. It can be shown that the ratio of the heterogeneous and homogeneous nucleation energy barriers is still given by the ratio of the corresponding volumes of the heterogeneous and homogeneous anisotropic nuclei. However, the function describing this ratio, which only depends on the ratio  $(\gamma_{lf} - \gamma_{sf})/\gamma_{sl0}$  for the isotropic case, where  $\gamma_{lf}$  and  $\gamma_{sf}$  are the liquid-foreign substrate and solid-foreign substrate interfacial energies, respectively, becomes a function of the orientation of the nucleus with respect to the substrate. In the case of zinc, it is shown that good wetting conditions, i.e.,  $(\gamma_{lf} - \gamma_{sf}) > 0$ , favor a basal orientation of the nucleus on the foreign substrate. Experimental evidence from several zinc-based systems will be presented to support this finding.

### 2:30 PM Invited

#### Phase-Field Simulations of Peritectic Growth in Ti-Al-B Including $TiB_2$ Inoculation: Markus Apel<sup>1</sup>; Janin Eiken<sup>1</sup>; Ulrike Hecht<sup>1</sup>; <sup>1</sup>Access e. V.

By varying the B content in a peritectic Ti45at%AlxB alloy the formation temperature of boride particles can be adjusted. For  $x > 1.47$ at%  $TiB_2$  is the first phase which forms during solidification. For  $0.58\text{at}\% < x < 1.47\text{at}\%$   $TiB_2$  becomes stable after  $\beta$ -Ti but before  $\alpha$ -Ti. In the first case boride particles can inoculate  $\beta$ -Ti, whereas in the latter case  $\alpha$ -Ti. We elucidate the effect of borides on microstructure formation by phase-field simulations coupled to a thermodynamic database. Nucleation and growth of small boride particles are explicitly taken into account on a scale below the phase-field interface thickness by using semi-analytical growth models. The simulation results show a variety of effects: grain refinement due to heterogeneous nucleation on  $TiB_2$  particles either of the  $\beta$  or  $\alpha$  phase, interactions between the growing Ti phases and the borides, as well as a pronounced dependency of the phase transformation rates on the dominant nucleation sites.

### 3:00 PM

#### Dispersion of Nanoparticles in Magnesium Using Contactless Electromagnetic Acoustic Transmission (EMAT) under High Magnetic Fields: Zachary Bryan<sup>1</sup>; Peiru Chen<sup>1</sup>; Hunter Henderson<sup>1</sup>; Orlando Rios<sup>2</sup>; Gail Mackiewicz-Ludtka<sup>2</sup>; Gerard Ludtka<sup>2</sup>; Michele Manuel<sup>1</sup>; <sup>1</sup>University of Florida; <sup>2</sup>Oak Ridge National Laboratory

Magnesium and its alloys have recently drawn significant attention due to their high specific strength. However, magnesium's inherently low ductility has prevented its wide spread integration into major engineering applications. It has been shown that the addition of ceramic nanoparticles to magnesium alloys can lead to dramatic increases in hardness, strength, and possibly ductility. This collaborative study focuses on the application of a novel contactless electromagnetic acoustical transmission (EMAT) technique to disperse dysprosium oxide nano-spheres and nano-rods in molten magnesium and throughout solidification. The magnesium and nano-particle composites, prepared at the University of Florida's Materials Design & Prototyping Laboratory, were induction melted using a custom apparatus developed at Oak Ridge National Laboratory (ORNL) in a 20 Tesla high magnetic field under controlled atmosphere at the National High Magnetic Field Laboratory (NHMFL). A detailed microstructural analysis characterizing the level and degree of nano-particle dispersion is presented and inferences will be provided regarding the nature of the solidification process. The authors acknowledge financial support from the US National Science Foundation award number DMR-0845868, Department of Energy DOE-EERE-ITP and Office of Science Graduate Fellowship Program administered by the Oak Ridge Institute for Science and Education, and General Motors Corporation.

### 3:20 PM

#### In-Situ Investigation of the Growth Dynamics of Floating and Locked Eutectic Grains during Thin-Sample Directional Solidification Using a Rotating Stage: Melis Serefoglu<sup>1</sup>; Sabine Bottin-Rousseau<sup>1</sup>; Silvère Akamatsu<sup>1</sup>; Gabriel Faivre<sup>1</sup>; <sup>1</sup>UPMC / CNRS

We investigated the directional-solidification dynamics of "floating" and "locked" eutectic grains (EGs) in a 12- $\mu\text{m}$  thick metallic samples (In-In2Bi) using a rotating stage. Our setup permits us to change the in-plane orientation of the crystals with respect to the thermal gradient continuously, while keeping the relative orientation of the two phases constant, and observing the solidification front in real time by videomicroscopy. We show that floating EGs correspond to the so-called regular eutectics generally observed in nearly isotropic systems with nonfaceted solid-liquid interfaces, i.e. the lamellae grow locally perpendicular to the front over the whole angular range. In contrast, in locked EGs, the lamellae keep, on average, a fixed orientation in the sample (i.e. crystal) reference frame during rotation. We usually observed a few locking orientations in a given EG. Assuming that they correspond to singular orientations, one can obtain valuable information on the gamma-plot of the interphase boundaries.

### Hume-Rothery Symposium Thermodynamics and Diffusion Coupling in Alloys - Application Driven Science: Modeling of Atomic Mobility

*Sponsored by:* The Minerals, Metals and Materials Society, TMS Electronic, Magnetic, and Photonic Materials Division, TMS: Alloy Phases Committee

*Program Organizers:* Zi-Kui Liu, The Pennsylvania State University; Larry Kaufman, CALPHAD, Inc.; Annika Borgenstam, Royal Institute of Technology; Carelyn Campbell, NIST

Monday PM  
February 28, 2011

Room: 31A  
Location: San Diego Conv. Ctr

*Session Chairs:* David Andersson, Los Alamos National Laboratory; Annika Borgenstam, Royal Institute of Technology

### 2:00 PM Invited

#### Assessment of Mobilities: Lars Hoglund<sup>1</sup>; <sup>1</sup>KTH

Simulations of diffusion controlled transformations have over the recent years become increasingly important for understanding the behaviour materials both in manufacturing and use. This applies both to new advanced material as well as materials that been long available. These simulations take advantage of the large availability of existing thermodynamic databases and software that with great accuracy can predict phase equilibria in a number of alloying systems. In order to perform accurate simulations of diffusion controlled processes, accurate descriptions of diffusion coefficients in the system must be assessed and stored in databases. The most convenient way in which to store this type of information is to assess and store the mobilities of the different diffusing components in databases. An overview on the methods used and the type of data that can be used to perform this task will be presented

### 2:30 PM Invited

#### Evaluation of the Uncertainty of Extrapolating Thermodynamic and Mobility Data in Temperature and Composition: Annika Borgenstam<sup>1</sup>; <sup>1</sup>KTH

It has for a very long time been debated if the bainitic transformation is formed by a diffusionless process or if it is controlled by carbon diffusion. If the transformation is controlled by carbon diffusion it should be possible to calculate the growth rate as controlled by carbon diffusion under paraequilibrium conditions. This has been done previously but must be done again for certain cases. When calculating the growth rate it is very important to have a proper thermodynamic description as well as correct mobility data. Since the bainitic transformation in steel takes place at rather low temperatures it is important that the extrapolations of both the thermodynamic and mobility data are correct. In the present work an attempt to evaluate the uncertainty in these extrapolations of temperature and composition are presented. It will be discussed from a general perspective and exemplified using new thermodynamic descriptions of Fe-C and Fe-Cr.

### 3:00 PM Invited

#### Development of a Reference Self-Diffusion Mobility Database: Carelyn Campbell<sup>1</sup>; <sup>1</sup>National Institute of Standards and Technology

Twenty years ago, John Ågren initiated the development of a CALPHAD-based approach to diffusion mobility databases. Since then, several multicomponent diffusion mobility databases have been developed for steels and Ni-base superalloys; however, the development of multicomponent diffusion mobility databases for other alloy systems has been slowed by the lack of standard references for the self-diffusion of the pure elements. In 2009, an international group began meeting at NIST to develop a set of standard reference diffusion mobilities. An overview of this group's work, including a set of initial recommendations for the self-diffusion in Al, Cu, Ni and Fe, will be presented. The recommendations are based on evaluation of the experimental data using a statistical meta-analysis, first principle calculations, and the use of previous assessments.

MONDAY PM



### 3:30 PM Break

### 3:50 PM Invited

**Atomistic and Meso-Scale Simulations of Diffusion in  $UO_{2+x}$ :** *David Andersson*<sup>1</sup>; Pankaj Nerikar<sup>1</sup>; Blas Uberuaga<sup>1</sup>; Michael Buksas<sup>1</sup>; Neil Carlson<sup>1</sup>; Cetin Unal<sup>1</sup>; Chris Stanek<sup>1</sup>; <sup>1</sup>Los Alamos National Laboratory

Species transport is a critical process in nuclear fuels and due to fission gas redistribution and evolution of the  $UO_{2+x}$  stoichiometry it is an important performance characteristic. Xe transport is studied by calculating the activation energy using density functional theory (DFT) techniques. By analyzing the Xe solution thermodynamics, the relevant migration barriers and the interaction of dissolved Xe atoms with U vacancies we demonstrate that Xe diffusion occurs via a vacancy-mediated ring-like mechanism. The interaction of Xe with grain boundaries and dislocations has previously been investigated via atomistic simulations and we apply these results to formulate a thermodynamic and kinetic model for Xe segregation that account for the unique boundary characteristics. The resulting transport model for bulk and boundaries is then solved for both idealized and realistic microstructures within a finite element code. Finally, using DFT and kinetic Monte Carlo simulations we study the diffusion of O in non-stoichiometric  $UO_{2+x}$ .

### 4:20 PM

**Ab Initio Determination of Point Defect Kinetics in Fe-Based Alloys:** Tilmann Hickel<sup>1</sup>; Roman Nazarov<sup>1</sup>; *Niko Sandschneider*<sup>1</sup>; Joerg Neugebauer<sup>1</sup>; <sup>1</sup>Max-Planck-Institut fuer Eisenforschung GmbH

Aiming at a weight reduction of Fe-based products, there is currently a great interest in various alloying concepts such as Fe-Mn or Fe-Al. However, in order to reduce failure mechanisms in these materials, the understanding of their defect kinetics needs to be significantly improved. We therefore extensively studied the diffusion of hydrogen, a prominent interstitial atom connected to brittle fracture. In addition we considered vacancy driven self- and impurity diffusion, which is often responsible for strength reduction and creep. Density functional theory has been used to determine the energetics and structures of the involved defects (including the complex interplay with the local magnetic environment) and to obtain the complete information on the relevant transition states. These data are combined with kinetic Monte-Carlo simulations, in order to achieve temperature dependent diffusion constants. We observe characteristic dependencies on the concentration of alloying elements, their spatial distribution and the resulting local strain.

### 4:50 PM

**Oxygen Diffusion in  $\alpha$ -Titanium Alloys:** *Henry Wu*<sup>1</sup>; Dallas Trinkle<sup>1</sup>; <sup>1</sup>University of Illinois at Urbana-Champaign

Titanium alloys are limited in high temperature applications by oxidation. To understand and inhibit oxygen penetration, we determine the mechanisms of oxygen diffusion through  $\alpha$ -titanium with *ab initio* calculations. Diffusion in both the c-axis and basal directions proceeds between octahedral interstitial sites, through metastable hexahedral and crowdion configurations. From the mechanisms and energy barriers, we calculate the diffusion coefficient and anisotropy in the c-axis and basal directions that match well to experimental measurements. We use DFT to compute the interaction energy between oxygen in  $\alpha$ -titanium and substitutional solutes such as Al, V, and Sc. Solute reduce oxygen diffusion: attractive solutes act as traps, and repulsive solutes induce the labyrinth effect for non-dilute concentrations. We use the diffusion model to compare the effect of solutes on oxygen diffusion through pure Ti and Ti-6Al-4V.

### 5:20 PM

**Phase Stability of Mg<sub>2</sub>X Intermetallic Phases in the Mg-X-X' (X, X': Si, Ge, Sn) Systems:** *Jean Claude Tedenac*<sup>1</sup>; Isabelle Martin<sup>1</sup>; Elodie Ruiz<sup>1</sup>; Abel Haidoux<sup>1</sup>; <sup>1</sup>ICG

The materials based on the intermetallic compounds Mg<sub>2</sub>X (X = Si, Ge, Sn) are widely studied for applications in thermoelectric energy conversion. The ternary systems from which they derive are not very well known. It appears that the stabilities of the solid solutions are not as obvious as it sounds. We present in this communication an experimental study on the sections Mg<sub>2</sub>Si-Mg<sub>2</sub>Ge and Mg<sub>2</sub>Si-Mg<sub>2</sub>Sn of the ternary systems. The

stability of alloys of composition between 10 and 30 at% are studied by the way of the solid state methods. A thermodynamic study is given and the kinetic of decomposition is described. This study concerns an experimental approach which will be included a Calphad procedure. First results on the modelling of the system Mg-Ge-Si are given.

## Hydrogen Storage in Materials: Theory and Experiment: Session II

*Sponsored by:* The Minerals, Metals and Materials Society, ASM Materials Science Critical Technology Sector, TMS: Energy Conversion and Storage Committee

*Program Organizer:* Louis Hector Jr, GM R&D Center

Monday PM

February 28, 2011

Room: 13

Location: San Diego Conv. Ctr

*Session Chair:* Dallas Trinkle, University of Illinois, Urbana-Champaign

### 2:00 PM

**Controlling the Kinetics and Decomposition Pathway of LiBH<sub>4</sub> and Mg(BH<sub>4</sub>)<sub>2</sub> via Confinement in Highly Ordered Nanoporous Carbon:**

*Xiangfeng Liu*<sup>1</sup>; David Peaslee<sup>1</sup>; Christopher Jost<sup>1</sup>; Eric Majzoub<sup>1</sup>; <sup>1</sup>University of Missouri-St. Louis

In addition to conventional strategies for improving kinetics and thermodynamics of metal hydrides, including the use of catalyst dopants or destabilization, the effect of nanoscale size, through confinement in templates or frameworks, has attracted increasing attention. The decomposition thermodynamics and kinetics of LiBH<sub>4</sub> and Mg(BH<sub>4</sub>)<sub>2</sub> has been investigated in the presence of highly ordered nanoporous carbon (NPC) with a 2D-hexagonal geometry, a narrow size distribution, and different pore sizes. LiBH<sub>4</sub> confined within 2 nm highly-ordered columnar pores becomes amorphous. The nano-confinement results in the disappearance of the structural phase transition and the melting transition, a significant decrease of the onset desorption temperature, and suppresses diborane release. The reaction pathway is likely altered through a strong interaction with the carbon template. We illustrate the wetting behavior of LiBH<sub>4</sub> on infiltration NPC using differential scanning calorimetry, and discuss the implications of the wetting behavior on the decomposition pathways.

### 2:20 PM

**Direct Line-of-Site Gas Desorption Study of LiBH<sub>4</sub> in Nanoporous Carbons: The Influence of Surface Chemistry and the Size Effect:**

*David Peaslee*<sup>1</sup>; Xiangfeng Liu<sup>1</sup>; E. Majzoub<sup>1</sup>; T. Baumann<sup>2</sup>; <sup>1</sup>University of Missouri - St. Louis; <sup>2</sup>Lawrence Livermore National Laboratory

Thermodynamic and kinetic properties of metal hydrides may differ between bulk and nano-sized particles. Studies of nano-structured carbon materials infiltrated with LiBH<sub>4</sub> reveal differences in the decomposition pathway that depend on the nano-pore size and the surface chemistry. We present results of gas desorption using a direct line-of-site residual gas analyzer mass-spectrometer (RGAMS) to characterize gas desorption species, and decomposition temperatures, and differences in reaction pathways for a variety of LiBH<sub>4</sub>, Ca(BH<sub>4</sub>)<sub>2</sub>, and Mg(BH<sub>4</sub>)<sub>2</sub> infiltrated carbons. We present results for 9-14 nm carbon aerogels and 2-4 nm highly ordered nano-porous carbons consisting of columnar pores packed in a hexagonal geometry. RGAMS results, together with XRD, FTIR, and calorimetry studies, indicate that pore size, non-crystallinity, and surface chemistry all play a role in formation of diborane (B<sub>2</sub>H<sub>6</sub>) during the infiltration process and also during desorption of melt-infiltrated materials.

### 2:40 PM

**Energetics and Microstructures in Mg/Nb Multilayers:** *Anchalee Junkaew*<sup>1</sup>; Byoungsoo Ham<sup>1</sup>; Xinghang Zhang<sup>1</sup>; Raymundo Arroyave<sup>1</sup>; <sup>1</sup>Texas A&M University

Nb has been proposed for improving the hydrogen sorption kinetics in Mg thin films. Microscopy studies show the formation of metastable phases

at interfaces. In this presentation, we examine the microstructure of Mg/Nb multilayers through first-principles calculations based on Density Functional Theory. The interfacial energies of different interface configurations are reported and the effect of chemistry and strain energy on the interfacial energies is quantified. The resulting interfacial structures are then compared to experimental investigations. The structures of bulk distorted bcc/hcp lattices will also be compared to the structures resulting from interfacial relaxations, and the underlying physical basis for the formation of these metastable interfacial phases will be discussed. Finally, the electronic structure of these interfacial structures will be compared to that of hydrogen-carrying bulk phases in order to determine likely sites for hydrogen occupation in Mg/Nb multilayer films.

### 3:00 PM

**Exploration of Mg and Ca Based Laves Phases for Hydrogen Storage:** *Beau Biller<sup>1</sup>; Yuwen Cui<sup>1</sup>; J.-C. Zhao<sup>1</sup>; Leonid Bendersky<sup>2</sup>; William Boettinger<sup>2</sup>*; <sup>1</sup>Ohio State University; <sup>2</sup>National Institute of Standards and Technology

Laves phases are well-known compounds for forming interstitial hydrides. Lightweight Laves phase based on Mg and Ca are attractive since lighter elements may improve the gravimetric density of the hydrides, which is key for hydrogen storage. For transition metal based Laves phases, empirical rules have been developed to correlate the hydriding and dehydriding properties to the interstitial site sizes. We are studying the mutual solubility and the dependence of lattice parameters with compositions using a high-efficiency diffusion-multiple approach. Two diffusion multiples made up of CaMg<sub>2</sub>, CaAl<sub>2</sub>, CaZn<sub>2</sub>, MgNi<sub>2</sub> and MgCu<sub>2</sub> are studied to determine the stability and composition space for the C14, C15 and C36 Laves phases of the pseudo binary and pseudo ternary systems. Results on the phase equilibria, interstitial sizes and hydrogen storage properties of selected compositions will be reported.

### 3:20 PM

**Hydrogen Absorption/Desorption Behavior of the MgH<sub>2</sub>-Ni/Al<sub>2</sub>O<sub>3</sub> Composite Prepared by High Energy Ball Milling:** *Natsuki Yamasaki<sup>1</sup>; Manshi Ohyanagi<sup>1</sup>*; <sup>1</sup>Ryukoku University

The effect of Ni/Al<sub>2</sub>O<sub>3</sub> composite additive on the hydrogen absorption/desorption kinetics of the magnesium hydride (MgH<sub>2</sub>) was studied. The Ni/Al<sub>2</sub>O<sub>3</sub> composite was prepared by the oxygen reduction of the NiO/Al<sub>2</sub>O<sub>3</sub> composite using hydrogen. The MgH<sub>2</sub> and 50wt% Ni/Al<sub>2</sub>O<sub>3</sub> were mechanically milled using a gear driven planetary ball mill for 10 min. In the case of the specimen heated with 1 °C/min under helium flow, the onset temperature of hydrogen desorption of the MgH<sub>2</sub>-Ni/Al<sub>2</sub>O<sub>3</sub> was 180 °C, which is 40 °C lower than that of MgH<sub>2</sub>-Al<sub>2</sub>O<sub>3</sub>. From the results of the hydrogen absorption measurement at 150 °C for 10 s, the Mg-Ni/Al<sub>2</sub>O<sub>3</sub> absorbed approximately 60% of the relative hydrogen desorption capacity, when the Mg-Al<sub>2</sub>O<sub>3</sub> absorbed only 10%.

### 3:40 PM Break

### 4:00 PM

**Improved Thermodynamics and Kinetics of Mg-based Hydrogen-Storage Materials Produced via Controlled Devitrification of a Metallic Glass:** *Eric Lass<sup>1</sup>*; <sup>1</sup>NIST

Mg-based hydrogen-storage materials are attractive because of their high gravimetric capacity and low cost. However, they exhibit poor kinetics and high absorption/desorption temperatures due to slow diffusion and a high formation enthalpy of the hydride. Ultra-fine grained materials show improved hydriding characteristics because of an increase in the density of short-circuit diffusion paths (i.e. grain/particle surfaces); and can destabilize the hydride phase when particle size is sufficiently reduced. In this work, nanocrystalline Mg-Ni based alloys for hydrogen-storage are produced via controlled devitrification of a metallic glass. The kinetics of hydriding/dehydriding are much improved compared to other bulk Mg-based materials. By adding small amounts of a ternary element, phase equilibria can be modified so that 4.5 to 5 wt. % H can be fully absorbed and desorbed at 473 K, about 100 K lower than other bulk Mg-based alloys.

### 4:20 PM

**Li-Mg Solid Solution Alloy for Reversible Hydrogen Storage:** *Bo Liu<sup>1</sup>; Zhigang Fang<sup>1</sup>; Jun Lu<sup>1</sup>; Peng Fan<sup>1</sup>*; <sup>1</sup>University of Utah

The search for onboard solid hydrogen storage materials have focused on complex metal hydride in recent years. The present work examines a new concept of hydrogen storage material based light metal solid solution alloys. Results of the experimental investigation of Li-Mg solid solution, which is a model system, are presented. Li-based solid solution can be prepared by using non-equilibrium processes such as rapid solidification and high energy mechanical alloying. The results showed that the temperature of dehydriding of the hydrogenated Li-Mg solid solution is much lower than that of monolithic LiH. The hydriding and dehydriding of the solid solution alloy of Li-Mg is reversible.

### 4:40 PM

**Nano-Chemo-Mechanics of Hydrogen Embrittlement of Metals under Extreme Conditions:** *Shan Huang<sup>1</sup>; David McDowell<sup>1</sup>; Ting Zhu<sup>1</sup>*; <sup>1</sup>Georgia Institute of Technology

Challenges associated with a hydrogen economy are substantial, ranging from hydrogen generation, storage and transportation. Hydrogen in high-pressure metallic containment systems causes the degradation that can result in sudden catastrophic fracture. A wide range of hydrogen embrittlement phenomena was attributed to the loss of cohesion of interfaces due to interstitially dissolved hydrogen. However, this concept has not been made sufficiently predictive, due to a lack of fundamental understanding of the chemo-mechanical processes of embrittlement. Here, by combining the atomistic simulation, thermodynamic theory of interfacial embrittlement, and electron theory of alloying, we analyze how the structure of grain boundaries influences the propensity of hydrogen chemisorption and consequent effects on embrittlement. Our results highlight the collective effects of multiple segregation sites in grain boundary embrittlement. Implications for efficient hydrogen storage are discussed by linking to a recent experiment showing that hydrogen embrittlement can be markedly reduced through grain boundary engineering.

### 5:00 PM

**Production and Characterization of Supported Transition Metal Nanoparticles on Multi-Walled Carbon Nanotubes Functionalized by Gamma Irradiation and Chemical Process:** *Jessika Rojas<sup>1</sup>; Carlos Castano<sup>1</sup>*; <sup>1</sup>Missouri University of Science and Technology

Recently, hydrogen has been the source of intense research and diverse methodologies to store it are being investigated. Single and multi-walled carbon nanotubes show promise as good options to achieve high storage. Although the current hydrogen storage capacity of CNTs does not fulfill the DoE requirements, further research is proposed about modifying the nanostructures to affect its properties. The main objective of this work is to evaluate mechanism of functionalization and purification by chemical and irradiation techniques to create functional groups in the surface and remove the caps at the end of the nanotubes to enhance the hydrogen storage capacity. Functional groups serve as a medium to attach metal nanoparticles to carbon nanotubes. SEM, STEM and XPS were used for morphological, chemical and structural characterization of the nanostructure.

### 5:20 PM Invited

**Thermodynamics of Nano-Cluster Complex Hydrides Using First-Principles Density Functional Theory:** *Eric Majzoub<sup>1</sup>; Vidvuds Ozolins<sup>2</sup>; Fei Zhou<sup>2</sup>*; <sup>1</sup>University of Missouri - St. Louis; <sup>2</sup>UCLA

While recent interest has focused on complex metal hydrides such as NaAlH<sub>4</sub> and Ca(BH<sub>4</sub>)<sub>2</sub>, these compounds are not as easily tunable as the interstitial metallic hydrides through alloying with other metal atoms. We investigate these materials at the nano-scale, where the ratio of surface to bulk atoms impacts the energetics. We present theoretical results for desorption energetics of nano-clusters of NaAlH<sub>4</sub>. Prototype geometries for the clusters were generated using a well-validated electrostatic ground state approach to a global optimization of the cluster total energy using a recently developed non-conventional Monte Carlo random walk in energy space. First-principles density functional theory applied to the prototype clusters

was used for full free energy calculations of the clusters and decomposition products. Results will be discussed with relation to recent experimental work on incorporation of complex hydrides in nanoporous framework materials, and the importance of the surface chemistry of the frameworks.

## ICME: Overcoming Barriers and Streamlining the Transition of Advanced Technologies to Engineering Practice -- The 12th MPMD Global Innovations Symposium: Modeling and Simulation Tools

*Sponsored by:* The Minerals, Metals and Materials Society, TMS Materials Processing and Manufacturing Division  
*Program Organizers:* Paul Mason, Thermo-Calc Software Inc; Mei Li, Ford Motor Company; James Warren, National Institute of Standards and Technology; Jeff Simmons, AFRL

Monday PM Room: 7A  
February 28, 2011 Location: San Diego Conv. Ctr

*Session Chairs:* Jeff Simmons, AFRL; David McDowell, Georgia Institute of Technology

### 2:00 PM Invited

**Open Source Calphad Software – Friend or Foe?:** *Ursula Kattner*<sup>1</sup>;  
<sup>1</sup>National Institute of Standards and Technology

In the early days of Calphad software was freely available, such as the Lukas' suite of programs or SOLGASMIX. Development of free packages has virtually stopped with Lukas' retirement and incorporation of SOLGASMIX into commercial software. Commercial software packages are constantly being extended and improved and have the benefit of the availability of support. Recently, Gibbs, a suite for the calculation and visualization, was introduced as open source software for thermodynamic calculations. A potential problem for developers of commercial Calphad software is the fairly small market size and that new products may have a negative impact on the sustainability of existing products. On the other hand, the advance cost of a license may deter newcomers from trying the method and/or restrict coupling of Calphad calculations with other calculations or simulations. The potential impact of open source software will be discussed using experience from thermodynamic databases for which similar issues apply.

### 2:25 PM Invited

**FiPy: PDE Performance in Python:** *Jonathan Guyer*<sup>1</sup>; *Daniel Wheeler*<sup>1</sup>;  
*James Warren*<sup>1</sup>; <sup>1</sup>NIST

FiPy is an open source, object oriented, partial differential equation (PDE) solver, written in Python. FiPy is particularly tailored to phase transformation simulations, focusing on the phase field and level set methods. The solution of coupled sets of PDEs is ubiquitous to the numerical simulation of science problems. Numerous PDE solvers exist, using a variety of languages and numerical approaches. Many are proprietary and difficult to customize. As a result, scientists spend considerable resources repeatedly developing limited tools for specific problems. FiPy takes advantage of Python's existing suite of open source tools for array calculations, sparse matrices and data rendering to provide a tool that is extensible, powerful and freely available. This talk focuses on our efforts to allow users to easily exploit parallel computing environments, sophisticated linear solvers, and advanced matrix preconditioners to obtain maximum performance without distracting them from their science.

### 2:50 PM

**Assessing Data Completeness and Predictive Potential in Magnesium Alloy Databases:** *Kim Ferris*<sup>1</sup>; *Dumont Jones*<sup>2</sup>; <sup>1</sup>Pacific Northwest National Laboratory; <sup>2</sup>Proximate Technologies, LLC.

Effective materials property databases need data completeness, which considers the range of property values and sufficiency of system

definitions. Property coverage and system definition are prerequisites for predictive structure-processing/property models. We have examined data completeness of Mg-alloy databases, finding current repositories do not exhibit full data completeness; however, their predictive capability can be substantially enhanced. Data completeness issues: 1) repositories do not completely specify individual alloy systems (e.g. processing); 2) reported Mg-alloy systems focus strongly on AZ series; and 3) measured properties show correlation in design and property spaces. Current information is sufficient to draw some conclusions for Mg-alloy design, and suggest design hypotheses. Improving predictive capability of repositories involves 1) better system definition (more detailed processing and post-treatment information), extracting basic mechanical measurements for "new" Mg-alloys, and testing hypotheses identified from current information. Authors acknowledge support from U.S. Department of Energy, Energy Efficiency and Renewable Energy, Office of Vehicle Technologies.

### 3:10 PM Invited

**Accelerated Insertion of Materials with Incomplete or Uncertain Information:** *Krishna Rajan*<sup>1</sup>; <sup>1</sup>Iowa State University

One of the critical barriers in transitioning new materials development into engineering practice is the uncertainty associated with the data that is used in the materials design process. While constitutive modeling strategies still form the foundations for computational materials design, uncertainty and incomplete information still pervades. Often intuition and/or heuristics experimentation is used to fill the gaps in evolving data needs. In this presentation we show how informatics methods helps to explore and analyze data where the information content and the taxonomy is not well defined. The talk aims to show that a formalism based on robust mathematical foundations, linked to materials engineering principles can be used to help in the design of materials in the context of their use in engineering practice. Suggestions on how this impacts the organization and use of databases to promote the philosophy of integrated computational materials engineering (ICME) are also discussed.

### 3:35 PM Break

### 3:50 PM Invited

**Code Validation and Qualification – The YMP Case:** *Patrice Turchi*<sup>1</sup>;  
<sup>1</sup>Lawrence Livermore National Laboratory

Having to tackle very challenging practical issues in an engineering-driven environment requires not only a quick solution but also in most cases code validation and qualification. For the purpose of illustration we will consider a series of studies conducted for the Yucca Mountain Project (YMP), although old and put on hold. One of the problems was to study the thermal integrity of the waste disposal canisters as a function of time with a combination of thermodynamic and kinetic modeling applied to complex multi-component alloys. After a brief review of the context of this project and the output of the materials study we will discuss the importance of code and results validation and qualification, and how it was done within this project. Then some general rules on how to qualify codes will be drawn. Work performed under the auspices of the U.S. DOE by LLNL under contract DE-AC52-07NA27344.

### 4:15 PM Invited

**A Phase Field Study on Static Strain Aging Kinetics of Dual Phase Linepipe Steel:** *Ning Ma*<sup>1</sup>; *Neeraj Thirumalai*<sup>1</sup>; *Nathan Nissley*<sup>2</sup>; *Rick Noecker*<sup>3</sup>; *William Lamberti*<sup>3</sup>; *Raghavan Ayer*<sup>1</sup>; <sup>1</sup>Corporate Strategic Research, ExxonMobil Research & Engineering Company; <sup>2</sup>ExxonMobil Upstream Research Company; <sup>3</sup>ExxonMobil Development Company

The increase of yield strength of steel during static strain aging is generally investigated following Cottrell's theory on Cottrell atmosphere formation. In the current study, we found that the time scale for strain aging of a dual-phase linepipe steel is several orders of magnitude longer than that needed for formation of "classical" Cottrell atmosphere. A Phase Field model was developed to study the kinetics of static strain aging considering the long range carbon diffusion. The observed strain aging kinetics can be rationalized by carbon diffusion across the ferrite grain from either trapped carbon in grain boundaries or neighboring carbon rich grains. The model was



extended to predict the increase in yield strength as a function of aging time and temperature. The predicted temperature dependence of yield strength produced by prolonged aging matches well with the experimental trend. Preliminary SIMS analysis in both aged and unaged samples will also be discussed.

#### 4:40 PM

**Determination of Microstructure-Property Correlations Using Phase Field Method:** *Saswata Bhattacharya*<sup>1</sup>; Tae Wook Heo<sup>1</sup>; Kunok Chang<sup>1</sup>; Ricardo Lebensohn<sup>2</sup>; Long-Qing Chen<sup>1</sup>; <sup>1</sup>Pennsylvania State University; <sup>2</sup>Los Alamos National Laboratory

Properties of materials, such as elastic stiffness, yield strength, dielectric and piezoelectric constants, diffusivity, thermal conductivity, etc. are affected by their microstructures. Therefore, establishment of microstructure-property relation is crucial for designing new materials and improving their performance. We developed an integrated computational framework based on phase field methodology to compute the effective properties of structurally inhomogeneous solids. We applied our technique to compute the effective properties of materials containing cavities or inclusions, composites, multiphase and polycrystalline microstructures. Moreover, our method can be used to calculate residual field distribution and the response behavior in inhomogeneous microstructures. As an example, we employed our method to computing the residual stress distribution and determining stress-strain relation in elastically and plastically anisotropic polycrystals undergoing deformation. Further, we studied grain growth and texture evolution under applied load and structural and diffusional phase transformations under applied field to demonstrate how the microstructural evolution affects the microstructure-property correlations.

#### 5:00 PM

**The Hierarchy of Fatigue Damage Accumulation:** *Sushant Jha*<sup>1</sup>; Christoph Szczepanski<sup>1</sup>; Craig Przybyla<sup>2</sup>; James Larsen<sup>2</sup>; <sup>1</sup>Universal Technology Corporation/Air Force Research Laboratory; <sup>2</sup>Air Force Research Laboratory

Fatigue damage is proposed to accumulate in an array of microstructural arrangements, which can be ranked in terms of the magnitude of deformation heterogeneity. These arrangements vary in size, combination of phases, and crystallographic orientations. This hypothesis rationalizes the dominance of crack growth lifetime (i.e., almost instantaneous crack-initiation) in the minimum fatigue behavior, which is often associated with an extreme microstructural arrangement. A computational study was conducted to explore the relationship between the occurrences of fatigue-critical microstructural arrangements and their rank, with the goal of predicting the probability of the life-limiting fatigue mechanisms. The analysis employed microstructures of a titanium alloy and a Ni-base superalloy simulated by an ellipsoid packing method. The computational study was complemented by detailed characterization of life-limiting microstructural configurations in both materials. The study also provided insights into the effect of microstructure, microtexture, and specimen volume on the probability of life-limiting failures in these materials.

#### 5:20 PM

**In-Situ Microscale Fatigue Study to Evaluate the Role of Microstructural Neighborhoods:** *Christopher Szczepanski*<sup>1</sup>; Sushant Jha<sup>1</sup>; Paul Shade<sup>1</sup>; Robert Wheeler<sup>2</sup>; James Larsen<sup>3</sup>; <sup>1</sup>UTC/AFRL; <sup>2</sup>UES/AFRL; <sup>3</sup>Air Force Research Laboratory/RX

A recent study of fatigue crack-initiation mechanisms and their relationship to lifetime variability in bulk samples of Ti-6Al-2Sn-4Zr-6Mo has revealed that crack initiation can occur in a variety of characteristic microstructural neighborhoods. These microstructural neighborhoods, which vary in size and frequency of occurrence, are observed at fatigue crack initiation sites through fractography. However, fractographic investigations do not allow one to identify the underlying nature of the fatigue damage accumulation and cracking mechanisms. To characterize these mechanisms under controlled conditions in a scanning electron microscope, an in-situ micro-scale tensile testing technique has been adapted to complete fatigue tests on micro-specimens extracted from representative fatigue-critical microstructural

neighborhoods. The results of these experiments will be presented, with an emphasis on identifying microstructurally driven cyclic damage accumulation processes leading to fatigue crack initiation. Additionally, the potential correlation between deformation severity and specific local microstructural configurations will be investigated to validate current mechanistic models.

---

## Magnesium Technology 2011: Casting and Solidification

*Sponsored by:* The Minerals, Metals and Materials Society, TMS Light Metals Division, TMS: Magnesium Committee  
*Program Organizers:* Wim Sillekens, TNO Science and Industry; Sean Agnew, University of Virginia; Suveen Mathaudhu, US Army Research Laboratory; Neale Neelameggham, US Magnesium LLC

Monday PM  
February 28, 2011

Room: 10  
Location: San Diego Conv. Ctr

*Session Chairs:* Baicheng Liu, Tsinghua University; Elhachmi Essadiqi, CANMET

---

#### 2:00 PM

**Simulation of Porosity and Hot Tears in a Squeeze Cast Magnesium Control Arm:** *Christoph Beckermann*<sup>1</sup>; Kent Carlson<sup>1</sup>; John Jekl<sup>2</sup>; R. Berkmortel<sup>2</sup>; <sup>1</sup>University of Iowa; <sup>2</sup>Meridian

Simulations are performed of the squeeze casting of AM60 and AZ91 automotive control arms. Advanced feeding flow and stress models are used within the casting simulation software to predict shrinkage porosity and hot tears. The simulations are validated through comparisons with observations made on experimental castings. Generally good agreement is obtained between the measured and predicted defect locations and extents. Design and process changes are introduced to mitigate the shrinkage and hot tear problems in these castings. The comparisons of the present study establish considerable confidence in the ability of casting simulation to predict shrinkage and hot tears in squeeze casting of magnesium alloys.

#### 2:20 PM

**Dendritic Microstructure in Directional Solidification of Magnesium Alloys:** *Morteza Amoorezaei*<sup>1</sup>; Sebastian Gurevich<sup>1</sup>; Nikolas Provatas<sup>1</sup>; <sup>1</sup>McMaster University

We demonstrate morphological transitions in Mg-Al alloy dendritic microstructure as the cooling conditions change during steady state and transient directional solidification. The effect of temperature gradient on the transition is investigated numerically using two-dimensional phase field simulations. The six-fold symmetry of Mg alloys leads to very different dendrite morphologies than those encountered in alloys exhibiting four-fold surface tension anisotropy. In particular, we find that at high temperature gradients primary dendrites become columnar in the direction of thermal gradient. In contrast, in the regions where surface energy anisotropy is dominant, primary stalks cross at 60-degree angles that characterize hexagonal crystal structure. Our modelling observations are compared to new Mg-Al experiments.

#### 2:40 PM

**Effect of Fraction Solid and Injection Speed on Microstructures and Casting Defects of Magnesium Alloy in New Type Semi-solid Injection Process:** *Yuichiro Murakami*<sup>1</sup>; Naoki Omura<sup>1</sup>; Mingjun Li<sup>1</sup>; Takuya Tamura<sup>1</sup>; Shuji Tada<sup>1</sup>; Kenji Miwa<sup>1</sup>; <sup>1</sup>Advanced Industrial Science and Technology

We have developed a new type semi-solid injection process, which can obtain high material yield of about 90% for magnesium alloy. In this process, generic magnesium billets are heated to the semi-solid temperature range in the injection cylinder without cover gasses and are injected into a mold. In this study, several billets were heated precisely in the cylinder to obtain desired fraction solid and the plate-like specimens were produced by injecting them under different injection speeds. The microstructures were observed by optical microscopy, and the casting defects were detected by

X-ray CT scanner. As increasing the injection speed, the shape and the size of alpha phase solid particles became more spherical, and smaller, and volume fraction of defects increased. Contrary, with higher fraction solid, volume fraction of defects decreased. Spheronization and miniaturization of solid particles was attributed to shear stress, and defects were affected by viscosity.

### 3:00 PM

**Macrostructure Evolution in Directionally Solidified Mg-RE Alloys:** Mario Salgado-Ordorica<sup>1</sup>; Willi Punessen<sup>1</sup>; Sangbong Yi<sup>1</sup>; Jan Bohlen<sup>1</sup>; Karl-Ulrich Kainer<sup>1</sup>; Norbert Hort<sup>1</sup>; <sup>1</sup>GKSS-Forschungszentrum

The mechanical properties of Mg-RE alloys, in particular their high strength at high temperatures, are well-known facts that make them promising materials for transport applications. However, since the quality of a specimen or the success of subsequent processing operations depends on the initial cast microstructure, an effort should be made on trying to understand and control the evolution of these alloy microstructures. To this end, Mg-RE alloys (where RE = Gd, Nd or Y) were cast by permanent mould direct chill casting. This process was performed in a specially optimized installation to ensure the obtention of ingots with homogeneous composition and free of porosity and inclusions. Different conditions were evaluated in order to better control the final grain size, orientation and distribution. The selection mechanisms operating during solidification, namely texturization and Columnar to Equiaxed Transition, were characterized and put into relation with the composition of the alloy and cooling conditions.

### 3:20 PM

**Microstructure and Mechanical Behavior of Cast Mg AZ31-B Alloy Produced by Magnetic Suspension Melting Process:** Nathan Rimkus<sup>1</sup>; Mark Weaver<sup>1</sup>; Nagy El-Kaddah<sup>1</sup>; <sup>1</sup>Univ of Alabama

Magnesium is the lightest of all structural metals and offers significant weight savings compared to traditional automotive materials. This paper describes macro/microstructure of Mg AZ31-B alloy produced via the Magnetic Suspension Melting (MSM) technique at a low superheat of 5°C. It was found that casting at this low superheat produced a fine cellular grain structure in comparison to a dendritic structure in conventionally cast alloys. The intermetallic phases were analyzed in detail and compared with the conventionally cast alloy. In the MSM cast alloy, the  $\gamma$ Mg17Al12 phase formed mainly at the grain boundaries, in contrast to typical dendritic entrapment of this phase within the grains in conventional castings. The formation of the Al-rich secondary- $\alpha$  phase during solidification was investigated. The effects of this morphology change on mechanical and fracture behavior of this material will be presented. These results will be discussed relative to conventionally cast Mg alloys.

### 3:40 PM

**Investigations on Hot Tearing of Mg-Zn-(Al) Alloys:** Le Zhou<sup>1</sup>; Yuanding Huang<sup>1</sup>; Pingli Mao<sup>2</sup>; Karl Ulrich Kainer<sup>1</sup>; Zheng Liu<sup>2</sup>; Norbert Hort<sup>1</sup>; <sup>1</sup>MagIC-Magnesium Innovation Centre, GKSS Research Centre; <sup>2</sup>Shenyang University of Technology

Mg-Zn alloys are widely used as wrought alloys such as ZM, ZK and ZE. It already had been reported that they are prone to hot tearing. The present work evaluates the hot tearing susceptibility (HTS) of binary Mg-Zn alloys using quantitative experimental methods and thermodynamic simulations based on Clyne's model. The results show that the curve of the HTS vs. the content of Zn has a typical "λ" shape. With increasing the content of Zn, the HTS increases firstly, reaches the maximum at 1.5% Zn and then decreases again. The addition of Al in Mg-Zn alloys influences the HTS. In the Mg-Zn-Al ternary system, the HTS decreases with the increase of Al content. The effect of Zn content on HTS in ternary Mg-Zn-Al systems is similar to that observed in binary Mg-Zn alloys.

### 4:00 PM Break

### 4:20 PM

**Proportional Strength-Ductility Relationship of Non-SF6 Diecast AZ91D Eco-Mg Alloys:** Shae K. Kim<sup>1</sup>; <sup>1</sup>Korea Institute of Industrial Technology

SF6 gas has been generally used for Mg alloys during melting and casting as a cover gas. The use of SF6 gas, however, will be limited owing to its

significant impact on global warming. Non-SF6 process during melting and casting in diecasting industry has been proved with Eco-Mg alloys, simple addition of small amount of CaO into AZ91D and AM60B Mg alloys. This paper will show non-SF6 diecasting procedures for AZ91D Eco-Mg alloys. Cold-chamber and hot-chamber diecasting mass productions were performed by using a Toshiba 135-ton cold chamber and a Frech 200-ton hot chamber diecasting machines under CO2 atmosphere without SF6 gas. An emphasis will be on proportional strength and ductility relationship of Eco-Mg alloys, in part, due to high-quality melt, refined grain size and Al2Ca second phase strengthening. Microstructures and mechanical properties of AZ91D Eco-Mg alloys will be evaluated in comparison with those of conventional AZ91D Mg alloy.

### 4:40 PM

**Estimation of Heat Transfer Coefficient in Squeeze Casting of Magnesium Alloy AM60 by Experimental Polynomial Extrapolation**

**Method:** Zhizhong Sun<sup>1</sup>; Xiaoping Niu<sup>2</sup>; Henry Hu<sup>1</sup>; <sup>1</sup>University of Windsor; <sup>2</sup>Promatek Research Centre, Cosma International

In this work, a different wall-thickness 5-step (with thicknesses as 3, 5, 8, 12, 20 mm) casting mold was designed and squeeze casting of magnesium alloy AM60 was performed in a hydraulic press. The casting-die interfacial heat transfer coefficient (IHTC) in 5-step casting was determined accurately based on thermal histories throughout the die and inside the casting which were recorded by fine type-K thermocouples. With measured temperatures, heat flux and IHTC were evaluated using the polynomial curve fitting method and numerical inverse method. For numerical inverse method, a solution algorithm is developed based on the function specification method to solve the inverse heat conduction equations. The IHTCs computed with these two techniques were compared. The results show that the peak values of IHTC at the thin steps are higher than those at the thick steps. However, the duration for IHTC remaining at the peak value increases as the step thickness increases.

### 5:00 PM

**Wide Strip Casting Technology of Magnesium Alloys:** Woo-Jin Park<sup>1</sup>; Jae-Joong Kim<sup>1</sup>; In-Joon Kim<sup>1</sup>; Dong-Kyun Choo<sup>1</sup>; <sup>1</sup>RIST

Extensive investigations relative to producing high performance and low cost magnesium sheet by strip casting have been performed for the applications to automotive parts and electronic devices. Research in order to develop magnesium sheet production technology has been begun from 2004 by RIST with support of POSCO. The POSCO has completed the plant to manufacture magnesium coil in the world's first. Big project in order to develop wide magnesium strip casting technology was started in succession. In this study, the recent results for wide magnesium strip casting are going to be presented. Wide magnesium coils of ~16 tons with 2,000mm width, 2,500mm diameter and 4~8mm thickness were successfully manufactured by strip casting process. Surface defects like inverse segregations could be minimized in the wide magnesium sheets by controlling adequately process parameters. As-strip cast microstructure consists of surface chill zone, dendritic columnar structure and central region.

### 5:20 PM

**Microstructural Analysis of Segregated Area in Twin Roll Cast Mg Alloy Sheet:** Jae Joong Kim<sup>1</sup>; Woo-Jin Park<sup>1</sup>; Dong Kyun Choo<sup>1</sup>; <sup>1</sup>RIST

Twin roll cast of magnesium alloy has been studied by various institutes since POSTECH started at the world first. RIST has done the R&D program of twin roll cast and reverse warm mill of magnesium sheet with 600 mm width. Presently, RIST is working on twin roll cast of magnesium sheet with 2,000 mm width. Twin roll cast magnesium alloy includes segregated area which is important due to controllable quality of final product. Here we present the microstructural analysis of segregated area of twin roll cast magnesium alloy to understand segregation phenomena. Especially, we studied on phase identification in segregated area, comparing the theoretical simulation. Our result shows that two kinds of phase morphologies are observed in the segregated area, not depending upon the position in the sheet. Phase identification shows that segregated area includes densely continuous or dispersed beta and phi phase, and dispersed Al<sub>3</sub>Mn<sub>3</sub> and Mg<sub>2</sub>Si.

5:40 PM

**Development of the Electromagnetic Continuous Casting Technology for Mg Alloys:** *Joonpyo Park*<sup>1</sup>; Myounggyun Kim<sup>1</sup>; Jong-Ho Kim<sup>1</sup>; Gyu Chang Lee<sup>1</sup>; U-Sok Yoon<sup>1</sup>; Woojin Kim<sup>1</sup>; <sup>1</sup>Research Institute of Industrial Science and Technology

Continuous casting technology for high-quality surface billets with fine-grained and homogeneous microstructure can be a solution for the cost barrier breakthrough. The latent heat of fusion per weight (J/g) of magnesium is similar to that of other metals. However, considering the heat emitted to the mould surface during continuous casting in meniscus region and converting it to the latent heat of fusion per volume, magnesium will be rapidly solidified in the mould during continuous casting, which induces subsequent surface defect formation. In this study, electromagnetic casting and stirring (EMC and EMS) techniques is proposed to control solidification process conveniently by compensating the low latent heat of solidification by volume and to fabricate magnesium billets of high quality surface. This technique was extended to large scale billets up to 300 mm diameter and continuous casting was successfully conducted. Then magnesium billet was used for the fabrication of prototype automobile pulley.

## **Magnesium Technology 2011: Primary Production; Characterization and Mechanical Performance**

*Sponsored by:* The Minerals, Metals and Materials Society, TMS Light Metals Division, TMS: Magnesium Committee

*Program Organizers:* Wim Sillekens, TNO Science and Industry; Sean Agnew, University of Virginia; Suveen Mathaudhu, US Army Research Laboratory; Neale Neelameggham, US Magnesium LLC

Monday PM  
February 28, 2011

Room: 6F  
Location: San Diego Conv. Ctr

*Session Chairs:* Neale Neelameggham, US Magnesium LLC; Adam Powell, Metal Oxygen Separation Technologies Inc.

2:00 PM

**The Development of the Multipolar Magnesium Cell: A Case History of International Cooperation in a Competitive World:** *Olivo Sivilotti*<sup>1</sup>; <sup>1</sup>Sigma Tau Technologies

The author conceived the first multipolar magnesium electrolytic cell in the late 1970s, in order to offset the impact of an 80kA monopolar cell being developed in cooperation with Osaka Titanium Company (OTC) being licenced by Alcan to a major competitor of OTC. During the 80s the commercial value of the multipolar magnesium cell technology was established. The 90s saw significant further progress in OTC, while attempts by Alcan to commercialize it in magnesium production plants met with technical difficulties and failure, due primarily to the lack of magnesium chloride feed of adequate quality. Now the author plans to commercialize a new multipolar cell design with a target productivity of 8.5-10 tons/day and a unit power consumption of 8.5-10 KWHR/kg of magnesium.

2:20 PM

**Effect of KCl on Liquidus of LiF-MgF<sub>2</sub> Molten Salts:** *Sh Yang*<sup>1</sup>; Fengli Yang<sup>1</sup>; Xianwei Hu<sup>2</sup>; Zhaowen Wang<sup>2</sup>; Zhingning Shi<sup>2</sup>; Bingliang Gao<sup>2</sup>; <sup>1</sup>Jiangxi University of Science and Technology; <sup>2</sup>School of Materials and Metallurgy117#, Northeastern University

Liquidus temperature of KCl-LiF-MgF<sub>2</sub> molten salts was determined based on cooling curve. The results proved the method of cooling curve was reliable and accurate by comparison liquidus temperatures of KCl. The measured value of KCl liquidus temperatures 769.27°C, and the documental value was 769.5°C. The different value was 0.23%, and the error ratio was 0.03%. The results were shown that effect of KCl on liquidus of molten salt was great for MgF<sub>2</sub>-LiF electrolyte. The liquidus temperatures were different with increasing of content of KCl in electrolyte. The liquidus temperature could be reduced 20°C with content of KCl in electrolyte from 0wt% to 50wt%. The experiments showed that the compound addition of

KCl into LiF-MgF<sub>2</sub> electrolyte not only reduced the liquidus temperature of electrolyte effectively but also decreased the aluminum-magnesium production cost and increased the economic benefits.

2:40 PM

**Efficiency and Stability of Solid Oxide Membrane Electrolyzers for Magnesium Production:** *Eric Gratz*<sup>1</sup>; Soobhankar Pati<sup>1</sup>; Jarrod Milshtein<sup>1</sup>; Adam Powell<sup>2</sup>; Uday Pal<sup>1</sup>; <sup>1</sup>Boston University; <sup>2</sup>Metal Oxygen Separation Technologies, Inc.

Solid oxide membrane (SOM) process has been successfully employed for the production of magnesium directly from its oxide. The process involves dissolving MgO in a fluoride based ionic flux and electrochemically pumping out the oxygen ions from the flux via an oxygen-ion-conducting SOM to the anode where they are oxidized, while reducing magnesium ions at the cathode. Understanding the long-term stability of the SOM in the flux is critical for the commercial success of this technology. This study utilizes electrochemical techniques such as impedance spectroscopy and linear sweep voltammetry to investigate key concepts related to MgO dissociation and current efficiency. Results show that the dissociation potential of MgO is dependent on the partial pressures at which magnesium is generated and the membrane stability is likely related to the current efficiency.

3:00 PM

**Magnesium Production by Vacuum Aluminothermic Reduction of a Mixture of Calcined Dolomite and Calcined Magnesite:** *Wenxin Hu*<sup>1</sup>; Naixiang Feng<sup>1</sup>; Yaowu Wang<sup>1</sup>; Zhihui Wang<sup>1</sup>; <sup>1</sup>Northeastern University

A new method of magnesium production was proposed that using a mixture of calcined dolomite and calcined magnesite with the molar ratio of MgO to CaO 6:1 as raw materials by vacuum aluminothermic reduction and extracted alumina from CaO·2Al<sub>2</sub>O<sub>3</sub>, the main phase of reduction slag analyzed by X-ray diffraction analysis. The results show that the reduction ratio of MgO was 86.18% at the conditions of 1414 K, 150 mins and was increased while reduction temperature and reduction time extended. The alumina leaching ratio of reduction slag reached 88% at the conditions of leaching temperature 95 °C and the concentration ratio of Na<sub>2</sub>CO<sub>3</sub> to NaOH was 100:75 in leaching Solution.

3:20 PM

**Multiphase Diffusion Study for Mg-Al Binary Alloy System:** *Young-Min Kim*<sup>1</sup>; Sazol Das<sup>1</sup>; Manas Paliwal<sup>1</sup>; In-Ho Jung<sup>1</sup>; <sup>1</sup>McGill University

Multiphase diffusion simulation and experimental studies are performed for Mg-Al binary alloy system at various temperatures. All simulations are based on the assumption that the inter-diffusion coefficients are composition independent and the interface always lies at equilibrium. Finite difference method (FDM) is used to solve diffusion equation and program is coded in FORTRAN with the evaluated self and inter diffusivity coefficients of Mg and Al. Annealing experiments of Mg-3wt% Al and Mg-6wt% Al were carried out at 330oC and 400oC for various times and the concentration profiles of Al were measured by Electron Probe Micro Analyzer (EPMA). The diffusion simulation results are in good agreement with both diffusion couple as well as annealing experiments.

3:40 PM

**Experiments and Modeling of Fatigue of an Extruded Mg AZ61 Alloy:** *J Jordan*<sup>1</sup>; J. Gibson<sup>1</sup>; M. Horstemeyer<sup>1</sup>; <sup>1</sup>Mississippi State University

In this study, structure-property relations with respect to fatigue of an extruded AZ61 magnesium alloy were experimentally quantified. Strain-life experiments were conducted in the extruded and transverse orientations under low and high cycle conditions. The cyclic behavior of this alloy displayed varying degrees of cyclic hardening depending on the strain amplitude and the specimen orientation. The fracture surfaces of the fatigued specimens were analyzed using a scanning electron microscope in order to quantify structure-property relations with respect to number of cycles to failure. Intermetallic particles were found to be the source of fatigue initiation on a majority of fracture surfaces. Finally, a multistage fatigue model based on the relative microstructural sensitive features quantified in this study was employed to capture the anisotropic fatigue damage of the AZ61 magnesium alloy.

MONDAY PM



#### 4:00 PM Break

#### 4:20 PM

**Low-Cycle Fatigue Behavior of Die-Cast Mg Alloy AZ91:** *Luke Rettberg*<sup>1</sup>; Warwick Anderson<sup>1</sup>; J. Wayne Jones<sup>1</sup>; <sup>1</sup>University of Michigan

An investigation has been conducted on the influence of microstructure and artificial aging response (T6) on the low-cycle fatigue behavior of super vacuum die-cast (SVDC) AZ91. Fatigue lifetimes were determined from total strain-controlled fatigue tests for strain amplitudes of 0.2%, 0.4% and 0.6%, under fully reversed loading at a frequency of 5 Hz. Cyclic stress-strain behavior was determined using incremental step test (IST) methods. Two locations in a prototype casting with different thicknesses and, therefore, solidification rates, microstructure and porosity, were examined. In general, at all total strain amplitudes fatigue life was unaffected by microstructure refinement and was attributed to significant levels of porosity. Cyclic softening and a subsequent increased cyclic hardening rate, compared to monotonic tests, were observed, independent of microstructure. These results, fractography and damage accumulation processes, determined from metallographic sectioning, are discussed.

#### 4:40 PM

**Small Fatigue Crack Growth Observations in an Extruded Magnesium Alloy:** *J. Bernard*<sup>1</sup>; J. Jordon<sup>1</sup>; M. Horstemeyer<sup>1</sup>; <sup>1</sup>Center for Advanced Vehicular Systems- Mississippi State University

The purpose of this paper is to quantify the microstructurally small/physically small crack growth behavior in an extruded AZ61 magnesium alloy. Fully-reversed, interrupted load control tests were conducted on notched specimens that were taken from the transverse direction with respect to the extrusion direction. In order to measure crack growth, replicas of the notch surface were taken at periodic intervals. Scanning electron microscopy analysis of the replica surfaces revealed multi site crack initiation and subsequent crack coalescence. The crack growth behavior of the small fatigue cracks was shown to have a strong dependence on the material microstructure as the crack was submitted to a tortuous growth path along grain boundaries and crystallographic slip planes. A multi-stage microstructurally dependent crack growth model that was previously calibrated for FCC metals was further developed by this research for HCP materials.

#### 5:00 PM

**Applicability of Mg-Zn-(Y, Gd) Alloys for Engine Pistons:** *Kazutaka Okamoto*<sup>1</sup>; Masato Sasaki<sup>2</sup>; Norikazu Takahashi<sup>2</sup>; Qudong Wang<sup>3</sup>; Yan Gao<sup>3</sup>; Dongdi Yin<sup>3</sup>; Changjiang Chen<sup>3</sup>; <sup>1</sup>Hitachi, R&D; <sup>2</sup>Hitachi Automotive Systems; <sup>3</sup>Shanghai Jiao Tong Univ

Commercial magnesium alloys have a great potential for structural applications in automotive due to their significant weight saving. However, they have poor creep resistance at temperature over 125°C, thus making them inadequate for power train applications such as engine pistons, which are operated at temperature up to 300°C. Recently, creep resistant magnesium alloys with rare earth elements and Zn have been developed, hence the applicability of Mg-Zn-(Y, Gd) alloys for engine pistons was investigated in this paper. Gravity casting was performed with Mg-Zn-(Y, Gd)-Zr ingot, followed by T6 treatment. High cycle fatigue tests were carried out and results were compared to the current aluminum cast alloy of A336 (JIS AC8A) for pistons. At room temperature, the fatigue strength is 27% lower than A336, while it is 35% higher at 300°C. The effects of microstructure on the mechanical properties will be discussed in the presentation.

#### 5:20 PM

**Compressive Creep Behaviour of Extruded Mg Alloys at 150°C:** *Michelle Fletcher*<sup>1</sup>; Lukas Bichler<sup>1</sup>; Dimitry Sediako<sup>2</sup>; Robert Klassen<sup>3</sup>; <sup>1</sup>University of British Columbia; <sup>2</sup>NRC-Canadian Neutron Beam Centre; <sup>3</sup>University of Western Ontario

Wrought Mg alloy bars, sections and tubes have been extensively used in the aerospace, nuclear and automotive industries, where component weight is of concern. The operating temperature of these components is typically limited to below 100°C, since appreciable creep relaxation of the alloys

takes place above this temperature. This study was focused on a selected wrought magnesium alloys developed for high temperature applications. Compressive creep behaviour of AE, ZE, AJ, AX and EZ rods was studied at room temperature and at 150°C using the microindentation creep technique. Measurements were obtained in the radial and transverse directions to observe the effect of texture on creep strain, hardness and elastic modulus. Microscopic examination of the alloys revealed that the distribution of second phases was critical to the alloy's creep resistance. Selected results were also related to in-situ compressive creep experiments carried out using neutron diffraction techniques.

#### 5:40 PM

**The Effect of Thermomechanical Processing on the Creep Behavior and Fracture Toughness of Thixomolded® AM60 Alloy:** *Zhe Chen*<sup>1</sup>; Amit Shyam<sup>2</sup>; Jane Howe<sup>2</sup>; Jack Huang<sup>3</sup>; Ray Decker<sup>3</sup>; Steve LeBeau<sup>3</sup>; Carl Boehlert<sup>1</sup>; <sup>1</sup>Michigan State University; <sup>2</sup>Oak Ridge National Laboratory; <sup>3</sup>Thixomat Inc.

The effect of thermomechanical processing and subsequent heat treatment on the small fatigue crack growth behavior of a nanoMAG AM60 magnesium alloy will be reported. The investigated alloys have a finer grain structure and higher levels of yield strength compared to similar alloys with conventional processing treatment. The effect of maximum stress and load ratio on the growth rate of cracks emanating from artificial notches will be characterized and modeled. The notches were of the same size scale as natural defects in these materials and were fabricated by electro-discharge machining. Microstructure and fracture surface characterization will be performed by electron microscopy to develop the microstructure-fatigue property relationships in this class of lightweight alloys.

### Magnetic Materials for Energy Applications: Magnetocaloric Materials

*Sponsored by:* TMS Electronic, Magnetic, and Photonic Materials Division, TMS: Energy Conversion and Storage Committee, TMS: Magnetic Materials Committee; JSPS 147th Committee on Amorphous and Nanocrystalline Materials; Lake Shore Cyrotronics, Inc.; AMT&C

*Program Organizers:* Victorino Franco, Sevilla University; Oliver Gutfleisch, IFW Dresden; Kazuhiro Hono, National Institute for Materials Science; Paul Ohodnicki, National Energy Technology Laboratory

Monday PM  
February 28, 2011

Room: 11A  
Location: San Diego Conv. Ctr

*Session Chair:* Oliver Gutfleisch, IFW Dresden

#### 2:00 PM Keynote

**Towards Better Magnetocaloric Materials:** *Vitalij Pecharsky*<sup>1</sup>; Karl Gschneidner<sup>1</sup>; <sup>1</sup>Iowa State University

Recent achievements in the design of robust near room temperature magnetic cooling devices signify paradigm shift in refrigeration, liquefaction and freezing technologies, and call for a much broader base of advanced magnetocaloric materials to support the quick realization of this environmentally friendly, energy efficient technology in a variety of markets. The latest materials discoveries and current trends in design of advanced magnetocaloric compounds will be reviewed. Work at the Ames Laboratory is supported by the U.S. Department of Energy – Basic Energy Sciences under contract No. DE-AC02-07CH11358.

#### 2:40 PM Invited

**Interplay between Structure and Magnetism in Gd<sub>5</sub>(Si<sub>x</sub>Ge<sub>1-x</sub>)<sub>4</sub>:** *Daniel Haskel*<sup>1</sup>; <sup>1</sup>Argonne National Laboratory

The connection between atomic structure and magnetism in giant magnetocaloric effect (MCE) material Gd<sub>5</sub>(Si<sub>x</sub>Ge<sub>1-x</sub>)<sub>4</sub> is explored using synchrotron radiation techniques. The element selectivity of x-ray absorption fine structure (XAFS) and additional orbital selectivity of x-ray magnetic circular

dichroism (XMCD) allow probing the magnetic polarization of conduction states responsible for mediating exchange interactions between localized Gd 4f electrons in the context of the magneto-structural phase transition. Furthermore, extension of these measurements to the diamond anvil cell allows a detailed comparison of the effects of chemical pressure (Si doping) and physical pressure upon the strength of magnetic interactions providing valuable insight into the role that Si/Ge p- Gd 5d hybridization plays in regulating the ferromagnetic ordering temperature of these materials. Work at Argonne is supported by the U.S. Department of Energy, Office of Science, Office of Basic Energy Sciences, under Contract No. DE-AC02-06CH11357.

### 3:05 PM Invited

#### **Novel Design of Magnetic Refrigerant Materials towards High Refrigeration Performance:** *Julia Lyubina*<sup>1</sup>; <sup>1</sup>Imperial College London

Materials showing a large magnetocaloric effect around room temperature are of increasing interest due to their possible application in magnetic refrigeration. Very attractive in this respect are materials with a first order transition, since the latter results in a large (giant) entropy change. However, these materials usually possess magnetic and thermal hysteresis and are prone to fracture due to crystal symmetry and/or volume change accompanying the transition that reduces the efficiency or even makes the refrigeration cycle impossible. Here, we discuss how the magnetic and mechanical properties can be improved by special processing. It is shown that the design of porous microstructure in La(Fe,Si)<sub>13</sub> materials is advantageous for the reduction of hysteresis and substantially improves mechanical stability. Practical implementation issues for the integration of La(Fe,Si)<sub>13</sub> in cooling engines are discussed. This research is in part supported by a Marie Curie Intra European Fellowship within the 7th FP of EC.

### 3:30 PM

#### **Adiabatic Temperature Change, Entropy Change and Magneto-Volume Effect in La-Fe-Si Alloys: A Study of Thermal and Magnetic Hystereses:** *Konstantin Skokov*<sup>1</sup>; James Moore<sup>1</sup>; Jian Liu<sup>1</sup>; Maria Krautz<sup>1</sup>; Oliver Gutfleisch<sup>1</sup>; <sup>1</sup>Leibniz Institute for Solid State and Materials Research

Compounds with the first-order ferromagnetic-paramagnetic transitions seem to be very promising for magneto magneto-cooling technique due to very high values of the magnetic entropy change. However in comparison with the second-order transition, the first-order transition is unavoidably accompanied by field- and temperature-hystereses as well as latent heat transfer. During operational field or temperature cycling this irreversibility appears as an undesirable heating of the magnetocaloric material. Thus, the study on the issue of hysteresis is extremely important for development of an efficient magnetic refrigerator prototype. A comparative study of the magnetic hysteresis from isothermal M-H loops, the magnetic entropy change, the adiabatic temperature change and the volume change of LaFe<sub>13-x</sub>Si<sub>x</sub> alloys undergoing the first-order magnetic transition has been carried out. Also, effects of temperature and field cycling on the magnetocaloric effect were investigated. By building the S-T diagram, a thermodynamic analysis of the first-order transition in LaFe<sub>13-x</sub>Si<sub>x</sub> alloys has been performed.

### 3:45 PM

#### **Magnetocaloric Study of Mechanically Alloyed LaFeSi:** *Mathieu Phejar*<sup>1</sup>; *Loffi Bessais*<sup>1</sup>; Valérie Paul-Boncour<sup>1</sup>; <sup>1</sup>CNRS

The room temperature magnetic refrigeration based on the magnetocaloric effect (MCE) is an alternative to conventional cooling. Much interest have been carried on La(Fe,Si)<sub>13</sub> compounds since the discovery of their giant MCE associated with low cost. These compounds is hardly formed by a peritectic reaction between the liquid La and the solid solution of Fe,Si resulting in a inhomogeneous microstructure. We have synthesized those compounds by ballmilling which until now haven't been used for this kind of samples. While a heat treatment of one month is necessary to obtain the crystallization of the NaZn<sub>13</sub> type structure for bulk alloys only 30 minutes is sufficient for ballmilled samples because of their finer microstructure. The magnetic properties of these compounds have been improved by substitution of Fe for Si and by insertion of hydrogen or carbon.

### 4:00 PM Break

### 4:15 PM

#### **Field Effect on Martensitic Transition and Magnetocaloric Effect in Ni<sub>50</sub>Mn<sub>35.5</sub>In<sub>14.5</sub> and Ni<sub>45.5</sub>Mn<sub>43</sub>In<sub>11.5</sub> Ribbons:** *Wagner Rosa*<sup>1</sup>; *Tatiana Sánchez*<sup>1</sup>; *Javier García*<sup>1</sup>; *Victor Vega*<sup>1</sup>; *Victor Prida*<sup>1</sup>; *Lluisa Escoda*<sup>2</sup>; *Joan Suñol*<sup>2</sup>; *Blanca Hernando*<sup>1</sup>; <sup>1</sup>Universidad de Oviedo; <sup>2</sup>Universidad de Girona

Ferromagnetic shape memory Ni-Mn-In Heusler alloys undergo a thermoelastic martensitic transformation (MT) from parent austenitic phase to a martensitic one on cooling [1]. The sensitivity of MT to the applied magnetic field becomes this material very suitable for alternative energy technologies due to magnetocaloric effect (MCE) [2]. We report on structural and magnetic properties for Ni-Mn-In melt-spun ribbons. Samples microstructure was checked by XRD and SEM together with their chemical composition by EDS. Magnetic properties were measured with a VSM in the temperature range of 50K-400K and up to 3 T. MT was characterized from the thermomagnetic measurements (ZFC-FC-FH) in different applied fields. MT behaves highly sensitive to the applied field and alloy composition. Direct and inverse MCE near Curie point and MT point, have been clearly revealed. [1] Z.D. Han, et al, Solid State Communications 146 (2008) 124. [2] B. Hernando, et al, Appl. Phys. Lett. 94 (2009) 222502.

### 4:30 PM

#### **In-Situ High-Energy X-Ray Studies of Magnetic-Field-Induced Functional Behaviors in Ferromagnetic Shape-Memory Alloys:** *Zhihua Nie*<sup>1</sup>; *Yandong Wang*<sup>1</sup>; *Yang Ren*<sup>2</sup>; <sup>1</sup>Beijing Institute of Technology; <sup>2</sup>Argonne National Laboratory

A large magnetic-field-induced strain (MFIS) found in ferromagnetic shape-memory alloys (FSMAs) has stimulated much attentions. The large MFIS can be achieved through (1) the rearrangement of martensite variants via twin boundary motion, such as NiMnGa, or (2) the phase transition from a phase with lower magnetization to a phase with higher magnetization, such as NiCoMnIn. Synchrotron-based high-energy X-ray diffraction (HEXRD) techniques provide an in-situ tool for tracing the microscopic evolution of structures under various environments. This talk will present our in-situ HEXRD studies of magnetic-field-induced functional behaviors in FSMAs. An internal-stress of ~8 MPa was uncovered in a NiMnGa single crystal after thermo-magnetic training, showing a new training mechanism by introducing internal-stress in FSMAs which aims to lower the twinning stress. In polymer-bonded NiCoMnIn composites, the magnetic-field not only induced an inverse martensitic phase transformation accompanied with a MFIS of ~1.76%, but also affected the phase fraction at low temperatures.

### 4:45 PM

#### **Room Temperature Magneto-caloric Effect In Fe Substituted Ni-Mn-Sn Alloy:** *Rahul Das*<sup>1</sup>; *Perumal Alagarsamy*<sup>1</sup>; *Ananthakrishnan Srinivasan*<sup>1</sup>; <sup>1</sup>Indian Institute of Technology Guwahati

Ferromagnetic shape memory alloys exhibiting high magnetic entropy change ( $\Delta S_M$ ) near room temperature are being developed for magnetic refrigeration application. Ni<sub>49</sub>Mn<sub>37</sub>Fe<sub>1</sub>Sn<sub>13</sub> (Ni<sub>47</sub>Mn<sub>37</sub>Fe<sub>3</sub>Sn<sub>13</sub>) exhibit highest  $\Delta S_M$  of ~6 Jkg<sup>-1</sup>K<sup>-1</sup> (11 Jkg<sup>-1</sup>K<sup>-1</sup>) for 2 T field change at 241 K (177 K) [1]. In this work, we altered the composition of Ni-Mn-Sn-Fe system and obtained  $\Delta S_M$  of 5.2 Jkg<sup>-1</sup>K<sup>-1</sup> for 2 T field change in Ni<sub>50</sub>Mn<sub>36</sub>Sn<sub>13</sub>Fe<sub>1</sub> alloy at 304 K.  $\Delta S_M$  obtained is larger than those reported for Fe substituted Ni-Mn-Sn alloys near room temperature for the same field change. Since the properties of these alloys are strongly influenced by the composition and processing conditions, it is possible to improve the  $\Delta S_M$  of these alloys further. Details of experiments and results obtained would be presented.[1] T. Krenke *et al. J. Appl. Phys.* 102 (2007) 033903.

### 5:00 PM

#### **The Magnetocaloric Effect in Ni-Mn-Ga Heusler Alloys:** *Mikhail Drobosyuk*<sup>1</sup>; *Vasily Buchelnikov*<sup>1</sup>; *Sergey Taskaev*<sup>1</sup>; <sup>1</sup>Chelyabinsk State University

In this work we study experimentally the positive magnetocaloric effect (MCE) in Ni<sub>2-x</sub>Mn<sub>1-x</sub>Ga (x = 0.02, 0.03, 0.04, 0.07, 0.09) Heusler alloys. The MCE have been measured by the direct method. For the magnetic field change

$\Delta H = 2$  T, the maximal adiabatic temperature change  $\Delta T_{ad}$  in  $Ni_{2-x}Mn_{1-x}Ga$  alloys is larger than 0.6 K. The results show that the studied Heusler alloys may be interesting from the practical application point of view.

5:15 PM

**Calorimetric and Magnetic Measurements of Magnetic Entropy Change in Pr<sub>0.5</sub>Sr<sub>0.49</sub>Ca<sub>0.01</sub>MnO<sub>3</sub>:** *Ramanathan Mahendiran*<sup>1</sup>; <sup>1</sup>National University of Singapore

Perovskite manganites are considered to be one of the likely candidates for magnetic refrigeration due to significant magnetic entropy change exhibited by them. Majority of the existing work focussed on extracting magnetic entropy change from magnetization isotherms using Maxwell's relation. However, application of Maxwell's equation overestimates magnetic entropy in first order transition and independent verification of magnetic entropy by thermal method is essential. We investigated magnetocaloric effect in Pr<sub>0.5</sub>Sr<sub>0.5-x</sub>CaxMnO<sub>3</sub> series (x = 0 to 1) using differential scanning calorimeter and magnetization isotherms. While magnetic measurement gave a large magnetic entropy change (= +10.9 J/kg K for a field variation of 5 T, calorimetric data gave smaller value (= +6.5 J/kg K) around the Neel temperature (TN = 140 K) but comparable values (= 4 J/kg K) around the Curie temperature (TC = 260 K). The large magnetic entropy around TN found by calorimetric method is promising for application.

5:30 PM

**Influence of Heat Treatment on the Structure and Magnetic Properties of Gd<sub>5</sub>Sn<sub>4</sub> Alloy for Magnetic Refrigeration:** *Xichun Zhong*<sup>1</sup>; H Zhang<sup>2</sup>; M Zou<sup>2</sup>; Zhongwu Liu<sup>1</sup>; Dechang Zeng<sup>1</sup>; K.A. Gschneidner Jr.<sup>2</sup>; V.K. Pecharsky<sup>2</sup>; <sup>1</sup>South China University of Technology; <sup>2</sup>The Ames Laboratory, Iowa State University

The effects of heat treatment on the structure and magnetic properties of Gd<sub>5</sub>Sn<sub>4</sub> alloy were investigated. In as-cast alloy, the main phase is orthorhombic Gd<sub>5</sub>Sn<sub>4</sub>, and two secondary phases are monoclinic Gd<sub>5</sub>Sn<sub>4</sub> and hexagonal Gd<sub>5</sub>Sn<sub>3</sub>. After 1300°C annealing, the content of main phase increased from 85.39% to 98.47% and the monoclinic Gd<sub>5</sub>Sn<sub>4</sub> phase disappeared. For as-cast alloy, an antiferromagnetism-ferromagnetism transition near 60K caused by Gd<sub>5</sub>Sn<sub>3</sub> phase was evident. Two magnetic transitions near 82K and 130K are caused by the Gd<sub>5</sub>Sn<sub>4</sub> main phase and monoclinic phase, respectively. For the annealed sample, the phase transitions near 60 and 130K are not significant due to the reduced secondary phases and the Tc of Gd<sub>5</sub>Sn<sub>4</sub> phase decreases from ~82 to ~80K. The maximum magnetic entropy change in a low field of  $\square H=20$ kOe increases from 21.5 to 24.65J/kgK after heat treatment. The results demonstrated that Gd<sub>5</sub>Sn<sub>4</sub> alloy is a good magnetocaloric material for refrigeration.

5:45 PM

**Bonded Magnetocaloric Powders for the Refrigeration Application:** *Spomenka Kobe*<sup>1</sup>; Benjamin Podmiljšak<sup>1</sup>; Marko Soderžnik<sup>1</sup>; Boris Saje<sup>1</sup>; Paul McGuinness<sup>1</sup>; <sup>1</sup>Jožef Stefan Institute

Magnetocaloric materials (MCM) based on Gd<sub>5</sub>Si<sub>2</sub>Ge<sub>2</sub> with Fe as an additive show that the refrigeration capacity (RC) can be optimized with processing methods and substitution of various atoms in the lattice. Modified alloy can be used at room temperature. The hysteresis losses are drastically decreased with small decrease of net refrigeration capacity (NRC). The final product for refrigeration application should not be in the powder form and the idea is to use the discs, which will rotate in the applied magnetic field. The discs should be mechanically hard, but the amount of the bonding material should be as low as possible to prevent the dilution of the active magnetocaloric material. We used MCM with the best properties achieved, and various bonding materials. With the systematic experimental work we determined the composition, which enabled us the highest density with simultaneously good mechanical strength and magnetocaloric properties.

### Massively Parallel Simulations of Materials Response: Session II

*Sponsored by:* The Minerals, Metals and Materials Society, TMS Materials Processing and Manufacturing Division, TMS Structural Materials Division, TMS/ASM: Computational Materials Science and Engineering Committee, TMS: High Temperature Alloys Committee  
*Program Organizers:* Diana Farkas, Virginia Tech; Susan Sinnott, University of Florida

Monday PM  
February 28, 2011

Room: 1A  
Location: San Diego Conv. Ctr

*Session Chair:* To Be Announced

2:00 PM Invited

**Status of the ReaxFF Reactive Force Field: Development and Applications:** *Adri van Duin*<sup>1</sup>; <sup>1</sup>Penn State

The ReaxFF method enables large-scale (>>1000 atoms) molecular dynamics simulations on chemically reactive systems. The method combines a bond order/bond distance concept with a polarizable charge method and employs relatively long-range bond orders, enabling an accurate description of transition state energies. While initially developed for hydrocarbons and first-row element chemistry, the method has currently been applied to a significant section of the periodic system, including covalent, metallic, ionic and ceramic materials. Furthermore, the ReaxFF program has been distributed to over 125 academic groups. In this presentation we will provide a status-report on the currently available ReaxFF force fields, the program environments that currently support ReaxFF, including a number of parallel options, and the plans for further method development. This includes recent extensions of ReaxFF to aqueous-phase chemistry, enabling applications to biochemical reactions, extensions and applications to combustion chemistry, applications to material failure and simulations on catalytic materials.

2:25 PM Invited

**LIGGGHTS – Open Source Discrete Element Simulations of Granular Materials Based on LAMMPS:** *Christoph Kloss*<sup>1</sup>; <sup>1</sup>JKU Linz

In this work, we present the development of an open-source software for modeling granular material by means of the Discrete Element Method. LIGGGHTS ([www.liggghts.com](http://www.liggghts.com)) stands for 'LAMMPS Improved for General Granular and Granular Heat Transfer Simulations' and is based on LAMMPS ('Large Atomic and Molecular Massively Parallel Simulator'), a successful open source Molecular Dynamics code written and distributed by Sandia National Laboratories for massively parallel computing on distributed memory machines. We first give a brief overview of implemented models and features. These comprise CAD geometry import, features for particle insertion and packing, contact models, wallstress analysis, moving mesh capability, a 6 DOF feature and non-spherical particle handling. Finally, we would like to focus on the simulation of coupled granular-fluid systems with the CFD-DEM approach.

2:50 PM Invited

**Parallel Parameterization of Models Using Noisy Simulation Data:** *Steven Stuart*<sup>1</sup>; Dheeraj Chahal<sup>1</sup>; Sebastien Goasguen<sup>1</sup>; <sup>1</sup>Clemson University

Although massively parallel simulations of materials are becoming increasingly routine, parallelization of the optimization of the potentials needed in those simulations generally lags far behind. This talk describes some advances in automated parameterization methods that make efficient use of large-scale parallel processing environments. Rather than performing a deterministic minimization of a noise-free objective function, as with most automated parameterization methods, this approach acknowledges the stochastic nature of the data obtained from finite-duration dynamics and sampling simulations. Consequently, potentials can be successfully fit to physically relevant thermodynamic data, rather than relying too heavily on zero-temperature quantum mechanical energetic and structural data. Each stage in the parameterization process terminates as soon as it can be



determined that the parameters are non-optimal, but continues sampling as long as the parameters remain viable, rather than terminating at an arbitrary cutoff. The parameterization approach interfaces easily with massively parallel simulation engines, including LAMMPS.

### 3:15 PM Invited

#### **Effect of the Stress Field of an Edge Dislocation on Carbon Diffusion in $\alpha$ -Iron: Coupling Molecular Statics and Atomistic Kinetic Monte Carlo:** *Michel Perez*<sup>1</sup>; <sup>1</sup>Université de Lyon - INSA de Lyon

Carbon diffusion near the core of a [111](101) edge dislocation in  $\alpha$ -iron has been investigated by means of an atomistic model that brings together molecular statics and atomistic kinetic Monte Carlo (AKMC). Molecular statics simulations with a recently developed embedded atom method potential have been carried out in order to obtain atomic configurations, carbon-dislocation binding energies, and the activation energies required for carbon hops in the neighborhood of the line defect. Using information gathered from molecular statics, on-lattice AKMC simulations have been performed for temperatures in the 300–600 K range, so as to study the behavior of a carbon atom as it interacts with the edge dislocation stress field. This model can be seen as a very first step toward the modeling of the kinetics of carbon Cottrell atmosphere formation in iron during the static aging process.

### 3:40 PM Break

### 3:55 PM

#### **Molecular Dynamics Simulation of Cavitation in Metallic Glass:** *Michael Falk*<sup>1</sup>; Shuo Lu<sup>2</sup>; Pavan Valavala<sup>1</sup>; Michael Spector<sup>1</sup>; <sup>1</sup>Johns Hopkins University; <sup>2</sup>Beihang University

Experimental investigations indicate that cavitation may play a critical role in determining the fracture toughness of amorphous solids such as metallic glasses. We have undertaken a series of molecular dynamics simulations of cavitation under hydrostatic tension in a binary metallic glass analog using pair-wise potentials. We compare the rate of cavity nucleation directly to homogeneous nucleation theory to extract the role of irreversible deformation in the cavitation process. In doing so we are able to estimate the effective free energy for cavitation. Our simulations indicate that the barrier to cavitation is several orders of magnitude lower than that expected in the liquid. The implication of these measurements for the observed fracture behavior in metallic glasses will be discussed.

### 4:15 PM

#### **Large Scale Simulation of 3D Nanocrystalline Mg by Molecular Dynamics:** *Dong-Hyun Kim*<sup>1</sup>; M. V. Manuel<sup>1</sup>; F. Ebrahimi<sup>1</sup>; S. R. Phillpot<sup>2</sup>; <sup>1</sup>Department of Materials Science and Engineering, University of Florida

So far, comparing with f.c.c metals, very little has been done in large scale simulation of mechanical behaviors of h.c.p. metals. To understand nucleation and interaction of dislocations by slip and twinning, here we take Mg as a prototypical nanocrystalline h.c.p. metal. Atomistic process of slip and twinning created by a tensile stress was observed in fully dense 3D structure with nano-grain sizes. We address a length-scale dependence of twinning and slip in plastic deformation of nc-Mg. This work was supported by DOE NERI contract DE-FC07-07ID14833 and by the DOE-BES Computational Materials Science Network (CMSN).

### 4:35 PM

#### **Large-Scale Molecular Dynamics Simulations of Tribology in Metallic Contacts:** *Michael Chandross*<sup>1</sup>; <sup>1</sup>Sandia National Laboratories

Materials that perform well in electrical contacts usually exhibit high adhesion during frictional contacts. An excellent example of this phenomenon is pure gold, which has extremely low electrical contact resistance, but generally has a high friction coefficient. The exception to this, however, is nanocrystalline gold alloyed with minute amounts of Ni or Co, which in addition to its low contact resistance can also show low friction. The mechanism for this remains poorly understood. We will present the results of large scale molecular dynamics (MD) simulations which study the tribological response of both single crystal and nanocrystalline gold films in contact with curved probe tips under a variety of sliding conditions. Results

from simulations of adhesion and friction in metallic alloys will also be presented.

### 4:55 PM

#### **Molecular Dynamics Simulations of Nanoindentation of Si/SiO<sub>2</sub> Systems using the Charge Optimized Many-Body (COMB) Potential:** *Tzu-Ray Shan*<sup>1</sup>; Simon Phillpot<sup>1</sup>; Susan Sinnott<sup>1</sup>; <sup>1</sup>University of Florida

Oxides such as SiO<sub>2</sub>, Al<sub>2</sub>O<sub>3</sub> and HfO<sub>2</sub>, are widely used together with Si in many high-performance electronic devices, including metal-oxide-semiconductor (MOS) devices/junctions and gate stacks. Since nanoindentation has been established as a primary tool for investigating the mechanical behavior of small volumes of materials, classical molecular dynamics simulation is used to examine the nanoindentation of Si/SiO<sub>2</sub> interfacial systems. Because these systems consist of heterogeneous interface with significant changes in bonding as one crosses from one side of the interface to the other, the empirical charge optimized many-body (COMB) potential as implemented in LAMMPS is used to model the structural evolution, mechanical response and charge transfer of Si/SiO<sub>2</sub> systems under the influence of a nanometer-scale spherical indenter. The SiO<sub>2</sub> layers considered include  $\alpha$ -quartz and amorphous silica with various thicknesses. Aspects of the Si/SiO<sub>2</sub> interface during nanoindentation, including dislocation formation and the mechanisms by which fracture occurs, will also be addressed.

### 5:15 PM Invited

#### **Shear Transformation Zone Dynamics Modeling of Metallic Glasses:** *Christopher Schuh*<sup>1</sup>; Eric Homer<sup>1</sup>; <sup>1</sup>MIT

A thorough understanding of deformation in metallic glasses has proven elusive as a result of the disparate time and length-scales that span between the unit processes of deformation and the macroscopic flow localization events that are experimentally observed. We attempt to model the deformation of metallic glasses using a meso-scale model that treats the “shear transformation zone” (STZ) as a fundamental unit of deformation. STZ dynamics combines finite element mechanics, to solve for the stress redistribution when STZs operate, with a kinetic Monte Carlo algorithm, to model the kinetics of their activation sequence. The method allows processing and deformation to be simulated on larger length-scales and longer time-scales than, e.g., atomistic simulations. The method can be implemented in two or three dimensions, and can provide insight on deformation in complex experimental situations, such as in the formation of shear bands or the development of microplasticity around stress concentrators.

### 5:40 PM Invited

#### **Modeling Shear Band Formation and Propagation in Bulk Metallic Glasses and Nanoglasses:** *Daniel Soper*<sup>1</sup>; Yvonne Ritter<sup>1</sup>; *Karsten Albe*<sup>1</sup>; <sup>1</sup>TU Darmstadt

Plastic deformation in metallic glasses is highly localized in shear bands and there is a broad consensus that shear transformation zones (STZs) are the basic units of plastic deformation. In this work, we study plastic deformation of bulk metallic glasses and nanoglasses by molecular dynamics simulation using LAMMPS. We investigate homogeneous shear band nucleation by simulating tensile deformation of a 3-dimensional-periodic metallic glass sample and compare it to shear band nucleation in the presence of free surfaces and interfaces as present in nanoglasses. In contrast to earlier studies, our results show only little influence of surfaces and interfaces on the shear band nucleation process and the stress-strain-behavior. We conclude that shear band formation involves the condensation of a critical number of STZs along a feasible shear path. Finally, we compare structural features present in shear bands to those found in internal interfaces present in nanoglasses.

## Materials for the Nuclear Renaissance II: Irradiation Effects

*Sponsored by:* The Minerals, Metals and Materials Society, TMS Structural Materials Division, TMS/ASM: Corrosion and Environmental Effects Committee, TMS/ASM: Nuclear Materials Committee

*Program Organizers:* Raul Rebak, GE Global Research; Brian Cockeram, Bechtel-Bettis; Peter Chou, Electric Power Research Institute; Micah Hackett, TerraPower, LLC

Monday PM Room: 4  
February 28, 2011 Location: San Diego Conv. Ctr

*Session Chair:* Micah Hackett, KAPL

### 2:00 PM Introductory Comments

#### 2:05 PM

**Evaluation of Scale Bridging Methodology for Performance Prediction:** *Dongsheng Li<sup>1</sup>; Yulan Li<sup>1</sup>; Fei Gao<sup>1</sup>; Ram Devanathan; Xin Sun<sup>1</sup>; Moe Kahleel<sup>1</sup>; <sup>1</sup>Pacific Northwest National Laboratory*

Effective property prediction is the cornerstone for performance evaluation of materials under irradiation condition. Molecular dynamics method is used to calculate atomic-level properties of materials, while phase field model is used to predict the microstructure evolution. Different methods have been developed to bridge low scale models with polycrystalline level models. Finite Element Analysis (FEA), microstructure informed FEA, self consistent models, Taylor models, Sachs models and statistical continuum mechanics are evaluated. Cost, efficiency and accuracy were compared for these methods. Pros and cons, depending on the problems studied, are discussed. While open to discussion, general recommendation on bridging methodology is presented based on different scenarios.

#### 2:25 PM

**Localized Deformation in Proton and Heavy Ion Irradiated Austenitic Stainless Steels:** *Zhijie Jiao<sup>1</sup>; Gary Was<sup>1</sup>; Terumitsu Miura<sup>2</sup>; Koji Fukuya<sup>2</sup>; <sup>1</sup>University of Michigan; <sup>2</sup>Institute of Nuclear Safety System*

Recent studies have shown that among the various features of the irradiated microstructure, localized deformation correlates most strongly with irradiation-assisted stress corrosion cracking (IASCC). The degree of localized deformation is influenced by irradiated microstructure and possibly by the irradiation depth if that depth is less than the grain size. In this study, two austenitic stainless steels, 304SS and 316SS, were irradiated to 5 dpa using 1.2 and 2 MeV protons and to 100 dpa using 2.8 MeV Fe<sup>++</sup> at 300/176C. Constant extension rate tensile tests were conducted on the irradiated samples to 2% strain in both argon and water environments. The degree of localized deformation (the weighted average dislocation channel height) was characterized using atom force microscopy and crack initiation was examined using scanning electron microscopy. The effect of the degree of localized deformation on IASCC and the influence of irradiation depth on localized deformation will be presented and discussed.

#### 2:45 PM

**Toward a Better Understanding of Heat-to-Heat Variations in Irradiation-Assisted Stress Corrosion Cracking:** *Peter Chou<sup>1</sup>; Raj Pathania<sup>1</sup>; Bob Carter<sup>1</sup>; <sup>1</sup>Electric Power Research Institute*

There are marked heat-to-heat variations in the susceptibility of materials to environmentally-assisted cracking in LWR environments. Although, in time, all heats will be affected by EAC, it is the "early" failures of a minority of heats in the field that consume attention and resources of the industry. Heat-to-heat variations imply a gap in knowledge between microstructure/microchemistry and materials performance; and better understanding will influence how the industry should approach testing, screening, and development of existing and new materials. This presentation will describe ongoing EPRI-sponsored research on the application of atom-probe

tomography to irradiated stainless steels and discuss how the observations serve as motivation for future research to support existing and new plants.

#### 3:05 PM

**Multiscale Simulation of the Effect of Irradiation-Induced Microstructure Evolution on Reactor Fuel Performance:** *Michael Tonks<sup>1</sup>; Paul Millett<sup>1</sup>; Derek Gaston<sup>1</sup>; Bulent Biner<sup>1</sup>; Anter El-Azab<sup>2</sup>; <sup>1</sup>Idaho National Laboratory; <sup>2</sup>Florida State University*

Fuel performance in nuclear reactors is highly dependent on irradiation-induced microstructure evolution. Therefore, a fuel performance code must consider atomistic and mesoscale effects in order to provide a predictive capability. In this work, we present the multiscale fuel performance modeling approach currently being employed at Idaho National Laboratory (INL). Atomistically-informed mesoscale phase field simulations are used to determine the effect of irradiation-induced microstructure evolution on bulk properties, such as thermal conductivity and density. Continuum expressions describing the effect of irradiation on the bulk properties as a function of temperature are then determined from the mesoscale simulations. Finally, these expressions are used in INL's BISON fuel performance code to model fuel pellet behavior.

#### 3:25 PM Break

#### 3:35 PM

**Mechanical Properties of Fresh and Neutron Irradiated U-Mo Fuels for the RERTR Application:** *Ramprasad Prabhakaran<sup>1</sup>; D Burkes<sup>1</sup>; A Robinson<sup>1</sup>; J-F Jue<sup>1</sup>; A DeMint<sup>2</sup>; J Gooch<sup>2</sup>; D Keiser<sup>1</sup>; D Wachs<sup>1</sup>; I Charit<sup>3</sup>; <sup>1</sup>Idaho National Laboratory; <sup>2</sup>Y-12 National Security Complex; <sup>3</sup>University of Idaho*

The Reduced Enrichment for Research and Test Reactors (RERTR) program was initiated to develop new nuclear fuels to enable the research and test reactors to use low-enriched uranium fuels instead of high-enriched uranium fuels, without significant loss in performance. Hence, a new monolithic fuel type that possesses the greatest possible uranium density in the fuel region is being developed, where the fuel region consists of a single foil encased inside an aluminum alloy cladding. Currently, efforts are ongoing to evaluate the mechanical properties and microstructure of fresh and irradiated fuels as a function of molybdenum content, carbon content, burn up and fabrication method (Friction Bond and Hot Isostatic Pressing). Small-scale specimen testing techniques, such as sub-size tensile testing, microindentation hardness testing and shear punch testing are being performed. Other materials characterization techniques, such as optical microscopy, XRD and SEM are being used in conjunction with the small-scale mechanical test methods.

#### 3:55 PM

**Micro-Displacement Measurement for Small Samples in the Advanced Test Reactor (ATR) National Scientific User Facility (NSUF):** *Anthony Santo Domingo<sup>1</sup>; Mitchell Meyer<sup>2</sup>; Denis Beller<sup>1</sup>; <sup>1</sup>Univ. of Nevada, Las Vegas; <sup>2</sup>ATR National Scientific User Facility*

The ATR NSUF at the Idaho National Laboratory (INL) provides a high-flux environment for long-term irradiation experiments. Battelle Energy Alliance (BEA) and the Electric Power Research Institute (EPRI) are fielding an experiment that will obtain data on the growth rate of zirconium alloys versus hydrogen content. This project will be conducted to investigate a postulated hydrogen-assisted irradiation growth rate mechanism that may be operative in zirconium alloys and that is associated with channel bowing in BWRs. In the project described herein, University of Nevada, Las Vegas faculty and students and INL personnel collaborated in an ATR NSUF Faculty-Student Research Project to design, build, and test a device that will accurately measure the micro-displacement of pre-irradiated and post-irradiated specimens of zirconium alloy. The design, fabrication, and operation of the micro-displacement measurement device will be described.

4:15 PM

**MC Calculation of Optimal Gd and B Containing Composition for Effective Protection from Gamma and Neutron Irradiation:** *Nikoloz Chikhradze*<sup>1</sup>; Leri Kurdadze<sup>2</sup>; Guram Abashidze<sup>1</sup>; <sup>1</sup>Mining Institute/Georgian Technical University; <sup>2</sup>G. Tsulukidze Mining Institute

The radiation materials have different applications, including: working in nuclear reactors, localization of uncontrolled radiation sources, safety storage of radiation wastes and etc. Accordingly, it is actual to create composite materials having the appropriate ratio mixtures of constituents, which can produce stable physical-chemical and radiation-resistant properties and characterized with abilities of inactivated absorption of various types of neutron and gamma irradiation. In the paper the results of calculation of sorption properties of Me-Gd and Me-B composite materials with various ratio of B and Gd are discussed. Calculations was performed by the Monte-Carlo method with a program package GEANT3 including a special package GCALOR for the simulation of the interaction of thermal and fast neutrons within the sample. During the neutron passage through the sample all main processes of the interaction of neutrons with matter are considered including: elastic and inelastic scattering, neutron fission of nuclei, radiation capture, etc.

4:35 PM

**Microstructure and Mechanical Properties of Irradiated Friction Stir Welded ODS Alloys:** *Ramprashad Prabhakaran*<sup>1</sup>; J Wang<sup>2</sup>; I Charit<sup>3</sup>; J Cole<sup>1</sup>; KL Murty<sup>4</sup>; R Mishra<sup>2</sup>; <sup>1</sup>Idaho National Laboratory; <sup>2</sup>Missouri University of Science and Technology; <sup>3</sup>University of Idaho; <sup>4</sup>North Carolina State University

Conventional fusion welding of oxide dispersion strengthened (ODS) alloys causes various undesirable effects, such as coalescence of oxide dispersoids and significant porosity. In this study, MA956 and MA754 alloys were friction stir welded in a bead-on-plate configuration. Microhardness, shear punch and mini-tensile testing of the base and processed materials were carried out to evaluate the mechanical properties. Optical microscopy and transmission electron microscopy were used to study the changes in the grain size and particle characteristics across the weld zone. Efforts are ongoing to study the effect of neutron irradiation (at the Advanced Test Reactor, Idaho Falls) on the friction stir welded MA956 and MA754 alloys. Microhardness and shear punch tests are being carried out on the irradiated samples (1 and 2 dpa), and will be compared with the properties of the unirradiated materials.

## Materials in Clean Power Systems VI: Clean Coal-, Hydrogen Based-Technologies, and Fuel Cells: Materials for Gasification and Turbines I

*Sponsored by:* The Minerals, Metals and Materials Society, TMS Electronic, Magnetic, and Photonic Materials Division, TMS Structural Materials Division, TMS/ASM: Corrosion and Environmental Effects Committee, TMS: Energy Conversion and Storage Committee, TMS: High Temperature Alloys Committee  
*Program Organizers:* Xingbo Liu, West Virginia University; Zhenguo "Gary" Yang, Pacific Northwest National Laboratory; Jeffrey Hawk, U.S. Department of Energy, National Energy Technology Laboratory; Teruhisa Horita, AIST; Zi-Kui Liu, The Pennsylvania State University

Monday PM  
February 28, 2011

Room: 33C  
Location: San Diego Conv. Ctr

*Session Chair:* Xingbo Liu, West Virginia University

2:00 PM Keynote

**Meeting the Materials Challenges to Enable Clean Coal Technologies:** *Cynthia Powell*<sup>1</sup>; <sup>1</sup>Office of Research and Development, National Energy Technology Laboratory, US Department of Energy

Realization that the environmental impact of energy production must be reduced on a global scale, combined with an increased desire in this country to reduce dependence on foreign energy sources, is driving significant

change in the way the United States will derive and produce power in the future. While renewable energy resources will continue to grow in importance, environmentally responsible fossil energy production will be necessary to provide a bridge to the next energy revolution. This drive to increase efficiencies and reduce environmental impact in fossil-based energy production will lead to increased operating temperatures and pressures and increasingly aggressive operating environments. The practical result is a requirement for affordable and reliable high-performance materials and materials systems to enable these next-generation fossil energy systems. This talk will focus on the research being performed at the National Energy Technology Laboratory to meet this requirement for high performance yet affordable materials.

2:30 PM Keynote

**Mechanistic Understanding of Materials Degradation Processes in Solid Oxide Fuel Cell (SOFC) Power Generation Systems: From Bulk to Interfacial Reactions:** *Prabhakar Singh*<sup>1</sup>; <sup>1</sup>University of Connecticut

High temperature operation of solid oxide fuel cells (600-1000C), exposure of cell components to dual atmosphere, and the presence of complex gas environment have been associated with severe surface and bulk corrosion and structural degradation conditions in cell and the balance of plant (BOP) components. This presentation provides an overview of materials degradation and corrosion processes operating in cell stack and BOP. Role of bi-polar exposure condition on accelerated corrosion has been investigated. Oxide evaporation in oxidizing and reducing atmospheres has also been investigated and its influence on the catalytic and electrocatalytic poisoning will be reported. Pertinent electrode structural changes and interfacial compound formation will be examined and discussed. Current research trend will be presented.

3:00 PM Invited

**The Impact of Mixed Carbon Feedstock on High Cr2O3 Refractory Liners Used in Commercial Gasifiers:** *James Bennett*<sup>1</sup>; Kyei-Sing Kwong<sup>1</sup>; Seetharaman Sridhar<sup>2</sup>; Jinichiro Nakano<sup>3</sup>; <sup>1</sup>NETL, US DOE; <sup>2</sup>Carnegie Mellon University; <sup>3</sup>URS Corp.

Gasifiers are high temperature/pressure reaction vessels used to contain interactions between a carbon feedstock, water, and oxygen (reducing environment); producing CO and H2 used in power generation or chemical production. Carbon feedstock includes coal and/or petcoke, with biomass considered a candidate to produce a carbon neutral process. Impurities in carbon feedstock materials vary from about 1-10 pct and liquefy during gasification (1325-1575°C, 10-8 O2 partial pressure), forming slags that interact with the high chrome oxide refractory liner by chemical corrosion and spalling, causing unpredictable and premature shutdown of a gasifier. Mixtures of carbon feedstock that include biomass will have an unknown impact on slag properties and refractory liners, and are the focus of ongoing research. Slag properties and slag/refractory interactions are being evaluated by post mortem analysis of commercial gasifier samples, in laboratory simulations, and by thermodynamic modeling. Results of these studies to date will be presented.

3:25 PM Break

3:40 PM

**Stability of Mullite and V2O3 in Synthetic Slags Based on Molten Coal/Petcoke Ash Mixtures:** *Jinichiro Nakano*<sup>1</sup>; Seetharaman Sridhar<sup>2</sup>; Kyei-Sing Kwong<sup>1</sup>; James Bennett<sup>1</sup>; Thomas Lam<sup>1</sup>; <sup>1</sup>NETL; <sup>2</sup>Carnegie Mellon University

In gasifiers, non-volatiles such as SiO2 in coal and petcoke carbon feedstock form slags that can impact gasifier efficiency and increase refractory corrosion. In this study, synthetic slags simulating coal-petcoke ash mixtures were evaluated for phases existing in a gasification environment at 1500°C and Po2=10-8atm. VxOy-bearing phases are of particular interest because their stabilities are governed by Po2. Slag mixtures of SiO2-Al2O3-Fe2O3-CaO-V2O5 containing 0-10wt.% of V2O5 were equilibrated at 1500oC and rapidly quenched to freeze high temperature phases. XRD analyses identified mullite (in Al2O3-rich slags) and V2O3 (in V2O5-rich slags) as stable

MONDAY PM



phases. TEM and EPMA analyses indicated that the mullite contained V and V<sub>2</sub>O<sub>3</sub> contained Al. Concentration depended on starting slag composition. XRD indicated that lattice parameters of the two crystalline phases were found to vary with elemental substitution. The presence of the solid phases is discussed in light of its impacts on slag fluidity and refractory erosion.

#### 4:00 PM

**Effect of Temperature Gradient on Slag Infiltration into Porous Refractory Material:** *Tetsuya Kaneko*<sup>1</sup>; *Junichiro Nakano*<sup>2</sup>; *Seetharaman Sridhar*<sup>1</sup>; *Kyei-Sing Kwong*<sup>2</sup>; *Rick Krabbe*<sup>2</sup>; *Hugh Thomas*<sup>2</sup>; *James Bennett*<sup>2</sup>; <sup>1</sup>Carnegie Mellon University; <sup>2</sup>US Department of Energy National Energy Technology Laboratory

Entrained-flow slagging gasifiers produce syngas (CO and H<sub>2</sub>) using coal, petcoke, and/or biomass as a carbon feedstock. The high operating temperatures (1325-1575°C) of these gasifiers, along with corrosive gases and slags from the carbon feedstock pose material challenges in the gasifier. Slags originating from mineral impurities in the carbon feedstock liquefy, corrode, and penetrate the porous refractory liner. The penetration characteristics of coal slag into alumina refractory have been studied using a temperature gradient along the slag's penetration direction, which are compared to those obtained under isothermal conditions. The studies were conducted with a hot face temperature of 1450°C and a CO/CO<sub>2</sub> ratio of 1.8 (corresponding to an oxygen partial pressure of approximately 10-8 atm). Slag-infiltrated refractory samples were studied using SEM-EDS to identify primary phases and to track the slag's changing chemical composition. Primary phases and slag compositions were compared to those calculated in using FactSage™ software.

#### 4:20 PM Invited

**Creep Strength Property of Advanced Ferritic Creep Resistant Steels for Fossil Energy Applications:** *Kazuhiro Kimura*<sup>1</sup>; *Kota Sawada*<sup>1</sup>; <sup>1</sup>National Institute for Materials Science

An overestimation of long-term creep strength was pointed out on creep strength enhanced ferritic (CSEF) steels and premature failure due to Type IV cracking and remarkable drop in creep rupture ductility were also recognized. Microstructural evolution is influenced by stress and that is different in the high- and low-stress regimes divided by a macroscopic elastic limit where successive plastic deformation of polycrystalline material initiates which corresponds to 50% of 0.2% offset yield stress. A region splitting analysis method was proposed for a reliable life prediction of CSEF steels and allowable stress was reduced. Creep rupture ductility drop is caused by a combination of high creep strength and stress dependence of creep deformation. In order to ensure strength and soundness, upper limit of aluminum was reduced from 0.04mass% to 0.02mass% and maximum level of 0.01mass% was specified on titanium and zirconium, as well as weld strength reduction factor.

#### 4:45 PM

**A Comparison of Creep-Rupture Tested Cast Alloys HR282, IN740 and 263 for Possible Application in Advanced Ultra-supercritical Steam Turbine and Boiler Components:** *Neal Evans*<sup>1</sup>; *Philip Maziasz*<sup>2</sup>; *Yukinori Yamamoto*<sup>2</sup>; *Paul Jablonski*<sup>3</sup>; <sup>1</sup>University of Tennessee, Knoxville; <sup>2</sup>Oak Ridge National Laboratory; <sup>3</sup>National Energy Technology Laboratory

Cast forms of traditionally wrought Ni-base precipitation-strengthened superalloys are being considered for service in the ultra-supercritical conditions (760°C, 35MPa) of next-generation steam boilers and turbines. After casting and homogenization, these alloys were given heat-treatments typical for each in the wrought condition to develop the gamma-prime phase. Specimens machined from castings were creep-rupture tested in air at 800°C. In their wrought forms, alloy 282 is expected to precipitate M<sub>23</sub>C<sub>6</sub> within grain boundaries, alloy 740 is expected to precipitate several grain boundary phases including M<sub>23</sub>C<sub>6</sub>, G Phase, and η phase, and alloy 263 has M<sub>23</sub>C<sub>6</sub> and MC within its grain boundaries. This presentation will correlate the observed creep-life of these cast alloys with the microstructures developed during creep-rupture tests, with an emphasis on the phase identification and chemistry of precipitated grain boundary phases. The suitability of these cast

forms of traditionally wrought alloys for turbine and boiler components will also be discussed.

#### 5:05 PM

**Mesososcopic Finite Element Analysis of Interfacial Failure in High Temperature Alloys:** *Changsoo Kim*<sup>1</sup>; *Keeyoung Jung*<sup>2</sup>; *Frederick Pettit*<sup>2</sup>; *Gerald Meier*<sup>2</sup>; <sup>1</sup>University of Wisconsin-Milwaukee; <sup>2</sup>University of Pittsburgh

A numerical model has been developed employing mesoscopic finite element analysis (FEA) to study interfacial failure in high temperature alloys and coatings. Using this model, the impacts of mesoscopic details on the thermo-mechanical performance such as different oxide compositions, types, sizes and shapes of encapsulated particles, and geometries of scales can be quantitatively estimated. The developed algorithm was applied to the scale buckling phenomena in an outward-growing thermal oxide that may occur in syngas-fired gas turbines assuming that brittle interfacial fracture occurs in Mode II. Experimentally observed microstructures with measured thermo-mechanical parameters were incorporated in the model. The presentation will discuss and elucidate the potential scale decohesion mechanism observed in experiments. This FEA model can be readily expanded to thermo-mechanical issues in other high temperature material applications that are integrated with clean energy systems such as scale spallation from metallic SOFC interconnects.

### Materials Processing Fundamentals: Process Modeling

*Sponsored by:* The Minerals, Metals and Materials Society, TMS Extraction and Processing Division, TMS: Process Technology and Modeling Committee

*Program Organizers:* Prince Anyalebechi, Grand Valley State University; Srikanth Bontha, Temple University

Monday PM

February 28, 2011

Room: 12

Location: San Diego Conv. Ctr

*Session Chair:* Prince Anyalebechi, Grand Valley State University

#### 2:00 PM

**Computational Modeling of Field-Assisted Sintering:** *Cristina Garcia Cardona*<sup>1</sup>; *Eugene Olevsky*<sup>1</sup>; *Veena Tikare*<sup>2</sup>; <sup>1</sup>San Diego State University; <sup>2</sup>Sandia National Laboratories

A three-dimensional multi-scale model of Field-Assisted Sintering is presented. The model captures the complexity of the multiphysics phenomena involved in field-assisted sintering by coupling: electrical, thermal, stress-strain and densification components. The calculations are based on the finite-element (macroscopic scale) and kinetic Monte-Carlo (mesoscopic scale) codes. Specimen's macroscopic behavior is described through a non-linear viscous constitutive relation. The simulation of the densification is based on local conditions, and micro-scale factors as grain growth are also taken into account. Thus not only distributions of current density, temperature and strain fields can be obtained but also a spatial density and grain size evolution can be computed. The sintering constitutive parameters are determined through Monte-Carlo simulations of the grain-pore structure evolution. This corresponds to a true 3D, multi-scale, multiphysics modeling of sintering. The modeling predictions are discussed via several examples and calculation results are compared with experimental data available.

#### 2:15 PM

**Simulation of Macroseggregation Due to Melt Convection and Grain Sedimentation in Steel Ingots Using a Mixture Model:** *Wensheng Li*<sup>1</sup>; *Houfa Shen*<sup>1</sup>; *Baicheng Liu*<sup>1</sup>; <sup>1</sup>Tsinghua University

In order to understand the formation of macroseggregation in steel ingots, a mixture solidification model has been developed which accounts for coupled mass, momentum, species, and energy transport and notably describes the sedimentation of free equiaxed grains. In this model, the mushy zone

is divided into the slurry and porous regimes according to a solid packing fraction. Settling velocity of equiaxed grains in the slurry regime is given by an explicit expression. The solidification of a binary steel ingot (Fe-0.36 wt pct C) with a two-dimensional geometry is numerically simulated. It is demonstrated that the predicted macrosegregation patterns agree to some extent with classical experimental results. Further refinement of this model is still necessary for realistically simulating steel ingot solidification.

**2:30 PM**

**Effect of Casting Speed on Temperature Difference between Copper Plate and Solidifying Shell in Meniscus of Slab Continuous Casting Mold:** *Xiangning Meng*<sup>1</sup>; <sup>1</sup>Northeastern University

A three-dimensional finite-element heat-transfer model was established to predict temperature of hot copper plate in a slab continuous casting mold and effect of casting speed on temperature difference between copper plate and solidifying shell was simulated in combination with process data. The results show that centre temperature of hot copper surface at casting speed 1.8 m·min<sup>-1</sup> and 2.0 m·min<sup>-1</sup> are higher than that of 1.6 m·min<sup>-1</sup> casting speed 4.7-5.2 °C and 11.2-12.2 °C respectively and temperature is not increased linearly with casting speed. Temperature difference in meniscus between mold wall and shell surface is influenced obviously by casting speed and increased 4.0-6.0 °C with increment of casting speed 0.2 m·min<sup>-1</sup>. Fluctuation of temperature difference in meniscus is a main reason to deteriorate casting effectiveness as increasing casting speed.

**2:45 PM**

**Numerical Simulation of Decarburization Reaction on the Surface of Liquid Iron:** *Hyunjin Cho*<sup>1</sup>; Sangjoon Kim<sup>1</sup>; Haegon Lee<sup>1</sup>; <sup>1</sup>POSTECH

Decarburization phenomena on the surface of liquid iron have been simulated by numerical method and the results were compared to the experimental data. During the DeC process in a converter, a large amount of splashed droplets are generated from the top surface of the bath and consequently the reaction surface area is increasing tremendously. Since the decarburization mainly occurs at the interface, it is important to understand the reactions on the liquid iron droplets. The flow and species concentration fields around liquid droplets taking into account the reaction of carbon with oxygen at the interface were calculated by a commercial CFD code FLUENT which solving multiphase Navier-Stokes equation with Volume Of Fluid method. The initial carbon concentration was fixed to 4 wt% and the concentrations of oxygen in the atmosphere were varied from 5 to 50 wt%. This numerical approach could allow predicting the decarburization rate of liquid iron.

**3:00 PM**

**3D Simulation of the Melting during an Electro-Slag Remelting Process:** *Abdellah Kharicha*<sup>1</sup>; <sup>1</sup>University of Leoben

The droplet formation during the melting of a 400 mm diameter electrode is simulated with a multiphase-MHD approach. The computational model includes a layer of slag and a layer of liquid steel. A VOF approach is used for the interface tracking, and a potential formulation is used for the electric and the magnetic field. The Lorentz force and the Joule heating is recalculated at each time step in function of the phase distribution. The first results provided by this model are presented.

**3:15 PM Break**

**3:30 PM**

**An Analysis of Electromagnetic Field and Joule Heating of Electroslag Remelting Processes with Two Series-Connected Electrodes:** *Fang Wang*<sup>1</sup>; *Baokuan Li*<sup>1</sup>; <sup>1</sup>Northeastern University

Comparing with single electrode in electroslag remelting processes, two series-connected electrodes have the advantage of small inductive, low power consumption and high efficiency, which was widely used to produce large scale steel. In the present work, a 3D finite element model was developed for the magnetic field, electromagnetic force, current density and Joule heating field of electroslag remelting processes (electrode, slag and ingot) with two series-connected electrodes using Maxwell equation, Lorentz law and Joule law. It was found through comparison that the modeling results

is in accord with the experimental results, thus verifying the reliability of the model developed and relevant computation program. The results show that the current distribute on internal surfaces of electrode is smaller than on external surfaces; the maximum electromagnetic force is at the upper surface of slag nearby the electrode and the maximum joule heating is at the middle bottom of two electrodes.

**3:45 PM**

**Modeling of Copper Converter Foamover and Operational Improvements:** *Pengfu Tan*<sup>1</sup>; <sup>1</sup>Xstrata Copper

The foamed converter charges were up to 38 per month in Xstrata Copper Smelter at Mount Isa. The issue of high converter foamover frequency had remained unsolved for many decades in Mount Isa. A thermodynamic model of copper P-S converter and a viscosity model of converter slag have been developed to simulate the slag blow and copper blow, in order to understand the mechanism of converter foamover. The model predicts the chemistry and viscosity of slag during slag blow and copper blow. The effects of oxygen potential, charge of dirty reverts, slag carry-over, under-blowing, over-blowing, and temperature on the foamover and viscosity of slag in copper blow have been discussed. A theory has been developed to understand the mechanism of converter foamover. The practical solutions have also been developed and implemented in Mount Isa Copper Smelter. Some improvements of the industrial operations have been presented. After a series of improvements, the number of foamed charges per month in the converter operations has been decreased significantly from 35 in Aug 2008 to only one per month in 2009/2010.

**4:00 PM**

**Modeling and Control of Copper Loss in Smelting Slag: Part I and Part II:** *Pengfu Tan*<sup>1</sup>; <sup>1</sup>Xstrata Copper

Xstrata Copper Smelter at Mount Isa in Australia had experienced the technical issue of high copper losses in smelting slag (or RHF slag) before 2008. The copper losses in RHF slag was more than 3% in 2006 and 2007. The thermodynamic models, viscosity model have been developed to simulate the process control, slag chemistry, slag viscosity, and matt-slag separations. The theory of RHF KPIs has also been developed to reduce the copper losses in RHF slag. The RHF KPIs Theory has been applied in Mount Isa Copper Smelter. The copper losses in RHF slag have been dropped from 3.1% in 2007 to 0.76% in Apr 2009. The average copper loss in RHF slag in 2009 and 2010 is about 0.9%.

---

**Microstructural Processes in Irradiated Materials: Microstructure Evolution: Experimental**

*Sponsored by:* The Minerals, Metals and Materials Society, TMS Structural Materials Division, TMS/ASM: Nuclear Materials Committee

*Program Organizers:* Gary Was, University of Michigan; Thak Sang Byun, Oak Ridge National Laboratory; Shenyang Hu, Pacific Northwest National Laboratory; Dane Morgan, UW Madison; Yasuyoshi Nagai, Tohoku University

Monday PM

February 28, 2011

Room: 3

Location: San Diego Conv. Ctr

*Session Chairs:* Dane Morgan, University of Wisconsin; Thak Byun, Oak Ridge National Laboratory

---

**2:00 PM Invited**

**In-Situ TEM Study on Elastic Interaction between a Prismatic Dislocation Loop and a Gliding Dislocation:** *Yoshi Matsukawa*<sup>1</sup>; Grace Liu<sup>1</sup>; Ian Robertson<sup>1</sup>; <sup>1</sup>University of Illinois

Due to its glissile character the prismatic dislocation loop is expected to be either swept or arrested by the strain-field of gliding dislocations, and the latter is believed to be a key mechanism whereby locking of dislocation source occurs in neutron-irradiated metals. In this talk we show the first successful in-situ TEM observation capturing trap and de-trap processes

MONDAY PM

of the prismatic loop to/from a gliding dislocation. The critical capture distance measured on a micrograph was ~8 nm, which was smaller than the loop diameter (~10 nm). The gliding dislocation was originally a mixed dislocation; however, its line direction changed to a screw configuration upon interaction. The dislocation eventually bypassed the loop via cross-slip to a plane with a resolved shear stress ~40% smaller than that of the original slip plane. The prismatic loop was certainly an obstacle for dislocation-slip though a single loop was insufficient to completely lock the dislocation.

#### 2:40 PM

**In-Situ Investigation of Microstructure Evolution in NF616 and HCM12A Alloys under Heavy Ion Irradiation:** *Cem Topbası<sup>1</sup>*; Arthur Motta<sup>1</sup>; Mark Kirk<sup>2</sup>; <sup>1</sup>Pennsylvania State University; <sup>2</sup>Argonne National Laboratory

The NF616 and HCM12A ferritic-martensitic alloys are candidate cladding and duct materials for Generation IV nuclear energy systems. In-situ investigation of radiation damage was conducted for these alloys using the IVEM-Tandem at Argonne National Laboratory, which is a transmission electron microscope interfaced with ion accelerators allowing observing the development of irradiation damage as it occurs. The alloys were irradiated in situ to 15 dpa with 1 MeV Kr<sup>++</sup> ions at temperatures between 50K and 673K. The number density and size distribution of irradiation induced defects were determined as a function of dose and temperature. Nano-sized defects (~1-2 nm) first appeared as white dots in dark-field TEM images between 0.5 to 1 dpa and later develop into resolvable loops. Dynamic observations show that black dots constantly appear and disappear under irradiation indicating a steady state of defect density. At high doses, complex defect superstructures including loop alignment were observed.

#### 3:00 PM

**Thermal Annealing Recovery Behavior of HT-9 Steel Irradiated to High Doses in FFTF:** *Thak Sang Byun<sup>1</sup>*; William Lewis<sup>1</sup>; Stuart Maloy<sup>2</sup>; <sup>1</sup>Oak Ridge National Laboratory; <sup>2</sup>Los Alamos National Laboratory

The Fuel Cycle R&D Program is investigating methods of burning minor actinides in a transmutation fuel, for which the fast reactor core materials must be able to withstand very high doses (>200 dpa). To investigate operating strategies to reduce the buildup of radiation-induced defects, thermal annealing behavior has been studied for irradiated HT-9 steel. Samples were taken from representative locations of the ACO-3 duct of Fast Flux Test Facility: their irradiation doses were in the range of 3 – 148 dpa and irradiation temperatures in the range of 379 – 503 °C. The samples were tested after each isochronal anneal for 1 hour at 300 – 650 °C or after each isothermal anneal at 510 or 550 °C. The radiation-induced hardening was nearly completely recovered by one-hour isochronal annealing above 550 °C or by isothermal annealing at 510 °C for about 20 hours or at 550 °C for 2 hours.

#### 3:20 PM

**Microstructural Study of Pure Iron and Fe-Cr Model Alloys Ion Irradiated within the Jannus Platform (In- and Ex-Situ Mode):** *Daniel Brimbal<sup>1</sup>*; Estelle Meslin<sup>1</sup>; Brigitte Décamps<sup>2</sup>; Jean Henry<sup>1</sup>; Alain Barbu<sup>1</sup>; <sup>1</sup>C.E.A. Saclay; <sup>2</sup>CNRS

Damage displacement cascades and helium production by transmutation reactions will result from the intense neutron irradiation in structural materials of future Fusion and GenIV reactors. In order to predict in-service properties of such materials, the microstructural evolution under irradiation of model materials (high purity iron and Fe-Cr alloys) has been studied using the JANNUS platform. Single- and dual-beam irradiations (Fe and Fe/He) have been performed ex-situ and in-situ (TEM) at high temperature. The TEM analysis leads to the following results: - In both materials irradiated ex-situ at 500°C up to 6 dpa, a coarse microstructure of large <100> dislocation loops, located in {100} planes, was formed. - Single-beam in-situ irradiations show a difference between iron and Fe-5at.%Cr: dislocation loops formed during irradiation display back-and-forth motion in iron but not in the alloy. They interact with dislocations in the alloy. - Dual-beam in-situ and ex-situ experiments are being analysed.

#### 3:40 PM

**Multiple-Beam Irradiation Effects in Ferritic Steels:** *Naoyuki Hashimoto<sup>1</sup>*; Norihito Yamaguchi<sup>1</sup>; Hiroshi Oka; Hiroshi Kinoshita<sup>1</sup>; Somei Ohnuki<sup>1</sup>; <sup>1</sup>Hokkaido University

Reduced-activation ferritic/martensitic steel F82H has been developed as one of prime candidate materials for experimental fusion reactors. To estimate irradiation effects in fusion reactor components, multiple-scale modeling has been studied. Modeling activities for irradiation induced microstructural change is quite effective to enhance the capability to predict mechanical properties of the materials during irradiation. Defect activation energies such as vacancy and interstitial migration energies should be estimated to obtain fundamental parameters for the modeling. And also, some of the key issues are the effects of helium and hydrogen on the microstructure evolutions such as swelling, and on the mechanical properties such as fracture toughness or embrittlement. In this study, TEM specimens of F82H, Fe-8Cr model alloy, and Pure Fe have been irradiated by electron and helium ion beams using a High Voltage Electron Microscope (HVEM) as the experimental evaluation of the modeling and simulations.

#### 4:00 PM Break

#### 4:20 PM

**The Effects of Mn on Microstructure and Hardness in A533B and Model Alloys:** *Hideo Watanabe<sup>1</sup>*; Naoaki Yoshida<sup>1</sup>; <sup>1</sup>RIAM, Kyushu University

It is well known that radiation hardening and embrittlement of A533B steels are very sensitive to minor solutes (namely, P, Cu, Ni, Si etc.) containing in the steels. To investigate the effect of these solutes on microstructural evolution and hardness changes due to irradiation, A533B steels and some model alloys were irradiated by neutron, Fe ion and electron at 290°C. After the irradiation, the microstructure of the specimens was observed by transmission electron microscopy. The recovery behavior of the hardness by post-irradiation annealing at 450°C was related with the disappearance of these dislocation loops. The study revealed that the formation of interstitial type dislocation loops, which can be seen by conventional weak-beam technique, was essential for irradiation hardening of these samples. In this study, microstructure and hardness of these samples were compared with the results of Fe ion and electron irradiation at room temperature and 290°C.

#### 4:40 PM

**Microstructural Changes by Thermal Aging and Neutron Irradiation in Stainless Steel Weld Overlay Cladding of Nuclear Reactor Pressure Vessels:** *Tomoaki Takeuchi<sup>1</sup>*; Jun Kameda<sup>2</sup>; Yasuyoshi Nagai<sup>3</sup>; Takeshi Toyama<sup>3</sup>; Yutaka Nishiyama<sup>1</sup>; Kunio Onizawa<sup>1</sup>; <sup>1</sup>Japan Atomic Energy Agency; <sup>2</sup>National Institute for Materials Science; <sup>3</sup>The Oarai Center, Institute for Materials Research, Tohoku University

Microstructural changes in thermally aged and neutron-irradiated stainless steel weld overlay cladding applied to the inner surface of nuclear reactor pressure vessels were investigated using three-dimensional atom probe (3DAP). The cladding material was composed mainly of austenitic phase and partly of ferritic phase. In the as-received cladding material, a slight fluctuation of Cr concentration probably due to spinodal decomposition was observed only in the ferritic phase. Moreover in the ferritic phase, thermal aging at 400°C for 10,000 h caused the precipitation of G phase with chemical composition of Ni:Si:Mn = 16:7:6 as well as increased spinodal decomposition. Significant hardening of the ferritic phase was induced by the thermal aging. A correlation between hardening and the microstructural changes will be discussed. The neutron irradiation effects will be also shown in this presentation.

#### 5:00 PM

**Dependence of Radiation Induced Segregation on Grain Boundary Structure in a 9 wt.% Cr Model Ferritic/Martensitic Steel:** *Kevin Field<sup>1</sup>*; James Bentley<sup>2</sup>; Chad Parish<sup>2</sup>; Jeremy Busby<sup>2</sup>; Todd Allen<sup>1</sup>; <sup>1</sup>University of Wisconsin - Madison; <sup>2</sup>Oak Ridge National Laboratory

Ferritic/Martensitic (F/M) steels containing 9 wt.% Cr, are candidate materials for structural components in the next generation of advanced nuclear and fusion reactors. Although it is known that these alloys exhibit



radiation induced segregation (RIS) at grain boundaries (GBs) while in-service, little is known about the mechanism behind RIS in F/M steels. Current understanding of RIS in F/M steels presents a model of point defect migration to GBs, which are considered perfect sinks. Changes in grain boundary character may influence the sink nature and migration processes. Proton irradiated 9 wt.% Cr model steel was investigated using STEM/EDS spectrum imaging and GB misorientation analysis to determine the role of GB structure on RIS at different GBs. This preliminary investigation found Cr preferentially segregates to specific GB structures. The preferential segregation to specific GB structures suggests a need to alter the understanding of how point defects interact at GBs in F/M steels.

**5:20 PM**

**Kinetic Lattice Monte Carlo Simulations of Radiation Induced Segregation of Chromium in Ferritic-Martensitic Steels:** *Brian Frisbie*<sup>1</sup>; Brian Wirth<sup>1</sup>; <sup>1</sup>University of California at Berkeley

Ferritic-martensitic steels with 8-12% Cr are leading candidates for advanced nuclear applications because of their superb thermal properties and swelling resistance. Irradiation of these steels introduces microstructural and microchemical changes in the material that can lead to degradation of their structural properties through processes such as radiation-induced embrittlement. In this work, we present a kinetic lattice Monte Carlo model intended to simulate the segregation behavior of Cr to grain boundaries in these ferritic-martensitic steels while under irradiation. The simulations confirm that the enrichment or depletion of Cr at grain boundaries is dependent on its diffusivity relative to that of Fe. While variations in input parameters including the temperature and local energy barriers influence the direction and rate of Cr enrichment, all simulation results display a tendency towards saturation in Cr content at the grain boundaries after a sufficiently high dose.

**5:40 PM**

**Application of Modified Inverse Kirkendall Model of Radiation-Induced Segregation to Ferritic-Martensitic Alloys:** *Janelle Wharry*<sup>1</sup>; Zhijie Jiao<sup>1</sup>; Gary Was<sup>1</sup>; <sup>1</sup>University of Michigan

Ferritic-Martensitic (F-M) alloys are leading candidates for fast reactor cladding and structural materials. This study is a combined experiment-modeling effort to understand radiation-induced segregation (RIS) of Cr in these alloys. Alloys T91 (9wt%Cr), HT9 (12wt%Cr), and HCM12A (11wt%Cr) were irradiated with 2.0 MeV protons at 400°C to 3, 7, and 10 dpa, and with 5.0 MeV Fe<sup>2+</sup> ions to 100 dpa at an equivalent temperature. Prior austenite grain boundary (PAGB) compositions were measured with scanning transmission electron microscopy using energy-dispersive X-ray spectroscopy (STEM/EDS). Results show Cr depletion at PAGBs in HT9 and HCM12A, and enrichment in T91. The modified inverse Kirkendall (MIK) model, which has successfully predicted RIS in austenitic alloys, was modified for the Fe-Cr system and used to predict the direction and magnitude of RIS in F-M alloys. Model results are compared to experimental results and are discussed in the context of the RIS mechanism in F-M alloys.

**6:00 PM**

**Ab Initio-Based Rate Theory Modeling of Radiation Induced Segregation in Ni-Cr Alloys:** *Leland Barnard*<sup>1</sup>; Samrat Choudhury<sup>2</sup>; Dane Morgan<sup>1</sup>; <sup>1</sup>University of Wisconsin-Madison; <sup>2</sup>Los Alamos National Lab

The fcc Ni-Cr alloy system forms the basis of an important class of structural materials in the nuclear power industry, both in existing reactors and for future reactor designs. Point defect diffusion under irradiation in this alloy results in a phenomenon known as radiation induced segregation (RIS), whereby Cr is depleted near grain boundaries, voids, and surfaces. Cr is essential to the corrosion resistance of these alloys, and depletion near these critical microstructural features potentially results in a vulnerability to corrosion damage. In this study, we construct a rate theory model to simulate RIS in Ni-Cr alloys parameterized entirely with data obtained through ab initio calculations. Our results indicate that details pertaining to the fate of radiation produced defects that are neglected in conventional RIS modeling, such as defect sink bias, production bias, and energetic defect trapping, may play a critical role in the evolution of Cr RIS.

---

## Neutron and X-Ray Studies of Advanced Materials IV Symposium: Brent Fultz Honorary Session I: Joint Session with Computational Thermodynamics and Kinetics Symposium

*Sponsored by:* The Minerals, Metals and Materials Society, TMS Structural Materials Division, TMS/ASM: Mechanical Behavior of Materials Committee, TMS: Chemistry and Physics of Materials Committee

*Program Organizers:* Rozaliya Barabash, Oak Ridge National Laboratory; Xun-Li Wang, Oak Ridge National Laboratory; Jaimie Tiley, Air Force Research Laboratory; Peter Liaw, The University of Tennessee; Erica Lilleodden, GKSS Research Center; Brent Fultz, California Institute of Technology; Y-D Wang, Northeastern University

Monday PM  
February 28, 2011

Room: 9  
Location: San Diego Conv. Ctr

*Session Chairs:* Xun-Li Wang, Oak Ridge National Laboratory; Michael Manley, Lawrence Livermore National Laboratory

---

*See page 133 for program.*

---

## Pb-Free Solders and Other Materials for Emerging Interconnect and Packaging Technologies: Whisker Growth

*Sponsored by:* The Minerals, Metals and Materials Society, TMS Electronic, Magnetic, and Photonic Materials Division, TMS: Electronic Packaging and Interconnection Materials Committee

*Program Organizers:* Indranath Dutta, Washington State University; Darrel Frear, Freescale Semiconductor; Sung Kang, IBM; Eric Cotts, SUNY Binghamton; Laura Turbini, Research in Motion; Rajen Sidhu, Intel Corporation; John Osenbach, LSI Corporation; Albert Wu, National Central Univ, Taiwan; Tae-Kyu Lee, Cisco Systems

Monday PM  
February 28, 2011

Room: 7B  
Location: San Diego Conv. Ctr

*Session Chairs:* Eric Cotts, Binghamton University; Peter Borgesen, Binghamton University

---

**2:00 PM Keynote**

**The Metallurgy of Sn Whisker and Hillock Growth:** *William Boettinger*<sup>1</sup>; <sup>1</sup>National Institute of Standards and Technology

Pb-free pre-tinned electronic components are subject to the spontaneous growth of Sn whiskers at room temperature. These whiskers are known to have caused shorts in various high reliability circuits. The metallurgical factors affecting whisker growth will be described. The columnar grain structure of Sn deposits combined with biaxial in-plane compressive stress cause either whiskers or hillocks to grow due to a grain boundary creep-type mechanism. Hillocks appear to grow when the grain boundaries of the Sn in the substrate are mobile whereas whiskers grow when the Sn grain boundaries in the substrate are pinned. The biaxial stress is due to the plating process as well as the growth of Cu<sub>3</sub>Sn<sub>5</sub> intermetallic particles. Remaining questions related to the location of nucleation sites for hillocks and whiskers as well as the details of the stress generation mechanisms will be discussed.

**2:40 PM Invited**

**Kinetic Mechanisms Controlling IMC Growth, Stress Evolution and Whisker Formation:** *Eric Chason*<sup>1</sup>; Nitin Jadhav<sup>1</sup>; Eric Buchovecky<sup>1</sup>; Fei Pei<sup>1</sup>; Allan Bower<sup>1</sup>; Sharvan Kumar<sup>1</sup>; <sup>1</sup>Brown University

Understanding the mechanisms controlling tin whisker formation is necessary for developing reliable mitigation strategies and for developing predictive models. Although stress is widely accepted as the driving force

MONDAY PM

for whisker growth, there are still many questions about how the stress is generated, what controls its evolution and how it leads to whisker formation. To address these issues, we present results from real-time studies that explore the correlation between the kinetics of IMC growth, stress evolution and whisker nucleation in films with different microstructures and layer morphologies. Comparisons among different measurements (e.g. varying layer structures, grain sizes, surface oxide layers and Pb content) help identify the different kinetic processes that play a role in their evolution. These mechanisms are used to develop a finite element analysis (FEA) model combining IMC growth, plastic deformation and grain boundary diffusion to simulate how the stress evolves and how it leads to whisker growth.

### 3:05 PM Invited

**Role of Stress and Oxidation on Metallic Whisker Growth:** *Elizabeth Hoffman*<sup>1</sup>; Yong Sun<sup>2</sup>; Poh-Sang Lam<sup>1</sup>; Xiaodong Li<sup>2</sup>; <sup>1</sup>Savannah River National Laboratory; <sup>2</sup>University of South Carolina

Preventing metallic whisker growth leading to electronic failures is particularly important in microelectronic circuits where devices are separated by spacings as small as tens of nanometers. Historically, lead has been added to solders to suppress whisker growth and to improve the manufacturing processes. With the understanding of lead's harmful effects on the environments and human health, this is no longer an acceptable solution. It is generally acknowledged that internal stresses arising in low melting point metals, such as Sn, promote whisker growth based on a creep-like process. Compressive stress resulting from metal oxidation is one of the theories that have been suggested to play a role in the growth of whiskers. To investigate the influence of oxidation on whisker formation and growth, a series of experiments are underway to correlate the oxygen uptake, the measured internal stress, and the whisker density that forms on specimens with particular thin film/substrate combinations.

### 3:30 PM

**Evidence of Plastic Deformation Adjacent to Sn Whiskers:** *John Osenbach*<sup>1</sup>; Robert Hilty<sup>2</sup>; <sup>1</sup>LSI Corporation; <sup>2</sup>Tyco

In this paper the results of indentation induced plastic deformation and Sn whisker growth is reported. Sn plating on a number of different substrate materials were subjected to indentation stresses. Post indentation, the microstructure and presence or absence of whiskers was evaluated using scanning and transmission electron microscopy. In all cases, independent of substrate alloy, plastic deformation as observed as evidenced by grain elongation and compression with no whiskers in the indentation region. Adjacent to the plastically deformed region whiskers are observed. Whiskers were typically found within 500um of the plastically deformed region. We interpret the results as being consistent with a theory that one of the authors has recently published "Creep and It's Affect on Sn Whisker Growth Whisker Formation".

### 3:50 PM Break

### 4:00 PM

**Whisker Formation Induced by Component and Assembly Ionic Contamination:** *Polina Snugovsky*<sup>1</sup>; Stephan Meschter<sup>2</sup>; Zohreh Bagheri<sup>1</sup>; Eva Kosiba<sup>1</sup>; Marianne Romankys<sup>1</sup>; <sup>1</sup>Celestica; <sup>2</sup>BAE Systems

The paper will describe the results of an intensive whisker formation study on Pb free assemblies with different level of cleanliness. Thirteen types of as-received surface mount (SMT) and pin-through-hole (PTH) components were cleaned and intentionally contaminated with solutions containing chloride, sulfate, bromide, and nitrate. Then the parts were assembled on double sided boards that were also cleaned or intentionally contaminated with three fluxes having different halide contents – ROL0, ROL1, and ORH1. The assemblies were subjected to high temperature/high humidity testing (85°C/85%RH). Periodic examination found that contamination triggers whisker formation on both exposed tin and solder fillets. Whisker occurrence, morphology, and length parameters depending on the type and level of contamination will be discussed. Sequential cross-sections were used to assess the metallurgical aspects of whisker formation and the microstructural changes occurring during corrosion.

### 4:20 PM

**Microstructure Formation and Whisker Growth in SAC105 Solder Joints with Rare Earth Elements:** *Polina Snugovsky*<sup>1</sup>; Zohreh Bagheri<sup>1</sup>; Stephan Meschter<sup>2</sup>; Leonid Snugovsky<sup>3</sup>; John Rutter<sup>3</sup>; Doug Perovic<sup>3</sup>; <sup>1</sup>Celestica; <sup>2</sup>BAE Systems; <sup>3</sup>University of Toronto

Rare earth elements (REE) such as Y, Ce, and La being added to Sn-Ag-Cu alloys may improve mechanical properties of solder joints. It was shown in literature that the addition of 0.2% REE refines the microstructure positively effecting drop/shock behavior. Unfortunately, it has also been demonstrated that Sn-Ag-Cu solders with REE are prone to whisker formation. In the present work, microstructure of SAC105 solder with 0.1 – 0.4 % Y, Ce, or La reflowed on the Cu substrate, is examined. The results of high temperature/high humidity testing that may trigger whisker formation is discussed. The similarities and differences in microstructure and whisker growth of SAC105 solder joints with different REE is examined from a metallurgical perspective using sequential microsectioning. The influence of flux type and cleanness on propensity of whiskering is discussed.

### 4:40 PM

**Tin Whisker Growth on the Surface of Sn-3.8Ag-0.7Cu-RE Solder Alloys:** *Hu Hao*<sup>1</sup>; Fu Guo<sup>1</sup>; Yonglun Song<sup>1</sup>; Guangchen Xu<sup>1</sup>; Yaowu Shi<sup>1</sup>; <sup>1</sup>Beijing University of Technology

Alloying approach by adding trace amount of rare earth (RE) elements in Sn-3.8Ag-0.7Cu solder alloy has been widely reported to show its ability on the improvement of processing and reliability properties. However, bulk RE-Sn phases, when adding excessive RE elements, can be observed inside the solder matrix. This study systematically investigated the tin whiskers growth (including the incubation time, growth rate, quantity, morphology, size, etc.) on the surface of CeSn<sub>3</sub>, LaSn<sub>3</sub>, (La<sub>0.4</sub>Ce<sub>0.6</sub>)Sn<sub>3</sub>, ErSn<sub>3</sub>, and YSn<sub>3</sub> by adding excessive Ce, La, La/Ce mixture, Er and Y, respectively, in the Sn-3.8Ag-0.7Cu solder. Most important, the finding of tin whiskers with a non-constant cross-section provided a better understanding to the spontaneous growth equation of tin whiskers. In addition, a hypothesis of "double stress zones" was proposed to demonstrate the underlying mechanism for tin whiskers growth on the bulk RE-Sn phases.

### 5:00 PM

**Effect of Sn Layer on Whisker Growth Kinetics: Modifying the Surface, Microstructure, Composition and Heat Treatment:** *Fei Pei*<sup>1</sup>; Gordon Barr<sup>2</sup>; Eric Chason<sup>1</sup>; Nitin Jadhav<sup>1</sup>; <sup>1</sup>Brown University; <sup>2</sup>EMC Corporation

Though it is well understood that compressive stress due to intermetallic (IMC) formation is the main driving force for whisker formation, the underlying mechanisms that control the stress distribution and cause whiskering are not clear. We present the results of studies done to understand how modification of the Sn layer (surface treatment, thickness, grain size, Pb-alloying, heat treatment) affects the growth and morphology of the IMC and the corresponding stress development in the Sn layers. We have quantified the whisker nucleation kinetics using an optical method so that we can relate the whisker growth to the underlying stress evolution. Changes in the Sn surface and bulk alter the mechanical properties and stress relaxation behavior and thus result in various whisker growth rates. The study also shows that a grain with a weaker oxide layer will not necessarily whisker, indicating that the underlying Sn microstructure plays a crucial role in whiskering.

---

## Physical and Mechanical Metallurgy of Shape Memory Alloys for Actuator Applications: Characterization of Shape Memory Alloys: Structure-Property Relationships

Sponsored by: The Minerals, Metals and Materials Society  
Program Organizers: S. Raj, NASA Glenn Research Center; Raj Vaidyanathan, University of Central Florida; Ibrahim Karaman, Texas A&M University; Ronald Noebe, NASA Glenn Research Center; Frederick Calkins, The Boeing Company; Shuichi Miyazaki, Institute of Materials Science, University of Tsukuba

Monday PM Room: 11B  
February 28, 2011 Location: San Diego Conv. Ctr

Session Chairs: Shuichi Miyazaki, University of Tsukuba; Huseyin Sehitoglu, University of Illinois

---

### 2:00 PM Invited Structure and Thermomechanical Behavior of NiTiPt Shape Memory Alloy Wires: Ken Gall<sup>1</sup>; <sup>1</sup>Georgia Tech

The objective of this work is to understand the structure property relationships in polycrystalline NiTiPt (Ti 42.7 at.% Ni 7.5 at.% Pt) with a composition showing pseudoelasticity at ambient temperatures. Structural characterization of the alloy includes grain size determination and texture analysis while the thermomechanical properties are explored using tensile testing. Variation in heat treatment is used as a vehicle to modify microstructure. The results are compared to experiments on Ni-rich NiTi alloy wires (Ti-51.0 at.% Ni), which are in commercial use in various biomedical applications. With regards to microstructure, both alloys exhibit a <111> fiber texture along the wire drawing axis; however, the NiTiPt alloy grain size is smaller than that of the Ni-rich NiTi wires, while the latter materials contain second-phase precipitates.

### 2:20 PM Training and the Two-Way Shape Memory Effect in TiNiPd and TiNiPdX High Temperature Shape Memory Alloys: Kadri Atli<sup>1</sup>; Brian Franco<sup>1</sup>; Ibrahim Karaman<sup>1</sup>; Ronald Noebe<sup>2</sup>; <sup>1</sup>Texas A&M University; <sup>2</sup>NASA Glenn Research Center

The relationship between thermomechanical cycling (training) and the two way shape memory effect (TWSME) was investigated for a number of shape memory alloy (SMA) systems including equiatomic TiNi, a ternary Ti<sub>50.5</sub>Ni<sub>24.5</sub>Pd<sub>25</sub> high temperature SMA (HTSMA), and its quaternaries TiNiPd<sub>25</sub>X (X = Sc, Ta replacing Ti). Training consisted of thermal cycling under various constant stress levels and stable and reproducible TWSME behavior was obtained for all materials after 100 thermal cycles. It was shown that training stress dictated the level of TWSME strain and thermal hysteresis behavior, which were in turn significantly affected by the strength of the material and the compatibility of the transforming phases. The work output capability of the TWSME was evaluated by constraining the "cold shape" under external stress-free conditions and heating above the transformation temperature. Improvements in TWSME strains and thermal hysteresis were found after microalloying TiNiPd<sub>25</sub> with Sc and Ta.

### 2:35 PM Thermomechanical Testing of NiTiPdPt High Temperature Shape Memory Alloy Springs: Douglas Nicholson<sup>1</sup>; Santo Padula<sup>2</sup>; Ronald Noebe<sup>2</sup>; Raj Vaidyanathan<sup>1</sup>; <sup>1</sup>UCF; <sup>2</sup>NASA GRC

Stroke in high temperature shape memory alloys (HTSMAs) can be limited in cases where stability and repeatability at elevated temperatures are required. However, these alloys can still be used in actuator applications that require large strokes, by fabricating them in the form of springs. Thus there is value in evaluating the thermomechanical performance of HTSMA helical actuators. Towards that goal, a test setup was designed to acquire stroke, moment, and temperature data during thermomechanical cycling of NiTiPdPt springs under load. The role of grip constraints was also systematically

investigated, i.e., by allowing the springs to freely rotate during actuation or fixing the ends of the springs. The experiments assessed the contributions of material behavior (i.e., microstructural evolution) and geometry (i.e., helical angle) to overall actuator performance. With appropriate assumptions, the mechanics of the spring behavior was approximately captured using spring theory and finite element analysis.

### 2:50 PM Structure-Property Relationships in a Ni-Rich Ni-25Pd-48Ti (at.%) High Temperature Shape Memory Alloy: Taisuki Sasaki<sup>1</sup>; B. C. Hornbuckle<sup>1</sup>; Glen Bigelow<sup>2</sup>; Ronald Noebe<sup>2</sup>; Mark Weaver<sup>1</sup>; Gregory Thompson<sup>1</sup>; <sup>1</sup>University of Alabama; <sup>2</sup>NASA Glenn Research Center

Ni-rich NiTi alloys, when properly processed, display relatively stable shape memory and superelastic behavior. However, their potential applications are severely limited because of low transformation temperatures. Recent efforts have focused on using ternary additions to raise the transformation temperatures, while simultaneously improving stability through nanoscale precipitation. In this work, we have investigated the effect of aging on the structure and shape memory behavior of an extruded Ni-48Ti-25Pd (at.%) alloy. After aging at 400°C, nanoscale precipitates formed within the matrix, resulting in an increase in transformation temperatures. Electron diffraction studies and atom probe analysis showed that the structure and the chemistry of the precipitate are similar to the P-phase seen in NiTiPt alloys. The mechanical responses of this aged alloy were tested via superelastic and load biased thermomechanical testing, demonstrating the stabilizing effect of the fine precipitate phase.

### 3:05 PM Structure-Property Relationships for Ni-Ti-Pt High Temperature Shape Memory Alloys: Grant Hudish<sup>1</sup>; Glen Bigelow<sup>2</sup>; Ronald Noebe<sup>2</sup>; Michael Kaufman<sup>1</sup>; <sup>1</sup>Colorado School of Mines; <sup>2</sup>NASA-GRC

Alloys of Ni and Ti in near equal amounts are commercially prevalent shape memory alloys (SMA's), but are limited to use near room temperature. Increasing the transformation temperature of traditional Ni-Ti SMAs, through ternary alloying of Pd, Pt, Au, Hf or Zr, would allow for their use in various higher temperature applications and industries including aerospace, automotive, and down hole energy exploration, to name a few. Pt is currently one of the most promising ternary additions for stable and predictable high temperature SMA's (HTSMA's), but little is understood about the effects of Pt on the microstructure and mechanical properties of Ni-Ti alloys. Using various techniques including scanning and transmission electron microscopy (SEM and TEM), differential thermal analysis (DTA), and load-biased thermally cycled compression tests, the current research explores the link between alloy microstructures and the shape memory properties of several Ni-Ti-Pt alloys.

### 3:20 PM Break

### 3:30 PM Invited A New Precipitate Phase in High-Temperature TiNiPt and Its Effect on Shape Memory Properties: F. Yang<sup>1</sup>; L. Kovarik<sup>1</sup>; Y. Wang<sup>1</sup>; P. M. Anderson<sup>1</sup>; A. Garg<sup>2</sup>; R.D. Noebe<sup>3</sup>; Michael Mills<sup>1</sup>; <sup>1</sup>The Ohio State University; <sup>2</sup>University of Toledo - and - NASA Glenn Research Center; <sup>3</sup>NASA Glenn Research Center

The effects of aging on mechanical and shape memory properties of the high-temperature shape memory alloy Ti<sub>50</sub>Ni<sub>30</sub>Pt<sub>20</sub> (at.%) were investigated in order to understand aging effects on transformation strain, work output and dimensional stability under cyclic load biased tests. Aging results in precipitation of a previously unidentified phase. The precipitate phase has been analyzed with electron diffraction and high-resolution STEM HAADF imaging. The precipitates are closely related to the high temperature cubic B2 phase, but have a unique structure due to their non-periodic character along one of the primary crystallographic directions. The importance of these precipitates in other high temperature shape memory alloys and their role in achieving optimal shape memory properties will be discussed.



3:50 PM

**Grain Size Distribution Effects on Phase Transformation Behavior of NiTi Thin Films:** *Xu Huang*<sup>1</sup>; David Wu<sup>2</sup>; Ainissa Ramirez<sup>3</sup>; <sup>1</sup>Yale University; <sup>2</sup>Institute of High Performance Computing

This presentation demonstrates the role of grain size and its distribution on phase transformations in sputter-deposited NiTi thin films. Two-step heat treatments—where growth and nucleation are both active in the first step, and nucleation is suspended in the second—narrow the grain size distribution, as determined by transmission electron microscopy. The associated transformation temperatures and actuation properties departed significantly from the Hall-Petch-like relationship of conventionally (one-step) annealed films. A change in texture was also apparent with two-step heat treatments. This presentation demonstrates a method for tailoring microstructures and illuminates the role of grain size distributions on properties.

4:05 PM

**Shape Memory Characteristics of Time Gradient Annealing Treated Ti-50.9 at.% Ni Alloy:** *Jae Il Kim*<sup>1</sup>; Su Ho Park<sup>1</sup>; Jun Hee Lee<sup>1</sup>; Yun-Jung Lee<sup>2</sup>; Tae-Hyun Nam<sup>3</sup>; <sup>1</sup>Dong-A University; <sup>2</sup>Gyungbook National University; <sup>3</sup>Gyungsang National University

In this study shape memory characteristics and superelasticity of a time gradient annealing treated Ti-50.9at%Ni alloy have been investigated by means of differential scanning calorimetry (DSC), thermal cycling tests under constant load and tensile tests. This method is an anneal within a time gradient after cold work, thus creating a structural gradient within the matrix of the alloy. By annealing 30% cold worked alloy under the time gradient from 3min to 20min at 773 K, 44K variation in R phase transformation interval (Rs - Rf) were obtained along the length of sample (80mm). Temperature dependence of R-phase transformation elongation (de/dT) of time gradient annealing treated sample at 773 K was 0.0068%/K. Also, it was found that the time gradient-anneal resulted in varying thermal transformation behavior along its length and a unique Lüders-type deformation behavior with a positive stress gradient. Such behavior provides improved controllability for actuation applications.

4:20 PM

**Crystal Structures, Phase Transformations and Microstructures of Rapidly Solidified Heusler Type CoNiGa(Al) Ferromagnetic Shape Memory Alloys for Micro-Actuator Applications:** *Shampa Aich*<sup>1</sup>; M. Vijaykumar<sup>2</sup>; I. Al-Omari<sup>3</sup>; M. Chakraborty<sup>4</sup>; D. Sellmayr<sup>3</sup>; <sup>1</sup>Indian Institute of Technology; <sup>2</sup>JSW Steel Ltd.; <sup>3</sup>University of Nebraska-Lincoln; <sup>4</sup>Indian Institute of Technology - Bhubaneswar

A series of arc-melted ingots of Heusler type  $\text{Co}_{50}\text{Ni}_{25}\text{Ga}_{25-2x}\text{Al}_{2x}$  ( $x = 0, 1, 2, 3,$  and  $4$ ) alloys were rapidly solidified by melt-spinning onto a copper wheel with a linear velocity of 25 m/s. The melt-spun ribbons were heat-treated at 800°C-1200 °C for 4 hours followed by water quenching. The occurrence of  $\text{L1}_2$  ordered structure and disordered  $\square$ -phase has been confirmed by XRD analysis in the as-spun and annealed alloys. The martensitic transformation temperature ( $T_m$ ) increases with annealing temperature and Al addition in all alloys with deterioration of ductility due to replacement of Ga with Al. The microstructural observations performed by HRTEM and FESEM reveal the martensitic twin bands at higher concentration of Ga in the as-spun as well as in heat-treated ribbons. High  $T_m$  (~ 390 K-440 K) and high Curie temperature  $T_c$  (~ 400K) make those alloys good enough to be used as Ferromagnetic Shape Memory Alloys.

4:35 PM

**Studies on Effect of Aging on Shape Memory Characteristics of Cu-Al-Fe Alloys:** *Sampath Vedamanickam*<sup>1</sup>; Raju T.N.<sup>1</sup>; <sup>1</sup>Indian Institute of Technology Madras

The most popular SMAs based on Ni-Ti cannot be used in service at  $T > 100^\circ\text{C}$ . In addition, they are difficult to produce and process and are also expensive. There is therefore a need for producing SMAs for high temperature actuator applications. With this as the background and impetus, Cu-Al-Fe shape memory alloys in the range of 10-12 wt% of Al and 0-2 wt % of Fe, exhibiting  $\beta$ -phase at high temperatures and manifesting shape memory effect upon quenching to lower temperatures, were prepared through

ingot metallurgy. The alloys were aged at 300°C and 500°C, respectively. The effect of ageing on the transformation temperatures and shape memory properties has been studied. The alloys aged at 300°C show an increase in the transformation temperatures. The results are presented and discussed in the paper.

4:50 PM

**Stoichiometry and Aging Effects on the Microstructure and Properties of NiTiHf Shape Memory Alloys:** *Daniel Coughlin*<sup>1</sup>; Ronald Noebe<sup>2</sup>; Glen Bigelow<sup>2</sup>; Anita Garg<sup>2</sup>; Michael Mills<sup>1</sup>; <sup>1</sup>Ohio State University; <sup>2</sup>NASA Glenn Research Center

Certain alloys belonging to the NiTiHf ternary system exhibit attractive high temperature shape memory properties, including relatively high transformation temperature, moderate transformation strain, and very small irrecoverable strain during load-biased, thermal-cycling tests at moderate to high stresses. Alloy compositions that span "stoichiometry", consisting of 20at.% Hf and varying Ti concentrations (from 29 to 30.5at.%) have been analyzed using SEM and TEM in the as-extruded condition. The phase constituents will be reported as a function of composition. The effect of aging on the Ni-29.7Ti-20Hf composition has also been explored using isothermal, constant strain rate testing above the austenite finish temperature. The results indicate that significant strengthening occurs upon aging due to the formation of a distribution of fine precipitates. The structure of these precipitates and their interaction with dislocations in the B2 phase will be discussed with relationship to the desirable shape memory properties.

5:05 PM

**Magnetic Shape Memory Effect in NiMnCo-Based Meta-Magnetic Shape Memory Alloy Micropillars:** *Nevin Ozdemir*<sup>1</sup>; Ibrahim Karaman<sup>1</sup>; Nathan Mara<sup>2</sup>; Douglas Pete<sup>3</sup>; <sup>1</sup>Texas A&M University; <sup>2</sup>Los Alamos National Laboratory; <sup>3</sup>Sandia National Laboratories

Magnetic Shape Memory Alloys (MSMAs) have recently emerged as an alternative to conventional Shape Memory Alloys (SMAs) due to their faster response, which is a consequence of the magnetic field-induced reversible shape change. NiMnCo-based SMAs show great promise for functional materials applications due to an order of magnitude higher actuation work output than other active materials and their potential for use in MEMS/NEMS devices. To the best of our knowledge, there is no work on the magnetic field-induced shape change via field-induced phase transformation on sub-micron structural length scales. Here, we studied the magnetic field-induced martensitic transformation on NiMnCoIn MSMAs at this size scale. The pillars were obtained from NiMnCoIn single- and polycrystals and deformed to various strain levels. Magnetic field was applied to recover the deformation via field-induced reverse martensitic transformation. The recovery strain levels and phase transformation characteristics were determined as a function of pillar size.

5:20 PM

**In-Situ Phase Transformation Behavior of Ni-Rich NiTi Shape Memory Alloys:** *Suresh Santharam*<sup>1</sup>; Dong-Ik Kim<sup>2</sup>; Subir Kumar Bhaumik<sup>3</sup>; Satyam Suwas<sup>1</sup>; <sup>1</sup>Indian Institute of Science; <sup>2</sup>Korea Institute of Science and Technology; <sup>3</sup>National Aerospace Laboratory (CSIR)

Ni-rich NiTi Shape memory alloy, characterized by room temperature austenite (B2) phase, was deformed in-situ in a Scanning Electron Microscope. The characteristic crystallographic features pertaining to B2 (austenite) to B19' (martensite) transformation were examined using Electron Back Scattered Diffraction. From the results, it has been shown that during stress induced transformation, different martensite variants appear within a single austenite grain. The Schmid factor calculations for different martensite variants indicate that in addition to the variants possessing the highest Schmid factor, certain variants with lower Schmid factor also get activated during stress induced martensitic transformation. The authors attribute the activation of different martensite variants with lower Schmid factor values as semi-coherent austenite-martensite interface. This proposition has been substantiated through transmission electron microscopic study.

5:35 PM End of Session

---

## Polycrystal Modelling with Experimental Integration: A Symposium Honoring Carlos Tome: Neutron Diffraction and Prediction of Internal Stresses

*Sponsored by:* The Minerals, Metals and Materials Society, TMS Structural Materials Division, TMS Materials Processing and Manufacturing Division, ASM-MSCTS: Texture and Anisotropy Committee, TMS/ASM: Mechanical Behavior of Materials Committee, TMS/ASM: Computational Materials Science and Engineering Committee

*Program Organizers:* Ricardo Lebensohn, Los Alamos National Laboratory; Sean Agnew, University of Virginia; Mark Daymond, Queen's University

Monday PM  
February 28, 2011  
Room: 6C  
Location: San Diego Conv. Ctr

*Session Chairs:* Mark Daymond, Queen's University; Bjoern Clausen, Los Alamos National Laboratory; Donald Brown, Los Alamos National Laboratory

---

### 2:00 PM Invited

#### Information Volumes in Diffraction Techniques for Strain Analysis: I Noyan<sup>1</sup>; <sup>1</sup>Columbia University

In this presentation we discuss how the modality (dynamical or kinematic) of scattering determines the volumes from which the information is obtained. In addition, this modality also impacts the uniqueness of the stress state measured. We use rigorous diffraction modeling to show that diffraction data obtained from weakly deformed crystals that scatter in the dynamical limit should not be used for validating continuum models. The "mean" strain obtained from polycrystalline continua and how this compares to the orientation-specific strain and mean-strain computed by mean-field models of deformation will also be discussed.

### 2:25 PM Invited

#### EPSC Modeling and Neutron Diffraction Measurements: Bjoern Clausen<sup>1</sup>; Donald Brown<sup>1</sup>; Levente Balogh<sup>1</sup>; Carlos Tomé<sup>1</sup>; <sup>1</sup>Los Alamos National Laboratory

Dr. Carlos Tomé has been one of the major contributors in developing and implementing the Elasto-Plastic Self-Consistent (EPSC) model throughout the years. Although the EPSC scheme was introduced in the 60's and 70's, the first publically released code implementing the EPSC model with full elastic and plastic anisotropy on both grain and polycrystal level originated in the 1994 Turner and Tomé paper. From the start, the predictions of the EPSC model were correlated with neutron diffraction measurements of internal strains and texture. In the following years there were many publications showing how internal strain measurements using diffraction can be used to verify the predictions of the EPSC model, and vice versa, how the EPSC model predictions can be used to interpret and deconvolute measured diffraction data. This symbiotic relationship between diffraction measurements and the EPSC model and how it has influenced the development of both techniques will be discussed.

### 2:50 PM Invited

#### Texture and Type-2 Strains in Rolled Zircaloy-2 and Their Relevance to In-Reactor Growth: Thomas Holden<sup>1</sup>; <sup>1</sup>Northern Stress Technologies

Zr-2 calandria tubes in CANDU reactors can grow by 0.1% in a fast neutron fluence thus creating an engineering problem. Neutron diffraction was used to measure the strain state of Zr-2 rolled plate, an analog for the tubes, in the late 1980's. The type-2 strains plus the texture determine the growth behaviour. The strong texture permits a practical estimate of the strain tensor of the material. With the aid of the elasto-plastic self-consistent model (EPSC), developed by C.N Tomé and his collaborators, one can compare experiment and theory for the strains in as-prepared or tensioned Zr-2 and incorporate this into the in-reactor growth model as set out by C. H. Woo. Carlos Tomé's contributions to the ever-improving EPSC, as well

as the problem of in-reactor growth, and his enthusiastic encouragement of experimentalists to test the polycrystal models are the mark of an outstanding scientist. His friendship is highly valued.

### 3:15 PM

#### Internal Stresses and Microstructure by Neutron Diffraction Profile Analysis: Comparison with Other Techniques: Vadim Davydov<sup>1</sup>; Petr Lukáš<sup>2</sup>; Helena Van Swygenhoven<sup>1</sup>; Martin Petrenc<sup>3</sup>; Ondrej Man<sup>4</sup>; Pavel Strunz<sup>2</sup>; Radomír Kužel<sup>5</sup>; <sup>1</sup>Paul Scherrer Institut; <sup>2</sup>Nuclear Physics Institute; <sup>3</sup>Institute of Physics of Materials; <sup>4</sup>Brno University of Technology; <sup>5</sup>Charles University

The neutron and X-ray diffraction techniques combined with electron microscopy methods has been used to study the internal microstresses and microstructure in low carbon steel. Since the real structure features affect the width and shape of the neutron or X-ray diffraction pattern, and, as these real structure aspects are very numerous and mutually superposed, diffraction effects in terms of real structure characteristics are not simple to interpret. Using the recently modified single-line profile analysis method, the dislocation content was addressed and compared in terms of dislocation density parameter with the results obtained by other microscopy methods. The single-line neutron diffraction profile analysis performed at NPI was extended using full diffraction patterns collected in time-of-flight mode on POLDI.

### 3:35 PM Break

### 3:50 PM Invited

#### On the Evolution of Crystal Stresses during the Elastic-Plastic Transition in FCC Polycrystals: Paul Dawson<sup>1</sup>; Su Leen Wong<sup>1</sup>; <sup>1</sup>Cornell University

Simulations based on crystal-scale elastoplasticity have proven to be a valuable tool for interpreting data measured by diffraction techniques. Diffraction measurements provide lattice strain data on subsets of the grains within the diffraction volume and offer insight into grain interactions. With finite element models the spatial arrangement of grains is included and interactions among the grains arise naturally in simulating an experiment. We discuss the roles of elastic and plastic anisotropies on grain interactions with attention to changes in the crystal stress distributions as the loading progresses through the elastic plastic transition. The simulations offer an explanation for the differences in lattice strain behaviors at the onset of yielding observed between metals of low and high elastic anisotropy under monotonic loading. We will show the implications of elastic and plastic anisotropies, as quantified by the directional strength-to-stiffness, on lattice strains during cyclic loading.

### 4:15 PM Invited

#### High Pressure Plastic Properties of Hcp Metals: Experiments and Elasto-Plastic Models: Sebastien Merkel<sup>1</sup>; <sup>1</sup>Universite Lille 1

Over the last few years, we developed new techniques for the study of plastic properties of materials under high pressure and temperature. Their physical properties are analyzed in-situ using x-ray diffraction to extract quantitative texture information and average elastic strains within the sample. Thanks to the contribution of Carlos Tomé, we now use EPSC models to relate the experimental observations and the plastic properties of the sample. In this presentation, I will show results on the hcp phase of Co deformed at 300 K between 0 and 42 GPa and results on the hcp phase of Fe deformed at pressures and temperatures reaching 19 GPa and 600 K. I will highlight how the combination of x-ray diffraction and EPSC modeling can be used to infer important information, such as the average stress within the sample, identify and constrain the plastic deformation activated, and evaluate stress heterogeneity with the sample.

### 4:40 PM Invited

#### A Decade Plus of Making Carlos Tomé Sweat: Donald Brown<sup>1</sup>; Bjoern Clausen<sup>1</sup>; Thomas Sisneros<sup>1</sup>; <sup>1</sup>Los Alamos National Lab

The Self-Consistent plasticity models developed by Carlos and his team are in the (un)enviable position of being readily, and robustly, validated by diffraction measurements, meaning the simulations can be easily tested. Since its inception, the SMARTS team has worked closely with Carlos to

“exercise” the models. Toward this end, we have moved to ever increasing complexity in the form of lower symmetry crystal structures (cubic to hexagonal to orthogonal) and more complicated thermo-mechanical histories (cycling, strain path changes, annealing, etc). Concomitantly, we have collected more diffraction data (e.g. during compression and tension) analyzed the data more aggressively, providing increased microstructural information to be used to constrain the model. This talk will use beryllium as an example material to discuss the evolution of both the modeling and experimental efforts toward improving the fidelity between the SC models and the actual physics occurring at the grain level during deformation.

5:05 PM

**Finite Element Diffraction Model for Spatially Resolved Strain Measurements in the Bulk of (Poly-) Crystals:** *Peter Reischig*<sup>1</sup>; Wolfgang Ludwig<sup>2</sup>; Andrew King<sup>3</sup>; Tilo Baumbach<sup>4</sup>; <sup>1</sup>TU Delft; <sup>2</sup>GEMPPM-MATEIS, INSA de Lyon; <sup>3</sup>GKSS-Forschungszentrum Geesthacht GmbH; <sup>4</sup>Institute for Synchrotron Radiation, Karlsruhe Institute of Technology

Measuring local strain state in the bulk of polycrystalline materials or single crystals is key to understanding their deformation processes and damage phenomena. We propose a linear model to spatially resolve the complete deformation tensor, i.e. 3 rotational and 6 elastic strain components, inside individual grains (diffraction contrast tomography) or a single crystal (rocking curve imaging) from full beam diffraction data. Practical implementation of the model comprises the concepts of finite elements, ray-tracing and kinematical diffraction. The linear approach of the crystal diffraction behavior under deformation enables fast and efficient computation and a rigorous analysis of the well-posedness of the inverse problem. The model allows for direct coupling with crystal plasticity simulation, hence for the verification of such models. Preliminary results on simulated and measured data will be presented.

5:25 PM

**The Bauschinger Effect in Austenitic (317L) Stainless Steel: Validating a Slip-System Based Non-Linear Kinematic Hardening Model with In-Situ Neutron Diffraction:** *James Wollmershauser*<sup>1</sup>; Bjørn Clausen<sup>2</sup>; Carlos Tome<sup>2</sup>; Sean Agnew<sup>1</sup>; <sup>1</sup>University of Virginia; <sup>2</sup>Los Alamos National Laboratory

Accurate prediction of the Bauschinger effect is considered a litmus test for the validity of strengthening theories. The effect is known to arise from ‘backstresses’ having intergranular and intragranular sources. Self-consistent polycrystal models inherently capture intergranular effects but typically fail to account for intragranular (dislocation-based) sources. This inadequacy is illustrated by comparisons of model predictions with in-situ neutron diffraction measurements of the hysteresis and internal stresses within a sample subjected to tension-compression fatigue. A single non-linear kinematic hardening rule, similar to the Armstrong-Frederick model, is implemented at the slip system level. With this simple adaptation, the polycrystal model accurately predicts the hysteresis loops and internal strains observed during the aforementioned in-situ low cycle fatigue tests, as well as monotonic stress strain curves and texture evolution after larger strain deformation. The physics-based polycrystal plasticity approach obviates the need for multiple kinematic hardening terms used in phenomenological models.

5:45 PM

**Study of Lattice Strain Based on the Finite Strain Elastic-Viscoplastic Self-Consistent Model for Polycrystalline Materials:** *Huamiao Wang*<sup>1</sup>; Peidong Wu<sup>1</sup>; Carlos Tome<sup>2</sup>; <sup>1</sup>McMaster University; <sup>2</sup>Los Alamos National Laboratory

The recently developed large strain elastic-viscoplastic self-consistent (EVPSC) model for polycrystalline materials is used to study the lattice strain measurements for conventionally extruded magnesium alloy AZ31 under uniaxial tension and compression. The EVPSC model is a completely general elastic-viscoplastic, fully anisotropic, self-consistent polycrystal model, applicable at large strain and to any crystal symmetry. At single crystal level, both the rate sensitive slip and twinning are included as the plastic deformation mechanisms, while elastic anisotropy is accounted in the

elastic moduli. The transition from the single crystal plasticity to polycrystal plasticity is based on a completely self-consistent approach. In the present study, effects of texture evolution, twinning activity and stress relaxation on lattice strain are interpreted by the EVPSC model. It is found that the stress relaxation has a significant effect on the lattice strain measurements.

6:05 PM

**High Pressure Deformation of Zirconium:** James Wilkerson<sup>1</sup>; *Sven Vogel*<sup>1</sup>; Donald Brown<sup>1</sup>; <sup>1</sup>Los Alamos National Laboratory

Uni-axial deformation of pure Zirconium and Zircaloy-2 was performed with the D-DIA apparatus at the APS. The transformation from  $\alpha$ -Zr to  $\omega$ -Zr during hydrostatic compression was observed at  $\sim 4.5$  GPa at room temperature with the applied pressure derived from the unit cell volume of  $\alpha$ -Zr and the known equation of state. A combination of texture analysis of the diffraction data and energy minimization-based variant selection during texture modeling allows to establish the orientation relationship between the two phases for the first time from a large number of grains. We found that both published orientation relationships, derived from TEM data, are needed to describe the texture change during the phase transformation. From the uni-axial deformation at applied pressure of Zircaloy-2 we found that the twin activity at elevated pressure is increased compared to deformation at ambient pressure, confirming predictions by Lebensohn & Tomé.

## Processing and Properties of Powder-Based Materials: Sintering Science and Technology

*Sponsored by:* The Minerals, Metals and Materials Society, TMS Materials Processing and Manufacturing Division, TMS: Powder Materials Committee

*Program Organizers:* K. Morsi, San Diego State University; Ahmed El-Desouky, San Diego State University

Monday PM

February 28, 2011

Room: 33A

Location: San Diego Conv. Ctr

*Session Chair:* Randall German, San Diego State University

2:00 PM Introductory Comments

2:05 PM

**Process Simulation of Cold Pressing and Sintering of Armstrong CP-Ti Powders:** Sarma Gorti<sup>1</sup>; *Adrian Sabau*<sup>1</sup>; William Peter<sup>1</sup>; Stephen Nunn<sup>1</sup>; Yukinori Yamamoto<sup>1</sup>; Wei Chen<sup>1</sup>; <sup>1</sup>Oak Ridge National Laboratory

A computational methodology is presented for the process simulation of cold pressing and sintering of Armstrong CP-Ti powders. Since the powder consolidation is governed by specific pressure-dependent constitutive equations, solution algorithms were developed for the ABAQUS user material subroutine, UMAT, for computing the plastic strain increments based on an implicit integration of the nonlinear yield function, flow rule, and hardening equations. Sintering was simulated using a model based on diffusional creep using the user subroutine CREEP. The initial mesh, stress, and density for the simulation of sintering were obtained from the results of the cold pressing simulation, minimizing the errors from decoupling the cold pressing and sintering simulations. Numerical simulation results are presented for the cold compaction followed by a sintering step of the Ti powders. The numerical simulation results for the relative density were compared to those measured from experiments before and after sintering, showing that the relative density can be accurately predicted.

2:25 PM

**Hot Isostatic Pressing of Beta Titanium Alloy Powders:** *Xinjiang Hao*<sup>1</sup>; Nicholas Wain<sup>1</sup>; Xinhua Wu<sup>1</sup>; <sup>1</sup>University of Birmingham

Hot isostatic pressing (“HIPping”) of Ti alloy powders is an effective near net-shape technique to produce complex parts which can have similar or even superior mechanical properties to wrought alloys. Ti alloy powders (such as Ti-6Al-4V) are normally HIPped at temperature below beta-transus to avoid excessive grain coarsening. However, the beta-transus of metastable beta or



beta titanium alloys is lower than alpha-beta alloys and this makes HIPping of beta alloys a challenge to produce a good bonding between powders and therefore good properties. In this work, powder bonding mechanisms in several beta titanium alloys (Ti-5553, Ti-6246 etc) were investigated and the HIPping parameters were optimized.

#### 2:45 PM

**Effect of Particle Size Particle Surface Modification Pressing Pressure and Sintering Temperature on Microstructure and Mechanical Properties P/M Al-B4C Composites:** *Fatih Toptan*<sup>1</sup>; *Isil Kerti*<sup>1</sup>; *Sibel Daglilar*<sup>1</sup>; *Ahmet Sagin*<sup>1</sup>; *Taner Hacioglu*<sup>1</sup>; <sup>1</sup>*Yildiz Technical University*

Al-Ti-B grain refiners are widely used as aluminium grain refiners despite the problems in application Al-Ti-C refiners have an increasing demand in recent years. In the present work, Al-Ti-C grain refiners with different Ti:C ratios were produced by in-situ method with the addition of elemental carbon into the Al-Ti master alloy and addition of K2TiF6 and elemental carbon powder mixture into the commercially pure aluminium. Microstructures were characterised by optic microscope and scanning electron microscope equipped with energy dispersive spectroscopy. The effects of production method and Ti:C ratio on the grain refinement process was investigated with Alcoa Coldfinger Test and optimum conditions were determined. Commercial Al-Ti-B grain refiners also tested with Alcoa Coldfinger Test in identical conditions and it has been stated that, in-situ Al-Ti-C refiners are more effective than commercial Al-Ti-B grain refiners in grain refining.

#### 3:05 PM

**Microstructure and Mechanical Properties of TiNbSn-HA Biocomposite Fabricated by Mechanical Alloying and Sintering:** *Xiaopeng Wang*<sup>1</sup>; *Yuyong Chen*<sup>1</sup>; *Kee-Do Woo*<sup>2</sup>; <sup>1</sup>*Harbin Institute of Technology*; <sup>2</sup>*Chonbuk National University*

Ti-based alloys have been used as biomaterials, due to their excellent properties. Recently nontoxic elements  $\beta$  type Ti-based alloys cause researchers' interest because of their lower elastic modulus. But poor bioactivity of Ti-based alloys becomes a problem. Hydroxyapatite(HA) has tightly combination ability with bones tissue. However, poor mechanical properties limit their application. In present paper,  $\beta$  type TiNbSn-HA composites were fabricated by mechanical alloying and sintering. These composites are expected to integrate advantages of TiNbSn alloy and HA. Elastic modulus, compression strength, wear resistance and microstructure of composites were investigated. XRD and DSC results showed that Ti was suggested to be fully transformed from  $\alpha$  phase to  $\beta$  phase after 12h milling, transform temperature was 380.06°C. TEM results indicated that nanostructure was obtained. With the increase of Sn content, composites' microstructure changed. Compression test and wear test results indicated that composites had lower elastic modulus and superior mechanical properties.

#### 3:25 PM

**Physical Principles and Technological Tools for the Control of Densification, Shape and Diffusion Bonding during HIP of Metal Powders And Ceramics:** *Charles Barre*<sup>1</sup>; *Viktor Samarov*<sup>1</sup>; *Dmitry Seliverstov*<sup>1</sup>; *Evgeny Khomyakov*<sup>1</sup>; *Roman Haykin*<sup>1</sup>; <sup>1</sup>*Synertech PM Inc.*

The process to manufacture complex-shaped homogeneous or diffusion bonded products using Hot Isostatic Pressing (HIP) of powder materials is utilizing a suit of the advanced technologies related to this consolidation process. The most essential of them is advanced computer modeling that enables to provide very complex shapes and a significant reduction of development and manufacturing costs. The suit also includes design of the HIP tooling to provide cost efficient manufacturing solutions and non-destructive inspection for complex shape parts with cavities. The paper analyses, the physical principles and technological tools for the control of densification, shape, mechanical properties and diffusion bonding of large and complex shape parts during HIP of various metal powders and ceramics.

#### 3:45 PM Break

#### 3:55 PM

**Effect of HCl Concentration on ZrB<sub>2</sub> Separation from a Self-Propagating High-Temperature Synthesis (SHS) Product:** *Burcu Akkas*<sup>1</sup>; *Murat Alkan*<sup>1</sup>; *Bora Derin*<sup>1</sup>; *Onuralp Yucel*<sup>1</sup>; <sup>1</sup>*Istanbul Technical University*

The self-propagating high-temperature synthesis (SHS) of zirconium diboride followed by hydrochloric acid leaching was carried out in this study. In the SHS stage, the initial mixture of B<sub>2</sub>O<sub>3</sub>, ZrO<sub>2</sub> and Mg powders were ignited and then a mixture of the ZrB<sub>2</sub>, MgO, Mg<sub>3</sub>B<sub>2</sub>O<sub>6</sub> and Mg<sub>2</sub>B<sub>2</sub>O<sub>5</sub> were formed. In the leaching step, the SHS product was leached in the acid solution to remove impurities i.e. MgO, Mg<sub>3</sub>B<sub>2</sub>O<sub>6</sub> and Mg<sub>2</sub>B<sub>2</sub>O<sub>5</sub>. The effects of temperature and acid concentration on the selective leaching were investigated. The obtained products were characterized by using X-ray diffraction and SEM techniques.

#### 4:15 PM

**Microwave Sintering of Different Aluminum Alloy Powders and Their Characterization:** *Padmavathi Chandran*<sup>1</sup>; *A Upadhyaya*<sup>1</sup>; *Dinesh Agrawal*<sup>2</sup>; <sup>1</sup>*Indian Institute of Technology, Kanpur, India*; <sup>2</sup>*The Pennsylvania State University*

Microwave processing has been emerged as a well recognized processing technique due to its advantages such as rapid heating rates, time savings, reduction in processing temperature, energy, and environmental friendly. The present work investigates the densification behaviour, microstructural and phase evolution during microwave sintering of various grades of aluminum alloy powders using multimode furnace operating at 2.45GHz. The microwave sintering resulted in approximately 55% reduction in processing time as compared with conventional sintering. The microwave sintered samples exhibited the higher densification response and absence of intermetallic phases as when compared with conventional counterparts. Keywords: P/M Al alloy, multimode-microwave sintering, densification behavior, microstructural aspects, phase transformation.

#### 4:35 PM

**Die-Press and Sinter Processing of Armstrong Process® CP-Ti and Ti-6Al-4V Powders for Near-Net-Shape Manufacturing:** *Wei Chen*<sup>1</sup>; *Yukinori Yamamoto*<sup>1</sup>; *Stephen Nunn*<sup>1</sup>; *Jim Kiggans*<sup>1</sup>; *Michael Clark*<sup>1</sup>; *Sarma Gorti*<sup>1</sup>; *Adrian Sabau*<sup>1</sup>; *William Peter*<sup>1</sup>; *Craig Blue*<sup>1</sup>; *Brian Fuller*<sup>2</sup>; *Kamal Akhtar*<sup>2</sup>; <sup>1</sup>*Oak Ridge National Laboratory*; <sup>2</sup>*Cristal US, Inc. / International Titanium Powder*

This work investigates the die-pressing and sintering processes of new titanium and titanium pre-alloyed powders made by Armstrong Process® technology. The CP-Ti and Ti-6Al-4V powders were uniaxially die-pressed at designated pressures up to 100 ksi to form disk samples with varying aspect ratios (thickness to diameter). Samples with high aspect ratios tended to exhibit non-uniform green density along the pressing axis. This led to non-uniform shrinkage after sintering, forming disks of an hourglass shape. In addition, the sintering shrinkage of diameter tended to be higher than that of thickness for all samples. Effects of multiple different die-pressing techniques such as holding and repeated pressure strikes were performed to obtain desired sample shape after sintering. In-situ and ex-situ sintering were also performed to record the powder morphology change. This research was sponsored by the U.S. DOE, Office of EERE Industrial Technologies Program, under contract DE-AC05-00OR22725 with UT-Battelle, LLC.

## Recent Developments in the Processing, Characterization, Properties and Performance of Metal Matrix Composites: Multimodal, Processing and Microstructure

Sponsored by: The Minerals, Metals and Materials Society  
Program Organizers: Martin Pech-Canul, Centro de Investigacion y de Estudios Avanzados del Instituto Politecnico Nacional; Zariff Chaudhury, Arkansas State University; Golam Newaz, Wayne State University

Monday PM Room: 6A  
February 28, 2011 Location: San Diego Conv. Ctr

Session Chair: Zariff Chaudhury, Arkansas State University

**2:00 PM**  
**Effect of Al+B4C Agglomerate Size on Mechanical Properties of Trimodal Aluminum Metal Matrix Composites:** *Bo Yao*<sup>1</sup>; Travis Patterson<sup>1</sup>; Yongho Sohn<sup>1</sup>; Matthew Shaeffer<sup>2</sup>; Cory Smith<sup>3</sup>; Mark van den Bergh<sup>3</sup>; Kyu Cho<sup>4</sup>; <sup>1</sup>University of Central Florida; <sup>2</sup>The Johns Hopkins University; <sup>3</sup>DWA Aluminum Composites; <sup>4</sup>U. S. Army Research Laboratory

Trimodal aluminum (Al) metal matrix composites (MMCs) consisting of a nanocrystalline Al (ncAl) phase, B4C reinforcement particles, and a coarse grain Al (cgAl) phase contain multiscale microstructure and interfacial features that contribute to exceptional mechanical properties. One of the hierarchical microstructural features within the composite, namely the ncAl+B4C agglomerates formed during cryomilling, is an important feature whose size can range from tens of micro-meters to millimeters. This paper reports a study on the influence of the ncAl+B4C agglomerate size on the dynamic compressive strength of the trimodal Al MMCs. A desired hierarchical microstructure for high-strength of Al MMCs is identified to contain uniformly distributed relatively small ncAl+B4C agglomerates. Commercial-scale fabrication process to achieve this microstructure includes size classification by sieving the cryomilled ncAl+B4C agglomerates.

**2:20 PM**  
**Alternate Processing of Trimodal Aluminum Composites:** *Joseph Paras*<sup>1</sup>; Deepak Kapoor<sup>1</sup>; Tony Zahrah<sup>2</sup>; Rod Rowland<sup>2</sup>; <sup>1</sup>U. S. Army ARDEC; <sup>2</sup>Matsys Inc.

The Trimodal Aluminum 5083-Boron Carbide (Al5083-B4C) system has generated much military interest due to the composite's light weight and high strength. The system has traditionally been processed through powder metallurgy means via cryomilling, resulting in long processing times. In an effort to make the process more efficient, we have explored dry high energy milling as an alternate process. Preliminary results indicate that there is very little difference between cryomilled Bimodal Al5083-B4C and dry milled Bimodal Al5083-B4C. It was also observed that poor bonding can exist between the bimodal composition and the coarse-grained Al5083 when consolidated. This was remedied by light milling of the coarse-grained Al5083 to break the nascent oxide layer and provide a clean metallurgical interface. Evidence of the increased bonding is seen in the fracture surfaces, and mechanical testing has shown a 10% increase in compressive strength and a 30-50% increase in ultimate failure strain.

**2:40 PM**  
**Effect of Layered Interface on Mechanical Behaviors in TiO2 Nano-Particle Reinforced Aluminum Matrix Composites:** *Jaehyuck Shin*<sup>1</sup>; Hyunjoon Choi<sup>1</sup>; Donghyun Bae<sup>1</sup>; <sup>1</sup>Yonsei University

Interface characteristics, with their mechanical behaviors, have been investigated for aluminum based composites reinforced with titanium dioxide nano-particles (TiO<sub>2</sub>, 20 nm). The composites are produced by hot rolling the ball-milled mixture of Al powders and TiO<sub>2</sub> nano-particles. During a milling process, TiO<sub>2</sub> nano-particles are gradually dispersed and embedded within the Al powders. After the subsequent annealing process, an interface layer composed of TiO and □-Al<sub>2</sub>O<sub>3</sub> has newly formed between the TiO<sub>2</sub>

nano-particles and the aluminum matrix. The composites show significant increase in yield strength with increasing volume fraction of TiO<sub>2</sub> nano-particles (514 MPa with 5vol.% TiO<sub>2</sub> nano-particle), and the semi-coherent interface layer between the Al matrix and the TiO<sub>2</sub> nano-particle enables the nucleation of dislocation at the particle/matrix interface during the plastic deformation. Mechanical properties with the variation of volume fraction of TiO<sub>2</sub> nano-particles and their deformation behaviors will be presented.

**3:00 PM**  
**Fabrication of Extruded Aluminum Composites Reinforced by Vapor Grown Carbon Nanofibers and Characterization, Modeling of Their Properties:** *Fumio Ogawa*<sup>1</sup>; Toshiyuki Nishimura<sup>2</sup>; Chitoshi Masuda<sup>1</sup>; <sup>1</sup>Waseda University; <sup>2</sup>National Institute for Materials Science

Aluminum composites reinforced by vapor grown carbon nanofibers (VGCNF) are expected to be used as thermal management devices and structural parts due to high strength and thermal conductivity of VGCNF e.g. about 2000W/mK along fiber direction. However, because of transverse anisotropy of VGCNF e.g. about 30W/mK transverses to fiber direction, it is expected their properties strongly depend on fiber orientation. In this study, composites were fabricated by powder metallurgy and extruded to control fiber orientation. Microstructure such as orientation, length of VGCNF, porosity in matrix was investigated. And relation of them with extrusion condition was discussed. Strength, thermal conductivity along and transverse to extrusion direction were measured and effect of orientation, anisotropy of VGCNF on them was studied. Modeling of their properties as function of fiber anisotropy, fiber aspect ratio, matrix and interface was conducted and mechanism of reinforcing and heat transfer in composites was discussed.

**3:20 PM**  
**Multi-Scale Modeling on the Mechanical Behavior of Aluminum-Based Metal-Matrix Nano Composites (MMNCs):** *Changsoo Kim*<sup>1</sup>; Pradeep Rohatgi<sup>1</sup>; Amirreza Sanaty-Zadeh<sup>1</sup>; <sup>1</sup>University of Wisconsin Milwaukee

A systemic, multi-scale computational model has been developed to describe mechanical behavior of metal-matrix nano composites (MMNCs). The modeling begins by using nano-scale (molecular dynamics, MD) simulations for the quantitative evaluation of material properties and dislocation movements. The results from MD simulations are then incorporated as a basis for the meso-scale (finite element analysis, FEA) simulations to predict mechanical performance and failure of MMNCs. Pseudo-plastic failure has been approximated for the fracture of MMNCs. Using this model, the influence of microstructural features such as fine, coarse grain sizes, fine-to-coarse heterogeneous multi-modal phase ratio, and the type, shape, contents of reinforcement particles on the macroscopic mechanical performance can be quantitatively characterized. The developed algorithm has been applied to Aluminum-based (Al) fine/coarse multi-modal MMNCs that are reinforced with SiC and/or B4C particles. The presentation will elucidate the potential failure mechanisms and propose optimized microstructures of these Al MMNC systems.

**3:40 PM Break**

**4:00 PM**  
**Strain Induced Grain Growth of Cryomilled Nanocrystalline Al in Tri-Modal Al Composites during Forging:** *Bo Yao*<sup>1</sup>; Cory Smith<sup>2</sup>; Mark van den Bergh<sup>2</sup>; Bhaskar Majumdar<sup>3</sup>; Yongho Sohn<sup>1</sup>; <sup>1</sup>University of Central Florida; <sup>2</sup>DWA Aluminum Composites; <sup>3</sup>New Mexico Institute of Mining and Technology

This report presents our study on the grain growth of nanocrystalline aluminum (NC-Al) in tri-modal Al metal-matrix-composites (MMCs) under forging process. The NC-Al phase formed through cryomilling in liquid nitrogen atmosphere exhibits an excellent thermal stability when annealed without applied stress. However, grain growth was observed when the Al MMCs were forged at temperatures where the NC-Al grain growth might have remained stable without applied stress. The influence of strain and temperature on the NC-Al grain growth during forging is presented. The grain growth activation energy with forging is lower than that without any

applied stress. The role of pinning effect by dispersoids and impurities at grain boundaries is presented and discussed.

#### 4:20 PM

**Origin of High Strength in a Micro-Alloyed Ferritic Steel:** *Hesamaldin Askari*<sup>1</sup>; Yong Shen<sup>2</sup>; C. Wang<sup>2</sup>; Xin Sun<sup>3</sup>; Hossein Zbib<sup>1</sup>; <sup>1</sup>Washington State University; <sup>2</sup>Northeastern University; <sup>3</sup>Pacific Northwest National Laboratory

The strengthening role of carbide precipitates in a high strength ferritic steel with finely dispersive precipitates was investigated using a combined experimental and modeling approach. Using EDXS and TEM, fine carbides with an average diameter of 10 nm were observed in the ferrite matrix of the 0.08%Ti steel, as well as some cubic M23C6 precipitates at the grain boundaries. The dual precipitate structure provides combined matrix and grain boundary strengthening. The increase in strength due to precipitation is 2-3 times higher than the conventional high strength steels depending on the average size and distance of the nanoscale precipitates. The effects of the particle size and density on the strength have been investigated through Dislocation Dynamics simulations. The DD simulations and experimental analysis showed that the finely dispersive precipitates can strengthen the steel by pinning the dislocations up to a critical shear stress and retarding the recovery and annihilation of dislocations.

#### 4:40 PM

**Synthesis of MWCNT Reinforced Al Based Nanocomposite Via Spark Plasma Sintering:** *Tapas Laha*<sup>1</sup>; Lakshmikanth Reddy<sup>1</sup>; Anup Keshri<sup>2</sup>; Devrupa Lahiri<sup>2</sup>; Anway Maiti<sup>1</sup>; <sup>1</sup>Indian Institute of Technology; <sup>2</sup>Florida International University

A trend has been perceived in the field of composite materials to employ carbon nanotubes as reinforcement in synthesizing composites of unique properties. In this endeavor, Al-based nanostructured composite with carbon nanotubes, as second phase particles, has been synthesized by combination of two novel processing techniques, viz. Cryomilling and Spark Plasma Sintering. Scanning electron microscopy and quantitative image analysis has been performed to understand the microstructural evolution and to verify the retention of carbon nanotubes. Nanoindentation and microhardness test have been carried out to obtain the effective elastic modulus and hardness of the consolidated samples. Tribological study on the nanocomposites has been done in order to understand the effect of CNT reinforcement on the mechanical properties. The characterization affirms the retention of carbon nanotubes in the nanocomposites. Raman spectroscopy revealed that the MWCNTs were partially damaged during cryomilling.

#### 5:00 PM

**Effects of SPS Parameters on the Mechanical Properties and Microstructures of Titanium Reinforced with Multi-Wall Carbon Nanotubes Produced by Hot Extrusion:** *Thotsaphon Threrujirapong*<sup>1</sup>; Katsuyoshi Kondoh<sup>1</sup>; Junko Umeda<sup>1</sup>; Bunshi Fugetsu<sup>2</sup>; <sup>1</sup>Osaka University; <sup>2</sup>Hokkaido University

The effects of spark plasma sintering (SPS) temperature and time on the mechanical properties and microstructures of titanium (Ti) reinforced with multi-wall carbon nanotubes (MWCNTs) were investigated. The Ti powders were coated with MWCNTs via a wet process using a zwitterionic surfactant solution containing 2.0 wt.% of MWCNTs. The coated Ti powders were consolidated by SPS process at various temperatures and times. All sintered billets were subsequently extruded at 1000°C. The mechanical properties responses of these extruded Ti composites showed the decrease of yield and tensile strength when higher consolidation temperatures were used. The microstructures of those Ti composites were observed using optical microscopy and scanning electron microscopy. All of the results were used to select the suitable condition for fabrication of Ti/MWCNTs composite materials.

#### 5:20 PM

**On the Methods for Grain Size Analysis and Grain Growth Kinetic Studies for a Thermally Stable Al 5083 Nanocomposite:** *Leyla Hashemi-Sadraei*<sup>1</sup>; S. E. Mousavi<sup>1</sup>; Rustin Vogt<sup>1</sup>; Ying Li<sup>1</sup>; Zhihui Zhang<sup>1</sup>; Enrique Lavernia<sup>1</sup>; Julie Schoenung<sup>1</sup>; <sup>1</sup>University of California Davis

A nanocomposite of Al 5083 and B<sub>4</sub>C was fabricated by cryomilling the powders for 24 hours. Powders annealed at temperatures as high as approximately 0.9 T<sub>m</sub> were investigated for grain growth and were found to exhibit superior thermal stability compared to Al 5083 powders without B<sub>4</sub>C that were cryomilled for shorter durations. The high thermal stability was attributed to the pinning effect of ultrafine secondary dispersoids residing on grain boundaries. Several approaches were evaluated, on the basis of X-ray diffraction and transmission electron microscopy, in order to determine average grain sizes. Grain size results from alternative X-ray-based methods were utilized in order to study grain growth mechanisms by fitting grain growth curves to established equations. Two distinct temperature-dependent grain growth regimes were observed. By comparing the kinetic results achieved when using different grain size calculation methods, the relevance and applicability of each method is described.

### Size Effects in Mechanical Behavior: Size Effects in Multilayer Structures

*Sponsored by:* The Minerals, Metals and Materials Society, Not Applicable, TMS: Nanomechanical Materials Behavior Committee  
*Program Organizers:* Erica Lilleodden, GKSS Research Center; Amit Misra, Los Alamos National Laboratory; Thomas Buchheit, Sandia National Laboratories; Andrew Minor, UC Berkeley & LBL

Monday PM  
February 28, 2011

Room: 2  
Location: San Diego Conv. Ctr

*Session Chairs:* Amit Misra, LANL; Jian Wang, Los Alamos National Laboratory

#### 2:00 PM

**A Quantized Crystal Plasticity Finite Element Model for Nanoindentation: Size Effect from Discrete Plasticity:** *Lin Li*<sup>1</sup>; Myoung-Gyu Lee<sup>2</sup>; Peter Anderson<sup>1</sup>; <sup>1</sup>The Ohio State University; <sup>2</sup>Pohang University of Science and Technology

Quantized crystal plasticity (QCP) simulations are employed to study a distinctive observation from an in-situ nanoindentation test on nanocrystalline Al. This displacement controlled indentation test shows that the sample surface recedes even faster than the rate of indenter as a consequence of incipient dislocation events. This direct experimental observation emphasizes the discrete nature of dislocation slip in a confined volume. The QCP model incorporates such a feature showing that the plastic shear strain can jump by discrete amounts that scale as 1/grain size. This unique feature is motivated by recent molecular dynamics results, showing that the grain averaged shear strain jumps ~1% as a dislocation unstably traverses a grain. This quantized aspect enables the QCP model to simulate the load-displacement trace and the underlying slip pattern during indentation. Also, the grain size effect on indentation response can be assessed through a comparison of the conventional and quantized simulations.

#### 2:20 PM

**Size Effects in Fatigue of Cu/Ta Multilayers:** *Guangping Zhang*<sup>1</sup>; Xiaofei Zhu<sup>1</sup>; Jiawei Yan<sup>1</sup>; Jin Xu<sup>1</sup>; <sup>1</sup>Chinese Academy of Sciences

Although strengthening and deformation mechanisms of metallic multilayers with different length scales ranging from microns to nanometers are investigated extensively, fatigue behavior of the metallic multilayers is known little. Here we present a systematic investigation of fatigue properties of Cu/Ta multilayers deposited on a flexible polyimide substrate. We will show that fatigue resistance of the multilayers gradually increases with decreasing individual layer thickness from 500 nm to 20 nm. Microscopic characterization reveals an evident transition of fatigue damage from typical



bulk-like extrusions/intrusions to boundary-localized behavior. Such size effects in fatigue are evaluated and compared with recent findings of fatigue of thin metal films constrained by a substrate as well as unconfined small-volume metals.

**2:40 PM**

**Microstructure and Strengthening Mechanisms of Highly Textured Cu/Ni Multilayers:** *Yue Liu*<sup>1</sup>; Dan Bufford<sup>1</sup>; Haiyan Wang<sup>1</sup>; Cheng Sun<sup>1</sup>; Xinghang Zhang<sup>1</sup>; <sup>1</sup>Texas A&M University

We report on the synthesis of sputtered, highly (111) and (100) textured Cu/Ni multilayers with individual layer thickness, *h*, varying from 1 to 200 nm. At greater *h*, XRD patterns of Cu and Ni (100) (or (111)) peaks are clearly separated indicating that the existence of semi-coherent interface. When *h* decreases to 10 nm or less, XRD spectra show significant peak distortions due to coherency stress. High resolution TEM studies confirm the coexistence of twin and coherent layer interfaces in highly (111) textured Cu/Ni multilayers. Multilayer hardnesses increase with decreasing *h*, approach a maxima at *h* of 2.5-5 nm, and show softening thereafter. A detail comparison between (111) and (100) textured Cu/Ni is made in both microstructure and strengthening mechanisms. The influences of both coherent layer interfaces and twin interfaces on strengthening mechanisms are discussed.

**3:00 PM**

**Hardening in He Ion Implanted V/Ag Multilayers:** *Qiangmin Wei*<sup>1</sup>; Nathan Mara<sup>1</sup>; Michael Nastasi<sup>1</sup>; Amit Misra<sup>1</sup>; <sup>1</sup>LANL

Hardness before and after irradiation as a function of layer thickness on sputter-deposited V/Ag multilayers, as well as pure Ag and V, was measured by nano-indentation. Radiation-induced hardening was found to decrease with decreasing individual layer thickness. No significant radiation hardening was observed at layer thickness less than 6 nm within the error limit of equipment. A model describing radiation effects on the hardness of multilayers with length scale from micrometer to less than one nanometer was developed on the basis of Freidel model and confined layer slip (CLS) model. At layer thickness larger than 50 nm, hardening from He bubbles dominates. With decreasing layer thickness, hardening from the interfaces becomes dominant with less contribution from He bubbles.

**3:20 PM Invited**

**Deformation Mechanisms of Nanoscale Multilayers:** *Jian Wang*<sup>1</sup>; Amit Misra<sup>1</sup>; <sup>1</sup>LANL

Nanoscale metallic multilayer composites exhibit relatively high flow strengths in comparison with bulk polycrystalline materials due to the presence of the high density of interfaces in composites. The flow strength of composite materials produced in this way increases as decreasing the thickness of individual layers. The systematic study regarding deformation mechanisms of layered composites from experimental measurements to theoretical and numerical studies, suggests that crossing of dislocations across interfaces becomes an important unit process at layer thicknesses in the range of a few nanometers, in turn, implying that interface structures and the resultant properties of interfaces play a vital role in determining material strength. The difficulty of crossing of dislocations across interfaces is ascribed to different mechanisms with respect to interface types. Using atomistic simulations, deformation mechanisms in nanolayered materials, such as Cu/Nb layered composites are discussed. Weak interface strengthening mechanisms are developed and examined.

**3:50 PM Break**

**4:20 PM**

**Fundamental Investigation of Deformation Using Spherical Indentations and 3D X-Ray Microscopy:** *Bennett Larson*<sup>1</sup>; Jon Tischler<sup>1</sup>; Yanfei Gao<sup>2</sup>; <sup>1</sup>Oak Ridge National Laboratory; <sup>2</sup>Oak Ridge National Laboratory, University of Tennessee Knoxville

3D x-ray microscopy measurements of the spatially confined lattice distortions under spherical indentations provide an opportunity for fundamental investigations of deformation on mesoscopic length scales and detailed testing of finite element crystal plasticity simulations of deformation in crystalline materials. Direct comparisons of 3D x-ray microscopy

measurements of deformation below 100 mN, 100 micron radius spherical indents in (100), (110), and (111) oriented Cu with crystal plasticity simulations have shown remarkable overall agreement. However, both qualitative and quantitative differences are found to exist between measured and simulated local rotational distortion components and geometrically necessary dislocation density patterns. Strong, depth dependent dislocation patterning under indents provides a further fundamental challenge to deformation simulations. Research sponsored by the Division of Materials Sciences and Engineering, Office of Basic Energy Sciences, U.S. Department of Energy.

**4:40 PM**

**Structure and Hardness of Aged Ti-W Multilayer Films:** *Ross Economy*<sup>1</sup>; Marian Kennedy<sup>1</sup>; <sup>1</sup>Clemson University

Metallic multilayer film systems are being studied for potential use in microelectromechanical systems and freestanding high-strength structures. Control of layer thickness has been shown to influence the mechanical response by controlling dislocation slip. Only a few groups, however, have looked at the influence of aging and porosity on the mechanical properties of these multilayer systems. As a result, this study will look at the influence of film porosity and thermal aging on the properties of Ti-W multilayer systems. 500nm Ti, W, and nano-porous Ti thin films, as well as multilayer Ti-W systems (20nm layers), were deposited onto Si(100) via magnetron sputtering. SEM and AFM were used to characterize film morphology and microstructure. Hardness was characterized using nanoindentation. Initial data shows that multilayer film systems exhibit an increase in hardness of ~200% when compared with bulk W and a slight decrease when compared to the W films.

**5:00 PM**

**Flow Stress Partitioning in Two-Phase Metallic Composites at Decreasing Phase Length Scales:** *Rainer Hebert*<sup>1</sup>; Girija Marathe<sup>1</sup>; <sup>1</sup>University of Connecticut

Repeated cold-rolling and folding of metallic multilayers generates two-phase composite materials with continuously decreasing length-scales in the layer thickness direction. Within a few rolling and folding passes, the layer thickness decreases for systems such as Cu-Ni from the micrometer to the nanometer scale. Instrumented indentation measurements are used to probe the hardness and flow stresses of the individual layers at increasing strain levels. During the initial stages, i.e. at the micrometer scale for the layer thickness, the indentation measurements allow for studies of the impact of the strain compatibility between the layers on the flow stress evolution. The strain compatibility between the layers modifies the work-hardening behavior and the observed changes in the flow stress evolution are discussed in light of crystal plasticity models based on geometrically necessary dislocations. The results reveal a mutual impact between the mechanical properties of the individual layers and the geometry of the layer arrangement.

**5:20 PM**

**Film Thickness Effects on Interfacial Failure in Polymer Metal Thin Film Structures:** *Neville Moody*<sup>1</sup>; Markus Ong<sup>2</sup>; E. David Reedy Jr.<sup>1</sup>; Edmundo Corona<sup>1</sup>; David Adams<sup>1</sup>; John Yeager<sup>3</sup>; David Bahr<sup>3</sup>; <sup>1</sup>Sandia National Laboratories; <sup>2</sup>Whitworth University; <sup>3</sup>Washington State University

Interfaces are the critical feature governing performance of polymer-metal thin film structures where differing properties between adjacent films can induce strong interlaminar stresses and catastrophic failure. We are studying these effects in a model system created by spin coating 10 to 650nm thick PMMA films onto copper coated silicon substrates followed with a sputter deposited overlayer of highly stressed tungsten. The high film stresses triggered spontaneous delamination and buckling along the PMMA-tungsten interface accompanied by intense deformation in the PMMA layers that varied markedly between each system studied and from model elastic behavior. In this presentation we will use crack growth simulations and comparison to metal film structures to show that film compliance provides a lower bound to behavior for all samples while constrained yielding accounts for the pronounced differences in behavior between samples. This work was

supported by Sandia National Laboratories through USDOE NNSA Contract DE-AC04 94AL85000.

#### 5:40 PM

**Size Effect in Cleavage Cracking in Polycrystalline Thin Films:** *Yu Qiao*<sup>1</sup>; Weiyi Lu<sup>1</sup>; <sup>1</sup>University of California San Diego

As a cleavage crack front propagates across a wide high-angle grain boundary, it would first penetrate across a number of break-through points, and the persistent grain boundary areas would then be separated through shear fracture or ligament bending. Therefore, as the film thickness is smaller than the characteristic distance between the break-through points, which is often in the range of 1-5 microns, the crack front transmission can be significantly confined by the film surfaces leading to an either beneficial or detrimental size effect. That is, the fracture toughness of the polycrystalline thin film is not a material constant; rather, it highly depends on the film thickness. This concept was recently validated in our bicrystal thin film testing.

### Surfaces and Heterostructures at Nano- or Micro-Scale and Their Characterization, Properties, and Applications: Growth, Characterization, and Devices II - and - Coatings, Surfaces, and Interfaces I

*Sponsored by:* TMS Electronic, Magnetic, and Photonic Materials Division, TMS Materials Processing and Manufacturing Division, TMS: Nanomaterials Committee, TMS: Surface Engineering Committee

*Program Organizers:* Nitin Chopra, The University of Alabama; Ramana Reddy, The University of Alabama; Jiyoung Kim, Univ of Texas; Arvind Agarwal, Florida International Univ; Sandip Harimkar, Oklahoma State University

Monday PM  
February 28, 2011

Room: 31B  
Location: San Diego Conv. Ctr

*Session Chairs:* Nitin Chopra, The University of Alabama; Jiyoung Kim, University of Texas at Dallas; Sandip Harimkar, Oklahoma State University; Arvind Agarwal, Florida International University

#### 2:00 PM Invited

**On the Role of Interface Engineering in Future Technology Applications:** *Aarthi Venkateshan*<sup>1</sup>; Rajendra Singh<sup>2</sup>; <sup>1</sup>Canon Anelva Corporation; <sup>2</sup>Clemson University

The global need for high performance, low power computing continues as a major driver of the semiconductor industry. A decade ago, Moore's Law scaling meant oxide thickness, transistor length and width were scaled by factor (1/k) to provide delay improvement 1/k at constant power density. In subsequent generations, performance enhancers were added to drive the transistor roadmap forward. The continued decrease in feature sizes means management of interfaces will play an important role in future scaling. High quality ZrO<sub>2</sub> high-k films were grown, EOT 1.4 nm 1V leakage current density 1.83 10<sup>-11</sup> A/cm<sup>2</sup> was observed. For Al<sub>2</sub>O<sub>3</sub> of EOT 1.04 nm at 1 V leakage current density 5.71 10<sup>-11</sup> A/cm<sup>2</sup> was achieved. We report results of EOT 0.39 nm HfO<sub>2</sub> with leakage current density 1.0 10<sup>-12</sup> A/cm<sup>2</sup> for gate voltage -3 to +3 V. Based on DOE and process variation data, process is robust and will transfer from laboratory to manufacturing environment.

#### 2:30 PM Invited

**Role of Rapid Photothermal Processing in Providing Homogenous Nanostructure of Silica Clad Silicon Fibers:** *Rajendra Singh*<sup>1</sup>; Nishant Gupta<sup>1</sup>; T. Wade Hawkins<sup>1</sup>; Paul Foy<sup>1</sup>; Colin McMillen<sup>1</sup>; Stephanie Morris<sup>1</sup>; Robert Rice<sup>2</sup>; Kelvin Poole<sup>1</sup>; John M. Ballato<sup>1</sup>; <sup>1</sup>Clemson University; <sup>2</sup>Northrop Grumman Space Technology

The recent realization of silicon core optical fibers has the potential for rack-to-rack optical interconnects in integrated optoelectronic applications. Incoherent light source based rapid photothermal processing was used to carry out ex-situ annealing on the as-drawn silicon core optical fibers. The

dark current-voltage characteristics of annealed silicon fibers diodes showed lower leakage current than the diodes based on as drawn fibers. X-ray diffraction examination of the crystal structure of as-drawn fiber of 5 mm length showed 3 mm stretch of single crystal Si and 2 mm of polycrystalline material. On the other hand, the entire 10 mm length of the annealed sample was crystalline. The role of rapid photothermal processing in obtaining homogenous nanostructure of the silica clad silicon fiber will be presented. Structural, electrical, and optical characterization of annealed and as-drawn fibers will be presented. This work is supported by Northrop Grumman Corporation.

#### 3:00 PM

**High Surface Metal/Metal Nano-Microstructured Porous Monoliths:** *Martin Bakker*<sup>1</sup>; Franchesca Maddox Saylor<sup>1</sup>; Amy Grano<sup>1</sup>; Keana Graves<sup>1</sup>; <sup>1</sup>The University of Alabama

Porous metal electrodes are of interest in a wide range of electrochemical processes. We report here on a versatile process for making a range of such electrodes using a porous silica template. The porous silica monoliths are produced by a sol-gel process with PEO polymer and cationic surfactant added to give porosity at nanometer and micrometer length scales. Metal nitrates are infiltrated into the silica monolith either as a saturated solution or as a melt. Decomposition under hydrogen results in formation of metal replicas. By controlling the number of infiltration cycles, the extent of replication can be controlled. By changing the metal salt used between infiltration cycles, heterostructures consisting of nanostructures of one metal on a continuous microstructure of a second metal can be produced. Typical surface areas are 40-90 m<sup>2</sup>/g. Significant variations in pore size distributions are found for different metals and for different methods of producing the metals.

#### 3:15 PM Break

**3:25 PM Introductory Comments for Coatings, Surfaces, and Interfaces I**

#### 3:30 PM Invited

**Microstructural Evolution in NiAlCrHf and NiAlCrZr Coated Superalloys:** *Mark Weaver*<sup>1</sup>; Joel Alfano<sup>1</sup>; <sup>1</sup>The University of Alabama

Coated Ni based superalloys are used for power generation due to their ability to function in oxidative and corrosive environments. However, it is well known that the microstructures of these coated systems change in service due to interactions with the environment and interdiffusion with the underlying substrate. In this study, NiAlCr-(Hf,Zr) overlay coatings were produced via dc magnetron sputtering. Post-deposition annealing in a mixture of Ar+5%H<sub>2</sub> and oxidation in laboratory air produced microstructural and chemical changes within the coating/substrate systems which significantly influenced their performance. The purpose this presentation is to describe the results of a study to quantify the microstructural changes occurring in NiAlCrHf and NiAlCrZr coated superalloys in comparison with (Ni,Pt)Al coated superalloys tested under the same conditions.

#### 4:00 PM Invited

**Nature of the B2 Phase in Sputter-Deposited 304 Stainless Steel + 10 wt.% Al Coatings:** U.M.R. Seelam<sup>1</sup>; C. Suryanarayana<sup>1</sup>; T. Ohkubo<sup>2</sup>; Kazuhiro Hono<sup>2</sup>; N. S. Cheruvu<sup>3</sup>; <sup>1</sup>University of Central Florida; <sup>2</sup>National Institute for Materials Science; <sup>3</sup>Southwest Research Institute

A Fe-18Cr-8Ni-10Al (wt.%) coating was deposited on a 304-type austenitic stainless steel substrate by magnetron sputtering technique using SS304 and Al targets. The as-deposited coatings were characterized by XRD, SEM, TEM, and 3DAP techniques. The coating consists of columnar grains with alpha-ferrite and B2 phase particles uniformly distributed. It also has a deposition-induced layered structure with two alternate layers (of 3.2 nm wavelength), one rich in Fe and Cr, and the other rich in Al and Ni. Conventional TEM techniques were able to provide the general microstructural features of the coating, but it was not able to determine the exact nature and chemistry of the B2 phase; 3DAP studies helped in unambiguously identifying that the B2 phase is NiAl. Based on the above

results, it was concluded that NiAl is the preferred phase over FeAl, further correlated with the heats of mixing among Fe, Ni, and Al elements.

#### 4:30 PM Invited

**The Solution Precursor Plasma Spray Process for Depositing Multi-Functional, Nanoscale Coatings:** *Maurice Gell*<sup>1</sup>; Eric Jordan<sup>1</sup>; <sup>1</sup>University of Connecticut

The Solution Precursor Plasma Spray Process (SPPS) is a highly flexible process that can deposit single- or multi-phase oxide coatings for functional applications. The coating microstructure is on the nanoscale and is compositionally homogeneous. In this presentation, the SPPS process and its utility to fabricate multi-functional materials will be described. Comparisons will be made to alternate plasma spray processing methods, including those using powder and suspensions. The applications include: (a) thermal barrier coatings with a unique strain-tolerant microstructure, (b) coatings with in-situ sensors on the atomic scale, and (c) two-phase transparent ceramics that meet stringent optical and elevated temperature mechanical properties.

#### 5:00 PM

**Tribological Behavior of Spark Plasma Sintered Iron-Based Bulk Amorphous Alloys:** *Ashish Singh*<sup>1</sup>; Sandip Harimkar<sup>1</sup>; <sup>1</sup>Oklahoma State University

Amorphous alloys (BMG's) exhibit high-micro hardness, fracture toughness, and yield strength at ambient temperature. These properties result in good tribological behavior of BMG's and make it a potential material for high performance wear resistance applications. Spark plasma sintering technique is used to fabricate fully amorphous and in-situ bulk amorphous matrix composites near crystallization temperature of the alloy. Sintered samples exhibited heterogeneous microstructure which involves nano crystallized phases embedded in-between amorphous matrix. Frictional and wear behavior of spark plasma sintered iron based BMG's are investigated under dry sliding conditions. Wear behavior of sintered specimens are analyzed at different normal loads and rotational speeds. The surface roughness, coefficient of friction, and wear loss of the wear tested samples are studied.

## The Second Symposium on the Recycling of Electronic Wastes: Management and Technology Overview of Electronic Wastes

*Sponsored by:* The Minerals, Metals and Materials Society, TMS Electronic, Magnetic, and Photonic Materials Division, TMS Extraction and Processing Division, TMS Light Metals Division, TMS: Electronic Packaging and Interconnection Materials Committee, TMS: Recycling and Environmental Technologies Committee  
*Program Organizers:* Lifeng Zhang, Missouri University of Science and Technology; Gregory Krumdick, Argonne National Laboratory; Jaan Kers, Tallinn University of Technology; Thomas P. Schuman, Missouri University of Science and Technology (Missouri S&T); Markus Reuter, Ausmelt Limited

Monday PM Room: 15B  
February 28, 2011 Location: San Diego Conv. Ctr

*Session Chairs:* Jaan Kers, Tallinn University of Technology; Thomas Schuman, Missouri S&T; Markus Reuter, Ausmelt Limited

#### 2:00 PM

**Willingness to Recycle Electronic Waste: Results from a National Survey of U.S. Households:** *Jean-Daniel Saphores*<sup>1</sup>; Oladele Ogunseitan<sup>1</sup>; Andrew Shapiro<sup>2</sup>; <sup>1</sup>University of California Irvine; <sup>2</sup>Jet Propulsion Laboratory, California Institute of Technology

The fate of used electronic products (e-waste) is of increasing concern because of the toxicity of e-waste, its growing volume, and the environmental and public health consequences of its inadequate handling. The U.S. EPA estimates that e-waste has become the main contributor of lead (Pb) to landfills. Households also store large volumes of e-waste, yet little is known

about their willingness to recycle e-waste at the national level. This paper starts filling this gap based on a 2006 survey of U.S. households. Using multivariate models, we find that gender, education, convenience, moral considerations, environmental beliefs, and knowledge of e-waste toxicity, but neither income nor political affiliation, are key factors explaining people's willingness to drop off e-waste at recycling centers. Our results suggest targeting e-waste public education programs at younger adults and making recycling more convenient for older adults.

#### 2:30 PM

**Development of Technology for Recycling Valuable Metals from Electronic Wastes in Korea:** *Jae-chun Lee*<sup>1</sup>; Byung-Su Kim<sup>1</sup>; Min-seuk Kim<sup>1</sup>; Jinki Jeong<sup>1</sup>; Banshi Pandey<sup>2</sup>; <sup>1</sup>Korea Institute of Geoscience and Mineral Resources (KIGAM); <sup>2</sup>National Metallurgical Laboratory, CSIR

The generation of electronic wastes in Korea has been increasing significantly over the years. These wastes viewed previously as the source of contaminants for environment due to the hazardous materials are now recognized as the new resources termed as "urbane ore" because of presence of the valuable metals. The development of a sustainable recycling technology for electronic wastes is urgently required with the aim of environmental protection and secured supply of resources simultaneously. The commercial recycling technology of electronic wastes uses pyrometallurgical process to recover copper, gold and silver partially in the existing smelters. This paper elaborates the development of a combined process involving mechanical pretreatment and hydrometallurgical reclamation which has the advantage to recover not only copper but most rare metals as well. The research focus is on the development of the liberation technology using various pulverization methods along with the eco-friendly and energy-saving metal extraction – separation technology.

#### 3:00 PM

**State of the Art in the Recycling of Waste Printed Wiring Boards:** *Lifeng Zhang*<sup>1</sup>; <sup>1</sup>Missouri University of Science and Technology

Printed Wiring Board (PWB) is a platform upon which microelectronic components such as semiconductor chips and capacitors are mounted. It is also called printed circuit board (PCB). In the PWBs, the organic substances are approximately 72%. The main composition of organic substances in PWBs is ethoxylated resin bromide or ethoxylated resin chlorinate. Depending on the different application and design of the PWB, various metals may be used in the manufacturing process, including precious metals such as copper, lead, silver, gold, platinum, and toxic metals such as mercury, cadmium, barium, gallium, cadmium, lead, bismuth. The current paper reviewed the recycling process for waste PWB materials, including mechanical recycling, combustion for energy recovery and different pyrolysis processes, such as vacuum pyrolysis, atmospheric inert pyrolysis and flux pyrolysis process, and hydrometallurgical recycling process.

#### 3:30 PM

**Overview of Electronics Waste Management in India:** *Sandip Chatterjee*<sup>1</sup>; Krishna Kumar<sup>1</sup>; <sup>1</sup>Department of Information Technology

Growth of electronics waste (e-waste) and lack of appropriate disposal mechanism are the great concern for developing countries like India. The domestic generation of e-waste in India is rapidly growing with the development. The imported substance is also substantially contributing to the e-waste inventory. Recycling of e-waste is mainly carried out in unorganized units in India. The primitive recycling technique used by the unorganized sector is a great threat to the environment and the health of the operators involved in these profession. Therefore, improvement of technology used by these units towards a cost effective, environmental friendly alternative could be the solution to the present crisis. Few initiatives of recycling have, however, come up in recent years in organized units. The precious metals are still recycled in the developed countries. This report discusses the inventory, technology status, legal legislative and existing practices of e-waste management in India.



#### 4:00 PM Break

#### 4:10 PM

**Prospective Scenario of E-Waste Recycling in India:** Manis Kumar Jha<sup>1</sup>; Abhishek Kumar<sup>1</sup>; Vinay Kumar<sup>1</sup>; Jae-chun Lee<sup>2</sup>; <sup>1</sup>National Metallurgical Laboratory; <sup>2</sup>Korea Institute of Geoscience and Mineral Resources (KIGAM)

However, India is rich in ores and minerals, but e-waste recycling is necessary due to the report of national and international studies, which cautioned on the generation, treatment and accumulation of e-waste in India. Current data indicate that the total domestic e-waste generation, including imports, is around 382979 MT. However, waste available for recycling and actually recycled are 144143 MT and 19000 MT, respectively, in which recycling by non-formal and formal sector are 95% and 5%, respectively. On the other hand, India has developed an expertise in handling varieties of metallic wastes in an organized and safe manner. The development of individual processes or combined processes for handling the e-waste is underway. Eco- friendly and energy-saving processes are necessary to comply with stringent environmental regulations. The paper includes the recent trend of e-waste generation, recycling process and its future prospects particularly in India.

#### 4:40 PM

**From a Technical Marvel to a Hazardous Box: An Estimate of the Volumes of Potentially Toxic Materials in Obsolete TVs Stored by US Households Based on National Survey:** Natalia Milovantseva<sup>1</sup>; Jean-Daniel Saphores<sup>1</sup>; <sup>1</sup>University of California, Irvine

The increasing popularity of consumer electronics continues to present tough challenges for policy makers concerned with the risks for human health and the environment of improperly disposing of electronic waste (e-waste). In 2007, the EPA estimates that approximately 26.9 million TVs were discarded in the US alone, yet only 18 percent by weight was recycled; unfortunately, these numbers are very uncertain. Discarded cathode ray tube (CRT) TVs contain large amounts of lead but flat panel TVs contain some mercury and present new recycling challenges. It is important for public policy to get better estimates of the number of TVs currently in storage and of the quantity of potentially toxic materials they contain. This paper relies on count models to analyze the data from a national survey (n=3165) of US households. Our models estimate the number and the size of obsolete TVs stored by US households using a set of behavioral, socio-economic and demographic variables, and we then approximate the volumes of potentially toxic materials they contain. Our findings provide information to support future state and national policy decisions on the management of hazardous materials.

#### 5:10 PM

**Methodology for Recovery Precious Metals: Gold, Silver and Platinum Group from Electronic Waste:** Oscar Restrepo<sup>1</sup>; Honorio Oliveros<sup>1</sup>; <sup>1</sup>National University of Colombia

Colombia produces nine tons of electronic waste per year and there are approximately 60 tons accumulation generated in the last nine years. This work aims to establish a general methodology in the laboratory to recover gold, silver and platinum groups present in electronic waste and also to explore other forms of recovery of metals contained in electronic waste. We selected seven types of electronic cards present in the computers, which have their parent desoldering electronic components. Initially, we characterized the components of the cards through x-ray diffraction and SEM to identify the metal species and composition. Tests were conducted in laboratory hydrometallurgical recovery of metals. This paper proposes a methodology for laboratory-scale work.

#### 5:40 PM

**WEEE: Obsolete Mobile Phones Characterization Aiming at Recycling:** Viviane Moraes<sup>1</sup>; Denise Espinosa<sup>1</sup>; Jorge Tenório<sup>1</sup>; <sup>1</sup>Escola Politécnica da Universidade de São Paulo

The development of mobile phone technology has increased the replacement of outdated equipment for more modern models, transforming the disposal of such devices into a serious environmental problem. Recycling

appears as an attractive alternative to minimize the environmental impact of disposing such large quantities. Recycling can be accomplished by treating the printed circuit boards of used mobile phones with the same techniques used in ore treatments with hammer mill: magnetic separation, electrostatic separation and grain size range. Before performing the recycling process, a PCB characterization was performed to identify the fraction with the higher metals concentration/content. This study demonstrated that the electrostatic separation was not the best metals concentration of PCB aiming the recycling, while the non-magnetic residue had presented a more significant metal concentration. Furthermore, after the magnetic separation, it was possible to separate the metals iron and nickel.

---

### Thermally Activated Processes in Plastic Deformation: Grain Boundary Evolution and Dislocation Core Effects

*Sponsored by:* The Minerals, Metals and Materials Society, TMS Materials Processing and Manufacturing Division, TMS/ASM: Computational Materials Science and Engineering Committee  
*Program Organizer:* Christopher Woodward, Air Force Research Laboratory

Monday PM  
February 28, 2011

Room: 1B  
Location: San Diego Conv. Ctr

*Session Chairs:* David Rodney, INP Grenoble; Gregory Rohrer, Carnegie Mellon University

---

#### 2:00 PM Invited

**Grain Boundary Diffusion: From Nearly Perfect Bicrystals to Severely Deformed Polycrystalline Materials:** Sergiy Divinski<sup>1</sup>; <sup>1</sup>University of Münster

An overview of recent advances in grain boundary (GB) diffusion and segregation in bi-crystalline, tri-crystalline, and poly-crystalline metals is presented with an emphasize on the relationship between the structure and kinetic properties. GB diffusion is strongly affected by the structural state of interfaces and segregation of residual impurities. The so-called 'non-equilibrium' GBs are introduced by severe plastic deformation of metals using deferent routes. These GBs are characterized by an increased free volume, larger excess free energy and, as a result, enhanced diffusivities. The kinetic and structure properties of the 'non-equilibrium' GBs are investigated for several pure metals (Cu, Ni, Ti) and Cu-based alloys severely deformed by equal channel angular pressing. The relaxation behavior of interfaces in ultra-fine grained metals is investigated by radiotracer diffusion measurements and differential scanning calorimetry.

#### 2:30 PM Invited

**Experimental Measurements of the Shear-Coupled Stress Driven Grain Boundary Migration in Al Bicrystals:** Dmitri Molodov<sup>1</sup>; Tatiana Gorkaya<sup>1</sup>; Günter Gottstein<sup>1</sup>; <sup>1</sup>RWTH Aachen University

Recent results of experimental research into stress induced grain boundary migration in aluminum bicrystals will be briefly reviewed. Boundary migration under a shear stress was observed to be coupled to a lateral translation of the grains for planar symmetrical <100> tilt boundaries. This coupling proved to be the typical migration mode of any <100> tilt boundary, no matter whether low- or high angle, low  $\Sigma$  CSL coincidence or non-coincidence boundary. The measured ratios of the normal boundary motion to the tangential displacement of the grains were in an excellent agreement with theoretical predictions. Measurements of the temperature dependence of coupled boundary migration revealed that there is a specific misorientation dependence of migration activation parameters. The experimental observations provide evidence that the investigated boundaries can act during their migration under stress as sources of lattice dislocations that results in the formation and growth of new grains in the boundary region.

### 3:00 PM Invited

#### **Evolution of the Grain Boundary Character Distribution during Grain Growth:** *Gregory Rohrer*<sup>1</sup>; Herbert Miller<sup>1</sup>; <sup>1</sup>Carnegie Mellon University

The grain boundary character distribution is the relative area of grain boundaries as a function of the lattice misorientation and grain boundary plane orientation. This paper will focus on experiments undertaken to assess the evolution of the grain boundary character distribution as a function of thermal annealing that leads to grain growth. The analysis is based upon electron backscatter diffraction (EBSD) data, which allows the crystallography and relative areas of all of the grain boundaries to be measured. Data from SrTiO<sub>3</sub> taken a range of grain sizes indicates that the grain boundary character distribution changes as the grains grow. Measurement of the relative grain boundary energies indicates that as grain growth proceeds, higher energy boundaries are preferentially eliminated from the distribution.

### 3:30 PM Break

### 3:45 PM Invited

#### **Grain Growth in 4D: A Comparison between Simulation and Experiment:** E. Lauridsen<sup>1</sup>; I. McKenna<sup>2</sup>; S. Poulsen<sup>1</sup>; W. Ludwig<sup>3</sup>; *Peter Voorhees*<sup>2</sup>; <sup>1</sup>Riso Laboratory for Sustainable Energy; <sup>2</sup>Northwestern University; <sup>3</sup>European Synchrotron Radiation Facility

The evolution of polycrystalline materials is examined using 3D imaging tools based on phase- and diffraction- contrast X-ray tomography and phase field simulations. Since the techniques are nondestructive, it is possible to record the morphological and topological evolution of an individual grain and compare this to the predictions of simulations using the experimentally measured structure as an initial condition. Through this comparison, we find that the phase field model can reproduce quite accurately grain morphology and topology in regions of the Ti-21S sample with isotropic grain boundary properties. However, in other regions, we find grain boundary mobilities that are orders of magnitude larger than the average, mobilities that depend strongly on the grain boundary normal, and clear influence of grain boundary energy anisotropy on the morphological evolution of grains.

### 4:15 PM

#### **A Comparison between Creep in Molybdenum and Iron toward Understanding Dynamic Abnormal Grain Growth:** *Phi Thanh*<sup>1</sup>; Daniel Worthington<sup>2</sup>; Cory Guebels<sup>1</sup>; J. P. Delplanque<sup>1</sup>; Joanna Groza<sup>1</sup>; <sup>1</sup>University of California Davis; <sup>2</sup>University of Texas

Dynamic abnormal grain growth (DAGG) is a phenomenon which produces abnormal grains during straining above a critical temperature. DAGG has been observed in molybdenum but not in iron at similar homologous temperatures ( $T = 0.4 TM$ ) and strain rates (strain-rate  $\square 10^{-3}$  to  $10^{-5} s^{-1}$ ). We compare high-temperature plastic deformation data of molybdenum and iron via creep and activation area analyses. Experiments for both materials were conducted under displacement-controlled tensile deformation. We utilize the present analyses to discuss the occurrence of DAGG in body-centered cubic metals.

### 4:35 PM Invited

#### **Quantum Dynamical Effects in Thermally-Activated Dislocation Glide: Origin of the Discrepancy between Experimental and Simulated Peierls Stresses:** *David Rodney*<sup>1</sup>; Laurent Provaille<sup>2</sup>; <sup>1</sup>INP Grenoble; <sup>2</sup>CEA Saclay

The Peierls stress is one of the most fundamental properties of a dislocation. In BCC crystals for example, it is appreciably high, causing a strongly temperature-dependent plasticity at low temperatures. Atomic-scale simulations are known to overestimate the Peierls stress. Indeed, calculations based on electronic structure theories and interatomic potentials predict Peierls stresses two to three times larger than experimental values. We show here that this discrepancy arises from quantum effects in atomic motion (zero-point motion and tunneling) so far neglected in atomistic calculations although the experiments were performed well below the Debye temperature. We used a Quantum Transition State Theory based on Path Integrals to evaluate how quantum dynamics alter the Peierls potential of several high-Peierls stress dislocations and find that the free energy barrier

against motion disappears at low temperatures for applied stresses below half the "classical" Peierls stress, thus in the experimental range.

### 5:05 PM

#### **Core Properties of Screw Dislocations in Fe and W Based Materials:** *Lisa Ventelon*<sup>1</sup>; François Willaime<sup>1</sup>; Emmanuel Clouet<sup>1</sup>; <sup>1</sup>CEA

A quantitative description of straight and kinked screw dislocations in iron and tungsten based materials from first principles is presented. We show that standard convergence criteria for relaxation in DFT calculations are not sufficient for a quantitative determination of the onset of glide and hence of the Peierls stress. We propose an alternative method, which consists in calculating the Peierls barrier for various strains, using a constrained minimization method. The calculation has been repeated for several crystal orientations to determine the deviation from Schmid law. We have also performed DFT simulations on the effect of rhenium on screw dislocations in tungsten using the VCA approximation, which confirm a recent prediction of the unexpected transition from symmetric to asymmetric core upon alloying. More insight into the stability of the core structure in tungsten alloys for different rhenium concentrations has been gained by looking at the response of the core polarization.

### 5:25 PM

#### **Thermal Activation in BCC Metals: Linking Local Atomistic Information to the Mesoscale:** *Kinshuk Srivastava*<sup>1</sup>; Daniel Weygand<sup>1</sup>; Peter Gumbsch<sup>1</sup>; <sup>1</sup>Karlsruhe Institute of Technology

High yield and flow stress in bcc metals is attributed to the large intrinsic resistance called Peierls stress experienced by the  $\langle 111 \rangle$  screw dislocations. This is because of the non-planar nature of the dislocation core. However, at finite temperatures, the screw dislocations overcome the intrinsic energy barriers at less than the theoretical stresses due to stress-assisted thermal activation of kink-pairs on screw dislocations and their subsequent migration along them. In this work, the activation enthalpies of kink-pair nucleation are obtained directly from atomistic data incorporating the effect of local non-glide stresses and orientation dependence of the Peierls barrier of the  $1/2\langle 111 \rangle$  screw dislocation. The effects of non-glide stresses and their importance on dislocation mobility in a three-dimensional discrete dislocation dynamics framework is presented. Simulations on micro-meter sized Tungsten pillars under bending show the effects of tension-compression asymmetry on dislocation micro-structure.

### 5:45 PM

#### **Thermally Activated Motion of $1/2\langle 111 \rangle$ Screw Dislocation in BCC Iron:** *Zhiming Chen*<sup>1</sup>; Matous Mrovec<sup>2</sup>; Peter Gumbsch<sup>2</sup>; <sup>1</sup>Karlsruher Institut für Technologie (KIT); <sup>2</sup>Fraunhofer-Institute Für Werkstoffmechanik IWM

The plastic deformation of body-centered cubic metals is governed by  $1/2\langle 111 \rangle$  screw dislocations. We perform atomistic computer simulations of the response of the  $1/2\langle 111 \rangle$  screw dislocation to various applied loadings in iron. The calculations have been made using tight-binding based bond-order potential, which also correctly accounts for magnetic effects. We study the orientation dependence of the critical resolved shear stress for pure shear stresses as well as the effect of non-glide stresses, which have a profound influence on the dislocation core structure. Our simulations show that iron possesses a significant twinning-antitwining and tension-compression asymmetries like other bcc metals and does not follow the Schmid law. The atomistic results are transferred to macroscopic level by formulating single crystal yield criteria which can be applied in discrete dislocation dynamics or continuum approaches.

## 2011 Functional and Structural Nanomaterials: Fabrication, Properties, Applications and Implications: Fabrication of Nanomaterials I

Sponsored by: The Minerals, Metals and Materials Society, TMS Electronic, Magnetic, and Photonic Materials Division, TMS: Nanomaterials Committee

Program Organizers: Jiyoung Kim, Univ of Texas; David Stollberg, Georgia Tech Research Institute; Seong Jin Koh, University of Texas at Arlington; Nitin Chopra, The University of Alabama; Suveen Mathaudhu, U.S. Army Research Office

Tuesday AM Room: 8  
March 1, 2011 Location: San Diego Conv. Ctr

Session Chairs: David Stollberg, Georgia Tech Research Institute; Greg Thompson, University of Alabama

### 8:30 AM Introductory Comments

#### 8:35 AM Invited

##### Atomic Layer Deposition for the Functionalization of Nanoporous Materials: Jeffrey Elam<sup>1</sup>; <sup>1</sup>Argonne National Laboratory

Atomic layer deposition (ALD) is a thin film growth technique that uses alternating, self-limiting chemical reactions to deposit materials in an atomic layer-by-layer fashion. Although this process is already used commercially for microelectronics manufacturing, ALD promises to have a much broader impact extending far beyond microelectronics. In particular, the capability to infiltrate and coat nanoporous substrates coupled with a broad palate of available materials make ALD a versatile technique for synthesizing nanostructured materials. At Argonne we are pursuing a variety of new applications for ALD including photovoltaics, catalysis, and energy storage. A central theme in these efforts is that we use ALD to apply precise, conformal coatings onto nanostructured scaffolds to impart the desired optical, electrical, or chemical properties to advance these technologies.

#### 9:05 AM Invited

##### One Dimensional Nanomaterials Synthesis Using Atomic Layer Deposition: Hyungjun Kim<sup>1</sup>; <sup>1</sup>Yonsei University

Atomic layer deposition (ALD) has been considered as a promising thin film deposition technique for nanoscale semiconductor device fabrication. Recently, however, the exclusive benefits of ALD make it viable tool for nanotechnology. In this presentation, I will present several examples on the one dimensional nanomaterials synthesis using ALD. Due to its excellent conformality, ALD is an ideal technique to produce nanomaterials with combination of nanopatterning techniques. Utilizing highly conformal Ru and ZnO ALD with nanotemplates, 1 D nanomaterials were fabricated. Moreover, by adding SiH<sub>4</sub> to the NH<sub>3</sub> plasma reactant during Co plasma-enhanced ALD process, Co nanorods array was formed on Si substrates without using nanotemplates. Also, by applying highly conformal ALD processes for transition metals followed by annealing, silicide nanowires were synthesized. The physical and structural properties of these nanomaterials were investigated by various analysis techniques.

#### 9:35 AM

##### Recent Progress on Synthesis and Characterization of Boron-based One-Dimensional Nanostructures: Terry Xu<sup>1</sup>; XiaoXia Wu<sup>1</sup>; Zhe Guan<sup>1</sup>; Youfei Jiang<sup>1</sup>; <sup>1</sup>UNC Charlotte

Boron-based (i.e., boron and metal boride) one-dimensional (1D) nanostructures have recently attracted much attention due to their predicted superior electrical and mechanical properties. Combining with other properties such as low density and high chemical stability, boron-based 1D nanostructures are appealing candidates for applications such as thermoelectric energy conversion, nanocomposites and nanoelectronics. In this presentation, our recent progress on synthesis and characterization of boron-based nanomaterials, such as  $\alpha$ -tetragonal boron, MB<sub>6</sub> (M=Ca, Sr and Ba), and B<sub>4</sub>C-type 1D nanostructures will be reviewed. Special discussion

will be on (1) the need of carbon to achieve high volume fabrication of  $\alpha$ -tetragonal boron nanostructures, (2) Young's modulus measurement of MB<sub>6</sub> 1D nanostructures and  $\alpha$ -tetragonal boron nanostructures, and (3) thermal stability of  $\alpha$ -tetragonal boron nanostructures. The thermoelectric property of these boron-based nanostructures will also be briefly discussed.

#### 9:50 AM

##### Superhydrophobicity of Boron Nitride Nanotubes Structures: Chee Huei Lee<sup>1</sup>; Jaroslav Drellich<sup>1</sup>; Yoke Khin Yap<sup>1</sup>; <sup>1</sup>Michigan Technological University

Boron nitride is a chemically inert, resistive to oxidation up to 900/176C, and transparent to visible-UV light, potentially attractive insulating material for applications under rigorous chemical and thermal conditions. Recently, we also demonstrated (Langmuir 25(9), 2009, 4853-4860) that boron nitride nanotubes can be structured into a superhydrophobic coating. Dense structures of partially vertically aligned boron nitride nanotubes demonstrate excellent water repellency, with advancing and receding contact angles exceeding 150 and 140 degrees, respectively. Boron nitride nanotubes demonstrate superhydrophobicity in both air environment and oil phase. Our results also show that the pH value of water does not affect wetting characteristics of boron nitride nanotubes. On a contrary, lowering the surface tension of liquid by adding ethanol to water reduces the receding contact angle to nearly zero value.

#### 10:05 AM Break

#### 10:20 AM Invited

##### Solution-Synthesized ZnO Nanomaterials for Hybrid Solar Cells: Julia Hsu<sup>1</sup>; <sup>1</sup>University of Texas at Dallas

There has been great interest in hybrid organic:inorganic solar cells due to their potential for large-scale, cost-effective solar cells. These devices commonly use zinc oxide (ZnO) as the electron acceptor and a conjugated polymer, e.g. poly(3-hexylthiophene), as the electron donor. ZnO nanomaterials are readily synthesized using solution methods. In this talk, I will review using various ZnO nanomaterials for hybrid solar cells. For example, by changing the pyrolysis temperature in the sol gel process, we are able to reduce the size of ZnO crystallites. Consequently, the band gap of the ZnO acceptor is increased due to greater quantum confinement, leading to a larger donor-acceptor energy level offset. We find that a direct correlation between the increase in ZnO Eg and device open-circuit voltage. Nanomaterials enables larger donor-acceptor interfacial area. I will also discuss the gain in device performance by using ZnO nanomaterials in the active layer.

#### 10:50 AM

##### Unipolar Assembly of ZnO Rods: Polarity Driven Collective Luminescence: Ujjal Gautam<sup>1</sup>; Masataka Imura<sup>1</sup>; Xiaosheng Fang<sup>1</sup>; Yoshio Bando<sup>1</sup>; Dmitri Golberg<sup>1</sup>; <sup>1</sup>National Institute for Materials Science

Crystal assemblies are omnipresent and are useful for many devices. Nature too has shown phenomenal control over biomineralization processes to produce exquisite looking crystal assemblies. We have discovered a new phenomenon associated with concentric assemblies of ZnO rods. Usually, a ZnO rod always has an intrinsically positive and a negative polar end induced by the non-centrosymmetric arrangement of Zn and O atoms. We found two distinct types of assemblies wherein all the rods in a single assembly emanate out of a central core maintaining a single polar direction. Due to growth along the two polar surfaces with different atomic arrangements, these assemblies are distinct in their intrinsic properties and exhibit strong UV luminescence in the exterior of Zn-polar assemblies, unlike the O-polar assemblies. While novel applications can be envisioned, these observations suggest that hierarchical organization with respect to internal asymmetry such as polarity might be widespread in natural crystal assemblies.

#### 11:05 AM

##### Hierarchical Graphene Nanomaterials and Applications: Cengiz Ozkan<sup>1</sup>; <sup>1</sup>University of California

I will first describe the patterning of DNA molecules and block copolymers on CVD grown large-area graphene layers to modulate their

TUESDAY AM



electronic properties. DNA molecules are found to act as negative potential gating agents that increase the hole density in single layer graphene. Highly sensitive and cost-effective field effect transistor biosensors are fabricated based on large area graphene layers. Next, I will describe new classes of CVD grown hierarchical graphene nanomaterials in the form of three dimensional architectures called pillared graphene nanostructures (PGN), which are combinations of graphene floors and carbon nanotube pillars. The dependence of the morphology of large-area PGN on the process conditions was investigated by Raman spectroscopy, SEM, TEM, and HRTEM techniques. The successful transfer of the large area PGN onto arbitrary substrates while keeping the 3D architecture intact is demonstrated. Hierarchical graphene nanomaterials are envisioned for future applications in fuel cells, ultracapacitors and hydrogen storage.

#### 11:20 AM Invited

**Atomic Layer Deposition of Al<sub>2</sub>O<sub>3</sub> and ZnO at Atmospheric Pressure in a Flow Tube Reactor:** Gregory Parsons<sup>1</sup>; Jesse S. Jur<sup>1</sup>; <sup>1</sup>North Carolina State University

Atomic layer deposition typically proceeds at ~ 1 Torr because the pressure is high enough to minimize precursor/reactant gas mixing, and the pressure is sufficiently low so that precursors with moderate vapor pressure can be delivered directly into the growth zone. Recently, to investigate capabilities of continuous ALD processes at under atmospheric pressure, our group developed a unique flow tube ALD reactor that operates at pressures between ~1 and 760 Torr. We have characterized ZnO and Al<sub>2</sub>O<sub>3</sub> film growth versus pressure, and used it on several soft material substrates, including polypropylene, nylon-6 and cellulose cotton. We find that ALD growth can be readily achieved for ZnO, whereas some excess growth is observed consistent with ALD+CVD for Al<sub>2</sub>O<sub>3</sub> growth under similar conditions. We will discuss likely mechanisms for these differences, and present possible new applications of ALD performed at atmospheric pressure.

#### 11:50 AM

**Boron Carbide-Nanowires/Carbon-Microfiber Hybrid Structures and Composites from Cotton T-shirts:** Xinyong Tao<sup>1</sup>; Lixin Dong<sup>2</sup>; Xinnan Wang<sup>1</sup>; Wenkui Zhang<sup>3</sup>; Bradley Nelson<sup>2</sup>; Xiaodong Li<sup>1</sup>; <sup>1</sup>University of South Carolina; <sup>2</sup>ETH Zurich; <sup>3</sup>Zhejiang University of Technology

Boron carbide-nanowire/carbon-microfiber hybrid structures have been fabricated using a cotton T-shirt as both the template and carbon source. The boron carbide nanowires exhibit a high elastic modulus of 428.1 GPa and elastic recovery after multiple high-strain bending cycles without brittle failure or obvious residual deformation for the strain up to 45%. The boron carbide-nanowire/carbon-microfiber hybrid structures can block 99.8% UV irradiation and achieve a superior reinforcing effect in their epoxy composites. The boron carbide-nanowire formation mechanisms and corresponding synthesis techniques presented here can be extended to other carbide nanowires such as SiC, TiC, MoC, and WC by introducing suitable carbide-sources and catalysts.

#### 12:05 PM Concluding Comments

## 2nd International Symposium on High-Temperature Metallurgical Processing: Refractories, Slag and Recycling

*Sponsored by:* The Minerals, Metals and Materials Society, TMS Extraction and Processing Division, TMS: Pyrometallurgy Committee, TMS: Energy Committee

*Program Organizers:* Jiann-Yang Hwang, Michigan Technological University; Jerome Downey, Montana Tech; Jaroslaw Drelich, Michigan Technological University; Tao Jiang, Central South University; Mark Cooksey, CSIRO

Tuesday AM  
March 1, 2011

Room: 18  
Location: San Diego Conv. Ctr

*Session Chairs:* Patrick Masset, TU Bergakademie Freiberg; Gabriella Tranell, Norwegian University of Science and Technology

#### 8:30 AM

**Study on Preparation of High-Quality Synthetic Rutile from Titanium Slag by Activation Roasting Followed by Acid Leaching:** Yufeng Guo<sup>1</sup>; Shuishi Liu<sup>1</sup>; Tao Jiang<sup>1</sup>; Guanzhou Qiu<sup>1</sup>; <sup>1</sup>Central South University

The preparation of high-quality synthetic rutile from electric furnace titanium slag was systematically investigated by activation roasting followed by acid leaching method. The results showed that impurities such as Ca and Mg in titanium slag can be effectively removed by roasting with phosphoric acid followed by acid leaching and TiO<sub>2</sub> grade of the product was markedly improved. High-quality synthetic rutile containing 88.54% TiO<sub>2</sub>, 0.42% (CaO+MgO) was obtained under the conditions that roasted with 7.5% (wt) H<sub>3</sub>PO<sub>4</sub> at 1000 \176C for 2h, two-stage leached in sulfuric acid of boiling for 2h. Mechanism studies showed that anosovite solid solution and silicate minerals were reacted with phosphoric acid in the roasting process, as a result, titanium components in titanium slag turned into rutile TiO<sub>2</sub>, impurities turned into acid-soluble phosphate and quartz, therefore, the structures of anosovite solid solution and silicate minerals were destroyed, which is favorable for impurities' removing.

#### 8:50 AM

**Calculation of Phase Equilibria Relations in CaO-SiO<sub>2</sub>-FeOx-MgO System:** Cuihuan Huang<sup>1</sup>; <sup>1</sup>Northeastern University

SiO<sub>2</sub>, CaO, Al<sub>2</sub>O<sub>3</sub>, Fe<sub>2</sub>O<sub>3</sub>, Na<sub>2</sub>O and MgO account for more than 90% by weight of the bottom ash slag from municipal solid waste incineration. These compositions have direct effect on the harmless disposal and efficient utilization of bottom ash slag. The phase transformation and phase relations of sub-systems in CaO-SiO<sub>2</sub>-FeOx-MgO system was considered to be important to provide essential data for the thermodynamic properties of the CaO-Al<sub>2</sub>O<sub>3</sub>-SiO<sub>2</sub>-FeOx-MgO-Na<sub>2</sub>O system. Based on FactSage software, a set of optimized parameters for the thermodynamic properties of CaO-SiO<sub>2</sub>-FeOx-MgO system was obtained, and the phase equilibria relations were calculated for different temperatures and oxygen partial pressures. Spinel solid solution emerged with the increase of partial pressure of oxygen, which changed the phase relations in FeOx-rich area, and the liquid phase region moved to the poor-FeOx area in MgO-SiO<sub>2</sub>-FeOx system. At 1873K and 10-8atm oxygen partial pressure, MgO solid phase can be found in CaO-SiO<sub>2</sub>-FeOx-MgO system.

#### 9:10 AM

**Dissolution Behavior of Rhodium into Molten Slag:** Chompunoot Wiraseranee<sup>1</sup>; Toru Okabe<sup>1</sup>; Kazuki Morita<sup>1</sup>; <sup>1</sup>The University of Tokyo

Due to very limited resources, recycling of rhodium becomes essential so that rhodium can be sustainably used. By the pyrometallurgical recycling process, rhodium can be separated from various impurities. However, the rhodium dissolution behavior in the process is not yet clarified; thus rhodium loss into slag cannot be estimated. Aiming at the development of more effective recycling processes, rhodium dissolution behavior into molten slag was investigated. Using a pure rhodium crucible and Na<sub>2</sub>O-SiO<sub>2</sub> slag system, equilibration experiments carried out for 18 h at 1423-1573 K, under oxygen

partial pressure 0.001-1 atm, and varying slag basicity. Rhodium solubility increases with increasing oxygen potential, slag basicity and temperature, and the dissolution reaction is determined as  $Rh + 3/4O_2 + 1/2O^{2-} = [RhO_2]$ . From this study, the correlations of rhodium solubility, the newly-defined rhodate capacity and optical basicity are discussed; and rhodium loss in the pyrometallurgical recycling process can be estimated.

**9:30 AM**

**“One Step” Technology to Separate Copper, Zinc, Lead from Iron in Metallurgical Slag and Pyrite Cinder: Part 2- Pilot Test:** *De-qing Zhu*<sup>1</sup>; Dong Chen<sup>1</sup>; Jian Pan<sup>1</sup>; Yu Cui<sup>1</sup>; Tie-jun Chun<sup>1</sup>; <sup>1</sup>Central South University

A study of processing pyrite cinder and metallurgical slag using “one step” technology in strand grate - rotary kiln is presented, which aims to efficiently recover valuable metals of iron, lead, zinc and copper. The effect of chlorination roasting parameters including roasting time and temperature on the nonferrous metal removal rate was investigated. It is shown that copper and zinc are low removed and lead is removed more easily. Then the preheated pellets were reduced in rotary kiln, which indicates zinc and lead can be removed easily and high iron grade and good metallurgical performance prereduced pellets can be obtained. Furthermore, the chlorination and reduction mechanisms of copper, lead and zinc are discussed. It is revealed that the phases of copper, lead and zinc in slag are complex and ferrite and silicate of metals are hardly removed.

**9:50 AM**

**Effect of Oxygen to Alumina Ratio on the Viscosity of Aluminosilicate and Aluminate Systems:** *Jifang Xu*<sup>1</sup>; Jieyu Zhang<sup>1</sup>; Chang Jie<sup>1</sup>; Fei Ruan<sup>1</sup>; Kuochih Chou<sup>1</sup>; <sup>1</sup>Shanghai Key Laboratory of Modern Metallurgy and Material Processing, Shanghai University

Viscosity is an important physical parameter of slag in metallurgical process. Most of studies of aluminosilicate and aluminate systems assume that aluminum occurs in tetrahedral coordination. In this case the O/Al value was utilized to describe the slag structure in terms of the network character of aluminosilicate and aluminate systems. Data of composition and viscosity were come from the literatures, and the trends have been analyzed according to the O/Al value and temperature. It is shown that the O/Al value can be used to explain the trends in more than ten systems successfully, containing more than 200 data points. In aluminosilicate system, the trend that viscosity value changed with the O/Al value implied that alumina works as network modifier such as basic oxides or works as network former. In aluminate system, irrespective of the system and temperature, viscosity would decrease steadily when O/Al value increasing.

**10:10 AM Break**

**10:20 AM**

**Blast Furnace Burdens Preparation from Blast Furnace Burdens Preparation from Metallurgical Dusts and Sludges with Composite Binder:** *Kecheng Zhang*<sup>1</sup>; *Yuanbo Zhang*<sup>1</sup>; Tao Jiang<sup>1</sup>; Guanghui Li<sup>1</sup>; Zhucheng Huang<sup>1</sup>; <sup>1</sup>Central South University

With rapid development of Iron and Steel industry, plenty of metallurgical dusts & sludges are generated, which have not been effectively utilized because of their poor hydrophilicity and bad ballability. Agglomeration and roasting of metallurgical dusts & sludges with a new-type composite binder are studied in this paper. The results indicate that the dosage of the new binders can be decreased to 2.5% from 3.5% when using the wet-grinding process. Under the optimal conditions of briquetting pressure 2070 N/cm<sup>2</sup>, briquetting moisture content 13%, roasting temperature 1000° and roasting time 40 min, the qualities of the green, dry and roasted briquettes meet the requirements of the industry production. The finished products have the compression strength of more than 2000 N/cm<sup>2</sup>, which can be used as high-quality burdens for blast furnaces.

**10:40 AM**

**Determination of FeO Containing Liquid Slag Surface Tensions Using the Sessile Drop Method:** *Clemens Schmetterer*<sup>1</sup>; Patrick Masset<sup>1</sup>; <sup>1</sup>TU Bergakademie Freiberg

Surface and interfacial tensions are important properties of slags for the virtualization of the blast furnace process, since they influence the interactions between the components in the blast furnace, e.g. at the slag – Fe interface. In this work the dependence of the surface tension of Al<sub>2</sub>O<sub>3</sub> – CaO – SiO<sub>2</sub> mixtures with varying Fe<sub>x</sub>O content and oxygen partial pressure was determined at different temperatures using the sessile drop technique with boron nitride (BN) as a substrate material under partial oxidation conditions. In addition, structural investigations using powder X-ray diffraction and Mössbauer spectroscopy (Fe<sup>3+</sup>/Fe<sup>2+</sup> ratio) on quenched specimens were performed as a start in developing a model combining the slag structure, the surface tension and its thermodynamic properties. The obtained experimental data will be discussed with respect to the slag structure and will be compared to results reported in the literature and obtained from modelling.

**11:00 AM**

**Preparation of Partially Stabilized Zirconia and Interface Structure Analysis:** *Dong Bo Li*<sup>1</sup>; Sheng Hui Guo<sup>1</sup>; Li Jun Liu<sup>1</sup>; Jin Hui Peng<sup>1</sup>; Li Bo Zhang<sup>1</sup>; Cheng Dong He<sup>1</sup>; <sup>1</sup>Kunming University of Science & Technology

In present study, partially stabilized zirconia (PSZ) was prepared from CaO doped fused zirconia heated by Microwave furnace at the temperature of 1450° and holding time of 120 min. The characterization of XRD results show that untreated fused zirconia mainly consists of crystalline compounds of cubic ZrO<sub>2</sub> phase; while the roasted one mainly composed of crystalline compounds of cubic ZrO<sub>2</sub> phase and monoclinic ZrO<sub>2</sub> phase. It is shown through the optimization of structures of two phases that structure of cubic ZrO<sub>2</sub> and monoclinic ZrO<sub>2</sub> reject, revealing its difficulty of forming coinciding interface and linkage of two phases being of Ca atom.

**11:20 AM**

**Characteristic of Mineralization of Specularite Iron Ores during Composite Agglomeration Processing:** *Helei Zhang*<sup>1</sup>; Heng Yu<sup>1</sup>; *Guanghui Li*<sup>1</sup>; Yuanbo Zhang<sup>1</sup>; Qian Li<sup>1</sup>; Tao Jiang<sup>1</sup>; <sup>1</sup>Central South University

Large reserves of specularite iron ores had been found all over the world, which is characterized as high total iron grade, low gangues content, as well as low commercial price. However, it has not been widely used in sinter or pellet production due to its inferior sintering and roasting characters. It has shown that the proportion of specularite ores reaches as high as 40%~50% and achieves good results by using Composite Agglomeration Process (CAP), an innovative agglomeration process invented by Central South University. But the mineralization of specularite is still unknown during composite agglomeration processing. In this paper, the induration characteristics of specularite ore is studied by simulating CAP in laboratory, as well as phase and microstructure analysis of CAP product. The results show that specularite pellet is mainly indurated through recrystallization of Fe<sub>2</sub>O<sub>3</sub>, calcium ferrite within high basicity sinters matrix interweaves with the recrystallized Fe<sub>2</sub>O<sub>3</sub> on the surface of the pellet, which forms an integral microstructure, and ensures high strength of CAP product for ironmaking.

**11:40 AM**

**Enrichment Behavior of Phosphorous in CaO-SiO<sub>2</sub>-FetO-P<sub>2</sub>O<sub>5</sub> Based Slag:** *Yingying Shen*<sup>1</sup>; <sup>1</sup>Northeastern University

As a by-product of steelmaking, not only environmental pollution can be removed, but also huge economical benefits can be created if reutilization of steel slag can be developed deeply. In order to enhance the reuse of convert slag to the metallurgical flowsheet, it's need to promote the enrichment of phosphorous to phosphorous-containing phase and separate the phosphorous-containing phase from steel slag to avoid the deterioration of refining process caused by the accumulation of phosphorous. In this paper, the enrichment behavior of phosphorous to CaO-SiO<sub>2</sub> particle in CaO-SiO<sub>2</sub>-FetO-P<sub>2</sub>O<sub>5</sub> based slag was studied and the phosphorous contents in the molten bulk slag, as well as the interior and surface of 2CaO·SiO<sub>2</sub> particle for different temperatures were also investigated. The enrichment process of phosphorous in CaO-SiO<sub>2</sub>-FetO-P<sub>2</sub>O<sub>5</sub> based slag can be considered to be mix-controlled

TUESDAY AM

by the two steps of diffusion in molten bulk slag and internal diffusion through  $2\text{CaO}\cdot\text{SiO}_2\text{-3CaO}\cdot\text{P}_2\text{O}_5$  solid solution reactant layer.

## Advances in Science-Based Processing of Superalloys for Cost and Sustainment: Residual Stress and NDE Technologies for Components

*Sponsored by:* The Minerals, Metals and Materials Society, TMS Materials Processing and Manufacturing Division, TMS Structural Materials Division, TMS/ASM: Computational Materials Science and Engineering Committee, TMS: High Temperature Alloys Committee, TMS: Advanced Characterization, Testing, and Simulation Committee

*Program Organizers:* Donna Ballard, US Air Force; David Furrer, Pratt & Whitney; Paul Jablonski, US Department of Energy; Christopher Woodward, Air Force Research Laboratory; Jeff Simmons, AFRL; Mark Blodgett, Wright-Patterson AFB

Tuesday AM  
March 1, 2011

Room: 33B  
Location: San Diego Conv. Ctr

*Session Chairs:* Mark Blodgett, Wright-Patterson AFB; Reji John, Air Force Research Laboratory

### 8:30 AM Introductory Comments

#### 8:35 AM Invited

#### Predicting and Managing Bulk Residual Stresses within Superalloys: Ronald Wallis<sup>1</sup>; <sup>1</sup>Wyman Gordon Forgings

The residual stresses developed in superalloy forgings during heat treatment result in a number of potential problems during subsequent manufacturing. They may lead to distortion of the forging which results in extra material being needed to ensure a part may be manufactured from it. The residual stress pattern may also lead to issues in machining the final component from the forging (the part moving during machining as the stresses attain a new equilibrium). A brief history of the numerical calculation of residual stresses during heat treatment (data needed and validation) is presented together with some examples of typical results obtained. The paper also gives examples where modifications to the manufacturing process have resulted in alleviating the problems. Finally the paper discusses more recent developments where models together with more versatile production equipment has been adopted to control the magnitude and distribution of residual stresses developed in a forging.

#### 9:05 AM Invited

#### Microstructural Effects on Electrical Resistivity in Comparison to Residual Stresses and the Implications for Eddy Current Methods in Measuring Residual Stress in IN718: Triplicane Parthasarathy<sup>1</sup>; Pavel Mogilevsky<sup>1</sup>; Sonya Boone<sup>1</sup>; Satish Rao<sup>1</sup>; Peter Nagy<sup>2</sup>; Mark Blodgett<sup>3</sup>; <sup>1</sup>UES, Inc.; <sup>2</sup>Univ. of Cincinnati; <sup>3</sup>Air Force Research Laboratory

As part of a sustainment program, the ability to measure residual stresses on the surface of turbine disks using eddy current methods has been of great interest. In IN718, a widely used disk alloy, initial results have shown that complex metallurgical phenomena interfere with this approach yielding an anomaly in eddy current measurements. The objective of this work was to determine the various possible metallurgical factors that might affect electrical resistivity and to identify the one that is responsible for the anomaly. A systematic investigation was carried out to evaluate and model the effects of chemistry, heat treatment, plastic deformation and recovery after cold work during annealing on the electrical resistivity of an IN718 alloy. The results were analyzed using semi-empirical models. The experimental results were fit to analytical models for use in calibrating eddy current methods for measuring residual stress in shot-peened or LPB treated engine parts.

#### 9:35 AM Invited

#### Modeling and Simulation of Residual Stresses Resulting from Superalloy Processing: Wei-Tsu Wu<sup>1</sup>; Ravi Shankar<sup>1</sup>; Alex Bandar<sup>1</sup>; Byung-Kwan Chun<sup>1</sup>; <sup>1</sup>Scientific Forming Technologies Corp

To meet the demands of increasing thrust and higher operating temperatures, sophisticated nickel based superalloy turbine disks are processed with spatially varying properties. Dual Microstructure Heat Treatment (DMHT) induces fine grained, high strength, fatigue resistant microstructure at the bore, while creating coarser grained, creep resistant microstructure at the rim. Accurate modeling of disks under thermal-mechanical loading require appropriate initial conditions, including variation of microstructure and properties resulting from forging, heat treatment, and machining. Current approach is to couple the multi-physics phenomena: heat transfer, non-linear deformation, and micro-structure evolution. The mechanical properties, such as flow stress, Young's modulus, creep property, etc evolve due to changes in microstructure during the thermo-mechanical processes. The microstructure evolution is impacted by changes in temperature and deformation history, and precipitation kinetics. To demonstrate the methodology, a dual microstructure heat treatment process (DMHT), followed by machining (material removal), and spinning process were simulated and presented.

#### 10:05 AM Break

#### 10:20 AM Invited

#### Probabilistic Fatigue Life-Prediction of Turbine Engine Materials: Reji John<sup>1</sup>; Sushant Jha<sup>2</sup>; Michael Caton<sup>1</sup>; James Larsen<sup>1</sup>; Patrick Golden<sup>1</sup>; <sup>1</sup>Air Force Research Laboratory; <sup>2</sup>Universal Technology Corporation

Physics-based probabilistic methods are essential in appreciably reducing the uncertainty in fatigue life prediction. Towards this objective, the role of competing mechanisms in producing dual-fatigue variability behavior in turbine engine materials is discussed. The competing modes could be related to randomly occurring microstructural configurations, differing in the degree of heterogeneous deformation accumulation in fatigue. The fatigue variability is described as a sequence of mechanisms, probabilistically originating from these configurations, in the order of decreasing heterogeneity level. These mechanisms separated into two primary contributions to the lifetime probability density: (i) the mean-lifetime response and (ii) the crack-growth-controlled, life-limiting behavior. A model incorporating this dual behavior was developed and provided reasonable predictions of the influence of material and extrinsic variables on the lifetime density and the probabilistic lifetime-limit.

#### 10:50 AM Invited

#### Advancements in NDE Technologies to Support Superalloy Component Lfing: R. Thompson<sup>1</sup>; Norio Nakagawa; Lisa Brasche<sup>1</sup>; <sup>1</sup>Iowa State University

NDE has a well established role in managing the lives of superalloy components such as the rotating disks in aircraft engines. Historically, this has been based on the detection of flaws, a capability that is quantified by the Probability of Detection. NDE techniques often employed for this purpose and the lifing strategies employed by the U.S. Air Force and Federal Aviation Agency, based on this strategy will be briefly reviewed. Attention will then turn to emerging NDE techniques that are intended to detect more subtle microstructural features that also influence component lifing, such as grain structure, dislocation density, inclusions, texture and residual stress. The current status of such techniques will be discussed. Finally, potential Bayesian strategies for integrating this information with the predictions of failure models to make lifetime predictions will be outlined.

#### 11:20 AM

#### Nondestructive Evaluation of Microstructure in Super Alloy Disk Material: James Blackshire<sup>1</sup>; Enrique Medina<sup>1</sup>; Jeong Na<sup>2</sup>; <sup>1</sup>Air Force Research Laboratory; <sup>2</sup>University of Dayton Research Institute

Nickel-based super alloy materials with dual-microstructure characteristics are being engineered to increase both fatigue and creep resistance properties in turbine engine disks. Nondestructive evaluation methods are needed to assess grain structure and size distributions, and for estimating material property



changes due to thermal and mechanical loads. Ultrasonic measurements represent one of the most promising candidates for characterization, where sound velocity, attenuation, and backscatter are known to be sensitive to microstructure in polycrystalline materials. The feasibility of three ultrasonic measurement approaches is investigated for grain size estimation in dual-microstructure materials including contact ultrasound, scanning immersion ultrasound, and scanning laser vibrometry detection of ultrasound energy. Finite element models are also used to study the ultrasonic forward problem, where the characteristic response of ultrasonic waves propagating through coarse and fine grain microstructures is investigated. Results indicate that qualitative measurements of coarse grain, transition, and fine grain regions are possible in realistic geometry samples.

#### 11:40 AM

**Application of Model-Based Inversion to Materials Characterization:** Harold Sabbagh<sup>1</sup>; R. Murphy<sup>1</sup>; Elias Sabbagh<sup>1</sup>; John Aldrin<sup>2</sup>; <sup>1</sup>Victor Technologies, LLC; <sup>2</sup>Computational Tools

Model-based inversion (MBI) is of increasing importance in eddy-current nondestructive evaluation (NDE). We apply MBI to two important problems: characterizing ferritic stainless steels and characterizing thermal barrier coatings. Ferritic stainless steels are being increasingly used in heat-exchanger tubes because of the increased resistance to chloride stress corrosion and intergranular attack. This presents interesting modeling opportunities for the eddy-current NDE of these tubes because their magnetic permeability is quite large, being of the order of 950 for low stress, decreasing to 500 for a state of shear stress. We will present examples of direct and inverse problems involving such tubes, using the proprietary code VIC-3D(c). The application of NDE to high-temperature coatings is one of the important factors in achieving a high level of structural integrity in advanced gas turbines. We will demonstrate that sophisticated eddy-current inverse techniques can be utilized to measure the thickness and remaining life of high-temperature coatings.

#### 12:00 PM

**Conductivity Profile Determination via Model-Based Inversion of Swept Frequency Eddy Current Data and Its Use for Near-Surface Material Characterization:** Norio Nakagawa<sup>1</sup>; Chester Lo<sup>1</sup>; Anatoli Frishman<sup>1</sup>; <sup>1</sup>Iowa State University

This paper reports on a nondestructive residual stress characterization methodology for superalloy components having residual stresses ranging in depth between tens of micrometers and an order of a millimeter. Using high frequency eddy current (EC) instrumentations, we measure the near-surface conductivity deviation profiles and relate them to the residual stress profiles via the piezoresistivity. We have been examining precipitation hardened superalloys such as Inconel 718, while recently adding other types of superalloys in the scope of applications. When inverting swept frequency impedance data into conductivity deviation profiles, we utilize the lift-off normalized vertical component signals for direct comparison with model predictions without being adversely affected by instrumentation and lift-off noise. The critical step is to convert conductivity profiles into residual stress profiles, where the apparent piezoresistivity is strongly affected by the specific material conditions. We will present recent findings regarding precipitation hardening and other material effects on residual stress characterization.

### Alumina and Bauxite: Bayer Process I

*Sponsored by:* The Minerals, Metals and Materials Society, TMS Light Metals Division, TMS: Aluminum Committee, TMS: Aluminum Processing Committee

*Program Organizers:* James Metson, University of Auckland; Carlos Suarez, Hatch Associates Consultants Inc

Tuesday AM  
March 1, 2011

Room: 17A  
Location: San Diego Conv. Ctr

*Session Chair:* To Be Announced

#### 8:30 AM

**Application of Operation Integrity Management to the Alumina Industry:** Carlos Suarez<sup>1</sup>; Daniel Welshons<sup>1</sup>; John McNerney<sup>2</sup>; Jim Webb<sup>2</sup>; <sup>1</sup>Hatch Associates Consultants Inc; <sup>2</sup>Warren-Fortought Inc

In today's economic environment the Safety of our industry assets – People, Equipment and Processes – have become even more demanding. This paper attempts to provide means to apply Operation Integrity Management System (OIMS) to the Alumina Industry. It discusses what OIM is about, its implementation parameters such as cost and time, as well as an effective way to integrate such a system into refineries day to day operations. A series of Key Process Performance Indicators (KPPIs) are presented as well as an Electronic Knowledge Support System (EKSS) Mockingbird ® as a tool to support the implementation of OIM.

#### 8:55 AM

**Influence of Solid Concentration, Particle Size Distribution, pH and Temperature on Yield Stress of Bauxite Pulp:** Carla Barbato<sup>1</sup>; Márcio Nele<sup>2</sup>; Silvia França<sup>3</sup>; <sup>1</sup>EQ/UFRJ/CETEM; <sup>2</sup>EQ/UFRJ; <sup>3</sup>CETEM

In Northern Brazil, bauxite pulp is transported through pipelines to the plant where alumina is produced. In slurry transportation through pipelines, knowing the yield stress value is essential for pumps and pipeline design. Yield stress is the minimum shear stress and corresponds to the first evidence of flow. This rheological property is influenced by some factors, such as: particle form, temperature, particle size distribution and interaction among the particles. Within the context above, the objective of this work is to verify the influence of solid concentration, particle size distribution, temperature and pH on the yield stress of bauxite pulp. It was verified that the yield stress of bauxite slurry increases as solid concentration goes up, decreases with particle size, temperature and pH.

#### 9:20 AM

**A New Method of Organics Removal in Bayer Process:** Bai Yingwei<sup>1</sup>; Gao Zhenwen<sup>1</sup>; Shen Mingliang<sup>1</sup>; Yi Xiaobing<sup>1</sup>; <sup>1</sup>CHALIECO

This article introduces briefly main organics sources at Bayer process alumina production and the harms due to accumulation during process flow, specifies the organics removal methods applied generally in world alumina refineries, and explains briefly advantages & disadvantages of each method. The article stresses the new super-concentrated organics removal method developed successfully by CHALIECO GAMI with Guizhou University together, which not only has good organics removal effect (total removal rate of 57~67%), but also removes the carbonates in the process flow.

#### 9:45 AM

**Alunorte Expansion 3 – The New Lines Added to Reach 6.3 Million Tons per Year:** Daryush Khoshnevis<sup>1</sup>; Luiz Corrêa<sup>2</sup>; Joaquim Ribeiro Alves Filho<sup>1</sup>; Hans Marius Berntsen<sup>3</sup>; Ricardo Carvalho<sup>2</sup>; Daryush Albuquerque Khoshnevis<sup>1</sup>; <sup>1</sup>Alumina do Norte do Brasil S.A.; <sup>2</sup>Vale S.A.; <sup>3</sup>Hydro Aluminium AS

Alunorte started operation in 1995 with a design production capacity of 1.1 Mtpy. Since then the plant was expanded three times and consists today of seven production lines with a total production capacity of 6.3 Mtpy. Expansion 3 was commissioned in 2008 and consists of process lines 6 and 7. Their nominal production capacity was reached after a short start-up phase. In Expansion 3 a number of new technology developments were

implemented. The impact of the process modifications applied in lines 6 and 7 compared to the previous lines are discussed with regard to effects on production volume, productivity, alumina quality and availability. However, a number of challenges are associated with the operation of a plant of the size of Alunorte which has grown very fast: the management of seven process lines, the operation of the plant with a very young organization and strong demand for training.

#### 10:10 AM Break

#### 10:20 AM

**One Green Field Megaton Grade Large Alumina Refinery with Successful Engineering and Operation Experience:** *Luo Xianqing*<sup>1</sup>; Yang Xiaoping<sup>1</sup>; Yi Xiaobing<sup>1</sup>; <sup>1</sup>CHALIECO

Phase I alumina project (1.6million tons/a metallurgical grade alumina) of Guangxi Huayin Aluminum Corporation Limited is one green field construction project with largest disposable investment in China alumina industry, and its diaspora bauxite is difficult to be ground and dissolved with high aluminum and low silicon content. Now two year's operation practice shows that the comprehensive energy consumption per ton alumina production is only 10.51GJ. This article introduces the process scheme and technical measures adopted in the engineering and operation stage for the features of this project.

#### 10:45 AM

**Advanced Process Control in the Evaporation Unit:** *C. Satish Kumar*<sup>1</sup>; Uttam Giri<sup>1</sup>; Rosalin Pradhan<sup>1</sup>; Tonmoy Banerjee<sup>1</sup>; Ramu Saha<sup>1</sup>; Pratichi Pattnaik<sup>1</sup>; <sup>1</sup>Vedanta Aluminium limited

Energy consumption is a significant constituent of production cost in an Alumina refinery. Indian refineries are striving to reach global benchmarks and have made conscious efforts to minimize energy consumption. Evaporation plays a significant role in conserving energy and is responsible for 30% of the thermal energy consumption. In the Evaporation unit, due to a large number of interacting processes, frequent disturbances and the presence of single line equipment, it is necessary to maximize the utilization of assets to ensure the production volumes at targeted efficiencies. The need for reduction in process variability resulting in optimizing operations, challenged by plant constraints, was derived by adopting Advanced Process Control (APC) application in the Evaporation unit. APC incorporates a matrix of modeled dynamic process responses with an optimizer to maintain the unit at the most profitable vertex of the allowable operating envelope. This paper will discuss the area selection criteria, activities carried out during the project tenure and post benefit analysis.

#### 11:10 AM

**Reduction in Metallic Impurities by Improvement in Process Control:** Ruth Headlam-Shaw<sup>1</sup>; <sup>1</sup>Alcoa Minerals of Jamaica

Alcoa's Clarendon Alumina Works recorded a significant improvement in the control of and reduction of impurities in its smelter grade alumina (SGA). This marked improvement came about as a result of a change in green liquor filter technology from gravity sand filtration to short cycle pressure filtration and improvement in process management systems.. This paper discusses the impact the change had on Iron,Chromium, Titanium, Phosphorous and Calcia in alumina product.

## Aluminum Alloys: Fabrication, Characterization and Applications: Solidification

*Sponsored by:* The Minerals, Metals and Materials Society, TMS Light Metals Division, TMS: Aluminum Processing Committee  
*Program Organizers:* Subodh Das, Phinix LLC; Zhengdong Long, Kaiser Aluminum; Tongguang Zhai, University of Kentucky

Tuesday AM  
March 1, 2011

Room: 14A  
Location: San Diego Conv. Ctr

*Session Chair:* Hiromi Nagaumi, Suzhou Research Institute for Nonferrous Metals

#### 8:30 AM

**Simulation of the Deformation of a Flexible Combo Bag in a DC Aluminium Casting:** *Abdellah Kharicha*<sup>1</sup>; <sup>1</sup>University of Leoben

In the latest years combo bags were introduced in the DC aluminium casting to give better production results. In order to understand why this is the case, hydrodynamic simulations are performed. The movement of the Combo bag surface is modelled though the introduction of particles markers. The particles are allowed to move according to a dynamic law using an assumed flow-bag drag interaction. An additional artificial elastic force is introduced between neighbour particles in order to keep the total bag surface constant. The specificity of the present liquid/bag drag is not only its dependence on the relative movements, but also on the relative liquid velocity/bag surface angle. This kind of fluid/structure approach allows a full coupling between the liquid flow hydrodynamic and the bag shape movement. The results will focus on the quantification of the impact of the bag on the global heat transfer and solidification pool shape.

#### 8:50 AM

**Solidification Analysis of Al-Si Alloys Modified with Addition of Cu Using In-Situ Neutron Diffraction:** *Dimitry Sediako*<sup>1</sup>; Wojciech Kasprzak<sup>2</sup>; Ian Swainson<sup>3</sup>; Ovidiu Garlea<sup>4</sup>; <sup>1</sup>National Research Council Canada ; <sup>2</sup>CANMET-MTL, Natural Resources Canada; <sup>3</sup>National Research Council Canada; <sup>4</sup>Oak Ridge National Lab

The potential of application of in-situ neutron diffraction for studies of solidification of Al alloys were earlier reported by the authors for the binary hypereutectic Al-Si system. This illustrated the potential of neutron diffraction for high resolution melt analysis at near-liquidus temperatures required for advanced studies of grain refining, eutectic modification, etc. The solid and liquid volume fractions were determined based on the change of intensity of neutron diffraction peaks over the solidification interval. The path of non-equilibrium solidification for the alloy modified with addition of copper and magnesium is very complex. Phase diagrams and FactSage-based computations give only approximate kinetics of solid phase(s) evolution during cooling and solidification. On the other hand, in-situ neutron diffraction, coupled with the results of thermal analysis, provided non-biased experimental data on phase evolution; for example, on formation of FCC Al-Cu-Si, diamond silicon, and Al-Cu theta phase during solidification of hypereutectic Al-Si-Cu alloy.

#### 9:10 AM

**Development of Novel Grain Refiner for Al-Si Alloys:** *Magdalena Nowak*<sup>1</sup>; Hari Babu Nadendla<sup>1</sup>; <sup>1</sup>BCAST

A novel effective grain refiner for aluminium alloys has been developed. The composition of the grain refiner has been optimised to produce a fine grain structure for Al-Si alloys. Effectiveness of grain size under various cooling conditions has also been investigated to simulate various practical casting conditions. For comparative purposes, a wide range of Al alloys have been produced with the addition of commercially available Al-5Ti-B master alloys. The results show that the addition of novel grain refiner reduces the grain size significantly when compared to that of the commonly used Al-5Ti-B grain refiner addition. As a result of fine grains, the porosity in the

solidified alloys is notably lower. A remarkable improvement in mechanical properties has also been observed.

#### 9:30 AM

**Application of Neutron Diffraction in Analysis of Residual Stress Profile in the Cylinder Web Region of As-Cast V6 Aluminum Engine Block with Cast-In Iron Liners:** *Dimitry Sediako*<sup>1</sup>; Ravi Ravindran<sup>2</sup>; Camden Hubbard<sup>3</sup>; Francesco D'Elia<sup>2</sup>; Anthony Lombardi<sup>2</sup>; Alan Machin<sup>2</sup>; Robert Mackay<sup>4</sup>; <sup>1</sup>National Research Council Canada ; <sup>2</sup>Ryerson University; <sup>3</sup>Oak Ridge National Laboratory; <sup>4</sup>Nemak of Canada

Nowadays aluminum alloys are widely used for production of gasoline engine blocks. In this study 319 aluminum is sand cast around Fe-liner cylinder inserts, then undergoes the T7 heat treatment process. One of the critical factors determining the quality of the final product is the type, level, and profile of residual stresses along the Fe liners (or extent of liner distortion) that are always present in a cast component. In this study neutron diffraction was used to characterize residual stresses along the Al and the liners in the web region of the cast engine block. The strains were measured both in aluminum and iron in hoop, radial, and axial orientations and stresses were determined using generalized Hook's law. The study gives invaluable insight on anticipated service properties of the engine block and demonstrates that neutron strain mapping is an efficient tool for optimization of manufacturing technologies.

#### 9:50 AM

**Surface Modification of Aluminum Alloys by Electrolytic Plasma Processing:** *Mark Liu*<sup>1</sup>; Xijin Li; Ben Li Luan<sup>1</sup>; <sup>1</sup>National Research Council Canada

Aluminum alloys are widely used as lightweight materials in the transportation industry. For applications in aggressive wear and corrosive environments, proper surface treatment and protection of aluminum alloys are required. Electrolytic plasma processing is a relatively new surface coating technology that offers an environmentally friendly and cost effective solution for the surface protection of lightweight materials. In this presentation, the effect of electrolyte chemistry and various processing parameters on the microstructure, phase constituents, and the properties of the surface coating of aluminum alloys is discussed.

#### 10:10 AM Break

#### 10:25 AM

**Solidification Characteristics of Aluminium Alloys under Electron Beam Fabrication Conditions:** *Ma Qian*<sup>1</sup>; Dacian Tomus<sup>2</sup>; <sup>1</sup>The University of Queensland; <sup>2</sup>Monash University

Wire-based electron beam direct manufacturing (EBDM) is a novel layer additive near-net shape metal fabrication technique. The process can be advantageous for aluminium alloys if new compositions can be created that leverage the near rapid solidification conditions inherent to the process. As most structural aluminium alloys utilize some form of precipitation strengthening, to capitalise on the EBDM attributes, it is important to understand the as-solidified microstructural characteristics under electron beam fabrication conditions. This paper describes the results of an investigation of the microstructures of electron beam processed AA 2219 and AA 6061 alloys and binary Al-Sc and Al-Ti alloys. Electron beam processing led to unique microstructural features in each alloy. The experimental observations are compared with Thermo-Calc predictions for metastable solidification. It will be demonstrated that electron beam processing offers promising alloy design opportunities for advanced aluminium alloy development.

#### 10:45 AM

**Formation of Intermetallic Compound Layer between A356 Al Alloy and Cast Iron in Isothermal Condition.:** *Kwang Suk Son*<sup>1</sup>; Sungmin Kang<sup>1</sup>; Jinsu Kim<sup>1</sup>; Donggyu Kim<sup>1</sup>; <sup>1</sup>Dong-A university

A356 alloy and cast iron have many advantages for industrial purpose despite of insufficient properties. Bonding of dissimilar materials which would compensate their weaknesses, could increase its applicability to the industrial usages. But some problems have been remained in bonding

these alloys by casting due to the role of graphite and the complexity of intermetallic compound layer of Al-Fe-Si system. This work, the interactions between liquid A356 alloy and cast iron, and the structural investigation of compound layer were performed with the variables of contact temperature and time by hot dip aluminizing. Microstructure of interlayer was investigated by TEM, FESEM and EDS. Intermetallic compound layer showed two growth steps, during and after dipping. Poly crystalline compound layer consisting of t1(Al<sub>10.42</sub>Fe<sub>0.39</sub>Si<sub>0.15</sub>) and □(FeAl<sub>2</sub>) was formed during dipping and columnar ternary phase of □(FeAl<sub>3</sub>) and t5(Al<sub>10.72</sub>Fe<sub>0.18</sub>Si<sub>0.10</sub>) was formed after dipping. In addition, the growth mechanisms of compound layer was also discussed.

#### 11:05 AM

**Effects of Al-8B Grain Refiner on the Structure, Hardness and Tensile Properties of a New Developed Super High-Strength Aluminum Alloy:** Mohammad Alipour<sup>1</sup>; Masuod Emamy<sup>1</sup>; Jafar Rassizadehghani<sup>1</sup>; Mostafa Karamouz<sup>1</sup>; Mortaza Azarbarmas<sup>1</sup>; <sup>1</sup>University of Tehran

In this study the effect of Al-8B grain refiner on the structural characteristics, hardness and tensile properties of Al-12Zn-3Mg-2.5Cu aluminum alloy was investigated. The results show that by adding 3.75 wt.% Al-8B grain refiner in the cast alloy, the grains can be refined to a fine degree. T6 heat treatment was applied for all specimens before tensile testing. In heat treated condition, the average tensile strength of 500 MPa was found to be increased to 590 MPa for sample refined with 3.75 wt.% Al-8B (0.3 wt.% B). SEM fractography of the fractured faces of several castings showed an overall macroscopically brittle appearance at low magnifications. At higher magnifications, unrefined specimens showed cracking along the grains, whereas B-refined specimens showed cracks in individual intermetallic compounds.

### Aluminum Reduction Technology: Environment-Emissions/ Anode Effect II

*Sponsored by:* The Minerals, Metals and Materials Society, TMS Light Metals Division, TMS: Aluminum Committee, TMS: Aluminum Processing Committee

*Program Organizers:* Mohd Mahmood, Aluminium Bahrain; Abdulla Ahmed, Aluminium Bahrain (Alba); Charles Mark Read, Bechtel Corporation; Stephen Lindsay, Alcoa, Inc.

Tuesday AM  
March 1, 2011

Room: 17B  
Location: San Diego Conv. Ctr

*Session Chair:* Marco Stam, Aluminium Delfzijl

#### 8:30 AM

**On Continuous PFC Unrelated to Anode Effects:** *Xiping Chen*<sup>1</sup>; Wangxing Li<sup>1</sup>; Jerry Marks<sup>2</sup>; <sup>1</sup>Zhengzhou Research Institute of Chalco; <sup>2</sup>J Marks & Associates

It was investigated what result in continuous PFC emission unrelated to anode effects in two smelters. Anode current distribution was measured in QY smelter, no obvious correlation was observed between non-homogenous anode current and continuous PFC emission. Bath temperature and alumina concentration were synchronously measured during PFC monitoring in LX smelter, no continuous PFC emit when cells are operated at stable bath temperature and alumina concentration. But no clear relationship among them was concluded and further survey need to be made in other smelters. The effect of feeding mechanism was also investigated. Metal tapping and anode exchange can disturb cells' balance, which result in cell voltage rising, then may cause continuous PFC emission. It is found out that continuous PFC emission only occurs in some particular cells and is different from cell to cell even with the same line current. It is only a small portion in total PFC emission.



8:50 AM

**Reduction of Anode Effect Duration in 400kA Prebake Cells:** *Wei Zhang*<sup>1</sup>; David Wong<sup>1</sup>; Michel Gilbert<sup>1</sup>; Yashuang Gao<sup>1</sup>; Mark Dorreen<sup>1</sup>; Mark Taylor<sup>1</sup>; Alton Tabereaux<sup>2</sup>; Melinda Soffer<sup>2</sup>; Xiaopu Sun<sup>2</sup>; Changping Hu<sup>3</sup>; Xuemin Liang<sup>4</sup>; Haitang Qin<sup>4</sup>; Jihong Mao<sup>5</sup>; Xuehui Lin<sup>5</sup>; <sup>1</sup>Light Metals Research Centre; <sup>2</sup>Institute for Governance and Sustainable Development; <sup>3</sup>China Nonferrous Metals Industry Association; <sup>4</sup>Henan Zhongfu Industrial Co. Ltd.; <sup>5</sup>Northeastern University

In order to improve energy efficiency and reduce green house gas emissions, the aluminum smelting industry has been continuously working on reducing both anode effect frequency (AEF) and duration (AED). However, there is still a long way to go to achieve zero anode effect (AE) on very high amperage, low specific power consumption cells due to the added complexity of the process. A new program to quickly terminate AEs has been developed by Light Metals Research Centre, the University of Auckland, in conjunction with the efforts of the Asia Pacific Partnership on Clean Development and Climate (APP) to facilitate investment in clean technologies and to accelerate the sharing of energy efficient best practices. A pilot project was initiated to test an automatic Anode Effect Termination (AET) program on 400kA cells in Zhongfu, China. This paper demonstrates the success of the new anode effect termination (AET) program in killing AEs on this cell technology without conflicting with normal cell operations. The resulting decrease in average anode effect duration (AED) is demonstrated.

9:10 AM

**Sustainable Anode Effect Based Perfluorocarbon Emission Reduction:** *Neal Dando*<sup>1</sup>; Lise Sylvain<sup>1</sup>; Janice Fleckenstein<sup>1</sup>; Ciro Kato<sup>1</sup>; Vince Van Son<sup>1</sup>; Laura Coleman<sup>1</sup>; <sup>1</sup>Alcoa

Alcoa has been performing plant-specific perfluorocarbon (PFC) emission testing at operating smelters for over 15 years and has the largest Tier 3 data base in the aluminum industry. From 2005-2009, Alcoa smelters have reduced anode effect (AE) based PFC emissions by over 0.48 T CO<sub>2</sub>e/T Al produced, resulting in an absolute annual reduction of 2.3 million tonne CO<sub>2</sub>e over this same time period. These PFC reductions were the result of 1) continuous local optimization at operating locations 2) focused monthly reporting on anode effect performance, 3) internal workshops regarding shared AE reduction efforts and 4) technology improvements. This paper will discuss examples of key enablers employed for sustaining AE-based PFC reductions of 15.9 million tonnes over the period 1990 to 2009.

9:30 AM

**The Initiation, Propagation and Termination of Anode Effects in Hall-Heroult Cells:** *Gary Tarcy*<sup>1</sup>; Alton Tabereaux<sup>2</sup>; <sup>1</sup>Alcoa; <sup>2</sup>Consultant

Anode effects in Hall-Heroult cells have been the subject of multiple investigations and studies. The current state of the knowledge is fairly well advanced and there is very little discrepancy or controversy with respect to many of the phenomena associated with anode effects. Included in this is the belief they are: 1) AE are the predominate emitter of PFC into the atmosphere 2) AE are triggered by low alumina concentrations near the anode surface 3) Short circuiting of at least part of the anode cathode inter electrode gap is required to terminate an anode effect. This paper will cover some of less discussed aspects of anode effect including the 1) the initiation at a single random anode in the circuit. 2) The propagation to multiple anodes until the whole circuit is on anode effect 3) The reason it is necessary to short circuit the anodes to terminate anode effect.

9:50 AM

**Towards Eliminating Anode Effects:** *Ali Al Zarouni*<sup>1</sup>; Barry Welch<sup>2</sup>; Maryam Al-Jallaf<sup>1</sup>; Arvind Kumar<sup>1</sup>; <sup>1</sup>DUBAL; <sup>2</sup>Welbank Consulting Ltd

It has been established that the atmosphere contains appreciable amount of per fluorocarbon (PFC) gases. These are powerful greenhouse gases and with extremely long lifetime. Although these gases are being used in the semiconductor industry, it has been established that aluminium smelters are the main source. Emissions of PFC Gases from the aluminium industry have therefore become an environmental issue. The PFCs are emitted from an aluminium reduction cell when it is on an 'anode effect'. The exact nature of the onset of an anode effect is still shrouded in mystery. However, an

astounding reduction in number of anode effects has been achieved by understanding, attributing and implementing a strict process control regime to eliminate assignable causes. Dubal's progress in reducing anode effect frequency to less than 0.05 AE/pot-day in a sustained manner in poline 5B has been discussed and presented.

10:10 AM Break

10:20 AM

**Monitoring Air Fluoride (F-) Concentration around ALUAR Smelter in Puerto Madryn (Chubut Province, Argentina):** *Jorge Zavatti*<sup>1</sup>; Claudio Lopez Moreno<sup>1</sup>; Juliana Lifschitz<sup>2</sup>; Gabriela Quiroga<sup>1</sup>; <sup>1</sup>ALUAR Aluminio Argentino SAIC

The emissions of F- is a significant environmental aspects of aluminum industry. Therefore the government have established regulations aimed at controlling the environmental performance of smelters through monitoring of F- emissions. Chubut Province (Argentina), sets emission limits, 1 kg F-/ton Al and following recommendations by the World Health Organization, they set a guideline for inmission at 16.0 µg F-/m<sup>3</sup>. In this paper we present: i)the monitoring network that ALUAR deployed in Puerto Madryn, 14 air sampling stations; ii)sampling procedures and analysis adopted; iii)the results of air fluoride concentration from July 2009 to June 2010; iv)the validation of these results by three scientific institutes of Argentina. The results show that in Puerto Madryn (100000 inhabitants; 2 km from ALUAR's Plant), the median concentration in air was 1.61 µg F-/m<sup>3</sup> (N = 471 - p95 = 5.32). These values met the inmission guideline level determined by the supervisory authority.

10:40 AM

**Correlation between Moisture and HF Formation in the Aluminium Process:** *Camilla Sommerseth*<sup>1</sup>; Karen Osen<sup>2</sup>; Thor Aarhaug<sup>2</sup>; Egil Skybakmoen<sup>2</sup>; Asbjørn Solheim<sup>2</sup>; Christian Rosenkilde<sup>1</sup>; Arne Ratvik<sup>1</sup>; <sup>1</sup>Norwegian University of Science and Technology, NTNU; <sup>2</sup>SINTEF

Hydrogen fluoride (HF) emission to the working atmosphere is still a problem in the aluminium industry. Moisture in secondary alumina fed to the cell and humidity in the ambient air reacts with fluorides in the bath and fluoride vapours to form hydrogen fluoride. The relation between the various sources of water and the resulting HF emission is still not well understood. In this work, industrial measurements have been done to determine where HF escapes from the bath. The quantities of HF and moisture at the specific sites have also been determined. Measurements were done in the duct during normal operation as well as during anode change, above the feeder hole and above an open hole in the crust. A strong correlation between feed cycle and HF levels was measured. Increased HF emissions were also recorded during anode change.

11:00 AM

**Particulate Emissions from Electrolysis Cells:** *Heiko Gaertner*<sup>1</sup>; Arne Ratvik<sup>1</sup>; Thor Aarhaug<sup>2</sup>; <sup>1</sup>NTNU; <sup>2</sup>SINTEF

In the dry cleaning of the exhaust gas from the aluminium cells impurities are accumulated in the finer fractions of secondary alumina from the dry scrubbers. The present work describes new methods for the determination of dust composition, aiming at increasing the understanding of the effect of cell operation on the amount and the composition of dust in the fume. New and advanced analysis methods are used to characterize a broad specter of emissions. An Electrical Low Pressure Impactor is used to sample and analyze the dust from the cells. The equipment enables real-time particle size distribution analysis of 12 particle classes in the range 30 nm - 10 µm. The size classified samples are analyzed by means of SEM/EDS and XRD to determine the characteristic chemical composition of the different fractions. Understanding the evolution, evaporation, and condensation of particulates in the cell emissions under different operational conditions may facilitate new standards for environmental friendly and energy efficient high amperage electrolysis cells.

11:20 AM

**Investigation of Solutions to Reduce Fluoride Emissions from Anode Butts and Crust Cover Material:** *Guillaume Girault*<sup>1</sup>; *Maxime Faure*<sup>1</sup>; *Jean-Marc Bertolo*<sup>1</sup>; *Stéphanie Massambi*<sup>1</sup>; *Georges Bertran*<sup>1</sup>; <sup>1</sup>Rio Tinto Alcan

For many aluminium smelters, reducing fluoride emissions is often a condition to increase production. Since they contribute up to 40% of the overall roof vent emissions, anode change operations are often targeted for improvements and specifically the emissions from the anode butts and crust cover. The Rio Tinto Alcan Research Centre, LRF, has been conducting an R&D programme over the past few years aimed at improving the understanding of the physical phenomena involved and ultimately minimising this specific contribution. On this basis, different conceptual solutions have been developed and their relative performance evaluated. These tests, associated with past experience of enclosed butt boxes and crust bins, concluded that any container receiving a hot butt and bath crust would require almost complete sealing to be effective. The next stage in this programme is engineering design with the aim of developing smelter technology with the lowest environmental footprint.

11:40 AM

**PFC Survey in Some Smelters of China:** *Wangxing Li*<sup>1</sup>; *Xiping Chen*<sup>1</sup>; <sup>1</sup>Zhengzhou Research Institute of Chalco

PFC survey was performed by CHALCO. Results of the first PFC survey from seven different Chinese potlines are discussed in this paper. This survey included normally-operated, newly-started, power-limitation and control-mode changing potlines. The measurement equipment used in the survey is MG2030 FTIR which comes from MKS Instruments. Gas sampling was directly pumped out of main exhaust duct before stack and transmitted into FTIR by Teflon tube. Fugitive PFC emission was not measured. The calculation of PFC amount was based on IPCC Tier 3a method. Total PFC emission was calculated from duct PFC emission divided by collection efficiency. Newly-started, control-mode changing and power-limitation potlines emitted much more PFC than normally-operated ones. PFC emission from power-limitation potline was the highest among seven. Three of seven potlines have PFC emission close to IAI 2010 target. Two potlines have similar PFC emission to Australia 2006 average level. The lowest PFC emission is 0.21 tCO<sub>2</sub>-e/t-Al.

## Approaches for Investigating Phase Transformations at the Atomic Scale: Transformations in Fe, Ni and Al Based Systems II

*Sponsored by:* The Minerals, Metals and Materials Society, ASM International, TMS Materials Processing and Manufacturing Division, TMS/ASM: Computational Materials Science and Engineering Committee, TMS/ASM: Phase Transformations Committee  
*Program Organizers:* Neal Evans, Oak Ridge National Laboratory; Francisca Caballero, Spanish National Research Center for Metallurgy (CENIM-CSIC); Chris Wolverton, Northwestern University; David Seidman, Northwestern University; Rajarshi Banerjee, University of North Texas

Tuesday AM  
March 1, 2011

Room: 32B  
Location: San Diego Conv. Ctr

*Session Chairs:* Rajarshi Banerjee, University of North Texas; Hamish Fraser, Ohio State University

8:30 AM Invited

**Nuclear Reactor Materials at the Atomic Scale:** *Emmanuelle Marquis*<sup>1</sup>; *Ceri Williams*<sup>2</sup>; *Nadine Baluc*<sup>3</sup>; *Samuel Humphry-Baker*<sup>2</sup>; <sup>1</sup>University of Michigan; <sup>2</sup>University of Oxford; <sup>3</sup>Paul Scherrer Institute

The development of next-generation fission and fusion reactors requires new and improved materials, which will withstand extreme combinations of temperature, stress and irradiation. In order to develop these materials,

fundamental understanding is required of the atomic-scale behaviour of candidate alloys subjected to extreme treatment. We report progress in the combined use of 3-D atom probe analysis and transmission electron microscopy to study the atomic processes occurring in Fe-Cr,oxide-dispersion-strengthened steels and W alloys after thermal and heavy ion irradiation treatments. In each case, the materials exhibit highly complex patterns of behaviour on the nanometre scale, including solute clustering, segregation to dislocations, grain boundaries and interphase interfaces, and the formation of second phase particles. These phenomena have been quantitatively investigated. Similarities and differences in the behaviour of the different materials will be described, and implications for the optimisation of future reactor materials design will be discussed.

8:55 AM Invited

**A Multiple Technique Approach for Understanding Phase Separation in Nanostructured Ferritic Steels:** *Michael Miller*<sup>1</sup>; *C.L. Fu*<sup>1</sup>; *C.M. Parish*<sup>1</sup>; *X.-L. Wang*<sup>1</sup>; <sup>1</sup>Oak Ridge National Laboratory

Nanostructured ferritic steels are under consideration for use in future generations of advanced nuclear systems due to their stability against high temperature creep and, more importantly, their remarkable tolerance to high dose neutron and ion irradiation. A synergistic combination of first principle calculations with atom probe tomography, transmission electron microscopy, and neutron scattering experiments have been used to understand the phase separation and diffusion processes that occur in these mechanically alloyed, nanostructured ferritic steels. From this multiple characterizations approach, the microstructural features responsible for these remarkable properties, including high number densities of nanoclusters and solute segregation to the grain boundaries, have been identified. This research was sponsored by the U.S. Department of Energy, Materials Sciences and Engineering Division. Research at the Oak Ridge National Laboratory SHaRE User Facility is sponsored by the Scientific User Facilities Division, Office of Basic Energy Sciences, U.S. Department of Energy.

9:20 AM Invited

**Atomic Scale Investigation of Y-Ti-O Nanoclusters in Nanostructured Ferritic Alloys:** *Brian Wirth*<sup>1</sup>; *Hyon-Jee Lee*<sup>2</sup>; *Lauren Marus*<sup>2</sup>; *G. Robert Odette*<sup>3</sup>; <sup>1</sup>University of Tennessee; <sup>2</sup>University of California, Berkeley; <sup>3</sup>University of California, Santa Barbara

Nanostructured ferritic alloys (NFAs) are characterized by very high tensile and creep strength, and resistance to neutron irradiation. These properties result from a very high number density dispersion of nm-scale Y-Ti-O rich features (NFs) that precipitate homogeneously at high consolidation temperatures from mechanically alloyed Fe-Cr-Ti-Y<sub>2</sub>O<sub>3</sub> powders. The NFs have been studied by small angle neutron scattering, atom probe tomography, transmission electron microscopy, positron annihilation spectroscopy, and x-ray absorption spectroscopy. NFs form rapidly at number densities, sizes and characters (compositions and structures) that are dictated by the processing temperature and alloy composition. However, the precise natures of various NFs are not well understood, and appear to range from coherent solute enriched GP-type zones to near stoichiometric complex oxides, such as Y<sub>2</sub>TiO<sub>5</sub> and Y<sub>2</sub>TiO<sub>7</sub>. In this presentation, atomic scale modeling results, developed from ab-initio electronic structure calculations, are presented that provide insight into the structure and composition of the NFs.

9:45 AM

**Characterization of Nanofeatures and Oxides in Nanostructured Ferritic Alloys – Cross Comparison SANS, SAXS, TEM, APT and Other Techniques:** *G. Robert Odette*<sup>1</sup>; *Nicholas Cunningham*<sup>1</sup>; *Takuya Yamamoto*<sup>1</sup>; *Yuan Wu*<sup>1</sup>; *Auriane Etienne*<sup>1</sup>; *Erich Stergar*<sup>1</sup>; <sup>1</sup>UC Santa Barbara

Nano-structured ferritic alloys (NFAs) have high tensile and creep strength permitting service up to 800°C and manifest remarkable resistance to radiation damage. These outstanding properties derive from an ultrahigh density of Ti-Y-O enriched nano-features (NFs) that provide dispersion strengthening, help stabilize dislocation and fine grain structures, reduce excess concentrations of displacement defects by enhancing vacancy-self-interstitial recombination and trap helium in fine, and relatively harmless, bubbles. However, the compositions and structures of the NFs, especially

TUESDAY AM

at the smallest sizes, are not well understood. The results of SANS, SAXS, TEM, APT and other characterization techniques are cross compared. The general trends in structure and composition suggest that the smallest NFs (less than 5 nm) are consistent with cubic Y<sub>2</sub>Ti<sub>2</sub>O<sub>7</sub>, while at larger sizes (5 to 25 nm) they are often more consistent with orthorhombic Y<sub>2</sub>TiO<sub>5</sub>. However many features cannot be identified with any known Y-Ti oxide and most often they are non-stoichiometric.

#### 10:00 AM

**Effect of Elastic Strain on Phase Separation in Fe-20% Cr-6% Al-0.5% Ti ODS Alloy:** *Carlos Capdevila-Montes*<sup>1</sup>; Mike Miller<sup>2</sup>; Isaac Toda<sup>1</sup>; Jesus Chao<sup>1</sup>; <sup>1</sup>CENIM-CSIC; <sup>2</sup>ORNL

The effect of elastic deformation on temporal evolution of the microstructure resulting from phase separation of an Fe-20% Cr-6% Al-0.5% Ti oxide dispersion strengthened (ODS) alloy at a temperature of 708 K has been analyzed by atom probe tomography (APT). Microstructures with high (as-cold rolled material) and low (coarse grained recrystallized material) dislocation densities have been tested at both 0.8 and 1 times the yield strength of this material during aging at 708 K. Microstructural analysis by APT revealed simultaneous phase separation kinetics into Fe-rich  $\alpha$ , Cr-rich  $\alpha'$  and Fe-Ti-Al phases. The roles of Al and Ti during the decomposition process have been investigated. Proximity histogram analysis revealed significant partitioning of Al and Ti, which is consistent with theoretical calculations. Research at the Oak Ridge National Laboratory SHaRE User Facility was sponsored by the Scientific User Facilities Division, Office of Basic Energy Sciences, U.S. Department of Energy.

#### 10:15 AM Break

#### 10:30 AM Invited

**Nano-Structural Characterizations Using Advanced Methods - A Case Study of Nanosized Cu Precipitates in C Containing Fe-1.2 Wt% Cu Alloys:** *Rajashekhara Shabadi*<sup>1</sup>; Roland Taillard<sup>1</sup>; <sup>1</sup>University of Science and Technology of Lille, France

This study deals with the sole effect of C on Cu precipitation in Fe-1.2 wt% Cu steels. Four C contents up to 750 ppm were studied. Addition of carbon substantially increases both the kinetics and magnitude of precipitation strengthening up to longer aging times. Advanced methods of characterization such as Small Angle X-ray Scattering (SAXS) and Tomographic Atom Probe (TAP) were adopted to precisely determine the composition, size, density and volume fraction of the nanometer sized precipitates after different aging periods. It was observed that C was not co-precipitated with Cu, but C agglomerations were present close to the precipitates. The accelerating effect on the Cu precipitation is discussed with regards to both the driving force of nucleation and the kinetics of Cu diffusion. Combining results of SAXS, TAP and TEM gave complementary results in following Cu precipitation sequence in the presence of the third alloying element.

#### 10:55 AM

**Anharmonic Phonon Behavior in  $\alpha$ -Fe at Temperatures near the Structural Phase Transition:** *Lisa Mauger*<sup>1</sup>; Matthew Lucas<sup>2</sup>; Jorge Munoz<sup>1</sup>; Brent Fultz<sup>1</sup>; <sup>1</sup>California Institute of Technology; <sup>2</sup>Air Force Research Laboratory

The phonon density of states (DOS) of bcc Fe was measured from room temperature up through the 1185K fcc phase transition using Nuclear Resonant Inelastic X-ray Scattering of <sup>57</sup>Fe. At higher temperatures all phonons shift to lower energies (soften) with thermal expansion. Above the 1043K Curie temperature, low energy transverse modes soften more rapidly, suggesting strongly anharmonic behavior before the  $\alpha$ -Fe to  $\gamma$ -Fe structural transition. Interatomic force constants for the bcc phase were obtained by iteratively fitting a Born von-Karman model to the experimental phonon spectra using a global optimizer. Trends in these force constants are used to interpret the thermal softening of the different phonon modes. The unusually large phonon anharmonicity of the transverse modes at elevated temperatures is assessed with the temperature dependences of the first and second-neighbor interatomic force constants.

#### 11:10 AM

**Atomic Scale Investigation of Gamma Prime Precipitation in Nickel Base Alloys Coupling Aberration-Corrected STEM with Atom Probe Tomography:** *Antariksh Singh*<sup>1</sup>; Gopal Viswanathan<sup>2</sup>; Soumya Nag<sup>1</sup>; Junyeon Hwang<sup>1</sup>; Jaimie Tiley<sup>2</sup>; Hamish Fraser<sup>3</sup>; *Rajarshi Banerjee*<sup>1</sup>; <sup>1</sup>University of North Texas; <sup>2</sup>Air Force Research Laboratory; <sup>3</sup>The Ohio State University

The compositional and microstructural evolution of gamma prime precipitates during continuous cooling at different rates, followed by isothermal aging, of a commercial nickel base superalloy, Rene 88DT, have been characterized by coupling multiple atomic scale characterization techniques. The primary focus was on investigating the mechanisms governing gamma prime precipitation as a function of cooling rate. Classical nucleation and growth is the dominant mechanism of precipitation in case of slower cooling rates, especially at lower undercoolings. In contrast, at faster cooling (quench) rates, the gamma prime precipitation appears to take place via a spinodal clustering (phase separation or compositional partitioning) within the disordered gamma matrix followed by chemical ordering. Direct experimental atomic scale evidence for such a mechanism will be presented based on results of aberration-corrected HAADF-STEM at atomic resolution and atom probe tomography.

#### 11:25 AM Invited

**Exploring Initial Stages of Precipitate Formation in Aluminum Alloys through Kinetic Lattice Monte Carlo Simulations:** *Marcel Suijter*<sup>1</sup>; <sup>1</sup>TU Delft

The very first stages of clustering that precede precipitation are still poorly understood. However, those stages can be important for the ultimate mechanical properties as empirical treatments such as spike pre aging prior to natural aging during storage in industrial alloys have shown. In order to augment atom probe experiments and to illuminate the role of vacancy-solute interactions, kinetic lattice Monte Carlo simulations have been employed for multicomponent Al alloys with realistic compositions, such as those based on Al-Mg-Cu and Al-Mg-Li. It is shown that these simulations, at least during the initial stages, can yield cluster distributions as function of time that resemble those from atom probe experiments provided that the solute-vacancy binding and vacancy dynamics are properly accounted for.

#### 11:50 AM

**Primary Crystallization Behavior Change Induced by Minor Element Substitution:** *Feng Yi*<sup>1</sup>; Seth Imhoff<sup>1</sup>; John Perepezko<sup>1</sup>; Paul Voyles<sup>1</sup>; <sup>1</sup>UW-Madison

Structural characterization by fluctuation electron microscopy (FEM), a technique sensitive to nanoscale order in glasses, combined with conventional techniques including BFTEM, XRD, and DSC, and computer simulations was applied to understand the primary crystallization reaction in Al-based metallic glasses. FEM shows that the glass contains nanoscale, Al-like medium range order (MRO) regions; other kinetics data demonstrate that these regions act as nucleation sites. Comparison of the FEM results to computer simulations indicates that the MRO size  $d$  and number density  $\rho_{961}$  are (1.92 $\pm$ 0.34) nm and (1.81 $\pm$ 1.67) $\times 10^{25}/m^3$  in Al<sub>88</sub>Y<sub>7</sub>Fe<sub>5</sub>. Substitution of 1 at.% Cu for Y decreases the crystallization onset,  $T_x$  by 50  $\pm$  176C with a doubling of  $\rho_{961}$  while substitution 1 at.% Cu for Al increases  $T_x$  by 10  $\pm$  176C, and reduces  $\rho_{961}$  by 30%. All the observations are consistent with a classical nucleation theory model including transient kinetics.



---

## Biological Materials Science: Surface Engineering and Biological Interactions

Sponsored by: The Minerals, Metals and Materials Society, TMS Electronic, Magnetic, and Photonic Materials Division, TMS Structural Materials Division, TMS: Biomaterials Committee  
Program Organizers: Jamie Kruzic, Oregon State University; Nima Rahbar, University of Massachusetts, Dartmouth; Po-Yu Chen, University of California, San Diego; Candan Tamerler, University of Washington

Tuesday AM  
March 1, 2011

Room: 15A  
Location: San Diego Conv. Ctr

Session Chairs: Candan Tamerler, University of Washington; Po-Yu Chen, University of California, San Diego

---

### 8:30 AM Introductory Comments

#### 8:35 AM Keynote

##### Role of Substrate Material Properties in Modulating Cell Fate and Function: *Shu Chien*<sup>1</sup>; <sup>1</sup>University of California, San Diego

Variations in physicochemical properties of the substrate can modulate the fate (proliferation and differentiation) of pluripotent stem cells (hPSCs) and the structure and function of adult cells such as vascular endothelial cells (ECs). Using a high-throughput screening approach, we have identified synthetic polymers that can be used as matrix macromolecules to support attachment, proliferation and self-renewal of several types of human hPSCs. Such findings can help to accelerate the translational applications of hPSCs in regenerative medicine. Variations in substrate rigidity under the extracellular matrix (ECM) can also regulate the proliferation and differentiation of hPSCs, with modulations of their mechanical properties. Culture of ECs on ECM seeded on substrates with different rigidity leads to alterations of their intracellular rheology and functional behavior, including signal transduction and gene expression. The material properties of the substrate can exert significant effects on the rheology of cells to modulate cell structure and function.

#### 9:15 AM Invited

##### Strategies to Promote Mammalian Cell Functions Pertinent to Tissue Formation at the Tissue-Implant Interface: A Materials Perspective: *Rena Bizios*<sup>1</sup>; <sup>1</sup>UTSA

Cellular and molecular events at tissue/implant interfaces dictate the fate of implants and, thus, have crucial clinical implications. The need (1) for biomaterials with properties similar to those of physiological tissues (characterized by surface grain sizes in the nanometer range) and (2) for identification/characterization of the optimal conditions, which maximize specific cell functions responsible for neotissue formation surrounding implants in the human body, has motivated investigation of chemical and topographical modifications of existing materials as well as design of nanostructured material formulations and of protein-engineered biomaterials. Biomaterials, which reliably and predictably promote specific interactions of biomolecules leading to targeted modulation of select mammalian cells and/or control of subsequent cell functions pertinent to new tissue formation and regeneration, have the potential of novel biotechnology-related and tissue-engineering-related applications as well as of major clinical impact. This presentation will highlight bio-inspired biomaterials-related accomplishments, current challenges and novel developments of great promise.

#### 9:45 AM

##### Protein Adsorption on Bioceramic Nanoparticles and Monoliths: *Kenneth Stanton*<sup>1</sup>; *Éilís McGrath*<sup>1</sup>; *John Gibbons*<sup>2</sup>; *Iseult Lynch*<sup>1</sup>; *Kenneth Dawson*<sup>1</sup>; <sup>1</sup>University College Dublin; <sup>2</sup>Royal College of Surgeons in Ireland

When a biomaterial is placed in-vivo, proteins will immediately adsorb to the surface and mediate the response of other biological entities such as cells. Over a short amount of time, a specific group of proteins will form a

quasi-equilibrium layer which has become known as the hard-corona while other less-tightly bound proteins comprise the soft corona. The nature of the corona will depend not only on the surface-charge distribution on the material but also on the way the material presents to the medium: i.e. as an effective monolithic surface or as a nano-particle and also on the specific proteins present and finally the nature of the suspension medium. Here, we present the results of protein adsorption experiments using human blood plasma and a range of bio-ceramic materials including hydroxyapatite, alumina and zirconia. Hard coronas are characterized using 1-D SDS-PAGE and the results from nano-particles are compared with those of monoliths.

#### 10:05 AM

##### Utilization of Diatoms to Collect Metallic Ions: *Itaru Jimbo*<sup>1</sup>; *Takahiro Sekiguchi*<sup>1</sup>; *Hiroaki Onizawa*<sup>1</sup>; <sup>1</sup>Tokai University

Microalgae have a capability to collect metallic ions from the aqueous solutions for their negatively charged surface. A number of works have already been published where heavy metals could be collected and contaminated water system was cleaned by biological measures. In the present study, diatoms are utilized to collect metallic ions such as silver and lead ions from the aqueous solution. Collecting processes are adsorption of ions on the diatoms surfaces and taking the ions inside the diatoms bodies through the cell membrane. Analyses were accomplished with the observation of the dried specimen with SEM and EPMA. Experimental results revealed that these processes depended both on illumination and temperature. These processes seem to be closely related to photosynthesis. Discussion will also include seasonal variations in the yields of the metals by the diatoms.

#### 10:25 AM Break

#### 10:35 AM Invited

##### Aligned TiO<sub>2</sub> Nanotubes for Strong Osseo-Integration in Orthopaedic Implants: *Sungho Jin*<sup>1</sup>; <sup>1</sup>UC San Diego

For improvement of the structural connection between living bone and implant, vertically aligned TiO<sub>2</sub> nanotubes with different dimensions were introduced on Ti implant surface by anodization and used for in vitro and in vivo studies. The presence of surface nanotube structure on titanium orthopaedic implants significantly enhances the kinetics of bone formation and interfacial bond strength as demonstrated by in vitro and in vivo experiments with rabbit and mice. It is also shown that the nanotube geometry has a profound effect on osteoblast and mesenchymal stem cell behavior, with the cell stretching and elongation becoming quite pronounced at a particular nanotube diameter regime, affecting the osseo-integration and bone bonding [1-2]. [1] Karla Brammer, et al, Acta Biomaterialia 5(8), 3215-3223 (2009). [2] Lars M. Bjursten, et al, J. Biomed. Mater. Res. 92A, 1218-24 (2010).

#### 11:05 AM

##### Surface Free Energy Modification of Titania for Bioactive Surfaces: *Kyle Krzywosinski*<sup>1</sup>; *Molly Gentleman*<sup>1</sup>; <sup>1</sup>Texas A&M University

Titanium implants have gained popular use in orthopedic implants, specifically hip implantation. As a result, effort is being made to increase the osseointegration between these load bearing artificial implants and native bone. In previous studies the observed wettability of a surfaces has been shown to be a good indicator of the quality and rate of osseointegration. In this study, the surface energy properties of titanium dioxide, the native oxide on titanium metal implants, is modified by to identify the relationship between surface energy and subsequent osseointegration. It has been demonstrated that thermal exposure increases the wettability of single crystal titania wafers by increasing both the acid and base components of surface free energy. XPS studies have been completed relating changes in surface energy to oxidation and reduction of the titania surface. These surfaces were then examined for cell adhesion to elucidate this relationship.

11:25 AM

**Cellular Response of Grain Boundary Grooved Nanograined/Ultrafine-grained Structures:** Pavan Challa<sup>1</sup>; Devesh Misra<sup>1</sup>; <sup>1</sup>University of Louisiana at Lafayette

We describe here the significance of grain boundary grooved nanograined/ultrafine-grained (NG/UFG) metallic substrates in comparison to planar (non-grooved) NG/UFG substrate in terms of improved surface and biological properties. In this regard, grooving of nano/ultrafine-grains by electrochemical etching is a potential approach to increase the biomechanical interlocking which results in improved cellular response. The differences in the cellular response of planar and grain boundary grooved NG/UFG surface are attributed to favorable surface topography that accelerates the cellular activity. Experiments on the effect of grain boundary grooved NG/UFG substrate indicated that cell attachment, proliferation, viability, morphology, and spread are favorably modulated and significantly different from planar (non-grooved) NG/UFG substrate.

11:45 AM

**Enhanced Bone Cell Response on Zirconium Oxide Nanotube Surface:** Christine Frandsen<sup>1</sup>; Karla Brammer<sup>1</sup>; Kunbae Noh<sup>1</sup>; Sungho Jin<sup>1</sup>; <sup>1</sup>University of California, San Diego

The present work investigates the bio-feasibility of a unique vertically-aligned, laterally-spaced nanotube nanostructure made of ZrO<sub>2</sub> fabricated by anodization. The growth, morphology, and functionality of osteoblasts cultured on ZrO<sub>2</sub> nanotubes have been examined. The initial cell response of adhesion and spreading was considerably improved on the nanotube surface as compared to a Zr surface without nanostructure. The morphology of adhered cells on the nanotube surface elicited a highly organized cytoskeleton with crisscross pattern actin, which was lacking on the flat Zr. Increased alkaline phosphatase levels, indicative of increased bone forming ability, and the formation of concentrated calcified extracellular matrix implied improved osteoblast functionality and mineralization on the nanotube substrate. This in vitro study shows that ZrO<sub>2</sub> nanotubes are highly promising as a biomedical implant surface because of their large surface area and unique nanoscale geometry which enhanced the osteoblast response and apparent role in providing a platform for bone growth.

12:05 PM

**Quantification of Osteoblast Adhesion Strength on Hydroxyapatite-Carbon Nanotube Coated Bioimplant Surface:** Debrupa Lahiri<sup>1</sup>; Ana Paula Benaduce<sup>1</sup>; Lidia Kos<sup>1</sup>; Arvind Agarwal<sup>1</sup>; <sup>1</sup>Florida International University

Adhesion of cells on orthopedic implant surface is important for integration of the implant with the bone. This study proposes the nanoscratch technique as an effective method to quantify the shear strength required to detach a single cell, from the underlying substrate. The method has been evaluated for osteoblast cells grown on plastic slides as well as hydroxyapatite (HA) coatings on Ti-6Al-4V alloy, with and without carbon nanotube (CNT) reinforcement. The cells were grown on the plastic slides and HA coatings for 1, 3 and 5 days. The measurement shows no change in the adhesion strength of osteoblast on plastic slides, with increasing culture-time. On the contrary, the adhesion strength of osteoblast increases with culture time for both HA and HA-CNT coated surfaces. Interaction of osteoblast cells with HA is responsible for such behavior. Addition of CNT to HA further increases the adhesion strength of osteoblast to the coating surface.

## Bulk Metallic Glasses VIII: Structures and Mechanical Properties I

*Sponsored by:* The Minerals, Metals and Materials Society, TMS Structural Materials Division, TMS/ASM: Mechanical Behavior of Materials Committee

*Program Organizers:* Gongyao Wang, University of Tennessee; Peter Liaw, Univ of Tennessee; Hahn Choo, Univ of Tennessee; Yanfei Gao, Univ of Tennessee

Tuesday AM  
March 1, 2011

Room: 6D  
Location: San Diego Conv. Ctr

*Session Chairs:* Takeshi Egami, University of Tennessee; John Lewandowski, Case Western Reserve Univ

8:30 AM Keynote

**Mechanical Properties of Metallic Glasses: An Atomistic View:** Takeshi Egami<sup>1</sup>; <sup>1</sup>University of Tennessee

Many mysteries surround the mechanical properties of metallic glasses, and make it a fascinating subject of study. For instance people assume that deformation occurs because of some defects, such as free-volume or shear transformation zones, but nobody seems to have seen them in action. I propose a rather different view, that the "potential" defects are abundant, as much as a quarter in volume fraction. But fluctuations, thermal or otherwise, statistically activate only a few of them, making precise prediction difficult. Defects are defined by topological instability of the nearest neighbor shell, and can be detected by simulation of the structure, static or dynamic under stress, or by diffraction measurements carried out with applied stress. In this view mechanical failure is the stress-induced glass transition, that can occur without heating nor volume dilation. This work was supported by the Department of Energy, Basic Science Program.

9:00 AM

**Structural Changes in BMG after Mechanical Fatigue and Pre-Loading:** Wei Guo<sup>1</sup>; Wojciech Dmowski<sup>1</sup>; Andrew Chuang<sup>1</sup>; Gongyao Wang<sup>1</sup>; Yoshihiko Yokoyama<sup>2</sup>; Yang Ren<sup>3</sup>; Peter Liaw<sup>1</sup>; Akihisa Inoue<sup>2</sup>; Takeshi Egami<sup>1</sup>; <sup>1</sup>University of Tennessee; <sup>2</sup>Tohoku University; <sup>3</sup>Advanced Photon Source

We studied changes in the atomic structure of bulk metallic glasses after a mechanical fatigue and elastic pre-loading below the yield stress. The Zr-based BMGs were fatigued for 10<sup>6</sup> cycles with mechanical load amplitude corresponding to 10, 50 and 70% of the elastic limit and 10<sup>5</sup> cycles at 80%. The mechanical preloading was done for 24 hrs at 1.5 GPa. The x-ray diffraction was carried out at APS using high energy x-rays and the structure function and PDF were determined. Measurements were performed at room temperature and at 5 K. In addition to statistical errors several sample cross-sections and spots were examined to assess systematic errors. Both room and low temperature data indicated small changes in the fatigued samples that were consistent with structural disordering. However, at the largest load amplitude we also observed that small volume of the sample was crystallized. Supported by the NSF-DMR-0906744 and U.S. DOE DE-AC05-00OR-22725

9:10 AM Invited

**X-Ray Strain Measurements in Metallic Glasses:** Todd Hufnagel<sup>1</sup>; <sup>1</sup>Johns Hopkins University

Several groups have recently used x-ray or neutron scattering to examine the structural effects of nominally elastic loading of metallic glasses. Most of the published data report x-ray elastic moduli that are uniformly larger (by some 5-20%) than the moduli determined by ultrasonic measurements. Furthermore, when strain is measured from shifts in the peak of the pair correlation function  $g(r)$ , a length-scale dependence of strain is observed, with the strain at small atomic separations being smaller than the macroscopic strain, increasing to asymptotically approach the macroscopic strain at large distances. In this talk, we review these results in light of several possible physical mechanisms, including local anelastic deformations and the

proposed presence of elastic heterogeneities in metallic glasses. We also discuss the application of scattering techniques to problems of interest, including x-ray measurements of the strain distribution around crack tips in metallic glasses under load.

#### 9:30 AM Invited

**Insights on Thermomechanical Deformation in Bulk Metallic Glasses from In-Situ X-Ray and Neutron Scattering Experiments:** Alexandru Stoica<sup>1</sup>; Dong Ma<sup>1</sup>; John Daniels<sup>2</sup>; Ken Littrell<sup>1</sup>; *Xun-Li Wang*<sup>1</sup>; <sup>1</sup>Oak Ridge National Laboratory; <sup>2</sup>European Synchrotron Radiation Facility

We have used in-situ neutron diffraction and synchrotron x-ray scattering to investigate the compressive deformation in several bulk metallic glass materials at temperatures below the glass transition temperatures. In situ, time resolved data revealed the structure evolution from atomic to nanometer length scales resulting from the thermomechanical deformation. In the case of a Ca-based metallic glass, after yielding the sample exhibits a transient softening stage that characterizes the homogeneous flow due to the local atomic structure rearrangement, followed by a hardening stage that originates from nano-scale crystallization. Our study provides insights for understanding homogeneous and inhomogeneous flows in metallic glasses from structure changes at multiple length scales.

#### 9:50 AM Invited

**Atomic Structure and Dynamics of BMG during Mechanical Deformation:** *Wojciech Dmowski*<sup>1</sup>; Andrew Chuang<sup>1</sup>; Wei Guo<sup>1</sup>; Konstantin Lokshin<sup>1</sup>; Yoshihiko Yokoyama<sup>2</sup>; Tatsuya Iwashita<sup>1</sup>; Yang Ren<sup>3</sup>; Matt Stone<sup>2</sup>; Peter Liaw<sup>1</sup>; Akihisa Inoue<sup>2</sup>; Takeshi Egami<sup>3</sup>; <sup>1</sup>University of Tennessee; <sup>2</sup>Tohoku University; <sup>3</sup>Advanced Photon Source; <sup>4</sup>SNS; <sup>5</sup>ORNL

We studied changes in the atomic structure and dynamics of metallic glasses during mechanical deformation below the yield stress. The x-ray diffraction was carried in-situ in tensile and compressive loading with applied stress up to 1.75 GPa. The inelastic neutron scattering was performed during compression up to 1.5 GPa. We obtained anisotropic components of the x-ray S(Q) and PDF in the nominal elastic mechanical regime as function of the applied load at room temperature and after the high temperature creep. Analysis of the anisotropic PDF showed that "elastic" deformation is not affine. However, the anisotropic PDF could be divided into elastic (affine) and anelastic components. Analysis showed that for any applied stress level about 24% of the apparent strain was anelastic. The inelastic neutron data show anisotropic component. We also observed changes in the inelastic part of the neutron scattering with the applied stress. Supported by the U.S. DOE, DE-AC05-00OR-22725.

#### 10:10 AM Break

#### 10:20 AM Invited

**Fracture Toughness of Bulk Metallic Glasses:** *John Lewandowski*<sup>1</sup>; <sup>1</sup>Case Western Reserve Univ

The effects of changes in chemistry and stress state on the fracture toughness has been determined for a number of different metallic glass systems. Both notched and fatigue precracked samples have been tested in order to determine the effects of changes in notch severity on the fracture energy/toughness of a number of systems. In addition, the effects of different loading rates and test temperatures on the fracture energy of a Zr-based bulk metallic glass have been determined. The results will be reviewed in the light of previous and ongoing work documenting the effects of such changes on damage tolerance of bulk metallic glass systems.

#### 10:40 AM

**Using Artificial Microstructures to Understand Microstructure Property Relationship in Metallic Glasses:** *Baran Sarac*<sup>1</sup>; Golden Kumar<sup>1</sup>; Jan Schroers<sup>1</sup>; <sup>1</sup>Yale University

Materials science seeks to correlate microstructure with (mechanical) properties. Various approaches have been employed to understand this correlation including conventional direct approaches where the microstructure is varied through processing parameters and composition and the effects on the mechanical properties determined. Technologically relevant materials have reached a level of complexity that conventional metallurgical strategies

as well as above mentioned model and simulation strategies are at their limit. Therefore, we propose a novel approach to study microstructure-property relationship; artificial microstructures, which allow us to individually and independently vary parameters and thereby determine their individual effects on mechanical properties. The artificial microstructure will be fabricated using our recently developed miniature fabrication method. Examples of this novel approach are toughening mechanism in metallic glasses, size effects, and the transition from plastic deformation to elastic buckling in metallic glass heterostructures.

#### 10:50 AM Invited

**Incipient Plasticity in Bulk Metallic Glasses at Elevated Temperatures and under Cyclic Loading:** *Oliver Franke*<sup>1</sup>; Christopher Schuh<sup>1</sup>; <sup>1</sup>MIT

Nanoindentation is used to study the initial yielding of bulk metallic glasses (BMG). The distribution of the pop-in events in the load displacement curves gives insight into the factors that control deformation. BMGs exhibit a high sensitivity to structural inhomogeneities which is studied at different rates, temperatures and different preconditions. One particular preconditioning of the BMGs is to cyclically load the sample in the elastic regime. At room temperature the passing of a critical threshold load causes significant hardening, while below the threshold several thousand cycles do not have any measurable effect. At elevated temperatures the emergence of thermal relaxation affects the ability of the glass to cyclically harden.

#### 11:10 AM Invited

**Inhomogeneous Deformation and Kinetics of Shear Banding in Metallic Glasses:** *Robert Maass*<sup>1</sup>; David Klaumünzer<sup>1</sup>; Jörg Löffler<sup>1</sup>; <sup>1</sup>Swiss Federal Institute of Technology (ETHZ)

Inhomogeneous flow in bulk metallic glasses is still an elusive topic with respect to the underlying deformation mechanisms which govern localized shear band operations. In this study we investigate the inhomogeneous flow both in the serrated and non-serrated regimes. In particular, we evaluate the characteristic times and velocities of the deformation kinetics during shear banding. Using temperature-dependent measurements we are able to show that the shear band propagation of an individual flow serration is a thermally activated process and not a catastrophic event. Electron microscopy investigations before and after an individual serration reveal that shear banding is not a nucleation-controlled mechanism, but rather that there is a one-to-one correspondence between flow serration and shear-offset formation. We also assess the behaviour of a single shear band operating at sub-ambient temperatures. These results indicate that stable flow at low temperatures is not an intrinsic property of cryogenic temperature plasticity.

#### 11:30 AM Invited

**Elastic, Plastic and Fracture Response of Bulk Metallic Glass Matrix Composites:** *Upadrashta Ramamurty*<sup>1</sup>; R. L. Narayan<sup>1</sup>; P.S. Singh<sup>1</sup>; K. Boopathy<sup>1</sup>; Indrani Sen<sup>1</sup>; D. C. Hofmann<sup>2</sup>; <sup>1</sup>Indian Institute of Science; <sup>2</sup>California Institute of Technology

Bulk metallic glasses (BMGs) exhibit extraordinary strengths but suffer from low ductility and fatigue resistance. A possible way to alleviate these problems is through the composite route. In the recent past, it has been shown that BMG matrix composites with tailored microstructures of crystalline dendrite phase in the amorphous matrix yield a combination of higher ductility, strength and toughness. The role of the constituent phases on the elastic, plastic and fatigue crack growth behaviors of several BMG matrix composites are investigated in this work. For this purpose, a variety of experimental tools such as nanoindentation, in-situ testing are employed. Further, the influences of temperature and strain rate are explored. The results of these experiments will be presented and the micromechanisms of deformation and fracture in BMG composites will be discussed.

#### 11:50 AM

**Mechanical Inhomogeneity in As-Cast Bulk Metallic Glass:** *John Plummer*<sup>1</sup>; Russell Goodall<sup>1</sup>; Ignacio Figueroa<sup>2</sup>; Iain Todd<sup>1</sup>; <sup>1</sup>University of Sheffield; <sup>2</sup>Universidad Nacional Autonoma de Mexico

A surface softening effect induced during copper-mould casting of bulk metallic glass is investigated as a function of rod diameter and kinetic glass



fragility index by nanoindentation. A reduction in hardness and reduced modulus at the rod surface is found to not be present in all rods and is favoured in small diameter castings and in fragile systems. Enhanced propensity for shear transformation zone nucleation in the low moduli surface is explained in terms of reduced atomic connectivity, arising from a reduction in local coordination number and a lowering of the shear modulus. Finally, the structure and mechanical diversity that is possible in a single as-cast bulk metallic glass rod is explored through a relative quantification of shear modulus and plastic zone size.

**12:00 PM Invited**

**Effect of Structure of  $\beta$  Phase on the Mechanical Properties of Ti-Based Bulk Metallic Glass Composites:** Chang Wook Bang<sup>1</sup>; Ka Ram Lim<sup>1</sup>; Jin Man Park<sup>1</sup>; Won Tae Kim<sup>1</sup>; *Do Hyang Kim*<sup>1</sup>; <sup>1</sup>Yonsei University

Ductile-phase-reinforced BMG composites show enhanced global plasticity and more graceful failure since soft crystalline inclusions stabilize the glass against the catastrophic failure associated with unlimited extension of a shear band. In the present study, role of ductile dendritic phase in optimizing the mechanical properties of Ti-rich Ti-Zr-Be-Cu-Ni-Nb BMG composites has been investigated from major two aspects: 1) quasi-stable equilibrium condition for beta phase and glass matrix and 2) effect of structure of beta phase on the mechanical properties of composites. As a result, combination of strength and plasticity is optimized by tailoring relative volume fraction of beta phase and glass matrix. The effect of martensitic transformation in beta phase during cooling and deformation has been investigated. Depending on the composition of beta phase, martensitic transformation occurs in the beta phase affecting the mechanical properties and deformation behavior of the bulk metallic glass matrix composites.

**12:20 PM Invited**

**In-Situ TEM/STEM Investigations on Crack Propagation with Plasticity in Zr-Based Metallic Glass:** Jingwei Deng<sup>1</sup>; *Manling Sui*<sup>2</sup>; <sup>1</sup>Shenyang National Laboratory for Materials Science, Institute of Metal Research, Chinese Academy of Sciences; <sup>2</sup>Beijing University of Technology

By in situ tensile test in a transmission electron microscope (TEM), the crack propagation with plasticity was observed in Zr-based metallic glass without nanocrystals formation. Different from that the dislocations generated at the crack tip and propagated along crystallographic planes in the crystalline materials, the plastic flow zone in front of crack presented in a zigzag trace in the monolithic metallic glass. Shear events were observed dynamically in the plastic flow zone by using a scanning imaging mode in TEM, i.e. STEM. It was found that the shear events were sensitive to the local sample thickness. The zigzag propagation of the crack is associated with every shear event in front of the crack. This work was supported by the Cheung Kong Scholars Programme of China and the Natural Sciences Foundation of China

**12:40 PM**

**In-Situ Studies of Micromechanical Behavior of Porous W/Zr-Based Amorphous Alloy Composite:** *Yunfei Xue*<sup>1</sup>; <sup>1</sup>Beijing Institute of Technology

The in-situ high energy X-ray diffraction (HEXRD) was employed to investigate the micromechanical behavior of the porous W/Zr-based amorphous alloy composite during compressive deformation. The lattice strain was measured by HEXRD along the loading direction for different  $\{h k l\}$  planes of W phase in the yielding stage. When the stress is less than 1250 MPa, the lattice strains responds linearly to the applied stress, indicating that only elastic deformation occurs during this stage in W phase. With the increment of stress, the lattice strains exhibit greater deformation, suggesting that the W phase still subjected to a great stress at this stage of deformation and it is an evidence of work-hardening for the W phase. The non-linearity was mainly due to the redistribution caused by interactions of grain-to-grain within W phase and phase-to-phase between the amorphous matrix and W phase.

## Cast Shop for Aluminum Production: Direct Chill Casting

*Sponsored by:* The Minerals, Metals and Materials Society, TMS Light Metals Division, TMS: Aluminum Committee, TMS: Aluminum Processing Committee

*Program Organizers:* Geoffrey Brooks, Swinburne University of Technology; John Grandfield, Grandfield Technology Pty Ltd

Tuesday AM  
March 1, 2011

Room: 16A  
Location: San Diego Conv. Ctr

*Session Chairs:* Dmitry Eskin, Delft University of Technology; Arild Hakonsen, Hydro Aluminium

### 8:30 AM Introductory Comments

**8:35 AM**

**Cold Cracking during Direct-Chill Casting:** *Dmitry Eskin*<sup>1</sup>; Mehdi Lalpoor<sup>1</sup>; Laurens Katgerman<sup>2</sup>; <sup>1</sup>Materials innovation institute; <sup>2</sup>Delft University of Technology

Cold cracking phenomenon is the least studied, yet very important defect occurring during direct-chill casting. The spontaneous nature of this defect makes its systematic study almost impossible, and the computer simulation of the thermo-mechanical behavior of the ingot during its cooling after the end of solidification requires constitutive parameters of high-strength aluminum alloys in the as-cast condition, which are not readily available. In this paper we describe constitutive behavior of high-strength 7XXX-series alloys in the as-cast condition based on experimentally measured tensile properties at different strain rates and temperatures, fracture and impact toughness at different temperatures, and thermal contraction. In addition fracture and structure of specimens and real cold-cracked billets are examined. As a result a fracture-mechanics-based criterion of cold cracking is suggested based on the critical crack length, and is validated upon pilot-scale billet casting.

**9:00 AM**

**Surface Defect Structures On Direct Chill Cast 6xxx Aluminum Billets:**

Mikael Erdegren<sup>1</sup>; *Torbjörn Carlberg*<sup>1</sup>; <sup>1</sup>Mid Sweden University

The surface zone in air-slip DC cast aluminum ingots of the alloys 6063, 6005 and 6082 have been analysed by metallographic methods and by chemical analysis. Inverse segregation to the surface was quantitatively analysed. The concentration profiles were coupled to the appearance of the defects and to microstructures from corresponding areas. Surface defects, of the type vertical drags (VD), were investigated and compared to defect free surfaces for the different alloys. It was shown, that for the 6005 VD defects, there was no change, neither for the segregation zone depth nor for the intermetallic phase particles, compared to undamaged surface areas. In the defect zones the grains started to come apart thus creating an increase in porosity. For the 6063 samples the defect zones had different particles compared to the general surface. The segregation in a defect free surface area contained mostly  $\beta$ -particles while at the defects  $\alpha$ -particles dominated.

**9:25 AM**

**Effect of Cooling Water Quality on the Dendrite Arm Spacing of DC Cast Billets:** *Satyra Mohapatra*<sup>1</sup>; Suvendra Nanda<sup>1</sup>; Anindya Palchowdhury<sup>1</sup>;

<sup>1</sup>National Aluminium Company

For a given alloy chemistry and casting technology, the quality of a billet produced through DC casting route is largely defined by the DAS (Dendrite arm spacing). DAS in turn is determined by the cooling rate and local solidification time. The cooling rate is influenced by the quality and quantity of water besides casting speed and melt temperature. This paper focuses on the relationship between the quality of cooling water and the resultant DAS during production of billets during DC casting process. An empirical relation is derived to indicate the influence of cooling water characteristics on the DAS, based on a mathematical model supplemented by experimental investigations. The model has been validated in plant scale trials.

9:50 AM

**Mould Wall Heat Flow Mechanism in a DC Casting Mould:** *Arvind Prasad*<sup>1</sup>; Ian Bainbridge<sup>1</sup>; <sup>1</sup>University of Queensland

Experiments have been performed to study the effect of the mode of heat transfer on the heat flow in the wall of a DC casting mould. Billet casting uses graphite as inner lining material within the mould-wall. Graphite being a black-body, provides a possible pathway for radiation to play a role in the mould-wall heat transfer. As such, experiments were performed with a graphite probe on the experimental apparatus presented at TMS 2010. An overview of these results will be presented together with the implications of the results for the DC casting process.

10:15 AM Break

10:25 AM

**Productivity Improvements at Direct Chill Casting Unit at Aluminium Bahrain (ALBA):** Abdulla Ahmed<sup>1</sup>; *Sukanta Chateeriji*<sup>1</sup>; A Rasool Maki<sup>1</sup>; <sup>1</sup>Aluminium Bahrain (Alba)

ALBA has been producing Rolling Ingots utilizing two DC casting units via., DC1 and DC6. Out of total annual production of 140,000 MT of Rolling Ingot, DC6 production was 100,000 MT (1XXX, 3XXX and 8XXX series alloys) while DC1 production was 40,000 MT of 5XXX series alloy. Due to higher cost of production and low productivity at DC1 ALBA management decided to close down DC1 as a part of restructuring exercise and maximizing production at DC6 to meet customers demand. An extensive study was carried out towards improving productivity. Four levers of improvement which has the maximum impact were identified e.g., furnace preparation practices, preparatory activities between casts, increasing casting speed etc. Various action plans were drawn up and were implemented. These actions were closely monitored by DC operators themselves by using trend charts. As a result a 30% improvement in productivity was achieved at DC6 on a consistent basis

10:50 AM

**The Coupling of Macroseggregation With Grain Nucleation, Growth and Motion in DC Cast Aluminum Alloy Ingots:** *Miha Založnik*<sup>1</sup>; Arvind Kumar<sup>1</sup>; Hervé Combeau<sup>1</sup>; Marie Bedel<sup>2</sup>; Philippe Jarry<sup>2</sup>; Emmanuel Waz<sup>2</sup>; <sup>1</sup>Institut Jean Lamour; <sup>2</sup>Alcan CRV

The phenomena responsible for the formation of macroseggregations and grain structures during solidification are closely intertwined. We present a model study of a DC cast extrusion ingot. The modeling of these phenomena in DC casting is a challenging problem due to the size of the products, the variety of the phenomena to be accounted for, and the nonlinearities involved. We used a two-phase multiscale model that describes nucleation on inoculant particles and grain growth, coupled with macroscopic transport: fluid flow driven by natural convection and shrinkage, transport of free equiaxed grains, heat transfer, solute transport. The roles of shrinkage, natural convection and grain motion on the sump shape and macroseggregation are analyzed. The formation and evolution of inoculated grains are discussed. We show that it is important to account for all these phenomena and the coupling of segregation and structure formation to be able to explain macroseggregation patterns observed experimentally.

11:15 AM

**Investment Casting of Surfaces with Microholes and Their Possible Applications:** *Todor Ivanov*<sup>1</sup>; Andreas Buehrig-Polaczek<sup>1</sup>; Uwe Vroomen<sup>1</sup>; Claudia Hartmann<sup>2</sup>; Arnold Gillner<sup>2</sup>; Kirsten Bobzin<sup>1</sup>; Jens Holtkamp<sup>2</sup>; Nazlim Bagcivan<sup>1</sup>; Sebastian Theiss<sup>1</sup>; <sup>1</sup>RWTH Aachen University; <sup>2</sup>Fraunhofer-Institute for Laser Technology

The common way to realize microstructured features on metallic surfaces is to generate the designated pattern on each single part by means of laser ablation, electro discharge machining or micromilling. The disadvantage of these process chains is the limited productivity due to the additional processing of each part. The approach to overcome this bottle neck is to replicate microstructured surfaces together with the parts. Therefore an investment casting process to produce functional 3D-surfaces with geometrical features in micrometer range on near-net-shape-cast parts is

investigated. The main research objective deals with the investigation of the single process steps of the investment casting process with regard to the molding accuracy. To demonstrate the potential of microcasted surfaces, current results of the casting of a microstructured hydrophobic surface are shown.

11:40 AM

**Using SEM and EDX for a Simple Differentiation of  $\alpha$ - and  $\beta$ -AlFeSi-Phases in Wrought Aluminum Billets:** *Marcel Rosefort*<sup>1</sup>; Christiane Matthies<sup>1</sup>; Hinrich Buck<sup>1</sup>; Hubert Koch<sup>1</sup>; <sup>1</sup>TRIMET ALUMINIUM AG

Aluminum 6xxx extrusions have considerable potential to make cars lighter. Thus there is a growing demand for high quality aluminum billets. Additionally there is a requirement to improve the aluminum properties. An important issue to fulfill these increasing requirements is the optimization of the microstructure. While utilizing 6xxx-alloys the formation and optimization of the AlFeSi-phase is important. The determination of  $\alpha$ - and  $\beta$ -AlFeSi-phases is a challenge, because  $\beta$ -AlFeSi-phases affect the mechanical properties negatively. A determination in wrought alloys via microscopy is often complicated and leads to questionable results due to the low amount of the phases. TRIMET has investigated one possibility of determining  $\alpha$ - and  $\beta$ -AlFeSi-phases with the help of scanning electron microscope and energy dispersive X-ray. The paper describes the first tests, the phase simulations and the casting experiments. Finally it presents the tests of such phase determinations in the production of 6xxx-alloys like the new TRIMAL 52.

## Characterization of Minerals, Metals and Materials: Characterization of Steel and Cast Iron

*Sponsored by:* The Minerals, Metals and Materials Society, TMS Extraction and Processing Division, TMS/ASM: Composite Materials Committee, TMS: Materials Characterization Committee  
*Program Organizer:* Sergio Monteiro, State University of the Northern Rio de Janeiro - UENF

Tuesday AM  
March 1, 2011

Room: 14B  
Location: San Diego Conv. Ctr

*Session Chairs:* Mingdong Cai, Exova; John Bridge, Maine Maritime Academy

8:30 AM

**Effect of Initial Structure on Grain Refinement of Medium Carbon Steel Processed by ECAP:** *Jozef Zrník*<sup>1</sup>; Sergey Dobatkin<sup>2</sup>; George Raab<sup>3</sup>; Martin Fujda<sup>4</sup>; Libor Kraus<sup>5</sup>; <sup>1</sup>Comtes FHT, Inc.; <sup>2</sup>Russian Academy of Science; <sup>3</sup>Ufa State University; <sup>4</sup>Technical University of Kosice; <sup>5</sup>COMTES FHT Inc.

The work deals with grain refinement of medium carbon steel having different initial microstructure modified by thermal and/or thermomechanical treatment. In case of TM treated steel preliminary structure refinement was achieved due to multistep open die forging. Fine recrystallized ferrite structure and with nest-like pearlite colonies was obtained. The further grain refinement of steel samples was accomplished during warm Equal Channel Angular Pressing (ECAP) at 400°C. Employment of this processing route resulted in extensive deformation of ferrite grains where mixture of subgrains and ultrafine grain was found regardless the preliminary treatment of steel. The dynamic polygonization and recrystallization became active to form mixture of polygonized subgrains and submicrocrystalline grains. The straining and moderate ECAP temperature caused the partial cementite lamellae fragmentation and spheroidization. The tensile behaviour was characterized by strength increase for both structural steel states. The work hardening behaviour was modified in steel where preliminary TM treatment was introduced.

TUESDAY AM

8:45 AM

**Effect of Test Temperature and Prior Straining on the Deformation Mode of Austenitic Stainless Steel during Tensile Testing:** Supratik Roychowdhury<sup>1</sup>; Suman Neogy<sup>1</sup>; Mayank Gupta<sup>2</sup>; Vivekanand Kain<sup>1</sup>; Dinesh Srivastava<sup>1</sup>; G.K. Dey<sup>1</sup>; R.C. Prasad<sup>3</sup>; *Raghvendra Tewari<sup>4</sup>*; <sup>1</sup>Bhabha Atomic Research Centre; <sup>2</sup>PEC; <sup>3</sup>IIT, Bombay; <sup>4</sup>Bhabha Atomic Resrach Centre

Austenitic stainless steels are an important material of construction for Boiling Water Reactors (BWR). These stainless steels are amenable to strengthening by strain hardening. Various deformation modes at different test temperatures and strain become active. In the present investigation type 304LN stainless steel was used in the annealed and strain hardened condition. Thin foils were prepared from gauge section for TEM investigation after tensile testing at room temperature and at 288°C. TEM investigation reveals that twinning is the major mode of deformation for the tests carried out at room temperature while dislocation cross slip is the major mode of deformation at higher temperature. Stacking faults were also observed to a limited extent. The extent of twinning was much higher for the tests carried out using the rolled material. The formation of martensite in the stainless steel due to straining was investigated by the analysis of selected area diffraction patterns.

9:00 AM

**Susceptibility of Low and High Manganese X70 Pipeline Steel to Hydrogen Embrittlement:** Daniel Hejazi<sup>1</sup>; Ayesha Haq<sup>1</sup>; Nima Yazdipour<sup>1</sup>; Druce Dunne<sup>1</sup>; Andrzej Calka<sup>1</sup>; Frank Barbaro<sup>2</sup>; *Elena Pereloma<sup>1</sup>*; <sup>1</sup>University of Wollongong; <sup>2</sup>BlueScope Steel

Hydrogen, even in very low concentrations, can diffuse to regions of high stress concentration resulting in a degradation of mechanical properties. The transport of hydrogen depends on the interaction between hydrogen atoms and the traps which, in turn, is related to microstructure. The influence of composition and microstructure on hydrogen embrittlement susceptibility was investigated by selecting pipeline steels with different Mn and S contents and in different conditions – normalized transfer bar, as-received strip and heat affected zone (HAZ). HAZ simulations were conducted using Gleeble thermo-mechanical machine to simulate a thermal cycle typical of in-service repairs. Notched and fatigue pre-cracked samples were subjected to electrochemical hydrogen charging using a solution of H<sub>2</sub>SO<sub>4</sub> and NaAsO<sub>2</sub> to achieve 2 and 4 ppm hydrogen content. Three point bend tests were conducted on as-received and hydrogen-charged samples. The results obtained are discussed in relation to the microstructure and fractography of the samples

9:15 AM

**Evaluation of Aging Embrittlement of Austenitic Stainless Steels JN1, JJ1 and JK2 by Cryogenic Small-Punch Testing:** Maribel Saucedo-Muñoz<sup>1</sup>; *Victor Lopez-Hirata<sup>1</sup>*; Shin-ichi Komazaki<sup>2</sup>; Toshiyuki Hashida<sup>3</sup>; <sup>1</sup>Instituto Politecnico Nacional (ESIQIE); <sup>2</sup>Muroran Institute of Technology; <sup>3</sup>Tohoku University

Small-punch tests were conducted at 4, and 77 K on three types of austenitic stainless steels JN1, JJ1 and JK2, which were solution treated, and then aged at 923-1073 K for 5 hours. Small-punch test energy was employed for the evaluation of the aging-induced embrittlement behavior in these materials. Fracture surface of small punch test specimen for the solution treated steels exhibited a ductile fracture, showing the highest SP test energy values. The presence of intergranular brittle fracture was observed in aged specimens. Small-punch test energy decreased significantly as the aging process progressed. The highest and lowest decrease in small-punch test energy with aging temperature occurred in JN1 and JK2 steels, respectively. The decrease in small-punch test energy showed to examine appropriately the aging-induced embrittlement in these materials. The difference in aging-induced embrittlement behavior for these steels was explained based on the volume fraction of intergranular precipitates in aged samples.

9:30 AM

**Investigations on the Cyclic Crack Growth Behaviour of Spring Steel Wire Reinforced EN AW-6082:** *Matthias Merzkirch<sup>1</sup>*; Kay Weidenmann<sup>1</sup>; Volker Schulze<sup>1</sup>; <sup>1</sup>Karlsruhe Institute of Technology

Unidirectional reinforced light weight materials such as the aluminium alloy EN AW-6082 are adequate partners for the future use in transportation means like automobiles and airplanes. Due to the occurring cyclic loads knowledge about the crack growth behaviour of these composites is needed. The investigations at a load ratio of R=0.18 show that the crack growth rate of the aluminium matrix is reduced if it is reinforced by spring steel wire with a reinforcing ratio of only about 1 Vol.-%. Further analyses with the help of a self designed capacitive travel measuring gauge show that the reinforcing element causes an increase of the stiffness resulting in a smaller crack opening in comparison to the pure matrix material. Additionally, the acoustic emission analysis allows to detect crack growth within the matrix material, crack propagation along the interface wire/matrix and crack closure. The qualitative results are verified by metallographic and SEM investigations.

9:45 AM Invited

**Effect of Cr Content on Corrosion Resistance of Fe-Based Alloys under SCW Condition:** *Jian Li<sup>1</sup>*; Wenyue Zheng<sup>1</sup>; William Cook<sup>2</sup>; <sup>1</sup>CANMET-MTL; <sup>2</sup>University of New Brunswick

Resistance to high temperature corrosion is one of the key challenges in future nuclear reactor material development. Iron based materials with low Cr content shows superior high temperature mechanical properties. However, due to relative low Cr content, their corrosion resistances under SCW conditions are generally poor. High-Cr alloys although show much improved corrosion resistance, often suffer from embitterment due to the pre-cipitation of sigma phase in the microstructure. In this study, corrosion resistance high Cr alloy (25%Cr) showed much better corrosion resistance compared to that of low Cr alloy (14%Cr). The high-Cr alloy was subsequently used as coating material for commercial P91 alloy.

10:15 AM Break

10:30 AM

**Variations of Elastic Modulus of Automotive Steels after Yielding:** Paolo Matteis<sup>1</sup>; Giorgio Scavino<sup>1</sup>; *Donato Firrao<sup>1</sup>*; <sup>1</sup>Politecnico di Torino

Numerical simulations of both production processes (e.g.: sheet cold forming) and service behavior (e.g.: low-speed car impact), used in the automotive industry to minimize the tests number and shorten the car design and industrialization, can be significantly affected by the variation of the steel elastic modulus due to plastic deformation. However, this phenomenon is not usually modeled, also for lack of specific data. Hence, five steel grades, belonging to different categories, were examined before and after several successive 4% true strain steps, and up to the uniform elongation. After each deformation step, the specimen was unloaded, the cross-section was re-measured, and the modulus was evaluated from a series of loading and unloading ramps in the elastic range. In most cases, the elastic modulus decreases approximately from 205 GPa in the as-received condition to 165 GPa after deformation, with most of this drop often occurring in the first deformation step alone.

10:45 AM

**The Development of a High Strength Microalloy Steel TiC Deposited by Reactive Magnetron Sputtering:** *Narayanna Ferreira<sup>1</sup>*; Edalmy Almeida<sup>1</sup>; Marcio Mendes<sup>1</sup>; Clodomiro Alves Júnior<sup>1</sup>; <sup>1</sup>UFRN

High strength low alloy steels (HSLA) are generally composed of micro-alloying elements Nb, V and Ti. Commonly are microalloyed with niobium and vanadium, however, the development of steels microalloyed with Ti have been objects of constant research. The mechanical properties of microalloyed steels result from the interaction between different hardening mechanisms involving dislocations, solid solution, ferritic grain refinement and precipitation of carbonitrides. The aim of this study was developed from a titanium microalloyed steel using the technique of enrichment by precipitation of TiC powder of iron deposition by reactive magnetron sputtering using different proportions of the mixture CH<sub>4</sub>, H<sub>2</sub>, Ar. This



work was realized on the microstructural characterization by SEM / EDX, XRD, XRF and microhardness. The results showed that the precipitation of titanium carbide by magnetron sputtering is viable and confirmed by the characterization techniques performed in this study.

**11:00 AM**

**Microstructure and Properties of New Wear Resistant Steel with High Strength and High Toughness:** *Li Hongbin*<sup>1</sup>; <sup>1</sup>Baosteel

A multi-element wear-resistant low-alloy steel with high strength and high toughness was developed. Microstructure, hardness, tensile properties and impact properties were carried out in order to establish a correlation amongst the parameters and to optimize the microstructural features and mechanical properties for superior wear performance. The results show that the optimal microstructure and mechanical properties were got when quenching at 880 °C and tempering at 180 °C. Fine martensite can be obtained, and the hardness is above 550HB, the tensile strength is above 1700MPa, the yield strength is above 1350MPa, the elongation is above 10%, and the impact energy is about 50J. The results obtained have been supplemented through the characteristics of the worn surfaces, subsurface regions, debris and fractured surfaces. These analyses also helped to understand the operative mechanisms of material removal and failure.

**11:15 AM**

**Evaluation of Growth Rates of Austenitic Transformation Products in Fe-C-Cr Alloys Using Laser Scanning Confocal Microscopy:** *Peter Kolmskog*<sup>1</sup>; *Peter Hedström*<sup>1</sup>; *Annika Borgenstam*<sup>1</sup>; <sup>1</sup>Royal Institute of Technology, KTH

An evaluation of the growth rates of the transformation products from austenite in three Fe-C-Cr alloys (Fe-1C-1Cr, Fe-1C-4Cr and Fe-0.15C-4Cr) during isothermal heat treatment has been performed in-situ using Laser Scanning Confocal Microscopy (LSCM) equipped with a hot-stage. The LSCM technique enables the clear observation of phase transformation that gives a surface relief e.g. Widmanstätten cementite and ferrite, bainite and inverse bainite. Specimens have been isothermally heat treated at temperatures from 275 to 700 °C and the growth rate of the different austenitic transformation products has been evaluated. The microstructures of the transformed specimens have been analyzed using LOM and SEM in order to verify the obtained results.

**11:30 AM**

**Internal Friction and Three Dimensional Atom Probe Analysis of Bake Hardening Phenomenon in Ultra-Low Carbon Bake Hardening Steel:** *Hua Wang*<sup>1</sup>; *Wen Shi*<sup>1</sup>; *Lin Li*<sup>1</sup>; <sup>1</sup>Shanghai University

Two samples of Ultra-Low Carbon Bake Hardening (ULC-BH) steel with different compositions were prepared by annealing and water quenching. These samples were pre-deformed with various levels from 2% to 10%, and further baked at 170 °C for 20min. The distribution of solute C in the processed samples was characterized by 3DAP, and the BH values of the samples with different pre-deformation were also determined. In addition, the relationship between the distribution of solute C in BH steels and the BH values was analyzed.

**11:45 AM**

**A New Understanding on the Initiation of Pitting Corrosion of Austenitic Stainless Steels in Salt Water:** *Xiu-Liang Ma*<sup>1</sup>; <sup>1</sup>Institute of Metal Research, Chinese Academy of Sciences

The pitting corrosion of stainless steels is generally believed to result from the local dissolution in MnS inclusions which are more or less ubiquitous in stainless steels. Nevertheless, the microstructure information on the local site where MnS dissolution preferentially occurs is lacking, which makes pitting corrosion remain the big headache for numerous engineering materials. We have applied in-situ ex-environment transmission electron microscopy and have identified the initial site, at an atomic scale, of MnS dissolution. We find that fine nano-octahedral precipitates of spinel MnCr<sub>2</sub>O<sub>4</sub> are dispersedly distributed in the MnS inclusions. In-situ TEM studies indicate that the MnS initially dissolves at the MnCr<sub>2</sub>O<sub>4</sub>/MnS interface in the presence of salt water. First-principles calculations indicate that the MnCr<sub>2</sub>O<sub>4</sub> nano-

octahedron with metal terminations is more reactive in catalyzing the MnS dissolution than O-terminated ones. This work sets up a new basis for understanding the initiation of pitting corrosion.

---

**Chloride 2011: Practice and Theory of Chloride-Based Metallurgy: Molten Salts, Magnesium and Aluminum**

*Sponsored by:* The Minerals, Metals and Materials Society, Canadian Institute of Metals, TMS Extraction and Processing Division, TMS: Magnesium Committee, TMS: Energy Committee  
*Program Organizers:* Dirk Verhulst, Consultant, Extractive Metallurgy; V.I. (Lucky) Lakshmanan, Process Research Ortech, Inc.

Tuesday AM  
March 1, 2011

Room: 19  
Location: San Diego Conv. Ctr

*Session Chairs:* Neale Neelameggham, US Magnesium LLC; Vladimirov Papangelakis, University of Toronto

---

**8:30 AM**

**Evaluation of 2.25Cr-1Mo Alloy for Containment of LiCl/KCl Eutectic during the Treatment of Used Nuclear Fuel:** *Brian Westphal*<sup>1</sup>; *S. Li*<sup>1</sup>; *G. Fredrickson*<sup>1</sup>; *D. Vaden*<sup>1</sup>; *T. Johnson*<sup>1</sup>; *J. Wass*<sup>1</sup>; <sup>1</sup>Idaho National Laboratory

Recovery of uranium from the Mk-IV and Mk-V electrorefiner vessels containing a LiCl/KCl eutectic salt has been on-going during the pyrometallurgical processing of used nuclear fuel for 14 and 12 years, respectively. Although austenitic stainless steels are typically utilized for LiCl/KCl salt systems, the presence of cadmium in the Mk-IV electrorefiner dictates an alternate material. A 2.25Cr-1Mo alloy (ASME SA-387) was chosen due to the absence of nickel in the alloy which has a considerable solubility in cadmium. Using the transition metal impurities (iron, chromium, nickel, molybdenum, and manganese) in the electrorefined uranium products, an algorithm was developed to derive values for the contribution of the transition metals from the various input sources. Weight loss and corrosion rate data for the Mk-V electrorefiner vessel were then generated based on the transition metal impurities in the uranium products. To date, the corrosion rate of the 2.25Cr-1Mo alloy in LiCl/KCl eutectic is "outstanding" assuming uniform (i.e. non-localized) conditions.

**8:50 AM**

**Numerical and Experimental Study of Fluid Flow during Electrolytic Process for Magnesium Production:** *Hyun Na Bae*<sup>1</sup>; *Myung Duk Seo*<sup>1</sup>; *Seon Hyo Kim*<sup>1</sup>; *Go-Gi Lee*<sup>2</sup>; *Jae Young Jung*<sup>2</sup>; <sup>1</sup>POSTECH; <sup>2</sup>RIST

Bubbles form at the anode during the electrowinning of magnesium and cause hydrodynamic acceleration and electrical field disturbance. A three-dimensional computational model was developed to investigate the effect of the geometry of the electrochemical chamber and the size distribution of bubbles on the fluid flow in the cell of a pilot plant. The results were validated by measurements of the surface characteristics of molten salt and of the formed bubbles. Fluid flow at the surface was recorded with a high speed camera, and the distribution of bubble size was determined by inspecting the video images frame by frame. The measured size distribution of the bubbles was entered into the computer simulation for multi-phase flow. A sloped roof was installed above the electrodes and enhanced the flow of the molten salt, resulting in higher current efficiency, lower energy consumption, and higher quality of magnesium metal.

**9:10 AM**

**Magnesium Removal from Secondary Aluminum Melts in Reverberatory and Rotary Furnaces:** *Eulogio Velasco*<sup>1</sup>; *Marcos Cardoso*<sup>2</sup>; *Jose Nino*<sup>2</sup>; <sup>1</sup>Texas State University; <sup>2</sup>NEMAK

Recycling of aluminum scrap for production of secondary alloys used for automotive applications is increasing continuously. Aluminum can be recycled with large energy and emission savings with minimal loss in material properties. Automotive alloys require a strict control to remove

TUESDAY AM

alloy impurities, inclusions and excess of magnesium. The aim of this work is to study the magnesium removal from recycled aluminum by chlorine injection in a reverberatory furnace, and removal by an oxidation process at high temperature in an industrial rotary furnace. The magnesium removal by gas injection is carried out by the reaction between chlorine and magnesium, with its efficiency associated to kinetic factors. In the rotary rapid oxidation of aluminum and magnesium elements at high temperature is characterized by the formation of surface films composed of magnesium oxide. Additionally this work reviews the benefits of an efficient demagging process.

**9:30 AM**

**Rapid Removal of Chlorine in Molten Salt Electrolysis of Magnesium Chloride:** *Gökhan Demirci*<sup>1</sup>; *Ishak Karakaya*<sup>2</sup>; <sup>1</sup>Aselsan Inc.; <sup>2</sup>Middle East Technical University

Energy consumption in electrolytic magnesium cells is well above the theoretical values. However, the mechanism of the back reaction, the main cause of the current losses, has not been fully understood yet. Magnesium dissolution into the melt is generally regarded as the limiting step for the back reaction. Accordingly, present cell designs are made with priority given to fast magnesium removal from the cell. However, experimental data and modeling results in this study indicate that the limiting step for the back reaction between magnesium and chlorine is the chlorine dissolution into the electrolyte when physical contact between electrolysis products was eliminated. Effects of chlorine bubbles on the current efficiency and the cell potential were investigated. Results show that the extent of back reaction is proportional to the chlorine surface area in contact with the electrolyte per unit time, and the cell potential increases with the amount of chlorine bubbles inside the electrolyte.

**9:50 AM**

**Preparation of Al-Ca Alloys by Molten Salt Electrolysis Method:** *Sh Yang*<sup>1</sup>; *Fengli Yang*<sup>1</sup>; *Mingzhou Li*<sup>1</sup>; *Xianwei Hu*<sup>2</sup>; *Zhaowen Wang*<sup>2</sup>; *Zhongning Shi*<sup>2</sup>; *Bingliang Gao*<sup>2</sup>; <sup>1</sup>Jiangxi University of Science and Technology; <sup>2</sup>School of Materials and Metallurgy117#, Northeastern University

Aluminum-calcium alloys were prepared by molten salt electrolysis method. 15w%KCl-80w%CaCl<sub>2</sub>-5w%MgF<sub>2</sub> was taken as electrolysis. Content of calcium in alloys was to be higher than 13w%, and tests were carried out with 0.80-1.20A•cm<sup>-2</sup> of cathode current density at 680-720°. The highest current efficiency was 80%. Aluminum-calcium alloys with different calcium contents could be prepared directly from the cell by molten salt electrolysis method. Compared with traditional method, the method not only could reduce the loss of calcium in the alloy manufacture process, but to reduce Greenhouse Gases and energy consumption. Moreover, component of alloys prepared by molten salt electrolysis method was even, and production could be carried out continuously.

**10:10 AM Break**

**10:25 AM**

**The Dissolution Behavior of TiCxO1-x Solid Solutions in Chloride Melt:** *Xiaohui Ning*<sup>1</sup>; *Chao Du*<sup>1</sup>; *Qiuyu Wang*<sup>1</sup>; *Shuqiang Jiao*<sup>1</sup>; *Hongmin Zhu*<sup>1</sup>; <sup>1</sup>University of Science and Technology Beijing

TiCxO1-x solid solutions were synthesized by sintering a mixture of titanium carbide and titanium monoxide at 1600 °C. The corresponding structures and morphologies of the TiCxO1-x solid solutions were characterized by XRD and SEM. A series of tests has been performed on the electrochemical dissolution behavior of TiCxO1-x solid solutions in NaCl-KCl molten salt. The influences of synthesis time and electrochemical parameters on the anodic dissolution behavior were also investigated in detail. The results showed that TiCxO1-x solid solutions can dissolve as Ti<sup>2+</sup> into alkali chloride melt. The tail gas on the anode was monitored by a mass spectrometer. And it was found the synthesis time significantly affects the components of the anodic gas. Titanium ion species dissolved from TiCxO1-x solid solutions changes between Ti<sup>2+</sup> and Ti<sup>3+</sup> depending on the applied potential.

**10:45 AM**

**Study on Mechanism of Alumina Carbothermic Reduction-Chlorination Process in Vacuum:** *Fulong Zhu*<sup>1</sup>; *Bin Yang*<sup>1</sup>; *Qingchun Yu*<sup>1</sup>; *Baoqiang Xu*<sup>1</sup>; *Yongnian Dai*<sup>1</sup>; <sup>1</sup>National Engineering Laboratory for Vacuum Metallurgy

In this paper, the mechanism of the carbothermic reduction-chlorination process to extract aluminum from alumina in vacuum was investigated. Content of CO in gas, phases of the reduction slag, surface morphology of the reduction slag and the product aluminum were measured by means of gas chromatography (GC), XRD, and SEM. The experimental results indicated that content of CO in gas decreased, but Al<sub>4</sub>C<sub>3</sub> increased with reduction time increasing at 1773K during carbothermic reduction process of alumina. AlCl(g) and C were produced by the reaction between Al<sub>4</sub>C<sub>3</sub> and AlCl<sub>3</sub>(g) at 1773K, then aluminum beads were generated after decomposition of AlCl(g). It implied that mechanism of alumina carbothermic reduction-chlorination process in vacuum should match with the following three steps: the carbothermic reduction process of Al<sub>2</sub>O<sub>3</sub> to produce Al<sub>4</sub>C<sub>3</sub>, the chlorination process of Al<sub>4</sub>C<sub>3</sub> by AlCl<sub>3</sub>(g) to produce AlCl(g), and the decomposition process of AlCl(g) to produce Al(l).

**11:05 AM**

**Investigation on the Corrosion Resistance of Several Steel Materials to LiCl-KCl Melt:** *Bing Li*<sup>1</sup>; <sup>1</sup>East China University of Science and Technology

In this paper the corrosion resistances of three steel materials including 304, 306, Q235A steels to the LiCl-KCl melt were investigated. The electrochemical impedance spectroscopies, Tafel curves and polarization curves of the three steel materials in the LiCl-KCl melt were measured and some dynamic parameters such as corrosion current, corrosion potential, exchange current density, transfer coefficient and electron transfer resistance were obtained. And then the corrosion resistances of the three steel materials were tested by immersing into the LiCl-KCl melt at 600° for 50h and then their surface morphology and composition were characterized by SEM and EDS, and their weight changes before and after immersion into the melt were compared. At the same time, electrolysis experiments were carried out in LiCl-KCl melt at about 450° by selecting the three steel materials as cathodes, respectively, and the corrosion of metal Li produced in-situ on them were analyzed.

**11:25 AM**

**Electrochemical Removal of Impurity Mg from LiCl-KCl Containing MgCl<sub>2</sub> Melt:** *Bing Li*<sup>1</sup>; *Miao Shen*<sup>1</sup>; *Jingwei Lou*<sup>1</sup>; <sup>1</sup>East China University of Science and Technology

As a main impurity in primary lithium metal, magnesium is difficult to remove because of the very close relative volatility of the two metals. Electrochemical refining provides a possibility to completely remove Mg in the LiCl-KCl melt prior to Li reduction. MgCl<sub>2</sub> reduction processes in LiCl-KCl-MgCl<sub>2</sub> melt were investigated by cyclic voltametry (CV) and square wave voltametry (SWV). The results showed that MgCl<sub>2</sub> is reduced in one step with two-electron transfer. The reduction potential was well defined. By constant potential electrolysis at the Mg reduction potential, Mg was reduced on a solid cathode (mild steel) and a liquid cathode (Zinc and Lead). Cyclic voltametry (CV) and square wave voltametry (SWV) were also employed to compare the removal effect after several hours of electrolysis. The dissolution kinetics of the deposited Mg in the above melt was investigated, and the relations between the activity and the dissolution kinetics of deposited Mg were discussed.

**11:45 AM**

**Direct Synthesis of Niobium Aluminides Powders by Sodiothermic Reduction in Molten Salts:** *Na Wang*<sup>1</sup>; *Chao Du*<sup>1</sup>; *Shuqiang Jiao*<sup>1</sup>; *Kai Huang*<sup>1</sup>; *Hongmin Zhu*<sup>1</sup>; <sup>1</sup>University of Science and Technology Beijing

Niobium aluminides were directly synthesized by a sodiothermic reduction process of NbCl<sub>5</sub> - AlCl<sub>3</sub> which was dispersed into LiCl - KCl - NaCl - CaCl<sub>2</sub> melts. The melt supplied a homogenous reaction medium which was substantially beneficial to the co-reduction of Nb and Al to form niobium aluminides in situ. The reduction was performed at 500° for 4 hours. The products were analyzed by X-ray diffraction (XRD) and scanning electron

microscope (SEM). The corresponding results indicated that niobium aluminides powders have been successfully synthesized.

### Computational Thermodynamics and Kinetics: Brent Fultz Honorary Session II

*Sponsored by:* The Minerals, Metals and Materials Society, ASM International, TMS Electronic, Magnetic, and Photonic Materials Division, TMS Materials Processing and Manufacturing Division, TMS: Alloy Phases Committee, TMS: Chemistry and Physics of Materials Committee, TMS/ASM: Computational Materials Science and Engineering Committee, ASM: Alloy Phase Diagrams Committee  
*Program Organizers:* Raymundo Arroyave, Texas A & M University; James Morris, Oak Ridge National Laboratory; Mikko Haataja, Princeton University; Jeff Hoyt, McMaster University; Vidvuds Ozolins, University of California, Los Angeles; Xun-Li Wang, Oak Ridge National Laboratory

Tuesday AM  
March 1, 2011

Room: 9  
Location: San Diego Conv. Ctr

*Session Chairs:* Matthew Lucas, Air Force Research Laboratory; Lee Roberson, Oak Ridge National Laboratory

#### 8:30 AM Invited

**Iron Alloys through the Lens of Nuclear Resonant Spectroscopy:**  
*Wolfgang Sturhahn*<sup>1</sup>; <sup>1</sup>Jet Propulsion Laboratory

In recent years, nuclear resonant scattering techniques that utilize synchrotron radiation have provided new opportunities for the study of vibrational and magnetic properties of condensed matter under extreme conditions. In particular, the determination of the vibrational density of states with nuclear resonant inelastic x-ray scattering (NRIXS) and the study of valencies and magnetic properties with synchrotron Mössbauer spectroscopy (SMS) provided unique results. In this presentation, the work of Prof. Brent Fultz on the vibrational and magnetic properties of iron and its alloys using these novel nuclear resonant scattering techniques will be highlighted. In particular, we will discuss the effects of particle size and high pressure in iron metal as well as chemical disorder in various iron alloys on atomic vibrations and magnetic properties. This work is supported by grants from the National Aeronautics and Space Administration (NASA).

#### 9:00 AM Invited

**Mixing Properties in Oxide Solid Solutions Relevant to Nuclear Fuels:**  
Ben Hanken<sup>1</sup>; *Mark Asta*<sup>2</sup>; Chris Stanek<sup>3</sup>; Fei Zhou<sup>4</sup>; Vidvuds Ozolins<sup>4</sup>; Niels Gronbech-Jensen<sup>1</sup>; <sup>1</sup>University of California, Davis; <sup>2</sup>University of California, Berkeley; <sup>3</sup>Los Alamos National Laboratory; <sup>4</sup>University of California, Los Angeles

Among Professor Fultz's many accomplishments are his important contributions to the field of alloy theory. His experimental measurements of vibrational entropy inspired an extensive body of theoretical work aimed at incorporating non-configurational contributions to the entropy of mixing and ordering in first-principles calculations of alloy phase diagrams. In this talk we discuss non-configurational contributions to the mixing thermodynamic properties of oxide solid solutions, originating from electronic degrees of freedom. The work focuses on urania-ceria solid solutions, a surrogate system for mixed-oxide nuclear fuels. First-principles calculations, combined with classical interatomic-potential modeling are used to investigate contributions to mixing thermodynamic properties associated with electronic disorder arising from charge transfer between uranium and cerium ions. The results are discussed in light of conflicting experimental measurements in the literature. Overall, our results suggest that charge disorder likely plays an important role in governing the thermochemical and phase stability properties in this system.

#### 9:30 AM Invited

**Time-Resolved Measurements of Transient Behaviors by Asynchronous In-Situ Neutron Diffraction at the Spallation Neutron Source:** *Ke An*<sup>1</sup>; Alexandru Stoica<sup>1</sup>; Harley Skorpenske<sup>3</sup>; Abhijit Pramanick<sup>1</sup>; Rick Riedel<sup>1</sup>; Steve Miller<sup>1</sup>; Hahn Choo<sup>2</sup>; Jabob Jones<sup>3</sup>; James Kohl<sup>1</sup>; Xun-Li Wang<sup>1</sup>; <sup>1</sup>Oak Ridge National Laboratory; <sup>2</sup>University of Tennessee; <sup>3</sup>University of Florida

Unlike the conventional histogram data collection method, the event-based data acquisition scheme at the Spallation Neutron Source (SNS) records neutrons with an intrinsic timing resolution of 100ns. A novel asynchronous neutron diffraction measurement technique has been demonstrated at VULCAN, the engineering diffractometer at SNS by making use of both neutron scattering and sample environment parameters in time event data acquisition mode. The asynchronous measurement strategy is an entirely new approach to study time-resolved phenomena such as in-situ phase transformation at elevated temperatures, lithiation and delithiation in rechargeable Li-ion batteries, and low cycle fatigue of stainless steel where the relevant time scales are minutes to milliseconds. The ultimate time resolution achievable with this technique is expected to be <10  $\mu$ s, which will enable the investigation of fast transition phenomena by neutron scattering. Details of this measurement methodology as well as its application in various scientific cases will be presented.

#### 10:00 AM Break

#### 10:20 AM

**Phonon Density of States and High Temperature Thermodynamics of MgB<sub>2</sub>:** *Jorge Munoz*<sup>1</sup>; Nikolay Markovskiy<sup>1</sup>; Matthew Lucas<sup>2</sup>; Olivier Delaire<sup>3</sup>; Chen Li<sup>1</sup>; Matthew Stone<sup>3</sup>; Douglas Abernathy<sup>3</sup>; Brent Fultz<sup>1</sup>; <sup>1</sup>California Institute of Technology; <sup>2</sup>Air Force Research Lab; <sup>3</sup>Oak Ridge National Lab

Inelastic neutron scattering spectra were measured from 7 to 750 K on polycrystalline MgB<sub>2</sub> and phonon density-of-states (DOS) curves were obtained. The thermal expansion was measured from 300 to 900 K using x-ray diffraction. First-principles calculations were conducted to study the phonon DOS curves and thermal expansion behavior in the quasi-harmonic approximation. The electronic DOS shows a peak at the Fermi level composed predominantly of in-plane boron hybridized states. These states couple strongly to the E<sub>2g</sub> phonon modes. Quantitative agreement was found between experiment and the quasi-harmonic simulations, suggesting a small role for anharmonicity in most modes. Nevertheless, the modes in the energy range from 60 to 75 meV, which include the E<sub>2g</sub> modes along the  $\Gamma$ -A direction, have different temperature dependence. This anomaly could be caused by the adiabatic electron-phonon interaction, which induces a broadening of sharp features in the electronic DOS and can alter the electronic screening behavior.

#### 10:40 AM Invited

**Phonon Studies with Inelastic Neutron Scattering and First-Principles Simulations:** *Olivier Delaire*<sup>1</sup>; <sup>1</sup>Oak Ridge National Laboratory

Inelastic neutron scattering is the preferred technique to measure phonons in materials, with recent advances allowing to fully map out the four-dimensional scattering function S(Q,E) for microscopic dynamics. First-principles calculations of the electronic structure and phonons have also reached a high level of accuracy, allowing for a powerful comparison with experiments. Studies combining these experimental and computational techniques will be presented. In particular, we have identified that the adiabatic coupling of phonons and electronic structure at high temperature significantly affects the thermodynamics in several classes of materials. This effect was investigated in details with temperature-dependent phonon measurements on powders and single-crystals, and with ab-initio molecular dynamics. We also present results on thermoelectric materials, where phonons are important to understand thermal transport, which directly relates to the thermoelectric efficiency. Work was partially supported by the US DOE, Basic Energy Sciences, as part of an Energy Frontier Research Center, DE-SC0001299.



## 11:10 AM Invited

**Phonon Thermodynamics of Binary Fe Alloys:** *Matthew Lucas*<sup>1</sup>; <sup>1</sup>Air Force Research Laboratory

The phonon density of states gives insight into interatomic forces and provides the vibrational entropy, making it a key thermodynamic function for understanding alloy phase transformations. The significance of phonon thermodynamics is discussed in the context of recent measurements on binary alloys of Fe with Al, Co, Cr, and V. For equiatomic B2 ordered FeAl, the vibrational entropy of vacancy formation counteracts the corresponding change in configurational entropy, destabilizing vacancies at higher temperatures. Changes in the phonon spectrum upon ordering in equiatomic FeCo are accurately captured using the cluster inversion method for measurements on random solid solutions. For FeCr alloys, the positive vibrational entropy of mixing helps to stabilize the random solid solution with respect to the unmixed phase. The change in vibrational entropy upon ordering for equiatomic FeV is found to be positive, which is consistent with recent calculations of the phonon density of states.

## 11:40 AM

**The Temperature Dependence of Phonons in Scandium Fluoride, a Material with Large Negative Thermal Expansion:** *Chen Li*<sup>1</sup>; *Xiaoli Tang*<sup>1</sup>; *Jorge Munoz*<sup>1</sup>; *Brandon Keith*<sup>1</sup>; *Doug Abernathy*<sup>2</sup>; *Sally Tracy*<sup>1</sup>; *Benjamin Greve*<sup>3</sup>; *Angus Wilkinson*<sup>3</sup>; *Brent Fultz*<sup>1</sup>; <sup>1</sup>California Institute of Technology; <sup>2</sup>Oak Ridge National Laboratory; <sup>3</sup>Georgia Institute of Technology

It has recently been discovered that cubic scandium tri-fluoride has a negative thermal expansion as large as  $1 \times 10^{-5}/\text{K}$  over a temperature range of 100 to 700 K. Inelastic neutron scattering experiments were performed to study the temperature-dependent lattice dynamics of  $\text{ScF}_3$  from 7 to 750 K. The measured phonon densities of states (DOS) shows a large non-harmonic behavior in the same range of temperature as the negative thermal expansion. Calculations of phonons with first-principles methods identified the individual modes in the DOS, indicating that the correlated rocking of the structural octahedra reduces the lattice parameter while preserving the cubic structure symmetry. First-principles molecular dynamics simulations showed that large thermal excursions of F atoms cause their neighboring Sc atoms to be drawn together with increasing temperature.

## David Pope Honorary Symposium on Fundamentals of Deformation and Fracture of Advanced Metallic Materials: Intermetallics III, Superalloys, and Gum Metal

*Sponsored by:* The Minerals, Metals and Materials Society, TMS Materials Processing and Manufacturing Division, TMS Structural Materials Division, TMS: High Temperature Alloys Committee, TMS/ASM: Mechanical Behavior of Materials Committee, TMS: Nanomechanical Materials Behavior Committee

*Program Organizers:* E. P. George, Oak Ridge National Laboratory; Haruyuki Inui, Kyoto University; C. T. Liu, The Hong Kong Polytechnic University

Tuesday AM  
March 1, 2011

Room: 32A  
Location: San Diego Conv. Ctr

*Session Chairs:* Ian Baker, Dartmouth College; Takayuki Takasugi, Osaka Prefecture University

## 8:30 AM Invited

**Stability and Structure of Transition Metal C14/C15 Laves Phases:** *Masao Takeyama*<sup>1</sup>; *Shigehiro Ishikawa*<sup>2</sup>; <sup>1</sup>Tokyo Institute of Technology; <sup>2</sup>Former graduate student (Currently Sumitomo Metal Co.)

Phase stability and crystal structure change between hexagonal C14 and cubic C15 Laves phases at elevated temperatures has been examined along the pseudo-binary lines of  $\text{A}_2\text{B}-\text{C}_2\text{B}$  and  $\text{A}_2\text{B}-\text{A}_2\text{C}$  in Fe-Nb-M and Co-Nb-Cr ternary systems (M: transition metals). In C14-C14 combinations, a continuous solid solution is formed between the two Laves phases in any

system. In C14-C15 combinations, the C14 phase region becomes enlarged extensively toward the counterpart, whereas the C15 region is limited to the binary edge. In C15-C15 combinations, however, the Laves phase region is limited to its binary edge and a large C14 region appears in between. These results suggest that C14 structure is thermodynamically more stable than C15 structure. The higher stability of C14 structure is associated with interaction energy among sublattices. The details will be discussed in terms of the site occupation of M and structure change of the tetrahedral unit in their crystal structures.

## 9:00 AM Invited

**Resemblance and Difference in Mechanical Properties between  $\text{L}_{12}$  and  $\text{E}_2$  Type Ordered Crystal Structures:** *Yoshisato Kimura*<sup>1</sup>; <sup>1</sup>Tokyo Institute of Technology

The ordered crystal structure of  $\text{E}_2$  can be regarded as ternary  $\text{L}_{12}$  stabilized by an interstitial carbon at the cell center. Objective of the present work, aiming at the heat resistant alloy design, is to understand mechanical properties of  $\text{E}_2$   $\text{M}_3\text{AlC}_{1-x}$  (M=Fe, Co, Ni) compounds from the viewpoint of resemblance and difference between  $\text{L}_{12}$  and  $\text{E}_2$  type ordered crystal structures. Single crystals of  $\text{M}_3\text{AlC}_{1-x}$  were prepared by directional solidification using optical floating zone melting and their mechanical properties were evaluated by compression tests. The operative slip systems of  $\text{E}_2$   $\text{Ni}_3\text{AlC}_{1-x}$  are the same as  $\text{L}_{12}$   $\text{Ni}_3\text{Al}$ ; octahedral slip at lower temperatures and cube slip at higher temperatures than 1073 K. Only cube slip operates in  $\text{Fe}_3\text{AlC}_{1-x}$  above 1073 K, while octahedral slip operates in a wide temperature range from 77 to 1373 K in  $\text{Co}_3\text{AlC}_{1-x}$  in which the extra ordering of carbon atoms plays quite important role.

## 9:30 AM Invited

**Microstructure Evolution and Solubility Change of Constituent Phases in Mo-Si-B Based Alloys at 1800 Degree C:** *Kyosuke Yoshimi*<sup>1</sup>; *Seong-Ho Ha*<sup>1</sup>; *Kouichi Maruyama*<sup>1</sup>; <sup>1</sup>Tohoku University

Microstructure evolution of as-cast Mo-rich Mo-Si-B alloys at 1800 degree C was experimentally investigated with referring some projection diagrams of the liquidus surfaces and some equilibrium phase diagrams of the alloys. As-cast microstructures of the alloys were drastically changed by heat treatment at 1800 degree C for 24 h, and thermally stable microstructures were developed during the heat treatment. For example, Mo2B crystallized out during solidification as the primary or secondary phase along with their solidification paths even though the alloy composition lied in the triangle of Mo-Mo3Si-Mo5SiB2. However, the unstable Mo2B was completely decomposed during the heat treatment and contributed to develop uniform, fine microstructures. The compositions of constituent phases after the heat treatment were carefully analyzed by EPMA with some Mo-Si-B alloy standards, and an equilibrium phase diagram in the Mo-rich side of the Mo-Si-B ternary system at 1800 degree C was established.

## 10:00 AM Break

## 10:15 AM Invited

**Overview of Creep Deformation of Nickel Base Superalloys and Intermetallics:** *Dilip Shah*<sup>1</sup>; <sup>1</sup>Pratt & Whitney

In comparison to tensile properties determined at high strain rate, diffusion controlled creep deformation is a far more complex process. The primary focus of the development of high temperature materials has been improvement in creep resistance. Creep deformation is not only a measure of temperature capability of the material but also affects other low strain rate deformation such as dwell fatigue and thermal-mechanical fatigue. This presentation provides an overview of creep deformation of nickel base superalloys and intermetallics. It will touch upon a variety of phenomena, such as primary creep, influence of crystal orientation, effects of alloying additions, role of phase instability, ordering, two phase structure and heat treatments. Also, the time has come to pay more attention to artifacts of load controlled creep testing of anisotropic single crystal alloys and to environmental interactions, even for nominal laboratory conditions.

10:45 AM

**Localized Shear Deformation in Gum Metal at Ideal Strength:** *Shigeru Kuramoto*<sup>1</sup>; *Tadahiko Furuta*<sup>1</sup>; *Naoyuki Nagasako*<sup>1</sup>; *John Morris*<sup>2</sup>; <sup>1</sup>Toyota Central R&D Labs., Inc.; <sup>2</sup>University of California, Berkeley

Experimental results on localized shear deformation in a multifunctional Ti-36Nb-2Ta-3Zr-0.3O alloy (mass%), Gum Metal, are summarized and the mechanism for the shear deformation is considered in relation to elastic softening in C11- C12. Very small value of C11- C12 in the alloy means sufficiently low Peierls stress required for dislocation motion. However, actual deformation strength of the alloy is much higher; resolved shear stress in nanopillars of the alloy has been reported to approach its ideal shear strength during compression test. Results of microstructural analyses in various size scales performed so far support that the key basic process of plastic deformation would be localized shear deformation accompanied by inhomogeneous crystal lattice rotation. The actual shear deformation stress at ideal strength along with elastic softening in the alloy implies that the localized shear deformation involves anisotropic shear melting process by local stress increase in specific crystal lattice orientation.

11:00 AM

**Microstructural Characterization and Deformation Behavior of Ideal Strength Metallic Materials:** *Tadahiko Furuta*<sup>1</sup>; *Shigeru Kuramoto*<sup>1</sup>; *Kaveh Edalati*<sup>2</sup>; *Zenji Horita*<sup>2</sup>; <sup>1</sup>Toyota Central R & D Labs., Inc.; <sup>2</sup>Kyushu University

The plastic deformation of metallic material is based on the dislocation theory, which well explains large difference between the ideal shear strength and the practical strength. We recently found that the actual deformation stress is considered to be closer to their ideal strength in Ti-23Nb-0.7%Ta-2%Zr-1.2O (in at%) and Fe-18.1%Ni-34.9%Co-9.3%Ti alloys. They are composed of body-centered cubic crystal with lattice softening along specific orientation and have nano-sized obstacles in their microstructures, which can suppress the dislocation motion up to high strength level, possibly near ideal strength. In this study, effects of phase stability on change in microstructure during severe plastic deformation and deformation behavior in both alloys and their deformation characteristics were compared. From these experimental results, requirements for ideal strength deformation will be discussed.

11:15 AM

**Non-Planar Deformation as a Dominant Deformation Mechanism Following Low Cycle Fatigue of a Ni-Based Superalloy:** *Patrick Phillips*<sup>1</sup>; *Libor Kovarik*<sup>2</sup>; *Raymond Unocic*<sup>3</sup>; *Dan Wei*<sup>4</sup>; *David Mourer*<sup>4</sup>; *Michael Mills*<sup>1</sup>; <sup>1</sup>Ohio State University; <sup>2</sup>PNNL; <sup>3</sup>ORNL; <sup>4</sup>GE Aviation

Many materials demonstrate strictly planar deformation during low cycle fatigue (LCF), which often takes the form of persistent slip bands. In the general case of Ni-based superalloys, these slip bands consist of paired dislocations traveling on {111} planes. However, extensive electron microscopy characterization has revealed non-planar deformation to be a dominant mode in polycrystalline R104, resulting from ample cross-slipping processes between {111} and {100} planes. Somewhat unexpectedly, this mechanism appears at both low and high temperatures, although the macroscopic material response is quite different. In addition to temperature effects, any deformation dependencies on grain orientation or cycle number will be discussed. Preliminary results comparing dwell fatigue deformation mechanisms to those observed during LCF will also be presented.

11:30 AM

**Investigation of Fatigue Crack Growth Mechanisms in a Ni-Based Superalloy:** *Clarissa Yablinsky*<sup>1</sup>; *Katharine Flores*<sup>1</sup>; *Michael Mills*<sup>1</sup>; *James Williams*<sup>1</sup>; <sup>1</sup>The Ohio State University

Historically, the critical design parameter for Ni-based superalloy turbine blades has been creep resistance. With modern airfoil designs and longer service times, fatigue resistance can also be a limiting factor. In this study, compact tension specimens of monocrystalline Ni-based superalloy René N5 were tested under cyclic loading conditions. Test temperature, environment, frequency, and orientation were varied in order to examine the effects of plastic zone size, recovery, and other time dependant processes on crack

growth. Fracture surfaces and microstructures were characterized using a high resolution scanning electron microscope in order to examine crack path selection, fracture topography, and the  $\gamma/\gamma'$  morphology along the crack wake and in the bulk material. Dislocation arrangements were characterized via transmission electron microscopy using site-specific foils prepared by focused ion beam techniques in order to understand the damage mechanisms active during fatigue crack growth.

11:45 AM

**Fatigue Life Modeling of Single Crystal Nickel-Base Superalloys:** *Clinique L. Brundidge*<sup>1</sup>; *Tresa M. Pollock*<sup>2</sup>; <sup>1</sup>University of Michigan; <sup>2</sup>University of California, Santa Barbara

Factors influencing the fatigue life of a single crystal nickel-base superalloy tested at 538/176C have been examined. The role of cooling rates during solidification has been investigated with the use of a liquid metal cooling (LMC) directional solidification process in comparison to a conventional Bridgman technique. Increases in cooling rates during solidification significantly decrease primary and secondary dendrite arm spacings as well as decrease the size of solidification shrinkage pores. Increases in cooling rates improve the fatigue life by as much as a factor of seven. Fatigue cracks originate from casting porosity, where the size of the largest pores in the samples scales with the secondary dendrite arm spacings. The development of a microstructure-based model to quantify the total life of single-crystals will be discussed.

12:00 PM

**The Effect of Temperature on the Microstructure and Mechanical Behavior of Two-Phase Fe<sub>30</sub>Ni<sub>20</sub>Mn<sub>20</sub>Al<sub>30</sub> Alloy:** *Xiaolan Wu*<sup>1</sup>; *Ian Baker*<sup>1</sup>; <sup>1</sup>Thayer School of Engineering, Dartmouth College

This paper describes the microstructures and mechanical properties of Fe<sub>30</sub>Ni<sub>20</sub>Mn<sub>20</sub>Al<sub>30</sub> at elevated temperatures. Both post-mortem and in-situ heating transmission electron microscopy (TEM) accompanied by energy dispersive X-ray spectroscopy were used to characterize the microstructures. At temperatures less than 723 K, the alloy Fe<sub>30</sub>Ni<sub>20</sub>Mn<sub>20</sub>Al<sub>30</sub> consisted of alternating Fe- and Mn-rich B2-ordered, and Ni- and Al-rich L<sub>2</sub><sub>1</sub>-ordered phases aligned along  $\langle 100 \rangle$ , which probably formed by spinodal decomposition. At  $\sim 723$  K, the L<sub>2</sub><sub>1</sub>-ordered Ni- and Al-rich phase started to disorder to a B2 structure. At  $\sim 773$  K only two B2 phases were present. Compression tests performed at temperatures up to 873 K at a strain rate of  $5 \times 10^{-4} \text{ s}^{-1}$  showed a brittle-to-ductile transition and a large drop in yield strength at  $\sim 773$  K, which was coincident with the L<sub>2</sub><sub>1</sub> to B2 temperature. Also, the deformation mechanism both at room temperature and at  $\sim 773$  K will be discussed in the paper.

## Deformation, Damage, and Fracture of Light Metals and Alloys: Session I

*Sponsored by:* The Minerals, Metals and Materials Society, MS&T Organization, TMS Light Metals Division, TMS: Chemistry and Physics of Materials Committee, TMS/ASM: Mechanical Behavior of Materials Committee

*Program Organizers:* Qizhen Li, University of Nevada, Reno; Xun-Li Wang, Oak Ridge National Laboratory; Yanyao Jiang, University of Nevada, Reno

Tuesday AM  
March 1, 2011

Room: 13  
Location: San Diego Conv. Ctr

*Session Chair:* Qizhen Li, University of Nevada, Reno

8:30 AM Invited

**Modeling Dislocation Slip Transmission across Alpha-Beta Interface in Ti-Alloy:** *Chen Shen*<sup>1</sup>; *Ju Li*<sup>2</sup>; *Yunzhi Wang*<sup>3</sup>; <sup>1</sup>GE; <sup>2</sup>University of Pennsylvania; <sup>3</sup>Ohio State University

We apply 3D microscopic phase field model to study dislocation transmission across alpha-beta interfaces with residual interfacial dislocations in Ti-alloys. The model employs complex alloy energetics directly from ab

TUESDAY AM

initio calculations, circumventing the need for fitting atomistic potential. We first compute the generalized stacking fault (GSF) energy surface of HCP (alpha) and BCC (beta) Ti. After matching the two GSFs at the alpha-beta interface with Burgers orientation relationship, we perform microscopic phase field simulations. These simulations have been previously checked against the Peierls model calculations and have been shown to agree with the Peierls model results completely. The new calculations in alpha-beta-alpha sandwich configurations reveal intricate dislocation pileup, transmission, storage and reaction mechanisms similar to what have been seen in atomistic simulations and experimental characterizations. A coarse-grained dislocation density based description coupled to continuum elasticity could be developed to predict the overall interface-strengthening behavior of the alloys.

#### 9:00 AM Invited

##### **Deformation and Fracture of Nanostructured fcc Materials under Monotonic and Cyclic Loading:** *Diana Farkas*<sup>1</sup>; <sup>1</sup>Virginia Tech

We present simulations using embedded atom method (EAM) potentials that investigate the deformation, fracture and fatigue behavior in nanocrystalline fcc materials. The simulations include deformation studies where strain localization and sustained emission of dislocations from the grain boundaries are shown to lead to crack initiation. Cracks nucleate preferentially in weak grain boundaries that are perpendicular to the loading direction. The simulation results also revealed a particular nanoscale mechanism of crack propagation as the main crack links with nano-voids nucleated ahead of the crack tip. Depending on the particular orientation relationships, cracks can also be stopped by grain boundaries. Under applied cyclic loading and show particular mechanisms of crack advance related to damage accumulation.

#### 9:30 AM

##### **Using Ab Initio Calculations in Designing BCC MgLi-X Alloys for Ultra-Lightweight Applications:** *Martin Friak*<sup>1</sup>; William Counts<sup>2</sup>; Dierk Raabe<sup>1</sup>; Joerg Neugebauer<sup>1</sup>; <sup>1</sup>Max Planck Institute for Iron Research

Body-center-cubic Mg-Li-based alloys are a promising light-weight structural material. In order to tailor the Mg-Li composition with respect to specific industrial requirements, systematic materials-design concepts need to be developed and applied. We have therefore performed a quantum-mechanical study of fundamental physical properties of bcc MgLi-X substitutional ternaries with solutes from the 3rd row (Na, Al, Si, P, S, Cl) and 4th row transition metal (Sc, Ti, V, Cr, Mn, Fe, Co, Ni, Cu, Zn) elements. The computed properties are used to determine engineering parameters such as (i) specific Young's modulus or (ii) bulk over shear modulus ratio (B/G) differentiating between brittle and ductile behavior. Analyzing these extensive and systematic ab initio data sets we derive chemical trends and explain why none is able to simultaneously improve both specific Young's modulus and ductility (see Counts et al., *Acta Materialia*, vol. 57, 69 (2009)).

#### 9:45 AM

##### **The Effect of Crystallographic Orientation on Void Growth: A Molecular Dynamics Study:** *Mehul Bhatia*<sup>1</sup>; *Kiran Solanki*<sup>1</sup>; *Amitava Moitra*<sup>1</sup>; *Mark Tschopp*<sup>1</sup>; <sup>1</sup>Mississippi State University

In ductile materials, fracture involves void nucleation, growth and coalescence. The objective of this research is to understand how crystallographic orientation influences void growth in Al for uniaxial tensile deformation. Molecular Dynamics simulation with Cubical specimens having periodic boundary condition were provided with one embedded spherical void and were subjected to remote uniaxial tension of different crystal orientation. The simulation results show how crystallographic orientation affects the yield stress and void growth corresponding to dislocation nucleation from surface of the void resulting in shear loops in perfect FCC lattice. The effect of crystallographic orientation was evident as very different dislocation patterns/shear loops occurred in the specimen with different orientations. The significance of this research is that atomistic simulations of this type can help to inform continuum void growth models for multiscale models.

#### 10:00 AM Break

#### 10:15 AM Invited

##### **Creep Deformation of Al-Sc-X Alloys:** *Matthew Krug*<sup>1</sup>; *David Seidman*<sup>1</sup>; *David Dunand*<sup>1</sup>; <sup>1</sup>Northwestern University

Three alloys (Al-0.12Sc, Al-2.9Li-0.11Sc, and Al-5.53Li-0.048Sc-0.0092Yb, at.%) were aged at 325°C to produce coherent, misfitting L12 Al<sub>3</sub>[Sc(Li,Yb)] nano-precipitates that are coarsening resistant. Compared to Al-0.12Sc, Al-2.9Li-0.11Sc has higher peak-strength, and the time to onset of over-aging is delayed from 24 to 96 h. The aged alloys were crept at 300°C in compression, over minimum steady-state strain rates between 10<sup>-9</sup> and 10<sup>-4</sup> s<sup>-1</sup>. The alloys exhibit high apparent stress exponents (n=14–33), indicative of threshold stress behavior. Calculated threshold stresses range between 8 and 20 MPa. The threshold stress normalized by the Orowan stress increases with precipitate size and lattice parameter mismatch due to elastic strains induced in the matrix, and their interactions with dislocations. Comparisons are made with past work on similar Al-Sc-RE alloys, helping to draw conclusions about the benefits of ternary additions to creep- and coarsening-resistant Al-Sc alloys.

#### 10:45 AM Invited

##### **Impression Creep – A Localized Technique for Characterizing Creep Deformation of Materials:** *Fuqian Yang*<sup>1</sup>; <sup>1</sup>University of Kentucky

The impression test using a flat-ended indenter has been developed to study the time-dependent plastic deformation of materials. In contrast to the sharp-instrumented indentation, the contact area remains constant during the impression allowing a constant average contact stress when subjected to constant loads. Steady-state creep of various materials has been observed. The impression creep tests of a precipitation hardenable Mg-8Zn-4Al-0.5Ca (wt.%) casting alloy were performed in the temperature range of 403–623 K and under the punching stress range of 1.68–60.4 MPa. Using a hyperbolic sine stress law between the steady-state impression velocity and the punching stress, a single activation energy was found to be 77.5 kJ/mol, which is about half of the activation energy for lattice diffusion in Mg. A single mechanism of grain boundary fluid flow was proposed to be the controlling mechanism for the creep behavior of the Mg-8Zn-4Al-0.5Ca alloy under the testing conditions.

#### 11:15 AM

##### **Creep Fatigue Behavior of 319 Aluminum Casting Alloys under Hot Compressive Dwell Conditions:** *Xiang Chen*<sup>1</sup>; *Diana Lados*<sup>1</sup>; *Richard Pettit*<sup>2</sup>; <sup>1</sup>Worcester Polytechnic Institute; <sup>2</sup>FractureLab

Fatigue crack growth under Hot Compressive Dwell (HCD) conditions is an important failure mode for many high temperature applications, such as cylinder heads for internal combustion engines. A new testing methodology was developed to study the creep mechanism that accelerates the growth of cracks loaded with a compressive dwell cycle. Tensile residual stress build up at the crack root is considered a key factor contributing to crack growth under HCD conditions. To evaluate this effect quantitatively, stress relaxation and crack growth tests were performed to determine the creep and crack growth responses of the material. A Blunt Compact Tension (BCT) specimen was then analyzed using FRANC2D to determine the stress distribution, and obtain a 2D weight function K-solution. The residual stress distribution is then applied via the weight function to determine residual K that builds up during the operating life of the part. These results will be presented and discussed.

#### 11:30 AM

##### **Room Temperature Creep and Substructure Formation in Pure Aluminum at Ultra-Low Strain Rates:** *Junjie Shen*<sup>1</sup>; *Iketa Ken-ichi*<sup>1</sup>; *Hata Satoshi*<sup>1</sup>; *Nakashima Hideharu*<sup>1</sup>; <sup>1</sup>Kyushu University

The creep behavior in highly pure aluminum (5N) and industrial pure aluminum (1070) with different grain sizes has been investigated by helicoid spring creep tests at ultra-low strain rates lower than 10<sup>-9</sup>s<sup>-1</sup> and room temperature. Obtained results show that different types of deformation mechanisms are closely related with grain sizes and impurity concentrations: when the average grain size was 24 μm, the stress exponent, n ~ 1. The



dominant deformation mechanism was considered to be grain boundary sliding; on the other hand when the average grain size was 1.6 mm, the stress exponent,  $n \sim 5$ , which was interpreted as dislocation creep. Microstructural observation shows dislocation tangle, cell formation; in an industrial pure aluminum with grain size of 25  $\mu\text{m}$ , the stress exponent,  $n = 2$ . Microstructure observations revealed dislocation emission from grain boundary acts as main deformation mechanism and intergranular dislocations tangle, cell formation as coordination mechanism.

**11:45 AM**

**Quantifying the Relationship Between Deformation-Induced Surface Roughness, Grain Orientation, and Strain Localization in Polycrystalline Aluminum:** *Mark Stouder*<sup>1</sup>; Joseph Hubbard<sup>1</sup>; Adam Creuziger<sup>1</sup>; Lyle Levine<sup>1</sup>; <sup>1</sup>National Institute of Standards and Technology

Since bulk plastic deformation in polycrystalline materials is strongly dependent on the character of the individual grains, careful examinations of surface morphology and grain orientations with strain can reveal considerable information about the active deformation mechanisms and directly quantify the morphological conditions that promote strain localization. High-resolution topographical analyses, performed *in-situ* on aluminum sheet that was incrementally strained in uniaxial tension, were used to construct maps of the localization potential as a function of strain. These maps were integrated with EBSD measurements of the initial grain orientations to yield a grain-by-grain assessment of the microstructural conditions required to produce the critical surface morphology. The results suggest the relationship between grain orientation and strain localization depends on multiple factors such as grain misorientation and Taylor factors. The methodologies used, and details regarding the nature of the relationships between strain, microstructure, and surface morphology shall be presented and discussed.

---

## Dynamic Behavior of Materials V: Spalling and Dynamic Fracture

*Sponsored by:* The Minerals, Metals and Materials Society, TMS Structural Materials Division, TMS/ASM: Mechanical Behavior of Materials Committee

*Program Organizers:* Marc Meyers, UCSD; Naresh Thadhani, Georgia Institute of Technology; George Gray, Los Alamos National Laboratory

Tuesday AM

March 1, 2011

Room: 5A

Location: San Diego Conv. Ctr

*Session Chair:* George Gray, Los Alamos National Lab

---

**8:30 AM Invited**

**Dynamic Necking of Structures Submitted to High Strain Rate Loadings:** *Alain Molinari*<sup>1</sup>; Sébastien Mercier<sup>1</sup>; <sup>1</sup>Université Paul Verlaine-Metz

The fragmentation of structures has received a large attention during the last decades. A large effort was recently made to understand the behavior of structures subjected to an intense blast. To ensure integrity of structures, the conditions for the onset of fragmentation as well as for delaying the occurrence of such phenomenon have to be understood. Experiments conducted on rings and cylinders under rapid expansion have shown that the ductility of materials and the fragmentation process are significantly affected by the loading rate. Our scope is to describe by theoretical means the process of multiple necking that leads to the failure of structural elements under dynamic loading (bars, plates, cylinders, rings and hemispherical shells). The effects of material parameters, material inertia, loading conditions and sample geometry are analysed by means of a linearized stability analysis. Results are compared to experimental data.

**9:00 AM**

**3-D Modelling of Local and Global Spall Damage in Shocked FCC Multicrystals:** *Kapil Krishnan*<sup>1</sup>; Leda Wayne<sup>1</sup>; Andrew Brown<sup>1</sup>; Pedro Peralta<sup>1</sup>; Shengnian Luo<sup>2</sup>; Darrin Byler<sup>2</sup>; Aaron Koskelo<sup>2</sup>; <sup>1</sup>Arizona State University; <sup>2</sup>Los Alamos National Laboratory

3-D finite element (FE) simulations were used to study effects of microstructure, e.g., grain boundaries (GBs), on spall damage in copper multicrystals. Laser-driven plate impact experiments were conducted at low pressures (2-6 GPa) to capture spall damage at the nucleation stage. The 3-D FE model was developed from serial sectioning of the tested samples. Analysis was performed with ABAQUS/EXPLICIT using anisotropic elasticity and the Steinberg-Guinan (SG) model, where plastic anisotropy was modeled using Hill's anisotropic yield criterion. A damage model based on a cut-off tensile pressure was incorporated for element removal to study interactions between release waves and existing voids. The global damage appeared at the expected spall plane and the difference between target and flyer diameters led to release waves from the corner of the flyer that localized damage zone towards this region. Locally, damage localized near GBs. The FE results were compared with the experimental observations.

**9:20 AM**

**Examination of the Damage and Failure Response of Tantalum and Copper under Varied Shock Loading Conditions:** Ellen Cerrata<sup>1</sup>; Darcie Dennis-Koller<sup>1</sup>; Neil Bourne<sup>1</sup>; George Gray<sup>1</sup>; *Curt Bronkhorst*<sup>1</sup>; Davis Tonks<sup>1</sup>; Irene Beyerlein<sup>1</sup>; Benjamin Hansen<sup>1</sup>; Ricardo Lebensohn<sup>1</sup>; <sup>1</sup>Los Alamos National Laboratory

A number of plate impact experiments have been conducted on high purity polycrystalline tantalum and copper samples using graded flyer plate configurations to alter the loading profile. These experiments are designed in a way so that a broad range of damage regimes are probed. The results show that the nucleation of damage primarily occurs at the grain boundaries of the materials. This affords us the opportunity to propose a porosity damage nucleation criterion which begins to account for the length scales of the microstructure (grain size distribution) and the mechanical response of the grain boundary regions (failure stress distribution). This is done in the context of a G-T-N type model for the ductile damage and failure response of both the materials examined. The role of micro-inertial effects on the porosity growth process is also considered.

**9:40 AM**

**Geometric and Microstructural 3-D Characteristics of Incipient Spall Damage in Shock Loaded Cu Multicrystals and Polycrystals:** *Andrew Brown*<sup>1</sup>; Leda Wayne<sup>1</sup>; Kapil Krishnan<sup>1</sup>; Pedro Peralta<sup>1</sup>; Shengnian Luo<sup>2</sup>; Scott Greenfield<sup>2</sup>; Darrin Byler<sup>2</sup>; Kenneth McClellan<sup>2</sup>; Aaron Koskelo<sup>2</sup>; <sup>1</sup>Arizona State University; <sup>2</sup>Los Alamos National Laboratory

Spall-induced void structures were analyzed in shock loaded copper samples to determine void size, shape, and spacing distributions. Copper samples (1000  $\mu\text{m}$  thick) were impacted by laser-driven flyer plates (500  $\mu\text{m}$  thick) at low pressures (2-6 GPa) to encourage incipient spall damage. Serial sectioning and Electron Backscattering Diffraction (EBSD), along with in-plane and through-thickness optical microscopy, were used to create 3-D renditions of the voids and their surrounding microstructure to characterize and compare their local and global geometrical and crystallographic characteristics. Analysis of regions of localized damage indicates that grain boundaries with misorientations between 30° and 50° are preferred sites for intergranular voids, which were typically shaped as sheets following the boundaries. Damage on the spall plane contained a spatial distribution of pores that was statistically uniform, indicating 1-D conditions. Effects of pre-existing plastic deformation on damage sites were also studied using half-hard and annealed samples with similar grain size.

TUESDAY AM

## 10:00 AM

**Instrumented Ring Expansion for the Measurement of High Strain Rate Constitutive and Fracture Behavior:** *Jason Johnson*<sup>1</sup>; Geoff Taber<sup>1</sup>; Gregg Fenton<sup>2</sup>; Glenn Daehn<sup>1</sup>; <sup>1</sup>Ohio State University; <sup>2</sup>Applied Research Associates

The study and development of high strain rate constitutive models is pertinent to several fields, yet the test methods utilized to probe this high strain-rate realm are limited in both number and standardization. New technologies have been leveraged to revive an old, under-utilized test method – the axisymmetric expanding ring. The combination of Photon Doppler Velocimetry (PDV) and one of several ring launch techniques allows the successful testing and instrumentation of samples loaded in tension without wave effects at strain rates in excess of 104 s<sup>-1</sup>. Design and construction of the embodiment of this test at OSU. Examples of expanding low ductility, modest conductivity metal (hardened steel) and a high conductivity, high ductility material will be discussed in depth. In the former case concurrent numerically modeling of the problem is necessary for accurate constitutive modeling, while simpler methods are acceptable in the latter case.

## 10:20 AM Break

## 10:30 AM Invited

**The Dependence of Dynamic Spall Strength on Flow Stress and Temperature:** *Roger Minich*<sup>1</sup>; <sup>1</sup>LLNL

A statistical void nucleation and growth model is presented that relates the dependence of dynamic spall strength on flow stress and temperature. The model is incorporated in a finite element code and compared to a wide range of plate impact experiments. The model successfully predicts the pressure dependence of the spall strength and emphasizes the role of stress fluctuations in determining the size distribution of nucleated voids. It also predicts the observation that the spall strength for two different microstructures are comparable when the corresponding flow stresses are comparable. Also, the temperature dependence of the dynamic spall strength is shown to be consistent with data for temperatures even approaching melt.

## 11:00 AM

**Laser-Shock Induced Spalling and Fragmentation in Vanadium:** *Marc Meyers*<sup>1</sup>; H. Jarmakani<sup>1</sup>; B. Maddox<sup>2</sup>; C. T. Wei<sup>1</sup>; D. Kalantar<sup>2</sup>; <sup>1</sup>University of California, San Diego; <sup>2</sup>Lawrence Livermore National Laboratory

Polycrystalline and monocrystalline vanadium was subjected to shock compression followed by tensile wave release to study spall and fragmentation behavior. The shock pulse was generated by a direct laser drive at energy levels ranging from 11 and 440 J/mm<sup>2</sup> and initial pulse durations of 3 and 8 ns (approximate initial pressures between 10 and 250 GPa). The effects of target thickness, laser energy, polycrystallinity, and pulse duration were studied. Calculations show melting at a pressure threshold of ~150 GPa. Consistent with the analytical predictions, the recovered specimens and fragments show evidence of melting at the higher energy levels. Spalling in the polycrystals occurred by a ductile tearing mechanism that favored grain boundaries. In the monocrystals, it occurred by a mixture of cleavage fracture along {010} planes and ductile dimple fracture. This lower spall strength in polycrystals contradicts predictions from the Hall-Petch equation. Experimentally obtained fragment sizes were compared with predictions from the Grady-Kipp model. The spall strength of vanadium under laser loading conditions was calculated from both VISAR pullback signals and using the spall thickness and found to be considerably higher than predictions from gas-gun experiments. This higher spall strength is suggestive of a strong time dependence of the phenomenon, consistent with the nucleation and growth kinetics of voids and the strain-rate sensitivity embedded in the Grady theory.

## 11:20 AM

**Micro-CT for the Quantification of 3D Voids within Damaged Structures:** *Brian Patterson*<sup>1</sup>; Christopher Hamilton<sup>1</sup>; Ellen Cerreta<sup>1</sup>; Darcie Dennis-Koller<sup>1</sup>; Curt Bronkhorst<sup>1</sup>; Benjamin Hansen<sup>1</sup>; <sup>1</sup>Los Alamos National Laboratory

Micro X-ray Computed Tomography (MXCT) is widely used in the materials community to examine the internal structure of materials for voids and cracks due to damage or casting, or other defects. Most research in this area focuses on the qualitative aspect of the image, simply answering: Are there voids present? Here we present an ongoing study of the quantified incipient spall voids in Cu with different grain sizes, using a gas gun with various velocities. Data analysis packages for MXCT are just now becoming able to dimensionally measure and produce statistics on the voids present. In order to make the size of the features in the 3D image quantifiable, the question, how many radiographs are required to render the object dimensionally accurate in 3D, must be answered. A series of data sets has been collected, varying the number of radiographs collected in order to determine the appropriate number required.

## 11:40 AM

**Shock-Induced Spallation Phenomena in Copper-Niobium Nanolayered Composites:** *Niraj Gupta*<sup>1</sup>; Alexander Stukowski<sup>2</sup>; Michael Baskes<sup>3</sup>; Srinivasan Srivilliputhur<sup>1</sup>; <sup>1</sup>University of North Texas; <sup>2</sup>Darmstadt University of Technology; <sup>3</sup>Los Alamos National Laboratory

Shock-induced spallation phenomena in Copper-Niobium nanolayered composites conforming to a Kurdjumov-Sach's orientation relation were simulated using molecular dynamics to determine both spallation strength and the nature of void formation. The copper and niobium system is of interest due to its immiscible nature and the orientational relation of the two lattices which creates an interface acting as an effective sink for dislocations and vacancies. The target structures consisted of varying numbers of alternating copper and niobium layers with thicknesses varying from 1 nm to 22 nm. Flyer velocities ranged from 3.5 to 11.5 Å/ps, corresponding to an approximate strain rate of 10<sup>9</sup> /s. Spallation occurs in the vicinity of the Cu-Nb interface, and always in the copper layer. The proposed factors contributing to spallation will be discussed, as well as what effect the layer morphology has on the strength of the target.

## 12:00 PM

**Materials Characterization of Railgun Erosion Phenomena:** *Brenda Machado*<sup>1</sup>; Lawrence Murr<sup>1</sup>; Edwin Martinez<sup>1</sup>; Sara Gaytan<sup>1</sup>; Sikhanda Satapathy<sup>2</sup>; <sup>1</sup>University of Texas at El Paso; <sup>2</sup>The University of Texas at Austin

Railguns, consisting of a Cu rail-stator system with a moving Al projectile armature, are able to launch large, light-weight (usually Al) projectiles hundreds of miles using a high current pulse creating a comparably large magnetic field. Rail erosion has been a limiting feature. In this research, we have examined the Cu rail surface erosion and mixing of rail and Al projectile debris using optical metallography and scanning electron microscopy. The observations illustrate a unique, elongated starting Cu rail grain structure with a high dislocation density observed by transmission electron microscopy (TEM). The rail surface debris coating exhibits a propensity of porous Al (or gas bubble structure) created by temperatures above the Al melting temperature. TEM representative of the Al/Cu interface illustrates little, if any, alloying. The Al projectile and Cu rail form a dynamically recrystallized zone where small Al and Cu grains (~20 nm diameter) allow for solid-state flow.

---

## Electrode Technology for Aluminium Production: Anode Raw Materials and Green Carbon

Sponsored by: The Minerals, Metals and Materials Society, TMS Light Metals Division, TMS: Aluminum Committee  
Program Organizers: Alan Tomsett, Rio Tinto Alcan; Ketil Rye, Alcoa Mosjøen; Barry Sadler, Net Carbon Consulting Pty Ltd

Tuesday AM Room: 16B  
March 1, 2011 Location: San Diego Conv. Ctr

Session Chair: Frank Cannova, BP Coke

---

### 8:30 AM Introductory Comments

#### 8:35 AM

**Property Profile of Lab- Scale Anodes Produced with 180°C Mettler Coal Tar Pitch:** Winfried Boenigk<sup>1</sup>; Claudia Boltersdorf<sup>1</sup>; Falk Lindner<sup>1</sup>; Jens Stiegert<sup>1</sup>; <sup>1</sup>RÜTGERS Germany GmbH

The PAH- induced toxicity of coal tar pitch decreases with increasing softening temperature. The use of high- melting pitches is however restricted due to operational challenges. One critical limitation is high-temperature mixing. Temperatures up to 300°C were now realised using a novel developed EIRICH mixer. A 180°C Mettler binder pitch resulted in anodes having a higher baked density (+ 0.03 g/cm<sup>3</sup>). Electrical resistivity and air permeability are reduced whereas compressive strength and Young's modulus are increased. The significantly lower baking loss allows a faster carbonisation process in the low temperature range potentially increasing the throughput of baking furnaces.

#### 9:00 AM

**Quality and Process Performance of Rotary Kilns and Shaft Calciners:** Les Edwards<sup>1</sup>; <sup>1</sup>Rain CII Carbon

Rotary kilns have been used successfully for many years to produce calcined coke for the aluminium industry and they offer a high level of automation, performance and flexibility. Shaft calciners make a high bulk density, coarse particle size product and several papers have been published recently highlighting these benefits. This paper presents a detailed comparison of the merits of these two different calcining technologies from a process and product quality perspective. It addresses several misconceptions about the technologies related to operability, product quality and their ability to handle a wide range of green coke qualities. Both technologies will continue to be used in a complimentary manner in the future.

#### 9:25 AM

**Sub-Surface Carbon Dioxide Reaction in Anodes:** Donald Ziegler<sup>1</sup>; <sup>1</sup>Alcoa Primary Metals

Formation of carbon dust in electrolysis is linked to reaction of the anodes with carbon dioxide. The general understanding is that the reaction takes place inside the anodes, below the bath surface and rather more toward the sides of the anodes than the bottom. Given this, a relevant question is the relative importance of transport through the anode compared to its intrinsic reactivity. To provide quantitative answers, a transport-reaction model has been developed. The key finding is that the extent of reaction is insensitive to the permeability. This is because the reaction produces two moles of CO for every mole of CO<sub>2</sub> consumed, so that there is a net flow away from the reaction locale. Consequently, fresh reactant must be supplied by diffusion rather than convection. Since these two processes are governed by different material properties, this finding opens the possibility of new approaches to optimization of anode structure.

#### 9:50 AM

**Paste Quality Improvements at Alcoa Poços de Caldas Plant:** Beatriz Vry<sup>1</sup>; Ciro Kato<sup>1</sup>; Jeronimo Araujo<sup>1</sup>; Fabiano José Ribeiro<sup>1</sup>; André Luís Abreu<sup>1</sup>; <sup>1</sup>Alcoa

Alcoa Poços de Caldas Soderberg Carbon Plant began its operation in 1965 and after a series of upgrades including the mixer heating system upgrade in

1989, fines control in 2000, mixing temperature optimization in 2004 and installation of coke pre heaters in 2009, the plant now has twice the original production capacity with near world-class paste quality. The benchmark paste quality characteristic is 1.55 g/cc of baked apparent density (BAD), while Poços results are about 1.45 g/cc. The Paste Plant is now challenged to meet Potroom requirements for anode performance (higher loads and dry anode top technology). This paper describes the enablers chosen to improve the baked properties, which includes the optimization of fines production, mixing process and recipe. The quality management system which includes a carbon laboratory with Soderberg baking furnace, sample preparation and baked analysis (BAD, Air Permeability, CO<sub>2</sub> Reactivity and Electrical Resistivity) is also described.

### 10:15 AM Break

#### 10:25 AM

**The Vertical Ball Mill for the Grinding of Calcined Petroleum Coke to Improve the Quality of the Anodes in the Aluminium Industry:** Stefan Gosau<sup>1</sup>; Andreas Wolf<sup>1</sup>; <sup>1</sup>Claudius Peters Projects GmbH

The carbon fines used in anode production have traditionally been generated using the "horizontal" ball mill concept. For carbon fines, the correct particle size distribution with low variation, and low impurity levels are required to produce high quality anodes. A new vertical ball ring mill concept has been developed based on the results of research on the grinding of calcined petroleum coke. Industrial vertical mills are now in operation in seven anode plants around the world. The benefits seen from the mill include lower capital expenditure, reduced variation in sizing and reduced wear of the mill. Results from the plants, showing reduced pitch level variation, improved anode quality and reduced operating costs will be presented in the paper.

#### 10:50 AM

**Prebaked Anode from Coal Extract (2) - Effects of the Properties of Hypercoal-Coke on the Performance of Prebaked Anodes:** Maki Hamaguchi<sup>1</sup>; Noriyuki Okuyama<sup>1</sup>; Nobuyuki Komatsu<sup>1</sup>; Jiro Koide<sup>2</sup>; Keisuke Kano<sup>2</sup>; <sup>1</sup>Kobe Steel, Ltd.; <sup>2</sup>Sumitomo Corporation

Preparation of prebaked anodes utilizing coal solvent extraction technology will be reported. We previously reported that the coal extract prepared from non-hydrogenative extraction of thermal coals using two-ring-aromatic solvent (Hyper-coal) is suitable for feedstock for anode coke. It contains very low levels of the impurities such as sulfur, sodium, nickel, and vanadium that are present in the coke normally used in anodes. In this paper, we will describe the results of detailed analyses of the Hyper-coal coke (HPCC), the effects of calcinating conditions of the Hypercoal, and the performance of prebaked anodes prepared from the HPCC.

#### 11:15 AM

**The New Generation of Vertical Shaft Calciner Technology:** Jingli Zhao<sup>1</sup>; <sup>1</sup>Jinan Aohai Carbon Products Co.,Ltd.

The vertical shaft calciner is widely applied in China for CPC calcination. Its application, however, is restricted by its lower capacity, less automation and no waste heat recuperation. A new generation of energy saving shaft calciner technology with higher capacity and power generation system has been developed recently and is illustrated in this paper. 75 kt of CPC annual production can be achieved by only one new shaft calciner, the waste heat from which can be recuperated to generate electricity of 28 million kWh. The major invention is calciner structure optimization by computer simulation for better volatile combustion and calciner heat balance, which brings about better CPC quality, higher capacity and provides more energy for power generation. The new shaft calciner technology is flexible to the size distribution and volatile content in the green coke and applicable for the pulverous coke and the coke with high volatile content.

TUESDAY AM



## Fatigue and Corrosion Damage in Metallic Materials: Fundamentals, Modeling and Prevention: Fatigue of Nanocrystalline Materials and Fatigue Property Enhancement

*Sponsored by:* The Minerals, Metals and Materials Society, TMS Structural Materials Division

*Program Organizers:* Tongguang Zhai, University of Kentucky; Zhengdong Long, Kaiser Aluminum; Peter Liaw, University of Tennessee

Tuesday AM                      Room: 31C  
March 1, 2011                      Location: San Diego Conv. Ctr

*Session Chairs:* Peter Liaw, University of Tennessee; E-Wen Huang, National Central University

**8:30 AM**  
**Monitoring and Characterization of the Fatigue Response of Nano-Crystalline Mg Composites Reinforced with Ti2AlC:** *Antonios Kotsos<sup>1</sup>; Kavan Hazeli<sup>1</sup>; Babak Anasori<sup>1</sup>; Theodoros Loutas<sup>2</sup>; Michel Barsoum<sup>1</sup>; <sup>1</sup>Drexel University; <sup>2</sup>University of Patras*

Herein we report on the mechanical and fatigue properties of nano-crystalline Mg-matrix composites reinforced with a Ti2AlC powder, fabricated by pressureless spontaneous melt infiltration of porous Ti2AlC preforms. Careful monotonic and cyclic tensile and compression experiments, combined with continuous acoustic emission (AE) monitoring are used to obtain vital information pertinent to the initiation and evolution of deformation and damage mechanisms related to this composite. The fatigue response is shown to be excellent over an extended period of time during which the recorded and extracted AE features are noticeably different from the initial and final stages of fatigue life. These results combined with the observed high damping are consistent with, and can be explained by invoking the formation and annihilation of incipient kink bands. The latter are fully reversible dislocation-based defects consisted of parallel coaxial dislocations formed on easy slip planes of kinking non-linear elastic solids such as Ti2AlC and Mg.

**8:50 AM**  
**Effects of Ultrasonic Nanocrystal Surface Modification on Fatigue Behavior of SUS316 Austenitic Stainless Steel Tube for Stents:** *Auezhan Amanov<sup>1</sup>; Young Sik Pyun<sup>1</sup>; Jun Hyong Kim<sup>1</sup>; Hak Du Kim<sup>1</sup>; Sang Ho Kim<sup>2</sup>; Chae Jong Park<sup>2</sup>; <sup>1</sup>Sun Moon University; <sup>2</sup>M.I. Tech Co., Ltd.*

The present paper describes the effect of Ultrasonic Nanocrystal Surface Modification (UNSM) treatment on fatigue behavior of SUS316 austenitic stainless steel tube for stents which is inserted into clogged heart, superficial femoral, carotid, and renal arteries. The surface hardness, surface integrity and compressive residual stress were compared before and after UNSM treatment. The fatigue test under room temperature is under carrying out and their results will be compared before and after UNSM treatment also. In addition, the possibility of replacement the expensive Co-Cr alloy tube by the UNSM treated SUS316 tube will be analyzed.

**9:10 AM**  
**Increasing the Fatigue Life of SAE52100 Steel by Ultrasonic Nanocrystal Surface Modification:** *Jong Soon Im<sup>1</sup>; Young Sik Pyun<sup>2</sup>; Auezhan Amanov<sup>2</sup>; Sung Jae Lee<sup>1</sup>; Jun Hyong Kim<sup>2</sup>; Chang Min Suh<sup>3</sup>; <sup>1</sup>ILJIN GLOBAL; <sup>2</sup>Sun Moon University; <sup>3</sup>Kyungpook National University*

To increase the fatigue strength of slim bearing rings, the Ultrasonic Nanocrystal Surface Modification (UNSM) treatment was applied to rotary bending fatigue test specimens which are made of bearing steel SAE52100. XRD analysis shows that the structure of subsurface layer has become a nano-grain structure till 100  $\mu\text{m}$  depth from the top surface. Surface structure and nano grain refinement were analyzed and compared before and after UNSM treatment by EBSD analyses as well as fatigue crack growth behavior of UNSM-treated specimens was compared with that of original specimens

which had not been UNSM-treated. It was also revealed from the surface analyses that surface hardness was increased by 20% and compressive residual stress was also induced up to 900 MPa of the UNSM-treated surface which are the main phenomena in prolonging fatigue life of bearings. RCF and friction characteristics after UNSM treatment were also explained.

**9:30 AM**  
**Research on HCF Tests and Damage Model of TC11 Alloy Welded Joints:** *Xiaogang Liu<sup>1</sup>; Guo Hai-ding<sup>1</sup>; <sup>1</sup>Nuaa*

In the paper, the loading controlled fatigue tests of TC11 alloy welded joints have been done; the micro characteristics of fatigue fracture surface have been studied by SEM (scan electron microscope) as well. According to the test results, two types of fatigue source on fracture surface of the welds are found, say, edge fatigue source and internal fatigue source. Then S-N curve of the two types are obtained respectively. The fatigue life of the edge fatigue source is 35-65% longer than that of the internal fatigue source. Moreover, based on the gray distribution of the fracture surface's SEM images, the fractal dimension of fatigue source rejoin on fracture surface has been calculated by box counting method, the relationship between fractal dimension and fatigue life is analyzed. Finally, a fractal damage model which concern macro and micro damage is established based on the combination of damage mechanics theory and fractal theory.

**9:50 AM**  
**Residual Stresses in Alloy CF8C Plus Coated with Iron Aluminide:** *Deepak Kumar<sup>1</sup>; Sebastien Dryepondt<sup>1</sup>; Philip Maziasz<sup>1</sup>; Bruce Pint<sup>1</sup>; Beth Armstrong<sup>1</sup>; Edgar Curzio<sup>1</sup>; <sup>1</sup>Oak Ridge National Laboratory*

CF8C plus is an economic, cast austenitic stainless steel that has creep resistance comparable to state-of-the-art wrought stainless steel and Ni-base alloy, such as alloy 617, but does not require any post processing heat treatments. In this paper we discuss the evolution of residual stresses when this alloy is coated with aluminide coatings applied by slurry-coating and pack cementation processes with the objective of improving its oxidation resistance. The near surface and bulk residual stresses during heating/cooling of the coated samples were determined by x-ray and neutron diffraction techniques for temperatures up to 900°C. Conventional tension-compression strain-controlled fatigue experiments were conducted on the bare and coated samples to assess the effect of residual stresses on the fatigue strength.

**10:10 AM Break**

**10:20 AM**  
**Fatigue Behavior of Al 6082-T4 and Al 7075-T73 after Ball Burnishing:** *Yasser Ahmed<sup>1</sup>; Mansour Mhaede<sup>2</sup>; Lothar Wagner<sup>2</sup>; <sup>1</sup>German University in Cairo; <sup>2</sup>Institute of Materials Science and Engineering (IWW), TU of Clausthal*

The effect of ball burnishing on the rotating beam fatigue strength of age-hardened 6082-T4 and 7075-T73 aluminum has been investigated. Deep rolled specimens were cyclically deformed at room temperature using push-pull stress controlled fatigue and compared to the electrically polished condition as a reference. Also Shot peened condition give better results compared to electrically polish. Optimization curve was produced for both SP and BB conditions, due to this optimization shot peened with Almen intensity of 0.2 mmA for both alloys was used. For ball burnishing (deep rolling) 40 bars was used for 6082-T4 and 75 bars for 7075-T73 by deep rolling tool HG13. The observed improvements were from about 45% for Al 6082-T4 while it was the double for Al 7075-T73 compared to electrically polish, while the improvement of fatigue for BB condition compared to SP was 5% for Al 6082-T4 and 28 % for Al 7075-T73. Data analysis shows that the fatigue behavior in these alloys affected by surface treatment. It was found that deep rolling can dramatically enhance the fatigue behavior of aluminum alloys as compared to the shot peening and polished condition due to near surface compressive residual stresses as well as work hardening states and increased hardness induced by mechanical surface treatment (deep rolling).

10:40 AM

**High Temperature Fatigue Behavior of Laser Shock Peened IN718Plus Superalloy:** *Vibhor Chaswal*<sup>1</sup>; S Mannava<sup>1</sup>; Dong Qian<sup>1</sup>; Vijay Vasudevan<sup>1</sup>; Kristina Langer<sup>2</sup>; <sup>1</sup>University of Cincinnati; <sup>2</sup>Wright Patterson Air Force Base

Service temperature fatigue testing is conducted on 2.5 and 5mm thick IN718Plus aeroengine superalloy after laser shock peening(LSP) with a double side patch overlay of 2.5mm spots at 5 to 8 GW/sq.cm using pulsed Nd:glass laser. Initially thermal relaxation of through thickness compressive residual stresses is established using conventional and Synchrotron X-Ray Diffraction. High temperature(HT) fatigue tests are then conducted at R=0.1 and monitored with an HT clip-on strain gauge and AC potential drop(ACPD). Subsequent fatigue induced residual stress relaxation is determined using a dedicated XRD system and correlated with nano and micro-indentation. While conditions for crack initiation and branching are investigated using scanning electron microscopy, ACPD is used to study final fracture. Microstructural evolution of Untreated, LSP treated, LSP + Fatigued samples is characterized using optical and Transmission electron microscopy. Based on dislocation substructures and precipitate morphologies that offer highest strengthening and fatigue resistance, optimum LSP parameters are recommended.

11:00 AM

**Mechanical Properties and Four-Point-Bending Fatigue Behaviors of Non-Heat Treated and Carburized Low-Carbon Steels for Load-Chain Materials:** *Wei Wu*<sup>1</sup>; Gongyao Wang<sup>1</sup>; David Huber<sup>2</sup>; Peter Hogan<sup>2</sup>; Rodney Reynolds<sup>2</sup>; Chris Hale<sup>2</sup>; Lee Whitted<sup>2</sup>; Joe Eudy<sup>2</sup>; John Stewart<sup>2</sup>; Jules Raphael<sup>3</sup>; Doug Fielden<sup>1</sup>; Peter Liaw<sup>1</sup>; <sup>1</sup>The University of Tennessee; <sup>2</sup>Columbus McKinnon Corporation; <sup>3</sup>J R Technical Services

The low-carbon steels, 10B22, 4615, and 4720, are used in electric hoists as load-chain materials. The mechanical properties of non-heat treated and carburized low-carbon steels were investigated. Four-point-bending-fatigue tests were conducted on cylindrical specimens to examine the fatigue behaviors of non-heat treated and carburized low-carbon steels at different stress levels. The four-point-bending-fatigue tests were performed at a stress ratio of 0.1 and a frequency of 10 Hz with a sinusoidal waveform. The fatigue results showed that the fatigue-strength of the carburized 10B22 steel was the highest at the reference cycles, 10<sup>7</sup>. Scanning-electron microscopy (SEM) fractography of tensile samples demonstrates the typical ductile fracture of the non-heat treated steels at room temperature. However, the mixture of the fracture mechanisms can be seen in the carburized steels; the ductile fracture at the core and the intergranular fracture in the hard layer were observed.

11:20 AM

**Sustained Peak Low Cycle Fatigue: The Role of Coatings:** *Britta Laux*<sup>1</sup>; Tresa Pollock<sup>1</sup>; <sup>1</sup>University of California, Santa Barbara

Turbine airfoil durability is often limited by low cycle fatigue, particularly when the cycle contains a compressive hold at elevated temperature. The initiation and growth of cracks in a single crystal superalloy have been studied during strain controlled fatigue at 1093\176C with a cycle that contained a 120s compressive hold. Samples which were fabricated from the SX nickel base superalloy Rene N5 were cycled in the uncoated condition and with aluminate coatings. All cracks initiated at sample surfaces and grew in a plane normal to the applied stress in the early stages of fatigue. Crack tips contained a layer of oxide. The growth process continued by a combined process of oxidation and creep. The role of the coating in this failure process is considered in the context of a model developed for crack growth during sustained peak low cycle fatigue.

11:40 AM

**S-N Fatigue and Fatigue Crack Propagation Behaviors of High Mn Steels:** *HyunJung Lee*<sup>1</sup>; Jackie Kwon<sup>2</sup>; Youngju Kim<sup>2</sup>; Sangshik Kim<sup>1</sup>; <sup>1</sup>Gyeong Sang National Univ.; <sup>2</sup>Korea Institute of Geoscience and Mineral Resources

The increasing concern on safety and economical issues in shipbuilding industry requires new steels with better fatigue behaviors. The efforts to increase yield strength of steel would increase S-N fatigue life, but may

decrease the resistance to fatigue crack propagation (FCP). In the present study, both S-N fatigue and FCP behaviors of high manganese steels were examined and compared to those of pearlite-ferrite and bainite steels. The S-N fatigue and FCP tests were conducted on high manganese steels, the microstructures of which were dominantly either martensitic or austenitic, at an R ratio of 0.1 and along L-T and T-L. It was found that the microstructure and yield strength affected both of fatigue behaviors of high Mn steels. Fatigue crack paths and fracture surfaces demonstrated that the crack tortuosity varied with different microstructure. The present study showed that yield strength alone could not explain the S-N fatigue behavior of steel specimens.

12:00 PM

**High Cycle Fatigue Behavior of Shot-Peened Steels:** *Alan Plumtree*<sup>1</sup>; Mehdi Mirzazadeh<sup>1</sup>; <sup>1</sup>University of Waterloo

The uniaxial fatigue behavior of four shot-peened engineering steels heat treated to the same hardness was investigated. Following long life (10<sup>7</sup>) cycling under fully reversed (R=-1) uniaxial loading conditions, cyclic softening of the surface was accompanied by a decrease in the depth of surface hardness. Neither cyclic softening nor hardening occurred in non shot-peened steels cycled under the same conditions. The greatest amount of cyclic softening occurred in the two(0.4C and 0.7C)shot-peened hot rolled steels, whereas the fatigue limit of a 0.5C powder metallurgical steel increased 14.0%. However, the fatigue limit of a shot-peened heat treated and tempered steel(0.5C) decreased 12.0% due to the relaxation of internal stresses. In general, the beneficial effects of shot-peening, such as those due to compressive residual stresses and work hardening balanced the effects of surface roughness. Crack initiation occurred below the surface.

---

## Friction Stir Welding and Processing VI: Aluminum and Magnesium Alloys I

*Sponsored by:* The Minerals, Metals and Materials Society, TMS Materials Processing and Manufacturing Division, TMS: Shaping and Forming Committee

*Program Organizers:* Rajiv Mishra, Missouri University of Science and Technology; Murray Mahoney, Retired from Rockwell Scientific; Yutaka Sato, Tohoku University; Yuri Hovanski, Pacific Northwest National Laboratory; Ravi Verma, General Motors

Tuesday AM  
March 1, 2011

Room: 5B  
Location: San Diego Conv. Ctr

*Session Chair:* Yutaka Sato, Tohoku University

8:30 AM

**Microstructure and Mechanical Properties of Friction Stir Welded (FSW) AA5454-Joints:** *Xavier Lang*<sup>1</sup>; Dietmar Eifler<sup>1</sup>; *Guntram Wagner*<sup>1</sup>; <sup>1</sup>University of Kaiserslautern

The industrial application of friction stir welding as a high quality joining process requires the understanding of the influence of the FSW process on the developing microstructure and the resulting mechanical properties. The present work provides a comparison of FSW butt welds of the aluminum alloy AA5454 in the states O and H22. The influence of the friction stir welding process on the microhardness profile in the joining areas and the changes of the grain size in the different welding zones in relation to the base material will be described in detail. Furthermore it will be shown that the ultimate tensile strength, the yield strength and the total elongation after friction stir welding are nearly identical independent of the initial state of the investigated Al-alloys. Finally the fatigue behavior of welded AA5454 in the states O and H22 will be discussed.

TUESDAY AM

8:50 AM

**The Effect of Friction Stir Welding on the Dispersoid Particles of Aluminium Alloy 2195:** Roy Crooks<sup>1</sup>; Jorge dos Santos<sup>2</sup>; Kati Savolainen<sup>3</sup>; Hannu Hänninen<sup>3</sup>; <sup>1</sup>Black Laboratories, L.L.C.; <sup>2</sup>GKSS-Research Centre GmbH; <sup>3</sup>Aalto University

Grain coarsening is observed in friction stir welded nuggets of AA2195 after post-weld anneals. One factor which may contribute to this behaviour is the modification of dispersoid particle distributions by friction stir welding (FSW). High volume fractions of small particles are desirable for impeding grain boundary motion, recrystallization and grain growth. The most effective dispersoid in this alloy is the coherent precipitate, Al<sub>3</sub>Zr, which is subject to loss of coherency during dynamic recrystallization and a consequent reduction in Zener drag. Loss of coherency implies an increase in the critical particle size and dissolution of particles below that size. The dispersoid distributions of the base plate were compared to those of the advancing side of the as-welded plate. The effect of FSW on the particle size distributions in FSW AA2195 was studied using small angle x-ray scattering (SAXS). Morphology and coherency changes of Al<sub>3</sub>Zr particles were studied by transmission electron microscopy.

9:10 AM

**Microstructural Characteristics of Sc-Modified Al-Zn-Mg-Cu Alloy Extrusions Joined by Friction Stir Welding:** Carter Hamilton<sup>1</sup>; Stanislaw Dymek<sup>2</sup>; Oleg Senkov<sup>3</sup>; <sup>1</sup>Miami University; <sup>2</sup>AGH University of Science and Technology; <sup>3</sup>UES, Inc

Extruded and T6 tempered plates of a Sc-modified Al-Zn-Mg-Cu alloy were joined by friction stir welding (FSW) at a constant weld velocity and various pin rotation speeds (PRS). At low PRS, hardness decreased from each edge of the weld to a local minimum at the weld center; however, at high PRS, the hardness initially decreased from each edge of the weld, but then rose toward the weld center. The transition in the hardness profile was related to different heating and cooling conditions during FSW. In particular, the peak temperature during FSW increased from ~250°C to 450°C as the PRS increased from 175 to 400 rpm. Differential scanning calorimetry of baseline and welded samples revealed that the volume fraction of GP zones and  $\eta'$  particles within the weld regions strongly depended on the weld conditions. For FSW heating rates, secondary phase dissolution/precipitation temperatures are in proximity to the welding temperatures.

9:30 AM

**AGG Suppression in Friction-Stir-Welded, Spun-Formed Al-Li 2195 Materials:** Stephen Hales<sup>1</sup>; Wesley Tayon<sup>1</sup>; <sup>1</sup>NASA

Currently, the Al 2219 dome caps for cryogenic propellant tanks are welded assemblies, where multiple panels are contoured to shape, heat treated, and joined. A new, single-piece fabrication approach being explored involves spin forming to final shape of Al-Li 2195 flat plates, which have been friction stir welded (FSW'd) together. The approach requires post-forming heat treatment to the T8 temper for service properties. Processing for the T8 condition involves solution heat treatment (SHT), cold water quenching, cold stretching and aging. The occurrence of abnormal grain growth (AGG) during SHT of 2195 FSW'd material has been problematic from the perspective of service properties. The objective of this work was to suppress AGG during SHT by post-forming thermal processing alone. Constraints on the experimental design included applicability to large, complex-shaped, thin-walled domes and the capabilities of commercial heat treatment facilities. In this presentation, the experiments conducted are outlined and research results discussed.

9:50 AM

**Analysis of Temperature and Residual Stress Evolution during Friction Stir Welding of Aluminum 7075-T6:** Yunfeng Cao<sup>1</sup>; Tyler Davis<sup>1</sup>; Yung Shin<sup>1</sup>; <sup>1</sup>Purdue University

In friction stir welding (FSW), it is well understood that the temperature can have a significant effect on the resultant weld quality. It is therefore necessary to examine the temperature evolution during FSW. In this work, a three dimensional model based on finite element analysis is used to investigate the temperature history and thermo-mechanical process in the welding of

aluminum alloy 7075-T6. The temperature history of the workpiece and the residual stress of the welded plate are measured by an infrared camera and the X-ray diffraction technique, respectively. The measured results are compared with the model predictions and a correlation between temperature and residual stresses is established. To achieve desirable residual stresses of the welded plate, a laser shock peening (LSP) process is subsequently applied on the workpiece. A complete LSP model is employed to predict the residual stresses after LSP and predictions are compared with experimental results.

10:10 AM

**Measurement of Residual Stress in Friction Stir Weld Joints:** Adrian DeWald<sup>1</sup>; Michael Hill<sup>2</sup>; Murray Mahoney<sup>3</sup>; <sup>1</sup>Hill Engineering, LLC; <sup>2</sup>University of California, Davis; <sup>3</sup>Consultant

Friction stir welding (FSW) is currently being used to join materials from plastics to high-strength steels in industries including automotive, aircraft, and shipbuilding. FSW employs a non-consumable pin that rotates at moderate speeds, which is plunged into the butting edges of the work pieces to be joined. Although the temperatures attained during FSW are relatively low compared with conventional fusion welding techniques, residual stresses still develop during FSW. The magnitude and distribution of these residual stresses can be detrimental to performance. This paper investigates the residual stresses generated by friction stir welding in a variety of materials including HSLA-65 steel, AA 2195, and AA 7075. Residual stress measurement data were obtained using the contour method and the slitting method. Using the contour method, residual stresses are obtained through the plate thickness for both the longitudinal and transverse orientations.

10:30 AM

**Development of Tatumaki Friction Stir Welding:** Seung Hwan C. Park<sup>1</sup>; Satoshi Hirano<sup>1</sup>; Shinichi Kaga<sup>2</sup>; Mitsuru Onose<sup>2</sup>; Noriaki Tominaga<sup>2</sup>; Yasutsugu Yoshimura<sup>3</sup>; <sup>1</sup>Hitachi Ltd.; <sup>2</sup>Mitsubishi-Hitachi Metals Machinery, Inc.

The authors have developed a double-sided friction stir welding (FSW) technology that consists of a dual-tool rotating mechanism arranged in face-to-face relation on the front and back surfaces of the joint. One rotating tool has a probe that protrudes from the shoulder, while the other rotating tool has a recess formed in the shoulder. The probe is inserted into the recess for receiving the probe during the FSW. With the shoulders pressed against both surfaces of the joint, the rotating tools move along the joint line. The main advantage of this process is the application of a wide range of weld thicknesses and high speed welding by controlling the motor power consumption. In this study, the effect of tool geometry on weld thickness, and its' possible application to continuous rolling system is described.

10:50 AM Break

11:00 AM

**The Role of Plastic Deformation in Suppressing Abnormal Grain Growth in Friction Stir Welded Al-Li 2195:** Eric Hoffman<sup>1</sup>; Robert Hafley<sup>1</sup>; Marcia Domack<sup>1</sup>; Ravi Shenoy<sup>2</sup>; Wesley Tayon<sup>1</sup>; Jessica Robinson<sup>1</sup>; <sup>1</sup>NASA Langley Research Center; <sup>2</sup>Lockheed Martin Space Systems

Traditional methods for producing large scale dome end caps for cryogenic propellant tanks utilize a multi-piece welded gore construction. To reduce the mass and fabrication costs and increase the reliability for these domes, a novel near-net manufacturing process is being explored in which a single-piece dome is spin formed from an Al-Li 2195-OM temper blank. The blank is friction stir welded (FSW) together from two commercial Al-Li 2195-OM temper plates to overcome plate size limitations. This manufacturing approach requires post-forming heat treatments to develop the required T8 temper properties. Abnormal grain growth (AGG) was observed in the FSW after solution heat treatment (SHT) and resulted in degraded mechanical properties. In this study, samples of FSW Al-Li 2195 were subjected to plastic deformation introduced by cold working and laser peening. The minimum level of cold work and laser peening intensity required to suppress AGG during SHT was determined.



11:20 AM

**The Effect of Dispersoid Modification on Abnormal Grain Growth in Friction Stir Welded Al-Li 2195:** Roy Crooks<sup>1</sup>; Ravi Shenoy<sup>2</sup>; Wesley Tayon<sup>3</sup>; Marcia Domack<sup>3</sup>; <sup>1</sup>National Institute of Aerospace; <sup>2</sup>Lockheed Martin Space Systems; <sup>3</sup>NASA Langley Research Center

Friction stir welded (FSW) AA2195 plates have been spun formed into large domes used as end caps for cryogenic tanks for space launch vehicles. After FSW, the plates are annealed, spun, solution treated and aged to peak strength. Solution heat treatment of the FSW and spun formed plates may result in excessive growth of nugget grains, particularly near the advancing side interface. Several factors are related to this growth, including stored strain energy, grain size and dispersoid particle size distributions. Samples of FSW AA2195 were studied after FSW and annealing to quantify the microstructural factors contributing to grain growth during the solution heat treatment. Electron backscattered diffraction (EBSD) systems in a scanning electron microscope (SEM) and in a transmission electron microscope were used. Heat treatments developed to modify these factors were assessed.

11:40 AM

**Friction Stir Welding of 25 mm Thick Al 6061-T651 Plates:** Guru Dinda<sup>1</sup>; Douglas Grant<sup>1</sup>; Matthew Scheid<sup>1</sup>; Ashish Dasgupta<sup>1</sup>; Sudip Bhattacharya<sup>2</sup>; Jyoti Mazumder<sup>2</sup>; <sup>1</sup>Focus: HOPE; <sup>2</sup>University of Michigan

Friction stir welding (FSW) was invented in 1991 by The Welding Institute as a solid-state joining method for a variety of metals and alloys, in particular aluminum alloys. Since the early discovery, FSW of aluminum alloys have been extensively investigated. However, very little work is reported on FSW of thick Al plates in the open literature. The objective of this work is to optimize the process parameters such as travel speed, forge force, rotational speed and tilt angle for butt welding of 25 mm thick Al 6061-T651 plates with a view to produce welds without any defects. A comprehensive design of experiments was conducted to establish a process parameter window for welding 25 mm thick Al 6061-T651 plates of various sizes. The weld quality was assessed via optical microscopy, SEM, XRD, microhardness and tensile testing. The effect of process parameters on the resulting weld properties was analyzed using statistical techniques.

12:00 PM

**Effects of Forge Axis Force and Backing Plate Boundary Condition on FSW of AA6056:** Piyush Upadhyay<sup>1</sup>; Anthony Reynolds<sup>1</sup>; <sup>1</sup>University of South Carolina

For a given set of welding parameters forge axis force can also have a significant effect on stir zone temperature, torque, and in-plane forces. Typically, for a given set of welding parameters, an FSW user chooses an appropriate but arbitrary forge axis force a posteriori based on weld surface quality. This qualitative adjustment of forge axis force can be affected by thermal boundary conditions that are applied to the work-piece. We seek to understand the effects of forge axis force coupled with the thermal boundary condition at the bottom of the work-piece on AA 6056 (4.2mm thick) plate. Forge axis force and backing plate conductivity are varied while holding other parameters constant. Resulting temperature, torque and in-plane forces are analyzed and correlated with the varied parameters. The result demonstrates that for the given gage thickness, metallurgically significant temperature variation can be achieved without changing the rotation/translation speed.

12:20 PM

**Friction Stir Welded "A" Frame For Dual Function Test Fixture:** Alan Handyside<sup>1</sup>; Farzad Baratzadeh<sup>1</sup>; Jeff Buller<sup>1</sup>; Hamid Lankarani<sup>2</sup>; Blair Carlson<sup>3</sup>; Dwight Burford<sup>1</sup>; <sup>1</sup>National Institute for Aviation Research; <sup>2</sup>Wichita State University; <sup>3</sup>General Motors Corporation

Advancements in friction stir welding (FSW) pin tool and joint design have been used to develop an automotive and aerospace test fixture. The fixture was designed and built for a case study analyzing functionality of an advanced bumper / crash box fabricated by FSW. The fixture "A" frame is fabricated using FSW of AA6063-T6 and AA6061-T6. The fixture is used as drop tower for constant acceleration tests and with crash sled for constant velocity tests. Butt welds, similar to those developed and tested for the crash box / bumper, were incorporated into the fixture. FEA simulations

on the "A" frame, including FSW joints, were used for analysis. Tensile test coupons made by FSW were prepared to determine weld parameters, parent and weld material properties. Summary of FSW process development is presented along with weld coupon test results. An overview of fixture function and preliminary fixture test results is presented.

12:40 PM

**Investigation of Lazy S Feature in Self Reacting Tool Welds in 2024-T4 Aluminum:** Karl Warsinski<sup>1</sup>; Michael West<sup>2</sup>; Jim Freeman<sup>3</sup>; Todd Curtis<sup>2</sup>; <sup>1</sup>Michigan Technological University; <sup>2</sup>South Dakota School of Mines and Technology; <sup>3</sup>MTS Systems Corporation

The current research is an examination of the "Lazy S" feature found in self-reacting tool (SRT) friction stir welds. The research objectives are to characterize the feature using scanning electron and optical microscopy and determine its effect on the mechanical properties of the welded material. Welds were conducted in 2024-T4 aluminum. Welding parameters were varied in an attempt to influence the size and location of the feature. Tensile tests were performed on each weld and were correlated with the total length of the feature. Preliminary results indicate that there is a correlation between decreasing feature length and decreasing tensile strength.

## Frontiers in Solidification Science: Experimental Studies

*Sponsored by:* The Minerals, Metals and Materials Society, TMS Electronic, Magnetic, and Photonic Materials Division, TMS: Chemistry and Physics of Materials Committee, TMS: Solidification Committee

*Program Organizers:* Jeffrey Hoyt, McMaster University; Daniel Lewis, Rensselaer Polytechnic Institute

Tuesday AM  
March 1, 2011

Room: 6E  
Location: San Diego Conv. Ctr

*Session Chair:* To Be Announced

8:30 AM Invited

**Simulation of Dendritic Growth Observed in Synchrotron X-ray Video Experiments:** Christoph Beckermann<sup>1</sup>; Pierre Delaleau<sup>1</sup>; Ragnvald Mathiesen<sup>2</sup>; Lars Arnberg<sup>2</sup>; <sup>1</sup>University of Iowa; <sup>2</sup>NTNU

A mesoscopic model is developed to simulate microstructures observed in situ by X-ray video microscopy during directional solidification of Al-Cu alloys in a Hele-Shaw cell. In the model, a volume-averaged species conservation equation is solved to obtain the solute concentration and solid fraction fields, and an analytical stagnant film model is used to predict the motion of the dendrite envelopes. Good agreement is found between the measured and predicted dendrite envelope shapes, solid fractions, and solute concentration fields. The predicted size of the mushy zone and the extent of the undercooled melt region ahead of the columnar front agree well with the in situ experimental observations. The simulation results show quantitative agreement with internal solid fraction variations measured from the radiographs. The model is also able to realistically simulate a primary dendrite trunk spacing adjustment that was observed in one of the experiments.

9:00 AM Invited

**Solidification of Metallic Alloys under Magnetic Fields:** Yves Fautrelle<sup>1</sup>; Xi Li<sup>1</sup>; Olga Budenkova<sup>1</sup>; Bachir Saadi<sup>1</sup>; Zhongming Ren<sup>1</sup>; <sup>1</sup>Grenoble Institute of Technology

Polyphase AC magnetic fields are used usually to generate either liquid metal stirring or electromagnetic vibrations. The electromagnetically-driven flows promote segregations and influence their distribution. The flow may also promote the CET thanks its effects on both the temperature and solute fields as well as the possible fragmentation mechanism. As far as DC magnetic fields are concerned, it was known that they usually exert a damping of the bulk fluid flows. Nevertheless, due to crystal anisotropy magnetic effects

TUESDAY AM

such that alignment or texturation appear during solidification under high magnetic fields. Furthermore, high-intensity magnetic field interacts with thermo-electric currents to create electromagnetic forces. Those forces are responsible for strong liquid metal flows both in the bulk and in the mushy zone. The forces act both on the liquid and the solid phase. Direct fragmentation of the dendrites are sometimes encountered, leading to equiaxed structures.

#### 9:30 AM Invited

**Two-Phased Spiral Dendrites:** *Silvere Akamatsu*<sup>1</sup>; Mikael Perrut<sup>2</sup>; Sabine Bottin-Rousseau<sup>1</sup>; Gabriel Faivre<sup>1</sup>; <sup>1</sup>CNRS - UPMC; <sup>2</sup>ONERA

We report for the first time experimental observations of a steady crystal growth shape called two-phased spiral dendrite in real-time directional solidification of a transparent SCN-DC base nonfaceted ternary alloy in glass-wall samples. Spiral dendrites arise from a ternary-component driven eutectic-cell instability of a two-phased solid. They exhibit an overall parabolic shape, and a lateral branching. Coupled growth occurs continuously from a spiral pattern on the tip, and delivers two intricate helices. The spiral step and the tip radius of curvature vary approximately as the reciprocal of the square root of the solidification rate, and fall close to the minimum-undercooling spacing of binary SCN-DC. The spiral geometry is compatible with a growth of the lamellae perpendicular to the solidification front envelope. In contrast to the one-phased dendrite, the growth direction of spiral dendrites is not determined by any surface tension anisotropy, and is initial-condition dependent.

#### 10:00 AM Break

#### 10:15 AM Invited

**Universality and the Pinch-off of Rods by Capillarity:** L. Aagesen<sup>1</sup>; A. Johnson<sup>1</sup>; J. Fife<sup>1</sup>; *Peter Voorhees*<sup>1</sup>; M. Miksis<sup>1</sup>; S. Poulsen<sup>2</sup>; E. Lauridsen<sup>2</sup>; F. Marone<sup>3</sup>; M. Stampanoni<sup>3</sup>; <sup>1</sup>Northwestern University; <sup>2</sup>Riso Laboratory for Sustainable Energy; <sup>3</sup>Swiss Light Source

The detachment of secondary dendrite arms during solidification processing has a significant influence on the resulting microstructure. To understand the fragmentation process when it is driven by capillarity, we examine the evolution of the interfacial morphology of liquid and solid rods in an Al<sub>15</sub> wt.% Cu alloy. Interfacial energy induces a rod develop undulations by the well-known Rayleigh instability. These undulations increase in amplitude and lead to pinching. We show theoretically that sufficiently close to the pinching event the interfacial morphology becomes universal; the interface shape is independent of the initial morphology of the rod-like phase and material system, and its evolution is described by a power law in time. We test this prediction using insitu x-ray tomography and find an excellent agreement between theory and experiment in both the morphology and the kinetics of the pinching process. The implications of this result to various solidification processes will be discussed.

#### 10:45 AM Invited

**Directional Growth Structures in Univariant Eutectics:** *Ralph Napolitano*<sup>1</sup>; <sup>1</sup>Iowa State University

Directional solidification and serial milling are employed here to investigate the three-dimensional features of multiphase microstructures in Al-Cu and Al-Cu-Ag alloys, focusing on univariant two-phase structures in the ternary. The relationships between local eutectic phase topology, crystallographic orientation/misorientation, eutectic fault configuration, faulted domain structure, and grain structure, relative to the constraints of specimen geometry and applied thermal field, are examined.

#### 11:15 AM

**Nucleation Catalysis Potency of Ceramic Nanoparticles in Aluminum Matrix Nanocomposites:** *Michael De Cicco*<sup>1</sup>; John Perepezko<sup>1</sup>; Lih-Sheng Turng<sup>1</sup>; Xiaochun Li<sup>1</sup>; <sup>1</sup>University of Wisconsin-Madison

The nanoparticles in metal matrix nanocomposites (MMNCs) were shown to catalyze nucleation of solidification. Nanoparticles of SiC, TiC, and  $\gamma$ -Al<sub>2</sub>O<sub>3</sub> were dispersed in an aluminum alloy A356 matrix using an ultrasonic processing technique. The droplet emulsion technique was used to examine the undercooling in each matrix-nanoparticle system. Despite

their small sizes, the nanoparticles demonstrated the ability to significantly reduce the necessary undercooling for nucleation. In general, the degree of undercooling in the MMNCs containing SiC, TiC and  $\gamma$ -Al<sub>2</sub>O<sub>3</sub> was in agreement with the free growth undercooling. The nucleation catalysis by the nanoparticles resulted in significantly refined microstructures. The grain refining effectiveness of nanoparticles was also examined in pure Al and Al-10Mg using TiC<sub>0.7</sub>N<sub>0.3</sub> nanoparticles. In both pure Al and Al-10Mg the nanoparticle addition significantly reduced the average grain size of the matrix. Comparison was made to the commonly used Al-5Ti-B grain refiner. At the addition levels used, the nanoparticles were more effective than the Al-5Ti-B grain refiner.

### Hume-Rothery Symposium Thermodynamics and Diffusion Coupling in Alloys - Application Driven Science: Diffusion Coefficients and Thermodynamics

*Sponsored by:* The Minerals, Metals and Materials Society, TMS Electronic, Magnetic, and Photonic Materials Division, TMS: Alloy Phases Committee

*Program Organizers:* Zi-Kui Liu, The Pennsylvania State University; Larry Kaufman, CALPHAD, Inc.; Annika Borgenstam, Royal Institute of Technology; Carelyn Campbell, NIST

Tuesday AM  
March 1, 2011

Room: 31A  
Location: San Diego Conv. Ctr

*Session Chairs:* Yongho Sohn, University of Central Florida; Gary Shiflet, University of Virginia

#### 8:30 AM Invited

**Influence of Thermodynamic Forces on Diffusion in Melts:** *Axel Griesche*<sup>1</sup>; Juergen Horbach<sup>2</sup>; Andreas Meyer<sup>2</sup>; <sup>1</sup>Federal Institute for Materials Research and Testing (BAM); <sup>2</sup>German Aerospace Center (DLR)

We report about diffusion measurements and molecular dynamic simulations in Al-Ni and Al-Cu melts. Capillary methods were used to measure Ni and Cu self diffusion and to measure interdiffusion. The combination of the capillary set-up with X-ray radiography allowed in-situ detecting of convective contributions to the interdiffusion transport by tracking the time dependence of diffusion. Thus, the determination of the interdiffusion coefficient can be restricted to convection-free experiment times resulting in an increased accuracy of the measured interdiffusion coefficient. Additionally, quasi-elastic neutron scattering was used to measure convection-free Ni and Cu self diffusion. Molecular dynamics simulations were used to determine all diffusion coefficients and the thermodynamic factor. The comparison between experiment and simulation shows an excellent agreement of the interdiffusion coefficients as a function of temperature. It was found that interdiffusion is enhanced by thermodynamic forces with a maximum around the stoichiometric composition.

#### 9:00 AM Invited

**Atomic Bond Defects; Thermodynamics and Diffusion in Metallic Glasses:** *Gary Shiflet*<sup>1</sup>; Aiwu Zhu<sup>1</sup>; S. Joseph Poon<sup>1</sup>; <sup>1</sup>University of Virginia

Diffusion in metallic glasses and deeply undercooled liquids will be atomistically developed and analyzed using the concept of 'atomic bond deficiency', i.e., cooperative movements of multiple adjacent atoms. Diffusion in metallic glasses and supercooled liquids is a fundamental process that controls the glass formability, thermal stability and viscosity and, to some extent, affects their ductility. Experimental measurements indicate that diffusion in amorphous metals is a thermal activation process with many similarities to crystalline solids, including: simple Arrhenius temperature-dependence of coefficient D; atomic size effect of diffusing species; and the annealing effect of quenched states. However, amorphous metal diffusion is significantly different from crystals, quantitatively in particular, as indicated in: a much larger slope of the Q versus the logarithm of D<sub>0</sub>, and more pronounced positive size effects of diffusing atoms on Q. Comparisons

with previous experimental data and rationalization with seemingly confusing disparate results will be presented and explained.

#### 9:30 AM Invited

**Application of Thermodynamic and Kinetic Modeling to Diffusion Simulations in Nickel-Base Superalloy Systems:** Anders Engström<sup>1</sup>; Henrik Larsson<sup>1</sup>; Johan Bratberg<sup>1</sup>; Lars Höglund<sup>1</sup>; Paul Mason<sup>2</sup>; <sup>1</sup>Thermo-Calc Software AB; <sup>2</sup>Thermo-Calc Software Inc

This paper presents a brief review, followed by some new results from recent diffusion simulations in Ni-base superalloy systems, performed by means of a thermodynamic and kinetic modelling approach as taken in the commercial finite-difference code DICTRA. The DICTRA code solves the multi-component diffusion equations, combining assessed thermodynamic and kinetic data in order to determine the full composition dependent interdiffusion matrix. The link between fundamental physics based models and critically assessed data allows simulations to be performed with realistic conditions and data on alloys of practical importance. Emphasis in this paper is on modelling and simulation of interdiffusion occurring between NiAl coatings and different Ni-base superalloy substrates. For this purpose we have used the so-called homogenization approach to diffusion in multi-phase systems, recently implemented into the DICTRA software. The simulation results obtained are validated against experimental data, and the agreement is very satisfactory given the complexity of the problem.

#### 10:00 AM Break

#### 10:20 AM Invited

**Selected Observations from Interdiffusion Study in U-Mo-Al System:** Yongho Sohn<sup>1</sup>; Emmanuel Perez<sup>1</sup>; Bo Yao<sup>1</sup>; Ashley Ewh<sup>1</sup>; Dennis Keiser, Jr.<sup>2</sup>; <sup>1</sup>University of Central Florida; <sup>2</sup>Idaho National Laboratory

Interdiffusion and microstructural development in the U-Mo-Al system with several additional alloying additions was examined using solid-to-solid diffusion couples in the temperature range of 500 to 600°C. In ternary U-Mo (7-12 wt.%) vs. Al diffusion couples annealed at 600°C for 24 hours, interdiffusion microstructure varied of finely dispersed UAl<sub>3</sub>, UAl<sub>4</sub>, U<sub>6</sub>Mo<sub>4</sub>Al<sub>14</sub>, and UMo<sub>2</sub>Al<sub>20</sub> phases while the average composition throughout the interdiffusion zone remained constant at approximately 80 at.% Al. The addition of Si (up to 5 wt.%) in Al significantly reduced the thickness of the intermetallic layer by changing the constituent phases within the interdiffusion zone. The formation of (U,Mo)(Al,Si)<sub>3</sub> with relatively large solubility for Mo and Si was observed. Concurrently, the UAl<sub>4</sub> and U<sub>6</sub>Mo<sub>4</sub>Al<sub>14</sub> phases with poor irradiation behavior were absent. Additional efforts to reduce the growth kinetics of the complex intermetallic layer including alloying additions to the U-Mo alloy and diffusion barriers such as Zr and Nb are presented and discussed.

#### 10:50 AM Invited

**Analysis of the Influence of Vacancy-Solute Interaction on Diffusion of Atomic Monomers and Clusters:** Piotr Warczak<sup>1</sup>; Jaroslav Zenisek<sup>2</sup>; Ernst Kozeschnik<sup>1</sup>; <sup>1</sup>Vienna University of Technology; <sup>2</sup>Materials Center Leoben Forschung GmbH

In the present paper, we investigate the dependence of the diffusional mobility of single solute atoms as well as clusters of atoms on the vacancy-solute binding characteristics with the Monte Carlo (MC) method. Existing work, mainly based on first-principles calculations and atomistic simulations, is reviewed first. Then, we compare these results to our simulations performed with MC and explore these effects in the light of macroscopic diffusive fluxes and atomic clusters movement in the sense of Brownian motion. Finally, we propose a numerical method for incorporation of the movement and potential collisions of clusters in a precipitation kinetics framework.

#### 11:20 AM

**Characterization of Phase Formation and Diffusion Behavior of the Cu-Zn Binary System:** Christopher Eastman<sup>1</sup>; John Kuper<sup>1</sup>; Ji-Cheng (J.-C.) Zhao<sup>1</sup>; <sup>1</sup>The Ohio State University

Diffusivity data are limited for the Cu-Zn binary system and it is still questionable whether β' undergoes a eutectoid decomposition at low temperatures. Zinc is a widely used element in copper alloys; therefore

the diffusion coefficient of Zn in Cu will be useful for simulating phase precipitation in Cu alloys. This paper characterizes phase formation and diffusion behavior in the Cu-Zn binary system through the use of infinite diffusion couples, transient liquid phase diffusion couples, solid-liquid conical diffusion couples by immersion of a Cu cone into molten Zn, and U.S. pennies which consist of a Zn core and an electroplated Cu outer layer. Heat treatments for different durations and at several temperatures were used to characterize the diffusion behavior of the Cu-Zn binary system. Optical microscopy, electron dispersive spectroscopy (EDS) and electron probe microanalysis were used to obtain composition profiles in order to extract the diffusivity values.

#### 11:50 AM

**Interdiffusion Investigation of Mo and Zr in Fe, Fe-Cr and Fe-Ni-Cr Alloys at 650, 750, and 850°C:** Ashley Ewh<sup>1</sup>; Judith Dickson<sup>1</sup>; Bulent Sencer<sup>2</sup>; John Kennedy<sup>2</sup>; Yongho Sohn<sup>1</sup>; <sup>1</sup>University of Central Florida; <sup>2</sup>Idaho National Laboratory

Interdiffusion between molybdenum or zirconium and iron alloys was studied using various solid-to-solid diffusion couples. The couples were assembled with disks of Mo, Zr, Fe, Fe-15Cr, and Fe-15Cr-15Ni, in wt.%, and were isothermally annealed at 650, 750, and 850°C for 45, 30, and 15 days, respectively. Following the diffusion anneal, the couples were water quenched to maintain the high temperature microstructure and were cross-sectioned for analysis. Microstructural observations of the interdiffusion zone were made via optical and scanning electron microscopy. Intermetallic layer phase constituents were identified using a combination of energy dispersive spectroscopy and transmission electron microscopy. Concentration profiles were also determined via electron probe microanalysis and were used to determine relevant interdiffusion coefficients of the individual components. The development and growth kinetics of the intermetallic phases developed in these couples are discussed with regard to the phase diagrams and compared with previous literature.

## ICME: Overcoming Barriers and Streamlining the Transition of Advanced Technologies to Engineering Practice -- The 12th MPMD Global Innovations Symposium: Emerging and Fundamental Techniques and the Advancement of ICME in Industry

*Sponsored by:* The Minerals, Metals and Materials Society, TMS Materials Processing and Manufacturing Division

*Program Organizers:* Paul Mason, Thermo-Calc Software Inc; Mei Li, Ford Motor Company; James Warren, National Institute of Standards and Technology; Jeff Simmons, AFRL

Tuesday AM  
March 1, 2011

Room: 7A  
Location: San Diego Conv. Ctr

*Session Chair:* Mei Li, Ford Motor Company

#### 8:30 AM

**Modeling and Simulation of Mechanical Properties of Magnesium Alloy Wheel Casting for Automobile:** Liang Huo<sup>1</sup>; Zhiqiang Han<sup>1</sup>; Xunming Zhu<sup>2</sup>; Junpeng Duan<sup>2</sup>; Aimin Wang<sup>2</sup>; Baicheng Liu<sup>3</sup>; <sup>1</sup>Key Laboratory for Advanced Materials Processing Technology (Ministry of Education), Department of Mechanical Engineering, Tsinghua University; <sup>2</sup>WANFENG Magnesium Co. Ltd., WANFENG Auto Holding Group; <sup>3</sup>State Key Laboratory of Automotive Safety and Energy, Department of Automotive Engineering, Tsinghua University

Modeling and simulation have become a powerful tool in optimizing casting process and predicting component microstructure. However, a further step is desirable for engineers to predict the mechanical properties based on the casting process and microstructure simulation, so as to optimize the structure of casting component and reduce the developing time. In



the present paper, the mechanical properties of a magnesium alloy wheel casting for automobile were predicted by integrating the model of as-cast microstructure with the model of tensile strength, as well as the simulation of mold filling process and temperature field during solidification. Considering the grain size variation due to different cooling rate, tensile strength was predicted based on Hall-Petch equation. The distribution of grain size and the variation of the tensile strength of the magnesium alloy wheel were predicted by the present model. Metallographic examination and mechanical property test were performed for validation.

#### 8:50 AM Invited

**Engineering Grain Boundary Populations and Connectivity in Polycrystalline Structures:** *Gregory Rohrer*<sup>1</sup>; Herbert Miller<sup>1</sup>; <sup>1</sup>Carnegie Mellon University

Efforts to control the populations of grain boundaries in polycrystals, and the structure sensitive properties that are linked to the grain boundary network structure, are usually referred to as grain boundary engineering. In this paper, I will review progress in understanding the mechanisms by which grain boundary populations and connectivity change during processing. Both the relative populations of different grain boundaries, and their connectivity, have been measured in Ni before and after repeated thermomechanical processing. When the observations are compared to recently measured grain boundary energies, it is observed that higher energy boundaries in the network are replaced by lower energy boundaries. A model for the evolution of the grain boundary populations will be presented. Finally, homology metrics are used to evaluate changes in the connectivity of grain boundaries as a function of processing.

#### 9:15 AM

**The Development of Tools for the Prediction of the Tensile and Fracture Toughness Properties in a/B Titanium alloys:** *Santhosh Koduri*<sup>1</sup>; Peter Collins<sup>2</sup>; Hamish Fraser<sup>1</sup>; <sup>1</sup>The Ohio State University; <sup>2</sup>University of North Texas

The development of tools to predict the mechanical properties based upon compositional and microstructural inputs in multi-component, multi-phase Ti-based alloys represents a significant challenge and a key element of Integrated Computational Materials Engineering. One such solution is the development of high-fidelity databases and the subsequent application of non-linear modeling tools such as neural networks based upon a Bayesian framework to extract the underlying composition-microstructure-property relationships. This talk will highlight the development of such rules-based models for the prediction of the tensile and fracture toughness properties of Ti6Al4V at room temperature. These models have been successfully used to isolate the influence of the individual microstructural features on the mechanical properties, potentially providing the basis for the development of more robust phenomenological models.

#### 9:35 AM

**Quantifying Interface Energetics and Kinetics using Atomic-scale Simulations:** *Moneesh Upmanyu*<sup>1</sup>; <sup>1</sup>Northeastern University

Predictive capabilities of microstructural evolution models are extremely sensitive to their properties, in particular their energetics and kinetics. In polycrystalline microstructures, the interfacial properties are set at the atomic-scale, necessitating the need for i) techniques that extract these properties for individual interfaces with well-known degrees of freedom, and ii) multiphysics integrated efforts that transfer of these properties to larger-scale evolution models. In this talk, I will present progress in computational frameworks that allow efficient extraction of interface free energies, stiffness and mobilities as relevant for fundamental annealing phenomena. A focus will be on techniques that allow us to quantify the effect of solutes for homophase interfaces such as grain boundaries. The relevance for ICME-based efforts will be discussed.

#### 9:55 AM Invited

**Integrated Computational Materials Design and Qualification: Making CyberSteel Fly:** *Greg Olson*<sup>1</sup>; <sup>1</sup>Northwestern University

The numerical implementation of established materials science principles in the form of purposeful engineering tools has brought a new level of integration of the science and engineering of materials. Parametric materials design integrating materials science, applied mechanics and quantum physics within a systems engineering framework has brought a first generation of designer "cyberalloys" that have now entered successful commercial applications, and a new enterprise of commercial materials design services led by QuesTek Innovations LLC has steadily grown over the past decade. The success of materials design established a basis for the DARPA-AIM initiative which broadened computational materials engineering to address acceleration of the full materials development and qualification cycle. The recent flight qualification of the Ferrium S53 CyberSteel for aircraft landing gear demonstrates the power of the integrated computational design + AIM methodology.

#### 10:20 AM Break

#### 10:35 AM Invited

**3-D Modeling of Machining Distortions of Aerospace Components:** *Shesh Srivatsa*<sup>1</sup>; <sup>1</sup>GE Aviation

Aircraft engine and airframe structural components that are machined from forgings represent a significant cost of both military and commercial aircraft. Typical component applications are rotating disks in aircraft engines and structural components in airframes. The buy-to-fly weight ratio, which is the ratio of the forged material weight to the finished part weight, is typically between 4 and 10 for such components. The excess material is removed by various machining operations, which are a major contributor to the cost of forged components. Machining distortions are a problem with most forged components which are quenched rapidly in order to generate the required mechanical properties. Distortion can be caused by material bulk stresses resulting from heat-treating operations, or from local near-surface machining-induced stresses. Typically additional machining operations and setups are added in a time-consuming and costly trial-and-error approach to minimize the effects of part distortion. Manufacturing residual stresses can adversely impact the behavior of the components during service. There is a need to understand the effects of heat treating and machining on distortion and to predict, minimize, and control these distortion-related processes. The objective of this program is to establish a modeling method that accurately predicts distortion during machining of 3-D shaped forgings used in aircraft engines and airframe structures. Prediction and validation of machining distortions due to bulk and surface residual stresses will be presented. This program is funded by the USAF Metals Affordability Initiative (MAI).

#### 11:00 AM Invited

**A Case for ICME - Ti Alloy Design Tool Development at Boeing:** *Donald Shih*<sup>1</sup>; <sup>1</sup>The Boeing Company

Titanium structures are critically important to Boeing. Advanced Ti alloys, e.g. lighter alloys and tougher/ stronger alloys are needed. But it commonly takes too long to develop such an alloy. New design concept and methodology that sharply reduce this cycle duration are a must. Atomic modeling, multiscale simulation and data-mining are proven useful to achieve such goals in other materials. However, they have not been applied in Ti alloys, mainly due to many key challenges. Boeing, with our academic partners, has been developing the concept and methodology to overcome these challenges using the ICME approaches. As a key part of multiscale modeling and simulation in the lighter Ti alloys and tougher/ stronger alloys design effort, DFT based first-principles and phase diagram calculations have been conducted. This presentation will give a case study of using of multiscale modeling and simulation and validation for Ti alloy design tool development will be presented.

11:25 AM Invited

**Application of Computational Modeling during Processing of Stainless Steels:** *Ashish Patel*<sup>1</sup>; <sup>1</sup>Carpenter Technology Corporation

These days process and alloy modeling is gaining prominence, largely due to the urgency in developing new alloys and optimizing the processes that are used in manufacturing these alloys. Currently, there are numerous efforts in both academia and in within the industry to model the effect of alloying elements on microstructure and to get an insight on the effect of processing parameters on properties of high performance alloys. This talk will provide a brief overview of the commonly used processing techniques used during manufacturing of high performance alloys followed by illustrations of typical outcomes from models used to simulate the entire processing sequence for manufacturing high nitrogen austenitic steels. The nitrogen solubility is determined from a CALPHAD based model, a CFD based model is used to simulate the melting and casting, an analytical model for simulating the heat treatment followed by a FEM based simulation for the thermo-mechanical processing.

11:50 AM Invited

**Fast Acting Models for Materials-Centric Engineering Design:** *Triplicane Parthasarathy*<sup>1</sup>; Y.S. Choi<sup>1</sup>; R. Goetz<sup>2</sup>; D. Furrer<sup>2</sup>; R. John<sup>3</sup>; R. Dutton<sup>3</sup>; <sup>1</sup>UES, Inc.; <sup>2</sup>Rolls Royce Engines; <sup>3</sup>Air Force Research Laboratory

Engineering design of turbine disks with complex heat treatment or heat treatment gradients are of interest in pushing the envelope of turbine disks in future aircraft design. The use of such complex process designs make it essential to incorporate material-centric models within the design space. UES has been working in collaboration with Rolls Royce, under Air Force funding, to develop fast acting models that are based on mechanism based higher order models towards property predictions from either microstructural inputs or heat treatment inputs. Results on these efforts are presented and implications discussed.

**Magnesium Technology 2011: Alloy Design/ Development; Grain Refinement and Severe Plastic Deformation**

*Sponsored by:* The Minerals, Metals and Materials Society, TMS Light Metals Division, TMS: Magnesium Committee  
*Program Organizers:* Wim Sillekens, TNO Science and Industry; Sean Agnew, University of Virginia; Suveen Mathaudhu, US Army Research Laboratory; Neale Neelameggham, US Magnesium LLC

Tuesday AM  
March 1, 2011

Room: 6F  
Location: San Diego Conv. Ctr

*Session Chairs:* Matthew Barnett, Deakin University; Suveen Mathaudhu, US Army Research Office

8:30 AM

**Effect of Zn/Gd Ratio on Phase Constitutions in Mg-Zn-Gd Alloys:** Song Zhang<sup>1</sup>; *Guangyin Yuan*<sup>1</sup>; Chen Lu<sup>1</sup>; Wenjiang Ding<sup>1</sup>; <sup>1</sup>Shanghai Jiao Tong University

The phase constitutions of Mg-Gd-Zn alloys in the Mg-rich corner were investigated using XRD, SEM and TEM. The effect of Gd/Zn ratio and contents of Gd, Zn element on the phase constitutions of Mg-Zn-Gd alloys were studied. Critical contents of Gd and Zn for the formation of long period stacking ordered (LPSO) structure and X phase in the Mg-Gd-Zn system in the Mg-rich corner have been confirmed using conventional cast process. When Zn%-Gd% = 0, LPSO structure and W phase were formed in Mg-Gd-Zn alloys. When Zn%-Gd% = 0.5%, only W phase was found in the alloys. When Zn%-Gd% = 1%, I phase and W phase were observed in the alloys.

8:50 AM

**Optimization of Magnesium-Aluminum-Tin Alloys for As-Cast Microstructure and Mechanical Properties:** Xiaoyu Kang<sup>1</sup>; *Alan Luo*<sup>2</sup>; Penghuai Fu<sup>1</sup>; Zhenzhen Li<sup>1</sup>; Tianyu Zhu<sup>1</sup>; Liming Peng<sup>1</sup>; Wenjiang Ding<sup>1</sup>; <sup>1</sup>National Engineering Research Center of Light Alloys Net Forming and State Key Laboratory of Metal Matrix Composite, Shanghai Jiaotong University; <sup>2</sup>General Motors Research & Development Center

The microstructure and mechanical properties of as-cast Mg-Al-Sn alloys have been investigated using computational alloy design and experimental approaches. The as-cast microstructure of Mg-Al-Sn alloys consists of a-Mg, Mg<sub>17</sub>Al<sub>12</sub> and Mg<sub>2</sub>Sn phases. The volume fractions of Mg<sub>17</sub>Al<sub>12</sub> and Mg<sub>2</sub>Sn phases increase with increasing Al/Sn contents, and show good agreement between computational thermodynamics modeling and the experimental results. Generally, the yield strength of as-cast alloys increases with Al/Sn alloying contents, while the ductility decreases. This study has confirmed an earlier development of Mg-7Al-2Sn alloy and led to a promising new Mg-7Al-5Sn alloy with significantly improved strength and ductility compared to commercial alloy AZ91 (Mg-9Al-1Zn).

9:10 AM

**Thermodynamic Analysis of As-Cast and Heat Treated Microstructures of Mg-Ce-Nd Alloys:** Mark Easton<sup>1</sup>; Suming Zhu<sup>1</sup>; Mark Gibson<sup>2</sup>; Jian-Feng Nie<sup>1</sup>; Joachim Groebner<sup>3</sup>; Artem Kozlov<sup>3</sup>; *Rainer Schmid-Fetzer*<sup>3</sup>; <sup>1</sup>CAST CRC, Monash University; <sup>2</sup>CAST CRC, CSIRO, Clayton; <sup>3</sup>Clausthal University of Technology

The phase relationships in the Mg-rich corner of the Mg-Ce-Nd system have been investigated through the evaluation of selected compositions in the as-cast and heat treated condition. Consistent thermodynamic CALPHAD-type assessments have also been generated for the Mg-Ce-Nd system. It is shown that this system reveals a significant degree of metastability under technologically relevant solidification conditions (i.e. permanent-mould or high pressure die casting). This is simulated in thermodynamic calculations by suppression of the RE<sub>5</sub>Mg<sub>41</sub> phase and reasonable agreement is found with the as-cast microstructures. After heat treatment these microstructures transform, depending on alloy composition, into phase assemblies consistent with the calculated stable equilibrium phase diagram. It is the elucidation of such metastable phase formation and the subsequent transformation from the as-cast to the heat treated state that is a particular strength of the thermodynamic approach and which makes it a powerful tool for alloy development.

9:30 AM

**Compressive Strength and Hot Deformation Behavior of TX32 Magnesium Alloy with 0.4% Al and 0.4% Si Additions:** *Pitchewara Kamineni*<sup>1</sup>; YVRK Prasad<sup>2</sup>; Suresh Kalidass<sup>1</sup>; Chalasani Dharmendra<sup>1</sup>; Norbert Hort<sup>3</sup>; Karl Kainer<sup>3</sup>; <sup>1</sup>City University of Hong Kong; <sup>2</sup>processingmaps.com; <sup>3</sup>GKSS Research Centre

Mg-3Sn-2Ca (TX32) alloy has good corrosion and creep resistance. In this paper, the influence of additions of 0.4%Al and 0.4%Si on its compressive strength and hot working characteristics is reported. It is observed that the compressive strength at higher-temperature dropped significantly. By comparing with the alloy having only 0.4% Al, it is clear that the Si addition is responsible for this deterioration. The hot working behavior as characterized by processing maps revealed that TX32 exhibits two domains of dynamic recrystallization occurring at (1) 300–350 °C and 0.003–0.001 s<sup>-1</sup>, and (2) 400–500 °C and 0.003–0.3 s<sup>-1</sup>. In Al and Si containing TX32, both the domains moved to higher temperatures and the flow instability is reduced. In both the domains, the apparent activation energy is higher than that for self-diffusion in magnesium implying that there is a significant contribution from the back stress generated by the hard particles.

9:50 AM

**An Analysis of the Grain Refinement of Magnesium By Zirconium:** Partha Saha<sup>1</sup>; *Srinath Viswanathan*<sup>1</sup>; <sup>1</sup>University of Alabama

A Design of Experiments approach was used to conduct a systematic study of the grain refinement of magnesium by zirconium: variables included the amount of zirconium, the pouring temperature, and the settling time prior to

TUESDAY AM

casting. Optical microscopy was used to measure the grain size. TEM was used to identify particles that are likely nucleation sites. The TEM results show that a range of particle sizes are likely substrates and that particles which are likely nucleation sites are faceted. Sample dissolution followed by SEM was used to characterize particle size and morphology while an AccuSizer 770 was used to measure particle size distributions, both in the master alloy and grain refined samples. While only 1 to 3% of the total particles serve as nucleation sites, a comparison of the grain density vs. faceted particle density shows close agreement, suggesting that only faceted particles are likely nucleation sites.

#### 10:10 AM

**Study on the Grain Refinement Behavior of Mg-Zr Master Alloy and Zr Containing Compounds in Mg-10Gd-3Y Magnesium Alloy:** *Guohua Wu<sup>1</sup>; Ming Sun<sup>1</sup>; Jichun Dai<sup>1</sup>; Wenjiang Ding<sup>1</sup>; <sup>1</sup>Shanghai Jiao Tong University*

The effects of Mg-Zr master alloy and potassium fluozirconate ( $K_2ZrF_6$ ) salts mixture (KSM) on the grain refinement behavior are studied. The results show that the Mg-10Gd-3Y alloy is well refined by Mg-Zr or KSM. The characteristic microstructure feature of the alloy refined by Mg-Zr master alloy is the Zr-rich cores that exist in most grains, while the Zr-rich cores are not observed in the alloy refined by KSM. It is suggested that the grain refinement mechanisms of zirconium in the two cases are different: the Zr released from Mg-Zr master alloy works by generating heterogeneous nucleation, while the Zr reduced from the in-situ reaction between Mg melt and  $K_2ZrF_6$  works by restricting grain growth. Compared with the Mg-30. wt%Zr master alloy, the KSM refiner shows much longer fading time during smelting.

#### 10:30 AM Break

#### 10:50 AM

**The Effect of Rare Earth Elements on the Texture and Formability of Asymmetrically Rolled Magnesium Sheet:** *David Randman<sup>1</sup>; Bruce Davis<sup>1</sup>; Martyn Alderman<sup>2</sup>; Govindarajan Muralidharan<sup>3</sup>; Tom Muth<sup>3</sup>; William Peter<sup>3</sup>; Tom Watkins<sup>3</sup>; Odis Cavin<sup>3</sup>; Edward Kenik<sup>3</sup>; <sup>1</sup>Magnesium Elektron North America; <sup>2</sup>Magnesium Elektron; <sup>3</sup>Oak Ridge National Laboratory*

The lack of formability is a serious issue when considering magnesium alloys for various applications. Standard symmetric rolling introduces a strong basal texture that decreases the formability; however, asymmetric rolling has been put forward as a possible route to produce sheet with weaker texture and greater ductility. It has also been shown in recent work that weaker textures can be produced through the addition of rare earth elements to magnesium alloys. Therefore, this study has been carried out to investigate the effect of rare earth additions on the texture changes during asymmetric rolling. Two alloys have been used (AZ31B and ZEK100). The effect that the rare earth additions have on the texture of asymmetrically rolled sheet and the subsequent changes in formability will be discussed.

#### 11:10 AM

**Improvement of Strength and Ductility of Mg-Zn-Ca-Mn Alloy by Equal Channel Angular Pressing:** *Mingyi Zheng<sup>1</sup>; <sup>1</sup>Harbin Institute of Technology*

Mg-Zn-CaMn alloys are low cost and have good creep resistance, high strength and excellent biocompatibility. In this research, equal channel angular pressing (ECAP) was performed on the as-extruded Mg-5.25wt%Zn - 0.6wt%Ca - 0.3wt%Mn magnesium alloy at 250°C and 300°C for 4 passes, respectively. With the decreasing of ECAP temperature, the grain size was reduced. After ECAP at 250°C for 4 passes, extremely fine grains with the average grain size of about 0.8 micrometer are formed. High UTS of 323 MPa and elongation to failure of 23% were achieved in the specimen ECAPed at 300°C, which was resulted from the fine grains, fine dispersed precipitates and the textures in which the basal plane is oriented parallel to the extrusion direction. While the specimens processed at 250°C have textures with the basal planes inclined at about 45° to the extrusion direction, leading to the lower yield strength.

#### 11:30 AM

**Deformation Behavior of a Friction Stir Processed Mg Alloy:** *Qi Yang<sup>1</sup>; Sergey Mironov<sup>2</sup>; Yutaka Sato<sup>3</sup>; Kazutaka Okamoto<sup>4</sup>; <sup>1</sup>Hitachi America, Ltd.; <sup>2</sup>Department of Materials Processing, Graduate School of Engineering, Tohoku University ; <sup>3</sup>Department of Materials Processing, Graduate School of Engineering, Tohoku University; <sup>4</sup>Hitachi Research Laboratory, Hitachi Ltd.*

Friction stir processing, as a derivative of friction stir welding, in which a non-consumable tool imparts severe plastic deformation to metallic materials, has been used for grain refinement and therefore ductility improvement. In this talk, deformation behavior of a friction stir processed Mg alloy is addressed. Analyses of grain size and crystallographic texture are made to interpret the characteristics of strength and ductility of friction stir processed Mg. Meanwhile, mechanical properties of a friction stir processed Mg alloy are compared with those of a friction stir processed 5083 Al alloy.

#### 11:50 AM

**Effect of Heat Index on Microstructure and Mechanical Behavior of Friction Stir Processed AZ31:** *Wei Yuan<sup>1</sup>; Rajiv Mishra<sup>1</sup>; <sup>1</sup>Missouri University of Science and Technology*

Friction stir processing modifies the microstructure and properties of metals through intense plastic deformation. The frictional heat input affects the microstructure evolution and resulting mechanical properties. 2 mm thick commercial AZ31B-H24 Mg alloy was friction stir processed under various process parameter combinations to investigate the effect of heat index on microstructure and properties. Recrystallized grain structure in the nugget region was observed for all processing conditions with decrease in hardness. Results indicate a reduced tensile yield strength and ultimate tensile strength compared to the as-received material in H-temper, but with an improved hardening capacity. The strain hardening behavior of friction stir processed material is discussed.

#### 12:10 PM

**Strengthening Mg-Al-Zn Alloy by Repetitive Oblique Shear Strain:** *Toshiji Mukai<sup>1</sup>; Hidetoshi Somekawa<sup>1</sup>; Alok Singh<sup>1</sup>; Tadanobu Inoue<sup>1</sup>; <sup>1</sup>National Institute for Materials Science*

Enhancing fracture toughness and/or ductility is requirement for reliability in structural application. It has been reported that the grain refinement is one of the possible ways to enhance the strength without losing the ductility. In this study, severe plastic working by caliber rolling has been demonstrated to refine the grain structure of a commercial AZ31 Mg-Al-Zn alloy effectively at a commercial processing speed with the formation of fine sub-grains in a sub-micro-meter scale and resulted in a high yield stress of more than 400 MPa. A simultaneous operation of oblique shear strain weakened the basal texture compared to that of the initial as-extruded alloy, and resulted in tensile ductility comparable to that of the commercially extruded alloy, and showed a higher asymmetry ratio of yield stress in compression/tension (0.82) than that of the as-extruded alloy (0.57).



## Magnetic Materials for Energy Applications: Nd-Fe-B Sintered Magnets

Sponsored by: TMS Electronic, Magnetic, and Photonic Materials Division, TMS: Energy Conversion and Storage Committee, TMS: Magnetic Materials Committee; JSPS 147th Committee on Amorphous and Nanocrystalline Materials; Lake Shore Cyrotronics, Inc.; AMT&C

Program Organizers: Victorino Franco, Sevilla University; Oliver Gutfleisch, IFW Dresden; Kazuhiro Hono, National Institute for Materials Science; Paul Ohodnicki, National Energy Technology Laboratory

Tuesday AM  
March 1, 2011

Room: 11A  
Location: San Diego Conv. Ctr

Session Chair: George Hadjipanayis, University of Delaware

### 8:30 AM Invited

**Materials for Motors of Hybrid Automobiles:** *Shigeru Konda*<sup>1</sup>; <sup>1</sup>Toyota Motor Corp., Inc.

It has passed over one hundred year after vehicle with gasoline engine had been released. Currently, environmental issues, such as global warming, greenhouse gas and so on, has been discussing. To realize the sustainable mobility society, Hybrid vehicle could be one of the good candidates as eco-friendly car. In this speech, the benefit of Hybrid vehicle could be described. Simultaneously, the needs and expectation for materials would be explained.

### 8:55 AM Invited

**Application of Nd-Fe-B Magnets to the Megawatt Scale Generator for the Wind Turbine:** *Takehisa Minowa*<sup>1</sup>; <sup>1</sup>Shin-Etsu Chemical Co. Ltd.

Wind power generation is cost effective compared to solar energy generation. Although energy efficiency increases with the size of generators, this makes the generator too heavy for installment. One solution is to use Nd-Fe-B based permanent magnets to make the generator smaller and lighter. Various technologies for wind power generators such as interior permanent magnet (IPM) motors and surface permanent magnet (SPM) motors have been proposed, but the best system has not been determined yet. In this talk, I will overview the technological trend and the required properties of permanent magnets for wind power generation.

### 9:20 AM Invited

**Enhancement of Coercivity of Nd-Fe-B Sintered Magnets by Grain Boundary Modifications:** *Kazuhiro Hono*<sup>1</sup>; <sup>1</sup>Tadakatsu Ohkubo<sup>1</sup>; <sup>1</sup>National Institute for Materials Science

Interest in the coercivity mechanism of Nd-Fe-B based permanent magnets has recently been revived in Japan due to the increasing demand for Dy-free Nd-Fe-B magnets for traction motors of (hybrid) electric vehicles, (H)EV. In the current Nd-Fe-B sintered magnets for the traction motors, 30% of Nd is substituted with Dy to use the increased anisotropy field of the (Nd,Dy)<sub>2</sub>Fe<sub>14</sub>B phase, but the natural abundance of Dy is only 10% of Nd. Thus, we are looking for a way to increase the coercivity of the Nd-Fe-B magnets with lower amount of Dy. For this purpose, we investigate the microstructure-coercivity relationships of Nd-Fe-B magnets by investigating the microstructures of commercial and experimental sintered magnets and hydrogen disproportionation desorption recombination (HDDR) powder by HRSEM, TEM and atom probe tomography (APT). In this talk, we will overview our recent work on the enhancement of coercivity of Nd-Fe-B based magnets by grain boundary modifications.

### 9:45 AM Invited

**Novel Approaches to Microstructural Characterisation in NdFeB Materials:** *Thomas Woodcock*<sup>1</sup>; *Nora Dempsey*<sup>2</sup>; *Dominique Givord*<sup>2</sup>; *Stefan Zaeferrer*<sup>3</sup>; *Oliver Gutfleisch*<sup>1</sup>; <sup>1</sup>IFW Dresden; <sup>2</sup>Institute Néel, CNRS-UJF; <sup>3</sup>Max Planck Institute for Iron Research

NdFeB sintered magnets have recently found important new applications in electric motors for hybrid electric vehicles and generators for wind

turbines. Magnet grades with Dy additions are typically used for such applications and this incurs a significant cost penalty. Much research effort has therefore recently been put into reducing the Dy content or eliminating Dy in NdFeB sintered magnets for high temperature applications. In addition to various experimental routes toward this, novel approaches yielding detailed microstructural characterisation are required in order to bring greater understanding of coercivity mechanisms. Recent developments include the use of aberration-corrected TEM to obtain highest spatial resolution images and the application of electron backscatter diffraction (EBSD) to obtain crystallographic orientation data on a local scale from all the phases present in the microstructure. The combination of EBSD and EDX with high resolution serial sectioning yields 3D orientation and chemical data which will also be discussed.

### 10:10 AM Invited

**Modeling of Magnetization Reversal in Nd-Fe-B Based Sintered Magnets:** *Thomas Schrefl*<sup>1</sup>; *Simon Bance*<sup>1</sup>; *Harald Oezelt*<sup>1</sup>; *Gino Hrkac*<sup>2</sup>; <sup>1</sup>St. Poelten University of Applied Sciences; <sup>2</sup>University of Sheffield

High remanent, sintered Nd-Fe-B magnets are a key material for energy saving technology. We study the magnetization reversal mechanism using a multi-scale approach. Atomistic simulations give the local distortion of the Nd<sub>2</sub>Fe<sub>14</sub>B crystal structure near grain boundaries and triple junctions. This translates into a change of the magneto-crystalline anisotropy. The thickness of the distorted region which shows a magnet-crystalline anisotropy that is considerably smaller than in the bulk depends on the composition of the intergranular phase and ranges from 0.6 nm to 1.8 nm. Taking into account these local defects, we apply finite element micromagnetics. The simulations show how reversed domains are nucleated near triple junctions. Domains expand over several grains. Domain walls are equally located at grain boundaries or go through the grains. The simulations show cascade type demagnetization in well-aligned sintered magnets.

### 10:35 AM

**Theoretical Investigation on Formation Mechanism of fcc-NdOx in Nd/Nd-Fe-B Interface:** *Ying Chen*<sup>1</sup>; *Satoshi Hirotsawa*<sup>2</sup>; *Shuichi Iwata*<sup>3</sup>; <sup>1</sup>Tohoku University; <sup>2</sup>NEOMAX Co., Hitachi Metals, Ltd.; <sup>3</sup>The University of Tokyo

The disordered fcc-NdOx phase formed at the interface of Nd/Nd-Fe-B is believed to take an important role in coercivity generation, and its appearance directly influenced by the oxygen concentration. To understand the formation mechanism and properties of this particular Nd oxides phase, the ground state stability analysis for a whole oxygen concentration in Nd-O has been performed based on LSDA + U calculations. It is revealed that at low oxygen concentration, the system tends to separate into dhcp-Nd and NdO-NaCl or NdO-ZnS, whereas at oxygen concentration over 50%, the Nd<sub>2</sub>O<sub>3</sub> becomes most stable. Further investigation is focused on the relation among Fluorite-NdO<sub>2</sub>, C-type(c180)-Nd<sub>2</sub>O<sub>3</sub> and ZnS-NdO which have same fcc-frame of cations and vary in configurations of oxygen anions due to introducing oxygen vacancies. Formation energies, electronic structures for various oxygen vacancies configurations are calculated along this line.

### 10:50 AM

**NdFeB Thick Films for Micro-System Applications:** *Nora Dempsey*<sup>1</sup>; *Mikhail Kustov*<sup>1</sup>; *Daniel O'Brien*<sup>1</sup>; *Yuepeng Zhang*<sup>1</sup>; *Luiz Zanini*<sup>1</sup>; *Georgeta Ciuta*<sup>1</sup>; *Frederic Dumas-Bouchiat*<sup>1</sup>; *Dominique Givord*<sup>1</sup>; <sup>1</sup>Institut Néel CNRS/UJF

For the same reasons (high magnetisation and high coercivity) that NdFeB based magnets are widely used in bulk applications such as hybrid and all electric vehicles and wind turbines, they have much potential for use in magnetic micro-systems. In addition, since the force exerted by a magnet depends of the field gradient it produces, a reduction in its size leads to an increase in the volume forces it exerts. Consequently, much effort has been put into the fabrication of NdFeB in film form. In this work we will present different aspects concerning their eventual use in micro-systems, namely their patterning at the micron-scale, the local characterisation of the magnetic fields they produce and the characterisation and control of strain in the films. Such films may be used in the generation of energy at the micron scale

(micro-generators) and to improve the efficiency of energy consumption at the macro-scale (micro-sensors, micro-actuators).

11:05 AM Break

## Magnetic Materials for Energy Applications: Magnetostrictive Materials

*Sponsored by:* TMS Electronic, Magnetic, and Photonic Materials Division, TMS: Energy Conversion and Storage Committee, TMS: Magnetic Materials Committee; JSPS 147th Committee on Amorphous and Nanocrystalline Materials; Lake Shore Cyrotronics, Inc.; AMT&C

*Program Organizers:* Victorino Franco, Sevilla University; Oliver Gutfleisch, IFW Dresden; Kazuhiro Hono, National Institute for Materials Science; Paul Ohodnicki, National Energy Technology Laboratory

Tuesday AM Room: 11A  
March 1, 2011 Location: San Diego Conv. Ctr

*Session Chair:* Michael McHenry, Carnegie Mellon University

11:20 AM

**Magnetostrictive Behavior of Fe-W Alloy Single Crystals:** *Gavin Garside<sup>1</sup>; Chai Ren<sup>1</sup>; Biswadeep Saha<sup>1</sup>; Meenakshisundaram Ramanathan<sup>1</sup>; Sivaraman Guruswamy<sup>1</sup>; <sup>1</sup>University of Utah*

A systematic examination of change in magnetostriction as a function of W content in the range of 0 to 10 at.% is presented in this paper. Fe-W alloy single crystals were prepared using vertical Bridgman growth technique. Single crystal samples with [001]-orientation were prepared with faces within 0.5 degrees from [001] orientation. The samples were annealed in the alpha-phase region and quenched. Longer annealing times and higher annealing temperatures increase the magnetostriction values obtained. Rapid increase in magnetostriction is observed with W additions of up to 4.4 at.% W. This is followed by a much slower increase with W content. This behavior is associated with the propensity for second phase formation at higher W contents in these alloys. \*Support of this work by NSF-DMR under the award DMR-0854166 is gratefully acknowledged.

11:35 AM

**Investigation of DO<sub>3</sub> and B2 Type Ordering in Quenched Magnetostrictive Fe-27.5 at.%Ga Alloy Single Crystals:** *Chai Ren<sup>1</sup>; Gavin Garside<sup>1</sup>; Biswadeep Saha<sup>1</sup>; Meenakshisundaram Ramanathan<sup>1</sup>; Sivaraman Guruswamy<sup>1</sup>; <sup>1</sup>University of Utah*

FeGa alloys with large low-field magnetostriction are attractive candidates in energy conversion and harvesting applications. The structural ordering in magnetostrictive Fe-27.5 at.% Ga alloy single crystals that were annealed in the alpha region and quenched was investigated using x-ray diffraction. The annealing temperatures used were 1100 and 1150 degree C. XRD examination as a function of depth in [100] or [111] oriented Fe-Ga samples show dominant existence of DO<sub>3</sub> type ordering arrangement on the top surface to B2 type ordering arrangement in the interior regions of the sample. The detailed examinations of scattering peaks in the XRD patterns suggest that the nature of short-range and long-range ordering present is influenced by sample size and thermal history. Thus sample size and shape will influence magnetostriction measurements. The observations are of importance in magnetostrictive device design. \*Support of this work by NSF through the award DMR-0854166 is gratefully acknowledged.

11:50 AM

**Influence of Plastic Deformation on the Magnetostrictive Behavior of [001]-oriented Fe-Ga Alloy Single Crystals:** *Biswadeep Saha<sup>1</sup>; Gavin Garside<sup>1</sup>; Meenakshisundaram Ramanathan<sup>1</sup>; Chai Ren<sup>1</sup>; Sivaraman Guruswamy<sup>1</sup>; <sup>1</sup>University of Utah*

Structural ordering, defects and second phases can influence the magnetostrictive behavior in Fe-Ga and other Fe-based magnetostrictive

alloys. In this study, the influence of dislocations on the magnetostrictive behavior of [001]-oriented Fe-20 at.% Ga single crystal is examined. Dislocation arrays were introduced through controlled deformation of rectangular parallelepiped single crystal samples with the faces oriented to within 0.25 degrees off the <100> orientation. Alloy single crystals were obtained through vertical Bridgman growth process. The crystals were plastically deformed to predetermined strain level. Magnetostriction measurements as well as TEM and x-ray examinations were performed prior to and after deformation. Results obtained show that deformation decreases magnetostriction values appreciably.\*Support of this work by NSF-DMR through the award DMR-0854166 is gratefully acknowledged.

12:05 PM

**Enhanced Magnetoimpedance Effect in Co89Zr7B4 Ribbon/Fe80Ni20 Bilayer Structures:** *N. Laurita<sup>1</sup>; A. Chaturvedi<sup>1</sup>; A. Leary<sup>2</sup>; P. Jayatilaka<sup>1</sup>; C. Bauer<sup>1</sup>; Casey W. Miller<sup>1</sup>; M.H. Phan<sup>1</sup>; M.E. McHenry<sup>2</sup>; H. Srikanth<sup>1</sup>; <sup>1</sup>University of South Florida; <sup>2</sup>Carnegie Mellon University*

We report the large enhancement of the magnetoimpedance (MI) effect in CoFe89Zr7B4 amorphous ribbon/Fe80Ni20 bilayers. The amorphous ribbons were prepared by rapid quenching. Atomic force microscopy indicate roughnesses for the free and wheel-side ribbon surfaces of 3-6 nm and 150-200 nm, respectively. 100 nm Fe80Ni20 layers were sputtered onto the ribbons; one sample was coated in zero field, another in 200 Oe applied transverse to the length. Magnetoimpedance measurements were carried out along the ribbon axis in applied dc magnetic fields up to 120 Oe over a frequency range of 0.1 ~ 13 MHz. We find that the MI effect is largely enhanced in the Fe80Ni20-coated ribbons. The 200 Oe-deposited sample shows the largest effect (19%), which is about twice that of the bare ribbon (11%). Our studies provide strong evidence for enhancing the MI effect in layered structures for sensor applications. Support: NSF-DMMI (HS). NSF-ECCS (CWM).

## Massively Parallel Simulations of Materials Response: Session III

*Sponsored by:* The Minerals, Metals and Materials Society, TMS Materials Processing and Manufacturing Division, TMS Structural Materials Division, TMS/ASM: Computational Materials Science and Engineering Committee, TMS: High Temperature Alloys Committee  
*Program Organizers:* Diana Farkas, Virginia Tech; Susan Sinnott, University of Florida

Tuesday AM Room: 1A  
March 1, 2011 Location: San Diego Conv. Ctr

*Session Chair:* To Be Announced

8:30 AM Invited

**Ultra-Large Scale Simulations of Deformation and Failure of Biological Protein Materials:** *Markus Buehler<sup>1</sup>; <sup>1</sup>Massachusetts Institute of Technology*

Deformation and failure of biological protein materials are critical to our understanding of injuries, disease state, and to reverse-engineer the functional design of biological materials. I will present a survey of recent materiomics studies in our laboratory based on ultra-large scale simulations using LAMMPS. The talk will include a discussion of investigations of intermediate filament fibrils and networks, beta-sheet structures as found in spider silk and amyloids, as well as collagenous tissues that form the structure of tendon and bone. Case studies will be presented that illustrate size effects in protein materials, flaw-tolerance mechanisms, and applications of materials science to genetic diseases, showing how structural defects at the molecular level can have profound effects at the material behavior at larger scales. A detailed analysis will be presented to explain how biological materials overcome the limitations of their building blocks, often functionally inferior, and yet display remarkable functional properties.

### 8:55 AM Invited

**Multilevel Atomistic Modeling of Grain Boundaries and Nanocrystals:** Garritt Tucker<sup>1</sup>; Shreevart Tiwari<sup>1</sup>; David McDowell<sup>1</sup>; <sup>1</sup>Georgia Institute of Technology

Deformation in nanocrystalline metals involves interface-mediated processes that depend on grain boundary network and structure, with atom shuffling/GB sliding/migration and dislocation nucleation as competing modes. As a step towards informing statistical descriptions of initial yield and plastic flow, and setting the stage to quantify percolation and scaling relations, we apply recently developed volume-averaged metrics of continuum kinematic quantities as post-processing “filters” to results of atomistic simulations of deformation using the LAMMPS MD code, computing vorticity, Green strain, dilatation, and lattice microrotation fields within nanocrystalline copper at a temperature of 10K. The results provide a new, alternative perspective into the role of competing deformation mechanisms as a function of boundary type in bicrystals and mean grain size in nanocrystals. Our results indicate potential utility of these continuum metrics in interpreting the wealth of information arising from atomistic simulations of nanocrystalline ensembles.

### 9:20 AM Invited

**Quantitative Studies of Nanoindentation: Coupled Experiments and Modeling:** Lyle Levine<sup>1</sup>; Richard Wagner<sup>1</sup>; Li Ma<sup>1</sup>; Francesca Tavazza<sup>1</sup>; Chandler Becker<sup>1</sup>; Douglas Smith<sup>1</sup>; Dylan Morris<sup>1</sup>; David Bahr<sup>2</sup>; Stefhanni Jennerjohn<sup>2</sup>; <sup>1</sup>National Institute of Standards and Technology; <sup>2</sup>Washington State University

Nanoindentation's ability to probe the local plastic mechanical properties at the surface of almost any specimen has made it the most widely used experimental technique for making such measurements at the nanoscale. However, standard test methods are limited and full traceability to primary reference standards is lacking. At low indentation loads, numerous potential experimental problems exist, including non-traceable force calibration at the nN level, uncharacterized irregular indenter tip shapes, and structural heterogeneities both on and below the sample surface. Similarly, attempts to back out quantitative mechanical properties often suffer from over-reliance on the Hertzian approximation and inaccurate boundary conditions for simulations. Example measurements and simulations (using FEA and LAMMPS-MD) for both new and heavily used indenters will be used to illustrate these problems for metal specimens. Finally NIST's recent efforts to provide quantitative experimental and modeling support for this valuable experimental technique will be described.

### 9:45 AM Invited

**Nanostructurally Small Cracks (NSC): Atomistic Modeling of Fatigue:** Mark Horstemeyer<sup>1</sup>; G. Potirniche<sup>2</sup>; S. Kim<sup>1</sup>; T. Tang<sup>1</sup>; Diana Farkas<sup>3</sup>; <sup>1</sup>Mississippi State University; <sup>2</sup>Univ. Idaho; <sup>3</sup>Virginia Tech

Molecular Dynamics simulations using EAM and MEAM potentials were conducted to study nanoscale fatigue cracks in nickel and copper crystals. Simulation results revealed that the cyclic plastic deformation at the crack tip was the main influencing factor for fatigue crack growth. Two main nanoscale mechanisms of crack propagation were observed: (1) the main cracks linked with the voids nucleated in front of crack tip due to high dislocation density generated by the cyclic loading; and (2) the main cracks broke the atomic bonds in the crack plane without much plasticity. For the bicrystals and polycrystals, the grain boundaries exerted resistance to the crack propagation. Fatigue crack growth rates for nanocracks were computed and compared with growth rates published in the literature. The atomistic simulations indicated that reversible plastic slip along the active crystallographic directions at the crack tip was responsible for advancing the crack during applied cycling.

### 10:10 AM Break

### 10:25 AM

**Atomistic Predictions of Age Hardening in Al-Cu Alloys:** Chandra Veer Singh<sup>1</sup>; Derek Warner<sup>1</sup>; <sup>1</sup>Cornell University

A large class of commercial alloys derive their strength from precipitation hardening. In many alloys, such as Al-Cu, hardening is a complex function of time and temperature as the precipitation process involves several types of competing metastable precipitates. Here we combine analytic models for microstructural kinetics with large-scale atomistic simulations (LAMMPS) of dislocation-precipitate and dislocation-solute interactions to examine the precipitation hardening process in an Al-Cu alloy. We compute the critical stresses for dislocations to overcome both GP zones and theta'' precipitates directly from atomistic simulations and use an improved Labusch model with atomistically computed interaction energies to calculate solute hardening. Combining strengthening effects, age hardening curves are then formulated and compared with experiments. By comprehensively examining the entire age hardening process, insight can be gained into the strengths and weaknesses of both common kinetics models and potential based atomistic simulations for broad application.

### 10:45 AM

**Massively Parallel Molecular Statics Simulations of the Percolation of Dislocations through a Random Array of Forest Dislocation Obstacles in FCC Nickel:** Satish Rao<sup>1</sup>; Dennis Dimiduk<sup>2</sup>; Jaafar El-Awady<sup>3</sup>; Triplicane Parthasarathy<sup>1</sup>; Michael Uchic<sup>2</sup>; Christopher Woodward<sup>2</sup>; <sup>1</sup>UES Inc.; <sup>2</sup>Air Force Research Laboratory; <sup>3</sup>Johns Hopkins University

This talk presents results from massively parallel molecular statics simulations, using LAAMPS with ~ 10,000 processors, of the percolation of dislocations through a random array of forest dislocation obstacles in face-centered cubic Nickel. A single gliding dislocation and 540 forest dislocations are inserted into a 0.6µm by 0.3µm by 0.3µm rectangular parallelepiped cell aligned along the [1-10], [11-2] and [111] directions, containing ~ 1 - 2 billion atoms. The behavior of the percolating dislocation under pure shear stresses applied on the (111) plane are simulated. Details of the percolating wave front and the critical stress required for percolation are obtained from the simulation results. These atomistic results representing the critical percolation stress for dislocations are compared with previous dislocation dynamics and point-obstacle pinning simulation results.

### 11:05 AM

**Atomic Scale Deformation Mechanisms of Amorphous Polyethylene under Tensile Loading:** Mark Tschoop<sup>1</sup>; Jean-Luc Bouvard<sup>1</sup>; Don Ward<sup>2</sup>; Mark Horstemeyer<sup>1</sup>; <sup>1</sup>Mississippi State University; <sup>2</sup>Sandia National Laboratory

Thermoplastic polymers, such as polyethylene and polypropylene, play an important role in components. However, to date, the molecular deformation behavior at an atomistic level involves coarse-graining potentials, such as the Dreiding potential. The objective of this research is to study the deformation mechanisms in full-atom amorphous polymer systems at the atomic scale under various loading conditions. We generated the amorphous structures and then used molecular dynamics simulations to equilibrate/deform the 3D periodic simulation cell. Various parameters like chain length, number of chain, strain rate were taken into consideration to study their influence on both the stress-strain behavior and the deformation mechanisms. Additionally, we analyzed how the energy associated with bond length, bond angle, dihedral angle, and non-bonding interactions evolved as a function of strain. The significance of this research is that understanding the deformation behavior at the atomic scale is vital to predicting bulk mechanical behavior via higher scale models.

### 11:25 AM

**Energy of Slip Nucleation and Transmission at Grain Boundaries:** Michael Sangid<sup>1</sup>; Huseyin Sehitoglu<sup>1</sup>; <sup>1</sup>University of Illinois, Urbana-Champaign

Grain boundaries (GBs) provide a strengthening mechanism in engineering materials by impeding dislocation motion. In a polycrystalline material,



there is a wide distribution of GB types with characteristic slip transmission and dislocation nucleation behaviors. There is a strong need to quantify the energy barriers of the individual GBs. We introduce a methodology to calculate the energy barriers during slip-GB interaction, in concurrence with the general stacking fault energy curve for slip in a perfect FCC material. By doing so, we calculate the energy barriers for slip transmission and nucleation from various classifications of GBs. The character and structure of the GB plays an important role in impeding slip within the material. From this analysis, we show that there is a strong correlation between the energy barrier and static interfacial boundary energy. The results have profound implications in understanding mechanical response influenced by the underlying grain boundary characters.

**11:45 AM**

**Molecular Dynamics Investigations of Polyurethane-Chrome Oxide Interfaces:** *Susanne Opalka*<sup>1</sup>; Kenneth Smith<sup>1</sup>; <sup>1</sup>United Technologies Research Center

Polyurethane-chrome oxide atomic-scale interfacial interactions were simulated with the LAMMPS molecular dynamics code to generate fundamental understanding of adhesion phenomena for component design and optimization. This modeling capability was implemented sequentially at several levels, creating models based upon experimentally-known material properties and validating modeling results with experimental tests. First, polymer models were refined by tuning both polymer characteristics and atomic force field parameters to achieve agreement with measured polymer thermal and mechanical properties. Then, hybrid force field parameters for the interactions of key polyurethane functional groups with the passivated chrome surface layer were customized to match interfacial surface tension measurements. Finally, virtual adhesion tests were conducted on conditioned polyurethane-chrome oxide interface models for comparison with nanoscale pull-test experimentation. The validated models will be used for molecular dynamics investigations of viscoelastic phenomena in a moving polyurethane-chrome oxide contact leading to material friction, wear, and transfer.

**12:05 PM**

**Tendency of Cooperative Grain Boundary Sliding in Nanocrystalline Materials:** *Shreevant Tiwari*<sup>1</sup>; David McDowell<sup>1</sup>; <sup>1</sup>Georgia Institute of Technology

The objective of this research is to identify the tendency of cooperative grain boundary (GB) sliding, leading to grain rotation in nanocrystalline metals. We use molecular dynamics (MD) simulations to uniaxially deform 3D nanocrystalline Cu ensembles in the elastic regime and visualize, for each grain, the rotational component of the atomic displacement vector field relative to the grain center. Our results suggest that the rotational component of the relative displacement is more pronounced in regions near certain preferred GBs and triple junctions, and that the extent of rotation in these favored boundary regions increases with temperature, thereby hinting at a thermally activated, cooperative GB sliding mechanism. Additionally, the rotational displacement field used as a part of this work can potentially help resolve GB sliding from a background of several other competing deformation mechanisms, and augment existing metrics of atomistic deformation kinematics.

## Materials for the Nuclear Renaissance II: Next Generation Reactors

*Sponsored by:* The Minerals, Metals and Materials Society, TMS Structural Materials Division, TMS/ASM: Corrosion and Environmental Effects Committee, TMS/ASM: Nuclear Materials Committee

*Program Organizers:* Raul Rebak, GE Global Research; Brian Cockeram, Bechtel-Bettis; Peter Chou, Electric Power Research Institute; Micah Hackett, TerraPower, LLC

Tuesday AM  
March 1, 2011

Room: 4  
Location: San Diego Conv. Ctr

*Session Chair:* Brian Cockeram, Bechtel Bettis

### 8:30 AM Introductory Comments

**8:35 AM**

**On the Prospects for Developing Advanced Alloys that Are Immune to Irradiation: Challenges and Opportunities:** *G. Robert Odette*<sup>1</sup>; Takuya Yamamoto<sup>1</sup>; <sup>1</sup>University of California, Santa Barbara

The approaches to developing alloys that are highly resistant to irradiation damage at high displacement damage (dpa) and helium levels are discussed. Nanostructured ferritic alloy class (NFAs) is the leading candidate for such irradiation tolerance. NFAs are Fe-Cr based ferritic stainless steels that contain an ultrahigh density of Y-Ti-O nanofeatures (NFs). The NFs are remarkably thermally stable and provide outstanding high temperature properties and remarkable tolerance to displacement damage as well as the degrading effects of transmutation product helium. The results of recent in situ injection experiments show that the NFs trap helium in ultrafine scale interface bubbles. The helium bubbles are effective sinks for point defects as well as additional helium, and at high densities can suppress almost all manifestation of radiation damage. It is argued that NFAs can be tailored to effectively transform helium from a liability to an asset, possibly leading to near immunity to irradiation damage.

**8:55 AM**

**A Multi-Layer Approach to a Stable Alpha Alumina Barrier Layer on Alloy 617:** *Elizabeth Clark*<sup>1</sup>; James Yang<sup>1</sup>; Gokce Gulsoy<sup>2</sup>; Deepak Kumar<sup>2</sup>; Gary Was<sup>2</sup>; Carlos Levi<sup>1</sup>; <sup>1</sup>University of California, Santa Barbara; <sup>2</sup>University of Michigan

Alloy 617 is a candidate material for heat exchangers in the GenIV very high temperature nuclear reactor concept. However, impurities in the He may lead to degradation by oxidation, carburization or decarburization of the alloy with deleterious effects on its structural integrity. Alpha-alumina is attractive as a protective barrier layer, but to assure that this phase forms (rather than transient aluminas) in the low pO<sub>2</sub> environment at the use temperature (T≤1000°C), surface modification is required. Lifetime requirements also demand stability of the modified surface layers against interdiffusion with the substrate, and the ability of the oxide to re-form in the event of cracking or spallation due to thermo-mechanical stresses in the prospective applications. This presentation will discuss concepts involving alloy 617 with combinations of aluminization and/or cladding, their oxidation and interdiffusion behavior, and preliminary results on their response to exposure to He with CO/CO<sub>2</sub> ratios conducive to carburization or oxidation/decarburization.

**9:15 AM**

**Order-Disorder Transformation in a Ni-Cr-Mo Alloy:** *Amit Verma*<sup>1</sup>; *Jung Singh*<sup>1</sup>; Mahadevan Sundararaman<sup>1</sup>; Nelia Wanderka<sup>2</sup>; <sup>1</sup>Bhabha Atomic Research Centre; <sup>2</sup>Helmholtz-Zentrum Berlin für Materialien und Energie GmbH

Ni-Cr-Mo alloys are potential candidates for structural materials application for high temperature reactors. These alloys form a long-range order (LRO) precipitates, Ni<sub>2</sub>(Cr,Mo) (Pt<sub>2</sub>Mo type structure), in the intermediate temperature range. The evolution of ordered precipitates has

been investigated in a Ni-Cr-Mo alloy using resistivity and transmission electron microscopy (TEM). The relative change in resistance as a function of temperature could be divided into 5 regimes, which could be attributed to different microstructural states. TEM investigations revealed the presence of two types of short-range order (SRO) in solution treated and quenched state: a  $\{1\ 1/2\ 0\}$  type SRO and a  $1/3\{110\}$  type SRO of Pt<sub>2</sub>Mo type. The formation of the LRO could be identified to initiate at  $\{1\ 1/2\ 0\}$  SRO which transformed first to  $1/3\{110\}$  type SRO followed by LRO transition. The SRO state also had an important influence on the kinetics of the transformation.

#### 9:35 AM

**Creep Characteristics of a Grade 91 Steel:** *Tirratna Shrestha*<sup>1</sup>; Mehdi Basirat<sup>1</sup>; Zachary Wuthrich<sup>1</sup>; Indrajit Charit<sup>1</sup>; Gabriel Potirniche<sup>1</sup>; Karl Rink<sup>1</sup>; <sup>1</sup>University of Idaho

Modified 9Cr-1Mo (Grade 91) steels are being considered as a potential candidate material for reactor pressure vessel applications for the Very High Temperature Reactor (VHTR). This research has been focused on studying the tensile creep behavior of as received and welded Grade 91 steel as a function of temperature (500–700 °C) and stress levels (50–200 MPa). The creep testing on the monolithic materials revealed a deformation regime with a stress exponent of ~10 at the higher stress levels. Microstructural analysis using transmission electron microscopy (TEM) is being carried out on the specimens before and after the creep deformation. TEM results will be correlated with the creep parametric dependencies to elucidate the underlying creep mechanisms.

#### 9:55 AM

**Microstructural Characterization of Nuclear Grade Graphites:** *Joshua Kane*<sup>1</sup>; Karthik Chinnathambi<sup>1</sup>; Rick Ubic<sup>1</sup>; Darryl Butt<sup>1</sup>; <sup>1</sup>Boise State University

Nuclear graphite is a prime candidate material for application in Generation IV Very High Temperature Reactor (VHTR) cores because of its high temperature thermo-mechanical properties, resilience to neutron absorption, and chemical resistance. Irradiation induced damage and creep are considered two primary degradation mechanisms for graphite and therefore major life-limiting issues for the VHTR core. This work reports preliminary transmission electron microscopy results of the microstructure characterization of Generation IV VHTR candidate virgin graphite grades PCEA and NBG-18 as well as historical grades IG-110 and PGX. Various microstructural features such as filler, binder, and quinoline insoluble particles have been identified for each grade and compared. Studies are currently underway to identify and analyze dislocations and pinning sites considered, in many theories, essential to irradiation creep in graphite.

#### 10:15 AM Break

#### 10:25 AM

**Evaluation of Nanofeature Evolution in the Sequence of Atomization to Consolidation Steps in Processing a Fe<sub>14</sub>Cr<sub>3</sub>W<sub>0.4</sub>Ti<sub>0.2</sub>Y Alloy:** *Nicholas Cunningham*<sup>1</sup>; Erich Stergar<sup>1</sup>; Auriane Etienne<sup>2</sup>; G. Robert Odette<sup>1</sup>; Yuan Wu<sup>1</sup>; Brian Wirth<sup>2</sup>; Stuart Maloy<sup>3</sup>; <sup>1</sup>UC Santa Barbara; <sup>2</sup>UC Berkeley; <sup>3</sup>Los Alamos National Laboratory

Nanostructured ferritic alloys (NFAs) contain an ultrahigh density of Y-Ti-O nanofeatures (NFs) that provide outstanding high temperature properties and remarkable tolerance to irradiation damage. NFA powders were produced by gas atomization from a melt containing Fe-14%Cr-3%W-0.4%Ti-0.2%Y. Electron probe microanalysis (EPMA), atom probe tomography (APT), small angle neutron scattering (SANS), transmission electron microscopy (TEM) and microhardness measurements were used to characterize the NFA in the as-atomized, ball milled, ball milled and annealed and hot isostatic pressed (HIP) consolidated conditions. Y is phase separated in the as atomized powders. However, attritor milling for 20 to 40 h mixes the Y and introduces O. Subsequent powder annealing and consolidation treatments, typically at 1150°C, result in the precipitation of a high density of NFs. All the annealed powder variants and consolidated alloys show a bimodal grain size distribution, but APT shows the presence of NFs in both large and small grains.

#### 10:45 AM

**Spatially-Dependent Cluster Dynamics Modeling of Vacancy and Interstitial Cluster Evolution in Ferritic/Martensitic Fe-Cr Alloys:** *Thibault Faney*<sup>1</sup>; Aaron Kohnert<sup>1</sup>; Brian Wirth<sup>1</sup>; Djamel Kaoumi<sup>2</sup>; Arthur Motta<sup>3</sup>; <sup>1</sup>UC Berkeley; <sup>2</sup>USC; <sup>3</sup>Penn State University

Computational materials modeling will investigate the mechanisms controlling microstructural evolution in ferritic/martensitic alloys following high dose, high temperature radiation exposure. The aim of this study is to understand and predict primary defects production and defects diffusion, clustering and interaction in a thin foil heavy ion irradiation of ferritic/martensitic steels. The model involves spatially dependent rate theory, or cluster dynamics, equations that describe the evolution of self-interstitial (mainly interstitial loops) and vacancy clusters (voids) in ferritic-martensitic steels under irradiation. The key parameters that are input to the model are determined from a combination of atomistic materials modeling and available experimental data. A new cascade dynamics model from molecular dynamics has been implemented which improves the accuracy of the results, as well as adaptive time stepping methods which allow to simulate up to higher doses. The Modeling predictions are compared with experimental results obtained at the IVEM facility in Argonne National Laboratory.

#### 11:05 AM

**Experimental and Modeling Studies on the Effects of a Wide Range of Flux on the Microstructures and Mechanical Properties of RPV Steels – Predicting Low Flux High Fluence Embrittlement:** *Takuya Yamamoto*<sup>1</sup>; G. Robert Odette<sup>1</sup>; Nicholas Cunningham<sup>1</sup>; Douglas Klingensmith<sup>1</sup>; Randy Nanstad<sup>2</sup>; <sup>1</sup>Univ. California Santa Barbara; <sup>2</sup>Oak Ridge National Laboratory

Transition temperature shifts (TTS) of reactor pressure vessels (RPV) steels must be predicted at extended life fluences that are far beyond the existing surveillance database. High fluences can be achieved only in test reactors at fluxes that are much higher than under vessel service. TTS are primarily caused by nm-scale hardening features including: a) thermally stable defect solute matrix features; b) thermally unstable matrix defects; c) and Cu-Mn-Ni rich precipitates. Flux affects both the concentrations and balance of these features, thus, the TTS for a given alloy and irradiation condition. We present a database and analysis of irradiation hardening and the evolution of the nm-scale features for a large set of alloys for a very wide range of fluxes and fluences in both the as-irradiated and annealed conditions. The database and analysis is used to develop a physically based model for predicting TTS at high fluence and low flux.

#### 11:25 AM

**Material Constraints on Accelerator Driven Sub-Critical Molten Salt Thorium Reactors:** *John Wallace*<sup>1</sup>; Ganapati Myneni<sup>2</sup>; <sup>1</sup>Casting Analysis Corp; <sup>2</sup>Thomas Jefferson Nat. Accelerator Facility

The development of linear superconducting accelerators has progressed so efficient and reliable machines can be used for neutron spallation sources. Future materials advances in these machines can be expected to improve their operating efficiencies. These hinge on understanding hydrogen and coatings in the niobium superconducting resonant cavities which provide the accelerating fields. Other than basic research these machines open the possibility of controlling thorium fission reactors as a heat sources for power generation and PWR nuclear waste digestion. This compact reactor is examined for long term materials stability both in the interface region of the spallation source, the long term integrity of the internal graphite structures and nickel based containers and piping. Historically there is limited data on materials degradation in the molten salt environment for periods of 40 years. Accelerated testing and monitoring of material degradation in a range of environments will be discussed along with preliminary experiments.

#### 11:45 AM

**Stress Corrosion Cracking Behavior of Ferritic and Austenitic Stainless Steels in High Temperature Water:** *Raul Rebak*<sup>1</sup>; Peter Andresen<sup>1</sup>; <sup>1</sup>GE Global Research

Austenitic stainless steels such as type 304 and 316 are used widely as core internals components in light water reactors. Under certain operation conditions these materials may be susceptible to stress corrosion cracking

and irradiation assisted stress corrosion cracking. Irradiation may produce hardening and alter the local chemistry of the alloys, which may increase their susceptibility to environmentally assisted cracking. Ferritic stainless steels are less susceptible to irradiation damage such as void swelling than the austenitic cousins. Ferritic stainless steels also offer higher thermal conductivity and lower expansion coefficients. Little is known however about the stress corrosion cracking behavior of ferritic steels in high temperature water. Crack propagation rate studies were conducted using four types of ferritic steels in high purity water at 288°C containing dissolved oxygen or dissolved hydrogen. The cracking susceptibility results obtained with the ferritic steels are compared with literature data for austenitic stainless steels.

12:05 PM

**Mechanical Properties of Advanced NF616 Steel:** *Mikhail Sokolov*<sup>1</sup>; *Lizhen Tan*<sup>1</sup>; <sup>1</sup>ORNL

Fracture toughness, Charpy impact and tensile properties of advanced ferritic-martensitic 9Cr-1.8WNbV steel NF616 were characterized in the wide temperature range from room temperature to 650C. This steel is one of the candidates of high-temperature structural materials in the next generation nuclear systems. Tensile properties are similar in transverse and longitudinal orientations. Strength was decreasing with increase of test temperature. This alloy exhibited considerable fracture toughness properties up to 650C. In addition, thermomechanical treatment is being developed on the as-received NF616. Preliminary results of Vickers microhardness and tensile tests showed enhancement in microhardness and both strength and ductility compared to the as-received NF616. Microstructural characterization is being performed to explain the properties enhancement induced by the thermomechanical treatment. The effects of thermomechanical treatment on fracture toughness will be discussed as well.

## Materials in Clean Power Systems VI: Clean Coal-, Hydrogen Based-Technologies, and Fuel Cells: Materials for Gasification and Turbines II

*Sponsored by:* The Minerals, Metals and Materials Society, TMS Electronic, Magnetic, and Photonic Materials Division, TMS Structural Materials Division, TMS/ASM: Corrosion and Environmental Effects Committee, TMS: Energy Conversion and Storage Committee, TMS: High Temperature Alloys Committee  
*Program Organizers:* Xingbo Liu, West Virginia University; Zhenguo "Gary" Yang, Pacific Northwest National Laboratory; Jeffrey Hawk, U.S. Department of Energy, National Energy Technology Laboratory; Teruhisa Horita, AIST; Zi-Kui Liu, The Pennsylvania State University

Tuesday AM  
March 1, 2011

Room: 33C  
Location: San Diego Conv. Ctr

*Session Chair:* Jeffrey Hawk, U.S. Department of Energy, National Energy Technology Laboratory

8:30 AM Invited

**Gas Turbines of the Future: Hydrogen and Oxy-Combustion Environments:** *Jeffrey Hawk*<sup>1</sup>; *Gordon Holcomb*<sup>1</sup>; <sup>1</sup>U.S. Department of Energy

Materials issues related to higher efficiency power plants, like hydrogen or oxy-fuel fired gas turbines, require materials with higher temperature capability than the current generation of turbines. Research to extend the usable critical temperature of nickel superalloys has focused on maintaining the strength and integrity of grain boundaries and the interface between the grain boundary phases (carbide and/or TCP) and the matrix, as well as improving the long-term stability of fine strengthening precipitates at the use temperature. Concurrent with achieving these goals is to understand how temperature, stress, and environment affect grain boundary, matrix and surface/coating interface stability as a consequence of exposure to the gas turbine environment. This presentation will focus on specific features of the microstructure and how these features are affected due to exposure to an

oxy-combustion type environment. The affect on low cycle fatigue will be discussed as well as the fracture morphology.

8:55 AM

**Tempered Martensitic Ferritic Steel Alloy Development for Ultrasupercritical Steam Applications:** *Christopher Cowen*<sup>1</sup>; *Jeffrey Hawk*<sup>1</sup>; *Paul Jablonski*<sup>1</sup>; <sup>1</sup>United States Department of Energy

Advanced 9-12% Cr tempered martensitic ferritic steels form the majority tonnage of components used in coal fired power plants that operate in the temperature range of 570-620°C. Computational and experimental alloy development efforts at NETL are focused on increasing the temperature capability of this class of alloy to 650°C in order to increase power plant efficiency while simultaneously decreasing the cost of construction and carbon footprint. This presentation focuses on microstructural stability issues and preservation of strengthening mechanisms that are keys to the successful development of advanced 9-12% Cr steels that meet minimum creep life requirements at 650°C for 100,000 hours and 100 MPa. Compositional, thermo-mechanical, weldability, and inspectability requirements for advanced 9-12% Cr steels are also discussed. Microstructural development and creep behavior determined in tandem for the newly developed NETL alloys as well as for COST E, B2, and FB2 alloys is presented.

9:15 AM Invited

**Accelerating High-Performance Materials Design: An Integrated Computational and Experimental Approach:** *Michael Gao*<sup>1</sup>; *De Nyago Tafen*<sup>1</sup>; *Kaisheng Wu*<sup>1</sup>; *Rongxiang Hu*<sup>1</sup>; *Vijay Jain*<sup>1</sup>; *Omer Dogan*<sup>1</sup>; *Jeff Hawk*<sup>1</sup>; *Chris Cowen*<sup>1</sup>; *Paul Jablonski*<sup>1</sup>; *Michael Widom*<sup>2</sup>; <sup>1</sup>NETL; <sup>2</sup>Carnegie Mellon University

In order to reduce harmful environmental emission from coal-fired power plants, National Energy Technology Lab has developed various high-performance materials. For example, high-temperature structural alloys based on Cr and Nb for components to be used in oxy-fuel or hydrogen combustion turbines; crystalline and non-Pd amorphous membrane alloys for hydrogen separation; ferritic Fe-based alloys capable of use at 650°C in advanced combustion systems to reduce the amount of CO<sub>2</sub> emission. We have adopted an approach that integrates computer simulations with critical experiments to accelerate new materials design. Balancing structure-property relationship require delicate tradeoffs and compromises by manipulating alloy system and composition, microstructure, coatings, and materials processing. During this talk, we will present ongoing research effort implementing this approach to design high-performance materials, using combination of computer simulation techniques such as first principles calculations, Molecular Dynamics simulations, CALPHAD modeling, microstructure simulations using phase field, and mechanical property simulations using discrete FFT.

9:40 AM Invited

**Effect of Oxy-Firing on Fireside Corrosion Rates:** *Michael Bestor*<sup>1</sup>; *Bruce Pint*<sup>1</sup>; <sup>1</sup>Oak Ridge National Laboratory

Oxy-firing has been suggested as a method to reduce NO<sub>x</sub> emissions and capture CO<sub>2</sub> from coal-fired power plants. This process involves recirculating the flue gas and will increase the CO<sub>2</sub>, and likely the H<sub>2</sub>O and SO<sub>2</sub> concentrations, in the boiler. In order to understand the role of substrate chemistry on corrosion behavior, commercial and model alloys are being exposed in standard fireside corrosion tests with and without synthetic ash. The gas composition is varied to reflect air-firing and various oxy-firing scenarios. The current testing was performed at 600°C with ferritic steels the primary focus; however, austenitic steels and Ni-base alloys also were exposed with the former showing the lowest corrosion attack. Research sponsored by the Office of Fossil Energy, Advanced Research Materials Program, U. S. Department of Energy.



**10:00 AM Break**

**10:15 AM Invited**

**Oxidation Kinetics Modeling Applying Phase Field Approach:** *Youhai Wen*<sup>1</sup>; Long-Qing Chen<sup>2</sup>; Jeff Hawk<sup>1</sup>; <sup>1</sup>National Energy Technology Laboratory; <sup>2</sup>Penn State University

Components in high temperature fossil energy applications are usually exposed to an aggressive environment containing H<sub>2</sub>O, CO, CO<sub>2</sub>, CH<sub>4</sub>, and O<sub>2</sub>. As service temperature of advanced fossil energy systems increase, chemical reaction rates will increase exponentially and environmental attack will become much more of a concern to designers and in life prediction models. In this work, a general phase-field model is formulated to model the oxidation kinetics. This model can be used to simulate the temporal evolution of oxide thickness and oxygen profile under various conditions such as microstructure dependent diffusivities and simultaneous scale formation and exfoliation. The long term goal of this project is to develop a quantitative tool to predict oxidation kinetics under realistic environmental conditions for certain materials. Pathway of achieving this goal will be discussed.

**10:40 AM**

**Cyclic Oxidation Behavior of HVOF MCrAlY Coatings Deposited on La- and Y-Doped Superalloys:** Michael Bestor<sup>1</sup>; Allen Haynes<sup>1</sup>; Bruce Pint<sup>1</sup>; <sup>1</sup>Oak Ridge National Laboratory

One suggested strategy for improving the performance of thermal barrier coating (TBC) systems used to protect hot section components in gas turbines is the addition of low levels of dopants to the Ni-base superalloy substrate. For the more aggressive environment expected for coal-derived, synthesis gas-fired turbines, this strategy may be effective in retaining TBC durability. To quantify the benefit of these dopants, coupons of three commercial alloys with different Y and La contents were coated with the same commercial NiCoCrAlYHfSi bond coating by high velocity oxygen flame spraying. Coupons were oxidized in cyclic tests at 1050°, 1100° and 1150°C and the oxidation rate and alumina scale adhesion were compared in an effort to better understand the benefit of superalloy dopants. This research was sponsored by the U.S. Department of Energy, Office of Coal and Power R&D, Office of Fossil Energy, (R. Dennis program manager).

**11:00 AM**

**An Investigation on Hot Corrosion Resistance of Plasma Sprayed YSZ-Ceria TBC in Na<sub>2</sub>SO<sub>4</sub>+V<sub>2</sub>O<sub>5</sub> at 1050 °C:** Mohsen Saremi<sup>1</sup>; M.H. Habibi<sup>1</sup>; <sup>1</sup>University of Tehran

Thermal Barrier Coatings are subjected to spallation and destabilization due to oxidation and hot corrosion. In this research, the hot corrosion behaviors of three types of composite coatings were investigated: (1) Conventional YSZ, (2) YSZ+CeO<sub>2</sub> (the composite layer of Ceria and YSZ), (3) CeO<sub>2</sub>/YSZ (The over layer of Ceria on YSZ). The treated samples were characterized using XRD and SEM equipped with EDS. Based on the microscopic observations, the formation of YVO<sub>4</sub> crystals and YSZ spallation, and the amount of phase transformations of tetragonal ZrO<sub>2</sub> to monoclinic, were the criteria for evaluating the resistance of composite coatings. It was observed that CeO<sub>2</sub>/YSZ the best resistant coating against hot corrosion test while conventional YSZ was the least among the three coatings. It was shown that the interaction of V<sub>2</sub>O<sub>5</sub> with yttria resulted in formation of YVO<sub>4</sub> which is detrimental to YSZ because of its accelerated destabilization.

**11:20 AM**

**An Investigation of the Electrochemical Properties of 3 Types PVD Coated on STS304:** *Min-Seok Moon*<sup>1</sup>; Woo KeeDo<sup>2</sup>; Chan-Won Kwak<sup>3</sup>; Sang-Hyuk Kim<sup>2</sup>; Joon-Hyuk Song<sup>1</sup>; Je-Ha Oh<sup>1</sup>; <sup>1</sup>Chonbuk National University, Jeonju Institute of Machinery Carbon Composites; <sup>2</sup>Chonbuk National University; <sup>3</sup>Se-Won Hard Facing Co., Ltd.

In the PEM fuel cell need to reduced weight and total fabrication cost of a fuel cell stack, and increased durability during the operating condition. Typically bipolar plates are a key component of PEMFC and other Fuel cells. In order to reduce both the weight and cost of the bipolar plates, nowadays consider attention is being paid to developing metallic bipolar plates to replace dense graphite. In this study, try to 3 types Nitride coating

process on an austenitic stainless steel (STS304) using a PVD technology (plasma enhanced reactive evaporation) to increase the corrosion resistance of the STS304. Contact angle, SEM, and potentiodynamic tests were used to characterize the 3 types Nitride coating process on the STS304. This study is focus on the best PVD nitride coating process for the corrosion resistance in the PEMFC operating conditions, and could potentially be used in PEMFCs as a bipolar plate material requirement.

**11:40 AM**

**Gaseous Hydrogen Embrittlement of Pipeline Steels:** *Nicholas Nanninga*<sup>1</sup>; Yaakov Levy<sup>2</sup>; Andrew Slifka<sup>1</sup>; <sup>1</sup>NIST; <sup>2</sup>NRCN

The tensile properties of x52, x65, x80 and x100 pipeline steels have been measured in a high pressure (13.6 MPa), high purity, hydrogen gas environment. Significant losses in elongation to failure and reduction in area were measured when testing in hydrogen compared to air (NTP), and these changes were accompanied by major changes in fracture morphology. For hydrogen charged specimens, surface crack initiation and growth was the primary failure mechanism, compared to a typical cup-and-cone failure for specimens tested in air. In addition to baseline characterization of the effects of strength and microstructure, several tests were conducted on the x100 alloy to determine the effects of strain rate and hydrogen gas pressure. Losses in ductility were observed with increases in pressure (up to 68 MPa) and decreases in strain rate, though a plateau in the effects of these variables was evident for the x100 alloy.

---

**Materials Processing Fundamentals: Powders and Composites**

*Sponsored by:* The Minerals, Metals and Materials Society, TMS Extraction and Processing Division, TMS: Process Technology and Modeling Committee

*Program Organizers:* Prince Anyalebechi, Grand Valley State University; Srikanth Bontha, Temple University

Tuesday AM  
March 1, 2011

Room: 12  
Location: San Diego Conv. Ctr

*Session Chair:* Prince Anyalebechi, Grand Valley State University

---

**8:30 AM**

**Exploratory Research in Reactive Spark Plasma Extrusion:** *P Mehra*<sup>1</sup>; K. Morsi<sup>1</sup>; <sup>1</sup>San Diego State University

Spark plasma sintering has gained a considerable amount of attention over the past decade, due to its rapid sintering rates, and low temperature requirements, but has so far been usually limited to the production of simple geometries. The present paper examines the current-activated production of extended geometries through the process of spark plasma "extrusion". Of interest in the present study is exploratory research into the effect of electrical current activation on the reactive consolidation of powder systems to form intermetallic materials.

**8:45 AM**

**Preliminary Investigations of the Effect of Particle Size and Tip Size in the Current Activated Tip-Based Sintering (CATS) of Nickel Powder Compacts:** *A. El-Desouky*<sup>1</sup>; K. Morsi<sup>1</sup>; K.S. Moon<sup>1</sup>; S.K. Kassegne<sup>1</sup>; <sup>1</sup>San Diego State University

Current Activated Tip-based Sintering (CATS) is a new process for the powder-based fabrication of macro, micro and possibly nano-scale features and shapes. This new and unique process enables selective sintering of powders by localizing electrically activated sintering conditions through a stationary or moving electrically conducting tip. We present preliminary experimental results on the effect of tip size in the CATS process as well as the effect of initial powder particle size on the sintering behavior of nickel powder.

TUESDAY AM

9:00 AM

**Determination of the Spark Plasma Sintering Fundamental Densification Mechanisms by Novel Cyclic Loading Approach:** *Wei Li*<sup>1</sup>; William Bradbury<sup>1</sup>; Joanna McKittrick<sup>1</sup>; Randall German<sup>2</sup>; Eugene Olevsky<sup>2</sup>; <sup>1</sup>University of California San Diego; <sup>2</sup>San Diego State University

Determination of fundamental densification mechanisms during spark plasma sintering (SPS) of particulate materials is critical in analyzing defect formation and density evolution. A new cyclic loading approach is applied to determine the dominant mechanism of material transport during SPS. The advantage of the cyclic loading technique is that only one experimental run is needed to determine the constitutive properties of a powder material for any given heating schedule, and no interrupted tests taking into account the grain growth kinetics are necessary. This methodology is employed for sintering compacts pressed from metal (pure spherical copper) and ceramic (alumina) powders. SPS experiments with different heating rates are conducted with the application of different load levels. The step-wise pressure cyclogram is utilized during processing. The determined material constitutive parameters serve as a basis for a full-scale modeling of spark-plasma sintering process.

9:15 AM

**Exploratory Investigations in Reactive Current Activated Tip-based Sintering (CATS):** *A Numala*<sup>1</sup>; K. Morsi<sup>1</sup>; K.S. Moon<sup>1</sup>; S.K. Kassegne<sup>1</sup>; <sup>1</sup>San Diego State University

Current Activated Tip-based Sintering (CATS) is a new process for the powder-based manufacturing of macro, micro and possibly nano-scale features and shapes. CATS enables the selective sintering of powders by localizing current activation conditions through an electrically conducting small tip (either in the stationary or moving mode). This paper presents preliminary experimental results on the CATS of reactive mixtures of Ni/Al powder to form nickel aluminide intermetallics. Preliminary investigations on the effect of current on the reaction characteristics is discussed.

9:30 AM

**Microstructural Evolution of Cu, Ni and Al Powder Particles Processed by Cold Spray:** *Yu Zou*<sup>1</sup>; Eric Irissou<sup>2</sup>; Jean-Gabriel Legoux<sup>2</sup>; Stephen Yue<sup>1</sup>; <sup>1</sup>McGill University; <sup>2</sup>Industrial Materials Institute (IMI), National Research Council Canada (NRC)

Cold spray is a relatively new coating technology by which coatings can be produced using high-velocity impact of powder particles without significant heating introduced. Micron-sized pure Cu, Ni and Al powder particles were processed by the cold spray, respectively. Microstructural evolutions of these particles were investigated using electron backscatter diffraction and transmission electron microscopy. The results show that non-uniform microstructures with elongated grains/subgrains in the size of microns, equiaxed grains in sub-microns and nanocrystalline grains appear in as-sprayed materials. Moreover, deformation twins in nano-scale are observed in the cold sprayed Cu. Formation of these structures is explained by high strain-rate deformation with the dynamic recovery/recrystallization in the complex thermo-mechanical process during cold spray.

9:45 AM

**Elucidating Microstructure Formations in Ta(x)C(1-x) at Various Carbon Contents:** Robert Morris<sup>1</sup>; *Gregory Thompson*<sup>1</sup>; <sup>1</sup>University of Alabama

TaC has a melting temperature near 4000°C and can precipitate out Ta-rich carbide precipitates with similar high melting temperatures. This offers the ability to engineer the microstructure for thermomechanical loading. A series of tantalum carbides have been hot isostatically pressed (HIP) from constituent TaC and Ta powders. Depending on carbon content various microstructures could be processed. These include equiaxed single phase TaC or Ta<sub>2</sub>C grains, equiaxed TaC grains which encased a hatch-pattern of Ta<sub>4</sub>C<sub>3</sub> laths, or acicular grains with very fine laths of TaC/Ta<sub>4</sub>C<sub>3</sub>/Ta<sub>2</sub>C running parallel to the major axis of the grain. To elucidate the microstructure formation mechanisms, a HIP diffusion couple of TaC – Ta metal powders was prepared. The HIP couple revealed the entire span of microstructures. The location of specific microstructures in relationship to the initial powder states provided insights

into the precipitation and reactions from which specific phases and grain morphologies formed.

10:00 AM Break

10:15 AM

**Fabrication, Characterization and Comparison of Spinel ZnFe<sub>2</sub>O<sub>4</sub> Obtained by Sonochemistry Way and Ceramic Way:** *Oscar Restrepo*<sup>1</sup>; Edgar Chavarriaga<sup>1</sup>; Juan Montoya<sup>1</sup>; Leidy Jaramillo<sup>1</sup>; Miguel Hernández<sup>1</sup>; <sup>1</sup>National University of Colombia

This paper provides an analysis of ZnFe<sub>2</sub>O<sub>4</sub> spinel type ceramic pigment obtained by the alternative manufacturing method sonochemistry and the ceramic way. The method sonochemistry appears as an attractive method with enormous advantages in ceramic chemistry, that is why in the synthesis of compounds of industrial interest is emerging as a possible route. The objective is to evaluate the influence that can produce the particle size with optical properties, which are of interest in ceramic pigments industry, also make a comparison with the ceramic way from colorimetric and physical properties. The methods used to characterize the ceramic pigments were x-ray diffraction (XRD), scanning electron microscopy (SEM) and UV-VIS spectrophotometry.

10:30 AM

**Properties and Performance of Composites Based on Superrefractories Cements:** *Ilyoukha Nickolai*<sup>1</sup>; Timofeeva Valentina<sup>1</sup>; Schabanov Alexander<sup>1</sup>; <sup>1</sup>Academic Ceramic Center

Superrefractories cements (1800-2700°C) is a new refractory insulating material and objective of this work is to enlarge our knowledge about this new product and to search solutions for problems the industry is facing. Based on this target, we realized several test to find answers to important questions about the application of this product in severe industrial conditions and to analyze how this material performs in high temperatures. High temperature composites and coatings based on superrefractories cements are meant to protect units from influence of temperature more than 2000°C and used for manufacturing monolithic lining, crucibles used in the melting of pure metals, including alloys on rare-earth elements, for closing one of ceramic modules of fire wall, in refractory lining of quartzglas tanks, petrochemistry reactors, in burial of radiation fuel by extreme environments in nuclear reactors.

10:45 AM

**Predicting the Mechanical Properties of Aluminium-SiC Functionally Graded Materials Processed by Centrifugal Rotation Method:** *Veerarajkumar Aparna*<sup>1</sup>; Savita Kaliya Perumal Veerapandian<sup>1</sup>; <sup>1</sup>College of Engineering, Guindy, Anna University

Materials characterized by variation in composition and structure gradually over volume, resulting in corresponding changes in properties are defined as functionally graded materials (FGM). Al-SiC FGM's were obtained by centrifugal rotation of die in a muffle furnace. The paper develops a reliable model to predict the functional gradient to the analyzed systems. The wear properties were studied using the pin-on tester. A fem code is employed to estimate the effective elastic properties along the gradient distribution. The obtained values were compared with the theoretical calculation acquired by the rule of mixtures. The results revealed that the properties were significantly influenced by the graded distribution of SiC in the matrix. The resultant FGM's were carefully characterized, a great attention devoted to micro structural investigation.

11:00 AM

**Improvement on the Tribological Characteristics of Particulate Copper Silicon Carbide Composites:** *David Esezobor*<sup>1</sup>; Atinuke Oladoye<sup>1</sup>; <sup>1</sup>University of Lagos

Particulate Cu-SiC composites find applications as wear and heat resistant materials in electrical sliding contacts such as in homopolar machines, railway overhead current collector systems where high electrical/thermal conductivity combined with good wear properties is required. However, challenges occur during machining due to the presence of hard reinforcement in the matrix this may lead to high turnover of tool wear and

poor surface finish. The adoption of near-net shape technology to produce such hard-to-machine metal matrix composites and subsequent finish machining with its attendant cost has reported limited success. This paper critically appraises the challenges and opportunities in the improvement of tribological characteristics of particulate Cu-SiC composites and identifies low cost reinforcement material that could be used to improve its tribological characteristics.

**11:15 AM**  
**Study on Preparation of High-Purity Magnesium Carbonate Whisker from Low-Grade Magnesite:** Caiyun Lu<sup>1</sup>; Min Chen<sup>1</sup>; Jingkun Yu<sup>1</sup>; <sup>1</sup>Northeastern University

Mg(HCO<sub>3</sub>)<sub>2</sub> solution was prepared through light burning, hydrous carbonation by using low-grade magnesite as the raw materials, and then the impurities were removed by using activated carbon as adsorbent. In this paper, the effect of different additives on the morphology of Mg(HCO<sub>3</sub>)<sub>2</sub> pyrolytic products and the effect of the heating rate on the morphology of the obtained magnesia were studied. The XRD result showed that the main components of Mg(HCO<sub>3</sub>)<sub>2</sub> pyrolytic products were 3MgCO<sub>3</sub>·Mg(OH)<sub>2</sub>·3H<sub>2</sub>O and MgCO<sub>3</sub>·3H<sub>2</sub>O, which contained less impurities such as CaO<0.04% and TFe<0.02% after adsorbing the impurities by activated carbon. SEM results showed that the morphology of magnesium carbonate was highly dependent to the preparation conditions, namely, without any additive, the flake-like pyrolytic product was obtained, petal shaped pyrolytic product was prepared with potassium dihydrogen phosphate additive, spherical pyrolytic product was obtained with ammonium carbonate additive, and whisker pyrolytic product was obtained while soluble magnesium salts was added, because the additives hindered the growth of crystals in one direction, while promoting the directions of crystal growth to without obstruction. The calcining system had a direct impact on the morphology of magnesia converted from the whisker precursor, while the calcining temperature was elevated at 5 °C·min<sup>-1</sup>, magnesia powder was obtained, while the calcining temperature was elevated at 2 °C·min<sup>-1</sup>, most magnesia maintained whisker morphology, because the decomposition of magnesium carbonate was divided into three stages, the calcination product could keep whisker morphology as precursor through control the decomposing speed.

**11:30 AM**  
**Preparation of Metal Cobalt Powder by Coprecipitation and Heat Decomposition Method:** Xue Ping<sup>1</sup>; Guo Xueyi<sup>2</sup>; Tian Qinghua<sup>2</sup>; Liang Sha<sup>2</sup>; <sup>1</sup>Jiangnan University; <sup>2</sup>central south university

This research provides a novel method to prepare the metal cobalt powder. This method prepared the precursor powder of Co(OH)<sub>x</sub>(CO<sub>3</sub>)<sub>y</sub> by the conventional chemical precipitation, the phase analysis made by X-ray and the infrared spectrum proved that component of the precursor powder was Co(OH)<sub>x</sub>(CO<sub>3</sub>)<sub>y</sub> adsorbing NH<sub>4</sub><sup>+</sup> and Cl<sup>-</sup> and the organic functional group. The precursor powder was prepared for metal cobalt powder through heat decomposition. Based on DSC-TGA analysis, influence of additive reagent and temperature factor to prepare for the cobalt powder were observed in heat decomposition. The results show when the amount of the additive reagent is 63.64%, calcination temperature is 500 °C, all the product is metal cobalt, and the properties are fine.

---

## Microstructural Processes in Irradiated Materials: Microstructure Evolution: Modeling

*Sponsored by:* The Minerals, Metals and Materials Society, TMS Structural Materials Division, TMS/ASM: Nuclear Materials Committee

*Program Organizers:* Gary Was, University of Michigan; Thak Sang Byun, Oak Ridge National Laboratory; Shenyang Hu, Pacific Northwest National Laboratory; Dane Morgan, UW Madison; Yasuyoshi Nagai, Tohoku University

Tuesday AM  
March 1, 2011

Room: 3  
Location: San Diego Conv. Ctr

*Session Chairs:* Yuri Osetsky, Oak Ridge National Laboratory; Shenyang Hu, Pacific Northwest National Laboratory

---

### 8:30 AM Invited

**Simulations of Voids and Gas Bubbles in Irradiated Materials:** Marius Stan<sup>1</sup>; Shenyang Hu<sup>2</sup>; <sup>1</sup>Argonne National Laboratory; <sup>2</sup>Pacific Northwest National Laboratory

The irradiation of nuclear reactor structural materials leads to the formation of voids that cause swelling while in nuclear fuels the accumulation and transport of fission products leads to the formation of gas bubbles that decrease the thermal transport. We review computer simulation techniques for predicting the evolution of voids and gas bubbles. To illustrate the challenges, we discuss phase-field simulations of the nucleation and growth of voids and gas bubbles, focusing on the role of the self-interstitial atoms and vacancies. The simulations show that a high rate of generating interstitials during displacement cascades delays the formation of void lattices. Phase field simulations of UO<sub>2</sub> show that gas bubble nucleation is favored at grain boundaries due to the trapping of fission products and the high mobility of vacancies and gas atoms. The effective thermal conductivity strongly depends on the bubble volume fraction but weakly on the morphology of the bubbles.

### 9:10 AM

**Modeling the Helium Transport, Fate in Tempered Martensitic Steels and Nanostructured Ferritic Alloys – Consequences to Void Swelling:** Takuya Yamamoto<sup>1</sup>; G. Robert Odette<sup>1</sup>; <sup>1</sup>Univ. California Santa Barbara

A rate theory cluster dynamics model that tracks helium transport and partitioning to, and recycling between, matrix sites, precipitates, dislocations and grain boundaries is applied to treat precipitation of helium bubbles in a tempered martensitic steel, F82H, and a nanostructured ferritic alloy, MA957. The model uses kinetic and thermodynamic parameters derived from atomistic simulations. The predictions are shown to be in good agreement with data from in-situ He implantation experiments. Recently, the model has been extended to treat void nucleation and growth. The model predicts significant swelling in F82H, even with conservative parameters: following an incubation dose of ~ 20 dpa at 40 appm He/dpa and 500°C swelling reaches 3.2 % at 100 dpa and 16.6 % at 200 dpa. The predictions of a more detailed and improved model will be compared to the in-situ He-implanter experiment up to 25 dpa and 1250 appm He.

### 9:30 AM

**Modeling He Behavior in Tungsten: Relevance of the Implantation Model:** Marc Hou<sup>1</sup>; Charlotte Becquart<sup>2</sup>; Andree De-backer<sup>2</sup>; Christophe Domain<sup>3</sup>; Christophe Ortiz<sup>4</sup>; <sup>1</sup>Physique des Solides Irradiés et des Nanostructures CP234; <sup>2</sup>UMET, UMR 8207, EM2VM; <sup>3</sup>EdF, R&D, EM2VM; <sup>4</sup>Laboratorio Nacional de Fusión por Confinamiento Magnético, CIEMAT

The binary collision approximation code Marlowe, and object kinetic Monte-Carlo simulations parameterized on Density Functional Theory (DFT) data have been used to investigate the fate of He atoms implanted in tungsten. The He atoms and the associated damage have been introduced either at random in the tungsten matrix or according to distributions provided by Marlowe, taking into account the crystalline nature of the matrix or considering it as an amorphous structure. The results indicate that



in order to reproduce the experimental results, one has to model properly the implantation sequence. They furthermore underline the significant contribution of the crystalline nature of the matrix.

**9:50 AM**

**Stability and Evolution of He Clusters and Complex Defect Clusters Investigated by Ab Initio Calculations and OKMC Simulations in Tungsten:** *Charlotte Becquart*<sup>1</sup>; *Andree De Backer*<sup>1</sup>; *Christophe Domain*<sup>2</sup>; <sup>1</sup>UMET, UMR 8207, EM2VM; <sup>2</sup>EdF, R&D, EM2VM

Understanding and predicting the behavior of helium in metals is an important issue in particular in the context of materials used in fusion reactors nowadays. Indeed in these conditions, two sources of He are present: transmutation and implantation from the plasma. In tungsten, which is a candidate for the divertor in fusion reactors, theoretical and experimental results indicate that helium is very mobile already below room temperature and can form He clusters very easily. We have used state of the art ab initio calculations to investigate the stability of He clusters associated or not with point defects in tungsten as well as impurities. Small He clusters are mobile and one notable result is that the smallest ones exhibit a 1D motion at low temperatures. The consequences on the evolution of the microstructure under irradiation conditions will be discussed in the framework of an object kinetic Monte Carlo model.

**10:10 AM**

**Mesoscale Simulation of Irradiation-Induced Gas Bubbles: Evolution and Impact on Macroscale Properties:** *Paul Millett*<sup>1</sup>; *Anter El-Azab*<sup>2</sup>; *Michael Tonks*<sup>1</sup>; <sup>1</sup>Idaho National Laboratory; <sup>2</sup>Florida State University

Nuclear materials used in fission and fusion applications can be subjected to simultaneously high displacement rates as well as gas production rates. The characteristics of the resultant gas bubble structure, i.e. internal gas density, bubble number density, and bubble distribution, are strongly dependent on the relative defect production rates as well as microstructure (e.g. grain size). Here, we implement a phase-field model capable of capturing multi-component defect (vacancies, self-interstitials, and gas atoms) diffusion, bubble nucleation and growth, and bubble/grain boundary interactions to investigate these processes throughout time and for varying irradiation conditions. Furthermore, we have utilized this simulation capability to develop models of bubble percolation and the effective thermal transport across heterogeneous microstructures. Interestingly, thermal conductivity is found to be strongly dependent on the relative distribution of intergranular versus intragranular bubbles. This research was supported by the Nuclear Energy Advanced Modeling and Simulation (NEAMS) program within DOE-NE.

**10:30 AM Break**

**10:50 AM**

**Simple Concentration-Dependent Pair Interaction Model for FeCr Alloys with Vacancy Supersaturation:** *Enrique Martinez Saez*<sup>1</sup>; *Maximilien Levesque*<sup>2</sup>; *Frederic Soisson*<sup>2</sup>; *Maylise Nastar*<sup>2</sup>; *Chu Chun Fu*<sup>2</sup>; <sup>1</sup>LANL; <sup>2</sup>CEA-Saclay

FeCr alloys are foreseen as strong candidates for fission and fusion applications as matrix for structural materials. A lattice pair interaction model based on the RedLich-Kister polynomial is presented. The interaction coefficients have been fitted to ab-initio data. The model captures the complex thermodynamics of the system, including the short-range order found experimentally for low Cr concentrations. The broken-bond model has been implemented into the synchronous parallel kinetic Monte Carlo algorithm [J. Comp. Phys. 227 (2008) 3804-3823] so to be able to extend the size of the system and therefore the statistics of the calculation as well as the total time studied. Correlation length and precipitate number density of voids and a' precipitates have been studied as well as their shape and size distributions and the results compared to the experimental results available in the literature. We have found a very good agreement between the kinetic model and the experiments.

**11:10 AM**

**Atomistic Study of Interstitial Migration in the Proximity of a Helium Bubble in the Fe-Cr System:** *Jeffery Hetherly*<sup>1</sup>; *Alfredo Caro*<sup>1</sup>; <sup>1</sup>Los Alamos National Laboratory

We investigate the effect that helium bubbles have on the diffusion of self interstitials in Fe-Cr alloys using atomistic techniques. Different bubble pressures and bubble locations (bulk versus grain boundaries) are explored. The results are interpreted in terms of the sink capture efficiency of a bubble for interstitials and the anisotropy of interstitial diffusion in the presence of a stress field. Coated bubbles, either depleted or enriched in solute, are also of interest and are expected to give a different behavior than plain voids.

**11:30 AM**

**Microstructure Evolution of Two Model Ferritic/Martensitic Steels Irradiated with Ions In-Situ in a TEM:** *Djamel Kaoumi*<sup>1</sup>; *Jimmy Adamson*<sup>1</sup>; *Athur Motta*<sup>2</sup>; *Mark Kirk*<sup>3</sup>; <sup>1</sup>The University of South Carolina; <sup>2</sup>The Pennsylvania State University; <sup>3</sup>Argonne National Laboratory

Two model steels (one ferritic/martensitic(Fe12Cr0.1C) and one fully martensitic(Fe9Cr0.1C)) were custom-made with the intent of reproducing the type of starting microstructure of F/M steels, but without the complications of additional alloying elements. The alloys were irradiated with 1-MeV Kr ions at 25°C, 200°C, 300°C to doses up to 10 dpa in-situ in a TEM. The microstructure evolution was followed and characterized at successive doses in terms of defect formation, black dot density, number density of defect clusters, and stability of as-fabricated microstructure using weak-beam dark-field imaging and g.b analysis. The effect of the irradiation temperature on the damage density and on the stability of the initial microstructure is assessed. The overall goal is to determine directly the spatial correlation of the time evolution of the irradiation-induced defect structures with the pre-existing alloy microstructure and to compare with calculations based on rate-theory modelling. The results are summarized in this paper.

**11:50 AM**

**Atomic-Scale Features of Strengthening Due to Impenetrable Obstacles in Iron:** *Yury Osetskiy*<sup>1</sup>; *Roger Stoller*<sup>1</sup>; <sup>1</sup>ORNL

Oxide dispersion strengthened (ODS) alloys are considered as promising structural materials and therefore are under study by different experimental, theoretical and modeling techniques. In this presentation we report the first results of an extensive atomic-scale study of mechanical properties of materials containing impenetrable obstacles simulating ODS particles. We have considered rigid spherical coherent precipitates embedded into bcc-iron matrix. At the first stage we simulated a  $\frac{1}{2}\langle 111 \rangle$  edge dislocation gliding in the plane intersecting precipitates of diameter from 1 to 6nm at different distances to their equator. Different interaction mechanisms were observed depending on the dislocation glide plane position and temperature. The conditions of maximum strength were investigated and the results were discussed in the view of existing experimental data.

**12:10 PM**

**Mobility of Low Energy Boundaries in FCC Copper during Irradiation:** *James Belak*<sup>1</sup>; *Bryan Reed*<sup>1</sup>; *Ming Tang*<sup>1</sup>; *Joel Bernier*<sup>1</sup>; *Vasily Bulatov*<sup>1</sup>; *Thomas LaGrange*<sup>1</sup>; *Mukul Kumar*<sup>1</sup>; <sup>1</sup>Lawrence Livermore National Laboratory

The mobility of ideal low energy boundaries (e.g. Sigma 3) in FCC copper has proven difficult to study using molecular dynamics due to the long time-scales involved. However, by introducing a small vicinal step or shear along the boundary (to nucleate a stepped region), these low energy boundaries readily move. Here we quantify the mobility of Sigma 3 boundaries in FCC copper as a function of vicinal angle and local boundary shear stress. These simulations are used to drive the boundary through regions of irradiation damage (vacancies, interstitials and defect clusters). The defect field initially enhances the step density and mobility, which saturates as the boundary roughens. The simulation results are used to parameterize a simplified model of boundary mobility during irradiation. \*Work performed under the auspices of the U.S. DOE by LLNL under Contract DE-AC52-07NA27344 and supported by the U.S. Department of Energy, Office of Basic Energy Sciences.

## Neutron and X-Ray Studies of Advanced Materials IV: Complex Materials

Sponsored by: The Minerals, Metals and Materials Society, TMS Structural Materials Division, TMS/ASM: Mechanical Behavior of Materials Committee, TMS: Chemistry and Physics of Materials Committee

Program Organizers: Rozaliya Barabash, Oak Ridge National Laboratory; Xun-Li Wang, Oak Ridge National Laboratory; Jaimie Tiley, Air Force Research Laboratory; Peter Liaw, The University of Tennessee; Erica Lilleodden, GKSS Research Center; Brent Fultz, California Institute of Technology; Y-D Wang, Northeastern University

Tuesday AM  
March 1, 2011

Room: 10  
Location: San Diego Conv. Ctr

Session Chairs: T.-C. Chiang, University of Illinois at Urbana-Champaign; Yang Ren, APS

### 8:30 AM Keynote

#### From Structure to Nano-Structure: Materials Research with X-Rays and Neutrons: *Gernot Kostorz*<sup>1</sup>; <sup>1</sup>ETH Zurich

X-rays and neutrons have served as probes for the study of structural and dynamic properties of materials for a long time. Improvements in X-ray and neutron sources and user-oriented research facilities continue to enhance possibilities for increasingly sophisticated experimentation. Some applications of neutron and X-ray scattering – diffraction, diffuse and small-angle scattering – will be presented, with emphasis on recent developments and combination with other methods.

### 8:55 AM Invited

#### Diffuse Scattering as an Aid to the Understanding of Polymorphism in Pharmaceuticals: *Richard Welberry*<sup>1</sup>; Darren Goossens<sup>1</sup>; Eric Chan<sup>1</sup>; Aidan Heerdegen<sup>1</sup>; <sup>1</sup>Australian National University

Polymorphism occurs when the same molecular compound can crystallise in more than one distinct crystal structure. Its study is a field of great interest and activity. This is largely driven by its importance in the pharmaceutical industry but polymorphism is also an issue in the pigments, dyes and explosives industries. The polymorph formed by a compound generally exerts a strong influence on its solid-state properties. The polymorphic form of a drug molecule may affect ease of manufacture and processing, shelf-life and most significantly, the rate of uptake of the molecule by the human body. They can even vary in toxicity; one polymorph may be safe, a second may be toxic. In this paper we show how diffuse scattering experiments coupled with Monte Carlo computer modeling can aid in the understanding of polymorphism. Examples of the two common pharmaceuticals benzocaine and aspirin, both of which are bimorphic, will be discussed.

### 9:15 AM Invited

#### Modeling Diffraction from Thin Film Structures: *I Noyan*<sup>1</sup>; Andrew Ying<sup>1</sup>; Braxton Osting<sup>1</sup>; Conal Murray<sup>1</sup>; <sup>1</sup>Columbia University

We present a rigorous model of kinematic diffraction of a coherent, monochromatic, X-ray beam, focused by a Fresnel zone plate onto a thin, perfect, single-crystal layer. In this model, we first calculate the coherent wave emanating from an ideal zone plate equipped with a direct-beam stop and order sorting aperture. Then, we compute the diffraction of the focused wavefront by a thin silicon film positioned at the primary focal spot. Finally, we propagate the diffracted wavefront to the position of an area detector, and map the intensity distribution in the detector plane. Our model showed that the data analysis of kinematic diffraction patterns obtained from area detectors have some differences from traditional radial scans. These differences were verified through experiments.

### 9:35 AM Invited

#### Multiple Diffraction in Quasicrystals: *Walter Steurer*<sup>1</sup>; Changzeng Fan<sup>1</sup>; <sup>1</sup>ETH Zurich

Multiple diffraction takes place when a crystal is oriented in a way that more than one set of atomic planes is in a position to diffract the incoming monochromatic radiation simultaneously. Because of the interaction between the excited reflections, the total amount of intensity will be redistributed among them. Multiple diffraction is omnipresent during a diffraction measurement on a quasicrystal as a result of its dense set of Bragg reflections. It can bias weak Bragg intensities, which are the key to the solution of the structure of quasicrystals. A complete understanding of multiple diffraction in quasicrystals will help us to get more accurate data sets. Therewith, quasicrystal structure refinement can be substantially improved. Here we report the first results of our study on multiple diffraction in quasicrystals and its influence on quasicrystal structure analysis.

### 9:55 AM Invited

#### Development of Ultrasmall-Angle X-Ray Scattering / X-Ray Photon Correlation Spectroscopy (USAXS/XPCS) for In Situ Studies of Equilibrium and Non-Equilibrium Dynamics over Extended Length and Time Scales: *Jan Ilavsky*<sup>1</sup>; Andrew Allen<sup>2</sup>; Fan Zhang<sup>2</sup>; Lyle Levine<sup>2</sup>; Alec Sandy<sup>1</sup>; Gabrielle Long<sup>1</sup>; <sup>1</sup>APS, Argonne National Laboratory; <sup>2</sup>National Institute of Standards and technology

Scattering and imaging techniques are applicable in static microstructural studies over the full nanometers-to-micrometers feature size range. The dynamics of materials, especially their response to abrupt changes in the sample environment, is on the other hand the domain of the X-ray photon correlation spectroscopy (XPCS). However, existing XPCS facilities are limited to microstructure length scales smaller than about 50 nanometers, thus eliminating large classes of materials that are of major technological importance. We have developed combined ultrasmall-angle X-ray scattering / X-ray photon correlation spectroscopy (USAXS/XPCS) technique to probe the slow equilibrium and non-equilibrium dynamics of optically opaque materials with prominent scattering features in the range 100 nm to several micrometers, i.e., between the ranges of dynamical light scattering and conventional XPCS. Presented example of USAXS-XPCS capabilities will be study of equilibrium dynamics of colloidal dispersions at various volume concentrations as a function of temperature.

### 10:15 AM Invited

#### X-ray Studies of the Lattice Dynamics of Cr across Its Antiferromagnetic Transition: *Tai Chiang*<sup>1</sup>; Ruqing Xu<sup>1</sup>; Mary Upton<sup>2</sup>; Hawoong Hong<sup>2</sup>; <sup>1</sup>University of Illinois; <sup>2</sup>Argonne National Laboratory

Spin-lattice coupling is a classic topic in solid state physics. While generally weak, it is relevant to the basic physics of how elementary excitations interact. A striking case is the Neel transition at  $T_c = 311$  K in chromium. Ultrasonic measurements revealed a substantial, anomalous softening in the elastic constants near  $T_c$ . However, this anomaly has not been detected by neutron scattering. To clarify this issue we have carried out both inelastic x-ray scattering (IXS) and x-ray thermal diffuse scattering (TDS) measurements of this system. IXS scans at several selected regions in reciprocal space did not find significant changes in phonon frequencies, in agreement with prior neutron scattering results. However, TDS measurements near a Brillouin zone center, where IXS measurements had difficulties, revealed an anomalous behavior of the phonons. Our findings suggest that the spin-lattice coupling in chromium is dominated by long-wavelength interactions.

### 10:35 AM Invited

#### Diffuse X-Ray Scattering of Bulk Au-50 at.% Pd and a Ni-23 at.% Pt(100) Surface: *Bernd Schoenfeld*<sup>1</sup>; <sup>1</sup>ETH Zurich

Experimentally no ground state structure is known for bulk Au-Pd, but a series of structures were suggested by electronic structure calculations. In search of plausible superstructures, diffuse x-ray scattering from single crystalline Au-50 at.% Pd was taken for a quenched state of thermal equilibrium. Maxima in short-range order scattering are seen at  $2k_F$  positions, repeatedly found with Au or Cu based alloys. Using the effective

pair interaction parameters, the existence of the suggested structures close to 1:1 stoichiometry is addressed, based on the values of the respective ordering energies. In the course of the ongoing research to characterize the near-surface microstructure of Ni-Pt by grazing incidence diffraction, Ni-23 at.% Pt(100) was measured at 970 K. In contrast to the (110) surface previously investigated, the (100) near-surface regime is connected with strong order leading to strong crystal truncation rods through 100 positions. A tetragonal model is applied to analyze diffuse scattering.

#### 10:55 AM Break

#### 11:05 AM Keynote

**Diffraction from Nanocrystalline Materials: Reciprocal Space versus Direct Space Methods:** *Paolo Scardi*<sup>1</sup>; Matteo Leoni<sup>1</sup>; Luca Gelisio<sup>1</sup>; Alberto Leonardi<sup>1</sup>; <sup>1</sup>University of Trento

Diffraction Line Profile Analysis (LPA) is commonly employed in the characterization of nanocrystalline materials, to gather information on nanocrystal size and shape, lattice defects and atomic-scale distortions. Despite the popularity of LPA in most nanomaterial studies, the applicability of traditional methods based on the reciprocal space approach down to the characteristic dimensions of a few nanometers is not so straightforward, and should be questioned when non-crystallographic structures are involved. The intrinsically discrete nature of the matter on the nanoscale is better described by direct space methods, like those based on the Debye equation. However, the change of paradigm - from reciprocal to direct space - opens new challenges in LPA, to develop computationally effective methods and to obtain a better understanding and representation of the real structure of nanocrystals.

#### 11:30 AM Invited

**Doing Neutron Scattering Science with the Multi-Axis Crystal Spectrometer at the NCNR:** *Jose Rodriguez-Rivera*<sup>1</sup>; <sup>1</sup>University of Maryland/NIST Center for Neutron Research

The Multi-Axis Crystal Spectrometer at the NIST Center for Neutron Research began commissioning operation on 2009 and is in the user program since January 2010. With a Energy range up to 20meV, the high neutron flux, up to  $5 \times 10^8$  neutrons/cm<sup>2</sup>/s will open new areas of condensed matter physics to exploration through inelastic neutron Scattering. The high neutron flux is obtained by using a doubly focusing monochromator subtending a solid angle of up to 0.005 Sr to the cold neutron source. The detector system consist of an array of 20 channels. Each detector channel is built around a vertically focusing double crystal analyzer. The MACS instrument is particularly powerful for probing the wave vector dependence of inelastic neutron scattering in select ranges of energy transfer to access the dynamic structure of fluctuating systems. The first experiment shows the instrument capabilities and opens a new horizon for neutron scattering science.

#### 11:50 AM

**Diffraction Measurements to Identify Structural Changes In Li[Li<sub>1/3-2x/3</sub>NixMn<sub>2/3-X/3</sub>]O<sub>2</sub> (x=1/5) Cathode Materials for Lithium Ion Batteries:** *Christopher Fell*<sup>1</sup>; Shirley Meng<sup>2</sup>; Jacob Jones<sup>1</sup>; <sup>1</sup>University of Florida; <sup>2</sup>Unveristy of California San Diego

The lithium-excess layered oxide compounds Li[NixLi<sub>1/3-2x/3</sub>Mn<sub>2/3-x/3</sub>]O<sub>2</sub> ( $0 < x < 1/2$ ) are of great interest as a new generation of positive electrode materials for high energy density lithium-ion batteries. Following lithium deintercalation and the associated oxidation of Ni<sup>2+</sup> to Ni<sup>4+</sup>, lithium may continue to be extracted from this material despite the fact that all the manganese and nickel ions are in their fully charged (+4) oxidation state. In order to understand the electrochemical processes in Li[Li<sub>0.2</sub>Ni<sub>0.2</sub>Mn<sub>0.6</sub>]O<sub>2</sub>, we investigated the structural changes in the bulk material quantitatively using synchrotron x-ray and neutron diffraction. Synchrotron X-ray diffraction data of electrochemically cycled electrode materials show an expanded c/a lattice ratio, peculiar cation migration and growth of a second phase. Neutron diffraction data following chemical delithiation confirms that not only the Li ions but the transition metal ions (i.e. Ni) are dynamically migrating during the delithiation process.

#### 12:00 PM Invited

**Site Occupation of Atoms in Crystal Lattice Determined by High-Pressure X-Ray Diffraction Technique:** *Zhihua Nie*<sup>1</sup>; Yandong Wang<sup>1</sup>; Zhenwei Huang<sup>2</sup>; Dongmei Liu<sup>2</sup>; Qiaoshi Zeng<sup>3</sup>; Wenge Yang<sup>3</sup>; Yang Ren<sup>4</sup>; <sup>1</sup>Beijing Institute of Technology; <sup>2</sup>Northeastern University; <sup>3</sup>Carnegie Institution of Washington; <sup>4</sup>Argonne National Laboratory

Both mechanical and functional behaviors of alloys rely greatly on their crystal lattice structure and lattice-site occupation (LSO) of atoms. The detailed LSO of added alloying elements in a crystalline phase can only be determined through the Rietveld refinement by fitting a theoretical line profile to experimental X-ray or neutron diffraction data or constructing the atomic pair distribution function in the real space. However, so far it is impossible to obtain the accurate information on the LSO of specified atoms with less difference in scattering factor between the alloying element and fundamental constitutive elements. Here we present a new method for determining the LSO through the change in lattice parameters and phase transition behavior under hydrostatic pressure by in-situ XRD, in comparison with that obtained by the first-principles calculations considering different LSOs of atoms. This method is successfully demonstrated through the high pressure XRD experiments of a NiCoMnIn magnetic-field-driven alloy.

#### 12:20 PM Invited

**In situ Neutron Diffraction Studies of Phase Transformations in Shape Memory Alloys:** *Raj Vaidyanathan*<sup>1</sup>; <sup>1</sup>UCF

We report on in situ neutron diffraction measurements performed on NiTi-based shape memory alloys during selected combinations of heating, cooling and mechanical loading at Los Alamos National Laboratory. The choice of alloy systems is motivated by the temperature range at which they exhibit phase transformations that result in the shape memory effect - from below room temperature for NiTiFe alloys and near room temperature for NiTi alloys to above room temperature for NiTiPd alloys. Micromechanical and microstructural changes, i.e., texture, strain and phase volume fraction evolution were quantified for the cubic B2 to trigonal R to monoclinic B19' phase transformations in NiTiFe, the cubic B2 to monoclinic B19' phase transformation in NiTi and the cubic B2 to orthorhombic B19 phase transformation in NiTiPd. The implications of these results for engineering shape memory alloys with useful ternary and quaternary elemental additions for aerospace applications is presented.

#### 12:40 PM Invited

**Temperature Dependence of Diffuse Scattering in PZN:** *Darren Goossens*<sup>1</sup>; Ross Whitfield<sup>1</sup>; T. Welberry<sup>1</sup>; <sup>1</sup>Australian National University

Structural disorder appears to relate to the useful physical properties of ferroelectrics and relaxors. One such material is PZN, PbZn<sub>1/3</sub>Nb<sub>2/3</sub>O<sub>3</sub>. To explore what aspects of the disorder are specific to the polarised state, the temperature dependence of diffuse scattering in PZN has been investigated. Data were collected using both neutron and X-ray single crystal experiments in a range of temperatures from 100K to 500K. It has been found that some features, like the diffuse scattering from the B-site ordering, remain unchanged with change of temperature in terms of both intensity and peak shape. However, other diffuse scattering features evolve with T, for example the size-effect scattering around the Bragg peaks. The size-effect becomes less pronounced with increasing temperature, with the diffuse scattering becoming more symmetric around the Bragg peaks. The diffuse rods caused by the planer domains change only slightly with temperature.



## **Pb-Free Solders and Other Materials for Emerging Interconnect and Packaging Technologies: Alloy and Microstructure Development**

*Sponsored by:* The Minerals, Metals and Materials Society, TMS Electronic, Magnetic, and Photonic Materials Division, TMS: Electronic Packaging and Interconnection Materials Committee  
*Program Organizers:* Indranath Dutta, Washington State University; Darrel Frear, Freescale Semiconductor; Sung Kang, IBM; Eric Cotts, SUNY Binghamton; Laura Turbini, Research in Motion; Rajen Sidhu, Intel Corporation; John Osenbach, LSI Corporation; Albert Wu, National Central Univ, Taiwan; Tae-Kyu Lee, Cisco Systems

Tuesday AM  
March 1, 2011

Room: 7B  
Location: San Diego Conv. Ctr

*Session Chairs:* Darrel Frear, Freescale Semiconductor; Thomas Bieler, Michigan State University

### **8:30 AM Invited**

**Structure and Transformation in Sn-Rich Sn-In Solders:** *John Morris*<sup>1</sup>; Kyu-Oh Lee<sup>2</sup>; Fay Hua<sup>2</sup>; <sup>1</sup>University of California Berkeley; <sup>2</sup>Intel Corporation

Of the Pb-free solders, Sn-rich InSn is unusually interesting in its structural and mechanical properties. The phases found for Sn-rich compositions include the  $\alpha$  (diamond) and  $\beta$  (tetragonal) structures of pure Sn, and the  $\square$  (hexagonal) structure of InSn. The  $\beta$ -Sn structure is notable for its complexity, which complicates the properties of all Sn-rich solders. The  $\square$ -InSn structure is notable for its simplicity; in ambient it is a solid solution rather than an ordered compound, and is one of few materials that crystallize in a simple hexagonal structure. Surprisingly, the  $\beta$ - and  $\square$ -structures of InSn have simple crystallographic connections, which not only facilitate transformation between them, but also permit martensitic transformation on cooling or under load. Here we describe the crystallographic relations and explore their influence on the microstructure and properties of Sn(7-13) In solders. Interestingly, transformation-induced plasticity (TRIP) occurs under appropriate conditions, including the first documented example of TRIP-mediated creep.

### **8:55 AM Invited**

**Optimization of Pb-Free Solder Joint Reliability from Metallurgical Perspective:** *Kejun Zeng*<sup>1</sup>; <sup>1</sup>Texas Instruments Inc.

Electronic packages with NEMI recommended Sn3.9Ag0.6Cu solder joints have shown poor performance in BLR tests. To improve package performance in board level drop test, a low Ag content of SnAgCu solder is preferred. On the other hand, the resistance of SnAgCu solder to thermal fatigue is dependant on the Ag content. Packages with low Ag content of SnAgCu solder have poor performance in thermal cycling test. In order for SnAgCu solder joints to perform well in both drop and thermal cycling tests, the key is to have better interfacial reliability. We will discuss how to optimize the Pb-free solder joint reliability by considering the effects of both solder alloys and surface materials on the metal pads. We will demonstrate that it is possible to keep a high content of Ag in the solder to get high resistance to thermal fatigue while the drop performance of the joints is not compromised.

### **9:20 AM Invited**

**On the Driving Force for Massive Spalling in Solder Systems:** W. M. Chen<sup>1</sup>; C. Robert Kao<sup>1</sup>; <sup>1</sup>National Taiwan University

To identify the driving force for the massive spalling phenomenon, well-designed experiments were carried out in this study. Copper-doped solder was reacted with Ni to form the Sn-0.6Cu/(Cu,Ni)6Sn5/Ni structure first. The original Sn-0.6Cu solder was then removed and replaced with Sn-0.3Cu, or with fresh Sn-0.6Cu. The swapping of solder to Sn-0.3Cu caused the massive spalling of (Cu,Ni)6Sn5. Without this swapping or in the case of swapping to fresh Sn-0.6Cu, the massive spalling did not occur. The results of this study unequivocally proved that the massive spalling reported in literature was caused by a driving force of pure thermodynamics in nature.

### **9:45 AM Invited**

**A Study of the Factors Affecting the  $\beta$  to  $\alpha$  Transition in Solder Alloys:** *Christopher Hunt*<sup>1</sup>; Davide Di Maio<sup>1</sup>; <sup>1</sup>National Physical Laboratory

With introduction of lead-free alloys into harsh conditions, there is some concern that these alloys will undergo the catastrophic solid state  $\beta$  to  $\alpha$  transformation. In this transformation, with an equilibrium temperature of 13°C, tin becomes a semiconductor and there is a 27% increase in volume. In this paper techniques that have been developed to monitor the transformation rate based on a time lapse technique and the application of electrical continuity measurements in the bulk tin. A technique for initiating the transformation based on the use of a seed is described. In this paper, various factors affecting the transformation rate were investigated: stress, alloy composition, and nucleating seed. Of very significant interest is the effect of flux and its residues, and that of oxides in influencing the transformation rates. Experiments are reported that show how these factors can affect the transformation rate.

### **10:10 AM**

**Effect of Solidification Temperature on the Microstructure of SnAgCu Solder Joints:** *Babak Arfaei*<sup>1</sup>; Eric Cotts<sup>1</sup>; <sup>1</sup>Binghamton University

Variations in the microstructure of SnAgCu solder joints resulting from changes in solidification temperatures are examined. Sample and pad size, thermal history and substrate finish all may affect the solidification temperature. Solder joint Sn grain morphology, and intermetallic precipitate size and number, are directly affected by solidification temperature; thus solder joint mechanical properties are strongly influenced by this parameter. The Sn grain morphologies and precipitate microstructures were examined in near eutectic SnAgCu solder joints solidified at undercoolings between ten and eighty degrees. Larger solder joints (e.g. ball grid array, 500 micron diameter) generally solidify at higher temperatures and show a beach ball twinning structure, however through the control of thermal history, the solidification temperature of such large solder joints was reduced thirty degrees. An interlaced twinning morphology was then observed. Corresponding changes in precipitate morphology are reported. Effects on creep and cyclic failure times of SnAgCu solder joints are discussed.

### **10:30 AM Break**

### **10:40 AM**

**Effect of the Ternary Quasiperitectic Reaction on the Formation of Microstructure during Freezing of Ternary Pb-Free Solder Alloys:** *Doug Perovic*<sup>1</sup>; Leonid Snugovsky<sup>1</sup>; Polina Snugovsky<sup>2</sup>; John Rutter<sup>1</sup>; <sup>1</sup>University of Toronto; <sup>2</sup>Celestica Inc.

The banning of Pb as a toxic material has led to the introduction of ternary solder alloys, such as the SAC series, to replace the traditional Pb-Sn eutectic solder. The addition of a third element to the solder alloy brings with it the possibility of the introduction of ternary solidification reactions, in addition to the usual binary reactions, during freezing of the solder. Such a ternary reaction, known as a quasiperitectic reaction, has been observed in the phase diagrams of certain Pb-free systems. In particular, these are alloy systems in which the phenomenon of "spalling" occurs in joints made with the associated solder alloys. It is the purpose of this paper to show the effect of the ternary quasiperitectic reaction on the formation of microstructure during freezing of such Pb-free solder alloys. Solder joint formation of Sn-Ag-Cu alloys and Sn-Zn-Cu Alloy on Cu/Ni substrate will be presented.

### **11:00 AM**

**Development of SAC3595 Solders Alloyed with Al, Mn, or Zn for High Reliability:** *Adam Boesenberg*<sup>1</sup>; Iver Anderson<sup>2</sup>; Joel Harringa<sup>2</sup>; <sup>1</sup>Iowa State University; <sup>2</sup>Ames Laboratory

As a robust replacement for leaded solders that can become environmental toxins, a family of near-eutectic Pb-free solder alloys based on Sn-Ag-Cu (SAC) compositions have shown promise worldwide for electronic assembly. However, reliability issues in divergent assembly methods and aggressive operating environments have arisen. Micro-alloying of Sn-3.5Ag-0.95Cu (wt.%) solder with Al, Mn, Zn was developed for reliable heterogeneous nucleation control in solder joint solidification to address drop impact and

thermal cycling issues. Cu substrate solderability of these SAC3595+X alloys was investigated at concentrations between 0.01-0.25wt% using globule wetting balance tests to quantify any increased oxidation during reflow. Composition dependence of these X additions also was explored in simplified Cu joints by differential scanning calorimetry, microstructure analysis, and X-ray diffraction to determine coupling between undercooling and joint microstructure development on single and multiple reflow cycles. Supported by Iowa State University Research Foundation and Nihon-Superior, Inc., through Ames Lab contract DE-AC02-07CH11358.

**11:20 AM**

**Effect of Gold Content on the Microstructural Evolution of SAC305 Solder Joints under Isothermal Aging:** *Mike Powers*<sup>1</sup>; Jianbiao Pan<sup>2</sup>; Julie Silk<sup>1</sup>; Patrick Hyland<sup>2</sup>; <sup>1</sup>Agilent Technologies; <sup>2</sup>California Polytechnic State University

Au over Ni on Cu is a widely used printed circuit board (PCB) surface finish, under bump metallization and component lead metallization. It is generally accepted that less than 2-3 weight percent Au in Sn-Pb solder joints will preclude reliability issues associated with the formation of Au based intermetallic compounds. However, the critical limit for Au content in Pb-free solder joints is not well established. This paper investigates the microstructural evolution of SAC305 solder joints with varying Au content under isothermal aging. Three surface mount package platforms with different Au thicknesses on their component leads were soldered to PCB with two different Au thicknesses, in a realistic manufacturing setting. The assembled boards were divided into three groups: one without thermal treatment, one isothermally aged at 125\176 C for 30 days and the third aged at 125\176 C for 56 days. The resulting microstructure of the test groups is compared.

**11:40 AM**

**Rare Earths Addition Effect on Microstructure and Intermetallic Layer Growth Kinetics on Lead-Free Solder Sn-Ag-Bi:** *Miguel Neri*<sup>1</sup>; Alberto Martinez-Villafañe<sup>1</sup>; Caleb Carreño<sup>1</sup>; <sup>1</sup>CIMAV, S.C.

Rare earths were added to Sn-Ag-Bi alloy in order to determine its effect on microstructure and Tin-Copper intermetallic layer growth kinetics. There were 3 different sample alloys prepared: Sn-Ag-Bi, Sn-Ag-Bi + Nd, and Sn-Ag-Bi + Pr. These alloys were applied to an electrolytic copper substrate and were given ageing heat treatments at temperatures between 50 to 150 °C at different times of permanence (0, 50, 150, 250 and 500 hours), in order to determine the Tin-Copper intermetallic layer growth kinetics and microstructure evolution on the soldered joints. These samples were prepared by metallographic techniques in order to measure the intermetallic layer thickness, and observe the microstructure thickening depending on temperature and time of ageing heat treatment, using optical microscopy, scanning electron microscopy, and EDS. The intermetallic layer thickness grew by increasing temperature and ageing treatment time, while microstructure was thickening with increasing temperature and ageing treatment time.

**12:00 PM**

**Magnetically-Driven Three-Dimensional Manipulation and Inductive Heating of Magnetic-Dispersion Containing Lead-Free Solders:** *Aimissa Ramirez*<sup>1</sup>; Xu Huang<sup>1</sup>; Joshua Calabro<sup>1</sup>; Brian Lewis<sup>1</sup>; <sup>1</sup>Yale University

Fundamental to the development of three-dimensional microfabrication is a material that enables vertical geometries. Here we show lead-free solders containing iron dispersions that can be remotely manipulated by magnetic fields to create vertical geometries and thus enable three-dimensional fabrication. These iron dispersions enhance the mechanical properties needed for strong, reliable interconnects, without significantly altering the electrical properties. Additionally, these iron dispersions act as susceptors during electromagnetic induction heating conditions, allowing the rapid melting of these novel materials at lower temperatures than those usually reported for conventional solder. Such capabilities have potential applications in the assembly of temperature-sensitive devices by localizing high temperatures and by reducing the temperature excursions associated with other lead-free solders.

## Physical and Mechanical Metallurgy of Shape Memory Alloys for Actuator Applications: Characterization of Shape Memory Alloys: Microstructural Transformation

*Sponsored by:* The Minerals, Metals and Materials Society  
*Program Organizers:* S. Raj, NASA Glenn Research Center; Raj Vaidyanathan, University of Central Florida; Ibrahim Karaman, Texas A&M University; Ronald Noebe, NASA Glenn Research Center; Frederick Calkins, The Boeing Company; Shuichi Miyazaki, Institute of Materials Science, University of Tsukuba

Tuesday AM  
March 1, 2011

Room: 11B  
Location: San Diego Conv. Ctr

*Session Chairs:* Ibrahim Karaman, Texas A&M University; Sai Raj, NASA Glenn Research Center

### 8:30 AM Introductory Comments

#### 8:35 AM Plenary

**Hysteresis, Reversibility, and Shape Memory:** *Richard James*<sup>1</sup>; Vijay Srivastava<sup>1</sup>; Yintao Song<sup>1</sup>; <sup>1</sup>University of Minnesota

We present some recent measurements of hysteresis, in materials undergoing first order phase transformations, that resulted from a systematic program of tuning of the lattice parameters by changing composition. The lattice parameters were tuned so that a certain non generic condition of compatibility between phases was satisfied. The tuned alloys exhibit thermal hysteresis as low as 2 C by careful bulk measurements, and in all cases less than 6 C. The procedures are effective for broad classes of hard materials undergoing diffusionless transformations, including metals and oxides. Studies of reversibility show improved stability of the transformation, measured by the migration of the hysteresis loop under repeated cycling. Some examples of this tuning in Heusler systems show fascinating convergence of shape memory and magnetism. Using these tuned Heuslers, we demonstrate new devices that 1) convert heat directly into electricity, 2) convert heat directly into kinetic energy.

#### 9:05 AM Invited

**Effects of Surface Modifications on Twinning Stress and the Stability of Twin Microstructures of Magnetic Shape-Memory Alloys:** *Peter Müllner*<sup>1</sup>; Markus Chmielus<sup>2</sup>; Cassie Witherspoon<sup>1</sup>; Rainer Schneider<sup>3</sup>; Kari Ullakko<sup>1</sup>; <sup>1</sup>Boise State University; <sup>2</sup>Boise State University and Helmholtz Centre Berlin for Materials and Energy; <sup>3</sup>Beuth Hochschule für Technik und VDI/VDE Innovation and Technik GmbH

Twinning is the primary deformation mechanism in magnetic shape-memory alloys (MSMA). Inclusions, precipitates and defects hinder or even prevent twin boundary motion in the bulk of MSMA single crystals. We study the effect of surface damage on the mechanical properties and twin structure of Ni-Mn-Ga single crystals. Surface damage was produced with spark erosion, ion implantation, shot blasting and abrasive wearing. The degree of surface modification was characterized with x-ray diffraction where the broadening of Bragg reflections and of rocking curves was taken as a measure of localized elastic and plastic strains. Surface deformation stabilizes a dense twin-microstructure and prevents twins from coarsening. The density of twins increases with increasing degree of deformation. With increasing surface deformation and twin density, twinning stress and hardening rate increase. The stabilization of a dense twin microstructure prevents damage accumulation in high-cycle magneto-mechanical actuation and is critical for technological applications of MSMA.

#### 9:25 AM Invited

**In-Situ Neutron Scattering Studies of Shape Memory Alloy Actuator Materials:** *Donald Brown*<sup>1</sup>; Bjorn Clausen<sup>1</sup>; Thomas Sisneros<sup>1</sup>; <sup>1</sup>Los Alamos National Lab

Neutrons are uniquely suited to probe the crystallographic response of materials to external stimuli because of their high penetration, which allows

them to sample the bulk of the material.. This is important for shape memory alloys (SMA's) as surface grains might be expected to behave differently from those in the bulk due to the different constraints. The SMARTS neutron diffractometer at the Lujan Center was built on the philosophy of studying materials under their operating conditions, and this philosophy has been aggressively applied to SMA's. The design of SMARTS allows for determination of the phase fraction, internal stress, and, to a degree, the texture evolution of SMA's under various conditions including tensile, compressive, or cyclic loading while simultaneously controlling temperature and/or magnetic field. This talk will highlight these capabilities, which are available to general users, by describing several examples of recent research on SMA's under multiple environmental conditions.

#### 9:45 AM Invited

**Nanocrystalline Shape Memory Alloys:** *Thomas Waitz*<sup>1</sup>; Wolfgang Pranger<sup>2</sup>; Clemens Mangler<sup>1</sup>; Martin Peterlechner<sup>1</sup>; Gerd Steiner<sup>1</sup>; Thomas Antretter<sup>3</sup>; Franz Dieter Fischer<sup>3</sup>; Peter Müllner<sup>4</sup>; <sup>1</sup>University of Vienna; <sup>2</sup>Materials Center Leoben Forschung GmbH; <sup>3</sup>Montanuniversität Leoben; <sup>4</sup>Boise State University

Martensitic phase transformations can be significantly affected by a grain size and specimen size on the micro- and nanoscale. Bulk nanocrystalline shape memory alloys for actuator applications can show large recovery stresses. Thin films and small pillars are promising candidates for actuators for micro- and nanoelectromechanical systems. In the present work, the effect of a grain size at the nanoscale on the martensitic phase transformation is studied using bulk materials processed by severe plastic deformation that include NiTi and high temperature NiTiHf shape memory alloys as well as NiMnGa and high temperature NiFeGaCo ferromagnetic shape memory alloys. Grain refinement causes a suppression of the martensitic phase transformation that can occur in burst like events. Considering a size dependent energy barrier opposing the transformation, the phase stability and unique martensitic morphology of the nanograins is explained.

#### 10:05 AM Break

#### 10:15 AM Invited

**New Microscopic Tools Applied for the Study of SMA:** *Dominique Schryvers*<sup>1</sup>; <sup>1</sup>University of Antwerp

In recent years several new electron microscopic tools have become available for the study of the crystallography and microstructure of functional materials. Atomic crystal structures can be refined with new optimization procedures including dynamic diffraction allowing focusing on nanoscale structures such as metastable Ni<sub>4</sub>Ti<sub>3</sub> precipitates in Ni-Ti SMA. Quantitative analysis of atomic resolution images and spectroscopic data yields three-dimensional views of concentration gradients and strain fields in the matrix surrounding such precipitates while tomographic slice-and-view techniques result in three-dimensional shape and distribution functions for the precipitates. More conventional techniques provide insight in the role of lattice parameter relations between parent and product for the lowering of the hysteresis and energy dissipation and the corresponding twin configurations. Site-specific sample preparation with FIB provides new ways for the study of surface and interior of micro-wires treated by a variety of processes. Examples of these and other applications will be presented.

#### 10:35 AM Invited

**Modulated Martensite: Why it Forms and Why it Deforms Easily:** *Sebastian Fähler*<sup>1</sup>; <sup>1</sup>IFW Dresden

The high strain up to 10% in magnetic shape memory alloys is only observed in martensitic phases exhibiting modulations. In order to understand the origin of modulated martensites and consequences for the twin boundary mobility we analyze epitaxial Ni-Mn-Ga films as a model system. In agreement with the concept of adaptive martensite modulations are induced by the geometrical constraints at the habit plane. Hence modulated martensite is build from nanotwinned tetragonal martensite. We observe coarsening of these twin variants by doubling of periodicity in discrete steps from the atomic to the micrometer scale. When the activation energy for this process is too high, a second hierarchy of mesoscopic twin boundaries forms.

In contrast to the common, atomically sharp twin boundaries, the complex unit cell of an adaptive phase results in diffuse, mesoscopic twin boundaries. The extraordinarily high mobility of mesoscopic twin boundaries can be attributed to their broad pinning potential

#### 10:55 AM Invited

**Transformation Characteristics of Ni-Mn-Ga High Temperature Shape Memory Alloys:** Ruben Santamarta<sup>1</sup>; *Jaume Pons*<sup>1</sup>; Catalina Picornell<sup>1</sup>; Eduard Cesari<sup>1</sup>; Joan Font<sup>2</sup>; Joaquim Muntasell<sup>2</sup>; Ibrahim Karaman<sup>3</sup>; Dimitris Lagoudas<sup>3</sup>; <sup>1</sup>University of the Balearic Islands; <sup>2</sup>Polytechnical University of Catalonia; <sup>3</sup>Texas A&M University

The martensitic transformation (MT) characteristics of several Ni-Mn-Ga alloys with high transformation temperatures (TTs) will be presented. The studied alloys with the highest TTs, ~750K, are unstable; the MT is degraded after a few cycles by intense precipitation of \947' phase or lath-shaped particles similar to the Ni<sub>5</sub>Al<sub>3</sub> phase. Alloys with Ni content close to stoichiometry show an excellent thermal stability upon ageing. For instance, the alloys Ni<sub>51.2</sub>Mn<sub>33.1</sub>Ga<sub>17.7</sub> (TT~485K) and Ni<sub>51.2</sub>Mn<sub>33.1</sub>Ga<sub>15.7</sub> (TT~575K) aged at 770 K for years do not experience any significant change in the TTs. In other alloys, like Ni<sub>55.2</sub>Mn<sub>29.1</sub>Ga<sub>15.7</sub> (TT~665K) and Ni<sub>58.3</sub>Mn<sub>15.5</sub>Ga<sub>25.8</sub> (TT~525K), precipitation of lath-shaped or \947' phases take place after several days at 670K or 770K, respectively. The superelasticity and shape memory characteristics will also be presented both in single phase alloys and in alloys with controlled precipitation of second phases introduced to improve the ductility. Finally, the effects of Cu additions will be discussed.

#### 11:15 AM

**Microstructural Instability in NiTi Based Shape Memory Alloy Actuators:** *Nicholas Jones*<sup>1</sup>; David Dye<sup>1</sup>; <sup>1</sup>Imperial College London

NiTi based shape memory alloy (SMA) actuators offer the potential for simple dynamic components that can reduce aerospace emissions. For these components to be structurally useful, they require a significant bias load. However, despite fabrication of successful demonstrator components, the cyclic instability of the martensitic transformation continues to prevent this technology from transferring into full scale production. The addition of copper can alter the transformation sequence including an orthorhombic martensite, which seems to decrease the rate of cyclic destabilisation. Using synchrotron X-ray diffraction we have studied the behaviour of both a near equiatomic and a copper containing NiTi SMA over several thermal cycles under different uniaxial loads. The martensitic microstructure is found to evolve during cycling and an accumulation of strain is observed, which appears to be driven by accommodation of the applied load. The observed effects are discussed, relating the transformation fundamentals to the instability of the material.

#### 11:30 AM

**The R Phase Transformation in Rapidly Solidified Ti-47.3Ni(at%) Alloy Ribbons:** *Tae-hyun Nam*<sup>1</sup>; Hyo-jung Mun<sup>1</sup>; Yinong Liu<sup>2</sup>; Hong Yang<sup>2</sup>; Yeon-wook Kim<sup>3</sup>; <sup>1</sup>Gyeongsang National University; <sup>2</sup>University of Western Australia; <sup>3</sup>Keimyung University

In the present study, Ti-47.3Ni(at%) alloy ribbons with a thickness of 32±1µm were prepared by melt spinning and then microstructures and transformation behavior were investigated by means of transmission electron microscopy(TEM), X-ray diffraction(XRD), electrical resistivity(ER) measurement and differential scanning calorimetry(DSC). Nano-sized Ti<sub>2</sub>Ni particles with a specific orientation relationship with matrix were observed in as-spun ribbons. The B<sub>2</sub>-R-B<sub>19'</sub> transformation occurred in as-spun ribbons and moreover the B<sub>2</sub>-R transformation was separated clearly from the R-B<sub>19'</sub> transformation. The two-stage B<sub>2</sub>-R-B<sub>19'</sub> transformation behavior was still preserved after annealing the as-spun ribbons at the temperature range from 673 K to 1223 K for 3.6 ks. When the annealing temperature was higher than 973 K, the B<sub>2</sub>-R and the R-B<sub>19'</sub> transformations were not separated clearly, which was ascribed to the fact that nano-sized Ti<sub>2</sub>Ni particles grew and lost the specific orientation relationship with matrix by high temperature annealing.



11:45 AM

**Characterization of Nanoscale Precipitates in a Ni-Rich Ni-29.7Ti-20Hf (at.%) High Temperature Shape Memory Alloy:** Taisuke Sasaki<sup>1</sup>; B. C. Hornbuckle<sup>1</sup>; Glen Bigelow<sup>2</sup>; Ronald Noebe<sup>2</sup>; Mark Weaver<sup>1</sup>; *Gregory Thompson*<sup>1</sup>; <sup>1</sup>University of Alabama; <sup>2</sup>NASA Glenn Research Center

Though Ni-rich Ni-Ti alloys have superior dimensional stability compared to Ti-rich compositions, after several thermomechanical cycles, retained strain can occur. The ternary addition of Hf has been observed to reduce this effect and has the added benefit of raising the transformation temperatures. The Hf addition has been shown to form nanoscale precipitates; however, little is understood with respect to the microstructure of this fine phase. In this work, we investigated the effect of aging on the transformation temperature and microstructure of an extruded Ni-29.7Ti-20Hf (at.%) alloy. The samples were solution treated at 1050°C for 0.5 hr followed by aging at 550°C for various times. Unlike the recent P-phase reported in NiTiPt, the NiTiHf alloys exhibit a different crystal structure. Transmission electron microscopy and atom probe tomography have been performed to quantify the structure.

12:00 PM End of Session

## Polycrystal Modelling with Experimental Integration: A Symposium Honoring Carlos Tome: Hexagonal Materials and Twinning

*Sponsored by:* The Minerals, Metals and Materials Society, TMS Structural Materials Division, TMS Materials Processing and Manufacturing Division, ASM-MSCTS: Texture and Anisotropy Committee, TMS/ASM: Mechanical Behavior of Materials Committee, TMS/ASM: Computational Materials Science and Engineering Committee

*Program Organizers:* Ricardo Lebensohn, Los Alamos National Laboratory; Sean Agnew, University of Virginia; Mark Daymond, Queens's University

Tuesday AM  
March 1, 2011

Room: 6C  
Location: San Diego Conv. Ctr

*Session Chairs:* Sean Agnew, University of Virginia; Jian Wang, Los Alamos National Laboratory; Irene Beyerlein, Los Alamos National Laboratory

8:30 AM Invited

**Role of Stress Fluctuations in the Nucleation of Deformation Twinning in Hcp Metals:** *Irene Beyerlein*<sup>1</sup>; Anand Kanjarla<sup>1</sup>; Carlos Tome<sup>1</sup>; Ricardo Lebensohn<sup>1</sup>; <sup>1</sup>Los Alamos National Laboratory

We present an experimental and theoretical approach for understanding the statistical nature of deformation twinning in hexagonal close packed (hcp) polycrystals. We first describe statistical studies of {1012} twinning in high-purity Zr and Mg that correlate deformation twinning with certain microstructural features, such as grain size, grain orientation, and grain boundary misorientation angle. To determine the impact of twinning on aggregate deformation behavior, these metallographic results are combined with a multi-scale constitutive model for hcp metals. The predictions indicate that the amplitude and variation in the stress fluctuations between the grain interior and grain boundary play a crucial role. In light of this, we consider two models, the second-order (SO) VPSC approach (Lebensohn et al., 2007) and Fast Fourier Transform method (FFT) (Lebensohn et al., 2004), both of which account for grain orientation in the calculation of stress states. We report on how the modeling results compare for various cases.

8:55 AM Invited

**Orthotropic Strain Rate Potential for Hexagonal Metals:** *Oana Cazacu*<sup>1</sup>; Ioan Ionescu<sup>2</sup>; <sup>1</sup>University of Florida; <sup>2</sup>LPMTM, University Paris 13

Existing strain rate potentials are applicable only to materials with cubic crystal structure. In this paper, an anisotropic strain rate potential for hexagonal metals is developed. First, an exact dual to the isotropic form of Cazacu et al. (2006) stress potential is derived. Next, this isotropic strain

rate potential is extended such as to account for orthotropic symmetry. The ability of the developed anisotropic strain rate potential to describe the complex behavior of hexagonal metals is demonstrated by comparison with experimental data on titanium.

9:20 AM

**Modeling Deformation Twinning with a Binary-Tree Based Polycrystal Model:** *Sivasambu Mahesh*<sup>1</sup>; <sup>1</sup>IIT Kanpur

A novel polycrystal model that explicitly accounts for intergranular interactions is described. In this model, the polycrystal is regarded as a binary tree. Leaf nodes of the binary tree represent the grains and successively higher nodes represent increasingly larger sub-aggregates of grains culminating with the root of the tree, which represents the entire polycrystalline aggregate. Traction and velocity continuity conditions are imposed across the interface between the children of each non-leaf node in the binary tree. The present model is employed to model deformation twinning of hcp magnesium and zirconium. Texture predictions from the present model are compared with those obtained using the VPSC model by Dr. Tome' and co-workers, and with experimental observations.

9:40 AM Break

9:55 AM Invited

**Effect of Texture on Anisotropic Creep of Zr-2.5Nb Tubes:** *Rick Holt*<sup>1</sup>; W. Li<sup>1</sup>; S. Tracy<sup>1</sup>; Ricardo Lebensohn<sup>2</sup>; <sup>1</sup>Queen's University; <sup>2</sup>Los Alamos National Laboratory

We have investigated the anisotropy of thermal creep of cold-worked Zr-2.5Nb tubes for a range of textures and stress states. The tests were performed on internally pressurized thin-wall standard capsules at a stress of 300MPa at 350C. The stress state was modified by applying a load to the ends of the capsules to give a stress ratio of  $0.25 < \sigma_{hoop} / \sigma_{axial} < 0.75$ . The tests showed an obvious correlation of creep anisotropy with the texture. A self-consistent visco-plastic polycrystalline model (SELPOLY) based solely upon crystallographic texture showed a poor correlation with the experimental results. A modified self-consistent model is introduced to take into account different pre-existing anisotropic dislocation distributions from cold-work. The anisotropic dislocation structures are calculated using an elasto-plastic self consistent model (EPSC). Much better agreement with the experimental creep anisotropy is found, indicating that individual dislocation distributions in grains with different orientations are important in controlling the creep anisotropy.

10:20 AM Invited

**Atomistic Modeling of Deformation Twinning Mechanisms in Hcp Metals:** *Jian Wang*<sup>1</sup>; Irene Beyerlein<sup>1</sup>; Carlos Tome<sup>1</sup>; <sup>1</sup>LANL

Twin propagation and growth are responsible for the hardening and texture evolution characteristic of Mg alloys subjected to plastic deformation. Propagation, however, does not take place unless it is preceded by twin nucleation. As a consequence, understanding nucleation and accounting for it in material models is a prerequisite for understanding the constitutive response of Mg alloys. Experimental observations indicate that twin formation tends to form in suitably oriented grains, and some studies report a positive grain size effect, wherein twinning appears to form more easily in larger grains. In this talk, some fundamental issues, such as grain boundary structures, twinning dislocations, and nucleation and propagation mechanisms of twins, are discussed. Finally, we propose a comprehensive approach for understanding deformation twinning from atomic-scale to micro-scale. Such approach relies on, and relates, molecular dynamics (MD) simulations, EBSD, and a nucleation model.

10:45 AM

**Grain Size and Neighbor Grain Effects on Deformation Twinning:** *Rodney McCabe*<sup>1</sup>; Irene Beyerlein<sup>1</sup>; Carlos Tome<sup>1</sup>; <sup>1</sup>Los Alamos National Laboratory

Whether or not twins nucleate and grow in a grain depends on several microstructural characteristics of the grain and its neighbors. Grain orientation is a good predictor of the probability of twinning. However, not all grains of similar orientation exhibit twins, and a considerable fraction of

observed twins are not of the twin variant with the highest resolved shear stress based on the orientation of the grain and the bulk stress state of the material. Here we examine the role that grain size and neighbor grain attributes (neighbor orientation, grain boundary misorientation) play in this statistical nature of twinning. We examine these effects using large numbers of twin statistics developed using electron backscatter diffraction (EBSD) for {1012} twinning in magnesium, {1012} and {1122} twinning in zirconium, and {130} twinning in uranium.

**11:05 AM**

**Texture Evolution during Thermo-mechanical Processing of Zircaloy-4:** *Christabel Evans*<sup>1</sup>; *David Dye*<sup>1</sup>; *Trevor Lindley*<sup>1</sup>; *David Rugg*<sup>2</sup>; *Nicholas Jones*<sup>1</sup>; <sup>1</sup>Imperial College London; <sup>2</sup>Rolls-Royce plc.

Zirconium alloys are widely used for nuclear reactor core internals due to their low neutron absorption cross section and good corrosion resistance. Zircaloy-4 is an alpha-Zr alloy which deforms at room temperature by both slip and twinning. The textures used are engineered so as to optimize service performance. In order to understand how texture can evolve in Zr under a variety of conditions, in situ synchrotron X-ray diffraction compression and tension tests have been performed on rolled Zry-4 under varying strain rates and temperatures up to 550 °C, along with post-hoc EBSD, to understand how the deformation mechanisms change from the texture evolution. The results are interpreted with the aid of Tome's now-famous VPSC model.

**11:25 AM**

**Crystal Plasticity Based Finite Element Simulations of Deformation in AM30 Magnesium Alloy Under Complex Strain Paths:** *Adel Izadbakhsh*<sup>1</sup>; *Kaan Inal*<sup>1</sup>; *Raja Mishra*<sup>2</sup>; <sup>1</sup>University of Waterloo; <sup>2</sup>General Motors R&D Center

Deformation of AM30 magnesium alloy subjected to complex strain paths has been simulated using a Crystal Plasticity based Finite Element Method (CPFEM). A new crystal plasticity framework that satisfies equilibrium and compatibility requirements throughout the polycrystal aggregate and incorporates the interaction between twinning and slip through the kinematics of deformation has been developed. The model includes contraction and double twinning mechanisms in addition to basal and non-basal slip and extension twinning. A rate-dependent crystal plasticity constitutive law calibrated with uniaxial tension and compression data at room temperature and at 2000C is implemented in a User defined MATerial subroutine (UMAT) in LS-DYNA. The deformation pattern of AM30 tubes, especially the initiation and propagation of localization during the "Ring Hoop Tension Test", simple shear and pure bending has been simulated. Simulations show that neglecting contraction and double twinning can significantly delay/defer the initiation of localized deformation and its propagation.

**11:45 AM**

**Experimental and Simulation Studies on the Evolution of Rolling Texture in a Two Phase Titanium Alloy:** *Nilesh Gurao*<sup>1</sup>; *Satyam Suwas*<sup>1</sup>; <sup>1</sup>Indian Institute of Science, Bangalore

The evolution of deformation texture and microstructure during rolling of a two phase (α+β) titanium alloy with a nominal composition Ti-13Nb-13Zr has been studied. Two different morphologies, namely, colony and equiaxed, were generated by suitable heat treatments prior to rolling. Microstructural evolution was examined using Electron Back Scatter Diffraction (EBSD) and textures were measured by X-ray diffraction. A characteristic texture evolution was noted in both the HCP α and the BCC β phase irrespective of the different initial morphology. The evolution of higher intragranular misorientations in the β phase indicates that the softer β phase carries most of the strain. Texture evolution was simulated using viscoplastic self-consistent (VPSC) model. The experimental textures were successfully reproduced using VPSC simulations that incorporated the different initial morphologies of both the phases.

**12:05 PM**

**Hardening Mechanisms upon Profuse Twinning in Pure Magnesium:** *Andrew Oppedal*<sup>1</sup>; *Haitham El Kadiri*<sup>1</sup>; *Carlos Tomé*<sup>2</sup>; *James Baird*<sup>1</sup>; *Sven Vogel*<sup>2</sup>; *George Kaschner*<sup>2</sup>; *Mark Horstemeyer*<sup>1</sup>; <sup>1</sup>Mississippi State University; <sup>2</sup>Los Alamos National Laboratory

Textured hexagonal close packed double-lattice structures show stronger anisotropy than textured single-lattice structures. The reason lies behind the necessity to activate glide twinning and hard slip dislocation modes. Although the mechanisms behind activation of dislocations with non-basal Burgers vectors are still not fundamentally understood, the effect of twinning on hardening presents the most substantial challenge to polycrystal plasticity modelers. The origin of the increasing strain hardening rate regime (Regime II) upon profuse twinning is still not fundamentally clear. Previous successful attempts to fit stress-strain behavior based on a Hall-Petch effect by twin segmentation led to discrepancies in predicting intermediate textures and/or twin volume fraction evolution. A recent dislocation-based hardening rule incorporated into the Visco-Plastic Self-Consistent (VPSC) model allows slip and twinning to be physically coupled in the simulations. In this paper, we investigate hardening mechanisms in pure magnesium and apply a dislocation based formalism to model anisotropy.

**12:25 PM**

**Micromechanical Model of Metals and Alloys of Low Symmetry Deforming by Slip and Twinning:** *Katarzyna Kowalczyk-Gajewska*<sup>1</sup>; <sup>1</sup>Institute of Fundamental Technological Research, Warsaw

The micromechanical model of finite plastic deformations of polycrystalline materials of low symmetry, characterized by high specific strength, is presented. As concerns texture evolution the model accounts for appearance of new twin related orientations using a new reorientation scheme called Probabilistic Twin Volume Consistent scheme. It takes into account the history of the deformation process and maintains the volume fraction of reoriented grains at a level consistent with the shear activity of twins contributing to the deformation. Within the proposed framework the hardening rule describing slip-twin interactions is developed. Evolution of critical shear stress for slip due to twin activity is described by the rule accounting for geometrical effects of twin boundaries in reducing main free path distance for dislocations. It also takes into account the lamellar substructure of single grain which evolves during twinning. Model predictions are verified for titanium alluminide intermetallic of near gamma microstructure and magnesium.

---

## Processing and Properties of Powder-Based Materials: Current-Activated and Conventional Sintering

*Sponsored by:* The Minerals, Metals and Materials Society, TMS Materials Processing and Manufacturing Division, TMS: Powder Materials Committee

*Program Organizers:* K. Morsi, San Diego State University; Ahmed El-Desouky, San Diego State University

Tuesday AM  
March 1, 2011

Room: 33A  
Location: San Diego Conv. Ctr

*Session Chair:* Javier Garay, University of California-Riverside

---

**8:30 AM Introductory Comments**

**8:35 AM Keynote**

**Coarsening Models Applicable to Sintering:** *Randall German*<sup>1</sup>; <sup>1</sup>San Diego State University

Treatments of sintering are analyzed to show grain size is determined by the microstructure contiguity during densification. Grain size determines the sintering rate. Thus, not only do properties pivot around grain size, but the rate of sintering traces to control of the interfaces during sintering. With nanoscale powders there is more demand for controlled coarsening during

TUESDAY AM

sintering. This treatment shows a simple model that links grain growth to interfacial features - pores, liquids, dispersoids, or other second phases. Since sintering converges toward a self-similar grain shape and grain size distribution, most of the relations are fairly simple. Then grain growth rates are predicted based on the fraction of each interface and the transport events associated with the evolving solid-liquid-vapor microstructure. Reviews of data from classic experiments to recent nanoscale SPS experiments are used to illustrate the model. Means to densify without extensive coarsening are extracted from the model.

### 9:05 AM

**Challenges in the Scalability of Field Assisted Sintering:** *Chris Haines*<sup>1</sup>; Darold Martin<sup>1</sup>; Deepak Kapoor<sup>1</sup>; William Bradbury<sup>2</sup>; Eugene Olevsky<sup>2</sup>; <sup>1</sup>US Army ARDEC; <sup>2</sup>San Diego State University

Field-Assisted Sintering Technology (FAST) aka Spark Plasma Sintering (SPS) is a revolutionary, game-changing technology which provides the ability to consolidate materials to full density in minutes, as opposed to hours with conventional sintering techniques. To date, most research has reported on sample sizes in the range of a few centimeters to a few inches. In order for the technology to mature as a viable manufacturing technology in the industrial base, significant scale-up is required. Scaling of such a highly energetic sintering technology is not trivial and presents many challenges. We have observed, both experimentally and in our modeling, a significant dependence on factors such as sample dimensions, geometry, and die design on the temperature and current distribution during sintering. These effects can subsequently be seen in the resulting microstructure of the sintered specimens. Proposed solutions to these challenges will be discussed.

### 9:25 AM

**Cryomilled Commercially Pure Ti Consolidated via Spark Plasma Sintering:** *Osman Ertoer*<sup>1</sup>; Troy Topping<sup>1</sup>; Ying Li<sup>1</sup>; Wes Moss<sup>2</sup>; Enrique Lavernia<sup>1</sup>; <sup>1</sup>University of California - Davis; <sup>2</sup>TRD

Cryomilled nanocrystalline CP-Ti powders were spark plasma sintered (SPS) using varied process parameters (i.e., heating rate, temperature, pressure, and dwell time) in order to study densification, microstructure, and mechanical behavior. Results were rationalized on the basis of the relevant literature and experimental results, and they reveal a strong dependence on SPS parameters. An interesting finding was that the measured high ductility was accompanied by a moderate strength (YS > 700 MPa, UTS > 840 MPa with elongation to failure values larger than 20%). The strain rate sensitivity of produced samples was also studied. The combinations of microstructure and mechanical response were attributed to the multi-step processing using various SPS parameters as well as to the presence of interstitial solutes introduced during cryomilling.

### 9:45 AM

**Microstructural Characterization of Mechanically Alloyed Lanthana-Bearing Oxide Dispersion Strengthened Steels:** *Somayeh Pasebani*<sup>1</sup>; Indrajit Charit<sup>1</sup>; Kerry Allahaar<sup>2</sup>; Brian Jaques<sup>2</sup>; Darryl Butt<sup>2</sup>; James Cole<sup>3</sup>; <sup>1</sup>University of Idaho; <sup>2</sup>Boise State University; <sup>3</sup>Idaho National Laboratory

Oxide dispersion strengthened (ODS) alloys are being considered for advanced reactor applications due to their excellent creep and radiation damage resistance imparted primarily due to the presence of fine oxide particles. The objective of this study is to develop a new ODS alloy by mechanical alloying (MA) followed by spark plasma sintering (SPS). Different amounts (0-1 wt.%) of lanthanum oxide were mixed with a base alloy composition of Fe-14Cr-0.9Ti-0.3Mo (in wt.%) and processed via MA for different durations using the stainless steel milling media. Differential scanning calorimetry (DSC) was performed on the MA powders to study the kinetics of any phase transformation occurring. Further, detailed phase analysis was carried out using X-ray diffraction (XRD). Scanning electron microscopy (SEM) was also used to determine the particle size, shape and distribution. SPS will be used to produce the bulk ODS samples and characterized for microstructure and mechanical properties.

### 10:05 AM

**Spark Plasma Sintering of Ultra-Fine Grained and Nanocrystalline WC Based Hard Metals:** *Milan Dopita*<sup>1</sup>; David Chmelik<sup>1</sup>; Anton Salomon<sup>1</sup>; C. Sriram<sup>2</sup>; Hans Seifert<sup>1</sup>; <sup>1</sup>Technical University of Freiberg; <sup>2</sup>National Institute of Technology Tiruchirappalli

Modern trends in the materials research emphasizing the increase of the materials serving life-time tend to the preparation of the materials with nanocrystalline microstructure as it has been shown that nanocrystalline hard metals have better mechanical properties in comparison to their coarse-grained counterparts. In our work we focused on sintering of the nanocrystalline WC based hard metals using the spark plasma sintering method. Two types of materials i) WC-Co composites and ii) binderless WC were studied. The main accent was focused on the study of individual sintering parameters (temperature, time and pressure) and their correlations with sintered specimens microstructure and mechanical properties. Sintered specimens were investigated using XRD, SEM/EBSD, TEM/HRTEM, hardness and fracture toughness measurements. We derived favourable conditions for sintering of fully dense nanocrystalline hard metals and proved that the specimens sintered using these conditions have significantly improved mechanical properties in comparison to classical coarse grained hard metals.

### 10:25 AM Break

### 10:35 AM

**Preliminary Investigations in Current-Activated Tip-Based Sintering (CATS): Modeling and Experiments:** *A. El-Desouky*<sup>1</sup>; S.K. Kassegne<sup>1</sup>; K.S. Moon<sup>1</sup>; K. Morsi<sup>1</sup>; <sup>1</sup>San Diego State University

Spark Plasma Sintering (SPS) has emerged as a process with unique advantages such as lower sintering temperatures and shorter holding times than conventional sintering, in addition to the production of materials with unique microstructures and properties. However, the process has been largely limited to the production of bulk materials with simple geometries on a relatively moderate size scale. In this presentation preliminary experimental and modeling results on novel current-activated tip-based sintering (CATS) powder compacts are presented. CATS enables the selective sintering of micro-scale (and potentially nano-scale) features using a moving or stationary (electrically conductive) tip configuration. Preliminary finite element modeling results on current and temperature distributions under typical CATS conditions is also presented, in addition to a discussion on the versatility and extended applications of this new process.

### 10:55 AM

**The Role of Sintering Methods (HP & SPS) on Substructure and Its Correspondence on Creep Properties in Alumina Based Ceramic Materials:** *Ebrahim Karamian*<sup>1</sup>; Alain Bataille<sup>2</sup>; Ahmad Monshi<sup>3</sup>; Ehsan Mohamadi Zahrani<sup>4</sup>; <sup>1</sup>Isfahan University of Technology; <sup>2</sup>UMET, Unité Matériaux et Transformations, UMR CNRS 8207, University of Lille Science and Technology; <sup>3</sup>Department of Materials Engineering, Isfahan University of Technology; <sup>4</sup>Department of Materials Engineering, University of British Columbia

Spark plasma sintering method (SPS) is more than a decade to be an interesting alternative to classical densification processes for ceramic materials. Owing to the advantage of rapid heating, the alumina ceramics obtained by SPS have a grain size and density comparable to those of HPed ones. This paper describes the effect of HP & SPS on substructure and its correspondence on creep properties in alumina based ceramic materials. Pure alumina (SM8, Baikowski) was densified SPS at 65 MPa (1200°C) and 45 MPa (1450 °C) by HP (hot pressing). The grain size of the HP alumina was more twice coarser than the grain size of SPS sample. The grain growth is more active during creep of SPS alumina (1300 °C,  $\sigma = 30$  MPa) than of HP alumina. Generally, the fineness of SPS materials microstructure shall speed up all processes related to diffusion. So, creep resistance shall be decreased.



11:15 AM

### Spark Plasma Sintering of Ferritic Oxide Dispersion Strengthened

**Alloys:** Kerry Allahar<sup>1</sup>; Jatuporn Burns<sup>1</sup>; Brian Jaques<sup>1</sup>; Indrajit Charit<sup>2</sup>; Darryl Butt<sup>1</sup>; James Cole<sup>3</sup>; <sup>1</sup>Boise State University; <sup>2</sup>University of Idaho; <sup>3</sup>Idaho National Laboratory

Oxide Dispersion Strengthened (ODS) alloys are candidate cladding materials due to their resistance to radiation, thermally induced creep, and swelling. Conventional powder metallurgy consolidation techniques have been primarily used in the development of ferritic ODS alloys with limited application of spark plasma sintering (SPS). Sintering by SPS is achieved by Joule heating using a pulsed DC coupled with uni-axial pressure. Advantages of SPS include faster heating rates, uniform heating condition, lower sintering temperature and shorter dwell time. The influences of SPS processing parameters on the microstructural evolution are presented for two pre-alloyed Fe/Cr/Al and Fe/Cr/Mo powders where the composition of Y<sub>2</sub>O<sub>3</sub> was varied (0 to 0.5%). Parameters included temperature (600 to 1100 oC), dwell time (5 to 30 minutes) and heating rate (50 to 200 oC/min). Characterization of the grain sizes and boundaries was performed using EBSD and SEM and the fate of the ceramic dispersions was studied using TEM.

11:35 AM

**Characteristics of Tin/Fe Cermet Fabricated by Mechanical Milling and Pulse Current Sintering:** Hiroyuki Nakayama<sup>1</sup>; Keizo Kobayashi<sup>1</sup>; Kotaro Kikuchi<sup>2</sup>; <sup>1</sup>National Institute of Advanced Industrial Science and Technology; <sup>2</sup>SS Alloy Co., Ltd.,

Titanium nitride (TiN) shows poor wettability with various liquid metals, thus the fabrication of TiN based cermets is difficult using conventional sintering. Therefore, in this study, we examined the fabrication of TiN based cermet by mechanical milling and subsequent pulse current sintering. The Fe as a binder phase was selected, because it is one of the most economical elements. The TiN powder (70 mass%) and Fe powder (30 mass%) were mechanically milled for 28.8 ks using planetary ball milling under Ar atmosphere. Subsequently, the milled powder was successfully consolidated using pulse current sintering method at 1473 K for 300 s under 60 MPa. The sintered compact was composed of TiN and Fe defined by X-ray diffraction, and the hardness achieved to HRA 91.5.

## Recent Developments in the Processing, Characterization, Properties and Performance of Metal Matrix Composites: Processing, Microstructure and Mechanical Properties I

**Sponsored by:** The Minerals, Metals and Materials Society  
**Program Organizers:** Martin Pech-Canul, Centro de Investigacion y de Estudios Avanzados del Instituto Politecnico Nacional; Zariff Chaudhry, Arkansas State University; Golam Newaz, Wayne State University

Tuesday AM  
March 1, 2011

Room: 6A  
Location: San Diego Conv. Ctr

**Session Chair:** Martin Pech-Canul, Cinvestav Saltillo

8:30 AM

**Effects of Zr on the Microstructure and Tensile Properties of Al-15wt%Mg2Si Metal Matrix Composite:** Ahmad Razaghian<sup>1</sup>; Amin Bahrami<sup>1</sup>; Masoud Emamy<sup>2</sup>; Nargues Nemati<sup>3</sup>; Hamid Reza Jafari Nodoshan<sup>4</sup>; <sup>1</sup>Imam Khomeini International University; <sup>2</sup>Center of Excellence for High Performance Materials, School of Metallurgy and Materials, University of Tehran; <sup>3</sup>Sahand University of Technology; <sup>4</sup>Islamic Azad University

The effects of Zr modification on the microstructure and tensile properties of an in situ prepared Al-15wt%Mg<sub>2</sub>Si composite have been investigated. Microstructural examinations were conducted by optical and scanning electron microscopy equipped with energy dispersive spectrometry. The optimum amount of Zr was selected as 1 wt. %. It was found that the addition

of Zr reduces the average size of Mg<sub>2</sub>Si primary particles. Adding Zr also raised both tensile strength (from 240MPa to 300MPa) and elongation values (from 2.4 to 6%). Fractographic examination of the unmodified composite also showed that large Mg<sub>2</sub>Si particles are responsible for fracture behavior.

8:50 AM

**Investigation of Wear Properties of Hot Extruded Al-15wt%Mg2Si In-Situ Metal Matrix Composite:** Hamid Reza Jafari Nodoshan<sup>1</sup>; Masoud Emamy<sup>2</sup>; Amin Bahrami<sup>3</sup>; Ashkan Zolriasatein<sup>4</sup>; <sup>1</sup>Islamic Azad University; <sup>2</sup>University of Tehran; <sup>3</sup>Imam Khomeini International University; <sup>4</sup>K. N. Toosi University of Technology

In recent years, lightweight metal matrix composites (MMC) have received wider attention for their technological application, such as automotive parts etc. For structural application, the wear properties are considered to be one of the major factors controlling the performance. In this study wear behavior of Al based composites reinforced with in-situ Mg<sub>2</sub>Si particles have been investigated. The composite was prepared by casting followed by extrusion at various temperatures with different ratio. The wear behavior of sample was investigated using a pin-on-disk technique under an applied load of 10N. In the extruded samples, the composite exhibited superior wear resistance than as cast in-situ composite.

9:10 AM

**Microstructural Development of Al-15wt.%Mg2Si in Situ Composite with Be Addition:** Mortaza Azarbarmas<sup>1</sup>; Masoud Emamy<sup>1</sup>; Jafar Rassizadehghani<sup>1</sup>; Mohammad Alipour<sup>1</sup>; Mostafa Karamouz<sup>1</sup>; <sup>1</sup>University of Tehran

In this study, the effects of Be additions on the microstructural development of an in situ Al-15wt.%Mg<sub>2</sub>Si composite were investigated. A study of the specimen's surfaces via scanning electron microscope (SEM) and optical microscope revealed that with increasing Be additions in the composites, the average size of primary Mg<sub>2</sub>Si particles was reduced, and that the amount of alpha phase surrounding the Mg<sub>2</sub>Si particles was increased, with a little change in morphology of this particles. Meanwhile the morphology of pseudo-eutectic phase was changed.

9:30 AM

**Microstructural Properties and Wear Behaviour of AlSi9Mg Matrix B4Cp Reinforced Composites:** Fatih Toptan<sup>1</sup>; Isil Kerti<sup>1</sup>; Ahmet Sagin<sup>1</sup>; Mustafa Cigdem<sup>1</sup>; Sibel Daglilar<sup>1</sup>; Fatih Yuksel<sup>1</sup>; <sup>1</sup>Yildiz Technical University

In the present work, AlSi<sub>9</sub>Mg alloy matrix composites reinforced with 10, 15 and 20% (wt.) B<sub>4</sub>Cp were produced by casting route at 850 °C. Titanium-containing flux (K<sub>2</sub>TiF<sub>6</sub>) was used to overcome the wetting problem between B<sub>4</sub>C and liquid aluminium metal. The microstructure of matrix/reinforcement interfaces were investigated with SEM studies. The reaction layer was also characterized with EDS analysis and X-ray mapping. It was found from the microstructural observations by high resolution field emission gun SEM (FEG-SEM) that the wetting improved by the formation of very thin (80-180 nm in thickness) TiC and TiB<sub>2</sub> reaction layers. The samples were subjected to pin-on-disc wear tests against AISI 4140 pin under dry sliding conditions. The worn surface was studied through SEM and EDS analysis. It has seen that, wear resistance increased as particle volume fraction increased.

9:50 AM

**Modification of Al-Mg2Si In Situ Composite by Boron:** Mortaza Azarbarmas<sup>1</sup>; Masoud Emamy<sup>1</sup>; Jafar Rassizadehghani<sup>1</sup>; Mostafa Karamouz<sup>1</sup>; Mohammad Alipour<sup>1</sup>; <sup>1</sup>University of Tehran

In this work, the effects of B additions on the microstructural development of an in situ Al-15wt.%Mg<sub>2</sub>Si composite were investigated. It was found from scanning electron microscope (SEM) and optical microscope images that with increasing B additions in the composites, the average size of primary Mg<sub>2</sub>Si particles was reduced, and that the amount of alpha phase surrounding the Mg<sub>2</sub>Si particles was increased. Meanwhile with the addition of B the pseudo-eutectic Al-Mg<sub>2</sub>Si was formed in a regular morphology

TUESDAY AM

in cells separated with the alpha phase. Moreover, a small amount of B-containing compounds were formed as a result of B additions .

#### 10:10 AM Break

#### 10:30 AM

**The Influence of Li on the Microstructure and Mechanical Properties of Hot Extruded Al-Mg<sub>2</sub>Si Metal Matrix Composite:** Amin Bahrami<sup>1</sup>; Masoud Emamy<sup>2</sup>; Ahmad Razaghian<sup>1</sup>; Hamid Reza Jafari Nodooshan<sup>3</sup>; Ashkan Zolriasatein<sup>4</sup>; <sup>1</sup>Imam Khomeini International University; <sup>2</sup>University of Tehran; <sup>3</sup>Islamic Azad University; <sup>4</sup>K. N. Toosi University of Technology

This article investigates the effect of Li as modifier on microstructure and mechanical properties of hot extruded the In-situ Al-15wt%Mg<sub>2</sub>Si composite. This composite have already been introduced as a new class of light materials but the brittle structure of the primary Mg<sub>2</sub>Si which is formed during solidification of these composites limits its application. Modified composite was directly extruded as rod by using three different dies with diameters 20, 10 and 5 mm and various temperature. Microstructures after this type of extrusion was studied by optical microscopy. Mechanical properties of the composite after various extrusions were tested by hardness and tensile tests. The results showed that Li addition were highly effective in reducing Mg<sub>2</sub>Si particle size from 30µm to about7µm and affects to the flow of material during the extrusion process and mechanical properties of extruded samples.

#### 10:50 AM

**Characterization of Composite Materials Interface Aimed to Suppress Vibration in Cast Parts:** M. David Hanna<sup>1</sup>; Shung Sung<sup>1</sup>; <sup>1</sup>General Motors

Damping performance of inserted castings is critically dependent on the nature of the interface between the insert and the casting. This investigation involved an attempt to analyze sound data over a wide frequency range and assess the damping performance with different insert coating properties for a grey cast iron component. Based on the measured frequency response function, characteristic damping behavior of different coatings has been identified. The graphite base coating material showed enhanced sound damping properties compared to another refractory type material when applied to a steel insert. The parts with the graphite-based coated inserts have shown significant improvements in: (a) modal frequency reduction, (b) sound pressure level (SPL) reduction at the most dominant circumferential modes, (c) 1/3 octave band SPL reduction over wide frequency bands and finally (d) a modal damping ratio increase.

#### 11:10 AM

**In-Situ Synthesis of AlN/Mg Matrix Composites:** Xiao Ma<sup>1</sup>; Salin Kuplin<sup>1</sup>; David Johnson<sup>1</sup>; Kevin Trumble<sup>1</sup>; <sup>1</sup>Purdue University

Magnesium matrix composites with AlN reinforcements are potential engineering materials for automobile and aerospace applications. Attractive properties of AlN include high thermal conductivity and hardness. AlN-reinforced Mg composites have been synthesized by in-situ reaction using pure Al and AZ31B and Si<sub>3</sub>N<sub>4</sub> powder as raw materials. Microstructures containing 15 vol.% AlN were obtained by heating the raw materials at 770°C for one hour under argon atmosphere. Composite microstructures were characterized by X-ray diffraction, optical microscopy, scanning electron microscopy. Final microstructures consisted of AlN particles 1-5 µm in size distributed within the Mg alloy matrix.

#### 11:30 AM

**Performance Evaluation of Particulate Reinforced Al-SiC Bolted Joints:** Gergis William<sup>1</sup>; Samir Shoukry<sup>1</sup>; Jacky Prucz<sup>1</sup>; <sup>1</sup>West Virginia University

The increasing requirements of weight savings and extended durability motivated the potential application of metal matrix composite technology into the heavy vehicle market. However, significant technical barriers such as joining are likely to hinder the broad applications of MMC materials in heavy vehicles. This paper examines the feasibility of manufacturing and the behavior of bolted joint connections made from aluminum reinforced with silicon carbide particles. Initially, the study concentrates on experimental evaluation of bolted joints of 20% and 45% MMC material. The behavior of joints is studied as a function of various design parameters. Then, a finite

element model is generated to predict the behavior of a double-lap joint of the same material. It is seen that experimental and numerical results agree well with each other. The results indicate that MMC joints are likely to fail early in the bearing mode, because of the brittle behavior of MMC materials.

#### 11:50 AM

**Synthesis and Mechanical Behavior of Ultrafine-Grained Al-B4C Composites:** Zhihui Zhang<sup>1</sup>; Ying Li<sup>1</sup>; Troy Topping<sup>1</sup>; Rustin Vogt<sup>1</sup>; Yizhang Zhou<sup>1</sup>; Julie Schoenung<sup>1</sup>; Enrique Lavernia<sup>1</sup>; <sup>1</sup>University of California Davis

The study of Al based ultrafine-grained (UFG) composites is prompted by the objective to develop ultrahigh strength (>1000 MPa), low density materials that also possess attractive high strain rate behavior. In this study, UFG Al/B<sub>4</sub>C composites with a B<sub>4</sub>C reinforcement size of ~1 µm and ~50 nm, respectively, were produced via cryomilling followed by consolidating via HIP and extrusion. The results showed that the mechanical milling process led to a homogeneous distribution of the micro- and nano-particles in the matrix and the matrix had an average grain size of ~300 nm after consolidation. HRTEM revealed a clean Al/B<sub>4</sub>C interface and no detrimental interfacial phase or defects such as voids were observed. The mechanical behavior of the UFG composites were studied and the strengthening mechanisms were discussed in the frame work of load transfer, Hall-Petch strengthening, geometry necessary dislocation strengthening and dispersion strengthening.

### Shape Casting IV: Light Metals Division Symposium in Honor of Prof. John T. Berry: Modeling

*Sponsored by:* The Minerals, Metals and Materials Society, TMS Light Metals Division, TMS: Aluminum Processing Committee, TMS: Solidification Committee

*Program Organizers:* Murat Tiryakioglu, University of North Florida; Paul Crepeau, General Motors Corporation; John Campbell, University of Birmingham

Tuesday AM  
March 1, 2011

Room: 15B  
Location: San Diego Conv. Ctr

*Session Chairs:* Mark Jolly, Univ of Birmingham; Daan Maijer, Univ of British Columbia

#### 8:30 AM Introductory Comments

#### 8:40 AM

**The History of Casting Process Simulation:** Christof Heisser<sup>1</sup>; <sup>1</sup>MAGMA Foundry Technologies, Inc.

An overview of significant steps in the development of casting process simulation will depict its development from simple "solidification-only" tools to comprehensive casting process simulation tools, which are irreplaceably integrated in the current product development process. The presentation will include topics like autonomous optimization and transfer of simulation results to FEA and lifetime prediction tools.

#### 9:05 AM

**State of the Art Review of Modelling Entrainment Defects in the Shape Casting Process:** Carl Reilly<sup>1</sup>; Nick Green<sup>2</sup>; Mark Jolly<sup>2</sup>; <sup>1</sup>University of British Columbia; <sup>2</sup>University of Birmingham

Entrainment of oxide films into liquid metals has been shown to be detrimental to casting integrity. A number of mechanisms have been shown to initiate the entrainment of oxide films including returning waves, plunging jets, bubble trails and fountains. Computational fluid dynamics (CFD) software packages allow foundry staff to improve casting systems using qualitative parameters. Optimization software is now a viable option for foundries. It does, however, require a measurable parameter which allows the quantification of defects. This is becoming an important research area to allow the optimization software manufacturers to meet the needs of industry. The current methods of modeling surface film and bubble generated casting

defects have been described and critically reviewed shedding light on the qualities and issues currently associated with the present available methods. However, it is clear that further investigations and developments are still required to allow the accurate and efficient modeling of casting defects.

**9:30 AM**

**Physical and Computational Models of Free Surface Related Defects in Low-Pressure Die-Cast Aluminum Alloy Wheels:** *Jianglan Duan*<sup>1</sup>; *Daan Maijer*<sup>1</sup>; *Steve Cockcroft*<sup>1</sup>; *Carl Reilly*<sup>1</sup>; *Ken Nguyen*<sup>2</sup>; *Dominic Au*<sup>2</sup>; <sup>1</sup>University of British Columbia; <sup>2</sup>Canadian Autoparts Toyota, Inc.

A water analogue model has been used to simulate the free surface behavior during mould filling of a low-pressure die-cast (LPDC) wheel. The water analogue has been used to validate a mathematical model of the filling process. A transparent die was manufactured with a 2D profile extracted from a typical production die, and the experimental parameters used were based upon the production process. The flow occurring in the model was recorded with camera. A mathematical model of the filling process was developed to reproduce the behavior observed in the water model. Both the experimental and modeled results have shown a relative tranquil fill of the sprue and the rim, while persistent returning waves were developed in the spoke. The results highlight the significant effects of venting, both in the water model and computational model. Future work is required to improve the accuracy of venting modeling of the mould cavity.

**9:55 AM**

**Solidification Model Coupling Lattice Boltzmann Method with Cellular Automaton Technique:** *Hebi Yin*<sup>1</sup>; *Liang Wang*<sup>2</sup>; *Sergio Felicelli*<sup>1</sup>; <sup>1</sup>Mississippi State University; <sup>2</sup>Mississippi State University

A two dimensional model combining the lattice Boltzmann method (LB) and the cellular automaton technique (CA) was developed to simulate dendrite growth during solidification. The LB method was used for the coupled-calculation of temperature, composition, and velocity fields while the liquid/solid interface was tracked by the CA method. The LB-CA model was validated by comparing tip velocity and equilibrium composition with analytical solutions. Single and multi- dendrite growth was simulated with energy and solute transport not only by diffusion but also by convection. In addition, the simulation morphology and computational time obtained with the LB-CA model was compared to that of a finite element – CA model.

**10:20 AM Break**

**10:40 AM**

**Physical Characterization of the Permeability of Equiaxed Eutectic Structures in Hypoeutectic Aluminum Alloys:** *Ehsan Khajeh*<sup>1</sup>; *Daan Maijer*<sup>1</sup>; <sup>1</sup>University of British Columbia

The permeability of hypoeutectic aluminum alloys during equiaxed eutectic solidification has been determined through physical modeling. The 3D geometries of primary phase obtained from X-ray microtomography (XMT) scans of solidified aluminum alloys have been used to generate computational domains for use in simulating the eutectic transformation. By applying the Cellular Automaton technique to simulate the growth of eutectic colonies, the evolution of the liquid channels has been modeled. Large-scale analogues of the simulated structures were produced by rapid prototyping for use as physical models. A glycerin-based solution was passed through the physical models and the permeability was calculated from measurements of the discharge flow rate and pressure drop. This work presents an alternative technique to determine permeability compared to conventional permeameters and shows a deviation from the conventional Carman-Kozeny expression at high eutectic grain density.

**11:05 AM**

**Foam Filters Used in Gravity Casting:** *Fu-Yuan Hsu*<sup>1</sup>; *Huey-Juan Lin*<sup>1</sup>; <sup>1</sup>National United University

Ceramic foam filters are normally used for reducing the velocity of liquid metal in the design of runner system. In this study four designs of runner systems with various orientations of foam filters were explored and their apparent velocities were estimated by casting experiment and computational modeling. In the casting experiment, trajectory and metal weighing methods

were employed for measuring apparent velocity and flow rate, respectively. Using Forchheimer's equation, a porous material such as a foam filter could be simulated in the modeling. The modeling result was validated by the casting experiment. For high efficient usage of a foam filter, through which liquid metal with high flow rate and low velocity was transformed, the optimized design is recommended in all of runner systems.

**11:30 AM**

**Simulation of Macrosegregation during Directional Solidification Using Mesh Adaptation:** *Udaya Sajja*<sup>1</sup>; *Sergio Felicelli*<sup>1</sup>; <sup>1</sup>Mississippi State University

Modeling of the formation of macroscopic segregation channels during directional solidification processes has important applications in the casting industry. Computations that consider thermosolutal convection involve different length scales ranging from the small solute boundary layer at the dendrite tips to the characteristic size of the casting. In general, numerical models of solidification in the presence of a developing mushy zone are computationally inefficient due to nonlinear transport in an anisotropic porous medium. In the present work, mesh adaptation with triangular finite elements is used in conjunction with an efficient fractional-step solver of the momentum equations to predict the occurrence of channel-type segregation defects or freckles. The triangulations are created dynamically using an unstructured grid generator and a refinement criterion that tracks the position of the channel segregates. The efficiency of mesh adaptation is illustrated with simulations showing channel formation and macrosegregation in directional solidification of a Pb-Sn alloy.

**11:55 AM**

**A Mathematical Model for Simulating the Microporosity of Squeeze Casting of Aluminum Alloy:** *Zhiqiang Han*<sup>1</sup>; *Jinxi Li*<sup>1</sup>; *Wen Yang*<sup>1</sup>; *Baicheng Liu*<sup>1</sup>; <sup>1</sup>Tsinghua University

A mathematical model for simulating the microporosity of squeeze casting of aluminum alloy has been developed, in which the heat transfer, solidification shrinkage, feeding flow, pressure transfer, and hydrogen conservation were taken into account. The shrinkage induced flow and the pressure drop in the mushy zone were calculated by solving continuity and momentum equations. A mechanical model was solved for obtaining the pressure transferred into the liquid core of the casting. By coupling the pressure drop and the pressure transferred into the liquid core, the pressure in the mushy zone was calculated. Based on the hydrogen conservation equation, the microporosity volume fraction was estimated by referring to the pressure in the mushy zone. The squeeze casting processes of aluminum alloy under different process conditions were simulated and the simulation results were compared with experimental results for assessment of the developed model.

---

### Size Effects in Mechanical Behavior: In Situ Characterization to Understand Mechanically Driven Size Effects

*Sponsored by:* The Minerals, Metals and Materials Society, Not Applicable, TMS: Nanomechanical Materials Behavior Committee  
*Program Organizers:* Erica Lilleodden, GKSS Research Center; Amit Misra, Los Alamos National Laboratory; Thomas Buchheit, Sandia National Laboratories; Andrew Minor, UC Berkeley & LBL

Tuesday AM  
March 1, 2011

Room: 2  
Location: San Diego Conv. Ctr

*Session Chairs:* Andrew Minor, UC Berkeley; Jun Lou, Rice University

---

**8:30 AM Invited**

**Quantitative In-situ TEM to Investigate Defect – Strength Relations:** *Daniel Kiener*<sup>1</sup>; <sup>1</sup>Austrian Academy of Science & University of Leoben

While reports consistently find that 'smaller is stronger', the governing mechanisms remain elusive due to lack of direct observations. *In-situ*

TUESDAY AM



TEM testing is ideally suited to provide this missing information, as the governing dislocation processes can be directly monitored. Experiments on FIB prepared samples depict that deformation is source controlled for compression samples, leading to single-slip deformation of small specimens oriented for multi-slip. With a novel tensile approach, we exclude effects from specimen taper and other compression boundary conditions and observe defect exhaustion with ongoing straining, resulting in strengths reported for whiskers. Significant changes in the 'mechanical annealing' behavior were observed for pre-deformed or proton irradiated samples. The proton irradiated material changes from a source controlled size-dependent strength at small dimensions to a size-independent strength governed by dislocation-defect interactions. Using *in situ* annealing, we achieved defect-free samples, which deformed at stresses near the theoretical strength of the material.

#### 9:00 AM

**Insights into Mg Plasticity From In Situ Nanomechanical Testing in the TEM:** *Qian Yu*<sup>1</sup>; Raj Mishra<sup>2</sup>; Andrew Minor<sup>3</sup>; <sup>1</sup>University of California Berkeley; <sup>2</sup>General Motors Corporation; <sup>3</sup>University of California Berkeley & Lawrence Berkeley National Laboratory

Magnesium is a lightweight metal that would be much more useful for structural applications than it currently is if not for its complicated and anisotropic plastic deformation behavior. The HCP structure of Mg has limited dislocation slip systems and, thus, twinning generally accompanies dislocation plasticity. Recently, we have run a series of *in situ* mechanical tests in a TEM on pure Mg where we have quantitatively measured and characterized the deformation behavior in both compression and in tension, and in both basal slip and non-basal slip orientations. By comparing the quantitative deformation behavior in these experiments we are able to provide significant insights into the twinning mechanisms and the origins of the compression-tension asymmetry in Mg.

#### 9:20 AM Invited

**In Situ TEM Studies of Plastic Deformation in Small-Volume Samples near Room Temperature:** *Evan Ma*<sup>1</sup>; <sup>1</sup>Johns Hopkins University

This talk reports on *in situ* TEM investigations of size effects in mechanical behavior carried out at our new research center, Center for Advancing Materials Performance from the Nanoscale (CAMP-Nano), founded in 2009 at XJTU. Recent projects at CAMP-Nano, led by Prof. Z. W. Shan, Prof. Ju Li and the speaker, have yielded interesting results. In this short talk, we will briefly describe two representative ongoing studies. For crystalline materials, an example will be given regarding the strong sample size effect on deformation twinning in a Ti alloy (Q. Yu et al., Nature 2010), illustrating a Hall-Petch type of dependence of deformation twinning on crystal size. For glassy materials, amorphous silica will be discussed as an example, demonstrating superplastic flow of nano-sized silica glass wires and particles near room temperature inside a TEM (in collaboration with K. Zheng, X.D. Han, Z. Zhang et al. at BJUT, Nature Communications, 2010).

#### 9:50 AM

**Dislocation Nucleation in Confined Crystalline Volumes: In-Situ TEM Observations and Micro-Mechanical Tests on Submicron Al Fibers:** *Frederic Mompiou*<sup>1</sup>; Marc Legros<sup>1</sup>; Daniel Caillard<sup>1</sup>; Daniel Gianola<sup>2</sup>; Andreas Sedlmayr<sup>3</sup>; Oliver Kraft<sup>3</sup>; <sup>1</sup>CEMES-CNRS; <sup>2</sup>University of Pennsylvania; <sup>3</sup>Karlsruher Institut für Technologie

Small crystals have an initial resistance to deformation much larger than their bulk counterpart, but the physical explanations for this multiplied yield stress are still highly debated. One critical step seems to be the nucleation of fresh dislocations and the nature of the sources. In the present work we present an extensive *in situ* TEM study of dislocation multiplication and shearing processes in sub-micrometer Al fibers that were kept free of FIB preparation. The size of operating sources and their production mode has been systematically analyzed and compared to the crystal dimensions and initial microstructure. In addition to the source operating regime, a very low ductility plastic regime has been observed in fibers containing no preexisting dislocations. These plastic behaviors have been correlated to stress and strain measurements obtained by micro-mechanical testing. Possible strengthening mechanisms and size effect on the mechanical properties will be discussed.

#### 10:10 AM Break

#### 10:40 AM

**Mechanical Annealing in Submicro-sized Molybdenum Crystals:** Ling Huang<sup>1</sup>; *Zhiwei Shan*<sup>1</sup>; Ju Li<sup>2</sup>; Jun Sun<sup>1</sup>; Evan Ma<sup>3</sup>; <sup>1</sup>Xi'an Jiaotong University; <sup>2</sup>University of Pennsylvania; <sup>3</sup>Johns Hopkins University

*In situ* TEM compression tests were carried out to investigate the mechanical behavior of single crystal molybdenum pillars with diameters ranging from 75 nm to 300 nm. Despite the high density initial defects, the flow stress of those focused ion beam (FIB) fabricated pillars increased monotonously as the size decreased, with the maximum value up to 8.5 GPa for pillars with a diameter of 75 nm. The power-law exponent of strength vs. pillar diameter is -0.92, about 2 times higher than that reported in previous works for larger pillars. More surprisingly, contrary to that predicated by computer simulation, significant mechanical annealing phenomena, followed by catastrophic failure, is observed during the compression test of these body centered cubic (BCC) metal pillars when their size is less than 200 nm. These striking findings shed new light on revealing the underlying physical mechanisms that are responsible for the plasticity of small scaled BCC crystals.

#### 11:00 AM

**A Length Scale Dependent Phase Transformation in Si:** *Aaron Beaber*<sup>1</sup>; Steven Girshick<sup>1</sup>; William Gerberich<sup>1</sup>; <sup>1</sup>University of Minnesota

The phase transformation of silicon during indentation has been widely studied over the past thirty years. The use of *in situ* indentation, particularly Raman microscopy and electrical characterization, has greatly clarified the transformation process. In the current work, TEM *in situ* indentation of Si nanospheres and *ex situ* indentation of confined nanotowers are used to propose a length scale dependent phase transformation. Below a critical dimension of approximately 100 nm, deformation of Si is dominated by dislocation plasticity rather than a phase transformation. This is shown to be consistent with multiple geometries, including spheres, towers, and wedges. Furthermore, the reverse transformation upon unloading is shown to occur at decreasing stresses for smaller geometries. These findings reinforce the importance of shear stresses during anisotropic loading and confirm the notion of enhanced ductility in Si at small scales.

#### 11:20 AM Invited

**Probing Size Dependent Mechanical Properties of Metallic Nanowires in Tension:** Yang Lu<sup>1</sup>; Cheng Peng<sup>1</sup>; Yogi Ganesan<sup>1</sup>; Hao Lu<sup>1</sup>; Jianyu Huang<sup>2</sup>; Jun Lou<sup>1</sup>; <sup>1</sup>Rice University; <sup>2</sup>Sandia National Laboratories

This talk presents some of our recent efforts to study the size dependent mechanical behaviors of metallic nanowires. We have developed a simple micro-device that allows *in situ* quantitative mechanical characterization of metallic nanowires, in SEM or TEM chamber equipped with a quantitative nanoindenter. The unique design of this device makes it possible to convert compression from nanoindentation to uni-axial tension at the sample stages. By utilizing this device, *in situ* results on deformation and fracture behavior of Ni and Au nanowires will be discussed. Also in this work, we performed *in situ* quantitative tensile tests on individual <111> single crystalline ultrathin gold nanowires (diameter ~7-15 nanometers) inside TEM. Significant load drop observed in stress-strain curve suggests the occurrences of dislocation nucleation. Corresponding high resolution TEM (HRTEM) imaging demonstrated that plastic deformation was indeed initiated and dominated by surface dislocation nucleation, mediating ultrahigh yield and fracture strength in gold nanowires.

#### 11:50 AM

**Micro-Cantilever Testing of Ti Alloys:** Jicheng Gong<sup>1</sup>; *Angus Wilkinson*<sup>1</sup>; <sup>1</sup>University of Oxford

Micro-cantilevers were machined using a focused ion beam from pure Ti(945), Ti-6Al (945) and Ti-6Al-4V (945+946) and tested in bending using a nano-indenter. The cantilevers had triangular cross-sections with widths varied across the range 10  $\mu$ m to 1  $\mu$ m. EBSD mapping of large areas allowed suitably oriented grains to be identified and the cantilevers cut so as to select specific slip systems. Strain-bursts and/or load-drops are much less

severe for the load-displacement curves for the cantilevers than for similarly sized compression pillars. Critical resolved shear stresses were extracted from the bend tests by fitting load-displacement data with crystal plasticity finite element simulations. All three systems exhibit a size effect consistent with a back stress from pile-up of dislocations against the low stress region at the neutral axis.

---

## Surfaces and Heterostructures at Nano- or Micro-Scale and Their Characterization, Properties, and Applications: Coatings, Surfaces, and Interfaces II - and - Magnetic Heterostructures I

*Sponsored by:* TMS Electronic, Magnetic, and Photonic Materials Division, TMS Materials Processing and Manufacturing Division, TMS: Nanomaterials Committee, TMS: Surface Engineering Committee

*Program Organizers:* Nitin Chopra, The University of Alabama; Ramana Reddy, The University of Alabama; Jiyoung Kim, Univ of Texas; Arvind Agarwal, Florida International Univ; Sandip Harimkar, Oklahoma State University

Tuesday AM  
March 1, 2011

Room: 31B  
Location: San Diego Conv. Ctr

*Session Chairs:* Arvind Agarwal, Florida International University; Sandip Harimkar, Oklahoma State University; Nitin Chopra, The University of Alabama; Ramana Reddy, The University of Alabama

---

### 8:30 AM Invited

**Thermal Annealing of ZnO Films Using High-Density Plasma Arc Lamps:** *Adrian Sabau*<sup>1</sup>; *Ralph Dinwiddie*<sup>1</sup>; *Jun Xu*<sup>1</sup>; *Joseph Angelini*<sup>1</sup>; *David Harper*<sup>1</sup>; <sup>1</sup>Oak Ridge National Laboratory

Nanostructured materials are rarely synthesized with appropriate phase and/or morphology. In this study, critical additional of as-synthesized nanostructured materials, such as annealing and/or activation of dopants, are addressed using infrared plasma arc lamps (PAL) over areas as large as 1,000 cm<sup>2</sup>. The broad spectral range of the PAL and the spectral variation of light absorption in nanostructured materials make the selection of processing parameters extremely difficult, posing a major technological barrier. In this study, the measurement of the surface temperature using various techniques for ZnO films on crystalline silicon wafers is discussed. An energy transport model for the simulation of rapid thermal processing using PAL is presented. The experimental and computational results show that the surface temperature cannot be measured directly and that computer simulation results are an effective tool for obtaining accurate data on processing temperatures.

### 9:00 AM

**Glass Transition at a Polymer Surface Monitored by Localized Surface Plasmon Resonance:** *Kaan Kalkan*<sup>1</sup>; *Ratan Putla*<sup>1</sup>; <sup>1</sup>Oklahoma State University

We investigate glass transition on a polymer surface by embedding gold nanoparticles (AuNP). The impregnation of AuNP into the polymer causes a spectral shift in the LSPR due to the changing dielectric environment. AuNP, at an average size of 8 nm, were synthesized on poly isobutyl methacrylate (PiBMA) films on glass by thermal evaporation. Subsequently, time series LSPR spectra of AuNP on PiBMA were acquired in a temperature controlled optical cell. The effective dielectric constant surrounding the AuNP was calculated from LSPR optical extinction peak. Depth and velocity of penetration were derived from the measured dielectric constant on the basis of dielectric mixing. The onset of AuNP penetration was found to be at 45 C, which is 10 C below the reported glass transition of "bulk" PiBMA. The penetration velocity was found to be fairly constant in time until complete embedding while temperature activated at 0.05 eV.

### 9:20 AM

**Oxidation and Interfacial Structure of Ti<sub>3</sub>Al:** *Muralidharan Ramachandran*<sup>1</sup>; *Ramana Reddy*<sup>1</sup>; <sup>1</sup>The University of Alabama

The isothermal oxidation of binary Ti<sub>3</sub>Al was studied as function of temperature in pure oxygen atmosphere. Weight gain data were acquired using thermo-gravimetric analyzer (TGA). The phase analysis of the base metal and the oxide layer were performed using x-ray diffraction, while the morphology and elemental composition were determined using scanning electron microscopy (SEM) and Transmission Electron Microscopy (TEM). The rate constant of the oxidation process increases from 9.75 X 10<sup>-4</sup> mg<sup>2</sup>/cm<sup>4</sup>/min at 1023K to 5.05 X 10<sup>-2</sup> mg<sup>2</sup>/cm<sup>4</sup>/min at 1223K. The activation energy for the oxidation process was determined to be 240.5 kJ/mol. The particle size in the oxide scale increased with the increase in temperature. At higher temperatures formation of layered structures was observed. The composition and structure of the metal/oxide interface was analyzed.

### 9:35 AM Break

### 9:45 AM

**Fabrication and Characterization of MWCNT Reinforced Aluminum Using Spark Plasma Sintering**

: *Vineet Yadav*<sup>1</sup>; *Sandip Harimkar*<sup>1</sup>; <sup>1</sup>Oklahoma State University

Spark plasma sintering (SPS) technique was used to fabricate aluminum-based metal matrix composites reinforced with MWCNT. The developments of composites properties such as hardness, strength, wear resistance, and corrosion resistance with reinforcement content and composite microstructure was investigated. In this presentation, the influence of CNT dispersing agents and SPS processing parameters on microstructure and properties of the Al-MWCNT composite will also be discussed.

### 10:00 AM

**Microstructure and Wear Behavior of Pulse Electrodeposited Nickel-Carbon Nanotube (Ni-CNT) Composite Coatings:** *Tushar Borkar*<sup>1</sup>; *Sandip Harimkar*<sup>1</sup>; <sup>1</sup>Oklahoma State University

Due to excellent mechanical properties such as high strength, high elastic modulus and large elastic, as well as fracture strain, carbon nanotubes (CNTs) are attracting significant interest as reinforcements in metallic coatings. In the present investigation, carbon nanotube (CNT) reinforced nickel composite coatings were deposited on a stainless steel substrate using pulse electrodeposition process employing a nickel Watts bath. The presence of CNTs in the composite coating prohibited the columnar growth of the nickel grains resulting in random/weak texture and smaller thickness of the composite coatings. The Ni-CNT composite coatings exhibited significantly improved microhardness (580±15 HV) compared to pure nickel coatings (320±15 HV). The pin-on-disc wear testing data indicated that the reinforcement of CNTs significantly improved wear resistance of the composite coatings compared to pure nickel coatings.

### 10:15 AM

**Synthesis and Characterization of Graphene after Ion Implantation:** *Tomoka Colon*<sup>1</sup>; *Cydale Smith*<sup>1</sup>; *Mohamed Seif*<sup>1</sup>; *Satilmis Budak*<sup>1</sup>; *Claudiu Muntele*<sup>1</sup>; *Lawrence Holland*<sup>1</sup>; *Robert Zimmerman*<sup>1</sup>; *Daryush Ila*<sup>1</sup>; <sup>1</sup>Alabama A&M University

Graphene is a flat monolayer of carbon atoms tightly packed into a two-dimensional (2D) honeycomb lattice and is a basic building block for graphitic materials of all other dimensionalities. It can be wrapped up into 0D fullerenes, rolled into 1D nanotubes, or stacked into 3D graphite. Graphene nanoribbons (GNRs) are essentially single layers of graphene that are cut in a particular pattern to give it certain electrical properties. Graphene's high electrical conductivity and high optical transparency make it a candidate for transparent conducting electrodes, required for such applications as touchscreens, liquid crystal displays, organic photovoltaic cells, and organic light-emitting diodes. In this study, we have synthesized graphene on silicon dioxide, used accelerated ion beams to induce defects, and then studied the effects those defects have on the properties of epitaxial graphene.

TUESDAY AM

10:30 AM

**A Facile Route to Synthesis and Characterisation of Hydrophobic Titania Nanofibres:** *T. Sundararajan*<sup>1</sup>; S. Abirami<sup>1</sup>; P. Manohar<sup>1</sup>; <sup>1</sup>Anna University

Polymer based hydrophobic titania nano fibers were fabricated using a simple Low Volume Medium Pressure (LVMP) spray gun. The FE-SEM studies showed that it resembled the nanofibers produced by electro spinning method. Spraying parallel to the length of the glass slide gave better contact angle values and the fibers were more entangled. The hydrophobicity was developed in the coating immediately after spraying. The contact angle measurements were done using Goniometer. Curing the fibers in hot air oven at 80°C reduced the contact angles. Three different sources of titania were experimented. Powder characterization was done by XRD, Raman spectroscopy. A set of nine experiments based on Taguchi's Method were also conducted for contact angle optimization. Even a small amount (0.03g) of hydrothermal titania with 0.7g of polystyrene gave a contact angle as high as 149.77°, which is close to super hydrophobic range.

10:45 AM

**Application of the Strong Contrast Technique to Thermoelastic Characterization of Nanocomposites:** *Majid Baniassadi*<sup>1</sup>; Akbar Ghazavizadeh<sup>1</sup>; David Ruch<sup>1</sup>; Yves Rémond<sup>1</sup>; Said Ahzi<sup>1</sup>; Hamid Garmestani<sup>1</sup>; <sup>1</sup>CRP Henri Tudor

The effective thermoelastic properties of composites filled with cylindrical nanofillers are evaluated using the statistical continuum theory of strong contrast. In terms of aspect ratio, the inclusions vary across a wide range from nanoplatelets to nanowires. As nanostructure descriptors, the statistical two-point correlation functions are calculated using the Monte Carlo method. Then the three-point correlation functions are estimated via an innovative technique. The resulting quadruple and sextuple integrals are calculated using the Monte Carlo integration. The final complex tensorial equations of the elastic part are solved by trial and error. Finally, to verify our proposed approach, it is implemented on a computer generated nanocomposite and the thermoelastic properties are compared with other results..

11:00 AM Break

11:10 AM **Introductory Comments for Magnetic Heterostructures**

11:15 AM **Invited**

**Multifunctional Plasmonic-Ferromagnetic Surface Nanocomposites Synthesized by Bilayer Liquid Self-Organization:** Hare Krishna<sup>1</sup>; Ritesh Sachan<sup>2</sup>; Nozomi Shirato<sup>2</sup>; Jeremy Strader<sup>2</sup>; Hernando Garcia<sup>3</sup>; Anup Gangopadhyay<sup>1</sup>; *Ramki Kalyanaraman*<sup>2</sup>; <sup>1</sup>Washington University in St. Louis; <sup>2</sup>University of Tennessee; <sup>3</sup>Southern Illinois University

Tunable ferromagnetic and resonant plasmon optical behavior in nanostructures provides opportunity to realize multifunctional materials. Here we will review the robust synthesis of such multifunctional surface nanostructures by self-organization via dewetting of bilayer films. Experimentally, such nanomaterials can be synthesized by nanosecond pulsed laser melting of ultrathin metallic films. We found that nanoscale bilayer films of immiscible metallic liquids show different self-organized patterning characteristics based on their arrangement on a substrate. The different bilayer arrangements change the signs of intermolecular interactions, which changes the mode of coupled deformations and the patterning characteristics. We will also discuss the physical properties of the Ag-Co nanocomposite particles created by this process which show tunable concentration dependent ferromagnetism and localized surface plasmon resonances. \* This work has been supported by NSF grants CAREER DMI-0449258, CMMI-0757589, and DMR-0805258 and by grants from CMI at Washington University and SEERC at the University of Tennessee.

11:45 AM **Invited**

**Nanocomposite Magnetic Materials: Improved Performance by Nanostructuring:** *Matthew Willard*<sup>1</sup>; Maria Daniil<sup>1</sup>; Keith Knipling<sup>1</sup>; Ramasis Goswami<sup>1</sup>; Ashish Baraskar<sup>2</sup>; Soack Yoon<sup>2</sup>; Vincent Harris<sup>2</sup>; <sup>1</sup>Naval Research Laboratory; <sup>2</sup>Northeastern University

Development of new magnetic materials, capable of providing higher energy products for permanent magnets and lower core losses for soft magnets, enables smaller, lighter, and more efficient devices. Over the past two decades, a major focus of research has been microstructure refinement to the nanoscale, which has advantages for each class of magnetic material, allowing permanent magnets to store more energy and soft magnets to dissipate less energy than alternative materials. These advantages originate in the exchange correlation length, a fundamental magnetic length scale determined by the strength of coupling between magnetic moments causing them to align, which has typical values with nanoscale dimensions. This presentation will highlight recent work on nanocomposite soft and hard magnetic materials produced by pulsed laser deposition and rapid solidification processing. The effect of nanostructure on the magnetic material performance will be shown experimentally and discussed from a theoretical perspective.

**Thermally Activated Processes in Plastic Deformation: Dislocation Ensemble Evolution**

*Sponsored by:* The Minerals, Metals and Materials Society, TMS Materials Processing and Manufacturing Division, TMS/ASM: Computational Materials Science and Engineering Committee  
*Program Organizer:* Christopher Woodward, Air Force Research Laboratory

Tuesday AM  
March 1, 2011

Room: 1B  
Location: San Diego Conv. Ctr

*Session Chairs:* Christopher Woodward, Air Force Research Laboratory; Ladislav Kubin, CNRS-ONERA

8:30 AM **Invited**

**On the Cross Slip of Dislocations in the Face-Centered Cubic Metals:** *Joël Bonneville*<sup>1</sup>; <sup>1</sup>University of Poitiers

Cross slip is the mechanism by which a screw dislocation changes from its primary glide plane to move on a locally more favourable stressed glide plane. Cross slip has been recognised to significantly contribute to plastic deformation by creating dislocation microstructure and causing dislocation annihilation, dynamic recovery, obstacle bypass, strain softening as well as strain hardening, etc. There has been in the recent years a renewed interest for studying the cross-slip of screw dislocations in the face-centered cubic structure. The main reasons originate from the development in computational power and algorithms allowing for realistic atomistic simulations and the need in integrated computational materials engineering for precise quantitative and predictive models. Our purpose is to present relevant models used for describing cross-slip processes from historical approaches up to the more recent theoretical developments. A particular emphasis will be placed to extract the significant characteristics deduced by the different approaches.

9:00 AM

**Measurement of Cross-Slip Activation Parameters in Pure Ni via Bonneville-Escaig Experiments:** *Jaafar El-Awady*<sup>1</sup>; Michael Uchic<sup>2</sup>; Sang-Lan Kim<sup>3</sup>; Paul Shade<sup>4</sup>; Satish Rao<sup>3</sup>; Dennis Dimiduk<sup>2</sup>; Christopher Woodward<sup>2</sup>; <sup>1</sup>Johns Hopkins University; <sup>2</sup>Air Force Research Laboratory; <sup>3</sup>UES, Inc.; <sup>4</sup>Universal Technology Corporation

To accurately incorporate the thermally-activated process of dislocation cross-slip into mobility laws of dislocation dynamics simulations, it is necessary to experimentally determine the activation volume and energy barrier for dislocation cross-slip. To achieve this we revisit the Bonneville-Escaig experiments to characterize cross-slip activation in pure-nickel single crystals. In this study, large Ni-single crystals were pre-strained in



compression to strains that correspond to the transition between stage-II and stage-III deformation. Meso-scale (5-80 micrometer diameter) and macro-scale (mm size) crystals were prepared from the pre-strained crystals, to explore whether modern microtesting methods can eliminate the need for 'large' single crystals in these experiments. The orientation of the compression axis of the children crystals is such that an avalanche of cross-slip events is produced at the yield stress. The results are interpreted in terms of the Escaig cross-slip model, and the recent molecular-statics simulations of cross-slip nucleation at screw-dislocation intersections with forest dislocations.

#### 9:20 AM Invited

**Atomistic Simulations of Cross-Slip Nucleation at Screw Dislocation Intersections in Face-Centered Cubic Nickel and Copper and L12 Ni3Al:** *Satish Rao*<sup>1</sup>; Dennis Dimiduk<sup>2</sup>; Jaafar El-Awady<sup>3</sup>; Triplicane Parthasarathy<sup>1</sup>; Michael Uchic<sup>2</sup>; Christopher Woodward<sup>2</sup>; <sup>1</sup>UES Inc.; <sup>2</sup>Air Force Research Laboratory; <sup>3</sup>Johns Hopkins University

We describe molecular-statics simulations of screw character dislocation intersections with forest dislocations, in FCC Ni and Cu and L12 Ni3Al, to illustrate a mechanism for cross-slip nucleation. The simulations show how such intersections readily produce cross-slip nuclei. There exists a finite activation barrier for the screw dislocation to transfer from the fully glide plane or the fully cross-slip plane state to the partially cross-slipped state at these intersections, which is a factor of 2 - 5 lower than without the presence of an intersection. The activation barrier for cross-slip at these intersections is shown to be linearly proportional to  $(d/b)\ln(1.732d/b)0.5$ , as with the case of no intersections, where 'd' is the Shockley partial spacing of the partial dislocations and 'b' is the Burger's vector of the screw dislocation. These results suggest that cross-slip should be preferentially observed at selected screw dislocation intersections in FCC materials as well as L12 Ni3Al.

#### 9:50 AM

**Dislocation Kinetics in Fe and Fe Alloys Investigated by In Situ TEM Straining Experiments:** *Daniel Caillard*<sup>1</sup>; <sup>1</sup>CNRS

Microsamples of pure Fe have been strained in a JEOL 2010HC transmission microscope, between 100K and 473K. At room temperature, dislocation loops exhibit straight screw portions moving slowly and steadily, and curved non-screw ones with a much higher mobility. The velocity of screw parts is proportional to their length, in agreement with the kink-pair model. The velocity-stress dependence of a single dislocation has been deduced from an in situ relaxation experiment. At low temperatures, the motion of screw dislocations becomes jerky. This change of kinetics has been interpreted by a change in the mechanism of motion of screw dislocations across the Peierls potential, and correlated to the change in the corresponding macroscopic activation parameters. The softening effect of carbon, and the hardening effect of silicon and chromium, are shown to result from the shift of the transition between the two mechanisms to respectively lower and higher temperatures.

#### 10:10 AM Break

#### 10:30 AM Invited

**Discrete Dislocation Dynamics: Principle and Recent Applications:** *Marc Fivel*<sup>1</sup>; <sup>1</sup>SIMaP-GPM2

The concept of three-dimensional discrete dislocation (DD) simulations has been imagined by L. Kubin, Y. Bréchet and G. Canova in the early 1990s. The first code MICROMÉGAS was a simple model for which dislocation lines of a f.c.c. single crystal are discretized in sets of edge and screw dislocation segments embedded in a continuum media. Typical output of DD simulations are obviously the dislocation microstructure but also many statistical data such as the dislocation densities, the cumulated shear strain, the stored energy, the local stresses and also the actual shape of any part of the crystal deformed by the dislocations. From some points of view, DD simulations can be seen as an ideal tool to fill the gap between atomic simulations (MD) and continuum modelling (FEM). This talk presents recent simulations performed at Grenoble using the edge-screw code Tridis derived from Canova's initial model.

#### 11:00 AM

**Forest Hardening in Materials with High Lattice Friction:** *Benoit Devincere*<sup>1</sup>; Ghiath Monnet<sup>2</sup>; Jonathan Amodeo<sup>3</sup>; <sup>1</sup>CNRS; <sup>2</sup>EDF; <sup>3</sup>Lille 1 University

In materials with high lattice friction like body centred cubic (bcc) crystals at low temperatures, the thermally activated motion of screw dislocations by the kink-pair mechanism governs the yield properties and also affects strain hardening. In this work, the problem of forest hardening at low temperature is revisited with DD simulations. Results are presented in the case of two illustrative materials, i.e. Iron and MgO. Unlike the classical picture of forest hardening in fcc crystal, calculations show that the strength of forest interaction is temperature and strain rate dependant. Hence, simplistic models based on the Taylor equation do not apply and alternative approaches must be considered. The results of massive simulations are compared with existing models. Finally, a new model accounting in a quantitative manner for the effects of temperature and dislocation density is proposed.

#### 11:20 AM

**Simulating the Evolution of the Dislocation Network under Irradiation:** *Dan Mordehai*<sup>1</sup>; Georges Martin<sup>2</sup>; <sup>1</sup>Technion; <sup>2</sup>CEA-Siège

The dislocation network evolution in metals under irradiation is a complex process, which is still a matter of controversy. While crystalline plasticity involves conservative motion of dislocations, the large concentration of point defects produced under irradiation contributes to plastic deformation either by eliminating at sinks (like climb of the existing dislocation network) or agglomerate into new defects. In this work, we propose a method to include dislocation climb in Dislocation Dynamics simulations, based upon the diffusion theory of point defects. In particular, we present an analytical model to calculate the climb rate of dislocations due to interstitial flux, in coordination with the dislocation network. We employ this model to demonstrate that when accounting for the dislocation network, the annihilation of dislocation pairs with opposite signs and the annihilation of low-angle tilt grain boundaries is accelerated under irradiation.

#### 11:40 AM

**Mobility of Dislocation Populations as a Thermally Activated Process:** *Craig Hartley*<sup>1</sup>; <sup>1</sup>El Arroyo Enterprises LLC

Dislocation Dynamics (DD) simulations offer an attractive means of providing basic input to Crystal Plasticity (CP) calculations by permitting micro-scale virtual experiments using models for dislocation behavior based on the physics of individual dislocations. While some of this information can be supplied by atomic models of lattice defects, modifications that employ the principles of stress-assisted, thermally activated motion of dislocations can expand the predictive power of such simulations. Deformation of an element is expressed as an appropriate average of unit processes over the volume of a representative element. To inform CP models, results of these virtual experiments must be expressed in terms of constitutive equations having parameters demonstrably related to the properties and behavior of the dislocation ensemble. This work describes a simple mathematical model for a constitutive relationship in terms of the motion of an ensemble of dislocations where individual dislocation behavior occurs by a thermally activated unit process.

## 2011 Functional and Structural Nanomaterials: Fabrication, Properties, Applications and Implications: Ultra-Fine Grained Materials I

Sponsored by: The Minerals, Metals and Materials Society, TMS Electronic, Magnetic, and Photonic Materials Division, TMS: Nanomaterials Committee

Program Organizers: Jiyoung Kim, Univ of Texas; David Stollberg, Georgia Tech Research Institute; Seong Jin Koh, University of Texas at Arlington; Nitin Chopra, The University of Alabama; Suveen Mathaudhu, U.S. Army Research Office

Tuesday PM Room: 8  
March 1, 2011 Location: San Diego Conv. Ctr

Session Chair: Suveen Mathaudhu, US Army Research Lab

### 2:00 PM Introductory Comments

#### 2:05 PM

**Deformation Twinning in Nanocrystalline HCP Mg Alloys:** *Yuntian Zhu*<sup>1</sup>; X.L. Wu<sup>2</sup>; K.M. Youssef<sup>1</sup>; C.C. Koch<sup>1</sup>; S.N. Mathaudhu<sup>3</sup>; L.J. Kecskes<sup>3</sup>; <sup>1</sup>North Carolina State Univ; <sup>2</sup>Institute of Mechanics; <sup>3</sup>U.S. Army Research Laboratory

Nanocrystalline (nc) hexagonal close-packed (hcp) metals are rarely observed to deform by twinning, although twinning is a major deformation mechanism in their coarse-grained counterparts. This behavior is contrary to what is observed in face-centered cubic metals. Here we report that by alloying Mg with other elements, deformation twins are observed in the nc Mg alloy processed by severe plastic deformation. The formation of deformation twins is attributed to the alloying effect, which may change the energy path for twinning. These results point to a promising approach to design nc hcp alloys for superior mechanical properties.

#### 2:35 PM

**Deformation Twins in Nanocrystalline Magnesium-Based Alloy:** *Marta Pozuelo*<sup>1</sup>; Wei Kao<sup>1</sup>; Jenn-Ming Yang<sup>1</sup>; <sup>1</sup>UCLA

Deformation twins are rarely observed in nanocrystalline hexagonal close-packed Mg mainly due to its high stacking fault energy. Here, we report transmission electron microscopy observations that provide evidence of deformation twins in a nanocrystalline magnesium-based alloy processed by cryomilling and spark-plasma-sintering. The cryomilled powders result in an average grain size of 25 nm. After spark-plasma-sintering, we found a bimodal grain size distribution with coarse-grains around 500 nm and fine-grains of 52 nm. Deformation twins have been observed in nanocrystalline grains smaller than 25 nm in the cryomilled Mg-based powders as well as in the spark plasma sintered sample. However, no evidence of twinning is observed in coarse-grains. These results indicate that the deformation twinning is directly related to the nanocrystalline structure. Deformation twins in nanocrystalline grains along with the reduced grain size presented in this work could lead to unique mechanical properties of nanocrystalline Mg-based alloys.

#### 2:50 PM

**Nanotechnology and the Army Research Laboratory:** *Suveen Mathaudhu*<sup>1</sup>; <sup>1</sup>U.S. Army Research Laboratory

U.S. Army Research Laboratory (ARL) programs on nanomaterials, nanoelectronics, nanophotonics and nanomagnetism have served as building blocks to innovative solutions for the future Army. Presented in this talk will be an overview of ARL research programs with key examples of successful applications of nanomaterials and nanotechnology, such as bulk nanostructured metals, nano-engineered additives for self-detoxifying surfaces, nano-porous glass-polymer composites and bio-inspired nanostructures.

#### 3:05 PM

**Solid Solutions in Ultra-Fine-Grained Al-Mg Alloys:** *Richard Karnesky*<sup>1</sup>; Nancy Yang<sup>1</sup>; Chris San Marchi<sup>1</sup>; Troy Topping<sup>2</sup>; Zhihui Zhang<sup>2</sup>; Ying Li<sup>2</sup>; Enrique Lavernia<sup>2</sup>; <sup>1</sup>Sandia National Laboratories; <sup>2</sup>University of California, Davis

The microstructure and mechanical properties of various binary ultra-fine-grained ( $d \approx 200$  nm) Al-Mg alloys is reported. The composition of alloys spans 0 wt.% Mg (pure Al) to 10.5 wt.% Mg (exceeding significantly the solubility limit). Powders are blended and mechanically alloyed during cryogenic milling in liquid nitrogen to obtain nanocrystalline structures. After cryomilling, powders are hot vacuum degassed and consolidated via hot isostatic pressing and extrusion. Local-electrode atom-probe tomography, X-ray diffraction, and electron microscopy are used with the goals of understanding microstructural evolution as a consequence of the various processing stages and Mg content. Alloys with the highest amounts of Mg exhibit strong Mg segregation to grain boundaries. The impact of this heterogeneous Mg distribution on microstructure and mechanical behaviors is discussed in the context of measured tensile and microhardness properties as a function of thermal exposure.

#### 3:20 PM

**Fabrication and Deformation of Bulk Lamellar Nanocomposites under Extreme Rolling Strains:** *Nathan Mara*<sup>1</sup>; Thomas Wynn<sup>1</sup>; Jonathan Ledonne<sup>2</sup>; Dhriti Bhattacharyya<sup>1</sup>; Duncan Hammon<sup>1</sup>; Anthony Rollett<sup>2</sup>; Irene Beyerlein<sup>1</sup>; <sup>1</sup>Los Alamos National Laboratory; <sup>2</sup>Carnegie Mellon University

In this work, we study composite systems consisting of two immiscible metals, Ag-Cu and Cu-Nb, wherein the individual phases are submicron to nanometer in scale, and the interfacial content is high. The bulk nanocomposites have been produced via severe plastic deformation techniques following three different processes: 1) Casting of nanolamellar eutectic and subsequent rolling (Ag-Cu), 2) Physical Vapor Deposition and subsequent rolling (Cu-Nb), and 3) Accumulative Roll-Bonding (Cu-Nb). We have found that changes in the texture and interface crystallography after SPD can be explained based on predominance of slip in the case of Cu-Nb or predominant twinning in the case of Cu-Ag, as described theoretically by Beyerlein et al. (in this symposium). Interfacial evolution in terms of layer morphology, chemical intermixing, crystallography, and interface plane normal is determined as a function of rolling strain, and then discussed in terms of dislocation/interface interactions.

#### 3:35 PM

**Thermal Stability of Nanocrystalline Cu 10at% Nb:** *Kris Darling*<sup>1</sup>; Suveen Mathaudhu<sup>1</sup>; Laszlo Kecskes<sup>1</sup>; <sup>1</sup>ARL

Interfacial energy reduction has been suggested to be a superior method to prevent grain growth in nanocrystalline materials. Recently, examples of thermally stabilized nanocrystalline alloys have emerged showing dramatic high temperature stability owing to grain boundary segregation of solutes and the associated interfacial energy reduction. Such samples are typically synthesized through high energy non equilibrium processes and therefore limited to small product geometries such as particles. Furthermore, the very same mechanism responsible for the high thermal stability can often lead to frustrated atomic diffusion and hinder the densification required for production of bulk samples. The primary objective of this study was to delineate the grain growth kinetics of thermally stabilized nanocrystalline Cu 10at% Nb by use of differential scanning calorimetry and micro structural analysis. Knowledge of such grain growth kinetics will establish the appropriate consolidation parameters for successful densification in the future.

### 3:50 PM Break

### 4:05 PM Invited

**Embedded Binary Eutectic Alloy Nanostructures:** *Daryl Chrzan*<sup>1</sup>; Swanee Shin<sup>1</sup>; Julian Guzman<sup>1</sup>; C.-W. Yuan<sup>2</sup>; Christopher Liao<sup>1</sup>; Cosima Boswell-Koller<sup>1</sup>; Peter Stone<sup>1</sup>; Oscar Dubon<sup>1</sup>; Andrew Minor<sup>1</sup>; Masashi Watanabe<sup>3</sup>; Jeffrey Beeman<sup>4</sup>; Kin Man Yu<sup>4</sup>; Joel Ager<sup>4</sup>; Eugene Haller<sup>1</sup>; <sup>1</sup>University of California, Berkeley; <sup>2</sup>Ludwig-Maximilians Universitat; <sup>3</sup>Lehigh University; <sup>4</sup>Lawrence Berkeley National Laboratory

Ion beam synthesis (IBS) is a powerful method for fabricating a wide variety of nanoparticles embedded within a matrix. Here we use IBS to fabricate GeSn and GeAu nanoclusters within amorphous SiO<sub>2</sub>. The as-formed nanocrystals assume a bi-lobed structure with one lobe nearly pure Ge, and the other nearly pure Sn or Au. Pulsed laser melting converts the bi-lobed nanoclusters into a nearly compositionally homogeneous amorphous alloyed state. Subsequent annealing recrystallizes the nanoclusters, and returns them to their initial bi-lobed state. The recrystallization temperature can be tuned by varying the net composition of the nanoclusters. It is suggested that embedded binary eutectic alloy nanostructures might form a basis for a new class of phase change materials with applications in optical storage and static RAM technologies. This research is funded primarily by the U. S. Department of Energy.

### 4:35 PM

**Molecular Dynamics of Fatigue Crack Growth in Nanocrystalline Aluminium:** *Y. Purohit*<sup>1</sup>; Ram Mohan<sup>1</sup>; <sup>1</sup>NCA&T State University

Comprehensive knowledge of fracture and fatigue of nano-crystalline metals and alloys is essential for their nano-structural applications. Limited experimental and computational studies have been conducted on fatigue damage of metals at nano-scale. Experimental techniques are prohibitive due to limitations of nano samples and advanced microscopic manipulators. In this study, crack propagation under cyclic loading in nano-crystalline Al is investigated via molecular dynamics (MD) simulations. The initial atomic configurations are generated using a Voronoi construction with the dynamic crack growth investigated via MD simulations using embedded atom method. Fatigue loading in a strain-controlled manner with a maximum strain (emax) of 0.035 and a load ratio (emin / emax) of 0.8 are considered. The plastic deformation mechanisms governing fatigue crack advancement such as the emission of dislocations from the crack tip and dislocation sub-structuring, as well as crack growth rates as a function of the stress intensity factor are analyzed and discussed.

### 4:50 PM

**Atomic-Scale Simulations of Straining of Nanocrystalline Palladium along Different Loading Paths:** *Dmitry Bachurin*<sup>1</sup>; Peter Gumbsch<sup>1</sup>; <sup>1</sup>Institut für Zuverlässigkeit von Bauteilen und Systemen (IZBS), Karlsruhe Institut für Technology (KIT)

We present the results of molecular dynamics investigations of stress release and repeated straining of fully 3D nanocrystalline palladium structures with mean grain size of 10 nm at room temperature. Previously the sample was uniaxially deformed by compression (up to 6%) at a constant strain rate. Thereafter stress was released at different stages of elastic and plastic deformation. It was found that the sample has an irreversible strain even after unloading from a region corresponding to the elastic stage. Following the stress release, repeated straining was performed in two different mutually perpendicular directions. Simulations revealed very significant differences in Young's modulus (up to 25%) for all predeformed samples. Mechanical behavior of computer simulated nanocrystalline palladium during repeated straining will be discussed in details.

### 5:05 PM

**Nanostructured Ti-alloys with Superior Fatigue Properties:** *Vladimir Zherakov*<sup>1</sup>; Irina Semenova<sup>1</sup>; Salavat Kusimov<sup>1</sup>; <sup>1</sup>Ufa State Aviation Technical University

This report is related to the enhancement of the fatigue properties in ultrafine-grained Ti alloys produced by severe plastic deformation (SPD) techniques. To process the Ti alloys, combined SPD techniques that include

equal channel angular pressing and thermo-mechanical treatments were used. As a result, the ultrafine-grained Ti materials with a similar grain size of about 300 nm but different in their shape and grain boundary structure (both low- and high-angle, equilibrium and non-equilibrium grain boundaries) were produced. It is shown that tailoring grain boundaries by SPD techniques makes it possible to considerably enhance the strength of Ti materials while preserving high ductility. In turn, ultrafine-grained materials with enhanced strength and ductility demonstrate superior fatigue endurance and life. High innovative potential of nanostructured Ti alloys is also considered and discussed.

### 5:20 PM

**Principles of Control over Fatigue Properties in Ultrafine Grain Ti Materials:** *Irina Semenova*<sup>1</sup>; A. Yu. Vinogradov<sup>2</sup>; V.V. Polyakova<sup>1</sup>; R.Z. Valiev<sup>1</sup>; <sup>1</sup>Ufa State Aviation Technical University; <sup>2</sup>Osaka City University

The purpose of this work is to understand the basic principles governing the fatigue behavior of ultrafine grain (UFG) materials manufactured by severe plastic deformation and to formulate the microstructure-based approaches towards controlling the fatigue life and achieving the enhanced durability under low and high cycle deformation. CP Ti Grade 4 was produced using equal channel angular pressing followed by thermal mechanical treatment and annealing. As a result, UFG Ti samples with grain sizes of 120 nm and 1 and 5 μm were produced. In discussion we argue that tailoring grain boundaries by severe plastic deformation techniques makes it possible to considerably enhance the strength of UFG Ti while preserving high ductility. In turn, UFG materials with enhanced strength and ductility demonstrate superior fatigue properties. Finally a simplified modeling framework is proposed to rationalize the experimental findings on the grounds of a dislocation kinetics approach adapted for cyclic deformation.

### 5:35 PM Concluding Comments

---

## 2nd International Symposium on High-Temperature Metallurgical Processing: Ferrous and Nonferrous Metals

*Sponsored by:* The Minerals, Metals and Materials Society, TMS Extraction and Processing Division, TMS: Pyrometallurgy Committee, TMS: Energy Committee

*Program Organizers:* Jiann-Yang Hwang, Michigan Technological University; Jerome Downey, Montana Tech; Jaroslaw Drellich, Michigan Technological University; Tao Jiang, Central South University; Mark Cooksey, CSIRO

Tuesday PM  
March 1, 2011

Room: 18  
Location: San Diego Conv. Ctr

*Session Chairs:* Mark Cooksey, CSIRO; Tao Jiang, Central South Univ

---

### 2:30 PM

**Enhancing the Pelletization of Brazilian Hematite by Adding Boron Bearing Additives:** *Wei Yu*<sup>1</sup>; *Deqing Zhu*<sup>1</sup>; *Tiejun Chun*<sup>1</sup>; *Jian Pan*<sup>1</sup>; <sup>1</sup>Central South University

One kind of Brazilian hematite is characterized by refractory balling and firing performance, such as poor ballability, higher firing temperatures and lower compressive strength of fired pellets. In this paper, improving the pelletization of Brazilian hematite by adding a boron bearing additive was carried out, and the pelletization parameters was also optimized. In the meantime, the mechanism of boron bearing additive was revealed in the kinetics of crystal grain growth by using LEICA microscopy and its software to measure hematite grain growth. Good qualities of green balls are manufactured with drop numbers above 5.7 times/0.5m, compressive strength higher than 13 Newton per pellet and thermal shock temperature over 620° under the following conditions: 1.2% bentonite, 0.4% boron bearing additive, 7% moisture and pelletizing in disc for 15min. When the green balls were preheated at 1000° for 8min and fired at 1280° for 15min, the



compressive strength of the fired pellets containing boron bearing additive is about 3096 Newton per pellet, which is far beyond the standard requirement for good quality pellets. Compared to the fired pellets without adding any boron bearing additives, the compressive strength of fired pellets containing boron bearing additive is increased by 1225N per pellet. It is revealed that adding boron additive into the hematite pellets help to form more liquid phases, lower the activation energy of the hematite grain growth by 135.24 kJ/mol and augment grain growth rate by 33.60%, leading to higher strength of fired pellets due to forming more coarse and dense recrystallized hematite and energy saving by firing at lower temperatures for shorten time.

**2:50 PM**

**Study on Improving the Quality of Pellet Made from Vale Hematite Pellet Feed:** *Vinicius Mendes*<sup>1</sup>; *Deqing Zhu*<sup>1</sup>; *Marcus Emrich*<sup>2</sup>; *Jian Pan*<sup>1</sup>; *Tiejun Chun*<sup>1</sup>; <sup>1</sup>Central South University; <sup>2</sup>CVRD

Some joint projects of studies of hematite acid pellet have been implemented to develop technological solutions for using CVRD hematite pellet feed in Chinese palletizing plant. Beneficial improvements on the pellets quality were achieved by adjusting the blends composition and using new technology of pre-treating the blended pellet feed with High Pressure Grinding Rolls (HPGR) on rotary kiln pellet technology. The drop strength of green balls increased from 3.4 to 6.0 times from 0.5m height, at the same time, the bentonite dosage decreased from 1.5% to 0.7%. The compressive strength of roasted pellets reaches 2500N/pellet. The reduction swelling index of roasted pellets is below 15%. The Reducibility of roasted pellets is also improved markedly.

**3:10 PM**

**Decomposition and Oxidation of Bismuthinite in Nitrogen-Oxygen Atmospheres:** *Rafael Padilla*<sup>1</sup>; *Ricardo Villa*<sup>1</sup>; *Maria Ruiz*<sup>1</sup>; <sup>1</sup>University of Concepcion

Bismuth is an impurity in copper minerals where it occurs mainly as the mineral bismuthinite ( $\text{Bi}_2\text{S}_3$ ). In smelting of copper minerals, most of the bismuth reports to the white metal, as a result, a substantial amount of bismuth accompanies the copper to the electrorefined cathodes. Thus understanding the behavior of  $\text{Bi}_2\text{S}_3$  at high temperatures is crucial to eliminate bismuth before electrorefining. In this paper, some experimental data on the decomposition/volatilization of bismuthinite in nitrogen-oxygen atmospheres is discussed. The results indicated that in nitrogen atmosphere, bismuth volatilization occurs through a fast decomposition of bismuthinite to metallic bismuth and sulfur with subsequent volatilization of bismuth in the range 850-1100 °C. Similarly, in the presence of oxygen, bismuthinite decomposes to bismuth too, followed by oxidation to the non-volatile bismuth trioxide at temperatures higher than 750 °C. Both, temperature and partial pressure of oxygen affect significantly the bismuth volatilization and oxidation rates.

**3:30 PM**

**Kinetic Study on Vanadium Oxidation in Low Vanadium Bearing Hot Metal during BOF Process:** *Qingyun Huang*<sup>1</sup>; *Bing Xie*<sup>1</sup>; *Xiaopeng Zhen*<sup>1</sup>; <sup>1</sup>Chongqing University

Extraction of vanadium from low V-bearing hot metal to slag by BOF process is a successful approach mainly used in China. In order to make oxidation of vanadium as more as possible, the kinetic behavior of vanadium oxidation was investigated under the laboratory condition. Firstly the paper summarized the oxidation mechanism of vanadium recovery from hot metal, then experiments were carried out in induction furnace to understand the oxidation behavior of vanadium. Also, the influence of the composition of final slag on oxidation rate of vanadium was researched. The restrictive step of vanadium oxidation and the expression of reaction rate were obtained. And reasonable temperature system and composition of vanadium slag at the end point were proposed.

**3:50 PM**

**Production of Strontium Metal from Strontium Oxide Using Vacuum Aluminothermic Reduction:** *Yeliz Demiray*<sup>1</sup>; *Onuralp Yücel*<sup>1</sup>; <sup>1</sup>Istanbul Technical University

In this present study production of strontium metal from its oxide was studied under the pressure of 1 mbar. In the experiments 99 % SrO was used. Effects of Al powder addition (100-200 % of stoichiometric ratio) and time were investigated on recovering of metallic strontium from SrO. Effects of BaO addition and additive concentrations were also investigated. The final residues were examined for their chemical composition. XRD, AAS and Flame Photometer devices were used for chemical analysis. More than 90 % of strontium metal recovery was observed.

**4:10 PM Break**

**4:20 PM**

**Pyrometallurgical Controls of Silver-residue Smelting in a Short Rotary Furnace:** *Atsushiro Nabei*<sup>1</sup>; *Ken-ichi Yamaguchi*<sup>1</sup>; <sup>1</sup>Mitsubishi Materials Corp. Central Research Institute

Wet chlorination process of de-copperized anode slimes is followed by de-chlorination stage in which lead sulphate and metallic silver form silver residue. The silver residue is subsequently reduced to  $\text{Ag}_2\text{Se}$  matte and  $\text{PbO-SiO}_2$  slag to remove lead to the slag in a short rotary furnace. Although this smelting process is proven well in actual operations, few papers have investigated its metallurgical aspect. This paper will describe the effectiveness of controlling parameters adopted at the Naoshima smelter and discuss decisive factors influencing silver loss to  $\text{PbO-SiO}_2$  slag.

**4:40 PM**

**A Study of Pelletization of Manganese Ore Fines:** *Deqing Zhu*<sup>1</sup>; *Vinicius Mendes*<sup>1</sup>; *Tiejun Chun*<sup>1</sup>; *Jian Pan*<sup>1</sup>; <sup>1</sup>Central South University

Comparing with the lump manganese ores, fine manganese fines are characterized by large amount and low price. However, they must be agglomerated as EAF (electric arc furnace) feed. In this paper, high quality fired pellets were produced by simulating grate-kiln process to supply the feed for EAF from some imported manganese ore fines containing high combined water, which was pretreated by high press roll grinding. Manganese ore fines assaying 44.47%Mn, 5.89%Fe, 12.09%LOI and with 72.67% ranging between 0.5mm and 8mm, are pretreated up to the specific surface areas of 2764  $\text{cm}^2/\text{g}$  and 84.74% passing 0.074mm by passing the fines through HPGR (high press grinding roller) twice in open circuit. The finely ground manganese fines were mixed with 1.2% bentonite, balled at 15% moisture for 7min in disc pelletizer, the drop numbers, compressive strength and thermal shock temperature of green balls reach 11 times/0.5m, 11 Newton per pellet and 360°, respectively. After the green balls drying in the oven, the dry pellets were preheated at 1050° for 12min and then fired at 1300° for 12min in electric tube furnace, and the compressive strength of fired pellets reaches 2621 Newton per pellet. Therefore, these pellets are high quality burden for blast furnace or electric furnace due to high mechanical strength and high Mn grade of 49.11% and low detrimental elements.

**5:00 PM**

**Microwave Induced Arcing of Metallic Sulfide Bearing Ore Particles:** *Matthew Andriese*<sup>1</sup>; <sup>1</sup>Michigan Technological University

It has been observed that ore particles of a metallic sulfide bearing ore are readily able to heat by microwave irradiation. Upon heating, an electric arc is often produced between particle interfaces containing chalcopyrite (Ccp), nickel-rich pyrrhotite (Ni-Po), and pyrrhotite (Po) minerals resulting in liquid formation and subsequent fusion of particles. Upon cooling, SEM imaging in back scatter mode shows new phases have formed within the melt. EDS examination of the new phases reveals incongruent melting ( $\text{Solid1} \rightarrow \text{Solid2} + \text{Liquid}$ ) of the peridotite host rock with the liquid containing some amounts of dissolved sulfur. Also formed is a solid solution of the sulfide-bearing minerals (Ccp + Ni-Po) dispersed within the liquid. The newly formed solid solution (or matte) has implication of yielding higher nickel recovery during hydro/pyro metallurgical processes as it may prove difficult or not feasible to separate Ni-Po from Po by conventional methods.

5:20 PM

**Reduction of Carbon-burdened Chromite Pellets in the Presence of Additives:** *Guanghui Li*<sup>1</sup>; Jianchen Li<sup>1</sup>; Mingjun Rao<sup>1</sup>; Guohua Bai<sup>1</sup>; Tao Jiang<sup>1</sup>; <sup>1</sup>Central South University

By using thermogravimetry, optical microscope and chemical phase analysis, the solid-state reduction of carbon-burdened chromite pellets in the absence and presence of additives were investigated in this paper. The effects of reduction temperature, reduction time and additives on the metallization of chromite pellet were studied. The results indicate that the pre-reduction ratio of carbon-burdened chromite pellets is improved with the increase of reduction temperature and the presence of additives. The metallization of chromium is increased from 63.9% to 92.8% reducing at 1300 oC for 4h with the addition of 2 wt.% of sodium borate. The reduction of carbon-burdened chromite pellets is diffusion controlled. The apparent activation energy of the reaction without sodium borate is 192.053kJ/mol, while that of the reaction with sodium borate decreases to 170.437kJ/mol.

5:40 PM

**Purification of Boron Trichloride by Decomposition of Phosgene in CO<sub>2</sub> Laser System:** *Duygu Agaogullari*<sup>1</sup>; Ismail Duman<sup>1</sup>; <sup>1</sup>Istanbul Technical University

In this study, COCl<sub>2</sub> was removed from the gas mixture by excitation and molecular level thermal decomposition with 250 W IR CO<sub>2</sub> laser beams. Different ratios of gas mixtures were provided from pure gases stored in steel cylinders. The effects of COCl<sub>2</sub> amount, flow rates of the gas mixtures and exposure time on the COCl<sub>2</sub> decomposition efficiencies were investigated. The decomposition was carried out in a glass reactor which was originally designed and equipped with gas inlet and outlet pipes on its barrel and NaCl windows on each end. Unattacked BCl<sub>3</sub> molecules in the gas mixture absorbed energy from CO<sub>2</sub> laser radiation that is followed by an intermolecular energy transfer to COCl<sub>2</sub> molecules. So, it results in decomposition and CO+Cl<sub>2</sub> formation. Decomposition products were separated by distillation in two different columns externally cooled by ethanol. The COCl<sub>2</sub> decompositions were interpreted with FTIR analysis.

## Alumina and Bauxite: Red Mud

*Sponsored by:* The Minerals, Metals and Materials Society, TMS Light Metals Division, TMS: Aluminum Committee, TMS: Aluminum Processing Committee

*Program Organizers:* James Metson, University of Auckland; Carlos Suarez, Hatch Associates Consultants Inc

Tuesday PM  
March 1, 2011

Room: 17A  
Location: San Diego Conv. Ctr

*Session Chair:* To Be Announced

2:00 PM

**Application of Nanofiltration Technology to Improve Sea Water Neutralisation of Bayer Process Residue:** *Kelvin Taylor*<sup>1</sup>; Mark Mullett<sup>1</sup>; Lee Fergusson<sup>2</sup>; Helen Adamson<sup>1</sup>; Juerg Wehrli<sup>1</sup>; <sup>1</sup>Hatch & Associates; <sup>2</sup>Vireotec Global Solutions

Sea Water Neutralization of alkaline Bayer Process Residue is a sustainable solution to turn a hazardous waste material into a benign, non-hazardous material that can be re-used in many applications. The concentrations of the active neutralizing agents in seawater, calcium and magnesium, are low and large volumes of sea water are required to neutralize the alkaline residue. Nanofiltration of seawater can produce a concentrate containing up to four times the calcium and magnesium levels in seawater, while the mono-valent ions, like sodium and chloride, are only marginally concentrated. This significantly reduces the volume of seawater required for the neutralization process and hence the size of neutralization equipment. Other advantages include improved reaction kinetics and reduced salinity of the neutralized residue, making it more suitable for certain applications. The nanofiltration

permeate, with lower scaling potential, is also an improved feed for sea water RO plants to produce potable water.

2:25 PM

**Caustic and Alumina Recovery from Bayer Residue:** *Songqing Gu*<sup>1</sup>; <sup>1</sup>Chalco

Bayer process is not suitable for alumina production from high silica bauxite due to too much caustic and alumina loss in the Bayer residue. The caustic and alumina recovery from the Bayer residue by various processes, such as sintering, lime treatment and hydration process etc, is analyzed and compared theoretically. The most important target to treat Bayer residue for the recovery is to find an efficient DSP containing less alumina and caustic soda by some suitable and less consumption processes.

2:50 PM

**Investigation on Alumina Discharge into Red Mud Pond at Nalco's Alumina Refinery, Damanjodi, Orissa, India:** *Birendra Kumar Mohapatra*<sup>1</sup>; Barada Kanta Mishra<sup>1</sup>; Chitta Ranjan Mishra<sup>2</sup>; <sup>1</sup>Institute of Minerals & Materials Technology(IMMT); <sup>2</sup>National Aluminium Company Limited(NALCO)

Around 14% of alumina gets discharged in to red mud pond from Nalco's alumina refinery, Damanjodi, Orissa. The minerals hosting alumina in red mud have been investigated using Scanning Electron Microscope (SEM) and Electron Probe Micro Analyzer (EPMA). The minerals identified are: gibbsite, goethite, sillimanite, muscovite and kaolinite. The average particle size of red mud is ~8µ except isolated grains of gibbsite, goethite and rutile which are > 20µ in size. The gibbsite invariably contains up to 60 mole % of boehmite. The nodular goethite contains over 30-mol % of 'Al' in its lattice and termed as alumo-goethite. Around 34% of Al<sub>2</sub>O<sub>3</sub> are present in muscovite/sillimanite. Studies reveal that most of the minerals in red mud have either alumina in their lattices or are undigested aluminium silicates that do not get dissolved during alumina refining, thus a considerable amount of alumina gets discharged through these phases into the red mud.

3:15 PM Break

3:25 PM

**Production of Ordinary Portland Cement(OPC) from NALCO Red Mud:** *Chitta Mishra*<sup>1</sup>; Devendra Yadav<sup>2</sup>; M All<sup>2</sup>; P Sharma<sup>2</sup>; <sup>1</sup>National Aluminium Company Limited; <sup>2</sup>National Council for Cement & Building Materials(NCB)

A unique process for production of Ordinary Portland Cement(OPC) from NALCO Red Mud has been successfully developed from a raw mix containing limestone, red mud, shale and fine coal. The raw materials are ground to the required fineness and then blended to prepare the raw mix. The raw mix is fed in to a kiln and fired to a temperature of 1400-1450 degree centigrade to obtain clinker. Clinker was cooled and gypsum was added in to it to obtain OPC. 3-4.5% of NALCO red mud was used for production of OPC. OPC prepared from this clinker confirmed to the requirements of three Indian Standard Specifications for 33, 43 & 53 grade of OPC. The process is most efficient, cost-economic and effectively addresses the environmental problems associated with the waste material red mud generated during the refining of bauxite for manufacture of alumina employing Bayer process.

3:50 PM

**Recovery of Metal Values from Red Mud:** *Puliyur Krishnaswamy Narasimha Raghavan*<sup>1</sup>; Nand Kumar Kshatriya<sup>1</sup>; <sup>1</sup>Bharat Aluminium Co. Ltd., (A Unit of Vedanta Resources Plc.), BALCO Nagar, Korba

In processing bauxite for production of alumina by Bayer's process, huge quantities of red mud is generated which are disposed of as a waste product. The red mud is normally disposed contains caustic soda and therefore poses pollution hazardous and requires storage in specially made large size ponds. This waste material at present does not find any use, hence, in addition to pollution hazardous, considerable expenditure and wastage of land is involved in disposal of this waste material. Hence, it is desirable to recover the oxides of iron, titanium and aluminium from red mud. The process applies to the recovery of alumina, titania and ferric oxide from red mud in Four Steps. Balco's red mud contains 45-47% Fe<sub>2</sub>O<sub>3</sub> and 16-25%

TUESDAY PM

of undigested alumina. The present papers provide an alternative and more environmentally acceptable process for the recovery of iron, titanium and aluminum from Balco's red mud.

#### 4:15 PM

**Red Mud Flocculants Used in The Bayer Process:** *Scott Moffatt*<sup>1</sup>; Frank Ballentine<sup>1</sup>; Morris Lewellyn<sup>1</sup>; <sup>1</sup>Cytec Industries

Flocculation and separation of red mud is an integral part of the Bayer process. Over the latter half of the 20th century, flocculant technology changed dramatically from natural starches to use of "rationally designed" synthetic polymers. Many of these advancements were due to the introduction of liquid or emulsion based flocculants which enabled elaborate post-reaction chemistry to be done on the polymer backbone. This paper presents a historical overview of milestones of flocculant technology used in the Bayer Process up to the present day. Discussion of flocculants is based on inventions in the published literature that have gained widespread use throughout the industry and will include the benefits/advantages of different flocculant technology for settling red mud.

#### 4:40 PM

**Reductive Smelting of Greek Bauxite Residues for Iron Production:** *Anthimos Xenidis*<sup>1</sup>; C. Zografidis<sup>1</sup>; I. Kotsis<sup>1</sup>; D. Boufounos<sup>2</sup>; <sup>1</sup>National Technical University of Athens; <sup>2</sup>Aluminium of Greece, SA

The reductive smelting of Greek bauxite residues was investigated for the production of an iron product that meets the minimum industrial requirements as a blast furnace feed. Fine-grained Greek bauxite residues -either as is or in the form of pellets- and solid fuel reducing agents -lignite and coke-, were used as raw materials. The effect of parameters such as the smelting temperature, the amount of the reducing agent in the mixture, the retention time and the addition of fluxes on the quality of the metallic product, as well as the basicity and the desulfurization capability of the slag, was investigated. The obtained results regarding the chemical properties of the metallic product were very promising, providing input for further research on the optimization of the proposed pyrometallurgical method for the production of an attractive ferrous raw material for the iron ore industry.

## Aluminum Alloys: Fabrication, Characterization and Applications: Thermal Mechanical Processing

*Sponsored by:* The Minerals, Metals and Materials Society, TMS Light Metals Division, TMS: Aluminum Processing Committee  
*Program Organizers:* Subodh Das, Phinix LLC; Zhengdong Long, Kaiser Aluminum; Tongguang Zhai, University of Kentucky

Tuesday PM  
March 1, 2011

Room: 14A  
Location: San Diego Conv. Ctr

*Session Chair:* Xiyu Wen, University of Kentucky

#### 2:00 PM

**Study of the Artificial Aging Kinetics of Different AA6013-T4 Heat Treatment Conditions:** *Josef Berneder*<sup>1</sup>; Ramona Prillhofer<sup>1</sup>; Josef Enser<sup>1</sup>; Peter Schulz<sup>1</sup>; Carsten Melzer<sup>1</sup>; <sup>1</sup>AMAG rolling

Aluminium alloy AA6013 was developed for aircraft fuselage applications and the transportation industry and its attractive combination of mechanical properties, formability, corrosion resistance and weldability makes it ideal for automotive sheet applications. Due to the high strength level of AA6013 in temper T6 it can be considered as a replacement option for commercial steel grades allowing maximum weight savings without losses in strength. In the present work an (i) improved heat treatment cycle for industrial production of alloy AA6013 in temper T4 is presented with the objective to reduce the subsequent time consuming and costly artificial aging. The hereby produced T4 temper sheet material is (ii) analyzed in comparison to standard T4 in terms of artificial aging kinetics and (iii) the process of formation and dissolution of precipitates is studied by using differential scanning calorimeter (DSC).

#### 2:20 PM

**Textures and Particle Structures of a Continuous Cast AA3004 Aluminum Alloy after Cold Rolling and Annealing:** *Xiyu Wen*<sup>1</sup>; Yansheng Liu<sup>2</sup>; Jingwu Zhang<sup>3</sup>; Shridas Ningileri<sup>1</sup>; Tongguang Zhai<sup>1</sup>; Zhong Li<sup>4</sup>; <sup>1</sup>University of KY; <sup>2</sup>Secat Inc.; <sup>3</sup>State Key Lab of Metastable Materials Science and Technology; <sup>4</sup>Aleris International Inc.

Measurements of textures of an AA3004 aluminum alloy sheets made from twin belt casting after cold rolling and annealing are carried out by use of the orientation distribution function (ODF) method. The particle structures of the sheet samples are observed and analyzed by use of scanning electronic microscopy (SEM) and Transmission electron microscopy (TEM) as well as X-ray diffractionmeter (XRD). The textures and particle structures resulting from the thermo-mechanical processing are studied and presented.

#### 2:40 PM

**Mechanical Properties of Bulk Nanostructured 7075 Al Alloy Prepared by Severe Plastic Deformation:** *Yonghao Zhao*<sup>1</sup>; Tory Topping<sup>1</sup>; Xiaozhou Liao<sup>2</sup>; Yuntian Zhu<sup>3</sup>; Enrique Lavernia<sup>1</sup>; <sup>1</sup>University of California, Davis; <sup>2</sup>The University of Sydney; <sup>3</sup>North Carolina State University, Raleigh

Age-hardened 7000 series Al alloys exhibit the highest strength amongst Al alloys and therefore are of interest in the aerospace, transportation, and sports industries. Grain refinement down to the nanometer region by severe plastic deformation is a promising technique for further enhancing the strength of Al alloys. However, precisely how to optimize the mechanical properties of nanostructured aged hardened Al alloys remains a challenge. In this study, the as-received 7075 Al alloys were first homogenized at 500 C for 5 h to form super saturated solid solution, then processed by equal-channel-angular pressing (ECAP), cryo-rolling and high pressure torsion (HPT) techniques, respectively, to form microstructures with different grain sizes ranging from nanometer to micrometer. Post-deformation aging treatments were then performed to introduce GP zones, metastable/stable phases. Precipitation kinetics and responding mechanical properties were finally measured and analyzed. Our work provides basic guidance for optimizing mechanical properties of the age-hardened nanostructured alloys.

#### 3:00 PM

**Investigation of High Strain Rate Flow of Aluminum Alloys:** *Yansheng Liu*<sup>1</sup>; Xiyu Wen<sup>2</sup>; Shridas Ningileri<sup>2</sup>; <sup>1</sup>SECAT Inc; <sup>2</sup>University of Kentucky

Industrial produced aluminum panels and parts are stamped or punched at a speed far beyond quasi-static state. Understand the deformation behavior of aluminum alloys at high strain rate is critical to determine the process parameters for a successful production. Both regular hydro-servo tensile test machine and foil tester were applied in the test. The dynamic properties of aluminum alloy sheets and foil were investigated at different strain rate from 0.01/s to 2.5/s. Filtration of wave signal is discussed. The results were used to derive the equations governing the strain-stress relationship at different strain rate. A combined exponent formula gives a good description from low to high strain rate. The test can provide important data for industrial simulation and production design.

#### 3:20 PM

**Estimating Response to Hot Rolling of Al-Mn-Mg Alloys from Hot Torsion Testing:** *Hugh McQueen*<sup>1</sup>; <sup>1</sup>Concordia University

Enhanced hot rolling and properties for additional forming can be designed from understanding the dependencies of flow stress, malleability, textures and microstructural evolution on temperature, strain rate, pass strains with related intervals and final cooling schedules. Recent hot torsion tests on Al-Mn-Mg at 250-550°C, 0.1-10 /s are made more applicable by comparison to a range of compositions, pretreatments and characterization methods. As in most Al alloys, dynamic recovery enhances the hot workability and subgrain size to such a degree that subsequent static recrystallization (SRX) requires long maintenance at or even above the finishing temperature. With variations dependent on slab thickness, segregation and homogenization, Al6Mn as fine dispersoid raises strength and retards SRX but when large stimulates nucleation; in contrast, Mg is a potent solute hardener reducing subgrain size and promoting SRX.



### 3:40 PM Break

### 3:55 PM

**A Study on Solute Redistribution during Solution Treatment and Aging Behavior in a Bi-Layer AA6xxx-AA3xxx Alloy System:** *Shahrzad Esmaeili*<sup>1</sup>; Ehsan Foroozmehr<sup>1</sup>; Lihua Liao<sup>1</sup>; Samuel Huberman<sup>1</sup>; David Lloyd<sup>2</sup>; Mark Gallerneault<sup>2</sup>; <sup>1</sup>University of Waterloo; <sup>2</sup>Novelis Global Technology Centre

AA6xxx alloy sheets are used for automotive skin panel applications for their light weight and high strength. The recent invention of Novelis Fusion™ technology has allowed the development of novel laminated alloy systems with AA6xxx alloys as the core layers and ductile alloys with superior surface properties as the clad layers. The resulting bi-layer alloy systems can be thermomechanically processed and/or strengthened through conventional thermal treatments. However, the microstructural changes during their processing constitute complex phenomena due to the inherent compositional gradients. The present work examines the effect of solution heat treatment on solute redistribution across the core-clad interfaces in an AA6xxx-AA3xxx system. The solute redistribution is modeled using a finite element analysis combined with physically-based descriptions for the precipitate dissolution and diffusion processes in the bi-layer system. The aging behavior across the interface and within the core layer is also examined using a combination of experimental and modeling approaches.

### 4:15 PM

**Interactive Processes during Non-Isothermal Annealing of an AA6xxx Alloy:** *Panthea Sepehrband*<sup>1</sup>; Xiang Wang<sup>2</sup>; Haiou Jin<sup>3</sup>; Shahrzad Esmaeili<sup>1</sup>; <sup>1</sup>University of Waterloo; <sup>2</sup>McMaster University; <sup>3</sup>Novelis Global Technology Centre

Annealing of precipitation hardening alloys involve interactions between precipitation and recovery-recrystallization processes. A broad range of such interactions in an AA6xxx alloy has been investigated through employing a non-isothermal annealing process during which precipitates nucleate, grow and coarsen. The interactive phenomena and microstructural evolution have been analysed using transmission electron microscopy (TEM), differential scanning calorimetry (DSC), microhardness measurements, and Electron backscatter diffraction (EBSD) analysis. A new computational method to quantify the EBSD results has also been developed. The method enables analysing the early stages of recrystallization, the spatial distribution of recrystallized grains and the evolution of grain size during recrystallization. The combined experimental and computational study has provided new knowledge on the strong effects of precipitate evolution on early stages of annealing processes.

### 4:35 PM

**Microstructural Characterization and Heat Treatments of Different Al-Zn-Mg/Zr Alloys:** *Paola Leo*<sup>1</sup>; Emanuela Cerri<sup>1</sup>; Hugh McQueen<sup>2</sup>; <sup>1</sup>Università del Salento; <sup>2</sup>Concordia University

Two Al-Zn-Mg alloys (Zr modified and not) were investigated by optical microscopy, hardness and tensile tests. The alloys were solutionized (2h at 490°C) and artificially aged at 130, 160, 190 and 210°C. Tensile tests were performed at room temperature on as-cast, solutionized and peak aged and the deformed samples annealed at 500°C. For both the alloys at room temperature, the solutionized samples exhibited the best ductility, the peak aged the highest strength and the as-cast alloy the highest strain-hardening rate. The higher average grain size of the Zr alloy does not lead to lower hardness and peak stresses during room temperature (RT) tensile tests. Recrystallization of Zr-modified alloy is incomplete and not homogeneous as compared with unmodified alloy.

### 4:55 PM

**Effect of Die Entry Angle on Extrusion Responses of Aluminum 6063 Alloy:** *Samson Adeosun*<sup>1</sup>; Sanmbo Balogun<sup>1</sup>; Olatunde Sekunowo<sup>1</sup>; Wasiu Ayoola<sup>1</sup>; Oluwashina Gbenedor<sup>1</sup>; <sup>1</sup>University of Lagos, Akoka

The effect of die entry angles on the mechanical properties of extruded 6063 aluminum alloy at 32°C has been investigated. Mild steel and tool steel dies with entry angles of 15, 30, 45, 60, 75 and 90° were used for the extrusion

and the extruded samples were subjected to mechanical and microstructural tests. The results show that peak extrusion pressure and hardness of extrudes increase with increasing die entry angle which is in agreement with the literature. Good extrusion response by samples was observed in mild steel dies over that of tool steel at entry angles of 45, 75 and 90°. Extrusion ratio for the die materials are practically the same except at 45° die entry angle where mild steel die exhibited superior extrusion ratio of 2.1 to that of tool steel of 1.8.

### 5:15 PM

**Hot Deformation Behaviour of 7075 Al Alloy:** Hossein Mohammadi<sup>1</sup>; *Mostafa Ketabchi*<sup>1</sup>; <sup>1</sup>Amirkabir University

7075 Al alloy is one of the most used high-strength materials for aircraft structural components. In the present work, the effect of hot deformation parameters such as temperature and strain rate on the dynamic restoration processes of a 7075 Al alloy was studied. Hot compression tests were performed in the temperature range of 300-500°C and the strain rate range of 0.001-0.1 s<sup>-1</sup>. The results show that the true stress–true strain curves exhibit a peak stress at a critical strain, after which the flow stresses decrease monotonically until high strains, showing a dynamic flow softening. The peak stress level decreases with increasing deformation temperature and decreasing strain rate, which can be represented by a Zener–Hollomon parameter in the hyperbolic-sine equation with the hot deformation activation energy of 125 kJ/mol.

### 5:35 PM

**Development of Microstructures and Mechanical Properties Aluminum Alloy after Equal Channel Angular Pressing:** Miroslav Greger<sup>1</sup>; *Ladislav Kander*<sup>2</sup>; <sup>1</sup>VSB-Technical University Ostrava; <sup>2</sup>Material & Metallurgical Research Ltd,

Microstructure and texture development of an aluminum alloy during equal channel angular pressing (ECAP) was investigated and correlated with the mechanical properties. The microstructure was effectively refined by ECAP, and the original fiber texture of the extruded aluminum alloy was disintegrated and a new texture was gradually developed by repetitive ECAP pressing. After 6 ECAP passes following route Bc, the yield stress is lower than for the as-extruded aluminum alloy, indicating that the texture softening is dominant over the strengthening due to grain refinement. Cross-section of original samples was 10 x 10 mm and their length was 45 mm. Deformation forces were measured during extrusion, resistance to deformation was calculated and deformation speed was determined approximately. Analysis of structure was made with use of light microscopy and SEM. Mechanical properties of samples after extrusion were determined by tensile test and by so called penetration test.

## Aluminum Reduction Technology: Cells Thermal Balance

*Sponsored by:* The Minerals, Metals and Materials Society, TMS Light Metals Division, TMS: Aluminum Committee, TMS: Aluminum Processing Committee

*Program Organizers:* Mohd Mahmood, Aluminium Bahrain; Abdulla Ahmed, Aluminium Bahrain (Alba); Charles Mark Read, Bechtel Corporation; Stephen Lindsay, Alcoa, Inc.

Tuesday PM  
March 1, 2011

Room: 17B  
Location: San Diego Conv. Ctr

*Session Chair:* Bernard Allais, Rio Tinto Alcan

2:00 PM

**Increasing the Power Modulation Window of Aluminium Smelter Pots with Shell Heat Exchanger Technology:** Pascal Lavoie<sup>1</sup>; Sankar Namboothiri<sup>1</sup>; Mark Dorreen<sup>1</sup>; John Chen<sup>1</sup>; Donald Zeigler<sup>2</sup>; Mark Taylor<sup>1</sup>; <sup>1</sup>Light Metals Research Centre, The University of Auckland; <sup>2</sup>Alcoa Primary Metals, Aluminerie Deschambault

With power prices constantly rising, and varying aluminium prices requiring operating flexibility, the financial incentive for smelters to adopt a power modulation strategy is becoming larger. However, the power modulation window, in which a smelter can safely operate its reduction cells, is limited. The Light Metals Research Centre has developed the Shell Heat Exchanger (SHE) technology for controlling the heat dissipation from aluminium smelting potshells. By varying the air flow through the SHE, the heat removal from the potshell can be increased or decreased as desired, allowing for an increased power modulation window with minimal disturbance to the pot thermal balance. This paper presents experimental results from LMRC's test facility, which show the shell temperature response when the SHE is operated in cooling or insulating mode. Steady state thermo-electric model results for these operating scenarios are also presented, outlining the impact on ledge thickness and other pot operating conditions.

2:20 PM

**New Approaches to Power Modulation at Trimet Hamburg:** Till Reek<sup>1</sup>; <sup>1</sup>Trimet Aluminium AG

Trimet Aluminium AG acquired the Reynolds technology smelter in Hamburg in 2006 after shut down. The 135 ktpa smelter was restarted successfully in 2007 and is in continuous operation since. The increasing spread of the energy price during night and day time, as well as long term price difference have lead to novel approaches to decrease the average energy price by operating the smelter with non linear energy input. Theoretical calculations were done to estimate the maximum energy difference of cell states. Experiences were gained of the impact on performance vs. modulation range. This paper will present theoretical background as well as practical data of a smelter operating with power modulation.

2:40 PM

**Some Aspects of Heat Transfer between Bath and Sideledge in Aluminium Reduction Cells:** Asbjorn Solheim<sup>1</sup>; <sup>1</sup>SINTEF

A literature review concerning the heat transfer coefficient between bath and sideledge (h) is given. Normally, the heat transfer is controlled mainly by the circulating bath motion due to gas drainage into the peripheral channel. After the introduction of slotted anodes that direct the gas towards the centre channel, it is likely that h will be determined by natural convection in some cases, and an equation is suggested to take this into account. The coupling between heat and mass transfer during melting and freezing of sideledge was studied in a numerical model involving multicomponent diffusion. During freezing, the concentration of bath components other than cryolite is higher at the ledge surface than in the bulk of the bath. The surface temperature of the ledge varies with the rate of freezing and melting in such a way that the variation of the ledge thickness is slower than thought earlier.

3:00 PM

**Heat Recovery from Aluminium Reduction Cells:** Yves Ladam<sup>1</sup>; Asbjorn Solheim<sup>1</sup>; Martin Segatz<sup>2</sup>; Odd-Arne Lorentsen<sup>2</sup>; <sup>1</sup>SINTEF; <sup>2</sup>Hydro PMT

About half of the energy spent in aluminium electrolysis is lost as heat. A preliminary study concerning the possibilities of recovering part of that heat was carried out, primarily focusing on electrical power production. The three main heat sources (cathode sides, anode yokes, and gas) were combined in different ways, using different types of power cycles. The potential for electric power production is significant (up to 9 percent of the total consumption). The two most promising families of power cycles appear to be 1) distributed open Brayton cycle based on a turbo charger and 2) centralised power production with a Rankine cycle. The temperature and amount of heat available in the anode match well with the heat from the sides, while the potential of integrating the flue gas is limited. The main aims in energy recovery may be increased productivity or reduced energy consumption, which gives different strategies for heat collection.

3:20 PM Break

3:30 PM

**Effects of Composition and Granulometry on Thermal Conductivity of Anode Cover Materials:** Hasini Wijayarane<sup>1</sup>; Margaret Hyland<sup>1</sup>; Mark Taylor<sup>1</sup>; Ionela Grama<sup>2</sup>; Tania Groutso<sup>1</sup>; <sup>1</sup>Light Metals Research Centre; <sup>2</sup>University of Auckland

Thermal conductivity of anode cover material is critical in determining cell top heat loss. It has been observed that thermal conductivity of cover material is strongly dependent on packing and particle size distribution. Granular material that is densely packed (lower voidage) has higher thermal conductivity. When two sizes of spherical particles are mixed at various size ratios, the theoretical voidage can be reduced from 0.4 to 0.2-0.3. This can be applied to a particle system of crushed bath and alumina that constitute cover material. Currently, many smelters produce cover material that is too fine with high voidages. This has the effect of lowering the thermal conductivity which can cause unnecessary operational problems within the cell. Additionally, the effect of cover composition on thermal conductivity is not obvious. This paper describes studies conducted in the laboratory to understand the effects of composition and voidage on thermal conductivity of cover material.

3:50 PM

**Multiblock Monitoring of Aluminum Reduction Cells Performance:** Jayson Tessier<sup>1</sup>; Carl Duchesne<sup>2</sup>; Gary Tarcy<sup>3</sup>; <sup>1</sup>STAS; <sup>2</sup>Aluminium Research Centre-REGAL; <sup>3</sup>Alcoa

Aluminum reduction cell performance are affected by many factors. In order to efficiently understand possible causes of performance upsets, all major sources of variations have to be monitored. This implies monitoring all anode and alumina properties, as well as pot state and manipulated variables, while also taking into account pot design or integrity after start-up. Considering the high number of variables involved in such a task, this is practically impossible using typical statistical process control tools. The problem is worst when applied on a pot basis. This paper proposes the use of multiblock PLS (MBPLS) to build a monitoring scheme on a pot basis, simultaneously taking into account the influence of alumina and anode properties, of pot state and manipulated variables, as well as the pot state following its start-up. Derived from a regression model, the monitoring policy ensures that only variations relevant to pot performance variations are highlighted.

4:10 PM

**Towards a Design Tool for Self-Heated Cells Producing Liquid Metal by Electrolysis:** Sophie Poizeau<sup>1</sup>; Donald Sadoway<sup>1</sup>; <sup>1</sup>Massachusetts Institute of Technology

As part of an effort to assess the technical feasibility of producing metals by molten salt electrolysis, a design tool is under development for the purposes of estimating the threshold cell size and current for self-heating operation. To make the model broadly applicable to the production of different metals, two major issues must be addressed. First, accurate values of the heat transfer

coefficient are required in order to model the position of the ledge. In the Hall-Héroult cell, the heat transfer coefficient is determined experimentally from industrial operation, an approach that is not possible for a cell that has never been built. Second, thorough treatment of transport phenomena in the cell involves solving the equations for liquid and gas flows simultaneously; however, the methods used to model the turbulent flows in the Hall-Héroult cell are usually not well coupled.

#### 4:30 PM

**Restart of 300kA Potlines after 5 Hours Power Failure:** *Xinliang Zhao*<sup>1</sup>; Bingliang Gao<sup>2</sup>; Hua Han<sup>1</sup>; Jie Liu<sup>1</sup>; Jiuyi Xiao<sup>1</sup>; Jianxun Qian<sup>1</sup>; <sup>1</sup>Keao Aluminium Company; <sup>2</sup>Northeastern University, China

A Chinese reduction plant has an installed capacity of 140 kt of metal per year and employs 180 pots with line current of 300kA. In May, 2008, power failure happened. The situation lasted 5 hours. The bath temperatures fell to 900°C below. Power was switched on after recovering the power system. At the initial stage of restart the anode effect frequency was high. The voltage and amperage of lines fluctuated severely, which caused higher anode effects. The situations may cause rectifier failure. We finally solved the problems and led the lines to the normal status. The paper discusses the strategies adopted; restart operations and the technological parameter normalization during restart.

### Approaches for Investigating Phase Transformations at the Atomic Scale: Other Systems and Transformations

*Sponsored by:* The Minerals, Metals and Materials Society, ASM International, TMS Materials Processing and Manufacturing Division, TMS/ASM: Computational Materials Science and Engineering Committee, TMS/ASM: Phase Transformations Committee  
*Program Organizers:* Neal Evans, Oak Ridge National Laboratory; Francisca Caballero, Spanish National Research Center for Metallurgy (CENIM-CSIC); Chris Wolverton, Northwestern University; David Seidman, Northwestern University; Rajarshi Banerjee, University of North Texas

Tuesday PM  
March 1, 2011

Room: 32B  
Location: San Diego Conv. Ctr

*Session Chairs:* Mark Asta, University of California - Berkeley; Jeffery Hoyt, McMaster University

#### 2:00 PM Invited

**A Molecular Dynamics Study of the Cavitation Pressure in Liquid Al:** *Jeffrey Hoyt*<sup>1</sup>; Alice Potter<sup>1</sup>; <sup>1</sup>McMaster University

During the casting of alloys density differences between the liquid and solid and/or thermal stresses establish a flow of liquid from the dendrite tips to the dendrite roots. If the pressure drop which drives the liquid filling is sufficiently large, voids can nucleate in the liquid, leading to a deleterious casting defect known as hot tearing. The critical pressure at which cavities can nucleate is an important parameter in models of hot tearing and in this study we have employed molecular dynamics simulations and an embedded atom description of Al to derive the cavitation pressure in the liquid. The cavitation pressure as a function of system size has been computed and the results are compared to classical nucleation theory. In addition, the cavitation pressure has been studied for heterogeneous void nucleation at the solid-liquid interface and with the addition of trace amounts of solute (Mg).

#### 2:25 PM

**Defect Structure at Rocksalt/Tetradymite-Telluride Interfaces:** *Douglas Medlin*<sup>1</sup>; J. Sugar<sup>1</sup>; N. Heinz<sup>2</sup>; T Ikeda<sup>2</sup>; G. Snyder<sup>2</sup>; <sup>1</sup>Sandia National Labs; <sup>2</sup>California Institute of Technology

Chalcogenide compounds based on the rocksalt and tetradymite structures possess good thermoelectric properties and are of emerging interest in thermoelectric nanocomposites, where the aim is to improve thermoelectric energy conversion efficiency by harnessing phonon scattering

processes at embedded heterophase interfaces. Here, we discuss our work on the interfacial structure of tetradymite precipitates in rocksalt-structured tellurides, focusing on Sb<sub>2</sub>Te<sub>3</sub> precipitates in PbTe and AgSbTe<sub>2</sub>. We discuss the particular aspects of interfacial coherency at rocksalt/tetradymite interfaces, laying out the formal crystallographic description of interfacial defects in these systems, and using this description to interpret transmission electron microscopy observations of the interfaces obtained through both HRTEM and weak-beam dark-field methods. From these results, we identify a defect that can accomplish the rocksalt-to-tetradymite phase transformation through diffusive-glide motion along the interface and we clarify the mechanisms of interfacial strain accommodation and the relationship of the step and dislocation structure to the tetradymite precipitate morphology.

#### 2:40 PM

**Phase Transformation Identification in Beta Titanium Alloys Using ETMT, Gleeble and SSDTA:** *Yufeng Zheng*<sup>1</sup>; Robert Williams<sup>1</sup>; Boian Alexandrov<sup>1</sup>; John Lippold<sup>1</sup>; Hamish Fraser<sup>1</sup>; <sup>1</sup>The Ohio State University

Beta titanium alloys are promising candidates for future biomedical implants as well as high temperature aerospace applications. Developing an understanding for the microstructural evolution in beta titanium alloys is critical for tailoring mechanical properties. Omega phase and b' phase are widely believed to be precursors of alpha precipitates during an intermediate temperature aging process. Using state of the art equipment, the onset of alpha precipitates formation in beta titanium alloys can be identified precisely using electrical resistivity measurement by the Electro-Thermo-Mechanical Tester (ETMT). Therefore, the ETMT has provided the ability for a detailed study of the microstructure and composition evolution during the initial stage of alpha precipitation formation with transmission electron microscopy (TEM). The phase transformation sequence is also compared with the result of the single sensor differential thermal analysis (SSDTA). The microstructure evolution in Ti-Xwt%Mo binary alloy will be introduced to illustrate the power of the method above.

#### 2:55 PM

**Investigating Omega Precipitation in Titanium Alloys at the Atomic Scale:** Arun Devaraj<sup>1</sup>; *Soumya Nag*<sup>1</sup>; Robert Williams<sup>2</sup>; Srinivasan Rajagopalan<sup>3</sup>; Srinivasan Srivilliputhur<sup>1</sup>; Hamish Fraser<sup>2</sup>; Rajarshi Banerjee<sup>1</sup>; <sup>1</sup>University of North Texas; <sup>2</sup>The Ohio State University; <sup>3</sup>Exxon Mobil Corporation

The omega phase is commonly observed in beta or near-beta titanium alloys on quenching from above the beta-solutionizing temperature. These omega precipitates are highly refined (nanometer scale), homogeneously distributed, and can potentially act as heterogeneous nucleation sites for the precipitation of the equilibrium alpha phase. The present study primarily focuses on omega precipitation within the beta (body-centered cubic or bcc) matrix of simple model binary titanium-molybdenum (Ti-Mo) alloys. Direct atomic scale observation of pre-transition omega-like embryos in quenched alloys, using aberration-corrected high-resolution scanning transmission electron microscopy coupled with 3D atom probe tomography will be presented. First-principles computations have been performed using the Vienna ab initio simulation package (VASP) to determine the minimum energy path for the beta to omega transformation in Ti-Mo alloys with upto 20wt%Mo and the results of these computations will be compared and contrasted with the results from the HAADF-HRSTEM and 3DAP characterization studies.

#### 3:10 PM Break

#### 3:25 PM Invited

**Computational and Experimental Investigations of Core-Shell Precipitates in Al-Sc-Li Alloys:** *Mark Asta*<sup>1</sup>; Colin Ophus<sup>2</sup>; Abhay Raj Singh Gautam<sup>2</sup>; Marta Rossell<sup>2</sup>; Emmanuelle Marquis<sup>3</sup>; Velimir Radmilovic<sup>2</sup>; Uli Dahmen<sup>2</sup>; <sup>1</sup>University of California, Berkeley; <sup>2</sup>Lawrence Berkeley National Laboratory; <sup>3</sup>University of Michigan

Two-step aging treatments in ternary Al-Sc-Li alloys have been shown to lead to the formation of highly monodisperse coherent core-shell precipitates with Al<sub>3</sub>Sc-based cores and Al<sub>3</sub>Li-based shells. In this talk we will discuss insights into the thermodynamic driving forces and kinetic pathways leading



to the formation of these precipitates, gained through a combination of advanced electron-microscopy techniques, small-angle X-Ray scattering, atom-probe tomography and first-principles computational modeling. Detailed measurements of compositional distributions within the precipitate establish the presence of appreciable levels of Li in the core phase, which is present even after very long annealing times. The origins of the observed Li partitioning and its effect on nucleation kinetics is analyzed with the aid of first-principles based Monte-Carlo simulations.

### 3:50 PM

**Remarkable Microstructural Stability of Cu-Based Ternary Alloys during High Temperature Annealing:** Xuan Zhang<sup>1</sup>; Nhon Vo<sup>1</sup>; Pascal Bellon<sup>1</sup>; Robert Averback<sup>1</sup>; <sup>1</sup>UIUC

The microstructural evolution of dilute Cu-based ternary Cu-W-Nb alloys under high temperature annealing was investigated by both experiments and Kinetic Monte Carlo simulations. Experiments using TEM/STEM and x-ray diffraction show that while annealing of Cu90Nb10 at 600C leads to extensive coarsening, with precipitate sizes greater than 40nm, the addition of only 1.5 at% of W dramatically suppresses this precipitate growth. The average precipitate size in the ternary alloy reaches only ~ 18nm at 700C, and then, surprisingly, decreases on annealing at higher temperatures. The precipitate size distribution, moreover, is bimodal. Kinetic Monte Carlo simulations provide insight for understanding these observations. Using kinetic and thermodynamic parameters representative of the experimental Cu-W-Nb system, we find that a subtle combination of the very low mobility of one of the solute components (W), and of its very low solubility, can explain the experimental results. Extension to other systems with refractory precipitates is discussed.

### 4:05 PM

**Ab-Initio Calculation of the Phase Stability of Mechanically Unstable High-Temperature Phases:** Nikolas Antolin<sup>1</sup>; Oscar Restrepo<sup>1</sup>; Wolfgang Windl<sup>1</sup>; <sup>1</sup>Ohio State University

Ab-initio calculations have been hugely successful in the past decade to provide the necessary free energies to predict phase transformations and phase stability for elemental and alloyed materials. The application of ab-initio methods, however, is problematic when it comes to model metals and their alloys with mechanically unstable high-temperature phases, such as the bcc high-temperature phases of Ti, Zr, Hf, or U. In this study, we propose an approximate first principles approach, considerably simpler and more efficient than previous methods, to calculate free energies of elemental and alloy phases, materials constants, and defect energies while addressing the problems of phase instability. We show examples for phase stability and transformations, defect energies and mechanical properties for systems with unstable high-temperature phases, including Ti alloys, metallic uranium, and NiTi shape memory alloys.

### 4:20 PM

**Effect of Dilute H on Phase Transformations near Hcp Zr Crack Tip:** Margarita Ruda<sup>1</sup>; Graciela Bertolino<sup>2</sup>; Diana Farkas<sup>3</sup>; Peter Evans<sup>3</sup>; <sup>1</sup>CAB-CNEA; <sup>2</sup>CONICET; <sup>3</sup>Virginia Tech

We present atomistic studies of the deformation mechanisms occurring in the crack tip region during low temperature fracture of hcp Zr. Several competing processes are involved, including the phase transformation to the bcc structure. Other major mechanisms which are responsible for ductility are twinning and dislocation emission. For the cases in which a phase transformation to bcc is observed, it results in a considerable improvement in ductility. A dilute amount of H impurities placed at different distances from the crack tip significantly affects the competition between crack propagation, twin generation and phase transformations in the crack tip region. In particular, the presence of H can modify the size of the transformation region and can lead to an increase in ductility.

### 4:35 PM

**Precipitation of Prismatic Plates in Mg-0.3Ca-(0.3-1)in (at%) Alloys:** Chamini Mendis<sup>1</sup>; Keiichiro Oh-ishi<sup>1</sup>; Tadakatsu Ohkubo<sup>1</sup>; Kazuhiro Hono<sup>1</sup>; <sup>1</sup>National Institute for Materials Science

Addition of over sized elements like RE and Ca in Mg alloys with a small amount of undersized elements like Zn and Al often cause the precipitation of basal plates, e.g., internally ordered GP zones in Mg-RE-Zn, Mg-Ca-Zn, and Mg-Ca-Al alloys. However, for effective age hardening response, precipitation of prismatic plates is proposed to be more effective. In this study, we report the precipitation of a high number density of thin prismatic plates in Mg-0.3Ca-In alloys. Optimized In additions led to the enhancement of age hardening response 3 times higher than that for the binary Mg-0.3Ca alloy. The peak aged Mg-0.3Ca-1.0In alloys consisted of uniformly dispersed prismatic plates with three atomic layers. The morphology, size and composition of the precipitates in the Mg-0.3Ca-1.0In alloys were characterized by TEM, HAADF and 3DAP, and the mechanism of the formation of the precipitates on the prismatic planes will be discussed.

### 4:50 PM

**Strengthening Precipitate Phases in the WE43 Alloy at Peak Hardness:** Shengjun Zhang<sup>1</sup>; Gregory Olson<sup>1</sup>; <sup>1</sup>Northwestern University

The precipitates in the WE43 alloy aged to peak hardness at 250°C have been characterized by local-electrode atom-probe (LEAP) tomography. The accurate chemical compositions of the matrix and the precipitates were determined and compared with the results calculated using the Mg-Nd-Y thermodynamic database. In parallel, the theoretical strengths of pure Mg and the Mg with yttrium along the prismatic and basal directions have been investigated by means of first-principles calculations with the highly-precise full-potential linearized augmented plane-wave (FLAPW) method within the method of ab initio tensile test. Both experimental and theoretical investigations show that the majority of yttrium and neodymium goes to the strengthening precipitates, and the remains in the hcp Mg-rich matrix contribute to the good toughness and ductility. This work provides an important calibration point for quantitative modeling of precipitation strengthening for high performance Mg alloys design. Work supported by U.S. Army Research Laboratory.

## Biological Materials Science: Biomedical Materials, Implants and Devices

*Sponsored by:* The Minerals, Metals and Materials Society, TMS Electronic, Magnetic, and Photonic Materials Division, TMS Structural Materials Division, TMS: Biomaterials Committee  
*Program Organizers:* Jamie Kruzic, Oregon State University; Nima Rahbar, University of Massachusetts, Dartmouth; Po-Yu Chen, University of California, San Diego; Candan Tamerler, University of Washington

Tuesday PM  
March 1, 2011

Room: 15A  
Location: San Diego Conv. Ctr

*Session Chairs:* Marian Kennedy, Clemson University; John Nychka, University of Alberta

### 2:00 PM Invited

**Biomaterial Advances and Failure in Total Joint Replacement:** Roy Bloebaum<sup>1</sup>; <sup>1</sup>University of Utah/ VA Medical Center

A historical review of the use and the application of biomaterials for cementless fixation and bearing surfaces in total joint replacement will be presented. An argument will be made that the history of what made the materials work is often ignored to the detriment of the patients and industry. Also experimental flaws that continue to be made when developing or selecting a material for cementless fixation or a load bearing surface in total joint replacement will be presented. The goal is that by understanding the history, success and failures of new and proven biomaterials that patient care

will no longer be compromised thereby preventing industry medical legal complications as well.

### 2:30 PM

**Can Mechanical Properties of Bioactive Glass-Ceramics be Improved Without Sacrificing Their Bioactivity?:** *John Nychka*<sup>1</sup>; *Satadru Kashyap*<sup>1</sup>; *Hamidreza Pirayesh*<sup>1</sup>; <sup>1</sup>University of Alberta

Whilst bioactive glasses have been used as implant materials for many years they lack sufficient mechanical properties for a wide range of applications. This presentation will discuss different strategies for processing fixed compositions of bioactive glasses in order to change their properties via phase transformations. For example, crack deflection and thermal shock resistance can be substantially increased. Analysis of the effects of phase transformations on bioactivity is presented along with characterization of the glass-ceramics.

### 2:50 PM

**Mechanical and In-Vitro Behaviour of Alumina and Zirconia Based Bioceramics:** *Ajoy Pandey*<sup>1</sup>; *Usha Jena*<sup>1</sup>; *Debika Mandal*<sup>1</sup>; *Koushik Biswas*<sup>1</sup>; <sup>1</sup>Indian Institute of Technology Kharagpur

Yttria/ceria stabilized zirconia (Y/C-SZ) and yttria/ceria stabilized zirconia toughened alumina (Y/C-SZTA) powders were synthesized by co-precipitation technique and conventionally sintered to full density. Polished ( $R_a=0.03/956\text{m}$ ) samples were subjected to fretting (ball on disc) and sliding (pin on disc) wear at different loads for  $10^5$  cycles taking (WC)/UHMWPE as counter body. The surface roughness, wear depths and wear volumes were estimated by surface profilometer from the surface scan of the worn profile. From the measured wear volume, specific wear rates were calculated. Hydrothermally treated (for 20-100 h in presence of simulated body fluid at  $134^\circ\text{C}/0.2\text{MPa}$ ) specimens were subjected to wear and found that the wear rates were different for different compositions and are influenced by the extent of phase transformation (tetragonal to monoclinic) during ageing. Biocompatibility (Osteoconduction) test of the developed materials were for various ageing times (1-4 weeks) by subjecting the specimens in SBF solution at  $37^\circ\text{C}$ .

### 3:10 PM

**Effects of Nanocrystalline Calcium Deficient Hydroxyapatite on the Resorption of Conventional Glass Ionomer Cements (GIC):** *Sumit Goenka*<sup>1</sup>; *Rajkamal Balu*<sup>2</sup>; *T. S. Sampath Kumar*<sup>2</sup>; <sup>1</sup>Visveswaraya National Institute of Technology (VNIT), Nagpur, India; <sup>2</sup>Indian Institute of Technology Madras (IITM), Chennai, India

The study focuses on developing a GIC-Calcium deficient hydroxyapatite (CDHA) composite with improved resorption properties of the cement. Nano-crystalline CDHA was synthesized via accelerated microwave synthesis and characterized using X-Ray Diffraction (XRD) and Fourier Transform Infrared Spectroscopy (FTIR). CDHA was mixed in 5%, 10%, and 15% with GIC as substitution, maintaining powder to liquid ratio and capsules of dimensions 8mm x 4mm diameter were made. XRD and FTIR of capsules showed increased crystallinity and characteristic apatite bands with increased CDHA content Scanning Electron Microscopy (SEM) showed the surface morphology. The capsules were kept at  $37^\circ\text{C}$  in deionized water ( $\text{pH}=7$ ) to check for ionic release via Inductive Coupled Plasma Spectroscopy (ICP) and demineralized solution ( $\text{pH}=5$ ) for weekly weight loss study of 4 weeks. The ionic release and %weight loss were found to increase with increasing CDHA, whereas micro-hardness was found to decrease with CDHA substitution using Vickers micro hardness test.

### 3:30 PM

**Spark Plasma Sintering of Complex Shape HAP-CNT Composites:** *Yen-Shan Lin*<sup>1</sup>; *Marc.A Meyers*<sup>1</sup>; *Eugene.A Olevsky*<sup>2</sup>; <sup>1</sup>UCSD; <sup>2</sup>SDSU

Hydroxyapatite ( $\text{Ca}_{10}(\text{PO}_4)_6(\text{OH})_2$  - HAP) is an attractive biocompatible material which can be utilized for implant fabrication. However, its insufficient mechanical strength limits its implementation in major load bearing components. In this study, carbon nanotubes were employed to enhance the mechanical properties of hydroxyapatite due to their unique mechanical properties. An HAP powder and carbon nanotubes were mixed

through ultrasonication and freeze drying; the produced composite powder mixtures were consolidated by spark plasma sintering (SPS) process. 2vol% CNT-HAP, 0.5vol% CNT-HAP and pure HAP powders were sintered at  $900^\circ\text{C}$  with dwelling time of 5 min. It is shown that the CNT-HAP composites exhibit higher nano-hardness values and elastic modulus in comparison with pure HAP-based components. The retention of the carbon nanotubes in the HAP matrix during SPS was confirmed by SEM analyses. Furthermore, the feasibility of the fabrication of complex shape CNT-HAP components via SPS is demonstrated as a possible venue for dental implant applications

### 3:50 PM Break

### 4:00 PM

**Nanopillared Metal Stent for Superior Endothelialization and Controlled Drug Release:** *Karla Brammer*<sup>1</sup>; *Mariana Loya*<sup>1</sup>; *Sungho Jin*<sup>1</sup>; <sup>1</sup>UC San Diego

Due to the late-stent-thrombosis concerns and limited endothelialization associated with drug-eluting stents, bare metal stents are receiving much attention in recent years. We have created radially emanating high aspect ratio metallic nanopillar structures on the surface of MP35N (Co-Ni-Cr-Mo) stent alloy wires using an argon RF plasma processing technique. It is shown that superior endothelial cell growth is also combined with a well organized monolayer formation and improved endothelialization on the nanopillar structure. Additionally, the nanopillar structure with deep grooves in between offers a much increased surface area and adds an important capability for trapping drugs and controlled release for therapeutics. We believe that these optimistic findings are likely to contribute to new surface design concepts for bare metal stents, eventually lead to medical advances toward mitigating stent thrombosis and restenosis, and eliminate the need for polymer modified stent surfaces.

### 4:20 PM

**Corrosion Products of Iron Wire Arterial Implants from In Vivo and In Vitro Studies:** *Daniel Pierson*<sup>1</sup>; *Jacob Edick*<sup>2</sup>; *Justine Farina*<sup>1</sup>; *Jonathan Zuidema*<sup>1</sup>; *Donisha Das*<sup>1</sup>; *Nikki Long*<sup>1</sup>; *Jon Stinson*<sup>2</sup>; *Heather Getty*<sup>2</sup>; *Jaroslav Drelich*<sup>1</sup>; *Jeremy Goldman*<sup>1</sup>; <sup>1</sup>Michigan Technological University; <sup>2</sup>Boston Scientific

Pure iron has been proposed as a bioabsorbable stent material due to its biocompatibility and mechanical strength. Presently, the degradation products and mechanisms of iron corrosion in an artery are largely unknown. In the present study, iron wire was implanted into either the abdominal rat aortic wall or lumen to simulate the implantation of an iron stent. In both implantation environments, the corrosion product hematite was produced on the surface of the implanted iron wire. In vitro studies revealed that iron plates submerged under culture medium or first encapsulated in fibrin exhibited similar corrosion product as the implant. The formation of the hematite corrosion product on the aortic wire implant, the submerged iron plate, and the iron plate encapsulated in fibrin suggests that cell culture medium may act as a realistic bio-simulating solution for investigating iron corrosion in vitro and that encapsulation within a networked extracellular matrix may promote bio-corrosion.

### 4:40 PM

**Surface Patterning Effects on Wear and Friction in Metal-Polymer and Metal-Metal Contact:** *Caleb Eljach*<sup>1</sup>; *Marian Kennedy*<sup>1</sup>; *John DesJardins*<sup>1</sup>; *Nathan Mitchell*<sup>1</sup>; <sup>1</sup>Clemson University

Interest in the friction and wear properties of joint materials has resulted in some studies on the effect of micropatterned surfaces on the frictional coefficient during sliding contact while under lubricated conditions. Our study focuses on the effect of pattern geometry and feature size using 316 steel. We will present data on the affect of the pattern geometry (holes, pillars and ovals) and surface feature size (10, 50 and 100  $\mu\text{m}$ ) of 316 stainless steel on its frictional when in contact with either a stainless steel or polyethylene. All samples were fabricated by a proprietary process by Hoowaki Inc and initial results will include characterized for surface uniformity and pattern aspect ratio. The coefficient of friction was measured for each surface (smooth, 10 $\mu\text{m}$  round holes, 50 $\mu\text{m}$  round holes, and 100 $\mu\text{m}$  round holes)

using a CETR system. All testing was done using both a stainless steel pin and a polyethylene pin.

**5:00 PM**

**Bi-functional Chimeric Peptide Coatings for Improved Osteointegration of Titanium Implants:** Hilal Yazici<sup>1</sup>; Mustafa Gungormus<sup>2</sup>; Mehmet Sarikaya<sup>2</sup>; Candan Tamerler<sup>2</sup>; <sup>1</sup>Istanbul Technical University; <sup>2</sup>University of Washington

The problems associated with osteointegration remains to be the main cause of failure of titanium implants into bone and dental tissues. To date, many of the surface modification techniques to improve integration of bone into implants rely on the chemical and physical tailoring of the substrates which otherwise contain biologically undesirable hostile surfaces leading to undesirable reactions. We demonstrate the use of chimeric peptide motifs as surface coatings towards improving osteointegration. The genetically designed, robust bi-functional peptide coatings require no specially prepared biological environment in binding to implant surfaces and could be linked to bioactive entities. The bi-functional peptides consist of both titanium-binding and mineralization-directing components. Solution and cell-based in vitro mineralization assays show that the peptides significantly increase the mineral formation on the implant creating an osteoconductive surface for cell attachment and proliferation. Research is supported by NSF-MRSEC, NSF-BIOMAT, TUBITAK-NSF IRES Joint Projects, and TR-SPO.

**5:20 PM**

**Mechanical Behavior of a Biological Beta-Ti Alloy:** Sudhakar Vadiraja<sup>1</sup>; <sup>1</sup>Montana Tech

$\beta$ -titanium alloys are developed as high-efficient biomedical alloys because of their high strength, high fracture toughness, good workability, low elastic modulus, and excellent corrosion resistance as opposed to commonly used  $\alpha+\beta$  type titanium alloys. The presently investigated  $\beta$ -titanium alloy (Ti-15V-3Al-3Cr-3Sn) was subjected to annealing treatment to maximize its forming characteristics. The mechanical properties; yield strength, tensile strength, %elongation in addition to hardness and impact strength were evaluated. The microstructural constituents were examined using HiRox digital microscope. The fracture morphology was also investigated using SEM to characterize the mode of fracture. The biological beta-Ti alloy exhibited a good combination of tensile and impact properties. The microstructure revealed the presence of stabilized beta phase with alpha particles. The fractography revealed a typical ductile fracture demonstrating its good level of toughness.

**5:40 PM**

**Effects of Extrusion and Heat Treatment on the Mechanical Properties and Bio-Corrosion Behaviors of Mg-Nd-Zn-Zr Alloy for Biomedical Applications:** Xiaobo Zhang<sup>1</sup>; Guangyin Yuan<sup>1</sup>; Lin Mao<sup>1</sup>; Guohua Wu<sup>1</sup>; Wenjiang Ding<sup>1</sup>; <sup>1</sup>Shanghai Jiaotong University

Room temperature mechanical properties and biocorrosion behaviors of Mg-3Nd-0.2Zn-0.4Zr (NZK) alloy prepared at different extrusion temperatures, as well as heat treatment, were studied. The mechanical properties of magnesium alloy at room temperature improve significantly after extrusion and heat treatment compared to as-cast alloy. The results of mechanical properties show that the yield strength (YS) decreases apparently with increasing extrusion temperature. The tensile elongation decreases a little while the ultimate tensile strength (UTS) has no obviously difference. The yield strength and ultimate tensile strength improve clearly after heat treatment at 200°C for 10 hours compared with that at extrusion state, which can be mainly contributed to the precipitation strengthening. The biocorrosion behaviors of the NZK alloy were studied using immersion tests and electrochemical tests. The results reveal that the extruded NZK alloy and the aging treatment on the extruded alloy show much better biocorrosion resistance than that at solid solution state (T4 treatment). The corrosion mechanism is regarded as uniform corrosion.

## Bulk Metallic Glasses VIII: Structures and Mechanical Properties II

*Sponsored by:* The Minerals, Metals and Materials Society, TMS Structural Materials Division, TMS/ASM: Mechanical Behavior of Materials Committee

*Program Organizers:* Gongyao Wang, University of Tennessee; Peter Liaw, Univ of Tennessee; Hahn Choo, Univ of Tennessee; Yanfei Gao, Univ of Tennessee

Tuesday PM  
March 1, 2011

Room: 6D  
Location: San Diego Conv. Ctr

*Session Chairs:* Katharine Flores, The Ohio State University; Michael Atzmon, University of Michigan

**2:00 PM Invited**

**High Heating Rate Crystallization Behavior of a Zr-Based Metallic Glass: Insights into Glass Structure:** Katharine Flores<sup>1</sup>; Hongqing Sun<sup>1</sup>; <sup>1</sup>The Ohio State University

Metallic glasses exhibit a pronounced asymmetry in their critical cooling and heating rates required to prevent crystallization. This has been attributed to the presence of pre-existing phase separation or quench-in nuclei that accelerate the crystallization process upon heating. The crystallization temperature increases with heating rate, suggesting that critical steps in the crystallization process may be bypassed at high heating rates. The present study examines the crystallization mechanisms for a Zr-based bulk metallic glass heated at 0.167 K/s–50 K/s. Crystallization at low heating rates results in nanocrystallization, while micro-scale spherulites form at high heating rates. The activation energy required for spherulite formation is markedly lower than that for nanocrystallization, contributing to the asymmetry in critical heating and cooling rates. TEM analysis reveals no compositional difference at the interface between the crystallized spherulite and amorphous parent material, suggesting that the structure of the spherulites may provide insight into the glass structure.

**2:20 PM**

**Investigation of Elevated Temperature Effect on the Mechanical Behaviors of a Thin Film Metallic Glass Cu<sub>52</sub>Zr<sub>48</sub>:** Jianjun Pang<sup>1</sup>; Yuchan Liu<sup>2</sup>; Ming-Jen Tan<sup>1</sup>; <sup>1</sup>Nanyang Technological University; <sup>2</sup>Singapore Institute of Manufacturing Technology

An amorphous thin film Cu<sub>52</sub>Zr<sub>48</sub> was grown on a Si substrate. The mechanical properties at the elevated temperatures were characterized through the instrumented nanoindentation. It was found that the displacement bursts in the loading process are facilitated as the temperature increases, i.e., very few burst events occur at the room temperature while they do more commonly at higher temperatures. Additionally, the indentation size effect (ISE) was probed. Interestingly, the reduced modulus shows more significant ISE rather than the hardness especially at higher temperatures. In other words, the modulus decreases with increasing indentation depth while the hardness holds almost constant throughout the range of test depths.

**2:30 PM Invited**

**Nanoscale Mechanics and Medium Range Order in Bulk Metallic Glasses:** Don Stone<sup>1</sup>; Zenon Melgarejo<sup>1</sup>; Jinwoo Hwang<sup>1</sup>; Jon Puthoff<sup>1</sup>; Joseph Jakes<sup>2</sup>; Hongbo Cao<sup>1</sup>; Chuan Zhang<sup>1</sup>; Eren Kalay<sup>3</sup>; Matthew Kramer<sup>3</sup>; Paul Voyles<sup>1</sup>; <sup>1</sup>University of Wisconsin; <sup>2</sup>USDA Forest Products Laboratory; <sup>3</sup>Iowa State University/Ames Laboratory

Broadband nanoindentation creep (BNC) measures hardness of Cu-Zr and Cu-Zr-Al metallic glasses across 5-6 decades in deformation rate. The experiments generate activation volume data across a wide enough range of flow stress to test atomistic theories of plastic deformation and to detect subtle differences in behavior depending on composition and annealing. For instance, BNC-based estimates place the shear transformation zone (STZ) size at between about 150 and 600 atoms, depending on composition, which falls in the regime of medium range order (MRO). Additional information about MRO is gained from fluctuation electron microscopy (FEM), which



reveals the “graininess” of the structure at nanometer length scales. FEM experiments demonstrate an ordering length scale of 1.7-2.5 nm in Zr-Cu metallic glass. Annealing experiments demonstrate quantitatively the structural relaxation of our metallic glass samples including an increase in STZ size.

### 2:50 PM

#### **Mechanical Polarization of Cu50Hf41.5Al8.5 Bulk Metallic Glass:** *Rainer Hebert*<sup>1</sup>; Arif Mubarak<sup>1</sup>; <sup>1</sup>University of Connecticut

Structurally relaxed Cu50Hf41.5Al8.5 bulk glasses were elastically compressed for up to 50 hours at loads of approximately 70 % of the yield strength. The effect of the static elastic compression on the bulk glass was examined with temperature-modulated thermomechanical analysis (MTMA) in directions parallel and perpendicular to the compression direction. The MTMA studies reveal anisotropy in the non-reversible length changes. Non-reversible length reductions with heating are more pronounced parallel to the loading direction and less pronounced perpendicular to the loading direction compared to structurally relaxed samples that were not elastically loaded. The MTMA results are compared with results of X-ray studies and are furthermore analyzed with an activation energy spectrum approach. It is proposed that the static elastic compression induces a re-orientation of atomic bond orientations and that the MTMA results reflect the tendency of the glass to regain an isotropic atomic bond distribution upon heating.

### 3:00 PM Invited

#### **Multiscale Mechanical Studies for Investigating the Role of the Metallurgical Structure on the Mechanical Properties of Metallic Glasses:** *Jian Lu*<sup>1</sup>; Y. Yang<sup>2</sup>; C.T. Liu<sup>2</sup>; Q. Wang<sup>2</sup>; J.C. Ye<sup>2</sup>; P. Liaw<sup>3</sup>; <sup>1</sup>City University of Hong Kong; <sup>2</sup>The Hong Kong Polytechnic University; <sup>3</sup>University of Tennessee

In this presentation, we summarize our recent works in the field of the mechanical behaviors of metallic glasses. The mechanisms of brittle and ductile transition as a function of the sample size will be studied using the multiscale mechanical testing techniques: compression test, micropillar compression test, nano-indentation and micro-bending tests. The newly developed high frequency dynamic micro-pillar tests have been used to probe both atomic clusters and flow defects in metallic-glasses. It is clearly revealed that atomistic free-volume zones are composed by two phases with distinguished characteristic dynamics signatures. The significant enhancement of ductility of Zr based; Cu based; Ti based; and Al based metallic glasses using the SMAT (Surface Mechanical Attrition Treatment) will be presented. The results show clearly the metallurgical structures play a key role for generating different toughening mechanisms.

### 3:20 PM

#### **Measurement of Viscosity of a Metallic Glass in the Inaccessible Temperature Region Using Rapid Joule Heating:** *Georg Kaltenboeck*<sup>1</sup>; Joseph Schramm<sup>1</sup>; Marios Demetriou<sup>1</sup>; William Johnson<sup>1</sup>; <sup>1</sup>California Institute of Technology

The lifetime of metallic glasses in the temperature region of the crystallization nose is so short that conventional heating techniques are far too slow to allow for the measurement of liquid properties. Therefore, a lack of physical data exists for metallic glasses in this temperature region. For example, a wide gap in the temperature-dependent viscosity exists around the crystallization nose even for the most robust glass formers. Recently, a novel joule heating method was developed that utilizes the unique electrical properties of the metallic glass to rapidly and uniformly heat to any temperature within the undercooled liquid region. Heating rates as high as 10<sup>6</sup> K/s were achieved, which enable the complete bypass of crystallization during the heating phase. Using parallel plate rheometry in combination with this heating technique, the viscosity of Zr<sub>41.25</sub>Ti<sub>13.75</sub>Cu<sub>12.5</sub>Ni<sub>10</sub>Be<sub>22.5</sub> was measured around the crystallization nose over a range inaccessible with conventional heating methods due to crystallization.

### 3:30 PM Break

### 3:40 PM Invited

#### **Properties of Shear Transformation Zones:** *Michael Atzmon*<sup>1</sup>; Jong Du Joo<sup>1</sup>; Dongchan Jang<sup>2</sup>; Amadi Nwankpa<sup>1</sup>; <sup>1</sup>University of Michigan; <sup>2</sup>Caltech

The different modes of time-dependent deformation of metallic glasses are believed to involve activation of shear transformation zones (STZs). Most studies of the subject focus on large local strains, with cross-interactions among STZs. In order to determine fundamental properties of STZ, it is advantageous to study them at low densities, when the probability of interactions among them is low. At low densities, STZs can be reversed by the elastically-deformed matrix upon release of external strain, resulting in macroscopic anelasticity. Therefore, we have measured anelastic relaxation in amorphous Al86.8Ni3.7Y9.5, using a combination of nanoindenter cantilever, and bend relaxation, measurements, spanning over 7 orders of magnitude in time. The resulting relaxation-time spectra indicate at least seven distinct processes. Using Argon's theory,\* we estimate the respective density of potential and active STZs, as well as their size. \*A. Argon, Acta Metall. 27, 47 (1979).

### 4:00 PM

#### **Microscale Characterization of Amorphous-Crystalline Metallic Composites:** J. Sosa<sup>1</sup>; K. Flores<sup>1</sup>; *Nicholas Hutchinson*<sup>1</sup>; <sup>1</sup>The Ohio State University

Bulk metallic glasses (BMG) are limited in application by their propensity for highly localized deformation that occurs with little to no ductile deformation when loaded in tension. To improve the toughness of these alloys, a number of Ti-Zr BMG composites have been created by a semi-solid processing technique that results in a two phase microstructure. The effectiveness of the reinforcement phase on improving toughness and ductility depends on both alloy composition and the microstructure. In the present work, we characterize two related composite compositions which exhibit vastly different mechanical properties. Microstructural variations are characterized 3-dimensionally using focused ion beam serial sectioning and a unique image processing technique. The effectiveness of the reinforcement phase is related to the ability to transfer deformation across the crystalline-amorphous interface, TEM characterization of the interface structure is also examined. Finally, the mechanical properties of the individual composite phases are characterized using a micro-compression technique.

### 4:10 PM Invited

#### **Understanding Roles of Secondary Amorphous Phases in Glassy Matrix:** *Eun Soo Park*<sup>1</sup>; <sup>1</sup>Seoul National University

Previous research on phase separating metallic glasses (PSMGs) suggests that exploring these paradigm shifting materials would be very fruitful for design of new types of composite structure. Thus, PSMGs have been actively studied not only to understand conditions for separation but also to investigate their unique properties. However, there has been no systematic approach to understand the role of secondary amorphous phase (SAP) in these PSMGs. In this study, we examine the effect of SAPs on their properties in various metallic glasses. We can fabricate SAP with different sizes in glassy matrix by controlling the kinds and amount of additional elements. Firstly, we will provide systematic discussion of the relationship between atomic scale SAPs and shear band formation. Secondly, we will discuss how nanometer scale SAP containing magnetic elements influences magnetic properties in PSMGs. Our results would contribute to a deeper understanding of various roles SAPs play in glassy matrix.

### 4:30 PM Invited

#### **Nanocrystallization of a Bulk Metallic Glass in the Zr-Al-CuNiCo System – Structure and Mechanical Properties:** Arnaud Caron<sup>1</sup>; Rainer Wunderlich<sup>2</sup>; *Hans Fecht*<sup>2</sup>; <sup>1</sup>Tohoku University; <sup>2</sup>Ulm University

A controlled two-phase mixture in terms of volume fraction and morphology of nanocrystalline and amorphous components offers the possibility of tailoring the ductility and mechanical strength of BMG forming complex alloys. This has been investigated in the Zr-Al-CuNiCo alloy system as a sole function of the Al-concentration varied between 7 and 20 at%. At the

composition limit of glass formation different amorphous to crystalline phase ratios and geometries have been obtained by casting and investigated by XRD, SEM, atomic resolution TEM (FIE Titan) and, in particular, AFAM. Minor compositional variations do result in a BMG exhibiting excellent glass forming ability and two widely separated crystallization peaks which allows a wide variation of the nanocrystalline / glassy microstructure and related properties.

**4:50 PM**

**On Interfacial Bonding in Mg-Cu-Gd Metallic Glass via High Pressure Torsion (HPT):** *Baolong Zheng*<sup>1</sup>; *Yizhang Zhou*<sup>1</sup>; *Chi Y.A. Tsao*<sup>2</sup>; *Ruslan Valiev*<sup>3</sup>; *Enrique Lavernia*<sup>1</sup>; <sup>1</sup>University of California, Davis; <sup>2</sup>National Cheng Kung University; <sup>3</sup>Ufa State Aviation Technical University

The nature of the interface between particles critically influences the mechanical properties of bulk Metallic glasses (MGs) consolidated from powder. However, the low atomic diffusion ability and low thermal stability under a favorable consolidation temperature window ( $T_g$  to  $T_x$ ), might hinder a good diffusion bonding. In this work, high pressure torsion (HPT) technique was applied to consolidate Mg-Cu-Gd amorphous powder via introduction of high pressure and severe plastic deformation, and to study fundamental phenomena associated with atomic diffusion and interfacial bonding during HPT consolidation of MG powder. The microstructural evolution at/near the interfaces of HPT'ed Mg-Cu-Gd BMG samples was characterized using SEM and TEM, and the phase transformation and thermal stability were analyzed with XRD and DSC. The influence of severe plastic deformation via HPT on interfacial bonding in bulk Mg-Cu-Gd and resultant mechanical response are discussed in an effort to provide insight into fundamental phenomena in MGs with HPT.

**5:00 PM Invited**

**Ni-Free Zr-Ti-Cu-Al Bulk Metallic Glasses: Tensile Property and Fracture Toughness:** *Jian Xu*<sup>1</sup>; *Qiang He*<sup>1</sup>; *Evan Ma*<sup>2</sup>; <sup>1</sup>Institute of Metal Research, Chinese Academy of Sciences; <sup>2</sup>Johns Hopkins University

In this work, we report an effort to simultaneously follow the three considerations/leads above, to reach a Ni-free, Zr-rich, high-toughness BMG with higher GFA. Specifically, concentrating on the Zr-rich compositions, we investigated the GFA of quaternary Zr(Ti)-Cu-Al alloys using the "3D pinpointing approach". A new Zr-Ti-Cu-Al BMG (denoted as ZT1) was discovered to have a good GFA to yield as-cast glassy rods of 10 mm in diameter, permitting the measurement of fracture toughness in accordance with ASTM standard E399. For this Ni-free BMG, yield strength ( $\sigma_y$ ) in tension at the strain rates of  $1 \times 10^{-4}/s$  and  $2 \times 10^{-1}/s$  was determined to be  $\sim 1590$  MPa and  $\sim 1400$  MPa, respectively. Furthermore, this Ni-free BMG exhibits a fracture toughness of  $\sim 100$  MPa $\sqrt{m}$ , together with a small variation. Summarizing the available toughness data for Zr-based BMGs, the previously suggested correlations between the fracture toughness and Poisson's ratio and shear modulus are discussed.

**5:20 PM**

**Mg-Cu/Ni-Nd Bulk Metallic Glasses: Glass Transition Temperature and Elastic Properties Versus Toughness:** *Ling Shi*<sup>1</sup>; *Jian Xu*<sup>1</sup>; <sup>1</sup>Institute of Metal Research, Chinese Academy of Sciences

Intrinsic brittleness of Mg-based BMGs correlates with lower Poisson's ratio ( $\nu \sim 0.31$ ). Meanwhile, the elastic constants of BMGs can be roughly estimated based on the weight-averaged elastic constants of the constituent elements. It is helpful for the alloy design to use the elastic constants as the indicators of ductility of BMGs. Among RE elements, Nd possesses the highest  $\nu$ . Thus, the Mg-Cu/Ni-Nd ternary BMGs are of interest for searching tough BMGs by tuning  $\nu$ . In this work, the optimized BMG-forming formers are located at the Mg<sub>57</sub>Cu<sub>34</sub>Nd<sub>9</sub> and Mg<sub>64</sub>Ni<sub>21</sub>Nd<sub>15</sub>, with shear modulus  $\mu$  and  $\nu$  determined to be 20.5 GPa and 0.322, and 17.9 GPa and 0.324, respectively. In addition, the Mg<sub>64</sub>Ni<sub>21</sub>Nd<sub>15</sub> BMG exhibits  $T_g$  around 37 K higher than that of the Mg<sub>57</sub>Cu<sub>34</sub>Nd<sub>9</sub> BMG which led to the increased the room temperature structural relaxation resistance. The low  $\mu$  and high  $T_g$  of Mg<sub>64</sub>Ni<sub>21</sub>Nd<sub>15</sub> BMG contribute to its higher notch toughness.

**5:30 PM Invited**

**Topological and Chemical Order in Liquids and Glasses – Influence on Phase Transitions:** *Ken Kelton*<sup>1</sup>; <sup>1</sup>Washington University

Recent studies have demonstrated significant short- and medium-range chemical and topological order in liquid alloys; some examples are discussed. Quantitative measurements of the time-dependent nucleation rate in a metallic glass (Zr<sub>59</sub>Ti<sub>3</sub>Cu<sub>20</sub>Ni<sub>8</sub>Al<sub>10</sub>) and associated structural studies of the supercooled liquid show that icosahedral short-range order grows significantly on supercooling and likely contributes to the glass transition. Recent studies of liquid Zr<sub>80</sub>Pt<sub>20</sub> demonstrate medium-range order at temperatures even above the melting temperature, suggesting that it is important in liquid solidification and glass formation in this alloy. Abrupt chemical ordering is observed in supercooled liquid Cu<sub>46</sub>Zr<sub>54</sub> near 850°C; it is correlated with a specific heat maximum, which yields information about the change in energy of the liquid with ordering. Nanoscale phase separation in Al<sub>88</sub>Y<sub>7</sub>Fe<sub>5</sub> glass explains the poor glass stability and the high crystal nucleation rates.

**5:50 PM Invited**

**Inhomogeneous Flow and Fracture of Glassy Materials:** *Akira Furukawa*<sup>1</sup>; *Hajime Tanaka*<sup>1</sup>; <sup>1</sup>University of Tokyo

Understanding the mechanism of the non-Newtonian rheological response in inhomogeneous flow of glassy materials, which eventually develops into macroscopic shear-band, fracture, and so on, has been a long-standing unresolved fundamental problem of science despite intensive efforts so far. On the basis of a novel rheological model of fracture, we demonstrate that nonlinear behavior associated with fracture is a consequence of the coupling between density fluctuations and deformation fields: shear-induced enhancement of density fluctuations is self-amplified by the resulting enhancement of dynamic and elastic asymmetry between denser and less-dense regions. This positive feedback may be the origin of fracture. We propose novel criteria for the onset of mechanical instability. The criteria enable us to predict and design fracture behavior of materials from the pressure or density dependence of their viscoelastic properties of glass formers.

## Cast Shop for Aluminum Production: Dross Formation, Control and Handling

*Sponsored by:* The Minerals, Metals and Materials Society, TMS Light Metals Division, TMS: Aluminum Committee, TMS: Aluminum Processing Committee

*Program Organizers:* Geoffrey Brooks, Swinburne University of Technology; John Grandfield, Grandfield Technology Pty Ltd

Tuesday PM  
March 1, 2011

Room: 16A  
Location: San Diego Conv. Ctr

*Session Chair:* Pierre Le Brun, Alcan CRV

**2:00 PM Introductory Comments**

**2:05 PM**

**Oxidation of AlMg in Simulated Dry and Humid Atmospheres:** *Anne Kvithyld*<sup>1</sup>; *Darcy Stevens*<sup>1</sup>; *Shawn Wilson*<sup>1</sup>; *Thorvald Engh*<sup>2</sup>; <sup>1</sup>SINTEF; <sup>2</sup>NTNU

The loss of aluminium is expected to be higher in cast houses that are hot and humid, due to increased oxidation. Al-Mg alloys are known to oxidise easily, and are investigated in our new thermo-gravimetric furnace with humidity control with possibility to measure evolved gases simultaneously. The effects of dry and humid atmospheres on aluminium oxidation are studied. Oxidation is compared for the given conditions and alloy composition as a function of time. Using the data from both the thermo-gravimetric furnace and mass spectrometer, the mechanisms of oxide formation can be described and modelled.

2:30 PM

**Study of Early Stage Interaction of Oxygen with Al; Methods, Challenges and Difficulties:** *Behrooz Fateh*<sup>1</sup>; Geoff Brooks<sup>1</sup>; M. Akbar Rhamdhani<sup>1</sup>; John Taylor<sup>2</sup>; Jeff. Davis<sup>3</sup>; Martin Lowe<sup>3</sup>; <sup>1</sup>Swinburne University of Technology; <sup>2</sup>CAST CRC; <sup>3</sup>The Centre for Atom Optics and Ultrafast Spectroscopy (CAOUS), Swinburne University of Technology

Aluminium is one of the metals with the greatest affinity for oxygen. Kinetics of early-stage oxidation are believed to have an important influence on the later steady-state oxide growth. Furthermore, there are many aspects of aluminium melt handling and casting processes that result in oxidation and dross formation. Sophisticated experimental studies such as scanning tunneling microscopy (STM), combined ellipsometry-auger electron microscopy and etc have clarified some aspects of the initial stage oxidation. However, most of the experimental data are not consistent and reproducible. Furthermore, the dynamics of absorption and oxidation processes are much less understood. This paper reviews the methods, techniques and the challenges of measuring and quantifying the oxidation of Al during its initial stages and also introduces a new method for studying the formation of an oxide layer upon solid aluminum, following ablation of the surface with an ultra-fast laser beam and a fast imaging techniques.

2:55 PM

**Quality Assessment of Recycled Aluminum:** *Derya Dispinar*<sup>1</sup>; Anne Kvithyld<sup>1</sup>; Arne Nordmark<sup>1</sup>; <sup>1</sup>SINTEF Materials and Chemistry

One of the significant aspects during remelting of aluminum is surface oxide also with contaminations such as coatings. In this work, a wrought and a cast alloy were selected and subjected to remelting experiments. Bifilm index was measured as a measure of metal quality; 3-point bending and tensile testing samples were collected for mechanical testing. 3105 wrought alloy sheets were collected from before anodising, between anodising and painting and after painting. It was found that the surface of all the charges were accumulated over the surface and skimmed off. Therefore, the quality of all three charges was same and the mechanical properties were also the same. For the cast alloy, A356 alloy was subjected to remelting for six times. The quality was decreased after three times of remelting with decreased mechanical properties. Overall, a good correlation between the mechanical properties and the bifilm index were found.

3:20 PM

**Preserving Metal Units Utilizing the Latest Generation of Aluminum Dross Press:** *James Herbert*<sup>1</sup>; Alan Peel<sup>2</sup>; <sup>1</sup>Altek LLC; <sup>2</sup>Altek Europe Ltd.

The proper handling and processing of dross at the generation site is critical to reclaiming maximum metal units from this valuable by-product. A widely used technology designed to cool dross and maximize metal recoveries is the dross press. Since its introduction to the industry in the early 1990's this technology has been significantly improved to meet the demands of the modern cast house and increasingly stringent environmental legislation. This paper describes developments that address the weaknesses and limitations of early systems and enhancements that have enabled the cooling of a wide variety of dross types including salt slag from rotary furnaces. Areas addressed include mechanical design/reliability, extended capacity, automation, safety and environmental compliance, and metal recovery. Data from recent installations will be discussed along with economic models showing the positive effect small improvements in dross recoveries can have on the bottom line.

---

## Characterization of Minerals, Metals and Materials: Characterization of Non-Ferrous Alloys

*Sponsored by:* The Minerals, Metals and Materials Society, TMS Extraction and Processing Division, TMS/ASM: Composite Materials Committee, TMS: Materials Characterization Committee  
*Program Organizer:* Sergio Monteiro, State University of the Northern Rio de Janeiro - UENF

Tuesday PM  
March 1, 2011

Room: 14B  
Location: San Diego Conv. Ctr

*Session Chairs:* Shadia Ikhmayies, Al Isra University; Augusta Isaac, Laboratório Nacional de Luz Síncrotron

---

2:30 PM

**Evolution of Crystallographic Texture of Cold Roll Bonding and Annealing Ti-Al-Nb Multilayer Sheets:** *Peng Qu*<sup>1</sup>; Liming Zhou<sup>1</sup>; Viola Acoff<sup>1</sup>; <sup>1</sup>the University of Alabama

Usually, the mechanical properties of sheet materials strongly rely on the crystallographic texture. Also, it is commonly known that cold rolling will affect the texture of a material extensively. A ternary Ti-46Al-9Nb intermetallic alloy (at. %) was produced by accumulative cold roll bonding (ARB) followed by reaction annealing in our previous research. In this paper, Electron Backscattered Diffraction (EBSD) was employed to explore the influence of deformation conditions on microstructure and texture evolution of Ti-Al-Nb multilayer sheets made by the ARB process. As the reduction amount increased, the textures of Al and Nb changed significantly. The texture of Ti became more random due to the increase in defects as a result of ARB. The rolling texture of thin sheet materials was found to be different from that of rolled bulk materials. The texture evolution of the sheet materials after annealing was also investigated.

2:45 PM

**Capillarity-Driven Migration of a Thin Ge Wedge on a Bicrystalline Au Substrate:** *Tamara Radetic*<sup>1</sup>; Andrew Minor<sup>1</sup>; Ulrich Dahmen<sup>1</sup>; <sup>1</sup>NCEM, Lawrence Berkeley National Lab

This work reports on the retraction of an anisotropic, solid thin Ge wedge in epitaxial contact with a bicrystalline Au film. Using TEM, we have observed striking crystallographic and morphological effects at the junction of the Ge-wedge with the Au substrate. In-situ microscopy and FIB-prepared cross-sectional samples allowed a 3D characterization of the observed morphological changes and enabled us to elucidate the mechanism of the transformation. We found that capillary forces at the Au/Ge interface result in ridge formation during wedge retraction. The bicrystalline Au substrate was not inert, but underwent abnormal grain growth in the area swept by the receding Ge-wedge. The morphological evolution of a solid wedge on a deformable substrate is of particular interest as a simple model system to investigate the stability of non-equilibrium configurations and its evolution under the influence of capillary forces and crystallographic anisotropy. This work is supported by DOE/BES/MSD under Contract No.DE-AC02-05CH11231.

3:00 PM

**Characterization of Laser Shock Peened IN718 SPF:** *Amrinder Gill*<sup>1</sup>; Vijay Vasudevan<sup>1</sup>; S.R. Mannava<sup>1</sup>; <sup>1</sup>University of Cincinnati

Laser shock peening improves service lifetimes of critical aero engine components. LSP introduces deep compressive residual stresses which improves fatigue strength, life and crack propagation resistance. This study aims to understand effects of LSP parameters on residual stress distributions and microstructural changes in an important aero-engine material, IN718 SPF. Coupons of alloy with and without sacrificial layer were peened with varying energy densities. Depth-resolved characterization of macro residual strains and stresses was achieved using high-energy synchrotron x-ray diffraction and conventional XRD. Near surface and through the depth changes in strain, texture and microstructure were also studied using EBSD

TUESDAY PM



in SEM and TEM. Local property changes were examined using micro and nano-indentation measurements. Studies were also done on thermal stability of residual stresses and microstructure

### 3:15 PM

**Classification of Precipitation Shapes in Nickel Base Gamma-Gamma Prime Alloys:** Jason Van Sluytman<sup>1</sup>; Tresa Pollock<sup>2</sup>; <sup>1</sup>University of Michigan; <sup>2</sup>University of California - Santa Barbara

Changes to the nominal compositions of nickel (Ni)-base superalloys provides a wide array of gamma prime ( $\gamma'$ ) morphology that has not typically been quantified. Two-dimensional moment invariants are implemented to classify morphologies and provide quantitative values for particle shapes. An experimental set of platinum group metal containing Ni-base superalloys, which contain variations in  $\gamma'$  morphology, has been examined using 2D moment invariants. Using the shape parameter ratio,  $\eta$ , it is demonstrated that Al, Cr, and Ta change  $\eta$  to a greater extent over Re and Ir. Plotting  $\eta$  as a function of lattice misfit magnitude results in a peak maximum at  $\eta$  approximately equal to 1 - indicative of a cuboidal morphology - when the misfit magnitude is 0.3%. This peak coincides with the misfit possessed by many highly creep resistant commercial superalloys. Thus, tailoring nominal compositions to provide  $\eta$  equal to 1 may be desirable in designing future superalloys.

### 3:30 PM

**Dynamic-Tensile-Extrusion of Zirconium: The Role of Texture:** Carl Trujillo<sup>1</sup>; George Gray III<sup>1</sup>; Ellen Cerreta<sup>1</sup>; Daniel Martinez<sup>1</sup>; <sup>1</sup>Los Alamos National Laboratory

The effect of high strain-rate and high strains on mechanical behavior has been observed primarily in isotropic, cubic materials. The behavior of low-symmetry, textured, materials is not as well understood. To examine the high strain and high strain rate response of structural metals a dynamic extrusion technique has been developed at Los Alamos National Laboratory. In this study, high-purity zirconium bullets were accelerated up to velocities of 615m/s and extruded through a high-strength steel die. A combination of in-situ and ex-situ characterization techniques has been used to study the response of Zr under this dynamic loading condition. For the first time, PDV (Photonic Doppler Velocimetry) has been employed to capture the time and velocity of the evolved deformation through the die. Quantitative examination of the influence of texture and extrusion velocity will be presented.

### 3:45 PM

**Effect of Ti Addition on Microstructure and Tensile Property of Aged Cu-Ni-Si Alloy:** Eungyeong Lee<sup>1</sup>; Sangshik Kim<sup>1</sup>; Kwangjun Euh<sup>2</sup>; Seungzeon Han<sup>2</sup>; <sup>1</sup>Gyeongang National University; <sup>2</sup>Korea Institute of Materials Science

Age-hardenable Cu-Ni-Si alloy is categorized as a high-electrical conductivity, high-strength copper alloy for the application of lead-frame and connector in the electronic devices, and the addition of trace amount of Ti, such as 0.09 wt.% and 0.18 wt.%, may improve both electrical conductivity and strength by increasing the driving force of  $\delta$ -Ni<sub>3</sub>Si precipitation during aging. In this study, the effect of trace amount of Ti addition on microstructure and tensile property of aged Cu-4.4Ni-1.0Si alloys at 450°C with varying time ranging from 10 to 360 minutes were examined. The tensile property of aged Cu-Ni-Si alloys was substantially influenced by small amount of Ti addition, as associated with a considerable microstructural evolution. The tensile behavior of Cu-4.4Ni-1.0Si-xTi alloys with different aging condition is discussed based on the detailed micrographic and fractographic observations.

### 4:00 PM Break

### 4:15 PM Invited

**Comparison of Ni-Cr and Co-Based Alloys for Fuel Injectors:** Giorgio Scavino<sup>1</sup>; Paolo Matteis<sup>1</sup>; Giovanni Mortarino<sup>1</sup>; Donato Firrao<sup>1</sup>; <sup>1</sup>Politecnico di Torino

A sintered Nickel-Chromium alloy (wt.% composition: Ni 50, Cr 48) is compared with cast or sintered Cobalt-based alloys (wt.% composition: Cr

25, W 5, C 1.2) for fuel injectors production. Each alloy underwent structural and microstructural examinations and tensile as well as fatigue tests at the maximum service temperature (500 °C). The 2 million cycles fatigue limit was estimated by the staircase method. Microscopic mechanisms for fatigue crack nucleation and growth and for overload fracture were also investigated. The Ni-Cr alloy is isotropic and homogeneous; it is biphasic, constituted by a Ni-rich FCC phase (about 70 vol.%) and a Cr-rich BCC one (30 vol.%), both with 2  $\mu$ m grain size. Its 500 °C tensile strength is intermediate between those of the sintered and cast Cobalt alloys, whereas its fatigue limit is somewhat lower than that of the sintered Cobalt alloy, but much higher than that of the cast Cobalt one.

### 4:45 PM

**Microstructural Characterization of 70Cu-30Ni Alloy Formed by Direct Metal Deposition (DMD®) Process:** Sudip Bhattacharya<sup>1</sup>; Jyotirmoy Mazumder<sup>1</sup>; Guru Prasad Dinda<sup>2</sup>; Ashish Dasgupta<sup>2</sup>; Bhaskar Dutta<sup>3</sup>; <sup>1</sup>University of Michigan, Ann Arbor; <sup>2</sup>Focus:HOPE; <sup>3</sup>POM

Direct Metal Deposition (DMD®) is a rapid prototyping technique used to generate near-net shape components from their computer aided design (CAD) files with very fine and controlled microstructures, and properties. In this investigation a 70Cu-30Ni alloy was deposited on a rolled C71500 alloy substrate using a CO<sub>2</sub> laser. The optical and scanning electron microscopy were used for microstructural investigation, the x-ray diffraction (XRD) technique was used for phase analysis, and the transmission electron microscopy (TEM) was used for crystal structure analysis. The microstructure consists of columnar dendrites. XRD analysis identified a CuNi solid solution phase in the sample. TEM selected area diffraction (SAD) patterns corroborated the phase analysis but the calculated lattice parameters were approximately 0.18% longer than the lattice parameters of the corresponding phase identified from XRD powder diffraction data file. This is caused by high residual stresses generated due to extremely high cooling rates during DMD®.

### 5:00 PM

**Characterization of the Manganese Oxide Scales Formed on a Grooved Cast Pb-Ag Anode from a Zinc Electrowinning Operation:** Tzong Chen<sup>1</sup>; John Dutrizac<sup>1</sup>; <sup>1</sup>CANMET-MMSL

Grooved cast Pb-Ag anodes are used by some zinc refineries to improve current efficiency. The manganese oxide scale formed on a grooved Pb-0.75% Ag anode consists mainly of MnO<sub>2</sub>, which occurs characteristically in rhythmically banded colloform structures. These adhere to a layer of "PbO<sub>2</sub>+PbSO<sub>4</sub>" that oxidized from the anode. The relatively homogeneous and nearly fracture-free morphology of the "PbO<sub>2</sub>+PbSO<sub>4</sub>" layer suggests the relatively uniform corrosion of the anode. Deposition of Mn oxide initially follows the contours of the anode surface, but the grooves eventually become filled with Mn oxide and gypsum. Hydrated Mn oxides and amorphous Mn oxides are believed to be also present in the manganese oxide scale. Tiny particles of PbSO<sub>4</sub> and SrSO<sub>4</sub>, together with gypsum, other impurities and micro-pores, tend to concentrate in the grooves.

### 5:15 PM

**Microstructure Evolution in Ultrafine-Grained CuZr Polycrystals Processed by High Pressure Torsion:** Miloš Janeček<sup>1</sup>; Ondrej Srba<sup>1</sup>; Petr Hrcubca<sup>1</sup>; Milan Dopita<sup>1</sup>; Jakub Cížek<sup>1</sup>; Radomír Kužel<sup>1</sup>; Hyoung Seop Kim<sup>1</sup>; <sup>1</sup>Charles University

Coarse grained CuZr polycrystals were processed by high pressure torsion (HPT) at room temperature with different number of rotations (N=1-15). The microstructure evolution and grain fragmentation as a function of strain induced by HPT was investigated by different experimental techniques, in particular electron backscatter diffraction (EBSD), transmission electron microscopy (TEM), positron annihilation spectroscopy (PAS) and X-ray diffraction (XRD). The evolution of microstructure with strain due to HPT was correlated with mechanical properties characterized by detail 2D-microhardness profile analysis throughout round disc specimens of 20mm in diameter.

5:30 PM

**The Effect of Rolling Mill Geometrical Parameters in Bulk Texture Analysis of Processed TiAl Based Multi-Layered Sheet Material:** *Liming Zhou*<sup>1</sup>; Peng Qu<sup>1</sup>; Viola Acoff<sup>1</sup>; <sup>1</sup>The University of Alabama

Multi-layered sheet materials processed by accumulative roll bonding technique are used to process lightweight materials such as TiAl-based alloy. Characteristics of cold roll bonded sheet materials using stacked Ti, Al, and Nb foils were studied by previous researchers, however, the texture evolution analysis of the cold rolled condition of the sheet materials is still unclear. Few studies reported the bulk texture changes and anisotropic characteristics that exist for the rolling direction and transverse direction as a function of layers along normal direction of multi-layered sheet materials. In this study, the bulk texture analysis will be investigated by both X-ray diffraction and electron back scattered diffraction techniques. Rolling mill geometrical parameters are treated as variables to impact anisotropic characteristics, like textures and disorientation distribution. The geometrical parameters influence on texture in ARB sheet materials consist of rolling speed, speed gear ratio, mean width, thickness of multi-layered specimens, reduction, and reduction ratio.

5:45 PM

**Thermophysical Properties of Platinum-Copper System:** *Shahid Mehmood*<sup>1</sup>; Ulrich E. Klotz<sup>2</sup>; Gernot Pottlacher<sup>1</sup>; <sup>1</sup>Institute of Experimental Physics TU Graz; <sup>2</sup>Fem Research Institute Precious Metals and Metals Chemistry

Platinum alloys are frequently used in technical applications and in jewellery. Their thermophysical properties such as density, heat capacity, thermal conductivity and surface tension play an important role in casting processes and are required as input data for casting simulation. Scope of this work was to investigate these properties by different methods. Platinum and four alloys namely, Pt-4Cu, Pt-32Cu, Pt-50Cu and Pt-75Cu were investigated. Thermal expansion was measured by dilatometry at fem, as well as surface tension by a sessile drop method. At TU Graz, wire shaped samples were investigated by an ohmic pulse heating technique. This technique allows the calculation of specific heat capacity and the temperature dependencies of electrical resistivity, enthalpy, and density of these alloys in the solid and liquid phase. Experimental results were compared with available literature and data from thermodynamic calculation using the SNOB1 database and ThermoCalc.

6:00 PM

**Processing and Characterization of Ultra-Fine Grain Structure in Al Alloy by Equal Channel Angular Pressing:** *Prasad Shanmugasandaram*<sup>1</sup>; Narayani Narasimhan<sup>2</sup>; Balasivanadha Prabhu<sup>3</sup>; <sup>1</sup>State University of New York, Stony Brook; <sup>2</sup>Stanford University; <sup>3</sup>Anna University

The grain refinement and mechanical properties of 6061 aluminium alloy produced by equal channel angular pressing (ECAP) have been analyzed in this present study. A innovative triple shear ECAP die was developed for the processing. It was observed that the grain refinement takes place for greater number of passes. It was also found that reducing the process temperature gives fine grain and high microhardness and hence improved properties.

6:15 PM

**Advances in Elemental Analysis, Characterization of Minerals and Ores, and Identification of Metal Alloys Using Handheld X-ray Fluorescence Technology:** *Jeff Walker*<sup>1</sup>; Chris Smith<sup>1</sup>; <sup>1</sup>Thermo Fisher Scientific

In recent years, elemental analysis using handheld x-ray fluorescence (XRF) has enjoyed significant growth in mineral analysis for mining and exploration, as well as for metal alloy characterization and identification. The introduction of large area silicon drift detectors (SDD) into handheld XRF instruments has produced significant performance improvements over traditional XRF capabilities, especially in the area of light element analysis such as Mg, Al, Si, P and S. Coupled with a high output, 50kV, miniaturized x-ray tube, the new systems can also perform light element analysis work without vacuum or helium purge. This paper will offer an explanation of the XRF technique and the evolution of handheld XRF systems. Performance considerations and specific applications will be explored.

**Computational Plasticity: Atomistic Modeling in Plasticity**

*Sponsored by:* The Minerals, Metals and Materials Society, TMS Materials Processing and Manufacturing Division, TMS Structural Materials Division, TMS/ASM: Computational Materials Science and Engineering Committee, TMS: High Temperature Alloys Committee  
*Program Organizers:* Remi Dingreville, Polytechnic Institute of NYU; Koen Janssens, Paul Scherrer Institute

Tuesday PM  
March 1, 2011

Room: 1A  
Location: San Diego Conv. Ctr

*Session Chair:* To Be Announced

2:00 PM Invited

**Deformation Mechanism in Nanocrystalline Metals: Experiments and Atomistic Simulations:** *Helena Van Swygenhoven*<sup>1</sup>; Mario Velasco<sup>1</sup>; Christian Brandl<sup>2</sup>; Andreas Elsener<sup>3</sup>; Steven Van Petegem<sup>1</sup>; Michael Weisser<sup>1</sup>; <sup>1</sup>Paul Scherrer Institut; <sup>2</sup>Los Alamos National Laboratory; <sup>3</sup>University of Zurich

Molecular dynamics deformation studies of nanocrystalline metals suggest a dislocation mechanism where dislocations travel through the grain, to be absorbed in the surrounding GBs. Cross-slip (PRL 100(2008)235501, Phil. Mag 2010-in press) is observed as a mechanism to avoid stress intensities in grain boundaries. On the other hand, many experimental observations often demonstrate grain coarsening during deformation, often referred as coupled grain boundary motion. This talk discusses the latest simulation results in terms of dislocation mediated mechanisms and coupled grain boundary motion. The influence of dilute oxygen in grain boundaries is addressed using a local chemical potential approach that optimizes the charge on only those atoms expected to be ionic (Acta Mat 57(2009)1988). Furthermore the simulation results are assessed in terms of experiments performed on nc Ni involving strain rate sensitivity measurements (APL 89(2006)73102), stress dip and in-situ tensile tests during X-ray diffraction (Scripta Mat 60(2009)297, Scripta Mat 58(2008)61).

2:30 PM

**Grain Boundary Migration as a Deformation Mechanism in Nanocrystalline Materials:** *Diana Farkas*<sup>1</sup>; <sup>1</sup>Virginia Tech

This talk will present results of atomistic simulation showing grain boundary motion in nanocrystalline materials as an important deformation mechanism. The simulations constitute virtual tensile tests of model nanocrystalline fcc materials described by empirical potentials. Grain boundary motion occurs as a response to applied stress, but not always coupled with grain boundary sliding. The atomistic mechanisms of the observed migration will be discussed. The simulation results also show that the presence of impurities in the grain boundaries can inhibit this process.

2:50 PM

**Extracting Dislocations and other Defects from Atomistic Simulations:** *Alexander Stukowski*<sup>1</sup>; Karsten Albe<sup>1</sup>; <sup>1</sup>Darmstadt University of Technology, Germany

We present a novel method for extracting dislocation lines from atomistic simulation data in a fully-automated way. Our algorithm delivers a geometric description of all dislocation lines contained in arbitrary crystalline model structures in a matter of seconds. Burgers vectors are determined reliably, and the extracted dislocation network fulfills the Burgers vector conservation rule at each node. All remaining crystal defects (grain boundaries, surfaces, etc.) are output as triangulated surfaces. In contrast to the recently proposed on-the-fly dislocation detection algorithm [Modelling Simul. Mater. Sci. Eng. 18 (2010), 015012], the new method is extremely robust, easy to use, and enables a detailed analysis of complex dislocation processes even in highly distorted crystal regions, as they occur, for instance, close to grain boundaries or in dense dislocation networks. We present applications of the

TUESDAY PM

new method to simulations of nanostructured metals and discuss prospects of a fully-automated analysis of secondary grain boundary dislocations.

**3:10 PM**

**Grain Boundary Kinetics in Molecular Dynamics: The Effect of the Driving Force on Mobility and Migration Mechanisms:** *Christopher Race*<sup>1</sup>; Johann von Pezold<sup>1</sup>; Joerg Neugebauer<sup>1</sup>; <sup>1</sup>Max-Planck-Institute for Iron Research

Molecular dynamics (MD) simulations of grain boundaries often employ some form of external driving force on the atoms to promote grain boundary motion. To obtain measurable motion of a boundary on the timescales accessible to MD, these forces must be much greater in magnitude than those responsible for real processes of microstructural evolution. Given this fact, we must take care that our externally imposed force, be it in the form of an elastic deformation or an artificial potential, does not fundamentally alter the atomic scale processes that give rise to the motion of the grain boundary. In this study we systematically investigate the effect of the strength and nature of the driving force on the mobility and migration mechanisms of representative tilt boundaries in Al. Based on an in-depth analysis of these results, we discuss possible schemes that guarantee the correct limit at zero driving force.

**3:30 PM Break**

**3:45 PM Invited**

**Slip Coupling in Crystal Plasticity:** *Vasily Bulatov*<sup>1</sup>; <sup>1</sup>Lawrence Livermore National Laboratory

The traditional computational crystal plasticity equates the plastic strain rate at a material point with the sum of component rates associated with the individual slip systems. However, experimental evidence and theoretical considerations suggest a stronger coupling between slip systems in BCC metals under certain straining conditions. When a BCC single crystal is deformed at a sufficiently low temperature and/or at a high straining rate, the fraction of screw dislocations in the total dislocation population is known to rapidly increase. Should the fraction of screws grow to become a majority, formation of (twist) dislocation networks can become the dominant mechanism by which the screw dislocations reduce their elastic energy. Such twist networks are indeed observed in BCC metals deformed at low temperatures. Each twist network ties together screw dislocations with two different  $\frac{1}{2}\langle 111 \rangle$  Burgers vectors for the total of six distinct Burgers vector pairs. In addition to a significant energy reduction through elastic screening, such tightly coupled dislocation networks can glide very easily along the  $\{110\}$  planes common to the two Burgers vectors of each couple. Careful analysis of atomic mechanisms and associated stress yield contours suggests that such cooperative network glide must be highly anisotropic in the  $\{110\}$  network planes and that the net effect of each network glide mode must be roughly equivalent to slip on a  $\langle 110 \rangle \{110\}$  pseudo-system. In BCC crystals, only three of such strongly coupled pseudo-systems are linearly independent. These observations suggest a novel interpretation of some of the known slip anomalies in BCC deformation and lead us to predict unusual new effects in crystal plasticity that can be verified by straining experiments.

**4:15 PM**

**Partial Dislocation Nucleation and Twinning in Aluminum:** Nitin Daphalapurkar<sup>1</sup>; *K.T. Ramesh*<sup>1</sup>; <sup>1</sup>The Johns Hopkins University

Recently, wide stacking fault (SF) ribbons with average widths as large as 3.5 nm have been reported in nanocrystalline Al. We use molecular dynamics (MD) simulations to investigate the widths of extended dislocations in aluminum, and demonstrate that the SF widths in aluminum are strongly dependent on the orientation of the applied stress and presence of stress-gradients. The results demonstrate a reasonable agreement between simulations, theoretical predictions, and experimental observations, and help explain recent observations of SFs in nanocrystalline-aluminum. Further, information on the Generalized Planar Fault Energy associated with Al (obtained from MD simulations) is used to arrive at orientation and temperature dependent stress required for nucleation of partial dislocations under initially homogeneous shear stress conditions, and equivalent values

for heterogeneous nucleation are derived. The qualitative and quantitative results will be useful in developing discrete models for incorporating nucleation of partial dislocation in a crystal plasticity framework.

**4:35 PM**

**Atomistic Simulations of Cu/Cu-Oxide Planar Interface Properties:** *Abdelmalek Hallil*<sup>1</sup>; Remi Dingreville<sup>2</sup>; Stéphane Berbenni<sup>1</sup>; Mohammed Cherkaoui<sup>1</sup>; <sup>1</sup>Georgia Tech - CNRS; <sup>2</sup>NYU-Poly

Preliminary work has been already carried-out for homogeneous interfaces by characterizing the general formula of Gibbs' interfacial excess energy (IEE) as a function of the interfacial excess stress. In the case of heterogeneous interfaces, the key issue is the matching of lattice vectors in the interface plane of each material, so that the overall strain is small when the interface is formed. Here, we focus on the extension of the global expression of the IEE by including the role of interfacial mismatch on the strained interfaces. Molecular Dynamics (MD) calculations are used to evaluate the role of this mismatch for a given heterogeneous interface. The Cu/Cu-oxide interface model is stretched along the interface plane regarding the length and angle of the surface-cell vectors. For each deformation process, Molecular Statics and MD simulations (NPT, NVT) are performed to compute the interfacial excess energy at the equilibrium state of the system.

**4:55 PM**

**Plastic Deformation of Au Nanoparticles and Thin-Films: A Comparative Experimental and Simulation Study:** *Dan Mordehai*<sup>1</sup>; Eugen Rabkin<sup>1</sup>; David Srolovitz<sup>2</sup>; <sup>1</sup>Technion; <sup>2</sup>Institute of High Performance Computing

We report a combined experimental/molecular dynamics study of the indentation of faceted Au nanoparticles and thin-films of similar dimensions on a sapphire surface. The particles were created via the dewetting of a polycrystalline Au film on sapphire substrate. Experiments show that the larger nanoparticles are softer, i.e. the strength is size dependent. The Molecular Dynamics simulations supply us with insights of the dislocation mechanisms within the nanoparticles during deformation and aide in rationalizing the size effect observed experimentally. The atomistic simulations show that deformation is controlled by dislocation nucleation near the tip. In nanoparticles, nucleation is followed by fast dislocation glide toward the lateral surfaces, leading to defect-free particles during indentation (dislocation starvation), while in thin films and elongated particles dislocations accumulated around and beneath the indenter. We conclude that the back-stress of the accumulated dislocations made the nucleation of new dislocations more difficult, which elucidates the experimentally-observed size effect.

**5:15 PM**

**Molecular Dynamics Analysis of Edge Dislocation Walls:** *Sebastian Echeverri Restrepo*<sup>1</sup>; Barend Thijssse<sup>1</sup>; <sup>1</sup>TU Delft

One of the simplest types of symmetrical tilt grain boundaries (GBs) can be described as a wall of equally spaced edge dislocations lying on the same plane and whose Burgers vectors are parallel to each other and perpendicular to the common plane. There exist analytical models, based mainly on the elastic isotropic theory of dislocations, to describe their structure, stress distribution and energy. We present an alternative approach to model this type of GB using molecular dynamics (MD). A new method of generating infinite dislocation walls is introduced. Edge dislocations are inserted into single aluminum crystals by selectively removing half-planes and applying the displacement field predicted by the elastic isotropic theory of dislocations. The system is subsequently relaxed to a temperature of 0K and a pressure of 0Pa using MD. The stress fields, energies and mechanical properties of the different configurations are calculated, analyzed and compared to the available models.



## Computational Thermodynamics and Kinetics: Energy Materials: Storage, Generation, Catalysis

Sponsored by: The Minerals, Metals and Materials Society, ASM International, TMS Electronic, Magnetic, and Photonic Materials Division, TMS Materials Processing and Manufacturing Division, TMS: Alloy Phases Committee, TMS: Chemistry and Physics of Materials Committee, TMS/ASM: Computational Materials Science and Engineering Committee, ASM: Alloy Phase Diagrams Committee  
Program Organizers: Raymundo Arroyave, Texas A & M University; James Morris, Oak Ridge National Laboratory; Mikko Haataja, Princeton University; Jeff Hoyt, McMaster University; Vidvuds Ozolins, University of California, Los Angeles; Xun-Li Wang, Oak Ridge National Laboratory

Tuesday PM  
March 1, 2011

Room: 9  
Location: San Diego Conv. Ctr

Session Chairs: Vidvuds Ozolins, UCLA; Stefano Curtarolo, Duke University

### 2:00 PM Invited

**First-Principles Approaches to Li-Air Batteries:** Donald Siegel<sup>1</sup>; Max Radin<sup>1</sup>; <sup>1</sup>University of Michigan

Of the many possible battery chemistries, the so-called "Li-air" system is noteworthy in that its theoretical capacity (~5 kWh/kg, including mass of O<sub>2</sub>) exceeds that of any electrochemical system. Perhaps more importantly, the simplified composition of its air cathode – involving only the inlet of oxygen from the atmosphere – has the potential to provide cost benefits in comparison to the Li-ion systems of today. Although the first rechargeable Li-air battery was demonstrated by Abraham and Jiang 13 years ago, performance in many dimensions remains poor, and relatively little work has been done to elucidate performance-limiting phenomena. This talk will introduce the basic properties and main performance issues associated with Li-air batteries. Opportunities for first-principles simulations to assist in overcoming these obstacles will be highlighted.

### 2:30 PM

**The Li-Graphite System and Surface Reactions from First-Principles:** Kristin Persson<sup>1</sup>; <sup>1</sup>LBNL

Graphitic carbon is the most commonly used anode in rechargeable Li batteries. We recently showed by kinetic Monte Carlo simulations that intralayer Li motion in bulk graphite is intrinsically very fast, even at high Li concentrations. However, carbonaceous anodes show relatively low rates, especially at low temperature. This indicates that transport through the graphite surfaces could be the slow step in the process. Furthermore, there are indications that water contamination of Li electrodes can cause damage to capacity retention [1]. In this context, we examine from first principles the graphite surfaces, and how different absorbing species and contaminants affect the Li potential at the surface, relevant for rechargeable Li batteries. [1] M. Kerlau, and R. Kostecki, J Elec. Soc. 153 (9), A1644-A1648, (2006).

### 2:45 PM

**A First Principles Study of Nanostructured Thermoelectric Materials:** Philippe Jund<sup>1</sup>; Romain Viennois<sup>1</sup>; Jean Claude Tédénac<sup>1</sup>; Mathieu Fèvre<sup>2</sup>; <sup>1</sup>Université Montpellier 2 - ICGM; <sup>2</sup>LEM - ONERA

We present DFT based simulations of magnesium silicide composites. After the determination of the energy of formation of the different structural defects, we compute the physical properties and in particular the phonon dispersion curves of Mg<sub>2</sub>Si containing various transition metal silicide nanoclusters with the aim of improving the thermoelectric properties of magnesium silicide.

### 3:00 PM

**Defects in Perovskites for Solid Oxide Fuel Cell Cathodes: Surface and Strain Effects:** Yueh-Lin Lee<sup>1</sup>; Milind Gadre<sup>1</sup>; Dane Morgan<sup>1</sup>; <sup>1</sup>University of Wisconsin-Madison

Understanding how interfaces, surfaces, and strain effects can alter defect and ionic transport properties of oxides is an area of increasing research interest in solid state ionics. In this talk we discuss *ab initio* modeling of how surfaces and strain can alter defect chemistry and kinetics in perovskites of interest as solid oxide fuel cell cathodes, such as (La,Sr)MnO<sub>3</sub> and (La,Sr)CoO<sub>3</sub>. We demonstrate that defect energy changes near surfaces are very large but can be understood in terms of a simple model based on defect charge and local oxidation level. We also show how strain can alter defect formation energies and integrate these results into a strain dependent thermodynamic defect model for (La,Sr)CoO<sub>3</sub> thin films.

### 3:15 PM Invited

**Data, Methods and Search Strategies for Metal Catalysts:** Stefano Curtarolo<sup>1</sup>; Gus Hart<sup>2</sup>; Ohad Levy<sup>3</sup>; Wahyu Setyawan<sup>1</sup>; <sup>1</sup>Duke University; <sup>2</sup>BYU; <sup>3</sup>NRCN

With a combination of "data-mining-high-throughput" and "cluster expansion" methods, we have parameterized the whole set of transition-metal binary intermetallics (435 alloys). In this talk, we introduce the method/tools [1], and we present examples for Rh-M [2], Hf-M [3] alloys, in addition to the automatic generation of *ab-initio* structure maps for hexagonal systems [4]. Furthermore, by tackling two test cases, we show the importance of the complete knowledge of the stable and metastable phases to understand deactivation in catalytic particles [5] and the solubility of species inside systems [6] leading to search strategies for novel catalytic materials with concurrent optimization of electronic [7] and thermodynamical properties [8]. [1] JACS 132, 4830 (2010)[2] JACS 132, 833 (2010)[3] Acta Mat. 58, 2887 (2010)[4] PRB 81 174106 2010[5] PRL 100, 195502 (2008)[6] Acta Mat. 57, 5314 (2009)[7] <http://dx.doi.org/10.1016/j.commatsci.2010.05.010>[8] JACS 132, 6851 2010

### 3:45 PM Break

### 3:55 PM Invited

**Self-Assembly of Stable Ti, Y, and O-Enriched Nanoclusters in Fe:** H. Zhao<sup>1</sup>; M. Krcmar<sup>2</sup>; C. L. Fu<sup>1</sup>; M. K. Miller<sup>1</sup>; <sup>1</sup>Oak Ridge National Laboratory; <sup>2</sup>Grand Valley State University

Stable nanoclusters (2-4 nm in diameter) in Fe-based alloys fabricated by mechanical alloying (MA) have been observed after isothermal aging up to 1400 C. Nanophase materials are known to be metastable in nature, because of coarsening processes that occur rapidly at elevated temperatures. These stable nanoclusters are an exception to this norm. First-principles theory has been used to investigate the defect mechanism and their formation and stability. The presence of preexisting vacancies (created during MA) is necessary for achieving high oxygen solubility and preventing the precipitation of FeO. This O-vacancy mechanism enables the nucleation of O-enriched nanoclusters with structures coherent with the underlying Fe lattice in the presence of solutes with high O affinities. An essential condition for stabilizing these nanoclusters is their exceptionally low interfacial energy in the Fe matrix. This research was sponsored by the U.S. Department of Energy, Office of Basic Energy Sciences, Materials Sciences and Engineering Division.

### 4:25 PM

**First-Principles Study of the Structure of RuO<sub>2</sub>\*xH<sub>2</sub>O:** Fei Zhou<sup>1</sup>; Yongduo Liu<sup>1</sup>; Mark Asta<sup>2</sup>; Vidvuds Ozolins<sup>1</sup>; <sup>1</sup>UCLA; <sup>2</sup>UC Berkeley

Hydrous ruthenia, RuO<sub>2</sub>\*xH<sub>2</sub>O, is a high-performance electrode material for electrochemical supercapacitors. Two different structural models for thermodynamically stable hydrous ruthenia have been proposed, differing in whether hydrogen is located inside or outside the bulk oxide. We present a theoretical examination of the validity of the bulk model using a combination of a systematic search algorithm based on electrostatics, database searching and density-functional theory calculations. We find that all the considered bulk model structures are unstable by ~0.3 - 0.4 eV per H<sub>2</sub>O molecule with

TUESDAY PM

respect to phase separation into anhydrous RuO<sub>2</sub> and water. Structures with hydroxyl groups or aggregate H<sub>2</sub>O are significantly lower in energy, demonstrating that the water prefers to agglomerate outside RuO<sub>2</sub>. This trend is shown to be present in other metal hydroxides with high valence and can be explained by qualitatively examining the water-metal oxide mixing energy. Our results strongly support the core+grain-boundary model of hydrous ruthenia.

**4:40 PM**

**Reaction Pathways of Methane Decomposition on Cu Surface from Ab Initio Calculations:** *Grzegorz Gajewski*<sup>1</sup>; Chun-Wei Pao<sup>1</sup>; <sup>1</sup>Research Center for Applied Sciences, Academia Sinica

Growth of large-area single- or few-layer graphene films has been reported recently by catalytic decomposition of methane on Cu surface at high temperature. However, the surface reaction pathways toward graphene formation have not been studied in detail. In this work, the minimum energy reaction pathways for successive dehydrogenation reactions of methane on Cu (111) surface have been investigated theoretically. Climbing image nudged elastic band method with spin-polarized DFT and periodic slab model have been used to identify geometries, energies of all reaction intermediates and transition states as well as activation barriers. The complete decomposition of isolated methane molecules on Cu surface is found endothermic. We also found activation barriers for methane decomposition on Cu surface are much lower than those in gas phase, which demonstrates the role of Cu as a catalytic material for large-area graphene film fabrication.

**5:00 PM Invited**

**Water Splitting on Reduced CeO<sub>2</sub>(111):** Heine Hansen<sup>1</sup>; *Chris Wolverton*<sup>1</sup>; <sup>1</sup>Northwestern University

Solar thermochemical cycles have the potential to convert solar energy into chemical fuels at high thermodynamic efficiency. This could for example be done by thermal reduction of CeO<sub>2</sub> to CeO<sub>2-x</sub> at high temperature followed by oxidation of CeO<sub>2-x</sub> in H<sub>2</sub>O at a lower temperature to produce H<sub>2</sub>. In this work we use density functional theory to identify the most stable surface structures on CeO<sub>2</sub>(111) containing surface or subsurface oxygen vacancies, H<sub>2</sub>O or H. We find the positions of Ce<sup>3+</sup> ions in the reduced surface affect the stability of vacancies and adsorbed hydrogen, but has only little effect on the adsorption of water. We calculate barriers for diffusion of oxygen vacancies from the bulk to the surface, for dissociation of water near surface oxygen vacancies, and for desorption of hydrogen from the surface. We use this information to derive a kinetic model of H<sub>2</sub> production from this reduced surface.

**5:30 PM**

**Thermodynamic Analysis of Phase Transformations in La<sub>c</sub>Sr<sub>1-c</sub>MnO<sub>3</sub> Perovskite Solid Solutions:** Royi Glass<sup>1</sup>; *David Fuks*<sup>1</sup>; Eugene Kotomin<sup>2</sup>; Joachim Maier<sup>2</sup>; <sup>1</sup>Ben Gurion University of the Negev; <sup>2</sup>Max Planck Institut für Festkörperforschung

Perovskite solid solutions La<sub>c</sub>Sr<sub>1-c</sub>MnO<sub>3</sub> of different compositions are widely used as cathodes for solid oxide fuel cells (SOFC). The phase diagram for the La<sub>c</sub>Sr<sub>1-c</sub>MnO<sub>3</sub> quasi-binary system is calculated combining the statistical thermodynamic approach with ab initio calculations. The temperature and concentration dependences of the long-range order parameters are calculated and used in constructing the phase diagram. The analysis of the competition between ordered structures (with the different states of order) and with the disordered state with different compositions, c and temperatures is carried out. Two-phase regions on the phase diagram are calculated. The critical temperatures for the order-disorder phase transformations are found and the type of the order-disorder phase transitions is determined. The particular La<sub>0.125</sub>Sr<sub>0.875</sub>MnO<sub>3</sub> and La<sub>0.25</sub>Sr<sub>0.75</sub>MnO<sub>3</sub> phases show extremely narrow homogeneity region and first-order type order-disorder transformation, in contrast to La<sub>0.5</sub>Sr<sub>0.5</sub>MnO<sub>3</sub> which reveals a rather extended homogeneity region and is characterized by the second-order type transformation.

**5:45 PM**

**Calculation of the Thermoelectric Power of Titanium, Zirconium, and Hafnium:** *Zhongliang Xiao*<sup>1</sup>; Hanli Yang<sup>1</sup>; Zhichao Ma<sup>1</sup>; Horst Brodowsky<sup>2</sup>; Qiyuan Chen<sup>3</sup>; <sup>1</sup>Changsha University of Science and Technology; <sup>2</sup>Christian-Albrechts-Universität zu Kiel; <sup>3</sup>Central South University

The thermoelectric power of titanium, zirconium, and hafnium has been calculated on the assumption, that number of electrons per atom as well as the pressure are constant in a temperature gradient and the electrochemical potential of the electrons is a unique function of the temperature in pure metals, and the local thermal equilibrium between electrons and metal ion cores is established. The diffusional thermopower is approximately equal to the gradient of the electrochemical potential of the electrons (calculated from the density of states), divided by the electronic charge. The calculated results agree with experimental results well.

## David Pope Honorary Symposium on Fundamentals of Deformation and Fracture of Advanced Metallic Materials: Deformation, Fracture, and Hydrogen Effects

*Sponsored by:* The Minerals, Metals and Materials Society, TMS Materials Processing and Manufacturing Division, TMS Structural Materials Division, TMS: High Temperature Alloys Committee, TMS/ASM: Mechanical Behavior of Materials Committee, TMS: Nanomechanical Materials Behavior Committee

*Program Organizers:* E. P. George, Oak Ridge National Laboratory; Haruyuki Inui, Kyoto University; C. T. Liu, The Hong Kong Polytechnic University

Tuesday PM  
March 1, 2011

Room: 32A  
Location: San Diego Conv. Ctr

*Session Chairs:* Dennis Dimiduk, Air Force Research Laboratory; Dilip Shah, Pratt & Whitney

**2:00 PM Invited**

**Non-Associated Flow of Crystalline Solids:** *John Bassani*<sup>1</sup>; <sup>1</sup>University of Pennsylvania

The structure of classical plasticity theory for crystalline materials is generally assumed to be associative in the sense that the flow potential is taken to be the yield function. Ample experimental evidence now exists that non-associated flow more appropriately characterizes dislocation glide. Indeed, in 1985, A. Cottrell remarked: "... for too long we have taken the FCC dislocation as the paradigm of all dislocation behaviour; but, as the studies of BCC screw dislocations have shown, the FCC structures and properties are the exception rather than the norm." Intermetallic compounds, in particular L12 alloys which were extensively studied by D. P. Pope, are another prominent example. Multislip models for single crystals are developed from atomistic simulations, and polycrystal behavior is estimated using simple homogenization techniques. At all levels, non-associated flow persists, and this is shown to significantly affect macroscopic deformations and failure mechanisms.

**2:30 PM Invited**

**The Ice-Structure Interaction Problem: Creep, Fracture and the Ductile-Brittle Transition of Ice:** *Erland Schulson*<sup>1</sup>; <sup>1</sup>Dartmouth College

Engineered structures situated within ice-infested waters must withstand loads that can exceed 100-year wave forces. The loads are induced through wind-and current-driven movement of floating ice sheets and icebergs, and, for a given feature, reach a maximum when the velocity of impact is great enough to activate a transition from ductile to brittle behavior of the ice. At still higher velocities where fracture dominates, structures can vibrate. This talk will review the problem, and then focus on ice and on the physical processes underlying its mechanical behavior. On scales both large and small, deformation mechanisms include dislocation climb, dynamic re-

crystallization, frictional sliding and crack initiation and propagation — processes common to all crystalline materials.

### 3:00 PM Invited

#### **Micro-Scale Investigations of Interfacial Delamination in Thermal Protection Systems:** *Kevin Hemker*<sup>1</sup>; <sup>1</sup>Johns Hopkins University

Modern thermal protection systems have multiple layers and functionalities; important phenomena governing the life of these systems occur in each layer and especially at the interfaces between disparate layers. Mechanical characterization of these systems is complicated by their reduced dimensionality. Micro-scale tensile and bending experiments provide direct routes for characterizing the constitutive properties of individual layers and for experimentally quantifying interfacial delamination. Results involving both commercial thermal barrier coatings for aircraft engines and developmental coatings for a solar probe satellite designed to fly within nine solar radii of the sun will be presented. The experimental insight gained in these experiments will be interpreted and used to facilitate hierarchical modeling of layered thermal protections systems.

### 3:30 PM Break

### 3:45 PM

#### **A TEM Study of the Micromechanisms Associated with Hydrogen Embrittlement in Steels:** *Srinivasan Rajagopalan*<sup>1</sup>; Neeraj Thirumalai<sup>1</sup>; Ning Ma<sup>1</sup>; Dakshina Valiveti<sup>1</sup>; Sanket Desai<sup>1</sup>; <sup>1</sup>ExxonMobil Research and Engineering

The study of hydrogen embrittlement of steels remains a focus area in the oil and gas industry. Several mechanisms, such as Hydrogen Enhanced Localized Plasticity (HELP) and Hydrogen Enhanced Decohesion (HEDE) have been proposed to explain the embrittling effect of hydrogen at the atomic level. Recently, another model, based upon the stabilization of vacancies in the presence of hydrogen, has also been proposed to explain this effect. However, a clear understanding of the effect of hydrogen on deformation mechanisms is still lacking. This study attempts to examine the micromechanisms associated with deformation in specific hydrogen-charged steels. Transmission Electron Microscopy (TEM) observations of deformation substructures from fracture surfaces of tensile and fracture toughness samples will be discussed. By coupling the understanding generated from these studies with observations of dislocation activity in controlled-strain tensile tests, an attempt is made to understand the effect of hydrogen on deformation and failure in specific steels.

### 4:00 PM

#### **Strain-Induced Metal-Hydrogen Interactions Across the First Transition Series – An Ab Initio Study of Hydrogen Embrittlement:** *Johann von Pezold*<sup>1</sup>; Ugur Aydin<sup>1</sup>; Tilmann Hickel<sup>1</sup>; Joerg Neugebauer<sup>1</sup>; <sup>1</sup>Max-Planck-Institut für Eisenforschung GmbH

The susceptibility of modern, high strength steels to H-embrittlement has spawned renewed interest in this long-standing, unresolved challenge in Materials Science. A key mechanism underlying all the currently discussed mechanisms of hydrogen-induced embrittlement of metals, such as hydrogen enhanced local plasticity (HELP), hydrogen enhanced decohesion (HEDE) and stress-induced hydride formation is the attractive interaction between hydrogen and distorted regions of the host matrix. In this study we systematically investigate these interactions by determining heat of solutions, H-H binding energies within the metal matrix, as well as phase diagrams as a function of the lattice strain and the H chemical potential across the first transition series (3d elements) using density functional theory (DFT) calculations. A careful analysis of the resulting extensive data sets provides direct insight into chemical trends and allows an identification whether the metal is susceptible to H-embrittlement and of the relevant embrittlement mechanism.

### 4:15 PM

#### **Influence of Hydrogen Loading on the Tensile Behavior of Fe-Ga Alloys:** *Meenakshisundaram Ramanathan*<sup>1</sup>; Biswadeep Saha<sup>1</sup>; Chai Ren<sup>1</sup>; Gavin Garside<sup>1</sup>; Sivaraman Guruswamy<sup>1</sup>; <sup>1</sup>University of Utah

Fe-Ga and other ferrous alloys exhibit large magnetostrictive behavior and are candidates for use in sensing, actuation and energy harvesting applications. Exposure to aqueous electrochemical environments is anticipated in some of these applications. This could potentially introduce hydrogen in to the alloy and cause severe ductility reduction due to hydrogen embrittlement effect. The present study examined the influence of electrochemical hydrogen loading on tensile behavior of FeGa alloys. Hydrogen was charged electrochemically prior-to and during the tensile test. The results show a dramatic reduction in the ductility with hydrogen charging. The fracture surfaces were examined using scanning electron microscope, to confirm the brittle failure in the presence of hydrogen. Influence of simultaneous presence of magnetic field during testing was also examined. \*Support of this work by NSF through the award DMR-0854166 is gratefully acknowledged.

### 4:30 PM

#### **Prismatic Cross-Slip in Mg from First Principles:** *Joseph Yasi*<sup>1</sup>; Louis Hector<sup>2</sup>; Dallas Trinkle<sup>1</sup>; <sup>1</sup>University of Illinois at Urbana-Champaign; <sup>2</sup>General Motors R&D Center

New ductile Mg alloys with high specific strength are of great interest to the transportation industry. At room temperature, forming is difficult due to the low ductility of Mg. Prismatic dislocations are two orders of magnitude stronger than basal dislocations at room temperature, but non-basal dislocation mobility is necessary to achieve the five independent slip systems required to handle an arbitrary deformation. Efficient, accurate computational models of dislocation/solute interactions provide insight into new Mg alloy development. We employ a first principles flexible boundary condition method to compute *a*-type basal and constricted prismatic screw and prismatic edge dislocation geometries in Mg. For these dislocations, we calculate solute binding energies for Al, Li, Y and Zn in the optimized dislocation cores. We predict changes in prismatic critical resolved shear stress with temperature and solute concentration from the differences in core energies on the basal and prismatic planes in the presence of solutes.

### 4:45 PM

#### **Substructure Evolution during Creep in Zirconium Alloys:** *Benjamin Morrow*<sup>1</sup>; Robert Kozar<sup>2</sup>; Kenneth Anderson<sup>2</sup>; Michael Mills<sup>1</sup>; <sup>1</sup>The Ohio State University; <sup>2</sup>Bechtel Bettis, Inc.

Zirconium alloys are commonly used for applications in nuclear reactors. Accurately predicting creep deformation of zirconium alloys throughout the lifecycle of a reactor depends on reliable deformation models. The Modified Jogged-Screw Model (MJSM) asserts that the motion of tall jogs in screw dislocations act as the rate controlling mechanism during creep in certain regimes. Previous studies have demonstrated the applicability of the MJSM to the thermal creep behavior of hcp metals, but effects of accumulated strain have never been fully explored. Scanning transmission electron microscopy (STEM) was used to directly observe and characterize the dislocation structure of creep tested Zircaloy-4 as a function of accumulated strain, and quantify pertinent model parameters such as jog height, jog spacing, and dislocation density. Thorough characterization will provide a better understanding of material behaviors in both primary and secondary creep regimes, which will ultimately result in more robust creep deformation predictions.



## Deformation, Damage, and Fracture of Light Metals and Alloys: Session II

Sponsored by: The Minerals, Metals and Materials Society, MS&T Organization, TMS Light Metals Division, TMS: Chemistry and Physics of Materials Committee, TMS/ASM: Mechanical Behavior of Materials Committee

Program Organizers: Qizhen Li, University of Nevada, Reno; Xun-Li Wang, Oak Ridge National Laboratory; Yanyao Jiang, University of Nevada, Reno

Tuesday PM  
March 1, 2011

Room: 13  
Location: San Diego Conv. Ctr

Session Chair: Qizhen Li, University of Nevada, Reno

### 2:00 PM Invited

#### Visualizing the 3D Microstructure Evolution during Deformation:

Henning Poulsen<sup>1</sup>; Masakazu Kobayashi<sup>2</sup>; Jette Oddershede<sup>1</sup>; Christian Wejdemann<sup>1</sup>; Ulrich Lienert<sup>3</sup>; Soeren Schmidt<sup>1</sup>; Ulrik Olsen<sup>1</sup>; Bettina Camin<sup>4</sup>; Grethe Winther<sup>1</sup>; Dorte Juul Jensen<sup>1</sup>; Hiroyuki Toda<sup>2</sup>; Walter Reimers<sup>4</sup>; <sup>1</sup>Risoe DTU; <sup>2</sup>Toyoashi University of Technology; <sup>3</sup>Argonne National Lab.; <sup>4</sup>TU Berlin

We present methodologies, limitations and examples of results for a coherent set of synchrotron based methods, primarily for in-situ studies of mm-sized samples during tension: • Grain mapping and grain-by-grain stresses: 3D maps with 1000+ grains have been made and compared to crack propagation as determined simultaneously by tomography. Likewise grain rotation studies of 1000+ bulk grains will be presented. • Plastic strain tomography: The strain field of an Al alloy was mapped in 3D to 10% strain and compared to the 3D grain structure and local rotations. • Orientation Imaging Microscopy. A non-destructive and 3D equivalent of the familiar EBSD technique has been established. • Formation and evolution of dislocation structures: Using a reciprocal-space approach focus will be on recent results for strain path changes. The methodologies can all be combined. The possible impact for plasticity modeling is outlined. (Experiments were performed at ESRF, APS and Spring-8.)

### 2:30 PM

#### Development of <111> Fiber Texture and {111}<112> Shear Bands in Pure Al Metal by Wire Drawing: Mohammad Shamsuzzoha<sup>1</sup>; <sup>1</sup>University of Alabama

Conventional transmission electron microscopy and x-ray diffraction techniques have been applied to study the microstructure of heavily wire drawn samples of pure Al metal. Samples thus drawn (~40% of the original value) have been found to be comprised of columnar grains with no evidence of any recrystallization and to exhibit a strong <111> texture. The microstructure of thus drawn samples contain deformation bands that are made of closely spaced parallel slip bands, which lie on {111} and extends along a <112>. Electron diffraction patterns taken from these slip bands yield very little evidence of twinning. This suggests that the slip bands in the microstructure are probably produced by coalescences of a group of parallel {111}<112> stacking faults. Most of the materials de-cohesions present in the deformed samples were found propagating along directions that are normal rather than parallel to the deformation bands.

### 2:45 PM

#### Effects of Spatial Locations of Nucleation Sites on Incipient Damage in High Purity Aluminum: Matthew Tucker<sup>1</sup>; John Bingert<sup>1</sup>; Timothy Ulrich<sup>1</sup>; Cheng Liu<sup>1</sup>; Ching-Fong Chen<sup>1</sup>; George Gray<sup>1</sup>; <sup>1</sup>Los Alamos National Lab

To accurately predict the failure of components, the mechanisms driving incipient damage nucleation must be more fully understood. This study aims to quantify the effect of the spatial location of nucleation sites on the earliest stages of damage evolution. A large-grained, high-purity aluminum provides a matrix with no significant level of homogeneous damage nucleation sites. OIM analysis will be employed to determine optimal sample extraction location with respect to grain orientation, shape, boundary inclusion, etc.

Once a suitable location is determined, a section will be extracted and prepared for the placement of designed damage nucleation sites and smaller tracer particles. The mating surfaces will then be diffusion bonded and a tensile specimen will subsequently be fabricated. The embedded nucleation and tracer particles will be monitored via XCMT and coupled with digital image correlation between interrupted tensile tests to capture the evolution of localized strain fields and damage nucleation.

### 3:00 PM

#### Fracture Behavior of Short Carbon Fiber Reinforced Aluminium Matrix Composite: Pengfei Yan<sup>1</sup>; Guangchun Yao<sup>1</sup>; Jianchao Shi<sup>1</sup>; Xiaolan Sun<sup>1</sup>; Hongjie Luo<sup>1</sup>; <sup>1</sup>School of Materials & Metallurgy, Northeastern University

The microstructure and fracture behavior of aluminum matrix composites reinforced with copper coated short carbon fiber were investigated. 4% carbon fibers were added to aluminium matrix through the stir casting method. The microstructure of composites showed that there was a uniform distribution of carbon fibers and good interfacial bonding with the matrix. The tensile test was carried out to evaluate the tensile strength of the composites. The microstructure of the fracture surface were observed by using scanning electron microscopy (SEM), and the fracture mechanism of the composites was discussed.

### 3:15 PM Break

### 3:30 PM

#### Microscale Discontinuous Displacement Measurement Techniques: Helena Jin<sup>1</sup>; Sandip Haldar<sup>2</sup>; Hugh Bruck<sup>2</sup>; Wei-Yang Lu<sup>1</sup>; <sup>1</sup>Sandia National Labs; <sup>2</sup>University of Maryland

This research is to develop a feasible technique to measure the discontinuous deformations at the microscale, such as those associated with crack tips. Both grid method and digital image correlation (DIC) technique were explored to measure the microscale and discontinuous displacements at the crack tip during the fracture test of aluminum specimens. Three point bending test of aluminum specimens were conducted inside a Scanning Electron Microscopy (SEM). A unique pattern which can be applied for both techniques was generated by sputtering gold films onto the specimen surface through copper mesh. The displacement fields calculated from both techniques are compared with each other to identify the strengths and weaknesses of each technique for the microscale and discontinuous displacement measurements.

### 3:45 PM

#### Microstructural Influence on the Mechanical Behaviour of Ti-5Al-5Mo-5V-3Cr: Nicholas Jones<sup>1</sup>; David Dye<sup>1</sup>; Trevor Lindley<sup>1</sup>; <sup>1</sup>Imperial College London

High strength titanium alloys, e.g. Ti-5Al-5Mo-5V-3Cr (Ti-5-5-5-3), are currently used in large components such as the truck beam in landing gear assemblies. Unlike other classes of titanium alloys, metastable beta alloys can be processed to develop a wide range of microstructures, all of which can influence the mechanical properties of the final component, e.g. strength, fatigue and fracture toughness. This ability to tailor the microstructure has resulted in significant interest into possible applications of these alloys into areas of the airframe traditionally dominated by other alloy classes. Thus, properties previously thought to be second order, such as high cycle fatigue (HCF) life have become important. Limited research concerning the fatigue behaviour of Ti-5-5-5-3 has been available in the public domain, with little or no consideration of the relationship between microstructure and micro-mechanisms of cracking. Here we consider the effect of different microstructures on the HCF properties of Ti-5-5-5-3.

### 4:00 PM

#### Effects of Rolling Induced Anisotropy on Fatigue Crack Initiation and Short Crack Propagation in Al 2024-T351 under Uniaxial and Biaxial States of Stress: Admir Makas<sup>1</sup>; Ikshwaku Atodaria<sup>1</sup>; Ross MacKinnon<sup>1</sup>; Pedro Peralta<sup>1</sup>; <sup>1</sup>ASU

The influence of rolling-induced anisotropy on fatigue properties is important for the prediction of useful life of aerospace structures via computational modeling. In this work, fatigue behavior is studied using

notched uniaxial samples with load axes along either the longitudinal or transverse direction, and biaxial samples (cruciforms), where local composition and crystallography are quantified using Energy Dispersive Spectroscopy and Electron Backscattering Diffraction. Subsequently, interrupted fatigue testing at stresses close to yielding is performed on the samples to nucleate and propagate short fatigue cracks and nucleation sites are located and characterized using standard optical and Scanning Electron Microscopy. Results indicate that scatter is higher for loading along the transverse direction. The 3-D geometry of the critical precipitates, obtained using ion beam machining, is correlated to local crystallography to understand the effects these variables have on cracking behavior. Work funded by Department of Defense, AFOSR Grant FA95550-06-1-0309, David Stargel program manager.

#### 4:15 PM

**Damage Evolution in Ultrasonic Welded Aluminum/Fiber-Reinforced Polymer Joints with Different Welding Geometries:** *Natalia Konchakova*<sup>1</sup>; Ralf Mueller<sup>1</sup>; Franz Josef Barth<sup>1</sup>; Frank Balle<sup>1</sup>; Dietmar Eifler<sup>1</sup>; <sup>1</sup>University of Kaiserslautern

This research aims at the investigation of damage evolution in light weight engineering structures, like aluminum/fiber-reinforced polymer welding joints. The finite element method is used for a numerical analysis of mechanical behavior of a single overlap tensile specimen, which is produced by ultrasonic welding. The influence of the welding geometry on the joint's damage is considered. An elastoplastic model with Lemaitre-type-damage is applied. The present work contains results for three different welding geometries: square, circle and moon. It is shown that the damage is lower in the specimen with circle welding zone as compared to square interface. The damage progress in the joint with moon welding domain takes place later than in the other specimens. The specimen with moon welding geometry has the highest point of maximal load. The simulated results show agreement with the experimental data for the ultrasonic welded joint with square welding area.

#### 4:30 PM

**Role of Austenite Plasticity in the Deformation of Superelastic Nitinol:** *David Xu*<sup>1</sup>; Robert Ritchie<sup>1</sup>; <sup>1</sup>UC Berkeley

Nitinol is an important biomedical shape memory alloy that can behave superelastically. It derives its superelasticity from transformation between austenite and martensite phases. The transformation occurs when local strain on the austenite phase exceeds 1.2%. Traditionally, the martensitic transformation is assumed to be the major source of strain. We loaded Nitinol tensile dogbone samples under X-ray microdiffraction to study the phase transformation and texture. It was found that numerous austenite grains went untransformed over 1.2% local strain. Beyond the orientation effects of transformation, it was found that martensite transformation is not the only contributing factor for strain. There are evidence of that some of the austenite phases are being plastically deformed instead of transformed into the martensite phase. The austenite plasticity can provide an explanation for the limits to the reversibility of transformation in cyclic loading of Nitinol.

#### 4:45 PM

**Deformation in Two-Phase Titanium Alloys Studied by Surface Strain Mapping Techniques:** *Rebecca Sandala*<sup>1</sup>; João Fonseca<sup>1</sup>; Michael Preuss<sup>1</sup>; <sup>1</sup>University of Manchester

The purpose of this study is to investigate the slip character at the  $\alpha/\beta$  interface in two phase titanium alloys. Detailed in situ deformation studies have been carried out on lamellar and bilamellar microstructures of Ti-6246. Digital Image Correlation was used to obtain the strain maps from optical images taken during loading where high localised strain was mainly observed close to grain boundary  $\alpha$  and in favourable  $\alpha$  orientations. It was found on further loading that high strain areas also coincided with slip traces. Several of these slip traces transferred across grain boundary  $\alpha$  regardless of the difference in neighbouring orientations. For further clarification CPFEM was used to predict the deformation by creating a virtual microstructure from the EBSD data. Furthermore studies of the  $a_1$ ,  $a_2$  and  $a_3$  slip were carried

out using EBSD and TEM to clarify why slip occurs in some regions of favourable orientations more than others.

#### 5:00 PM

**Vanadium Effects on a BCC Iron Sigma 3 Grain Boundary Strength:** *Sungho Kim*<sup>1</sup>; Seong-Gon Kim<sup>1</sup>; Mark Horstemeyer<sup>1</sup>; <sup>1</sup>Center for Advanced Vehicular Systems

The effects of micro-alloying element, vanadium, on a BCC Fe sigma 3 (111)[1-10] symmetric tilt grain boundary strength are studied using Density Functional Theory calculations. The lowest energy configuration of the grain boundary structure are obtained from the first-principles calculations. The substitutional and interstitial point defect formation energies of vanadium in the grain boundary are compared. The substitutional defect is preferred to interstitial one. The segregation energies of vanadium onto the grain boundary and its fractured surfaces are computed. The cohesive energy calculation of the grain boundary with and without vanadium show that vanadium strengthen the BCC iron grain boundary. The tensile and shear tests on the grain boundary with and without vanadium segregation are carried out to study the vanadium effect on the grain boundary.

### Dynamic Behavior of Materials V: Shock Compression

*Sponsored by:* The Minerals, Metals and Materials Society, TMS Structural Materials Division, TMS/ASM: Mechanical Behavior of Materials Committee

*Program Organizers:* Marc Meyers, UCSD; Naresh Thadhani, Georgia Institute of Technology; George Gray, Los Alamos National Laboratory

Tuesday PM  
March 1, 2011

Room: 5A  
Location: San Diego Conv. Ctr

*Session Chair:* Jerry La Salvia, US Army Research Lab

#### 2:00 PM Invited

**Material Deformation Dynamics at Ultrahigh Pressures and Strain Rates:** *Bruce Remington*<sup>1</sup>; <sup>1</sup>Lawrence Livermore National Laboratory

Solid state dynamics experiments at extreme pressures,  $P > 1000$  GPa (10 Mbar), and strain rates ( $1.e6 - 1.e8$  1/s) are being developed for the NIF laser. The experimental methods are being developed on the Omega laser facility. VISAR measurements establish the ramped, high pressure conditions. Recovery experiments offer a look at the residual microstructure. Dynamic diffraction measurements allow phase, shear stress (strength), and possibly twin volume fraction and dislocation density to be inferred with  $< 1$  ns time resolution. Constitutive models for material strength are currently being tested at  $\sim$ Mbar pressures by comparing 2D simulations with experiments measuring the Rayleigh-Taylor instability evolution in solid state samples of vanadium and tantalum. We suggest that the material deformation at these conditions falls into the phonon drag regime, and make an estimate of the (microscopic) phonon drag coefficient, by relating to the (macroscopic) effective lattice viscosity.

#### 2:30 PM

**Length- and Timescales for Dynamic Deformation in Materials:** *Neil Bourne*<sup>1</sup>; <sup>1</sup>AWE Aldermaston

Materials respond to dynamic loading with a variety of mechanisms. Each has its own mechanical threshold for operation including discrete stress levels. However it also responds with a defined kinetics to the impulse applied. When a crystalline material is exposed to extremes of pressure such mechanisms include martensitic phase transformation, dislocation nucleation and propagation, twinning and potentially melting. The mechanical environment and the thermodynamics of the mechanisms determine the kinetics and the effect upon the microstructure. Energy considerations define timescales and thus lengthscales over which such mechanisms can operate. Thus lengthscale regimes exist within which certain mechanisms are

TUESDAY PM

confined. Examples are drawn from a variety of metallic responses showing the suite of available mechanisms and the range of observables that result.

### 2:45 PM

**Extracting Plastic Flow Properties from Shock Velocimetry:** *Bryan Reed*<sup>1</sup>; James Stolken<sup>1</sup>; Roger Minich<sup>1</sup>; Mukul Kumar<sup>1</sup>; <sup>1</sup>Lawrence Livermore National Laboratory

We present a coherent set of analysis methods designed to deduce the evolution of plasticity inside a shocked material from measurements of free surface velocities. While the problem is inherently underconstrained, much information may still be deduced with these methods, provided one may apply a few fairly modest assumptions about the wave propagation (a statement we support in part through analysis of simulated data sets in which the correct answers are known). This is particularly challenging when one is concerned with rate-dependent effects in nonsteady waves, which invalidates many assumptions commonly made in such analysis. Instead, we derive an estimate of the full deviatoric-stress/plastic-strain-rate relation for every point in the material. Viewing the data in this way provides insights into the coupling among elastic precursor decay, post-shock relaxation, and the speed of the plastic wave.

### 3:00 PM

**High Strain Rate and Pressure Induced Twinning in Tantalum:** *Jeffrey Florando*<sup>1</sup>; James McNaney<sup>1</sup>; Luke Hsiung<sup>1</sup>; Nathan Barton<sup>1</sup>; Mukul Kumar<sup>1</sup>; <sup>1</sup>Lawrence Livermore National Laboratory

Experiments on both single crystal and polycrystalline Ta deformed under various high rate loading conditions were performed to help determine the twinning threshold. For the single crystal samples, recovery experiments under gas gun plate impact loading conditions were conducted at two shock pressures, 25 and 55 GPa, and for four orientations {(100), (110), (111), (123)}. For the polycrystalline Ta samples, compression experiments were conducted at liquid nitrogen temperatures at strain rates ranging from  $10^4$  to  $10^6$  s<sup>-1</sup>. In addition, samples were cold-rolled and then tested at liquid nitrogen temperatures to determine the effect of dislocation density on the overall twin fraction. Recovered samples were characterized using EBSD orientation mapping along with a limited amount of transmission electron microscopy to assess the occurrence of twinning under each test condition.

### 3:15 PM

**Isomorphic Phase Transformation of Cerium under Shock Loading Using Molecular Dynamics:** *Virginie Dupont*<sup>1</sup>; Timothy Germann<sup>1</sup>; Shaoping Chen<sup>1</sup>; <sup>1</sup>Los Alamos National Laboratory

Cerium (Ce) has an atypical phase diagram with an isomorphic phase transition between two FCC structures that induces a volume collapse of ~16%. We present an Embedded Atom Method (EAM) potential for Ce and its use in shock loading via MD simulations. The samples studied are single crystalline and defect-free. The velocity profiles of the shocked samples show a split wave structure typical of a phase transition. Two waves are observed, an elastic precursor followed by a plastic wave. The plastic wave causes the expected phase transition. Comparisons to experiments on Ce and MD simulations on Cesium (Cs) indicate that three waves could be observed, one elastic precursor, a first shock compression wave in the gamma phase, and finally the phase transition wave from gamma to alpha. The construction of the potential is believed to be responsible for the two-wave structure.

### 3:30 PM

**Laser Compression of Monocrystalline Tantalum:** *Chia-Hui Lu*<sup>1</sup>; Bruce Remington<sup>2</sup>; Brian Maddox<sup>2</sup>; Bimal Kad<sup>1</sup>; Fabienne Gregori<sup>3</sup>; Hye-Sook Park<sup>2</sup>; Marc Meyers<sup>1</sup>; <sup>1</sup>University of California, San Diego; <sup>2</sup>Lawrence Livermore National Laboratory; <sup>3</sup>Université Paris Nord

Monocrystalline tantalum with orientations [100] and [111] was subjected to laser compression at energies of 350 to 685 J, generating shock amplitudes varying from 15 to 100 GPa. The laser beam, with a diameter slightly higher than 1 mm, created a crater of significant depth, on the surface of which traces of twins were visible by back-scattered SEM. The decay of the pulse through the specimens was accompanied by an attendant decrease in the density of shock-generated dislocations. Microhardness

measurements paralleled this decay. TEM revealed profuse mechanical twinning within a distance from the energy deposition surface of ~1.5 mm at 684 J compression power, corresponding to an approximate pressure of 40 GPa. The experimentally measured dislocation densities and threshold stress for twinning are compared with predictions using an analysis based on the constitutive response and the similarities and differences are discussed in terms of the mechanisms of defect generation.

### 3:45 PM Break

### 3:55 PM Invited

**Shock Response and Recovery of Cu-Nb Nanolayer Composites:** *Timothy Germann*<sup>1</sup>; <sup>1</sup>Los Alamos National Laboratory

Large-scale classical molecular dynamics (MD) simulations and laser-launched flyer plate experiments have been used to study the shock response of Cu-Nb nanolayered composites. At a layer thickness of 5 nm, the hardness of such metallic multilayers (as measured by quasistatic indentation or compression tests) reaches a maximum due to the difficulty of dislocation transmission across the interfaces. We observe a similar strengthening effect under dynamic shock loading, both in the MD simulations and in post mortem examinations of shock-recovered samples subjected to 10-20 GPa shock loading. The MD simulations provide insight into the dislocation nucleation and transmission processes that occur under compression, as well as the subsequent annihilation upon release. The Cu-Nb interfaces serve both as dislocation sources during shock compression, and dislocation sinks upon release, and thus lead to a greater degree of recovery as compared to either constituent Cu or Nb single crystal.

### 4:25 PM

**Mode Transitions in Shocked Single-Crystal Tantalum:** *Luke Hsiung*<sup>1</sup>; Brian Maddox<sup>1</sup>; Bruce Remington<sup>1</sup>; <sup>1</sup>Lawrence Livermore National Laboratory

TEM studies of shocked single-crystal tantalum recovered from gas-gun impact and laser-shock experiments are presented to reveal the transitions of deformation mode from dislocation glide to twinning and shear transformation. The transitions take place to accommodate insufficient dislocation flow resulting from the exhaustion of dislocation sources when dynamic-recovery reactions for dislocation annihilation and cell formation are largely suppressed under dynamic pressure conditions. The exhaustion of dislocation sources is proposed to occur when the stress for dislocation multiplication exceeds the threshold stresses for twinning and shear transformation. This work was performed under the auspices of the U.S. Department of Energy by Lawrence Livermore National Laboratory under Contract DE-AC52-07NA27344.

### 4:40 PM

**Analytical Models for Predicting Pressure-Volume Compressibility of Low-Density Compacts of Iron Nano-Particles:** Chengda Dai<sup>1</sup>; Daniel Eakins<sup>2</sup>; Naresh Thadhani<sup>3</sup>; <sup>1</sup>Southwest Institute of Fluid Physics; <sup>2</sup>Imperial College; <sup>3</sup>Georgia Institute of Technology

The shock compression behavior of nano-sized powders is investigated to determine the applicability of analytical models for predicting the pressure-volume compressibility of nano-particles of iron, pre-pressed to ~35% and ~45% TMD compacts. Time-resolved experiments were performed to measure the pressure-volume Hugoniot using piezoelectric stress gauges which monitored the input and propagating stress profiles and the shock velocity. The results show a densification-distension transition at ~2 GPa for the ~35% TMD, and ~6 GPa for the ~45% TMD compacts. Correlations of the model calculations with the measured data indicate that the shock Hugoniot of pre-pressed nano-iron powder compacts cannot be correctly described by the analytical models, which are otherwise capable of predicting the Hugoniot of highly porous materials (pre-pressed compacts) of micron-sized powders of similar density. The principal cause for the ineffectiveness is the lack of incorporating the difference in internal energy between the powder compact and the solid.



4:55 PM

**Simultaneous Contour Forming and Shock Hardening in Planar Impact Forming:** *Huimin Wang*<sup>1</sup>; Yuan Zhang<sup>1</sup>; Geoff Taber<sup>1</sup>; Glenn Daehn<sup>1</sup>; <sup>1</sup>Ohio State University

Nominally flat components with a number of features are desired for a range of components ranging from heat exchangers, to bipolar plates, to micro-reactors to micro-fluidics. To fabricate such components in standard presses, the forming pressure must often exceed the flow stress of the workpiece by a factor of 2 to 3, requiring very large presses. In contrast, impact velocities beyond 100 m/s collisions can provide impact pressures large enough to cause the workpiece to fully conform. Such a manufacturing process, driven by electromagnetic discharge is very viable and has two very interesting advantages: 1) dimensional reproduction is exceptional and 2) rates of hardening at the strain rates seen at surface impact (often in excess of  $10^6$  s<sup>-1</sup> cause much greater rates of strain hardening than press forming. Detailed experiments with copper will show variations in material microstructure and properties that result from this high strain rate impact forming process.

5:10 PM

**Spatial Distribution of Damage after Shock Loading:** *Veronica Livescu*<sup>1</sup>; John Bingert<sup>1</sup>; Davis Tonks<sup>1</sup>; <sup>1</sup>Los Alamos National Laboratory

The quantification of shock damage in polycrystalline materials is critical for the understanding of mechanisms controlling failure under dynamic conditions. Ductile fracture in metals occurs by the nucleation, growth, and coalescence of voids. Most damage models characterize the distribution of the voids by volume fraction and assume uniform porosity, but voids in a real material are neither uniform in size nor spatial distribution, and vary with experimental parameters. Physically-based damage models must statistically reproduce this heterogeneity of void damage to accurately model ductile failure of materials under shock loading. This work investigates void damage distributions and clustering of void damage by using a correlation function-based approach to produce quantitative descriptors of microstructural damage. Damage statistics were obtained from three-dimensional reconstructions of experimentally shock-induced damage in plate impact and high-explosive driven specimens. Discussion will include evolution of damage statistics with experimental parameters, and plastic flow localization due to non-uniform void distribution.

5:25 PM

**The Effect of Cold Work on the Shock Response of Tantalum:** *Jeremy Miller*<sup>1</sup>; Glenn Whiteman<sup>1</sup>; Neil Bourne<sup>1</sup>; Nigel Park<sup>1</sup>; <sup>1</sup>AWE

The response of the body centred cubic metal tantalum to shock loading has been studied for several decades, due to its use by the military in explosively formed projectiles. Previous studies on well controlled, annealed specimens has shown that deformation is controlled by the motion of rather than the generation of  $a/2\langle 111 \rangle\{110\}$  screw dislocations in straight segments, which result in little if any post shock hardening. In situ-shear strength measurements have also shown a significant strength reduction behind the shock front, suggesting that the motion of these dislocations acts as a stress relief mechanism. Similar effects have also been noted in tungsten and its alloys. In this presentation, we return to tantalum, investigating the differences in shock response between a low dislocation density (annealed) and high dislocation density (cold rolled) material. Results are discussed in terms of the shear strength and its variation with time behind the shock front.

5:40 PM

**The Role of the Structure of Grain Boundary Interfaces during Shock Loading:** *Alejandro Perez-Bergquist*<sup>1</sup>; Juan Escobedo<sup>1</sup>; Carl Trujillo<sup>1</sup>; Ellen Cerreta<sup>1</sup>; George Gray<sup>1</sup>; Saryu Fensin<sup>1</sup>; Timothy Germann<sup>1</sup>; <sup>1</sup>Los Alamos National Laboratory

In order to understand the role of interfaces in the shock tolerance of metals, three specific copper bi-crystal boundaries have been studied under shock loading and incipient spall conditions. These boundaries, two 001/111 boundaries and a 001/001 tilt boundary and their structures have been characterized prior to deformation using both electron back scattered diffraction (EBSD) and transmission electron microscopy (TEM) to obtain

their axis/angle pair relationship and the structure at the boundary. This characterization has been utilized as input for MD simulations to examine in-situ dislocation/grain boundary interactions. These boundaries were then shocked at 2.5 and 10GPa in an 80mm gas gun and soft recovered. Post-mortem characterization, EBSD and TEM, has revealed that typical grain boundaries readily form damage during shock loading but the special boundaries (S3) are resistant to failure. This is linked to differences in slip transmissibility across these types of boundaries.

5:55 PM

**Role of Twinning in Shock Related Deformation:** *Veronica Livescu*<sup>1</sup>; John Bingert<sup>1</sup>; Thomas Mason<sup>1</sup>; George Gray III<sup>1</sup>; <sup>1</sup>Los Alamos National Laboratory

Twinning is observed under shock loading conditions in metals that do not twin under conventional loading conditions. The occurrence of twinning depends on both material properties and experimental parameters. However, real time diagnostics used currently in shock experiments are insufficient to identify and characterize specific deformation and damage processes and their precise sequence in time. The post-mortem microstructure characterization presented here provides insight on the progression of deformation in high-explosive driven Tantalum and validates deformation and damage mechanisms under shock loading. Crystallographic aspects that contribute the most to the twinning behavior will be presented, as well as effects of shock obliquity on the twinning behavior. Spatial distribution and morphology of twins found in high-explosive driven Tantalum show that twinning is a critical deformation mechanism and must be incorporated into dynamic deformation models for an accurate description of shock damage.

---

## Electrode Technology for Aluminium Production: Petroleum Coke VBD

*Sponsored by:* The Minerals, Metals and Materials Society, TMS Light Metals Division, TMS: Aluminum Committee

*Program Organizers:* Alan Tomsett, Rio Tinto Alcan; Ketil Rye, Alcoa Mosjøen; Barry Sadler, Net Carbon Consulting Pty Ltd

Tuesday PM  
March 1, 2011

Room: 16B  
Location: San Diego Conv. Ctr

*Session Chair:* Angelique Adams, Alcoa

---

2:00 PM Introductory Comments

2:10 PM Invited

**Historical and Future Challenges with the Vibrated Bulk Density Test Methods for Determining Porosity of Calcined Petroleum Coke:** *Jignesh Panchal*<sup>1</sup>; Mark Wyborney<sup>1</sup>; Jeffrey Rolle<sup>1</sup>; <sup>1</sup>A.J.Edmond Company

Over several decades, calcined petroleum coke producers and the aluminum industry have been using various techniques such as Vibrated Bulk Density (VBD), Mercury Intrusion Porosimetry (MIP), and Mercury Apparent Density to predict the porosity of calcined petroleum coke. Better knowledge of the coke porosity allows a more accurate estimation of coke quality and pitch demand for fabricating anode of optimum performance. Industry has had limited success in accurately predicting porosity using the existing VBD methods. Direct measurement of porosity by MIP is an alternative way to measure porosity accurately. Currently there is limited correlation between VBD and MIP. Any improvements to the VBD test method should demonstrate improved correlation to the results obtained from MIP. This paper covers the historical and traditional approach to predict calcined coke porosity, correlation study of VBD test method and porosity by MIP, and input to the development of superior test methods to meet industry requirements.

TUESDAY PM

### 2:35 PM Invited

**Prediction of Calcined Coke Bulk Density:** *Marie-Josée Dion*<sup>1</sup>; Hans Darmstadt<sup>1</sup>; Nigel Backhouse<sup>1</sup>; Frank Cannova<sup>2</sup>; Mike Canada<sup>2</sup>; <sup>1</sup>Rio Tinto Alcan; <sup>2</sup>BP

The vibrated bulk density (VBD) is an important calcined coke property. Due to changing green coke quality, a reliable forecast of the calcined coke VBD from small green coke samples is required. The VBD can be predicted from green coke properties, like the Hardgrove Grindability Index (HGI) and volatiles content but the precision of this forecast is often not sufficient for procurement decisions. Several laboratory calcination techniques were studied including the use of two different laboratory rotary kilns at BP Coke and a contractual facility. When compared to RTA's Arvida calciner it was determined certain methods could achieve good agreement for VBD and coke calcination level (Lc) and it was also possible to replicate phenomena that cause problems at an industrial scale such as coke ring formation. The methods will be used in the future to support the RTA calcining operations.

### 3:00 PM Invited

**Calcined Coke Particle Size and Crushing Steps Affect Its VBD Result:** Frank Cannova<sup>1</sup>; *Mike Canada*<sup>1</sup>; Bernie Vitichus<sup>1</sup>; <sup>1</sup>BP Coke

The size of a calcined coke particle used in the Vibrated Bulk Density (VBD) test and the size of the particle before crushing affects its VBD analysis. That is, naturally occurring particles usually have a higher packing density and VBD compared with particles that are crushed to the same size. Consequently, calcined coke preparation crushing steps can dramatically affect the VBD result. Data, showing how calcined coke particle size and crushing steps affect the VBD result will be presented. These data help explain why the roll crushing steps need to be controlled to improve VBD repeatability and reproducibility. In addition, data will be presented showing how the roll crusher operation and maintenance affects the VBD result.

### 3:25 PM Invited

**Bulk Density - Overview of ASTM and ISO Methods with Examples of between Laboratory Comparisons:** *Lorentz, Petter Lossius*<sup>1</sup>; Bill Spencer<sup>2</sup>; Harald A. Øye<sup>3</sup>; <sup>1</sup>Hydro Aluminium AS; <sup>2</sup>Oxbow Calcining; <sup>3</sup>Norwegian University of Science and Technology

The bulk density of petroleum coke is recognized as a key coke property for the density of anodes in primary aluminum electrolysis, and this makes the bulk density important in petroleum coke trade. ASTM and ISO have standards for testing; ASTM with the two VBD methods D4292 and D7454, and ISO with the TBD method, ISO 10236. There is a concern in anode production that it is difficult to obtain good between-laboratory comparisons. The paper will compare the methods, give results from several interlaboratory studies and discuss the observed within- and between-laboratory results.

### 3:50 PM Break

### 4:00 PM Invited

**Improving the Repeatability of Coke Bulk Density Testing:** *Les Edwards*<sup>1</sup>; Marvin Lubin<sup>1</sup>; James Marino<sup>1</sup>; <sup>1</sup>Rain CII Carbon

The "Pechiney" mercury apparent density test was used by the aluminium industry for many years to measure the density/porosity of calcined petroleum coke. Over the last 5 years, the industry has moved away from this test for occupational health and safety reasons. The current alternative tests are based on vibrated or tapped bulk density methods. The value of measuring bulk density is reduced due to poor reproducibility caused by differences in equipment and sample preparation. This paper reviews different bulk density test methods and presents repeatability data on a new method for measuring coke bulk density. The method is based on automated equipment which uses transverse axial pressure to measure bulk volume and hence bulk density, of calcined coke samples. The new equipment shows improved repeatability compared to existing equipment.

### 4:25 PM Invited

**ASTM D7454 Vibrated Bulk Density Method – Principles and Limitations:** *Francois Laplante*<sup>1</sup>; Luc Duchesneau<sup>1</sup>; <sup>1</sup>RioTinto Alcan

This method proposed by Rio Tinto Alcan and approved by ASTM in 2008, differs from method D4292 by the introduction of a semiautomated

equipment and also by referring to a tighter sample preparation procedure. The performance expressed in terms of repeatability is = 0.008 g/mL when the preparation variance is not included and 0.01 g/mL when the preparation variance is included. The intralaboratory reproducibility over a two-year period came out to 0.02 g/mL. The interlaboratory reproducibility has not yet been systematically determined but appears to be high considering the large punctual differences observed between coke providers and coke purchasers. The underlying principles of D7454 will be presented, the factors causing differences between laboratories will be discussed and a mitigation strategy will be proposed.

### 4:50 PM Invited

**Vibrated Bulk Density (VBD) of Calcined Petroleum Coke and Implications of Changes in the ASTM Method D4292:** *Bill Spencer*<sup>1</sup>; Laura Johnsen<sup>1</sup>; David Kirkpatrick<sup>1</sup>; Desiree Clark<sup>1</sup>; Miguel Baudino<sup>1</sup>; <sup>1</sup>Oxbow Calcining LLC

Vibrated bulk density (VBD) is a quantitative measurement used in the aluminum industry to evaluate the density of calcined petroleum coke. In the calcining industry, the reproducibility and ambiguity of the current ASTM International (ASTM) method D4292 generates a wide range of VBD data. Therefore, Oxbow Calcining LLC (Oxbow) made an investigation into the VBD procedure - D4292. Issues with D4292 include the use of the appropriate crushing equipment, crushing of the gross sample, sieving of the prepared sample, determination of the sample volume using appropriate graduated cylinder vibration time, and apparatus setup. This investigation led to a revision in the ASTM D4292 method to remove the ambiguities.

### 5:15 PM Panel Discussion

## Fatigue and Corrosion Damage in Metallic Materials: Fundamentals, Modeling and Prevention: Fatigue and Corrosion Interaction and Materials Corrosion

*Sponsored by:* The Minerals, Metals and Materials Society, TMS Structural Materials Division

*Program Organizers:* Tongguang Zhai, University of Kentucky; Zhengdong Long, Kaiser Aluminum; Peter Liaw, University of Tennessee

Tuesday PM  
March 1, 2011

Room: 31C  
Location: San Diego Conv. Ctr

*Session Chairs:* Chengjia Shang, University of Science and Technology Beijing; Soo Yeol Lee, The University of British Columbia

### 2:00 PM Invited

**Effect of Sensitized Microstructure on Corrosion Fatigue Crack Growth in Al 5083:** *Peter Pao*<sup>1</sup>; Ramasis Goswami<sup>2</sup>; Robert Bayles<sup>1</sup>; Ronald Holtz<sup>1</sup>; <sup>1</sup>Naval Research Laboratory; <sup>2</sup>SAIC

The influence of  $\beta$  phase (Al<sub>3</sub>Mg<sub>2</sub>) at the grain boundaries on the corrosion fatigue crack growth of sensitized (175 °C/1 – 1000 hrs) and as-received (H131) Al 5083 was investigated. TEM investigations reveal, while  $\beta$  is absent at the grain boundaries of as-received Al 5083, small and discontinuous  $\beta$  precipitates at the grain boundaries after few hours at 175 °C. On prolonged aging at 175 °C,  $\beta$  grows and coalesces and most grain boundaries are covered with continuous  $\beta$ . The presence of  $\beta$  at the grain boundaries significantly reduces the high stress ratio corrosion fatigue crack threshold and increases the crack growth rates in saltwater. Such corrosion fatigue degradation is proportional to the amount of  $\beta$  present at the grain boundaries. The observed fatigue crack growth responses are discussed in terms of differences in microstructure and the interplay between stress-corrosion and corrosion fatigue cracking thresholds.

2:20 PM

**The Effect of Hot Corrosion Pits on Fatigue Crack Initiation and Fatigue Life of a Disk Superalloy:** *Yoshiki Yamada*<sup>1</sup>; Ignacy Telesman<sup>2</sup>; Timothy Gabb<sup>2</sup>; Louis Ghosn<sup>2</sup>; <sup>1</sup>Ohio Aerospace Institute; <sup>2</sup>NASA GRC

Type II Hot Corrosion pitting can occur for disk superalloys having salt deposits and exposures near 700°C. These pits act as stress concentrators and thus can significantly reduce low cycle fatigue life at both low and high temperatures. In this study, the effect of hot corrosion pits on fatigue crack initiation and low cycle fatigue life was investigated. In order to understand a mechanism of crack initiation around corrosion pits, FEA model was used to estimate the localized elevation in stress concentrations. The FEA models were based on SEM observations of the type and size of the corrosion pits initiating cracks. In addition, fatigue life prediction based on equivalent initial flow size was attempted and compared with test results.

2:40 PM

**Effect of Proximity and Dimension of Two Artificial Pitting Holes on the Fatigue Endurance of Aluminum Alloy 6061-T6 under Rotating Bending Fatigue Tests:** *Gonzalo Dominguez Almaraz*<sup>1</sup>; Victor Hugo Mercado<sup>1</sup>; J. Jesus Villalon<sup>1</sup>; <sup>1</sup>University of Michoacan

This work is oriented to study the effect of two artificial pitting holes, its dimensions and proximity, on the fatigue endurance of aluminum alloy 6061-T6 under rotating bending fatigue tests. Stresses concentration induced by artificial pitting holes is analyzed and correlated with the experimental fatigue life. It is found that the stresses concentration increases exponentially when the two pitting holes approaching and this induces an important reduction on the fatigue life. Concerning the dimensions variation of one pitting in regard the second, no important influence was observed on fatigue life for a given separation between them; this implies that separation between the two artificial pitting holes and the associated stress concentration is the principal parameter on the fatigue life under these conditions. The results are discussed and conclusions are presented involving the fatigue life, proximity and dimension of pitting holes, stress concentration and the fracture surfaces related to failure origin.

3:00 PM

**Microstructural and Environmental Effects on Fatigue Crack Growth in 7075 Aluminum Alloy:** *Amir Bonakdar*<sup>1</sup>; Fengjiang Wang<sup>1</sup>; Jason Williams<sup>1</sup>; Nikhilesh Chawla<sup>1</sup>; <sup>1</sup>Arizona State University, School of Mechanical, Aerospace, Chemical, and Materials Engineering

The fatigue behavior of aluminum alloys is greatly influenced by environment and precipitate structure. In this talk, the role of moisture on fatigue crack growth behavior of 7075 Al alloy was investigated. In particular, the role of crystallographic slip, as dictated by precipitate structure, was studied. Rolled 7075 Al alloy was heat-treated to underaged, peak-aged, and overaged conditions. Fatigue crack growth rates were measured under various partial pressures of water vapor. Standard compact tension specimens along the S-T orientation were used, and testing was performed under load ratios of  $R = 0.1$  and  $R = 0.8$ . The experimental results were analyzed by the two parameter approach ( $\square K-K_{max}$ ). The microstructure and morphology of the fracture surfaces were examined by scanning electron microscopy (SEM) and correlated with the crack growth behavior.

3:20 PM Invited

**A Study of Corrosion of Pure Aluminum and AA2037 Al Alloy in a NaOH Solution by Positron Annihilation:** *Yichu Wu*<sup>1</sup>; *Tongguang Zhai*<sup>2</sup>; <sup>1</sup>University of Wuhan; <sup>2</sup>University of Kentucky

Pure Al and a continuous cast AA 2037 Al alloy were analyzed with positron beam-based Doppler broadening spectroscopy after corrosion in 1mol/L NaOH for various periods of time. By varying the incident positron energy, corrosion-induced defects in different depth from the surface could be detected by measuring the S parameter in these samples. It was found that the S parameter near the surface was significantly increased in pure Al after corrosion. This was likely to be due to the interaction between positrons and the nanometer-sized voids formed in the Al surface during corrosion. AFM examination indicated that many cavities were formed on the Al surface after corrosion. A significant decrease in S parameter was observed in the AA

2037 Al alloy, which was cold-rolled, solid solution heat-treated and water-quenched, after corrosion. This could be caused by Cu enrichment occurred at the metal-oxide interface during corrosion in this alloy.

3:40 PM Break

3:50 PM Invited

**Constituent Particle Clustering and Pitting Corrosion:** *D Gary Harlow*<sup>1</sup>; <sup>1</sup>Lehigh University

Corrosion in aluminum alloys results from local galvanic coupling between constituent particles and the metal matrix; it is a complex stochastic process. Severe pitting is caused by particle clusters, of which are dependent on the spatial statistics of particles. Critical statistics include location, size, density and chemical composition. The localized corrosion growth rate is primarily dependent on the galvanic process perpetuated by particle-to-particle interactions and electrochemical potentials. Frequently, severe pits are millimeters in length, and these pits have the dominant impact on structural prognosis. To accommodate large sizes, a model for three-dimensional constituent particle microstructure is proposed. The model employs a fusion of classic stereological techniques, spatial point pattern analyses, and qualitative observations to describe the constituent particle microstructure in three-dimensions. The methodology can be carried out using standard optical microscopy and image analysis techniques.

4:10 PM Invited

**Life Prediction of a New Developed Ferrite Stainless Steel for Automobile Muffler:** *Chengjia Shang*<sup>1</sup>; <sup>1</sup>University of Science and Technology Beijing

The ferrite stainless steel has been used in automobile exhaust system for many years. However, the damage of muffler is severely by using low Cr content stainless steel, especially serving in poor oil quality district. The corrosion mechanism of the condensate water in muffler shows that pin corrosion by chloride and sulfur are the main reasons, and with Cr content increasing the pin corrosion resistance can be improved dramatically. In this paper, the life prediction of different Cr content ferrite stainless steels were invested by simulating tests. The life prediction shows that as the Cr content reached about 17%, the life of muffler can be increased about 50% comparing with 409L type ferrite stainless steel (11%Cr content). The newly developed 439M was used in passenger car in Chinese automobile work. The road testing result of muffler life show that it can be more than 100,000km, which satisfy specified requirements.

4:30 PM

**A Versatile Component Testing Method for the Life Time Determination of Automotive Exhaust Mufflers:** *Muhammad Yasir*<sup>1</sup>; Gregor Mori<sup>1</sup>; Helmut Wieser<sup>2</sup>; Martin Schattenkirchner<sup>2</sup>; Manuel Hognl<sup>2</sup>; <sup>1</sup>Christian Doppler Laboratory of Localized Corrosion, University of Leoben, Austria; <sup>2</sup>Faurecia Emissions Control Technologies, Germany

The problem originates in the automotive exhaust industry where a manufacturer has to perform number of tests on different types of samples before selection of a right material. Correlations of these testing methods often lead to a disagreement. All these tests provide information about relative ranking of different grades under different conditions. To predict the life time of a complete system under real conditions is always a difficult task and sometimes also uncertain. There is no test available in which simulation of external and internal corrosion can be performed simultaneously. The objective of this study was to develop a type of testing procedure that can determine the combined effect of salt corrosion, condensate corrosion and high temperature corrosion. Corrosion resistance of different materials and designs are studied in this research. A comparative study was performed between field systems and test systems to establish a relation for the life time calculation.

4:50 PM Invited

**Effect of Hydrogen on the Localized Corrosion of Steels:** *Lijie Qiao*<sup>1</sup>; <sup>1</sup>University of Science and Technology Beijing

This paper presents our recent work on the effects of hydrogen on the properties of steels. The results show that hydrogen enhances nucleation of micro-cracks, increases propagation rates of stress-corrosion cracks, and

TUESDAY PM



reduces the threshold stress in stainless steel. Hydrogen decreases corrosion and pitting potentials, and increases passivation current of 2507 duplex stainless steels in 0.5mol/LH<sub>2</sub>SO<sub>4</sub>+3%NaCl solution. Hydrogen promotes pitting initiation in ferrite phase in duplex stainless steel in which increase in hydrogen density decreases the time for pitting initiation and growth rate. Both hydrogen and Cl<sup>-</sup> decrease linearly corrosion and pitting potentials, and increase the passivation current of carbon steel in boric acid buffer solution.

5:10 PM

**Studying Properties of Zn-Coated Carbon Steel:** *Ruqaya Khammas<sup>1</sup>*;  
<sup>1</sup>Technical College

This study includes coating low carbon steel, with pure Zn, Zn-0.2Al for one coat layer and two coat layer using batch hot dip galvanizing method and studying the coating properties, to protect the base metal from corrosion in several medias. Microstructure shows series of Fe-Zn alloy layer with a surface of free Zn, and the effect of adding (0.2%Al) is to suppressing the alloying layers and increase the bath fluidity. The coating phases presents, gamma  $\gamma$  (Fe<sub>3</sub>Zn<sub>10</sub>), delta  $\delta$  (FeZn<sub>7</sub>), zeta  $\zeta$  (FeZn<sub>13</sub>) and eta  $\eta$  (Zn). Coating thickness Zn one coat layer is (55 $\mu$ m), Zn two coat layer is (180 $\mu$ m), that's mean when we doubled the immersing time the coating thickness is almost trebled. For Zn-0.2Al one coat layer the thickness mean was about (45 $\mu$ m), the double coat of Zn-0.2Al was failed. Corrosion test done by potentiostat system with two different medias, tap water and sea water.

## Friction Stir Welding and Processing VI: Aluminum and Magnesium Alloys II

*Sponsored by:* The Minerals, Metals and Materials Society, TMS Materials Processing and Manufacturing Division, TMS: Shaping and Forming Committee

*Program Organizers:* Rajiv Mishra, Missouri University of Science and Technology; Murray Mahoney, Retired from Rockwell Scientific; Yutaka Sato, Tohoku University; Yuri Hovanski, Pacific Northwest National Laboratory; Ravi Verma, General Motors

Tuesday PM  
March 1, 2011

Room: 5B  
Location: San Diego Conv. Ctr

*Session Chair:* Murray Mahoney, Retired from Rockwell Scientific

2:00 PM Invited

**Novel Techniques for Corner Joints Using Friction Stir Welding:** *Jonathan Martin<sup>1</sup>*; Chris Stanhope<sup>1</sup>; Sam Gascoyne<sup>2</sup>; <sup>1</sup>TWI; <sup>2</sup>Centre for Doctoral Training in Advanced Metallic Systems

Most commercial FSW applications use simple butt joint configurations and alternative designs such as T-sections and corner welds are very rarely considered. This paper presents the development of novel techniques which have demonstrated the ability to produce high quality internal and external corner welds using an adaption of Stationary Shoulder Friction Stir Welding. Further enhancements using a shaped shoulder have also allowed fillet radii to be added to internal corners and a consumable filler wire to provide the material for the fillet. The principles of these techniques are explained including the results of process development trials on a range of aluminium alloys including metallurgical examinations, mechanical property evaluations and how they are related to the thermal weld cycles. The development of these techniques has the potential to be applied to a range of new joint geometries and extend the product design possibilities.

2:25 PM

**Investigation of the Material Shear Layer in Bobbin Tool Friction Stir Welding:** *Jakob Hilgert<sup>1</sup>*; Jorge dos Santos<sup>1</sup>; Norbert Huber<sup>1</sup>; <sup>1</sup>GKSS Forschungszentrum GmbH

In bobbin tool FSW the material flow around the tool is of great importance for the process stability and weld seam quality. This study presents a CFD model of the shear layer implemented in Comsol-Multiphysics. The material used is AA2024-T3. The metal is treated as a highly viscous shear thinning liquid governed by an inverse hyperbolic sine relationship for the viscosity.

The boundary condition at the interface between tool and work piece can be either sticking or slipping in any ratio. This information is part of the output of the model. The temperature information as well as the applied machine torque are taken from previous numerical and experimental work. The predicted shear layer shape and velocity profile are experimentally validated. The shear rate distribution and contact state predicted by the model for parameter sets that result in sound welds are compared to those that result in defective or instable welds.

2:45 PM

**Effect of Tool Geometry and Process Condition on Static Strength of Magnesium Friction Stir Lap Linear Weld:** *Qi Yang<sup>1</sup>*; Xiang Li<sup>1</sup>; Ke Chen<sup>1</sup>; Yijing Shi<sup>1</sup>; <sup>1</sup>Hitachi America, Ltd.

Friction stir lap linear welding is conducted on overlapped AZ31 Mg plates with different welding tools. Welds are made mainly with the orientation such that the weld retreating side on the upper plate is to be placed under load. Welding tools consist of a concave shoulder and a pin having a cylindrical, or triangular, or pie shape. This work addresses the effects of tool geometry and process condition on lap shear strength of welds. The shape of hook formed due to upward bending of the plate interface is examined. Compared to the cylindrical tool, the triangular tool effectively suppresses the hook on the retreating side due to an enhanced horizontal material flow, and this primarily leads to a 78% increase in optimized weld strength. A 'pure' shear surface present on the tool pin significantly reduces weld strength.

3:05 PM

**Effect of Tool Feature on the Joint Strength of Dissimilar Friction Stir Lap Welds:** *Saumyadeep Jana<sup>1</sup>*; Yuri Hovanski<sup>1</sup>; Glenn Grant<sup>1</sup>; Karl Mattlin<sup>1</sup>; <sup>1</sup>PNNL

Several variations of friction stir tools were used to investigate the effects on the joint strengths of dissimilar friction stir lap welds. In the present lap weld configuration the top sheet was 2.32 mm thick AZ 31 alloy. The bottom sheet consisted of two different steels, a (i) 0.8 mm thick electro-galvanized (EG) mild steel, or a (ii) 1.5 mm thick hot dip galvanized (HDG) high strength low alloy (HSLA) steel. Initially the tool shape was modified to accommodate the material, at which point the tool geometry was fixed. With a fixed tool geometry an additional feature was added to the pin bottom on one of the tools by incorporating a short hard insert, which would act as a stronger bottom sheet cutter. The effects of such modification on the unguided lap shear strength, and associated microstructural changes are discussed in this study.

3:25 PM

**Friction Stir Fabrication of Spar T-Joints Made from 7075 Aluminum:** *Jeremy Brown<sup>1</sup>*; Dwight Burford<sup>1</sup>; <sup>1</sup>Wichita State University

Corrosion or mechanical damage may result in the removal of an aircraft from service. The grounded aircraft must wait until replacement parts can be located and delivered or fabricated. Since many aircraft are out of production, the replacement parts may be difficult and costly to procure. Friction Stir Welding presents a cost-effective and timely alternative to create one-off structures from plate material. An evaluation was undertaken on the feasibility of joining plates of AA7075 aluminum into T-beams with friction stir welding. The fabrication approach involves lap welding through a top horizontal plate into a bottom vertical plate. Different forms of cooling to control heat input were also evaluated. Mechanical and metallurgical properties for these joints show the viability of using friction stir welding to create structures for aircraft.

3:45 PM

**A Study Of a Versatile Method To Attach a Portable FSW System To an Aluminum Structure Using Adhesives:** *Jordan Walser<sup>1</sup>*; Tracy Nelson<sup>1</sup>; Carl Sorensen<sup>1</sup>; Murray Mahoney<sup>1</sup>; <sup>1</sup>Brigham Young University

This study demonstrates a versatile method to attach a portable FSW system to an aluminum structure using adhesives. After preliminary tests of a number of adhesive candidates, Acrylic DP 820 epoxy was chosen because of its high strength, ease of application, and repeatability. Tests were developed to determine adhesive characteristics for all stages of friction stir welding

associated with repair of an aluminum structure. Tests included tensile strengths over a range of temperatures, peel strength, and dynamic loading that simulates a friction stir loading environment. Further, practical issues such as the effects of non parallel attachment and gaps between the fixture and the structure on adhesive performance were examined. Procedures for proper application and removal of the adhesive were developed. The results demonstrate that an adhesive approach meets the requirements to attach a portable FSW system to aluminum structures.

#### 4:05 PM

**Microstructural and Mechanical Properties of Friction Stir Welding Joints of 6082-T6 with 6063-T6:** *Farzad Baratzadeh*<sup>1</sup>; Alan Handyside<sup>1</sup>; Enkhsaikhan Boldsaikhan<sup>1</sup>; Hamid Lankarani<sup>2</sup>; Blair Carlson<sup>3</sup>; Dwight Burford<sup>1</sup>; <sup>1</sup>National Institute for Aviation Research; <sup>2</sup>Wichita State University; <sup>3</sup>General Motors Corporation

Friction stir welding (FSW) offers a "green" alternative to fusion welding automotive bumpers. Therefore, a case study was initiated to compare a friction stir welded bumper design to a conventional fusion welded bumper design. To that point, a unique set of FSW tools were designed, fabricated and coupons were prepared for developing the process parameters through a Design of Experiment (DOE). Once the coupons were completed, a mechanical and metallurgical characterization study of the friction stir welded butt joints of aluminum alloy 6082-T6 with 6063-T6 was carried out. Sheets of 3.5 mm (0.138 inch) thick were friction stir welded with a set of optimized welding parameters. The work included microstructural examination and tensile testing of 1) as-welded coupons, 2) naturally aged coupons, and 3) post-weld heat treated coupons. In addition, the feedback signals gathered during the welding process were analyzed by e-NDE method that is used for detecting weld anomalies

#### 4:10 PM Break

#### 4:20 PM Invited

**Microstructure and Corrosion Behavior of Friction Stir Welded Mg/Al- and Mg/Mg-Joints:** *Guntram Wagner*<sup>1</sup>; Otmar Klag<sup>1</sup>; Dietmar Eifler<sup>1</sup>; <sup>1</sup>University of Kaiserslautern

Friction stir welding (FSW) is a well suited solid state welding process to produce high-quality light weight metal joints. In the present work the developing microstructure and the monotonic stress-strain behavior of dissimilar joints between AZ91-Mg-alloy and AA5454-Al-alloy are presented. SEM investigations, EDX element mappings and electron probe microanalysis (EPMA) as well as temperature measurements during the welding process have been carried out to describe the welding zone in detail and to develop a phase-diagram which indicates the possible fracture of the different phases. Microstructural investigations showed that under load the cracks are predominantly initiated at the intermetallic phases precipitated as interlayers in the contact areas between of the two alloys. Furthermore the corrosion behavior of the friction stir welding zone of the hybrid joints and of die casted Mg/Mg-joints (AZ91D, MRI 153M and MRI 230D) will be discussed.

#### 4:45 PM

**Corrosion and Mechanical Behavior of Friction Stir Processed Mg-CeO<sub>2</sub> Surface Composite:** *Kumar Kandasamy*<sup>1</sup>; Gourav Argade<sup>1</sup>; Sushanta Panigrahi<sup>1</sup>; Rajiv Mishra<sup>1</sup>; <sup>1</sup>Missouri University of Science and Technology

Rare-earth conversion coatings are proven to improve corrosion properties of magnesium alloys. The mechanism behind the improvement is precipitation of oxides and hydroxides of rare-earth elements. In this study, friction stir processing was used to add 50-80 nm size cerium oxide particles at the magnesium alloy plate surface. The improvement in corrosion property has been attributed to the presence of cerium oxide, and as well as the formation of fresh cerium oxide/hydroxide which forms from the reduced cerium from cerium oxide during friction stir processing. The advantages of this approach include flexibility of second phase volume fraction and the depth of surface layer. In addition, the refined microstructure and the nano sized cerium oxide particles in the matrix enhance the compressive strength

of the material from 210 MPa to 380 MPa, and the hardness from 74 VHN to 160 VHN.

#### 5:05 PM

**Mechanical Properties of Al and Mg Alloy Welds Made by Friction Stir Lap Welding:** *Shamzin Yazdanian*<sup>1</sup>; Zhan Chen<sup>1</sup>; Guy Littlefair<sup>1</sup>; <sup>1</sup>AUT university

The unfavourable effect of hooking or softening, respectively, on fracture strength of joints made using friction stir lap welding (FSLW) is known but the combined effect on the magnitude of strength reduction is not clear. In this study, FSLW experiments using AA6060-T5 and AZ31B-H24 alloys were conducted. For both alloys, rotation speed has a dominant effect on increasing the hook size due to increasing the stir flow volume thus lifting more the original lapping surfaces. In AA6060 welds, FS softening has limited the strength, when hook size approaches zero. Meanwhile hook starts to reduce the strength significantly, when its size reaches a critical value. The maximum strength of AA6060 FSL welds reaches ~ 70% of the base metal UTS when hook size approaches zero. This is in contrast to ~30% for AZ31B FSL welds. This can be explained by the local plastic deformation behaviour during lap tensile testing.

#### 5:25 PM

**Microstructure and Tensile Fracture Characteristic of 7005 Aluminum Alloys with Friction Stir Processes:** *Ming-Hsiang Ku*<sup>1</sup>; Fei-Yi Hung<sup>1</sup>; Truan-Sheng Lui<sup>1</sup>; Li-Hui Chen<sup>1</sup>; <sup>1</sup>National Cheng Kung University

In this study, the structures and the tensile properties of 7005 aluminum alloys containing lower Mg content after friction stir process (FSP) were investigated. After aging treatments, the friction stir process induced behaviors in the mechanical properties were compared. The ZM35 alloy (Zn/Mg ratio was 3.5) and the ZM57 alloy had different fracture characteristics. After FSP and then natural aging for 12 days, the experiment results showed that the strengths of ZM35 and ZM57 were lower than that of the base metal (extruded material with T6, no FSP). Notably, the strength of as-FSP specimen was promoted after aging treatments. The one-step (80□/16hr) and two-step (80□/16hr+T6) treatments exhibited the similar results for ZM35 and ZM57 alloys. However, the three-step (T4+80□/16hr+T6) treatments, the strength and the ductility of the ZM57 alloy had reduced, and the deterioration rate of the ductility reached 65%. The ZM35 alloy possessed a better ductility.

#### 5:45 PM

**Evaluation of Microstructure and Mechanical Properties of Aluminum / Copper Friction Stir Butt Welds:** *Rouzbeh Sarrafi*<sup>1</sup>; Amir Hossein Kokabi<sup>1</sup>; Majid Abbasi Gharacheh<sup>1</sup>; Babak Shalchi<sup>1</sup>; <sup>1</sup>Department of Materials Science and Engineering, Sharif University of Technology

In this research, the friction stir welding of aluminum to copper is studied. A sound Al/Cu butt joint was achieved with a relatively high strength in uniaxial tensile tests. Mechanical properties (tensile strength and microhardness) and microstructure of the obtained sound FSW welds were examined. The ultimate tensile strength of the joints reached about 75 percent of that of the aluminum base metal, with the fracture occurring at aluminum side. The metallurgical study of the welds showed that the heat affected zone of aluminum controls the strength of the joints in tensile loading. Microscopy of the stir zone (SZ) showed the relatively small volume fraction of intermetallic compounds and their discreteness. The presence of these phases did not to have a considerable harmful effect on the tensile properties of the welds. The formation of the observed microstructure in the SZ is discussed in the paper.

## Frontiers in Solidification Science: Phase Field and Phase Field Crystal Modeling

Sponsored by: The Minerals, Metals and Materials Society, TMS Electronic, Magnetic, and Photonic Materials Division, TMS: Chemistry and Physics of Materials Committee, TMS: Solidification Committee

Program Organizers: Jeffrey Hoyt, McMaster University; Daniel Lewis, Rensselaer Polytechnic Institute

Tuesday PM  
March 1, 2011

Room: 6E  
Location: San Diego Conv. Ctr

Session Chair: To Be Announced

### 2:00 PM Invited

**Phase Field Crystal Modelling of Solidification:** Ken Elder<sup>1</sup>; <sup>1</sup>Oakland University

In this talk I would like to discuss methods for modelling solidification on atomic length scales and diffusive time scales. The main advantage of such an approach is that elasticity, dislocations and multiple crystal orientations are naturally incorporated. This allows modelling of elastically strained solids, such as occurs in liquid phase epitaxially growth or the creation of grain boundaries when grains of different orientation collide during solidification. Additionally the method can be used to evaluate the mechanical properties of the final solidified product. Connection of this approach with others will also be discussed.

### 2:30 PM Invited

**Phase-Field Crystal Modeling of Homogeneous and Heterogeneous Crystal Nucleation:** Laszlo Granasy<sup>1</sup>; Gyorgy Tegze<sup>1</sup>; Gyula Toth<sup>1</sup>; Gergely Toth<sup>2</sup>; Tamas Pusztai<sup>1</sup>; <sup>1</sup>Research Institute for Solid State Physics and Optics; <sup>2</sup>Eotvos University

We address crystal nucleation in non-equilibrium fluids using atomistic phase-field crystal (PFC) methods (original PFC and eight-order-fitting version by Jaatinen et al.) via solving (i) the equation of motion supplemented with Langevin noise to model thermal fluctuations and (ii) the Euler-Lagrange equation. Relying on approach (i), it will be shown that in these PFC models crystal nucleation at high supersaturations happens via an amorphous precursor. Remarkably, the effective pair potentials corresponding to these PFC models, evaluated from structural data for the glassy state (obtained by deep quenching the liquid), differ significantly. These findings support the view that the two-stage nucleation process observed here might be fairly general. Next we apply approach (ii) to explore the microscopic aspects of Greer's free growth model of liquid inoculation by solid particles, and study the role played by the structure and shape of the foreign particles, and the effect of lattice mismatch.

### 3:00 PM Invited

**Spacing Characterization in Al-Cu Alloys Directionally Solidified under Transient Growth Conditions:** Morteza Amoozazei<sup>1</sup>; Sebastian Gurevich<sup>1</sup>; Nikolas Provatas<sup>1</sup>; <sup>1</sup>McMaster University

We examine primary spacing in Al-Cu alloys grown under transient conditions. The mean value of the primary spacing is shown, both experimentally and numerically, to evolve between characteristic incubation-like periods during which the array configuration is statistically stable. Our results display a rapid, but continuous, transition period from one spacing range to another, consistent with the fact that the sharp doubling of spacing predicted by the transient theory of Warren and Langer affects different wavelengths of a distribution at different times. This transition is shown to depend on the rate of change in growth speed using phase field simulations of directional solidification where the pulling speed is ramped at different rates. For high rates of change of the pulling speed we observe temporary marginally stable array configuration separated by relatively short-lived transitions, while for lower rates of change of the pulling speed, the distinction between incubation and transition periods disappears.

### 3:30 PM Break

### 3:45 PM Invited

**Thermodynamic and Mechanical Properties of Hot Grain Polycrystalline Evolution during Late-Stage Solidification:** Alain Karma<sup>1</sup>; Ari Adland<sup>1</sup>; <sup>1</sup>Northeastern University

This talk will discuss recent progress made using phase-field-crystal and amplitude-equation based simulation methods to characterize the interaction between solid-liquid interfaces that come into close contact during the late stages of solidification. When interfaces belong to different crystal grains, this interaction can be either attractive or repulsive depending on the relative orientation of the two grains. For strong repulsion, crystal cohesion is retarded and interface bridging only occurs substantially below the liquidus temperature. The thin liquid films that persist in between the liquidus and bridging temperatures are believed to promote strain localization and hot cracking through a reduction of shear resistance of wet grain boundaries. Results will be presented that shed light on complex factors that control interface bridging as well as grain boundary shearing as a function of temperature and grain boundary bicrystallography.

### 4:15 PM Invited

**Unified Derivation of Phase-Field Models for Alloy Solidification:** Mathis Plapp<sup>1</sup>; <sup>1</sup>CNRS/Ecole Polytechnique

In the literature, two quite different phase-field formulations for the problem of alloy solidification can be found. In the first, the material in the diffuse interfaces is assumed to be in an intermediate state between solid and liquid, with a unique local composition. In the second, the interface is seen as a mixture of two phases that retain their macroscopic properties, and a separate concentration field for each phase is introduced. It is shown that both types of models can be obtained by the standard variational procedure if a grand potential functional is used as a starting point instead of a free energy functional. The dynamical variable is then the chemical potential instead of the composition. In this framework, a complete analogy with phase-field models for the solidification of a pure substance can be established. This analogy is exploited to formulate quantitative phase-field models for alloys with arbitrary phase diagrams.

### 4:45 PM Invited

**Phase-Field Model for Strong Non Equilibrium Solidification:** Ingo Steinbach<sup>1</sup>; <sup>1</sup>Ruhr-University

A multi-phase-field model is developed where the interface condition between the different phases is treated out of chemical equilibrium. This results in a finite interface dissipation rate dependent on the deviation from equilibrium. The model is based in the standard multi-phase-field model with separate phase concentration fields in solid and liquid. These concentration fields are coupled via a dynamic equation accounting for finite interface dissipation. The model is shown to converge towards the standard model with equal diffusion potentials in the interface for infinitely fast relaxation. It can be applied to investigate the initial state of contact of a solid with a melt in an arbitrary off equilibrium state. Applications are melt coating of sheet products of soldering. The model is also shown to be applicable to rapid solidification.

### 5:15 PM

**Phase-Field Simulations of Stress-Induced Twin Formation during Solidification:** Shenyang Hu<sup>1</sup>; Chuck Henager Jr.<sup>1</sup>; <sup>1</sup>Pacific Northwest National Laboratory

Twin formation during crystal growth from the melt due to crucible contact stresses or growth stresses can be problematic for processing of single crystals, such as the case of CZT growth via the vertical gradient freeze method. In this talk, we present a phase-field model to describe twin evolution in an FCC polycrystalline material. The model assumes that twin nucleation and growth is a process of partial dislocation nucleation and slip on successive habit planes. Stacking fault energies, energy pathways, critical stresses for the formation of stacking faults, and dislocation core energies are used to construct the thermodynamic model. With the model, twin formation and evolution during crystal growth from the melt is simulated. The effect



of grain orientation and cooling rate on the twin structure is systematically studied. The potential application of the model in studying the deformation twinning in polycrystalline materials will also be discussed.

## Hume-Rothery Symposium Thermodynamics and Diffusion Coupling in Alloys - Application Driven Science: Diffusion Theory and Diffusion in Grain Boundary

Sponsored by: The Minerals, Metals and Materials Society, TMS Electronic, Magnetic, and Photonic Materials Division, TMS: Alloy Phases Committee

Program Organizers: Zi-Kui Liu, The Pennsylvania State University; Larry Kaufman, CALPHAD, Inc.; Annika Borgenstam, Royal Institute of Technology; Carelyn Campbell, NIST

Tuesday PM  
March 1, 2011

Room: 31A  
Location: San Diego Conv. Ctr

Session Chairs: Jian Luo, Clemson University; Sybrand van der Zwaag, Technical University Delft

### 2:00 PM Invited

**Development of a Theory of Solute Diffusion Enhancement for Analyzing Interdiffusion Experiments:** Irina Belova<sup>1</sup>; Alan Allnatt<sup>2</sup>; Yongho Sohn<sup>3</sup>; Nagraj Kulkarni<sup>4</sup>; Sarah Brennan<sup>3</sup>; Graeme Murch<sup>1</sup>; <sup>1</sup>The University of Newcastle; <sup>2</sup>University of Western Ontario; <sup>3</sup>University of Central Florida; <sup>4</sup>Oak Ridge National Laboratory

Recently, the accuracy of interdiffusion measurements has increased greatly. The SIMS technique allows for very precise determination of interdiffusion concentration profiles down into the ppm range. At such small concentrations of solute, an interdiffusion enhancement theory becomes relevant. However, previous development of a diffusion enhancement theory has focused exclusively on tracer solute diffusion and not interdiffusion. Here, we consider the steps for undertaking the development of an interdiffusion enhancement theory applicable to interdiffusion data. These include: the 5-frequency vacancy mechanism in fcc (or related mechanisms for other lattices) with expansion of this model to higher order vacancy-solute atoms clusters, asymptotic analysis of the phenomenological coefficients, vacancy concentration and thermodynamic factor. It is shown that a correct diffusion enhancement theory for the interdiffusion coefficient must involve consideration of clusters of vacancy and two solute atoms (triplets) in order to assess the contribution of off-diagonal phenomenological coefficients.

### 2:30 PM Invited

**The 17 Diffusion Path Theorems by Kirkaldy and Brown Revisited:** John Morral<sup>1</sup>; <sup>1</sup>Ohio State University

In a 1963 review paper by Kirkaldy and Brown a list of 17 theorems were given for diffusion paths in multicomponent diffusion couples. These same theorems were repeated in the 1987 text entitled Diffusion in the Condensed State by Kirkaldy and Young. In the nearly 50 years since they were first published, these theorems have withstood the test of time. However now it is possible to formulate additional theorems that are more specific about what happens to diffusion paths in multiphase regions. The theorems are based on theoretical work that was developed to explain features seen in DICTRA simulations and experimental work. Examples are theorems about how boundaries in diffusion couples can be classified and identified on diffusion paths and also when zigzag features and horns occur on diffusion paths. Both the original and new theorems will be discussed in this work

### 3:00 PM Invited

**Determination of the Intrinsic Interface Mobility in Binary Ferrous Alloys Using Reversible Partial Transformation Experiments:** Sybrand van der Zwaag<sup>1</sup>; Hao Chen<sup>1</sup>; <sup>1</sup>Technical University Delft

The kinetics of the principal austenite to ferrite phase transformation is determined both by the kinetics of the diffusional solute partitioning and

the intrinsic interface mobility. However, the determination of the interfacial mobility is not straightforward due to the fact that the usual transformation kinetics are determined by nucleation and growth kinetics simultaneously and can not be separated. In this work we will present the transformation kinetics for incomplete phase transformation in the two phase region which do allow a far more accurate determination of the interface mobility as nucleation effects can be excluded. The data are interpreted in the context of both the TU Delft mixed mode model and the diffusional transformation model developed at KTH by Agren and colleagues.

### 3:30 PM Break

### 3:50 PM

**Diffusion Coefficients in Liquid and Grain Boundary Predicted by Ab Initio Molecular Dynamics:** Zi-Kui Liu<sup>1</sup>; Huazhi Fang<sup>1</sup>; Bill Wang<sup>1</sup>; <sup>1</sup>The Pennsylvania State University

Molecular dynamics (MD) is a powerful tool to probe the thermodynamic and kinetic properties of solid, glass and liquid phases. In classical molecular dynamics (CMD), empirical models are used to describe the force by considering bond, bend and dihedral angle contributions with parameters fitted to experimental data or first-principles calculations of small clusters. In the ab initio molecular dynamics (AIMD), the forces are calculated on the fly using the first-principles density functional theory as discussed above. In the present work, we use AIMD simulations to follow the random walk of atoms in the liquid state. Based on the mean square displacements (MSD), the diffusion coefficients are calculated from the Einstein equation. Furthermore, we extend this approach to understand the diffusion in grain boundaries.

### 4:20 PM

**Grain Boundary "Phase" Diagrams and Their Applications in Predicting Activated Sintering and Microstructure Development:** Jian Luo<sup>1</sup>; <sup>1</sup>Clemson University

Our recent HRTEM studies revealed that impurity-based, nanometer-thick, quasi-liquid, intergranular films can be thermodynamically stabilized well below the bulk solidus lines at grain boundaries in W and Mo based alloys [Acta Mater. 55:3131 (2007); APL 94:251908 (2009)]. Enhanced diffusion in such liquid-like grain boundaries explained a long-standing mystery regarding the mechanism of "solid-state activated sintering". Similar impurity-based interfacial films have been widely observed in other materials (especially ceramic materials), where they often control the microstructural evolution as well as mechanical and electronic properties [Crit. Rev. Solid State Mater. Sci. 32:67 (2007)]. We propose a long-range scientific goal of developing grain boundary "phase" diagrams as a new materials science tool [APL 92:101902 (2008); Curr. Opin. Solid State Mater. Sci. 12:81 (2008); APL 95: 071911 (2009)]. Most recent results on Mo-Ni and Mo-Si-B based alloys will be presented, with an emphasis on the correlation among grain boundary disordering, diffusion and sintering.

### 4:50 PM

**Finding Critical Nucleus Configuration and Activation Energy for Heterogeneous Nucleation at Grain Boundaries:** Ning Zhou<sup>1</sup>; Yipeng Gao<sup>1</sup>; Yunzhi Wang<sup>1</sup>; <sup>1</sup>The Ohio State University

A free-end nudged elastic band (NEB) algorithm is used to explore the free-energy landscape of phase field models of Ni<sub>4</sub>Ti<sub>3</sub> precipitation in a polycrystal Ni-Ti shape memory alloy. The saddle-point configuration and energy for heterogeneous nucleation of a coherent Ni<sub>4</sub>Ti<sub>3</sub> precipitate on large angle B2 grain boundaries are determined. Thermodynamic inputs such as the Gibbs free energy of the B2 phase are obtained from databases developed using the CALPHAD method. The elastic strain energy contribution from the coherency stress due to the lattice mismatch is calculated using experimentally measured lattice constants and lattice correspondence. The influences of grain boundary plane inclination with respect to precipitate habit plane and grain boundary segregation on nucleation barrier and critical nucleus configuration are investigated. The simulation results could provide insights on how to control Ni<sub>4</sub>Ti<sub>3</sub> precipitation to tailor the property of NiTi-based shape memory alloys. The work is supported by NASA under grant NNX08AB49A.

5:20 PM

**Influence of Porosity on Grain Boundary Diffusion of Fe in Ultrafine-Grained 14YWT Steel Produced by Mechanical Alloying:** *Reeti Singh*<sup>1</sup>; Sergiy Divinski<sup>1</sup>; Joachim Schneibel<sup>2</sup>; Gerhard Wilde<sup>1</sup>; <sup>1</sup>Institute of Material Physics, Westfälische Wilhelms-University Münster, Germany; <sup>2</sup>Institute for Materials and Joining Technology, University of Magdeburg

The diffusion of Fe in nanocluster-strengthened ferritic 14YWT steel has been investigated. The grain boundary penetration at lower temperatures was found to reveal a specific time dependence, which indicates the existence of interconnected porosity in the ferritic steel. The solid state diffusion along boundaries and the penetration along interconnected cavities were verified by <sup>59</sup>Fe diffusion measurements as well as by room temperature penetration of the liquid <sup>110m</sup>Ag tracer. The presence of porosity in the given material affected the diffusion kinetics introducing a hierarchy of short-circuit diffusion paths. The grain boundary diffusion coefficient and the diffusivity along internal surfaces were determined in the so-called type C C, C-B and B-B kinetic regimes of interface diffusion in the hierarchical microstructure, according to the Divinski's classification. The results of the diffusion analyses are discussed with respect to the high creep strength of the material at high temperatures.

## Magnesium Technology 2011: High-Temperature Alloys; High-Strength Alloys; Precipitation

*Sponsored by:* The Minerals, Metals and Materials Society, TMS Light Metals Division, TMS: Magnesium Committee  
*Program Organizers:* Wim Sillekens, TNO Science and Industry; Sean Agnew, University of Virginia; Suveen Mathaudhu, US Army Research Laboratory; Neale Neelameggham, US Magnesium LLC

Tuesday PM  
March 1, 2011

Room: 6F  
Location: San Diego Conv. Ctr

*Session Chairs:* Alan Luo, General Motors; Alok Singh, National Institute for Materials Science

2:00 PM

**Creep and Elemental Partitioning Behavior of Mg-Al-Ca-Sn Alloys with the Addition of Sr:** *Jessica TerBush*<sup>1</sup>; Olivia Chen<sup>1</sup>; J.Wayne Jones<sup>1</sup>; Tresa Pollock<sup>2</sup>; <sup>1</sup>University of Michigan; <sup>2</sup>University of California

The partitioning of elements during solidification can strongly affect precipitation and solute strengthening during creep, especially in alloys where creep is controlled by viscous glide of dislocations. Elemental partitioning during solidification and its influence on creep behavior has been examined for Mg-6.5Al-2.25Ca-0.8Sn with and without 0.25wt% Sr additions. The alloy containing Sr experienced increased partitioning of Al and Ca to the  $\alpha$ -Mg phase. However, the creep behavior in compression at 110 MPa and 180°C was not significantly different from that of the alloy without Sr. In addition, it was determined that the elemental partitioning profiles of permanent mold cast specimens were representative of the grain interiors of die-cast specimens, although greater disagreement was observed for interdendritic regions of the microstructure. These observations are discussed in terms of current models for solid solution and precipitation strengthening.

2:20 PM

**Effect of Mn Addition on Creep Property in Mg-Al-Ca Systems:** *Tomoyuki Homma*<sup>1</sup>; S. Nakawaki<sup>1</sup>; K. Oh-ishi<sup>2</sup>; Kazuhiro Hono<sup>2</sup>; Shigeharu Kamado<sup>1</sup>; <sup>1</sup>Nagaoka University of Technology; <sup>2</sup>National Institute for Materials Science

The effect of Mn addition on creep property in Mg-2Al-2Ca (mass%) alloys has been investigated by analytical transmission microscopy and atom probe tomography. The Mn addition can reduce the minimum creep rate of the Mg alloys so that fine and dense precipitates are dispersed during the creep deformation at 175-225 °C. The fine precipitates are Al<sub>2</sub>Ca phases and G.P. zones. Nevertheless, while the creep temperatures are high, these

precipitates are stable at the high temperature. Mn tends to be involved in the fine precipitates, leading to the dense distribution of the precipitates. The measured number density of the fine precipitates is one order of magnitude higher than that in Mn-free alloy.

2:40 PM

**The Effect of Precipitate State on the Creep Performance of Mg-Sn Alloys:** Mark Gibson<sup>1</sup>; Xi-ya Fang<sup>2</sup>; Colleen Bettles<sup>3</sup>; *Christopher Hutchinson*<sup>4</sup>; <sup>1</sup>CSIRO Manufacturing and Infrastructure Technology; <sup>2</sup>Monash Centre for Electron Microscopy; <sup>3</sup>ARC Centre of Excellence for Design in Light Metals; <sup>4</sup>Monash University

The Mg-Sn system has recently received attention as a potential base for the development of creep resistant alloys. In this work we report our efforts at using alloying additions to modify both the shape and the number density of the Mg<sub>2</sub>Sn precipitates and our measurements of the resulting effects on the creep behaviour. Under a load of 60MPa, it is shown that the secondary creep rates can be improved by at least five orders of magnitude compared to the binary alloy. Transmission electron microscopy observations show that the origin of the excellent creep properties is a remarkable thermal stability of the precipitate structure. The possible origins of the stability are discussed.

3:00 PM

**Microstructure and Mechanical Properties of Mg-Zn-Y-M (M: Mixed RE) Alloys with LPSO Phase:** *Jonghyun Kim*<sup>1</sup>; Yoshihito Kawamura<sup>2</sup>; <sup>1</sup>Kumamoto Technology & Industrial Foundation; <sup>2</sup>Kumamoto University

Magnesium alloys are emerging as potentially good candidates for numerous applications, especially in automotive, aerospace and electronic industry. Their advantages, such as low density and high specific strength, make them promising structural materials for applications. Among the various alloy systems developed, the commonly used magnesium alloys, such as AZ91 and AM60, are based on Mg-Al system. However, the use of these Mg alloys has been limited to temperatures below 120° because of their poor heat resistance, especially creep property at elevated temperatures. Therefore, it is necessary to develop some heat-resistant magnesium alloys for elevated temperature applications. Recently, Kawamura et al. have developed the Mg-Zn-Y alloys with the LPSO phase. These alloys have the excellent mechanical properties. The investigation reported here focused on the influence of mixed RE, which was also effective in strengthening Mg-Zn-Y alloys at elevated temperature, on the microstructure and mechanical properties of the Mg-Zn-Y-M (M: Mixed RE) alloys.

3:20 PM

**Analysis of Texture Evolution during High-Temperature Creep in Magnesium Alloys with Application of Neutron Diffraction:** *Dimitry Sediako*<sup>1</sup>; Scott Shook<sup>2</sup>; Sven Vogel<sup>3</sup>; Anton Sediako<sup>4</sup>; <sup>1</sup>National Research Council Canada; <sup>2</sup>Applied Magnesium International; <sup>3</sup>Los Alamos Neutron Science Center; <sup>4</sup>McGill University

Although a large share of the material used in industry is in the form of castings, the use of wrought products in automotive applications is on the rise. Extrudability and high temperature performance of wrought material became critical factors in developing new wrought alloys and processing technologies. This paper shows some results received in creep testing and studies of in-creep texture evolution for several wrought magnesium alloys developed for use in elevated-temperature applications. These studies were performed using E3 neutron spectrometer of the Canadian Neutron Beam Centre in Chalk River, Ontario, and HIPPO time-of-flight spectrometer at Los Alamos Neutron Science Center, NM. It was confirmed that there is a notable difference in the strength of extrusion-type texture for the extruded samples of studied alloys, that represent four alloying systems; namely, Mg-Al-RE, Mg-Al-Ca, Mg-Al-Sr, and Mg-Zn-RE. This difference in texture likely affected material performance in high-temperature creep tests.

3:40 PM

**Improved Processing of Mg-Zn-Y Alloys Containing Quasicrystal Phase for Isotropic High Strength and Ductility:** *Alok Singh*<sup>1</sup>; *Yoshiaki Osawa*<sup>1</sup>; *Hidetoshi Somekawa*<sup>1</sup>; *Toshiji Mukai*<sup>1</sup>; <sup>1</sup>National Institute for Materials Science

The stable quasicrystal phase in Mg-Zn-Y alloys has been proved to be beneficial for strength and ductility and has also been shown to impart high fracture toughness. However, the strength of these alloys has been limited by effective dispersion of the quasicrystal phase by wrought processing. Yield strengths have been limited to 300MPa with a grain size of 1  $\mu\text{m}$ . We show a simple procedure in which a  $\text{Mg}_{90}\text{Zn}_6\text{Y}_4$  alloy was chilled cast and then extruded. Yield strengths of up to 400 MPa in tension and compression, accompanied by ductility of  $\approx 14\%$  were obtained with grain of size of about 1  $\mu\text{m}$ . Compression to tension yield anisotropy ratios were in the narrow range of 0.95 to 1.03. These alloys also showed ageing response with two peaks. The effect of ageing on mechanical properties has been studied. Precipitation effects slip more than twinning, decreasing the yield asymmetry ratio.

4:00 PM Break

4:20 PM

**Precipitation Hardenable Mg-Ca-Al Alloys:** *J. Jayaraj*<sup>1</sup>; *C.L. Mendis*<sup>1</sup>; *T. Ohkubo*<sup>1</sup>; *K. Oh-ishi*<sup>1</sup>; *K. Hono*<sup>1</sup>; <sup>1</sup>National Institute for Materials Science

The combinations of oversized element like RE and Ca and undersized element like Zn in Mg causes the formation of plate like precipitates on the basal plane. Both Mg-RE-Zn and Mg-Ca-Zn alloys exhibit age hardening response and good creep properties, which are attributed to the formation of plate like GP zones. It is intriguing to see whether or not other undersized elements like Al exhibit the similar effect. Thus, the effect of Al additions in a Mg-0.5Ca(wt.%) alloy on age hardening responses have been investigated. The Mg-0.5Ca-0.3Al alloy showed peak hardness (72 HV) higher than that for the Mg-1Ca-1Zn alloy. TEM and 3DAP analyses confirmed the dense distribution of ordered G.P. zones on the basal planes and the subsequent formation of  $\text{Al}_2\text{Ca}$  causes the over-aging. Since only a trace addition of inexpensive alloying elements contribute to the age hardening, this alloy may be suitable for wrought applications.

4:40 PM

**Microstructure, Phase Evolution and Precipitation Strengthening of Mg-3.1Nd-0.45Zr-0.25Zn Alloy:** *Galit Atiya*<sup>1</sup>; *Menachem Bamberger*<sup>1</sup>; *Alexander Katsman*<sup>1</sup>; <sup>1</sup>Technion - Israel Institute of Technology

The microstructure of the Mg-3.1%Nd-0.45%Zr-0.27%Zn (wt) alloy has been investigated after solution treatment at 540°C for 24hr followed by isothermal aging at 175°C up to 32 days. After solution treatment the bct ( $\text{Mg}_3\text{Zn}$ )<sub>12</sub>Nd phase dissolved and small tetragonal  $\text{Zn}_2\text{Zr}_3$  rod-like particles precipitated at  $\alpha$ -Mg grain interiors. Precipitation during isothermal aging involves the formation of metastable phases  $\beta''$  ( $\text{Mg}_3\text{Nd}$ )<sub>hcp</sub> ( $\text{DO}_{19}$  structure) and  $\beta'$  ( $\text{Mg}_3\text{Nd}$ )<sub>fcc</sub> ( $\text{DO}_3$  structure). The  $\beta''$  precipitates formed during the first 8 days of aging have a platelet shape and are fully coherent with Mg matrix. During 16-32 days of aging, the  $\beta''$  precipitates transform to  $\beta'$  precipitates with an FCC structure. The  $\beta'$  precipitates are semi-coherent with the Mg matrix and have the following orientation relationship:  $[0001]_{\text{Mg}} \parallel [101]_{\beta'}$  and  $[-1100]_{\text{Mg}} \parallel [-112]_{\beta'}$ . After prolonged aging of 32 days, the  $\beta'$  precipitates transform to the stable incoherent  $\beta$  ( $\text{Mg}_3\text{Zn}$ )<sub>12</sub>Nd phase. The growth, coarsening and phase transformations were followed by microhardness tests.

5:00 PM

**Precipitation Process in Mg-Nd-Zn-Zr-Gd/Y Alloy:** *Jiehua Li*<sup>1</sup>; *Gang Sha*<sup>2</sup>; *Peter Schumacher*<sup>1</sup>; *Simon Ringer*<sup>2</sup>; <sup>1</sup>Chair of Casting Research, Department of Metallurgy, the University of Leoben; <sup>2</sup>Australian Centre for Microscopy and Microanalysis, The University of Sydney

Transmission electron microscopy (TEM) and atom probe tomography (APT) were employed to investigate the solute cluster and precipitates formed in different Mg-Nd-Zn-Zr-Gd/Y alloys aged at 200°C up to 100h. TEM characterizations confirmed the precipitation microstructure evolution and the precipitation sequence in these alloys, which involved the formation

of phase such as  $\beta''$ ,  $\beta'$ ,  $\beta_1$  and  $\beta$ . These precipitates had ideal-shaped and distribution, with the plate lying on (01-10) a-Mg and very thin plate lying on (0001) a-Mg. APT analyses, for the first time, revealed that the precipitates were enriched with Nd, Zn and Gd. Moreover, Nd partitioned more strongly into the precipitates than Gd and Zn. In contrast, Y was less prone to partition into precipitates than any other alloying element in these alloys. These careful TEM characterizations and quantitative atom probe data analyses elucidated the precipitation behavior of Mg-Nd-Zn-Zr-Gd/Y alloys.

5:20 PM

**Mechanical Properties and Microstructures of Twin-Roll Cast Mg-2.4Zn-0.1Ag-0.1Ca-0.16Zr Alloy:** *Chamini Mendis*<sup>1</sup>; *Jun Ho Bae*<sup>2</sup>; *Nack Kim*<sup>2</sup>; *Kazuhiro Hono*<sup>1</sup>; <sup>1</sup>National Institute for Materials Science; <sup>2</sup>Pohang University of Science and Technology

In our previous study, we reported that the additions of 0.1 at.% Ag and 0.1 at.% Ca to Mg-2.4Zn-0.16Zr (at.%) alloy enhanced the age hardening response, and extruded alloy showed tensile yield strength of 325 MPa with the T6 heat treatment. Considering its excellent age hardenability, we attempted to develop high strength sheets from the alloy by twin-roll casting (TRC). TRC sheet of 2 mm in thickness were hot rolled to  $\sim 1.2$  mm. The TRC Mg-2.4Zn-0.1Ag-0.1Ca-0.16Zr alloy sheet showed tensile yield strength of  $\sim 320$ MPa and an elongation to failure of 17% after T6 heat treatment. EBSD study indicated the average grain size is  $\sim 18 \pm 2.5 \mu\text{m}$  and the grains have a weak basal texture. TEM, showed a uniform distribution of  $\sim 5$  nm diameter  $\text{MgZn}_2$  phase. The dispersion of rod-like precipitates was attributed to the high yield strength observed.

5:40 PM

**The Solidification Microstructure and Precipitation Investigation of Magnesium-Rich Alloys Containing Zn and Ce:** *Chuan Zhang*<sup>1</sup>; *Alan A. Luo*<sup>2</sup>; *Y. Austin Chang*<sup>1</sup>; <sup>1</sup>UW-Madison; <sup>2</sup>General Motors Research & Development Center

Solidification microstructure and precipitation of Mg-Zn-Ce alloys were investigated to develop high-strength and high-ductility lightweight magnesium alloys for structural applications. The characterized microstructures of four directionally solidified Mg-Zn-Ce alloys agree well with the calculated solidification paths using computational thermodynamics coupled with the Scheil model. Equilibrium calculations were also performed on these Mg-Zn-Ce alloys. The precipitation of Mg<sub>12</sub>Ce intermetallic phase was predicated thermodynamically, and characterized using high-resolution transmission electron microscopy (HRTEM).

## Magnetic Materials for Energy Applications: Soft Magnetic Materials

*Sponsored by:* TMS Electronic, Magnetic, and Photonic Materials Division, TMS: Energy Conversion and Storage Committee, TMS: Magnetic Materials Committee; JSPS 147th Committee on Amorphous and Nanocrystalline Materials; Lake Shore Cytronics, Inc.; AMT&C

*Program Organizers:* Victorino Franco, Sevilla University; Oliver Gutfleisch, IFW Dresden; Kazuhiro Hono, National Institute for Materials Science; Paul Ohodnicki, National Energy Technology Laboratory

Tuesday PM  
March 1, 2011

Room: 11A  
Location: San Diego Conv. Ctr

*Session Chair:* Paul Ohodnicki, National Energy Technology Laboratory

2:00 PM Keynote

**Soft Magnetic Materials Fabricated by Rapid Quenching Technique for Energy Applications:** *Motoki Ohta*<sup>1</sup>; *Yoshihito Yoshizawa*<sup>1</sup>; <sup>1</sup>Hitachi Metals Ltd.

Recently, the Fe-based amorphous alloys have been coming into use for iron core materials because of their low iron loss. However, since there is problem of noise due to their large saturation magnetostriction, the magnetic

TUESDAY PM



flux density for operating,  $B_m$  is limited. To enlarge  $B_m$ , improving squareness of B-H curve becomes key. Moreover, recent progresses of high saturation magnetic flux density nanocrystalline alloys are also introduced.

#### 2:40 PM Invited

**Recent Advances in Non-oriented Electrical Steel for EV/HEV Traction Motor:** *Ichiro Tanaka*<sup>1</sup>; Hiroyoshi Yashiki<sup>1</sup>; <sup>1</sup>Sumitomo Metal Industries, Ltd.

To improve efficiency of traction motors for environmentally friendly vehicles, we have developed two kinds of non-oriented electrical steels: low core loss and high magnetic induction grades for stator core and high-strength grades highly suitable for rotor core of IPM motors. Excellent magnetic properties of the developed steel for stator core were ascribed to recrystallization texture control by phosphorus addition. Phosphorus segregation at initial grain boundaries enhances beneficial texture evolution. High-strength of the developed steel for rotor core of IPM motors was achieved by dislocation strengthening through niobium addition. Solute niobium moderately retards recrystallization kinetics; then the retardation leads to specific microstructure favorable for great strength. The newly developed electrical steels of notable characteristics will significantly contribute to an improvement in performance of traction motors for electric vehicles and hybrid electric vehicles, and furthermore, motors for appliances, particularly compressor motors for air conditioners.

#### 3:05 PM Invited

**The Requirements of Soft Magnetic Materials for Industrial Applications:** *Francis Johnson*<sup>1</sup>; Satish Prabhakaran<sup>1</sup>; Ayman El-Refai<sup>1</sup>; <sup>1</sup>GE Global Research

Advanced magnetic materials are required to enhance the performance of electrical power generation, distribution, and conversion systems. The complementary needs of high power density and high system efficiency demand components that exhibit low power loss at high frequencies. The trend in power conversion technology is to move away from all-passive low frequency transformers to modular power electronic systems with high frequency transformers. New magnetic materials operable from the MW-level-20 kHz range up to the kW-level -MHz range with operating temperatures up to 300 °C will be required. Advanced electric machines and drives, often with permanent magnet architectures, are being developed to operate at continually higher speeds and temperatures. In addition to excellent magnetic properties, these rotating machines place demands on the mechanical and thermal properties of the material. Strategies for improved material performance include nanoscale structure control, novel device geometries, and improved processing methods to maintain a sustainable value chain.

#### 3:30 PM Invited

**Soft Magnetic Materials for Improved Energy Performance:** *Matthew Willard*<sup>1</sup>; Maria Daniil<sup>1</sup>; Keith Knippling<sup>1</sup>; Ramasis Goswami<sup>1</sup>; <sup>1</sup>Naval Research Laboratory

Recent activity to improve the sustainability of our energy use has resulted in increased awareness of the impact of energy efficiency on the performance of devices. Magnetic materials play an important role in improving the efficiency due to their widespread use in electric power generation, conditioning, conversion, transportation, and other technology-based sectors of the economy. This presentation will focus on state-of-the-art amorphous and nanocrystalline soft magnetic alloys optimized for energy applications, including electricity generation, conditioning, conversion, refrigeration, and transportation applications. Our recent work on Fe-based nanocrystalline alloys for high temperature applications and (Fe,Si,Al)-based nanocrystalline alloys for cryogenic applications will be highlighted.

#### 3:55 PM Break

#### 4:25 PM Invited

**FeCo and FeNi-based Nanocomposite Magnets for Energy Applications.:** *Michael McHenry*<sup>1</sup>; <sup>1</sup>Carnegie Mellon University

Magnetic nanocomposites and derived magnetic properties impact energy applications: (1) FeCo nanocomposites for power conversion

applications. (2) High Co-containing alloys for magnetic sensors for deep well oil exploration. (3) Ni- and FeCoCr-based alloys for magnetocaloric cooling. FeCo-based nanocomposites have large saturation inductions and Curie temperatures. Field crystallization impacts high frequency core losses. AC power conversion applications in hybrid vehicles will be discussed. In Co-rich nanocomposites 2- and 3-phase nanocrystallization impacts induced magnetic anisotropy. Low loss, linear B(H) and and corrosion resistance of makes these alloys candidates for high temperature fluxgate and giant magnetoimpedance magnetometers for oil and strategic mineral exploration and well-leak remediation. FeCoCr-based alloys have sizeable magnetocaloric effects near room temperature. The synthesis of low  $T_c$  Fe-Ni nanocomposites require stabilization of the metastable  $\gamma$  phase at Fe-rich compositions discussed in light of the  $T_0$  construction in the Fe-Ni eutectoid phase diagram.

#### 4:50 PM Invited

**Field-Annealed FeCo-Based Amorphous and Nanocrystalline Alloys with Improved Magnetic Softness:** *Ivan Skorvanek*<sup>1</sup>; Jozef Marcin<sup>1</sup>; Peter Svec<sup>2</sup>; <sup>1</sup>Institute of Experimental Physics; <sup>2</sup>Institute of Physics

The continuing interest in the development of FeCo-based amorphous and nanocrystalline alloys is mainly due to their ability to combine a high saturation magnetic flux density with relatively good magnetic softness. In this work, a controllable field annealing induced magnetic anisotropy is produced in series of Fe-Co-Nb-B and Fe-Co-B-Cu amorphous and (nano) crystalline alloys. We show that the specimens annealed without the presence of external magnetic field show an appreciable increase of the coercivity with crystallization. A heat treatment under the presence of longitudinal magnetic field results for the Fe-Co-Nb-B alloy in squared hysteresis loops characterized by very low coercive field values in the range of 2 - 8 A/m. The saturation magnetic flux density for the optimum field annealed amorphous  $Fe_{63}Co_{21}B_{15}Cu$  alloy reaches 1.83 T and the value of coercive field is 1.7 A/m. Such low  $H_c$  values are superior to those previously reported for FeCo-based amorphous and nanocrystalline alloys.

#### 5:15 PM

**Effect of Different Annealing Methods on Structure and Texture of Primary Recrystallization of Grain-oriented Silicon Steel:** *Lijuan Li*<sup>1</sup>; Li-hua Liu<sup>1</sup>; Xue-liang Wu<sup>1</sup>; Wen Shi<sup>1</sup>; Qi-jie Zhai<sup>1</sup>; <sup>1</sup>Shanghai University

The effects of different annealing methods which include pulse current annealing, salt bath annealing and conventional furnace annealing on microstructure and texture of primary recrystallization of grain-oriented silicon steel were studied. Comparing with the sample treated by conventional furnace annealing, pulse current annealing and salt bath annealing increase the intensity of (110), which may means more Goss grains (secondary nucleus) forming and will be good for the development of structure and texture of secondary recrystallization. Pulse current annealing can obviously decrease the proportion of  $\Sigma 1$  grain boundary which is harm for secondary recrystallization, however, salt bath annealing increases  $\Sigma 1$  grain boundary. There are strong  $\{111\}<112>$  texture in the samples of pulse current annealing, salt bath annealing and conventional furnace annealing. The results show that by pulse current annealing we can obtain better structure and texture of primary recrystallization of grain-oriented silicon steel.

#### 5:30 PM

**Solute Effects on Magnetic Properties and Thermal Stability in Fe-Mo-B-P-Si Metallic Glasses:** *Gary Shiflet*<sup>1</sup>; S. Bhattacharya<sup>1</sup>; S. Joseph Poon<sup>1</sup>; <sup>1</sup>University of Virginia

The role of gallium, copper and cobalt on the size and morphology of BCC iron crystals forming from an amorphous matrix will be discussed in this presentation. Among the metallic glasses, the Fe-based systems with high glass formability (GFA) are of significant interest for their possible excellent soft magnetic properties. This talk will focus on the above listed element's effects, as well as the role of metalloids on the thermal stability and magnetic properties of Fe-X-B-C-P-Si metallic glasses (X=Ga, Cu, Co, or Mo). The beneficial effect of controlling the BCC nanocrystalline iron phase (ca. 10 nm) will also be shown and discussed. Time-temperature-transformation (TTT) studies and investigation of nano-crystallization properties will be

presented based on results using transmission electron microscopy and magnetic measurements.

#### 5:45 PM

##### **Fabrication of High Performance Fe-Si-Al Soft Magnetic Composites:**

*Junhua You*<sup>1</sup>; <sup>1</sup>Shenyang University of Technology

The Fe-Si-Al soft magnetic composites were produced by cold pressing of water-atomized Fe-Si-Al powder using organic binder. The effect of shaping pressure, annealing temperature, magnetic annealing and dielectric content on properties of Fe-Si-Al soft magnetic composites was investigated. The results showed that increasing shaping pressure increases density and radial crushing strength of Fe-Si-Al soft magnetic cores, and decreases coercivity and total loss. Increasing annealing temperature can increase effective permeability and decrease total loss owing to decreasing hysteresis loss, and overannealing (>660°) can deteriorate magnetic properties. The magnetic annealing can decrease total loss of Fe-Si-Al magnetic powder core. Increasing dielectric content can reduce the eddy current loss of Fe-Si-Al magnetic powder core and decrease the real part of permeability. Fe-Si-Al magnetic powder core with shaping pressure of 1800 MPa, annealing temperature of 660° and dielectric content of 0.7% presented the optimum magnetic properties with an effective permeability of 127, a total loss of 78 mW/cm<sup>3</sup> and a radial crushing strength of 18MPa.

## **Materials for the Nuclear Renaissance II: Zirconium and Fuel**

*Sponsored by:* The Minerals, Metals and Materials Society, TMS Structural Materials Division, TMS/ASM: Corrosion and Environmental Effects Committee, TMS/ASM: Nuclear Materials Committee

*Program Organizers:* Raul Rebak, GE Global Research; Brian Cockeram, Bechtel-Bettis; Peter Chou, Electric Power Research Institute; Micah Hackett, TerraPower, LLC

Tuesday PM  
March 1, 2011

Room: 4  
Location: San Diego Conv. Ctr

*Session Chair:* Peter Chou, EPRI

#### 2:00 PM Introductory Comments

#### 2:05 PM

##### **Determination of Zircaloy Liquidus and Solidus with an Instrumented Transvaerstraint Test:** *Micah Hackett*<sup>1</sup>; George Young<sup>1</sup>; <sup>1</sup>KAPL

Zirconium alloys are commonly welded for nuclear and chemical process applications, but they can be susceptible to solidification cracking during fusion welding. Determining the liquidus and solidus temperatures is of fundamental importance to an alloy's weldability since the extent of the two-phase 'mushy' zone defines the region susceptible to solidification cracking. However, the high melting temperature and reactivity of molten zirconium makes conventional methods (e.g. differential thermal analysis) to determine the liquidus and solidus impractical. An instrumented transvaerstraint test was developed to determine the liquidus and solidus via a series of thermocouples attached to zircaloy test plates outside of the weld fusion zone. At high applied strains, solidification cracks span the length of the mushy zone and can be used in conjunction with temperature measurements and finite element modeling to estimate the solidus and liquidus temperatures. Details of the experimental setup and results for industrial alloys will be discussed.

#### 2:25 PM

##### **Development of Microstructure and Irradiation Hardening of Zircaloy during Low Dose Neutron Irradiation at Nominally 300C:** *Brian Cockeram*<sup>1</sup>; Lance Sneed<sup>2</sup>; Richard Smith<sup>1</sup>; <sup>1</sup>Bechtel-Bettis; <sup>2</sup>ORNL

Wrought Zircaloy-2 and Zircaloy-4 were neutron irradiated at nominally 300C in the High Flux Isotope Reactor (HFIR) at relatively low neutron fluences between 1X10<sup>23</sup> and 6X10<sup>25</sup> n/m<sup>2</sup> (E>0.1 MeV). The irradiation hardening and change in microstructure were characterized following

irradiation using tensile testing, hardness and examination of microstructure using Analytical Electron Microscopy. Small increments of dose were used in the range where the saturation of irradiation hardening is typically observed so that the role of microstructure evolution, <a> loop formation, and change in precipitate structure on irradiation hardening may be understood. An incubation dose between 1X10<sup>23</sup> and 2X10<sup>24</sup> n/m<sup>2</sup> was needed for loop nucleation to occur that resulted in irradiation hardening, but saturation of the <a> loop number density to values within the range of those reported in literature was observed to occur over the fluence range in this work.

#### 2:45 PM

##### **Fabrication and Irradiation of LWR Hydride Mini-Fuel Rods:** *Kurt Terrani*<sup>1</sup>; Mehdi Balooch<sup>1</sup>; Donald Olander<sup>1</sup>; <sup>1</sup>University of California, Berkeley

Benefits of incorporation of hydride fuels into the current fleet of light water reactors (LWRs) have been previously investigated by the means of calculations and laboratory-scale experiments. Recognizing the necessary shift from laboratory scale experiments to more relevant environments, an irradiation experiment is underway to evaluate the feasibility of LWR hydride fuel concept. The irradiation experiment is supported by US DOE's Advanced Test Reactor National Scientific User Facility program. The present work focuses on demonstrating the viability of the combination of hydride fuel (U(30wt%)-ZrH1.6), liquid metal bond, and Zircaloy cladding by long-term irradiation of multiple mini-fuel elements in the MIT reactor. The fuel-cladding gap that is conventionally filled with helium, is replaced with liquid metal of eutectic lead-bismuth alloy. Each mini-fuel is instrumented with thermocouples at fuel- centerline and cladding surface. Rods are kept inside the core at various times in order to generate burnup dependent information upon post-irradiation investigation.

#### 3:05 PM

##### **Vanadium and Zirconium Interaction with HT-9 Stainless Steel:** *Randall Fielding*<sup>1</sup>; James Cole<sup>1</sup>; <sup>1</sup>Idaho National Laboratory

Metallic nuclear fuel is a candidate fuel form for advanced high burnup fuel cycles. To achieve high burnups metallic fuel will require an advanced cladding resistant to fuel cladding chemical interaction. Zirconium/HT-9 stainless steel and vanadium/HT-9 stainless steel diffusion couples were fabricated and heated to the tempering temperature of 704°C for 50, 100, and 200 hours. Diffusion couples were also heated to 815°C for 100 hours. After heating the samples were microstructurally examined to determine the amount of interaction. The main interaction seen was decarburization of the HT-9 by the vanadium. Zirconium diffusion couples showed some iron/zirconium interactions, but to a much lower extent than the vanadium decarburization. Based on these results although vanadium has been shown to be a better diffusion barrier zirconium has much less interaction with the cladding material.

#### 3:25 PM Break

#### 3:35 PM

##### **Fuel-Cladding Development for Sodium Fast Reactor Metallic Transmutation Fuels:** *James Cole*<sup>1</sup>; Randall Fielding<sup>1</sup>; Jian Gan<sup>1</sup>; Haiyan Wang<sup>2</sup>; Todd Allen<sup>3</sup>; Kumar Sridharan<sup>3</sup>; <sup>1</sup>Idaho National Laboratory; <sup>2</sup>Texas A&M University; <sup>3</sup>University of Wisconsin

As part of the US Department of Energy's Fuel Cycle R&D (FCRD) program, metallic transmutation fuels have been extensively studied. One issue that remains to be fully resolved in metallic fuel is fuel-cladding chemical interaction. Past studies have shown that as fission product content increases due to carry over from separation processes and build up due to higher burn-up of the fuel, fuel constituents will diffuse into the cladding and cladding constituents will diffuse into the fuel alloy. Of particular concern is cladding wastage when brittle phases form in the cladding, which reduces the maximum allowable stress that can build up in the fuel element. To overcome these issues, liner and coating materials have been examined which will act as diffusion barriers, effectively stopping or greatly slowing FCCI. An overview of efforts to identify, test and fabricate liner and coating options for fuel cladding tubes will be provided.

3:55 PM

**Rapid Synthesis of Nuclear Nitride Fuels at Low Temperatures:** *Brian Jaques*<sup>1</sup>; *Daniel Osterberg*<sup>1</sup>; *Cole Smith*<sup>1</sup>; *Mike Hurley*<sup>1</sup>; *Darryl Butt*<sup>1</sup>; <sup>1</sup>Boise State University

According to the advanced fuel cycle, energy must be harvested from spent fuel and future fuels must reach higher burn-ups. Accordingly, complex fuels comprised of fissile materials must be developed. Although disadvantages exist, nitride fuels have advantages such as: high actinide loadings, high thermal conductivities, and compatibility with candidate inert matrices. Phase pure nitrides were formed from their elements in one hour by milling at ambient temperatures, as confirmed with XRD, EDS, and elemental combustion analysis. The kinetics of nitride synthesis (UN and surrogates for AmN, PuN) through high energy reaction milling in nitrogen was quantified. The extent of the reaction was monitored using in-situ pressure and temperature measurements and the Benedict-Webb-Rubin equation of state. An actinide recycling facility designed around pyro-processing, reactive milling, and SPS would be a relatively closed, proliferation resistant facility with a small footprint. Such a facility would enable simple, quick, and inexpensive partitioning and transmutation.

4:15 PM

**Statistics of Grain Boundary Crystallography in Surrogates for Oxide Nuclear Fuels and its Effects on Mass Transport: Comparison between 2-D and 3-D Measurements and Models:** *Karin Rudman*<sup>1</sup>; *Kapil Krishnan*<sup>1</sup>; *Pedro Peralta*<sup>1</sup>; *Chris Stanek*<sup>2</sup>; *Kenneth J. McClellan*<sup>2</sup>; <sup>1</sup>Arizona State University; <sup>2</sup>Los Alamos National Laboratory

Mass transport in oxide nuclear fuels can be strongly influenced by grain boundary (GB) crystallography. In particular, diffusion of fission products can be enhanced or suppressed depending on the GB misorientation and character (tilt, twist, mixed). However, experimental data are scarce on full GB crystallography of oxide fuels and their surrogates. This study aims to characterize the full GB crystallography in Yttria stabilized Zirconia and depleted Urania using Electron Backscattering Diffraction (EBSD) and serial sectioning. For each section, three parameters for the GB misorientation were collected using EBSD. These EBSD maps were used to create 3D reconstructions and obtain the GB normal. Then, 2-D and 3-D finite element models were created with these data to account for actual microstructure and model local and global diffusion of chosen fission products. The 2-D and 3-D results are compared and contrasted to elucidate role of GB crystallography on mass transport in oxide fuels.

4:35 PM

**The Development of Crystalline Ceramic Wasteforms for an Advanced Nuclear Fuel Cycle:** *Kyle Brinkman*<sup>1</sup>; *Amanda Billings*<sup>1</sup>; *Kevin Fox*<sup>1</sup>; *James Marra*<sup>1</sup>; *Ming Tang*<sup>2</sup>; *Kurt Sickafus*<sup>2</sup>; <sup>1</sup>Savannah River National Laboratory (SRNL); <sup>2</sup>Los Alamos National Laboratory (LANL)

Crystalline materials with potentially enhanced thermodynamic stability as compared to glass wasteforms are currently being developed and evaluated for the encapsulation of species for repository disposal. Ceramic waste forms based on titanate and alumina were investigated for cesium and lanthanide (CS/LN) waste streams; titanate, alumina and calcium based oxides were targeted for cesium and lanthanide streams with transition metal additions (CS/LN/TM). Wasteform processing involved a melting and solidification approach as well as conventional ceramic sintering and sparks plasma sintering. This approach allows for a comparison of amorphous to crystalline phase formation that occurs via the melt versus solid state reactions encountered in conventional sintering and spark plasma sintering. Conclusions to date include i) identification of crystalline phase assemblage in ceramics by XRD and SEM/EDS as a function of composition, waste loading, and processing conditions ii) initial product consistency "dissolution" tests for crystalline ceramics and iii) room temperature irradiation studies.

4:55 PM

**Alloy Optimization for Metallic Inert Matrix Nuclear Fuels:** *Vincenzo Lordi*<sup>1</sup>; *James Belak*<sup>1</sup>; *Patrice Turchi*<sup>1</sup>; <sup>1</sup>Lawrence Livermore National Lab

Inert matrix nuclear fuels (IMF) are promising advanced fuel forms exhibiting high tolerance for fission gases (FG) and irradiation dose, while

maintaining high fuel density and thermal conductivity. IMF in a dispersed metallic matrix form, fabricated by impregnation with molten matrix metal as suggested by Savchenko *et al.*, may meet these requirements by providing space for FG and a direct metallurgical bond between fuel and cladding. Impregnation must occur below 950°C to maintain the integrity of the fuel meat. Computational optimization based on coupling between thermodynamic software and a global constrained search engine was performed for a series of Zr-based metal matrix alloys to achieve low melting temperatures, while incorporating constraints on phases formed during solidification to ensure strength and reliability. Optimized alloys were identified, including an example that promotes formation of precipitates in a ductile matrix, providing both strength and FG gettering. Prepared by LLNL under Contract DE-AC52-07NA27344.

5:15 PM

**Initial Microstructure Formation and Evolution in U-Pu-Zr Alloys:** *Dawn Janney*<sup>1</sup>; *Rory Kennedy*<sup>1</sup>; <sup>1</sup>Idaho National Laboratory

The United States Department of Energy (DOE) is developing actinide alloys (primarily U, Pu, and Zr, with lower concentrations of Np, Am and lanthanides) as metal fuels for transmuting minor actinides as part of a closed nuclear fuel cycle. Previous research suggests that U-Pu-Zr alloys form a continuous solid solution at the solidus, and that this solid solution may include Np. This paper reports results of scanning electron microscope (SEM) examinations in several actinide alloys. Microstructures in rapidly cooled 4-mm cylinders demonstrate phase segregation on a sub-micron scale; those in a more slowly cooled sample are coarser. Although the mechanism of unmixing is not yet understood in detail, some geometrical relationships appear consistent with heterogeneous nucleation. This presentation will discuss results from ongoing studies of early nucleation and phase-segregation mechanisms and processes in these important materials.

5:35 PM

**Modeling of Molten Salt Mixtures: Thermodynamic Assessment of CeBr<sub>3</sub> and MBr-CeBr<sub>3</sub> Systems (M=Li, Na, K, Rb):** *Yue Wu*<sup>1</sup>; *Weiping Gong*<sup>2</sup>; *Leszek Rycerz*<sup>2</sup>; *Ewa Ingier-Stocka*<sup>3</sup>; *Ida Chojnacka*<sup>3</sup>; *Jan Kapala*<sup>3</sup>; *Slobodan Gadzuric*<sup>4</sup>; *Marcelle Gaune-Escard*<sup>5</sup>; <sup>1</sup>Central South University; <sup>2</sup>a)State Key Laboratory of Powder Metallurgy, Central South University and b) Huizhou University; <sup>3</sup>Wroclaw University of Technology; <sup>4</sup>University of Novi Sad; <sup>5</sup>Polytech

Lanthanide halides and their mixtures with alkali metal halides play a significant role in a number of industrial applications largely based on molten salt technologies, many still under development. Their thermodynamic and transport properties can provide basic information for process development and optimization. However these data are scarce and not easily accessible in literature. Accordingly, intensive efforts are being made at an international level both in R&D aspects and also in database development. The thermodynamic properties (temperature and enthalpy of phase transition, heat capacity of solid and liquid phases) of CeBr<sub>3</sub> and MBr-CeBr<sub>3</sub> mixtures as the phase diagrams were experimentally investigated by Differential Scanning Calorimetry (DSC). Assessment and optimization were performed over the whole temperature/composition range. Two different models and two optimization procedures were used for the thermodynamic description of the liquid phase. A critical discussion is given.



---

## Materials in Clean Power Systems VI: Clean Coal-, Hydrogen Based-Technologies, and Fuel Cells: SOFC I - Interconnects

*Sponsored by:* The Minerals, Metals and Materials Society, TMS Electronic, Magnetic, and Photonic Materials Division, TMS Structural Materials Division, TMS/ASM: Corrosion and Environmental Effects Committee, TMS: Energy Conversion and Storage Committee, TMS: High Temperature Alloys Committee  
*Program Organizers:* Xingbo Liu, West Virginia University; Zhenguo "Gary" Yang, Pacific Northwest National Laboratory; Jeffrey Hawk, U.S. Department of Energy, National Energy Technology Laboratory; Teruhisa Horita, AIST; Zi-Kui Liu, The Pennsylvania State University

Tuesday PM                      Room: 33C  
March 1, 2011                  Location: San Diego Conv. Ctr

*Session Chairs:* Paul Jablonski, US Department of Energy; Jeffrey Fergus, Auburn University

---

### 2:00 PM Invited

#### On the State of the Art of Metal Interconnects for SOFC Application:

*Paul Jablonski*<sup>1</sup>; <sup>1</sup>US Department of Energy

One of the recent developments for Solid Oxide Fuel Cells (SOFC) is oxide component materials capable of operating at lower temperatures such as 700-800C. This lower temperature range has provided for the consideration of metallic interconnects which have several advantages over ceramic interconnects: low cost, ease in manufacturing, and high conductivity. Most metals and alloys will oxidize under both the anode and cathode conditions within an SOFC, thus a chief requirement is that the base metal oxide scale must be electrically conductive since this constitutes the majority of the electrical resistance in a metallic interconnect. Common high temperature alloys form scales that contain chrome, silicon and aluminum oxides among others. Under SOFC operating conditions chrome oxide is a semi-conductor while silicon and aluminum oxides are insulators. In this talk we will review the evolution in candidate alloys and surface modifications which constitute an engineered solution for SOFC interconnect applications.

### 2:25 PM Invited

#### Development of a New Alloy for SOFC Interconnects:

*Nobutaka Yasuda*<sup>1</sup>; Toshihiro Uehara<sup>2</sup>; Shigenori Tanaka<sup>1</sup>; Kazuhiro Yamamura<sup>1</sup>; <sup>1</sup>Hitachi metals, Ltd.; <sup>2</sup>Hitachi Metals, Ltd.

Recently, metallic materials, especially Fe-Cr ferritic alloys (ex. ZMG232L, our current alloy), are promising as interconnect materials of solid oxide fuel cells (SOFCs) operated at around medium temperatures such as 700 – 850°C. These metallic materials are usually machined or pressed into various shapes of interconnect parts, and thickness of these parts is often thin. As for these alloys, good oxidation resistance and good electrical conductivity in very thin sheets are required. Moreover, it is needed to reduce Cr evaporation from Cr<sub>2</sub>O<sub>3</sub> layer of alloy surface, because Cr evaporation causes the degradation of the cell. In this study, the effect of chemical compositions on required properties at elevated temperature was investigated on the basis of our previously developed alloy, and a new alloy with excellent oxidation resistance and reduced Cr-evaporation was developed. This study was supported by New Energy and Industrial Technology Research Development Organization (NEDO).

### 2:50 PM

#### Chromium Poisoning and Degradation of Cathodes for Solid Oxide Fuel Cells:

*Teruhisa Horita*<sup>1</sup>; DoHyong Cho<sup>1</sup>; Taro Shimonosono<sup>1</sup>; Haruo Kishimoto<sup>1</sup>; Katsuhiko Yamaji<sup>1</sup>; Manuel Brito<sup>1</sup>; Harumi Yokokawa<sup>2</sup>; <sup>1</sup>AIST; <sup>2</sup>Tokyo City University

Chromium poisoning is one of the major degradation factors in Solid Oxide Fuel Cells (SOFCs). The vaporization of chromium can occur from the metallic components surface with very low Cr-vapor pressures (less than 10-8 atm at 1073 K). To correlate the Cr poisoning and electrochemical degradation at cathodes, we have analyzed the Cr concentration in cathodes

by using Secondary Ion Mass Spectrometry (SIMS). This technique enabled us to determine the distribution of Cr and its concentration lower than 1 ppm. We examined the degradation tests of cathodes under Cr vapor supply; (La,Sr)MnO<sub>3</sub> and (La,Sr)FeO<sub>3</sub> on Gd<sub>0.2</sub>Ce<sub>0.8</sub>O<sub>2</sub>. It was found that the location of Cr-deposition and the degradation of cathodes are different due to the difference of electrochemical reaction and chemical reactivity. We will show the relationship between the Cr-concentration levels and the performance of LSM cathode. The effects of Cr poisoning and estimation of long-term degradation will be also discussed.

### 3:10 PM Break

### 3:25 PM Invited

#### Degradation of Manganese Cobalt Spinel SOFC Interconnect Coatings:

*Jeffrey Fergus*<sup>1</sup>; Yingjia Liu<sup>1</sup>; Yu Zhao<sup>1</sup>; <sup>1</sup>Auburn University  
The reduced operating temperatures of intermediate temperature solid oxide fuel cells allows for the use of metallic alloys as interconnects. Although most materials degradation processes become significantly less severe with decreasing temperature, the formation of chromium oxyhydroxide gases remains significant even at relatively low operating temperatures. To reduce this volatilization and the associated cathode poisoning ceramic coatings are applied to the metal interconnects. The interaction of these coatings with the alloy over long periods of time can lead to the formation of reaction layers, which can affect the coating performance. This paper will focus on the degradation of coatings based on the manganese cobalt spinel. The reaction mechanism and the effect of the reaction on relevant properties, such as electrical conductivity and coefficient of thermal expansion, will be presented.

### 3:50 PM Invited

#### Development of Protective Coating on Alloy Interconnect for SOFCs:

*Yoshitaka Baba*<sup>1</sup>; Harukuni Kameda<sup>1</sup>; Yoshio Matsuzaki<sup>1</sup>; Satoshi Yamashita<sup>1</sup>; Nobutaka Yasuda<sup>2</sup>; Toshihiro Uehara<sup>2</sup>; Katsuhiko Yamaji<sup>3</sup>; Teruhisa Horita<sup>3</sup>; Harumi Yokokawa<sup>3</sup>; <sup>1</sup>TOKYO GAS CO., LTD.; <sup>2</sup>Hitachi Metals, Ltd.; <sup>3</sup>National Institute of Advanced Industrial Science and Technology (AIST)

In intermediate temperature operation SOFCs, metallic interconnects are often used in order to increase in strength of the stack and to reduce material cost. However, there are many problems remaining such as a cathode degradation by Cr-poisoning from the alloy and an increase of the electrical resistance by growth of oxide scale. Therefore, in the SOFCs using metallic interconnects the stability of the alloy at the operation temperature is the greatest technical challenge. We have examined manganese-cobalt spinel coating on metallic interconnects for improvement of the stability of the alloy and reported the manufacture methods of the spinel coating made a difference to the oxide scale growth rate. In this study, we investigate the cause of the difference to the oxide scale growth rate by focusing on the oxide scale, and improve the more protective coating in order to reduce further not only the oxide scale growth but Cr evaporation.

### 4:15 PM

#### Electrophoretic Deposition of (Mn,Co)3O4 Spinel for SOFC Interconnects Application:

*Hui Zhang*<sup>1</sup>; Zhaolin Zhan<sup>2</sup>; Xingbo Liu<sup>1</sup>; <sup>1</sup>West Virginia University; <sup>2</sup>Kunming University of Science and Technology

(Mn,Co)<sub>3</sub>O<sub>4</sub> spinel is a promising coating for SOFC interconnect application due to its high conductivity and capability of blocking Cr evaporation, as well as good CTE match with stainless steel and YSZ electrolyte. Slurry coating, PVD, and electroplating have been reported to apply the (Mn,Co)<sub>3</sub>O<sub>4</sub> spinel for SOFC interconnect application. Electrophoretic Deposition (EPD) offers another fast and cost-effective coating method. In this research, we investigated the effects of deposition parameters and sintering environments on the morphology, microstructure, and area specific resistance (ASR) of Mn-Co spinel coatings by EPD. By varying the deposition voltage, time, and sintering atmosphere, the dense spinel coating was successfully deposited onto stainless steel, whose surface and cross section was characterized by SEM/EDX and XRD. ASR of coatings are about 45–90 mΩ cm<sup>2</sup> at 800 °C after more than 10,000 minutes, indicating the long-term stability of spinel layer.

4:35 PM

**Electrodeposited Mn-Co Alloy Coating For SOFC Interconnects:** Heather McCrabb<sup>1</sup>; Tim Hall<sup>1</sup>; Junwei Wu<sup>2</sup>; Hui Zhang<sup>2</sup>; Xingbo Liu<sup>2</sup>; EJ Taylor<sup>1</sup>; <sup>1</sup>Faraday Technology; <sup>2</sup>West Virginia University

The decrease in the SOFC operating temperatures from 1000°C to 850 °C has enabled the use of ferritic stainless steels as interconnects instead of ceramics. However, even newly developed ferritic alloys such as SS441, cannot completely eliminate the chromia scale growth and chromium evaporation into cells that can cause degradation in the SOFC electrochemical performance. One attractive method to resolve the scale growth and diffusion issues is to coat the interconnect surface. Faraday Technology and WVU are developing an electrodeposition process that can produce uniform dense, crack-free, well-adhered Mn-Co alloy coatings of various alloy compositions and thickness onto a SS441 interconnect surface. A post-deposition thermal treatment converts the alloy coating to (Mn,Co)<sub>3</sub>O<sub>4</sub> spinels. The electrodeposited spinel coatings have demonstrated a low ASR after 500 hours of thermal treatment and EDX analysis suggests the coating has the potential to prevent chrome diffusion to the interconnect surface.

4:55 PM

**Electrodeposited Metal Ni Coating on Ferritic Stainless Steel for Intermediate Temperature SOFC Interconnect Application:** Shuijiang Geng<sup>1</sup>; Fuhui Wang<sup>2</sup>; <sup>1</sup>Northeastern University; <sup>2</sup>Institute of Metal Research, Chinese Academy of Sciences

Ferritic stainless steels (FSS) have been widely employed as solid oxide fuel cell (SOFC) interconnects. However, the evaporation of chromia scale might migrate to and poison the cathode. In this study, Ni, Ni-Fe and Ni-Fe-Co coatings were deposited on FSS by means of a cost-effective technique of electroplating method. They were evaluated at 800°C in air corresponding to the cathode environment of SOFC. The surface and cross-sectional morphologies of the steel with these coatings after thermal exposure were observed using scanning electron microscopy (SEM) with an energy dispersive X-ray spectroscopy (EDX). The phase structures of oxide scale formed on them were identified by X-ray diffraction (XRD). NiO/(Ni,Fe)3O<sub>4</sub>, (Ni,Fe)3O<sub>4</sub> and (Ni,Fe,Co)3O<sub>4</sub> outer layer with chromia inner layer were developed on the steel with Ni, Ni-Fe and Ni-Fe-Co coatings, respectively. Long-term area specific resistance (ASR) of oxide scales was measured. The promising electrodeposited metal/alloy coatings as SOFC interconnect application was discussed.

## Materials Processing Fundamentals: Smelting, Refining, and Liquid Processing

*Sponsored by:* The Minerals, Metals and Materials Society, TMS Extraction and Processing Division, TMS: Process Technology and Modeling Committee

*Program Organizers:* Prince Anyalebechi, Grand Valley State University; Srikanth Bontha, Temple University

Tuesday PM  
March 1, 2011

Room: 12  
Location: San Diego Conv. Ctr

*Session Chair:* Prince Anyalebechi, Grand Valley State University

2:30 PM

**Removal of Textile Dye using Electrocoagulation:** Jewel Gomes<sup>1</sup>; Sadia Jame<sup>1</sup>; Daniel Chen<sup>1</sup>; Venkata Palla<sup>1</sup>; Paul Bernazzani<sup>1</sup>; David Cocke<sup>1</sup>; <sup>1</sup>Lamar University

Textile industries use various kinds of chemicals including dyestuffs and pigments during dyeing and finishing processes. The effluent from these processes includes suspended particles, strong color, high pH and high chemical oxygen demand (COD) that are extremely toxic and make environmental hazard. Although physical, chemical, photochemical, and biological methods are available for treating such wastewater, the electrochemical technique, electrocoagulation (EC), has emerged as an

efficient, simple, and cost-effective technology in the last few decades. In this study we present the applicability of EC technique for removing dye, such as direct red dye using iron electrodes, and the optimized conditions such as dye concentration, current density, conductivity, no. of cycles and pH. The degradation of dye molecules was investigated using HPLC and UV-visible spectroscopy. The EC-floc was also characterized using SEM/EDS, XRD and FTIR.

2:45 PM

**A Study On Ferromolybdenum Production By Metallothermic Reduction Process:** Güvenç Güven<sup>1</sup>; Murat Alkan<sup>1</sup>; Bora Derin<sup>1</sup>; Onuralp Yücel<sup>1</sup>; <sup>1</sup>Istanbul Technical University

In this study, production conditions of ferromolybdenum alloys by metallothermic reduction process were investigated. Metallothermic reduction process was carried out producing ferromolybdenum alloys that suits for the standarts by using a mixture of technical grade molybdenum trioxide, Fe based components, aluminium, ferrosilicon (75 wt.% Si) and calcium oxide powders in open air. In the experimental studies, different ratios of Al/Fe/Si powder mixtures and different amounts of calcium oxide and steel scrap additions were used and the effects of these parameters on the molybdenum recovery efficiency and final chemical compositions were carried out. The obtained alloys and slags were characterized by wet chemical analysis (AAS), XRD and EPMA techniques and due to the molybdenum recovery and ferromolybdenum production efficiency, production parameters were also optimized.

3:00 PM

**Development of a Surface Micro Texturing Process Based on the Ablation at Cathode Spots of Atmospheric Arc:** Rouzbeh Sarrafi<sup>1</sup>; Mehdi Asgharifar<sup>1</sup>; Radovan Kovacevic<sup>1</sup>; <sup>1</sup>Research Center for Advanced Manufacturing, Southern Methodist University

This paper investigates the application of atmospheric GTAW arc for surface texturing of aluminum alloy in micro scale. The evolution of cathode spots, which occur during electron emission from non-thermionic materials, is used for roughening the smooth surface of aluminum. Surface microscopy and real-time observation by high-speed camera are used to understand the process. SEM microscopy of arc-treated surfaces shows the evolution of a very dense texture with the micro-scale feature size on the aluminum surface under the effect of numerous cathode spots of the arc. The roughness is generated by the combined effect of material evaporation and melt ejection at cathode spots. By using variable-polarity GTAW arc and the adjustment of the duty cycle of polarities, the issue of damage to the tungsten electrode (which is observed in DC arc) is resolved, and the same equipment used for AC GTAW arc welding can be used for high-speed surface texturing.

3:15 PM

**DRI Carburization in the Reduction and Transition Zones of a Shaft Furnace MIDREX Type:** Ferry Benique<sup>1</sup>; Jose D'Abreu<sup>1</sup>; Hélio Kohler<sup>2</sup>; Mauricio Otaviano<sup>3</sup>; <sup>1</sup>Pontifical Catholic University; <sup>2</sup>Independent Consultant; <sup>3</sup>Samarco Mineração SA

Nowadays the MIDREX process is one of the most important iron ore direct reduction routes. Aiming to a better understanding of the carburization phenomenology of the DRI into the industrial reactor, the current work is a result of the cooperative program between SAMARCO Mining Company and the Pontifical Catholic University of Rio de Janeiro / PUC-Rio. It presents the methodology utilized for the laboratory scale tests and they were a simulation for the reactor seen as divided into three zones: Reduction, Transition and Cooling zones. For each of these ones, a set of experiments were designed in a way to permit kinetic measurements of the carburization. The experimental methodology, encompassing pellet reduction and carburization, employed gaseous mixtures similar to those present in the industrial process, obeying the scale fluidodynamic similarities.

3:30 PM

**Low Grade Ore Leaching to Produce Cheap Dry Cell:** *Alphonse Djorgbenoo*<sup>1</sup>; <sup>1</sup>Mining

My work presents column leaching to the treatment of low grade rhodochrosite (MnCO<sub>3</sub>) ore using spent solution of sulfuric acid to establish on a preliminary basis essential design parameters for heap leaching plant, and using the leachate to produce dry cell (battery). The physical and chemical characteristics of the low grade (MnCO<sub>3</sub>) ore, the tonnage or volume to be handled, the economics and safety of operations were discussed. The porosity of the ore was found to be 5% indicating that the material has been sufficiently weathered for heap leaching. Consequently, when it was leached with 1M H<sub>2</sub>SO<sub>4</sub>, about 20% of the total dissolved material (1000g) was found to be manganese after 12 hours of leaching and 30% was found after 15 days of leaching. It was found out that some of the material precipitated and the exact composition determined analytically. The leached solution was also used to produce dry cell.

3:45 PM

**Preparation and Properties of CuInS<sub>2</sub> Thin Films by Electrodeposition and Sulfurization:** *Min Li*<sup>1</sup>; *Huimin Lu*<sup>1</sup>; *Lisha Yang*<sup>1</sup>; <sup>1</sup>Beihang University

CuInS<sub>2</sub> thin films solar cells have been drawn much attention due to their potential prospects for its low-cost, high conversion efficiency and high stability. The electrodeposition of Cu-In precursor films, as the first step in making CuInS<sub>2</sub> solar cells electrochemically in the air-and water-stable ionic liquid based on choline chloride/urea eutectic mixture has been investigated at constant potential. Compared with aqueous electrolytes, the large electrochemical window as well as the high thermal stability of this ionic liquid allow the direct electrodeposition of Cu-In precursor films. Then the precursor films were sulfuretted in a tube furnace at different sulfurization temperatures to optimize the films properties. The films obtained were characterized by X-ray diffraction (XRD), scanning electron microscope (SEM), energy dispersive spectroscopy (EDS).

4:00 PM Break

4:15 PM

**Effect of Technological Conditions on Enrichment of Phosphor during Melting Adjustment Process of Converter Slag:** *Min Chen*<sup>1</sup>; *Hong-xu Cui*<sup>1</sup>; *Zhen Tian*<sup>1</sup>; <sup>1</sup>Northeastern University

Many studies have focused on dephosphorization of the slag for its internal reuse inside metallurgical enterprises, but little has considered the phosphor resource in the slag. On the other hand, as one of the strategy resources, the mining and application of phosphate rock have been causing much attention. The present work investigated the effect of adjustment technologies on enrichment of phosphor using molten converter slag as starting material. The result showed that the grain size of 2CaO•SiO<sub>2</sub> containing high-grade phosphor increased slightly with decrease the cooling rate, with the proper one around 1.0°C/min. In addition, the morphology of the phosphor-rich 2CaO•SiO<sub>2</sub> phase changed from granular in high basicity slag to coexistence of granular and rod-like in lower basicity of the adjusted slag. By melting adjustment treatment, phosphor was effectively enriched into 2CaO•SiO<sub>2</sub> phase, with P<sub>2</sub>O<sub>5</sub> content over 30%.

4:30 PM

**Experimental Study on the Production of Nitrogen-bearing Stainless Steel by Injecting Nitrogen Gas:** *Liyuan Sun*<sup>1</sup>; *Jingshe Li*<sup>1</sup>; *Lifeng Zhang*<sup>2</sup>; <sup>1</sup>University of Science and Technology Beijing; <sup>2</sup>Missouri University of Science and Technology

Instead of nickel-based stainless steel, nitrogen-containing stainless steel was developed to reduce the production cost stemming from the shortage of nickel resources. Thermodynamic model to calculate the saturation nitrogen content in the stainless steel was developed and the model was validated by experiments. In these experiments with a high temperature induction furnace, nitrogen gas under constant pressure was injected by which the nitrogen was transferred to the nitrogen-containing stainless steel. The effects of chemical compositions, temperature, superficial active elements and nitrogen-flow rate on transferring nitrogen to the steel were investigated and discussed.

4:45 PM

**A New Method of Synthesis of Rod-like Magnetite:** *Xiyun Yang*<sup>1</sup>; *Xichang Shi*<sup>1</sup>; *Hui Xu*<sup>1</sup>; *Xiaofeng Zhang*<sup>1</sup>; *Xiang Xiao*<sup>1</sup>; *Liwen Ma*<sup>1</sup>; <sup>1</sup>Central South University

Rod-like magnetite particles were prepared by precipitation of iron salts with urea under the induction of magnetic field. Temperature and initial Fe<sup>3+</sup>/Fe<sup>2+</sup> ratio have a significant effect on the composition of the product. Magnetite particles change from spherical into rod shape in the presence of 0.35T magnetic field. The addition of a small amount of spherical seeds increases the rod-like magnetite particles yield. The seeds are prepared by aging ferrous and ferric solution with sodium hydroxide as precipitator. The aspect ratio of the rod is controlled by varying the ratio of seed to iron salt.

5:00 PM

**Preparation of Fibrous CoO Particles by Thermal Decomposition of a New Precursor:** *Jing Zhan*<sup>1</sup>; *Difei Zhou*<sup>1</sup>; *Chuanfu Zhang*<sup>1</sup>; *Jianfeng Yue*<sup>1</sup>; <sup>1</sup>Central South University

A novel precursor of fibrous CoO powders has been synthesized by coordination-precipitation process using oxalic acid and cobalt chloride as starting materials, and ammonia as coordinator. The phase, composition and morphology of the novel precursor were characterized by XRD, IR, DTA/TGA and SEM analysis. The results show that the precursors obtained at pH=9.0 is different from that of β-CoC<sub>2</sub>O<sub>4</sub>•2H<sub>2</sub>O precipitated at pH=1.0, which indicates that the existence of ammonia in the precursor formed at pH=9.0 and the formula of the new precursors was inferred as [Co(NH<sub>3</sub>)<sub>x</sub>]C<sub>2</sub>O<sub>4</sub>•yH<sub>2</sub>O•nNH<sub>3</sub> in reaction system Co(II)-C<sub>2</sub>O<sub>4</sub><sup>2-</sup>-NH<sub>3</sub>-NH<sub>4</sub><sup>+</sup>-H<sub>2</sub>O. The fibrous CoO particles with about 0.3~0.5μm in diameter and 20~40 in aspect ratio were produced in the condition of 800°C for thermal decomposition and nitrogen atmosphere with sufficient oxygen.

5:15 PM

**Direct Observation of Al Drop and Gas Bubbles in the Anode-Cathode Space during Aluminum Electrolysis:** *Jilai Xue*<sup>1</sup>; *Yifang Zheng*<sup>1</sup>; *Zhu Jun*<sup>1</sup>; *Lin Li*<sup>1</sup>; <sup>1</sup>University of Science and Technology Beijing

Al drops and gas bubbles in the anode-cathode space of aluminum electrolysis cell are of great importance for cell operation improvement in metal loss, current efficiency and energy consumption. A direct observation on the Al drop, gas bubble and ultrasound was carried out through a see-through cell. The Al drop immersed into the cryolitic melt was found moving up and down irregularly in the anode-cathode space without electrolysis, which was then completely dissolved into the melt. During electrolysis, the Al drop came to the anode area and reacted with the gas bubbles generated on the anode. Under ultrasound, the gas bubbles were removed from the anode surface while the Al drop was kept on the side of anode. The observed phenomena were useful for reducing anode-cathode distance or lower the energy consumption.

5:30 PM

**Extracting Al<sub>2</sub>O<sub>3</sub> from Coal Gangue by Carbonthermal Reduction - Alkaline Leaching Process:** *Jun Zhu*<sup>1</sup>; *Jilai Xue*<sup>1</sup>; *Tao Li*<sup>1</sup>; <sup>1</sup>University of Science and Technology Beijing

Coal gangue is industrial waste containing Al<sub>2</sub>O<sub>3</sub> and SiO<sub>2</sub> with great recycling and reuse values. This work is aimed at extracting Al<sub>2</sub>O<sub>3</sub> content in the coal gangue by a process of carbonthermal reduction - alkaline leaching. The Al<sub>2</sub>O<sub>3</sub> and SiO<sub>2</sub> contents first became a mixture of SiC and Al<sub>2</sub>O<sub>3</sub> in the process of carbonthermal reduction, and then Al<sub>2</sub>O<sub>3</sub> was separated by leaching in NaOH solution, thus producing the sodium aluminate solution for Al(OH)<sub>3</sub> precipitation. The products generated at various stages in the process were inspected using XRD and chemical analysis. The effects of parameters such as reduction temperature, carbon ratio, NaOH concentration, leaching time, leaching temperature, stirring speed, etc will be presented in details.

TUESDAY PM



5:45 PM

**ESP Dust Recovery Process Test Works, Plant Trial, Commissioning, Operations and Metallurgical Performance:** Pengfu Tan<sup>1</sup>; <sup>1</sup>Xstrata Copper

Arsenic enters the Mount Isa copper circuit in the form of arsenic rich minerals in concentrates from both the Mount Isa and Ernest Henry copper mines. Arsenic is a volatile metal, and will partition in the copper smelter between smelter off gases, slag and anode. Most of the volatile arsenic will report to Isasmelt Electrostatic Precipitator (ESP) or Waste Heat Boiler dusts where it will form a re-circulating load within the smelter. ESP dust is produced at a rate of 15,000 – 20,000 t/y and is currently removed from the precipitator and leached in the new ESP Dust Recovery Plant to separate copper and arsenic from the ESP dust. This paper describes the lab test works of ESP dust leaching, neutralisation and cementation processes. The plant trial, commissioning and operation have been presented as well.

**Microstructural Processes in Irradiated Materials: Phase Stability**

*Sponsored by:* The Minerals, Metals and Materials Society, TMS Structural Materials Division, TMS/ASM: Nuclear Materials Committee

*Program Organizers:* Gary Was, University of Michigan; Thak Sang Byun, Oak Ridge National Laboratory; Shenyang Hu, Pacific Northwest National Laboratory; Dane Morgan, UW Madison; Yasuyoshi Nagai, Tohoku University

Tuesday PM  
March 1, 2011

Room: 3  
Location: San Diego Conv. Ctr

*Session Chairs:* Emmanuelle Marquis, University of Michigan; Philippe Pareige, Université et INSA de Rouen

2:00 PM Invited

**Characterization of Solute Atom Distribution in Grain Interior of Neutron-Irradiated 304L and 304 Stainless Steels:** Naoki Soneda<sup>1</sup>; Kenji Nishida<sup>1</sup>; Akiyoshi Nomoto<sup>1</sup>; Kenji Dohi<sup>1</sup>; Peter Chou<sup>2</sup>; <sup>1</sup>Central Research Institute of Electric Power Industry; <sup>2</sup>Electric Power Research Institute

Solute atom distribution of 304L and 304 stainless steels irradiated by neutrons was investigated by means of atom probe tomography (APT). The materials were retrieved from control-rod blades or removed from the top guide of commercial boiling water reactors. The doses of materials range from 3.6 to 13 dpa. As the first step of the characterization of these materials, solute atom distribution in grain interior was investigated. Features enriched with Ni and Si atoms were clearly and commonly identified in all samples examined. Many of such Ni-Si features at low dose are not very well shaped like precipitates. Some Ni-Si features show the form of ring lying on a plane. We attribute such features to dislocation loops segregated with Ni and Si atoms. In 304L materials, formation of Al clusters was also observed. The size and number density of such clusters are 2~3 nm in diameter and  $3\sim 6 \times 10^{23} \text{m}^{-3}$ , respectively.

2:40 PM

**Grain Boundary Chemistry in Irradiated Fe-Cr Alloys:** Rong Hu<sup>1</sup>; Emmanuelle Marquis<sup>2</sup>; <sup>1</sup>University of Oxford; <sup>2</sup>University of Michigan

Ferritic Fe-Cr alloys are the base for structural steels currently considered for Gen IV nuclear plants and future fusion reactors. Among the outstanding issues related to the use of these alloys under irradiation are a' precipitation (and the uncertainty of the position of the solvus line at low temperatures) and radiation induced segregation (RIS) or depletion (RID) of grain boundaries. These phenomena could indeed significantly affect the properties of these alloys. Past observations reported grain boundary Cr depletion or segregation without any clear correlation to irradiation conditions (Lu et al. Scripta Mater. 2008). Moreover, common impurities such as carbon are expected to affect the integrity of grain boundaries and modify the extent of radiation induced segregation phenomena. The experimental approach using atomic scale characterization techniques as well as the role of carbon will be

described and the effect of irradiation discussed as function of carbon content and grain boundary orientation.

3:00 PM

**Precipitation and Grain Boundary Segregation under Neutron Irradiation in Fe-12at%Cr Based Alloy:** Philippe Pareige<sup>1</sup>; Viacheslav Kuksenko<sup>1</sup>; Brigitte Décamps<sup>2</sup>; Pierre Desgardin<sup>3</sup>; Cristelle Pareige<sup>1</sup>; <sup>1</sup>GPM - UMR 6634 CNRS, University and INSA of Rouen; <sup>2</sup>CSNSM, UMR CNRS 8609, Université Paris-Sud; <sup>3</sup>CEMHTI/CNRS site Cyclotron

High-chromium ferritic-martensitic steels are up to now candidates as structural materials in the next Generation IV power plants. For the first time, a nanoscale description of an industrial purity Fe-12at%Cr model alloy, neutron irradiated at 300°C, was performed using the 3D atom probe technique. This paper presents a quantitative description of intragranular  $\alpha'$  clusters and NiSi complexes formed under the neutron irradiation, as well as low-angle grain boundary segregations. These atomic scale results are compared to those obtained by complementary techniques such as SANS [1] and TEM [2] performed on the same model alloy. These results are important for the understanding of the basic mechanisms at the origin of the decomposition of these alloys under irradiation and for comparison or improvement of multi-scale modelling. [1] F.Bergner, A.Ulbricht and C.Heintze, Scripta mater.61 (2009) 1060. [2] M.Matijasevic, A.Almazouzi, J.Nucl.Mater.377 (2008) 147.

3:20 PM

**Characterization of Radiation-induced Precipitation in Ferritic-Martensitic Alloys by Different Particle Types:** Zhijie Jiao<sup>1</sup>; Gary Was<sup>1</sup>; <sup>1</sup>University of Michigan

Ferritic-martensitic (F-M) alloys are of great interest as cladding and structural materials in fast fission and fusion reactors. However, they are prone to hardening and embrittlement caused by radiation-induced precipitates. In this study, three F-M alloys, T91, HT-9 and HCM12A, were irradiated to 7 dpa at 400\176C using 2 MeV protons, to 100 dpa at 500\176C using heavy ions, and to 3 dpa at 500\176C using neutrons. Radiation-induced precipitates were characterized using atom probe tomography. Preliminary results have showed that Ni/Si/Mn-rich, Cu-rich and Cr-rich precipitates form under proton or heavy ion irradiations. This study will compare the types and nature of precipitates formed by different particle irradiations.

3:40 PM Break

4:00 PM

**Effects of Helium on Cavity and Microstructural Evolution in Tempered Martensitic Steels and Nanostructured Ferritic Alloys – In Situ Helium Implantation Studies:** G. Robert Odette<sup>1</sup>; Danny Edwards<sup>2</sup>; Yuan Wu<sup>1</sup>; Takuya Yamamoto<sup>1</sup>; Richard J. Kurtz<sup>2</sup>; <sup>1</sup>University of California, Santa Barbara; <sup>2</sup>Pacific Northwest National Laboratory

Two-step thermal neutron ( $n_{th}$ )  $^{58}\text{Ni}(n_{th},\gamma)^{59}\text{Ni}(n_{th},\alpha)$  reactions in micron scale NiAl layers injected high-energy  $\alpha$ -particles to a depth of ~ 5 to 8  $\mu\text{m}$  into adjacent alloys simultaneously undergoing fast neutron induced displacement (dpa) damage in HFIR irradiations. The implantations were carried out for a large matrix of alloys over a wide range of temperatures and dpa at controlled He/dpa ratios from  $\ll 1$  to 40 appm He/dpa. Earlier studies showed that 9Cr tempered martensitic steels contain a bimodal distribution of bubbles and voids for irradiations to 9 dpa and 380 appm He at 500°C. In contrast, the same irradiations Y-Ti-O nanostructures in nanostructured ferritic alloys trap He in ultrafine scale interface bubbles. Building on the earlier studies, we compare the cavity structures in a 14Cr NFA, MA957, to those in an 8Cr TMS, F82H, following HFIR irradiations up to 25 dpa and 1200 appm He.

4:05 PM

**Ni-Si Clusters in Neutron-irradiated 304 Stainless Steel Studied by Three-dimensional Atom Probe:** *Takeshi Toyama*<sup>1</sup>; Yoshitaka Matsukawa<sup>1</sup>; Yasuko Nozawa<sup>1</sup>; Masahiko Hatakeyama<sup>1</sup>; Yasuyoshi Nagai<sup>1</sup>; Wouter Van Renterghem<sup>2</sup>; Steven Van Dyck<sup>2</sup>; Abderrahim Al Mazouzi<sup>3</sup>; <sup>1</sup>Tohoku University; <sup>2</sup>SCK•CEN; <sup>3</sup>EDF R&D

Ni-Si clusters such as  $\gamma'$  precipitate ( $\text{Ni}_3\text{Si}$ ) are the typical irradiation-induced solute clusters in stainless steel (SS). They are considered to contribute to the changes of mechanical properties. In this study, the morphologies of Ni-Si clusters in neutron-irradiated 304 SS were characterized using laser-assisted local electrode-type three-dimensional atom probe. The studied sample was irradiated to a neutron fluence of  $1.6\text{E}+22$  n/cm<sup>2</sup> ( $E>1\text{MeV}$ ): 24 dpa at  $\sim 300^\circ\text{C}$  in the fuel wrapper plate of a commercial pressurized water reactor. A high number density ( $3\text{E}+17$  /cm<sup>3</sup>) of Ni-Si enriched and Cr-Fe depleted clusters was observed. In some clusters, Mn enrichment and P segregation at the cluster-matrix interface were observed as well. The average chemical composition of the clusters was Ni: 55%, Si: 20%, Mn: 5%, Cr: 5%, Fe: 10% (at.%), close to that of a  $\gamma'$  precipitate. Effects of these clusters on the irradiation-hardening will be presented.

4:25 PM

**Microstructure Evolution in Irradiated Austenitic Stainless Steels:** *Gary Was*<sup>1</sup>; Zhijie Jiao<sup>1</sup>; <sup>1</sup>University of Michigan

The evolution of radiation induced segregation and radiation induced precipitation in austenitic stainless steels is characterized using atom probe tomography (APT) and STEM-EDS. Types 304 and 316 stainless steels were irradiated with 2 MeV protons to a dose of 5 dpa at  $360^\circ\text{C}$  and with 5 MeV Ni<sup>++</sup> to 100 dpa. Boron segregation to the grain boundary prior to irradiation is not affected by the irradiation while phosphorus segregation is enhanced by irradiation and carbon depletes. Segregation at dislocations mirrors that at the grain boundary with the exception of Si. The composition varies within the grain boundary plane and along the dislocation loop core. Ni/Si-rich clusters formed in irradiated commercial purity 304 were likely precursors of  $\gamma'$  or other Si- and Ni-rich phases. Copper clusters were observed to form adjacent to Ni/Si-rich clusters and copper depletion was observed at both the grain boundary and at dislocation loops.

4:45 PM

**Phase Stability of Solution Strengthened 316 Stainless Steel Under Fast Neutron Irradiation Using a Diffusion Couple Approach:** *Luke Brewer*<sup>1</sup>; Khalid Hattar<sup>2</sup>; Joseph Puskar<sup>2</sup>; Steven Goods<sup>2</sup>; Mark Reece<sup>2</sup>; <sup>1</sup>Naval Postgraduate School; <sup>2</sup>Sandia National Laboratories

Austenitic stainless steels are critical materials for the structural components of fast neutron reactors and must be able to withstand prolonged exposure to fast neutrons at high temperatures. The phase stability of refractory element-based solution strengthened stainless steels under high dose irradiation (up to and greater than 100 dpa) is not known. This talk will discuss a diffusion couple approach that allows for the rapid assessment of many compositions and irradiation levels. 316L steel substrates were diffusion bonded with tantalum, tungsten, molybdenum, and niobium plates and then annealed at  $1100^\circ\text{C}$  for 400 hours. A suite of spatially-registered, microscale techniques such as x-ray microanalysis, electron backscatter diffraction, and nanoindentation was used to map out the phase stability, elastic modulus, hardness and other properties as a function of composition. This microscale, structure-property assessment will be discussed for several irradiation levels from 1 dpa to 100 dpa.

5:05 PM

**Solute Rich Clusters Formation under Neutron Irradiation of Fe Dilute Alloys Representative of Model and RPV Steels by Atomic Kinetic Monte Carlo:** *Christophe Domain*<sup>1</sup>; Raoul Ngayam Happy<sup>1</sup>; Charlotte Becquart<sup>2</sup>; <sup>1</sup>EDF R&D; <sup>2</sup>UMET, UMR8207

The embrittlement and the hardening of pressure vessel steels under radiation has been correlated with the formation of more or less dilute clusters containing Cu, Ni, Mn and Si which are investigated in this work using a multiscale approach based on ab initio and atomistic kinetic Monte Carlo simulations. The parameterisation of the interactions is based on DFT

calculations and some of the parameters have been adjusted on binary alloys isochronal annealing experiments. The model has been used to simulate the medium term evolution of different Fe dilute alloys under neutron irradiation. Alloys of growing complexity have been simulated allowing an investigation of the synergetic roles of the different solutes. The influence of dose and dose rate on the point defect clusters and solute clusters.

5:25 PM

**The Role of Carbon in Copper Precipitation Process in Neutron Irradiated Fe-Cu Binary Alloys:** *Milan Konstantinovic*<sup>1</sup>; <sup>1</sup>SCK.CEN

In spite of general understanding of the copper precipitation in neutron irradiated Cu-rich alloys, the role of carbon in the precipitation process, and their overall effect to the dislocation dynamics, as well as to the hardening and embrittlement, are not yet fully elucidated. The ability of internal friction (IF) technique to detect both the carbon relaxation and dislocation-related relaxation processes makes the IF experiment as one of the most suitable techniques to study afore mentioned problems. The behaviour of the Snoek-Koster peak intensities in the temperature dependent IF spectra of neutron-irradiated Fe-Cu binary alloys indicate the existence of carbon redistribution as a function of dose. By correlating the IF and results of mechanical tests, we argue that carbon is not a passive observer of the copper precipitation process and estimate the contribution of the carbon redistribution to the hardening in these alloys.

## Neutron and X-Ray Studies of Advanced Materials IV: Dislocations, Strains and Stresses I

*Sponsored by:* The Minerals, Metals and Materials Society, TMS Structural Materials Division, TMS/ASM: Mechanical Behavior of Materials Committee, TMS: Chemistry and Physics of Materials Committee

*Program Organizers:* Rozaliya Barabash, Oak Ridge National Laboratory; Xun-Li Wang, Oak Ridge National Laboratory; Jaimie Tiley, Air Force Research Laboratory; Peter Liaw, The University of Tennessee; Erica Lilleodden, GKSS Research Center; Brent Fultz, California Institute of Technology; Y-D Wang, Northeastern University

Tuesday PM

March 1, 2011

Room: 10

Location: San Diego Conv. Ctr

*Session Chairs:* Klaus-Dieter Liss, The Bragg Institute<sup>1</sup>; E-Wen Huang, National Central University of Taiwan

2:00 PM Keynote

**Pursuing 3DXRD at the Sub-Micron Scale:** *Henning Poulsen*<sup>1</sup>; Erik Lauridsen<sup>1</sup>; Wolfgang Ludwig<sup>2</sup>; Alexei Snigirev<sup>2</sup>; Ulrik Olsen<sup>1</sup>; Soeren Schmidt<sup>1</sup>; Haihua Liu<sup>1</sup>; Xiaoxu Huang<sup>1</sup>; Gavin Vaughan<sup>2</sup>; <sup>1</sup>Risoe DTU; <sup>2</sup>ESRF

We present several approaches being explored at beamline ID11, ESRF, for generalising the 3DXRD & DCT grain and orientation mapping methodologies towards the sub-micron scale: • **C o n v e n t i o n a l** 3DXRD. By going to the limit of the existing detector technology a resolution of 400 nm has been achieved. • **F u l l** field microscopy for tomography and DCT. Using compound refractive lenses as an objective, and placing the detector 52 m from the sample, this set-up comes with  $\sim 50\text{cm}$  of free space around the sample and a 100 nm spatial imaging resolution. • **N e w** detectors. A 3D detector has been commissioned, with enhanced possibilities for 3D orientation mapping of deformed specimens. At the time of writing a new detector principle with nominal 100 nm resolution is being tested. The latter is directly compatible with parallel beam tomography, holography and 3DXRD. • Stochastic type experiments on grains in the 20-100 nm range.

TUESDAY PM

2:25 PM Invited

**3D Orientation Imaging Microscopy Based on Monochromatic Beam Synchrotron X-Ray Diffraction and Imaging Techniques:** *Wolfgang Ludwig*<sup>1</sup>; Andrew King<sup>2</sup>; Peter Reischig<sup>3</sup>; Michael Herbig<sup>1</sup>; Henry Proudhon<sup>4</sup>; <sup>1</sup>Université de Lyon; <sup>2</sup>ESRF; <sup>3</sup>Karlsruhe Institute of Technology; <sup>4</sup>Mines Paristech

3D X-ray diffraction (3DXRD) is a methodology, which combines the principles of X-ray diffraction imaging (topography) and image reconstruction from projections (tomography) for investigation of polycrystalline materials. We present a new acquisition strategy aiming at the reconstruction of local orientation and elastic strain distribution via a combination of full-field imaging and micro-beam diffraction techniques. Associating this 3D orientation mapping with conventional attenuation and/or phase contrast tomography yields a non-destructive characterization technique, enabling time-lapse observation of crystal growth, deformation and damage mechanisms in the bulk of structural materials. The capabilities and limitations, as well as perspectives of this combined characterization approach will be discussed and illustrated on selected application examples.

2:45 PM Invited

**Measuring Complete Strain Tensors from Individual Dislocation Cells in Deformed Cu:** *Lyle Levine*<sup>1</sup>; Peter Geantil<sup>2</sup>; Bennett Larson<sup>3</sup>; Jonathan Tischler<sup>3</sup>; Francesca Tavazza<sup>1</sup>; Michael Kassner<sup>4</sup>; Wenjun Liu<sup>5</sup>; <sup>1</sup>National Institute of Standards and Technology; <sup>2</sup>University of Southern California; <sup>3</sup>Oak Ridge National Laboratory; <sup>4</sup>Director of Research, Office of Naval Research; <sup>5</sup>Argonne National Laboratory

The use of depth resolved, sub-micrometer X-ray beams for studying dislocation structures in plastically deformed metals has advanced considerably over the past five years. Thus, we previously measured elastic strains (and thus stresses) from individual cell interiors and cell walls in plastically deformed Cu specimens and compared these results with model calculations. However, these measurements included just a single component ( $\epsilon_{11}$ ) of the elastic strain tensor, since only a single X-ray reflection could be examined with the necessary accuracy. Recently, additional detectors were installed to allow multiple reflections to be measured over a wide range of angles, enabling us to measure both the crystallographic orientation and the complete elastic strain tensor (and thus the stress tensor) from spatially resolved, sub-micrometer sample volumes within deformed metal specimens. The first results of these experiments will be presented along with model-based simulations of the stress tensor in cell walls and cell interiors.

3:05 PM Invited

**Synchrotron X-Ray Laue Microdiffraction for the Study of Materials Micromechanics:** *Nobumichi Tamura*<sup>1</sup>; Martin Kunz<sup>1</sup>; Kai Chen<sup>1</sup>; <sup>1</sup>Lawrence Berkeley National Lab.

Laue X-ray microdiffraction is a powerful tool which allows mapping crystal orientation and elastic strains in 2D and 3D at the mesoscopic scale (0.1 - 10  $\mu\text{m}$ ). Small displacements of the reflection positions with respect to their calculated "unstrained" positions allows determining the deformation of the unit cell and thus the elastic strain (in effect the deviatoric component of the elastic strain). Plastic deformation on the other hand manifest itself as broadening of the Laue reflections. Symmetric broadening is linked to statistically stored dislocations (SSD) but asymmetric broadening in the form of peak streaking can be explained in term of geometrically necessary dislocations (GND) causing local bending of the lattice. Examples of the application of x-ray microdiffraction to the study of deformation in polycrystalline thin films and single crystal nanopillars will be given.

3:25 PM

**A Study of Casting Residual Stress:** *Thomas Watkins*<sup>1</sup>; Eric Johnson<sup>2</sup>; Camden Hubbard<sup>1</sup>; Joshua Schmidlin<sup>1</sup>; <sup>1</sup>ORNL; <sup>2</sup>Deere and Company

Stringent regulatory requirements, such as Tier IV norms, have pushed the cast iron for automotive applications to its limit. As such, castings need to be designed with closer tolerances by incorporating hitherto unknowns, such as residual stresses. In the present work, a benchmark study was undertaken for casting residual stress measurements through neutron diffraction, which was subsequently used to validate the accuracy of a simulation prediction.

Castings of lattice specimen geometry were made such that adequate residual compressive and tensile stresses were generated during solidification, without any cracks. The residual stresses in the cast specimen were measured using neutron diffraction. Simulations were performed using the identical geometry and casting condition for predictions of residual stresses. The simulation predictions were found to agree well with the experimentally measured residual stresses.

3:40 PM

**Laue Microdiffraction Measure of Crystal Distortion and Dislocation Density Profile in a Plastically Deformed Multi-Crystal:** *Gael Daveau*<sup>1</sup>; Benoit Devincré<sup>2</sup>; Thierry Hoc<sup>3</sup>; Odile Robach<sup>4</sup>; <sup>1</sup>LEM (CNRS-ONERA) / MSSMAT (ECP); <sup>2</sup>LEM (CNRS-ONERA); <sup>3</sup>LTDS (EC-Lyon); <sup>4</sup>CEA-Grenoble DSM/INAC/SP2M/NRS

In this study, a dislocation density based model [1] initially developed for fcc single crystal is extended to strain hardening in polycrystal. For this reason, the early stages of plastic deformation in a Cu tri-crystal are investigated with Laue microdiffraction. Measures are made in the vicinity of a triple node after approximately 0.5% of compression. The existence of extended rotation and strain gradients at the grain boundaries (GBs) is shown. Peak broadening analysis provides qualitative and quantitative evolutions of the GNDs density distribution during deformation. The GB impact on strain hardening is thus clearly revealed. Those results are compared with simulations of dislocation dynamics that calculate the reduction of dislocation mean free path imposed by GBs. This information serves as an input to a crystal plasticity code reproducing the tri-crystal plastic deformation. [1] Devincré, Hoc, Kubin, Science, 320 (2008) p 1745-1748.

3:50 PM

**Pair Distribution Function of a High Entropy Alloy: A Neutron Scattering Study:** *Wei Guo*<sup>1</sup>; Peter Liaw<sup>1</sup>; Takeshi Egami<sup>1</sup>; <sup>1</sup>university of tennessee, knoxville

A ZrNbHf high entropy alloy is prepared. Laboratory X-ray diffraction indicates the lattice structure is body center cubic. Since this material is composed of different elements with various dimensions and valences, it is compelling to study the local structure of the alloy to unveil how the atoms construct this structure. Samples deformed at different strains and as-cast samples with no deformation are investigated by neutron scattering with high-intensity powder diffractometer. Pair distribution functions of the samples are obtained and compared. The local structural features of the high entropy alloy are discussed, and the deformation mechanism is suggested.

4:00 PM Break

4:10 PM Invited

**Cyclic-loading Effects on Lattice-Strain Asymmetry Behavior in Loading and Transverse Directions:** *E-Wen Huang*<sup>1</sup>; Kyle Woods<sup>2</sup>; Bjorn Clausen<sup>3</sup>; Rozaliya Barabash<sup>4</sup>; Peter Liaw<sup>2</sup>; <sup>1</sup>National Central University; <sup>2</sup>Univ. of Tennessee; <sup>3</sup>Los Alamos Neutron Science Center; <sup>4</sup>Oak Ridge National Laboratory

Cyclic loading and the subsequent fatigue-induced structural transformations have been investigated using in-situ neutron-diffraction experiments at elevated temperatures. In-situ neutron-diffraction measurements identify the development of different fatigue stages in the cyclic-deformation-induced structural transformations, such as bulk hardening, softening, and eventual saturation. A transition is observed during the saturation cycles, which is characterized by the emergence of the lattice-strain asymmetry in the loading and transverse directions. An anomaly during saturation cycles is believed to arise from dislocation self-organization – possibly during the formation of microcracks. The single-phase, polycrystalline nickel-based alloy is selected for the present study of the loading and transverse asymmetry subjected to cyclic loading at both room and high temperatures. In this investigation, we compare the deformation at room and elevated temperatures. The identical loading and transverse -asymmetry feature is found to be valid at both room and high temperatures.



#### 4:30 PM

**Twin Boundaries and Dislocation Densities in  $\langle 111 \rangle$ ,  $\langle 100 \rangle$  and  $\langle 211 \rangle$  Textured Ni Thin Films Determined by X-Ray Line Profile Analysis:** Gábor Csiszár<sup>1</sup>; Karen Pantleon<sup>2</sup>; Hossein Alimadadi<sup>2</sup>; Tamás Ungár<sup>1</sup>; <sup>1</sup>Eötvös University Budapest; <sup>2</sup>Technical University of Denmark

Ni thin films were grown by electrochemical deposition resulting in  $\langle 111 \rangle$ ,  $\langle 100 \rangle$  and  $\langle 211 \rangle$  textures and about 15  $\mu\text{m}$  thickness. The X-ray diffraction measurements were carried out in a special high resolution diffractometer with a plane Ge (220) primary monochromator. The Co  $K\alpha 1$  beam of 0.1x2 mm size hit the specimen under different angles selected in order to obtain diffraction always from the same texture component. The dislocation density and the frequency of twin boundaries was determined by the extended Convolutional Multiple Whole Profile (eCMWP) line profile analysis procedure. The dislocation densities are found to be relatively high and the twin boundary densities are varying between zero and a few percent. The X-ray results are discussed in relation to electron microscopy investigations and the different growth conditions.

#### 4:45 PM Invited

**Grain Resolved Strain Evaluation Using Hard X-Rays:** Marcin Moscicki<sup>1</sup>; Andras Borbely<sup>2</sup>; Jonathan Wright<sup>3</sup>; Anke Pyzalla<sup>4</sup>; <sup>1</sup>Max-Planck Institut für Eisenforschung; <sup>2</sup>Ecole des Mines de Saint-Etienne; <sup>3</sup>ESRF; <sup>4</sup>Helmholtz Zentrum für Materialien und Energie Berlin

In situ diffraction experiments during uniaxial straining of OFHC copper and stainless steel of grade 1.4301 were performed at beamline ID11 of the European Synchrotron Radiation Facility. The crystallographic orientation change, location of center of mass and the strain tensor of individual grains have been evaluated. The accuracy of strain tensor elements is discussed based on simulated and experimental 2D diffractograms. Issues related to the calibration of the 3DXRD setup are presented and a two-step calibration method based on the use of reference powder and single crystal specimens is presented. Problems concerning the stress free lattice parameter "a0" are highlighted and a solution based on the minimization of the elastic energy of the polycrystal aggregate is proposed. The experimentally obtained strain tensor elements characterizing single grains show a large scatter, but their average values are in good agreement with the macroscopically imposed strain state and known Poisson's ratio.

#### 5:05 PM Invited

**High Resolution Reciprocal Space Mapping of Individual Grains within Deformed Polycrystals:** Ulrich Lienert<sup>1</sup>; Matthew Brandes<sup>2</sup>; Joel Bernier<sup>3</sup>; Peter Kenesei<sup>1</sup>; Michael Mills<sup>2</sup>; Matthew Miller<sup>4</sup>; <sup>1</sup>Argonne National Laboratory; <sup>2</sup>Ohio State University; <sup>3</sup>Lawrence Livermore National Laboratory; <sup>4</sup>Cornell University

The High Energy Diffraction Microscopy program at the 1-ID beamline of the Advanced Photon Source employs high energy x-rays for the structural characterization of polycrystalline bulk materials on individual grain and subgrain scales during themomechanical loading. The status of distinct techniques that enable orientation mapping and the measurement of strain tensors and centroid positions of hundreds to thousands of individual grains will be summarized. Emphasis will be put on high resolution reciprocal space mapping which has been demonstrated to provide orientation and strain information on the subgrain scale. A case study of Ti-7Al after tensile deformation will be presented. The combination with electron microscopy investigations of the same grains will be discussed. Use of the Advanced Photon Source was supported by the U. S. Department of Energy, Office of Science, Office of Basic Energy Sciences, under Contract No. DE-AC02-06CH11357.

#### 5:25 PM

**Evolution of Internal Strain with Temperature in Depleted Uranium in the Presence of Hydrides:** Michael Hemphill<sup>1</sup>; Elena Garlea<sup>2</sup>; Jonathan Morrell<sup>2</sup>; Don Brown<sup>3</sup>; Thomas Sisneros<sup>3</sup>; Sven Vogel<sup>3</sup>; G Powell<sup>2</sup>; Peter Liaw<sup>1</sup>; <sup>1</sup>University of Tennessee; <sup>2</sup>Y-12 National Security Complex; <sup>3</sup>Los Alamos National Laboratory

The effects of temperature and hydrogen corrosion on the mechanical behavior of depleted uranium (DU) were investigated by neutron diffraction

to relate the grain-level behavior to the observed macroscopic behavior. Three cylindrical compression specimens of rolled depleted uranium were charged with 0 wppm, 0.3 wppm, and 1.8 wppm of hydrogen and compared to a reference specimen that remained in the as-rolled condition. Uniaxial compression was performed at room temperature, 100°C, and 150°C to measure the macroscopic stress versus strain. In-situ neutron diffraction was performed during the loading sequence to measure the internal strain evolution at the grain level. Additionally, a series of unloading sequences was used to measure the residual strain build-up. Texture measurements were performed before and after loading to describe texture changes due to temperature and loading. These micro- and macroscopic results provide insight into the effect temperature and hydrogen/hydrides has on the activation of deformation modes.

#### 5:35 PM

**Measuring Single Crystal Diffuse Neutron Scattering on the Wombat High Intensity Powder Diffractometer:** Ross Whitfield<sup>1</sup>; Darren Goossens<sup>1</sup>; Andrew Studer<sup>2</sup>; Jennifer Forrester<sup>3</sup>; <sup>1</sup>Australian National University; <sup>2</sup>Australian Nuclear Science and Technology Organisation; <sup>3</sup>The University of Newcastle

Single crystal diffuse scattering was collected on the Wombat high-intensity powder diffractometer at the OPAL reactor at the Bragg Institute. The difficulty in measuring diffuse scattering come from its relative low intensity compared to the Bragg peaks, some  $10^3$ - $10^4$  factor smaller. Wombat allows collection of diffuse scattering due to its high intensity and large two-dimensional detector. Diffuse scattering data from yttria-stabilised cubic zirconia and PZN ( $\text{PbZn}_{1/3}\text{Nb}_{2/3}\text{O}_3$ ) have been successfully collected, the latter at a range of temperatures. The data have been processed, normalised and background subtracted to reconstruct flat reciprocal space sections with a minimum of artefacts. The strategies used to tackle the collection of neutron diffuse scattering and the way in which they are implemented will be discussed.

#### 5:45 PM

**Validation of Predicted Residual Stresses within DC Cast Magnesium Alloy WE43 Slab:** Mark Turски<sup>1</sup>; Anna Paradowska<sup>2</sup>; Shu Yan<sup>2</sup>; Dag Mortensen<sup>3</sup>; Hallvard Fjaer<sup>3</sup>; John Grandfield<sup>4</sup>; Tim Wilks<sup>1</sup>; Bruce Davis<sup>5</sup>; Richard DeLorme<sup>5</sup>; <sup>1</sup>Magnesium Elektron; <sup>2</sup>Rutherford Appleton Laboratory; <sup>3</sup>Institute for Energy Technology; <sup>4</sup>Grandfield Technology Pty Ltd; <sup>5</sup>Magnesium Elektron North America

During direct chill (DC) casting of the high strength magnesium alloy Elektron WE43, a significant level of cold cracking has been observed. In order to ensure good slab yields for this alloy, the effect of casting parameters on the residual stress field within the cast material has been investigated. A finite element modeling (FEM) code, called ALSIM, has been used to determine the residual stress within DC cast slab. Validation of FEM simulations were carried out using neutron diffraction measurements of the residual stress field within a slab of cross section 870 x 315 mm. Given that measurements in such large scale components using diffraction measurements are particularly challenging and expensive, efficient use of neutron diffraction measurements is emphasized. These measurements allowed validation of the FEM code. The use of this validated model has allowed optimized casting parameters to be developed to produce crack-free Elektron WE43 slab via DC casting.

## **Pb-Free Solders and Other Materials for Emerging Interconnect and Packaging Technologies: Thermo-Mechanical Behavior I**

*Sponsored by:* The Minerals, Metals and Materials Society, TMS Electronic, Magnetic, and Photonic Materials Division, TMS: Electronic Packaging and Interconnection Materials Committee

*Program Organizers:* Indranath Dutta, Washington State University; Darrel Frear, Freescale Semiconductor; Sung Kang, IBM; Eric Cotts, SUNY Binghamton; Laura Turbini, Research in Motion; Rajen Sidhu, Intel Corporation; John Osenbach, LSI Corporation; Albert Wu, National Central Univ, Taiwan; Tae-Kyu Lee, Cisco Systems

Tuesday PM  
March 1, 2011

Room: 7B  
Location: San Diego Conv. Ctr

*Session Chairs:* Tae-Kyu Lee, Cisco Systems; Hongtao Ma, Cisco Systems, Inc.

### **2:00 PM Invited**

**Comparison of Extensive Thermal Cycling Effects on Microstructure Development in Micro-Alloyed Sn-Ag-Cu Solder Joints:** *Iver Anderson*<sup>1</sup>; Adam Boesenber<sup>2</sup>; Joel Harringa<sup>1</sup>; David Riegner<sup>2</sup>; Andrew Steinmetz<sup>2</sup>; David Hillman<sup>3</sup>; Tim Pearson<sup>4</sup>; <sup>1</sup>Ames Laboratory; <sup>2</sup>Iowa State University; <sup>3</sup>Rockwell-Collins; <sup>4</sup>Rockwell-Collins

Pb-free solder alloys based on the Sn-Ag-Cu (SAC) ternary eutectic have promise for widespread adoption across assembly conditions and operating environments, but enhanced microstructural control is needed. Micro-alloying with elements like Zn was demonstrated for promoting a preferred solidification path and joint microstructure both in simple (Cu/Cu) solder joints studies for different cooling rates and in (reworked) ball grid array (BGA) joints, using dissimilar, Sn-3.5Ag-0.5Cu (SAC305), solder paste. In addition to this industrial assembly operation, the BGA joints made with a preferred Sn-3.5Ag-0.74Cu-0.21Zn (SAC3595+0.21Zn) solder were tested in thermal cycling (-55°C/+125°C) along with baseline SAC305 BGA joints, beyond 3000 cycles with continuous failure monitoring. A correlation of thermal cycle lifetime with initial as-solidified BGA joint microstructure features, i.e. large Ag<sub>3</sub>Sn "blades" and distributed pro-eutectic Cu<sub>6</sub>Sn<sub>5</sub> phase, was attempted to compare these SAC305 and SAC3595+0.21Zn joints. Support from Iowa State University Research Foundation and Nihon-Superior through Ames Lab Contract No. DE-AC02-07CH11358

### **2:25 PM Invited**

**The Role of Elastic and Plastic Anisotropy on Microstructure Evolution and Strain History during Thermomechanical Cycling of Lead-Free Solder Joints:** *Thomas Bieler*<sup>1</sup>; Bite Zhou<sup>1</sup>; Payam Darbandi<sup>1</sup>; Farhang Pourboghrat<sup>1</sup>; Guilin Wu<sup>2</sup>; Stefan Zaefferer<sup>2</sup>; Tae-kyu Lee<sup>2</sup>; Kuo-Chuan Liu<sup>3</sup>; <sup>1</sup>Michigan State University; <sup>2</sup>Max-Planck-Institut für Eisenforschung; <sup>3</sup>Cisco Systems, Inc.

Because failures in lead-free solder joints occur in locations other than the most highly shear strained regions, reliability prediction is challenging, requiring physically based understanding of how the microstructure and properties evolve during thermomechanical cycling. Sn-Ag-Cu solder joints can be initially single, tri- or multi-crystals, depending on the composition of the solder and underbump metallurgy and melting history. The evolution of microstructures and properties are characterized using optical and orientation imaging microscopy and in-situ synchrotron x-ray measurements during thermal cycling. With time and thermal history, microstructural evolution unique to each joint occurs, due to the interaction between local boundary conditions and strong anisotropic elastic, plastic, expansion, and diffusional properties of Sn crystals. Initial efforts to simulate well-characterized joint microstructures and strain histories measured with synchrotron measurements with crystal plasticity finite element modeling will be compared to assess the effectiveness of constitutive models. Supported by NSF-GOALI contract with Cisco Systems, Inc.

### **2:50 PM Invited**

**Studies of Impact Fracture Modes on Pb-Free Solder Joint Reliability:** T. Kobayashi<sup>1</sup>; Andre Lee<sup>1</sup>; K. Subramanian<sup>1</sup>; <sup>1</sup>Michigan State University

Fracture modes encountered during impact can have important influences on the capabilities of as-reflowed, as well as reliability during service, of electronic solder joints. Such considerations arise due to damages resulting from field influences and their relative orientations of such damage with respect to the direction of impact loading. An analysis based on impact strength and energy indicates potential fracture modes that can improve the solder joints reliability, both for shipping and service scenarios. The fracture initiation plays important roles during early stages of services, while propagation plays important roles during the later stages. The interplay of these features in different alloy systems, as well as modes of impact fracture, affects the overall impact reliability during service. Findings of this study may provide significant insights into the interconnect design strategies for microelectronic applications.

### **3:15 PM Invited**

**Damage and Fracture in SnAgCu Solder Alloys:** Dennis Chan<sup>1</sup>; Ganesh Subbarayan<sup>1</sup>; <sup>1</sup>Purdue University

Cyclic fatigue damage leading to crack initiation and propagation in solder joints is very challenging to model on account of extensive plasticity and large crack area relative to the size of the joint. We present in this talk a non-empirical approach to modeling damage accumulation and fracture based on two experimentally observed facts: (1) cracks result from irreversible, dissipative process, and (2) fracture has an inherent length-scale, time-scale, and/or spatial hierarchy influenced by the microstructural state. The proposed single-parameter, geometry-independent, failure model, the hierarchical fracture process model, is founded on the theoretical principles of Information Theory and Maximum Entropic dissipation. The model maximally accounts for microstructural uncertainty in relating entropic dissipation to material's loss of load bearing capacity. We present detailed experiments and finite element simulations of fracture initiation and propagation in Wafer-Level CSP (WL CSP) and Quad-Flat Nolead (QFN) packages with significantly different joint geometries to validate the failure model.

### **3:40 PM Break**

### **3:50 PM Invited**

**Dynamic Recrystallization in Pb-Free Solder Joints during Fatigue Tests:** *Liang Yin*<sup>1</sup>; Luke Wentlent<sup>2</sup>; Linlin Yang<sup>2</sup>; Babak Arfaei<sup>2</sup>; Awni Osaimeh<sup>2</sup>; Peter Borgesen<sup>2</sup>; <sup>1</sup>Universal Instruments Corp; <sup>2</sup>Binghamton University

The dynamic recrystallization of beta-Sn profoundly affects deformation and failure of Pb-free, SnAgCu solder joints under cyclic stressing. The numerous grain boundaries of recrystallized beta-Sn enable grain boundary sliding. Strain localization is also augmented by the thermal mismatches due to the anisotropy of recrystallized grains. Fatigue cracks initiate at, and propagate along, recrystallized grain boundaries, eventually leading to intergranular fracture. A better understanding of these phenomena could help to develop more accurate constitutive relations for these materials. Thus the dynamic recrystallization behavior of SnAgCu solder joints was examined during thermo-mechanical fatigue and isothermal mechanical fatigue tests. The degree of recrystallization was observed to depend on fatigue loading conditions, alloy composition and the thermal history of joints. The results suggested a relation between recrystallization behavior and the morphology and distribution of secondary precipitates. Discussions are presented on microstructure evolution during the fatigue tests, including dynamic recovery and persistent slip bands.

### **4:15 PM**

**Creep of Bi-Containing Pb-Free Solders:** *David Witkin*<sup>1</sup>; <sup>1</sup>The Aerospace Corporation

SAC-Bi and Sn-Ag-Bi alloys have demonstrated superior performance in thermal cycling reliability tests of printed circuit boards, but due to their Bi content they have not been widely used in electronics manufacturing. Constant-stress creep tests were performed on bulk samples of these alloys at 25, 75, 100 and 125°C, with emphasis on comparison of properties in

as-solidified and aged microstructures. The addition of Bi results in shear strain rates that are relatively unaffected by thermal aging, while creep rates of SAC305 and SAC-Sb increase by more than an order of magnitude after aging. At a given temperature, the applied shear stress at which the power law exponent changed was not altered by aging in Bi-containing alloys, while for SAC305 and SAC-Sb after aging the change in exponent was shifted to lower stress. These differences suggest that thermal fatigue reliability of solder joints may be enhanced by addition of Bi.

#### 4:35 PM

**Fracture Mechanics of Solder Joint under Mechanical Fatigue: Selection and Transition of Failure Location with Microstructure:** *Woong Ho Bang*<sup>1</sup>; Emil Zin<sup>1</sup>; Huili Xu<sup>1</sup>; Choong-Un Kim<sup>1</sup>; Hong-Tao Ma<sup>2</sup>; Tae-Kyu Lee<sup>2</sup>; Kuo-Chuan Liu<sup>2</sup>; <sup>1</sup>University of Texas Arlington; <sup>2</sup>Cisco Systems, Inc.

Mechanics of solder joint failure under various loading conditions has been investigated in numerous recent studies, yet these studies often show several inconsistencies especially on the location of failure site. While some report the solder/IMC to be predominant fracture site, the others identify IMC or solder matrix to be the crack growth path. Structural similarities in solder joint used in these studies yet varying locations of cracking site suggest that fracture in solder joint is affected greatly by a subtle change in microstructure and geometry of the solder. This paper reports experimental and theoretical findings that the weakest link of fracture in solder joint changes sensitively with local constraints resulted by inhomogeneous distribution of mechanical strength of solder. Specifically, transition in fracture site within an identical lead-free solder joint by a simple change in aging condition will be presented along with mechanistic analysis of fracture on each case.

#### 4:55 PM

**Impact of Isothermal Aging on Sn-Ag-Cu Solder Interconnect Board Level Mechanical Shock Performance:** *Tae-Kyu Lee*<sup>1</sup>; Weidong Xie<sup>1</sup>; Kuo-Chuan Liu<sup>1</sup>; <sup>1</sup>Cisco Systems, Inc.

The mechanical stability of solder joints with SnAgCu was an issue since the material was applied to the consumer electronic field. Various shock test methods were developed and standardized tests are used in the industry worldwide. Although it is applied for several years, the detailed mechanism of the shock induced failure mechanism is still under investigation. The work reported here concerns the impact of isothermal aging on board level shock performance. A test vehicle is developed to have various strain and shock level conditions. Along with no aged 17x17mm CABGA package samples, isothermal aging were applied to the samples to observe the impact of different microstructures. The result revealed a clear indication of the strain and shock correlation with a trend of isothermal aging induced degradation. A test condition by eliminating the strain and maintaining the shock level revealed interesting aspects which will be presented and discussed.

## Phase Stability, Phase Transformations, and Reactive Phase Formation in Electronic Materials X: Solder-Related Reliability Issues

*Sponsored by:* The Minerals, Metals and Materials Society, TMS Electronic, Magnetic, and Photonic Materials Division, TMS: Alloy Phases Committee

*Program Organizers:* Chih-Ming Chen, National Chung Hsing University; Hans Flandorfer, University of Vienna; Sinn-Wen Chen, National Tsing Hua University; Jae-ho Lee, Hongik University; Yee-Wen Yen, National Taiwan Univ of Science & Tech; Clemens Schmetterer, TU Bergakademie Freiberg; Ikuo Ohnuma, Tohoku University; Chao-Hong Wang, National Chung Cheng University

Tuesday PM  
March 1, 2011

Room: 7A  
Location: San Diego Conv. Ctr

*Session Chairs:* Chih-Ming Chen, National Chung Hsing University; Ikuo Ohnuma, Tohoku University

### 2:00 PM Introductory Comments

#### 2:05 PM Invited

**Whisker Growth Behavior in a High Vacuum with Thermal Cycling:** *Keun-Soo Kim*<sup>1</sup>; Jung-Lae Jo<sup>1</sup>; Ki-Ju Lee<sup>1</sup>; Alongheng Baated<sup>1</sup>; Katsuaki Suganuma<sup>1</sup>; Norio Nemoto<sup>2</sup>; Tsuyoshi Nakagawa<sup>3</sup>; Toshiyuki Yamada<sup>3</sup>; <sup>1</sup>Osaka University; <sup>2</sup>Japan Aerospace Exploration Agency; <sup>3</sup>Nippon Avionics Co., Ltd.

Aerospace electronics are placed in a very special environment compared to consumer electronics used on the ground. They exposed severe thermal cycling and vacuum conditions. The temperature range between -30 °C and 125 °C, and the vacuum ranges from 10-2 Pa to 10-4 Pa. In this work, the influence of vacuum environment on tin whisker growth was examined by means of a specially designed vacuum thermal cycling chamber. 42 alloy lead-frames with matte tin plating were tested in a high vacuum (10-4 Pa) and in an air conditions with thermal cycling (-40 °C ~ 125 °C). As compared with thermal cycling in the air condition, the substantial influence of environment was found on the whisker growth. Tin whiskers grow thinner and longer in a high vacuum with thermal cycling compared to air. The details mechanism of thermal cycling whisker growth both in air and vacuum will be discussed.

#### 2:30 PM

**Investigation of Tin Whisker Growth on Patterned Surface:** *Chien Hao Su*<sup>1</sup>; Li-Wei Zou<sup>1</sup>; Hao Chen<sup>1</sup>; Albert T. Wu<sup>1</sup>; <sup>1</sup>National Central University

The reaction between Sn and Cu forms Cu<sub>6</sub>Sn<sub>5</sub> intermetallic compound (IMC) at room temperature. The IMC provided compressive stress and induced the growth of tin whiskers on Sn coatings over Cu substrate. One of the required conditions to grow whisker is the weak surface oxide. Cracks on the oxide served as weak spots that were essential for the protrusion of whiskers to release the stresses. In this paper, we intentionally induced "weak spots" on the surface by lithography process, which was utilized to define arrayed of dots on Sn substrates. The whiskers could be found only from the patterned area. Since the number and the location of the whiskers could be predicted, the kinetics of the whisker growth could be calculated. The growth model could thus be verified or modified based on the growth rate.

#### 2:45 PM

**Oxidation Behaviors and Cosmetic Discolor of Pb-Free Solders:** *Chi-Hang Tsai*<sup>1</sup>; Yun-Min Cheng<sup>2</sup>; Jenn-Ming Song<sup>2</sup>; Shih-Yun Chen<sup>1</sup>; <sup>1</sup>National Taiwan University of Science and Technology; <sup>2</sup>National Dong Hwa University

Considering that solders may encounter oxidation problems, this study aims to investigate the thermal oxidation properties of Pb-free solders in both the liquid and solid states. With the oxidation of molten solders, a commonly-used die-attach solder, Pb-Sn, and its potential high temperature Pb-free alternatives (Bi-Ag and Zn-Sn) are investigated. The additions of Ag can significantly reduce the oxidation of Bi and thus Bi-11Ag has a



comparable performance with Pb-5Sn. As for the oxidation of solid solders, this study also deals with the oxidation behaviour and surface discolor of a commonly-used level 2 Pb-free solder, Sn-Cu-Ni. The effect of trace alloying additions (Al and P) was examined by using TGA and UV-visible spectroscopy. The results show the addition of P formed P<sub>2</sub>O<sub>5</sub> on the solder surface. SnCuNi0.01P exhibits the greatest light reflection and thus a superior brightness. This may contribute to the effect of P to retard the formation of SnO.

### 3:00 PM

#### **The Change of Melting Temperature after Soldering at Sn-10wt.%Sb and Bi-2wt.%Sn Alloys:** *Minoru Ueshima*<sup>1</sup>; <sup>1</sup>Senju Metal Industry

Some solder joints start to melt from less than solidus line of their solders because of the segregation of the solidification and the reaction with the electrode. The melting temperatures and microstructures of Sn-10wt.%Sb and Bi-2wt.%Sn solders jointed at the lead-frame with Ag, Cu and Ni electrodes are researched. Ag and Cu electrodes easily dissolve into Sn-10Sb alloy during the die-bonding and then each solidus line decrease from 245 to 228C and 237C, respectively. In the results, the molded joints are torn after reflow at 240C peak temperature. However, the molded joint with Ni finishing doesn't be torn after reflow because the solidus line keeps 245C after die-bonding. On the other hands, the solidus line increase to more than 250C after die-bonding at Bi-2Sn alloy.

### 3:15 PM

#### **Electroless-Plated Ni Layer as a Barrier Layer for a Cu Bump/Sn/Cu Bump Bonding Structure for the Applications of 3D Integration:** *Byunghoon Lee*<sup>1</sup>; *Jongseo Park*<sup>1</sup>; *Hoo-Jeong Lee*<sup>1</sup>; <sup>1</sup>Sungkyunkwan University

For 3D integration, searching for bonding materials with high mechanical and electrical reliabilities is a key issue. Cu bump /Sn layer/Cu bump is a widely-adopted bonding structure; nevertheless, a strong material interaction between Cu and Sn that occurs during the bonding process is potentially a serious problem for both electrical and mechanical reliabilities. In this study, we employed electroless-plated Ni as a barrier layer to suppress metallurgical interaction between Cu and Sn. We carried out material characterization using SEM and TEM on the samples bonded at different temperatures to examine the effects of inserting a bonding layer. We also examined the mechanical properties using lap-shear testing. Our analysis discloses that the Ni barrier layer effectively suppressed interdiffusion between Cu and Sn up to 250° and that at a higher temperature, however, the Ni layer succumbs to the strong interdiffusion and allowed the rapid progress of intermetallic compound formation.

### 3:30 PM Break

### 3:50 PM

#### **Effects of Surface Finish Conditions and Loading Speeds on Shear Strengths of Sn-3.0Ag-0.5Cu BGA Solder Bump:** *Jae-Myeong Kim*<sup>1</sup>; *Myeong-Hyeok Jeong*<sup>1</sup>; *Schoon Yoo*<sup>2</sup>; *Chang-Woo Lee*<sup>2</sup>; *Young-Bae Park*<sup>1</sup>; <sup>1</sup>Andong National University; <sup>2</sup>Korea Institute of Industrial Technology

Fundamental understanding on the BGA Pb-free solder joint reliability under high speed loading condition is still needed. In order to evaluate the mechanical joint reliability of the solder ball joint, the most popular testing method is the ball shear test due to its convenient and simple experiment method. In this study, the effect of surface finish conditions and applied loading speeds on the shear strength of SAC305 BGA solder bump were systematically investigated under varying thermal aging temperature and time. The surface finishes of the electrodes of PCB were ENIG and OSP and the samples were subject to thermal aging at 150° up to 1000 hours with shear speed from 10mm/s to 1,000mm/s. The shear force increased with increasing shear speed while ductility and toughness decreased. Fundamental joint reliability with respect to thermal aging time, surface finish, and loading speed will be discussed in detail.

### 4:05 PM

#### **Electromigration of SnZn and SnBi Solders:** *Chih-Ming Chen*<sup>1</sup>; <sup>1</sup>National Chung Hsing University

With the size shrinkage of the solder joints, electric current that passes through the solder joints increases in its density, and therefore electromigration becomes an unavoidable reliability issue. The SnZn and SnBi alloys are promising Pb-free solders and have been used in microelectronic packaging. Electromigration of these two Pb-free solders were investigated with current stressing at the density range of 1000~10000 A/cm<sup>2</sup>. Effects of minor addition of third element into the solders upon their electromigration behavior were also studied.

### 4:20 PM

#### **Study of EM-Induced Ni(P) Consumption of ENIG and ENEPIG Bond-Pads:** *C. T. Lu*<sup>1</sup>; *Cheng Yi Liu*<sup>1</sup>; <sup>1</sup>National Central University

Electromigration tests on (1) Ni(P) bond-pad (ENIG) and (2) on Ni(P)/Pd bond-pad (ENEPIG) joined with Sn solder bumps were performed with a high current density of 10<sup>4</sup> A/cm<sup>2</sup>. We found that a serious EM-induced Ni(P) consumption and an unusual electromigration-enhanced diffusion of the interfacial Ni<sub>3</sub>Sn<sub>4</sub> compound layer are observed in the Ni(P) bond-pads (ENIG) sample. Intriguingly, by introducing an additional electroless Pd layer on the Ni(P) layer, i.e., (ENEPIG), the EM-induced Ni(P) consumption was greatly reduced. In addition, the interfacial compound layer is analyzed to be the NiSn<sub>4</sub> phase dissolved with very limited Pd atoms. Since, no equilibrium NiSn<sub>4</sub> phase exists in the binary Ni-Sn phase diagram, so, we tend to believe that the formation of the (Ni,Pd)Sn<sub>4</sub> phase should be induced by the current stressing or the presence of dissolved Pd.

### 4:35 PM

#### **Interfacial Reactions between High-Pb Solders and Ag Metallization:** *Chi-pu Lin*<sup>1</sup>; *Chih-ming Chen*<sup>1</sup>; *Yee-wen Yen*<sup>2</sup>; <sup>1</sup>National Chung Hsing University; <sup>2</sup>National Taiwan University of Science and Technology

Although the ban of Pb-containing solders in microelectronics is a global trend, high-Pb solders with weight compositions of 95Pb5Sn and 97Pb3Sn are still used in some specific applications like high-end microprocessors. Therefore, the understanding of interfacial reactions between high-Pb solders and different metallizations is important when evaluating the reliability of the high-Pb solder joints. Immersion Ag is a promising candidate of the Pb-free surface finish. In this presentation, the interfacial reactions between high-Pb solders and Ag metallization will be discussed. During the reflow, the intermetallic compound formation transforms from Ag<sub>3</sub>Sn to Ag<sub>4</sub>Sn when the composition of Sn in solder decreases. With increasing the reflow time, part of the immersion Ag layer dissolves and Pb penetrates into the gap between the Ag layer and underlying Cu substrate.

### 4:50 PM

#### **Influence of Pd Concentration on the Interfacial Reaction and Mechanical Reliability of the Ni/Sn-xPd System:** *Sheng-Wei Lin*<sup>1</sup>; *Yen-Chen Lin*<sup>1</sup>; *Ling-Huang Hsu*<sup>1</sup>; *Cheng-En Ho*<sup>1</sup>; <sup>1</sup>Yuan Ze University

The Pd concentration effect on the interfacial reaction of the Ni/Sn-xPd (x = 0 - 1 wt.%) system and the mechanical reliability were investigated in this study. We found that a slight variation in the Pd concentration produced a completely different reaction product(s) in spite of only a 0.1 wt.% difference. When the Pd concentration was high (more than 0.2 wt.%), a Pd-Ni-Sn layer over Ni<sub>3</sub>Sn<sub>4</sub> was created. The Pd-Ni-Sn was identified to be the PdSn<sub>4</sub>-based structure through electron backscattered diffraction (EBSD) analysis. In contrast, the Ni<sub>3</sub>Sn<sub>4</sub> replaced the (Pd,Ni)Sn<sub>4</sub> when the Pd concentration was below 0.05 wt.%. A Pd-Ni-Sn isotherm simulated by the CALPHAD method was utilized to rationalize the above transition. Additionally, the mechanical reliability in response of the interfacial microstructure was evaluated through a high speed ball shear test. The correlation of the interfacial strength with various Pd concentrations will be established in this study.

---

## Physical and Mechanical Metallurgy of Shape Memory Alloys for Actuator Applications: Fundamental and Engineering Modeling of Shape Memory Alloys

*Sponsored by:* The Minerals, Metals and Materials Society  
*Program Organizers:* S. Raj, NASA Glenn Research Center; Raj Vaidyanathan, University of Central Florida; Ibrahim Karaman, Texas A&M University; Ronald Noebe, NASA Glenn Research Center; Frederick Calkins, The Boeing Company; Shuichi Miyazaki, Institute of Materials Science, University of Tsukuba

Tuesday PM  
March 1, 2011

Room: 11B  
Location: San Diego Conv. Ctr

*Session Chairs:* Dimitris Lagoudas, Texas A&M University; Richard James, University of Minnesota

---

### 2:00 PM Invited

#### Structural Anisotropy, Orientational Flexibility and Superelasticity of a Premartensitic State: Armen Khachaturyan<sup>1</sup>; Wei-Feng Rao<sup>1</sup>; <sup>1</sup>Rutgers University

A theory and 3D modeling of a giant superelasticity in a pre-martensitic state which is a coherent system of low-symmetry nano-precipitates is developed. We took into consideration two new concepts inherent to displacively transforming phase, the structural anisotropy and orientational flexibility. Both automatically follow from a generalization of the existing theory of coherent systems by considering the transformation strain as a relaxing thermodynamic parameter. The structural anisotropy is a notion that is similar to magnetic anisotropy of ferromagnetics. It determines the crystal lattice symmetry and orientation relations of the phases. The systems with low structural anisotropy have extremely high orientation flexibility and display giant and mostly non-hysteretic strain responses. Vanishing structural anisotropy results in a new glass-like state with random orientation relations and unlimited orientational flexibility. Using 3D and 2D modeling, we formulated conditions leading to a drastic amplification of non-hysteretic strain responses that may reach orders of magnitude.

### 2:20 PM Invited

#### Basic Properties of Shape Memory Materials from First-Principles Calculations: Peter Entel<sup>1</sup>; Mario Siewert<sup>1</sup>; Antje Dannenberg<sup>1</sup>; Markus Gruner<sup>1</sup>; <sup>1</sup>University of Duisburg-Essen

The mutual influence of phase transformations, magnetism and electronic properties of magnetic shape memory materials is a basic issue of electronic structure calculations based on density functional theory (DFT). In this contribution we show that the DFT calculations can be pursued to finite temperatures which allows to derive on a first-principles basis the temperature versus composition phase diagram of the pseudo-binary Ni-Mn-(Ga, In, Sn, Sb) system. The DFT calculations allow also to make predictions of magnetostructural and magnetic field induced properties of other (new) magnetic Heusler alloys not based on manganese such as Co-Ni-(Ga-Zn) and Fe-Co-Ni-(Ga-Zn) intermetallic compounds. We will give a systematic description in how far the magnetic shape memory effect associated with magnetic anisotropy and twin mobility in tetragonal martensite depends on composition, atomic disorder and competing ferro- and antiferromagnetic interactions between the magnetic transition metal elements.

### 2:40 PM Invited

#### Modeling Martensitic Phase Transformations Using the Self-Consistent Lattice Dynamics Approach: Ryan Elliott<sup>1</sup>; Venkata Guthikonda<sup>1</sup>; <sup>1</sup>University of Minnesota

Few accurate models exist for martensitic phase transformations (MPTs) based on atomic composition and crystal structure. This work develops a model using a first-order self-consistent lattice dynamics approach. A renormalization of the frequencies of atomic vibration (phonons) via a set of self-consistent equations allows the model to accurately capture how atomic

vibrations affect the thermomechanical properties of the material. The model is applied to a one-dimensional bi-atomic chain. The Morse pair potential and its parameters are chosen to demonstrate the model's capabilities. The model is evaluated by generating bifurcation diagrams corresponding to thermal and mechanical loading. A first-order MPT is predicted between an entropically stabilized high symmetry phase to a low symmetry phase. It is found that the MPT can be both temperature- and stress-induced. This qualitative prediction of an MPT indicates the likelihood that the current modeling technique can be used for the computational discovery of new SMAs.

### 3:00 PM

#### A Generalized Ginzburg-Landau Model for Martensitic Transformations in Shape Memory Alloys: Rajeve Ahluwalia<sup>1</sup>; Srikanth Vedantam<sup>2</sup>; Turab Lookman<sup>3</sup>; Avadh Saxena<sup>3</sup>; <sup>1</sup>Institute of High Performance Computing; <sup>2</sup>Indian Institute of Technology; <sup>3</sup>Los Alamos National Lab

The Ginzburg-Landau theory has been demonstrated to be an effective approach to describe phase transformations in shape memory materials. Recently, such models have also been used to simulate microstructure and mechanical properties. In this approach, the free energy is phenomenologically expressed as a symmetry allowed expansion in the strain components. The approach has been extensively used to study cubic to tetragonal transformations. Clearly, there is a need to extend the approach to transformations from cubic to lower symmetry phases such as orthorhombic, trigonal and monoclinic. We have developed a generalized free energy functional that can, in different parameter ranges, describe these transformations. We present simulations of microstructural evolution and mechanical response.

### 3:15 PM

#### Chemical Trends for Phase Transitions in Magnetic Shape Memory Alloys Derived from First Principles: Tilmann Hickel<sup>1</sup>; Ali Al-Zubi<sup>1</sup>; Joerg Neugebauer<sup>1</sup>; <sup>1</sup>Max-Planck-Institut fuer Eisenforschung GmbH

The Heusler alloy Ni<sub>2</sub>MnGa is a prototype system for a magnetic shape memory alloy, but its martensitic transition temperature is too low for practical applications. In order to systematically improve the performance of this class of materials, an accurate prediction of the critical temperature as function of the chemical composition is crucial. We have, therefore, developed an ab initio scheme based on density functional theory (DFT) to derive the free energies for the austenitic, the martensitic and (modulated) pre-martensitic phases of magnetic Heusler alloys. All relevant temperature effects such as quasiharmonic phonons, electronic excitations, fixed-spin magnons and chemical disorder are computed within DFT. Using this approach we successfully described the phase transition in Ni<sub>2</sub>MnGa. We extended the concept to non-stoichiometric alloys with Ni or Mn excess, determined the resulting increase of the transition temperatures and revealed that a delicate interplay of vibrational and magnetic excitations is responsible for the observed trends.

### 3:30 PM Break

### 3:40 PM Invited

#### Mechanics of Shape-Memory Alloys: Kaushik Bhattacharya<sup>1</sup>; <sup>1</sup>California Institute of Technology

This talk will describe recent advances in understanding and modeling the mechanics of shape-memory alloys. It will focus specifically on (a) multiscale modeling that seeks to understand the interplay between microstructure, polycrystalline texture and macroscopic properties and (b) a constitutive relation that implicitly accounts for the microstructure and polycrystalline texture. Illustrative examples and comparison with experiments will be provided.

### 4:00 PM Invited

#### Multivariate Modeling and Experiments of Shape Memory Alloys: L. Catherine Brinson<sup>1</sup>; Aaron Stebner<sup>1</sup>; <sup>1</sup>Northwestern University

As the number of shape memory alloys (SMAs) and applications continues to increase and the significance of texture evolution in shape memory behaviors becomes more evident, the need for models that simulate

the relationships between microstructural and macroscopic responses becomes more apparent. The Simplified Multivariant Model is the most recent among several generations of multivariant, micromechanical models that have been formulated and numerically implemented to address this need in both single crystal and polycrystalline SMA systems. Most recently, additional methodologies have been developed to couple these simulations with neutron diffraction data as a way to concurrently validate micro and macro scale predictions of the model, and also gain further insight into the diffraction data, such as inter-granular configurations of habit plane and correspondence variants. The model and methodologies are presented and illustrated through isothermal reorientation of NiTi martensite variants, as well as thermo-mechanical cycling.

**4:20 PM**

**Multivariant and Rate-Dependent Calculation of Martensitic Phase Transformation:** *Seung Yong Yang*<sup>1</sup>; Tae-Hyun Nam<sup>2</sup>; <sup>1</sup>Korea University of Technology and Education; <sup>2</sup>Gyeongsang National University

In continuum crystalline description of martensitic phase transformation, the analogy with crystal plasticity can be used. But, unlike crystal plasticity, the sum of the volume fractions of all phases should remain one. To impose this constraint in a multivariant description of martensitic transformation, a kinetic relation is used based on an Arrhenius equation. The kinetic law is capable of calculating rate-dependent behavior. We hypothesized that temperature induced self-accommodating variants form a separate phase in addition to the individual stress-induced variants. Low misfit strain energy or activation energy barrier was taken into consideration by allowing different kinetic constants for the self-accommodation group. The constitutive equations were implemented in the finite element code ABAQUS user material subroutine. Strain vs. temperature curve of NiTi shape memory alloy was calculated.

**4:35 PM**

**Simulating Load Biased Thermal Cycling of Polycrystalline NiTi:** Sivom Manchiraju<sup>1</sup>; Darrell Gaydos<sup>2</sup>; Ronald Noebe<sup>2</sup>; Shipeng Qiu<sup>3</sup>; Raj Vaidyanathan<sup>3</sup>; *Peter Anderson*<sup>1</sup>; <sup>1</sup>The Ohio State University; <sup>2</sup>N. A. S. A. Glenn Research Center; <sup>3</sup>University of Central Florida,

A joint research program involving NASA, Ohio State University, University of Central Florida, and Northwestern University aims to couple experimental and computational materials science techniques across a range of length scales, to study and quantify shape memory actuator performance. An outcome is a finite element approach to simulate the thermomechanical response of polycrystalline NiTi, by coupling a crystallographic description of the B2-to-B19' transformation with crystal-based plasticity. It is informed by recent density functional theory calculations for the martensite (B19') elastic moduli, as well as experimental characterization of the texture, pseudoelastic behavior, and stress-biased thermal cycling response of solutionized polycrystalline NiTi (55wt% Ni). Key model outcomes are the ability to capture the (1) initial increase and subsequent decrease in actuator strain with increasing bias stress, and (2) evolution of martensite texture with stress-biased thermal cycling. Some significant challenges remain, including under prediction of strain ratcheting and the effect of upper cycle temperature.

**4:50 PM**

**Modeling the Shape Memory Effect: Comparison and Validation of Two Constitutive Models:** *Marco Fabrizio Urbano*<sup>1</sup>; <sup>1</sup>SAES Getters

In order to properly exploit the functional properties of Shape Memory Alloys, a good design is necessary. Especially if complex geometries (and consequently stress-strain states) are involved, modeling could be an extremely effective tool for engineers. Although many constitutive models describing the thermomechanical behavior of Shape Memory Alloys have been developed in the last two decades, a thorough validation of their performances is still missing. In this presentation some recent works aiming at filling this gap are presented: two constitutive models are described and compared. Results predicted by the models are compared to experiments. In particular, temperature cycles at constant tension load and three point

bending at constant load. Some simulations of their implementation in Ansys and Abaqus will be shown.

**5:05 PM End of Session**

## Polycrystal Modelling with Experimental Integration: A Symposium Honoring Carlos Tome: Orientation Imaging Techniques and Related Models

*Sponsored by:* The Minerals, Metals and Materials Society, TMS Structural Materials Division, TMS Materials Processing and Manufacturing Division, ASM-MSCTS: Texture and Anisotropy Committee, TMS/ASM: Mechanical Behavior of Materials Committee, TMS/ASM: Computational Materials Science and Engineering Committee

*Program Organizers:* Ricardo Lebensohn, Los Alamos National Laboratory; Sean Agnew, University of Virginia; Mark Daymond, Queens's University

Tuesday PM  
March 1, 2011

Room: 6C  
Location: San Diego Conv. Ctr

*Session Chairs:* Brent Adams, Brigham Young University; Robert Wagoner, Ohio State University; David Field, Washington State University

**2:00 PM Invited**

**A High Resolution EBSD Study of Deformation near Twins in Ti:** *Benjamin Britton*<sup>1</sup>; Angus Wilkinson<sup>1</sup>; <sup>1</sup>University of Oxford

Twinning makes an important contribution to the deformation of many hexagonal close packed metals including Ti and its alloys. Pure Ti is particularly prone to twinning. Cross-correlation based analysis of EBSD patterns allows intra-granular lattice rotations and elastic strain variations at the 10<sup>-4</sup> (rads) level to be mapped. Additionally the lattice curvature can be used to assess the density and nature of geometrically necessary dislocations present. We have investigated various compression twins in large grained grade 1 CP Ti using the hi-res EBSD method and AFM. We will present maps of elastic strain variations, lattice rotations and GND distributions around such twins and correlate results with AFM maps of surface topography. Examples showing the interactions of twin tips with grain boundaries and at twin-twin intersections will be given.

**2:25 PM Invited**

**High-Resolution EBSD Characterization and Analysis of Defect Structure of In-Situ Deformations of Steel:** *Brent Adams*<sup>1</sup>; Samikshya Subedi<sup>1</sup>; Sadeh Ahmadi<sup>1</sup>; David Fullwood<sup>1</sup>; Robert Wagoner<sup>2</sup>; <sup>1</sup>Brigham Young University; <sup>2</sup>The Ohio State University

This paper describes recent developments in high-resolution electron backscatter diffraction (HR-EBSD) characterizations and analysis of the development of defect structure during in-situ deformations of columnar steel. Cross correlations of EBSD patterns with strain-free reference patterns is used to recover the spatial fields of the elastic displacement gradient tensor. Corrections for varying pattern center (PC) are essential to minimize non-physical contributions. Application of new geometrical corrections to the cross correlations, based upon motions of the PC, are described. In-situ deformation experiments on steels in the elastic and plastic regimes are described. Comparisons of the measured elastic fields with Green's function based solutions to the equilibrium equation are shown. Novel methods for recovery of the full Nye tensor of geometrically necessary dislocations are described.



2:50 PM

**Meso-Scale Treatment of Dislocation-Grain Boundary Interactions 2: Single Crystal Constitutive Model without Tacit Grain Boundary Effects:** *Hojun Lim*<sup>1</sup>; Robert Wagoner<sup>1</sup>; Myoung-Gyu Lee<sup>2</sup>; Brent Adams<sup>3</sup>; John Hirth<sup>4</sup>; <sup>1</sup>The Ohio State University; <sup>2</sup>Pohang University of Science and Technology; <sup>3</sup>Brigham Young University; <sup>4</sup>-

Single crystal constitutive equations based on dislocation density (SCCE-D) were developed from Orowan's strengthening equation and simple geometric relationships of the operating slip systems. The multiplication of dislocations on each slip system incorporated standard 3-parameter dislocation density evolution equations applied to each slip system independently. In contrast, the most widely used single crystal constitutive equations for texture analysis (SCCE-T) feature 4 or more adjustable parameters that are usually back-fit from a polycrystal flow curve. Tensile tests of single crystals oriented for single slip were simulated using CPFEM. Best-fit parameters were determined using either multiple or single slip stress-strain curves for copper and iron from the literature. Tensile tests of single crystals oriented to favor the remaining combinations of slip systems were then simulated. The SCCE-D method provides an improved representation of single-crystal plastic response with fewer adjustable parameters, better accuracy, and better predictivity than the SCCE-T.

3:10 PM Invited

**Meso-Scale Treatment of Dislocation-Grain Boundary Interactions 3: Prediction of Dislocation Densities, Lattice Curvatures, and the Hall-Petch Effect:** *Robert Wagoner*<sup>1</sup>; Hojun Lim<sup>1</sup>; Ji Hoon Kim<sup>2</sup>; Myoung-Gyu Lee<sup>3</sup>; Brent Adams<sup>4</sup>; <sup>1</sup>The Ohio State University; <sup>2</sup>Korea Institute of Materials Science; <sup>3</sup>Pohang University of Science and Technology; <sup>4</sup>Brigham Young University

A practical two-scale method has been developed and implemented to predict quantitatively the Hall-Petch effect and local microstructural details such as dislocation densities and lattice curvatures. The first scale is a FE model of a polycrystal using novel single-crystal constitutive equations based on dislocation density and incorporating a back stress. The second scale redistributes mobile dislocation density consistent with the plastic strain distribution, and enforces slip transmission criteria at grain boundaries that depend on local grain and boundary properties. The following advances were demonstrated: 1) Quantitative prediction of the Hall-Petch slopes without imposing unrealistic or unobserved dislocation configurations. 2) Quantitative prediction of dislocation densities consistent with grain-dislocation and dislocation-dislocation interactions. 3) Computationally tractable meso-scale treatment of large numbers of dislocations, their interactions, and the relationship between their redistribution and strain. 4) A simple quantitative model and method to treat grain boundaries as impediments to slip depending on local configurations.

3:35 PM Break

3:50 PM Invited

**Measuring Misorientations and Grain Sizes in Severely Deformed Metals through Orientation Mapping on a Transmission Electron Microscope:** *Edgar Rauch*<sup>1</sup>; Muriel Veron<sup>1</sup>; <sup>1</sup>SIMAP Laboratory

Severe plastic deformations are known to modify drastically the structural state of metals. However, measuring grain size or dislocation densities after large strains is not a straightforward task. Consequently, the hardening related to grain refinement is usually discussed with rather imprecise data and poor descriptions of the structural state. The present work proposes an experimental approach that gives a better insight in the structural evolution for severely deformed materials. Misorientations are measured with a dedicated TEM tool (ACOM/TEM) that will be described with some details. With this attachment, grain sizes are estimated despite the fact that they are ill-defined at very large strains. Moreover, it is demonstrated that the large dislocation densities may be reasonably approximated from the misorientations. The results are used to discuss the validity of both the Hall-Petch and Taylor/Friedel law and to propose an alternative formulation of the flow law.

4:15 PM Invited

**Quantification of Dislocation Structure Heterogeneity in Deformed Polycrystals:** *David Field*<sup>1</sup>; <sup>1</sup>Washington State University

Plastic deformation in polycrystalline materials involves a complex interaction of dislocations with defects in the lattice. A dislocation density based crystal plasticity finite element model was developed for both FCC and BCC materials. Based upon the kinematics of crystal deformation and dislocation interaction laws, and adopting information from discrete dislocation dynamics calculations, dislocation generation and annihilation are modeled. Dislocation densities evolve and are tracked as state variables in the model, leading to spatially inhomogeneous dislocation densities. These are compared against measurements obtained using electron backscatter diffraction wherein the excess component of dislocation density can be obtained. A study of the effects of different minimization schemes shows that measured densities for specific slip systems varies considerably depending upon which minimization scheme is used, but the overall densities are reasonably consistent. The experimental technique is shown on various structures and compared against modeled structures.

4:40 PM

**Determining Correlations between Crystallography and Mechanical Response in a 3D Polycrystalline Material:** *Alexis Lewis*<sup>1</sup>; Siddiq Qidwai<sup>2</sup>; Andrew Geltmacher<sup>1</sup>; <sup>1</sup>Naval Research Laboratory; <sup>2</sup>SAIC

Three-dimensional reconstructions of a polycrystalline BCC microstructure were derived from serial sectioning experiments combined with electron backscatter diffraction measurements of crystallography. These reconstructed datasets were used as input for image-based finite element simulations of mechanical response at low strains. Using experimentally-measured 3D microstructure and crystallography data allowed for the direct observation of correlations between crystallography and mechanical response, most notably the relationship between the axis of applied load and the crystallographic orientation of each grain under that load. Due to the large size of the 3D dataset, representative volume elements, extracted from the microstructure based on 2-point correlations of crystallographic texture, were used in the FE simulations.

5:00 PM

**Three-Dimensional Interface Curvature as a Function Crystallographic Grain Boundary Character:** *David Rowenhorst*<sup>1</sup>; Alexis Lewis<sup>1</sup>; <sup>1</sup>Naval Research Lab

Grain coarsening describes the curvature driven process wherein polycrystalline systems decrease their surface energy by increasing the average grain size. In isotropic systems, the interfaces between domains are assumed to always be spherical sections where the two principle curvatures are equivalent. The results of optical serial sectioning of approximately 2100 grains in Ti-21S (a beta stabilized titanium alloy), combined with EBSD scans are used to determine the grain boundary character as a function of the five macroscopic degrees of freedom of the grain boundary as well as the local curvature of the interface. We will show that not only are there preferences for particular types of boundaries, but also that the assumption of equivalent curvatures is not valid in anisotropic systems, especially near high symmetry boundaries.

5:20 PM

**On the Role of Grain Size Distribution on the Heterogeneity of Plastic Deformation:** *Francis Wagner*<sup>1</sup>; Nathalie Allain-Bonasso<sup>1</sup>; Stephane Berbenni<sup>1</sup>; David Field<sup>2</sup>; <sup>1</sup>Universite de Metz; <sup>2</sup>Washington State University

Plastic deformation in polycrystals is well known to be a heterogeneous process due to crystallographic texture, but the role of the grain size distribution is generally neglected. Nevertheless some calculations including grain size effects have shown that it is also an important source of heterogeneity. In this paper the role of grain sizes is considered from an experimental point of view. An IF steel has been submitted to a tensile test for several deformation degrees. The grain size distribution as well as the orientation distribution have been determined from EBSD measurements before and after plastic deformation. Several quantities such as the GOS (Grain Orientation Spread), the GAM (Grain Average Misorientation) and the GND (Geometrically

TUESDAY PM

Necessary Dislocation) density have been calculated. Mean values of these quantities were calculated for several classes of grain size. The role of grain size in plastic deformation is evident in these measures.

**5:40 PM**

**Microstructure Effects on Local Plasticity: Closing the Loop between Experiment and Simulation:** *Michael Groeber*<sup>1</sup>; Paul Shade<sup>2</sup>; Michael Uchic<sup>1</sup>; <sup>1</sup>AFRL; <sup>2</sup>UTC/AFRL

There is a demand for both accurate virtual representations of material microstructure and microscale experimental results to validate simulations of structures. In this work, we have attempted to close this loop by testing and investigating the same sample. A micro-sized tensile sample was prepared in a Dual Beam FIB microscope and tested in-situ while strain mapping the surface. The surfaces of the sample were investigated with Electron Backscatter Diffraction (EBSD) prior to, as well as after the test. Following the test, the sample was sectioned and mapped with EBSD to collect the true 3D microstructure of the entire microsample. The sample was tested to only a few percent strain in order to limit the change in microstructure. Thus, the collected microstructure can reasonably serve as the input structure to a Crystal Plasticity Finite Element Model (CPFEM). This presentation will focus on the analysis of local deformation to compare with simulations.

**6:00 PM**

**3D EBSD Characterization of Deformed Polycrystalline Micro-Scale Tensile Samples:** *Paul Shade*<sup>1</sup>; Michael Groeber<sup>2</sup>; Michael Uchic<sup>2</sup>; Robert Wheeler<sup>3</sup>; Dennis Dimiduk<sup>2</sup>; <sup>1</sup>UTC / AFRL; <sup>2</sup>Air Force Research Laboratory; <sup>3</sup>UES / AFRL

This presentation describes the application of a dual beam focused ion beam-scanning electron microscope (DB FIB-SEM) outfitted with an electron backscatter diffraction (EBSD) system to characterize the internal microstructure and local lattice rotations within micro-scale test samples that have been deformed via in-situ SEM tensile testing. The objectives of this study are to develop an experimental methodology that can provide a high-fidelity 3D characterization of the internal grain structure of mechanical test samples that contain a limited number of grains (< 1000 grains); obtain knowledge of the external boundary conditions and measurement of the resultant stress-strain behavior of the same test samples; and, perform a 3D characterization of the internal lattice rotations that develop after a modest amount of plastic deformation. Such information is needed to assess and guide the further development of modeling and simulation methods that predict the local plastic deformation response of polycrystalline ensembles.

### Processing and Properties of Powder-Based Materials: Powder Fabrication and Processing

*Sponsored by:* The Minerals, Metals and Materials Society, TMS Materials Processing and Manufacturing Division, TMS: Powder Materials Committee

*Program Organizers:* K. Morsi, San Diego State University; Ahmed El-Desouky, San Diego State University

Tuesday PM  
March 1, 2011

Room: 33A  
Location: San Diego Conv. Ctr

*Session Chair:* Iver Anderson, Iowa State University

**2:00 PM Introductory Comments**

**2:05 PM**

**Characterization of Copper Open Cellular Structures Fabricated by Electron Beam Melting:** *Diana Ramirez*<sup>1</sup>; L Murr<sup>1</sup>; S Li<sup>2</sup>; E Martinez<sup>1</sup>; D Hernandez<sup>1</sup>; J Martinez<sup>1</sup>; F Medina<sup>3</sup>; P Frigola<sup>4</sup>; R Wicker<sup>3</sup>; <sup>1</sup>University of Texas at El Paso; <sup>2</sup>Institute of Metal Research, Chinese Academy of Sciences; <sup>3</sup>W.M. Keck Center for 3D Innovation; <sup>4</sup>Radiabeam Technologies

Copper open cellular foams and meshes were fabricated by additive manufacturing (AM) using electron beam melting (EBM). Foam models developed from CT-scans of aluminum foams and mesh elements were

embedded in CAD models for EBM. These structures are the first directly fabricated Cu foams and meshes with low density and high porosity (densities ranging from 0.8 to 1.7 g/cm<sup>3</sup>). Corresponding stiffness or Young's modulus values measured using a resonant frequency-damping analysis technique ranged from ~1.2 to 3.7 GPa, respectively. Plotting relative stiffness (E/E<sub>0</sub>) versus relative density (d/d<sub>0</sub>) produced a slope of ~1.6 in contrast to ~2 for aluminum and aluminum alloys using the Gibson-Ashby model for open cellular materials ((E/E<sub>0</sub>) = (d/d<sub>0</sub>)<sup>n</sup> where E<sub>0</sub> and d<sub>0</sub> are solid Cu modulus and density, respectively). Corresponding ligament hardness (H) averaged 1.6 GPa (using a Vickers indenter), corresponding to an approximate yield strength (Y) of 0.5 GPa based on assumption that Y ~ H/3.

**2:25 PM**

**Comparative Study of Production of Boron Carbide Powder by: Resistance Furnace and Arc Furnace:** *Habibollah Amini Rastabi*<sup>1</sup>; Ayoub Karimi Dehcheshmeh<sup>1</sup>; <sup>1</sup>Islamic Azad University

Boron carbide is the third hardest known material next to diamond and boron nitride. Reasonable cost of production, low density, and high chemical inertness makes boron carbide an attractive material for micro-electronic, military, space and medical applications. At present work, B<sub>4</sub>C, free of impurities, was produced using reduction reaction of boron oxide by carbothermal process. Boron loss during the process, in the form of B<sub>2</sub>O<sub>2</sub> gas; a common problem in B<sub>4</sub>C production, was minimized by adjusting the stoichiometry of feeding materials. Likewise, carbon residue was eliminated by taking appropriate composition at the starting point. The result of number of experiments showed that production of boron carbide is highly dependent on the phase change of reactant boron oxide from solid to liquid and from liquid to gaseous boron hypo-oxides. Also, the results show that the production of pure boron carbide by resistance furnace is more suitable than that by arc furnace.

**2:45 PM**

**Prediction and Control of Nucleation Kinetics of Mono-Sized Spherical Copper Droplets:** *Mehmet Islier*<sup>1</sup>; Teiichi Ando<sup>1</sup>; <sup>1</sup>Northeastern University

Production of copper balls with quality suitable for electronics packaging applications by droplet solidification depends on an ability to control the kinetics of droplet nucleation during droplet cooling. Controlling the in-flight nucleation kinetics requires information on how droplets cool during their flight and a method to predict their nucleation temperatures given their cooling schedules. A recently developed droplet cooling and nucleation simulation model was used to determine and predict the in-flight nucleation kinetics of mono-size copper droplets produced by the uniform-droplet spray (UDS) process, a capillary jet breakup process, that produces mono-size metal droplets. Initial inputs needed to evaluate the values of materials specific constants in the model were obtained experimentally from the deformation morphologies of UDS droplets quenched on substrates at various heights. Continuous-cooling transformation (CCT) curves were computed for the heterogeneous nucleation on both internal and surface catalysts. Predicted CCT curves were verified by additional droplet quenching experiments.

**3:05 PM**

**Characterization and Properties of Titanium Alloy Powder Produced by Close-Coupled Gas Atomization and of Resulting Consolidated Samples:** *Andrew Heidloff*<sup>1</sup>; Joel Rieken<sup>1</sup>; Iver Anderson<sup>2</sup>; David Byrd<sup>2</sup>; <sup>1</sup>Iowa State University; <sup>2</sup>Ames Laboratory

The capabilities of a new induction skull melting close-coupled gas atomizer utilizing a novel ceramic composite melt pouring tube has proven to be capable of producing fine, spherical Ti alloy powder with minimal impurities. Resulting powder from the atomization process was characterized using X-ray, SEM, TEM, as well as ICP-AES and LECO inert gas fusion for chemical analysis. Sieved powders were consolidated using hot isostatic pressing and post-consolidation analysis of the samples was conducted to determine the mechanical properties and to characterize the microstructure. Mechanical tests included room temperature tensile and low cycle fatigue. Work supported by Iowa State University Research Foundation, the Grow Iowa Values Fund, and Quad Cities Manufacturing Laboratory and performed at Ames Lab under contract no. DE-AC02-07CH11358.

3:25 PM

**Microstructural Investigation of D2 Tool Steel during Rapid Solidification Using Impulse Atomization:** *Pooya Delshad Khatibi*<sup>1</sup>; Arash Ilbagi<sup>1</sup>; Hani Henein<sup>1</sup>; <sup>1</sup>University of Alberta

D2 tool steels are widely used in industry because of their good wear and abrasion properties. It is believed that excellent mechanical properties can be achieved from reduced microsegregation and good distributed carbides during the solidification process. Rapid solidification yields significant enhancement in properties through reduced microsegregation and formation of metastable phases. An understanding of the evolution of microsegregation and carbide formation during rapid solidification is necessary to control the microstructure and hence the properties of these alloys. Impulse Atomization has been used to produce D2 powders. Microstructural investigation on D2 powders shows that because of rapid solidification during Impulse Atomization, there is no carbide inside the microstructure and all the alloying elements are supersaturated inside the austenite phase. XRD results shows both small and large powders mainly contain retained austenite and small amount of ferrite phases. Further phase and microstructural investigation is going on the D2 Impulse Atomized powders.

3:45 PM Break

3:55 PM

**Mechanism of Thermal Decomposition of Zinc Hydroxide Carbonate and Preparation of Complexional Ultra-Fine Zinc Oxide:** *Z. F. Tong*<sup>1</sup>; L. X. Lian<sup>1</sup>; Y. L. Li<sup>1</sup>; <sup>1</sup>Jiangxi University of Science and Technology

The thermal decomposition process of zinc hydroxide carbonate ( $Zn_3CO_3(OH)_4 \cdot H_2O$ ) absorbed  $NH_4^+$  is studied by TG, DTA, DTG. The results show mechanism model of thermal decomposition process accords with one-dimension diffusion model. The zinc hydroxide carbonate ( $Zn_3CO_3(OH)_4 \cdot H_2O$ ) decomposes into complexional ultra-fine zinc oxide under the conditions of calcination temperature 350°C and 1.5h. The structure and appearance of complexional ultra-fine zinc oxide are studied by XRD and SEM. The results show the zinc oxide is particle size about 200nm and complexional and flake and hexagonal zinc oxide. Key words: zinc hydroxide carbonate; complexional ultra-fine zinc oxide; mechanism of thermal decomposition

4:15 PM

**Synthesis of Silver Plating Nano-Copper Bimetallic Powders:** *Wei Liu*<sup>1</sup>; Qionghua Zhou<sup>1</sup>; <sup>1</sup>Henan University of Science and Technology

The silver plating nona-copper bimetallic powders were synthesized by substitution reaction method and chemical deposition method with  $AgNO_3$  as main salt. Transmission electron microscopy (TEM) and Energy Dispersive Spectrometer (EDS) were used to characterize the as-prepared bimetallic powders. Three kinds of preparation processes (direct substitution reaction with  $AgNO_3$ , substitution reaction method with  $[Ag(NH_3)_2]^+$  and chemical deposition method) were compared with each other. The experimental results indicate that the silver plating nano-copper bimetallic powders can be synthesized by direct substitution reaction method with relatively simple procedure. The silver content on the surface of the bimetallic powders prepared by direct substitution reaction can reach 74.78 at%. The silver content on the powders prepared with  $[Ag(NH_3)_2]^+$  after depositing once and twice are 35.46 at% and 70.16 at%, respectively. The bimetallic powders synthesized by chemical deposition method show a mixture structure with nano-copper and nano-silver powders rather than silver plating nano-copper structure.

4:35 PM

**Effect of Pore Size on High Temperature Oxidation Behavior of Ni-Fe-Cr-Al Porous Metal:** *Kee-Ahn Lee*<sup>1</sup>; Sung-Hwan Choi<sup>1</sup>; Song-Yi Kim<sup>1</sup>; Jung-Yeul Yun<sup>2</sup>; Hye-Moon Lee<sup>2</sup>; Byung-Kee Kim<sup>3</sup>; <sup>1</sup>Andong National University; <sup>2</sup>Korea Institute of Machinery and Materials; <sup>3</sup>University of Ulsan

This study investigated the effects of the pore size of Ni-22.4%Fe-22%Cr-6%Al porous metal on its high-temperature oxidation behaviors. Two types of open porous metals with pore sizes of 800  $\mu m$  and 580  $\mu m$  were used. The results of the high-temperature oxidation test showed that porous metals

compared to bulk metal exhibited far lower levels of oxidation resistance, and that the decreasing pore size led to the weakening of oxidation resistance characteristics. The relationship between  $\log K_p$  (oxidation rate constant) and  $1/T$  as identified during the oxidation test was found to be linear. Activation energy values were calculated to be 198 KJ/mol and 220 KJ/mol in the 580  $\mu m$  and 800  $\mu m$  samples, respectively. This indicates its effect of compromising the overall oxidation characteristics of the porous metal. In addition, Ni-Fe-Cr-Al porous metal's high-temperature oxidation microscopic mechanism was discussed. [supported by the Fundamental R&D program for Core technology, Korea]

4:55 PM

**WC Alloys Technology:** *Alex Li*<sup>1</sup>; <sup>1</sup>Glorytek Industry(Beijing)Co., Ltd

The technology of Glorytek industry Co.,Ltd ([www.alloys-welding.com](http://www.alloys-welding.com)) is based on a chemical process for the synthesis of WC and WC/Co powders, in which the individual W, C, and/or Co precursors are intimately mixed at the molecular level, yielding a uniquely homogeneous product with exceptional high performance. Glorytek industry has developed exceptionally hard bulk consolidated composite materials, with hardness measured up to 2300 VHN. These sintered materials exhibit unparalleled fracture toughness at this level of hardness. These materials are compression sintered in inert gas or vacuum furnaces to form highly homogeneous monoliths. The hardness of the sintered products is found to be a function of cobalt content. Typically, cutting tool applications force the minimum Co content level to be above 6%, below which the material cannot be sintered.

## Properties, Processing, and Performance of Steels and Ni-Based Alloys for Advanced Steam Conditions: Alloy Design, Selection, Qualification, and Processing

*Sponsored by:* The Minerals, Metals and Materials Society, TMS Structural Materials Division, TMS/ASM: Corrosion and Environmental Effects Committee, TMS: High Temperature Alloys Committee

*Program Organizers:* Peter Tortorelli, Oak Ridge National Laboratory; Bruce Pint, Oak Ridge National Laboratory; Paul Jablonski, National Energy Technology Laboratory; Xingbo Liu, West Virginia University

Tuesday PM  
March 1, 2011

Room: 33B  
Location: San Diego Conv. Ctr

*Session Chair:* Bruce Pint, Oak Ridge National Laboratory

2:00 PM Invited

**U. S. Program on Advancing the Materials Technology for Advanced Ultrasupercritical Steam Boilers and Turbines:** *John Shingledecker*<sup>1</sup>; R. Viswanathan<sup>1</sup>; R. Purgert<sup>2</sup>; P. Rawls<sup>3</sup>; <sup>1</sup>Electric Power Research Institute; <sup>2</sup>Energy Industries of Ohio; <sup>3</sup>National Energy Technology Laboratory

One method for achieving reduced emissions (including CO<sub>2</sub>) in pulverized coal-fired (PC) power plants is to increase plant efficiency by increasing steam temperatures and pressures. The current materials of construction (steels) for ultrasupercritical (USC) PC power plants limit maximum steam temperature to ~620°C (1150°F). To increase temperatures further and reduce emissions by an estimated 20% compared to a standard PC boiler, nickel-based alloys will be required. A consortium of U.S. steam boiler and turbine manufacturers, the Electric Power Research Institute (EPRI), Energy Industries of Ohio (EIO), Oak Ridge National Laboratory (ORNL) and the National Energy Technology Laboratory (NETL) supported by the U. S. Department of Energy Office of Fossil Energy and the Ohio Coal Development Office (OCDO) has been conducting a research program to develop the materials technology necessary to construct and operate an Advanced-USC (A-USC) Steam Boiler and Turbine with maximum steam conditions of 760°C (1400°F) and 35 MPa (5,000 psi). The comprehensive program, focused on nickel-based alloys, includes studies on: materials

TUESDAY PM



selection, high-temperature material behavior, oxidation, corrosion, fabrication, weldability, weld performance, and application to codes and standards. For this paper the overall structure of the consortium, the major materials issues, the research areas, results, and ongoing research work and needs will be presented and discussed.

### 2:30 PM Invited

**Ultra-Super-Critical (USC) Power Plant Development and High Temperature Materials Research and Application in China:** *Fusheng Lin*<sup>1</sup>; Xishan Xie<sup>2</sup>; <sup>1</sup>Shanghai Power Equipment Research Institute; <sup>2</sup>University of Science and Technology Beijing

The USC fossil power plants are developing rapidly since the first USC power plant had put in service on the end of 2006. Up to May 2010 there are 26 USC power plants with the steam temperature of 600° and 51 units (600-1000MW) for service in China. For further improvement of thermal efficiency and decreasing CO<sub>2</sub> emission China intends to develop the advanced USC power plant with the steam temperature of 700°. The key issue for USC power plant development is high temperature material. This paper will review today's high temperature materials used for 600° USC power plants in China and the high temperature materials research and development for 700° A-USC in the near future.

### 3:00 PM Invited

**Alloy Design for Improved High-Temperature Performance:** *Philip Maziasz*<sup>1</sup>; <sup>1</sup>Oak Ridge National Laboratory

High temperature alloys are essential for many demanding advanced energy production applications, including advanced steam conditions for coal-fired power plants. One of the most critical performance criteria for such applications is creep-rupture resistance, which critically depends on microstructural development during the early stages of service, and the stability of such structures for very long periods of time. Some principles relating alloying effects to precipitation behavior so as to create appropriate microstructures for better creep-resistance in austenitic stainless steels and ferritic steels have been developed. Some examples will be summarized, including the development of CF8C-Plus cast stainless steel. The applicability of this alloy design approach to Ni-based superalloys will also be described. Research sponsored by the U.S. Department of Energy, Office of Fossil Energy, Advanced Research Materials Program under contract DE-AC05-00OR22725 with UT-Battelle, LLC.

### 3:30 PM Invited

**The Metallurgy and Engineering of USC and A-USC Steam Turbines:** *Jeffrey Hawk*<sup>1</sup>; <sup>1</sup>U.S. Department of Energy

Steam turbines have provided electricity for well over 100 years. However, large-scale generation has only dominated energy production since 1950. Since the 1990's there has been pressure to increase the efficiency of large steam turbines, partly to improve the rate of return on initial investment, but also to decrease the amount of greenhouse gases emitted to the environment. Increasing efficiency means the temperature and/or pressure must be increased. Doing either means current materials of construction are no longer adequate in meeting the stresses generated by the moving and stationary parts. The presentation provides background information on the direction steam turbine technology has taken during the last couple of decades, addressing the way new materials have been identified and selected for use. The presentation will conclude with discussion on current strategies of alloy design for the next generation of steam turbines designed to operate at temperatures in excess of 700°C.

### 4:00 PM Break

### 4:10 PM

**Ni-Base Alloys for Use as Components in Advanced-USC Steam Turbines:** *Jeffrey Hawk*<sup>1</sup>; Paul Jablonski<sup>1</sup>; Christopher Cowen<sup>1</sup>; <sup>1</sup>U.S. Department of Energy

Experience with nickel-base alloys in the NETL sponsored 760°C steam turbine program has shown that commercial, "off-the-shelf" nickel superalloys exist, and while promising, may not provide for all long-term mechanical needs associated with the steam turbine environment. One alloy, Haynes

282, has shown robust capability in terms of starting microstructure (gamma prime precipitate size and volume fraction). Another alloy, Nimonic 105, has exhibited the potential for improved creep behavior upon extended aging. In addition to the forged components in the steam turbine, cast materials for the turbine shell and valve chest also pose significant manufacturing challenges, primarily in terms of casting size and environment. This presentation will summarize the progress to date in identifying the most promising alloys, providing information on mechanical behavior and assessing their potential for use in A-USC steam turbines.

### 4:30 PM

**Castability of Traditionally Wrought Ni-Based Superalloys for USC Steam Turbines:** *Paul Jablonski*<sup>1</sup>; Christopher Cowen<sup>1</sup>; Jeffrey Hawk<sup>1</sup>; Neal Evans<sup>2</sup>; Philip Maziasz<sup>2</sup>; <sup>1</sup>US Department of Energy; <sup>2</sup>ORNL

The high temperature components within conventional coal fired power plants are manufactured from ferritic/martensitic steels. In order to reduce greenhouse gas emissions the efficiency of pulverized coal steam power plants must be increased. The proposed steam temperature in the Advanced Ultra Supercritical (A-USC) power plant is high enough (760°C) that ferritic/martensitic steels will not work due to temperature limitations of this class of materials; thus Ni-based superalloys are being considered. The full size castings are quite substantial: ~4in thick, several feet in diameter and weigh 5-10,000lb each half. Experimental castings were quite a bit smaller, but section size was retained and cooling rate controlled in order to produce relevant microstructures. A multi-step homogenization heat treatment was developed in order to better deploy the alloy constituents. The castability of two traditionally wrought Ni-based superalloys to which minor alloy adjustments have been made in order to improve foundry performance is further explored.

### 4:50 PM

**Castability of HAYNES 282 Alloy:** *Henry White*<sup>1</sup>; Zenon Pirowski<sup>2</sup>; Robert Purgert<sup>3</sup>; <sup>1</sup>Haynes International; <sup>2</sup>Foundry Research Institute; <sup>3</sup>Energy Industries of Ohio

Excellent high temperature mechanical properties, weldability, and fabricability makes HAYNES 282 alloy an attractive material for high temperature/ high pressure boiler and turbine components in Advanced Ultrasupercritical Power Plants. Several programs are in place in the United States and Overseas to gather the necessary data in order to utilize the material in plant construction. In this presentation we report on casting trials for the turbine program which was funded by the Energy Industries of Ohio and performed at Foundry Research Institute in Poland. Optical light and scanning electron microscopy were used to evaluate the structure and processing of the as cast material. A comparison between cast and wrought properties will be provided.

### 5:10 PM

**Simplified Production of Ni-Based Oxide Dispersion Strengthened (ODS) Alloys via Gas Atomized Precursor Powder Approach:** *John Meyer*<sup>1</sup>; Iver Anderson<sup>2</sup>; Joel Rieken<sup>1</sup>; David Byrd<sup>2</sup>; <sup>1</sup>Iowa State University; <sup>2</sup>Ames Laboratory - US DOE

Oxide dispersion strengthened (ODS) Ni-base superalloys have been considered promising candidate materials to fulfill the corrosion, erosion, oxidation and creep challenges imposed by proposed power plant environments. Current processing of Ni-based ODS materials is very time, energy and cost intensive as well as susceptible to contamination. Gas atomization reaction synthesis (GARS) with a mixed (Ar/O<sub>2</sub>) atomization gas is being developed as a simplified route for generation of ODS precursor powders on a small scale. Already, hot consolidation conditions that encourage the necessary oxide exchange reactions have been verified for Fe-based ODS alloy billets and a preliminary kinetic study determined Ni-base, Ni-Cr-Y-(Hf or Ti) containing, alloys viable for this production method. Results of experimental trials will be reported in terms of powder characterization and consolidation results. Supported by Carpenter Technology and USDOE-FE-ARM Program through Ames Laboratory contract no. DE-AC02-07CH11358.

---

## Recent Developments in the Processing, Characterization, Properties and Performance of Metal Matrix Composites: Processing, Microstructure and Mechanical Properties II

Sponsored by: The Minerals, Metals and Materials Society  
Program Organizers: Martin Pech-Canul, Centro de Investigación y de Estudios Avanzados del Instituto Politécnico Nacional; Zariff Chaudhury, Arkansas State University; Golam Newaz, Wayne State University

Tuesday PM  
March 1, 2011

Room: 6A  
Location: San Diego Conv. Ctr

Session Chair: Martin Pech-Canul, Centro de Investigación y de Estudios Avanzados del Instituto Politécnico Nacional

---

### 2:00 PM

#### Deformation and Cavitation in Non-Contact Creep Studies for a Nb-Based Superalloy: Robert Hyers<sup>1</sup>; Xiao Ye<sup>1</sup>; Jan Rogers<sup>2</sup>; Laurent Cretegy<sup>3</sup>;

<sup>1</sup>University of Massachusetts; <sup>2</sup>NASA/MSFC; <sup>3</sup>GE Global Research

A non-contact method for measuring creep at extremely high temperatures has been developed. Samples are high-precision machined spheres, levitated in the NASA MSFC Electrostatic Levitation Facility and heated with a laser. An induction motor rotates samples up to 30,000 revolutions per second. The rapid rotation loads the sample through centripetal acceleration, producing a shear stress of about 60 MPa at the center, causing the sample to deform. Deformation of the sample is captured on high-speed video and analyzed. This method has been applied to new materials, including a niobium-based superalloy, which is a metal and silicide composite (MASC). Microstructural analysis of crept samples provides insight into creep mechanisms. An overview of the method and results from these studies will be presented.

### 2:20 PM

#### Effect of MgAl<sub>2</sub>O<sub>4</sub> on the Superficial Hardness of Hybrid-Multimodal Al/SiC Composites Processed by Reactive Infiltration: Miguel Montoya-Davila<sup>1</sup>; Martin Pech-Canul<sup>2</sup>; Maximo Pech-Canul<sup>2</sup>; Rodrigo Escalera-Lozano<sup>3</sup>;

<sup>1</sup>Universidad Autónoma de Zacatecas; <sup>2</sup>Centro de Investigación y de Estudios Avanzados del Instituto Politécnico Nacional; <sup>3</sup>Universidad del Istmo

The effect of MgAl<sub>2</sub>O<sub>4</sub> formed at the reinforcement/matrix interface, on the superficial hardness of hybrid Al/SiC composites processed by reactive infiltration was investigated. Composites were prepared from porous preforms of a-SiC and silica-coated a-SiC powders of 10, 86, and 146 μm. The preforms, with particle size distribution from monomodal to trimodal, contained 0.6 volume fraction of SiC. The infiltration tests with the alloy Al-13.3Mg-1.8Si (wt. %) were carried out in Ar->N<sub>2</sub> atmosphere at 1100°C for 60 min. The composites were characterized by X-ray diffraction (XRD) and scanning electron microscopy (SEM). In addition to density and residual porosity, superficial hardness measurements were performed. Results show that with spinel at the interfaces, residual porosity decreases and density and superficial hardness are slightly improved. This is attributed to the increase in the metal/ceramic interfacial joints by formation of the spinel phase and to an enhanced matrix/reinforcement load transmission.

### 2:40 PM

#### Corrosion and Wear Behaviour of Aluminum Alloy 6061-Fly Ash Composites: Ajit Bhandakkar<sup>1</sup>; B. Balaji<sup>1</sup>; R. C. Prasad<sup>1</sup>; Shankar Sastry<sup>1</sup>;

<sup>1</sup>Indian Institute of Technology

The environmental degradation of aluminium metal matrix composites has been a subject of research for the damage tolerant design requirement in aerospace and automobile components. In the present investigation AA6061 aluminium alloy as matrix material and up to 10 wt% of low cost fly ash particulate composite were fabricated using liquid metallurgy stir casting route. Potentiodynamic and cyclic polarization studies were carried out in 3.5% NaCl solution on AA6061 and AA6061-fly ash composites to study

their corrosion behavior. Polarization results in 3.5% NaCl solution indicates that the composites are more susceptible to corrosion than the base alloy. However, the base alloy and composite have same pitting and repassivation potential. The wear rate, frictional force and the frictional coefficient of composite was found to decrease with the increase in the reinforcement from 5 to 10 wt%. The environmentally degraded and worn out samples of base alloy and composites were analyzed using optical and scanning electron microscopes.

### 3:00 PM

#### Interface Evolution in Tungsten Wire Reinforced Stainless Steel Composites: Pawan Kumar<sup>1</sup>; Milo Kral<sup>1</sup>;

<sup>1</sup>University of Canterbury

There is potential for improving creep properties of high temperature steels by tungsten wire reinforcement. Fiber/matrix interfaces have a significant influence on the properties of metal matrix composites, especially when they are used for high temperature applications, for example due to differences in thermal expansion coefficients. The present study investigated interactions between tungsten wires in two cast stainless steel matrices. Intermetallic phases develop at the wire-matrix interface during solidification. When the composite is aged at high temperatures, these phases further develop as a function of temperature, time and matrix composition. A combination of scanning electron microscopy, energy dispersive spectroscopy and electron backscatter diffraction was used to identify the constituents present at the interface, their chemistry and interface growth kinetics.

### 3:20 PM Break

### 3:40 PM

#### Effects of Annealing on the Growth Behavior of Intermetallic Compounds on the Interface of Copper/Aluminum Clad Metal Sheets: Li Xiaobing<sup>1</sup>; Zu Guoyin<sup>1</sup>; Deng Qiang<sup>2</sup>;

<sup>1</sup>Northeastern University; <sup>2</sup>Pangang Group Company LTD

The growth behavior and composition of intermetallic compound (IMC) on the interface of copper/aluminum clad sheets fabricated by the asymmetrical cold rolling on the different annealing process were investigated by means of OM, SEM, EDS and XRD techniques. The effect of temperature on the morphology and distribution of IMC is obvious at elevated temperature from 200°C to 500°C. The IMC begin to appear on the local area at 300°C and the thickness of the IMC layer increases rapidly with the rise of temperature. The growth rate of the IMC layer is slow for the annealing time from 20 min to 180 min. The composition of inter-layer varies into complicated with the rise of temperature. According to the results, the optimal annealing process can be chosen at 400°C for 20 min.

### 4:00 PM

#### Contribution of Different Strengthening Mechanisms in Particulate-Metal Matrix Nanocomposites: Z. Razavi Hesabi<sup>1</sup>; J. Gracio<sup>2</sup>; S. Ahzi<sup>3</sup>;

Hamid Garmestani<sup>3</sup>;

<sup>1</sup>Georgia Institute of Technology - and - University of Aveiro; <sup>2</sup>University of Aveiro; <sup>3</sup>Georgia Institute of Technology

The relative contribution of different strengthening mechanisms in particulate metal matrix composites, namely, load-bearing, grain boundary strengthening, Orowan and enhanced dislocation density strengthening due to thermal expansion mismatch between ceramic particles and metal matrix, has been evaluated for a wide range of particle sizes varying from micrometer to nanometer. On the basis of the dislocation theory, a critical particle size (dc) was determined below which thermal expansion mismatch strengthening is absent in metal matrix nanocomposites (MMNCs). Nanoparticles located at grain boundaries may not play any role in strengthening by Orowan mechanism, however, they significantly affect grain size leading to increase of relative contribution of grain boundary strengthening. The data analysis shows an increase in the slope of Hall-Petch equation (K value) when nanoparticles are located at grain boundaries. In this work, we show that different strengthening mechanisms should be weighted as a function of microstructural features dependent on the volume fraction, size, and strongly distribution and location of nanoparticles.

4:20 PM

**Manufacturing of an Aluminum Composite Structure Using a New Method and Its Comparison with Two Different Conventional Methods:**

*Atefeh Nabavi*<sup>1</sup>; J. Vahdati Khaki<sup>1</sup>; <sup>1</sup>Ferdowsi University of Mashhad

In this study, a novel method for manufacturing of metal foam sandwich panels via self-propagating high temperature synthesis (SHS) has been introduced and investigated. In this method, a powder mixture of metallic aluminum and copper oxide was placed in core-sheet interface and then sandwich panel was heated under static pressure. During heating, SHS reaction ( $3\text{CuO}+2\text{Al}=\text{Al}_2\text{O}_3+3\text{Cu}$ ,  $H<0$ ) occurred in the sheet-core interface and the generated heat from this exothermic reaction caused sheets to join the core by melting the interface and nearby. By plotting the hardness values of the panels' sheets across distance, it was found that the generated heat of the exothermic reaction caused a local melting of the panel sheets and the core. In addition, in order to evaluate the shear strength of the interface, the shear test was applied to manufactured sandwich panels and its results were compared with sandwich panels which were produced by two different conventional methods; diffusion and adhesive bonding processes. Furthermore, by the aid of energy dispersive spectrometer (EDS) and x-ray diffraction (XRD) analyses, the formation of copper in the core-sheet interface and its diffusion into the sheets and the core were investigated. The results showed that metal foam sandwich panels produced by using SHS method have higher joint strength than those which were produced by diffusion and adhesive bonding processes, and the maximum shear strength of the interface was achieved in shorter heating time. Significantly, this innovating method for manufacturing metal foam sandwich panels can be applied as a proper and alternative method.

4:40 PM

**Joining of Advanced Aluminum-Graphite Composite:**

*Wayne Hung*<sup>1</sup>; Manasa Velamati<sup>1</sup>; Mauricio Garza<sup>2</sup>; Edgar Aguilar<sup>2</sup>; Mike Powers<sup>3</sup>; <sup>1</sup>Texas A&M University; <sup>2</sup>COMIMSA; <sup>3</sup>Agilent Technologies

Advanced aluminum graphite (Al-Gr) composites have unique thermal properties due to opposite coefficients of thermal expansion of aluminum and graphite. The thermal and mechanical properties of such composites are anisotropic due to directional properties of graphite fibers and their designed orientation. A joint of components with different fiber orientations would theoretically produce an isotropic material for thermal management purpose. This paper presents research results for welding and brazing of Al-Gr composites using different joining techniques. A laser beam melts the matrix and delaminates graphite fibers. The molten aluminum reacts with graphite to form aluminum carbide Al<sub>4</sub>C<sub>3</sub>. The joint strength is compromised when laser welding at optimal conditions to minimize the carbide formation. Brazing is preferred since the low melting temperature of a filler material suppresses the formation of Al<sub>4</sub>C<sub>3</sub> while minimizing shrinkage cavities in the joint. Exceptional joint strength is obtained when resistance brazing Al-Gr composites with Al-Zn filler.

**Refractory Metals 2011: Refractory Metal-Based Alloys**

*Sponsored by:* The Minerals, Metals and Materials Society, TMS Structural Materials Division, TMS: Refractory Metals Committee  
*Program Organizers:* Omer Dogan, DOE National Energy Technology Laboratory; Jim Ciulik, University of Texas, Austin

Tuesday PM  
March 1, 2011

Room: 19  
Location: San Diego Conv. Ctr

*Session Chairs:* Omer Dogan, National Energy Technology Laboratory; Evan Ohriner, Oak Ridge National Laboratory

2:00 PM Invited

**Potential Next Generation Airfoil Alloys for Advanced Land-Base Gas Turbines:**

*Jeffrey Hawk*<sup>1</sup>; <sup>1</sup>U. S. Department of Energy  
Advanced, super high efficiency gas turbine systems will necessarily need to operate at conditions that correspond to blade metal temperatures in excess

of the melting temperature of current state-of-the-art Ni-base superalloys (i.e., hydrogen or oxy-combustion firing conditions). Consequently, any and all high melting temperature alloys systems must be investigated to determine which might be suitable for manufacture and testing. This presentation outlines the current NETL path forward in developing these substrate materials. A short introduction to NETL's materials development program will be given, followed by a discussion of several possible systems of interest (e.g., Nb-based refractory metal silicides, Nb-based alloys, ceramic matrix composites). The merits of each system, as well as, the research required for development will be described. The path forward is discussed next with emphasis on reducing the development time by utilizing computational materials modeling to pre-screen potential materials before attempting to produce those materials in the laboratory.

2:20 PM

**Strengthening in High Entropy Alloys:**

*Garth Wilks*<sup>1</sup>; Oleg Senkov<sup>1</sup>; Daniel Miracle<sup>1</sup>; <sup>1</sup>Air Force Research Laboratory

High Entropy Alloys (HEAs) represent a novel shift in strategy for alloy development. In conventional alloys, complex formulations are usually avoided in order to prevent the formation of intermetallic compounds that degrade material properties, whereas HEAs capitalize on the high entropy of a cocktail of constituents to frustrate formation of the same. Often, this strategy results in an alloy with a single phase consisting of a simple crystal structure. While strength in these materials has been suggested to operate under the agency of a solid-solution like strengthening mechanism, a critical analysis of available HEA data in the literature will be presented which broadly discusses observed trends in properties (e.g. lattice parameter and yield strength) as a function of constitution and highlights experimental observations from the authors' studies of refractory-based HEAs.

2:40 PM Invited

**Processing Methods for Iridium and Iridium Alloys:**

*Evan Ohriner*<sup>1</sup>; <sup>1</sup>Oak Ridge National Laboratory

Iridium and iridium alloys have a combination of properties that recommend them for a variety of applications. Their high melting temperature, resistance to oxidation, and strength at elevated temperature have led to their use in crucibles, spark plugs, nuclear fuel containers, and coatings for rocket thrusters. However, these same properties, combined with potential sensitivity of material properties to impurities and microstructure, result in a material that is often difficult to fabricate. The variety of methods used to fabricate iridium and iridium alloys are reviewed, including both traditional and novel methods. Metal purification, melting, forming and joining are traditional methods that have continued to develop. Powder metal processing and iridium coating technology are now also available as fabrication methods. This research was sponsored by the Office of Space and Defense Power Systems, U. S. Department of Energy, under Contract DE-AC05-00OR22725 with UT-Battelle, LLC.

3:00 PM

**Surface Processing of an Iridium Alloy for Control of Emissivity:**

*Evan Ohriner*<sup>1</sup>; G. B. Ulrich<sup>1</sup>; R. G. Miller<sup>1</sup>; W. Zhang<sup>1</sup>; <sup>1</sup>Oak Ridge National Laboratory

The effects of surface processing on the microstructure and properties of DOP-26 iridium alloy (Ir-0.3% W-0.006% Th-0.005% Al) are investigated. Surface processing is used to control emissivity of components operating at elevated temperature. The surface treatments include grit blasting with tungsten carbide media and pulse laser heating. The effects of processing parameters on surface morphology, grain structure, and emissivity are evaluated. The results are compared to those from numerical modeling of surface processing and material grain growth behavior. Recrystallization and grain growth is evaluated for both as-treated surfaces and following post-treatment annealing. This research was sponsored by the Office of Space and Defense Power Systems, U. S. Department of Energy, under Contract DE-AC05-00OR22725 with UT-Battelle, LLC.



### 3:20 PM Break

### 3:40 PM

**Improving Chromium Ductility:** Hailey Murdock<sup>1</sup>; Jamie Kruzic<sup>2</sup>; Omer Dogan<sup>1</sup>; <sup>1</sup>National Energy Technology Laboratory; <sup>2</sup>Oregon State University

The next generation of high temperature structural alloys for gas-turbines must exhibit exceptional resistance to fracture, creep, oxidation and fatigue at high temperatures. Chromium is being considered due to its high melting point (>1800°C), relatively low density (~7.2 g/cc), high temperature strength, and oxidation resistance. Limiting chromium is its high ductile-to-brittle transition temperature (DBTT). First principles calculations revealed elements, when alloyed with chromium, which have potential to reduce the ductile-to-brittle transition temperature. Experiments investigating room and elevated temperature deformation behavior of Cr-V alloys are presented. Cr-V samples (0 – 75% V) were prepared from powders, hot isostatically pressed, annealed at 1300°C for 120 hours, and extruded at 130 MPa and 1250°C. Extrusion achieved better homogeneity of the alloys as confirmed by electron microprobe data. Results of room and elevated temperature hardness tests, three-point bend tests, tensile tests and the effect of vanadium on the ductile-to-brittle transition temperature are described.

### 4:00 PM

**High-Temperature Oxidation Behaviour of Co-Re-Cr-Based Alloys:** Bronislava Gorr<sup>1</sup>; Steffen Burk<sup>1</sup>; Hans-Jürgen Christ<sup>1</sup>; <sup>1</sup>University Siegen

Co-Re-Cr-based model alloys have been developed for high-temperature applications beyond 1200°C. The purpose of the present investigation is to gain an insight into the oxidation mechanisms of the model Co-Re-Cr alloys and to find ways to improve oxidation resistance of this class of materials. The first generation of this class of alloys showed a rather poor oxidation resistance during exposure to laboratory air. As a consequence of the lacking protectiveness of the oxide layer, the vaporization of rhenium oxide takes place during oxidation. It has been found that Si stabilizes the Cr<sub>2</sub>O<sub>3</sub> scale, enhancing the oxidation resistance significantly. Other concepts to improve the oxidation resistance of this class of materials are discussed, such as the formation of a borosilicate layer or protective Al<sub>2</sub>O<sub>3</sub> scale on the substrate surface.

### 4:20 PM

**Computational Study of Microstructure-Property Relationships in High Temperature Materials for Fossil Energy Applications: An Integrated Phase Field and Numerical Viscoplasticity Approach:** Kaisheng Wu<sup>1</sup>; Omer Dogan<sup>1</sup>; <sup>1</sup>National Energy Technology Laboratory

An integrated computational approach has been developed to investigate the correlations between complex microstructures and mechanical properties. In this approach, a phase field model was utilized to simulate the evolution of the complex microstructures in response to a variety of processing conditions such as different heat treatment schedules. Microstructure features including grain boundary segregation, grain growth, and second phase precipitations, etc., were taken into account in multi-component and multiphase systems. The results were incorporated into a numerical viscoplasticity model which was modified based on Fast Fourier Transform (FFT) algorithm to simulate the overall mechanical and microstructural response of the materials subjected to plastic deformation. Several examples of applying the developed model to high temperature materials, including refractory metals, for fossil energy applications will be discussed.

### 4:40 PM

**Characterization of Osmium-Ruthenium Thin Films for Cathode Coatings:** Phillip Swartzentruber<sup>1</sup>; T. John Balk<sup>1</sup>; Scott Roberts<sup>2</sup>; <sup>1</sup>University of Kentucky; <sup>2</sup>Semicon Associates

Osmium-Ruthenium (OsRu) alloy thin film coatings were characterized to understand the effects of film structure on thermionic emission from dispenser cathodes. Electron microscopy and x-ray diffraction of coated dispenser cathodes were used to characterize the various film structures, and life testing was conducted to gauge the improvement in cathode emission due to each film structure. In collaboration with industrial partner Semicon Associates, three novel film structures were studied in addition to the standard

Semicon film. Different film architectures were created, with varying levels of substrate bias during film deposition. The films were simultaneously magnetron sputtered on porous tungsten pellets for characterization and on cathode assemblies for life testing. The cathode assemblies were life tested for 1000 hours. Cathode performance will be discussed in light of the microstructural features of each film.

---

## Shape Casting IV: Light Metals Division Symposium in Honor of Prof. John T. Berry: Solidification

*Sponsored by:* The Minerals, Metals and Materials Society, TMS Light Metals Division, TMS: Aluminum Processing Committee, TMS: Solidification Committee

*Program Organizers:* Murat Tiryakioglu, University of North Florida; Paul Crepeau, General Motors Corporation; John Campbell, University of Birmingham

Tuesday PM  
March 1, 2011

Room: 15B  
Location: San Diego Conv. Ctr

*Session Chairs:* William Griffiths, Univ of Birmingham; Peter Schumacher, Univ of Leoben

---

### 2:00 PM Introductory Comments

#### 2:10 PM

**Review of Defect Behavior in Ni-Based Superalloys:** John Campbell<sup>1</sup>; <sup>1</sup>University of Birmingham

The Ni-base superalloys, normally melted and cast in vacuum, entrain their surface oxide film during turbulent pouring of the melt, which unfortunately at this time, is universally practiced for investment castings of these materials. The entrained film automatically becomes a bifilm crack, so that cast alloys have a large population of cracks that controls their failure behavior. The problems of the growth of single crystals, and the welding of polycrystalline alloys are reviewed to illustrate the central role of bifilms in the cracking of turbine blades, the heat affected zones of welds and the reliability of properties. It has been demonstrated that improved gravity pouring systems can significantly reduce these problems, but only counter-gravity filling of molds is expected to result in defect-free castings.

#### 2:35 PM

**Premium Quality Super Duplex Stainless Steel Castings without Secondary Refining:** Bob Puhakka<sup>1</sup>; <sup>1</sup>Alloy Casting Industries

The ASTM A890/ A995 super duplex stainless steels are a popular family of high alloy cast steels used extensively in the power generation and energy sectors. The manufacturing steps for these alloys have, up to now, required the use of costly secondary refining processes such as Argon Oxygen Decarburization (AOD). This paper will describe and validate a set of process parameters that obviate the need for secondary refining. Initial results indicate that the principle embrittling features, carbides and sigma phases, are not found, confirming the proposal that these phases form on bifilms entrained by pouring turbulence. Other significant benefits from the absence of bifilms appear to include the elimination of cracking and leakage defects.

#### 3:00 PM

**Direct X-Ray Observation of High Temperature Deformation in Aluminum Alloy Composites:** Richard Hamilton<sup>1</sup>; Andre Phillion<sup>2</sup>; Alex Leung<sup>1</sup>; Thomas Connolly<sup>3</sup>; Peter Lee<sup>1</sup>; <sup>1</sup>Imperial College London; <sup>2</sup>University of British Columbia; <sup>3</sup>Diamond Light Source

The development of a novel tension/compression rig capable of loading samples at high temperature during x-ray observation has enabled in-situ imaging of semi-solid deformation using both laboratory and synchrotron sources. This study focuses on phenomena of interest to the aluminum alloy processing industry, where defects formed in the mushy zone during processing can result in significant costs. Experiments were devised to apply

a measured, controlled load to the specimen to enable direct observation of the formation and deformation of the microstructure and flow of interdendritic fluid. The effect of composite additions, along with cooling rate and strain rate on the mechanisms of failure, initiation, growth, and liquid healing were studied whilst monitoring the load. The localization of strain followed by void formation and coalescence was observed. Finally, post failure x-ray tomography allows 3D characterization of the final fracture helping to explain the failure mechanism.

### 3:25 PM

**In-Mold Thermal Analysis of Ductile Cast Iron:** *Morten Onsoien*<sup>1</sup>; <sup>1</sup>SINTEF

The objective of the present work is to study characteristic solidification data of three experimental ductile irons produced using a flow-through in-mould melt treatment technique, by means of in-mould thermal analysis. All produced irons were, in addition, subjected to chemical analysis and quantitative metallography, as well as an evaluation of shrinkage porosity and carbide forming propensity. Applied melt treatment alloys were based on FeSiMg with small contents of cerium, lanthanum or misch-metal. Based on the obtained results, it was concluded that in-mould thermal analysis provides an effective way of monitoring the graphite nucleation throughout the solidification. Furthermore, the selected melt treatment resulted in ductile irons having very high nodule counts, up to 1162 nodules mm<sup>-2</sup>, very low shrinkage porosity and very low carbide forming propensity.

### 3:50 PM Break

### 4:10 PM

**Modeling of Hot Tearing and Its Validations in Metal Castings:** *Jianzheng Guo*<sup>1</sup>; *J. Z. Zhu*<sup>1</sup>; *Sam Scott*<sup>2</sup>; <sup>1</sup>ESI US R&D, Inc.; <sup>2</sup>ESI NA

Hot tearing is one of the most serious defects for a metal casting. The nucleation and propagation of the hot tearing can result in permanent defects in the casting, which may cause the final cast product to be unusable. It is believed that the imposed strains and stresses on the solid framework in the mushy zone by the solidification shrinkage and thermal contraction create the conditions for hot tearing. It has been very well documented that the composition of the alloy and the mechanical properties of the metals in the semisolid state play critical roles in the formation of hot tears. To predict the susceptibility of hot tearing in a casting, a hot tearing indicator is proposed which is based on the Gurson's constitutive model and uses the thermophysical and thermomechanical properties obtained from the thermodynamic calculation in the final stage of the solidification. The numerical implementation of the hot tearing indicator is described in details and the numerical modeling of the hot tearing formation is validated by experiments.

### 4:35 PM

**Effect of Alloying Elements (Magnesium and Copper) On Hot Cracking Susceptibility of AlSi7MgCu-Alloys:** *Salar Bozorgi*<sup>1</sup>; *Katharina Haberl*<sup>1</sup>; *Christian Kneissl*<sup>2</sup>; *Thomas Pabel*<sup>2</sup>; *Peter Schumacher*<sup>1</sup>; <sup>1</sup>University of Leoben; <sup>2</sup>Austrian Foundry Research Institute

Hot cracking during solidification can be a serious problem in aluminium casting alloys under certain conditions. This feature is well known, but still insufficiently investigated in shape casting. This study gives a brief overview on the factors influencing hot cracking during shape casting. Five different AlSi7MgCu-alloys with varying Mg and Cu contents were examined. Theoretical models including the cracking susceptibility coefficient (CSC) from Clyne and Davies have been considered. Thermodynamic calculations of the behaviour of the fraction solid during solidification have been compared to an experimental based hot cracking indexing (HCI) method. Scanning electron microscopy (SEM) was used to compare existing microstructure and precipitated thermodynamic phases. Furthermore, SEM was used to investigate crack surfaces initiated by a dog bone shaped mold during casting. A good correlation between theoretical models and experimental hot cracking index method was observed.

### 5:00 PM

**Hydrogen and Cooling Rate Effects on Microporosity Formation in the Production of Defect-Controlled Fatigue Specimens:** *Rosario Squatrito*<sup>1</sup>; *Ivan Todaro*<sup>1</sup>; *Lorella Ceschini*<sup>1</sup>; *Luca Tomesani*<sup>1</sup>; <sup>1</sup>University of Bologna

In experiments aimed at the production of fatigue specimens, the increased number of nearly identical specimens needed for each processing condition, together with the high sensitivity to pore size, call for very strict requirements of both the casting tool and the processing conditions. An experiment for producing aluminium alloy fatigue specimen by gravity casting with controlled microstructure and defects is here presented. The main requirements to be obtained on a set of specimens (extracted from a single casting block) were to have the same microstructure and gas porosity content. The main process parameters were the hydrogen level of the melt, the addition of oxides for improving the number of pore nucleation sites and the cooling rate within the casting mould. The distribution of the relevant properties (SDAS, %area of porosity) was measured throughout the casting plates in order to validate the design criteria of the both experiment and the mould.

### 5:25 PM

**Effects of Gravity on the Columnar to Equiaxed Transition in Directional Solidification:** *Wajira Mirihanage*<sup>1</sup>; *David Browne*<sup>1</sup>; <sup>1</sup>University College Dublin

In industrial casting processes, microstructure plays a major role in determining the properties of the final cast product. Columnar to equiaxed transition (CET) is a frequent result of the evolving grain structure during alloy solidification. In this contribution, we analyze CET in directional solidification via numerical simulations. The numerical model employs front tracking to track columnar growth and a volume average approach to track the evolution of the equiaxed zone. The effects of gravity, thermal natural convection and dendrite transport were integrated into the model. Simulations of vertical directional solidification of an Al-7%wt.Si alloy both in and opposite the direction of gravity were conducted for different cooling conditions. Here, we present a preliminary analysis of these numerical simulations and a comparison of the predictions with previously published theoretical and experimental work.

## Size Effects in Mechanical Behavior: Capturing the Size Effect through Modeling and Simulation

*Sponsored by:* The Minerals, Metals and Materials Society, Not Applicable, TMS: Nanomechanical Materials Behavior Committee  
*Program Organizers:* Erica Lilleodden, GKSS Research Center; Amit Misra, Los Alamos National Laboratory; Thomas Buchheit, Sandia National Laboratories; Andrew Minor, UC Berkeley & LBL

Tuesday PM  
March 1, 2011

Room: 2  
Location: San Diego Conv. Ctr

*Session Chairs:* Thomas Buchheit, Sandia National Laboratories; Srinivasan Srivilliputhur, University of North Texas

### 2:00 PM

**Gradient Theory and Size Effects:** *Elias Aifantis*<sup>1</sup>; <sup>1</sup>Aristotle University of Thessaloniki

Various forms of gradient theory are used to interpret size effects at micron and nano scales. They include size-dependent material moduli, size-dependent strength and fracture criteria, as well as size-dependent stress-strain curves.

### 2:20 PM

**Deformation of Polycrystalline Magnesium Thin Film Size Effects:** *Mark Horstemeyer*<sup>1</sup>; *Amitava Moitra*<sup>1</sup>; *Kiran Solanki*<sup>1</sup>; <sup>1</sup>Mississippi State University

The inelastic behavior of columnar nanocrystalline magnesium has been studied using molecular dynamics simulation. Polycrystalline materials

are analyzed using Voronoi tessellation in which the randomness of the microstructure is generated using a Delaunay network from which a random distribution of grains is generated. Different specimen sizes and grain sizes were examined under different applied stress states (tension, compression, and shear). We have found that the grain reorientation occurs within the elastic regime to release the stored energy by local plastic deformation in grain boundary (GB) regions. The effect of thermal fluctuations in dislocation formation and nucleation leading to the yielding mechanism has been observed and analyzed. Evolution of twin and dislocation densities are also been estimated. A size scale effect related to the volume averaged yield stress in the specimen was evidenced.

### 2:40 PM

**Controlling the Strength of Nanocrystalline Metals and Alloys: On the Importance of the Grain Boundary Relaxation State:** Jonathan Schäfer<sup>1</sup>; Alexander Stukowski<sup>1</sup>; Karsten Albe<sup>1</sup>; <sup>1</sup>TU Darmstadt

Plastic deformation in various nanocrystalline fcc metals and their alloys is studied by means of atomic scale computer simulations. The distribution of solutes is equilibrated using a hybrid Monte-Carlo/Molecular Dynamics scheme before samples are deformed under uniaxial load. The relaxation state of the grain boundary is measured by means of the atomic free volume and the evolution of line defects within the grains is monitored using a novel dislocation extraction algorithm. By comparing chemically and structurally relaxed samples we find that the relaxation state of the GBs is controlling the maximum strength of all studied material systems and for all grain sizes. The (chemical) equilibration is proven to raise the barrier for GB mediated processes. Also in the case of grain sizes, where the major carrier of plastic deformation is dislocation slip, the relaxation state of the GB is shown to have a significant effect.

### 3:00 PM

**A Continuum Theory of Dislocation Dynamics - Microstructure Evolution, Size Effects and Comparison With DDD:** Stefan Sandfeld<sup>1</sup>; Thomas Hochrainer<sup>2</sup>; Michael Zaiser<sup>3</sup>; Peter Gumbsch<sup>1</sup>; <sup>1</sup>Karlsruhe Institute of Technology; <sup>2</sup>Florida State University; <sup>3</sup>The University of Edinburgh

Progressive miniaturization of components further increases the demand for physically-based continuum theories of plasticity, which can predict size-dependent behaviour by accounting for length scales associated with the dislocation microstructure. An important recent development has been the formulation of a Continuum-Dislocation-Dynamics theory (CDD) which provides a kinematically consistent continuum description of the dynamics of systems of curved dislocations. This theory overcomes the limitations of classical continuum methods while it is not constricted by the number of interacting line segments. We outline the theoretical foundations of CDD and demonstrate the applicability by presenting several model systems, among them bending and shearing of a thin single crystalline film, torsion of a wire, and shearing of a composite material. The microstructure evolution along with size-effects will be compared to results from DDD-simulations and classical plasticity models.

### 3:20 PM

**Effect of Precipitate Morphology on Chemical Mixing during Severe Plastic Deformation:** Nhon Vo<sup>1</sup>; Robert Averback<sup>1</sup>; Pascal Bellon<sup>1</sup>; Yinon Ashkenazy<sup>1</sup>; <sup>1</sup>University of Illinois Urbana Champaign

The effect of precipitate morphology on atomic mixing during severe plastic deformation (SPD) was investigated using molecular dynamics (MD) computer simulations. Different initial precipitate morphologies in fcc A75B25 alloys with heats of mixing ranging from 0 to 21 kJ/mol were cyclically deformed to strains up to  $\epsilon = 200$ . For highly immiscible alloys (~16 kJ/mol), the precipitates always acquired a platelet structure during shear, independent of their initial microstructures. We attribute this tendency to dislocation localization on the interface and enhanced local atomic rearrangements. We also examined SPD in Cu-Nb for which bcc precipitates reside in an fcc matrix. In this case the shear-induced mixing depends strongly on the specific interface, with Kurdjumov-Sachs (KS) interfaces behaving very differently than non-KS interfaces. The role of temperature in the mixing mechanism is also discussed.

### 3:40 PM Break

### 4:00 PM Invited

**Deformation of Nanoscale Single Crystal Gold by Atomistic Simulation:** Shivraj Karewar<sup>1</sup>; Niraj Gupta<sup>1</sup>; Alex Stukowski<sup>2</sup>; Michael Baskes<sup>3</sup>; Srinivasan Srivilliputhur<sup>1</sup>; <sup>1</sup>University of North Texas; <sup>2</sup>Technical University of Darmstadt; <sup>3</sup>Los Alamos National Laboratory

We compare the deformation behaviour of gold single crystal nanoparticles with 6 ~ 30 nm diameters with that of gold spherical shells of varying inner to outer diameter ratios. Gold nanoparticles were modelled with an EAM potential and the indenter was described by repulsive potential. Yield strength dependence on sample size, geometry, and temperature was studied in these nanoparticles. Yield strength increases with increase in size from 6 nm to 20 nm and decreases after that until 30 nm. An increase in temperature lowers the yield strength in the nanoparticles, and the effect is more pronounced for larger radii. The deformation mechanism is aided by the continuous displacement burst accompanying dislocation escape from the nanoparticles. Based on this, a dislocation starvation mechanism has been discussed. Extended dislocations were found to be the prominent defect type. Spherical shell calculations are under way.

### 4:30 PM

**Two-Dimensional Discrete Dislocation Plasticity Incorporating Anisotropic Elasticity:** Siamak Shishvan<sup>1</sup>; Erik Van der Giessen<sup>2</sup>; <sup>1</sup>University of Tabriz; <sup>2</sup>University of Groningen

The modeling of discrete dislocation plasticity (DDP) has become a powerful tool to study the size-dependent behavior of materials and (sub) micron-size devices. By construction, plastic deformation in DDP is anisotropic, but almost all current implementations treat dislocations as line singularities in an isotropic elastic crystal. This unbalance in anisotropy originates from the fact that the three dimensional anisotropic elastic fields of a dislocation are extremely complex. Here we present a DDP method for two-dimensional problems, which relies on the fact that plane-strain plastic deformation of cubic crystals is possible in specific orientations when described in terms of edge dislocations on three effective slip systems. The long-range fields of such dislocations are known and recapitulated. To handle polycrystalline problems, we follow O'Day and Curtin in treating each grain as a separate plastic domain, and adopt superposition to determine the overall response taking into account the boundary conditions.

### 4:50 PM

**Frank Read Sources in the Continuum Theory of Dislocations:** Thomas Hochrainer<sup>1</sup>; Stefan Sandfeld<sup>2</sup>; Jochen Senger<sup>2</sup>; Peter Gumbsch<sup>1</sup>; <sup>1</sup>The Florida State University; <sup>2</sup>Karlsruher Institut fuer Technologie

Several small scale experiments revealed that size effects in plasticity are not always tied to strain gradients, but may also appear in largely homogeneous deformations, e.g. as in micro-compression tests. We recently introduced the continuum theory of dislocations which features natural boundary conditions, dislocation fluxes and source limitation. In the current paper we present the treatment of Frank-Read sources in this framework. We note that this approach properly accounts for the plastic slip introduced while forming a new loop from a source. Discrete dislocation dynamics simulations are used to deduce laws for the triggering of existing sources and for the creation of new sources from dislocation reactions. Small numerical examples illustrate the resulting microstructure evolution which is compared with DDD results.

### 5:10 PM

**A Discrete Dislocation Analysis of Size Effects on Void Growth in Single Crystals:** Shyam Keralavarma<sup>1</sup>; Javier Segurado<sup>2</sup>; Javier LLorca<sup>2</sup>; Ahmed Benzerga<sup>1</sup>; <sup>1</sup>Texas A&M University; <sup>2</sup>Polytechnic University of Madrid

The growth of sub-micron sized voids in single crystals is analyzed using discrete dislocation dynamics. A two dimensional plane strain analysis of self-similar square crystals containing circular voids in the center and subjected to uniaxial and biaxial deformation is performed. Edge dislocations, modeled as discrete points in two dimensions, move along well-defined slip systems and interact through their long range elastic



fields. Physics-based constitutive rules are implemented to model their short range interactions including junction formation and dynamic evolution of the source and obstacle population, allowing for an adequate representation of strain hardening. Two types of boundary conditions for dislocation slip are analyzed: (i) free boundaries simulating deformation of free-standing crystals and (ii) slip blocking at the boundaries to simulate the deformation of a grain in a polycrystal. We discuss possible micro-mechanisms for the observed size effects in the stress-strain response and the void growth rates.

### 5:30 PM Invited

**Dislocation Core Spreading in Gum Metals:** *Daryl Chrzan*<sup>1</sup>; Matthew Sherburne<sup>1</sup>; Yuranan Hanlumuang<sup>1</sup>; Tianshu Li<sup>2</sup>; John Morris<sup>1</sup>; <sup>1</sup>University of California Berkeley; <sup>2</sup>University of California Davis

The structure of dislocation cores in elastically anisotropic (nominally) BCC alloys is considered. A definition of the dislocation core radius based on linear elasticity theory and the ideal strength of a material is introduced. For screw dislocations in BCC crystals, the core radius so obtained scales inversely with  $(C_{11}-C_{12})^{-1/2}$ . The design criteria for the Ti-Nb alloys known as Gum Metals was aimed at driving  $(C_{11}-C_{12})$  towards zero. This has the immediate consequence that dislocation core radii in Gum Metals are driven towards infinity. The implications of the diverging dislocation core radii are explored using atomic scale calculations of dislocation core structures in Ti-V approximants to Gum Metal. The atomic scale structures predicted to arise from core overlap in TiV alloys are reminiscent of the nanodisturbances observed in Gum Metals. This research is supported by the National Science Foundation and Toyota Research and Development.

## Surfaces and Heterostructures at Nano- or Micro-Scale and Their Characterization, Properties, and Applications: Magnetic Heterostructures II - and - Energy and Catalysis Technologies I

*Sponsored by:* TMS Electronic, Magnetic, and Photonic Materials Division, TMS Materials Processing and Manufacturing Division, TMS: Nanomaterials Committee, TMS: Surface Engineering Committee

*Program Organizers:* Nitin Chopra, The University of Alabama; Ramana Reddy, The University of Alabama; Jiyoung Kim, Univ of Texas; Arvind Agarwal, Florida International Univ; Sandip Harimkar, Oklahoma State University

Tuesday PM Room: 31B  
March 1, 2011 Location: San Diego Conv. Ctr

*Session Chairs:* Nitin Chopra, The University of Alabama; Ramana Reddy, The University of Alabama

### 2:00 PM Invited

**Green Magnetic Energy: Mn(Bi,Al) Nanomagnets:** *Yang-Ki Hong*<sup>1</sup>; <sup>1</sup>University of Alabama

The figure of merit for permanent magnet is the maximum energy product (BH)<sub>max</sub> in the units of MGOe. Sintered Nd<sub>2</sub>Fe<sub>14</sub>B and SmCo magnets show high 64 and 28 MGOe of theoretical (BH)<sub>max</sub>, respectively. However, low operation temperature of NdFeB, which may lead to loss of machine power, and availability of rare-earth and transition elements are potential barriers to EV motor and other applications. Thus, aiming at developing high temperature magnets without rare-earth and transition elements, we have theoretically calculated the (BH)<sub>max</sub> for MnBi and t-phase MnAl alloys using density functional theory and modified Skomski's equation. Our calculations predict 20 MGOe (3.66 μB/f.u.; H<sub>k</sub> = 53 kOe) and 12.5 MGOe for MnBi and MnAl alloys, respectively. Accordingly, it is envisioned that core-shell MnBi-soft metal and MnAl-soft metal micro/nanoparticles will exhibit large remanent magnetization, thereby increasing the (BH)<sub>max</sub> to 51 MGOe and 53 MGOe for MnAl and MnBi core-shell nanoparticles, respectively.

### 2:30 PM

**HR-STEM Imaging and EELS Characterizing of Nano-Scale Defects in Sputter Deposited Thin Films of Double-Perovskite Sr<sub>2</sub>FeMoO<sub>6</sub> (SFMO):** *Robert Williams*<sup>1</sup>; Jeremy Lucy<sup>1</sup>; Rebecca Riccardo<sup>1</sup>; Patrick Woodward<sup>1</sup>; Fengyuan Yang<sup>1</sup>; Hamish Fraser<sup>1</sup>; Adam Hauser<sup>1</sup>; Manisha Dixit<sup>1</sup>; <sup>1</sup>The Ohio State University

Oxides are promising candidates in the emerging field of spintronics. Some oxide systems of interest include single perovskites such as SrTiO<sub>3</sub> (STO) and double perovskites such as Sr<sub>2</sub>FeMoO<sub>6</sub> (SFMO). The magnetic properties of these systems have been found to depend on the amount of disorder present as well as defects. The major challenge during processing is the obtaining of the necessary long-range order while preventing defect formation due to processing parameters. This requires structural and chemical characterization ranging from identification of defects and morphology as well as correlating microstructure-property relationships. For this work thin films of SFMO have been sputter deposited on STO with varying parameters and HAADF-STEM imaging and EELS analyses have been conducted using an aberration-corrected FEI Titan<sup>TM</sup>80-300 STEM to provide microstructural and chemical information. HAADF-STEM images of SFMO ordering are presented as well as characterization of interfacial defects. NSF Materials Research Science and Engineering Center (DMR-0820414).

### 2:45 PM Break

### 2:55 PM Introductory Comments for Energy and Catalysis Technologies

### 3:00 PM Invited

**High Efficiency Photolytic Nanostructures for Hydrogen Production:** *Kaan Kalkan*<sup>1</sup>; <sup>1</sup>Oklahoma State University

Conversion of sunlight to chemical fuels by artificial photosynthesis has been a long-sought goal. In particular, significant research activity was stimulated towards photolytic cells producing hydrogen in 1972, when Fujishima and Honda demonstrated water could be split into hydrogen and oxygen under sunlight (photolysis) using a light-absorbing semiconductor electrode. Since then, however, the development of efficient photolytic devices has been hindered by the challenge of meeting the following requirements all in one device: i) efficient channeling of photogenerated electrons and holes to redox reactions at the interfaces; ii) efficient absorption of sunlight; and iii) avoidance of photo-oxidation of the semiconductor electrode. The present work demonstrates a hydrogen generating photolytic device, which consists of a low band gap oxide semiconductor nanowire decorated with metal nanoparticles. The multifunctional (i.e., electronic, photonic, and plasmonic) nanowire-nanoparticle conjugates are synthesized via sol-gel and reduction chemistries, respectively. A quantum efficiency of 0.8 is measured for the photolysis.

### 3:30 PM Invited

**Visible Light Photoreduction of CO<sub>2</sub> Using Heterostructures of Nanocrystalline TiO<sub>2</sub> and Semiconductor Quantum Dots:** *Christopher Matranga*<sup>1</sup>; Congjun Wang<sup>1</sup>; Robert Thompson<sup>1</sup>; John Baltrus<sup>1</sup>; <sup>1</sup>US DOE - NETL

The design of photocatalysts for converting CO<sub>2</sub> into value-added chemicals and fuels is a critical area of research supporting our nation's development of new CO<sub>2</sub> management technologies. Historically, titanium oxide photocatalysts have been investigated for this application, however, the large band gap of this material limits it to the UV region of the solar spectrum and rapid charge carrier recombination can reduce this material's catalytic efficiency. We report on the use of heterostructures of semiconductor quantum dots (QDs), such as CdSe, with nanocrystalline TiO<sub>2</sub> for the photocatalytic reduction of CO<sub>2</sub>. These heterostructures simultaneously improve the visible light activity of this catalyst system and spatially separate the photogenerated charge carriers, thereby reducing recombination. Our results show that these heterostructures are capable of photoreducing CO<sub>2</sub> using only visible light ( $\lambda > 420$  nm) to produce CH<sub>4</sub>, CH<sub>3</sub>OH, and trace amounts of CO and H<sub>2</sub>.

#### 4:00 PM Invited

**Controlling Defect Density in Polymer-Fullerene Bulk Heterojunction Solar Cells by Optimizing Growth Conditions:** Kanwar Nalwa<sup>1</sup>; Rakesh Mahadevapuram<sup>1</sup>; Yuqing Chen<sup>1</sup>; Santosh Pandey<sup>1</sup>; *Sumit Chaudhary*<sup>1</sup>; <sup>1</sup>Iowa State University

Although promising, the performance of polymer:fullerene bulk-heterojunction solar cells is still limited by several factors including recombination at interfacial states. Hence, it is important to study and quantify the factors that govern the density of defects states (DODS). To understand the effect of growth rate on the DODS of poly(3-hexyl thiophene (P3HT) based solar cells, three types of P3HT:fullerene cells (A, B, and C) were fabricated with growth rate (solvent drying time upon spin coating) of ~ 40, 7 and 1 minutes, respectively. Capacitance and sub-band gap characterizations showed that slowest growth of device A led to reduction of DODS by an order of magnitude as compared to fastest grown device C. The slow growth assists the formation of self-organized ordered structure in the P3HT/fullerene blend system diminishing morphological defects. These observations were also confirmed by analysis of dark current-voltage curves.

#### 4:30 PM

**Photovoltaics Using Doped and Undoped Amorphous Silicon Heterojunctions with Conjugated Polymers:** Rakesh Mahadevapuram<sup>1</sup>; Kanwar Nalwa<sup>1</sup>; Vikram Dalal<sup>1</sup>; *Sumit Chaudhary*<sup>1</sup>; <sup>1</sup>Iowa State University

Polymer based photovoltaic (PV) technology is an exciting solar-electric conversion paradigm due to high extinction coefficient of polymers and low-cost manufacturability. Amorphous Silicon (a-Si:H) based solar technology is another emerging thin-film technology that promises to alleviate the cost issues of traditional crystalline Si based PVs. It is natural to think that marriage of a-Si:H and organics may open new avenues in PV device architecture. However, recent research efforts in this area are few and there is a need for in-depth analysis of Si-organic interfaces. In this direction, we fabricated polymer PVs in a bilayered configuration with a-Si:H, both doped and undoped. We observed that intrinsic a-Si:H based cells produced highest photocurrent; n-type a-Si:H based device shows highest fill factors implying efficient electron collection, whereas the p-type a-Si:H based device shows worst performance due to energy level mismatch. Detailed understanding of the Si/organic interfaces and future prospects will be presented.

#### 4:45 PM Invited

**Characterization and Modeling of 3D Photovoltaics:** *Jonathan Guyer*<sup>1</sup>; Daniel Josell<sup>1</sup>; <sup>1</sup>NIST

First generation (thick layers of crystalline silicon) and second generation (thin films of CdTe, CIGS, etc.) PV devices are both well established, with well defined techniques for fabrication and characterization. Third generation PV encompasses a wide diversity of materials and nanostructures and commercially viable technologies, and means of fabrication are yet to be determined. Many of the proposed structures have considerable microstructural variability that complicate interpretation of macroscopic device measures. We are developing idealized, three-dimensionally patterned templates that can serve as test structures to enable measurement of critical device and materials properties. Initial heterostructures are based around electrodeposited CdTe. To guide and interpret the experimental measurements we are developing open source models of carrier and light transport within arbitrary 2D and 3D device geometries. This talk will compare experimental measurements with simulation results and discuss how the model is used to guide new device geometries.

#### 5:15 PM Invited

**Engineering Carbon Nanomaterials for Energy Application:** *Wonhong Choi*<sup>1</sup>; <sup>1</sup>Florida International University

This talk will focus on engineering of carbon nanomaterials, carbon nanotubes (CNTs), and graphene for various applications in future energy. Particularly, the interfaces of CNT-CNT, CNT-substrate, graphene-substrate and graphene-CNT will be used to highlight the challenges towards energy applications. Our recent results of electrical functionality in carbon nanomaterials will be presented. Some of these results offer excellent opportunity to have high efficiency devices and systems, high efficiency

Li-ion battery based on interfacial controlled CNTs and flexible solar electrode based on large graphene structure. Our efforts on the strategies of manipulation of carbon nanomaterials interface and its characterization at nanoscale will be reviewed and critical issues will be discussed.

### Thermally Activated Processes in Plastic Deformation: Deformation Mechanisms and Polycrystal Plasticity

*Sponsored by:* The Minerals, Metals and Materials Society, TMS Materials Processing and Manufacturing Division, TMS/ASM: Computational Materials Science and Engineering Committee  
*Program Organizer:* Christopher Woodward, Air Force Research Laboratory

Tuesday PM  
March 1, 2011

Room: 1B  
Location: San Diego Conv. Ctr

*Session Chairs:* Dennis Dimiduk, Air Force Research Laboratory; Yoon-Suk Choi, UES Inc

#### 2:00 PM Invited

**High Energy X-Ray Diffraction Methods for Dynamic Characterization of Non-Linear Material Behaviors:** *Matthew Miller*<sup>1</sup>; <sup>1</sup>Cornell University

The current generation of engineering material behavior models has created an incredible challenge for the experimental characterization community. Traditional experiments are pre-deformation and post-mortem snapshots of microstructure coupled with macroscopic stress-strain behaviors. New high energy synchrotron x-ray diffraction tools, capable of structural and mechanical characterization on the grain and subgrain size scale, are currently coming online. This talk presents an overview of the current generation of experiments beginning with a general diffraction primer followed by specific descriptions of the classes of experiments that are currently available and soon coming online for quantifying microstructure and mechanical response at the size scale of the grain and below. The talk emphasizes the potential that exists for combined experiment/simulation methodologies. The establishment of a community around the diffraction experiment that would encourage and enable the mechanics community to move upstream, closer to the actual scattering event, is proposed.

#### 2:30 PM Invited

**Physics Based Single Crystal Deformation Material Modeling for Aerospace Applications:** *Alexander Staroselsky*<sup>1</sup>; Brice Cassenti<sup>2</sup>; <sup>1</sup>Pratt & Whitney; <sup>2</sup>University of Connecticut

In this presentation we discuss modeling of high temperature creep, plasticity, and fatigue using physics based crystal-plasticity methods. The work is focused on prediction of elastic-visco-plastic response of Ni-based superalloys using finite element methods. Damage accumulation causes tertiary creep and shear localization around local concentrators, which is essential for airfoil life prediction. We analyze the relative importance of each of the damage modes at different temperatures and stress levels. A computational transient thermal analysis of a turbine airfoil provides the illustration of the TMF/LCF life prediction for different engine operating conditions such as rotor speed, compressor discharge pressure, turbine inlet temperature and pressure at different mission points such as take-off, climb, end-climb, cruise and descent. We close the presentation by reviewing the current status of physics based FE modeling from the perspective of aerospace industry and discuss the current challenges in validation and modeling development.

#### 3:00 PM Invited

**Modeling the Orientation Dependence and Nonlinearity in the Creep of Single Crystal Superalloys Using a Semi-Mechanistic Approach:** *Y. Sun*<sup>1</sup>; <sup>1</sup>Rolls Royce

This paper will demonstrate the role of creep and rupture of single crystal superalloys in life models for gas turbine engine airfoils and the use of a

semi-mechanistic approach for modeling the orientation dependence and nonlinearity of creep. In a turbine engine deformation by creep is responsible, not just for failure by rupture, but also for the forces that drive fatigue crack initiation and propagation at stress risers. In the semi-mechanistic approach creep is modeled using strain-hardening and strain-rate sensitivity. The approach gives a single, explicit solution for the creep strain that covers the primary "steady-state" and tertiary stages of creep. Orientation dependence is addressed through the anisotropy in the work hardening rate and slip multiplicity. The model is applied to CMSX-4 single crystals and is shown to provide good representation of the orientation dependence of creep and rupture in this material as well as single crystal superalloys in general.

### 3:30 PM

**Local Strain Accommodation in Polycrystalline Ni-Base Superalloys:** *Jennifer Walley*<sup>1</sup>; Robert Wheeler<sup>2</sup>; Michael Uchic<sup>3</sup>; Michael Mills<sup>1</sup>; <sup>1</sup>The Ohio State University; <sup>2</sup>UES; <sup>3</sup>Air Force Research Laboratory

A new in-situ experimental methodology was used to characterize local strain heterogeneities in nickel-based superalloys that have relatively fine grain size (Dave < 50 μm). Initial work was performed on Rene 104 that was heat treated to produce two sets of samples with similar grain size distributions, but different γ distributions and grain boundary morphologies. One sample set has planar boundaries and a bimodal γ distribution, the other has serrated boundaries and a trimodal γ distribution. Quasi-isostatic tensile tests were performed at elevated temperatures in a scanning electron microscope, with images acquired at regular strain intervals. Samples were processed prior to testing using electron beam lithography techniques to produce a suitable speckle pattern to facilitate local strain analysis by digital image correlation techniques using Correlated Solutions VIC-2D software. The initial data indicates that interesting strain heterogeneities develop and correlate with grain size, orientations, and boundary relationships between the tensile axis and other boundaries.

### 3:50 PM

**Comparison of Deformation Mechanisms for Constant Strain Rate and Creep Testing of a Ni-Based Superalloy:** *Hallee Deutchman*<sup>1</sup>; Patrick Phillips<sup>1</sup>; Michael Mills<sup>1</sup>; <sup>1</sup>The Ohio State University

The effect of strain rate on deformation mechanisms was investigated under creep and constant strain rate conditions on an advanced polycrystalline Ni-based disk superalloy. A detailed microstructure characterization aimed at measuring the gamma-prime precipitate size, morphology, distribution, as well as grain size and degree of grain boundary serration, was performed prior to mechanical testing experiments so that the effects of microstructure can be correlated with the deformation response. Constant load creep tests and constant strain rate tests were performed at the same temperature so that the influence of strain rate on deformation substructure can be assessed. Following mechanical testing, a thorough TEM characterization study was done to determine the operative deformation mechanisms. Significant differences have been observed with dislocation-mediated mechanisms at higher strain rates and microtwinning and faulting of precipitates at low strain rates. Funding for this work has been provided by AFOSR through the Metals Affordability Initiative (MAI) program.

### 4:10 PM Break

### 4:25 PM Invited

**Challenges in the Micromechanical Modelling of Hot Deformation:** *David Dye*<sup>1</sup>; Nicholas Jones<sup>1</sup>; <sup>1</sup>Imperial College

Micromechanical models, both self-consistent homogenization schemes (see the Tome symposium at this meeting) and spatially-explicit crystal plasticity FE, have developed rapidly over recent years. The methods are briefly introduced and some popular underlying single crystal flow rules examined, along with their application to room temperature deformation. Hot deformation presents additional challenges, as the microstructure evolves under the influence of defects such as dislocation networks. This evolving microstructure often dominates the flow behaviour. Examples include recrystallisation, the break-up of precipitates, hard body rotation and phase evolution. Of particular interest is the rapidly evolving ability to examine

these processes in situ using diffraction techniques and microscopy, with time resolutions of ~1ms now becoming achievable. Thus, it is now possible to imagine developing micromechanics models that go beyond empirical flow rules. Examples from nickel superalloys, from beta, alpha-beta and near-alpha Ti alloys, from TWIP steels and from Zry-4 will be examined.

### 4:55 PM

**Thermal Aging of IN718Plus Superalloy and Relaxation of Laser Shock Peened Residual Stresses:** *Vibhor Chaswal*<sup>1</sup>; S. Mannava<sup>1</sup>; Dong Qian<sup>1</sup>; Vijay Vasudevan<sup>1</sup>; Kristina Langer<sup>2</sup>; <sup>1</sup>University of Cincinnati; <sup>2</sup>Air Force Research Laboratory

Thermal aging is conducted on as-received IN718Plus aeroengine superalloy at 923K, 973K, 1023K, 1073K up to 1000h under ambient conditions to replicate in service exposure and on laser shock peened (LSP) coupons at 973K to investigate operative stress relaxation mechanisms. Microstructural evolution of gamma prime precipitates and eta-Ni3Ti is investigated using transmission electron microscopy and convergent beam electron diffraction. Based on quantitative measurements and image analysis, gamma prime coarsening is found to follow LSW kinetics with average activation energy of 318 kJ/mol. At smaller precipitate sizes, higher activation energy is observed and a procedure for goodness of data is arrived at employing Johnson Mehl Avrami formulation. At longer aging, gamma prime transforms to hexagonal eta-Ni3Ti involving a faulting mechanism. Up to 50% thermal relaxation of residual stresses was measured between LSP treated and LSP+Aged samples using both conventional and synchrotron x-ray diffraction techniques. Results are correlated with dislocation substructure and dislocation-precipitate interactions involved.

### 5:15 PM

**Localized Deformation during Macroscopically Uniform Plastic Flow of a Dynamically Strain Aging Alloy:** *R. Storer*<sup>1</sup>; M. Lebyodkin<sup>2</sup>; P. Kurath<sup>1</sup>; A. Beaudoin<sup>1</sup>; C. Fressengeas<sup>2</sup>; <sup>1</sup>University of Illinois at Urbana Champaign; <sup>2</sup>Universite Paul Verlain-Metz/CNRS

Dynamic strain aging presents a competition between the interaction of solute atoms with dislocations and plastic strain rate, through the thermal breakaway of dislocations from obstacles. The Portevin - Le Chatelier (PLC) effect presents evidence of the collective dislocation activity in the presence of dynamic strain aging: continuously propagating and hopping bands are vivid examples of plastic bursts at sample length scale, with allied serrations in the stress-time curve. Closer study, through digital image correlation and analysis of (small) transients in the stress response, suggests that dislocation-solute interaction extends to regimes of "uniform" plastic response. The present effort provides an experimental study of an Al-Mg alloy, with spatio-temporal resolution sufficient to reveal patterns of localized deformation with stress transients much less than those typically associated with the PLC effect.

### 5:35 PM

**Comparative Hot-Work Constitutive Analyses of Carbon/HSLA and Stainless Steels with Linkage to Microstructural Evolution:** *Hugh McQueen*<sup>1</sup>; Yong Li<sup>1</sup>; I. Rieiro<sup>2</sup>; M. Carsi<sup>3</sup>; O. Ruano<sup>3</sup>; <sup>1</sup>Concordia University; <sup>2</sup>Universidad de Castilla-La Mancha; <sup>3</sup>Centro Nacional de Investigaciones Metalúrgicas

Constitutive analysis (Garofalo's sinh equation) for torsion test peak stresses of 0.29C, 0.15V steel over 850-1200°C, 0.6-30/s was conducted by an integrated automatic program (RCR) without pre-specifying any empirical constants. Here the tuning data has been analyzed using the traditional practice of selecting stress multiplier (SM) values previously employed for C/HSLA steels; this allows plotting data on common graphs to compare changes including Q due to composition. Although the activation energies Q vary very little, the RCR method predicted the stresses beyond the tuning set extremes. The similarities confirm that the RCR results can be linked to the previously derived flow curve models and to the related microstructural evolution determined optically and substructures (SEM-EBS, TEM of austenitic stainless steels). In turn the structures can be related to magnetically measured rates of transformation to ferrite and to bainite.



5:55 PM

**A Crystalline Law for Thermally Activated Plastic Deformation:** *Ghiath Monnet*<sup>1</sup>; <sup>1</sup>EDF

Based on Dislocation Dynamics (DD) simulations in iron at low temperature, we propose constitutive equations providing the strain rate intensity on a given slip system as a function of the shear stress, temperature, obstacle density and strength. The model differs from the Kocks-Mecking formalism in the sense that strengthening is not always conditioned by applied work against the dislocation line tension. In this model the kink-pair kinetics is integrated into the flow rule. DD simulations show that the difference in mobility between dislocations of different characters induces a strong curvature on non-screw dislocations, leading to a significant decrease in the interaction strength. Depending on the obstacle nature and concentration, two strengthening components may prevail: one is due to the decrease of the average length of screw dislocation segments and the other appears only when all dislocations, including screw dislocations, are curved under the effect of the applied stress.

# NOTES

TUESDAY PM

## 2011 Functional and Structural Nanomaterials: Fabrication, Properties, Applications and Implications: Ultra-Fine Grained Materials II

*Sponsored by:* The Minerals, Metals and Materials Society, TMS Electronic, Magnetic, and Photonic Materials Division, TMS: Nanomaterials Committee

*Program Organizers:* Jiyoung Kim, Univ of Texas; David Stollberg, Georgia Tech Research Institute; Seong Jin Koh, University of Texas at Arlington; Nitin Chopra, The University of Alabama; Suveen Mathaudhu, U.S. Army Research Office

Wednesday AM                      Room: 8  
March 2, 2011                      Location: San Diego Conv. Ctr

*Session Chair:* Suveen Mathaudhu, U.S. Army Research Laboratory

### 8:30 AM Introductory Comments

#### 8:35 AM Invited

**SPD-Processed Nanostructured Metals for Innovative Applications:** *Ruslan Valiev*<sup>1</sup>; *Georgy Raab*<sup>1</sup>; *Maxim Murashkin*<sup>1</sup>; *Nail Zaripov*<sup>1</sup>; <sup>1</sup>Ufa State Aviation Technical University

Among main requirements for application of nanostructured metals and alloys as advanced functional and structural nanomaterials, one should emphasize their bulk form (rods, wires or sheets) for fabrication of different articles and parts. Secondly, nanometals should possess enhanced properties. In the paper we report new results of our R&D works showing that the use of severe plastic deformation (SPD) techniques allows one to meet these requirements. For this goal equal-channel angular pressing (ECAP) and its recent modifications were used, which allowed to produce rods and wires out of a number of commercial alloys. By changing SPD processing regimes we could also control the nanostructural features of the processed materials. The report also provides examples of successful realization of these principles applied to several commercial Al and Ti alloys and steels for enhancement of their properties. The first pilot articles for innovative applications in medicine and engineering are presented as well.

#### 9:05 AM Invited

**Understanding the Role of Interfaces in the Deformation of Lamellar Nanocomposites Fabricated via Severe Plastic Deformation Techniques:** *Irene Beyerlein*<sup>1</sup>; *Jian Wang*<sup>1</sup>; *Ruifeng Zhang*<sup>1</sup>; *Nhon Vo*<sup>2</sup>; *Pascal Bellon*<sup>2</sup>; *Robert Averback*<sup>2</sup>; *Anthony Rollett*<sup>3</sup>; *Nathan Mara*<sup>1</sup>; <sup>1</sup>Los Alamos National Laboratory; <sup>2</sup>University of Illinois; <sup>3</sup>Carnegie Mellon University

In this work, we study the evolution and role of hetero-phase interfaces in slip and twinning in nanolayered composites during severe plastic deformation. The composite systems studied consisted of two immiscible metals, Ag-Cu or Cu-Nb, wherein the individual phases are submicron to nanometer in scale, and the interfacial content is high. Through a variety of modeling techniques, we have found that changes in the texture and interface crystallography after SPD can be explained based on the predominance of slip in the case of Cu-Nb or the predominance of twinning in the case of Cu-Ag. Polycrystal modeling is employed to predict bulk microstructural properties, such as texture, while atomistic and dislocation-density-based models are applied to study the interactions between the interface and lattice glide and twinning dislocations. Experimental results are interpreted in these models in terms of the influence of interface crystallography on the nucleation of both lattice and twinning dislocations.

#### 9:35 AM

**On the Hall-Petch Contribution in a Bulk Nanostructured Al-4Cu Alloy:** *Shanmugasundaram Thangaraju*<sup>1</sup>; *Martin Heilmaier*<sup>1</sup>; *Subramanya Sarma*<sup>2</sup>; *B.S. Murty*<sup>2</sup>; <sup>1</sup>Technical University Darmstadt; <sup>2</sup>Indian Institute of Technology Madras

Bulk nano-crystalline (NC) materials produced by powder metallurgy show very high strength and follow the Hall-Petch (HP) relation but with both, a higher HP slope and frictional stress as compared to their coarse

grained counterparts. In view of this, considering only the experimentally measured yield strength for evaluating the strength-grain size correlations may not be appropriate to determine HP constants for the original mechanism of grain boundary dislocation pile-up. In the present study, Al-4Cu alloys with grain sizes from 47 to 105 nm (synthesized by mechanically alloying followed by vacuum hot pressing at different temperatures) were deformed at room temperature to study the Hall-Petch relation: the analysis revealed a high frictional stress (170 MPa) and a high positive slope (0.13 MPavm) as compared to pure Al. From a detailed evaluation of the different strengthening mechanisms it is inferred that the oxide particles are the likely reason for these high values.

#### 9:50 AM

**Direct Production of Sheet from Alloys of Limited Workability Using Machining-Based Processes:** *Wilfredo Moscoso*<sup>1</sup>; *Mert Efe*<sup>1</sup>; *Dale Compton*<sup>1</sup>; *Kevin Trumble*<sup>1</sup>; *Srinivasan Chandrasekar*<sup>1</sup>; <sup>1</sup>Purdue University

Large Strain Extrusion Machining (LSEM), a constrained chip formation SPD process, is demonstrated as a method for producing ultrafine grained sheet/foil from alloys of limited workability. By appropriate choice of tool geometry and deformation rate, the hydrostatic pressure, temperature and shear strain in the deformation zone are set, locally, such that metals that would otherwise be difficult to work show significant formability, with minimal or no pre-heating. The process is illustrated using the production of sheet/foil directly from cast alloys (e.g., Cu, brass), and alloys with limited slip systems operative at room temperature (e.g., Mg AZ31). The mechanics underlying the process is also explored both theoretically and experimentally.

#### 10:05 AM Break

#### 10:20 AM Invited

**Ductility and Strategies for Improving Ductility of Bulk Nanostructured Materials:** *Yonghao Zhao*<sup>1</sup>; *Enrique Lavermia*<sup>1</sup>; <sup>1</sup>University of California, Davis

The limited ductility of bulk nanostructured materials has emerged as an important obstacle to widespread application of bulk nanostructured materials, despite their other attributes, such as ultra high strength levels, in some cases. This talk will first analyze the intrinsic and extrinsic reasons for the low ductility of the bulk nanostructured materials, and then summarize effective strategies for improving the poor ductility of bulk nanostructured materials. Finally we report on recent successful results by applying some of these strategies in nanostructured 7075 Al, NiFe, Ni to obtain both high strength and ductility.

#### 10:50 AM

**Grain Boundary Segregation of Carbon and Formation of Nanocrystalline Iron-Carbon Alloys by Ball Milling:** *Reiner Kirchheim*<sup>1</sup>; *Yuzeng Chen*<sup>1</sup>; *Andreas Herz*<sup>1</sup>; <sup>1</sup>University of Goettingen

According to a novel DEFECTANT (DEFect ACTing AgeNT) concept, attractive interaction between solute atoms and defects lowers defect energies which is a generalization of Gibbs Adsorption Isotherm. Thus synthesizing nanocrystalline (NC) material by severe plastic deformation is described by a reduced energy of dislocation and grain boundary (GB) formation in the presence of defectants. The iron-carbon system was chosen as a model system where carbon acts as the defectant. Iron powders mixed with different amount of carbon were ball milled to prepare NC iron-carbon alloys with different carbon concentrations (C0). The microstructures of the powders were examined by means of transmission electron microscopy and X-ray diffraction. The results indicated that once the saturation of GBs is achieved, the grain size of the NC iron-carbon powders will be strongly dependent on C0 described by the assumption of zero grain boundary energy and partitioning of carbon between grains and their boundaries.

11:05 AM

**Investigation of Mechanical Properties of Silica/Epoxy Nano-Composites by Molecular Dynamics and Finite Element Modeling:** *Bohayra Mortazavi<sup>1</sup>; Julien Bardon<sup>1</sup>; Said Ahzi<sup>2</sup>; David Ruch<sup>1</sup>; <sup>1</sup>Centre de Recherche Public Henri Tudor; <sup>2</sup>University of Strasbourg*

Materials filled with particles of at least one dimension in the nanosize range are of high interest in numerous areas, such as structural adhesive applications. Inorganic nanoparticles incorporation can impart attractive properties in epoxy matrices by increasing its stiffness and its thermal resistance, among other properties. In this study Molecular Dynamics (MD) and Finite Elements (FE) modeling were performed in order to study the mechanical properties of nano-composites obtained from silica nanoparticles incorporation into an epoxy polymer. To this aim, MD modeling of tensile test was carried out to obtain the elastic modulus and Poisson's ratio of an alfa quartz silica crystal. In a next step, the 3-dimensional FE model of Representative Volume Element (RVE) of the nano-composite was developed by introducing the materials properties of silica obtained by MD simulations. Finally, the validity of the used technique was discussed by comparing the obtained results with experimental measurements.

11:20 AM

**Mechanical Properties and Microstructure Evolutions of Ultrafine-Grained Al during Recovery via Annealing:** *Yonghao Zhao<sup>1</sup>; Tory Topping<sup>1</sup>; John Bingert<sup>2</sup>; Y. Li<sup>1</sup>; Peiling Sun<sup>3</sup>; Xiaozhou Liao<sup>4</sup>; Yuntian Zhu<sup>5</sup>; Enrique Lavernia<sup>1</sup>; <sup>1</sup>University of California, Davis; <sup>2</sup>Los Alamos National Laboratory; <sup>3</sup>Feng Chia University; <sup>4</sup>The University of Sydney; <sup>5</sup>North Carolina State University Raleigh*

Ultrafine grained (UFG) metals and alloys usually have mechanical and thermal instabilities which limit their practical engineering applications. Annealing is a simple and effective way to regain strain hardening and stabilize UFG structures. In this work, we systematically investigated the mechanical properties and microstructural evolutions of UFG Al during recovery. In details, we found that low-temperature annealing at 250 °C for 20 min increases ultimate strength from 190 to 208 MPa by 10 % and tensile ductility from 4.5 to 6.8 % by 50 % without changing yield strength. Microstructural analyses indicate that upon annealing the average grain size increases from 740 to 840 nm, dislocation density decreases from 5 to 10<sup>14</sup> m<sup>-2</sup>, while the GB type was not changed. Moreover, annealing changes statistically stored dislocations to low-energy dislocation wall (subgrain boundaries). The mechanical properties evolution upon annealing was finally rationed based on the microstructural evolutions, fracture and deformation mechanisms.

11:35 AM

**Microstructural Evolution of 316L Stainless Steel during ECAP Process:** *Suk Hoon Kang<sup>1</sup>; Hyung-Ha Jin<sup>1</sup>; Jinsung Jang<sup>1</sup>; Do Hyun Kim<sup>2</sup>; Kyu Hwan Oh<sup>2</sup>; Xinghang Zhang<sup>3</sup>; David Foley<sup>3</sup>; Karl Hartwig<sup>3</sup>; <sup>1</sup>Korea Atomic Energy Research Institute; <sup>2</sup>Seoul National University; <sup>3</sup>Texas A&M University*

316L stainless steel samples with 1 x 1 x 6 inch in size were processed by equal channel angular pressing (ECAP) to develop a nano grain microstructure with a higher fraction of coherent site lattice (CSL) boundaries. Two different paths of ECAP were applied, and the corresponding microstructure evolutions were studied using electron backscattered diffraction (EBSD) and transmission electron microscopy (TEM). The results indicate that the shear band has an inclination of about 45 degree from the shear direction; as the more shear deformation is given to the sample material, the shear band width becomes narrower and the grains are more aligned to shear band direction. In the meantime, large amounts of secondary twin boundaries were developed within the shear deformed grains, and the boundaries alignment appeared to have orientation a relationship with the initial twin patterns and also with the shear band direction.

11:50 AM

**Microstructure Characterization of Grain Boundaries in Al 5083/B4C Ultrafine Grained Composites:** *Ying Li<sup>1</sup>; Zhihui Zhang<sup>1</sup>; Rustin Vogt<sup>1</sup>; Enrique Lavernia<sup>1</sup>; Julie Schoenung<sup>1</sup>; <sup>1</sup>University of California Davis*

The purpose of this study was to characterize the grain boundaries in Al 5083/B4C ultrafine grained composites fabricated by cryomilling, degassing, cold isostatic pressing and extrusion. The grain boundaries in the ultrafine-grained (UFG) and coarse-grained (CG) Al 5083 regions, and the interfaces between the UFG and CG regions, were investigated by transmission electron microscopy (TEM), high resolution TEM (HRTEM), energy dispersive X-ray spectroscopy (EDX), electron energy loss spectroscopy (EELS) and energy filtered TEM (EFTEM) method. High/low angle grain boundaries, equilibrium and non-equilibrium grain boundaries, elemental segregation and dislocation storage at the grain boundaries were studied in detail. The coincidence site lattice model was also used to analyze the grain boundaries.

12:05 PM Concluding Comments

## 2nd International Symposium on High-Temperature Metallurgical Processing: Treatment of Metals and Pellets

*Sponsored by:* The Minerals, Metals and Materials Society, TMS Extraction and Processing Division, TMS: Pyrometallurgy Committee, TMS: Energy Committee

*Program Organizers:* Jiann-Yang Hwang, Michigan Technological University; Jerome Downey, Montana Tech; Jaroslaw Drelich, Michigan Technological University; Tao Jiang, Central South University; Mark Cooksey, CSIRO

Wednesday AM  
March 2, 2011

Room: 18  
Location: San Diego Conv. Ctr

*Session Chairs:* Jeffrey Schoonover, GE Global Research; Stephen Kampe, Michigan Technological University

8:30 AM

**The Production of LaB<sub>6</sub> by "Hot-Powder" CVD and Subsequent Milling:** *Duygu Agaogullari<sup>1</sup>; Özge Balci<sup>1</sup>; Ismail Duman<sup>1</sup>; <sup>1</sup>Istanbul Technical University*

In this study, LaB<sub>6</sub> were synthesized by a combined method of gas phase reduction of BCl<sub>3</sub> with H<sub>2</sub> on the substrates of fine La grains and high-energy ball milling. An externally heated horizontal quartz tube was used as reactor. Gas mixtures were passed through the reactor at the temperature ranges of 800 to 1000 °C with a 1/4 BCl<sub>3</sub>/H<sub>2</sub> molar ratio, where Ar was used as carrier gas. La particles were reacted with deposited boron on their contact surfaces. Subsequently, mechanical alloying was carried out to the coated powder with a duration of 30 minutes. Products were characterized by using X-ray diffraction technique (XRD) and scanning electron microscope (SEM). The purity was determined by Atomic Absorption Spectrometer (AAS). The exhaust gases were analyzed by Fourier Transform Infrared Spectroscopy (FTIR).

8:50 AM

**Fundamentals of Spark-Plasma Sintering: Net-Shaping and Size Effects:** *Eugene Olevsky<sup>1</sup>; Evan Khaleghi<sup>1</sup>; Cristina Garcia<sup>1</sup>; William Bradbury<sup>1</sup>; Randall German<sup>1</sup>; Cnris Haines<sup>2</sup>; Darold Martin<sup>2</sup>; Deepak Kapoor<sup>2</sup>; <sup>1</sup>San Diego State University; <sup>2</sup>US Army ARDEC*

Spark-plasma sintering is an emerging powder consolidating technique which provides significant advantages to the processing of materials into configurations previously unattainable. Net-shaping capabilities and size effects on spark-plasma sintering are analysed both theoretically and experimentally. Modeling and experimentation are conducted for cylindrical, prismatic, and complex powder specimen shapes. The impact of the shape and size factors on the non-uniformity of electric current density, temperature, relative density, and grain size spatial distributions is analysed.

WEDNESDAY AM



The modeling includes the novel constitutive concept of spark plasma sintering and the finite-element analysis with coupled electrical, thermal, and mechanical boundary conditions. The modeling results are compared to the experimentally obtained data on the spark plasma sintering of conductive and non-conductive powder-based specimens of various shapes and sizes. The conducted research indicates the promising capabilities and addresses the challenges of spark-plasma sintering of complex-shape parts.

#### 9:10 AM

**Microwave Brazing of Gas Turbine Components:** *Jeffrey Schoonover*<sup>1</sup>; Laurent Cretegnny<sup>1</sup>; <sup>1</sup>GE Global Research

Microwave heating was investigated for braze repair of gas turbine components such as shrouds and nozzles. A novel process using a ceramic susceptor and a locally-generated plasma was developed to selectively heat and melt the braze material while keeping the component relatively cool. Epitaxial growth of braze metal on a monocrystalline substrate was demonstrated. An advantage of this energy efficient process over conventional brazing is that parent or near-parent braze compositions may be locally melted to fill a crack while the component remains below the recrystallization temperature, resulting in improved braze joint properties.

#### 9:30 AM

**Spark Plasma Sintering of Tantalum Carbide:** *Evan Khaleghi*<sup>1</sup>; <sup>1</sup>San Diego State University

A tantalum carbide powder was consolidated by spark plasma sintering. The specimens were processed under various temperature and pressure conditions and characterized in terms of relative density, grain size, hardness, and rupture strength (measured using a novel measurement technique). The results are compared to hot pressing conducted under similar settings. It is shown that high densification is accompanied by substantial grain growth. Carbon nanotubes were added to mitigate grain growth; however, while significantly increasing specimens' rupture strength and final density, they had little effect on grain growth.

#### 9:50 AM

**Heats of Reaction in the Formation of TiB<sub>2</sub> Reinforced Titanium Aluminide Composites:** *Andrew Baker*<sup>1</sup>; Stephen Kampe<sup>1</sup>; Tony Zahrah<sup>2</sup>; <sup>1</sup>Michigan Tech; <sup>2</sup>Matsys Inc.

Reaction synthesis is a technique to produce ceramics, intermetallics, and in-situ composite materials. The technique, and the resulting microstructures of the product, rely upon a large enthalpy reduction during the reaction, and also the relatively high temperatures that are characteristic of the process. This research presents experimental heats of reaction for the formation of various volume relative proportions of TiB<sub>2</sub>-reinforced titanium aluminide composites utilizing bomb calorimetry. To overcome the kinetic constraints and achieve ignition in these formulations, a boron (B)/potassium nitrate (KNO<sub>3</sub>) initiation aid was incorporated within the blended reactant compact. The heat contribution from the initiation aid was regressed to provide estimates of the heat of reaction of the nominal formulations. Powder x-ray diffraction was utilized to identify the products of the reaction and discern any differences between the predicted equilibrium products from formulation and the actual products.

#### 10:10 AM

**A Path Planning Study of Multi-pass Heat Treatment using High Power Direct Diode Laser:** *Soundarapandian Santhanakrishnan*<sup>1</sup>; Radovan Kovacevic<sup>1</sup>; <sup>1</sup>Southern Methodist University

This study is focused on the development of a coupled finite element (FE) thermo-kinetic (TK) phase transformation model to minimize tempering effect of multi-pass laser heat treatment (MPLHT) process. The model predicts the temperature history, phase transformations, and the hardness of MPLHT process. A 2-kW high power direct diode laser (HPDDL) of 808 nm in wavelength is used to heat treat the tool steel AISI S7 by changing the laser power and scanning speeds while keeping a constant size of overlap. The tempering effect of the MPLHT process is studied for different lengths of scan. The numerical results are experimentally evaluated to study the

effect of length of scans on the variation of tempering temperature, phase transformations and the change of hardness.

#### 10:30 AM

**Hot Workability of 1.2690 Ledeburitic Tool Steel and Development Of Microstructure:** *Milan Terceelj*<sup>1</sup>; Goran Kugler<sup>1</sup>; <sup>1</sup>University of Ljubljana, NTF-OMM

The 1.2690 high alloyed tool steel is usually applied for cold working and is alloyed with carbide-forming elements Cr, V, W and Mo. It exhibits very poor hot deformability. Since there is no enough available data in literature for elucidation of this problem, hot workability and development of microstructure during hot deformation was studied. Hot compression tests were carried out in temperature range 850-1200°C and strain rates range 0.001-6s<sup>-1</sup>. SEM and OM were used for observation of microstructure. Results revealed very complex precipitation of carbides that depends on deformation temperature as well as on strain rate. It was found that especially at lower temperatures of hot working range the precipitation of carbides strongly depends on strain rate. Three different hot deformation behaviours were observed depending on temperature and strain rate range.

#### 10:50 AM

**Effect of TiO<sub>2</sub> on the Conduction Heat Transfer of Mold Flux:** *Xuemei Qing*<sup>1</sup>; *Bing Xie*<sup>1</sup>; Jiang Diao<sup>1</sup>; <sup>1</sup>Chongqing University

Based on non-stationary hot wire method, a testing device was established, and the lattice conductivities of the mold fluxes which have different integration basicity (0.9, 1.1, 1.3) and different TiO<sub>2</sub> content (0~8%) were measured at different temperatures (400~1300°C) by this mechanism. The results showed that when the TiO<sub>2</sub> content was held constant, the lattice conductivities of the mold fluxes increased with the basicity increased, and when the basicity remained constant, the lattice conductivities of the mold fluxes decreased with the increase of the content of TiO<sub>2</sub>. At the same time, the lattice conductivities of all the mold fluxes increased firstly and decreased afterward with increasing the temperature from 400°C to 1300°C, and the peak value always appeared at 700°C to 800°C. XRD results showed that CaTiO<sub>3</sub>, Ca(Si<sub>1.5</sub>Ti<sub>0.5</sub>)O<sub>5</sub>, Ca<sub>2</sub>Ti<sub>5</sub>O<sub>12</sub> were precipitated after adding TiO<sub>2</sub>, and these phases will decrease the conduction heat transfer ability of the mold flux in various degree.

#### 11:10 AM

**Flow Stress and Microstructural Evolution during Single and Double Hit Isothermal Forging of Waspaloy:** *Ahmad Chamanfar*<sup>1</sup>; Mohammad Jahazi<sup>1</sup>; Javad Gholipour<sup>2</sup>; Priti Wanjara<sup>2</sup>; Stephen Yue<sup>3</sup>; <sup>1</sup>AMTC-IAR-NRC and McGill University; <sup>2</sup>AMTC-IAR-NRC; <sup>3</sup>McGill University

The high temperature deformation behavior of the nickel-base superalloy, Waspaloy, using single and double hit isothermal compression testing was investigated at 1373 K (1100°C), above the  $\gamma'$  solvus, and constant strain rate of 0.01 s<sup>-1</sup>. For single hit deformation, the applied strain was 0.84 and for double hit compression, the strain per pass and inter pass time were respectively 0.42 and 60 seconds. Flow softening and microstructure investigation indicated that dynamic recrystallization (DRX) took place during deformation in the single hit compression and each pass of the double hit compression. Furthermore, about 15% flow stress relaxation was observed in the second pass of the double hit compression because meta-dynamic recrystallization (MDRX), static recrystallization (SRX) and grain growth occurred during the inter pass time. The solution heat treatment at 1373 K for 15 minutes conducted before starting the deformation, resulted in full dissolution of  $\gamma'$  precipitates and grain growth from 10  $\mu$ m to 173  $\mu$ m. The incidences of MDRX, SRX and grain growth during inter pass time in the double hit deformation led to an increase of the DRX grain size from 24  $\mu$ m to 60  $\mu$ m.

11:30 AM

**Effects of Binders on Oxidized Pellets Preparation from Vanadium/Titanium-Bearing Magnetite:** Guihong Han<sup>1</sup>; Yuanbo Zhang<sup>1</sup>; Yanfang Huang<sup>1</sup>; Zengqing Sun<sup>1</sup>; Guanghui Li<sup>1</sup>; *Tao Jiang<sup>1</sup>*; <sup>1</sup>School of Minerals Processing & Bioengineering, Central South University

Because of small specific surface area and poor ballability, vanadium/titanium-bearing magnetite is difficult for production of oxidized pellet. A novel organic copolymer binder, modified humic acid (MHA), has been authorized recently in China. Effects of the novel MHA binder on the quality of V/Ti-bearing magnetite pellets are studied in this research. Experimental results show the MHA binder can obviously improve the strength of green pellet. Because of better heat endurance, the MHA binder pellet has a higher strength than Peridur pellet under the same preheating conditions. Moreover, TFe grade of pellet with the MHA binder is much higher than that of the bentonite pellet. The strength of preheated pellet containing MHA binder of 0.25%~1.0% meets the requirements of oxidized pellet production by grate-kiln process. Comparatively, MHA is a promising organic binder for iron ore pellets, the price of which is only one tenth as that of Peridur and about 3 times as that of bentonite.

11:50 AM

**Constituents and Porosity of Lead Concentrate Pellets Produced in the Trepcë Plant:** *Ahmet Haxhija<sup>1</sup>*; Jaroslaw Drellich<sup>2</sup>; <sup>1</sup>University of Pristina; <sup>2</sup>Michigan Technological University

Porosity of pellets is one of the main parameters in reductive melting process in water-jacket furnace during the roasting of sulfide lead concentrate in a smelter located in Trepcë. Roasting is done at about 900°C, for pellets which are composed of PbS, CaCO<sub>3</sub>, Fe<sub>2</sub>O<sub>3</sub>, and SiO<sub>2</sub>. In order to facilitate the formation of slag in the reductive melting, the pellets must have proper content of CaO, SiO<sub>2</sub>, and FeO, and porosity. Pellets with porosity of 18% do not melt adequately in the water-jacket furnace. The optimal porosity for pellets melting was found to be 35-55% and is achieved with loading of pellets with more than 10 wt.% CaO. The pellets with less than 10% CaO have not enough pores for the gasses to penetrate their entire structure. The composition of the pellets must satisfy the ratio of CaO : SiO<sub>2</sub> : FeO = 1 : 1.2 : 1.8.

12:10 PM

**Experimental Research on Increasing Hematite Concentrate Proportion in Oxide Pellet:** *Xiaohui Fan<sup>1</sup>*; Lishun Yuan<sup>1</sup>; Yi Wang<sup>1</sup>; Luben Xie<sup>1</sup>; <sup>1</sup>Central South University

Effect of 3 inorganic bentonite, 5 composite bentonite, as well as hematite proportion on pelletizing and induration are studied in this paper. The results show that on the premise of small range adjusting and guaranteed pellet quality, the proportion of hematite concentrate can be increased to 50%.

12:30 PM

**Oxidized Pellet Preparation from Refractory Specularite Concentrates Using Modified Humic Acid (MHA) Binders:** Guohua Bai<sup>1</sup>; Daoyuan Zhang<sup>1</sup>; *Yuanbo Zhang<sup>1</sup>*; Guihong Han<sup>1</sup>; Zijian Su<sup>1</sup>; Guanghui Li<sup>1</sup>; <sup>1</sup>School of Minerals Processing & Bioengineering, Central South University

Specularite concentrates have poor hydrophilicity and ballability as well as bad high-temperature reactivity, which restrict the large-scale application of them in the pelletizing and sintering production. Modified humic acid (MHA) organic binders are firstly used for pellet preparation from specularite in this paper. The results show when using 1.0% MHA binder, the drop strength of green pellets is 3.7 times/0.5m and compression strength is 12.5 N/P. Under the optimal experimental conditions of preheating temperature 980°C, preheating time 12 min, roasting temperature 1280°C and roasting time 10 min, the preheated pellets have the compression strength of more than 400 N/P, and that of roasted pellets is 2747 N/P. The strength of finished pellets meet the requirements of blast furnace iron-making. MHA is a kind of more effective organic binder for specularite pellets compared with the inorganic bentonite.

## Advances in Mechanics of One-Dimensional Micro/Nano Materials: Nanomechanics: Pillars and Wires

*Sponsored by:* The Minerals, Metals and Materials Society, TMS Materials Processing and Manufacturing Division, TMS Electronic, Magnetic, and Photonic Materials Division, TMS: Nanomechanical Materials Behavior Committee

*Program Organizers:* Reza Shahbazian-Yassar, Michigan Technological University; Seung Min Han, Korea Advanced Institute of Science and Technology; Katerina Aifantis, Aristotle University

Wednesday AM

March 2, 2011

Room: 1B

Location: San Diego Conv. Ctr

*Session Chairs:* Reza Shahbazian Yassar, Michigan Technological University; Katerina Aifantis, Aristotle University

8:30 AM Invited

**Deformation and Failure of Phosphide- and Boride-Based Nanofilaments:** Melisa Steighner<sup>1</sup>; Humberto Gutierrez<sup>1</sup>; *Christopher Muhlstein<sup>1</sup>*; <sup>1</sup>The Pennsylvania State University

Theoretical predictions of unique physical and mechanical properties for compound nanofilaments with novel morphologies have motivated countless nanomaterials research programs. However, in some case empirical confirmations of the predictions have been elusive, either due to the difficulty to synthesize the predicted nanostructures or due to the complexity of the experiments needed to unambiguously demonstrate their physical properties. In this presentation we explore the structural and mechanical properties of phosphide- and boride-based nanofilaments that were synthesized using chemical vapor deposition techniques. Their deformation and fracture behaviors were evaluated using a micromachined loadframe and correlated one-to-one with their structure, morphology and chemical composition studied by transmission electron microscopy. Combining micro-Raman spectroscopy and direct stress measurements, we studied the mechanical behavior of nanofilaments in the presence of strain. These experiments provided insight into when and how nanoscale size effects are observed.

8:55 AM Invited

**The Brittleness Transition in 1-D Pillars:** *William W. Gerberich<sup>1</sup>*; A. Beaber<sup>1</sup>; <sup>1</sup>University of Minnesota

A transition-state modeling effort has been recently posed for dislocation nucleation. Parallel to that, several experimental efforts have been mounted to measure the yield and fracture characteristics of 1-D structures, in our laboratories emphasizing silicon. We conclude that both yield and flow stresses as well as fracture toughness are length scale dependent and plan to illustrate how a transition-state model might be applied to the brittle to ductile transition in strain-rate sensitive materials. Some in-situ transmission electron studies of the flow stress in nanopillars will illustrate the progress towards this goal.

9:20 AM Invited

**Deformations in Nano-Sized Pillars of Metallic Glasses:** *Jeff De Hosson<sup>1</sup>*; Alexey Kuzmin<sup>1</sup>; ChangQiang Chen<sup>1</sup>; YuTao Pei<sup>1</sup>; <sup>1</sup>Univ of Groningen

Size effect, or the lack thereof, during deformation of nano-sized metallic glassy objects has recently drawn great attention. It is not only of fundamental interest when scrutinizing shear localization processes, but also of practical significance for the incorporation of small size components in micro-/nano- electromechanical systems. An intriguing question is why and how nucleation and propagation of these shear bands (SBs) are affected by the size of the system, and would it be possible to suppress brittleness and enhance ductility by changing the size of the samples? Therefore, we have carried out quantitative in-situ TEM compression and bending experiments of metallic glass pillars with diameters ranging from 50 nm to 500 nm. A micromechanical model based on quantitative description of shear banding events explains the size-dependent deformation behavior and a statistical analysis of strength reveals the physical picture defined by the interactions between stress fields of flow defects.

WEDNESDAY AM

9:45 AM

**Elastic and Plastic Deformation of Nano- and Micro- Pillars:** *Katerina Aifantis*<sup>1</sup>; <sup>1</sup>Aristotle University

Experimental evidence will be presented on the deformation of polymeric and metallic nano-cones and nano-pillars, through atomic force microscopy indentation and nanoindentation. It will be shown that gradient plasticity can capture the deformation of such nanoscale configurations and estimates will be provided for the key material parameters, namely the elastic modulus and the internal length, that come into play in elasticity and gradient plasticity.

10:00 AM Invited

**Dislocation Sources in Micro-Pillars:** *Wei Cai*<sup>1</sup>; <sup>1</sup>Stanford University

The size-dependent yield stress observed in recent experiments of sub-micrometer metallic pillars provides a unique opportunity in which the predictions from defect dynamics simulations can be directly compared with mechanical strength measurements. The balance between the dislocation multiplication rate and depletion rate (at the surface) may be the key to understand the observed size effect in flow stress. Here we report two counterintuitive observations concerning dislocation multiplication in small volumes from Molecular Dynamics and Dislocation Dynamics simulations. In body-centered-cubic (BCC) metals, the surface itself can induce dislocation multiplication as a single dislocation moves across the pillar. In face-centered-cubic (FCC) metal pillars and thin films, however, even jogs of the Lomer-Cottrell type are not strong enough pinning points to act as permanent dislocation sources. These results highlight the need for better calibration of Dislocation Dynamics models against the more fundamental atomistic models.

10:25 AM

**Numerical Study of Fracture of Si-NWs Subjected to Lithiation/Delithiation:** *Ill Ryu*<sup>1</sup>; William Nix<sup>1</sup>; <sup>1</sup>Stanford University

There is currently a great amount of work devoted to the development of electrodes for Li-ion batteries. Silicon is one of the most promising candidates, because it shows high charge capacity and low discharging rates. However, silicon experiences a huge volume expansion about 400% during the lithiation/delithiation process. As shown recently, silicon nano-wires are attractive candidates for electrodes because they provide less constraint on the volume changes that occur during Li charging. In the present study, we have tried to estimate the critical size below which fracture does not occur in silicon nano-wires.

10:40 AM Break

11:05 AM Invited

**Deformation Mechanisms In Single Crystalline fcc Nanowhiskers:** *Daniel Gianola*<sup>1</sup>; Andreas Sedlmayr<sup>2</sup>; Lisa Chen<sup>1</sup>; Gunther Richter<sup>3</sup>; Reiner Mönig<sup>2</sup>; Oliver Kraft<sup>2</sup>; <sup>1</sup>University of Pennsylvania; <sup>2</sup>Karlsruhe Institute of Technology; <sup>3</sup>Max Planck Institute for Metals Research

The emerging picture in the size-dependent deformation of small-scale fcc metals suggests that the relationships between density and character of defects, discrete source statistics, and free surface/defect interactions, governs the mechanical response. Theoretical and simulation results also predict a shift in the rate-controlling mechanisms at small specimen size towards deformation modes that require thermal activation. We present results from quantitative in situ experiments on near defect-free fcc nanowhiskers in electron microscopes. Cu and Au nanowhiskers endure stresses near the limit of their ideal strength during tensile straining and the resulting deformation behavior suggests a lack of conventional dislocation-dislocation interactions. Transient and non-ambient temperature nanomechanical experiments are employed to extract activation parameters for plastic deformation. These results will be discussed in the context of thermal activation of nanoscale plastic deformation, which has recently been predicted to be important in ultra-strength materials.

11:30 AM

**Mechanics of Nanotubes/Nanowires: In Situ Microscopy:** *Reza Shahbazian-Yassar*<sup>1</sup>; Kasra Momeni<sup>1</sup>; Hessam Ghassemi<sup>1</sup>; Anjana Asthana<sup>1</sup>; Yoke Yap<sup>1</sup>; <sup>1</sup>Michigan Technological University

The correct estimation of mechanical properties in nanotubes and nanowires has been a challenging task due to complexity of stress state and end-support boundary conditions. Here we utilized simple beam formulations and buckling theories to explain the deformation and mechanics of boron nitride (BN) nanotubes and zinc oxide (ZnO) nanowires. Size scale effects were observed in ZnO nanowires and were explained by the modification of atomic structure at the nanowire surface. In addition, the rippling and bifurcation of multiwalled BN nanotubes were observed upon buckling and were quantified in terms of number of walls and nanotube's diameter.

11:45 AM Invited

**Structure-Elastic Property Relations in One-Dimensional Nanostructures:** *Gheorghe Stan*<sup>1</sup>; Robert Cook<sup>1</sup>; <sup>1</sup>National Institute of Standards and Technology

Nanoscale mechanical property measurements enable the link between atomistic simulations and micromechanical models to be defined and established. In this talk discussion will focus on the applicability of contact-resonance atomic force microscopy (CR-AFM) for quantitative measurements of the elastic modulus of one-dimensional nanostructures. By using CR-AFM we have systematically investigated the size-dependence of the elastic modulus of various nanowires and nanotubes: ZnO nanowires, Te nanowires, and AlN nanotubes. The observed increases in elastic moduli with reduction in nanowire diameter directly proved the stiffening enhancement that occurs in the outer layers of nanowires of reduced diameter. A distinctive CR-AFM application of enhanced compositional sensitivity has been demonstrated in measuring the mechanics of nonplanar subsurface Si-SiO<sub>2</sub> interfaces in partially oxidized Si nanowires. Such examples demonstrate the unique spatial resolution and compositional sensitivity of CR-AFM in investigating structure-mechanical property relationships at the nanoscale.

12:10 PM

**A Study of the Mechanical Properties of Nanowires Using Nanoindentation:** *Gang Feng*<sup>1</sup>; Davood Askari<sup>2</sup>; <sup>1</sup>Villanova University; <sup>2</sup>University of Texas at Brownsville and Texas Southmost College

A nanoindenter with scanning capabilities was used to perform nanoindentations on several nanowires with radii in the range of 20–500 nm, positioned on a substrate. Since the geometry of indentation of a nanowire differs significantly from the indentation of a half-space, a two interface contact model has been developed for the nanoindentation of a nanowire on a flat substrate, with the two interfaces, indenter/nanowire and nanowire/substrate, being in a series. The model has been used to analyze the nanoindentation data for several types of nanowires. Furthermore, to evaluate the analytical model, 3-dimensional finite element analysis (FEA) is performed, indicating significant nanowire-receding, a large deformation at the nanowire/substrate contact, and the insignificance of the adhesion at the contact. We also find that the sphere (indenter)/cylinder contact cannot be well approximated by a Hertzian elliptical contact.

12:25 PM

**Mechanical Behavior of the Ag Nanowires for Transparent Electrode Application:** *Chansun Park*<sup>1</sup>; Hui Wu<sup>2</sup>; Yi Cui<sup>2</sup>; Seung Min Han<sup>1</sup>; <sup>1</sup>KAIST; <sup>2</sup>Stanford University

In this study, we utilized nanoindentation to study the mechanical behavior of both single crystalline and polycrystalline Ag nanowires synthesized using a solution based synthesis and an electrospinning method, respectively. The solution synthesis method involves a poly reduction reaction, which is a common method of producing colloidal particles of metal elements, then selective growth of single crystalline nanowires along the (100) orientation. The electrospinning method involves using polymer based solutions with Ag precursors, then extracting out the fibers that are removed the polymer and therefore produce polycrystalline Ag nanowires. Both synthesis methods are tuned to fabricate wires of different diameters, and their hardnesses were determined using the Hysitron Ti-750 nanoindenter. Instead of using Oliver



and Pharr method for indentation hardness, we utilized a method where is calculated by utilizing the measured stiffness that was reported by Feng et al. I. I. G. Feng et al, Journal of Applied Physics 99, 74304(2006).

## Alumina and Bauxite: Precipitation, Calcination and Properties

Sponsored by: The Minerals, Metals and Materials Society, TMS Light Metals Division, TMS: Aluminum Committee, TMS: Aluminum Processing Committee

Program Organizers: James Metson, University of Auckland; Carlos Suarez, Hatch Associates Consultants Inc

Wednesday AM  
March 2, 2011

Room: 17A  
Location: San Diego Conv. Ctr

Session Chair: To Be Announced

### 8:30 AM Introductory Comments

#### 8:35 AM

**Effect of Technological Parameters on PSD of Aluminum Tri-Hydroxide from Seed Precipitation in Seeded Sodium Aluminate Solution:** Yusheng Wu<sup>1</sup>; Li Mingchun<sup>1</sup>; Qu Yanping<sup>1</sup>; <sup>1</sup>shenyang university of technology

Abstract: Periodical attenuation of particles, which interferes seriously with the normal alumina production, exists in Bayer process. In order to construct A mathematical model of total number of particles and particle size distribution (PSD) which is helpful to broadcast and control the PSD of aluminum tri-hydroxide for alumina refinery, the PSD of aluminum tri-hydroxide from seeded precipitation process in deferent technological parameters has been investigated under industrial conditions modeled in laboratory. The results show that PSD of the direction of translation to the small particle size with the initial precipitation temperature decreasing and molecule ratio of Na<sub>2</sub>O/Al<sub>2</sub>O<sub>3</sub> increasing. The volume fraction of particles below 44μm first increased and then decreased With the initial concentration of Na<sub>2</sub>O increasing. The PSD has a opposite variation tendency in different initial seed amount compared with the initial concentration of Na<sub>2</sub>O. Keywords: Bayer process, Sodium aluminate solution, Periodically attenuating, Particle size distribution, Aluminum tri-hydroxide

#### 9:00 AM

**Methods to Reduce Operating Costs in Circulating Fluidized Bed Calcination:** Cornelis Klett<sup>1</sup>; Michael Missalla<sup>1</sup>; Bernd Reeb<sup>1</sup>; Hans Schmidt<sup>1</sup>; <sup>1</sup>Outotec GmbH

Calcination of Gibbsite or Hydrate to Alumina needs approximately 30% of the energy input to an alumina refinery. Over the years Circulating Fluidized Bed (CFB) Calciners by Outotec (formerly Lurgi) have reduced energy consumption for calcination significantly. Until 1961 rotary kilns were standard technology for calcination of alumina. Since 1961 CFB technology reduced fuel consumption up to 30%. Since then, CFB calciners have been constantly improved and methods have been developed to reduce fuel consumption further. Some of these methods have resulted in increasing process complexity and operator and maintenance demand. However, also a lot of measures have been introduced to mitigate the negative effects of the increased process complexity and to improve operability and maintainability even beyond. In this paper different options and methods for reduction of fuel consumption, but also increase of operability and maintainability are compared and evaluated in their effects on installation costs and operating costs.

#### 9:25 AM

**Pressure Calcination Revisited:** Fred Williams<sup>1</sup>; C Misra<sup>2</sup>; <sup>1</sup>CMIS Corp; <sup>2</sup>AluminaTech

Twenty-five years ago at the TMS 100th anniversary meeting of the Hall-Heroult Process, two Alcoa scientists, S. W. Sucech and the co-author of this paper, C. Misra presented a paper on an improvement to the alumina calcination process – pressure calcination. The improved process offered an

opportunity for a net energy reduction in fluid flash calciners of 1.6 GJ/ton alumina (and the subsequent green house gas reductions). The improved process could be retrofitted into existing fluid flash calciners and produce an alumina meeting smelting requirements with the added advantage of high attrition resistance and thus low dust generation. The question is: Why hasn't this improvement been incorporated into today's alumina plants? Technical data in the previous paper will be reviewed and updated in the present paper.

#### 9:50 AM

**Dynamic Simulation of Gas Suspension Calciner (GSC) for Alumina:** Benny Raahauge<sup>1</sup>; Susanne Wind<sup>1</sup>; Mengzhe Wu<sup>1</sup>; Torsten Jensen<sup>1</sup>; <sup>1</sup>FLSmidth

Training of plant operational personnel is becoming more important today than ever, to sustain high availability and productivity of high capacity equipment. The Gas Suspension Calcination process for production of Smelter Grade Alumina is very easy to operate and control regardless of calcining capacity. But increasing calcining capacity of single GSC units exceeding 4500 tpd of SGA makes it increasingly costly to loose operating time. The process dynamics of GSC units are very fast with some true response times in fraction of seconds. To train GSC operators, FLSmidth has developed a dynamic Calciner Simulator which serves the primary purpose of training both new operators, as well as maintaining the skills of experienced ones. The dynamic Calciner Simulator has been developed from supply of more than 75 Pyro process simulators by FLSmidth to the global cement. The first Calciner Simulator for Alumina will be commissioned in Australia later this year.

#### 10:15 AM Break

#### 10:25 AM

**Physical Simulation and Numerical Simulation of Mixing Performance in the Seed Precipitation Tank with a Improved Intermig Impeller:** Zhang Ting-an<sup>1</sup>; Liu Yan<sup>1</sup>; Wang Shuchan<sup>1</sup>; Zhao Hongliang<sup>1</sup>; Zhang Chao<sup>1</sup>; Zhao Qiuyue<sup>1</sup>; Dou Zhihe<sup>1</sup>; Lv Guozhi<sup>1</sup>; <sup>1</sup>Northeastern University

The C6D fiber optic reflection probe was used to measure the local solid concentration distributions in the seed precipitation tank with a new-style impeller—Improved intermig impeller and the commercial software FLUNET 12.0 was used to simulate numerically its flow fields. The physical simulation results show that the high rotation and viscosity high-speed particles are more conducive to uniform distribution. When  $\square=3.50\text{cp}$   $\square n=172\text{rpm}$ , the multiple relationships of the average value of the practice and theory is 1.011 times. The numerical simulation results show that the too longer or shorter impeller off-bottom clearance height(C) is not conducive to the suspending of Al(OH)<sub>3</sub> particles. Enlarging the blade diameter is good for the suspending of Al(OH)<sub>3</sub> particles. The blade diameter (D) has big influence on the stirring power, and the longer blade diameter need the more power consumption. The physical simulation results compare well with the numerical simulation ones.

#### 10:50 AM

**Two Perspectives on the Evolution and Future of Alumina:** Linus Perander<sup>1</sup>; James Metson<sup>1</sup>; Cornelis Klett<sup>2</sup>; <sup>1</sup>Light Metals Research Centre; <sup>2</sup>Outotec GmbH

Over the 125 year history there have been a number of step-changes in the Hall-Heroult process, despite a remarkable adherence to the original concepts of the inventors. In addition to the steady increment in scale, most noteworthy perhaps have been the introduction and impending disappearance of Soderberg technology, the introduction of magnetically compensated cell design, changes in dynamics of alumina feeding and the introduction of dry-scrubbers for HF control and fluoride recovery. The Bayer process has also seen some significant advances, driven by the demands of energy and environmental imperatives and the steadily narrowing window of product specifications, driven in turn by refinements in the Hall-Heroult process. Demands for coarser particle size distribution and higher specific surface areas have been accompanied by changes in precipitation strategy and conversion to more energy efficient stationary calcination processes. The properties of a "typical" metallurgical alumina have thus changed. Indeed

the term "alumina" is now more indicative of stoichiometry than it is of structure, and even in this, it is less than precise. In this paper we discuss how new scientific tools and insights are changing the way we define (and perhaps should specify) this material.

**11:15 AM**

**Significant Improvement of Energy Efficiency at Alunorte's Calcination Facility:** *Michael Missalla*<sup>1</sup>; Hans Schmidt<sup>1</sup>; Joaquim Ribeiro<sup>2</sup>; Reiner Wischniewski<sup>3</sup>; <sup>1</sup>Outotec GmbH; <sup>2</sup>Alunorte-Alumina do Norte do Brasil S.A.; <sup>3</sup>Hydro Aluminium AS

The Alunorte refinery produces 6.3 million t/a of alumina with seven Circulating Fluid Bed (CFB) calciners. The calcination facility only needs about one third of the total energy for the refinery. The CFB calcination system has implemented several preheating and cooling stages with cyclones for the separation of gas and solids. If the cyclones were more efficient, it would lead to an increase in heat recovery thus decreasing energy consumption. The paper presents a process to improve efficiency of these cyclones and the solid dust load significantly by using new method of simulation technology. With the optimised process considerably lower energy consumption figures are achieved. Results of these improvements regarding fuel and electrical energy consumption as well as return on investment are presented. Alunorte has already installed the improvements at two of their seven calciners and has received the energy efficiency award 2010 from the German Energy Agency.

**11:40 AM**

**Attrition of Alumina in Smelter Handling and Scrubbing Systems:** *Stephen Lindsay*<sup>1</sup>; <sup>1</sup>Alcoa, Inc.

Smelting customers place various levels of importance upon the Attrition Index of Smelter Grade Alumina, SGA. Concerns are generally associated with the content of alumina fines in fluorinated alumina as it arrives to the reduction cell. In this paper the author discusses factors of importance related to the design and operation of the alumina handling systems. Examples will be given in which the attrition of alumina particles has been minimal. Discussion will include techniques on how to estimate the contribution of fine particles of bath evolved by the pots from attrition of alumina particles.

## Aluminum Alloys: Fabrication, Characterization and Applications: Materials Characterization

*Sponsored by:* The Minerals, Metals and Materials Society, TMS Light Metals Division, TMS: Aluminum Processing Committee  
*Program Organizers:* Subodh Das, Phinix LLC; Zhengdong Long, Kaiser Aluminum; Tongguang Zhai, University of Kentucky

Wednesday AM  
March 2, 2011

Room: 14A  
Location: San Diego Conv. Ctr

*Session Chair:* Tongguang Zhai, University of Kentucky

**8:30 AM**

**Transmission Electron Microscopic Investigations of Grain Boundary Beta Phase Precipitation in Al-5083:** *Ramasis Goswami*<sup>1</sup>; Peter Pao<sup>2</sup>; Ronald Holtz<sup>2</sup>; <sup>1</sup>SAIC/Naval Research Laboratory; <sup>2</sup>Naval Research Laboratory

The fine scale microstructure of Al-5083 sensitized at 70, 100 and 175°C and at ambient temperature for different durations has been investigated using transmission electron microscopy (TEM) to study the evolution of the  $\beta$  phase (Al<sub>3</sub>Mg<sub>2</sub>) at grain boundaries. TEM observations showed that, at 100°C, the grain boundary precipitation of  $\beta$ -phase was discrete between 3 to 14 days of aging, and no segregation of Mg at the grain boundary was observed between two discrete  $\beta$  islands. Considerable portion of grain boundaries were fully covered by the  $\beta$ -phase after 30 to 45 days of aging at 100°C. Grain boundaries were also observed to be migrated by diffusion induced grain boundary migration (DIGM) after aging for 90 days at 100°C. The nucleation and growth of  $\beta$ -phase at grain boundaries at different

temperatures, 70, 100, 175°C and ambient temperature, will be discussed in detail.

**8:50 AM**

**Effect of Ultrasonic Impact Treatment on a 5456 Aluminum Alloy Characterized through Micro-Specimen Testing and X-Ray Tomography:** *Caroline Scheck*<sup>1</sup>; Kim Tran<sup>2</sup>; Christopher Cheng<sup>1</sup>; Marc Zupan<sup>1</sup>; <sup>1</sup>University of Maryland, Baltimore County; <sup>2</sup>Naval Surface Warfare Center, Carderock Division

Ultrasonic impact treat (UIT) is a surface treatment that causes uniform, but severe, plastic deformation. UIT gives excellent parameter control and has a high energy efficiency, unlike similar processes such as shot peening. The objective of this work is to show the measured hardness, strength, and void properties of an ultrasonically impacted 5456-H116 aluminum. Micro-indentation is used to map the hardness properties while microsample specimens directly measure tensile mechanical properties. The micro species (3mm in length by 1mm wide with a gage section of 250 mm square) are made at varying distances from the UIT treated surface and tested to characterize the Young's modulus and yield strength. Voids in the gage section of the micro specimens are analyzed before and after testing using a novel X-ray topography. These void characteristics are linked to the yield and plastic deformation behavior of the material.

**9:10 AM**

**Effect of Extrusion Microstructure on the Corrosion Behavior of AA6005A Aluminum Alloy:** *Dan Seguin*<sup>1</sup>; Calvin White<sup>1</sup>; Richard Dickson<sup>2</sup>; <sup>1</sup>Michigan Technological University; <sup>2</sup>Hydro Aluminum

Extrusions of AA6005A alloy have a duplex grain structure consisting of a thin recrystallized layer near the extrusion surface and a fibrous layer at the core. The recrystallized layer in underaged AA6005A is known to be susceptible to intergranular corrosion when containing more than about 0.12% Cu. No study on the corrosion behavior of the fibrous core structure exists to date. For the present work, specimens of thin-walled AA6005A extrusion with a range of thermal and surface treatments were prepared and exposed to an accelerated corrosion solution. Within the fibrous structure, surfaces cut normal to the extrusion direction were found to be much more susceptible to pitting attack than surfaces cut parallel to the extrusion direction.

**9:30 AM**

**Failure Loads and Deformation in 6061-T6 Aluminum Alloy Spot Welds:** *Radu Florea*<sup>1</sup>; Kiran Solanki<sup>1</sup>; Douglas Bammann<sup>1</sup>; Brian Jordon<sup>1</sup>; Matt Castanier<sup>1</sup>; <sup>1</sup>Mississippi State University

Failure loads and deformation in 6061-T6 aluminum alloy resistance spot welded joints were experimentally investigated. The welding experiments were carried out using different process parameters such as electrode forces, welding times, and currents. Nugget and microstructure characteristics were quantified using laser beam profilometry, electron back scatter diffraction technique (EBSD), and quasi-static shear tests. Mechanical tests were used to characterize the failure forces in spot welded specimens to elucidate the influence of process parameters. Finally, the microstructure of the weld nugget was discussed based on the process parameters, and the modeling results were compared with measurements obtained by electron back scatter diffraction mapping.

**9:50 AM**

**Magnesium Diffusivity Measurement in AA5083 Alloys:** *Soumya Kar*<sup>1</sup>; Michael Free<sup>1</sup>; <sup>1</sup>University of Utah

AA5083 alloys are widely used for marine application. However, these alloys are susceptible to intergranular corrosion after prolonged exposure at moderate temperature. Formation of Mg rich beta phase is the primary concern in this type of material degradation. We investigated Mg diffusion behavior to quantify the amount of beta phase formation. AA5083 alloy was investigated with O and H131 temper. 5456-H116 alloys were also investigated for comparative study. High resolution scanning electron microscopy images were taken to identify the beta phase. Beta phase thickness was estimated from the etch trench thickness distribution profile. The model was developed

based on the fundamental assumption that increase of Mg along the grain boundary is due to the depletion of Mg from the bulk. Solving a mass balance equation, the model can provide beta phase thickness for a range of thermal exposure time and temperature. Mg diffusivity parameters can be estimated from this information.

#### 10:10 AM Break

#### 10:25 AM

##### Surface Energy, Electronic Structure, and Complexity of Al-Based

**Intermetallics:** *Jean-Marie Dubois*<sup>1</sup>; *Esther Belin-Ferré*<sup>2</sup>; <sup>1</sup>Institut Jean Lamour, CNRS; <sup>2</sup>LCPMR, CNRS

Many compounds based on aluminum alloyed with transition elements or simple metals contain a large number of atoms in their crystal unit cell. As a consequence of the resulting complexity, their properties depart significantly from the ones of the elemental constituents. In this paper, we will examine one such important property, namely surface energy, which we will assess based on friction experiments against steel in vacuum. We will show how it correlates to partial densities of electronic states deduced from soft x-ray emission spectroscopy. Complexity will be shown to play the key role, via Hume-Rothery and hybridization effects.

#### 10:45 AM

##### Measurement of Resistivity/Conductivity of Aluminium Oxide-Film by Electrochemical Impedance Spectroscopy (EIS): *Khaled Habib*<sup>1</sup>; <sup>1</sup>KISR

The technique of Electrochemical Impedance Spectroscopy (EIS) is widely used in laboratories and industries for materials evaluation. The aim of this investigation is to measure, for the first time, the resistivity/conductivity of the anodized (oxide) aluminium sheets (samples) by using the EIS in a laboratory in 0-10 % sulphuric acid. In order to achieve such task, the alternating current (AC) impedance and the thickness of the anodized (oxide) aluminium samples will be measured at low frequency in 0-10 % sulphuric acid. In other words, the absolute value of the AC impedance will be equivalent to the direct current resistance of the anodized (oxide) aluminium samples. As a result, the resistivity/conductivity of the anodized (oxide) aluminium samples can be determined by knowing the resistance and the thickness of the samples in 0-10 % sulphuric acid.

#### 11:05 AM

##### Effect of Conical and Cylindrical Tool with Grooves Pin Profiles on Tensile Strength in Friction Stir Welding Process: *C. N. Suresha*<sup>1</sup>; *B. M. Rajaprakash*<sup>1</sup>; *Sarala Upadhyay*<sup>1</sup>; <sup>1</sup>Bangalore University

Friction stir welding (FSW) is an innovative solid-state material joining method invented by The Welding Institute (TWI). It has evolved into a process focused on joining arc weldable (5xxx and 6xxx) and unweldable (2xxx and 7xxx) aluminum alloys where it can be implemented by the aerospace and automotive industries for their joining needs. The present study has aimed to investigate the influence of tool profile on tensile strength and joint efficiency of welded joints of AA 7075-T6 Aluminum alloy by FSW process. Tool profiles like conical and cylindrical with grooves are used in this study. Experiments were carried to find contribution of the main welding parameters, such as tool rotational speed, weld traverse speed and plunge depth on tensile strength of welded joint. It has been observed that the use of tool having conical grooved profile has resulted better results than the tool having cylindrical grooved profile.

## Aluminum Reduction Technology: Cells Technology, Development and Sustainability

*Sponsored by:* The Minerals, Metals and Materials Society, TMS Light Metals Division, TMS: Aluminum Committee, TMS: Aluminum Processing Committee

*Program Organizers:* Mohd Mahmood, Aluminium Bahrain; Abdulla Ahmed, Aluminium Bahrain (Alba); Charles Mark Read, Bechtel Corporation; Stephen Lindsay, Alcoa, Inc.

Wednesday AM  
March 2, 2011

Room: 17B  
Location: San Diego Conv. Ctr

*Session Chair:* Gilles Dufour, Aluminerie de Deschambault

#### 8:30 AM

##### High Amperage Operation of AP18 pots at Karmøy: *Marvin Bugge*<sup>1</sup>; *Haakon Haakonsen*<sup>1</sup>; *Ove Kobbeltvedt*<sup>1</sup>; *Knut Paulsen*<sup>1</sup>; <sup>1</sup>Hydro Aluminium

The AP18 potline at Karmøy has increased the amperage to 230 kA. This has increased the productivity and reduced the specific production costs. The operation showed some lack of performance at high amperage for the old pots designed for lower amperage. The old pots had too high heat input resulting in thin ledge and higher Si content in the metal. To improve the heat balance the pot voltage had to be reduced for the old pots, and this resulted in reduced CE. The cathode life was reduced to ~2250 days due to use of graphitized cathode blocks and the increased amperage. The new cathodes designed for 230 kA show good operational results. The young pots show 94-94.5% current efficiency and 13.1 kWh/kg Al energy consumption. Due to less bath volume in the new pots it has been a challenge to reduce the anode effect frequency.

#### 8:50 AM

##### Aluminium Smelter Manufacturing Simulation – Can These Bring Real Cost Savings?: *Maarten Meijer*<sup>1</sup>; <sup>1</sup>Hencon

Incorporating logistics tools at the smelter design stage: implications for capex and opex Optimising interaction between smelter units and processes for additional cost savings The use of simulation in achieving “lean thinking” in new smelters or upgrades

#### 9:10 AM

##### Simultaneous Preheating and Fast Re-Start of 50 Aluminium Reduction Cells in an Idled Pot Line- A New Soft Re-Start Technique for a Pot Line: *Albert Mulder*<sup>1</sup>; *Anita Folkers*<sup>1</sup>; *Marco Stam*<sup>1</sup>; *Mark Taylor*<sup>2</sup>; <sup>1</sup>Aluminium Delfzijl; <sup>2</sup>The Light Metals Research Centre

Due to the global economical crisis a significant amount of primary aluminium production capacity has been shut-down. A number of different strategies to restart idled aluminium reduction cells have been discussed in the literature. This paper describes the successful development and execution of the start-up of 50 cells simultaneously in one pot line. The procedure is based on restarting reduction cells using a cold metal plate. Contrary to electrical preheating of new cells with use of cokes or graphite, these cells have been prepared with anodes positioned in direct contact and on top of the cold metal plate. The rate of preheating of the cells and associated melting of metal is controlled by a gradual line current increase. The actual start-up of the cells is performed sequentially by the addition of liquid electrolyte and moving the anode beam upwards. In this respect 50 cells have been started in 8 days.

#### 9:30 AM

##### SWOT Perspectives of Mid-age Prebaked Aluminium Smelter: *Pradip Choudhury*<sup>1</sup>; *Arun Sharma*<sup>1</sup>; <sup>1</sup>National Aluminium Company Ltd.

Aluminium smelters in nineties witnessed radical changes in technology of electrolysis, carbon manufacturing and casting. The pace of transformation in Aluminium industries posed different challenges specifically to the mid-age smelters operating with relatively lower amperage. Enduring needs to match the demands of evolving technology, socio-cultural and environment issues forced mid-age Smelters to adopt appropriate strategies as long-



term business imperatives. With structured approach, the threat perception could be turned into vast opportunities of innovation and improvements. Energy conservation, waste management, recycling, emission control and customer orientation remained specific focus areas to enhance productivity and retain profitability in the backdrop of global economic recession. Process optimization and system upgradation through customised solutions, motivating and retaining high employee morale became the order of the day. The paper is a case study on the sustainable achievements of the state owned Indian Aluminium major, NALCO, through well-coined strategies and pragmatic investment.

### 9:50 AM Break

### 10:00 AM

#### **Integrated Approach for Safe and Efficient Plant Layout Development:** Rafael Pires<sup>1</sup>; Robert Baxter<sup>1</sup>; Laszlo Tikasz<sup>1</sup>; Robert McCulloch<sup>1</sup>; <sup>1</sup>Bechtel

Aluminium complex layout development usually involves dealing with an intricate mix of operations (e.g. smelter, refinery, rolling mill, port). The choice of a layout can significantly impact the success of the envisaged operation, in terms of safety, life-cycle cost and environmental impact. This paper is a continuation of last year's publication, exploring the application of safety by design and lean manufacturing methods on the layout design of a fully integrated aluminium complex. An innovative approach, derived from lessons learnt to assist plant layout development and resource analysis, is presented. This approach is able to quickly and effectively assess safety and efficiency in a proposed layout. The dynamic feature of this approach provides the capability of closely mimicking the future traffic operation, allowing to monitor how the traffic evolves in time. Throughout this paper, the design of access roads, choice of transportation modes, and planning of resource are discussed.

### 10:20 AM

#### **Improving Current Efficiency of Aged Reduction Lines at Aluminium Bahrain (Alba):** Abdulla Ahmed<sup>1</sup>; Ragahavendra K.S.R<sup>1</sup>; Hasanain Hassan<sup>1</sup>; <sup>1</sup>Aluminium Bahrain (Alba)

The side worked end-on-end pre-bake anode technologies install during 1970's at Alba achieved a current efficiency of 90%. During the early nineties, the potlines were retrofitted from side break to point fed cell arrangement, along with an increase of 7% and 10% in line current. The retrofits included anode gas collection system, a changed anode setting pattern, and installation of alumina and aluminium fluoride feeders controlled using individual cell controller, which increased the current efficiency to 92.5%. During the last 6 years, improvements done in the alumina feeding control, thermal control and stability of cell operations has increased the current efficiency to 94.5%. Close monitoring and follow up of quality of work and key parameters on daily basis by the new employees forum introduced at Alba in 2004 called SMART Centres (See My Actions Reflect Targets) has also contributed towards this improvement and maintaining it.

### 10:40 AM

#### **Current Efficiency for Aluminium Deposition from Molten Cryolite-Alumina Electrolytes in a Laboratory Cell:** Geir Martin Haarberg<sup>1</sup>; Joseph Armoo<sup>1</sup>; Henrik Gudbrandsen<sup>2</sup>; Egil Skybakmoen<sup>2</sup>; Asbjørn Solheim<sup>2</sup>; Trond Eirik Jentoftsen<sup>3</sup>; <sup>1</sup>Norwegian University of Science and Technology; <sup>2</sup>SINTEF; <sup>3</sup>Hydro Aluminium

The current efficiency with respect to aluminium can be as high as 96 % in modern Hall-Heroult cells. The loss in current efficiency is strongly linked to the fact that aluminium is soluble in the electrolyte. In addition the presence of dissolved sodium must be considered. The back reaction between dissolved metals and the anode product is responsible for the major loss in current efficiency. The rate of the reaction is controlled by diffusion of dissolved metals (Al and Na) through the diffusion layer. A laboratory cell was used to determine the current efficiency for aluminium during constant current electrolysis. Standard conditions were NaF/AlF<sub>3</sub> (CR=2.5), Al<sub>2</sub>O<sub>3</sub> (sat), 5 wt% CaF<sub>2</sub> at 980°C and 0.85 A/cm<sup>2</sup>. Current efficiencies ranging from ~ 90 - 97 % were obtained. The current efficiency was found to increase

slightly by increasing cathodic current density. Increasing excess AlF<sub>3</sub> gave higher current efficiencies.

### 11:00 AM

#### **New Progress on Application of NEUI400kA Family High Energy Efficiency Aluminum Reduction Pot ("HEEP") Technology:** Dingxiong Lv<sup>1</sup>; Xiquan Qi<sup>1</sup>; Junman Qin<sup>1</sup>; Zijin Ai<sup>1</sup>; Yungang Ban<sup>1</sup>; <sup>1</sup>Northeastern University Engineering & Research Institute Co. Ltd

China's first 400kA class potline was put into operation in August 2008 with NEUI400(I) cell technology. The annual design production capacity of the potline is 230kt. The present amperage is 420kA, average working voltage is less than 3.88V, DC energy consumption is less than 12.8 kW·h/kg-Al, and the anode effect frequency is below 0.015. Based on the successful application and testing results of NEUI400(I) cells, further research work was carried out on the structural optimization, energy saving and environment protection. The improved NEUI400 (II-IV) cells were successfully applied in the potlines of LinFeng, NanShan and JinNing smelters, and the annual design production capacity is 250kt, 250kt and 300kt respectively. All the NEUI400 potlines amperage reached 430~450kA after start-up. Excellent technical-economic indexes were obtained after the cells putting into operation three months, such as average working voltage is less than 3.85V, DC energy consumption is less than 12.5 kW·h/kg-Al, anode effect frequency is well below 0.01.

### 11:20 AM

#### **Development of NEUI500kA Family High Energy Efficiency Aluminum Reduction Pot ("HEEP") Technology:** Dingxiong Lv<sup>1</sup>; Yungang Ban<sup>1</sup>; Xiquan Qi<sup>1</sup>; Jingxiong Liu<sup>1</sup>; <sup>1</sup>Northeastern University Engineering & Research Institute Co. Ltd

Based on the successful development and commercial application experience of NEUI400kA class reduction cells, also combined with testing results and proprietary numerical simulation softwares, NEUI developed NEUI500kA class high-efficient reduction cell technology, and successfully resolved the problems with increasing of amperage capacity, current density and cell span. Compared with NEUI400kA class cell technology, better simulation results were obtained. The economic and security of busbar is more better; and the cell current deviation of two sides is less than 0.5%, cathode busbar voltage is lower than 200mV, |Bz|ave is less than 3.14Gs, and vertical magnetic gradient is less than 3.1Gs. Interface deformation is more smaller, and MHD stability is further improved. Ideal thermal balance and uniform pressure distribution of the cell were obtained. Furthermore, more greater intensity and economical tube truss superstructure was adopted.

### 11:40 AM

#### **An Innovative Approach to Improving the Operational Performance of Aluminum Smelters:** Nelson Dubé<sup>1</sup>; Thiago Heitling<sup>1</sup>; <sup>1</sup>SNC-Lavalin

The efficient operation of an aluminum smelter necessitates that all production activities have to be executed perfectly to ensure an optimum operation. In today's competitive environment, all aluminum smelters need to continually look for improvement opportunities in order to achieve better profitability and market position. The innovative Plant Optimization Services, developed by SNC-Lavalin, is aimed at assisting aluminum smelter personnel in their plant operational debottlenecking and performance improvement processes. The methodology takes an integrated approach - combining the elements of process management, production process analysis, and equipment management. This paper presents the methodology, the analysis outputs, and the implementation of changes.

## Battery Recycling: Session I

Sponsored by: The Minerals, Metals and Materials Society, TMS Extraction and Processing Division, TMS Light Metals Division, TMS Electronic, Magnetic, and Photonic Materials Division, TMS: Recycling and Environmental Technologies Committee, TMS: Energy Conversion and Storage Committee

Program Organizers: Gregory Krumdick, Argonne National Laboratory; Linda Gaines, Argonne National Laboratory

Wednesday AM  
March 2, 2011

Room: 12  
Location: San Diego Conv. Ctr

Session Chairs: Gregory Krumdick, Argonne National Laboratory; Linda Gaines, Argonne National Laboratory

### 8:30 AM Introductory Comments

#### 8:35 AM

**Taking a Life Cycle Approach to Battery Management:** *Mira Inbar*<sup>1</sup>; <sup>1</sup>Dow Kokam

The end of a battery's life is a topic of much interest and debate. Will batteries be recycled or reused after they have reached 80% capacity in vehicles? We argue that the end of a battery's life must be conceived in the early design of the battery system and implemented throughout the battery's life cycle. Inherent in good battery design is a deep understanding of the environmental tradeoffs involved in a battery life cycle: from material sourcing, to manufacturing, to use, to end-of-life management. Dow Kokam is undertaking a Life Cycle Analysis, using the GaBi software, to quantify the environmental impacts and benefits (greenhouse gases, water, particulates, etc) from cradle to grave. This analysis will give us a detailed understanding of the "hot spots" in the environmental profile of our battery systems and how certain parameters in battery production influence the environmental profile.

#### 8:55 AM

**Role of Recycling in the Life Cycle of Batteries:** *John Sullivan*<sup>1</sup>; Linda Gaines<sup>1</sup>; Andrew Burnham<sup>1</sup>; <sup>1</sup>Argonne National Laboratory

Over the last few decades, rechargeable battery production has increased substantially. Applications including phones, computers, power tools, power storage, and partially to fully electric vehicles are either commonplace or will be in the next decade or so. Because advanced rechargeable batteries, like nickel metal hydride or lithium ion systems, consist of less-plentiful and comparatively expensive materials (e.g., nickel, cobalt, cadmium, misch metal) that often require considerable energy to be formed into battery components, battery recycling has the potential to significantly reduce the burdens associated with the life cycle of batteries. The key issue is, therefore, to determine the most practical type of recycling. Is it feasible to recover such components as anodes, cathodes, and electrolytes, or should the elements be recovered? Estimates of the impacts of battery recycling are given.

#### 9:15 AM

**Treatment or Recycling End-Of-Life (H)EV Battery Packs:** *Mark Caffarey*<sup>1</sup>; <sup>1</sup>Umicore USA

To understand the processing options for an end-of-life (H)EV battery pack, it is important to compare the Treatment process as it is known today with the Umicore UHT process. The Ultra High Temperature process allows for maximum recycling while allowing minimal air emissions and waste generation. The UHT process is the only process that returns the metals contained to their elemental phase thus allowing for a recycled battery material equal to primary material. A description of the new Umicore facility is given (7,000 tons of batteries per year) with its inputs and outputs as well as a Life Cycle Analysis illustrating process benefits on the short and long term for the battery industry and society as a whole. Opportunities to build on the UHT process with additional recycling options such as for Lithium and Rare Earths show that this can serve as a building block for further recycling improvements

#### 9:35 AM

**Evaluation of Environmental Tradeoffs in Portable Battery Recycling:** *Elsa Olivetti*<sup>1</sup>; Gabrielle Gaustad<sup>2</sup>; Randolph Kirchain<sup>1</sup>; <sup>1</sup>Massachusetts Institute of Technology; <sup>2</sup>Rochester Institute of Technology

Approximately 80% of portable batteries manufactured in the US are primary alkaline batteries with a global annual production >10 billion. The majority of these batteries go to landfills at end-of-life (EOL). An increased focus on environmental issues related to disposal combined with recently implemented EOL directives in the EU and Canada, has intensified interest in quantifying optimal EOL routes for both primary and secondary batteries. Careful evaluation of the environmental impacts of battery recycling is critical to determining the conditions under which recycling is most beneficial. The magnitude of portable batteries that are retired each year, variation in material composition between different battery types, and the broad dispersion of those batteries makes the logistics of efficient battery collection challenging. This research investigates environmental tradeoffs within collection and recycling systems for the recovery of materials in EOL batteries. Analysis compares alkaline battery recycling challenges to other chemistries, including rechargeable Li-ion systems.

#### 9:55 AM

**Managing Hybrid Electric Batteries at End of Life:** *Todd Coy*<sup>1</sup>; <sup>1</sup>Kinsbursky Brothers /Toxco

Hybrid systems are commonplace with a variety of models available from different manufacturers. As these vehicles start to age, the management of the battery system has surpassed the contingency planning stage and is now a reality that the auto manufacturer, dealership service centers, must take into consideration when replacing older hybrid battery systems. Automotive Dismantlers must also be aware of the hazards that these batteries present if batteries are not removed prior to their receipt at a dismantlers facility. The recovery and proper handling of batteries is a complicated task for persons not aware of the regulatory requirements for managing hazardous materials. This is true for companies located in California, as California maintains one of the strictest regulatory code systems in the United States. Navigating these environmental regulations, as they pertain to the proper management and disposal of end of life batteries can be an arduous undertaking.

#### 10:15 AM Break

#### 10:25 AM

**The 10 Obstacles to a Successful Battery Recycling Program: The North American Experience:** *Lisa Pollack*<sup>1</sup>; *Carl Smith*<sup>1</sup>; <sup>1</sup>Call2Recycle

Battery recycling in North America has reached adolescence. Retailers are demanding collection programs that can be incorporated into overall corporate sustainability programs. Consumer education is difficult to track and expensive. Municipalities are slow to take action, but require world-class results. There are no uniform success metrics. Furthermore, the effort required to indulge politicians, corporate sustainability executives, manufacturers, consumers and environmentalists isn't paying off in collection results. How can battery recyclers overcome the obstacles of "puberty" and ensure a successful, long-term program? Carl Smith, CEO of Call2Recycle®, will offer an overview of the battery recycling industry's evolving landscape including: how recent legislation in North America will affect international battery recycling initiatives; why product stewards must work together to develop measurement standards; why the latest battery chemistry advancements aren't as exciting as they seem; and how battery industry stakeholders can help lift the burden from manufacturers and share end-of-life responsibilities.

#### 10:45 AM

**Product Stewardship Pressures on the Lead and Motive Power Battery Industries:** *David Weinberg*<sup>1</sup>; <sup>1</sup>Wiley Rein LLP

This presentation will address challenges to the world's most successful recycling programs – those related to lead acid batteries – and the quickly expanding realm of EV, HEV and other motive power batteries that arise from the uniformed fervor of "product stewardship" advocates and outdated hazardous materials transportation regulations. It will cover legislative and

regulatory activities throughout North America and efforts to craft reasonable responses to them. Mr. Weinberg is Washington Counsel of the Battery Council International and General Counsel of PRBA-The Rechargeable Battery Association and the Rechargeable Battery Recycling Corporation.

**11:05 AM**

**A Preliminary Investigation for Spent LIBs Recycling:** Mengjun Chen<sup>1</sup>; Fu-shen Zhang<sup>2</sup>; Jianxin Zhu<sup>2</sup>; <sup>1</sup>Southwest University of Science and Technology; <sup>2</sup>Research Center for Eco-Environmental Sciences, Chinese Academy of Sciences

Spent lithium-ion secondary battery (LIB) is one important kind of waste electric and electronic equipment (WEEE). At present, technologies available for spent LIBs recycling include chemical deposition, solvent extraction, Etoile-Rebatt process, electrodeposition, floatation and ion-exchanging. In this paper, a novel vacuum-aided pyro-metallurgical process for recovery metallic Co directly from waste LIBs was presented. The experiment results showed that 1) the decomposition and reduction rates of LiCoO<sub>2</sub> increased with the increase of experiment temperature; and 2) metallic Co can be recovered successfully when the experiment temperature was higher than 700° and the system pressure was maintained at 10 Pa. XRD and SEM results obtained at different temperatures showed that, in this paper, LiCoO<sub>2</sub> was first reduced to CoO at a lower temperature and then it was reduced to metallic Co as the increase of temperature. This vacuum-aided pyrometallurgical process might be a promising one for spent LIBs recycling.

**11:25 AM**

**Recovery of Metal Values from Waste Cathode Active Material Using Organic Acid as Leachant and Its Application to Synthesis of LiCoO<sub>2</sub>:** Hyun-Jong Kim<sup>1</sup>; Seong Ho Son<sup>1</sup>; Chi Ho Shin<sup>1</sup>; Howard Lee<sup>2</sup>; <sup>1</sup>Korea Institute of Industrial Technology; <sup>2</sup>OSC Co., Ltd.

Since lithium ion batteries (LIBs) consist of heavy metals, organic chemicals and plastics, the recovery of major spent cell components is beneficial in terms of environmental protection and also for the provision of raw materials. In this study, environmentally benign organic acids were used to recover the cobalt and lithium from cathode materials of LIBs. Various organic acids, including acetic acid, citric acid, and taurine, etc., were tested as a function of leachant/reductant concentration and temperature. As a heating process, autoclave could highly improve the leaching efficiency up to over 90%. In a view point of the LiCoO<sub>2</sub> synthesis, acetic acid was favorable since the metal acetate could be easily used in sol-gel reaction. The leached cobalt acetate solution was directly supplied to prepare the LiCoO<sub>2</sub> powder. Battery charge-discharge experiments showed very promising results for the recycle of LIBs.

**11:45 AM Concluding Comments**

## Biological Materials Science: Mechanical Behavior of Biological Materials I

*Sponsored by:* The Minerals, Metals and Materials Society, TMS Electronic, Magnetic, and Photonic Materials Division, TMS Structural Materials Division, TMS: Biomaterials Committee  
*Program Organizers:* Jamie Kruzic, Oregon State University; Nima Rahbar, University of Massachusetts, Dartmouth; Po-Yu Chen, University of California, San Diego; Candan Tamerler, University of Washington

Wednesday AM  
March 2, 2011

Room: 15A  
Location: San Diego Conv. Ctr

*Session Chairs:* Po-Yu Chen, University of California, San Diego; David Kisailus, University of California, Riverside

**8:30 AM Keynote**

**Turning Weakness into Strength: Explaining the Great Strength and Extensibility of Spider Silk:** Markus Buehler<sup>1</sup>; <sup>1</sup>Massachusetts Institute of Technology

Biology creates hierarchical structures, where initiated at nano scales, are exhibited in physiologically materials to provide structural support, force generation, catalytic properties or energy conversion. Spider silk is one of the strongest, most extensible and toughest biological materials, exceeding the properties of many engineered materials including steel. The issue is particularly puzzling since despite its great strength, spider silk is made of weak hydrogen bonds. We discovered that the great strength and extensibility of spider silk can be explained based on the particular structural makeup of the material, which involves several hierarchical levels from the nano- to the macro-scale. Our work unveils the material design strategy that enables silks to achieve superior material performance despite simple and inferior material constituents. This concept could lead to a new materials design paradigm, where enhanced functionality is not achieved using complex building blocks but rather through the utilization of simple repetitive constitutive elements.

**9:10 AM Invited**

**Biomechanics of Cancer Cells:** Chwee Teck Lim<sup>1</sup>; <sup>1</sup>National University of Singapore

During the onset of a disease, a cell may experience alterations in both the composition and organization of its cellular structures. These alterations may eventually manifest as changes in the mechanical properties such as cell deformability and cell adhesion. With the recent advancements in micro/nanotechnology and biophysical techniques, we can now probe and study mechanical property changes in individual cells and even proteins. In fact, knowing the effect of mechanical forces acting on cells can reveal ways by which diseased cells differ from healthy ones. This can help us better understand and establish possible connections between change in mechanical properties of cells and the onset and progression of human diseases. Here, we will highlight studies on cancer using techniques such as atomic force microscopy, microfluidics, cell migration and cell adhesion assays among others. It is hoped that from these studies, new and effective diagnostics for disease detection may be developed.

**9:40 AM**

**On the Structure and Mechanical Behavior of Scales from Cyprinus Carpio:** Adriana Garrano<sup>1</sup>; Dwayne Arola<sup>2</sup>; <sup>1</sup>University of Catania; <sup>2</sup>University of Maryland Baltimore County

In this investigation the microstructure and mechanical behavior of scales from Cyprinus Carpio (i.e. the common freshwater carp) were evaluated. Uniaxial tensile specimens were prepared from extracted scales and the constitutive behavior was characterized in the hydrated and dehydrated conditions and as a function of anatomic position (i.e. from head to tail). Dehydration was achieved using selected polar solvents. In the hydrated condition the scales exhibited an average tangent modulus of  $E < 0.5$  GPa, ultimate strength of  $\sim 60$  MPa and strain to failure of  $\epsilon_{max} \sim 12\%$ . Though dehydration caused significant changes in the elastic modulus (factor of 2



or more), the change in strength and strain to fracture was less substantial. There was some variation in the properties as a function of location, which appeared to correlate with the microstructure. Fish scales may provide a new model for compliant material designs requiring toughness and penetration resistance.

#### 10:00 AM

##### **Mechanical Properties and Laminate Structure of Arapaimas Gigas Scale:** Yen-Shan Lin<sup>1</sup>; Marc.A Meyers<sup>1</sup>; Eugene.A Olevsky<sup>1</sup>; <sup>1</sup>UCSD

The Arapaimas is one of the largest freshwater fish with a length of more than 2m, living in Amazon river. Their armor-like scales with laminate structure protects them from being attacked by the piranha. The scales are made by collagen and composed of highly mineralized external layer and soft internal layers. In this study, the mechanical properties and structure were investigated. The micro-hardness value of the external layer (550MPa) is higher than internal layer (200MPa) due to the higher mineral content in external layer. Tensile strength is higher in dry condition (53MPa) than in wet condition showing that hydration plays an important role in mechanical properties of the scales. The fracture surface investigated by SEM indicates that the pull-out collagen fibers is the main fracture mechanism. The structure of the demineralized scale exhibits 67-nm periodicity on the collagen fiber. And the deproteinized scale shows randomly orientation plate with 10nm thickness.

#### 10:20 AM Break

#### 10:30 AM Invited

##### **Biological Materials: A Materials Science Approach:** Marc Meyers<sup>1</sup>; Po-Yu Chen<sup>1</sup>; Maria Lopez<sup>1</sup>; Yasuaki Seki<sup>1</sup>; Albert Lin<sup>1</sup>; Joanna McKittrick<sup>1</sup>; <sup>1</sup>University of California, San Diego

The approach used by Materials Science and Engineering is revealing new aspects in the structure and properties of biological materials. The integration of advanced characterization, mechanical testing, and modeling methods can rationalize heretofore unexplained aspects of these structures. As an illustration of the power of this methodology, we apply it to biomineralized shells, avian beaks and feathers, and fish scales. We discuss removable attachment devices, focusing on the gecko, the abalone, and the Brazilian tree frog. We also present a few selected bioinspired applications: Velcro, an Al<sub>2</sub>O<sub>3</sub>-PMMA composite inspired on the abalone shell, and synthetic attachment devices inspired by the gecko. Research is supported by the NSF Grant DMR 1006931.

#### 11:00 AM

##### **Dynamic Mechanical Behavior of Shark Tesselated Skeleton:** Xiaoxi Liu<sup>1</sup>; Hamed Youssefpour<sup>1</sup>; Mason Dean<sup>2</sup>; Adam Summers<sup>3</sup>; James Earthman<sup>1</sup>; <sup>1</sup>University of California, Irvine; <sup>2</sup>Max Planck Institute of Colloids and Interfaces; <sup>3</sup>University of Washington

Much of the skeleton of sharks is characterized by a tessellated structure, comprised of mineralized tiles of hydroxyapatite called tesserae covering a soft hyaline cartilage core. The significance of this skeletal tissue type has not been well understood, particularly with regard to any mechanical advantages provided by the tiled structure. In the present work, dynamic mechanical behavior of blue shark tessellated cartilage was studied by performing both stress relaxation and percussion tests. Results from these tests indicate that tessellation strongly influences the dynamic stiffness and damping capacity of shark cartilage under loading that is parallel to the tessellated layer, while it has little effect on either of these properties under normal loading or impact. These findings reveal plausible advantages of shark tessellated skeletons: 1) allowing efficient movement and feeding activity; 2) reducing the risk of failure by lowering impact forces normal to the surface and effectively dissipating impact energy.

#### 11:20 AM

##### **Structure and Mechanical Behavior of Saxidomus Purpuratus Shells:** Wen Yang<sup>1</sup>; Marc Meyers<sup>1</sup>; Guang-Ping Zhang<sup>2</sup>; Xiao-Wu Li<sup>3</sup>; <sup>1</sup>University of California, San Diego; <sup>2</sup>Institute of Metal Research, Chinese Academy of Sciences; <sup>3</sup>College of Sciences, Northeastern University

The structure and mechanical behaviour of Saxidomus purpuratus bivalve shell were investigated. The inner and middle layers have a cross-lamellar structure, while the outer layer has porosity and does not have tiles, but 'blocky' regions. That leads to structure-dependent hardness. The hardness of outer layer decreases significantly compared with those of inner and outer layers, especially in the plane view. The compressive strength along the three different loading directions exhibits a significant difference. The cracking paths were found to be closely related to the loading direction. The Weibull strength at 50% of the probability of failure, with the loading direction perpendicular to the surface of the shell is much less than those in the other two orientations in shell plane loading. These differences are interpreted in terms of the anisotropic structures. Moreover, high cycle fatigue behavior was also investigated by three point bending testing through gradually increasing load method.

#### 11:40 AM

##### **Unveiling the Deformation and Toughening Mechanisms of Nacre – Lessons from Nature:** Xiaodong Li<sup>1</sup>; <sup>1</sup>University of South Carolina

Nacre is a natural nanocomposite with superior mechanical strength and toughness. What is the secret recipe that Mother Nature uses to fabricate nacre? What roles do the nanoscale structures play in the inelasticity and toughening of nacre? Can we learn from this to produce nacre-like nanocomposites? The recent discovery of nanoparticles in nacre is summarized, and the role these nanoparticles play in nacre's toughness is elucidated. It was found that rotation and deformation of aragonite nanoparticles are the two prominent mechanisms contributing to energy dissipation in nacre. The biopolymer spacing between nanoparticles facilitates the particle rotation process. Individual aragonite nanoparticles are deformable. Stacking fault and dislocation formation together with deformation twinning were found to play an important role in the plastic deformation of individual nanoparticles. This talk also presents future challenges in the study of nacre's nanoscale structure and mechanical properties.

#### 12:00 PM

##### **On the Growth and Mechanical Behavior of Abalone Nacre: Role of Organic Constituent:** Maria Lopez<sup>1</sup>; Po-Yu Chen<sup>1</sup>; Laura Connelly<sup>1</sup>; Ratnesh Lal<sup>1</sup>; Joanna McKittrick<sup>1</sup>; Marc Meyers<sup>1</sup>; <sup>1</sup>UCSD

Characterization of the growth surfaces removed from red abalone (*Haliotis rufescens*) shells is performed. Abalone shell is demineralized exposing the chitin matrix and its structural and mechanical components are analyzed. The details of the mineral and organic layer surface are revealed by atomic force microscopy (AFM) and scanning electron microscopy. AFM pull-off and nanoindentation experiments are performed on the organic interlayer. Indentation of the organic layer provides a force-deflection curve that can be expressed as tension on a centrally-loaded membrane. The effect of hydration of organic layer is revealed. Results allow insight to the biomineralization mechanism, further explaining the influence of the organic component in the process.

## **Bridging Microstructure, Properties and Processing of Polymer Based Advanced Materials: Session I**

*Sponsored by:* The Minerals, Metals and Materials Society, TMS Extraction and Processing Division, TMS Materials Processing and Manufacturing Division, TMS: Materials Characterization Committee, TMS: Shaping and Forming Committee, ASM-MSCTS: Texture and Anisotropy Committee

*Program Organizers:* Dongsheng Li, Pacific Northwest National Laboratory; Said Ahzi, University of Strasburg; Moe Kahleel, Pacific Northwest National Laboratory

Wednesday AM                      Room: 32B  
March 2, 2011                        Location: San Diego Conv. Ctr

*Session Chair:* Said Ahzi, University Louis Pasteur, Strasbourg

### **8:30 AM Introductory Comments**

#### **8:35 AM Keynote**

**Constitutive Modeling of Deformation Behaviour of Semicrystalline Polymers under Small Strains:** Stanislav Patlazhan<sup>1</sup>; Yves Remond<sup>2</sup>; <sup>1</sup>Russian Academy of Sciences; <sup>2</sup>University of Strasbourg

The constitutive modelling of tensile deformation behaviour of semicrystalline polymers under small strains is discussed. The heterogeneous materials are treated within the two-phase model comprised of the crystalline elastoplastic component imbedded into the soft amorphous domain. Structural transformations between the hard and soft components are assumed to obey thermofluctuation mechanisms. The plastic flow is supposed to occur within the hard component due to the inter- and intralamellar sliding. One-dimensional basic structural-mechanical element (BSME) as the structure-sensitive model of the deformed material is analysed in the limits of linear and nonlinear dependences on the applied stresses. Our analysis and results suggest that instead of a single element, the spectrum of the interacting BSME of different structural-mechanical properties reflecting strong heterogeneity of semicrystalline polymers should be considered. This approach is shown to provide the best fitting of tensile behaviour of iPP at different strain rates below the yield point.

#### **9:05 AM**

**Molecular Dynamics Simulation of Diffusion of Atmospheric Penetrates in Polydimethylsiloxane based Nanocomposites:** Alexander Sudibjo<sup>1</sup>; Varun Ullal<sup>1</sup>; Douglas Spearot<sup>1</sup>; <sup>1</sup>University of Arkansas

Molecular dynamics (MD) simulations are used to study the nanoscale mechanisms associated with diffusion of small atmospheric penetrates in polydimethylsiloxane (PDMS) based nanocomposites with metallic inclusions. PDMS is modeled within the MD framework using a hybrid coarse-grained interatomic potential which retains atomic distinction along the siloxane backbone but models the methyl side groups as united atoms. In a novel contribution, crosslinking is incorporated into the nanocomposite model via the introduction of tetra(dimethylsiloxy)silane crosslinking agents combined with silanol-terminated PDMS chains. Diffusion-related material properties are extracted over a range of temperatures for both N<sub>2</sub> and O<sub>2</sub> penetrates, allowing for the calculation of diffusion constants and activation energies using an Arrhenius style equation. Ultimately, these calculations are motivated by the need to calibrate a recently developed PDMS-based sensor, where metallic nanoparticles are embedded within a PDMS matrix.

#### **9:25 AM**

**Nanostructuring of Polymers for Energy, Drug Delivery and Bio-Implant Systems:** Frédéric Addiego<sup>1</sup>; Marc Michel<sup>1</sup>; Valérie Toniazzo<sup>1</sup>; David Ruch<sup>1</sup>; <sup>1</sup>CRP Henri Tudor

The search for a method to design nanostructures from a variety of materials is of growing interest. As the commercialization of nanotechnology continues to expand, the ability to translate design methods from a laboratory to applications is of increasing significance. In our Institute, we examine

several of the most readily scalable bottom-up methods for the fabrication of such structures made of particles and polymers. In this frame, we propose to employ versatile and straightforward methods of processing (layer-by-layer, plasma polymerization and extrusion) allowing to fabricate materials whose architectures and properties make them suitable for energy, drug delivery and bio-implants development.

#### **9:45 AM**

**A Bilinear Semi-Empirical Constitutive Model for an Orthotropic Material:** Edmond Saliklis<sup>1</sup>; Jorien Baza<sup>1</sup>; <sup>1</sup>California Polytechnic State University

This study developed a nonlinear constitutive model for a sustainable orthotropic material. The model is semi-empirical in that it is grounded in mechanics principles but it was slightly modified to capture the behavior of a specific nonlinear material. The material is an extruded composite made of a recycled polypropylene homopolymer reinforced with the agricultural fiber kenaf. Fifty-six tension tests were performed to solve for Young's modulus at various angles to the primary axis of the material. These experimentally obtained values formed the basis of the body of data used to create the new constitutive model. The new constitutive model simplified the nonlinear stress-strain relationships into bilinear stress-strain curves. The "break" in the bilinear curve is based on strain energy principles. The proposed constitutive model captures the modulus of elasticity through any angle from the primary extruded axis and comparisons of the model to experimental data will be shown.

#### **10:05 AM Break**

#### **10:20 AM**

**Fabrication and Characterization of Super Strong Cellulose Nanowhisker Paper:** Dongsheng Li<sup>1</sup>; Hamid Garmestani<sup>2</sup>; <sup>1</sup>Pacific Northwest National Laboratory; <sup>2</sup>Georgia Institute of Technology

Effective property prediction is the cornerstone for performance evaluation of materials applied under irradiation condition. Phase field model and molecular dynamics model are used to predict the microstructure and local properties. Different methods have been developed to bridge low scale models with polycrystalline level models. Finite Element Analysis (FEA), microstructure informed FEA, self consistent models, Taylor models, Sachs models and statistical continuum mechanics are evaluated. Cost, efficiency and accuracy were compared for these methods. Pros and cons, depending on the problems studied, are discussed. While open to discussion, general recommendation on bridging methodology is presented based on different scenarios.

#### **10:40 AM**

**Fully Recoverable High Strain Shape Memory Polymers:** Walter Voir<sup>1</sup>; Taylor Ware<sup>1</sup>; Ken Gall<sup>2</sup>; <sup>1</sup>UT Dallas; <sup>2</sup>Georgia Tech

Shape-memory polymers (SMPs) with recoverable strains of more than 800%, twice the previously published literature value, are demonstrated. SMPs are self-adjusting, smart materials in which shape changes are controlled at specific, tailored temperatures. We adjust the glass transition temperature (T<sub>g</sub>) between 28 °C and 55 °C through synthesis of copolymers of methyl acrylate, methyl methacrylate and isobornyl acrylate. SMPs with both crosslinker densities and photoinitiator concentrations optimized at fractions of a mole percent, demonstrate fully recoverable strains at 807% for a T<sub>g</sub> of 28 °C, at 663% for a T<sub>g</sub> of 37 °C and at 553% for a T<sub>g</sub> of 55 °C. We synthesized a novel compound, 4,4'-di(acryloyloxy)benzyl, polymerized it into acrylate SMPs and characterized the resulting polymer which yielded fully recoverable strains above 500%. These materials are intended to enable future applications where recoverable high strain capacity and the ability to accurately and independently position T<sub>g</sub> are required.

11:00 AM

**Hydroxyapatite Reinforced Polymer Biocomposites with Tailored Mechanical Properties through Microstructure Design:** *Ryan Roeder*<sup>1</sup>; Timothy Conrad<sup>1</sup>; Jeffrey Vitter<sup>1</sup>; Justin Deuerling<sup>1</sup>; <sup>1</sup>University of Notre Dame

Hydroxyapatite (HA) reinforced polymers were first conceived as a bone-analog biomaterial enabling mechanical properties to be tailored to mimic those of bone tissue, but have generally fallen short of bone tissue at comparable levels of porosity and HA content. Recently, dense or porous HA whisker reinforced polyaryletherketone (PAEK) biocomposites have been engineered to mimic the elastic properties human bone tissue. Novel powder processing and compression molding methods enabled the dispersion of high volume fractions of HA reinforcements. Single crystal HA whiskers enabled improved load-transfer from the matrix to reinforcement, resulting in significantly improved static and fatigue properties when directly compared to equiaxed powder reinforcements. A multiscale, micromechanical model was also developed to accurately predict the anisotropic elastic constants from the HA whisker volume fraction, aspect ratio distribution, and orientation distribution.

11:20 AM

**Computer-Aided Design, Processing and Characterization of Polymer-Matrix Magnetic Composites:** *Tianle Cheng*<sup>1</sup>; Jie Zhou<sup>1</sup>; Yu Wang<sup>1</sup>; <sup>1</sup>Michigan Technological University

Diffuse interface field models of magnetic particle self-assembly and polymer-matrix magnetic composites are developed to study the processing-microstructure-property relationships and the underlying mechanisms. Ferro-colloidal processing under external magnetic field is investigated as a fabrication route to particle-matrix microstructure control. Directed self-assembly of dipolar interacting particles in uncured polymer matrix is simulated to understand the mechanisms responsible for controlled formation of particulate microstructures. The simulated evolution of particle microstructures during composite fabrication process is seamlessly incorporated into the magnetic composite model to perform in-situ property characterization, which provides a way for real-time monitoring of microstructure optimization. It is shown that, with the gradual formation of aligned particles into fibrous microstructures along external field direction from randomly-dispersed initial state, the effective composite properties develop strong magnetic anisotropy. The effects of composite microstructures on the effective magnetic properties are discussed.

11:40 AM

**Effects of Filler Microstructures on Effective Properties of Magnetic Composites: Phase Field Modeling and Simulation:** *Jie Zhou*<sup>1</sup>; Tian-Le Cheng<sup>1</sup>; Yu Wang<sup>1</sup>; <sup>1</sup>Michigan Technological University

Phase field model is developed to calculate heterogeneous distributions of magnetization and magnetic field and effective susceptibility of magnetic composites with arbitrary multi-component microstructures, where inter-phase boundary conditions are automatically satisfied without explicitly tracking inter-phase interfaces in the composites. Computer simulation is performed to study the relationships between filler microstructures and effective properties of magnetic composites. Composites composed of paramagnetic, superparamagnetic and non-magnetic (diamagnetic) constituent components are considered. Various factors associated with filler microstructures are investigated, including particle size, shape, orientation, volume fraction, spatial arrangement and directional alignment. It is found that dipole (and multipole) interactions among high-susceptibility fillers and the resultant effective demagnetization factors of filler ensembles play critical roles in determining the composite properties, which sensitively depend on filler arrangement and, especially, directional alignment into fibrous microstructures (chains). Such microstructurally engineered composites, whose fillers are not randomly dispersed, exhibit strong magnetic anisotropy despite all constituent components are isotropic.

**Bulk Metallic Glasses VIII: Fatigue and Corrosion**

*Sponsored by:* The Minerals, Metals and Materials Society, TMS Structural Materials Division, TMS/ASM: Mechanical Behavior of Materials Committee

*Program Organizers:* Gongyao Wang, University of Tennessee; Peter Liaw, Univ of Tennessee; Hahn Choo, Univ of Tennessee; Yanfei Gao, Univ of Tennessee

Wednesday AM

March 2, 2011

Room: 6D

Location: San Diego Conv. Ctr

*Session Chairs:* Y. Yokoyama, Institute for Materials Research; Jamie Kruzic, Oregon State University

8:30 AM Invited

**Fracture and Fatigue in Monolithic and Composite Metallic Glasses:**

*Robert Ritchie*<sup>1</sup>; Maximillien Launey<sup>2</sup>; Douglas Hofmann<sup>3</sup>; William Johnson<sup>3</sup>; <sup>1</sup>University of California Berkeley; <sup>2</sup>Lawrence Berkeley National Laboratory; <sup>3</sup>California Institute of Technology

The mechanical properties of bulk metallic glasses (BMG) are often plagued by low fracture and fatigue resistance. Correspondingly, much effort in recent years has been devoted to improving their damage tolerance properties, either through compositional changes or by introducing some degree of microstructure. By matching the microstructural length scales (of a second phase) to mechanical crack-length scales, metallic glass matrix composites can demonstrate strongly improved tensile ductility, toughness, and fatigue resistance. These improvements are explained by the effect of the mechanically soft and ductile second phase, which acts stabilizing against shear localization and critical crack propagation; it results in extensive plastic shielding, which further stabilizes crack growth. In this talk, the fracture and fatigue behavior of semi-solidly processed Zr- and Ti-based BMG matrix composites with in-situ dendritic phase were examined. Specifically resistance-curve, fatigue crack-growth, and stress-life behavior are here presented in light of the relevant toughening and fatigue mechanisms involved.

8:50 AM

**Zr-Based Glass-Forming Film for Fatigue-Property Improvements of 316L Stainless Steel: Annealing Effects:** *Jinn P. Chu*<sup>1</sup>; *Cheng-Min Lee*<sup>1</sup>;

*R. T. Huang*<sup>2</sup>; *Jia-Hong Zhu*<sup>1</sup>; *Peter K. Liaw*<sup>3</sup>; <sup>1</sup>Nation Taiwan University of Science and Technology; <sup>2</sup>National Taiwan Ocean University; <sup>3</sup>The University of Tennessee

When annealed in the supercooled liquid region ( $\square T$ ),  $Zr_{53}Cu_{29}Al_{12}Ni_6$  metallic glass thin film exhibits a uniform structure relative to the metastable as-deposited film because of the annihilation of the columnar structure. Microstructure became condensed due to the structure relaxation and free volume equilibrated in the annealed film. Therefore, it is expected that the annealed Zr-based glass-forming film would improve mechanical properties such as high strength, enhanced ductility, and smooth surface, along with good adhesion to the substrate. These properties are considered to be key factors that will improve the fatigue resistance of materials. A fatigue test of coated 316L stainless steel was carried out. Under a stress of 750 MPa, the fatigue life was improved from  $4.4 \times 10^5$  cycles of the uncoated sample by  $\sim 10$  times to  $4.5 \times 10^6$  cycles, and further improved by more than 22 times to  $10^7$  cycles when the annealing was applied.

9:00 AM Invited

**Fatigue of Zr-Based Bulk Metallic Glass under Cyclic Shear Stress:**

*Yoshikazu Nakai*<sup>1</sup>; *Kenich Nakagawa*<sup>1</sup>; *Kohei Mikami*<sup>1</sup>; <sup>1</sup>Kobe University

Fatigue strength of Zr-based bulk metallic glass plate with rectangular cross-section was conducted under cyclic torsion to reconcile the applicability of fracture criteria. A computer-controlled direct drive motor driven fatigue testing machine was developed for the tests. The stress ratio, R, was -1 and the loading frequency was 10 Hz. It was found that fatigue cracks initiated from the center of the side surface although the maximum shear stress was higher at the center of plate surface than that at the center of side surface for

WEDNESDAY AM



the shape of specimen which was employed for the present study. It suggests that the fatigue strength of BMG is considered to depend on the cooling rate in the casting process of the material, which is different along the thickness direction. Then, the criteria for fatigue limit under combined stress for metallic glass should be constructed by considering the crack initiation site.

### 9:20 AM Invited

**Fatigue Crack Growth in Zr-Based Bulk Metallic Glasses:** *Jamie Kruzic*<sup>1</sup>; Sarah Philo<sup>1</sup>; Maximilien Launey<sup>2</sup>; <sup>1</sup>Oregon State University; <sup>2</sup>Lawrence Berkeley National Laboratory

Fatigue crack growth rates were measured for  $Zr_{44}Ti_{11}Ni_{10}Cu_{10}Be_{25}$  and  $Zr_{58.5}Nb_{2.8}Cu_{15.6}Ni_{12.8}Al_{10.3}$  bulk metallic glasses (BMGs). Growth rate data overlapped considerably for both. The former BMG was tested in different initial free volume states, different residual stress states, and in both ambient air and dry nitrogen environments. Fatigue crack growth rates were relatively unaffected by the initial free volume state. This was attributed to the formation of a fatigue transformation zone of increased local free volume at the fatigue crack tip. When residual stresses were not annealed out, it was found that the fatigue threshold and fracture toughness increased due to residual compressive stresses at the sample surfaces. Finally, it was observed that testing in a dry nitrogen environment significantly increased the fatigue threshold, suggesting a corrosion fatigue mechanism in ambient air. A similar environmental effect was observed for the Zr-Nb-Cu-Ni-Al BMG in ambient air, but at very different growth rates.

### 9:40 AM

**The Effect of Structural Ordering on Active, Passive and Localized Corrosion in an Amorphous Cu75Hf20Dy05 Alloy:** *Derek Horton*<sup>1</sup>; John Scully<sup>1</sup>; <sup>1</sup>University of Virginia

The role of structural change on the corrosion properties of amorphous alloys is unclear. An amorphous material that undergoes devitrification without changing composition is an ideal specimen to reveal the effect of structural ordering on corrosion properties in the absence of an accompanying chemical partitioning. This study focuses on the Cu75Hf20Dy05 amorphous alloy systems which undergoes single phase devitrification to a stoichiometrically equivalent solid solution. The global corrosion behavior of this system was studied during active, passive, and passive/pitting conditions. The results indicate that the ordered crystal structure plays a dominant role in the corrosion behavior due to the periodic presence of beneficial solute atoms which can enhance (a) oxide formation, (b) impeded dissolution, (c) and alter surface diffusion.

### 9:50 AM Invited

**Why Can't The Excellent Corrosion Resistance of Amorphous and Amorphous-Nanocrystalline Melt Spun Alloys be Achieved in Thermally Sprayed Coatings?:** *J.R. Scully*<sup>1</sup>; N. Tailleart<sup>1</sup>; T. Aburada<sup>1</sup>; D. Horton<sup>1</sup>; R. Huang<sup>1</sup>; A. Lucente<sup>1</sup>; <sup>1</sup>University of Virginia

We have previously investigated the corrosion resistance of selected aluminum, transition metal, rare earth metallic glass alloys (Al-Co-Ce, Al-Fe-Gd, Al-Ni-Y) in the form of ribbons spun from the molten state. These have been analyzed in the as-spun amorphous, relaxed amorphous, amorphous + nano-crystalline, and fully crystalline states. Results suggest that certain structural and/or chemical non-uniformities strongly affect corrosion resistance while other defects are not detrimental at certain length scales. These findings were compared to results on low porosity Al-Co-Ce metallic coatings applied to various substrates deposited using a pulsed thermal spray (PTS) process. Coating thicknesses ranged from 100 to 500  $\mu\text{m}$ . Coatings were characterized using a variety of metallurgical and corrosion methods. The localized corrosion properties of the PTS applied coating samples were inferior to those of compositionally equivalent fully amorphous melt spun ribbons even when synthesized using the same feedstock powders. The inferior corrosion behavior in coatings was traced to presence of certain metallurgical and physical defects but not others.

### 10:10 AM Break

### 10:20 AM

**Investigation of the Corrosion Behavior of a Zr-Based Bulk Metallic Glass:** *Courtney Harmon*<sup>1</sup>; Mary Cavanaugh<sup>1</sup>; Katharine Flores<sup>1</sup>; Rudolph Buchheit<sup>1</sup>; <sup>1</sup>The Ohio State University

While research has proven the exceptional mechanical properties of bulk metallic glasses (BMG's), little is known about the corrosion properties of Zr-based BMG's. The corrosion behavior of a  $Zr_{58.5}Nb_{2.8}Cu_{15.6}Ni_{12.8}Al_{10.3}$  BMG exposed to dilute chloride solutions with pH values ranging from 2 to 12 was characterized by cyclic polarization. Results showed that the glass is spontaneously passive across this pH range exhibiting passive current densities less than  $1 \mu\text{A}/\text{cm}^2$  between pH 2 and 10, and only slightly greater at pH 12. Passive film breakdown occurred during anodic polarization with breakdown potentials ranging from -0.05 to -0.15  $V_{\text{sec}}$  from pH 2 to 10 with a significant increase to +0.45  $V_{\text{sc}}$  at pH 12. Repassivation occurred at about -0.20  $V_{\text{sc}}$  and did not appear to vary with solution pH. Additionally, free corrosion exposure experiments were performed to characterize corrosion mode and morphology as a function of pH and results are to follow.

### 10:30 AM Invited

**Characterization of Shear Bands Induced by Three-Point Bending Fatigue Test in Zr-Cu-Al Bulk Metallic Glass:** *Pei-Ling Sun*<sup>1</sup>; Gongyao Wang<sup>2</sup>; Peter Liaw<sup>2</sup>; <sup>1</sup>Feng Chia University; <sup>2</sup>University of Tennessee

Zr50Cu40Al10 bulk metallic glass was deformed by three-point bending fatigue test. Shear bands appeared on the tension and compression sides after deformation. Characterization of these shear bands by scanning electron microscopy (SEM) reveals the presence of different fracture modes: river pattern and smooth fracture path. Cross sections of the shear bands were then cut by focused ion beam (FIB) for transmission electron microscopy (TEM) observation. The microstructure of the shear bands will be investigated in detail and the deformation mechanism will be discussed.

### 10:50 AM

**Four-Point-Bending Fatigue Study on a Tough Fe-Based Bulk-Metallic Glass:** *Gongyao Wang*<sup>1</sup>; Marios Demetriou<sup>2</sup>; Peter Liaw<sup>1</sup>; William Johnson<sup>2</sup>; <sup>1</sup>University of Tennessee; <sup>2</sup>Keck Laboratory

Amorphous steel alloys of Fe-(Mo,Ni,Cr)-(C,B)-P have recently been developed. These Fe-based bulk metallic glasses exhibit low shear moduli, high toughness, and good glass-forming ability. In the current investigation, Fe70Mo5Ni5C5B2.5P12.5 glassy rods with 3 mm in diameter were fabricated and then polished to  $2 \times 2 \times 25 \text{ mm}^3$  rectangular beam samples. Four-point-bending fatigue experiments are performed on these Fe70Mo5Ni5C5B2.5P12.5 beam samples in air. The applied stress versus cycles to failure (S-N) curve will be presented. Moreover, a mechanistic insight into the mechanism governing the fatigue failure in a low-shear-modulus high-toughness Fe-based bulk-metallic glasses will be proposed. Acknowledgement: This work is financially supported by the US National Science Foundation, under CMMI-0900271 and DMR-0909037, with Drs. C. V. Cooper, Dr. D. Finotello, and Dr. A. Ardell as contract monitors.

### 11:00 AM Invited

**Compression-Compression Fatigue Behaviour of Zr-Based Bulk Metallic Glass (BMG): The Effects on the Near-Surface Residual-Stresses:** *Bartłomiej Winiarski*<sup>1</sup>; Gongyao Wang<sup>2</sup>; Yoshihiko Yokoyama<sup>3</sup>; Peter Liaw<sup>2</sup>; Philip Withers<sup>1</sup>; <sup>1</sup>University of Manchester; <sup>2</sup>The University of Tennessee; <sup>3</sup>Tohoku University

The influence of compression-compression fatigue conditions on evaluation of near-surface residual stresses (RS) in rod-like  $Zr_{50}Cu_{30}Al_{10}Ni_{10}$  bulk metallic glass (BMG) was studied. The fatigue tests were conducted at ambient temperature, with a maximum stress of 1525 MPa. After the fatigue experiment residual-stresses were inferred locally, in volumes about  $20 \times 20 \times 5 \mu\text{m}^3$ , by applying a focused ion beam (FIB)-based micro-slotting semidestructive mechanical relaxation method. The results show that the compression-compression fatigue increases beneficial compressive residual-stresses depending on the maximum fatigue stress, and mapped locations on the sample. The compressive residual stress elevates with higher fatigue

stress and reaches its maximum near the sample grips. Whereas, in the middle of the sample, the compressive RS experience minor improvement.

#### 11:20 AM

**Effects of Frequency on Fatigue Behavior of Zr-Base Bulk Metallic Glasses:** *Qingming Feng*<sup>1</sup>; Gongyao Wang<sup>1</sup>; Lu Huang<sup>2</sup>; Peter Liaw<sup>1</sup>; <sup>1</sup>University of Tennessee; <sup>2</sup>Beijing University of Aeronautics & Astronautics

Fatigue tests were conducted on Zr-base Bulk Metallic Glasses (BMGs) using a state-of-the-art high-frequency, 1000-Hz, material test system. Fatigue experiments were conducted at high (1000 Hz), mid-high (100 Hz) and conventional (10 Hz) frequencies in air at room temperature. The effects of the test frequency, and temperature increase during fatigue are discussed. Following the completion of fatigue tests, the samples were examined by scanning electron microscopy (SEM) to identify the failure mechanisms and transition regions, several possible explanations are presented to explain the observed frequency effects. Acknowledgement: G. Y. Wang and P. K. Liaw very much appreciate the financial support of the US National Science Foundation, under DMR-0909037, and CMMI-0900271, with Drs. A. Ardell, Dr. D. Finotello, and Dr. C. V. Cooper as contract monitors. Q. M. Feng wishes to gratefully acknowledge the financial support provided for this study by the National Science Foundation.

#### 11:30 AM Invited

**Investigating the Effects of Fatigue on Annealed and As-Quenched Zr-Based Bulk Metallic Glasses:** *Peng Tong*<sup>1</sup>; Despina Louca<sup>1</sup>; Peter Liaw<sup>2</sup>; Gongyao Wang<sup>2</sup>; Yoshihiko Yokoyama<sup>3</sup>; <sup>1</sup>University of Virginia; <sup>2</sup>University of Tennessee; <sup>3</sup>Tohoku University

Bulk metallic glasses (BMGs) exhibit unique physical properties and understanding their mechanical response is central to their application as engineering materials. In order to look for a structural signature resulting from changes brought upon by fatigue, the local atomic structures of Zr-glasses Zr<sub>50</sub>Cu<sub>40</sub>Al<sub>10</sub> (Zr541) and Zr<sub>60</sub>Cu<sub>30</sub>Al<sub>10</sub> (Zr631) were investigated via the pair density function analysis of synchrotron X-ray diffraction data. A comparison of the local atomic configuration of as-quenched and annealed alloys indicated that annealing induces some local ordering in the structure of Zr631. For Zr541, a weaker change on the local structure from annealing was observed. However, the local structure changes after cyclic loading are more dramatically observed in the annealed sample than in the as-quenched one. Our results indicate that the physical properties of BMGs following fatigue loading conditions may be influenced by structural relaxation, with annealing leading to observable differences at the atomic level under fatigue.

#### 11:50 AM

**Interpreting Temperature Change in Shear Bands of a Bulk-Metallic Glass Using Spatial-Temporal Analysis:** *Jiajia Luo*<sup>1</sup>; Gongyao Wang<sup>1</sup>; Hairong Qi<sup>1</sup>; Yoshihiko Yokoyama<sup>2</sup>; Peter Liaw<sup>1</sup>; Akihisa Inoue<sup>2</sup>; <sup>1</sup>University of Tennessee; <sup>2</sup>Institute for Materials Research

Infrared imaging represents an innovative sensing modality to study interior structure of metallic glasses such that hidden defects like fracture can be identified and handled in a controlled way. However, how to interpret the temperature change from infrared images across the entire glass over certain period of time remains a challenging problem. This paper formulates the temperature evolution over time across spatial domain using a linear mixing model and presents robust unsupervised unmixing algorithm such that joint effects of hidden (or source) events (or defects) can be identified, providing prevailing support to the understanding of IR image of Bulk-Metallic Glass. Besides characterizing the internal structural change under pressure, the proposed unmixing algorithm also has the potential to reveal depth information of the defect, which is a breakthrough to functional infrared imaging.

#### 12:00 PM Invited

**Fatigue and Fracture Behavior of a Ca-Based Bulk-Metallic Glass:** *Julian Raphael*<sup>1</sup>; Gongyao Wang<sup>2</sup>; Peter Liaw<sup>2</sup>; Oleg Senkov<sup>3</sup>; Dan Miracle<sup>3</sup>; <sup>1</sup>J R Technical Services, LLC; <sup>2</sup>University of Tennessee; <sup>3</sup>Air Force Research Laboratory

The compression and fatigue behavior of a Ca<sub>65</sub>Mg<sub>15</sub>Zn<sub>20</sub> bulk-metallic glass (BMG) was studied in air at room temperature. During the preparation of cubical samples of the Ca<sub>65</sub>Mg<sub>15</sub>Zn<sub>20</sub> for compression and fatigue investigations, small spherical cavities were found. Under both monotonic and cyclic compression loadings of the samples, fractures initiated at these cavities and propagated in a direction generally parallel to the loading axis. Finite-element analysis (FEA) was used to model the fracture behavior. The FEA of a centrally located spherical void showed that under compression loading, large tensile stresses evolved in the cavities. The orientation of the maximum principal stress (P1) was found to be normal to the direction of crack propagation, which is consistent with the experimental finding. Stresses in deeply embedded adjacent voids and those in superficial voids were also studied. The influence of the void location in the cubical sample on the fracture behavior was quantitatively discussed.

#### 12:20 PM

**Studying Fatigue-Crack-Propagation Behavior of Zr-Based Bulk-Metallic Glasses:** *Gongyao Wang*<sup>1</sup>; P. Liaw<sup>1</sup>; Y. Yokoyama<sup>2</sup>; Q. Feng<sup>1</sup>; T Toll<sup>1</sup>; A. Inoue<sup>2</sup>; <sup>1</sup>University of Tennessee; <sup>2</sup>Institute for Materials Research

The fatigue-crack-propagation behavior is very critical for predicting the fatigue life of structural materials. Various compositions of zirconium (Zr)-based bulk-metallic glasses (BMGs) were fabricated by an arc-melt tilt-casting technique. The casting rods were cut into disk-shaped compact-tension specimens. Fatigue-crack-growth-rate experiments were performed on these BMG samples in air. The experiments were conducted at a frequency of 10 Hz, using an electrodynamic test instrument with an R ratio of 0.1, where  $R = \sqrt[963]{\min/\max}$ ,  $\sqrt[963]{\min}$  and  $\sqrt[963]{\max}$  are the applied minimum and maximum absolute stresses, respectively. The crack-growth rates of Zr-based BMGs with different compositions will be presented. A mechanistic understanding of the fatigue behavior of these Zr-based BMGs is suggested. Acknowledgement: This work is financially supported by the US National Science Foundation, under CMMI-0900271 and DMR-0909037, with Drs. C. V. Cooper, Dr. D. Finotello, and Dr. A. Ardell as contract monitors.

### Cast Shop for Aluminum Production: Melt Quality Control

*Sponsored by:* The Minerals, Metals and Materials Society, TMS Light Metals Division, TMS: Aluminum Committee, TMS: Aluminum Processing Committee  
*Program Organizers:* Geoffrey Brooks, Swinburne University of Technology; John Grandfield, Grandfield Technology Pty Ltd

Wednesday AM  
March 2, 2011

Room: 16A  
Location: San Diego Conv. Ctr

*Session Chairs:* Claude Dupuis, Rio Tinto Alcan; Steinar Benum, Alcoa Norway

#### 8:30 AM Introductory Comments

#### 8:35 AM

##### In-Line Salt-ACD™:

**A Chlorine-Free Technology for Metal Treatment:** *Patrice Robichaud*<sup>1</sup>; Claude Dupuis<sup>1</sup>; Alain Mathis<sup>2</sup>; Pascal Coté<sup>3</sup>; Bruno Maltais<sup>3</sup>; <sup>1</sup>Rio Tinto Alcan, Arvida Research & Development Centre; <sup>2</sup>Rio Tinto Alcan, Aluval; <sup>3</sup>STAS

A new generation of the Alcan Compact Degasser (ACD™), the Salt-ACD™, based on the utilization of salt fluxes in replacement of chlorine gas, was introduced to the aluminum industry [1]. This unique technology has been developed by Rio Tinto Alcan (RTA) since 2003 and in collaboration

with La Société des Technologies de l'Aluminium du Saguenay (STAS). Its utilization in combination with the Rotary Flux Injector (RFI<sup>TM</sup>) for furnace preparation and/or the Treatment of Aluminum in Crucible (TAC<sup>TM</sup>) for aluminum pre treatment eliminates the use of chlorine in casthouses. The Salt-ACD<sup>TM</sup> technology has been successfully implemented and operated in RTA casthouses. It supports the objective of eliminating chlorine from the casthouse for health, safety and environmental reasons. This paper presents recent developments in terms of equipment, key components and retrofittability to existing ACD<sup>TM</sup> units. The operating experience and metallurgical performance are reviewed.

### 9:00 AM

**The Effect of TiB<sub>2</sub> Granules on Metal Quality:** Maryam Al Jallaf<sup>1</sup>; Margaret Hyland<sup>2</sup>; Barry Welch<sup>3</sup>; Ali Al Zarouni<sup>1</sup>; Fahimi Abdullah<sup>1</sup>; <sup>1</sup>DUBAL; <sup>2</sup>University of Auckland; <sup>3</sup>Welbank Consulting

TiB<sub>2</sub> granules were added to a fully graphitized electrolytic cell in a trial to provide a barrier coating on the carbon cathode to prolong cathode life. The consequential impact on metal cleanliness was evaluated by a detailed metallographic analysis using the PoDFA technique. Metal produced from the test cell was mixed with regular potline metal and cast into billets. Samples were taken from different locations in the process stream and also for three different types of metal charged into the furnace, namely regular potline metal, 10 tons of metal from test cell mixed with regular potline metal, and 20 tons of metal from test cell mixed with regular metal. The PoDFA analysis shows that samples containing metal from test cell had more grain refiner inclusions than regular potline metal but fewer carbide inclusions. However, there was no overall significant negative impact on the specified requirements of metal cleanliness.

### 9:25 AM

**Thermodynamic Analysis of Ti, Zr, V and Cr Impurities in Aluminium Melt:** Abdul Khaliq<sup>1</sup>; Muhammad Rhamdhani<sup>1</sup>; Geoffrey Brooks<sup>1</sup>; <sup>1</sup>Swinburne University of Technology

Aluminium has been considered as an alternative for copper conductor applications. Metal impurities in particular Ti, Zr, V and Cr in the solution affect the electrical conductivity of aluminium significantly. Industrially boron treatment has been used to remove these impurities through the formation of borides. However solution thermodynamics and reaction mechanics of the borides formation in an aluminium melt are not well understood. In the present study, thermodynamic analysis has been carried out to investigate and elaborate the formation of various borides in aluminium melt. It has been shown in this study that diborides (MB<sub>2</sub>) were the most thermodynamically stable boride compounds of these impurities in the given working conditions. The ZrB<sub>2</sub>, TiB<sub>2</sub> and VB<sub>2</sub> particles were more stable compared to AlB<sub>2</sub> and CrB<sub>2</sub> hence did not dissolve readily. It is also shown that the relative stability of boride particles has been affected by the presence of other metal diborides.

### 9:50 AM

**Current Technologies for the Removal of Iron from Aluminum Alloys:** Lifeng Zhang<sup>1</sup>; Jianwei Gao<sup>2</sup>; <sup>1</sup>Missouri University of Science and Technology; <sup>2</sup>Shanghai Jiao Tong University

In the current paper, the Fe-rich phases in and their detrimental effect on aluminum alloys are summarized. The use of high cooling rate, solution heat treatment and addition of elements such as Mn, Cr, Co, Be and Sr are reported to modify the platelet Fe-rich phases in aluminum alloys. Technologies to remove iron from aluminum are extensively reviewed, including gravitational separation, electromagnetic separation, and centrifuge. Other methods include electrolysis, electro-slag refining, fractional solidification, fluxing refining, and three-layer cell electrolysis process.

### 10:15 AM Break

### 10:25 AM

**Electromagnetically Enhanced Filtration of Aluminum Melts:** Mark Kennedy<sup>1</sup>; Shahid Akhtar<sup>1</sup>; Ragnhild Aune<sup>1</sup>; Jon Bakken<sup>1</sup>; <sup>1</sup>Norwegian University of Science and Technology

The major drawback of the use of Ceramic Foam Filters (CFF) for purification of aluminum is their low efficiency for particles in the range of

10-30 µm. The application of electromagnetic force from an induction coil in combination with a filter can cause back mixing and recirculation through the filter media. In the present work an experimental set-up has been designed, built and verified by studying the meniscus behavior of molten aluminum under varying magnetic field strength. Batch type filtration experiments with 30 ppi CFF were also conducted with and without a magnetic field using an A356 aluminum alloy containing 20% anodized and lacquered plates, as well as 20% composite material (A356 base and 15% SiC particles with size range 10-50 µm). The presence of a magnetic field has proven to have both an effect on the build up of the filter cake, as well as on the re-distribution of particles within the filter.

### 10:50 AM

**A Review of the Development of New Filter Technologies Based on the Principle of Multi Stage Filtration with Grain Refiner Added in the Intermediate Stage:** John Courtenay<sup>1</sup>; Stephen Instone<sup>2</sup>; Frank Reusch<sup>3</sup>; <sup>1</sup>MQP Limited; <sup>2</sup>Hydro Aluminium Deutschland GmbH; <sup>3</sup>Drache Umwelttechnik GmbH

Recent developments in filtration technology based on the principle of using a three stage process where a ceramic foam filter is operated in cake mode in the first stage; grain refiner is added in a second chamber and a further filtration means is used in the third stage to remove oxide inclusions or agglomerates originating from the grain refiner addition are reviewed. The first development – the XC Filter, was presented by Instone et al in 2005 and described a system where a small deep bed filter (DBF) was successfully applied in the third chamber. A second prototype multi stage filter was described at TMS 2008 based on the same principle but with a cyclone deployed in the final chamber. An industrial prototype was constructed based on water modeling work and plant trials were undertaken. The current stage of development of each system and their relative merits are evaluated.

### 11:15 AM

**Wettability of Aluminium with Sic and Graphite in Aluminium Filtration:** Sarina Bao<sup>1</sup>; Anne Kvithyld<sup>2</sup>; Thorvald Engh<sup>1</sup>; Merete Tangstad<sup>1</sup>; <sup>1</sup>NTNU; <sup>2</sup>SINTEF

The aim of aluminium filtration is to remove inclusions such as Al<sub>3</sub>C<sub>4</sub>. For inclusions to be removed they have to come in close contact with the filter walls composed of Al<sub>2</sub>O<sub>3</sub> or SiC. It is therefore important that the molten aluminium has close contact with the filter wall. In addition to wetting properties between inclusions (Al<sub>4</sub>C<sub>3</sub>) and molten aluminium, the wettability of the filter (SiC) by aluminium is determined in sessile drop studies in the temperature range 1000-1300°C. Wettability changes with time in three successive steps and improves with time. To describe wettability at filtration temperatures employed in the industry of around 700°C, the results will be extrapolated to this temperature in future work.

### 11:40 AM

**Study of Microporosity Formation under Different Pouring Conditions in A356 Aluminum Alloy Castings:** Lu Yao<sup>1</sup>; Steve Cockcroft<sup>1</sup>; Daan Majjer<sup>1</sup>; Jindong Zhu<sup>1</sup>; Carl Reilly<sup>1</sup>; <sup>1</sup>University of British Columbia

In this work, the formation of microporosity has been examined under different casting conditions aimed at manipulating the tendency to form and entrain oxide films in small directionally cast A356 samples. Porous disc filtration analysis (PoDFA) was used to assess the melt cleanliness and identify the inclusions in the castings. The porosity volume fraction and size distribution were measured using X-ray micro-tomography (XMT) analysis. By fitting a pore formation model to the experimental results, an estimate of the pore nucleation population has been made. The results from the model predictions indicate that increasing the tendency to form and entrain oxide films not only increases the number of nucleation sites but also reduces the supersaturation necessary for pore nucleation in A356 castings.



## Characterization of Minerals, Metals and Materials: Structural Characterization

Sponsored by: The Minerals, Metals and Materials Society, TMS Extraction and Processing Division, TMS/ASM: Composite Materials Committee, TMS: Materials Characterization Committee  
Program Organizer: Sergio Monteiro, State University of the Northern Rio de Janeiro - UENF

Wednesday AM  
March 2, 2011

Room: 14B  
Location: San Diego Conv. Ctr

Session Chairs: Jiann-Yang Hwang, Michigan Technological University;  
Jeonguk Kim, Korea Railroad Research Institute

### 8:30 AM

#### Micro-Computerized Tomography of Ti-5111 Friction Stir Welded

**Microsamples:** Christopher Cheng<sup>1</sup>; Jennifer Wolk<sup>2</sup>; Marc Zupan<sup>1</sup>;  
<sup>1</sup>University of Maryland Baltimore County; <sup>2</sup>Naval Surface Warfare Center, Carderock Division

The use of Ti and Ti alloys in marine applications can deliver improved mechanical, physical, and corrosion properties. These material performance gains when put into service can be significantly reduced by the difficulties of conventional welding of joints. Friction stir welding (FSW) is an alternate welding process that overcomes some of the difficulties, but localized mechanical characterization of the various regimes of FSW joints are still immature. Previous measurements of the mechanical properties of the weld, transition, and base regimes of friction stir welded Ti-5111 microsamples showed significant differences in stiffness, yield strength, and ultimate tensile strength. Micro-Computerized Tomography (micro-CT) is utilized to document the internal gage structure of the microsample before and after tensile testing. The micro-CT information is linked to fractography of the failure surfaces, the microstructural textural information, and crystallographic slip which are used to explain the variations in the different FSW zone mechanical properties.

### 8:45 AM

#### Application of Novel Techniques to the Three-Dimensional Characterization of Microstructural Features in $\alpha+\beta$ Titanium Alloys:

John Sosa<sup>1</sup>; Santhosh Koduri<sup>1</sup>; Vikas Dixit<sup>1</sup>; Peter Collins<sup>2</sup>; Stephen Niezgod<sup>3</sup>; Surya Kalidindi<sup>3</sup>; Hamish Fraser<sup>1</sup>; <sup>1</sup>The Ohio State University; <sup>2</sup>University of North Texas; <sup>3</sup>Drexel University

Advanced three-dimensional data collection techniques such as Robo. Met-3D™ have permitted rapid acquisition of robust datasets on optical length scales. Implementation of such datasets may improve the accuracy of neural networks and phase-field models. However, the accurate statistical representation of three-dimensional microstructural features is challenging, requiring continual improvement to analytical methods. This work addresses the serial two-dimensional collection, three-dimensional processing, and analysis of datasets containing microstructural features such as equiaxed- $\alpha$  and colony- $\alpha$  in  $\alpha+\beta$  titanium alloys. In regards to equiaxed- $\alpha$ , rigorous dataset collection, along with novel 3-D feature-find and separation algorithms have allowed for robust three-dimensional quantification that was subsequently compared to 2-D stereological measurements, providing new insights into their validity. With regard to colony- $\alpha$ , collaboration with Dr. Surya Kalidindi's group at Drexel University has led to advanced automated colony segmentation permitting 3-D visualization of their interpenetrating morphology and three-dimensional quantification. Crystallographic information has been incorporated using electron backscatter diffraction (EBSD).

### 9:00 AM

#### Application of Conical Beam X-Ray Tomography to Multi-Phase Materials:

Jason Wolf<sup>1</sup>; Anthony Rollett<sup>1</sup>; Marc De Graef<sup>1</sup>; <sup>1</sup>Carnegie Mellon University  
We report on the use of a new, custom-designed conical x-ray tomography instrument, consisting of a Phoenix 160 kV multi-focal x-ray source, a 3056x3056 fiber optically coupled CCD camera with 12 micron pixel size and a GdOS poly-crystalline scintillator, with optimal operation around 40 kV. This setup, mounted inside a lead sarcophagus on an air-bearing table, is capable of a resolution of about 400 nm. Tomographic reconstructions are carried out using the SnapCT tomography code (Digisens) on a multi-GPU platform; the reconstruction occurs in near real time. The system employs a cylindrical or rod-shaped sample with a diameter of 1-2 mm, mounted on a five-axis precision stage. We will report on a number of material data sets, ranging from carbon foams to biological materials to two-phase alloy systems. We will also discuss a number of segmentation methods used for post-processing of the tomographic reconstructions.

### 9:15 AM

#### High Temperature X-ray Diffraction Characterization of Thermal Energy Storage Materials – The Binary Phase Diagram Study:

Wen-Ming Chien<sup>1</sup>; Vamsi Kamisetty<sup>1</sup>; Ivan Gantan<sup>1</sup>; Prathyusha Mekala<sup>1</sup>; Anjali Talekar<sup>1</sup>; Dhanesh Chandra<sup>1</sup>; <sup>1</sup>University of Nevada, Reno  
Thermal energy storage materials (organic crystalline materials) undergo a solid-solid phase transition before melting which will store large amounts of thermal energy. Three materials [tris(hydroxymethyl)aminomethane (TRIS) and 2-Amino-2-methyl-1, 3-propanediol (AMPL) and Pentaglycerol (PG)] were used for this study. High temperature X-ray diffraction characterization and differential scanning calorimetric (DSC) methods were used to develop the binary AMPL-TRIS and AMPL-PG phase diagrams. The high temperature solid-state phases of AMPL and TRIS were characterized as a disordered BCC structure, and PG was characterized as FCC. Lattice and volume expansion calculations on single phase of AMPL, TRIS and PG have been performed. Calculation of Phase Diagrams (CALPHAD) modeling technique is used to calculate the AMPL-TRIS and AMPL-PG binary phase diagrams by using the Thermal-Calc software. The detail of the thermal properties and excess Gibbs energies will present.

### 9:30 AM

#### Non-Invasive X-Ray Imaging of Paint Layers in Old Master Paintings:

Peter Reischig<sup>1</sup>; Lukas Helfen<sup>2</sup>; Tilo Baumbach<sup>2</sup>; Arie Wallert<sup>3</sup>; Joris Dik<sup>1</sup>; <sup>1</sup>Delft University of Technology; <sup>2</sup>Institute for Synchrotron Radiation, Karlsruhe Institute of Technology; <sup>3</sup>Rijksmuseum Amsterdam  
To develop conservation procedures for a certain type of painting, as well as for a thorough art historical study or conservation of a specific work of art, it is of crucial importance to look under the surface and visualize its paint stratigraphy. We propose synchrotron based x-ray laminography to explore the fine details of the microstructure, which are hard to detect by conventional (non-destructive) techniques. The method can provide three-dimensional high-resolution local maps of the paint layers without the need of invasive sample removal. The rotation axis is perpendicular to the sample surface and inclined to the incident beam, enabling scanning of whole paintings. For the reconstruction, filtered backprojection algorithms are used, based on radiographs that exhibit absorption contrast (from local variations in density) and/or phase contrast (from interfaces). The technique enables visualization of fine structure (pigment particles, voids, cracks) in underlying paint layers and the substrate.

### 9:45 AM

#### Characterization of Residual Stress Distributions and Microstructural Changes in Laser Shock Peened Ti-6Al-4V Alloy:

Yixiang Zhao<sup>1</sup>; Ulrich Lienert<sup>2</sup>; Jon Almer<sup>2</sup>; Yang Ren<sup>2</sup>; David Lahrman<sup>3</sup>; Dong Qian<sup>1</sup>; S. Mannava<sup>1</sup>; Vijay Vasudevan<sup>1</sup>; <sup>1</sup>University of Cincinnati; <sup>2</sup>Advanced Photo Source, Argonne National Laboratory; <sup>3</sup>LSP Technologies, Inc.,  
Laser shock peening (LSP) is a novel surface treatment process that generates deep compressive residual stresses and microstructural changes and thereby dramatically improves fatigue strength of critical metal

aircraft engine parts. The present study was undertaken to develop a basic understanding of the effects of LSP parameters on the residual stress distributions and microstructural changes in Ti-6Al-4V alloy. Coupons of the alloy with and without a sacrificial/ablative layer were LSP-treated using the LSP systems at GE Aviation and LSP Technologies, Inc. Depth-resolved characterization of the macro residual strains and stresses was achieved using high-energy synchrotron x-ray diffraction, as well as by conventional XRD. The near-surface and through-the-depth changes in strain, texture and microstructure were studied using EBSD/OIM and by TEM. Local property changes were examined using microhardness and nanoindentation. The results showing the relationship between LSP processing parameters, microstructure, residual stress distributions and hardness are presented and discussed.

#### 10:00 AM Break

#### 10:15 AM Invited

**In Situ Tomographic Characterization of Single Cavity-Growth during High-Temperature Creep of Metallic Materials:** *Augusta Isaac*<sup>1</sup>; Federico Sket<sup>2</sup>; Krzysztof Dzieciol<sup>3</sup>; Andras Borbely<sup>3</sup>; <sup>1</sup>Laboratório Nacional de Luz Síncrotron; <sup>2</sup>Madrid Institute for Advanced Studies of Materials; <sup>3</sup>École Nationale Supérieure des Mines de Saint-Étienne

The service lifetime of metallic components for high temperature applications is usually controlled by creep damage consisting of nucleation, growth and coalescence of grain boundary voids. This work presents a conceptually new approach to void growth characterization based on synchrotron microtomographic measurements performed in-situ during creep. We show that the average growth rates of voids in leaded brass and copper are larger by a factor of about 25 and 46 than predicted by the continuum theory, respectively. The distorted shape of voids reconstructed by nanotomography suggests that the enhanced growth rate is related to the crystallographic nature of creep deformation.

#### 10:45 AM

**EBSD Analysis Strategies for Quantitative Characterization of 'Multi-Phase' Steel Microstructures:** *Eric Payton*<sup>1</sup>; Shenja Dziazyk<sup>1</sup>; Gunther Eggeler<sup>1</sup>; <sup>1</sup>Ruhr-Universität Bochum

Quantitative characterization of the volume fractions, sizes, and spatial arrangements of major microstructural components is necessary for further development of advanced low-alloy steels, such as TRIP steels, which are important in automotive manufacturing. Automated EBSD is capable of producing data that can be used to simultaneously characterize the crystallographic texture as well as the volume fraction and size of grains of ferrite and retained austenite. However, several challenges remain in distinguishing martensite, bainite, ferrite, and the local state of recrystallization by EBSD. To assess the quality of EBSD data analysis strategies suggested by various authors for identifying these microstructural components, EBSD, nanoindentation, and other characterization techniques were performed on the same regions of several 'multi-phase' steels. EBSD simulations were used to better explain experimental observations. The conclusions are applicable to EBSD-based characterization of microstructural evolution during processing of many engineering alloys.

#### 11:00 AM

**EBSD Ferrite Fraction in Austenitic Welds:** *Carl Necker*<sup>1</sup>; John Milewski<sup>1</sup>; John Elmer<sup>2</sup>; <sup>1</sup>Los Alamos National Laboratory; <sup>2</sup>Lawrence Livermore National Laboratory

In this study we test the potential of electron backscatter diffraction (EBSD) as a delta ferrite quantification technique in austenitic stainless steel welds. Quantification of ferrite in welds presents issues as existing techniques (magnetic permeability, ferrite scopes, x-ray diffraction) sample volumes larger than the welds. EBSD sub-micron resolution and millimeter scan sizes overcome the volumetric averaging issues. Optical image analysis allows for local analysis but relies on sufficient differential phase contrast. With proper surface preparation EBSD should clearly differentiate austenite from ferrite. Centrifugally cast stainless steel weld ferrite secondary standards were used in this study. EBSD results were compared to optical image analysis, ferrite

scope, and the standard's Magne Gage ferrite numbers. EBSD results were lower than the other characterization techniques. Although EBSD clearly differentiated austenite and ferrite, it was clear that surface topography, total area scanned and scan step size play significant roles in properly capturing the ferrite morphology.

#### 11:15 AM

**Characterization of Twin Boundaries in Twinning-Induced Plasticity Steels Using Electron Backscatter Diffraction Electron Microscopy:** *Erin Diedrich*<sup>1</sup>; David Field<sup>1</sup>; <sup>1</sup>Washington State University

This experiment uses electron backscatter diffraction (EBSD) performed in a field emission scanning electron microscope (FESEM) to characterize and quantify twin boundaries in mechanically deformed TWIP steel samples in order to relate the presence of twins to the mechanical properties of the material. EBSD scans were performed at magnifications of 2,400x and 20,000x on samples that were mechanically deformed to 3%, 9% strain and to failure, as well as a specimen of as-received material. The twin fractions within the low-strain value specimens remained relatively constant, however this fraction increased from 1.4% in the as-received material to 3.6% in the sample pulled to failure at 34% true strain. However, the suspected presence of bundles of nano-scale twins that behave as lattice defects resulted in poor diffraction patterns and it was determined that these percentages are not an accurate representation of the twin fraction.

#### 11:30 AM

**EBSD Detail Extraction for Greater Spatial and Angular Resolution in Material Characterization:** *Jay Basinger*<sup>1</sup>; David Fullwood<sup>1</sup>; Brent Adams<sup>1</sup>; <sup>1</sup>Brigham Young University

Orientation imaging methods have been a mainstay of characterization efforts for crystalline materials for nearly two decades. Electron backscatter diffraction images provide statistical data regarding atomic alignment to create relatively large scale (up to several mm) orientation maps in crystalline and polycrystalline materials. However, recent work has highlighted that the information in such images has generally been under-used. Advances in high-resolution strain measurement, dislocation densities, and defect detection have begun to utilize this often ignored detail. This paper presents a review of recent developments in detail extraction from EBSD, including new developments in pattern center determination (a critical enabling technique that facilitates many other high-resolution techniques) and image separation methods as a basis for improved spatial resolution in material characterization.

#### 11:45 AM

**Segmentation of Three-Dimensional EBSD Data through Fast Multiscale Clustering:** *Cullen McMahon*<sup>1</sup>; Cassandra George<sup>1</sup>; Md. Zakaria Quadir<sup>2</sup>; Michael Ferry<sup>2</sup>; Lori Bassman<sup>1</sup>; <sup>1</sup>Harvey Mudd College; <sup>2</sup>University of New South Wales

Complete and accurate analysis of subgrain microstructural features must include three-dimensional information. Three-dimensional electron backscatter diffraction (EBSD) data can be used to characterize these features, however their boundaries first must be determined. This cannot be accomplished simply with pixel-to-pixel misorientation thresholding because many of the boundaries are gradual transitions in crystallographic orientation. Fast Multiscale Clustering (FMC) is an established image processing technique that we have combined with quaternion representation of orientation to segment this kind of data. Segmentation algorithms often have issues handling images with both distinct and subtle boundaries. Our implementation of FMC addresses this by using a novel distance function and statistical analysis to take into account the variance in orientation of each feature. Although FMC was originally a two-dimensional image processing algorithm we have extended it to analyze three-dimensional data sets. As an example, a segmentation of microbands in cold-rolled aluminum will be presented.

12:00 PM

**Characterization and Processing Ultramafic Nickel Ore after Acid Attack to Disintegrate Fibres:** *Salah Uddin*<sup>1</sup>; *Mitra Mirmezami*<sup>1</sup>; *Ram Rao*<sup>1</sup>; *James Finch*<sup>1</sup>; <sup>1</sup>McGill University

Ultramafic ores are a potential major resource of nickel. The primary processing challenge is posed by fibrous minerals such as chrysotile. These minerals create physical entanglement which increases pulp viscosity and hinders selectivity in flotation. The proposal in this paper is to disintegrate the fibres by adapting technology pursued in CO<sub>2</sub> sequestration. The concept is to release Mg by acid attack (the Mg is reacted with CO<sub>2</sub> in the sequestration process) which destabilizes the fibres enabling them to be broken by grinding. Structural changes in the ore due to combined acid (H<sub>2</sub>SO<sub>4</sub>) and grinding treatment was characterized using SEM-EDAX, XRD, Micro-Raman and FT-IR. Based on the analysis, a possible mechanism of fibre disintegration and consequent change in slurry rheology is proposed. The possibility of collectorless flotation through the use of H<sub>2</sub>SO<sub>4</sub> and elimination of frother due to the high ionic strength liquor produced (due to released Mg ions) is demonstrated. Significant improvement in Ni grade-recovery with higher MgO rejection was achieved compared to untreated ore. The process has environmental attractions: the H<sub>2</sub>SO<sub>4</sub> can be derived from SO<sub>2</sub> smelter off-gas and the tailings are candidates for CO<sub>2</sub> sequestration.

12:15 PM

**Microwave Sintering of CaO Stabilized Nature Baddeleyite:** *Li Jing*<sup>1</sup>; *Peng Jinhui*<sup>1</sup>; *Guo Shenghui*<sup>1</sup>; *Li Wei*<sup>1</sup>; *Zhang Libo*<sup>1</sup>; <sup>1</sup>Faculty of Metallurgy and Energy Engineering, Kunming University of Science and Technology

Partially stabilized zirconia ceramics (PSZ) were prepared by microwave sintering using natural baddeleyite which was obtained by flotation of baddeleyite ore as starting materials. Because of using natural baddeleyite as raw and the process producing no waste, it realized shorter process, energy saving, environmentally-friendly and non-damage processing. In this work natural baddeleyite stabilized with 3.8 wt.% CaO were sintered at 1300 °C for 60 min in a multi-mode 2.45 GHz microwave furnace. Microwave sintering could fast heating and sintering. Besides that, microwave sintering could heat materials wholly, low the sintering temperature, improve the materials properties and save energy. X-ray spectrum displayed the product composed by the tetragonal phase and monoclinic phase that also showed the product was PSZ. Fine and uniform microstructures were observed in the product through scanning electron microscopy. PSZ which was with high density was confirmed by the method of the Archimedes technique.

## Coatings for Structural, Biological, and Electronic Applications II: Process-Property-Performance Correlations - I; Metallic Coatings

*Sponsored by:* The Minerals, Metals and Materials Society, TMS Electronic, Magnetic, and Photonic Materials Division, TMS: Thin Films and Interfaces Committee

*Program Organizers:* Nuggehalli Ravindra, New Jersey Institute of Technology; Choong Kim, University of Texas at Arlington; Nancy Michael, University of Texas at Arlington; Gregory Krumdick, Argonne National Laboratory; Roger Narayan, Univ of North Carolina & North Carolina State Univ

Wednesday AM  
March 2, 2011

Room: 6E  
Location: San Diego Conv. Ctr

*Session Chairs:* Nuggehalli Ravindra, New Jersey Institute of Technology; Nancy Michael, University of Texas at Arlington

### 8:30 AM Symposium Overview

8:35 AM Invited

**Improved Mechanical Properties of Coatings and Bulk Components as a Function of Grain Size:** *Robert Gansert*<sup>1</sup>; *Chris Melynk*<sup>2</sup>; *David Grant*<sup>2</sup>; *David Lukan*<sup>2</sup>; *Brian Weinstein*<sup>2</sup>; <sup>1</sup>Advanced Materials & Technology Services, Inc.; <sup>2</sup>California Nanotechnologies, Inc.

Thermal sprayed coatings produced from nano- and near-nano grained powders provide improved properties as compared to conventional powders. These nano- and near-nano grained materials show great potential for applications in the aerospace, energy, and many other industries. A study is proposed to investigate the influence of grain size on mechanical properties by examining nano-, near-nano, and micro-grained materials. Powders, coatings and consolidated components of tungsten carbide based materials (WC-Co-Cr, WC-Co) will be examined. Thermal spray coatings will be produced of carbides of various grain sizes, from nano to micron sized grains. An examination of consolidated forms will be performed using these materials. Spark Plasma Sintering (SPS) will be used to provide consolidated forms of these materials. A comparison will be made of the influence of grain size in thermal spray coatings to that of bulk consolidated materials using these materials.

9:00 AM Invited

**Residual Stresses in Coatings Measured at Micro Scale:** *Jeff De Hosson*<sup>1</sup>; *Vasek Ocelik*<sup>1</sup>; *Ivan Furar*<sup>1</sup>; <sup>1</sup>Univ of Groningen

In this contribution we demonstrate a novel approach of measuring internal stresses at the micron scale in coatings scale. The new method is based on applying of dual beam microscopy like imaging-milling semidestructive instrument to realize mechanical relaxation for measuring internal stress. Focused Ion Beam is used as a knife to release the local strain induced by internal stresses. Surface relaxation in the vicinity of such cut is mapped by the Digital Image Correlation of scanning electron microscope images and released stresses are calculated on the base of displacement maps. Measurements were performed on laser clad coatings with different thicknesses. 3.3 kW IPG fiber laser was used to create different metallic coatings. Numerical and statistical methods are used to calculate the stress components inside the laser treated coatings.

9:25 AM Invited

**Factors Influencing the Formation of Oxide Layer on AZ91 Mg Alloy Coated by Electrochemical Plasma Coating:** *Dong H. Shin*<sup>1</sup>; *In Jun Hwang*<sup>1</sup>; *Kang Min Lee*<sup>1</sup>; *Young Gun Ko*<sup>2</sup>; <sup>1</sup>Hanyang University; <sup>2</sup>Yeungnam University

A study was made to study the formation of oxide layer on AZ91 Mg alloy coated by electrochemical plasma coating (EPC) process as functions of various electrical parameters such as frequency, wave form, and current density. The formation of coating layer was characterized by scanning electron microscope and X-ray photoelectron spectroscopy for their structural

WEDNESDAY AM



features and constituent phase fractions, which were strongly influenced by electrical parameters. Optimum conditions suitable for coatability including internal stress, dense layer, and high MgO content were suggested. In addition, the corrosion response of the EPC-treated sample was examined by potentiodynamic polarization and electrochemical impedance tests.

#### 9:50 AM Invited

**Phase Stability and Surface Rumpling during Cyclic Oxidation of Pd/Pt-Modified Ni-Al Bond Coats at 1150°C:** *Raghavendra Adharapurapu*<sup>1</sup>; Jun Zhu<sup>1</sup>; Don Lipkin<sup>2</sup>; Varamon Dheeradhada<sup>2</sup>; Tresa Pollock<sup>3</sup>; <sup>1</sup>University of Michigan; <sup>2</sup>General Electric Global Research Center; <sup>3</sup>University of California Santa Barbara

Phase stability, surface rumpling and interdiffusion behavior of Pd/Pt-modified Ni-Al-Hf-Cr bond coats were investigated during cyclic oxidation via a combinatorial approach. Bond coats with compositions in the range of Ni-(33-39)Al-5Cr-(1-8)Pd/Pt were deposited on RenéN5 substrates and subjected to both short-term and long-term cyclic oxidation experiments at 1150°C. The Pt- and Pd-modified overlay coatings exhibited comparable oxidation kinetics with intermediate Pt/Pd+Hf additions exhibiting the best cyclic oxidation properties. The oxidation lives of the Pd-modified overlays exceeded those of Pd-modified diffusion aluminides with a positive synergistic effects between Pd/Pt and Hf+Cr additions. Transformations from B2-phase- $\rightarrow$ 3R+7R-martensites- $\rightarrow$  $\gamma'$ - $\rightarrow$  $\gamma$ + $\gamma'$  occurred in both Pd- and Pt-modified coatings due to Al depletion to substrate and surface oxide. Rumpling or surface roughening occurred for all the coating compositions at 1150°C. A greater depletion of Pd to the substrate compared to Pt was also observed; the interdiffusion coefficients were consistent with those measured in NiAl-NiAl+Pt/Pd diffusion couples.

#### 10:15 AM Break

#### 10:25 AM Invited

**The Benefits of the Thermal Properties and Durability of Alodine EC2 Coated Aluminum in the Heat Transfer Industry:** *Jianhui Shang*<sup>1</sup>; Ryan Brune<sup>1</sup>; Wesley Sprague<sup>1</sup>; Larry Wilkerson<sup>1</sup>; Steve Hatkevich<sup>1</sup>; <sup>1</sup>American Trim LLC

The heat exchanger industry currently employs the high thermal conductivity of aluminum to produce efficient coils at a low cost. These systems often deteriorate over time as the aluminum coils oxidize or their protective coating wears away, leading to a decreased effectiveness for transferring heat. Recently, Henkel Corporation developed a new coating for aluminum that increases the thermal transfer capability and prevents surface oxidation and abrasive damage. This coating, called Alodine EC2™, will allow for the replacement of expensive copper coil systems with low cost aluminum coils, and the increased thermal properties will allow for smaller heat exchangers to be constructed that exhibit the same heat transfer capabilities as larger traditional systems. This will result in systems with lower cost and decreased weight. This paper presents the thermal properties of Alodine EC2™ to validate the potential applications to the heat transfer industry.

#### 10:50 AM

**Characterization of Electroless Ni-B Coating for Tribological Application:** *Soupitak Pal*<sup>1</sup>; Nisha Verma<sup>1</sup>; Vikram Jayaram<sup>1</sup>; Sanjay Biswas<sup>1</sup>; Yancy Riddle<sup>2</sup>; <sup>1</sup>Indian Institute of Science; <sup>2</sup>UCT Coatings, Inc

The crystalline counterpart of amorphous electroless Ni-B coatings are generally regarded as low friction and wear resistant materials in which the major crystalline phases are Ni<sub>3</sub>B and Ni<sub>2</sub>B whose evolution occurs through a multi-stage crystallization process due to the presence of composition fluctuation in the as deposited coating induced by the deposition process. This study mainly focuses on the role of individual crystalline phases on the overall tribological behaviour of the coating. Microstructural developments are carefully probed in conjunction with heat treatments. Ball (alumina, steel) on disk tribometer has been used to evaluate the overall tribological properties while the response of individual phases has been analyzed through lateral force microscopy using a silicon nitride cantilever. Though scaling of contact area and the nature of the counterface influence the results, it is found

that increase in the ratio of Ni<sub>2</sub>B to Ni<sub>3</sub>B leads to a decrease in coefficient of friction.

#### 11:05 AM

**Improving High Temperature Performance of Aluminum Foams by Nickel Coating:** *Zhuokun Cao*<sup>1</sup>; Huan Liu<sup>1</sup>; *Yihan Liu*<sup>1</sup>; Guangchun Yao<sup>1</sup>; <sup>1</sup>Northeastern University, China

To meet the application of aluminum foams as high temperature acoustic absorbers, nickel coating was formed on the surface of aluminum foams by direct electroplating. Microstructure of the pretreated and nickel coated specimens was observed by SEM, and influences of pretreatment, current density, operating time and additives on the property of coating were discussed. Flat and smooth coating was obtained by electroplating for 2 hours at a current density of 0.02A/m<sup>2</sup> with certain additives. Compressive tests were performed on the specimens both with and without nickel coating at room temperature and at 540, 660 and 700 °C. The results show the fact that nickel coating can effectively improve the compressive property of aluminum foams, especially at high temperature near and beyond the melting point of aluminum.

#### 11:20 AM

**Studies on Ni-Ti Thin Films Grown by Bias Assisted Magnetron Sputtering:** *B Geetha Priyadarshini*<sup>1</sup>; Shampa Aich<sup>1</sup>; Madhusudan Chakraborty<sup>2</sup>; <sup>1</sup>Indian Institute of technology (IIT),Kharagpur; <sup>2</sup>Indian Institute of technology (IIT), Bhubaneswar

Co-sputtering from Ni and Ti elemental targets was employed to deposit Ni-Ti thin films on Si (100) substrates. The influence of energetic particle bombardment on the microstructure of sputtered deposited Ni-Ti alloy films has not been well understood by the researchers. Attempts are made here to investigate the microstructural and structural evolution taking place during the ion-bombardment on Ni-Ti thin films using Field Emission Scanning Electron Microscopy (FE-SEM), High Resolution Transmission Electron microscopy (HR-TEM) and Grazing Incidence X-ray diffraction (GIXRD). Films deposited at -100 V substrate bias, were amorphous exhibiting smooth and continuous microstructure. At 600 °C annealing temperature, the films were polycrystalline with grain size of 15-25 nm containing mixture of B19' and B2 phases.

## Commonality of Phenomena in Composite Materials II: Development of New Composite Materials

*Sponsored by:* The Minerals, Metals and Materials Society, ASM International, TMS Structural Materials Division, TMS/ASM: Composite Materials Committee

*Program Organizers:* Meisha Shofner, Georgia Institute of Technology; Carl Boehlert, Michigan State University

Wednesday AM  
March 2, 2011

Room: 6A  
Location: San Diego Conv. Ctr

*Session Chair:* Nik Chawla, Arizona State University

#### 8:30 AM Invited

**Tuning the Properties of Nanocrystalline Semiconductors: Producing Bulk Sized Nanocomposites Using Electric Currents:** *J. Alaniz*<sup>1</sup>; *J. Morales*<sup>1</sup>; *C. Dames*<sup>1</sup>; *J. Garay*<sup>1</sup>; <sup>1</sup>UC Riverside

Improving the performance of devices such as thermoelectric power generators often hinge producing materials with a precise blend of properties. Nanocrystalline oxides and semiconductors offer a route for attaining new functionalities, yet their direct application in products has been hindered by the difficulty in producing them reliably. One reason is that consolidation of nanocrystalline powders usually results in grain growth and therefore loss of enhanced nanocrystalline properties. Recently, the versatile material processing technique of current activated pressure assisted densification has proven effective in overcoming the grain growth challenge; it is now possible

to efficiently produce materials large enough to be viable nanocrystalline parts. The materials produced have very different properties than traditional materials including improved tailorable conductivity, and magnetic coupling and can be used for energy scavenging, cooling and magnetic sensing. The results will be discussed in terms of crystal length scale effects and proximity of nanoscale phases.

#### 9:10 AM

**Initial Characterization of an Aluminum Based Syntactic Foam:** Oliver Strbik<sup>1</sup>; Satyendra Kumar<sup>1</sup>; Chris Smith<sup>1</sup>; *Todd Osborn*<sup>1</sup>; Joe Cochran<sup>2</sup>; Thomas Sanders<sup>2</sup>; Naresh Thadhani<sup>2</sup>; Laura Cerully<sup>2</sup>; Tammy McCoy<sup>2</sup>; Liang Quan<sup>2</sup>; Vincent Hammond<sup>3</sup>; Kyu Cho<sup>3</sup>; <sup>1</sup>Deep Springs Technology; <sup>2</sup>Georgia Tech; <sup>3</sup>Army Research Lab

Continued progress in the development of metallic, high-strength, hollow spheres has generated renewed interest in syntactic metal foams. These foams, when composed of hollow spheres in a lightweight metallic matrix, possess low density, high specific stiffness, high strength to weight ratios, and greatly increased energy absorbing capabilities. As a result, they are of interest for applications ranging from ballistic armor to aircraft structures to automotive structural components and crumple-zones. Recently, a metallic foam composed of AA5083 filled with 60% (Vol) of M350 spheres has been produced using conventional casting methods. Following fabrication, the foam microstructure was characterized using both optical and electron microscopy. Quasi-static compression and microhardness testing was performed to determine the change in properties resulting from the incorporation of the spheres. Finally, limited ballistic testing has been performed to determine the ability of the foam to provide protection against low caliber threats.

#### 9:30 AM

**Machinable Aluminum Matrix Composite:** *William Harrigan*<sup>1</sup>; <sup>1</sup>Gamma Technology

One of the impediments to widespread use of aluminum matrix composites has been the difficulties in machining parts at an acceptable cost. Gamma Technology has refined the production of spherical aluminum oxide particles and has incorporated the new particles into aluminum matrix composites. These composites have mechanical and physical properties similar to the SiC or B4C reinforced composites made for the past 20 years by powder metallurgy techniques. This new composite has the ability to be machined with carbide inserts. This paper will discuss the mechanical properties of several composites containing the spherical alumina particles. One composite has strength values that are similar to 2618 aluminum at temperatures up to 350°C. Another composite has yield strength properties greater than 650 MPa at room temperature. The microstructure of these composites and the fracture surfaces will be presented to demonstrate the role of the spherical particles in developing the mechanical properties.

#### 9:50 AM

**Stability and Lithium Adsorption Property of LiMn2O4-LiSbO3 Composite in Aqueous Medium:** *Li-Wen Ma*<sup>1</sup>; Xi-Chang Shi<sup>1</sup>; Bai-Zhen Chen<sup>1</sup>; Kun Zhang<sup>1</sup>; <sup>1</sup>School of Metallurgical Science and Engineering

LiMn2O4-LiSbO3 composite with the molar ratio Mn/Sb=3 was obtained by solid state reaction. The synthesis process of the LiMn2O4-LiSbO3 composite was analyzed by TG-DSC. The structure, stability and Li<sup>+</sup> extraction/adsorption properties of the composites obtained at various temperatures were characterized by X-ray diffraction (XRD), scanning electron microscopy (SEM) and atomic absorption spectrophotometer (AAS). The results show that the LiMn2O4-LiSbO3 composite has a combined structure of LiMn2O4 (spinel) and LiSbO3 (perovskite) in which manganese and antimony ions diffuse mutually into perovskite and spinel to form complex solid solutions. The lithium in the LiMn2O4-LiSbO3 composite can be extracted from its framework with the structure and morphology maintained during acid treatment. After acid treatment the composite can adsorb Li<sup>+</sup> from an aqueous lithium solution, which demonstrates that it can be used as lithium inorganic adsorbent.

#### 10:10 AM Break

#### 10:30 AM Invited

**Nanotube Based Composites: A Matrix of Understanding:** *Enrique Barrera*<sup>1</sup>; <sup>1</sup>Rice University

Inventing nanotube-based nanocomposites can take on several pathways. These pathways are further enabled when a matrix of understanding is established and the properties of nanotubes in broad array of materials are considered. Certainly, advancement of nanosystems is fostered by the knowledge base created in completely different materials. The leveraging of new ideas for polymer-based nanocomposites is an attractive approach for producing metal matrix nanocomposites. Likewise, the ability to advance nanoceramics is not far removed from the advancement of polymeric or metal matrix nanocomposites. In this presentation, the philosophy, design considerations, approaches, and achievements of nanocomposites will be overviewed and the use of a matrix of understanding will be identified that has fostered a broad range of nanotechnology advances.

#### 11:10 AM

**Impact Damage Sensing of Multiscale Glass/Epoxy Composite Structures:** *Luciana Arronche*<sup>1</sup>; *Valeria La Saponara*<sup>1</sup>; <sup>1</sup>University of California, Davis

Carbon nanotubes provide increased conductivity to polymer matrix composites, and have been the object of much attention. Changes of conductivity offer a method to monitor structural health. This work investigates the effect of impact damage on the electrical properties of composite samples prepared with epoxy resin, multi-walled carbon nanotubes (MWCNT), and glass fiber woven reinforcement. The current work follows an investigation of counter-intuitive results (Yesil et al., Surfactant-modified multiscale composites for improved tensile fatigue and impact damage sensing, accepted by Materials Science and Engineering A, July 2010): higher resistivity changes were measured on the impacted surface, while damage occurs close to the opposite surface. The effects of manufacturing and resistance measurement methods are studied: a) variability between impacted and bottom surfaces and between batches; b) difference between 2 and 4 points probe methods. Moreover, the damage sensing performance of specimens with as-received MWCNT or with treated MWCNT are discussed.

#### 11:30 AM

**Temperature-Sensitive Shape Memory Polymer Based Acoustic Metamaterials:** *Brayden Ware*<sup>1</sup>; *Walter Voit*<sup>1</sup>; <sup>1</sup>University of Texas at Dallas

Shape-memory polymer (SMP) acoustic metamaterials are dynamic composites containing local sonic resonators with variable stiffness coatings that change controllably as a function of temperature. The resonators absorb incident sound waves in specific frequency ranges. Modeling: we use multiple scattering theory to describe viscoelastic wave propagation through the composites to demonstrate negative effective mass density and a frequency band gap that moves with changing temperature. Sound transmission through the material is an order of magnitude less than predicted by the conventional mass-density law. Experimental: we synthesize several versatile acrylic SMP coatings around 5 to 15 mm lead and tungsten balls to create materials with tunable resonant frequencies. We can adjust the glass transition temperature (between about -20°C and 80°C) and stiffness in the rubbery regime (between about 300 KPa and 20 MPa). Dynamic mechanical analysis and impedance tube tests are used to confirm the predicted temperature-sensitive sound attenuation.

#### 11:50 AM

**Reinforced Steel/Polymer/Steel Sandwich Composites with Improved Properties:** *Heinz Palkowski*<sup>1</sup>; *Olga Sokolova*<sup>1</sup>; *Adele Carradó*<sup>2</sup>; <sup>1</sup>TU Clausthal; <sup>2</sup>Institut de Physique et Chimie des Matériaux de Strasbourg

Composite parts as sandwich structures are specifically used in applications for automotive, aerospace and vehicle industries. 316L/PP-PE/316L composites were investigated because of high stiffness and strength, good forming behaviour and damping properties. For thermal and mechanical joining additionally local plate reinforcing elements (RE) in the polymer core of the sandwich were placed and their forming behaviour and limits

were studied by deep drawing and bending processes. The experimental and theoretical analyses of failure mechanisms of sandwich plates without and with various RE were also investigated. Due to the material, size, shape and position of the local inlays the forming behaviour of the sandwich composites by deep drawing is strongly influenced. The position of local inlays e.g. in head, edge or flange regions of sandwich cup after deep drawing strongly influences the forming and flow behaviour of RE as well as sandwich composite areas. Results will be given.

## 12:10 PM

**Fatigue Damage Identification in Glass/Epoxy Composite Structures through Embedded Piezoelectrics and Wavelet Transforms:** *Valeria La Saponara*<sup>1</sup>; *Wahyu Lestari*<sup>2</sup>; *Charles Winkelmann*<sup>1</sup>; *Luciana Arronche*<sup>1</sup>; <sup>1</sup>University of California, Davis; <sup>2</sup>Embry-Riddle Aeronautical University

This work investigates signal processing and interpretation of waveforms acquired from cross-ply woven fiberglass/epoxy specimens with surface-mounted and embedded piezoelectric (PZT) transducers. The specimens are loaded under axial tensile fatigue in load control. The PZTs' pitch-catch signals are recorded at set intervals while the specimens are loaded at the mean stress in the testing machine, at low ultrasonic frequencies. Therefore, the waveform captures cumulative global damage of the specimens. In some samples, edge replications were taken concurrently to the waveforms. We discuss a signal processing technique based on wavelet transforms, where the denoised signal is processed with Gabor wavelet transforms, and the area of one of its contours is measured at set fatigue intervals, throughout the specimens' life. Results seem to indicate the presence of a steady-state condition which may be correlated to the characteristic damage state typical of cross-ply composites, and to the nonlinear accumulation of transverse cracks.

---

## Computational Plasticity: Continuum Computational Plasticity

*Sponsored by:* The Minerals, Metals and Materials Society, TMS Materials Processing and Manufacturing Division, TMS Structural Materials Division, TMS/ASM: Computational Materials Science and Engineering Committee, TMS: High Temperature Alloys Committee  
*Program Organizers:* Remi Dingreville, Polytechnic Institute of NYU; Koen Janssens, Paul Scherrer Institute

Wednesday AM  
March 2, 2011

Room: 1A  
Location: San Diego Conv. Ctr

*Session Chair:* To Be Announced

---

## 8:30 AM Invited

**Microstructural Evolution and Its Effect on Plastic Flow and Strain Localization:** *John Bassani*<sup>1</sup>; <sup>1</sup>University of Pennsylvania

We consider a class of elastic-plastic materials possessing local orthotropic symmetries that evolve with deformation. Microstructural spin, i.e. the spin of the orthotropic axes, is defined to be the difference between the material spin and plastic spin. At finite strain, flow rules are defined in the intermediate configuration in terms of a thermodynamically-consistent non-symmetric stress and two second-order orientation tensors. A fundamental relationship between plastic stretching and spin is derived utilizing representation theory for tensor-valued functions, and that result is the basis of phenomenological constitutive relations for plastic spin which have been implemented in finite element simulations. Significant effects of microstructural evolution on limits to ductility are predicted from analyses of necking and shear banding. Comparisons with experimental data for textured polycrystals under both uniaxial tension and shear are very promising.

## 9:00 AM Invited

**Advances in the Constitutive Equation Parameter Identification Procedure: Why Experiments Should Discuss With Numerical Simulations:** *Jerôme Crépin*<sup>1</sup>; *Eva Héripé*<sup>2</sup>; *Arjen Roos*<sup>3</sup>; *Dominique Geoffroy*<sup>3</sup>; <sup>1</sup>MinesParistech; <sup>2</sup>Ecole Polytechnique; <sup>3</sup>ONERA

The topic of this talk concerns a methodology for identifying mechanical parameters of constitutive equations thanks to an optimization procedure based on multiscale coupling between microstructure characterizations (morphology, crystallographic texture, chemical composition, etc...), mechanical strain field analysis obtained during in situ or ex situ tests and finite element simulations. Special interest is given to the effects of different boundary conditions (homogeneous strain, homogeneous stress, experimental strain field) applied to the finite element mesh and in particular the sensitivity of these simulations on the optimum set of parameters. Moreover, global 3D simulations performed on an RVE will be compared to the results of 2D extruded mesh from experimental characterization. Discussions about recent tools dedicated to virtual 3D microstructures in respect to real microstructure will be introduced.

## 9:30 AM

**On the Origin of Plastic Instability of Al-Mg Alloy 5052 during Stress Rate Change Test:** *Chen-Ming Kuo*<sup>1</sup>; *Chi-Ho Tso*<sup>1</sup>; <sup>1</sup>I-Shou University

Plastic instability or Portevin-Le Chetelier effect is observed during stress rate change test of Al-Mg alloy 5052 at room temperature. In the stress rate change experiments, strain retardation and plastic instability are observed between the initial and final stress levels, that is, although the applied stress rate changes from the initial stress level, plastic strain is insignificant until the plastic instability occurs. By gradually increasing the final stress level from initial stress level at fixed applied stress rate, plastic instability is also observed and could be modeled by the typical plastic deformation mechanism, that is, thermally activated kinetic flow theory of dislocations coupled with structural evolution law. By changing the values of suitable parameters to simulate the microstructure change of instability, the origin of plastic instability could be understood.

## 9:50 AM Invited

**Probabilistic Simulation of Incubation and Nucleation of Fatigue Cracks in AA 7075-T651:** *Anthony Ingrassia*<sup>1</sup>; *Jacob Hochhalter*<sup>2</sup>; *Michael Veilleux*<sup>1</sup>; *Jeffrey Bozek*<sup>1</sup>; <sup>1</sup>Cornell University; <sup>2</sup>NASA

Microstructurally small fatigue cracking in AA 7075-T651 includes incubation, nucleation, and microstructurally small propagation stages. The first part of this work addresses incubation through identification of particles prone to cracking, and predicting particle cracking frequency, given a distribution of particles and crystallographic texture. For the nucleation event, it is hypothesized that nucleation can be predicted by computing a non-local metric near the crack front. The hypothesis is tested by experimentation and 3D finite element modeling. Slip- and energy-based nucleation metrics are tested for validity. Each metric is derived from a continuum crystal plasticity formulation. Good agreement is found between the predicted frequency of particle cracking and two preliminary validation experiments. For nucleation, it is found that a continuum crystal plasticity model and a non-local nucleation metric can be used to predict the nucleation event. However, nucleation metric threshold values that correspond to various nucleation-governing mechanisms must be calibrated.

## 10:20 AM

**A Stochastic-Based Modified Gurson Model for Modeling Void Growth in Metallic Alloys:** *Huiyang Fei*<sup>1</sup>; *Kyle Yazzie*<sup>1</sup>; *Nikhillesh Chawla*<sup>1</sup>; *Hanqing Jiang*<sup>1</sup>; <sup>1</sup>Arizona State University

The Modified Gurson Model, also known as Gurson-Tvergaard-Needleman Model, is widely used to study ductile fracture in metallic materials where microvoid formation is prevalent. In Gurson's theory, the void volume fraction (VVF) is the only parameter representing a void, while the size of void is ignored. In the FEA package ABAQUS, the initial VVF is an average value assigned to an area. In this talk, we developed a stochastic method that could generate a random distribution of VVF as the initial configuration for FEA simulation. The numerical simulations were



conducted with ABAQUS/Standard using Gurson parameters obtained from experiments. This stochastic enhancement method better characterizes the real distribution of microvoids in porous metals, and better predicts the failure than non-randomized Modified Gurson Model in ABAQUS, compared to the experiments. Moreover, this stochastic enhancement can also be applied to other Gurson parameters, such as nucleation strain, critical failure VVF, etc..

#### 10:35 AM Break

#### 10:55 AM Invited

**Approaching Statistically Significant Correlations through Reduced Modeling of Initial Yielding Behavior:** Siddiq Qidwai<sup>1</sup>; Alexis Lewis<sup>2</sup>; Andrew Geltmacher<sup>2</sup>; <sup>1</sup>SAIC; <sup>2</sup>Naval Research Laboratory

Image-based 3D modeling techniques have been used to examine the role of microstructure on the initial yielding behavior of a beta titanium alloy. The determination of statistically significant microstructure-property correlations among the many measured parameters require analysis of data from large 3D microstructural reconstructions, and in many cases, these analyses exceed the computational power of the available hardware and software. In this paper, two techniques are examined to increase computational efficiency by decreasing image-based model sizes. The first technique involves the evaluation of reduced-parameter constitutive relationships. The second technique involves the use of 2-point cross-correlation method based on crystal orientation probability function to identify smaller sub-volume sets within the large sample that when properly weighted are statistically representative of the entire microstructure. It was found that each of these approaches was effective in reducing the computational resources necessary to analyze statistically significant volumes of material.

#### 11:25 AM Invited

**Deformation and Microrotation in the Vicinity of Grain Boundaries: Continuum Analysis of Atomistic Simulations:** Garritt Tucker<sup>1</sup>; Jonathan Zimmerman<sup>2</sup>; David McDowell<sup>1</sup>; <sup>1</sup>Georgia Institute of Technology; <sup>2</sup>Sandia National Laboratories

Grain boundaries and their deformation accommodation mechanisms impact the mechanical behavior of polycrystalline materials, particularly when grain size is at the nanometer scale. Some commonly observed processes in nanocrystalline metals include heterogeneous dislocation nucleation, grain boundary sliding, and migration. Here, we apply metrics from continuum mechanics to atomistic simulations to develop a theoretical understanding of deformation mechanisms in grain boundaries. Expressions for deformation gradient and vorticity are evaluated for simulations of 3-dimensional symmetric tilt grain boundaries of Cu subject to uniaxial tension and simple shear loading conditions. Numerous grain boundary orientations are analyzed with respect to deformation mechanisms and our metrics for deformation and microrotation. Our analysis also compares how the microrotation varies with distance from the grain boundary and with increasing applied strain. Sandia is a multiprogram laboratory operated by Sandia Corporation, a Lockheed-Martin Company, for the United States Department of Energy's National Nuclear Security Administration under contract DE-AC04-94AL85000.

#### 11:55 AM

**An Attempt to Express Isotropic Yield Functions of Metals Based on the Invariants of Stress Tensor:** Mohammad Habibi Parsa<sup>1</sup>; Kamal Azimi<sup>1</sup>; Payam Matin<sup>2</sup>; <sup>1</sup>University of Tehran; <sup>2</sup>Sciences University of Maryland

Different yield functions have been proposed for describing metals yield points and there are many kind of yield function that is used for different types of metals. Many of proposed yield function have been originated from extensive experiments and curve fitting of resulted data. Few theoretical based yield functions have been also suggested. Such different yield functions are source of confusion for applicant of these functions for predicting of yield phenomena. In the present work, it has been tried to describe yield function of metals using stress tensor invariants in order to describe all different kind of yield functions by one equation. Based on mentioned idea, general form of polynomial yield function based on the stress tensor invariants has been developed and then using geometrical tool and existing experimental results,

a general polynomial yield function has been proposed that can express all of existing yield functions.

#### 12:15 PM

**Three Dimensional Visualization and Microstructure-Based Modeling of Plasticity**

**and Void Growth in Pb-Free Solder Alloys:** Vaidehi Jakkali<sup>1</sup>; Ling Jiang<sup>1</sup>; Jason Williams<sup>1</sup>; Nikhilesh Chawla<sup>1</sup>; M Pacheco<sup>2</sup>; V Novitski<sup>2</sup>; S Lau<sup>3</sup>; Luke Hunter<sup>3</sup>; <sup>1</sup>Arizona State University; <sup>2</sup>Intel; <sup>3</sup>Xradia

Pb-free interconnects are being used extensively in Electronic Packaging. One of the significant defects introduced during processing of the solder joints is voids. The presence of porosity affects the mechanical performance of solder joints. 3D X-Ray Tomography is an effective non destructive technique of characterizing the nature of porosity in Solder joints. In this study, 3D X-Ray Tomography was used to visualize and re-construct the microstructure of Sn-3.9Ag-0.7Cu/Cu solder joints. This reconstructed micro-structure was incorporated into a Finite Element Model, using Modified Gurson criterion to simulate shear deformation and eventual failure of the joint due to void nucleation, growth, and coalescence. The effectiveness of this technique in understanding the effect of size, shape, and distribution of pores on local and global plasticity of the solder joints will be discussed.

### Computational Thermodynamics and Kinetics: Microstructural Evolution

*Sponsored by:* The Minerals, Metals and Materials Society, ASM International, TMS Electronic, Magnetic, and Photonic Materials Division, TMS Materials Processing and Manufacturing Division, TMS: Alloy Phases Committee, TMS: Chemistry and Physics of Materials Committee, TMS/ASM: Computational Materials Science and Engineering Committee, ASM: Alloy Phase Diagrams Committee  
*Program Organizers:* Raymundo Arroyave, Texas A & M University; James Morris, Oak Ridge National Laboratory; Mikko Haataja, Princeton University; Jeff Hoyt, McMaster University; Vidvuds Ozolins, University of California, Los Angeles; Xun-Li Wang, Oak Ridge National Laboratory

Wednesday AM  
March 2, 2011

Room: 9  
Location: San Diego Conv. Ctr

*Session Chairs:* Min Soo Park, Texas A&M University; Nele Moelans, Katholieke Universiteit Leuven

#### 8:30 AM Invited

**Role of Elastostatic Interaction in Domain Processes of Magnetic Shape Memory Alloys:** Yongmei Jin<sup>1</sup>; <sup>1</sup>Michigan Technological University

A phase field micromagnetic micromagnetic model is employed to study the role of elastostatic interaction in magnetic domain evolution and field-induced deformation of magnetic shape memory alloys. The model explicitly treats magnetic and elastic domain microstructures and takes into account multiple thermodynamic driving forces, including magnetostatic, elastostatic, magnetocrystalline, exchange, chemical, and applied magnetic and mechanical loadings. Computer simulations reveal details of coupled magnetic and elastic domain evolutions, and show that the competition between elastostatic and magnetostatic interactions governs domain processes and the resultant field-induced strain behaviors in magnetic shape memory alloys. The different contributions from twin shear strain and magnetostrictive strain to elastostatic interactions are analyzed. The effects of twin boundary mobility on domain processes are discussed.

#### 9:00 AM Invited

**Phase-field Modeling of Deformation Twinning:** Taewook Heo<sup>1</sup>; Yi Wang<sup>1</sup>; Saswata Bhattacharya<sup>1</sup>; Xin Sun<sup>2</sup>; Shenyang Hu<sup>2</sup>; Long Qing Chen<sup>1</sup>; <sup>1</sup>Pennsylvania State University; <sup>2</sup>Pacific Northwest National Lab

We propose a phase-field model for modeling microstructure evolution during deformation twinning. Using a face-centered cubic aluminum as an

example, the deformation energy as a function of shear strain is obtained using first-principle calculations. The gradient energy coefficients are fitted to the twin boundary energies along the twinning planes and to the dislocation core energies along the directions that are perpendicular to the twinning planes. The elastic strain energy of a twinned structure is included using the Khachatryan's elastic theory. We simulated the twinning process and microstructure evolution under a number of fixed deformation magnitudes and predicted the twinning plane orientations and microstructures. It is shown that twinning may take place through either nucleation and growth or spinodal mechanism, and the relative volume fractions of twin variants has approximate linear dependence on the magnitude of deformation strain.

**9:30 AM**

**Microstructure Evolution and Analysis of Single Crystal Nickel-Based Superalloy During Compression Creep:** Shu Zhang<sup>1</sup>; Sugui Tian<sup>1</sup>; <sup>1</sup>Shenyang University of Technology

Through creep property test and microstructure observation, the microstructure evolution of [001] orientation single crystal nickel-based superalloy during compressive creep is identified as the cubical  $\gamma'$  phase being transformed into the rafted structure along the direction parallel to the applied stress axis. By the calculation of von Mises stress distribution of the  $\gamma'$  phase with the three-dimensional stress-strain finite element method, it indicates that the applied compressive stress may change the stress distribution of the cubical  $\gamma'$  phases, and the coarsening orientation of  $\gamma'$  phase is closely related to the von Mises stress distribution of the  $\gamma'$  matrix channel. Under the action of the applied compressive stress, the bigger von Mises stress is produced on (001) crystal plane of the cubical  $\gamma'$  phase, which is the main reason for microstructure evolution. The driving forces of the elements diffusion and directional coarsening of  $\gamma'$  phase during compressive creep are further discussed.

**9:45 AM**

**Combining Phase-Field and CALPHAD for Systems Containing Intermediate Phases with Low Solubility:** Nele Moelans<sup>1</sup>; Bo Sundman<sup>2</sup>; <sup>1</sup>K.U. Leuven, Belgium; <sup>2</sup>INSTN, CEA, France

Reactive growth of intermediate phases with low solubility is important for many applications, for example IMC growth in solder joints, growth of silicide layers and oxidation. Gibbs energies developed according to the CALPHAD approach, using a regular solution model, can be combined with the phase-field technique to study microstructure evolution in multi-component systems. Phases with low solubility, however, are usually modeled as stoichiometric or using a sublattice model defined for a restricted composition range. This format is not directly compatible with the free energies used in a phase-field model. We have compared 3 approaches to combine CALPHAD thermodynamic descriptions of multi-component systems with the phase-field technique, applicable for systems containing phases with limited solubility. The methodologies are illustrated for binary and ternary systems.

**10:00 AM Break**

**10:10 AM Invited**

**Modeling of Crystal Defects and Interactions at Diffusive Time Scales:** Jon Dantzig<sup>1</sup>; <sup>1</sup>University of Illinois

Many important aspects of the mechanical behavior of materials are manifested at the atomic length scale, but at diffusive time scales. This combination makes these phenomena inaccessible to both molecular dynamics and continuum approaches. The phase-field crystal (PFC) method is able to capture this portion of parameter space using a continuous function to represent density resolved at the atomic length scale, coarse-grained in time to diffusive scales. Modifications to the original PFC model that stabilize vacancies are described, and the mechanical response of defected structures under mechanical loading will be presented.

**10:40 AM**

**Free Energy Functionals for Efficient Phase Field Crystal Modeling of Structural Phase Transformations:** Michael Greenwood<sup>1</sup>; Nikolas Provatas<sup>2</sup>; Joerg Rottler<sup>1</sup>; <sup>1</sup>University of British Columbia; <sup>2</sup>McMaster University

The phase field crystal (PFC) method is a promising technique for modeling materials with atomic resolution on mesoscopic time scales. While numerically more efficient than classical density functional theory (CDFT), its single mode free energy limits the complexity of structural transformation that can be simulated. We introduce a new PFC model inspired by CDFT, which uses a systematic construction of two-particle correlation functions that allows for a broad class of structural transformations, including bcc, fcc and hcp lattices. Our approach allows for control and parameterization of temperature effects and anisotropy of the surface energy and elastic coefficients of the material.

**10:55 AM**

**Control of Domain Configurations and Sizes in Crystallographically Engineered Ferroelectric Single Crystals: Phase Field Modeling:** Jie Zhou<sup>1</sup>; Tian-Le Cheng<sup>1</sup>; Ke-Wei Xiao<sup>2</sup>; Wei-Feng Rao<sup>2</sup>; Yu Wang<sup>1</sup>; <sup>1</sup>Michigan Tech. Univ.; <sup>2</sup>Virginia Tech

Phase field modeling and simulation is performed to study the mechanisms of crystallographic domain engineering technique for ferroelectrics. It is found that both domain configurations and domain sizes in ferroelectric single crystals can be controlled through sophisticated thermal and electrical conditions imposed on the materials during ferroelectric phase transformations. The simulations reveal that minimal domain sizes and highest domain wall densities are obtained with intermediate magnitude of electric field applied along non-polar axis of ferroelectric crystals, while lower and higher fields produce coarser domains and lower domain wall densities. It is found that temperature also plays an important role in domain size control. The simulations show that selection of polar domain variants by external electric field during nucleation stage of ferroelectric phase transition significantly affects subsequent domain growth and evolution kinetics and controls the formation and sizes of twin-related lamellar domains. This technique can be used to develop high-performance piezoelectrics.

**11:10 AM**

**Phase Field Modeling of Nanoparticles for Medical Applications:** Jonathan Guyer<sup>1</sup>; David Saylor<sup>2</sup>; James Warren<sup>1</sup>; <sup>1</sup>NIST; <sup>2</sup>FDA

Nano-particulate silver systems are widely used in wound dressings, surgical masks, and catheter coatings as anti-microbial agents. We have shown that a phase field model of the electrochemical interface captures behaviors including electrocapillary phenomena, differential capacitance curves that resemble experimental measurements, and non-linear kinetics consistent with the empirical Butler-Volmer relation. Although numerical constraints limit the applicability of this model to dimensions of a few nanometers, the model is capable of making predictions at precisely the spatial and temporal scale that we are interested in for studying medical applications of silver nano-particles. We will discuss the impact of particle size, solution concentration, and particle aggregation on ion release and surface charge, which not only impact the anti-microbial efficacy and system stability, but may also affect biocompatibility. Finally, we will discuss our efforts to extend the length and time scales of the model.

**11:25 AM**

**Phase-Field Crystal Modeling of Compositional Domain Formation in Ultrathin Films:** Srevatsan Muralidharan<sup>1</sup>; Raika Khodadad<sup>2</sup>; Mikko Haataja<sup>1</sup>; <sup>1</sup>Princeton University; <sup>2</sup>California State University Northridge

Bulk-immiscible binary systems often form stress-induced miscible alloy phases when deposited on a substrate. Both alloying and surface dislocation formation lead to the decrease of the elastic strain energy, and the competition between these two strain-relaxation mechanisms leads to the emergence of compositional nanoscale domains. We develop a phase-field crystal model for compositional domain formation of binary metallic systems. We demonstrate that the model naturally incorporates the competition between alloying and misfit dislocations, and quantify the effects of misfit and line tension on

equilibrium domain size. Then, we quantitatively relate the parameters of the PFC model to a specific system, CoAg/Ru(0001), and demonstrate that the simulations capture experimentally observed morphologies. We find that a Co rich system is pseudomorphic with the underlying substrate, while in an Ag rich system, the excess Ag phase displays dislocations and stacking faults that is in equilibrium with the 50-50 pseudomorphic alloy phase.

**11:40 AM**

**Quantitative Phase-Field Predictions of  $\beta''$  Precipitate Size Distribution as a Function of Heat Treatment Conditions and Alloying Composition in AA6111:** *Junsheng Wang*<sup>1</sup>; *Shiyao Huang*<sup>1</sup>; *Ruijie Zhang*<sup>1</sup>; *William Donlon*<sup>1</sup>; *Mei Li*<sup>1</sup>; *Long-Qing Chen*<sup>2</sup>; *John Allison*<sup>3</sup>; <sup>1</sup>Ford Research and Advanced Engineering Lab, Ford Motor Company; <sup>2</sup>Department of Materials Science and Engineering, Penn State University; <sup>3</sup>Department of Materials Science and Engineering, The University of Michigan

A phase-field model was used to simulate precipitate nucleation and growth during the heat treatment of AA6111 (Al-Mg-Si) alloys. The influence of forming prior to heat treatment is also included in this analysis. After the forming process, the dislocation density is calculated which is then related to the nucleation density of precipitation. The distribution of critical  $\beta''$  precipitate nuclei in AA6111 alloys were stochastically assigned and the potential for nucleation was calculated as a function of local supersaturation. Therefore, we calculate the nucleation and growth kinetics of  $\beta''$  precipitate during age hardening of AA6111 alloys. We studied the effects of initial Mg and Si concentrations on the  $\beta''$  size distribution. In addition, both aging time and temperature alter the precipitate size and thus affect the final yield strength of AA6111 components. Transmission electron microscopy was performed to quantify the size and number density of precipitates for model development and validation.

**11:55 AM**

**Phase-Field Simulations of Bainitic Phase Transformation in 100Cr6:** *Wenwen Song*<sup>1</sup>; *Ulrich Prah*<sup>1</sup>; *Wolfgang Bleck*<sup>1</sup>; *Krishnendu Mukherjee*<sup>1</sup>; <sup>1</sup>RWTH Aachen University

Bainite structure is of considerable importance in the design of high strength steels which contribute a lot in automotive industry. In order to better understand the mechanisms of bainite structure formation and its microstructure evolution controlling parameters, 2D phase-field simulations of the bainitic phase transformation are performed coupling with CALPHAD method. In the present work, high carbon bearing steel EN DIN 100Cr6 is used to investigate the bainite transformation and the bainitic growth mode is considered to be faceted in the phase-field simulations. The results show the bainitic microstructure evolution and its growth kinetics. Carbon diffusion as well as the interfacial mobility during bainitic phase transformation is stressed. The phase-field predicted phase fraction and microstructure evolution results are compared against the dilatometry and HRTEM experimental results. The isothermal bainitic phase transformation kinetics is successfully modeled.

**12:10 PM**

**Transmission Electron Microscopy and Modeling of Carbide Precipitation in Tempered Martensitic Steels:** *Peter Hedström*<sup>1</sup>; *Joakim Odqvist*<sup>1</sup>; *Fredrik Lindberg*<sup>2</sup>; <sup>1</sup>KTH - Royal Institute of Technology; <sup>2</sup>Swerea KIMAB AB

Carbide precipitation during tempering of martensite has a significant effect on the final mechanical properties of alloyed steels. Hence, detailed knowledge of carbide precipitation sequences, element partitioning and size distribution evolution is essential. The recent advancement in modelling strategies has opened up the possibility to perform modeling of carbide precipitation with predictive capability, but more detailed experimental work is required to assess the necessary thermodynamic and kinetic data for the relevant alloy systems. The purpose of this work is to provide such an experimental assessment for some selected model and industrial alloys. The experimental results from transmission electron microscopy and atom probe are used to evaluate modeling of carbide precipitation using a Langer-Schwartz approach.

---

## David Pope Honorary Symposium on Fundamentals of Deformation and Fracture of Advanced Metallic Materials: Deformation, Fracture, and Advanced Characterization Techniques

*Sponsored by:* The Minerals, Metals and Materials Society, TMS Materials Processing and Manufacturing Division, TMS Structural Materials Division, TMS: High Temperature Alloys Committee, TMS/ASM: Mechanical Behavior of Materials Committee, TMS: Nanomechanical Materials Behavior Committee  
*Program Organizers:* E. P. George, Oak Ridge National Laboratory; Haruyuki Inui, Kyoto University; C. T. Liu, The Hong Kong Polytechnic University

Wednesday AM  
March 2, 2011

Room: 32A  
Location: San Diego Conv. Ctr

*Session Chairs:* Tresa Pollock, University of California Santa Barbara; Erland Schulson, Dartmouth College

---

**8:30 AM Invited**

**Forensic Applications of Materials Science-An Overview:** *Michael Smith*<sup>1</sup>; <sup>1</sup>Federal Bureau of Investigation

Forensic science serves as an umbrella term for a broad range of technical activities that also entail a legal element. While many are familiar with such disciplines as DNA analysis and latent fingerprints, the role of materials science in the legal system is relatively less known. Nevertheless, materials issues commonly arise in both civil and criminal legal proceedings. To illustrate this, a range of examples will be presented along with an explanation of how the information provided by the forensic analysis of materials is used in investigative and judicial settings.

**9:00 AM Invited**

**Investigations of Zirconium Alloy Deformation and Fracture:** *Jake Ballard*<sup>1</sup>; *John Sutliff*<sup>1</sup>; *Tom Angelis*<sup>1</sup>; *Robert Mulford*<sup>1</sup>; *Joseph Pyle*<sup>1</sup>; <sup>1</sup>Knolls Atomic Power Lab

Zirconium-based alloys have been the backbone of commercial nuclear power generation for over half a century, but unexpected behaviors are still observed during service. Fundamental understanding of zirconium alloy deformation and fracture, especially during power transients is growing in its importance to better predicting long-term performance and minimizing testing and post irradiation examination costs. The complexity of events controlling deformation and fracture require both mechanical and chemistry focused studies. For example, one hypothesis attributes fuel rod failure to fission product release from cracked fuel promoting iodine stress corrosion cracking. Results from several fundamental studies will be presented, including Zircaloy fracture mechanism maps, atomistic modeling of iodine at grain boundaries and surfaces, and electron backscattered diffraction analysis of iodine SCC crack tips and fracture surfaces. A goal of these studies is to better guide development of modeling tools to enhance prediction capabilities and better guide future testing.

**9:30 AM Invited**

**Crack Growth on Basal Planes in Zn Single and Bicrystals: Experiments and Computations:** *Sharvan Kumar*<sup>1</sup>; *Dhiraj Catoor*<sup>2</sup>; <sup>1</sup>Brown University; <sup>2</sup>Dassault Systèmes Simulia Corp

Crack propagation on the basal planes in zinc was examined by means of in-situ fracture testing of pre-cracked single crystals, with attention paid to the fracture mechanism. Crack propagation occurred in bursts of dynamic extension followed by periods of arrests, the latter accompanied by plastic deformation. The crystallographic orientation of the crack growth direction on the basal plane influenced the fracture load and deformation at the crack-tip, producing noticeably different fracture surfaces. In-situ crack propagation experiments across grain boundaries of controlled "twist misorientation" in bicrystals confirmed significant resistance to

WEDNESDAY AM



crack propagation across such boundaries through extrinsic toughening mechanisms that operate when the crack stagnates at the boundary. A strong dependence of the crack propagation resistance on the twist angle was observed. Finite element models incorporating crystal plasticity were used to explain the micromechanisms of crack propagation in the single crystals, and capture several features of crack-grain boundary interaction in bicrystals.

**10:00 AM Invited**

**JIM INTERNATIONAL SCHOLAR AWARD WINNER: Crack Tip Dislocations and the Sequential Multiplication Process of Dislocation Sources along the Crack Front Revealed by HVEM-Tomography:** Masaki Tanaka<sup>1</sup>; S. Sadamatsu<sup>1</sup>; G.S. Liu<sup>2</sup>; H. Nakamura<sup>1</sup>; K. Higashida<sup>1</sup>; I.M. Robertson<sup>2</sup>; <sup>1</sup>Kyushu University; <sup>2</sup>University of Illinois

Previous investigations have revealed that the brittle-to-ductile transition (BDT) behavior often exhibited in metals is influenced by the activity of crack tip dislocations—but the exact processes governing dislocation multiplication at the crack tip remains experimentally ambiguous. This study elucidates the three-dimensional structure of crack tip dislocations via a novel combined approach of high-voltage electron microscopy and tomography (HVEM-tomography) in single crystal silicon. It was revealed that dislocations cross-slipped proximal to the crack tip even in the initial stages of plastic deformation. The local stress intensity factor along the crack front was calculated, taking into account the experimentally determined dislocation character. Based on these results, a model to account for the sequential multiplication of dislocation sources along the crack front is proposed.

**10:30 AM Invited**

**Improving Surfboards through the Adaptation of Metallic Honeycomb Sandwich Structure Technology:** Edison Conner<sup>1</sup>; <sup>1</sup>N/A

Edison Conner was a Materials Science undergraduate student of Dr. Pope, graduating from the University of Pennsylvania in 2005. Mr. Conner's senior project proposed fundamental design changes that could dramatically improve the performance of surfboards. Traditional surfboard construction techniques were developed in the 1960's and do not employ many of the major technological advances that have occurred in the advanced composites industry over the past half-century. Mr. Conner's talk will discuss a hypothesis for creating a higher-performance surfboard followed by a discussion of how his newly-developed aluminum honeycomb core surfboards have met those needs.

**11:00 AM Invited**

**Fundamental Research to Discover Amazing Metals through the "Nano-Metallurgy":** Kenji Abiko<sup>1</sup>; <sup>1</sup>Tohoku University

Recently, due to the remarkable technological progress in industries, the demand for the development of higher performance metals has been accelerated. It is, however, not easy to discover such metals of desirable properties. Fortunately, we know the incredible properties and phenomena of metals appear sometimes by the ultra-purification. After our investigation of such facts, I proposed the new concept of "Nano-Metallurgy" in the UHPM International Conference at Helsinki, 2000, to discover amazing metals. The properties of conventional metals are strongly affected by the impurity atoms. After the removal of the impurity effects by ultra-purification, the incredible properties are revealed as the inherent properties. After the nano-control of beneficial elements by doping to the ultra-purified matrix and then the nano-control of structure by heat treatment, amazing metals of very interesting properties will be born. In my talk, the development of innovative stainless alloys will be present through the concept of "Neno-Metallurgy".

**11:30 AM**

**Subsonic Edge Dislocation near Interface Solved with Discrete Image Edge Dislocation Components:** Johannes Weertman<sup>1</sup>; <sup>1</sup>Northwestern University

The use of ordinary image edge dislocations to solve the problem of an edge dislocation near an interface is thwarted because of the impossibility of simultaneously satisfying the two traction continuity conditions. However, using only discrete edge image dislocations components (some dependent

on the shear wave velocity and others on the longitudinal wave velocity) the problem is solved of an edge dislocation moving near a welded interface separating material of different elastic constants or moving near a free surface.

**11:45 AM**

**Fundamentals of Fatigue Crack Initiation and Propagation:** Chandra Pande<sup>1</sup>; <sup>1</sup>Naval Research Laboratory

A basic understanding of the fundamental nature of fatigue crack initiation and growth in metals has long been a major scientific challenge starting with the first dislocation model of fatigue crack growth of Bilby et al. (1963). Understanding the process of emission of dislocations from cracks, and determining precise expressions for the size of the plastic zone size, the crack-tip opening displacement and the energy release rate of the crack are some of the major technical issues for this purpose. We summarize briefly some of the significant results obtained in our investigations towards this goal.

**12:00 PM**

**Intelligent Microscopy for the Study of Fracture and Fatigue:** David Fullwood<sup>1</sup>; Brent Adams<sup>1</sup>; Travis Rampton<sup>1</sup>; Ali Khosravani<sup>1</sup>; <sup>1</sup>Brigham Young University

A fundamental goal in the investigation of fracture and fatigue mechanisms is the development of methods for recording critical event inception. The development of in-situ test equipment, and high-resolution microscopy techniques (such as high-resolution orientation imaging microscopy, HROIM) have placed invaluable tools into the hands of researchers. Nevertheless, practical considerations limit the volume of material that can be carefully monitored during a given testing regime. Machine learning techniques offer a promising framework for enhancing efficiency in the search for critical events. This paper presents initial efforts to develop an intelligent microscopy environment for the study of fracture and fatigue, based upon machine learning methods, in general, and reinforcement learning, in particular. The test bed for the study will include ductility studies in magnesium, exploiting recent advances by the authors in the area of HROIM.

---

## Deformation, Damage, and Fracture of Light Metals and Alloys: Session III

*Sponsored by:* The Minerals, Metals and Materials Society, MS&T Organization, TMS Light Metals Division, TMS: Chemistry and Physics of Materials Committee, TMS/ASM: Mechanical Behavior of Materials Committee

*Program Organizers:* Qizhen Li, University of Nevada, Reno; Xun-Li Wang, Oak Ridge National Laboratory; Yanyao Jiang, University of Nevada, Reno

Wednesday AM  
March 2, 2011

Room: 13  
Location: San Diego Conv. Ctr

*Session Chair:* Qizhen Li, University of Nevada, Reno

---

**8:30 AM Invited**

**Confining Shear Bands and Fracture to Improve Plasticity in an Amorphous Mg Alloy Reinforced with Mo Particles:** Taigang Nieh<sup>1</sup>; Jason Jang<sup>2</sup>; Jacob Huang<sup>3</sup>; <sup>1</sup>University of Tennessee; <sup>2</sup>National Central University; <sup>3</sup>National Sun Yat-Sen University

Amorphous alloys are intrinsically brittle because of the formation of plastically unstable shear bands. By adding ductile crystalline phase to arrest shear bands is an effective method to improve plasticity. We synthesized amorphous Mg alloy (Mg<sub>58</sub>Cu<sub>28.5</sub>Gd<sub>11</sub>Ag<sub>2.5</sub>) reinforced with porous Mo particles with different volume fractions and particle sizes by casting technique. It was found that the presence of porous Mo particles (20-50 μm) could effectively block/deflect shear band propagation. For a given volume fraction of Mo particles, smaller particles or more volume fraction would lead to shorter inter-particle spacings, thus smaller confinement zone sizes

for shear band, and consequently the improvement of compression plasticity (up to 27%). We will also discuss the criterion and mechanism for plasticity improvement in amorphous alloys.

#### 9:00 AM

**Formability of Wrought Magnesium Sheet for Various Temperatures and Strain Conditions:** Michael Miles<sup>1</sup>; David Fullwood<sup>1</sup>; Brent Adams<sup>1</sup>; Jonathan Scott<sup>1</sup>; Ali Khosravi<sup>1</sup>; <sup>1</sup>Brigham Young University

Formability of wrought magnesium alloys at or near room temperature is not favorable. The hexagonal close packed structure of Mg has few active slip systems at lower forming temperatures, limiting ductility. Much greater levels of ductility can be reached at higher temperatures but this is expensive and inconvenient for a high-volume production environment. A series of forming experiments will be conducted at room temperature and at slightly elevated temperatures, up to 150°C. Limit strains will be measured in uniaxial tension, plane strain, and biaxial tension. Microstructure evaluation will be performed on samples formed at different temperatures and strain paths, in order to determine how twinning and dislocation density are correlated localization and failure under these forming conditions. High-resolution EBSD will be used to generate data on twinning and dislocation density in order to find links between forming conditions, initial texture, and forming ductility.

#### 9:15 AM

**Utilizing HR-OIM and In-Situ Tensile Tests for Studying Crack Initiation in AZ31 Magnesium Alloys:** Ali Khosravi<sup>1</sup>; Brent L. Adams<sup>1</sup>; David T. Fullwood<sup>1</sup>; Mike Miles<sup>1</sup>; Stuart Rogers<sup>1</sup>; Jonathan Scott<sup>1</sup>; <sup>1</sup>Brigham Young University

The magnesium alloys, including AZ31 alloys, are being increasingly used in structural applications. However, poor ductility of the hcp materials due to limited numbers of slip systems is a major issue preventing faster deployment of AZ31 alloy. Several parameters, collectively known as FIPs, failure initiation parameters, have been reported as the main reasons for the nucleation of cracks within the microstructure. These FIPs often include tensile, compression, and double twinning, triple junction, grain boundary sliding, and their intersections. The objective of this paper is to clarify the importance of each FIP in crack initiation using HR-OIM. By utilizing in-situ tensile test in the SEM and applying different levels of strain up to failure, the stress and dislocation maps of the microstructure can be obtained at each step. The dislocation maps can further be refined to consider basal slip and non-basal slip maps which can help us in the investigation.

#### 9:30 AM

**Stress Intensity Factor Solutions for Friction Stir Spot Welds of Magnesium AZ31 Alloy:** Tian Tang<sup>1</sup>; Mark F. Horstemeyer<sup>1</sup>; Brian Jordan<sup>1</sup>; Paul Wang<sup>1</sup>; <sup>1</sup>Mississippi State University

The focus of the present study is to investigate the stress intensity solutions for friction stir spot welds of magnesium AZ31 alloy using finite element method. Three dimensional finite element models are constructed to thoroughly analyze the distribution of stress intensity factors including both global and local values. For the local stress intensity factors, we considered two cases, namely, infinitesimal kinked crack and finite length kinked crack. The local stress intensity factors at the critical points of infinitesimal length kinked crack are determined using the global stress intensity factors and analytical expressions of Cotterell and Rice (1980). In comparison to the stress intensity factor solutions of resistant spot weld with solid nuggets, the nonsymmetrical geometry of friction stir spot welds with respect to the faying face cause the distribution of stress intensity factors significantly different from those of resistant spot welds with symmetric structure.

#### 9:45 AM

**Deformation Induced Phase Transformation during Machining of Ti-5Al-5Mo-5V-3Cr:** David Yan<sup>1</sup>; Guy Littlefair<sup>1</sup>; Tim Pasang<sup>1</sup>; <sup>1</sup>AUT University

Ti-5553 is a relatively new titanium alloy with applications particularly in the aerospace industry for such key structural components as landing gear. However, during machining of Ti-5553, the elevated temperature and high

strain at the tool-workpiece interface may alter workpiece microstructure and result in  $\beta$  to  $\alpha$  phase transformation. During phase transformation, some intermediated phase such as  $\omega$  phase may form which is brittle and hard to machine, and it could reduce the fatigue life of machined components. The aim of this research work is to optimize the machining condition for Ti-5553, in which the  $\beta$  to  $\alpha$  phase transformation could be fully understood. Analysis of variables such as micrographs of phase components and cutting zone temperature demonstrates that the cutting temperature governs the formation of final phase components and to some extent this variation has been quantified to allow for further and more detailed investigation.

#### 10:00 AM Break

#### 10:15 AM Invited

**Fatigue Modeling in Nickel-Base Superalloys:** Bradley Fromm<sup>1</sup>; Chen Shen<sup>1</sup>; Timothy Hanlon<sup>1</sup>; Yan Gao<sup>1</sup>; Liang Jiang<sup>1</sup>; <sup>1</sup>GE Global Research

Fatigue is a leading cause of damage in gas turbine components. Tremendous progress has been made in understanding fundamental mechanisms of fatigue and in methods for fatigue life prediction and damage tolerant design of engineering components. Recent advances in three-dimensional microstructural characterization, e.g., serial sectioning and high-energy x-ray, and in microstructure-based fatigue modeling are enabling a more mechanistic understanding of the fatigue process. These techniques are demonstrated here in nickel-base superalloys, a key class of materials within the hot-section of aero and land-based gas turbines. Discussed herein are the characterization techniques used to interrogate the fatigue initiation process, the microstructure-based fatigue modeling approach, and the key challenges involved in modeling and mechanistic understanding of fatigue behavior.

#### 10:45 AM Invited

**Fatigue Deformation of Nanocrystalline NiFe Alloy:** Sheng Cheng<sup>1</sup>; Yonghao Zhao<sup>2</sup>; Xun-Li Wang<sup>3</sup>; Sooyeol Lee<sup>1</sup>; Li Li<sup>1</sup>; Jon Almer<sup>4</sup>; Peter Liaw<sup>1</sup>; Enrique Lavernia<sup>2</sup>; <sup>1</sup>University of Tennessee, Knoxville; <sup>2</sup>University of California, Davis; <sup>3</sup>Oak Ridge National Laboratory; <sup>4</sup>Argonne National Laboratory

Materials fatigue is one of the fundamental problems in application, and has remained an active research subject for decades. As a group of emerging materials, the fatigue deformation of nanocrystalline materials has been poorly understood. Recently, we have conducted a series of studies on fatigue deformation of nanocrystalline NiFe alloy. Advanced characterization using both electron transmission microscopy and in-situ high-energy X-ray diffraction has been performed to study the structure stability during fatigue crack propagation. It is found that significant grain growth can be induced by the local plastic deformation around crack tip. The in-situ diffraction technique further demonstrates the internal strain distribution, and correlates it with the microstructure variation near crack tip. Our study indicates that the crack propagation behavior in nanocrystalline materials is not only different from that in conventional materials, but also different from these computer predictions.

#### 11:15 AM

**Mechanical Properties and Deformation Mechanisms of Ultrafine Grained Al and Ti:** Yonghao Zhao<sup>1</sup>; Troy Topping<sup>1</sup>; Y. Li<sup>1</sup>; Peiling Sun<sup>2</sup>; Ruslan Valiev<sup>3</sup>; <sup>1</sup>University of California, Davis, CA 95616, USA; <sup>2</sup>Feng Chia University, Taichung 40724, Taiwan; <sup>3</sup>Ufa State Aviation Technical University, Ufa 450000, Russia

The high strength of ultrafine grained (UFG) materials is particularly attractive for light-weight structural materials such as Al, Mg and Ti alloys used in aerospace, transportation and biomedical industries. However, UFG metals and alloys usually have mechanical and thermal instabilities, due to a high density of lattice defects, which limit their practical engineering applications. Annealing is a simple and effective way to regain strain hardening/ductility and stabilize UFG structures. In this work, we systematically investigated the mechanical properties and microstructural evolutions of UFG Al and Ti during annealing. The UFG Al and Ti were prepared by equal-channel-angular pressing (ECAP). Annealing formed multi-modal grain structure in UFG Ti and polygenized dislocation walls

in UFG Al. Mechanical results indicate that both structures improved the combination of strength and ductility. The improved mechanical properties were finally rationed based on the microstructures, fracture and deformation mechanisms.

**11:30 AM**

**Investigation of the Fatigue Crack Growth Behavior of Wrought and Cast Light Metals:** *Anastasios Gavvas*<sup>1</sup>; *Brendan Chenelle*<sup>1</sup>; *Diana Lados*<sup>1</sup>; <sup>1</sup>Worcester Polytechnic Institute

The response of light metals under fatigue crack growth conditions was investigated. Fatigue crack growth experiments were conducted on cast and wrought aluminum alloys (A535 and 6061), wrought titanium alloys (Ti-6Al-4V), and alloys processed by novel techniques (6061 aluminum alloys processed by cold spray and friction stir welding). Microstructural effects on the resistance to fatigue crack propagation within each class of materials were evaluated by altering the microstructure through heat treatment, chemistry, and processing. In addition, initial crack size effects were studied for each material under various stress ratios ( $R=0.1$ ,  $R=0.5$ , and  $R=0.7$ ). The mechanisms of fatigue crack growth at the microstructural scale were identified and will be discussed. The differences in the behavior and controlling crack growth mechanisms between long and small cracks, in the near-threshold regime, and their importance in design are also discussed. Recommendations for integrating materials knowledge into a new design approach for fatigue crack growth resistance are provided.

**11:45 AM**

**An Experimental Study on Cyclic Deformation and Fatigue of Extruded ZK60 Magnesium Alloy:** *Qin Yu*<sup>1</sup>; *Jixi Zhang*<sup>1</sup>; *Yanyao Jiang*<sup>1</sup>; *Qizhen Li*<sup>2</sup>; <sup>1</sup>Department of Mechanical Engineering, University of Nevada, Reno; <sup>2</sup>Department of Chemical and Metallurgical Engineering, University of Nevada, Reno

Cyclic deformation and low-cycle fatigue properties of extruded ZK60 Mg alloy were experimentally investigated by conducting fully reversed strain-controlled fatigue experiments along the extrusion direction. The material shows marginal cyclic hardening. Under larger strain amplitudes ( $>0.52\%$ ), asymmetric hysteresis loop and significant tensile mean stress develop. With an immediate strain amplitude ( $0.45\% \sim 0.52\%$ ), asymmetric hysteresis loop evolves with loading cycles to become symmetric at about 10% fatigue life, accompanied by moderate saturated mean tensile stresses. Symmetric hysteresis shape without mean stress is observed for lower strain amplitudes ( $<0.45\%$ ). The strain-life curve shows a kinking plateau at the strain amplitude of  $0.52\%$ . Tensile cracking is exhibited and the SWT fatigue parameter is appropriate to describe the mean stress effect. The fatigue-fractured surfaces and the residual twins were microscopically observed. The microscopic features strongly depend on the strain amplitudes and are discussed with respect to the possible crack initiation and propagation mechanisms.

**12:00 PM**

**Effect of Strain Ratio on Cyclic Deformation and Fatigue of Extruded Magnesium Alloy AZ61A:** *Jixi Zhang*<sup>1</sup>; *Qin Yu*<sup>1</sup>; *Yanyao Jiang*<sup>1</sup>; *Qizhen Li*<sup>1</sup>; <sup>1</sup>Department of Mechanical Engineering, University of Nevada, Reno

Strain-controlled fatigue tests at a variety of strain amplitudes combined with three levels of strain ratio ( $R=0$ ,  $-1$ ,  $-8$ ) were conducted on an extruded magnesium alloy AZ61A using smooth tubular specimens. As the strain ratio decreased, stronger cyclic hardening rate, more asymmetric hysteresis loop, smaller stress amplitude, and lower mean stress were observed. This is considered to be associated with the twinning-detwinning processes during cyclic deformation and the accumulation of residual twins with the number of loading cycles. At the same strain amplitude, fatigue life increased with decreasing strain ratio. The strain-fatigue life curves exhibited a distinguishable kink at the strain ratios of  $-1$  and  $-8$ , but the kink disappeared at the strain ratio of  $0$ . Fatigue crack initiation was dependent on strain amplitude and strain ratio, while fatigue crack propagation was dominated by mechanical twins.

## Dynamic Behavior of Materials V: Dynamic Deformation

*Sponsored by:* The Minerals, Metals and Materials Society, TMS Structural Materials Division, TMS/ASM: Mechanical Behavior of Materials Committee

*Program Organizers:* Marc Meyers, UCSD; Naresh Thadhani, Georgia Institute of Technology; George Gray, Los Alamos National Laboratory

Wednesday AM  
March 2, 2011

Room: 5A  
Location: San Diego Conv. Ctr

*Session Chair:* William Proud, U. Cambridge

**8:30 AM Invited**

**A New Paradigm for Lowering the Ductile-to-Brittle Transformation Temperature in Steels:** *Morris Fine*<sup>1</sup>; *Semyon Vaynman*<sup>1</sup>; *Dieter Isheim*<sup>1</sup>; *Yip-Wah Chung*<sup>1</sup>; *Shrikant Bhat*<sup>2</sup>; <sup>1</sup>Northwestern University; <sup>2</sup>ArcelorMittal

Inspired by the early work of Weertman, we will present results of a theoretical study on the effect of slightly misfitting nanoscale precipitates on dislocation configurations in metals. The study shows that coherent and coplanar precipitates can twist nearby screw dislocations to locally reduce the Peierls stress, giving rise to improved dislocation mobility at low temperatures. Experimental results will be presented on copper precipitation-strengthened low-carbon steels that have remarkably high Charpy impact fracture energies at cryogenic temperatures. These results suggest a new paradigm for markedly reducing the ductile-to-brittle transformation temperatures in materials.

**9:00 AM**

**Deformation Twinning in Tantalum:** *Changqiang Chen*<sup>1</sup>; *Kaliat Ramesh*<sup>1</sup>; *Kevin Hemker*<sup>1</sup>; *Mukul Kumar*<sup>2</sup>; *Jeffrey Florando*<sup>2</sup>; <sup>1</sup>Johns Hopkins University; <sup>2</sup>Lawrence Livermore National Laboratory

The competition between deformation twinning and dislocation slip in bcc metals, such as tantalum, has been a long standing issue. The conditions under which twinning occurs are not clearly understood. In this work, we use transmission electron microscopy (TEM) and atomic scale high resolution microscopy (HREM) to characterize deformation twins in tantalum deformed under a wide range of loading conditions (quasistatic, dynamic and shock loading) and temperatures (down to 77K). The competition between dislocation slip and mechanical twinning is analyzed from both the micromechanical and crystallographic points of view, and possible twinning criteria are discussed.

**9:15 AM**

**Dynamic Deformation Response of High-Strength Ni-Containing Steels:** *Ramesh Gupta*<sup>1</sup>; *Sharvan Kumar*<sup>1</sup>; <sup>1</sup>Brown University

In this study, the effect of Ni content and heat treatment on microstructure and mechanical properties of Fe-xNi ( $x=2.5\%-10\%$ )-(0.1C/no Cu or 0.04C+1.2Cu)-Cr,Mo,V/Nb steels were examined. Plates were heat-treated to achieve high quasi-static yield strengths varying from 860 to 1100 MPa. The dynamic deformation behavior of these steels was examined in compression in the strain rate regime 2000 s<sup>-1</sup> to 3000 s<sup>-1</sup> using a split-Hopkinson bar. Optical microscopy of deformed specimens confirmed shear localization to varying extents in these steels, the extent depending on the quasi-static yield strength. Thus, under comparable deformation conditions, whereas a 3.5%Ni steel did not show shear localization, the 10%Ni steel showed fully developed shear band(s) with microcracks within the shear band. Transmission electron microscopy characterization of specimens extracted from within the shear band and without, enabled a recognition of the microstructure evolution within the band. These observations will be presented and implications discussed.



9:30 AM

**Dynamic Properties of Ultrafine-Grained Magnesium Alloys:** *Bin Li*<sup>1</sup>;  
<sup>1</sup>Center for Advanced Vehicular Systems

Dynamic testing was performed on ultrafine-grained (UFG) Mg alloys (ZK60 and AZ31B) processed by severe plastic deformation with grain size ranging from tens of microns to 250 nm, at strain rates from quasi-static (0.0001/s) to dynamic (10000/s). The dynamic properties of hcp Mg alloys present a strong rate dependence. At quasi-static rates, the deformation was dominated by dislocation slip with a moderate strain hardening, whereas at high strain rates, a sharp increase in strain hardening was observed, indicative of a transition from dislocation slip at quasi-static rates to twinning at dynamic rates. The dislocation structure of the UFG Mg alloys was analyzed by transmission electron microscopy (TEM) before and after testing.

9:45 AM Break

10:00 AM Invited

**Lighter, Stronger, Faster: Materials for an Insecure Future:** *K Ramesh*<sup>1</sup>;  
<sup>1</sup>Johns Hopkins University

In a near future dominated by energy insufficiency and global insecurity, structural materials are increasingly being required to be strong as well as light and to survive dynamic loads as a consequence of impact, explosions, and high-speed transportation. In this talk we explore the behavior of lightweight materials (in particular, metals and ceramics) subjected to dynamic loads. The dynamic behaviors of these materials are discussed in terms of the inertia associated with mass transport, the inertia associated with failure processes, and the inertia associated with deformation mechanisms. We develop specific insights through a combination of careful high strain rate experiments, transmission electron microscopy and high-resolution electron microscopy and fundamental analytical modeling of the deformation and failure processes. As specific examples, we examine the dynamic behavior of nanostructured aluminum alloys and of aluminum nitride.

10:30 AM Invited

**Small Scale Experiments to Support Strength and Damage Modeling:** *Ellen Cerreta*<sup>1</sup>; *Darcie Koller*<sup>1</sup>; *George Gray*<sup>1</sup>; *Curt Bronkhorst*<sup>1</sup>; *Carl Trujillo*<sup>1</sup>; *Juan Escobedo*<sup>1</sup>; *Alex Bergquist*<sup>1</sup>; *Benjamin Hansen*<sup>1</sup>; *Davis Tonks*<sup>1</sup>; *Ricardo Lebensohn*<sup>1</sup>; <sup>1</sup>Los Alamos National Laboratory

The limited understanding of the stochastic way in which polycrystalline materials fail prevents accurate prediction of their performance. Understanding these processes allows for prediction of their response in service and can lead to the design of more failure resistant materials. Characterization of these processes can be difficult, particularly within the dynamic strain rate regime due to limitations in experimental platforms, in-situ diagnostics, and understanding of path dependent processes. In this talk, current studies to investigate dynamic damage evolution in bulk metals will be discussed. Through the use of novel wave shock wave shaping experiments and combinations of dynamic test platforms (gas guns, laser shock and direct high explosive drive), the kinetic and spatial effects on dynamic damage can be examined. Soft recovery of these specimens enables post mortem characterization. In this way, relationships between dynamic loading conditions and deterministic damage processes are revealed.

11:00 AM

**Influence of Cryogenic Processing on Dynamic Tensile Response of High-Purity Copper:** *Joel House*<sup>1</sup>; *Michael Nixon*<sup>1</sup>; *Philip Flater*<sup>1</sup>; *James O'Brien*<sup>2</sup>; *William Hosford*<sup>3</sup>; *Robert De Angelis*<sup>4</sup>; <sup>1</sup>Air Force Research Laboratory; <sup>2</sup>O'Brien & Associates; <sup>3</sup>University of Michigan; <sup>4</sup>University of Florida, REEF

It was demonstrated in the work by Wang et al (2002) that cryogenic temperature processing could be used to increase the overall toughness of high-purity copper. Increased material toughness was attributed to coherent twin boundaries introduced via the cryogenic processing and retained by low temperature recrystallization annealing, Ma et al (2004). The current research seeks to extend that characterization by processing high-purity copper using severe plastic deformation at cryogenic temperatures. The severe plastic deformation was introduced by equal channel angular pressing. A series

of experiments to characterize the mechanical properties were conducted using a commercially available copper as a baseline for comparison with cryogenic ECAP copper. The Dynamic Tensile Extrusion experiment, see Gray et al (2005), was the principle source of data. Optical microscopy, scanning electron microscopy, and electron backscattered diffraction were used to characterize the grain morphology and the texture evolution.

11:15 AM

**High Plasticity and Substantial Deformation in Nanocrystalline NiFe Alloys under Dynamic Loading:** *Yonghao Zhao*<sup>1</sup>; *Sheng Cheng*<sup>2</sup>; *Yazhou Guo*<sup>3</sup>; *Ying Li*<sup>1</sup>; *Qiuming Wei*<sup>3</sup>; *Xun-Li Wang*<sup>4</sup>; *Yang Ren*<sup>5</sup>; *Peter Liaw*<sup>2</sup>; *Enrique Lavernia*<sup>1</sup>; <sup>1</sup>University of California, Davis; <sup>2</sup>University of Tennessee; <sup>3</sup>University of North Carolina, Charlotte; <sup>4</sup>Oak Ridge National Laboratory; <sup>5</sup>Argonne National Laboratory

High strength of bulk nanocrystalline materials (with an average grain size < 100 nm) has been widely reported, but their plasticity is disappointingly low. In this paper, by dynamically deforming a nanocrystalline NiFe alloy, we achieved a highly improved plasticity (from 8% deformation strain under quasi-static deformation to a maximum strain of ~22%) accompanied by a much enhanced yield strength (33% enhancement compared with quasi-static deformation). Microstructure investigation indicates that the high plasticity was mainly resulted from dynamic deformation induced significant grain coarsening due to grain rotation and grain boundary sliding. In addition, de-twinning (e.g. a great reduction of twin density) occurred driven by dynamic loading. Both grain coarsening and de-twinning led to a unique texture as compared to conventional deformation texture. Our work demonstrates ways of improving plasticity of nanocrystalline materials and their potential technological applications in dynamic loading atmosphere (Adv. Mater. 21, 2009, 5001).

11:30 AM

**Micromechanical Modelling of the Dynamic Behavior of Amorphous and Crystalline Polymers:** *Said Ahzi*<sup>1</sup>; *Nadia Bahlouli*<sup>1</sup>; <sup>1</sup>University of Strasbourg

In a first part of this work, we will discuss the cooperative model for the yield behavior of amorphous polymers as well as the micromechanically based extension of this model to semi-crystalline polymers. This model is valid for a wide range of strain rates (from quasi-static to dynamic) and temperatures. Applications and comparison of predicted results to experimental ones from the literature will be shown and discussed. The second part of this work describes the experimental characterization and the modeling of the thermo-mechanical behavior of two thermoplastics polyolefins: a polypropylene and an impact polypropylene. Several dynamic strain rates and temperatures were considered. The effect of the adiabatic heating on the flow stress is analyzed and discussed in terms of molecular motion. The micromechanically-based cooperative model was then used to model the yield behavior and the large deformation response. A good correlation between our tests results and the model was obtained.

11:45 AM

**High-Strain Rate Behavior of Nanostructured Niobium Processed by Severe Plastic Deformation to Very Large Strains:** *Suveen Mathaudhu*<sup>1</sup>; *Zhiliang Pan*<sup>2</sup>; *Weihua Ying*<sup>2</sup>; *Laszlo Kecskes*<sup>1</sup>; *Qiuming Wei*<sup>2</sup>; <sup>1</sup>U.S. Army Research Laboratory; <sup>2</sup>University of North Carolina - Charlotte

We have investigated the high-strain rate, uni-axial compressive behavior of nanostructured niobium (Nb), a refractory metal with body-centered cubic lattice structure. The material was processed by equal channel angular extrusion (route C) to a maximum number of passes of 24. The microstructure of the processed billets was analyzed using electron back-scattering diffraction (EBSD). We have performed mechanical testing within a wide range of strain rates: from quasi-static loading to high-rate (strain rate >103 /s) loading. It was found that nanostructured Nb exhibits reduced strain rate sensitivity (~0.02) in comparison with the coarse-grained counterpart (~0.04). Unlike many other nanostructured bcc metals such as Fe and W, nanostructured Nb exhibits homogeneous plastic flow under high-rate uni-axial compression. Flow softening is primarily caused by uniform adiabatic temperature rise of the whole specimen.

WEDNESDAY AM

12:00 PM

**Strain-Rate and Temperature Dependent Tensile Behavior of Pb-Sn and Sn-Ag-Cu Solder Alloys:** *Brad Boyce*<sup>1</sup>; Mike Neilsen<sup>1</sup>; Luke Brewer<sup>2</sup>; <sup>1</sup>Sandia National Labs; <sup>2</sup>Naval Postgraduate School

The present study examines the thermomechanical strain-rate sensitivity of eutectic 63Sn-37Pb and Pb-free 95.5Sn-3.9Ag-0.6Cu solder over a broad range of strain rates from 0.0002/s to 200/s at temperatures ranging from -60°C to +100°C. A recently developed servohydraulic tensile method enabled this span of 6-orders of magnitude in strain-rate with a single technique, thereby eliminating ambiguity caused by evaluation across multiple experimental methods. As expected, the tensile behavior of both alloys exhibited strong temperature and strain-rate sensitivity. Microstructural characterization using backscatter electron imaging and electron backscatter diffraction revealed very little intragranular rotation after deformation, suggesting the dominance of a grain boundary sliding deformation mechanism. Finally, a unified-creep-plasticity (UCP) constitutive model for solder deformation has been developed to describe the observed behavior with much higher fidelity than the common Johnson-Cook model.

12:15 PM

**Deformation and Failure Behavior of Al/Si Nanocomposites at Atomic Scales:** *Avinash Dongare*<sup>1</sup>; B. LaMattina<sup>2</sup>; A.M. Rajendran<sup>3</sup>; M.A. Zikry<sup>4</sup>; D.W. Brenner<sup>5</sup>; <sup>1</sup>North Carolina State University, Department of Materials Science and Engineering, Department of Mechanical and Aerospace Engineering; <sup>2</sup>University of Mississippi, Department of Mechanical Engineering; <sup>3</sup>U. S. Army Research Office; <sup>4</sup>North Carolina State University, Department of Mechanical and Aerospace Engineering; <sup>5</sup>North Carolina State University, Department of Materials Science and Engineering

Nanostructured composites materials comprised of metal/ceramic interfaces show significant promise for use in energy, defense, and nuclear applications. Functionally graded ceramic particle reinforced composites are an emerging class of materials for protective structures and are often referred to as blast and penetration resistant materials. The improved damage mitigation is attributed to the compositional gradients introduced through the variation of the concentration of the reinforcing ceramic particles in the matrix. Nanolayered metal-ceramic composites have also shown superior mechanical properties as compared to the conventional-engineered materials. The design and optimization of these composites for extreme environments requires a fundamental understanding of the links between the atomic scale microstructure and mechanical behavior under dynamic loading conditions. Large scale molecular dynamics simulations are used to understand the micro-mechanisms related to deformation and failure of Al/Si interfaces at high strain rates and impact loading conditions. The effect of microstructure (grain size, layer thickness, distribution, etc.) and loading conditions on the strengthening and failure behavior of metal-ceramic composites will be discussed.

**Electrode Technology for Aluminium Production: Anode Quality and Rodding Processes**

*Sponsored by:* The Minerals, Metals and Materials Society, TMS Light Metals Division, TMS: Aluminum Committee

*Program Organizers:* Alan Tomsett, Rio Tinto Alcan; Ketil Rye, Alcoa Mosjøen; Barry Sadler, Net Carbon Consulting Pty Ltd

Wednesday AM  
March 2, 2011

Room: 16B  
Location: San Diego Conv. Ctr

*Session Chair:* Nigel Backhouse, Rio Tinto Alcan

8:30 AM **Introductory Comments**

8:35 AM

**Multivariate Monitoring of the Baked Anode Manufacturing Process:**

*Julien Lauzon-Gauthier*<sup>1</sup>; Carl Duchesne<sup>1</sup>; Jayson Tessier<sup>2</sup>; Katie Cantin<sup>3</sup>; Isabelle Petit<sup>3</sup>; <sup>1</sup>Aluminium Research Centre – REGAL; <sup>2</sup>STAS; <sup>3</sup>Alcoa

Producing consistent high quality baked anodes is important for improving performance of the Hall-Héroult aluminum reduction process. Reducing variability is, however, challenging □ variations are introduced by both the raw materials and the plant itself, the former constantly fluctuate (supplier transitions, natural variability), and little feedback on anode quality is available before their use in reduction cells since lab quality assessment is destructive, time consuming and costly. Partial Least Squares (PLS) regression was used for developing a plant-wide monitoring scheme for the baked anode manufacturing process. Relationships are established between raw material properties, process conditions, and baked anode quality attributes. The model was built using weekly averaged data available at the Alcoa Deschambault smelter. Good prediction results and traceability were obtained for several anode properties. Model interpretation based on carbon plant knowledge will be discussed, and its intended use for plant monitoring, troubleshooting and decision making will be illustrated.

9:00 AM

**Characterization of a Full Scale Pre-Baked Carbon Anode Using X-Ray Computerized Tomograph:** *Donald Picard*<sup>1</sup>; Houshang Alamdari<sup>1</sup>;

Donald Ziegler<sup>2</sup>; Pierre-Olivier St-Arnaud<sup>1</sup>; Mario Fafard<sup>1</sup>; <sup>1</sup>NSERC/Alcoa Industrial Research Chair MACE3 and Aluminium Research Centre-REGAL, Laval University; <sup>2</sup>Alcoa Canada Primary Metals

In the conventional Hall-Héroult electrolysis process, the carbon anode is formed either by compaction or vibro-compaction. The final properties of an anode are influenced by many parameters such as the raw material properties, which may change from day to day. To minimize the effects of the raw materials property variation on the final product, one may want to model numerically the forming process. However, it is imperative that information on real anodes is gathered in order to calibrate those models. Some of the most valuable information is the density and porosity distribution of a full scale baked anode obtained with the computed tomography method. To test the method, three cored samples of 300 mm diameter were taken from a real anode and scanned with a Somatom Sensation 64. Calibrations standards were also used to fit the CT scan results with the experimental results.

9:25 AM

**FEM Analysis of the Anode Connection in Aluminium Reduction Cells:**

*Susann Beier*<sup>1</sup>; John J. J. Chen<sup>1</sup>; Mario Fafard<sup>2</sup>; <sup>1</sup>University of Auckland; <sup>2</sup>University of Laval

Achieving voltage savings over the anode assembly in an aluminium reduction cell, particularly at the anode connection, is a worthwhile approach within a wider programme of improvement in energy efficiency. Experiments carried out using operating cells are very difficult and expensive, however finite element method (FEM) simulations as used in this study are a cost efficient and accurate method to understand the behaviour of the anode connection, and to identify the constraints to voltage savings. This study investigates the impacts of stub deterioration and yoke stiffness on the anode connection and hence the performance of the anode assembly. An ideal stub

diameter for the investigated configuration was found, and the increased voltage drops for various level of stub deterioration were identified. The results show that a yoke cross-bar with reduced height and hence reduced stiffness decreases the tensile stress developed in the anode carbon, which lowers the risk of anode cracks. A limit for stub service life is suggested, showing a potential saving of US\$0.8m annually. A limit for a stub service life was suggested, showing a potential saving of US\$1m annually.

#### 9:50 AM

**Development of Industrial Benchmark FEA Model to Study Energy Efficient Electrical Connections for Primary Aluminium Smelters:** *David Molenaar*<sup>1</sup>; Kan Ding<sup>2</sup>; Ajay Kapoor<sup>2</sup>; <sup>1</sup>CSIRO; <sup>2</sup>Swinburne University of Technology

Process improvements of 5MW per plant (50,000tCO<sub>2</sub>e pa for coal based electricity) are possible through optimisation of the complex cast iron to carbon contacts within aluminium smelter anode and cathode assemblies. Finite element analysis is considered the tool of choice within industry for assessing potential improvements; however there are limitations with existing models regarding handling of contact resistance and carbon stress state. A study has been undertaken using thermo-electrical-mechanical finite element analysis of the cast iron to carbon contact for an anode assembly. The contact pressure and electrical resistance and its dependence on temperature have been derived from data available in the public domain. This paper presents development of the benchmark model including results. The benchmark model will be used as the reference point for the development of more advanced models in ongoing studies to assist primary aluminium smelters achieve these substantial savings in energy efficiency and reduced greenhouse gasses.

#### 10:15 AM Break

#### 10:25 AM

**Real Time Temperature Distribution during Sealing Process and Room Temperature Air Gap Measurements of a Hall-Héroult Cell Anode:** *Olivier Trempe*<sup>1</sup>; Daniel Larouche<sup>1</sup>; Donald Ziegler<sup>2</sup>; Michel Guillot<sup>1</sup>; Mario Fafard<sup>1</sup>; <sup>1</sup>Université Laval; <sup>2</sup>Alcoa

An experimental investigation of the sealing process of an anode assembly used in electrolysis cells has been performed to better define the thermal and mechanical aspects of the cast iron thimble solidification between the steel stub and carbon hole. Three holes of a baked anode have been thoroughly measured with a Coordinate Measuring Machine (CMM) to obtain a high precision three-dimensional map of the carbon interface. These measurements were then compared to the outer surface of the frozen thimbles to obtain a room temperature air gap dimension. Thirty-nine thermocouples, placed in a strategic configuration, allowed the reconstruction of the temperature field in the steel stub, carbon block and solidifying cast iron thimble from the pouring to room temperature. Hence, heat transfer coefficients can be evaluated at the carbon/cast iron and steel/cast iron interfaces with a thermal model. Metallographic analysis is matched with the cooling curves.

#### 10:50 AM

**Effects of High Temperatures and Pressures on Cathode and Anode Interfaces in a Hall-Heroult Electrolytic Cell:** *Lyne St-Georges*<sup>1</sup>; Laszlo I. Kiss<sup>1</sup>; Jens Bouchard<sup>1</sup>; Mathieu Rouleau<sup>1</sup>; Daniel Marceau<sup>1</sup>; <sup>1</sup>UQAC

This paper deals with the physical modifications occurring at high temperatures and pressures at the interfaces found in the anode and cathode of a Hall-Heroult electrolytic cell. The anode and the cathode are fabricated with carbon blocks, where steel bars are inserted and sealed with cast iron. Consequently, their interfaces are composed of cast-iron and steel and of cast-iron and carbon. For the investigation presented here, an experimental setup was built to heat and load anodic and cathodic samples. A specific attention was put on the samples preparation, to reproduce real cathode/anode sealing conditions. During the heating and the loading of the samples, fluctuations of electrical and thermal contact resistances are observed and related to physical transformations at the interfaces. These transformations could explain the fluctuations of electrical and thermal contact resistances

observed and potentially the non-homogeneities of voltage and current distribution occurring in a Hall-Heroult electrolytic cell.

#### 11:15 AM

**New Apparatus for Characterizing Electrical Contact Resistance and Thermal Contact Conductance:** *Nedelcho KandeV*<sup>1</sup>; *Hugues Fortin*<sup>1</sup>; Sylvain Chénard<sup>1</sup>; Guillaume Gauvin<sup>2</sup>; Marie-Hélène Martin<sup>2</sup>; Mario Fafard<sup>2</sup>; <sup>1</sup>Hydro-Quebec; <sup>2</sup>Laval University

A new apparatus for characterizing the electrical contact resistance and the thermal contact conductivity of connections has been developed and tested. Samples have been heated by induction heating of a stainless steel billet, which creates a powerful heat generator, instead of the commonly used convection furnace. With this apparatus, the thermo-electro-mechanical (TEM) behavior of metal-carbon and metal-metal interfaces can be reproduced. Using a controlled inert gas environment, temperature up to 1000°C and mechanical pressure up to 2 MPa can be achieved. A major advantage is that the temperature equilibrium of the samples can be reached quickly (within 2 or 3 hours) while precisely controlling the heat flux. Recent experimental results performed on steel-carbon samples showed that this concept is feasible and very efficient. This apparatus will be used to establish the constitutive laws of interfaces to support numerical modeling of the aluminium reduction cell.

#### 11:40 AM

**Carbon Anode Modeling for Electric Energy Savings in the Aluminium Reduction Cell:** *Dag Herman Andersen*<sup>1</sup>; Z. L. Zhang<sup>2</sup>; <sup>1</sup>Hydro Primary Metal Technology; <sup>2</sup>Norwegian University of Science and Technology (NTNU)

The carbon anode geometrical design influences the energy consumption in aluminium production. A 2D finite element model (FEM) of an anode immersed in an aluminium reduction cell has been developed to study how the anode geometry affects the variation in the anode to cathode distance (ACD). Large variation in ACD will prevent a systematic reduction of the average ACD and thereby hindering a reduction of electrical power loss in the bath. Another modelling example focuses on the large amount of energy loss occurring at the anode-cast iron interface due to the roughness-induced contact resistance. An analytical equation for the real contact area has been established to link the electrical power loss from the contact resistance with the pressure-dependent interface properties. The proposed contact model can be implemented in a full scale electrical FEM analysis of an anode, and used to optimize energy savings.

### Fatigue and Corrosion Damage in Metallic Materials: Fundamentals, Modeling and Prevention: Materials Corrosion and Prevention

*Sponsored by:* The Minerals, Metals and Materials Society, TMS Structural Materials Division

*Program Organizers:* Tongguang Zhai, University of Kentucky; Zhengdong Long, Kaiser Aluminum; Peter Liaw, University of Tennessee

Wednesday AM  
March 2, 2011

Room: 31C  
Location: San Diego Conv. Ctr

*Session Chairs:* Yoshiki Yamada, Ohio Aerospace Institute; Zhefeng Zhang, Institute of Metal Research, Chinese Academy of Sciences

#### 8:30 AM

**The Zinagizado Processes as New Electrochemical Alternative to Prevent the Corrosion:** *S. R. Casolco*<sup>1</sup>; A. Zanatta A.<sup>1</sup>; H. Castañeda<sup>2</sup>; S. Valdez<sup>2</sup>; <sup>1</sup>ITESM-Campus-Puebla; <sup>2</sup>Battelle, Applied Energy Systems; <sup>3</sup>Instituto de Ciencias Físicas-UNAM

The corrosion is the principal cause of metallic deteriorates. Corrosion originates the fracture, pitting, crack by the oxidation and weakening of the surface. For all this, several anticorrosive processes have been developed



to prevent corrosion. In the present work, is described the electrochemical deposition process called Zinagizado, which is based in to add a thin layer of Zn-Al-Ag alloy, previously called ZINAG. This alloy has been studied for their excellent mechanical properties, additionally is been proposed as an alternative of anticorrosive material. Due to the Zinag is consumed first, such as a sacrificial anode. The deposition of Zinag provides the environmental protection against the corrosion and could be used to covering all kind of steel metallic materials in contact with corrosive medium. The anticorrosive properties, has been obtained by the corrosion resistance of zinc achieve by the aluminium and silver addition, which is cathodically respect to the iron and steel.

#### 8:50 AM

**Corrosion Control by Natural Alkaloids in Silicone Coatings on Mild Steel in Simulated Seawater:** *Sandy Tran*<sup>1</sup>; James Earthman<sup>1</sup>; <sup>1</sup>University of California, Irvine

Protective coatings are typically applied to improve corrosive and fouling resistance but often fail to satisfactorily prevent corrosive damage, especially in aqueous settings where microbiologically influenced corrosion (MIC) is common. MIC and fouling are often coupled mechanisms that involve the settlement of microorganisms that attach and grow on immersed surfaces. Alkaloids are chemicals used by plants for defensive purposes, but which exhibit properties favorable for MIC inhibition, such as anti-microbial and chemisorption properties. Immersion testing with nicotine in a simulated seawater solution was performed to evaluate the potential effectiveness of natural alkaloids for reducing corrosion rate. Nicotine was also incorporated into two silicone coatings that were evaluated for corrosion resistance. Relative to a control sample of a coated mild steel, a coated sample in the presence of nicotine in seawater decreased the corrosion rate by over eight-fold. Electrochemical impedance spectroscopy and electrochemical noise analysis are being performed to confirm results.

#### 9:10 AM

**Electrochemical Evaluation of Martensitic-Austenitic Stainless Steel in Sulfuric Acid Solutions:** *Mosaad Sadawy*<sup>1</sup>; <sup>1</sup>University of Technology

The electrochemical behavior of martensitic-austenitic stainless steel has been evaluated in sulfuric acid solution by weight loss and electrochemical techniques. The results indicated that, increasing sulfuric acid concentration leads to increasing the corrosion rate and decreasing the passive region. Also the results showed that solution heat treated at 1050 °C and as-received specimens gave the highest corrosion resistance, while the tempering process has an adverse effect on martensitic-austenitic stainless steel, showing that the corrosion current increased by increasing tempered temperature.

#### 9:30 AM

**The Preparation of Imidazoline Corrosion Inhibitor:** *Daowu Yang*<sup>1</sup>; Yunyun Zhang<sup>1</sup>; Zhuo Ren<sup>1</sup>; <sup>1</sup>ChangSha University of Science & Technology

2 - phenyl-imidazoline was improved to enhance its water solubility and inhibition efficiency, and then composite corrosion inhibitor was manufactured with 2 - phenyl-imidazoline quaternary ammonium salt, potassium iodide, triethanolamine, polyoxyethylene nonylphenyl ether and peregol. An efficient, environmentally friendly Hydrochloric acid composite corrosion inhibitor was selected by orthogonal gravimetric measurements. The static corrosion rate of the composite inhibitor is less than 0.5 g / (m<sup>2</sup> · h), and the inhibition efficiency steel reached above 95%, which can increase by 1.1% compared with imidazoline inhibitor. The corrosion inhibition effect of the composite inhibitor have been investigated by weight loss measurements, Tafel polarization curve methods and electrochemical impedance spectroscopy (EIS). The result shows that the composite corrosion inhibitor efficiency is high in process temperature range of Hydrochloric acid cleaning; The composite corrosion inhibitor restrain the process of cathode and anode, which belongs to cathode control-oriented and charge transfer-controlled.

#### 9:50 AM

**Effect of Temperature on The Loss of Ductility of S-135 Grade Drill Pipe Steel and Characterization of Corrosion Products in CO<sub>2</sub> Containing Environment:** *Arshad Bajvani Gavanluei*<sup>1</sup>; Brajendra Mishra<sup>1</sup>; David Olson<sup>1</sup>; <sup>1</sup>Colorado School of Mines

Evaluation of loss of ductility of the API S-135 grade drill pipe steel was studied at different temperatures from 25 - 175 °C in CO<sub>2</sub> containing solution using constant extension rate test in connection with a high temperature/high pressure autoclave. Besides, the effect of temperature on the composition and morphology of corrosion product layers of this steel were investigated using X-ray diffraction (XRD), scanning electron microscopy (SEM). Results indicated the change of loss of ductility with temperature and the maximum was observed at 175 °C. XRD studies of the specimens revealed the formation of iron carbonate on the surface. SEM study of surface of the specimens showed a rhombohedral crystalline iron carbonate layer above 100 °C while no FeCO<sub>3</sub> was detected at temperatures below 100 °C. Compactness of films increased with temperature.

#### 10:10 AM Break

#### 10:20 AM

**Corrosion Behavior and Galvanic Corrosion Studies of Ti-6Al-4V Alloy GTA Weldment in HCl Solution:** M. Atapour<sup>1</sup>; E. Zahrani<sup>1</sup>; M. Shamanian<sup>1</sup>; M. H. Fathi<sup>1</sup>; <sup>1</sup>Isfahan University of Technology

The corrosion behavior and galvanic coupling of Ti-6Al-4V alloy in its welded and unwelded conditions were investigated in 5% HCl solution. Welded samples were fabricated using the conventional continuous current gas-tungsten arc welding process. Open circuit potential and potentiodynamic polarization tests were used for corrosion examinations. In addition, open circuit conditions in a zero-resistance ammeter were used to examine the galvanic corrosion behavior of the base metal – weld metal pair. The results indicated that the welded sample exhibited higher corrosion rate compared to the base metal. The galvanic corrosion evaluations showed that the welded sample was the anode of the base metal – weld metal pair. The inferior corrosion behavior of the weld sample is attributed to the coarse prior  $\beta$  grains and acicular  $\alpha/\beta$  microstructure.

#### 10:40 AM

**Comparative Study of Hot Corrosion Behavior of Plasma Sprayed Ytria and Ceria Stabilized Zirconia Thermal Barrier Coatings in Na<sub>2</sub>SO<sub>4</sub>+V<sub>2</sub>O<sub>5</sub> at 1050 °C:** Mohammad Sadegh Mahdipour<sup>1</sup>; Mohammad Reza Rahimipour<sup>1</sup>; *Mohammad hamed Habibi*<sup>2</sup>; <sup>1</sup>Materials and Energy Research Center; <sup>2</sup>University of Tehran

Thermal Barrier Coatings are subjected to spallation and destabilization due to hot corrosion. Ceria Stabilized Zirconia (CSZ)-based TBCs have been intensively investigated for the YSZ replacement because CSZ has a much lower thermal conductivity and a higher expected thermal expansion coefficient than those of YSZ. In this research, Ytria stabilized zirconia (YSZ) and ceria stabilized zirconia (ZrO<sub>2</sub> 25CeO<sub>2</sub> 2.5Y<sub>2</sub>O<sub>3</sub>) TBCs were fabricated, followed by hot corrosion tests with a Na<sub>2</sub>SO<sub>4</sub>+V<sub>2</sub>O<sub>5</sub> salt at 1050 °C. The treated samples were characterized using XRD and SEM equipped with EDS. From studies on microscopic failure behavior, the formation of YVO<sub>4</sub> crystals and the amount of phase transformations of tetragonal ZrO<sub>2</sub> to monoclinic lead to degradation of coatings. Results revealed that CSZ TBCs were better resistant to hot corrosion than YSZ TBCs. The amount of YVO<sub>4</sub> crystals and monoclinic ZrO<sub>2</sub> in YSZ are much more than CSZ which leads sooner degradation of YSZ than CSZ.

#### 11:00 AM

**The Effect of Temperature on the Corrosion Behavior of 625 Superalloy in PbSO<sub>4</sub>-Pb<sub>3</sub>O<sub>5</sub>-PbCl-ZnO Molten Salt System with 10 wt. % CdO:** E. Zahrani<sup>1</sup>; A. M. Alfantazi<sup>1</sup>; <sup>1</sup>The University of British Columbia

Corrosion behavior of 625 superalloy under 47.288PbSO<sub>4</sub> -12.776 Pb<sub>3</sub>O<sub>5</sub> -6.844 PbCl -23.108 ZnO -10 CdO (wt.%) molten salt mixture and dynamic air atmosphere were studied at 600, 700 and 800°C. Electrochemical impedance spectroscopy(EIS), open circuit potential measurements and potentiodynamic polarization technique were used to

evaluate the degradation mechanisms and characterize the corrosion behavior of the alloy. Morphology, chemical composition and phase structure of the corrosion products and surface layer of the corroded specimens were studied by SEM/EDX and x-ray map analyses. Results confirmed that during the exposure of the alloy to the molten salt, Cr was mainly dissolved through an active oxidation process as CrO<sub>3</sub>, Cr<sub>2</sub>O<sub>3</sub> and CrNbO<sub>4</sub> while Ni dissolved only as NiO in the system. Formation of a porous and non-protective oxide layer with decreased resistance should be responsible for the weak protective properties of the barrier layer at high temperatures of 700 and 800°C.

## Friction Stir Welding and Processing VI: Friction Stir Processing

*Sponsored by:* The Minerals, Metals and Materials Society, TMS Materials Processing and Manufacturing Division, TMS: Shaping and Forming Committee

*Program Organizers:* Rajiv Mishra, Missouri University of Science and Technology; Murray Mahoney, Retired from Rockwell Scientific; Yutaka Sato, Tohoku University; Yuri Hovanski, Pacific Northwest National Laboratory; Ravi Verma, General Motors

Wednesday AM  
March 2, 2011

Room: 5B  
Location: San Diego Conv. Ctr

*Session Chair:* Ravi Verma, General Motors

### 8:30 AM Invited

**Friction Stir Processing to Enable High Peak Combustion Pressures in Mid-sized and Heavy Duty Diesel Engines:** *Glenn Grant*<sup>1</sup>; Saamyadeep Jana<sup>1</sup>; Mark Veliz<sup>2</sup>; Brad Beardsley<sup>2</sup>; <sup>1</sup>Pacific Northwest National Laboratory; <sup>2</sup>Caterpillar Technical Center

As the internal combustion engine has gained efficiency, peak combustion pressures (PCP) have been steadily rising. Since 2003, however, PCP has plateaued around 190 to 200 bar because above this, conventional engine materials in pistons, cylinder liners, and heads will be beyond strength and fatigue limits. In order to increase engine efficiency further, either unconventional expensive materials must be used, or conventional materials must be modified in a way that increases their durability. This presentation describes efforts to develop Friction Stir Processing (FSP) as a method of surface modification for better durability. Data will be presented showing that FSP can produce up to 15 times fatigue life improvement and up to 80% improvement in fatigue strength. This work, a partnership between the US-DOE and Caterpillar, Inc., is developing the FSP process required to engineer the surface of engine components for improved properties, and fabricating prototype parts for testing in-engine.

### 8:55 AM Invited

**Mechanical Properties of Friction Stir Processed, Friction Stir Welded, and Gas Metal Arc Welded AA5083 Aluminum Plate:** *Christopher Smith*<sup>1</sup>; Murray Mahoney<sup>2</sup>; Rajiv Mishra<sup>3</sup>; <sup>1</sup>Friction Stir Link; <sup>2</sup>Consultant; <sup>3</sup>Missouri University of Science and Technology

Friction Stir Processing (FSP) can be used to locally modify material properties of aluminum, such as room temperature ductility. Ductility is increased due to the resulting fine grain microstructure and localized surface annealing. This allows FSP to locally improve the formability of aluminum, normally limited, without altering the properties of the bulk of the structure. Typically, forming of aluminum is restricted, with most aluminum fabrications composed primarily of flat components and excessive joining. Alternatively, FSP can enable the forming of complex shapes, reducing the number of detail parts and the subsequent joining steps. One such example is the fabrication of angles or C-channels. This paper will describe the results of a qualification program of FSP on 5083-H116 aluminum to form angles or C-channels. Static and dynamic material property test results on FSP'ed material, base material, and GMAW'ed material in both formed and unformed conditions will be presented.

### 9:20 AM Invited

**Friction Stir Powder Processing (FSPP) in Al/Cu and Fe/C Systems:** *Hidetoshi Fujii*<sup>1</sup>; Koji Inada<sup>1</sup>; YuFeng Sun<sup>1</sup>; Yoshiaki Morisada<sup>2</sup>; <sup>1</sup>Osaka University; <sup>2</sup>Osaka Municipal Technical Research Institute

Friction Stir Powder Processing (FSPP) has been developed, based on the principle of FSW (friction stir welding). The FSPP is a method to design the properties of the welded area as well as to prevent the defect formation, by performing FSW after powder with a controlled composition is placed in the gap between two plates. AA1050 was used as the plates and pure Al powder (89µm average grain diameter) and pure Cu powder (106µm average grain diameter) were used as the powder. When using pure Al powder as the filler material, the formation of defects is prevented. When using pure Cu powder, Al<sub>2</sub>Cu precipitates were formed in the stir zone, and consequently, the hardness significantly increased. In addition, when carbon powder is added into a steel plate, stirring and diffusion of carbon and the transformation occur simultaneously, leading to significantly harden the FSPPed area.

### 9:45 AM

**Mechanical Interlock of Thin Metallic Wire Using Friction Stir Forming:** *Koshi Yamamura*<sup>1</sup>; Kazuya Torikai<sup>2</sup>; Tadashi Nishihara<sup>2</sup>; <sup>1</sup>Yamamura Mfg. Co., Ltd.; <sup>2</sup>Kokushikan University

Friction Stir welded (FSW) is attracting attention as solid-state joining process using friction heating. In recent author's study, noting excellent fluidity of aluminum alloy at FSW, micro-forging and its application to mechanical interlocking were investigated. We call this new process friction stir forming (FSF). In this study, a novel method of mechanical interlock of a thin metallic wire using FSF is proposed. The FSF process uses the friction heat and plastic deformation generated between a rotating tool and the material being forged. Trial with friction stir interlocking of aluminum alloys and various thin wires were carried out using a modified milling machine. The results were discussed in terms of pulling out characteristics. We concluded that a thin metallic wire has been successfully interlocked with aluminum alloy by friction stir technique.

### 10:05 AM

**Friction Stir Fabrication - An Additive Friction Stir Technology:** *Jeffrey Schultz*<sup>1</sup>; Peter Ferek<sup>1</sup>; <sup>1</sup>Schultz-Creehan, LLC

Friction stir fabrication (FSF) is an additive solid state, friction stir coating and joining method being developed at Schultz-Creehan, LLC (Blacksburg, VA, www.schultz-creehan.com). The FSF process uses shear-induced interfacial heating and plastic deformation to deposit wrought metal and metal matrix composite (MMC) coatings onto metal and MMC substrates. In this process, the coating alloy (in rod or powder form) is forced through a rotating spindle onto the substrate surface. Frictional heating occurs at the filler-rod/substrate interface due to the rotational motion of the filler rod and the downward force applied. The mechanical shearing that occurs at the interface acts to disperse any oxides or boundary layers, resulting in a metallurgical bond between the substrate and coating. As the substrate moves, the coating is extruded under the rotating shoulder of the stirring tool at the nose of the spindle.

### 10:25 AM

**Friction Consolidation of Aluminum Chips:** *Wei Tang*<sup>1</sup>; Anthony Reynolds<sup>1</sup>; <sup>1</sup>University of South Carolina

In this paper, friction consolidation was applied on various aluminum chips (2xxx, 5xxx, 6xxx, and 7xxx series) with a rotating die and a stationary 'billet' chamber. For consolidation aluminum, both components were made with H13 tool steel, and the die had a scroll pattern on the working end: similar to a 0° friction stir welding tool shoulder. In the friction consolidation process, the Z axis force was remained constant and different rotational speeds were applied from 100 rpm to 400 rpm, and solid aluminum disks were obtained. The consolidation quality was evaluated from the cross section after grinding, polishing and etching processes, and micro-hardness testing was performed along the mid-plane of the cross section. The die rotation rate, consolidating time cost, consolidating torque and power, consolidating quality, grain size, micro-hardness distribution, and relationship among those factors were discussed in this paper.

10:45 AM

**Friction Stir Processing as a Base Metal Preparation Technique for Modification of Fusion Weld Microstructures:** *Jeff Rodelas*<sup>1</sup>; John Lippold<sup>1</sup>; James Rule<sup>1</sup>; Jason Livingston<sup>1</sup>; <sup>1</sup>The Ohio State University

Friction stir processing was applied as a technique to modify the base metal microstructure of Ni-base Alloy 600 prior to fusion welding. Following FSP, autogenous gas tungsten arc welds were placed atop the stir-processed region. The resulting weld microstructure was characterized using various techniques. Grain refinement produced from FSP increased the extent of epitaxial nucleation and led to grain refinement of the weld metal. Grain size within the heat affected zone was also reduced by a factor of 3 near the fusion boundary relative to unprocessed base metal. The combination of fusion zone and heat affected zone grain refinement is a unique characteristic of friction stir processing and is not otherwise achievable using conventional weld microstructure refinement methods.

11:05 AM Break

11:15 AM

**Thermal Stability of Friction Stir Processed Ultrafine Grained Al-Mg-Sc Alloy:** *Nilesh Kumar*<sup>1</sup>; Rajiv Mishra<sup>1</sup>; <sup>1</sup>Missouri University of Science & Technology

Friction stir processing of coarse grained (initial average grain size ~ 50 μm) Al-Mg-Sc resulted into ultrafine grained alloy (average grain size ~ 0.4 μm). This alloy was subjected to annealing heat treatment at varying temperatures from 200 °C – 600 °C for 1 h duration at each temperature to study the stability of ultrafine grained microstructure. To understand the role of Al<sub>3</sub>Sc precipitates in this alloy, another Al-Mg alloy was friction stir processed using the same processing parameters and subjected to identical annealing conditions. EBSD and TEM were employed to investigate the grain growth and precipitate coarsening as a result of annealing heat treatment.

11:35 AM

**Effect of Friction Stir Processing on Constituent Particles in a Commercial 2024Al:** *Somayeh Pasebani*<sup>1</sup>; Indrajit Charit<sup>1</sup>; Rajiv Mishra<sup>2</sup>; <sup>1</sup>University of Idaho; <sup>2</sup>Missouri University of Science and Technology

Almost all commercial aluminum alloys have primary constituent particles that are often harmful to their mechanical properties. Friction stir processing (FSP) leads to substantial changes in the constituent particle size and distribution, lessening the deleterious effects of the constituent particles. FSP was carried out on AA 2024Al alloy with a combination of different parameters (tool rotation speed of 200-1000 rpm and traverse speed of ~25-152 mm/min). Backscattered Electron (BSE) imaging mode was used to detect and analyze the relevant constituent particles in 2024 Al. Energy Dispersive X-ray Spectrometry (EDXS) experiments were conducted in the SEM to characterize the chemical identity of the constituent particles. It has been observed that the insoluble constituent particles (Al-Cu-Mn-Fe) were fragmented into particles of smaller sizes and more rounded shapes. Conversely, the soluble particles (Al-Cu-Mg) in most cases went into solution during FSP. Different possible mechanisms are proposed to explain the phenomenon behind these changes.

11:55 AM

**Obtaining Sub-Micron Grain Size in AM60 Magnesium Alloy Using Friction Stir Processing:** *Daniel Gesto*<sup>1</sup>; David Verdera<sup>1</sup>; Paz Miniño<sup>2</sup>; Pilar Rey<sup>1</sup>; Gloria Pena<sup>2</sup>; <sup>1</sup>AIMEN Technology Centre; <sup>2</sup>Universidad de Vigo

Friction Stir Processing has gained importance in recent years as a very useful tool to produce UFG microstructures in cast and wrought magnesium and aluminum alloys, achieving superplastic behaviour. In this work, the influence of initial material condition and cooling rate on microstructure (in particular in the final grain size) of an AM60-6 mm thick magnesium alloy was carried out. A MP159 fix pin tool for 3 mm butt joints was used. FSP tests were conducted on as-cast and solubilized plates. Particular attention was paid to the level of grain refinement when a cooper backing plate and a cooling agent are used. A clearly homogenized structure and sub-micron grain sizes were obtained when these vigorous cooling systems were employed.

12:15 PM

**Effect of Friction Stir Processing on Corrosion Behavior of AA5083 Aluminum Alloy:** *Gaurav Argade*<sup>1</sup>; Rajiv Mishra<sup>1</sup>; Chris Smith<sup>2</sup>; Murray Mahoney<sup>3</sup>; <sup>1</sup>Missouri University of Science and Technology; <sup>2</sup>Friction Stir Link; <sup>3</sup>Consultant

The corrosion behavior of AA5083 depends on microstructural features such as matrix grain size, second phase size, and distribution of (β-Al<sub>3</sub>Mg<sub>2</sub>) and the nature of Al-Fe-Mn complex dispersoids. In the present work, the effect of grain size on the corrosion behavior of the alloy was studied in a 3.5 wt% NaCl solution. The grain size was varied via friction stir processing (FSP) by adopting different combinations of tool rotation rate and tool traverse speed. Corrosion behavior was characterized using potentiodynamic polarization measurements and the free corroding potential response with respect to time. In addition, a galvanostatic technique was applied to estimate the pit nucleation and pit repassivation potential of processed alloy samples. The fine grain microstructure, obtained using FSP, exhibited improved corrosion response vs. the base material. Overall corrosion response is presented on a process map.

12:35 PM

**Evaluation of Rotational Speed and Post Annealing Effect on the Microstructural Homogeneity of Friction Stir Processed 5083 Aluminum Alloy:** *Chun-Yi Lin*<sup>1</sup>; Truan-Sheng Lui<sup>1</sup>; Li-Hui Chen<sup>1</sup>; <sup>1</sup>National Cheng Kung University

The effect of rotational speed and post annealing on the microstructural homogeneity of friction stir processed 5083 aluminum alloy was evaluated. In the stir zone grain size increased with the rotational speed from 450 to 850 rpm. While the rotational speed further arising up to 1650 rpm, the grain size was almost invariant. With a rotational speed of 450 rpm grains grew up to extremely large size and occupied nearly half area in SZ. Before 850 rpm increasing rotational speed could reduce extreme grain growth in post annealing. However, the post annealed microstructure of the specimens 850-1650 rpm was similar, in which the survived initial fine grains occupied about 60% area of SZ. The effect of stored energy induced by the different rotational speeds on the microstructural homogeneity of post annealed FSPed specimens was also discussed in this study.

## Furnace Efficiency – Energy and Throughput: Session I

*Sponsored by:* The Minerals, Metals and Materials Society, TMS Light Metals Division, TMS: Energy Committee

*Program Organizers:* Thomas Niehoff, Linde Gas; Cynthia Belt, Consultant; Russell Hewertson, Air Products and Chemicals Inc; Robert Voyer, Hatch

Wednesday AM  
March 2, 2011

Room: 4  
Location: San Diego Conv. Ctr

*Session Chairs:* Russell Hewertson, Air Products and Chemicals, Inc.; Thomas Niehoff, Linde Gas

8:30 AM

**Furnaces Designed for Fuel Efficiency:** *David White*<sup>1</sup>; <sup>1</sup>The Schaefer Group, Inc.

This presentation will discuss the optimum furnace designs. Why they work and what you can do as purchasers to enhance that efficiency. Topics include refractory selection, circulation, preheat hearths, heat exchangers and operating procedures. Mainly large wet bath reverberatory furnaces will be presented with some information on tilters and immersion element melters and holders. Actual case studies will be presented of the energy savings.



### 8:50 AM

#### **Latest Trends in Post Consumer and Light Gauge Scrap Processing to Include Problematic Processing Material such as UBC, Edge Trimmings and Loose Swarf:** Franz Niedermair<sup>1</sup>; Guenther Wimroither<sup>1</sup>; <sup>1</sup>Hertwich Engineering

Melting of Post Consumer Aluminum Scrap is a challenging issue, with ever increasing requirements in terms of efficiency and environmental impact. In today's competitive world the following topics are of particular importance: Highest possible metal yield; Low energy/fuel consumption; Reduction of residues and emissions; Safe working and operational conditions. Hertwich Engineering, Braunau, Austria, a member of the SMS group, has recently developed a remelt furnace type for the processing of such scrap. The "HE-Ecomelt" furnace series is designed to accept a wide range of post consumer and light gauge scrap and to efficiently recycle the product into molten metal. Integrated high efficiency preheating and delacquering, thermal reclamation of organics and the applied submerge melting process ensure the best recoveries and lowest fuel consumption in the industry. At the same time, the ever increasing emission constraints in industrialized countries are easily met.

### 9:10 AM

#### **Investigation of Heat Transfer Conditions in a Reverberatory Melting Furnace by Numerical Modeling:** Andreas Buchholz<sup>1</sup>; John Rødseth<sup>2</sup>; <sup>1</sup>Hydro Aluminium Rolled Products GmbH; <sup>2</sup>Hydro Aluminium as

A numerical model based on the commercial software Fluent was used to analyze the heat transfer conditions in an industrial reverberatory melting furnace. The model comprises different physical phenomenon as gas flow, chemical reactions, i.e. combustion, conduction, radiation and latent heat release in the metal. The gas circulation was analyzed for different metal loads and burner arrangements. The melting process inside the furnace is inherently time-dependent, and a complete transient analysis is very time-consuming. To study the impact of varied burner positions on the energy utilization, stationary solutions were applied, where the effect of melting heat was approximated by artificial heat sinks inside the metal. The results of the stationary solutions were compared with fully transient results to guarantee the transferability of the cost-efficient steady state calculations. The results stress the dominant effect of radiative heat transfer in the melting process.

### 9:30 AM

#### **Oxyfuel Optimization Using CFD Modeling:** Thomas Niehoff<sup>1</sup>; Sreenivas Viyyuri<sup>1</sup>; <sup>1</sup>Linde Gas

Before converting production furnaces to different combustion technologies it is essential to understand all related changes and side effects. An experienced team will be able to successfully conclude a conversion like this. However, CFD Modeling will enable to make informed decisions in terms of effort and results of furnace retrofitting with new combustion equipment. This paper will give insight of how Oxyfuel together with CFD can impact energy balance and productivity of production furnaces.

### 9:50 AM

#### **Operational Efficiency Improvements Resulting from Monitoring and Trim of Industrial Combustion Systems:** Jim Oakes<sup>1</sup>; <sup>1</sup>Super Systems Inc

Combustion is the exothermic chemical reaction (a reaction in which heat is given off) of hydrogen and carbon atoms contained in fuels with oxygen. Excess O<sub>2</sub> makes heating inefficient, thus requiring more gas for the same results. In addition, excess air also allows for the formation of pollutants such as Nitrous Oxide (NO) and Nitrogen Dioxide (NO<sub>2</sub>). It is estimated that precise control of air to fuel ratio will yield 5 to 25% or more savings in heat generation. The air gas ratio can be determined by analyzing the flue gas and the mixture for combustion can be altered to produce the most clean and efficient heat for the process. Periodic checking and resetting of air-fuel ratios is one of the simplest ways to get maximum efficiency out of fuel-fired process heating equipment. In heat treatment facilities, the customer would find potential efficiency improvements on generators, radiant tubes, furnaces, ovens, heaters, and boilers.

### 10:10 AM Break

### 10:30 AM

#### **50% Reduction of Energy and CO2 Emission in Metallurgical Furnaces by Burners:** Michael Potesser<sup>1</sup>; B. Holleis<sup>2</sup>; M. Demuth<sup>2</sup>; D. Spoljaric<sup>2</sup>; J. Zauner<sup>3</sup>; <sup>1</sup>Superior Industries International; <sup>2</sup>MESSER AUSTRIA GmbH; <sup>3</sup>University of Leoben

The efficiency of industrial combustion processes can be raised in two ways, either by preheating the fuel and combustion air or by oxyfuel. The most important issue of the usage of oxygen burners is the substantially increasing melting rate by lowering the specific production costs because of the higher combustion efficiency. The flameless combustion (internal offgas recirculation) and the external offgas recirculation solves the problem with the high flame temperature and leads to cold combustion and lower dross formation or alloying elements combustion. The Oxipyr®-Air combines the technology of diluted combustion during air and oxygen usage decreasing the emission of pollutants. Constitutive of the Oxipyr®-Air development a fuel-oxygen-burner, Oxipyr®-Flex, was designed for a maximum of flexibility for the customer. The Oxipyr®-Air and Oxipyr®-Flex have been developed for the specific needs of melting and recycling companies for all non ferrous metals. The paper shows the theory, practical installations and economical outlook.

### 10:50 AM

#### **New Technology for Electromagnetic Stirring of Aluminum Reverberatory Furnaces:** James Herbert<sup>1</sup>; Alan Peel<sup>2</sup>; <sup>1</sup>Altek LLC; <sup>2</sup>Altek Europe Ltd.

The benefits of circulation in aluminum reverberatory furnaces are well documented and include higher productivity, and reduced fuel consumption and dross generation. One popular method to achieve the benefits of circulation is electromagnetic stirring. That said, this technology has certain drawbacks preventing its universal acceptance: high capital cost, high operating cost (especially power consumption and maintenance of water cooled copper tubes), reluctance to use water in close proximity to molten metal, and in some cases the inability to operate through full thickness refractory hearths. This paper describes a technology which amounts to the reinvention of traditional electromagnetic stirring devices, effectively addressing all of the above negative aspects of traditional systems. In this paper we will describe how these issues are addressed and results documented in recent installations

### 11:10 AM

#### **Evaluation of Effects of Stirring in a Melting Furnace for Aluminum:** Kunio Matsuzaki<sup>1</sup>; Steve Iijima<sup>2</sup>; <sup>1</sup>National Institute of Advanced Industrial Science and Technology, Japan; <sup>2</sup>Zmag America, Ltd.

The purpose of this paper is to investigate commercialization of an integrated melting furnace and stirrer for molten aluminum. The concept was tested via installation of a new type of permanent magnet stirrer to an existing furnace. The end goal is to improve the quality of aluminum through bath temperature homogenization and to reduce energy usage and dross generation while providing a reduction in melt loss. Traditionally, molten aluminum has been mechanically or electromagnetically stirred; however the former is both inefficient and can be dangerous, and the latter requires excessive energy and complicated components. In this research, molten aluminum was stirred by setting a permanent magnet circuit beside a furnace. This report also incorporates thoughts on more effective shapes of furnaces, compared to ordinary furnaces.

### 11:30 AM

#### **Business Analysis of Total Refractory Costs:** Cynthia Belt<sup>1</sup>; <sup>1</sup>Consultant

Refractory is a critical component of a furnace. Both planned and unplanned downtime due to refractory wear or failure can detrimentally affect production. Refractory materials, design, and maintenance can improve or degrade energy efficiency and melt rate. In addition, the cost of refractory is typically the largest maintenance expense of a melt or hold furnace. Total refractory costs include refractory materials, installation, energy, and downtime. Many attempts have been made by companies to hold

down these costs in various ways. This paper compares several methods and gives relative cost savings based on a benchmark furnace.

**11:50 AM**

**Improved Furnace Efficiency through the Use of Refractory Materials:** James Hemrick<sup>1</sup>; Angela Rodrigues-Schroer<sup>2</sup>; Dominick Colavito<sup>2</sup>; Jeffrey Smith<sup>3</sup>; <sup>1</sup>Oak Ridge National Laboratory; <sup>2</sup>MINTEQ International, Inc.; <sup>3</sup>Missouri University of Science and Technology

This paper will describe efforts performed at Oak Ridge National Laboratory (ORNL), in collaboration with industrial refractory manufacturers, refractory users, and academic institutions, to improve energy efficiency of U.S. industry through increased furnace efficiency brought about by the employment of novel refractory systems and techniques. Work in furnace applications related to aluminum, gasification, and lime will be discussed. The energy savings strategies discussed are achieved through reduction of chemical reactions, elimination of mechanical degradation caused by the service environment, reduction of temperature limitations of materials, and elimination of costly installation and repair needs. Key results of several case studies resulting from US Department of Energy (DOE) funded research programs will be discussed with emphasis on applicability of these results to high temperature furnace applications.

**12:10 PM**

**Study on the Energy-Saving Technology of Chinese Shaft Calciners:** Guanghui Lang<sup>1</sup>; Chongai Bao<sup>1</sup>; Shoulei Gao<sup>1</sup>; Ronald Logan<sup>1</sup>; Yan Li<sup>1</sup>; Jingou Wu<sup>1</sup>; <sup>1</sup>Sunstone

Shaft calcining technology is widely used in China for the calcination of green petroleum coke. It has the advantages of lower energy consumption and lower carbon burning loss compared to the rotary kilns. In this paper, a method of further reducing carbon burning loss using integrated technology is discussed.

## Hume-Rothery Symposium Thermodynamics and Diffusion Coupling in Alloys - Application Driven Science: Diffusion and Phase-Field Simulations

*Sponsored by:* The Minerals, Metals and Materials Society, TMS Electronic, Magnetic, and Photonic Materials Division, TMS: Alloy Phases Committee

*Program Organizers:* Zi-Kui Liu, The Pennsylvania State University; Larry Kaufman, CALPHAD, Inc.; Annika Borgenstam, Royal Institute of Technology; Carelyn Campbell, NIST

Wednesday AM  
March 2, 2011

Room: 31A  
Location: San Diego Conv. Ctr

*Session Chairs:* Katsuyo Thornton, University of Michigan; Ingo Steinbach, Ruhr-University

**8:30 AM Invited**

**Thermodynamics and Ionic/Electronic Transport in Oxides:** Ye Cao<sup>1</sup>; Saswata Bhattacharya<sup>1</sup>; Jie Shen<sup>2</sup>; Clive Randall<sup>1</sup>; Long Qing Chen<sup>1</sup>; <sup>1</sup>Pennsylvania State University; <sup>2</sup>Purdue University

Ionic and electronic transport is an important process that can influence the applications of many oxides. For example, one of the primary limiting factors for the life time of multi-layer dielectric capacitors is long-term resistance degradation. It is characterized by slowly increasing leakage currents under a constant voltage stress. In this presentation, a general thermodynamic formulation for the total free energy of an inhomogeneous system containing both electronic and ionic species as well as microstructures will be described within the phase-field formulation. The ionic/electronic transport equations as well as the electrostatic Poisson equation and the elasticity equation are then derived from the thermodynamic free energy. Implementation of spectral methods to solving the systems of equations under non-periodic boundary conditions will be presented. Application of the set of transport

equations to resistance degradation behavior of ferroelectric dielectrics and domain/defect interactions will be discussed.

**9:00 AM Invited**

**Stress Induced Diffusion of Voids and Interstitials in Solids:** Ingo Steinbach<sup>1</sup>; <sup>1</sup>Ruhr-University

Diffusion in solids is caused not only by gradients in the local concentration, but also by gradients in the local stress distribution in the microstructure if the material exhibits a non negligible influence of its volume on the composition. A multi-phase-field model is developed to account for the effect of concentration on volume in Vegard's approximation. The model is applied to diffusion of carbon in the austenite phase in a pearlitic steel grade and to diffusion of voids in a multi-grain structure. It is demonstrated, how stress driven diffusion in steel determines the growth kinetics of pearlite. In polycrystalline material it is shown how void diffusion controls grain growth for nano-sized structures. It is highlighted that the contribution of stress to diffusion in solids is crucial for the quantitative understanding of microstructure evolution.

**9:30 AM Invited**

**Modeling Displacive-Diffusional Coupling in Phase Transformation and Plastic Deformation:** Yunzhi Wang<sup>1</sup>; Ju Li<sup>2</sup>; <sup>1</sup>Ohio State University; <sup>2</sup>University of Pennsylvania

Microstructural evolution in materials often involves coupled displacive and diffusional processes. For example, structural phase transformations often involve coupled lattice shear, shuffle, and diffusion, while creep deformation often involves coupled dislocation glide, climb and atom diffusion. Mechanistic studies of these mechano-chemically coupled processes require modeling capabilities at micrometer, nanometer and even atomistic length scales but diffusional time scales. In this presentation, recent efforts in developing multi-scale modeling approaches by integrating ab initio calculations and atomic potentials into continuum phase field method at all length scales will be reviewed. Examples will be given to demonstrate quantitative aspects of the approaches in (a) predicting defect size and energy, and thermally activated processes of defect nucleation and migration, utilizing directly ab initio information as model input, (b) studying deformation/transformation mechanisms at atomic resolution but at diffusion time scales, and (c) identifying and incorporating transformation and deformation mechanisms in combination with advanced experimental characterizations.

**10:00 AM Break**

**10:20 AM Invited**

**Diffuse Interface Modeling and Simulations: Conventional and Rigorous Treatments of Diffusion Accompanied by the Kirkendall Effect:** Hui-Chia Yu<sup>1</sup>; Katsuyo Thornton<sup>2</sup>; <sup>1</sup>University of Michigan - Department of Material Science & Engineering; <sup>2</sup>University of Michigan - Department of Material Science & Eng.

The Kirkendall effect arises in substitutional alloys when various atomic species exchange with vacancies at different rates. Vacancies that facilitate diffusion are generated and eliminated at their sources and sinks, resulting in lattice shifts and deformations. The conventional model of the Kirkendall effect assumes that vacancy sources and sinks are distributed uniformly and thus the vacancy concentration remains at its equilibrium value throughout the solid. We simulate interdiffusion and Kirkendall-effect-induced deformation based on the conventional interdiffusion equation using the Smoothed Boundary Method. Bulging, grooving and bending due to the Kirkendall effect are studied. In a more rigorous model, free surfaces and grain boundaries are treated as the dominant vacancy sources and sinks, such that vacancy concentration remains at its equilibrium value only at these locations. We investigate the interdiffusion process, void growth, and deformation using simulations based on this rigorous model, again using the Smoothed Boundary Method.

#### 10:50 AM Invited

**Evaluation of Ordering Mobility from Antiphase Domain Growth Rate in Fe<sub>3</sub>Al Using Phase-Field Simulation:** *Yuichiro Koizumi*<sup>1</sup>; Samuel Allen<sup>2</sup>; Masayuki Ouchi<sup>3</sup>; Yoritoshi Minamino<sup>3</sup>; <sup>1</sup>Tohoku University; <sup>2</sup>Massachusetts Institute of Technology; <sup>3</sup>Osaka University

The phase-field method (PFM) is becoming the premier method for predicting the microstructural evolution. For accurate prediction, reliable data of free energy and mobility are required. Although the free energies for major alloys are available in thermodynamic databases; the mobility for solute-atoms are derived from diffusivity data, the mobility for phase transformations is unavailable in many cases. In this study, the mobilities for ordering transformation in Fe<sub>3</sub>Al have been evaluated by comparing the rates of experimentally measured antiphase domains (APDs) growth and that simulated by PFM. The apparent ordering mobility experimentally evaluated for Fe-24at%Al alloy was approximately one half of that for Fe-26at%Al alloy. The difference was ascribed to the solute-drag by the PFM [Koizumi et al. *Acta Mater.* 2009;57:3039.]; the ordering mobilities re-evaluated by taking the solute-drag into account were in good agreement. This suggests that PFM is useful to extract underlying intrinsic mobility from experimentally measured extrinsic mobility.

#### 11:20 AM

**Phase Field Modeling of Beta to Alpha Transformations in Ti-6Al-4V:** *Rongpei Shi*<sup>1</sup>; Ning Zhou<sup>1</sup>; Ning Ma<sup>2</sup>; Yunzhi Wang<sup>1</sup>; <sup>1</sup>The Ohio State University; <sup>2</sup>ExxonMobil Research & Engineering Company

Microstructure evolution during beta to alpha transformation in Ti-6Al-4V is investigated using a quantitative 3D phase field modeling. The model takes into account crystallography of the BCC to HCP transformation, misfit dislocations at the alpha/beta interfaces, and coherency stresses. In addition, model inputs are linked directly to available thermodynamic and mobility databases. Effects of local stress, existing precipitate and grain boundary on variant selection during nucleation and growth of alpha phase are studied. The spatial distribution of different variants of the alpha phase is found to correlate strongly with local stress, existing precipitate and grain boundary in a pre-existing microstructure. Various morphologies of intersecting alpha plates captured during their growth are compared with experimental observations.

#### 11:50 AM

**Thermotransport in  $\gamma$ (bcc) U-Zr Alloys: A Phase-field Model Study:** *Rashmi Mohanty*<sup>1</sup>; *Joshua Bush*<sup>1</sup>; *Maria Okuniewski*<sup>2</sup>; *Yongho Sohn*<sup>1</sup>; <sup>1</sup>University of Central Florida; <sup>2</sup>Idaho National Laboratory

Atomic transport in the presence of temperature gradient or the thermotransport phenomenon was simulated for U-Zr alloys using a phase-field model derived from irreversible thermodynamics. The free energy of the system was directly incorporated from the available thermodynamic database, and the kinetic parameters such as atomic mobility and heat of transport terms were obtained from experimental values reported in the literature. The model was applied to a single-phase (bcc- $\gamma$ ) alloy and to a diffusion couple consisting of two single-phase ( $\gamma$ ) alloys of different compositions, both subjected to a constant temperature gradient. An enrichment of Zr at the hot end of the single-phase alloy, with a corresponding depletion of U, was observed from an initially homogeneous single-phase alloy. A similar atomic transport was observed in the diffusion couple, where the magnitude and direction of the final composition gradient was dictated by a combination of atomic mobility and heat of transport.

## Magnesium Technology 2011: Deformation Mechanisms I

*Sponsored by:* The Minerals, Metals and Materials Society, TMS Light Metals Division, TMS: Magnesium Committee  
*Program Organizers:* Wim Sillekens, TNO Science and Industry; Sean Agnew, University of Virginia; Suveen Mathaudhu, US Army Research Laboratory; Neale Neelameggham, US Magnesium LLC

Wednesday AM  
March 2, 2011

Room: 6F  
Location: San Diego Conv. Ctr

*Session Chairs:* Carlos Caceres, University of Queensland; Eric Nyberg, Pacific Northwest National Laboratory

#### 8:30 AM

**Crystal Plasticity Analysis on Compressive Loading of Magnesium with Suppression of Twinning:** *Tsuyoshi Mayama*<sup>1</sup>; Tetsuya Ohashi<sup>2</sup>; Kenji Higashida<sup>3</sup>; Yoshihito Kawamura<sup>1</sup>; <sup>1</sup>Kumamoto university; <sup>2</sup>Kitami Institute of Technology; <sup>3</sup>Kyushu University

In this study, the compressive loading behavior of single crystals and bi-crystals of magnesium without consideration of deformation twinning has been investigated by crystal plasticity finite element analysis method with the aim of fundamental understanding of kink band formation in magnesium alloys with long period stacking ordered structure (LPSO) phase. First, the basal plane of the single crystal model is set to be parallel to the compressive direction. For this analysis model, the effects of grain boundary, slight change of loading direction and heterogeneity of the initial dislocation density have been studied. Secondly, the analysis to clarify the influence of the angle between basal plane and the loading axis is performed. The results of the analysis are discussed in terms of active slip system and heterogeneity of deformation.

#### 8:50 AM

**Crystal Plasticity Modeling of Pure Magnesium Considering Volume Fraction of Deformation Twinning:** *Yuichi Tadano*<sup>1</sup>; <sup>1</sup>Saga University

In this study, a novel crystal plasticity model for pure magnesium involving the deformation twinning is presented. The deformation twinning is an important deformation mechanism of magnesium and other HCP metals. The deformation twinning has two important issues: first, large rotation of crystal lattice caused by twinning occurs. Second, in the crystalline scale, twinned and untwinned regions may simultaneously exist in a grain. Therefore, a crystal plasticity analysis of magnesium should introduce both of them, and the present framework takes into account these two key features. To represent the second issue, the volume fraction of deformation twinning is considered, and a material behavior of a grain is described as mixed state of twinned and untwinned regions. This paper provides some numerical examples with the present model, and it is shown that a smooth transition from untwinned to twinned states can be represented.

#### 9:10 AM

**Nucleation Mechanism for Shuffling Dominated Twinning in Magnesium:** *Sungho Kim*<sup>1</sup>; Haitham Kadiri<sup>1</sup>; Mark Horstemeyer<sup>1</sup>; <sup>1</sup>Center for Advanced Vehicular Systems

We observed for the first time spontaneous nucleation of {10-12} twinning under tensile loading in magnesium crystal using atomistic molecular dynamic simulation. The system is a rectangular rod and rod axis is normal to basal plane of Mg crystal. The tensile deformation in c-axis nucleates {10-12} twinning starting at the corner of square of cross section of the rod. The twin boundary is spherical at the beginning and become a linear boundary in {10-12} planes as time goes by. The twinning and shuffling processes are described. The nucleation mechanism of the shuffling dominated twinning is explained.



9:30 AM

**On the Impact of Second Phase Particles on Twinning in Magnesium Alloys:** *Matthew Barnett*<sup>1</sup>; <sup>1</sup>Deakin University

Deformation twinning is an important deformation mode in magnesium alloys. Despite this, little is known on the extent to which the stress for twinning can be altered by a dispersion of second phase particles. The current paper presents a series of findings on the role of differently shaped particles on both the stress required for twinning and the characteristics of the twins that form. It is shown that plate shaped particles are, as one might expect, an effective strengthener to {10-12} twinning. When precipitate plates form on the basal planes, the relative hardening of basal slip is minor in comparison to that seen for twinning. This provides opportunity for the alloy designer to control the apparent critical resolved shear stresses (CRSS) for the different deformation modes. Possible sources for the hardening of twins are discussed.

9:50 AM

**Influence of Crystallographic Orientation on Twin Nucleation in Single Crystal Magnesium:** *Christopher Barrett*<sup>1</sup>; *Mark Tschopp*<sup>1</sup>; *Haitham El Kadiri*<sup>1</sup>; *Bin Li*<sup>1</sup>; <sup>1</sup>Mississippi State University

Deformation twinning plays a vital role in the mechanical behavior of polycrystalline magnesium alloys. To understand twinning in complex polycrystals, we need to first understand twinning phenomena in single crystals and bicrystals. This project studies twinning nucleation and propagation at the atomic scale for magnesium under various loading conditions. We used molecular dynamics to study the effect of loading orientation (in single crystals) and grain boundary structure on twinning or slip nucleation. We ran simulations at various strain rates, temperatures, and simulation cell sizes. The mechanisms are coupled with the stress-strain response and initial conditions to fully comprehend twinning nucleation. A better understanding of twin nucleation can elucidate how twinning phenomena occurs in more complex polycrystalline magnesium microstructures for inclusion in macroscopic constitutive models.

10:10 AM

**Twinning Multiplicity in an AM30 Magnesium Alloy under Uniaxial Compression:** *Q. Ma*<sup>1</sup>; *H. El Kadiri*<sup>1</sup>; *A.L. Oppedal*<sup>1</sup>; *J.C. Baird*<sup>1</sup>; *M.F. Horstemeyer*<sup>1</sup>; <sup>1</sup>Mississippi State University

Twinning under compression along two perpendicular directions of an AM30 alloy with a {10-10} fiber texture was investigated. The primary extension {10-12} twinning occurred for both compression normal to the fiber and compression parallel to the fiber. These primary extension twins took the forms of fully residual twins parallel to the fiber and "stopped elastic" twins normal to the fiber. Both the {10-11}-{10-12} and {10-13}-{10-12} double twinning occurred in the matrix grains at the last stage of compression normal or parallel to the fiber, but as the "combined two shears mode" of the double twinning. Another time-sequence type of {10-11}-{10-12} double twin also activated early normal to the fiber. The primary extension twinning and contraction twinning seem to obey the Schmid law according to the texture evolution.

10:30 AM Break

10:50 AM

**Inhomogeneous Deformation of AZ31 Magnesium Sheet in Uniaxial Tension:** *Jidong Kang*<sup>1</sup>; *David Wilkinson*<sup>1</sup>; *Raja Mishra*<sup>2</sup>; <sup>1</sup>McMaster University; <sup>2</sup>General Motors R&D

Inhomogeneous plastic deformation during uniaxial tensile test of AZ31 magnesium sheet has been studied using digital image correlation and electron backscatter diffraction. Simultaneous examination of the strain distributions on both the flat and the through thickness surfaces of the sample loaded along the rolling direction reveals very little deformation in the thickness direction and strain gradients on the sheet surface parallel and perpendicular to the loading direction. The lack of thinning leads to the abrupt fracture right after a premature but profound diffuse necking without transitioning to localized necking. Such inhomogeneous deformation arises from the strong basal texture and the resultant high critical resolved shear stress for slip as well as

the need for contraction and double twinning. The strain distribution on the sheet surface evolves nonlinearly with strain, impacting the measurement of the r-value. The relationship between the inhomogeneity of deformation and the deformation mechanism will be presented.

11:10 AM

**Limitation of Current Hardening Models in Predicting Anisotropy by Twinning in hcp Metals: Application to a Rod-Textured AM30 Magnesium Alloy:** *Andrew Oppedal*<sup>1</sup>; *Haitham El Kadiri*<sup>1</sup>; *Carlos Tomé*<sup>2</sup>; *James Baird*<sup>1</sup>; *Sven Vogel*<sup>2</sup>; *Mark Horstemeyer*<sup>1</sup>; <sup>1</sup>Mississippi State University; <sup>2</sup>Los Alamos National Laboratory

When a strongly textured hexagonal close packed (HCP) metal is loaded under an orientation causing profuse twinning or detwinning, the stress-strain curve is sigmoidal in shape and inflects at some threshold. Authors have largely attributed the dramatic stress increase in the lower-bound vicinity of the inflection point to a combined effect of a Hall-Petch mechanism correlated to grain refinement by twinning, and twinning-induced reorientation requiring activation of hard slip modes. We experimentally and numerically demonstrate that these two mechanisms alone are unable to reproduce the stress-strain behaviors obtained under intermediate loading orientations correlated to in-between profuse twinning and nominal twinning. We argue based on adopting various mechanistic approaches in hardening model correlations from the literature. We used both a physics dislocation based model and a phenomenological Voce hardening model. The HCP material is exemplified by an extruded AM30 magnesium alloy with a <10-10>-fiber parallel to the extrusion direction.

11:30 AM

**Deformation Behavior of Mg from Micromechanics to Engineering Applications:** *Erica Lilleodden*<sup>1</sup>; *Jörn Mosler*<sup>2</sup>; *Malek Homayonifar*<sup>2</sup>; *Mintesnot Nebebe*<sup>2</sup>; *Gyu Kim*<sup>2</sup>; *Norbert Huber*<sup>2</sup>; <sup>1</sup>GKSS-Research Centre; <sup>2</sup>Helmholtz-Zentrum Geesthacht

We have investigated the influence of the underlying microstructure of Mg on the macroscopic deformation behavior. Using microcompression experiments on Mg single crystals, we have identified the orientation dependent deformation slip and twinning systems. These have aided the development of an energy based crystal plasticity model for the twinning in polycrystals. This model has been applied to representative volume elements to identify the flow surface for a macroscopic model, which is used to predict the forming limit diagram. Validation of the results has been realised through Nakazima tests. Additionally an outlook will be given on the prediction of the forming behavior of laser beam welded Mg sheets and its dependence on welding direction.

11:50 AM

**Effect of Substituted Aluminum in Magnesium Tension Twin:** *Kiran Solanki*<sup>1</sup>; *Amitava Moitra*<sup>1</sup>; *Mehul Bhatia*<sup>1</sup>; <sup>1</sup>Mississippi State University

Atomistic simulations are performed in order to study the Aluminum substitution effect on Magnesium twinning mechanism. Multiple twin boundaries are found in pure Mg single crystal under tensile loading condition involving {10-12} twinning plane. However, no twinning has occurred under compression loading. Al substitution has been done for 2, 5, 7, and 10% doping. For 2 and 5% Al substitution, number of twins increase when the system is monitored under tensile loading. On the other hand, for 7 and 10% Al doping under tensile loading, no twin has been found. We found that dislocation-twin and dislocation-dislocation interaction are majorly responsible for this behavior and it is important that which one is prevalent.

12:10 PM

**Influence of Solute Cerium on the Deformation Behavior of an Mg-0.5wt.%Ce Alloy:** *Lan Jiang*<sup>1</sup>; *John Jonas*<sup>1</sup>; *Raj Mishra*<sup>2</sup>; <sup>1</sup>McGill University; <sup>2</sup>General Motors

Some researchers have found that the nucleation of recrystallization at shear bands plays a role in the formation of the RE texture component. In steel rolling, it is well known that the formation of shear bands is favored by increasing the amount of solute carbon and rolling at temperatures where dynamic strain aging (DSA) occurs, leading to flow localization. The

question therefore arises whether Ce in solution can play a similar role in Mg alloys. Compression tests were therefore performed on samples taken from extruded bars of Mg-0.5 wt.% Ce. It was found that the effect of DSA on increasing the flow stress was stronger than that of extension twinning. The occurrence of DSA also led to a decrease in the ductility. In addition, after heat treatment and conventional cooling, the supersaturation of Ce resulting from such cooling increases the strength of the DSA effect during subsequent deformation.

## Magnetic Materials for Energy Applications: Amorphous and Nanostructured Magnetocaloric Materials

*Sponsored by:* TMS Electronic, Magnetic, and Photonic Materials Division, TMS: Energy Conversion and Storage Committee, TMS: Magnetic Materials Committee; JSPS 147th Committee on Amorphous and Nanocrystalline Materials; Lake Shore Cryotronics, Inc.; AMT&C

*Program Organizers:* Victorino Franco, Sevilla University; Oliver Gutfleisch, IFW Dresden; Kazuhiro Hono, National Institute for Materials Science; Paul Ohodnicki, National Energy Technology Laboratory

Wednesday AM  
March 2, 2011

Room: 11A  
Location: San Diego Conv. Ctr

*Session Chair:* Victorino Franco, Sevilla University

### 8:30 AM Invited

**Effect of Magnetic Cluster Size on the Magnetocaloric Effect in a Magnetic Spin Glass:** Eric Lass<sup>1</sup>; Virgil Provenzano<sup>1</sup>; Robert Shull<sup>1</sup>; <sup>1</sup>National Institute of Standards and Technology

A number of years ago, it was predicted and subsequently demonstrated that the magnetocaloric effect of a material could be enhanced when the material's independent magnetic spins were replaced by groups of magnetic spins. At that time, a paramagnetic garnet,  $Gd_5Ga_3O_{12}$ , was modified by the addition of Fe to transform the garnet into a superparamagnet. This magnetic state transformation occurred because the Fe atoms enabled a magnetic superexchange interaction between the Gd spins. As a consequence, the magnetocaloric effect of the material increased by a factor of 4-5. As a test of how generic this effect is, we have investigated a classic spin glass material, Cr-Fe, sequentially aged to grow larger magnetic clusters in the material. Here, a review of the origins of the enhancement will be presented along with a report on the response of the magnetocaloric effect in such a material as the cluster size is sequentially changed.

### 8:55 AM Invited

**Nanostructured Materials for Magnetic Refrigeration:** Christian Binek<sup>1</sup>; Rathagata Mukherjee<sup>1</sup>; Ralph Skomski<sup>1</sup>; David Sellmyer<sup>1</sup>; Steven Michalski<sup>1</sup>; Renat Sabirianov<sup>2</sup>; <sup>1</sup>University of Nebraska-Lincoln; <sup>2</sup>University of Nebraska-Omaha

Alternatives to conventional cooling technology harnessing the electrocaloric or magnetocaloric effect (MCE) will play an important role in energy-efficient and environmentally-friendly technologies of the future. We focus on magnetocaloric materials which are cost-effective, stable, environmentally-friendly, and maximize the MCE in the vicinity of room-temperature while minimizing hysteretic losses. We use nanotechnology to harness the MCE of simple magnetic materials by tailoring interactions in and between ultra-thin films or particles. As an example, Co/Cr superlattices are realized by molecular beam epitaxial growth where finite-size scaling effects tailor the  $T_c$  of Co and RKKY inter-layer coupling is tuned via Cr thickness into antiferromagnetic coupling between Co layers. Isothermal entropy changes are deduced from the temperature and field dependence of the magnetization using the Maxwell and Clausius-Clapeyron relations. The experimental results are discussed in the light of our theoretical findings.

Future improved nanostructures are discussed. Support by NRI, Career-DMR0547887, and MRSEC-0820521.

### 9:20 AM Invited

**Magnetocaloric Effect in Oxide Nanostructures:** Hariharan Srikanth<sup>1</sup>; Manh-Huong Phan<sup>1</sup>; <sup>1</sup>University of South Florida

A grand challenge in magnetic refrigeration is to fabricate refrigerant materials as thin films and nanostructures preserving their magnetocaloric properties. We will discuss the magnetocaloric effect (MCE) in oxide magnetic nanostructures from the spinel ( $Fe_3O_4$ ,  $CoFe_2O_4$ ,  $NiFe_2O_4$ ), garnet ( $Gd_3Fe_5O_{12}$ ) and perovskite ( $La, Pr, Ca$ ) $MnO_3$  families. We will demonstrate that particle size distribution and interparticle interactions lead to broadening of MCE over a wide temperature range thus offering the potential to enhance refrigeration capacity (RC). While blocking is detrimental to achieving large magnitude in MCE, surface spin disorder enhances the effect under high applied fields. We also show that the interesting coupling between the magnetic, structural and electronic degrees of freedom in manganites plays a critical role in enhancing the MCE in nanostructures. Our observations provide strong evidence for control of the surface spin ordering as a viable route to increase the MCE and RC in nanostructured materials. Supported by DoE and ARO.

### 9:45 AM Invited

**Ordered Arrays of Magnetic CoNi-Base Nanowires and Nanodots: Magnetization and Transport:** Manuel Vazquez<sup>1</sup>; Laura Vivas<sup>1</sup>; Victor Prida<sup>2</sup>; Victor Vega<sup>2</sup>; <sup>1</sup>Spanish Council for Research; <sup>2</sup>University of Oviedo

The magnetic behaviour of ordered arrays of magnetic nanowires is of general interest for the development of new generation of functional nanostructures, with properties for magnetocaloric effect, sensing devices or magnetic storage media [1]. Hexagonally-ordered arrays of magnetic nanopillars are prepared by electrochemical route filling self-assembled pores of anodic alumina templates. We introduce last achievements on ordered arrays of such CoNi-base single and multilayer nanowire arrays (20-80 nm diameter, 65 nm interwire distance, and 120 to 2,000 nm long). Magnetization and magnetic transport properties are studied as a function of geometry parameters and composition. The magnetic anisotropy is particularly investigated in view of its decisive role in all magnetic behavior including magnetic and energy related effects. [1] V. Franco, K. Pirota et al. Phys. Rev. B 77 (2008) 104434; K. Pirota, M. Vázquez et al. "Magnetic Nanowires", Handbook of Nanoscience and Nanotechnology, Ed. A. Narlikar, Oxford Un. Press (2010) 772.

### 10:10 AM

**Magnetocaloric Effect in Gd-Based Thin Film Heterostructures:** Casey Miller<sup>1</sup>; Christopher Bauer<sup>1</sup>; Daryl Williams<sup>1</sup>; Brian Kirby<sup>2</sup>; <sup>1</sup>University of South Florida; <sup>2</sup>NIST Center for Neutron Research

To understand the impact of nanostructuring on the magnetocaloric effect, we have investigated  $W(300\text{\AA})/Gd(2000\text{\AA})/W(300\text{\AA})$  and  $[W(50\text{\AA})/Gd(400\text{\AA})]_8/W(50\text{\AA})$ . The samples were sputtered onto  $MgO(001)$  at 300K. Post-deposition annealing was performed sequentially from 150°C to 600°C, with structural and magnetic characterization between each step. For the 2000Å Gd film, the entropy peak shifts from about 276K in the as-deposited film to the bulk value by 450°C; further annealing to 600°C improves the magnitude to ~4.4J/kg-K for a 0-4T field change. Differences with bulk behavior will be discussed in terms of grain size and strain. The multilayer sample's entropy peak is significantly broadened relative to bulk Gd. Polarized neutron reflectometry results indicate a suppression of  $T_c$  at the W-Gd interface, which is the likely cause of the peak broadening. Supported by AFOSR-YIP; use of the Center for Nanoscale Materials for magnetometry was supported by the US DOE under Contract No. DE-AC02-06CH11357.

### 10:25 AM Break

### 10:55 AM

#### Optimization of the Refrigerant Capacity in Multiphase Magnetocaloric

**Materials:** Rafael Caballero-Flores<sup>1</sup>; Victorino Franco<sup>1</sup>; Alejandro Conde<sup>1</sup>; K. Knipling<sup>2</sup>; M. Willard<sup>2</sup>; <sup>1</sup>Sevilla University; <sup>2</sup>U.S. Naval Research Laboratory

One of the key parameters for enhancing the performance of magnetocaloric materials is the refrigerant capacity, RC, i.e. the heat that can be transferred between the cold and hot reservoirs. In order to optimize it, two strategies are possible: either to look for new materials with large RC, or to use known materials as building blocks of composites for achieving a large RC. In this work we will present numerical simulations which prove that there exist optimal values of Curie temperatures, fractions of phases and applied field values which can enlarge RC with respect to the starting phases as much as ~90%. As a proof of concept, it will be shown that the combination of experimental data of two FeCoNiZrBCu alloys produces an enhancement in RC of ~37%, making it ~92% larger than that of the Fe-doped GdSiGe.

### 11:10 AM

#### The Magnetocaloric Effect of Fe-B-Cr-Gd Amorphous Alloys: J

Law<sup>1</sup>; Raju Ramanujan<sup>1</sup>; V Franco<sup>2</sup>; <sup>1</sup>Nanyang Technological University; <sup>2</sup>Universidad de Sevilla

The magnetocaloric effect of Fe<sub>80-x</sub>B<sub>12</sub>Cr<sub>8</sub>Gd<sub>x</sub> (x = 1 to 11) amorphous alloys was studied by magnetometry, TEM, DSC and XRD techniques. Gd addition can be used to tune the Curie temperature, addition of Gd also increases the crystallization temperature. A linear relationship between the magnetic entropy change and the magnetic moment of the alloys was observed. The experimental values of magnetic field dependence of the magnetic entropy change were consistent with a phenomenological universal curve. The maximum magnetic entropy change, for x = 1, was ~33% larger than Fe<sub>80</sub>B<sub>12</sub>Cr<sub>8</sub>, the refrigerant capacity (RC) is ~29% larger than Gd<sub>5</sub>Si<sub>2</sub>Ge<sub>1.9</sub>Fe<sub>0.1</sub> and within 10% of Fe<sub>82.5</sub>Zr<sub>7</sub>B<sub>4</sub>Co<sub>2.75</sub>Ni<sub>2.75</sub>Cu<sub>1</sub>, which is one of the best Fe-based amorphous magnetocaloric material. The tunable Curie temperature can be used to increase RC and the temperature span of layered multi-composition magnetocaloric regenerators. These results as well as the development of a novel active transient cooling magnetocaloric system will be presented.

### 11:25 AM

#### Tunable Magnetocaloric Properties of Gd-Based Metallic Glasses:

Charlotte Mayer<sup>1</sup>; Stéphane Gorsse<sup>2</sup>; Bernard Chevalier<sup>1</sup>; <sup>1</sup>ICMCB/CNRS Bordeaux 1 University; <sup>2</sup>ICMCB/CNRS IPB

Since the recent discovery of large second-order paramagnetic to ferromagnetic transitions upon cooling in rare earth and transition metal (TM) based amorphous alloys; magnetocaloric effect (MCE) and refrigeration capacity (RC) of Gd-rich metallic glasses has been intensively studied. They have shown that, additions and/or substitutions of alloying elements (mainly TM) to Gd, have a great influence on MCE properties of these materials. To have a better understanding of this tuning ability, we have synthesised a series of amorphous ribbons of compositions Gd<sub>60</sub>TM<sub>30</sub>In<sub>10</sub> and Gd<sub>60</sub>TM<sub>30-x</sub>TM'<sub>x</sub>In<sub>10</sub>, with TM or TM' = Mn, Fe, Co, Ni, Cu. This family of metallic glasses gives impressive results: a huge range of accessible Curie temperatures (87 K < T<sub>c</sub> < 220 K) and a magnetic entropy change peak value (ΔS<sub>M</sub><sup>peak</sup>) that can go to double. Finally, adequate TM and TM' mixing leads to the enlargement of the magnetic transition thus increasing the RC of the material.

### 11:40 AM

#### Magnetocaloric Studies in Binary Gd-X (X = B, Ga, & Mn) Alloys:

Tanjore Jayaraman<sup>1</sup>; Laura Langemeier<sup>1</sup>; Mark Koten<sup>1</sup>; Jeffrey Shield<sup>1</sup>; <sup>1</sup>University of Nebraska

Magnetic refrigeration based on the magnetocaloric effect has attracted attention as it is energy efficient and a "greener" alternative to the existing vapor-compression refrigeration technology. Gd as a room temperature magnetic refrigerant has a narrow working temperature region. Identifying suitable alloying additions and processing techniques that can alter the Curie

temperature (T<sub>c</sub>), improve near-room temperature magnetocaloric properties and extend the useful range of Gd-based alloys is of significant importance. This paper reports the variation of T<sub>c</sub>, peak value of ΔS<sub>M</sub>/(ΔS<sub>M</sub><sup>max</sup>), refrigerant capacity (q) and relative cooling power (RCP) on a series of Gd<sub>100-y</sub>X<sub>y</sub> (X = B, Ga and Mn; 0 = y = 20 at.%) alloys prepared by conventional melting and melt spinning. The T<sub>c</sub> and ΔS<sub>M</sub><sup>max</sup> for these alloys were controllable by alloying and processing. Improvement in ΔS<sub>M</sub><sup>max</sup>, q and RCP for these alloys over Gd suggests their potential application as room temperature magnetic refrigerants.

### 11:55 AM

#### Magnetocaloric Effect and Enhanced Refrigeration Efficiency in

(La<sub>0.7</sub>Sr<sub>0.3</sub>MnO<sub>3</sub>/SrRuO<sub>3</sub>) Superlattices: Qiang Zhang<sup>1</sup>; S. Thota<sup>1</sup>; F. Guillou<sup>1</sup>; P. Padhan<sup>1</sup>; V. Hardy<sup>1</sup>; A. Wahl<sup>1</sup>; W. Prellier<sup>1</sup>; <sup>1</sup>CRISMAT

Currently, the search for the magnetocaloric materials was limited mainly to polycrystalline systems or superparamagnetic nanoparticles. In this work, we reported the magnetic and magnetocaloric effect in a series of (La<sub>0.7</sub>Sr<sub>0.3</sub>MnO<sub>3</sub>/SrRuO<sub>3</sub>) superlattices where the SrRuO<sub>3</sub>(SRO) layer thickness is varying. Compared with the polycrystalline La<sub>0.7</sub>Sr<sub>0.3</sub>MnO<sub>3</sub> (LSMO) compound, the TC of different (La<sub>0.7</sub>Sr<sub>0.3</sub>MnO<sub>3</sub>/SrRuO<sub>3</sub>) superlattices is decreased to 325 K due to the finite size effect and the magnetization is significantly enhanced, leading to remarkable MCE modulated by the SRO layers. While the working temperature ranges are enlarged, ΔS(Max to Min) values retain comparable with the values in polycrystalline La<sub>0.7</sub>Sr<sub>0.3</sub>MnO<sub>3</sub>. As a consequence, the relative cooling powers (RCP) are significantly improved, the microscopic mechanism of which is related to the effect of the interfaces at La<sub>0.7</sub>Sr<sub>0.3</sub>MnO<sub>3</sub>/SrRuO<sub>3</sub> and higher nanostructural disorder. These studies indicate that artificial oxide superlattices/multilayers may provide an alternative pathway in searching for efficient room-temperature magnetic refrigerators for (nano)microscale systems.

## Material Science Advances Using Test Reactor

### Facilities: Session I

Sponsored by: The Minerals, Metals and Materials Society, TMS Structural Materials Division, TMS/ASM: Nuclear Materials Committee

Program Organizer: Todd Allen, University of Wisconsin-Madison

Wednesday AM

Room: 3

March 2, 2011

Location: San Diego Conv. Ctr

Session Chair: Todd Allen, University of Wisconsin

### 8:30 AM Introductory Comments

### 8:40 AM

#### In-Reactor Oxidation of Zircaloy and Surface-Modified Zircaloy in

Water Vapor at Low Partial Pressures: David Senor<sup>1</sup>; Stan Pitman<sup>1</sup>;

Mitch Cunningham<sup>1</sup>; Clark Carlson<sup>1</sup>; Walter Luscher<sup>1</sup>; Kevin Clayton<sup>2</sup>;

Glen Longhurst<sup>3</sup>; <sup>1</sup>Pacific Northwest National Laboratory; <sup>2</sup>Idaho National

Laboratory; <sup>3</sup>Southern Utah University

The TMIST-1 irradiation experiment at the Advanced Test Reactor evaluated oxidation and nascent hydrogen uptake of Zircaloy-2, Zircaloy-4, and surface-modified Zircaloy-4. Zircaloy-4 specimens with two different microstructural textures, resulting from different manufacturing processes, were included in the experiment. The surface-modified material consisted of Zircaloy-4 that was coated on one surface with electroplated Ni in four different thicknesses, followed by heat treatment to fully react the Ni with the substrate, forming a layered surface of Zr-Ni intermetallics. The specimens were exposed to a flowing oxidant consisting of He carrier gas with D<sub>2</sub>O at either 300 or 1000 Pa partial pressure. Exposure temperatures were either 330 or 370°C, and the exposure continued for approximately 131 days at temperature. Duplicate sets of specimens were exposed to the same conditions in-reactor and ex-reactor. Post-irradiation examination included dosimetry, mass gain measurements, Fourier-transform infrared



spectroscopic measurement of oxide thickness, deuterium assay, optical microscopy, and SEM/EDS.

#### 9:00 AM

**Effect of Neutron Radiation on Mechanical Properties of Nanograin Structured Copper:** *Walid Mohamed*<sup>1</sup>; Korukonda Murty<sup>1</sup>; Jacob Eapen<sup>1</sup>; <sup>1</sup>North Carolina State University

With the abundance of interfaces and grain boundaries, materials with nanograin structures are expected to be relatively more radiation resistant than their conventional (micrometer) grain sized counterparts. We report here some preliminary results on conventional grained (38 micrometers) and nanocrystalline (28 nm) copper following neutron irradiation in PULSTAR reactor at the NCSU to relatively low fluence of  $6 \times 10^{17}$  n/cm<sup>2</sup> corresponding to 0.34 dpa. While radiation hardening and decreased ductility were noted in conventional Cu, nano-Cu revealed softening and ductility increase following radiation. Microstructural observations in nano-Cu revealed in-reactor grain growth accompanied by dislocation and twin structures. Grain size dependence of strength followed Hall-Petch relation. Materials irradiated in ATR to higher neutron fluences corresponding to a maximum 2 dpa are being tested and the results to-date will be presented. This work is supported by ATR/NSUF program and we acknowledge the encouragement and support by Drs. Mitch Meyer and Todd Allen.

#### 9:20 AM

**Program for Irradiation of Reactor Structural Materials at the ATR-National Scientific User Facility:** *Heather MacLean Chichester*<sup>1</sup>; Kumar Sridharan<sup>2</sup>; Ramprasad Prabhakaran<sup>1</sup>; Yong Yang<sup>2</sup>; Peng Xu<sup>2</sup>; Todd Allen<sup>2</sup>; <sup>1</sup>Idaho National Laboratory; <sup>2</sup>University of Wisconsin-Madison

Under the University of Wisconsin Pilot Project, neutron irradiation experiments have been designed to understand the irradiation performance of structural materials for advanced nuclear power systems. Twenty-six materials are being irradiated in the ATR, including ferritic/martensitic steels, HT-9, T91, NF616, HCM12A, 9% Cr ODS steel, Fe-Cr binary alloys, and austenitic alloys 800H, D9, NF709, super 304 stainless steel and HT-UPS-AX-6 alloy. Additionally, grain boundary engineered alloys, SiC and MgO-ZrO<sub>2</sub> ceramics, as well as Fe-Cr-B amorphous alloys are also being irradiated. The samples are mostly 3 mm diameter TEM disks, but for some alloys miniature tensile samples are also being irradiated. Targeted temperatures are 300°C to 700°C, and doses are 3 and 6 dpa. Issues pertaining to irradiating such a large matrix of sample materials, geometries, and irradiation conditions will be discussed. Post-irradiation examination will include tensile, microhardness, and shear punch testing, along with transmission electron microscopy.

#### 9:40 AM

**MAX Ceramics for Nuclear Applications: A New Material for a New Generation of Power:** *Darin Tallman*<sup>1</sup>; Elizabeth Hoffman<sup>2</sup>; Dennis Vinson<sup>2</sup>; Robert Sindelar<sup>2</sup>; Gordon Kohse<sup>3</sup>; Michel Barsoum<sup>1</sup>; <sup>1</sup>Department of Materials Science and Engineering, Drexel University; <sup>2</sup>Savannah River National Laboratory; <sup>3</sup>Department of Nuclear Engineering, Massachusetts Institute of Technology

Gen IV nuclear reactors need materials that can withstand harsher environments than in current reactors. The Mn+1AX<sub>n</sub> (MAX) phases are a group of layered machinable ternary compounds, where M is an early transition metal, A is a group 13 to 16 element, and X is C and/or N. These compounds possess mechanical properties atypical for ceramics. Data about their irradiated properties are required to fully realize their potential. Research is thus ongoing to characterize their irradiated properties. The pre-irradiated characterization, as well as neutron activation of several MAX compounds exposed to fast and thermal spectra will be presented. The specific activities of Ti<sub>3</sub>SiC<sub>2</sub>, Ti<sub>3</sub>AlC<sub>2</sub> and Ti<sub>2</sub>AlC were similar to SiC and three orders of magnitude less than Alloy 617 for three activation times in both fast and thermal spectra. Like SiC, the main radioisotopes, after a decay period of 10 years are tritium and C14.

#### 10:00 AM Break

#### 10:30 AM

**Status of UCSB ATR-1 and ATR-2 Experiments:** *Takuya Yamamoto*<sup>1</sup>; G. Robert Odette<sup>1</sup>; Douglas Klingensmith<sup>1</sup>; David Gragg<sup>1</sup>; Ben Sams<sup>1</sup>; Mitchell Meyer<sup>2</sup>; Gregg Wachs<sup>2</sup>; Julie Foster<sup>2</sup>; James Cole<sup>2</sup>; Dan Ogden<sup>2</sup>; Michael Sprenger<sup>2</sup>; Thomas Maddock<sup>2</sup>; Paul Murray<sup>2</sup>; Joseph Nielsen<sup>2</sup>; Randy Nanstad<sup>3</sup>; William Server<sup>4</sup>; <sup>1</sup>Univ. California Santa Barbara; <sup>2</sup>Idaho National Laboratory; <sup>3</sup>Oak Ridge National Laboratory; <sup>4</sup>ATI Consulting

Two UCSB ATR irradiation experiments are described. About 1400 specimens for a large alloy matrix were irradiated up to 6 dpa at 8 temperatures from 300 to 750 °C in the UCSB ATR-1, experiment. An innovative passive capsule thermal design minimized irradiation temperatures uncertainties, which were evaluated by SiC monitors. UCSB ATR-1 will provide a specimen lending library for studies of irradiation hardening/softening, embrittlement, microstructural evolutions and basic mechanisms, including helium injection and diffusion multiple experiments. UCSB ATR-1 will support the development of irradiation effects models for advanced fission and fusion applications. The UCSB ATR-2 experiment will be carried out in an instrumented capsule at a lower flux location in ATR. It is aimed at providing a similar database on irradiation embrittlement for a large matrix of RPV steels at temperatures from 250 to 310°C up to extended life doses of 0.15 dpa.

#### 10:50 AM

**In-Situ Measurement of Tritium Permeation Through Stainless Steel:** *David Senor*<sup>1</sup>; Walter Luscher<sup>1</sup>; Mitch Cunningham<sup>1</sup>; Clark Carlson<sup>1</sup>; Kevin Clayton<sup>2</sup>; Glen Longhurst<sup>3</sup>; <sup>1</sup>Pacific Northwest National Laboratory; <sup>2</sup>Idaho National Laboratory; <sup>3</sup>Southern Utah University

The TMIST-2 irradiation experiment at the Advanced Test Reactor evaluated tritium permeation through Type 316 stainless steel. The interior of the cylindrical test specimen was exposed to a He carrier gas with T<sub>2</sub> at 0.1, 5, or 50 Pa partial pressure. Extraneous permeation was minimized from the ends of the test specimen by temperature control and Al coatings. The active length of the test specimen was approximately 10 cm, and temperature in this region was maintained at either 292 or 330°C. Temperature and tritium concentration changes were made online during the test. Tritium permeation was measured in-situ by sweeping the outside surface of the test specimen with a He/Ne mixture that was carried out of the reactor vessel in Cu tubing to ion chambers and bubblers for scintillation counting. Post-irradiation examination included dosimetry, Auger spectroscopy of the stainless steel surface, residual He-3 assay, and optical and scanning electron microscopy.

#### 11:10 AM

**Target Development Initiatives at SINQ Applying Neutron Techniques:** *Werner Wagner*<sup>1</sup>; Peter Vontobel<sup>1</sup>; Yong Dai<sup>1</sup>; Michael Wohlmuther<sup>1</sup>; <sup>1</sup>Paul Scherrer Institut

SINQ is a continuous spallation neutron source, driven by PSI's 590 MeV proton accelerator which routinely delivers 2.2 mA of proton beam (of which SINQ receives 1.5 mA), making SINQ a Megawatt-class spallation source. The neutron production target at SINQ is a stationary solid so-called 'cannelloni' type target, i.e. it consists of an array of steel or Zircaloy tubes filled with lead, cooled by heavy water. Target development towards optimized neutron production efficiency for the neutron users always was a primary endeavour of PSI. One of the mayor tools to investigate the target rods before and after service is neutron imaging, done at the SINQ radiography station NEUTRA, which is equipped to investigate highly radioactive samples. These investigations turned out to be indispensable for assessing the condition and integrity of the target rods after service, in support of further improvements and for the sake of radiological safety and lifetime prediction.

11:30 AM Invited

**Criticality Validation and Reactor Physics Experiment for the Advanced Test Reactor (ATR) National Scientific User Facility (NSUF):** Kimberly Clark<sup>1</sup>; Denis Beller<sup>1</sup>; John Bess<sup>2</sup>; <sup>1</sup>Univ. of Nevada, Las Vegas; <sup>2</sup>Idaho National Laboratory

The ATR Critical facility at the Idaho National Laboratory (INL) provides a criticality experiment capability that has not been certified in the International Criticality Safety Benchmark Evaluation Project (ICSBE). The qualification of the ATRC would be highly desirable as a general-purpose thermal-spectrum facility to complement other U.S. facilities for nuclear criticality safety experiments. In the project described herein, University of Nevada, Las Vegas faculty and students and INL personnel are collaborating in an ATR NSUF project to develop, evaluate, and validate a physically accurate radiation transport model of the ATRC in accordance with guidelines of the ICSBE. To validate the radiation transport modeling effort, which is in progress, and to provide data for the International Reactor Physics Experiment Evaluation Project, a series of experiments will be conducted using a cassette containing one to eight precision aluminum bars. The design, fabrication, and status of the experiment will be described.

11:50 AM Concluding Comments

## Materials in Clean Power Systems VI: Clean Coal-, Hydrogen Based-Technologies, and Fuel Cells: SOFC II

*Sponsored by:* The Minerals, Metals and Materials Society, TMS Electronic, Magnetic, and Photonic Materials Division, TMS Structural Materials Division, TMS/ASM: Corrosion and Environmental Effects Committee, TMS: Energy Conversion and Storage Committee, TMS: High Temperature Alloys Committee  
*Program Organizers:* Xingbo Liu, West Virginia University; Zhenguang "Gary" Yang, Pacific Northwest National Laboratory; Jeffrey Hawk, U.S. Department of Energy, National Energy Technology Laboratory; Teruhisa Horita, AIST; Zi-Kui Liu, The Pennsylvania State University

Wednesday AM Room: 33C  
March 2, 2011 Location: San Diego Conv. Ctr

*Session Chairs:* Teruhisa Horita, AIST; Kathy Lu, Virginia Tech

8:30 AM

**The Growth of the Oxide Scale on Alloy Interconnects under Electrical Current Supply:** Kenichi Kawamura<sup>1</sup>; Mitsutoshi Ueda<sup>1</sup>; Toshio Maruyama<sup>1</sup>; <sup>1</sup>Tokyo Institute of Technology

The usage of alloy interconnects differ from general usage of high temperature alloy. That is, the alloy interconnects must conduct an electrical current. The electrical conductivity is decreased by the formation of oxide scale on the surface of alloy. Since the oxide scale, generally Cr<sub>2</sub>O<sub>3</sub> scale, is grown by diffusion of ionic species, the growth of oxide scale is influenced by the electrical current. In this study, we demonstrate the oxidation behavior of Fe-Cr alloy with or without electrical current supply, and analyzed quantitatively. This study was supported by New Energy and Industrial Technology Research Development Organization (NEDO).

8:55 AM

**Oxidation Behavior of (CoMn)3O4 Coatings on Preoxidized 441HP Stainless Steel:** Kathryn Hoyt<sup>1</sup>; Paul Gannon<sup>1</sup>; Preston White<sup>1</sup>; Rukiye Tortop<sup>1</sup>; <sup>1</sup>Montana State University

Ceramic coatings are being explored to extend the lifetime of the stainless steel interconnects in planar Solid Oxide Fuel Cells (SOFC). One promising coating is CoMn oxide, (CoMn)<sub>3</sub>O<sub>4</sub>, which is deposited in various ways. In this study, stainless steel 441HP samples were subjected to four levels of preoxidation prior to coating with magnetron sputtered metallic CoMn, and subsequently annealed to (CoMn)<sub>3</sub>O<sub>4</sub> in 800°C air for various times. The oxidation behavior and electrical resistance were evaluated as a function of these exposures. Preoxidation was found to inhibit Fe transport from the

stainless steel into the coating. Preoxidized samples maintained a slightly lower area specific resistance (ASR) after 1650 hours compared to non-preoxidized samples. Oxidation behaviors and possible implications for SOFC interconnects are presented and discussed.

9:15 AM

**Influence of CeO<sub>2</sub> Coating on Fe-Cr Base Alloys for SOFC Interconnect Applications:** Keeyoung Jung<sup>1</sup>; Nazik Yanar<sup>1</sup>; Frederick Pettit<sup>1</sup>; Gerald Meier<sup>1</sup>; <sup>1</sup>University of Pittsburgh

A model Fe-13.5Cr and a commercial Fe-26Cr-1Mo alloy were coated with CeO<sub>2</sub> via pulsed laser deposition (PLD) and sol-gel coating technique in order to suppress the growth kinetics of the thermally-grown chromia and to avoid chromia evaporation. The coated alloys were isothermally exposed at 800°C in dry air up to 500h and their oxidation characteristics were compared with those of uncoated alloys. It was found that fine-grained Ce-rich oxides were formed on the surface whereas a pure coarser-grained chromia scale was formed on the uncoated alloys. Overall growth kinetics of the thermal oxides were decreased, in the presence of a CeO<sub>2</sub> layer, by up to 50% in specific mass changes depending on oxidation time. Other microstructural features and a proposed mechanism to explain the difference in the observations will be discussed.

9:35 AM

**Advanced Conductive Spinel Coating on SOFC Interconnect Frames with One-Step Heat Treatment:** Jung Pyung Choi<sup>1</sup>; Jeffrey Stevenson<sup>1</sup>; Matt Chou<sup>1</sup>; Josh Templeton<sup>1</sup>; Gordon Xia<sup>1</sup>; <sup>1</sup>Pacific Northwest National Laboratory

Low-cost, chromia-forming ferritic stainless steels are usually used for making interconnect plates in planar SOFCs. However, volatile Cr-containing species, which originate from the steel's oxide scale, can poison the cathode material in the cells and subsequently cause power degradation in the device. A conductive MnCo spinel coating has been developed for preventing cathode materials poisoning. However, this coating is not compatible with the formation of hermetic seals between interconnect frame components and the ceramic cell. Thus, a new aluminizing process has been developed to enable durable sealing, prevent Cr evaporation, and maintain electrical insulation between stack repeat units. However, the coating processes for the conductive and non-conductive material are very different. Therefore, it is challenging to fabricate these two coatings at the same time. The authors have previously reported success in preparing simultaneous coatings. However, to reduce cost and time, additional modifications are under development.

9:55 AM

**Fabrication of Metal-Supported Micro-SOFC:** Gyeong Man Choi<sup>1</sup>; Younki Lee<sup>1</sup>; Sunwoong Kim<sup>1</sup>; <sup>1</sup>POSTECH

Micro-SOFC, fabricated with thin film processes, is being developed for supplying electrical power for portable electronics. Lithography and etching processes are generally used for the miniaturization of the cell. As the cell components become thinner with reduced size, the cell becomes mechanically weaker. The use of metal support for micro-SOFC is one of the solutions to improve mechanical strength. In this study, we will review the status of micro-SOFC fabrication and our approach for the fabrication process. We have fabricated micro-SOFC on Ni support using simple fabrication process. A porous metal film was fabricated either in free-standing form or on top of glass substrate. Electrolyte film was further deposited on the porous metal. Details of fabrication procedure will be discussed.

10:15 AM Break

10:25 AM Invited

**Search and Study of a Solid Oxide Fuel Cell Seal Material:** Kathy Lu<sup>1</sup>; <sup>1</sup>Virginia Tech

Solid oxide fuel cells are electrochemical devices that convert chemical energy into electric power. High temperature hermetic seal is essential for utilizing the full potentials of planar solid oxide fuel. In this talk, seal requirements will be first discussed from thermal, chemical, mechanical, and electrical property point of view. Based on these considerations, our glass composition design approaches will be explained in search of the best seal

glass that can offer all the desired sealing properties and thermal stabilities. A boron-free SrO-La<sub>2</sub>O<sub>3</sub>-Al<sub>2</sub>O<sub>3</sub>-SiO<sub>2</sub> seal glass will be specifically discussed because it has met all the thermal and chemical properties along with high thermal and chemical stabilities. Long-term thermochemical stability and interfacial compatibility of the seal glass with Crofer 22 APU and AISI441 interconnects will be analyzed. The results show excellent thermal stability and interface compatibility of the SrO-La<sub>2</sub>O<sub>3</sub>-Al<sub>2</sub>O<sub>3</sub>-SiO<sub>2</sub> glass with the Crofer 22APU interconnect.

#### 10:50 AM

**In-Situ Neutron Diffraction Study of Porous NiO-YSZ Composite under Uniaxial Loading:** *Ling Yang*<sup>1</sup>; *Ke An*<sup>1</sup>; *Alexandru Stoica*<sup>1</sup>; *Harley Skorpenske*<sup>1</sup>; *Xunli Wang*<sup>1</sup>; <sup>1</sup>Oak Ridge National Laboratory

Porous cermet composites consisting of Ni and Y<sub>2</sub>O<sub>3</sub>-stabilized ZrO<sub>2</sub> (YSZ) are commonly used as anode in solid oxide fuel cells (SOFCs). This type of anode-supported SOFCs has many advantages such as high electrical conductivity, low operating temperature, compatible thermal expansion behavior and reliable mechanical properties. The pores in the composite are essential to the integrity of SOFCs as they provide the diffusion path to the fuel and reaction products as well as the triple phase boundary where the charge transfer occurs, but the existence of pores can also weaken the mechanical properties due to local stress concentration. In this study, we performed in-situ neutron diffraction measurement on NiO-YSZ composites of various porosity ratios under uniaxial loading at the engineering diffractometer VULCAN. With in-situ neutron diffraction, the deformation mechanisms at micro-structural level of each single phase, inter-phase lattice strain/stress evolution and the impact of porosities are characterized and discussed.

#### 11:10 AM

**Design on Elevated-Temperature and Methanol-Blocking Proton Exchange Membrane for Fuel Cell Application:** *Yan Xiang*<sup>1</sup>; <sup>1</sup>Beihang University

In the filed high temperature proton exchange membrane fuel cells, we successfully explored a series of Elevated-Temperature proton exchange membranes with high performance based on engineering plastics. The ET-PEMs show high proton conductivity (rang from 0.05~0.15S/cm) and good mechanical strength (tensile strength > 5MPa) under high temperature operation conditions of 110°C~200°C. Single HT-PEMFC based on this HT-PEM show excellence out-put performance, and the maximum power density of 500mW/cm<sup>2</sup> can be obtained at 160°C, which is comparable to the similar products of BASF. For the issue of Methanol permeability of DMFC, we invented both surface modification and in-situ structural modification for Nafion membrane, HPW and bacteriorhodopsin were involved as methanol-blocking agents using LBL techniques and bulk modification. The methanol crossover could be deduced more than 70%, meanwhile, the power density of single cell has improved.

#### 11:30 AM

**Magnetic Analysis of Nickel Nano-Particles in Solid Oxide Fuel Cell Materials:** *James O'Brien*<sup>1,2</sup>; <sup>2</sup>Quantum Design; <sup>1</sup>UCSD

Reaction sintering can reduce large-scale production costs of SOFC material 8YSZ. Addition of 1%NiO lowers the temperature for rapid yttria diffusion into zirconia, but leaves dissolved Ni<sup>2+</sup> ions. During operation of the fuel cell in reducing environments, nickel particle formation occurs. This process does not alter the level of ionic conduction when 10YSZ is adopted. Magnetic analysis will determine Ni<sup>2+</sup> ion solubility limits, monitor rate of reduction and characterize the formation of metallic nano-particles. Superparamagnetic properties confirm one synthesis technique yields roughly 3 nm Ni particles. The temperature and DC field dependence of SQUID based AC susceptibility will establish particle size distribution on the bulk scale. Infusion of metallic nano-particles into environmentally robust, stable oxide host lattices could impact many areas, from electronic component design to catalysis.

#### 11:50 AM

**Investigation of 5 MOL% YSZ Electrolyte for SOFC:** *Nilufer Evcimen*<sup>1</sup>; *Ahmet Ekerim*<sup>1</sup>; <sup>1</sup>Yildiz Technical University

To investigate the performance of electrolyte for intermediate temperature SOFC, commercially available 5 mol% YSZ powder was used. Average particle size was measured as 0.3 μm by using TEM. The sintering attitude of the powder was studied on pellets with conventional ceramic processing methods by means of mixing, pressing (110 MPa) and sintering. Sintering temperatures were determined as 1200, 1300 and 1400 °C for 3 h. Density measurements were done by using Archimedes technique. Sintered samples were observed via SEM and AFM and the best sintering temperature was selected as 1400 °C. Electrical property of YSZ pellets were measured after coating with platinum paste onto surface of the samples sintered at 1400 °C to serve as electrode. After that, pellets were heated at 800 °C for 1 h. This process was repeated for the other side. The ionic conductivity was measured by impedance spectroscopy in air between 500-900 °C.

### Neutron and X-Ray Studies of Advanced Materials IV: Resolving Time

*Sponsored by:* The Minerals, Metals and Materials Society, TMS Structural Materials Division, TMS/ASM: Mechanical Behavior of Materials Committee, TMS: Chemistry and Physics of Materials Committee

*Program Organizers:* Rozaliya Barabash, Oak Ridge National Laboratory; Xun-Li Wang, Oak Ridge National Laboratory; Jaimie Tiley, Air Force Research Laboratory; Peter Liaw, The University of Tennessee; Erica Lilleodden, GKSS Research Center; Brent Fultz, California Institute of Technology; Y-D Wang, Northeastern University

Wednesday AM

March 2, 2011

Room: 10

Location: San Diego Conv. Ctr

*Session Chairs:* Erica Lilleodden, GKSS Research Center; Zahir Islam, APS

#### 8:30 AM Keynote

**Time-Resolved X-Ray Scattering Techniques for Sub-picosecond to Millisecond Investigation of The Dynamics of Atomic Displacement Cascades\*:** *Bennett Larson*<sup>1</sup>; *Jon Tischler*<sup>1</sup>; *Roger Stoller*<sup>1</sup>; *Matthew Perkins*<sup>2</sup>; <sup>1</sup>Oak Ridge National Laboratory; <sup>2</sup>Oak Ridge High School

Information on the dynamics of atomic displacement cascades, formed by the direct collision of fast neutrons or energetic ions with lattice atoms, has until now been obtained entirely from molecular dynamics simulations. In this talk, x-ray diffuse scattering techniques to be used for the first experimental measurements of the dynamical structure of energetic-ion induced cascades on sub-picosecond to millisecond time-scales using the Linac Coherent Light Source (LCLS) and the Advanced Photon source (APS) will be discussed. Methods for analyzing time-resolved diffuse scattering measurements from cascades using molecular dynamics simulations and numerical x-ray diffuse scattering calculations will be presented for cascades in iron and copper. Methods for measurements and simulations of cascade evolution in the nanosecond to millisecond regimes will be considered. \*Research supported by the US DOE, Office of Basic Energy Sciences within the Center for Defect Physics Energy Frontier Research Center, and the DOE Academies Creating Teacher Scientists (ACTS) program (MPP).

#### 8:55 AM

**Three-Dimensional Reciprocal Space Mapping of Martensitic Transformations in Bulk Single Crystals by In-Situ High-Energy Synchrotron X-Ray Diffraction:** *Yu Wang*<sup>1</sup>; *Xin Zhao*<sup>1</sup>; *Tian-Le Cheng*<sup>1</sup>; *Yang Ren*<sup>2</sup>; <sup>1</sup>Michigan Tech; <sup>2</sup>Argonne National Laboratory

Martensitic transformations in bulk single crystals of NiMnGa magnetic shape memory alloys are studied by in-situ X-ray diffraction at Argonne National Laboratory. High-energy X-ray beam of Advance Photon Source provides the required penetration depth for probing structural transformations in bulk specimens. 3D reciprocal space mappings of various



phases along transformation paths (temperature, stress) are constructed from sequences of 2D diffraction patterns at in-situ incremental specimen rotation. 2D experiment by in-situ specimen rocking is also performed, which reduces data collection time from hours for 3D diffraction at each experimental condition to seconds, thus enabling detailed studies along phase transformation paths. Combining 3D and 2D diffraction techniques allows accurate interpretation of diffraction data and provides detailed information of martensitic transformations in bulk single crystals. The observed diffraction features are further explained in light of recent observation by high-resolution transmission electron microscopy as well as theoretical modeling and computation of nanotwin microstructure refinement.

### 9:10 AM Invited

**In-Situ X-Ray Diffraction Observations of Silver-Nanoink Sintering and High Temperature Eutectic Reaction with Copper:** *John Elmer*<sup>1</sup>; Eliot Specht<sup>2</sup>; <sup>1</sup>LLNL; <sup>2</sup>ORNL

Nanoinks contain nm sized metallic particles suspended in an organic dispersant fluid and are finding numerous microelectronic applications. These nanoinks sinter at much lower temperatures than their conventional counterparts due to their high surface area to volume ratio and small radius of curvature that reduces their melting points drastically below their bulk values. The unusually low melting and sintering temperatures have great potential for materials joining since their melting points increase dramatically after initial sintering. In this presentation, Ag nanoink is studied using in-situ synchrotron based x-ray diffraction to follow the kinetics of the initial sintering step, and to directly observe their high remelt temperature. Ag nanoink is further explored as a possible eutectic bonding medium with copper by tracking phase transformations to high temperatures using in-situ x-ray diffraction, and is demonstrated as a less expensive bonding medium than alternative physical vapor deposition or electroplating methods.

### 9:30 AM Invited

**In-Situ Neutron and Synchrotron X-Ray Diffraction for the Investigation of Thermo Mechanical Processes in Materials Science:** *Klaus-Dieter Liss*<sup>1</sup>; <sup>1</sup>ANSTO

Physical thermo-mechanical simulation is widely used to evaluate microstructural changes in metals as they occur in production, manufacturing or application processes. Neutron radiation bears the advantage to average over larger sample volumes and therefore provide a good powder average, as needed for quantitative phase analysis and the determination of global texture. Synchrotron high energy X-rays around 100 keV allow to investigate the local structure of the specimen. Large and fast two-dimensional detectors are employed for a multi-dimensional exploitation of the diffraction patterns. The different scattering lengths between the two types of radiation can be used to enhance the contribution of particular species of atoms and, in some cases, be particularly sensitive to atomic order and disorder. Selected metallic systems are presented undergoing thermo-mechanical load. Features like grain correlations upon phase transformations, grain refinement, subgrain formation, grain rotation, dynamic recovery, dynamic recrystallization, grain growth and the evolution of texture are revealed.

### 9:50 AM Invited

**Using In-Situ Neutron Diffraction and Mesoscale Modeling to Understand Texture Evolution during Recrystallization of Metallic Polycrystals Simulate Texture Evolution during Recrystallization of Metallic Polycrystals:** *Bala Radhakrishnan*<sup>1</sup>; Grigoreta Stoica<sup>1</sup>; Govindarajan Muralidharan<sup>1</sup>; Sarma Gorti<sup>1</sup>; Xun-Li Wang<sup>1</sup>; <sup>1</sup>Oak Ridge National Laboratory

Structural and functional materials often derive their unique properties through crystallographic texture that evolves during thermo-mechanical processing. Despite years of research, a comprehensive understanding of texture evolution during recrystallization has been elusive. Even with the availability of the most sophisticated computers and simulation tools, a direct dislocation level simulation of recrystallization is nearly impossible. The proposed research exploits the unique features of the VULCAN diffractometer at SNS, ORNL, to perform in-situ neutron diffraction investigation of the nucleation and growth steps associated with recrystallization. The texture

data in conjunction with advanced microstructure evolution modeling are used to develop an integrated, predictive, tool for texture evolution in structural materials. The application of the tool to develop lightweight materials for the energy and automotive sectors will be discussed.

### 10:10 AM Invited

**In-Situ High-Energy X-Ray Study of Advanced Materials for Energy Storage:** *Yang Ren*<sup>1</sup>; Zonghai Chen<sup>1</sup>; Yugang Sun<sup>1</sup>; Tu Truong<sup>1</sup>; Jian Xie<sup>2</sup>; <sup>1</sup>Argonne National Laboratory; <sup>2</sup>IUPUI

The increasing demand in safer and higher performance rechargeable batteries for broad applications has led to global efforts to develop advanced electrode materials, electrolyte components and additives, and other cell components. There is a critical need in understanding key material issues in batteries under realistic conditions and in real time. We will present here a recent application of synchrotron high-energy x-ray diffraction (HEXRD) for in-situ structural characterization of advanced battery materials. Our experimental work includes in-situ HEXRD studies of cathode materials during solid-state synthesis, time-resolved measurements during hybrid pulse characteristic test (HPPC) of a full battery, in-situ study of Si-Li interaction and nondestructive material characterization of commercial 18650 cells during cycling and long term aging tests. Our results provide important property-structure-performance information for in-depth understanding of advanced energy materials and the safety and performance of batteries. (Use of APS was supported by the U.S. DOE under Contract No. DE-AC02-06CH11357.)

### 10:30 AM

**A Study of the Deformation Modes in B2 Intermetallics CoTi and CoZr Using In-Situ Neutron Diffraction and Electron Backscattered Diffraction:** *Rupalee Mulay*<sup>1</sup>; Sean Agnew<sup>1</sup>; <sup>1</sup>University of Virginia

Many B2 compounds, like NiAl, are known to exhibit slip primarily on the  $\langle 001 \rangle \{110\}$  slip systems, which provide only 3 independent slip systems and, hence, fail to satisfy the von Mises criterion for polycrystalline ductility. B2 CoTi and CoZr have been examined by in-situ neutron diffraction and the results reiterate that the primary slip systems are  $\langle 001 \rangle \{110\}$ . In spite of the apparent violation of the von Mises criterion, CoZr and CoTi have shown significant ductility. Neutron diffraction also exposed a transition in strain hardening and possible explanations for the anomalous ductility include the slip of  $\langle 110 \rangle$  or  $\langle 111 \rangle$  dislocations and the formation of kink bands. The present study makes use of a combination of in-situ neutron diffraction, crystal plasticity modeling, slip trace analysis, and electron backscattered diffraction (to determine both the orientation of the grains and the in-grain misorientation axes) to establish the active deformation modes in these alloys.

### 10:40 AM Break

### 10:50 AM Invited

**In Situ Studies of Engineering Processes with Synchrotron Radiation and Neutrons:** *Andreas Schreyer*<sup>1</sup>; Torben Fischer<sup>1</sup>; Jorge Dos Santos<sup>1</sup>; Andreas Stark<sup>1</sup>; Robert Gerstenberger<sup>2</sup>; Peter Staron<sup>1</sup>; Martin Müller<sup>1</sup>; Florian Pyczak<sup>1</sup>; Walter Reimers<sup>2</sup>; Norbert Huber<sup>1</sup>; <sup>1</sup>GKSS Research Center; <sup>2</sup>TU Berlin

High-energy X-rays and neutrons offer the large penetration depths that often are required for determination of bulk properties in engineering materials research. In addition, new sources provide very high intensities on the sample which can be used not only for high spatial resolution using very small beams, but also for high time resolution in combination with a fast detector. This opens up possibilities for a wide range of engineering specific in situ experiments. Typical examples that are already widely used are heating or tensile testing in the beam. However, there are also more challenging in situ experiments in the field of engineering materials research like e.g. friction stir welding, dilatometry, or cutting. Selected examples of such experiments will be presented.

### 11:10 AM Invited

**Energy Research on the HIPPO Beam-Line at LANSCE:** *Sven Vogel*<sup>1</sup>; Yusheng Zhao<sup>1</sup>; <sup>1</sup>Los Alamos National Laboratory

The HIPPO beam-line at LANSCE is a general purpose neutron diffractometer and in this presentation we provide an overview of energy-related research. We will present our recently commissioned battery cell nSEC for in situ studies of anode, cathode and electrolyte materials as well as studies of charge and discharge behaviour of commercial Li-ion battery cells. HIPPO's high neutron flux allows for time-resolved studies and we will present recent results of chemical segregation in U-10wt.% Mo fuel foils during simulated bonding cycles, where a temporal resolution of one minute was achieved on two 250  $\mu\text{m}$  foils as samples. We will briefly touch upon our research in hydrogen storage materials and present results from high pressure investigations of ammonia borane and on the high pressure behaviour of a metal-organic framework structure as a function of pressure medium.

### 11:30 AM Invited

**In-Situ Intergranular Strains in Extrusion Textured 304L Stainless Steel:** 18 Students<sup>1</sup>; Harley Skorpenske<sup>1</sup>; Ke An<sup>1</sup>; Sheng Cheng<sup>2</sup>; Ercan Cakmak<sup>2</sup>; *Thomas Holden*<sup>1</sup>; Hahn Choo<sup>2</sup>; Peter Liaw<sup>2</sup>; Xun-Li Wang<sup>1</sup>; <sup>1</sup>Oak Ridge National Laboratory; <sup>2</sup>University of Tennessee

Many measurements have been reported of intergranular strains in austenitic stainless steel alloys, but none for the case of extruded material nor for 304 stainless steel. This case serves to emphasize how the crystallographic texture can affect which grain orientations [hkl] in the material show non-zero intergranular strains. The measurements were made on the new VULCAN engineering diffractometer at the Spallation Neutron Source at Oak Ridge National Laboratory as part of the "National Neutron and X-ray School" to demonstrate to 18 students the capabilities of the instrument. The texture was a cylindrically symmetric extrusion texture and there were already residual strains in the material prior to subjecting the samples to tensile strains between 1 and 5.5%. The experimental results are compared with an elasto-plastic self-consistent model taking into account the texture and the  $\{111\}<110>$  slip system operating in austenitic alloys.

### 11:50 AM

**In-Situ Study of Plastic Deformation in 316LN Stainless Steel by Fast Neutron Diffraction:** *Alexandru Stoica*<sup>1</sup>; Sheng Cheng<sup>1</sup>; Ke An<sup>1</sup>; Harley Skorpenske<sup>1</sup>; Xun-Li Wang<sup>1</sup>; <sup>1</sup>ORNL

A novel data acquisition system based on event mode data storage is currently implemented at SNS. By using time-of-flight diffractometer VULCAN, this data acquisition system provides exquisite capabilities to observe fast structural changes in materials subjected to plastic deformation. Unlike the conventional holding approach, the diffraction data are collected continuously during constant strain rate deformation tests. This new approach allows adjustable data histogramming and stroboscopic data processing. We report the evolution of lattice strain during tensile and cyclic deformation of 316LN stainless steel. The intergranular (type II) strains are unambiguously separated from the elastic macroscopic contribution. By monitoring the broadening of the diffraction peaks we were also able to observe the accumulation of intragranular (type III) strains. The density of residual dislocations induced by plastic deformation was estimated from these data. Under deep plastic deformation we observed characteristic grain orientation changes, which influence the residual intergranular strains.

### 12:05 PM

**In-situ Phase Transformation Studies of High Strength Beta Titanium Alloys:** *Xinjiang Hao*<sup>1</sup>; Nicholas Wain<sup>1</sup>; Chao Yang<sup>1</sup>; Xinhua Wu<sup>1</sup>; <sup>1</sup>University of Birmingham

The addition of C to beta Ti alloys has a significant effect on the phase transformations and leads to homogeneous and fine microstructures and to better mechanical properties, but at present the mechanisms underlying these effects are not understood, partly because only limited dynamic observations of the phase transformations have been made. This work, using in-situ high temperature synchrotron diffraction experiments, is aimed at identifying the mechanisms underlying the effect of C through direct observations of the

influence of C on the transformations so that a less empirical approach can be developed for the improvement of the properties of Ti alloys.

### 12:20 PM Invited

**Texture Evolution and Phase Transformation in Titanium Investigated by In-Situ Neutron Diffraction:** *Dong Ma*<sup>1</sup>; A.D. Stoica<sup>1</sup>; K. An<sup>1</sup>; L. Yang<sup>1</sup>; H. Bei<sup>1</sup>; R.A. Mills<sup>1</sup>; H. Skorpenske<sup>1</sup>; X.-L. Wang<sup>1</sup>; <sup>1</sup>ORNL

In-situ neutron diffraction has been carried out to study texture evolution and the  $\alpha(\text{hcp}) \rightarrow \beta(\text{bcc})$  phase transformation in titanium upon continuous heating and cooling. It was found that the recrystallization of  $\alpha$  resulted in the development of a new texture component, which facilitated the texture formation in  $\beta$  in the beginning of the  $\alpha \rightarrow \beta$  transformation. However, surprisingly, the transformation-induced texture started to diminish upon completion of the transformation. This new observation is explained in terms of competitive  $\beta$ -grain growth. The texture changes upon the  $\beta \rightarrow \alpha$  transformation during cooling will be also discussed.

---

## Pb-Free Solders and Other Materials for Emerging Interconnect and Packaging Technologies: Thermo-Mechanical Behavior II

*Sponsored by:* The Minerals, Metals and Materials Society, TMS Electronic, Magnetic, and Photonic Materials Division, TMS; Electronic Packaging and Interconnection Materials Committee  
*Program Organizers:* Indranath Dutta, Washington State University; Darrel Frear, Freescale Semiconductor; Sung Kang, IBM; Eric Cotts, SUNY Binghamton; Laura Turbini, Research in Motion; Rajen Sidhu, Intel Corporation; John Osenbach, LSI Corporation; Albert Wu, National Central Univ, Taiwan; Tae-Kyu Lee, Cisco Systems

Wednesday AM

Room: 7B

March 2, 2011

Location: San Diego Conv. Ctr

*Session Chair:* Sung Kang, IBM Corporation

---

### 8:30 AM Invited

**Local Mechanical Properties of Microstructural Constituents in Pb-Free Solders by Micropillar Compression:** Ling Jiang<sup>1</sup>; *Nikhilesh Chawla*<sup>1</sup>; <sup>1</sup>Arizona State University

Micropillar compression using a nanoindenter is a unique technique for probing the local mechanical properties of microconstituents in Pb-free solders. This methodology was used to perform uniaxial compression experiments on Sn, Sn-Ag3Sn eutectic, and Cu6Sn5. Focused Ion beam (FIB) was employed to mill the microconstituents. The pillars were tested using a nanoindenter with a flat tip in compression, to determine the stress-strain behavior. The effect of aspect ratio and taper of pillars on mechanical properties will be discussed. The crystallographic orientation of pillars was examined using electron back-scattered diffraction. The relationship between orientation and mechanical properties of pillars will be discussed. A knowledge of local microconstituent behavior can be used to develop "composite models" that predict the behavior of the solder as a whole.

### 8:55 AM Invited

**Coupled Effect of Electric and Mechanical Load on the Fracture Behavior of Lead-Free Solder Joint:** *Choong-Un Kim*<sup>1</sup>; Woong Ho Bang<sup>1</sup>; Hong-Tao Ma<sup>2</sup>; Tae-Kyu Lee<sup>2</sup>; Kuo-Chuan Liu<sup>2</sup>; <sup>1</sup>University of Texas Arlington; <sup>2</sup>Cisco Systems, Inc.

Mechanical reliability of solder joint has been a subject of extensive studies in recent years. These studies have addressed various contributing factors to the fracture reliability such as thermo-mechanical load conditions, and microstructural evolutions due to aging and electromigration. However, all these studies have failed to consider the most critical aspect of solder reliability, that is the fact that mechanical load is combined with electrical load in real solder joint. Our recent investigation on this subject reveals that the current and mechanical load (and thus fracture) couples in completely unexpected manner. Specifically, it is found that there exists a condition where high density electric current can retard the joint failure. Our theoretical

analysis on the fracture process further strengthens our experimental findings with a result showing high build-up of compressive stress at the crack-tip. This paper presents experimental data showing the coupled effect and discusses possible mechanistic mechanisms.

#### 9:20 AM Invited

**Effects of Aging on Pb-Free Solder Properties in Long Term Service:** *Peter Borgesen*<sup>1</sup>; Babak Arfaei<sup>1</sup>; Tariq Tashtoush<sup>1</sup>; Younis Jaradat<sup>1</sup>; Awni Qasameh<sup>1</sup>; <sup>1</sup>Binghamton University

Practical SnAgCu solder joint microstructures are inherently unstable, and resulting properties have been shown to keep changing over periods of years. In the absence of loading, this is primarily a result of ongoing coarsening of the secondary precipitates. The sensitivity to this varies with alloy composition, including the addition of Pb in so-called backward compatible assembly, and solder pad finishes as do dependencies on aging temperature. This is further complicated by systematic dependencies on solder volume and reflow parameters. Comparisons between alternatives by accelerated testing may, therefore, easily be misleading. Effects on life in long-term service are, however, not easily simulated by accelerated preconditioning. In addition, cyclic loading leads to pile-up of dislocations between precipitates, providing for particularly rapid diffusion paths and, thus, both faster coarsening and different temperature dependencies. Finally, recrystallization and subsequent crack growth are affected strongly by the coarsening. Consequences for long term reliability are discussed.

#### 9:45 AM Invited

**Electromigration-Enhanced Stress Relaxation of Sn and Sn-Ag-Cu Alloy:** H. Liu<sup>1</sup>; Q. Zhu<sup>1</sup>; Z. Wang<sup>1</sup>; J. Shang<sup>2</sup>; <sup>1</sup>Institute of Metal Research; <sup>2</sup>University of Illinois

Solder interconnects are often subject to both electric and mechanical forces which may combine to cause device failures. In this study, the mechanisms of electromigration-induced softening of solder interconnects were investigated by examining the electromigration damage and the stress relaxation behavior in Sn and Sn-Ag-Cu solder joints. With pure Sn, electromigration favored the grain boundary processes such as grain rotations and grain boundary sliding so that the dominant mechanism of stress relaxation changed from dislocation climb to grain boundary diffusion. For Sn-Ag-Cu, electromigration produced excess vacancies and numerous hillocks on the alloy surface. The interaction of excess vacancies with dislocations led to enhanced stress relaxation in the solder joint.

#### 10:10 AM Break

#### 10:20 AM

**Time-Dependent Mechanical Properties of Thermomechanically Fatigued Pb-Free Solder Joints:** *Andre Lee*<sup>1</sup>; K. Subramanian<sup>1</sup>; <sup>1</sup>Michigan State University

Evolution of microstructures and the cyclic mechanical loading attributed to thermal expansion coefficient mismatches of various entities presence in electronic interconnects are some of the known factors that affect the service reliability of Pb-free electronic solder joints. Residual mechanical property evaluation invariably destroys the specimens, without providing any means for following the progress of damage accumulation within the same solder joint. Time-dependent stress relaxation behavior in such joints will be highly sensitive to the internal changes. Small-amplitude oscillatory shear stress relaxation measurements can provide means to continuously characterize the damage accumulation resulting from thermomechanical fatigue (TMF). Studies based on series of strain-controlled experiments at different temperature regimes were used to evaluate time-dependent mechanical properties of Pb-free solder joints exposed to varying extents of TMF. Results from these experiments are used to address some critical issues in the accelerated tests employed for long-term service reliability of Pb-free solders.

#### 10:40 AM

**Life Prediction of Sn-3.0Ag-0.5Cu/ENIG and OSP Pb-Free Solder Joints of Chip Scale Package for Automotive Electronics:** *Won Sik Hong*<sup>1</sup>; Chulmin Oh<sup>1</sup>; <sup>1</sup>Korea Electronics Technology Institute

Due to ELV (End-of-Life Vehicle) banning, it is necessary to use Pb-free solder in car electronics. Therefore, in this study, we have predicted solder joints life of chip scale package (CSP) for automotive cabin electronics. For the experiment, 84 ball CSP was soldered with Sn-3.0Ag-0.5Cu on OSP and ENIG finish PCB. To investigate the fracture time of solder joints, we have conducted three kinds test under thermal shock conditions: -40~110, -25~125, -40~140 deg.C. Also, we continuously monitored the resistance of daisy-chained CSP solder joints. Failure criterion was 300 ohms of loop resistance. From these results, we have analyzed fracture mechanism and interfacial reaction of CSP solder joints. Finally, using the Norris-Landzberg modification of the Coffin-Manson equation, we have estimated solder joint life due to thermo-mechanical fracture of automotive electronics.

#### 11:00 AM

**Lead-Free Solder Joint Reliability under Wide Range of Thermal Cycling Conditions:** *Hongtao Ma*<sup>1</sup>; Mudasir Ahmad<sup>1</sup>; Kuo-Chuan Liu<sup>1</sup>; <sup>1</sup>Cisco Systems, Inc.

In lead-free solder joints reliabilities, there is a common understanding that the different temperature range of temperature cycle test may result into different results, especially the failure modes. Unfortunately, the differences in failure modes for lead-free packages across these different test conditions have not been fully studied and documented. In this study, a comprehensive set of tests was performed on test vehicles with different package types, sizes, pitches, and solder joints metallurgies. Accelerated Thermal Cycling (ATC) testing was performed using four different thermal cycling profiles: 0-100 °C, -40-125 °C, -55-125 °C, and -60-150 °C. Data from the tests were analyzed for failure mode and failure rate using Weibull statistics, and the characterized life for each test condition was determined and analyzed. The data will help quantify discrepancies due to test condition variations and will also provide valuable guidance on effects of package types, size, pitches, and solder joints metallurgies.

#### 11:20 AM

**Microstructural and Damage Evolution in Thermally Cycled Sn-3.5Ag Solder Joints:** *Govindarajan Muralidharan*<sup>1</sup>; Kanth Kurumaddali<sup>1</sup>; Andrew Kercher<sup>1</sup>; Larry Walker<sup>1</sup>; Scott Leslie<sup>2</sup>; <sup>1</sup>Oak Ridge National Laboratory; <sup>2</sup>Powerex Inc

There is a significant need for next-generation, high-performance power electronic packages and systems with wide band gap devices that operate at high temperatures in automotive and electric grid applications. Sn-3.5Ag solder is a candidate for use in such packages with potential operating temperatures up to 200°C. However, there is a need to understand thermal cycling reliability of Sn-3.5Ag solders. Damage evolution occurring in large area Sn-3.5Ag solder joints between silicon dies and Direct Bonded Copper (DBC) substrates subject to thermal cycling between 200°C and 5°C was followed using high resolution X-ray radiography techniques. This study will highlight the effect of thermal cycling conditions and stress state on damage evolution in these solder joints. \*Research was sponsored by the U. S. Department of Energy, Office of Electricity Delivery and Energy Reliability, and by the Assistant Secretary for Energy Efficiency and Renewable Energy, Propulsion Materials Program, Office of Vehicle Technologies.

#### 11:40 AM

**Effects of Reflow Parameters and Aging on Fracture Toughness of a Lead-Free Solder Joint under Dynamic Loading Conditions:** *Zhe Huang*<sup>1</sup>; Praveen Kumar<sup>1</sup>; Indranath Dutta<sup>1</sup>; Rajen Sidhu<sup>2</sup>; Mukur Renavikar<sup>2</sup>; Ravi Mahajan<sup>2</sup>; <sup>1</sup>Washington State University; <sup>2</sup>Intel Corp.

The fracture behavior of solders at high strain rates is a critical design parameter for the reliability of microelectronic packages as solder joints are prone to failure during drop. A methodology for measuring mixed-mode fracture toughness of Sn3.5Ag0.7Cu solder/Cu joints under dynamic loading conditions was developed. This method was applied to investigate the effect of reflow parameters (dwell time and cooling rate) and aging on the fracture



toughness of solder joints at different strain rates (0.1 to 100 s<sup>-1</sup>) and at various loading angles (0 – 75° at an interval of 15°). The results show that critical strain energy release rate, GC, decreased with an increase in the strain rate, dwell time and the cooling rate. A fracture mechanism map was developed to describe the correlation between the yield strength (dependent on the microstructure of solder), the IMC morphology, the mode mixity and the fracture toughness.

## Phase Stability, Phase Transformations, and Reactive Phase Formation in Electronic Materials X: Interfacial Reactions of the Pb-Free Solder Joints

*Sponsored by:* The Minerals, Metals and Materials Society, TMS Electronic, Magnetic, and Photonic Materials Division, TMS: Alloy Phases Committee

*Program Organizers:* Chih-Ming Chen, National Chung Hsing University; Hans Flandorfer, University of Vienna; Sinn-Wen Chen, National Tsing Hua University; Jae-ho Lee, Hongik University; Yee-Wen Yen, National Taiwan Univ of Science & Tech; Clemens Schmetterer, TU Bergakademie Freiberg; Ikuo Ohnuma, Tohoku University; Chao-Hong Wang, National Chung Cheng University

Wednesday AM  
March 2, 2011

Room: 7A  
Location: San Diego Conv. Ctr

*Session Chairs:* Sinn-Wen Chen, National Tsing Hua University; Yee-Wen Yen, National Taiwan Univ. of Sci. & Tech.

### 8:30 AM Invited

**Effect of Ag on Growth Behavior of Cu<sub>6</sub>Sn<sub>5</sub> Formed between Molten Sn-xAg-0.5Cu Solders and Cu UBMs:** Moon Gi Cho<sup>1</sup>; Sun-Kyoung Seo<sup>1</sup>; Hyuck Mo Lee<sup>2</sup>; <sup>1</sup>Samsung Electronics; <sup>2</sup>KAIST

Cu<sub>6</sub>Sn<sub>5</sub> intermetallic compounds (IMCs) formed at the interface of Sn-3.0Ag-0.5Cu solders with Cu exhibit much smaller grains, but their thickness is not substantially different from that of IMCs formed in Sn-0.5Cu and Sn-1.0Ag-0.5Cu solders with Cu. More specifically, the ripening growth of Cu<sub>6</sub>Sn<sub>5</sub> grains during reflow is reduced by the addition of 3.0 wt% Ag into Sn-rich solders. The measurement of the angles of two neighboring Cu<sub>6</sub>Sn<sub>5</sub> grains indicates that the interfacial energy of Cu<sub>6</sub>Sn<sub>5</sub>/molten solders in Sn-3.0Ag-0.5Cu is much smaller than that of Sn-0.5Cu and Sn-1.0Ag-0.5Cu, respectively. The Cu<sub>6</sub>Sn<sub>5</sub> IMCs formed at the interface of Sn-3.0Ag-0.5Cu with Cu during reflow retain small grain size even after aging for 500 h, and the small Cu<sub>6</sub>Sn<sub>5</sub> grains induce slower growth of Cu<sub>3</sub>Sn IMCs during aging.

### 8:55 AM Invited

**Influence of Alloying Elements on Solid-State Reactive Diffusion at Interconnection between Sn and Pd:** Masanori Kajihara<sup>1</sup>; <sup>1</sup>Tokyo Institute of Technology

Tin-base solders are widely used in the electronics industry. If a multilayer Pd/Ni/Cu conductor is interconnected with the Sn-base solder, Pd-Sn compounds are formed by reactive diffusion at the interconnection during soldering and then gradually grow during energization heating at solid-state temperatures. However, the Pd-Sn compounds are brittle and possess high electrical resistivities. Thus, the growth of the compounds deteriorates the electrical and mechanical properties of the interconnection. In order to inhibit the deterioration of the interconnection, influence of various alloying elements on the growth behavior of the compounds during the solid-state reactive diffusion was experimentally observed at temperatures of T = 433-473 K in the present study. According to the observation, the addition of Ag into Pd decelerates the growth. For the addition of Ni into Sn, however, the deceleration works at T < 473 K but not at T = 473 K.

### 9:20 AM

**Solid-Solid Reaction between Sn<sub>3</sub>Ag<sub>0.5</sub>Cu Alloy and Au/Pd/Ni(P) Metallization Pad with Various Pd Thicknesses:** Wei-Hsiang Wu<sup>1</sup>; Yen-Chen Lin<sup>1</sup>; Cheng-Shiuan Lin<sup>1</sup>; Cheng-En Ho<sup>1</sup>; <sup>1</sup>Yuan Ze University

In the past ten years, there has been a growing concern over “black pad” in the electroless nickel/immersion gold [Ni(P)/Au] surface finishing applications. In order to diminish such reliability concern, the deposition of a protective layer of Pd [or Pd(P)] between the Ni(P) and Au has gained a great attention and was readapted very recently. The thickness of Pd layer is customarily deposited within a range of 0.05 – 0.3 micron based on the cost-effective consideration. However, the effect of Pd thickness on the solderability has not been well established yet. In this study, the solid-solid reaction between 96.5 wt.% Sn – 3 wt.% Sn – 0.5 wt.% Cu (SAC305) alloy and the Au/Pd/Ni(P) with various Pd thickness (0, 0.1, 0.25 micron) was investigated. The growth kinetics of the reaction product(s) and the mechanical reliability in response of the different Au/Pd/Ni(P) will be presented in this talk.

### 9:35 AM

**Phase Equilibria of the Sn-Fe-Ni Ternary System and Interfacial Reactions at the Sn/Fe-xNi Alloys Couples:** Yee-wen Yen<sup>1</sup>; Hsien-Ming Hsiao<sup>1</sup>; Shih-Wei Lin<sup>1</sup>; Chen-Kuan Lin<sup>1</sup>; Chiapying Lee<sup>1</sup>; <sup>1</sup>National Taiwan University of Science and Technology

In this study, the phase equilibria of the Sn-Fe-Ni ternary system and interfacial reactions in Sn/Fe-Ni alloys couples were experimentally investigated. The experiment indicated that the isothermal section of the Fe-Ni-Sn ternary system at 270° had eight tie triangles, seventeen two-phase regions, ten single-phase regions and without any ternary intermetallic compounds (IMCs). One FeSn<sub>2</sub> phase was formed at the Sn/Fe-xNi interface, when the Ni concentration was less 60 at.%. When the Ni content was between 80-90 at.%, both the FeSn<sub>2</sub> and Ni<sub>3</sub>Sn<sub>4</sub> phases were formed on the interface. When the Ni content in the Fe-Ni alloy was up to 95 at.%, only the thick layer of the Ni<sub>3</sub>Sn<sub>4</sub> phase could be found. The IMC growth mechanism of the Sn/Alloy 42 and Sn/Fe-60 at.%Ni couples was diffusion-controlled. The reaction path of the Sn/Fe-80at.%N couple was Sn/Sn+FeSn<sub>2</sub>/Ni<sub>3</sub>Sn<sub>4</sub>/Fe-80 at.%Ni.

### 9:50 AM

**Modeling of Alternating Reaction Phases in Sn/Ni-V Couples:** Chun-Chong Fu<sup>1</sup>; Chih-chi Chen<sup>1</sup>; <sup>1</sup>Chung Yuan Christian University

Ni-V alloys are barrier materials in flip chip technology, and Sn is the primary constituent of Pb-free solders. It is demonstrated that unusual alternating reaction phases, T/Ni<sub>3</sub>Sn<sub>4</sub>/T/Ni<sub>3</sub>Sn<sub>4</sub>, are formed in solid/solid Sn/Ni-V couples. T phase is an amorphous Sn-Ni-V ternary phase. In this study, a mathematical model was formulated to describe the alternating phenomenon. The basic assumption of the model is that Sn is the dominant diffusion species, and that V is immobile. The parameters of the model were determined by the least square method, and the correlation coefficient (R<sup>2</sup>) demonstrated a good agreement between the experimental and calculated results. The differential equations can be solved by using some assumptions. The alternating phenomenon is represented by the none-zero imaginary part of the eigen value, which is caused by the relative high mobility difference between Sn and V in the diffusion zone.

### 10:05 AM Break

### 10:25 AM Invited

**Phase Evolution and Growth at the Interface of Sn/Cu-xZn under Liquid and Solid Reaction:** Chi-Yang Yu<sup>1</sup>; Jenq-Gong Duh<sup>1</sup>; <sup>1</sup>National Tsing Hua University

Cu-Zn is a potential substrate material to improve the reliability of solder/Cu-Zn solder joints. In this study, three kinds of solder joints, i.e. Sn/Cu, Sn/Cu-15Zn, and Sn/Cu-30Zn (wt.%), were fabricated to probe the formation mechanism of intermetallic compounds (IMCs). At the Sn/Cu interface, thick Cu<sub>6</sub>Sn<sub>5</sub> and Cu<sub>3</sub>Sn grew rapidly during liquid and solid reaction. Kirkendall voids formed between Cu<sub>3</sub>Sn and Cu substrate after solid state aging. In contrast, no void was observed at these Sn/Cu-Zn interfaces. The

Sn/Cu-15Zn and Sn/Cu-30Zn solder joints revealed slow growth rate of interfacial IMCs, and the formation of Cu<sub>3</sub>Sn was evidently suppressed. Cu<sub>6</sub>(Sn,Zn)<sub>5</sub>, Cu(Zn,Sn), and CuZn were the dominant IMCs. The phase evolution is attributed to the atomic diffusion and elemental re-distribution at the Sn/Cu-xZn interfaces under liquid and solid reaction. With regards to the thickness variation of interfacial IMCs, the growth mechanisms of IMC and related phases are proposed.

**10:50 AM**

**Metallurgical Reaction in Sn-Cu-Ni Solder Alloys:** Han-wen Lin<sup>1</sup>; Chih Chen<sup>1</sup>; <sup>1</sup>National Chiao Tung University

Sn-Pb alloys have been used in packaging industry due to its favorable physical, mechanical and metallurgical properties. However, since the RoHS was adopted in 2003 and it took effect in 2006, new Pb-free alloys, such as Sn-Ag, Sn-Cu, Sn-Ag-Cu, have been developed. Among these systems, Sn-Ag and Sn-Ag-Cu are the most common candidates as Pb-free solder materials in packaging industry. However, as the bumps get smaller and smaller, the brittle intermetallic compounds of tin and silver, Ag<sub>3</sub>Sn, might become a fatal factor to joints. Therefore, alloy system of Sn-Cu-Ni is proposed. In this paper, different composition of Sn-Cu-Ni are prepared, including SnCu<sub>2</sub>Ni<sub>1</sub>, SnCu<sub>3</sub>Ni<sub>1.5</sub>, SnCu<sub>4</sub>Ni<sub>2</sub> (weight percent). The metallurgical reactions of the solder alloys with Ni and Cu foils will be investigated.

**11:05 AM**

**Microstructure Effect of Electroplated Cu Foils on Interfacial Reaction with Pb-Free Sn-Based Solders:** T. S. Huang<sup>1</sup>; Cheng Yi Liu<sup>1</sup>; <sup>1</sup>National Central University

The interfacial reaction between Pb-free Sn-based solders and Cu substrate has been studied for decades. Yet, how does the microstructure of Cu affect the interfacial reaction is still an issue to be understood. In this study, we will investigate the correlation between the microstructure of Cu substrate and the interfacial reaction. Cu substrates with different orientations are prepared by electroplating. Then, reflowing solder balls on the electroplated Cu substrates and aging the Sn/Cu solder joint samples under 150°. The aged Sn/Cu samples were examined by the metallurgical examination, XRD and FIB analysis to investigate (1) the grain morphology and preferred orientation of electroplated Cu substrates. (2) Cu-Sn compound layers and Kirkendall voids distribution at the joint interfaces. The results indicate that the growth kinetics of the interfacial Cu<sub>3</sub>Sn and Cu<sub>6</sub>Sn<sub>5</sub> layer strongly depends on the prefer-orientation of the electroplated Cu substrates, i.e., (111) and (220). In addition, the detail growth kinetics of the Cu-Sn intermediate phases, (Cu<sub>3</sub>Sn and Cu<sub>6</sub>Sn<sub>5</sub>) layers are modeled by analyzing the three interfaces (Cu/Cu<sub>3</sub>Sn, Cu<sub>3</sub>Sn/Cu<sub>6</sub>Sn<sub>5</sub>, and Cu<sub>6</sub>Sn<sub>5</sub>/Sn) movement. The detail kinetics would be presented in this talk.

## Physical and Mechanical Metallurgy of Shape Memory Alloys for Actuator Applications: Alloy Design and Development

*Sponsored by:* The Minerals, Metals and Materials Society  
*Program Organizers:* S. Raj, NASA Glenn Research Center; Raj Vaidyanathan, University of Central Florida; Ibrahim Karaman, Texas A&M University; Ronald Noebe, NASA Glenn Research Center; Frederick Calkins, The Boeing Company; Shuichi Miyazaki, Institute of Materials Science, University of Tsukuba

Wednesday AM  
March 2, 2011

Room: 11B  
Location: San Diego Conv. Ctr

*Session Chairs:* Sebastian Fähler, IFW Dresden; Petr Sittner, Institute of Physics of the Academy of Sciences

**8:30 AM Introductory Comments**

**8:35 AM Plenary**

**New Experimental Results on the Role of Alloy Composition and Microstructure on Thermodynamic and Mechanical Properties of NiTi Shape Memory Alloys:** Gunther Eggeler<sup>1</sup>; <sup>1</sup>Ruhr-Universität Bochum

NiTi shape memory alloys are well known for many years. They show fascinating properties like the one way effect (1-WE) and pseudoelasticity (PE) which are technically exploited in different areas of engineering and medical technology. These properties rely on thermally or stress induced martensitic transformations as has been reported on many occasions. However, a number of open issues remain which hamper the breakthrough of these high potential functional materials. Thus, there are no precise data on the concentration dependence of the phase transition temperatures in the binary alloy. The elementary processes which govern the formation of microstructure during ingot metallurgy processing routes are only poorly understood. And the role of dislocations during the martensitic transformation and their effect on functional fatigue remains unclear. Moreover, basic micro mechanical aspects like crack propagation and the stress induced formation of R-phase have not been fully rationalized. The brief overview reports on progress in these areas made by the collaborative research center on shape memory technology (SFB 459) funded by the German research foundation (DFG) at the Ruhr-Universität Bochum in the last two years. Areas in need of further research are outlined.

**9:05 AM Invited**

**Characteristic Features of Ni- and Fe-Based Magnetic Shape Memory Alloys:** Ryosuke Kainuma<sup>1</sup>; <sup>1</sup>Tohoku University

In the past decade, many kinds of Ni-based magnetic shape memory alloys, such as Ni-Co-Al[1], Ni-Fe-Ga[2], Ni-Co-Mn-In[3], besides the Ni-Mn-Ga alloy have been reported. Very recently, our research group has found new magnetic shape memory alloys in ferrous alloy systems, Fe-Mn-Ga[4] and Fe-Ni-Co-Al[5]. In the presentation, characteristic features on magnetic, martensitic and mechanical properties for these advanced Ni- and Fe-based magnetic shape memory alloys are reviewed and their ability for actuator applications will be discussed. (References) [1] K. Oikawa et al., Appl. Phys. Lett., 79 (2001) 3290. [2] K. Oikawa et al., Appl. Phys. Lett., 81(2002) 5201. [3] R. Kainuma et al., Nature, 439 (2006) 957. [4] T. Omori et al., Appl. Phys. Lett., 95 (2009) 082508. [5] Y. Tanaka et al., Science, 327 (2010)1488.

**9:25 AM Invited**

**Design of Ferromagnetic Shape Memory Alloy (FSMA) Composites:** Minoru Taya<sup>1</sup>; <sup>1</sup>University of Washington

I will discuss the design of a set of new FSMA composites based on "hybrid mechanism of actuation" under magnetic field gradient. Originally, we discovered this Hybrid Mechanism based on FePd. Due to its higher cost, we is now designing lower-cost FSMA composites made of Ferromagnetic (soft magnetic) material and Superelastic SMA, which can exhibit larger strain at faster speed under the applied magnetic field gradient. I will

discuss several cases of such FSMA composite actuators following first the fundamental hybrid mechanism which includes both modeling, processing and characterization.

**9:45 AM**

**Thermoelastic and Non-Thermoelastic Martensitic Transformations in Fe-Mn-Al and Fe-Mn-Ga bcc Alloys:** *Toshihiro Omori*<sup>1</sup>; Ikuo Ohnuma<sup>1</sup>; Kiyohito Ishida<sup>1</sup>; Ryosuke Kainuma<sup>1</sup>; <sup>1</sup>Tohoku University

Martensitic transformations (MTs) from the  $\gamma$ -fcc parent phase to the  $\alpha'$ -bcc or -bct martensite phase are commonly recognized in Fe-based alloys. Recently, we have reported that MTs from the  $\alpha$ -bcc phase occur in Fe-Mn-Al and Fe-Mn-Ga systems, and that these transformations are thermodynamically reasonable. In the Fe-Mn-Al system, the  $\alpha$  phase has a disordered A2 structure and the MT is non-thermoelastic, in which the martensite phase has a fcc structure. On the other hand, the Fe-Mn-Ga alloy has a L2<sub>1</sub> ordered structure, showing thermoelastic MT to a fct structure. It is interesting to note that these two alloy systems show opposite magnetic properties. Those parent and martensite phases are ferromagnetic and weak magnetic (probably antiferromagnetic) in Fe-Mn-Al alloy, but ferromagnetic and paramagnetic in Fe-Mn-Ga alloy, respectively. Stress- and magnetic-field induced properties will also be presented.

**10:00 AM Break**

**10:10 AM**

**Phase Transformation and Shape Memory Effect of Ti(Pt, Ir):** *Yoko Yamabe-Mitarai*<sup>1</sup>; Toru Hara<sup>1</sup>; Seiji Miura<sup>2</sup>; Hideki Hosoda<sup>3</sup>; <sup>1</sup>National Institute for Materials Science; <sup>2</sup>Hokkaido University; <sup>3</sup>Tokyo Institute of Technology

We have focused on the alloys combining with Ti and platinum group metals such as TiPt or Ti(Pt, Ir) as high-temperature shape memory alloys due to their high martensitic transformation temperature above 1273 K. In the previous study, phase transformation and shape memory effect were investigated in the alloy with 50at% of Ti. The 2% of the strain recovery was found in ternary compounds by heating above Af after compression test. In this study, phase boundary of the B2 phase was first investigated in Ti-Pt-Ir ternary system. Based on the obtained phase boundary, several alloys with Ti-rich composition were prepared. Composition dependence of phase transformation and shape recovery effect was investigated in Ti-Pt-Ir with a variety of composition.

**10:25 AM**

**New Ferrous Polycrystalline Shape Memory Alloy Showing Huge Superelasticity:** *Yuuki Tanaka*<sup>1</sup>; Toshihiro Omori<sup>1</sup>; Ryosuke Kainuma<sup>1</sup>; Yui Sutou<sup>1</sup>; Kiyohito Ishida<sup>1</sup>; <sup>1</sup>Tohoku University

Recently, we have developed a polycrystalline Fe-Ni-Co-Al based alloy exhibiting a large superelasticity of about 13% due to a thermoelastic  $\square$  (fcc) /  $\alpha'$  (bct) transformation, which is almost twice than that of the Ni-Ti-based shape memory alloys. This ferrous alloy shows a very large mechanical damping capacity about 5 times larger than that in the Ni-Ti alloy and exhibits some unique properties, such as a large reversible change in magnetization during tensile loading and unloading and a magnetic-induced strain of about 1% at room temperature[1]. In this presentation, details on the alloy design and the fundamental physical properties of the Fe-Ni-Co-Al-based alloys are introduced. [1] Y. Tanaka, Y. Himuro, R. Kainuma, Y. Sutou, T. Omori, K. Ishida, Science, 327 (2010) 1488.

**10:40 AM**

**The Effect of Aluminum Additions on the Shape Memory Behavior in NiTiZr Alloys:** Derek Hsen Dai Hsu<sup>1</sup>; Taisuke Sasaki<sup>2</sup>; Gregory Thompson<sup>2</sup>; Michele Manuel<sup>1</sup>; <sup>1</sup>University of Florida; <sup>2</sup>The University of Alabama

The NiTiZr shape memory alloy system is of interest due to zirconium's ability to significantly change transformation temperatures as a function of composition. The addition of aluminum to this system provides the opportunity to form coherent Heusler phase precipitates. The present work reports the change in the thermomechanical, transformation, and microstructural behavior of the alloy system with the addition of aluminum as a quaternary alloying element to NiTiZr alloy with zirconium contents up

to 20 at.%. An overview of NiTiZr and NiTiAl alloys is provided and the results will be used to develop a new thermodynamic framework for alloy design. The authors would like to acknowledge support from the National Science Foundation under award number CMMI-0824352.

**10:55 AM**

**Characterization of New Phases in the Ti-Pt System Relevant to High Temperature Shape Memory Alloys:** *Karem Tello*<sup>1</sup>; Scott Cochran<sup>1</sup>; Jacob Neuchterlein<sup>1</sup>; Keith Roman<sup>1</sup>; Dana Drake<sup>1</sup>; Heather Rosin<sup>1</sup>; Anita Garg<sup>2</sup>; Ronald Noebe<sup>2</sup>; Michael Kaufman<sup>1</sup>; <sup>1</sup>Colorado School of Mines; <sup>2</sup>NASA Glenn Research Center

Nitinol (Ni-Ti) shape memory alloys (SMAs) are used widely in superelastic and shape memory applications near ambient temperatures. Platinum increases the martensitic transformation temperatures responsible for the shape memory properties and makes them potentially attractive as high temperature SMAs (HTSMAs). Unfortunately, the Ti-Pt phase diagram is poorly understood in the range 30-50 at. % Pt making the development of HTSMAs difficult. In this investigation, alloys in this range cast and heat treated and characterized using DTA, SEM and TEM methods. The alloys frequently contained more than two phases even after equilibration treatments; since this violates the phase rule, it was concluded that interstitial contamination must be complicating matters. Furthermore, one of the new phases of approximate composition Ti5Pt3, which appears to be interstitially stabilized, is related structurally to what appears to be a complex, lower-symmetry and equilibrium Ti4Pt3 phase. The results will be examined and a modified phase diagram proposed.

**11:10 AM**

**Influence of Precipitation on the Phase Transformation Temperatures of High Temperature Shape Memory NiMnCoIn Films:** *Steven Rios*<sup>1</sup>; Ibrahim Karaman<sup>1</sup>; Xinghang Zhang<sup>1</sup>; <sup>1</sup>Texas A&M University

Amorphous Ni<sub>30</sub>Mn<sub>38</sub>Co<sub>6</sub>In<sub>6</sub> films 20  $\mu$ m in thickness were fabricated using DC magnetron sputtering. Films crystallized during annealing in a differential scanning calorimeter (DSC). Crystallized films retained a nonmodulated L1<sub>0</sub> martensite structure at room temperature. DSC studies were used to determine the crystallization activation energy and showed that as the annealing temperature increased, the martensitic phase transformation temperature decreased substantially. The formation of precipitates and evolution of grain size are investigated by scanning transmission electron microscopy. Mechanisms that lead to the reduction of phase transformation temperature are discussed.

**11:25 AM**

**Phase Transformation and Microstructure Evolution in Rapidly Solidified Co-Ni-Ga Ferromagnetic Shape Memory Alloys:** *Haamun Kalaantari*<sup>1</sup>; Reza Abbaschian<sup>1</sup>; <sup>1</sup>University of California, Riverside (UCR)

Co-Ni-Ga ternary alloys are good candidates as Ferromagnetic Shape Memory Alloys (FSMAs) for modern applications such as sensing and actuating devices. The alloys have magnetic properties similar to Ni-Mn-Ga system, but with improved ductility since these Co and Ni based alloys generally consist of dual-phase structure with the phase imparting enhanced room temperature ductility significantly. In this investigation, Electromagnetic Levitation (EML) technique is applied to explore the effects of rapid solidification and bulk supercooling in a Co2NiGa and some of its off stoichiometric alloys. The effects of these solidification processing variables on the phase transformation, microstructure and FSM properties will be discussed.

**11:40 AM**

**Plasticity Enhanced Martensite Transformation in Ni-Ti Shape Memory Alloys:** *Harshad Paranjape*<sup>1</sup>; Sivom Manchiraju<sup>1</sup>; Peter Anderson<sup>1</sup>; <sup>1</sup>The Ohio State University

The response of polycrystalline shape memory actuators depends in part on the internal stress state that is induced by plastic deformation. This deformation may occur during preprocessing or during subsequent operation of the actuator. This work uses a recently developed finite element approach to study how plasticity in the austenite (B2) phase affects transformation



during both pseudoelastic and load-biased thermal cycling conditions for a solutionized Ti-50.9at.%Ni polycrystal. An outcome is that plasticity may be viewed as “good” or “bad”, depending on whether it enhances or suppresses martensite formation. The particular outcome at a grain level depends on the local texture. This knowledge is used to synthesize model polycrystals that manipulate the nature of plasticity in an effort to optimize actuator performance.

**11:55 AM End of Session**

## Polycrystal Modelling with Experimental Integration: A Symposium Honoring Carlos Tome: Dislocation Dynamics, Geomaterials, Nanoscale

*Sponsored by:* The Minerals, Metals and Materials Society, TMS Structural Materials Division, TMS Materials Processing and Manufacturing Division, ASM-MSCTS: Texture and Anisotropy Committee, TMS/ASM: Mechanical Behavior of Materials Committee, TMS/ASM: Computational Materials Science and Engineering Committee

*Program Organizers:* Ricardo Lebensohn, Los Alamos National Laboratory; Sean Agnew, University of Virginia; Mark Daymond, Queens's University

Wednesday AM Room: 6C  
March 2, 2011 Location: San Diego Conv. Ctr

*Session Chairs:* Laurent Capolungo, Georgia Tech; Amit Misra, Los Alamos National Laboratory; Olivier Castelnau, ENSAM

### 8:30 AM Invited

#### Scaling Laws for Dislocation Microstructures in Cyclic Deformation:

*Ladislav Kubin*<sup>1</sup>; *Sauzay Maxime*<sup>2</sup>; <sup>1</sup>CNRS; <sup>2</sup>CEA

The dislocation microstructures formed during the monotonic deformation of fcc crystals follow two well-known scaling laws. These laws relate the flow stress to the square root of the mean dislocation density and to the inverse of the wavelength of dislocation patterns. A compilation of literature results on the cyclic deformation of fcc single and polycrystals shows that these scaling laws also apply to persistent slip bands (PSBs) and dislocation cell structures. The two scaling constants are, however, three times smaller than in monotonic deformation. This result seems to arise from the partial reversibility of cyclic plastic flow, as modeled by Essmann in the 1980's. The saturation stress for PSBs and the critical stress for the onset of dynamic recovery in monotonic deformation appear to exhibit very similar temperature dependencies. This shows that the two stresses are governed by the same mechanism, specifically the mutual annihilation of screw dislocations by cross-slip.

### 8:55 AM Invited

#### Dislocation Dynamics Enhanced Single Crystal Constitutive Law:

*Laurent Capolungo*<sup>1</sup>; *Carlos Tome*<sup>2</sup>; *irene Beyerlein*<sup>2</sup>; <sup>1</sup>Georgia Institute of Technology; <sup>2</sup>Los Alamos National Laboratory

Hexagonal closed packed (hcp) metals deform plastically via the simultaneous activation of several different deformation modes (i.e. twinning, slip). As in the case of cubic crystals, interactions between slip systems, which translate into latent hardening or softening at the macroscopic scale, are of particular interest. Indeed, these slip system interactions control microstructure development- and in particular the magnitude and strength of strain gradients. In order to precisely quantify the effects of such dislocation interactions, a new constitutive model is developed. The model is directly informed with results obtained from discrete dislocation dynamics simulations of the strength and chance of junction formation for each junction type. Mobile, statistically stored and geometrically necessary dislocations evolutions are accounted for as well as their directionality. Latent hardening between different slip modes are captured via the introduction of a new dislocation storage model

### 9:20 AM

#### Experimental and Simulation Study of Grain Boundary Influence on Dislocation Mean Free Path: *Gael Daveau*<sup>1</sup>; *Benoit Devincré*<sup>2</sup>; *Thierry Hoc*<sup>3</sup>; *Odile Robach*<sup>4</sup>; <sup>1</sup>LEM (CNRS-ONERA) / MSSMAT (ECP); <sup>2</sup>LEM (CNRS-ONERA); <sup>3</sup>LTD (EC-Lyon); <sup>4</sup>CEA-Grenoble DSM/INAC/SP2M/NRS

In this study, a dislocation density based model [1] initially developed for fcc single crystal is extended to strain hardening in polycrystal. The early stages of plastic deformation in a Cu tri-crystal are investigated as an ideal validation test. Crystal rotation and elastic strain are measured by Laue microdiffraction in the vicinity of grain boundaries (GBs). In addition, the storage of GND density induced by the existence of GBs is evaluated at increasing deformation. The corresponding profiles are used to test predictions made with DD simulation. From that comparison, a decrease of the dislocation mean free path is determined as a function of GB distances. Following a multiscale modeling approach, this information is finally included in a “storage-recovery” constitutive law part of a crystal plasticity code. The latter is used to simulate deformations at larger scale. [1] Devincré, Hoc, Kubin, Science, 320 (2008) p 1745–1748.

### 9:40 AM Invited

#### Slip Systems Interactions in Ice Single Crystals: *Benoit Devincré*<sup>1</sup>; <sup>1</sup>CNRS

With dislocation dynamics simulation we examine the nature and the strength of slip systems interactions in ice single crystals. As an hcp material with plastic deformation dominated by basal slip, focus is on basal-basal, basal-pyramidal and basal-prismatic slip interactions. Based on the results of large-scale 3D simulations of latent hardening tests, an interaction matrix is proposed for crystal plasticity modelling.

### 10:05 AM Break

### 10:20 AM Invited

#### Polycrystal Plasticity: Linking the Microscopic and Macroscopic Scale:

*Hans-Rudolf Wenk*<sup>1</sup>; <sup>1</sup>University of California

Material scientists are generally concerned about deformation of objects meters in size and over time spans of hours. Similar processes take place in the Earth but on a much larger scale of thousands of kilometers and lasting for millions of years. We will illustrate how the visco-plastic self-consistent theory successfully predicts texture development in the lower mantle that are compatible with seismic observations of anisotropy. While modeling of flow in the deep Earth is on a large scale, it requires information about deformation mechanisms in the phases perovskite, postperovskite and magnesiowuestite that can only be determined at the microscopic (micron) level with diamond anvil experiments. Also here VPSC is needed to interpret active slip systems from experimental textures of these phases which are unstable at ambient conditions. This micro-macro linking has attracted materials researchers such as Gilles Canova and later Carlos Tomé to engage in geophysical research.

### 10:45 AM Invited

#### The Transient Creep of Polycrystalline Ice Inferred from Theoretical, Numerical, and Experimental Micromechanical Approaches: *Olivier Castelnau*<sup>1</sup>; *Claudiu Badulescu*<sup>2</sup>; *Renald Brenner*<sup>3</sup>; *Paul Duval*<sup>4</sup>; *Fanny Grennerat*<sup>4</sup>; *Noel lahellec*<sup>2</sup>; *Maurine Montagnat*<sup>4</sup>; *Hervé Moulinec*<sup>2</sup>; *Pierre Suquet*<sup>2</sup>; *Quoc Huy Vu*<sup>3</sup>; <sup>1</sup>PIMM-CNRS; <sup>2</sup>LMA-CNRS; <sup>3</sup>LPMTM-CNRS; <sup>4</sup>LGGE-CNRS

The significant overall hardening occurring during the transient creep of polycrystalline ice strongly depends on the elastic and viscoplastic behaviors at the grain scale but also on dislocation processes at the slip system level. The local viscoplastic anisotropy, which is particularly large for ice crystals, plays a crucial role in the development of intra- and inter-granular stress and strain field heterogeneities. One difficulty for the description of transient creep behavior comes from the coupling between elastic and viscoplastic responses, and the subsequent memory effect that has to be considered. We will present our ongoing work on the topic in which full-field modeling (based on a FFT approach), mean-field modeling (homogenization), and experimental characterization of intragranular strain heterogeneities (image

correlation) on 2-D specimens, are compared with each other. Presented results will focus on the link between local grain microstructures, strain heterogeneities, and effective behavior.

**11:10 AM**

**Rheologic Anisotropy Associated with Flow-Induced Texturing of Earth's Mantle:** Donna Blackman<sup>1</sup>; Olivier Castelnau<sup>2</sup>; <sup>1</sup>UCSD; <sup>2</sup>CNRS

We investigate feedbacks between upper mantle flow and associated texturing of polycrystalline mineral aggregates. A multi-scale (nanometer-100's km), linked numerical procedure allows us to assess local rheological anisotropy that could alter the mantle flow. Results to date use an 'intermediate coupling' approach. Mantle flow is computed assuming isotropic viscosity. Anisotropic rheology due to flow-induced textures is determined at local positions throughout the model space. These local viscosity tensors update the stiffness matrix and a new steady-state flow-field is solved. In low gradient areas, deviation from isotropic results is small. In high strain-rate gradient areas, notable rheologic anisotropy is predicted. Differences in flow velocities reach ~25% of the spreading rate in these regions of this interim case. We expect to report results for successive iterative runs, where updated viscosity tensors are computed at each step and introduced to the subsequent flow model calculation.

**11:30 AM Invited**

**Studying the Mechanical Response of Regions within Grains and near Grain Boundaries Using Spherical Nanoindentation:** Siddhartha Pathak<sup>1</sup>; Surya Kalidindi<sup>2</sup>; <sup>1</sup>Mechanics of Materials and Nanostructures Laboratory, EMPA; <sup>2</sup>Drexel University

We discuss the capabilities of spherical nanoindentation stress-strain curves, extracted from the measured load-displacement dataset, in characterizing the local mechanical behavior within individual grains and near grain boundaries of polycrystalline samples. Since nanoindentation length scales are smaller than the typical grain sizes in polycrystalline samples, this technique is an ideal tool for detailed characterization of the microscale heterogeneities present in these materials and their evolution during various metal shaping/working operations. Using a series of examples, we demonstrate the tremendous capabilities of our data analyses procedures in a) characterizing the local indentation yield strengths in individual grains of deformed polycrystalline metallic samples and relating them to increases in the local slip resistances, b) correlating the stored energy differences of individual grains to their Taylor factors as a function of imposed cold work, and c) understanding the role of interfaces such as grain boundaries in the deformation of a multi-phase polycrystalline sample.

**11:55 AM**

**Ab-Initio Based Study of the Elastic Properties of Dual-Phase Ti-Nb Polycrystalline Composites:** Martin Friak<sup>1</sup>; Benedikt Sander<sup>1</sup>; Duancheng Ma<sup>1</sup>; William Counts<sup>1</sup>; Dierk Raabe<sup>1</sup>; Joerg Neugebauer<sup>1</sup>; <sup>1</sup>Max Planck Institute for Iron Research

We present a scale-bridging approach for modeling the integral elastic response of polycrystalline composites that is based on a multi-physics combination of (i) parameter-free first-principles calculations of thermodynamic phase stability and single-crystal elastic stiffness, and (ii) homogenization schemes developed for polycrystalline aggregates and composites. The modeling is used as a theory-guided bottom-up materials design strategy and applied to Ti-Nb alloys as a promising candidate for biomedical implant applications. The theoretical results (i) show an excellent agreement with experimental data and (ii) reveal a decisive influence of the multi-phase character of the polycrystalline composites on their integral elastic properties. The study shows that the results based on the density-functional-theory calculations at the atomistic level can be directly used for predictions at the macroscopic scale, effectively scale-jumping several orders of magnitude without using any empirical parameters (see e.g. Raabe et al., *Acta Materialia*, vol. 55, 4475, (2007)).

**12:15 PM**

**Plasticity of Metallic Nanolayered Composites: Shrinking Tomé to Nanoscales:** Amit Misra<sup>1</sup>; <sup>1</sup>Los Alamos National Laboratory

Metallic nanolayered composites synthesized via physical vapor deposition possess ultra-high strengths. Although the individual layer thickness is on the order of nanometers, foils with total thickness on the order of a few tens to a hundred micrometers can be readily produced and deformed to large plastic strains via room temperature rolling. A symmetric slip model will be presented to account for preservation of the initial crystallographic relations after large strain deformation. The VPSC model developed by Carlos Tomé was used to model texture evolution in Cu-Nb nanolayered composites. At this length scale, the model accounts for the interface between Cu and Nb layers by computing the aggregate response of composite grains using a visco-plastic self-consistent scheme. The model was later extended to interpret similar observations of preservation of initial out-of-plane textures at nanoscales in other nanolayered systems such as nanotwinned Cu and Cu-metallic glass composites.

**12:35 PM**

**Assessment of the Hertzian Estimate of Dislocation Nucleation Stresses from Nanoindentation Experiments:** Li Ma<sup>1</sup>; Dylan Morris<sup>2</sup>; Stephani Jennerjohn<sup>3</sup>; David Bahr<sup>3</sup>; Lyle Levine<sup>1</sup>; <sup>1</sup>NIST; <sup>2</sup>Michelin North America; <sup>3</sup>Washington State University

The dislocation nucleation stress of crystalline materials is frequently estimated from the maximum shear stress assuming Hertzian contact up to the first "pop-in" event, which is a sudden displacement burst during load-controlled nanoindentation. However, the irregular indenter tip shape will significantly change the stress distribution, and therefore the maximum shear stress from Hertzian estimation. In this work, the near-apex shape of two real Berkovich indenters, one lightly and another heavily used, were measured by SPM and directly input into FEA models for "virtual" nanoindentation experiments on <100>-oriented single-crystal tungsten. Simultaneously, experiments were carried out using the same indenters. The load-displacement curves from FEA simulation show good agreement with those from the experiments. However the discrepancies between Hertzian and FEA estimates of the shear stresses are larger than 30%. This indicates that small irregularities of indenter tips may cause significant deviations from Hertzian estimation of dislocation nucleation stress from nanoindentation experiments.

---

**Processing and Properties of Powder-Based Materials: Powder and Laser Processing**

*Sponsored by:* The Minerals, Metals and Materials Society, TMS Materials Processing and Manufacturing Division, TMS: Powder Materials Committee

*Program Organizers:* K. Morsi, San Diego State University; Ahmed El-Desouky, San Diego State University

Wednesday AM  
March 2, 2011

Room: 33A  
Location: San Diego Conv. Ctr

*Session Chair:* David Bourell, University of Texas-Austin

---

**8:30 AM Introductory Comments**

**8:35 AM**

**Effect of Heat Diffusion in Interparticle Micro-Welding for 3-D Particle Assembly:** Kenta Takagi<sup>1</sup>; Kimihiro Ozaki<sup>1</sup>; Keizo Kobayashi<sup>1</sup>; <sup>1</sup>National Institute of Advanced Industrial Science and Technology

We have developed a particle assembly method to build up arbitrary 3-D structures for novel functional materials and devices. The key technique in this method was interparticle bonding in terms of accurate locating of particles. Micro-laser and resistance weldings would be preferred approaches because both of good connectivity and spot heating. The welding tests to single point were conducted using monosized micro-particles of

WEDNESDAY AM

various materials. Highly thermal conductive materials were hard to be bonded without distortion, because local melting at the contact point could not be attained due to fast heat diffusion. FEM analysis revealed that the thermal problem became more serious in multipoint bonding. As a result, the materials with the conductivity smaller than several tens W/mK were found to be adequately bonded. Eventually, 3-D structures with diamond lattice were successfully assembled using the lowly thermal conductive particles such as Bi alloy and polymer by the developed method.

## 8:55 AM

**Thermal Characterization of Powder-Based Selective Laser Sintering of Nylon-12:** *Tim Diller*<sup>1</sup>; Rameshwar Sreenivasan<sup>1</sup>; David Bourell<sup>1</sup>; Joseph Beaman<sup>1</sup>; <sup>1</sup>University of Texas

Precise thermal control of selective laser sintering (SLS) is desirable for improving geometric accuracy, mechanical properties, and surface finish of nylon parts. A measurement system was set up to monitor thermal aspects. A SinterStation 2500 SLS machine was the test-bed for studying part builds made of Duraform(tm) nylon-12 powder. Thermal characterization included resistance temperature detectors embedded in the part bed powder to monitor the temperature during the build process. Part bed surface temperature was measured with an infrared camera aimed through the front window. A two-part, macro-scale, time-dependent multi-physics computational thermal model was developed. Boundary conditions were chosen to match the observed conditions in the test-bed machine. In this presentation, initial results are shared, including insights into the material properties and their evolution during the build and the importance of tight control of the pre-heating process. This research was funded by the Department of Defense under Grant Number GRT00015778.

## 9:15 AM

**Characterization of Al-Ni Composites Produced by Ultrasonic Powder Consolidation:** *Dinc Erdeniz*<sup>1</sup>; Teichi Ando<sup>1</sup>; <sup>1</sup>Northeastern University

Reactive composites, applicable to localized heating applications, were produced from Al and Ni powders by ultrasonic powder consolidation (UPC) at temperatures = 573K in 1 s. The composites exhibited a fully dense microstructure consisting of a metallurgically bonded Al matrix and nearly undeformed Ni particles distributed in the Al matrix. No indications of reactions were noted between the elements. Differential scanning calorimetry (DSC) revealed two exothermic and one endothermic peaks. The phase evolution during DSC was investigated by X-ray diffraction (XRD). The first exothermic peak initiated at 830 K was due to solid-state formation of Al<sub>3</sub>Ni and Al<sub>3</sub>Ni<sub>2</sub>. At 913 K, an endothermic peak formed due to eutectic melting of Al<sub>3</sub>Ni and Al which triggered ignition, producing the second exothermic peak at 925 K. The final reacted materials consisted of Al<sub>3</sub>Ni, Al<sub>3</sub>Ni<sub>2</sub>, AlNi and unreacted Ni.

## 9:35 AM

**Comparison of the Effect of Particle Size on the Compressive Strength of Sintered Wollastonite - And Chemically Bonded Phosphate - Ceramics:** *H. A. Colorado*<sup>1</sup>; J. Juanri<sup>1</sup>; Clem Hiel<sup>2</sup>; H. T. Hahn<sup>1</sup>; J-M Yang<sup>1</sup>; <sup>1</sup>University of California, Los Angeles; <sup>2</sup>Composite Support and Solutions Inc

The effects of different wollastonite powders size distributions on the compressive strength of both sintered and chemically bonded phosphate ceramics (CBPC) is currently being investigated. Wollastonite powder samples were compressed at 5000lb and then sintered at 1050°C for 30h. Compression tests were conducted to evaluate the effectiveness of the sintering treatment. For comparison proposes, CBPCs were fabricated by mixing a phosphoric acid formulation (from CS&S) with different wollastonite powders size. Curing and compression tests were conducted for the CBPCs to evaluate the powder processing effects on their final mechanical properties. The micro-structure in all cases was studied with Scanning Electron Microscopy.

## 9:55 AM

**Laser Cladding of Functional Coatings for Biomedical Applications:** *Shaodong Wang*<sup>1</sup>; Lijue Xue<sup>1</sup>; <sup>1</sup>National Research Council Canada

Surface coating can be used to enhance and/or optimize the functionalities of medical implants and devices. Blown powder laser cladding, a material additive technology, has a potential to apply various functional coatings on the metallic materials for biomedical applications. Two laser clad coatings have been investigated for medical implant applications: (1) Ti-6Al-4V alloy coating laser-clad on porous titanium foams; and (2) Composite coating of Ti-6Al-4V combined with Co-Cr-Mo alloy laser-clad on Ti-6Al-4V substrates. The microstructure of the laser-clad coating was examined by optical microscope (OM) and SEM. Micro-hardness was measured in the laser-clad coating. Sliding wear testing was particularly performed to evaluate the wear resistance of (Ti-6Al-4V + Co-Cr-Mo) composite coating using pin-on-disc wear testing. Initial results show that laser-clad Ti-6Al-4V coating on porous titanium foams is dense and crack-free. The addition of a small fraction of Co-Cr-Mo alloy will significantly increase the wear resistance of the Ti-6Al-4V composite coating.

## 10:15 AM Break

## 10:25 AM

**Millimeter-Wave Beam Sintering of Ceramic Laser Host Materials:** *Arne Fliflet*<sup>1</sup>; Steven Gold<sup>1</sup>; Spencer Miller<sup>2</sup>; M. Imam<sup>1</sup>; C. Feng<sup>1</sup>; <sup>1</sup>Naval Research Laboratory; <sup>2</sup>Directed Energy Professional Society Scholar

Millimeter-wave beam sintering of ceramic laser host materials such as neodymium-doped yttrium aluminum garnet (Nd:YAG) and ytterbium-doped yttria (Yb:Y<sub>2</sub>O<sub>3</sub>) has been under investigation at the Naval Research Laboratory (NRL) for high-energy laser (HEL) applications. Compacts pressed from high-purity micron and submicron grain-size powders are placed in closed insulating caskets and heated by an 83 GHz beam to temperatures of 1600–1800°C using a combination of direct and indirect heating. Over 99% theoretical density has been achieved with moderate grain growth; however, imperfections in the sintered compact microstructure have as yet prevented full transparency. As an aid to designing insulating caskets with low thermal gradients and consistent processing temperatures, we have compared temperature profile calculations based on an inhomogeneous slab model for millimeter-wave beam heating of the casket/work-piece system with experimental measurements. The implications of these calculations and measurements for improving the millimeter-wave sintering process will be discussed.

## 10:45 AM

**Characterization of Particle-Interface Structure and Its Effect on Tensile Fracture in Bulk Copper Produced by Cold Gas Dynamic Spray Processing:** *Paul Eason*<sup>1</sup>; Phillip Brooke<sup>1</sup>; Timothy Eden<sup>2</sup>; Gerald Bourne<sup>3</sup>; Michael Kaufman<sup>4</sup>; <sup>1</sup>University of North Florida; <sup>2</sup>Pennsylvania State University; <sup>3</sup>University of Florida; <sup>4</sup>Colorado School Of Mines

Cold gas dynamic spray processing is employed as a coating technology in many alloy systems. It has been proposed that improved control over process variables could permit the freeform fabrication of bulk parts. In this investigation, bulk copper samples were sprayed using either nitrogen or helium process gas, allowing comparison of the effects of particle velocities. The helium sprayed samples exhibit recrystallized grains smaller than 100 nm in diameter in regions adjacent to prior particle boundaries. These regions are the subject of investigation into the mechanisms of bonding resulting from high velocity impact. Tensile specimens were produced from samples in the as-sprayed and annealed condition. Field-emission scanning electron microscopy was performed to relate the fracture response to the presence and extent of interfacial bonding. Focused ion beam sectioning and transmission electron microscopy were also employed to establish the extent of interfacial mixing/bonding by examining the fracture path.



11:05 AM

**A Feasibility Study of Multi-Pass Cladding Using High-Power Direct Diode Laser:** *Soundarapandian Santhanakrishnan*<sup>1</sup>; Radovan Kovacevic<sup>1</sup>; <sup>1</sup>Southern Methodist University

In this study, a multi-pass cladding by high power direct diode laser (HPDDL) is performed to study the hardness uniformity in the clad to the substrate. A 2-kW HPDDL of 808 nm in wavelength is used to clad the tool steel H13 on the substrate of AISI 4140 steel. A number of experiments are carried out by changing the laser power and scanning speeds while keeping a constant powder feed rate and the size of overlap to produce different sizes of clad. A coupled thermo-kinetic (TK) hardening model is developed to predict the temperature history, rates of heating and cooling, temperature gradient, rate of solidification and the hardness. The study of microstructure, energy dispersive X-ray spectroscopy (EDX), and hardness measurements are performed to quantify the effect of process parameters on the variation of solidification and the change of hardness.

### **Properties, Processing, and Performance of Steels and Ni-Based Alloys for Advanced Steam Conditions: Mechanical Behavior and Physical Metallurgy**

*Sponsored by:* The Minerals, Metals and Materials Society, TMS Structural Materials Division, TMS/ASM: Corrosion and Environmental Effects Committee, TMS: High Temperature Alloys Committee

*Program Organizers:* Peter Tortorelli, Oak Ridge National Laboratory; Bruce Pint, Oak Ridge National Laboratory; Paul Jablonski, National Energy Technology Laboratory; Xingbo Liu, West Virginia University

Wednesday AM  
March 2, 2011

Room: 33B  
Location: San Diego Conv. Ctr

*Session Chair:* Paul Jablonski, National Energy Technology Laboratory

8:30 AM

**Creep Properties of Fe-20Cr-30Ni-2Nb Austenitic Heat Resistant Steels Strengthened by Intermetallics Designed for A-USC Power Plant:** *Masao Takeyama*<sup>1</sup>; Imanuel Tarigan<sup>2</sup>; Naoya Kanno<sup>2</sup>; <sup>1</sup>Tokyo Institute of Technology, Consortium of the Japan Research and Development Center for Materials (JRCM); <sup>2</sup>Tokyo Institute of Technology

Carbon free Fe-20Cr-30Ni-2Nb (at%) austenitic steels newly designed for A-USC power plant exhibit excellent creep properties at 973 K. The creep rupture strength is twice as high as that of SUH 347 steel and could meet the requirement of 10<sup>5</sup>-hour creep rupture strength higher than 100 MPa at 973 K. In these steels, two types of intermetallic phases of Ni<sub>3</sub>Nb (GCP) and Fe<sub>2</sub>Nb Laves (TCP) precipitate with different kinetics and morphology; the former precipitates homogeneously within grain interiors in short-time range, whereas the latter mainly at grain boundaries in long-term range. The higher the grain-boundary area fraction of the Laves phase, the lower the creep rate, and the creep rate decreases continuously even though the GCP phase coarsens. Thus, the superior long-term creep strength is attributed to the Laves phase at grain boundaries. The novel strengthening mechanism called "Grain-boundary precipitation strengthening (GBPS)" will be given.

8:50 AM

**Development and Evaluation of High Mn Containing Alumina-Forming Austenitic Stainless Steel Alloys for Advanced Steam Conditions:** *Yukinori Yamamoto*<sup>1</sup>; Michael Santella<sup>1</sup>; Michael Brady<sup>1</sup>; Neal Evans<sup>2</sup>; Philip Maziasz<sup>1</sup>; <sup>1</sup>Oak Ridge National Laboratory; <sup>2</sup>University of Tennessee

A series of alumina-forming austenitic (AFA) stainless steel alloys, based on Fe-(12-14)Cr-(2.5-4)Al-(10-25)Ni-(2-10)Mn-(0.6-2.5)Nb-(0.05-0.1)C, wt%, are currently under development for use at 600-900°C. The alloys exhibit superior oxidation resistance to chromia-forming stainless steel alloys, in water-vapor containing environments. This presentation

focuses on the development of a low-cost grade of AFA alloys utilizing Mn substituting for Ni to both stabilize the austenite matrix relative to the ferrite phase and reduce raw material costs. Preliminary results indicated that alloys based on Fe-14Cr-2.5Al-(5-10)Mn-(10-12)Ni exhibited a good combination of oxidation resistance at 650°C in air with 10% water vapor and creep resistance at 750°C/100MPa comparable to that of type 347 stainless steel (Fe-18Cr-12Ni base). Details of microstructure, creep, and oxidation resistance will be presented. This research is sponsored by the U.S. DOE, Office of EERE Industrial Technologies Program, and the LDRD Program of Oak Ridge National Laboratory, under contract DE-AC05-00OR22725 with UT-Battelle, LLC.

9:10 AM

**New Ferritic Steels with Combined Optimal Creep Resistance and Ductility Designed by Coupling Thermodynamic Calculations with Focused Experiments:** *Zhenke Teng*<sup>1</sup>; Fan Zhang<sup>2</sup>; Michael Miller<sup>3</sup>; Chain Liu<sup>4</sup>; Austin Chang<sup>2</sup>; Shenyan Huang<sup>1</sup>; Robert Tien<sup>5</sup>; Ye Chou<sup>5</sup>; Peter Liaw<sup>1</sup>; <sup>1</sup>University of Tennessee, Knoxville; <sup>2</sup>CompuTherm LLC; <sup>3</sup>Oak Ridge National Laboratory; <sup>4</sup>Hong Kong Polytechnic University; <sup>5</sup>Multi-Phase Services Inc.

Two critical issues restricting the applications of NiAl precipitate-strengthened ferritic steels are their poor room temperature ductility and insufficient creep resistance at temperatures higher than 600°C. In this study, thermodynamic modeling approach is integrated with focused experiments to investigate the ductility and creep resistance of steel alloys based on the Fe-Ni-Al-Cr-Mo system. The mechanical property studies showed that the creep resistance increases with increasing the volume fraction of B2-ordered precipitates, while the opposite trend was observed for the ductility. Low solubility of Al in the Fe matrix was found to favor a ductility increase. Thermodynamic calculations were used to predict the volume fraction of B2-ordered precipitates and the elemental partitioning to guide the selection of alloy compositions which may exhibit the balanced creep resistance and ductility. Key experiments were then conducted to validate the prediction. This integrated approach was found to be very effective in the alloy design and development.

9:30 AM

**Alloy 740 Weld Strength Optimization:** *John deBarbadillo*<sup>1</sup>; Brian Baker<sup>1</sup>; <sup>1</sup>Special Metals Corporation

If the goals of the USA A-USC project are to be met, age hardened nickel-base alloys will be required for a number of welded components such as headers and reheaters. These alloys pose new issues for large pressure containing systems because their homogenization temperatures are too high to permit full heat treatment of weldments in the field. Extensive testing has shown that age hardened alloys have reduced creep strength, described by the term "weld strength reduction factor" (WSRF). The WSRF is on the order of 0.7-0.8 for nickel-base alloys. This loss of strength can be compensated for in some joints, but not in others. There are several active programs underway in the USA to address this issue. This paper reviews microstructural information and relates it to the predicted cast structure, computed thermal cycles and the phase stability for alloy 740. Potential solutions are proposed and initial results presented.

9:50 AM

**Creep Rupture Testing of Inconel™ 740 Weldments:** *Michael Santella*<sup>1</sup>; John Shingledecker<sup>2</sup>; Oleg Barabash<sup>1</sup>; <sup>1</sup>Oak Ridge National Laboratory; <sup>2</sup>EPRI

Creep-rupture testing at 750 and 800°C was performed on cross-weld specimens of gas-tungsten-arc welded Inconel™ 740 tubes. In one case, the weldments were given a post-weld heat treatment of 800°C for 4 h. For fixed time conditions, these specimens failed in the weld deposits at rupture times averaging near 75% of those for base metal, i.e., the average weld strength factor was about 0.75. In the second case, before testing, the weldments were solution treated at 1120°C for 1 h and then aged at 800°C for 4 h. Failures in these specimens occurred in base metal at rupture times near those of unwelded base metal. Solution treatment caused the original dendritic microstructures of the weld deposits to recrystallize into equiaxed

WEDNESDAY AM

structures of grain sizes larger than those of base metal. Orientation image mapping was used to relate the rupture properties to the grain structure and crystallographic orientation.

### 10:10 AM Break

### 10:30 AM

#### Effect of Steam Exposure on the Creep Properties of Ni-Based Alloys: *Sebastien Dryepondt*<sup>1</sup>; Bruce Pint<sup>1</sup>; Edgar Lara-Curzio<sup>1</sup>; <sup>1</sup>ornl

Advanced coal-fired ultrasupercritical steam conditions of 760°C and 350 bar have been targeted to meet the future demand for high-efficiency, low emission power generation. This is a dramatic increase compared to the current targets of 600-625°C and ~245 bar. The durability of current candidate Fe- and Ni-based alloys under such harsh conditions needs to be determined and creep testing in air as well as oxidation testing in steam is being conducted. Lifetime models based on these tests cannot accurately integrate the effect of steam exposure on the alloy creep resistance, or the influence of stress on the material oxidation rate. To estimate the effect of steam environment on creep properties, Ni-based specimens have been exposed from 2000 to 5000 h in steam or inert gas prior to creep testing in air. These results were compared to creep data from a new environmental creep rig that allows testing in steam.

### 10:50 AM

#### High Temperature Fatigue Life of Coated and Uncoated Valve Materials: *Jeffrey Evans*<sup>1</sup>; Seth Farrington<sup>1</sup>; Sebastien Dryepondt<sup>2</sup>; Bruce Pint<sup>2</sup>; <sup>1</sup>University of Alabama in Huntsville; <sup>2</sup>Oak Ridge National Laboratory

In many power generation applications, the search for higher system efficiency has resulted in a progressive increase in operating temperatures. A direct consequence is a decrease of some components' durability due to the appearance of new types of failure. In the case of exhaust valves in natural-gas fired reciprocating engines, high temperature oxidation assisted cracking has been suggested as a rupture mechanism. The presence of water vapor in the exhaust gas accelerates the depletion of Cr from the valve material. The Ni-based alloy 31V is currently one material used in this application, however, its fatigue life has not been reported in the open literature. Aluminide coatings have demonstrated their ability to protect Ni-based alloys from high temperature corrosion, but their impact on the substrate mechanical properties needs to be assessed. This study evaluates the fatigue life of coated and uncoated samples of alloy 31V when tested at elevated temperature.

### 11:10 AM

#### A Study on Constitutive Model for Alloy IC10: *Hongjian Zhang*<sup>1</sup>; Weidong Wen<sup>1</sup>; Haitao Cui<sup>1</sup>; <sup>1</sup>Nanjing University of Aeronautics and Astronautics

Alloy IC10, a newly developed Ni3Al-based superalloy, is a typical multiphase alloy with about 65% volume fraction of Gama' phase. As IC10 exhibit unusual thermo-mechanical flow behaviors, a constitutive model was developed to describe the features of IC10. It is well known that the deformation mechanism of different phase is different. So, two assumes are proposed in this model: (i) the contributions to the yield and hardening of different phases are different; (ii) the yield and hardening is the effect of obstacles opposing the motion of mobile dislocations. The flow stress of IC10 can be calculated by building the relationships between the contributions and the evolution of the mobile dislocation density in different phases. The model is used to simulate flow behaviors of IC10 under different experiment conditions. The results show that it is valid.

### 11:30 AM

#### A Study on Constitutive Model for the Recrystallization Behaviors of Alloy IC10: *Hongjian Zhang*<sup>1</sup>; Weidong Wen<sup>1</sup>; Haitao Cui<sup>1</sup>; Ying Xu<sup>1</sup>; <sup>1</sup>Nanjing University of Aeronautics and Astronautics

IC10 is a newly developed Ni3Al-based superalloy, with its nominal composition (wt %): .07-0.12% C 11.5-12.5% Co 6.5-7.5% Cr 5.6-6.2% Al 4.8-5.2% W 1.0-2.0% Mo 6.5-7.5% Ta 1.3-1.7% Hf 0.01-0.02% B and Bal. Ni. As IC10 shows typical dynamic recrystallization behaviors above 1173K, a mechanism-based constitutive model was developed to describe the recrystallization features of IC10. It is well known that the deformation

is the results of the movement of mobile dislocations. In this paper, the recrystallization behaviors can be described by building evolution of mobile dislocations. The model is used to simulate recrystallization behaviors of IC10 under different experiment conditions. The results show that it is valid.

### Refractory Metals 2011: Tungsten-Based Alloys

*Sponsored by:* The Minerals, Metals and Materials Society, TMS Structural Materials Division, TMS: Refractory Metals Committee  
*Program Organizers:* Omer Dogan, DOE National Energy Technology Laboratory; Jim Ciulik, University of Texas, Austin

Wednesday AM  
March 2, 2011

Room: 19  
Location: San Diego Conv. Ctr

*Session Chairs:* Gary Rozak, H.C. Starck, Inc.; John Shields, Pentamet Associated, LLC

### 8:30 AM

#### New Refractory High-Entropy Alloys: *Oleg Senkov*<sup>1</sup>; Garth Wilks<sup>1</sup>; Daniel Miracle<sup>1</sup>; C. (Andrew) Chuang<sup>2</sup>; Peter Liaw<sup>2</sup>; <sup>1</sup>Air Force Research Laboratory; <sup>2</sup>University of Tennessee

Microstructure and properties of two refractory high entropy alloys,  $W_{25}Ta_{25}Mo_{25}Nb_{25}$  and  $W_{20}Ta_{20}Mo_{20}Nb_{20}V_{20}$ , are reported. The alloys were produced by vacuum arc-melting. Despite containing many constituents both alloys have a single-phase body-centered cubic (BCC) structure. The lattice parameters  $a = 3.2134(3) \text{ \AA}$  for the quaternary alloy and  $a = 3.1832(2) \text{ \AA}$  for the quinary alloy were determined with high-energy X-ray diffraction using a scattering vector length range from 0.7 to 20  $\text{\AA}^{-1}$ . The alloy density and Vickers microhardness were  $\rho = 13.75 \text{ g/cm}^3$  and  $H_v = 4455 \text{ MPa}$  for the  $W_{25}Ta_{25}Mo_{25}Nb_{25}$  alloy and  $\rho = 12.36 \text{ g/cm}^3$  and  $H_v = 5250 \text{ MPa}$  for the  $W_{20}Ta_{20}Mo_{20}Nb_{20}V_{20}$  alloy. The exceptional microhardness in these alloys is greater than that of the individual constituents, suggesting the operation of a solid-solution-like strengthening mechanism.

### 8:50 AM

#### Mechanical Properties of Refractory High-Entropy Alloys: *Oleg Senkov*<sup>1</sup>; Garth Wilks<sup>1</sup>; Daniel Miracle<sup>1</sup>; <sup>1</sup>Air Force Research Laboratory

Compression properties of two refractory high entropy alloys,  $W_{25}Ta_{25}Mo_{25}Nb_{25}$  and  $W_{20}Ta_{20}Mo_{20}Nb_{20}V_{20}$ , determined in the temperature range from 20°C to 1600°C, are reported. The alloys were produced by vacuum arc-melting and had a single phase bcc crystal structure. Compression test samples were 3 mm in diameter and 6 mm in length. The compression tests were conducted in vacuum using a constant strain rate of 0.001  $s^{-1}$ . The room temperature yield strength of the four-component alloy was 1050 MPa and it slowly decreased from 560 MPa to 405 MPa in the temperature range of 600 to 1600°C. The addition of V increased the yield strength by ~200 MPa in this temperature range. The compression strain of the alloys was ~5% at 20°C and above 20% in the temperature range of 600°C – 1600°C. The very high elevated temperature yield strength was suggested to be controlled by a solid-solution-like strengthening mechanism.

### 9:10 AM

#### Creep, Oxidation and Intermetallic Phase Formation: Assessing the High Temperature Performance of a Tungsten-Stainless Steel Hybrid: *Ben Reynhoud*<sup>1</sup>; Milo Kral<sup>1</sup>; <sup>1</sup>University of Canterbury

The purpose of this study was to investigate the feasibility of a hybrid material comprised of stainless steel reinforced with tungsten wire. The single greatest threat to the success of this composite is the volatile oxidation behaviour of tungsten. Various strategies to protect the tungsten from oxidation were investigated, while simultaneously assessing if there was sufficient ductility and durability to manage thermal cycling and mismatches in thermal expansion coefficients. Creep tests were conducted under isothermal and cyclic conditions at temperatures as high as 1100°C. SEM, EDS, EBSD and TEM were utilized to characterize the formation of cracks, voids, intermetallic phases and oxides.

9:30 AM

**WC(100) Surface and Co/WC(100) Interface: Spin-Polarized Ab Initio Study:** *Victor Zavodinsky*<sup>1</sup>; <sup>1</sup>Russian Academy of Sciences

Ab initio methods of the density functional theory and pseudopotentials were used to study the clean WC(100) surface and the formation of the Co/WC(100) interface. It has been found that the first Co monolayer repeats the geometry of the WC(100) surface with the same value of the lattice constant. The second Co monolayer also repeats the fcc-cubic WC geometry, however the distance between the first and second Co layers is rather less than the distance between planes in the WC cubic crystal. The binding energy grows but the separation energy decreases with transfer from 1ML to 2 ML cobalt covering. The density of states for the WC/Co system looks like the superposition of DOSes for bulk fcc-WC and Co layers. All Co layers are ferromagnetic, however, the magnetization does not influence essentially on their energetics and geometry.

9:50 AM Break

10:10 AM

**A Bimodal Distribution of W Grain Size in a Mechanically Alloyed Bulk Tungsten Heavy Alloy:** *Andrew Zeagler*<sup>1</sup>; Alex Aning<sup>2</sup>; <sup>1</sup>Virginia Polytechnic Institute and State University; <sup>2</sup> Virginia Polytechnic Institute and State University

A tungsten heavy alloy (W-4wt.%Ni) was mechanically alloyed by SPEX mill for various milling times. Cold isostatically pressed powders were solid-state sintered for 1 hour at 1200°C, yielding densities 90–95% of the theoretical value. Scanning electron microscopy revealed a bimodal distribution of W grain size; grains 1–3 μm in diameter are observed to surround regions of submicron grains. Subsequent sets of samples were mechanically alloyed with 2 and 6 wt.% Ni, and the effects of Ni content and milling time on the composition, grain size and volume fraction of each region were analyzed by microscopy and energy dispersive x-ray spectroscopy.

10:30 AM

**Spark Plasma Sintering of Tungsten-Rhenium Alloys for Very High Temperature Nuclear Reactor Applications:** *Cory Sparks*<sup>1</sup>; John Youngsman<sup>1</sup>; Jonathan Webb<sup>2</sup>; Steve Howe<sup>2</sup>; Indrajit Charit<sup>3</sup>; Megan Frary<sup>1</sup>; Darryl Butt<sup>1</sup>; <sup>1</sup>Boise State University; <sup>2</sup>Idaho National Laboratory; <sup>3</sup>University of Idaho

Very high temperature nuclear reactors require materials capable of withstanding elevated temperatures. Refractory alloys, such as tungsten-rhenium, have been identified as suitable materials due to their excellent high temperature capabilities, but difficulties associated with conventional processing techniques have limited their development. In this study, the tungsten-rhenium microstructure was optimized using alternative techniques such as high energy ball milling and spark plasma sintering, which can control initial particle size and subsequent grain growth. The microstructure and thermo-mechanical properties of the sintered samples were characterized and the results compared to traditionally consolidated alloy data. This comparison illustrates the advantages of using spark plasma sintering to process tungsten-rhenium alloys for very high temperature nuclear applications.

10:50 AM

**Physical and Mechanical Properties of Tungsten-Rhenium Alloys Produced Via Spark Plasma Sintering:** *Jonathan Webb*<sup>1</sup>; Indrajit Charit<sup>2</sup>; Cory Sparks<sup>3</sup>; Darryl Butt<sup>3</sup>; Megan Frary<sup>3</sup>; Mark Carroll<sup>4</sup>; <sup>1</sup>Center for Space Nuclear Research; <sup>2</sup>University of Idaho; <sup>3</sup>Boise State University; <sup>4</sup>Idaho National Laboratory

Future fast spectrum fission reactors used in both terrestrial and space applications will require materials with very high melting temperatures such as tungsten and tungsten-rhenium alloys. In order to support refractory alloy development for fission reactors, tungsten-rhenium alloys of varying rhenium compositions were mechanically alloyed via high energy ball milling technique. The mechanically alloyed tungsten-rhenium powders were then spark plasma sintered at 1600 K and 1700 K for 20 minutes to

produce W-Re alloys with high bulk density (92-97% of theoretical density). The specific heat, thermal conductivity, thermal expansion coefficient, and creep properties of these materials are tested at temperatures ranging from 300 K to 1300 K. The research is supported by the US Nuclear Energy University Program (NE-UP).

11:10 AM

**Characterization and Sintering of Open-Cell Ceramic Foams Infiltrated with Tungsten Powder:** *Eric Faierson*<sup>1</sup>; Kathryn Logan<sup>1</sup>; <sup>1</sup>Virginia Polytechnic Institute and State University

Extreme environments require materials that retain adequate mechanical properties at elevated temperatures, and in other hostile conditions such as radiation. Tungsten has a high melting point (3422° C), and retains good mechanical properties at elevated temperatures. This study investigates the use of open-cell ceramic foams to provide a continuous network of reinforcement in a composite material. Silicon carbide and tantalum carbide foams with reticulated vitreous carbon (RVC) cores were infiltrated with tungsten powder by applying vibration, vacuum, and/or isostatic pressure. The infiltrated foam was densified through vacuum sintering. Microstructural analysis was conducted on the foam prior to infiltration and after densification. Mechanical tests were conducted to determine the influence of foam pore and ligament size on the strength and fracture behavior of the foams. Measurements of neutron transmittance through the foam were also conducted.

11:30 AM

**Comparative Study of Grain Boundary Impurity Effects in Tantalum and Tungsten Based on First-Principles Calculations:** *Zhiliang Pan*<sup>1</sup>; Laszlo Kecskes<sup>2</sup>; *Qiuning Wei*<sup>1</sup>; <sup>1</sup>University of North Carolina Charlotte; <sup>2</sup>U. S. Army Research Laboratory

We used density functional theory to systematically calculate the separation energy of symmetric tilt S3(111) GBs of tungsten and tantalum, with and without impurity atoms (H, B, C, N, O, F, Al, Si, P, S, Cl, Fe). We found that although the effects of various interstitial impurity atoms on the specific GB are different, the influence of certain impurity atoms on the GBs is similar. Boron and carbon both enhance the GBs, whereas oxygen, sulfur and silicon etc, weaken the GBs. More importantly, despite the existence of interstitial impurities, GB separation energy of tungsten is always higher than that of tantalum given similar atomic configurations. These findings suggest that it is not yet convincing to attribute the poor ductility of tungsten only to the decreased GB separation energy. We need to consider the competition between brittle deformation mechanisms such as GB separation and plastic deformation mechanisms such as dislocation activities.

11:50 AM

**Atomistic Modelling of Complex Phases in Refractory Alloys:** *Thomas Hammerschmidt*<sup>1</sup>; Bernhard Seiser<sup>2</sup>; Ralf Drautz<sup>1</sup>; David Pettifor<sup>2</sup>; <sup>1</sup>ICAMS Ruhr-Universität Bochum; <sup>2</sup>University of Oxford

The group of topologically close-packed (TCP) phases plays an important role in modern alloys and steels. While their precipitation in single-crystal Ni-based superalloys has a detrimental effect on the mechanical properties, the TCP phases are desirable in precipitation-hardened steels. The formation of the TCP phases is attributed to high local concentrations of refractory elements. We discuss that the trend of the structural stability of TCP phases in refractory elements is captured by a simple tight-binding model. We carried out extensive density-functional theory calculations of the tcp phases A15, C14, C15, C36, mu, sigma, and chi in binary refractory alloys and summarize the influence of band-filling and atomic size on TCP phase stability.



## Shape Casting IV: Light Metals Division Symposium in Honor of Prof. John T. Berry: Properties

*Sponsored by:* The Minerals, Metals and Materials Society, TMS Light Metals Division, TMS: Aluminum Processing Committee, TMS: Solidification Committee

*Program Organizers:* Murat Tiryakioglu, University of North Florida; Paul Crepeau, General Motors Corporation; John Campbell, University of Birmingham

Wednesday AM                      Room: 15B  
March 2, 2011                        Location: San Diego Conv. Ctr

*Session Chairs:* Glenn Byczynski, Nematik Europe; Sergio Felicelli, Mississippi State Univ

### 8:30 AM Introductory Comments

#### 8:40 AM

**On Faceted Fatigue Fracture in Castings:** *Murat Tiryakioglu*<sup>1</sup>; John Campbell<sup>2</sup>; <sup>1</sup>University of North Florida; <sup>2</sup>University of Birmingham

Facets are intriguing features observed on the fracture surfaces in some high-cycle fatigue specimens. There exist several hypotheses on their formation and how they contribute to the fatigue failure. An extensive literature survey on faceted fatigue fracture in castings is presented in this study. A new hypothesis is proposed based on the experimental observations presented in the literature, which states that facets form as a result of casting defects. The implications on the true fatigue life potential of castings are discussed in the paper.

#### 9:00 AM

**Effect of Holding Time before Solidification on Double-Oxide Film Defects and Mechanical Properties of Aluminium Alloys:** Mahmoud El-Sayed<sup>1</sup>; Hanadi Salem<sup>2</sup>; Abdel-Razik Kandeil<sup>1</sup>; *William Griffiths*<sup>3</sup>; <sup>1</sup>Arab Academy for Science, Technology & Maritime Transport; <sup>2</sup>American University Cairo; <sup>3</sup>University of Birmingham

Double oxide films (bifilms) have been held responsible for the variability in the mechanical properties of aluminium castings. It has been suggested that the air entrapped inside the bifilm reacts with the surrounding melt leading to its consumption, which might improve the mechanical properties of the castings. In this work, the effect of the holding time of the melt before solidification on the entrained double oxide films for different aluminium alloys was investigated. The Weibull moduli of the plate castings were determined under tensile conditions, and their fracture surfaces examined for evidence of oxide films. The results suggested the occurrence of two competing mechanisms during the holding treatment. The consumption of air inside the bifilms due to reaction with the surrounding molten metal improves the mechanical properties, but this may be followed by hydrogen passing into the bifilms, which has a deleterious effect on properties.

#### 9:20 AM

**Weibull Analysis of Thin A356 Plates Cast with an Electromagnetic Pump Green Sand Process:** *Ratessia Lett*<sup>1</sup>; Sergio Felicelli<sup>1</sup>; John Berry<sup>1</sup>; Rafael Cuesta<sup>2</sup>; Jose Maroto<sup>2</sup>; Ruth San Jose<sup>2</sup>; <sup>1</sup>Mississippi State University; <sup>2</sup>CIDAUT

Four multiple gated configurations were utilized with an electromagnetic pump green sand process in order to produce quiescently-filled thin A356 plates that minimize melt surface damage during casting and defect formation during solidification. Eight cast plates were examined, two from each gating design. The method of four point bend testing was used to obtain information about the mechanical properties of the castings, as this method produces a uniform distribution of the bending stress within the central span. From these results, a Weibull statistical analysis was performed in order to quantify specimen failure rate for each of the configurations. The specimen fracture surfaces were then examined using Scanning Electron Microscopy in order to locate possible locations of failure initiation as well as the presence of

oxide bifilms. This project is funded by the National Science Foundation (NSF) under the International Research and Education in Engineering (IREE) program.

#### 9:40 AM

**Guidelines for 2-Parameter Weibull Analysis for Castings:** *Murat Tiryakioglu*<sup>1</sup>; <sup>1</sup>University of North Florida

Mechanical properties of castings have been analyzed generally by using the two-parameter Weibull distribution for more than a decade. The statistics of this Weibull analysis has received much attention recently. These recent results will be summarized and a step-by-step procedure will be introduced to conduct a proper Weibull analysis for castings. The use of the procedure will be demonstrated on actual datasets.

#### 10:00 AM

**Melt Cleanliness, Hydrogen Content and Tensile Properties of A356:** *Derya Dispinar*<sup>1</sup>; Arne Nordmark<sup>1</sup>; Freddy Syvertsen<sup>1</sup>; <sup>1</sup>SINTEF

Degassing of aluminium melts is one of the most important stages in a casting operation. Main reason for this treatment is the removal of hydrogen from the melt, and thereby the ultimate goal is the achievement of a pore-free casting. However, it was shown that the interaction between the bifilms and the hydrogen plays a significant role on pore formation. Therefore, series of degassing experiments were carried out with commercially available A356. Two melts were prepared and one melt was upgassed gradually and the other was degassed gradually. Tensile samples were collected and bifilm index measurements were compared at each treatment sequences. Weibull analysis was used and it was found that the turbulence and vortex (increase in bifilm index) during rotary degassing caused an increase in the scatter irrespective of the hydrogen content.

#### 10:20 AM Break

#### 10:40 AM

**The Origin of Griffith Cracks:** *John Campbell*<sup>1</sup>; <sup>1</sup>University of Birmingham

The presence any pre-existing Griffith crack or a pore is not necessarily to be expected in solidified metals as a result of the extremely high interatomic forces. It seems likely that pores and cracks may not be created intrinsically by the atomic mechanisms involved in the formation of a solid by solidification from liquid, or condensation from vapor phases nor, probably, by mechanisms of plastic deformation. It is proposed here that initiation sites for pores and cracks for most, if not all failures of metals, can only be introduced into metals via extrinsic (entrainment) mechanisms resulting from production processes, particularly melting and casting, but also spraying and powder metallurgy processes. It seems probable that only entrainment processes can create unbonded interfaces that can explain microstructures containing cracked (apparently 'brittle') intermetallics and decohered phases, and the initiation of tensile fracture and fatigue.

#### 11:00 AM

**The Use of the Weibull Statistical Method to Assess the Reliability of Cast Aluminium Engine Blocks made from Different Casting Processes:** *Glenn Byczynski*<sup>1</sup>; Robert Mackay<sup>1</sup>; <sup>1</sup>Nematik Canada

The use of aluminum cast engine blocks has grown considerably within the automotive industry due to their lighter weight when compared to traditional materials such as cast iron. In this investigation, three aluminum cast engine block processes: High Pressure Die Cast, Precision Sand Cast Process-Zircon and Precision Sand Cast Process-Silica/Chill are evaluated in terms of reliability (Weibull Plots) of the mechanical strength determined from tensile test samples extracted from the bulkhead region. Metallographic analysis was performed on the tensile test samples to provide interpretative feedback on the statistical analysis of the mechanical test results.

#### 11:20 AM

**Ultra-High Strength Sand Castings from Aluminum Alloy 7042:** O. Senkov<sup>1</sup>; *Alan Druschitz*<sup>2</sup>; S. Senkova<sup>1</sup>; K. Kendig<sup>1</sup>; J. Griffin<sup>2</sup>; <sup>1</sup>Air Force Research Laboratory; <sup>2</sup>University of Alabama Birmingham

Ultra-high strength, aluminum alloy castings with very good ductility have been successfully produced using the combination of chemically

bonded sand molds, an Al-Zn-Mg-Cu-Sc alloy (aluminum alloy 7042) and solidification under pressure. In the T6 condition, castings had the following mechanical properties: 585-595 MPa ultimate tensile strength, 505-520 MPa yield strength and 5-10% elongation. HIP'ing slightly increased the tensile strength (to 590-610 MPa) and increased the elongation (to 8-12%). In the T4 condition, castings had the following mechanical properties: 490-540 MPa ultimate tensile strength, 340-360 MPa yield strength and 10-13% elongation.

#### 11:40 AM

##### **Relationship between Structures and Properties of Al-Cu Alloys:** *Alicia Ares*<sup>1</sup>; *Liliana Gassa*<sup>1</sup>; *Carlos Schvezov*<sup>1</sup>; <sup>1</sup>CONICET

The objective of the present research consist on studying the type of structure (columnar, equiaxed or with columnar to equiaxed transition, CET) using parameters of the solidification process and electrochemical parameters in Al, Cu and Al-Cu alloys with different concentrations. In order to obtain columnar, equiaxed and CET structures, the alloys were directionally solidified upwards in an experimental set up with a set of thermocouples in the samples which permit to determine the time dependent profiles during the process. From these profiles and the location of thermocouples it was possible to calculate the cooling rates, growth velocities and temperature gradients along the samples. The electrochemical studies of the samples were realized by using an electrochemical impedance spectroscopy (EIS) technique and potentiodynamic polarization curves immersed in 3% NaCl solution at room temperature. It was found a higher susceptibility to the corrosion as the Cu content increased in the alloy.

#### 12:00 PM

##### **Microstructure Characterization of Magnesium Control Arm Castings:** *Liang Wang*<sup>1</sup>; *Ratessiea Lett*<sup>2</sup>; *Sergio Felicelli*<sup>2</sup>; *John Berry*<sup>2</sup>; <sup>1</sup>Mississippi State University; <sup>2</sup>Mississippi State University

Microstructural and mechanical property data were generated from several control arm castings of Mg alloy AZ91 produced for the High Integrity Magnesium Automotive Components (HIMAC) project. The castings were made by four different processes: squeeze cast, low pressure permanent mold, T-Mag, and Ablation. Ten control arms were examined from each of the four casting groups. The microstructure, grain size, pore fraction, and pore size were measured with optical microscopy and image analyzer. Different types of defects are identified to evaluate the four casting processes. In order to explore the presence of oxide films, a series of four-point bend (FPB) tests were performed, and the maximum load was measured. The mechanical properties of the castings were quantitatively evaluated for reliability using a two-parameter Weibull distribution function. A detailed metallographic analysis of the fracture surfaces of FPB samples was performed using SEM. This project was sponsored by the United States Automotive Materials Partnership (USAMP).

## Size Effects in Mechanical Behavior: Indentation Size Effects

*Sponsored by:* The Minerals, Metals and Materials Society, Not Applicable, TMS: Nanomechanical Materials Behavior Committee  
*Program Organizers:* Erica Lilleodden, GKSS Research Center; Amit Misra, Los Alamos National Laboratory; Thomas Buchheit, Sandia National Laboratories; Andrew Minor, UC Berkeley & LBL

Wednesday AM  
March 2, 2011

Room: 2  
Location: San Diego Conv. Ctr

*Session Chairs:* Erica Lilleodden, GKSS Research Center; Khalid Hattar, Sandia National Laboratories

#### 8:30 AM

##### **Stress-Strain Responses from Spherical Nano-Indentation and Micro-Pillar Compression Experiments: A Comparative Study:** *Siddhartha Pathak*<sup>1</sup>; *Rejin Koodakal*<sup>2</sup>; *Surya Kalidindi*<sup>3</sup>; *Johann Michler*<sup>2</sup>; <sup>1</sup>California Institute of Technology; <sup>2</sup>EMPA - Swiss Federal Laboratories for Materials Testing and Research; <sup>3</sup>Drexel University

Spherical nano-indentation and micro-pillar compression experiments were conducted on individual grains (grain size ~mm) of varying orientations in two sets of Fe-3%Si (BCC) polycrystalline samples of different deformation levels - as-cast and 30% deformed. The local indentation loading modulus and yield strength values, as well as certain aspects of post-yield strain hardening behavior, were obtained by transforming the raw load-displacement data obtained using spherical indenters of two different radii (1 and 13.5  $\mu\text{m}$ ) into indentation stress-strain curves. Micro-pillars of varying diameters were FIB machined on the same grains and compressed in-situ SEM to identify their uniaxial elastic modulus, yield strength and strain hardening behavior. The advantages and limitations of each technique in capturing the effects of lattice orientation and the level of plastic deformation in their respective stress-strain responses are discussed. An analysis on the similarities, as well as individual insights from each of the two techniques, is also presented.

#### 8:50 AM

##### **Nanoscale Behavior of Ta Single Crystals – Temperature and Orientation Dependence:** *Zhi-Chao Duan*<sup>1</sup>; *Juergen Biener*<sup>2</sup>; *Monika Biener*<sup>2</sup>; *Andrea Hodge*<sup>1</sup>; <sup>1</sup>University of Southern California; <sup>2</sup>Lawrence Livermore National Laboratory

The study of Ta at elevated temperatures presents new insights into the nanoscale flow behavior of BCC materials. Here we will report on the deformation behavior of BCC single crystals Ta (100), (111) and (110) studied by a combination of nanoindentation and atomic force microscopy. Nanoindentation at temperatures ranging from 25 – 200°C was used to study the plastic flow behavior of Ta. For all three crystal orientations the onset of plasticity is marked by a discontinuity in the load displacement curve, which is most pronounced on the (100) surface. We will discuss the origin of the “pop-in” event, as well as the atomistic mechanism of the deformation process during nanoindentation. Most notably, we find that the shape of the load displacement curves changes with increasing temperature and multiple pop-ins separated by elastic reloading segments were observed at 200°C.

#### 9:10 AM

##### **The Effect of Point Defects on the Nucleation Plasticity in Small Volumes:** *David Bahr*<sup>1</sup>; *Veronica Perez*<sup>1</sup>; *Iman Salehinia*<sup>1</sup>; *Marc Weber*<sup>1</sup>; <sup>1</sup>Washington State University

In small structures, the chances that relatively defect free volumes control the mechanical performance of materials increases. Nanoindentation has been used to measure the onset of plasticity in Ni single crystals with differing point defect (vacancy and hydrogen impurities) concentrations. The effect of increased vacancy concentration is to statistically lower the yield point, similar to the effects of increasing sampled volume by changing the probe tip radius. Hydrogen also appears to slightly lower the yield point in these materials. These results are compared to EAM simulations which

show similar trends with non-equilibrium vacancy concentrations imposed in the solid. Similar results are found for BCC metals. The balance between softening the yield point, but hardening subsequent flow will be discussed.

#### 9:30 AM

**Length Scale Effect on the Mechanical Properties of Irradiated Metals:** *Khalid Hattar*<sup>1</sup>; Thomas Buchheit<sup>1</sup>; Brad Boyce<sup>1</sup>; Luke Brewer<sup>2</sup>; <sup>1</sup>Sandia National Laboratories; <sup>2</sup>Naval Postgraduate School

Length scale effect on mechanical properties is important in the development of a validation technique to simulate end of life irradiation damage in metals relevant to nuclear reactors. This technique utilizes heavy-ion irradiation to generate extensive damage, but is limited in volume. Nanoindentation and micropillar compression is implemented to elucidate the change in properties as a function of irradiated microstructure produced. The nanoindentation work investigates the geometric effect through the comparison of pyramidal and spherical indentations. Finite element modeling of various tip geometries and implantation conditions provides assistance in distinguishing between a perceived increased hardness of the irradiated region and the classic indentation size effect. The effect of length scale testing is also observed in the mechanical response of irradiated micropillars. Both measurements are susceptible to geometrically driven size effects and methods to distinguish between geometrical influences and radiation damage on will be discussed.

#### 9:50 AM

**Plastic Flattening of a Sinusoidal Surface:** Fengwei Sun<sup>1</sup>; Erik Van der Giessen<sup>2</sup>; *Lucia Nicola*<sup>1</sup>; <sup>1</sup>Delft University of Technology; <sup>2</sup>University of Groningen

When two rough surfaces are pressed into contact, plastic deformation occurs at rather small loads. During further loading, the forces between contacting asperities, as well as the true contact area, evolve in a non trivial way. This evolution is not properly calculated by the current statistical contact models, like Persson's and Mueser's, since in those models the plastic behavior of the asperities is neglected. Other studies focus instead on an accurate description of the material behavior, but are limited to a single deforming contact. The aim of this work is to extend those studies to a collection of asperities. The numerical technique used is discrete dislocation plasticity, which has proven successful to capture size dependent plastic behavior of isolated contacts, as well as arrays of flat contacts. The description of the surface is kept simple; the roughness is represented by a sinusoidal wave of varying amplitude and period.

#### 10:10 AM Break

#### 10:40 AM Invited

**Statistical Effects in Nanoindentation and Nanopillar Compression:** *James Morris*<sup>1</sup>; Hongbin Bei<sup>1</sup>; Easo George<sup>1</sup>; <sup>1</sup>Oak Ridge National Laboratory

Experimental probes such as nanoindentation, or nanopillar compression, only stress a small volume. When this highly stressed region is comparable to the density of defects, the number and arrangement of defects in the region is highly variable, and the response of the material is similarly stochastic. Simple statistical models are formulated to describe these distributions of behavior. In the case of nanoindentation, close agreement between the model and experiment is shown using only the defect density and a single defect strength. Scaling behavior of the results is observed, breaking down when pop-in is primarily determined by the theoretical strength of the material. For nanopillar deformation, the distribution of defect strengths becomes important. Thus, experiments on different geometries may provide complementary information on both defect densities and defect strength distribution. This research was sponsored by the Division of Materials Sciences and Engineering, U.S. Department of Energy, Office of Basic Energy Sciences.

#### 11:10 AM

**Size Effects in Yield Instabilities:** *William Gerberich*<sup>1</sup>; <sup>1</sup>University of Minnesota

Plastic instability in indentation has been studied via decades of research. Load control produces displacement excursions, and displacement control

produces load drops. The magnitude of the plastic instability, e.g. the displacement jump to arrest, depends on the driving force when indenting single crystals. But does it also depend on the indenter tip shape or contact radius? Similarly, the magnitude of the plastic instability occurring in the compression of nanopillars also depends on the driving force. But does this also depend on size through the pillar diameter? The role of back stress, if any, is explored to demonstrate differences and similarities between indentation and pillar compression. Size effects aware demonstrate in FCC, BCC, and HCP systems. Generally, increasing size of indentation contact diameters or compressed pillar diameters produce increased instabilities. Caveats associated with the stochastic nature of nucleation sites are emphasized as well.

#### 11:30 AM

**Time-Dependent Plasticity in the Small-Scale: Influence of Initial Strain:** Byung-Gil Yoo<sup>1</sup>; In-Chul Choi<sup>1</sup>; Kyu-Sik Kim<sup>1</sup>; Jun-Hak Oh<sup>1</sup>; Yong-Jae Kim<sup>1</sup>; *Jae-il Jang*<sup>1</sup>; <sup>1</sup>Hanyang University

Recently, many nanomechanical studies have reported that the mechanical responses of materials can be significantly dependent on both the size and time of deformation. One more interesting finding is that in some materials, e.g. nanocrystalline materials and amorphous alloys, the time-dependent deformation (often simply referred to as "creep") can occur even at room temperature. Analyzing the creep in the small-scale can be valuable not only for solving scientific curiosity, but also for obtaining practical engineering information, e.g. life-time and reliability of BMG-based MEMS. In this talk we would like to report our recent observations that the initial strain at the onset of creep does seriously affect the small-scale time-dependent deformation in a somewhat interesting way.

## Surfaces and Heterostructures at Nano- or Micro-Scale and Their Characterization, Properties, and Applications: Energy and Catalysis Technologies II - and - Biological Applications

*Sponsored by:* TMS Electronic, Magnetic, and Photonic Materials Division, TMS Materials Processing and Manufacturing Division, TMS: Nanomaterials Committee, TMS: Surface Engineering Committee

*Program Organizers:* Nitin Chopra, The University of Alabama; Ramana Reddy, The University of Alabama; Jiyoun Kim, Univ of Texas; Arvind Agarwal, Florida International Univ; Sandip Harimkar, Oklahoma State University

Wednesday AM  
March 2, 2011

Room: 31B  
Location: San Diego Conv. Ctr

*Session Chairs:* Ramana Reddy, The University of Alabama; Arvind Agarwal, Florida International University; Nitin Chopra, The University of Alabama

#### 8:30 AM

**Silicon-Coated Carbon Nanotube Anodes for Lithium-Ion Batteries:** *Michelle Gaines*<sup>1</sup>; Samuel Karpowicz<sup>1</sup>; Deborah Williams<sup>2</sup>; <sup>1</sup>Georgia Institute of Technology; <sup>2</sup>DM Therrell School for Technology, Engineering, Math, and Science

Current rechargeable lithium-ion batteries contain graphite anodes. Although adequate for powering small, portable electronics, graphite anodes don't possess enough storage capacity to power larger devices. Silicon has a much higher storage capacity, providing the potential for much more energy storage during charging. The only challenge with using silicon lies in its resulting pulverized structure after repeated charge/discharge cycles. In this work, multi-walled carbon nanotubes (MWCNT) were used as mechanical reinforcements for amorphous silicon. MWCNT were grown using thermal CVD on copper foil. Two catalyst systems were compared: 1) Iron(III) p-toluenesulfonate, reduced to form iron nanoparticles on the surface and 2) metal tri- and bi- diffusion layers with an iron coating on top. Amorphous



silicon was deposited on top of the carbon nanotubes using plasma enhanced chemical vapor deposition. Full and half cells were constructed from commercially available cathodes, and electrical impedance and galvanic cycling were performed.

**8:45 AM**

**Fundamental Studies on Morphological Evolution of Multi-Functional Carbon Nanotubes-Nickel/Nickel Oxide Core/Shell Nanoparticle Heterostructures:** Wenwu Shi<sup>1</sup>; Anshuman Bansal<sup>2</sup>; Nitin Chopra<sup>1</sup>; <sup>1</sup>The University of Alabama; <sup>2</sup>Alabama School of Fine Arts

A simple and facile method was utilized to fabricate carbon nanotubes-nickel/nickel oxide core-shell nanoparticles (CNC) heterostructures. Nickel nanoparticles from thermal decomposition of nickel salt were nucleated on well-dispersed carbon nanotubes to form heterostructures. Various chemical synthesis parameters, post-fabrication processing, and carbon nanotube surface chemistries were studied to manipulate nanoparticle coverage density, size, shape, oxide shell thickness, and magnetic properties. Alignment of these heterostructures on a large area substrate was also achieved. Such a patterning of heterostructures is of great importance for magnetic devices, supercapacitors, and 3-D nanoarchitectures.

**9:00 AM Break**

**9:10 AM Introductory Comments for Biological Applications**

**9:15 AM Invited**

**Cytokine Nanotechnology:** Venkat Sharma<sup>1</sup>; <sup>1</sup>University of West Alabama

Therapeutic usage of cytokines has been widely established in the medical field. Cytokines are a group of proteins that elicit their biological effects similar to hormones and serve as intercellular messenger molecules of the immune system. Therefore, cytokines and their receptors are increasingly considered as therapeutic drug targets. Although usage of cytokines is theoretically ideal, an obstacle in the way of treatment is due to its characteristics; therefore, actual treatment with cytokines needs more improvement over its delivery system and prolongation of cytokine life span. Combination of cytokine to nanotechnology techniques might accomplish what would otherwise be impossible in drug delivery. By manipulating nanoparticle surface characteristics, it is theorized that cytokines can efficiently be delivered to the target place. In this presentation, I will survey the variety of applications of formulating therapeutic agents with nanotechnology and further provide a survey of the actual effect of nanoparticles on cytokine secretion.

**9:45 AM Invited**

**Surface Modification of Microneedles for Antimicrobial Activity:** Roger Narayan<sup>1</sup>; Shaun Gittard<sup>1</sup>; Boris Chichkov<sup>2</sup>; Aleksandr Ovsianikov<sup>2</sup>; Shane Stafstien<sup>3</sup>; Bret Chisholm<sup>3</sup>; <sup>1</sup>University of North Carolina & North Carolina State University; <sup>2</sup>Laser Zentrum Hannover; <sup>3</sup>North Dakota State University

Microneedles with antimicrobial properties may be prepared by coating microneedles with materials that exhibit antimicrobial activity. Silver exhibits broad-spectrum activity against bacteria; this activity is attributed to disruption of electron transport, as well as interruption of deoxyribonucleic acid replication. In this study, silver thin films were deposited on the surfaces of polymer microneedles at room temperature using pulsed laser deposition. We fabricated silver-coated microneedles using a two-step process, which involved two photon polymerization-micromolding and pulsed laser deposition. In the first step, solid microneedle arrays were prepared using organically-modified ceramic material by means of two photon polymerization-micromolding. In the second step, pulsed laser deposition was used to deposit silver thin films on these microneedle arrays. An absence of *S. aureus* growth was noted beneath the silver-coated microneedle array. In addition, inhibited growth was observed in the region surrounding the microneedle array, which suggested that silver was released into the agar.

**10:15 AM Invited**

**Functionalized Quantum Dots for Molecular Profiling of Cancer Biomarkers:** Peter Searson<sup>1</sup>; <sup>1</sup>Johns Hopkins University

Quantum dots have received considerable attention for applications in biomedicine, particularly in imaging and sensing. In contrast, cellular

targeting using quantum dots has remained challenging. Quantum dots exhibit high quantum yield, narrow emission peak, broad excitation range, and are resistant to photobleaching. We report on different surface modification schemes and show how surface modification is key to producing stable suspensions of quantum dots in water. We show results for profiling of cancer biomarkers using quantum dots conjugated with targeting antibodies.

**10:45 AM Invited**

**Autonomous Nano/Microscale Motion through Catalysis:** Ayusman Sen<sup>1</sup>; <sup>1</sup>Pennsylvania State University

Self-powered nano and microscale moving systems are currently the subject of intense interest due in part to their potential applications in nanomachinery, nanoscale assembly, robotics, fluidics, and chemical/biochemical sensing. We will demonstrate that one can build nanomotors that mimic biological motors by using catalytic reactions to create forces based on chemical gradients. These motors are autonomous in that they do not require external fields as energy sources. Instead, the input energy is supplied locally and chemically. By appropriate design, the chemical gradients can be translated into anisotropic body and/or surface forces. Depending on the shape of the object and the placement of the catalyst, different kinds of motion can be achieved. The resulting nanomotors can be tethered or coupled to other objects to act as the "engines" of nanoscale assemblies. It is also possible to control the movement of nanomotors by: (a) chemotaxis, (b) phototaxis, and (c) magnetic steering.

**11:15 AM**

**Precipitation and Crystallization of Hydroxyapatite on Boron Nitride Nanotubes Immersed in Simulated Body Fluid:** Debrupa Lahiri<sup>1</sup>; Virendra Singh<sup>2</sup>; Anup Keshri<sup>1</sup>; Sudipta Seal<sup>2</sup>; Arvind Agarwal<sup>1</sup>; <sup>1</sup>Florida International University; <sup>2</sup>University of Central Florida

Success of Boron Nitride Nanotubes (BNNT) as reinforcement in orthopedic implant/scaffold or structural mimic of collagen in bone repair depends on mineralization and integration of hydroxyapatite (HA) on BNNT surface to form an integrated bone-like structure. Present study investigates precipitation and crystallization-ability of HA on BNNT, immersed in simulated body fluid (SBF) for 7, 14 and 28 days. Presence of phosphate peak of HA in Raman Spectrum proves the formation of HA precipitate on BNNTs immersed in SBF. The SEM and EDS results reveal linear increase in calcium content on BNNT between 7 -28 days. The quantitative EDS results suggest an initial threshold period for starting the precipitation. HRTEM study shows amorphous HA covering the BNNT surface initially (7 days), which forms well defined crystal structure with increasing time (28 days). Analysis of lattice images at interface provides further insight into the crystallographic arrangement of HA crystals on BNNT surface.

**11:35 AM**

**Synthesis of Magnetic and Fluorescent Bifunctional Nanoparticles:** Yaolin Xu<sup>1</sup>; Soubantika Palchoudhury<sup>1</sup>; Yuping Bao<sup>1</sup>; <sup>1</sup>The University of Alabama

Magnetic nanoparticles (MNP) have significantly advanced cancer treatments through targeted drug delivery and localized therapy. MNPs further make simultaneous therapy and diagnosis possible as magnetic resonant imaging (MRI) contrast agents. Unfortunately, the studies of simultaneous therapy and diagnosis of MNPs are limited by the expensive MRI equipment. Currently, fluorescence imaging remains the primary choice for bio-imaging because of its high sensitivity. Here, we reported magnetic-fluorescent integrated nanoparticles using iron oxide as the magnetic component and metallic nanoclusters as the fluorescent component. Iron oxide nanoparticles were synthesized using a modified co-precipitation method by introducing a capping molecule during synthesis. Subsequently, these iron oxide nanoparticles were used as seeds for the synthesis of Ag metallic nanoclusters. Around 10 nm iron oxide nanoparticles were successfully produced, followed by attachment of fluorescent clusters with a broad emission in the range of 600 -650 nm. This work is funded by NSF-DMR 0907204

11:50 AM

**Synthesis of Multiple Platinum Attached Iron Oxide Nanoparticles:** *Soubantika Palchoudhury*<sup>1</sup>; Yaolin Xu<sup>1</sup>; Yuping Bao<sup>1</sup>; <sup>1</sup>The University of Alabama

We report the synthesis and detailed structural analysis of multiple Pt attached iron oxide nanoparticles (NPs). Two different routes were carried out to obtain water soluble, Pt attached iron oxide NPs. First, Pt NPs were attached onto iron oxide NP surfaces in organic solvent followed by a phase transfer process; second, a surfactant exchange process was performed first, prior to the deposition of Pt NPs. The presence of Pt NPs is evident based on the contrast in the transmission electron microscopy images. High-angle annular dark field (HAADF) and energy dispersive x-ray (EDX) analysis were further performed to confirm the presence of Pt.

12:05 PM

**Colloid-Chemical Nanoprocesses and Nanotechnologies on the Basis of Oxyhydrate Systems of Rare-Earth Elements:** *Tatiana Prolubnikova*<sup>1</sup>; Yuri Sucharev<sup>1</sup>; Tatiana Ukolkina<sup>1</sup>; Konstantin Nosov<sup>1</sup>; <sup>1</sup>Chelyabinsk State University

Research of oxyhydrate gel systems of rare-earth elements showed that the processes of structure formation are nonlinear dynamic processes. Oxyhydrates have emission-wave duality behavior. Due to this fact, you can discover and understand colloid-chemical phenomena occurring in the gels. It was researched pulsating spontaneous splashes of oxyhydrate gel's nanocurrent. It was proved antimicrobial activity of these currents in a wide range of microorganisms. The reason for current ripple is self-organization gel over time. Research of rheological properties of oxyhydrates from the position Nonlinear Dynamics discovered anomaly viscosity and the possibility of establishing nanomicroscopy for monitoring structural changes during ageing. We have a digital phase molecular microscope to examine colloid chemical state of oxyhydrate systems based on stochastic coherent resonance. Nanodimension of colloid oxyhydrate structures proved studies of their optical density. Consecutive kinetic experiments give maximum size of nanocluster, which are registered in the system at different wavelengths.

12:20 PM **Concluding Comments**

### 2011 Functional and Structural Nanomaterials: Fabrication, Properties, Applications and Implications: Characterizations of Nanomaterials and Session in Honor of Prof. T. Kang

*Sponsored by:* The Minerals, Metals and Materials Society, TMS Electronic, Magnetic, and Photonic Materials Division, TMS: Nanomaterials Committee

*Program Organizers:* Jiyoung Kim, Univ of Texas; David Stollberg, Georgia Tech Research Institute; Seong Jin Koh, University of Texas at Arlington; Nitin Chopra, The University of Alabama; Suveen Mathaudhu, U.S. Army Research Office

Wednesday PM  
March 2, 2011

Room: 8  
Location: San Diego Conv. Ctr

*Session Chairs:* Jiyoung Kim, University of Texas at Dallas; Seung Kang, Qualcomm

2:00 PM **Introductory Comments**

2:05 PM **Invited**

**Tailored Fabrication and Characterization of Nanostructures:** *Moon Kim*<sup>1</sup>; <sup>1</sup>University of Texas at Dallas

As the scaling of silicon integrated circuits continues, the future of electronics will rely on both top-down and bottom-up approaches. In addressing both of these approaches, nanoscale fabrication, manipulation, and characterization become ever more important. The electron beam lithography approach for nanowire fabrication provides a top-down method that allows us to control their orientation and size. In the same manner, future

nanowires can be fabricated from different materials such as Ge and GaAs. This will allow us to explore these materials' properties when scaled down to the quantum regime. This talk will present our recent research efforts on several key electronic material systems of current and future interests including lithographically defined Si nanowires and nanodots and in-situ manipulation and characterization of graphene sheets and functional nanostructured devices. Single CMOS and HEMT transistors were also characterized by in-situ TEM with nanometer scale spatial resolution.

2:35 PM

**Scanning Tunneling Microscopic Characterization of Electron Transport in Pi-Conjugated Organic Self-Assembled Monolayer:** *Govind Mallick*<sup>1</sup>; Shashi Karna<sup>1</sup>; <sup>1</sup>Army Research Laboratory

Surface topology and electron transport properties of self-assembled monolayer (SAM) of an engineered molecule 4,4'-[1,4-phenylenebis(methylidynenitro)]bisbenzenethiol (PMNBT), 1-dodecanethiol (DDT) and 1-hexadecanethiol (hDT) adsorbed on Au substrates have been investigated by scanning tunneling microscopy (STM) under ambient condition. The estimated differential conductance,  $(dI/dV)_V=0.75 = 123.91nS$  for PMNBT, is over an order of magnitude larger than the corresponding value (7.15nS) for dDT and two order of magnitude larger (0.078nS) than hDT. The tunneling current (I) as a function of the applied bias (V) between STM tip and SAM of PMNBT exhibits asymmetric behavior. A combination of electronic and geometrical effects in the molecule and at the molecule-metal interface is proposed to be responsible for the observed asymmetric I-V characteristics. The increased conductance in PMNBT is also explained in terms of its nearest available electronic states.

2:50 PM

**Tunneling Spectroscopy with Near Zero Line-Width Broadening:** Ramkumar Subramanian<sup>1</sup>; *Pradeep Bhadrachalam*<sup>1</sup>; Taejoo Park<sup>2</sup>; Jiyoung Kim<sup>2</sup>; Seong Jin Koh<sup>1</sup>; <sup>1</sup>University of Texas at Arlington; <sup>2</sup>University of Texas at Dallas

For practical application of nanoparticles/quantum dots in the field of energy harvesting, bio-labeling and treatment, in opto-electronic devices and in photonic crystals it is imperative to know their electronic structure. Currently available tunneling spectroscopic techniques, however, are accompanied by a large linewidth broadening, typically ~100meV even at cryogenic temperatures (~5K). We present a novel tunneling spectroscopy technique in which electronic structure of individual quantum dots can be directly measured with extremely small linewidth broadening even at room temperature. The spectroscopic measurement units are composed of double-barrier tunneling junctions and were fabricated using CMOS-compatible processes. Using the lock-in technique, direct differential conductance measurements were carried out to obtain the electronic structure of 6nm and 7nm CdSe quantum dots. The spectroscopic measurements were done at 77K, 150K, 225K and room temperature. Clear peaks were observed even at room temperature with a linewidth(FWHM) of ~20meV. At 77K, the FWHM linewidth was only ~3meV.

3:05 PM

**Sub-Nanometer Resolution 3D Mapping of Isotopically Modulated Si Multilayers by Atom-Probe Tomography:** *Oussama Moutanabbir*<sup>1</sup>; Dieter Isheim<sup>2</sup>; Yoko Kawamura<sup>3</sup>; Kohei Itoh<sup>3</sup>; David Seidman<sup>2</sup>; <sup>1</sup>Max Planck institute of Microstructure Physics; <sup>2</sup>Department of Materials Science and Engineering, Northwestern University; <sup>3</sup>School of Fundamental Science and Technology, Keio University

The introduction of enriched and stable semiconductor isotopes as an additional degree of complexity in nanofabrication processes provides a wealth of opportunities in the manipulation of the properties of the emerging nanomaterials. In spite of the crucial information it could provide, there are only a few theoretical studies on the influence of the isotopic content on the physical properties of nanoscale systems. Tackling this promising area requires characterization techniques that are sensitive to one of the isotopic effects besides having the spatial resolution needed to probe nanoscale structures. In this work, we demonstrate that UV-laser assisted local-electrode atom-probe tomography is a unique instrument capable of

achieving an atomic resolution and having a detectability of <10 atomic ppm for each isotope. As a model system, we used isotopically modulated Si layers of <sup>28</sup>Si and <sup>30</sup>Si isotopes having a thickness below 10 nm. 3D atom-by-atom isotopic maps with sharp interfaces are achieved.

**3:20 PM**

**Electronic Structure of Bimetallic Nanowires and Implications for Catalytic Activity:** *Regina Ragan*<sup>1</sup>; <sup>1</sup>University of California, Irvine

Self-organization of atomic ensembles on surfaces using atomic structure on nanowire templates is used to fabricate metal nanoassemblies having feature size and atomically controlled interfaces that are typically unattainable using lithographic technique. Core-shell nanowires consisting of an outer layer of Au coating a rare earth disilicide nanowire have unique electronic structure that is very promising for various applications such as nanocatalysis. Using synergistic first principles and scanning probe techniques, we have characterized atomic and electronic properties of Au-disilicide core-shell nanowires on Si(100) substrates. Calculations of electronic structure predict that electrons deplete from Au adatoms on disilicide nanowire surfaces; Scanning Kelvin probe force microscopy measures a reduced work function for Au on disilicide nanowires in agreement with electron depletion on the surface. The chemical properties of Au-disilicide nanostructures will also be discussed in terms of charge density, density of states and adsorption energy of CO molecules.

**3:35 PM Break**

**3:50 PM Introductory Comments**

**3:55 PM Invited**

**Nano-Scale Multilayer Mask for EUV Lithography Applications and Its Extendability:** *Jinho Ahn*<sup>1</sup>; Tak Kang<sup>2</sup>; <sup>1</sup>Hanyang University; <sup>2</sup>Seoul National University

Extreme ultra violet lithography (EUVL) using 13.5nm wavelength is an extreme technology in the point of optical material preparation, which consists of nano-scale multilayer structure for EUV Bragg reflection. This is expected to be the most promising patterning process for 22nm half pitch and below. To extend the patterning capability below 16nm, a phase shift concept might be required to improve the image contrast with a thinner absorber stack. However, there are many fabricating issues to be solved before it can be applied to manufacturing. In this paper, we suggest an optimal attenuated phase shift mask (PSM) structure. The changes of phase shift and reflectivity depending on the structure were studied using aerial image simulation. In addition, the lithographic performances of manufactured attenuated PSM were investigated using coherent scattering microscopy (CSM).

**4:25 PM Invited**

**Aminosilane Monolayer-Assisted Patterning of Conductive Poly(3,4-Ethylenedioxythiophene) PEDOT Source/Drain Electrodes for Bottom Contact Pentacene Thin Film Transistors, and the Effects of the Surface Morphology of PEDOT on the Electrical Performance:** *Kyunghoon Jeong*<sup>1</sup>; *Hyunjung Shin*<sup>1</sup>; *Jaegab Lee*<sup>2</sup>; <sup>1</sup>Kookmin University; <sup>2</sup>Center for Materials and Processes of Self-Assembly

Organic thin film transistors (OTFTs) with conducting poly(3,4-ethylenedioxythiophene)(PEDOT) electrodes have been fabricated using a bottom-up process consisting of the selective growth of PEDOT on a pre-patterned (3-aminopropyl)trimethoxysilane (APS) monolayer. The newly developed bottom-up process produced strongly adherent, selectively and uniformly patterned PEDOT films on oxidized substrates. In addition, the PEDOT/APS double structure showed an approximately one order of magnitude lower leakage current and contact resistance than the Au/Ti electrodes. Furthermore, smooth PEDOT films produced well-oriented pentacene islands while rough PEDOT films randomly oriented islands. In addition, PEDOT electrodes provided morphological continuity at the electrode-channel interface, making the accumulation channel of the pentacene formed on the electrodes a main contributor to the contact resistance. As a result, the smooth PEDOT surface yielded the low contact resistance, approximately half of that obtained with the rough surface.

**4:55 PM**

**Electrochemical Characterization of CdSe and CdTe Electrodeposits:** *Jae-Ho Lee*<sup>1</sup>; *Ju-Young Lee*<sup>1</sup>; <sup>1</sup>Hongik University

The electrodeposition in acidic aqueous electrolyte bath of cadmium selenide and cadmium telluride on gold electrodes has been studied by electrochemical analysis. Conventional cyclic voltammetry using potentiostat is considered as a reliable method to study electrochemical behavior of electrodeposition of CdSe and CdTe. The mechanism of CdSe and CdTe deposition and its cyclic voltammetry were studied in the Se and Te ion concentration, temperature, potential, scan rate and also we investigated changing surface morphology and atomic composition of Cd and Te(Se) by applied potential (versus Ag/AgCl). Atomic composition of Se and Te by EDS(energy dispersive spectroscopy) were varied with Se and Te ion in electrolyte. Check surface morphology by FeSEM. Structure information about those materials was obtained by X-ray diffraction

**5:10 PM**

**Electrochemical Migration of Cu on Printed Circuit Board; Mechanism and Sn Surface Finish Effect:** *Young-Chang Joo*<sup>1</sup>; *Min-Suk Jung*<sup>1</sup>; *Shin-Bok Lee*<sup>1</sup>; *Ho-Young Lee*<sup>1</sup>; *Tak Kang*<sup>1</sup>; <sup>1</sup>Seoul National University

Electrochemical migration (ECM) phenomenon, defined as the formation of conducting filaments under an applied voltage, high temperature and humidity, leads to short-circuit failure of electronic devices. To secure the disadvantages of Cu, which is the most widely used for metal electrode, Sn coating was introduced because Sn has stronger corrosion resistance compared to Cu and forms inter-metallic compounds (IMCs). Results revealed that time to failure (TTF) increased dramatically in the sample with Sn coating and 160 nm-thick Sn coating was more effective than 90 nm-thick coating in terms of increasing the TTF from water drop test (WDT). By anodic polarization test, it was found that IMCs, formed between Sn and Cu layers, enhanced the corrosion resistance with passivity behavior. By introducing WDT and anodic polarization test, it was understood that dissolution step controlled entire ECM process corresponding to the rate determining step in ECM.

**5:25 PM**

**Biosensor Applications of Functionalized Singular TiO<sub>2</sub> Nanotubes:** *Mingun Lee*<sup>1</sup>; *Jie Huang*<sup>1</sup>; *Moon Kim*<sup>1</sup>; *Hyunjung Shin*<sup>2</sup>; *Jiyoung Kim*<sup>1</sup>; <sup>1</sup>University of Texas at Dallas; <sup>2</sup>Kookmin University

Nanotubular structures are highly regarded in biological sensor applications for the high detection sensitivity stemming from their inherently high surface area per volume. Most notably, TiO<sub>2</sub> nanotubes have an added benefit of nontoxicity, making them an invaluable candidate. In this study, we have evaluated TiO<sub>2</sub> nanotube functionalization for specific chemical detection. To accommodate selectivity for streptavidin, the surface was treated with biotin; selective binding between the two chemicals ensures excellent results. Precise control over the nanotube wall thickness is critical in fine-tuning performance parameters of the resulting biosensor, hence ALD was employed in nanotube fabrication. Finally, singular nanotubes rather than nanotube bundles were selected for study, as the former has a brighter prospect in miniaturization and multichannel device application. This research was supported by a grant (code #:2010K000351) from 'Center for Nanostructured Materials Technology' under '21st Century Frontier R&D Programs' of the Ministry of Education, Science and Technology, Korea.

**5:40 PM Concluding Comments**



## 2nd International Symposium on High-Temperature Metallurgical Processing: Raw Materials Processing

*Sponsored by:* The Minerals, Metals and Materials Society, TMS Extraction and Processing Division, TMS: Pyrometallurgy Committee, TMS: Energy Committee

*Program Organizers:* Jiann-Yang Hwang, Michigan Technological University; Jerome Downey, Montana Tech; Jaroslaw Drelich, Michigan Technological University; Tao Jiang, Central South University; Mark Cooksey, CSIRO

Wednesday PM                      Room: 18  
March 2, 2011                        Location: San Diego Conv. Ctr

*Session Chairs:* Ismail Duman, Istanbul Technical University; Wei Li, Kunming University of Science and Technology

### 2:00 PM

#### An Innovative Process on Beneficiation of Superfine Low Grade Hematite Ore: *Deqing Zhu*<sup>1</sup>; Yongzhong Xiao<sup>1</sup>; Tiejun Chun<sup>1</sup>; Jian Pan<sup>1</sup>; <sup>1</sup>Central South University

In this paper, an innovative process of reverse floatation-direct reduction-low intensity magnetic separation was developed to effectively beneficiate the superfine run-of-mine (ROM) ore mined from Hunan Province, China. Mineralogy was measured that the ROM ore is of superfine low grade hematite ore type, assaying 27.23%Fe<sub>2</sub>O<sub>3</sub> and with main valuable minerals of hematite occurring at size between 3~5 $\mu$ m. The upgrading results show that the final iron concentrate, assaying 88.31%Fe total and 94.45% metallization degree was obtained at an overall iron recovery of 69.92% under the following conditions: rough concentration by grinding of ROM up to 88.72% passing 0.074mm and reverse floatation at pH=9.4, 100g/t starch and 200g/t dodecylamine(DDA), and coal reducing the rough concentrate pellets containing 12% calcium containing complex additive at 1200° for 120min and 2.5 coal-to-pellet mass ratio, and finally magnetic separation of the reduced pellets by grinding up to 89.20% passing 0.043mm at 0.08T field intensity.

### 2:20 PM

#### Calcination Behavior of Sivrihisar Laterite Ores of Turkey: *Ender Keskinilic*<sup>1</sup>; Saeid Pournaderi<sup>2</sup>; Ahmet Geveci<sup>2</sup>; Yavuz A. Topkaya<sup>2</sup>; <sup>1</sup>Atilim University; <sup>2</sup>Middle East Technical University

This study investigated calcination behavior of one of the Turkish laterite deposits, which was recently found in Sivrihisar region. Representative limonitic laterite samples (1.26% Ni) taken from Yunusemre Karasivritepe and Kucuksivritepe location were first subjected to drying. Removal of chemically bound water and other volatiles were then studied, in detail. In the calcination experiments, temperature and time were the main experimental variables. Thermal treatment was conducted at the specific temperatures in 250°C - 800°C range. The weight losses due to elimination of chemically bound water and other volatiles were reported to be approximately 10 per cent of the weight of the ore. For the particle size used in the current work, 700°C and 40 minutes were determined to be the optimum calcination temperature and time, respectively.

### 2:40 PM

#### Function of High Pressure Roll Grinding in Producing Magnetite Oxidized Pellets: *Yu-feng Guo*<sup>1</sup>; Hai-zheng Hao<sup>1</sup>; Tao Jiang<sup>1</sup>; Jan-jun Fan<sup>1</sup>; <sup>1</sup>Central south University

Function of High Pressure Roll Grinding(HPRG) was systematically studied in producing oxidized pellets by using magnetite concentrate as raw material, with results that the bentonite dosage was massively reduced,when specific surface area of magnetite concentrate pretreated by HPRG was controlled at 2553.41 cm<sup>2</sup>.g<sup>-1</sup> approximately,the bentonite dosage was decreased to 0.8% compared with 1.3% without pretreating. The green ball quality was also obviously improved,due to the marked increase of specific surface area and fine particles content of pretreated material ,as well as the

improvement of granulometric distribution and the static pelletizability index of pelletfeed.With decrease of pellet porosity and increase of pellet compactness, the primary solid phase reaction and oxidation reaction were accelerated, which made the pellets surface form compaction layer which handicapped the diffusion and migration of oxygen, promoting the double layer structure of pellet forming, consequently, the compression of preheated and roasted pellets was not markedly improved by HPRG.

### 3:00 PM

#### Magnetic and Floatability Behaviors of Nonstoichiometric Pyrrhotites: Vladimir Luganov<sup>1</sup>; Shinibai Baiysbekov<sup>1</sup>; Tatyana Chepushtanova<sup>1</sup>; Viktor Ermolayev<sup>1</sup>; <sup>1</sup>The K.I. Satpayev Kazakh National Technical University

Using Faraday method of magnetic scale, it was found that magnetic pyrrhotites are formed in the result of roasting. When temperature increasing up to 220°C, magnetic permeability of pyrrhotites Fe<sub>0.855</sub>S, Fe<sub>0.888</sub>S, Fe<sub>0.909</sub>S dramatically increases, then falls to zero at temperatures of 310-320°C. At temperatures above Curie point (till 570°C) an abrupt drop of magnetic permeability had been observed, followed by consistent increases in magnetic permeability until reaching its peak at Fe<sub>0.855</sub>S = 3,75; Fe<sub>0.888</sub>S = 5,43; Fe<sub>0.909</sub>S = 2,18 point CI at 700-800°C. Curie temperature depends on pyrrhotites composition. Temperature hysteresis of magnetic properties has been observed within the temperature interval of up to 240°C. Results of investigations show that electro kinetic potentials of the pyrrhotites increases with pH rising within the interval 5-13, and decreases with reduction of sulfur content from 52,1 mV for pyrrhotite Fe<sub>0.85</sub>S till ~ 40,8 mV for pyrrhotites Fe<sub>0.89</sub>S.

### 3:20 PM

#### Improving the Pelletization of Fluxed Hematite Pellets by Hydrated Lime: *Deqing Zhu*<sup>1</sup>; Wei Yu<sup>1</sup>; Tiejun Chun<sup>1</sup>; Jian Pan<sup>1</sup>; <sup>1</sup>Central South University

In this paper, the technology of producing fluxed pellets by using hydrated lime as binder instead of bentonite was carried out. The results show that the drop numbers of 4.8 to 5.0 times/0.5m, compressive strength of 19.7 to 24.2 Newton per pellet and thermal shock temperature of 280 to 385°C for green balls with 0.8% bentonite and green balls containing 2% hydrated lime were obtained under the same conditions of 8.5% moisture, 1.45 basicity and balling for 10min in disc pelletizer. Comparing with bentonite as binder, the compressive strength of fired pellets with hydrated lime is elevated by 13.82% and climbs up to 3113 Newton per pellet under the following conditions: preheating at 1050°C for 15min and firing at 1300°C for 15min. The hydrated lime also improves the metallurgical performance of fired pellets, the reduction index being enhanced from 68.55% to 70.58%, RDI+3.15 increased from 90.12% to 98.79% and reduction swelling index dropped from 22.35% to 7.39%, respectively.

### 3:40 PM

#### Microwave Assisted Breakage of Metallic Sulfide Bearing Ore: *Matthew Andriese*<sup>1</sup>; <sup>1</sup>Michigan Technological University

An mafic ore body contains high concentrations of nickel and copper chiefly occurring in the minerals pyrrhotite, chalcopyrite, and pentlandite. Refractory ore bodies are difficult to treat by conventional mineral processing methods thus it is of interest to find other processing methods that increase metallic-particle/host rock liberation. One such proposed method to improve particle liberation is microwave-pretreatment of the ore. Differential heating properties of the constituent mineral phases produce cracks in ore particles by tension. Preliminary experiments have shown the ore particles heat rapidly when exposed to 1000W microwave power for short durations of time (30, 60, 90s). SEM imaging shows fracture occurring along grain boundaries and throughout host rock matrix. Preliminary ball milling experiments show promising results for increased grindability of the ore. Further work would be to investigate the effect microwave treatment has on the work index and washability of the ore after the grinding stage.

#### 4:00 PM Break

#### 4:10 PM

**Research on the Ball Milling and Followed by Microwave Reduction of Panzihua Low Grade Ilmenite Concentrate:** Ying Lei<sup>1</sup>; Yu Li<sup>1</sup>; Jinhui Peng<sup>1</sup>; Libo Zhang<sup>1</sup>; Shenghui Guo<sup>1</sup>; Wei Li<sup>1</sup>; <sup>1</sup>Key Laboratory of Unconventional Metallurgy, Ministry of Education

In this work, the Panzihua low grade ilmenite and graphite were milled for 1, 2, 4 and 8 h firstly, then the temperature rising behavior of milled sample in microwave field were studied. The average heating rate of samples milled for 1, 2, 4, 8 h were 1.86, 4.08, 2.82, and 2.32 K/s; Before optimize the microwave reduction process, several experiments were conducted in order to confirm the parameters range. After milled for 4 or 8 h and reduced above 930°, the Fe metallization are higher than 90%; Then the optimization was investigated by using response surface methodology (RSM), the significance of predict model and each terms were analyzed, and the optimization parameters were given as: milling time is 4 h; reduction temperature is 1001 or 1070°; the holding time is 37.5 or 26.9 min. Under these conditions, the Fe metallization given by predict model is 91 or 92 %.

#### 4:30 PM

**Research on the Recovery of Vanadium from Low-Grade Vanadium Slag by the Calcium Roasting Process:** Xiaojun Li<sup>1</sup>; <sup>1</sup>Chongqing University

The recovery of vanadium from low-grade vanadium slag (V2O3 8%) by means of calcium roasting and acid leaching was investigated. XRD analysis shown that there are three different of calcium vanadate formed during roasting process. The acid leaching of the roasted slag indicated that the content of CaO in roasted slag plays an important role in the roasting process, vanadium extraction ratio was increased from 55.3% to 69.2% when CaO/V2O3 increased from 0.5 to 1.125, but the ratio would be decreased when CaO/V2O3 exceed 1.125. When the roasting temperature was increased from 750° to 825°, vanadium extraction ratio would be increased from 56.3% to 69.7%. However, the slag would be sintered when the roasting temperature is higher than 825°, which would lead to the decrease of vanadium extraction ratio.

#### 4:50 PM

**Study of Strengthen Pelletization of Nickel Laterite:** Jian Pan<sup>1</sup>; Xian Zhou<sup>1</sup>; De Zhu<sup>1</sup>; Guo Zheng<sup>1</sup>; <sup>1</sup>Central South University

In ferronickel production, it is one economical and efficient technology that the nickel oxide and part of the iron oxide are reduced to metal by agglomeration and smelting in blast furnace. Due to the physical and chemical properties of the laterite ores, a large fraction of fines is generated during the pre-treatment stages and the strength of agglomeration is weakened, which results in low productivity and bad quality. In this paper, the process of pelletization of nickel laterite was developed firstly, and some parameters to strengthen the pelletization of nickel laterite has been optimized. The result showed that the compressive strength of fired nickel laterite pellet can reach over 2000 Newton per pellet while firing at the temperature of 1220°~1250° and induration for 12min under the optimization conditions, and the product pellet can be used as high-quality burden for blast furnace to manufacture ferronickel.

#### 5:10 PM

**Waste to Wealth: Production of Fe-Ni from Lateritic Ore/ Chromite over Burden of Sukinda Deposit in Orissa, India:** Bhagyadhar Bhoi<sup>1</sup>; Chitta Mishra<sup>2</sup>; Hara Mishra<sup>3</sup>; <sup>1</sup>Institute of Minerals and Materials Technology; <sup>2</sup>Natal Aluminium Company Ltd.; <sup>3</sup>Industrial Promotion and Investment Corporation of Orissa Ltd.(IPICOL)

In the Sukinda Valley of Orissa, India, the total quantity of nickel ore reserves comprising of both lateritic and overburden have been estimated at around 231 million tonnes containing 0.3 to 0.9 % Ni. While mining of one tonne of Chromite ore, around 6-7 tonnes of chromite overburden are removed. These overburden materials are disposed off as waste materials causing lot of environmental hazards and ecological imbalance. India imports a large amount of nickel and ferro-nickel to meet its growing demands in various sectors. For import substitution, efforts have been made to produce

ferro nickel from the lean deposits of nickel bearing lateritic ores / chromite overburden materials by reduction roasting followed by magnetic separation and then the nickel rich magnetic fraction is smelted to produce ferro-nickel. It has been possible to produce ferro-nickel of grade varying from 4-25% nickel.

#### 5:30 PM

**Mineralization Behavior of Fluxes during Iron Ore Sintering:** Min Gan<sup>1</sup>; Xiaohui Fan<sup>1</sup>; Tao Jiang<sup>1</sup>; <sup>1</sup>Central South University

The mineralization behavior of common fluxes is studied by investigating the microstructures with optical microscope. The results show that the reactions start between iron ore and lime, small particle limestone, which form the primary liquid. Then coarse limestone, dolomite and serpentine take part in reaction under the action of primary liquid. Limestone is the easiest to mineralization, then dolomite, and the last one is serpentine. In order to mineralize dolomite and serpentine completely, either the basicity of sinter should be increased or the size of them should be reduced.

### Advances in Mechanics of One-Dimensional Micro/Nano Materials: Nanomechanics: Size Scale and Theory

*Sponsored by:* The Minerals, Metals and Materials Society, TMS Materials Processing and Manufacturing Division, TMS Electronic, Magnetic, and Photonic Materials Division, TMS: Nanomechanical Materials Behavior Committee

*Program Organizers:* Reza Shahbazian-Yassar, Michigan Technological University; Seung Min Han, Korea Advanced Institute of Science and Technology; Katerina Aifantis, Aristotle University

Wednesday PM

March 2, 2011

Room: 1B

Location: San Diego Conv. Ctr

*Session Chairs:* Xiaodong Li, University of South Carolina; Julia Greer, California Institute of Technology

#### 2:00 PM Invited

**Measurement of Size-Scale Effects in Pure Ni: Effect of Initial Dislocation Density:** Jaafar El-Awady<sup>1</sup>; Paul Shade<sup>2</sup>; Sang-Lan Kim<sup>3</sup>; Michael Uchic<sup>4</sup>; Satish Rao<sup>3</sup>; Dennis Dimiduk<sup>4</sup>; Chris Woodward<sup>4</sup>; <sup>1</sup>Johns Hopkins University; <sup>2</sup>Universal Technology Corporation; <sup>3</sup>UES, Inc.; <sup>4</sup>Air Force Research Laboratory

The importance of the initial dislocation density on the mechanical response of microcrystals has been the subject of both recent experimental and simulation-based studies. However, there is little experimental examination of the changes to either the size-dependent flow response or the observed strain intermittency in pure FCC metals as a function of the initial dislocation density. We have performed long annealing treatments that have reduced the initial dislocation density in pure Ni single crystals to extremely low levels, approaching 10<sup>8</sup> m<sup>-2</sup>. These low dislocation density crystals enabled studies of size-scale effects in pure FCC metals that contain essentially no grown-in dislocations. Furthermore, we have pre-deformed <110> oriented crystals to selected stages of substructure development: Stage II, the transition between Stage II-to-III, and Stage III. The talk presents experimental measurements from these crystals to characterize the effect that the starting substructure has on size-affected flow response as well as plastic intermittency.

#### 2:25 PM Invited

#### 3:00 PM

**Atomistic Simulations of the Strength of Gold Nanowires:** Christopher Weinberger<sup>1</sup>; <sup>1</sup>Sandia National Labs

Molecular dynamics simulations of nanostructures can be used to estimate strength but are limited by the timescale resolution. To overcome this, we use energy barrier calculations of dislocation nucleation to estimate the strength of gold nanowires. Crystal orientation, size and surface termination

types are included in this study to predict strengths, which can be compared to experiments.

## 2:50 PM Invited

### Gradient Theory for One-Dimensional Configurations and Objects: *Elias Aifantis*<sup>1</sup>; <sup>1</sup>Aristotle University of Thessaloniki

Various forms of gradient theory are used to discuss one-dimensional configurations and objects. They include interfaces, layers, fibers, nanowires and nanotubes.

## 3:15 PM

### Size Effects on Strength and Plasticity of Vanadium Nanopillars: *Seung Min Han*<sup>1</sup>; Tara Bozorg-Grayeli<sup>2</sup>; James Groves<sup>2</sup>; Yi Cui<sup>2</sup>; William Nix<sup>2</sup>; <sup>1</sup>Korea Advanced Institute of Science and Technology; <sup>2</sup>Stanford University

A size effect study was conducted on vanadium BCC nanopillars that were synthesized from both the thin film and the bulk crystal in (100) orientations. Our results indicate that the size dependent deformation behavior exists for V; the smaller nanopillars displayed discrete bursts and higher stresses during deformation. The size effect exponent was calculated to be -0.79, and our results were compared with the previous reports on Nb, Ta, Mo and W. Our V results reported a higher size effect exponent compared to those of Ta, Mo, and W, and this trend is in agreement with the critical temperature dependent size effect theory. V poses a unique opportunity in conducting in-situ TEM deformation study due to its high electron transparency. Our report on both ex-situ and in-situ studies will be discussed.

## 3:30 PM Invited

### Size Dependent Deformation Mechanism Transition in a Titanium Alloy: *Zhiwei Shan*<sup>1</sup>; <sup>1</sup>Xi'an Jiaotong University

Using micro-compression and in situ nano-compression experiments, we find that the stress required for deformation twinning (DT) increases drastically with decreasing sample dimension (d) of a titanium alloy single crystal, until d is reduced to a critical value (~1 micrometer), below which the DT is overtaken altogether by less correlated, ordinary dislocation plasticity (ODP). Accompanying the transition in deformation mechanism, the maximum flow stress of the submicron-sized pillars was observed to saturate at a value close to titanium's ideal strength. A "stimulated slip" model is developed to explain the strong size dependence of DT. The large sample size in transition is easily accessible in experiments, making our understanding of size dependence highly significant for applications (Q. Yu, Z. W. Shan, J. Li, X. X. Huang, L. Xiao, J. Sun and E. Ma, Nature 463, 335-338, 2010).

## 3:55 PM Break

## 4:10 PM Invited

### Size Matters: Size-Dependent Mechanical Properties of Metallic Systems: *Julia Greer*<sup>1</sup>; Dongchan Jang<sup>1</sup>; Andrew Jennings<sup>1</sup>; Ju-Young Kim<sup>1</sup>; <sup>1</sup>California Institute of Technology

When microstructural (intrinsic) or external material dimensions are reduced to nano-scale, they exhibit unique behaviors. We fabricate nanopillars with different initial microstructures ranging from 50 nm to 1 micron by using Focused Ion Beam and E-beam lithography/electroplating approaches. Their strengths in uniaxial compression and tension are subsequently measured in in-situ mechanical deformation instrument, SEMentor. We discuss nano-mechanical behavior in four distinct metallic systems: single crystals, nano-crystalline metals, nano-twinned metals, and metallic glasses. We observe SMALLER is STRONGER phenomenon in single crystals while nano-crystalline metals exhibit SMALLER is SOFTER trend. Metallic glasses show strength increase and ductility when reduced to nano-scale. Unlike in bulk, nano-scale materials exhibit discretized stress-strain relationships. We attribute these dissimilarities to free surface effects, leading to unique dislocation interactions with internal interfaces (grain and twin boundaries) in the presence of free surfaces and shear transformation zones in metallic glasses, serving as fundamental reason for observed deformation mechanisms.

## 4:35 PM Invited

### Environmental Effects on the Mechanical Behavior and Function Performance of Nanostructures: *Xiaodong Li*<sup>1</sup>; <sup>1</sup>University of South Carolina

Nanostructures are often mechanically tested and/or functionally operated in various severe environments, such as at high humidity levels and electron beam radiation conditions. We found that humidity and electron beam radiation remarkably affect the mechanical behavior and function performance of nanostructures. The mechanical properties such as elastic modulus vary significantly at different humidity levels and electron beam radiations, in turn affecting the function performance of the nanostructures which utilize the elastic modulus as the function base. We also found that functions of the mechanically damaged nanostructures can be recovered by self healing in the nanostructures in situ over a period of time.

## 5:00 PM Invited

### Transition from Deterministic to Stochastic Deformation: *Alfonso Ngan*<sup>1</sup>; <sup>1</sup>University of Hong Kong

The deformation of small material volumes is often jerky, with discrete strain jumps occurring in a stochastic manner. In this paper, the condition for the stochastic model of deformation is analyzed theoretically. The model used considers a large ensemble of macroscopically identical but microscopically different experiments each of which emits bursts randomly according to a rate law that depends on the history of emission and the instantaneous stress. The model predicts that if burst sources get depleted on continuous emission, the stress-strain behavior will be stochastic, and if burst sources get multiplied on continuous emission, the stress-strain behavior will be deterministic. The strength at the same strain in the stochastic regime is also higher than in the deterministic regime. The condition for sources getting depleted on continuous emission corresponds to "dislocation starvation", and so the model predicts that dislocation starvation is always accompanied by the stochastic mode of deformation.

## 5:25 PM Invited

### Structural Transformations in Bulk Nanocrystalline Materials, Nanorods, and Nanoparticles Triggered by Disclinations: *Alexey Romanov*<sup>1</sup>; Anna Kolesnikova<sup>2</sup>; Leonid Dorogin<sup>3</sup>; Ilmar Kink<sup>3</sup>; Elias Aifantis<sup>4</sup>; <sup>1</sup>Ioffe Physical-Technical Institute RAS; <sup>2</sup>Institute of Problems of Mechanical Engineering; <sup>3</sup>University of Tartu; <sup>4</sup>Aristotle University of Thessaloniki

Present talk gives the analysis of structural transformations caused by disclinations and leading to grain refinement in bulk nanocrystalline materials (BNCMs), emerging 1D nanowhiskers (NWs), and structural changes in pentagonal nanorods (PNRs) and nanoparticles. The model developed for BNCMs qualitatively and quantitatively describes the effect of grain size diminishing in the course of plastic deformation and explains the peculiarities of the flow stress dependence on the grain size. A new model of NW formation operates with prismatic dislocation loops that condensate on the disclination defect placed in the triple junction of grain boundaries of a polycrystal. To understand the transformations in nanoparticles and PNRs their internal organization is explained in terms of disclinations. It is demonstrated that initial multiple twinned structure of particles or PNRs is unstable with respect to dislocation formation above a certain critical diameter of a particle or radial phase separation in case of two-phase PNR.

## 5:50 PM

### Vibration Analysis of Nano-Structures Using Wavelets and Gradient Theory: *Avraam Konstantinidis*<sup>1</sup>; <sup>1</sup>Aristotle University of Thessaloniki

The vibration of cantilevers used in nano-electromechanical systems (NEMS) is studied using gradient theory, first proposed by Aifantis and co-workers in 1984. Wavelets are then proposed to extract the noise from the vibration signals. The same is sought for the vibration of single walled carbon nanotubes (SWCNTs).



## Alumina and Bauxite: Energy and Environment

Sponsored by: The Minerals, Metals and Materials Society, TMS Light Metals Division, TMS: Aluminum Committee, TMS: Aluminum Processing Committee

Program Organizers: James Metson, University of Auckland; Carlos Suarez, Hatch Associates Consultants Inc

Wednesday PM  
March 2, 2011

Room: 17A  
Location: San Diego Conv. Ctr

Session Chair: To Be Announced

### 2:00 PM

**Perspective on Bayer Process Energy:** *Don Donaldson*<sup>1</sup>; <sup>1</sup>Alumina Consultant

The three most important cost items in the production of alumina are bauxite, caustic soda and energy. Alumina energy cost will rise more than other costs as energy prices increase and energy related environmental issues impact alumina production. Many refineries will need to adjust process to maintain or improve their position on the world cost curve. The Bayer Process is simple but the use of energy in the process can be complex. The uses of energy in the Bayer process and their interrelationship will be discussed.

### 2:20 PM

**Optimization of Heat Recovery from the Precipitation Circuit:** *Rashmi Singh*<sup>1</sup>; *Sushant Hial*<sup>1</sup>; *Michael Simpson*<sup>1</sup>; <sup>1</sup>Vedanta Aluminium Ltd.

In the Bayer process, temperature profile across the precipitation circuit plays a major role to maximize the precipitation yield while maintaining product quality. For this reason, plate heat exchangers are used both at inlet to Precipitation and in between precipitation stages at Vedanta Aluminium's Lanjigarh alumina refinery. For the Heat Interchange Department (HID), cooling media is spent liquor while for the Interstage Coolers (ISCs) of Precipitation both spent liquor and cooling water are used. A simple model was built using existing heat exchanger performance data along with heat and mass balances across Heat Interchange Department (HID) and Precipitation. This was then used to determine feasible modifications for improving heat recovery in the Precipitation circuit. The results obtained have indicated process steam reduction of 3 % can be achieved with minor modifications.

### 2:40 PM

**Alunorte Global Energy Efficiency:** *Arthur Monteiro*<sup>1</sup>; *Reiner Wischniewski*<sup>2</sup>; *Cleto Azevedo*<sup>1</sup>; *Emerson Moraes*<sup>1</sup>; <sup>1</sup>Alumina do Norte do Brasil S.A.; <sup>2</sup>Hydro Aluminium AS

Alunorte is the largest alumina refinery in the world with a production capacity of 6.3 Mtpy. The plant has a specific energy consumption of less than 8 GJ per ton of alumina which defines the world-wide benchmark for energy efficiency in alumina production. The high energy efficiency is achieved by taking advantage of a good process design, the utilization of state-of-the-art technologies, good operation and the processing of high quality bauxite. The technologies which are applied in Alunorte to contribute to the global energy efficiency of the plant are reviewed and its heat integration and its water balance are discussed.

### 3:00 PM

**Opportunities for Improved Environmental Control in the Alumina Industry:** *Richard Mimma*<sup>1</sup>; *John Kildea*<sup>2</sup>; *Everett Phillips*<sup>1</sup>; *Wayne Carlson*<sup>1</sup>; *Bruce Keiser*<sup>1</sup>; <sup>1</sup>Nalco Company; <sup>2</sup>Nalco Australia

Alumina production from bauxite offers a unique set of environmental concerns that affect air, water, and solids. Governments and industry have recognized that reductions in plant emissions and environmental impacts are necessary. The alumina industry is not the only industry that has been subjected to, and responded to, such regulatory scrutiny over the past decade. A number of industry sectors are actively developing innovative ways to control a broad range of potential environmental hazards. A number of these technologies may have direct application in alumina refineries. Methods to significantly reduce mercury emissions in both air and water have recently

been developed for use in a range of industries. In addition, powerhouse emissions of NO<sub>x</sub>, SO<sub>x</sub>, and particulate matter can now be significantly reduced. This paper reviews a number of these new technologies now in commercial use in non-alumina plants and considers how they may be applicable within the alumina industry.

### 3:20 PM

**Alumina Refinery Water Management: When Zero Discharge Just Isn't Feasible.....:** *Lucy Martin*<sup>1</sup>; *Steven Howard*<sup>1</sup>; <sup>1</sup>Bechtel

Management and treatment of liquid effluents are determinant considerations in the design of alumina refineries. Rainfall, evaporation rate, proximity to the coast, process design and layout, ore mineralogy, the local environment, and potential impact on contiguous communities are all integral to the development of an appropriate refinery water management strategy. The goal is to achieve zero discharge of liquid effluent to the environment. However this is not always the most feasible solution under the extreme rainfall conditions in tropical and subtropical locations. This paper will explore the following issues for both inland and coastal refineries: •Methods to reduce and control refinery discharges •Treatment design criteria •Socioeconomic aspects relating to surface water use in settlements adjacent to the refinery.

### 3:40 PM Break

### 3:50 PM

**High Purity Alumina Powders Extracted from Aluminum Dross by the Calcining—Leaching Process:** *Liu Qingsheng*<sup>1</sup>; <sup>1</sup>Jiangxi University of Science and Technology

A new calcining-leaching process was used to extract high purity alumina (Al<sub>2</sub>O<sub>3</sub>) powders from aluminum dross in this study. The aluminum dross was mixed with soda (Na<sub>2</sub>CO<sub>3</sub>) and calcined at 900°C to yield soluble aluminates. Subsequently the calcined dross was leached with sulfuric acid (H<sub>2</sub>SO<sub>4</sub>) to produce a solution containing aluminum. The unwanted metal ions including Fe<sup>3+</sup> and Na<sup>+</sup> were removed by ethylene diamine tetraacetic acid (EDTA) and water washing. Then added the proper dispersant, controlling the crystallization of aluminum trihydroxide precipitation, and the drying and calcining process was carried out, resulting in ultra fine Al<sub>2</sub>O<sub>3</sub> powders with high purity. The characteristics of the Al<sub>2</sub>O<sub>3</sub> powders were examined by means of XRD, TEM and Brunauer-Emmet-Teller (BET) surface analysis method. The extraction efficiency of Al<sub>2</sub>O<sub>3</sub> can surpass 98% by optimization of the calcination and lixiviation processes. Well-dispersed fibriform Al<sub>2</sub>O<sub>3</sub> powders were obtained by calcining at 800°C and the purity of the ultra fine Al<sub>2</sub>O<sub>3</sub> powders was more than 99.6%.

### 4:10 PM

**Effect of Calcium/Aluminium Ratio on MgO Containing Calcium Aluminate Slags:** *Wang Bo*<sup>1</sup>; *Sun huilan*<sup>1</sup>; *Guo Dong*<sup>1</sup>; *Bi Shiwen*<sup>2</sup>; <sup>1</sup>Hebei University of Science and Technology; <sup>2</sup>Northeastern University

MgO is the main impurity in calcium aluminate slag. The existence of MgO will change the occurrence state of alumina and decrease the alumina leaching property of slag. In order to remove or reduce the negative effect of MgO, the method of changing C/A of calcium aluminate slag was studied and the effect mechanism was also analyzed. The results showed that the formation of quaternary compound 20CaO•13Al<sub>2</sub>O<sub>3</sub>•3MgO•3SiO<sub>2</sub> (C<sub>20</sub>A<sub>13</sub>M<sub>3</sub>S<sub>3</sub>) would be inhibited with the increasing of C/A of calcium aluminate slag, and the MgO crystallized in the form of periclase independently under this condition. There is an optimal C/A to improve the alumina leaching property of calcium aluminate slag. The increase of C/A could not remove the negative effect of MgO on calcium aluminate slag completely, and the optimal C/A of slag will increase with the increase of MgO content.

### 4:30 PM

**Study on Extracting Aluminum Hydroxide from Reduction Slag of Magnesium Smelting by Vacuum Aluminothermic Reduction:** *Wang Yaowu*<sup>1</sup>; *Feng Naixiang*<sup>1</sup>; *You Jing*<sup>1</sup>; *Hu Wenxin*<sup>1</sup>; *Peng Jianping*<sup>1</sup>; *Di Yuezong*<sup>1</sup>; *Wang Zhihui*<sup>1</sup>; <sup>1</sup>Northeastern University

Feng Naixiang invent a new producing magnesium method, which mainly include two steps, the first step is producing magnesium with vacuum

aluminothermic reduction, the second step is extracting aluminum hydroxide from reduction slag. In the reduction slag, the alumina is more than 65% and it is mainly in the form of  $\text{CaO} \cdot 2\text{Al}_2\text{O}_3$ . The process of producing aluminum hydroxide from the slag leached by the mixture solution of sodium hydroxide and sodium carbonate was studied. It showed that the leaching rate of alumina is more than 85% when leaching temperature is  $85^\circ\text{C}$ , L/S is 5 and leaching time is 2h. The magnesia-alumina spinel which generated in the reduction process and  $3\text{CaO} \cdot \text{Al}_2\text{O}_3 \cdot 6\text{H}_2\text{O}$  which generated in the leaching process are the two main ways caused loss of alumina. The chemical composition of aluminum hydroxide products which obtained after desilicisation and carbonation precipitation can meet the quality standard of the alumina plant.

#### 4:50 PM

**Application of Thermo-Gravimetric Analysis for Estimation of Tri-Hydrate Alumina in Central Indian Bauxites --- An Alternative for Classical Techniques:** *Yarlagadda Ramana*<sup>1</sup>; Rajesh Patnaik<sup>1</sup>; <sup>1</sup>Vedanta Aluminium Limited

Tri-hydrate alumina ( $\text{Al}_2\text{O}_3 \cdot 3\text{H}_2\text{O}$ ) content in bauxite is a fundamental quality parameter in Bayer alumina process using low temperature digestion. Classical techniques available for its estimation are mainly time consuming and prone to standard and non-standard sources of error. Extensive studies on analysis of samples from Central Indian bauxite sources using thermo-gravimetry at varied temperature ranges and comparing it with that of the data obtained from classical techniques have revealed that loss of molecular water at different temperatures in thermo-gravimetry provides a meaningful tool to correlate with tri-hydrate alumina content by applying relevant correction factors derived from the experimental data at different concentrations of tri-hydrate alumina. The studies also have found that the thermo-gravimetric analysis can be used as a very fast and dependable technique with higher levels of accuracy over classical methods and free from other interferences. The accuracy levels of the method developed were checked using reference standards.

#### 5:10 PM

**Determination of Oxalate Ion in Bayer Liquor Using Electrochemical Method:** Seval Turhan<sup>1</sup>; Betül Usta<sup>1</sup>; Yücel Sahin<sup>2</sup>; Oktay Uysal<sup>3</sup>; <sup>1</sup>ENTEKNO Industrial Technological and Nano Materials Ltd.& Anadolu University, Faculty of Science, Department of Chemistry; <sup>2</sup>Anadolu University, Faculty of Science, Department of Chemistry; <sup>3</sup>ENTEKNO Industrial Technological and Nano Materials Ltd

The Bayer process can be summarized as the digestion of bauxite with caustic liquor and the subsequent precipitation of hydrated alumina [1]. Most bauxite contains organic compounds in various amounts. Depending upon the digestion conditions, 5–10% of the organic carbon is converted to sodiumoxalate [2]. When sodiumoxalate, if not controlled in Bayer process, builds up to a certain level of supersaturation, it precipitates out in the hydrate precipitator tank. This co-precipitation affects the quality of alumina [3]. In this study, we investigated the electrochemical determination of oxalate ion by using differential puls voltammetry in Bayer liquor. A linear relationship between oxalate concentration and current response was obtained with good reproducibility of the current. [1] T.G. Pearson, The chemical background of the aluminium industry, Monograph No. 5, Royal Institute of Chemistry, London, UK, 137-143, 1955. [2] G. Lever, Travaux, 13, 335 (1983). [3] R. Calalo, T. Tran, Light Metals, 125(1993).

## Aluminum Alloys: Fabrication, Characterization and Applications: Emerging Technologies

*Sponsored by:* The Minerals, Metals and Materials Society, TMS Light Metals Division, TMS: Aluminum Processing Committee  
*Program Organizers:* Subodh Das, Phinix LLC; Zhengdong Long, Kaiser Aluminum; Tongguang Zhai, University of Kentucky

Wednesday PM  
March 2, 2011

Room: 14A  
Location: San Diego Conv. Ctr

*Session Chair:* Subodh Das, Phinix LLC

#### 2:00 PM

**Microstructure Evolution Of Cryomilled Nanostructured Light Weight Al 5083 During SPS:** *Yuhong Xiong*<sup>1</sup>; Dongming Liu<sup>1</sup>; Ying Li<sup>1</sup>; Baolong Zheng<sup>1</sup>; Troy Topping<sup>1</sup>; Yizhang Zhou<sup>1</sup>; Deepak Kapoor<sup>2</sup>; Chris Haines<sup>2</sup>; Joseph Paras<sup>2</sup>; Darold Martin<sup>2</sup>; Julie Schoenung<sup>1</sup>; Enrique Lavernia<sup>1</sup>; <sup>1</sup>University of California; <sup>2</sup>US Army

Al alloys are widely used because they provide the combination of light weight and high strength. In recent years, spark plasma sintering (SPS) technology has emerged as a viable approach to sinter materials due to its rapid heating and high pressure application features. In this study, SPS was chosen to produce dense ultrafine-grained bulk samples using cryomilled nanostructured powder. A bimodal microstructure and banded structures were observed through TEM investigation. The evolution of such microstructures can be attributed to the starting powder and the process conditions, which are associated with the thermal, electrical and pressure fields present during SPS. A finite element method (FEM) was also applied to investigate distributions in temperature, current and stress between metallic powder particles. The FEM results reveal that the localized heating, deformation and thermal activation occurring at inter-particle regions are associated with the formation of the special microstructure.

#### 2:20 PM

**Design and Optimization of Innovative High Performance Aluminum Sandwich Structures:** Antonio Valente<sup>1</sup>; *Edward Chen*<sup>2</sup>; <sup>1</sup>PLY Engenharia, Lda; <sup>2</sup>Transition45 Technologies, Inc.

An innovative technique to manufacture high performance aluminum sandwich structures has been developed. A sheet metal is cut and bent to form the skin and the core of the sandwich. This element is joined to the plain sheet to form the panel. With intelligent layout the new solution can outperform traditional metal sandwich structures in specific stiffness and provide multi-functionality. This presentation describes the evolution of the Opencell™ concept from an idea, to a product, and then software implementation that meets a variety of requirements for the preliminary design of structures. Manufacturing aspects served as design drivers and numerical simulations by Finite Element Analysis (FEA) were used to improve mechanical performance. The panel bending and out-of-plane shear stiffness were used as design objectives to start. A variety of panel configurations were optimized, by integrating commercial FEA code in a process integration and design optimization environment, for the most effective use of material.

#### 2:40 PM

**Effects of Spark Plasma Sintering (SPS) on Cryomilled Nanostructured Al 5083 Alloy:** *Dongming Liu*<sup>1</sup>; Yuhong Xiong<sup>1</sup>; Troy Topping<sup>1</sup>; Yizhang Zhou<sup>1</sup>; Chris Haines<sup>2</sup>; Joseph Paras<sup>2</sup>; Deepak Kapoor<sup>2</sup>; Darold Martin<sup>2</sup>; Julie Schoenung<sup>1</sup>; Enrique Lavernia<sup>1</sup>; <sup>1</sup>UC Davis; <sup>2</sup>US Army, RDECOM-ARDEC, Picatinny Arsenal, NJ 07806, USA

Fundamental studies have been conducted to investigate the influence of SPS processing variables on densification behaviors for cryomilled nanostructured Al 5083 powders and the mechanical properties of the subsequent compacts. It has been found that: pressure-loading mode has a significant effect on mechanical properties and bonding between powders: in comparison with that loaded at room temperature, pressure loaded at

target sintering temperature can enhance bonding between particles and thus improve the mechanical properties; surface activation at pores and other interfaces can help break up the oxide layers existing on particle surfaces and release absorbed gases; grain size as well as powder size play important roles in shrinkage of samples; pulse pattern shows an insignificant influence on the consolidation of SPS processed samples unless using a pulse pattern with on:off ratio less than one; the cryomilled powder is more easily consolidated than the atomized one.

**3:00 PM**

**Microstructural and Electrochemical Characterization of Anodic Oxide Films Formed on Spray-Deposited Al-Si Alloys:** *Hector Herrera*<sup>1</sup>; Manuel Palomar<sup>1</sup>; Mario Romero<sup>1</sup>; Jose Juárez<sup>2</sup>; <sup>1</sup>Metropolitan Autonomous University (UAM); <sup>2</sup>Centro Nacional de Metrología (CENAM)

In this research, aluminum oxide films were grown on one spray-deposited Al-Si alloy and its extrudate product using an anodizing treatment. The electrochemical behavior of the oxide-films was investigated by electrochemical impedance spectroscopy (EIS) technique and potentiodynamic polarization measurements in chloride media. The surface morphology was examined by scanning electron microscopy (SEM). Anodizing was performed in H<sub>2</sub>SO<sub>4</sub> by means of standard procedures and sealed in either boiling water, or potassium dichromate. Finally, the effect of the anodic-surface modification by immersion in boiling CeCl<sub>3</sub> for 2 hours on the pitting corrosion resistance was also investigated. The results of the electrochemical characterization demonstrate that anodizing followed by a simple hot water sealing was less effective, so pits were detected on the anodic oxide film in less than 2 days, as denoted by characteristic changes in the EIS spectra at the lowest frequencies. Improved results were achieved with the hot cerium surface modification.

**3:20 PM**

**Preparation of Al - Li Alloys for Lithium-Air Secondary Battery by Solid Diffusion Method:** Tao Cheng<sup>1</sup>; Zijian Lv<sup>1</sup>; *Xiujing Zhai*<sup>1</sup>; Mingjie Zhang<sup>1</sup>; Ganfeng Tu<sup>1</sup>; <sup>1</sup>Northeastern University

In present work, Al-Li alloys used as lithium-air battery anode material were prepared by solid diffusion method. In the system of molten LiCl-KCl-LiF with molar compositions of 55%-45%-5%, electrolytic reduction of Li-ion on solid aluminum plate was conducted; And Al-Li alloys were formed by the diffusion of metal Li into the plate. The effects of influencing factors, such as electrolysis time, cell voltage and current density, were all studied. The characteristics of Al-Li alloys were analyzed by X-ray diffraction and scanning electron microscopy. It was found that the lithium content of 15%wt. in Al-Li alloys can be obtained by solid diffusion method for 4.0 h with the current density of 0.125 A.cm<sup>-2</sup> at 480 °C; and the phase compositions of the Al-Li alloys were alpha- and beta-aluminum lithium from X-ray diffraction analysis.

**3:40 PM Break**

**3:55 PM**

**Effects of Process Parameters on Rolled Precursor of Aluminum Foam Sandwich Panel:** *Binna Song*<sup>1</sup>; Guangchun Yao<sup>1</sup>; Guoyin Zu<sup>1</sup>; Lei Wang<sup>1</sup>; Zhihao Guan<sup>1</sup>; <sup>1</sup>Northeastern University

The small size preforms of aluminum foams sandwich panel were prepared by a powder rolling method using the powders of AlSi12 alloy, Mg and TiH<sub>2</sub> as raw materials. Effects of foaming temperature and time on rolled foamable sandwich panel were investigated in details using SEM, OM analysis and a scanner at a resolution of 300 dpi. The results show that deformation of Al face sheet of the aluminum foams sandwich panel completely disappears. Furthermore, the local melting of Al face sheet can also be hardly found. The bonding between Al face sheet and foam core is good. No macro and micro defects exist in the cell structures and 225% of the expansion rate is achieved. The metallurgical bonding between Al face sheet and foam core can be absolutely obtained as the optimum foaming process of the small size preforms are guaranteed, viz., foaming temperature is 700° and the range of foaming time is between 90 and 120 seconds.

**4:15 PM**

**Preparation and Characterization of Short Carbon Fiber Reinforced Aluminium Matrix Composites:** Pengfei Yan<sup>1</sup>; Guangchun Yao<sup>1</sup>; Jianchao Shi<sup>1</sup>; Xiaolan Sun<sup>1</sup>; *Hongjie Luo*<sup>1</sup>; <sup>1</sup>School of Materials & Metallurgy, Northeastern University

Aluminium matrix composites reinforced by short carbon fibers were prepared through stir casting process. The carbon fibers coated with copper by using electrolysis plating were characterized by using scanning electron microscopy (SEM). The composites with different levels of carbon fibers were prepared through stir casting method. The microstructure and mechanical properties of composites were evaluated. The microstructure results showed that the carbon fibers were reasonably uniformly distributed within the aluminium matrix and exhibited good interfacial bonding with the matrix. The mechanical properties testing results indicated that the tensile strength and hardness increases with the increase of carbon fiber level. The results demonstrated that the stir casting is a promising method to prepare aluminium matrix composites.

**4:35 PM**

**Preparation of Aluminum Foam Using a Novel Gas-Generating Agent:** Deng-Wei Huo<sup>1</sup>; *Xiang-yang Zhou*<sup>1</sup>; Tai-kang Zhang<sup>1</sup>; Jin Qin<sup>1</sup>; Jie Li<sup>1</sup>; Huan Zhao<sup>1</sup>; <sup>1</sup>School of Metallurgical Science and Engineering, Central South University

The thermal decomposition behavior of a novel gas-generating agent (NA) and its effect on the viscosity of aluminum melt were investigated, as well as the preparation technology of aluminum foam by using NA as foaming agent and viscosifier was presented. The results show that NA has a wide decomposition temperature range and a gentle decomposition rate, and NA can effectively increase the viscosity of aluminum melt, as a result, the drier-metal foaming agents such as TiH<sub>2</sub> and ZrH<sub>2</sub> can be replaced by NA and an extra viscosifier such as Ca is unnecessary during preparation process of aluminium foam by melt foaming method. The aluminum foam with porosity of 60%-85% can be prepared while the additive amount of fine NA powder as viscosifier is in the range from 0.6wt% to 1.0wt%, and the additive amount of coarse NA powder as foaming agent is in the range from 1.6wt% to 2.2wt%.

**4:55 PM**

**High Temperature Dry Sliding Wear Behaviour of Aluminium-Silicon/Graphite Composite Processed by Stir Casting:** G. Rajaram<sup>1</sup>; *S. Kumaran*<sup>1</sup>; <sup>1</sup>National Institute of Technology Tiruchirappalli

Aluminum metal matrix composites are extensively used for tribological applications due to excellent wear resistance especially during sliding under dry, wet and high temperature environments. In this present study, aluminum silicon alloy and aluminum silicon alloy /graphite (3 wt.%) composite were prepared by stir casting method and their dry sliding wear behaviour was investigated by using Pin on Disc wear tester with temperatures up to 350°C in air. Incorporation of graphite and its distribution was confirmed with optical microscopy. Wear rate of alloy and composite was decreased with increasing temperature due to formation of oxide and glazing layers on the sliding surfaces. However, the wear behaviour of composite is better than that of alloy for all temperature conditions due to formation of rich tribo film between sliding surfaces by smeared graphite particulates. The worn surfaces of alloy and composite were characterized by scanning electron microscope to understand the wear mechanism.



## Aluminum Reduction Technology: Improvement in Cell Equipment and Design

*Sponsored by:* The Minerals, Metals and Materials Society, TMS Light Metals Division, TMS: Aluminum Committee, TMS: Aluminum Processing Committee

*Program Organizers:* Mohd Mahmood, Aluminium Bahrain; Abdulla Ahmed, Aluminium Bahrain (Alba); Charles Mark Read, Bechtel Corporation; Stephen Lindsay, Alcoa, Inc.

Wednesday PM  
March 2, 2011

Room: 17B  
Location: San Diego Conv. Ctr

*Session Chair:* Stephan Broek, Hatch Ltd

### 2:00 PM

#### Retrofit of a Combined Breaker Feeder with a Chisel Bath Contact Detection System to Reduce Anode Effect Frequency in a Potroom:

*Jonathan Verreault<sup>1</sup>; René Gariépy<sup>1</sup>; Bernard Desgroseilliers<sup>1</sup>; Claude Simard<sup>1</sup>; Xavier Delcorde<sup>2</sup>; Christophe Turpain<sup>2</sup>; <sup>1</sup>Rio tinto Alcan; <sup>2</sup>ECL*

Chisel bath contact detection is a feedback system provided on aluminium reduction cell alumina point feeders to ensure that the crust breaker (or chisel) contacts liquid bath. The benefits of chisel bath contact detection on anode effect reduction are well known on AP technology™ operating with a separate system of breaker and feeder. The present paper describes the technology adaptation for a safe hot change installation of chisel bath contact detection applied to the combined breaker/feeder in a P-155 cell while at the same time introducing a longer pneumatic cylinder stroke. Mechanical modifications allowing the reuse of most of the existing breaker/feeder parts as well as the results obtained on four experimental cells during the development phase are presented. The retrofit procedure is also described in the context of a hot change while controlling HSE related aspects. AP technology™ is trade-mark of Rio Tinto Innovations Ltd.

### 2:20 PM

#### Anode Dusting from a Potroom Perspective at Nordural And Correlation with Anode Properties: Halldor Gudmundsson<sup>1</sup>; <sup>1</sup>Century - Nordural

Anode performance in the cells is ultimately the most important measure of the anode quality and is not always reflected in the quality certificates. Nordural has through the years developed some tools to measure anode performance in the cells to use as feedback to anode suppliers so that they may improve the anode performance. Anode dusting in the cells leading to anode spikes and loss of current efficiency can be the biggest issue in the supplier - customer relationship. This paper shows some examples of anode dusting excursions experienced with three anonymous anode suppliers, how it was measured in the cells and how it was reduced or resolved in cooperation with the suppliers.

### 2:40 PM

#### The Application of Continuous Improvement to Aluminium Potline Design and Equipment: William Paul<sup>1</sup>; <sup>1</sup>Rio Tinto Alcan

The design and supply of technologies to a large number of aluminium smelter projects, over the last two decades, has provided a unique opportunity to benefit from continuous improvement. This improvement process starts with feedback from customers and suppliers, combined with input from R&D and internal reviews, to identify, validate and then incorporate experiences and innovation from many areas. The process can be described as systematic continuous improvement and the results are superior technology packages that incorporate the latest enhancements and better meet clients' needs. This paper describes the methodology used to manage the continuous improvement of technology packages. It includes examples of improvements, including ancillary equipment redesign to improve safety and reduce forklift truck usage. Also discussed are the challenges and opportunities of working with potline equipment suppliers. Effective cooperation enables the development of fit for purpose solutions that minimise potline commissioning issues and maximise pot performance.

### 3:00 PM

**Alcoa STARprobe:** Xiangwen Wang<sup>1</sup>; Bob Hosler<sup>1</sup>; Gary Tarcy<sup>1</sup>; <sup>1</sup>Alcoa, Inc.

Alcoa STARprobe is a probe device/system used to measure cryolitic bath properties including Superheat, Temperature, Alumina concentration, and cryolite Ratio (acidity), STAR, all together in real time for active pot control. The patented measurement principle is based on differential thermal analysis (DTA). This paper shows the fundamentals of operation along with the correlation of all the analysis with the accepted methods (XRD and pyrotitration for acidity, thermal couples for Bath Temperature and LECO and XRF analysis for alumina). The timing of the measurement will be shown to be equal to the traditional methods and the reliability (including reusable use of the probes) will also be described.

### 3:20 PM Break

### 3:30 PM

**Active Pot Control Using Alcoa STARprobe:** Xiangwen Wang<sup>1</sup>; Gary Tarcy<sup>1</sup>; Eliezer Batista<sup>1</sup>; <sup>1</sup>Alcoa, Inc.

To run an aluminum smelting cell, routine bath sampling and subsequent chemistry analysis are required along with pot temperature measurement. The sampling and analytical process is lengthy and tedious and very often, results are delayed as long as 24 hours. In addition the results are not coupled to the other critical information (e.g. noise, automatic resistance adjustments etc) at the time of the sample. Alcoa STARprobe™, which was previously described, corrects these deficiencies while providing a means to more efficiently and effectively control a smelting pot. This paper presents the background philosophy for an advanced control that has been enabled by the new measurement technique. The control method has been applied in multiple plants and demonstration of improved performance will be shown.

### 3:50 PM

**Applications of New Structure Reduction Cell Technology in Chalco's Smelters:** Fengqin Liu<sup>1</sup>; Songqing Gu<sup>1</sup>; Jiangmin Wang<sup>1</sup>; <sup>1</sup>Chalco

A new generation of key energy saving technology for aluminum reduction – the new structure aluminum reduction cell technology has been successfully developed by Chalco and widely applied in Chalco's smelters, which includes such key technologies, as the new specially designed cathode installation, heat preservation lining and low voltage operation control system. The molten metal fluctuation driven by the great magnetic field is greatly restrained in the cells, based on which reducing ACD without any loss of current efficiency is realized for lower energy consumption and less emission. The industrial tests and applications of this technology have been carried out successfully in the various scale aluminum reduction cells in Chalco's smelters and about 12000 kWh of DC consumption per ton of aluminum and 3.70 V of cell voltage have been achieved.

### 4:10 PM

**Transport Numbers in the Molten System NaF-KF-AIF3-Al2O3:** Pavel Fellner<sup>1</sup>; Jan Hives<sup>1</sup>; Jomar Thonstad<sup>2</sup>; <sup>1</sup>Slovak University of Technology in Bratislava; <sup>2</sup>NTNU

Transport numbers in the molten system NaF – KF – AIF3 (Al2O3, CaF2) were investigated by the Hittorf method. It was confirmed that in molten cryolite, Na3AlF6, 1010 °C, the current is transported almost exclusively by the Na+ cations ( $t(\text{Na}+) = 0.99$ ). When AIF3 is added to a Na3AlF6 melt, the transport number of sodium cations decreases to 0.74 at the composition corresponding to NaAlF4. In molten K3AlF6 the transport number of K+ cations equals 0.836 at 1005 °C. In melts containing both Na+ and K+, the cations contribute to the charge transport approximately in the ratio of the squares of their ionic radii.

### 4:30 PM

**Study on Solution of Al2O3 in Low Temperature Aluminum Electrolyte:** Hongmin Kan<sup>1</sup>; Ning Zhang<sup>1</sup>; Xiaoyang Wang<sup>1</sup>; <sup>1</sup>Shenyang University

Current efficiency can be increased and energy consumption can be lowered by low temperature aluminum electrolysis. However, many problems will occur, such as low electrical conductivity, cathode shell, low alumina solubility and alumina-solution rates if the temperature is too low. Of

these problems, low alumina solubility and alumina-solution rate are difficult problems. In this paper, a novel method which can measure the solubility and dissolution rate of  $Al_2O_3$  is introduced based on early researches. The double rooms' transparent quartz electro bath is used for low temperature aluminum electrolysis. The image sequence is gained by taking from the double rooms' transparent quartz electro bath. Image analysis techniques are used to compute the change of solubility and dissolution rate of  $Al_2O_3$ . The method can analyze the influence factors of solubility and dissolution rate of  $Al_2O_3$  intuitively and roundly by transparent quartz electro bath and image analysis techniques.

## Biological Materials Science: Mechanical Behavior of Biological Materials II

*Sponsored by:* The Minerals, Metals and Materials Society, TMS Electronic, Magnetic, and Photonic Materials Division, TMS Structural Materials Division, TMS: Biomaterials Committee  
*Program Organizers:* Jamie Kruzic, Oregon State University; Nima Rahbar, University of Massachusetts, Dartmouth; Po-Yu Chen, University of California, San Diego; Candan Tamerler, University of Washington

Wednesday PM                      Room: 15A  
March 2, 2011                      Location: San Diego Conv. Ctr

*Session Chairs:* Dwayne Arola, University of Maryland Baltimore County; Ryan Roeder, University of Notre Dame

### 2:00 PM Invited

**Energy Absorption in Natural Materials:** *Joanna McKittrick*<sup>1</sup>; Po-Yu Chen<sup>1</sup>; Ekaterina Novitskaya<sup>1</sup>; Maria Lopez<sup>1</sup>; Irene Chen<sup>1</sup>; Marc Meyers<sup>1</sup>; <sup>1</sup>University of California, San Diego

Some of the most remarkable materials in terms of energy absorption and impact resistance are not found through human processing but in nature. Solutions to the continuing problems of improved composite technologies may lie in replicating naturally occurring systems. In this presentation, several mammalian structural materials: bones (bovine femur, elk antler), teeth and tusks from various taxa, armadillo and turtle carapaces, horns from the desert big horn sheep, and equine hooves are examined. The relationships between structural and mechanical properties for these materials, with an emphasis on energy absorption mechanisms are established. Energy absorbing strategies utilized in these materials will be identified. Implementation of these bioinspired design strategies can serve as a basis for the design of new energy absorbent synthetic composite materials. This research is supported by NSF Grant (Ceramics and Biomaterials Program) 1006931.

### 2:30 PM Invited

**High Performance Impact-Tolerant and Abrasion-Resistant Materials: Lessons from Nature:** *David Kisailus*<sup>1</sup>; Qianqian Wang<sup>1</sup>; Michiko Nemoto<sup>1</sup>; Dongsheng Li<sup>1</sup>; Brian Weden<sup>1</sup>; <sup>1</sup>University of California at Riverside

Chitons are marine mollusks found worldwide in the intertidal or subtidal zones of cold water as well as in tropical waters. These organisms have evolved an amazing feeding structure called a Radula. The Radula is a ribbon-like structure that consists of abrasion resistant teeth anchored to a flexible stylus that the organism uses to abrade rocky substrates to reach algae. We investigate the structure and mineralization process in *Cryptochiton stelleri*, the largest of the chitons. Using various microscopy and spectroscopy techniques as well as synchrotron analyses, we have uncovered critical structure-function relationships in the mineralized teeth and insights into the mineralization processes in these unique structures. Investigation of the mechanical properties of the fully mineralized teeth have revealed that the combination of ultrahard minerals and templating organics, architected in a unique microstructure, lead to a damage tolerant composite that is of the hardest known biominerals known in nature.

### 3:00 PM

**Anatomic Variability in the Elastic Anisotropy of Human Cortical Bone Tissue is Governed by the Orientation Distribution of Apatite Crystals:**

*Justin Deuerling*<sup>1</sup>; *David Rudy*<sup>1</sup>; *Ryan Roeder*<sup>1</sup>; <sup>1</sup>University of Notre Dame

Computational models commonly account for elastic inhomogeneity in cortical bone using power-law scaling relationships with tissue or mineral density, and assume elastic isotropy or homogeneous anisotropy due to inadequate experimental data. Therefore, the objectives of this work were to characterize anatomic variation in the elastic anisotropy of human cortical bone and identify the governing structural parameters. Elastic constant magnitudes decreased and anisotropy increased from the mid-diaphysis toward the epiphyses of human femora. Tissue exhibited orthotropy toward the epiphyses, but was reasonably approximated as transversely isotropic near the mid-diaphysis. A specimen-specific micromechanical model accounting for seven structural parameters across multiple length scales identified the apatite crystal volume fraction and orientation distribution to be the most influential structural parameters governing the elastic constant magnitude and anisotropy, respectively. Model results were verified by experimental measurements of the elastic anisotropy, mineral density, tissue porosity, and apatite orientation distribution on the same tissue specimens.

### 3:20 PM

**Ab Initio Study of Thermodynamic, Structural, and Elastic Properties of Mg-Substituted Crystalline Calcite:**

*Martin Friak*<sup>1</sup>; *Pavlina Elstnerova*<sup>1</sup>; *Liverios Lymperakis*<sup>1</sup>; *Michal Petrov*<sup>1</sup>; *Tilmann Hickel*<sup>1</sup>; *Helge Fabritius*<sup>1</sup>; *Andreas Ziegler*<sup>2</sup>; *Svetoslav Nikolov*<sup>3</sup>; *Sabine Hild*<sup>4</sup>; *Dierk Raabe*<sup>1</sup>; *Joerg Neugebauer*<sup>1</sup>; <sup>1</sup>Max Planck Institute for Iron Research; <sup>2</sup>University of Ulm; <sup>3</sup>Bulgarian Academy of Sciences; <sup>4</sup>Johannes Kepler University Linz

Arthropoda, that represent nearly 80 % of all known animal species, are protected by an exoskeleton formed by their cuticle. The cuticle represents a hierarchically structured multifunctional bio-composite based on chitin and proteins. Some groups like Crustacea reinforce the load-bearing parts of their cuticle with calcite. As the calcite sometimes contains Mg it was speculated that Mg may have a stiffening impact on the mechanical properties of the cuticle. We present a theoretical parameter-free quantum-mechanical study of phase stability and structural and elastic properties of Mg-substituted calcite. Our results show that substituting Ca by Mg causes an almost linear decrease in the crystal volume with Mg concentration and of substituted crystals. As a consequence the calcite crystals become stiffer giving rise e.g. to substantially increased bulk moduli.

### 3:40 PM Break

### 3:50 PM

**Crack Propagation in Biocomposites: A Phase Field Study:**

*Murali Palla*<sup>1</sup>; *Tanmay Bhandakkar*<sup>2</sup>; *Wei Cheah*<sup>3</sup>; *Mark Jhon*<sup>1</sup>; *Huajian Gao*<sup>2</sup>; *Rajeev Ahluwalia*<sup>1</sup>; <sup>1</sup>Institute of High Perform. Computing; <sup>2</sup>Brown University; <sup>3</sup>Institute of Materials Research and Engineering

We investigate, using a phase field approach, the crack propagation in systems akin to biological composites which have layered microstructures of stiff mineral and a soft organic phase. We find crack bifurcation at the interfaces of the soft phase, which is distinct from the usual dynamic crack branching. The crack tip shape shows extensive blunting due to the presence of the soft strip. We also find a significant increase in the fracture toughness due to the presence of the thin layer of soft material. The effect of geometrical distribution of the soft and stiff phases on the crack propagation behavior is of interest and extrinsic mechanisms that enhance the toughness would be investigated using phase field approach.

### 4:10 PM

**Fracture Behaviour of Whole Teeth and Dentine at Different Hierarchical Levels:**

*Claudia Fleck*<sup>1</sup>; *Tania Traykova*<sup>1</sup>; *Paul Zaslansky*<sup>2</sup>; *Anke Maerten*<sup>2</sup>; <sup>1</sup>Technische Universitaet Berlin; <sup>2</sup>Max-Planck-Institute of Colloids and Interfaces

We investigated the interaction of cracking and damage with the microstructure of dentine on different hierarchical levels. Micro-tomography and histological sectioning of compression loaded whole premolars served

to characterise failure patterns in different dentine areas on the whole tooth level. Cracks developed in the dentine and in the enamel even though the teeth were not visibly broken. Bending and notch tensile tests on wet bar-like specimens were performed to better understand the material properties of dentine itself. ESEM and XRD showed profound differences in the spatial strain distribution round the tip of advancing cracks. The observation of crack propagation during fracture of dentine revealed differences in the strain distribution within the microstructural elements of the hierarchical levels. We believe that similar strain fields, modified by the graded structure of dentine and the layered structure of the tooth, are responsible for crack initiation and propagation in dentine in the whole tooth.

#### 4:30 PM

**Depth, Tubule Density and the Fatigue Crack Growth Resistance of Dentin:** *Juliana Ivancik*<sup>1</sup>; Dwayne Arola<sup>1</sup>; <sup>1</sup>University of Maryland Baltimore County

Dentin is a complex hierarchical mineralized tissue that occupies the majority of the human tooth by both weight and volume. The most distinct structural feature of this tissue is the dentin tubules, which is a system of microscopic channels extending in almost a radial arrangement from the pulp. The number, orientation and size of the tubules varies as a function of depth within the tooth. In this experimental investigation contribution from the tubule characteristics, including geometry and density, on the fatigue crack growth properties of dentin were characterized. There was a significant correlation between the tubule density and the relative resistance to fatigue crack initiation and growth; decreasing resistance was associated with greater depths. Overall, there was nearly a 1000 times increase in the incremental fatigue crack growth rate over the depth of tissue examined. This behavior appears attributed to the mechanisms in which crack extension occurs from adjacent tubules.

#### 4:50 PM

**Nanoscale Dynamic Mechanical Properties of a Mineralized Tissue: Human Dentin:** Dwayne Arola<sup>1</sup>; *Heonjune Ryou*<sup>1</sup>; <sup>1</sup>University of Maryland Baltimore County

In this study intertubular and peritubular components of dentin were evaluated by Dynamic Mechanical Analysis (DMA) using nanoindentation. The complex (E), loss (E''), and storage (E') moduli of intertubular and peritubular dentin were measured using a Hysitron Triboindenter over a range of dynamic frequencies (1 to 100 Hz). As expected, the storage modulus of the peritubular cuff (22.19 GPa < E' < 34.71 GPa) was significantly greater (p < 0.001) than for the intertubular dentin (16.08 GPa < E' < 22.79 GPa) over the range of frequencies, due to the higher relative mineral content. The loss modulus of the intertubular dentin (1.31 GPa < E'' < 2.28 GPa) was greater than that of the peritubular cuffs (0.70 GPa < E'' < 1.60 GPa), but the differences were not significant (p > 0.05). While the moduli increased with loading frequency they were not dependent on the mean load. The intertubular and peritubular dentin exhibit significant differences in the time-dependent aspects of mechanical behavior when measured using a dynamic mechanical analysis.

#### 5:10 PM

**The Effects of High Doses of Irradiation on the Fracture Behavior of Human Cortical Bone:** *Holly Barth*<sup>1</sup>; Maximilien Launey<sup>2</sup>; Robert Ritchie<sup>1</sup>; <sup>1</sup>UC Berkeley; <sup>2</sup>Lawrence Berkeley National Laboratory

Human bone is exposed to irradiation for a wide range of medical and scientific reasons. In the medical community bones are sterilized through irradiation for bone allograft surgery. For scientific studies the effects of irradiation is a concern with experiments that use *in situ* testing with high-energy synchrotron radiation diffraction and tomography imaging. Bone's mechanical behavior is a function of its' multi-dimensional hierarchical nature. To better predict the effects of irradiation on bone's fracture behavior it is important to investigate changes at each significant size scale. The findings in this study show that bone exposed to high levels of irradiation can cause serious deleterious effects to the collagen which leads to drastic losses in strength, ductility and toughness. It was shown that the plasticity in

bone was suppressed after as little as 70 kGy and the fracture toughness was decreased by a factor of 5 after 210 kGy of irradiation.

#### 5:30 PM

**Quantitative and Qualitative Changes in the Structure and Properties of Demineralized and Deproteinized Compact Bone:** *Ekaterina Novitskaya*<sup>1</sup>; Joshua Vasquez<sup>1</sup>; Robert Urbaniak<sup>1</sup>; Steve Lee<sup>1</sup>; Po-Yu Chen<sup>1</sup>; Ana Castro<sup>2</sup>; Gustavo Hirata<sup>2</sup>; Joanna McKittrick<sup>1</sup>; <sup>1</sup>UCSD; <sup>2</sup>Centro de Investigación Científica y de Educación Superior de Ensenada

Bone loss (osteoporosis) and demineralization occur as bones age and are major causes of bone fractures. The mineral/collagen interaction is important for understanding how this affects the bone fracture. A method of partial demineralization of bone was established through aging in 0.6N hydrochloric acid (HCl), monitored by inductively coupled plasma optical emission spectroscopy on the acid solution. Compression and bending mechanical tests of partially demineralized, completely deproteinized and untreated bovine femur bone were investigated with different strain rates. Fracture surfaces were analyzed by optical microscopy, scanning electron microscopy, micro-CT scanning, and atomic force microscopy. Compression tests showed that the sum of the stress-strain curves for completely demineralized and completely deproteinized bone was far lower than that of the untreated bone, indicating a strong molecular interaction between a collagen matrix and a mineral phase. This research is supported by the National Science Foundation grant DMR 0510138 and UC-MEXUS 2009 grant.

### Bridging Microstructure, Properties and Processing of Polymer Based Advanced Materials: Session II

*Sponsored by:* The Minerals, Metals and Materials Society, TMS Extraction and Processing Division, TMS Materials Processing and Manufacturing Division, TMS: Materials Characterization Committee, TMS: Shaping and Forming Committee, ASM-MSCTS: Texture and Anisotropy Committee

*Program Organizers:* Dongsheng Li, Pacific Northwest National Laboratory; Said Ahzi, University of Strasburg; Moe Kahleel, Pacific Northwest National Laboratory

Wednesday PM  
March 2, 2011

Room: 32B  
Location: San Diego Conv. Ctr

*Session Chairs:* Dongsheng Li, Pacific Northwest National Laboratory; Frédéric Addiego, CRP Henri Tudor

#### 2:00 PM Keynote

**Amorphous and Semi-Crystalline Blends of Poly(Vinylidene Fluoride) and Poly(Methyl Methacrylate): Characterization and Modeling of the Mechanical Behavior:** *Jean Halary*<sup>1</sup>; <sup>1</sup>ESPCI ParisTech

After extensive studies in the 1970s in relation to miscibility and piezoelectric properties, the blends of poly(methyl methacrylate) (PMMA) and poly(vinylidene fluoride) (PVDF) have been revisited with the aim of assessing their mechanical behavior. Depending on the amount of PVDF, either amorphous or semi-crystalline blends are produced: typically, the blends remain amorphous when their PVDF content does not exceed 50 wt%. Emphasis is put on the low deformation range covering the anelastic and plastic behaviors. The reported data depend, as expected, on temperature and strain rate and also, markedly, on blend composition and degree of crystallinity. Molecular arguments, based on the contributions of the glass transition motions and of the PMMA motions associated by the secondary relaxation are proposed to account for the observed features. Thanks to this understanding of the phenomena on the molecular level, accurate models can be selected in the view of stress-strain curve modeling.



2:30 PM

**Mechanical Behavior of Melt Mixing Polypropylene Organoclay Nanocomposites:** *Said Ahzi<sup>1</sup>; Nadia Bahloui<sup>1</sup>; Kui Wang<sup>1</sup>; Rodrigue Matadi<sup>1</sup>; Rene Muller<sup>1</sup>;* <sup>1</sup>University of Strasbourg

This work aims to investigate the mechanical behavior of polypropylene organoclay nanocomposites under quasistatic and dynamic loading conditions. The nanocomposite was obtained by mixing the polypropylene matrix with a master batch of polypropylene modified anhydride maleic and montmorillonite organoclay (pp-nanocor). The obtained nanocomposite exhibits a good dispersion and an exfoliated morphology. To study the effect of the nanocomposite dispersion and morphology, another nanocomposite was prepared by melt mixing of polypropylene and a modified montmorillonite (dellite) (pp-dellite). The dynamic behaviour was investigated by using a split Hopkinson pressure bars, at different strain rates and different temperatures. The obtained results for pp-nanocor, showed an increase of both Young's modulus and yield stress with the increasing organoclay concentration. However pp-dellite nanocomposites presented poor mechanical properties compared to those of pp-nanocor.

2:50 PM

**Microstructural Characterization of Plastic-Bonded Explosives:** *John Yeager<sup>1</sup>; Daniel Hooks<sup>1</sup>; David Bahr<sup>2</sup>;* <sup>1</sup>Los Alamos National Laboratory; <sup>2</sup>Washington State University

Plastic-bonded explosives (PBX's) consist of hard, anisotropic molecular crystals in a polymer matrix. Historical studies have shown PBX's fail prematurely via crack propagation along the crystal-polymer interface. Characterization of the interface is therefore important for the development of predictive failure models. Additionally, study of the interface reveals the importance of wetting and dewetting phenomena which relate mechanical and explosive properties to the manufacturing process. Here, the interface is characterized using several methods. The adhesion of the crystal to several polymers has been characterized by surface energy measurements and a novel mechanical test, revealing that the practical adhesion is orders of magnitude higher than the calculated work of adhesion. The physical nature of the interface has been probed with atomic force microscopy and nanoindentation and is compared to pristine crystal surfaces. The interfacial chemistry has been analyzed with neutron reflectometry, differentiating between a clean interface and a compositionally graded interphase region.

3:10 PM

**An Electron Microscopy Study of Nanoscale Surface and Sub-Surface Deformation Response of Polymer Nanocomposites:** *Qiang Yuan<sup>1</sup>;* Devesh Misra<sup>1</sup>; <sup>1</sup>University of Louisiana at Lafayette

The objective of the presentation is to elucidate the nanoscale surface and sub-surface deformation response of polymer nanocomposites. The commonality in surface deformation behavior between nano- and microscale deformation is studied in order to reinforce the underlying fundamental principles governing surface deformation. An understanding of mechanics of surface deformation is accomplished via electron microscopy analysis of scratch damage at and beneath the surface in conjunction with physical and mechanical properties.

3:30 PM Break

3:50 PM

**Investigation on Modified Humic Substances Based Binders for Iron Ore Agglomeration:** *Tao Jiang<sup>1</sup>; Guihong Han<sup>1</sup>; Yuanbo Zhang<sup>1</sup>; Yanfang Huang<sup>1</sup>; Guanghui Li<sup>1</sup>;* <sup>1</sup>School of Minerals Processing & Bioengineering, Central South University

Characterization of modified humic substances based binders for iron ore agglomeration was examined by chemical analysis, optical density, FTIR and TG-DSC. Chemical analysis displays the proportion of fulvic acid (FA) to humic acid (HA) in the binders is 1:10. Compared with the HA, the FA possesses more functional groups. Meantime, optical density ratio analysis shows that molecular weight and aromatization degree of the FA are smaller than those of the HA. FTIR spectra further confirm aromatic and aliphatic fractions are associated with various types of oxygen-rich groups

including carboxyl and hydroxyl groups. TG-DSC and chemical analysis indicate structural changes of the binder including thermal decomposition, dehydroxylation and/or decarboxylation are caused during heating. The structural characterization of the binder ensures its good performance in the field of iron ore agglomeration.

4:10 PM

**Triple Shape Memory Polymers Based on Self-Complimentary Hydrogen Bonding:** *Taylor Ware<sup>1</sup>; Keith Hearon<sup>2</sup>; Duncan Maitland<sup>2</sup>; Walter Voit<sup>1</sup>;* <sup>1</sup>The University of Texas at Dallas; <sup>2</sup>Texas A&M University

Triple-shape polymers (TSPs) are a growing subset of a class of smart materials known as shape memory polymers. TSPs can store one permanent and two metastable shapes. We describe a novel TSP system, comprised of both permanent covalent crosslinks and reconfigurable hydrogen bonding crosslinks, which enables broad and independent control of both glass transition temperature ( $T_g$ ) and crosslink density. Triple shape properties arise from the combination of (meth)acrylate copolymers and the dissociation of self-complimentary hydrogen bonding moieties. Specifically, ureidopyrimidone methacrylate and a novel monomer, ureidopyrimidone acrylate, were copolymerized with methyl acrylate, butyl acrylate and bisphenol A ethoxylate diacrylate. Control of  $T_g$  from 10-70°C was demonstrated; concentration of hydrogen bonding moieties was varied from 0-40mol%; concentration of the diacrylate was varied from 0-20mol%. The effects of varying concentration of each crosslink type were observed through changes in shape-memory characteristics including stress-strain response and changes in modulus as a function of temperature.

4:30 PM

**Thermomechanical Properties of Epoxy Nanocomposites Using Surface Functionalized Silica Nanoparticles:** *Muhammad Sajjad<sup>1</sup>;* Bernhard Feichtenschlager<sup>1</sup>; Silvia Pabisch<sup>2</sup>; Thomas Koch<sup>1</sup>; Sabine Seidler<sup>1</sup>; Herwig Peterlik<sup>2</sup>; Guido Kikelbick<sup>3</sup>; <sup>1</sup>TU wien; <sup>2</sup>University of Vienna; <sup>3</sup>Saarland University,

Surface functionalized silica nanoparticles have been utilized in order to enhance better interaction with the epoxy matrix to produce homogenous nanocomposite films of epoxy. The resulting nanocomposites were characterized by DSC, DMA, TGA and micro hardness techniques. The dispersibility of the particles in organic media and within the polymer matrix was investigated by transmission electron microscopy (TEM) and SAXS. Diglycidylether of Bisphenol F epoxy matrix was embedded with two sized silica nanoparticles (big and small which were prepared by in situ polymerization (via Stoeber process). Silica nanoparticles (one fraction in the lower nanoscale "small" and one in the higher nanorange "big") have been surface functionalized with 3 glycidylpropyltrimethoxysilane (Gly-C3-TMEOs). Due to the surface modification of the silica nanoparticles better dispersibility was achieved throughout the whole matrix which resulted in homogenous and transparent films even at higher nanoparticle loadings. SAXS results confirmed the better structural properties with both sized particles. The mechanical properties of the resulting nanocomposites were generally superior to the pure epoxy matrix. The prepared nanocomposite films showed increase in micro hardness and higher elastic moduli. On the other hand, incorporation of the modified nanoparticles was responsible for some decrease in the glass transition temperature as was evidenced during DSC study and thermal degradation behaviour was almost unaffected by even the use of modified particles.

4:50 PM

**Electrospun Polymer Nanofiber Composite as Thermal Neutron Scintillators:** *Stephen Young<sup>1</sup>;* Indraneel Sen<sup>1</sup>; Dayakar Penumadu<sup>1</sup>; <sup>1</sup>University of Tennessee, Knoxville

Electrospun polymer nanofibers are attractive due to their volume-to-space, chemical, electrical and unique optical properties. Homeland security has great interest in applications with polymeric scintillation detectors that directly discriminate between neutron and gamma radiations using manufacturing techniques that are inexpensive and which can be effectively implemented to produce large area detectors. Lithium-6 isotope has a significant thermal neutron cross-section and produces high energy charged

particles on thermal neutron absorption. In this research, lithium-6 fluoride ( $^6\text{LiF}$ ) loaded polymer composite was successfully spun onto a stationary aluminum target creating a thermal neutron scintillator made of randomly oriented fibers. Fiber mats thus obtained were characterized for morphology, optical properties, polymeric properties like glass transition and response to thermal neutrons, alpha, beta and gamma radiation. Fiber matrix was made out of an aryl vinyl polymer and a wavelength shifting fluor with efficient resonant energy transfer characteristics.

## 5:10 PM

**Environmental Reliability Analysis of Mobile Phone Based on Active Disassembly Using Smart Materials:** Liu Zhifeng<sup>1</sup>; Zhao Liuxian<sup>1</sup>; Li Xinyu<sup>1</sup>; <sup>1</sup>Hefei University of Technology

Active disassembly using smart material (ADSM) is a method using shape memory material to replace fastener, when it is heated to the stimulated temperature, the product can be disassembled actively. ADSM can enhance the disassembly efficiency greatly; therefore, it gets more and more attention. When the method of ADSM is applied to practical electronic products, such as mobile phone, we need to conduct environmental reliability analysis of the product before it is put into market. This paper is about the environmental reliability analysis of mobile phone based on active disassembly using smart materials. Firstly, establishing the active disassembly model of mobile phone. Then analyzing the impacts of temperature, vibration and collision on the mobile phone. Comparing it with the environmental reliability of ordinary mobile phone. Finally, modifying the structure of mobile phone rationally by analysis.

## 5:30 PM

**Epitaxial and Confinement Effects in Hybrid Organic-Inorganic Nanostructured Composites:** Qiang Yuan<sup>1</sup>; Devesh Misra<sup>1</sup>; <sup>1</sup>University of Louisiana at Lafayette

We described here the fundamental mechanisms underlying nucleation and growth of polymer crystals in polymer-carbon nanotube composites. The periodic patterning of polymer lamellar crystals decorated along the carbon nanotube axis is discussed in terms of epitaxial and nanoparticle confinement effect. Furthermore, the dependence of crystallization conditions including pressure and temperature on this novel structure is investigated. As a result, by controlling pressure and crystallization temperature, a high degree of structural control may be achievable, which has profound effect on mechanical properties.

## 5:50 PM Keynote

**Bio-Based Nanocomposites Formed by Nanoparticle-Catalyzed Polymerization of Furfuryl Alcohol:** Rina Tannenbaum<sup>1</sup>; <sup>1</sup>Georgia Institute of Technology, School of Materials Science and Engineering

Bio-based polyfurfuryl alcohol (PFA) matrix nanocomposites have been fabricated by in-situ polymerization of furfuryl alcohol (FA), using montmorillonite nanoclays (MMT) or cellulose whiskers (CW) both as catalysts and matrix modifiers, to enhance thermal performance. The present work describes the polymerization of FA in the presence of MMT and CW and the resulting structure-property relationships. Fabricated nanocomposites were characterized by FTIR and TGA. Both nanocomposites afford a notable increase in the onset of degradation temperature compared to pure PFA. CW-PFA nanocomposites show improved mechanical toughness over previously reported PFA systems. To realize MMT-PFA nanocomposites with increased thermal stability, organomodified MMT clay must be selected. These results also highlight the importance of investigating both the non-oxidative and oxidative degradation behavior of a given material.

## Bulk Metallic Glasses VIII: Simulation and Modeling

*Sponsored by:* The Minerals, Metals and Materials Society, TMS Structural Materials Division, TMS/ASM: Mechanical Behavior of Materials Committee

*Program Organizers:* Gongyao Wang, University of Tennessee; Peter Liaw, Univ of Tennessee; Hahn Choo, Univ of Tennessee; Yanfei Gao, Univ of Tennessee

Wednesday PM

March 2, 2011

Room: 6D

Location: San Diego Conv. Ctr

*Session Chairs:* Dan Miracle, AF Research Laboratory; Ju Li, University of Pennsylvania

## 2:00 PM Invited

**Partial Coordination Numbers in Solute-Rich Glasses:** Dan Miracle<sup>1</sup>; Oleg Senkov<sup>2</sup>; Garth Wilks<sup>3</sup>; <sup>1</sup>AF Research Laboratory; <sup>2</sup>UES, Inc.; <sup>3</sup>General Dynamics

A clear description of the atoms in the first coordination shell surrounding each constituent atom is essential for a structural description of metallic glasses. Only limited experimental data are available for these partial coordination numbers. The efficient cluster packing (ECP) model enables prediction of partial coordination numbers, but this has only been developed for solute-lean glasses. The most stable metallic glasses are generally solute-rich, so that the first coordination shells around solute and solvent sites are expected to contain both solute and solvent atoms. We extend the earlier model to enable prediction of partial coordination numbers in solute-rich binary glasses. Results from predictions of this new model are compared with available experimental data. This analysis enables bond counting and packing efficiencies to be estimated. Results from these calculations will be presented and discussed with regard to the recent topological fluctuation theory (TFT) of metallic glasses.

## 2:20 PM

**Atomic-Scale Modeling of Chemical Effects on the Glass-Forming Ability of Metallic Glass Alloys:** Logan Ward<sup>1</sup>; Katharine Flores<sup>1</sup>; Wolfgang Windl<sup>1</sup>; <sup>1</sup>The Ohio State University

Atomic size ratio, number of constituents, and enthalpy of mixing are well-known rules for selecting constituents for metallic glasses. The role of atomic size ratio in the glass-forming ability has been examined through several experimental and computational studies. However, there has been little research into other aspects of atomic interactions, such as bond energy and the curvature of the potential well. In this research, the influence of these interactions on glass-forming ability was studied through molecular dynamics simulations. A method for determining the fragility of a supercooled metallic liquid was developed to indicate glass-forming ability. These methods were then applied to systems with modified potentials to determine the effects of curvature and bond energy changes. A major goal of this work is to develop new rules for constituent selection, as the bond energy and well shape can be directly linked to many thermal and elastic properties of the constituent materials.

## 2:30 PM Invited

**Cold Versus Hot Shear Banding in Metallic Glass: A Stick-Slip Model Compared with Experiments:** Evan Ma<sup>1</sup>; <sup>1</sup>Johns Hopkins University

Recent experiments (e.g., by T.G. Nieh et al., Y. Li et al., F. Dalla Torre et al.) have revealed that for some BMGs, the serrations in the compressive stress-strain curve correspond to the sliding of a single shear band in a stop-and-go fashion. The details of the serration (e.g., the step size of the growing shear offset and the stability of the shear) depend on the sample size and machine stiffness. Here we illustrate a stick-slip model to explain the origin of the serration and the effects of sample size and machine stiffness. The model also predicts the regime where the shear band becomes hot and unstable from the get-go. The predicted striation spacing, size of the shear offset, sliding speed, as well as the temperature reached and the duration

of the shear band stop-and-go cycle, all quantitatively agree with the experimental observations.

### 2:50 PM

**Condensed Bond Enthalpies in Metal-Nonmetal and Metal-Semimetal Compounds:** *Amanda Dahlman*<sup>1</sup>; Daniel Miracle<sup>1</sup>; Garth Wilks<sup>1</sup>; <sup>1</sup>Air Force Research Laboratory

Bond enthalpies are widely used measures of the energy contained in a bond between atoms in molecular gases and have recently been extended to metallic systems in the condensed state. The further extension of this concept to metal-semimetal and metal-nonmetal compounds is performed using readily available thermodynamic and crystallographic data. These determined values will be critically examined by exploring trends and relationships between compounds.

### 3:00 PM Invited

**Effects of the Potential Landscape on Metallic Liquids and Alloys:** *James Morris*<sup>1</sup>; <sup>1</sup>Oak Ridge National Laboratory

One approach to understanding the transition between the liquid and glass states has been through the concept of the potential landscape, which has been used to demonstrate that there are three distinct temperature regimes: the high-temperature liquid, the low-temperature glass, and an intermediate "potential dominated" regime. This will be reviewed, with a particular emphasis on recent simulation results on metallic glasses. We demonstrate that there are experimentally measurable signatures of the associated transition from the high temperature regime to the intermediate regime, which show up in simulations of both model systems and more realistic potentials. The different regions show different diffusive, structural and thermodynamic signatures. The fragility of the liquid is shown to be correlated with the Poisson ratio of the glass phase, in accordance with recent experimental and theoretical results. This research was sponsored by the Division of Materials Sciences and Engineering, U.S. Department of Energy, Office of Basic Energy Sciences.

### 3:20 PM

**Continuum Modeling of Bulk Metallic Glasses and Composites:** *Fadi Abdeljawad*<sup>1</sup>; Max Fontus<sup>2</sup>; Lisa Manning<sup>1</sup>; Mikko Haataja<sup>1</sup>; <sup>1</sup>Princeton University; <sup>2</sup>Prairie View A&M University

At low temperatures, monolithic bulk metallic glasses (BMGs) exhibit high strength and large elasticity limits. On the other hand, BMGs lack overall ductility due to highly localized deformation mechanisms. Recent experimental findings suggest that the problem of catastrophic failure by shear band propagation in BMGs can be mitigated by tailoring microstructural features at different length scales to promote more homogeneous plastic deformation. Herein, based on a continuum approach capable of capturing strain softening, we present a quantitative analysis of the effects of microstructure on the deformation behavior of monolithic BMGs and BMG composites. In particular, simulations highlight the importance of short-ranged structural correlations on ductility in monolithic BMGs and demonstrate that ductile phase morphology and its associated length scales control the ductility of BMG composites. In broader terms, our results provide new avenues for further improvements to the mechanical properties of BMGs.

### 3:30 PM Break

### 3:40 PM Invited

**Stress and Fracture Analyses of Bulk Metallic Glasses under Compressive Loading:** *Leon Keer*<sup>1</sup>; Xiaoqing Jin<sup>1</sup>; Gongyao Wang<sup>2</sup>; Oleg Senkov<sup>3</sup>; Daniel Miracle<sup>3</sup>; Peter Liaw<sup>2</sup>; Jules Raphael<sup>1</sup>; <sup>1</sup>Northwestern University; <sup>2</sup>The University of Tennessee, Knoxville; <sup>3</sup>Air Force Research Laboratory; <sup>4</sup>Columbus McKinnon Corporation

Fracture under compressive loading exhibits distinct behaviors than that under tensile loading. Various crack-propagation modes have been identified for compression failure of bulk metallic glasses (BMGs). Experiments on Ca-based BMG under uniaxial compression indicate that cracks initiate from micro porosity and propagate in a direction generally parallel to the loading axis. Micromechanical stress analysis shows that pores cause axial tensile

splitting microcracks emanating from the pore. A simplified computational model based on the linear elastic fracture mechanics (LEFM) is proposed to investigate the crack-extension behaviors under compressive load. The stable crack length is characterized by a dimensionless fracture-mechanics quantity required to attain the associated crack length. The stability of crack growth is examined based on the stress-intensity-factor (SIF) calculation, and its dependence on the loading and geometric conditions is discussed in this study. The present modeling provides heuristic insights into the different failure modes under compression.

### 4:00 PM Invited

**Deformation and Failure of Glasses at Nanoscale:** *Ju Li*<sup>1</sup>; <sup>1</sup>University of Pennsylvania

Recent experiments on nanoscale amorphous materials have suggested interesting ductility - size scale dependencies (PNAS 104, 11155; PRB 77, 155419). Such size effect may shed light on the connection between plastic deformation and underlying spatio-temporal hierarchies of structural flow defects, the smallest of which is a single shear transformation zone  $\sim 1\text{nm}^3$ . A mesoscale computational model on the same level as discrete dislocation dynamics for crystalline materials is constructed, which utilizes detailed statistical information about shear transformations, damage accumulations and damage repairs from atomistic simulations.

### 4:20 PM

**Correlation between Elastic Modulus and Intrinsic Plasticity of Metallic Glass: The Roles of Atomic Configuration and Alloy Composition:** *Yongqiang Cheng*<sup>1</sup>; Ajing Cao<sup>1</sup>; Evan Ma<sup>1</sup>; <sup>1</sup>Johns Hopkins University

Recent experiments revealed intriguing correlations between elastic modulus and plasticity of MGs. The shear modulus (G) to bulk modulus (B) ratio G/B was found to be a useful indicator of the intrinsic plasticity. We will discuss how the structural order (atomic configuration) and the composition (constituent elements) influence the intrinsic mechanical properties of monolithic MGs, and what common basis underlies the apparent property correlations. Using computer simulation, it is found that B is primarily determined by the constituent elements and the composition, while G is more sensitive to the degree of structural order. Using more ductile metals (in its crystalline form) and/or creating more disordered structure would therefore result in a lower G/B ratio of the MG, as well as less strain localization (enhanced intrinsic plasticity). Such a microscopic picture for the macroscopic property correlation is expected to facilitate the search of MGs with desired properties.

### 4:30 PM Invited

**Equation of State of Metallic Glasses:** *Mo Li*<sup>1</sup>; <sup>1</sup>Georgia Institute of Technology

Equation of state (EOS) relates pressure, volume and other thermodynamic variables in a material system under hydrostatic loading. The EOS of metallic glasses exhibits marked features that are different from those of many crystalline phases: a softer regime at low pressure and a harder regime at high pressure, and a hysteresis loop. There are also reports of polymorphic transitions between different amorphous phases. In this talk, I will present our recent work using both atomistic and analytical work on EOS in model metallic glasses. We show that the EOS is closely related to the topological packing of the glassy phases and the physical properties of constituent alloy elements; there exist two regimes under hydrostatic pressure, which are connected by a topological phase transition. We will discuss and put forward a measure for the transition. The EOS from the atomistic simulation and those from various models will be compared and discussed.

### 4:50 PM Invited

**Molecular Dynamics Simulations of Metallic Glasses under Cyclic Loading:** *Yunfeng Shi*<sup>1</sup>; Despina Louca<sup>2</sup>; Gongyao Wang<sup>3</sup>; Peter Liaw<sup>3</sup>; <sup>1</sup>Rensselaer Polytechnic Institute; <sup>2</sup>University of Virginia; <sup>3</sup>The University of Tennessee

We present a molecular dynamics study of cyclic loading tests on model metallic-glass nanowires. Both compression-compression and tension-tension cyclic loading are imposed on the testing sample up to 100 cycles.



The maximum strain is chosen to be 4 %, which is above the linear elastic regime but without shear band formation. The cyclic-loaded samples exhibit spatially uncorrelated shear band formation, which indicates the absence of accumulated structural damages. Upon compression-compression cyclic loading, it was found that the metallic-glass nanowire hardens in compression tests, while softens in tensile tests. However, upon tension-tension cyclic loading, it was found that the metallic-glass nanowire softens in compression tests, while hardens in tensile tests. Such asymmetric hardening behavior can be explained in terms of anisotropic distribution of icosahedral pairs, which evolves during cyclic loading.

**5:10 PM**

**Phase-Field Modeling of Phase Transformations in Glass Forming Alloys:** *Tao Wang*<sup>1</sup>; Ralph Napolitano<sup>2</sup>; <sup>1</sup>Ames Lab; <sup>2</sup>Ames Lab & Iowa State University

A phase-field model is presented for phase transformations in glass forming alloys. The competitions among stable and metastable phases are simulated for Cu-Zr alloys. The free-energy density is developed from atomistic calculations and thermodynamic modeling and some kinetic properties are extracted from molecular dynamics simulations. The simulation results provide a better understanding of the influences of the underlying thermodynamic and kinetic factors.

**5:20 PM Invited**

**Molecular Dynamics Studies of Cu-Zr-Al Metallic Glasses in Connection with In-Situ Synchrotron Experiment:** *Yunche Wang*<sup>1</sup>; Chun-Yi Wu<sup>1</sup>; Feng Jiang<sup>2</sup>; Jinn Chu<sup>3</sup>; Peter Liaw<sup>2</sup>; <sup>1</sup>National Cheng Kung University; <sup>2</sup>The University of Tennessee; <sup>3</sup>National Taiwan University of Science and Technology

Cu-Zr-Al glass-forming alloys have received increased attentions due to minor changes in the aluminium content drastically affecting the plasticity of the metallic glass. Molecular dynamics (MD) thin-film models of the alloys have been constructed by sputter-deposition simulation with argon as working gas on substrate. The simulated, as-deposited films were amorphous. Results from uniaxial loading/unloading MD simulations were compared with data from in-situ synchrotron experiments on radial distribution functions, Young's modulus and Poisson's ratio of the (Cu<sub>50</sub>Zr<sub>50</sub>)<sub>100-x</sub>Al<sub>x</sub> (in atomic percent, at%) amorphous alloys with x less than 12. Young's modulus and Poisson's ratio of the cube samples were calculated from the MD simulations, and they were found to be in agreement with experimental data. Strong correlations between the loose-packing local structures and the plasticity of the glass-forming alloys were found. Atomic structures at short and medium range orders of the alloys will be discussed.

**5:40 PM**

**Correlations between Local Stresses and Moduli in Model Metallic Glasses:** Karimi Kamran<sup>1</sup>; *Craig Maloney*<sup>1</sup>; <sup>1</sup>Carnegie Mellon University / Civil & Environmental Engineering

Molecular dynamics (MD) simulations of sheared model metallic glasses have long shown evidence for localized flow events. However, meaningful ways for defining flow defects where the system has a propensity to yield have been elusive. We present results of MD simulations of slowly sheared Lennard-Jones glasses. We show that the deviatoric component of the coarse grained stress tensor shows a non-trivial power-law decay with coarse-graining size reflecting a scale-invariant local anisotropy. We furthermore discuss how these scalings of the stress field are related to similar scalings in the elastic moduli. The results call into question the naive use of the stress field to identify defective regions in a glass.

**5:50 PM Invited**

**Local Atomic Structure of Ca-Mg-Zn Bulk Metallic Glasses:** *Oleg Senkov*<sup>1</sup>; Emma Barney<sup>2</sup>; Yongqiang Cheng<sup>3</sup>; Daniel Miracle<sup>1</sup>; Evan Ma<sup>3</sup>; Alex Hannon<sup>2</sup>; <sup>1</sup>Air Force Research Laboratory; <sup>2</sup>ISIS, Rutherford Appleton Laboratory; <sup>3</sup>John Hopkins University

Amorphous structure of ternary Ca<sub>60</sub>Mg<sub>x</sub>Zn<sub>40-x</sub> metallic glasses (X = 10, 15, 20, and 25 at.%) was modeled by Reverse Monte Carlo (RMC) and *ab initio* Molecular Dynamics (MD) techniques. The RMC and MD modeled

structures were statistically the same and consistent with experimental neutron and X-ray diffraction data. The amorphous structure was described as a mixture of Mg and Zn centered atomic clusters, with Ca dominating in the first shell. A coordination number (CN) of 10 (with about 7 Ca and 3 (Mg+Zn) atoms) was most common for the Zn-centered clusters. CN = 11 and 12 (with about 7-8 Ca and 4 (Mg+Zn) atoms) were most common for Mg-centered clusters. Analysis of the neighbor environment and bond angle distributions suggested near-equilateral triangles and pentagonal bipyramids to be the most common nearest atom configurations. The results were compared with recently proposed cluster packing models.

**6:10 PM**

**Predicting the Properties of High Entropy Alloys from Electronic Structure:** *Andrew Cunliffe*<sup>1</sup>; Colin Freeman<sup>1</sup>; Iain Todd<sup>1</sup>; <sup>1</sup>University of Sheffield

The electronic structures of the High Entropy Alloys (HEAs); CoCrFeNiAl (bcc) and CoCrFeNiTi (fcc) have been modelled using Density Functional Theory (DFT). The Fermi energy and free electron density from the model have been used to predict mechanical and physical properties of the alloys. This approach has allowed prediction of resistivity, heat capacity, thermal expansion coefficient and bulk modulus of the alloys. The predicted bulk moduli for CoCrFeNiAl and CoCrFeNiTi are 58.7 GPa and 41.36 GPa respectively. The adoption of different crystal symmetries is also explained in terms of the different free electron densities of the alloys. The properties of HEAs are difficult to predict, as they have no obvious base metal to extrapolate from. The use of DFT modelling in the treatment of HEAs allows the prediction of properties from composition and gives a better understanding of the behaviour of these novel materials.

**6:20 PM Invited**

**Predicating the Bulk Elastic Modulus and Density of Metallic Glasses by First Principles Calculation:** *X. Hui*<sup>1</sup>; Z. P. Lu<sup>1</sup>; G. L. Chen<sup>1</sup>; Z. K. Liu<sup>2</sup>; <sup>1</sup>University of Science and Technology Beijing; <sup>2</sup>The Pennsylvania State University

Metallic glasses are generally regarded as elastically isotropic, and they behave as an elastic continuum at low temperatures. Here we present a new way for the predication of bulk moduli and densities of metallic glasses by *ab initio* molecular dynamics and first principles calculation. Using this approach, we obtained the bulk moduli and densities for Zr-, Cu-, Co, and Ti based bulk metallic glasses, and found that the predicated results are in good agreement with the experimental data. Additionally, some other physical properties can be also deduced from this work.

## Cast Shop for Aluminum Production: Grain Refinement, Alloying, Solidification and Casting

*Sponsored by:* The Minerals, Metals and Materials Society, TMS Light Metals Division, TMS: Aluminum Committee, TMS: Aluminum Processing Committee

*Program Organizers:* Geoffrey Brooks, Swinburne University of Technology; John Grandfield, Grandfield Technology Pty Ltd

Wednesday PM  
March 2, 2011

Room: 16A  
Location: San Diego Conv. Ctr

*Session Chairs:* Peter Schumacher, University of Leoben; Arild Hakonsen, Hydro Aluminium Hycast a.s.

**2:00 PM Introductory Comments**

**2:05 PM**

**Hycast Gas Cushion (GC) Billet Casting System:** Idar Steen<sup>1</sup>; Arild Hakonsen<sup>1</sup>; <sup>1</sup>Hydro Aluminium

The Hycast GC Billet Casting System for casting of extrusion billets has been in use in Hydro Aluminium casthouses (both primary and remelt) for more than 20 years. The technology is based on a patented mould construction utilizing dual graphite rings for optimal distribution of oil

and gas into the mould. Annual production capacity in existing casthouses equipped with Hycast GC is more than 2 million tons /year. The diameter range is from 152mm up to 405mm (6"-16"). The Hycast GC casting system produces excellent and consistent metal quality in combination with high productivity, excellent metal recovery and low maintenance cost. The technology is now available for the aluminium industry also outside Hydro Aluminium. This paper describes the main technical achievements of the technology with focus on operational issues as HES, metal recovery, metal quality and productivity.

#### 2:30 PM

**Studies of Fluid Flow and Meniscus Behavior during Horizontal Single Belt Casting (HSBC) of Thin Metallic Strips:** *Donghui Li*<sup>1</sup>; *Jaspreet Gill*<sup>1</sup>; *Mihaiela Isac*<sup>1</sup>; *Roderick Guthrie*<sup>1</sup>; <sup>1</sup>McGill Metals Processing Centre

Horizontal Single Belt Casting (HSBC) of strips is a green strip casting technology potentially capable of replacing current slab caster operations. As-cast strip bottom surface quality is a key factor for near-net shape casting operations. The meniscus behavior at the triple point of gas, substrate, and liquid metal when the melt first touches the moving belt is important to surface quality, as is the way in which the melt is in subsequent contact with the chill substrate. In this paper, meniscus behavior and fluid flow mechanisms were analyzed and predicted through mathematical modeling, using ANSYS Fluent software. The mathematical modeling of meniscus behavior and fluid flow was further supported by physical water modeling, and was validated through HSBC simulator tests using aluminum alloys.

#### 2:55 PM

**Development of Alba High Speed Alloy:** *Abdulla Ahmed*<sup>1</sup>; *Jalal Hassan*<sup>1</sup>; <sup>1</sup>Aluminium Bahrain (Alba)

Aluminium Bahrain has developed inhouse an alloy called "ALBA HIGH SPEED 6063.10", which is a variant of alloy AA 6063. The driving force behind this has been, the ever standing requirement of extruders to attain progressively higher extrusion speeds, thereby boosting productivity. Small and controlled amount of Mn and Mg addition to alloy 6063 was found to help in improving extrusion speeds and reduce die pick-up thereby improving the surface appearance. The reason was attributed to improved beta to alpha transformation rates at the microstructure level. This was achieved by having tight control of Mn addition to reduce the band from 0 - 0.10 % in normal 6063 alloy to 0.03% - 0.06 % in 6063.10. In addition controlling the Mg addition to 0.45 % - 0.51 % in the new alloy, assisted in better distribution of Mg<sub>2</sub>Si precipitates in the matrix during the cooling process post soaking at 580C.

#### 3:20 PM

**Dissolution Studies of Si Metal in Liquid Al under Different Forced Convection Conditions:** *Mehran Seyed Ahmadi*<sup>1</sup>; *Stavros Argyropoulos*<sup>1</sup>; *Markus Bussmann*<sup>1</sup>; *Don Doutré*<sup>2</sup>; <sup>1</sup>University of Toronto; <sup>2</sup>Novelis Global Technology Center

The dissolution of Silicon metal into liquid Aluminum is a very slow process. The main focus of this research is to develop procedures which contribute to speeding up the dissolution of Silicon metal into Aluminum bath. Experimental dissolution studies of Silicon metal in liquid Aluminum will be reported under natural and forced convection conditions. A unique Revolving Liquid Metal Tank (RLMT) is being used, capable of stirring approximately 50 kg of liquid Aluminum to create desired tangential velocities. In addition experimental work on Silicon dissolution in liquid Aluminum under conditions of two-phase flow, utilizing Nitrogen gas, in liquid Aluminum will also be reported. Silicon dissolution into liquid Aluminum under single-phase flow will be compared with results obtained in two-phase flow conditions. Finally, the commercial software FLOW-3D is being adapted to predict the various transport phenomena involved; comparisons will be presented between experimental and predicted results.

#### 3:45 PM Break

#### 3:55 PM

**Modification and Grain Refinement of Eutectics to Improve Performance of Al-Si Castings:** *Milan Felberbaum*<sup>1</sup>; *Arne Dahle*; <sup>1</sup>The University of Queensland

The formulation of alloy compositions for aluminium castings has not changed significantly for decades. Strontium (Sr) modification is commonly used to obtain a refined fibrous morphology of eutectic in Al-Si foundry alloys, and grain refinement can be used to refine the primary Al dendrites. Compared to the coarse plate-like unmodified silicon morphology, the refined fibrous eutectic structure can substantively improve the mechanical properties particularly ductility and fatigue. However, a problem often associated with Sr modification is a change in porosity - distribution and amount. A new alloy technology has been developed to produce castings combining a well-modified eutectic with reduced porosity. This can be achieved by providing effective substrates for the nucleation and growth of eutectic cells. Further, the additions do not change the overall alloy specification, ie. they involve trace level additions. This paper will present the current status in the development and commercialisation of the new eutectic grain refiner and modifier.

#### 4:20 PM

**Production of Al-Ti-C Grain Refiners with the Addition of Elemental Carbon and K<sub>2</sub>TiF<sub>6</sub>:** *Fatih Toptan*<sup>1</sup>; *Isil Kerti*<sup>1</sup>; *Sibel Daglilar*<sup>1</sup>; *Ahmet Sagin*<sup>1</sup>; *Omer Faruk Karadeniz*<sup>1</sup>; *Aysin Ambarkutuk*<sup>1</sup>; <sup>1</sup>Yildiz Technical University

Al-Ti-B grain refiners are widely used as aluminium grain refiners despite the problems in application Al-Ti-C refiners have an increasing demand in recent years. In the present work, Al-Ti-C grain refiners with different Ti:C ratios were produced by in-situ method with the addition of elemental carbon into the Al-Ti master alloy and addition of K<sub>2</sub>TiF<sub>6</sub> and elemental carbon powder mixture into the commercially pure aluminium. Microstructures were characterised by optic microscope and scanning electron microscope equipped with energy dispersive spectroscopy. The effects of production method and Ti:C ratio on the grain refinement process was investigated with Alcoa Coldfinger Test and optimum conditions were determined. Commercial Al-Ti-B grain refiners also tested with Alcoa Coldfinger Test in identical conditions and it has been stated that, insitu Al-Ti-C refiners are more effective than commercial Al-Ti-B grain refiners in grain refining.

#### 4:45 PM

**Effect of Mechanical Vibrations on Microstructure Refinement of Al-7Mass% Si Alloys:** *Takuya Tamura*<sup>1</sup>; *Toshiro Matsuki*<sup>2</sup>; *Kenji Miwa*<sup>1</sup>; <sup>1</sup>National Institute of Advanced Industrial Science and Technology (AIST); <sup>2</sup>Yamagata Research Institute of Technology

Mechanical vibration treatment is known to induce microstructure refinement. However, it is not completely understood which factor of vibrations is important for microstructure refinement. Factors of vibrations include frequency, acceleration, velocity and amplitude. Thus, this study aims to investigate effect of mechanical vibrations on microstructure refinement of Al-7mass%Si alloys by a systematic study. As a result, it was found that velocity of vibrations is important factor for primary crystals refinement. The square of the velocity corresponds to the energy of mechanical vibrations. Thus, the energy of mechanical vibrations promotes microstructure refinement during solidification. Moreover, it was found that primary crystal particles become rosette-like and fine when the mechanical vibrations are applied to the melt from about 923K to 888K (liquidus - 2K). This result is considered to indicate that the mechanical vibrations promote heterogeneous nucleation.

#### 5:10 PM

**Predicting the Response of Aluminum Casting Alloys to Heat Treatment:** *Chang-Kai Wu*<sup>1</sup>; *Makhlouf Makhlouf*<sup>1</sup>; <sup>1</sup>Worcester Polytechnic Institute

The mechanical properties of aluminum alloy castings can be greatly improved by a precipitation hardening. Typically, this heat treatment consists of three steps: (1) solutionizing, (2) quenching, and (3) aging; and is

performed by first heating the casting to and maintaining it at a temperature that is a few degrees lower than the solidus temperature of the alloy in order to form a single-phase solid solution. Then rapidly quenching the casting in a cold (or warm) fluid in order to form a supersaturated non-equilibrium solid solution; and finally, reheating the casting to the aging temperature where nucleation and growth of the strengthening precipitate(s) can occur. Obviously, these processing steps involve significant thermal changes that may be different from location to location in the casting. The objective of this project is to develop a finite element model and the necessary material database that allow predicting these physical and material property changes.

## Characterization of Minerals, Metals and Materials: Nanomaterials, Nanotechniques and Thin Films

*Sponsored by:* The Minerals, Metals and Materials Society, TMS Extraction and Processing Division, TMS/ASM: Composite Materials Committee, TMS: Materials Characterization Committee  
*Program Organizer:* Sergio Monteiro, State University of the Northern Rio de Janeiro - UENF

Wednesday PM Room: 14B  
March 2, 2011 Location: San Diego Conv. Ctr

*Session Chairs:* Shadia Ikhmayies, Al Isra University; Jozef Zrnik, Comtes FHT, Inc.

### 2:00 PM

**Microstructural Characterization of Nanomaterials Produced from Co-Products of the Ethanol Production (DDGS):** Joner Alves<sup>1</sup>; Chuanwei Zhuo<sup>2</sup>; Yiannis Levendis<sup>2</sup>; Jorge Tenório<sup>1</sup>; <sup>1</sup>University of Sao Paulo; <sup>2</sup>Northeastern University

Reduction of combustion-emitted greenhouse gases, which are associated with global warming, may be achieved by use of CO<sub>2</sub>-neutral alternative fuels, such as bio-ethanol. Distillers Dried Grains with Solubles (DDGS) are the main co-products of the corn-grain-based ethanol industries. In 2009, the North American production of ethanol from corn was about 38 billion liters, which generated approximately 31.5 million tons of DDGS. Samples of DDGS were pyrolysed at temperatures of 600-1000 °C in a two-stage laminar-flow horizontal furnace, and a catalyst system was used to synthesize nanomaterials. This work presents a microstructural characterization of these nanomaterials by scanning electron microscopy (SEM) and transmission electron microscopy (TEM). Results showed that the nanomaterials produced from pyrolysis of DDGS were in the form of long, entangled, rope-like structures with rugged walls, lengths in the tens of microns, and axially non-uniform diameters in the range of 100-300 nm.

### 2:15 PM

**Photoluminescence of the Interface of SnO<sub>2</sub>:F/CdS:In/CdTe Thin Film Solar Cells Prepared Partially by the Spray Pyrolysis Technique:** Shadia Ikhmayies<sup>1</sup>; Riyad Ahmad-Bitar<sup>2</sup>; <sup>1</sup>Al Isra University; <sup>2</sup>Al-Hussain Ben Talal University, Ma'an Jordan

CdS/CdTe solar cells were built by depositing a 200 nm layer of SnO<sub>2</sub>:F on glass substrates by the spray pyrolysis (SP) technique, a 500 nm CdS:In layer by the same technique and a 1-1.5 μm CdTe layer by vacuum evaporation. The cells were CdCl<sub>2</sub> heat-treated in nitrogen atmosphere for 30 minutes at 350°C. The photoluminescence (PL) spectra were measured at the CdS/CdTe interface for two cells with different values of the CdTe layer's thickness at temperature T = 60 K. A deconvolution peak fit was performed from which it is found that the peaks are characteristic of the solid solution CdS<sub>x</sub>Te<sub>1-x</sub>. The parabolic relation that relates the bandgap energy with the composition was used to estimate x, where x is [S]/([Te]+[S]) and [Te], [S] are the concentrations of Te and S atoms respectively. The results show that the interface is smooth and the change of the bandgap occurs gradually.

### 2:30 PM

**Particle Size Analysis of Metallic Nanoparticles Using Ultra-High Resolution Mass Sensors:** Kerri-Ann Hue<sup>1</sup>; Ken Babcock<sup>2</sup>; Patrick O'Hagan<sup>1</sup>; Larry Unger<sup>1</sup>; <sup>1</sup>Particle Sizing Systems; <sup>2</sup>Affinity Biosensors

Metallic nanoparticles exhibit properties that are significantly different from individual atoms or bulk materials. Their applications are diverse and have varying applications in areas such as cancer treatment, biochemical sensors, nanoelectronics, and drug delivery. For each of these applications extensive characterization must be performed in order to probe the unique properties of these nanoparticles. In this study, ultra-high resolution mass sensors consisting of MEMs-fabricated, suspended microchannel resonators were used to determine the size and concentration of metallic nanoparticles. With femtogram (10E-15 g) mass resolution, ultra-high resolution mass sensors can weigh individual particles suspended in fluid, and so measure their mass, density, and size. Particle size analysis with these sensors provides excellent accuracy and resolution compared to mature technologies such as light scattering. This technique also provides quantitative information via the ability count particles.

### 2:45 PM

**Observation of Heterogeneous Deformation in Commercial Purity Ti Using Nano-Indentation:** Yiyi Yang<sup>1</sup>; Claudio Zambaldi<sup>2</sup>; Leyun Wang<sup>1</sup>; Philip Eisenlohr<sup>2</sup>; Thomas Bieler<sup>1</sup>; Martin Crimp<sup>1</sup>; <sup>1</sup>Michigan State University; <sup>2</sup>Max-Planck-Institut für Eisenforschung

Nano-indentation is widely applied to measure mechanical properties on a local scale, providing an opportunity to understand how the local structure, such as grain boundary and grain orientation is linked to observed local deformation behavior. In this work, a series of conical nano-indentations were performed on a patch of grains in polycrystalline titanium of commercial purity (and hexagonal lattice structure). Atomic force microscopy (AFM) was then used to observe the resulting surface topography due to the dislocation pile-up formation, which is heterogeneous in different grains. The driving mechanism for pile-ups is almost crystallographically dependent in that the influence of stress concentrations due to indenter shapes is negligible. The dependence of nanohardness and plastic zone size upon different grain orientation was studied. Support was provided by NSF grant DMR-0710570 and DFG grant EI 681/2-1.

### 3:00 PM

**Production of CdS<sub>1-x</sub>Te<sub>x</sub> Thin Films and Bandgap Investigation of the Produced Solid Solution:** Shadia Ikhmayies<sup>1</sup>; Riyad Ahmad-Bitar<sup>2</sup>; <sup>1</sup>Al Isra University; <sup>2</sup>Al-Hussain Ben Talal University, Ma'an Jordan

CdS<sub>1-x</sub>Te<sub>x</sub> thin films with 0 < x < 0.3 were prepared on glass substrates by the annealing of CdS:In thin films produced by the spray pyrolysis technique. The annealing was performed in nitrogen atmosphere at 400°C in the presence of Te vapor. The compositions of the films were determined by energy dispersive X-ray detection (EDAX) measurements. Scanning electron microscopy (SEM) was used to investigate the morphology of the films. The transmittance of the films was measured at room temperature in the wavelength range 400-1100 nm and used to produce the absorbance of the films. The first derivative of the absorbance was used to estimate the optical bandgap energy E<sub>g</sub> by using the minima in the first derivative. The relation between the bandgap energy and the fraction x was found to fit with a parabola and bandgaps in the range 2.196 = E<sub>g</sub> = 2.480 eV were obtained. Urbach tailing in the bandgap was also investigated.

### 3:15 PM

**Studying the Microstructural Evolution of Nanocrystalline Metals in Response to External Straining by Automated Acquisition and Indexing of Diffraction Patterns in the TEM:** Kai Zweier<sup>1</sup>; Andreas Kulovits<sup>1</sup>; Jorg Wiecek<sup>1</sup>; <sup>1</sup>University of Pittsburgh

Nano-crystalline Ni with an average grain size of 40nm has been cold deformed at room temperature by rolling to thickness reductions of up to 85%. In this grain size regime plastic deformation is facilitated by dislocation activity. Dislocation-grain boundary interactions dominate during plastic flow, resulting in grain boundary character evolution and inducing grain coalescence. We used automated acquisition and indexing of precession



diffraction patterns and hollow-cone dark-field imaging in the transmission electron microscope to monitor the evolution of populations of grains orientations in these nanocrystalline aggregates. The high spatial resolution of the TEM allowed us to monitor these changes on the nanoscale, which was previously not possible with SEM based approaches. We acknowledge use of the facilities of the Materials Micro-Characterization Laboratory of the Department of Mechanical Engineering and Materials Science, University of Pittsburgh, and support by a grant from the National Science foundation NSF-CMS 0140317.

### 3:30 PM Break

### 3:45 PM Invited

**An Investigation of the Photoluminescence and Transmittance of CdS1-xTex Thin Films:** *Shadia Ikhmayies*<sup>1</sup>; Riyad Ahmad-Bitar<sup>2</sup>; <sup>1</sup>Al Isra University; <sup>2</sup>Al-Hussain Ben Talal University, Ma'an Jordan

CdS1-xTex thin films were prepared by first producing CdS:In thin films by the spray pyrolysis (SP) technique and then annealing the films in the presence of Te vapor in nitrogen atmosphere. X-Ray diffraction (XRD) measurements showed that the films are polycrystalline with the wurtzite structure. Transmittance measurements were recorded at room temperature in the wavelength range 400-900 nm and used to deduce the absorbance. The first derivative of the absorbance was calculated and used to find the values of the bandgap energy, where more than one bandgap was obtained for each film. These results show that the films are inhomogeneous or the composition differs with location. The photoluminescence (PL) was recorded at T = 60 K and a deconvolution peak fit was performed for each spectrum. The results of the PL spectra are consistent with those obtained from the first derivative and confirm the inhomogeneity of the films.

### 4:15 PM

**Convergent Beam Electron Diffraction of Nanomaterials:** Karen Henry<sup>1</sup>; Richard Vanfleet<sup>2</sup>; *Gregory Thompson*<sup>1</sup>; <sup>1</sup>University of Alabama; <sup>2</sup>Brigham Young University

The most readily available technique for the determination of long-range order parameter S is X-ray diffraction. Experimentally, S is determined by measuring the total integrated peak intensities of the superlattice and fundamental reflections according to kinematical scattering theory. However, X-ray scattering from thin films and nanoparticles can be very small and difficult to measure with laboratory diffractometers. In contrast, electron scattering can be more amenable for diffraction studies of small volumes, though strong interaction of electrons with the material results in multiple scattering events. As a result, the scaling of the ratio of integrated intensities is no longer valid and S determination becomes more complex. To correctly account for multiple electron scattering events, a multislice simulation is necessary to predict the convergent beam electron diffraction (CBED) intensities for a given order parameter, orientation and thickness. This talk will address these techniques for thin films and nanoparticles.

### 4:30 PM

**Measuring the Elastic Modulus of Polymers by Nanoindentation with an Atomic Force Microscope:** Daniel Hoffman<sup>1</sup>; Ibrahim Miskioglu<sup>1</sup>; Katerina Aifantis<sup>2</sup>; *Jaroslav Drellich*<sup>1</sup>; <sup>1</sup>Michigan Technological University; <sup>2</sup>Aristotle University of Thessaloniki

A new method to determine the elastic modulus of a material using the atomic force microscope (AFM) has been proposed by Pethica et al. (Nanotechnology 19, 2008, 495713). This method models the cantilever and the sample as two springs in a series. The ratio of the cantilever spring constant (k) to diameter of the tip (2a) is treated in the model as one parameter ( $\alpha=k/2a$ ). The value of  $\alpha$ , along with the cantilever sensitivity, are determined on two reference samples with known mechanical properties and then used to find the elastic modulus of an unknown sample. To determine the reliability and accuracy of this technique it was tested on several polymers. Traditional depth-sensing nanoindentation was performed for comparison. Using both methods, the elastic modulus of the polymers tested was calculated. The elastic modulus values from the AFM were within  $\pm(5-20)\%$  of the nanoindenter results.

### 4:45 PM

**Microstructural Analysis of Nanomaterials Synthesized from Unserviceable Tires:** Jone Alves<sup>1</sup>; *Chuanwei Zhuo*<sup>2</sup>; Yiannis Levendis<sup>2</sup>; Jorge Tenório<sup>1</sup>; <sup>1</sup>University of Sao Paulo; <sup>2</sup>Northeastern University

The ever increasing number of automobiles and the consequential increase in consumption of tires have generated a pressing environmental issue, concerning the disposal of unserviceable tires. The worldwide disposed of waste tires is approximately 1 billion units per year and this amount is expected to increase by 2% each year. This work presents a microstructural characterization of nanomaterials synthesized in a catalyst system from the effluent of burning waste tire chips in a horizontal two-stage laminar-flow furnace. Controlled combustion of waste tire chips took place at temperatures of 900 or 1000°C, and stainless steel meshes were used to synthesize the nanomaterials at 1000°C. Produced materials were analyzed by scanning electron microscopy (SEM) and transmission electron microscopy (TEM). The catalyst meshes were covered by materials with diameters of 20 to 200 nm and lengths of about 40  $\mu$ m. They possessed structures similar to those of carbon nanotubes.

### 5:00 PM

**Synthesis of Sr-Doped LaP<sub>3</sub>O<sub>9</sub> Films in Phosphoric Acid Solutions and Their Proton Conduction Properties:** *Takayuki Onishi*<sup>1</sup>; Naoyuki Hatada<sup>1</sup>; Kazuaki Toyoura<sup>1</sup>; Yoshitaro Nose<sup>1</sup>; Tetsuya Uda<sup>1</sup>; <sup>1</sup>Kyoto University

Lanthanum polyphosphate, LaP<sub>3</sub>O<sub>9</sub>, is considered as a potential solid electrolyte in fuel cells. It exhibits relatively high proton conductivity when doped with alkaline earth metals such as Sr. For practical use, however, further enhancement of the conductivity is necessary while the proton conductivity mechanism has not been understood. For example, it is not clear whether the bulk conduction or grain boundary conduction is dominant. It is also unknown which crystallographic direction is the best for the proton conduction. To determine them, we aimed at measuring the proton conductivity of polycrystalline Sr-doped La<sub>2</sub>O<sub>9</sub> with different grain sizes or specific crystallographic orientations. However it is difficult to obtain these samples by solid-state synthesis. In this study, therefore, we attempted to synthesize polycrystalline films of Sr-doped La<sub>2</sub>O<sub>9</sub> in condensed phosphoric acid solutions. Then the grain size, crystallographic orientation, and the conductivity of the samples were analyzed and compared with previously reported values.

### 5:15 PM

**Effects of Heat Treatment Schedule on the Crystallization Behavior and Thermal Expansion of a LiS<sub>2</sub> Based Glass-Ceramic:** *Onder Guney*<sup>1</sup>; Erdem Demirkesen<sup>1</sup>; <sup>1</sup>Istanbul Technical University

In this study, the crystallization and thermal expansion coefficient behavior of a lithium disilicate (LiS<sub>2</sub>) based glass-ceramic which is derived from SiO<sub>2</sub>-Li<sub>2</sub>O-Al<sub>2</sub>O<sub>3</sub>-K<sub>2</sub>O-ZrO<sub>2</sub> system was investigated by using x-ray diffraction (XRD), high temperature x-ray diffraction (HTXRD), differential thermal analysis (DTA) and dilatometer techniques. Analytical reagent grade chemicals were used as raw materials for preparing glass batches. Nucleation and crystal growth heat treatments were planned according to DTA results. Amorphous and crystalline phases developed during the heat treatments, were determined by quantitative XRD. Applied heat treatments showed the formation of metastable lithium silicate (LS) and its transformation to stable LS<sub>2</sub>. The thermal expansion coefficients of glass-ceramics were also measured depending on the applied heat treatments.

### 5:30 PM

**Characterization of Nanocrystalline Silver Fabricated by Warm-Vacuum-Compaction Method:** *Wei Liu*<sup>1</sup>; Qionghua Zhou<sup>1</sup>; <sup>1</sup>Henan University of Science and Technology

Nanocrystalline silver bulk material with average grain size of 20.3 nm was prepared by warm-vacuum-compaction method. The as-prepared nanocrystalline silver was characterized by X-ray diffraction (XRD), differential scanning calorimetry analysis (DSC), thermogravimetric analysis (TG), and 6157 type Electrometer test, respectively. The experimental results show that the average grain size and microstrain of the nanocrystalline silver are 20.3 nm and 0.088%. The melting point and melting enthalpy are

955.7°C and 82.34 J/g, which are lower than that of coarse-grained silver by 6 K and 22.6J/g, respectively. The electrical resistivity of nanocrystalline silver increases with higher temperature when the range of temperature is between 233K and 293K. The electrical resistivity at 293 K is  $1.475 \times 10^{-7}$   $\Omega \cdot m$ , which is higher than that of coarse-grained silver by a factor of 9.

## Characterization of Nuclear Reactor Materials and Components with Neutron and Synchrotron Radiation: Development of Nuclear Energy Systems and Fuels

*Sponsored by:* The Minerals, Metals and Materials Society, TMS Structural Materials Division, TMS/ASM: Nuclear Materials Committee

*Program Organizers:* Matthew Kerr, US Nuclear Regulatory Commission; Meimei Li, Argonne National Lab; Jonathan Almer, Argonne National Laboratory; Donald Brown, Los Alamos National Lab

Wednesday PM                      Room: 4  
March 2, 2011                      Location: San Diego Conv. Ctr

*Session Chairs:* Meimei Li, Argonne National Lab; Matthew Kerr, US Nuclear Regulatory Commission

### 2:00 PM Keynote

**Using Synchrotron Radiation to Study Nuclear Energy Systems:** *Lynda Soderholm*<sup>1</sup>; <sup>1</sup>Argonne National Laboratory

The realization of advanced nuclear reactors as a national source of reliable energy awaits materials research on fuels, reactor components under extreme environments, and options for waste treatment and storage. As described in a recent workshop, [1] third generation synchrotrons such as the Advanced Photon Source (APS) provide a high-flux of coherent, variable-energy x-rays that can be used to probe in situ a wide range of chemical, physical, and materials problems of relevance to nuclear energy production. Experimental opportunities will be highlighted within the context of techniques that provide new information. Also presented will be guidance on how to access these techniques at the APS. This work was performed with the support of DOE-OBES, under contract number DE-AC02-06CH11357[1] Workshop on the Role of Synchrotron Radiation in Solving Scientific Challenges in Advanced Nuclear Energy Systems, 27-28 January 2010

### 2:30 PM Invited

**Zirconium Alloy Oxide Structure Studied Using Microbeam Synchrotron Radiation Diffraction and Fluorescence:** *Arthur Motta*<sup>1</sup>; Aylin Kucuk<sup>2</sup>; Marcelo Gomes da Silva<sup>3</sup>; Robert Comstock<sup>4</sup>; Barry Lai<sup>5</sup>; Zhonghou Cai<sup>6</sup>; <sup>1</sup>Penn State University; <sup>2</sup>EPRI; <sup>3</sup>Universidade Federal do Ceara; <sup>4</sup>Westinghouse Electric Co.; <sup>5</sup>Argonne National Laboratory

Corrosion can often limit the service life of materials in nuclear power plants. To better understand the corrosion resistance of Zr-based alloys in light water reactors and in supercritical water reactors, techniques were developed to characterize oxide corrosion films using synchrotron radiation. Cross-sections of oxides formed in high temperature water or steam were probed by a microbeam (200 nanometers) of synchrotron radiation to provide both diffraction and fluorescence data. The diffraction data provided information on oxide phases, grain size, and crystallographic texture as a function of distance from the oxide-metal interface, while the fluorescence results provided chemical information at the ppm level. Results from the characterization of these oxides will be presented and linked to the protective or non-protective character of the oxide layers, thus highlighting the contributions made by the synchrotron radiation studies in improving our understanding of mechanisms of corrosion protection in these materials.

### 3:00 PM

**Texture and Intergranular Stresses of Hydrides Precipitated in Zr-2.5%Nb and Zircaloy-4:** *Javier Santisteban*<sup>1</sup>; MA Vicente-Alvarez<sup>1</sup>; Pablo Vizcaino<sup>2</sup>; A. D. Banchik<sup>2</sup>; Jon Almer<sup>3</sup>; <sup>1</sup>CONICET; <sup>2</sup>Comision Nacional de Energia Atómica; <sup>3</sup>Argonne National Laboratory

We have measured texture and intergranular stresses of hydrides precipitated in Zr-2.5%Nb pressure tube material and Zircaloy-4 plates of different microstructures by synchrotron X-Ray diffraction experiments. Results show large in-plane compressive stresses in hydride platelets precipitated in pressure tube material and in Zircaloy-4 of ~30  $\mu m$  grain size, whilst no stresses are observed for hydrides in Zircaloy-4 of ~100  $\mu m$  grain size. The origin of these stresses and the effect of tensile stress on hydride texture were investigated by performing in-situ hydride dissolution/precipitation under external loads. Some of the loads were high enough to produce hydride reorientation as seen under the optical microscope. Small changes in hydride texture were observed for all loads, whilst clear differences in hydride intergranular stresses emerged only for samples presenting hydride reorientation. The observed stresses can be explained by the constraint imposed by grain boundaries to the planar growth of hydride platelets.

### 3:20 PM

**A High Energy Synchrotron X-Ray Study of Biaxial Thermal Creep of AISI 316L Steel:** *Hsiao-Ming Tung*<sup>1</sup>; Kun Mo<sup>1</sup>; Xiang Chen<sup>1</sup>; Jonathan Almer<sup>2</sup>; Meimei Li<sup>2</sup>; James F. Stubbins<sup>1</sup>; <sup>1</sup>University of Illinois; <sup>2</sup>Argonne National Laboratory

A study of the thermal creep properties of Type 316L stainless steel was performed using pressurized tube specimens. Creep tubes of 8.12mm outside diameter (OD) by 0.25 mm wall thickness were subject to constant load generated with a high-pressure high-purity argon gas. Specimens were heated to 650 and 700\176C in an air environment. Macro-strain due to the change in OD was measured with a high-precision laser profilometer. To evaluate creep damage due to microstructural change of the creep tubes, high energy synchrotron X-ray diffraction was used to determine the lattice strains of the creep tube during deformation at the temperature of 650 and 700\176C. Fracture surface of the creep tubes was characterized using scanning electron microscopy (SEM). The grain boundaries with chromium-rich carbide precipitated are likely the path for crack propagation during fracture.

### 3:40 PM

**Synchrotron X-Ray Characterization of the Oxide Structure Formed on Ferritic-Martensitic Alloys Exposed to 500°C Steam and Supercritical Water:** *Jeremy Bischoff*<sup>1</sup>; Arthur Motta<sup>1</sup>; Guoping Cao<sup>2</sup>; Robert Comstock<sup>3</sup>; Zhonghou Cai<sup>4</sup>; <sup>1</sup>Penn State University; <sup>2</sup>University of Wisconsin-Madison; <sup>3</sup>Westinghouse Electric Co.; <sup>4</sup>Argonne National Laboratory

The Supercritical Water Reactor (SCWR) is a Generation IV design envisioned for its high thermal efficiency and simplified core. One of the major materials issues for its development is the corrosion resistance of the cladding and structural materials when exposed to supercritical water at temperatures between 500°C and 600°C. Candidate alloys include ferritic and martensitic steel alloys and the protective oxide layers formed during corrosion determine the overall corrosion rate. In this study oxide layers formed on these alloys during exposure to 500°C steam and supercritical water were analyzed using microbeam synchrotron x-ray diffraction and fluorescence. This technique enables the examination of the oxide layer microstructure with a spatial resolution up to 0.2  $\mu m$ , with simultaneous acquisition of elemental and phase information. The results of these examinations in various alloys will be shown and compared to corrosion kinetics with a view to determining corrosion mechanisms.

### 4:00 PM Break

### 4:10 PM Keynote

**Microbeam, Timing and Wavelength-Dispersive Studies of Nuclear Materials with Synchrotrons:** *Gene Ice*<sup>1</sup>; <sup>1</sup>Oak Ridge National Laboratory

Synchrotron sources allow for nondestructive 3D studies of materials structure and evolution at unprecedented time and length scales. These new

capabilities are essential to understand the underlying materials physics needed to make transformational materials with tailored physical properties. For activated samples, high-brilliance synchrotron sources are particularly important and will allow for small samples to be studied after doses that would make larger samples difficult to handle. We describe ongoing 3D x-ray microscopy studies of materials structure, and describe how these studies provide new insights into materials structure evolution, with direct ties to emerging models. We also describe emerging opportunities with sources of the future. Work sponsored by the U.S. Department of Energy (DOE), Office of Basic Energy Sciences, Division of Materials Sciences and Engineering. Experiments performed on Beamline 34-ID at the Advanced Photon Source Argonne II, supported by the DOE Office of Basic Energy Science, Division of User Facilities.

#### 4:40 PM

**Synchrotron Radiation Study of Hydride Reorientation in Zircaloy under In Situ Stress and Temperature Cycles:** Kimberly Colas<sup>1</sup>; Arthur Motta<sup>1</sup>; Mark Daymond<sup>2</sup>; Jonathan Almer<sup>3</sup>; Zhonghou Cai<sup>3</sup>; <sup>1</sup>Pennsylvania State University; <sup>2</sup>Queen's University; <sup>3</sup>APS Argonne National Laboratory

Hydrogen ingress into zirconium alloy fuel cladding during operation in nuclear reactors can degrade cladding performance due to formation of brittle hydrides. At temperature and under stress, hydrogen redistribution and reorientation can occur, reducing cladding resistance to failure. Thus, it is crucial to understand the kinetics of hydride dissolution and reprecipitation under load and at temperature. In the current study we have used high energy synchrotron radiation diffraction to study the kinetics of hydride reorientation in previously hydrided Zircaloy-4 sheet. Micro-beam diffraction was performed on samples containing hydrides grown at stress concentrations such as crack tips to study their state of strain and their orientation relationship with the matrix. In addition the strain was measured in hydrides formed near the crack with a spatial resolution of 50 microns, to provide a map of hydride precipitation and straining. The results are discussed in terms of previous measurements in the literature.

#### 5:00 PM

**SAXS and ASAXS Studies of Nanoscale Features in Reactor Pressure Vessel Steels and Nanostructured Ferritic Alloys:** Takuya Yamamoto<sup>1</sup>; Nicholas Cunningham<sup>1</sup>; G. Robert Odette<sup>1</sup>; Carlo Segre<sup>2</sup>; Shanshan Liu<sup>2</sup>; Sonke Seifert<sup>3</sup>; <sup>1</sup>Univ. California Santa Barbara; <sup>2</sup>Illinois Institute of Technology; <sup>3</sup>Argonne National Laboratory

Small angle and anomalous small angle X-ray scattering (SAXS/ASAXS) measurements were on RPV steels and model alloys aged at 350°C for 13000 h as well as nanostructured ferritic alloys (NFA) at the ANL APS. Aging the RPV steels and model alloys resulted in precipitation of Cu(Mn-Ni-Si) rich nm-scale phases. The NFA contain nm-scale Y-Ti-O features. ASAXS was performed on ~ 15 μm samples near the K-edges of Mn, Fe, Ti and Y (depending on the alloy composition) while SAXS was performed at 18 keV on 50 μm thick specimens. Control specimens without NF were also measured. The data analysis is currently under way and has proven to be challenging, especially due to X-ray fluorescence. The size distribution of a RPV model alloy has been analyzed and is in good agreement with SANS results. The status of the analysis of the overall experimental matrix will be presented, along with lessons learned.

#### 5:20 PM

**Design of Materials Testing Capsule in PULSTAR Reactor for High Temperature Irradiations:** Santosh Sahoo<sup>1</sup>; Kalyan Chitrada<sup>1</sup>; Jacob Eapen<sup>1</sup>; Timothy Burchell<sup>2</sup>; K. Murty<sup>1</sup>; <sup>1</sup>North Carolina State University; <sup>2</sup>Oak Ridge National Laboratory

A limited number of thermo-mechanical experiments have been conducted in the past at high temperatures in a nuclear reactor. An irradiation capsule is currently being fabricated in the PULSTAR reactor at the North Carolina State University which is capable of conducting irradiations tests at temperatures in excess of 1000 deg.C. In this design, concentric alumina tubes separated by nitrogen gas enclose a tubular graphite electrical heater (in lieu of gamma heating) containing disk shaped materials samples. Extreme care is taken for maintaining thermal and electrical insulation as well as minimizing the

activation from nuclear radiations. A pressurized inert gas environment is maintained inside the capsule to avoid the risk of graphite oxidation. We report the main features of the irradiation capsule design and results from thermal/stress analysis using the Finite Element software – ANSYS. We acknowledge financial support from the Department of Energy (DoE).

#### 5:40 PM

**Microtomographic Investigation of Damage in E911 Steel after Long Term Creep:** Federico Sket<sup>1</sup>; Andras Borbely<sup>2</sup>; Karl Maile<sup>3</sup>; Rudy Scheck<sup>3</sup>; <sup>1</sup>IMDEA Materials; <sup>2</sup>Ecole des Mines de Saint-Etienne; <sup>3</sup>Materialprüfungsanstalt Universität Stuttgart

Damage distribution in a notched hollow cylinder made of E911 steel and crept for 26,000 h under multi-axial stress state was assessed. High-resolution tomographic reconstructions allowed characterization of the size, shape and spatial distribution of cavities along the notch of the cylinder. Cross-correlation analysis between the corresponding distributions of cavities number density and different stress parameter indicate that the highest similarity is obtained for stress triaxiality. The maximum principal stress and the von Mises stress show also strong correlation with damage distribution. The analysis of the size distribution of non-coalesced cavities in terms of general power-law functions describing nucleation and growth, led to the conclusion that cavity growth in E911 steel is dominated by the constrained diffusion mechanism.

---

## Coatings for Structural, Biological, and Electronic Applications II: Process-Property-Performance Correlations - II; Metallic, Semiconducting and Insulating Coatings

*Sponsored by:* The Minerals, Metals and Materials Society, TMS Electronic, Magnetic, and Photonic Materials Division, TMS: Thin Films and Interfaces Committee

*Program Organizers:* Nuggehalli Ravindra, New Jersey Institute of Technology; Choong Kim, University of Texas at Arlington; Nancy Michael, University of Texas at Arlington; Gregory Krumdick, Argonne National Laboratory; Roger Narayan, Univ of North Carolina & North Carolina State Univ

Wednesday PM

March 2, 2011

Room: 6E

Location: San Diego Conv. Ctr

*Session Chairs:* Gregory Krumdick, Argonne National Laboratory; Roger Narayan, Univ of North Carolina & North Carolina State Univ

---

#### 2:00 PM

**The Development of a Non-Destructive Multiple Partial Unloading Micro-Indentation Technique for Thermal Barrier Coating Spallation Prediction:** Jared Tannenbaum<sup>1</sup>; Kwangsoon Lee<sup>1</sup>; Bruce Kang<sup>1</sup>; Mary Anne Alvin<sup>2</sup>; <sup>1</sup>West Virginia University; <sup>2</sup>National Energy Technology Laboratory

Failure of TBCs applied to gas turbine combustor components currently limits the maximum temperature at which these engines operate. In this research, a non-destructive load-based micro-indentation methodology for damage assessment of these coatings is presented. A multiple-loading/partial-unloading evaluation procedure has been developed wherein stiffness responses of TBC coupons subjected to thermal loads have been analyzed. At various thermal cycles time-series color maps were developed correlating accumulated degradation to overall TBC residual stress states. Through this procedure regions having relatively higher stiffness are correlated to elevated out-of-plane tensile residual stress states. A high temperature exposure testing plan was conducted where after each thermal loading, microstructural analyses were carried out identifying damage accumulation. Results indicate this test methodology is capable of predicting spallation sites on TBCs before its occurrence. In addition, FEM analyses of interfacial stresses produced upon cooling has provided explanation to the experimentally observed failure patterns within this region.



## 2:15 PM Invited

**Study of the Nanocomposites for Superalloy Thermal Barrier Coatings:** *Shiqiang Qian*<sup>1</sup>; <sup>1</sup>School of Materials Engineering, Shanghai University of Engineering Science

High temperature alloy can be plated on metal bonding coat layer, by magnetron sputtering or electrophoresis, and thermal barrier layer, by high-speed jet electrodeposition or electrophoresis. We can get nanocomposites on alloy by plating metal bonding coat layer first and then thermal barrier layer. The surface morphology, phase composition and element of these two layers can be observed through OM, XRD, SEM. We placed the K17 high temperature alloy into melting sodium chloride at 900° for 1h then air-cooled for 10 minutes and did 15 cycles hot corrosion test. For metal bonding coat layer, magnetron sputtering is better than electrophoresis while for thermal barrier, electrophoresis better than high-speed jet electrodeposition. We found that it has better anti-hot-corrosion performance for nanocomposites through plating NiCrCoAlY, a metal bonding coat layer, by magnetron sputtering and then YSZ, a thermal barrier layer, by electrophoresis on K17 alloy.

## 2:40 PM

**Effect of Solubilizer on Low-Temperature Stability of Organic Solderability Preservative:** *Zhongliang Xiao*<sup>1</sup>; Yan Shi<sup>1</sup>; Yu Ding<sup>1</sup>; Daoxin Wu<sup>1</sup>; Guojun Xu<sup>2</sup>; <sup>1</sup>Changsha University of Science and Technology; <sup>2</sup>Shenzhen Yicheng Electronic Technology Co., Ltd

Organic solderability preservative(OSP) become more and more important in PCB producing process because of requirements on environment protection and reducing cost. An organic solderability preservative(OSP) against low temperature was prepared by adding a kind of solubilizer. The effect of the content of OSP solubilizer on the low-temperature stability of the OSP solution and OSP film thickness, OSP film hydrophobic, and Solderability. The results showed that the storage temperature of the OSP lower than the common OSP 10-15°C while the other properties have no obvious change.

## 2:55 PM

**Failure Mechanisms of Strained Copper Films on Polyimide:** *Megan Cordill*<sup>1</sup>; Gerhard Dehm<sup>2</sup>; <sup>1</sup>University of Leoben; <sup>2</sup>Erich Schmid Institute of Materials Science

Mechanical properties and interfacial phenomena of thin films on compliant substrates are important to understand in order to design reliable flexible electronic devices. Thin films of Cu with an interlayer of Ti on polyimide substrates will be examined for their use as interconnects in flexible electronic devices. Using an in-situ tensile device inside a scanning electron microscope the mechanical behavior can be observed. With this technique, the initial fracture and buckling of the film can be observed and correlated to the strain. The strain of initial failure and subsequent delamination are observed to increase with film thickness. However, when the films are annealed the adhesion decreases as well as the fracture strain. The difference in mechanical behavior is examined using TEM, EBSD, and FIB to uncover the mechanisms defining the mechanical behavior of these films systems.

## 3:10 PM

**High-Performance Organic-Inorganic Thin Film Structural Adhesive Interphases:** *Jeffrey Yang*<sup>1</sup>; Reinhold Dauskardt<sup>1</sup>; <sup>1</sup>Stanford University

High-performance bonding plays an integral role in the reliability of thin-foil structural laminates. Novel organic-inorganic thin films with a through-thickness composition gradient have been developed to create complex metal / silane interphase regions engineered to form durable bonds between metal oxides and structural adhesive organic resins. Despite the efficacy of these hybrid films, much remains unknown about the fundamental processing-structure-property relationships that govern their performance and reliability. Strategies for forming strong adhesive bonds using a conditioned oxide, an optimized sol-gel layer and a high-performance epoxy resin are described. Micro and nanoscale mechanisms of interphase degradation and failure have been characterized under a range of loading and environmental conditions, revealing significant improvements in adhesion strength and enhanced resistance to moisture-assisted crack growth over traditional

bonded joints. The influence of metal oxide isoelectric point and epoxy functionality on fracture energy and network connectivity will also be discussed.

## 3:25 PM

**Effect of the Duty Cycle on the Microstructural, Mechanical and Tribological Properties of TiN Layers Deposited by PACVD:** Mohammad Sadegh Mahdipoor<sup>1</sup>; Mani Montazeri<sup>2</sup>; Mansour Soltanie<sup>2</sup>; Farzad Mahboubi<sup>1</sup>; *Mohammad Hamed Habibi*<sup>3</sup>; Shahrokh Ahangarani<sup>4</sup>; <sup>1</sup>Amirkabir University of Technology; <sup>2</sup>Iran University of Science and Technology; <sup>3</sup>University of Tehran; <sup>4</sup>Iranian Research Organization for Science and Technology

The PACVD process by pulsed-DC plasma in a TiCl<sub>4</sub>-N<sub>2</sub>-H<sub>2</sub>-Ar gas mixture to deposit TiN layer is investigated. The heat treatment of quench and temper carried out on hot work steel samples. Then TiN layers were deposited on all samples at 540 °C, 3-5 mbar pressure, and N<sub>2</sub>/H<sub>2</sub>= 0.22 gas flow ratio for 90 min. Deposition process were carried out under three different duty cycles, 40%, 50%, and 60%, to investigate the effect of this parameter on the microstructural, mechanical, and tribological properties of the coatings. Coatings properties were characterized using XRD, SEM, AFM, and Hardness tester with nano indenter and pin-on-disk wear test. The results indicate that by decreasing the duty cycle, the TiN layer shows an isotropic growth, smoother surface, more thickness and more surface hardness. As a result of wear tests, TiN coating deposited at 40% duty cycle showed the best wear resistant.

## 3:40 PM Break

## 3:50 PM

**The Influence of Pre-Treatment Plasma Nitriding on Tribological Properties of TiN Coatings Produced by PACVD:** Mohammad Sadegh Mahdipoor<sup>1</sup>; Farzad Mahboubi<sup>1</sup>; Mahdi Raoufi<sup>2</sup>; Hasan Elmkhah<sup>3</sup>; *Mohammad Hamed Habibi*<sup>4</sup>; <sup>1</sup>Amir Kabir university; <sup>2</sup>Iran University of Science and Technology; <sup>3</sup>Tarbiat Modarres University; <sup>4</sup>University of Tehran

The aim of this study was to investigate the effect of pre-treatment plasma nitriding (PN) on mechanical and tribological behavior of TiN coatings deposited by plasma assisted chemical vapor deposition (PACVD). A group of hot work steel samples were plasma nitrided at 500 °C for 4 h. Then TiN layer was deposited on all of samples at 520 °C temperature, 8 kHz frequency and 33% duty cycle. The microstructural, mechanical and tribological properties of the coatings were investigated using SEM, WDS, AFM, microhardness tester and pin-on-disc wear test. The load of wear test was 10 N and the samples were worn against different pins, ball-bearing steel WC-Co. The results indicate that the difference of hardness between the samples with PN-TiN layer and those samples with only TiN layer without PN was 450 HV and the former samples showed a significant amount of wear resistance in comparison to the latter ones.

## 4:05 PM

**The Effects of Annealing on the Charge-Discharge Characteristics of Al-Si Thin Film with Pre-Deposited Al Layer:** *Chao-Han Wu*<sup>1</sup>; Fei-Yi Hung<sup>2</sup>; Truan-Sheng Lui<sup>1</sup>; Li-Hui Chen<sup>1</sup>; <sup>1</sup>Department of Materials Science and Engineering, National Cheng Kung University; <sup>2</sup>Institute of Nanotechnology and Microsystems Engineering, Center for Micro/Nano Science and Technology, National Cheng Kung University

In this study, radio frequency magnetron sputtering was used to prepare Al-Si film anodes and the effect of both pre-sputtered Al thin film and oxygen fraction (17 ~ 7 at. %) within the Al-Si film on the charge-discharge capacity characteristics are discussed. The pre-sputtered 40nm Al thin film not only reduced the resistivity of the composite anode film, but also diffused to prevent peeling between the Al-Si films and Cu foils after annealing in the vacuum. Owing to the above reasons, the stability for the charge-discharge cycling life at high temperature (55°) was achieved. The reduction of oxygen fraction in the Al-Si film also led to an improvement on capacity of the anode.

#### 4:20 PM Invited

**Morphology Evolution during the Growth of Polycrystalline Thin Films:** *Ramanathan Krishnamurthy*<sup>1</sup>; Mikko Haataja<sup>2</sup>; <sup>1</sup>Purdue University; <sup>2</sup>Princeton University

Growth models for polycrystalline films, commonly used in optoelectronic applications, ignore time-dependent lateral grain size effects. We address this through a thermodynamics-based method that incorporates both grain boundary grooving and lateral grain growth effects. In prior work, we studied the annealing of a film with polydisperse grain sizes, and successfully reproduced several experimental observations, including microscopic features (e.g. 'ghost' lines, groove asymmetry, grooving-grain growth interactions), and aggregate characteristics of the grains of the film (e.g. surface roughness evolution). Here, we study film growth / deposition. We demonstrate that film grooving / grain growth is considerably enhanced / impeded when a large deposition flux is employed, owing to the enhanced chemical potential driving grooving. We examine spatially varying fluxes, using physical vapor deposition & electrodeposition as examples, and find that film morphology evolution depends critically upon the ratio of length scales associated with growth instabilities and grain growth respectively.

#### 4:45 PM

**Characterization of Nanospherical ZnO: Al Films and ZnO: Al/p-Si Structure:** *Nilgun Baydogan*<sup>1</sup>; O. Karacasu<sup>2</sup>; H. Cimenoglu<sup>2</sup>; <sup>1</sup>Istanbul Technical University, Energy Institute; <sup>2</sup>Istanbul Technical University, Metallurgical & Materials Engineering Department

Multilayer transparent conducting aluminium doped zinc oxide films have been deposited on p type silicon wafers by the sol-gel dip coating process to fabricate ZnO:Al/p-Si heterojunction. Each layer was pre-heated at 400 °C in a conventional furnace for 10 min. and the final films were annealed at different temperatures in oxygen, vacuum and nitrogen ambient. The surface of ZnO:Al films on p-Si substrates were characterized by using XRD, SEM and EDS analysis. Results showed that the films consist of almost spherical nanoparticles with a size range of 25-50 nm. The thickness measurements were performed by a surface profilometer (Dektak- 6M surface profilometer) at different parts of the films. The optical properties of nanospherical ZnO:Al thin films were performed by UV/VIS Spectrophotometer in the wavelength range from 192.5 to 950 nm. The resistivity of ZnO:Al the film on p-type silicon wafer was investigated by Dispensible Four Point Resistivity Probe with Mounting Stand (SIGNATONE).

### Commonality of Phenomena in Composite Materials II: Understanding Composite Performance

*Sponsored by:* The Minerals, Metals and Materials Society, ASM International, TMS Structural Materials Division, TMS/ASM: Composite Materials Committee

*Program Organizers:* Meisha Shofner, Georgia Institute of Technology; Carl Boehlert, Michigan State University

Wednesday PM  
March 2, 2011

Room: 6A  
Location: San Diego Conv. Ctr

*Session Chair:* Enrique Barrera, Rice University

#### 2:00 PM Invited

**Microstructural Optimization of Hybrid Materials for Multifunctional Performance:** *Jonathan Spowart*<sup>1</sup>; <sup>1</sup>Air Force Research Laboratory

Hybrid materials can be defined in various ways, including functional hybrids and structural hybrids. Often, the differences between these two definitions become blurred. Moreover, the microstructures of hybrid materials can range over many orders of magnitude in length scale - from the nanoscale at the interface, up to the macroscale at the structural component level. Microstructural characterization over multiple length scales therefore remains a challenge. In this presentation, we focus on optimizing the combination of different materials to provide new and improved

functionalities for the resulting hybrid. Methods for microstructural optimization from the literature and our own research are discussed, in the context of providing optimized multifunctional performance. Abstract Cleared for Public Release | Distribution Unlimited | 88ABW-2010-3965

#### 2:40 PM

**Stiffness Based Failure Predictions in Composite Structures:** *Chandra Veer Singh*<sup>1</sup>; <sup>1</sup>Cornell University

Presently, composite structures are designed against strength failure. The criteria used are often empirical and overly conservative, as recognized by recent world wide failure exercise (WWFE-III). Moreover, many applications involve design functions such as structural deflections, vibrations, etc., where critical performance is determined by material stiffness. Design of these structures with strength criteria alone is inaccurate as subcritical damage in form of ply cracking and interfacial debonding occurs well before ultimate failure. Here we present a stiffness based failure criterion which accounts for progressive damage. Initiation and progression of damage is analyzed using a fracture mechanics based energy model. Subsequent stiffness reduction is computed using our newly developed synergistic damage mechanics. The structure fails when its stiffness properties reduce below a critical level. Above model is implemented in commercial FEA package ABAQUS via user subroutine. The model is then applied to practical problems and verified with available experimental data.

#### 3:00 PM

**Ablation Properties of Glass Ceramic Matrix/C and Glass Ceramic/SiC Matrix Composites during Oxyacetylene Torch Test:** *Julien Beauder*<sup>1</sup>; Jonathan Cormier<sup>1</sup>; André Dragon<sup>1</sup>; <sup>1</sup>PPRIME

The ablative properties of two laminated composites, having the same glass matrix and architecture with different kind of fibers, are evaluated and compared. Ablation tests are performed using an oxyacetylene torch on samples having two different thicknesses. Mass loss and ablation depth are measured after flame exposure. The results obtained shows that the decomposition of SiC fibres during thermal exposure has a significant impact on ablation behavior. The oxidation process of SiC produces a liquid SiO<sub>2</sub> film at the top of the material during ablation. This leads to an improved ablation resistance compared to a glass ceramic / C composite, especially in case of successive flame exposures where the SiO<sub>2</sub> film consumes a substantial fraction of the heat flow during its liquefaction.

#### 3:20 PM

**Higher-Order Micromechanics and Effective Elastic Moduli of Particle Reinforced Composites:** *Keiji Yanase*<sup>1</sup>; Jiann-Wen Ju<sup>2</sup>; <sup>1</sup>Fukuoka University; <sup>2</sup>University of California, Los Angeles

A novel higher-order micromechanical formulation is proposed to predict the effective elastic moduli of particle reinforced composites. By considering the direct particle interactions, micromechanical field equation is systematically presented, and the near-field particle interactions are accounted for in the effective elastic moduli of spherical particle reinforced composites. Specifically, the focus is upon the effective elastic moduli of two-phase composites containing randomly distributed isotropic spherical particles. To demonstrate the predictive capability of the proposed micromechanical framework, comparisons between the theoretical predictions and the available experimental data on effective elastic moduli are rendered.

#### 3:40 PM Break

#### 4:00 PM Invited

**Enhancing Performance, Durability and Properties of Engineering Resins through the Use of Nanotechnology:** *Michael Meador*<sup>1</sup>; <sup>1</sup>NASA Glenn Research Center

Future NASA missions will require materials with durability, properties and performance that far exceed that of today's materials. Developments in nanotechnology over the past decade have demonstrated that addition of nanoscale additives to engineering resins and composites can significantly enhance their mechanical properties and durability. This paper will review NASA's plan for development of nanostructured materials and their potential use in NASA missions and recent results from research efforts in this area.

4:40 PM

**Modelling Shear Fracture of Hybrid CFRP/Ti Laminates with Cohesive Elements; Effects of Geometry and Material Properties:** Parya Naghipour<sup>1</sup>; Marion Bartsch<sup>1</sup>; Joachim Hausmann<sup>1</sup>; Karola Schulze<sup>1</sup>; <sup>1</sup>German Aerospace Research Center (DLR)

Hybrid laminates made of Carbon Fibre Reinforced Plastic (CFRP) and metal foil plies (e.g. titanium) have been investigated numerically and experimentally to be considered for applications in aerospace industry. The numerical FE model of the hybrid laminate, subjected to lap shear fracture, is composed of a CFRP core between two titanium layers with cohesive elements lying within CFRP/Ti interface. In the FE model, the CFRP laminate is assumed as an orthotropic homogenized continuum under plane stress, and titanium face sheets are modelled as an elastic-plastic continuum. The constitutive law for the quadratic CFRP/Ti interface elements, implemented as User Element in ABAQUS, is an exponentially decaying law representing the degrading behaviour of the interface. The influence of geometry (e.g. overlap length and total length), interface cohesive properties, and plastic deformation of the adherent metal foils on the lap shear fracture response are analyzed in detail in this study.

5:00 PM Invited

**Deformation Mechanisms in Carbon Nanotube/Epoxy Composites:** Scott Brownlow<sup>1</sup>; Alexander Moravsky<sup>2</sup>; Bhaskar Majumdar<sup>1</sup>; <sup>1</sup>New Mexico Tech; <sup>2</sup>MER Corporation

This presentation will highlight our understanding of load transfer in double wall carbon nanotube/epoxy composites obtained by a combination of in situ FTIR and Raman measurements. Emphasis will be focused on FTIR measurements of spectral shifts of the epoxy matrix under mechanical load, and a theoretical basis for such stress induced shifts using recent quantum mechanical analysis of a modular epoxy-hardener molecule combination will be provided. Some of the problems of using Raman measurements to interpret load transfer in the randomly oriented nanotube reinforcement will be pointed out. The final part of the presentation will focus on application of carbon nanotubes in hybrid carbon-fiber-nanotube composites. The beneficial effect of interply nanotube layers on interlaminar fracture toughness and delamination damage resistance, and the associated failure mechanisms, will be discussed.

## Computational Plasticity: Crystal Plasticity

*Sponsored by:* The Minerals, Metals and Materials Society, TMS Materials Processing and Manufacturing Division, TMS Structural Materials Division, TMS/ASM: Computational Materials Science and Engineering Committee, TMS: High Temperature Alloys Committee  
*Program Organizers:* Remi Dingreville, Polytechnic Institute of NYU; Koen Janssens, Paul Scherrer Institute

Wednesday PM  
March 2, 2011

Room: 1A  
Location: San Diego Conv. Ctr

*Session Chair:* To Be Announced

2:00 PM Invited

**A Methodology for Simulating Microtexture Evolution in Deformed Aluminum and Titanium Polycrystals:** Paul Dawson<sup>1</sup>; Romain Quey<sup>1</sup>; <sup>1</sup>Cornell University

Crystal plasticity models implemented in finite element formulations have been used successfully to predict the effects of plastic anisotropy on deformation and to predict the evolution of crystallographic texture. Currently, efforts are focussed on predicting the spatial variations in lattice orientations within individual grains (microtextures) that are observed experimentally in deformed samples. Several challenges arise in making such predictions accurately. Samples of sufficient size (number of crystals) and sufficient resolution (number of elements discretizing each crystal) must be instantiated and deformed to large strains. The results must be abstracted for comparison to experimental data. We discuss the simulation of

microtexture evolution in metallic alloys, focusing on comparison of metrics that quantify microtextures: average lattice misorientations, crystallographic spread of misorientations, and its crystallographic dependence. We compare predicted trends to ones measured in deformed aluminum and contrast the behaviors of aluminum and titanium polycrystals.

2:30 PM Invited

**A Modular Crystal Plasticity Framework Applicable from Component to Single Grain Scale:** Philip Eisenlohr<sup>1</sup>; Denny Tjahjanto<sup>1</sup>; Christoph Kords<sup>1</sup>; Franz Roters<sup>1</sup>; Dierk Raabe<sup>1</sup>; <sup>1</sup>Max-Planck-Institut für Eisenforschung

The solution of a continuum mechanical boundary value problem requires a constitutive response connecting deformation and stress at each material point. Such connection can be regarded as three separate hierarchical problems. First, partitioning of the (mean) boundary values of the material point among its microstructural constituents and the associated homogenization of their response. Second, based on an elastoplastic decomposition of (finite strain) deformation, these responses follow from explicit or implicit time integration of the plastic deformation rate per constituent. Third, to establish the latter a state variable-based constitutive law needs to be interrogated and its state updated. We demonstrate the versatility of such framework, which has been implemented into finite element packages, by considering three scenarios. Component-scale forming simulations comparing different homogenization schemes, selective refinement of the constitutive material description within a single geometry, and gradient-dominated deformation of an oligocrystalline patch using a non-local constitutive law.

3:00 PM Invited

**An Efficient Strategy to Take Texture-Induced Anisotropy Point-By-Point into Account during FE Simulations of Metal Forming Processes:** Paul Van Houtte<sup>1</sup>; Jerzy Gawad<sup>1</sup>; Philip Eyckens<sup>1</sup>; Bert Van Bael<sup>1</sup>; Samaey Giovanni<sup>1</sup>; Dirk Roose<sup>1</sup>; <sup>1</sup>Katholieke Universiteit Leuven

Focus will be on the implementation of texture-induced plastic anisotropy in FE simulations of metal forming. The crystallographic texture can be introduced as a state variable in every integration point. A multi-scale model is then called to calculate the stress-strain response and the local texture evolution in every integration point and for every strain increment. Less calculation-intensive is to use anisotropic analytical constitutive models, identified in advance from mechanical tests. These can also be done in a "virtual" way, i. e. using measured texture data and a multi-scale model. However, texture evolution is then not taken into account. An adaptive scheme for updating the texture and the anisotropy has been developed recently. Texture and anisotropy were updated by the ALAMEL-model. Results for a cup drawing process will be shown. The calculation time was reduced from months to days. Predicted fields of plastic anisotropy and textures will be discussed including experimental validation.

3:30 PM Invited

**Crystal Plasticity Computations Using Real Grain Arrangements to Simulate Deformation and Fracture:** Henry Proudhon<sup>1</sup>; Samuel Forest<sup>1</sup>; Wolfgang Ludwig<sup>2</sup>; <sup>1</sup>MINES ParisTech; <sup>2</sup>INSA Lyon

Progress with Finite Elements (FE) codes, more robust meshing algorithms and larger computer power make Crystal Plasticity FE simulations suitable to simulate the deformation and fracture of complete specimens. This becomes of primary interest when those specimens can also be characterized experimentally in the form of the 3D arrangement of their grain microstructure and damage evolution. Two examples of applications of those large scale simulations are described in this paper. In the first example, Crystal Plasticity simulations are conducted on sample imaged by Diffraction Contrast Tomography, which allows to resolve the 3D shape and orientation of the grains constituting the specimen. It is shown how to explicitly take into account the presence of a crack within the microstructure and its effect on the strain/stress distribution. The second example aims at simulating 3D coherent X-ray diffraction patterns in a polycrystalline gold sample to help interpreting the complex results obtained experimentally.



4:00 PM

**A Rate-Dependent Polycrystal Model for Evaluation of the Creep Deformation in the Heat Affected Zone of the Modified 9Cr-1Mo Steels:** *Mehdi Basirat*<sup>1</sup>; *Gabriel Potirniche*<sup>1</sup>; *Triratna Shrestha*<sup>1</sup>; *Indrajit Charit*<sup>1</sup>; *Karl Rink*<sup>1</sup>; <sup>1</sup>University of Idaho

The high creep resistance at the elevated temperature has made the modified 9Cr-1Mo steels an excellent choice for power plant reactor pressure vessels. Modeling creep based on classical inelastic approaches is predominant in creep literature. While these efforts have a certain practical importance, they are essentially phenomenological in nature. In this paper a rate-dependent polycrystal plasticity model has been developed for computing the creep deformation of the modified 9Cr-1Mo steels in the weld heat affected zone. The constitutive behavior of tertiary creep at the crystal level has been modeled through evolution equations for three simultaneous degradation processes: (i) subgrain and dislocation network coarsening, (ii) a decrease in dislocation density, and (iii) solute depletion at the subgrain level. A user subroutine has been developed to compute the resulting creep strains; furthermore the numerical results have been validated experimentally. Finally a User MATerial Subroutine (UMAT) has been implemented in the ABAQUS software.

4:15 PM Break

4:30 PM Invited

**Use of Spectral Databases for Crystal Plasticity Finite Element Simulations of Bulk Deformation Processing of Cubic Metals:** *Hamad Al-Harbi*<sup>1</sup>; *Josh Shaffer*<sup>1</sup>; *Surya Kalidindi*<sup>1</sup>; <sup>1</sup>Drexel University

In recent work, we have demonstrated the viability and computational advantages of DFT-based spectral databases for facilitating rigid-viscoplastic crystal plasticity solutions in cubic metals subjected to arbitrary deformation paths. In this paper, we report the first incorporation of our novel spectral crystal plasticity databases into a commercial finite element package for simulating bulk deformation processing operations on face centered and body centered cubic metals. The evolution of the underlying crystallographic texture in the work-piece and its associated macroscale anisotropic properties predicted from our new Spectral Crystal Plasticity Finite Element Approach (SCP-FEA) will be compared against the corresponding results from the conventional crystal plasticity finite element method. It will be shown that SCP-FEA produces excellent predictions with about two orders of magnitude savings in the computational time.

5:00 PM

**Modeling Mesoscopic Plastic Flow Heterogeneities of 3D Polycrystalline Microstructures Using Crystal-Plasticity FEM and FFT-Based Viscoplastic Model:** *Yoon Suk Choi*<sup>1</sup>; *Benjamin Anglin*<sup>2</sup>; *Michael Groeber*<sup>3</sup>; *Paul Shade*<sup>4</sup>; *Michael Uchic*<sup>3</sup>; *Christopher Woodward*<sup>3</sup>; *Dennis Dimiduk*<sup>3</sup>; *Anthony Rollett*<sup>2</sup>; *Ricardo Lebensohn*<sup>3</sup>; *Triplicane Parthasarathy*<sup>1</sup>; <sup>1</sup>UES, Inc.; <sup>2</sup>Carnegie Mellon University; <sup>3</sup>Air Force Research Laboratory; <sup>4</sup>UTC; <sup>5</sup>Los Alamos National Laboratory

The initiation and development of mesoscopic plastic flow heterogeneities have been the objective of numerous numerical studies because of their significance in understanding and identifying critical microstructural features for microscopic instability and damage initiation. Numerical approaches widely used for such studies include crystal plasticity FEM and the image-based FFT-based viscoplastic model. However, there are few experimental validations of these numerical approaches in the 3D mesoscopic space. Recently, some of the authors obtained 3D microstructure data using EBSD mapping and FIB-based serial sectioning from micro-tension specimens of polycrystalline nickel. Elasto-viscoplastic FEM modeling and FFT-based viscoplastic modeling were performed for these real 3D microstructures. The heterogeneities that develop within simulations of plastic responses were analyzed using various statistical characterization techniques, and compared between the two numerical approaches. An effort was also made to compare simulated plastic flow heterogeneities to the limited 3D plasticity information obtained from micro-tension specimens.

5:20 PM Invited

**Efficient Methodologies for Determining Temperature-Dependent Parameters of Crystal Viscoplasticity:** *Daniel Smith*<sup>1</sup>; *Richard Neu*<sup>1</sup>; <sup>1</sup>Georgia Institute of Technology

The current limitations of widespread use of crystal viscoplasticity in industry for modeling complex thermomechanical loading are often tied to the difficulty in the calibration of the temperature-dependent material parameters. The conventional approach typically involves conducting multiple sets of isothermal deformation experiments at different temperatures. This is highly costly and time consuming, often requiring months to establish the parameters. This paper outlines protocols aimed at efficiently determining microstructure-sensitive temperature-dependent material parameters. These protocols include minimal, carefully planned calibration experiments and the judicious use of optimization software for identifying material parameters. The approach is demonstrated on Ni-base superalloys with application of modeling the influence of microstructure on the thermomechanical fatigue and creep-fatigue response of hot section components in gas turbines. ModelCenter is used along with some MATLAB intermediary routines to assist the user in determination of material parameters for a crystal viscoplasticity model that is coded as a UMAT for ABAQUS.

5:50 PM

**A Dislocation Density Based Crystal Plasticity Model for  $\alpha$ -Titanium:** *Alankar Alankar*<sup>1</sup>; *Philip Eisenlohr*<sup>1</sup>; <sup>1</sup>Max-Planck Institute for Iron Research

A constitutive model for single crystal plasticity of hexagonal  $\alpha$ -titanium is developed. In the model framework, pure edge and screw dislocation densities evolve on basal, prismatic  $\langle a \rangle$ , and pyramidal  $\langle a \rangle$  slip families. For non-basal slip systems, a spread out core is assumed for screw segments, leading to much higher mobility of edge compared to screw dislocations, similar to the behavior found in body-centered cubic crystals. This enables the model to reflect the observed transition of stress evolution from stage I to stage II in single crystals oriented for prismatic slip. The basal slip behavior is modeled as in face-centered cubic metals. Calibration of the model is done based on experimental results of titanium single crystals with varying commercial purity. Further, the model is employed for analysis of microstructure evolution in a polycrystal. A reasonable agreement is found between experimentally observed slip and twinning activity in different grains.

6:10 PM

**Numerical Eulerian Modeling in Dynamic Crystal Plasticity:** *Ioan Ionescu*<sup>1</sup>; *Oana Cazacu*<sup>2</sup>; <sup>1</sup>University Paris 13; <sup>2</sup>University of Florida

A robust numerical algorithm for an Eulerian rigid-visco-plastic crystal model that accounts for high-strain rates, large strains, and large material and lattice rotations, was developed. The viscoplastic law is obtained from Schmid law by using an overstress approach; the numerical instabilities associated to the classical power law are thus eliminated. To handle the non differentiability of the plastic terms an iterative decomposition-coordination formulation coupled with the augmented Lagrangian method was adopted. A mixed finite element-finite volume strategy was adopted: the equation for the velocity field is discretized using the finite element method while a finite volume method, with an upwind choice of the flux, is adopted for the hyperbolic equation related to the lattice orientation. Several two-dimensional boundary value problems are selected to analyze the robustness of the numerical algorithm. The grains interaction during channel die compression of a multi-crystal was analyzed using an ALE description.

## Computational Thermodynamics and Kinetics: Thermodynamics, Phase Stability and Phase Transformations

*Sponsored by:* The Minerals, Metals and Materials Society, ASM International, TMS Electronic, Magnetic, and Photonic Materials Division, TMS Materials Processing and Manufacturing Division, TMS: Alloy Phases Committee, TMS: Chemistry and Physics of Materials Committee, TMS/ASM: Computational Materials Science and Engineering Committee, ASM: Alloy Phase Diagrams Committee  
*Program Organizers:* Raymundo Arroyave, Texas A & M University; James Morris, Oak Ridge National Laboratory; Mikko Haataja, Princeton University; Jeff Hoyt, McMaster University; Vidvuds Ozolins, University of California, Los Angeles; Xun-Li Wang, Oak Ridge National Laboratory

Wednesday PM                      Room: 9  
March 2, 2011                        Location: San Diego Conv. Ctr

*Session Chairs:* Patrice Turchi, Lawrence Livermore National Laboratory; Michael Gao, National Energy Technology Lab/URS Corp

### 2:00 PM Invited

#### Thermomechanical Processing Design of Nanoprecipitate Strengthened Alloys Employing Genetic Algorithms: *Pedro Rivera-Diaz-del-Castillo*<sup>1</sup>; University of Cambridge

A modelling strategy for designing nanoprecipitation strengthened alloys is presented here. This work summarises the application of a new thermokinetics approach wherein multiple design criteria are enforced: corrosion resistance and high strength combined with affordable thermomechanical processing schedules. The methodology presented here iteratively performs thermodynamic and kinetic calculations, these are aimed at determining the best precipitate nanostructures following multiple design objectives. A genetic algorithm is employed to more rapidly finding optimal alloy compositions and processing parameters consistent with the design objectives. It was possible to computationally design new alloys strengthened by Ni-based nanoprecipitates and carbides with yield strengths exceeding 1.6 GPa and good corrosion resistance. A major limitation in the methodology is the determination of optimum processing times, which require the computation of formation energies of non-equilibrium precipitates employing other techniques. A method to circumvent such limitation is discussed.

### 2:30 PM

#### Thermodynamic Assessment and Experimental Investigation of the Ternary Ti–Al–Cr System: *Mario Kriegel*<sup>1</sup>; Damian Cupid<sup>1</sup>; Olga Fabrichnaya<sup>1</sup>; Dmytro Pavlyuchkov<sup>1</sup>; Kostyantyn Korniyenko<sup>2</sup>; Vera Khorujaya<sup>2</sup>; Fereshteh Ebrahimi<sup>3</sup>; Hans Seifert<sup>1</sup>; <sup>1</sup>Freiberg University of Mining and Technology; <sup>2</sup>I.N. Frantsevich Institute for Problems of Materials Science; <sup>3</sup>University of Florida

Titanium aluminides alloyed with Cr are promising materials for high temperature applications because of their expected improved processability and high temperature oxidation resistance in comparison to the non-alloyed titanium aluminides. A thermodynamic description for the Ti–Al–Cr system was developed using experimental data on phase stabilities and phase equilibria from the literature. The ternary  $\text{Ti}_{0.96}\text{Al}_{0.04}\text{Cr}_{0.32}\text{Al}_{2.68}$  phase was modelled as a stoichiometric phase for the first time, and ternary mixing parameters of the  $\text{Ti}_{0.96}\text{Al}_{0.04}\text{Cr}_{0.32}\text{Al}_{2.68}$  phase were optimized. Using this dataset, the liquidus and solidus surfaces and several key isothermal sections were calculated. In order to assess the reliability of the calculated liquidus and solidus surfaces, several alloys in the Ti–Al–Cr system were arc-melted and the as-cast structures were evaluated using the techniques of SEM, XRD, and thermal analysis (DTA / DSC).

### 2:45 PM

#### First-Principles Prediction of Partitioning of Alloying Elements between Cementite and Ferrite: Chaitanya Krishna Ande<sup>1</sup>; Marcel Sluiter<sup>2</sup>; <sup>1</sup>Materials Innovation Institute, Delft University of Technology; <sup>2</sup>Delft University of Technology

At long tempering times in steels when both cementite ( $\text{Fe}_3\text{C}$ ) and ferrite (bcc-Fe-rich solid solution) phases are present, alloying elements tend to segregate to either of the two phases. V, Cr, Mn, Mo and W are found to partition to the cementite phase while the elements Al, Si, P, Co, Ni and Cu partition to ferrite. We show that partitioning of alloying elements and cementite (de)stabilization by alloying in mixtures of bcc-Fe and cementite are intimately related through the introduction of a partitioning enthalpy. The formation enthalpy of alloying element substituted cementite is shown not to be a proper gauge for addressing these questions and that magnetism plays an important role in describing the partitioning correctly.

### 3:00 PM

#### Ab Initio Aided CALPHAD Thermodynamic Modeling of Ionic Systems: Application to $\text{La}_{1-y}\text{MnO}_{3-3y}$ : *Shih-kang Lin*<sup>1</sup>; Dane Morgan<sup>1</sup>; <sup>1</sup>University of Wisconsin-Madison

Defect concentrations vs. temperature and gas partial pressures play a fundamental role in the properties of ionic systems. Defect models can be constructed through the conventional calculation of PHase Diagram (CALPHAD) approach using the Compound Energy Formalism (CEF). However, determining the large number of model parameters in the CEF from typical experimental data sets requires many, often poorly justified, approximations. *Ab initio* energies offer a way to reduce the approximations used in applying the CEF to complex ionic systems. However, the required *ab initio* energies are often end-members that are not stable and can involve non-neutral cells. Here we discuss approaches to treat these problems to enable *ab initio* energetics to be applied in the CALPHAD CEF. Initial results for  $\text{La}_{1-y}\text{MnO}_{3-3y}$ , a base oxide for many important cathode materials in SOFC and other applications, will be presented.

### 3:15 PM

#### Phase Formation in Actinide Alloys: Why Ab Initio?: *Patrice Turchi*<sup>1</sup>; Alexander Landa<sup>1</sup>; Larry Kaufman<sup>2</sup>; Per Söderlind<sup>1</sup>; <sup>1</sup>Lawrence Livermore National Laboratory; <sup>2</sup>CALPHAD, Inc.

Nuclear fuels for fast spectrum nuclear reactors raise challenging questions on the role of minor actinides and fission products and gases on properties and performance. Hence, prediction of phase stability trends and phase diagrams of complex actinide-based alloys is undoubtedly the Holy Grail of materials properties simulations. We show that CALPHAD, combined with appropriate first-principles electronic structure results, is a powerful tool to predict the thermodynamic properties of actinide-based multi-component alloys. For the sake of clarity the presentation focuses on {Am,Np,Pu,U,Zr} that are the basis for candidate metallic fuels. Since experiments on this class of alloys are costly and challenging, we show that *ab initio* input provides useful guidance for well-chosen experiments that can lead to full validation and verification of the thermodynamic driving force that is critically needed for subsequent work on materials evolution and performance. Work performed under the auspices of the U.S. DOE by LLNL under contract DE-AC52-07NA27344.

### 3:30 PM Break

### 3:40 PM Invited

#### Topological Modelling of Martensitic Transformations: Robert Pond<sup>1</sup>; <sup>1</sup>University of Exeter

According to the topological model (TM), a martensitic interface exhibits a partially coherent structure where the coherent segments are bounded by disconnections (line defects having both step and dislocation character) and crystal defects (slip or twinning dislocations) [1]. In this way the coherency strains are removed at long range. The transformation strain arises from the motion of the interfacial defects, laterally along the interface in the case of the disconnections, and along glide or twin planes in the wake of the moving interface for the crystal defects. It can be demonstrated that this

transformation mechanism is diffusionless. The orientation relationship (OR) between the adjacent crystals is determined by the superposition of the coherency strain and the elastic fields of the defects in the static interface. In general, the OR deviates by a small tilt and/or twist deviation from the reference OR of the coherent segments. Experimental evidence supporting this model is accumulating, particularly from TEM observations, and will be presented. In addition, the TM provides mechanistic insights, in contrast to the earlier phenomenological model (PM). For example, the TM distinguishes between the reversible plastic transformation strain and the elastic distortion field. Whereas the former is determined by purely geometrical parameters, the latter depends on the relative elastic moduli of the parent and product crystals. This analysis also shows why the PM provides a good first approximation to transformation crystallography in cases such as Ti alloys, but fails for other cases such as lath martensite in steel. In the former instance, small tilt deviations are present so the invariant line concept is approximately valid, but in the latter case small twists are present, violating the invariant plane notion.[1] R.C. Pond, X. Ma, Y.W. Chai and J.P. Hirth, in *Dislocations in Solids*, edited by F.R.N. Nabarro and J.P. Hirth, Vol. 13 (Elsevier, Amsterdam, 2007), p. 225.

#### 4:10 PM Invited

**Ginzburg-Landau Modeling of Martensitic and Multifunctional Materials:** *Avadh Saxena*<sup>1</sup>; <sup>1</sup>Los Alamos National Lab

Strain plays a central role in phase transformations in martensites, ferroelastics as well as multifunctional materials such as ferroelectrics, multiferroics and magnetoelectrics. A variety of microstructures observed in these materials can be systematically modeled and understood by means of a crystal symmetry based Landau free energy in relevant strain tensor components. Since the strain components are not independent, the elastic compatibility constraint provides an anisotropic long-range force which governs the microstructure. In multifunctional materials lattice distortion (or strain) acts as an elastic template to which magnetization, polarization and other functionalities couple. The long range elastic force competes with other forces, e.g. polar (or magnetic) short range dipolar forces resulting in multiple competing states and a multiscale microstructure. The consequences of the resulting microstructure on various materials properties will be discussed.

#### 4:40 PM

**Simulation of Liquid/Solid Phase Transformations - How Thin Is a Sharp Interface?:** *Markus Rettenmayr*<sup>1</sup>; <sup>1</sup>Friedrich-Schiller-University Jena

Different techniques for simulating phase transformations as e.g. the Phase Field Method incorporate a finite width of the interface, which is said to correspond closely to a natural interface. In contrast, sharp interface models generally assume the interface to be mathematically sharp or infinitely thin. However, if interface kinetics such as trans-interface diffusion is considered, sharp interface models still define the interface position precisely, but for the kinetic processes through the interface a finite width is implicitly assumed. If interface kinetics is included in solid/liquid phase transformation models, both solidification and melting can be modeled for a wide range of parameters, and the asymmetry between the two types of phase transformations is accounted for. The implications of the interface width in such simulations are discussed.

#### 4:55 PM

**A Molecular Dynamics Study of the Austenite-Ferrite Interface Mobility in Pure Fe:** *Huajing Song*<sup>1</sup>; *Jeff Hoyt*<sup>1</sup>; <sup>1</sup>McMaster University

Molecular dynamics (MD) simulations performed on two phase simulation cells were used to compute the FCC/BCC boundary mobility in pure Fe over the temperature range 400-1000K. An embedded atom method interatomic potential was used to model Fe and the driving force for interface motion is the free energy difference between the two phases, which was computed as a function of temperature using a thermodynamic integration technique. For low index FCC/BCC crystallographic orientations no interface motion is observed, but for slight misorientations steps are introduced at the interface and sufficient mobility is observed over MD time scales. The interface velocity can reach 2 m/s and the mobility at 1000K is approximately 0.001

mol-m/J-s. In agreement with previous MD studies of grain boundary mobility, we find that the activation energy for the austenite-ferrite boundary mobility is much lower than values found in experiment.

#### 5:10 PM

**Phase Stability of Fe-Nb-M (M=Cr, Mn, Si, Ti): A First Principles Approach:** *Michael Gao*<sup>1</sup>; *Paul Jablonski*<sup>1</sup>; <sup>1</sup>NETL

Metallic interconnects are the cost enabling technological leap for solid oxide fuel cells. Presently, the ferritic steel 441ss is the alloy of choice for this application. What seems to distinguish this alloy from other medium level Cr stainless steels is that 441ss forms C14 Fe<sub>2</sub>Nb Laves phase (Pearson Symbol hP12, prototype MgZn<sub>2</sub>) that provides additional precipitate strengthening. Furthermore, solute (namely Cr, Mn, Si, and Ti) partitioning in the Laves phase is controversial. In this work, we use ab initio density functional theory calculations to predict the energies of substituting alloying elements in the ferritic steel 441ss for Fe or Nb in the Laves phase. Based on the energy calculations of this Laves alone, it is found that Si atoms favor substituting for the Fe sites while Ti atoms for the Nb site. In order to compare with experimental phase diagrams, we also calculate the energies of the Fe-Nb-M ternaries.

#### 5:25 PM

**Thermodynamic Modeling of the Cu-Hf System:** *Yu Zhong*<sup>1</sup>; *Arkapol Saengdeejeing*<sup>1</sup>; *Laszlo Kecskes*<sup>2</sup>; *Zi-Kui Liu*<sup>1</sup>; <sup>1</sup>Pennsylvania State University; <sup>2</sup>US Army Research Laboratory

The complete thermodynamic description of the Cu-Hf binary system is modeled using the CALPHAD approach that combines both first-principles calculations and experimental investigations. The enthalpy of formation for all the compounds in the system are calculated via first-principles calculations, based on density functional theory (DFT), using the Vienna Ab-initio Simulation Package (VASP). The projector augmented-wave (PAW) method is used and the exchange and correlation energy are described with the supplied generalized gradient approximation pseudopotentials (PBE). In addition to the recent work between 38 to 60 at.% Hf[1], further experimental investigations, including differential thermal analysis and scanning electron microscopy, were used to extend and study the phase equilibrium between 13 to 40 at.% Hf. References: [1] R. H. Woodman, B. R. Klotz, and L. J. Kecskes, *J. Phase Equilib. Diffus.* 27, 477 (2006).

---

### David Pope Honorary Symposium on Fundamentals of Deformation and Fracture of Advanced Metallic Materials: Grain Boundaries, Phase Transformations, and Steels

*Sponsored by:* The Minerals, Metals and Materials Society, TMS Materials Processing and Manufacturing Division, TMS Structural Materials Division, TMS: High Temperature Alloys Committee, TMS/ASM: Mechanical Behavior of Materials Committee, TMS: Nanomechanical Materials Behavior Committee  
*Program Organizers:* E. P. George, Oak Ridge National Laboratory; Haruyuki Inui, Kyoto University; C. T. Liu, The Hong Kong Polytechnic University

Wednesday PM  
March 2, 2011

Room: 32A  
Location: San Diego Conv. Ctr

*Session Chairs:* Michael Mills, The Ohio State University; Robert Mulford, Knolls Atomic Power Laboratory

---

#### 2:00 PM Invited

**Physical Metallurgy Insights into the Effects of Grain-Boundary Segregants on Ductility and Fracture:** *E. P. George*<sup>1</sup>; *C. T. Liu*<sup>2</sup>; *D. P. Pope*<sup>3</sup>;

<sup>1</sup>Oak Ridge National Laboratory; <sup>2</sup>Hong Kong Polytechnic University; <sup>3</sup>University of Pennsylvania

Elements that segregate to grain boundaries in metals can be harmful, beneficial, or benign. Some of these effects are manifested at low temperatures, others at elevated temperatures. Some at slow strain rates,



others at high strain rates. Some act on their own while others act in concert with or to counteract the effects of other segregants. Because of the sheer number of different mechanisms by which grain boundary segregants act, simple physical metallurgy insights gleaned from clever experiments are needed to isolate the operative mechanisms. A more comprehensive understanding will have to wait until multiscale models of deformation and fracture can properly account for trace (ppm level) changes in alloy composition. In this talk we will use examples of trace elements that exhibit beneficial and harmful effects on the ductility and fracture behavior of high-temperature materials to highlight what we know and do not yet know about the underlying mechanisms.

## 2:30 PM

### **Study of Grain Boundary Strength in AA2198 Using Notched Micro-Beam Bending:** Daniel Kupka<sup>1</sup>; Erica Lilleodden<sup>1</sup>; <sup>1</sup>GKSS Research Center

Al-Li alloys are of great interest due to their high strength and low specific weight. However, these alloys show complicated fracture behavior, motivating fundamental studies of grain boundary strength and its dependence on thermo-mechanical processing. In the present work, we have studied the fracture of grain boundaries in rolled AA2198 sheets in the T8 ("heat treated") and T351 ("as-rolled") conditions using microbeam bending experiments. Micron-scale cantilever beams were fabricated by focused ion beam (FIB) milling, with single grain boundaries aligned within a semi-cylindrical notch. The beams were then loaded using a nanoindenter, and finite element simulations were carried out to help in the analysis of the load-displacement data. Intergranular fracture was shown to occur at the grain boundaries positions within the notch, as expected. Significant differences in normalized load and fracture morphology were observed between the T8 and T351 samples.

## 2:45 PM

### **In Situ TEM Observations of Reverse Dislocation Motion upon Unloading of Ultrafine-Grained (UFG) Aluminium Strained in the Microyield Region:** Daniel Caillard<sup>1</sup>; Frederic Mompou<sup>1</sup>; Marc Legros<sup>1</sup>; Hael Mughrabi<sup>2</sup>; <sup>1</sup>CNRS; <sup>2</sup>University Erlangen-Nürnberg

When strained in the microyield region and subsequently unloaded, UFG materials exhibit unusually large inelastic reverse strains which are not observed in similarly strained material of conventional grain (CG) size. In situ experiments have been carried out to find the origin of such an effect. Sources emitting dislocations which interacted with adjacent grain boundaries (GBs) have been observed. Depending on the character of the dislocations emitted, different behaviours have been observed: i) intensive cross-slip and rapid insertions in GBs for screw and mixed dislocations, and ii) pile-up formation in front of GBs for pure edge dislocations. Upon unloading, the release of stress induces a substantial reverse motion of dislocation pile-ups in case ii), whereas in case (i) only a relaxation of the source was observed. On the basis of these results, the origin of the inelastic behaviour in the bulk material and the possible role of dislocation pile-ups are discussed.

## 3:00 PM

### **Grain Boundary Based Plasticity: In-Situ TEM Experiments and Modelling:** Frederic Mompou<sup>1</sup>; Marc Legros<sup>1</sup>; Daniel Caillard<sup>1</sup>; <sup>1</sup>CEMES-CNRS

Ultrafine grains (UFG) and nanocrystalline (nc) metals are unstable and tends to evolve by grain growth even at a relatively low temperature. This behaviour seems also favoured by the application of a mechanical stress. However few studies have been focused on the elementary mechanisms that promote this instability and on the role of grain growth in the overall deformation process. We present here the results of in situ TEM straining experiments on self standing nc Al films at room temperature and on UFG Al at moderate temperature. All the results show unambiguously fast grain boundary motion assisted by the applied stress. The associated deformation has been found to be in the range of few percents in UFG Al, in contradiction with the available shear-migration coupling models. A tentative geometrical model (SMIG model) based on atom shuffling in the core of interfacial step-dislocation has been tentatively proposed.

## 3:15 PM

### **Truncated Dislocation Sources in Nanometric Aluminum Crystals: A Molecular Dynamics Study:** Bulent Biner<sup>1</sup>; L. P. Kubin<sup>2</sup>; <sup>1</sup>Idaho National Laboratory; <sup>2</sup>LEM CNRS/ONERA

In this study, the evolution behavior of truncated dislocation sources by free surfaces in small finite volumes is elucidated for aluminum using molecular dynamics simulations. Under zero stress and without dislocations, very large stress gradients arising from surface effects, of the order of several GPa, were observed. The formation of very large stacking faults due to the operation of partial dislocations and the development of full and helix dislocations were recorded during the evolution of the truncated dislocation loops under an applied shear strain. In addition, cross-slip by the Fleischer mechanism, twin formation and detwinning with two different mechanisms were identified. These dislocation mechanisms were strongly influenced by the initial configuration of the truncated dislocation loops and the geometry of the simulation cell.

## 3:30 PM

### **Geometrical Construction and Structure of Quasi-Periodic Grain Boundaries in Cubic Materials:** Mohammad Shamsuzzoha<sup>1</sup>; <sup>1</sup>University of Alabama

Geometrical construction and the structure of a special type of quasi-periodic boundary in cubic materials based on vector representation of lattice sites is proposed. The construction of these quasi-periodic crystals is achieved when mutual rotation of a unique vector termed as sigma generating vector and its square root counterpart found in identically oriented orthogonal lattice network of the participating crystals brings mutual superposition. Grain boundary in such quasi-crystals appears to comprise of structural units. Experimental evidences such as HREM images and double diffracted electron diffraction pattern supporting the existence of such structural units for a [001]45° twist quasi-periodic grain boundary are presented.

## 3:45 PM Break

## 4:00 PM

### **Mechanism of Creep Deformation in Alumina-Forming Stainless Steel Fe-25Ni-14Cr-3.5Al-2.5Nb-0.1wt%C:** Deepak Kumar<sup>1</sup>; Yukinori Yamamoto<sup>1</sup>; Michael Santella<sup>1</sup>; Michael Brady<sup>1</sup>; Edgar Curzio<sup>1</sup>; <sup>1</sup>Oak Ridge National Laboratory

Alloy Fe-25Ni-14Cr-3.5Al-2.5Nb-0.1wt%C belongs to a family of creep resistant, Al<sub>2</sub>O<sub>3</sub> film forming austenitic stainless (AFA) steel with intended applications in the range of 600-900°C. Al, Nb, Cr, and Ni level was optimized to promote the formation of an adherent and slow growing alumina film in this alloy, which is expected to provide better oxidation resistance than conventional Cr<sub>2</sub>O<sub>3</sub> film forming stainless steel and Ni-base alloys in water vapor, C, and/or S rich environments. Strengthening is achieved via stable nano-scale MC and intermetallic phases. In the present study creep deformation and rupture behavior of alloy OC4 were investigated at stresses between 100 and 170 MPa and temperatures between 650°C and 800°C, and the results were compared with those for other precipitation strengthened alloys. Norton's law was used to model the creep response of the alloy. Long term microstructure stability was evaluated via up to 5000h aging studies.

## 4:15 PM

### **Evolution and Modeling for Fatigue Damage Initiation of Thermal-Mechanically Processed High-Strength Steel:** Angelika Brueckner-Foit<sup>1</sup>; Benjamin Bode<sup>1</sup>; Yibin Xue<sup>2</sup>; <sup>1</sup>Kassel University; <sup>2</sup>Utah State University

The fatigue damage initiation of a differential thermal-mechanical processed (DTMP) high strength, functionally graded steel was evaluated numerically by implementation of a crystal plasticity constitutive model to a series of representative realistic microstructures. Most of the high cycle fatigue life is spent in fatigue damage initiation, which is susceptible to the variations in microstructural features. In-situ fatigue experiments were conducted to evaluate the microstructure-fatigue damage incubation properties. A three-dimensional simulation model was developed based on the realistic microstructure of the newly developed steel that includes phases, textures, and residual stresses from the thermo-mechanical processing. A crystal

plasticity constitutive model is implemented to evaluate microplasticity for accessing fatigue damage incubation mechanisms and predict the cycles needed for incubation. The directly application of the model will reduce the need to evaluate each individual part of the graded alloy and enhances the design and application of the novel steel.

#### 4:30 PM

**Influences of Material and Process Parameters on Delayed Fracture in TRIP-Aided Austenitic Stainless Steels:** Xiaofei Guo<sup>1</sup>; Wolfgang Bleck<sup>1</sup>; <sup>1</sup>RWTH Aachen University

The effects of material and process parameters on delayed fracture susceptibility of three AISI 301 steels have been studied by Slow Strain Rate Tests (SSRT) and Deep Drawing Tests (DDT). The parameters of austenite stability, presence of prior martensite nuclei and hydrogen content have been evaluated through analyzing the tensile strength, ductility, time to fracture and fracture surface of hydrogen pre-charged SSRT and DDT specimens. Steels having prior martensite nuclei or more unstable austenite were found more sensitive to delayed fracture. Besides, the time to fracture declined with increasing diffusive hydrogen content in a power-law manner. In addition, delayed fracture in DDT specimens could be prohibited by raising the forming temperature and punch velocity, owing to the suppressed phase transformation and partial residual stress relief. Fractographic studies revealed the transition of fracture mode from ductile to quasi-cleavage/intergranular fracture depending on hydrogen content and stress triaxility.

#### 4:45 PM

**In-Situ EBSD Study of Micromechanical Behavior of TRIP Steel:** Nan Li<sup>1</sup>; Yandong Wang<sup>1</sup>; Xin Sun<sup>2</sup>; Guilin Wu<sup>1</sup>; Kang Yuan<sup>1</sup>; <sup>1</sup>Beijing Institute of Technology; <sup>2</sup>Pacific Northwest National Laboratory

The deformation-induced martensitic transformation behaviors have been investigated for several decades, while the origin of plasticity enhancement is less understood so far. Transformation-induced-plasticity (TRIP) steels are a typical class of multiphase steels, of which contains metastable austenite transforming into martensite lately during deformation, offering an attractive combination of strength and plasticity. In this presentation, we will report the in-situ experimental investigations of micro-mechanical behavior of the TRIP steel using Electron Back-Scattered Diffraction (EBSD) technique, which accounts for the quantitative information on contribution of the transformation-induced plasticity to the total plasticity. EBSD orientation mapping of all phases at different applied strains provide not only the transformation kinetics from austenite to martensite, but martensitic transformation crystallography, grain rotation, and strain partitioning of individual grains as well. Our investigations are important for in-depth understanding the role of martensite variant selection in the TRIP effect during plastic flow in the alloys with metastable phase.

#### 5:00 PM

**Patterning of Alloy Precipitation through External Pressure:** Jack Franklin<sup>1</sup>; Jennifer Lues<sup>1</sup>; <sup>1</sup>University of Pennsylvania

Industrial heat treating has been developed to optimize the selection of final microstructures, and therefore material properties, across products as a whole. However as engineering problems become more complex and require multi-functional solutions it is desirable to fabricate 'architected' or designed components whose microstructure and properties may vary across the sample. In this talk, I present an innovative processing technique designed to control the location of formation and growth rate of precipitates within metallic alloys in order to create multiple patterned areas of unique microstructure within a single sample. Control over precipitation is achieved by an additional surface pressure applied to selected locations during precipitate heating. The applied pressure changes both the enthalpic and chemical potential landscapes, which in turn control the rate and directionality of atomic diffusion in regions close to the loaded surfaces. Experimental results displaying a dependence on quench rate and thermal history are presented.

## Dynamic Behavior of Materials V: Dynamic Effects in Materials

*Sponsored by:* The Minerals, Metals and Materials Society, TMS Structural Materials Division, TMS/ASM: Mechanical Behavior of Materials Committee

*Program Organizers:* Marc Meyers, UCSD; Naresh Thadhani, Georgia Institute of Technology; George Gray, Los Alamos National Laboratory

Wednesday PM  
March 2, 2011

Room: 5A  
Location: San Diego Conv. Ctr

*Session Chair:* Ellen Cerreta, Los Alamos National Laboratory

#### 2:00 PM Invited

**The Use of Diagnostics in Determining the High-Rate Response of Granular and Porous Materials:** W.G. Proud<sup>1</sup>; D.J. Chapman<sup>1</sup>; W. Neal<sup>1</sup>; D. Eakins<sup>1</sup>; <sup>1</sup>Cavendish Laboratory

Granular and porous materials are widely encountered in nature, industrial products and engineering applications. These materials are often used for their lightweight or shock absorbing properties. Characterising them at high-strain rates is difficult due to a number of factors; they tend to have very low strengths in the initial part of their crushing behaviour resulting in low initial signals in most diagnostics when most of the compaction is occurring; they display a marked ramping effect on any mechanical stimulus, resulting in incomplete compaction during the loading pulse and a strongly variable mechanical impedance; they show relatively large movements before becoming compact producing marked strain for in-material diagnostics which then produce incorrect signal levels; as well as these diagnostic-related issues, it has been found that in looking for trends in behaviour that while granular materials generally change their properties slowly over a large range of porosities they can manifest a step change in their behaviour when a critical porosity is reached. This paper will outline some of the difficulties in studying these materials, review progress made, discuss the use of multiple diagnostics to understand the fundamental processes in these materials.

#### 2:30 PM

**Determination of Bulk Modulus and Shear Modulus of Human Thoracic Organ Tissue and Biosimulants at High Strain Rates:** Morgan Trexler<sup>1</sup>; Andrew Lennon<sup>1</sup>; Adam Maisano<sup>1</sup>; Alexis Wickwire<sup>1</sup>; Timothy Harrigan<sup>1</sup>; Quang Luong<sup>1</sup>; Andrew Merkle<sup>1</sup>; <sup>1</sup>Johns Hopkins University Applied Physics Laboratory

Modeling human body response to dynamic loading events and developing human surrogates require accurate high rate material properties of organ tissues. This work describes characterization of dynamic mechanical behavior of human thoracic organ tissues, including liver, lung and spleen, as well as biosimulants. Modified split Hopkinson pressure bar techniques were developed for measuring bulk and shear moduli under hydrostatic pressure and shear loading, respectively. Hydrostatic pressure was achieved via use of a steel confinement cylinder around a disc-shaped specimen. Shear specimens were tested in a double lap shear configuration. Shear tests require establishment and maintenance of a uniform state of stress in the sample, which was achieved via pulse shaping and verified using piezoelectric quartz force gages on the input and output sides of the specimens. Results of bulk and shear tests of thoracic organ tissues and silicone-based biosimulant materials are reported. Comparisons are made between tissues and simulants.

#### 2:45 PM

**Electrically Driven Expanding Plasma as a Means to Drive High Velocity and High Strain Rate Experiments:** Anupam Vivek<sup>1</sup>; Jason Johnson<sup>1</sup>; Gregg Fenton<sup>2</sup>; Geoff Taber<sup>1</sup>; Glenn Daehn<sup>1</sup>; <sup>1</sup>Ohio State University; <sup>2</sup>Applied Research Associates

When directed properly, plasma created by rapid vaporization of a metallic wire or foil by passing a very high current through them is an efficient medium for converting electric energy into kinetic energy. This energy can

then be used to propel sheets, tubes etc. at very high speeds. This method can provide considerable simplification in the experimental system as compared to electromagnetic solenoid actuators, and the consumable component can be very inexpensive. In this work, copper and aluminum tubes are expanded using fast, capacitor bank driven, vaporization of coaxially placed wires. Diameter, length and material of wire are varied for optimization purposes. Pressure is calculated from the velocity-time measurements done by Photon Doppler Velocimetry. Currents and voltages are also recorded. The pressure, current and voltage data would be compared against a multi-physics numerical model. Applications of the method will be discussed as will design rules for efficient system design.

### 3:00 PM

**Shear-Rate Dependence in Dislocation Pile-up Simulations at Asymmetric Tilt Boundaries in Aluminum:** *Steven Valone<sup>1</sup>; Jian Wang<sup>1</sup>; Richard Hoagland<sup>1</sup>; Timothy Germann<sup>1</sup>*; <sup>1</sup>Los Alamos National Laboratory

Materials deformation processes are increasingly approachable through atomistic methods. In one deformation process, dislocation pile-up at a grain boundary, how dislocations transmit through grain boundaries is of intense interest. Here dislocation pile-ups in an aluminum bicrystal with an asymmetric sigma-11 tilt grain boundary are simulated. Dislocations are initially distributed according to linear elastic estimates from a far-field stress of 40 MPa. The system is propagated for different periods of time, representing different shear rates. Incremental loading occurs every 40 ps or every 80 ps. In spite of the factor of two difference in shear rate, differences in the events are quite marked. At the higher rate, dislocations are transmitted on both available slip systems. The entities transmitted are perfect dislocations. At the slower rate, transmission and reflection events consist of multiple Shockley partial dislocations, parallel to each other, on one of the slip planes.

### 3:15 PM

**Thermal Stability of Commercially Pure Ultra-fine Grained Al at High Strain Rates:** *Emily Huskins<sup>1</sup>; K Ramesh<sup>1</sup>*; <sup>1</sup>Johns Hopkins University

Materials with ultra-fine grained (UFG) nanostructures are of interest due to their improved strengthening over their coarse-grained counterparts. However, these materials also exhibit different strain rate sensitivity and deformation mechanisms, both of which affect the stability of plastic deformation and therefore ultimate failure. One such example is thermal stability of UFG materials. While the thermal stability of coarse grain Al is available in ASM Handbooks this data cannot be applied for UFG and nanocrystalline Al due to changes in deformation mechanisms as a result of grain size reduction. In addition, there are limited studies of either UFG or coarse grained materials at elevated temperatures and high strain rates. In this work an UFG commercially pure Al (obtained through ECAP) is tested under dynamic compression ( $10^3 \text{ s}^{-1}$ ) at elevated temperatures (298K – 573K). The thermal stability of this material is investigated and a physics-based internal variable constitutive model is presented.

### 3:30 PM

**The Implications of Loading History on Grain Size Effects in Polycrystalline Copper Spallation Damage from Hydrocode Simulations:** *Davis Tonks<sup>1</sup>; Ellen Cerreta<sup>1</sup>; Darcie Dennis-Koller<sup>1</sup>; John Bingert<sup>1</sup>; Veronica Livescu<sup>1</sup>; Curt Bronkhorst<sup>1</sup>*; <sup>1</sup>Los Alamos National Lab

New incipient damage spallation experiments are being done at LANL on polycrystalline copper exploring the effects of grain size and loading rate on incipient damage morphology. The emphasis is on metallurgical and tomographic examination of the damage state in recovered samples, supplemented by VISAR records of the free surface velocity. However, a full understanding of the recovered damage morphology and its evolution requires a knowledge of the stress and strain histories of the damage process which are not measured in the experiment but must be calculated. This work presents calculated stress and strain histories of the gas gun shots together with their implications about the damage structures. The calculations will include 1D hydrocode simulations and some FEM simulations with more detailed grain microstructure included. The 1D simulations will reveal

spatially averaged loading histories while the FEM calculations will reveal crystal grain effects investigation.

### 3:45 PM

**Dynamic Characterization of Cast and Wrought Uranium-Niobium Metals:** *Carl Cady<sup>1</sup>; George Gray<sup>1</sup>; Ellen Cerreta<sup>1</sup>; Robert Aikin<sup>1</sup>; Dan Thoma<sup>1</sup>; Robert Field<sup>1</sup>*; <sup>1</sup>Los Alamos National Laboratory

A uranium-6wt% niobium alloy with different processing paths was investigated as a function of strain rate, temperature and stress state. The “wrought” material was produced by forging and forming and the second material was generated using direct cast methods. Characterization over a range of rates and temperatures was used to generate a constitutive material model and Taylor impact testing was used to validate the model. The yield and flow stresses of the U-Nb materials was found to exhibit a pronounced strain rate sensitivity, while the hardening rates were found to be insensitive to strain rate and temperature. Twin dominated deformation processes are seen in U-6Nb at low strain rates. High strain rate and shock loading can be dominated by twinning or phase transformation. Evaluation of explosively driven hemispheres will provide insight into the relative difference between the two processing paths and an interpretation of the test results will be presented.

### 4:00 PM Break

### 4:10 PM Invited

**Characteristic Responses of Thick Ceramic Bodies to High-Velocity Impact:** *Jerry LaSalvia<sup>1</sup>; James McCauley<sup>1</sup>; Jeffrey Swab<sup>1</sup>; Parimal Patel<sup>1</sup>*; <sup>1</sup>U.S. Army Research Laboratory

Characteristic responses of ceramics to high-velocity impact by hard and ductile projectiles have been the recent subject of investigation. Most investigations have focused on ballistic response by determining the penetration-depth history of the projectile through the ceramic as a function of impact velocity. This enables penetration onset velocity, penetration velocities, and dwell durations to be estimated. Other investigations included post-mortem examination of the ceramics. These have provided insight into the fundamental processes governing both ballistic and material responses of ceramics. Because high-velocity impact involves the generation of transient, large amplitude, spatially and temporally varying stresses, these responses are complex, involving processes that span macro-to-nano length-scales driven primarily by shear and tension. Mechanistically, microcracking, microcracking, comminution and fragmentation, solid-state amorphization, shear localization, microplasticity, twinning, grain boundary slip, stacking faults, and phase transformations have been observed. The characteristic responses of ceramics to high-velocity impact by hard and ductile projectiles will be reviewed.

### 4:40 PM Invited

**Effects of Strain Rate and Stacking-Fault Energy on Microstructures and Mechanical Properties of Deformed Cu and Cu-Al Alloys:** *Y. Zhang<sup>1</sup>; N.R. Tao<sup>1</sup>; K. Lu<sup>1</sup>*; <sup>1</sup>SYNL, Institute of Metal Res.

Pure Cu and Cu-Al alloys were subjected to quasi-static compression (QSC) and dynamic plastic deformation (DPD) in order to investigate the effects of strain rate and stacking fault energy (SFE) on the microstructures and mechanical properties. For low SFEs, deformation twinning occurs in the QSC samples, and the amount of twins increases with decreasing SFEs. The twin thickness and sizes of refined grains decrease with a reduction of SFEs. For the DPD samples, the amount of twins is insensitive to SFE. However, the twin thickness and grain sizes decrease significantly with smaller SFEs. The microstructure characteristics of DPD samples with different SFEs are determined including twin thickness, grain size, volume fraction of nanoscale twins, etc. Tensile strength and ductility of the QSC and DPD sample are analyzed in terms of their microstructure features.



## 5:10 PM

**The Critical Role of Shock Melting in Ultrafast Laser Machining:** *Ben Torralva*<sup>1</sup>; S. Ma<sup>1</sup>; A. Kumar<sup>1</sup>; S. M. Yalisove<sup>1</sup>; T. M. Pollock<sup>2</sup>; K. Thornton<sup>1</sup>; <sup>1</sup>University of Michigan; <sup>2</sup>University California, Santa Barbara

The interaction of ultrashort laser pulses (ULP) with materials holds fundamental importance. To understand the damage and the dynamic deformation behavior under these unique conditions, we combine computational modeling and experimental characterization of the collateral damage in CMSX-4. Hydrodynamics modeling is employed to simulate the interaction of ULP with metals to gain understanding of the state of the material during deformation, and a combination of experimental techniques is used to characterize the damage. We observe that the dislocation distribution is confined to the region beneath the laser-irradiated region, unlike with nanosecond lasers. Moreover, the amount of damage injected can be dramatically enhanced or suppressed depending on laser fluence. We propose that the initiation of shock melting is the origin of the sharp transition in ablation efficiency and in the amount of damage injected into the bulk. The importance of d-state scattering in the electron thermal transport model will be discussed.

## 5:25 PM

**Blast Wave Mitigation Using a Nanoporous Functionalized Liquid Materials:** *Yu Qiao*<sup>1</sup>; Douglas Giese<sup>2</sup>; <sup>1</sup>UCSD; <sup>2</sup>AgileNano

The use of bombs and blasts are the number one threat to the U.S. troops in Iraq and Afghanistan. Recently, we developed a novel, nanoporous functionalized material, AgileZorb, that can react within microseconds to sufficiently affect a shock front. AgileZorb is formed by immersing nanoporous particles in a liquid phase. The inner nanopore surface is specially treated so that it is nonwettable to the liquid. Under ambient condition, due to the capillary effect, the nanopores remain empty. At a blast wave front, the local high pressure can rapidly compress the liquid into the nanopores, converting a significant amount of energy into heat as well as interfacial tension. Our experiments have shown encouraging results.

## 5:40 PM

**Effects of Grain Size and Boundary Structure on the Dynamic Response of Polycrystalline Copper:** *Juan Escobedo*<sup>1</sup>; Ellen Cerreta<sup>1</sup>; Darcie Dennis-Koller<sup>1</sup>; Curt Bronkhorst<sup>1</sup>; Benjamin Hansen<sup>1</sup>; Ricardo Lebensohn<sup>1</sup>; Davis Tonks<sup>1</sup>; Brian Patterson<sup>1</sup>; <sup>1</sup>Los Alamos National Laboratory

Plate-impact experiments were conducted to examine the effect of grain size (30, 60 and 200  $\mu$ m) on the dynamic tensile response of high purity copper samples. The preceding compressive stress was  $\sim 1.5$  GPa for all tests, low enough to cause early stage incipient spall. The free-surface velocity histories show no significant effect of the grain size on the initial pull-back signal. The quantitative metallography of the recovered samples shows the volume fraction of voids to be 0.4% for all cases. Nevertheless, the void size distribution is different, with the void size increasing with increasing grain size. In the 200  $\mu$ m samples, void coalescence was observed along the grain boundaries, whereas in smaller grained specimens individual voids dominated the deformation. EBSD observations show that voids preferentially nucleate/grow at grain boundaries with high angle misorientation, while the boundaries corresponding to low angle ( $<5^\circ$ ) or  $\mu$ 3 type were more resistant to damage.

## Electrode Technology for Aluminium Production: Cathode Design and Operation

*Sponsored by:* The Minerals, Metals and Materials Society, TMS Light Metals Division, TMS: Aluminum Committee

*Program Organizers:* Alan Tomsett, Rio Tinto Alcan; Ketil Rye, Alcoa Mosjøen; Barry Sadler, Net Carbon Consulting Pty Ltd

Wednesday PM

March 2, 2011

Room: 16B

Location: San Diego Conv. Ctr

*Session Chair:* Richard Jeltsch, Consultant

## 2:00 PM Introductory Comments

### 2:05 PM

**Preheating Collector Bars and Cathode Blocks Prior to Rodding with Cast Iron by Passing an Ac Current through the Collector Bars:** *Erik Jensen*<sup>1</sup>; Hans Petter Bjørnstad<sup>2</sup>; Jan Hansen<sup>2</sup>; <sup>1</sup>EAJ Consulting; <sup>2</sup>ALMEQ

Three basic methods for heating collector bars and cathode blocks prior to pouring cast iron are in use today; gas burners directly impinging on the collector bars, ovens for heating bars and blocks separately, and third, passing an alternating electrical current through the collector bars to heat bars and blocks simultaneously. This paper examines electrical heating using the collector bar as the heating element. Passing an alternating current through the collector bar produces an easily regulated and uniform temperature throughout the bar. Radiant energy from the bar heats the slot area of the cathode block. Temperature levels are adjusted by time and voltage selection. Electrically heating collector bar/cathode block assemblies uses less than 15% of the energy required for propane gas burner heating. The method is quiet, requires little or no supervision, has no products of combustion to exhaust, and temperatures are highly repeatable.

### 2:30 PM

**Development and Application of an Energy Saving Technology for Aluminum Reduction Cells:** *Peng Jianping*<sup>1</sup>; Feng Naixiang<sup>1</sup>; Feng Shaofeng<sup>2</sup>; Liu Jun<sup>3</sup>; Qi Xiquan<sup>4</sup>; <sup>1</sup>Northeastern University; <sup>2</sup>Zhejiang Huadong Aluminum Corporation Ltd.; <sup>3</sup>East Hope Baotou Xitu Aluminum Ltd.; <sup>4</sup>Northeastern University Engineering & Research Institute Co. Ltd

An energy saving technology based on novel structure cathodes in aluminum reduction cells has got wide application and development in many smelters in recent years. Structure characteristic of the cells are described in this paper. Some details, such as lining structure and wear of cathodes, are discussed according to the present applications. And the effect of bath component on energy consumption is also studied.

### 2:55 PM

**Study of Electromagnetic Field in 300kA Aluminium Reduction Cells with Innovation Cathode Structure:** *Baokuan Li*<sup>1</sup>; Xiaobo Zhang<sup>1</sup>; Suirui Zhang<sup>1</sup>; Fang Wang<sup>1</sup>; Naixiang Feng<sup>1</sup>; <sup>1</sup>Northeastern University

The flow field of molten aluminum is divided by the novel structure that there are twenty-six pairs of convex blocks on the innovation cathode surface, as thus, the flow velocity decreases significantly, which weaken effectively the effect of gravity waves of molten aluminum so as to reduce the volatility of molten aluminum. The novel cathode structure can make the current distribution in the molten aluminum more uniform, which can reduce the flow power of molten aluminum. Small current in horizontal direction come into being on the convex surfaces, the current force the molten aluminum to form a loop around the convex plates, which is not only to weaken the action of vertical wave in aluminium reduction cells, but also is conducive to the dissolution of alumina. The aluminium reduction cells with innovation cathode structures have smaller fluctuations, stronger stability and improve the current efficiency of aluminum reduction cells.

## 3:20 PM Break

### 3:30 PM

**Evaluation of the Thermophysical Properties of Silicon Carbide, Graphitic and Graphitized Carbon Sidewall Lining Materials Used in Aluminium Reduction Cell in Function of Temperature:** *Ayesha Khatun*<sup>1</sup>; Martin Desilets<sup>1</sup>; <sup>1</sup>University of Sherbrooke

The thermal properties of the sidewall lining materials are required to ensure good predictions of the dynamic thermal behavior of Hall-Héroult cells. A precise estimation of energy losses and location of the side freeze, are made possible when the sidewall lining materials are well characterized as a function of temperature. The present work uses transient characterization techniques to measure the thermal diffusivity, heat capacity and thermal conductivity of silicon carbide, graphitic and graphitized carbon materials. The thermal diffusivity and the heat capacity are measured by state-of-the-art transient laser flash analyzer and a differential scanning calorimeter respectively. The thermal conductivity is calculated by assuming a constant density. Finally, based on the calculations conducted with a 2-D numerical model, the effect of the temperature varying thermal properties of the sidewall materials on the dynamic behavior of a laboratory scale phase change reactor is presented.

### 3:55 PM

**Advanced Numerical Simulation of the Thermo-Electro-Mechanical Behaviour of Hall-Héroult Cells under Electrical Preheating:** Daniel Marceau<sup>1</sup>; Simon Pilote<sup>1</sup>; *Martin Desilets*<sup>2</sup>; Lyès Hacini<sup>3</sup>; Jean-François Bilodeau<sup>3</sup>; Yves Caratini<sup>3</sup>; <sup>1</sup>Université du Québec à Chicoutimi; <sup>2</sup>Sherbrooke University; <sup>3</sup>Rio Tinto Alcan

In today's context, aluminum producers strive to improve their position regarding energy consumption and production costs. To do so, mathematical modeling offers a good way to study the behavior of the cell during its life. This paper deals with the numerical simulation of the electrical preheating of a Hall-Héroult cell using a quarter model of the cell. The fully coupled thermo-electro-mechanical model includes material non linearities and multiphysical behavior at interfaces allowing accurate evaluation of the stress distribution in the cathode blocks and surrounding components. The baking of the ramming paste as well as the evolution of its thermo-electro-mechanical properties are updated via the baking index computed using a kinetic of reaction. The model is initially calibrated with in situ measurements and then used to estimate the effect of preheating on the behavior of the cell including temperature, current, deformations as well as the contact conditions at critical interfaces.

### 4:20 PM

**Creep Behaviors of Industrial Graphitic and Graphitized Cathodes during Modified Rapoport Tests:** *Wei Wang*<sup>1</sup>; Jilai Xue<sup>1</sup>; Jianqing Feng<sup>2</sup>; Qingsheng Liu<sup>2</sup>; Lei Zhan<sup>2</sup>; Hua He<sup>2</sup>; <sup>1</sup>University of Science and Technology Beijing; <sup>2</sup>Ningxia Qingtongxia Energy Aluminium Group, China Power Investment Corporation

Creep is of importance for reduction cell design and cathode construction. The purpose of this work is to obtain the creep data for various cathode products under the conditions close to the industrial operation in reduction cells. A modified Rapoport equipment was used for measuring the creep behaviors during aluminum electrolysis with CR=4.0 and at temperature of 965°. Testing samples were taken from industrial semi-graphitic, full graphitic and graphitized carbon products and characterized for their graphitized degree using XRD method. The values of d200 for all cathode samples were lowered after aluminum electrolysis, and the graphitized cathode made in an energy saving heat-treatment process still showed smaller creep deformation than those of semi-graphitic and full graphitic cathode samples. The obtained data will be useful for quality control of cathode product and improvement in cathode performance.

## Friction Stir Welding and Processing VI: Process Modeling and Verification

*Sponsored by:* The Minerals, Metals and Materials Society, TMS Materials Processing and Manufacturing Division, TMS: Shaping and Forming Committee

*Program Organizers:* Rajiv Mishra, Missouri University of Science and Technology; Murray Mahoney, Retired from Rockwell Scientific; Yutaka Sato, Tohoku University; Yuri Hovanski, Pacific Northwest National Laboratory; Ravi Verma, General Motors

Wednesday PM  
March 2, 2011

Room: 5B  
Location: San Diego Conv. Ctr

*Session Chairs:* Guntram Wagner, University of Kaiserslautern; Carl Sorensen, Brigham Young University

### 2:00 PM

**Effect of Plasticized Material Flow on the Tool Feedback Forces during Friction Stir Welding:** *Enkhsaikhan Boldsaikhan*<sup>1</sup>; Dwight Burford<sup>1</sup>; Pedro Gimenez Britos<sup>1</sup>; <sup>1</sup>Wichita State University

The goal of this study is to characterize the dynamic nature of the friction stir welding process by examining time series data of the tool feedback forces. The tool feedback forces are generated by the resistance of the material to deformation in direct response to the rotational and translational motion of the weld tool during the welding process. While traveling from the leading face to the trailing face of the weld tool, a "pulse" flow of plasticized material usually imposes dynamic shear stresses and normal stresses on the weld tool surfaces. These dynamic stresses constitute the resultant tool feedback forces and the spindle torque that can be captured during the process. In this study, a 2D model, based on a pseudo shear stress concept, is established to characterize oscillations of the feedback forces with the dynamics of the material flow, including erratic flow associated with flaw formation.

### 2:20 PM

**Weld Flaw Analysis of High Speed Friction Stir Processed Magnesium AZ31:** *Leon Hütsch*<sup>1</sup>; Jorge dos Santos<sup>1</sup>; Norbert Huber<sup>1</sup>; <sup>1</sup>GKSS Forschungszentrum GmbH

In the present study processing parameters in a range of welding speeds varying from 1 to 10m/min have been investigated in combination with different vertical forces and tool rotational speeds. The welding has been carried out on 2mm thick rolled AZ31 sheets employing a Tricept 805 robot. The tool consisted of a threaded shoulder and a pin with three flats. The obtained welds were analysed by optical and electron scanning microscopy. The results have been compiled in the form of correlations between welding speed and vertical force as well as rotational speed, whereby regions of defect-free and defective welds could be identified. These results allow the determination of a stable process window. The verification and further refinement of the process window has been performed based on hardness and tensile testing of the produced welds. Additionally, an artificial neural network was trained to correlate the processing parameters with the observed weld flaws.

### 2:40 PM

**Developing an Alternative Heat Indexing Equation for FSW:** *Joseph Querin*<sup>1</sup>; Judy Schneider<sup>1</sup>; <sup>1</sup>Mississippi State University

In friction stir welding (FSW), a non-consumable, rotating weld tool is used to impart large shear deformations under simultaneous compressive stress states to join the faying surfaces of a weld joint. As a result of the process, the workpiece material microstructure is altered due to heat and plastic deformation. The peak temperature experienced in the weldment is guided by the workpiece material, weld tool geometry, friction stir weld tooling, and process parameters. This temperature is believed to be an important parameter in determining the characteristics of the weld and resultant weld properties. As there are currently no reliable analytical methods for determining process parameters, an alternative heat indexing equation is formulated based on maintaining a constant peak temperature.

### 3:00 PM Invited

#### **Finite Element Modeling of Friction Stir Welding:** Paul Dawson<sup>1</sup>; Donald Boyce<sup>1</sup>; <sup>1</sup>Cornell University

Friction stir welding is a complex process that severely alters the microstructure as metal is deformed by the action of the probe. Modeling the mechanical response involves solving coupled equations for the plastic flow, heat transfer, and evolution of critical descriptors of the state, especially the strength and damage. We summarize the components of a three-dimensional formulation for friction stir welding that incorporates of these elements. It utilizes an Eulerian reference frame and is limited to a steady-state approximation, but provides fully-coupled solutions for the flow field, temperature distribution, and state variables for strength and porosity. Of particular importance is the choice of constitutive equations that represent the viscoplastic behavior of the metal including strain hardening and softening. We illustrate the formulation with simulations of the welding of a titanium alloy and conclude with a discussion of remaining challenges for robust and useful simulation capability for the welding community.

### 3:25 PM

#### **Investigation of Methods to Control Friction Stir Weld Power with Spindle Speed Changes:** Kenneth Ross<sup>1</sup>; Carl Sorensen<sup>1</sup>; <sup>1</sup>Brigham Young University

Process zone temperatures in FSW determine the properties of the resulting weld and dramatically effects tool life in PCBN tools. Therefore an active control system to control weld temperature is desirable. Spindle power is a key factor in temperature control because it is the primary power input to the stir zone. Temperature control is achieved by using an outer control loop to set the desired power based on temperature feedback and an inner loop to adjust spindle speed to achieve the desired power. The inner loop can be achieved using a power feedback PID loop. Alternatively torque feedback can be used to change spindle speed to achieve the desired power. The choice of control scheme will affect the ability to control the process temperature. This paper investigates the dynamics of power control using the different control schemes and describes the implications of the control scheme on the temperature control process.

### 3:45 PM

#### **Materials Design for Joinable, High Performance Aluminum Alloys:** Ryan Glamm<sup>1</sup>; Greg Olson<sup>1</sup>; <sup>1</sup>Northwestern University

A systems based approach is used to design an aluminum alloy which has compatibility with friction stir welding, sufficient strength, resistance to stress corrosion cracking, and low cost of processing. As part of the systems approach, quantitative models are used to enhance predictive capabilities. PrecipiCalc software is used to model nucleation, growth, and coarsening to characterize the relationship between processing and structure. A strength model is utilized from previous literature to model the relationship between structure and properties. Prototype alloys are designed and then characterized using atom probe tomography. Modeling parameters are calibrated from atom probe characterization of isothermal aging treatments. Friction stir weld thermal cycles are input into PrecipiCalc to gain insight on microstructural evolution during welding. The resulting microstructures are input into the strength model and compared to experimental hardness data. These predictions are validated by experimental friction stir welding time-temperature cycles and microhardness measurements.

### 4:05 PM

#### **Transient Heat and Material Flow Modeling of Friction Stir Processing of Magnesium Alloy:** Zhenzhen Yu<sup>1</sup>; Hahn Choo<sup>1</sup>; Wei Zhang<sup>2</sup>; Zhili Feng<sup>2</sup>; <sup>1</sup>University of Tennessee; <sup>2</sup>Oak Ridge National Laboratory

A three-dimensional transient model with a threaded pin tool was developed to investigate material flow and heat transfer during friction stir processing (FSP) of AZ31B Mg plate. The material was considered as a non-Newtonian viscoplastic fluid, and constitutive law was employed to describe the dependence of viscosity on temperature and strain rate, with the material constants determined from compression test under a wide range of temperatures and strain rates. A dynamic mesh method, combining Lagrangian and Eulerian formulations, was used to capture the material flow

induced by the stirring motion of the pin. Temperature profiles recorded from actual FSP experiments were used to validate simulation results. Furthermore, massless inert particles were embedded in the model to track the detailed material flow history. Finally, a model with a smooth pin surface was established as well, in order to compare the influence of thread on the simulated thermal history and material flow.

### 4:25 PM Break

### 4:35 PM

#### **Approaches to In-Situ Data Monitoring of FSW Quality:** Haley Doude<sup>1</sup>; Judy Schneider<sup>1</sup>; <sup>1</sup>Mississippi State University

Since the development of friction stir welding (FSW) in 1991, researchers have seen the need for ways to better understand and predict FSW results. Current practices use a trial and error method to develop weld parameters for new materials to the FSW process and thorough destructive and non-destructive testing to prove that the weld is acceptable. Because of the time and expense of testing, other ways of developing parameters and determining weld quality are necessary. One such area of research is processing of the output signals from the FSW machine. If successful, weld quality could be determined real time or post-weld without destructive testing of the weld panel. Process parameters could also be adjusted real time to improve the weld quality as the material is being welded. This paper evaluates current research approaches and their effectiveness in determining weld quality.

### 4:55 PM

#### **A Comparison of Experimental Data and Model Predictions with Constitutive Laws Commonly Used to Model Friction Stir Welding:** Katherine Kuykendall<sup>1</sup>; Carl Sorensen<sup>1</sup>; Tracy Nelson<sup>1</sup>; <sup>1</sup>Brigham Young University

Numerical modeling of friction stir welding is dependent on the constitutive law used to determine flow stress as a function of strain rate, temperature, and strain. Commonly used constitutive laws include Sheppard and Wright, Johnson-Cook, and Kocks and Mecking. Material constants were determined for AA5083 for these laws from constant strain rate and temperature compression data found in the Atlas of Formability. Two-dimensional Lagrangian models of axial compression tests identical to source data tests were developed. The modeled stress-strain curves were compared with curves from the Atlas of Formability. The Sheppard and Wright law is capable of capturing saturation but incapable of capturing strain hardening, which can account for up to 20% plastic strain. The Johnson-Cook law is capable of capturing strain hardening; however, its inability to capture saturation causes overpredictions of stress at large strains. The Kocks and Mecking model is capable of capturing strain hardening and saturation.

### 5:15 PM

#### **Long Range Oscillations in Friction Stir Welding Tool Travel Speed:** Mike Brendel<sup>1</sup>; Judith Schneider<sup>1</sup>; <sup>1</sup>Mississippi State University

Oscillations in the weld travel speed were observed during Friction Stir Welding (FSW) of Al-Li 2195-O panels. These oscillations can be explained as a beat frequency occurring between the frequency of the inverse weld pitch and the frequency of feedback correction to the weld table travel speed to maintain the initial set-point. The frequency of table correction was found to be constant in the inverse distance domain, but not in the inverse time domain. Measurements of the spacing between individual tooling marks on the FSW surface confirm these travel speed oscillations. Measured forces during the welding process were also influenced by these travel speed oscillations. The changing of the tool rotation rate from 170 to 200 RPM at constant travel of 13 IPM shifted the wavelength of the oscillations such that the inverse weld pitch at 200 RPM closely matched the frequency of table correction.

### 5:35 PM

#### **Tool Load and Torque Study for Portable Friction Stir Welding in Aluminum:** Scott Rose<sup>1</sup>; Murray Mahoney<sup>2</sup>; Tracy Nelson<sup>1</sup>; Carl Sorensen<sup>1</sup>; <sup>1</sup>Brigham Young University; <sup>2</sup>Consultant

As Friction Stir Welding (FSW) broadens its applications, the need for portable equipment has arisen. Minimizing both loads and torques is



necessary to fabricate a truly versatile and portable FSW system. In order to do this, a tool study was done to find the minimal loads needed to achieve a feasible portable system. This study evaluated optimal loads, torque and surface temperature profiles in AA 5083 through the variation of RPM, IPM, and different pin and shoulder configurations of two-piece FSW tools. Plunge studies were also done to evaluate different approaches to further reduce the high loads typically seen during the plunging of an FSW tool. Typical consolidated welds in this study were produced with around 2000 lbs of load and 20 ft-lbs of torque. Results from these studies will be presented illustrating the optimum tool design and weld parameters to minimize the load requirements for a portable FSW system.

### 5:55 PM

**Towards Process Control of Friction Stir Welding for Different Aluminum Alloys:** Axel Fehrenbacher<sup>1</sup>; Edward Cole<sup>1</sup>; Michael Zinn<sup>1</sup>; Nicola Ferrier<sup>1</sup>; Neil Duffie<sup>1</sup>; Frank Pfefferkorn<sup>1</sup>; <sup>1</sup>Univ. Wisconsin-Madison

The real-time temperature measurement of aluminum alloy 6061-T6 friction stir welds (FSW) has shown that spindle speed has a greater influence on the tool-workpiece interface temperature than travel speed. This process knowledge allows for spindle speed to be used as a control method for maintaining weld temperature. However, spindle speed dominance has not been shown to be true for all aluminum alloys. Additional parametric studies have been performed on aluminum alloys 2024-T3, 5083-H116, and 7075-T6, where alloy 5083 is the only alloy of which neither spindle speed or travel speed has a significant effect on the interface temperature. Among the alloys, not only does the average interface temperature vary, but also the amplitude in temperature change, depending on the alloy and chosen weld parameters (spindle or travel speed).

### General Abstracts: Structural Materials Division: Applications

*Sponsored by:* The Minerals, Metals and Materials Society, TMS Structural Materials Division, TMS: Advanced Characterization, Testing, and Simulation Committee, TMS: Alloy Phases Committee, TMS: Biomaterials Committee, TMS: Chemistry and Physics of Materials Committee, TMS/ASM: Composite Materials Committee, TMS/ASM: Corrosion and Environmental Effects Committee, TMS: High Temperature Alloys Committee, TMS/ASM: Mechanical Behavior of Materials Committee, TMS/ASM: Nuclear Materials Committee, TMS: Refractory Metals Committee, TMS: Titanium Committee

*Program Organizers:* Roger Narayan, Univ of North Carolina & North Carolina State Univ; Judith Schneider, Mississippi State University

Wednesday PM  
March 2, 2011

Room: 31C  
Location: San Diego Conv. Ctr

*Session Chair:* To Be Announced

### 2:00 PM

**Steel Design for Blast and Fragment Protection:** Zechariah Feinberg<sup>1</sup>; <sup>1</sup>Northwestern University

In light of the general increase in terrorist attacks, there is a pressing need to design high performance, blast resistant steels that are capable of withstanding high impact explosions. The ultimate goal of this research is to develop a blast resistant steel from a materials science perspective by fully understanding the interrelation between the processing, structure, properties, and performance. In this project, a systems-based approach using predictive models has been implemented to design a high-performance transformation-induced plasticity (TRIP) steel. An experimental alloy called TRIP-120 has been designed, created, optimized, and experimentally tested to verify the predicted property objectives of high strength, high toughness, shear localization resistance, and high uniform ductility to maximize energy absorption and deliver maximum blast resistant performance. By combining computational tools with experimental data, predictive models have been

used to design optimized steel alloys for high strain rate loading conditions for improved blast and fragment penetration resistance.

### 2:15 PM

**Effects of Differential Oxygen Access on the Corrosion Behavior of Zinc Relevant to Mechanically Stabilized Earth Walls:** Victor Padilla<sup>1</sup>; Akram Alfantazi<sup>1</sup>; <sup>1</sup>UBC

The purpose of this work is to study the effect of differential oxygen access on the corrosion performance of zinc, the most commonly used material used as protection system on Mechanically Stabilized Earth (MSE) walls. Uneven soil compaction creates differential oxygen access, which promotes corrosion macrocells. High purity zinc (99.6%) was immersed in solutions with varied concentration of Na<sub>2</sub>SO<sub>4</sub> to simulate the conditions in soils and ground water, while the concentration of NaCl was kept at 3.5 wt%. Corrosion rates were measured using potentiodynamic anodic polarization method in different concentrations of oxygen. Scanning Electron Microscope (SEM), and X-Ray Diffraction (XRD) were used to characterize the corroded samples. The results indicate an increase on the corrosion rate with increasing amount of Na<sub>2</sub>SO<sub>4</sub>, as well as a potential difference between samples at different oxygen concentrations, which indicates the possibility for macrocell formation under the studied conditions.

### 2:30 PM

**Analysis of Eutectically Soldered Silicon Chips on a Copper Flanges with Innovative "Ductile Layer" Technology:** Pu Zhou<sup>1</sup>; Michael Zimmerman<sup>1</sup>; Anil Saigal<sup>1</sup>; <sup>1</sup>Tufts University

Managing thermal performances of high power silicon devices is critical in assuring long term reliability. For LDMOS power transistors, thermal performance has traditionally been optimized using hard "AuSi" eutectic solder, whereas, the flange is made of copper. Copper is a much more thermally conductive material, but it has a CTE mismatch with the silicon die that can result in large stresses and potential cracking of the die. A "ductile layer" technology has been developed to mitigate this problem. This paper presents the finite element analysis of stresses and deformation of eutectically soldered silicon chips to a copper flange incorporating the ductile layer technology. In this study different geometric and material characteristics of the ductile layer are considered. The analysis shows that the stresses in the silicon chips are significantly reduced due to the existence of the ductile layer, and the stresses decrease even further as the thickness of the ductile layer increases.

### 2:45 PM

**Influence of Sulfide on Internal-Fracture-Type Rolling Contact Fatigue Life of Bearing Steels:** Kazuya Hashimoto<sup>1</sup>; Kazuhiko Hiraoka<sup>1</sup>; Katsuyuki Kida<sup>2</sup>; <sup>1</sup>Sanyo Special Steel; <sup>2</sup>Kyushu University

Energy saving is an important driving force to reduce of the size and weight of bearing components. Since bearings are expected to stand higher loads, it is desirable to substantially improve rolling contact fatigue (RCF) life of bearing steels and to develop the techniques to predict RCF life accurately. Flaking failure in RCF under well-controlled lubrication is originated from non-metallic inclusions. The factors to control this type of RCF life have not been clarified, except inclusion size, due to the difficulties in visualization of RCF processes. The authors have investigated the RCF processes through experiments on artificial-cavity-bearing materials, stress simulation and the evaluation of oxide-caused failure. The influences of sulfides on crack initiation and propagation behavior, and RCF life was examined in this paper.

### 3:00 PM

**Stress-Rupture Behavior of Single Crystal Superalloy M09A:** Qi Zheng<sup>1</sup>; Jinxia Yang<sup>1</sup>; Hongyu Zhang<sup>1</sup>; Xiaofeng Sun<sup>1</sup>; Hengrong Guan<sup>1</sup>; Zhuangqi Hu<sup>1</sup>; <sup>1</sup>IMR

M09A, a nickel-base single crystal (SC) superalloy was lately developed by IMR, CAS. Its hot corrosion-resistance is equivalent to that of IN738 and the stress-rupture property reach the level of first generation SC superalloys. It does not contain precious elements so that it is cheaper and lighter. It is a candidate used for turbine blade material working in marine environment

and advanced IGT. The excellent stress-rupture property of M09A as a hot corrosion-resistant superalloy is resulted from the alloy design combined with the solidification control and heat treatment processes. Higher level of alloying strengthening was realized to obtain higher volume fraction of Ni3Al phase and avoid TCP phase formation. The grain boundary is removed by SC process to further improve the stress-rupture property and the hot corrosion-resistance at high temperature. More uniform and finer Ni3Al precipitates were obtained by the heat treatment process in the alloy.

### 3:15 PM

**Tensile Deformation Characteristics of a Ferrite/Austenite Two Phase Steel Containing the High Mn and Al Contents:** *Kyung-Tae Park*<sup>1</sup>; Si Woo Hwang<sup>2</sup>; Jung Hoon Ji<sup>1</sup>; Sera Kim<sup>1</sup>; Youngil Son<sup>3</sup>; <sup>1</sup>Hanbat National University; <sup>2</sup>Steel Research Institute; <sup>3</sup>Agency for Defense Development

High Mn austenitic steels usually exhibit an excellent combination of strength and ductility, mainly due to twinning induced plasticity (TWIP). In this study, in order to produce the steel grade with the reduced specific weight as well as a good combination of strength-ductility, Al was added to a high Mn steel and its tensile characteristics were examined. The steel (Fe-20Mn-9Al-0.6C (in wt.)) consisted of austenite and ferrite in a wide range of annealing temperatures. A special focus was made on identifying the deformation mode of austenite in relation to the SFE. This is because austenite deformation is primarily determined by the SFE and Al significantly increases the SFE of austenite. The results showed that austenite deformation was dominated by dislocation planar glide rather than TWIP even with the high SFE. The planar glide with the high SFE was rationalized in terms of the Fisher interaction.

### 3:30 PM

**Shear Capacity of Reinforced Concrete Beams Using Recycled Coarse Aggregates:** *Efe Ewaen Ikponmwosa*<sup>1</sup>; Musbau Salau<sup>1</sup>; <sup>1</sup>University of Lagos

An investigation into the shear capacity of reinforced concrete beams using recycled coarse aggregate from crushed graded inorganic particles processed from used construction materials and demolition debris is reported. Eighty (80) beams 150 x 150mm cross-sectional area and 1000mm length and twelve (12) cubes were cast. The concrete mix adopted was 1:2:4 (cement: sand: granite/recycled aggregate) with w/c ratio of 0.55 by weight. The percentage replacement of normal coarse aggregate by recycled aggregate was 0% for forty (40) beams and 30% for the remaining forty (40) beams. Six (6) cubes for each mix were cast. The specimens are subjected to line loads to determine their failure behaviour, deflection, crack patterns and post-crack performance. The results showed that the average density and strength of recycled aggregate concrete were slightly lower than that of normal aggregate concrete as the recycled aggregate concrete cubes densities and strengths averaged 97.8% and 88.7% of that of normal aggregate concrete. Each test beam specimen exhibited initial flexural failure at mid span. Diagonal cracks also propagated from each of the supports to the point of the application of load, indicating shear failure. The failure mode of the test specimens varied with the shear span – effective depth ratio as well as the concrete mix type.

### 3:45 PM Break

### 4:00 PM

**Hot Deformation Behavior of Ti-6Al-4V Alloy with a' Martensite Starting Microstructure:** *Hiroaki Matsumoto*<sup>1</sup>; Bin Liu<sup>1</sup>; Sang-Hak Lee<sup>2</sup>; Yunping Li<sup>1</sup>; Kazuhisa Sato<sup>1</sup>; Yoshiki Ono<sup>2</sup>; Akihiko Chiba<sup>1</sup>; <sup>1</sup>Institute for Materials Research, Tohoku university; <sup>2</sup>NHK Spring Co., Ltd

Hot deformation behavior and microstructural evolution of Ti-6Al-4V alloy in case of a' martensite starting microstructure were examined by comparing the case in equilibrium (a+β) starting microstructure. In compression test in temperature region of (a+β), Equiaxed grained structure is exhibited for both starting microstructures of a' martensite and equilibrium (a+β) after compression test. Then, distortion-less ultrafine grained microstructure is obtained in case of a' martensite starting microstructure after hot compression especially under conditions of higher Z (Zener-Hollomon parameter). The apparent activation energy of hot deformation in temperature region of (a+β)

is 395 kJ/mol for the case of a' martensite starting microstructure and 320 kJ/mol for the case of (a+β) starting microstructure, respectively. This result indicates that hot deformation behavior in the cases of a' martensite- and (a+β) starting microstructure is different.

### 4:15 PM

**Hot Ductility of Near-Alpha and Alpha + Beta Titanium Alloys:** *Jeff Rodela*<sup>1</sup>; John Lippold<sup>1</sup>; <sup>1</sup>The Ohio State University

Titanium alloy 5111 (5Al-1Sn-1Zr-1V-0.8Mo [wt%]) is a near-alpha intermediate-strength Ti alloy with excellent fracture toughness and low-temperature creep resistance. Elevated temperature mechanical behavior (up to ~1620 °C) has not been studied in great detail and is of great interest to many applications such welding. The hot ductility of β-processed Ti-5111 was measured using a Gleeble thermomechanical simulator. Samples were tested at temperatures from 600-1620°C using thermal cycles representative of welding. Ti-5111 exhibited a significant decrease in ductility when tested at temperatures below the β transus temperature exhibiting mixed inter/transgranular fracture with some ductile features. The sharp decrease in ductility for Ti-5111 below β transus likely contributes to processing-related issues such the poor friction stir weldability. Hot ductility of Ti-5111 was also compared to β-processed Ti-6Al-4V a + β alloy.

### 4:30 PM

**Influence of Heterogeneous Deformation on Microstructural Cracking in Alpha-Titanium Alloys:** *Motoaki Morita*<sup>1</sup>; Satoshi Moroka<sup>1</sup>; Osamu Umezawa<sup>1</sup>; <sup>1</sup>Yokohama National University

Subsurface crack initiation in high-cycle fatigue has been detected as a transgranular cracking in alpha-titanium alloys at and below room temperature. Strain incompatible due to heterogeneous deformation may cause the cracking and form a crystallographic facet. In the present study, both neutron diffraction and Taylor analyses under tension mode were adopted to discuss the influence of heterogeneous deformation on the cracking. The stress distribution on grains was clearly detected and divided into soft and hard grains. The lowest rate of plastic work appeared at tensile axis of between [-12-11] and [-12-12]. The movable slip systems were determined as {01-10}<11-20> and {0001}<11-20>. The grain in which the highest rate of plastic work was around tensile stress axis of <0001> was hardly relaxed, since the slip systems of {10-11}<11-23> were not in active at all. Thus the tensile stress was accumulated normal to (0001) plane, and may assist to the microstructural cracking.

### 4:45 PM

**Deformation Behavior of Biomedical Co-Cr-Mo Alloy:** *Hiroaki Matsumoto*<sup>1</sup>; Shingo Kurosu<sup>1</sup>; Byong-soo Lee<sup>1</sup>; Yunping Li<sup>1</sup>; Yuichiro Koizumi<sup>1</sup>; Akihiko Chiba<sup>1</sup>; <sup>1</sup>Institute for Materials Research, Tohoku university

Cobalt-chromium-molybdenum (Co-Cr-Mo)-based alloys have been used as many kinds of biomedical applications due to their excellent biocompatibility and mechanical properties. The deformation behaviors of Co-27Cr-5.5Mo-0.16N (in mass%) alloy consisting of ε phase (fcc) and Co-27Cr-5Mo (in mass%) alloy consisting of ε phase (hcp) were summarized in this study. Stacking fault formation followed by evolution to ε phase with increasing strain was dominant deformation mode in γ Co-27Cr-5.5Mo-0.16N alloy. Excellent tensile ductility at room temperature more than 20% was seen in ε Co-27Cr-5.5Mo-0.16N alloy. However, fracture occurred under quasi-brittle manner. Then, crack propagated preferentially at interface between ε phase and strain induced ε phase which is due to the highly-accumulated strain at the interface. While, in ε Co-27Cr-5Mo alloy, simultaneous activation of basal <a> slip and prismatic <a> slip is dominant deformation mode, and fracture occurred dominantly by intergranular fracture.

5:00 PM

**Cyclic Oxidation Of Co-Al-W-Based Alloys At 900°C And 1000°C:** *Raghavendra Adharapurapu*<sup>1</sup>; *Sara Perez-Bergquist*<sup>1</sup>; *Jennifer Dibbern*<sup>1</sup>; *Akane Suzuki*<sup>2</sup>; *Tresa Pollock*<sup>3</sup>; <sup>1</sup>University of Michigan; <sup>2</sup>General Electric Global Research Center; <sup>3</sup>University of California Santa Barbara

New Co-Al-W-based alloys containing  $\gamma'$ -Co<sub>3</sub>(Al,W) have been developed with superior high-temperature strength. Effect of quaternary additions of X=Ta/Mo/V/Ni on the phase stability and oxidation properties of Co-Al-W-X alloys have been investigated. Alloys were subjected to cyclic oxidation to a maximum temperature of 900°C/1000°C in air and SEM and XRD investigations of the oxidation products at various stages of oxidation have been conducted. A duplex oxide layer consisting of outer porous cobalt-oxide above a metal-rich complex oxide Co-W-Al-X-O was observed in all alloys. Compared to the Ni-based superalloys, the cobalt-based alloys have inferior oxidation resistance since the cobalt-oxide is not protective like alumina in Ni-based alloys. Among the quaternary elements, cobalt alloys with Ni additions exhibited the best oxidation resistance. Additions of V/Mo led to extensive spallation due to the formation of W-rich CoWO<sub>4</sub>-spinel. Protective coatings or alternative alloying strategies may be necessary to improve the oxidation resistance of Co-based alloys.

5:15 PM

**Effects of Solution Temperatures on Creep Properties and Fracture Mechanism of FGH95 Nickel-Base Superalloy:** *Jun Xie*<sup>1</sup>; *Sugui Tian*<sup>1</sup>; <sup>1</sup>Shenyang University of Technology

By means of the enduring properties measurement and microstructure observation, an investigation has been made into the influence of the microstructure on the enduring properties and fracture mechanism of FGH95 superalloy. After solution treated at 1150°C, the thicker  $\gamma'$  phase is distributed in wider boundary regions. When temperature raised to 1160°C, the thicker  $\gamma'$  phase is fully dissolved, and the particles of (Nb, Ti)C are discontinuously precipitated along the boundaries. After solution treated at 1165°C, the grain size grown up obviously, and carbide films are continuously precipitated along boundaries. The carbide particles which are discontinuously precipitated along boundary can effectively restrain boundaries sliding. As the creep goes on, the deformation characteristic of the alloy is single and double orientation slipping. The slipping trace on the sample surface increase to bring out the stress concentration, which result in the initiating and propagating of the micro-cracks along the boundaries up to rupture.

5:30 PM

**Novel Opencell™ Metal Sandwich Panels:** *Antonio Valente*<sup>1</sup>; *Mika Sirén*<sup>2</sup>; *Jukka Säynäjäkangas*<sup>3</sup>; *Edward Chen*<sup>4</sup>; <sup>1</sup>PLY Engenharia, Lda; <sup>2</sup>VTT Technical Research Centre of Finland; <sup>3</sup>Outokumpu Stainless Tornio Works; <sup>4</sup>Transition45 Technologies, Inc.

All-metal sandwich panels offer numerous outstanding properties allowing the designer to develop lightweight and efficient structural configurations for diverse applications. The most established type of all-metal sandwich panels is using directional stiffeners between solid surface sheets. Characteristic of these panels, however, is the heterogeneity of strength and/or stiffness properties in longitudinal and transverse directions. Sandwich panel technology development towards lattice truss concepts has resulted in a completely new metal panel idea called Opencell™. Instead of a conventional three constituent panel structure (sheet/core/sheet), a combination of cut-and-formed core and single solid sheet element is used, resulting in higher degree of design variables for tailored properties. Other key benefits of the Opencell™ technology are reduction of the number of elements, and hence manufacturing phases and eventually weight. This presentation describes the design and optimization of prototype Opencell™ panels, their manufacture, and test results from static and fatigue bending type tests.

5:45 PM

**Effect of Hydrogen on Tensile Properties of a Ductile Cast Iron:** *Hisao Matsunaga*<sup>1</sup>; *Kenshin Matsuno*<sup>1</sup>; *Katsuya Hayashida*<sup>2</sup>; <sup>1</sup>Fukuoka University; <sup>2</sup>Toppan Printing Co., Ltd.

Effect of hydrogen-charging and strain rate was investigated on the tensile properties of a ductile cast iron having spheroidal graphite, pearlite and ferrite structures. Hydrogen-charging accelerated the crack-growth from graphite. The crack-growth acceleration resulted in a decrease in reduction of area (RA) by ~40%. In the uncharged specimens RA was nearly constant regardless of strain rate, whereas in the hydrogen-charged specimens RA was gradually decreased with a decrease in strain rate. Hydrogen microprint technique and thermal desorption spectroscopy revealed that most of the charged hydrogen was diffusive and segregated at the graphite and pearlite. Considering all the obtained results together, the hydrogen-induced degradation was attributed to the following three mechanisms: (i) hydrogen supply to the crack tip from the graphite/matrix interface, (ii) Hydrogen-enhanced pearlite cracking and (iii) hydrogen emission from the graphite and supply to the crack tip.

6:00 PM

**Analysis of Sandwich Composite Chassis Using Multiscale Modeling Technique:** *Arslan Siddiqui*<sup>1</sup>; <sup>1</sup>Pakistan Navy Engineering College - NUST

Our aim was to design a vehicle chassis that provides an ideal balance between strength and weight. The analysis approach was based on the multi-scale modeling technique. A unit cell of facesheet and core was modeled in detail; this unit cell was then arrayed as per adequate size to overcome the non-linear effects of the honeycomb geometry itself. The materials used for the core were Aluminum honeycomb that was bonded by woven glass fabric laminates. The sandwich was analyzed under different boundary conditions, to obtain the bulk properties of composite. These bulk properties were then applied to the chassis of the vehicle as homogenized solid properties. The variable that was given primary importance was the thickness of honeycomb core.

## Hume-Rothery Symposium Thermodynamics and Diffusion Coupling in Alloys - Application Driven Science: Materials Design and Diffusional Simulations

*Sponsored by:* The Minerals, Metals and Materials Society, TMS Electronic, Magnetic, and Photonic Materials Division, TMS: Alloy Phases Committee

*Program Organizers:* Zi-Kui Liu, The Pennsylvania State University; Larry Kaufman, CALPHAD, Inc.; Annika Borgenstam, Royal Institute of Technology; Carelyn Campbell, NIST

Wednesday PM  
March 2, 2011

Room: 31A  
Location: San Diego Conv. Ctr

*Session Chairs:* Richard Sisson, Worcester Polytechnic Institute; Roger Reed, University of Birmingham

2:00 PM Invited

**Thermodynamics-Based Materials Design:** *Greg Olson*<sup>1</sup>; <sup>1</sup>Northwestern University

The development of the Thermocalc/DICTRA toolset at KTH raised the accuracy of the CALPHAD method and its supporting databases to sufficient accuracy to enable an approach to materials design. Thermodynamics-based parametric materials design integrating materials science, applied mechanics and quantum physics within a systems engineering framework has brought a first generation of designer "cyberalloys" that have now entered successful commercial applications, and a new enterprise of commercial materials design services has steadily grown over the past decade. As the central engine of the AIM methodology for accelerated qualification, the PrecipiCalc microstructural simulator, built on the multicomponent Thermocalc/DICTRA platform, has demonstrated both accelerated thermal process optimization at



the component level and the effective forecast of manufacturing variation with efficient fusion of minimal datasets. Flight qualification of the computationally designed Ferrium S53 landing gear steel using the AIM methodology heralds a new era of Integrated Computational Materials Engineering grounded in accurate multicomponent thermodynamics.

#### 2:30 PM Invited

##### **New Nickel-Based Superalloys By CALPHAD-Driven Design Methods:** Roger Reed<sup>1</sup>; Nils Warnken<sup>1</sup>; <sup>1</sup>University of Birmingham

New grades of superalloys are needed in the aerospace, power generation and oil/gas sectors. Design rules are proposed by which new compositions can be chosen systematically, using models for the most important characteristics: e.g. creep resistance, microstructural stability, castability, density and cost. Application of the rules allows the very large compositional space to be reduced to just a few ideal compositions, so that optimal ones for given applications can be isolated. Much depends upon the accuracy of the underlying sub-models; the ones based upon CALPHAD are critical - developments and limitations of these are emphasised. It is demonstrated that the procedures have the potential to remove much of the traditional reliance upon empiricism and trial-and-error-based testing.

#### 3:00 PM Invited

##### **High-Throughput Measurements for Accelerated Establishment of Materials Databases:** Ji-Cheng Zhao<sup>1</sup>; Xuan Zheng<sup>2</sup>; David Cahill<sup>2</sup>; <sup>1</sup>The Ohio State University; <sup>2</sup>University of Illinois

This talk will use recent examples to illustrate high-throughput measurements for fast establishment of materials databases. The methodology is based on a simple idea of taking advantage of the compositional gradients and phase formation in diffusion couples and diffusion multiples to perform localized property measurements. Such measurements require a new suite of materials property microscopy tools with micron-scale resolution, but would greatly accelerate the efficiency of data gathering as compared to traditional measurements on individual alloys. The local equilibrium at the phase interfaces allows fast evaluation of phase diagrams which are essential input to CALPHAD modeling. Micron-scale resolution tools were developed to measure thermal conductivity, elastic modulus, and coefficients of thermal expansion (CTE). These tools can be applied not only to accelerate the development of structural materials, but also to discover new multifunctional materials.

#### 3:30 PM Break

#### 3:50 PM Invited

##### **Atomic Defects in Alloys and Compounds: The Effect of a Macroscopic State:** Pavel Korzhavyi<sup>1</sup>; Andrei Ruban<sup>1</sup>; Oleg Gorbato<sup>2</sup>; Yuri Gornostyrev<sup>2</sup>; Borje Johansson<sup>1</sup>; <sup>1</sup>Royal Institute of Technology (KTH); <sup>2</sup>Institute of Quantum Materials Science

Case ab-initio studies of atomic defects in concentrated metallic (Fe-based) alloys and compound semiconductors (GaAs- and ZnO-based alloys) are presented. The general picture emerging from these studies is quite interesting and complex: The microscopic parameters of point defects (such as the energies of their formation, interaction, and migration) are found to be strongly dependent upon the macroscopic state (i.e., the electronic and magnetic structure) of the host. For example, we show that the solute-solute and vacancy-solute interactions are quite different in the fully ordered ferromagnetic state and the completely disordered paramagnetic state of the Fe-based alloy matrix. Also, we show that by changing (through alloying) the electronic structure of a metallic alloy or a compound semiconductor one may "tune" the chemical and magnetic exchange interactions of point defects in these hosts. We discuss how these effects are treated within the existing atomistic (e.g., cluster expansion) and continuum (e.g., Calphad) approaches.

#### 4:20 PM

##### **Modeling the Microstructural Development during the Nitriding of Low Alloy Steels:** Mei Yang<sup>1</sup>; Danielle Belsito<sup>1</sup>; Richard Sisson<sup>1</sup>; <sup>1</sup>Worcester Polytechnic Institute, Center for Heat Treating Excellence

The microstructural development during the nitriding of quenched and tempered low alloy steels has been theoretically and experimentally investigated. These results will be compared with those of CALPHAD calculations from Thermo-Calc, which use thermodynamic data to predict multicomponent phase behavior during nitriding. Isoleths with nitrogen content will be presented for steels with and without added aluminum. Customized Lehrer diagrams will be developed to predict the relationship between the nitriding potential and the phase development at different temperatures. In addition, a computational model is being developed to predict the nitriding behavior. The methodology and preliminary results for this model will be presented and compared with experimental results.

#### 4:50 PM

##### **Phase Field and DICTRA Simulations of Type 3 Boundaries:** Xiaojin Ke<sup>1</sup>; John Morral<sup>1</sup>; Yunzhi Wang<sup>1</sup>; <sup>1</sup>Ohio State University

Boundaries between layers that form in diffusion couples can be characterized by the number of phases that change on crossing the boundary. Accordingly a type 3 boundary is one in which 3 phases change. In the present work, attempts were made to simulate type 3 boundaries using both a phase field model and the newly available homogenization model in DICTRA. It was found that type 3 boundaries could not be successfully simulated with the homogenization model, because of problems that will be presented. However type 3 boundaries could be simulated with the phase field method. All simulations were performed on a prototype A-B-C ternary system in which elements A, B and C form regular solutions with each other.

#### 5:20 PM

##### **Thermodynamics Test of the Mixed Enthalpy TiCxOy System:** Bo Jiang<sup>1</sup>; Chengjun Gao<sup>1</sup>; Zhanmin Cao<sup>1</sup>; Kai Huang<sup>1</sup>; Hongmin Zhu<sup>1</sup>; <sup>1</sup>USTB

The combustion enthalpy  $\Delta H$ , and  $C_p$  of the TiC, TiO and Ti<sub>2</sub>CO were investigated by the differential scanning calorimeter (DSC) method. And the effects of parameters such as the start combustion temperature, the flow rate of oxygen, the heating rate and the sample preparation were discussed in detail. It was found that the results of  $\Delta H_{TiC}$  and  $\Delta H_{TiO}$  have a good agreement with the JANAF data. The mixed enthalpy of the reaction  $TiO + TiC = Ti_2CO$  was calculated in this article. Furthermore, the standard formation Gibbs free energy of the solid solution  $Ti_xC_xO_y$  ( $x+y=1$ ) were obtained from the basis of regular solution model.

---

## **Magnesium Technology 2011: Deformation Mechanisms II; Formability and Forming**

*Sponsored by:* The Minerals, Metals and Materials Society, TMS Light Metals Division, TMS: Magnesium Committee

*Program Organizers:* Wim Sillekens, TNO Science and Industry; Sean Agnew, University of Virginia; Suveen Mathaudhu, US Army Research Laboratory; Neale Neelameggham, US Magnesium LLC

Wednesday PM  
March 2, 2011

Room: 6F  
Location: San Diego Conv. Ctr

*Session Chairs:* Paul Krajewski, General Motors; Wim Sillekens, TNO Science and Industry

---

#### 2:00 PM

##### **Texture Weakening Effect of Y in Mg-Zn-Y System:** Seyed Amir Farzadfar<sup>1</sup>; Mehdi Sanjari<sup>1</sup>; In-Ho Jung<sup>1</sup>; Elhachmi Es-Sadiqi<sup>2</sup>; Steve Yue<sup>1</sup>; <sup>1</sup>McGill University; <sup>2</sup>CANMET- Materials Technology Laboratory

The CALPHAD (Calculation of Phase Diagram) method was successfully used in this study to select the alloys from Mg-Zn-Y system, aimed at determining the mechanism(s) of texture weakening in Y-containing Mg alloys: PSN (particle-stimulated nucleation of recrystallization) and/or solute

effects. The selected alloys are Mg-6Zn-1.2Y, Mg-5Zn-2Y, Mg-2.9Y and Mg-2.9Zn (in wt%). After heat treatment, the ternary alloys contain (nearly) the same amount of ternary intermetallics in equilibrium with a Mg at 350 °C, and the microstructure of the binary alloys is composed of a-Mg solid solution at 350 °C containing the same solute amount as that in the ternary alloys. The hot deformation and post-deformation annealing of these alloys at a constant temperature (i.e., 350 °C) showed that the texture weakening happens during growth of recrystallized grains in deformed and annealed samples where Y element is in a-Mg solid solution.

#### 2:20 PM

**In-Situ Scanning Electron Microscopy Comparison of Microstructure and Deformation Behavior between WE43-F and WE43-T5 Magnesium Alloys:** *Tomoko Sano*<sup>1</sup>; Jian Yu<sup>1</sup>; Bruce Davis<sup>2</sup>; Richard DeLorme<sup>2</sup>; Kyu Cho<sup>1</sup>; <sup>1</sup>US Army Research Laboratory; <sup>2</sup>Magnesium Elektron North America

In-situ tensile testing in the scanning electron microscope was used to investigate the quasi-static deformation behavior and fracture mechanism of WE43 magnesium alloys. The in-situ tensile experiments were conducted at room temperature at a constant crosshead speed of 0.5 mm / min. One set of samples was a rolled and quenched F temper alloy and the other set was an artificially aged T5 temper alloy. The objective of this research was to determine the effect of tempering on precipitates chemistries, microstructure, and mechanical properties. The sample orientation is known to affect the tensile properties. Hence tensile specimens with different sample orientation were tested. The crystallographic orientations were characterized by electron backscattered diffraction. Strong textures were observed with rolling plane crystals indicating a basal plane orientation.

#### 2:40 PM

**A Molecular Dynamics Study of Fracture Behavior in Magnesium Single Crystal:** *Tian Tang*<sup>1</sup>; Sungho Kim<sup>1</sup>; Mark F. Horstemeyer<sup>1</sup>; Paul Wang<sup>1</sup>; <sup>1</sup>Mississippi State University

The analysis of crack growth in magnesium crystals was performed using molecular dynamics simulation with Embedded Atom Method (EAM) potentials. Four specimens with increasing sizes were used to investigate the influences of material length scale on crack growth of magnesium single crystals. Furthermore, the effects of temperature, loading strain rate, and the size of the initial crack were also verified. The specimens were subjected to uniaxial tension strain up to the total strain level of 0.2 with a constant strain rate. In the simulation of each specimen, the uniaxial stress strain curve was monitored. The simulation results show that the specimen size, loading strain rate, temperature, and the size of initial crack have strong influences on the yield strength at which the twin nucleated followed by the crack growing. The initial slope of the uniaxial stress strain curve is independent of the loading strain rate and temperature. Moreover, the stress at the crack tip was released by the reorganization of atoms as a result of the high mobility of atoms caused by high temperature.

#### 3:00 PM

**Microstructural Relationship in the Damage Evolution Process of an AZ61 Magnesium Alloy:** *Marcos Lugo*<sup>1</sup>; J Jordan<sup>2</sup>; M Horstemeyer<sup>1</sup>; M Tschopp<sup>1</sup>; <sup>1</sup>Mississippi State University; <sup>2</sup>The University of Alabama

The damage evolution process of magnesium AZ61 alloy under monotonic tensile loading conditions is investigated. Specimens that had been subjected to interrupted tensile loading were examined under optical microscopy to quantify the number density of cracked intermetallic particles as a function of applied strain. Digital image analysis of the optical images was employed to automatically quantify damage by separating cracked from non-cracked particles. Lastly, an internal state variable damage model was shown to adequately capture the experimentally-observed damage of intermetallic particles in the magnesium AZ61 alloy.

#### 3:20 PM

**Formability Enhancement in Hot Extruded Magnesium Alloys:** *Raja Mishra*<sup>1</sup>; Anil Gupta<sup>2</sup>; Rajiv Sikand<sup>3</sup>; Anil Sachdev<sup>1</sup>; Li Jin<sup>4</sup>; <sup>1</sup>General Motors; <sup>2</sup>Advanced Materials and Processes Research Institute; <sup>3</sup>National Physical Laboratory; <sup>4</sup>Shanghai Jiao Tong University

The effects of cerium (Ce), aluminum (Al) and manganese (Mn) additions on the microstructure and mechanical properties of hot extruded magnesium alloy rods have been investigated. Seven different compositions of Mg alloys - Pure Mg, Mg-0.2Ce, Mg-0.5Ce, AM30, AM50, Mg-3Al-0.2Ce and Mg-5Al-0.2Ce were hot extruded under optimized process conditions. Minor addition of Ce to Mg was found to enhance its ductility from <10% to >30% and 3 - 5% Al addition resulted in ~40% and 50% increase in strength respectively, compared to pure Mg. A combination of 5% Al and 0.2% Ce addition resulted in concurrent improvement in strength and ductility as a result of concurrent grain size refinement, texture randomization and solute strengthening.

#### 3:40 PM

**Deformation and Evolution of Microstructure and Texture during High Speed Heavy Rolling of AZ31 Magnesium Alloy Sheet:** *Tetsuo Sakai*<sup>1</sup>; Akinori Hashimoto<sup>1</sup>; Go Hamada<sup>1</sup>; Hiroshi Utsunomiya<sup>1</sup>; <sup>1</sup>Osaka University

An AZ31 magnesium alloy sheet was rolled to 60% by one pass operation at 473K at a rolling speed of 500m/min. During rolling, the mill was suddenly stopped and the sheet was withdrawn from the work rolls. The evolution of microstructure and texture of the AZ31 magnesium alloy sheet during rolling deformation was revealed by observing microstructure and texture at the plane perpendicular to the transverse direction from the entry to the exit of the zone of deformation of the withdrawn sheet. Crystals aligned their 0001 planes oblique to the sheet plane preferentially deforms near the entry of the deformation zone. Dynamically recrystallized grains are observed in the deformation zone. The double peak texture developed during recrystallization.

#### 4:00 PM Break

#### 4:20 PM

**Formability of Magnesium Sheet ZE10 and AZ31 with Respect to Initial Texture:** *Lennart Stutz*<sup>1</sup>; Jan Bohlen<sup>1</sup>; Dietmar Letzig<sup>1</sup>; Karl Ulrich Kainer<sup>1</sup>; <sup>1</sup>GKSS Forschungszentrum Geesthacht GmbH

The commercial application of conventional magnesium alloy sheets is hindered by their low formability and therefore technological and economic constraints. Tailoring the texture has been identified as playing a major role in enhancing the formability of magnesium sheets. In this study, the formability of magnesium sheet ZE10 and AZ31 was investigated. While the texture of AZ31 is of unfavourable basal type, ZE10 shows a significantly different texture with the basal planes being randomly distributed. More basal planes are oriented favourably for basal slip, promising higher formability and thus, lower process temperature. Formability is assessed by means of forming limit diagrams as a representation of material response to various strain paths. Nakajima tests were carried out from room temperature to 250°C. Local strain data is correlated with the microstructural evolution. This study reveals a significant influence of texture on formability with ZE10 sheet showing superior formability compared to AZ31.

#### 4:40 PM

**Hot Workability of Alloy WE43 Examined using Hot Torsion Testing:** *Frederick Polesak*<sup>1</sup>; Bruce Davis<sup>2</sup>; Rick DeLorme<sup>2</sup>; Sean Agnew<sup>1</sup>; <sup>1</sup>University of Virginia; <sup>2</sup>Magnesium Elektron North America Inc.

While rare earth additions can impart a variety of property improvements in magnesium alloys, they can also limit the processing parameter window inside which the alloys may be successfully wrought in commercial production routes such as extrusion and rolling. In the present work, hot torsion testing is used to explore the temperature and rate sensitivity of the flow stress of the alloy WE43 in order to establish the boundaries of this processing window. Two mechanisms appear to be important from a fundamental perspective: first, dynamic recrystallization appears to be a prerequisite for significant plastic flow; second, serrated flow and negative

strain rate sensitivity are observed at lower deformation temperatures ( $T \sim 150\text{--}250^\circ\text{C}$ ). The Sellars-Tegart model and simple power law, both of which have been successfully applied to describe the temperature/strain-rate/flow stress relationship in AZ31 and many other Mg alloys, are explored in the context of WE43.

#### 5:00 PM

**Enhancement of Superplastic Forming Limit of Magnesium Sheets by Counter-Pressurizing:** *Wonkyu Bang*<sup>1</sup>; Hyun-Seok Lee<sup>1</sup>; Hyung-Lae Kim<sup>2</sup>; Young-Won Chang<sup>2</sup>; <sup>1</sup>RIST; <sup>2</sup>POSTECH

As often reported in various metallic materials, fine-grained wrought magnesium can exhibit extensive superplasticity at the elevated temperature, which makes superplastic forming (SPF) of magnesium as a promising process for manifesting complex-shaped, lightweight thin-walled structural components. The superplastic tensile deformation of magnesium is commonly accompanied by substantial cavitation in its failure stage, which is also typical to quasi-single phase aluminum alloys. In this regard, a series of bulge test have been conducted with independent inflating/counter-pressure control setup. From the evaluation of superplastic forming limit along Limit Dome Height (LDH), considerable improvement was reproduced by counter-pressurized conditions. Constitutive modeling and microstructural analysis implies that it is mainly achieved by the retardation of nucleation and growth of cavities under hydrostatic stress.

#### 5:20 PM

**Microstructural Evolution during Roller Hemming of AZ31 Magnesium Sheet:** *Amanda Levinson*<sup>1</sup>; Raja Mishra<sup>2</sup>; John Carsley<sup>2</sup>; Roger Doherty<sup>1</sup>; Surya Kalidindi<sup>1</sup>; <sup>1</sup>Drexel University; <sup>2</sup>General Motors

The evolution of microstructure and texture during multi-pass roller hemming (prehemming and flat hemming) of commercial grade AZ31-O sheet has been studied using electron backscatter diffraction (EBSD). The prehemming and hemming operations were performed with and without local heating using a laser source. Dynamic recrystallization (DRX) occurred on the outer and inner diameter of the hem at all temperatures up to  $200^\circ\text{C}$ , with the center of the sheet exhibiting no DRX. The texture in the outer and inner diameter regions are rotated by  $90^\circ$  in the hemmed sample. It is observed that samples prehemmed at room temperature could not be flat hemmed even after applying heat. The results suggest that the large stored energy in the roller hemmed sheet induces recrystallization at room temperature but the damage in this prehemmed sample leads to failure even if heat is applied during subsequent roller passes.

#### 5:40 PM

**The Warm Forming Performance of Mg Sheet Materials:** *Paul Krajewski*<sup>1</sup>; Peter Friedman<sup>2</sup>; Jugraj Singh<sup>3</sup>; <sup>1</sup>General Motors; <sup>2</sup>Ford Motor Company; <sup>3</sup>Chrysler Group, LLC

The warm forming performance of five different magnesium sheet materials was evaluated using a heated pan die. Forming maps were generated to determine the optimum temperature and die conditions for successful forming. All five materials exhibited excellent formability above  $325^\circ\text{C}$ , with a robust forming window. Below  $300^\circ\text{C}$ , significant differences in the materials were observed. Some materials could be formed into a pan at temperatures as low as  $175^\circ\text{C}$  while others could not be formed below  $300^\circ\text{C}$ . The differences in forming performance were investigated considering material properties, tribology, and microstructure. These trials included both continuously cast and direct chill cast materials, and demonstrated that the continuously cast materials can be successfully warm formed.

## Magnetic Materials for Energy Applications: Nanocrystalline and Nanocomposite Nd-Fe-B Magnets

*Sponsored by:* TMS Electronic, Magnetic, and Photonic Materials Division, TMS: Energy Conversion and Storage Committee, TMS: Magnetic Materials Committee; JSPS 147th Committee on Amorphous and Nanocrystalline Materials; Lake Shore Cytronics, Inc.; AMT&C

*Program Organizers:* Victorino Franco, Sevilla University; Oliver Gutfleisch, IFW Dresden; Kazuhiro Hono, National Institute for Materials Science; Paul Ohodnicki, National Energy Technology Laboratory

Wednesday PM

March 2, 2011

Room: 11A

Location: San Diego Conv. Ctr

*Session Chair:* Kazuhiro Hono, National Institute for Materials Science

#### 2:00 PM Keynote

**High Performance Magnets for Energy Efficient Devices:** *George Hadjipanayis*<sup>1</sup>; <sup>1</sup>University of Delaware

For the past twenty years, the Magnetics Lab at the University of Delaware has been involved in the development of materials for high performance permanent magnets. These materials are currently used in a vast number of commercial and military applications. These include advanced motors, generation and distribution of electrical power, the automotive and aviation industry, the information storage industry, medical surgical and diagnostic equipment, bioengineering, and numerous military weapons, guidance and communications systems. In this talk, I will summarize our latest efforts to develop high performance nanocomposite magnets with much higher energy products ( $(BH)_{\text{max}} > 60$  MGOe) using the bottom-up approach. The high strength of these magnets will allow lighter, more compact, lower cost and more energy efficient devices to be developed which will help us to reduce our dependency on fossil fuels and enable "more electric" product commercialization. Supported by DOE ARPA-E DE-AR0000046

#### 2:40 PM Invited

**Coercivity Enhancement in Sintered Nd-Fe-B Magnets Annealed under High Magnetic Fields:** *Hiroaki Kato*<sup>1</sup>; Takahiro Akiya<sup>2</sup>; Kunihiro Koike<sup>1</sup>; <sup>1</sup>Yamagata University; <sup>2</sup>Tohoku University

The coercivity ( $H_c$ ) mechanism in sintered Nd-Fe-B magnets is one of the most important issues in this research field with relation to a reduction of Dy usage for high-temperature applications. Although morphology of intergranular phases is thought to be strongly correlated with  $H_c$  values, there is no quantitative evidence for it. We found [1, 2] that a coercivity enhancement occurs by annealing the sintered Nd-Fe-B magnets under high magnetic fields at particular temperatures where a liquid phase appears in the grain boundary, which was confirmed by an endothermic anomaly in the DSC curve. In this presentation, we review our recent high-field experiments on a series of Nd-Fe-B-type sintered magnets with different values of Dy content and Cu additive concentration. [1] H. Kato, *et al.*, *J. Magn. Mater.*, 310 (2007) 2596. [2] T. Akiya, *et al.*, *IOP Conf. Series: Mater. Sci. & Eng.* 1 (2009) 012034.

#### 3:05 PM Invited

**Toward Development of Anisotropic Nanocomposite Permanent Magnets:** *Satoshi Hiroasawa*<sup>1</sup>; <sup>1</sup>Hitachi Metals, Limited

Researches aiming at realization of anisotropic nanocomposite permanent magnets on the basis of Nd<sub>2</sub>Fe<sub>14</sub>B have been facing a tremendous difficulty in obtaining a sizable coercivity ( $H_cJ$ ). One of approaches to possibly solve this problem is to develop a nanometer-sized internal microstructure in the hard magnetic Nd<sub>2</sub>Fe<sub>14</sub>B phase to hinder propagation of the magnetization reversal. Such a material with a built-in microstructure may be consolidated by itself to develop high- $H_cJ$  Nd-Fe-B magnets for the electric vehicle applications without relying on rare elements such as Dy. For these purposes, intensive researches are currently conducted on the hydrogenation-



disproportionation-desorption-recombination (HDDR) process that generates a textured fine-grained microstructure in Nd<sub>2</sub>Fe<sub>14</sub>B in order to clarify the mechanisms that control coercivity and microstructure formation. The HcJ values of HDDR powders were increased by up to 25 % with newly developed grain-boundary modification processes. Toward nanocomposite, processes to combine and consolidate HDDR powder with nano-sized Fe are being developed.

### 3:30 PM Invited

**Development of High Coercivity Nd-Fe-B Permanent Magnets:** *Matahiro Komuro*<sup>1</sup>; *Yuichi Satsu*<sup>1</sup>; *Hiroyuki Suzuki*<sup>1</sup>; *Akira Nambu*<sup>1</sup>; *Kazuhiro Ueda*<sup>1</sup>; *Akira Sugawara*<sup>1</sup>; *Hideyuki Matsuoka*<sup>1</sup>; <sup>1</sup>Hitachi, Ltd.

Nd-Fe-B permanent magnets are widely applied for various products including motors, generators and hard disk drives. Temperature resistant is especially demanded in the automotive application in various products. In order to get high temperature resistant, large amount of heavy rare-earth elements has been added in Nd-Fe-B magnets. Recently, effective processes for reducing the amount of heavy rare-earth elements have been developed to protect heavy rare-earth resources. In these new processes, heavy rare-earth elements which are supplied by vaporizing, slurry or solution are diffused along grain boundaries in Nd-Fe-B magnets. Among these processes, the effect of the magnetic properties improvement using the fluoride solution will be explained in detail. Segregation of the heavy rare-earth elements along grain boundaries with fluorine contributes to coercivity increase, leading to the great reduction of the heavy rare-earth elements consumption. The evaluation results for the motor with the high coercivity magnets will be introduced.

### 3:55 PM Invited

**High Coercivity Nd-Fe-B Thin Films:** *Toshiyuki Shima*<sup>1</sup>; <sup>1</sup>Tohoku Gakuin University

Nd-Fe-B based permanent magnets have been used in a variety of applications such as sensors, actuators and motors because of their high magnetocrystalline anisotropy and high coercivity. In order to keep up with the recent trend of environmental and energy issues, a considerable number of magnets are adopted for the motors of electric and hybrid vehicles. However, it is well known that a practical value of coercivity in the Nd-Fe-B magnet is much smaller than that was predicted by the theory. In order to improve the hard magnetic properties of Nd-Fe-B magnet, understanding of the magnetization process is essential and important. We reported that the magnetic properties of Nd-Fe-B thin films were remarkably changed by the morphology and also by the addition of additive elements. In this talk, the recent studies of Nd-Fe-B thin films including in-field magnetic force microscope observation will be reviewed.

### 4:20 PM Invited

**Current Status of Permanent Magnet Research and Market in China:** *Aru Yan*<sup>1</sup>; <sup>1</sup>Ningbo Institute of Material Technology and Engineering

The past decades have witnessed an impressive progress of permanent magnets in China. In 2008, China supplied 77.6% of Nd-Fe-B, 55.2% of ferrite and 55.3% of AlNiCo for global permanent magnets market. Financial crisis since 2008 has spurred Chinese magnet manufacturers to turn to products with high added value. This requirement further catalyzed the R&D on permanent magnets. Today both fundamental and application research have been carried out in China. New material systems including Nd-Fe-N and nanocrystalline composites were studied. Mechanisms were explored for the exchanged coupling between hard and soft nanocrystallines in composite magnet. Traditional synthesis methods were improved and novel ones were developed. Especially, permanent magnet films attracted intense attention since their potential grand applications. Recently, Chinese government announced a plan to facilitate the popularization of electric vehicles and renewable wind power to reduce CO<sub>2</sub> release, which provided a new large market for permanent magnets.

### 4:35 PM

**Grain Refinement in Nd<sub>2</sub>Fe<sub>14</sub>B Powders by High Hydrogen Pressure Reactive Milling and Desorption:** *Konrad Güth*<sup>1</sup>; *Julia Lyubina*<sup>2</sup>; *Ludwig Schultz*<sup>1</sup>; *Oliver Gutfleisch*<sup>1</sup>; <sup>1</sup>IFW Dresden; <sup>2</sup>Imperial College London

Recently, high performance permanent magnets undergo a renaissance in the scientific research. The magnetic properties, e. g. remanence, coercivity and consequently energy product, are strongly dependent on their microstructure and crystallographic orientation. One simple way to produce highly coercive powders for inexpensive Nd-Fe-B resin bonded magnets is the HDDR process (Hydrogenation Disproportionation Desorption Recombination). This process is carried out under carefully controlled hydrogen atmosphere at elevated temperature resulting in Nd<sub>2</sub>Fe<sub>14</sub>B crystallites with a size of about 300 nm well-oriented within micrometer-sized particles. A further increase in energy product of the HDDR powders may be achieved via inter-grain exchange coupling, which requires the decrease of grain size by one order of magnitude. Here, the combination of high pressure reactive milling (HPRM) technique prior to the hydrogen desorption and recombination process will be discussed on the basis of the structure and magnetic properties.

### 4:50 PM

**Coercivity Mechanism in Hydrogenation-Disproportionation-Desorption-Recombination Processed Nd-Fe-B Base Powders:** *T. Ohkubo*<sup>1</sup>; *H. Sepehri-Amin*<sup>1</sup>; *T. Nishiuchi*<sup>2</sup>; *S. Hirosawa*<sup>2</sup>; *K. Hono*<sup>1</sup>; <sup>1</sup>National Institute for Materials Science; <sup>2</sup>Hitachi Metals Ltd

Since the grain size of Nd-Fe-B HDDR powders is close to the single domain size of Nd<sub>2</sub>Fe<sub>14</sub>B phase, coercivity values exceeding 20kOe should be achieved if grains can be magnetically decoupled. However, the coercivity of the HDDR powders is much lower for their ultrafine grain size. Hence, the aim of this work is to understanding the reasons for the low coercivity of HDDR processed powders. The microstructure of HDDR processed Nd-Fe-B powders with different HD and DR times were studied using HRSEM, HRTEM and 3D atom probe. Based on the experimental results, we discuss the mechanisms of the formation of ultrafine grained structure and the roles of microalloyed elements like Ga. We also discuss the way to process fully dense high coercivity magnets from HDDR powders.

### 5:05 PM

**Texture Investigation in Melt-Spun High Temperature Mixed Rare Earth-Iron-Boron Alloys:** *Nathaniel Oster*<sup>1</sup>; *Iver Anderson*<sup>2</sup>; *Matthew Kramer*<sup>2</sup>; *R.W. McCallum*<sup>2</sup>; *Wei Tang*<sup>2</sup>; *Yaqiao Wu*<sup>2</sup>; *Kevin Dennis*<sup>2</sup>; <sup>1</sup>Iowa State University; <sup>2</sup>Ames Laboratory

To gain energy product and manufacturing efficiency, anisotropic polymer (PPS) bonded Nd-Fe-B (2-14-1) magnets have been identified for possible cost-effective use in automotive traction motors, especially if their operating temperature limit was raised to 200°C. Mixed rare earth (MRE) 2-14-1 alloy particulate for isotropic nanocrystalline bonded magnets was developed for 200°C, but translation to suitable anisotropic high temperature PPS bonded magnets remains a challenge. Modification of melt-spinning parameters and grain refining additions (such as TiC) are both possible methods to produce suitable directional growth. Thus, microstructure scale and degree of texturing were varied as a function of quench rate, temperature gradient, ribbon thickness, and alloy design. Analysis of results from scanning electron microscopy with orientation imaging, x-ray diffraction, and TEM of the resulting particulate will be presented, along with SQUID magnetometer characterization of aligned and unaligned magnets. Funding provided by DOE-EERE-FCVT Office through Ames Lab Contract No. DE-AC02-07CH11358.

### 5:20 PM

**Structure and Magnetic Properties of Mechanically Milled Melt Spun Rare Earth-based Permanent Magnets:** *Farhad Golkar*<sup>1</sup>; *Jeffrey Shield*<sup>1</sup>; <sup>1</sup>University of Nebraska-Lincoln

One challenge in developing "bulk" nanocomposite permanent magnets is increasing the soft magnetic phase fraction. One method is to utilize eutectic and near-eutectic compositions in the Sm-Co alloy system. The eutectic transformation naturally produces a two-phase structure with a ~0.21 soft magnetic phase fraction, and melt spinning results in a structural refinement

to 20-25 nm. Subsequent mechanical milling further reduced the scale, although the milled material retained crystallinity, as peaks characteristic of the TbCu<sub>7</sub>-type structure were observed up to 6 h of milling. An increase in coercivity with milling time was observed. Annealing somewhat changed the phase distribution, leading to an increase in coercivity. Additionally, alloying elements resulted in the refinement of the microstructure during melt spinning, producing dramatic increases in coercivity to 5-10 kOe. These ternary and quaternary alloys were also mechanically milled in order to study the combined processing effects on the microstructures and magnetic properties.

**5:35 PM**

**Effects of Cu Addition on Microstructures and Magnetic Properties of Nd-Fe(Co,Cu)-B Nanocomposite Magnets:** *Junhua You*<sup>1</sup>; <sup>1</sup>Shenyang University of Technology

The microstructure and magnetic properties of Nd<sub>4</sub>.5Fe<sub>73-x</sub>Co<sub>4</sub>Cu<sub>x</sub>B<sub>18.5</sub> (x=0,0.2,0.5,0.8,1.0) nanocomposite magnets prepared by melt spinning have been investigated by X-ray diffraction (XRD), differential thermal analysis (DTA), transmission electron microscope (TEM) and vibrating sample magnetometer (VSM). The results show that Cu can promote the nucleation rate of Fe<sub>3</sub>B phase, decrease the crystallizing temperature of Fe<sub>3</sub>B and Nd<sub>2</sub>Fe<sub>14</sub>B phases, refine the nanocomposite microstructure and enhance the magnetic properties. The optimum content of Cu is 0.2at%. The Nd<sub>4</sub>.5Fe<sub>72.8</sub>Co<sub>4</sub>Cu<sub>0.2</sub>B<sub>18.5</sub> ribbon made at roll speed of 35 m/s obtained the better magnetic properties: Br=0.98 T, iHc =357 kA•m<sup>-1</sup>, (BH)<sub>max</sub>=89 kJ•m<sup>-3</sup> after annealed at 690° for 10min.

**5:50 PM**

**NdFeB Thick Films as Model Systems for Coercivity Analysis:** *Ciuta Georgeta*<sup>1</sup>; Fruchart Olivier<sup>1</sup>; Zhang Yuepeng<sup>1</sup>; Woodcock Thomas<sup>2</sup>; Gutfleisch Oliver<sup>2</sup>; Dempsey Nora<sup>1</sup>; Givord Dominique<sup>1</sup>; <sup>1</sup>CNRS/Institut Neel; <sup>2</sup>IFW

The increasing demand for NdFeB-based permanent magnets for applications in electric vehicles and wind turbines combined with insecurity in sourcing of heavy rare earth elements has stimulated research into the development of Dy-free magnets. In this work, the preparation, characterization and analysis of Dy-free NdFeB films, which serve as model systems, will be described. The 5 μm thick films are deposited using high rate triode sputtering, in a two step process: deposition + annealing. Varying different processing parameters influences the microstructure, which in turn determines the coercivity. Strong out of plane texture and coercivity values as high as 2.8 T have been achieved. Magnetization reversal in low coercivity and high coercivity films has been studied using both global (vibrating sample magnetometry) and local (magnetic force microscopy) techniques. The understanding of magnetization reversal in these model systems should contribute to the development of Dy-free bulk magnets with the required properties.

## Materials in Clean Power Systems VI: Clean Coal-, Hydrogen Based-Technologies, and Fuel Cells: Membranes and Materials for Renewable Energies

*Sponsored by:* The Minerals, Metals and Materials Society, TMS Electronic, Magnetic, and Photonic Materials Division, TMS Structural Materials Division, TMS/ASM: Corrosion and Environmental Effects Committee, TMS: Energy Conversion and Storage Committee, TMS: High Temperature Alloys Committee  
*Program Organizers:* Xingbo Liu, West Virginia University; Zhenguo "Gary" Yang, Pacific Northwest National Laboratory; Jeffrey Hawk, U.S. Department of Energy, National Energy Technology Laboratory; Teruhisa Horita, AIST; Zi-Kui Liu, The Pennsylvania State University

Wednesday PM

March 2, 2011

Room: 33C

Location: San Diego Conv. Ctr

*Session Chair:* Yan Xiang, Beihang University

**2:00 PM**

**Novel Metallic Membranes for Hydrogen Separation:** *Omer Dogan*<sup>1</sup>; <sup>1</sup>DOE National Energy Technology Laboratory

To reduce dependence on oil and emission of greenhouse gases, hydrogen is favored as an energy carrier for the near future. Hydrogen can be converted to electrical energy utilizing fuel cells and turbines. One way to produce hydrogen is to gasify coal which is abundant in the U.S. The coal gasification produces syngas from which hydrogen is then separated. Designing metallic alloys for hydrogen separation membranes which will work in a syngas environment poses significant challenges. In this presentation, a review of technical targets, metallic membrane development activities at NETL and challenges that are facing the development of new technologies will be given.

**2:20 PM**

**Pd-Based Membrane Reactor for Simultaneous CO<sub>2</sub> Sequestration and Hydrogen Production from Syngas Produced from IGCC:** *Yi Ma*<sup>1</sup>; <sup>1</sup>Worcester polytechnic Institute

An integrated catalytic membrane reactor-separator process for producing pure hydrogen with high pressure CO<sub>2</sub> for sequestration requires membranes with long-term chemical, thermal and mechanical stability at high temperatures and pressures. The basis of composite Pd and Pd/alloy membranes for hydrogen separations and productions will be discussed. Our patented technology for improving the long-term thermal stability of composite Pd- and Pd/alloy-porous-metallic-substrate membranes by the controlled in-situ oxidation of the substrate and bi-metal multi-layer (BMML) deposition to generate an intermetallic diffusion barrier layer will be demonstrated. Experimental results from a Pd-based catalytic membrane reactor for water gas shift (WGS) reaction using simulated Syngas composition from a coal gasifier showed superior performance exceeding thermodynamic equilibrium CO conversion, achieving 98% conversion at 450oC and clearly demonstrating the beneficial effects of a membrane reactor. A thinner membrane synthesized by the same technology showed a permeance exceeding the 2015 DOE target.

**2:40 PM**

**Structure/Property Relations in Proton Conducting Ceramics of the Form SrCe<sub>0.95</sub>Yb<sub>0.05</sub>O<sub>3</sub> With Applications in Membrane Separations: The Role of Microstructure and Second Phase Additions to Enhance Electronic Conductivity:** *Kyle Brinkman*<sup>1</sup>; Frank Chen<sup>2</sup>; Kevin Huang<sup>2</sup>; Sung Gu Kang<sup>3</sup>; David Sholl<sup>3</sup>; <sup>1</sup>Savannah River National Laboratory (SRNL); <sup>2</sup>University of South Carolina (USC); <sup>3</sup>Georgia Institute of Technology

Membrane separations are a key enabling technology for future energy conversion devices. In this study, the model proton conducting system "SrCe<sub>0.95</sub>Yb<sub>0.05</sub>O<sub>3</sub>" was produced by conventional mixed oxide ceramic techniques and a chemical solution route to i) alter the microstructure and explore ii) second phase additions consisting of conductive oxide or metallic elements to enhance electronic conductivity. Microstructural modification was performed by using Spark Plasma Sintering (SPS) in order to densify

WEDNESDAY PM

crystalline material without the grain growth associated with conventional sintering. Dual phase ionic and electronic conductive materials were fabricated from conventionally processed SrCe<sub>0.95</sub>Yb<sub>0.05</sub>O<sub>3</sub> and metallic additions of noble metals palladium (Pd) and (Rh). In addition, calculations using Density Functional Theory (DFT) in model proton conducting ceramics were performed to understand the role of defects and structure on proton transport. The results obtained will be discussed in terms of applications as gas separation membranes in commercial and nuclear arenas.

### 3:00 PM

**Ternary CuPdM Alloys for Hydrogen Separation Membranes:** *Rongxiang Hu*<sup>1</sup>; Michael Gao<sup>1</sup>; Ömer Dogan<sup>2</sup>; Bret Howard<sup>2</sup>; Bryan Morreale<sup>2</sup>; <sup>1</sup>URS at National Energy Technology Laboratory; <sup>2</sup>National Energy Technology Laboratory

CuPd alloys are among the most promising candidate materials for hydrogen separation membranes and membrane reactor applications due to their high hydrogen permeability. In order to reduce the Pd content and, therefore, the cost of the membrane materials, efforts have been initiated to develop CuPdM ternary alloys having a bcc structure. Searching for alloying elements is done using first principles electronic density functional theory calculations. Potential ternary alloys are synthesized via arc melting, followed by a homogenization heat treatment and equilibrium annealing. The phase stability and bcc phase boundary in Cu-Pd-M systems are investigated by microstructural observation (Optical microscopy and SEM), thermal analysis, and XRD. Finally, the hydrogen permeability of promising alloys is determined.

### 3:20 PM

**Electrodeposition of ZnO Nanocrystallines on ITO Mesoporous Films and Application to Photoelectrochemical Cells:** *Haining Chen*<sup>1</sup>; Liqun Zhu<sup>1</sup>; Weiping Li<sup>1</sup>; Huicong Liu<sup>1</sup>; <sup>1</sup>Beihang University, Key Laboratory of Aerospace Materials and Performance (Ministry of Education), School of Materials Science and Engineering

ZnO nanocrystallines doped indium-tin-oxide (ITO) mesoporous films were prepared by electrodepositing ZnO nanocrystallines on ITO mesoporous films in the electrolyte of 0.1 M Zn(NO<sub>3</sub>)<sub>2</sub>. To function as a photoelectrode, the CdS quantum dots as sensitizers were synthesized on the surface of ZnO nanocrystallines doped ITO mesoporous films. Both SEM and TEM images showed that ZnO nanocrystallines were successfully electrodeposited on the ITO mesoporous films. XRD pattern and selective area electron diffraction pattern revealed that the ZnO nanocrystallines were hexagonal (wurtzite) phase. The results of UV-Vis adsorption spectra analysis demonstrated that absorbance in visible region was enhanced with the deposition of ZnO and CdS on ITO mesoporous films. Photocurrent-voltage measurement results indicated that the ITO mesoporous film/ZnO/CdS photoelectrodes were efficient as a working electrode and its performance was superior to that of ITO mesoporous film/CdS photoelectrodes because of the suppression of recombination by ZnO coating.

### 3:40 PM Break

### 3:50 PM

**Catalysts Decorated ZnO/Si Branched Nano-heterostructure Electrodes for Solar Water Splitting:** *Ke Sun*<sup>1</sup>; Kristian Madsen<sup>1</sup>; Khaleda Banu<sup>1</sup>; Deli Wang<sup>1</sup>; <sup>1</sup>University of California, San Diego

Si is low-cost, abundant, and most broadly used for both electronics and photovoltaics. Nanostructure-enabled alternative renewable energy solutions promise high conversion efficiencies and low-cost, particularly for photoelectrochemical cells (H<sub>2</sub> generation from solar energy using semiconductor photoelectrodes). In this application, advantages, such as gigantic surface area-to-volume ratio and large solid/liquid interface, nanoscale hetero-epitaxy and band engineering, enhanced light absorption, etc., are exhibited from nanostructured photoelectrodes. We recently applied low-cost solution-based techniques to integrate ZnO nanowires (NW) to SiNW arrays forming a branched NW photocathode. This interesting structure provides improved performances for H<sub>2</sub> production compared to SiNW-based photoelectrode, mainly due to the increased absorption,

enhanced charge generation, and improved electron transportation. In this work, additive photocatalysts including semiconductor quantum dots or metal nanoparticles, are applied to ZnO/SiNW heterostructures through a cost-effective scalable electrodeposition or a spray electropyrolysis method. Photocatalytic activities are investigated, targeting further enhancement of photoelectrochemical responses and suppression of corrosion.

### 4:10 PM

**Competitive Adsorption of CO<sub>2</sub> from Binary Gas Mixtures in a Structurally Dynamic Porous Coordination Polymer:** *Kristi Kauffman*<sup>1</sup>; Jeffrey Culp<sup>2</sup>; Angela Goodman<sup>1</sup>; Thomas Brown<sup>1</sup>; Mark Bernardo<sup>1</sup>; Russell Pancoast<sup>1</sup>; Christopher Matranga<sup>1</sup>; <sup>1</sup>National Energy Technology Laboratory; <sup>2</sup>URS

Porous-Coordination-Polymers (PCPs), commonly referred to as Metal-Organic-Frameworks, are highly crystalline and exhibit large surface areas and pore volumes. They have attracted much attention for gas storage and separation applications. Yet, because measuring adsorption from mixtures is technologically challenging, most studies focus on single-component gases or simulations. Traditional gravimetric/volumetric methods cannot easily discriminate between gases in mixtures and are ineffective for evaluating gas selectivity. Here, we report a new method using Fourier-transform infrared spectroscopy (FTIR) and headspace Gas Chromatography (GC) to analyze adsorption from binary gas mixtures (CO<sub>2</sub>/N<sub>2</sub>, CO<sub>2</sub>/CH<sub>4</sub>, and CO<sub>2</sub>/N<sub>2</sub>O) in a flexible PCP, catena-bis(dibenzoilmethanato)-(4,4'-bipyridyl)nickel(II), (NiDBMBpy). We evaluated the isothermal adsorption of infrared-active gases into the NiDBMBpy sorbent bed at elevated pressures using FTIR. GC analysis was applied to determine the headspace composition following adsorption. NiDBMBpy preferentially adsorbs CO<sub>2</sub> over N<sub>2</sub> and CH<sub>4</sub> but CO<sub>2</sub> and N<sub>2</sub>O are adsorbed equally. This trend is confirmed by both independent analytical techniques.

### 4:30 PM

**Direct Deposition of Nanostructured Platinum Cluster on Gas Diffusion Layer for Highly Durable Polymer Electrode Membrane Fuel Cell (PEMFC):** *Hyun-Jong Kim*<sup>1</sup>; Ji-Eun Ahn<sup>1</sup>; Ho Nyun Lee<sup>1</sup>; Myung Keun Han<sup>1</sup>; Hong Kee Lee<sup>1</sup>; <sup>1</sup>Korea Institute of Industrial Technology

In this study, electrodeposition of platinum cluster was investigated, and especially the pulsed electro-deposition (PED) technique was found to be a versatile method for the preparation of nanostructured Pt deposits due to its simple operation, high purity of deposits, and improvement of energy density per volume. The pulse electro-deposition processes created the nanostructured Pt cluster directly on the surface of gas diffusion layer (GDL). By localizing platinum on the surface of a gas diffusion layer (GDL), it is possible to decrease the thickness of the catalyst layer and increase the efficiency of platinum usage. Experimentally, the Pt cluster was well dispersed in GDL and composed of Pt nanosheet. The growth mechanism was carefully monitored. By increasing the current density for pulse electrodeposition, the size of Pt cluster decreased, result in the enhancement of ESA. And, all showed very promising results.

### 4:50 PM

**Optimization of the Concentrated V(IV)/V(V) Electrolytes in a Vanadium Redox Battery:** *Feng Shi*<sup>1</sup>; Huimin Lu<sup>1</sup>; Yuan Yuan<sup>1</sup>; <sup>1</sup>Beihang University

The higher vanadium concentration is required to reduce the size and weight of the battery and the main limitation for the vanadium electrolyte concentration is the precipitation of V(IV) ion. In this paper, the electrode process of concentrated V(IV) species has been studied at a Pt electrode using cyclic voltammetry and linear polarization techniques. The results have revealed that the solubility of VOSO<sub>4</sub> decreases continuously with increasing H<sub>2</sub>SO<sub>4</sub> concentration. In 2mol/l VOSO<sub>4</sub> solution containing 3mol/l H<sub>2</sub>SO<sub>4</sub>, the V(IV) electrolyte has the highest peak current and the best reversibility. Adding alkali metal sulfates and organics, the additive effect on the electrolyte properties was discussed and the electrode process was investigated. The results indicate that the hydrophilic organics improve the stability of V(IV)/V(V) species, the alkali metal sulfates elevate the peak



current a little, and there is no adverse effect of the additives on the redox reaction in vanadium sulfate solution.

#### 5:10 PM

**Thermo-mechanical Reliability of Proton Exchange Membranes in Fuel Cells:** *Ruiliang Jia*<sup>1</sup>; Binghong Han<sup>1</sup>; Takuya Hasegawa<sup>2</sup>; Jiping Ye<sup>3</sup>; Reinhold Dauskardt<sup>1</sup>; <sup>1</sup>Stanford University; <sup>2</sup>Nissan Motor Co., Ltd.; <sup>3</sup>NISSAN ARC LTD.

Nafion perfluorosulfonic acid (PFSA) polymer thin films are currently the most popular material for proton exchange membranes in PEM fuel cells. A common failure mode that limits the operational life of fuel cells involves the mechanical degradation of the membranes. In the present work, we describe a number of thin film testing methods to characterize the mechanical and fracture properties of PFSA membranes under simulated fuel cell operational environments. Moreover, the role of the PFSA molecular structure together with selected composite forms made with the addition of oxide particles on mechanical and fracture behavior is demonstrated. The study not only reveals significant factors that influence the mechanical behavior and fracture properties of PFSA membranes in operation, such as water diffusion, foreign cation contamination and chemical degradation, but also investigates methods to improve thermo-mechanical reliability for fuel cell applications.

#### Microstructural Processes in Irradiated Materials: Nanostructured Alloys, Mechanical Properties

*Sponsored by:* The Minerals, Metals and Materials Society, TMS Structural Materials Division, TMS/ASM: Nuclear Materials Committee

*Program Organizers:* Gary Was, University of Michigan; Thak Sang Byun, Oak Ridge National Laboratory; Shenyang Hu, Pacific Northwest National Laboratory; Dane Morgan, UW Madison; Yasuyoshi Nagai, Tohoku University

Wednesday PM

Room: 3

March 2, 2011

Location: San Diego Conv. Ctr

*Session Chairs:* Robert Odette, University of California Santa Barbara; Peter Hosemann, University of California Berkeley

#### 2:00 PM Invited

**Radiation Response of Nanostructured Ferritic Steels to High Dose Ion Irradiation:** *Michael Miller*<sup>1</sup>; Yanwen Zhang<sup>1</sup>; <sup>1</sup>Oak Ridge National Laboratory

The microstructures of a 14YWT nanostructured ferritic steel in the unirradiated state and after several high dose ion irradiations have been characterized by atom probe tomography in order to evaluate the radiation response of this material. The ultrafine Ti-, Y- and O-enriched nanoclusters were found to be present in the ferrite matrix in high number densities from doses between 3 and 450 displacements per atom (dpa). The microstructural changes that occur at these nanoclusters and at grain boundaries during ion irradiation will be discussed in detail with particular emphasis on the solute distributions in the vicinity of these microstructural features. This research was sponsored by the U.S. Department of Energy, Materials Sciences and Engineering Division. Research at the Oak Ridge National Laboratory SHaRE User Facility is sponsored by the Scientific User Facilities Division, Office of Basic Energy Sciences, U.S. Department of Energy.

#### 2:40 PM

**On the Stability of Nanofeatures in Nanostructured Ferritic Alloys – the Effects of Long Term High Temperature Thermal Aging and Friction Stir Welding:** *Nicholas Cunningham*<sup>1</sup>; Auriane Etienne<sup>1</sup>; Yuan Wu<sup>1</sup>; Doug Klingensmith<sup>1</sup>; G. Robert Odette<sup>1</sup>; Erin Haney<sup>1</sup>; Erich Stergar<sup>1</sup>; <sup>1</sup>UC Santa Barbara

Nano-structured ferritic alloys (NFAs) have high tensile and creep strength permitting service up to 800°C or more, manifest remarkable resistance to radiation damage and can manage high concentrations of helium. These outstanding properties derive from an ultrahigh density of Ti-Y-O enriched

nano-features (NFs) that provide dispersion strengthening, help stabilize dislocation and fine grain structures, reduce excess concentrations of displacement defects by enhancing vacancy-self-interstitial recombination and trap helium in fine, and relatively harmless, bubbles. We present multi-technique characterization studies demonstrating the remarkable stability of the NFs during long-term thermal aging (e.g., for >19kh at 1000°C) and after severe plastic deformation experienced in friction stir welding (FSW). The characterization tools include atom probe tomography (APT), small angle neutron scattering (SANS), transmission electron microscopy (TEM), and micro-hardness. The various techniques are generally consistent with one another and with finite but modest decreases observed in microhardness of ~10% (aging) and 20% (FSW).

#### 3:00 PM

**Atomistic Studies on Y-Ti-O Nanoclusters in Ferritic Alloys:** *Lauren Marus*<sup>1</sup>; Hyon-Jee Voigt<sup>1</sup>; Brian Wirth<sup>2</sup>; <sup>1</sup>University of California-Berkeley; <sup>2</sup>University of Tennessee-Knoxville

Nanostructured ferritic alloys demonstrate high creep strength and irradiation resistance in high temperature irradiation environments of interest for advanced nuclear energy systems. The presence of a high number density of Y-Ti-O nanometer scale clusters (NCs) is responsible. However, the structure and composition of the NCs are not yet well understood. Through the systematic atomistic simulations we are beginning to understand and prioritize the effects of magnetism, strain energy, and vacancy and solute concentrations on the NCs. Interaction potentials are obtained by ab initio calculations of Fe-Y-Ti-O alloys. Lattice Monte Carlo (LMC) and off-lattice techniques have been used to simulate NC precipitation within the iron lattice. These results provide insight into features and necessary conditions for NC formation and are compared with available experimental data, although the modeling assumptions do have a substantial impact on the predicted NC structure.

#### 3:20 PM

**HRTEM Study of Oxide Nanoparticles in Fe-Cr MA/ODS Steels:** *Luke Hsiung*<sup>1</sup>; Micheal Fluss<sup>1</sup>; <sup>1</sup>Lawrence Livermore National Laboratory

Structures of oxide nanoparticles in MA956, MA957, and K3 ODS steels produced by a mechanical alloying (MA) method have been studied using high-resolution transmission electron microscopy techniques to better understand the formation mechanism of oxide nanoparticles in ODS steels. Partially crystallized nanoparticles with a core/shell structure were frequently observed in all three ODS steels. While the crystalline nanoparticles in K3 and MA956 steels are mainly Y4Al2O9, those in MA957 steel are mainly Y2TiO5 and Y2Ti2O7. HRTEM observations of crystalline nanoparticles larger than ~2 nm and amorphous or disordered cluster-domains smaller than ~2 nm provide us an insight into the formation mechanism of oxide nanoparticle in MA/ODS steels, which involves fragmentation, amorphization, and recrystallization. This work was performed under the auspices of the U.S. Department of Energy by Lawrence Livermore National Laboratory under Contract DE-AC52-07NA27344.

#### 3:40 PM Break

#### 4:00 PM

**Radiation Response the Nanostructured Ferritic Alloy 14YWT to High Dose Irradiation:** *Alicia Certain*<sup>1</sup>; Jim Bentley<sup>1</sup>; Shuttha Shutthanandan<sup>2</sup>; David Hoelzer<sup>3</sup>; Todd Allen<sup>1</sup>; <sup>1</sup>University of Wisconsin-Madison; <sup>2</sup>Pacific Northwest National Laboratory; <sup>3</sup>Oak Ridge National Laboratory

Ferritic–martensitic (F/M) alloys are expected to play an important role as cladding or structural components in Generation IV and other advanced nuclear systems operating in the temperature range 350–700°C and to doses up to 200 displacements per atom (dpa). Nanostructured ferritic alloys (NFA) have been developed to operate at higher temperatures than traditional F/M steels. These steels contain nanometer-sized Y–Ti–O nanoclusters for additional strengthening. Heavy ion irradiations have been performed on 14YWT up to 100 dpa at two temperature ‘extremes’ (-75°C and 60 °C) in order to evaluate the stability of the nanoclusters at high doses. Energy-

filtered transmission electron microscopy (EFTEM) has been used to analyze the evolution of the nanoclusters post-irradiation.

**4:20 PM**

**Microstructural Evolution by Helium Irradiation and Its Desorption in ODS Alloy:** Jinsung Jang<sup>1</sup>; Yitao Yang<sup>2</sup>; Hyung-Ha Jin<sup>1</sup>; Suk-Hoon Kang<sup>1</sup>; Chonghong Zhang<sup>2</sup>; <sup>1</sup>Korea Atomic Energy Research Institute; <sup>2</sup>Institute of Modern Physics, CAS

Due to the superior thermal creep properties and the high resistance to neutron irradiation, oxide dispersion strengthened (ODS) steels are considered as potential candidate alloys for high temperature applications in advanced nuclear or fusion reactor. The accumulation of helium after neutron irradiation has a substantial influence on the mechanical properties and it would be of technical importance to understand the helium behavior and its consequences in the microstructure. In this work, lower energy helium ions are implanted into a commercial ODS alloy (MA956TM) samples with different fluences. Thermal helium desorption spectroscopy (THDS) and transmission electron microscopy (TEM) are used to study the helium irradiation and its release behavior, corresponding evolution of cavities, and surface morphology of the samples at different helium concentrations. For comparison, a high Cr steel will be also considered. \* MA956TM is a trademark of SMC (Special Metals Corporation).

**4:40 PM Invited**

**Nano-Mechanical Testing and Post Testing Investigation on Ion Beam Irradiated Single Crystal Cu:** Peter Hosemann<sup>1</sup>; Daniel Kiener<sup>2</sup>; Stuart Maloy<sup>3</sup>; Osman Anderoglu<sup>3</sup>; Eric Olivas<sup>3</sup>; Yongqiang Wang<sup>3</sup>; <sup>1</sup>UC Berkeley; <sup>2</sup>University of Leoben; <sup>3</sup>LANL

Ion beam irradiation is widely used to study the effects of radiation on structural materials. In this work we performed proton irradiation (1dpa, 150°C) on single crystal Cu. Before and after proton irradiation, in-situ nanoscale compression tests in a transmission electron microscope were performed to evaluate the mechanical properties of the irradiated material. It was found that the nano pillars changed their deformation behavior fundamentally after irradiation and behaved more bulk like. The failure of the irradiated pillars was strongly localized. In addition, to gain bulk like data for comparison to the nano compression tests and to validate the method of cross-sectional nano indentation on ion beam irradiated materials, nanoindentation experiments were carried out on 10µm deep irradiated single crystal Cu. It was found that the hardness data followed the irradiation profile. Moreover, the deformed area underneath different indents was examined using TEM.

**5:20 PM**

**Point Defect Mediated Radiation Induced Creep in Nano-Crystalline Metal:** Yvon Ashkenazy<sup>1</sup>; Tai Kai-Ping<sup>1</sup>; Pascal Bellon<sup>1</sup>; Robert Averback<sup>1</sup>; <sup>1</sup>University of Illinois at Urbana Champaign

Various mechanisms, such as Stress Induced Preferential Nucleation (SIPN) and Stress Induced Preferential Absorption (SIPA) have been proposed in the past to account for radiation induced creep (RIC). Here we consider a new mechanism of for RIC in irradiated nanocrystalline materials. The different time scales involved in creep and radiation damage present a challenge in simulating them in unison. We use a new simplified atomistic model or describing RIC. The model is based on introducing defects at grain boundaries and simulating short-time relaxations. A similar model was used successfully for simulating radiation induced viscous flow [PRL 90,055505(2003)]. We compare the resulting RIC rates for copper with those measured by a bulge test and show reasonable agreement. We further show that neither SIPN or SIPA are required. Using the same methods we explore the origins of lowered RIC rates caused by introducing of precipitates at quad-points.

**5:40 PM**

**Stress, Temperature, and Dose Rate Dependence of Proton Irradiation Creep of Ferritic-Martensitic Steel T91:** Cheng Xu<sup>1</sup>; Gary Was<sup>1</sup>; <sup>1</sup>University of Michigan

Developing an understanding of irradiation creep in ferritic martensitic steels has become a major objective for the fuel cladding and core

internal design of the next generation sodium fast reactor. The in-situ irradiation creep apparatus at the Michigan Ion Beam Laboratory has been benchmarked against existing literature through thermal creep experiments. Through single variable change experiments, the dose rate dependence, stress dependence, and temperature dependence of irradiation creep for T91 were determined. Results show that the creep rate varies linearly with the dose rate, as expected. TEM was used to quantify the dislocation network and loop densities of T91 after irradiation creep and provide insight into the possible mechanisms driving irradiation creep of T91. Results of the creep experiments and the microstructure of the crept samples will be presented in the context of possible creep mechanisms.

## Neutron and X-Ray Studies of Advanced Materials IV: Dislocations, Strains and Stresses II

*Sponsored by:* The Minerals, Metals and Materials Society, TMS Structural Materials Division, TMS/ASM: Mechanical Behavior of Materials Committee, TMS: Chemistry and Physics of Materials Committee

*Program Organizers:* Rozaliya Barabash, Oak Ridge National Laboratory; Xun-Li Wang, Oak Ridge National Laboratory; Jaimie Tiley, Air Force Research Laboratory; Peter Liaw, The University of Tennessee; Erica Lilleodden, GKSS Research Center; Brent Fultz, California Institute of Technology; Y-D Wang, Northeastern University

Wednesday PM  
March 2, 2011

Room: 10  
Location: San Diego Conv. Ctr

*Session Chairs:* Karen Pantleon, Denmark Technical University; Phil Ryan, APS

**2:00 PM Keynote**

**In-Situ Laue Diffraction of Deforming Mo Pillars:** Helena Van Swygenhoven<sup>1</sup>; Julien Zimmermann<sup>1</sup>; Steven Van Petegem<sup>1</sup>; Cecile Marichal<sup>1</sup>; Daniel Grolmund<sup>1</sup>; Hongbin Bei<sup>2</sup>; Hongbin Bei<sup>2</sup>; Michael Weisser<sup>1</sup>; <sup>1</sup>Paul Scherrer Institut; <sup>2</sup>Oak Ridge National Laboratory

In-situ Laue diffraction is applied during compression of bcc single crystals. Pillars of 1 micron diameter are obtained from a directionally solidified (DS) NiAl-Mo eutectic grown. DS Mo pillars in as-grown and pre-strained conditions, as well as DS pillars treated with FIB are investigated. To obtain free standing single pillars for Laue analysis, a special specimen preparation procedure was developed [Scripta Mat. 62 (2010) 746]. Among the results presented will be the macroscopic yield stress in as-prepared DS, pre-deformed and FIBed pillars and its relation to the mobility of screw dislocations, the character of the activated slip planes i.e. (112) and (110) planes, the difference in initial dislocation structure between pillars obtained from a deformed composite and pillars that are compressed free standing starting from the DS pillars, the formation of substructures in pillars compressed till high strains and the influence of FIB on the deformation behavior.

**2:25 PM Invited**

**Depth-Resolved Phase Identification and Internal Stress Analysis after High Temperature Corrosion in Power Plants:** Karen Pantleon<sup>1</sup>; <sup>1</sup>Technical University of Denmark

During long-term high temperature exposure of superheater tubes in power plants various oxides are formed on the inner side (steamside) of the tubes and oxide spallation is a serious problem, because it causes blockage of loops and, consequently, overheating and failure due to insufficient steam flow. Instead of laboratory studies just mimicking the actual conditions in the power plant for simplified sample geometries, rather the investigation of real plant exposed tubes is essential for understanding phase transformations and stress evolution as a function of operating conditions, material influences and real sample geometries. Although X-ray diffraction including grazing incidence and microdiffraction techniques on real industrial samples is not straightforward, the present work demonstrates the need of those

measurements. Depth-resolved phase analysis and phase-dependent stress analysis in the inner side of superheater tubes considerably contributed to understanding high temperature corrosion in power plants and allow evaluation of the risk of oxide spallation.

#### 2:45 PM Invited

**Developing Links Between the Microstructure and Lattice Strain Uncertainties:** Jay Schuren<sup>1</sup>; Matthew Miller<sup>1</sup>; Alexander Kazimirov<sup>1</sup>; <sup>1</sup>Cornell University

Even though failure mechanisms such as yielding and fracture initiate on the scale of the individual crystal, most life prediction models for polycrystals continue to be formulated on macroscale. Enormous opportunities exist, therefore, in the area of micromechanical testing of engineering materials to close this gap. In conjunction with the Cornell High Energy Synchrotron Source, we have developed a method for measuring lattice strain pole figures on deforming samples using synchrotron x-rays. This talk describes recent efforts focused on quantifying the link between each lattice strain measurement and the material microstructure. In particular we have found that experimental uncertainty is intimately linked to microstructure. In addition, we present a method for using grain size, texture measurements, and the range of specimen orientations to design in-situ loading / high energy x-ray diffraction experiments. We demonstrate the method on monotonic and cyclic loading of AA7075 aluminum and nickel-base superalloys.

#### 3:05 PM Invited

**Full Local Elastic Strain Tensor from Laue Microdiffraction: A White-Beam Method to Measure the Lattice Expansion:** Odile Robach<sup>1</sup>; Jean-Sébastien Micha<sup>2</sup>; Olivier Ulrich<sup>1</sup>; Patrice Gergaud<sup>3</sup>; <sup>1</sup>CEA-Grenoble / INAC; <sup>2</sup>CNRS / SPrAM UMR 5819; <sup>3</sup>CEA-Grenoble / LETI

In sample-scanning Laue microdiffraction, the local crystal orientation and local deviatoric strain tensor are obtained by illuminating the polycrystalline sample with a broadband "white" (5-30 keV) x-ray microbeam, and analyzing the spot positions in the resulting local Laue pattern. Mapping local lattice expansion is usually slower, due to the need to alternate between white and variable-energy monochromatic microbeam. A method was developed to measure lattice expansion in the white beam mode. The energy of one of the "side" diffracted beams of the grain of interest is measured using an energy-resolved point detector, while recording the Laue pattern on the "top" 2D detector. The experimental peak energy,  $E_{exp}$ , is therefore measured simultaneously with  $E_{theor}(HKL)$ , the theoretical peak energy for zero lattice expansion. In several cases, this leads to an improved accuracy on  $da/a = -(E_{exp}-E_{theor})/E_{theor}$  compared to the monochromatic beam method, as incertitude on beam position is avoided.

#### 3:25 PM Invited

**X-Ray Diffraction Evaluation of the Hardening State of Various Cubic and Hexagonal Materials after Large Strains:** Brigitte Bacroix<sup>1</sup>; Thierry Chauveau<sup>1</sup>; Guy Dirras<sup>1</sup>; Olivier Castelnaud<sup>2</sup>; Renald Brenner<sup>1</sup>; Akrum Abdul-Latif<sup>3</sup>; Christophe Le Bourlot<sup>1</sup>; Aurélie Wauthier<sup>1</sup>; <sup>1</sup>CNRS - LPMTM; <sup>2</sup>CNRS - PIMM; <sup>3</sup>SUPMECA - LISMM

A high resolution X-Ray Diffraction technique, developed in our laboratory, enables us to characterize in some details the deformed state and especially to estimate, from the shape of the peaks measured within individual texture components, the dislocation density as well as the size of the formed subgrains / dislocation cells as a function of plastic strain and orientation. Some data recently obtained on several materials (Al, Fe, Mg and Zr) after different loading paths (severe deformation or classical rolling process) are presented and analyzed in some details and the comparison of these data with some calculations performed with advances micromechanical models enables us to identify the hardening, softening and fragmentation mechanisms operating in each case.

#### 3:45 PM Invited

**Extending Line Profile Analysis to Neutron Diffraction:** Tamás Ungár<sup>1</sup>; <sup>1</sup>Eötvös University Budapest

X-ray line profile analysis is a powerful tool for characterizing the microstructure of crystalline materials in terms of (i) grain size, (ii)

dislocation structure and (iii) planar defects either in bulk polycrystalline samples or on the single grain level. The angular or spatial resolution of recently commissioned neutron beamlines at spallation neutron sources open up new scopes for the characterization of microstructures by the method of neutron line profile analysis. The challenges and possibilities provided by neutron line profile analysis will be discussed on the basis of first experimental results.

#### 4:05 PM

**Comprehensive Characterization of the Effects of Composition, Temperature, Flux and Fluence on the Evolution of Cu-Mn-Ni Precipitates in Reactor Pressure Vessel Steels:** G. Robert Odette<sup>1</sup>; Nicholas Cunningham<sup>1</sup>; Brian Wirth<sup>2</sup>; Matthew Alinger<sup>3</sup>; Takuya Yamamoto<sup>1</sup>; Doug Klingensmith<sup>1</sup>; <sup>1</sup>UC Santa Barbara; <sup>2</sup>UC Berkeley; <sup>3</sup>GE Global Research

Irradiation embrittlement of RPV steels is caused by radiation enhanced solute diffusion driven accelerated evolution of Cu (CRPs) and Mn-Ni (MnPs) rich precipitates, along with defect-solute complexes. A large SANS database on the effects of metallurgical (Cu, Mn, Ni and P) and irradiation (temperature, flux and fluence) variables on the evolution of the precipitate size, number density, volume fraction and composition is presented. The volume fractions of the precipitates increase with the alloy Cu, Mn and Ni contents. At high Mn and Ni levels the precipitates contain more Mn and Ni than Cu; and Mn-Ni-Si precipitates can form even in Cu free steels. The number densities and volume fractions of precipitates generally decrease with increasing temperature. The precipitate volume fractions increase with increasing fluence and decreasing flux. The fluence dependence of the precipitation often manifests stages of nucleation, growth and coarsening. Increasing flux delays precipitation to higher fluence.

#### 4:15 PM Invited

**Study of Precipitate and Recrystallization in Ti-Added Low Carbon Steels by SANS:** Baek Seok Seong<sup>1</sup>; <sup>1</sup>KAERI

SANS is very powerful tool to understand the precipitation on the recrystallization behavior in low carbon steels. The recrystallization temperature of the higher Ti-added is higher than that of the lower Ti-added steel. SANS measurements were performed both for cold rolled samples and for annealed samples. The size distribution and the volume fraction of the nano-sized precipitates were determined using a direct model fitting with a sphere. SANS results revealed no additional carbo-nitrides precipitation during the recrystallization annealing procedure in the low Ti-added steel. However, in higher Ti-added steel, new TiC precipitates, with a size range of several nm to several tens of nms, form during the recrystallization annealing process. This dynamic interaction of the precipitation of fine TiC particles with the recovery of dislocations seems the primary source of the retardation of the recrystallization in the higher Ti-added low carbon steel.

#### 4:35 PM Break

#### 4:45 PM Invited

**Nanostructure of Surrogate Nuclear-Reactor Pressure Vessel Steels:** Davor Balzar<sup>1</sup>; <sup>1</sup>University of Denver

It is believed that the embrittlement of ferritic steels used in nuclear-reactor pressure vessels is caused by formation of small (1-2 nm) copper-rich precipitates (CRPs). Small CRPs are coherent with the bcc matrix, which causes local matrix strain and interaction with the dislocation strain fields, thus impeding dislocation mobility. As CRPs grow, at some critical size the bulk crystal structure of copper (fcc) is achieved, the CRPs are no longer coherent with the matrix, and the matrix strain is relieved. We prepared a series of surrogate low-alloy ferritic-steel specimens. SANS measurements showed that the precipitate size distribution broadens and shifts toward larger sizes as a function of annealing time. Diffraction line broadening analysis showed that the strain-related broadening dominated and correlated with mechanical hardness and precipitate volume fraction, as determined from the SANS measurements. A model of strain broadening was developed to explain these results.



5:05 PM

**Microstructure of MgGeO<sub>3</sub> Post-Perovskite at 84 GPa Determined by 3D X-Ray Diffraction:** *Gabor Ribarik*<sup>1</sup>; *Carole Nisr*<sup>2</sup>; *Tamás Ungár*<sup>1</sup>; *Gavin Vaughan*<sup>3</sup>; *Patrick Cordier*<sup>2</sup>; *Sebastien Merkel*<sup>2</sup>; <sup>1</sup>Eotvos Lorand University, Institute of Physics, Budapest, Hungary; <sup>2</sup>Université Lille 1; <sup>3</sup>European Synchrotron Research Facility

MgGeO<sub>3</sub> post-perovskite is a lower pressure analogue of MgSiO<sub>3</sub>, the major mineral in Earth's D'' layer. Plastic deformation has an important role for convection in the Earth's mantle. Moreover, observations of seismic anisotropy are likely linked to anisotropic lattice defects, like dislocations. A recently developed 3D X-ray diffraction technique was used at the ID11 beamline of ESRF to extract the microstructure of individual grains in a polycrystalline aggregate of post-perovskite samples. A special geometry was used to measure high resolution single crystal peak profiles. The dislocation structure of MgGeO<sub>3</sub> was determined by X-ray line profile analysis. Our results suggest <110> glide in {110} or (001) and [010](001) as the most probable slip systems for this material, with a smaller contribution of [100] and [001] dislocations types. The results are compared to the most probable slip systems based on the magnitude of the Peierls stress, determined by numerical simulations.

5:20 PM

**Influence of Recrystallization Texture on Tensile Behavior of Friction Stir Processed Magnesium Alloy:** *Zhenzhen Yu*<sup>1</sup>; *Hahn Choo*<sup>1</sup>; *Zhili Feng*<sup>2</sup>; *Ke An*<sup>2</sup>; <sup>1</sup>University of Tennessee; <sup>2</sup>Oak Ridge National Laboratory

In order to investigate the influence of thermo-mechanical input during friction stir processing (FSP) on the resulting texture and tensile behavior in an AZ31B Mg alloy, a series of FSP were conducted by varying its key parameters, i.e., rotation and travel rates of the weld processing tool. Neutron diffraction texture measurements show that, with the systematic changes in the thermo-mechanical input factor, there is corresponding changes in crystallographic texture that correlates well with the expected changes in deformation and recrystallization mechanisms. In order to investigate the influence of texture changes on tensile behavior of the stir zone (SZ), in-situ neutron diffraction tensile test along the longitudinal direction of the Mg plate was conducted on subsize tensile samples machined from the SZ of FSP plates. Tensile behavior showed dramatic changes in the strength and ductility in a way consistent with the changes in the FSP textures and the dominant deformation mechanisms.

5:30 PM

**Investigation of Microstrain near the Fracture Surface in the Tensile-Overloaded Corrosion Resistant Hastelloy C-2000 Alloy:** *Gabor Csizsar*<sup>1</sup>; *Soo Yeol Lee*<sup>2</sup>; *Tamas Ungar*<sup>1</sup>; *Peter K. Liaw*<sup>2</sup>; *Lee M. Pike*<sup>3</sup>; <sup>1</sup>Eötvös University Budapest; <sup>2</sup>The University of Tennessee; <sup>3</sup>Haynes International, Inc.

Fatigue-crack-propagation experiments following a tensile overload were carried out on compact-tension specimens of the corrosion-resistant Hastelloy C-2000 alloy. After the tensile overload, a large crack-growth retardation phenomenon was observed. In this work, the fracture surfaces of the fatigue-tested samples were studied by high-resolution X-ray diffraction for the purpose of line profile analyses. The X-ray beam was the size of 0.2 x 2 mm enabling the spatial resolution with 0.5 micron step size. Electron microscopy reveals about 5 nm coherent precipitates producing large coherency strains. The coherency strains are given in terms of dislocation densities determined by line profile analyses. The results are discussed in light of the overloading effect on the fatigue-crack-growth behavior.

5:45 PM

**Neutron Diffraction Studies of Intercritically Austempered Ductile Irons:** *Alan Druschitz*<sup>1</sup>; *Ricardo Aristizabal*<sup>1</sup>; *Edward Druschitz*<sup>1</sup>; *Camden Hubbard*<sup>2</sup>; *Thomas Watkins*<sup>2</sup>; *Larry Walker*<sup>2</sup>; *Mel Ostrander*<sup>3</sup>; <sup>1</sup>University of Alabama at Birmingham; <sup>2</sup>Oak Ridge National Laboratory; <sup>3</sup>Rex Heat Treat

Intercritically austempered ductile irons have a unique combination of excellent mechanical properties (particularly fatigue durability) and excellent manufacturing characteristics (excellent castability, low production energy requirements, reduced greenhouse gas emissions and excellent

machinability). In the present study, four different ductile iron alloys were produced using manganese and nickel as the primary austenite-stabilizing elements. The intercritical austenitizing temperatures were experimentally determined and two different heat treatments were performed on each alloy to obtain different quantities of austenite in the final microstructure. This paper reports the microstructures, phases present and tensile properties of these alloys. Further, lattice strains and diffraction elastic constants in various crystallographic directions and the transformation characteristics of the austenite as a function of applied stress were determined using neutron diffraction at the NRSF2 at the High Flux Isotope Reactor (HFIR) at Oak Ridge National Laboratory.

5:55 PM

**Analysis of the Initial Oxidation of Gamma-TiAl by Non-Destructive Ion Beam Analysis:** *Hans-Eberhard Zschau*<sup>1</sup>; *Michael Schütze*<sup>1</sup>; *Dechema e. V.*

The gamma-Titanium Aluminides are one of the most important materials in high temperature technology. This material can be protected against oxidation at high temperatures by a dense alumina scale using the so-called fluorine effect. The non-destructive ion beam analysis was applied to study the oxide layer composition of F-implanted gamma-TiAl during the heating process up to 1000°C. The depth profiles of O, Al and Ti obtained by the Rutherford Backscattering Spectrometry (RBS) show the formation of an initial thin (1 micrometer) alumina scale already after oxidation of 1h/800°C/air. The F-depth profiles measured with the Proton Induced Gamma-ray Emission (PIGE) reveal the F-loss during the heating process, whereas a relatively small amount of fluorine remains at the metal/oxide interface. The potential of both methods to establish a non-destructive quality assurance of the formed alumina scale is pointed out.

6:10 PM

**Crack Trafficking across Borders: Imaging Fatigue Crack Propagation In Situ at Grain Boundaries with Synchrotron Radiation:** *Naji Hussein*<sup>1</sup>; *Martina Zimmermann*<sup>2</sup>; *Clinique Brundige*<sup>1</sup>; *Jason Geathers*<sup>1</sup>; *Christopher Torbet*<sup>3</sup>; *Wah-Keat Lee*<sup>4</sup>; *Tresa Pollock*<sup>3</sup>; *J Jones*<sup>1</sup>; *Roy Clarke*<sup>1</sup>; <sup>1</sup>University of Michigan; <sup>2</sup>Universität Siegen; <sup>3</sup>University of California, Santa Barbara; <sup>4</sup>Argonne National Laboratory

Grain boundaries can form during the growth of single-crystal, nickel-base superalloys, and they are omnipresent in polycrystalline materials. Synchrotron x rays can produce quasi-three-dimensional, in-situ radiographs that reveal the micron-scale evolution of fatigue cracks through such grain boundaries. With a custom-built ultrasonic fatigue instrument operating at 20 kHz, we imaged crack propagation in thin microfoils under tension. The crack morphology at bicrystal grain boundaries depended on the load amplitude: cracks deflected by intergranular misorientation angles to remain on {111} planes at high amplitudes but became pinned to the grain boundaries at low amplitudes. In polycrystalline metals, cracks grew through or along grain boundaries depending on the orientation with respect to the load axis. In all cases, the crack growth rate decelerated, and then accelerated, when traversing a grain boundary. Accumulation of dislocations at the grain boundaries, mapped with rocking curves about Bragg angles, contribute to this change in growth rate.

6:20 PM

**Particle Size Analysis of Multimodal Gamma-Prime ( $\gamma'$ ) Distributions in an Advanced Polycrystalline Nickel-Base Superalloy by a Peak Broadening Approach:** *David Collins*<sup>1</sup>; *Howard Stone*<sup>1</sup>; <sup>1</sup>University of Cambridge

Diffraction line profile analysis can yield information on the structure, microstructure or micromechanics of materials. However, analysis of line profiles from materials with complex microstructures and multiple phases, particularly those that contain overlapping diffraction patterns, can be non-trivial. This is true of materials containing superlattice structures such as nickel-base superalloys. A theoretical diffraction pattern has been constructed for a nickel-base superalloy, accounting for the  $\gamma$  matrix and a trimodal distribution of  $\gamma'$  precipitates. Each  $\gamma'$  distribution was modelled independently, accounting for the differences in composition and therefore lattice parameters, along with the peak broadening from the particle

size within each distribution. With this model, it was demonstrated that multimodal precipitate size distributions in these alloys may not be reliably determined from diffraction line profile analysis. This was supported by measurements made of the nickel-base superalloy RR1000 using high resolution synchrotron X-ray diffraction.

## **Pb-Free Solders and Other Materials for Emerging Interconnect and Packaging Technologies: Interfaces and Electromigration**

*Sponsored by:* The Minerals, Metals and Materials Society, TMS Electronic, Magnetic, and Photonic Materials Division, TMS: Electronic Packaging and Interconnection Materials Committee  
*Program Organizers:* Indranath Dutta, Washington State University; Darrel Frear, Freescale Semiconductor; Sung Kang, IBM; Eric Cotts, SUNY Binghamton; Laura Turbini, Research in Motion; Rajen Sidhu, Intel Corporation; John Osenbach, LSI Corporation; Albert Wu, National Central Univ, Taiwan; Tae-Kyu Lee, Cisco Systems

Wednesday PM  
March 2, 2011

Room: 7B  
Location: San Diego Conv. Ctr

*Session Chairs:* Laura Turbini, Research In Motion; Polina Snugovsky, Celestica

### **2:00 PM Invited**

**Interfacial Reactions in the Sn-(Pb)/Ni-7wt%V Couples:** *Sinn-wen Chen*<sup>1</sup>; Yu-ren Lin<sup>1</sup>; Hsin-jay Wu<sup>1</sup>; Hong-ming Lin<sup>2</sup>; <sup>1</sup>National Tsing Hua University; <sup>2</sup>Tatung University

The interfacial reactions in the Sn-(Pb)/Ni-7.0wt%V couples are examined at temperatures varied from 210oC to 450oC, and the interfacial reaction mechanisms are proposed. Although Pb does not react with the Ni-7.0wt%V substrate, the Sn-(Pb)/Ni-7.0wt%V interfacial reactions are affected with the Pb addition. Unlike the reaction results in the Sn/Ni-7.0wt%V couples, the Ni<sub>3</sub>Sn<sub>4</sub> phase is formed in the early stage and the T phase is formed later in the Sn-40.0wt%Pb/Ni-V and Sn-90.0wt%Pb/Ni-V couples reacted at 210oC to 250oC. The T phase is formed first in the Sn-10.0wt%Pb/Ni-V couples and the results are similar to those in the Sn/Ni-V couples. A two distinguishable regions are observed in the T phase layer in the Sn/Ni-V couple reacted at 250oC. It is also observed that the region in the T phase layer adjacent to the solder is Ni-depletion layer and is primarily composed of fine grains of V<sub>2</sub>Sn<sub>3</sub> phase.

### **2:25 PM Invited**

**Fundamental Studies on Electromigration in Eutectic Sn-Based Solder Joints:** *Fu Guo*<sup>1</sup>; Guangchen Xu<sup>1</sup>; Ruihong Zhang<sup>1</sup>; Hongwen He<sup>1</sup>; <sup>1</sup>Beijing University of Technology

Electromigration (EM) induced failures have become a great threat with the miniaturization trend in microelectronic products. In practice, failure mechanisms of EM are associated with many factors such as Joule heating effects, thermomigration, and interfacial reactions, etc., hence the real root cause cannot be easily detected and understood. Therefore, fundamental studies by decoupling the complex failure modes using simply eutectic solders have become a necessity in an effort to advance a better understanding of the mechanisms of EM. This talk will summarize our recent progress in such efforts and present a critical overview of the basis of microstructural evolution, temperature evolution, and electrical resistivity evolution during current stressing. In addition, materials modification by introducing the alloying elements and reinforcing phases into the conventional solder alloys will be discussed to demonstrate their potential roles on retarding the EM process.

### **2:50 PM Invited**

**Effect of the Cu Thickness in Ti/Ni(V)/Cu under Bump Metallization on Interfacial Reaction and Mechanical Test of Sn<sub>3.0</sub>Ag<sub>0.5</sub>Cu Solder Joint:** I-Tai Wang<sup>1</sup>; Kai-Jheng Wang<sup>1</sup>; Chi-Yang Yu<sup>1</sup>; *Jenq-Gong Duh*<sup>1</sup>; <sup>1</sup>National Tsing Hua University

In the Ti/Ni(V)/Cu under bump metallization (UBM), the Sn-patch is observed in the Ni(V) layer after reflow and aging. The Sn-patch growth may cause the IMCs detaching from the interface of solder joint and then reduces the reliability. In this study, the Sn<sub>3.0</sub>Ag<sub>0.5</sub>Cu solder was reflowed on the Ti/Ni(V)/Cu UBM with various Cu thickness at 250 deg. C for 60 s, and then aged at 150 deg. C for various periods of duration. It was revealed that the Sn-patch growth could be controlled by increasing the Cu thickness in Ti/Ni(V)/Cu UBM. As a result, the mechanical property of SnAgCu solder joint with thick-Cu UBM was superior to that with thin-Cu UBM via a high-speed impact tester. The coupling factor in the Cu thickness of UBM and mechanical property of solder joint was discussed. Besides, the optimal Cu thickness in Ti/Ni(V)/Cu UBM was proposed.

### **3:15 PM**

**Electroless Fe-Ni under Bump Metallurgy for Solder Interconnects:** H. Zhou<sup>1</sup>; J. Guo<sup>1</sup>; *J. Shang*<sup>2</sup>; <sup>1</sup>Institute of Metal Research; <sup>2</sup>University of Illinois

Fe-Ni alloys are attractive Under Bump Metallurgy because of their excellent metallurgical stability against liquid and solid solder alloys. However, traditional Fe-Ni wrought alloys, such as Fe-42Ni, have shown poor wettability with liquid solders. In this study, electroless Fe-Ni alloys were prepared by overcoming the difference in the reduction potential between Fe<sup>2+</sup> and Ni<sup>2+</sup> and by preventing Fe<sup>2+</sup> from early oxidation. Electroless deposition of Fe-Ni alloys with high Fe concentrations was achieved on the copper substrate. The electroless Fe-Ni alloys were found to have excellent wettability, very slow reaction rates with liquid and solid solders, and excellent oxidation resistance.

### **3:35 PM Break**

### **3:45 PM**

**Effect of Solder Bump Heights on Cu Dissolution Rate in Pb-Free Flip Chip Solder Joints by Electromigration:** *Fan-Yi Ouyang*<sup>1</sup>; Pilin Liu<sup>1</sup>; Matt Pharr<sup>2</sup>; Kejie Zhao<sup>2</sup>; Zhigang Suo<sup>2</sup>; Intel Corporation; <sup>2</sup>Harvard University

Solder joint reliability has long been a concern in the microelectronic packaging industry. As microelectronic circuit dimensions continue to reduce, some reduction in package feature dimensions is also anticipated. To effectively use the limited space and meet the Z-height requirements in hand-held devices, dramatic change in package design and shrinkage of solder bump dimensions is expected. With continuing reduction on the dimension of solder bump, the volume fraction of intermetallic compound (IMC) due to Cu-Sn reaction will increase. This will change the physical properties and diffusion behavior inside the solder bump, thus making it more important to understand the mechanism of Cu dissolution in Sn-based solder. The Cu dissolution in Pb-free solder joint under electromigration will be discussed here. We will focus on the role of solder bump height on Cu dissolution rate. A theory will also be proposed on relationship between Cu dissolution rate and solder bump height.

### **4:05 PM**

**Effects of Cu-Bearing Flux on Sn-3.5Ag Soldering with Electroless Ni-P/Au Surface Finish: Microstructure and Joint Reliability:** *Hitoshi Sakurai*<sup>1</sup>; Keun-Soo Kim<sup>1</sup>; Youichi Kukimoto<sup>2</sup>; Katsuaki Sukanuma<sup>1</sup>; <sup>1</sup>Osaka University; <sup>2</sup>Harima Chemicals, Inc.

The microstructure and joint reliability for Sn-3.5Ag soldering on an electroless Ni-P/Au surface finish by using the fluxes containing Cu(II) stearate were investigated. The content of the Cu compound in a flux varies from 0 wt.% to 40 wt.%. The study of the interfacial microstructure revealed that the thickness of a P-rich layer became thinner with increasing Cu content in a flux. According to the qualitative analysis of the joint interface, Cu was detected in the interfacial intermetallic layer formed by the use of the Cu-bearing flux. Additionally, joint strength tests showed that the Cu-bearing

flux gave relatively higher joint strength than a baseline flux without Cu compound. It is presumed that the intervention of Cu derived from a flux in an interfacial reaction led to a small growth of a P-rich layer, and this may help to improve the joint strength when using the Cu-bearing flux.

4:25 PM

**Effect of Cu Electroplating Process on the "Kirkendall Voiding" in SnAgCu-Cu Solder Joints:** *Liang Yin*<sup>1</sup>; *Nikolay Dimitrov*<sup>2</sup>; *Peter Borgesen*<sup>2</sup>; <sup>1</sup>Universal Instruments Corp; <sup>2</sup>Binghamton University

Soldering to Cu surface finish with Sn-containing alloys usually leads to the formation of a layered interfacial  $Cu_3Sn/Cu_6Sn_5$  structure. Frequently microscopic voids within  $Cu_3Sn$  have been observed to develop during extended thermal aging or current stressing. Excess impurity incorporation during Cu electroplating has been shown to cause this phenomenon. In this study, crystallographic orientation analysis by X-ray diffraction (XRD) was performed on samples plated by various electroplating additive combinations and plating process parameters. The results suggested that the level of impurity incorporation and the associated voiding propensity were greatly affected by applied over-potential and the texture of electroplated Cu films. A general picture was proposed, based on the parabolic adsorption behavior of organic molecules as a function of the applied over-potential.

4:45 PM

**Correlations of Microstructure and Electromigration Behavior in Eutectic Sn-Pb Solder Joints:** *Andre Lee*<sup>1</sup>; *Y. Lee*<sup>1</sup>; *K. Subramanian*<sup>1</sup>; <sup>1</sup>Michigan State University

Atomic movements within a multi-phase alloy attributed to the direct-current stressing will depend on size, shape and distribution of phases present. However, most of current stressing studies are carried out with solder joints possessing as-reflowed microstructures. To better understand the role of microstructure on materials movement resulting from direct current stressing, electromigration studies were carried out on eutectic Sn-Pb joints with coarsened microstructures produced by varying extents of isothermal aging treatments. These studies characterized the evolution of microstructural features at the bulk region of solder joints, as well as at the interface of solder/Cu substrates of anode and cathode. Results of this study indicate the electromigration behavior in a two-phase alloy is significantly influenced by the initial microstructure, evolution of microstructures and concentration gradients of moving atomic species under the influence of high current density. These events indirectly affect the type of interfacial intermetallic compounds formed at the solder/substrate interfaces.

5:05 PM

**The Effect of Pd Thickness in the Interfacial Reaction between Sn-3.0Ag-0.5Cu Solder and Electroless Nickel/Electroless Palladium/Immersion Gold Surface Finish and Their Mechanical Properties:** *Youngmin Kim*<sup>1</sup>; *Jin-Young Park*<sup>1</sup>; *Young-Ho Kim*<sup>1</sup>; <sup>1</sup>Hanyang University

Electroless Nickel/immersion gold (ENIG) surface finish has been widely used in electronic packaging industries, however, ENIG easily causes black pad issue. Recently, electroless nickel/electroless palladium/immersion gold (ENEPIG) has been developed to overcome the weak solder joint by introducing a Pd between Ni and Au layer. Pd acts an efficient protector against corrosion in the Ni-P layer. ENEPIG offers an excellent solder joint even in higher thermal conditions. In this study, the thickness effect of Pd in the interfacial reaction between ENEPIG and Sn-3.0Ag-0.5Cu solder was investigated systematically by varying the thickness of Pd ranging from 0 to 0.5  $\mu\text{m}$ . In all specimens, (Cu, Ni) $_6\text{Sn}_5$  formed at the SAC/ENEPIG interfaces after reflow at 260°C. For Pd thickness of 0.5  $\mu\text{m}$ , monoclinic structure of (Pd, Ni) $_4\text{Sn}_4$  formed over (Cu, Ni) $_6\text{Sn}_5$ . The relationship between the interfacial reaction of SAC/ENEPIG with different thickness of Pd and their mechanical properties will be discussed.

## Phase Stability, Phase Transformations, and Reactive Phase Formation in Electronic Materials X: Conductors, Dielectrics, Interconnects, Phase Change Memory, and Polymer Materials

*Sponsored by:* The Minerals, Metals and Materials Society, TMS Electronic, Magnetic, and Photonic Materials Division, TMS: Alloy Phases Committee

*Program Organizers:* Chih-Ming Chen, National Chung Hsing University; Hans Flandorfer, University of Vienna; Sinn-Wen Chen, National Tsing Hua University; Jae-ho Lee, Hongik University; Yee-Wen Yen, National Taiwan Univ of Science & Tech; Clemens Schmetterer, TU Bergakademie Freiberg; Ikuo Ohnuma, Tohoku University; Chao-Hong Wang, National Chung Cheng University

Wednesday PM

March 2, 2011

Room: 7A

Location: San Diego Conv. Ctr

*Session Chairs:* Alexandre Kodentsov, Eindhoven University of Technology; Jae-Ho Lee, Hongik University

2:00 PM Invited

**Phase Transformation of PVP-Protected Noble Metallic Nanoparticle Deposits upon Heating in Air:** *Jenn-Ming Song*<sup>1</sup>; *Guan-Di Chiou*<sup>2</sup>; *Wei-Ting Chen*<sup>1</sup>; *Shih-Yun Chen*<sup>2</sup>; *Tzu-Hsuan Kao*<sup>3</sup>; *In-Gann Chen*<sup>3</sup>; *Hsin-Yi Lee*<sup>4</sup>; <sup>1</sup>National Dong Hwa University; <sup>2</sup>National Taiwan University of Science and Technology; <sup>3</sup>National Cheng Kung University; <sup>4</sup>National Synchrotron Radiation Research Center

By utilizing a proper deposition technique, e.g. drop-on-demand ink jet printing, inks containing noble metallic nanoparticles have been widely used to fabricate conductive lines and electrodes for electronic devices. For the transportation of power and signal, the nanoparticle deposits (NPDs) should be consolidated and well jointed with the contacts of the devices. This study prepared polyvinylpyrrolidone (PVP)-protected Ag and Au nanoparticles and observed their structural evolution upon heating using in-situ synchrotron radiation X-ray diffraction (SR-XRD). Due to the difficult desorption of the surfactant, low temperature melting of NPDs did not occur. Instead, particle coarsening and coalescence were verified by gradual intensification of the X-ray diffractions. This talk will also discuss the interactions between NPDs and the commonly used electronic metallic substrates, and how they influenced the phase transitions and oxidation of the NPDs, as well as the degree of thermal expansion.

2:25 PM

**Synthesis of Ag Nanoparticles for the Fabrication of Highly Conductive Ink:** *Inyu Jung*<sup>1</sup>; *Yun Hwan Jo*<sup>1</sup>; *Hyuck Mo Lee*<sup>1</sup>; <sup>1</sup>KAIST

A various size of Ag nanoparticles were synthesized by using a thermal decomposition process for low temperature electronic devices. Mono-dispersed Ag nanoparticles with diameters of 6 nm, 8 nm and 12 nm were synthesized by incubation and ripening stages related with nucleation and growth. After Ag nanoparticles were made into ink with a proper solvent, the inkjet printing and thermal sintering methods were employed to form a metal thin film with thickness of 50nm. The electrical resistivity was examined by a 4-point probe system and compared with the resistivity of bulk Ag. As a result, the resistivity of the Ag film has reached around 50  $\mu\Omega\cdot\text{cm}$ , which is much higher than that of bulk Ag. To improve the electrical stability and properties, we applied surface treatment on the substrate and plasma ashing. Both treatments had the effect of diminishing the resistivity of the printed conductive films.

2:40 PM

**Influence of Post Annealing Ambient on the Microstructure and Contact Resistance of Screen-Printed Silver Contacts of Silicon Solar Cells:** *Sungbin Cho*<sup>1</sup>; *Jung-Woo Chun*<sup>1</sup>; *Bo-Mook Chung*<sup>1</sup>; *Joo-Youl Huh*<sup>1</sup>; *Byung-Chul Lee*<sup>2</sup>; *Kuninori Okamoto*<sup>2</sup>; <sup>1</sup>Korea University; <sup>2</sup>Cheil Industries Inc.

Screen-printed Ag thick-film metallization is commonly used in photovoltaic industry for front-side emitter contacts of commercial Si solar



cells. During firing process, glass frit contained in Ag paste plays a crucial role in contact formation. In order to achieve good-quality ohmic contacts to Si emitters, thin glass layer formed in between Ag crystallites on Si surface and bulk Ag after firing must provide a certain path for current transport. Recently, it was shown that firing ambient has a strong influence on microstructure and contact resistance of fire-through contacts. In this study, we carried out post annealing treatments of fired contact samples at various temperatures above and below glass softening temperature under various ambient gases with different oxygen partial pressures. The precipitation of Ag particles in glass layer depending on annealing ambient was examined. In the presentation, we will discuss how the annealing ambient affects contact microstructure and thus contact resistance.

#### 2:55 PM

**Low Resistivity Ru-Ta-C Barrier for Cu Interconnection:** *Jau-Shiung Fang*<sup>1</sup>; J. Lin<sup>1</sup>; B. Chen<sup>1</sup>; G. Chen<sup>1</sup>; T. Chin<sup>1</sup>; <sup>1</sup>National Formosa University

Ultrathin Ru-Ta-C film on silicon substrate is evaluated as a barrier for copper metallization. The films were deposited by magnetron sputtering using Ru and TaC targets so that composition and structure can be adjusted by tuning the respective deposition power. The characterization of Ru-Ta-C and its barrier properties were elucidated by four-point probe measurement, x-ray diffractometry, field emission electron probe microanalysis, Auger electron spectroscopy (AES) and transmission electron microscopy. Structure of Ru-Ta-C films gradually changes from Ru<sub>4</sub>Ta(C) to amorphous when increasing TaC. The failure temperatures are 800°C in a sandwiched scheme Si/Ru<sub>82</sub>Ta<sub>12</sub>C<sub>5</sub> (10 nm)/Cu and Si/Ru<sub>77</sub>Ta<sub>15</sub>C<sub>7</sub> (10 nm)/Si, and are at least 750°C for 5 nm Ru-Ta-C barriers. Because of its low resistivity (92 μΩcm for Ru<sub>82</sub>Ta<sub>12</sub>C<sub>5</sub> film) and high thermal stability, the Ru-Ta-C film is promising as a barrier and capable of directly Cu electroplating without Cu seed.

#### 3:10 PM Break

#### 3:30 PM

**Metal-Induced Crystallization and the Diffusion Behavior of Al/Ge Thin Film:** *Chao Nan Yeh*<sup>1</sup>; Kewin Yang<sup>1</sup>; Albert T. Wu<sup>1</sup>; <sup>1</sup>National Central University

Metal-induced crystallization (MIC) is a rapid process for crystallization in semiconductor materials, such as Si and Ge. In this paper, Al/Ge thin films were deposited by sputtering technique. Layer exchange and surface morphology evolution accompanied by MIC of Ge film induced by Al were investigated. Ge films were deposited on top of Al layer to avoid oxidation of Al. Complete layer exchange could be found after annealing at 300°C for 10 days. The interdiffusion coefficient of Al and Ge films that were annealed between 200°C to 400°C for various duration of time were calculated by Boltzmann-Matano analysis based on the ESCA depth profiling measurement. The diffusivities were in the range between the orders of 10<sup>-22</sup>-20 (m<sup>2</sup>/s) for heat treatment at different temperatures. From the SEM image, mushroom-shaped hillocks formed on the surfaces of the films at the annealing temperature at 400°C. We proposed a mechanism to explain the growth mechanism of the hillocks and discussed the phase stability after thermal treatment.

#### 3:45 PM

**Measurement of Warpage for Chips on Si Interposer:** *Hsueh-Hsien Hsu*<sup>1</sup>; Tao-Chih Chang<sup>2</sup>; Chih Chen<sup>3</sup>; Hsin-Yi Lee<sup>4</sup>; Albert T. Wu<sup>1</sup>; <sup>1</sup>National Central University; <sup>2</sup>Industrial Technology Research Institute; <sup>3</sup>National Chiao Tung University; <sup>4</sup>National Synchrotron Radiation Research Center

For the demand of electronic devices with high performance, 3D stacking IC in the vertical direction is a new trend for electronic packaging. 3D IC used Si as interposer. Due to the decreasing chip size, the thickness of the dies and the choices of underfill were critical to the mechanical properties of the chip. The test samples had microbump with the dimension of 25μm. Both the dies and the substrates are Si. The samples were placed on a heating stage. The current was stressed at different temperatures while the chips were scanned by synchrotron radiation X-ray. The deformation of the dies was recorded in situ. The glass transition temperature, T<sub>g</sub>, greatly affected the

warpage of the dies. Based on the out-of-plane strain, the deformation of the chips could be measured and the in-plane stress in the dies could be determined.

#### 4:00 PM

**Dynamic Transmission Electron Microscope Investigation of Coupled Laser Absorption, Phase Transformation, and Nanoscale Morphology in e<sub>2</sub>Sb<sub>2</sub>Te<sub>5</sub>:** *Bryan Reed*<sup>1</sup>; Melissa Santala<sup>1</sup>; Stefan Meister<sup>2</sup>; Thomas LaGrange<sup>1</sup>; Geoffrey Campbell<sup>1</sup>; Nigel Browning<sup>1</sup>; <sup>1</sup>Lawrence Livermore National Laboratory; <sup>2</sup>Stanford University

Morphology changes during cycling of phase change materials are detrimental to their stability as nanoscale memory systems. While x-ray and optical investigations can reveal much about the spatially-averaged kinetics, the Dynamic Transmission Electron Microscope provides complementary information because of its unique combination of abilities: single shot nanosecond/nanometer-scale real space imaging, in situ laser drive for direct, rapidly iterated before-during-after comparisons, and collection of diffraction data from very small volumes of material. We show that: (1) the amorphous phase shows some evolution of structure prior to obvious nucleation of the crystalline phase, (2) once crystal nucleation begins, the nucleation density is extremely high, and (3) while morphology changes are most pronounced when the material is partially melted for several microseconds, striations accumulate over a large number of laser shots below the threshold intensity for melting. This occurs at the same time as grain coarsening, so these processes may be coupled.

#### 4:15 PM

**Thermal Treatment of a Ni/Pt Bi-Layer Deposited on a Polyimide Film for Dye-Sensitized Solar Cells:** *Sheng-Jye Cherng*<sup>1</sup>; Chih-Ming Chen<sup>1</sup>; <sup>1</sup>National Chung Hsing University

A Ni/Pt bi-layer coated on a polyimide (PI) film is prepared as an efficient counterelectrode for dye-sensitized solar cell (DSSC). Surface metallization of Ni/Pt on the PI film is carried out via a specific wet process, where the surface Pt is the catalyst and the bottom Ni is the conduction/light-reflection layer. Thermal treatment of the Ni/Pt bi-layer is performed to investigate the interaction between Ni and Pt. Surface morphology, interfacial microstructure, and phase evolution are studied using a scanning electron microscope, X-ray diffractometer, and transmission electron microscope. DSSCs employing the annealed Ni/Pt counterelectrodes are fabricated. Their photovoltaic performance and electrochemical impedance spectroscopy (EIS) are examined and the correlation between the thermal treatment of the Ni/Pt counterelectrode and the cell's performance is discussed.

#### 4:30 PM

**Synthesis of Carbon Nanomaterials from Paper Phenolic Board:** *Yu Ting Huang*<sup>1</sup>; YiWei Lin<sup>1</sup>; Chih Ming Chen<sup>1</sup>; <sup>1</sup>National Chung Hsing University

Due to the advantages of low cost and easy fabrication of printed circuit board (PCB), they have been widely used and manufactured in a variety of electronic products. The prototype of PCB is a bilayer copper (Cu)/polymer laminate, also named paper phenolic board. Two different methods are addressed to synthesize the carbon nanomaterials using the paper phenolic board as the carbon source. A patterned Cu trace is served as localized heating source. Thermal decomposition of the paper phenolic board takes place primarily near the Cu trace, and the products contain carbon nanosheets and tubular carbon nanofibers. Other than the above, we also use chemical vapor decomposition (CVD) method to synthesize the carbon nanomaterials. Tubular carbon nanofibers are successfully synthesized using different catalysts.

## Physical and Mechanical Metallurgy of Shape Memory Alloys for Actuator Applications: Effect of Processing on the Properties of Shape Memory Alloys

*Sponsored by:* The Minerals, Metals and Materials Society  
*Program Organizers:* S. Raj, NASA Glenn Research Center; Raj Vaidyanathan, University of Central Florida; Ibrahim Karaman, Texas A&M University; Ronald Noebe, NASA Glenn Research Center; Frederick Calkins, The Boeing Company; Shuichi Miyazaki, Institute of Materials Science, University of Tsukuba

Wednesday PM                      Room: 11B  
March 2, 2011                        Location: San Diego Conv. Ctr

*Session Chairs:* Gunther Eggeler, Ruhr-Universität Bochum; Thomas Waitz, University of Vienna

### 2:00 PM Invited

**On the Processes Involved in Shape Setting of SMA:** *Petr Sittner*<sup>1</sup>; J. Pilch<sup>1</sup>; L. Heller<sup>1</sup>; <sup>1</sup>Institute of Physics of the ASCR

Although shape setting of shape memory alloys has been performed for decades, the physical processes responsible for it are still not completely clear. The properly shape set SMA element displays functional properties (e.g. superelasticity) and, at the same time, its parent austenite shape is memorized. Both happens due to the microstructure changes brought about by thermomechanically driven processes at high temperatures and stress. Both cold worked and annealed SMAs can be shape set but strategies are different. In large extent, same processes as those involved in shape setting are responsible for degradation and strain drift of high temperature SMA actuators. In this work, results of recently performed in-situ experiments (thermomechanical, electrical resistivity, X-ray and TEM) during shape setting of NiTi wires by short DC electric pulses will be reviewed. Practical implications for industrial shape setting treatments as well as for optimization of high temperature actuation will be discussed.

### 2:20 PM

**An In Situ Neutron Diffraction Study of Shape Setting NiTi:** *Othmane Benafan*<sup>1</sup>; Santo Padula<sup>2</sup>; Ronald Noebe<sup>2</sup>; Raj Vaidyanathan<sup>1</sup>; <sup>1</sup>UCF; <sup>2</sup>NASA GRC

A bulk polycrystalline NiTi shape memory alloy specimen was shape set while neutron diffraction spectra were simultaneously acquired. The temperature and shape of the specimen were controlled in a load frame while the stress exerted by the specimen on the grips was monitored during these in situ neutron diffraction experiments. The objective was to correlate internal stress, phase volume fraction, and texture measurements (determined from neutron diffraction spectra), with the macroscopic stress and shape changes (from a load cell and extensometry) during the shape setting procedure and subsequent shape recovery. Comparisons were made between the pre-shape set specimen and the post-shape set specimen, both with and without external constraints. Emphasis was placed on capturing the texture evolution in inverse pole figures and comparing the measured macroscopic blocking or actuation stress with direction dependent intergranular stresses determined from the neutron spectra.

### 2:35 PM Invited

**The Effect of Inclusion Content on the Mechanical and Physical Properties of Binary NiTi Shape Memory Alloys:** *Giorgio Vergani*<sup>1</sup>; Frank Sczerzeniec<sup>1</sup>; Graeme Paul<sup>1</sup>; <sup>1</sup>SAES Smart Materials

Binary nickel titanium alloys with transformation temperature in the range of 95 degrees centigrade are being used for several actuator applications. We have observed that higher transformation temperature binary alloys have larger inclusion size and greater area fraction of inclusions than superelastic alloys. Actuator performance is affected by the response to cyclic strain and by variations in strain recovery. Historically, higher inclusion content has been correlated to reductions in strain recovery. This paper will present

new data on the structure, physical properties and mechanical behavior of standard 95 degrees centigrade alloy and alloy processed to minimize inclusion content. We will compare transformation temperature, active austenite finish temperature, static and cyclic mechanical properties and strain recovery of these materials.

### 2:55 PM

**Characterization of Low Inclusions NiTi Shape Memory Wires for Industrial Applications:** *Alberto Coda*<sup>1</sup>; Luca Fumagalli<sup>1</sup>; Giorgio Vergani<sup>2</sup>; Frank Sczerzeniec<sup>2</sup>; <sup>1</sup>SAES Getters S.p.A.; <sup>2</sup>SAES Smart Materials Inc.

Inclusions content is important for the mechanical behavior and performances of Nitinol wires particularly in fatigue rated devices. This includes high transformation temperature wires that are thermally or electrically actuated for industrial applications. Higher inclusions content has been correlated to reductions in strain recovery under thermo-mechanical cycling. Moreover, most fatigue fractures show inclusions at the initiation site. As lower the wire diameter is, as more important the size and concentration of inclusions become. Therefore, a general reduction of inclusions may have a beneficial effect in improving the shape memory properties of such devices. In this work, the functional behavior of standard 95°C binary NiTi wires and wires processed to minimize inclusion content will be compared. Possible explanations for the observed differences and their significance will be given and discussed.

### 3:10 PM

**Study of the Influence of Inclusions on the Behavior of NiTi Shape-Memory Alloys in Thermal Cycling by Means of FEM:** *Marco Fabrizio Urbano*<sup>1</sup>; <sup>1</sup>SAES Getters

Despite the number of papers on the subject, the influence of inclusions on the behavior of Nitinol is still controversial. Numerical simulations can play a fundamental role in providing insight into this subject. As far as superelastic materials are concerned, other authors have shown by means of Finite Element simulations that, in wires loaded in rotary bending conditions, the presence of inclusions greatly increases the stress distribution in the cross section, and that the maximum stress increases as the distance between the inclusion and the neutral axis increases. In this work a similar approach is utilized to analyze the effect of inclusions on thermal cycles of wires loaded in tension. By means of a thermo mechanical constitutive model implemented in Ansys, the stress strain field in presence of a particle is computed. Both particle diameter and position are varied in the analysis. The influence on fatigue behavior is estimated.

### 3:25 PM Break

### 3:35 PM Invited

**Shape Memory Alloy Cables:** *John Shaw*<sup>1</sup>; <sup>1</sup>The University of Michigan

Common structural cables (or wire ropes) are hierarchical constructions of straight and helical wire filaments and strands that have desirable mechanical properties as tension elements in terms of load carrying redundancy and increased bending compliance for spooling/packaging. Experiments on new cables made from NiTi shape memory alloy (SMA) wires show interesting thermomechanical phenomena as measured by infrared imaging and digital image correlation. Different mechanical responses and load-rate sensitivities are observed, depending on the particular construction and layup. SMA cables leverage the excellent properties of SMA wires in a scalable and tailorable form, and thus hold promise for new adaptive and enhanced structural properties over a broad range of applications.

### 3:55 PM Invited

**Shape-Memory Nitinol with Micro-Channel Networks:** Anselm J. Neurohr<sup>1</sup>; *David Dunand*<sup>1</sup>; <sup>1</sup>Northwestern University

NiTi powders containing parallel layers of steel wire meshes were densified into dense NiTi/steel composites. Subsequent electrochemical dissolution of the meshes results in parallel layers of orthogonally interconnected micro-channels, with 24-34 vol.% and ~400 µm diameters, exactly replicating the steel meshes. For low carbon steel wires, iron diffuses into the surrounding NiTi creating a Fe-enriched zone. For high carbon steel wires, TiC forms at the steel/NiTi interface thus inhibiting iron diffusion while also depleting

some titanium from the adjacent NiTi. In both cases, phase transformation characteristics of the NiTi regions near the micro-channels are altered, but not sufficiently to affect adversely the mechanical properties of porous NiTi which shows superelastic and shape-memory recovery. These NiTi structures with networks of micro-channels have potential as bone implants (where channels reduce stiffness and stress-shielding, while allowing bone in-growth) and as actuators (where channels enable rapid heating and cooling, reducing actuation time.)

#### 4:15 PM

**Joining Strategies for Shape Memory Alloy Actuators:** *Konstantin Lygin*<sup>1</sup>; Sven Langbein<sup>1</sup>; Tim Sadek<sup>1</sup>; <sup>1</sup>Ruhr University Bochum

During the transformation from deformed to primal form shape memory alloys (SMA) display high forces. These forces are usable in actuators based on SMA technology. To transfer the actuating force of SMA elements it is necessary to connect them to the system environment. Basically three connection types are used: form locked, material bonded and friction locked. An example for a form locked connection is a SMA element sealed in a polymer matrix. With laser welding it is possible to create a material bonded connection. A force locked connection can be created by locking a SMA element with a screw. This paper presents the mentioned and several other connection methods for SMA components and categorizes those methods in terms of actuating forces, lifetime, interaction with system environment, geometry of actuating elements and joining elements. Finally SMA connection methods were recommended for different use cases with specific restrictions.

#### 4:30 PM

**Fabrication of Neck Ache Prevent Tool Applying Ti-Ni Superelastic Alloy:** *Kazuhiro Kitamura*<sup>1</sup>; Hiraku Tsuboi<sup>2</sup>; Katsuyoshi Chino<sup>3</sup>; Yu Takeuchi<sup>4</sup>; Kimio Satou<sup>5</sup>; <sup>1</sup>Aichi University of Education; <sup>2</sup>Nagano Techno Foundation; <sup>3</sup>C. K. Techno Co, Ltd.; <sup>4</sup>Misuya Industry Co, Ltd.; <sup>5</sup>Suzaka city

Ti-Ni alloy had excellent shape memory and superelastic effect. Especially, superelastic effect showed unique mechanical properties. We were developed the neck ache prevent tools applying Ti-Ni superelastic alloy. The superelastic wire was made from Ti-Ni wires of 1.5mm in diameter and 70mm in length. The components were arranged right and left side of the shoulder. The composition of this wire was Ti-50.8at%Ni. The transformation temperatures were measured by differential scanning calorimetry (DSC). From DSC measurement, this alloy showed the superelastic behavior at room temperature. The bending fatigue characteristics of superelastic wire were investigated by fatigue tester. Fatigue lives of the superelastic components were about 100,000 times at 1.8% strain.

#### 4:45 PM

**Severe Plastic Deformation of a Beta-Titanium Shape Memory Alloy:** *Ji Ma*<sup>1</sup>; Ibrahim Karaman<sup>1</sup>; <sup>1</sup>Texas A&M University

Because of their biocompatibility and ease of cold working,  $\beta$ -titanium SMAs, such as Ti-Nb are being investigated as possible alternatives to the commonly-used Nitinol in biomedical applications. However, they suffer from low yield strength in the solution-treated condition. Equal Channel Angular Extrusion (ECAE) strengthens the alloy through grain refinement, increase in dislocation density, and possibly stress-induced precipitations of the  $\beta$  phase. After appropriate post-extrusion heat treatments, fully reversible shape memory effect and superelasticity were attained. Curiously, while the texture of cold-rolled specimens was similar to the expected BCC rolling texture, ECAE texture of the alloy was quite different from that expected for a typical BCC material undergoing ECAE. We suspect this discrepancy is related to stress-induced martensitic transformation taking place during processing, as well as the intermittent nature of cold rolling, where strain is applied incrementally throughout several passes, as opposed to ECAE, where all strain were applied at once.

#### 5:00 PM

**Self-Assembled Ti Nanowires on Single Crystal NiTi Shape Memory Alloys:** *Xu Huang*<sup>1</sup>; Yuriy Chumlyakov<sup>2</sup>; Ainissa Ramirez<sup>1</sup>; <sup>1</sup>Yale University; <sup>2</sup>Siberian Physical and Technical Institute

Self-assembled Ti nanowires were fabricated by electro-polishing a NiTi single crystal in a solution of 20% H<sub>2</sub>SO<sub>4</sub>-80% methanol at 1 A for 60 seconds. The resulting Ti nanowires were approximately 480X480 nm<sup>2</sup> in cross section and 50  $\mu$ m in length. The nanowire orientations were determined and found to grow perpendicularly along the <110> and <100> planes of the single crystal substrate. Although most of them were oriented perpendicular to the surface, some presented an incline at a specific angle. Their composition was determined using microprobe methods and diffraction, and their electrical properties were investigated using four-point probe measurements. These methods for producing Ti nanowires could provide new routes for generating nanostructures.

#### 5:15 PM End of Session

---

### Polycrystal Modelling with Experimental Integration: A Symposium Honoring Carlos Tome: Steels, Damage

*Sponsored by:* The Minerals, Metals and Materials Society, TMS Structural Materials Division, TMS Materials Processing and Manufacturing Division, ASM-MSCTS: Texture and Anisotropy Committee, TMS/ASM: Mechanical Behavior of Materials Committee, TMS/ASM: Computational Materials Science and Engineering Committee

*Program Organizers:* Ricardo Lebensohn, Los Alamos National Laboratory; Sean Agnew, University of Virginia; Mark Daymond, Queen's University

Wednesday PM  
March 2, 2011

Room: 6C  
Location: San Diego Conv. Ctr

*Session Chairs:* Jose Gracio, Universidade de Aveiro; Thomas Bieler, Michigan State University; Chad Sinclair, University of British Columbia

---

#### 2:00 PM Invited

**Plastic Anisotropy in Multiphase Steels:** Young Ung Jeong<sup>1</sup>; *Frederic Barlat*<sup>1</sup>; <sup>1</sup>Pohang University of Science and Technology

In advanced steels, which are mostly multiphase alloys, plastic anisotropy depends on many parameters, in particular crystallographic texture, slip properties and volume fraction of each phase. In this work, the stress-strain curves and flow anisotropy of multiphase steels are measured in uniaxial tension, in-plane biaxial tension and through-the-thickness disk compression. The yield loci are assessed using an in-plane biaxial tensile machine. For each material, the locus is determined at different amounts of plastic work. Continuum and simple crystal plasticity models are used to predict plastic properties. Because of the number of experiments conducted in this work, some data are used for constitutive model identification while others are used for validation purpose. The objective of this work is to compare the ability of simple continuum and crystal plasticity models to describe the plastic behavior of multiphase materials.

#### 2:25 PM Invited

**Effect of Asymmetric Rolling on the Mechanical Behavior of Low Carbon Steel under Shear Tests: A Simple Modelling Approach:** *Jose Gracio*<sup>1</sup>; <sup>1</sup>University of Aveiro

In this work we analyzed the mechanical behaviour of low carbon steel pre-deformed in conventional, continuous asymmetric and inverse asymmetric rolling and reloaded in simple shear at different orientations with respect to the previous rolling direction. In essence, the mechanical behavior in simple shear seems to be not strongly affected by the different rolling conditions imposed during pre-strain. The behavior was modelled with a simple approach based on the evolution of the dislocation microstructures. A



parameter which measures the amplitude of the strain path change as well as textural effects were incorporated in this approach.

## 2:50 PM

**Comparison of Experimental and Computational Texture Evolution in Steel under Multi-Axial Loads:** *Adam Creuziger*<sup>1</sup>; Thomas Gnäupel-Herold<sup>1</sup>; Lin Hu<sup>2</sup>; Anthony Rollett<sup>3</sup>; <sup>1</sup>National Institute of Standards and Technology; <sup>2</sup>Carnegie Mellon University; <sup>3</sup>Carnegie Mellon University

In this study, as received High Strength Low Alloy (HSLA) and Transformation Induced Plasticity (TRIP) steel sheets are deformed under uniaxial, plane strain and balanced biaxial strain conditions. After deformation the texture evolution was investigated using neutron diffraction to determine both the phase fractions in the deformed material and how the crystallographic texture evolves as a function of strain for each deformation mode. Additionally, the texture evolution was modeled using a viscoplastic self-consistent (VPSC) model. Comparisons between the experimental and computational texture evolution show while there is good qualitative agreement, the VPSC model over predicts the amount of texture sharpness.

## 3:10 PM

**Micromechanical Modelling of Strength and Deformation of Advanced High Strength Steels on the Grain Level:** Christian Krempaszky<sup>1</sup>; *Ewald Werner*<sup>2</sup>; Andreas Pichler<sup>3</sup>; Thomas Hebesberger<sup>3</sup>; <sup>1</sup>CD Laboratory of Material Mechanics of High Performance Alloys, TU-Munich; <sup>2</sup>Technische Universität München; <sup>3</sup>voestalpine Stahl Linz GmbH

A micromechanical model on the grain level is presented to describe the strength and deformational behaviour of advanced high strength steels based on microstructural and phase specific properties. The topology of the microstructure is modelled by Voronoï tessellation and appropriate coloring algorithms are presented to simulate the topology of the constituting phases ferrite, bainite and martensite. The effect of the geometrical arrangement of these phases in the microstructure and the strength ratio of the phases on formability is discussed in comparison with experimental results from tensile and hole expansion tests performed with industrially produced dual-phase and complex-phase steels. Special emphasis is placed on the comparison of two approaches, namely the finite element analysis and a discrete Fourier transform based algorithm.

## 3:30 PM Break

## 3:50 PM Invited

**Roping of Ferritic Stainless Steels: Models and Experiments:** *Chad Sinclair*<sup>1</sup>; Guillaume Lefebvre<sup>1</sup>; Ricardo Lebensohn<sup>2</sup>; Jean-Denis Mithieux<sup>3</sup>; <sup>1</sup>University of British Columbia; <sup>2</sup>Los Alamos National Laboratory; <sup>3</sup>ArcelorMittal

Roping of ferritic stainless steel sheet results in an anisotropic surface roughening parallel to the prior rolling direction. While this may appear to be a surface phenomenon, it is in fact a collective through thickness deformation pattern leading to a "corrugation" of the sheet. While many important factors associated with roping have been identified, many questions remain regarding what constitutes a "sufficient" set of conditions leading to "strong" or "weak" level of roping. At this time it is not possible, from experiment alone, to predict the severity of roping in a given material prior to testing it. This talk will review experimental and modelling efforts aimed at understanding the relationship between roping and local texture, grain (orientation) clustering and the collective deformation behaviour of groups of grains. Simulation results examining the morphological rotation of grains via 1-site and N-site viscoplastic model calculations will be discussed in relation to experimental observations.

## 4:15 PM Invited

**Integrated Experimental and Crystal Plasticity Investigations of Heterogeneous Deformation and Damage Nucleation in Titanium:** *Thomas Bieler*<sup>1</sup>; Philip Eisenlohr<sup>2</sup>; Martin Crimp<sup>1</sup>; Leyun Wang<sup>1</sup>; A. Alankar<sup>2</sup>; Yiyi Yang<sup>1</sup>; Rozaliya Barabash<sup>3</sup>; Gene Ice<sup>3</sup>; Wenjun Liu<sup>4</sup>; <sup>1</sup>Michigan State University; <sup>2</sup>Max-Planck-Institut für Eisenforschung; <sup>3</sup>Oak Ridge National Laboratory; <sup>4</sup>Argonne National Laboratory

Predicting heterogeneous deformation and the likelihood of damage nucleation in polycrystalline metals requires knowledge of the history of slip system activity and its interaction with microstructural features such as interfaces. These processes are dependent on the strain path, which can be locally complex due to heterogeneous deformation arising from different orientations of neighboring grains, and effects of slip resistance and slip transfer across boundaries. To assess the ability of crystal plasticity finite element models to predict heterogeneous deformation, experimental characterization using several modern experimental characterization tools to quantify the activity of slip systems is used to directly compare with crystal plasticity finite element computational models. Comparisons between local and non-local models are used to identify where improvements in computational modeling are needed using illustrative microstructural patches from titanium and titanium alloys. Supported by NSF, DOE and DFG.

## 4:40 PM Invited

**Role of Crystallographic Texture in the Delamination and Fracture of Al-Li Alloys:** *Armand Beaudoin*<sup>1</sup>; Rebecca Storer<sup>1</sup>; Wesley Tayon<sup>2</sup>; Sean Hamel<sup>1</sup>; Peter Kurath<sup>1</sup>; <sup>1</sup>University of Illinois at Urbana-Champaign; <sup>2</sup>NASA Langley

Driven by savings in weight, application of Aluminum-Lithium alloys in aerospace structures is increasing. Considering fracture of these alloys, the crack path may deviate from the Mode I direction toward the direction of elongated grain boundaries, a phenomena called delamination. Even in the absence of a "crack", uniaxial and cyclic failures are observed at elongated grain boundaries. To provide insight into fracture tolerant design, this work explores the relationship between crystallographic orientation and stress state about a primary crack. Coordinated use of experiment and modeling (crystal plasticity) are pursued to evaluate the contribution of anisotropy to the nucleation and propagation of delamination. In general, results indicate the key role of slip incompatibility: a grain oriented favorably for slip sharing a boundary with another 'less favorable' crystallographic orientation promotes the development of shear stress which sustains delamination. This work is supported by the NASA Marshall Flight Center through grant NNX09AN21G.

## 5:05 PM

**Ductile Failure of Metals: The Initiation and Growth of Nanovoids:** *Marc Meyers*<sup>1</sup>; Eduardo Bringa<sup>2</sup>; Yizhe Tang<sup>1</sup>; <sup>1</sup>UCSD; <sup>2</sup>U. Nacional de Cuyo

It has been known since the 1940s that the ductile failure of metals proceeds by the initiation, growth, and coalescence of voids. In spite of the rigorous mechanical and metallurgical understanding of the processes involved gained in the past sixty years, the fundamental deformation mechanisms had not been understood. The postulation of special shear and prismatic dislocation loops to accomplish the outward matter transfer required for void formation, in 2004, has been followed by significant efforts, worldwide, in molecular dynamics. The generation and expansion of shear loops has been observed in simulations in copper and tantalum. A specific requirement is that the extremities of the dislocations have to remain attached to the void surface. In some cases these loops react and form prismatic loops which glide away from the void. In copper, partial dislocation loops generate extended stacking faults that impede cross slip. In tantalum, twinning can also occur, in some cases. We review our most recent research on the formation of these voids in both mono and nanocrystals.

## 5:30 PM

**Roles of Stress and Strain in IG Cracking of Irradiated Stainless Steel in Supercritical Water:** *Elaine West*<sup>1</sup>; Gary Was<sup>1</sup>; <sup>1</sup>University of Michigan

The Schmid factors of grains in irradiated 316L stainless steel were used as indicators of their deformation propensities to determine the role of stress

and strain on intergranular cracking in 400°C supercritical water. Variations in grain deformation propensities resulted in heterogeneous cracking that was promoted by strain incompatibilities, and ultimately determined by normal stress. The formation of cracks along grain boundaries perpendicular to the tensile axis and adjacent to grains with low Schmid factors indicated normal stress dependence. The Schmid-Modified Grain Boundary Stress Model was developed to evaluate the grain boundary normal stress as a function of the orientation of the grain boundary plane with respect to the tensile axis and Schmid factor. This model confirmed the normal stress dependence of intergranular cracking, and demonstrated that the Schmid factor dependence of the cracking could be predicted from the distribution of cracked grain boundary surface trace inclinations to the tensile axis.

#### 5:50 PM

**The Effect of Asymmetric Rolling on the Mechanical Properties of Interstitial Free Steel:** *Saeed Tamimi*<sup>1</sup>; Gabriela Vincze<sup>1</sup>; Augusto Lopes<sup>2</sup>; Jose Gracio<sup>1</sup>; Edgar Rauch<sup>3</sup>; Frédéric Barlat<sup>4</sup>; <sup>1</sup>TEMA; <sup>2</sup>Departamento de Engenharia Ceramica e do Vidro; <sup>3</sup>Génie Physique et Mécanique des Matériaux ENSPG-INPG (ESA CNRS 5010); <sup>4</sup>Graduate Institute of Ferrous Technology

Asymmetric rolling (ASR) of sheet metals has been used to improve the mechanical properties. Present work deals with the perspective of crystallographic texture and microstructure and their relevance with the mechanical properties of interstitial free steel using ASR. The effect of rolls velocity ratio on the properties of the samples was investigated. It was found that the speed ratio 1.5 can make better condition for shearing and consequently rising more shear texture. The samples were deformed for 60% strain and annealed in 550-700 °C for 1, 8 and 24 hours. The results indicate that 650 °C for one hour can be considered as an optimum heat treatment condition for applied strain. Improvement in the mechanical responses and the texture evolution during ASR and conventional rolling are observed using numerical simulation of ideal texture based on a polycrystal plasticity model. The results were compared with the experimental results.

#### 6:10 PM

**Simulations for Fatigue Damage Incubation Mechanisms of Textured Al Alloy Using Crystal Plasticity Model:** *Yibin Xue*<sup>1</sup>; Chong Teng<sup>1</sup>; Tong Li<sup>1</sup>; <sup>1</sup>Utah State University

The high-cycle fatigue life of a textured Al alloy is consumed primarily during fatigue damage formation or incubation stage. The vital fatigue damage forms at the micrometer-sized intermetallic particles located at or near the surfaces or the change of geometries, as commonly observed. In this paper, micromechanical simulations are implemented to assess the crystallographical textured effects on the fatigue-life critical damage formation, which are difficult or impossible to obtain experimentally. The representative unit cell (UC) models are set with an intermetallic particle located in typical grain orientations, sizes, and grain boundary mismatches of the textured 7075-T651 Al alloy. Crystal plasticity constitutive model is applied to quantify the micronotch-root plasticity and such to quantify and classify the severity of texture effects to the fatigue damage incubation. Eventually, the uncertainty and statistical distribution of the fatigue incubation life induced by the texture are obtained.

## Processing and Properties of Powder-Based Materials: Mechanical Alloying/Milling, Reactions and Consolidation

*Sponsored by:* The Minerals, Metals and Materials Society, TMS Materials Processing and Manufacturing Division, TMS: Powder Materials Committee

*Program Organizers:* K. Morsi, San Diego State University; Ahmed El-Desouky, San Diego State University

Wednesday PM  
March 2, 2011

Room: 33A  
Location: San Diego Conv. Ctr

*Session Chair:* K. Morsi, San Diego State University

### 2:00 PM Introductory Comments

#### 2:05 PM

**Effect of Milling Process on Mechanical Properties of Fully Consolidated Titanium and Titanium Alloy Powders Made by Armstrong Process® Technology:** *Yukinori Yamamoto*<sup>1</sup>; Wei Chen<sup>1</sup>; Stephen Nunn<sup>1</sup>; Jim Kiggans<sup>1</sup>; Michael Clark<sup>1</sup>; Sarma Gorti<sup>1</sup>; Adrian Sabau<sup>1</sup>; Ronald Swain<sup>1</sup>; Craig Blue<sup>1</sup>; Brian Fuller<sup>2</sup>; Kamal Akhtar<sup>2</sup>; <sup>1</sup>Oak Ridge National Laboratory; <sup>2</sup>Cristal US, Inc./ International Titanium Powder

Press-and-sinter processing of new titanium and titanium alloy powders produced by the Armstrong Process® technology has been systematically investigated, in order to develop the optimized near-net-shape manufacturing process. This study focuses on the effect of different types of milling processes and the length of time the powder was milled on the mechanical properties and the chemistry after the consolidation process. Milling significantly improves the tap density and the density after sintering for both CP-Ti and Ti-6Al-4V powders when compared to un-milled powders. However, extended milling time tends to increase the oxygen and carbon contents in the powder which degrades the ductility of the consolidated materials. Effects of several different milling processes on the microstructure, the chemistry and the room-temperature tensile properties will be discussed. This research is sponsored by the U.S. DOE, Office of EERE Industrial Technologies Program, under contract DE-AC05-00OR22725 with UT-Battelle, LLC.

#### 2:25 PM

**Fabrication of Ultrafine-Grained Al-Mg Alloy via ECAP Consolidation of Nanostructured Powder:** *Zhihui Zhang*<sup>1</sup>; Xiaolin Wu<sup>2</sup>; Ying Li<sup>1</sup>; Troy Topping<sup>1</sup>; Wei Xu<sup>2</sup>; Yizhang Zhou<sup>1</sup>; Kenong Xia<sup>2</sup>; Enrique Lavernia<sup>1</sup>; <sup>1</sup>UC Davis; <sup>2</sup>University of Melbourne

Nanostructured Al powder produced by cryomilling showed good microstructural stability against thermal exposure. However, the grain growth behavior in a stress/strain field during thermomechanical processing is less understood. In this work, the microstructure evolution in an Al-7.5Mg alloy was studied via direct ECAP consolidating the cryomilled powder with an average grain size of 25 nm. The ECAP was conducted at 200 and 325 °C and after 4 passes, the samples showed averaged grain sizes of 170 and 450 nm, respectively. However, the bulk sample by HIP consolidating the annealed (24 hrs at 400 °C) cryomilled powder at 400 °C only showed an average grain size of 100 nm, indicating that plastic strain introduced during ECAP may have played a role in grain growth. TEM examination revealed that grain rotation and coalescence contributed to the observed grain growth. Finally, the mechanical behavior of the ultrafine-grained Al-7.5 Mg alloys was discussed.

#### 2:45 PM

**Investigation of Mechanical Alloying Process Parameters on Fe-Mn-Si Based System:** *A. Umut Soyler*<sup>1</sup>; Burak Özkal<sup>1</sup>; Leandru G. Bujoreanu<sup>2</sup>; <sup>1</sup>Istanbul Technical University; <sup>2</sup>The "Gh. Asachi" Technical University

In this work, Fe-Mn-Si based powder mixture having shape memory alloy composition prepared by mechanical alloying and systematically studied with different milling conditions. Effect of ball to powder ratio (BPR), type and amount of binder addition and milling time were investigated as

process parameters. All mechanical alloying studies performed under argon atmosphere and stainless steel balls and vials were used as milling media. X-Ray diffraction (XRD), laser particle size analysis (LPSA), scanning electron microscopy (SEM) and optical microscopy (OM) techniques used to characterize the powders. Results were discussed to show that powder metallurgy can be an alternative technique to obtain Fe-Mn-Si based shape memory alloys with the required composition and microstructural homogeneity in contrast to classical metallurgy.

### 3:05 PM

**The Effects of Boron Sources on the Mechanochemical Synthesis of  $\text{AlB}_2$  from Chloride-Based Powders:** Duygu Agaogullari<sup>1</sup>; Hasan Gökçe<sup>1</sup>; Ismail Duman<sup>1</sup>; M. Lütfi Öveçoglu<sup>1</sup>; <sup>1</sup>Istanbul Technical University

The mechanochemical process to synthesize aluminum diboride ( $\text{AlB}_2$ ) powder from  $\text{AlCl}_3$ - $\text{B}_2\text{O}_3$ -Mg and  $\text{AlCl}_3$ -B-Mg system at room temperature was investigated systematically in this study. The reaction was driven by high-energy ball milling of powder mixtures in Spex 8000 D Mixer/Mill performed at different durations. Milled powders were subsequently annealed in a tube furnace to obtain  $\text{AlB}_2$  phases. After obtaining  $\text{AlB}_2$ , by-products of the reaction i.e. MgO and  $\text{MgCl}_2$ , and impurities released by the milling vial (Fe, Ni, Cr) were removed by leaching and washing with distilled water and ethanol. The phases, morphologies and thermal properties of the milled, leached and annealed powders were characterized by X-ray diffraction (XRD), scanning electron microscope (SEM), differential thermal analyzer (DTA) and atomic absorption spectrometer (AAS).

### 3:25 PM Break

### 3:35 PM

**Deformation-Induced Ductility in Cryomilled Nanostructured Nickel:** Yonghao Zhao<sup>1</sup>; Qian Zhan<sup>2</sup>; Troy Topping<sup>1</sup>; Y. Li<sup>1</sup>; Enrique Lavernia<sup>1</sup>; <sup>1</sup>University of California, Davis, CA 95616, USA; <sup>2</sup>University of Science and Technology Beijing, Beijing 100083, People's Republic of China

When bulk nanostructured (NS) materials are prepared via consolidation of individual particles, agglomerates or clusters, extraneous defects, such as porosity, and impurities are sometimes introduced leading to the degradation of ductility. In this study we propose to examine the hypothesis that deformation can be used to ameliorate negative effects of these artifacts on the ductility of NS alloys. The approach involved cryomilling and forging to synthesize bulk NS nickel with porosity (95.5% theoretical density) and nitrogen grain boundary (GB) segregation. The results demonstrate that cold rolling resulted in increased tensile ductility from 2 to ~4%, with slight decrease in yield strength from 1150 to 1050 MPa. Microstructural analyses suggest that the elimination of nano-porosity together with the physical breakdown of a continuous nitrogen layer at GBs during cold rolling are responsible for the observed ductility enhancement, and in the case of the latter phenomena, also a corresponding decrease in strength.

### 3:55 PM

**The Effects of Ti Addition on the Microstructural and Physical Properties of Cu-SiC Composite Powders:** Ceren Dudubi<sup>1</sup>; Hasan Gokce<sup>1</sup>; A. Umur Soyler<sup>1</sup>; M. Lutfi Ovecoglu<sup>1</sup>; Burak Ozkal<sup>1</sup>; <sup>1</sup>ITU

In this study, the effects of Ti addition on the microstructural properties and hardness values of the mechanically alloyed Cu-SiC based metal matrix composites were investigated. The Cu-SiC vol. % 20 matrix composites reinforced with different amounts of Ti such as 1, 2, 3, 5 vol. % were fabricated via mechanically alloying using a Spex Mixer/mill at room temperature. Powders were mechanically alloyed for 4 h using stainless steel milling media which closed under purified Argon atmosphere. Mechanically alloyed powders were characterized by using X-Ray diffractometer, Scanning Electron Microscope, Optical Microscope and Laser Particle Size Analyser. Moreover, micro-hardness measurements performed on the mechanical alloyed powders.

### 4:15 PM

**The Effect of Ball-to-Powder Weight Ratio on the Synthesis of Aluminum Diboride:** Hasan Gökçe<sup>1</sup>; Duygu Agaogullari<sup>1</sup>; Ismail Duman<sup>1</sup>; M. Lütfi Öveçoglu<sup>1</sup>; <sup>1</sup>Istanbul Technical University

In this study,  $\text{AlB}_2$  powders were synthesized by using a combined method of mechanical alloying (MA) and annealing of elemental aluminum (Al) and boron (B) powders mixed in stoichiometric amounts. Mechanical alloying was performed up to 15 h under Ar atmosphere in a vibratory ball-mill (Fritsch Pulverisette 7 Premium Line) using hardened steel vial and balls. Subsequently, milled powders were annealed in a tube furnace under flowing Ar atmosphere at 650°C for 6 h. The effects of ball-to-powder weight ratios (BPR) on the synthesis of  $\text{AlB}_2$  were examined in the experimental studies. Milled and annealed powders were characterized by using X-ray diffraction (XRD) technique, Scanning Electron Microscope (SEM) and Differential Thermal Analyzer (DTA).

### 4:35 PM

**Investigation of Solid State Reaction Mechanism for Sodium Metaborate ( $\text{NaBO}_2$ ) Production:** Aysel Kanturk Figen<sup>1</sup>; Hatice Ergüven<sup>1</sup>; Sabriye Piskin<sup>1</sup>; <sup>1</sup>Yildiz Technical University

Sodium metaborate ( $\text{NaBO}_2$ ), is a compound derivative of borax, is used in the chemical industry as photographic and textile chemicals, detergents, cleansers, and adhesives. Literature on  $\text{NaBO}_2$  used as sources of boron in the production of the  $\text{NaBH}_4$  methods is available. Therefore, the use of anhydrous  $\text{NaBO}_2$  in the energy field and the importance of both commercial borates class are growing gradually. In this study, solid-state preparation of  $\text{NaBO}_2$  was investigated based on thermal analysis. Therefore, anhydrous borax ( $\text{Na}_2\text{B}_4\text{O}_7$ ) and sodium hydroxide ( $\text{NaOH}$ ) were mixed at mole ratio of 1:2 and thermal analysis was performed at different heating rates. There were four endothermic peaks in the DTA plots, corresponding to four reactions that explain the solid state reaction stage as: diffusion stage, reaction stage, nucleation stage and growth stage. Keywords: Sodium metaborate; hydrogen; solid state; mechanism; thermal analysis

## Properties, Processing, and Performance of Steels and Ni-Based Alloys for Advanced Steam Conditions: High Temperature Oxidation and Design for Resistance

*Sponsored by:* The Minerals, Metals and Materials Society, TMS Structural Materials Division, TMS/ASM: Corrosion and Environmental Effects Committee, TMS: High Temperature Alloys Committee

*Program Organizers:* Peter Tortorelli, Oak Ridge National Laboratory; Bruce Pint, Oak Ridge National Laboratory; Paul Jablonski, National Energy Technology Laboratory; Xingbo Liu, West Virginia University

Wednesday PM  
March 2, 2011

Room: 33B  
Location: San Diego Conv. Ctr

*Session Chairs:* Peter Tortorelli, Oak Ridge National Laboratory; Xingbo Liu, West Virginia University

### 2:00 PM

**High Temperature Corrosion Resistance of Fe-Ni-Cr Alloys in  $\text{CO}_2$ - $\text{H}_2\text{O}$  Atmospheres:** Thomas Gheno<sup>1</sup>; Jianqiang Zhang<sup>1</sup>; David Young<sup>1</sup>; <sup>1</sup>University of New South Wales

In the oxyfuel process, heat exchanger materials will be exposed to  $\text{CO}_2$ / $\text{H}_2\text{O}$  mixtures. The corrosion behaviour at 800°C of Fe-Ni-Cr alloys in these atmospheres has been investigated. Binary Fe-9Cr, Fe-20Cr and Fe-25Cr alloys, and ternary alloys containing 10 and 20 wt. % Ni were exposed to dry and wet Ar- $\text{CO}_2$ . Additions of Ni significantly slowed metal consumption rates for Fe-9Cr alloys, whereas the opposite effect was observed for high chromium alloys. Low chromium alloys formed iron-rich oxide scales, and underwent severe carburisation. Overall weight uptakes followed linear



kinetics in dry CO<sub>2</sub>, but additions of H<sub>2</sub>O caused a transition to parabolic kinetics. In contrast, high chromium alloys formed a protective chromia layer in all atmospheres, although mild internal attack also took place. Resistance to corrosion was good, except for ternary alloys containing 10 wt.% Ni, which failed during long exposures. These observations are discussed in terms of reaction morphologies.

#### 2:20 PM

**Oxidation and Corrosion Resistance of Structural Alloys in Supercritical Water for Generation IV Reactor Systems:** Peng Xu<sup>1</sup>; Liang Zhao<sup>1</sup>; Lizhen Tan<sup>1</sup>; Todd Allen<sup>1</sup>; <sup>1</sup>University of Wisconsin

The supercritical water reactor (SCWR) is considered to be one of the promising Generation IV nuclear reactor designs worldwide. The high outlet temperature (500-600C), high pressure (25 MPa), and a rather aggressive chemical environment in the SCWR require materials to be highly corrosion resistant. This paper reviews the oxidation and corrosion resistance of candidate alloy materials proposed for use in the SCWR environment, with a focus on grain boundary engineering. The talk will review how grain boundary engineering of the bulk metal dramatically changed the oxide formation in alloys 800H and 617. Additionally, recent work on grain boundary engineered Ni alloy 690 will be presented. Samples were tested at 500°C from 2 to 12 weeks. Selected samples were characterized using weight change, glancing angle XRD, SEM, EDS, EBSD and TEM. The relationship between material chemistry, grain boundary character, and oxidation performance will be discussed.

#### 2:40 PM

**Steam Oxidation of Fe-20Cr-30Ni-2Nb Austenitic Steel at 973 K:** Toshio Maruyama<sup>1</sup>; Masakazu Yamashita<sup>1</sup>; Mitsutoshi Ueda<sup>1</sup>; Kenichi Kawamura<sup>1</sup>; Masao Takeyama<sup>1</sup>; <sup>1</sup>Tokyo Institute of Technology

Steam oxidation of Fe-20Cr-30Ni-2Nb austenitic steel which is a promising material for advanced power generation was examined at 973 K. Although oxidation in air provided a protective Cr<sub>2</sub>O<sub>3</sub> scale, the duplex scale of magnetite and iron-chromium spinel was formed in steam oxidation. The microstructure of the steel which was varied by heat treatments of homogenization and aging affected the oxidation behavior.

#### 3:00 PM

**Austenitic Steel Oxidation in Steam: Alloy Composition and Surface Modification Solutions:** Bruce Pint<sup>1</sup>; <sup>1</sup>Oak Ridge National Laboratory

Oxidation in the presence of water vapor has become a major research topic in the past decade as material degradation has become a concern for current and future power generation systems. With or without free oxygen, the presence of water vapor has a dramatic effect on the oxidation behavior of both Fe- and Ni-base alloys. In current coal-fired systems, austenitic steel tubing can experience catastrophic scale spallation leading to blockages and tube failures. Potential solutions to this problem include (1) modifying initial service conditions to alter the spallation events, (2) using more expensive, higher-alloyed steels and (3) employing surface modifications such as coatings or shot peening. Current projects are evaluating the steam oxidation resistance of various commercial and model alloys as well as the durability of thin aluminide coatings on austenitic steels. The viability of the potential solutions will be discussed.

#### 3:20 PM

**Moisture Effects on the Oxidation Behavior of Ni-Based Alloys:** Wei Zhao<sup>1</sup>; Brian Gleeson<sup>1</sup>; <sup>1</sup>University of Pittsburgh

The effects of moisture on the 1000°C oxidation behavior of model Ni-based alloys were studied using dry air and air + 30% water vapor ("wet air" in short) gas environments. It was found that the critical concentration of Al (N<sub>Al</sub><sup>\*</sup>) to form a continuous alumina scale on Ni-Al-Cr alloys increases when the environment is wet air. Further study also showed that the growth rate of NiO is enhanced, which was inferred to contribute to the N<sub>Al</sub><sup>\*</sup> increase. This enhanced NiO growth rate was the result of an increased amount of oxidation within the metal consumption zone. Internal oxidation experiments revealed that the increase in N<sub>Al</sub><sup>\*</sup> for wet air conditions could not be attributed to enhanced oxygen permeability. The presence of water vapor could also

lead to instability of the NiO scale surface, which was found to be related to preferred oxide growth along certain crystallographic directions.

#### 3:40 PM Break

#### 4:00 PM

**Oxidation Behavior of Alumina-Forming Austenitic Steel in Steam:** Kinga Unocic<sup>1</sup>; Michael Brady<sup>1</sup>; Yukinori Yamamoto<sup>1</sup>; Bruce Pint<sup>1</sup>; <sup>1</sup>ORNL

Alumina-forming austenitic (AFA) stainless steels exhibit a unique combination of high temperature creep strength and corrosion resistance. By forming a protective alumina scale, AFA steels exhibit significantly better corrosion resistance than conventional, chromia-forming stainless steels and even Ni-base alloys. This improvement in oxidation resistance is a significant benefit for advanced steam applications where materials are often limited by their oxidation resistance rather than their creep resistance. Steam exposures have been conducted at several temperatures from 550\176-800\176C and the rate of oxidation is compared to conventional candidate alloys as well as model alumina-forming alloys. In addition, the reaction product on AFA steel has been characterized using a range of low- to high-resolution techniques. Research sponsored by the U. S. Department of Energy, Office of Energy Efficiency and Renewable Energy, Industrial Technologies Program.

#### 4:20 PM

**Hydrogen Ingress in Stainless Steels during High-Temperature Oxidation in Water Vapor:** James Keiser<sup>1</sup>; <sup>1</sup>Oak Ridge National Laboratory

High-temperature environments containing water vapor are encountered in energy production systems. Accelerated oxidation by water vapor is a limiting factor for stainless steels in these applications. It is well established that hydrogen derived from water vapor can penetrate oxidizing alloys. The complexities of tracking hydrogen species have hampered direct profiling and correlation of hydrogen ingress with the oxidized microstructure. Tracer studies were performed using SIMS in combination with XPS and TEM. Materials studied include Fe-20Cr, type 347 SS, and developmental alumina-forming austenitic SS which were exposed 24 h at 800°C in air + 10% D<sub>2</sub>O. The resultant D profiles were found to vary markedly among the alloys examined. Details of oxidized alloy microstructures and correlation of findings with alloy chemistry will be discussed. Research sponsored by the Laboratory Directed Research and Development Program of Oak Ridge National Laboratory, managed by UT-Battelle, LLC, for the U. S. Department of Energy.

#### 4:40 PM

**Steam Oxidation of New PVD Nano-Structured and Microstructured Coatings on P92 Steels:** Francisco Pérez Trujillo<sup>1</sup>; Maria Hierro<sup>1</sup>; Maria Mato<sup>1</sup>; Juan Sanchez<sup>1</sup>; Marta Brizuela<sup>1</sup>; <sup>1</sup>Universidad Complutense de Madrid

The steels with chromium contents between 9 and 12% wt are used for power plants with advanced steam oxidation conditions. In the last years numerous investigation in development of coatings has been realized with the aim the protected them against the oxidation in order to allow operation of steam turbines at 650°C. In this study, nano-structured coatings based in Cr-Al forming oxides were developed by PVD and deposited on P92 steel, have shown to be protective at 650°C under steam exposure under atmospheric pressure, comparing with the previously data reported in the literature on micro-structured coatings based in Fe-Al design. Experiment for 2.000 h exposure time shown a very promising application of nano-structured coatings for steam environments. Those coatings have similar corrosion rates than micro-structured, avoiding problems of inter-diffusion. Morphology and composition of coatings were characterized by different techniques, such as scanning electron microscopy will be shown.

#### 5:00 PM

**Characterization of Amorphous/Nanocrystalline Steel Coatings Developed by Different Thermal Spray Processes:** Vikram Varadaraajan<sup>1</sup>; Ramesh Kumar Guduru<sup>1</sup>; Pravansu Mohanty<sup>1</sup>; <sup>1</sup>Univ of Michigan

Amorphous/nanocrystalline coatings are very useful for wear and corrosion protection applications. Here, we report structure – property correlation of amorphous/nanocrystalline high performance steel coatings

developed by plasma, high velocity oxy fuel (HVOF), arc as well as a new hybrid spray process. The hybrid spray process combines the arc and HVOF techniques. Microstructural, mechanical, corrosion and tribological characterization of the coatings was done and compared. The mechanical testing data from shear punch and impact tests indicated that the amorphous coatings obtained via plasma and HVOF techniques had lower strength compared to the nanocrystalline hybrid and arc spray coatings. Corrosion properties revealed an influence of chemical composition of the coatings on the measured impedance and corrosion behavior. Tribology data showed similarities between the HVOF, plasma and hybrid coatings although the microstructure of hybrid coating was noticeably different from the other two. Arc coating showed higher coefficient of friction and weight loss.

## Recycling General Session: Metals

*Sponsored by:* The Minerals, Metals and Materials Society, TMS Extraction and Processing Division, TMS Light Metals Division, TMS: Recycling and Environmental Technologies Committee  
*Program Organizer:* Joseph Pomykala, Argonne National Laboratory

Wednesday PM  
March 2, 2011

Room: 12  
Location: San Diego Conv. Ctr

*Session Chair:* Joseph Pomykala, Argonne National Laboratory

### 2:00 PM Introductory Comments

#### 2:05 PM Keynote

#### 2011 Vittorio de Nora Award Winner: Recycling of Contaminated Aluminium Scrap: *Anne Kvithyld*<sup>1</sup>; <sup>1</sup>SINTEF

Recycling is important in the aluminum industry. Removal of contaminants such as the coat and organic materials- applied for protection and appearance- are the tail that wags the recycling dog. Successful removal of contaminants from scrap would ensure that more aluminum be recycled, minimize losses and prevent downgrading of the resource. Performing decoating in a closed system, efficient cleaning of the evolved gases and reuse of the energy is possible. Motivation for removal of contaminants on aluminium scrap will be presented. A sum up of fundamental studies will be given. De-coating may be described as two distinct regimes: Scission and Combustion, regardless of metal substrate and coating. This is studied by methods: (i) mass and enthalpy change together with the off-gas composition recorded simultaneously and (ii) hot stage microscope to give a visual record of the surface. In conclusion a more fundamental understanding of the decoating process should enable the metallurgical industry to process post consumer aluminium scrap in a more efficient and sustainable manner.

#### 2:25 PM

#### Recycling and Material Price: An Exploration of the Effects of Secondary Substitutability on Price Stability: *Nathan Fleming*<sup>1</sup>; *Randolph Kirchain*<sup>1</sup>; *Elisa Alonso*<sup>1</sup>; *Richard Roth*<sup>1</sup>; *Frank Field*<sup>1</sup>; <sup>1</sup>Massachusetts Institute of Technology

High material prices and price uncertainty can be harmful to manufacturing firms. Increased use of recycled materials, industry-wide, can lower both material prices and price variability; moreover, increased recycling decreases the use of primary material, which mitigates price increases due to scarcity effects. These stabilizing and price lowering effects are explored using an Aluminum industry model. We show that (a) increased recycling leads to smaller price fluctuations in the presence of a primary metal supply perturbation, and (b) that the more substitutable the secondary metal is for the primary metal, the lower the overall material price is.

#### 2:45 PM

#### Increased Recycled Aluminum Content during Remelting by Incorporating Compositional Uncertainty: *Tracey Brommer*<sup>1</sup>; *Elsa Olivetti*<sup>1</sup>; *Britt Elin Gihleengen*<sup>2</sup>; *Geir Øyen*<sup>2</sup>; *Hans Ole Riddervold*<sup>2</sup>; *Randolph Kirchain*<sup>1</sup>; <sup>1</sup>Massachusetts Institute of Technology; <sup>2</sup>Norsk Hydro

Although significant environmental and economic gains result from remelting secondary materials during aluminum alloy production, high concentrations of alloying elements and compositional uncertainty limit their incorporation. Incorporation of secondary materials increases the likelihood a batch will not satisfy the compositional specifications of its intended final product. Such "batch errors" are inefficient and expensive prompting remelters to cautiously incorporate secondary materials, resulting in scrap underutilization and higher cost products. Remelters adopt deterministic batch planning algorithms to inform production portfolios, complementing manual batch planning by plant managers. Uncertainty-aware batch planning algorithms are an alternative to deterministic; potentially allowing remelters to simultaneously increase secondary material utilization and decrease batch errors by incorporating the compositional uncertainty of individual secondary materials into the optimization algorithm. This investigation characterizes the conditions under which uncertainty-aware batch planning algorithms outperform the deterministic and manual equivalents for a variety of remelting conditions in the context of interlinked production portfolios.

#### 3:05 PM

#### On In-Process Separation of Zinc from EAF Dust: *Naiyang Ma*<sup>1</sup>; <sup>1</sup>ArcelorMittal

EAF dust is categorized as a hazardous solid waste. EPA approves only two treatment methods: either sending the dust to zinc recycling facility, or stabilizing it first and then disposing it to a specially-lined landfill. Both treatment methods are costly to EAF steelmakers. In order to reduce the cost and even better to make profit from the dust, EAF steelmakers need to find a cost-effective technology to separate zinc from EAF dust. This paper is dedicated to discussion of a novel recycling strategy: in-process separation of zinc from EAF dust. The concept of in-process separation of zinc from EAF dust is first defined, and then a simple Zn concentration model is developed. From this model, two approaches of in-process separation of zinc from EAF dust are derived: (1) prematurely capturing dust at very high temperature when zinc is still in vapor status, (2) prematurely collecting dust immediately after quickly cooling EAF off-gas from high temperature to low temperature. Next, thermodynamic analysis is conducted to understand zinc behavior in EAF off-gas. It is demonstrated in theory that zinc is in vapor status while it exits from electric arc furnaces. At last, recycling routes and economics of in-process separation of zinc from EAF dust are discussed.

#### 3:25 PM

#### The Removal of Nickel from Leachate of Galvanic Sludge with Titanium Dioxide: *Muge Sari Yilmaz*<sup>1</sup>; *Sibel Kasap*<sup>1</sup>; *Ozgul Dere Ozdemir*<sup>1</sup>; *Sabriye Piskin*<sup>1</sup>; <sup>1</sup>Yildiz Technical University

Galvanic sludge is generated at the end of the waste water treatment process of metal plating system. The waste sludge is one of the main hazardous solid wastes produced by metallurgical industries. It is caused the harm of human health and damage of the environment due to containing reasonable amounts of toxic metals (e.g., nickel, zinc, copper, chromium, iron, lead, cadmium, etc.). The concentration of those toxic metals in the wastewater might reach 30% (w/w, dry weight) making their removal and recovery an interesting issue. In this study, synthesized titanium dioxide is used as adsorbent to remove nickel in leachate of galvanic sludge. The adsorption experiments were carried out isothermally at four different temperatures. The effects of pH, temperature, and contact time on nickel adsorption efficiency were investigated, and the optimum parameters were determined from the experimental studies. The experimental results indicated that pH, temperature, and contact time played a significant role on the adsorption capacity of nickel.

3:45 PM Break

3:55 PM

**Recycling of High Quality Steel Scraps Directly in Electroslag Remelting Process (ESR):** *Burak Birol*<sup>1</sup>; Muhlis Saridede<sup>1</sup>; <sup>1</sup>Yildiz Technical University

The scraps of high quality steels generally contain expensive alloying elements such as chromium, vanadium, nickel, etc. These scraps are melted in an induction or an electric arc furnace and refined in ESR (Electroslag Remelting) purification process. A significant amount of alloying elements are lost during these processes. In order to avoid these losses, scraps can be utilized directly in ESR by skipping the melting step. In this study, 316L stainless steel scraps were refined in ESR with selected synthetic slags. The products were analyzed by optic emission spectrometry and the effects of slag compositions on the alloying element losses were examined. According to the analysis of the scrap and the products, generally chromium, nickel and manganese losses were encountered. It was determined that the alloying element losses has no connection with electrical conductivity. The slag containing CaF<sub>2</sub>, Al<sub>2</sub>O<sub>3</sub>, and FeO gives the optimum Cr and Ni losses.

4:15 PM

**Recycling of Wastes Generated during the Steelmaking Process:** *Victor Telles*<sup>1</sup>; *Joner Alves*<sup>1</sup>; *Denise Espinosa*<sup>1</sup>; *Jorge Tenório*<sup>1</sup>; <sup>1</sup>University of Sao Paulo - USP

The world production of crude steel in 2009 reached 1.2 billion tons. For each ton of steel produced, 150 kg of steelmaking slag and 20 kg of steelmaking dust are generated. These are wastes with considerable production and limited applications, therefore this work studied the recovery of these wastes into useful sub-products. The slag was used as raw material in the production of mineral wools (a thermo-acoustic insulator) and the dust was inserted in the iron ore sintering process. Results showed that produced materials have exceptional proprieties, therefore the recovery of these wastes can contribute to decrease extraction of non-renewable resources, reduce the costs and impact of disposals, and aggregate value to the slag and dust.

4:35 PM

**Differential Removal of Copper and Iron from Acidic Polymetallic Aqueous Solutions:** *Jinhui Li*<sup>1</sup>; *Youjun Xiao*<sup>1</sup>; *Daoling Xiong*<sup>1</sup>; *Ruixiang Wang*<sup>1</sup>; *Hao Chen*<sup>1</sup>; <sup>1</sup>Jiangxi University of Science and Technology

Leaching solution prepared from spent battery materials contains large quantities of valuable metals, such as Cu, Ni, Co, Mn and Fe. Therefore, recovery of valuable metals from acidic polymetallic aqueous solutions is of great importance for every plant. In this work, a method is introduced of recovery of Ni, Co and Mn from polymetallic solution prepared by leaching spent battery material. The basic concept includes copper was removed through replacement by iron powder followed by iron precipitation in goethite method. The experimental results show that Cu can be removed 99% at least through replacement by Fe powder, and the removal of Fe can achieve 99% by goethite method. At the same time, the loss of Ni, Co and Mn are about 2%, 3% and 2%, respectively. The purified solution which only contains Ni, Co and Mn can be used to prepare Ni<sub>x</sub>Co<sub>y</sub>Mn<sub>z</sub> ternary system precursor.

4:55 PM

**High Purity Alumina Powders Extracted from Aluminum Dross by the Calcining—Leaching Process:** *Liu Qingsheng*<sup>1</sup>; <sup>1</sup>Jiangxi University of Science and Technology

A new calcining-leaching process was used to extract high purity alumina (Al<sub>2</sub>O<sub>3</sub>) powders from aluminum dross in this study. The aluminum dross was mixed with soda (Na<sub>2</sub>CO<sub>3</sub>) and calcined at 900°C to yield soluble aluminates. Subsequently the calcined dross was leached with sulfuric acid (H<sub>2</sub>SO<sub>4</sub>) to produce a solution containing aluminum. The unwanted metal ions including Fe<sup>3+</sup> and Na<sup>+</sup> were removed by ethylene diamine tetraacetic acid (EDTA) and water washing. Then added the proper dispersant, controlling the crystallization of aluminum trihydroxide precipitation and the drying and calcining process was carried out resulting in ultra fine Al<sub>2</sub>O<sub>3</sub> powders with high purity. The characteristics of the Al<sub>2</sub>O<sub>3</sub> powders were examined by means of XRD, TEM and Brunauer-Emmet-Teller (BET) surface analysis

method. The extraction efficiency of Al<sub>2</sub>O<sub>3</sub> can surpass 98% by optimization of the calcination and lixiviation processes. Well-dispersed fibriform Al<sub>2</sub>O<sub>3</sub> powders were obtained by calcining at 800°C and the purity of the ultra fine Al<sub>2</sub>O<sub>3</sub> powders was more than 99.6%.

5:15 PM

**Research on Effect of Recombination Action of Rare Earth Metals La, Ce and Y on Soil Enzymatic Activities:** *Nie Jinxia*<sup>1</sup>; *Chen Yunnan*<sup>1</sup>; <sup>1</sup>Jiangxi University of Science and Technology

Rare earth resources are strategic and non-renewable resources. But disordered exploitation on rare earth metals leads to resources waste, environmental pollution and ecosystem destroyed. In this paper, soil collected from garden was cultured in thermostated incubator. Adding exogenous rare earth to the soil and the effects of recombination action of rare earth lanthanum, cerium and yttrium on soil enzymatic activities were studied. The results showed that single metal La and Ce can increase urease activity, but Y inhibits its. Coexist La/Y or La/Ce in soil inhibit the urease activity, coexist Y/Ce or coexist three metals promote its. Single metal La, Y and Ce can promote catalase activity, and that of coexist three metals. Pairwise coexist La, Y, Ce in soil inhibit catalase activity. With certain concentration of rare earth recombination action, urease activity in soil has been very significant direct proportion to ionic impulse, but catalase activity been insignificant inverse proportion to its.

---

## Refractory Metals 2011: Refractory Metal-Based Composites I

*Sponsored by:* The Minerals, Metals and Materials Society, TMS Structural Materials Division, TMS: Refractory Metals Committee  
*Program Organizers:* Omer Dogan, DOE National Energy Technology Laboratory; Jim Ciulik, University of Texas, Austin

Wednesday PM

March 2, 2011

Room: 19

Location: San Diego Conv. Ctr

*Session Chairs:* James Ciulik, University of Texas at Austin; Michael Gao, URS at National Energy Technology Laboratory

2:00 PM Invited

**Optimization of Mo-Ni-Al-X Alloys for High Temperature Oxidation:** *Matthew Kramer*<sup>1</sup>; *Pratik Ray*<sup>1</sup>; *Travis Brammer*<sup>1</sup>; *Kevin Severs*<sup>1</sup>; *Mufit Akinc*<sup>1</sup>; <sup>1</sup>Iowa State University

Using a series of computational methodologies ranging from semi-empirical methodologies to more accurate ab initio methods we have identified the Mo-Ni-Al system as a potential base alloy for high temperature applications. Of the a refractory metals, Mo appears to be the best candidate for combining a “skeleton” of a creep resistant metal with a high temperature intermetallic as a source of the oxidatively stable elements. Initial oxidation tests at 1150°C and above, while promising, shows that additional Platinum group metals, designated as X, are required to boost oxidation stability above 1300°C. Key to maintaining fracture toughness, creep strength and a prime-reliant oxidation protection will be synthesis methods to assemble the refractory metal and the oxidatively protective phases at the appropriate length scales. We are adopting a computational approach to optimize the Mo grain size and distribution in order to maximize the Mo fraction in the alloy without compromising oxidation stability.

2:20 PM Invited

**Effect of Zr Micro-Alloying Additions on Microstructure and Mechanical Properties of Mo-Si(-B) Alloys:** *Martin Heilmaier*<sup>1</sup>; *Manja Krüger*<sup>2</sup>; *Nelia Wanderka*<sup>3</sup>; <sup>1</sup>Technische Universität Darmstadt; <sup>2</sup>University of Magdeburg; <sup>3</sup>Helmholtz Zentrum Berlin für Materialien und Energie GmbH

We review our current understanding of the effect of Zr-microalloying on the deformation behavior of mechanically alloyed Mo-Si(-B) alloys: addition of 0.5 and 1 at% Zr to Mo-Si solid solutions leads to both, an increase in bend strength and plastic deformability. Auger analyses yielded a change



in fracture mode from intercrystalline to transgranular failure indicating Si segregation to cause grain boundary embrittlement. Complementing atom probe tomography and transmission electron microscopy investigations, however, reveal the formation of nano-scale Mo<sub>2</sub>Zr intermetallics decorating the grain boundaries was observed in ternary Mo-Si-Zr alloys, thereby suppressing the Mo<sub>5</sub>Si<sub>3</sub> and Mo<sub>3</sub>Si intermetallics found at grain boundaries in binary Mo-Si solid solutions. It is concluded that this phenomenon may be responsible for the observed decrease of the brittle-to-ductile transition temperature by Zr-addition in Mo-Si solid solutions as well as in complex 3-phase Mo-Si-B alloys.

**2:40 PM**

**Fracture Behavior of Mo-Si-B Alloys at Elevated Temperatures in Air and Inert Atmospheres:** *Joseph Lemberg*<sup>1</sup>; Michael Middlemas<sup>2</sup>; Joseph Cochran<sup>2</sup>; Robert Ritchie<sup>1</sup>; <sup>1</sup>University of California Berkeley; <sup>2</sup>Georgia Institute of Technology

Refractory metal silicides, such as Mo-Si-B, have been proposed as possible successors to current nickel superalloys. These alloys have the potential to operate in temperatures greater than 1300°C. Two alloys (Mo-3Si-1B wt%) processed in vastly differing manners, but with similar “duplex” microstructures, are studied. A “duplex” microstructure couples the oxidation resistance of the intermetallic Mo<sub>5</sub>Si<sub>3</sub> & Mo<sub>5</sub>SiB<sub>2</sub> (T<sub>2</sub>) phases with the fracture resistance of the ductile Mo-945-Mo phase. Within the framework of fracture resistance, the effect of processing route is examined. In inert atmospheres at 1300°C both alloys exhibited initiation toughnesses more than four times higher than at room-temperature, though the reaction-synthesized material described by Middlemas and Cochran (JOM, 2008) is much more ductile above 1100°C. The influence of an oxidizing environment on the fracture resistance of these alloys, a relatively unexplored consideration, is also analyzed. The present results are compared to previously-reported behavior exhibited by much-coarser grained materials.

**3:00 PM**

**Effect of Alloying on Phase Stability and Deformation Behavior of Mo-Si-B System:** *Oleg Kontsevoi*<sup>1</sup>; Arthur Freeman<sup>1</sup>; <sup>1</sup>Northwestern University

Mo-base alloys are promising materials for ultra-high temperature applications (>1400 °C), while one of the main drawbacks is poor ductility. By means of density-functional theory calculations we investigated the effect of alloying with 3d, 4d and 5d metals on phase stability and deformation behavior of 3-phase system T<sub>1</sub>(Mo<sub>5</sub>Si<sub>3</sub>) – T<sub>2</sub>(Mo<sub>5</sub>SiB<sub>2</sub>) – A15(Mo<sub>3</sub>Si). We determine site preference, phase partitioning of alloying elements, and their effect on shear behavior and preferred deformation modes. We show that alloying with early 3d transition metals results in softening, while most 4d and 5d elements lead to hardening. The results are discussed in conjunction with possible pathways to ductility enhancement through alloying.

**3:20 PM Break**

**3:40 PM**

**Molybdenum - Silicate Multiphase Composites: Mechanical Considerations:** *Peter Marshall*<sup>1</sup>; Joe Cochran<sup>1</sup>; Will Daloz<sup>1</sup>; <sup>1</sup>Georgia Institute of Technology

Multiphase, molybdenum based materials have received considerable attention for structural applications above 1150°C in oxidizing environments. In the MoSiB system a protective scale is accomplished by oxidation of molybdenum-silicides. However these composites suffer from poor fracture toughness at ambient temperatures due to the segregation of dissolved silicon to molybdenum grain boundaries and dislocations. In a novel approach presented here, the coating develops from a silicate glass phase present a priori in the composite. By avoiding a solid solution of silicon, the molybdenum matrix maintains ductility at room temperature. The glass is introduced through powder processing techniques as a fine, thermodynamically stable phase; taking care to minimize additional oxygen content. Additionally, powder processing allows for the introduction of other components to improve the high and low temperature mechanical properties. These include titanium and zirconium, commonly used in molybdenum

alloys, as well as mullite, a refractory ceramic capable of pinning grain boundaries.

**4:00 PM**

**Molybdenum-Silicate Multiphase Composites: Oxidation Concerns:** *William Daloz*<sup>1</sup>; Joe Cochran<sup>1</sup>; Peter Marshall<sup>1</sup>; <sup>1</sup>Georgia Institute of Technology

A new powder processing approach to produce oxidation resistant molybdenum alloys for high temperature is under development. Oxidation protection is provided by fine dispersion of silica glass particles within a molybdenum matrix. As the molybdenum oxidizes, the glass is exposed and melts to form a self-healing protective oxide coating. A third phase of homogeneously dispersed Mo<sub>2</sub>B provides boron which reduces glass viscosity so that the coating can be formed more rapidly at lower temperatures. Internal Mo<sub>2</sub>B also provides internal oxidation resistance. This is similar to the oxidation protection used in Mo-3Si-1B (wt%) systems; however embedding the glass directly into the Mo matrix and eliminating the Mo<sub>3</sub>Si (A15) provides the same volume of glass at lower volume fractions of brittle phases. Additionally the glass composition can be tailored for different applications and different temperatures beyond that achievable in Mo-Si-B based systems. A variety of microstructures for improved oxidation protection are explored.

**4:20 PM**

**Microstructures and Oxidation Behavior of W Substituted Mo-Si-B Alloys:** *Pratik Ray*<sup>1</sup>; Mufit Akinc<sup>1</sup>; Matthew Kramer<sup>1</sup>; <sup>1</sup>Iowa State University

The drive for increased Carnot efficiencies requires the development of alloys that can withstand harsh environments. Mo-Si based alloys, with a multitude of high melting intermetallics, have attracted considerable attention as candidates for ultra-high temperature applications. Boron doped Mo<sub>5</sub>Si<sub>3</sub> has been shown to have excellent oxidation resistance at high temperatures. The mechanical behavior of Mo<sub>5</sub>Si<sub>3</sub> intermetallics is relatively poor. Hence, a microstructure containing Mo<sub>5</sub>Si<sub>3</sub> along with Mo metal is thought to be more advantageous from the viewpoint of mechanical properties. Due to the nature of the Mo-Si-B phase diagram, co-existence of Mo, Mo<sub>5</sub>Si<sub>3</sub> and Mo<sub>5</sub>SiB<sub>2</sub> will require destabilization of Mo<sub>3</sub>Si, an intermetallic that has very low fracture toughness and poor oxidation resistance. Keeping this in mind, a combination of experimentation and computational techniques were used to determine optimal solute additions for destabilizing Mo<sub>3</sub>Si. The alloys thus designed were then tested for high temperature oxidative stability.

**4:40 PM**

**Oxidation Performance of Mo-Si-B Alloys: Implications through Alloying and Pre-Treatment:** *Steffen Burk*<sup>1</sup>; Bronislava Gorr<sup>1</sup>; Hans-Jürgen Christ<sup>1</sup>; <sup>1</sup>Universität Siegen

Mo-Si-B alloys melt around 2000°C and exhibit good mechanical properties and oxidation resistance at very high temperatures. Mo-9Si-8B-X alloys show excellent oxidation behaviour between 900°C-1300°C as a consequence of a protective silica scale. Below 900°C, volatile Mo-oxide formation leads to catastrophic oxidation. A protective oxide layer is not formed as a consequence of simultaneous and competitive Mo- and Si-oxide formation. Implications through alloying additions as well as pre-treatment prior to oxidation in air were examined. Classical alloying with Cr is a suitable means for protective Cr-oxide scale formation at intermediate temperatures, whereas additions of small amounts of reactive elements was found to have a strong impact on the silica scale forming abilities. Furthermore, the oxidation behaviour can be controlled by selective oxidation of silica in oxygen-deficient atmospheres prior to operation in air. Sufficient oxidation protection for Mo-Si-B alloys from room temperature up to 1300°C requires a combination of these approaches.

**5:00 PM**

**The Systematic Control of Polyhedral Mo Powder Formation with Different Particle Sizes:** *Xian Qin Wang*<sup>1</sup>; Fei Zhuang<sup>1</sup>; Yuan Jun Sun<sup>1</sup>; Jun Huai Liu<sup>1</sup>; Jing Li<sup>1</sup>; Hu Zhao<sup>1</sup>; <sup>1</sup>Jin Dui Cheng (JDC) Molybdenum Group Co. Ltd.

The icositetrahedron molybdenum powder showed great advantage in high performance of molybdenum materials with the ultra-low oxygen

content, regular crystalline boundary and good flowability etc. Investigation indicated polyhedral Mo powder with different size should have unique property in alloying and catalyst application. The MoO<sub>3</sub> decomposed from crystalline ADM was employed as start material. H<sub>2</sub> dewpoint, flowrate and temperature profile, residence time combinatorially performed to achieve microstructure with different sub-particle size during MoO<sub>3</sub>-MoO<sub>2</sub> reaction stage. In MoO<sub>2</sub>-Mo reaction stage, the MoO<sub>2</sub> sub-particle size always could be inherited. However there was flexibility for large MoO<sub>2</sub> sub-particles which could be separated into small Mo particles under the condition of slow reaction rate caused by low H<sub>2</sub> flowrate, suitable H<sub>2</sub>O partial pressure and temperature with feeding rate. The growth regime of polyhedral Mo was discussed by bonding the experiment results with related theory to make the production programmed in future.

## Sensors, Sampling, and Simulation for Process Control: Liquid Metal Sensing and Online Measurement

*Sponsored by:* The Minerals, Metals and Materials Society, TMS Extraction and Processing Division, TMS: Process Technology and Modeling Committee, TMS: Solidification Committee  
*Program Organizers:* Brian Thomas, University of Illinois at Urbana-Champaign; Andrew Campbell, WorleyParsons; Srinath Viswanathan, University of Alabama; Lifeng Zhang, Missouri University of Science and Technology; James Yurko, 22Ti LLC; Thomas Battle, Midrex Technologies

Wednesday PM  
March 2, 2011  
Room: 13  
Location: San Diego Conv. Ctr

*Session Chairs:* Brian Thomas, University of Illinois at Urbana-Champaign; Lifeng Zhang, Missouri University

### 2:00 PM Introductory Comments

#### 2:10 PM Keynote

**In-Situ Sensors for Liquid Metal Quality:** *Roderick Guthrie*<sup>1</sup>; Mihaiela Isac<sup>1</sup>; <sup>1</sup>McGill Metals Processing Centre

The development of effective methods for directly measuring liquid metal quality, prior to casting and final solidification, has been a goal for Process Metallurgists. Most techniques now in use either freeze a sample of the metal, or first concentrate the inclusions through filtering the metal through a porous frit, before then freezing the metal, and subjecting it to microscopic examination (e.g. PoDFA). The alternative method is to take a sample of metal, freeze it, and then dissolve the metal to release the particles (inclusions) through elutriation (The Slime Technique). The only true on-line, in-situ, methods are the Ultrasonic Liquid Metal Sensors (Mansfield Molten Metal Sensor), and the Electric Sensing Zone Approach (LiMCA and ESZ-pas). A brief history of the developments in these two approaches will be presented, and their long term prospects will be assessed versus other techniques.

#### 2:40 PM Keynote

**Sensors for On-Line Monitoring of Molten Metal Quality:** *Jeffrey Fergus*<sup>1</sup>; <sup>1</sup>Auburn University

The dissolution of gases in molten metals can lead to porosity and/or formation of inclusions in the resulting product. Real-time control of the process to minimize these defects requires information on the quality of the melt during processing. Electrochemical-based techniques can provide information on the chemical properties of the melt, while electromagnetic or acoustic-based techniques are used for physical properties, such as the presence of inclusions. The aggressive environments in molten metals create challenges in the development of reliable sensors. In particular, materials that are stable and provide the needed transduction properties at these high-temperature reactive conditions must be identified or developed. In this paper, techniques for measuring dissolved gas and inclusion contents in molten metals are reviewed.

#### 3:10 PM

**Development of an Aqueous Particle Sensor (APSIII) System as a Research Tool for Studying the Behavior of Inclusions in Water Models of Tundish Operations:** *Mihaiela Isac*<sup>1</sup>; *Abhishek Chakraborty*<sup>1</sup>; *Luis Calzado*<sup>1</sup>; *Roderick Guthrie*<sup>1</sup>; <sup>1</sup>McGill Metals Processing Centre

The control of liquid metal cleanliness during refining operations is an effective procedure used to improve the material properties of the final product. Low temperature simulation studies of inclusion behavior in steelmaking tundish operations have recently been carried out to develop techniques to float out as many inclusions as possible, prior to casting. The inclusions are simulated by glass microspheres submerged in water, and their behavior was studied with a new Aqueous Particle Sensor (APS III) recently constructed using digital based micro-computing technology. The working principle of the APS is identical to the well known Liquid Metal Cleanliness Analyzer (LiMCA) used worldwide for the detection of inclusion in molten aluminum. Both are based on the Resistive Pulse, or Electric Sensing Zone (ESZ) approach. The present "water LiMCA" has a wide particle size measurement capability, ranging between 25 to 170 microns, gathering on-line or off-line data with high accuracy.

#### 3:35 PM Break

#### 3:55 PM

**Lorentz Force Velocimetry – A Contactless Technique for Flow Measurement in High-Temperature Melts:** *Andre Thess*<sup>1</sup>; *Yurii Kolesnikov*<sup>2</sup>; *Christian Karcher*<sup>1</sup>; *Rico Klein*<sup>2</sup>; <sup>1</sup>Ilmenau University of Technology; <sup>2</sup>Ilmenau University of Technology

We describe a non-contact technique for velocity measurement in electrically conducting fluids. The technique, which we term Lorentz force velocimetry (LFV), is based on exposing the fluid to a magnetic field and measuring the force acting upon the magnetic-field-generating system. We illustrate the physical principles of LFV and report results of comprehensive laboratory experiments which characterise the sensitivity of LFV. We then present results of an industrial test of the technique in the aluminium industry which demonstrates that LFV performs well under harsh industrial conditions. We finally outline some future developments and argue that LFV, if properly designed, has a wide range of potential metallurgical applications.

#### 4:20 PM

**The Development of a Sensor to Determine the Direction of Velocity in Liquid Aluminum:** *Mitren Sukhran*<sup>1</sup>; *Stavros Argyropoulos*<sup>1</sup>; <sup>1</sup>University of Toronto

This paper shows that the temperature distribution within a cylindrical rod, while inserted into flowing liquid aluminum (Al), produces different heating profiles regarding the direction of flow. One can deduce the direction of velocity in the metal by understanding the heating pattern of the cylinder. Specifically, by being able to track the temperature as a function of spatial and temporal coordinates within the cylindrical rod, one can infer the direction of velocity. Experimental research work involving liquid Al has been conducted using this sensor in the Revolving Liquid Metal Tank (RLMT) at the University of Toronto. The RLMT is capable of melting approximately 50 kg of Al and imposing specified tangential velocities up to 0.35 m/s. It will be shown that our cylindrical rod sensor records different heating patterns under different fluid flow conditions. This temperature information is then used to infer the direction of velocity in the bath.

#### 4:45 PM

**New Sensors for the Velocity Measurement in Liquid Metal Processes:** *Klaus Timmel*<sup>1</sup>; *Sven Eckert*<sup>1</sup>; *Thomas Wondrak*<sup>1</sup>; *Frank Stefani*<sup>1</sup>; *Gunter Gerbeth*<sup>1</sup>; <sup>1</sup>Forschungszentrum Dresden-Rossendorf

In many technological processes involving liquid metals or semiconductor melts the velocity fields cannot be measured due to the lack of commercial measuring techniques for opaque melts. We present two measuring techniques which have proven recently as providing reliable velocity measurements in liquid metals, at least in the temperature range up to about 700°C: the ultrasonic Doppler Velocimetry (UDV) and the contactless inductive flow tomography (CIFT). UDV is capable of delivering velocity profiles along the

ultrasonic beam with a time-resolution of about 20 Hz. CIFT is based on the flow-induced modification of some externally applied magnetic field, which is measured by some array of magnetic field sensors outside of the melt. We present measurements with both techniques at the small-scale liquid metal model Mini-LIMMCAST of the continuous steel casting process. Both measuring methods give consistent results for the jets evolving from the nozzle outlets.

#### 5:10 PM

**Measurement of Molten Steel Surface Velocity with SVC and Nail Dipping during Continuous Casting Process:** Joydeep Sengupta<sup>1</sup>; Rui Liu<sup>2</sup>; Don Crosbie<sup>1</sup>; S. Chung<sup>1</sup>; M. Trinh<sup>1</sup>; Brian Thomas<sup>2</sup>; <sup>1</sup>ArcelorMittal Dofasco; <sup>2</sup>University of Illinois at Urbana Champaign

Surface velocity of the molten steel is critical to final product quality during continuous casting of steel. Plant experiments using two different new sensors, Sub-meniscus Velocity Control (SVC) devices and nail boards, are performed to evaluate their performance, and to quantify liquid steel velocities at locations 50 mm apart on the surface of ArcelorMittal Dofasco's No. 1 continuous caster under different casting conditions, including different throughputs, mold widths, Submerged Entry Nozzle (SEN) depths and SEN designs. A relation between the height difference of the solidified lump on the nail and surface velocity is confirmed and extended. Reasonable agreement between the two sensing methods of surface velocity is obtained, both in trends and magnitudes for both time-averaged velocity and transient flows. Correlations between surface velocity and throughput are developed using computational fluid dynamics (CFD) models and the performances for different casting conditions are compared and evaluated based on the velocity measurements.

#### 5:35 PM

**Measurement of Transient Meniscus Flow in Steel Continuous Casters and Effect of Electromagnetic Braking:** Seong-Mook Cho<sup>1</sup>; Hyoung-Jun Lee<sup>1</sup>; Seon-Hyo Kim<sup>1</sup>; Rajneesh Chaudhary<sup>2</sup>; Brian Thomas<sup>2</sup>; Duck-Hee Lee<sup>3</sup>; Yong-Jin Kim<sup>3</sup>; Woong-Ryul Choi<sup>4</sup>; Sung-Kwang Kim<sup>4</sup>; Hui-Soo Kim<sup>4</sup>; <sup>1</sup>Pohang University of Science and Technology; <sup>2</sup>University of Illinois at Urbana Champaign; <sup>3</sup>POSCO Gwangyang Steel Works; <sup>4</sup>POSCO Gwangyang Works

Unstable meniscus flow leads to slab surface defects during continuous casting of steel, due to level fluctuations and vortex formation, which causes entrapment of argon bubbles and mold flux. Applying electromagnetic fields across the liquid steel pool, such as the "ruler" or "FC-mold" braking system, has been commercialized to stabilize meniscus flow. Plant measurements were performed using nail boards to quantify meniscus flow in a typical steel slab-casting mold with a slide gate system. Meniscus level shape, surface velocity, the direction of meniscus flow, and the variations of all of these parameters with time and location are all quantified by analyzing the shape of the skull of solidified steel that encases each dipped nail. The results reveal interesting time-variations in the flow pattern, which cannot and should not be detected with a standard mold-level sensor used for flow control. Finally, the effect of applying the electromagnetic field on the flow pattern is revealed.

## Shape Casting IV: Light Metals Division Symposium in Honor of Prof. John T. Berry: Methods and Systems

*Sponsored by:* The Minerals, Metals and Materials Society, TMS Light Metals Division, TMS: Aluminum Processing Committee, TMS: Solidification Committee

*Program Organizers:* Murat Tiryakioglu, University of North Florida; Paul Crepeau, General Motors Corporation; John Campbell, University of Birmingham

Wednesday PM  
March 2, 2011

Room: 15B  
Location: San Diego Conv. Ctr

*Session Chairs:* Alan Druschitz, Univ of Alabama; Derya Dispinar, SINTEF

#### 2:00 PM Introductory Comments

#### 2:10 PM

**The Effect of Reducing the Molecular Weight of the Foam Pattern in the Lost Foam Casting Process:** Kiavash Siavashi<sup>1</sup>; Clare Topping<sup>2</sup>; William Griffiths<sup>3</sup>; <sup>1</sup>University of Birmingham; <sup>2</sup>Isotron; <sup>3</sup>University of Birmingham

In lost foam casting there can be a reduction in casting quality if the liquid polymer byproducts from the foam pattern become entrapped in the liquid metal. However, these are absorbed by the permeable pattern coating, once degradation has sufficiently reduced their molecular weight. This suggests that beginning with a lower molecular weight pattern may give higher quality castings, because less reduction in molecular weight will be required before absorption of the liquid polymer byproduct into the pattern coating. The initial molecular weight of expanded polymethylmethacrylate-polystyrene copolymer foam patterns was reduced by  $\gamma$ -radiation. The properties of castings made with these irradiated foam patterns, such as porosity, fluidity length, tensile and fatigue properties, (in the case of aluminium castings), and carbon pick up, (ferrous castings), were compared with the properties of castings made from unirradiated foam, to show the advantages of using the former.

#### 2:30 PM

**Classical Nondestructive Testing Techniques Do Not Correlate with Strength as Does Process Compensated Resonant Testing:** Robert Nath<sup>1</sup>; Marvin Johnson<sup>2</sup>; Clifford Grupke<sup>2</sup>; Chuck Leonard<sup>3</sup>; <sup>1</sup>Magnaflux Quasar; <sup>2</sup>Retired/Consultant; <sup>3</sup>Diversified Machine, Inc.

Process Compensated Resonant Inspection (PCRT) outperforms classical nondestructive testing (NDT) on aluminum parts based not just upon the significantly better results obtained from testing millions of automotive parts in production operations with achieved near-zero failures, but also insight gained from destructive testing and analysis. Several different destructive testing efforts were performed. Applicable classical NDT and PCRT were used. The PCRT relies on defining as "acceptable" those parts that are structurally acceptable, as measured by metallurgical, destructive and other nondestructive testing. Castings tested and accepted with classic NDT indications often have structural weakness and are accepted because their major defects are often the result of damaging thermal history or invisible oxide bifilms. Conversely, structurally acceptable castings are often rejected for negative classic NDT indications. Key previously assumed "facts" dealing with the parts and how they are accepted/rejected do not always stand up to more thorough destructive testing and analysis.

#### 2:50 PM

**Advanced Methoding Concepts for the Gravity Casting of Steel Alloys:** Bob Puhakka<sup>1</sup>; <sup>1</sup>Alloy Casting Industries

Wlodawer and Chvorinov provided invaluable early guidelines for the feeding of steel castings, but technology has moved on. This paper describes a new set of concepts that apply to the filling conditions for the entire family of steel casting alloys, from plain carbon to super duplex stainless steels. Application of the concepts is achieving new standards of quality together with reduced costs.



3:10 PM

**Advanced Mold Design Technology of the LCS Waterjet (WJ) Entry Edge Casting Components Assisted by Flow, Solidification and Stress Modeling:** *Laurentiu Nastac*<sup>1</sup>; John Romanelli<sup>1</sup>; <sup>1</sup>Concurrent Technologies Corporation

In order to reduce cost, increase performance and ensure quality, this Navy Metalworking Center (NMC) project utilized an advanced casting simulation-based optimization approach to assist in the improvement of the mold design of LCS Waterjet (WJ) entry edge components. This approach helped to minimize mold filling and solidification related defects (misruns, coldshuts, shrinkage and porosity and hot tears), as well as post-solidification related defects (hot and cold cracks, distortion and residual stresses). The results of this optimization were used to more readily achieve first time quality on the geometrically challenging WJ components.

3:30 PM

**Evaluation of the Distortion of a Hydro Turbine Blade during Heat Treatment Process:** *Jinwu Kang*<sup>1</sup>; <sup>1</sup>Tsinghua University

Hydro turbine blade castings are susceptible to distortion during heat treatment process for their thin and curved shapes. By the numerical simulation method, the distortion of the castings can be acquired. However, the distortion values depend on the selection of reference points which are selected only by experience. In this paper, a distortion evaluation method is presented, in which the normal direction change of local triangle areas with respect to the original shape is utilized. By this method, the distribution of distortion degree of the whole casting is obtained and the reference points are selected in the smallest distortion areas. Then, the dynamic distortion of the casting represented by the displacement values during heat treatment process is acquired. The distortion mainly concentrates on the two corners and the inner sides of root areas of the two corners are intensively cooled to avoid distortion. The simulated results show its validity.

3:50 PM Break

4:10 PM

**The Capability Enhancement of Aluminium Casting Process by Application of the Novel CRIMSON Method:** *Xiaojun Dai*<sup>1</sup>; Mark Jolly<sup>1</sup>; <sup>1</sup>University of Birmingham

The conventional foundry frequently uses the batch casting process where the aluminium alloys are melted and held in a furnace for a long time, sometimes as long as a complete shift. The long holding time increases the level of hydrogen absorption and the thickness of oxide films which are often the main reasons for casting defect generation. In this paper, a novel CRIMSON aluminium casting method is introduced which has a number of advantages. Instead of the batch casting method, it uses the single shot casting method to realize the rapid melting and rapid counter-gravity-filling mould operations, which reduce the contact time between the melt and environment, thus reducing the possibility of defect generation. Another advantage is the drastic reduction of energy consumption due to shortened melting and filling time. An actual case is used to compare the CRIMSON process and the conventional casting process.

4:30 PM

**Optimization of the Process Parameters and Tooling Improvement for the Rheocasting of High Quality Aluminum Components Using the SEED Process:** Chang-Qing Zheng<sup>1</sup>; *Ehab Samuel*<sup>1</sup>; Alain Simard<sup>1</sup>; Florentin Laplume<sup>1</sup>; <sup>1</sup>National Research Council Canada

The SEED (Swirled Enthalpy Equilibrium Device) rheocasting method, developed by Rio Tinto Alcan in collaboration with NRC Canada, was analyzed in an attempt to optimize parameters which affect the final casting quality. The SEED process has already proven successful in producing sound aluminum castings having an excellent combination of strength and ductility. However, in many of the existing semi-solid processes which make use of billets as feedstock, it is often found that the outer surface of the billets is contaminated. The use of such a contaminated billet can often result in an increased rejection rate of castings. To avoid the presence of a contaminated surface inside the casting, the paths along which the billet skin evolves must

be controlled during the filling stage. Simultaneously, there was an ongoing effort to enhance the mechanical properties of the aluminum alloys studied.

4:50 PM

**Shaped Castings and Machining:** *John Wyatt*<sup>1</sup>; John Berry<sup>1</sup>; <sup>1</sup>Mississippi State University

This paper will discuss three aspects of the machining of shaped castings: a) machinability, b) machining sequence, and c) residual stresses, the principal thrust being that of machinability. Currently, there is a growing movement to reconsider the whole process of machining from the standpoint of fracture mechanics. This has resulted from the groundbreaking work of Atkins at Reading University (UK), which is relevant to cast alloys and which, invariably, are multiphase materials. Although secondary and tertiary phases have been blamed for tool wear, they are, in fact, intrinsically tied into the cutting process. The premise of Atkins is that ductile rupture takes place near the tool tip. These ductile tears manifest as dimples associated with the secondary and tertiary phases. Although some secondary phases will cleave (silicon particles in AlSi type alloys), some will decohere from the matrix leaving dimples. The authors will describe some experiments confirming the theories of Atkins.

5:10 PM

**The Estimable Value of "Clever" Experiments:** *John Berry*<sup>1</sup>; <sup>1</sup>Mississippi State University

The inexorable growth of computational modeling in materials science and engineering has initiated a serious decline in the number of "clever", or genuinely useful experiments. Experimental evidence, if provided, is often second-hand and merely placed there to validate a model, thus not stimulating further study. Many established concepts in materials science have been overturned as a result of careful experiments. These experiments have often nucleated new concepts and have started a sequence of experiment pacing theory and vice-versa. In his long career, the writer has witnessed many examples of this pacing effect, some of which he lists. Several of these resulted in viable industrial processes. He describes unpublished work concerning the heat extractive capacity of molds, which is relevant to current processing developments. The experiments concerned spawned further analytical work providing examples of the said pacing effect.

5:35 PM Concluding Comments

**Dr. Berry will have the opportunity to reflect on the symposium, metal casting and life.**

---

**Size Effects in Mechanical Behavior: Observing Size Effects Using the Microcompression Method**

*Sponsored by:* The Minerals, Metals and Materials Society, Not Applicable, TMS: Nanomechanical Materials Behavior Committee  
*Program Organizers:* Erica Lilleodden, GKSS Research Center; Amit Misra, Los Alamos National Laboratory; Thomas Buchheit, Sandia National Laboratories; Andrew Minor, UC Berkeley & LBL

Wednesday PM  
March 2, 2011

Room: 2  
Location: San Diego Conv. Ctr

---

*Session Chairs:* Andrew Minor, UC Berkeley; Cynthia Byer, Johns Hopkins University

---

2:00 PM Invited

**Achieving Ultra-High Strength and Strain-Hardening Rate by Trapping Dislocations in Small Material Volumes:** Kwok-Sing Ng<sup>1</sup>; *Alfonso Ngan*<sup>1</sup>;

<sup>1</sup>University of Hong Kong

The deformation of metallic micro-pillars is, in general, jerky and of a stochastic nature. The jerky flow is due to a source-depleted condition specific to small material volumes; therefore, confining the dislocations instead of allowing them to annihilate at free surfaces may change the deformation mode. In this work, a number of methods were used to confine

WEDNESDAY PM

dislocations inside micro-sized aluminum pillars. First, the pillar was coated with a thin layer of tungsten by focused-ion-beam (FIB) induced, chemical vapor deposition (CVD) on its free surface. Secondly, a cavity was milled inside the pillar by FIB, and this was then filled with tungsten by FIB-CVD. The third method involved including a grain boundary inside the pillar to form a micro-bicrystal. In these cases, the coating, filling, or grain boundary was found to hold the dislocations inside the micro-specimen resulting in much smoother deformation with very high strength and strain-hardening rate.

#### 2:30 PM Invited

**Size Effects on Strength and Hardening in Cu Micropillars:** P. J. Guruprasad<sup>1</sup>; Daniel Kiener<sup>2</sup>; Gerhard Dehm<sup>2</sup>; Shyam Keralavarma<sup>3</sup>; *Amine Benzerga*<sup>2</sup>; <sup>1</sup>Ecole des Mines de Paris; <sup>2</sup>Austrian Academy of Sciences; <sup>3</sup>Texas A&M University

The stress-strain response under compression of single crystalline Cu micropillars is investigated. The crystals are oriented for double slip, and the size of the pillars studied fall in the range 0.4–10 microns. The experiments reveal a size effect on the crystal strength. The hardening rates are extracted from the experiments and compared with those from the simulations. A two-dimensional discrete dislocation dynamics framework is used to model the experiments with additional constitutive rules for junction formation and dynamic source operation. It is observed that the simulations using a relatively large initial density of Frank-Read sources yield good quantitative agreement with the experiments for all specimen sizes investigated. Moreover, the simulations predict the correct scaling of both the flow stress, as well as the strain hardening rate with the pillar size. Possible micro-mechanisms for the observed size effects are discussed in light of the DD simulations.

#### 3:00 PM

**Effect of Initial Dislocation Density on Microcompression Experiments of HCP Single-Crystal Magnesium:** *Cynthia Byer*<sup>1</sup>; K. T. Ramesh<sup>1</sup>; <sup>1</sup>Johns Hopkins University

The size effects and orientation dependence of deformation mechanisms associated with single crystals under uniaxial compression are becoming an increasingly popular area of study. Microcompression literature shows that, for some materials, decreasing the diameters of these micro-scale pillars increases the yield stresses and strain hardening rates; however, many questions remain, especially for hexagonal close packed (hcp) materials. In this study, we focus on the impact of initial dislocation density on deformation mechanisms and size effects in single crystal magnesium. Microcompression experiments are conducted on micropillars (1–10 micrometers in diameter) fabricated using focused ion beam (FIB) milling on both chemically etched and unetched samples. Specimens are loaded along the [0001] c-axis and reveal that etched samples with lower initial dislocation densities fail at lower stresses than unetched micropillars. Post-mortem microscopy is used to examine the details of the deformation mechanisms that are involved.

#### 3:20 PM

**Size Effects in Slip and Twinning in Mg Single Crystals:** *Erica Lilleodden*<sup>1</sup>; Gyu Seok Kim<sup>1</sup>; <sup>1</sup>GKSS Research Center

Microcompression testing has been performed on magnesium single crystals with [0001], [2-1-12], [10-11], [11-20] and [10-10] compression axes in order to investigate the slip and twinning mechanisms in Mg. In all cases a size effect in flow stress is observed, although the deformation mechanisms are varied between samples. While columns compressed along the [0001], [2-1-12], and [10-11] axes undergo dislocation plasticity, the columns compressed along the <11-20> and <10-10> axes are dominated by deformation twinning. While the basis for the size effect in the former cases can be explained by a finite volume effect on dislocation interactions, it is less clear why such a significant size effect occurs in the case of twinning. We will offer two possible explanations for the behavior, based on a mechanistic picture of the deformation behavior as revealed through SEM, EBSD and TEM characterizations.

#### 3:40 PM Break

#### 4:10 PM

**Size Effects on Plasticity and Martensitic Transformation in Shape Memory Alloy Microcrystals:** *Matthew Bowers*<sup>1</sup>; Michael Mills<sup>1</sup>; John Carpenter<sup>1</sup>; Peter Anderson<sup>1</sup>; Sivom Manchiraju<sup>1</sup>; <sup>1</sup>The Ohio State University

The present study investigates the effects of crystal orientation and specimen size on the pseudoelasticity and shape memory response of Ni-Ti based shape memory alloys. Previous work has shown a dramatic increase in strength for pure nickel when reduced to micron and submicron test volumes, leading to the hypothesis that small sample sizes may influence dislocation plasticity. Experimental evidence exists which links residual strain caused by dislocation plasticity to degradation of the pseudoelastic effect in shape memory alloys. This suggests that enhancement of the pseudoelastic response with small sample dimensions may be possible. To investigate these size effects, FIB-machined single crystal micropillars are tested in compression and analyzed via mechanical response measurements and post-mortem TEM observations. An additional feature is that micropillar testing can activate specific martensite plates, allowing for the isolation and investigation of particular variants in the absence of interaction effects between competing plates.

#### 4:30 PM

**Anomalous Features of the Nanoscale Deformation of “Gum Metal”:** *John Morris*<sup>1</sup>; Elizabeth Withey<sup>1</sup>; Rohini Sankaran<sup>1</sup>; Andrew Minor<sup>1</sup>; Daryl Chrzan<sup>1</sup>; Shigeru Kuramoto<sup>2</sup>; <sup>1</sup>University of California Berkeley; <sup>2</sup>Toyota Central R&D Laboratory

The name “gum metal” has been given to a set of  $\beta$ -Ti alloys that, with appropriate preparation, appear to deform by a dislocation-free mechanism involving elastic instability at the limit of strength. We have studied the nanodeformation of these materials through nanoindentation and via instrumented, in situ compression in high resolution TEM. A number of unusual deformation mechanisms and patterns are observed. This paper will discuss three topics: (1) The initial deformation of nanopillars that yield at near ideal strength is local and nanoscaled, with the consequence that there is no significant size effect to the smallest sizes tested. (2) Nanopillar deformation sometimes involves the “shear bands” that dominate deformation at larger sizes, but these are secondary, post-yielding deformation features. (3) The material in the depths of nanoindentation pits contains no well-defined dislocations or other defects, but is rather deformed by continuous rotation about some preferential axis.

#### 4:50 PM

**A Microcompression Study of Gum Metal:** *Julia Hapke*<sup>1</sup>; Shigeru Kuramoto<sup>2</sup>; Erica Lilleodden<sup>1</sup>; <sup>1</sup>GKSS-Research Center; <sup>2</sup>Toyota Central R&D Laboratory

We have investigated a unique beta-Ti alloy called gum metal using microcompression testing. In the cold-worked state, this alloy has been reported to fail at its ideal strength without contribution of dislocation plasticity. In order to understand the effects of cold work on the deformation, a sample without cold working was also investigated. Microcompression specimens with diameters in the range of 300 nm to 10  $\mu$ m were fabricated within single crystalline volumes, where possible. In contrast to the non-worked sample, which showed a nominal grain size of 100  $\mu$ m, the cold-worked sample displayed no clear grain structure. While the non-worked sample displayed a size effect in flow stress, no significant size effect was observed in the cold-worked sample. Both samples showed shear bands, but with significantly different shear band spacing. The resultant stress-strain responses and deformation morphologies will be further discussed in terms of the governing microstructural length scales.

5:10 PM

**High Resolution Imaging of Gum Metal Defect Structure:** *Rohini Sankaran*<sup>1</sup>; *Velimir Radmilovic*<sup>2</sup>; *Daryl Chrzan*<sup>1</sup>; *Andrew Minor*<sup>1</sup>; *John Morris*<sup>1</sup>; <sup>1</sup>University of California Berkeley; <sup>2</sup>Lawrence Berkeley National Laboratory

Gum metal, a set of beta-Ti alloys, has remarkable mechanical properties that occur upon severe cold working, the most prominent being that it plastically deforms at its theorized ideal strength. Previous studies have indicated that plastic deformation is not achieved through conventional dislocation motion. However, the details of the precise mechanism to achieve this deformation are not yet well understood. Here, we aim to clarify the deformation mechanisms through high resolution TEM imaging of the defect structure in gum metal. The HRTEM images reveal a highly distorted lattice of non-discrete defects. Geometric phase analyses of the images reveal complex atomic displacements which may be indicative of an overlapping dislocation core structure in the cold worked gum metal. The relationship of these atomic displacements to theorized "nanodisturbances" as a possible deformation structure is discussed along with the atomic nature of possible dislocation pinning sites.

---

### Waste Heat Recovery: Session I

*Sponsored by:* The Minerals, Metals and Materials Society, TMS Extraction and Processing Division, TMS Light Metals Division, TMS: Energy Committee

*Program Organizers:* Cynthia Belt, Consultant; Mark Jolly, University of Birmingham; Xingbo Liu, West Virginia University; Rachel DeLucas, H.C. Starck

Wednesday PM  
March 2, 2011

Room: 31B  
Location: San Diego Conv. Ctr

*Session Chairs:* Rachel De Lucas, HC Starck Inc; Xingbo Liu, West Virginia Univ

---

2:00 PM

**Waste Heat Utilization to Increase Energy Efficiency in the Metals Industry:** *Elizabet Cruz*<sup>1</sup>; *Maytinee Vatanakul*<sup>1</sup>; *Rory Hynes*<sup>1</sup>; *Jim Sarvinis*<sup>1</sup>; <sup>1</sup>Hatch

Energy efficiency improvements achieved using heat recovery processes offer benefits to both the business case and environmental impact of metallurgical facilities. Global demand drives the development of lower and lower grade ore bodies. This trend results in higher energy intensity and consequently increased waste heat. Waste heat boilers and Organic Rankine Cycle (ORC) processes are becoming cost competitive methods of utilizing this waste heat. This study analyzes heat recovery from available sources to produce power using:

- High grade: waste heat boiler and steam turbine generator. This system will produce electricity, and/or process steam.
- Low grade: ORC to produce electricity. The cycle is well adapted to low-moderate temperature heat sources. Processes from metallurgical plants, hot exhaust streams, cooling and condensers could benefit from application of these systems. The study demonstrates:
- The energy and cost saving potential of waste heat recovery technologies
- The environmental benefit

2:20 PM

**Waste Heat Reduction and Recovery Options for Metals Industry:** *Arvind Thekdi*<sup>1</sup>; *Cynthia Belt*<sup>2</sup>; <sup>1</sup>E3M Inc.; <sup>2</sup>Consultant

Waste heat from industrial operations in metals industry represents 20% to 50% of the total energy used in most manufacturing plants. Reduction and recovery of waste heat offers the most attractive and cost effective method of reducing energy intensity for an industrial plant to meet corporate energy saving goals. It is possible to reduce or recover 30% to 60% of the available waste heat by using conventional and readily available technologies. Projects to reduce or recover waste heat may offer less than 3 years payback to as short as a few months. This paper presents information on most commonly used methods for waste heat reduction and recovery in the metals industry

operations. It describes the methods and use of analysis tools that would allow a user to estimate energy savings, CO<sub>2</sub> or GHG reduction potential, and economic benefit and includes appropriate case histories.

2:40 PM

**Development of a Direct Evaporator for the Organic Rankine Cycle:** *Donna Guillen*<sup>1</sup>; *Helge Klockow*<sup>2</sup>; *Matthew Lehar*<sup>2</sup>; *Sebastian Freund*<sup>2</sup>; *Jennifer Jackson*<sup>2</sup>; <sup>1</sup>Idaho National Laboratory; <sup>2</sup>General Electric Company

Research and development is currently underway to place the evaporator of an Organic Rankine Cycle (ORC) system directly in the path of a hot exhaust stream produced by a gas turbine engine. The main goal of this research effort is to improve cycle efficiency and cost by eliminating the usual secondary heat transfer loop. The project's technical objective is to eliminate the pumps, heat exchangers and all other added cost and complexity of the secondary loop by developing an evaporator that resides in the waste heat stream, yet virtually eliminates the risk of a working fluid leakage into the gaseous exhaust stream. The research team comprised of Idaho National Laboratory and General Electric Company engineers leverages previous research in advanced ORC technology to develop a new direct evaporator design that will reduce the ORC system cost by up to 15%, enabling the rapid adoption of ORCs for waste heat recovery.

3:00 PM

**The Application of Industrial Waste Heat to ORC Waste Heat Generators:** *Bob Miller*<sup>1</sup>; <sup>1</sup>Calnetix, Inc.

The Organic Rankine Cycle (ORC) has been used for waste heat turbines to turn heat into electricity. The goal of this paper is to show as many practical applications of ORC technology to industrial waste heat streams. The cycle will be explained using a high speed radial expander along with discussion of heat exchangers and waste heat gas streams. Specific examples from chemical, petroleum, metals, and materials industries will be discussed. Project economics will be reviewed for industrial use.

3:20 PM

**Topological Considerations for Thermoelectric Capture of Waste Heat:** *Jan Beck*<sup>1</sup>; *David Nemir*<sup>1</sup>; *Manuel Alvarado*<sup>1</sup>; <sup>1</sup>TXL Group, Inc.

Thermoelectric generation using special N-doped and P-doped semiconductors is well known as a means for direct heat energy to electrical energy conversion. However, while the technology is scalable and appropriate for energy capture from both small scale (milliwatt) and large scale (megawatt) heat streams, the choice of topology must be tailored to the power generation requirements. This paper describes a simulation study to define the optimal aspect ratios for the active thermoelements and the electrical interconnect. By using a finite element model that incorporates the intercoupled heat and electrical energy flows, a set of empirical rules is presented to guide successful generator deployments. A discussion is provided on using these rules for evaluating the costs and trade-offs in thermoelectric generator design.

3:40 PM

**Waste Heat Recovery in the Aluminum Melting Furnaces:** *John W. Norton*<sup>1</sup>; <sup>1</sup>Norton Engineering, LLC

This presentation will cover the physical properties of waste heat recovery. It is a two part presentation. The first deals with actually recovering the heat with new state of the art heat exchangers and applying that heat to the furnace combustion and the second part will cover what other processes you can enhance with this "free" heat. It will also talk about converting it to steam, hot air or electricity to be used or sold back to the utility company. The economics of various schemes will be reviewed. A brief discussion on state and federal grants and subsidies will be presented.

4:00 PM

**Energy Efficiency Improvement by Implementation of the Novel CRIMSON Aluminium Casting Process:** *Mark Jolly*<sup>1</sup>; *Xiaojun Dai*<sup>1</sup>; <sup>1</sup>University of Birmingham

Foundry engineers in the traditional foundry usually regard the quality of casting component as the most important issue and leave the energy saving or energy efficiency as the subsidiary one. This frequently causes



disproportionate energy consumption as a result of the inefficient casting processes used and increases the production costs. This paper presents the novel CRIMSON aluminium casting process and compares its facility and melting process with traditional melt furnaces and aluminium alloy melting process. A real example is investigated to demonstrate quantitatively how the traditional foundry wastes energy and what the improvement of energy efficiency can be achieved using the novel CRIMSON method. The results of this investigation will help the foundry engineer recognize the importance of energy saving and demonstrate how to use this new technology to reduce production costs and carbon footprint without decreasing the quality of the cast component.

**4:20 PM**

**Waste Heat Recovery Trial from Aluminum Reduction Cell Exhaust Gases:** *Hadi Fanisalek*<sup>1</sup>; Mohsen Bashiri<sup>1</sup>; Reza Kamali<sup>1</sup>; <sup>1</sup>Hormozal

Half of the input energy to aluminum reduction cell will be lost as waste heat which could be studied for possible recovery. Since the price of energy is increasing and the main production cost in primary aluminum industry is energy, waste heat recovery consideration will be interesting. One of the possible choices for recovery is from aluminum exhaust gases that need minimum modifications for reduction cell and has no influence on cell heat balance which is vital for the operation. By using heat exchangers with in-line and staggered tube arrangements placed before fume treatment plant (FTP) we will be able to recover enough amount of heat. The main challenging problem which is necessary to overcome will be the heat exchanger material and its design because of corrosive and dusty exhaust gases from potroom. In this paper, a desalination system with six effects of evaporator is proposed for producing distilled water by using recovered heat from hot exhaust gases. The calculated amount of produced distilled water is around 27,000 kg/hr in this specific suggested desalination plant. The suggested desalination plant is based on Hormozgan Aluminum Company data (Hormozal) in Bandar Abbas, Iran which is constructed by the Persian Gulf.

**4:40 PM**

**The Study of Coal Gasification by Molten Blast Furnace Slag:** *Peng Li*<sup>1</sup>; Qingbo Yu<sup>1</sup>; <sup>1</sup>Northeastern University

A new heat recovery system is proposed. This system uses the endothermic heat of gasification reaction instead of sensible heat to recover the energy of molten blast furnace slag. The gasification technological parameter in molten blast furnace was calculated and the exergy of the system was analyzed. The gasification reactions were studied kinetically by the isothermal thermogravimetry using STA409PC thermal analyzer. The results showed that, according to different gasification agent, this system can produce syngas with different C-H ration. The exergy efficiency of this system is high and its internal exergy loss rate is about 5%. This method can bring huge economic and environmental benefits which are important to the survival and sustainable development of iron-steel enterprises. The molten BF slag acts as not only thermal media but also good catalyst. The kinetic parameters on gasification reaction with different types of coal used differ from each other, e.g.

**5:00 PM**

**System for Recovering Waste Heat from High Temperature Molten Blast Furnace Slag:** *Junxiang Liu*<sup>1</sup>; Qingbo Yu<sup>1</sup>; Qin Qin<sup>1</sup>; <sup>1</sup>Northeastern University

Dry-granulation is a new process of molten blast furnace slag treatment and air is used as heat exchange medium. There are some shortages: poor effectiveness of granulation, high air-slag ratio and high energy consumption, which are the obstacles to popularize dry-granulation. Based on rotary cup atomization, the technique of recovering waste heat of molten blast furnace slag through waste heat boiler producing high pressure steam is exploited. The molten blast furnace slag is granulated to uniform small slag granules with high temperature, and slag granules pour into the waste heat boiler. It could produce steam, obtained in first row and second row tubes, when descending velocity of slag granules equaled 1.1mm/s and the Reynolds

number equaled 7100. The application of the system for recovering waste heat from high temperature molten blast furnace slag has a significant meaning.

**5:20 PM**

**Stability and Thermoelectric Properties of Transition Metal Silicides from First Principles Calculations:** *Philippe Jund*<sup>1</sup>; Xiaoma Tao<sup>1</sup>; Romain Viennois<sup>1</sup>; Catherine Colinet<sup>1</sup>; Jean Claude Tédénac<sup>1</sup>; <sup>1</sup>Université Montpellier 2 - ICGM

We report an ab-initio study of the stability and electronic properties of transition metal silicides in order to study their potential for high temperature thermoelectric applications. We focus on the family M5Si3 (M = Ta, W) which is stable up to about 2000 °C. We first investigate the structural stability of the two compounds and then determine the thermopower of the equilibrium structure using the electronic density of states and Mott's law. We find that W5Si3 has a relatively large thermopower but probably not sufficient enough for thermoelectric applications.

## 2011 Functional and Structural Nanomaterials: Fabrication, Properties, Applications and Implications: Fabrication of Nanomaterials II

Sponsored by: The Minerals, Metals and Materials Society, TMS Electronic, Magnetic, and Photonic Materials Division, TMS: Nanomaterials Committee

Program Organizers: Jiyoun Kim, Univ of Texas; David Stollberg, Georgia Tech Research Institute; Seong Jin Koh, University of Texas at Arlington; Nitin Chopra, The University of Alabama; Suveen Mathaudhu, U.S. Army Research Office

Thursday AM  
March 3, 2011

Room: 8  
Location: San Diego Conv. Ctr

Session Chairs: Jud Ready, Georgia Institute of Tech; Vijay Singh, University of Kentucky

### 8:30 AM Introductory Comments

#### 8:35 AM

**Synthesis of Discrete Aluminum Nanoparticles:** *Christopher Crouse*<sup>1</sup>; Eunsung Shin<sup>2</sup>; P. Terry Murray<sup>2</sup>; Jonathan Spowart<sup>1</sup>; <sup>1</sup>Air Force Research Laboratory; <sup>2</sup>University of Dayton Research Institute

Conventional, "top-down" methods used to prepare commercial grade aluminum nanoparticles often yield a highly aggregated, polydisperse product. Due to the pyrophoric nature of nano-sized aluminum it is also necessary to passivate these particles, achieved through the formation of a thin amorphous oxide layer at the surface of the particle, to impart stability. In an effort to reduce aggregation and minimize loss of active aluminum, due to oxide formation, we have explored the synthesis of discrete aluminum nanoparticles through the use of conventional laser ablation in the presence of organic solvent and stabilizing ligands. Highly soluble, discrete aluminum nanoparticles, average particle size of 21nm, have been prepared in tetrahydrofuran using oleic acid as a stabilizing ligand. TEM and EDS analysis were used to confirm the metallic nature of the particles. Our investigation concerning chemical effects on particle size and morphology in addition to potential applications will be presented.

#### 8:50 AM

**Microstructure of Ball Milled Nanostructured Cu:** *Daria Setman*<sup>1</sup>; Michael Kerber<sup>1</sup>; Hamed Bahmanpour<sup>2</sup>; Ronald Scattergood<sup>2</sup>; Carl Koch<sup>2</sup>; Michael Zehetbauer<sup>1</sup>; <sup>1</sup>Research group Physics of Nanostructured Materials, University Vienna, Austria; <sup>2</sup>Department of Materials Science and Engineering, North Carolina State University, USA

Copper powder of 99.9% purity and an initial particle size in the micrometer range was subjected to high energy ball milling in a Spex 8000 mixer with ball to powder ratio of 10. Two different surfactants (NaCl solution and stearic acid) of different concentrations were used during milling. The evolution of the microstructure with respect to different processing parameters was determined using differential scanning calorimetry (DSC) and X-ray line profile analysis (XPLA). DSC measurements show a decreasing stored energy of lattice defect annealing with increased ballmilling time. This indicates a surprising decrease of lattice defects concentration of more than one order of magnitude. XPLA measurements allow determining the grain size and the density and arrangement of dislocations. A decrease of grain size with decreasing dislocation density may indicate that in nanometals with grain sizes 30 nm and below dislocation based deformation mechanisms become less important.

#### 9:05 AM

**Growth of Bulk, Nano-Composite (RE)-Ba-Cu-O Single Grain Superconductors:** *Hari babu Nadendla*<sup>1</sup>; YunHua Shi<sup>2</sup>; Sandeep Pathak<sup>2</sup>; Anthony Dennis<sup>2</sup>; David Cardwell<sup>2</sup>; <sup>1</sup>Brunel University; <sup>2</sup>University of Cambridge

Bulk RE-Ba-Cu-O (where RE = Rare earth) superconductors fabricated in the form of large, single grains have the potential to trap magnetic fields than

are significantly greater than those produced by hard, Nd-Fe-B permanent magnets (~ 1 T). Recently, we have introduced successfully nano-scale (RE)2Ba4CuMOy (RE-2411, where M = W, Nb, Ag and Bi) second phase inclusions into the REBa2Cu3O7-d superconducting phase matrix and have shown that these nano-scale inclusions enhance critical current density and trapped magnetic fields in these materials. Achieving a homogeneous distribution of these nano-scale particles in the bulk microstructure is crucial for achieving improved trapped fields. In this paper, we report the pushing/trapping behavior of various RE-2411 particles by the (RE)Ba2Cu3O7-d growth front during large grain growth and discuss the conditions under which a relatively homogeneous distribution of nano-scale RE-2411 phases within the RE-123 superconducting single grain matrix can be achieved.

#### 9:20 AM

**Inkjet Printed Gold Nanoparticulate Pads for Surface Finish in Electronic Package:** *Seonhee Jang*<sup>1</sup>; Kyoung-Jin Jeong<sup>1</sup>; Sungkoo Kang<sup>1</sup>; Donghoon Kim<sup>1</sup>; <sup>1</sup>Samsung Electro-Mechanics

Gold (Au) pads for surface finish in electronic package were developed by inkjet printing method. The microstructures of inkjet-printed Au film were investigated by various thermal treatment conditions. The film showed the grain growth as well as bonding between nanoparticles (NPs). The film became denser with pore elimination when NPs were sintered under gas flows of N2-bubbled through formic acid (FA/N2) and N2, which resulted in improvement of electrical conductance. The resistivity of film was 4.79  $\mu\text{O-cm}$ , about twice of bulk value. From organic analyses of FTIR, Raman spectroscopy, and TGA, the amount of organic residue in the film was 0.43 % which meant considerable removal of the solvent or organic capping molecules. The solder ball shear test was adopted for solderability and shear strength value was 820 gf on average. This shear strength is good enough to substitute the inkjet-printed Au nanoparticulate film for electroplating in electronic package.

#### 9:35 AM

**Synthesis of Anisotropic Nanoporous Platinum Structures:** *Yuan Li*<sup>1</sup>; Antonia Antoniou<sup>1</sup>; <sup>1</sup>Georgia Institute of Technology

We report on the synthesis of anisotropic porous structures of platinum formed by the preferential dealloying of an amorphous Pt-Si alloy. The nanoporous Pt structures (pores and ligaments 5-30nm in size and grain sizes of 5 nm) are formed in a two-step process involving Pt-Si co-sputtering and subsequent selective electrochemical etching in HF solution. We examine the conditions that can influence the level of anisotropy in the porous structures. The effect of the anisotropy on the mechanical behavior will also be discussed.

#### 9:50 AM

**Tailoring the Structure of Iron-Carbon Nanocomposites by Laser Power Variation Throughout the Laser Pyrolysis Process:** *Ion Morjan*<sup>1</sup>; Florian Dumitrache<sup>1</sup>; Rodica Alexandrescu<sup>1</sup>; Claudiu Fleaca<sup>1</sup>; Ruxandra Birjega<sup>1</sup>; Catalin-Romeo Luculescu<sup>1</sup>; Iuliana Soare<sup>1</sup>; Victor Kuncser<sup>1</sup>; Victor Ciupina<sup>1</sup>; <sup>1</sup>National Institute for Lasers, Plasma and Radiation Physics

The laser pyrolysis, as a single step synthesis method has been developed to prepare Fe@C nanocomposites with Fe/Fe3C nanoparticles/cores embedded in layered carbon. Fe (CO)5 and pure or Ar-diluted C2H4 were used as the iron and carbon sources, respectively. Ethylene serves also as an energy transfer agent towards the gaseous mixture. The incident laser power, as main experimental parameter was successively varied in order to optimize the chemical structure of the iron-based cores without a deleterious effect on the carbon coverage (which assures the passivation against the ambient). The control of the composition and crystallinity of the nanocomposites was performed by different analytical techniques such as EDAX, XRD, TEM and Moessbauer spectroscopy. In all samples, crystalline phases of alpha-iron and iron carbides (mainly cementite) (with varying relative content) were identified. The decrease of the laser power leads to the decreased carbon content and consequently to the slight superficial powder oxidation.

**10:05 AM Break**

**10:20 AM**

**Mechanomutable Nanomaterials: Multiscale Computational and Experimental Studies:** *Markus Buehler*<sup>1</sup>; Steven Cranford<sup>1</sup>; Christine Ortiz<sup>2</sup>; <sup>1</sup>Massachusetts Institute of Technology

Mutable materials are found widely in biology, characterized by a material's capacity to change its properties under external cues based on directed structural changes at specific material levels. Here we focus on a class of mechanomutable materials, which change their mechanical properties such as elasticity, deformability, strength and toughness based on external signals. A hierarchical approach, implemented through coarse-grain molecular modeling, is utilized to develop a powerful framework that can successfully collaborate atomistic theory and simulations with material synthesis and physical experimentation, and facilitate the design of mechanomutable structural materials. We review studies of PAA/PAH polymer systems, where a first principles based bottom-up approach is used to predict the structure and mutability of large-scale material properties from the nanoscale up. We demonstrate hierarchical material designs, validated by experimental studies, to realize mechanomutable polymer nanotubes and films. Experimental approaches towards the design of adaptable, mutable and active nanomaterials will be presented.

**10:35 AM**

**Fabrication of Gold-Platinum Nanoalloy by High-Intensity Laser Irradiation of Solution:** *Takahiro Nakamura*<sup>1</sup>; Yuliati Herban<sup>1</sup>; Shinichi Sato<sup>1</sup>; <sup>1</sup>IMRAM, Tohoku University

Gold-platinum nanoalloys were fabricated by high-intensity femtosecond laser irradiation of aqueous solutions of auric and platinum ions with different mixing ratio. The resulting particles were characterized by UV-visible spectroscopy, TEM and XRD. After irradiation, absorption peak arise from surface plasmon resonance of gold nanoparticles were observed in the spectrum of auric solution, and the peak position shifted to shorter wavelength range and the absorption peak in the spectrum decreased with decreasing the composition of auric ion in the solution. The position of XRD peaks of the particles shifted from that of pure gold to platinum, and XRD peaks of the particles prepared in the solutions with a certain mixing ratio of auric and platinum ions were observed between the peak positions of gold and platinum. This finding demonstrates gold-platinum nanoalloy of are successfully fabricated only by high-intensity laser irradiation of aqueous solution of auric and platinum ions.

**10:50 AM**

**Enhancement of CFRP Composites' Lateral Strength by Means of Magnetically Aligned CNTs:** *Saud Aldajah*<sup>1</sup>; Yousef Haik<sup>1</sup>; <sup>1</sup>United Arab Emirates University

Carbon Reinforced Polymer (CFRP) composites have outstanding mechanical properties in the longitudinal direction due to their light weight and excellent strength. However, they have poor transverse mechanical properties which limit their use in many structural applications. This paper presents a new technique to substantially enhance the transverse mechanical properties of CFRP composites. Multi-wall carbon nanotubes (CNTs) will be added to the CFRP composite aligned in the transverse direction by means of a magnetic field. The CNTs alignment process will be aided by the addition of magnetic nanoparticles which will adhere to the carbon nanotubes by surface adsorption during the curing process. This will result in increasing the transverse stiffness of the CFRP composites. In order to assess the impact of this technique on the mechanical properties, three-point bending tests were carried out. The results showed that the aligned CNTs increased the stiffness and the maximum load carrying capacity.

**11:05 AM**

**Effective Elastic Properties of Solids Containing Imperfectly Bonded Nano-Inhomogeneities Based on Atomistic-Continuum Interphase Model:** *Bhasker Paliwal*<sup>1</sup>; Mohammed Cherkaoui<sup>1</sup>; <sup>1</sup>Unité Mixte Internationale (UMI) Georgia Tech-CNRS & Georgia Institute of Technology

The classical micromechanics is revised to study elastic properties of heterogeneous materials containing nano-inhomogeneities. Contrary to the previous studies, this work introduces the concept of interphase instead of sharp interface to account for the surface/interface excess stress effect at the nano-scale. The interphase's constitutive properties are derived within the continuum framework from atomistics. These properties are then incorporated in micromechanics-based interphase model to compute the effective properties of the nanocomposite. This approach bridges the gap between discrete systems (atomic level interactions) and continuum mechanics. An advantage of this approach is that it combines atomistic with a three-phase micromechanical model that considers inhomogeneity shape. It thereby enables both the shape and the anisotropy of nano-inhomogeneity and nano-interphase to be simultaneously accounted for in computing overall properties.

**11:20 AM**

**Carbon Nanotube and Thin Film RF Antenna:** *David Stollberg*<sup>1</sup>; <sup>1</sup>Georgia Tech Research Institute

There is a need a smaller, more efficient, steerable RF antennas. Microstrip antennas (MSAs) have several advantages compared with conventional microwave antenna: lower weight, ease of integration with other microwave integrated circuits, and multiband operations. However, MSAs have several disadvantages compared to other microwave radiators: narrow bandwidth, and lower gain and power handling capability. This work endeavors to overcome these issues with non-conventional materials having superior, tailored electromagnetic properties suitable for applications in RF antennas. The specific design is a carbon nanotube (CNT) or thin metal film patch MSA in a novel design. The prototype MSA is composed of thin film iron or multi-walled carbon nanotubes on a silicon substrate. The two prototype antennas showed excellent response in the X-band, for which it was designed. In addition, an observed left-shift resonance effect points towards significant potential for miniaturization.

**11:35 AM**

**Metallic Nanoparticles in a Polysaccharide Thin Film:** *Patricia Farias*<sup>1</sup>; Josivandro Silva<sup>1</sup>; Igor Cavalcanti<sup>2</sup>; Beate Santos<sup>1</sup>; Adriana Fontes<sup>1</sup>; Rosa Dutra<sup>2</sup>; <sup>1</sup>Federal University of Pernambuco - UFPE; <sup>2</sup>RENORBIO

Gold and Silver nanoparticles (NAu and NAg) embedded in thin films of the polysaccharide Chitosan (Ch) were obtained by the heating at 70 Celsius degree of Ch aqueous solution containing NAu and NAg precursors. NAu and NAg were obtained directly into the polymeric matrix. X-Ray Diffractometry and Transmission and Scanning Electronic Microscopies (TEM and SEM), as well as spectroscopic and electrochemical methods (cyclic voltametry and impedimetric measurements) were performed in order to characterize the obtained materials. UV-Vis spectra presented typical plasmons bands which are not observed in the UV-Vis spectra of Ch without NAu and NAg. FT-IR spectroscopy results showed changes in amine groups modes. These features strongly suggest that the NH<sub>2</sub> groups effectively actuate on the reduction of the metallic precursors. The films are 25µm thick. MEV images showed that the obtained films are highly homogeneous. The results point to the feasibility of the obtained nanocomposites as potential biosensing substrates.

**11:50 AM Concluding Comments**



## 2nd International Symposium on High-Temperature Metallurgical Processing: Sintering and Synthesis

Sponsored by: The Minerals, Metals and Materials Society, TMS Extraction and Processing Division, TMS: Pyrometallurgy Committee, TMS: Energy Committee

Program Organizers: Jiann-Yang Hwang, Michigan Technological University; Jerome Downey, Montana Tech; Jaroslaw Drellich, Michigan Technological University; Tao Jiang, Central South University; Mark Cooksey, CSIRO

Thursday AM  
March 3, 2011

Room: 18  
Location: San Diego Conv. Ctr

Session Chairs: Xiaohui Fan, Central South University; Xuewei Lv, Chongqing University, China

### 8:30 AM

#### Crystallization Behavior of Calcium Ferrite during Iron Ore Sintering: Xiaohui Fan<sup>1</sup>; Lin Hu<sup>1</sup>; Min Gan<sup>1</sup>; <sup>1</sup>Central South University

Crystal precipitation behavior of calcium ferrite (CF) during iron ore sintering process along with the effect of cooling rate, SiO<sub>2</sub> and Al<sub>2</sub>O<sub>3</sub> on crystalline condensation were studied. The results show that CF, whose ability of precipitation was strong, and barely affected by external factors, began to precipitate when the liquid phase cooling down to about 1200°C. CF could crystallize rapidly at the cooling speed of 150°/min. Furthermore, slowing down the cooling rate was obviously favorable for development of crystal. Binder phase transformed from CF system to silicate system when SiO<sub>2</sub> content was increased to 5~6%, with a constant basicity (R) 2.0. Increasing Al<sub>2</sub>O<sub>3</sub> content could promote precipitation of CF and development of crystal.

### 8:50 AM

#### Numeric Simulation of the Cooling Process of the Iron Ore Sinter: Jiaqing Yin<sup>1</sup>; Xuewei Lv<sup>1</sup>; Chenguang Bai<sup>1</sup>; <sup>1</sup>Chongqing University, China

The iron ore sinter is one of the main raw materials for the blast furnace (BF) process. In the production of iron ore sinter, the cooling speed of the sinter determines the quality of the iron ore sinter. In addition, the heat recovery devices are installed in the cooling machine for energy saving. The cooling parameters like gas flow rate and location of the gas blower should be optimized for getting the gas with a higher temperature and a good quality of sinter at the same time. In this study, the commercial simulation software COMSOL was used to establish a model simulating the cooling process of the iron ore sinter. Several factors including gas flow rate, the size of sinter ores and its distribution in the cooling machine were investigated with the model.

### 9:10 AM

#### Study on Sintering Properties of A Fine Iron Concentrate Containing Hematite and Limonite: Tao Jiang<sup>1</sup>; Zheng-wei Yu<sup>1</sup>; Yu-feng Guo<sup>1</sup>; Yong-bin Yang<sup>1</sup>; Jian-jun Fan<sup>2</sup>; <sup>1</sup>Central South University; <sup>2</sup>Taiyuan Iron and Steel (Group) Corp.

A fine iron concentrate containing hematite and limonite was used to sinter in sinter pot. It was found that productivity of sinter is only 1.16 t/(m<sup>2</sup>·h) when using 100% iron concentrate of this kind. However, productivity is increased to 1.53 t/(m<sup>2</sup>·h) with addition of partial magnetite concentrate, meanwhile, tumble index of sinter is improved from 64.67% to 67.20%. Granulation properties and reactivities at high temperature of the two kinds of iron concentrate were studied. The results indicated that permeability index and liquid fluidity of iron concentrate containing hematite and limonite are much lower than those of magnetite concentrate, which are the key reasons for poor yield and quality of sinter.

### 9:30 AM Break

### 9:40 AM

#### Kinetics Studies of the Zinc Ferrite Synthesis: Mery Gómez<sup>1</sup>; José D'Abreu<sup>1</sup>; Helio Kohler<sup>1</sup>; <sup>1</sup>Puc-rio

This work deals with the kinetics of the zinc ferrite synthesis, occurring through a solid-solid reaction in a selected range of temperatures, using as reactants an equimolar mixture of pure iron oxide- Fe<sub>2</sub>O<sub>3</sub> and zinc oxide - ZnO. This equimolar mixture was thermally characterized using the DTA and TGA techniques. In sequence the zinc ferrite produced were examined using X-Ray Diffraction, Scanning and Transmission Electronic Microscopy. Finally the software Topas 3.0, Difrac Plus, using the Rietveld XRD method was applied to calculate the amount of zinc ferrite generated during the synthesis reaction. The results showed that at the low temperature (873 to 1003 K), the best fitting model was Phase Boundary Reaction, with apparent activation energy of 272 kJ/mol. On the other hand, for the high temperature (1023 to 1273 K), the results showed that Modified Logistic Equation had the best agreement with apparent activation energy of 67 kJ/mol.

### 10:00 AM

#### Vitrification of the Thermal State during Iron Ore Sintering: Xuling Chen<sup>1</sup>; Xiaohui Fan<sup>1</sup>; Tao Jiang<sup>1</sup>; Xiaoming Mao<sup>1</sup>; Hongming Long<sup>2</sup>; <sup>1</sup>central south university; <sup>2</sup>Anhui university of technology

On the basis of deep analysis to characters of iron ore sintering, the three-dimensional temperature distribution model was built using temperature of pallet sides and waste gas in windbox. The sintering bed was divided into four parts: wet mix zone, drying and preheating zone, burning zone and sinter zone according to temperature distribution. Some parameters, such as burn through point, rising point of temperature, vertical sintering speed, were soft-sensed. Based on these parameters, the thermal state during iron ore sintering was evaluated comprehensively. The model has been applied successfully in Baoshan Iron and Steel Group Corporation.

### 10:20 AM

#### Improving of Compression Strength of Preheated Pellets by High Pressure Roll Grinding: Jianjun Fan<sup>1</sup>; Guanzhou Qiu<sup>1</sup>; Tao Jiang<sup>1</sup>; Yufeng Guo<sup>1</sup>; <sup>1</sup>Central South University

The experiments were conducted on pellets roasting properties of one kind of iron concentrate with complicated mineralogical composition. It was found that this pellets required higher preheating temperature and longer time during roasting process, so it is difficult for such preheated pellets to withstand the mechanical collision when roasted in rotary kiln. More research work was carried out on how to improve preheated pellets compression strength by processing this iron concentrate with High Pressure Roll Grinding (HPRG). The researches revealed that not only the compression strength of preheated pellets would improve but that of finished pellets would increase even at lower temperature and shorter time. With the help of HPRG, the preheating and roasting temperature would decrease by 70° and 50°, preheating and roasting time would decrease by 2 and 4 minutes, but compression strength for preheated and roasted pellets would increase by 200 N/P and 220 N/P respectively.

### 10:40 AM Concluding Comments

## Advances in Mechanics of One-Dimensional Micro/Nano Materials: Nanomechanics: In-Situ Techniques

*Sponsored by:* The Minerals, Metals and Materials Society, TMS Materials Processing and Manufacturing Division, TMS Electronic, Magnetic, and Photonic Materials Division, TMS: Nanomechanical Materials Behavior Committee

*Program Organizers:* Reza Shahbazian-Yassar, Michigan Technological University; Seung Min Han, Korea Advanced Institute of Science and Technology; Katerina Aifantis, Aristotle University

Thursday AM  
March 3, 2011

Room: 1B  
Location: San Diego Conv. Ctr

*Session Chairs:* En Ma, John Hopkins University; Paulo Ferreira, The University of Texas at Austin

### 8:30 AM Invited

#### In Situ Mechanical Testing in the TEM as a Window into Small-Scale Plasticity Phenomena: *Andrew Minor*<sup>1</sup>; <sup>1</sup>UC Berkeley & LBL

Recent progress in both in situ and ex situ small-scale mechanical testing methods has greatly improved our understanding of mechanical size effects in volumes from a few nanometers to a few microns. Besides the important results related to the effect of size on the strength of small structures, the ability to systematically measure the mechanical properties of small volumes through mechanical probing allows us to test samples that cannot easily be processed in bulk form, such as a specific grain boundary or a single crystal. This talk will describe recent technique developments for experimentally probing nanoscale volumes and the resulting insights into dislocation plasticity and small-scale deformation mechanisms. Specifically, the hardening behavior of Cu samples during in situ compression and in situ tension will be compared and the critical stress for basal slip and twinning in Mg will be discussed.

### 8:55 AM Invited

**Application of In-Situ Electron Microscopy in Nanoscience and Energy Research:** *Jianyu Huang*<sup>1</sup>; *Li Zhong*<sup>2</sup>; *Chongmin Wang*<sup>3</sup>; *Ju Li*<sup>4</sup>; *Liang Qi*<sup>4</sup>; *John Sullivan*<sup>1</sup>; *Wu Xu*<sup>3</sup>; *Jie Yu*<sup>3</sup>; *Liqiang Zhang*<sup>2</sup>; *Scott Mao*<sup>2</sup>; *Nicholas Hudak*<sup>1</sup>; *Xiaohua Liu*<sup>1</sup>; *Arunkumar Subramanian*<sup>1</sup>; *Hongyu Fan*<sup>1</sup>; *Akihiro Kushima*<sup>4</sup>; <sup>1</sup>Sandia National Laboratories; <sup>2</sup>University of Pittsburgh; <sup>3</sup>Pacific Northwest National Laboratory; <sup>4</sup>University of Pennsylvania; <sup>5</sup>Harbin Institute of Technology

By integrating an atomically sharp scanning tunneling microscopy (STM) probe into a transmission electron microscope (TEM), the atomic structure and physical properties of individual nanostructures can be directly probed in real time at the atomic length-scale. Such studies have revealed a number of unexpected phenomena that only present themselves at the nano-scale. Cold-welding and surface mediated plasticity were revealed in ultrathin Au nanowires. A nanobattery comprised of an individual nanowire electrode was constructed inside a TEM, and the charge and discharge process was revealed in real time, pushing the forefront of knowledge in the highly technologically relevant area of Li-ion batteries.

### 9:20 AM Invited

**Deformation in Metallic Nanowires under In-Situ TEM:** *Scott Mao*<sup>1</sup>; *He Zheng*<sup>1</sup>; *J. Luo*<sup>1</sup>; *Jianyu Huang*<sup>2</sup>; <sup>1</sup>University of Pittsburgh; <sup>2</sup>Sandia National Lab

The mechanical behavior of bulk metals is usually characterized as smooth continuous plastic flow following by yielding. Here we show, by using in-situ TEM and molecular dynamics simulations, that the mechanical deformation behaviors of single-crystalline Ag and Ni nanowires are quite different from their bulk counterparts. Correlation between the obtained stress-strain curves and the visualized defect evolution during deformation processes clearly demonstrates that a sequence of complex dislocation slip processes results in dislocation starvation, involving dislocation nucleation, propagation and finally escaping from the wire system, so that the wires deformed elastically

until new dislocation generated. This alternating starvation of dislocations is unique in small-scale structures. Furthermore, the magnitude of yield stress of these nanowires is strongly dependent of the wire size.

### 9:45 AM Invited

**In-Situ Mechanical Testing of Nanowires and Nanodots:** *Johann Michler*<sup>1</sup>; <sup>1</sup>EMPA, Swiss Federal Laboratories for Materials Science and Technology

We developed recently several instruments for mechanical testing of nanowires in the SEM: an AFM for resonance and bending experiments, a MEMS-tensile tester, a nanoindenter, and a femtoprogram mass sensor. The fracture strength of monocrystalline Si and ZnO was found to be close to the theoretical strength. Similarly, the yield stress of monocrystalline Rhenium was found to be close to E/10. Nanocompression tests on gold nanodots were found to be mediated through large strain bursts. The released strain energy can be correlated to the new surface created during the burst in an simple model. Electrodeposited nanocrystalline Cobalt nanowires were loaded in tension and revealed surprisingly low Young's modulus values of around 70GPa. Resonance excitation of the wires in a bending mode allows to assess the ratio of Young's modulus to mass density. Using the Young's modulus from the tensile testing revealed a low mass density of the nanowires.

### 10:10 AM

**In-Situ SEM Micro-Compression Behavior of 1-D Nanostructure Arrays:** *Siddhartha Pathak*<sup>1</sup>; *William Mook*<sup>1</sup>; *Mikhael Bechelany*<sup>1</sup>; *Johann Michler*<sup>1</sup>; <sup>1</sup>EMPA - Swiss Federal Laboratories for Materials Testing and Research

We study the mechanical response of one-dimensional arrays of highly dense small-diameter (1-3 nm) non-catalytic multiwall (2-4 walls) carbon nanotube (CNT) brushes, measured using SEM in-situ micro-pillar compression testing. These dense CNT pillars, fabricated using focused ion beam (FIB) micromachining, were found to exhibit significantly higher modulus (~150 GPa) and orders of magnitude higher resistance to buckling (~6 GPa) than CNT brushes produced using other methods. Van der Waals' interactions in such dense brushes provide them with the added ability to dissipate energy while withstanding such elevated stresses. In comparison, lower density forests of Si nanowires (SNWs) have also been fabricated by metal induced chemical etching of silicon wafers (to avoid FIB-induced damages). A comparative study of the buckling and failure behavior during compression in these two unique material systems is expected to provide valuable insights into the cluster strengthening characteristics of such 1-D turfs.

### 10:25 AM Break

### 10:40 AM Invited

**Quantitative In Situ Mechanical Characterization of Carbon Nanotube/Epoxy Interface and Individual Carbon Nanotube Using Novel Micromechanical Devices:** *Yogi Ganesan*<sup>1</sup>; *Cheng Peng*<sup>1</sup>; *Yang Lu*<sup>1</sup>; *Phillip Loya*<sup>1</sup>; *Jun Lou*<sup>1</sup>; <sup>1</sup>Rice University

The knowledge of carbon nanotube (CNT) strength and fundamental mechanisms that govern mechanical behavior at the nanotube-matrix interface are critical for CNT reinforced nanocomposite development. We have recently developed a simple micro-fabricated device that could be used within a scanning electron microscope (SEM) chamber in order to perform in situ tensile tests of individual CNTs treated with different functional groups and nanoscale CNT pullout experiments using different matrices quantitatively. In this work, we report on the usage of such device that works in conjunction with a quantitative inSEM nanoindenter, for the in situ quantitative tensile testing of an individual multi-wall carbon nanotube (MWNT) and for an individual MWNT pullout experiment from an epoxy matrix. The insights gained from this research could potentially help engineer superior CNT reinforced nanocomposites by enabling the development of powerful predictive models.

11:05 AM Invited

**Superplastic Shaping of Silica Glass Nanowires and Nanoparticles: Electron-Beam-Assisted Flow Near Room Temperature:** *Evan Ma*<sup>1</sup>; <sup>1</sup>Johns Hopkins University

At or near room temperature, oxide glasses (with SiO<sub>2</sub> as a prototype) are brittle and fracture upon any mechanical deformation for shape change. As structural and functional members, low-dimensional oxide glasses are widely used in today's electronic devices and microelectromechanical systems, fabricated in the forms of thin films, wires/fibers, pillars, particles and cantilever beams. One may want to plastically deform these glass components to alter their dimensions and configuration, and use the shape change to control properties (e.g., optical performance). In this talk, we demonstrate that with moderate exposure to low-intensity (<1.8×10<sup>-2</sup> A/cm<sup>2</sup>) electron beam, dramatic shape changes can be achieved for amorphous silica at strain rates as high as 10<sup>-4</sup>/s, not only in compression for nanoparticles but also superplastic elongation larger than 200% in tension for nanowires. We also report the first quantitative comparison with and without the beam, revealing dramatic difference in the flow stress.

11:30 AM Invited

**Recent Advances in Characterization with In Situ SPM-TEM Instruments:** *Oleg Lourie*<sup>1</sup>; <sup>1</sup>Nanofactory Instruments Inc.

In situ SPM-TEM instruments such as AFM-TEM, STM-TEM and TEMNanoIndenter are used for characterization of the electrical and mechanical properties of various nanomaterials. Piezo actuated and having force or current feedback, the SPM probe in these instruments is also employed for sample surface imaging combined with conventional TEM imaging of the samples. SPM-TEM system is aimed to correlate the electro-mechanical measurements with on-line HRTEM observations of structural changes in the materials during the experiment. Such combination of SPM and TEM techniques in one instrument becomes especially valuable for in situ studies of various nanoscale structures like nanotubes, nanoparticles or nanowires. This presentation will outline the recent progress in the instrumentation development aimed to expand the range of available SPM-TEM systems employed to study mechanical properties of nanostructures.

11:55 AM

**Quantitative Tensile Testing of Free-Standing Thin Films in a TEM:** *Claire Chisholm*<sup>1</sup>; *Zhiwei Shan*<sup>2</sup>; *Jason Oh*<sup>3</sup>; *S.A. Syed Asif*<sup>3</sup>; *O.L Warren*<sup>3</sup>; *Andrew Minor*<sup>1</sup>; <sup>1</sup>University of California, Berkeley and National Center for Electron Microscopy; <sup>2</sup>Xi'an Jiaotong University and Hysitron, Inc.; <sup>3</sup>Hysitron, Inc.

In situ transmission-electron-microscopy (TEM) tensile testing is a powerful tool for revealing the underlying physical mechanisms of deformation in materials. Here we report a novel technique for quantitative, in-situ tensile testing of free standing metallic films inside a TEM. Freestanding thin films of Au were loaded onto a microfabricated "push-to-pull" (PTP) device and pulled in tension with a quantitative in-situ nanoindentation/nanocompression holder. The (PTP) device allows for quantitative load-displacement data in parallel with real time images of the microstructural behavior. Results from the uniaxial tensile testing of Au thin films will be presented including observations of the transition from elastic to plastic loading and the related deformation phenomena. With this technique, it is possible to observe the deformation of thin films with correlated mechanical and microstructural data at high resolution.

12:10 PM Invited

**Are Dislocations Possible in Nanoparticles?:** *C.E. Carlton*<sup>1</sup>; *Paulo Ferreira*<sup>1</sup>; <sup>1</sup>University of Texas at Austin

The deformation behavior of nanoscale metals continues to be an exciting area for materials research. However, in the case of single crystal 0-D nanoscale metals, no deformation experiments, to our knowledge, have been performed at the nanoscale. The one experiment closest to the nanoscale was an in-situ TEM compression of ~200 nm Si nanoparticles. However, the particle tested was too large to extract relevant information at the nanoscale and the mechanical deformation of Si is also expected to be different from that of metals. For nanoparticles it is claimed there is a conspicuous lack

of dislocations, regardless of the materials processing history, even after significant deformation. Therefore, it has been suggested that dislocations cannot exist or/ do not play a role on the deformation of 0-D nanomaterials. To address this issue of the role played by dislocations in the deformation of 0-D nanomaterials, nanoparticles with diameters <20nm were compressed in-situ under phase-contrast in a transmission electron microscope (TEM). Two phase-contrast TEM experiments were done, one in a conventional TEM and the other in an aberration corrected TEM. Evidence for nucleation of dislocations and dislocation motion was observed during in-situ TEM nanoindentation, but upon unloading dislocations were no longer visible. A new model for explaining dislocation instability is introduced. In this model we consider the change in Gibbs free energy of an edge dislocation, as it moves through the nanoparticle, towards the surface. The nanoindentation experiments seem to confirm the model proposed.

---

## Aluminum Reduction Technology: Cells Process Modeling

*Sponsored by:* The Minerals, Metals and Materials Society, TMS Light Metals Division, TMS: Aluminum Committee, TMS: Aluminum Processing Committee

*Program Organizers:* Mohd Mahmood, Aluminium Bahrain; Abdulla Ahmed, Aluminium Bahrain (Alba); Charles Mark Read, Bechtel Corporation; Stephen Lindsay, Alcoa, Inc.

Thursday AM  
March 3, 2011

Room: 17B  
Location: San Diego Conv. Ctr

*Session Chair:* Marc Dupuis, GéniSim Inc

---

8:30 AM

**Development and Application of an ANSYS Based Thermo-Electro-Mechanical Collector Bar Slot Design Tool:** *Marc Dupuis*<sup>1</sup>; <sup>1</sup>GéniSim Inc

After the successful development and application of an ANSYS based thermo-electro-mechanical anode stub hole design tool, an ANSYS based thermo-electro-mechanical collector bar slot design tool has been developed. Since the average contact resistance at the cast iron/cathode block interface is higher than the contact resistance at the cast iron/anode carbon interface, the potential for mV saving is even greater. A demonstration model has been developed and used to study different collector bar slot configurations, results obtained are presented.

8:50 AM

**Impact of Amperage Creep on Potroom Busbars and Electrical Insulation: Thermal-Electrical Aspects:** *Andre Schneider*<sup>1</sup>; *Daniel Richard*<sup>1</sup>; *Olivier Charette*<sup>1</sup>; <sup>1</sup>Hatch

Busbars electrical insulation is a critical aspect of aluminium smelters potrooms electrical safety. With amperage creep, busbars are typically running hotter than they were at start-up. The long-term reliability of busbars and the integrity of insulating materials is therefore of concern. To assist smelters evaluate the performance of the busbars systems under realistic operating conditions, a methodology was developed using ANSYS/8482-based numerical simulation, laboratory testing and *in situ* measurements. This approach has been validated on different pot technologies and smelters. A realistic test case based on a demonstration busbar system is presented and the typical impact of line current, ambient temperature and selected operational procedures on thermal-electrical performance and reliability is discussed.

9:10 AM

**Modern Design of Potroom Ventilation:** *Anastasiya Vershenya*<sup>1</sup>; *Umesh Shah*<sup>1</sup>; *Stephan Broek*<sup>1</sup>; *Tom Plikas*<sup>1</sup>; *Jennifer Woloshyn*<sup>1</sup>; *Andre Felipe Schneider*<sup>1</sup>; <sup>1</sup>Hatch Limited

A typical natural ventilation design of a pot room incorporates incoming ambient air flow dividing into two main streams. The 'under the pot' stream passes through basement infrastructure and sweeps the heat/emissions from

THURSDAY AM



the pots upward to roof. The 'over the pot' one flows through the Claustra wall and pushes the emissions/heat away from the working zone. This paper describes the use of CFD modeling to accurately predict the ventilation air flow split between these two main streams and improve the ventilation design, thus meeting the defined workplace hygiene standards. The model's success greatly depends on reliable input conditions such as cell emissions and heat release rates. An innovative approach for the calculation of cell emission rates is thus introduced. Furthermore, the ventilation model can be coupled with pot heat balance and busbars thermoelectric analyses in order to obtain proper Joule heat generation and release rates.

**9:30 AM**

**Modeling of Energy Savings by Using Cathode Design and Inserts:** *René von Kaenel*<sup>1</sup>; Jacques Antille<sup>1</sup>; <sup>1</sup>KAN-NAK SA

The use of modified cathode shape and inserts in the cathode allow drastically redistributing the current density in the aluminium liquid pool. As a result both the cathode voltage drop and the anode to cathode voltage drop can be significantly decreased. Electrical modeling can easily explain the energy savings in the cathode. Magneto-hydrodynamic modeling shows why and how specific energy can be saved in the anode to cathode distance. The energy saving inside the cell depends on the cell initial design but may exceed 1 kWh/kg.

**9:50 AM Break**

**10:00 AM**

**A Preliminary Finite Element Electrochemical Model for Modelling Ionic Species Transport in the Cathode Block of a Hall-Héroult Cell:** *Frédéric Gagnon*<sup>1</sup>; Donald Ziegler<sup>2</sup>; Mario Fafard<sup>1</sup>; <sup>1</sup>NSERC/Alcoa Industrial Research Chair MACE3 and Aluminium Research Centre-REGAL, Laval University; <sup>2</sup>Alcoa Primary Metals

A first 2D transient isothermal model was developed for the modelling of bath penetration in a Hall-Héroult cell cathode block. The model simulates the 'non convective' ionic species transport. The molten cryolite solution system is defined with an ionic model. The migration and diffusion of the ionic species is followed in the cathode block pores and in an overlying bath layer. The evolution of the potential is simultaneously obtained using charge conservation equations. The model includes a linear kinetic model for the electrochemical formation of metallic aluminum. The porous cathode behaviour is modelled using volume averaging based methods. The aluminofluoride ionic equilibrium is implemented by the penalty method and the electroneutrality criterion as a constraint on the FEM weak form. This is the first application of porous electrode theory, adapted for a molten salt, to Hall-Héroult cell cathodes. The results show the early stage evolution of voltage and ions distribution.

**10:20 AM**

**Anodic Voltage Oscillations in Hall-Héroult Cells:** *Kristian Etienne Einarsson*<sup>1</sup>; Espen Sandnes<sup>2</sup>; <sup>1</sup>Norwegian University of Science and Technology; <sup>2</sup>Hydro Aluminium AS

Experiments on lab- and industrial scale cells have been conducted in order to study the behaviour of anodic gas bubbles under various operating conditions. Traditional voltage measurements have been supplied with high-speed video recordings of the bath surface showing a good correspondence between voltage fluctuations and escaping gas bubbles. On average, 0.5 and 2 bubbles were observed per second in each respective case. Average frequencies obtained by a FFT of the voltage signal however show significantly lower values, approximately half of that observed. It is shown that this discrepancy can be due to large variations in the bubble release times and observed bubble events can be related to FFT frequencies by means of a frequency based on statistically significant periods. For industrial anodes, the possibility of overlapping bubbles is investigated as alternative effect resulting in the mismatch between observed and calculated frequencies.

**10:40 AM**

**CFD Modelling of Alumina Mixing in Aluminium Reduction Cells:** Yuqing Feng<sup>1</sup>; Mark Cooksey<sup>2</sup>; Phil Schwarz<sup>1</sup>; <sup>1</sup>CSIRO Mathematics, Informatics and Statistics; <sup>2</sup>Process Science and Engineering

More uniform alumina concentration in an aluminium reduction cell can improve cell performance substantially. Control of alumina dissolution and distribution is more critical for modern cells, given that they are often operated at low anode-cathode distances (ACDs) and increased anode size and current density. This paper presents a numerical study of possible methods to improve alumina feeding system by use of a computational fluid dynamics (CFD) model. Using a typical full-scale industrial cell as a test bed, a simulation was first conducted based on a conventional multi-point alumina feeding method with uniform alumina feeding through each feeder. Following quantification of the alumina concentration over the whole cell and identification of the poor feeding region, a simulation was further conducted with an optimised feeding through each feeder. A better alumina concentration was achieved with the improved feeding strategy, which demonstrates the effectiveness of CFD modelling for improving cell performance.

**11:00 AM**

**Bubble Transport by Electro-Magnetophoretic Forces at Anode Bottom of Aluminium Cells:** *Valdis Bojarevics*<sup>1</sup>; Alan Roy<sup>1</sup>; <sup>1</sup>University of Greenwich

Particles and bubbles experience additional forcing in an electric current-carrying liquid. The electro-magnetophoretic forces are well known in metallurgical applications, like metal purification in vacuum-arc remelting, electro-slag processes, impurity concentration change in castings. However, this effect appears to be never considered for aluminium cells. We present models to estimate the effect of electric current in the vicinity of the bubbles and the additional pressure distribution resulting from the magnetic forces in liquid electrolyte. According to the estimates, the electro-magnetophoretic force becomes important for the bubbles of size exceeding 2 mm to overcome a typical drag force of electrolyte flow, and potentially can oppose the bubble motion along a mild slope of the nearly horizontal anode bottom. The effect could explain certain features of the anode effect onset. Numerical results are presented, a further implementation in the general MHD code for the aluminium cell design is discussed.

---

## Biological Materials Science: Mechanical Behavior of Biological Materials III

*Sponsored by:* The Minerals, Metals and Materials Society, TMS Electronic, Magnetic, and Photonic Materials Division, TMS Structural Materials Division, TMS: Biomaterials Committee  
*Program Organizers:* Jamie Kruzic, Oregon State University; Nima Rahbar, University of Massachusetts, Dartmouth; Po-Yu Chen, University of California, San Diego; Candan Tamerler, University of Washington

Thursday AM  
March 3, 2011

Room: 15A  
Location: San Diego Conv. Ctr

*Session Chairs:* Nima Rahbar, University of Massachusetts Dartmouth; Jamie Kruzic, Oregon State University

---

**8:30 AM Invited**

**Adhesion in Biomaterials: From BioMEMS to Nanoparticles for Cancer Detection and Treatment:** *Winston Soboyejo*<sup>1</sup>; <sup>1</sup>Princeton University

This talk explores the role that adhesion can play in the design of interfaces in biomaterials that are relevant to cancer detection and treatment. These include: bio-electro-mechanical systems (BioMEMS) and ligand-conjugated nanoparticles for the early detection and treatment of breast cancer. Dip-coating and atomic force microscopy techniques are used to measure the adhesion between gold/magnetite nanoparticles and cancer drugs or molecular recognition units that enable them to attach specifically

to breast cancer cells. The adhesion between cancer cells and BioMEMS surfaces is also elucidated via shear assay and atomic force microscopy techniques. The implications of the results are discussed for the design of BioMEMS interfaces and nanoparticle clusters that are being explored for the early detection and treatment of cancer via combinations of localized drug delivery and hyperthermia.

#### 9:00 AM

**Micro Tribology of Compression Molded Ultrahigh Molecular Weight Polyethylene Reinforced with Aluminum Oxide, Hydroxyapatite and Carbon Nanotubes:** Ankur Gupta<sup>1</sup>; Debrupa Lahiri<sup>2</sup>; Sanat Ghosh<sup>2</sup>; Garima Tripathi<sup>1</sup>; Bikramjit Basu<sup>1</sup>; Arvind Agarwal<sup>2</sup>; Kantesh Balani<sup>1</sup>; <sup>1</sup>Indian Institute of Technology, Kanpur; <sup>2</sup>Florida International University, Miami

Ultrahigh-molecular-weight-polyethylene (UHMWPE) is used as a liner in acetabular cups for total hip and knee replacement. In the present work, compression molding of UHMWPE has been carried out with varying content of nanocrystalline Hydroxyapatite (HAp) (2-5wt%), nanocrystalline Aluminum Oxide (Al<sub>2</sub>O<sub>3</sub>) (2-5wt%) and multi-walled-carbon-nanotube (MWNT) (2-4wt%). HAp addition is expected to impart biocompatibility, Al<sub>2</sub>O<sub>3</sub> to improve compressive strength and stiffness, and MWNT to enhance strength and wear resistance. Presence of HAp and Al<sub>2</sub>O<sub>3</sub> create additional interfaces leading to poor interfacial bonding eliciting poor mechanical/tribological properties. Modulus and hardness of 0.66543GPa and 39.08 MPa is observed for UHMWPE-5HAp, increases to 0.97213GPa and 54.17 MPa respectively for UHMWPE-5HAp-2MWNT-2Al<sub>2</sub>O<sub>3</sub>. MWNT has shown to significantly reduce the coefficient of friction (from 0.23 for UHMWPE-5HAp to 0.12 for UHMWPE-2HAp-2MWNT-5Al<sub>2</sub>O<sub>3</sub>). Pareto charts were developed from quantitative analysis of tribological properties in conjunction with various reinforcements. Cytocompatibility of the UHMWPE-HAp-Al<sub>2</sub>O<sub>3</sub>-MWNT biocomposites was confirmed via SAOS-2 cell line.

#### 9:20 AM

**Determination of Micro-Mechanical Properties of Bovine Cortical Bone by Uniaxial Compression Testing:** Pravin Ramesh<sup>1</sup>; Katrina Altman<sup>1</sup>; Elise Morgan<sup>2</sup>; Katharine Flores<sup>1</sup>; <sup>1</sup>The Ohio State University; <sup>2</sup>Boston University

Bone is an anisotropic, hierarchically structured material, and as a result, its mechanical behavior is highly statistical in nature. The application of microscale compression testing to bone will permit modeling of the aggregate material to predict effects of age, disease, or injury on the mechanical properties. The present work analyzes the mechanical behavior of 15-25  $\mu$ m diameter uniaxial compression pillars prepared by a femtosecond laser micromachining technique. Pillars are selectively machined within regions of interest in the cross-section, for example within osteons near the periosteal and endosteal surfaces. The pillars are then compressed with a modified nanoindenter in wet or dry conditions. Both monotonic and cyclic loading are considered. Modulus, strength, and modes of deformation are compared as functions of specimen size and position. The potential influences of chemical and thermal damage to the bone structure by the femtosecond laser micromachining process are also considered.

#### 9:40 AM

**Advanced Mechanical Characterization of Biomaterials by Nanoindentation:** Nicholas Randall<sup>1</sup>; Bo Zhou<sup>1</sup>; <sup>1</sup>CSM Instruments

Various conventional methods are currently used to characterize the mechanical behaviour of biomaterials but have major drawbacks. Nanoindentation is particularly appropriate because it allows the characterization of very small material volumes. However, the main drawback of nanoindentation is linked to the low thermal stability of most instruments. The recent development of the Ultra Nanoindentation Tester now permits a precise investigation of the creep behaviour of the sample using very long duration tests. Such results are made possible thanks to a quasi elimination of the thermal drift. A series of long term quasi static tests on several viscoelastic biomaterials will be used to demonstrate the efficiency of this novel instrument design and its ability to almost totally eliminate the thermal drift. This study therefore demonstrates that nanoindentation testing, when performed in good conditions with appropriate apparatus,

constitutes a reliable tool to study the time-dependent mechanical properties of biomaterials.

#### 10:00 AM

**Broadband Nanoindentation Spectroscopy for Biological Materials:** Joseph Jakes<sup>1</sup>; Daniel Yelle<sup>1</sup>; Charles Frihart<sup>1</sup>; Donald Stone<sup>2</sup>; <sup>1</sup>USDA Forest Products Laboratory; <sup>2</sup>University of Wisconsin - Madison

Nanoindentation has increasingly been used for probing mechanical properties of biological materials at microscopic length scales. We propose nanoindentation to be used as a tool for mechanical spectroscopy in which detailed information about deformation mechanisms can be gained by characterizing viscoplastic properties across 4-6 decades of strain rate using broadband nanoindentation creep (BNC) and viscoelastic properties across 8 decades in time-scale with broadband nanoindentation viscoelasticity (BNV). In validation studies on poly methyl methacrylate, polycarbonate, and polystyrene the data generated from nanoindentation agree closely with more conventional viscoplastic and viscoelastic measurements. BNC is applied to study wood-adhesive interactions in individual components of the wood cell walls. BNC discriminates among different types of wood-adhesive interaction including formation of covalent bonds with wood polymers, bulking, and formation of interpenetrating networks. Unambiguous chemical information showing formation of covalent bonds between adhesive components and wood polymers is provided by two-dimensional solution-state nuclear magnetic resonant spectroscopy.

#### 10:20 AM Break

#### 10:30 AM

**Fiber Reinforced Tough Hydrogels:** Animesh Agrawal<sup>1</sup>; Dapeng Li<sup>1</sup>; Nima Rahbar<sup>1</sup>; Paul Calvert<sup>1</sup>; <sup>1</sup>University of Massachusetts

A 3D rapid prototyping technique is used to form crossed "logpiles" of elastic fibers that are then impregnated with an epoxy-based hydrogel in order to form a fiber-reinforced gel structure resembling natural cartilage. The presence of the fibers increases the gel modulus and toughness and constrains the swelling. The fracture properties of the gel are expressed in terms of a critical strain energy release rate and compared with theories of gel strength.

#### 10:50 AM

**Microstructural and Mechanical Investigation of Macadamia Nutshells on Different Hierarchical Levels:** Claudia Fleck<sup>1</sup>; Ruth Loprang<sup>1</sup>; Paul Schüler<sup>1</sup>; Paul Zaslansky<sup>2</sup>; Dietmar Meinel<sup>3</sup>; <sup>1</sup>Technische Universität Berlin; <sup>2</sup>Max-Planck-Institute of Colloids and Interfaces; <sup>3</sup>Bundesanstalt für Materialforschung und -prüfung BAM

Macadamia nutshells exhibit surprisingly high strength and toughness making them interesting model materials for impact resistant engineering structures. The properties of the nutshell are assumed to be due to the hierarchically organised microstructure. Up to now, the degree of anisotropy of the microstructure and the relationship between microstructure and mechanical properties has not been clear. In the present work, by means of light and scanning electron microscopy and micro-tomography, the anisotropic, hierarchical microstructure of the nutshells was clearly shown. The layered composite structure with local variations in the degree of orientation gives the shell a high resistance against compressive as well as tensile stresses. This was demonstrated on different hierarchical levels in compression tests on whole and half nutshells, C-rings and cylindrical specimens. First results of crack growth tests on notched specimens allow to assume that this structure also lends a rather high resistance against crack growth to the nutshell.

#### 11:10 AM

**Characterization of Brazil Nut Shell Fiber:** Nelida Lucia del Mastro<sup>1</sup>; Patricia Inamura<sup>1</sup>; Felipe Kraide<sup>1</sup>; Maria Aguirre<sup>1</sup>; Marcos Scapin<sup>1</sup>; Esperidiana Moura<sup>1</sup>; <sup>1</sup>IPEN-CNEN/SP

The fruit from Brazil nut (*Bertholletia excelsa*) is characteristically a spherical capsule, with a thick and hard surface dark brown in color. When mature, the capsule releases seeds through the lower portion. Each capsule contains between 14 and 24 seeds. The Brazil nut seeds are angular nuts with

a very hard hull. Although the Brazil nuts market grows, the nut shell fiber residues have no further application. In this work, an attempt has been made to characterize the Brazil nut shell fiber by various instrumental techniques like thermogravimetric analysis (TGA) and scanning electron microscopy (SEM). The organic composition was established and elemental composition was determined by the methods of Instrumental Neutron Activation Analysis (INAA) and Energy Dispersive X-ray Fluorescence Spectrometry (EDXRF). Some perspectives for these fibers are also presented, as novel markets for lignocellulosics have been identified in recent years, representing an exceptional opportunity of sustainable technological development.

11:30 AM

**Armadillo Armor: Mechanical Testing and Micro-Structural Evaluation:** Irene Chen<sup>1</sup>; James Kiang<sup>1</sup>; Joshua Yee<sup>2</sup>; Maria Lopez<sup>1</sup>; Po-Yu Chen<sup>1</sup>; Joanna McKittrick<sup>1</sup>; Marc Meyers<sup>1</sup>; <sup>1</sup>University of California at San Diego; <sup>2</sup>University of California at Irvine

The armadillo has a unique protective bony armor, called the osteoderm, which confers to its shell-like skin with distinctive mechanical properties. The top layer of the shell is made out of a dark-brownish keratin layer, arranging in a bimodal random pattern. Beneath the keratin layer, the osteoderm consists of hexagonal and triangular tiles with both tiles having a composition that is the same as bone (mainly collagen type I fibers and hydroxyapatite minerals). The tiles are connected by non-mineralized collagen fibers, called Sharpey fibers. The hierarchical structure of armadillo osteoderm is characterized using optical microscopy, SEM, and AFM. Various mechanical tests (tensile, shear, impact, and flexural) are performed and fracture surface is examined under SEM. Toughening mechanisms will be discussed and compared with other mineralized tissues. This research is supported by NSF Grant (Ceramics and Biomaterials Program) 1006931.

11:50 AM

**Feathers in Flexure: Why Buckling Up is for the Birds:** Sara Bodde<sup>1</sup>; James Kiang<sup>1</sup>; Joanna McKittrick<sup>1</sup>; Marc Meyers<sup>1</sup>; <sup>1</sup>UCSD

Having studied microstructure and mechanical properties of feather in a piecewise fashion, we will now present investigations of the mechanical behaviour of the intact system in flexure. We will present data on sandwich-structured feather segments subjected to four-point bending until the buckling with an emphasis on gradient in loading limit from the proximal to the distal end. We will correlate this with geometric characterization of the medulloid pith at the core of the feather. In this study, we will compare the flexural strength of primary flight feathers from two North American Owl species of the same taxonomic family: one a large Horned Owl (~1.4 kg in mass) and the other a small Screech Owl (~200 g in mass). By this intra-familial and inter-specific comparison, we attempt to intimate scaling effects of microstructure on flexural strength. Research support: N.S.F. Biomaterials Program (Grant DMR 0510138).

12:10 PM

**Quasi-Static and Dynamic Characterization of Agar:** Vinod Nayar<sup>1</sup>; James Weiland<sup>1</sup>; Andrea Hodge<sup>1</sup>; <sup>1</sup>University of Southern California

Nanoindentation is used to quasi-statically and dynamically characterize agar. Using a Hysitron Triboscope nanoindenter, the reduced, storage, and loss moduli of agar are presented. Quasi-static tests are performed on agar samples ranging from 0.5 to 5% concentrations using both open and closed-loop methodologies as the effects of proper loading conditions and adhesion are discussed. Dynamic properties, storage and loss modulus, are measured on the softer agar samples to observe the viscoelastic properties of a low modulus biologically-based polymer. Agar concentration, quasi-static load, and dynamic oscillation frequency were controlled to determine the linearity of the viscoelastic response, which was determined to be primarily affected by the frequency of oscillation. Agar is a principally an elastic polymer, with a smaller frequency-dependent viscoelastic response.

## Bulk Metallic Glasses VIII: Mechanical and Other Properties I

*Sponsored by:* The Minerals, Metals and Materials Society, TMS Structural Materials Division, TMS/ASM: Mechanical Behavior of Materials Committee

*Program Organizers:* Gongyao Wang, University of Tennessee; Peter Liaw, Univ of Tennessee; Hahn Choo, Univ of Tennessee; Yanfei Gao, Univ of Tennessee

Thursday AM  
March 3, 2011

Room: 6D  
Location: San Diego Conv. Ctr

*Session Chairs:* Ralph Napolitano, Iowa State Univ; Jianzhong Jiang, International Center for New-Structured Materials (ICNSM)

8:30 AM Invited

**Devitrification Kinetics and Phase Selection Mechanisms in Cu-Zr: I.** Kalay<sup>1</sup>; Y. Kalay<sup>2</sup>; M. Kramer<sup>2</sup>; *Ralph Napolitano*<sup>1</sup>; <sup>1</sup>Iowa State University; <sup>2</sup>Ames Laboratory

Devitrification dynamics and phase selection mechanisms in melt-spun amorphous Cu<sub>50</sub>Zr<sub>50</sub>, Cu<sub>56</sub>Zr<sub>44</sub>, and Cu<sub>45.5</sub>Zr<sub>54.5</sub> alloys are investigated using in-situ high-energy synchrotron X-ray diffraction (HEXRD), conventional/high resolution transmission electron microscopy (TEM/HRTEM), and differential scanning calorimetry (DSC). Crystallization sequences and nanoscale structures are analyzed and discussed in terms of binary system thermodynamics, nucleation and growth kinetics, crystal-orientation relationships, solute partitioning, and chemical diffusion. This research is supported by U.S. DOE-OS, Ames Laboratory contract No.DE-AC02-07CH11358.

8:50 AM

**Crystallization Behavior and Magnetic Properties of FeCoSiBn BMG with Cu Additions:** Mihai Stoica<sup>1</sup>; Ran Li<sup>2</sup>; Stefan Roth<sup>1</sup>; Gavin Vaughan<sup>3</sup>; Jürgen Eckert<sup>1</sup>; <sup>1</sup>IFW Dresden; <sup>2</sup>BUAA University; <sup>3</sup>ESRF Grenoble

Fe-Co-B-Si-Nb bulk metallic glasses (BMGs) exhibit high glass-forming ability (GFA) as well as good mechanical and soft magnetic properties. The soft magnetic properties can be enhanced by nanocrystallization. To force the nanocrystallization, small content of Cu was added to the starting composition. Cu has positive heat of mixing with both main constituents, Fe and Co. In this way, the desired fine-tuned nanostructures may be obtained even directly upon casting. In this paper,  $\{[(\text{Fe}_{0.5}\text{Co}_{0.5})_{0.75}\text{Si}_{0.05}\text{B}_{0.20}]_{0.96}\text{Nb}_{0.04}\}_{100-x}\text{Cu}_x$  glassy alloys ( $x = 1, 2$  and  $3$ ) were chosen for investigation. The effects of crystallization during heat-treatment processes on the phase evolution, the kinetic parameters and the magnetic properties, including  $M_s$ ,  $H_c$  and  $T_c$ , in these alloys were investigated. The phase analyses were done with the help of the X-ray diffraction patterns recorded in-situ by using the synchrotron radiation in transmission configuration.

9:00 AM

**Viscosity Measurement and Fragility Calculation in Fe-Based Amorphous Alloys:** Jong Hyun Na<sup>1</sup>; Marios D. Demetriou<sup>1</sup>; Won Tae Kim<sup>2</sup>; Do Hyang Kim<sup>3</sup>; William L. Johnson<sup>1</sup>; <sup>1</sup>California Institute of Technology; <sup>2</sup>Cheongju University; <sup>3</sup>Yonsei University

Since bulk metallic glasses (BMGs) have discovered in several multicomponent alloys, viscosity studies of BMGs have been conducted in the past two decades. However, though large-scale Fe-based amorphous alloys have successfully developed by enormous efforts for last six years to apply structural components, there is a limited rheological data due to the experimental difficulties such as their very brittle manner. In the present study, the rheological measurements of Fe-based amorphous alloys are performed in isothermal three-point beam-bending experiments. The experiments lead to the determination of the equilibrium viscosity, which can evaluate the fragility by means of one parameter law proposed by Johnson et al. Finally, the correlation between fragility and glass forming ability in Fe-based amorphous alloys has been investigated.



**9:10 AM Invited**

**Structural Relaxation, Glass-Transition, Viscous Formability and Crystallization of Bulk Metallic Glasses on Heating Including Microwave Treatment:** *Dmitri Louzguine<sup>1</sup>; Akihisa Inoue<sup>1</sup>; <sup>1</sup>WPI-AIMR, Advanced Institute for Materials Research, Tohoku University*

Here we summarize our recent findings on relaxation, glass transition, viscous flow and crystallization of various metallic glasses on heating. We also present structure changes upon microwave treatment of powders. At least two processes related to the diffusivities of different alloying elements take place in the glass-transition region of a Zr-Cu-Al-Ni glassy alloy. Also we report an unusual solidification behavior of the bulk glassy alloy produced using low-purity Zr in which both primary and eutectic-type structural constituents were formed simultaneously during solidification of the melt. As the mechanical properties are not deteriorated these glassy-crystal composites can be used instead of the monolithic glassy alloys. In addition viscous flow of the Cu-Zr-Al-Ag glassy alloy is examined in both the glass-transition and supercooled liquid regions and this alloy is found to exhibit phase separation prior to crystallization. This process opens up possibilities for innovative processing which causes an increase in room-temperature plasticity.

**9:30 AM**

**Effect of Tantalum Substitution on the Crystallization Kinetics and Hydrogen Permeability of Ni-Nb-Zr Amorphous Alloys:** *Sang-Mun Kim<sup>1</sup>; Narendra Pal<sup>1</sup>; Wen-Ming Chien<sup>1</sup>; Joshua Lamb<sup>1</sup>; Anjali Talekar<sup>1</sup>; Dhanesh Chandra<sup>1</sup>; Michael Dolan<sup>2</sup>; Stephen Paglieri<sup>3</sup>; Ted Flanagan<sup>4</sup>; <sup>1</sup>University of Nevada, Reno; <sup>2</sup>Commonwealth Scientific and Industrial Research Organisation; <sup>3</sup>TDA Research; <sup>4</sup>The University of Vermont*

Amorphous ternary Ni-Nb-Zr and quaternary Ni-Nb-Zr-Ta alloys are promising hydrogen permeable membranes. Amorphous alloy membranes were prepared by melt-spinning technique. The crystallization temperature and kinetics of amorphous membranes were examined by using differential scanning calorimetry (DSC) under various heating rates. It was observed that crystallization of amorphous  $(\text{Ni}_{0.6}\text{Nb}_{0.4})_{70}\text{Zr}_{30}$  and  $(\text{Ni}_{0.6}\text{Nb}_{0.4}\text{Ta}_{0.1})_{70}\text{Zr}_{30}$  alloys proceed through two exothermic reactions. Ta substitution resulted in slight decrease in the primary crystallization temperature ( $T_{x1}$ ) but increase in secondary crystallization temperature ( $T_{x2}$ ). The activation energies,  $E_a$ , of amorphous alloys have been calculated using Kissinger and Ozawa equations based on DSC data. The activation energies for crystallization of amorphous  $(\text{Ni}_{0.6}\text{Nb}_{0.4})_{70}\text{Zr}_{30}$  alloy are determined as 548 kJ/mol and 534 kJ/mol, respectively. The  $(\text{Ni}_{0.6}\text{Nb}_{0.4}\text{Ta}_{0.1})_{70}\text{Zr}_{30}$  membrane shows slightly higher values of  $E_a$  (579 kJ/mol and 563 kJ/mol). Ta substitution on the crystallization kinetics and hydrogen permeability of amorphous alloys will be discussed in detail.

**9:40 AM Invited**

**Plastic Deformation Behaviors of Metallic Glasses under Multiaxial Loadings:** *Zhefeng Zhang<sup>1</sup>; F. F. Wu<sup>1</sup>; J. X. Zhao<sup>1</sup>; R. T. Qu<sup>1</sup>; <sup>1</sup>Institute of Metal Research*

The plastic deformation behaviors and evolution of shear bands in a Zr<sub>52.5</sub>Ni<sub>14.6</sub>Al<sub>10</sub>Cu<sub>17.9</sub>Ti<sub>5</sub> metallic glass were systematically investigated under multiaxial loadings, including tension, compression and small punch tests. First, we find that the Zr-based metallic glass can be controlled to create regularly arrayed fine multiple shear bands under small punch test. Second, we report on the macroscopically tensile plasticity up to ~25% in the Zr-based metallic glass sample with dimension of ~100 nanometers at room temperature. Third, the tensile ductility or brittleness of metallic glasses is found to strongly depend on the critical shear offset. Finally, following the dislocation theory in crystalline materials, we find that the plasticity of Zr-based metallic glass could be improved to a high value of ~10% under compression tests through installing two symmetrical semi-circular notches due to the steady shear deformation by the large-scale stress gradient around the two symmetrical notches.

**10:00 AM Break****10:10 AM**

**Interface Properties of Crystalline-Amorphous Metallic Multilayers:** *Christian Brandl<sup>1</sup>; Timothy Germann<sup>1</sup>; Amit Misra<sup>1</sup>; <sup>1</sup>Los Alamos National Laboratory*

The combination of amorphous layers with crystalline layers showed extraordinary high toughness, i.e. ultra-high strength in conjunction with high elongation-to-failure. The plastic deformation, moreover, is confined by the crystalline-amorphous interface, which additionally has to maintain deformation compatibility to mediate homogeneous plastic flow. In nanocrystalline metals molecular dynamics (MD) simulation showed huge varieties of ordered fine structures in the interface, which can be related to the observed dislocation mediated deformation mechanism in the vicinity of the interface structure. Contrary to crystalline-crystalline interfaces, where crystalline phases exhibit long range order, the amorphous structure is characterized by a lack of long-range order. Using MD methods the compensation mechanism of the lacking long-range order at the interface is studied for metallic systems. The observed structural features are discussed in terms of dislocation-based deformation mechanisms such as dislocation transmission, nucleation, and absorption.

**10:20 AM Invited**

**Effect of Minor Additives on Nucleation and Grain Growth Behaviors in Zr-Al-Ni-Cu-Based Metallic Glass:** *Junji Saida<sup>1</sup>; Albertus Setyawan<sup>1</sup>; Mitsuhide Matsushita<sup>2</sup>; Akihisa Inoue<sup>1</sup>; <sup>1</sup>Tohoku University; <sup>2</sup>JEOL Co., Ltd.*

Recently, formation of various nanocrystalline phases as primary precipitation phases has been found by addition of minor elements, which deviate from the best composition for glass-forming ability (GFA) in metallic glasses. Especially, nano icosahedral quasicrystalline (QC) phase formation is important for the investigation of mechanism of high GFA as well as the improvement of mechanical properties in Zr-based metallic glasses. The authors have reported that the nano QC phase is easily precipitated by addition of a small amount of elements such as noble metals, Nb, V, Ta, Mo etc.. In this study, we report the transformation kinetics of nucleation and grain growth behaviors of the primary QC phase in Zr-Al-Ni-Cu metallic glasses by addition of Pd and Nb. The results bring us the useful information on nucleation and grain growth controlling for nanostructure formation with minor additives for the improvement of mechanical properties of bulk metallic glasses (BMGs).

**10:40 AM**

**Electrochemical and Wear Properties of Zr<sub>55</sub>Cu<sub>30</sub>Ni<sub>5</sub>Al<sub>10</sub> Bulk Metallic Glass with Respect to Use as a Medical Implant Material:** *Steven Savage<sup>1</sup>; Maysam Nezafati<sup>2</sup>; Magnus Skjellerudsveen<sup>3</sup>; Dan Persson<sup>2</sup>; Ragnhild Aune<sup>3</sup>; <sup>1</sup>FOI; <sup>2</sup>Swerea KIMAB AB; <sup>3</sup>NTNU*

Bulk Metallic Glasses (BMG) are known to have excellent corrosion resistance in aqueous media. However, when a material is used as a medical implant other properties including abrasive wear, tribocorrosion and leaching of metallic ions are also important. Relevant properties of the BMG Zr<sub>55</sub>Cu<sub>30</sub>Ni<sub>5</sub>Al<sub>10</sub> have been compared with those of surgical grade Co-Cr-Mo (F75) and stainless steel 316 LVM. All measurements have been made under conditions which approximate those experienced by implants, using a phosphate buffer solution at pH 7.4, with and without the addition of protein (albumin), at 37°C. Abrasive wear measurements using the ball-on-disc method have been made and show that the wear resistance of the BMG is inferior to F75. However, the corrosion resistance measured by potentiodynamic tests was improved, and the amount of metallic ions leached into solution was much reduced. In particular it is noteworthy that nickel-ion release was greatly reduced.

10:50 AM

**In-Vitro Biocompatibility of Ni-Free Zr-Al-Cu-Nb-Pd Bulk Metallic Glasses:** *Lu Huang*<sup>1</sup>; *Wei He*<sup>2</sup>; *Yoshihiko Yokoyama*<sup>3</sup>; *Shujie Pang*<sup>1</sup>; *Peter Liaw*<sup>2</sup>; *Akihisa Inoue*<sup>3</sup>; *Tao Zhang*<sup>1</sup>; <sup>1</sup>Beihang University; <sup>2</sup>University of Tennessee; <sup>3</sup>Tohoku University

Zr-based bulk metallic glasses (BMGs) possess attractive properties for their prospective biomedical applications. The present work investigated the in-vitro biocompatibility of Ni-free Zr-Al-Cu-Nb-Pd BMGs by studying bio-corrosion behaviors and cellular responses. Ti-6Al-4V alloy was used as a reference material. Surface composition and wettability were characterized. Electrochemical tests were performed in a physiologically relevant environment using cyclic anodic polarization technique. Cellular behaviors including cell attachment and proliferation activity were investigated with three different types of cells (RAW 246.7 macrophages, NIH3T3 fibroblasts, and MC3T3-E1 pre-osteoblasts). It was found that the Zr-based BMGs exhibited low corrosion penetration rates (CPRs) representing good corrosion resistance. The general biosafety of the Zr-based BMGs were revealed by normal cell responses. This study concluded that the Ni-free Zr-based BMGs demonstrated favorable electrochemical properties and biocompatibility, which made them a potential alternative as a biomedical material. This work was supported by NSFC, NSF, and IMI program.

11:00 AM Invited

**Microstructure Evolution and Mechanical Properties of Zr-Cu-Ni-Al Bulk Metallic Glasses by the Bridgman Solidification:** *Jialin Cheng*<sup>1</sup>; *Guang Chen*<sup>1</sup>; *Hongwei Xu*<sup>1</sup>; <sup>1</sup>Nanjing University of Science and Technology

Microstructure evolution was experimentally studied at growth velocity between 0.1 and 6 mm/s by a Bridgman technique in Zr51.7Cu30Ni8.3Al10. Our results show that the critical growth velocity of the glassy sample was 4 mm/s for Zr51.7Cu30Ni8.3Al10, the critical growth velocities of the full crystalline sample were 1 mm/s for the alloy. When the growth velocities are between 1 mm/s and 4 mm/s, the in-situ formed eutectic phase/ bulk metallic glass matrix composites could be acquired. Moreover, compressive tests were performed on these samples. The results show that as the growth velocity decreases and the precipitation of eutectic phase, plastic strain decreases, indicating that the precipitated eutectic phase can not block the fast propagation of the localized shear bands and the macroscopically brittle failure.

11:20 AM

**Shear Band Patterns in Metallic Glasses under Vickers Indentation:** *Zhinan An*<sup>1</sup>; *Yanfei Gao*<sup>1</sup>; *Fengxiao Liu*<sup>1</sup>; *Peter Liaw*<sup>1</sup>; <sup>1</sup>University of Tennessee

Vickers indentation was conducted on Zr-based bulk metallic glasses and metallic glass thin films. Both semi-sphere shear bands and radial shear bands were discovered in free-bond metallic glasses, yet only radial shear bands could be seen in non-free-bond metallic glasses. The radial shear bands were generated due to in-plane shear stresses and were in agreement with the maximum shear stress direction according to our finite element analysis. While the semi-sphere shear bands were caused by out-of-plane shear stresses. Shear bands were blocked by the film/substrate. Instead of penetrating into the substrate, the radial shear bands were reflected back into the metallic glass thin film. This phenomenon was both discovered experimentally and predicted in our modeling.

11:30 AM

**Effects of Laser-surface Melting Treatment on the Mechanical Behaviors of Zr-Based Bulk Metallic Glasses:** *Haoling Jia*<sup>1</sup>; *Gongyao Wang*<sup>1</sup>; *Junwei Qiao*<sup>1</sup>; *Bingqing Chen*<sup>2</sup>; *Tao Zhang*<sup>2</sup>; *Peter Liaw*<sup>1</sup>; <sup>1</sup>University of Tennessee; <sup>2</sup>Beihang University

Laser-surface melting (LSM) is a precision manufacturing technique capable of producing materials with highly nonequilibrium microstructures. Due to the localized heat input and high cooling rate inherent to the process, this technology is attractive for the production of metallic glasses. In the present work, an effort has been made to study the effects of LSM on the mechanical behaviors of a Zr55Cu30Al10Ni5 bulk metallic glass. The results of high-energy synchrotron diffraction, differential scanning calorimeter, and

scanning electron microscopy indicated that the solidification microstructure in the laser-melted zone was still a single-phase amorphous structure. After the laser-surface remelting, Zr-based alloys exhibited an enhancement in both the compressive strength and plasticity, compared with the as-cast samples. The improvement in mechanical behavior of the LSM-treated metallic glasses may result from complex residual stress distributions and different amorphous structure in the surface layer induced by the LSM treatment.

11:40 AM

**Viscosity Measurement of Fe-Based Metallic Glass by Single Particle Compressive Test:** *Rui Yamada*<sup>1</sup>; *Noriharu Yodoshi*<sup>1</sup>; *Akira Kawasaki*<sup>1</sup>; <sup>1</sup>Tohoku University

Fe-based metallic glasses have attracted much attention due to their excellent properties and are expected to be utilized as micro-components. However, Fe-based metallic glasses have insufficient resistance against crystallization and are difficult to fabricate into the required shape within the incubation time before crystallization. Therefore, we need to investigate the optimal processing conditions and material properties of Fe-based metallic glasses. The viscosity is an important parameter in determining the stresses during processing and the shape of the final products. Conventional viscosity measurement methods, however, cannot be applied to most Fe-based metallic glasses because of their size limitation. To overcome this, we propose a new method in which viscosities are derived from the viscous flow behavior on the micrometer scale of a single metallic glassy particle during the compressive test. Our studies have shown that temperature dependence of the viscosities of [(Fe0.5Co0.5)0.75Si0.05B0.2]96Nb4 metallic glass in the supercooled-liquid region can be measured.

## Carbon Dioxide and Other Greenhouse Gas Reduction Metallurgy - 2011: Electrochemical Reduction Methods - CO2 Use and Other Metal Production

*Sponsored by:* The Minerals, Metals and Materials Society, TMS Extraction and Processing Division, TMS Light Metals Division, TMS: Energy Committee

*Program Organizers:* Neale Neelameggham, US Magnesium LLC; Ramana Reddy, The University of Alabama; Maria Salazar-Villalpando, National Energy Technology Laboratory; James Yurko, 22Ti LLC; Malti Goel, INSA

Thursday AM  
March 3, 2011

Room: 15B  
Location: San Diego Conv. Ctr

*Session Chairs:* Aldo Steinfeld, Solar Technology Lab; Mahesh Jha, Department of Energy

8:30 AM Introductory Comments

8:35 AM

**Concentrated Solar Power for Producing Liquid Fuels from CO2 and H2O:** *Peter Loutzenhiser*<sup>1</sup>; *Anastasia Stamatou*<sup>1</sup>; *Daniel Gstoehl*<sup>2</sup>; *Anton Meier*<sup>2</sup>; *Aldo Steinfeld*<sup>1</sup>; <sup>1</sup>ETH Zurich; <sup>2</sup>Paul Scherrer Institute

A two-step solar thermochemical cycle for producing synthesis gas from H2O and CO2 with Zn/ZnO redox reactions is considered. The first, endothermic step is the thermolysis of the ZnO to Zn and O2 using concentrated solar energy as the source of process heat. The second, non-solar, exothermic step is the reaction of Zn with mixtures of H2O and CO2 yielding synthesis gas and ZnO; the latter is recycled to the first solar resulting in the net reaction of CO2 + H2O = CO + H2 + O2. Syngas is further processed to liquid fuels via Fischer-Tropsch or other catalytic reforming processes. Second law analysis is used to determine the solar-to-chemical efficiencies attainable for molar ratios of CO to H2 of 0.2-5 and a summary of the experimentation on both steps, including the solar reactor technology and kinetic analyses, is provided.

8:55 AM

**CO<sub>2</sub> Electrochemical Reduction by Specifically Adsorbed Anions:** Korato Ogura<sup>1</sup>; Jack Ferrell<sup>2</sup>; *Maria Salazar-Villalpando*<sup>3</sup>; <sup>1</sup>Research and Engineering Services; <sup>2</sup>ORISE; <sup>3</sup>National Energy Technology Laboratory

Due to concerns of global climate change and depleting fossil fuel resources, there have been many attempts to efficiently electrochemically reduce CO<sub>2</sub>. However, the net current densities for CO<sub>2</sub> reduction described in the literature are very small; this has limited practical applications. Here, we describe a CO<sub>2</sub> reduction electrochemical set up which yields a high current density on a Cu-mesh electrode. The CO<sub>2</sub> reduction occurs in an acidic solution containing a high concentration of a halide ion. Weakly solvated ions, such as a halide anion, can strip part of their solvation shell and form a direct chemical bond with the metal electrode. This effect has been shown to play an important role in electrochemical reactions. Here, the observed high current density for electrochemical CO<sub>2</sub> reduction is caused by the specifically adsorbed anion, bonded with a covalent character on the Cu electrode. This anion effectively captures CO<sub>2</sub> and accelerates the electro-reduction.

9:15 AM

**Photo-Electro-Catalytic Conversion of CO<sub>2</sub> to Synthetic Fuels on Surface Modified Nanowires:** *Jung-Kum Lee*<sup>1</sup>; Mengjin Yang<sup>1</sup>; *Maria Salazar-Villalpando*<sup>2</sup>; <sup>1</sup>University of Pittsburgh; <sup>2</sup>National Energy Technology Laboratory

The photo-electro-catalytic conversion of CO<sub>2</sub> to synthetic fuels is one of the very environment-friendly ways to reduce CO<sub>2</sub> concentrations in the air. This is also an energy storage process that converts solar into chemical energy. Here, we report the recent results on the reuse of CO<sub>2</sub> by the surface modified TiO<sub>2</sub> and ZnO nanowires. The surface of the nanowires is coated with a very thin layer of highly active materials by using an atomic layer deposition (ALD) technique to decrease kinetic reaction barriers. Electron hole recombination is the main challenge to overcome in the photo-electro-catalytic reduction of CO<sub>2</sub>. Compared with the nanoparticle counterpart, the arrays of 1-dimensional nanomaterials have higher carrier mobility due to the decrease in the concentration of the trapping sites, which allows for the efficient use of the photo-generated carriers. We will show the correlation between carrier transport and CO<sub>2</sub>-photo-electro-catalytic conversion in the nanowire arrays.

9:35 AM

**Solar Thermo-Chemical Splitting of Carbon Dioxide by Metal Oxide Redox Pairs:** Martin Roeb<sup>1</sup>; Sebastian Stenger<sup>1</sup>; *Martina Neises*<sup>1</sup>; Christian Sattler<sup>1</sup>; <sup>1</sup>DLR

A two-step thermo-chemical cycle process has been developed and investigated. It is based on metal oxide redox pair systems, which can split carbon dioxide as well as water molecules by abstracting oxygen atoms and reversibly incorporating them into their lattice. If concentrated solar radiation is used as the heat source one has a promising method in hand to produce synthesis gas from water and CO<sub>2</sub>. An easy way of operation is gained by the combination of a ceramic substrate as absorber structure, which can be heated to high temperatures with concentrated solar radiation, and of a metal oxide coating which is capable to carry out the reactions. Different redox materials as powders and coated on ceramic substrates were investigated in a laboratory set-up. CO<sub>2</sub> could be reduced to CO with significant yields. In addition several side reactions were observed like the formation of carbon and like the Boudouard reaction.

9:55 AM

**Recent Progress in Molten Oxide Electrolysis for Iron Production:** *Antoine Allanore*<sup>1</sup>; Felipe Carillo<sup>1</sup>; Luis Ortiz<sup>1</sup>; Donald Sadoway<sup>1</sup>; <sup>1</sup>MIT

The steelmaking industry has drastically reduced its energy consumption in the last fifty years, and today's technologies are considered to operate at their optimal efficiency with respect to energy needs. To cope with new constraints related to green-house gases emissions, a change of paradigm is necessary. One of the future technologies which could be deployed to reach CO<sub>2</sub> mitigation targets relies on the intensive use of electricity: molten oxide electrolysis. One possible electrolyte contains molten iron oxide, to directly

produce liquid iron. This talk will present the recent progress obtained in the development of molten oxide electrolysis of iron and will discuss the potential energy and CO<sub>2</sub> impact of the process.

10:15 AM

**Perfluorocarbon Generation during Electrolysis in Molten Fluorides:** Xiangsheng Wang<sup>1</sup>; Zuoju Huang<sup>1</sup>; Guihua Wang<sup>1</sup>; *Hongmin Zhu*<sup>1</sup>; <sup>1</sup>University of Science & Technology Beijing

During the electrolysis in oxide-fluoride melts with carbon anode, the main anode products are carbon oxides (CO<sub>2</sub>, CO), under normal potential. However, when the anode potential exceeds a certain value, the generation of perfluorocarbons (PFC) CF<sub>4</sub> and C<sub>2</sub>F<sub>6</sub> happens accompanying with the anode effect. The current behavior of the carbon electrode under high potentials largely depends on the composition of the fluoride melts, and temperature.

10:35 AM Break

10:45 AM

**Climate Change and Metal and Mining Sector: An Overview of Trends, Project Potential and Its Abatement:** *Puliyur Krishnaswamy Narasimha Raghavan*<sup>1</sup>; <sup>1</sup>Bharat Aluminium Co. Ltd.

This paper identifies potential technologies for Carbon dioxide abatement from the mining and metal industry with special reference to the Aluminium industry. Mine reclamation could contribute to this effort to successfully reach the greenhouse gas (GHG) emissions reduction commitments for a nation. An overview of GHG production by the mining and metal industry together with a review of principles used to set the context in which specific options for GHG reduction are described. Options for GHG reduction in the mining and metal industry include reforestation, Addition of soil amendments or neutralizing agents, CO<sub>2</sub> capture and storage, initiatives towards energy reduction, waste heat recovery and alternative energy use. An analysis and quantification of the potential GHG reduction of potential carbon sinks and sequestration options for the mining and metal industry are provided. Cost estimates for different options are provided. The paper also identifies sources that could fund research regarding GHG reduction options. The paper concludes with recommendations.

11:05 AM

**Fundamental Thermodynamics of Aqueous Carbon Dioxide Systems:** *Dave Tahija*<sup>1</sup>; H.H. Huang<sup>2</sup>; <sup>1</sup>Gehenna Corp; <sup>2</sup>Montana Tech

Many investigations are being performed with the goal of removing carbon dioxide from the atmosphere and permanently storing it in geologically stable settings. At the same time, carbon dioxide in the form of dissolved carbonate is steadily accumulating in the world's oceans. Both carbon dioxide sequestration and oceanic accumulation are constrained by the aqueous thermodynamics of the carbonate system. These constraints are illustrated using the STABCAL computer model to generate potential-pH and aqueous distribution diagrams of seawater in contact with various pressures of carbon dioxide gas. STABCAL diagrams and titration simulations are also used to model some potentially useful cation-carbonate sequestration systems.

11:25 AM

**Electrodeposition of PbTe Thermoelectric Materials in NaOH Solutions:** *Zhongning Shi*<sup>1</sup>; Ramana Reddy<sup>2</sup>; <sup>1</sup>School of Materials and Metallurgy, Northeastern University; <sup>2</sup>The University of Alabama

The thermoelectric materials such as PbTe are becoming useful material for alternative energy production which helps reduce CO<sub>2</sub> emissions. The electrodeposition of lead telluride (PbTe) is reported. Electrochemical behavior on Ag electrode in electrolyte 0.2M NaOH+0.01MPb(NO<sub>3</sub>)<sub>2</sub>, 0.2M NaOH +0.01M TeO<sub>2</sub> and 0.2M NaOH +0.01MTeO<sub>2</sub> +0.01M Pb(NO<sub>3</sub>)<sub>2</sub> solution were carried out at 298K by cyclic voltammetry. The results showed that two different underlying processes are occurring depending on deposition potential. One process involves the reduction of TeO<sub>2</sub> to Te<sup>0</sup> and a subsequent interaction between reduced Te<sup>0</sup> and Pb<sup>2+</sup> to form PbTe at -0.92V. A second process at more negative reduction potentials involves reduction of TeO<sub>2</sub> to H<sub>2</sub>Te at -1.29V followed by the chemical interaction with Pb<sup>2+</sup>. Both processes result in the production of crystalline PbTe in

THURSDAY AM



the potential range  $-1.38V < E < -0.9V$  (vs.Hg/HgO) on Ag substrates. The electrodeposition in 0.2M NaOH +0.01TeO<sub>2</sub> +0.01M Pb(NO<sub>3</sub>)<sub>2</sub> is described by the reaction  $TeO_2 + Pb^{2+} + e^- + H^- > PbTe + H_2O$ .

**11:45 AM**

**Study of Bamboo Charcoal Load Ce-Doped Nano-TiO<sub>2</sub> Photochemical Catalysis Oxidation Degradation of Formaldehyde Device:** *Daowu Yang*<sup>1</sup>; Zhuo Ren<sup>1</sup>; Hui Liu<sup>1</sup>; Yu Su<sup>1</sup>; <sup>1</sup>ChangSha University of Science & Technology

The Nano - TiO<sub>2</sub> / bamboo charcoal adsorption of formaldehyde, as well as the influences of a certain amount of formaldehyde after adsorption on its photochemical catalysis effect were discussed in this paper. The sol preparation process of Ce-doped Nano-TiO<sub>2</sub> was described. Results indicated that: the surface of bamboo Charcoal still has a strong formaldehyde adsorption capacity after Supported by Nano TiO<sub>2</sub>. After adsorbing formaldehyde, the photochemical catalysis degradation efficiency of formaldehyde of the catalyst at a steady state is basically the same with new prepared catalysts'. When the thickness of the catalyst layer of the multi-ladder-type structure photoreactor is 2mm, the interval is 20mm, the absorption efficiency of formaldehyde of Nano-TiO<sub>2</sub> / bamboo charcoal is the best. Nano-TiO<sub>2</sub> undoped Ce responded with no degradation of formaldehyde after 2 hours, the formaldehyde decontamination of the equipment reached 94%.

## Challenges in Mechanical Performances of Materials in Next Generation Nuclear Power Plants: Session I

*Sponsored by:* The Minerals, Metals and Materials Society, American Nuclear Society, ASM International, Japan Institute of Metals, National Science Foundation, TMS Materials Processing and Manufacturing Division, TMS Structural Materials Division, ASM Materials Science Critical Technology Sector, TMS: Advanced Characterization, Testing, and Simulation Committee, TMS/ASM: Composite Materials Committee, TMS: Energy Committee, TMS: High Temperature Alloys Committee, TMS/ASM: Mechanical Behavior of Materials Committee, TMS/ASM: Nuclear Materials Committee

*Program Organizer:* Faramarz Zarandi, CANMET-Materials Technology Laboratory

Thursday AM  
March 3, 2011

Room: 5A  
Location: San Diego Conv. Ctr

*Session Chairs:* Amit Misra, Los Alamos National Laboratory; Milo Kral, University of Canterbury

**8:30 AM Invited**

**Materials Selection and Qualification for Advanced Nuclear Reactors:** *R. N. Wright*<sup>1</sup>; <sup>1</sup>Idaho National Laboratory

The Next Generation Nuclear Plant (NGNP) is a helium cooled high temperature reactor that is being developed in the United States to deliver process heat to industrial processes or for hydrogen generation. The goal of the project is to design and demonstrate a plant that can be licensed for commercial operation for 60 years. In addition to components like fuel cladding that will see nuclear service, selection and qualification of metallic materials focused on the intermediate heat exchanger or steam generator, reactor pressure vessel, and control rod assemblies is critical. The goals for the NGNP of long term operation at high temperature under a commercial license are fairly typical for new reactor systems under development and can be used as a framework for discussing new material development. It is highly desirable for example to design the reactor system using materials that are approved for nuclear service in the ASME Boiler and Pressure Vessel Code, have a well developed experience base, and exhibit stable properties with respect to aging and environmental effects. The ability to fabricate appropriate size and shape components, and joining and inspection are additional significant considerations. The approach to material selection and qualification that is being carried out by the NGNP program will be discussed

and key properties of the materials under consideration will be reviewed. The important role of international collaboration on technology development and university programs in the US will be discussed. In addition, elevated temperature design rules that are incorporated in the ASME Code will be discussed and suggestions for extension or modification of the design rules will be presented.

**9:10 AM**

**Creep Behavior of High Temperature Alloys for Generation IV Nuclear Power Plant Applications:** *Xingshuo Wen*<sup>1</sup>; Laura Carroll<sup>2</sup>; Richard Wright<sup>2</sup>; T.-L. (Sam) Sham<sup>3</sup>; Vijay Vasudevan<sup>1</sup>; <sup>1</sup>University of Cincinnati; <sup>2</sup>Idaho National Laboratory; <sup>3</sup>Oak Ridge National Laboratory

Alloy 617 and 800H were selected as candidate materials for Intermediate Heat Exchangers in the Next Generation Nuclear Plant project with operating temperature in the range of 800 to 950°C and service life of 60 years. In this work, thermomechanically processed plates of alloys 617 and 800H were produced and their creep behavior over the temperature range of 750 to 1050°C and stresses ranging from 5 to 100 MPa was studied. The creep data was analyzed to decipher the various stages, and the stress exponents and activation energies were determined and diffusional versus dislocation creep mechanisms were discriminated. Microstructural changes, deformation structures and damage processes following creep were characterized using electron microscopy techniques, with particular attention given to the evolution of grain size, grain boundaries, second phase precipitates, dislocation structures and void formation. The results relating the creep behavior to microstructural changes in these alloys will be presented and discussed.

**9:30 AM**

**The Influence of a VHTR Environment on the Creep-Fatigue Behavior of Alloy 617:** *Laura Carroll*<sup>1</sup>; Celine Cabet<sup>2</sup>; Rachael Madland<sup>3</sup>; Richard Wright<sup>1</sup>; <sup>1</sup>Idaho National Laboratory; <sup>2</sup>CEA, DEN, DPC, SCCME; <sup>3</sup>Colorado School of Mines

Alloy 617 is the leading candidate material for an intermediate heat exchanger (HX) application of the Very High Temperature Nuclear Reactor (VHTR), which may have an outlet temperature as high as 950°C. Previous work on corrosion of nickel base alloys in impure helium has shown that this environment is far from inert with respect to Alloy 617. A series of experiments have been conducted to elucidate the effect of environment, both laboratory air and VHTR impure helium, on the creep-fatigue behavior and the associated deformation mechanisms. The creep-fatigue behavior was investigated at a 0.3% total strain range and tensile hold times of up to 30 minutes at 950°C. Similarly, experiments with the corresponding time, temperature, and environment "no load" condition were conducted for comparison. The microstructural evolution, corrosion layer, and depleted surface region of the controlled chemistry exposures in both the "no load" and creep-fatigue conditions have been analyzed.

**9:50 AM**

**The Effect of Grain Size and Annealing Twin Density on the Creep Properties of Alloy 800H:** *Ben Gardiner*<sup>1</sup>; Milo Kral<sup>1</sup>; <sup>1</sup>University of Canterbury

The overall purpose of the present work is to identify an optimal grain size for an austenitic alloy (INCOLOY Alloy 800H) in a creep susceptible application. In order to accomplish this, an algorithm for measuring grain size in austenite must be developed in conjunction with an understanding of the influence of annealing twins. While the use of Electron Backscatter Diffraction (EBSD) to measure grain size would seem to be an obvious method due to advantages such as automatic identification of  $\Sigma 3$  boundaries, there are many subtle but significant technical issues with using EBSD for this purpose. This presentation will describe how these issues have been addressed as well as progress towards the relationships between grain size and annealing twin density on the creep properties of INCOLOY Alloy 800H.

#### 10:10 AM Break

#### 10:20 AM Invited

##### **On the Scientific and Engineering Challenges Facing the Development of Irradiation Tolerant Nanostructured Ferritic Alloys:** *G. Robert Odette*<sup>1</sup>;

<sup>1</sup>University of California Santa Barbara

Nanostructured ferritic alloys (NFAs) have the potential to make transformational contributions to developing advanced sources of fission and fusion energy. NFAs are Fe-Cr based ferritic stainless steels that contain an ultrahigh density of Y-Ti-O nanofeatures (NFs). The NFs provide outstanding high temperature properties and remarkable tolerance to irradiation induced displacement damage as well as the degrading effects of transmutation product helium. Indeed, the results of recent in situ injection experiments suggest that the NFs can be tailored to effectively transform helium from a liability to an asset. This is accomplished by trapping helium in ultrafine scale bubbles at the interfaces of the NFs, thereby increasing point defect sink strengths and providing deep trap reservoirs for very high concentrations of managed helium that protects grain boundaries and prolongs incubation doses for void and creep cavity formation. However, NFAs are in the very early stages of development. Important challenges and opportunities they face including fundamental issues of: a) determining the structures of the NFs and their interface with the matrix, as well as their compositions, that is their 'character'; b) relating the NF characteristics to their ability to provide sustained high temperature strength and irradiation tolerance; c) demonstrating and understanding the thermal and irradiation stability of far-from-equilibrium NFs and NFA microstructures. After a brief review of the status of these scientific issues, focus will be on a number of other engineering challenges including: a) identifying alloy composition-synthesis designs and thermal mechanical processing paths that optimize the NFs and the balance of NFA microstructures; b) developing practical fabrication and joining methods that preserve optimal NFA microstructures, provide a balanced suite of outstanding and isotropic properties and yield defect free components; c) reducing costs; d) improving alloy homogeneity and reproducibility; e) establishing industrial scale supply sources; and, f) developing protocols needed to qualify new alloys for nuclear service.

#### 11:00 AM

##### **Microstructure and Creep Behavior of Nanocluster-Strengthened Ferritic Steels:** *M Brandes*<sup>1</sup>; *Libor Kovarik*<sup>2</sup>; *Glenn Daehn*<sup>1</sup>; *Joachim Schneibel*<sup>3</sup>; *Martin Heilmaier*<sup>4</sup>; *Michael Mills*<sup>1</sup>; *Michael Miller*<sup>3</sup>; <sup>1</sup>The Ohio State University; <sup>2</sup>Pacific Northwest National Lab; <sup>3</sup>Oak Ridge National Laboratory; <sup>4</sup>University of Magdeburg

Mechanically-alloyed, nanostructured ferritic steels represent a class of alloys that can display high resistances to radiation and creep deformation. Their excellent high temperature creep performance derives from the presence of nanoclusters. The microstructure of a Fe-14YWT alloy was investigated by probe-corrected STEM imaging and electron energy loss spectroscopy. The structure of matrix and grain boundary nanoclusters are presented. The homogeneously-dispersed nanoclusters have faceted interfaces consistent with low index planes of the Fe matrix. The attractive interaction of dislocations with the nanoclusters was studied using bright-field STEM imaging. In light of these observations, a model of the creep response using a modified Frost-Ashby approach will be discussed. With this approach, it is possible to explain the low creep rates and small stress exponents that have been measured in these alloys. This research was sponsored by the U.S. Department of Energy, Materials Sciences and Engineering Division, Office of Basic Energy Sciences.

#### 11:20 AM

##### **On the High Temperature Creep and Crack Growth Studies of Nanostructured Ferritic Alloys:** *E. Steggar*<sup>1</sup>; *M. Salston*<sup>1</sup>; *G.R. Odette*<sup>1</sup>; *K. Fields*<sup>1</sup>; *D. Gragg*<sup>1</sup>; <sup>1</sup>UC Santa Barbara

Nano-structured ferritic alloys (NFAs) have high tensile and creep strength permitting service up to 800°C and manifest remarkable resistance to radiation damage. These outstanding properties derive from an ultrahigh density of Ti-Y-O enriched nano-features (NFs) that provide dispersion strengthening, help stabilize dislocation and fine grain structures, reduce

excess concentrations of displacement defects and trap helium in fine, and relatively harmless, bubbles. The first part of the presentation summarizes an extensive database on the viscoplastic creep properties of the MA957 and other NFAs. The creep strength is anisotropic in extruded product forms with higher and lower strengths in the axial and transverse directions. Note the strong and weak directions for creep are opposite to those for fracture toughness of extruded NFAs, which are lower in the axial versus transverse directions. The second part of the presentation focuses on the low ductile tearing toughness of NFAs at elevated temperatures.

#### 11:40 AM

##### **Characterization of Nano-scale Features in Mechanically Alloyed and HIP-ed Oxide Dispersion Strengthened Steel U14YWT:** *Dhriti Bhattacharyya*<sup>1</sup>; *Patricia Dickerson*<sup>1</sup>; *Stuart Maloy*<sup>1</sup>; *G. Robert Odette*<sup>2</sup>; *Michael Nastasi*<sup>1</sup>; *Amit Misra*<sup>1</sup>; <sup>1</sup>Los Alamos National Laboratory; <sup>2</sup>University of California, Santa Barbara

An Oxide-Dispersion-Strengthened ferritic steel with a high density of nano-features, designated U14YWT, is studied in order to understand the nature of the nano-features. This alloy has a composition Fe - 14Cr - 3W - 0.4Ti - 0.25Y<sub>2</sub>O<sub>3</sub> (wt%), and was processed by Hot Isostatic Pressing. The authors examine the morphology, crystal structure and chemistry of the different nano-scale oxide particles existing in these alloys and their orientation relationship with the BCC-Fe matrix using conventional and high-resolution Transmission Electron Microscopy (TEM), Energy Dispersive X-Ray Spectroscopy (EDS) and Energy Filtered TEM (EFTM). Three different types of precipitates or features were observed - (a) 50-300 nm, irregular shaped faceted particles, (b) 10-50 nm square shaped particles, and (c) small, spherical particles <5nm in diameter. The study revealed nano-features with hitherto unobserved crystal structures and varying chemical compositions, which, because of their relative abundance, may influence the radiation damage resistance of these ferritic alloys.

##### **Characterization of Minerals, Metals and Materials: Characterization of Polymers, Composites and Natural Materials**

*Sponsored by:* The Minerals, Metals and Materials Society, TMS Extraction and Processing Division, TMS/ASM: Composite Materials Committee, TMS: Materials Characterization Committee  
*Program Organizer:* Sergio Monteiro, State University of the Northern Rio de Janeiro - UENF

Thursday AM  
March 3, 2011

Room: 14B  
Location: San Diego Conv. Ctr

*Session Chairs:* Fernando Rizzo, PUC Rio de Janeiro; Jian Li, CANMET-MTL

#### 8:30 AM

##### **Characterization of Tensile Properties of Piassava Fiber Reinforced Polyester Composites:** *Denise Nascimento*<sup>1</sup>; *Isabela da Silva*<sup>1</sup>; *Felipe Lopes*<sup>1</sup>; *Sergio Monteiro*<sup>1</sup>; <sup>1</sup>State University of the Northern Rio de Janeiro - UENF

The piassava fiber is one of the most rigid natural lignocellulosic fibers, which has since the last decade been investigated as possible reinforcement for polymeric composites. In the present work, the tensile properties of polyester composites reinforced with piassava fibers with different diameters were investigated. Composites with volume fractions up to 30% of continuous and aligned piassava fibers were tensile tested at room temperature to evaluate the ultimate strength, elastic modulus and total strain. For each volume fraction, separated fibers with smaller larger diameters were tested. The results indicated that the tensile properties tend to improve with increasing volume fraction of the thinnest piassava fibers. The role played by the fiber/matrix interaction was analyzed by scanning electron microscopy.

8:45 AM

**Characterization of Tensile Tested Continuous Bamboo Stripped Fiber Reinforced Epoxy Composites:** *Lucas da Costa*<sup>1</sup>; Romulo Loiola<sup>1</sup>; Sergio Monteiro<sup>1</sup>; <sup>1</sup>State University of the Northern Rio de Janeiro - UENF

Composites with DGEBA/TETA epoxy matrix reinforced with thinner and continuous bamboo fibers stripped from culms were mechanically characterized by tensile tests. Specimens with up to 30% in volume of aligned fibers were tensile ruptured at room temperature. The results showed a steady increase in both the ultimate strength and the elastic modulus of the composites with the amount of incorporated bamboo fibers. The fractographic analysis by scanning electron microscopy showed evidence of moderate adhesion between the bamboo fiber and the epoxy matrix. This fiber/matrix adhesion by interaction mechanism apparently justifies the improved tensile properties of the composites.

9:00 AM

**Characterization of Thermal Behavior of Polyester Composites Reinforced with Curaua Fibers by Differential Scanning Calorimetry:** Ailton Ferreira<sup>1</sup>; *Felipe Lopes*<sup>1</sup>; Sergio Monteiro<sup>1</sup>; Teresa Castillo<sup>1</sup>; Ruben Rodriguez<sup>1</sup>; <sup>1</sup>State University of the Northern Rio de Janeiro - UENF

Polyester composites reinforced with natural lignocellulosic fibers have, in recent times, been gaining attention in engineering areas as lighter and cheaper alternatives for traditional composites such as the "fiberglass". One of the strongest, the curaua fiber, is today being considered as reinforcement of composites for automobile interior parts. In fact, several research works are currently being dedicated to curaua fiber composites since physical and mechanical properties are required for practical uses. In this work, the thermal behavior of polyester composites reinforced with up to 40% in volume of curaua fibers was investigated by differential scanning calorimetry, DSC. The results showed endothermic events associated with water release and possible molecular chain degradation. Comparison with similar composites permitted to propose mechanisms that explain this DSC thermal behavior.

9:15 AM

**Characterization of Thermogravimetric Behavior of Polyester Composites Reinforced with Coir Fiber:** *Helvio Santafé*<sup>1</sup>; Sergio Monteiro<sup>1</sup>; Ruben Rodriguez<sup>1</sup>; Teresa Castillo<sup>1</sup>; <sup>1</sup>State University of the Northern Rio de Janeiro - UENF

The coir fiber extracted from the husk of the coconut fruits are worldwide available in tropical regions as a low cost lignocellulosic by-product for many applications including composite filler in automobile parts. Possible uses above room temperature require information on the thermal behavior of coir fiber composites. Therefore, the objective of this work was to perform thermogravimetric, TGA and DTG, analysis on polyester matrix composites incorporated with coir fiber with different intervals of diameter. In general, it was found that thermal degradation associated with weight loss occurred in two stages. Changes were also observed in the DTG peaks for the different diameters investigated.

9:30 AM

**Characterization of Aluminum Composite Reinforced with ZrO<sub>2</sub> Nanoparticles Produced by Mechanical Alloying and Sintering Process:** *Jose de Jesus Cruz Rivera*<sup>1</sup>; Jorge Garcia Rocha<sup>1</sup>; Luis Salvador Hernandez Hernandez<sup>1</sup>; Esperanza Elizabeth Martinez Flores<sup>1</sup>; Roberto Martinez Sanchez<sup>1</sup>; Hector Javier Dorantes Rosales<sup>1</sup>; <sup>1</sup>Instituto de Metalurgia

Because of their high specific strength and elastic modulus, aluminum matrix composites have been studied extensively and are regarded as light weight / high strength materials. The Mechanical Alloying (MA) technique belong to process in that a solid state reaction takes place when the nanometric size is arise and the contact between the fresh powder surfaces of the reactant materials at room temperature. In this work it have been tried to take the advantages of using powder metallurgy processes to produce 2024 aluminum composite starting from alloy in powders and dispersing ZrO<sub>2</sub> nanoparticles as reinforcement with the aim to increase mechanical properties and to avoid the drawbacks of liquid processes. The composite was obtained through mechanical alloying, sintering and hot extrusion

processes. The characterization was made using X ray diffraction, scanning electron microscopy and transmission electron microscopy.

9:45 AM

**Flexural Mechanical Characterization of Polyester Composites Reinforced with Continuous Buriti Fibers:** Tammy Portela<sup>1</sup>; *Lucas da Costa*<sup>1</sup>; Rômulo Loiola<sup>1</sup>; Sergio Monteiro<sup>1</sup>; <sup>1</sup>State University of the Northern Rio de Janeiro - UENF

The fibers extracted from the petiole of the buriti palm tree are relatively strong as compared to other lignocellulosic fibers, with a potential for composite reinforcement. In this work, polyester matrix composites incorporated with these fibers were investigated for their flexural behavior. Specimens with up to 35% in volume of continuous and aligned buriti petiole fibers were bend-tested until rupture. The results showed an increase in the composite mechanical strength and stiffness with incorporation of these fibers. A fractograph analysis by scanning electron microscopy disclosed an effective adhesion mechanism between the buriti petiole fiber and the polyester matrix. This mechanism is apparently responsible for the improved performance of the composites.

10:00 AM Break

10:15 AM

**Tensile Failure Characterization of Polymer Matrix Composites:** *Jeongguk Kim*<sup>1</sup>; Sung Cheol Yoon<sup>1</sup>; Jung-Seok Kim<sup>1</sup>; Hyuk-Jin Yoon<sup>1</sup>; Sung-Tae Kwon<sup>1</sup>; <sup>1</sup>Korea Railroad Research Institute

In this investigation, the failure behavior of glass fiber reinforced epoxy polymer matrix composites (PMCs) was characterized during tensile testing. The PMCs have been used for railway bogie materials application. Through tensile testing, the fracture initiated at the epoxy matrix, and the brittle failure mode was observed. In order to monitor tensile damage evolution of PMC sample, a high-speed infrared camera was used to measure surface temperature changes during tensile testing. Through the thermographic image analysis, crack initiation and propagation were qualitatively monitored. Moreover, the thermographic images were helpful to provide the information on fracture mode and mechanisms in PMC sample. In this investigation, an IR camera was used to facilitate a better understanding of damage evolution and failure mode of PMC materials during tensile testing.

10:30 AM

**Rheological and Dynamic Strain Rate Studies of Wax-Coated Granular Composites Used in Sports Surfaces:** *John Bridge*<sup>1</sup>; Alper Kiziltas<sup>2</sup>; Douglas Gardner<sup>2</sup>; Michael Peterson<sup>2</sup>; Wayne McIlwraith<sup>3</sup>; <sup>1</sup>Maine Maritime Academy; <sup>2</sup>University of Maine; <sup>3</sup>Colorado State University

Dynamic mechanical thermal analysis (DMTA) tests were conducted on high-oil content, paraffin-based wax used in wax-coated granular composites. These composites make up the surface of synthetic Thoroughbred horse racetracks used in North America. The modulus and damping response from the DMTA tests were correlated with the dynamic triaxial shear strength response of the bulk track material taken at two different operational temperatures and at four strain rates. The purpose of these tests is to understand the mechanisms of shear strengthening of the bulk track material as the wax is heated through the first crystalline solid to liquid nominal transition temperature. Previous work using differential scanning calorimetry confirmed that under common operational surface temperatures, the wax coatings undergo distinct thermal transitions. The resulting increase in triaxial shear strength values affects the consistency of the racetrack which, in turn, can potentially affect Thoroughbred racing performance and safety of the track surface.

10:45 AM

**Characterization of Plastic Materials Used by Automotive Industry (Impact-Stress):** *Alejandro Rojo*<sup>1</sup>; Nora Ramirez<sup>1</sup>; Jorge Salgado<sup>1</sup>; <sup>1</sup>ITESM Toluca

This work gives a different procedure to characterize the plastics used in the car body interior and improve its design process to be able to predict its behavior when subjected to impact tests involving human casualties. The standard Izod configurations are used on unnotched specimens for



characterization by impact tests. From these tests we obtain the movement curves and the absorption energy estimations. Through stress analysis at high speeds and a video camera set-up, the area reduction of the specimen is obtained from the image analysis, allowing us to get the stress-strain real curve of the material. The proposed testing procedure allows the acquisition of force and displacement data through time at various strain rates, which are indispensable for the characterization of dynamic events. A specimen with a special configuration is used that shows the more detailed dynamic behavior resulting in more accurate numerical analysis in the design process.

**11:00 AM**

**Dynamic-Mechanical Characterization of Polyester Matrix Composites Reinforced with Banana Fibers:** Nathalia Rosa<sup>1</sup>; Lucas Martins<sup>1</sup>; Felipe Lopes<sup>1</sup>; Lucas da Costa<sup>1</sup>; Sergio Monteiro<sup>1</sup>; Rubén Rodriguez<sup>1</sup>; <sup>1</sup>State University of the Northern Rio de Janeiro - UENF

The fibers extracted from the stem of the banana plant are relatively stronger and have been used as reinforcement of polymer matrix composites. In addition to quasi-static mechanical properties, there is a need to characterize the dynamic behavior of banana fiber composites under thermal constraints. In this work, the temperature variation of the dynamic-mechanical parameters of polyester composites incorporated with up to 30% in volume of banana fibers were investigated by DMA tests. The storage and loss moduli as well as then tan delta were measured from 20 to 200°C in a TA Instrument operating with the flexural mode at 1 Hz. The results showed that the incorporation of banana fibers tends to increase the viscoelastic stiffness of the polyester matrix. It was also observed changes in the T<sub>g</sub> and the structure dumping capacity of the composites with increasing fraction of banana fibers.

**11:15 AM**

**Characterization of Thermal Properties of Curaua Fibers by Photothermal and Photoacoustic Techniques:** Felipe Lopes<sup>1</sup>; Leonardo Mota<sup>1</sup>; Marcelo da Silva<sup>1</sup>; Helion Vargas<sup>1</sup>; Sergio Monteiro<sup>1</sup>; <sup>1</sup>State University of the Northern Rio de Janeiro - UENF

Natural fibers, as a class of materials, are attracting the interest of engineering sectors owing to specific advantages such as lower cost and density as well as environmental benefits associated with renewability and biodegradability. For industrial applications, thermal properties, among others, are required especially in the case of an insulating natural fiber. In the present work, thermal properties of the curaua fibers were investigated by photothermal techniques, i.e., the open photoacoustic cell and a method based upon the monitoring of the temperature evolution as a function of time. This investigation, in turn, permitted to evaluate two important thermal properties (thermal diffusivity and specific heat capacity) of the curaua fibers. Indirectly, by means of simple mathematical relations, thermal conductivity and thermal effusivity were obtained. The results were compared with other materials and characterize the curaua fiber as an efficient insulator.

**11:30 AM**

**Photoacoustic Thermal Characterization of a Natural Biofoam Extracted from the Buriti Palm Tree:** Lucas da Costa<sup>1</sup>; Leonardo Mota<sup>1</sup>; Marcelo da Silva<sup>1</sup>; Tammy Portela<sup>1</sup>; Helion Vargas<sup>1</sup>; Sergio Monteiro<sup>1</sup>; <sup>1</sup>State University of the Northern Rio de Janeiro - UENF

A natural biofoam extracted from the buriti palm tree (*Mauritia flexuosa*) has shown characteristics for potential substitution of synthetic foams. In the present work, a photoacoustic thermal characterization was performed on buriti biofoam samples. An open photoacoustic cell technique and a photothermal rise method under continuous laser illumination were employed in order to determine the thermal diffusivity and the specific heat capacity of such material. Beyond their intrinsic values (finger print), these physical parameters represent the light-into-heat conversion efficiency and the amount of heat stored per unit volume, respectively. The results showed that the buriti biofoam presents thermal properties that permit its use as an effective insulation material.

**11:45 AM**

**Pullout Test of Jute Fiber to Evaluate the Interface Shear Stress in Polyester Composites:** Isabela da Silva<sup>1</sup>; Alice Bevitori<sup>1</sup>; Felipe Lopes<sup>1</sup>; Sergio Monteiro<sup>1</sup>; <sup>1</sup>State University of the Northern Rio de Janeiro - UENF

Jute fibers have in the past decades being investigated as possible reinforcement of polymer composites. However, information is still needed on the fiber interaction with a polymeric matrix for a complete evaluation of the capacity of load transference inside the composite. The present work investigated the interaction of jute fibers with polyester matrix by means of the critical length assessment through pullout tests. Tensile tests of polyester sockets embedded with different fiber lengths allowed the critical length to be determined and then the interface shear stress to be calculated. It was found a relatively low interfacial strength indicating a weak adhesion between the ramie fiber and the polyester matrix. The SEM analysis of pulled out fibers corroborates this result.

**12:00 PM**

**Thermal Analysis Characterization of Ramie Fibers with Different Diameters:** Ruben Rodriguez<sup>1</sup>; Alice Bevitori<sup>1</sup>; Isabela da Silva<sup>1</sup>; Felipe Lopes<sup>1</sup>; Sergio Monteiro<sup>1</sup>; <sup>1</sup>State University of the Northern Rio de Janeiro - UENF

The fibers extracted from the stem of the ramie plant are among the strongest natural lignocellulosic fibers with potential to be used as reinforcement of polymer matrix composites. Characterization of the ramie fiber has recently been conducted for physical and mechanical properties. However, the effect of increasing temperature on the ramie fiber behavior has not yet been fully investigated. Therefore, the objective of this work was to perform a thermal analysis on ramie fibers with different diameters within the naturally found range in practice. The analysis was conducted by thermogravimetric, TGA and DTG, as well as differential scanning calorimetric, DSC, techniques. It was found that the ramie fibers present thermal stability up to 200°C and then suffer a sharp deterioration between 300 and 500°C, resulting in characteristic peaks.

**12:15 PM**

**Characteristics of Cementitious-Based Materials When Subjected to Microwave Energy:** Natt Makul<sup>1</sup>; <sup>1</sup>Phranakhon Rajabhat University

In this study, microwave energy at a frequency of 2.45 GHz with a multi-mode applicator was used to accelerate early-age hydration reaction of Portland cement pastes with/without pozzolan materials. Influences of water-to-cementitious ratios (w/c), pozzolan materials and aggregates were investigated. Delay time (30 minutes after mixing), microwave power (390 watt) and time of application (45 minutes), the phases and microstructural characteristics scanning electron microscope (SEM) with dispersive X-ray (EDX), X-ray diffraction (XRD) and thermal analysis (TG). Furthermore, the efficiency of curing procedures was evaluated by comparing the compressive strengths with the pastes that were cured by soaking in lime-saturated deionized water. From test results it can be concluded that water-to-cementitious strongly affect to rise in temperatures inside the pastes to be process, and to develop microstructures and to gain higher compressive strengths.

## Characterization of Nuclear Reactor Materials and Components with Neutron and Synchrotron Radiation: Mechanical Characterization and Modeling

*Sponsored by:* The Minerals, Metals and Materials Society, TMS Structural Materials Division, TMS/ASM: Nuclear Materials Committee

*Program Organizers:* Matthew Kerr, US Nuclear Regulatory Commission; Meimei Li, Argonne National Lab; Jonathan Almer, Argonne National Laboratory; Donald Brown, Los Alamos National Lab

Thursday AM Room: 4  
March 3, 2011 Location: San Diego Conv. Ctr

*Session Chairs:* Matthew Kerr, US Nuclear Regulatory Commission; Don Brown, Los Alamos National Lab

### 8:30 AM Invited

#### Studies of Deformation Modes in Zirconium Alloys for Nuclear Power Applications by Diffraction: *Mark Daymond*<sup>1</sup>; Fei Long<sup>1</sup>; Don Brown<sup>2</sup>; Rick Holt<sup>1</sup>; <sup>1</sup>Queen's University; <sup>2</sup>Los Alamos National Lab

Understanding the performance of materials in the complex stress-temperature-radiation damage environment of a reactor requires predictive capabilities, and hence micromechanical models for prediction of material behaviour. Diffraction experiments, both texture and strain measurement, play a key role in the validation of such models. Internal stresses, generated between differently oriented grains, or between phases, greatly affect the mechanical performance of zirconium alloys. A study of the development of internal stresses by diffraction, coupled with micromechanical models, can provide insights into the deformation mechanisms operating as a function of applied strain and/or temperature. Radiation damage changes the dislocation structures present in a material, and hence the subsequent micromechanics of deformation. This paper demonstrates the application of the technique in understanding deformation modes operating in a zirconium alloy at room temperature. Results obtained on un-irradiated material are compared with those obtained from material irradiated over several years of service in a commercial reactor.

### 9:00 AM

#### In-Situ Observation of the Dissolution and Precipitation of Hydrides in Zircaloy-4: *Olivier Zanellato*<sup>1</sup>; Michael Preuss<sup>2</sup>; Fabienne Ribeiro<sup>1</sup>; Jean-Yves Buffiere<sup>3</sup>; Jean Desquines<sup>4</sup>; Axel Steuwer<sup>4</sup>; <sup>1</sup>IRSN Cadarache, France; <sup>2</sup>The University of Manchester; <sup>3</sup>INSA Lyon; <sup>4</sup>ESSS

Zircaloy-4 is used for fuel assemblies in Pressurised Water Reactors. In the reactor core, the material corrodes and picks up hydrogen that leads to precipitation of hydrides. These hydrides can impair the integrity of the structure, especially after temperature transients. This paper presents observations of in-situ temperature cycles using synchrotron x-ray diffraction carried out on Zircaloy-4 plates charged to different levels of hydrogen content. The diffraction experiment allowed following the evolution of phase fractions, crystallographic structures and lattice strains during the heating cycle. The presence of a strong solubility/precipitation hysteresis of hydrides during temperature cycling was confirmed, as observed by some authors using more indirect methods. It was also possible to study the precipitation kinetics of the hydrides and solve some controversies found in the literature. Self consistent modelling was performed to understand the evolution of the elastic strain in the matrix and the hydrides.

### 9:20 AM

#### Effects of Altering Bulk Hydride Phase and Orientation on DHC Behaviour in Zr-2.5wt% Nb: *Eric Tulk*<sup>1</sup>; Matthew Kerr<sup>2</sup>; Mark Daymond<sup>1</sup>; <sup>1</sup>Queen's University; <sup>2</sup>US Nuclear Regulatory Commission

Delayed Hydride Cracking (DHC) is a time dependant fracture mechanism that has caused both compromise and failure in zirconium reactor core

components. DHC entails the repeated formation, growth and fracture of a brittle hydrides at a notch tip. Although there is extensive experimental data collected on DHC, there is still no consensus on the mechanism of hydride precipitation and growth at the notch tip. A study is presented of how the hydride orientation (affected by the microstructure/texture and by applied stress) and phase (delta vs gamma; affected by quench rate and quantified with synchrotron techniques) of the bulk hydrides affects subsequent DHC behaviour. The different hydride phases have different volume expansions compared to the parent matrix, while a hydride precipitated under stress, and hence in a non-microstructure favoured orientation, presumably has a higher energy than a hydride precipitated under no stress. Initial results indicate that DHC behavior is affected.

### 9:40 AM Invited

#### Validation of Models and Simulations of Nuclear Fuels: *Marius Stan*<sup>1</sup>; Bogdan Mihaila<sup>2</sup>; Mark Bourke<sup>2</sup>; <sup>1</sup>Argonne National Laboratory; <sup>2</sup>Los Alamos National Laboratory

In the reactor, nuclear fuels are subjected to extreme radiation, temperature, and chemical environments that can severely damage their properties. Multi-scale theoretical models and computer simulations are often used to predict these effects. We discuss recent simulations of coupled heat transfer, chemical species diffusion and thermal expansion of UO<sub>2</sub>+x fuel elements with metallic clad. The simulations demonstrate that accounting for the dependence of thermal conductivity and density on local composition leads to changes in the predicted temperature profile that exceed 5%. Such predictions are difficult to validate due to the uncertainty associated with the models and the challenges related to the in situ measurements of the temperature profile in the fuel element. Recent developments and demonstration experiments at synchrotron X-ray and neutron user facilities are discussed to evaluate their potential for model validation. We also speculate on what future facilities might offer for making in situ measurements, including temperature profiles.

### 10:10 AM

#### Chemical Segregation of U-10wt.% Mo Fuel Foils during Simulated Bonding Cycles: *Sven Vogel*<sup>1</sup>; Donald Brown<sup>1</sup>; Maria Okuniewski<sup>2</sup>; Jan-Fong Jue<sup>2</sup>; Blair Park<sup>2</sup>; <sup>1</sup>Los Alamos National Laboratory; <sup>2</sup>Idaho National Laboratory

The mission of the Global Threat Reduction Initiative of the National Nuclear Security Administration in the U.S. DOE is to reduce and protect vulnerable nuclear and radiological material located at civilian sites worldwide by providing support for countries' own national programs. The GTRI Reactor Convert program converts research reactors from the use of highly enriched uranium to low enriched uranium. The baseline fuel for conversion of high performance research reactors is monolithic uranium-10wt.% molybdenum, encased in an aluminum cladding. During fabrication, the aluminum cladding is hot isostatic pressed so that it bonds to the rolled U10Mo foil. However, the final crystal structure of the U10Mo foil is dependent on the HIP'ing temperature and profile. The  $\gamma$  phase is preferred for the fuel application and it is stable in U10Mo above ~560°C. However the fuel transforms to  $\alpha$ ,  $\gamma$ , and  $\gamma'$  crystal structures if held at temperatures below this point.

### 10:30 AM

#### Microstructure Characterization and Processing of U-Mo Alloy Fuels for Nuclear Reactors: *Amy Clarke*<sup>1</sup>; Robert Field<sup>1</sup>; Deniece Korzekwa<sup>1</sup>; Robert Aikin<sup>1</sup>; Duncan Hammon<sup>1</sup>; David Alexander<sup>1</sup>; Kester Clarke<sup>1</sup>; Ann Kelly<sup>1</sup>; Pallas Papin<sup>1</sup>; Rodney McCabe<sup>1</sup>; Carl Necker<sup>1</sup>; Robert Forsyth<sup>1</sup>; Joel Katz<sup>1</sup>; David Dombrowski<sup>1</sup>; <sup>1</sup>Los Alamos National Laboratory

Monolithic, low enriched uranium (LEU)-10 wt.% molybdenum (Mo) fuels have been identified as a potential replacement for highly enriched uranium (HEU) dispersion fuels in high performance research reactors. The microstructures of cast and rolled U-Mo alloys were characterized using optical and electron microscopy to understand the influence of processing on microstructure evolution during the production of monolithic foils. The as-cast microstructure was examined using light optical microscopy (LOM) and electron backscatter diffraction (EBSD) and Mo segregation was quantified using electron microprobe analysis (EMPA). Homogenization heat-

treatments of the as-cast material were performed to evaluate possible time/temperature combinations to reduce the extent of Mo segregation. EBSD of rolled microstructures was also performed to determine the influence of processing and chemical banding on microstructure evolution and texture. The results from this work support the Global Threat Reduction Initiative (GTRI) Convert Fuel Development Program.

#### 10:50 AM Break

#### 11:00 AM

**Dissimilar Metal Weld Residual Stress Mappings by Neutron and X-ray Diffraction and Incremental Hole Drilling Methods:** *Camden Hubbard*<sup>1</sup>; Josh Schmidlin<sup>1</sup>; Matthew Klug<sup>2</sup>; James Pineault<sup>3</sup>; Shane Van De Car<sup>3</sup>; Zhili Feng<sup>1</sup>; Fei Ren<sup>1</sup>; Wei Zhang<sup>1</sup>; <sup>1</sup>Oak Ridge National Laboratory; <sup>2</sup>Dominion Engineering, Inc.; <sup>3</sup>PROTO Manufacturing

The US Nuclear Regulatory Commission (NRC) and the Energy Power Research Institute (EPRI) are conducting a weld residual stress validation program aimed at both (1) refining computational procedures for residual stress simulations in dissimilar metal welds, and (2) developing and categorizing the uncertainties in the resulting residual stress predictions. This program currently consists of four phases, with each phase increasing in complexity from lab size specimens to component mock-ups. The US NRC and EPRI are working cooperatively on this effort under a memorandum of understanding, with this talk focusing on the characterization of residual stresses in dissimilar metal welds by the incremental hole drilling (IHD), X-ray diffraction (XRD) and neutron diffraction (ND) methods conducted by Oak Ridge National Laboratory (ORNL). The three methods provide stress maps at the surface (XRD), near surface (IHD) and through thickness (ND).

#### 11:20 AM

**2D Mapping of Weld Residual Stresses Using the Contour Method:** *Adrian DeWald*<sup>1</sup>; Michael Hill<sup>2</sup>; <sup>1</sup>Hill Engineering, LLC; <sup>2</sup>University of California, Davis

Residual stresses play a significant role in the performance of welded joints, which are often critical locations in nuclear reactor components. Accurate information regarding the magnitude and distribution of residual stress in welded joints is required for assessment of structural integrity. The contour method has become a useful tool for generating two-dimensional maps of residual stress in weldments. This paper provides a description of the contour method and presents the results of recent contour method measurements on weld joints. Comparisons with residual stress data obtained using complementary techniques (e.g., neutron diffraction and slitting) are also provided.

#### 11:40 AM

**Eliminating Do in Neutron Diffraction Weld Residual Stress Measurement:** *Zhili Feng*<sup>1</sup>; Wei Zhang<sup>1</sup>; Paul Crooker<sup>2</sup>; Howard Rathbun<sup>3</sup>; David Rudland<sup>3</sup>; Raj Iyengar<sup>3</sup>; Xun-Li Wang<sup>1</sup>; Ke An<sup>1</sup>; Camden Hubbard<sup>1</sup>; <sup>1</sup>Oak Ridge National Laboratory; <sup>2</sup>Electric Power Research Institute; <sup>3</sup>U.S. Nuclear Regulatory Commission

Neutron diffraction is a unique tool for non-destructive measurement of residual stresses of welded structures. The conventional approach generally requires the knowledge of stress-free lattice spacing a priori. For multiple-pass dissimilar metal welds, the stress-free lattice parameter is a complex function of position due to the chemistry inhomogeneity in the weld region that can be challenging to determine experimentally. This paper presents a new approach to determine the weld residual stress field without the use of the stress-free lattice parameter and any presumption of the residual stress conditions. The theoretical basis is presented first. The new approach is applied to a multi-pass dissimilar metal weld consisting of a stainless steel base metal and a nickel alloy filler metal. The residual stress results as determined from the new approach are compared with finite element modeling results. The general applicability of the new approach for neutron diffraction residual stress measurement is discussed.

#### 12:00 PM Invited

**Neutron Diffraction Measurements in Thick Section Nuclear Reactor Piping Systems:** *Thomas Holden*<sup>1</sup>; D.W. Brown<sup>2</sup>; T. Sisneros<sup>2</sup>; M. Kerr<sup>3</sup>; <sup>1</sup>Northern Stress Technologies; <sup>2</sup>Los Alamos National Laboratory; <sup>3</sup>US Nuclear Regulatory Commission

Time-of-flight neutron diffraction measurements were conducted at the SMARTS diffractometer at Los Alamos National Laboratory on a welded pressurizer safety nozzle which had been retired from service and decontaminated. Thick sections present experimental difficulties due to long neutron path lengths, difficult scattering geometries, and alloy concentration gradients at the weld interface. The safety nozzle studied was composed of carbon steel, stainless steel, and nickel based Alloy 182 weld metal with a large neutron absorption and scattering cross sections. This talk describes the efforts made to measure the stresses in the safety nozzle, specifically the use of a method akin to the  $\sin^2\Psi$  method to minimize the neutron path length and recommendations are given for attempting problems of this kind. Finally comparisons will be made to measurements in a smaller plate specimen, fabricated from similar material and characterized with multiple techniques (neutron diffraction, contour method, incremental hole drilling, and a finite element weld model).

### Coatings for Structural, Biological, and Electronic Applications II: Metallic, Semiconducting, Insulating Coatings - Applications

*Sponsored by:* The Minerals, Metals and Materials Society, TMS Electronic, Magnetic, and Photonic Materials Division, TMS: Thin Films and Interfaces Committee

*Program Organizers:* Nuggehalli Ravindra, New Jersey Institute of Technology; Choong Kim, University of Texas at Arlington; Nancy Michael, University of Texas at Arlington; Gregory Krumdick, Argonne National Laboratory; Roger Narayan, Univ of North Carolina & North Carolina State Univ

Thursday AM  
March 3, 2011

Room: 6E  
Location: San Diego Conv. Ctr

*Session Chairs:* Choong-un Kim, University of Texas at Arlington; Sudhakar Shet, National Renewable Energy Laboratory

#### 8:30 AM Introductory Comments

#### 8:35 AM Invited

**Thin Film Coatings for Silicon Solar Cells: Requirements and Challenges:** *Bhushan L. Sopor*<sup>1</sup>; <sup>1</sup>National Renewable Energy Laboratory  
Abstract not available.

#### 9:00 AM Invited

**Effect of Gas Ambient on the Synthesis of Al and N Co-Doped ZnO:(Al,N) Films and Their Influence on PEC Response for Photoelectrochemical Water Splitting Application:** *Sudhakar Sher*<sup>1</sup>; Le Chen<sup>1</sup>; Houwen Tang<sup>1</sup>; Todd Deutsch<sup>1</sup>; Heli Wang<sup>1</sup>; Nuggehalli Ravindra<sup>2</sup>; Yanfa Yan<sup>1</sup>; John Turner<sup>1</sup>; Mowafak Al-Jassim<sup>1</sup>; <sup>1</sup>National Renewable Energy Laboratory; <sup>2</sup>New Jersey Institute of Technology

Al and N co-doped ZnO thin films, ZnO:(Al,N), are synthesized by radio-frequency magnetron sputtering in mixed Ar and N<sub>2</sub> and mixed O<sub>2</sub> and N<sub>2</sub> gas ambient at 100°C. The ZnO:(Al,N) films deposited in mixed Ar and N<sub>2</sub> gas ambient did not incorporate N, whereas ZnO:(Al,N) films grown in mixed O<sub>2</sub> and N<sub>2</sub> gas ambient showed enhanced N incorporation and crystallinity as compared to ZnO:N thin films grown in the same gas ambient. As a result, ZnO:(Al,N) films grown in mixed O<sub>2</sub> and N<sub>2</sub> gas ambient showed higher photocurrents than the ZnO:(Al,N) thin films deposited in mixed Ar and N<sub>2</sub> gas ambient. Our results indicate that the gas ambient plays an important role in N incorporation and crystallinity control in Al and N co-doped ZnO thin films.



**9:25 AM Invited**

**Viscoplastic Deformation in Porous Low-k Dielectrics:** Nancy Michael<sup>1</sup>; Emil Zin<sup>1</sup>; Woong Ho Bang<sup>1</sup>; Sean King<sup>2</sup>; Todd Ryan<sup>3</sup>; Choong-Un Kim<sup>1</sup>; <sup>1</sup>University of Texas at Arlington; <sup>2</sup>Intel; <sup>3</sup>Global Foundries

One of the key advances in microelectronics technology is the implementation of porous low-k dielectrics (PLK) in interconnect structures. The use of PLK is necessary to increase the device operation speed, yet its implementation has been seriously delayed due mainly to the reliability failure of interconnects integrated with PLK. While several reliability failure mechanisms instigated by PLK have been identified, the linkage between those mechanisms and properties of PLK itself has been illusive. In recent investigation, we find that the root cause of those failures is related to viscoplasticity of PLK. According to theoretical silicate structure properties, PLK should not show plasticity at interconnect processing temperatures, yet our experiment produces evidence showing the opposite. A significant level of viscoplasticity occurs under a mild mechanical and thermal load. The mechanism of such deformation and its linkage to pore structure and molecular bond properties will be discussed in this paper.

**9:50 AM**

**Nanostructured Zinc Oxide Coatings Developed Via Solution Precursor Plasma Spray Technique:** Raghavender Tummala<sup>1</sup>; Ramesh Guduru<sup>1</sup>; Pravansu Mohanty<sup>1</sup>; <sup>1</sup>The University of Michigan - Dearborn

Zinc Oxide (ZnO) is a wide band gap semiconducting material that has various applications including optical, electronic, biomedical and corrosion protection. It is usually synthesized via processing routes, such as vapor deposition techniques, sol-gel, spray pyrolysis and thermal spray of pre-synthesized ZnO powders. However, production of ZnO coatings using an inexpensive and a single step process which is also capable of producing nanostructures is of technological importance. Here, we report synthesis of nanostructured ZnO coatings directly from a liquid solution precursor in a single step using plasma spray technique, for the first time. Adherent and nanostructured ZnO coatings were deposited from the solution precursor prepared using zinc acetate and water/isopropanol. An axial liquid atomizer was employed in a DC plasma spray torch to create fine droplets of precursor for faster thermal treatment in the plasma plume to form ZnO. The microstructures of coatings revealed ultrafine particulate agglomerates. X-ray diffraction confirmed polycrystalline nature and hexagonal Wurtzite crystal structure of the coatings. Transmission electron microscopy studies showed fine grains in the range of 10–40 nm. Observed optical transmittance (~65–80%) and electrical resistivity (48.5–50.2 mΩ-cm) of ZnO coatings are attributed to the ultrafine particulate morphology of the coatings.

**10:05 AM Break**

**10:15 AM**

**Thin Al Doped ZnO Films for Si Heterojunction Solar Cells:** Sudhakar Shet<sup>1</sup>; Bhushan L. Sopori; <sup>1</sup>National Renewable Energy Laboratory

Ga-N co-doped ZnO thin films with reduced bandgaps were deposited on F-doped tin-oxide-coated glass by radio-frequency magnetron sputtering at different substrate temperatures in mixed N<sub>2</sub> and O<sub>2</sub> gas ambient. We found that Ga-N co-doped ZnO films exhibited enhanced crystallinity compared to undoped ZnO films grown under the same conditions. Furthermore, Ga-N co-doping ensured enhanced N-incorporation in ZnO thin films as the substrate temperature is increased. As a result, Ga-N co-doped ZnO thin films exhibited much improved photoelectrochemical (PEC) response, compared to ZnO thin films. Our results therefore suggest that the passive co-doping approach could be a means to improve PEC response for bandgap-reduced wide-bandgap oxides through impurity incorporation.

**10:40 AM Invited**

**Spin Coated Er<sub>2</sub>O<sub>3</sub>-SiO<sub>2</sub> Films on Silicon Substrates:** Sufian Abedrabbo<sup>1</sup>; Bashar Lahlouh<sup>1</sup>; Anthony Fiory<sup>2</sup>; Nuggehalli Ravindra<sup>2</sup>; <sup>1</sup>University of Jordan; <sup>2</sup>New Jersey Institute of Technology

Optically active Er<sup>3+</sup> in silica films, which are suitable for silicon-based optical applications, have been produced by a sol-gel deposition process with high Er atomic concentrations of 6 and 12 %, followed by

furnace annealing. Films were characterized for their thickness, index of refraction, and photoluminescence at room temperature. Photoluminescence yield is strongly enhanced for vacuum annealing in the temperature range 500 – 750°C. Reasonable room-temperature photoluminescence is also observed for annealing at 1000°C. These results demonstrate the viability of incorporating Er at high concentrations.

**11:05 AM**

**Magnetic Material Interactions for the Method of Magnetic Field Directed Assembly:** Rene Rivero<sup>1</sup>; Michael R. Booty<sup>1</sup>; Anthony T. Fiory<sup>1</sup>; Nuggehalli M. Ravindra<sup>1</sup>; <sup>1</sup>New Jersey Institute of Technology

Magnetic Field Directed Assembly is a method that offers a non-statistical solution to the problem of assembly via parallel processing. The method requires the use of magnetic layers on top of devices and in recesses within wafers where they need to be located. We have developed a model that allows us to select magnetic materials that minimize their total weight contribution to the system while maximizing magnetization. We apply the model to a range of magnetic materials of high permeability that are often used as magnetic layers on semiconductors.

**11:20 AM Invited**

**Bioactive Hydroxyapatite Coatings on Titanium Implants:** Hadeer Ibrahim Mohammed<sup>1</sup>; Adele Carradò<sup>2</sup>; Thierry Roland<sup>3</sup>; Genevieve Pourroy<sup>2</sup>; Wafa Abdel-Fattah<sup>4</sup>; <sup>1</sup>Biophysics Department, Ain-Shams University; <sup>2</sup>IPCMS; <sup>3</sup>INSA; <sup>4</sup>NRC

This study presents an alternative coating method based on biomimetic techniques which are designed to form a crystalline hydroxyapatite (HA) layer very similar to the process corresponding to the formation of natural bone. The deposition route is electroless and based on redox reaction having several advantages of controlled conditions, application to complicated shapes, without adverse effect of heating besides being cost effective. The oxidant, alkaline (pH 9.2 at 60 °C) and acidic (pH 5.3 at 80 °C) baths were performed. The HA formations on the surface of titanium alloy pre-treated were investigated by means of Scanning Electron Microscopy (SEM) and Energy Dispersive Spectroscopy (EDS), FT-IR (Fourier Transform Infrared) Spectroscopy, Atomic Force Microscopy (AFM) and Simulated Body Fluids (SBF) for several periods. The data suggest that the method utilized in this study can be successfully applied to obtain deposition of uniform coatings of crystalline hydroxyapatite on titanium substrates.

**11:45 AM Invited**

**Flame Spray Deposition of Composite Titanium Alloy and Bioactive Glass Coatings:** Greg Nelson<sup>1</sup>; Andre McDonald<sup>1</sup>; John Nychka<sup>1</sup>; <sup>1</sup>University of Alberta

Flame spray deposition development and characterization of a composite coating for use in bone fixation implants is described. The composite coating was deposited using a mixture of TiAl6V and bioactive glass 45S5 powders to produce a porous coating. Porosity, phase distribution, and in vitro bioactivity will be discussed for these promising biomaterial coatings.

---

## Commonality of Phenomena in Composite Materials II: Characterization and Processing Techniques for Composites

Sponsored by: The Minerals, Metals and Materials Society, ASM International, TMS Structural Materials Division, TMS/ASM: Composite Materials Committee

Program Organizers: Meisha Shofner, Georgia Institute of Technology; Carl Boehlert, Michigan State University

---

Thursday AM  
March 3, 2011

Room: 6A  
Location: San Diego Conv. Ctr

Session Chairs: Meisha Shofner, Georgia Institute of Technology; Erica Corral, University of Arizona

---

### 8:30 AM Invited

**Characterization of Composite Materials: Thermal Analysis of ROMP-Based Thermosets:** Michael Kessler<sup>1</sup>; Xia Sheng<sup>1</sup>; Timothy Mauldin<sup>1</sup>; Wonje Jeong<sup>1</sup>; Jong Lee<sup>2</sup>; <sup>1</sup>Iowa State University; <sup>2</sup>Kumoh National Institute of Technology

Ring-opening metathesis polymerization (ROMP) has become a powerful tool for producing linear and networked polymers and their composites. In this work, we describe various monomers and catalysts that are being developed for ROMP-based thermosets for applications ranging from adhesives to structural composites. Differential scanning calorimetry and oscillatory shear rheology experiments are used to describe the kinetics of cure and gelation, as well as catalyst dissolution, for various ROMP-active monomers. The influence of multifunctional crosslinking agents, surface modified carbon nanotubes, and structurally modified vegetable oils on the cure behavior of the resins and the resulting thermo-mechanical properties of the cured thermosets are examined in detail using various thermal analysis techniques.

### 9:10 AM

**Nanoparticle Shape Effects in Polymer Composites:** Meisha Shofner<sup>1</sup>; Ji Hoon Lee<sup>1</sup>; Jasmeet Kaur<sup>1</sup>; <sup>1</sup>Georgia Institute of Technology

Polymer nanocomposites have been widely studied in the past 20 years in order to elucidate and exploit changes in polymer behavior at the particle-polymer interface. The excess specific surface area of nanoparticles provides increased opportunity for polymer-particle interactions and changes to polymer morphology in the interfacial zone. The quantity and structure of interfacial material is influenced by many nanoparticle attributes such surface chemistry and size. In this research, the effect of nanoparticle shape was studied. Nanocomposites containing chemically similar calcium phosphate nanoparticles with different shapes have been synthesized and characterized to further understand how particle shape affects nanocomposite structure and properties. Three nanoparticle shapes have been used: near-spherical, nanofiber, and platelet. When blended into the same polymer matrix, trends in thermal and mechanical properties showed different sensitivities to changes in nanoparticle shape that may be understood in terms of aspect ratio and specific surface area.

### 9:30 AM

**Effect of Piassava Fiber Incorporation In Morphological, Thermal and Viscoelastic Behavior of HDPE Composites:** Esperidiana Moura<sup>1</sup>; Thiago Luiz Souza<sup>1</sup>; Anne Chinellato<sup>2</sup>; Walker Drummond<sup>3</sup>; Beatriz Nogueira<sup>1</sup>; <sup>1</sup>Instituto de Pesquisas Energeticas e Nucleares - IPEN-CNEN/SP; <sup>2</sup>Mash: Tecnologia em Compostos e Masters; <sup>3</sup>Departamento de Engenharia Metalúrgica e de Materiais da Universidade de São Paulo

In the present work, the morphological, thermal and viscoelastic behavior of high-density polyethylene (HDPE) matrix composites were investigated. HDPE reinforced with the piassava fiber weight fractions varying to 10 % to 40 % were prepared and characterized by means of scanning electron microscopy (SEM), differential scanning calorimetry analysis (DSC), thermogravimetric analysis (TGA) and melt flow index (MFI) tests. The

results showed that there were significant changes ( $p < 0.05$ ) in surface morphology, melting enthalpy, crystallinity percentage variation and initial degradation temperature of the HDPE and HDPE/fiber composites content different piassava fractions. HDPE MFI values presented a significant reduction around 60 %, due to piassava fiber incorporation, confirming that fiber addition significantly affects the dynamic viscoelastic melt.

### 9:50 AM

**Thermo-Mechanical Behavior of HDPE/Sugarcane Bagasse Fiber/Organoclay Nanocomposites:** Anibal V Castillo<sup>1</sup>; Alejandra Teran<sup>1</sup>; Anne Chinellato<sup>2</sup>; Maria de Fátima Nascimento<sup>3</sup>; Francisco Rolando Díaz<sup>4</sup>; Esperidiana Moura<sup>3</sup>; <sup>1</sup>Laboratorio Tecnológico del Uruguay; <sup>2</sup>Mash: Tecnologia em Compostos e Masters; <sup>3</sup>Instituto de Pesquisas Energeticas e Nucleares - IPEN-CNEN/SP; <sup>4</sup>Universidade de São Paulo

In recent years, studies have shown that the addition of natural fiber or proper filler is an effective strategy for achieving improved properties in polymer composites. Moreover, is especially important if such fibers are residues of agro-industrial processes. In this work a promising technique to develop HDPE matrix nanocomposites by addition natural fibers and clay nanoparticles prepared by extrusion process is described. The HDPE with 20 % (w/w) of sugarcane bagasse fiber from agro-industrial residues and 3 % (w/w) of bentonite chocolate organophilic nanoclay (Brazilian smectitic organophilic clay) addition were obtained using a twin-screw extruder machine type. After extrusion process, the composites were characterized by tensile and flexural tests, SEM, Vicat and HDT tests. The MFI tests were determined to evaluate the effects of fiber and organoclay addition on dynamic viscoelastic melt of the HDPE. The results showed that the thermo-mechanical properties of nanocomposites obtained were superior to those of the pure HDPE.

### 10:10 AM Break

### 10:30 AM Invited

**Three Dimensional (3D) Microstructure Visualization and Modeling of Deformation in Composites by In situ X-ray Synchrotron Tomography:** Jason Williams<sup>1</sup>; Vijesh Tanna<sup>1</sup>; Vaidehi Jakkali<sup>1</sup>; Nikhilesh Chawla<sup>1</sup>; Xianghui Xiao<sup>2</sup>; Francesco De Carlo<sup>2</sup>; <sup>1</sup>Arizona State University, School of Mechanical, Aerospace, Chemical, and Materials Engineering; <sup>2</sup>Advanced Photon Source, Argonne National Laboratory, Argonne, IL

Characterization of composite materials is often conducted by mechanical testing followed by laborious cross-section, characterization, etc. X-ray tomography provides a wonderful means of characterization damage in composites non-destructively. In this talk, we report on a methodology that addresses the critical link between microstructure and deformation behavior, by using a three-dimensional (3D) microstructure obtained by x-ray synchrotron tomography. The approach involves capturing the microstructure by sophisticated in situ tensile testing in an x-ray synchrotron, followed by x-ray tomography and image analysis, and 3D reconstruction of the microstructure. Incorporation of the microstructure into a powerful finite element modeling code for simulation was also conducted. We will present a case study based SiC particle reinforced Al alloy matrix composites, as an illustration of how this technique can be used for a variety of composites. The evolution of damage in the form of particle fracture, interfacial debonding, and void growth will be described.

### 11:10 AM Invited

**Spark Plasma Sintering of Ultra-High Temperature Ceramic Composites:** Erica Corral<sup>1</sup>; <sup>1</sup>The University of Arizona

The development of next generation hypersonic flight vehicles requires new thermal protection system (TPS) materials that are capable of withstanding extreme aerothermal heating loads. Transition metal borides are attractive materials for use in harsh environments due to their high temperature properties. However, the application of diboride-based ceramics has been limited due to poor sinterability using conventional sintering techniques. Therefore, our approach couples using spark plasma sintering (SPS) and high temperature sintering additives in order to reduce the sintering temperature of ZrB<sub>2</sub>-SiC composites from 1900 to 1700°C, while maintaining density

values >99% of theoretical density. The effect of adding small amounts sintering additives on the densification and refinement of the ZrB<sub>2</sub>-SiC microstructure using SPS will be discussed. In addition, high temperature oxidation behavior of ZrB<sub>2</sub>-SiC composites will be presented up to, 1650°C.

## Computational Plasticity: Dislocations Structures and Dynamics during Plasticity

*Sponsored by:* The Minerals, Metals and Materials Society, TMS Materials Processing and Manufacturing Division, TMS Structural Materials Division, TMS/ASM: Computational Materials Science and Engineering Committee, TMS: High Temperature Alloys Committee  
*Program Organizers:* Remi Dingreville, Polytechnic Institute of NYU; Koen Janssens, Paul Scherrer Institute

Thursday AM  
March 3, 2011

Room: 1A  
Location: San Diego Conv. Ctr

*Session Chair:* To Be Announced

### 8:30 AM Invited

**Plasticity at Small Scales:** *Richard LeSar*<sup>1</sup>; *Caizhi Zhou*<sup>2</sup>; <sup>1</sup>Iowa State University; <sup>2</sup>Ames Laboratory

Deformation in small systems offers a unique environment in which to apply computational methods of plasticity at the mesoscale, specifically, in our case, discrete dislocation dynamics. The number of dislocations is relatively small, making the simulations tractable on modest computational platforms. The increasing number of experiments at this scale make it possible to use discrete dislocation simulations to first verify the calculations and then to provide important details that add to the understanding of the fundamental physical processes. In this talk, we will review the computational approaches for applying discrete dislocation dynamics at this scale, including boundary conditions, sub-scale dislocation mechanisms (e.g., cross slip), etc. We will then discuss the applicability of these methods to the plasticity in small pillars and single-crystal and polycrystalline thin films.

### 9:00 AM Invited

**Applications of Phenomenological Mesoscale Field Dislocation Mechanics:** *Armand Beaudoin*<sup>1</sup>; *Koenraad Janssens*<sup>2</sup>; <sup>1</sup>University of Illinois at Urbana-Champaign; <sup>2</sup>Paul Scherrer Institute

Phenomenological Mesoscale Field Dislocation Mechanics (Acharya & Roy, JMPS 2006) provides a platform for introducing constitutive theories for plastic deformation into a continuum setting. The continuum formulation provides for evolution and transport of the excess (geometric) dislocation density and continuity of the plastic strain rate. In this work, we present examples of dislocation evolution at the mesoscale in the compression of pillars, and in the cyclic loading of layered structures.

### 9:30 AM

**Binary and Ternary Interaction Coefficients and Strain Hardening in BCC Single Crystals:** *Ronan Madec*<sup>1</sup>; *Ladislav Kubin*<sup>2</sup>; <sup>1</sup>CEA, DAM, DIF; <sup>2</sup>LEM (CNRS/ONERA)

Dislocation dynamics simulations have now reached a stage where they are able to tackle such problems as the formation of dislocation microstructures and forest hardening in bulk single crystals. The connection between mesoscopic and continuum approaches of plasticity is based on the knowledge of the interaction matrix between slip systems and of the dislocation mean free paths, from which a hardening matrix can be derived. The objective of the present work is to establish this connection in the case of BCC crystals, using a dislocation dynamics simulation that is briefly described. Emphasis is put on the determination of the interaction matrix in the high temperature regime, above the so-called "athermal temperature" at which the lattice friction vanishes. Results on binary and ternary dislocation reactions are discussed. Preliminary crystal plasticity computations using these coefficients and stress vs. strain curves for various orientations are presented and discussed.

### 9:50 AM Invited

**Continuity Constraints at Interfaces and Scale Dependence of the Mechanical Behavior of Crystalline Materials:** *Claude Fressengeas*<sup>1</sup>; *Thiebaut Richeton*<sup>2</sup>; *Guofeng Wang*<sup>3</sup>; <sup>1</sup>University Paul Verlaine - Metz / CNRS; <sup>2</sup>CNRS / Arts et Metiers ParisTech; <sup>3</sup>Harbin Institute of Technology

We analyze the implications on the mechanical behavior of metal matrix composites of tangential continuity conditions on the elastic distortion obtained from the balance of lattice incompatibility across a material surface of discontinuity by using both conventional crystal plasticity, appended with this continuity condition, and a field dislocation dynamics model. The latter features the long-range interactions due to the presence of geometrically necessary dislocations and the short range interactions arising from dislocation transport. Solution of the boundary value problems is obtained via a mixed finite element approach where balance of momentum is solved via a Galerkin scheme, while the transport problem is solved by a Galerkin-Least Squares method. The results in the simple shear of a Al-SiC particle strengthened composite demonstrate the effects of particle size, shape and distribution on the hardening behavior of the composite, as well as the role of the continuity constraints at the matrix-inclusion interfaces.

### 10:20 AM Break

### 10:35 AM Invited

**Entropic Effect on Dislocation Nucleation:** *Wei Cai*<sup>1</sup>; *Seunghwa Ryu*<sup>1</sup>; *Keonwook Kang*<sup>1</sup>; <sup>1</sup>Stanford University

Dislocation nucleation plays an important role in the plasticity of sub-micron and nano-scale samples. However, the prediction of the dislocation nucleation rate from atomistic simulations by computing the nucleation free energy barrier at finite temperature has been lacking. Here we present the first atomistic predictions of the free energy barrier and nucleation rate for homogeneous and heterogeneous nucleation of dislocations in EAM Cu. The data exhibits anomalously large entropy, the neglect of which would cause an underestimate of the nucleation rate by many orders of magnitude. The origin of this entropic effect is discussed.

### 11:05 AM Invited

**On Particle Size Effects: An Internal Length Mean Field Approach Using Field Dislocation Mechanics Simulations:** *Vincent Taupin*<sup>1</sup>; *Stephane Berbenni*<sup>1</sup>; *Claude Fressengeas*<sup>1</sup>; *Olivier Bouaziz*<sup>1</sup>; <sup>1</sup>LPMM, CNRS, Univ Metz, ENSAM

A mean field approach including an internal length scale is developed in order to capture the particle size effects on the overall material's behavior of particle-reinforced alloys. A generalized self-consistent scheme (with coated particles) is employed, with a new "phase" representing the coatings where orderly dislocations between the matrix and the particles are present. The thickness of these "layers" is supposed constant and constitutes the internal length scale [1]. It is determined dynamically by field dislocation mechanics [2], where orderly dislocations accommodate lattice incompatibility between matrix and inclusions. The beneficial influence of this scheme, as compared to classical mean field approaches, is shown from comparisons with experimental data on the particle size effects in Al/SiC composites. [1] V. Taupin, S. Berbenni, C. Fressengeas, O. Bouaziz. Acta Materialia, In Press, 2010. [2] A. Acharya, A. Roy, J. Mech. Phys. Solids 54, 1687, 2006.

### 11:35 AM

**Interaction between Edge Dislocations and Voids in bcc Iron Investigated Thanks to a Multiscale Approach:** *Sylvain Queyreau*<sup>1</sup>; *Brian Wirth*<sup>1</sup>; *Jaime Marian*<sup>2</sup>; *Anastasios Arsenlis*<sup>2</sup>; <sup>1</sup>University of California at Berkeley; <sup>2</sup>Lawrence Livermore National Laboratory

This work focuses on the strengthening associated to nanometer-sized vacancy clusters, or voids, which are formed in bcc Iron under irradiation. We propose a new Dislocation Dynamics (DD) modeling for dislocation - void interactions based on complementary atomistic calculations. The following mechanisms are assumed to control the void strengthening: (i) the surface step creation, (ii) the removal of dislocation segments inside voids and (iii) the distant interaction between the stress field of the dislocation and the voids. A coupling with Boundary Element Method is performed for this



last mechanism. The DD model is able to reproduce the effect of void size and the temperature dependence on the strengthening obtained in atomistic simulations. The strengthening contribution related to the line energy of the removed dislocation segments is twice larger than the surface energy contribution. However, the temperature dependence appears to be mainly controlled by the decrease in the surface energy.

**11:55 AM**

**3-Dimensional Dislocation Dynamics Simulation of Low-Angle Grain Boundary Migration:** Adele Lim<sup>1</sup>; Wei Cai<sup>2</sup>; Mikko Haataja<sup>1</sup>; David Srolovitz<sup>3</sup>; <sup>1</sup>Princeton University; <sup>2</sup>Stanford University; <sup>3</sup>Institute of High Performance Computing

Using dislocation dynamics simulations, we investigate the migration of a mixed low-angle grain boundary (LAGB) composed of a network of two intersecting dislocation arrays. The migration of this boundary was examined as a function of applied stress, dislocation climb mobility, and misorientation between grains adjacent to the boundary. Under an applied stress that gives rise to boundary migration, the dislocation network that comprises the boundary also translates along the boundary plane, i.e., migration normal to the boundary plane is coupled to tangential motion in the plane of the boundary. From the simulations, we find the boundary migration velocity to be directly proportional to the applied stress. At the same applied stress, the migration velocity increases with increasing dislocation climb mobility. We derive analytical expression for the mobility as well as the ratio of tangential to normal motion for a mixed LAGB having a simple and well-defined dislocation structure.

**12:10 PM**

**Discrete Dislocation Simulations of Plasticity of Polycrystalline Thin Films:** Caizhi Zhou<sup>1</sup>; Richard LeSar<sup>1</sup>; <sup>1</sup>Iowa State University

The mechanical properties of metallic thin films are of great importance in determining the reliability of microelectronic devices and have thus attracted much attention in materials research. One of the most important phenomena is that their strength differs significantly from that of the corresponding bulk materials when their dimensions become comparable to the length scales of the underlying dislocation microstructures. In our study, 3-D discrete dislocation dynamics (DDD) simulations have been used to investigate the size-dependent plasticity of polycrystalline thin films. We consider both cross-slip of dislocations and stress relaxation at grain boundaries. In this talk, we will relate the plastic deformation of polycrystalline thin films to such quantities as thin film thickness, grain size and dislocation density. In addition, we will compare the simulation results to experiment to guide the development of simple, accurate models for predicting thin film behavior.

---

## Computational Thermodynamics and Kinetics: Thermodynamics and Microstructure Evolution in Soft Matter

*Sponsored by:* The Minerals, Metals and Materials Society, ASM International, TMS Electronic, Magnetic, and Photonic Materials Division, TMS Materials Processing and Manufacturing Division, TMS: Alloy Phases Committee, TMS: Chemistry and Physics of Materials Committee, TMS/ASM: Computational Materials Science and Engineering Committee, ASM: Alloy Phase Diagrams Committee  
*Program Organizers:* Raymundo Arroyave, Texas A & M University; James Morris, Oak Ridge National Laboratory; Mikko Haataja, Princeton University; Jeff Hoyt, McMaster University; Vidvuds Ozolins, University of California, Los Angeles; Xun-Li Wang, Oak Ridge National Laboratory

Thursday AM  
March 3, 2011

Room: 9  
Location: San Diego Conv. Ctr

*Session Chairs:* Mikko Haataja, Princeton University; James Morris, Oak Ridge National Laboratory

---

**8:30 AM Invited**

**Continuum-Level Simulations of Two-Phase Lipid Membranes Coupling Composition with Deformation:** Chloe Funkhouser<sup>1</sup>; Francisco Solis<sup>2</sup>; Katsuyo Thornton<sup>3</sup>; <sup>1</sup>University of Michigan - Department of Biomedical Engineering; <sup>2</sup>Arizona State University West - Division of Mathematical and Natural Sciences; <sup>3</sup>University of Michigan - Department of Material Science & Engineering

We examine the formation and evolution of lipid raft-like domains in two-phase lipid membranes using a continuum-level simulation method. Our model couples composition with membrane deformation using a modified Helfrich free energy. The compositional evolution is modeled with a phase-field method and is described by a Cahn-Hilliard-type equation, while the shape changes are described by relaxation dynamics in which surface area is conserved. Our objective is to investigate how various physical input parameters such as spontaneous curvature, bending rigidity, and phase fraction affect the dynamics and equilibrium morphological phases formed in lipid membrane vesicles and tubules. We find that the compositional and shape evolution are significantly altered when mechanical coupling is present by comparing the results with those of systems where this coupling is absent. Both dynamics and equilibria are examined to elucidate the link between the morphologies of the membranes with their physical properties.

**9:10 AM Invited**

**Lateral Segregation in Lipid Bilayer Membrane Modulated by Curvature:** Tobias Baumgart<sup>1</sup>; <sup>1</sup>University of Pennsylvania

Lateral segregation of lipids and proteins in lipid bilayer membranes lies at the heart of fundamental biological phenomena such as organelle homeostasis, membrane signaling, and trafficking. Our research is directed at understanding how membrane curvature affects lateral segregation in both weak and strong segregation limits in the phase diagram of mixed model membranes. We will discuss the biophysical method of micropipette aspiration of giant unilamellar vesicles, which are bilayer membranes with spherical topology. These vesicles can be used to generate tubular membranes with adjustable radius that allow quantitatively investigating the role of curvature in modulating local membrane composition. In the strong segregation limit we introduce the phenomenon of curvature-induced nucleation and growth of lipid phases. In the weak segregation limit, we observe segregation with qualitative differences along two roughly orthogonal directions in the lipid mixing phase diagram.

THURSDAY AM

9:50 AM

**Modeling the Self-Assembly of Arbitrary-Shaped Ferro-Colloidal Particles in Bulk Liquid and at Fluid Interface:** *Tianle Cheng*<sup>1</sup>; Yu Wang<sup>1</sup>; Paul Millet<sup>2</sup>; <sup>1</sup>Michigan Technological University; <sup>2</sup>Idaho National Laboratory

Development of a novel diffuse interface field approach to modeling and simulation of self-assembly of ferro-colloidal particles in bulk liquid (e.g. uncured polymer melt) and at fluid interface (e.g. multi-phase fluid) is presented. The model employs diffuse interface fields to describe arbitrary particle shapes and sizes as well as dipole and charge properties. Particle interactions of long-range (electrostatic) and short-range (contact) as well as with fluid interface (capillary) are taken into account. In particular, electrostatic force is accurately treated (conventional point-dipole/charge approximation is not applicable due to non-spherical particle shapes and small inter-particle distances). Evolving microstructures of particle self-assembly and fluid interfaces with/without applied external field (used to tune self-assembling forces and control particle microstructures) are simulated without explicitly tracking the boundaries of arbitrary-shaped particles and multi-phase fluid. Various simulation examples are presented to demonstrate the new model's capability and potential to engineer advanced material microstructures.

10:10 AM Break

10:20 AM Invited

**Lipid Rafts Reach a Critical Point:** *Sarah Veatch*<sup>1</sup>; Benjamin Machta<sup>2</sup>; <sup>1</sup>University of Michigan; <sup>2</sup>Cornell University

Multicomponent lipid bilayer membranes can contain two coexisting liquid phases, named liquid-ordered and liquid-disordered. Recently, we demonstrated that large (micron-scale) and dynamic critical fluctuations are found in ternary lipid bilayer membranes prepared with critical compositions. Remarkably, robust critical behavior is also found in compositionally complex vesicles isolated directly from living cell plasma membranes. This finding strongly suggests that cells tightly regulate plasma membrane protein and lipid content to reside near a critical point and that critical fluctuations provide a physical basis of functional membrane heterogeneity in living cells at physiological temperatures. We are currently probing for signatures of critical fluctuations in intact cells using high resolution imaging techniques (scanning electron microscopy and super-resolution fluorescence localization microscopy). In addition, we are investigating possible structural and functional consequences of plasma membrane criticality using computational approaches.

11:00 AM Invited

**Mesoscale Computational Studies of the Compositional and Morphological Heterogeneities of Biomembranes:** *Mohamed Laradji*<sup>1</sup>; <sup>1</sup>University of Memphis

Biomembranes are complex quasi-two dimensional fluids composed of various types of lipids and proteins. Experiments showed that plasma membranes of animal cells exhibit compositional and morphological organization. These include, nanoscale lipid domains, known as rafts, which are rich in saturated lipids and cholesterol. Lipid rafts are implicated in signaling, recruitment and endocytosis. Reasons for the finite size of lipid rafts remain elusive. This emphasizes the importance of understanding both the phase behavior and kinetics of multicomponent membranes while incorporating as many ingredients present in the plasma membrane. In this talk, I will review some of the computational work done by us for studies of both compositional and morphological heterogeneities in lipid membranes using mesoscale modeling either explicit or implicit solvent. This work is supported by NSF (DMR 0812470 and DMR 0755447) and the Research Corporation (CC6689).

11:40 AM Invited

**Solid Domains on Fluid Lipid Vesicles Induced by pH:** *Stavroula Sofou*<sup>1</sup>; <sup>1</sup>Polytechnic Institute of New York University

Lipid bilayer membranes in the form of giant unilamellar vesicles (GUVs) were prepared. Lipid mixtures were composed of two lipid types - a lipid

with a titratable headgroup and a non-titratable headgroup - and variable levels of cholesterol. GUVs were prepared using the gentle hydration method and were imaged at room temperature using fluorescence microscopy. We show that lowering pH induces increase of the extent of formation of phase separated solid (gel) domains with size, shape and number that depend on the final pH value and the cholesterol content. Phase separation with lowering pH seems to be mostly driven by hydrogen bonding among the titratable lipid headgroups. At the lowest pH studied all mixtures exhibit formation of "florets". We suggest that this is mostly driven by the decrease of the overall membrane area per GUV arising from the shrinkage of the area in the gel phase domains at lower pH.

## Electrode Technology for Aluminium Production: Cathode Materials and Wear

*Sponsored by:* The Minerals, Metals and Materials Society, TMS Light Metals Division, TMS: Aluminum Committee

*Program Organizers:* Alan Tomsett, Rio Tinto Alcan; Ketil Rye, Alcoa Mosjøen; Barry Sadler, Net Carbon Consulting Pty Ltd

Thursday AM  
March 3, 2011

Room: 16B  
Location: San Diego Conv. Ctr

*Session Chair:* Frank Hiltmann, SGL Carbon GmbH

## 8:30 AM Introductory Comments

8:35 AM

**Measurement of Cathode Surface Wear Profiles by Laser Scanning:** *Egil Skybakmoen*<sup>1</sup>; Stein Rørvik<sup>1</sup>; Asbjorn Solheim<sup>1</sup>; Knut Ragnar Holm<sup>2</sup>; Priska Tiefenbach<sup>2</sup>; Oyvind Ostrem<sup>2</sup>; <sup>1</sup>SINTEF Materials and chemistry; <sup>2</sup>NTNU

The service life time for high amperage aluminium reduction cells with graphitized cathodes is limited by cathode wear. The wear is normally very non-uniform, and it is commonly documented by photography and/or point measurements by levelling. In an attempt to record the wear surface in a much more detailed way, a laser scanning procedure was developed. A laser scanner with an accuracy of  $\pm 0.5$  cm has been used to produce a 3D model based on three overlapping scans with an average resolution of about 1 cm. The same cathodes was also measured with a leveller for comparison. The method developed gives detailed information regarding the wear at different positions within the cell, and it may become a valuable tool for investigating the influence of different parameters on the cathode wear.

9:00 AM

**Coke Selection Criteria for Abrasion Resistant Graphitized Cathodes:** Raymond Perruchoud<sup>1</sup>; Werner Fischer<sup>1</sup>; *Markus Meier*<sup>1</sup>; Ulrich Mannweiler<sup>2</sup>; <sup>1</sup>R&D Carbon Ltd.; <sup>2</sup>Mannweiler Consulting

The high abrasion rate of the graphitized cathodes became a major limitation of the pot lining life time for high amperage cells. This is related to the usage of low Sulfur anode grade petroleum coke resulting in too soft a cathode after graphitization. A review of the effects of the coke characteristics on the cathode abrasion and on the other pot lining relevant properties has been performed on a pilot scale. The selection of more isotropic calcined coke prepared by delayed coking of appropriate soft pitches allowed to decrease the abrasion rate by four times. No detrimental effects on the graphitization behaviour nor on the cathode relevant properties have been observed. Dedicated tar pitch feedstocks in optimized delayed coking have the potential, together with shaft kiln calcinations, to solve the W shaped wear of graphitized cathodes responsible of the short pot life time.

9:25 AM

**Determination of the Effect of Pitch-Impregnation on Cathode Erosion Rate:** *Pretesh Patel*<sup>1</sup>; Yoshinori Sato<sup>2</sup>; Pascal Lavoie<sup>1</sup>; <sup>1</sup>Light Metals Research Centre; <sup>2</sup>SEC Carbon, Ltd

In recent years, a number of smelters have adopted or trialed higher density, pitch impregnated cathode blocks as a measure to counter the decreasing cell life trend due to line current increases. To date, the true

benefits of pitch impregnated cathode blocks are not fully understood. A collaboration between SEC CARBON Limited and the Light Metals Research Centre has therefore endeavored to understand the effects of pitch impregnation on cathode block performance. It was previously reported that pitch impregnated materials were found to have detrimental effects in regards to electrochemical wear resistance, and it was proposed that pitch impregnation increases reactivity of the cathode material. This paper will concentrate on recent work which was carried out firstly to characterize the difference between the pitch impregnation phase and the bulk cathode matrix and secondly to determine the reactivity of these phases under electrolysis conditions.

#### 9:50 AM

**Simplifying Protection System to Prolong Cell Life:** *Maryam Al Jallaf*<sup>1</sup>; Margaret Hyland<sup>2</sup>; Barry Welch<sup>3</sup>; Ali Al Zarouni<sup>1</sup>; <sup>1</sup>DUBAL; <sup>2</sup>University of Auckland; <sup>3</sup>Welbank Consulting Ltd.

Cathode materials are mainly deteriorated by physical erosion, chemical and electrochemical corrosion. The wear patterns are characterised by "W-shaped wear" and localised potholes. A variety of materials such as alpha alumina and refractory hard materials have been used for protecting conventional cathodes. TiB<sub>2</sub> based refractory hard materials are well suited for this. They satisfy the electrical conductivity requirements, have a very low solubility in molten aluminium and are wetted by aluminium providing potential benefit. The focus of study was to explore the potential of increasing life of graphitised cathodes using TiB<sub>2</sub> grains without compromising on metal purity or cell performance and lining design. Statistical tools were used to determine the significance of erosion rate in operating cells. The study revealed that cathode life could be increased by at least 2 years. Increase in Ti and B impurities in pot metal was within the tolerance limits of the casthouse.

#### 10:15 AM Break

#### 10:25 AM

**Aluminate Spinels as Sidewall Linings for Aluminum Smelters:** Xiao Yan<sup>1</sup>; Reiza Mukhlis<sup>2</sup>; M. Rhamdhani<sup>2</sup>; *Geoffrey Brooks*<sup>2</sup>; <sup>1</sup>CSIRO; <sup>2</sup>Swinburne University of Technology

There is a need for ledge-free sidewalls due to about 30% energy savings for the Hall-Heroult process. However, this approach poses great material challenges because such sidewalls are in direct contact with oxidizing, corrosive and reducing environments at different cell locations. Here, NiAl<sub>2</sub>O<sub>4</sub>, MgAl<sub>2</sub>O<sub>4</sub> and Ni<sub>0.5</sub>Mg<sub>0.5</sub>Al<sub>2</sub>O<sub>4</sub>, were identified and tested in cryolite-based baths at 980 °C under air and CO<sub>2</sub>. Both specimens and baths were characterized using XRD, XRF and SEM-EDS methods. This study revealed that the NiAl<sub>2</sub>O<sub>4</sub> and MgAl<sub>2</sub>O<sub>4</sub> spinels had good corrosion resistances towards a molten cryolite-AlF<sub>3</sub>-Al<sub>2</sub>O<sub>3</sub>-CaF<sub>2</sub> bath under CO<sub>2</sub>, with solubility of Ni from NiAl<sub>2</sub>O<sub>4</sub> being 100ppm and Mg from MgAl<sub>2</sub>O<sub>4</sub> being 700ppm. Dissolutions of Ni and Mg into the bath were lowered to 70ppm Ni and 500ppm Mg by forming a Ni<sub>0.5</sub>Mg<sub>0.5</sub>Al<sub>2</sub>O<sub>4</sub> solid solution due to reduced activities of NiO and MgO in the spinel solution. The corrosion behaviour of the Fe spinels is also discussed.

#### 10:50 AM

**A New Ramming Paste with Improved Potlining Working Conditions:** *Bénédicte Allard*<sup>1</sup>; Régis Paulus<sup>1</sup>; Gérard Billat<sup>2</sup>; <sup>1</sup>Carbone Savoie - Vénissieux - France; <sup>2</sup>Carbone Savoie - Aigueblanche - France

The ramming paste used in the aluminium electrolysis pots has long been a concern regarding health, safety and environment. While the situation has improved over the last 20 years, pastes on the market today still contain either carcinogenic products as PaH components or phenol, or other hazardous components. Health regulations in many regions require substitution of these hazardous components as soon as an acceptable alternative becomes available. A new paste, NeO<sup>2</sup>, has been developed which contains no hazardous component, according to the present regulations. Standard physico-chemical properties of the paste have been studied, with some

specific characterizations which will be detailed. This paper will provide a summary of paste developments and provide the latest results achieved with the NeO<sup>2</sup> paste.

#### 11:15 AM

**Towards a Better Understanding of Carburization Phenomenon:** Martin Lebeuf<sup>1</sup>; *Marc-André Coulombe*<sup>1</sup>; Bénédicte Allard<sup>2</sup>; Gervais Soucy<sup>1</sup>; <sup>1</sup>Université de Sherbrooke; <sup>2</sup>Carbone Savoie

Cathode wear in aluminum electrolysis cells is an undesirable phenomenon which decreases potlife. Although it has been the subject of many studies, it is not yet satisfactorily understood. One major factor of this wear is the formation and dissolution of aluminum carbide, for which the mechanisms still remain to be thoroughly explained. Laboratory scale electrolysis experiments were performed under different operating conditions, namely the current density, the presence or absence of an aluminum metallic layer on the cathode surface and the atmosphere type. The aluminum carbide formation was then studied using X-ray Photoelectron Spectroscopy (XPS), Scanning Electron Microscopy-Energy Dispersive Spectroscopy (SEM-EDS), X-Ray fluorescence (XRF) and optical microscopy. In particular, the XPS analysis permitted further investigation of the chemical species present in bath-penetrated veins of the carbon cathode.

#### 11:40 AM

**Characterization of Sodium and Fluorides Penetration into Carbon Cathodes by Image Analysis and SEM-EDS Techniques:** *Yuanling Gao*<sup>1</sup>; Jilai Xue<sup>1</sup>; Jun Zhu<sup>1</sup>; Kexin Jiao<sup>1</sup>; <sup>1</sup>University of Science and Technology Beijing

The porous structure in carbon cathodes is materials dependent, which can provide channels for sodium and fluorides penetration during aluminum electrolysis. This work is aimed to develop a better digital method for characterization of the pores and the penetration resistance of the cathode products. The profiles of penetrated Na, F, Al vs. penetration depth in the cathode samples after aluminum electrolysis were obtained using SEM-EDS analysis. The internal porosity, pore size distribution, pore shape and direction, pore connectivity, etc. were also characterized by image analysis. It was found that the pore connectivity, not the total porosity, contribute the most to Na and F penetration into the carbon cathodes. The chemical resistance to Na and F penetration varied with change in cathode materials (from semi-graphitic, full graphitic to graphitized carbons). Other detailed information about the correlation between the pore structures and Na-fluoride penetration will be presented.

### Friction Stir Welding and Processing VI: Friction Stir Spot Welding

*Sponsored by:* The Minerals, Metals and Materials Society, TMS Materials Processing and Manufacturing Division, TMS: Shaping and Forming Committee

*Program Organizers:* Rajiv Mishra, Missouri University of Science and Technology; Murray Mahoney, Retired from Rockwell Scientific; Yutaka Sato, Tohoku University; Yuri Hovanski, Pacific Northwest National Laboratory; Ravi Verma, General Motors

Thursday AM  
March 3, 2011

Room: 5B  
Location: San Diego Conv. Ctr

*Session Chairs:* Tony Reynolds, University of South Carolina; Michael West, South Dakota School of Mines and Technology

#### 8:30 AM Invited

**Fatigue Behavior of Dissimilar Friction Stir Spot Welds between Aluminum and Steel Sheets:** Van-Xuan Tran<sup>1</sup>; *Jwo Pan*<sup>1</sup>; <sup>1</sup>University of Michigan

Fatigue behavior of dissimilar friction stir spot welds in lap-shear specimens of aluminum 6000 series alloy and coated steel sheets is investigated based on experiments, analytical solutions and three-dimensional finite element analyses. The Al/Fe welds were tested under cyclic loading conditions.



Optical micrographs of the failed welds show that the Al/Fe welds mainly fail along the interfacial surface between the aluminum and steel sheets. Three-dimensional finite element analyses were conducted to obtain the stress intensity factor and J integral solutions for the welds with complex geometry, bend and gap. Analytical solutions for the equivalent welds with consideration of the bend and gap were also derived. The computational and analytical solutions suggest that the J integral and in-plane effective stress intensity factor solutions at the critical locations of the welds can be used as fracture mechanics parameters to correlate the fatigue crack growth patterns of the Al/Fe welds in lap-shear specimens.

8:55 AM

**Material Flow and Temperature Distribution in Friction Spot Welding of Al and Steel:** *Yingchun Chen*<sup>1</sup>; Phil Prangnell<sup>1</sup>; <sup>1</sup>The University of Manchester

The material flow in friction spot welding of Al to steel has been investigated by differential etching after welding a split top sheet consisting of two Al-alloys with similar mechanical properties, but different copper contents. The temperature distribution was studied using an infrared thermal camera and thermocouples. The effect of rotation speed, plunge depth, dwell time, surface condition of steel sheet (un-coated and galvanized), and tool coupling on the material flow and temperature distribution are systematically discussed. The aim of the work was to better understand the effect of coupling with the spot welding tool and, between the top and bottom sheets, as a function of the tool geometry and the welding conditions, on the relationship between material flow and the temperature distribution, and the formation of weld defects and intermetallic reaction layers at the joint interface during welding.

9:15 AM

**Continued Development of Friction Stir Spot Welding for Advanced High Strength Steels**

: *Yuri Hovanski*<sup>1</sup>; Michael Santella<sup>2</sup>; Glenn Grant<sup>1</sup>; <sup>1</sup>Pacific Northwest National Laboratory; <sup>2</sup>Oak Ridge National Laboratory

With successful research in friction stir spot welding of advanced high strength steel alloys demonstrating that tool materials do exist that can be utilized to rapidly produce spot joints in a variety of high strength automotive sheet materials, heightened interest continues to further development of process parameters and tooling for production ready applications. As such a specific list of targeted alloy and thickness combinations were investigated for joinability by means of friction stir spot welding. Combinations of hot-stamp boron steels, transformation induced plasticity steels and dual-phase alloys were utilized to investigate spot joints between dissimilar alloy and thickness combinations. Mechanical properties of the lap joints along with an investigation of the sheet interfaces are presented. Low cost versions of both polycrystalline cubic boron nitride and silicon nitride tools were used during the evaluation, and their potential for high volume production is reported.

9:35 AM

**Structure-Property Relationships of Fatigue in Friction Stir Spot Welding of AZ31 Mg Alloy:** *J Jordan*<sup>1</sup>; <sup>1</sup>Mississippi State University

In this present work, structure-property relations are quantified in regards to fatigue performance of friction stir spot welding. Lap-shear coupons of AZ31 magnesium alloy were spot welded using two sets of tooling and welding parameters. Optical microscopy of the initial state of the microstructure of each set of spot welds revealed differences in the weld interface in both size and shape. Both sets of welds were fatigue tested in load control until failure at various load ratios. Fractography analysis revealed differences in the failure modes and the number of cycles to failure for the two sets of coupons. Direct correlations were made between the structure of the weld interface and the number of cycles to failure.

9:55 AM

**Mechanical and Microstructural Investigation of Dissimilar Resistance and Friction Stir Spot Welds in AA5754-H22 and AA6082-T6 Aluminium Alloys and 22MnB5 Hot-Stamped Boron Steel:** *Antonio da Silva*<sup>1</sup>; Egoitz Aldanondo<sup>1</sup>; Pedro Alvarez<sup>1</sup>; Alberto Echeverría<sup>1</sup>; Martin Eierseber<sup>2</sup>; <sup>1</sup>Research Centre LORTEK; <sup>2</sup>FRONIUS International GmbH

The aim of this investigation is to evaluate and compare two distinct spot joining processes suitable for dissimilar welding aluminium and steel for mass production applications in the automotive industry: Friction Stir Spot Welding (FSSW) and Resistance Spot Welding (RSW). The effect of joining parameters on the mechanical and microstructural properties of dissimilar 1 mm-thick aluminium alloys (AA5754-H22 and AA6082-T6) and 22MnB5 hot-stamped boron steel joints produced by both processes has been investigated. Microstructural features of FSSW and RSW connections have been analysed; while mechanical performance has been investigated in terms of hardness and shear testing. Failure modes of shear specimens have been also investigated. Maximum failure loads close to 3 kN have been obtained in RSW connections; while FSSW has shown lower failure loads. Interfacial failure mode has been observed in RSW conditions; while a mixture of interfacial and nugget pullout failure modes have been found for FSSW connections.

10:15 AM

**Effect of Coating on Mechanical Properties of Magnesium Alloy Friction Stir Spot Welds:** *Wei Yuan*<sup>1</sup>; R.S. Mishra<sup>1</sup>; B. Carlson<sup>2</sup>; R. Verma<sup>2</sup>; R. Szymanski<sup>2</sup>; <sup>1</sup>Missouri University of Science and Technology; <sup>2</sup>General Motors R&D Center

Magnesium alloy AZ31 sheets with a 25 µm coating layer were friction stir spot welded. Compared to bare AZ31 sheet, the coated material exhibited lower tool plunge force for similar process parameters. Lap-shear tests indicated a much lower separation load for the coated AZ31 spot welds. The coated specimens separated in a nugget pull-out mode as a result of bottom-sheet cracking in the thermomechanically affected zone adjacent to the nugget. The initial crack started from the under surface of the bottom sheet and appeared to be dependent on thermal stress and strain gradient. The length of the crack varied as the tool rotation rate changed, and the crack moved away from the weld center as nugget size increased.

10:35 AM Break

10:45 AM Invited

**Process-Properties Relationship in Friction Spot Welds on Aircraft Al-Alloys:** *Gabriel Pieta*<sup>1</sup>; *Jorge dos Santos*<sup>1</sup>; Ana Paula Camilo<sup>2</sup>; Sergio Amancio<sup>1</sup>; Marcelo Beltrao<sup>1</sup>; Sebastiao Kury<sup>2</sup>; Nelson de Alcantara; Nelson de Alcantara<sup>2</sup>; <sup>1</sup>GKSS Forschungszentrum; <sup>2</sup>Federal University of Sao Carlos

Friction Spot Welding (FSpW) is a new solid-state joining process able to produce similar and dissimilar overlap connections in different classes of materials. Advantages of this new technique are: short production cycles, high performance joints, absence of filler materials and good surface finishing supported by material refilling in the spot area. Although few authors have addressed the microstructural and mechanical behavior of friction spot welds of Aluminum alloys, there is still a lack of a systematic evaluation on the process-properties relationship. In this work aircraft aluminum alloy (rolled sheets) were investigated. Design of experiment (DOE) and analyses of variance (ANOVA) techniques were applied to evaluate joint shear strength under static loading. Sound joints with elevated shear strength were achieved and the influence of the main process parameters on joint strength evaluated.

11:10 AM

**Retractable vs. Fixed Probe Tools in Swept Friction Stir Spot Welding:** *Jeremy Brown*<sup>1</sup>; James Gross<sup>1</sup>; Jeff Buller<sup>1</sup>; Dwight Burford<sup>1</sup>; <sup>1</sup>Wichita State University

Swept Friction Stir Spot Welding is a variation of Friction Stir Spot Welding (FSSW). In contrast to conventional plunge and retract FSSW, in swept FSSW the tool is programmed to travel along a closed path following the plunge. The advantages of swept FSSW over the conventional FSSW

include a larger joint shear area and the minimization of hooking defects. A disadvantage of creating a FSSW joint with a Fixed Probe Tool (FPT) is the exit hole left in the joint. A potential method for removing the exit hole is to use a Retractable Probe Tool (RPT) where the probe may be retracted from the workpiece during welding. In this study the relative advantages and disadvantages of using RPT technology instead of FPT technology in swept FSSW have been examined by comparing the lap shear strength and fatigue life of joints produced by both technologies in 1mm thick AA7075 on AA2024.

**11:30 AM**

**Friction Stir Spot Welding of Magnesium to Aluminum Alloys with a Cold Sprayed Interlayer:** *Dustin Blossmo*<sup>1</sup>; *Todd Curtis*<sup>1</sup>; *Timothy Johnson*<sup>1</sup>; *Nicholas Prociwe*<sup>1</sup>; *Christian Widener*<sup>1</sup>; *Blair Carlson*<sup>2</sup>; *Robert Symanski*<sup>2</sup>; *Michael West*<sup>1</sup>; <sup>1</sup>South Dakota School of Mines and Technology; <sup>2</sup>General Motors

The research focus is to join thin sheet magnesium to aluminum. Magnesium AZ-31 alloy was joined to Al 5754 alloy using both plunge spot welding and refill friction stir spot welding. A design of experiments was conducted to study the affect of welding parameters including plunge rate, plunge depth, and rotation speed on the joint strength and failure mode. Welds made on bare metal were compared to welds using different interlayers deposited using the cold spray process. Microstructural analysis was also performed to characterize grain size and intermetallic formation.

**11:50 AM**

**Swept FSSW in Aluminum Alloys through Sealants and Surface Treatments:** *Karin Withar*<sup>1</sup>; *Jeremy Brown*<sup>1</sup>; *Dwight Burford*<sup>1</sup>; <sup>1</sup>Wichita State University

The objective is to investigate the effects that surface treatments have on the faying surface of 7075-T73 to 2024-T3 friction stir spots welds. The effects studied include mechanical properties and corrosion resistance. This experiment generates Friction Stir Spot Welded aluminum sheets of 0.040" thick 2024-T3 to 7075-T73. The dissimilar alloy sheets are treated with Alodine 600, and a sealant placed on the faying surface of the welds. The sealants chosen for this experiment are PRC-DeSoto PR-1432 GP and PRC-DeSoto PS 870 GRV. Coupons without sealants are also evaluated to establish a baseline statistical comparison. Four pin tools are used for these experiments. These pin tools have varying flow direction relative to the shoulder – neutral, additive, subtractive, and mixed. Mechanical properties of coupons with a guided 4-spot configuration are tested through ultimate lap shear and fatigue testing. Corrosion tested coupons are welded in a single spot configuration.

## General Abstracts: Light Metals Division: Metal Matrix Composites

*Sponsored by:* The Minerals, Metals and Materials Society, TMS Light Metals Division, TMS: Aluminum Committee, TMS: Aluminum Processing Committee, TMS: Energy Committee, TMS: Magnesium Committee, TMS: Recycling and Environmental Technologies Committee

*Program Organizers:* Alan Luo, General Motors Corporation; Eric Nyberg, Pacific Northwest National Laboratory

Thursday AM  
March 3, 2011

Room: 17A  
Location: San Diego Conv. Ctr

*Session Chair:* Alan Luo, General Motors Global Research & Development

**8:30 AM**

**Preparation and Characterization of Cast Hypereutectic Al-20wt.%Si-4.5wt.%Cu Nanocomposites with Al<sub>2</sub>O<sub>3</sub> Nanoparticles:** *Hongseok Choi*<sup>1</sup>; *Xiaochun Li*<sup>1</sup>; <sup>1</sup>University of Wisconsin-Madison

Hypereutectic Al-20Si-4.5Cu nanocomposites were cast with various percentages of  $\gamma$ -Al<sub>2</sub>O<sub>3</sub> nanoparticles that were dispersed by an ultrasonic

method. The as-cast Al-20Si-4.5Cu-Al<sub>2</sub>O<sub>3</sub> nanocomposites showed marked enhancements in both strengths and ductility when compared with those of the original alloy without the nanoparticles. The ductility was significantly increased for more than 10 times with an addition of 0.5wt.%  $\gamma$ -Al<sub>2</sub>O<sub>3</sub> nanoparticles. Microstructural analysis with optical and scanning electron microscopy (SEM) revealed that both the primary and eutectic silicon phases were significantly refined. The primary silicon phases were refined from star shapes to polygon or blocky shapes, and their edges and corners were much smoother. The large plate eutectic silicon phases were also modified into the fine fibrous ones.

**8:55 AM**

**An Investigation of Nanoparticle Wetting, Grain Refinement and Mechanical Property Enhancement in Aluminum Matrix Nanocomposites:** *Michael De Cicco*<sup>1</sup>; *Dake Wang*<sup>1</sup>; *Xiaochun Li*<sup>1</sup>; <sup>1</sup>University of Wisconsin-Madison

Nanoparticle wettability and incorporation during ultrasonic processing was studied in a pure aluminum (Al) matrix with TiC<sub>0.7</sub>N<sub>0.3</sub> and Al<sub>2</sub>O<sub>3</sub> nanoparticles. Additions of wetting elements of magnesium (Mg) and titanium (Ti) were used to enhance nanoparticle incorporation and wetting. In the pure Al without wetting elements significant TiC<sub>0.7</sub>N<sub>0.3</sub> incorporation was observed however there was no observed incorporation of the Al<sub>2</sub>O<sub>3</sub> nanoparticles. Additions of 0.2% Ti and 0.8% Mg (weight %) did not improve the incorporation of the TiC<sub>0.7</sub>N<sub>0.3</sub> nanoparticles however with 10% Mg addition there was improvement in TiC<sub>0.7</sub>N<sub>0.3</sub> nanoparticle incorporation. Additions of 0.2% Ti resulted in good incorporation of Al<sub>2</sub>O<sub>3</sub> nanoparticles. Adding Mg resulted in Mg containing oxides in the samples due to reaction with the Al<sub>2</sub>O<sub>3</sub> nanoparticles. The Al-10Mg+TiC<sub>0.7</sub>N<sub>0.3</sub>, which had the most significant nanoparticle incorporation, showed significant grain refinement and mechanical property enhancement. This grain refinement and mechanical property enhancement was maintained when pieces of the original 1.5% TiC<sub>0.7</sub>N<sub>0.3</sub> nanocomposites were added to additional Al-10Mg for a final 0.5% TiC<sub>0.7</sub>N<sub>0.3</sub> nanocomposite. This illustrates the potential of a master nanocomposite approach for metal matrix nanocomposite (MMNC) processing.

**9:20 AM**

**Influence of Processing Parameters on Distribution of Fibers in Cast Aluminium Matrix:** *Pengfei Yan*<sup>1</sup>; *Guangchun Yao*<sup>1</sup>; *Jianchao Shi*<sup>1</sup>; *Xiaolan Sun*<sup>1</sup>; *Hongjie Luo*<sup>1</sup>; <sup>1</sup>School of Materials & Metallurgy, Northeastern University

In this paper, 5% short carbon fibers reinforced aluminium matrix composites were prepared by stir casting method, using different stirring times and stirring speeds. The microstructure of the composites was observed through optical microscope and scanning electron microscopy (SEM), the tensile test was carried out. The results demonstrated that stirring time and stirring speed influence the microstructure and mechanical properties of the composites. The higher stirring time and stirring speed make the distribution of the fibers uniform and improved the mechanical properties. But beyond certain parameter, the fibers cluster and breakage, and the mechanical properties fall.

**9:45 AM**

**In Situ Fabrication of Ceramic Containing Metal Matrix Composite onto a TC4 Ti Alloy by Laser Cladding:** *Kemin Zhang*<sup>1</sup>; *Jianxin Zou*<sup>2</sup>; <sup>1</sup>Shanghai University of Engineering Science; <sup>2</sup>National Engineering Research Center of Light Alloy Net Forming, Shanghai Jiao Tong University

In the present work, a Ti based ceramic containing composite was successfully produced onto a TC4 Ti alloy by using laser surface cladding. TiC and Ti powders were mixed with a ratio of 1:3 and were put onto the TC4 alloy samples. They were then treated by laser beam with different scanning speed. The microstructure and composition modifications of the surface layer were investigated in details by using SEM, EDX and XRD techniques. The results have shown that, the laser clad layers have graded microstructures and compositions originated from the rapid heating, melting and cooling during laser processing. The maximum hardness of the laser

clad layer can research as high as 4.5 times of the initial one while the wear resistance was significantly improved after laser cladding.

#### 10:10 AM Break

#### 10:40 AM

**Stability of Nanoparticle Dispersion and Property Enhancement in Aluminum Matrix Nanocomposites during Repeated Casting Cycles:** *Dake Wang*<sup>1</sup>; Michael De Cicco<sup>1</sup>; Xiaochun Li<sup>1</sup>; <sup>1</sup>University of Wisconsin-Madison

It was shown that aluminum metal matrix nanocomposites (MMNCs) can be simply recast and maintain good nanoparticle dispersion and property enhancement. Pure aluminum nanocomposites with 1.5 volume %  $\text{TiC}_{0.7}\text{N}_{0.3}$  nanoparticle addition were produced by ultrasonic dispersion and cast in a permanent mold. The initial castings showed a significantly refined grain structure as well as 20% enhancement in yield strength, 24% enhancement in tensile strength and 7% enhancement in elongation. The materials were then remelted and cast four additional times. Scanning electron microscopy (SEM) analysis showed the nanoparticles remained well dispersed, and tensile testing showed maintained mechanical property enhancement.

#### 11:05 AM

**Study of Sputtering Deposition of Aluminum Boride-Based Composite:** *Glorimar Ramos*<sup>1</sup>; O. Marcelo Suárez<sup>1</sup>; <sup>1</sup>University of Puerto Rico-Mayaguez Campus

New polymer/Al-based hybrid composites were proposed for device fabrication, which require precise formulation of sputtered Al/AlB<sub>2</sub> composite layers due to their tunable elastic modulus. Two methods were investigated to this purpose. In the first one the sputtering targets utilized were cast via centrifugal casting with added silicon to improve the part (target) castability. Particle gradient concentration allowed fabricating several sputtering targets in just one centrifugal casting process. In the second method, deposition of alternating Al and AlB<sub>2</sub> layers were analyzed. The deposited films obtained through both methods were compared and investigated using atomic force microscopy to observe surface grain morphology while a stylus profiler allowed measuring the film roughness and overall topography.

#### 11:30 AM

**Corrosion Behavior of Metal-Matrix Composite AlMg-SiCp:** M.A. Hernandez<sup>1</sup>; S. Valdez<sup>2</sup>; <sup>1</sup>E.T.S.E.I., Universidade de Vigo; <sup>2</sup>UNAM-ICF

The AlMgSiC metal-matrix composite, obtained by Vortex Technique and the AlMg unreinforced alloy, have been studied in order to know their electrochemical response. The Vortex technique, generate a material composite with homogenous distribution of SiC particles and less casting porosity. The specimen tests were conducted in NaCl solution at 3.5 wt % for both the weight loss and potentiodynamic polarization measurements. The corrosion phenomena in unreinforced AlMg alloy were inhibited by the addition of silicon carbide particles, due to a slowing down the oxygen reduction reaction and the limiting cathodic current in function of time. The anodic dissolution in the alloy was proved by the formation of a non-stable oxide layer exhibiting partial protection having small resistance to polarization conditions.

#### 11:55 AM

**Preparation Process of Aluminum Foam Reinforced by Carbon Fibers:** *Hongjie Luo*<sup>1</sup>; Yihan Liu<sup>1</sup>; <sup>1</sup>Northeastern university

In this paper, it shows the fabrication process of aluminum foam reinforced by carbon fibers, and effects of mass percentage and length of carbon fiber on aluminum foam structure and properties in detail. The results show that aluminum foam with uniform structure was prepared by copper-coated carbon fibers as the stabilizer, and the apparent density of aluminum foam gradually decreases along with increasing the copper-coated carbon fiber content. The apparent density and porosity were not influenced by carbon fiber length regularly. The compression performance results indicate that the quantity of carbon fiber has a remarkable influence on plateau stress and the platform width of aluminum foam. The plateau stress increases with the addition of carbon fiber obviously. The compressive strength of aluminum

foam reinforced by carbon fiber is more than 5MPa generally, which is much higher than that of ordinary aluminum foam.

## Hydrometallurgy Fundamentals and Applications: Session I

*Sponsored by:* The Minerals, Metals and Materials Society, TMS Extraction and Processing Division, TMS: Hydrometallurgy and Electrometallurgy Committee

*Program Organizer:* Michael Free, University of Utah

Thursday AM  
March 3, 2011

Room: 16A  
Location: San Diego Conv. Ctr

*Session Chair:* Michael Free, University of Utah

#### 8:30 AM Keynote

**2011 EPD DISTINGUISHED LECTURER: The Removal of Arsenic, Selenium and Metals from Aqueous Solution by Iron Precipitation and Reduction Techniques:** *Larry Twidwell*<sup>1</sup>; <sup>1</sup>Montana Tech of The University of Montana

The removal of arsenic, selenium, and metal species from hydrometallurgical solutions and waste water has been and continues to be an important research topic. This presentation includes a discussion of the research conducted at Montana Tech of the University of Montana during the past twenty years and current literature studies. The discussion will be focused on removal of arsenic by co-precipitation with Fe(III) and Fe(II), co-precipitation with Fe(III) and Al(III), reduction using elemental iron; the removal of selenium by elemental iron and catalysed iron; and the removal of cadmium, copper, nickel, zinc by co-precipitation with Fe(III) and Al(III).

#### 9:10 AM

**Enhanced Pressure Dissolution of Enargite Using Pyrite or Ferrous Sulfate:** *Maria Ruiz*<sup>1</sup>; Oscar Jerez<sup>1</sup>; Jonathan Retamal<sup>1</sup>; Rafael Padilla<sup>1</sup>; <sup>1</sup>University of Concepcion

Enargite ( $\text{Cu}_3\text{AsS}_4$ ) is hard to leach mineral in acid media, which requires high oxygen overpressures and high temperatures for fast dissolution rates. To improve the leaching kinetics of enargite in milder conditions, additions of pyrite or ferrous sulfate has been proposed. In this research, mixtures of enargite/pyrite, with 10 to 50 weight percent of pyrite, were leached in  $\text{H}_2\text{SO}_4\text{-O}_2$  media, while pure enargite was leached in  $\text{H}_2\text{SO}_4\text{-O}_2$  and  $\text{H}_2\text{SO}_4\text{-FeSO}_4\text{-O}_2$  media. The results showed that mixtures of enargite/pyrite leached faster than pure enargite and the rate enhancement increased with higher pyrite content. For a mixture with 50% pyrite, size 46  $\mu\text{m}$ , complete dissolution could be obtained in 20 min at 180 °C and 690 kPa  $\text{P}_{\text{O}_2}$ . In the same conditions, the dissolution of pure enargite was less than 15%. Similarly, adding  $\text{FeSO}_4$  to the leaching solution augmented the enargite leaching rate and again the rate enhancement increased with larger additions.

#### 9:35 AM

**Model and Simulation of Ion Exchange of Antimony:** *Gerardo Cifuentes*<sup>1</sup>; Jaime Simpson<sup>2</sup>; Cesar Zúñiga<sup>1</sup>; Leoncio Briones<sup>1</sup>; Alejandro Morales<sup>3</sup>; <sup>1</sup>USACH; <sup>2</sup>ProPipe S.A.; <sup>3</sup>UCN

A model is proposed for the removal of Sb by ion exchange from copper refining electrolytes that fits the data from the literature. The correction factors for the MX-2, UR-3300S and Duolite C-467 resins were 0.5531; 0.2839 and 0.5455, respectively. The following variables were studied: volume of resin (bed height), volumetric matter transfer coefficient, and initial antimony concentration in the solution. The model's average percentage error was 3.01%.



#### 10:00 AM Break

#### 10:15 AM

##### **Analysis of the Adsorption of Gold and Silver on Magnetic Species Formed in the Electrocoagulation Process:** *Jose Parga*<sup>1</sup>; *Jesus Valenzuela*<sup>2</sup>;

<sup>1</sup>Institute Technology of Saltillo; <sup>2</sup>University of Sonora

In metallurgical operations, cyanidations is the predominant process by which gold and silver are recovered from their ores and it is recognized that the Carbon in Pulp, Merrill-Crowe process or the Ion Exchange resins are used for the concentrations and purification of gold and silver from cyanide solutions. Among several options are available for recovery precious metals from cyanide solutions, Electrocoagulation (EC) is a very promising electrochemical treatment technique that does not require high concentrations of gold and silver in solutions. First, this study will provide an introduction to the fundamental concepts of the EC method for recovery precious metals from cyanide solutions. In this research, X-ray Diffraction, SEM and Transmission Mossbauer Spectroscopy were used to characterize the solid products formed at iron electrodes during the EC process. The results suggest that magnetite particles and amorphous iron oxyhydroxides present in the EC products remove gold and silver in 5 minutes.

#### 10:40 AM

##### **Characterization and Performance of Smart Anode for Cobalt Electrowinning:** *Masatsugu Morimitsu*<sup>1</sup>; *Katsuya Kawaguchi*<sup>1</sup>; <sup>1</sup>Doshisha University

Smart anodes for cobalt electrowinning were developed by thermal decomposition of a precursor solution containing ruthenium and titanium compounds. Low temperature decomposition produced less crystalline composite oxide on a titanium substrate, and the oxide showed a high catalytic activity for chlorine evolution and suppressed the anodic deposition CoOOH in cobalt electrowinning solutions. These properties were effective to reduce the cell voltage of cobalt electrowinning and the sludge as deposited on the crystalline oxide surface.

#### 11:05 AM

##### **Treatment of Acid Mine Drainage by Electrodialysis:** *Daniella Buzzi*<sup>1</sup>; *Lucas Viegas*<sup>2</sup>; *Flávia Silvas*<sup>1</sup>; *Marco Antônio Rodrigues*<sup>3</sup>; *Ivo André Schneider*<sup>2</sup>; *Andréa Bernardes*<sup>2</sup>; *Denise Espinosa*<sup>1</sup>; *Jorge Alberto Tenório*<sup>1</sup>;

<sup>1</sup>Universidade de São Paulo; <sup>2</sup>Universidade Federal do Rio Grande do Sul;

<sup>3</sup>Universidade Feevale

One of the major impacts caused by coal mining activity is water pollution from acid mine drainage (AMD). AMD is produced by the reaction of pyrite, water and oxygen, that is intensified in the acidophilic bacteria presence. This solution acts as a leaching agent of minerals present in the residue, producing a solution with dissolved metals and sulfuric acid. Conventional treatment of AMD consists of neutralization and precipitation of heavy metals, but is technically deficient. The electrodialysis (ED) has emerged as an attractive process for effluents treatment since it does not need reagents addition and generates no waste polluting in the environment. The ED used to treat the AMD is a membrane process that consists in the separation of cations and anions by the application of an electric field on a process cell. In this study the possibility of using ED to the AMD treatment was evaluated aiming water reuse.

#### **Magnesium Technology 2011: New Applications (Biomedical and Other)**

*Sponsored by:* The Minerals, Metals and Materials Society, TMS Light Metals Division, TMS: Magnesium Committee

*Program Organizers:* Wim Sillekens, TNO Science and Industry; Sean Agnew, University of Virginia; Suveen Mathaudhu, US Army Research Laboratory; Neale Neelameggham, US Magnesium LLC

Thursday AM  
March 3, 2011

Room: 6F  
Location: San Diego Conv. Ctr

*Session Chairs:* Norbert Hort, Helmholtz-Zentrum Geesthacht; Michele Manuel, University of Florida

#### 8:30 AM

##### **Current Research Activities of Biomedical Mg Alloys in China:** *Yufeng Zheng*<sup>1</sup>; <sup>1</sup>Peking University

The potential biomedical application of Mg alloys as bioabsorbable/biodegradable implant in human body had been extensively studied worldwide, and becomes an emerging and promising application direction. Based on the presentations at a symposium on Biomedical Mg alloys in December 2009 at the 12th Annual Conference on Biomaterials, Chinese Society of Biomedical Engineering, and a symposium on Biodegradable Metallic Materials in May 2010 at Peking University, in these two conferences the present author served as the Chairman and the abstract numbers are about 50 for each conference, the frontier research activities of biomedical Mg alloys in China as the orthopedic and cardiovascular implants will be systematically summarized and comprehensively reviewed in this paper. The research highlights on the alloying system design, novel structure, degradation rate control, surface modification methods of Bio-Mg will be demonstrated via plenty of in vitro and in vivo study data.

#### 8:50 AM Invited

##### **Design Considerations for Developing Biodegradable Magnesium Implants:** *Harpreet Brar*<sup>1</sup>; *Benjamin G. Keselowsky*<sup>2</sup>; *Malisa Sarntinoranont*<sup>3</sup>; *Michele V. Manuel*<sup>1</sup>;

<sup>1</sup>University of Florida, Department of Materials Science and Engineering; <sup>2</sup>University of Florida, Department of Biomedical Engineering; <sup>3</sup>University of Florida, Department of Mechanical and Aerospace Engineering

The integration of biodegradable and bioabsorbable magnesium implants into the human body is a complex undertaking that faces major challenges. The complexity arises from the fact that biomaterials must meet both engineering and physiological requirements to ensure the desired properties. Historically, efforts have been focused on the behavior of commercial magnesium alloys in biological environments and their resultant effect on cell-mediated processes. Developing causal relationships between alloy chemistry and microstructure, and its effect on cellular behavior can be a difficult and time intensive process. A systems design approach driven by thermodynamics has the power to provide significant contributions in developing the next generation of magnesium alloy implants with controlled degradability, biocompatibility, and optimized mechanical properties, at reduced time and cost. This approach couples experimental research with theory and mechanistic modeling for the accelerated development of materials. The aim of this article is to enumerate this strategy, design considerations and hurdles for developing new magnesium alloys for use as biodegradable implant materials [1].

#### 9:10 AM

##### **Coating Systems for Magnesium-Based Biomaterials - State of the Art:** *Mark Staiger*<sup>1</sup>; *Jay Waterman*<sup>1</sup>;

<sup>1</sup>University of Canterbury

Magnesium and its alloys have the potential to be used for biodegradable orthopedic implants. However, the corrosion rate in physiological conditions is too high for most applications. For this reason, surface modification to slow the corrosion rate is of great interest. Such modifications must remain biologically compatible as well as protective in corrosive environments.

What follows is a brief review of recent research in inorganic coatings and surface modifications to create coatings for magnesium-based biomaterials.

**9:30 AM**

**Corrosion, Surface Modification and Biocompatibility of Mg and Mg Alloys:** *Sannakaisa Virtanen*<sup>1</sup>; Ben Fabry<sup>1</sup>; <sup>1</sup>University of Erlangen

Mg-based materials corrode in aqueous biological environments and are of growing interest for use as biodegradable implants. For a successful and biologically safe application, a thorough understanding of the corrosion behavior in vivo is required but is currently lacking. In particular, the effects of proteins and cells on Mg corrosion are unknown. Moreover, the effect of Mg dissolution on the biological environment needs to be characterized, as the corrosion reaction is coupled with H<sub>2</sub> gas evolution and surface alkalization. The aim of our study was to elucidate the interactions between corroding Mg (alloy) surfaces and cells, by an interdisciplinary approach of electrochemistry, surface modification and analysis, and cell culture testing. Of a special interest is the development of novel chemical and biological surface functionalization, to tailor the corrosion rate and biocompatibility.

**9:50 AM**

**Magnesium Alloys for Bioabsorbable Stents: A Feasibility Assessment:** *Charles Deng*<sup>1</sup>; Rajesh Radhakrishnan<sup>1</sup>; Steve Larsen<sup>1</sup>; Dennis Boismier<sup>1</sup>; Jon Stinson<sup>1</sup>; Adrienne Hotchkiss<sup>1</sup>; Jan Weber<sup>1</sup>; Torsten Scheuermann<sup>1</sup>; <sup>1</sup>Boston Scientific

Cardiovascular disease is the leading cause of the death in US. Stents are used to keep arteries open preventing cardiovascular disease related deaths. Presently, most stents consist of a stainless steel or other permanent metal alloy framework. Bioabsorbable stents are expected to provide scaffolding for the vessels for 3-6 months and then get fully absorbed within 1-2 years. They should ideally leave nothing behind, except the healed natural vessel, allowing restoration of healthy vessel properties. In this way, late stent thrombosis is unlikely, and prolonged anti-platelet therapy is not necessary. Also, bioabsorbable stents can be used as a delivery device for drugs such as Everolimus or Paclitaxel. Magnesium is a suitable candidate for bioabsorbable stent material. This presentation includes mechanical and electrochemical properties of magnesium alloy stents. In addition, it provides correlation between in vivo animal study and in vitro corrosion testing.

**10:10 AM Break**

**10:30 AM**

**Processing Aspects of Magnesium Alloy Stent Tube:** Robert Werkhoven<sup>1</sup>; Wim Sillekens<sup>1</sup>; Koos van Lieshout<sup>1</sup>; <sup>1</sup>TNO Science and Industry

Biomedical applications are an emerging field of interest for magnesium technology, envisioning biodegradable implants that dissolve in the human body after having cured a particular medical condition (such as clogging of arteries or bone fractures). This challenges research in a sense that the materials to be used need to dissolve in vivo in a controlled fashion without leaving harmful remainders and while maintaining sufficient strength and other (mechanical) attributes as long as necessary. To comply to the requirements, magnesium alloys as well as their processing routes into implants need to be tailored. While new alloy compositions are receiving ample attention, the paper at hand addresses the latter issue. The application of choice is the (cardio)-vascular stent. The different steps in manufacturing magnesium AZX-alloy stent tube are considered, including extrusion and subsequent drawing operations. Strategy for development is that the microstructure of the stent tube should be rendered possibly fine.

**10:50 AM**

**Ballistic Analysis of New Military Grade Magnesium Alloys for Armor Applications:** *Tyrone Jones*<sup>1</sup>; Katsuyoshi Kondoh<sup>2</sup>; <sup>1</sup>U.S. Army Research Laboratory; <sup>2</sup>Joining and Welding Research Institute

Since 2006, the U.S. Army has been evaluating magnesium (Mg) alloys for ballistic structural applications. While Mg-alloys have been used in military structural applications since WWII, very little research has been done to improve its mediocre ballistic performance. The Army's need for ultra-lightweight armor systems has led to research and development of high strength, high ductility Mg-alloys. The U.S. Army Research Laboratory

(ARL) and the Joining and Welding Research Institute (JWRI) of Osaka University collaborated through International Technology Center-Pacific (ITC-PAC) Contract Number FA-5209-09-P-0158 to develop the next generation of high strength, high ductility Mg-alloys using a novel Spinning Water Atomization Process (SWAP) for rapid solidification. New alloys AMX602 and ZAXE1711 in extruded bar form are characterized for microstructure, mechanical, corrosion, and ballistic response. Increases in ballistic performance and favorable corrosion resistance were evident when compared to the baseline alloy AZ31B.

**11:10 AM**

**Mg17Al12 Intermetallic Prepared by Bulk Mechanical Alloying:** Kenji Sakuragi<sup>1</sup>; *Masashi Sato*<sup>1</sup>; Takamitsu Honjo<sup>1</sup>; Toshiro Kuji<sup>1</sup>; <sup>1</sup>Tokai University

The properties of the metal hydrides are traditionally controlled by the nature and relative amount of the constituent elements. However, this straight forward way does not affect the thermodynamic properties of Mg-based hydrides in all cases, because the thermodynamic stability of Mg-based alloy is governed by the strong Mg-H bonding. In a last decade, nano-crystallised materials are widely investigated. The nano-crystalline provides other directions for solving many issues in the field of materials science. Ball milling process is general tool for preparing the nano-structured materials. The samples, however, show the fine powder form and the most of those are very sensitive against circumstance around. The bulk-form samples are desirable. In this study, it will be demonstrated that Mg17Al12 phase was prepared by newly developed Bulk Mechanical Alloying.

**11:30 AM**

**Corrosion Behaviour of Mg Alloys in Various Basic Media: Application of Waste Encapsulation of Fuel Decanning from UNGG Nuclear Reactor:** *David Lambertin*<sup>1</sup>; Adrien Blachere<sup>1</sup>; Fabien Frizon<sup>1</sup>; Florence Bart<sup>1</sup>; <sup>1</sup>CEA Marcoule

The dismantling of UNGG nuclear reactor generates a large volume of fuel decanning. These materials are based on Mg-Zr alloy. The strategy could be to encapsulate these wastes into an ordinary Portland cement (OPC) or geopolymer (aluminosilicate material) in a form suitable for storage. Studies have been performed on Mg or Mg-Al alloy in basic media but no data are available on Mg-Zr behaviour. The influence of representative solution of OPC and geopolymer with Mg-Zr alloy has been studied on corrosion behaviour. Electrochemical methods have been used to determine the corrosion densities at room temperature. Results show that the corrosion densities of Mg-Zr alloy in OPC solution is one order of magnitude more important than in geopolymer solution environment and effect of inhibiting agent has been undertaken with Mg-Zr alloy. Evaluation of encapsulation of Mg-Zr alloy in OPC and geopolymer has been done in term of corrosion hydrogen production.

## Magnetic Materials for Energy Applications: Other Magnets

Sponsored by: TMS Electronic, Magnetic, and Photonic Materials Division, TMS: Energy Conversion and Storage Committee, TMS: Magnetic Materials Committee; JSPS 147th Committee on Amorphous and Nanocrystalline Materials; Lake Shore Cyrotronics, Inc.; AMT&C

Program Organizers: Victorino Franco, Sevilla University; Oliver Gutfleisch, IFW Dresden; Kazuhiro Hono, National Institute for Materials Science; Paul Ohodnicki, National Energy Technology Laboratory

Thursday AM  
March 3, 2011

Room: 11A  
Location: San Diego Conv. Ctr

Session Chair: Iver Anderson, Ames Laboratory

### 8:30 AM Invited

**Nanoscaling like Noodles — A Novel Approach to Fabrication Nanocomposite Magnets with High Energy Density:** *J.Ping Liu*<sup>1</sup>; Chuanbing Rong<sup>1</sup>; Ying Zhang<sup>1</sup>; M.J. Kramer<sup>2</sup>; <sup>1</sup>University of Texas-Arlington; <sup>2</sup>Ames Laboratory

Exchange-spring hard/soft phase nanocomposite magnets have extremely high energy density owing to the inter-phase exchange coupling. The precondition for the effective exchange coupling is the nanoscale soft phase grains homogeneously distributed in the hard-phase matrix. Recently we found that by severe plastic deformation, the soft phase a-Fe grains in a SmCo/Fe composite system with the Fe concentration up to 35% can be “self-nanoscaled” to ~10 nm from the original particle size of 10  $\mu\text{m}$ . The ~1000 times size reduction is a result of a brittle/ductile composite deformation that leads to the elongation of the ductile component into noodle-like grains. The “noodles” then breakdown into nanoscale grains with further deformation. Subsequent warm compaction processing of the deformed nanocomposite particles produces fully dense bulk magnets with retained nanoscale morphology of the hard/soft phase composites. The energy density of the composite magnets is as double higher as the single-phase counterparts.

### 8:55 AM Invited

**Intergranular Diffusion in Exchange-Coupled Sm-Co/Fe Nanocomposites and Thin Films:** *Matthew Kramer*<sup>1</sup>; Ying Zhang<sup>1</sup>; J Liu<sup>2</sup>; Chuanbing Rong<sup>2</sup>; Ichiro Takeuchi<sup>3</sup>; Debjani Banerjee<sup>3</sup>; <sup>1</sup>Ames Lab/ISU; <sup>2</sup>University of Texas at Arlington; <sup>3</sup>University of Maryland

The nanostructural features, especially grain sizes, soft phase distribution and their grain boundaries are critical features to be controlled in exchange coupled permanent magnets. Using advanced microscopy techniques, we have investigated the Co-Fe interchange in  $\text{SmCo}_5+\text{Fe}$  and  $\text{Sm}_2\text{Co}_7+\text{Fe}$  nanocomposites and thin films. We find that the behavior of the interdiffusion between the bcc soft phase and the magnetically hard phases are similar in thin films and bulk samples under similar annealing conditions: Co and Fe interdiffuse forming a  $\text{Co}_{40}\text{Fe}_{60}$  bcc soft phase while the balance of the Fe forms a ternary Sm-Co-Fe phase of the initial phase. If the initial bcc phase has optimal Co content, substantial interdiffusion of Fe into the Sm-Co phases is not observed nor was the initial phase distributions retained. The magnetic properties of these alloys are inferior suggesting that optimal grain boundary chemistry is dependent on the appropriate local chemical driving forces.

### 9:20 AM

**Hard Magnetic PrCo<sub>3</sub> Structural and Magnetic Properties:** *Lotfi Bessais*<sup>1</sup>; Khedidja Younsi<sup>1</sup>; Vincent Russier<sup>1</sup>; Jean-Claude Crivello<sup>1</sup>; <sup>1</sup>CNRS

The structure and magnetic properties of nanocrystalline  $\text{PrCo}_3$  obtained from high energy milling technique and investigated by X-ray diffraction. Curie temperature determination and magnetic properties measurements are reported. The as-milled samples have been annealed in a temperature range of 1023K to 1273K for 30mn to optimize the extrinsic properties. The Curie temperature is 349K and coercive fields of 55kOe at 10K and 12kOe at 293K

are obtained on the samples annealed at 1023K. A simulation of the magnetic properties in the framework of micromagnetism has been performed in order to investigate the influence of the nanoscale structure. A composite model with hard crystallites embedded in an amorphous matrix, corresponding to the as-milled material, leads to satisfying agreement with the experimental magnetization curve. The microscopic scale is also considered from DFT calculations of the electronic structure of  $\text{RCo}_x$  compounds where  $R=(\text{Y},\text{Pr})$  and  $x=2,3$  and 5.

### 9:35 AM

**Directional Annealing Induced Texture in Melt-Spun Sm-Co Based Alloys:** *Tanjore Jayaraman*<sup>1</sup>; Paul Rogge<sup>1</sup>; Jeffrey Shield<sup>1</sup>; <sup>1</sup>University of Nebraska

Developing texture in nanocrystalline permanent magnet alloys is important for continued development in permanent magnet materials. This paper reports texture development in melt-spun alloys using directional annealing, a novel approach that utilizes anisotropic grain growth for texture development. Melt spinning of  $(\text{Sm}_{88}\text{Co}_{12})_{100-x-y}\text{Nb}_x\text{C}_y$  ( $x, y = 5$ ) alloys produced isotropic grain structures of the  $\text{SmCo}_7$  phase. The conventional and directional annealing formed the equilibrium  $\text{Sm}_2\text{Co}_{17}$  phase. While conventional annealing resulted in random crystallographic orientations, directional annealing with appropriate combinations of annealing temperature and translational velocity resulted in the development of (0006) in-plane texture as determined by x-ray diffraction analysis. Magnetization measurements along different directions corroborate the texture development, and suggested that the degree of texture was on the order of 25-40 percent. Coercivity values above 2 kOe were maintained. The texture development via directional annealing while minimizing exposure to elevated temperatures provides a promising route to anisotropic high-energy permanent magnets.

### 9:50 AM

**Magnetic Hardening of Nanocrystalline Sm-Fe-Mo Synthesized by Mechanical Alloying:** Lotfi Bessais<sup>1</sup>; Salwa Khazzan<sup>1</sup>; Najeh Miki<sup>2</sup>; Gustaaf Van Tendeloo<sup>3</sup>; <sup>1</sup>CNRS; <sup>2</sup>University of Tunisia; <sup>3</sup>EMAT, University of Antwerp

Materials based on rare-earth and iron have drawn much attention due to their high performance properties for permanent magnet application. The structural and magnetic properties of  $\text{Sm}_2(\text{Fe},\text{Mo})_{17}$ , its out of equilibrium precursor and their carbides are investigated by means of powder X-ray diffraction, magnetic measurements and HRTEM. In this work, the Rietveld analysis shows that the stoichiometry for the hexagonal phase is 1/9. Moreover, it points out a lattice expansion along the c axis after Mo substitution for Fe and reveals 2e preferential occupation for Mo atoms the out of equilibrium hexagonal precursor. Upon carbonation, the lattice expansion favors the Curie temperature increase up to 49% for the metastable 1/9C carbide. The Curie temperature and the coercive field of the 1/9 carbides are higher than those of 2/17 ones. This makes the hexagonal precursor a competitive candidate for use as permanent magnet.

### 10:05 AM

**Understanding and Control of Coercivity in Non-Rare Earth Alnico Permanent Magnets:** *Scott Long*<sup>1</sup>; Iver Anderson<sup>2</sup>; R.W. McCallum<sup>2</sup>; Matthew Kramer<sup>2</sup>; Wei Tang<sup>2</sup>; Yaqiao Wu<sup>2</sup>; <sup>1</sup>Iowa State University; <sup>2</sup>Ames Lab

Due to expanding Chinese markets & manufacturing capacity and subsequent decline in rare earth (RE) exports from this dominant RE source (97% world market), suitable alternatives to rare earth magnets are desired. Alnico alloys were the premier permanent magnet material before the development of Sm-Co and, especially Nd-Fe-B. Although coercivities are relatively low, Alnico magnets have the highest remanence of commercially available non-RE permanent magnets. Alnico magnets have superior thermal properties to Nd-Fe-B and, with modest improvements in coercivity, could be a viable alternative in many electric motor and generator applications. Alnico alloys rely on shape anisotropy of nano-scale precipitates as a main coercivity mechanism. The effects on coercivity of precipitate shape/spacing and alignment of parent grains (prior to precipitation) will be investigated. Characterization methods will include SEM, TEM, and SQUID



magnetometry and the results will be presented. Funding provided by DOE-EERE-FCVT Office through Ames lab Contract DE-AC02-07CH11358.

10:20 AM Break

## Magnetic Materials for Energy Applications: Requirements of Magnetic Materials for Current Technological Applications

*Sponsored by:* TMS Electronic, Magnetic, and Photonic Materials Division, TMS: Energy Conversion and Storage Committee, TMS: Magnetic Materials Committee

*Program Organizers:* Victorino Franco, Sevilla University; Oliver Gutfleisch, IFW Dresden; Kazuhiro Hono, National Institute for Materials Science; Paul Ohodnicki, National Energy Technology Laboratory

Thursday AM  
March 3, 2011

Room: 11A  
Location: San Diego Conv. Ctr

*Session Chair:* Paul Ohodnicki, National Energy Technology Laboratory

10:30 AM Invited

## The Transformational Potential of Magnetic Materials: ARPA-E Investment: Rajevee Ram<sup>1</sup>; <sup>1</sup>ARPA-E

Producing electricity is the largest sink of primary energy in the US - consequently electricity production is the largest contributor to atmospheric carbon dioxide. The ARPA-E ADEPT program is focused on improvements in electrical energy efficiency from lower cost, more efficient, solid-state lighting to lighter weight electrical vehicles to a flexible electricity grid. Program targets include converters utilizing magnetic materials with high operating flux exceeding 0.5T (15x greater than MnZn) with electrical resistivity exceeding 1mOhm-cm (5-10x MnZn) and high thermal conductivity. For chip-scale power conversion, novel magnetic materials deposited as CMOS compatible laminates or as ink-jet printed and sintered nanocolloids are being developed. At the kW scale, module integrated converters employing advanced thick-film magnetic nanocomposites as well as transformer geometries are being explored. At MW scale, approaches include creating greater flexibility in grid assets such as transformers by employing advanced converter architectures that leverage bipolar SiC.

10:55 AM Panel Discussion

**Requirements of Magnetic Materials for Current Technological Applications:** *Moderator:* Paul R. Ohodnicki<sup>1</sup>; <sup>1</sup>National Energy Technology Laboratory

**Panelists:**

*Karl Gschneidner<sup>1</sup>; <sup>1</sup>Ames Laboratory: Critical Parameters for the Utilization of First Order Magnetocaloric Regenerator Materials in Magnetic Cooling Machines*

*Takehisa Minowa<sup>1</sup>; <sup>1</sup>Shin-Etsu Chemical Co. Ltd.: Application of Nd-Fe-B Magnets to the Megawatt Scale Generator for the Wind Turbine*

*Jinfang Liu<sup>1</sup>; <sup>1</sup>Electron Energy Corporation: Industrial Requirements and Applications of Hard Magnetic Materials*

*Aru Yan<sup>1</sup>; <sup>1</sup>Ningbo Institute of Material Technology and Engineering: Current Status of Permanent Magnet Research and Market in China*

*Francis Johnson<sup>1</sup>; <sup>1</sup>General Electric Global Research: Industrial Needs and Applications for Soft Magnetic Materials*

*Ryusuke Hasegawa<sup>1</sup>; <sup>1</sup>Metglas, Inc: Soft Magnetic Materials in Energy Applications*

*Sarah Bedair<sup>1</sup>; <sup>1</sup>US Army Research Laboratory: Low Loss, High Power Density Magnetics in Inductor/Transformer Cores for Army Applications*

12:35 PM

**Industrial Requirements and Applications of Hard Magnetic Materials:** *Jinfang Liu<sup>1</sup>; <sup>1</sup>Electron Energy Corporation*

The selection of hard magnetic materials for industrial applications depends on many factors but is primarily determined by the trade off between cost and performance. Magnetic performance of interest includes residual induction (Br), coercivity (Hc) and intrinsic coercivity (Hci). Br and Hc are normally pre-determined by electromagnetic design. Application environment (temperature, humidity, and pH of the service environment) is a critical factor for the selection of hard magnetic materials. Applications of hard magnetic materials can be found everywhere, from cell phones, computers, automobiles, office appliances, to fighter jets, missiles, and space vehicles. In recent years, green technologies attracted a lot of attention. Hard magnetic materials play a significant role in many green technologies, such as electric or hybrid vehicles and wind turbines. Demand for hard magnetic materials is said to surge in the coming years.

12:45 PM

**Low Loss, High Power Density Magnetics in Inductor/Transformer Cores for Army Applications:** *Sarah Bedair<sup>1</sup>; Wesley Tipton<sup>1</sup>; Damian Urciuoli<sup>1</sup>; Brian Morgan<sup>1</sup>; <sup>1</sup>US Army Research Laboratory*

The Army Research Laboratory (ARL) currently has efforts in high efficiency power conversion for unique, military specific applications in the power ranges: 1) 1-100kW, 2)mW-10W. The former power requirements motivate high efficiency materials for use in bulk scale inductors and transformers. The magnetic material requirements include high  $B_{sat}$  with high operating temperatures (>120°C) and minimal switching losses (20-200kHz switching frequencies). There is also an ARL thrust for power conditioning units (mW-10W scale), where the vision is an ultra-miniature, mm<sup>3</sup> scale, distributed power supply. Increasing the switching frequency (20-500MHz) of DC-DC converters would lead to size reduction of the magnetic passives which dominate the converter size. High inductance densities in a miniature form factor on integrated, single chip platforms necessitate novel, thin film ( $\mu\text{m}$ -10's  $\mu\text{m}$  thick), CMOS-process compatible (<400°C thin-film deposition) magnetic materials. The material requirements for high frequencies include low eddy current losses and minimization of  $\mu''$  (complex permeability).

12:55 PM

**Soft Magnetic Materials in Energy Applications:** *Ryusuke Hasegawa<sup>1</sup>; <sup>1</sup>Metglas, Inc*

In light of energy generation and efficient use of it, development of pertinent soft magnetic materials based on amorphous and nanocrystalline alloys is discussed. These materials have lower magnetic losses and faster flux reversal than crystalline counterparts. This increases devices' operating frequency, which enables smaller and more efficient devices. The impact of this is evidenced in magnetic switches and pulse generation and compression. Examples are pulse sources for lasers and charged-particle accelerators. The latter application is noteworthy as it could lead to nuclear fusion for energy generation. In the area of energy efficiency, these materials contribute considerably in reducing energy distribution system loss with the resultant reduction of CO2 emission at power plants. In power management, non-crystalline alloys are widely used in power electronics including switch-mode power supplies for e.g. PCs, inductors in inverters in wind/solar power generators and power supplies in hybrid cars.

1:05 PM

**Industrial Needs and Applications for Soft Magnetic Materials:** *Francis Johnson<sup>1</sup>; <sup>1</sup>GE Global Research*

Research and development trends in soft magnetic materials will be discussed from the perspective of an industrial research organization. Key application drivers will be reviewed, included modular power electronic systems for mobile and stationary applications, traction motor systems, and power generation systems. Unique challenges are faced when selecting and engineering magnetic materials for operation in the kilohertz frequency band at Megawatt power levels as compared to the Megawatt frequency bands at the kilowatt power level. The impact of recently enhanced emphasis on

materials sustainability, when applied to the value chain of components in an integrated power system, will be discussed.

1:15 PM

**Critical Parameters for the Utilization of First Order Magnetocaloric Regenerator Materials in Magnetic Cooling Machines:** Karl Gschneidner<sup>1</sup>;

<sup>1</sup>Iowa State University

Materials which undergo a first order magnetic transition exhibit a number of properties which may prohibit or limit their utilization as regenerator materials for magnetic refrigerators, freezers, air conditioners, etc. These include hysteresis, time for the completion of the transition, adiabatic temperature change, ductility/brittleness, and magnetostriction. Other properties may include corrosion resistance, environmental concerns, vapor pressure, and friability. Since an operating cooling machine will undergo about a trillion cycles in its lifetime there are many challenges for the materials design engineer to ameliorate these obstacles for a reliable magnetocaloric refrigerant.

---

**Microstructural Processes in Irradiated Materials: Nuclear Fuel Materials**

*Sponsored by:* The Minerals, Metals and Materials Society, TMS Structural Materials Division, TMS/ASM: Nuclear Materials Committee

*Program Organizers:* Gary Was, University of Michigan; Thak Sang Byun, Oak Ridge National Laboratory; Shenyang Hu, Pacific Northwest National Laboratory; Dane Morgan, UW Madison; Yasuyoshi Nagai, Tohoku University

Thursday AM

Room: 3

March 3, 2011

Location: San Diego Conv. Ctr

*Session Chairs:* Dieter Wolf, Argonne National Laboratory; Maria Okuniewski, Idaho National Laboratory

---

8:30 AM Invited

**Multi-Scale Modeling of Irradiation Effects on Nuclear Fuel**

**Microstructure:** Dieter Wolf<sup>1</sup>; <sup>1</sup>Argonne National Laboratory

In spite of the well-known existence of microstructural phenomena in nuclear materials, such as void swelling and fission-gas release, a comprehensive understanding of how microstructural processes control the thermo-mechanical behavior of nuclear materials remains to be developed. This lecture provides a vision on how a predictive nuclear fuel modeling capability can be developed by an atomistically-informed mesoscale approach. Two critical elements of the approach are: (i) capturing irradiation effects within an atomistically-informed mesoscale modeling framework, and (ii) developing a comprehensive theoretical and computational mesoscale approach that considers all the various, simultaneously occurring and highly coupled microstructural process within a unified framework. The critical need for experiments will be emphasized. Work supported by the Energy Frontier Research Center for Materials Science of Nuclear Fuels and by Argonne National Laboratory's LDRD program.

9:10 AM

**Formation and Incorporation Energies of Fission Gases He, Xe, and Kr in bcc Uranium:** Benjamin Beeler<sup>1</sup>; Benjamin Good<sup>1</sup>; Chaitanya Deo<sup>1</sup>;

Sergey Rashkeev<sup>2</sup>; Michael Baskes<sup>3</sup>; Maria Okuniewski<sup>2</sup>; <sup>1</sup>Georgia Institute of Technology; <sup>2</sup>Idaho National Laboratory; <sup>3</sup>University of California-San Diego

Various metallic nuclear fuels are bcc alloys of uranium that swell under fission conditions, creating fission product gases such as helium, xenon and krypton. An analysis is performed on He, Xe, and Kr point defects in metallic uranium using two methodologies. Defects are investigated within a density functional theory framework utilizing projector augmented-wave pseudopotentials and also with Modified Embedded Atom Method potentials. Formation and incorporation energies of He, Xe, and Kr are calculated at various defect positions for the prediction of fission gas behavior in the bcc

phase of uranium. The most likely position for dilute Xe and Kr atoms in bcc uranium is the substitutional site. Helium atoms are likely to be found in a wide variety of defect positions due to the comparable formation energies of all defect configurations analyzed. This is the first detailed study of the stability and incorporation of fission gases in uranium.

9:30 AM

**Recent Results of Microstructural Characterization of Irradiated**

**RERTR Fuels:** Dennis Keiser<sup>1</sup>; Jan-Fong Jue<sup>1</sup>; Adam Robinson<sup>1</sup>; Pavel Medvedev<sup>1</sup>; <sup>1</sup>Idaho National Laboratory

The Reduced Enrichment for Research and Test Reactor (RERTR) program is developing low enriched U-Mo fuels for use in reactors that currently employ fuels containing highly enriched uranium. Two different fuel types are being developed: a dispersion fuel and a monolithic fuel. A large part of this fuel development involves irradiation testing in the Advanced Test Reactor. This presentation will discuss the microstructural development that occurs during the irradiation of these two types of fuel. Emphasis will be given to the recent results from the microstructural characterization of irradiated nuclear fuel plates using electron microscopy.

9:50 AM

**Phase Field Modeling of Void Growth in Irradiated Two-Phase U-Zr**

**Alloys:** Ximiao Pan<sup>1</sup>; Morral Morral<sup>1</sup>; Y. Wang<sup>1</sup>; <sup>1</sup>OSU

Void growth in irradiated, two-phase U-Zr alloys was investigated using a phase field model. The phase field model was linked to a thermodynamic and kinetic database that included vacancies (Va) to represent the U-Zr-Va system. The thermodynamic database was created from an established one for binary U-Zr alloys and by treating the U-Va and Zr-Va binaries as regular solutions with a 40 kJ/mole interaction energy. There were no ternary interaction parameters. A solute mobility database was created from experimental measurements and is composition dependent, while the vacancy mobility was taken as a constant. The phase field model predicts void growth under irradiation in two-phase, gamma + gamma prime alloys. The change in vacancy concentration with time due to irradiation was assumed to be a function of the local vacancy concentration. This assumption was suggested by a plume model prediction, as an alternative to using the mean field approximation for damage.

10:10 AM

**Lanthanides Migration and Immobilization in U-Zr Based Nuclear**

**Fuels:** Guillermo Bozzolo<sup>1</sup>; Gerard Hofman<sup>1</sup>; Abdellatif Yacout<sup>1</sup>; Hugo Mosca<sup>2</sup>; <sup>1</sup>Argonne National Laboratory; <sup>2</sup>CNEA

Redistribution of fission products such as minor actinides and lanthanides leads to migration to the surface of U-Zr based fuels, generating concern due to their interaction with the cladding. The existing remedy for preventing this effect is the introduction of diffusion barriers on the cladding inner surface or by adding thermodynamically stable compound-forming elements to the fuel. Exploring this second option, in this work we introduce atomistic modeling using the BFS method for alloys to study the formation of lanthanide-rich precipitates in U-Zr fuel and the segregation patterns of all constituents to the surface. Surface energies for all elements were computed and, together with the underlying concepts of the BFS method and large scale simulations, the migration of lanthanides to the surface region in U-Zr fuels is explained. The role of additions to the fuel such as In, Ga, and Tl for immobilization of lanthanides is discussed.

10:30 AM Break

10:50 AM

**Fission Induced Fuel Swelling, Creep and Sintering of U-Mo Alloy Fuel:**

Gerard Hofman<sup>1</sup>; Yeon Soo Kim<sup>1</sup>; <sup>1</sup>Argonne National Laboratory

U-Mo alloy fuel is currently under development for the use of high-power research and test reactors. Irradiation tests of this fuel have been conducted in the Advanced Test Reactor for the US GTRI-Convert program, formerly known as the RERTR (Reduced Enrichment for Research and Test Reactors) and worldwide. Detailed analysis of metallographic sections of irradiated U-Mo fuel plates has shown that the apparent fuel swelling contains a significant fuel creep component induced by high fission. Some of the

fuel particles with a high fission density and a fission rate show sintering with neighbour particles due to fission induced diffusion. Analysis results of fission induced swelling, creep and sintering of U-Mo alloy fuel are presented. A comparison with other ceramic fuels is also given.

#### 11:10 AM

**Simulation of Recrystallization in Uranium Dioxide Nuclear Fuels:** Jonathan Madison<sup>1</sup>; Veena Tikare<sup>1</sup>; Elizabeth Holm<sup>1</sup>; <sup>1</sup>Sandia National Laboratories

Uranium Dioxide (UO<sub>2</sub>) high burn-up structures found in the rim of light water reactor fuels demonstrate marked differences in yield as well as a variety of additional microstructural markers such as Xe depletion, decreased hardness, increased porosity and extensive recrystallization. In an effort to more clearly understand the microstructural evolution in the formation and development of the rim structure, a kinetic Monte Carlo model incorporating a probabilistic cellular-automata approach has been developed. This model treats dynamic recrystallization while utilizing a position and time-dependent damage accumulation in both two and three-dimensional domains. Results will be provided offering insights into local percolation thresholds, mechanisms for damage migration and implications for continued irradiation of fuel materials beyond currently established NRC regulations.

#### 11:30 AM

**The Influence of Temperature on the Evolution of Irradiation-Induced Defect Structure in CeO<sub>2</sub>:** Bei Ye<sup>1</sup>; Wei-Ying Chen<sup>1</sup>; Mark Kirk<sup>2</sup>; James Stubbins<sup>1</sup>; Abdellatif Yacout<sup>2</sup>; Jeffery Rest<sup>2</sup>; <sup>1</sup>U of Illinois at Champaign-Urbana; <sup>2</sup>Argonne National Lab

Microstructure evolution of ceria (CeO<sub>2</sub>) during irradiation has been investigated through transmission electron microscopy (TEM) under in-situ irradiation. Single crystal CeO<sub>2</sub>, grown by molecular beam epitaxy, is used to simulate fluorite-structure UO<sub>2</sub>, which is a very important nuclear fuel. 500 keV xenon ions were implanted into CeO<sub>2</sub> thin foils at a range of temperatures (room temperature, 600°C and 800°C) to reveal the temperature effects in defect structure development (to 5x10<sup>15</sup> ions/cm<sup>2</sup>). Experiment results show a clear impact of temperature on irradiation damage production. At room temperature, defect clusters appear in irregular shapes, and gas bubbles are hardly observed. On the contrary, at elevated temperatures, defect clusters tend to form circular-shaped dislocation loops while gas atoms precipitate in high-density (~ 1.5x10<sup>17</sup> ions/cm<sup>2</sup>) gas bubbles with a size of ~ 1 – 2 nm in diameter. The differences are attributed to the correlation between defect diffusion ability and temperature.

#### 11:50 AM

**Influence of Radiation Damage on Strontium Diffusion in Silicon Carbide:** Erich Friedland<sup>1</sup>; Nic van der Berg<sup>1</sup>; Johan Malherbe<sup>1</sup>; Elke Wendler<sup>2</sup>; Werner Wesch<sup>3</sup>; <sup>1</sup>University of Pretoria; <sup>2</sup>Institute for solid state physics; <sup>3</sup>Friedrich-Schiller-Universitaet

Fuel elements of gas cooled nuclear reactors and those studied under the International Generation IV Reactor Program are commonly based on TRISO fuel particles. These particles are encapsulated by pyrolytic carbon and silicon carbide layers to reduce fission product release. This study aims to obtain information on strontium diffusion in silicon carbide and the influence of radiation damage on it. For this purpose strontium was implanted in silicon carbide wafers at temperatures ranging from 300 to 900 K. Diffusion coefficients were obtained from the broadening of the implantation profile after thermal annealing studies up to 1700 K using ion beam analysis. Structural information was obtained by electron microscopy. Comparison of profile broadening in annealed single and poly-crystalline samples yielded information on the importance of volume and grain boundary diffusion. Information on the influence of radiation damage was extracted by comparing results from samples implanted at room and elevated temperatures.

#### 12:10 PM

**Atomistic Modeling of Fission Products Transport in SiC and ZrC TRISO Fuels:** Sungtae Kim<sup>1</sup>; David Shrader<sup>1</sup>; Sarah Khalil<sup>1</sup>; Andrew Heim<sup>1</sup>; Dane Morgan<sup>1</sup>; Izabela Szlufarska<sup>1</sup>; <sup>1</sup>University of Wisconsin - Madison

SiC is used as the primary barrier layer to metallic fission product release in TRISO nuclear fuels, but release of Ag and Cs at higher temperatures has been reported. Some studies have suggested the ZrC can provide improved fission product retention compared to SiC and ZrC is presently under consideration for use with, or even in place of, SiC. We have used ab initio methods to determine the structure, mobility, and energetics of Ag and Cs defects in bulk, and to a lesser extent, grain boundaries of SiC and ZrC. We find an important role for impurity – vacancy clusters, charged defect states, and dramatic changes possible in comparing grain boundary and bulk diffusion. Predicted diffusion behavior agrees with measured values where comparisons can be made but solubility predictions suggest that other processes than those considered here may be playing a role in measured fission product release.

### Neutron and X-Ray Studies of Advanced Materials IV: Dislocations, Strains and Stresses III

*Sponsored by:* The Minerals, Metals and Materials Society, TMS Structural Materials Division, TMS/ASM: Mechanical Behavior of Materials Committee, TMS: Chemistry and Physics of Materials Committee

*Program Organizers:* Rozaliya Barabash, Oak Ridge National Laboratory; Xun-Li Wang, Oak Ridge National Laboratory; Jaimie Tiley, Air Force Research Laboratory; Peter Liaw, The University of Tennessee; Erica Lilleodden, GKSS Research Center; Brent Fultz, California Institute of Technology; Y-D Wang, Northeastern University

Thursday AM  
March 3, 2011

Room: 10  
Location: San Diego Conv. Ctr

*Session Chairs:* Jaimie Tiley, Air Force research Laboratory; Peter Liaw, UTK

#### 8:30 AM Invited

**Development of Recrystallization Texture during Friction Stir Processing of Magnesium Alloy:** Hahn Choo<sup>1</sup>; Zhenzhen Yu<sup>1</sup>; Wei Zhang<sup>2</sup>; Zhili Feng<sup>2</sup>; Sven Vogel<sup>3</sup>; Edward Kenik<sup>2</sup>; <sup>1</sup>Univ of Tennessee; <sup>2</sup>Oak Ridge National Laboratory; <sup>3</sup>Los Alamos National Laboratory

The influence of thermo-mechanical input during friction stir processing (FSP) on texture development was investigated for AZ31B Mg alloy. By varying key processing parameters systematically, i.e., rotation speed and travel rate of the tool, a series of FSP specimens were prepared with a wide range of thermo-mechanical input that can be represented in terms of Zener-Hollomon parameter (Z). Neutron diffraction results show a dramatic change in volume-averaged texture in the stir zone as Z parameter was increased, clearly indicating the influence of processing parameters on the deformation and recrystallization mechanisms. Using the neutron diffraction results, in combination with electron backscattering diffraction and three-dimensional transient modeling, the deformation and recrystallization mechanisms responsible for the microstructure development during FSP of Mg alloy were investigated.

#### 8:50 AM

**Neutron Diffraction Measurements of Residual Stresses in a 50-mm Thick Weld Plate:** Wanchuck Woo<sup>1</sup>; Vyacheslav EM<sup>1</sup>; Jeong-Ung Park<sup>2</sup>; Gyu-Baek An<sup>3</sup>; Baek-Seok Seong<sup>1</sup>; <sup>1</sup>KAERI (Korea Atomic Energy Research Institute); <sup>2</sup>Chosun University; <sup>3</sup>POSCO Steel

Most of the engineering neutron diffractometers have a difficulty in increasing their penetration capability over 25 mm thickness in plate. In order to decrease the beam attenuation, we optimized the configurations of the diffractometer. Specifically, the bent perfect crystal monochromator Si (111) at the take-off angle of 45° provides the wavelength of 2.4 Å and



the bcc ferrite (110) peak at the diffraction angle of  $71.7^\circ$ . It constitutes the wavelength located at the lower neutron cross-section of iron (avoid the 112 Bragg edge) and enables us to obtain the enhanced peak resolution and intensity. We have successfully determined through thickness variations of the residual stresses in the 50-mm thick, 300-mm width/length weld plate without any cutting. Used gauge volumes were  $2 \times 2 \times 8 \text{ mm}^3$  (longitudinal) and  $2 \times 2 \times 20 \text{ mm}^3$  (transverse/normal), and 'stress-free' do measurements were considered. Significant amounts of the tensile longitudinal stresses (over 300 MPa) were observed along the heat-affected zone.

#### 9:05 AM

**Deformation Behavior of Nanostructured Metals Over Different Strain Rates and Temperatures:** *Ryan Ott*<sup>1</sup>; *Yinmin Wang*<sup>2</sup>; *Matthew Besser*<sup>1</sup>; *Jonathan Almer*<sup>3</sup>; *Matthew Kramer*<sup>1</sup>; <sup>1</sup>Ames Laboratory (USDOE); <sup>2</sup>Lawrence Livermore National Laboratory; <sup>3</sup>Argonne National Laboratory

For most metals the length-scale of the microstructure can significantly affect both the bulk macroscopic mechanical response and the atomic-scale deformation mechanisms. Furthermore, the mechanical behavior can also depend on the strain rate and deformation temperature. We have examined the deformation mechanisms of different nanostructured metals (e.g. Ni, Cu) using real-time high-energy X-ray diffraction. We report on the effects of both strain rate and test temperature on the grain and twin-boundary stability, the lattice strain, and dislocation-mediated plasticity. From the experiments we find that the lattice strain and the peak broadening are dependent on the deformation conditions. The interconnection between the deformation mechanisms measured by in situ X-ray diffraction and the mechanical responses measured by bulk tests are discussed.

#### 9:20 AM

**Deformation Studies of a Creep Resistant Bainitic Steel Using Synchrotron and Neutron Diffraction:** *Michael Weisser*<sup>1</sup>; *Alexander Evans*<sup>1</sup>; *Steven Van Petegem*<sup>1</sup>; *Stuart Holdsworth*<sup>2</sup>; *Helena Van Swygenhoven*<sup>1</sup>; <sup>1</sup>Paul Scherrer Institut; <sup>2</sup>EMPA

Creep resistant bainitic steels are commonly used for power plant applications, experiencing both static and cyclic stresses at typical operating temperatures of  $565^\circ\text{C}$ . The strengthening mechanisms at both ambient and elevated temperatures are governed by the complex microstructure comprising ductile ferrite matrix and hard carbides. Synchrotron X-rays and neutrons provide an insight to the phase specific behaviours of the main microstructural components during deformation. Residual lattice strain measurements on ex-situ deformed samples with two different deformation histories have shown opposing trends for the ferrite matrix: i) large ferrite phase strain when tensile deformed at ambient temperature and ii) balanced phase strain when creep deformed at operating temperatures. This supports the operation of different deformation mechanisms. Complementary tensile loading tests performed in-situ at ambient temperature suggests that the residual ferrite phase strain originates from load-transfer of the plastifying ferrite matrix to a cementite phase with the onset of macroscopic plasticity.

#### 9:35 AM

**MikroGap Area Detector for Stress and Textures Analysis:** *Bob He*<sup>1</sup>; <sup>1</sup>Bruker AXS

Two-dimensional X-ray diffraction is an ideal method for examining the residual stress and texture. The most dramatic development in two-dimensional x-ray diffractometry involves three critical devices, including x-ray sources, x-ray optics and detectors. The recent developments in brilliant X-rays sources and high efficiency X-ray optics provide high intensity X-ray beam with the desired size and divergence. Correspondingly, the detector used in such a high performance system requires the capability to collect large two-dimensional images with high counting rate and high resolution. This presentation introduces an innovative large area detector based on the MikroGap™ technology and the diffraction vector approach for processing the data for stress and texture analysis. The fundamental equations for stress and texture analysis are derived from the unit vector expression. The stress is given by the distortion of the diffraction ring and the texture is given by the intensity variation along the diffraction ring.

#### 9:50 AM

**Micromechanical Behavior Evolution of Twinning-Induced Plasticity Steels Studied by Neutron Diffraction and Self-Consistent Modeling:** *Xiaopeng Liu*<sup>1</sup>; *Ru Lin Peng*<sup>2</sup>; *Xiangyuan Wang*<sup>1</sup>; *Yandong Wang*<sup>3</sup>; *Yongfeng Shen*<sup>1</sup>; *Shuyan Zhang*<sup>4</sup>; *Xin Sun*<sup>5</sup>; *Sten Johansson*<sup>2</sup>; <sup>1</sup>Northeastern University; <sup>2</sup>Linköping University; <sup>3</sup>Beijing Institute of Technology; <sup>4</sup>Rutherford Appleton Laboratory; <sup>5</sup>Pacific Northwest National Laboratory

TWIP (Twinning-Induced Plasticity) steels exhibit good ductility at a very high strength level and are therefore promising materials for making automotive parts with complex geometry. The enhanced formability of such steels is attributed to the formation of mechanical twins during plastic deformation. To understand the twinning-related micromechanical behaviors, in-situ time-of-flight (TOF) neutron diffraction experiments under tensile loading were performed at ISIS to study the change in lattice strains for different hkl-planes of a Fe-30Mn-4Si-3Al TWIP steel. The micromechanical behavior in the TWIP steel is further simulated by the self-consistent model considering both dislocation-slipping and twinning activities. The parameters used for describing the micromechanical behavior of the TWIP steels are directly derived from the TOF experiments and TEM observation. A reliable prediction on evolution of hkl lattice strains and grain orientation distribution is achieved while the interaction of slipping and twinning is considered in the studied material undergoing uniaxial tensile deformation.

#### 10:05 AM

**Study of Material Deformation at High Pressure Using Synchrotron X-Rays:** *Jiuhua Chen*<sup>1</sup>; *Jennifer Girard*<sup>1</sup>; <sup>1</sup>Florida International University

Developments of high pressure apparatus in conjunction with ultra-brilliant third-generation synchrotron X-ray sources have significantly advanced our capability to study material properties under extreme conditions. Here we report some recent developments in characterization of mechanical properties of materials at high pressure and temperature. In these experiments, x-ray diffraction is used to measure the differential stress and x-ray radiograph imaging is used to determine the strain/strain rate of specimens. The maximum pressure and temperature generated by the deformation high pressure apparatus can reach above 10 GPa and  $1300^\circ\text{C}$  respectively. Accuracy of stress and strain rate measurements are about 50 MPa and  $10^{-6}$ . While experiments are routinely conducted on polycrystalline specimens, latest advances enable experiments on single crystalline samples as well. Pressure/water induced transitions of active slip system along different crystallographic orientations have been observed in recent experiments.

#### 10:15 AM

**Micromechanical and Neutron Diffraction Studies of Intergranular Strain Development near a Fatigue Crack Tip:** *Lili Zheng*<sup>1</sup>; *Yanfei Gao*<sup>1</sup>; *Rozaliya Barabash*<sup>2</sup>; *Sooyeol Lee*<sup>3</sup>; *Jinhaeng Lee*<sup>1</sup>; *Ewen Huang*<sup>1</sup>; *Hahn Choo*<sup>1</sup>; *Peter K Liaw*<sup>1</sup>; <sup>1</sup>University of Tennessee; <sup>2</sup>Oak Ridge National Laboratory; <sup>3</sup>The University of British Columbia

The general deformation characteristics near a fatigue crack tip include a plastic zone in front of the crack tip and a plastic wake left behind, where the cyclic loading and fatigue crack growth lead to a compressive strain. The magnitude and distribution of the compressive strain in this plastic wake depend on the stress multiaxiality, material properties, and crack growth increment in each loading cycle. We compare lattice strain measurements by the neutron diffraction technique and simulations by an irreversible and hysteretic cohesive-interface model, which is developed to simulate the fatigue crack nucleation and growth. Crystal plasticity simulations have been conducted to relate the macroscopic and lattice strains. This method also allows us to quantitatively analyze the grain-orientation-dependent lattice strain. Excellent agreement between micromechanical models and neutron strain measurements has been reached. We also discuss implications on fatigue behavior of nanocrystalline or superplastic polycrystals where grain boundary plasticity dominates.

10:25 AM

**In-Situ Observations of Martensitic Transformation and Precipitation in Blast Resistant Steel:** *Xinghua Yu*<sup>1</sup>; Sudarsanam Babu<sup>1</sup>; John Lippold<sup>1</sup>;

<sup>1</sup>The Ohio State University

BlastAlloy 160 (BA160) is a Naval steel strengthened by lath martensite, Cu precipitates, and M<sub>2</sub>C carbides. Previous martensite morphology investigation shows that martensite sub-structure has a significant impact on the strength of BA160. In order to understand the martensitic transformation kinetic, time-resolved X-ray diffraction using synchrotron diffraction is performed at Spring-8 in Japan. The martensite morphology change during transformation is also in-situ observed laser scanning confocal microscope. Specimens are heated to different peak temperatures to achieve different prior austenite grain size. Results reveal prior austenite grain size has an influence on both martensitic transformation and amount of retained austenite. Cu Precipitates and carbides in steel are ex-situ characterized by 3D atom probe.

10:35 AM Break

10:45 AM Invited

**High P-T nanoMechanics and Molecular Physics:** *Yusheng Zhao*<sup>1</sup>; <sup>1</sup>Los Alamos National Laboratory

Nano-crystalline materials show drastic differences in physical properties compared with their bulk counterparts under high pressure (P) and temperature (T) conditions. We show a model to explain the observed contrasts between nano-metals and nano-ceramics, in the sense that the surface tension and compression of nanocrystals are the underlying cause of the differences in elasticity, yield strength, and work hardening and weakening. This nano-mechanics model has been tested by the comparative study of constitutive property and elastic modulus of nano-/micron- crystalline materials under high pressure and high temperature conditions. These studies provide fundamental understanding for metal/ceramics performances at nano-scales. Our study on molecular inclusion compounds consisting of host frameworks with guest hydrogen molecules trapped inside nano-scale cages reveals that a strong densification/pressurization effect that the nano-scale molecular cages may exert on the enclosed hydrogen molecules.

11:05 AM

**Fast X-Ray Microdiffraction and X-Ray Phase-Contrast Imaging Studies of Self-Propagating Reactions in Nanolayered Metals:** *Todd Hufnagel*<sup>1</sup>; Stephen Kelly<sup>1</sup>; Timothy Weihs<sup>1</sup>; Sara Barron<sup>1</sup>; Eric Dufresne<sup>2</sup>; Kamel Fezzaa<sup>2</sup>; <sup>1</sup>Johns Hopkins University; <sup>2</sup>Argonne National Laboratory

Self-propagating exothermic reactions in nanoscale metallic multilayers occur as localized (~100  $\mu\text{m}$  wide) reaction fronts that propagate at velocities on the order of 10 m/s. These reactions are extremely challenging to study because they require experimental techniques with excellent spatial (<100  $\mu\text{m}$ ) and temporal (<100  $\mu\text{s}$ ) resolution. Here we describe two complementary techniques. In time-resolved x-ray microdiffraction we focus a high flux (~10<sup>14</sup> ph/s) "pink" beam to a small (<10  $\mu\text{m}$ ) spot and use a fast shutter to produce a short (<75  $\mu\text{s}$ ) pulse of x-rays and collect the resulting diffraction patterns. With x-ray phase-contrast imaging we can examine the real-space structure of the reaction front with excellent spatial (~2  $\mu\text{m}$ ) and temporal (~0.5  $\mu\text{s}$ ) resolution. This research was supported by the U.S. Department of Energy, Office of Basic Energy Sciences, Division of Materials Sciences and Engineering under award DE-FG02-09ER46648.

11:20 AM

**Strain Heterogeneity in Deformed Polycrystals Inferred from Neutrons, Synchrotron, and Laboratory Diffraction Experiments -- Application to a Duplex Steel:** *Christophe Le Boullo*<sup>1</sup>; Olivier Castelnau<sup>2</sup>; Brigitte Bacroix<sup>1</sup>; Thierry Chauveau<sup>1</sup>; Marie-Hélène Mathon<sup>3</sup>; Veijo Honkimäki<sup>4</sup>; Thomas Buslaps<sup>4</sup>; Dominique Thiaudière<sup>5</sup>; <sup>1</sup>LPMTM; <sup>2</sup>Arts et Métiers ParisTech; <sup>3</sup>CEA-LLB; <sup>4</sup>ESRF; <sup>5</sup>Synchrotron SOLEIL

In order to investigate the local response of polycrystals, which is heterogeneous owing to elastic and plastic anisotropies of grains, and to validate mean- and full-field micromechanical models, we have performed elastic strain measurements using several diffraction techniques (neutrons, transmission and reflexion under synchrotron radiation, Laue

microdiffraction, and laboratory X-ray) during which the specimen was tensile deformed in-situ. Those techniques are providing different spatial and instrumental resolution, and also different gauge volumes that can range from cubic micrometers up to cubic centimeters. Application has been performed on a duplex steel (ferrite and austenite) as an example of two-phase high-strength polycrystals. The uncertainty and relevance of the different measurements will be discussed and compared with simulations based on an elasto-viscoplastic self-consistent model.

11:30 AM

**Mapping the Strain Distributions in Deformed Bulk Metallic Glasses Using Hard X-Ray Diffraction:** *Jozef Bednarcik*<sup>1</sup>; Hermann Franz<sup>1</sup>; Lianyi Chen<sup>2</sup>; Xiaodong Wang<sup>2</sup>; Jianzhong Jiang<sup>2</sup>; <sup>1</sup>Deutsches Elektronen Synchrotron DESY; <sup>2</sup>ICNSM, Zhejiang University and Laboratory of New-Structured Materials

Bulk metallic glasses (BMGs) represent relatively new class of materials which exhibit many interesting properties. Compared with crystalline counterparts, BMGs have some superior properties, such as high yield strength, hardness, large elastic limit, high fracture toughness and corrosion resistance, and hence are considered as promising engineering materials. It was recently demonstrated that X-ray diffraction utilizing high-energy photons can be used to measure the elastic strain under compression and tension. The main objective of this work was to follow the strain distribution within Cu-Zr-Al-Ti bulk metallic glass undergoing bend deformation using in-situ hard X-ray diffraction. The special emphasis was placed at the observation of differences between the strain distributions within Cu-Zr-Al-Ti bulk metallic glass when exposed to different levels of bending deformation. X-ray diffraction experiments using high-energy photons (100 keV) were performed at the BW5 wiggler beamline of DORIS III positron storage ring at DESY (Hamburg, Germany).

11:45 AM

**X-Ray Diffraction Analysis of the Dislocation Structure of Cu-Nb Interfaces:** *Gábor Csizsár*<sup>1</sup>; Amit Misra<sup>2</sup>; Tamás Ungár<sup>1</sup>; <sup>1</sup>Eötvös University Budapest; <sup>2</sup>Los Alamos National Laboratory

The Burgers vector population and dislocation densities are determined in strongly textured Cu-Nb multilayers by the method of X-ray line profile analysis. In a high-resolution diffractometer dedicated for line profile analysis the specimens are mounted on a crystal-goniometer. For each hkl reflection the samples are oriented in such a manner that always the major texture component is in reflection conditions. The strain part of line broadening is evaluated in terms of individual measured dislocation contrast factors. The Burgers vector population is evaluated by matching the measured and the theoretically calculated contrast factors. When the total specimen thickness is less than about a few micrometers, the prevailing Burgers vectors are either within the plane parallel to the interface of close to these directions.

11:55 AM

**Stress Field in Deformed Polycrystals at the Micron Scale:** *Johann Petit*<sup>1</sup>; *Olivier Castelnau*<sup>1</sup>; Michel Bornert<sup>2</sup>; Christophe Le Boullo<sup>3</sup>; Odile Robach<sup>4</sup>; Jean-Sébastien Micha<sup>4</sup>; Olivier Ulrich<sup>4</sup>; <sup>1</sup>PIMM-CNRS; <sup>2</sup>Unité de Recherche NAVIER; <sup>3</sup>LPMTM-CNRS; <sup>4</sup>CEA-Grenoble

The overall elastic and plastic straining of polycrystals leads to the build up of strong stress and strain heterogeneities inside and between grains. These heterogeneities have to be considered for many issues, e.g. onset of microplasticity, crack propagation, phase transformation, ... The white beam X-ray Laue microdiffraction technique under synchrotron radiation is in principle perfectly adapted for stress field characterizations in deformed polycrystals at the micron scale. The shape of the resulting Laue diffraction patterns reveals many features relative to the specimen deformation including the elastic strain of interest. We will present new results obtained during in situ tensile tests on tungsten (for which the stress field is expected to remain homogeneous upon incremental loading) and duplex steel (in which strong heterogeneities arise). The presentation will focus on a new data treatment method making use of state-of-the-art image processing and allowing reaching a stress accuracy adapted to micromechanical investigations.

12:10 PM

**Study of Microstrain Evolution during Creep of a Ferritic Superalloy:** *Shenyang Huang*<sup>1</sup>; Bjørn Clausen<sup>2</sup>; Donald Brown<sup>2</sup>; Zhenke Teng<sup>1</sup>; Gautam Ghosh<sup>3</sup>; Morris Fine<sup>3</sup>; Peter Liaw<sup>1</sup>; <sup>1</sup>University of Tennessee; <sup>2</sup>Los Alamos National Laboratory; <sup>3</sup>Northwestern University

In-situ neutron diffraction has been utilized to monitor the microstrain evolution during creep deformation of ferritic superalloys. The ferritic superalloy designed for ultra supercritical steam turbine applications at elevated temperatures was strengthened by a secondary phase of coherent coplanar ordered (Ni,Fe)Al B2-type precipitates. Isothermal creep experiments under constant loading were carried out at different stress levels for various compositions. The temporal evolutions of the elastic phase strain, plane-specific strain (intergranular strain), lattice misfit between the matrix and precipitates, and peak width as a representative of dislocation density were determined. Insights into the micromechanism of creep deformation were achieved with the microstructural information obtained by in-situ neutron diffraction measurements as well as scanning-electron microscopy and transmission-electron microscopy characterizations of grain boundaries, B2 precipitates, and dislocations.

12:20 PM

**EXAFS Study of Local Atomic Environment in Annealed and Quenched Fe-27.5 at.% Ga Single Crystals:** *Gavin Garside*<sup>1</sup>; Sivaraman Guruswamy<sup>1</sup>; <sup>1</sup>University of Utah

Extended x-ray absorption fine structure (EXAFS) measurements were made at the Advanced Photon Source at ANL on Fe-27.5 at % Ga single crystals that were long-term annealed and quenched. These EXAFS measurements were taken at the K-edges of Fe, and Ga to determine the Fe-Ga, Fe-Fe, and Ga-Ga atom distances and short range ordering pair correlations. The magnetoelastic coupling, the source of magnetostrictive strain, is sensitive to the interatomic spacing of the magnetic ion core. The measurements of local inter-atomic distances is therefore of interest to gain an improved understanding of how solutes influence magnetostriction in alpha-Fe-based alloys. Annealing was done at 1150 degree C for 70 days followed by quenching in water to room temperature. The paper presents estimated Fe-Fe, Fe-Ga and Ga-Ga near neighbor distances.

12:35 PM

**SANS to Evaluate Precipitate Morphology Degradation in Creep Exposed Single Crystal Nickel Base Superalloy:** *Jozef Zrnik*<sup>1</sup>; Pavel Strunz<sup>2</sup>; Alexander Epishin<sup>3</sup>; Thomas Link<sup>3</sup>; <sup>1</sup>Comtes FHT, Inc.; <sup>2</sup>Nuclear Physics Institute; <sup>3</sup>Technical University Berlin

Turbine blades in gas turbines, fabricated of Ni base superalloys, operate under the creep and creep-fatigue conditions. One of the main changes which appear in microstructure during creep exposure is the directional coarsening (rafting) of originally cubic gamma prime ( $\gamma'$ ) precipitates embedded in gamma ( $\gamma$ ) matrix. For residual lifetime estimation, it is desirable to have a non-destructive method which could reliably evaluate the progress in  $\gamma'$  degradation in dependence on exposure time and relate these changes to the magnitude of stress the blade is experiencing. The available literature indicates that necessary information can be obtained from the analysis of geometrical parameters of the  $\gamma'$  microstructure and  $\gamma/\gamma'$  misfit [1, 2]. Using the bulk sensitive small-angle neutron scattering (SANS), morphological changes of  $\gamma'$  phase resulting from the operation condition can be detected. SANS method [3] has proved to contribute successfully to the morphology assessment of  $\gamma'$  in nickel base superalloys [4]. The aim of this investigation was to evaluate the morphological changes of  $\gamma'$  in creep-exposed single-crystal Ni-base superalloy CMSX4 using SANS method and relate them to the various applied stress levels. The secondary aim of the experiment was to test a possibility to investigate the microstructural parameters using a new special sample design: a conic specimen. As a result of the diameter change along the longitudinal axis, a continuous change of applied stress magnitude acting during the creep test exists, which contributes substantially to  $\gamma'$  morphology modification and causes different microstructural change at different positions along the specimen.

12:50 PM Invited

**Investigation of Welding Residual Stresses Before and After Post-Weld Heat Treatment:** *Anna Paradowska*<sup>1</sup>; John W.H. Price<sup>2</sup>; Trevor R. Finlayson<sup>3</sup>; R. Ibrahim<sup>2</sup>; <sup>1</sup>ISIS, Rutherford Appleton Laboratory; <sup>2</sup>Monash University, Department of Mechanical Engineering; <sup>3</sup>The University of Melbourne, School of Physics

In welded structures residual stresses are formed primarily as the result of differential contractions which occur as the weld metal solidifies and cools to ambient temperature. RS have a significant effect on corrosion, fracture resistance, creep and corrosion/fatigue performance and a full understanding of these stresses is desirable. The aim of this paper is to investigate residual stresses in various weldments using the non-destructive neutron diffraction technique. This research is focused on characterization of the residual stress distribution: in the original weld and after conventional post-weld heat treatment. The focus of the measurements is on the values of the sub-surface strain/stress variations across the weld and through the thickness of the weld.

### **Pb-Free Solders and Other Materials for Emerging Interconnect and Packaging Technologies: Processing and Reliability Issues**

*Sponsored by:* The Minerals, Metals and Materials Society, TMS Electronic, Magnetic, and Photonic Materials Division, TMS: Electronic Packaging and Interconnection Materials Committee  
*Program Organizers:* Indranath Dutta, Washington State University; Darrel Frear, Freescale Semiconductor; Sung Kang, IBM; Eric Cotts, SUNY Binghamton; Laura Turbini, Research in Motion; Rajen Sidhu, Intel Corporation; John Osenbach, LSI Corporation; Albert Wu, National Central Univ, Taiwan; Tae-Kyu Lee, Cisco Systems

Thursday AM  
March 3, 2011

Room: 7B  
Location: San Diego Conv. Ctr

*Session Chairs:* Kejun Zeng, Texas Instruments Inc; Andre Lee, Michigan State University

8:30 AM Invited

**Impact of Isothermal Aging and Sn Grain Orientation on Long Term Reliability of SnAgCu Solder Interconnects in 5.0wt% NaCl Solution Environment:** *Tae-Kyu Lee*<sup>1</sup>; Bo Liu<sup>1</sup>; Bite Zhou<sup>2</sup>; Thomas R. Bieler<sup>2</sup>; Kuo-Chuan Liu<sup>1</sup>; <sup>1</sup>Cisco Systems, Inc.; <sup>2</sup>Michigan State University

Understanding the sensitivity of Pb-free solder joint reliability on various environmental conditions becomes a critical topic while deploying Pb-free products in various markets and applications. The work reported here concerns the impact of marine environment to SnPb and SnAgCu interconnects. Both SnPb and SnAgCu solder alloy wafer level packages with and without 5% NaCl salt spray pre-condition with various isothermal aging are thermal cycled to failure. These tests consistently show three interesting results. First, the corrosion path in SnAgCu exactly aligned with a preferred Sn grain orientation. Second, the salt spray test didn't degrade the lifetime of SnPb solder joints but reduces the life of SnAgCu. Third, salt spray applied solder joints after thermal aging show an even further degradation, which turns out more than 50%. The potential mechanisms leading to these results are presented and dependency of the degradation on different solder alloys are discussed.

8:55 AM

**In-Situ 2D X-Ray Study of Pb-Free Solder Joints and Next Generation Thermal Interface Material in Flip Chip Packages:** *Yan Li*<sup>1</sup>; Rahul Panat<sup>1</sup>; Bin Li<sup>1</sup>; Rose Mulligan<sup>1</sup>; Purushotham Kaushik Muthur Srinatha<sup>1</sup>; Arun Raman<sup>1</sup>; <sup>1</sup>Intel Corp

In-situ observations of the soldering process in microelectronic packages can reveal the effect of input process parameters on the joint formation. A hot stage was placed inside a 2D X-ray machine to perform in situ X-ray study at temperature as high as 300°C. This apparatus was employed to understand the root cause of corner thermal resistance degradation of a next generation

THURSDAY AM



thermal interface material after temperature cycle B stress. First level interconnect solder bump bridging during chip attach in a flip chip package with large die area substrate warpage was also studied. Lastly, the in-situ X-ray system was used to analyze second level interconnects ball grid array solder joint bridging in a large die package with integrated heat spreader during surface mounting solder reflow. By being able to study failures in-situ at high temperatures, a new dimension to the package failure analysis has been presented in this paper.

9:15 AM

**The Stability Window and Mechanical Properties of the Interfacial Intermetallic in Lead-Free Solder Joints:** *Keith Sweatman*<sup>1</sup>; Kazuhiro Nogita<sup>2</sup>; Hideaki Tsukamoto<sup>2</sup>; Tetsuro Nishimura<sup>1</sup>; <sup>1</sup>Nihon Superior Co., Ltd.; <sup>2</sup>University of Queensland

The trend to copper UBM for lead-free area array packages subjected to drop impact means that the properties of the intermetallic that forms at the solder/copper interface are major determinants of joint reliability. The transformation of the Cu<sub>6</sub>Sn<sub>5</sub> from the close packed hexagonal  $\eta$  to the monoclinic  $\eta'$  at 186°C can reduce the impact resistance and long term reliability of the solder joint. In this paper the authors will report new studies on the effect of Ni over the range 0-9% on the stabilization of the  $\eta$  phase. The distribution of the Ni in the Cu<sub>6</sub>Sn<sub>5</sub> and its crystal structure, lattice dimensions and thermal stability have been studied using SEM/EDS, TEM/EDS, synchrotron micro-XRF mapping techniques, synchrotron XRD, DSC and dilatometry. The mechanical properties of the intermetallic as a function of nickel content have been measured by nanoindentation. The data collected provides basis for lead-free alloy formulation for area array attachment.

9:35 AM

**Effect of Temperature and Strain Rate on Flow and Fracture Behavior of Pb-Free Solder Joints:** *Andre Lee*<sup>1</sup>; Deep Choudhuri<sup>1</sup>; K. Subramanian<sup>1</sup>; <sup>1</sup>Michigan State University

Isothermal mechanical characterization of Pb-free solder joints was carried out at various temperatures between -55C and 150C at strain rates ranging from 0.001 s<sup>-1</sup> to 0.1 s<sup>-1</sup>. Grain boundary sliding was the dominant mode of deformation at high temperatures and low strain rates, where as debonding at intermetallic compounds (IMC)/ solder interfaces was dominant at low temperatures and high strain rates. Shear banding was noted at the intermediate temperatures and strain rates. The extents of overlap between these modes of deformation depend on both temperatures and strain rates. Higher strain rates at a given temperature resulted in a mode of deformation representative at a lower temperature with a slower strain rate. These findings are significant with respect to thermomechanical fatigue reliability evaluation by accelerated tests since the range of temperatures and ramp rates encountered during service encompasses similar transitions between different modes of deformation.

9:55 AM

**Printing of Functionally Graded, Pb-Free Braze Layers for Use in High Temperature Die Attach Applications:** *Jared McCoppin*<sup>1</sup>; Thomas Reitz<sup>2</sup>; Ryan Miller<sup>2</sup>; *Henry Young*<sup>1</sup>; <sup>1</sup>Wright State University; <sup>2</sup>Wright Patterson Air Force Base

Functional gradation of a die-attach has the potential to mitigate thermal stress in high temperature environments. Our current research uses an aerosol-based printing system to print functionally graded, Pb-free die attach layers.

10:15 AM Break

10:25 AM

**Joule Heating Effect Caused by Continuous Al Trace Damage under Electromigration on Physical and Statistical Failure Analysis of Solder Joints:** *Jung Kyu Han*<sup>1</sup>; Daechul Choi<sup>1</sup>; King-Ning Tu<sup>1</sup>; <sup>1</sup>University of California Los Angeles

In reliability concerns of flip-chip Pb-free solder joint, under-bump-metallization structure has a strong impact. To investigate physical failure mode and mean-time-to-failure of different under-bump-metallization structure, three different test vehicles were used: Pb-free solder with thick Cu

(7.5 um), e-less Ni (5 um), and thin Cu (0.5 um) under-bump-metallization. In an accelerated test condition ( $> 7.5 \times 10^3$  A/cm<sup>2</sup>), Al trace also has continuous damage with time while solder joint forms void at the interface. In order to correlate Joule heating effect with physical and statistical failure analysis, temperature change of the chip and resistance change of the solder was measured by in-situ monitoring. Joule heating due to Al trace finally leads to the melting of solder and affects the mean-time-to-failure. Focused-ion-beam images give good understanding of the behavior.

10:45 AM

**Erosion Behavior of Stainless Steels in Molten Lead-Free Solder:** *Hiroshi Nishikawa*<sup>1</sup>; Songai Kang<sup>1</sup>; Tadashi Takemoto<sup>1</sup>; <sup>1</sup>Osaka University

The dissolution of iron and stainless steel during soldering presents a serious issue for manufacturing equipment such as wave soldering baths and soldering-iron tips. Severe erosion damage of stainless steel wave solder equipment has been encountered in operation. Therefore, it is necessary to study the erosion mechanism of stainless steel by molten lead-free solders. A method for evaluating the erosion depth of stainless steel by molten lead-free solder has been investigated using micro-focus X-ray systems for fluoroscopic and computed tomography (CT) to establish a method for measuring the maximum erosion depth. In this study, the effect of immersion test parameters and surface condition of the test sample on the erosion behavior of 304 and 316 stainless steels into a molten solder was investigated and the interface reaction between the lead-free solder and stainless steel was studied.

11:05 AM

**Influence of Solder Microstructure and Cu<sub>6</sub>Sn<sub>5</sub> Interfacial Intermetallic on Mechanical Shock Resistance of Sn-rich Solders:** *Kyle Yazzie*<sup>1</sup>; Huiyang Fei<sup>1</sup>; Hanqing Jiang<sup>1</sup>; Nikhilesh Chawla<sup>1</sup>; <sup>1</sup>Arizona State University

Pb-free solder alloys are routinely subjected to mechanical shock and drop conditions in service. While these solder alloys are susceptible to dynamic loading, a fundamental understanding of mechanical shock is lacking. Quantifying the contributions of intermetallic layer thickness and solder microstructure to the mechanical shock behavior of the solder specimen is extremely important and needs to be studied. In this study, dynamic strength of Sn-3.9Ag-0.7Cu solder joints was quantified as a function of strain rate, solder microstructure, and intermetallic layer thickness. The morphology and distribution of intermetallic precipitates in Pb-free solder joints was observed using X-ray tomography and radiography. Digital image correlation was used in conjunction with high-speed video, and nanoindentation of Sn grains in solder joints, to measure constitutive data for high-fidelity finite element models. The mechanisms for deformation and the interplay between solder-controlled and intermetallic controlled fracture will be discussed.

11:25 AM

**Interdiffusion of Aluminum/Germanium Bi-Layer Thin Film:** *Chao-Nan Yeh*<sup>1</sup>; Kewin Yung<sup>1</sup>; Albert T. Wu<sup>1</sup>; <sup>1</sup>National Central University

Al/Ge bi-layer thin film is a possible candidate for hermetic sealing in the application of MEMS devices. Al/Ge thin film was deposited on Si substrates by sputter. The interdiffusion coefficient of Al/Ge film that was annealed at 200°C, 300°C, 400°C for various duration of times was calculated by Boltzmann-Matano analysis with depth profiling distributions. The diffusivities have the values in the range of 10<sup>-22</sup>, 10<sup>-21</sup>, 10<sup>-20</sup> (m<sup>2</sup>/s) for the found that the diffusivity decreased as the annealing time heat treatment temperatures of 200°C, 300°C, and 400°C, respectively. We increased annealing times at the same annealing temperature. The depth profile showed layer-exchange phenomenon for the samples that were annealed at 300°C for 10 days. Two glass substrates were bonded by Al/Ge thin film along the edges of the substrates and immersed in red ink for several days, and the results showed that Al/Ge film provides good hermetic sealing property.

11:45 AM

**Influence of Dynamic Recovery and Recrystallization on the Fatigue Fracture Mechanics of Lead-Free Solder Joint:** *Huili Xu*<sup>1</sup>; Woong Ho Bang<sup>1</sup>; Choong-un Kim<sup>1</sup>; Tae-Kyu Lee<sup>2</sup>; Hongtao Ma<sup>2</sup>; Kuo-Chuan Liu<sup>2</sup>; <sup>1</sup>University of Texas Arlington; <sup>2</sup>Cisco Systems, Inc.

The mechanism of solder joint failure under various fatigue conditions has emerged as one of the critical research subjects in device packaging industry. While recent studies address a few failure mechanisms, it is not yet clear how fatigue failure interacts with dynamic microstructural changes possible in solder joint. With low homologous temperature, solder has an ability of releasing the fatigue damage, yet its influence on the failure mechanism is not well understood. Utilizing high cycle bending and shear fatigue tester, we have conducted series of investigations to better understand such mechanism. This study reveals that dynamic recovery is the most active form of damage relaxation at room temperature while recrystallization is at higher temperature and that such mechanism is effective only when their kinetics can keep up with the rate of damage accumulation. This paper presents our findings along with mechanistic analysis of fatigue fracture process.

### **Phase Stability, Phase Transformations, and Reactive Phase Formation in Electronic Materials X: Phase Equilibria and Transformation of the Pb-Free Solders and Thermoelectric Materials**

*Sponsored by:* The Minerals, Metals and Materials Society, TMS Electronic, Magnetic, and Photonic Materials Division, TMS: Alloy Phases Committee

*Program Organizers:* Chih-Ming Chen, National Chung Hsing University; Hans Flandorfer, University of Vienna; Sinn-Wen Chen, National Tsing Hua University; Jae-ho Lee, Hongik University; Yee-Wen Yen, National Taiwan Univ of Science & Tech; Clemens Schmetterer, TU Bergakademie Freiberg; Ikuo Ohnuma, Tohoku University; Chao-Hong Wang, National Chung Cheng University

Thursday AM  
March 3, 2011

Room: 7A  
Location: San Diego Conv. Ctr

*Session Chairs:* Hyuck Mo Lee, Korea Advanced Institute of Science and Technology; Albert T. Wu, National Central University

8:30 AM Invited

**Ni-Sb-Sn Alloys as Possible High-Temperature Solders: Phase Equilibria and Thermochemistry:** *Herbert Ipser*<sup>1</sup>; Ratikant Mishra<sup>1</sup>; <sup>1</sup>University of Vienna

Ternary Sb-Sn alloys are being considered as high-temperature solders where the liquidus temperature can be adjusted by varying amounts of a third element. Therefore, the ternary Ni-Sb-Sn phase diagram, with particular emphasis on the Sn-rich corner, was investigated by X-ray powder diffraction, electron microprobe analysis and thermal analyses. A number of isothermal sections, different isopleths, as well as the liquidus projection will be presented. Partial pressures of Sb were determined by an isopiestic vapor pressure method along three sections through the ternary system. From these measurements it was possible to derive partial Gibbs energies (i.e. thermodynamic activities) of Sb, and from their temperature dependence the other partial thermodynamic properties could be obtained. All these experimental data will provide an input for a CALPHAD-type optimization of the ternary Ni-Sb-Sn system.

8:55 AM Invited

**The Effect of Sb Addition on Sn-Based Alloys for High-T Lead-Free Solders: An Investigation of the Ag-Sb-Sn System:** *Simona Delsante*<sup>1</sup>; Dajian Li<sup>1</sup>; Gabriella Borzone<sup>1</sup>; Andy Watson<sup>2</sup>; <sup>1</sup>University of Genoa; <sup>2</sup>University of Leeds

Today there is a renewed interest in alloys belonging to Sb-Sn-X (X = Cu, Ag, Bi) ternary systems and their phase equilibria, phase transformation and thermodynamic properties because of their possible use as high temperature

lead-free solders in the electronic industry. The integral mixing enthalpy of Ag-Sb-Sn liquid alloys has been measured along five different sections (25Ag75Sn, 50Ag50Sn, 30Sb70Sn, 50Sb50Sn and 70Sb30Sn) at 530, 600 and 630°C using a high temperature Calvet calorimeter by dropping pure elements (Ag or Sb) in the binary liquid bath. The ternary extrapolation models of Kohler, Muggianu and Toop were used to calculate the integral enthalpy of mixing and to compare measured and extrapolated values. Selected ternary alloys have been prepared for a thermal investigations by using a differential scanning calorimeter at different heating/cooling rate in order to clarify the temperature of the invariant reactions and the crystallization path.

9:20 AM

**Phase Field Simulations of Growth and Coarsening in the Interdiffusion Zone of Lead Free Ag-Cu-Sn/Cu Joints:** *Nele Moelans*<sup>1</sup>; <sup>1</sup>Katholieke Universiteit Leuven, Belgium

Solute transport and the growth of intermetallic layers, precipitates and voids in the interdiffusion zone of solder joints is highly affected by temperature and solder and substrate compositions, but also by the current size, shape and arrangement of the grains and precipitates. A quantitative phase-field model for multi-component alloys is developed that distinguishes different phases and grain orientations and considers the effect of both bulk and grain boundary diffusion. CALPHAD expressions for the bulk Gibbs energy and diffusion mobilities of the ternary Ag-Cu-Sn system are directly used in the phase-field model. The effect of temperature, composition and grain and precipitate size and spatial distribution on the growth and coarsening of intermetallic layers and precipitates in polycrystalline solder joints are studied by means of phase-field simulations. This work fits within the activities of COST MP0602 "Advanced Solder Materials for High Temperature Application".

9:35 AM

**Phase Equilibria in the Au-Ag-X (X= Sn and Zn) Systems:** *Yoshikazu Takaku*<sup>1</sup>; Eri Sato<sup>1</sup>; Ikuo Ohnuma<sup>1</sup>; Toshihiro Omori<sup>1</sup>; Ryosuke Kainuma<sup>1</sup>; Kiyohito Ishida<sup>1</sup>; <sup>1</sup>Tohoku University

Au as well as Ni is usually plated on the surface of the Cu substrate to prevent it from being oxidized due to atmospheric exposure. Therefore, the equilibrium relationship between Au and Pb-free solders, such as Sn-Ag-Cu and Sn-Zn-Bi alloys, are of practical importance. In this study, the phase equilibria of the Au-Ag-X (X=Sn and Zn) systems were investigated experimentally. Making use of experimental results, the thermodynamic assessment was carried out based on the CALPHAD (Calculation of Phase Diagrams) method. In the Au-Ag-Sn system, experimental results have shown that the stability of the  $\epsilon$ -Ag<sub>3</sub>Sn is enhanced by Au, which was taken into account in the thermodynamic evaluation. In the Au-Ag-Zn system, an A2/B2 order-disorder transition boundary was determined. Now, 11 elements, namely, Sn, Ag, Cu, Pb, Sb, Bi, Zn, In, Ni, Al and Au, are available in the thermodynamic database ADAMIS (Alloy Database for Micro-Solders), which we developed in 1999.

9:50 AM

**Thermodynamic Modeling of the Ag-Cu-In-Sn System:** *Wojciech Gierlotka*<sup>1</sup>; Kai-chien Zhang<sup>1</sup>; <sup>1</sup>YuanZe University

The binary Cu-Sn system is the basis for various emerging Pb-free solders and for most of the important solder-related materials systems. With the increasing demand for Pb-free solders and more advanced applications of soldering technology in electronic products, the Cu-Sn system has become one of the most important material systems. The ternary Ag - Cu - Sn system is promising replacement of classic Pb-Sn solder due to favorable solder ability and wetting properties. Unfortunately, the temperature of melting of ternary Ag - Cu - Sn eutectic (217oC) is much higher than lead solder eutectic (183oC). Some other elements, like In or Bi can decrease temperature of the eutectic point. The Calphad method has been used for thermodynamic modeling of the Ag - Cu - Sn - In quaternary system. The set of thermodynamic parameters were obtained and good agreement between experimental results and calculation was found.

THURSDAY AM

#### 10:05 AM Break

#### 10:20 AM Invited

**High Temperature Lead-Free Solder: Phase Relations in (Cu,Ni)-Sn-Zn:** *Clemens Schmetterer*<sup>1</sup>; Hans Flandorfer<sup>2</sup>; Divakar Rajamohan<sup>2</sup>; Herbert Ipser<sup>2</sup>; <sup>1</sup>TU Bergakademie Freiberg; <sup>2</sup>University of Vienna

The issue of lead-free high temperature solders with melting temperatures > 230 °C, which are required for e.g. die-attach, chip scale package and multi-chip modelling, remains unsolved. Alloys of the systems Cu-Sn-Zn and Ni-Sn-Zn have been contemplated as promising solders. Phase diagrams of these systems provide detailed information to the solidification behavior and formation of intermetallic compounds, which is necessary for the control of the microstructure of alloys and alloy interfaces. The systems Cu-Zn, Ni-Zn and Ni-Sn-Zn have been investigated by means of XRD, DTA and metallography including EPMA. In the binary systems significant changes of the phase relations compared to previous versions were found. The ternary system has been investigated above 700 °C; the phase relations have been represented as isothermal and vertical sections, as well as a liquidus surface and reaction scheme. Furthermore, the crystal structures of three ternary compounds were determined and compared to neighboring phases.

#### 10:45 AM

**Sn-Bi-Te Phase Equilibria and Interfacial Reactions in the Sn/Bi<sub>2</sub>Te<sub>3</sub> Couples:** Chen-nan Chiu<sup>1</sup>; *Chia-ming Hsu*<sup>1</sup>; Sinn-wen Chen<sup>1</sup>; <sup>1</sup>National Tsing Hua University

This study investigates the phase equilibria of the ternary Sn-Bi-Te system and interfacial reactions in the Sn/Bi<sub>2</sub>Te<sub>3</sub> reaction couples. The Bi<sub>2</sub>Te<sub>3</sub> is an important thermoelectric compound, and Sn is the primary constituent element of electronic solders. Various Sn-Bi-Te alloys were prepared and equilibrated at 160 and 500°C, and the equilibrium phases were determined. In addition to the already known SnBi<sub>2</sub>Te<sub>4</sub> and SnBi<sub>4</sub>Te<sub>7</sub> compounds, three new ternary compounds were found in the Sn-Bi-Te system. Interfacial reactions between Sn and Bi<sub>2</sub>Te<sub>3</sub> at 150 and 160°C were studied. A Sn-Bi liquid layer was formed between Sn and Bi<sub>2</sub>Te<sub>3</sub> at 150 and 160°C. The reaction path is Sn/L/SnTe+L/SnTe+Bi/Bi<sub>2</sub>Te<sub>3</sub>, and could be well illustrated with the determined isothermal Sn-Bi-Te isothermal section.

#### 11:00 AM

**Microstructures and Liquidus Projection of the Ternary Ag-Sb-Te System:** *Hsin-jay Wu*<sup>1</sup>; Sinn-wen Chen<sup>1</sup>; <sup>1</sup>National Tsing Hua University

Ag-Sb-Te alloys are important for thermoelectric applications. Fifty-one Ag-Sb-Te ternary alloys were prepared, and their primary solidification phases were analyzed. The liquidus troughs of the liquidus projection of the ternary Ag-Sb-Te system are determined based on the experimental results and the phase diagrams of the three binary constituent systems. There are thirteen primary solidification phase regions. In addition to the three terminal solid solution phases and nine binary compounds, there is one ternary compound, AgSbTe<sub>2</sub>. A unique microstructure with bright spherical phases uniformly dispersed in a matrix caused by a miscibility gap in the liquid phase is found in the  $\gamma$ -Ag<sub>2</sub>Te primary solidification phase regime. A very fine microstructure with nanometer size Ag<sub>2</sub>Te is also observed, resulting from the class I reaction, liquid =  $\delta$  + Ag<sub>2</sub>Te + AgSbTe<sub>2</sub>, at 496.5°C, and the liquid composition of Ag-40.0at%Sb-36.0at%Te.

#### 11:15 AM

**A Study on the Phase Transformation and Microstructure Evolution of Sputtered Bi-Te Thermoelectric Films with Different Compositions during Post-Annealing:** *Minsub Oh*<sup>1</sup>; Seong-jae Jeon<sup>1</sup>; Seungmin Hyun<sup>2</sup>; Hoo-jeong Lee<sup>1</sup>; <sup>1</sup>Sungkyunkwan University; <sup>2</sup>Korea Institute of Machinery and Materials

This study examined the fundamental aspect of the phase transformation and the microstructure evolution of Bi-Te films during post-annealing. Bi-Te Films of various compositions were grown by co-sputtering deposition and annealed at 200°C for different durations. We examined the microstructure of the films using X-ray diffraction and transmission electron microscopy and also measured the electrical and thermoelectric properties. The effects of the post-annealing on the thermoelectric properties and their variations with the film composition were found remarkable: The film with a composition

close to that of Bi<sub>2</sub>Te<sub>3</sub> shows the very sensitive improvement of the Seebeck coefficient (56  $\mu$ V/K to 250  $\mu$ V/K) with the annealing while the films with a composition away from that of Bi<sub>2</sub>Te<sub>3</sub> show little changes in Seebeck coefficient. Our careful characterization using XRD and TEM disclosed that such interesting behavior is a direct consequence of a phase transformation involving a metastable phase and the stable Bi<sub>2</sub>Te<sub>3</sub> phase.

#### 11:30 AM

**Fabrication Process of Half-Heusler Compound TiNiSn Based on the Solid-Liquid Reaction:** *Shinya Otani*<sup>1</sup>; Yoshisato Kimura<sup>1</sup>; Yaw-Wang Chai<sup>1</sup>; Yoshinao Mishima<sup>1</sup>; <sup>1</sup>Tokyo Institute of Technology

Half-Heusler compound TiNiSn is one of the most promising thermoelectric materials which can be used to directly convert waste heat into clean electric energy at around 1000K. The objective of this work is to establish the basis of new fabrication process for both n-type TiNiSn and p-type doped Ti(Ni,Co)Sn. We have proposed to apply the solid(TiNi)/liquid(Sn) reaction for the powder metallurgy process focusing on the low melting of Sn. The formation behavior of Ti(Ni,Co)Sn phase was observed using diffusion couples. We have found that Ti(Ni,Co)Sn phase layer forms at the Ti(Ni,Co)(S)/Sn(L) interface not only as continuous layers but also as faceted grains growing toward the liquid Sn phase. Nearly single-phase Ti(Ni,Co)Sn alloys can be fabricated by the proposed process which is based on the reactive sintering between Ti(Ni,Co) and Sn powders, where Ti(Ni,Co) powders with averaged grain size of 30 $\mu$ m were prepared by gas atomization.

#### 11:45 AM

**Formation of Intermetallic Compounds between Lead-free Solder Systems and Thermoelectric Materials:** *Tai-Yin Lin*<sup>1</sup>; Chien-Neng Liao<sup>2</sup>; Albert Wu<sup>1</sup>; <sup>1</sup>National Central University; <sup>2</sup>National Tsing Hua University

SnTe intermetallic compound rapidly formed at the interfaces between p-type bismuth telluride (Bi<sub>0.5</sub>Sb<sub>1.5</sub>Te<sub>3</sub>) thermoelectric materials and lead-free solders. The intermetallic compound affects the mechanical and electrical properties of the joints. Different lead-free solder alloys, Sn-3.5Ag, Sn-3Ag-0.5Cu, Sn-0.7Cu, were used. Bi<sub>0.5</sub>Sb<sub>1.5</sub>Te<sub>3</sub> slices were immersed in the molten solder baths when the reaction temperature was at 250°C for various duration of time. The results suggested that the joints of Sn-Ag solder had thinner interfacial compounds than those of Sn-Cu and Sn-Ag-Cu solders. Furthermore, the existence of antimony in p-type thermoelements affected the growth rate of the interfacial compounds. Solid state aging was conducted to investigate the stability of the intermetallic compound. Electroless nickel is plated at the interfaces to serve as diffusion barrier. The results could provide the understanding of the growth kinetics of the intermetallic compounds in the thermoelectric material systems.

### Physical and Mechanical Metallurgy of Shape Memory Alloys for Actuator Applications: Applications of Shape Memory Alloys

*Sponsored by:* The Minerals, Metals and Materials Society  
*Program Organizers:* S. Raj, NASA Glenn Research Center; Raj Vaidyanathan, University of Central Florida; Ibrahim Karaman, Texas A&M University; Ronald Noebe, NASA Glenn Research Center; Frederick Calkins, The Boeing Company; Shuichi Miyazaki, Institute of Materials Science, University of Tsukuba

Thursday AM  
March 3, 2011

Room: 11B  
Location: San Diego Conv. Ctr

*Session Chairs:* F. Calkins, The Boeing Company; Santo Padula II, NASA Glenn Research Center

#### 8:30 AM Invited

**Shape Memory Actuation: Pitfalls and Opportunities:** *Tom Duerig*<sup>1</sup>; <sup>1</sup>Nitinol Devices and Components

More than 50 years after the discovery of shape memory alloys, and after investments of millions of dollars, there are very few successful examples of



using the effect to perform mechanical work. Much of the reason for this is simply the unrealistic expectations that are created once engineers first see a metal that “magically” changes shape with temperature, or sees a nitinol spring effortlessly lift a heavy weight. These disappointments can be almost invariably attributed to just a few technical issues. This presentation will present a few hypothetical engineering examples that highlight some of these commonly encountered pitfalls. It discusses potential solutions when available, but is also intended to help engineers recognize when memory alloys are simply not the right solution.

#### 8:50 AM Invited

**Selected Applications of Aeropropulsion Actuation and Shape Control Devices Using HTSMAs:** *Todd Quackenbush*<sup>1</sup>; Robert McKillip<sup>1</sup>; <sup>1</sup>Continuum Dynamics, Inc.

Recent research has seen the relatively rapid development of High Temperature Shape Memory Alloys (HTSMAs), materials that combine useful work output with transition temperatures well in excess of the range of typical binary NiTi SMAs. The proposed paper will describe recent demonstration applications of HTSMAs in devices representative of mechanisms useful for a variety of aeropropulsion applications. The work to date has chiefly featured application of Pt-doped NiTi alloys in wire form, though some data on Pd- and Hf-doped alloys will also be presented. The paper will describe bench top and wind tunnel experiments of demonstration devices employing HTSMA wire actuators. The test results validate operation at 300+ C and document the force and strain capability of the new alloys. Ongoing and projected work in pertinent areas will also be described.

#### 9:10 AM

**Optimization of Ferromagnetic Shape Memory Alloys for Strain Detection:** *Terryl Wallace*<sup>1</sup>; John Newman<sup>1</sup>; William Leser<sup>2</sup>; Patrick Leser<sup>2</sup>; Michael Horne<sup>2</sup>; <sup>1</sup>NASA Langley Research Center; <sup>2</sup>North Carolina State University

The safety of aerospace vehicles is largely dependent on the ability of modern nondestructive evaluation (NDE) tools to detect structural damage before it reaches a critical size. However, existing NDE technologies are inherently limited by the physical response of the structural material being inspected and are therefore not generally effective at the identification of small discontinuities, making the detection of incipient damage difficult. One innovative solution to this problem is to add particles or coatings of a second material with an enhanced NDE response to damage. Ferromagnetic shape-memory alloys (FSMAs) are an ideal material for this application as they undergo a uniform and repeatable change in both magnetic properties and crystallographic structure (martensitic transformation) when subjected to strain and/or temperature changes which can be detected using conventional NDE techniques. In this study, the NDE response of a FSMA as a function of composition and processing was investigated.

#### 9:25 AM

**Fabrication and Characterization of Porous Meta-Magnetic Shape Memory Alloys:** *James Monroe*<sup>1</sup>; Josue Perez<sup>1</sup>; Ibrahim Karaman<sup>1</sup>; Kohei Ito<sup>2</sup>; Ryosuke Kainuma<sup>2</sup>; <sup>1</sup>Texas A&M University; <sup>2</sup>Tohoku University

NiMn based meta-magnetic shape memory alloys (MMSMAs) exhibit reversible magnetic field induced martensitic phase transformation due to the differences between the austenite and martensite magnetic saturation levels. Most mechanical experimentation on these alloys has been confined to single crystals due to the low fracture toughness caused by intergranular incompatibility. Powder metallurgy techniques, such as pressureless and spark plasma sintering, have been used on NiCoMnSn to introduce small pores between grains that relax the geometric constraints improving both the toughness and shape memory recovery. Introducing pores can also make these alloys attractive for micropump and magnetocaloric applications. Space holders and Ni43Co7Mn39Sn11 pre-alloyed powders are used to create a bi-modal pore size distribution with small pores <50µm to improve ductility and large interconnected pores 300-500µm to allow the transport of fluids. The effects of porosity and processing on the MMSMA foam's magnetic, thermal and mechanical response are then characterized.

#### 9:40 AM

**New Concepts for Shape Memory Actuator Systems:** *Sven Langbein*<sup>1</sup>; Konstantin Lygin<sup>1</sup>; Tim Sadek<sup>1</sup>; <sup>1</sup>Ruhr University Bochum

The existing actuator systems based on shape memory alloys (SMA) are characterized mainly by the alignment to specific applications. The adoption of the solutions for other applications is admitted in only a few cases. In order to improve the flexibility and the critical properties of actuators that are based on SMA, different kinds of concepts can be found. Beyond the conventional form of an actuator there is the possibility to create integrated or adaptive shape memory actuator systems for example by using agonist-antagonist principle or other adaptive resetting principles. Another emphasizing feature of SMAs is their potential to produce different functional effects, for example thermal shape memory or superelasticity, in one component. Separated from the former point of view a new perspective with extreme integral and standardized set up is opened up. The aim of this study is to show and to analyze such integrated and adaptive SMA components.

#### 9:55 AM Break

#### 10:05 AM Invited

**A Hyper-Elastic Thin Film Nitinol Flow Diverter for Brain Aneurysms:** *Greg Carman*<sup>1</sup>; Y.J. Chun<sup>1</sup>; K.P. Mohanchandra<sup>1</sup>; D. Levi<sup>1</sup>; C. Kealey<sup>1</sup>; C.S. Hur<sup>1</sup>; D. DiCarlo<sup>1</sup>; F. Vinuela<sup>1</sup>; <sup>1</sup>UCLA

This presentation describes the fabrication of a hyperelastic thin film (~5 microns) Nitinol material attached to a stent for use a flow diverter in the treatment of brain aneurysms. The thin film Nitinol is sputter deposited with transformation temperatures at or near body temperature (37C). The thin film Nitinol is micromachined using a lift off method to produce a film containing fenestrations of different sizes. The geometry of the fenestrations are chosen with a finite element model to produce a film providing a 400% recoverable elongation. The film is attached to a commercially available stent and tested both in vitro and in vivo. Particle image velocimetry data demonstrate that the flow diverter dramatically reduces the flow into a simulated aneurysm sac. In vivo data using a swine with surgically created aneurysms demonstrate occlusion of the aneurysm sac within as little as 2 minutes.

#### 10:25 AM

**Development of a SMA-Based Drive Unit for Prehension Orthoses to Support Disabled People:** *Yukiharu Yoshimi*<sup>1</sup>; Shunji Moromugi<sup>2</sup>; Kazuhiro Kitamura<sup>2</sup>; Tsunaki Ikeda<sup>2</sup>; Takakazu Ishimatsu<sup>2</sup>; <sup>1</sup>Yoshimi, Inc.; <sup>2</sup>Nagasaki University; <sup>3</sup>Aichi University of Education

Most conventional assistive devices use hydraulic motors or pneumatic rams in order to assist the human bodily motion. Their structures are robotic and mechanical, making the devices heavy and tricky to put on. We believed by replacing the motor, a widely used traditional driving source, with shape-memory alloy, we can utilize shape-memory alloy's super-elastic property and shape memory property to improve assistive devices and create a more silent, compact device that allows more natural movements. Devices that use super-elastic material operate according to the strength applied by the user. This makes the device very safe. The other characteristic of shape-memory alloy, which is its shape memory property, is activated by electrical heating. This means operation speed can be adjusted by controlling the current.

#### 10:40 AM

**Antagonistic SMA Actuator with Bowden Cable Housing for Orthosis Systems:** *Hyung-Min Son*<sup>1</sup>; Dong-Hyun Jeong<sup>1</sup>; Yun-Jung Lee<sup>1</sup>; <sup>1</sup>Kyungpook National Univ.

This paper proposes an orthosis system driven by a new antagonistic SMA actuator with bowden cable housing. Many attempts on the actuator of orthosis have been researched to overcome the limitation of electric motor-driven orthosis which is usually bulky and heavy. In contrast to conventional approaches, the SMA actuator has attractive features such as light weight, high power density, and silent actuation. In terms of the mechanical configuration, there have been winding-type, weaving-type, straight-line-type, coil-type, and bowden-cable-type actuators. Among these alternatives of the SMA actuation, the winding-type is superior with respect to force generation, amount of displacement within a restricted volume. The mechanical design

including new winding method of the SMA wire and control system are investigated in this study. The proposed SMA actuator is applied to an arm orthosis and its performance is verified through experiments.

**10:55 AM**

**Modeling of Improved Frequency Shape Memory Alloy Actuation Structures:** Aaron Stebner<sup>1</sup>; James Mabe<sup>2</sup>; Joseph Kreuger<sup>1</sup>; Frederick Calkins<sup>2</sup>; L. Catherine Brinson<sup>1</sup>; <sup>1</sup>Northwestern University; <sup>2</sup>The Boeing Company

While SMA actuators have proven a successful means for creating adaptive aerospace structures in many demonstrations, including live flight tests, maximum operational frequencies have been identified as a property that could inhibit their commercial implementation in some circumstances. The maximum cyclic frequency of aerospace actuation structures is primarily limited by cooling time, thus several approaches to increase the surface area and reduce the mass of existing actuator forms are being examined. To understand these approaches and enhance their design processes, actuator performance is being modeled using a 3D SMA constitutive law that has been developed and implemented into ABAQUS via a user subroutine. The resulting characterization of the work capability-cooling time relationships of the different approaches is presented.

**11:10 AM**

**Control Loops of Shape Memory Actuators by Detection of the Electrical Resistance:** Horst Meier<sup>1</sup>; Alexander Czechowicz<sup>1</sup>; <sup>1</sup>Ruhr-University Bochum

Due to their ability to change into a previously imprinted actual shape through the means of thermal and electrical activation, shape memory alloys (SMA) are suitable as actuators. To apply these smart materials to a wide range of industrial applications, a simple method of controlling the actuator effect is required. The detection of inner electrical resistance allows to gauge the actuator's movement. By usage of a microcontroller a smart system without any hardware sensors can be realized. Changing outer boundary conditions and the material fatigue (affecting the control loop) can be compensated by software. The paper gives an overview about different controlling methods for SMA-actuators, experiments concerning the resistance behaviour of SMA and the development of automotive actuator systems using a resistance control feedback signal.

**11:25 AM**

**Computer-Aided Development and Simulation Tools for Shape Memory Actuator Systems:** Horst Meier<sup>1</sup>; Alexander Czechowicz<sup>1</sup>; <sup>1</sup>Ruhr-University Bochum

This paper deals with the dynamic properties of SMA-actuators (Shape Memory Alloy) -characterized by their rate of heating and cooling procedures- that today can only be described insufficiently for different boundary conditions. Based on an analysis of energy fluxes into and out of the actuator, a numerical model, implemented in MATLAB/SIMULINK is presented. Besides the fluxes, the time variable parameters like the latent heat of transformation or the influence of stress on the transformation temperatures are also included in the model. These parameters, depending on the actuator-geometry and temperature, the fraction of martensite and the environmental conditions are considered in the simulation in real time. The SMA-wire based actuation system, can be configured by drag and drop tools and finally simulated and graphically displayed for different actuator-systems. The development of such tools, from the theoretical equations to the verification on real elements, is the main topic of this article.

**11:40 AM**

**Problems and Solutions for Shape Memory Actuators in Automotive Applications:** Sven Langbein<sup>1</sup>; Konstantin Lygin<sup>1</sup>; Tim Sadek<sup>1</sup>; <sup>1</sup>Ruhr University Bochum

The increased automation of technical applications in automobiles requires the use of simple and effective actuator components. The interior of vehicles offer numerous opportunities where mechanical actuators can be or have already been replaced by electrical actuators, e.g. unlocking functions for cup holders or glove boxes. The growing application range of electrical

actuators leads to new problems. The need for optimisation can be located in fields of weight, sounds and costs. Because of the high power density, the simple design and the noiseless actuation of shape memory alloys, they are a solution for this problem. But the use of SMAs leads to new problems, too. The requirements of a short reactivation time, of a high durability and for an operability in ambient temperatures between -40 and +80°C have been identified as critical for SMA actuators. Therefore, ways to increase these properties by technical means are presented in this study.

**11:55 AM Conclusion of Symposium**

---

## Polycrystal Modelling with Experimental Integration: A Symposium Honoring Carlos Tome: Emerging Polycrystal Models with Experimental Integration II

*Sponsored by:* The Minerals, Metals and Materials Society, TMS Structural Materials Division, TMS Materials Processing and Manufacturing Division, ASM-MSCTS: Texture and Anisotropy Committee, TMS/ASM: Mechanical Behavior of Materials Committee, TMS/ASM: Computational Materials Science and Engineering Committee

*Program Organizers:* Ricardo Lebensohn, Los Alamos National Laboratory; Sean Agnew, University of Virginia; Mark Daymond, Queens's University

Thursday AM  
March 3, 2011

Room: 6C  
Location: San Diego Conv. Ctr

*Session Chairs:* Anthony Rollett, Carnegie Mellon University; Craig Hartley, El Arroyo Enterprises; Philip Eisenlohr, Max-Planck Institut fuer Eisenforschung

---

**8:30 AM Invited**

**Full-Field Modeling with Experimental Integration of 3-D Polycrystalline Materials Deforming in Different Regimes Using Fast Fourier Transforms:** Ricardo Lebensohn<sup>1</sup>; <sup>1</sup>Los Alamos National Laboratory

We present a recent extension of a numerical formulation based on Fast Fourier Transforms to obtain the evolution of micromechanical fields in 3-D polycrystals during the elastoplastic transition. This formulation, originally developed [1] as a fast algorithm to compute the elastic and elastoplastic response of composites using input from a digital image of their microstructures, has been in turn adapted to deal with 3-D polycrystals deforming either elastically or by dislocation glide in a rigid-viscoplastic regime (e.g [2]). The present extension to elasto-viscoplasticity allows us to predict, e.g., the evolution of the full stress field in polycrystalline microstructures, with intragranular resolution. The relevance of this formulation to the interpretation of 3-D space-resolved measurements obtained with emerging experimental methods will be discussed. [1] H. Moulinec, P. Suquet, *Comput. Methods Appl. Mech. Eng.* 157, 69 (1998). [2] R.A. Lebensohn R. Brenner, O. Castelnau, A.D. Rollett, *Acta Mater.* 56, 3914 (2008).

**8:55 AM Invited**

**Solving Finite-Deformation Crystal Elasto-Viscoplasticity with a Fast Fourier Transformation-Based Spectral Method:** Philip Eisenlohr<sup>1</sup>; Martin Diehl<sup>1</sup>; Franz Roters<sup>1</sup>; Ricardo Lebensohn<sup>2</sup>; <sup>1</sup>Max-Planck-Institut fuer Eisenforschung; <sup>2</sup>Los Alamos National Laboratory

We extend the spectral framework introduced by Lebensohn (*Acta Materialia* 49, 2001, pp. 2723--37) to the case of finite-deformation hyperelasticity. Here, the connection between the total deformation gradient and its work-conjugate (first Piola-Kirchhoff) stress is found at each Fourier grid point by invoking a crystal plasticity framework which internally decomposes deformation into elastic and plastic parts. The partitioning between both contributions is established by implicit integration of a state variable-based constitutive material law and associated update of its internal state. This flexible framework is applied to the problem of curling, which

occurs in wire drawing of body-centered cubic polycrystals, and is contrasted to the purely viscoplastic infinitesimal-strain solution.

#### 9:20 AM Invited

**Problem Solving with Viscoplasticity:** *Anthony Rollett*<sup>1</sup>; ricardo lebensohn<sup>2</sup>; Francis Wagner<sup>3</sup>; David Field<sup>4</sup>; <sup>1</sup>Carnegie Mellon University; <sup>2</sup>Los Alamos national laboratory; <sup>3</sup>University of Metz; <sup>4</sup>Washington State Univ

Carlos Tomé has made many contributions to the problem of relating mechanical response to microstructure but it remains an interesting challenge. Euclidean distance maps have proven to be a useful tool for quantifying the proximity of hot spots to grain boundaries, for example. We report on recent results that show that the development of local misorientation is also strongly related to the presence of grain boundaries. In this case, the relationship between local misorientation around each point and distance to the nearest boundary is monotonic: the largest misorientations are found close to boundaries. No direct relationship, however, emerged between misorientation development and grain size. Both simulation with the FFT model and EBSD maps of lightly deformed IF-steel show this trend in a very similar way. These findings are intended to illustrate the general way in which the study of viscoplasticity can help one to understand microstructure-property relationships.

#### 9:45 AM

**Modeling Slip and Twinning Induced Plastic Deformation: Comparison between a Crystal Plasticity Finite Element and a Self Consistent Approach:** *Hamidreza Abdolvand*<sup>1</sup>; Charles Mareau<sup>1</sup>; Mark R. Daymond<sup>1</sup>; <sup>1</sup>Queen's University

Results from a crystal plasticity finite element (CPFE) code used to model elasto-plastic deformation in an HCP material are compared to those obtained from self-consistent (SC) approach. In the constitutive equations of both models, it is assumed that slip and twinning deformations can be described using a rate dependent formulation. The predictions of both models in terms of average strain-stress response, lattice strain and texture development, and twinning volume fraction for uniaxial compression loading along the axial direction of a magnesium alloy AZ31 rod are compared with experiment. Excellent agreement is achieved. Due to different grain geometry assumptions, the results of the CPFE model are softer than that of the SC model if the same material constitutive law parameters are used. The inclusion of more realistic grain-grain interactions in the CPFE approach resulted in better prediction of texture development than with the SC model.

#### 10:05 AM Break

#### 10:20 AM Invited

**Modeling Non-Conservative Deformation in Crystal Plasticity:** *Craig Hartley*<sup>1</sup>; <sup>1</sup>El Arroyo Enterprises LLC

Restricting crystal plasticity models to conservative deformation is inadequate to describe situations where dislocation climb can occur in addition to glide. Both occur in response to a virtual force due to the local effective stress due to mechanical sources and an excess or deficit of point defects. It is convenient to express these forces in terms of the projections of the local effective stress tensor onto the slip plane in the slip direction, using the Schmid Tensor, and onto the extra half plane of edge and mixed dislocations, using a similar construct called the Climb Tensor. Because this latter quantity only acts on the edge components of mixed dislocations, it depends on the character of the dislocation population in a manner that is conveniently described by a Dislocation Density Vector. These concepts can be employed in a natural manner to develop expressions that expand crystal plasticity models to include creep.

#### 10:45 AM Invited

**Improving Texture Predictions by Introducing Microstructurally Based Spin Continuity on Grain Boundaries:** *Raúl Bolmaro*<sup>1</sup>; Andrea Fourty<sup>1</sup>; Javier Signorelli<sup>1</sup>; <sup>1</sup>IFIR

Texture evolution predictions are usually assertive on the description of components and general trends but lack a proper quantitative output for their severity. Moreover, if we attempt to rationalize the results in function of modern quantitative experiments describing grain fragmentation

and misorientations, the limitations of the models become evident. The current paper presents an implementation of certain rules stemming from continuity of spin on grain boundaries in an FCC polycrystal subject to large deformations. Continuity of spins together with shear stress continuity and strain assumptions on a pair of grains are further used on a Taylor like homogenization scheme. The main results of experiments, accumulated along the last decade, describing misorientations at fragment boundaries, distribution of misorientations for selected texture components and misorientation evolution vs. deformation are remarkably well reproduced. The model can also give hints on the process of development of dislocation arrays on geometrically necessary dislocation boundaries.

#### 11:10 AM

**Grain-Scale Interactions and Correlations: Effects on Yield Strength and Flow Stress:** *James Stolken*<sup>1</sup>; Bryan Reed<sup>1</sup>; Mukul Kumar<sup>1</sup>; <sup>1</sup>LLNL

The influence of micro-plasticity phenomena on yielding and subsequent work hardening is considered in the context of Grain-Boundary Engineered microstructures. Samples of commercial purity copper and nickel were subjected to thermal-mechanical processing that produced microstructures with varying fractions of low "Sigma" grain-boundaries over a modest range of grain size and with nearly identical (random) crystallographic texture. A four-fold variation in grain-boundary effectiveness (Hall-Petch effect) is observed. Finite element simulations were performed to specifically access the role of stress concentrations and cooperative slip near grain boundaries. Conventional crystal plasticity calculations coupled with high resolution EBSD data are ideally suited to address these two issues and thereby deduce some of the unique grain-scale phenomena upon comparison with experiments. Nearest neighbor and larger-scale twin-related domain correlations are examined and new directions in model development are identified.

#### 11:30 AM

**Grain Boundary Engineered Materials as Correlated Networks:** *Bryan Reed*<sup>1</sup>; Ming Tang<sup>1</sup>; James Belak<sup>1</sup>; Joel Bernier<sup>1</sup>; Vasily Bulatov<sup>1</sup>; Thomas LaGrange<sup>1</sup>; Mukul Kumar<sup>1</sup>; <sup>1</sup>Lawrence Livermore National Laboratory

This presentation will describe an emerging viewpoint that considers the extended network of grain boundaries as an entity unto itself. Especially in grain boundary engineered materials, these networks exhibit correlations that can extend over many grain diameters, and these correlations are very important for the clustering and percolation properties that determine the ability of the microstructure to withstand a variety of insults. We will describe ongoing efforts to capture the mathematical essence underlying grain boundary network correlations in a way that translates well into computer simulation. Prior work has shown that purely mathematical models can reproduce these correlations surprisingly well, producing microstructures that look much like real grain boundary engineered materials, provided they correctly represent the network constraints governing the formation, growth, and interaction of twins. Now we have implemented phase field simulations built on these same mathematical models, showing the importance of special boundary mobility in controlling coarsening.

#### 11:50 AM

**Multiscale Modeling of the Mechanical Response of Dislocation Structures Developed Using High Straining at Low Deformation Temperatures:** *Krzysztof Muszka*<sup>1</sup>; Janusz Majta<sup>1</sup>; <sup>1</sup>AGH University of Science and Technology

Metals subjected to high deformation at low temperature are characterized by ultrafine/nano structure, high volume fraction of high-angle grain boundaries and high fraction of dislocation structure in the form of cells and/or subgrains. The stored energy present in such materials, as elastic energy in dislocation structure and as boundary energy in the high-angle grain boundaries, affects in a complex way annealing processes leading to more stable structures. Upon annealing, both dynamic recovery, and recrystallization can take place, as well as structural (abnormal) coarsening. All of these mechanisms lead to dislocation structures' rearrangements into more stable high angle grain boundaries. In the present work, FEM multiscale physically-based model is proposed to predict the mechanical behavior



of ultrafine-grained materials developed using severe plastic deformation process (MaxStrain deformation) with or without subsequent annealing. An approach, relating macroscopic stress to dislocation cell size and dislocation density at submicron scale, is used.

**12:10 PM**

**Study Microstructure Evolution in FCC Polycrystalline Materials Using a New Eulerian Continuity Model:** *Sadegh Ahmadi*<sup>1</sup>; Brent Admas<sup>1</sup>; David Fullwood<sup>1</sup>; <sup>1</sup>Brigham Young University

A new model for predicting the evolution of microstructure in FCC polycrystalline materials is presented. The proposed model was developed based upon the continuity relations by which motion of grain particles in the mass space and rotation of orientations in the orientation space are monitored in an Eulerian framework. To study the accuracy of the proposed model, rolling process of a commercially pure nickel material was simulated using this model. Then, textural and statistical analyses of the experimental and simulated microstructures were carried out. Based on the obtained results, it was found that the new model predicts the statistical features of the microstructure for low and intermediate levels of rolling reductions, but for deformations above 70% because of not including complicated physical phenomena (i.e. grain fragmentation and inhomogeneities) in simulations, the accuracy of the continuity model on predicting the statistics of the real microstructure was decreased.

**12:30 PM Invited**

**Strain Hardening Behavior of HPDC Mg-Al Alloys at Low Strains:** *K. Vanna Yang*<sup>1</sup>; C. H. Caceres<sup>1</sup>; A. V. Nagasekhar<sup>2</sup>; M. A. Easton<sup>3</sup>; <sup>1</sup>ARC Centre of Excellence for Design in Light Metals, The University of Queensland; <sup>2</sup>Carpenter Technologies; <sup>3</sup>CAST Co-operative Research Centre

The Kocks-Mecking method of analysis was applied to quantify the contribution of the eutectic microstructure to the strain hardening behaviour of high pressure die cast Mg-Al and Mg-RE alloys at low strains. The strain hardening rate was proportional to the volume fraction of the eutectic phases for 7 binary Mg-Al and 3 Mg-RE binary alloys. The results indicate that a large share of the specimens remains elastic at low strains, suggesting that the softer core yields first. The strain hardening rate of each alloy is commensurate with the amount of intermetallic in the eutectic.

## Recycling General Session: Waste Utilization

*Sponsored by:* The Minerals, Metals and Materials Society, TMS Extraction and Processing Division, TMS Light Metals Division, TMS: Recycling and Environmental Technologies Committee  
*Program Organizer:* Joseph Pomykala, Argonne National Laboratory

Thursday AM  
March 3, 2011

Room: 12  
Location: San Diego Conv. Ctr

*Session Chair:* Jeffrey Spangenberg, Argonne National Laboratory

**8:30 AM Introductory Comments**

**8:35 AM**

**Designing a Collaborative System for Socio-Environmental Management of Industrial Waste:** *Marisa Borges*<sup>1</sup>; Fabio Baldini<sup>2</sup>; <sup>1</sup>Universidade Federal do Paraná; <sup>2</sup>Excel Solutions

The proposed method emphasizes the optimization of waste management with regard to the exploitation of raw materials incorporated in the remains of industry, as well as the economics of natural resources as an environmental impact assessment. This system [tool] allows: (a) the conversion of an environmental liability into an asset by finding a line of appropriate research for each type of waste and the development of new materials applicable to other industries, (b) performs internal control of the waste generated (production, storage, final destination) as well as legal conformity.

**8:55 AM**

**Analysis of Carbon Fiber Recovered from Optimized Processes of Commercial Scale Recycling Facilities:** *Joseph Heil*<sup>1</sup>; Davis Litzenger<sup>1</sup>; Jerome Cuomo<sup>1</sup>; <sup>1</sup>North Carolina State University

Carbon fiber reinforced polymer composites (CFRPs) are highly desired materials exhibiting superior strength to weight properties. Aerospace grade carbon fiber, once recycled, is still a valuable material. By evaluating properties of carbon fibers from commercial facilities, target applications in both the aerospace industry and within consumer goods such as automobiles and sporting goods can be identified. In 2009 NC State University characterized fibers recovered from initial production batches of commercial recycling facilities; in 2010 characterization of carbon fibers recovered from optimized processes was conducted. Special attention was paid to recycled intermediate modulus (IM) fibers versus virgin standard modulus (SM) fibers; as previous work as shown better or comparable mechanical properties from recycled IM fibers compared to virgin SM fibers. Characterization focuses on morphology by using scanning electron microscopy, surface chemistry (derived from x-ray photoelectron spectroscopy analysis), and mechanical testing on the tow and filament level.

**9:15 AM**

**Analysis and Control of Light Hydrocarbon Gases in the Pyrolysis/Combustion Process of Several Solid Wastes:** *Joner Alves*<sup>1</sup>; *Chuanwei Zhuo*<sup>2</sup>; Yiannis Levendis<sup>2</sup>; Jorge Tenório<sup>1</sup>; <sup>1</sup>University of Sao Paulo; <sup>2</sup>Northeastern University

The disposal of wastes is a serious environmental problem, since available landfill space is dwindling. Their treatment by pyrolysis or combustion has merit, and the corresponding fuel or power production is of technological interest. However, such processes need a rigid control of emissions. This work addresses the gaseous light hydrocarbons (LHCs) generated during sequential pyrolysis and partial oxidation of unserviceable tires, PET bottles, corn wastes (DDGS) and sugarcane bagasse in a two-stage laminar-flow horizontal furnace, kept at 1000°C. Gas chromatography was used to identify and quantify the components of the emitted gaseous light hydrocarbons. The results showed that the biomass residues generated the highest emissions of aliphatic hydrocarbons, whereas PET generated the most aromatic hydrocarbons. When stainless steel meshes were inserted in the exhaust flow, it was found that hydrocarbon emissions were curtailed; as such meshes catalyzed partial conversion of these carbon-bearing gases to carbonaceous nanomaterials.

**9:35 AM**

**Reduction Properties of Iron Ore Composite Pellets Bearing Waste Plastics:** *Burak Birol*<sup>1</sup>; Muhlis Saridede<sup>1</sup>; <sup>1</sup>Yildiz Technical University

Plastic wastes become a huge problem day after day due to the growth of plastic industry. Hence, plastic wastes are used as a raw material for other industries to eliminate this problem. Polyethylene Terephthalate (PET), which is a commonly used for plastic bottles, may be used as a reductant for iron production because of its C and H content. In this study, composite pellets containing iron ore concentrate, flux and reductant were prepared. Crystallized PET bottles and coke were used as reductant after ground. The prepared pellets were reduced at 1400°C for 30 min. and iron nuggets were produced successfully. Usage of waste PET purely as reductant in composite pellets gives a higher metallization degree and proper carbon content than coke or PET and coke mixture.

**9:55 AM**

**Recycling Charge and Subsidy for Waste Packaging Containers in Taiwan:** *Esher Hsu*<sup>1</sup>; Chen-Ming Kuo<sup>2</sup>; <sup>1</sup>National Taipei University; <sup>2</sup>I-Shou University

Under the 4-in-1 recycling system, Taiwan producers and importers who using packaging containers have the responsibility to pay the recycling fees for recycling the waste packaging containers they produced or imported, while the collectors/recycling plants who collect/sort/recover waste packaging containers receive subsidy for conducting recycling. A reasonable pricing for recycling charge and subsidy is a way for sustainability of the recycling. The objective of this study is to provide an amending mechanism

for product charge and recycling subsidy in response to the social economic changes. This study employs a regression analysis and cost adjusting model to link the factors used for calculating product charge and recycling subsidy on recycling waste packaging containers with socio-economic indicators, raw material prices, wholesale prices, and secondary material prices. Study results provide estimated models to EPA in Taiwan for amending product charge and recycling subsidy in response to the social economic changes.

#### 10:15 AM Break

#### 10:25 AM

**Treatment of Waste Leaching Liquor of a SHS Produced Tungsten Boride:** M. Seref Sonmez<sup>1</sup>; Sertac Yazici<sup>1</sup>; Bora Derin<sup>1</sup>; <sup>1</sup>Istanbul Technical University

In this study, the recycling conditions of waste liquor obtained after the production of tungsten boride powder from calcium tungstate by self-propagating high temperature synthesis (SHS) and the following hydrochloric acid leaching were investigated in detail. Environmentally unfriendly and extremely acidic (pH~ -0.3) liquor consisting of calcium, magnesium, and boron ions was treated with 1 M sodium carbonate solution to precipitate magnesium carbonate and calcium carbonate phases. The obtained amorphous precipitates were heated up to the temperature of 400°C for re-crystallization. As a result, MgO, CaCO<sub>3</sub> and CaMg(CO<sub>3</sub>)<sub>2</sub> phases were obtained, while sodium, boron, chlorine ions were remain in the solution. The present study is still in progress.

#### 10:45 AM

**The Effect of CO<sub>2</sub> Carbonation Reaction on the Behavior Leaching of Heavy Metals and Chlorine in the Industrial Waste Incineration Ash:** Ji-Whan Ahn<sup>1</sup>; Kwangsuk Yoo<sup>1</sup>; Seong-Young Nam<sup>1</sup>; <sup>1</sup>Korea Institute of Geoscience and Mineral Resources

Industrial waste incineration ash (IWIA) is the residue generated during the incineration of municipal solid waste. In Korea, approximately 100 thousand tons of IWIA ash was generated in 2008, with nearly 93.7% of the generated bottom ash landfilled. The ash consists of glasses, ceramics, ferrous metals and slag typically including a small amount of unburnt, non ferrous metals such as aluminum and copper. Many studies have found that the physical properties of the ash are suitable for aggregate substitutes in road materials. Environmental problems, however, such as the leaching of heavy metals and salts must be also considered. In this study, it has been researched to the behaviors of ferrous and non-ferrous materials, heavy metals, and chlorine in the ash under recycling process including carbonation system.

#### 11:05 AM

**Study on the Treatment of Wastewater Containing High Concentration of Ammonia Nitrogen:** Ding Lichao<sup>1</sup>; Chen Yunnen<sup>1</sup>; <sup>1</sup>Jiangxi University of Science and Technology

With the development of industrial production, more and more wastewater containing high concentration ammonia nitrogen was discharge into the environment, which caused serious harm to the environment. Treating the wastewater has great significance to protect water resources. Using air-stripping combined with oxidation to uptake high concentration of ammonia nitrogen wastewater. The influence of operating parameters was investigated. Experimental results revealed that pH of solution, aeration time and aeration strength showed heavy influence on ammonia nitrogen removal. Air-stripping combined with oxidation can be considered as an alternative approach for the removal of high concentration of ammonia nitrogen from practical metallurgical wastewater. When pH was 11, aeration time 20 min, aeration strength 1040 L/h, and oxidation with 10 % NaClO solution 10 min, the initial ammonia nitrogen 2130 mg/L could reduce to 12 mg/L. Other items could also be removed to meet the "Integrated wastewater discharge standard (GB8978-88)".

## Refractory Metals 2011: Refractory Metal-Based Composites II

*Sponsored by:* The Minerals, Metals and Materials Society, TMS Structural Materials Division, TMS: Refractory Metals Committee  
*Program Organizers:* Omer Dogan, DOE National Energy Technology Laboratory; Jim Ciulik, University of Texas, Austin

Thursday AM  
March 3, 2011

Room: 19  
Location: San Diego Conv. Ctr

*Session Chairs:* S.K. Varma, University of Texas at El Paso; Panos Tsakiroopoulos, University of Sheffield

#### 8:30 AM Invited

**Computational Design of Oxidation and Creep-Resistant Ductile Refractory Alloys for High Temperature Applications:** Abhijeet Misra<sup>1</sup>; <sup>1</sup>QuesTek Innovations LLC

Computational materials design integrates targeted materials process-structure-property models within a systems framework to meet specific engineering needs. A key component to design models is a basis on fundamental thermodynamics, phase equilibria, and diffusion, implemented in a multicomponent framework applicable to real systems. The application of computational materials design is especially advantageous to systems that must operate in environments or for lifetimes that are difficult to validate in a laboratory setting. QuesTek Innovations LLC is applying its *Materials by Design*<sup>®</sup> technology to the computational design and development of oxidation- and creep-resistant ductile multicomponent refractory-based superalloys for use at 1300°C and above. Fundamental design tools have been developed and used to design microstructural concepts with the potential of achieving critical performance requirements simultaneously. The computational design approach for these systems will be discussed along with some results from QuesTek's DOE-NETL and DARPA-funded programs on the development of niobium and molybdenum-based refractory alloys.

#### 8:50 AM

**First-Principles Calculation and Thermodynamic Modeling of Cr-Al-Ni-Ti Quaternary System:** Michael Gao<sup>1</sup>; Omer Dogan<sup>1</sup>; <sup>1</sup>National Energy Technology Laboratory

Enhancement of creep resistance of structural alloys for high-temperature applications largely rely on presence of finely dispersed high-strength second phase particles that are resistant to oxidation. In this study, the phase stability in Cr-Al-Ni-Ti system was investigated using first principles calculations, CALPHAD modeling, and characterization tools such as SEM and TEM. There are several technologically important strengthening compounds in this system, namely, Laves C15-Cr<sub>2</sub>Ti, Heusler L21-AlNi<sub>2</sub>Ti, and B2-AlNi. The alloying partitioning behavior of these compounds in the ternaries and quaternary were theoretically studied using DFT calculations. Their elastic constants and theoretical strength were also predicted. Phonon calculations were carried out to predict the temperature dependence of their structural, thermodynamic, elastic, and plastic properties, for example, heat capacity and coefficient of thermal expansion. Based on the present DFT calculations, previous thermodynamic assessment, and available experimental data, the thermodynamic descriptions of the quaternary system was optimized using CALPAHD approach.

#### 9:10 AM

**Effect of Various Ternary Additions on Cr-Cr<sub>2</sub>Ta Based Alloys:** Ayan Bhowmik<sup>1</sup>; Howard Stone<sup>1</sup>; <sup>1</sup>University of Cambridge

Alloys based upon Cr-Cr<sub>2</sub>X (X being Ta, Nb, Hf etc) have been considered for a while as alternative materials for high temperature service. In this study, we present the effect of alloying additions of Mo, Al and Si on Cr-Cr<sub>2</sub>Ta two phase alloys. The ternary additions have been made in 5 and 10 atomic percents to a master alloy of Cr-10at% Ta. Mo has been added for increased strength, Al for superior oxidation resistance and Si for improved

toughness and oxidation resistance. The binary Cr-10at% Ta alloy comprises of Cr<sub>2</sub>Ta dendrites and a eutectic mixture of Cr(Ta) solid solution and Cr<sub>2</sub>Ta. The composition and stability of the individual phases upon alloying have been determined using electron probe microanalysis and scanning electron microscopy. The microhardness and room temperature fracture toughness of the alloys have also been determined using three point bend tests.

#### 9:30 AM

**Microwave Sintering of Nb/Nb5Si3 Composite Material:** Yi Liu<sup>1</sup>; Huimin Lu<sup>1</sup>; Jingru Dai<sup>1</sup>; <sup>1</sup>Beihang University

Based on the high melting point, low density, a balance of high-temperature strength and room-temperature toughness, Nb/Nb5Si3 composite material has become a super-alloy for the next generation of aircraft engine. Nb/Nb5Si3 composite material was sintered by the method of direct microwave heating and SiC auxiliary heating, and the effects of peak sintering temperature and sintering time on the density and microstructure of the material were investigated. Compared with conventional sintering, microwave sintering time is only its 20%, and the energy consumption has been reduced by about 70%. Nb5Si3 phase appears in the sample and the grain size is between 1~2 μm, after sintering at 1600° for 5 min. In the meantime, the mechanism of microwave sintering was systematically studied.

#### 9:50 AM Break

#### 10:10 AM

**Oxidation Behavior of Nb-25Cr-20Si-15Mo-5B and Nb-25Cr-20Mo-15Si-10B in Air from 700 to 1300°C:** Benedict Portillo<sup>1</sup>; Shailendra Varma<sup>1</sup>; <sup>1</sup>University of Texas El Paso

Nb-25Cr-20Si-15Mo-5B and Nb-25Cr-20Mo-15Si-10B (at.%) have been subjected to oxidation in air for 24 hours and 168hrs of cyclic oxidation in a range of temperatures from 700 to 1300°C. The as cast microstructures of both alloys contained a molybdenum rich solid solution, Nb<sub>5</sub>Si<sub>3</sub>, and NbCr<sub>2</sub>. The 10%B alloy exhibited better oxidation resistance than the 5%B alloy after 24hrs of oxidation. Samples were characterized by XRD, x-ray mapping, and EDS on SEM. A semi continuous intermediate oxide layer containing molybdenum was found to develop in both alloys at high temperature and was not observed to spall after cooling. The 10%B alloy was also found to have significantly better performance after long term cyclic oxidation test.

#### 10:30 AM

**Study of the Effect of Al, Cr, Mo and Ta Additions on the Microstructure and Properties of Nb Silicide Based Alloys:** Panayiotis Tsakiroopoulos<sup>1</sup>; <sup>1</sup>The University of Sheffield

Niobium silicide based alloys could replace Ni based superalloys in some structural applications at high temperatures. Alloy development must address the improvement of environmental behaviour and mechanical properties at room, intermediate and high temperatures. Alloying and processing have sought to enhance the performance of the Nbss, to identify optimum microstructures in terms of phase selection, stability and microstructural architecture and to understand how the latter affect performance. In this work, the role of Al, Cr and Mo and Ta in the microstructures of Nb-24Ti-18Si (at %) based alloys has been studied. The phases observed in the alloys were the Nbss, the Nb3Si and αNb5Si3 and βNb5Si3 silicides and Laves phase. The role of the alloying elements on the stability of Nb3Si, the structure of Nb5Si3 and on the Nb3Si > Nbss + αNb5Si3 and βNb5Si3 > αNb5Si3 + (Nb,Ti)ss transformations and the formation of the C14-Cr2Nb Laves phase will be discussed.

#### 10:50 AM

**Thermomechanical Processing and Microstructure Evolution in Nb-Si-Ti-Al-Cr-X Alloys for High Temperature Aeroengine Applications:** Raghvendra Tewari<sup>1</sup>; Hyojin Song<sup>2</sup>; Amit Chatterjee<sup>3</sup>; Vijay Vasudevan<sup>2</sup>; <sup>1</sup>Bhabha Atomic Research Centre; <sup>2</sup>University of Cincinnati; <sup>3</sup>Rolls-Royce Corporation

The present paper reports the development of selected Nb-Si-Ti-Cr-Al-X alloys subjected to various conditions. Detail microstructural investigations have revealed a strong tendency for solute partitioning and the formation of the laves phases. Thermomechanical processing was quite

effective in breaking down the cast-structure and refining microstructure. The morphological distribution, structure and chemical composition of the various phases were investigated. The β phase exhibits B2 ordering. Dissolution and re-precipitation of the Laves phase, which has been encountered during various heat treatments, has been studied in detail and characterized in terms of elemental distribution in the phase and mechanistic aspects. The results reveal that additional strengthening of the β matrix can be achieved by precipitation of the Laves phase. Mechanical properties of these alloys in different conditions were also evaluated and interesting results were obtained. The role of microstructure, in particular the Laves phase, in controlling mechanical properties is discussed.

#### 11:10 AM

**Consolidation of Tantalum Materials by the Cold Spray Process:** Matthew Trexler<sup>1</sup>; Robert Carter<sup>1</sup>; Victor Champagne<sup>1</sup>; <sup>1</sup>U. S. Army Research Laboratory

Cold spray is a novel process used to consolidate metal powders to which ceramic particulates may be added to form both thin coating and large bulk materials. Cold spray relies on the large deformation that occurs when small particles that have been entrained in a super sonic gas stream impact upon a substrate. Cold spray eliminates the need for more complex methods of forming parts such as liquid infiltration and/or sintering, which can be difficult given the high processing temperatures needed to form refractory metals. This work examines the use of cold spray as it pertains to the consolidation of refractory Ta powder for use as structural components. Cold spray was able to create fully dense near-net shaped powder parts that exhibit excellent tensile properties with limited post-processing.

#### 11:30 AM

**Ta/Al2O3 Based Coatings Produced by Thermal Spraying:** Marcio Mendes<sup>1</sup>; Eraldo Souza<sup>2</sup>; Narayanna Ferreira<sup>2</sup>; Clodomiro Alves, Jr.<sup>2</sup>; <sup>1</sup>Universidade Federal do Rio Grande do Norte ; <sup>2</sup>Universidade Federal do Rio Grande do Norte

Thermal spraying is a group of processes in which metallic or nonmetallic particles are deposited on a substrate properly prepared, provided or semi-molten melt, thus forming a surface coating. The heating necessary for the operation is generated by a spray torch using a combustible gas, electrical arc or plasma. The aim of this paper is soaking, using a plasma torch arc not transferred, particulate mixture of tantalum oxide and aluminum prepared in a stoichiometry manner and with excess of Al +5% and +10%, with flows of 10, 20 and 30 l / min on a 316 stainless steel substrate, producing a coating with high microhardness composed of nanometric particles of tantalum in an alumina matrix. The products of the sprays were characterized by XRD, SEM and electron temperature of the plasma jet was obtained by optical emission spectroscopy.

#### 11:50 AM

**Micropillar Compression of Nanocrystalline and Ultra-Fine-Grained BCC Metals Processed by Severe Plastic Deformation:** Jonathan Ligda<sup>1</sup>; Brian Schuster<sup>2</sup>; Qiuming Wei<sup>1</sup>; <sup>1</sup>University of North Carolina Charlotte; <sup>2</sup>U. S. Army Research Laboratory

We report on the mechanical properties of nanocrystalline (NC) and ultra-fine-grained (UFG) tantalum and other bcc metals processed using high pressure torsion (HPT). HPT samples have an inherent gradient in structure and properties along a radius of a bulk platen; grains are UFG near the center and NC near the edge. Using site-specific FIB we have examined the properties of micro-compression and tension specimens with grain sizes ranging from tens to hundreds of nanometers and have probed the balance between specimen strength, toughness, strain rate sensitivity and the deformation mode (e.g. homogenous or localized plastic deformation). Observations of the proposed mechanism will be supported through microstructural examinations with transmission electron microscopy. This study will aid in the understanding of how the deformation occurs in bcc metals when the grain size is reduced to the nanoscale.



---

## Sensors, Sampling, and Simulation for Process Control: Temperature-Related Process Monitoring Systems

*Sponsored by:* The Minerals, Metals and Materials Society, TMS Extraction and Processing Division, TMS: Process Technology and Modeling Committee, TMS: Solidification Committee  
*Program Organizers:* Brian Thomas, University of Illinois at Urbana-Champaign; Andrew Campbell, WorleyParsons; Srinath Viswanathan, University of Alabama; Lifeng Zhang, Missouri University of Science and Technology; James Yurko, 22Ti LLC; Thomas Battle, Midrex Technologies

Thursday AM  
March 3, 2011

Room: 13  
Location: San Diego Conv. Ctr

*Session Chairs:* Hani Henein, University of Alberta; Srinath Viswanathan, University of Alabama

---

### 8:30 AM

#### **Dynamic Run-Out Table Cooling Simulator and Temperature Controllers:** *Nicolas Pethe*<sup>1</sup>; Kai Zheng<sup>1</sup>; Didier Huin<sup>1</sup>; Christian Moretto<sup>1</sup>; Evgueni Poliak<sup>1</sup>; <sup>1</sup>ArcelorMittal

Intense competition in steel market has led to the development of a number of high strength steel grades which pose new serious challenges in their manufacturing. One of the major challenges lies in the control of strip cooling after hot rolling, which has become a key step in delivering products with desired microstructure and mechanical properties. To meet this need, SimROT, a dynamic run out table cooling simulator has been developed. Based on a coupling between physical principle based thermal and metallurgical models, SimROT is able to predict temperature and mechanical property accurately over a wide range of products. In addition, a control system has been developed by introducing adaptation to compensate for unmodeled dynamics and a model-based dynamic controller. Implementation has been carried out in the ArcelorMittal USA Riverdale plant to have replaced the old commercial system. Production data have shown significant performance improvement for the entire product mix.

### 8:55 AM

#### **Real-Time Model-Based Spray-Cooling Control System for Steel Continuous Casting:** *Bryan Petrus*<sup>1</sup>; Kai Zheng<sup>2</sup>; X. Zhou<sup>1</sup>; Brian Thomas<sup>1</sup>; Joseph Bentsman<sup>1</sup>; <sup>1</sup>University of Illinois at Urbana Champaign; <sup>2</sup>Mittal Steel Company

A new system to control secondary cooling water sprays in continuous casting of steel slabs, CONONLINE, is presented. It features use of a real-time numerical simulation of heat transfer and solidification within the strand as a software sensor in place of unreliable pyrometer sensors. The one-dimensional finite-difference model, CON1D is adapted to create the real-time predictor of the slab temperature and solidification state. During operation, the model is updated with data collected by the caster Level 2 automation system, including measured mold heat flux. A decentralized controller configuration based on a bank of PI (Proportional-Integral) controllers with antiwindup is developed to maintain the shell surface temperature profile at a desired setpoint. A user-friendly monitor accepts setpoint changes from the caster operator and visualizes the state of the caster for the operators. Example simulations demonstrate how better shell surface temperature control is achieved. The system has been implemented to control the Nucor Steel casters in Decatur, Alabama.

### 9:20 AM

#### **Measurement of the Solidification Front inside a Metallurgical Reactor:** *Clement Bertrand*<sup>1</sup>; Marc-Andre Marois<sup>1</sup>; Martin Desilets<sup>1</sup>; Gervais Soucy<sup>1</sup>; <sup>1</sup>University of Sherbrooke

Recent amperage increase programs in aluminium smelters generally aim at boosting the metal production using a slightly modified design of an electrolytic cell while keeping its thermal equilibrium unchanged. It is sometimes difficult to evaluate the dynamic cell behaviour with regards

to those changes in design and operating point. Sensors are thus needed to diagnose and control the thermal state of modern electrolysis cells. Due to the aggressiveness of the electrolytic bath and high temperatures, solidification front thickness measurements are tedious, imprecise and time consuming. A new measurement technique intended at the evaluation of the solidification front inside an experimental phase change reactor close to a typical aluminium reduction cell is developed. The study of its thermal behaviour is used here to show the possibilities and challenges brought by this new technique. Direct measurements and numerical simulations support the development of such a sensor.

### 9:45 AM

#### **Inverse Prediction and Control of the Bank Thickness in High Temperature Metallurgical Reactors:** *Marc LeBreux*<sup>1</sup>; Martin Désilets<sup>1</sup>; Marcel Lacroix<sup>1</sup>; <sup>1</sup>Université de Sherbrooke

An inverse heat transfer procedure for predicting the time-varying bank thickness in high temperature metallurgical reactors is presented. A Kalman filter coupled with a recursive least-square estimator (inverse method) is employed to estimate the time-varying solidification front position from the data collected by a temperature and/or heat flux sensor located in the reactor wall. The inverse method, known also as a virtual sensor, is then combined to a proportional-integral (PI) controller in order to control the bank thickness by regulating the air forced convection cooling of the reactor external wall. The inverse prediction and the control strategy are thoroughly tested for typical phase change conditions that prevail inside industrial facilities. It is seen that the discrepancy between the exact and the estimated bank thickness remains smaller than 5% at all times, and that the controller performance is much better when the virtual sensor uses a heat flux sensor at the wall/bank interface.

### 10:10 AM Break

### 10:25 AM

#### **Online Imaging Pyrometer for Laser Deposition Processing:** *James Craig*<sup>1</sup>; Thomas Wakeman<sup>1</sup>; Richard Grylls<sup>2</sup>; James Bullen<sup>3</sup>; <sup>1</sup>Stratronics, Inc.; <sup>2</sup>Optomec, Inc.; <sup>3</sup>Optomec, Inc.

An online imaging pyrometer has been developed to monitor the temperature distribution of the melt pool in laser additive manufacturing processes. The imaging pyrometer uses two CCD cameras with "long and short" wavelength filters in the NIR waveband. The intensity ratio is formed and the two wavelength temperature is determined from a calibration, relating the ratio to the temperature. In the experiment, deposit strips are formed over a variation of laser power levels, ranging from standard levels for a superalloy to about half the initial level. As the power is lowered, the deposit efficiency is reduced, as is its dimensions. Melt pool temperature distributions are measured in the final 6 through 10 passes and their properties will be presented and described. Peak temperatures of about 1800 C are noted for standard power levels, and in general lower temperatures are observed at lower power levels.

### 10:50 AM

#### **Optimization of Continuous Hot Dipped Galvanization Lines through the Addition of a Hot Coating Weight Sensor:** *Christopher Burnett*<sup>1</sup>; Andreas Quick<sup>1</sup>; <sup>1</sup>Thermo Scientific

The ability to reliably measure the zinc coating directly above the pot allows for dramatic improvements in hot dipped galvanizing line performance. The feedback time for air knife control is nearly instantaneous. When coupled with intelligent control software in a complete coating weight Autocontrol system, a "hot" coating weight gauge can reduce overcoating to save raw materials, avoid overcoating and increase overall mill yield. While this location significantly improves coating weight autocontrol performance due to short dead time between air knife and measurement, the environment presents electrical, mechanical, and thermal challenges that must be considered in the final sensor design.

11:15 AM

**Monitoring of Meniscus Thermal Phenomena with Thermocouples in Continuous Casting of Steel:** *Brian Thomas*<sup>1</sup>; *Mary Wells*<sup>2</sup>; *Dianfeng Lee*<sup>3</sup>; <sup>1</sup>University of Illinois at Urbana Champaign; <sup>2</sup>Waterloo University; <sup>3</sup>Belvac Metal Forming Company

Many steel quality problems are related to mold level fluctuations, stickers, deep oscillation marks, and other events at the meniscus, and can be detected by monitoring temperature signals in the wall of the copper mold. This work applies an inverse heat conduction model to investigate the potential capabilities of mould thermocouples to detect such phenomena by computing the sensitivity of the detected signal to heat flux variations at the meniscus. The model is first validated with temperature data recorded in a commercial slab casting mold, and in a previous laboratory measurement. The method is capable of monitoring meniscus level, and to detect large level fluctuations. However, its ability to detect temperature fluctuations decreases with the frequency of the fluctuations and the distance of the thermocouple from the hotface. Sensitivity calculations with the model are presented to quantify these detection limits.

11:40 AM

**Implementation of Temperature and Strain Micro-Sensors into a Casting Mold Surface:** *Brian Thomas*<sup>1</sup>; *Michael Okelman*<sup>2</sup>; <sup>1</sup>University of Illinois at Urbana Champaign; <sup>2</sup>ArcelorMittal Inc.

Microfabricated thin-film thermocouples (TFTCs) and Fiber Bragg Grating (FBG) sensors can be embedded in the coating layers of the mold to measure temperature, heat flux, and strain during continuous casting. Embedding sensors within 1mm near the surface has the advantages of sensitive real-time monitoring of thermal behavior without damping by the copper mold, and protection from hostile environments. A novel TFTC suited for use in continuous casting molds has been designed and a method to embed TFTCs in a coating layer was developed, as well as a computational model to quantify the effect of air gaps between the sensor strip and the copper mold on heat transfer and stress in the coating layer. Finally, a method to successfully embed FBG sensors has been proposed. The signal output by FBG sensors embedded in a nickel coating layer on a copper mold has been investigated and can be predicted with simple equations.

12:05 PM

**Simulated Temperature Profile Control of a Laminar Cooling System Using the Genetic Algorithms:** *Baher Bineshmarvasti*<sup>1</sup>; *J. Barry Wiskel*<sup>1</sup>; *Amos Ben-Zvi*<sup>1</sup>; *Hani Henein*<sup>1</sup>; <sup>1</sup>University of Alberta

The Genetic Algorithms optimization method, in conjunction with a finite element thermal model, was used to simulate control of the temperature profile (i.e. both cooling rate and coiling temperature) of a steel skelp during laminar cooling. Simulated optimization parameters include skelp velocity and laminar cooling configuration. As an example case, the Genetic Algorithms was used to obtain a simulated laminar cooling configuration for an imposed skelp cooling rate of 11.5°C/s and a coiling temperature of 600°C. The ability to achieve the desired skelp cooling profile was found to be sensitive to the control point location (e.g. temperature location inside skelp) used in the Genetic Algorithms.

## Silicon Production, Purification and Recycling for Photovoltaic Cells: Session I

*Sponsored by:* The Minerals, Metals and Materials Society, TMS Extraction and Processing Division, TMS Light Metals Division, TMS: Energy Conversion and Storage Committee, TMS: Recycling and Environmental Technologies Committee

*Program Organizers:* Anne Kvithyld, SINTEF; Gregory Hildeman, Consultant; Gabriella Tranell, Norwegian University of Science and Technology (NTNU); Arjan Ciftja, SINTEF; Shadia Ikhmayies, Al Isra University

Thursday AM  
March 3, 2011

Room: 14A  
Location: San Diego Conv. Ctr

*Session Chair:* Gabriella Tranell, Norwegian University of Science and Technology

8:30 AM

**Polysilicon in Photovoltaics: Market Conditions & Competing PV Technologies:** *David Lynch*<sup>1</sup>; *Byron Cocilovo*<sup>2</sup>; *Mario Marquez*<sup>2</sup>; *Akram Amooali*<sup>2</sup>; *Andrew Shroods*<sup>2</sup>; *Scott De Valle*<sup>2</sup>; *Rochellee Manyoats*<sup>2</sup>; *Chad Munich*<sup>2</sup>; <sup>1</sup>Solar Technology Research Corporation; <sup>2</sup>University of Arizona

Material requirements and technical issues impacting several photovoltaic (PV) technologies are examined. That data, along with projections regarding the growth in installed PV capacity, are used to predict demand the solar industry will place on materials used in producing solar cells. Those figures are compared to current production figures and available reserves.

8:50 AM

**Agglomeration as a Minor Mechanism for Polycrystalline Silicon Grown in a Fluidized Bed Reactor:** *Mohamad Zbib*<sup>1</sup>; *Uttara Sahayam*<sup>1</sup>; *Wayne Osborne*<sup>2</sup>; *Grant Norton*<sup>1</sup>; *David Bahr*<sup>1</sup>; <sup>1</sup>Washington State University; <sup>2</sup>REC Silicon

Polycrystalline silicon, grown using fluidized bed reactors, produces crystalline granular beads, as well as fine (sub 100 nm) amorphous nanopowders. The microstructure of this material was analyzed using scanning and transmission electron microscopy to determine if agglomeration of the nanopowders in the granular material is a significant growth mechanism, in part due to concerns regarding pores in the material. The granular material is primarily crystalline with a high twin density, but some amorphous regions appear around 100-500 nm sized pores, while the porosity larger than 1000 nm exhibits a crystalline structure to the edge of the pore. Total volume fraction of porosity varied between 1.5-4%; pores less than 500 nm represent 0.3 volume %; therefore, it appears agglomeration of nanopowders to the granular beads exists, but is only a minor contributor to the total mass of silicon produced.

9:10 AM

**Preparation of Polysilicon by the Reaction of Zinc and Silicon Tetrachloride:** *Tao Zhang*<sup>1</sup>; *Huimin Lu*<sup>1</sup>; *Jingbo Xu*<sup>1</sup>; <sup>1</sup>Beihang University

Polysilicon is the cornerstone of the photovoltaic industry as more than 80% of the solar cell chips are manufactured by the silicon material (monocrystalline silicon and polysilicon). In this paper, polysilicon is produced through a reaction between silicon tetra-chloride and zinc in a reaction furnace. The experiment results indicate that this method is promising and lays a good foundation for industrial application. The conditions of this reaction were studied including temperature, reaction time, reaction atmosphere and the ratio of zinc and silicon tetrachloride. The polysilicon produced meets the requirements of solar cells. The energy consumption of this method has been reduced by about 60%, as compared with traditional polysilicon production methods.

**9:30 AM**

**Macrosegregation of Impurities during Solidification of Metallurgical Grade Silicon in a Vertical Bridgman Furnace:** *Marcelo Martorano*<sup>1</sup>; João Ferreira Neto<sup>2</sup>; Theógenes Oliveira<sup>1</sup>; Tomoe Tsubaki<sup>2</sup>; <sup>1</sup>University of São Paulo; <sup>2</sup>Instituto de Pesquisas Tecnológicas do Estado de São Paulo

Directional solidification of metallurgical-grade Si was carried out in a vertical Bridgman furnace. The effects of a change in mold velocity on the macrosegregation of impurities were investigated. Macrostructures of cylindrical Si ingots consist mostly of columnar grains parallel to the ingot axis. Neither dendrites, nor cells, were observed although there is some indication of their presence in the microstructures obtained at the largest velocities. Measured concentrated profiles of impurities showed that ingot bottom and middle are purer than the metallurgical Si. Impurities accumulate at the ingot top creating the typical normal macrosegregation. When mold velocity decreases, macrosegregation and ingot purity increase, changing abruptly below  $20\mu\text{m}^{-1}$ . A mathematical model of solute transport shows that, for mold velocities  $\geq 20\mu\text{m}^{-1}$ , macrosegregation is caused mainly by diffusion in a stagnant liquid layer assumed at the solid-liquid interface, while for lower velocities, macrosegregation increases owing to convective solute transport.

**9:50 AM Break****10:10 AM**

**Removal of Inclusions from Solar Grade Silicon Using Electromagnetic Field:** *Anping Dong*<sup>1</sup>; Lucas Damoah<sup>1</sup>; Lifeng Zhang<sup>1</sup>; <sup>1</sup>Missouri University of Science and Technology

SiC and Si<sub>3</sub>N<sub>4</sub> are the main non-metallic particles in the solar grade silicon impair the conversion efficiency of the solar cell. Since the non-metallic particles and the metallic impurity elements are non- or less-conductive while the molten silicon is well conductive, under EM field, the Lorenz force will push the particles to the boundary layer, thus remove these inclusions. A laboratory-scale electromagnetic purification unit was used to remelt the silicon scraps and remove inclusions from the melt. The effects of frequency and the current on the inclusion removal are discussed.

**10:30 AM**

**Effect of Calcium Addition and Microstructure of Metallurgical Grade Silicon on Its Leaching Behavior:** *Yulia Meteleva-Fischer*<sup>1</sup>; Yongxiang Yang<sup>1</sup>; Rob Boom<sup>1</sup>; <sup>1</sup>Delft University of Technology

Leaching is a very attractive method of purification for metallurgical grade silicon due to its low costs. However, quantitative published results and proposed treatment conditions remarkably differ from each other. The true reason for the various explanations is in the origin of silicon. Specific microstructure and impurities set result in specific leaching behavior of silicon. In present work leaching behavior has been analyzed based on microstructure of metallurgical grade silicon and concentration of calcium addition. It is shown that leaching behavior and efficiency of metallurgical grade silicon depends very much on microstructure of grain boundaries, which is affected by calcium content. It has been detected that increase of calcium concentration and slow cooling rate result in favorable microstructure of grain boundaries, which is possible to remove more easily by using only diluted hydrochloric acid.

**10:50 AM**

**Effect of Solidification Conditions on Si Growth from Si-Cu Melts:** *Yosuke Ohshima*<sup>1</sup>; Takeshi Yoshikawa<sup>1</sup>; Kazuki Morita<sup>1</sup>; <sup>1</sup>University of Tokyo

To develop a new silicon refining process for solar cells, solidification refining of silicon with Si-Al melt has been investigated in our research group. This process is considered to be more effective than conventional solidification refining from thermodynamic prediction. However, refined Si with needle-like shape was highly dispersed in a directional solidification refining. Accordingly, the solidification conditions to obtain bulk Si crystal were investigated with various temperature gradients and cooling rates, and bulk Si crystal was obtained under limited conditions. Since cooling rates were still slow, further development was required for the practical process. In

this study, solidification conditions to obtain bulk Si crystal by solidification refining with Si-Cu melt were investigated under various conditions, such as temperature range, temperature gradient, solidification rate, etc. Bulk Si crystal was found to be obtained when the flat interface was observed. Also, the condition to obtain facet Si growth was discussed.

**11:10 AM**

**Structure Silicon Deposits Obtained by Electrolytic Refining in Salt Melt:** *Oleg Chemezov*<sup>1</sup>; Oleg Vinogradov-Jabrov<sup>1</sup>; Yuriy Zaikov<sup>1</sup>; Aleksey Apisarov<sup>1</sup>; Andrey Isakov<sup>1</sup>; <sup>1</sup>Russian Academy of Sciences

Silicon deposits containing up to 99.99 of main component were obtained by electrowinning from salt melts. Substrates were used from glass-carbon, graphite and nickel. The operating temperature was varied from 550 to 800°C. Structure silicon deposits were investigated by ESM method.

**11:30 AM**

**Silicon Electrodeposition Process in Molten Fluorides:** *Anne-laure Bieber*<sup>1</sup>; Laurent Massot<sup>1</sup>; Laurent Cassayre<sup>1</sup>; Pierre Chamelot<sup>1</sup>; Mathieu Gibilaro<sup>1</sup>; Pierre Taxil<sup>1</sup>; <sup>1</sup>Laboratoire de génie Chimique

With the exponential growth of solar industry for the photovoltaic panel, the silicon demand is exceeding the supply. So developing new processes able to produce Solar Grade Silicon (SoG-Si) is a major stake. Electrodeposition seems to present many advantages for the production of SoG-Si. The aim of this work is the achievement of an acceptable purity deposit of silicon suitable for the photovoltaic industry in molten salts between 700 and 900°C by electrochemical way in molten fluorides. First, the silicon ions reduction mechanism was studied using cyclic and square wave voltammetries. These experiments, correlated to a bibliography study, allow asserting that Si(IV) ions are reduced in a one-step process exchanging four electrons:  $\text{Si(IV)} + 4 e^- = \text{Si}$ . Deposits of silicon were obtained after electrolysis under different conditions (nature of the solvent, temperature, current density, cathode material) and characterized by scanning electron microscopy (SEM) and energy dispersive spectroscopy (EDS).

---

### Size Effects in Mechanical Behavior: Combined Approaches Applied to Size Scale Dependent Experimental Problems

*Sponsored by:* The Minerals, Metals and Materials Society, Not Applicable, TMS: Nanomechanical Materials Behavior Committee  
*Program Organizers:* Erica Lilleodden, GKSS Research Center; Amit Misra, Los Alamos National Laboratory; Thomas Buchheit, Sandia National Laboratories; Andrew Minor, UC Berkeley & LBL

Thursday AM  
March 3, 2011

Room: 2  
Location: San Diego Conv. Ctr

*Session Chairs:* Thomas Buchheit, Sandia National Laboratories; T. John Balk, University of Kentucky

---

**8:30 AM**

**The Behavior of Nanoporous Au and Cu Foams with Controllable Pore Size:** *I-Chung Cheng*<sup>1</sup>; Andrea Hodge<sup>1</sup>; <sup>1</sup>University of Southern California

Monolithic nanoporous copper and gold foams prepared by dealloying processes are investigated. The pore and ligament size are controllable by using either free corrosion or electrochemically driven methods. The ligament size of the samples dealloyed by free corrosion is ~ 50 nm, while the ligament size of the samples dealloyed by electric driven method is ~ 15nm. Electron backscatter diffraction (EBSD) inverse pole figure maps show the grain morphology and orientation of the base alloy before and after dealloying. The mechanical behavior of nanoporous foams is tested by nanoindentation. Hardness and modulus values are compared in order to determine the effect of oxide formation to the overall material behavior.



8:50 AM Invited

**Nanoporous FCC Metals: Effects of Nanoscale Structure on Mechanical Behavior:** *T. John Balk*<sup>1</sup>; <sup>1</sup>University of Kentucky

Nanoporous metals with nanoscale ligaments offer a unique opportunity to explore the deformation behavior of highly confined metallic volumes. The ligaments provide an extreme constraint on the motion of dislocations. This presentation will discuss several FCC metals in nanoporous form that were mechanically tested. Thin film and bulk samples of nanoporous Au, Pd, Ir and Ni exhibit mechanical properties much different from those of their fully dense counterparts. Hardness testing of nanoporous Au suggests equivalent strength values that may approach the theoretical level. While the measured stress in thin films corresponds to an equivalent stress of one-half the theoretical shear strength, the equivalent elastic modulus appears to be underestimated for porous materials. In nanoporous Pd films, hydrogen was absorbed more quickly than in dense Pd films, leading to large compressive stresses and a gradual phase transformation. These measurements will be interpreted in light of the nanoporous structure of each metal.

9:20 AM

**Scaling Behavior of Nanoporous Bcc Materials:** *Ralph Spolenak*<sup>1</sup>; Flavio Mornaghini<sup>1</sup>; <sup>1</sup>ETH Zurich

The scaling behavior of fcc metals, with regard to yield strength, has been well established, whereas the sub 100 nm regime has been explored by including nanoporous gold into the scaling plots of solid pillar geometries. Recently, bcc materials have also been explored in pillar geometry, and their scaling behavior has been found to be less sensitive to pillar diameter than fcc systems. Pillar geometries, however, are difficult to fabricate below 100 nm diameters. Here, we present a study on nanoporous tungsten as fabricated by a novel thermal dealloying process. Stud sizes of below 20 nm exhibit strength levels close to the theoretical yield strength.

9:40 AM

**Internal Friction Measurements in Nanocrystalline and Nanoporous Metals:** *Nicolas Briot*<sup>1</sup>; <sup>1</sup>University of Kentucky

Several mechanisms have been proposed to account for internal friction in metals at various temperatures, including interactions between dislocations and point defects, nucleation of kink/antikink pairs and grain boundary diffusion. In this study, damping properties of free-standing cantilever samples were investigated using a home-built system composed of a vacuum chamber and a laser vibrometer connected to an acquisition system. The cantilever's deflection was observed in real time, and the evolution of logarithmic decrement of free decay was determined between -150°C and +150°C. Internal friction peaks were observed for nanocrystalline and coarse grain nickel samples, as well as for nanoporous metals obtained by dealloying. The damping peaks for nanocrystalline Ni appear to arise from interactions between dislocations and point defects. Because the ligament size of the nanoporous structure (between 5 and 15 nm) makes dislocation nucleation more difficult, different relaxation mechanisms may be involved.

10:00 AM

**Measurement and Analysis of Internal Friction in Sputtered Thin Films of Aluminum:** *Guruprasad Sosale*<sup>1</sup>; Luc Frechette<sup>2</sup>; Srikar Vengalatore<sup>1</sup>; <sup>1</sup>McGill University; <sup>2</sup>Universite de Sherbrooke

Measuring internal friction in deposited thin films can provide useful insight into the effects of scale and confinement on the mechanisms of anelasticity and guide the design of high-performance microresonators used in microelectromechanical systems for sensing and communications. To this end, we have developed a new approach for accurate measurement of internal friction based on a silicon microcantilever platform that uses thermoelastic damping for calibration. This approach has been implemented to measure the effects of thickness (50–500 nm), frequency (100–1500 Hz), and adhesion layers (15 nm thick chromium) on internal friction in sputtered films of aluminum at room temperature. Our measurements suggest that damping is dominated by mechanisms within the film, rather than at the interface or free surface. We have used our results to critically evaluate previously proposed theories for damping due to grain-boundary sliding in thin Al films. Results from measurement and modeling will be presented.

10:20 AM Break

10:40 AM

**Augmentation of Micro-Tension Testing Methods: New Parallelized Sample Fabrication Techniques and Development of Elevated Temperature Micro-Heater Grips:** *Paul Shade*<sup>1</sup>; Robert Wheeler<sup>2</sup>; Sang-Lan Kim<sup>2</sup>; Michael Uchic<sup>3</sup>; Sabyasachi Ganguli<sup>4</sup>; Jianjun Hu<sup>2</sup>; <sup>1</sup>Universal Technology Corporation; <sup>2</sup>UES Inc.; <sup>3</sup>AFRL; <sup>4</sup>UDRI / AFRL

Mechanical testing of micron-size samples provides distinct advantages over macroscopic testing for quantifying selected fundamental processes that govern plastic flow. However, the application and utilization of micron-scale tension testing methods has been paced by a number of factors. One factor is that sample fabrication can be both slow and expensive if an extensive amount of focused ion beam (FIB) milling is required. Another factor is a lack of suitable methods that can locally heat the micro-scale test samples while keeping temperature-sensitive components on a micro-mechanical test frame at room temperature. The present study aims to address these two deficiencies. We demonstrate a novel technique for parallelized specimen fabrication that utilizes high-aspect-ratio Si stencil masks in conjunction with a broad ion beam milling system. Furthermore, we present progress toward the development of MEMS-based microheater grips that can be used to conduct high temperature micro-tensile experiments within a scanning electron microscope.

11:00 AM

**Casting and Testing of Cast metallic Microsamples:** *Jerome Krebs*<sup>1</sup>; Csilla Miko<sup>1</sup>; Nadja Marxer<sup>1</sup>; Andreas Mortensen<sup>1</sup>; <sup>1</sup>EPFL

Under pressure, molten metal can be made to fill cavities significantly smaller than one micrometer in width. Pressure casting processes may, therefore, offer an alternative approach towards preparing net-shape metallic samples having dimensions sufficiently small for plasticity size effects to be manifest. We present results of a project aimed at the production of microsamples by pressure infiltration of molten metal into shaped micrometric cavities produced within salt-based molds, followed by directional solidification and leaching of the mold. Our goal is to define a new class of small-scale monocrystalline samples different from micromachined “nanopillars”, or vapor-grown whiskers, that can be tested for mechanical behavior on the scale of plasticity size effects. Recent results on microcast samples of aluminum and copper will be presented, with focus on their processing and mechanical properties.

11:20 AM

**Understanding Mechanical Behaviors of Indium Nanostructures through Synchrotron Laue X-Ray Microdiffraction:** *Michael Burek*<sup>1</sup>; *Arief Budiman*<sup>2</sup>; Gyuhyon Lee<sup>1</sup>; Ju-Young Kim<sup>3</sup>; Nobumichi Tamura<sup>4</sup>; Martin Kunz<sup>2</sup>; Julia Greer<sup>3</sup>; Ting Tsui<sup>1</sup>; <sup>1</sup>University of Waterloo; <sup>2</sup>Los Alamos National Laboratory; <sup>3</sup>California Institute of Technology; <sup>4</sup>Lawrence Berkeley National Laboratory

Indium is a key material in lead-free solder applications for microelectronics due to its ductility, wetting properties, and high electrical conductivity. With electronic devices continuing to shrink and the promise of indium-based nanotechnologies, it is important to develop an understanding of the mechanical properties of indium nanostructures. Studying how dislocation configurations and densities evolve in particular during deformation will be crucial in understanding the mechanical behaviors of indium nanostructures and this is enabled by the synchrotron Laue x-ray microdiffraction ( $\mu$ SXRD) technique. Using this approach, we found significant Laue peak broadening of indium after the deformation which indicates accumulation of dislocations much like in bulk metals during deformation. These observations, coupled with post-compression scanning electron microscopy, as well as in situ uniaxial compression tests, suggest thermally activated deformation processes in low-melting temperature indium, such as diffusion and dislocation climbs act to suppress the size effect commonly reported in other metal nanostructures.

---

## 2011 Functional and Structural Nanomaterials: Fabrication, Properties, Applications and Implications: Nanomaterials-Characteristics

Sponsored by: The Minerals, Metals and Materials Society, TMS Electronic, Magnetic, and Photonic Materials Division, TMS: Nanomaterials Committee

Program Organizers: Jiyoung Kim, Univ of Texas; David Stollberg, Georgia Tech Research Institute; Seong Jin Koh, University of Texas at Arlington; Nitin Chopra, The University of Alabama; Suveen Mathaudhu, U.S. Army Research Office

Thursday PM  
March 3, 2011

Room: 8  
Location: San Diego Conv. Ctr

Session Chairs: Seong Jin Koh, University of Texas at Arlington; Nitin Chopra, U. of Alabama

---

### 2:00 PM Introductory Comments

#### 2:05 PM

**Engineered Electronic Transport in Assembled Carbon Nanotube (CNT) Thin Films: Role of CNT-scale Properties and Network Topology:** *Moneesh Upmanyu*<sup>1</sup>; Hailong Wang<sup>1</sup>; Yung Jung<sup>1</sup>; Myung Hahn<sup>1</sup>; <sup>1</sup>Northeastern University

Nanoelectronic devices that rely on the superior electronic transport in individual CNTs are typically beleaguered by reliability and scalability issues, the primary reason for the ongoing paradigm shift towards CNT thin films as active elements. In this talk, we present coarse-grained computations on understanding the role CNT-scale mechanics and assembled network topology on the form of electronic transport across the thin films. In particular we explore the effect of nanoscale confinement that arises during template-assisted directed assembly of CNT solutions. Our results show that the width and thickness of the nanoscopic trenches result in a topology that acts to alleviate the effect of the electrical heterogeneity in the networks. We also presents results on the effect of extrinsic deformation, via densification or prescribed strain, on the electronic transport. Validation of the results is achieved through electrical characterization of fluidic assembly of ultra-thin CNT thin films on micropatterned silica substrates.

#### 2:20 PM

**Calculating the Relative Density of Nanoporous Metal Structures:** *Ran Liu*<sup>1</sup>; Antonia Antoniou<sup>1</sup>; <sup>1</sup>Georgia Institute of Technology

In cellular materials the relative density controls different material properties, from mechanical response to resistivity. We report on a simple phenomenological model that can predict the relative nanoporous metal density using a geometrical consideration. The dependence of relative density on ligament diameter and length is also examined. We finally report on the dependence of yield strength on relative density for isotropic nanoporous platinum structures.

#### 2:35 PM

**Fundamental Interactions between Au Nanoparticles and Deoxyribonucleic Acid:** Govind Mallick<sup>1</sup>; *Milleshree Karna*<sup>2</sup>; Shashi Karna<sup>1</sup>; <sup>1</sup>Army Research Laboratory; <sup>2</sup>University Southern California

In recent years, there has been increased interest in the application of semiconductor quantum dots (QDs) and metal nanoparticles (NPs) in biomedical research as fluorescent labels and sensors. The optical properties of QDs and NPs allow them to be effective imaging agents and also allow them to bind with target biomolecules, such as the deoxyribonucleic acid (DNA) through a linker, followed by change in color and/or electrical conductivity. The focus of this research is the understanding of fundamental interactions between gold (Au) NPs and single-strand (ss) DNA. Spectroscopic and surface probe microscopic techniques were used to investigate and understand fundamental interactions between Au NPs and ss-DNA. Uv-Vis spectra suggest complexation between Au NPs and ss-

DNA, which is also validated by Atomic force microscopic images. Further analysis of the results will be discussed.

#### 2:50 PM

**Large 3D Oxides with Length Scale Dependent Magnetic Properties:** *J. Morales*<sup>1</sup>; J. Garay<sup>1</sup>; <sup>1</sup>UC Riverside

Materials with length scale confinement have been shown to have very different magnetic properties than traditional materials. Polycrystalline bulk materials usually have the advantage of lower costs required for synthesis, but bulk materials with grain sized in the true nanoscale have been notoriously difficult to fabricate. A processing method is presented for the production of macroscopic nanocomposites that display length scale dependent magnetic properties. Depending on the composition, the nanocomposites have soft or hard magnetic hysteresis, display exchange bias or have antiferromagnetic/ferrimagnetic (AFM/fM) coupling. Possible applications of our nanocrystalline oxides are permanent magnets, magnetic sensors and in magneto-optical devices. The results are discussed in terms of length scale and composition of magnetic phases.

#### 3:05 PM

**Thermoelectric Circuits Based on Single Bismuth Telluride and Bismuth Nanowires as Bolometric Detectors:** *Tito Huber*<sup>1</sup>; K. Owusu<sup>1</sup>; <sup>1</sup>Howard University

Bismuth and Bismuth Telluride compounds are thermoelectrics of high efficiency. Films and nanowires of these materials are interesting as building blocks of thermoelectric circuits that can measure the incident electromagnetic energy, such as infrared light and X-rays. We will discuss our method for the fabrication of individual nanowires and the preparation of thermoelectric circuits based on them. Our fabrication method is based on several steps, namely, synthesis of nanowire array composites, isolation of the individual nanowires in solution, deposition of the nanowires on patterned electrodes, and contact making using focused ion beam and other techniques. Results of measurements of the electronic transport and thermoelectric properties of the circuits will be presented. The implication of these technology advances in the field of bolometric detection will be discussed.

#### 3:20 PM

**Crystallization Kinetics and Giant Magneto Impedance Behavior of FeCo Based Amorphous Wires:** *Rajat Roy*<sup>1</sup>; Partha Sarkar<sup>1</sup>; Satnam Singh<sup>1</sup>; Ashish Panda<sup>1</sup>; Amitava Mitra<sup>1</sup>; <sup>1</sup>National Metallurgical Laboratory

The effects of Nb addition on crystallization kinetics and giant magneto impedance (GMI) properties of  $\text{Fe}_{39}\text{Co}_{39}\text{Si}_8\text{B}_{14}$  amorphous wires prepared by in-water quenching system have been investigated. Thermal behaviors of the wires have been investigated by thermal electrical resistivity measurement and differential scanning calorimetry. The substitution of 4 at% Nb for Fe and Co increases crystallization temperature and merges two crystallization peaks into one peak, leading to a significant increase in thermal stability against crystallization for  $\text{Fe}_{37}\text{Co}_{37}\text{Nb}_4\text{Si}_8\text{B}_{14}$  wire. The formation of  $\text{Fe}_2\text{Nb}$  phase due to addition of Nb increases the activation energy for crystallization from 425 to 550 kJ/mol. The GMI properties of the alloys are evaluated at driving current amplitude of 10 mA and a frequency of 400 kHz. The alloys show the single peak behavior in the GMI profile. The change in GMI properties increases from 10% at 0 at% Nb to 25% at 4 at% Nb.

#### 3:35 PM Break

#### 3:50 PM

**Utilization of Fe-Based Nanocomposite Materials for Industrial Applications:** *Ryan Dehoff*<sup>1</sup>; Andrew Klarnar<sup>1</sup>; Wei Chen<sup>1</sup>; Peter Blau<sup>1</sup>; Louis Aprigliano<sup>2</sup>; Dave Novotnak<sup>3</sup>; William Peter<sup>1</sup>; <sup>1</sup>Oak Ridge National Laboratory; <sup>2</sup>Strategic Analysis, Inc.; <sup>3</sup>Carpenter Powder Products

Nanomaterials are typically not utilized for structural applications due to size scale limitations and difficulty producing bulk quantities of material. The current research examines the production of Fe-based amorphous or nanocrystalline powder materials via the gas atomization process and subsequent utilization of these powder materials for the production of bulk components and coatings. High cooling rates associated with the gas

atomization process allow for increased quantities of Boron and Carbon to be incorporated into the material than would be tolerable during conventional alloy processing such as casting. Devitrification of the amorphous material resulted in a nanoscale or submicron distribution of complex carbides and borides distributed in an iron based matrix. The resulting material is extremely hard and abrasion resistant, making it an ideal material for high wear applications. The microstructure and mechanical behavior of the material is discussed including material function in field applications.

4:05 PM

**Silicon Coated Vertically Aligned Carbon Nanotubes as High Capacity Anodes for Lithium Ion Batteries:** *Kara Evanoff*<sup>1</sup>; Thomas Fuller<sup>1</sup>; W. Jud Ready<sup>2</sup>; Gleb Yushin<sup>1</sup>; <sup>1</sup>Georgia Institute of Technology; <sup>2</sup>Georgia Tech Research Institute

The development of thick, high specific capacity anodes with long cycle lifetime is an attractive route to increase the energy and power storage characteristics of Li-ion batteries with reduced cost and weight. Silicon (Si) has a theoretical capacity nearly ten times greater than graphitic anodes. However utilizing Si in a non-destructive manner has been a challenge due to the large volume changes that occur during Li insertion and extraction. Without sufficient mechanical robustness of Si-based anodes and without free space available in the electrode for Si volume expansion during electrochemical alloying with Li, the significant stresses generated during cell operation commonly lead to rapid mechanical degradation of the anode. Here, we present a novel, robust anode architecture consisting of Si coated vertically aligned carbon nanotubes to achieve a high specific capacity, large thickness, and greatly improved anode stability.

4:20 PM

**Engineering Shapes in Nanotechnology: Helicity on Demand:** *Zi Chen*<sup>1</sup>; Carmel Majidi<sup>2</sup>; David Srolovitz<sup>3</sup>; Mikko Haataja<sup>1</sup>; <sup>1</sup>Princeton University; <sup>2</sup>Harvard University; <sup>3</sup>Institute of High Performance Computing

The formation of helical nanostructures continues to be a subject of intense fundamental and applied research. Though usually modeled as one-dimensional space curves, natural and synthetic helices often exhibit behavior that can only be captured with two-dimensional models. In this work, the pitch angles, chiralities, and radii of such helices are determined within a novel theoretical framework combining continuum mechanics and differential geometry. The theory can be specialized to study a broad range of natural and engineered helical shapes. As a concrete example, the deformation of a thin, elastically isotropic ribbon under prescribed surface stress on one or both surfaces is resolved, with the morphology of resulting helix quantitatively related to the surface stresses. Furthermore, the theoretical predictions are shown to be in excellent quantitative agreement with table-top experiments. In more general terms, we anticipate this framework will enable the design of engineered helical structures in, e.g., biology and nanotechnology.

4:35 PM

**Nanoimprinting and Piezoresponse Force Microscopy of Ferroelectric Poly(Vinylidene Fluoride-Trifluoroethylene) Copolymer Films:** *Yuanming Liu*<sup>1</sup>; Dirk Weiss<sup>1</sup>; Jiangyu Li<sup>1</sup>; <sup>1</sup>University of Washington

Patterned poly(vinylidene fluoride-trifluoroethylene) [P(VDF-TrFE)] ferroelectric films with feature size down to nanometer scales have their scientific and technological significances. In this talk, we demonstrate an enhanced rapid nanoimprinting process on P(VDF-TrFE) copolymer films with feature size down to 100nm in just 3 minutes. The structure and crystallinity of the thin film were measured by scanning electron microscope, and atomic force microscope. The ferroelectricity of the imprinted films was investigated by surface potential measurement and piezoresponse force microscopy. Electrical properties of P(VDF-TrFE) films were also studied utilizing switching spectroscopy PFM (SSPFM) mode, which allowed real-space mapping of switching behavior and electromechanical activity. The SSPFM measurements were carried out at different temperatures. The effects of imprinting conditions have been investigated, and the optimal imprinting parameters for excellent pattern transfer have been identified.

4:50 PM

**Synthesis of Vertical Ultra-long Platinum Nanolawns via Thermally Assisted Photoreduction:** *You-Lin Shen*<sup>1</sup>; Shih-Yun Chen<sup>1</sup>; Jenn-Ming Song<sup>2</sup>; Tzu-Kang Chin<sup>2</sup>; Chu-Hsuan Lin<sup>2</sup>; In-Gann Chen<sup>3</sup>; <sup>1</sup>National Taiwan University of Science and Technology; <sup>2</sup>National Dong Hwa University; <sup>3</sup>National Cheng Kung University

Among the Pt nanostructures, nanowires attract more attention because of their great potential as 3D electrodes for highly active electrocatalysts. Several methods have been reported to synthesize Pt nanowires, but there is no template and surfactant-free routes available so far for obtaining Pt nanowires with the aspect ratio higher than 50. In this study, the thermally-assisted photoreduction process, is developed to prepare vertically grown ultra-long Pt nanowires via the photocatalytic ability and semiconductor characteristics of the TiO<sub>2</sub> substrate. The remarkable aspect ratio of up to 200 is the greatest value reported. TEM analytical results suggest that the Pt nanowires are single-crystalline with a preferred <111> growth direction. The ultra-long Pt NWs can also be prepared on TiO<sub>2</sub> coated carbon fibers. The results of electrochemical tests indicate that such a Pt NWs/TiO<sub>2</sub> hybrid structure could be applied as the electrocatalyst for methanol oxidation, which provides high catalytic activity and CO tolerance.

5:05 PM Concluding Comments

## Advances in Mechanics of One-Dimensional Micro/Nano Materials: Nanomechanics: Multilayers, Composites, Wires, and Sensors

*Sponsored by:* The Minerals, Metals and Materials Society, TMS Materials Processing and Manufacturing Division, TMS Electronic, Magnetic, and Photonic Materials Division, TMS: Nanomechanical Materials Behavior Committee

*Program Organizers:* Reza Shahbazian-Yassar, Michigan Technological University; Seung Min Han, Korea Advanced Institute of Science and Technology; Katerina Aifantis, Aristotle University

Thursday PM  
March 3, 2011

Room: 1B  
Location: San Diego Conv. Ctr

*Session Chairs:* Ali Shokuhfar, K.N.T University; Seung Min Han, Korea Advanced Institute of Science and Technology

2:00 PM

**Plasticity in the Nanoscale Cu/Nb Single Crystal Multilayers as Revealed by Ex Situ Synchrotron X-Ray Microdiffraction:** *Arief Budiman*<sup>1</sup>; Seung-Min Han<sup>2</sup>; Patricia Dickerson<sup>1</sup>; Martin Kunz<sup>3</sup>; Nobumichi Tamura<sup>3</sup>; John Hirth<sup>1</sup>; Amit Misra<sup>1</sup>; <sup>1</sup>Los Alamos National Laboratory (LANL); <sup>2</sup>Stanford University; <sup>3</sup>Advanced Light Source (ALS), Berkeley Lab

There is much interest in the recent years in the nanoscale metallic multilayered composite materials due to their unusual mechanical properties such as very high flow strength and stable plastic flow to large strains. These unique mechanical properties have been proposed to result from the interface-dominated plasticity mechanisms in nanoscale composite materials. Studying how the dislocation configurations and densities evolve during deformation will be crucial in understanding the mechanics of the nanolayered materials. To shed light on these topics, uniaxial compression experiments on nanoscale Cu/Nb single crystal multilayer pillars using ex situ synchrotron Laue X-ray microdiffraction technique were conducted. Using this approach, we found significant Laue peak broadening in the Cu phase after deformation while none was observed in the Nb phase. These observations suggest that the plasticity here is achieved by storage and recovery of dislocations by the many interfaces in the multilayers during the course of the deformation.



2:20 PM

**Enhanced Tensile Strength and Ductility in Nano-Multilayer:** *Ju-Young Kim*<sup>1</sup>; Julia Greer<sup>1</sup>; <sup>1</sup>Caltech

We have performed the in-situ tensile and compressive testing and microstructural characterizations of nano-multilayer of Cu-Zr metallic glass and nanocrystalline (nc) Cu. They show enhanced strength and ductility at the nano-scale compared to single amorphous Cu-Zr layer. We found nc Cu layers play a key role in attaining ductility in these composites by preventing shear bands from transferring into the neighboring Cu-Zr layer. The initial films were deposited via RF magnetron-sputtering, and dog-bone shaped one-dimensional micro-tensile/compressive samples were patterned using photolithography, directional ion milling, and undercutting of Si substrate by selective dry etching. We analyze the specific deformation mechanisms leading to the nano-multilayers' improved mechanical properties by focusing on the non-trivial contribution of interfaces to defect activity during deformation with TEM images.

2:40 PM

**In-Situ Observation of Ultra-Strong but Ductile Deformation Behavior of Single Crystalline Metallic Nanowires:** Jong Hyun Seo<sup>1</sup>; Youngdong Yoo<sup>2</sup>; Sang Won Yoon<sup>1</sup>; Tae-Yeon Seong<sup>3</sup>; *In-Suk Choi*<sup>4</sup>; Kon Bae Lee<sup>5</sup>; Bongsoo Kim<sup>2</sup>; Jae-Pyoung Ahn<sup>4</sup>; <sup>1</sup>Korea Institute of Science and Technology - and - Korea University; <sup>2</sup>KAIST; <sup>3</sup>Korea University; <sup>4</sup>Korea Institute of Science and Technology; <sup>5</sup>Kookmin University

We experimentally observed ultra-strong but ductile deformation behavior of single crystalline Au, Pd and PdAu nanowires resulting from deformation twinning process. In-situ tensile tests were performed using Nanomanipulator and AFM force measurement equipped in FEI DualBeam system. Microstructural change was also characterized using TEM at different deformation stages. The real time observation of twin nucleation and twin migration of metallic nanowires was accomplished with quantitative stress-strain measurement. The yield stress of a  $\langle 110 \rangle$  rhombic Au nanowire reaches up to 1.54 GPa at 4% elastic strain and then twin nucleation occurs with a sudden load drop down to 200 MPa. Followed by twin migration, structural reorientation of the  $\langle 110 \rangle$  rhombic nanowires into the  $\langle 100 \rangle$  square nanowires results in ductile elongation at about 41% at the constant stress of 200 MPa. The ultra-strong but ductile deformation by twinning process was also observed for Pd and PdAu nanowires.

3:00 PM

**Artificial Neural Network for Solving Large Deflection of Micro/Nano-Beams:** *Payam Heidary*<sup>1</sup>; Ali Shokuhfar<sup>1</sup>; <sup>1</sup>K.N.Toosi University of Technology

A technique based on artificial neural network (ANN) is developed for solving large deflection of micro/nano beams. The proposed method is designed to be simple and is accessible to users with minimal experience with multi-layer feed forward ANN. Additionally, this ANN method produces a continuous solution, which can be evaluated at any point within the domain and satisfies the boundary conditions. Traditional training methods of ANN for solving nonlinear Euler Bernoulli beams consisting a system of Fourth order nonlinear boundary value problem are inappropriate and those cannot reach to best approximation. In this paper, to overcome the limitation associated with the current training algorithm, a hybrid of two optimization methods, i.e. sequence quadratic programming (SQP) and particle swarm optimization (PSO) have been used for training adjustable parameters in approximation function. Some of the numerical results are described to validate the proposed technique and to compare with finite difference method.

3:20 PM

**Geometric Nonlinear Effects on the Micro/Nano-cantilever Biosensors:** Ali Shokuhfar<sup>1</sup>; *Payam Heidary*<sup>1</sup>; <sup>1</sup>K.N.Toosi Univ. of Technology

In this study the influence of geometrically nonlinear deformation on the response of microsensors based on tension or displacement detection was investigated. Although the large deflection of micro/nano-scale sensor can improve the signal to noise ratio, it can be expected that nonlinear response create poor scale factor linearity. Nonlinear Euler-Bernoulli beams theory

for the geometrically nonlinear deformation was utilized. The introduced nonlinear model has been compared with the effect of behavior on the performances of the microsensors with tension or displacement detector. Based on the introduced model for both silicon and polymeric sensors, the opportunities and challenges of nonlinear microsensors and the designed guidelines are discussed. The results were compared with existing simulation data and the sources of errors were discussed.

3:40 PM Break

4:00 PM

**Synthesis and Mechanical Properties of AL/ $\gamma$ -Al12Mg17 Nanocomposite Prepared by Ball Milling and Hot Pressing:** *Ali Shokuhfar*<sup>1</sup>; Ashkan Zolriasatein<sup>1</sup>; Narguess Nemati<sup>2</sup>; Abbas Sabahi<sup>2</sup>; <sup>1</sup>Advanced Materials and Nanotechnology Research Laboratories, Department of Mechanical Engineering, K.N.Toosi University of Technology; <sup>2</sup>Sahand University of Technology

Aluminium based metal matrix composites reinforced with  $\gamma$ -Al12Mg17 intermetallic nano particle were prepared by mechanical milling and hot pressing methods.  $\gamma$ -Al12Mg17 intermetallic nano particle was synthesized by mechanical milling (MM) of Pre-alloyed  $\beta$ -Al13Mg2 intermetallic compound ingot in attritor ball mill. The content of reinforcement in the composite was varied from 0 to 15% (by weight). Powders were mixed by planetary ball mill for 10 hour. Hot pressing of milled samples was executed at 380°C under 800MPa pressure in a uniaxial die. Nanocomposite samples were prepared in sizes 10 mm in diameters and 20 mm in height. Investigation of density, hardness and compression test properties has carried out on the nano composite sample to study the effect of particles concentration on mechanical properties. The  $\gamma$ -Al12Mg17 reinforcement remarkably improves the mechanical properties of pure Al.

4:20 PM

**Effect of Intermetallic Reinforcement Particle Size on Wear Behaviour of Al/ $\gamma$ -Al12Mg17 Nanocomposite Prepared by Ball Milling and Hot Pressing:** Ashkan Zolriasatein<sup>1</sup>; *Ali Shokuhfar*<sup>1</sup>; Narguess Nemati<sup>2</sup>; <sup>1</sup>Advanced Materials and Nanotechnology Research Laboratories, Department of Mechanical Engineering, K.N.Toosi University of Technology; <sup>2</sup>Sahand University of Technology

In this work, the wear behaviour of aluminium matrix composites reinforced with  $\gamma$ -Al12Mg17 intermetallic particles was evaluated. Composite samples were manufactured by ball milling and hot pressing method using different amounts of  $\gamma$ -Al12Mg17 intermetallic particles having various sizes (nano and micro particles) were mixed with micrometric Al powder particles. Attrition milling time of prealloyed intermetallic powder particles was optimized to prepare nano and micro  $\gamma$ -Al12Mg17 intermetallic particles. Hot pressing of milled samples was executed at 380°C under 800MPa pressure in a uniaxial die. After the manufacturing, samples were tested in terms of wear. Volumetric wear rate was determined by the measurement of difference in weight of the pin sample before and after the test using a high precision balance. The effects of intermetallic reinforcement particle size on wear behaviour of nanocomposite were investigated. Based on the SEM observation of the worn surfaces the plausible wear mechanisms were discussed.

## Aluminum Reduction Technology: Energy Savings by Cell Design Improvements

Sponsored by: The Minerals, Metals and Materials Society, TMS Light Metals Division, TMS: Aluminum Committee, TMS: Aluminum Processing Committee

Program Organizers: Mohd Mahmood, Aluminium Bahrain; Abdulla Ahmed, Aluminium Bahrain (Alba); Charles Mark Read, Bechtel Corporation; Stephen Lindsay, Alcoa, Inc.

Thursday PM  
March 3, 2011

Room: 17B  
Location: San Diego Conv. Ctr

Session Chair: Bjorn Moxnes, Hydro Aluminium AS

2:00 PM

**Experimental Investigation of Single Bubble Characteristics in a Cold Model of a Hall-Héroult Electrolytic Cell:** Subrat Das<sup>1</sup>; Yos Morsi<sup>1</sup>; Geoffrey Brooks<sup>1</sup>; William Yang<sup>2</sup>; John Chen<sup>3</sup>; <sup>1</sup>Swinburne University of Technology; <sup>2</sup>CSIRO Light Metals National Research Flagship; <sup>3</sup>University of Auckland

Understanding the characteristics of the bubbles generated within a Hall-Héroult electrolytic cells, can assist greatly in the optimization and the operation of the process. One of the significant factors that greatly influence the bubbles formation is the vertical walls formed by the anodes. In this paper we used a high speed camera to investigate the effect of vertical walls on the shape of a single bubble rising in two liquids of high and low viscosity namely glycerol and water respectively under various offsets of the vertical wall and gas injection rates. The images of the bubble rising were recorded at the speed of 5000 frames per second and subsequently processed using the classical image-processing algorithms incorporated with MATLAB. The data related to various parameters such as aspect ratio, equivalent diameter of the bubble and bubble distance from the vertical wall are presented and discussed for various flow rate regimes. The findings showed that the presence of a vertical wall on one side of the bubble has a significant effect on the bubble shape, orientations and the trajectory path. In addition, it was found that as the bubble moved away from the wall, the velocity of the fluid between the bubble and the wall increased relative to the surrounding fluid, which created an asymmetric flow field around the bubble. Still the aspect ratios of the bubbles were found to be a function of the rate of gas injection as well as wall offset.

2:20 PM

**Large Gas Bubbles under the Anodes of Aluminum Electrolysis Cells:** Alexandre Caboussat<sup>1</sup>; Laszlo Kiss<sup>2</sup>; Jacques Rappaz<sup>3</sup>; Klára Vékony<sup>4</sup>; Alexandre Perron<sup>5</sup>; Steeve Renaudier<sup>6</sup>; Olivier Martin<sup>7</sup>; <sup>1</sup>Ycoor Systems SA; <sup>2</sup>Université du Québec à Chicoutimi; <sup>3</sup>École Polytechnique Fédérale de Lausanne; <sup>4</sup>Universitat Politècnica de Barcelona; <sup>5</sup>Rio Tinto Alcan - CRDA; <sup>6</sup>Rio Tinto Alcan - LRF; <sup>7</sup>Rio Tinto Alcan - LRF

The gas bubble laden layer under the anodes during the electrolysis of alumina plays an important role in the hydrodynamics and the voltage balance of the reduction cells. Under certain geometrical and operational conditions, very large gas pockets can be formed. The particular shape of these large gas bubbles was first described by Fortin et al in 1984. In the present paper the results of a combined experimental and numerical approach are described. In the experiments, the shape and the kinematics of the Fortin bubbles were analyzed by videography and Particle Image Velocimetry (PIV). A finite element method (FEM) combined with a Volume of Fluid (VOF) method was used to reproduce the experimentally observed phenomena, with particular attention to the reduction of the numerical diffusion of the liquid-gas interfaces. The morphology of the large bubbles and their movement including the velocity field around them are described.

2:40 PM

**Initiatives To Reduction Of Aluminum Potline Energy Consumption Alcoa Poços De Caldas/Brazil:** André Abreu<sup>1</sup>; Mauro Salles<sup>1</sup>; Ciro Kato<sup>1</sup>; <sup>1</sup>Alcoa

Energy is one of the most important inputs for aluminum production and is responsible for approximately 40% of the cost of aluminum production (CAP) in Soderberg pots. Facing the 2008/09 global economic downturn, Alcoa Poços de Caldas Plant, Brazil, has focused its efforts on a planned project, counting on its personnel's potential, to reduce the energy consumption. Main initiatives taken along this process were: workshops on energy (thermal balance and energy consumption), STAR Probe measurements (pot control focused on thermal balance), new cathode design, financial model development and changes in automatic pot control. Through this project a reduction of 77mV/pot and 0.30 kWh/kg Al were achieved, the best ever result reached at the plant at the present load level. In financial terms, in 2008/09, US\$ 1 million was saved without any extra investment.

3:00 PM

**Electrical Conductivity of the KF-NaF- AlF<sub>3</sub> Molten System at Low Cryolite Ratio with CaF<sub>2</sub> Additions:** Alexander Redkin<sup>1</sup>; Alexander Dedyukhin<sup>1</sup>; Alexei Apisarov<sup>1</sup>; Pavel Tin'ghaev<sup>1</sup>; Yurii Zaikov<sup>1</sup>; <sup>1</sup>Institute of High Temperature Electrochemistry

Calcium fluoride is brought to cryolite-alumina melts with alumina. The CaF<sub>2</sub> content does not exceed 5 wt.%. It increases density and depress the electrical conductivity of cryolite-alumina melts. The influence of calcium fluoride on physicochemical properties is investigated only for high cryolite ratio (2.5-3.0). At lower CR the electrical conductivity of cryolite melts containing CaF<sub>2</sub> was not investigated yet. The electrical conductivity of the NaF-KF-AlF<sub>3</sub> system at CR=1.3-1.7 was investigated depending on the CaF<sub>2</sub> content and [KF]/([NaF]+[KF]) molar ratio. The CaF<sub>2</sub> concentration did not exceed 16 wt. %. The [KF]/([NaF]+[KF]) molar ratio was varied from 0 to 0.5. The electrical conductivity was found to decrease with calcium fluoride addition at all electrolytes under investigation. The cryolite ratio effect on the electrical conductivity of NaF-KF-AlF<sub>3</sub>-CaF<sub>2</sub> melts has been discussed.

3:20 PM Break

3:30 PM

**Study of ACD Model and Energy Consumption in Aluminum Reduction Cells:** Tian Yingfu<sup>1</sup>; Wang Hang<sup>1</sup>; <sup>1</sup>Chongqing Tiantai Aluminum Industry Co., Ltd

A model of anode-cathode distance (ACD) is built according to actual production in traditional reduction cells. And the limit ACD is study in this paper. Based on the ACD model and the limit ACD it can be described why some cells can normal produce under low cell voltage at present aluminum industry. And it is possible that only 9500kW•h/t of the DC energy will be required at 2.0 cm of ACD and 0.8 A/cm<sup>2</sup> of anode current density.

3:50 PM

**Cell Voltage Noise Reduction Based on Wavelet in Aluminum Reduction Cell:** Binchuan Li<sup>1</sup>; Jianshe Chen<sup>1</sup>; <sup>1</sup>Northeastern University

For line current fluctuation, cell voltage signals collected in aluminium electrolysis process are with high noise, which have a significant impact on the electrolyzer cell voltage and precision of alumina feeding amount. Based on wavelet de-noising theory, this paper analyses and compares different wavelet bases and threshold conditions for signal de-noising effect by application of MATLAB modeling simulation and field research. Simulation and processing results of field data show that 5-step Harr Wavelet is a good choice for filtering cell voltage signal, with better prospects.

## Bulk Metallic Glasses VIII: Mechanical and Other Properties II

Sponsored by: The Minerals, Metals and Materials Society, TMS Structural Materials Division, TMS/ASM: Mechanical Behavior of Materials Committee

Program Organizers: Gongyao Wang, University of Tennessee; Peter Liaw, Univ of Tennessee; Hahn Choo, Univ of Tennessee; Yanfei Gao, Univ of Tennessee

Thursday PM  
March 3, 2011

Room: 6D  
Location: San Diego Conv. Ctr

Session Chairs: Dongchan Jang, California Institute of Technology; Yuri Petrusenko, National Science Center - Kharkov Institute of Physics & Technology

### 2:00 PM Invited

**Transition from Strong-Yet-Brittle to Stronger-and-Ductile by Size Reduction in Metallic Glasses:** Dongchan Jang<sup>1</sup>; Julia Greer<sup>1</sup>; <sup>1</sup>California Institute of Technology

A combination of high strength and extended deformability of materials is favorable for engineering applications, as the former assures optimal performance under extreme environments while the latter increases the reliability by protecting the system from a sudden breakdown. In this work we report the attainment of both high strength and superior deformability in Zr-based metallic glass by using sample dimensions as key property-controlling parameter. We report that once the lateral dimension is decreased to 100 nm, the formation of shear bands ceases, and the material shows significant homogeneous plasticity (25%) while maintaining its high strength (2.25 GPa). Furthermore, unlike in other engineering materials, we observe a distinct difference between the transition from lower, bulk-like strength to higher one and that from brittle to ductile deformation, as strength and ductility appear to be de-coupled in these metallic glass nano-pillars. A phenomenological model for size dependence and brittle-to-homogeneous deformation is provided.

### 2:20 PM Invited

**Local Structures of Supercooled Ni-Nb, Cu-Zr, and Cu-Hf Melts at Eutectic and Bulk Metallic Glass-Forming Compositions:** Victor Wessels<sup>1</sup>; Kevin Laws<sup>2</sup>; Kisor Sahu<sup>1</sup>; Nicholas Mauro<sup>3</sup>; Anup Gangopadhyay<sup>3</sup>; Kenneth Kelton<sup>3</sup>; Jörg Löffler<sup>1</sup>; <sup>1</sup>ETH Zurich Laboratory of Metal Physics and Technology; <sup>2</sup>University of New South Wales; <sup>3</sup>Washington University in St. Louis

The development of stable, efficiently-packed clusters has been proposed to form the basis of improved glass-forming ability in certain alloy compositions. The observation of similar cluster formation in supercooled liquids of binary eutectic compositions may provide a solution to the longstanding puzzle of Stockdale, Hume-Rothery and Anderson regarding the preferential occurrence of eutectics at certain whole-number composition ratios. Recently, a rapid chemical and topological ordering in a supercooled Cu<sub>46</sub>Zr<sub>54</sub> liquid was measured using the beamline electrostatic levitation (BESL) technique, consistent with the results of MD simulations that predict the development of atomic-scale ordered clusters in supercooled melts prior to the glass transition. Here, BESL studies were conducted on various eutectic and glass-forming compositions in Ni-Nb, Cu-Zr, and Cu-Hf alloys. By comparing the results of the BESL analysis with predictions from a stable cluster packing model, the influence of atomic-scale clustering on liquid stability and glass-forming ability was studied.

### 2:40 PM

**Sliding Wear Behavior of Cu<sub>50</sub>Hf<sub>41.5</sub>Al<sub>8.5</sub> Bulk Metallic Glass:** Rainer Hebert<sup>1</sup>; Dharma Maddala<sup>1</sup>; <sup>1</sup>University of Connecticut

The sliding wear and friction behavior of Cu<sub>50</sub>Hf<sub>41.5</sub>Al<sub>8.5</sub> bulk metallic glass has been studied at different devitrification stages. Hardness and wear volume loss are linearly related for the fully amorphous condition and the early devitrification stage. For longer annealing times, the crystallization

products remain below about 50-80 nm in size, the wear behavior improves marginally while the hardness increases about twice as much for samples annealed at 515°C for between 60 min and 300 min annealing than for the first 60 min. Fracture toughness measurements suggest that the wear behavior changes from hardness controlled to fracture toughness controlled with devitrification. Transmission electron microscopy studies showed moreover that nanocrystals developed during sliding for as-cast sample and structurally relaxed samples. The results of this study suggest that wear behavior of the Cu<sub>50</sub>Hf<sub>41.5</sub>Al<sub>8.5</sub> metallic glass can be improved with careful annealing treatments and then exceeds the wear behavior of 304 stainless steel.

### 2:50 PM Invited

**Residual Stresses Induced by Laser Shock Peening on Zr-Based Bulk Metallic Glass and Its Effect on Plasticity:** Yunfeng Cao<sup>1</sup>; Xie Xie<sup>2</sup>; Bartłomiej Winiarski<sup>3</sup>; Gongyao Wang<sup>2</sup>; Yung Shin<sup>1</sup>; Philip Withers<sup>3</sup>; Peter Liaw<sup>2</sup>; <sup>1</sup>Purdue University; <sup>2</sup>University of Tennessee; <sup>3</sup>University of Manchester

Zr-based bulk metallic glasses (BMGs) are a new family of attractive materials with good glass-forming ability and excellent mechanical properties. However, BMGs typically show near-zero ductility in tension and limited plasticity in compression, which significantly impedes the wide industrial application of BMGs. It was recently reported that the plasticity of BMG can be improved by controlling the residual stress in BMGs. In this study, laser shock peening (LSP) under a water-confinement configuration is employed to impart compressive residual stresses into the BMG material and hence to improve the plasticity of BMG. An improvement of plasticity is demonstrated via static compression tests. A complete LSP model, while considering the LSP-induced plasticity, is employed to predict the residual stresses by LSP for the first time, which are compared with the experimental data measured by the focused-ion-beam micro-slitting method. A reasonable agreement is obtained, especially in the region close to the workpiece surface.

### 3:10 PM

**Relaxation and Nanocrystallization of Bulk Amorphous Niti Processed by Severe Plastic Deformation:** Martin Peterlechner<sup>1</sup>; Joachim Bokeloh<sup>2</sup>; Gerhard Wilde<sup>2</sup>; Thomas Waitz<sup>1</sup>; <sup>1</sup>University of Vienna, Faculty of Physics; <sup>2</sup>University of Münster

Metallic glasses can be obtained by processing routes that drive an initial crystalline phase far from thermal equilibrium. In the present work, bulk amorphous NiTi alloys were processed by severe plastic deformation. At relatively low degrees of the deformation, specimens contain a mixture of crystalline and amorphous phases. The crystalline volume fraction decreases with increasing degree of deformation until an almost completely amorphous structure is obtained. Upon heating, nanocrystallization occurs by three-dimensional growth at a constant rate. The overall activation energy of the crystallization is significantly lower than that observed in the case of thin ribbons of amorphous NiTi processed by sputter deposition or melt spinning. The results of the crystallization obtained from isothermal calorimetry were modelled in terms of the Johnson-Mehl-Avrami theory. This requires a careful analysis of the data with respect to the overall exothermic heat flow caused by crystallization and relaxation of the amorphous phase.

### 3:20 PM Break

### 3:30 PM Invited

**Manifestation of the Bulk Metallic Glass Structure Features in the Compression-Compression Fatigue Experiments:** Yuri Petrusenko<sup>1</sup>; Alexander Bakai<sup>1</sup>; Ivan Neklyudov<sup>1</sup>; Sergij Bakai<sup>1</sup>; Peter K. Liaw<sup>2</sup>; Gongyao Y. Wang<sup>2</sup>; Lu Huang<sup>3</sup>; Tao Zhang<sup>3</sup>; <sup>1</sup>National Science Center - Kharkov Institute of Physics & Technology; <sup>2</sup>The University of Tennessee; <sup>3</sup>Beihand University

We have performed extensive experiments using the electron irradiation and fatigue technique, which study the bulk metallic glass (BMG) structure-defect stability and their role in the anelastic and plastic deformations. These data in combination with results of the field emission microscopy lead to a conclusion that BMGs possess stable points and extended structure defects. This conclusion is important for the interpretation of results of the low (10



Hz) and high (20 kHz) frequency compression-compression fatigue and fracture experiments. The low-frequency fatigue has comparatively large fatigue-endurance limits, and the fracture is controlled by the initiated from the surface catastrophic crack propagating at a direction of 45° to the applied stress. At the high-frequency fatigue the BMG fracture is a result of several stages, which includes anelastic boundary slip, slip-layers formation and propagation, branching and development of the inner nano-cracks, resulting in the catastrophic crack formation mainly along the applied stress direction.

#### 3:50 PM

**Structural Characterization of Iron Based Bulk Metallic Glass by Dilatometric Measurements:** Fatemeh Saedi<sup>1</sup>; Mahmoud Nili-Ahmadaadi<sup>2</sup>; Amir Seifoddini<sup>1</sup>; <sup>1</sup>University of Tehran

Bulk metallic glasses (BMGs) are a relatively new class of materials with a specific combination of interesting properties. Understanding the structure of BMGs is an attractive issue in material science, due to its close connection with glass forming ability and mechanical properties. The structural inhomogeneous nature and the structural stability of BMGs greatly affect their mechanical properties. In the present study, dilation measurements were conducted on samples of a Fe-Co-Cr-Mo-Y-C-B bulk metallic glass to calculate the structural stability and the activation energy of the alloy by heating samples with different heating rates and routes. Dilation curves and thermal behavior of the samples are analyzed based on the structural relaxation and free volume theory. In addition some thermal parameters such as glass transition temperature and crystallization temperatures are obtained by dilatometric curve and compared with temperatures derived from differential thermal analysis (DTA).

#### 4:00 PM

**Effect of Li on the Microstructure and Mechanical Properties of an Mg-Based BMG:** Ignacio Figueroa<sup>1</sup>; John Plummer<sup>2</sup>; Iain Todd<sup>2</sup>; <sup>1</sup>National Autonomous University of Mexico; <sup>2</sup>University of Sheffield

Though Mg-based glassy alloys typically fail in a brittle manner, with cracking often occurring before yielding, they display high specific strengths making them a potential option for engineering applications. Li has the ability to lower the density of the alloy further though limited data is present in the literature as to the effect it has on structure, with no reports of its impact on mechanical response. Here, between 3-15 at% Li is added to a base Mg-Cu-Gd BMG with XRD and TEM implemented to characterise the structural response to the alloying addition. Adding Li in increasing proportions is found to favour the formation of a glass-crystal composite and induce plastic flow. Finally, a fully crystalline alloy results with maximum plastic flow, whilst retaining the high failure strength of the base alloy. It is thus illustrated that amorphous pre-cursors can lead to crystalline alloys with improved mechanical properties.

#### 4:10 PM Invited

**Selective Nanocrystallization of Metallic Glasses Induced by Nanoindentation:** Jordi Sort<sup>1</sup>; Jordina Fornell<sup>1</sup>; Aida Varea<sup>1</sup>; Emma Rossinyol<sup>1</sup>; Luiz Bonavina<sup>2</sup>; Carlos Souza<sup>2</sup>; Walter Botta<sup>2</sup>; Claudemiro Bolfarini<sup>2</sup>; Claudio Kiminami<sup>2</sup>; Santiago Suriñach<sup>1</sup>; Josep Nogués<sup>3</sup>; Maria D Baró<sup>1</sup>; <sup>1</sup>Universitat Autònoma de Barcelona; <sup>2</sup>Universidade Federal de Sao Carlos; <sup>3</sup>ICREA/ICN-CSIC

Nanocrystallization of  $Zr_{62}Cu_{18}Ni_{10}Al_{10}$  and  $Fe_{67.7}B_{20}Cr_{12}Nb_{0.3}$  (at %) metallic glasses can be locally induced by nanoindentation. While in the first alloy this phenomenon causes significant increases in hardness and plasticity, nanocrystallization of the Fe-based alloy constitutes an effective magnetic patterning procedure. Indeed, periodic arrays of micrometer-sized ferromagnetic structures with perpendicular-to-plane magnetic anisotropy and enhanced saturation magnetization are obtained at the surface of the Fe-based glassy ribbon (initially showing in-plane magnetic anisotropy) after nanoindentation. Detrimental effects caused by the dipolar/exchange interactions between the dots and the matrix can be avoided by heating the indented ribbon beyond  $T_c$  of the glass (340 K), since the crystallized regions (consisting of  $\alpha$ -Fe) remain ferromagnetic up to very high temperatures. The inverse magnetostriction effect seems to be the main factor contributing to the observed perpendicular anisotropy. Our results pave the way for new

strategies to fabricate miniaturized magnetic devices or patterned magnetic recording media.

#### 4:30 PM

**Phase Formation and Mechanical Properties of Cu-Zr-Co alloys:** Fatemeh A. Javid<sup>1</sup>; Norbert Mattern<sup>1</sup>; Simon Pauly<sup>1</sup>; Jürgen Eckert<sup>1</sup>; <sup>1</sup>Leibniz Institute for Solid State and Materials Research Dresden

Cu<sub>50</sub>Zr<sub>50</sub> B2 phase is a stable phase at temperatures above 715oC. On the other hand Co<sub>50</sub>Zr<sub>50</sub> is a B2 phase which is stable at room temperature. It seems that adding cobalt to binary Cu-Zr stabilizes Cu<sub>50</sub>Zr<sub>50</sub> B2 phase at room temperature. In this work the effect of cobalt on phase formation and mechanical properties of Cu-Zr alloy is investigated. Rods with composition of Cu<sub>50-x</sub>Zr<sub>50</sub>Cox (x=2, 5, 10, 20 at.%) and 3mm Ø were suction casted into a copper mould. X-ray analysis showed a martensite CuZr phase for 2 & 5 at.% Co compositions, while compositions with 10 & 20 at.% Co had stabilized B2 phase. DSC measurements declared a martensitic transformation for 2 & 5 at.% Co samples in which increasing the Co content, decreased the transformation temperatures. Under compression test 10 & 20 at.% Co compositions showed deformation-induced martensitic transformation and plastic strains up to 15%.

#### 4:40 PM

**Temperature Effects on Flow of Several Metallic Glasses:** Lisa Deibler<sup>1</sup>; John Lewandowski<sup>1</sup>; <sup>1</sup>Case Western Reserve University

Several different test techniques were utilized to examine the effects of changes in test temperature and/or prior thermal exposure on the flow behavior of a variety of different amorphous metal alloys. Melt spun ribbons of magnesium-, iron-, and zirconium-based metallic glasses were evaluated as well as zirconium-based bulk metallic glasses. The effects of changes in test temperature and strain rate on the flow/viscosity were determined at temperatures approaching T<sub>g</sub> for the various systems. Fracture surface morphologies for the different metallic glasses and test conditions were also characterized. The results will be reviewed in the light of ongoing work on the behavior of amorphous systems.

#### 4:50 PM

**Study of Activation Parameters of Deformation by Broadband Nanoindentation Creep in Structural Relaxed Zr-Cu-Al Bulk Metallic Glasses:** Zenon Melgarejo<sup>1</sup>; Joseph Jakes<sup>2</sup>; Jonathan Puthoff<sup>1</sup>; Hongbo Cao<sup>1</sup>; Chuan Zhang<sup>1</sup>; Donald Stone<sup>1</sup>; Paul Voyles<sup>1</sup>; <sup>1</sup>University of Wisconsin-Madison; <sup>2</sup>Performance Enhanced Biopolymers, United States Forest service, Forest Products laboratory

Models of plastic deformation in BMGs hypothesize shear transformation zones (STZs) as the elementary units of plastic deformation. Activation energy for shear of an STZ depends on stress; activation parameters should vary systematically with atomic structure including short and medium range order and should be sensitive to composition, quenching rate, and annealing. In the present work we employ broadband nanoindentation creep (BNC) to characterize activation volume and energy for plastic deformation in Zr-Cu-Al BMGs. BNC measures hardness across 5-6 decades of strain rate, and is therefore capable of mapping out the shape of the activation barrier. BMGs studied include Zr<sub>54</sub>Cu<sub>38</sub>Al<sub>8</sub>, Zr<sub>45</sub>Cu<sub>49</sub>Al<sub>6</sub>, and Zr<sub>36</sub>Cu<sub>58</sub>Al<sub>6</sub>. STZ sizes estimated from activation volume measurements vary between 170 and 600 atoms depending on composition and annealing. Annealing generally increases both activation energy and STZ volume. Structural relaxation of Zr<sub>54</sub>Cu<sub>38</sub>Al<sub>8</sub> is studied in detail by measuring BNC in specimens annealed in a differential scanning calorimeter (DSC).

#### 5:00 PM

**Enhanced Plasticity of a Zr-Cu-Ni-Al Bulk Metallic Glass by Micro Nb Additions:** Shuang-shuang Chen<sup>1</sup>; John Plummer<sup>1</sup>; Iain Todd<sup>1</sup>; <sup>1</sup>The university of Sheffield

Zr-based bulk metallic glasses have been extensively studied because of their high glass forming ability and prominent mechanical properties. In this work, the effect of micro Nb additions on plasticity of a Zr-Cu-Ni-Al bulk metallic glass is explored. In compression testing, the base alloy showed limited plasticity of 2.2%; however, this significantly increased to

19.7% upon addition of 0.5 at.% Nb, with the alloy exhibiting typical strain softening during deformation. The large plasticity was attributed to shear band interaction with a phase separated structure.

#### 5:10 PM

**A Study on Crystalline Phases Present in the As-Solidified and Crystallized Microstructures in  $Zr_{53}Cu_{21}Al_{10}Ni_8Ti_8$  Alloy:** *Raghvendra Tewari*<sup>1</sup>; Suman Neogy<sup>1</sup>; Gautam Dey<sup>1</sup>; Srikumar Banerjee<sup>2</sup>; S. Ranganathan<sup>3</sup>; <sup>1</sup>Bhabha Atomic Resrach Centre; <sup>2</sup>Department of Atomic Energy; <sup>3</sup> Indian Institute of Science

In the present study the as-solidified and subsequently crystallized microstructures of  $Zr_{53}Cu_{21}Al_{10}Ni_8Ti_8$  alloy have been examined in detail using transmission electron microscopy. Solidification was carried out by melt spinning, suction casting and copper mould casting techniques. The last technique yielded a partially crystalline microstructure comprising 'big cube phase' in dendritic morphology and bct  $Zr_2Ni$  phase, whereas the other two techniques resulted in amorphous microstructures. The crystallography of the dendritic growth and that of the instabilities at the crystal/liquid interface has been examined and it has been established that the dendrites grew by the formation of atomistic ledges. The bct- $Zr_2Ni$  phase formed during solidification also appeared during crystallization and showed various types of internal faults depending upon the crystallite size, crystallography of which has been examined. The present study also brought out the role of oxygen in controlling the degree of medium range order and crystallization behavior of glasses.

## Carbon Dioxide and Other Greenhouse Gas Reduction Metallurgy - 2011: CO<sub>2</sub> and GHG Reduction in Metal Industries

*Sponsored by:* The Minerals, Metals and Materials Society, TMS Extraction and Processing Division, TMS Light Metals Division, TMS: Energy Committee

*Program Organizers:* Neale Neelameggham, US Magnesium LLC; Ramana Reddy, The University of Alabama; Maria Salazar-Villalpando, National Energy Technology Laboratory; James Yurko, 22Ti LLC; Malti Goel, INSA

Thursday PM

Room: 15B

March 3, 2011

Location: San Diego Conv. Ctr

*Session Chairs:* Maria salazaar - Villalpando, National Energy Technology Laboratory; Malti Goel, Jawaharlal Nehru University

#### 2:00 PM Introductory Comments

#### 2:05 PM

**Vacuum Distillation of Aluminum and Silicon via Carbothermal Reduction of Their Oxides with Concentrated Solar Energy:** *Peter Loutzenhiser*<sup>1</sup>; Enrico Guglielmini<sup>1</sup>; Alwin Frei; Aldo Steinfeld<sup>1</sup>; <sup>1</sup>ETH Zurich

Using concentrated solar radiation as the energy source of high-temperature process heat, the carbothermal reductions of  $Al_2O_3$  to Al and  $SiO_2$  to Si were examined thermodynamically and demonstrated experimentally at vacuum pressures. Reducing the system pressure favors Al(g) and Si(g) formation, enabling their vacuum distillation and avoiding contamination by carbides and/or oxycarbides. Exploratory experimentation in a solar reactor was performed with mixtures of charcoal with alumina and silica in the ranges of 1300–2000 K and 1997–2263 K, respectively, at 10–3 bar by direct exposure to concentrated thermal radiation. Distilled samples contained up to 19 wt% of Al in Al- $Al_2O_3$  mixtures and 79 wt% of Si in Si- $SiO_2$  mixtures. When the reducing agent is derived from a biomass source, the solar-driven carbothermal processes are CO<sub>2</sub> neutral.

#### 2:25 PM

**The Alkali Roasting of Complex Oxide Minerals for High Purity Chemicals – Beyond Le Chatelier into 21st Century:** *Animesh Jha*<sup>1</sup>; <sup>1</sup>University of Leeds

It was in 1855 when Le Chatelier invented the alkali roasting and leaching process for the extraction of alumina from natural minerals. However, his process was replaced by the Bayer process since 1888. Was the aluminium industry short-sighted to reject Le Chatelier in favour of Bayer's process? This paper critically examines the impact of Le Chatelier's proposal for the extraction two important inorganic chemicals, aluminium hydroxide from bauxite and gibbsite and sodium chromate from chromite minerals. The paper reviews past research in alumina and chromium chemicals and adds new dimension to the chemicals processing, by considering Le Chatelier's approach for the extraction of very high purity aluminium hydroxide, chromium chemicals and titanium dioxide, using high-temperature alkali roasting followed by leaching. The emphasis of new research is on zero-waste process, including CO<sub>2</sub> sequestration, which was the beautiful characteristic of Le Chatelier's process chemistry but lost through the generations.

#### 2:45 PM

**The Alkali Roasting and Leaching of Ilmenite Minerals For the Extraction of High Purity Synthetic Rutile and Rare-Earth Oxides:** *Animesh Jha*<sup>1</sup>; *Graham Cooke*<sup>1</sup>; <sup>1</sup>University of Leeds

CO<sub>2</sub> reduction by alternative energy devices such as wind-power, electric vehicles utilize rare-earth elements (REE) in several forms; such as in piezo-electric devices, batteries and magnetic materials. In 2010, the 95% of Rare Earth supply is controlled by China, compared to USA being dominant supplier in the 1980s. The dependence upon a single source of lanthanides has prompted the utilization of lower grades of titaniferous mineral concentrates, which often have rich seams of REE. We propose a new methodology, which utilizes the low-grade minerals for the extraction of synthetic rutile and also significant quantities of REE. We demonstrate the alkali roasting of lower grades of mineral concentrates and subsequent leaching in an aqueous medium for preferential flocculation of REE during the extraction of synthetic rutile. Changes in mineral structure during alkali roasting and leaching determine flocculation of REE and permit their separation at the front end of unit process.

#### 3:05 PM

**Hydrogen-Rich and Carbon-Neutral Gas as Reducing Agent for Heavy Metal Containing Residues:** *Thomas Griessacher*<sup>1</sup>; Jürgen Antrekowitsch<sup>1</sup>; <sup>1</sup>University of Leoben

Heavy metal containing residues are typically hazardous wastes why on the one hand side a deposition gets more and more complicated and on the other hand side the large amounts of metals like Zn, Cu, Fe and Pb represent a significant value. So a post-treatment of these materials with the recovery/recycling of the metals and stabilization of the waste is not even ecological but often also economical. The therefore typically applied recycling processes utilize pyrometallurgical steps, where carbon or carbon monoxide from fossil coal and coke is used as reducing agent, which results in large amounts of CO<sub>2</sub>-emissions. An alternative option is the application of a hydrogen-rich gas emitted at biomass utilization processes as carbon-neutral reducing agent. Investigations at a retort process which were done at different temperatures and times showed excellent results concerning the achievable reduction rates and final contents of the heavy metals for various residues.

#### 3:25 PM

**Bauxite Residue Use to Remove SO<sub>2</sub> from Gas Effluents:** *Luis Venancio*<sup>1</sup>; Paulo Santos<sup>1</sup>; José Antonio Souza<sup>1</sup>; Emanuel Macedo<sup>1</sup>; Wanderson Rodrigues<sup>1</sup>; <sup>1</sup>Federal University of Pará

The production of alumina from bauxite using the Bayer process generates 0.7 to 2.0 ton of the residue known by red mud per ton of alumina. This material has no large scale current use and is usually stored. This paper shows that it can be used in a suspension with water as a gas effluent cleaner with high efficiency to remove SO<sub>2</sub>. It can substitute other materials currently

used reducing the overall environmental impact and potentially reducing the cost of gas treatment.

3:45 PM

**Greenhouse Gas Emission Reduction from Aluminum Industry in India: Challenges and Prospects:** Malti Goel<sup>1</sup>; <sup>1</sup>INSA

Ferrous and non-ferrous metals industries are source of both direct and indirect greenhouse gas (GHG) emissions. Indian metal industry accounted for 29.7% of the total GHG emitted from the industry sector in 2007 and is moving towards low carbon economy. Aluminum is second largest contributor after steel. Indian Aluminum industry is growing and is adopting several effective measures for better efficiencies through process change and waste utilization. Improvement in the energy efficiency is expected to optimize energy use and realize material efficiencies as well. It can form the basis of monitoring reduction in emissions. National Mission for Enhanced Energy Efficiency (NMEEE) seeks to upscale the efforts to unlock the market for energy efficiency on a public private partnership (PPP) basis to achieve up to 25% saving in energy. In this paper an attempt is made to overview recent developments in Indian Aluminum industry as well as summarizes challenges and prospects.

4:05 PM Break

4:15 PM

**Dissolution Kinetics of Steelmaking Slag and Its Promotion for the Growth of Algae:** Chunfang Zi<sup>1</sup>; Kai Huang<sup>1</sup>; Lianyun Liu<sup>1</sup>; Xiaohui Li<sup>1</sup>; Hongmin Zhu<sup>1</sup>; <sup>1</sup>University of Science and Technology of Beijing

In this study, the dissolution kinetics of steelmaking slag in water was studied. It was found that the silicon extraction increases with temperature, and decreasing in the particle size of slag enhanced silicon dissolution. A simple dissolution model was proposed to describe and explain the dissolution behavior of the slag particles in water. The external film diffusion was determined to be the controlling step of the whole dissolution process. The model described experimental data well in the whole process of dissolution. The apparent activation energy determined to be 4.8 kJ/mol, and the concentration of silicon produced a linear relationship with the specific surface area of slag, which also supports the assumption of external film diffusion control. Further experiments by using pH meter to monitoring the pH variation for the slag particle samples showed more proofs that the leaching behavior observed the physical dissolution process.

4:35 PM

**Life Cycle Assessment of China's Alumina Manufacturing by Bayer Process:** Li Hongxi<sup>1</sup>; Duan Ge<sup>1</sup>; Bai Hao<sup>1</sup>; Cang Daqiang<sup>1</sup>; <sup>1</sup>University of science and technology, Beijing

In this paper LCA was newly used to evaluate the environmental impact of alumina manufacturing by Bayer process in china from two aspects of matter and energy flow, Gabi software acted as analysis tools with evaluation model established, and five environmental impact assessment criteria were selected based on the actually typical date of manufacturing. Evaluation results show that alumina manufacturing has a great impact on the global warming and human health of respiration, even roasting process gives rise to the greatest impact of winter fog index. Scenario analysis has proposed possible ways of reducing environmental load caused by Bayer process including: (1) the economic and efficient use of mineral processing technology; (2) optimization of energy use, saving power consumption or the use of new more economical source of energy; (3) actively promote the use of innovated technology and equipment in alumina manufacturing and waste such as red mud utilization process.

4:55 PM

**Analysis of Carbon Emission Reduction of China's Integrated Steelworks:** Hao Bai<sup>1</sup>; <sup>1</sup>University of Science and Technology Beijing

Coal, as the main energy in ferrous metallurgy, is consumed on a large scale and great amount of CO<sub>2</sub> is emitted likewise. In this paper, a model, based on carbon balance, was developed for CO<sub>2</sub> emission analysis, with data obtained from a typical integrated steelworks in China. The result shows that, CO<sub>2</sub> emissions increase almost constantly with the growth of

steel production. However, coals of different classes and product variety in the steelworks exerted an influence on CO<sub>2</sub> emissions. Furthermore, three scenarios, including natural gas instead of coal for power generation, EAF process partly replacing integrated steelmaking, and feasible techniques applied to achieve lowest process energy consumption (LPEC), were assumed to seek possible ways of carbon emission reduction. The result proves that the second scenario is most effective. If 40% of the steel product could be from EAF process, CO<sub>2</sub> emissions would be reduced by 45.07%.

---

**Challenges in Mechanical Performances of Materials in Next Generation Nuclear Power Plants: Session II**

*Sponsored by:* The Minerals, Metals and Materials Society, American Nuclear Society, ASM International, Japan Institute of Metals, National Science Foundation, TMS Materials Processing and Manufacturing Division, TMS Structural Materials Division, ASM Materials Science Critical Technology Sector, TMS: Advanced Characterization, Testing, and Simulation Committee, TMS/ASM: Composite Materials Committee, TMS: Energy Committee, TMS: High Temperature Alloys Committee, TMS/ASM: Mechanical Behavior of Materials Committee, TMS/ASM: Nuclear Materials Committee

*Program Organizer:* Faramarz Zarandi, CANMET-Materials Technology Laboratory

Thursday PM  
March 3, 2011

Room: 5A  
Location: San Diego Conv. Ctr

*Session Chairs:* G. Robert Odette, University of California, Santa Barbara; Laura Carroll, Idaho National Laboratory

---

2:00 PM

**Simplified Powder Processing of ODS Ferritic Stainless Steels:** Joel Rieken<sup>1</sup>; Iver Anderson<sup>2</sup>; Matthew Kramer<sup>2</sup>; <sup>1</sup>Iowa State University; <sup>2</sup>Ames Laboratory

Precursor ferritic stainless steel powders (i.e., Fe-16.0Cr-(0.2-0.4)(Ti,Hf)-0.2Y at.%) were oxidized in situ using a novel gas atomization reaction synthesis technique. During this process, a metastable Cr-enriched oxide layer formed and enveloped the rapidly solidified powder particles. Upon consolidation, this metastable oxide phase was used as an internal oxygen reservoir, which was continuously dissolved during elevated temperature heat treatment, through oxygen exchange reactions with Y and other reactive alloying additions (i.e., Ti or Hf). These exchange reactions resulted in the formation of nano-metric mixed oxide dispersoids (i.e., Y-Ti-O or Y-Hf-O) throughout the alloy microstructure. Subsequent thermal-mechanical processing was then used to develop fine dislocation sub-structures for increased alloy strengthening. Transmission electron microscopy coupled with high-energy X-ray diffraction was used to evaluate phase evolution and thermal stability of the dispersoids within these ODS ferritic stainless steel alloys. Support from the USDOE-FE (ARM program) through Ames Laboratory contract no. DE-AC02-07CH11358 is gratefully acknowledged.

2:20 PM

**Degradation of High Temperature Mechanical Performance in Ferritic-Martensitic Steels:** Meimei Li<sup>1</sup>; Saurin Majumdar<sup>1</sup>; Ken Natesan<sup>1</sup>; <sup>1</sup>ANL

Ferritic-martensitic steels are the lead structural materials for next-generation nuclear energy systems. Due to increased operating temperatures required in advanced high-temperature reactor concepts, the high temperature performance of the alloys and reliable high temperature structural design methodology have become increasingly urgent issues. This paper discusses the critical code qualification issues identified for applications of advanced ferritic-martensitic steels with the focus on extension of design allowables to the 60-year design life and need for an improved creep-fatigue design rule. Efforts in developing a fundamental understanding of microstructural evolution and associated mechanical property change during long-term aging processes to assist development of mechanism-based predictive models for



reliable data extrapolation will be discussed. Detailed analysis of archive fatigue and creep-fatigue data of ferritic-martensitic steels to improve the understanding of creep-fatigue interaction and establishment of improved creep-fatigue models will also be addressed.

#### 2:40 PM

**Optimized Thermomechanical Treatment for High Strength 9Cr Ferritic-Martensitic Steels:** *Lizhen Tan*<sup>1</sup>; Edward Kenik<sup>1</sup>; Jeremy Busby<sup>1</sup>; <sup>1</sup>Oak Ridge National Laboratory

Ferritic-martensitic (F-M) steels, e.g., 9-12 wt.%Cr, are important structural materials for use in advanced nuclear reactors due to their tolerance of irradiation and swelling resistance. However, their strength is less than that of other candidate alloy systems. Many efforts have focused on controlling alloying compositions during the development of such steels. Recently, thermomechanical treatment (TMT) showed significant improvement in mechanical properties on several high-Cr F-M steels by introducing high density of dislocations and fine precipitates. This work primarily studies the effect of TMT on a commercial 9Cr F-M steel NF616. The NF616 in an optimized TMT condition showed more than 35% enhancement in strength, which had strength comparable and ductility superior to PM2000 oxide-dispersion-strengthened (ODS) steel. A variety of characterization techniques were employed to elucidate the strengthening mechanism induced by the TMT. Additionally, model 9Cr F-M steels were developed with the guidance of computational thermodynamics. Preliminary results of the model steels in TMT conditions showed significant enhancement in strength.

#### 3:00 PM

**Nitride-Strengthened Reduced Activation Martensitic Steels:** *Yiyin Shan*<sup>1</sup>; Ping Hu<sup>1</sup>; Wei Yan<sup>1</sup>; Wei Wang<sup>1</sup>; Wei Sha<sup>2</sup>; Ke Yang<sup>1</sup>; <sup>1</sup>Institute of Metal Research; <sup>2</sup>Queen's University of Belfast

Two nitride-strengthened reduced activation martensitic (RAFM) steels with different Mn contents were investigated. The experimental steels were designed, based on the Eurofer 97 steel, but the C content was reduced to an extremely low level. The steel with low Mn content (0.47 wt.%) could not obtain a full martensitic microstructure due to the inevitable  $\delta$ -ferrite independent of cooling rate after soaking. This steel showed similar room temperature strength and higher strength at 600°C, but lower impact toughness, compared with Eurofer 97 steel. Fractography of the Charpy-V notch (CVN) impact specimen revealed that the low room temperature toughness should be related to the Ta-rich inclusions initiating the cleavage fracture. The large amount of V-rich nitrides and more dissolved Cr in the matrix could be responsible for the similar strength to Eurofer 97 steel. In the second steel the Mn content was increased to 3.73 wt.% and obtained a full martensitic microstructure.

#### 3:20 PM

**Inclusion Initiated Cleavage Fracture in a Nitride-Strengthened Reduced Activation Martensitic Steel:** *Wei Yan*<sup>1</sup>; Wei Wang<sup>1</sup>; Ping Hu<sup>1</sup>; Lifeng Deng<sup>1</sup>; Yiyin Shan<sup>1</sup>; Ke yang<sup>1</sup>; <sup>1</sup>Institute of Metal Research

The nitride-strengthened reduced activation martensitic steel is a novel and promising heat-resistance structural steel for the future fusion reactor. The experimental steel in this work contained much Mn element and showed high strength at both room temperature and 600°. The inclusion morphology analysis in the steel revealed that the inclusions mainly consisted of Al<sub>2</sub>O<sub>3</sub> and MnS. Fractography on the surface of the broken Charpy V-notch (CVN) specimens showed that the inclusions in this steel initiated cleavage fracture, which should be responsible for the poor impact toughness. The inferior tolerance of the steel to inclusions is explained from the views of the high strength enhanced by the addition of too much Mn and the detrimental characteristics of the inclusions.

#### 3:40 PM Break

#### 4:00 PM

**Determination of Ion Bombardment, in Reactor Irradiation and Post Irradiation Fatigue Properties:** *Z. W. Zhang*<sup>1</sup>; Suiqiong Li<sup>1</sup>; Wen Shen<sup>1</sup>; C. T. Liu<sup>1</sup>; Xun-Li Wang<sup>1</sup>; Xun-Li Wang<sup>2</sup>; Bryan Chin<sup>1</sup>; <sup>1</sup>Auburn University; <sup>2</sup>Oak Ridge National Laboratory

Energetic neutron irradiation and associated transmutation reactions cause significant damage and deterioration in material properties. Any one of a number of material properties may limit the reactor performance and lifetime. Because of the cyclic nature of reactors and because cracks will inevitably be present, fatigue crack propagation as well as the influence of irradiation on fatigue behavior become one of the concerns for the designing of the fusion devices. With the development of experimental reactor and accelerator-based irradiation facilities world-wide, the development of testing technology, particularly for scoping properties of irradiated materials is of particular significance in light of the current fusion reactor materials development program. In this paper, we concentrate on some of the advance on fatigue properties testing of irradiated materials, as they conduct under the conditions of ion bombardment, in reactor irradiation and post irradiation. Some example test module designs and limitations were discussed.

#### 4:20 PM

**Oxidation and Diffusion Investigation of the Carbides Used as Cladding Materials in TRISO-Coated Fuel Particles:** *John Youngsman*<sup>1</sup>; Brian Gorman<sup>2</sup>; Ivar Reimanis<sup>2</sup>; Darryl Butt<sup>1</sup>; <sup>1</sup>Boise State University; <sup>2</sup>Colorado School of Mines

The continued development of Generation IV nuclear reactors is dependent upon advancing the fundamental understanding of TRISO-coated particle fuels under various working conditions. The present work investigates the interaction of cesium, palladium, and silver with silicon carbide and zirconium carbide in order to suggest a kinetic model for the behavior. The metals are uranium fission products and the carbides are used as cladding materials that form the containment vessel in the TRISO particle. Ion implantation is used to deposit the metals into the carbide substrates which are then subjected to high temperatures. Diffusion properties and microstructure development are characterized with SIMS, EBSD, XRD, SEM, and TEM. Thermogravimetric analysis of the carbides at elevated temperatures under CO-CO<sub>2</sub> environments is used to supplement the diffusion and microstructural data to propose a kinetic model for the degradation of the SiC and ZrC substrates.

#### 4:40 PM

**Forming 6061 Al HIP-Clad DU10Mo Monolithic Fuel Plates:** *Kester Clarke*<sup>1</sup>; David Alexander<sup>1</sup>; Cheng Liu<sup>1</sup>; Hunter Swenson<sup>1</sup>; <sup>1</sup>Los Alamos National Laboratory

A significant goal for the Global Threat Reduction Initiative (GTRI) is converting high performance research reactors from highly enriched (HEU) to low enriched (LEU) uranium, requiring development, qualification, and production of high-density, monolithic LEU10Mo foils. These foils are to be co-rolled with Zr and clad with 6061Al using hot isostatic pressing (HIP). Some reactor designs, for example the Advanced Test Reactor (ATR), require a forming/bending operation after HIP processing. The selected method for bending fuel plates is press brake forming with solid punches and flexible bottom dies. Small scale trials with multi-layer 6061 Al HIP-clad DU10Mo (depleted uranium), co-rolled with Zr, have been performed. Important results include springback evaluation in the multi-layer plates and examination of the interaction/diffusion zone integrity as a function of strain. Experiments also provided samples for evaluation of radius measurement techniques and plate relaxation as a function of time and temperature.

## Characterization of Nuclear Reactor Materials and Components with Neutron and Synchrotron Radiation: Irradiated Materials and Technique Development

*Sponsored by:* The Minerals, Metals and Materials Society, TMS Structural Materials Division, TMS/ASM: Nuclear Materials Committee

*Program Organizers:* Matthew Kerr, US Nuclear Regulatory Commission; Meimei Li, Argonne National Lab; Jonathan Almer, Argonne National Laboratory; Donald Brown, Los Alamos National Lab

Thursday PM Room: 4  
March 3, 2011 Location: San Diego Conv. Ctr

*Session Chairs:* Jonathon Almer, Argonne National Lab; Don Brown, Los Alamos National Lab

### 2:00 PM Invited

#### Characterization of Radioactive Materials Using the MARS Beamline at the Synchrotron SOLEIL: *Bruno Sitaud*<sup>1</sup>; *Pier Lorenzo Solari*<sup>1</sup>; *Sandrine Schlutig*<sup>1</sup>; <sup>1</sup>Synchrotron SOLEIL

Since 2004 numerous efforts have been done at the new French synchrotron SOLEIL to construct a beamline for studying radioactive matter in general and nuclear materials in particular. This Multi Analyses on Radioactive Samples beamline (MARS) has been designed and built thanks to a close partnership with CEA. The optics and the experimental stations has been optimized for performing X-ray characterizations (diffraction, scattering, absorption spectroscopy, fluorescence imaging) for a very large variety of radioactive elements. The special infrastructure of this beamline has been defined to be in accordance with the safety regulations for analysing of relatively high activity samples (up to 2 GBq for gamma emitters and 18.5 GBq for other emitters). Several relevant results obtained during the commissioning of the experimental end stations are presented and discussed in the frame of the near future characterisations of nuclear materials from X-ray diffraction and absorption spectroscopy.

### 2:30 PM

#### Neutron Imaging for Non-Destructive Testing of Nuclear Materials: *Peter Vontobel*<sup>1</sup>; *Eberhard Lehmann*<sup>1</sup>; *Yong Dai*<sup>1</sup>; *Mirco Grosse*<sup>2</sup>; <sup>1</sup>Paul Scherrer Institut; <sup>2</sup>Forschungszentrum Karlsruhe

Unlike X-rays thermal neutrons transmit heavy metals like  $UO_2$  or lead easily and provide high sensitivity for small amounts of hydrogen containing compounds like  $ZrH_2$ . Neutron radiography is therefore an ideal probe for non-destructive, post-irradiation examination of fuel rods from nuclear power plants or lead target rods from a spallation neutron source. After irradiation such samples are strong  $\gamma$  sources themselves. At the spallation neutron source SINQ of the Paul Scherrer Institute operates a unique neutron imaging facility allowing highly radioactive samples to be positioned in a neutron beam for radiography. The main advantage of this method is to highlight regions in a sample with peculiar material changes e.g. cracks or fissures, cladding corrosion, material swelling, etc.. Well-directed destructive investigations in a hot cell can subsequently be applied to such material zones. The capabilities of our facility will be demonstrated with selected results.

### 2:50 PM Invited

#### From In-Core to BOP to Waste, Neutrons Characterize Nuclear Materials and Components: *Ron Rogge*<sup>1</sup>; <sup>1</sup>National Research Council

From the advent of materials engineering applications of neutron scattering, the Canadian Neutron Beam Centre has been applying neutron scattering techniques for the nuclear industry. Over this period stress mapping, powder diffraction, texture and other neutron scattering techniques have been employed to study materials from in the reactor core to the balance of plant (BOP). Studies have characterized in-core component materials,

nuclear fuels, studied hydrogen ingress/egress, examined components of heat transport system and evaluated materials used for waste storage. The presentation will present how results have been used to further fundamental understanding of the materials, aid failure analysis, evaluate fitness-for-service and predict component lifetime.

### 3:20 PM

#### SANS and TEM Investigation of Phase Precipitation in HT-9 at High Neutron Irradiation Dose Levels: *Joris Van den Bosch*<sup>1</sup>; *Osman Anderoglu*<sup>1</sup>; *Tobias Romero*<sup>1</sup>; *Patricia Dickerson*<sup>1</sup>; *Robert Dickerson*<sup>1</sup>; *Peter Hosemann*<sup>1</sup>; *Rex Hjelm*<sup>1</sup>; *Stuart Maloy*<sup>1</sup>; <sup>1</sup>LANL

Phase precipitation caused by neutron irradiation is known to strongly influence the mechanical properties of the structural materials and forms one of the lifetime limiting factors for high Cr steel cladding. Most phases can be analyzed using TEM but fully coherent, isostructural phases such as alpha prime are very difficult to image with TEM and more easily observed using small angle scattering measurements. Therefore, TEM and SANS specimens of ferritic-martensitic alloy HT-9 were taken from a duct irradiated in the FFTF reactor up to 155 dpa at a temperature of 380-510°C. In this presentation we will discuss the microstructure of the HT9 steel duct after long term irradiation based on Small Angle Neutron Scattering (SANS) and TEM results from 5 different locations along the length of the duct.

### 3:40 PM

#### Synchrotron Radiation Study of Unirradiated and Irradiated Ferritic-Martensitic Steels: *Meimei Li*<sup>1</sup>; *Jonathan Almer*<sup>1</sup>; *Yang Ren*<sup>1</sup>; *Jeff Terry*<sup>2</sup>; *Stuart Maloy*<sup>3</sup>; *Ken Natesan*<sup>1</sup>; <sup>1</sup>ANL; <sup>2</sup>Illinois Institute of Technology; <sup>3</sup>Los Alamos National Lab

Ferritic-martensitic steels are the lead structural materials for various types of advanced fission and fusion energy systems. The high performance of this class of alloys heavily relies on complex dislocation and subgrain structure and second-phase precipitate particles. The stability of these microstructural features is the key for maintaining the superior properties over an extended reactor service life. To develop a quantitative understanding of microstructural evolution and mechanical property degradation during long-term thermal aging, unirradiated mod.9Cr-1Mo and NF616 were investigated by in situ synchrotron x-ray diffraction (XRD) under thermal and thermo-mechanical loading and by ex situ thermal and mechanical testing and microstructural characterization by synchrotron radiation and electron microscopy. Microstructural change under irradiation was characterized by synchrotron extended x-ray absorption fine structure (EXAFS) spectroscopy in irradiated mod.9Cr-1Mo to understand the different roles of alloying elements in the evolution of local atomic environments during irradiation.

### 4:00 PM Break

### 4:10 PM

#### X-ray Absorption Spectroscopy Study of Irradiated ZrC and ZrN: *Daniel Olive*<sup>1</sup>; *Yong Yang*<sup>2</sup>; *Jeff Terry*<sup>1</sup>; <sup>1</sup>Illinois Institute of Technology; <sup>2</sup>University of Wisconsin-Madison

In complex alloys, radiation-induced segregation and the creation of other stable phases can lead to irradiation hardening and embrittlement. The mechanisms of radiation damage are much less clear in simple, stable binary compounds. Samples of ZrC and ZrN were irradiated to 1 dpa at 800 °C in the Advanced Test Reactor, and shipped to the MRCAT beamline for XAS measurements. The data indicates that no new phases formed in the material. The ZrC retained the overall cubic NaCl structure, with no detectable expansion of the lattice. The number of nearest neighbors remained saturated, as extra carbon in the grain boundaries, adventitious carbon, etc. will find and repair unterminated Zr caused by irradiation. However, at larger interatomic distances, the coordination was significantly reduced indicating that defect sites have resulted in smaller regions of perfect crystallinity. The measurements on ZrN showed similar results to that of ZrC.

4:30 PM

**Cold Neutron Prompt-Gamma Activation Analysis of Hydrogen Pickup during Zirconium Alloy Corrosion:** *Adrien Couet*<sup>1</sup>; Arthur Motta<sup>1</sup>; Robert Comstock<sup>2</sup>; Rick Paul<sup>3</sup>; <sup>1</sup>Penn State University; <sup>2</sup>Westinghouse Electric Company; <sup>3</sup>National Institute of Standards and Technology

Zirconium alloy fuel cladding corrosion and the associated hydrogen pickup is a critical life-limiting degradation mechanism for nuclear fuel in existing and advanced nuclear reactors, since the ingress of hydrogen can cause embrittlement. Past studies used destructive techniques, such as hot vacuum extraction, to measure hydrogen but knowledge of the pickup variation with corrosion and the pickup mechanism is lacking. This research investigates the mechanistic link between hydrogen pickup, oxidation rate, alloy chemistry, and microstructure on a wide selection of zirconium alloys. With the usual destructive techniques, we combine the non destructive technique of Cold-Neutron Prompt-Gamma Activation Analysis. This technique allows precise determinations of hydrogen content, (and thus the hydrogen pickup fraction at various stages of corrosion), and the ability to perform several measurements on a single sample, thus removing the sample-to-sample variability. The results obtained are discussed and related to the overall corrosion kinetics and to the oxide structure.

4:50 PM

**Comparison of Proton, Benchtop X-Ray and Synchrotron X-Ray Radiography of Surrogate Urania and Thoria/Ceria Composite Fuel Samples:** *Mark Bourke*<sup>1</sup>; Donald Brown<sup>1</sup>; Darrin Byler<sup>1</sup>; Christopher Chen<sup>1</sup>; Jeremy Kropf<sup>2</sup>; James Hunter<sup>1</sup>; Fesseha Mariam<sup>1</sup>; Christopher Morris<sup>1</sup>; Andrew Saunders<sup>1</sup>; <sup>1</sup>Los Alamos National Laboratory; <sup>2</sup>Argonne national laboratory

Two surrogate nuclear fuel types were examined with three radiographic probes. The samples were rods (a few cm long) of urania and thoria-ceria that were 5mm and 10mm in diameter respectively. Spatial and density heterogeneities were introduced with inclusions during sintering and by altering the sintering conditions during powder consolidation. Three radiographic tools were used; benchtop (425 KeV ) X-rays, synchrotron (225KeV) X-rays and 800 MeV protons. Tomographic reconstructions were produced. The spatial and density resolutions achieved with the different techniques are compared as well as the potential for their improvement. The potential application of the different techniques to highly radioactive samples will also be considered.

5:10 PM

**Crystallographic Texture Contrast in Neutron Radiography of Zirconium Based Components:** *Javier Santisteban*<sup>1</sup>; Sven Vogel<sup>2</sup>; Anton Tremsin<sup>3</sup>; Winfried Kockelmann<sup>4</sup>; Eberhard Lehmann<sup>5</sup>; <sup>1</sup>Comision Nacional de Energia Atómica; <sup>2</sup>Los Alamos National Laboratory; <sup>3</sup>University of California at Berkeley; <sup>4</sup>Rutherford Appleton Laboratory; <sup>5</sup>Paul Scherrer Institut

The microstructure and crystallographic texture of metal objects affect the transmission of thermal neutrons. As a result the Bragg edges departs largely from those found on isotropic polycrystalline materials, with some Bragg edges even absent along certain specimen directions. A clear understanding of the wavelength dependence of the neutron transmission of textured materials can be directly exploited in energy-resolved neutron imaging. Here, we present the wavelength-dependent transmission of different Zr-based components of nuclear reactors such as pressure tubes, rolled plates and welds, in order to interpret the intensity variations observed in neutron radiographies of such components. The discussion is based on energy-resolved transmission measurements and radiographies taken at ISIS (UK) and PSI (Switzerland), and theoretical calculations of the elastic coherent total cross section from the orientation distribution function (ODF) of the crystallites composing a sample.

5:30 PM

**Spatially Resolved Strain Fields in Nuclear Fuel Plates Determined by Synchrotron X-Ray Diffraction:** *Maria Okuniewski*<sup>1</sup>; Don Brown<sup>2</sup>; Levente Balogh<sup>2</sup>; Jeff Terry<sup>3</sup>; Daniel Olive<sup>3</sup>; Yulia Trenikhina<sup>3</sup>; John Okasinski<sup>4</sup>; Pavel Medvedev<sup>1</sup>; Hakan Ozaltun<sup>1</sup>; Soenke Seifert<sup>4</sup>; Soma Chattopadhyay<sup>3</sup>; Tomohiro Shibata<sup>3</sup>; Hasitha Ganegoda<sup>3</sup>; Jan-Fong Jue<sup>1</sup>; Barry Rabin<sup>1</sup>; Glenn Moore<sup>1</sup>; Blair Park<sup>1</sup>; <sup>1</sup>Idaho National Laboratory; <sup>2</sup>Los Alamos National Laboratory; <sup>3</sup>Illinois Institute of Technology; <sup>4</sup>Argonne National Laboratory

The U.S. Reduced Enrichment for Research and Test Reactors program converts research reactors which utilize highly enriched uranium fuel to low enriched uranium fuel in order to prevent proliferation. The fuel that is utilized for the conversion of the high performance research reactors is U-10wt.%Mo (U10Mo) alloy foil encased in an Al-6061 cladding. Hot isostatic pressing (HIP'ing) is used to fabricate the reactor fuel. During the fabrication process, residual stresses are introduced to the plates via the difference in thermal expansion coefficients in the U10Mo and Al. Synchrotron x-ray diffraction was utilized to measure the spatially resolved residual strain in two HIP cooling processes. Diffraction measurements were conducted in Laue geometry with ~90 keV x-rays. Elastic strains were calculated from the fractional change in the lattice parameter of the HIP'ed specimen to the bare U10Mo foil. Finite element calculations are compared to the strain results obtained from the diffraction experiments.

5:50 PM

**Diffraction Studies of Irradiated Cladding and Duct Reactor Materials:** *Tarik Saleh*<sup>1</sup>; Stuart Maloy<sup>1</sup>; Tobias Romero<sup>1</sup>; Joris Van Den Bosch<sup>1</sup>; Sara Perez-Bergquist<sup>1</sup>; Donald Brown<sup>1</sup>; <sup>1</sup>Los Alamos National Laboratory

Qualifying materials for use in reactors with fluences greater than 200 dpa requires development of advanced alloys and irradiations in fast reactors to test these alloys. Research into the mechanical behavior of these materials under reactor conditions is conducted under the Fuel Cycle Research and Development program. Specimens of a ferritic/martensitic alloy (HT-9) from a duct previously irradiated in the FFTF reactor to doses of up to 155 dpa at temperatures from 370 to 510°C are presently being tested. In order to probe deformation mechanisms in these materials, samples of HT-9 were tested in tension in situ on the SMARTS beamline at the Los Alamos Neutron Science Center. Results showed load sharing between the carbides and parent phase of the steel beyond yield, displaying the critical role of carbides during deformation. Complimentary measurements of radiation induced microstructural effects using Pair Distribution Function and Orientation Imaging Microscopy will also be discussed.

---

## Computational Plasticity: Multiscale Modeling in Plasticity

*Sponsored by:* The Minerals, Metals and Materials Society, TMS Materials Processing and Manufacturing Division, TMS Structural Materials Division, TMS/ASM: Computational Materials Science and Engineering Committee, TMS: High Temperature Alloys Committee  
*Program Organizers:* Remi Dingreville, Polytechnic Institute of NYU; Koen Janssens, Paul Scherrer Institute

Thursday PM

March 3, 2011

Room: 1A

Location: San Diego Conv. Ctr

*Session Chair:* To Be Announced

---

2:00 PM Invited

**Effective Elastic Properties of Solids Containing Imperfectly Bonded Nano-Inhomogeneities Based on Atomistic-Continuum Interphase Model:** *Mohammed Cherkaoui*<sup>1</sup>; Bashkar Paliwal<sup>1</sup>; <sup>1</sup>Georgia Institute of Technology

The classical micromechanics is revised to study elastic properties of heterogeneous materials containing nano-inhomogeneities. Contrary to the previous studies, this work introduces the concept of interphase instead of sharp interface to account for the surface/interface excess stress effect

THURSDAY PM



at the nano-scale. The interphase's constitutive properties are derived within the continuum framework from atomistics. These properties are then incorporated in micromechanics-based interphase model to compute the effective properties of the nanocomposite. This approach bridges the gap between discrete systems (atomic level interactions) and continuum mechanics. An advantage of this approach is that it combines atomistic with a three-phase micromechanical model that considers inhomogeneity shape, thereby enabling both the shape and anisotropy of the nano-inhomogeneity and nano-interphase to be simultaneously accounted for in computing overall properties.

**2:30 PM**

**Kinetics of Deformation Mechanisms in Nanocrystalline Copper:** *Mathieu McPhie*<sup>1</sup>; Stéphane Berbenni<sup>2</sup>; Mohammed Cherkaoui<sup>1</sup>; <sup>1</sup>Georgia Tech Lorraine, GT-CNRS UMI 2958; <sup>2</sup>Laboratory of Physics and Mechanics of Materials (LPMM), CNRS, ENSAM

A multiscale micromechanical model is developed to describe the new physics present in the deformation behaviour of nanocrystalline materials, in particular the breakdown of the Hall-Petch law. This model includes the effects of the emission and absorption of dislocations from grain boundaries, and the coupled grain boundary sliding and migration. Numerical input for this model is given by atomistic simulations of bicrystal layers of fcc-copper using the nudged elastic band technique. Using this technique, zero-temperature, stress-dependent activation energies and saddle point configurations are found for a wide variety of grain boundary misorientations. Additionally, the effect of defects in the grain boundary structure (voids, ledges, dislocations) is studied.

**2:50 PM**

**Experimental and Microstructurally Based Computational Investigation of the High Strain-Rate Behavior of High Strength Aluminum Alloys:** *William Lee*<sup>1</sup>; Khalil El-Khodary<sup>1</sup>; H. Salem<sup>2</sup>; Mohammed Zikry<sup>1</sup>; <sup>1</sup>North Carolina State University; <sup>2</sup>American University of Cairo

The objective of this study is to identify the dominant microstructural and dislocation-density mechanisms related to the high strength and ductile behavior of high strength aluminum alloys, and how high strain-rate loading conditions would affect the overall behavior. Characterization techniques and specialized microstructurally-based finite-element (FE) analyses based on a dislocation-density based multiple-slip crystalline plasticity formulation that accounts for an explicit crystallographic and morphological representation of different precipitates and their rational orientation relations was conducted. As the microstructural FE predictions have indicated, and consistent with the experimental observations, the interrelated effects of precipitates, dispersoids, and grain-boundaries acting on different crystallographic orientations, enhance the strength, the ductility, and reduce the susceptibility of 2139-Al to shear strain localization and dynamic crack propagation.

**3:05 PM Break**

**3:20 PM Invited**

**Lengthscale, Orientation and Morphology Effects in Fatigue Crack Nucleation in Polycrystals:** *Fionn Dunne*<sup>1</sup>; <sup>1</sup>University of Oxford

A crystal plasticity model for near-alpha hcp titanium alloys embodying a quasi-cleavage failure mechanism is presented and employed to investigate the conditions necessary in order for facet nucleation to occur in cold-dwell fatigue. A model polycrystal is used to investigate the effects of combinations of crystallographic orientations, lengthscale effects, and the essential role of (cold) creep during hold periods in the loading cycle. Direct comparisons of model predictions are made with dwell fatigue test results. The crystal model for faceting is found to be consistent with a range of experimental observations.

**3:50 PM Invited**

**Quantifying the Microstructure-Induced Uncertainty in Strain Concentrations at Engineered Defects:** *Corbett Battaile*<sup>1</sup>; Luke Brewer<sup>2</sup>; John Emery<sup>1</sup>; Brad Boyce<sup>1</sup>; <sup>1</sup>Sandia National Laboratories; <sup>2</sup>Naval Postgraduate School

Materials properties are usually assumed to be either independent of the details of the materials' microstructure, or perhaps sensitive only to the structure's average characteristics (e.g. the Hall-Petch effect in metals). However, this assumption is sometimes inadequate. In particular, when the length scale of the relevant mechanism(s) is comparable to that of the microstructure itself, the resulting properties can depend strongly on the particular, local, microstructural environment in which the relevant mechanism(s) operate. To illustrate this, we have used electron backscatter diffraction and digital image correlation to measure the influence of microstructure on deformation near engineered defects in brass, and polycrystal plasticity finite element analysis to simulate the statistical dependence of local deformation on microstructure. We will present the results of this study, and discuss the concept of microstructure-induced uncertainty in materials properties in general.

**4:20 PM**

**Modeling the Evolution of the Microstructure in Magnesium by Means of Incremental Energy Minimization:** *Joern Mosler*<sup>1</sup>; Malek Homayonifar<sup>1</sup>; <sup>1</sup>GKSS-Forschungszentrum Geesthacht

Magnesium alloys exhibit a relatively poor formability for traditional metal forming processes. This is directly related to the complex interplay between slip and twinning observed in magnesium single crystals. In the present contribution, slip and twinning as well as the evolution of the subgrain microstructure in magnesium are analyzed by means of a variational principle. Within the proposed model, every single aspect is driven by energy minimization, i.e., the energetically most favorable microstructure is obtained. In contrast to previous approaches, the twinning's interface energy as well as an energy related to the misfit of the crystal in a boundary layer is also considered. This introduces implicitly a size effect within the model allowing to determine the thickness of the aforementioned twin lamellas. The novel approach is verified by comparing numerically computed results to their experimental counterparts observed within the channel die.

**4:40 PM**

**Studying Dislocation Nucleation from Different Shaped Notches Using a Multiscale Model:** *Steffen Brinckmann*<sup>1</sup>; Dhiraj Mahajan<sup>1</sup>; Alexander Hartmaier<sup>1</sup>; <sup>1</sup>ICAMS

Engineering materials have rough surfaces. This surface roughness acts as stress concentrator and dislocations nucleation site. The dislocations move into the material and might lead to irreversible plastic deformation, which may trigger fracture of the engineering material. While the dislocation dynamics model has been used to study dislocations motion and free surface interaction, that model is a continuum representation. Molecular dynamics, on the other hand, accurately describe dislocation - notch interaction. However, molecular dynamics alone might lead to numerical artifacts. We present a novel approach that combines molecular dynamics and dislocation dynamics in a domain separating concurrent approach. The notch domain is simulated using molecular dynamics while the outer domain is simulated with dislocation dynamics. We study how dislocations are nucleated repeatedly at the notch and how they propagate into the surrounding area. Furthermore, we investigate how the notch shape influences the incipient irreversible deformation.

**5:00 PM**

**A Microstructure Sensitive Crystal Plasticity Model for a-Iron:** *Alankar Alankar*<sup>1</sup>; David Field<sup>2</sup>; <sup>1</sup>Max-Planck Institute for Iron Research; <sup>2</sup>Washington State University

A dislocation density based crystal plasticity finite element model (CPFEM) is developed for a-iron which tracks dislocation densities on 12 no. of {112} slip systems. Based upon the kinematics of crystal deformation and dislocation interaction laws, dislocation generation and annihilation laws are modeled. Screw dislocations velocity is modeled such as they move in

kink-pairs. This leads to capture the typical phenomenon of low mobility of screw dislocations as compared to their edge counterparts in bcc metals. The CPFEM model is calibrated using literature data of single crystals oriented with tensile axis along [-111], [001], and [011] directions. Simulation results of texture evolution and slip activity in a multicrystal show reasonably good agreement with experimental observations.

**5:20 PM**

**Statistical Modeling of Elastic Strain, Lattice Rotation and Dislocation Density Tensor in FCC Crystals:** Mamdouh Mohamed<sup>1</sup>; Jie Deng<sup>1</sup>; Anter El-Azab<sup>1</sup>; Ben Larson<sup>2</sup>; <sup>1</sup>Florida State University; <sup>2</sup>Oak Ridge National Laboratory

A computational technique to characterize the statistics of internal elastic fields of 3D dislocation systems in deforming crystals is presented. The internal elastic fields are computed based on 3D dislocation realizations generated by the method of dislocation dynamics. The results show that the elastic strain components exhibit nearly symmetric probability density functions with zero mean values, which depend on the level of crystal strain. The probability density function for the lattice rotation, however, is found to be non-symmetric. The correlation of all elastic field components are found to be highly anisotropic and tend to be enhanced as the crystal strain is increased. The importance of the current analysis is demonstrated by the relevance of the simulations to the development of a mesoscale plasticity theory, and the direct comparison of the simulations with spatially resolved 3D X-ray microscopy measurements of lattice rotation and the dislocation density tensor at the mesoscale.

---

## Electrode Technology for Aluminium Production: Inert Anodes and Wettable Cathodes

*Sponsored by:* The Minerals, Metals and Materials Society, TMS Light Metals Division, TMS: Aluminum Committee  
*Program Organizers:* Alan Tomsett, Rio Tinto Alcan; Ketil Rye, Alcoa Mosjøen; Barry Sadler, Net Carbon Consulting Pty Ltd

Thursday PM  
March 3, 2011

Room: 16B  
Location: San Diego Conv. Ctr

*Session Chairs:* Veronique Laurent, Rio Tinto Alcan; Jilai Xue, Department of Nonferrous Metallurgy

---

### 2:00 PM Introductory Comments

**2:05 PM**

**Pressureless Sintering of TiB<sub>2</sub>-Based Composites Using Ti and Fe Additives for Development of Wettable Cathodes:** Hamed Heidari<sup>1</sup>; Houshang Alamdari<sup>1</sup>; Dominique Dubé<sup>1</sup>; Robert Schulz<sup>2</sup>; <sup>1</sup>Université Laval; <sup>2</sup>Hydro-Quebec

Titanium diboride is the most promising candidate material for development of wettable cathodes for aluminum smelting. It is considered as an alternative for carbon cathodes in order to reduce the anode cathode distance resulting in higher energy efficiency in electrolysis cells. In this work, TiB<sub>2</sub>-based ceramic specimens were consolidated using metallic additives followed by pressureless sintering. Different proportions of iron and titanium (= 10wt%) were used as low melting point sintering additives. Sintering was conducted at 1400–1650°C under controlled atmosphere. The effects of composition, sintering temperature, milling time and pre-alloying of the additives on densification, microstructure, and mechanical properties were investigated. It was found that pre-alloying and milling time have significant influence on densification, microstructure uniformity and bending strength. Uniform crack-free microstructure with even distribution of pores as well as maximum relative density of 91% and bending strength of 300 MPa were obtained using pre-alloyed additives, milling time of 30 min and sintering for 1 h at 1650°C.

**2:30 PM**

**Furan Resin and Pitch Blends as Binders for TiB<sub>2</sub>-C Cathodes:** Hongliang Zhang<sup>1</sup>; Jinlong Hou<sup>1</sup>; Xiaojun Lü<sup>1</sup>; Yanqing Lai<sup>1</sup>; Jie Li<sup>1</sup>; <sup>1</sup>School of Metallurgical Science and Engineering, Central South University

Blends of furan resin and pitch were applied for the binder of TiB<sub>2</sub>-C cathodes. Some characteristic properties of binder and furan/pitch based TiB<sub>2</sub>-C cathodes were studied. The actual coking value of furan/pitch binder was higher than theoretical value that simply adding up. There was a synergistic effect between pitch and furan resin. Such synergistic effect leads to ameliorative TiB<sub>2</sub>-C cathode materials with lower open porosity, electrical resistivity and higher bulk density, compressive strength than those of pure pitch based TiB<sub>2</sub>-C cathode materials. In addition, the low-temperature electrolysis expansion of TiB<sub>2</sub>-C samples were tested also, furan/pitch based TiB<sub>2</sub>-C samples showed lower electrolysis expansion than pitch based TiB<sub>2</sub>-C samples (1.68% and 1.87%, respectively). Molecular structure (FTIR) and semicoke morphology (SEM) analysis results indicated that after adding appropriate amount of furan resin, the pitch binder was modified by furan resin effectively, the cohesion and flexibility of pitch binder were significant enhanced.

**2:55 PM**

**Influence of Cobalt Additions on Electrochemical Behaviour of Ni-Fe-Based Anodes for Aluminium Electrowinning:** Vivien Singleton<sup>1</sup>; Barry Welch<sup>2</sup>; Maria Skyllas-Kazacos<sup>1</sup>; <sup>1</sup>University of New South Wales; <sup>2</sup>Welbank Consulting Ltd.

The anodic behaviour of surface-oxidised Ni-Fe-Co alloys was investigated over short-term periods of aluminium electrolysis in an alumina-saturated bath. Additions of 10wt% Co were found to significantly improve the anodic wear resistance, due to suppression of Fe<sub>2</sub>O<sub>3</sub> formation. Anodes having cobalt contents =30wt% exhibited poor performance due to rapid outwards diffusion of cobalt to the reaction interface. In general, the protective ability of the pre-formed oxide scales was greatly affected by the level of porosity and surface adhesion. In electrolytes containing <4wt% Al<sub>2</sub>O<sub>3</sub>, catastrophic failure of the anodes was observed due to concentration polarisation at the reaction interface. Under these conditions, the metal was rapidly destroyed by a combination of dissolution and fluorination events.

**3:20 PM Break**

**3:30 PM**

**Effects of the Additive ZrO<sub>2</sub> on Properties of Nickel Ferrite Cermet Inert Anode:** Xiao Zhang<sup>1</sup>; Guangchun Yao<sup>1</sup>; Yihan Liu<sup>1</sup>; Jia Ma<sup>1</sup>; Zhigang Zhang<sup>1</sup>; <sup>1</sup>Northeastern University

The objective of this paper is to study a new attempt on preparing Cu-Ni-NiO-NiFe<sub>2</sub>O<sub>4</sub> ceramic inert anodes by adding trace ZrO<sub>2</sub> (0–1.50 wt%), carrying out high temperature solid-phase process. NiFe<sub>2</sub>O<sub>4</sub> spinel, the matrix material, was prepared firstly with extra 18wt% NiO and Fe<sub>2</sub>O<sub>3</sub> as the raw materials. The product was crushed to fines, and then mixed uniformly with Cu-Ni and ZrO<sub>2</sub> powders to prepare Cu-Ni-NiO-NiFe<sub>2</sub>O<sub>4</sub> ceramic inert anodes by cold-pressing sintering method. The impact of ZrO<sub>2</sub> addition on the relative density, the bend strength and the corrosion resistance of Cu-Ni-NiO-NiFe<sub>2</sub>O<sub>4</sub> ceramic inert anodes was investigated. The results show that, with the addition of 0.5% ZrO<sub>2</sub>, the relative density slightly increases and the corrosion resistance decreases a little while the bending strength improves remarkably from 55.50MPa of the sample without ZrO<sub>2</sub> additive to 105.26MPa.

**3:55 PM**

**Effect of Sintering Atmosphere on Phase Composition and Mechanical Property of 5Cu/(10NiO-NiFe<sub>2</sub>O<sub>4</sub>) Cermet Anodes for Aluminum Electrolysis:** Zhong Zou<sup>1</sup>; Juan Wei<sup>1</sup>; Liang Tian<sup>1</sup>; Kai Liu<sup>1</sup>; Liang Zhang<sup>1</sup>; Qing Lai<sup>1</sup>; Jie Li<sup>1</sup>; <sup>1</sup>Central South University

5Cu/(10NiO-NiFe<sub>2</sub>O<sub>4</sub>) cermet anodes for aluminum electrolysis were prepared by the cold-pressing sintering method in different atmosphere, and their phase composition, microstructure and mechanical property were also investigated. The results reveal that 5Cu/(10NiO-NiFe<sub>2</sub>O<sub>4</sub>) cermet can be obtained by sintering in the low vacuum or atmosphere with oxygen content

of 10ppm, 200ppm, 2000ppm, and 10000ppm respectively, and O<sub>2</sub> content brings great effect on the content of phase composition of materials. Cermet tend to have a high content of NiO sintered under atmosphere with low O<sub>2</sub> content, and a high content of metallic phase sintered under atmosphere with high content of O<sub>2</sub>. When O<sub>2</sub> content in the atmosphere is 10ppm, the grain size of 5Cu/(10NiO-NiFe<sub>2</sub>O<sub>4</sub>) cermet is 5.43μm, the bending strength can reach 80.05Mpa at the room temperature.

## Electrometallurgy Fundamentals and Applications: Session I

*Sponsored by:* The Minerals, Metals and Materials Society, TMS Extraction and Processing Division, TMS: Hydrometallurgy and Electrometallurgy Committee

*Program Organizer:* Michael Free, University of Utah

Thursday PM  
March 3, 2011

Room: 18  
Location: San Diego Conv. Ctr

*Session Chair:* Michael Free, University of Utah

### 2:00 PM

#### Electrochemical Reduction of Tantalum Oxide in a CaCl<sub>2</sub> – CaO Molten Salt Electrolyte: Roger Barnett<sup>1</sup>; Derek Fray<sup>1</sup>; <sup>1</sup>University of Cambridge

Tantalum is usually prepared by the sodium reduction of potassium heptafluorotantalate. However, this route is relatively expensive and this paper reports the direct electro-deoxidation of tantalum oxide (Ta<sub>2</sub>O<sub>5</sub>). When tantalum oxide is immersed in a melt of CaCl<sub>2</sub> containing CaO, a series of calcium tantalum oxides formed with orientations in the direction of the CaO concentration gradient. These include CaTa<sub>4</sub>O<sub>11</sub>, Ca<sub>2</sub>Ta<sub>2</sub>O<sub>6</sub> and Ca<sub>2</sub>Ta<sub>2</sub>O<sub>7</sub>. The morphology varied with the compound leading to a sample with reduced strength. Reduction experiments, where the tantalum oxide was made the cathode in a bath of CaCl<sub>2</sub> – CaO resulted in a similar series of calcium tantalum compounds with Ca<sub>3</sub>(CaTa<sub>2</sub>)O<sub>9</sub> as the final stage before the formation of tantalum. Final oxygen contents of 6700 ppm were achieved with carbon contamination in 1200 ppm range from the carbon anode. The use of inert anodes is discussed.

### 2:25 PM

#### Molten Oxide Electrolysis Application to Steelmaking: A New Approach of Slag Science?: Ghazal Azimi<sup>1</sup>; Antoine Allanore<sup>1</sup>; Donald Sadoway<sup>1</sup>; <sup>1</sup>MIT

Molten oxide electrolysis (MOE) is a new steelmaking technique that does not rely on the use of carbon in the step of chemical conversion of iron oxide to metal. However, the fundamental chemical knowledge developed in slag science is of critical importance to design a mixture of molten oxides that is adapted to the development of an electrolysis operation with high selectivity. Starting from thermodynamic evaluation and discussion of available data on iron speciation in molten slag, the recent results and developments obtained by MOE will be presented. These show that a fundamentally new approach using iron oxide chemistry in molten oxide and the corresponding change in energy vector used for the conversion of iron oxide will not require the development of new science, but could help physico-chemists in the development of new characterization methods.

### 2:50 PM

#### Direct Electroreduction of Oxides in Molten Fluorides: Laurent Cassayre<sup>1</sup>; Mathieu Gibilaro<sup>1</sup>; Jacques Pivato<sup>1</sup>; Laurent Massot<sup>1</sup>; Pierre Chamelot<sup>1</sup>; Olivier Dugne<sup>2</sup>; <sup>1</sup>Université de Toulouse; <sup>2</sup>CEA Marcoule

In the last decade, a great amount of work has been dedicated to the study of the so-called direct reduction reaction, which aims at the conversion of a solid oxide into its metal by electrochemical reduction in a molten salt. The considered applications are for instance titanium production and conversion of spent nuclear oxide fuels in molten chloride salts (CaCl<sub>2</sub> and LiCl respectively). However, up to now, the use of chloride salts is still problematic partially because of the anodic reaction. In the present work,

an attempt to use fluoride salts in replacement of chlorides was carried out in order to reduce SnO<sub>2</sub>, Fe<sub>3</sub>O<sub>4</sub>, TiO<sub>2</sub>, TiO and UO<sub>2</sub> solid pellets. After intensiostatic electrolyses, metal conversion was obtained for all oxides except TiO, and the structure of the metal observed by SEM had a typical coral-like structure. An overview of the results is presented here.

### 3:15 PM

#### Thermodynamic Studies on the Preparation of Titanium Alloys by Molten Salt Electrolysis: Du Jihong<sup>1</sup>; Shenghong Yang<sup>1</sup>; Qingyu Li<sup>1</sup>; Chengben Yang<sup>1</sup>; Mingxia Sun<sup>1</sup>; Zhengping Xi<sup>1</sup>; <sup>1</sup>Northwest Institute for Nonferrous Metal Research

The high cost of raw materials limits more applications of the titanium and titanium alloys. However, preparation of titanium alloy by molten salt electrolysis has advantages of low cost and low pollution, by far, the formation mechanism of titanium alloy prepared by this method has not yet been studied in-depth. In this paper, we selected the binary titanium alloy preparation for research object, and the calculated results show that the decomposition voltage for the formation of titanium alloy not only relates to the Gibbs free energy for each oxide formed, but also relates to the Gibbs free energy for the alloying reaction. We gave the thermodynamic explanations for the experimental results of alloying process of different types of mixed-oxide electrolysis, and concluded the deoxidation laws and alloying pathways during the electrolysis of mixed oxides which has theoretical predictability on the preparation of titanium alloys by molten salt electrolysis.

### 3:40 PM Break

### 3:55 PM

#### Preparation of TiFe Alloy by Electrolysis in Molten Salt: Hu Meilong<sup>1</sup>; Bai Chenguang<sup>1</sup>; Shi Ruimeng<sup>1</sup>; Lv Xuwei<sup>1</sup>; Liu Xuyang<sup>1</sup>; <sup>1</sup>Chongqing University

FeTi alloy was prepared directly by electrolysis in molten CaCl<sub>2</sub> at 1173K and 3.1V using titanium concentrate as feed material, graphite rod as anode. The mechanism of electro-deoxidation of titanium concentrate was studied preliminarily. The results showed that FeTi alloy can be prepared by electrolysis using titanium concentrate in molten salt. Fe is first deoxidized product and titanium oxides are deoxidized gradually. And temperature has great effect on the product. Fe<sub>2</sub>Ti was obtained at 1133K and FeTi was obtained at 1173K.

### 4:20 PM

#### Recapturing Metals from Electrocoagulation Floc: Jewel Gomes<sup>1</sup>; Md Islam<sup>1</sup>; Paul Bernazzani<sup>1</sup>; George Irwin<sup>1</sup>; Dan Rutman<sup>1</sup>; David Cocke<sup>1</sup>; Mohammad Islam<sup>1</sup>; <sup>1</sup>Lamar University

Electrocoagulation (EC) is an emerging technology mainly used for wastewater treatment. In this process, in situ coagulants are produced by passing electric current through a conductive aqueous media in presence of sacrificial electrodes. When iron is used as electrodes, layered double hydroxides (LDH) or green rust are formed as intermediates that turns into iron metallic oxides/hydroxides/oxyhydroxides with time. LDH has a very effective capacity to absorb different kinds of water contaminants, such as arsenic, lead, cadmium, and copper in its structure. In this study, we present our work to treat the EC-floc to recapture the metals, such as copper. Both thermal and electrochemical methods have been applied for the treatment. The floc and recovered metals have been characterized using XRD, SEM/EDS, FTIR, and Moessbauer spectroscopy. A cost analysis is also presented for the treatment and recovery processes.

### 4:45 PM

#### Mechanism of Antimony Deposition in Alkaline Solution Containing Xylitol: Wei Liu<sup>1</sup>; Tianzu Yang<sup>2</sup>; Qionghua Zhou<sup>1</sup>; <sup>1</sup>Henan University of Science and Technology; <sup>2</sup>School of Metallurgical Science and Engineering, Central South University

The mechanism of antimony deposition in alkaline solution containing xylitol was investigated by cyclic voltammetry, linear sweep voltammetry and alternating current impedance techniques. The theoretical kinetics equations of electrode reaction velocity were also derived. Cyclic voltammograms with different scan rates indicate that the antimony electrodeposition process



is an electrocrystallization which is an irreversible electrode process. The apparent activation energy, apparent transfer coefficient and exchange current density of cathodic electrode process are calculated to be 46.33 kJ mol<sup>-1</sup>, 0.64 and 4.40×10<sup>-6</sup> A m<sup>-2</sup>, respectively. The values of the kinetics parameters calculated from the theoretical kinetics equations are agreed well with the experimentally measured ones.

#### 5:10 PM

**Preparation of Ti-Al Intermetallic by Electrolytic Reduction from TiO<sub>2</sub> and Al<sub>2</sub>O<sub>3</sub>:** Chengbeng Yang<sup>1</sup>; Du Jihong<sup>1</sup>; Zhengping Xi<sup>1</sup>; <sup>1</sup>Northwest Institute for Nonferrous Metal Research

An investigation into preparation of Ti-Al intermetallic by electrolytic reduction from TiO<sub>2</sub> and Al<sub>2</sub>O<sub>3</sub>. Electroanalysis process and thermodynamics mechanism was discussed. The results shows that, in 1223K and 3.1 V electrolytic conditions in molten salt of CaCl<sub>2</sub>. Electrolysis process can be divided into three stages: the initial reaction exist Ca<sub>3</sub>Al<sub>2</sub>O<sub>6</sub>, TiO and so on. Middle, exist Al<sub>2</sub>Ca, Ti<sub>2</sub>O and so on. At last, Al<sub>2</sub>Ca reacts with Ti<sub>x</sub>O<sub>y</sub> to form Ti-Al intermetallic. The main reaction is electrolytic reduction of TiO<sub>2</sub> or Al<sub>2</sub>O<sub>3</sub>, and metallothermic reduction of Al<sub>2</sub>Ca to form Ti-Al intermetallic. There is no oxygen and other impurities in reduction by SEM inspection. Current efficiency could be arrived 40%.

### General Abstracts: Electronic, Magnetic and Photonic Materials Division: Session II

*Sponsored by:* The Minerals, Metals and Materials Society, TMS Electronic, Magnetic, and Photonic Materials Division, TMS: Alloy Phases Committee, TMS: Biomaterials Committee, TMS: Chemistry and Physics of Materials Committee, TMS: Electronic Materials Committee, TMS: Electronic Packaging and Interconnection Materials Committee, TMS: Energy Conversion and Storage Committee, TMS: Magnetic Materials Committee, TMS: Nanomaterials Committee, TMS: Thin Films and Interfaces Committee

*Program Organizers:* Long Qing Chen, Pennsylvania State University; Sung Kang, IBM Corporation; Mark Palmer, Kettering University

Thursday PM  
March 3, 2011

Room: 9  
Location: San Diego Conv. Ctr

*Session Chair:* To Be Announced

#### 2:00 PM

**Processing Parameter Optimization to Synthesize High Quality Single Phase CZTS Film:** Prashant Sarswat<sup>1</sup>; Michael Free<sup>1</sup>; Ashutosh Tiwari<sup>1</sup>; <sup>1</sup>University of Utah

Synthesis of Cu<sub>2</sub>ZnSnS<sub>4</sub> (CZTS) photovoltaic absorber material from an electrodeposition-annealing route can be considered as promising production methodology. In the present work, single-phase Cu<sub>2</sub>ZnSnS<sub>4</sub> thin film synthesis using a single-stage electrochemical deposition, followed by Sulfurization at elevated temperature, is reported. Electrodeposition of Cu-Zn-Sn was carried out on a conducting substrate using a platinum counter electrode and a saturated calomel reference electrode. Single phase CZTS is formed over a narrow range of bath concentrations, and a slight deviation may lead to formation of various secondary phases. The processing parameters are optimized to minimize the secondary phase formation and achieve high quality CZTS film. Detailed structural, morphological, electrochemical, and optical properties of film were investigated using several techniques including x-ray diffraction, Raman and UV-visible spectroscopy, electrochemical impedance spectroscopy and scanning electron microscopy.

#### 2:20 PM

**Tantalum Nitride For Efficient Visible-Light-Driven Photocatalyst:** Zheng Wang<sup>1</sup>; Jiangting Wang<sup>1</sup>; Lianyun Liu<sup>1</sup>; Kai Huang<sup>1</sup>; Jungang Hou<sup>1</sup>; Hongmin Zhu<sup>1</sup>; <sup>1</sup>University of Science and Technology Beijing

Tantalum nitride (Ta<sub>3</sub>N<sub>5</sub>) nanoparticles as a visible light photocatalyst were prepared by nitriding the amorphous tantalum nitride nanoparticles under ammonia atmosphere at 1073 K. The production of well-crystallized Ta<sub>3</sub>N<sub>5</sub> nanoparticles have primary particles 40-60 nm in size and a broad absorption band in the vicinity of 600 nm. The as-synthesized materials exhibit good activity for H<sub>2</sub> and O<sub>2</sub> evolution from pure water under visible light irradiation (λ = 420nm).

#### 2:40 PM

**Failure Mechanism of Electrode in Crystalline Photovoltaics:** Oh Chulmin<sup>1</sup>; Park Nochang<sup>1</sup>; Han Changwoon<sup>1</sup>; Hong Won Sik<sup>1</sup>; <sup>1</sup>KETI/Reliability Physics Research Center

In this study, the electrode used for the path of electron generated by solar energy was subjected to identify the failure mechanism. The crystalline solar cell with electrode was prepared without EVA and backsheet to eliminate the effect of other parts. Several environment test were conducted with measuring various the solar parameters each constant interval time to monitor the degradation of electrode performance affected by various environment condition. After environment test, the Auger analysis was conducted to identify failure site with various position of electrode. Therefore, we established the failure mechanism of electrode and made an opportunity to build the acceleration test for reliability performance of photovoltaics electrode.

#### 3:00 PM

**Property-Structure Relations II Oxide Thin Films Used in Light Sensing Applications:** J. Wilde<sup>1</sup>; Y. Kodera<sup>2</sup>; C. Dames<sup>2</sup>; J. Garay<sup>2</sup>; <sup>1</sup>Raytheon Vision Systems; <sup>2</sup>UC Riverside

Over the past few years, uncooled infrared bolometer arrays have been reaching performance levels previously thought possible only with the cooled detectors. One of the most important bolometer design parameter is the bolometer temperature sensing material. This material must necessarily have a high temperature coefficient of resistance (TCR) with low 1/f noise properties with a sufficiently low bolometer thermal time constant. One well known thermistor material is Vanadium Oxide (VO<sub>x</sub>). Although some important physical properties of bulk VO<sub>x</sub> are known, the effective properties of VO<sub>x</sub> thin films are not well understood. We present result of our on-going investigations of the effects of VO<sub>x</sub> thin film microstructure and composition on material properties (electrical and thermal conductivity). We discuss the results in light of grain morphology, grain size, defects and defect length scales.

#### 3:20 PM

**The Investigation of Chemical Vapor Deposited Antimony Doped SnO<sub>2</sub> Thin Films by Synchrotron Grazing Incidence X-Ray:** Yang Yi Lin<sup>1</sup>; Albert T. Wu<sup>1</sup>; <sup>1</sup>National Central University

In recent years, transparent conductive oxides (TCO) films have been widely used for the solar cell due to its high transmission, low sheet resistance and highly texture structure that could increase the efficiency of the solar cell. The purpose of this study is to investigate the amount of antimony that was doped into tin oxide thin films by synchrotron radiation grazing incidence X-Ray diffraction. The films were prepared by CVD deposition by using SnCl<sub>4</sub> and SbCl<sub>5</sub> as precursors. Films were deposited at 450 and 500° for various times. The results suggested that the lattice constant of the film varied with the amount of dopant. The measurement of opto-electrical properties indicated that the films would have higher transmittance and lower resistivity by doping antimony in tin oxide films.

**3:40 PM Break**

**4:00 PM**

**Synthesis of Nano-sized Tantalum Nitrides with Various Morphology:**

Lianyun Liu<sup>1</sup>; Chunhong Ma<sup>1</sup>; Zheng Wang<sup>1</sup>; Kai Huang<sup>1</sup>; Shuqiang Jiao<sup>1</sup>; Hongmin Zhu<sup>1</sup>; <sup>1</sup>University of Science and Technology Beijing

Tantalum nitrides (Ta<sub>n</sub>X<sub>n</sub>) nanoparticles with different crystal phase and various morphology were synthesized through low temperature homogenous sodium reduction route with the subsequent assistance of heat-treatment process. X-ray diffraction and TEM results demonstrated that the tantalum nitrides had the morphology of sphere, rectangle or square with the average particle size below 100nm. The specific surface area of the tantalum nitrides powders measured by BET was around 9.87-13.49m<sup>2</sup>•g<sup>-1</sup>, which indicated such nano-sized tantalum nitrides are the promising candidate for capacitor with high specific capacitance.

**4:20 PM**

**Properties of Perfect GaP Crystals:** *Sergei Pyshkin*<sup>1</sup>; John Ballato<sup>2</sup>;

Andrea Mura<sup>3</sup>; <sup>1</sup>Academy of Sciences of Moldova; <sup>2</sup>Clemson University; <sup>3</sup>University of Cagliari

Here we discuss over 40 year evolution of GaP single crystal properties and their convergence to the behavior of GaP nanoparticles. We show that migration of host and impurity atoms to their proper equilibrium positions leads to creation of an impurity superlattice inside the host lattice. Essential role of the photomechanical effect in the final formation of perfect crystals also has been observed. We demonstrate that the highly ordered nature that develops throughout the decades facilitates stimulated emission, increases the radiative recombination efficiency and spectral range of luminescence. In GaP doped by N substituted P with the period of 10 nm we observe a new type of crystal lattice where nitrogen divides it in short P chains. Highly optically excited GaP:N single crystal turns into the crystalline bound exciton phase - a unique accumulator of optic energy and a prospective medium for non-linear optic phenomena.

**4:40 PM**

**Development of New Transparent Conductive Material of Mg(OH<sub>1-x</sub>Cx)<sub>2</sub> ( x = 0.1-0.35 ) by Magnetron Sputtering:** *Takamitsu Honjo*<sup>1</sup>;

Toshiro Kujji<sup>1</sup>; <sup>1</sup>Tokai university

It is well known that transparent conductive materials are key materials for FPD (Flat Panel Display). Indium Tin Oxide (ITO) consisting of indium - tin oxides have been widely used for practical applications. However, indium is a typical rare element so that the price has increased rapidly over the last several years. Therefore, many research works for developments of the alternative-material without including indium have been actively done. We are reporting that, Mg(OH<sub>1-x</sub>Cx)<sub>2</sub> ( x = 0.1-0.35 ) is an excellent electrical conductor with high optical transparency. The compound has approximately 80% of optical transmission and conductivity of approximately 10-2 ohm cm. The compound was fabricated through two consecutive processes. First Mg-C films were prepared by magnetron sputtering. Then, post-treatment was done in the moist air. These processes yielded Mg(OH<sub>1-x</sub>Cx)<sub>2</sub> ( x = 0.1-0.35 ). In this study, the fabrication processes, optical and electrical conductive properties of the compound.

**5:00 PM**

**Synthesis of Ultrafine Single Crystals and Nanostructured Coatings of Indium Oxide from Solution Precursor:** *Nagaswetha Pentylala*<sup>1</sup>;

Ramesh Kumar Guduru<sup>1</sup>; Pravansu Mohanty<sup>1</sup>; <sup>1</sup>University of Michigan Dearborn

Indium oxide (In<sub>2</sub>O<sub>3</sub>) has been widely used in sensors, solar cells and microelectronics. There are several techniques available for making In<sub>2</sub>O<sub>3</sub> crystals and coatings. Here we present, for the first time, inexpensive and straightforward synthesis of micron/submicron size single crystals, as well as nanostructured adherent coatings of In<sub>2</sub>O<sub>3</sub> from InCl<sub>3</sub> precursor via calcination and DC plasma spray technique, respectively. In<sub>2</sub>O<sub>3</sub> crystals were made by heating the precursor on different substrates at different temperatures, whereas nanostructured films were deposited by feeding atomized liquid directly into the plasma plume. The coatings had ultrafine particles with grain size ranging between 40 – 75 nm. The crystallinity,

phase of the crystals and coatings were characterized by X-ray Diffraction. The coatings with a thickness of 25 micron showed 60% transmission in the visible region and the electrical resistivity(6.5mO-cm) was comparable to the literature. The nanostructured coatings with large surface area could be useful in sensors.

**5:20 PM**

**Reliability of Wedge Wire Bonds Subjected to Ultrasonic Welding and Thermal Cycling:** *Anil Saigal*<sup>1</sup>; Michael Zimmerman<sup>1</sup>; James Battaglia<sup>1</sup>;

<sup>1</sup>Tufts University

Ultrasonic welding is being increasingly used to attach plastic lids as part of integrated circuit packages to replace metal and ceramic lids in hermetic packages. This paper presents the effect of the ultrasonic welding lid attachment process on the reliability and mechanical strength of 1.0 and 1.5 mil gold wedge wire bonds in LDMOS integrated circuit packages. Theoretical modeling of the system including wirebonds and package geometry showed that the natural frequencies of the system were significantly different than the natural frequencies of the wirebonds. This indicates that the ultrasonic welding process does not cause significant stresses in the wirebonds, and therefore doesn't effect wire bond reliability. This hypothesis was tested by exposing the wirebonded packages to thermal air-to-air cycling of the MIL-spec temperature extremes of -65°C and +150°C. Results showed that thermal cycling caused degradation of wirebond pull strengths, but the lid attachments did not cause any deterioration.

**General Abstracts: Light Metals Division: General Light Metals**

*Sponsored by:* The Minerals, Metals and Materials Society, TMS Light Metals Division, TMS: Aluminum Committee, TMS: Aluminum Processing Committee, TMS: Energy Committee, TMS: Magnesium Committee, TMS: Recycling and Environmental Technologies Committee

*Program Organizers:* Alan Luo, General Motors Corporation; Eric Nyberg, Pacific Northwest National Laboratory

Thursday PM  
March 3, 2011

Room: 14B  
Location: San Diego Conv. Ctr

*Session Chair:* Alan Luo, General Motors Global Research & Development

**2:00 PM**

**The Effect of Residual Chloride on the Sintering and Sintered Properties of Titanium and Its Alloys:** *Ma Qian*<sup>1</sup>; <sup>1</sup>The University of Queensland

The commercial production of titanium since 1948 has been based on the tetrachloride route. As a reaction product, residual MgCl<sub>2</sub> or NaCl exists in most titanium products. Commercially available titanium powder can contain chlorine, for example, ranging from < 10 ppm to 2 wt.% (under-separated). This paper reviews the effect of the residual chloride on the sintering and sintered properties of titanium and its alloys. A detailed literature survey indicates that vacuum sintering is able to produce highly dense (> 98%TD) Ti-6Al-4V with tensile properties equivalent to wrought levels from titanium powders containing up to 0.36 wt.% chloride. This offers a potential cost-effective near-net shape fabrication route for many applications where fatigue is not critical. However, sintering in argon results in much inferior properties or densification versus in high vacuum with respect to various levels of chlorine. The effect of the residual chloride on titanium powder metallurgy is discussed.

**2:20 PM**

**High Strain Rate Behavior of 2139-T8 Al Alloy:** *Buyang Cao*<sup>1</sup>; K. Ramesh<sup>1</sup>;

<sup>1</sup>The Johns Hopkins University

The high strain rate behavior of the age hardenable Al-Cu-Mg-Ag alloy known as Al 2139 has been measured over a wide range of strain rates. We obtain dynamic flow stresses of 450 MPa at quasi-static strain rates and flow stress of 550 MPa at dynamic strain rates. We explored the contributions of

several strengthening mechanisms to the total strength of the material, using quantitative TEM together with existing models for each mechanism. Using the results of atomistic calculations, we show that the O phase is the primary strengthening phase in this alloy.

#### 2:40 PM

**Determination of Heat Treatment Effect on 6XXX Series Aluminum Foams by Design of Experiment:** Deniz Polat<sup>1</sup>; B. Ozkal<sup>1</sup>; O. Keles<sup>1</sup>; <sup>1</sup>Istanbul Technical University

In recent years, there is a high demand for light-weight metals foams. Aluminum foams being one of the most commonly preferred metallic foam have been utilized in a wide range of sectors such as health, construction, defense and automotive due to its properties such as industrial advantages (raw material cost, availability and ability to be worked on), melting temperature, specific strength and corrosion resistance. In this work, first 6XXX series of aluminum alloy foams are produced from elemental powders via compact powder melting methods. The alloying elements, Si, Mg and foaming agent titanium hydride powders are added in aluminum powder. Each powder mixture's composition is determined by response surface methodology. 3 levels and 3 parameters are chosen in order to investigate the effects of alloying elements. Then, in order to evaluate their mechanical properties heat treatment is applied at 540°C for 40 min and aged naturally. The results are evaluated by microstructural analysis and hardness tests. A response surface methodology is employed to analyze the hardness results. OM (optical microscopy) and SEM (Scanning Electron Microscopy) are utilized to investigate their microstructures. The formation of AlFeSi and Mg<sub>2</sub>Si intermetallics are seen within the aluminum foam structure. Also, the hardness values of the samples are increased after heat treatment.

#### 3:00 PM

**Effect of Reacted Layer on Galvanic Corrosion Phenomenon at Interface between Ti Dispersion and Mg-Al Alloy:** Katsuyoshi Kondoh<sup>1</sup>; Nozomi Nakanishi<sup>1</sup>; Rei Takei<sup>1</sup>; Junko Umeda<sup>1</sup>; <sup>1</sup>Osaka University

It was previously clarified pure titanium (Ti) particles were effective reinforcements of magnesium (Mg) composites because of their higher hardness, Young's modulus and suitable ductility. When Mg-Al alloy was used as matrix material, Ti-Al reacted layer was formed at the interface between Ti dispersoids and matrix. In general, standard electrode potential (SEP) of Ti is -1.63V, which is much larger compared to Mg (SEP: -2.363V), and results in galvanic corrosion at the interface between Ti and Mg due to the large difference of the SEP. In this study, the effect of the Ti-Al intermetallic layer on the galvanic corrosion of Mg-Al composites reinforced with Ti particles was investigated by salt immersion test. On the other hand, Scanning Kelvin Probe Force Microscopy (SKPFM) analysis was applied to directly measure the surface potential difference at the interface. By comparing these measurements, the galvanic corrosion phenomenon of the Mg composite was quantitatively investigated.

#### 3:20 PM

**Compressive Capacity and Fracture Mechanism of Aluminum Foam:** Hai Hao<sup>1</sup>; Guoqiang Lu<sup>1</sup>; Mouhamadou Diop<sup>1</sup>; Hanwei Dong<sup>1</sup>; Xingguo Zhang<sup>1</sup>; <sup>1</sup>Dalian University of Technology

The tests of compressive capacity of aluminum foam samples manufactured by the melt foaming method were carried out and the compressive curves of stress-strain were obtained. The behavior of deformation by compression and the energy absorption of the aluminum foam were studied. The test results show that there are three regions during the deformation: linear elastic deformation region, collapse region and densification region. As the porosity increases, the capacity of elastic strain resistance reduced significantly, and the specimen with a porosity of 75% has the highest energy absorption capacity. The aluminum foam failed due to a mixture mechanism of malleable tearing and brittle fracture, moreover the slit develops along the crystal border.

#### 3:40 PM Break

#### 4:00 PM

**LiAl Alloy Prepared by Bulk Mechanical Alloying:** Takamitsu Honjo<sup>1</sup>; Toshiro Kuji<sup>1</sup>; <sup>1</sup>Tokai University

LiAl alloy has a high potential as cathode materials of Li-ion battery. In this study we have successfully prepared LiAl alloy by newly developed Bulk Mechanical Alloying (BMA). This MA process has a great advantage for Ball-Milling type MA because everything was in a die and handling of fine powders are not necessary. In general, Ball-milling type MA is time consuming process. In this paper, we will demonstrate that BMA is effectively yielding alloying Li and Al elements compared to Ball-Milling MA even for active element like Li. Prepared alloy has a nano-sized morphology.

#### 4:20 PM

**Multistage Fatigue Model for High-Strength Textured Al Alloys:** Yibin Xue<sup>1</sup>; Chong Teng<sup>1</sup>; Brian Jordan<sup>2</sup>; Mark Horstermeyer<sup>3</sup>; David McDowell<sup>4</sup>; Elias Anagnostou<sup>5</sup>; <sup>1</sup>Utah State University; <sup>2</sup>University of Alabama; <sup>3</sup>Mississippi State University; <sup>4</sup>Georgia Tech; <sup>5</sup>Northrop Grumman

Physically motivated mechanistic MultiStage Fatigue (MSF) model is extended for structural health prognosis to evaluate the extended fatigue life of aging aircrafts. Typically military airframes undergo variable loading conditions with certain severe overloads that induce plastic deformations at the rivet holes or the location of extreme geometry changes, which often serve as fatigue damage initiation sites. Therefore, the structural health prognosis requires an excellent cyclic plasticity, damage incubation and fatigue crack-growth life prediction model that is capable of accurately accounting for the effects of 1) multiaxial loads, 2) notch effects, and 3) overload. The deformation gradient at the macroscopic notch root is integrated into the loading transfer function for fatigue damage incubation model. The overload effects to small-crack growth are further evaluated both experimentally and numerically. A high-order MSF model was developed consider uncertainty induced by the combination effects of microstructure and loading.

#### 4:40 PM

**Super Plasticity of Magnesium Alloys after Rolling and ECAP:** Miroslav Greger<sup>1</sup>; Radim Kocich<sup>1</sup>; <sup>1</sup>VSB-Technical University Ostrava

The paper is focused on investigation of structure and properties of Mg alloys with fine-grained nano-structure. Forming of magnesium alloys with usual grain size 250 to 500 μm is difficult as they are characterised by low plastic properties. Application of SPD processes (Severe Plastic Deformation) enables us to achieve in these alloys as well an ultra-fine grains – nano-grains – and thus also high mechanical properties. Influence of accumulation of deformation by the ECAP process on grain size and mechanical properties of the alloys AZ61 and AZ91 was determined experimentally. Application of the ECAP technology generated nano-structure with an average grains size around approx.  $d \sim 0.7 \mu\text{m}$ . After the ECAP deformation  $\epsilon = 6$  these alloys gained super-plastic behaviour. Ductility of the alloy AZ91 was around 420 %. Experiment proved influence of extreme plastic deformations on grain refinement and on final values of mechanical properties.

#### 5:00 PM

**Tomographic Reconstruction of Microstructures in Al-Ni-Y-Based Alloys:** Mauricio Gordillo<sup>1</sup>; Lichun Zhang<sup>1</sup>; Thomas Watson<sup>2</sup>; Mark Aindow<sup>1</sup>; <sup>1</sup>University of Connecticut; <sup>2</sup>Pratt and Whitney Aircraft

Recently, there has been significant interest in the use of metastable vitreous intermediates in the development of new high strength Al alloys. Such intermediates have higher solubility limits than crystalline Al. Thus, by careful control of alloy composition and thermal history during devitrification, one can obtain fine-grained microstructures with higher volume fractions of precipitates than can be achieved in conventional Al Alloys. We have investigated Al-Ni-Y-based alloys that can be produced in the glassy state by gas atomization. These alloys devitrify to a give a matrix of FCC Al with laths of Al<sub>19</sub>Ni<sub>5</sub>Y<sub>3</sub> and secondary Al<sub>3</sub>Ni or Al<sub>3</sub>Y precipitates. Here we report the use of serial section FIB tomography to study microstructural development in these alloys during powder consolidation and subsequent forging. It is shown that the Al<sub>19</sub>Ni<sub>5</sub>Y<sub>3</sub> laths retain their integrity during



forging and rotate with the flowing Al matrix, rather than breaking up as one might expect.

5:20 PM

**Improved Properties of Light Alloys Using Near-Nano and Nano-Based Materials in Bulk Consolidation Processing:** *Robert Gansert*<sup>1</sup>; Chris Melnyk<sup>2</sup>; David Grant<sup>2</sup>; David Lukan<sup>2</sup>; Brian Weinstein<sup>2</sup>; <sup>1</sup>Advanced Materials & Technology Services, Inc.; <sup>2</sup>California Nanotechnologies, Inc.

Near-nano and nano-grained light alloys (Al, Ti, Mg) show great potential for applications in a variety of industries (e.g., energy, automotive and aerospace). The Hall-Petch relationship cites the strengthening of materials by reducing the average crystallite (grain) size. A study is proposed to investigate the increase in mechanical properties provided by near-nano and nano-grained powders used in powder metallurgical applications. Nanocrystalline powders of light alloys (aluminum, titanium, magnesium) will be produced from cryomilling operations. Consolidated forms of near-nano and nanocrystalline materials will be produced using Spark Plasma Sintering (SPS). The mechanical properties of the near-nano and nanocrystalline materials will be compared to consolidated forms of conventional materials. Initial testing of aluminum and titanium based materials shows a significant increase in hardness and shear from use of near-nano and nano-crystalline materials. Cryomilled powders and consolidated forms of these powders will be examined using microstructural analysis and mechanical property testing.

## General Abstracts: Materials Processing and Manufacturing Division: Casting, Surface Modification, and Powder Processing

*Sponsored by:* The Minerals, Metals and Materials Society, TMS Materials Processing and Manufacturing Division, TMS/ASM: Computational Materials Science and Engineering Committee, TMS: Global Innovations Committee, TMS: Integrated Computational Materials Engineering Committee, TMS: Nanomechanical Materials Behavior Committee, TMS/ASM: Phase Transformations Committee, TMS: Powder Materials Committee, TMS: Process Technology and Modeling Committee, TMS: Shaping and Forming Committee, TMS: Solidification Committee, TMS: Surface Engineering Committee  
*Program Organizers:* Corbett Battaile, Sandia National Laboratories; Joy Forsmark, Ford Motor Company; Amit Misra, Los Alamos National Laboratory

Thursday PM  
March 3, 2011

Room: 2  
Location: San Diego Conv. Ctr

*Session Chair:* To Be Announced

2:00 PM

**Application of Thermodynamics in Nucleation of Secondary Graphite on Heat Treated Ductile Cast Iron:** *Fabian Imanasa Azof*<sup>1</sup>; Eung Ryul Baek<sup>1</sup>; <sup>1</sup>Yeungnam University

Microstructure gives significant effect on the mechanical properties of ductile cast iron. Secondary graphite which occurs during the tempering of martensitic ductile cast iron can deteriorate the elastic modulus and hardness property of the material. Current research presents some application of thermodynamics in nucleation of secondary graphite on heat treated ductile cast iron. The nucleation of secondary graphite in 3.7C-3Si on several austenitization and tempering temperatures were examined using TGA-DTA analysis to ensure the validity of calculation.

2:15 PM

**Evaluation of Microstructures and Mechanical Properties on the Effects of Build Orientation and Building Parameters on Manufactured Ti6Al4V Specimens by EBM:** *Karina Puebla*<sup>1</sup>; Sara Gaytan<sup>1</sup>; Lawrence Murr<sup>1</sup>; Ryan Wicker<sup>1</sup>; <sup>1</sup>The University of Texas at El Paso

Titanium alloys are the preferred metallic biomaterials for implants due to their mechanical properties, biocompatibility, and corrosion resistance.

Ti6Al4V is one of the employed metal powders in electron beam melting (EBM), an additive manufacturing technology capable of fabricating complex 3-dimensional end-use products layer-by-layer. The current investigation was performed to determine the effects of build orientation and scan rate on the microstructure and mechanical properties of EBM manufactured specimens. Microscopic characterization and mechanical testing was performed. Electron microscopy analysis demonstrated the existence of  $\alpha$  and  $\beta$  phases and grain size variations in the microstructure. The different melt scan rate created dissimilarities and produced zones with defects such as porous and voids of non-melting or sintering of Ti6Al4V powder. These effects produced variations affecting physical and mechanical properties of the manufactured specimens. The suggestions to meet specific mechanical properties of EBM manufactured products will be discussed.

2:30 PM

**Calciumsilicate-Graphite-Compound, a New Material for the Flow Control of Liquid Aluminium Alloys:** *Wolf Huettnner*<sup>1</sup>; Tobias Hoelscher<sup>1</sup>; Mark Quackenbush<sup>2</sup>; Rusty Smith<sup>3</sup>; <sup>1</sup>Calsitherm International; <sup>2</sup>Prime Material Sales; <sup>3</sup>Industrial Products International

Graphite and Calciumsilicate are standard materials in casting processes, especially in direct contact with liquid aluminium alloys. The new material is a compound of Calciumsilicate and various amounts of Graphite. It combines the advantageous properties of both materials. The thermal conductivity of the Calciumsilicate increases significantly, whereas the thermal expansion, especially in the plane of the graphite lattice orientation becomes small. The properties are dependent upon the amount of graphite and can be tailored close to required values. Both properties results in an improved thermal shock resistance. The graphite particles also reduce significantly the oil absorption without any additional coating, which is of importance for the use as transition-plate. Furthermore the graphite particles in the compound act as a self-lubricating agent, also at operational temperatures, as the graphite consists of a high oxidation resistance. The material has a high potential to reduce costs especially in the billet production.

2:45 PM

**Influence of a Direct Current on the Solidification Behavior of Pure Aluminum:** *Yunhu Zhang*<sup>1</sup>; Changjiang Song<sup>1</sup>; Liang Zhu<sup>1</sup>; Hongxing Zheng<sup>1</sup>; Qijie Zhai<sup>1</sup>; <sup>1</sup>Shanghai University

To well understand the action mechanism of electric current on the solidification structures of metals and alloys, the effect of a direct current (DC) on the solidification behavior of pure aluminum was investigated experimentally. The experiments show that the measure accuracy of an unarmored K-Type thermocouple is clearly affected by the electric current, but an armored one is not. Therefore, an armored K-Type thermocouple was used to examine the effect of a DC on the solidification behavior of pure aluminum. The results reveal that the freezing temperature decreases by about 1.5° with the application of an 8A/cm<sup>2</sup> DC during the solidification of pure aluminum. The reason for this change is simply discussed.

3:00 PM

**Influence of Heating Effect on the Solidified Structure of Pure Aluminum by Electric Current Pulse:** *Zhenxing Yin*<sup>1</sup>; Bo Li<sup>1</sup>; Yongyong Gong<sup>1</sup>; Qijie Zhai<sup>1</sup>; <sup>1</sup>Shanghai University

This paper investigated the effect of electric current pulse (ECP) on solidification structure of pure aluminum under different pulse parameters. The results exhibit that the area ratio of equiaxed zone increases sharply with the increase of peak value of electric current; however the area ratio varies slowly with the increase of pulse frequency. Additionally, the effect of ECP on solidification structure of aluminum under slower cooling rate was studied, which was attained by imposing thermal insulator on the top of ingot. The results show that the shrinkage cavities of ingots become smaller to varying extents, especially under high current peak value. The structure refinement effects however all weaken too. Based on these findings above, the conclusions can be drawn that current peak value plays a more important role in the refinement of solidified structure than pulse frequency and Joule heat effect isn't the main cause for structure refinement.

3:15 PM

**Influence of Silicon to (Fe,Si)Al Island Formation in Fe<sub>2</sub>Al<sub>5</sub> Aluminide Layer during Heat Treatment of Al-Si Coated Steel Sheets:** *Nandyo Alpalmy*<sup>1</sup>; Baek Eung-Ryul<sup>1</sup>; Kim Tai-Ho<sup>2</sup>; <sup>1</sup>Yeungnam University; <sup>2</sup>POSCO

Aluminide layers (i.e. Fe<sub>3</sub>Al, FeAl, FeAl<sub>2</sub>, Fe<sub>2</sub>Al<sub>5</sub>, FeAl<sub>3</sub>) grew between the melt and the surface of steel sheets coated with Al-Si alloy during heat treatment. It is assumed that silicon affects the morphology of these aluminide layers. (Fe,Si)Al intermetallic islands were formed in Fe<sub>2</sub>Al<sub>5</sub> aluminide layer. In order to observe the morphology, two different alloy, 5 wt% and 10 wt% silicon was added in molten aluminum. Besides, steel sheets coated with pure Al were prepared and analyzed for comparison. The growth behavior of (Fe,Si)Al islands after heat treatment at temperatures ranging from 400 – 800 oC was analyzed by scanning electron microscope (SEM), energy dispersive spectroscopy (EDS), and X-ray diffraction (XRD). It is revealed that no (Fe,Si)Al islands formed in a specimens coated with pure-Al. With the addition of silicon into the aluminum melt, the growth of (Fe,Si)Al islands becomes more severe. Furthermore, the most severe islands exist in specimen coated with higher silicon content.

3:30 PM

**Manufacturing Methods and Properties of Powder-Based Parts with Inherently Saved Information:** Bernd-Arno Behrens<sup>1</sup>; *Najmeh Vahed*<sup>1</sup>; Fabian Lange<sup>1</sup>; Edin Gastan<sup>1</sup>; <sup>1</sup>Institute of Metal Forming and Metal-Forming Machines of the Leibniz University of Hannover

As it is common in the production industry the produced components are physically separated from their related information. Inherently stored specific data in a component facilitates its identification, processing and reproduction during its lifecycle. Especially the powder metallurgy offers great potentials to realize this concept. Developing a method to manufacture and utilize sintered parts with inherent data is one of the main incentives of the Collaborative Research Centre 653 “Gentelligent Components in Their Lifecycle”. The term “gentelligent” refers to the genetic and intelligent character of these components as they carry the essential information about their properties. As data carrier, foreign material in particle or powder form is embedded in the part body prior to consolidation and sintering process. The information readout is based on radiographic methods. The research is focused on the manufacturing methods and the impact of the embedded foreign materials on the mechanical properties of the part.

3:45 PM

**Microstructure and Mechanical Properties of Al Based Composite Coatings Produced by the Cold Gas Dynamic Spraying Process:** *Onur Meydanoglu*<sup>1</sup>; Murat Baydogan<sup>1</sup>; Eyup Kayali<sup>1</sup>; Huseyin Cimenoglu<sup>1</sup>; <sup>1</sup>Istanbul Technical University

In this study, microstructure and mechanical properties (hardness and wear) of Al-B<sub>4</sub>C composite coatings prepared on structural steel substrate by cold spraying were investigated. Feeding powder compositions of Al and B<sub>4</sub>C were 100:0, 80:20, 60:40 and 40:60 in volume. Al and B<sub>4</sub>C powders used in this study were 10 μm and 60 μm in diameter, respectively. Air at room temperature is used as a propellant gas under a pressure of 6 bar. Hardness measurements were made on coatings using Vickers micro hardness tester and wear tests were conducted under dry sliding wear testing conditions on a ball-on disc wear tester by rubbing alumina and stainless steel balls. Addition of B<sub>4</sub>C improved hardness and wear resistance of the coatings. Hardness of coatings increased with increasing B<sub>4</sub>C content; however, wear resistances did not show any significant change with B<sub>4</sub>C content. Alumina balls caused higher wear rate on coatings when compared to steel balls.

4:00 PM

**Optimization of Fiber Laser Produced Hastelloy C-276 Single Track Clad:** *Perry Leggett*<sup>1</sup>; Prabu Balu<sup>1</sup>; Radovan Kovacevic<sup>1</sup>; Syed Hamid<sup>2</sup>; <sup>1</sup>SMU; <sup>2</sup>Halliburton

The present study involves laser cladding of steel substrate with Hastelloy C-276, a nickel super alloy that is highly resistant to chemical corrosion. The laser cladding system consists of four main components: 1) a 4 kW fiber laser; 2) a carrier gas assisted powder feeder; 3) a five-axis CNC

vertical machining center and; 4) a heater. A grey based Taguchi method is used to optimize the key factors that determine the percentage dilution, circularity expressed as a ratio of height and width, and microhardness with minimal number of experiments. The circularity index and percent dilution are determined through optical microscopy; microhardness is measured using a Clark Microhardness tester, the results are then analyzed using a statistical approach. The results show the optimum Laser Power is 350 W, the optimum Powder Flow Rate is 0.13 g/s, and the optimum Scanning Velocity is 13.5 mm/s. A conformal experiment demonstrates the efficiency of the optimization procedure.

4:15 PM

**Preparation of Nanocrystalline Aluminium by Warm-Vacuum-Compaction Method:** *Wei Liu*<sup>1</sup>; Qionghua Zhou<sup>1</sup>; <sup>1</sup>Henan University of Science and Technology

The nano-sized aluminium particles were prepared by flow-levitation technology firstly, and then the particles were compacted with warm-vacuum-compaction method to fabricate the nanocrystalline aluminium with average grain size of 25.2 nm. The influences of experimental parameters, such as pressure, temperature and pressure duration, upon the density and microhardness of the nanocrystalline aluminium were investigated in detail. The experimental results show that both the density and microhardness of the nanocrystalline aluminium increase significantly with higher pressure or elevated temperature, while the duration of pressure has a little effect to the density or microhardness. The average microhardness of the as-prepared nanocrystalline aluminium is 1.65 GPa, which is 11 times higher than that of coarse-grained aluminium.

4:30 PM

**The Effect of Sintering Conditions on the Properties of WC-Co Hard Metal Fabricated by Powder Injection Molding Process:** *Sung-Hyun Choi*<sup>1</sup>; Kyoung-Rok Do<sup>1</sup>; Dong-Wook Park<sup>1</sup>; Young Sam Kwon<sup>2</sup>; Kwon Koo Cho<sup>1</sup>; In-Sup Ahn<sup>1</sup>; <sup>1</sup>GNU; <sup>2</sup>CetaTech, Inc

This study was investigated for microstructure and mechanical properties of WC-10%Co insert tool fabricated by PIM process. The feedstock fabricated by two blade mixer. The debinding process was carried by two-steps methods with solvent extraction and thermal debinding. After debinding process, the specimens were sintered at hydrogen-nitrogen mixed gas or vacuum atmosphere. The microstructure and phase were observed and the hardness and TRS were measured by vickers hardness tester and 3-point bending tester. The density of sintered at 1380° in mixed gas atmosphere was 87.5% and the hardness was 1400Hv. In the case of sintering at 1380° in a vacuum atmosphere after argon gas purging, the hardness was 1850Hv, and the relative density was 99.5%. The density of specimen sintered at 1350° in vacuum atmosphere was 99% and hardness was 1930Hv. In the case of sintered specimen at 1380°, the TRS result was 1100MPa.

4:45 PM

**Annealing Characteristics of Cold Sprayed Pure Cu and Ni Coatings Using EBSD Technique:** *Ahmad Rezaeian*<sup>1</sup>; A. Changizi<sup>1</sup>; Y. Zou<sup>1</sup>; E. Irissou<sup>2</sup>; J.-G. Legoux<sup>2</sup>; S. Yue<sup>1</sup>; <sup>1</sup>McGill University; <sup>2</sup>National Research Council Canada(NRC) – Industrial Materials Institute(IMI)

The cold spray process produces a coating by mechanical deformation of sprayed particles. This heavily cold worked structure needs recrystallization heat-treatment in order to gain back the normal microstructure and ductility of the material. In this study, the effect of heat treatment of cold sprayed coatings was investigated for pure Copper and Nickel powders on mild steel as substrate, using N<sub>2</sub> gas. As-sprayed coatings were then annealed for one hour at a range of temperatures up to 600°C. These were then compared to as-sprayed specimens in terms of microstructure, hardness, and porosity. It was found that 200°C was enough to decrease the hardness of heavily cold deformed pure copper due to restoration processes. The corresponding temperatures were around 600°C for pure Ni. The microstructures were evaluated using EBSD technique.

5:00 PM

**Microstructure Evolution of Amorphous/Nanocrystalline Steel Coatings by Hybrid Spray Process:** Vikram Varadaraajan<sup>1</sup>; Ramesh Kumar Guduru<sup>1</sup>; Pravansu Mohanty<sup>1</sup>; <sup>1</sup>University of Michigan

Amorphous/nanocrystalline coatings are very useful in wear and corrosion protection applications. Here, we report microstructural evolution of an amorphous/nanocrystalline high performance steel coating developed by a novel "hybrid thermal spray" technique. This process combines the arc and high velocity oxy fuel (HVOF) techniques, in which the molten metal at the arcing tip is atomized and rapidly propelled to the substrate by HVOF jet. This so-called "hybrid" concept combines the benefits of productivity of arc spray with improved coating densities of HVOF. The microstructural characterization of the hybrid spray coatings was done by different materials characterization techniques and then compared with the coatings of the same material developed by plasma, HVOF and arc spray processes. The HVOF and plasma spray coatings showed amorphous structures, whereas hybrid and arc spray techniques yielded nanocrystalline coatings. The final microstructures could be attributed to the process temperatures and cooling rates during the spray process.

5:15 PM

**Surface Characteristics and High Temperature Oxidation Resistance Performance of Stainless Steel Foam Modified by Pack Aluminizing and Moderate Oxidation:** Deng-Wei Huo<sup>1</sup>; Xiang-Yang Zhou<sup>1</sup>; Hui Wang<sup>1</sup>; Jie Li<sup>1</sup>; Hong-Yu Song<sup>1</sup>; Peng Zhu<sup>1</sup>; <sup>1</sup>School of Metallurgical Science and Engineering, Central South University

The composition, phase structures and morphology of surface coating of stainless steel foam modified by pack-aluminizing and moderate oxidation were characterized by EDX, XRD and SEM, the effects of pack aluminizing and moderate oxidation on the oxidation resistance performance of stainless steel foam at 800° were also investigated. The main inter-metallic phases present in aluminizing coating on the surface of aluminized stainless steel foam are NiAl and Ni3Al, and the aluminizing coating is well-integrated with the foam substrate. The aluminized and oxidized foam displays excellent high temperature oxidation resistance performance, which may be due to the fact that the compact and uniform Al<sub>2</sub>O<sub>3</sub> film formed on the outer layer of aluminizing coating obstructs the diffuse of oxidizing gas into matrix metal. Additionally, the surface layer reveals good property of thermal shock resistance, the treatment of pack aluminizing and moderate oxidation has little effect on the bending strength of foam.

5:30 PM

**Development of Copper Coating on Austenitic Stainless Steel through Microwave Hybrid Heating:** Dheeraj Gupta<sup>1</sup>; Apurbha Sharma<sup>1</sup>; <sup>1</sup>Indian Institute of Technology Roorkee

Coating of copper on austenitic stainless steel (Fe-Cr-Ni) is useful in electrical and electronic fields where high thermal conductivity as well as high electrical conductivity along with high strength is desirable. Usually, chemical vapor deposition (CVD) and physical vapor deposition (PVD) techniques are employed for developing such coatings. In the present work, copper coatings have been developed by a novel route, where microwave irradiation has been used as a heating source. The copper coating with average thickness of 230 microns were successfully deposited on austenitic stainless steel substrates by microwave hybrid heating process. The copper powder of size 5 microns were melted and deposited on austenitic stainless steel substrates. The deposited coatings exhibit dense and homogeneous microstructure. It was found that the coatings so developed had a mean hardness of 272±30 (Hv). Coatings were analyzed through Field emission scanning electron microscope (FE-SEM), X-ray diffraction (XRD) and X-ray elemental mapping.

5:45 PM

**Anodization of Aluminum Alloys with Novel Anodizing Additive:** Alp Manavbasi<sup>1</sup>; <sup>1</sup>METALAST International, Inc.

Application of additives has been gaining great interest in contemporary aluminum hard anodizing technologies. The purposes for utilization of additives are to enhance the performance of anodizing processes and

resultant anodic coatings while minimizing the environmental impact. Comparative studies showed that the developed additive provides a variety of functions including minimization of burning and blistering, improvement of current and conversion efficiency, enhancement of hardness and wear resistance as well as corrosion resistance. The results also show that the developed technology is capable of significantly improving the uniformity and consistency of anodic coatings. Additionally, aluminum alloys hard-anodized at relatively high temperatures can meet or exceed the abrasion resistance and weight requirements per military specs when the additive is used in the anodizing electrolyte.

## General Abstracts: Materials Processing and Manufacturing Division: Forging, Forming, and Machining

*Sponsored by:* The Minerals, Metals and Materials Society, TMS Materials Processing and Manufacturing Division, TMS/ASM: Computational Materials Science and Engineering Committee, TMS: Global Innovations Committee, TMS: Integrated Computational Materials Engineering Committee, TMS: Nanomechanical Materials Behavior Committee, TMS/ASM: Phase Transformations Committee, TMS: Powder Materials Committee, TMS: Process Technology and Modeling Committee, TMS: Shaping and Forming Committee, TMS: Solidification Committee, TMS: Surface Engineering Committee  
*Program Organizers:* Corbett Battaile, Sandia National Laboratories; Joy Forsmark, Ford Motor Company; Amit Misra, Los Alamos National Laboratory

Thursday PM  
March 3, 2011

Room: 5B  
Location: San Diego Conv. Ctr

*Session Chair:* To Be Announced

2:00 PM

**Profile of Electrochemically Machined Microcomponents:** Wayne Hung<sup>1</sup>; Laxmi Viswanathan<sup>1</sup>; Mike Powers<sup>2</sup>; <sup>1</sup>Texas A&M University; <sup>2</sup>Agilent Technologies

Traditional micromachining uses silicon to fabricate microcomponents. Since silicon is not suitable for applications that demand high strength, robustness and biocompatibility, alternative micromanufacturing processes are sought. The non-traditional electrochemical micromachining ( $\mu$ ECM) process is precise, non-contact, repeatable, and applicable to all conductive materials regardless of their mechanical properties. This paper examines effects of  $\mu$ ECM parameters on profiles of micropatterns. A square-wave current forms micropatterns on an anodic workpiece with a slight undercut due to anisotropic electrochemical mechanism. The undercut is largest between the electrodes but is reduced outwardly. This micromachining uses a megahertz-wave to produce sharp profiles and reduces undercut at the expense of material removal rate. Although sharp corners can be formed on a convex pattern, rounded corners on concave patterns result due to combined edge effects. When utilized at a high frequency and an enhanced material removal rate, the  $\mu$ ECM could become a suitable process for robust microsystems.

2:15 PM

**A New Method for the Determination of Formability Limit in Tube Drawing Process:** Hien Bui<sup>1</sup>; Reza Bihanta<sup>1</sup>; Michel Guillot<sup>1</sup>; Guillaume D'Amours<sup>2</sup>; Ahmed Rahem<sup>2</sup>; Mario Fafard<sup>1</sup>; <sup>1</sup>Laval University; <sup>2</sup>National Research Council Canada, Aluminium Technology Centre

A new method for determination of formability limit in the tube drawing process was developed using the position controlled mandrel technique. In this method the mandrel has conical angle in a way that with change of mandrel position, the distance between die and mandrel will be changed and various combinations of thicknesses can be obtained using just one conic mandrel. The advantage of this method is determining the limit cross-sectional reduction for each tube dimension with just one experiment. The



realized drawing limit tests on the aluminium tubes show that the average maximum area reduction of AA6063 tubes is about 40%. An optimal tube drawing schedule for production of the constant wall thickness aluminium tubes with high cross-sectional reduction in one pass was successfully established based on the proposed formability limit test.

### 2:30 PM

**A Novel Method for Joining of Stainless Steel (SS-316) through Microwave Energy:** *M Srinath*<sup>1</sup>; Apurbba Sharma<sup>1</sup>; Pradeep Kumar<sup>1</sup>; <sup>1</sup>IIT Roorkee

In the present work, microwave processing of metallic materials in the form of joining of bulk stainless steel (SS-316) has been successfully carried out by using multimode applicator with 2.45GHz and 900W power. Nickel based powder was used as a sandwich layer in between the interface surfaces. Samples were exposed to microwave radiation upto a maximum of 390s in multimode applicator. Principle of hybrid heating was employed to initiate microwave coupling with the metals. Stainless steel plates were also joined through TIG welding process. Joints have been characterized through field emission scanning electron microscopy (FESEM), X-ray diffraction (XRD), microhardness and porosity measurement. Microstructure study showed the faying surfaces are well fused and got bonded with base material. The observed Vicker's microhardness of microwave processed SS-316 joints was observed to be 290±14Hv, which is higher than the TIG welded joints (210±5Hv). The porosity of microwave processed joints was 0.78%.

### 2:45 PM

**A Reliable Method for Determining the Solidification Force of Steel for Continuous Casting Conditions:** *Matthew Rowan*<sup>1</sup>; <sup>1</sup>University of Illinois at Urbana-Champaign

Determining the stress profile in a solidifying steel shell is difficult given the nonuniform temperature and stress profiles. Experimental methods such as the Submerged Split Chill Tensile (SSCT) and Contraction (SSCC) tests can measure solidification forces in the shell under controlled conditions identical to continuous casting. A computational model of the SSCC test using an austenite constitutive equation was created in ABAQUS to outline the correct methodology of obtaining the forces that develop in a shell during solidification. By using the nodal force output, it was determined that previous descriptions of the behavior of the solidifying shell during the SSCC test were incomplete. This fundamental change in the understanding of the SSCC test illustrates a case study when combining computational and experimental tools is more insightful than using these two tools separately.

### 3:00 PM

**An Investigation into the Laser Micro-Welding of Aluminum and Copper in Lap Joint Configuration:** *Prabu Balu*<sup>1</sup>; B Carlson<sup>2</sup>; Rouzbeh Sarrafi<sup>1</sup>; Radovan Kovacevic<sup>1</sup>; <sup>1</sup>SMU; <sup>2</sup>GM

Miniaturization, properties tailoring, weight reduction and high automation trends emerging in electrical and electronics industries necessitate successful application of laser micro welding technology to join similar and dissimilar aluminum and copper foils. A single mode fiber laser and a disc laser are used to obtain micro welds of these materials in different combinations (Al-Al, Cu-Cu, Al-Cu, Cu-Al, Cu-Al-Cu, and Al-Cu-Cu) with overlap configuration. The weld quality is quantified based on the electrical resistance, micro hardness and shear strength. The cross-sectional view of the dissimilar welds revealed that placement of aluminum or copper on the top dictates the weld quality. Different microstructural features and defects associated with micro welding of these materials are discussed in the light of optical metallography.

### 3:15 PM

**Carbothermal Production of ZrB<sub>2</sub>-ZrO<sub>2</sub> Composite Powders from ZrO<sub>2</sub>-B<sub>2</sub>O<sub>3</sub>/B System by High-energy Ball Milling and Annealing Assisted Process:** *Duygu Agaogullari*<sup>1</sup>; Özge Balci<sup>1</sup>; Ismail Duman<sup>1</sup>; <sup>1</sup>Istanbul Technical University

The purpose of this study was to produce zirconium diboride-zirconium dioxide composite powders by comparing two different boron sources as boron oxide and elemental boron. The production method was high-energy ball milling and subsequent annealing of powder mixtures containing

stoichiometric amounts of zirconium dioxide, boron oxide/boron powders in the presence of graphite as a reductant. Milling was performed in a vibratory ball-mill using hardened steel balls with 10:1 ball-to-powder weight ratio. The milled products were placed in alumina boats and annealed in a tube furnace held in Argon atmosphere. Milled/annealed products were leached for removing the impurities released by the vial (Fe, Ni, and Cr). ZrB<sub>2</sub>-ZrO<sub>2</sub> composite powders were obtained after centrifuging, washing and drying treatments. The effects of milling duration and annealing temperature on the formation and microstructure of composite powders were investigated. The milled and annealed products were characterized by XRD, SEM and DTA analyses.

### 3:30 PM

**Deformation of High Purity Copper Specimens in Compression between Flat and Grooved Dies:** *Bashir Raddad*<sup>1</sup>; <sup>1</sup>University of Alfatrah, Mechanical Department

Experiments were carried out to generate data on cold compression of high purity copper specimens having different height-to-diameter (Ho/Do) ratios (0.5 to 1.5) between two flat dies having various degrees of surface condition (knurled, dry and lubricated) and between grooved dies having different groove numbers (1 to 3). Different Ho/Do ratios, die surface conditions and number of grooved resulted in different loading characteristics and also different modes of deformation. The latter case resulted forward and backward extrusion modes plus the radial flow resulting from ordinary compression. Three shapes of deformed specimen were obtained according to the number of grooves. Load values decreased as Ho/Do increased and friction condition improved. For a fixed load, displacement increased for higher Ho/Do ratio. Surface strains were apparently affected by the above variables. In case of compression between grooved dies, in spite of the different mode of deformation, the same trends were obtained.

### 3:45 PM

**Improved Shear Zone Quality by an Oscillating Shear Blade:** *Michael Lücke*<sup>1</sup>; <sup>1</sup>IPH

One of the most important factors of influence by forging without flash is the mass constancy of the billet. Because of large reachable quantities and low costs shearing of bar stock is an established proceeding in forging industry. Due to shearing faults the dimensional steadiness of sheared slugs is limited. Therefore the improvement of the shear surface is a desirable goal. The shear zone quality can be improved by an oscillating shear-cutter. Forming and cutting processes were found to be improved by the oscillation of the shear blade. An increased dislocation density, accelerated dislocation motions within the crystal lattice and an expedient friction rate suggest similar quality improvements and extensions of process limits in billet shearing processes. Primary goal of the analysis was the improvement of the slugs' shear zones. Shearing faults like ears, guides, nicks or deformations of pressure loaded areas were observed.

### 4:00 PM

**Local Strain Hardening of Massive Forming Components by Means of Martensite Generation:** *Bernd-Arno Behrens*<sup>1</sup>; *Julian Knigge*<sup>1</sup>; <sup>1</sup>Institute of Metal Forming and Metal-Forming Machines

The investigations presented in this paper are done within the scope of the collaborative research centre 675 „Creation of high strength metallic structures and joints by setting up scaled local material properties“. The production of massive forming components made of metastable austenitic steels with local strengthening by means of forming-induced \945'-martensite is examined. The aim is the forming-induced setting of high-strength martensitic areas beside ductile austenitic regions for the realisation of locally load-adapted components. Different forming processes were performed for the basic determination of the dependence of the phase transformation on the forming parameters. It was found out that the forming-induced martensite formation essentially depends on the degree of deformation and the forming temperature. The phase transition during the forging process could be influenced by locally different degrees of deformation as well as a temperature difference between tool and specimen. Especially temperatures below ambient temperature increased the phase transformation.

4:15 PM

**Machinable Tricalcium Phosphate / CaTiO<sub>3</sub> Composites:** *Celaletdin Ergun*<sup>1</sup>; <sup>1</sup>Istanbul Technical University

Synthetic calcium phosphates have chemical composition very close to that of the inorganic component of bone. Therefore, it is widely used in many biomedical applications. One of the important shortcomings of calcium phosphate is its very restricted ability to be machined to appropriate shapes and sizes in the manufacturing stage due to its high brittleness. In order to evaluate the machinability of tricalcium phosphate (TCP) /CaTiO<sub>3</sub> composites, TCP composites with CaTiO<sub>3</sub> were prepared with pressureless air sintering between 500 and 1300°C for 2 hrs. The composites were characterized with XRD, SEM, and simple pole drilling. Results showed that β-TCP tricalcium phosphate and CaTiO<sub>3</sub> composites were stable up to 1100°C. As a result they fulfilled the requirement of phase stability to insure the weak interface for machinability. Pole drilling test also proved this results.

4:30 PM

**Some Studies on Performance of a Natural Polymer Media for Abrasive Flow Machining:** *S. Rajesha*<sup>1</sup>; Apurbba Kumar Sharma<sup>1</sup>; Pradeep Kumar<sup>1</sup>; <sup>1</sup>Indian Institute of Technology Roorkee

In abrasive flow machining (AFM) process, the media is one of the key components because of its ability to precisely abrade the selected areas along its flow path. Many researchers have developed their own media apart from a few available commercially. However, prohibitively longer time of preparation, its non-reusability and considerably high cost necessitates development of alternate media. In the present work, a new natural polymer based media was used to machine brass work pieces. Performance of the new reusable media has been evaluated by considering extrusion pressure, abrasive grit size, and processing time as process parameters and 'surface finish improvement' and 'material removal' as process responses. Experimentation scheme was planned using design of experiments with twenty sets of trials. The study reveals that the new media yields good improvement in surface finish as well as material removal. Further, preparation of the media and cost are significantly less.

4:45 PM

**Surface Characterization of Laser Machined and Electropolished Metal Micro-Parts:** *Lysle Serna*<sup>1</sup>; Bradley Jared<sup>1</sup>; Brad Boyce<sup>1</sup>; Gerald Knorvosky<sup>1</sup>; <sup>1</sup>Sandia National Labs

Laser micro-machining is the fabrication of parts with feature dimensions approaching 1 micron. As a thermally driven process, the laser/material interaction produces a "recast" layer of melted and re-solidified material on the part surface. Thus, while feature resolution can be exceptional, the resulting surface finish of the part is poor. Recast is generally undesirable, resulting in excessive wear and wear induced debris generation. Electropolishing is a post-machining process typically used for surface remediation by selective dissolution of the recast layer, resulting in improved material performance. In this talk, examples of laser machined stainless steel micro-parts and the as machined surface morphology will be presented, as well as the results of surface remediation by electropolishing. Sandia National Laboratories is a multi-program laboratory managed and operated by Sandia Corporation, a wholly owned subsidiary of Lockheed Martin Corporation, for the U.S. Department of Energy's National Nuclear Security Administration under contract DE-AC04-94AL85000.

5:00 PM

**Effect of Particle Size on the Microstructure and Hardness of TiC and ZrC Reinforced Al-4 wt. %Cu Metal Matrix Composites Fabricated by a Novel Casting Method:** *Hulya Kaftelen*<sup>1</sup>; Lütfi Öveçoğlu<sup>1</sup>; Hani Henein<sup>2</sup>; Necip Ünlü<sup>1</sup>; <sup>1</sup>Istanbul Technical University; <sup>2</sup>Alberta University

The effect of particle size on microstructure and physical properties of Al-4wt.% Cu alloys reinforced with both the 10 wt.% TiC and ZrC particles were evaluated. The TiC having in mean size of 13 μm, 93 μm and ZrC particles having in mean size of 8 μm, 157 μm were introduced into Al-4wt.% Cu as reinforcements using a novel flux-assisted casting method. Studies indicated that TiC particles within the Al-4wt.% Cu matrix were uniformly distributed,

whereas the cluster formation exists in composites including small size of ZrC particles (8 μm). Clustering of fine ZrC particles within the Al-4wt.%Cu matrix leads to a decrease in the hardness of composite compared to coarse ZrC particles reinforced composite. Hardness of Al-4wt.% Cu alloy increased by a factor of two with the addition of 10 wt.% TiC particles; hardness of 1.3 GPa was obtained for the composite containing small TiC (13 μm) reinforcements.

5:15 PM

**Effects of Coil Configurations on Electromagnetic Tube Compression:** *Jianhui Shang*<sup>1</sup>; Allen Jones<sup>1</sup>; Larry Wilkerson<sup>1</sup>; Steve Hatkevich<sup>1</sup>; <sup>1</sup>American Trim LLC

Electromagnetic forming is a complex mechanical-thermal-electromagnetic forming process. During electromagnetic forming, the coil is placed close to the workpiece to produce repulsive electromagnetic force between the coil and the workpiece. The coil design varies largely depending on the geometries of parts and the required forces to deform and accelerate workpiece. Tube compression is one of the major applications of electromagnetic forming. There are several coil configurations for electromagnetic tube compression in the literatures, but the detailed comparison between them is lacked. To investigate the effects of coil configurations, a series of experiments were carried out in this study for electromagnetic compression of Al 6061-T6 tube. This paper presents the detailed experimental results and discusses the advantages and disadvantages of the different coil configurations. Besides, computer simulations of the electromagnetic forming process were carried out to better understand the effects of coil configurations, which will be also presented.

## General Abstracts: Materials Processing and Manufacturing Division: Modeling, Simulation, Ceramics, and Chemical Processing

*Sponsored by:* The Minerals, Metals and Materials Society, TMS Materials Processing and Manufacturing Division, TMS/ASM: Computational Materials Science and Engineering Committee, TMS: Global Innovations Committee, TMS: Integrated Computational Materials Engineering Committee, TMS: Nanomechanical Materials Behavior Committee, TMS/ASM: Phase Transformations Committee, TMS: Powder Materials Committee, TMS: Process Technology and Modeling Committee, TMS: Shaping and Forming Committee, TMS: Solidification Committee, TMS: Surface Engineering Committee  
*Program Organizers:* Corbett Battaile, Sandia National Laboratories; Joy Forsmark, Ford Motor Company; Amit Misra, Los Alamos National Laboratory

Thursday PM  
March 3, 2011

Room: 7B  
Location: San Diego Conv. Ctr

*Session Chair:* To Be Announced

2:00 PM

**A Finite Element-Phase Field Study of Solid State Phase Transformation: Coarsening of Coherent Precipitates and Instability of Multilayer Thin Films:** *Mohsen Asle Zaeem*<sup>1</sup>; Haitham El Kadiri<sup>1</sup>; Sinisa Mesarovic<sup>2</sup>; Paul Wang<sup>1</sup>; Mark Horstemeyer<sup>1</sup>; <sup>1</sup>Mississippi State University; <sup>2</sup>Washington State University

Governing equations for solid state phase transformation are derived by coupling Cahn-Hilliard type of phase field model to elasticity equations. The governing equations include 2nd order partial differential equations for elasticity coupled with a 4th order evolution partial differential equation for the conserved phase field variable. A mixed order finite element model is developed for the computations with C0 interpolation functions for displacement and C1 interpolation functions for the phase field variable. Developed finite element-phase field model is used to study coarsening of systems of coherent particles and also investigate morphological instabilities of multilayer thin films in solid state binary systems. It was shown that

compositional mismatch elastic stresses in precipitates-matrix systems and multilayer thin films significantly affect the instability of these systems and alter the kinetics of transformations.

**2:15 PM**

**Developing a New Method for Prediction of the Inhomogeneity of Stored Energy Based on the Recrystallization Phenomenon:** *Peyman Saidi*<sup>1</sup>; <sup>1</sup>Ferdowsi University

A new criterion based on recrystallization kinetics proposed in order to predict the inhomogeneity of stored energy. For this purpose, kinetic of static recrystallization and the interfacial area between recrystallized and unrecrystallized material per unit volume are considered. The Differential Scanning Calorimetry (DSC) method is utilized to determine the stored energy and for verification of the model. The effect of strain on the stored energy investigated. Good agreement between the prediction of proposed model and experimental results was observed.

**2:30 PM**

**FEM Analysis of a Channel-Compression Process to Produce a Severe-Plastically Deformed Sheet:** *Jong Jin Park*<sup>1</sup>; <sup>1</sup>Hongik University

Recently, a new process for severe plastic deformation was proposed by A. Ghosh and R. Lee in which a round bar is pushed through a channel against a flat surface to be a pancake in shape. In the present study, the rigid-plastic finite-element method was used for the analysis of the process where an Al-1100 bar with the diameter of 20 mm was compressed and forced to flow through a gap of 1.5 mm. The punch force increased to 350 KN. Thickness of the pancake was 1.5 mm up to a certain radius, beyond which it decreased. Since the periphery of the pancake was elongated in the circumferential direction, it would be cracked at certain stage during the process. The effective strain increased smoothly in the radial direction but drastically in the thickness direction. The outer area of the pancake was noted to be wrinkled in the radial direction.

**2:45 PM**

**Investigation on Electrohydraulic Servo Valve through a Finite Element Method:** *Somashekhar S. Hiremath*<sup>1</sup>; M. Singaperumal<sup>1</sup>; <sup>1</sup>Indian Institute of Technology Madras

The analyzed electrohydraulic servo valve is a jet pipe type, is one of the mechatronics component used for precision flow control application. Electrohydraulic servo valves (EHSV) promise unique application opportunities and high performance, unmatched by other drive technologies. Typical applications include aerospace, robotic manipulators, motion simulators, injection molding, CNC machines and material testing machines. EHSV available are either a flapper/nozzle type or a jet pipe type. In the present paper an attempt has been made to study the dynamics of jet pipe EHSV with built-in mechanical feedback using Finite Element Method (FEM). In jet pipe EHSV, the dynamics of spool greatly depends on pressure recovery and hence the fluid flow at spool ends. The effect of pressure recovery on spool dynamics is studied using FEM by creating the fluid-structure-interaction. The mechanical parts were created using general purpose finite elements like shell, beam, and solid elements while fluid cavities were created using hydrostatic fluid elements. The analysis was carried out using the commercially available FE code ABAQUS. The jet pipe and spool dynamics are presented in the paper.

**3:00 PM**

**Mathematical Modeling for Analysis of the Burden Distribution and Gas Flow:** *Jong-in Park*<sup>1</sup>; Hun-je Jung<sup>1</sup>; Min-Kyu Jo<sup>1</sup>; Jeong-Whan Han<sup>1</sup>; <sup>1</sup>Inha university

Process efficiency in the blast furnace is influenced by gas flow pattern which is under the control of burden profile. Therefore, it is important to control the burden distribution for reasonable gas flow. In this study, the falling trajectory of burden is decided by several variables. After falling, the burden stacked on the surface has the angle of repose due to the falling trajectory and falling velocity. The stock lines of each burden type in upper part of shaft move to the low part. And then, the burden profile of the blast is completed. Each section of burden profile was separated into cells which

have information, such as diameter, porosity and shape factor for calculation of the gas flow. The analysis model was developed by using the Excel program based on visual basic. The mathematical formulas for developing this model was modified by the 1/12 scale model experiment.

**3:15 PM**

**Development of a New Modeling Technique for Die Geometry for Extrusion of LCP Films:** *Arash Ahmadzadegan*<sup>1</sup>; *Michael Zimmerman*<sup>1</sup>; *Anil Saigal*<sup>1</sup>; <sup>1</sup>Tufts University

It is known that a liquid crystal polymer (LCP) melt aligns in the direction of the shear flow when it passes through an extrusion die. This alignment causes thin films of the anisotropic LCP material to display different properties in different directions. To overcome this problem, many complex die design technologies have been developed that involve moving surfaces. However, there is a clear need to develop a method of predicting crystal orientation (alignment) to aid in die design. This paper investigates different modeling methods, and develops a numerical modeling technique using FLUENT, to predict molecular alignment by correlating it to streamlines of flow. This model also incorporates the complex rheology of the LCP in predicting the resulting alignment. Using this tool, newer and simpler designs are proposed, which result in more favorable orientations of the crystals.

**3:30 PM**

**Microwave Drying of Silica Sand: Modeling, Kinetics, and Energy Consumption:** *Yu Li*<sup>1</sup>; *Ying Lei*<sup>1</sup>; *Hao Niu*<sup>1</sup>; *Libo Zhang*<sup>1</sup>; *Jinhui Peng*<sup>1</sup>; *Huilong Luo*<sup>1</sup>; *Wenwen Qu*<sup>1</sup>; <sup>1</sup>Key Laboratory of Unconventional metallurgy, Ministry of Education

A ratio of sample mass and power level(g/W) was used as power density to measure the effects on moisture content, drying rate and moisture ratio. The power densities used in this work were 4.167 (500 g, 120 W), 1.190 (500 g, 420 W), 0.714 (500 g, 700 W), 0.429 (300 g, 700 W) and 1.000 (700 g, 700 W) g/W, respectively. The experimental data and computational data were estimated by nine empirical models, and the Page model was observed be perfect fit for all experimental data with values for the of greater than 0.9970 and the and lower than 0.0035 and 3.6E-4, respectively. The activation energy was estimated as 0.279 W/g for power density=1 (1.000~4.167) g/W and 3.493 W/g for power density =1 (0.429~1.000) g/W. The obtained theoretical and practical specific energy consumption were 3.92 and 7.14 MJ/kg water, approximate or smaller than the similar literature report.

**3:45 PM**

**Structural and Thermal Stability of Microwave Synthesized Nano-Hydroxyapatite:** *M Bilal Khan*<sup>1</sup>; *Rafaqat Hussain*<sup>2</sup>; *Muhammad Aftab Akram*<sup>1</sup>; *Nida Iqbal*<sup>2</sup>; <sup>1</sup>National University of Sciences and Technology (NUST), SCME; <sup>2</sup>COMSATS

Thermally stable bioactive hydroxyapatite (HAP) is synthesized by coprecipitation reaction between calcium nitrate tetrahydrate and diammonium hydrogen phosphate under microwave irradiation. The solution is refluxed in modified microwave oven and the effect of microwave power output and irradiation time is investigated in regard to thermal stability of synthesized HAP and the results are found in agreement with the earlier research (Zhengwen Yang et al, 2004). XRD indicated the minimum limit for microwave exposure to get thermally stable HAP inferred from appearance of additional identifiable peaks. Irradiation time is varied from 1 to 5 minutes at the rated powers of 600W and 1000W. Powders were treated for one hour in the 900 to 1100°C range. The treated nano HAP is analyzed for structural stability using XRD.

**4:00 PM**

**A Study on the Hydrophobicity and Investigation of Physical and Chemical Properties of Produced Zinc Borate:** *Mehmet Burcin Piskin*<sup>1</sup>; *Nil Baran Acarali*<sup>1</sup>; *Nurcan Tugrul*<sup>1</sup>; *Emek Moroydor Derun*<sup>1</sup>; *Orzlem Akgun*<sup>1</sup>; <sup>1</sup>Yildiz Technical University

Zinc borate which has different crystal structures is a synthetic hydrate metal borate. Zinc borates are widely used in rubber, plastic, ceramic, paint, electric insulation, wood applications, cement, medicine and flame retardant industries. Zinc borate has relatively high dehydration on-set temperature



which property permits processing in a wide range of polymer system. Zinc borate particles are hardly dispersed in a polymer matrix. Thus, hydrophobic zinc borate is used in different applications. In this study, zinc borate was synthesized by the reaction of zinc oxide and boric acid in the presence of kerosen and seed. In conclusion, physical and chemical analyses of products were carried out. The analysis results were compared with reference values. The results showed that the physical and chemical properties of produced zinc borate effected the hydrophobicity.

#### 4:15 PM

**Investigation of Reaction Conditions Effecting Hydrophobicity on Zinc Borate Yield:** *Sabriye Piskin*<sup>1</sup>; Nil Baran Acarali<sup>1</sup>; Emek Moroydor Derun<sup>1</sup>; Nurcan Tugrul<sup>1</sup>; <sup>1</sup>Yildiz Technical University, Chemical Engineering Department

Zinc borate has been the subject of significant research for applications including the polymer additive which serves as the flame retardant synergist, the preservative in wood composites because of its high thermal stability, the smoke and afterglow suppressant due to its ability to undergo endothermic dehydration in fire conditions, and optical properties, and the additive for lubrication. It can be isolated as crystalline material in various forms having different chemical compositions, structures and there are no toxicity, low cost, and good performance in particular in halogen-free systems. In this study, the synthesis of zinc borate was carried out by the reaction of zinc oxide and boric acid in the presence of kerosen, seed. The effects of reaction conditions as reaction time, reactant ratio on yield were investigated. Optimum points for each parameter were determined. In conclusion, it was seen that changing reaction conditions effected the hydrophobicity of zinc borate.

#### 4:30 PM

**The Role of Energy Sinks in Discontinuous Reactions and the Approach to Equilibrium in U-Nb Alloys:** *Robert Hackenberg*<sup>1</sup>; Kester Clarke<sup>1</sup>; Robert Forsyth<sup>1</sup>; Ann Kelly<sup>1</sup>; Tim Tucker<sup>1</sup>; Pallas Papin<sup>1</sup>; Robert Field<sup>1</sup>; Heather Volz<sup>1</sup>; GERALYN Hemphill<sup>1</sup>; <sup>1</sup>Los Alamos National Lab

Lamellar decomposition products result when U-Nb alloys are transformed between about 300C and the 650C monotectoid temperature. As such microstructures give undesirable properties, the kinetics of these cellular reactions were investigated for U-5.6 wt% Nb and U-7.7 wt% Nb alloys. This study will evaluate the magnitudes of the chemical and interfacial energy sinks before and during the discontinuous precipitation (DP) and discontinuous coarsening (DC) reactions. The role of age hardening reactions taking place in the matrix prior to the passage of the DP growth front, diminishing the free energy available for the DP reaction, will be given particular attention. This will provide insight into the degrees to which different modes of decomposition relieve the initial supersaturation and drive the system toward equilibrium.

#### 4:45 PM

**Effect of Iron Additions on the Shape Memory Characteristics of Cu-Al Alloys:** *T.N. Raju*<sup>1</sup>; Sampath Vedamanickam<sup>1</sup>; <sup>1</sup>Indian Institute of Technology Madras

Even though binary Cu-Al alloys with Al≥10 wt% exhibit shape memory effect and higher transformation temperatures, they are prone for poor workability. This is especially the case with polycrystalline alloys. This limits their practical applications. Attempts have therefore been made by researchers in the past to improve their mechanical and shape memory properties by ternary and quaternary additions, such as Mn and Ni, leading to improved ductility and shape memory properties. A similar trend is observed by adding Fe to Ni-Al alloys so as to overcome their brittleness. The effect of Fe addition on Cu-Al SMAs has not been explored so far. In the present work, therefore, the effect of Fe on the transformation temperatures and shape memory properties has been studied. The alloy shows excellent shape memory properties and higher transformation temperatures. The results are presented and discussed in the paper.

#### 5:00 PM

**Improved Wear Resistance by DLC Coatings:** *Andreas Krause*<sup>1</sup>; <sup>1</sup>IPH - Institut für Integrierte Produktion

Warm forged parts are favourable due to their good surface quality and close tolerances. The main disadvantage of warm forging compared to hot forging is the higher flow stress causing high mechanical loads and hence die wear. Diamond-like carbon coatings (DLC) are extremely hard and have good tribological properties which qualify them to reduce die wear. This capability is analysed in forging trials. These trials are supported by preceding FEA simulations to perceive the conditions causing wear of the coatings. Abrasive wear of DLC is mainly bred to conversion of diamond-like sp<sup>3</sup> to graphitical sp<sup>2</sup> bonding which is to be reduced by doping the DLC with metallic elements. The cavity of the forging tools is designed to reflect the main influencing factors on die wear like high relative velocity and high normal stresses. A developed model mapping the wearing-process helps to improve the design and usage of DLC coatings for warm forging.

#### 5:15 PM

**Asphalt Fatigue Damage Characterization Based on Laser Scanning Detection and Energy Dissipation:** *Hossein Ajideh*<sup>1</sup>; James Earthman<sup>1</sup>; <sup>1</sup>University of California, Irvine

Fatigue damage is one of the major distresses in pavement and has been evaluated using various approaches over the last two decades. A better understanding of fatigue behavior in asphalt materials is needed for better design methods to minimize fatigue failures. The primary objective of the present research was to develop a laser scanning detection system that detects changes in surface properties in order to monitor damage and characterize fatigue behavior of asphalt mixtures. This technique characterizes the surface state using a parameter called defect frequency by rapidly scanning a laser beam along the specimen. The results of laser scanning method have been compared to data for other traditional (50% reduction in stiffness) and dissipated energy approaches. This system provides the opportunity to quantify micro-crack formation rate and evaluate fatigue performance of asphalt mixtures in situ.

### General Abstracts: Structural Materials Division: Microstructure

*Sponsored by:* The Minerals, Metals and Materials Society, TMS Structural Materials Division, TMS: Advanced Characterization, Testing, and Simulation Committee, TMS: Alloy Phases Committee, TMS: Biomaterials Committee, TMS: Chemistry and Physics of Materials Committee, TMS/ASM: Composite Materials Committee, TMS/ASM: Corrosion and Environmental Effects Committee, TMS: High Temperature Alloys Committee, TMS/ASM: Mechanical Behavior of Materials Committee, TMS/ASM: Nuclear Materials Committee, TMS: Refractory Metals Committee, TMS: Titanium Committee

*Program Organizers:* Roger Narayan, Univ of North Carolina & North Carolina State Univ; Judith Schneider, Mississippi State University

Thursday PM  
March 3, 2011

Room: 11B  
Location: San Diego Conv. Ctr

*Session Chair:* To Be Announced

#### 2:00 PM

**Grain Size Dependence of Fracture Toughness of Fine Grained Alumina Sintered by Spark Plasma Sintering:** *Wenlong Yao*<sup>1</sup>; Jing Liu<sup>1</sup>; Troy Holland<sup>1</sup>; Lin Huang<sup>1</sup>; Yuhong Xiong<sup>1</sup>; Julie Schoenung<sup>1</sup>; Amiya Mukherjee<sup>1</sup>; <sup>1</sup>University of California, Davis

Fully dense fine grained alumina was prepared by spark plasma sintering. A series of alumina with grain sizes varying from ~300nm to ~3µm were obtained. The fracture toughness was measured by Vickers indentation and Surface Crack in Flexure method, a 2007 ASTM standard. More than 50 fracture toughness values from Surface Crack in Flexure with different grain

sizes were statistically analyzed based on the Weibull distribution. It was found that the fracture toughness in fine grained alumina is independent of grain size and the fracture toughness calculated from Weibull distribution is 3.37 MPam<sup>1/2</sup>.

#### 2:15 PM

**Formation and Thermal Stability of Nanosized Oxide Precipitates in NiAl Alloys:** *Yongdeog Kim*<sup>1</sup>; Hyon-Jee L. Voigt<sup>1</sup>; Zuhair A. Munir<sup>2</sup>; Brian D. Wirth<sup>3</sup>; <sup>1</sup>University of California, Berkeley; <sup>2</sup>University of California, Davis; <sup>3</sup>University of California, Berkeley/University of Tennessee

We have produced NiAl oxide dispersion strengthened (ODS) super alloys by mechanical alloying of NiAl with Y<sub>2</sub>O<sub>3</sub> and Ti powders, followed by spark plasma sintering, with the objective of improving the high temperature strength and creep resistance. These target properties are expected due to a presence of high number density of stable nano-meter scale clusters (NCs), akin to those recently observed to improve creep strength and radiation resistance in nano-structured ferritic alloys. In this presentation, the alloy production process and high temperature mechanical properties of the NiAl ODS alloys will be summarized. The improved mechanical properties will be explained in connection with the size, structure, and number density of the precipitated oxide particles, which are obtained using transmission electron microscopy (TEM) and atomistic simulation methods. Finally, the thermal stability of oxide precipitate will be discussed using the mechanical properties of NiAl ODS alloys as a function of thermal annealing condition.

#### 2:30 PM

**The Effect of Hafnium Addition on the Microstructure and Phase Equilibria in Cr-Si Based Alloys:** *Amir Nanpazi*<sup>1</sup>; Panos Tsakiroopoulos<sup>1</sup>; <sup>1</sup>IMMPETUS, Department of Engineering Materials, The University of Sheffield, Sir Robert Hadfield Building, Mappin Street, Sheffield S1 3JD, England, UK

This study focussed on the effect of Hf addition on the microstructure and phase equilibria of the as cast and heat-treated Cr-45Si-5Al-5Hf (AN1) and Cr-25Si-25Al-5Hf (AN2) (at %) alloys. There was no macrosegregation in the as cast alloys AN1 and AN2 the microstructures of which respectively contained the (Hf,Cr)<sub>5</sub>Si<sub>4</sub>, Cr<sub>5</sub>(Si, Al)<sub>3</sub> and Cr (Si, Al)<sub>2</sub>, and the Cr<sub>3</sub>(Si, Al), Cr<sub>5</sub>(Al, Si)<sub>8</sub> and (Hf,Cr)<sub>5</sub>Si<sub>4</sub> intermetallics. A key result of this study was the destabilization respectively of the CrSi and Cr<sub>5</sub>Si<sub>3</sub> silicides in the alloys AN1 and AN2 and the stabilization of the (Hf,Cr)<sub>5</sub>Si<sub>4</sub> silicide via the addition of Hf. The Vickers microhardness of the phases present in the as cast and heat-treated alloys AN1 and AN2 and their macrohardness were measured.

#### 2:45 PM

**Microstructural Properties of Gamma Titanium Aluminide Manufactured by Electron Beam Melting:** *Sanna Fager Franzén*<sup>1</sup>; Joakim Karlsson<sup>1</sup>; Ryan Dehoff<sup>2</sup>; Ulf Ackelid<sup>1</sup>; Orlando Rios<sup>2</sup>; Chad Parish<sup>2</sup>; William Peter<sup>2</sup>; <sup>1</sup>Arcam AB; <sup>2</sup>Oak Ridge National Laboratory

Gamma titanium aluminides ( $\gamma$ -TiAl) have been recognized for decades to be suitable for aerospace applications due to their low density and high strength at elevated temperatures. However, TiAl is limited in application due to difficulties during machining which arise from the inherent brittle nature associated with intermetallic phases. Electron Beam Melting (EBM) has recently been proven as a processing method to produce complex, near net shape  $\gamma$ -TiAl parts with short lead times. We present the results from investigation of mechanical and microstructural features of EBM built  $\gamma$ -TiAl, Ti-48Al-2Cr-2Nb. The results include characterization of the unique, small grained, microstructure obtained and suggestions of heat treatment paths to obtain various microstructures. Microstructural investigations were conducted using standard optical and scanning electron microscopy techniques in conjunction with newly emerging techniques such as FIB-SEM to closely map the microstructure. In addition to microstructural characterization, the mechanical properties of EBM built material are presented.

#### 3:00 PM

**Microstructure of a' Martensites in Ti-V-Al Alloys Studied by High-Resolution Transmission Electron Microscopy:** *Kazuhisa Sato*<sup>1</sup>; Hiroaki Matsumoto<sup>1</sup>; Akihiko Chiba<sup>1</sup>; Toyohiko Konno<sup>1</sup>; <sup>1</sup>Tohoku University

Titanium alloys are widely used in various fields due to their high specific strength and corrosion resistance. Among the Ti-alloy systems, Ti-V-Al alloys composed of hexagonal a' martensites possess low Young's moduli and high strength. In this study, atomic structure and morphology of a' martensites in Ti-12%V-2%Al and Ti-6%Al-4%V alloys were studied by aberration-corrected (AC) high-resolution transmission electron microscopy (HRTEM). The {10-11}-type twin formed by martensitic transformation remained in a Ti-12%V-2%Al alloy aged at 400°C. The alloy was once solution treated at 950°C and then quenched into ice water. The twin boundaries are free from precipitates or stacking faults in spite of substantial age-hardening. In contrast, thin layers of stacking faults, 1-2nm in thickness, were observed at the {10-11} twin boundaries of a Ti-6%Al-4%V alloy quenched from 1100°C. AC-HRTEM benefits from smaller optimal defocus values due to small spherical aberration, which enables unambiguous identification of interface structures.

#### 3:15 PM

**Precipitation and Growth of Omega Phase and Alpha Phase during Aging of Alpha-Beta Solution Treated Ti-6.8Mo-4.5Fe-1.5Al:** *Jana Smilauerova*<sup>1</sup>; Milos Janecek<sup>1</sup>; Radomir Kuzel<sup>1</sup>; Petr Harcuba<sup>1</sup>; Josef Strasky<sup>1</sup>; Henry Rack<sup>2</sup>; <sup>1</sup>Charles University; <sup>2</sup>Clemson University

Precipitation of omega and alpha particles in TIMETAL LCB (Ti-6.8Mo-4.5Fe-1.5Al, wt. %) during aging after alpha-beta solution treatment was examined. Initially alpha-beta solution treatment between 700 and 745°C was used to control the volume fraction, size and contiguity of grain boundary alpha. Subsequent aging at 400, 450 and 500°C for times between at 0.5 and 256 hrs was monitored by superficial hardness measurements, the changes in response being correlated with size, volume fraction and spatial distribution of the omega and alpha phase as defined by x-ray diffraction, transmission and scanning electron microscopy.

#### 3:30 PM

**Abnormal Phase Stability in a Ru-Containing Ni-Base Single Crystal Superalloy:** *Jingyang Chen*<sup>1</sup>; Yanhui Chen<sup>1</sup>; Yunrong Zheng<sup>2</sup>; Zuqing Sun<sup>1</sup>; *Qiang Feng*<sup>1</sup>; <sup>1</sup>University of Science and Technology Beijing; <sup>2</sup>Beijing Institute of Aeronautical Materials

Ru addition has been reported to suppress the precipitation of topologically close-packed phases (TCPs) in Ni-base single crystal superalloys during thermal exposures. However, the mechanisms by which Ru enhances microstructural stability remain debatable. In this study, high Ru (4.9 wt.%) addition was found to significantly promoted the formation of TCPs in a high Cr-containing (5.7 wt.%) alloy due to higher Re partitioning ratio and high Re supersaturation in the  $\gamma$  matrix. The time-temperature-transformation (TTT) curves for TCP phase formation indicated that Ru addition accelerated the onset of TCPs precipitation during thermal exposures (900-1200°C). After long-term annealing at 1100°C, the TCPs in Ru-free and Ru-containing alloys were different in morphology and density, while Ru addition significantly enhanced the kinetics for transforming  $\sigma$  phase to P phase. The mechanisms by which Ru promoted the TCPs formation have been clarified on high-temperature phase stability, elemental partitioning behavior and TCPs/ $\gamma$  interface misfit.

#### 3:45 PM Break

#### 4:00 PM

**Comparison of Point-Defect Evolution in Irradiated UO<sub>2</sub> and CeO<sub>2</sub> from Molecular Dynamics Simulation:** *Dilpuneet Aidhy*<sup>1</sup>; Dieter Wolf<sup>1</sup>; <sup>1</sup>Argonne National Laboratory

We elucidate the degree to which CeO<sub>2</sub> can serve as a surrogate material for UO<sub>2</sub> in understanding the evolution of irradiation-induced point defects. Using a new methodology to atomistically capture long-time evolution of point defects in UO<sub>2</sub> (Aidhy, et. al., PRB, 2009) we observed that, in the presence of defects on the U sublattice, annihilation of oxygen defects

via mutual recombination is hindered. The surviving defects form clusters including O vacancies forming Schottky defects, and O interstitials forming cuboctahedral clusters. However, in the absence of U defects, the O defects annihilate completely. We employ a similar methodology to CeO<sub>2</sub> to predict the underlying point-defect evolution in the two sublattices and elucidate the mechanism of cluster formation in CeO<sub>2</sub> (interstitial type dislocation loops lying on {1 1 1} planes, Yasunaga et al., NIM B, 2006). Work supported by the Energy Frontier Research Center for Materials Science of Nuclear Fuels.

#### 4:15 PM

##### **A New Method for Constructing Coincident Site Lattices for Cubic Crystals:** *Mohammad Shamsuzzoha*<sup>1</sup>; <sup>1</sup>University of Alabama

A simple method for geometrical construction of two-dimensional coincidence site lattices (CSL) in cubic crystals based on vector representation of lattice sites is put forward. The construction of such CSLs is achieved by mutual rotation of unique vectors, termed sigma generating vectors, found in the identically projected orthogonal lattice network of both the constituting crystals of the same species. The angle of rotation of the bi-crystal is expressed in terms of some unique nonprime integers that describe the orientation of the sigma generating vector within the lattices of each constituting crystal. The cell parameters of the two-dimensional CSL thus formed can be described in terms of both the magnitude (termed as S) of the square root of the sigma generating vector as well as the lattice parameters of the constituting crystals. Addition of a third axis along the rotation axis of these two-dimensional CSLs yields related three dimensional CSLs.

#### 4:30 PM

##### **Martensite Strain Induced Phase Transformation and Corrosion Resistance of AISI 201 and AISI 304 Stainless Steel:** *Viviane de Moraes*<sup>1</sup>; <sup>1</sup>MAHLE

The increase in the application demand of austenitic stainless steels and the constant pressure for cost reduction in the steelmaking industry, due to the high instability of nickel price, has conduced to new developments of the AISI 200 series steels. This new austenitic stainless steel series employes high manganese and nitrogen contents in substitution to nickel. Samples of these steels were heat treated and cold rolled to different strains for subsequent microstructural evaluation. Strain hardening versus strain, martensite volume fraction versus strain, as well as microstructure evolution and its respective phase identification with strain are some of the main results obtained in this study. The AISI 201 steel presented higher susceptibility to induced phase transformation in comparison to the AISI 304 steel due to its lower stacking fault energy. Electrochemical impedance spectroscopy and anodic potentiondynamic polarization were the techniques used to evaluate the corrosion resistance and passivation behavior, respectively.

#### 4:45 PM

##### **Mechanical Twinning Investigation in a 17.5%Mn TWIP Steel. A Physically-Based Phenomenological Model:** *Ayoub Soulami*<sup>1</sup>; Xin Sun<sup>1</sup>; Moe Khaleel<sup>1</sup>; <sup>1</sup>Pacific Northwest National Laboratories

TWining Induced Plasticity (TWIP) steel combines both high strength and extended ductility due to TWIP effect. In this work, the principal features of deformation twinning in Faced-Centered Cubic (FCC) austenitic steels are discussed. A physically-based phenomenological model derived from microscopic consideration is presented. The model contains internal variables: dislocations density and micro-twins volume fraction, representing the microstructure evolution during deformation process. The contribution of this work is to use physically-based criterion for twin's nucleation and twin's volume fraction evolution in a conventional approach. Model's predictions are compared to experimental tensile data at different strain levels for a 17.5%Mn TWIP steel. Microstructure investigation, using SEM and TEM, are also used to validate and verify modeling assumptions.

#### 5:00 PM

##### **Mechanical Properties and Strain Mechanisms Analysis in Ti-5553 Titanium Alloy:** *Timothée Duval*<sup>1</sup>; Patrick Villechaise<sup>1</sup>; Sandra Andrieu<sup>2</sup>; <sup>1</sup>Institut P<sup>2</sup> - ENSMA; <sup>2</sup>Messier Dowty

This study focuses on the mechanical behaviour of the Ti-5553 beta-titanium alloy used in aerospace industries for structural components. Tensile and fatigue tests were performed to evaluate the macroscopic mechanical characteristics of this alloy at room temperature. Strain mechanisms will be analyzed from post mortem investigations and by performing in-situ tensile tests in a scanning electron microscope. The crystallographic orientation of both alpha and beta phases was measured by Electron Back Scattered Diffraction. This allows to identify the activated slip bands and to investigate the validity of a Schmid factor approach. The plasticity mechanisms will be detailed at the different scales that characterize the metallurgical microstructure: beta grain, primary alpha nodules, beta matrix with secondary fine alpha lamellae. The discussion will focus on the relative contribution on the macroscopic behaviour of each scale and plasticity mechanism.

#### 5:15 PM

##### **Creep Studies of Misoriented Grains in René N4 and GTD 444 Superalloy Bicrystals:** *Kaitlin Gallup*<sup>1</sup>; Tresa Pollock<sup>1</sup>; <sup>1</sup>UCSB

The transverse creep properties of samples containing misoriented (m/o) grains in the nickel-based superalloys René N4 and GTD444 have been studied. Bicrystal slabs were cast using the liquid metal cooled directional solidification method, with seeds rotated about the [001] growth axis to yield bicrystals with low and high angle boundaries with <10°m/o, 20°, >30°m/o. The role of carbides at the boundary and effect of the grain boundary strengthening additions of boron and carbon are explored. Further, creep mechanisms are compared between single crystal bars and bars loaded transverse to the grain boundaries at 982C/207MPa and 760C/690MPa. Up to a 99% reduction in creep rupture lifetime is found. Damage accumulates in interdendritic regions in both the single crystal and bicrystal samples during high temperature creep. At the lower temperature, fracture follows crystallographic planes in single crystals and transitions to the interdendritic grain boundary region at high misorientations.

#### 5:30 PM

##### **Static Recrystallization Behavior of Co-Ni-Cr-Mo Superalloy after Cold Rolling and Subsequent Heat Treatment:** *Takuma Otomo*<sup>1</sup>; Shingo Kurosu<sup>1</sup>; Yunping Li<sup>1</sup>; Hiroaki Matsumoto<sup>1</sup>; Shigeo Sato<sup>1</sup>; Yuichiro Koizumi<sup>1</sup>; Kazuaki Wagatsuma<sup>1</sup>; Akihiko Chiba<sup>1</sup>; <sup>1</sup>Institute for Materials Research, Tohoku University, Japan

The recrystallization behavior of Co-33Ni-20Cr-10Mo (CNCM) superalloy due to heat treatment after cold rolling was studied. The alloy CNCM is used as a spring of mechanical watch; thus a refined structure is required to improve the mechanical properties. The alloy CNCM was cold-rolled from 15% to 90% reduction. The deformed alloy was heat treated at 700 and 800 °C. Microstructural evolution of the alloy was characterized by means of TEM, HRTEM, XRD and EBSD. The Goss {110}<001> texture was dominantly formed after conventional cold rolling. The microstructure was refined after the cold rolling by the reduction higher than 70%. It is suggested that the refined structure was formed due to the strain induced grain subdivision during cold rolling. The average grain size after the recrystallization was submicron meter and the texture did not change after the recrystallization. It is indicated that the alloy CNCM exhibits the continuous recrystallization behavior.

#### 5:45 PM

##### **Oxidation Behavior of Copper Thin Films with Nanoscale Twins:** *Pi-Hua Lee*<sup>1</sup>; Chan Tsung-Cheng<sup>1</sup>; Liao Chien-Neng<sup>1</sup>; <sup>1</sup>Department of Materials Science and Engineering, National Tsing-Hua University

Copper with a high density of nanoscale twins has attracted extensive research attention in the last decade due to its excellent mechanical strength and decent electrical conductivity. Nanotwinned Cu is considered as a candidate of interconnect material in nanoelectronic devices. However, the oxidation behavior of nanotwinned Cu has to be evaluated for process integration considerations. In this study, we deposited Cu films on a Si



substrate by e-gun evaporation. The activation energy of oxidation of Cu films was determined using the ramping technique that measured the change of electrical resistivity of the Cu film exposed to air with different temperature ramping rates. The preliminary results showed that the Cu films with higher deposition rate appeared to have lower oxidation temperature and smaller activation energy than the typical Cu films. The effect of nanotwin and grain size on the oxidation kinetics of Cu films will be investigated.

## General Abstracts: Structural Materials Division: Processing

*Sponsored by:* The Minerals, Metals and Materials Society, TMS Structural Materials Division, TMS: Advanced Characterization, Testing, and Simulation Committee, TMS: Alloy Phases Committee, TMS: Biomaterials Committee, TMS: Chemistry and Physics of Materials Committee, TMS/ASM: Composite Materials Committee, TMS/ASM: Corrosion and Environmental Effects Committee, TMS: High Temperature Alloys Committee, TMS/ASM: Mechanical Behavior of Materials Committee, TMS/ASM: Nuclear Materials Committee, TMS: Refractory Metals Committee, TMS: Titanium Committee

*Program Organizers:* Roger Narayan, Univ of North Carolina & North Carolina State Univ; Judith Schneider, Mississippi State University

Thursday PM  
March 3, 2011

Room: 6A  
Location: San Diego Conv. Ctr

*Session Chair:* To Be Announced

### 2:00 PM

**Using Resistance Heating to Create Full-Scale API RP2Z CTOD Samples:** Morgan Gallagher<sup>1</sup>; Sudarsanam Suresh Babu<sup>2</sup>; Jerry Gould<sup>1</sup>; <sup>1</sup>Edison Welding Institute; <sup>2</sup>The Ohio State University

API RP2Z testing is used by the oil and gas industry to qualify steel plate for service in offshore environments. Part of this qualification process involves assuring "that the steel to be supplied is inherently suitable for welding". Suitability for welding is demonstrated in part through CTOD testing of the HAZs of plates welded over a wide range of heat-inputs. Unfortunately, the time and cost associated with welding CTOD samples can become burdensome as the qualified plate thickness increases. Additionally, the current RP2Z welding procedure may not lead to uniform microstructures in the HAZ of new generation steels. Consequently, EWI has begun to study resistance heating to manufacture full-scale CTOD samples with microstructures identical to samples produced through welding. Initial trials used A36 steel and two peak temperatures. The resultant cross-sections were metallurgically uniform and consisted of microstructures expected for CGHAZs and FGHAZs for peak temperatures of 1200°C and 1000°C.

### 2:15 PM

**Brazing of Titanium Alloys Using Low-melting Eutectic Zr-Ti-Ni(Cu) Filler Alloys:** Dong-Myoung Lee<sup>1</sup>; Gerhard Welsch<sup>1</sup>; Yong-Soo Kim<sup>2</sup>; Seung-Yong Shin<sup>3</sup>; <sup>1</sup>Case Western Reserve University; <sup>2</sup>Yosan Eng.; <sup>3</sup>KITECH

The Zr-Ti-Ni(Cu) alloy system consists of several ordered intermetallic phases, and shows low-melting alloys containing intermetallic phases. Upon rapid solidification these enable glass-forming ability and produce flexible ribbon sheets suitable as filler alloy for brazing. In this study low-melting-point filler alloys in the Zr-Ti-rich side of the Zr-Ti-Ni(Cu) alloy system were investigated for brazing of titanium alloys. Low-melting ternary and quaternary eutectic alloys with melting temperatures below 800° were discovered. Using eutectic as well as off-eutectic braze alloys, CP-Ti and Ti-6Al-4V alloys were successfully brazed at 830° and 850°. The braze joints exhibited interdiffusion-modified structure with intermetallic and solid-solution phases, and the bond strengths were close to the base metal strengths (CP Ti: 438MPa, Ti-6Al-4V: 1007MPa).

### 2:30 PM

**Development of Coatings on Titanium Aluminide Alloys Using Chemical and Physical Deposition Methods:** Patrick Masset<sup>1</sup>; Laurent Bortolotto<sup>2</sup>; Ludovic Charpentier<sup>1</sup>; Michael Schütze<sup>3</sup>; Hans Jürgen Seifert<sup>1</sup>; <sup>1</sup>TU Bergakademie Freiberg; <sup>2</sup>Dechema; <sup>3</sup>DECHEMA

Due to their low density and good mechanical properties even at high temperatures titanium aluminide intermetallics are candidates to replace nickel based super alloys in jet engines. However, they still suffer from environmental embrittlement, which deteriorates their mechanical properties at elevated temperatures. The development of ductile intermetallic coatings with gradient composition constitutes an interesting alternative to repress the environmental embrittlement by creating a physical barrier against hot gases, and to suppress or at least to reduce to an acceptable level the oxygen ingress into the alloy. Coatings on technical alloys were produced using MO-CVD and PVD techniques. They contain elements which favour the coating ductility on the top of the substrate whereas other alloying elements enhance its oxidation and corrosion resistance. The coatings were characterised by XRD, SEM-EDX, EPMA, nano-hardness. In addition, the developed coatings were tested under isothermal and thermocyclic conditions in air.

### 2:45 PM

**Precipitation-Strengthened Ferritic Steels with Increased Strength and Ductility:** Monica Kapoor<sup>1</sup>; Semyon Vaynman<sup>1</sup>; Gautam Ghosh<sup>1</sup>; Dieter Isheim<sup>1</sup>; Yip-Wah Chung<sup>1</sup>; <sup>1</sup>Northwestern University

High-strength, low-carbon, ferritic steels with yield strength up to 1600 MPa and elongation-to-fracture up to 25% were achieved by addition of Cu, Ni, Mn and Al via solution treatment, followed by water quench, and aging. Precipitation strengthening appears to be the primary strengthening mechanism. Atom probe and transmission microscope studies demonstrate that two types of coherent slightly misfitting nanosized precipitates are formed in the steel: Cu-rich and NiAl-type. In this talk, we will discuss the need to reduce the amount of retained austenite to maximize the effect of alloying elements on the yield strength. This can be achieved by appropriate choice of the steel composition and the aging temperature.

### 3:00 PM

**Role of Heat Treatments on the Mechanical Properties of Dual-Phase Steel Sheet:** Hossein Seyedrezai<sup>1</sup>; Keith Pilkey<sup>1</sup>; Doug Boyd<sup>1</sup>; <sup>1</sup>Queen's University

The mechanical behaviour of dual-phase (DP) steel depends on various factors, mainly the size, spatial distribution and volume fraction of the non-ferritic phase (e.g. martensite). To understand the effect of these parameters, a series of pre-treatments were performed on DP600 steel prior to inter-critical annealing. These pre-treatments served to change the spatial distribution of carbides before the inter-critical annealing step, thereby producing distinctly different final microstructures. One pre-treatment involved austenitizing, quenching and tempering (at various temperatures). The second pre-treatment was an austempering process. Optical and scanning electron microscopy observations confirm that both pre-treatments produce a very fine and uniform distribution of carbides, which later lead to a more uniform distribution of fine martensite particles in the final DP microstructures. Uniaxial tensile testing demonstrates that the application of these pre-treatments results in improved mechanical properties as compared to the base-line material without any pre-treatment history.

### 3:15 PM

**Friction Stir Processing of Cast Superalloys:** Edward Chen<sup>1</sup>; Bharat Jasthi<sup>2</sup>; Douglas Bice<sup>1</sup>; William Arbogast<sup>2</sup>; Matthew Heringer<sup>2</sup>; Stanley Howard<sup>2</sup>; <sup>1</sup>Transition45 Technologies, Inc.; <sup>2</sup>South Dakota School of Mines and Technology

This presentation examines the feasibility of incorporating friction stir processing (FSP) with casting to produce higher performance yet cost affordable near-net shape Ni-based superalloy components. Casting is one of the most inexpensive fabrication methods in existence. Friction stir processing is an emerging microstructural modification technique based on friction stir welding (FSW) that can be applied to enhance the microstructure-properties. It can be used to refine cast microstructures such as to improve

properties such as damage tolerance. This added step could be used to allow cast superalloy components to be employed without casting factors. If successfully developed and implemented, this technology could have the tremendous potential for reducing the weight and cost of Ni-based superalloy castings that are used in industries as diverse as rocket propulsion, aircraft engines, land-based gas turbines, and chemical process industry pumps and valves. It could also be used for part repair and refurbishment.

#### 3:30 PM

**Characterization of Ni-Base Superalloy Die Materials:** *Alvaro Mendoza Jr.<sup>1</sup>; Krishna Ganesan<sup>1</sup>; Gerhard Fuchs<sup>1</sup>; <sup>1</sup>University of Florida*

A case study was undertaken to examine the premature failure of a set of IN718 forging dies. Detailed microstructural characterization of the failed dies indicated that they were exposed to higher temperatures than initially expected. Higher use temperatures resulted in a significant strength reduction of the IN718 dies, and failure of the dies. This led to rising costs, as the dies had to be replaced more often than expected. Rather than changing the forging conditions, a new die material with higher temperature capabilities was identified. IN-100 was selected as the replacement die material due to the higher temperature capabilities of the IN-100. To validate the new material selection, samples of both IN718 and IN-100 were given thermal cycles to replicate the expected die lifetime. The microstructural stability of each alloy was characterized by optical and SEM metallographic techniques. Hardness testing was also used to characterize the microstructure and properties.

#### 3:45 PM Break

#### 4:00 PM

**Metal (Fe-Al)- Fullerene Nanocomposites Made by Powder Metallurgy Methods:** *Hector Calderon<sup>1</sup>; <sup>1</sup>ESFM-IPN*

Nanocomposites have been produced by using a metal (Fe or Al) together with pure C60 or a mixture of fullerenes (C60 + C70) and soot. The synthesis includes mechanical milling and spark plasma sintering (SPS). Different milling media produce a variety of transformations of the carbon phases, depending on the energy input, nanodiamonds, metallic carbides or well dispersed fullerenes can be obtained after relatively short milling times (up to 2 h). Sintering develops considerable increases of mechanical strength without reducing the ductility of the sintered composites. During sintering further phase transformations occur involving the carbon phases. Carbides are normally produced, however diamonds in nanometric dispersions can also be found after highly energetic milling of the original powders particularly in the presence of Fe. The soot in the fullerene mixture transforms during sintering to other phases including fullerenes, particularly in Fe based materials. High temperature rolling of the composites gives rise to transformation of the remaining fullerenes to more stable phases i.e., carbides or diamonds. Electron microscopy, Raman spectroscopy, and X-ray diffraction are mainly used for characterization.

#### 4:15 PM

**Preparing Titanium Powders by Calcium Vapor Reduction Process of Titanium Dioxide:** *Baoqiang Xu<sup>1</sup>; Bin Yang<sup>1</sup>; Heli Wan<sup>1</sup>; Wei Sen<sup>1</sup>; Yongnian Dai<sup>1</sup>; Dachun Liu<sup>1</sup>; <sup>1</sup>National Engineering Laboratory for Vacuum Metallurgy, Kunming*

In this paper, thermodynamic equilibrium calculations on the system of Ca-O<sub>2</sub>-N<sub>2</sub>-TiO<sub>2</sub> were carried out and the calciothermic reduction process of titanium dioxide to prepare titanium powders in the closed graphite vessel was investigated by means of XRD, SEM and EDS. The thermodynamic calculation results indicated that the sum of partial pressures of gas O<sub>2</sub> and gas N<sub>2</sub> would equal to 10<sup>-6</sup>–10<sup>-10</sup> that is much less than the saturated vapor pressure of metal calcium at the same temperature during the range of 298K-1500K in the same system, which implied the metal calcium would become vapor to reduce TiO<sub>2</sub> at certain temperature after exhausting O<sub>2</sub> and N<sub>2</sub> in the closed system. Experimental results indicated with reduction temperature risen and reduction time increased calcium vapor reduction process of TiO<sub>2</sub> was improved and on the condition of reduction temperature in the range of 1273K-1473K and reduction time 6h the TiO<sub>2</sub> was reduced

effectively, then titanium powders (purity: >95%Ti, particle size: 3-5 $\mu$ m, shape: irregular) were prepared.

#### 4:30 PM

**Partial Melting Homogenization of Thick Section Austempered Ductile Iron Containing 2% Mn:** *Seid Ata Sheikholeslami<sup>1</sup>; Mahmoud Nili-Ahmadabadi<sup>1</sup>; Jafar Rassizadehghani<sup>1</sup>; <sup>1</sup>University of Tehran*

Ductile iron castings are usually alloyed with elements such as Mn and Mo to improve mechanical properties and hardenability. Inasmuch as conventional homogenization of ductile iron does not change segregation of Mn or Mo considerably, in particular in thick section castings, in this study partial melting homogenization (PMH) was applied to reduce the deteriorative segregation effects. Thick section ductile iron castings containing 2% Mn was processed by PMH in as cast and austempered condition. Homogenization just above the intercellular eutectic temperature causes melting of the highly Mn segregated regions. Isothermal solidification of this region causes diffusion of Mn from liquid pool to the surrounding solid region while Si diffuses in the reverse direction. The microstructure of homogenized specimens by PMH were found to be more uniform with a reduced amount of segregation when compared to the as cast samples. Tensile tests demonstrated the improving effects of PMH heat treatment.

#### 4:45 PM

**Formability Evaluation of TRIP Steel Sheets:** *Joong Eun Jung<sup>1</sup>; Jong Bae Jeon<sup>1</sup>; Young Won Chang<sup>1</sup>; <sup>1</sup>POSTECH*

Multiphase TRIP steels provide high potential for applications to automotive bodies and frames due to their excellent combination of strength and elongation resulted from deformation induced martensitic transformation (DIMIT). There have been extensive works on DIMIT kinetics and the role of retained austenite (RA) on tensile properties, but formability of these steel grades has not been well clarified to date. The characteristics of RA have been reported to be an important parameter for formability as in the case of uniaxial tensile test. It is thus attempted in the present study to investigate the formability of TRIP steels in relation to the transformation behavior of RA during forming tests. Forming tests were performed using an Erichsen machine and forming limit diagrams were obtained under uniaxial and biaxial stress state. Phase fractions were evaluated on the sample surface and the results were then mapped as a function of stress states.

#### 5:00 PM

**Environment-Friendly Corrosion Inhibition of A20 Carbon Steel By 2-Mercaptobenzimidazole For Citric Acid Pickling:** *Yunyun Zhang<sup>1</sup>; Daowu Yang<sup>1</sup>; Zhuo Ren<sup>1</sup>; Jin-hui Li<sup>1</sup>; <sup>1</sup>Changsha University of Science and Technology*

The corrosion inhibition effect of 2-mercaptobenzimidazole (2MBI) on the A20 carbon steel in citric acid has been investigated in relation to the concentration of the inhibitor by weight loss measurements, polarization curve methods and electrochemical impedance spectroscopy (EIS). Weight loss results obtained revealed that 2MBI is a good corrosion inhibitor whose efficiency can reach 98%. The addition of increasing concentrations of 2MBI moves the corrosion potential towards positive values and reduces the corrosion rate. Polarization curve results show that the corrosion inhibitor restrain the process of cathode and anode, belonging to anode control-oriented and charge transfer-controlled. EIS results show that the changes in the impedance parameters (R<sub>p</sub> and C<sub>d</sub>) with concentrations of 2MBI is indicative of the adsorption of the molecules leading to the formation of a protective layer on A20 carbon steel surface. The adsorption of 2MBI is also found to obey Langmuir's adsorption isotherm in citric acid.

#### 5:15 PM

**Synthesis and Application of Imidazolylquaternary-Ammonium-Salt Corrosion Inhibition for Hydrochloric Acid Pickling:** *Yunyun Zhang<sup>1</sup>; Daowu Yang<sup>1</sup>; Yi Liu<sup>1</sup>; Yang Sun<sup>1</sup>; <sup>1</sup>Changsha University of Science and Technology*

To enhance the water solubility and inhibition efficiency of 2-phenyl-imidazoline, a type of imidazolylquaternary-ammonium-salt was synthesized from 2-phenyl-imidazoline and benzyl chloride. And then the

compound pickling inhibitor was manufactured with imidazolylquaternary-ammonium-salt, potassium iodide, triethanolamine, polyoxyethylene nonylphenyl ether and peregal by weight loss through orthogonal experiment. The effect of the compound inhibitor on corrosion of A20 carbon steel in hydrochloric acid have been investigated in relation to its concentration by various corrosion monitoring techniques. It was found that the corrosion inhibition efficiency increased with the increase of compound inhibitor concentration by gravimetric measurements. Polarization studies showed depression of cathodic and anodic polarization curves in the presence of the compound inhibitor, indicating mixed type compound inhibition. EIS results show that the changes in the impedance parameters ( $R_p$  and  $C_d$ ) with concentrations of the compound inhibitor are indicative of the adsorption of these molecules leading to the formation of a protective layer on carbon steel surface. The adsorption of the compound inhibitor is also found to obey Langmuir's adsorption isotherm in hydrochloric acid.

### 5:30 PM

**Additive Manufacturing of Nickel-Base Superalloys:** John Wooten<sup>1</sup>; Ulf Ackelid<sup>2</sup>; Frank Medina<sup>3</sup>; Shane Collins<sup>4</sup>; Ryan Wicker<sup>3</sup>; Larry Murr<sup>3</sup>; <sup>1</sup>CalRAM; <sup>2</sup>Arcam AB; <sup>3</sup>University of Texas El Paso; <sup>4</sup>Paramount Inc

Additive manufacturing is being developed to produce functional hardware without the use of tooling. Components can be built one layer at a time making the technology ideal for complex hardware where low volume or low-rate production is needed. For structural aerospace applications where low-rate production quantities are often the norm, nickel-base superalloys are used. If the combination of layer building and nickel-base superalloys for aerospace applications can be successfully developed, then additive manufacturing will replace traditional methods of building such hardware. However, the acceptance of additive manufacturing will require a reference body of material property data. A study was undertaken to compare and contrast candidate additive manufacturing technology capable of producing nickel-base superalloys. Specifically, alloy 625 was fabricated by electron beam melting manufacturing, and a microstructural analysis was performed and a limited amount of tensile data was developed. These results were compared to other techniques capable of producing alloy 625.

## Hydrometallurgy Fundamentals and Applications: Session II

*Sponsored by:* The Minerals, Metals and Materials Society, TMS Extraction and Processing Division, TMS: Hydrometallurgy and Electrometallurgy Committee

*Program Organizer:* Michael Free, University of Utah

Thursday PM  
March 3, 2011

Room: 16A  
Location: San Diego Conv. Ctr

*Session Chair:* Michael Free, University of Utah

### 2:00 PM

**Investigations on the Mechanism of Acid Leaching of Alkali-Activated Ilmenite Concentrate and Titanium-Rich Slag:** Qian Xu<sup>1</sup>; Yajun Fu<sup>1</sup>; Jianfeng Jin<sup>1</sup>; Jihong Du<sup>2</sup>; <sup>1</sup>Northeastern University; <sup>2</sup>Northwest Institute for Non-ferrous Metal Research

Ilmenite is one of the primary sources of titanium dioxide, while titanium-rich slag generally is one product of ilmenite concentrate smelting reduction. In the present investigation, ilmenite concentrate and titanium-rich slag are pretreated by an alkali activation, then leached by moderate acid solutions in order to decrease the environmental loads arising from the titanium dioxide production. The mechanism of the alkali activation process is studied by X-Ray diffraction and chemical composition analyses. The structure and composition of intermediates of the alkali activation obviously affect the acid leaching efficiency of titanium and iron, following the alkali activation. The effects of temperature, time, mixture composition, acid concentration and stirring intensity on titaniferous iron oxide dissolution are studied, as well as optimization of the leaching process.

### 2:25 PM

**Kinetics Study of Alkaline Decomposition of Rubidium Jarosite in Ca(OH)<sub>2</sub> Media:** Eduardo Cerecedo<sup>1</sup>; Eleazar Salinas<sup>1</sup>; Luis Longoria<sup>2</sup>; Francisco Carrillo<sup>3</sup>; Juan Hernández<sup>1</sup>; <sup>1</sup>Universidad Autónoma del Estado de Hidalgo; <sup>2</sup>National Institute of Nuclear Researches; <sup>3</sup>Universidad de Coahuila

Rubidium jarosite was synthesized, leading a single phase product, composed principally by particles of spherical morphology with sizes varying from 25 to 40 microns forming aggregates of rhombohedral crystals strongly soldered in a compact texture. This compound has the following contents: 28.31% Fe, 35.30% SO<sub>4</sub>, 13.62% Rb, 5.57 ppm Ag and 22.74% (H<sub>3</sub>O + OH). Leading the approximated formula: [Rb<sub>0.2722</sub>(H<sub>3</sub>O)<sub>0.1423</sub>Ag<sub>0.000039</sub>]Fe<sub>3</sub>(SO<sub>4</sub>)<sub>2</sub>(OH)<sub>6</sub>. By the other hand, the nature of alkaline decomposition process of rubidium jarosite is characterized by an induction period followed by a progressive conversion period where sulphate and rubidium ions go to solution, leaving in residue the iron as amorphous hydroxide. Finally, the global process of alkaline decomposition of rubidium jarosite in Ca(OH)<sub>2</sub> media, has an order of reaction with respect to Ca(OH)<sub>2</sub> concentration of  $n=0.42$ , with an activation energy found of 99.10 kJ/mol, which can confirm that the process is controlled by chemical reaction.

### 2:50 PM

**Leaching Behavior of Secondary Zinc Oxide Dusts in Ammonia Solutions:** Yang Yong Bin<sup>1</sup>; Wang Wen Juan<sup>1</sup>; Jiang Tao<sup>1</sup>; Qian Li<sup>1</sup>; <sup>1</sup>Central South University

Leaching of secondary zinc oxide dusts is an important process in recovery of zinc from solid wastes to produce zinc based products. Ammonia leaching has been accepted as a more promising method for zinc leaching. The leaching behaviors of two secondary zinc oxide samples in ammonia leaching systems were investigated. The results indicated that, different samples had different leaching property. At the condition of L/S=5:1, [NH<sub>3</sub>] total:[CO<sub>3</sub>]<sup>2-</sup>=4:1(mol/mol), the optimum leaching conditions are 20min, 400r/min; 30min, 500r/min and 60min for pure ZnO, sample A and sample B respectively. Under their respective optimum leaching conditions, [NH<sub>3</sub>] total:[Zn<sup>2+</sup>]total ratio in pregnant solutions were 8.06:1, 9.32:1, and 10.01:1 for pure ZnO, sample A and sample B respectively. The main cause for these differences in leaching behavior lies in the species and contents of impurities occurred in the samples, higher contents of Pb, Fe, Cd are responsible for lower zinc leaching ratio in sample B.

### 3:15 PM

**Leaching of Gold in Acid Thiourea-Thiocyanate Solutions Using Ferric Sulfate as Oxidant:** Xiyun Yang<sup>1</sup>; Xichang Shi<sup>1</sup>; Hui Xu<sup>1</sup>; Michael S Moats<sup>1</sup>; Jan D Miller<sup>1</sup>; Xiang Xiao<sup>1</sup>; Liwen Ma<sup>1</sup>; <sup>1</sup>central south university

The leaching of gold in ferric-thiourea-thiocyanate solutions has been studied by the rotating-disk technique. The effects of initial concentrations of ferric, thiourea, thiocyanate, temperature and pH value on gold dissolution rate were studied. Determinations of apparent activation energy indicate that the process is controlled by a combination of chemical reaction and diffusion in the mixed lixiviant system. The gold dissolution rate in the mixed ligand solutions is higher than either lixiviant alone, even the sum of each individual lixiviant. In the presence of thiourea, thiocyanate shows considerable stability towards oxidation.

### 3:40 PM Break

### 3:55 PM

**Studies on the Dissolution of Platinum Powder by Electro-Generated Chlorine in Hydrochloric Acid Solution:** Min-Seuk Kim<sup>1</sup>; Jae-chun Lee<sup>1</sup>; Eun-Young Kim<sup>1</sup>; Jinki Jeong<sup>1</sup>; Banshi. D. Pandey<sup>2</sup>; <sup>1</sup>Korea Institute of Geoscience and Mineral Resources (KIGAM); <sup>2</sup>National Metallurgical Laboratory, CSIR

The dissolution of platinum powder by electro-generated chlorine has been investigated in hydrochloric acid solutions. The electro-generated chlorine in 1.0 mol/L HCl solution was supplied into a leaching reactor containing platinum powder suspended in HCl solution. Platinum dissolution was observed to be dependant on the concentration of hydrochloric acid, the



reaction temperature, and dissolved aqueous chlorine species. The results show negligible amount of platinum solubilization when less than 4 mol/L HCl was used; only 1.85 wt.% dissolution occurred in 4 mol/L HCl solution at 343 K and 2 g/L pulp density in 220 min. However, the dissolution of platinum increased abruptly to 95 wt.% within 45 min by raising the acid concentration to 5 mol/L. Raising the temperature has significantly improved the platinum dissolution rate. An activation energy of 46 kJ/mol was acquired for platinum dissolution in 5 mol/L HCl with 15 mmol/L aqueous chlorine in the temperature range 323-343K.

#### 4:20 PM

**Modeling of Cobalt and Nickel Extraction by Solvent Extraction in Sulfate Media with D2EHPA in Isoparaffin (17/21):** *Clenilson Sousa Junior*<sup>1</sup>; *Marisa Nascimento*<sup>2</sup>; *Ivan Masson*<sup>2</sup>; *Oswaldo Cunha*<sup>3</sup>; <sup>1</sup>Federal Institute of Education, Science and Technology of Rio de Janeiro; <sup>2</sup>Centre for Mineral Technology - CETEM; <sup>3</sup>Federal University of Rio de Janeiro - UFRJ

The divalent metals (Co<sup>2+</sup> and Ni<sup>2+</sup>) extraction, from the system MSO<sub>4</sub> - H<sub>2</sub>SO<sub>4</sub> - H<sub>2</sub>O - D2EHPA, in isoparaffin, was studied by a thermodynamic model based on balance equations of mass and charge. The activity coefficients of all solutes in the aqueous phase were calculated by modified Davies's equation. By applying this model, the concentrations of solutes in the equilibrium were calculated from the values of total concentration of cobalt and nickel in solution and pH. The metal extracted species was determined to be CoH<sub>0.25</sub>A<sub>2.25</sub> and NiH<sub>0.25</sub>A<sub>2.25</sub> (where HA is D2EHPA) and the equilibrium constant of the extraction was found to have a value, respectively, of 2,10x10<sup>-5</sup> and 2,40x10<sup>-5</sup>, from the calculation of non-linear regression Quasi-Newton method realized with the experimental data. The values of distribution coefficients predicted by the model for Co(II) and Ni(II) extraction were a good agreement when compared with experimental results.

### Magnesium Technology 2011: Advanced Materials and Processing

*Sponsored by:* The Minerals, Metals and Materials Society, TMS Light Metals Division, TMS: Magnesium Committee

*Program Organizers:* Wim Sillekens, TNO Science and Industry; Sean Agnew, University of Virginia; Suveen Mathaudhu, US Army Research Laboratory; Neale Neelameggham, US Magnesium LLC

Thursday PM  
March 3, 2011

Room: 6F  
Location: San Diego Conv. Ctr

*Session Chairs:* Karl Kainer, Helmholtz-Zentrum Geesthacht; Venkata Anumalasetty, Carpenter Technology Corporation

#### 2:00 PM

**Characterization of Hot Extruded Mg/SiC Nanocomposites Fabricated by Casting:** *Sunya Nimityongskul*<sup>1</sup>; *Noé Alba-Baena*<sup>1</sup>; *Hongseok Choi*<sup>1</sup>; *Milton Jones*<sup>1</sup>; *Tom Wood*<sup>2</sup>; *Mahi Sahoo*<sup>3</sup>; *Roderic Lakes*<sup>1</sup>; *Sindo Kou*<sup>1</sup>; *Xiaochun Li*<sup>1</sup>; <sup>1</sup>University of Wisconsin-Madison; <sup>2</sup>GS Engineering Inc; <sup>3</sup>CANMET Materials Technology Laboratory

Mg-1%SiC nanocomposites were fabricated using an ultrasonic-cavitation based casting method, resulting in the dispersion of the reinforcing SiC nanoparticles to form Mg-metal matrix nanocomposite (Mg-MMNC) billets. The MMNC billets were then processed using hot extrusion at 350°C. Micrographic observations illustrate a significant grain size reduction and the presence of micro-bands that align the SiC nanoparticles parallel to the direction of extrusion for the Mg-MMNCs. Observations from the cross-section at 90° of the extrusion direction show uniform nanoparticles dispersion contrasting previous observations. Results from the extruded Mg-MMNCs tensile testing at different temperatures (25°C, 125°C and 177°C) reveal an increase of the yield strength, ultimate tensile strength, and ductility values as compared to the un-reinforced and extruded Mg-alloy; such increase was also observed from the microhardness testing results where an increase from 19 to 34% was measured.

#### 2:20 PM

**Effects of Silicon Carbide Nanoparticles on Mechanical Properties and Microstructure of As-Cast Mg-12wt.%Al-0.2wt.%Mn Nanocomposites:** *Hongseok Choi*<sup>1</sup>; *Hiroshi Konishi*<sup>1</sup>; *Xiaochun Li*<sup>1</sup>; <sup>1</sup>University of Wisconsin-Madison

Microstructure and tensile properties of as-cast Mg-12Al-0.2Mn alloys with SiC nanoparticles were studied. SiC nanoparticles were dispersed into Mg-12Al-0.2Mn melts through an ultrasonic based nanoparticle-dispersion method. The content of SiC nanoparticles varied from 0 to 2 wt.%. The microstructural analysis with optical and scanning electron microscopy (SEM) showed that the massive brittle intermetallic phase ( $\beta$ -Mg<sub>17</sub>Al<sub>12</sub>) as well as  $\alpha$ -Mg grain was significantly refined, resulting in the enhancement of both strengths and ductility of as-cast Mg-12Al-0.2Mn alloys. Transmission electron microscopy (TEM) showed that there were SiC nanoparticles in both  $\alpha$ -Mg and  $\beta$ -Mg<sub>17</sub>Al<sub>12</sub> phases of the Mg-12Al-0.2Mn nanocomposites. It was found that there was a partial reaction between Mg/Al and SiC nanoparticles, producing Mg<sub>2</sub>Si intermetallic phases. X-ray diffraction (XRD) analysis confirmed also that the content of Mg<sub>2</sub>Si phases increased with increasing SiC content, limiting further enhancement of ductility of Mg-12Al-0.2Mn-SiC nanocomposite.

#### 2:40 PM

**Thermally-Stabilized Nanocrystalline Mg-Alloys:** *Suveen Mathaudhu*<sup>1</sup>; *Kristopher Darling*<sup>1</sup>; *Laszlo Kecskes*<sup>1</sup>; <sup>1</sup>U.S. Army Research Laboratory

Advanced nanocrystalline alloys have shown remarkable property improvements, particularly, order-of-magnitude strength increases, when compared to their coarse-grained counterparts. However, a major obstruction to the widespread application of such materials is the degradation of properties via rapid grain growth at even ambient temperatures. Conventional methods for circumvention of this problem at low temperatures have largely steered toward kinetically pinning the boundaries with dispersoids, or through misorientation of grain boundaries, yet even these methods have limited utility at elevated temperatures needed for routine sintering and forming operations. In this work, we will present a synergistic approach to the development of thermally stable nanostructured Mg-alloys which incorporates elements of predictive modeling of suitable alloy systems, fabrication of nanostructured alloy powders by high energy ball milling and consolidation of the powders at elevated temperatures to bulk ultrahigh strength alloys.

#### 3:00 PM

**TiNi Reinforced Magnesium Composites by Powder Metallurgy:** *Ziya Esen*<sup>1</sup>; <sup>1</sup>Çankaya University

Rod shaped Mg-TiNi composite samples were manufactured by powder metallurgical route in which the samples were heated and deformed simultaneously using rotary hot swaging technique. Firstly, encapsulated argon filled copper tubes which contained compacts of pure magnesium and pre-alloyed TiNi alloy powder mixtures were deformed about 45% in two steps at 450°C. Pre/post annealing heat treatments were applied at 450°C for 20 mins between the stages of coaxial deformation to enhance the sintering degree and to homogenize the heavily deformed composite structures. Next, copper peeled and machined samples were compression tested under quasi-static conditions to investigate the mechanical properties, i.e. yield and peak strength, and ductility. Transmission and Scanning Electron Microscopy studies were carried out to examine the Mg-TiNi interface and fracture surfaces of the compression tested composites, respectively.

#### 3:20 PM

**Nanocrystalline Mg-Matrix Composites with Ultrahigh Damping Properties:** *Babak Anasori*<sup>1</sup>; *Shahram Amini*<sup>1</sup>; *Volker Presser*<sup>1</sup>; *Michel Barsoum*<sup>1</sup>; <sup>1</sup>Drexel University

Recently, we reported on the processing of 50 vol.% Ti<sub>2</sub>AlC-nanocrystalline magnesium, nc-Mg, matrix composites using a pressureless melt infiltration method. Herein we report on composites with up to 80 vol.% Mg. These composites are readily machinable, relatively stiff, strong and light, and exhibit ultrahigh damping. Increasing the nc-Mg volume fraction leads to lighter composites with higher damping characteristics at lower stresses (~30% of the mechanical energy is dissipated at 250 MPa). In some cases,

the Mg nanograins are also extraordinarily thermally stable, which renders these composites good candidates for applications at temperatures higher than ambient. Due to the simple inexpensive melt infiltration technique used to fabricate these novel nanocomposites, it is possible to produce samples as large as ones made via normal powder metallurgy methods.

#### 3:40 PM Break

#### 4:00 PM

**Effect of Fiber Reinforcement on Corrosion Resistance of Mg AM60 Alloy-based Composites in NaCl Solutions:** *Qiang Zhang*<sup>1</sup>; Henry Hu<sup>1</sup>; <sup>1</sup>University of Windsor

There is great interest in developing low-cost, magnesium-based MMCs because of their high stiffness-to-weight ratio for aerospace and automotive applications. However, corrosion resistance of MMC is often a concern for components to be used in harsh environment. In this study, the corrosion behaviour of Al<sub>2</sub>O<sub>3</sub> fibres reinforced magnesium AM60 composite, in aqueous solutions containing various concentrations of NaCl, was studied in comparison to that of matrix alloy by potentiodynamic polarization measurements. The microstructure of the composite and matrix alloy AM60 before and after corrosion testing was analyzed by optical microscopy, and scanning electron microscopy. The results show that the presence of Al<sub>2</sub>O<sub>3</sub> fiber deteriorates the corrosion resistance of the matrix magnesium alloy AM60. The effect of Al<sub>2</sub>O<sub>3</sub> fiber reinforcement and NaCl concentrations on the corrosion behavior of the composites are discussed. The corrosion mechanisms of the composite are proposed in light of metallographic observation on the formation of corrosion products.

#### 4:20 PM

**The Production of Powder Metallurgy Hot Extruded Mg-Al-Mn-Ca Alloy with High Strength and Limited Anisotropy:** *Ayman Elsayed*<sup>1</sup>; Junko Umeda<sup>1</sup>; Katsuyoshi Kondoh<sup>1</sup>; <sup>1</sup>Osaka University

Rapidly solidified Mg-Al-Mn-Ca alloy produced by Spinning Water Atomization Process (SWAP) was hot extruded into rectangular bars, from which tensile and compression samples have been cut at 0°, 45° and 90° from the extrusion direction to study their anisotropy. Electron Back Scattered Diffraction (EBSD) has been used to investigate the texture evolution during the hot extrusion process. Both the Schmid factor and the intensity of the basal plane in the pole figure have been evaluated and correlated to the mechanical properties. Results have shown that the extruded rods exhibit high strength and limited anisotropy compared to many previously reported values for magnesium alloys. The reasons for that limited anisotropy were both the fine grained microstructure of the extruded material and the transverse component of the texture evolution.

#### 4:40 PM

**Thermal Effects of Calcium and Yttrium Additions on the Sintering of Magnesium Powder:** Paul Burke<sup>1</sup>; Chloe Petit<sup>2</sup>; Sonia Yakoubi<sup>2</sup>; *Georges Kipouros*<sup>1</sup>; <sup>1</sup>Dalhousie University; <sup>2</sup>ICAM

Magnesium and its alloys are attractive materials for use in automotive and aerospace applications because of the low density and good mechanical properties. Powder metallurgy P/M can be used to alleviate the formability problem through near-net-shape processing, and also allows unique chemical compositions that can lead to new alloys with novel properties. However, the surface layer formed on the Mg powders during processing acts as a barrier to diffusion and sintering is problematic. The layer, characterized using focused ion beam milling and transmission electron microscopy, as well as x-ray photoelectron spectroscopy, contains oxides, hydroxides and carbonates of magnesium, formed by reactions with the atmosphere. To overcome this barrier, small additions were made of calcium and yttrium the oxides of which are thermodynamically more stable than magnesium oxide. The present work reports on the thermal effect of Ca and Y additions to magnesium powder during sintering, utilizing differential scanning calorimetry (DSC).

#### 5:00 PM

**Microstructure and Mechanical Properties of Solid State Recycled Mg Alloy Chips:** *Kunio Matsuzaki*<sup>1</sup>; Youich Murakoshi<sup>1</sup>; Toru Shimizu<sup>1</sup>; <sup>1</sup>National Institute of Advanced Industrial Science and Technology

Mg alloy chips generated in machining process such as turning and sawing are hard to recycle through melting process because the chips are very fine and easily burned during the heating. In this paper, several machined Mg alloy chips were solid state recycled into a bar using hot-pressing and hot-extrusion, and mechanical properties of recycled chips were examined. The recycled AZ91 and AZX911 alloy show a fine microstructure with a grain size below 10 micrometers. The compressed yield stress at R.T. is 208MPa and 210 MPa for the AZ91 and AZX911, respectively, and higher than that of virgin samples. The backward extrusion test reveals that the recycled AZ91 and AZX911 alloys have good formability at above 573K. Therefore, the solid state recycled Mg alloys have high strength with formability and would be expected as materials for forging.

#### 5:20 PM Concluding Comments

**Presentation of the Best Poster Award 2011 by Eric Nyberg**

### Magnesium Technology 2011: Corrosion and Coatings

*Sponsored by:* The Minerals, Metals and Materials Society, TMS Light Metals Division, TMS: Magnesium Committee  
*Program Organizers:* Wim Sillekens, TNO Science and Industry; Sean Agnew, University of Virginia; Suveen Mathaudhu, US Army Research Laboratory; Neale Neelameggham, US Magnesium LLC

Thursday PM  
March 3, 2011

Room: 10  
Location: San Diego Conv. Ctr

*Session Chairs:* Robert McCune, Robert C. McCune and Associates LLC; Neale Neelameggham, US Magnesium LLC

#### 2:00 PM

**Salt Spray Corrosion of Mechanical Junctions of Magnesium Castings:** Sabrina Grassini<sup>1</sup>; Paolo Matteis<sup>1</sup>; Giorgio Scavino<sup>1</sup>; Marco Rossetto<sup>1</sup>; *Donato Firrao*<sup>1</sup>; <sup>1</sup>Politecnico di Torino

The corrosion of cast, 3 mm thick, AE44 magnesium-alloy plates fastened to aluminum-alloy threaded counterparts, either constituting the screw or the nut, were tested in neutral salt spray for 48 hours, with or without interposed AA5051 spacers (washers). Steel nuts or screws were used, respectively, always insulating from corrosion the steel sides. Couplings between magnesium alloy plates and coated steel counterparts (screw heads) with interposed AA5051 washers were also tested, while insulating the nut side. Every 4 or 8 hours the test was halted and the samples were rinsed and photographed for manual image analysis. Then the plates were unmounted, slightly polished (highlighting the deep corrosion pits), and scanned for automatic image analysis. Different image analysis methods were compared. The least corrosion occurs, in couplings with aluminum alloy counterparts, when AA5051 washers are interposed; whereas the most effective coupling with steel counterparts is the one with nylon coated steel heads.

#### 2:20 PM

**Comparing the Corrosion Effects of Two Environments on As-Cast and Extruded Magnesium Alloys:** *Holly Martin*<sup>1</sup>; M. Horstemeyer<sup>1</sup>; Paul Wang<sup>1</sup>; <sup>1</sup>Center for Advanced Vehicular Systems, Mississippi State University

Magnesium is easily corroded in the presence of saltwater, limiting its use in the automotive industry. The magnesium microstructure greatly affects the corrosion rate, due to various additional elements. In the Center for Advanced Vehicular Systems at Mississippi State University, the effects of immersion and cyclical salt spray testing on various as-cast and extruded magnesium alloys is currently being examined. Previous work on an as-cast AE44 magnesium alloy has demonstrated that individual pit characteristics, such as pit depth, pit area, and pit volume, were deeper and larger following

exposure to the immersion environment. However, the data elucidating the corrosion effects on individual pit characteristics has only been seen on as-cast magnesium containing rare earth elements, not on extruded magnesium alloys or zinc-containing magnesium alloys, both common magnesium forms. The research presented here will cover the effects of individual pit characteristics formed on various magnesium alloys due to the different environments.

#### 2:40 PM

**Influence of Lanthanum on the Corrosion Behaviour of Binary Mg-La Alloys:** *Daniel Hoeche*<sup>1</sup>; Rosario Silva Campos<sup>1</sup>; Carsten Blawert<sup>1</sup>; Karl Ulrich Kainer<sup>1</sup>; <sup>1</sup>GKSS Research Centre

Different contents of Lanthanum have been added to Magnesium and have been investigated on their influence on the microstructure and the corrosion properties. The microstructure was studied by means of SEM and optical microscopy. Corrosion performance was evaluated using potentiodynamic polarization measurements. Immersion tests were carried out using distilled water and 0.1% sodium chloride solution. The corrosion products were investigated by X-ray induced photoelectron spectroscopy (XPS), Auger electron spectroscopy (AES) and X-ray diffraction (XRD) which lead to detailed information on phase formation and mass transport. The oxide and hydroxide formation have been correlated to the chemical states and formed intermetallics, i.e. by taking into account the XPS peak shift and peak splitting of the La-3d, O-1s and the Mg-2p state. Additionally, the results have been verified by means of AES on the Mg-KLL, O-KLL and La-MNN excitation and by XRD. Latter suggests the supplemental formation of a nanocrystalline phase.

#### 3:00 PM

**Cryogenic Burnishing of AZ31B Mg Alloy for Enhanced Corrosion Resistance:** *Z. Pu*<sup>1</sup>; Guang-Ling Song<sup>2</sup>; S. Yang<sup>1</sup>; O. Dillon, Jr.<sup>1</sup>; D. Puleo<sup>1</sup>; I. Jawahir<sup>1</sup>; <sup>1</sup>University of Kentucky; <sup>2</sup>GM Global Research & Development

Poor corrosion resistance is limiting applications of Mg alloys. However, the corrosion performance of a Mg alloy can be enhanced through modification of its microstructure. It has been reported in the literature that the microstructure, especially grain size of AZ31 Mg alloy, has a significant influence on its corrosion resistance. In this study, AZ31B discs were subjected to a novel mechanical processing method—cryogenic burnishing; the surface of AZ31B workpiece was burnished with a custom tool under a liquid nitrogen spraying condition. The processing led to a more than 2 mm thick surface layer with remarkably changed microstructures formed on the disc surface. Significant grain refinement occurred within this surface layer due to dynamic recrystallization induced by severe plastic deformation and effective cooling by liquid nitrogen. Electrochemical measurements indicate that the corrosion resistance of the burnished surface was significantly improved.

#### 3:20 PM

**Advanced Conversion Coatings for Magnesium Alloys:** *Syam Nibhanupudi*<sup>1</sup>; Alp Manavbasi<sup>1</sup>; <sup>1</sup>Metalast International

Magnesium and its alloys have excellent physical and mechanical properties due to their high strength-to-weight ratio and are ideal for various applications in automotive, aerospace and defense sectors. However, Mg alloys are also highly susceptible to corrosion under harsh environments. Owing to the carcinogenicity as well as environmental impact of hexavalent chromium fueled by stringent environmental regulations, an environmentally green alternative to the carcinogenic hexavalent chromium coatings on magnesium is due. In this work, a novel trivalent chromium based conversion coating has been developed to improve the corrosion resistance and paint adhesion properties of Mg alloys. Surface characterizations were conducted using SEM/EDX and anti corrosive properties have been investigated via hydrogen evolution and electrochemical corrosion analysis techniques. Results have shown that the novel environmentally green trivalent chromium based coating on magnesium has indeed performed comparable to hexavalent chromium and thus establishing a viable alternative.

#### 3:40 PM Break

#### 4:00 PM

**Development of Zirconium-Based Conversion Coatings for the Pretreatment of AZ91D Magnesium Alloy Prior to Electrocoating:** *James Reck*<sup>1</sup>; Yar-Ming Wang<sup>1</sup>; Hong-Hsiang Kuo<sup>1</sup>; <sup>1</sup>General Motors

This work examines the use of hexafluorozirconic acid based solutions at concentrations from 0.025 M to 0.100 M and pH values of 2.0 to 4.0 for the creation of a zirconia-based conversion coating less than 1 micron thick to protect magnesium alloy AZ91D. Similar coatings have been found to give excellent protection for steel and aluminum alloys, but little research has been conducted on its application to magnesium. Work was performed to gain an understanding of the film formation mechanisms and related kinetics using x-ray photo-electron spectroscopy, scanning electron microscopy, and open circuit potential monitoring techniques. A design of experiments approach was taken to determine the effects of acid concentration, pH, and soak time on the corrosion properties both as-deposited and with an application of electrocoat. It was found that the application of the zirconia-based coating significantly increased corrosion resistance, and allowed for an acceptable e-coat application with excellent adherence.

#### 4:20 PM

**Use of an AC/DC/AC Electrochemical Technique to Assess the Durability of Protection Systems for Magnesium Alloys:** *Sen Song*<sup>1</sup>; *Robert C. McCune*<sup>2</sup>; Weidian Shen<sup>1</sup>; Yar-Ming Wang<sup>3</sup>; <sup>1</sup>Eastern Michigan University; <sup>2</sup>Robert C McCune & Associates LLC; <sup>3</sup>General Motors Company

One task under the U.S. Automotive Materials Partnership (USAMP) "Magnesium Front End Research and Development" (MFERD) Project has been the evaluation of methodologies for the assessment of protective capability for a variety of proposed protection schemes for this hypothesized multi-material, articulated structure. Techniques which consider the entire protection system, including both pretreatments and topcoats are of interest. In recent years, an adaptation of the classical electrochemical impedance spectroscopy (EIS) approach using an intermediate cathodic DC polarization step (viz. AC/DC/AC) has been employed to accelerate breakdown of coating protection, specifically at the polymer-pretreatment interface. This work reports outcomes of studies to employ the AC/DC/AC approach for comparison of protective coatings to various magnesium alloys considered for front end structures. In at least one instance, the protective coating system breakdown could be attributed to the poorer intrinsic corrosion resistance of the sheet material (AZ31) relative to die-cast AM60B.

#### 4:40 PM

**Effects of Oxidation Time on Micro-Arc Oxidized Coatings of Magnesium Alloy AZ91D in Aluminate Solution:** *Weiyi Mu*<sup>1</sup>; Zhengxian Li<sup>1</sup>; Jihong Du<sup>1</sup>; Ruixue Luo<sup>1</sup>; Zhengping Xi<sup>1</sup>; <sup>1</sup>Northwest Institute for Nonferrous Metal Research

Micro-arc oxidation coatings were prepared on magnesium alloy AZ91D at different oxidation times in aluminate solution. The effects of the oxidation time on the microstructure, growth rate and corrosion resistance of the coatings were investigated. The results indicate that the coatings are uniform in thickness and mainly composed of MgAl<sub>2</sub>O<sub>4</sub> and MgO. There were many residual discharging channels on the coatings surface. The coatings improved the corrosion resistance of magnesium alloy AZ91D considerably. With increased oxidation time, the crystalline substances content and thickness of the coatings increased, while the growth rate of the coatings decreased, and the resulting coatings surface had lower porosity and larger pore sizes. In addition, the corrosion resistance of the coatings on magnesium alloy AZ91D surfaces is superior to the magnesium alloy AZ91D substrate in the NaCl solution, and the effect is more remarkable with longer oxidation times.

#### 5:00 PM

**Composite Coatings Combining PEO Layer and EPD Layer on Magnesium Alloy:** *Yongfeng Jiang*<sup>1</sup>; Huashan Yang<sup>1</sup>; Yefeng Bao<sup>1</sup>; <sup>1</sup>Hohai University

Protective composite coatings were prepared by combining plasma electrolytic oxidation (PEO) treatment and cathodic electrophoretic



deposition (E-coat) on magnesium alloy AZ91D. The corrosion protection of composite coatings were evaluated by using potentiodynamic polarization measurements in 3.5% NaCl solution, copper accelerated acetate salt spray (CASS) test and immersion test in acid solution. The adhesion of composite coatings was evaluated by means of cross-cut test and pull-off test. It is indicated that the corrosion resistance of magnesium alloy AZ91D with the composite coatings is improved obviously compared to it merely with PEO coating, and it is also shown pitting corrosion PEO coating on magnesium alloy is decreased by EPD posttreatment. The adhesion of composite coatings can attain 11.3 N/mm<sup>2</sup> in quantitative method due to the interlocking effect of organic layer in pores of PEO layer.

#### 5:20 PM Concluding Comments

#### Presentation of the Best Poster Award 2011 (in Room 6F)

### Magnetic Materials for Energy Applications: Experimental and Modelling Techniques for the Magnetocaloric Effect

*Sponsored by:* TMS Electronic, Magnetic, and Photonic Materials Division, TMS: Energy Conversion and Storage Committee, TMS: Magnetic Materials Committee; JSPS 147th Committee on Amorphous and Nanocrystalline Materials; Lake Shore Cyrotronics, Inc.; AMT&C

*Program Organizers:* Victorino Franco, Sevilla University; Oliver Gutfleisch, IFW Dresden; Kazuhiro Hono, National Institute for Materials Science; Paul Ohodnicki, National Energy Technology Laboratory

Thursday PM  
March 3, 2011

Room: 11A  
Location: San Diego Conv. Ctr

*Session Chair:* Francis Johnson, GE Global Research

#### 2:00 PM Invited

**First to Second Order Magnetocaloric Transition: on Correct Analysis of Experimental Data:** *Daniel Fruchart*<sup>1</sup>; Mohamed BALLI<sup>1</sup>; <sup>1</sup>CNRS - Institut Néel

In the vicinity of magnetic transition a magnetocaloric (MC) material behaves under external field sollicitations in metastable conditions. This means that the used magnetisation cycle applied versus time, temperature, field...has a dramatic impact on the received experimental data. Moreover, recent papers display variations of magnetic entropy measured on first order type materials exceeding by very far what was measured elsewhere and reported accordingly. This proves that a carefull use of the most appropriated phenomenological model must be applied. Based on several experimental data sets recorded on different type materials exhibiting a first order MC transition, our report aims demonstrate correctness application of the models.

#### 2:25 PM Invited

**Magnetocaloric Parameters from Measurements of Heat and Temperature:** *Ramón Burriel*<sup>1</sup>; Elías Palacios<sup>1</sup>; <sup>1</sup>CSIC - Universidad de Zaragoza

A correct determination of the magnetocaloric parameters is of crucial importance for the evaluation of efficient cooling materials. Most of the interesting compounds present first-order transitions that give frequent problems in the estimation of the isothermal entropy change,  $\Delta S_T$ , through magnetic determinations of  $M(T,H)$ . Adiabatic calorimetry and modifications of this technique provide valuable determinations of  $\Delta S_T$  and also of the adiabatic entropy change,  $\Delta T_S$ , through entropy calculations from field dependent heat capacity  $C_p(T,H)$ , or with direct measurements of  $\Delta S_T$  and  $\Delta T_S$ . The determination of the cooling efficiency in hysteretic compounds requires control of the thermal and field history, considering the Field-Temperature phase diagram. The possible coexistence of different phases in the hysteretic region can give erroneous results from the magnetic measurements and from direct determinations. Also the direction when crossing the transition line has

to be considered, and the irreversible entropy creation at the transition when estimating the heat exchanges.

#### 2:50 PM Invited

**Experimental Methods of the Magnetocaloric Effect Studies:** *Youri Spichkin*<sup>1</sup>; <sup>1</sup>AMTC

The methods of experimental investigations of the magnetocaloric parameters (adiabatic temperature change and isothermal magnetic entropy change caused by external magnetic field) are reviewed and discussed. The direct and indirect methods are compared and their advantages and disadvantages are considered. Possible influence of the used methods on the obtained results is regarded. The main attention is paid to the direct methods of measurements. The realization of the dynamic mode of the direct adiabatic temperature change measurement is considered. Importance of the magnetocaloric measurements in dynamic mode for characterization of the magnetocaloric materials suitable for using as working bodies in magnetic heat machines is shown. The methods of the experimental data processing are discussed. Recent experimental results of the magnetocaloric parameters on some materials are presented.

#### 3:15 PM Invited

**First Principles Modeling of Magnetocaloric Gd<sub>5</sub>Ge<sub>4</sub> Based Materials:** *Durga Paudyal*<sup>1</sup>; Y. Mudryk<sup>1</sup>; V. K. Pecharsky<sup>1</sup>; K. A. Gschneidner, Jr.<sup>1</sup>; <sup>1</sup>The Ames Laboratory, U. S. Department of Energy

We present the first principles modeling of structural and magnetic properties of Gd<sub>5</sub>Ge<sub>4</sub> based magnetocaloric materials. The total energy as a function of the shear displacement of slabs confirms stability of experimentally observed crystal and magnetic structures. Small substitutions of the Gd by Y and Lu lead to a catastrophic loss of ferromagnetism, but the substitutions by La have no effect on the magnetism. Furthermore, substitutions of the Ge by Si exert chemical pressure and transform the antiferromagnetic O(II) to the ferromagnetic O(I) ground state. In addition, we present a pathway for estimating the magnetic entropy change in the room temperature giant magnetocaloric compounds, i.e. Gd<sub>5</sub>Si<sub>2</sub>Ge<sub>2</sub>, by coupling first principles outputs with the established magneto-thermodynamic models. The theoretical values of the magnetic entropy change compare well with experimental results. This work was supported by the Office of Basic Energy Sciences, Materials Sciences Division of the Office of Science.

#### 3:40 PM

**Monte Carlo Simulations of the Magnetocaloric Effect and Exchange Bias Effect in Heusler Ni-Mn-Sb Alloys:** *Vladimir Sokolovskiy*<sup>1</sup>; Vasily Buchelnikov<sup>1</sup>; Ivan Taranenko<sup>1</sup>; Sergey Taskaev<sup>1</sup>; Peter Entel<sup>2</sup>; <sup>1</sup>Chelyabinsk State University; <sup>2</sup>University of Duisburg-Essen

Heusler Ni-Mn-Sb alloys have unique properties such as the shape memory effect, magnetocaloric effect (MCE), and exchange bias effect (EB). The reason of these properties is a magnetostructural phase transition. In this work, we present a theoretical model for investigation of the EB and MCE in Ni<sub>50</sub>Mn<sub>25-x</sub>Sb<sub>25-x</sub> alloys by Monte Carlo method. In the model, we use a cubic lattice with real unit cell. In the case of the MCE modeling, we choose the 3-5 state Potts model for magnetic transitions and Blume-Emery-Griffiths model allowing to describe a structural transformation. For the EB modeling, the model Hamiltonian includes Heisenberg's spin interactions with an anisotropy term. The temperature dependences of positive and negative MCE for Ni<sub>50</sub>Mn<sub>25-x</sub>Sb<sub>25-x</sub> alloys are obtained. Our simulations have shown that EB field depends on a concentration of excess Mn atoms. We have found a blocking temperature of EB for Ni<sub>50</sub>Mn<sub>37.5</sub>Sb<sub>12.5</sub> which is closer to experimental value.

#### 3:55 PM

**Structural Entropy Contributions to the Total Magnetocaloric Effect in Materials Which Exhibit a First Order Transition:** *Karl Gschneidner*<sup>1</sup>; Yaroslav Mudryk<sup>1</sup>; Vitalij Pecharsky<sup>1</sup>; <sup>1</sup>Iowa State University

A few magnetic materials have been observed to exhibit a first order magnetic transition which is coupled with a crystal structure change, or with a large volume change. The entropy associated with the structural transformation or volume change is comparable to the entropy associated

with the purely magnetic transition for 50 kOe field changes. Since the magnetic and structural changes are coupled, it is difficult to directly measure the two contributions to the total entropy change independently, since normal measurements of the magnetocaloric effect yield only the total entropy change. However, by doping it is possible to destroy the structural transition and thus measure the purely magnetic entropy. Using this information one can determine the structural entropy associated with the first order transition. By heat treating or by high pressure measurements it is also possible to determine the structural entropy. The structural entropy changes for various materials will be compared.

#### 4:10 PM

##### **Environmentally Friendly New Air-Conditioning Magnetocaloric System:** Christian Muller<sup>1</sup>; Carmen Vasile<sup>2</sup>; <sup>1</sup>Cooltech Applications; <sup>2</sup>INSA

The concept, the design and the manufacture of a new magnetocaloric air-conditioning system is based on the intimate knowledge of the active magneto-thermodynamic materials properties. The needed characteristics of the magneto-caloric materials are adiabatic temperature change, heat capacity and magnetisation. It is also of great interest the understanding of the behaviour of these active elements submitted to the permanent magnet alternative magnetising field and demagnetising field. This paper presents a new system environmentally friendly and energy efficient, based on a recent technological breakthrough: "magnetocaloric cooling around room temperature". The expected benefits are: increased energy efficiency, reduced consumption of energy, reduction of corresponding pollutant emissions and of any direct emission of pollutants. A magnetocaloric demonstrator will be presented and its performance described. The energy performance, the range of ambient temperatures and the temperature span, as well as the useful power will also be presented and explained.

#### **Microstructural Processes in Irradiated Materials: Non-Metals**

*Sponsored by:* The Minerals, Metals and Materials Society, TMS Structural Materials Division, TMS/ASM: Nuclear Materials Committee

*Program Organizers:* Gary Was, University of Michigan; Thak Sang Byun, Oak Ridge National Laboratory; Shenyang Hu, Pacific Northwest National Laboratory; Dane Morgan, UW Madison; Yasuyoshi Nagai, Tohoku University

Thursday PM  
March 3, 2011

Room: 3  
Location: San Diego Conv. Ctr

*Session Chairs:* Ming Tang, Los Alamos National Laboratory; Yong Yang, University of Wisconsin-Madison

#### 2:00 PM Invited

**Radiation Stability of GFR Candidate Ceramics:** Yong Yang<sup>1</sup>; Clayton Dickerson<sup>1</sup>; Jian Gan<sup>2</sup>; Todd Allen<sup>1</sup>; <sup>1</sup>University of Wisconsin-Madison; <sup>2</sup>Idaho National Laboratory

Determining and predicting the stability in response to radiation is a key part in developing a practical ceramics-based fuel for a gas cooled fast reactor (GFR). The hot pressed ceramics including ZrC, ZrN, TiC and TiN were irradiated in Cd shrouded capsule in the Advanced Test Reactor (ATR) to a dose of 1 dpa at 800 °C, and the materials were procured from the ATR irradiated sample library. The radiation stability of these ceramics were examined using transmission electron microscopy (TEM) to understand the effect of radiation on lattice stability, phase change, void growth, and other microstructural features such as dislocation loops and Stacking Fault Tetrahedra (SFTs). The irradiation induced hardening is also evaluated using Vickers hardness test. The irradiation response of neutron irradiated ceramics is further compared with that from proton irradiation at a comparable condition.

#### 2:40 PM

**Microstructure and Radiation Damage Tolerance of TiO<sub>2</sub> Thin Films:** Mujin Zhuo<sup>1</sup>; Engang Fu<sup>1</sup>; Wang Yongqiang<sup>1</sup>; Yingying Zhang<sup>1</sup>; Blas Uberuaga<sup>1</sup>; Amit Misra<sup>1</sup>; Michael Nastasi<sup>1</sup>; Quanxi Jia<sup>1</sup>; <sup>1</sup>Los Alamos national Lab

Ion irradiation damage effects in TiO<sub>2</sub> thin films with different polymorphs were investigated using X-ray diffraction (XRD) and TEM. The TiO<sub>2</sub> film grown on LaAlO<sub>3</sub> (001) has anatase structure with [004] orientation while that on Al<sub>2</sub>O<sub>3</sub> (102) substrate is rutile with {101} parallel to the substrate surface. The films were irradiated at room temperature with 600 keV Kr<sup>2+</sup> ions to a fluence of 1.5 10<sup>15</sup> Kr/cm<sup>2</sup>. Extensive XRD and TEM analyses reveal that no amorphization transformation occurs under such irradiation conditions and both anatase and rutile films remain crystalline after irradiation. Coupled with Rutherford Backscattering Spectroscopy in channeling geometry, it is observed that the damage accumulation within TiO<sub>2</sub> films is very low despite that the substrates are heavily damaged. Moreover, no significant denuded area was found in either irradiated anatase or rutile TiO<sub>2</sub> films. This study reveals that grain boundary plays a critical role in the irradiation tolerance of TiO<sub>2</sub>.

#### 3:00 PM

**Computational Studies of Radiation Damage near Grain Boundaries in TiO<sub>2</sub>:** Xian-Ming Bai<sup>1</sup>; Blas Uberuaga<sup>1</sup>; <sup>1</sup>Los Alamos National Laboratory

Grain boundaries (GBs) can serve as sinks for absorbing radiation-induced defects. However, the role of GBs in promoting radiation tolerance in ceramics not well understood, and is complicated by the facts that the defects in ceramics are charged. Here, we use three atomistic modeling methods to examine the role of GBs in a model system. TiO<sub>2</sub>, in modifying defect thermodynamics and defect production. TiO<sub>2</sub> has multiple polymorphs, including rutile and anatase, which have different radiation tolerances. We use molecular statics and temperature accelerated dynamics to investigate the defect thermodynamics and kinetics in these two polymorphs and predict their long-time damage annealing behaviors. We use molecular dynamics to investigate defect production near GBs and find that the damage production is sensitive to the knock-on atom position. GBs also can induce more residual damage than if the boundary was not present. The properties of defect clusters of various forms are also investigated.

#### 3:20 PM

**Interstitial Loading Effects during Irradiation in MgO:** Blas Uberuaga<sup>1</sup>; Xian-Ming Bai<sup>1</sup>; <sup>1</sup>Los Alamos National Laboratory

It is well established that boundaries in materials can promote radiation tolerance. However, the atomic-scale mechanisms responsible for this improved tolerance are still not clear. This is especially true for oxide ceramics. Even at low temperatures where vacancy are immobile, nanocrystalline oxides have been observed to have significantly more radiation tolerance than larger grained materials [1]. The recently-discovered interstitial emission mechanism, observed in Cu [2], may provide insight into the enhanced tolerance in oxides. Using atomistic simulation methods, we explore the interaction between grain boundaries and irradiation-induced defects in MgO, a model ceramic. We focus on the interstitial emission mechanism and the role it plays in enhancing the radiation tolerance of oxides. We find that there is a significant propensity for low-barrier interstitial mechanisms to occur in MgO, possibly explaining the experimental observations. [1] Shen et al. APL 90, 263115 (2007). [2] Bai et al. Science 327, 1631 (2010).

#### 3:40 PM Break

#### 4:00 PM

**Structure and Mechanical Properties of Swift Heavy Ion Irradiated Tungsten-bearing Delta-phase Oxides Y<sub>6</sub>W<sub>10</sub>O<sub>12</sub> and Yb<sub>6</sub>W<sub>10</sub>O<sub>12</sub>:** Ming Tang<sup>1</sup>; Thomas Wynn<sup>1</sup>; Maulik Patel<sup>1</sup>; Nathan Mara<sup>1</sup>; Kurt Sickafus<sup>1</sup>; <sup>1</sup>Los Alamos National Laboratory

We report on the relationship between structure and mechanical properties of complex oxides whose structures are derivatives of fluorite, following irradiation with swift heavy ion (92 MeV Xe) which approximately simulates fission product irradiation. The two compounds of interest in this presentation

are the compounds, Y6W1O12 and Yb6W1O12. These compounds possess an ordered, fluorite derivative crystal structure known as the delta phase, a rhombohedral structure belonging to space group R-3. Structural changes induced by irradiation were examined using X-ray diffraction (XRD) and transmission electron microscopy (TEM). Post-irradiation characterization experiments revealed irradiation induced amorphization in these compounds. The mechanical properties of both irradiated samples, determined by cross-sectional nano-indentation measurements as a function of ion penetration depth, can be related to their microstructures. Post-irradiation annealing experimental results on the structure and mechanical properties of these compounds will also be discussed.

#### 4:20 PM

**Atomistic and Rate Theory Modeling of Radiation Damage and Amorphization of Nanocrystalline Silicon Carbide:** Narasimhan Swaminathan<sup>1</sup>; Dane Morgan<sup>1</sup>; Izabela Szlufarska<sup>1</sup>; <sup>1</sup>University of Wisconsin-Madison

Cubic silicon carbide (3C-SiC) is being considered as a structural material for nuclear fission and fusion reactors. Polycrystalline SiC is already known for its excellent mechanical properties and low neutron cross section, and improvements in mechanical and radiation resistance properties may be possible through use of nanocrystalline (nc) SiC. This work uses modeling techniques from multiple length scales to understand the effects of radiation on SiC as a function of grain size. Molecular dynamics cascade simulations, ab initio formation and migration energies, and rate theory modeling have been combined to study defect production rates and amorphization trends with grain size, radiation dose, and temperature. Initial results suggest little impact on in-grain defect production rates from using nc-SiC but a complex coupling between grain size and temperature is seen for the dose to amorphization.

#### 4:40 PM

**Microstructure and Mechanical Property Characterization of Self-Ion Irradiated 3C-SiC with Novel Micromachined Samples:** Chansun Shin<sup>1</sup>; Hyung-ha Jin<sup>1</sup>; Suk Hoon Kang<sup>1</sup>; Junhyun Kwon<sup>1</sup>; Ji Yeon Park<sup>1</sup>; <sup>1</sup>KAERI

This work investigated the microstructural and mechanical response of chemically vapor-deposited 3C-SiC irradiated with self-ion. SiC samples were irradiated up to ~20 dpa at temperatures up to ~400 degrees Celsius. Multiple-step irradiations were performed with different self-ion energies to obtain a roughly rectangular damage profile. Electron backscatter diffraction measurement showed that grains are columnar along the growth direction and {111} fibre textures. The irradiated 3C-SiC samples were examined by transmission electron microscopy for the specimens prepared by focused ion beam milling. The microstructure consists of black dots. The mechanical response of the irradiated 3C-SiC samples were characterized by means of both nano-indentation technique and micro-compression tests on micromachined SiC pillars. SiC micropillars were fabricated by using lift-off process and inductively coupled plasma-reactive ion etching technique. Irradiation effects and size effects in the fracture strength of micro-pillars were investigated, and will be discussed in relation with the observed microstructures.

#### 5:00 PM

**TEM Observation of Crack Tip in Heavily Neutron Irradiated Ceramics:** Masashi Watanabe<sup>1</sup>; Tatsuo SHIKAMA<sup>1</sup>; Yoshiaki TACHI<sup>2</sup>; <sup>1</sup>Tohoku University; <sup>2</sup>Japan Atomic Energy Agency

Inert matrix fuels (IMFs) are an attractive component of advanced nuclear fuel cycles, as they provide of burning plutonium and transmuting the minor actinides. Candidate materials of inert matrix are mainly magnesia (MgO), zirconia (ZrO<sub>2</sub>), and spinel (MgAl<sub>2</sub>O<sub>4</sub>). For better performance of the IMFs in the fast reactor, fracture behavior of neutron irradiated inert matrix, including change of mechanical properties such as fracture toughness, need to be investigated in relation with irradiation induced microstructural changes. In the present study, we focused on the relation between crack propagation and irradiated induced defects. Cracks were introduced by Vickers indentations on heavily neutron irradiated ceramics of the ZrO<sub>2</sub> and the MgAl<sub>2</sub>O<sub>4</sub>. Both specimens were irradiated at 710 °C to 5.5×10<sup>26</sup>n/m<sup>2</sup>

and at 680 °C to 3.9×10<sup>25</sup>n/m<sup>2</sup> in the experimental fast reactor of JOYO in JAEA. Microstructure beneath and near the crack tip were examined by the transmission electron microscopy.

#### 5:20 PM

**Proton Irradiation-Induced Creep Effects in Pyrolytic Carbon and Graphite:** Anne Campbell<sup>1</sup>; Gary Was<sup>1</sup>; <sup>1</sup>University of Michigan

The creep behavior of pyrolytic carbon and graphite under high temperature neutron irradiation is critical to predicting the integrity of both fuel and structural components of the Very High Temperature Reactor. Proton irradiation-induced creep experiments were performed on graphite samples at 900°C at applied tensile stresses of 6MPa and 20.7MPa, and doses of 0.35 dpa and 0.23 dpa respectively. Preliminary results show a linear dependence of creep rate on both applied stress and dose rate. The primary creep behavior of graphite and pyrolytic carbon will be presented in the context of irradiation induced microstructural changes, including the effect of unrestrained proton irradiation and the effect of proton irradiation-induced creep on the sample density, Young's modulus, and anisotropy.

#### 5:40 PM

**Structural Modifications and Mechanical Degradation of Ion Irradiated Glassy Polymer Carbon:** Malek Abunaemeh<sup>1</sup>; mohameh Seif<sup>1</sup>; abdalla Elsamadicy<sup>2</sup>; Claudiu Muntele<sup>1</sup>; young yang<sup>3</sup>; Daryush ILA<sup>1</sup>; <sup>1</sup>Alabama A&M University; <sup>2</sup>University of Alabama in Huntsville; <sup>3</sup>University of Wisconsin

The TRISO fuel that is planned to be used in the GenerationIV nuclear reactor consists of a fuel kernel of UOx coated in several layers of materials with different functions. We are looking at the ion irradiation induced structural modifications of the glassy polymeric carbon (GPC) microstructure and their effect on the mechanical and physical properties. GPC is considered as a potential replacement for the pyrolytic carbon coatings, with a function of diffusion barrier for the fission products. We irradiated GPC samples with 1 MeV protons, 5 MeV Ag and Au ions. We chose protons to simulate the effects of neutrons. During the nuclear fission of <sup>235</sup>U, the fission fragment mass distribution has two maxima around 98 and 137 that would best fit Rb and Cs. However, both ions are hard to produce from our SNICS source therefore we chose Ag (107 amu) and Au (197 amu) as best replacements.

### Phase Stability, Phase Transformations, and Reactive Phase Formation in Electronic Materials X: Electrode, Ceramic, Optical, Spintronic, and Coating Materials

*Sponsored by:* The Minerals, Metals and Materials Society, TMS Electronic, Magnetic, and Photonic Materials Division, TMS: Alloy Phases Committee

*Program Organizers:* Chih-Ming Chen, National Chung Hsing University; Hans Flandorfer, University of Vienna; Sinn-Wen Chen, National Tsing Hua University; Jae-ho Lee, Hongik University; Yee-Wen Yen, National Taiwan Univ of Science & Tech; Clemens Schmetterer, TU Bergakademie Freiberg; Ikuo Ohnuma, Tohoku University; Chao-Hong Wang, National Chung Cheng University

Thursday PM  
March 3, 2011

Room: 7A  
Location: San Diego Conv. Ctr

*Session Chairs:* Clemens Schmetterer, TU Bergakademie Freiberg; Wojciech Gierlotka, YuanZe University

#### 2:00 PM Invited

**Electroless Nickel Plating on Carbon Fibers for Ultra Porous Nickel Electrode:** So-Young Chun<sup>1</sup>; So-Youn Park<sup>1</sup>; Jae-Ho Lee<sup>1</sup>; <sup>1</sup>Hongik University

Electroless nickel plating on carbon fibers was investigated. The carbon fibers were selected as the substrate since it has high surface area. Acidic and alkaline bath were used for the electroless nickel plating. Sonosmashing method was applied to disassemble carbon fibers. The effects of pH and



temperature on the electroless nickel were investigated. Inhibitor was added to achieve the uniform nickel coating on the surface. Wettability of the substrate was improved by surface treatment prior to the activation process. Highly porous nickel electrode was fabricated after pressing electroless nickel coated carbon fibers.

#### 2:25 PM Invited

**Phase Stabilities and Equilibria in the Lithium–Manganese–Oxygen System:** *Damian Cupid*<sup>1</sup>; Toni Lehmann<sup>1</sup>; Olta Cakaj<sup>2</sup>; Hans Seifert<sup>1</sup>; <sup>1</sup>Freiberg University of Mining and Technology; <sup>2</sup>University of Tirana

Several phases in the lithium–manganese–oxygen system such as  $\text{LiMn}_2\text{O}_4$ ,  $\text{Li}_2\text{MnO}_3$ , and  $\text{LiMnO}_2$  are promising for the development of cathode materials for rechargeable lithium ion batteries due to their low costs, environmental friendliness, and safety. Consequently, phase diagrams in this system are critical for optimizing processing conditions to be able to produce cathode materials with improved electrochemical performance properties. The type two phase diagram where one axis is a thermodynamic potential function such as temperature, partial pressure, or chemical potential and the second is the ratio of extensive variables is suitable for representing phase stabilities and phase equilibria in such a system. To investigate such diagrams for the lithium–manganese–oxygen system, several samples were prepared and equilibrated at various temperatures and oxygen partial pressures to examine the phase stability ranges of the phases produced. Additionally, thermogravimetric analysis was performed to investigate observed decomposition reactions.

#### 2:50 PM

**Crystallization Kinetics of SiO<sub>2</sub>-Bi<sub>2</sub>O<sub>3</sub> Glass-Ceramics:** *Guo Hongwei*<sup>1</sup>; <sup>1</sup>Shaanxi University of Science and Technology

The SiO<sub>2</sub>-Bi<sub>2</sub>O<sub>3</sub> glasses were prepared by melt-quench technique. The non-isothermal crystallization kinetics and the phase transition kinetics of the BS glasses were analyzed by the Kissinger equation and the equation of Augis-Bennett with the applying of differential scanning calorimetric X-ray diffraction and scanning electron microscopy. The experimental results showed that the three main crystal phases of Bi<sub>12</sub>SiO<sub>20</sub>, Bi<sub>2</sub>SiO<sub>5</sub> and Bi<sub>4</sub>Si<sub>3</sub>O<sub>12</sub> were generated sequentially in the heat treatment process, as crystallization exothermic peak can be seen from the DSC curves. The corresponding activation energies are  $E_{p1}=150.6\text{kJ/mol}$ ,  $E_{p2}=474.9\text{kJ/mol}$ ,  $E_{p3}=340.3\text{kJ/mol}$ ; the average crystallization indexes are  $p_1=2.5$ ,  $p_2=2.1$ ,  $p_3=2.2$ . The crystal phases were generated by volume nucleation, and grew in the one-dimensional pattern. The activation energy of phase transition of BS glasses is calculated by Kissinger equation. And the meta-stable phase of Bi<sub>2</sub>SiO<sub>5</sub> is easy to be transitioned into the stable phase of Bi<sub>4</sub>Si<sub>3</sub>O<sub>12</sub>.

#### 3:05 PM

**Phase-Transformation Induced Changes in the Optical and Electrical Properties of W<sub>0.95</sub>Ti<sub>0.05</sub>O<sub>3</sub> Films:** *Narasimha Kalidindi*<sup>1</sup>; C. Ramana<sup>1</sup>; <sup>1</sup>University of Texas El Paso

Tungsten oxide (WO<sub>3</sub>) is an intensively studied optical material; the ability to exhibit variable optical and electrical properties under ion-insertion, radiation-irradiation, and gas-phase interaction makes WO<sub>3</sub> interesting for application in electrochromic displays, smart windows, temperature control of space vehicles, and sensors. The present work was performed on the microstructure, optical and electrical conductivity evaluation of the W<sub>0.95</sub>Ti<sub>0.05</sub>O<sub>3</sub> films made by radio-frequency magnetron sputtering. The effect of temperature and Ti was significant on the microstructure. The Ti-incorporation affects the crystallization of WO<sub>3</sub> and induces the changes in optical and electrical properties. An amorphous-to-crystalline transition occurs in W<sub>0.95</sub>Ti<sub>0.05</sub>O<sub>3</sub> at 300°C, where the films crystallize in monoclinic phase. At 300°C, monoclinic-to-tetragonal phase transformation is induced in W<sub>0.95</sub>Ti<sub>0.05</sub>O<sub>3</sub> films. The corresponding changes in the electronic properties are significant; band gap decreases from 2.92 to 2.00 eV while electrical conductivity increases from 0.63 to 7.4 Ω-m. The results will be presented and discussed.

#### 3:20 PM Break

#### 3:40 PM

**Transparent Conductive Properties of Manganese Zinc Oxide Film Deposited by Chemical Bath Deposition:** *Jau-Shiung Fang*<sup>1</sup>; W. Luo<sup>1</sup>; C. Hsu<sup>1</sup>; J. Yang<sup>1</sup>; T. Tsai<sup>1</sup>; <sup>1</sup>National Formosa University

Manganese-doped Zinc Oxide thin film was prepared using Chemical Bath Deposition (CBD), and the effect of manganese-doped content on the structural change, electrical resistivity, optical transmission and magnetic property were studied using x-ray diffraction, electron probe x-ray microanalyzer, Hall measurement system, field emission scanning electron microscope, ultraviolet-visible-near infrared spectrophotometer and vibrating sample magnetometer. The manganese-doped amount in the film affects the properties critically, and the 7.1 at.% Mn-doped film has resistivity of  $4.29 \times 10^{-1} \text{ Ohm-cm}$ , transmittance of 74.7% in the visible range and bandgap of 3.17 eV when the film was annealed at 600°C in Ar+H<sub>2</sub>. The magnetic properties of the film can be enhanced by annealing so that the film has a saturation magnetization of 20.6 emu/c.c. and coercivity of 54.9 Oe. Because of its electrical, optical and magnetic properties, the film is promising to be used in spintronic devices.

#### 3:55 PM

**Electroplating of Nano Silica Dispersed Permalloy Composite Coating:** Myung-Won Jung<sup>1</sup>; Jong-Hun Kim<sup>1</sup>; Heung-Yeol Lee<sup>2</sup>; Tai-Hong Yim<sup>2</sup>; *Jae-Ho Lee*<sup>1</sup>; <sup>1</sup>Hongik University; <sup>2</sup>Korea Institute of Industrial Technology

Nickel alloys have been extensively used in packaging and electronic industries and then electro and electroless nickel plating have been investigated by many researchers. Nickel alloy, especially Ni-Fe alloy, was used as shadow mask for its low coefficient of thermal expansion. Even Ni-Fe alloy has high yield stress and hardness, its values are reduced after heat treatment. Silica was uniform sized spherical nano material. Silica dispersed permalloy composite coating was fabricated with electroplating method. Surface modified silica was suspended in the Ni-Fe electrolytes and then silica and Ni-Fe alloy was codeposited. The optimum condition for the silica suspension was investigated. The electrical and mechanical properties of composite coating were also investigated. The surface of composite coating was analyzed by AES and EDS.

#### 4:10 PM

**Optical Properties of the Al<sub>2</sub>O<sub>3</sub>-NiP Spectrally Selective Composite Coatings Prepared by Electroless Composite Coating:** *Ting Kan Tsai*<sup>1</sup>; Chiao Yin Hsu<sup>1</sup>; Shun Jen Hsueh<sup>1</sup>; Jiing Herng Lee<sup>1</sup>; Jau Shiung Fang<sup>1</sup>; <sup>1</sup>National Formosa University

Al<sub>2</sub>O<sub>3</sub>-NiP spectrally selective composite coatings were deposited on Al substrates to form Al<sub>2</sub>O<sub>3</sub>-NiP/Al solar absorbers by electroless composite coating. This work aims at studying effects of the Al<sub>2</sub>O<sub>3</sub> particle size, the Al<sub>2</sub>O<sub>3</sub> content, the thickness of Al<sub>2</sub>O<sub>3</sub>-NiP composite coating and the anti-reflection(AR)layer on the optical properties of Al<sub>2</sub>O<sub>3</sub>-NiP composite coatings. The optical properties including absorptance(Asol)and thermal emittance(etherm)were measured in the wavelength interval of 0.3-2.5 and 2.5-20 μm by using the UV/VIS/NIR and FTIR spectrophotometers equipped with integral spheres, respectively. The Al<sub>2</sub>O<sub>3</sub>-NiP composite coatings containing 70 nm Al<sub>2</sub>O<sub>3</sub> have better optical properties than that containing 300 nm Al<sub>2</sub>O<sub>3</sub>. The Asol and etherm of Al<sub>2</sub>O<sub>3</sub>-NiP composite coatings increase with the increasing of Al<sub>2</sub>O<sub>3</sub> content. Increasing the thickness of Al<sub>2</sub>O<sub>3</sub>-NiP composite coating and adding the AR layer obviously improve the optical properties of Al<sub>2</sub>O<sub>3</sub>-NiP/Al absorbers.

#### 4:25 PM

**Plasma Spray Deposition of CdS Thin Films via Liquid Precursor Route:** *Raghavender Tummala*<sup>1</sup>; Ramesh Guduru<sup>1</sup>; Pravansu Mohanty<sup>1</sup>; <sup>1</sup>University of Michigan

Thin film Cadmium sulfide (CdS) coatings are used in solar cells, sensors and microelectronics. We report a comparatively inexpensive process for depositing nanostructured CdS films, in which a solution precursor is thermally decomposed by a DC plasma jet. The solution precursor prepared from cadmium chloride, thiourea and distilled water is fed through an

atomizer in the spray torch to create ultrafine droplets for instantaneous thermal decomposition in the plasma plume to form ultrafine/nano particles of CdS. Thus formed CdS are then rapidly propelled towards the substrate to form the coating. The microstructures exhibited ultrafine particulate morphology comprising of nanostructured grains. X-ray diffraction studies confirmed hexagonal Wurtzite structure. Optical measurements showed a decreasing transmittance in the visible light with increasing the film thickness. The electrical characterization of the coatings will be presented. These polycrystalline coatings could find applications in sensing due to their nanostructures.

## Recycling General Session: Building Materials

Sponsored by: The Minerals, Metals and Materials Society, TMS Extraction and Processing Division, TMS Light Metals Division, TMS: Recycling and Environmental Technologies Committee  
Program Organizer: Joseph Pomykala, Argonne National Laboratory

Thursday PM  
March 3, 2011

Room: 12  
Location: San Diego Conv. Ctr

Session Chairs: Jeffrey Spangenberg, Argonne National Laboratory;  
Joseph Pomykala, Argonne National Laboratory

### 2:00 PM Introductory Comments

#### 2:05 PM

**The Effect of Binder and Pressure in the Preparation of Recycled Soda Lime Silica Glass Composite Bodies:** *Adele Garkida*<sup>1</sup>; Jiann-Yang Hwang<sup>2</sup>; Xiaodi Huang<sup>2</sup>; <sup>1</sup>Ahmadu Bello University; <sup>2</sup>Michigan Technological University

This study exploited the use of waste soda lime silica glass as substitute for clay in ceramic tile making. Powder compacts comprising at least 90% recycled glass content were made using the uniaxial press method. Compositions containing 106 microns and minus 75 microns soda lime silica glass powder were made in various proportions. Sodium silicate and bentonite were added as the binders and three sets of compacts were made. The first containing no binder, the second containing sodium silicate and the third set containing bentonite, pressed at 5,000 psi and 10,000 psi. The compacts were sintered at a temperature range of 600°C – 800°C and tested using the American Standard Test Methods for shrinkage, warpage, absorption and imperviousness. Results show that the composite body containing bentonite pressed at 10,000 psi, which fused at 750°C meets the standard specification for ceramic glazed structural clay facing tile according to C 126 -99.

#### 2:25 PM

**Production of Rock Wool from Ornamental Rock Wastes:** *Joner Alves*<sup>1</sup>; Girley Rodrigues<sup>1</sup>; Denise Espinosa<sup>1</sup>; Jorge Tenório<sup>1</sup>; <sup>1</sup>University of Sao Paulo

Rock wools are mineral fibers composed of amorphous silicates, due to their thermo-acoustic characteristics this material has a broad consumer market in the construction, automotive, and electric-electronics industries. This work studied the recovery of wastes from ornamental rocks (granite and marble) as partial raw materials in the production of rock wools. Residues from granite and marble cuttings are industrial wastes with considerable production and limited applications. These wastes should be appropriately managed because when discharged in rivers or lakes can cause siltation, and also they can cause serious human health problems, such as silicosis. Samples of produced materials with thickness smaller than 500µm were characterized by chemical analyses, XRD, SEM, EDS and DTA. Results showed that the rock wools produced using granite or marble wastes have important properties, especially the melting point. This process decreases the extraction of mineral resources and provides a profitable destination for the ornamental rock wastes.

#### 2:45 PM

**Recycling of Fluorescent Lamp Glass into Clayey Ceramic:** *Alline Morais*<sup>1</sup>; Thais Caldas<sup>1</sup>; Sergio Monteiro<sup>1</sup>; Carlos Maurício Vieira<sup>1</sup>; <sup>1</sup>State University of the North Fluminense

This work has as its objective to evaluate the effect of the incorporation of glass powder waste of fluorescent lamp into clayey ceramics used to fabricate bricks and roofing tiles. Formulations were prepared with incorporation of the waste up to 10 wt.% into the clayey body. Rectangular specimens were prepared by uniaxial mold-press at 20 MPa to fire at 850 and 1050°C. The physical and mechanical properties evaluated were: linear shrinkage, water absorption and flexural rupture strength. The microstructure of the fired ceramics was evaluated by optical microscopy. The results showed that the waste significantly changed the evaluated properties.

#### 3:05 PM

**Clayey Ceramic Incorporated with Powder from the Sintering Plant of a Steel-Making Industry:** *Mônica Ribeiro*<sup>1</sup>; Sergio Monteiro<sup>2</sup>; Carlos Vieira<sup>2</sup>; <sup>1</sup>Fluminense Federal Institute of Education, Science and Technology; <sup>2</sup>State University of the North Fluminense

This work has as its objective to evaluate the effect of incorporation of the powder retained in the electrostatic precipitator of the sintering stage from an integrated steel making plant on the physical and mechanical properties of a red ceramic. Formulations were prepared with incorporation of the waste up to 20 wt.% into a kaolinitic clay. Rectangular specimens were prepared by uniaxial mold-press at 20 MPa and then fired at 750, 900 and 1050°C. The evaluated physical and mechanical properties were: linear shrinkage, water absorption and flexural rupture strength. The microstructure of the ceramics was evaluated by optical microscopy. The results showed that the waste enhanced the properties of the ceramic, decreasing the water absorption and increasing the mechanical strength at all investigated temperatures.

#### 3:25 PM

**Recycling of Ornamental Rock Waste into Clayey Ceramics:** *Carlos Maurício Vieira*<sup>1</sup>; Mariane Costalonga de Aguiar<sup>1</sup>; Sergio Neves Monteiro<sup>1</sup>; <sup>1</sup>State University of the North Fluminense

This work evaluates the effect of incorporation of an ornamental rock waste into an industrial clayey body used for roofing tiles fabrication. Formulations with 0, 10, 20 and 30 wt.% of waste were prepared by replacing the sand in the industrial clayey body. The plasticity of the formulations was determined by the Atterberg limits. Specimens were fabricated by 18 MPa press-molding and then fired from 850, 950 and 1050°C. The specimens were tested to determine the water absorption, linear shrinkage and three points bending flexural strength. The results indicated that the waste improves the extrusion performance of the clayey body by decreasing its plasticity. The use of the waste was beneficial to the water absorption and mechanical strength of the fired clayey ceramic at 1050°C.

#### 3:45 PM Break

#### 3:55 PM

**Use of Ash from the Incineration of Urban Garbage into Clayey Ceramic:** *Carlos Maurício Vieira*<sup>1</sup>; Ana Paula de Sá<sup>1</sup>; Jhonatas Vitorino<sup>1</sup>; Sergio Monteiro<sup>1</sup>; <sup>1</sup>State University of the North Fluminense

This work has as its objective to characterize a waste for incorporation into a clayey ceramic. The waste is a type of fly-ash resulting from the incineration of a selected part of urban garbage, which basically constituted of organic matter and plastics. The waste was submitted to mineralogical, physical, morphological and chemical characterization. Formulations were prepared with incorporation of the waste up to 10 wt.% into the clayey ceramic body. Rectangular specimens were prepared by uniaxial mold-press at 20 MPa to fire in a laboratory furnace at 900°C. The physical and mechanical properties evaluated were: linear shrinkage, water absorption and flexural rupture strength. The results showed that the waste is predominantly composed of quartz and calcium compounds. Although, the use of the waste has enhanced the water absorption of the clayey ceramic, it is suggested to incorporate amount around 5 wt.% to avoid deleterious effect in the mechanical strength.

4:15 PM

**Gas Emission Analysis of Clay Incorporated with Rejected Sanitary Ware Mass:** Shirley Cosin<sup>1</sup>; Francisco Diaz<sup>1</sup>; Vanessa Souza<sup>2</sup>; Roberto Faria Jr.<sup>2</sup>; <sup>1</sup>Escola Politécnica da Universidade de São Paulo; <sup>2</sup>Universidade Estadual do Norte Fluminense Darcy Ribeiro

The search of the quality is a question of survival, regulated for the environment and technical requirements. The necessary ceramic industry needs to adjust to this reality. In this work gas emission of clay incorporated with rejected sanitary ware mass was measured and analyzed during the firing process in the point of view of microstructure and thermal behavior. The used method is the photothermal technique with the help of a commercial infrared gas analyzer. Gases under study were CO, CO<sub>2</sub>, SO<sub>2</sub>, CH<sub>4</sub> and NO. The ceramic sample contains about 30% of the sanitary wastes. Gases were monitored as in function of the following temperatures: 150, 300, 450, 550, 650, 800, 950, 1050 and 1100°C. The total firing cycle took about 10h. The results suggested that the addition of sanitary waste allows a substantial decrease of the pollutant gas emissions.

4:35 PM

**Purification of Vegetable Oils Post-Consumption Residential and Commercial Clay with Two Brazilian:** Elaine Araújo<sup>1</sup>; Edcleide Araújo<sup>1</sup>; Marcus Fook<sup>1</sup>; Shirley Cavalcanti<sup>1</sup>; Divânia Silva<sup>1</sup>; Arthur Mesquita<sup>1</sup>; <sup>1</sup>Federal University of Campina Grande

In this study, bentonite clay (Tonsil and Aporofo) Brazil were evaluated in the purification process of post-consumer vegetable oil collected in residential and dinner in the city of Campina Grande-PB/Brazil. A sample of virgin oil was used for comparison purposes. The XRD of clay, after the purification process showed that the clay Tonsil retained on the filter showed a more amorphous structure and a higher intensity peak (identified as an organic part of oil) in relation to Aporofo, possibly due to greater adsorption of pigments in oil. The viscosity residential treated with clay Tonsil was lower compared to the crude oil and oil-treated clay and oil Aporofo snacks. A decrease in acidity of the oils was observed in treated compared to untreated oil. According to the results, it was concluded that the clays used in this study, clay Tonsil showed better results in the treatment of the oils analyzed.

4:55 PM

**Influence of Fly Ash and Fluorgypsum on Hydration Heat and Mortar Strength of Cement:** Daowu Yang<sup>1</sup>; Yan Yao<sup>1</sup>; Julian Zeng<sup>1</sup>; Yi Liu<sup>1</sup>; <sup>1</sup>Changsha University of Science & Technology

The mixing cement hydration exothermic process were studied at different temperatures and different content of fly ash and fluorgypsum with 8-channel micro-calorimeter (TAM Air). The results show that: the heat of hydration of cement hydration heat is lower than the pure cement, but the lower range is not in proportion with the content. As the temperature decreases, reducing the peak heat of hydration of cement hydration heat is also reduced, and the peak time of heat is delayed. The strength test results show that: in the same dosage conditions, the double-doped mortar compressive strength is higher than the fly ash single. Replaced with equal parts fluorgypsum fly ash, it can significantly improve the early strength of mortar (3d intensity), maintained at baseline 80% to 87%, and the late mortar strength has been growing steadily, 28d of compressive strength reached a benchmark of 87% ~ 92%.

5:15 PM

**Study on Solidification/Sintering Brick Making with EMD Residue:** Wang Jia<sup>1</sup>; Peng Bing<sup>1</sup>; Chai Li-yuan<sup>1</sup>; Zhang Jin-long<sup>1</sup>; Zhang Qiang<sup>1</sup>; <sup>1</sup>Central South University

Electrolytic manganese dioxide (EMD) residue was mixed with shale and fly ash as the main materials to make solidification/sintering brick for the utilization of the residue from EMD production. The effects of sintering temperature, sintering time, solid waste content and cooling process on its mechanical properties and toxic elements solidification were investigated according to compressive strength and leaching toxicity. The results showed that the calcined residue had capability of solidifying toxic metals and exhibited perfect strength after treated in the optimal parameters of EMD

residue below 50%, temperature at 1000-1100°, time 3-5h, and semi-quenched at 600°.

## Refractory Metals 2011: Molybdenum, Niobium, Tantalum, Rhenium

*Sponsored by:* The Minerals, Metals and Materials Society, TMS Structural Materials Division, TMS: Refractory Metals Committee  
*Program Organizers:* Omer Dogan, DOE National Energy Technology Laboratory; Jim Ciulik, University of Texas, Austin

Thursday PM  
March 3, 2011

Room: 19  
Location: San Diego Conv. Ctr

*Session Chairs:* Todd Leonhardt, Rhenium Alloys; Thomas Bieler, Michigan State University

2:00 PM

**Dynamic Abnormal Grain Growth and the Production of Single Crystals in Tantalum:** Nicholas Pedrazas<sup>1</sup>; Daniel Worthington<sup>1</sup>; Eric Taleff<sup>1</sup>; Elizabeth Holm<sup>2</sup>; <sup>1</sup>University of Texas Austin; <sup>2</sup>Sandia National Laboratories

Dynamic abnormal grain growth (DAGG) is a phenomenon which produces large "abnormal" grains during plastic deformation. It is the dynamic aspect of DAGG that distinguishes it from previously-studied abnormal grain growth phenomena, which can be generally categorized as static, i.e., do not occur during plastic deformation. DAGG was previously reported to occur in commercial-purity molybdenum materials. This presentation is the first report of DAGG in tantalum. DAGG was observed in tantalum by tensile deformation of sheet material at elevated temperatures, above approximately 1870 K. DAGG was used to produce, in the solid state, single crystals of approximately 1 cm length and width in a thin tantalum sheet. The temperatures and critical strains required for initiation and propagation of DAGG in tantalum will be presented. Factors affecting DAGG in the tantalum material investigated will be discussed.

2:20 PM

**Factors Affecting Dynamic Abnormal Grain Growth in Molybdenum:** Daniel Worthington<sup>1</sup>; Eric Taleff<sup>1</sup>; <sup>1</sup>University of Texas Austin

Dynamic abnormal grain growth (DAGG) is a phenomenon which produces large "abnormal" grains during plastic deformation. It is the dynamic aspect of DAGG that distinguishes it from previously-studied abnormal grain growth phenomena, which can be generally categorized as static, i.e., do not occur during plastic deformation. DAGG was observed in several commercial-purity molybdenum materials at elevated temperatures, generally greater than 1800 K, and was used to produce quite large single crystals in the solid state. Recent experimental results from molybdenum sheet material provide additional understanding of the DAGG phenomenon. We will report new data on 1. a mechanism for nucleation of DAGG; 2. the relative rates of abnormal grain growth under static and dynamic conditions; and 3. the effects of accumulated strain, at temperature, and annealing on DAGG.

2:40 PM

**Effects of Processing Methods on the Properties and Structure of Molybdenum:** Gary Rozak<sup>1</sup>; Dincer Bozkaya<sup>1</sup>; Mark Zody<sup>1</sup>; <sup>1</sup>H. C. Starck Inc.

Most mill products of molybdenum and molybdenum alloys are produced with powder metallurgical processing techniques. H. C. Starck additionally uses Arc Casting and E-Beam melting as alternative techniques for producing molybdenum mill products. Liquid metallurgical techniques produce molybdenum with different microstructures and properties than those produced by powder metallurgy. Advantageous properties and specific applications will be discussed for molybdenum and molybdenum alloys produced through the melt processing.



**3:00 PM**

**Hot Extruding Powder Metallurgy Rhenium:** *Todd Leonhardt*<sup>1</sup>; James Ciulik<sup>2</sup>; <sup>1</sup>Rhenium Alloys Inc.; <sup>2</sup>University of Texas Austin

This study explored the different densification/compaction processes and their effect on the microstructures and mechanical properties of hot isostatically pressed rhenium and hot extruded rhenium to determine if extrusion is a viable method for manufacturing fully dense rhenium rods. Rhenium is a heavy transition metal with a melting point of 3180°C and has the highest modulus of elasticity of all the refractory metals (420 GPa). It is extremely sensitive to processing conditions because of its high work-hardening coefficient. In this study, two 45mm diameter rhenium rods were processed through sintering; one rod was subsequently hot isostatically pressed and the other rod was hot extruded to 23mm diameter. The two processing methods are compared and contrasted through the differences in the resulting microstructures, morphologies of the fracture surfaces, and mechanical properties obtained from tensile testing at room temperature and at 1927°C.

**3:20 PM Break****3:40 PM**

**Work Hardening Behavior of Commercial-Purity Rhenium Sheet:** *James Ciulik*<sup>1</sup>; *Todd Leonhardt*<sup>2</sup>; <sup>1</sup>University of Texas Austin; <sup>2</sup>Rhenium Alloys, Inc.

In many published articles it is stated that rhenium has the highest work hardening coefficient of any metal, but the value is not usually provided. In this study, annealed commercial-purity rhenium sheet was tested in uniaxial tension to obtain stress versus strain plots. Testing was performed using both mechanical extensometers attached to the test coupons and a noncontact video extensometer. The results obtained were used to calculate the work hardening coefficient of rhenium using two methods: (1) based upon the traditional Holloman analysis and (2) using the differential Crussard-Jaoul analysis with a Ludwik power relationship. These results show that the tensile behavior of rhenium does not exhibit a single value of work hardening coefficient. The value changes as strain accumulates and the range of the work hardening coefficient of rhenium in uniaxial tensile is much lower than 0.78.

**4:00 PM**

**Textural Evolution during Dynamic Recovery and Static Recrystallization of Molybdenum:** *Sophie Primig*<sup>1</sup>; *Harald Leitner*<sup>1</sup>; *Wolfram Knabl*<sup>2</sup>; *Alexander Lorich*<sup>2</sup>; *Helmut Clemens*<sup>1</sup>; *Roland Stickler*<sup>3</sup>; <sup>1</sup>Montanuniversität Leoben; <sup>2</sup>Plansee Metall GmbH; <sup>3</sup>University of Vienna

During the last decades, a special interest on the microstructural and textural evolution during processing of refractory metals has awakened because of several new applications. In the present investigation, sintered molybdenum specimens were deformed in compression in a deformation dilatometer over a range of temperatures from warm to hot deformation and deformation ratios between 0.3 and 1.1. Subsequent annealing treatments were carried out in order to study static recrystallization phenomena. EBSD scans of deformed and recrystallized specimens revealed that the microstructure after hot deformation is a recovered structure with two strong textural components, [111] parallel to the loading direction exhibiting a high Taylor factor and [100] parallel to the loading direction with a low one. The fraction of the first component increases at lower deformation temperatures, while recrystallization leads to a higher frequency of the second component. Results are discussed employing models for textural evolution and recrystallization in bcc metals.

**4:20 PM**

**Recrystallization Microstructures in High Purity Niobium:** *Shreyas Balachandran*<sup>1</sup>; *Richard Griffin*<sup>2</sup>; *Karl Hartwig*<sup>1</sup>; <sup>1</sup>Texas A&M University; <sup>2</sup>Texas A&M University Qatar

Pure Niobium (RRR Nb 99.99+%), is a technologically important material for the superconductor and High Energy Physics communities because of the combination of Type II superconductivity behavior and the ease of formability. However, to attain optimum performance in terms of forming, specific microstructures are preferable, including a uniform grain

size distribution and texture. Previously, the authors successfully showed that thermo-mechanical processing involving severe plastic deformation can produce refined Nb microstructures. The present study focuses on the recrystallization behavior of RRR Nb and lower purity (RG) Nb processed via two different processing routes; the main variables of the study are: annealing time and temperature. We will report on grain growth and microstructural uniformity. Preliminary observations indicate a high correlation between microstructural banding and higher temperature heat treatments, and certain texture components nucleate at higher rates than others during the onset of recrystallization.

**4:40 PM**

**Simulation of Tensile Testing of Single Crystal Niobium Using an Optimized FEM:** *Payam Darbandi*<sup>1</sup>; *Farhang Pourboghra*<sup>1</sup>; *Derek Baars*<sup>1</sup>; *Thomas Bieler*<sup>1</sup>; *Chris Compton*<sup>1</sup>; <sup>1</sup>Michigan State University

In this study a crystal plasticity model for Niobium single crystal is developed taking into account the plastic anisotropy due to non-planar spreading of skew dislocation cores. In view of the longstanding inconsistent statements on the deformation of BCC single crystals, recent insights and developments are considered in this model. The flow stress of Niobium single crystals shows a significant dependence on the crystal orientation. This phenomena leads to violation of Schmid's law in this material which is not observed in, for example, FCC materials. An optimized method based on combined constraints is used to identify orientation dependent critical resolved shear stresses and work hardening parameters. Uniaxial tension simulations are done for Nb single crystals and compared with experiments. Material parameters are calibrated from experimental results using a proper identification method. The model is validated for different crystal orientations.

**5:00 PM**

**The Swelling, Microstructure, and Hardening of LCAC, TZM, and ODS Molybdenum Following Neutron Irradiation:** *Brian Cockeram*<sup>1</sup>; *R. Smith*<sup>1</sup>; *L. Snead*<sup>2</sup>; <sup>1</sup>Bechtel-Bettis; <sup>2</sup>Oak Ridge National Laboratory

Transmission Electron Microscopy (TEM) examinations are used to characterize the microstructure of wrought Low Carbon Arc Cast (LCAC), Oxide Dispersion Strengthened (ODS), and TZM molybdenum following irradiation in the High Flux Isotope Reactor (HFIR) at 300C, 600C, and 870-1100C to neutron fluences between 10.5 to 247 X 10<sup>20</sup> n/cm<sup>2</sup>. The size and number density of the dislocation loops and voids are determined. Models for the increase in strength are evaluated by comparing measured tensile strength values to values that are predicted using the microstructural data. Irradiation of all alloys at 300C results in the formation of a high number density of fine loops (about 1-3nm) and voids (1nm). A relatively high number density of small voids (5-6nm) are observed after irradiation at 600C. A low number density of coarse voids (10-20nm) are observed after irradiation at 870-1100C. The evolution of microstructure with respect to fluence is discussed.

**5:20 PM**

**Micron-Scale Resistance Spot Welding of Mo-Re Alloys:** *Tongguang Zhai*<sup>1</sup>; *Jianhui Xu*<sup>2</sup>; <sup>1</sup>University of Kentucky; <sup>2</sup>Smith International Inc.

Small-scale resistance spot welding (SSRSW) of a refractory alloy 50Mo-50Re thin sheet (0.127 mm thick) was investigated. The effects of seven important welding parameters, such as hold time, electrode material, electrode shape, ramp time, weld current, electrode force and weld time, were studied systematically, in an attempt to optimize the welding quality. The diameter of a weld nugget was found to be only 30-40% of the electrode diameter in SSRSW, which was due to the relatively low electrode force used in SSRSW, compared with the high electrode force employed in large-scale resistance spot welding (LSRSW) where the diameter of nugget was almost 100% of the electrode diameter. Large pores often found in the nugget during SSRSW could be due to shrinkage during solidification as a result of fast cooling or due to agglomeration of residual volatile elements absorbed during powder metallurgy processing of the material.

## Sensors, Sampling, and Simulation for Process Control: Steel Processing; Online Sensors

*Sponsored by:* The Minerals, Metals and Materials Society, TMS Extraction and Processing Division, TMS: Process Technology and Modeling Committee, TMS: Solidification Committee

*Program Organizers:* Brian Thomas, University of Illinois at Urbana-Champaign; Andrew Campbell, WorleyParsons; Srinath Viswanathan, University of Alabama; Lifeng Zhang, Missouri University of Science and Technology; James Yurko, 22Ti LLC; Thomas Battle, Midrex Technologies

Thursday PM  
March 3, 2011

Room: 13  
Location: San Diego Conv. Ctr

*Session Chairs:* James Yurko, 22Ti LLC; Robert Hyers, University of Massachusetts Amherst

### 2:00 PM Introductory Comments

#### 2:05 PM

### High Impact Computer Integrated Level 2 Melt Shop Management Systems: *John Middleton*<sup>1</sup>; <sup>1</sup>Multon Process Technology Ltd

Based upon 30+ years experience in the development, implementation and on-going support of computer-based melt shop systems in about 40 plants in the UK, Europe and the USA, consideration of : • the facilities and functionality of a state-of-the-art, comprehensive Level 2 Integrated Melt Shop System covering melting and secondary processes for all grades of steels and superalloys; • the application of mathematical models and optimisation within those systems; and • interfaces to plant and laboratory instrumentation and control.

#### 2:30 PM

### Analysis of the Transient Phenomena during Steel Continuous Casting through the On-Line Detection Data: *Lifeng Zhang*<sup>1</sup>; <sup>1</sup>Missouri University of Science and Technology

The transient phenomena during steel continuous casting are analyzed through the on-line detection data of casting speed, top level fluctuation, and mold temperature. The macro-fluctuation and the micro-fluctuation are differentiated. The macro-fluctuation is found to relate to the casting operation and the micro-fluctuation is related to the turbulent fluctuation in the continuous casting mold. The fluctuation itself induces the asymmetrical flow in the continuous casting vessels. The CFD modeling and the water modeling are also used to investigate the transient phenomena during continuous casting process.

#### 2:55 PM

### Advancements in Process Optimization and Process Control in the Youngstown, Ohio Melt Shop of V&M Star: *Eric Schmidt*<sup>1</sup>; <sup>1</sup>Vallourec Research Aulnoye

Vallourec and Mannesman is a leading international supplier of seamless steel pipe, including the North American oil country tubular goods producer V&M Star. Melting and casting operations of V&M Star occur at the Youngstown, Ohio melt shop, consisting of a 100 ton AC electric arc furnace, a two-stand ladle metallurgical furnace, and a three-strand round billet caster. Two process optimization projects will be the focus for this presentation. An instrumented mold investigation was employed in selecting the mold taper for an updated caster configuration. Integral flux, circumferential homogeneity, and time stability of heat transfer were analyzed using molds of two diameters and two taper profiles, containing up to 40 thermocouples each. An energy and material optimization of the electric furnace has included the installation of arc stability analysis, slag analysis, and gas flow/composition sensing equipment. A thermodynamic modelling of slag evolution during foaming was used to improve carbon injection practices.

#### 3:20 PM

### Use of Statistical Process Control in the Manufacture of HSLA Line Pipe: *Richard Hill*<sup>1</sup>; *Felipe Ramirez*<sup>2</sup>; <sup>1</sup>Consultant ; <sup>2</sup>Consultant

The use of statistical process control (SPC) has been used in the manufacture of high strength low alloy plate and pipe material used for the conveyance of sour and non-sour hydrocarbons. Incorporating SPC into the hot plate mill has enabled critical rolling parameters, such as slab soak time and temperature, roughing mill reduction, resume temperature, finishing temperature and reduction ratio, as well as cooling temperature, to be optimized and ensure uniformity in mechanical, toughness and dimensional properties. Within the pipe mill real time (in line) SPC is being used to assess dimensional tolerances and facilitate changes to the manufacturing process that insure consistent properties. For mechanical and toughness properties historical data is being evaluated and a probability assessment conducted to evaluate the characteristics of the entire production population. The data is being shared by all stakeholders through statistical assessment programs.

#### 3:45 PM Break

#### 4:05 PM

### High-Temperature Sensors from Aerospace: *Robert Hyers*<sup>1</sup>; <sup>1</sup>University of Massachusetts

NASA's Aerospace Research Mission Directorate recently commissioned a review of high-temperature sensors relevant to materials and structures for hypersonic aircraft. Many of the underlying technologies and some of the sensors themselves are relevant to other high-temperature environments, including those present in materials processing operations. An overview of the results of this study relevant to materials processing and stationary energy conversion will be presented.

#### 4:30 PM

### Rugged, Verifiable In-Situ Oxygen Analyzers for Combustion Optimization in Steel Reheat Operations and Process Chemical Production: *Yvonne Boltz*<sup>1</sup>; *Eric Boltz*<sup>1</sup>; *Justin Clark*<sup>1</sup>; <sup>1</sup>Marathon Monitors Inc.

Combustion optimization has always proved difficult. Extractive analyzers are prone to clogging; introducing both measurement offsets and time delays. Conventional, heated in-situ sensors must be located in cooler furnace regions far from combustion and have similar time delays, a need for frequent calibration and are easily fouled by combustion and process by-products. Non-heated, "high-temperature," in-situ oxygen analyzers have been used in this application but are fragile; requiring time-consuming insertion and removal processes to avoid thermal shock of the sensing element. Typical installation can mean hours on a hot furnace. Finally, conventional non-heated analyzers do not meet zero-and-span criteria for regulatory compliance, requiring a downstream unit. Marathon Monitors will present a new, robust analyzer, based on a ceramic-composite electrolyte, providing thermal toughness, allowing for fast insertion and removal. The new design also incorporates a patent-pending focused flow system which provides zero and span capability in accordance with regulatory guidelines.

#### 4:55 PM

### High Performance Wireless Sensors System for Structural Health Monitoring: *Gerges Dib*<sup>1</sup>; *Janardhan Padiyar*<sup>2</sup>; *Lassaad Mhamdi*<sup>1</sup>; *Nizar Lajnef*<sup>1</sup>; *Tariq Khan*<sup>1</sup>; *Jung-Wuk Hong*<sup>1</sup>; *Lalita Udpa*<sup>1</sup>; *Krishnan Balasubramaniam*<sup>2</sup>; <sup>1</sup>Michigan State University; <sup>2</sup>IIT Madras

Continuous structural health monitoring (SHM) uses permanently mounted sensor networks on critical locations of a structural component. In-situ wired sensors require a large amount of cabling for power and data transfer, which can drive up costs of installation and maintenance. Hence the need for developing wireless sensors for SHM. The major obstacles preventing the widespread use of wireless sensor networks (WSN) for SHM is the availability of portable, low cost, low powered, low footprint, and high SNR based instrumentation. This paper presents a high performance data acquisition unit that is interfaced with the Imote2 wireless module for the use in active WSN. Piezoelectric sensors are integrated with this system for the identification of anomalous events using ultrasonic techniques. Power aware

algorithms are used to coordinate the actuator-sensor network interaction with a central processing server, where appropriate signal processing techniques may be used to quantify the damage in terms of severity.

## **Silicon Production, Purification and Recycling for Photovoltaic Cells: Session II**

*Sponsored by:* The Minerals, Metals and Materials Society, TMS Extraction and Processing Division, TMS Light Metals Division, TMS: Energy Conversion and Storage Committee, TMS: Recycling and Environmental Technologies Committee

*Program Organizers:* Anne Kvithyld, SINTEF; Gregory Hildeman, Consultant; Gabriella Tranell, Norwegian University of Science and Technology (NTNU); Arjan Ciftja, SINTEF; Shadia Ikhmayies, Al Isra University

Thursday PM  
March 3, 2011

Room: 14A  
Location: San Diego Conv. Ctr

*Session Chair:* Shadia Ikhmayies, Al Isra University

### **2:00 PM**

#### **Review of Developments in Production of Silicon for Photovoltaics:**

*David Lynch*<sup>1</sup>; Wade Ben<sup>1</sup>; Xiaoyang Ji<sup>1</sup>; Feng Jiang<sup>1</sup>; Alex Salce<sup>1</sup>; Evan Morey<sup>1</sup>; Yubo Jiao<sup>1</sup>; <sup>1</sup>University of Arizona

Polysilicon photovoltaics are expected to play a significant role in meeting the world's shortfall in electrical energy that is estimated to be 1.4 terawatts per year by 2030. The photovoltaic industry relies on high-purity silicon produced using the Siemens process. New Siemens-like processes, as well as metallurgical processes for producing solar silicon, are under development. Technological advancements in the Siemens and Siemens-like processes are reviewed, and their energy payback time, as well as lifetime carbon emissions, are examined. Those values are compared to the corresponding figures for photovoltaics (PVs) manufactured using solar silicon produced by a metallurgical route.

### **2:20 PM**

#### **Distribution Measurements of Dopants in Compensated Silicon Ingots by Fast-Flow High Resolution Glow Discharge Mass Spectrometry:**

*Xinwei Wang*<sup>1</sup>; *Karol Putyera*<sup>1</sup>; Johnny Liu<sup>1</sup>; Dominic Leblanc<sup>2</sup>; <sup>1</sup>Evans Analytical Group LLC; <sup>2</sup>Becancour Silicon Inc.

The distribution of trace and ultra-trace levels of multiple dopants and/or unwanted impurities was evaluated in directionally solidified compensated silicon ingots by the direct sampling fast-flow glow discharge mass spectrometry technique. A power fitting of the observed dopant mass fractions versus the ingot length was applied to each of these dopants according to the Scheil's equations. All showed consistent fitting curves, with  $R^2 = 0.9$ . From the fitting results, the experimental distribution coefficient values for all dopants were determined. This paper introduces a simple and very robust evaluation analytical tool to evaluate, experimentally, the directionally solidified ingot dopant characteristics when considerable donor and acceptor impurities exist simultaneously in the starting melt.

### **2:40 PM**

#### **Preparation of High Purity Silicon by Electrolysis-Vacuum Distillation:**

*Jidong Li*<sup>1</sup>; *Mingjie Zhang*<sup>1</sup>; *Zhuo Zhang*<sup>1</sup>; *Yaowu Wang*<sup>1</sup>; <sup>1</sup>Liaoning University of Science and Technology

Solar energy is the most abundant renewable resource. Polysilicon is the major raw material of solar cell, and preparation of polysilicon by metallurgical technique will reduce production costs greatly. In this paper, Mg-Zn-Si alloys were prepared by electrolysis in electromagnetic stirring using high purity silicon dioxide as raw material and high purity silicon obtained was separated from Mg-Zn-Si alloys by vacuum distillation. The conditions such as current density, electrolysis time and electromagnetic stirring effecting on back electromotive force, silicon content and current efficiency were well investigated. Finally, at 1000°C, magnetic field intensity 28mT, the silicon content of 35.7%(mass fraction) in Mg-Zn-Si alloy can

be obtained by electrolyzing for 4h in the current density of 0.56A.cm<sup>-2</sup>. Then, at 1050°C, the high purity silicon of 99.98% was obtained by vacuum distillation for 3h.

### **3:00 PM**

#### **Effect of Calcium Addition and Solidification Conditions on the Microstructure of Metallurgical Grade Silicon:** *Yulia Meteleva-Fischer*<sup>1</sup>; *Yongxiang Yang*<sup>1</sup>; *Rob Boom*<sup>1</sup>; <sup>1</sup>Delft University of Technology

Metallurgical refining of metallurgical grade silicon (MG-Si) currently is one of the most developing areas in research for production of solar grade silicon (SoG-Si). However, choice of refining method and conditions depends on impurities and microstructure of metallurgical grade silicon, where alloying with calcium is one of the perspective refining steps. In the present work a detailed analysis of transformation of phases on the grain boundaries has been carried out, focusing on behavior of impurities during solidification and using calcium addition. Depending on cooling rate and concentration of calcium, different silicide and non-silicide phases have been found in studied silicon. It was shown, that calcium addition promotes segregation of other metallic impurities. Such enhanced segregation will result in improved efficiency of acid leaching as a next refining step. It has been determined, that some impurity phases enhance phosphorus segregation: up to 0.4 wt% of phosphorus was found in Si-Al-Ca, Si-Ba-Cr and FeSi<sub>2</sub>Ti phases.

### **3:20 PM**

#### **Purification of Silicon by Electron Beam Melting Technique:** *Takashi Nagai*<sup>1</sup>; *Tomoki Kageyama*<sup>1</sup>; *Masafumi Maeda*<sup>1</sup>; <sup>1</sup>The University of Tokyo

The production of solar cells is increasing rapidly and the shortage of silicon for solar cells becomes a serious problem. Developing a low-cost production process for solar grade silicon is required. An electron beam melting technique is known to be effective for the removal of phosphorus from molten silicon. Although phosphorus is removed from the silicon by preferential evaporation in this process, the removal rate is not sufficient. In order to improve the removal rate, the effects of four experimental factors on this rate were investigated. Raising temperature of the surface of molten silicon provide effective, neither residual gas pressure in a vacuum chamber nor stirring molten silicon improve the rate, while supplying reactant gas to molten silicon had some effect. In this research, the potential of the electron beam melting technique to remove boron from molten silicon was also investigated.

### **3:40 PM Break**

### **4:00 PM**

#### **STRC's Process for Producing Low Cost Solar Silicon:** *David Lynch*<sup>1</sup>; <sup>1</sup>Solar Technology Research Corporation

Solar Technology Research Corporation has developed a patented process for manufacturing solar-grade silicon that will bring the cost of electricity generated by PV cells closer to grid parity. STRC's new process brings silicon production cost down to less than \$10 per kg resulting in a projected reduction in the cost of producing solar power by \$0.22 per watt. STRC's approach to producing solar silicon is to use high purity starting materials that are exceptionally free of B and P. By using high purity materials and STRC's technology, savings in downstream refining costs more than compensate for the additional expense of the raw materials. STRC has located suitable quartz deposits of a quantity large enough to cover the world's projected shortfall in electrical energy needs for 50 years. Processing these ores will yield silicon with a B content of <0.10ppmw and P content of <0.075ppmw, concentrations characteristic of superior solar silicon.

### **4:20 PM**

#### **The Rate of Boron Elimination from Molten Silicon by Slag and Cl<sub>2</sub> Gas Treatment:** *Hiroshi Nishimoto*<sup>1</sup>; *Kazuki Morita*<sup>1</sup>; <sup>1</sup>The University of Tokyo

Among production techniques of solar grade silicon at low cost, the purification of metallurgical grade silicon has been developed. The key process of pyrometallurgical refining of silicon is removal of B from molten silicon because of large segregation coefficient and low vapor pressure. In this study, the possibility of B elimination from molten silicon through slag by chlorination was investigated. At first in order to discuss the kinetics of



total reaction, the rate of B elimination from molten silicon by the use of CaO-SiO<sub>2</sub> slag was investigated at 1823 K in Ar atmosphere. As a result the rate of B elimination was controlled by mass transport in molten slag and the mass-transfer coefficient of B in molten slag was determined to be  $1.4 \times 10^{-6}$  m/s. Moreover, some studies on chlorination of B in silicon and borate in slag by gaseous chlorine have been carried out.

**4:40 PM**

**Silicon Surface Texturing by Electro-Deoxidation of a Thin Silica Layer in Molten Salt:** Eimutis Juzeliunas<sup>1</sup>; Antony Cox<sup>1</sup>; Derek Fray<sup>1</sup>; <sup>1</sup>University of Cambridge

Solar energy can be converted to electricity with no impact on the environment; however, the process is expensive. The major part of its costs is related to materials, mainly silicon. Silicon with improved surface properties is urgently needed in many semiconductor and solar-energy devices. A new method of silicon surface texturing is reported, which is based on thin silica layer electrochemical reduction in molten salts. A thermal silica layer grown on p-type silicon was potentiostatically reduced in molten calcium chloride at 850°C. Typical nano-micro formations, obtained at different stages of electrolysis, were demonstrated by SEM. X-ray diffraction measurements confirmed conversion of the amorphous thermal silica layer into crystalline silicon. The proposed approach shows promise in photovoltaic applications, for instance, for production of antireflection coatings in silicon solar cells.

**5:00 PM**

**Solid Oxide Membrane Process for Solar Grade Silicon Production Directly from Silicon Dioxide:** Alexander Roan<sup>1</sup>; Soobhankar Pati<sup>1</sup>; Soumendra Basu<sup>1</sup>; Uday Pal<sup>1</sup>; <sup>1</sup>Boston University

Solar grade silicon (SoG-Si), at a small fraction of its current cost, can be produced by employing the Solid Oxide Membrane (SOM) electrolysis process. The SOM electrolyzer consists of a cathode immersed in a molten fluoride flux with dissolved silicon dioxide (SiO<sub>2</sub>) on one side of an oxygen-ion-conducting stabilized zirconia membrane. On the other side of the membrane, a coating of yttria-stabilized zirconia plus strontium-doped lanthanum manganite or nickel acts as the anode. The SOM electrolyzer is operated by applying an electrical potential between the electrodes. Upon exceeding the dissociation potential of SiO<sub>2</sub>, silicon metal is deposited on the cathode and the oxygen ions from the melt are transported through the membrane and are oxidized at the anode. This investigation reports flux composition, cathode materials used, operating temperature, applied potential, and other relevant operating parameters for the production of SoG-Si.

## General Poster Session

Sponsored by: The Minerals, Metals and Materials Society, TMS Electronic, Magnetic, and Photonic Materials Division, TMS Extraction and Processing Division, TMS Light Metals Division, TMS Materials Processing and Manufacturing Division, TMS Structural Materials Division

Program Organizer: Mark Palmer, Kettering University

Mon PM-Wed PM  
Feb 28-Mar 2, 2011

Room: Exhibit Hall  
Location: San Diego Conv. Ctr

### A Low Cost Method for Manufacturing of Aluminum/Alumina Composite by Anodizing and CRB Process: Roohollah Jamaati<sup>1</sup>; Mohammad Reza Toroghinejad<sup>1</sup>; E. Zahrani<sup>1</sup>; <sup>1</sup>Isfahan University of Technology

In this work, Al/Al<sub>2</sub>O<sub>3</sub> composite strips are manufactured by a low cost method consist cold roll bonding (CRB) process of anodized aluminum strips. This technique has the flexibility to control the volume fraction of metal matrix composites (MMCs) by varying the oxide layer thickness on the anodized aluminum strip. Meanwhile pre- and post-rolling annealing treatment was performed on some produced MMCs. Microstructure, hardness, tensile strength, and elongation of composite strips are investigated as a function of alumina quantity and the applied production method. It is found that higher quantities of alumina improve hardness and tensile strength, while the elongation value decreases negligibly. Furthermore, pre-rolling annealing was found to be as the best method for producing this composite via the anodizing and CRB processes. Finally, it was found that both monolithic aluminum and aluminum/alumina composite exhibited a ductile fracture, having dimples and shear zones.

### A Model for Diffusion Bonding of Cu and Al Plate by Hot Compression: Yong-Shin Lee<sup>1</sup>; Sang-Hun Yoon<sup>1</sup>; Sangmok Lee<sup>2</sup>; <sup>1</sup>Kookmin University; <sup>2</sup>KITECH

It is well known that bonding of bimetal such as Cu and Al plates by hot compression is accomplished by diffusion. Here, hot compression experiments with Cu and Al plates are carried out for the wide ranges of experimental conditions such as temperature, and compressive load, and load holding time, which are known as the most important factors for the success of diffusion bonding. It is very difficult to observe the bonding and deformation behaviour near the contact surface. Finite element simulations for hot compression tests are also performed to examine the detailed behaviours of state variables near the bonded surfaces. Eventually, the bonding criterion for Cu and Al plates by hot compression is given in terms of temperature, compressive load, and holding time, which will be used to design a combined process of hot compression and hydrostatic extrusion of Cu clad Al bar.

### A Study on the Characteristics of Truck Materials Using Structural Steel: Sung Cheol Yoon<sup>1</sup>; <sup>1</sup>Korea Railroad Research Institute

The truck of railroad vehicle is major part affecting the operational performance of vehicle and supporting the vehicle load. A truck is composed of frame, wheel, axle, suspension, and damping device. Among these parts, the truck supporting vehicle weight is considered one of the most important parts. This study aims to check out problems related to the characteristics of truck materials by measuring the stress in each truck location after giving maximal vertical load, right and left load, and front and rear load. Before the test, a stress distribution analysis of the truck was performed after conducting a structural analysis. A material test was then performed after deciding on the measuring location by referring to the structural analysis findings. As a result of the material characteristic test, it was verified that the truck meets safety requirements of a railroad vehicle.

### A Study on the Effect of Sintering Atmosphere on the Microstructural Properties of Injection Molded T42 High-Speed Steel: Kyoung-Rok Do<sup>1</sup>; Sung-hyun Choi<sup>1</sup>; Jinhwa Kim<sup>1</sup>; Young-Sam Kwon<sup>2</sup>; Young-Sam Kwon<sup>2</sup>; Kwon-Koo Cho<sup>1</sup>; In-Shup Ahn<sup>1</sup>; <sup>1</sup>Gyeongsang National University; <sup>2</sup>Cetatech, Inc

HSS have high strength, wear resistance, and hardness together with an appreciable toughness and fatigue resistance. PIM was received attention owing to shape without additional processes. The experimental specimens were manufactured using the PIM with T42 powders (59 vol.%) and polymer (41 vol.%). The green parts were solvent debinded in n-Hexan at 60° for 24 hours and thermal debinded at N<sub>2</sub>-H<sub>2</sub> mixed gas atmosphere for 18 hours. Specimens were sintered in high vacuum (10-5mtorr), low vacuum (10-2mtorr), N<sub>2</sub>, H<sub>2</sub>, and Ar gas atmosphere. When sintering at 1240°, the specimen sintered at high vacuum had highest hardness (520Hv). The Carbides were smaller (1µm) and well distributed. The grain size was 10µm. When sintering at high vacuum over 1260°, the carbides were changed to eutectic carbide and located at grain boundary. The grain growth was observed. The specimen sintered at other atmosphere had lower density and hardness than high vacuum.

### A Study on the Structural Safety of the High-Speed Railroad: Sung Cheol Yoon<sup>1</sup>; Jeongguk Kim<sup>1</sup>; Joon Hyung Ryu<sup>1</sup>; Kang Youn Choe<sup>1</sup>; Gyeong Hoan Park<sup>2</sup>; <sup>1</sup>Korea Railroad Research Institute; <sup>2</sup>Hyundai Rotem

This study describes the structural analysis and load test to evaluate the safety of the high-speed railroad frame. It aims to evaluate the structural safety of the high-speed railroad frame when adding tare weight and passenger load to it. The high-speed railroad frame is considered an important railroad vehicle structure supporting major equipment such as electrical devices and heavy machines. It is composed of an underframe, side frame, roof, and interior materials. The load test was performed based on the loading conditions of "The guide on safety standard of railroad vehicle" of the Railroad Safety Act currently being used in Korea. The internal stress measuring location of the load test was selected by referring to the structural analysis findings. The high-speed railroad frame was found to be safe in terms of design load as a result of seven types of load tests such as the load test on operational condition.

### Abnormal Grain Growth in Alloy 2195 Friction Stir Welds: Anupam Kundu<sup>1</sup>; Tony Reynolds<sup>1</sup>; <sup>1</sup>University of South Carolina

In this study we examine the effects of welding parameters, post weld deformation levels, and deformation temperature, on the propensity for AGG in 2195 friction stir welds. Three welding parameters sets were used. The welding speed was held constant while high, medium, and low tool rotation rates were applied resulting in three different power levels and, consequently, three different initial weld nugget grain sizes. Subsequently, deformations in compression up to engineering strains of 50% were imposed at room temperature, 200°C, and 340°C. Deformed specimens were solution heat treated in a salt bath for times up to 1 hour and the grain growth was characterized by optical microscopy. Depending on the starting condition and the deformation conditions, varying levels of secondary recrystallization, normal grain growth, and AGG were observed.

### Aerosol Route Synthesis of Lithium Borate Spheres Using Lithium Nitrate and Boric Acid Solution: Burcak Ebin<sup>1</sup>; Sebahattin Gurmen<sup>1</sup>; Cuneyt Arslan<sup>1</sup>; <sup>1</sup>Istanbul Technical University

Lithium borate has a potential to use various field from solid state batteries to sensors owing to its high conductivity and piezoelectricity. In this study, lithium borate spheres were synthesized by thermal decomposition of lithium nitrate and boric acid aerosols droplets atomized in ultrasonic nebulizer under air atmosphere. Energy dispersive spectroscopy (EDS) was performed to determine the chemical composition of prepared structures. Boron detected in the EDS analysis, and peaks of possible impurities were not observed. Also, size, shape, and surface morphology of samples were characterized by scanning electron microscope (SEM). Images revealed that non-agglomerated lithium borate particles were produced in spherical morphology with smooth surface, but particles had relatively wide size distribution between 50 nm and 1100 nm. The X-ray diffraction measurement was employed to identify

the crystalline phase, and the absence of clear diffraction peaks in the pattern indicates that obtained lithium borate particles have amorphous structure.

**Aging Effect of Aluminized Coating Layer for Ni-Base Superalloy:** *Tae Sun Jo*<sup>1</sup>; Jeong Hun Lim<sup>1</sup>; Dae kyung Kim<sup>1</sup>; Young Do Kim<sup>1</sup>; <sup>1</sup>Hanyang University

Ni-base superalloy is a candidate material for the high temperature applications such as turbine blades, structural materials for nuclear reactors, and high-temperature gas-cooled reactors. In this work, aluminized Ni-base superalloy was investigated about the formation and growth of coating layer by high temperature aging. Al-pack cementation was carried out at 1000° C for 1 h in Ar using an Al<sub>2</sub>O<sub>3</sub> crucible containing the specimen and a powder mixture of Al : Al<sub>2</sub>O<sub>3</sub> : NH<sub>4</sub>Cl = 15g : 83g : 2g. The aluminized Ni-base superalloy was aged at 950°C for 480 h in air. The phase analysis of coating layer was carried out by XRD, SEM, EPMA and TEM. The hardness of coating layer was measured by nanoindentation. This work was financially supported by Ministry of Education, Science and Technology (MEST) through the Nuclear Hydrogen Technology Development (NHTD) program.

**An Empirical Model of Rehydration/Rehydroxylation Kinetics for Archaeological Ceramics:** *Patrick Bowen*<sup>1</sup>; Timothy Scarlett<sup>1</sup>; Jaroslaw Drelich<sup>1</sup>; <sup>1</sup>Michigan Technological University

Fired-clay ceramic rehydroxylation dating has recently been proposed as a new chronometric dating tool for use on archaeological ceramics. The technique relies upon the well-known characteristic of fired clay objects to take up water in a slow manner, which has been shown to follow a (time)<sup>1/4</sup> power law. Experiments were conducted in which the mass measurements taken from 19th century ceramic artifacts revealed a deviation from the (time)<sup>1/4</sup> power law over a wide range of temperatures. These findings have led to the formation of a general empirical equation which describes the observed rehydration/rehydroxylation behavior.

**An Investigation of the Electrochemical Properties of TiAlCrN PVD Coated in STS304:** *Min-Seok Moon*<sup>1</sup>; Kee-Do Woo<sup>2</sup>; Chan-Won Kwak<sup>3</sup>; Jin-Won Han<sup>3</sup>; Myeong Han Yoo<sup>2</sup>; Dae Up Kim<sup>4</sup>; <sup>1</sup>Chonbuk National University, Jeonju Institute of Machinery Carbon Composites; <sup>2</sup>Chunbuk National University; <sup>3</sup>Se-Won Hard Facing Co., Ltd.; <sup>4</sup>KITECH

In the PEM fuel cell need to reduced weight and total fabrication cost of a fuel cell stack, and increased durability during the operating condition. Typically bipolar plates are a key component of PEMFC and other Fuel cells. In order to reduce both the weight and cost of the bipolar plates, nowadays consider attention is being paid to developing metallic bipolar plates to replace dense graphite. In this study, try to TiAlCrN nitride coating process on an austenitic stainless steel (STS304) using a PVD technology (plasma enhanced reactive evaporation) to increase the corrosion resistance of the STS304. Contact angle, SEM, and potentiodynamic tests were used to characterize the TiAlCrN Nitride coating process on the STS304. This study is focus on the best PVD nitride coating process for the corrosion resistance in the PEMFC operating conditions, and could potentially be used in PEMFCs as a bipolar plate material requirement.

**An Investigation of Wire Drawing of Hyper-eutectoid Steel Wires:** *Byung In Jung*<sup>1</sup>; <sup>1</sup>POSCO

The mechanical properties of high strength steel wires are affected tremendously by wire-drawing process. Among the parameters of drawing process, the approach angle of drawing die is one of the most important parameters in the process. It can create microstructural inhomogeneity inside the material, resulting in the loss of strength and the degradation of ductility. The degradation of ductility in drawn steel wires often causes “delamination,” the longitudinal fracture during stranding wires for tire cords or bridge cables. The optimized wire drawing conditions effectively increased the attainable tensile strength and minimized the occurrence of delamination. The effects of several wire drawing parameters on the mechanical properties and microstructures were investigated by finite element analysis and the simulated results were compared to the wire drawing experiments.

**Analysis of Human Osteoporosis Compact Bones by Neutron Scattering and X-Ray Diffraction Methods:** *Yong Choi*<sup>1</sup>; A. Pirogov<sup>1</sup>; Doo Jin Baik<sup>1</sup>; E. J. Shin<sup>1</sup>; B.S. Seong<sup>1</sup>; <sup>1</sup>Sunmoon University

Neutron scattering and X-ray diffraction methods were applied to analyze nano-structure of normal and osteoporosis Korean compact bones to give a criterion for more precise decision and find a unique healing method about bone diseases like osteoporosis. The SANS profiles of the bones show a directional and regular distribution of plate-like bony crystals and bundles of bony crystals between collagen fibers. Lattice parameters of the bones depend on the type of bones and sex. Osteoporosis compact bones have less amounts of the bony crystal than normal compact bones. The change of the lattice parameters of the bony crystal is observed, especially, in case of the bones with low bone mineral density(BMD). It is related to mineralization process and the extraction of calcium and oxygen ions at special sites of the unit cell.

**Application of the Creep Continuum Damage Mechanics Unified Law for a Gas Turbine Rotor:** *Ali Nayebi*<sup>1</sup>; Hamid Ranjbar<sup>1</sup>; <sup>1</sup>Iran

In this research the unified creep continuum damage mechanics model was used to model the stress – strain behavior of a gas turbine rotor. The unified damage law can be applied for the creep and LCF damage. It is based on the increment of the accumulated inelastic strain which can be due of creep damage or of the low cycle fatigue damage. Based on the relaxation tests, the parameters of the unified CDM model, including S and s and Norton constants, were optimized and determined. Creep damage was modeled and stress – strain evolution in the gas turbine rotor was obtained. A careful three dimensional thermal analysis permitted to determine the thermal stresses which was superposed on the mechanical stresses of the gas turbine rotor. The Replica tests were done on the four points of the rotor surface and the formation of the creep voids was verified by an SEM.

**CALPHAD and DFT Assessment of Metallic Alloy Fuel Materials:** *Saurabh Bajaj*<sup>1</sup>; Raymundo Arroyave<sup>1</sup>; Alexander Landa<sup>2</sup>; Patrice Turchi<sup>2</sup>; <sup>1</sup>Texas A&M University; <sup>2</sup>Lawrence Livermore National Laboratory

A promising choice for fuel in Gen-IV reactors are metallic alloys where an actinide is alloyed with a high-melting transition element. The burn-up process in these systems leads to transmutation to minor actinides and variability in fuel chemistry and thus, a phase stability study would be beneficial in improving our understanding of alloy formation in these alloys. In the present work, phase diagram calculation (CALPHAD) and the DFT based EMTO-CPA methods are employed to investigate heats of formation of the bcc and intermetallic  $\delta$ -phase. This  $\delta$ -phase forms in a hexagonal C32 structure and is analogous to the high-pressure  $\omega$ -phase in pure Zr. Examples include UZr<sub>2</sub>, NpZr<sub>2</sub> and U<sub>2</sub>Ti. A random occupation of atomic sites makes these phases non-stoichiometric in nature. The work at LLNL was performed under the auspices of U.S. Department of Energy by the Lawrence Livermore National Laboratory under Contract DE-AC52-07NA27344.

**Characteristics of the Gas Dispersion Generated through a Jet Sparger in Aqueous Media:** *Ramiro Garcia*<sup>1</sup>; *Francisco Tavera*<sup>1</sup>; <sup>1</sup>Universidad Michoacana

In the gas-liquid and gas-liquid-solid systems where chemical reactions and mass transfer phenomena take place, the efficiency of such process depends on the characteristics of the dispersions. Four jet spargers with variable gas discharge were installed in both a flotation laboratory cell and a 0.50 m flotation column, in order to produce a gas dispersion in liquid media. Experimental data of bubble diameter, gas holdup, and bubble surface area rate were obtained. The average Sauter bubble diameter was measured for every experimental point through the photography-image analysis technique, whereas the estimated bubble diameter was calculated by applying the drift flux model. The gas holdup was measured through a sensor based on conductivity. A mathematical from experimental data was derived relating the bubble diameter with the pressure drop inside the bubble generator, the superficial flowrate in the tailings stream, the surface tension of the media, and the dimensional characteristics of the sparger. The model was validated by running a set of experiments in a 0.50 m flotation column with the same four spargers installed. Experimental results show that there



is possible to scale-up or design bubbles for a given application using the spargers described in this work.

**Characterization and Synthesis of Adsorption Material with Hematite and Polystyrene:** *He Dewen*<sup>1</sup>; Zhou Huannian<sup>1</sup>; <sup>1</sup>Central South University

In this study, a three dimensionally ordered macroporous (3DOM) hematite was prepared with a polystyrene template and characterized by X-ray diffraction (XRD), scanning electron microscope (SEM), transmission electron microscope (TEM), and nitrogen adsorption isotherm. The 3DOM hematite has a porous structure with macropores of 200-nm in diameter and walls of 20-nm in thickness. The adsorption of Pb<sup>2+</sup> and Cd<sup>2+</sup> ions in aqueous solution by 3DOM hematite was also evaluated. At room temperature, each gram hematite adsorbs 12.5 mg of Pb<sup>+</sup> and 7.0 mg of Cd<sup>+</sup>. The results suggest that 3DOM hematite may be a promising adsorbent to remove Pb<sup>+</sup>, Cd<sup>+</sup>, and possibly other heavy metal ions from aqueous solution.

**CO<sub>2</sub>-Corrosion of Steels Exposed to Saline Water Environment:** *Anja Pfennig*<sup>1</sup>; <sup>1</sup>HTW Berlin

With CO<sub>2</sub> being one reason for climate change carbon capture and storage (CCS) is discussed to mitigate climate change. When emission gases are compressed into deep geological layers CO<sub>2</sub>-corrosion can easily cause failure of injection pipes. Different steels used as injection pipe X46Cr13 and X20Cr13 were tested as well as X35CrMo17 and X5CrNiCuNb16-4 in a laboratory environment similar to the conditions of the CCS engineering site at Ketzin, Germany. Samples were exposed to synthetic aquifer saturated with technical CO<sub>2</sub> at a flow rate of 3 l/h. After 1000 h of exposure time pits are found on all 3 with maximum pit heights around 20 μm. Corrosion rates obtained via mass loss vary in a wide range (0,005 to 2.5 mm/year). The precipitations within the corrosion scale revealed a complicated multiphase layer containing siderite FeCO<sub>3</sub>, goethite α-FeOOH, lepidocrocite γ-FeOOH, mackinawite FeS and akaganeite Fe<sub>8</sub>O<sub>8</sub>(OH)<sub>8</sub>Cl<sub>11,34</sub> and spinelphases of various compositions.

**Coarsening of Beta' Precipitates in an Isothermally-Aged Fe75-Ni10-Al15 Alloy:** Orlando Soriano Vargas<sup>1</sup>; *Victor Lopez-Hirata*<sup>2</sup>; Hector Dorantes-Rosales<sup>2</sup>; Maribel Saucedo-Muñoz<sup>2</sup>; Erika Avila-Davila<sup>3</sup>; Susana Lezama-Alvarez<sup>2</sup>; <sup>1</sup>Universidad Autonoma del Estado de Mexico; <sup>2</sup>Instituto Politecnico Nacional (ESIQIE); <sup>3</sup>Instituto Tecnologico de Pachuca

The coarsening process of the beta prime precipitates was studied in an isothermally aged Fe75-Ni10-Al15 alloy. The aging treatments at 750, 850, and 920 °C caused the precipitation of the beta prime phase with the B2 type crystalline structure in a bcc ferritic matrix phase. As the aging progressed, the initial rounded shape changed to cuboids aligned in the <100> directions of the ferritic matrix, and finally to rectangular plates also aligned in the same direction. The coarsening process of the beta prime phase was faster as the aging temperature increased. Nevertheless, the highest hardness and slowest overaging process took place during the aging at 920°C. This increase in hardness seems to be associated with the more rapid formation of the cuboid precipitates aligned in the <100> direction of the ferritic matrix.

**Combined Processing of ECAP and Cold Rolling to Enhance the Performance of Metallic Materials:** *Hiroyuki Miyamoto*<sup>1</sup>; <sup>1</sup>Doshisha University

The effect of simple shear deformation by equal-channel angular pressing (ECAP) for one pass on the texture and ridging of ferritic stainless steel sheets with 16 mass% chromium has been investigated. Hot rolled and annealed sheets of 4 mm thickness were ECA-pressed for one pass, prior to cold rolling and final annealing. The grains were subdivided by grain-scale heterogeneous plastic deformation, namely, deformation bands, during simple shear by ECAP. Deformation bands appear to contribute to the fragmenting layered structure after cold rolling and facilitate recrystallization of the so-called colonies having {hkl}<110> texture, which are otherwise difficult to recrystallize in final annealing. In other words, strain energy can be stored more effectively by combining simple shear and cold rolling than by cold rolling alone. Recrystallization occurred at a much lower temperature in the process including ECAP than in a conventional cold-rolling only process, thus

enhancing its formability and reducing ridging.

**Composition Control of CaO-MgO-Al<sub>2</sub>O<sub>3</sub>-SiO<sub>2</sub> and CaS Inclusions in Pipe Line Steel:** *Suzhou Wu*<sup>1</sup>; Jiongming Zhang<sup>2</sup>; Pan Gao<sup>2</sup>; Zhizheng Li<sup>2</sup>; <sup>1</sup>Wuhan University of Science and Technology; <sup>2</sup>University of Science and Technology Beijing

Non-metallic inclusions in ultra-low sulfur pipeline steel during refining and continuous process were investigated. The result shows that during the initial stage of LF refining, the inclusion in steel mainly are spherical, polygonal and clusters of Al<sub>2</sub>O<sub>3</sub>. After alloying treatment, some Al<sub>2</sub>O<sub>3</sub> inclusions contain SiO<sub>2</sub> and MgO in steel. Most of Al<sub>2</sub>O<sub>3</sub> inclusions transformed to mCaO-nAl<sub>2</sub>O<sub>3</sub> containing SiO<sub>2</sub> and MgO, and some of them are CaS. Thermodynamic calculations get best window for calcium treatment and show that it is not only to generate CaS inclusion easily, but also to generate aluminum calcium inclusions of high Al<sub>2</sub>O<sub>3</sub> content when aluminum content in high sulfur steel is relatively high.

**Correlation of Porosity Detected by Computed Tomography and Fatigue Strength of Aluminium Alloys:** Thomas Pabel<sup>1</sup>; Georg Geier<sup>1</sup>; Daniel Habe<sup>1</sup>; Joerdis Rosc<sup>1</sup>; Peter Schumacher<sup>1</sup>; Tose Petkov<sup>1</sup>; <sup>1</sup>Austrian Foundry Research Institute

The aim of the current research was to verify the impact of a suboptimal melt quality on the static and dynamic mechanical properties of aluminium castings. The particular interest was to use the possibilities of computed tomography to describe volumetric casting defects and to compare these results with measured mechanical properties. The results of static materials testing and the S/N curve are in excellent correlation with that of the CT evaluations as well as the density index. The selected resolution in the CT gave an adequate description from the pore space. In the future it should be possible to forecast the reduction of the mechanical properties due to an increased gas content based solely on NDT using CT. The results can now be implemented in FEM analysis to calculate a maximum pore level for a given load situation.

**Determination of Coating Thickness of Anti-Fingerprint Steel Coils Using Ultraviolet Spectra:** *Chi-Hyuck Jun*<sup>1</sup>; Yong Sun Shim<sup>1</sup>; Sang Moo Hwang<sup>1</sup>; <sup>1</sup>POSTECH

Coating thickness is one of target variables for quality control in steel industry. To determine the coating thickness of anti-fingerprint steel coils rapidly, ultraviolet-visible spectra can be utilized. We propose a variable selection procedure based on the variable importance in projection of partial least square regression in order to build an efficient calibration model. It is found that the prediction performance appears better in the reduced model using the proposed variable selection than the full model with full spectra absorbance. It is also shown that the first differencing as a data preprocessing technique works well for the prediction of coating thickness. Keywords: Partial least square, variable importance in projection, data preprocessing.

**Development and Characterization of Milled Silver Powder Addition to Polypropylene Feedstock for Injection Molding:** *Kübra Yumagil*<sup>1</sup>; A. Umut Söyler<sup>1</sup>; Gizem Yilmaz<sup>1</sup>; Candan Tamerler<sup>1</sup>; Burak Özkal<sup>1</sup>; <sup>1</sup>Istanbul Technical University

In the present study, polypropylene-silver composites were prepared via addition of milled Ag powder to polypropylene (PP) matrix and subsequently injection molding was applied for final shaping. In order to add the milled Ag powders to granular PP feedstock two different approaches were studied prior to mixing them in extruder to obtain homogeneous dispersion in PP matrix. The effects of different ratio of silver on the properties of composites were analyzed by using different characterization techniques (DSC, FTIR, SEM and XRD). DSC analysis was used for determination of crystallinity that highly affects the antibacterial behavior of composites. Moreover, the thermal analysis and FTIR studies showed there is no degradation on the polypropylene matrix with addition of the silver content.

**Development on Management Information System on Cleaner Production Assessment in Electrolytic Aluminum Industry:** *He Dewen*<sup>1</sup>; Liu Lei<sup>1</sup>; Zhou Huangnian<sup>1</sup>; <sup>1</sup>Central South University

In this paper, the impact to environment and society by electrolytic aluminum industry were studied, and evaluation index and method of cleaner production in electrolytic aluminum industry is put forwards, and the management information system are developed by VB and SQL, and database of cleaner production indicators and enterprise information is built. Then the functional structure of management information system is consisted of four parts as follows: system management, cleaner production assessment indexes management, enterprise information management and cleaner production assessment method management. By the ways of checking, modifying and renovating the indicators' information, the management information system can be used as effective tool not only for the government to carry out management of enterprise cleaner production, but also for electrolytic aluminum enterprises to provide with concretely action promoting cleaner production.

**Diffusion Bonding Process for Aerospace Components:** *Ho-Sung Lee*<sup>1</sup>; Jong-Hoon Yoon<sup>2</sup>; Dong-Hyuk Shin<sup>2</sup>; <sup>1</sup>Korea Aerospace Research Institute; <sup>2</sup>Hanyang University

In diffusion bonding process, the metal components being joined undergo only microscopic deformation and the joining region is homogeneous and complete metallurgical bonding is possible without secondary materials or liquid phases. In the present work, diffusion bonding of titanium in an inert environment has been investigated to fabricate several aerospace components with various complex configure. Micrographs of diffusion bonded titanium alloys show grain boundary rearrangement and complete bonding and therefore homogeneous microstructure can be obtained. The optimum condition for diffusion bonding of Ti-6Al-4V in an inert environment was obtained at 875°C with applying gas pressure of 4MPa for 1 hour.

**Effect of Beam Width on Melt Pool Geometry and Solidification Microstructure in Beam-Based Solid Freeform Fabrication:** *Srikanth Bontha*<sup>1</sup>; Nathan Klingbeil<sup>2</sup>; <sup>1</sup>Temple University; <sup>2</sup>Wright State University

Laser and electron beam-based deposition of titanium alloys is currently under consideration for application to aerospace comments. The success of these promising technologies will depend on the ability to control geometric and mechanical properties of fabricated parts, which requires an understanding and control of melt pool size and microstructure. As such, the focus of this work is the effect of beam width on melt pool geometry and thermal conditions controlling microstructure in beam-based solid freeform fabrication. Process maps that relate deposition process variables to solidification cooling rates and thermal gradients have been previously developed using the Rosenthal solution for a moving point heat source. Present work, extends the approach to include the effects of beam width by superposition of the Rosenthal solution for both 2-D thin-wall and bulky 3-D geometries. Results suggest that intentional variations in beam width could potentially enable significant changes in melt pool geometry without affecting microstructure.

**Effect of Cooling Rates and Mn Content on Grain Boundary Serration of Silicon Steel:** *Xianyong He*<sup>1</sup>; *Qin Peng*<sup>1</sup>; *Quanzhi Sun*<sup>1</sup>; *Lei Wang*<sup>1</sup>; *Changjiang Song*<sup>1</sup>; *Qijie Zhai*<sup>1</sup>; <sup>1</sup>Shanghai University

To investigate the effect of cooling rates and Mn content on grain boundary serration, four groups of silicon steel samples with different Mn contents and thicknesses which corresponding to different cooling rates were prepared for this research. It was observed that the lower the cooling rates, the easier the occurrence of serration and the more the proportion of equiaxed grains zone. Also it can be found that serration is more prominent and grains are more refined with the increasing of Mn content. It is suggested that Mn segregation which affected by cooling rates and Mn content is responsible for occurrence of grain boundary serration. The serration is formed by hindrance of Mn solute element to the interface tension of residual liquid at the end of solidification process.

**Effect of Magnesium Ion on Electrodeposited Zinc:** *Gang Xie*<sup>1</sup>; Yu Xiaohua<sup>1</sup>; Li Rongxing; <sup>1</sup>Technology Center of Yunnan Metallurgy Group Co.Ltd.

the effect of Mg<sup>2+</sup> on current efficiency and electrical power consumption of electrodeposited zinc was researched through changing temperature of sulfate electrolyte and Mg<sup>2+</sup> Concentration. Sulfate electrolyte density, viscosity and electrical conductivity were determined at the difference of temperature and Mg<sup>2+</sup> Concentration. The result shows that at certain Mg<sup>2+</sup> Concentration, electrical conductivity increases and electrical power consumption decreases with increasing temperature. At certain temperature, electrical conductivity increases and electrical power consumption decreases with decreasing Mg<sup>2+</sup> Concentration. Sulfate Electrolyte density and Viscosity show increasing trend with decreasing temperature and increasing Mg<sup>2+</sup> Concentration. Sulfate electrolyte electrical conductivity increases with increasing temperature and decreasing Mg<sup>2+</sup> Concentration.

**Effect of Microstructure Change on Magnetic Property of Nd-Fe-B Sintered Magnets:** *Jin Woo Kim*<sup>1</sup>; Se Hoon Kim<sup>1</sup>; Dae-Gun Kim<sup>1</sup>; Young Do Kim<sup>1</sup>; <sup>1</sup>Hanyang University

Sintered Nd-Fe-B magnets have been widely used due to their excellent magnetic properties. They are normally composed of Nd<sub>2</sub>Fe<sub>14</sub>B hard magnet phase as matrix and Nd-rich phase on grain boundary. According to several authors, it was reported that the distribution of Nd-rich phase was affected to the magnet property. Thus, the magnetic properties of sintered Nd-Fe-B magnets will be improved by modification of microstructure. In this study, the modification of microstructure was carried out by modified sintering process. The modified-sintering process was repeated to apply the liquid phase sintering by heating and cooling between certain temperatures. Consequently, the modified sintering process led to uniform Nd-rich distribution which had the improved magnetic properties

**Effect of Ni Addition on the Production of As-Cast Bainitic Ductile Iron:** *Alex Ossa*<sup>1</sup>; Sandra Murcia<sup>1</sup>; Marco Paniagua<sup>1</sup>; <sup>1</sup>Eafit University

Ductile iron is widely used due to its low cost and higher ductility than other cast irons. There has been an increased interest during the last years in increasing the strength of these irons by means of heat treating. This work study the fabrication of ductile cast irons with martensitic and bainitic structures in the as cast condition, reducing costs related to heat treating processing and improving the mechanical behavior of the material. Cast irons alloyed with Ni ranging from 0% up to 5% were fabricated in order to evaluate the effect of Ni content on the phase transformations and mechanical properties of the material. The effect of cooling speed in the phase transformations and properties was studied using moulds with different wall thicknesses. Optical and electronic microscopy, tensile testing and Charpy impact testing were used to characterize the ductile cast irons.

**Effect of Predeformation and Heat Treatment Conditions in the Modified SIMA Process on Microstructural of a New Developed Super High-Strength Aluminum Alloy Modified by Al-8B Grain Refiner:** *Mohammad Alipour*<sup>1</sup>; *Masoud Emamy*<sup>1</sup>; *Jafar Rasizadeh*<sup>1</sup>; *Mostafa Karamouz*<sup>1</sup>; *Mortaza Azarbarmas*<sup>1</sup>; <sup>1</sup>Kargar street

This study was undertaken to investigate the influence of Al-8B master alloy on the structural characteristics of Al-12Zn-3Mg-2.5Cu aluminum alloy. The optimum amount of B containing master alloy for proper grain refining was selected as 3.75 wt.%. In order to examine the effectiveness of the modified SIMA process, structure of the alloy prepared by the modified SIMA process were studied. The microstructure evolution of reheated Al-12Zn-3Mg-2.5Cu aluminum alloy was characterized by SEM and optical microscopy. In this study the relation between the induced strain with size and shape of grain size has been studied. Results indicated that with the increase of strain, sphericity of particles, their size decreases and sphericity takes place in less reheating time. Optimum combinations of average globule size and shape factor were obtained in holding time of 20 min and 590 °C for the samples predeformed up to 60%.

**Effect of Pulse Magnetic Field on Normal Grain Growth of Grain Oriented Silicon Steels during Primary Recrystallization Annealing:** *Qiangqiang Xia*<sup>1</sup>; Lijuan Li<sup>1</sup>; Junjun Huang<sup>1</sup>; Lihua Liu<sup>1</sup>; Qijie Zhai<sup>1</sup>; <sup>1</sup>School of Materials Science and Engineering, Shanghai University

Pulsed magnetic field was applied to investigate the normal grain growth of grain oriented silicon steels during primary recrystallization annealing. Three pieces of cold-rolled sheet were firstly annealed at 700° for 10 minutes; then two of them were annealed with and without a pulsed magnetic field of 1T with the direction parallel to the rolling direction at 700° for 30 minutes respectively. Microstructures and textures of the three annealed samples mentioned above were finally characterized by optical microscopy and Electron Backscatter Diffraction (EBSD) technique. The results indicate that pulsed magnetic field can promote the normal grain growth, and can affect the texture development by increasing the intensity of {001}<120> component and decreasing the intensity of a and  $\square$  fibers. Magnetocrystalline anisotropy energy and grain boundary mobility are employed to account for the pulsed magnetic field annealing mechanism.

**Effect of Soldering Flux in Sn3.0Ag0.5Cu on Electrochemical Migration:** *Junghwan Bang*<sup>1</sup>; <sup>1</sup>Korea Institute of Industrial Technology(KITECH)

Recently, there is a growing tendency that fine-pitch electronic devices are increased due to higher density and very large scale integration. This finer pitch of printed circuit board decreases the insulation resistance between patterns or electrical components, which will induce electrical short in electronic circuit by electrochemical migration when it exposes to long-term in high temperature and high humidity. In this research, the effect of soldering flux acting as an electrical carrier between conductors on electrochemical migration was investigated. The surface of PCB was treated with OSP finished. Solder paste of Sn3.0Ag0.5Cu was screen printed on the PCB and then the PCB was reflowed. Thereby, specimen for ion migration test was fabricated. Electrochemical migration test was conducted under the condition of DC 48 V, 85 degree Celsius, and 85 % relative humidity. The fundamentals and mechanism of electrochemical migration was discussed depending on the existence of flux after reflow process.

**Effect of Tungsten on the Microstructure and Mechanical Properties of the Ni-Base Superalloy Inconel 740:** *Sung-yong Lee*<sup>1</sup>; Kyoung Soo Shin<sup>1</sup>; Sun Jin Kim<sup>1</sup>; <sup>1</sup>Hanyang Univ.

The energy crisis and the environmental restriction have been serious issues in the recent society. It could be solutions for these problems to increase operating temperature and pressure in the pulverize coal-fired power plants since higher operating temperature and pressure can improve the efficiency and reduce the emission of harmful gases like CO<sub>2</sub>. In addition, it is required to develop new material which can support in the target steam condition (more than 700°, 37.5MPa). For this reason, SMC(Special Metals Corporation) developed "Inconel 740" used in the ultrasupercritical steam boiler tubes. In this study, we succeeded in improving the stability of Inconel 740 by adding tungsten, and also the effect of tungsten on the coarsening rate of gamma prime precipitates was investigated. Furthermore, the microstructural changes and mechanical properties with tungsten content, aging time, and aging temperature were examined.

**Effects of Al-5Ti-1B Grain Refiner on The Structure, Hardness and Tensile Properties of Al-12Zn-3Mg-2.5Cu Aluminum Alloy:** Mohammad Alipour<sup>1</sup>; Masoud Emamy<sup>2</sup>; *Jaafar Rasizadeh*<sup>1</sup>; Mortaza Azarbarmas<sup>2</sup>; Mostafa Karamouz<sup>2</sup>; <sup>1</sup>Kargar street; <sup>2</sup>Tehran University

In this study the effect of Al-5Ti-1B grain refiner on the structural characteristics, hardness and tensile properties of Al-12Zn-3Mg-2.5Cu aluminum alloy was investigated. The optimum amount for Ti containing grain refiners was selected as 2 wt.%. T6 heat treatment was applied for all specimens before tensile testing. Significant improvements in mechanical properties have been obtained with a combination of grain refiner and T6 heat treatment. After heat treated specimens, the average tensile strength of 495 MPa was found to be increased to 605 MPa for sample refined with 2 wt.% Al-5Ti-1B. The fractography of the fractured faces and microstructure evolution of Al-12Zn-3Mg-2.5Cu aluminum alloy was characterized by SEM (Scanning electron microscopy) and optical microscopy.

**Effects of Silicon Content and Cooling Rate on Distribution and Size of Inclusion in Silicon Steel Thin Strip:** *Qin Peng*<sup>1</sup>; Lei Wang<sup>1</sup>; Xianyong He<sup>1</sup>; Rong Yang<sup>1</sup>; Changjiang Song<sup>1</sup>; Qijie Zhai<sup>1</sup>; <sup>1</sup>Shanghai Key Laboratory of Modern Metallurgy & Materials Processing, Shanghai University

The twin roll thin strip continuous casting is a technology with near rapid solidification, which can be used to produce high performance silicon steel. To physically simulate the fabrication of silicon steel thin strips, the suction casting experiment was carried out by a vacuum casting apparatus. Strips with different silicon content and cooling rate were prepared, and the inclusion distribution of the strips was observed by scanning electron microscope (SEM). The experimental results show that the number of inclusions increases with the increasing of silicon content and the decreasing of cooling rate. Moreover the size of the biggest inclusions decreases with the increasing of silicon content and cooling rate.

**Electrical Properties of SiOC Low-k Films:** *Teresa Oh*<sup>1</sup>; <sup>1</sup>Cheongju University

SiOC films made by the chemical vapor deposition were analyzed the chemical shift by the Fourier transform infrared spectra and photoluminescence spectra. The chemical shift obtained in Fourier transform infrared spectra resulted from the increase of right shoulder Si-O bond in the main bond due to the delocalization and lowering polarization of carbon in Si-CH<sub>3</sub>. The right shoulder bond of Si-O increased after annealing because of the delocalization due to the charge dispersion of carbocation, so the final materials became more stability than as deposited film. The phenomenon of the delocalization in the carbon bond of Si-CH<sub>3</sub> was also confirmed by the chemical shift in the photoluminescence spectra. The PL intensity decreased due to the delocalization after annealing. However, the sample due to the localization of carbon showed higher intensity and moved to higher wavelength, and the shapes of the main bond also involved the strong shoulder bonds.

**Electron Backscatter Diffraction of Ni and Cu Powder Particles Impacted at High Velocity:** *Yu Zou*<sup>1</sup>; Eric Irissou<sup>2</sup>; Jean-Gabriel Legoux<sup>2</sup>; Stephen Yue<sup>1</sup>; <sup>1</sup>McGill University; <sup>2</sup>Industrial Materials Institute (IMI), National Research Council Canada (NRC)

Micron-sized Ni and Cu powder particles were deposited at supersonic velocity on steel substrates to form coatings using the method of cold spraying, respectively. The microstructural evolution was investigated using electron backscatter diffraction and nanoindentation. We found non-uniform microstructure with ultrafine grains in the size of 200 nm with relatively higher hardness appeared in the cold sprayed Ni coating. However, the cold sprayed Cu shows more uniform microstructure and homogeneous hardness distribution. These formed microstructures and corresponding hardness are interpreted in terms of dynamic recrystallization in cold spraying and static recrystallization during the cooling process.

**Electron Beam Melting and Recycling of Hafnium:** *Katia Vitova*<sup>1</sup>; Vania Vassileva<sup>1</sup>; Georgi Mladenov<sup>1</sup>; Elena Koleva<sup>1</sup>; Tirthalli Prakash<sup>2</sup>; Nagegownivari Munirathnam<sup>2</sup>; <sup>1</sup>Institute of electronics, Bulgarian Academy of Sciences; <sup>2</sup>Centre for Materials for Electronics technology

In this paper, experimental results for different regimes, data for chemical analysis and theoretical investigation of the process parameters at electron beam melting and refining (EBMR) of hafnium samples are presented and discussed. Thermodynamics conditions and mechanisms as possibilities for the refining process Hf are described and analyzed. Calculated data for the refining kinetics of EBMR of Hf shows that the refining rate is determined not only by the process of mass transport of the impurities through the liquid metal and by the evaporation from the molten pool surface, but also by a great extent by other processes. The results show that the minimal impurities' concentrations are obtained at 12 kW electron beam power and short heating time.



**Electrosynthesis, Characterization, and Thermal Property Analysis of Pentakis(Diethylamido)Tantalum:** *Yang Jian-guang*<sup>1</sup>; <sup>1</sup>Central South University

Pentakis(diethylamido)tantalum (PDEAT) was synthesized by electrochemical reaction involving diethylamide with a sacrificial tantalum anode and stainless steel cathode in the presence of tetraethylammonium bromine as the conductive additive and acetonitrile as the inert support electrolyte. The condensates were isolated by the reduced pressure distillation of as-synthesized crude PDEAT below 5 kPa. The final product was characterized by FT-IR and NMR spectroscopy. The thermal properties of the resulting PDEAT were analyzed by TG-DTG. Results indicate that the resulting compound was indeed PDEAT. The vapor pressure of the compound was calculated from the Langmuir equation, while the enthalpy of vaporization was calculated from vapor pressure-temperature data using the Clausius-Clapeyron equation. The concentration of the impurities in the sample were detected via ICP-Mass spectroscopy, and it was found that the purity of the compound synthesized could reach 99.995%.

**Evaluation of the Effect of Residual Silver in Copper on the Cementation Process by Factorial Design and Multiple Regression Analysis:** *Duygu Aogaogullari*<sup>1</sup>; *Ismail Duman*<sup>1</sup>; *Özgül Keleş*<sup>1</sup>; <sup>1</sup>Istanbul Technical University

Residual silver in cementator copper was studied to examine its effect on the efficiency of cementation process in form of reduced silver (process output) by considering reaction duration, silver content and rotation speed of copper electrodes. The experiments were conducted at room temperature with 100 mm<sup>2</sup> non-rotating and rotating disc copper electrodes (0 and 500 rpm) alloyed with different Ag ratios (0.5 and 10 %). The reactions were carried out in nitrate solutions in certain reaction time (10 min. and 2 h). Experiments were designed by full factorial design (2k) method and analyzed using ANOVA and multiple regression analysis. The maximum amount of reduced silver was obtained at a silver content of 0.5 % with non-rotating disc copper electrode in 2 h reaction duration. The most effective parameter on the cementation process was determined as reaction duration. Correlation coefficients ( $R^2$  and  $R^2_{adj}$ ) were calculated as 0.978 and 0.948, respectively.

**Evaluation of the Structural Strength in Railroad Car:** *Sung Cheol Yoon*<sup>1</sup>; *Jongguk Kim*<sup>1</sup>; <sup>1</sup>Korea Railroad Research Institute

To check the structural strength of the body of the railroad car, load was added to the underframe of the railroad car. The objective of this study is to evaluate whether or not the underframe of a railroad car under the maximal strength is safe. The carbody of rolling stock is a principal structure that supports major equipment of the underframe and the freight. Therefore, the strength evaluation of this structure is important. Both structural analysis and loading test were performed under the loading condition. Prior to the evaluation of structural strength, finite element method was used for structural analyses on stress distribution in a carbody of a railroad car. The strain gauges were attached on the car based on FEM results. The test results showed that the carbody is safe under the condition of the designed load.

**Explosive Generation of High Pressures and Temperatures and Areas of Their Application:** *Nikoloz Chikhradze*<sup>1</sup>; *V. Kabulashvili*<sup>1</sup>; <sup>1</sup>Georgian Technical University

The possibilities for generation of ultra-high pressures and temperatures using the different schemes of detonation of an explosives are discussed. It is demonstrated that ultra-high pressures and temperatures generated by explosives of different shape could be effectively used for the industrial production of super hard materials and ultra-disperse powders.

**Flux Effect on Electrochemical Migration of Sn<sub>3.0</sub>Ag<sub>0.5</sub>Cu Solders:** *Junghwan Bang*<sup>1</sup>; *Sehoon Yoo*<sup>1</sup>; *Changwoo Lee*<sup>1</sup>; <sup>1</sup>Korea Institute of Industrial Technology(KITECH)

Flux effects on the electrochemical migration (ECM) were investigated in this study. Flux in solder paste is the source of the impurities like halogen species, which influences the ECM properties. Generally, flux is not cleaned after soldering process in recent automotive electronic industries. However, most ECM researches on solder interconnection have performed with solder-dipped or flux-cleaned samples which were not able to understand the flux

effect. In the present study, “no-clean” and “flux-cleaned” samples were used to understand the flux effect for ECM. In this study, Sn<sub>3.0</sub>Ag<sub>0.5</sub>Cu solder pastes were printed and reflowed on OSP-treated Cu pad. ECM test was conducted under the condition of DC 48 V, 85°C, and 85 % RH. Both Sn and Cu was migrating species in the ECM test of Sn-3.5Ag-0.5Cu solder/Cu pad structure. As compared with flux cleaned test samples, solders with flux residue showed high rate of ECM failures.

**Generation and Control of Two Way Shape Memory Effect for SMA Coil Spring:** *Kwang Jee*<sup>1</sup>; *Jun Han*<sup>1</sup>; *Woo Jang*<sup>2</sup>; *Je Min Park*<sup>3</sup>; <sup>1</sup>Korea Institute of Science and Technology; <sup>2</sup>Chosun Univ.; <sup>3</sup>Hongik University

A coil spring has a peculiar demerit that it works only in one direction when it is closed. Since no further compression can be applied to the closed coil, there are some difficulties in generating TWSME. One of example is a SMA coil spring which expands on heating and contracts on cooling. An open coil spring should be severely contracted to generate the TWSME. However, contraction is limited to the initial stroke of the coil, so it is difficult to obtain such TWSME. In this work, we introduce a new method of compression of closed coil by reversing the coil winding orientation. According to our invention, a severe compression can be attained by reversing the coil orientation and extending severely. Some more applications of the ‘reverse of coil orientation’ to TWSME are presented.

**High Temperature Corrosion of Ni-25Cr-20Co Alloys at 1073-1373 K in SO<sub>2</sub> Gases:** *JaeHo Lee*<sup>1</sup>; *SangHwan Bak*<sup>1</sup>; *Minjung Kim*<sup>1</sup>; *DongBok Lee*<sup>1</sup>; <sup>1</sup>Sungkyunkwan University

Structural components are exposed to highly corrosive environments containing sulfur and oxygen in high-temperature gas turbines, petrochemical units, and coal gasification systems. Thus, the SO<sub>2</sub>-gas corrosion-resistance is of considerable industrial interest for practical applications. In this study, the corrosion performance of INCONEL 740 whose composition is Ni-25Cr-20Co-2Nb-1.8Ti-0.9Al-0.7Fe-0.5Si-0.5Mo-0.03C was investigated at 1073-1373K for up to 100 hr in an Ar-0.2% SO<sub>2</sub> atmosphere. The INCONEL 740 alloy corroded parabolically at 1073 and 1173K for up to 10 hr, and no scale spallation occurred. However, the parabolic law was not obeyed at 1273 and 1373K. The formed scales consisted of Cr<sub>2</sub>O<sub>3</sub>, (Ni,Co)Cr<sub>2</sub>O<sub>4</sub> and TiO<sub>2</sub>. Sulfur was distributed at the scale/matrix interface and internal precipitates. Acknowledgement. This work was supported by the Human Resources Development of the Korea Institute of Energy Technology Evaluation and Planning (KETEP) grant funded by the Korea government Ministry of Knowledge Economy (No. 20101020300460).

**Horizontal Directional Solidification of Zn-Al Alloys:** *Alicia Ares*<sup>1</sup>; *Sergio Guejman*<sup>2</sup>; *Carlos Schvezov*<sup>1</sup>; <sup>1</sup>CONICET/FCEQyN-UNaM; <sup>2</sup>FCEQyN-UNaM

Zinc-Aluminum alloys were solidified in horizontal form and the results obtained analyzed. During solidification the distribution of temperatures were measured by using thermocouples located strategically. From the measured temperatures the following parameters were derived; the local temperature gradient, the cooling rate and the velocities of the liquid and solidus fronts. Comparing the location of the transition and the values of these parameters it was found that the temperature gradient reaches minimum values of as low as 1 °C/cm, and velocities of the fronts of around 0.1 cm/s. In addition the grain size and secondary dendritic arm spacing was measured along the samples. The spacings and grain sizes are correlated with thermal parameters and compared with the predictions from available models. The results are presented and discussed in the frame of the results obtained for other alloys.

**How to Control Strength and Grain Structure of 304L Stainless Steel during Forging:** *Nathan Switzer*<sup>1</sup>; *Jamie McQueen*<sup>1</sup>; *Wayne McLaren*<sup>1</sup>; *Robert Bergen*<sup>2</sup>; *Chris San Marchi*<sup>3</sup>; <sup>1</sup>Honeywell FM&T; <sup>2</sup>Precision Metal Products; <sup>3</sup>Sandia National Labs - Livermore

304L forgings were made using a High Energy Rate Forging (HERF) press at hot working temperatures 843 °C (1550 °F) and 941 °C (1725 °F). Strain was varied from 0.4 to 1.8 EQPS (calculated using ABAQUS). Mechanical testing and microstructural analysis were conducted on the forgings. Room temperature yield strength increased with strain from about 0 to 0.7 EQPS.

However, higher strain levels of 1.4 to 1.8 EQPS decreased yield strength due to recrystallization. Material deformed at 843 °C (1550 °F) began to recrystallize at a strain value of about 1.1 EQPS, but material deformed at 941 °C (1725 °F) began to recrystallize at about 0.7 EQPS. ABAQUS coupled thermal simulation estimated a temperature increase of 80-120 °C (150-200 °F) due to rapid deformation in the HERF press. Therefore the strength and grain structure of 304L forgings may be controlled using two parameters—forging temperature and shape change, i.e. strain.

**Improved Dual Duct Boosted Suction (DDBS) System Doubles Pot Suction, Reduces Roof Emission:** *Peter Klut<sup>1</sup>; Erik Dupon<sup>1</sup>; Danieli-Corus*

Potroom emission and working environment within the potroom are becoming more and more an issue with the authorities and the potroom workers. A large portion of the potroom emission is emitted during pot maintenance or during tapping when the covers of the pot are removed. By doubling the gas flow from the pot during these periods the emission can be brought back to normal levels. The DDBS system doubles the gas flow by using the existing pressure differential over the restriction orifice or control damper to direct the gas to the DDBS ducting instead of using dedicated DDBS dampers. For combined pots the required number of dampers can be reduced up to 70% compared to existing systems. Test executed at an Australian smelter proved that this is a feasible technology which reduces Smelter Potroom Emissions significantly, and requires minimal investment and operating costs.

**Influence of Cr Addition on Crystallization Behaviour and GMI Properties of FeCoBSi Amorphous Wire:** *Rajat Roy<sup>1</sup>; Satnam Singh<sup>1</sup>; Partha Sarkar<sup>1</sup>; Ashis Panda<sup>1</sup>; Amitava Mitra<sup>1</sup>; <sup>1</sup>National Metallurgical Laboratory (CSIR)*

The effect of Cr addition on crystallization behaviour, electrical resistivity and giant magneto impedance (GMI) in amorphous wires with a nominal composition of  $(\text{Fe}_{0.5}\text{Co}_{0.5})_{78-x}\text{Cr}_x\text{Si}_8\text{B}_{14}$  ( $x = 0, 4, 7$  and  $10$  at%) has been investigated. The quality of the wires improves with increasing Cr content owing to the Cr-oxide layer at the surface of wire. During isochronal annealing of the wires, crystallization behaviour is examined by DSC thermograms and electrical resistivity. The substitution of a small amount of Fe and Co with Cr increases the thermal stability and GMI properties of amorphous wires. It is interesting to note that the crystallization peak shifts to the highest temperature and thermal stability is also higher when Cr addition increases from 7 to 10 at%. The GMI properties of all wires are maximized at the frequency of 400 kHz and at driving current amplitude of 10 mA.

**Influence of Limestone Composition on Lime Desilication of Green Liquors:** *Andrey Panov<sup>1</sup>; Alexander Suss<sup>1</sup>; Natalia Kuznetsova<sup>1</sup>; Irina Paromova<sup>1</sup>; <sup>1</sup>RUSAL VAMI*

At processing of mixed type/monohydrate bauxites traditional ways of desilication are less effective due to peculiarities of silica containing minerals. Introduction of calcium compounds in the head of process makes excessive scaling of heating surfaces. As alternative, desilication of green liquor with reduced amount of lime milk with subsequent reuse of the residue at digestion in order to capture more silica, is considered. During the tests, influence of composition of initial limestone, method of Ca-containing compound preparation, impurities, etc. on desilication efficiency and sediment particle size has been studied.

**Influences of Alloying Elements on Grain Sizes in Friction Stir Processed Pure Aluminum and Aluminum Alloys:** *Tomotake Hirata<sup>1</sup>; Taiki Morishige<sup>2</sup>; Masato Tsujikawa<sup>2</sup>; Kenji Higashi<sup>2</sup>; <sup>1</sup>Technology Research Institute of Osaka Prefecture; <sup>2</sup>Department of Materials Science, Osaka Prefecture University*

A friction stir processing (FSP) technique has been developed for use with aluminum and magnesium alloys. The microstructure was evolved into fine grains by the dynamic recrystallization during FSP. In this study, FSP was used to pure aluminum and aluminum alloys and the influence of alloying element on the grain size was investigated. In addition, the relationship between the grain size and the Zener–Hollomon parameter was

investigated. There was observed difference in grain size between these materials. The recrystallized grain of FSP-ed ultra-high-purity (99.999%) aluminum was particularly large, compared to the grain sizes of other materials, when subjected to the same processing conditions. In contrast, grain sizes decreased with an increase in the Zener–Hollomon parameter in all materials. However, the grain size reached a certain minimum value at high-strain-rates of processing. Compared to other processed aluminum materials, the minimum grain size was found for each material.

**Interfacial Microstructure and Mechanical Properties of the Friction Stir Welds between AA6061 and Ti-6Al-4V Alloy Sheets:** *Kwang-jin Lee<sup>1</sup>; <sup>1</sup>Korea Institute of Industrial Technology*

Butt joining was carried out using a friction stir welding method for 5mm-thick AA6061-T6 and Ti-6Al-4V alloy plates. Sound joints were successfully obtained. Mechanical properties were evaluated using tensile test and Vickers hardness test. Interfacial microstructure, in particular, newly formed interfacial region and the distribution of additional elements at the weld interface was precisely examined using TEM-HAADF (High Angle Annular Dark Field) technique and element mapping method, respectively. Thin foils were prepared using a Focused Ion Beam (FIB) method. Root area of probe in stir zone (SZ) revealed a mixture of fine recrystallized grains of aluminum alloy and lots of titanium alloy particles pushed away from the base metal due to strong stirring by the tool fabricated by WC-Co. Interestingly, segregation of Si was detected at the weld interface. Fracture surface revealed very complicate sequence according to the tool position.

**Interfacial Reactions at the Sn-xBi/Au Couples:** *Yee-wen Yen<sup>1</sup>; Wei-Kai Liou<sup>2</sup>; Chao-Ming Chen<sup>3</sup>; Meng-Kuang Huang<sup>3</sup>; <sup>1</sup>National Taiwan University of Science and Technology; <sup>2</sup>Lunghwa University of Science and Technology; <sup>3</sup>National Taipei University of Technology*

The interfacial reactions between Sn-50wt%Bi, Sn-57wt%Bi, Sn-65wt%Bi, and Au substrate, aged at 80, 100, 120°C for 12 to 350 h had been investigated in this study. The Bi contents were 57 and 65wt% in the Sn-Bi alloys, the Au-Sn intermetallic compounds (IMCs) were observed at the interface. The Au-Sn IMCs and ternary Sn-Bi-Au metastable phases were formed at the Sn-50wt%Bi/Au couple. However, this ternary Sn-Bi-Au metastable phase was transferred into the AuSn4 phase, when the reaction was extended over 72 h. Increasing the Bi contents in the Sn-Bi alloys could make the large (Bi) phases be segregated on the solder/Au interface to decrease the IMCs growth. The IMC growth mechanism in all reaction couples is diffusion-controlled. The lowest value of the reaction activity energy could be found in the Sn-57 wt%Bi couples.

**Intermetallic Phases and Microstructure in AlSi Alloys Influenced by Fluid Flow:** *Piotr Mikolajczak<sup>1</sup>; Lorenz Ratke<sup>2</sup>; <sup>1</sup>German Aerospace Center, Poznan University of Technology; <sup>2</sup>German Aerospace Center*

In secondary AlSi alloys, the presence of small amounts of Fe causes the formation of intermetallic phases, which have a negative effect on the mechanical and physical properties of castings. To understand the effect of fluid flow on the microstructure and intermetallic phases, Al-5/7/9 wt pct Si 0.2/0.5/1.0 wt pct Fe alloys have been directionally solidified under defined thermal and fluid flow conditions (rotating magnetic field). The primary Al-phase, interdendritic eutectic and intermetallic phases were studied using light microscopy and SEM with EDX. An essential observation is that fluid flow can shorten the length of the  $\beta$ -Al<sub>5</sub>FeSi plates accompanied with an increase in the density number. The presence of broken and curved  $\beta$ -phases was observed, beside common straight ones. The secondary dendrite arm spacing is not effected by fluid flow, probably due to the presence of intermetallics in the interdendritic space.

**Investigation of Inclusion Evolution Mechanism during the Refining and Continuous Casting Process of 28MnCr5 Steel:** *Suzhou Wu<sup>1</sup>; Zhizheng Li<sup>2</sup>; <sup>1</sup>Wuhan University of Science and Technology; <sup>2</sup>University of Science and Technology, Beijing*

By means of SEM, EDS and other experimental means, 28MnCr5 gear steel produced in a steel plant was researched. The size, appearance and number of inclusions in LF refining process, VD vacuum refining process and

casting billet were studied. The results show that the independent manganese sulfide were mostly massive, some spherical or rod-like. Compound manganese sulfide were a core part of inclusion spinel or calcium aluminate, manganese sulfide outside. The size of manganese sulfide inclusions were in  $5\mu\text{m}\sim 15\mu\text{m}$ . By using of thermodynamic calculation software FactSage, the relationship between steel elements and slag composition and inclusions in steel was calculated. The results show that according to the thermodynamic calculation of the low melting point area and lower oxygen content in selected area, the range of inclusion area was selected:  $\text{SiO}_2$  0%~9%,  $\text{Al}_2\text{O}_3$  33%~51%,  $\text{CaO}$  49%~58%.

**Investigation of Molybdenum Double Perovskites for Use in Anode Supported Solid Oxide Fuel Cells:** *Adam Weisenstein*<sup>1</sup>; Stephen Sofie<sup>1</sup>; <sup>1</sup>Montana State University

In this study molybdenum-based double perovskites were investigated for application as electrochemical fuel electrodes, e.g.  $\text{Sr}_x\text{MMoO}_6$ , where M represents Ni, Ti and V. Also, A-site deficiencies were investigated as  $\text{Sr}_x$  varied from  $\text{Sr}_{1.8}$  to  $\text{Sr}_2$ . Double perovskite powders were synthesized by ball milling for 48 hours, flash freezing, sublimation and calcination at  $1000^\circ\text{C}$  for 6 hours. Pellets were then made and sintered under reducing conditions for 24 hours in temperatures ranging from  $1200^\circ\text{C}$  to  $1400^\circ\text{C}$ . The phase composition and phase evolution were characterized by x-ray diffraction and DC electrical conductivity was measured at temperatures ranging from  $20^\circ\text{C}$  to  $800^\circ\text{C}$  in 95% N and 5% H. Thermal analysis was also utilized to characterize thermal and dimensional stability.

**Investigation of the Thermodynamic Factor of Diffusion Coefficient for Lithium Ion Migration in Lithium Titanium Dioxide:** *Zheng Liang*<sup>1</sup>; Guangsha Shi<sup>1</sup>; <sup>1</sup>University of Michigan

The chemical diffusion coefficient for the Li-ion diffusion within the host crystal structure depends on the overall Li concentration. This coefficient can be factored as a product of a self-diffusion coefficient  $D^*$ , and a thermodynamic factor  $\theta$ , according to  $D = \theta D^*$ . The thermodynamic factor serves as a measure for the deviation of the Li chemical potential from thermodynamic ideality. It can be expressed as a function of Li chemical potential  $\mu$ , absolute temperature T, and Li concentration x derived from our model. Curve of  $\theta$  is plotted as a function of lithium concentration at a given temperature from numerical methods. Also, this quantity can be obtained from grand canonical monte carlo simulation as the fluctuation of the number of lithium ions within a reference volume. Both the two methods agree with each other and we can gain further information from the thermodynamic factor – Li concentration curve.

**Libyan Industrial Complex Case Study and Gear Failure:** *Ali Tajouri*<sup>1</sup>; *Mosbah Akreem*<sup>2</sup>; <sup>1</sup>Faculty of Engineering, University of Alfatah; <sup>2</sup>Libyan Industrila Research Center

Gears are the necessary parts for transmissions of power and has wide spread in various machines, such as metal cutting machines, mixers, vehicles, heavy duty machinery and lifting machines as well. The main cause and reasons of gear failures are error in design, manufacturing, and applications. This investigation considers the fracture of gear on mixer machine it cause sudden stop of main Libyan industrial complex production. Samples were tested, an interpretation of results was performed, in order to identify the cause of failure, it was found that the gear material is medium carbon steels and its selection is according to the standards. Microstructure investigation clearly indicate that hardness and materials microstructure greatly affected by heat treatment and it was performed in good manner. The main cause of this case failure is contributed to non precise gear mounting during periodical maintenance.

**Libyan Made Steels Quality and Standers:** *Ali Tajouri*<sup>1</sup>; <sup>1</sup>Faculty of Engineering, University of Alfatah

LISCO established in 1989, designed to produce 2.3 million tons liquid steel per year .Direct Reduction of iron (DRI) with Medrix process. EAF LISCO steel making utilizing the abundant supply of locally natural gas .Where Imported high quality prefluxed iron pellets is reduced .The complex produces various steel products such as Hot and Cold Rolled

Sheets. Libyan manufacturing companies uses local made sheets for different commercial use. During cutting of LISCO sheets using automatic cutter, final product was deformed. Steel samples have been subjected for chemical analysis, mechanical tests (hardness and tensile tests), heat treatment and finally microstructure was studied. The investigated samples, considered in accordance with the use for heavy duty trucks, tension and Vickers hardness testing as well. Those testing and examinations, confirm that crucial deformation problem of plate during the shaping depends mainly on the asymmetry of residual stresses, related principally to the difference of work-hardening intensity.

**Liquid Phase Sintering and Age Hardening of Different P/M Aluminum Alloys:** *Padmavathi Chandran*<sup>1</sup>; Anish Upadhyaya<sup>1</sup>; <sup>1</sup>Indian Institute of Technology, Kanpur, India

The P/M aluminum alloys offers light weight combined with excellent specific properties such as high strength, thermal stability that are attractive for structural applications in automotive and aerospace industries. The main objective of the present work is to study the sintering and age hardening of 2712 and 6711 aluminum alloys. The powders were pressed at 200 and 400 MPa followed by sintering in a range of temperature under high vacuum (10-6 torr)and nitrogen. The 6711 alloy compacts under supersolidus liquid phase sintering (SLPS) leading to better densification and mechanical properties. One striking contrast was remarkably higher ductility observed for 6711 alloy under vacuum. It interesting to note that T6 condition not only enhanced tensile strength by about 75% without any reduction in ductility. As highlighted above, the retention of ductility levels in the naturally aged 6711 alloy was noticed.

**Manufacture and Properties of Cold Spray Deposited Large Thickness Cu Coating Material for Sputtering Target:** *Jin-Hyeon Cho*<sup>1</sup>; *Young-Min Jin*<sup>1</sup>; *Dong-Yong Park*<sup>2</sup>; *Hyung-Jun Kim*<sup>3</sup>; *Ik-Hyun Oh*<sup>4</sup>; *Kee-Ahn Lee*<sup>1</sup>; <sup>1</sup>Andong National University; <sup>2</sup>Tae-Kwang Tech.; <sup>3</sup>RIST; <sup>4</sup>KITECH

This study attempted to manufacture a large thickness Cu coating layer as sputtering target material via a cold-spray coating process. The result of observation of the layer's purity and microstructure showed that a purity level (99.47%) similar to that of early powder 2N5 was maintained, and that the manufacture of cold spray deposited, a thick ~20 mm Cu coating material for sputtering target was successfully performed. As a result of EBSD mapping, the average grain size near the interface and around the center measured 1.48  $\mu\text{m}$  and 1.49  $\mu\text{m}$ ; they were small and non-uniform compared to the 1.91  $\mu\text{m}$  near the surface. Post annealing heat treatment, overall porosity declined, and grain size & texture became uniform. Based on the aforementioned findings, this study suggests that using cold-spray deposition, large thickness Cu-coating layers as sputtering target is practically applicable.[supported by "the program for the Industrial Strategic Technology Development" and "the program for the Training of Graduate Students in Regional Innovation", Korea]

**Manufacturing and Macroscopic Properties of Cold Sprayed Cu-In Coating Material for Sputtering Target:** *Kee-Ahn Lee*<sup>1</sup>; *Young-Min Jin*<sup>1</sup>; *Jin-Hyeon Cho*<sup>1</sup>; *Dong-Yong Park*<sup>2</sup>; *Ju-Ho Kim*<sup>2</sup>; <sup>1</sup>Andong National University; <sup>2</sup>Tae-Kwang Tech

This study attempted to manufacture a Cu-In coating layer via the cold spray process and to investigate the layer's applicability as a sputtering target material. To examine the microstructural and property changes made to the Cu-In coating layer and Cu coating layer (comparison material), ICP, XRD, SEM, and other tests were conducted; purity, density, hardness, porosity, and bond-strength were measured. The results showed that coating layers with thickness of 20 mm (Cu) and 810  $\mu\text{m}$  (Cu-In) could be manufactured via cold spraying under optimal process conditions. Pure Cu and intermetallic compounds of  $\text{Cu}_7\text{In}_3$  and  $\text{CuIn}_4$  were found to exist inside the layer regardless of annealing heat treatment. The Cu-In coating layer manufactured via cold spraying and annealing can be said to be applicable as sputtering target. [supported by "the program for the Industrial Strategic Technology Development" and "the program for the Training of Graduate Students in Regional Innovation", Korea]



**Measurement of Fatigue Damage in Al/Ni and TiW/Ni Metal Interconnections on Glass by Nanoindentation:** *Jae Ho Kim*<sup>1</sup>; Chul Min Joe<sup>1</sup>; Yeo Hyoun Yun<sup>1</sup>; Yong Jun Oh<sup>1</sup>; <sup>1</sup>Hanbat university

Chip-on-glass packages require highly reliable bonding of interconnect materials to glass. We performed fatigue test with two metal multilayer interconnects-Al/Ni and TiW/Ni-on glass, and evaluated the fatigue damage in the materials by nanoindentation. The Al/Ni interconnect was prepared by anodic bonding of Al to glass, Ni plating, and then patterning into lines. The TiW/Ni interconnect was prepared by TiW sputtering, Ni plating and patterning. The two types of interconnects were then subjected to three-point bending fatigue tests. The tests were interrupted at regular time intervals for the nanoindentation measurement. The Al/Ni interconnect showed greater fatigue resistance than the TiW/Ni one. From the nanoindentation measurements, the hardness and Young's modulus of both types of interconnects gradually decreased as the fatigue cycle progressed; however, the degradation was severer in the case of the TiW/Ni than the Al/Ni. The correlation between fatigue damage and indentation response was discussed in detail.

**Mechanical Performance of Tungsten Inert Gas Welded Aluminum Alloy 6061-T6:** *Daniel Steves*<sup>1</sup>; *Jahan Rasty*<sup>1</sup>; <sup>1</sup>Texas Tech University

The use of aluminum welding is used in everyday applications from manufacturing small brackets to commercial airliner fittings. Due to its light weight and resistance to corrosion, aluminum has become one of the leading materials used today. The fusion of aluminum parts by means of welding is a complex process and takes a very skilled welder to make sure the integrity of the material is not susceptible to failure. Different studies have taken place on welded aluminum, in particular type Al 6061-T6, to test whether this alloy meets the standard requirements. Researchers have conducted numerous experiments quantifying the hardness and tensile strength of the weld area, however there is very little done on time dependent trials. Because welded AA 6061-T6 ages naturally, these changes must be accounted for in cases such as static and dynamic loading conditions. These tests are required to understand the properties that welded structures take.

**Mechanical Property of In-Situ Particulate Reinforced Titanium Matrix Composites by Investment Casting:** *Bong-Jae Choi*<sup>1</sup>; *Seul Lee*<sup>1</sup>; *Jeong-Il Youn*<sup>1</sup>; *Young-Jig Kim*<sup>1</sup>; <sup>1</sup>Sungkyunkwan University

The aim of this research is to evaluate the microstructure and tensile property of in-situ (TiB+TiC) particulate reinforced titanium matrix composites (TMCs) synthesized by investment casting process. Boron carbide (1,500° and 150°) was added to the titanium matrix during vacuum induction melting which can provide the in-situ reaction of 5Ti + B4C -> 4TiB + TiC. 0.94, 1.88 and 3.76wt% of B4C were added into the melt. The phases identification of in-situ synthesized TMCs were examined using scanning electron microscopy, X-ray diffractometer, electron probe micro-analyzer and transmission electron microscopy. Tensile property of TMCs was investigated in accordance with the reinforcements size and volume fraction. The improvement of tensile property of titanium matrix composites were caused by load transfer from the titanium matrix to reinforcement and grain refinement of titanium matrix and reinforcements.

**Membranes Obtained from PA6/HDPE Blends Via Precipitation by Immersion:** *Carlos Cunha*<sup>1</sup>; *Gustavo Brito*<sup>1</sup>; *Pankaj Agrawal*<sup>1</sup>; *Helio Lira*<sup>1</sup>; *Tomas Melo*<sup>1</sup>; <sup>1</sup>Federal University of Campina Grande - UFCG

Currently the use of polymeric membranes has grown considerably, so research in this area has been following this development. Alternatives have been sought for the separation processes due to economic and environmental issues. The use of polymer blends to obtain membranes appears to be differential, since we can add features such as processing, improvement of properties and low cost. In this study, Polyamide 6 (PA6) and High Density Polyethylene (HDPE) blends in various compositions were prepared in a counter-rotating twin screw extruder at 240°C and 50 rpm. The influence of the compatibilizing agent was also investigated. To obtain the membranes, the blends were dissolved in formic acid and then immersed on a coagulant liquid for precipitation. The membranes were characterized by SEM. The results showed the characteristic pores for microfiltration process.

**Microstructural and Mechanical Performance of Cold-Rolled Al Base Alloys:** *S.R. Casolco*<sup>1</sup>; *S. Valdez*<sup>2</sup>; <sup>1</sup>ITESM-Puebla; <sup>2</sup>UNAM-ICF

The Al base alloys could be strongly influenced by the microalloying elements, modifying the microstructural and mechanical performance. An Al alloy added with zinc and silver was studied in as-cast and cold-rolled conditions by means of tensile testing machine, scanning and transmission electron microscopy. The flow stress and elongation were improved by the alloying addition, especially by the Ag content. The Ag-solute in low concentration, is homogeneously distributed in the AlZn matrix, which should contribute to increase the deformation. However, a high content of Ag decreases the solubility and precipitate as Ag<sub>2</sub>Zn<sub>3</sub>. This microstructural evolution, influenced the deformation mechanism in aluminum alloys. In addition, microstructural performance of Al base alloys added with Zn and Ag show the presence of solid solution zinc-rich hexagonal close-packed (hcp) crystal structure, named η-phase and α-Al solid solution with Zn dissolved into the matrix. The silver concentration in AlZn alloy modifies the ε-type precipitates.

**Microstructural and Mechanical Properties (Hardness) Investigations of 0.61%Al-1.11%Si Austempered Ductile Iron:** *Ali-Reza Kiani-Rashid*<sup>1</sup>; *Behdash Hashemi*<sup>1</sup>; <sup>1</sup>Ferdowsi University of Mashhad

The effect of aluminium as a strong graphitizing element is known. A lot of investigations have been made by researchers to replace silicon with aluminium in gray and ductile cast irons. The influence of aluminium in increasing the oxidation resistance at high temperatures is increasing the hardness and strength of material. So, in this research, by adding a few values of aluminium in presence of silicon, that is tried to determine the microstructure of sand mould casting samples by using optical and electron microscopes. Thus, the phase transformations are investigated by doing suitable heat treatments by austenitising at 890°C and austempering at 350, 400 and 450°C. Furthermore, hardness measurements are used for determining the mechanical properties of the material.

**Microstructural Characterization of Sintered Fe-Mn-Si Based Shape Memory Alloy Prepared Via Mechanical Alloying Technique:** *A. Umut Soyler*<sup>1</sup>; *Burak Özkal*<sup>1</sup>; *Leandru G. Bujoreanu*<sup>2</sup>; <sup>1</sup>Istanbul Technical University; <sup>2</sup>The "Gh. Asachi" Technical University

In this study, microstructural characterizations of Fe-Mn-Si based shape memory alloys fabricated via mechanically alloying and sintering were investigated. Powders were mechanically alloyed for 4 h using a Spex mixer/mill at room temperature and compacted powders were sintered at 1150 °C for 2 h under Ar atmosphere. Microstructural and phase characterizations of the sample was performed using SEM/EDS and XRD analysis. Moreover, X-ray photoelectron spectroscopy (XPS) studies were conducted in order to obtain a quantitative composition analysis with depth profiling. On the basis of the performed characterization studies, it is revealed that Fe-Mn-Si sample MA'd for 4 h has almost uniform homogeneity in its microstructure.

**Microstructural Evolution in Fe-based Oxide Dispersion Strengthened Alloys - A Computational Study:** *Samrat Choudhury*<sup>1</sup>; *Christopher Stanek*<sup>1</sup>; *Blas Uberuaga*<sup>1</sup>; <sup>1</sup>Los Alamos National Laboratory

Nanostructured ferritic alloys (NFAs) (with usual composition 12– 14 wt% Cr, 0.25 wt% Y and 0.5 wt% Ti) are considered excellent candidate materials for structural applications in nuclear reactors as they exhibit exceptionally high creep strength due to the presence of highly stable nanometer sized Y-Ti-O precipitates (NPs). Understanding the high stability of these NPs requires an investigation of the precise structure, compositions, and stages of nucleation and growth of these NPs. Experimentally it has been observed that Y<sub>2</sub>O<sub>3</sub> precipitates exhibit similar structural features as these NPs, such as formation of core-shell structures. In this work, as a first step, we will present the possibility of applying a phase-field model to understand the nucleation and growth of Y<sub>2</sub>O<sub>3</sub> precipitates under an applied stress in Fe-Cr alloys. We will also present ab-initio calculated thermokinetic parameters and diffusion coefficients of atomic species and compare them with experimental measurements wherever available.

**Microstructural Observations and Electromagnetic Interference Shielding Characteristics of Tin Based Alloy Thin Films:** Hung Fei-Yi<sup>1</sup>; Hung Fei-Shuo<sup>2</sup>; Chiang Che-Ming<sup>2</sup>; <sup>1</sup>Institute of Nanotechnology and Microsystems Engineering, Center for Micro/Nano Science and Technology, National Cheng Kung University; <sup>2</sup>Department of Architecture, National Cheng Kung University

The elements Sn, Al and Cu not only possess electromagnetic interference (EMI) shield efficiency, but also have acceptable costs. In this study, the sputtered Sn-Al thin films and Sn-Cu thin film were used to investigate the effects of the annealed, film thickness and the compounds properties on the electromagnetic interference (EMI) characteristics. The results show that Sn-xAl film increased the electromagnetic interference (EMI) shielding after annealed. For as-sputtered Sn-xCu films with higher Cu atomic concentration, the low frequency EMI shielding could not be improved. After annealing, the Sn-Cu thin film with lower Cu content possessed excellent EMI shielding at lower frequencies, but had an inverse tendency at higher frequencies. For both the Sn-xAl-0.5Ni and Sn-xCu-0.5Ni thin films, after crystallized treatment, the sputtering films had higher electric conductivity and saturation magnetization, however the EMI shielding was not enhanced completely.

**Microstructural Properties and TEM Analysis of Amorphous Reinforced Aluminum Matrix Composite by Friction Stir Processing:** Liu Peng<sup>1</sup>; <sup>1</sup>Shandong Jianzhu University

A novel aluminium matrix composite reinforced with Al-based amorphous was fabricated by friction stir processing (FSP). The hardness of composite has shown increase to a certain extent. The maximum tensile strength of composite was about 410MPa. A large number of ultrafine grained structures with size 90~400nm constitutes the composite. These ultrafine grained structures are composed of a-Al and a-Al amorphous structure. The existence of ultrafine grained structures will contribute greatly to improving the structure and properties of this composite.

**Microstructure and Properties of Laser Shock Processed Ti6Al4V, X5CrNi18-10 Steel and Pure Aluminum Materials:** Kusinski Jan<sup>1</sup>; Magdalena Rozmus-Górnikowska<sup>1</sup>; <sup>1</sup>AGH University of Sciences and Technology

The effect of the Laser Shock Processing on the microstructure and properties of Ti6Al4V, X5CrNi18-10 steel and aluminum was studied. Examination of the treated surfaces showed that the laser shock processing caused an ablation and melting of thin surface layer of all isamples. It indicates that process was not purely mechanical but thermo-mechanical. However, TEM micrographs revealed that under the thin melting layer, there were a high density of dislocations observed in the treated surface of all investigated materials. Presence of high density of dislocations, stacking faults and deformation twins testified that the laser shock processing caused sever plastic deformation of the surface layer of the investigated materials. Compressive residual stresses were measured using x-Ray diffractometry technique. The increase in hardness was observed and related to an increase in the dislocation density, microtwinning and grain refinement.

**Modeling and Experimental Activities for Heavy Castings and Forgings:** Dianzhong Li<sup>1</sup>; Mingyue Sun<sup>1</sup>; <sup>1</sup>Institute of Metal Research, Chinese Academy of Sciences

The Materials Process Modeling Division, IMR, CAS has been promoting for more than 10 years research activities on multi-scale modeling of materials for hot-processing. In the following, we highlight some selected achievements and impacts in this area: To satisfy domestic strategic requirements, such as nuclear and hydraulic power, marine projects and high speed rail, we have developed several casting and forging technologies, which combine advanced computing simulations, X-ray real time observation techniques and industrial-scaled trial experiments. These technologies have been successfully applied in various industrial areas and yielded a series of scientific and technological breakthroughs and innovation. Important examples of this strategic research include the hot-processing technologies of the Three Gorge water turbine runner, marine crankshaft manufacturers, backup rolls for hot rolling mills and the production of huge steel ingot.

**Modeling of Weld Penetration in High Velocity GTAW:** Ustun Duman<sup>1</sup>; Patricio Mendez<sup>2</sup>; <sup>1</sup>Colorado School of Mines; <sup>2</sup>University of Alberta

This work presents a scaling analysis to predict penetration depth in high current and high travel speed Gas Tungsten Arc Welding (GTAW). Scaling laws based on the governing equations of heat transfer phenomena provide closed form expressions that capture the essence of a welding process explicitly. In high productivity GTA welding, the pressure and shear stress of the plasma results in a gouging region under the welding torch. Experimental studies were performed to estimate the range of validity of the gouging penetration model using D.C. GTAW on five different metals (A36 structural steel, AISI304 stainless steel, CP Aluminum and AA5083 Aluminum alloys, and CP Titanium grade 3). The welds were generated with the bead-on-plate technique using a map of welding parameters of travel speed and current values, where travels speeds varied between 2-19 mm/s and the current values varied between 225-700A.

**Modulation of the Degree of Heterogeneity with Compositional Control and Heat Treatment in Cu-Zr-(Y, Gd)-Al Bulk-Forming Metallic Glasses:** Jin Woo Kim<sup>1</sup>; Eun Soo Park<sup>1</sup>; <sup>1</sup>Seoul National University

In the present study, we systematically explored the heterogeneity in Cu-Zr-(Y, Gd)-Al bulk-forming metallic glasses. Firstly, we will report a large amount of substitution over 15 at.% can lead to nanometer-scale phase separation in Cu-Zr-rich and Cu-(Y, Gd)-rich glass phases, which exhibit extreme brittleness. Secondly, a small amount of substitution under 5 at.% generates atomic scale heterogeneity in monolithic BMGs, which can be detected with small/wide angle X-ray scattering. In this case, the plasticity of BMGs is improved by heterogeneous viscous flow. This atomic scale local heterogeneity grows with elevating temperature and is preferentially crystallized in supercooled liquid region. The results suggest that heterogeneity in amorphous matrix can be modulated by both the optimization of tailoring combinations of constituent elements and heat treatment, which can enhance plasticity of BMGs. These concepts could prove to be useful in the design of a novel composite material with desirable properties.

**Modulus Dependence on Large Scale Porosity:** Paul Allison<sup>1</sup>; Mark Horstemeyer<sup>2</sup>; Hayley Brown<sup>2</sup>; <sup>1</sup>US Army Engineer Research and Development Center; <sup>2</sup>Mississippi State University

This work compares the existing theoretical expressions for the porosity dependence on elastic constants to experimental data for a commercially available FC-0205 powder metallurgy (PM) steel. The modulus of compression, tension, and ultrasound based data at varying porosity levels are plotted graphically against the theoretical expressions. An equation by McAdam (1950) was able to most accurately predict the experimental data with the adjustment of only one material constant.

**MWCNT Based Structures as Negative Electrodes for High Capacity Lithium Ion Batteries:** Indranil Lahiri<sup>1</sup>; Sung-Woo Oh<sup>2</sup>; Yang-Kook Sun<sup>2</sup>; Wonbong Choi<sup>1</sup>; <sup>1</sup>Florida International University; <sup>2</sup>Hanyang University

Among different varieties of rechargeable batteries, Li-ion batteries have become most popular. Despite their established market, researchers have shown great deal of interest in developing new, improved electrode materials for lithium ion batteries leading to higher specific capacity, longer cycle life and extra safety. The present study deals with development of multiwall carbon nanotubes (MWCNT) based anodes for Li-ion batteries. The novel anodes were prepared from interface-controlled MWCNTs, directly grown on copper current collectors. The anode structures have shown very high specific capacity (almost three times as that of graphite), excellent rate capability, nil capacity degradation in long-cycle operation and introduced a higher level of safety by avoiding organic binders. Enhanced properties of the anode were well related to high Li-ion intercalation on the walls of CNTs, as observed in HRTEM. These MWCNT based anode structures may be considered as best suitable materials for application as anode in Li-ion batteries.

**Nanocomposites Based on Polymer Blends: Effect of the Organoclay on the Thermo-Mechanical Properties and Morphology of PA6/HDPE and PA6/Compatibilizer/HDPE Blends:** Pankaj Agrawal<sup>1</sup>; Akidauna Oliveira<sup>1</sup>; Gustavo Brito<sup>1</sup>; Carlos Cunha<sup>1</sup>; Edcleide Araujo<sup>1</sup>; Tomas Melo<sup>1</sup>; <sup>1</sup>Federal University of Campina Grande - UFCG

The effect of the organoclay on the thermo-mechanical properties and morphology of PA6/HDPE and PA6/compatibilizer/HDPE blends was investigated. The blends and nanocomposites were prepared by extrusion followed by injection molding at 240°C and characterized by X-Ray diffraction, Thermogravimetry, mechanical properties and Scanning Electron Microscopy. The results showed that when the organoclay was added to PA6/HDPE blend, the clay peaks were shifted to lower 2θ angles indicating that the polymers were intercalated between the clay platelets. When the organoclay was added to PA6/compatibilizer/HDPE blend, the clay peaks almost disappeared, indicating that an exfoliated structure was formed. The organoclay decreased the thermal stability of PA6/HDPE blend and has little effect on that of PA6/compatibilizer/HDPE blend. The addition of the clay increased the modulus and decreased the impact strength of the blends. The presence of the clay decreased the HDPE particles size on PA6/HDPE blend and changed the morphology of PA6/compatibilizer/HDPE blend.

**Al<sub>2</sub>O<sub>3</sub>/Al<sub>2</sub>O<sub>3</sub> Nanoparticles with Perfect Catalytic Activity:** S. F. Rahnemaye Rahsepar<sup>1</sup>; H. Dastjerd<sup>2</sup>; E. Zahrani<sup>2</sup>; <sup>1</sup>Islamic Azad University, Shareza; <sup>2</sup>Isfahan University of Technology

Steam reforming of methane was carried out to make synthesis gas and hydrogen on the NiAl<sub>2</sub>O<sub>4</sub>/Al<sub>2</sub>O<sub>3</sub> catalysts with perfect activity. The experimental results indicated that the modification of impregnation samples at various calcination temperatures led to the formation of nanoparticles of NiAl<sub>2</sub>O<sub>4</sub>/Al<sub>2</sub>O<sub>3</sub>. It means that NiO with Al<sub>2</sub>O<sub>3</sub> could be transformed into the surface spinel structure of nickel aluminate during heat treatment at high temperature, which was confirmed by TPR, XRD and TG/DTA patterns. The TG/DTA measurements showed thermal decomposition was a three-step process with crystallization of the spinel phase started at a temperature 443°C. The nanoparticles' size was calculated from the line broadening of X-ray diffraction peaks, they are between 5.7-8.4 nm. These results were confirmed by SEM and TEM. The NiAl<sub>2</sub>O<sub>4</sub>/Al<sub>2</sub>O<sub>3</sub> catalysts had high conversions and selectivity for SRM reaction. This is due to structural surface properties of NiAl<sub>2</sub>O<sub>4</sub> and the ability to reduce of the carbon deposition.

**Nondestructive Characterization of Railway Bogies Using Infrared Thermography Technique:** Jeongguk Kim<sup>1</sup>; <sup>1</sup>Korea Railroad Research Institute

The railway bogies are composed of weldments with reinforced materials. Therefore, the nondestructive inspection of the weldments is required for the integrity of railway bogies. In this paper, the railway bogies were nondestructively characterized using the infrared thermography technique. The thermographic detection of the weldments of bogies was performed using the lock-in thermography method with an infrared camera. Through lock-in thermography, the optimal frequency of heat source was determined for the best flaw detection. In this investigation, the lock-in thermography was employed to develop a nondestructive evaluation tool for the detection of flaws in railway bogies. Moreover, the nondestructive evaluation results for railway bogies have been presented.

**Optical Properties and Electrical Properties of Transparent Conductive Films of Magnesium Hydroxide Based Compounds:** Masafumi Chiba<sup>1</sup>; Mikiteru Higashi<sup>1</sup>; Hideo Kiyota<sup>1</sup>; Mikihiko Maizono<sup>1</sup>; Toshiro Kuji<sup>1</sup>; <sup>1</sup>Tokai University

Indium oxide doped with tin oxide, or ITO, has been widely used as an electrode material for flat panel displays. However, the rare metal in ITO is a limited natural resource. We succeeded in developing a material composed solely of elements with abundant reserves. We would like to present the results of analyzing the optical properties and the electronic structure of an Mg-based compound films based on its electrical conductivity. On average, its transmittance of visible light was 90%. The structures were observed by X-ray photoelectron spectroscopy (XPS). In addition, a comparison between the calculated electronic state around the valence band and

the result measured by XPS of the obtained film reveals that they are in extremely close agreement. Part of this work was supported by Grant-in-Aid for Challenging Exploratory Research (22656076) of Japan Society for the Promotion of Science.

**Oxidation Behavior of Spark Plasma Sintered ZrB<sub>2</sub>-SiC Composites:** Ipek Akin<sup>1</sup>; Filiz Sahin<sup>1</sup>; Onuralp Yuce<sup>1</sup>; Gultekin Goller<sup>1</sup>; <sup>1</sup>Istanbul Technical University

ZrB<sub>2</sub>-SiC composites containing 40 and 60 mass% SiC were prepared by spark plasma sintering (SPS) at 1770°C for 300 s under a pressure of 40 MPa. Oxidation behavior of these samples was characterized by exposing them to 1400, 1500, and 1600°C in an ambient atmosphere for 180 min, and by measuring the weight gains of the sample. The oxide layers were characterized by field emission scanning electron microscopy with energy dispersive spectroscopy analysis. At 1400 and 1500°C, layered structures consisted of a SiO<sub>2</sub> rich outer layer, a thin ZrO<sub>2</sub>-SiO<sub>2</sub> layer, ZrO<sub>2</sub>-containing layer and unaffected ZrB<sub>2</sub>-SiC. However, at 1600°C, active oxidation of SiC was observed and changed oxidation mechanism significantly. The consumption of SiC particles resulted in a formation of oxide regions mainly composed of SiO or SiO<sub>2</sub> and ZrO<sub>2</sub>. Unaffected ZrB<sub>2</sub>-SiC region was not observed at 1600°C.

**Phase Change Materials in Thermal Energy Storage for Concentrating Solar Power (CSP):** Corey Hardin<sup>1</sup>; Anoop Mathur<sup>2</sup>; Rajan Kasetty<sup>2</sup>; Chris Dames<sup>1</sup>; Reza Abbaschian<sup>1</sup>; Javier Garay<sup>1</sup>; <sup>1</sup>UC Riverside; <sup>2</sup>Terrafore Inc.

States of the art concentrating solar power (CSP) plants use molten inorganic salts for thermal energy storage (TES). Utilizing latent heat storage in addition to sensible heat storage systems can potentially result in a 30% reduction in amount of molten salt, 60% reduction in container size, and a 2-3% improvement in overall system efficiency. One of the main issues with using phase change materials is that solidification often reduces total heat transfer, reducing the efficiency of the storage system. The natural affinity of the salt is to solidify onto the cold heat exchanger tubes and even a very thin layer of this solid on the heat exchanger can lead to an order of magnitude drop in heat transfer. By analyzing surface energies and nucleating agents solid accumulation in the heat exchanger can be prevented. Results from these analysis and experimental data will be presented.

**Phase Diagram Calculation and Its Applications to Materials Design and Development:** Fan Zhang<sup>1</sup>; Weisheng Cao<sup>1</sup>; Shuanglin Chen<sup>1</sup>; Y. Austin Chang<sup>1</sup>; <sup>1</sup>CompuTherm, LLC

Phase diagrams are the road maps for materials scientists and engineers in materials design and process optimization. Traditionally, phase diagrams were determined primarily by meticulous and costly experiments. Nowadays, complex multi-component, multi-phase equilibria can be calculated by the CALPHAD approach. Moreover, this approach has in recent years been applied to a broader field of materials science and engineering beyond phase diagrams, such as solidification, coating, joining, and phase transformation. It has therefore become increasingly important in materials design and development and process optimization. In this presentation, I will use examples to demonstrate how phase diagram calculation can be integrated with key experiments in accelerating materials design and development. I will also demonstrate that the applications of this approach can be further extended by integrating it with kinetic models and microstructural models for the prediction of phase transformations and microstructure evolution of multi-component alloys.

**Phase Transformation and Magnetic Properties of Pr<sub>2</sub>Co<sub>7</sub> Intermetallics:** Najeh Mliki<sup>1</sup>; Riadh Fersi<sup>2</sup>; Lotfi Bessais<sup>3</sup>; <sup>1</sup>LMOP, Faculté des Sciences de Tunis; <sup>2</sup>(1) LMOP, Faculté des Sciences de Tunis, (2) CMTR, ICMPE, UMR7182; <sup>3</sup>CMTR, ICMPE, UMR7182, CNRS-UPEC

Pr<sub>2</sub>Co<sub>7</sub> alloys with high coercivity were synthesized by mechanical alloying and subsequent annealing. X-ray diffraction analysis by Rietveld method was used to determine their structure and lattice constants. The crystallization, phase components and magnetic properties of the alloys were investigated systematically. For samples annealed at TA= 800°C, the main phase of those alloys is hexagonal of the Ce<sub>2</sub>Ni<sub>7</sub> type structure whereas at



TA= 1050°C, the main one is rhombohedral of the Gd<sub>2</sub>Co<sub>7</sub> type structure. The coercivity increases with annealing temperature reaching a maximum for TA =800°C. The highest is equal to 18 kOe at 293K and 23 kOe at 10K. This leads to the formation of a magnetically hard Pr<sub>2</sub>Co<sub>7</sub> phase. This high coercivity is attributed to the high anisotropy field of the Pr<sub>2</sub>Co<sub>7</sub> phase and its nanoscale grain size. Its Curie temperature is about 600K.

**Prediction of Hexagonal Lattice Parameters of Non-Stoichiometric Apatites by Artificial Neural Networks:** *Zafer Evis*<sup>1</sup>; *Umit Kockan*<sup>1</sup>; *Midde East Technical University*

Hexagonal lattice parameters and unit cell volumes of non-stoichiometric apatites (A<sub>10</sub>(BO<sub>4</sub>)<sub>6</sub>C<sub>2</sub>), were predicted from their ionic radii by artificial neural networks. Multilayer perceptron network was used for training. Best results were obtained with Bayesian regularization method with four neurons in the hidden layer with 'tansig' activation function and one neuron in the output layer with 'purelin' function. Errors of lattice parameters for the predicted data with approximate formulas were less than 1% for a and 2% for c. Non-stoichiometric apatites with exact formulas generated up to around 3% errors for both lattice parameters because of their complex B sites.

**Preparation and Current Distribution Performance of Pb-Al Layered Composite Anode Materials:** *Shenggang Zhou*<sup>1</sup>; *Peixian Zhu*<sup>1</sup>; *Yong Sun*<sup>1</sup>; *Lida Sun*<sup>2</sup>; *Kunming University of Science and Technology*; *Honghe University*

Taking Sn as the third element in the Pb-Al immiscible system, the Al-Sn-Pb layered composite materials at different temperatures were prepared by solid-liquid coating method. Microstructure of the layered composite materials was studied by scanning electron microscope (SEM) and Energy Dispersive Spectrometer (EDS), and then the current distribution performance as the anode material for zinc electrowinning in ZnSO<sub>4</sub>-MnSO<sub>4</sub>-H<sub>2</sub>SO<sub>4</sub> system was characterized by electric analysis module of ANSYS program. The results showed that, introducing of Sn reduced the enthalpy heat of mixing of Pb-Al system to be negative, and inter-diffusion of elements in the interface region occurred, and a metallurgical bonding interface between Pb and Al formed. Compared with the traditional Pb alloy anode, the Pb-Al layered composite anode showed a more uniform current distribution performance.

**Preparation and Electrochemical Properties of Nanostructured Lithium Manganese Oxide Based Cathode Particles:** *Burcak Ebin*<sup>1</sup>; *Sebahattin Gurmen*<sup>1</sup>; *Cuneyt Arslan*<sup>1</sup>; *Istanbul Technical University*

Novel lithium-ion battery cathode materials based on layered manganese oxides was developed by a single step fabrication process. In this research, carbon / lithium manganese oxide nanocomposite particles were prepared by ultrasonic spray pyrolysis method from the stoichiometrically dissolved tartaric acid, lithium and manganese nitrate. It is intended to improve the cycling performance of the cathode materials by decreasing particle size and increasing electrical conductivity by carbon addition to the structure. The particle morphology, size, crystallinity and chemical composition were investigated by field emission scanning electron microscopy (FE-SEM), X-ray diffraction (XRD) and energy dispersive spectroscopy (EDS). Analyses show that porous submicron particles obtained by nanoparticles with graphite and cubic crystalline structured lithium manganese oxide was successfully fabricated. Electrochemical measurement demonstrated that cells containing carbon / lithium manganese oxide nanocomposite particles could improve capacity and cycling stability of the battery.

**Preparation of (Ti<sub>0.8</sub>Mo<sub>0.2</sub>)C-Ni Cermets by Mechanical Alloying:** *Hiroyuki Hosokawa*<sup>1</sup>; *Kiyotaka Kato*<sup>1</sup>; *Koji Shimojima*<sup>1</sup>; *Akihiro Matsumoto*<sup>1</sup>; *National Institute of Advanced Industrial Science and Technology*

The microstructural evolution of (Ti<sub>0.8</sub>Mo<sub>0.2</sub>)C-Ni powders by mechanical alloying of pure titanium, nickel, carbon and molybdenum as starting powder were investigated by both X-ray diffraction (XRD) using CuK $\alpha$  radiation and electron microscopy with energy-dispersive X-ray spectroscopy (EDS). The powders were mixed gradually and the size of the mechanically alloyed particles was submicrometer order. The C peak, the Ni peaks and the Mo peaks disappeared and the TiC peaks appeared after several hundred hour

milling time. The peaks of the TiC structure in this work showed a trend toward higher angles, compared with the referenced TiC peaks. The particles consisted of nano ordered grains. The nickel might be transformed from crystallized phase into an amorphous phase by mechanical alloying.

**Probing Li-Ni Cation Disorder in Li<sub>1-x</sub>Ni<sub>1+x-y</sub>Al<sub>y</sub>O<sub>2</sub> Cathode Materials by Neutron Diffraction:** *Lu Cai*<sup>1</sup>; *Zengcai Liu*<sup>1</sup>; *Ke An*<sup>1</sup>; *Chengdu Liang*<sup>1</sup>; *Xun-Li Wang*<sup>1</sup>; *Oak Ridge National Laboratory*

The power of neutron diffraction to detect lithium and its ability of differentiating cations enables the probing of cation disorder in cathode materials of lithium-ion batteries. We will present the research on probing the cation mixing of LiNiO<sub>2</sub> with and without Al<sup>3+</sup> substitution. LiNi<sup>3+</sup>O<sub>2</sub> is an attractive cathode material, but the cycling properties has been greatly depressed by the Ni<sup>2+</sup> entering into Li<sup>+</sup> sites. Al<sup>3+</sup> substitution of Ni<sup>3+</sup> stabilizes the structure of lithium nickelate (LiNi<sub>1-y</sub>Al<sub>y</sub>O<sub>2</sub>) and reduces the formation of Ni<sup>2+</sup>, therefore mitigating the migration of Ni<sup>2+</sup> into the Li<sup>+</sup> sites. The Rietveld refinement of the powder neutron diffraction patterns will be used to determine the cation disorder of Li and Ni in samples synthesized at different conditions. The correlation of structure with synthesis conditions will be discussed in details. We expect the results will provide guidance on the development of new materials to meet the needs of lithium-ion batteries.

**Process Modeling and Reduction of Copper Loss in Smelting Slag:** *Pengfu Tan*<sup>1</sup>; *Xstrata Copper*

A series of technical improvements have been implemented to address the issue of high copper losses in Rotary Holding Furnace (RHF) slag, which experienced in Xstrata Copper Smelter at Mount Isa in 2007 and 2008. The copper losses in RHF slag was more than 3% in 2006 and 2007. The thermodynamic models, viscosity model have been applied in the operation of Xstrata Copper Smelter in Mount Isa. The theory of RHF KPIs has also been developed to reduce the copper losses in RHF slag. The RHF KPIs Theory has been applied in Mount Isa Copper Smelter. The copper losses in RHF slag have been dropped from 3.1% in 2007 to 0.76% in Apr 2009. The average copper loss in RHF slag in 2009 and 2010 is about 0.9%.

**Processing of Multifunctional Oxides for Photonic Applications:** *Elias Penilla*<sup>1</sup>; *Javier Garay*<sup>1</sup>; *UC Riverside*

Polycrystalline ceramics are desired materials for applications in demanding environments because they offer high hardness, high melting points and chemical stability. Moreover, their development as transparent materials has seen a recent resurgence in activity due to their viability as optical-structural materials as well as for light emitting applications such as laser host materials. We report the development of a novel processing procedure for the derivation of bulk nanocrystalline yttrium aluminum garnet (YAG) and neodymium-doped YAG optically transparent ceramics via a reactive-CAPAD approach. We have investigated the effects of processing temperature, and pressure on the resultant sample density, densification rate, microstructure, and ultimately on the resultant optical properties, e.g. transmission, reflectance, absorbance, etc.

**Reactive Sintering Behaviors of the Formation of ZrC in Tungsten Matrix Composites:** *Tae-Woo Kang*<sup>1</sup>; *Hyun-Joo Choi*<sup>1</sup>; *Dong-Hyun Bae*<sup>1</sup>; *Yonsei University*

Dense ZrC/W composites have been fabricated by sintering the ball-milled mixture of W powders, MWNTs and Zr<sub>2</sub>Cu powders at 1400°C. While the milling process, Zr<sub>2</sub>Cu powders are effectively dispersed in MWNTs embedded W powders. During the subsequent sintering process, at first, WC particles are formed by decomposition and reaction of carbon atoms in MWNTs. Secondly, Zr<sub>2</sub>Cu particles react with newly formed WC particles resulting in the uniform dispersion of ZrC particles in W matrix. Hardness of the composite increase with increasing volume fraction of MWNTs and Zr<sub>2</sub>Cu, exhibiting more than two times enhanced hardness, as compared to that of pure W. Mechanical properties, according to the process variables, such as particle morphology, volume fraction, milling condition, sintering temperature and time, will be presented.

**Research on the Carbothermic Reduction Conditions of Mill Scale from Continuous Casting Processes:** *Fahri Demirci*<sup>1</sup>; *Onuralp Yucel*<sup>1</sup>; <sup>1</sup>Istanbul Technical University

This study concerns itself with the carbothermic reduction of mill scale, which is an iron oxide layer that forms on the surface of materials subjected to hot rolling or continuous casting. The mill scale is pelletized before undergoing reduction in a rotary kiln. The final product is direct reduced iron pellets with different amounts of metallic iron. Chemical and XRD analyses are carried out on samples obtained at different periods of time during the reaction. The effect of temperature, reductant type and amount of reductant is investigated by comparing the results reached by performing experiments with different parameters. Metallization degree, which is the ratio of metallic iron to total iron, and phase structure of the samples provide the necessary data to determine the effect of the parameters. It was found out that different types of reductants offered different temperature and stoichiometry dependency with regards to the reduction potential they provide.

**Separation of Antimony from a Stibnite Concentrate through a Low-Temperature Smelting Process to Eliminate SO<sub>2</sub> Emission:** *Yang Jian-guang*<sup>1</sup>; *Tang Chao-bo*<sup>1</sup>; <sup>1</sup>Central South University

The main purpose of this study is to characterize and separate antimony from a stibnite concentrate through a low-temperature sulfur-fixing smelting process. This paper reports on a study conducted on optimization of process parameters, such as flux and zinc oxide weight percentage, in charging, smelting temperature, smelting duration on the antimony yield, resultant crude antimony grade, and sulfur fixing rate. A maximum antimony recovery of 97.07%, crude antimony grade of 96.45%, and 98.61% sulfur fixing rate are obtained when a charge is smelted at 880°C for 120 minutes. This smelting operation is free from atmospheric pollution because zinc oxide is used as the sulfur fixing agent. Based on the results of the chemical content analysis of as-resultant zinc sulfide, more than 90% zinc sulfide can be recovered, and the recovered zinc sulfide grade can reach 66.7%.

**Simultaneous Heat and Moisture Transfer and Shrinkage during Drying of Ceramic Materials:** *José Nascimento*<sup>1</sup>; *Ariosvaldo Sobrinho*<sup>1</sup>; *Luiz Pontes*<sup>2</sup>; *Marcos Baracho*<sup>1</sup>; <sup>1</sup>UAEMA / UFCG; <sup>2</sup>UFPP

The ceramic industry presents industrial processes with a large consumption of energy and high environmental impact. These industries are developing products of low quality due to inadequate drying and firing processes. Therefore, the purpose of this study is to contribute for the improvement of drying process by presenting a drying experimental study of the samples of clay for red ceramics (hollow and solid bricks), with different dimensions and initial moisture contents. In the drying processes, several air temperatures and air relative humidity were used, and thus several curves of the drying kinetics and volumetric retraction are shown and analyzed. Mathematical equations for predict lost of water and dimension variations during the process were obtained. It was verified that drying process takes place in the falling rate period and shrinkage happens in two distinct periods.

**Simultaneous Recovery of Valuable Metals from Wastes with Reducing Metal Bath Technologies:** *Juergen Antrekowitsch*<sup>1</sup>; *Stefan Steinlechner*<sup>1</sup>; *Thomas Griessacher*<sup>1</sup>; <sup>1</sup>University of Leoben

Heavy metal containing wastes from metallurgical industry today generally offer more than one valuable metal to recover. To make a simultaneous recovery possible from the technical and economical point of view, special technologies have to be developed mainly based on metal bath technologies. Such processes, tending to be zero waste solutions, are evaluated by their mass and energy balances. Furthermore typical difficulties and limits for an feasible processing are discussed within the paper. Especially zinc containing wastes are investigated which offer the special situation that valuable products can be recovered in the metal bath and in the off gas. First of all the amount of energy necessary for such a combined recycling of metals are an indication for their feasibility in future. Beside this some results of lab-scale investigations are described, showing first experiences concerning possible yields and product qualities for some selected residues treated with the mentioned processes.

**Spatially-Correlated Microstructural Characterization: From Centimeters to Nanometers:** *Dawn Janney*<sup>1</sup>; *Timothy McJunkin*<sup>1</sup>; *Tammy Trowbridge*<sup>1</sup>; *Jill Scott*<sup>1</sup>; <sup>1</sup>Idaho National Laboratory

The Idaho National Laboratory uses a variety of analytical instruments to characterize the chemistry, crystal structures, and microstructures in nuclear and other solid materials. With recent procurement of micro-X-ray diffractometer (MXRD) and focused ion beam (FIB) instruments it is possible in principle to analyze exactly the same volume of material on spatial scales spanning seven orders of magnitude (centimeters to nanometers). In practice, however, each instrument is operated independently, and it is difficult to ensure that each instrument collects data from the same area or to correlate data from the same area collected by different instruments. This presentation describes recently developed techniques for correlating data from instruments including scanning electron microscopes and an X-ray micro-focus diffractometer with video camera.

**Study of Dislocation Density Field and Local Elastic Strain around the Triple Junction:** *Samikshya Subedi*<sup>1</sup>; *Brent Adams*<sup>1</sup>; *Sadegh Ahmadi*<sup>1</sup>; <sup>1</sup>Brigham Young University

In this poster, measurement of dislocation density and local elastic strain is demonstrated using High resolution electron backscatter diffraction (HR-EBSD) technique. A large grain (average of 3mm) columnar iron sample having three grains and a triple junction within the gage section was prepared, decorated with four platinum-based fiducial markers. Cross correlation of the fiducials before and after the load gives the measure of macroscopic strain within the material. In order to find the local elastic strain the simulated pattern method is applied, where strain-free reference patterns are compared with experimental patterns, recovering strain by cross-correlating selected regions of interest within the EBSD patterns. Local elastic strain and dislocation density is recovered at each scan point. These data are presented as fields on the microstructure geometry.

**Study on Microstructure and Mechanical Properties of Ti-Nb-(Zr, Mo)-CPP Composites Consolidated by Spark Plasma Sintering:** *Kee-Do Woo*<sup>1</sup>; *Duck-Soo Kang*<sup>1</sup>; *Sang-Hyuck Kim*<sup>1</sup>; *Sang-Hoon Park*<sup>1</sup>; *Ji-Young Kim*<sup>1</sup>; <sup>1</sup>Chonbuk National University

Ti and its alloys such as Ti-6Al-4V alloy have been widely used for biomaterials due to their excellent biocompatibility, low density, excellent corrosion resistance and good balance of mechanical properties. However, some problems of Al and V, which are contained in mostly used Ti-6Al-4V have been reported. Calcium phosphate (CPP) materials have gained clinical acceptance for bone substitution because of their similarity to the mineral part of bone and their recognized biocompatibility. The aim of this study is to fabricate superior biocompatible Ti-Nb-(Zr, Mo)-CPP composites using SPS. Microstructure and phase composition of Ti-Nb-(Zr, Mo)-CPP composites were investigated by scanning electron microscopy (SEM) and X-ray diffractometer (XRD). Wear behavior, strength and corrosion resistance of the sintered Ti-Nb-(Zr, Mo)-CPP composites and Ti-6Al-4V ELI alloy have been observed.

**Study on Preparation of ZnO/TiO<sub>2</sub> and Its Photocatalytic Activity:** *Wu Daoxin*<sup>1</sup>; <sup>1</sup>Changsha University of Science and Technology

With Ti(C<sub>4</sub>H<sub>9</sub>O)<sub>4</sub> and Zn(Ac)<sub>2</sub>•2H<sub>2</sub>O used as raw materials, oxalic acid as the complexing agent and anhydrous ethanol as solvent, the ZnO/TiO<sub>2</sub> photocatalytic nanocomposite materials was prepared by Sol-gel method and characterized by XRD, DRS and FS, and catalyst for photodegradation experiments. The results showed a good absorption performance of ZnO/TiO<sub>2</sub> when TiO<sub>2</sub> composite was 40% (mole fraction), calcination temperature was 400°C, which indicated that red shift occurred. With sunlight as the light source, pH=5.0, catalyst concentration was 1.0mg.L<sup>-1</sup>, concentration of methyl orange was 5.0mg.L<sup>-1</sup>. The result showed that ZnO/TiO<sub>2</sub> powders(40%, 400°C) had the most photodegradation efficiency, and the degradation efficiency of 96.5% after 4 hours.

**Study on Reactor Selecting with Indigestible Ore and Suspension Digestion:** *Cao Wenzhong*<sup>1</sup>; Tian Weiwei<sup>1</sup>; Wang Lei<sup>1</sup>; Zhong Hong<sup>1</sup>; <sup>1</sup>Environmental and chemical engineering institute, Nanchang university

Suspension digestion of bauxite, digestion equipment and new technology have been studied. In the vertical reactor system, the experimental particle size range of criteria was determined by the flow pattern around the particles, so that velocity of suspended particles in the slurry was calculated more simply and accurately. The flow mechanism of suspended mineral particles and digestion kinetics were investigated in laboratory. That predicted design parameters of the bauxite digestion. The results show that digestion of diasporic bauxite. Bayer alumina process should adopt the suspended digestion process. Key words: suspension digestion, design parameters, Indigestible ore, suspension velocity

**Study on the Characteristic of Crystalline Silicon Solar Cells:** Teresa Oh<sup>1</sup>; Gil Jae Jung<sup>2</sup>; *Jae Jun Lee*<sup>2</sup>; <sup>1</sup>Cheongju University; <sup>2</sup>Young Sung Middle School

In recent years, the problem of silicon feedstock shortage is a major concern for most solar cell manufacturers. One of the solutions is to realize a high output conversion efficiency and low processing cost. Material costs account for about half the price of energy generated by a solar module built according to the current industrial technologies. From the electronics point of view, the same efficiency could be achieved by thin films of semiconductor supported by inexpensive substrates, thereby reducing the cost per kilowatt. In this study, the phosphorus oxychloride for n+ type doping were diffused on a p+ Si, SiC and poly Si using the carrier gas of N<sub>2</sub> by LPCVD. Recombination losses are related to the metal to semiconductor contact areas and the series resistance losses are due to the resistance contributed by the metal fingers, metal to semiconductor contact resistance, bus bar and emitter region.

**Study on the Interface Behavior of Ore Powder in Organic Media:** *Li Dan*<sup>1</sup>; <sup>1</sup>Central South University

In this paper, the interface behavior of pyrite powders dispersed in acetone, chloroform, cyclohexane, cyclohexanol, toluene, tetrahydrofuran, sodium dodecyl sulfate with n-dodecanethiol as modifier was studied. The dispersion nature of pyrite powder is also investigated in solvents through ultraviolet spectroscopy, oscillation, scanning electron microscopy, and electron spin resonance method. Ultraviolet spectrum analysis illustrates the sequence of dispersion as: sodium dodecyl sulfate > tetrahydrofuran > cyclohexanol > cyclohexane > toluene > acetone > chloroform. Dispersion property of powder were measured with Oscillation method. It was found that the dispersion properting of modified pyrite powder is better than that of the unmodified powders. The smaller the particle size the better the dispersion. Powder's particle SEM morphology shows that the particles of pyrite modified with sodium dodecyl sulfate are uniform and agglomeration of particles is not obvious. Surface activity of powder modified with n-dodecanethiol surfactant is large. Pyrite powders are more easily dispersed in other organic solvents.

**Study on the Microstructure Evolution of Fe-6.5wt.%Si Powders Fabricated by High Pressure Gas Atomization:** *Liang Zhu*<sup>1</sup>; Kefeng Li<sup>1</sup>; Yuanyi Guo<sup>1</sup>; Changjiang Song<sup>1</sup>; Qijie Zhai<sup>1</sup>; <sup>1</sup>Shanghai Key Laboratory of Modern Metallurgy & Materials Processing

Silicon steel with 6.5wt.%Si have a great potential application in electric fields because of good properties such as high permeability, high electric resistivity, and low anisotropy. However, due to the brittleness of high silicon Fe-Si alloy, the silicon content is generally less than 3.5wt.% for the conventional silicon steel. In this paper, high pressure gas atomization technology was used to produce Fe-6.5wt.%Si powders so as to obtain desired components by powder compacting. During atomization process, the size of atomized droplets is in a wide range. The specific surface area of the droplet would be sharply changed with the change of droplet diameter, which results in significant difference of heat transfer and cooling rate. This paper mainly studied the microstructure evolution of Fe-6.5wt.% Si powders with the change of powder size. At last, the microstructure forming course was theoretically analyzed.

**Study on the Photocatalytic Oxidation of Water Splitting Over W<sup>6+</sup>-Dopant of Rutile TiO<sub>2</sub>:** Wu Daoxin<sup>1</sup>; *Yin Zhoulan*<sup>1</sup>; <sup>1</sup>Central South University

In this paper, W<sup>6+</sup>-doping rutile titania were prepared by low temperature hydrolysis using Tetrabutyl titanate (C<sub>16</sub>H<sub>36</sub>O<sub>4</sub>Ti) as raw material. Powers were characterized by XRD,DRS,PL,BET. The photocatalytic activity of W<sup>6+</sup>-dopant of r-TiO<sub>2</sub> was investigated with Fe<sup>3+</sup> as electron acceptor at pH=2.0 under 365nm UV irradiation. The O<sub>2</sub> production rate reached 480μmol.L<sup>-1</sup>h<sup>-1</sup>. Results show that rutile titania were finally transformed at sintering temperature 850°. The photocatalytic activity of W<sup>6+</sup>-doping rutile titania increases with higher photoluminescence performance and photo absorption. The photoinduced electrons are easily captured by oxygen vacancy so that the recombination of photoinduced electron and hole pairs is effectively inhibited. These are responsible for the enhancement in the photocatalytic activity.

**Study on Thermal Decomposition of Precursor of Nb<sup>5+</sup> Doped Rutile TiO<sub>2</sub> Treated by Ultrasonic:** *Wu Daoxin*<sup>1</sup>; <sup>1</sup>Changsha University of Science and Technology

In many applications, anatase TiO<sub>2</sub> powders consisting of particles with a large surface area are used as the photocatalysts. In contrast to these compounds, oxidation of water efficiently proceeds on large rutile TiO<sub>2</sub> particles. The thermal decomposition behavior of precursor of Nb<sup>5+</sup> doped rutile TiO<sub>2</sub> were prepared by sol-gel method. With ultrasonic treatment of 100W and 30min were investigated in TG-DSC, XRD, SEM and DRS. It has been shown that Ultrasonic treatment could be made use of the phase transition. Ultrasonic treatment could facilitate the growing of crystal. Ultrasonic-treated doped TiO<sub>2</sub> phase transformation from anatase to rutile at 400°~500°, which was 100° lower than untreated ones. The absorbing performance of Nb<sup>5+</sup> doped rutile TiO<sub>2</sub> powders treated by ultrasonic was better than that of without treatment while wavelength above 400nm. The ultrasonic treatment could also lead to the decrease of catalyst size. The doped catalysts will have been shown better catalytic activity.

**Synthesis and Characterization of Flame Retarding UV-Curable Boron Containing Hybrid Coatings:** *Bihter Zeytuncu*<sup>1</sup>; *Vezir Kahraman*<sup>2</sup>; *Onuralp Yucel*<sup>1</sup>; <sup>1</sup>Istanbul Technical University; <sup>2</sup>Marmara University

A series of UV-curable boron containing hybrid coatings were prepared by anhydrous sol-gel technique. The chemical structure of hybrid coatings was characterized by FT-IR, RT-IR, 1H-NMR and 29Si-CP MAS-NMR techniques. UV curable coatings were applied on polycarbonate substrates. The physical and mechanical properties of UV-cured coatings such as pendulum hardness, pencil hardness, contact angle, gel content, MEK rubbing test, tensile test, abrasion resistance, chemical resistance, flame retardant, anti-stain and gloss were examined. Thermal gravimetric analysis (TGA) was made. Results of all analysis conducted on free films and coatings were discussed. The morphology of the hybrid materials was examined by SEM. The hybrids were nanocomposites.

**Synthesis of Nanocrystalline Cu<sub>3</sub>B<sub>2</sub>O<sub>6</sub> Particles by Ultrasonic Spray Pyrolysis Method:** *Burcak Ebin*<sup>1</sup>; *Sebahattin Gurmen*<sup>1</sup>; *Cuneyt Arslan*<sup>1</sup>; <sup>1</sup>Istanbul Technical University

The copper boron oxide (Cu<sub>3</sub>B<sub>2</sub>O<sub>6</sub>) attracts great attention due to the combination of its structural and unique physicochemical properties such as high thermal and chemical stability. The other interesting behaviors of the Cu<sub>3</sub>B<sub>2</sub>O<sub>6</sub> structure are its antiferromagnetism, non-toxicity and hydrophobic properties, which allow it several potential applications. In this research, nanocrystalline Cu<sub>3</sub>B<sub>2</sub>O<sub>6</sub> particles were produced by ultrasonic spray pyrolysis (USP) method using aqueous solution of copper nitrate and boric acid in desired concentration. Particles obtained thermal decomposition of precursor under constant air flow rate at 1000°C furnace temperature. Then samples were structurally characterized by X-ray diffraction (XRD), scanning electron microscope (SEM) and energy dispersive spectroscopy (EDS). The results show that nanocrystalline Cu<sub>3</sub>B<sub>2</sub>O<sub>6</sub> particles in nearly spherical morphology were prepared successfully. Also, XRD analysis reveals that obtained Cu<sub>3</sub>B<sub>2</sub>O<sub>6</sub> particles have an orthorhombic crystal structure and their crystalline size are nearly 29 nm, which are calculated by Scherrer equation.



**Technical Developments and Improvements in Xstrata Copper Smelter in Australia:** Pengfu Tan<sup>1</sup>; <sup>1</sup>Xstrata Copper

Xstrata Copper Smelter at Mount Isa in Australia has operated one copper Isasmelt furnace, two Rotary Holding Furnaces (RHF), four Peirce-Smith P-S converters, two anode furnaces, one casting wheel, slag crushing and screening plant, and ESP dust recovery plant. Some recent technical developments and improvements have been presented and discussed in this paper. Those improvements include: development of smelting and converting process models, slag chemistry models and slag viscosity model; reduction of copper loss in RHF slag; reduction of converter foamover frequency; improvement of yields and throughput; ESP dust recovery plant trials, lab tests, commissioning and operations; and improvement of Isasmelt brick campaign life.

**Texture Evolution during Annealing on a Hot Rolled AISI 310 Austenitic Stainless Steel:** Jesús Sandoval<sup>1</sup>; Maribel De la Garza<sup>1</sup>; Rafael Colás<sup>1</sup>; Víctor Páramo<sup>2</sup>; Adriana Salas<sup>1</sup>; Martha Guerrero<sup>1</sup>; Ivan Houbaert<sup>3</sup>; <sup>1</sup>Universidad Autónoma de Nuevo León; <sup>2</sup>Frisa Aerospace S.A. de C.V.; <sup>3</sup>Ghent University

This work presents the study of the texture evolution during annealing on a hot rolled AISI 310 austenitic stainless steel. As received, the material presented the typical hot rolling texture components with similar intensities; however in the annealed samples, the major texture components are concentrated on the  $\beta$  fiber, primarily the Brass  $\{110\}\langle 1-12 \rangle$  and Sulfur components  $\{123\}\langle 63-4 \rangle$ , as well as the Goss component  $\{110\}\langle 001 \rangle$ . The results show that at higher annealing temperatures and times, an increment on the intensity of such texture components take place. Similar results were obtained by Electron Backscattering Diffraction (EBSD) analysis technique. The inverse pole figures showed an increase on the fraction area of with  $\langle 634 \rangle$  and  $\langle 211 \rangle$  direction,  $\langle 100 \rangle$  direction was found to be constant during the annealing.

**The Carbonation Reaction of Waste Cement and the Sequestration of CO<sub>2</sub>:** Kwangsuk Yoo<sup>1</sup>; Seong-Ho Lee<sup>1</sup>; Sung-Ho Hwang<sup>1</sup>; Ji-Hwan Ahn<sup>1</sup>; <sup>1</sup>Korea institute of geoscience and mineral resources

The rate of CO<sub>2</sub> emission has kept increasing every year and the global warming is now a major issue. The generation rate of construction waste increased drastically in Korea, reaching 65 million tons in 2008. This study research discusses on the ability of waste cement for the fixation of CO<sub>2</sub> gas and the property changes of the surface of waste cement during carbonation reaction. Especially, in this study, there was an investigation on the effect of the physicochemical properties of the carbonated surface of waste cement. The specific surface area and CEC of carbonated waste cement had linearly increased with the increase in the carbonation percentage. It can be seen that Si component was transformed from linear polysilicate anions in C-S-H gel into a silica with 3-dimension and the formation of Al(OH)<sub>3</sub> gel. And the carbonation percentage in the base of CaO content also increased up to 35%.

**The Corrosion of (Fe, Ni)-Alloys in N<sub>2</sub>-H<sub>2</sub>S-H<sub>2</sub>O Mixtures at 600-800°C:** Min Jung Kim<sup>1</sup>; Chenguang Zhao<sup>1</sup>; Dong Bok Lee<sup>1</sup>; <sup>1</sup>Sungkyunkwan University

The corrosion of (Fe, Ni)-alloys in simulated IGCC gas atmospheres were studied at 600-800°C in N<sub>2</sub>/H<sub>2</sub>S/H<sub>2</sub>O gases. IGCC is a key technology to realize high efficiency and good environmental performance for electricity generation. The corrosion resistance increased in the order of SUS 430, SUS 310, Alloy 800, and IN 625. Ni and Cr increased the corrosion resistance of the alloys. The scale formed consisted primarily of an outer (Fe, Ni)S scale plus an inner CrS scale in the case of SUS310, an outer FeS scale plus an inner (CrS, Cr<sub>2</sub>O<sub>3</sub>)scale in the case of SUS 430, an outer (Fe, Ni)S scale plus an inner CrS scale in the case of Alloy 800, and an outer (Fe, Ni)S scale plus an inner (CrS, Cr<sub>2</sub>O<sub>3</sub>)scale in the case of IN 625. This work was supported by New & Renewable Energy R&D program under the Ministry of Knowledge Economy, Republic of Korea.

**The Effect of ARB Parameters on Mechanical Properties of Ultra Fine Grained Cu, Al and Fe:** Saeed Tamimi<sup>1</sup>; Amir Chegini<sup>2</sup>; Mostafa Ketabchi<sup>3</sup>; Nader Parvin<sup>3</sup>; <sup>1</sup>TEMA; <sup>2</sup>Department of Mechanical Engineering; <sup>3</sup>Mining and Metallurgical Eng. Dep.

Present work deals with Accumulative Roll Bonding (ARB) in low Carbon steel, pure copper and Al-1100. A number of passes of ARB were performed at 500°C for steel, 350°C for copper and 250°C for Al-1100, with 50% reduction in area in each rolling pass. The hardness distribution along the thickness was directly dictated by grain size in each point. It was found that both the ultimate grain size achieved, as well as the degree of bonding, depend on the number of rolling pass and reduction in area as a whole. Mean grain size of samples were determined about 225nm for steel, 1-3 $\mu$ m for copper and 500-700nm for Al-1100. The rolling process was stopped when cracking of the edges became pronounced. Finally, the effect of process temperature and wire brushing were investigated. Moreover, the effect of process temperature on the hardness was investigated.

**The Effect of Irreversible Losses on the Structure of NdFeB Magnets:** Levent Vural<sup>1</sup>; Feriha Birol<sup>2</sup>; Gultekin Goller<sup>1</sup>; <sup>1</sup>Istanbul Technical University; <sup>2</sup>Arcelik R&D Center

In recent years, magnet materials having permanent and high magnetic properties are widely used in a wide variety of applications such as white and electronic goods, medical field and automotive industry. Generally NdFeB magnets are used in permanent magnet motors. The magnetic and aging properties of these magnets can be affected by material properties. In this study, the detailed characterization of NdFeB magnet materials was performed and the changes on the material properties after magnetic aging were investigated. The composition of the materials and phase analysis were carried out by using XRF and XRD techniques, respectively. The Curie temperature of the materials was determined by differential scanning calorimetry (DSC) and the magnetic properties determination was carried out by permeagraph device. The additive elements and phases caused different magnetic properties on NdFeB magnets. A great magnetic losses were observed and these losses could be reduced by the existence of some phases.

**The Effect of Pressure and Temperature on Densification Rates in Current Activated Densification:** Alexander Dupuy<sup>1</sup>; Joseph Alaniz<sup>1</sup>; Javier Garay<sup>1</sup>; <sup>1</sup>University of California Riverside

Current Activated Pressure Assisted Densification (CAPAD) techniques have shown great promise in efficiently consolidating a wide range of materials systems. This efficiency manifests itself in the form of a high densification rate, which is influenced by the processing parameters and material properties. To better understand these influences, a wide range of materials (ionic, covalent, and metallic solids) were densified using the CAPAD technique. By calibrating the device, it was possible to eliminate the effects of thermal expansion and determine the true densification rate of the materials. This data was examined in order to determine the effect that pressure and homologous temperature have on densification rate as well as their sensitivity to material bonding type. In particular, the connection between pressure and bonding type on densification rate was investigated by processing zirconia, silicon, and aluminum at a variety of pressures.

**The Effect of Sintering Conditions on the Properties WC-Co Hard Metal by Powder Injection Molding Process:** Sung-Hyun Choi<sup>1</sup>; Dong-Wook Park<sup>1</sup>; Young-Sam Kwon<sup>2</sup>; Kwom-Ku Cho<sup>1</sup>; In-Shup Ahn<sup>1</sup>; <sup>1</sup>School of nano and advanced Materials Engineering, I-Cube Center, K-MEM R&D cluster, Gyeongsang National University; <sup>2</sup>CetaTech, Inc

Powder injection molding (PIM) is an advanced technology for processing metal and ceramic powders for forming desired shapes at a relatively low processing cost. Tungsten carbide-cobalt hard materials (WC-Co) are widely used for a variety of applications. The WC-10Co feedstock mixed with wax binder was fabricated by two blade mixer. After feedstocks were injection molded, debinding process was carried by two-steps methods with solvent extraction and thermal debinding. After debinding process, the specimens were sintered at vacuum in difference temperature. The microstructure and phase were observed by FE-SEM. In the case of sintered at 1380° in

vacuum atmosphere, The hardness was 1840Hv, and the relative density of WC-10%Co was 95%. The density of specimen sintered at 1400° in vacuum atmosphere was 96.5% and hardness was 1880Hv. In case of heating rate 3° per minute to 1380°, The hardness and density were observed 1910Hv and 97.5%.

**The Effects of Al-5Ti-1B Grain Refiner and Heat Treatment on the Microstructure and Dry Sliding Wear Behavior of a New Developed Super High-Strength Aluminum Alloy:** Mohammad Alipour<sup>1</sup>; Masoud Emamy<sup>1</sup>; *Jafar Rassizadeh*<sup>1</sup>; Mostafa Karamouz<sup>1</sup>; Mortaza Azarbarmas<sup>1</sup>; <sup>1</sup>Kargar street

In this study the effect of Al-5Ti-1B grain refiner on the structural characteristics and wear properties of Al-12Zn-3Mg-2.5Cu aluminum alloy was investigated. The optimum amount for Ti containing grain refiners was selected as 2 wt.%. T6 heat treatment, heating at 460°C for 1 h and water quenching to room temperature and aging at 120°C for 24 h, was applied for all specimens before wear testing. Dry sliding wear performance of the alloy was examined in normal atmospheric conditions. The experimental results showed that the T6 heat treatment considerably improved the resistance of Al-12Zn-3Mg-2.5Cu aluminum alloy to dry sliding wear.

**The Effects of Be on Mechanical Properties of Al-Mg2Si In Situ Composite:** Mortaza Azarbarmas<sup>1</sup>; Masoud Emamy<sup>1</sup>; *Jafar Rassizadehghani*<sup>1</sup>; Mohammad Alipour<sup>1</sup>; Mostafa karamouz<sup>1</sup>; <sup>1</sup>University of Tehran

The influence of Be content on the mechanical properties of Al-15%Mg2Si composite was investigated. The results showed that with the addition of 0.5%Be, the ultimate tensile strength (UTS) and elongation values reached from 252 to 280 MPa and 2.2 to 3.8%, respectively. A study of the specimen's fracture surfaces via scanning electron microscope (SEM) showed that adding Be increase the number of fine dimples that is consistent with results from tensile tests.

**The Effects of Cooling Rate on the Microstructure and Hardness of Al-15wt.%Mg2Si In Situ Composite with Boron:** Mortaza Azarbarmas<sup>1</sup>; Masoud Emamy<sup>1</sup>; *Jafar Rassizadehghani*<sup>1</sup>; Mostafa Karamouz<sup>1</sup>; Mohammad Alipour<sup>1</sup>; <sup>1</sup>University of Tehran

The effect of cooling rate was investigated by the use of two molds with different section test bars. The results showed an increase in hardness values with reduction in section thicknesses corresponding to increasing cooling rates. This influence was observed in both with and without Boron specimens. Optical and SEM images show that with increasing of cooling rate the size of primary Mg2Si particles decreased. The results demonstrate that the cooling rate affected the amount of alpha phase and the size of pseudo-eutectic cells.

**The Effects of Li Additions on the Microstructure and Mechanical Properties of 380 Aluminum Casting Alloys:** Mostafa Karamouz Ravari<sup>1</sup>; Masoud Emamy<sup>1</sup>; *Jafar Rassizadehghani*<sup>1</sup>; Mohammad Alipour<sup>1</sup>; Mortaza Azarbarmas<sup>1</sup>; <sup>1</sup>University of Tehran

The effects of Li on the microstructure and mechanical properties of Type 380A aluminum casting alloys have been examined. It is shown that, as the Li content is increased up to 0.1 wt.pct in the baseline alloy (Al-8.5 wt.%Si-3.5 wt.%Cu-1 wt.%Fe), Li successfully modifies the morphology of the  $\beta$ -Al5FeSi and eutectic Si phases from coarse intersected and branched platelets into finer and independent ones. The Li-containing alloy exhibits higher strength and elongation to failure, presumably due to both finer  $\beta$ -Al5FeSi and eutectic Si phases.

**The Effects of Ni and Mn on the Solid Particle Erosion Resistance of Austenitic Fe-12Cr-0.4C-xNi/Mn Alloys:** *Ki Nam Kim*<sup>1</sup>; Tae Ho Kim<sup>1</sup>; Jun Ki Kim<sup>2</sup>; Seon Jin Kim<sup>1</sup>; <sup>1</sup>Hanyang Univ.; <sup>2</sup>Korea Institute of Industrial Technology

Solid particle erosion implies the removal of material from component surfaces due to successive impacts of hard particles, and has been recognized as a serious problem for many years in various engineering applications such as hydrotransport lines, power plants and gas turbine blades. Recently, it was confirmed that strain-induced martensitic transformation improved abrasive, adhesive wear and cavitation erosion resistance in Fe-base austenitic alloys.

The damage was decreased due to the absorption of external energy and the hardened surface formed by the strain-induced martensitic transformation. So, it is considered that the strain-induced martensitic transformation may have significant effect on improving solid particle erosion resistance due to absorbing impact energy of particles. In this study, the effect of Ni and Mn on the solid particle erosion resistance of Fe-12Cr-0.4C-xNi/Mn (x = 5, 10) alloys was investigated in term of the strain-induced martensitic transformation.

**The Extended Q-Range Small Angle Neutron Scattering Diffractometer at the SNS:** *Yang Gao*<sup>1</sup>; Dazhi Liu<sup>1</sup>; Jinkui Zhao<sup>1</sup>; <sup>1</sup>Oak Ridge National Laboratory

The Extended Q-Range Small Angle Neutron Scattering Diffractometer (EQ-SANS) at the Spallation Neutron Source (SNS) is a high intensity instrument with a wide neutron momentum transfer (Q) coverage and a good wavelength resolution. It has a variable sample to detector distance of ~1.3 to 10 m and an accessible neutron momentum transfer (Q) range of ~0.001 to 1 Å<sup>-1</sup>. The neutron flux on sample is greater than 106 n/cm<sup>2</sup>/s/Å at the collimation length of four meters. The standard sample environment equipment on the EQ-SANS is a 45-position automated sample changer with temperature control between -2 and 80°C. The instrument are used to study proteins, polymers, metal alloys, and many other nanocomposites. Experimental results are shown to demonstrate the instrument ability.

**The Influence of Li on Properties of 380 Aluminum Casting Alloys:** Mostafa Karamouz Ravari<sup>1</sup>; Masoud Emamy<sup>1</sup>; *Jafar Rassizadehghani*<sup>1</sup>; Mortaza Azarbarmas<sup>1</sup>; Mohammad Alipour<sup>1</sup>; <sup>1</sup>university of tehran

This study was undertaken to investigate the influence of Li on the structural characteristics and hardness properties of Al-8.5Si-3.5Cu-1Fe aluminum alloy. A study of the specimen's surfaces via optical and scanning electron microscope (SEM) revealed that in the Li-containing alloys the eutectic Si is well refined and the  $\beta$ -phase has a finer and individual structure. It was revealed from hardness tests that the addition of Li decreases the hardness values.

**The Materials Accelerator: A New Working Model to Promote Commercialization of Multi-Materials through a National Network in Manufacturing Materials:** *Karnika De Silva*<sup>1</sup>; Ralph P. Cooney<sup>1</sup>; Mark P. Taylor<sup>1</sup>; <sup>1</sup>Materials Accelerator, University of Auckland, Tamaki Innovation Campus, Auckland, New Zealand

The Materials Accelerator (MA) is a national capability network which seeks to develop transformational multi-material products in cooperative R&D partnership with innovative high-technology companies. MA has teams of researchers drawn from eight NZ research institutions with multi-materials expertise in composites, plastics, conducting polymers, nanotechnology, metals and also expertise in prototyping, virtual manufacturing, materials analysis and characterization, modeling, interfacial analysis etc. MA Network includes contributions from universities and government laboratories with ~100 researchers associated with the network. Some research projects administered by MA that are beneficial to the MA commercial platforms and to NZ generally will be presented. These proposals are interfacial in its materials focus and bridges more than one type of materials and include mechanisms for preserving the knowledge within the MA business model, its strategy, and its aspirations for new product and market development, as well as outlining the technical and research issues raised by potential R&D projects.

**The Universality Class of Avalanches in Plasticity: Integrated Exponents from Relaxation Processes:** *Stefanos Papanikolaou*<sup>1</sup>; <sup>1</sup>Cornell University

Crackling noise in plastically deformed materials has been suggested to display mean-field behavior, where the histograms of strain jumps show a critical exponent of 3/2. However, there is strong experimental evidence that as the strain-rate decreases, the exponent drifts to higher values, suggesting that the simple mean-field picture is not complete. Here, we present a coarse-grained model of avalanches where an additional slow stress diffusion process takes place in between the fast avalanche events. This model displays the observed rate dependence, which is due to a periodic

integration over hardening levels. Our model suggests that the true universal behavior of avalanches is described by integrated mean-field avalanches, and relaxation processes are important in explaining the experimental behavior.

**The Use of the Multi-Axial Parameter for Fretting Fatigue Assessment of Titanium Alloys:** *Hyukjae Lee*<sup>1</sup>; <sup>1</sup>Andong National University

Fretting fatigue occurs when two mating components are subjected to oscillating loading and can facilitate crack initiation at very low stresses leading to premature failure in components such as spline joint and blade and disk attachment in dovetail joint. Since its multi-axial nature, fretting fatigue is generally depicted better with multi-axial parameters. In this presentation, a critical plane based fatigue crack initiation parameter is computed from the results of finite element analysis and then used to predict fretting fatigue life of titanium alloys. In addition, the multi-axial parameter is used to understand the different fretting fatigue behaviors of titanium alloys with various conditions, such as different surface treatment, material composition, etc. The results show that the multi-axial parameter is very effective to predict fretting fatigue life of titanium alloys from the conventional fatigue life and it can be a very useful tool for analyzing complex fretting fatigue behaviors.

**Thermodynamic Modeling of Chemical Soluble Copper Loss and Liquidus Temperature of High Magnesia Slag:** *Pengfu Tan*<sup>1</sup>; <sup>1</sup>Xstrata Copper

Xstrata Copper Smelter at Mount Isa in Australia had experienced the technical issue of high copper losses in the Rotary Holding Furnace (RHF) slag before 2008. The copper losses in RHF slag was more than 3% in 2006 and 2007. The thermodynamic models, viscosity model have been developed to simulate the process control, slag chemistry, slag viscosity, and matt-slag separations. The effect of SiO<sub>2</sub>/Fe ratio, CaO%, MgO%, and Al<sub>2</sub>O<sub>3</sub>% in slag on the liquidus temperature of slag has been predicted. The effect of slag compositions, matte grade, oxygen potential, and temperature on the soluble copper loss in the copper smelting slag has been modeled and discussed.

**Thermodynamic Study for Cleaning Water Contaminated with Cu, Pb, and Ni:** *Ramiro Garcia*<sup>1</sup>; Francisco Tavera Miranda<sup>1</sup>; Eunice Espinoza<sup>1</sup>; <sup>1</sup>Universidad Michoacana

Flotation devices originally designed for minerals recovery are considered as alternative for waste water treatment (i.e., water contaminated with heavy metals). This work proposes to study the mechanisms of precipitation of lead, copper, and nickel species in a liquid media, in order to design a procedure of cleaning waste water through a flotation-sedimentation route. Copper, lead, and nickel salts were dissolved into distilled water, and according to the thermodynamic analysis of the corresponding metal-water system, the precipitation of solid species were predicted after changing both the electrochemical potential and the pH of the liquid media. Experimental results show the possibility to remove completely copper, nickel, and lead from contaminated water, and to establish a sedimentation procedure for cleaning waste water.

**Thermoelectric Properties of  $\beta$ -Zn<sub>4</sub>Sb<sub>3</sub> Synthesized by Mechanical Alloying and Vacuum Hot Pressing:** *Pee-Yew Lee*<sup>1</sup>; <sup>1</sup>National Taiwan Ocean University

The  $\beta$ -Zn<sub>4</sub>Sb<sub>3</sub> compound has become the focus of attention as a thermoelectric material applicable to thermoelectric power generation around 700 K. It has a relatively low cost and can potentially substitute for high performance lead tellurides which contain toxic lead. In this research, a method combining the mechanical alloying with the vacuum hot pressing was adopted to obtain the bulk sample of  $\beta$ -Zn<sub>4</sub>Sb<sub>3</sub>. It is found single-phase  $\beta$ -Zn<sub>4</sub>Sb<sub>3</sub> were successfully prepared by mechanical alloying of elemental powders containing 0.6 at.% excess Zn. Thermoelectric properties as a function of temperature were investigated from room temperature to 600 K and compared with results of other studies. Transport properties at room temperature were also evaluated. Thermoelectric properties of single-phase  $\beta$ -Zn<sub>4</sub>Sb<sub>3</sub> materials produced by present method were measured and are comparable to the published data. Synthesis by mechanical alloying and vacuum hot pressing provides an optional processing route in this material.

**Thermographic Analysis of Braking in Railway Brake Disc:** *Jeongguk Kim*<sup>1</sup>; Sung-Tae Kwon<sup>1</sup>; Sung Cheol Yoon<sup>1</sup>; Byung Choon Goo<sup>1</sup>; <sup>1</sup>Korea Railroad Research Institute

The damage evolution due to generation of hot spots on railway brake disc has been considered the main degradation mechanism in brake disc. Therefore, the understanding of hot spots, also called hot judder, which is undesirable low frequency vibrations developed by non-uniform contact area between brake pad material and brake disc, is important for a better understanding of material design as well as enhancement of materials properties in railway brake disc. In this investigation, during braking, the thermographic temperature analysis of railway brake disc was quantitatively performed to investigate the degradation mechanism of brake disc. The analysis of surface temperature changes on railway brake disc was conducted using a high-speed infrared camera. Through the analysis of thermographic monitoring images, the temperature evolution with different braking speeds was qualitatively evaluated. In this paper, the qualitative investigation results on the temperature evolution of railway brake disc was summarized and presented.

**Thermographic Monitoring of Fracture Behavior in Railway Steels:** *Jeongguk Kim*<sup>1</sup>; <sup>1</sup>Korea Railroad Research Institute

The tensile failure behavior of different types of railway steels, which are used for railway vehicle components such as wheel and axle, was characterized using high-speed infrared camera. The tensile specimens were obtained from the actual railway vehicle parts, which were used for over 20 years. An infrared camera was used to monitor damage evolution in terms of surface temperature measurements with the camera speed of 100 Hz. A qualitative image analysis was conducted to explain failure mode and mechanisms in different railway steel samples based on infrared thermographic images obtained during tensile testing. Moreover, the microstructural characterization using scanning electron microscope (SEM) was performed to correlate the mechanical failure mode with thermographic results. In this investigation, an IR camera and SEM characterization method were used to facilitate a better understanding of fracture behavior of different types of railway steels during tensile testing.

**Three-Dimension Electrode Device Assembled from Bamboo Char Loaded Nano Ferric Oxide for Catalytic Treatment of Organic Wastewater:** *Li Dan*<sup>1</sup>; <sup>1</sup>Central South University

Three-dimension electrode device assembled from foam nickel and bamboo char loaded nano ferric oxide electrode was investigated for catalytic treatment of organic wastewater. The influence of the following parameters, namely calcination temperature, organic pollutant concentration, voltage, amount of electrolyte, was the main focus. The optimum value of calcination temperature (400°), organic pollutant concentration (5mg/L), voltage (1V), amount of electrolyte (0.7g/L), were obtained, corresponding to the best elimination rate of 96.5% with good durability. The order of the treatment effect for different organic wastewater is as follow: basic fuchsine > Methyl orange > Rhodamine B > Acid fuchsine.

**Three-Dimension Electrode Device with Bamboo Char Loaded Nano-Cobalt Oxide for Catalytic Degradation of Organic Pollutant in Wastewater:** *Zhang Ling*<sup>1</sup>; <sup>1</sup>College of Chemistry and Bioengineering, Changsha University of Science and Technology

Bamboo char loaded nano-cobalt oxide catalyst was prepared by sol-gel method from bamboo char, cobalt nitrate, and citric acid. The catalytic performance of the obtained catalyst contained in three-dimension electrode device for catalytic degradation of organic pollutant in wastewater was investigated. The prepared catalyst with uniform particle size was fine. Orthogonal experiments were performed to achieved the optimum conditions, namely calcination temperature of 600°, voltage of 7V, and amount of electrolyte of 0.7g/L. The order of the degradation effect for different organic pollutant was as follow: methyl orange > basic fuchsine > rhodamine B > acid fuchsine > phenol. The test of the effect of catalyst under the optimum conditions indicates that the catalyst exhibited best degradation rate to acid fuchsine (91.36%) with catalyst concentration of



1.0g/L, calcination temperature of 600°, catalytic degradation time of 5h, and acid fuchsine concentration of 1mg/L.

**Toughened Poly (Acid Lactic): Mechanical and Morphological Characterizations:** Gustavo Brito<sup>1</sup>; Tomas Melo<sup>1</sup>; Pankaj Agrawal<sup>1</sup>; Carlos Cunha<sup>1</sup>; Edcleide Araújo<sup>1</sup>; <sup>1</sup>Federal University of Campina Grande - UFCG

The poly (acid lactic) has attracted great attention of researchers due to it come from renewable source, and possess characteristics like biodegradability and good processability. However, the PLA presents some drawbacks, like brittleness, that should be overcome to make possible its wide application. In this work, PLA was blended with an impact modifier. The blends were tested by impact and tensile tests. Scanning Electronic Microscopy was realized in the fracture surface of the impact samples. Results showed that a toughened PLA was obtained.

**Toughening of ADI Austenitized in Intercritical Region:** J.K. Chen<sup>1</sup>; B.T. Chen<sup>1</sup>; J.S. Tsai<sup>1</sup>; <sup>1</sup>National Taipei Univ. Technology

The current article investigates the influences of intercritical austenitizing temperatures on microstructures and mechanical properties of austempered ductile irons. A series of intercritical austenitizing temperatures ranging from 775 to 900°C are used and austempering is performed at 400°C on a conventional FCD700 ductile iron. Experimental results show that mechanical properties, including strength, ductility, and the toughness, all increase with intercritical austenitizing temperatures till an optimum austenitizing temperature of 830°C. At this optimum processing condition, strength of 974MPa, impact energy of 166 J, and 16.4% ductility is achieved which is compared with the non-treated ductile iron with 790MPa strength, 42J impact energy, and 8.2% ductility. Microstructure refining via well distributed sub-micron ausferrite structure is essential for the increase of strength. Furthermore, the increased carbon content of retained austenite and austenite volume fraction combines to increase toughness through martensitic transformation and gives rise to transformation induced plasticity (TRIP) effect.

**Ultrasonic-Assisted Soldering of Aluminum Alloy under Liquidus Temperature of Zn-Al Alloy:** Toru Nagaoka<sup>1</sup>; Yoshiaki Morisada<sup>1</sup>; Masao Fukusumi<sup>1</sup>; Tadashi Takemoto<sup>2</sup>; <sup>1</sup>Osaka Municipal Technical Research Institute; <sup>2</sup>Joining and Welding Research Institute, Osaka University

To obtain butt-joints of aluminum alloy containing 4.5 to 5.6 mass % magnesium, an ultrasonic-assisted soldering process using Zn-xAl (x = 5, 13, and 38 mass %) solder alloys was investigated. Each solder foil was inserted between faying surfaces of the aluminum rods. Ultrasonic vibration was propagated to the solder foil through the aluminum rod for 4 seconds at soldering temperatures. As the results of tensile tests for obtained joints, the joint strength increased with decrease of soldering temperature and with increase of Al content of Zn-Al solder alloy. The results of XRD on the fracture surface and SEM-EDX analysis of the solder layer revealed that the improvement of joint strength was due to the decreased amount of MgZn<sub>2</sub> phase in the solder layer. The generation of MgZn<sub>2</sub> phase should be decreased by suppression of the dissolution of 5056-Al substrates during the soldering process.

**Use of Polymeric Residues from the Footwear Industry in Layers of Asphalt Composites:** Ariosvaldo Sobrinho<sup>1</sup>; Fábio Rios<sup>1</sup>; Karine Santos<sup>2</sup>; Marcos Baracho<sup>2</sup>; Luiz Pontes<sup>3</sup>; José Nascimento<sup>1</sup>; <sup>1</sup>UAEMA / UFCG; <sup>2</sup>UAEC/UFCG; <sup>3</sup>LMPC / DTM / UFPB

Technological innovation, analysis of the life cycle of materials, development of new alternative products such as composites and asphalt blanket, using materials from industrial waste for use in construction, are constant challenges for researchers. In general, the reasons that motivate these researchers are: reducing the environmental impact, gradual reduction of deposit areas, depletion of non-renewable raw materials, reducing costs and energy consumption and improvement in quality of life. The demands of current management, and proper management of waste and tariffs imposed by environmental legislation, and bring great concern and cost to entrepreneurs, have also motivated research on recycling and reprocessing.

**Utilizing SST and Ultrasonic NDT for Microstructure Analysis of the Irradiated Steel Structure:** Mohammad Allazadeh<sup>1</sup>; <sup>1</sup>University of Pannonia

The radiation, particularly neutron radiation, can have deleterious effects on material properties such as formation of internal voids or bubbles. Modification of microstructural configuration may cause catastrophic results in the soundness of the irradiated heavy section ferritic-martensitic steels structure (e.g. nuclear pressure vessels). The small specimen technique (SST) method is a technique used to predict the standard mechanical properties of heavy section components and structures under operational loading conditions. Defect distributional map provided by the ultrasonic nondestructive testing (NDT) can be analyzed to specify the type of the defect and to assess the level of the defects in the microstructure. A microstructural analysis method is suggested to study the microstructural variability based on a combination of SST and signal processing analysis of ultrasonic NDT. This method can be applied to monitor catastrophic flaw formation and crack propagation in large steel structure due to microstructural degradation by irradiation.

**Water Modeling of Optimization of Two-Strand Tundish Configuration for Slab Continuous Casting with Gas Bubbling:** Shu-guo Zheng<sup>1</sup>; <sup>1</sup>Northeastern University

The effects of various flow control devices on melt flow in a two-strand tundish with gas bubbling were investigated in water modeling experiments. The results showed that the bubbling flowrate had an effect on the melt flow in the tundish. And within a reasonable range of bubbling flowrates, the melt flow was improved. While too large bubbling flowrates not only seemed to be inefficient in the improvement of melt flow, but also lead to reoxidation by exposing the metal to air. For the present research, the optimal bubbling flowrate range is from 1.18 to 2.36 Nl/min. With reasonable arrangements of turbulence inhibitor with gas bubbling curtains, weirs and dams or without dams showed good control on the melt flow. While the arrangement of turbulence inhibitor with gas bubbling curtains was poor in the improvement of melt flow. In present study, an optimal proposal was presented by physical modeling.

**WCLES: An Innovative Environmental Friendly Combustionless Engines For Marine Applications Based On Low-Current Electrolysis Technology:** Saad Sharaf<sup>1</sup>; <sup>1</sup>MOMCO

A new innovative engine design is proposed. The design offers a radical solution for the design of safe, environmental friendly, energy efficient engines. The engine is based on water power. The poster discusses aspects related to energy generation, retrieval and storage. The discussion emerges from a designer point of view, offering design formulas and qualitative comparisons with existing fuel technologies. Case studies are used to demonstrate the advantages and challenges associated with the proposed solution. The concept behind water power generation is based on the following arguments. When water electrolyzed, it converts to hydrogen and oxygen. For the same mass, the volume of generated gases is higher than the original amount of water. This large increase in the pressure can work as a power stroke in internal combustion engine.

**Wettability Testing for Ni/Ti(CN) System in High Temperature:** Koji Shimojima<sup>1</sup>; Hiroyuki Hosokawa<sup>1</sup>; Kiyotaka Kato<sup>1</sup>; Akihiro Matsumoto<sup>1</sup>; <sup>1</sup>AIST

The titanium carbide (TiC) based cermet is one of the candidates for the alternative material of WC-Co cemented carbide and has been known its higher resistance to wear than that of WC-Co cemented carbide in the use of tools for working steels. Cermet was made from hard particles such as TiC or Ti(CN), metal binders, such as Ni / Co and some additives such as Mo. For improve of strength and toughness of the cermet, it is important to know the wettability of the hard particles with the binder materials. In this paper, we show the wettability testing equipment with HDTV system under high temperature in Ar / N<sub>2</sub> / vacuum atmosphere. We also show some experimental results of the wettability test for various Ti(CxNx-1) with Ni at 1727 K and they showed that substrate materials affects the wet angle.

**Work of Adhesion and Thermodynamic Stability of Metal/Oxide Interface:** Hongmei Jin<sup>1</sup>; Ping Wu<sup>1</sup>; <sup>1</sup>Institute of High Performance Computing

By using density functional theory (DFT) and semi-empirical approach, the thermodynamic stability of metal/oxides interface including Ni/ZrO<sub>2</sub>, Cu/ZrO<sub>2</sub> and Au/TiO<sub>2</sub> were evaluated. The work of adhesion and stability of Ni/ZrO<sub>2</sub> and Cu/ZrO<sub>2</sub> which are the function of the total energy of the interacted system and the oxygen partial pressure were calculated. An empirical model for work of adhesion and interfacial stability was developed by using DFT calculations results as a reference. The developed empirical model was further extended to Au/TiO<sub>2</sub> system and the stability of different crystallographic orientations of Au/TiO<sub>2</sub> was predicted.

# NOTES

# TMS2011

## 140th Annual Meeting & Exhibition

**A**

|                          |   |   |   |                        |   |
|--------------------------|---|---|---|------------------------|---|
| Aagesen, L.....          | 202   | Ahn, J.....                                       | 353, 392, 457, 465, 519                   | Al-Omari, I.....       | 162   |
| Aarhaug, T.....          | 122, 180  | Ahzi, S... 106, 230, 283, 293, 304, 321, 362, 363 |   | Alonso, E.....         | 406   |
| Abashidze, G.....        | 155   | Aich, S.....                                      | 85, 162, 312                              | Alonso, M.....         | 13  |
| Abbaschian, R.....       | 31, 341, 515  | Aidhy, D.....                                     | 487                                       | Alpalmy, N.....        | 481   |
| Abbasi, A.....           | 75  | Aifantis, E.....                                  | 286, 356                                  | Alpay, P.....          | 49  |
| Abbasi Gharacheh, M..... | 259   | Aifantis, K.....                                  | 295, 296, 355, 369, 418, 464              | Altman, K.....         | 421   |
| Abbasi, M.....           | 141   | Aikin, R.....                                     | 380, 430                                  | Alvarado, M.....       | 413   |
| Abdel-Fattah, W.....     | 432   | Aindow, M.....                                    | 49, 479                                   | Alvarez, P.....        | 438   |
| Abdeljawad, F.....       | 365   | Ai, Z.....  | 300                                       | Alves, J.....          | 130, 368, 369, 407, 456, 499                        |
| Abdel-Malek, S.....      | 78  | A. Javid, F.....                                  | 468                                       | Alves, Jr., C.....     | 458   |
| Abdolrahim, N.....       | 15  | Ajideh, H.....                                    | 486                                       | Alves Júnior, C.....   | 188   |
| Abdolvand, H.....        | 455   | Akamatsu, S.....                                  | 31, 143, 202                              | Alvin, M.....          | 71, 371   |
| Abdullah, F.....         | 308   | Akgun, O.....                                     | 485                                       | Al Zarouni, A.....     | 180, 308, 437                                       |
| Abdul-Latif, A.....      | 395   | Akhtar, K.....                                    | 165, 403                                  | Al-Zubi, A.....        | 277   |
| Abedrabbo, S.....        | 432   | Akhtar, S.....                                    | 98, 308                                   | Amancio, S.....        | 438   |
| Abe, G.....              | 82  | Akinc, M.....                                     | 407, 408                                  | Amani Hamedani, H..... | 18  |
| Abernathy, D.....        | 191, 192  | Akin, I.....                                      | 515                                       | Amanov, A.....         | 24, 198   |
| Abiko, K.....            | 318   | Akiya, T.....                                     | 389                                       | Amaral, C.....         | 26  |
| Abirami, S.....          | 230   | Akkas, B.....                                     | 165                                       | Ambarkutuk, A.....     | 367   |
| Abreu, A.....            | 197, 466  | Akram, M.....                                     | 24, 485                                   | Amini Rastabi, H.....  | 280   |
| Abunaemeh, M.....        | 497   | Akreem, M.....                                    | 512                                       | Amini, S.....          | 21, 31, 492   |
| Aburada, T.....          | 306   | Alagarsamy, P.....                                | 151                                       | Ammar, H.....          | 30  |
| Ackelid, U.....          | 487, 491  | Alamdari, H.....                                  | 30, 322, 475                              | Amodeo, J.....         | 231   |
| Acoff, V.....            | 245, 247  | Alam, M.....                                      | 32  | Amoali, A.....         | 460   |
| Adams, A.....            | 255   | Alaniz, J.....                                    | 312, 519                                  | Amoozezaei, M.....     | 147, 260  |
| Adams, B.....            | 72, 278, 279, 310, 318, 319, 517  | Alankar, A.....                                   | 375, 402, 474                             | Anagnostou, E.....     | 479   |
| Adams, D.....            | 168   | Alba-Baena, N.....                                | 492                                       | Anasori, B.....        | 21, 198, 492  |
| Adamson, H.....          | 235   | Albe, K.....                                      | 153, 247, 287                             | Ande, C.....           | 376   |
| Adamson, J.....          | 216   | Aldajah, S.....                                   | 416                                       | Anderoglu, O.....      | 394, 472  |
| Adams, S.....            | 111   | Aldanondo, E.....                                 | 438                                       | Andersen, D.....       | 323   |
| Addiego, F.....          | 304, 362  | Alderman, M.....                                  | 206                                       | Anderson, I.....       | 83, 94, 116, 133, 219, 274, 280, 282, 390, 443, 470 |
| Adeosun, S.....          | 237   | Aldrin, J.....                                    | 177                                       | Anderson, K.....       | 251   |
| Adham, K.....            | 132   | Al-Dubaisi, A.....                                | 120                                       | Anderson, P.....       | 134, 161, 167, 278, 341, 412                        |
| Adharapurapu, R.....     | 312, 386  | Aleksov, A.....                                   | 47  | Anderson, W.....       | 150   |
| Adjanor, G.....          | 23  | Alexander, D.....                                 | 430, 471                                  | Andersson, D.....      | 143, 144  |
| Adland, A.....           | 260   | Alexander, S.....                                 | 214                                       | Ando, D.....           | 33  |
| Admas, B.....            | 456   | Alexandrescu, R.....                              | 14, 415                                   | Ando, T.....           | 280, 344  |
| Agaoğullari, D.....      | 235, 293, 404, 483, 510   | Alexandrov, B.....                                | 239                                       | Andresen, P.....       | 211   |
| Agarwal, A.....          | 55, 110, 169, 184, 229, 288, 350, 351, 421  | Alfano, J.....                                    | 169                                       | Andriese, M.....       | 62, 117, 234, 354                                   |
| Agarwal, R.....          | 110   | Alfantazi, A.....                                 | 324, 384                                  | Andrieu, S.....        | 488   |
| Ager, J.....             | 233   | Al-Harbi, H.....                                  | 375                                       | An, G.....             | 446   |
| Agnew, S.....            | 32, 52, 92, 105, 147, 149, 163, 164, 205, 222, 262, 278, 329, 336, 342, 387, 388, 401, 441, 454, 492, 493 | Al Hosni, S.....                                  | 138                                       | Angelini, J.....       | 229   |
| Agrawal, A.....          | 421   | Alimadadi, H.....                                 | 273                                       | Angeliu, T.....        | 317   |
| Agrawal, D.....          | 165   | Alingur, M.....                                   | 395                                       | Anglin, B.....         | 54, 375   |
| Agrawal, J.....          | 91  | Alipour, M.....                                   | 179, 225, 508, 509, 520                   | Aning, A.....          | 347   |
| Agrawal, P.....          | 513, 515, 522   | Al Jallaf, M.....                                 | 180, 308, 437                             | An, K.....             | 44, 140, 191, 335, 337, 396, 431, 516               |
| Agren, J.....            | 87  | Aljarrah, M.....                                  | 33  | An, P.....             | 102   |
| Ågren, J.....            | 54  | Al-Jassim, M.....                                 | 431                                       | Antille, J.....        | 420   |
| Aguilar, E.....          | 284   | Alkan, M.....                                     | 165, 268                                  | Antolin, N.....        | 240   |
| Aguirre, M.....          | 421   | Allahar, K.....                                   | 224, 225                                  | Antoniou, A.....       | 415, 463  |
| Ahangarani, S.....       | 372   | Allain-Bonasso, N.....                            | 279                                       | Antonyraj, A.....      | 34  |
| Ahluwalia, R.....        | 277, 361  | Allais, B.....                                    | 238                                       | Antrekowitsch, H.....  | 121   |
| Ahmad-Bitar, R.....      | 368, 369  | Allanore, A.....                                  | 60, 425, 476                              | Antrekowitsch, J.....  | 469, 517  |
| Ahmadi, S.....           | 278, 456, 517   | Allard, B.....                                    | 437                                       | Antretter, T.....      | 221   |
| Ahmad, M.....            | 338   | Allazadeh, M.....                                 | 522                                       | Anumalasetty, V.....   | 492   |
| Ahmadzadegan, A.....     | 485   | Allen, A.....                                     | 217                                       | An, X.....             | 28  |
| Ahmed, A.....            | 22, 122, 179, 187, 238, 299, 300, 360, 367, 419, 466  | Allen, S.....                                     | 329                                       | Anyalebechi, P.....    | 39, 97, 156, 213, 268                               |
| Ahmed, S.....            | 16  | Allen, T.....                                     | 40, 43, 158, 265, 332, 333, 393, 405, 496 | An, Z.....             | 424   |
| Ahmed, Y.....            | 198   | Alli, M.....                                      | 235                                       | Aparna, V.....         | 214   |
| Ahn, B.....              | 20  | Allison, J.....                                   | 89, 317                                   | Apelian, D.....        | 95  |
| Ahn, I.....              | 505, 519  | Allison, P.....                                   | 514                                       | Apel, M.....           | 143   |
| Ahn, I.....              | 481   | Allnatt, A.....                                   | 261                                       | Apisarov, A.....       | 461, 466  |
|                          |   | Al Maawali, S.....                                | 137                                       | Aprigliano, L.....     | 463   |
|                          |   | Al Mazouzi, A.....                                | 271                                       | Araujo, E.....         | 515   |
|                          |   | Almeida, E.....                                   | 188                                       | Araújo, E.....         | 500, 522  |
|                          |   | Almeida Neto, L.....                              | 65  | Araujo, J.....         | 197   |
|                          |   | Almer, J.....                                     | 309, 319, 370, 371, 430, 447, 472         | Arbegast, W.....       | 81, 489   |



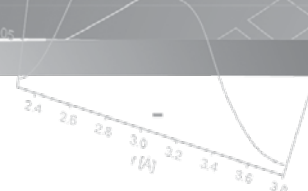
|                         |   |                           |                                  |                       |  |
|-------------------------|---|---------------------------|----------------------------------|-----------------------|--|
| Ardell, A.....          | 59  | Bacon, D.....             | 99                               | Banerjee, D.....      | 443  |
| Ares, A.....            | 349, 510  | Bacroix, B.....           | 395, 448                         | Banerjee, R.....      | 17, 23, 66, 124, 181, 182, 239                               |
| Arfaei, B.....          | 219, 274, 338   | Badarinarayan, B.....     | 39                               | Banerjee, S.....      | 469  |
| Argade, G.....          | 259, 326  | Badulescu, C.....         | 342                              | Banerjee, T.....      | 178  |
| Argyropoulos, S.....    | 367, 409  | Bae, D.....               | 35, 166, 516                     | Bang, C.....          | 186  |
| Ari, M.....             | 72  | Bae, H.....               | 189                              | Bang, J.....          | 509, 510   |
| Aristizabal, R.....     | 396   | Bae, J.....               | 36, 263                          | Bang, W.....          | 37, 275, 337, 389, 432, 451                                  |
| Armoo, J.....           | 300   | Baek, E.....              | 480                              | Baniassadi, M.....    | 230  |
| Armstrong, B.....       | 198   | Bagcivan, N.....          | 187                              | Banovic, S.....       | 121  |
| Arnberg, L.....         | 55, 201   | Bagheri, Z.....           | 160                              | Bansal, A.....        | 351  |
| Arola, D.....           | 302, 361, 362   | Baharuddin, H.....        | 52                               | Bansil, R.....        | 125  |
| Arquis, E.....          | 30  | Bahloui, N.....           | 363                              | Banu, K.....          | 392  |
| Arronche, L.....        | 313, 314  | Bahlouli, N.....          | 321                              | Ban, Y.....           | 300  |
| Arroyave, R.....        | 27, 46, 74, 133, 144,<br>191, 249, 315, 376, 435, 506 | Bahmanpour, H.....        | 17, 18, 20, 415                  | Bao, C.....           | 328  |
| Arsenlis, A.....        | 434   | Bahrami, A.....           | 108, 225, 226                    | Bao, S.....           | 308  |
| Arslan, C.....          | 505, 516, 518   | Bahr, D.....              | 15, 168, 209, 343, 349, 363, 460 | Bao, Y.....           | 351, 352, 494  |
| Artola, J.....          | 138   | Bai, C.....               | 61, 116, 417                     | Barabash, O.....      | 100, 345   |
| Arulkumar, M.....       | 52  | Bai, G.....               | 235, 295                         | Barabash, R.....      | 44, 100, 135, 159, 217,<br>271, 272, 335, 394, 402, 446, 447 |
| Asadi, M.....           | 98  | Bai, H.....               | 470                              | Baracho, M.....       | 517, 522   |
| Asefa, T.....           | 16  | Baik, D.....              | 506                              | Baran Acarali, N..... | 485, 486   |
| Asgharifar, M.....      | 25, 39, 268   | Baik, S.....              | 96                               | Barandiaran, J.....   | 105  |
| Ashkenazy, Y.....       | 66, 287, 394  | Bainbridge, I.....        | 187                              | Barashev, A.....      | 99   |
| Askari, D.....          | 296   | Baird, J.....             | 223, 330                         | Baraskar, A.....      | 230  |
| Askari, H.....          | 167   | Bai, X.....               | 100, 496                         | Baratzadeh, F.....    | 201, 259   |
| Asle Zaeem, M.....      | 76, 484   | Baiysbekov, S.....        | 354                              | Barbadikar, D.....    | 15   |
| Asokamani.....          | 24  | Bajaj, S.....             | 506                              | Barbaro, F.....       | 188  |
| Asta, M.....            | 79, 82, 83, 191, 239, 249                             | Bajvani Gavanluei, A..... | 324                              | Barbato, C.....       | 177  |
| Asthana, A.....         | 296   | Bakai, A.....             | 467                              | Barbu, A.....         | 158  |
| Atapour, M.....         | 324   | Bakai, S.....             | 467                              | Bardou, J.....        | 293  |
| Athènes, M.....         | 23  | Bakavos, D.....           | 114                              | Barlat, F.....        | 401, 403   |
| Atiya, G.....           | 263   | Baker, A.....             | 294                              | Barmak, K.....        | 118  |
| Atli, K.....            | 161   | Baker, B.....             | 345                              | Barnard, L.....       | 159  |
| Atodaria, I.....        | 252   | Baker, I.....             | 134, 192, 193                    | Barnett, M.....       | 106, 205, 330  |
| Atsumi, K.....          | 74  | Bakir, M.....             | 103                              | Barnett, R.....       | 476  |
| Atwater, M.....         | 17  | Bakken, J.....            | 98, 308                          | Barney, E.....        | 366  |
| Atwood, R.....          | 31  | Bakker, M.....            | 110, 169                         | Baró, M.....          | 468  |
| Atzmon, M.....          | 242, 243  | Bak, S.....               | 510                              | Barre, C.....         | 63, 165  |
| Aubery, L.....          | 129   | Balachandran, S.....      | 501                              | Barraera, E.....      | 313, 373   |
| Au, D.....              | 227   | Balaji, B.....            | 283                              | Barrett, C.....       | 330  |
| Aune, R.....            | 98, 308, 423  | Balani, K.....            | 23, 421                          | Barr, G.....          | 160  |
| Averback, R.....        | 43, 66, 240, 287, 292, 394                            | Balasubramaniam, K.....   | 502                              | Barron, S.....        | 67, 448  |
| Avila-Davila, E.....    | 507   | Balasubramanian, K.....   | 91                               | Barsoum, M.....       | 21, 198, 333, 492  |
| Aydelotte, B.....       | 137   | Balci, Ö.....             | 293, 483                         | Bart, F.....          | 442  |
| Aydin, U.....           | 251   | Baldini, F.....           | 456                              | Bart, F.....          | 253  |
| Ayer, R.....            | 146   | Bale, H.....              | 108                              | Barth, H.....         | 362  |
| Ayhan, T.....           | 65  | Balk, T.....              | 285, 461, 462                    | Bartol, L.....        | 105  |
| Ayoola, W.....          | 237   | Ballard, D.....           | 62, 63, 118, 119, 176            | Barton, N.....        | 254  |
| Azarbarmas, M.....      | 179, 225, 508, 509, 520                               | Ballard, J.....           | 317                              | Bartsch, M.....       | 106, 374   |
| Azari Dorcheh, K.....   | 30  | Ballato, J.....           | 169, 478                         | Bashiri, M.....       | 414  |
| Azevedo, C.....         | 357   | Balle, F.....             | 114, 115, 253                    | Basinger, J.....      | 310  |
| Azimi, G.....           | 476   | Ballentine, F.....        | 236                              | Basirat, M.....       | 211, 375   |
| Azimi, K.....           | 315   | BALLI, M.....             | 495                              | Baskes, M.....        | 100, 196, 287, 445   |
| Azizi, A.....           | 12, 14  | Balogh, L.....            | 35, 53, 163, 473                 | Bassani, J.....       | 76, 250, 314   |
| <b>B</b>                |   | Balog, J.....             | 30                               | Bassman, L.....       | 310  |
| Baars, D.....           | 501   | Balogun, S.....           | 237                              | Bastrygin, V.....     | 61   |
| Baated, A.....          | 275   | Balooch, M.....           | 265                              | Basu, B.....          | 421  |
| Babapour Naseri, M..... | 18  | Baltrus, J.....           | 288                              | Basu, R.....          | 51   |
| Baba, Y.....            | 267   | Baluc, N.....             | 181                              | Basu, S.....          | 504  |
| Babb, J.....            | 141   | Balu, P.....              | 481, 483                         | Bataille, A.....      | 224  |
| Babcock, K.....         | 368   | Balu, R.....              | 241                              | Batista, E.....       | 123, 360   |
| Babu, S.....            | 66, 448, 489  | Balzard, D.....           | 395                              | Battaglia, J.....     | 478  |
| Bacakova, L.....        | 24  | Bamberger, M.....         | 263                              | Battaile, C.....      | 474, 480, 482, 484   |
| Bachelet, C.....        | 43  | Bammann, D.....           | 88, 298                          | Battle, T.....        | 409, 459, 502  |
| Bachurin, D.....        | 233   | Bance, S.....             | 207                              | Baudino, M.....       | 256  |
| Backhouse, N.....       | 138, 256, 322   | Banchik, A.....           | 370                              | Baudin, T.....        | 107  |
|                         |   | Bandar, A.....            | 176                              | Baudrenghien, J.....  | 129  |
|                         |   | Bandaru, P.....           | 110                              | Bauer, C.....         | 208, 331   |
|                         |   | Bando, Y.....             | 173                              |                       |  |

# TMS2011

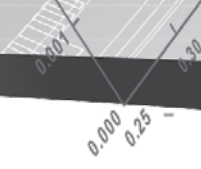
## 140th Annual Meeting & Exhibition

|                     |                            |                        |   |                         |  |
|---------------------|----------------------------|------------------------|---|-------------------------|--|
| Baumann, T.....     | 144                        | Bernhard, C.....       | 98  | Blaesing, J.....        | 102                                      |
| Baumbach, T.....    | 164, 309                   | Bernier, J.....        | 216, 273, 455                                   | Blau, P.....            | 463                                      |
| Baumgart, T.....    | 435                        | Berntsen, H.....       | 177   | Blawert, C.....         | 494                                      |
| Baxter, R.....      | 122, 300                   | Berry, J.....          | 348, 349, 411                                   | Bleck, W.....           | 317, 379                                 |
| Baydogan, M.....    | 481                        | Bertolino, G.....      | 240   | Blodgett, M.....        | 62, 118, 176                             |
| Baydogan, N.....    | 373                        | Bertolo, J.....        | 181   | Blöebaum, R.....        | 240                                      |
| Bayer, M.....       | 23                         | Bertrand, C.....       | 459   | Blosmo, D.....          | 439                                      |
| Bayles, R.....      | 256                        | Bertran, G.....        | 181   | Blue, C.....            | 165, 403                                 |
| Baza, J.....        | 304                        | Bessais, L.....        | 151, 443, 515                                   | Bobzin, K.....          | 187                                      |
| Beaber, A.....      | 228, 295                   | Besseghini, S.....     | 105   | Bodde, S.....           | 422                                      |
| Beaman, J.....      | 344                        | Besser, M.....         | 447   | Bode, B.....            | 378                                      |
| Beardsley, B.....   | 325                        | Bess, J.....           | 334   | Boehlert, C.....        | 150, 312, 373, 433                       |
| Beaudet, J.....     | 373                        | Bestor, M.....         | 212, 213  | Boenigk, W.....         | 197                                      |
| Beaudoin, A.....    | 290, 402, 434              | Bettles, C.....        | 262   | Boesenberg, A.....      | 219, 274                                 |
| Bechelany, M.....   | 418                        | Bevitori, A.....       | 429   | Boettinger, W.....      | 145, 159                                 |
| Becker, C.....      | 209                        | Beyerlein, I.....      | 16, 53, 195, 222, 232, 292                      | Bogdan, A.....          | 95                                       |
| Beckermann, C.....  | 147, 201                   | Bhadrachalam, P.....   | 352   | Bohlen, J.....          | 35, 148, 388                             |
| Beck, J.....        | 413                        | Bhandakkar, A.....     | 283   | Boismier, D.....        | 442                                      |
| Becquart, C.....    | 42, 94, 215, 216, 271      | Bhandakkar, T.....     | 361   | Bojarevics, V.....      | 420                                      |
| Becze, L.....       | 132                        | Bhat, A.....           | 128   | Bokeloh, J.....         | 127, 467                                 |
| Bedair, S.....      | 444                        | Bhatia, M.....         | 194, 330  | Boldsakhan, E.....      | 259, 382                                 |
| Bedel, M.....       | 187                        | Bhat, S.....           | 320   | Bolfarini, C.....       | 20, 69, 468                              |
| Bednarcik, J.....   | 448                        | Bhattacharya, K.....   | 277   | Bolmaro, R.....         | 23, 455                                  |
| Beeler, B.....      | 445                        | Bhattacharya, S.....   | 115, 147, 201, 246, 264, 315, 328               | Bolon, A.....           | 71                                       |
| Beeman, J.....      | 233                        | Bhattacharyya, D.....  | 232, 427  | Boltersdorf, C.....     | 197                                      |
| Behraves, S.....    | 39                         | Bhaumik, S.....        | 162   | Boltz, E.....           | 502                                      |
| Behrens, B.....     | 481, 483                   | Bhoi, B.....           | 355   | Boltz, Y.....           | 502                                      |
| Beier, S.....       | 322                        | Bhole, S.....          | 39  | Bonakdar, A.....        | 257                                      |
| Bei, H.....         | 100, 337, 350, 394         | Bhowmik, A.....        | 457   | Bonavilla, L.....       | 468                                      |
| Beiss, P.....       | 17                         | Bian, M.....           | 35  | Bonneville, J.....      | 77, 107, 230                             |
| Belak, J.....       | 78, 216, 266, 455          | Bice, D.....           | 81, 489   | Bonta, S.....           | 19                                       |
| Belin-Ferré, E..... | 299                        | Bichler, L.....        | 150   | Bontha, S.....          | 39, 97, 156, 213, 268, 508               |
| Beller, D.....      | 154, 334                   | Bieber, A.....         | 461   | Boom, R.....            | 461, 503                                 |
| Bellet, M.....      | 30                         | Bieler, T.....         | 47, 135, 219, 274, 368, 401, 402, 449, 500, 501 | Boone, S.....           | 176                                      |
| Bellon, P.....      | 43, 66, 240, 287, 292, 394 | Biener, J.....         | 349   | Boopathy, K.....        | 185                                      |
| Bell, W.....        | 62, 117                    | Biener, M.....         | 349   | Booty, M.....           | 432                                      |
| Belova, I.....      | 113, 261                   | Bigelow, G.....        | 104, 105, 161, 162, 222                         | Borbely, A.....         | 273, 310, 371                            |
| Belsito, D.....     | 387                        | Bigot, J.....          | 138   | Borgenstam, A.....      | 29, 54, 87, 143, 189, 202, 261, 328, 386 |
| Belt, C.....        | 326, 327, 413              | Bihamta, R.....        | 482   | Borgesen, P.....        | 103, 159, 274, 338, 398                  |
| Beltramino, L.....  | 138                        | Billat, G.....         | 437   | Borges, M.....          | 456                                      |
| Beltrao, M.....     | 438                        | Billet, B.....         | 89, 145   | Borkar, T.....          | 55, 229                                  |
| Benaduce, A.....    | 184                        | Billings, A.....       | 266   | Bornert, M.....         | 448                                      |
| Benafan, O.....     | 400                        | Bilodeau, J.....       | 382   | Bortolotto, L.....      | 489                                      |
| Bendersky, L.....   | 101, 145                   | Binek, C.....          | 331   | Boryczko, B.....        | 62                                       |
| Ben Hamouda, H..... | 31                         | Biner, B.....          | 154, 378  | Borzone, G.....         | 451                                      |
| Benique, F.....     | 268                        | Bineshmarvasti, B..... | 460   | Boswell-Koller, C.....  | 233                                      |
| Ben Khalifa, N..... | 122                        | Bingert, J.....        | 252, 255, 293, 380                              | Botta, W.....           | 20, 69, 468                              |
| Bennett, J.....     | 155, 156                   | Bingsman, J.....       | 500   | Böttcher, H.....        | 121                                      |
| Benson, D.....      | 137                        | Bin, Y.....            | 26, 491   | Bottin-Rousseau, S..... | 31, 143, 202                             |
| Bentley, J.....     | 158, 393                   | Birjega, R.....        | 415   | Bouaziz, O.....         | 434                                      |
| Bentsman, J.....    | 459                        | Birmie, D.....         | 16  | Bouchard, J.....        | 323                                      |
| Benum, S.....       | 307                        | Birol, B.....          | 407, 456  | Bouchard, P.....        | 122                                      |
| Ben, W.....         | 503                        | Birol, F.....          | 519   | Boufounos, D.....       | 236                                      |
| Benzerger, A.....   | 287, 412                   | Bischoff, J.....       | 370   | Bourell, D.....         | 343, 344                                 |
| Ben-Zvi, A.....     | 460                        | Bishay, A.....         | 13  | Bourges, G.....         | 26                                       |
| Berbenni, S.....    | 248, 279, 434, 474         | Biswas, B.....         | 112   | Bourgier, A.....        | 129                                      |
| Bergen, R.....      | 510                        | Biswas, K.....         | 241   | Bourke, M.....          | 430, 473                                 |
| Bergquist, A.....   | 321                        | Biswas, S.....         | 312   | Bourne, G.....          | 344                                      |
| Berkmortel, R.....  | 147                        | Bitzek, E.....         | 113   | Bourne, N.....          | 195, 253, 255                            |
| Berkovich, A.....   | 138                        | Bizios, R.....         | 183   | Bourricaudy, E.....     | 73                                       |
| Berlioux, J.....    | 129                        | Bjarno, O.....         | 123   | Bouvard, C.....         | 121                                      |
| Berman, T.....      | 37                         | Bjørnstad, H.....      | 381   | Bouvard, J.....         | 209                                      |
| Bermudez, K.....    | 32                         | Blachere, A.....       | 442   | Bo, W.....              | 21, 357                                  |
| Bernardes, A.....   | 441                        | Blackman, D.....       | 343   | Bowen, P.....           | 506                                      |
| Bernard, J.....     | 150                        | Blackshire, J.....     | 176   | Bower, A.....           | 159                                      |
| Bernardo, M.....    | 392                        |                        |   | Bowers, M.....          | 134, 412                                 |
| Bernazzani, P.....  | 268, 476                   |                        |   | Boyce, B.....           | 322, 350, 474, 484                       |
| Bernerder, J.....   | 236                        |                        |   |                         |  |

$Q(\phi, \sigma)$



$$kT_g = \frac{2(B)(V)(\epsilon_1)}{K_a}$$



|                         |   |                          |   |                          |  |
|-------------------------|---|--------------------------|---|--------------------------|--|
| Boyce, D.....           | 383   | Buchelnikov, V.....      | 151, 495                                      | Cai, W.....              | 296, 434, 435                              |
| Boyd, D.....            | 489   | Buchheit, R.....         | 306   | Cai, Z.....              | 370, 371                                   |
| Bozek, J.....           | 314   | Buchheit, T.....         | 108, 167, 227, 286, 349, 350, 411, 461        | Cakaj, O.....            | 498  |
| Bozkaya, D.....         | 106, 500  | Buchholz, A.....         | 327   | Cak, M.....              | 76   |
| Bozorg-Grayeli, T.....  | 356   | Buchovecky, E.....       | 159   | Cakmak, E.....           | 337  |
| Bozorgi, S.....         | 286   | Buck, H.....             | 187   | Calabro, J.....          | 220  |
| Bozzolo, G.....         | 445   | Budak, S.....            | 229   | Caldas, T.....           | 499  |
| Bradbury, W.....        | 19, 214, 224, 293   | Budenkova, O.....        | 30, 201                                       | Calder, A.....           | 99   |
| Bradley, C.....         | 15  | Budiman, A.....          | 103, 462, 464                                 | Calderon-Colon, X.....   | 125  |
| Bradshaw, T.....        | 96  | Budruk, A.....           | 51  | Calderon, H.....         | 490  |
| Brady, M.....           | 345, 378, 405   | Buehler, M.....          | 208, 302, 416                                 | Calderón, J.....         | 71   |
| Brammer, K.....         | 25, 184, 241  | Buehrig-Polaczek, A..... | 187   | Calixto, J.....          | 123  |
| Brammer, T.....         | 407   | Buekens, A.....          | 133   | Calka, A.....            | 188  |
| Brandes, M.....         | 273, 427  | Buffiere, J.....         | 430   | Calkins, F.....          | 50, 104, 161, 220, 277, 340, 400, 452, 454 |
| Brandl, C.....          | 78, 247, 423  | Buffière, J.....         | 80  | Calvert, P.....          | 125, 126, 421                              |
| Brankovic, S.....       | 85  | Bufford, D.....          | 109, 168                                      | Calzado, L.....          | 409  |
| Brar, H.....            | 25, 441   | Bugaev, V.....           | 76  | Camilo, A.....           | 438  |
| Brasche, L.....         | 176   | Bugge, M.....            | 299   | Camin, B.....            | 252  |
| Bratberg, J.....        | 203   | Bui, H.....              | 482   | Campbell,.....           | 112  |
| Bravo, J.....           | 26  | Bujoreanu, L.....        | 403, 513                                      | Campbell, A.....         | 409, 459, 497, 502                         |
| Brechet, Y.....         | 88  | Buksas, M.....           | 144   | Campbell, C.....         | 87, 113, 143, 202, 261, 328, 386           |
| Breczewski, T.....      | 105   | Bulatov, V.....          | 216, 248, 455                                 | Campbell, G.....         | 31, 67, 399                                |
| Breidenich, J.....      | 125, 126  | Bullen, J.....           | 459   | Campbell, J.....         | 226, 285, 348, 410                         |
| Brendel, M.....         | 383   | Buller, J.....           | 201, 438                                      | Campos, B.....           | 57   |
| Brennan, S.....         | 32, 261   | Bunin, I.....            | 130   | Campos, R.....           | 494  |
| Brenner, D.....         | 322   | Burchell, T.....         | 371   | Campoy-Quiles, M.....    | 13   |
| Brenner, R.....         | 342, 395  | Burek, M.....            | 462   | Canada, M.....           | 256  |
| Brewer, L.....          | 271, 322, 350, 474  | Burford, D.....          | 201, 258, 259, 382, 438, 439                  | Cannova, F.....          | 197, 256                                   |
| Bridge, J.....          | 187, 428  | Burke, P.....            | 493   | Cantin, K.....           | 322  |
| Brimbal, D.....         | 158   | Burkes, D.....           | 154   | Cao, A.....              | 365  |
| Brinckmann, S.....      | 474   | Burk, S.....             | 285, 408                                      | Cao, B.....              | 478  |
| Bringa, E.....          | 78, 94, 402   | Burnett, C.....          | 459   | Cao, G.....              | 370  |
| Brinkman, K.....        | 266, 391  | Burnham, A.....          | 301   | Cao, H.....              | 242, 468                                   |
| Brinson, L.....         | 277, 454  | Burns, J.....            | 96, 225                                       | Cao, W.....              | 119, 515                                   |
| Briones, L.....         | 440   | Burriel, R.....          | 495   | Cao, X.....              | 44   |
| Briot, N.....           | 462   | Burton, B.....           | 29  | Cao, Y.....              | 200, 328, 467                              |
| Brito, G.....           | 513, 515, 522   | Busby, J.....            | 158, 471                                      | Cao, Z.....              | 98, 312, 387                               |
| Brito, M.....           | 267   | Bush, J.....             | 329   | Capdevila-Montes, C..... | 182  |
| Britton, B.....         | 79, 278   | Buslaps, T.....          | 448   | Capolungo, L.....        | 342  |
| Brizuela, M.....        | 405   | Bussmann, M.....         | 367   | Caratini, Y.....         | 382  |
| Brock, J.....           | 100   | Butt, D.....             | 43, 96, 211, 224, 225, 266, 347, 471          | Cardoso, M.....          | 189  |
| Brodowsky, H.....       | 250   | Butz, A.....             | 90  | Cardwell, D.....         | 85, 415                                    |
| Broek, S.....           | 123, 360, 419   | Buzzi, D.....            | 441   | Carillo, F.....          | 425  |
| Brommer, P.....         | 83  | Byczynski, G.....        | 348   | Carillo, J.....          | 96   |
| Brommer, T.....         | 406   | Byer, C.....             | 411, 412                                      | Carlberg, T.....         | 186  |
| Bronkhorst, C.....      | 195, 196, 321, 380, 381                                   | Byler, D.....            | 195, 473                                      | Carlson, B.....          | 201, 259, 438, 439, 483                    |
| Brooke, P.....          | 344   | Byrd, D.....             | 280, 282                                      | Carlson, C.....          | 332, 333                                   |
| Brooks, G.....          | 129, 186, 244, 245, 307, 308, 366, 437, 466               | Bystrov, V.....          | 62  | Carlson, K.....          | 147  |
| Brown, A.....           | 195   | Byun, K.....             | 103   | Carlson, N.....          | 144  |
| Brown, D.....           | 53, 104, 163, 164, 220, 273, 370, 430, 431, 449, 472, 473 | Byun, T.....             | 40, 41, 99, 157, 158, 215, 270, 393, 445, 496 | Carlson, W.....          | 357  |
| Brown, E.....           | 79, 114   | <b>C</b>                 |   | Carlton, C.....          | 419  |
| Browne, D.....          | 286   | Caballero, F.....        | 23, 66, 124, 125, 181, 239                    | Carman, G.....           | 453  |
| Brown, H.....           | 514   | Caballero-Flores, R..... | 332   | Caro, A.....             | 29, 93, 94, 216                            |
| Browning, N.....        | 399   | Cabet, C.....            | 426   | Caron, A.....            | 243  |
| Brown, J.....           | 258, 438, 439   | Caboussat, A.....        | 466   | Carozzani, T.....        | 55   |
| Brownlow, S.....        | 374   | Caceres, C.....          | 329, 456                                      | Carpenter, J.....        | 16, 412                                    |
| Brown, R.....           | 92  | Cady, C.....             | 380   | Carpenter, R.....        | 85   |
| Brown, T.....           | 392   | Caffarey, M.....         | 301   | Carradó, A.....          | 313  |
| Bruck, H.....           | 252   | Cahill, D.....           | 387   | Carradó, A.....          | 432  |
| Brueckner-Foit, A.....  | 378   | Cahn, J.....             | 101   | Carreño, C.....          | 220  |
| Brüggemann, T.....      | 65  | Cai, L.....              | 44, 516                                       | Carrillo, F.....         | 491  |
| Brundidge, C.....       | 193, 396  | Caillard, D.....         | 105, 228, 231, 378                            | Carrillo, J.....         | 96   |
| Brune, R.....           | 312   | Cai, M.....              | 187   | Carroll, L.....          | 426, 470                                   |
| Brunet-Gauthier, V..... | 107   | Cairns, E.....           | 12  | Carroll, M.....          | 347  |
| Bryan, Z.....           | 143   |                          |   | Carsí, M.....            | 290  |
| Bucci, R.....           | 90  |                          |   | Carsley, J.....          | 64, 389                                    |
|                         |   |                          |   | Carter, B.....           | 154  |



# TMS2011

## 140th Annual Meeting & Exhibition

|                       |                                       |                        |  |                      |   |
|-----------------------|---------------------------------------|------------------------|--|----------------------|---|
| Carter, R.....        | 458                                   | Chason, E.....         | 159, 160                               | Chevalier, B.....    | 332   |
| Carvalho, R.....      | 177                                   | Chaswal, V.....        | 199, 290                               | Chiang, T.....       | 217   |
| Casolco, S.....       | 323, 513                              | Chateeriji, S.....     | 187                                    | Chiba, A.....        | 76, 385, 487, 488                           |
| Cassayre, L.....      | 461, 476                              | Chatterjee, A.....     | 458                                    | Chiba, M.....        | 515   |
| Cassenti, B.....      | 289                                   | Chatterjee, S.....     | 170                                    | Chickov, B.....      | 351   |
| Castañeda, H.....     | 323                                   | Chattopadhyay, S.....  | 473                                    | Chien-Neng, L.....   | 488   |
| Castanier, M.....     | 298                                   | Chaturvedi, A.....     | 208                                    | Chien, S.....        | 183   |
| Castano, C.....       | 44, 145                               | Chatzigeorgiou, G..... | 104                                    | Chien, W.....        | 88, 89, 309, 423                            |
| Castelnau, O.....     | 342, 343, 395, 448                    | Chaudhari, G.....      | 20                                     | Chikhradze, N.....   | 155, 510                                    |
| Castillo, A.....      | 433                                   | Chaudhary, R.....      | 410                                    | Chin, B.....         | 124, 471                                    |
| Castillo, T.....      | 428                                   | Chaudhary, S.....      | 289                                    | Chinella, J.....     | 121   |
| Castro, A.....        | 69, 362                               | Chaudhury, Z.....      | 107, 166, 225, 283                     | Chinellato, A.....   | 433   |
| Caton, M.....         | 176                                   | Chauveau, T.....       | 395, 448                               | Chinnathambi, K..... | 43, 211                                     |
| Catoor, D.....        | 317                                   | Chavariaga, E.....     | 214                                    | Chino, K.....        | 401   |
| Cavalcanti, I.....    | 416                                   | Chawla, N.....         | 32, 47, 49, 257, 312,                  | Chin, T.....         | 399, 464                                    |
| Cavalcanti, S.....    | 500                                   | .....                  | 314, 315, 337, 433, 450                | Chiou, G.....        | 398   |
| Cavanaugh, M.....     | 306                                   | Cheah, W.....          | 361                                    | Chisholm, B.....     | 351   |
| Cavin, O.....         | 206                                   | Chegini, A.....        | 52, 519                                | Chisholm, C.....     | 419   |
| Cazacu, O.....        | 222, 375                              | Chegini, Z.....        | 52                                     | Chisholm, M.....     | 110   |
| Cederqvist, L.....    | 141                                   | Chemezov, O.....       | 461                                    | Chitrada, K.....     | 371   |
| Cerecedo, E.....      | 131, 491                              | Che-Ming, C.....       | 514                                    | Chiu, C.....         | 116, 452                                    |
| Cerný, R.....         | 88, 89                                | Chemisky, Y.....       | 104                                    | Chiu, P.....         | 137   |
| Cerreta, E.....       | 79, 195, 196, 246,                    | Chénard, S.....        | 323                                    | Chiu, Y.....         | 46  |
| .....                 | 255, 321, 379, 380, 381               | Chen, B.....           | 46, 131, 313, 399, 424, 522            | Chmelik, D.....      | 224   |
| Cerri, E.....         | 64, 237                               | Chen, C.....           | 41, 45, 46, 47, 49, 150,               | Chmielus, M.....     | 220   |
| Certain, A.....       | 393                                   | .....                  | 252, 275, 276, 295, 320, 339,          | Cho, D.....          | 267   |
| Cerully, L.....       | 313                                   | .....                  | 340, 398, 399, 451, 473, 497, 511      | Choe, K.....         | 505   |
| Cesari, E.....        | 221                                   | Chen, D.....           | 39, 175, 268                           | Cho, H.....          | 157   |
| Ceschini, L.....      | 286                                   | Chen, E.....           | 81, 358, 386, 489                      | Choi, B.....         | 513   |
| Chae, J.....          | 126                                   | Chenelle, B.....       | 320                                    | Choi, C.....         | 25  |
| Chagelishvili, E..... | 136                                   | Chen, F.....           | 391                                    | Choi, D.....         | 450   |
| Chahal, D.....        | 152                                   | Chen, G.....           | 118, 134, 366, 399, 424                | Choi, E.....         | 51  |
| Chai, Y.....          | 452                                   | Cheng, C.....          | 48, 103, 141, 298, 309                 | Choi, G.....         | 334   |
| Chakraborty, A.....   | 409                                   | Cheng, F.....          | 140                                    | Choi, H.....         | 36, 166, 439, 492, 516                      |
| Chakraborty, M.....   | 162, 312                              | Cheng, I.....          | 461                                    | Choi, I.....         | 34, 350, 465                                |
| Challa, P.....        | 25, 68, 184                           | Cheng, J.....          | 36, 424                                | Choi, J.....         | 28, 334                                     |
| Chamanfar, A.....     | 294                                   | Cheng, K.....          | 12                                     | Choi, M.....         | 61  |
| Chamelot, P.....      | 461, 476                              | Cheng, S.....          | 319, 321, 337                          | Choi, P.....         | 124   |
| Champagne, V.....     | 458                                   | Cheng, T.....          | 84, 305, 316, 335, 359, 436            | Choi, S.....         | 36, 54, 84, 281, 481, 505, 519              |
| Chan, D.....          | 274                                   | Chenguang, B.....      | 476                                    | Choi, W.....         | 17, 18, 289, 410, 514                       |
| Chanda, A.....        | 122                                   | Cheng, Y.....          | 38, 275, 365, 366                      | Choi, Y.....         | 116, 205, 289, 375, 506                     |
| Chandler, J.....      | 138                                   | Chen, H.....           | 28, 46, 49, 261, 275, 392, 407         | Cho, J.....          | 53, 65, 512                                 |
| Chandra, D.....       | 88, 89, 309, 423                      | Chen, I.....           | 361, 398, 422, 464                     | Chojnacka, I.....    | 266   |
| Chandran, P.....      | 165, 512                              | Chen, J.....           | 22, 59, 89, 238,                       | Cho, K.....          | 20, 34, 37, 39, 166,                        |
| Chandrasekar, S.....  | 34, 292                               | .....                  | 322, 447, 466, 487, 522                | .....                | 313, 388, 481, 505, 519                     |
| Chandross, M.....     | 153                                   | Chen, K.....           | 103, 258, 272                          | Cho, M.....          | 339   |
| Chan, E.....          | 217                                   | Chen, L.....           | 42, 48, 84, 115, 147, 213, 259, 296,   | Choo, D.....         | 148   |
| Chang, A.....         | 345                                   | .....                  | 315, 317, 326, 328, 372, 431, 448, 477 | Choo, H.....         | 35, 69, 127, 140, 184, 191, 242,            |
| Chang, C.....         | 76                                    | Chen, M.....           | 56, 57, 215, 269, 302                  | .....                | 305, 337, 364, 383, 396, 422, 446, 447, 467 |
| Chang, H.....         | 70                                    | Chen, O.....           | 262                                    | Chopra, N.....       | 12, 55, 59, 110, 111,                       |
| Changizi, A.....      | 481                                   | Chen, P.....           | 23, 67, 68, 69, 125, 143,              | .....                | 115, 169, 173, 229, 232, 288,               |
| Chang, K.....         | 147                                   | .....                  | 183, 240, 302, 303, 361, 362, 420, 422 | .....                | 292, 350, 351, 352, 415, 463                |
| Chang, T.....         | 399                                   | Chen, Q.....           | 29, 250                                | Cho, S.....          | 110, 398, 410                               |
| Chang, W.....         | 84                                    | Chen, S.....           | 28, 119, 254, 275, 339,                | Choubey, P.....      | 112   |
| Changwoon, H.....     | 477                                   | .....                  | 397, 398, 451, 452, 464, 468, 497, 515 | Choudhuri, A.....    | 15  |
| Chang, Y.....         | 47, 119, 127, 133, 263, 389, 490, 515 | Chen, T.....           | 246                                    | Choudhuri, D.....    | 450   |
| Chan, L.....          | 72                                    | Chen, W.....           | 22, 40, 45, 99, 128, 164,              | Choudhury, A.....    | 32  |
| Chanturiya, V.....    | 130                                   | .....                  | 165, 219, 398, 403, 446, 463           | Choudhury, P.....    | 299   |
| Chan, Y.....          | 68                                    | Chen, X.....           | 89, 179, 181, 194, 370, 417            | Choudhury, S.....    | 159, 513                                    |
| Chao-bo, T.....       | 517                                   | Chen, Y.....           | 18, 82, 114, 127, 130,                 | Chou, K.....         | 175   |
| Chao, J.....          | 182                                   | .....                  | 165, 207, 289, 292, 438, 487           | Chou, M.....         | 334   |
| Chao, Z.....          | 297                                   | Chen, Z.....           | 40, 150, 172, 259, 336, 464            | Chou, P.....         | 95, 154, 210, 265, 270                      |
| Chapman, D.....       | 379                                   | Chepushtanova, T.....  | 354                                    | Chou, Y.....         | 345   |
| Chapman, K.....       | 101                                   | Cherkaoui, M.....      | 248, 416, 473, 474                     | Christ, H.....       | 285, 408                                    |
| Charette, O.....      | 419                                   | Chernenko, V.....      | 105                                    | Chrzan, D.....       | 233, 288, 412, 413                          |
| Charit, I.....        | 96, 154, 155, 211,                    | Cherng, S.....         | 399                                    | Chuang, A.....       | 184, 185                                    |
| .....                 | 224, 225, 326, 347, 375               | Chernova, L.....       | 106                                    | Chuang, C.....       | 346   |
| Charpentier, L.....   | 489                                   | Cheruvu, N.....        | 169                                    | Chuang, H.....       | 45  |

Chu, J..... 84, 101, 127, 305, 366  
 Chulmin, O..... 477  
 Chumlyakov, Y..... 50, 105, 401  
 Chun, B..... 176  
 Chung, B..... 398  
 Chung, C..... 45, 96  
 Chung, Q..... 103  
 Chung, S..... 410  
 Chung, Y..... 51, 320, 489  
 Chun, J..... 398  
 Chun, S..... 497  
 Chun, T..... 116, 175, 233, 234, 354  
 Chun, Y..... 453  
 Chupas, P..... 101  
 Ciappina, M..... 27  
 Ciftja, A..... 55, 460, 503  
 Cifuentes, G..... 440  
 Cigdem, M..... 225  
 Cimenoglu, H..... 24, 373, 481  
 Çimenoglu, H..... 23  
 Ciulik, J..... 284, 346, 407, 457, 500, 501  
 Ciupina, V..... 415  
 Ciuta, G..... 207  
 Cížek, J..... 246  
 Clark, D..... 256  
 Clark, E..... 210  
 Clarke, A..... 104, 430  
 Clarke, K..... 430, 471, 486  
 Clarke, R..... 396  
 Clark, J..... 502  
 Clark, K..... 334  
 Clark, M..... 165, 403  
 Clark, S..... 67  
 Clausen, B..... 53, 163, 164, 220, 272, 449  
 Clayton, K..... 332, 333  
 Clemens, H..... 501  
 Cloue, J..... 43  
 Clouet, E..... 172  
 Cobo, E..... 138  
 Cochran, J..... 313, 408  
 Cochran, S..... 341  
 Cocilovo, B..... 460  
 Cockcroft, S..... 227, 308  
 Cocke, D..... 72, 268, 476  
 Cockeram, B..... 95, 154, 210, 265, 501  
 Coda, A..... 400  
 Colas, K..... 371  
 Colás-Ortiz, R..... 21  
 Colás, R..... 519  
 Colavito, D..... 328  
 Cole, E..... 384  
 Cole, J..... 96, 155, 224, 225, 265, 333  
 Coleman, G..... 141  
 Coleman, L..... 180  
 Colinet, C..... 414  
 Colla, M..... 108  
 Collar, K..... 30  
 Collins, D..... 396  
 Collins, P..... 66, 135, 204, 309  
 Collins, S..... 491  
 Colon, T..... 229  
 Colorado, H..... 44, 344  
 Combeau, H..... 30, 187  
 Compton, C..... 501  
 Compton, D..... 292  
 Comstock, R..... 370, 473  
 Conde, A..... 332  
 Conley, R..... 102

Connelly, L..... 303  
 Conner, E..... 318  
 Connolley, T..... 31, 285  
 Conrad, T..... 305  
 Cooke, G..... 469  
 Cook, R..... 296  
 Cooksey, M..... 60, 116, 174, 233,  
 ..... 293, 354, 417, 420  
 Cook, W..... 188  
 Cooley, J..... 30  
 Cooney, R..... 520  
 Cooper, K..... 37, 60  
 Coppack, J..... 130  
 Cora, O..... 36  
 Cordes, N..... 110  
 Cordier, P..... 396  
 Cordill, M..... 372  
 Cormier, J..... 373  
 Cornella, M..... 73  
 Cornide, J..... 125  
 Corona, E..... 168  
 Corral, E..... 433  
 Corrêa, L..... 177  
 Cosin, S..... 500  
 Costalonga de Aguiar, M..... 499  
 Coté, P..... 307  
 Cotts, E..... 45, 47, 102, 103, 159,  
 ..... 219, 274, 337, 397, 449  
 Couet, A..... 473  
 Coughlin, D..... 162  
 Coulaud, C..... 138  
 Coulombe, M..... 437  
 Counts, W..... 74, 194, 343  
 Coupeau, C..... 77  
 Courchee, R..... 129  
 Courtenay, J..... 308  
 Couvy, H..... 89  
 Cowen, C..... 87, 212, 282  
 Cox, A..... 504  
 Cox, B..... 108  
 Cox, W..... 113  
 Coy, T..... 301  
 Craig, J..... 459  
 Cranford, S..... 416  
 Crepeau, P..... 226, 285, 348, 410  
 Crépin, J..... 314  
 Cretegy, L..... 283, 294  
 Creuziger, A..... 105, 195, 402  
 Crimp, M..... 135, 368, 402  
 Crivello, J..... 443  
 Crone, W..... 105  
 Crooker, P..... 431  
 Crooks, R..... 200, 201  
 Crosbie, D..... 410  
 Crouse, C..... 415  
 Crozier, P..... 94  
 Cruz, E..... 413  
 Cruz Rivera, J..... 428  
 Csiszar, G..... 396  
 Csiszár, G..... 273, 448  
 Cuesta, R..... 348  
 Cui, H..... 269, 346  
 Cui, J..... 33  
 Cui, Y..... 145, 175, 296, 356  
 Culp, J..... 392  
 Cunha, C..... 513, 515, 522  
 Cunha, O..... 492  
 Cunliffe, A..... 366

Cunningham, M..... 332, 333  
 Cunningham, N..... 41, 181, 211, 371, 393, 395  
 Cuomo, J..... 456  
 Cupid, D..... 376, 498  
 Curtarolo, S..... 249  
 Curtis, T..... 201, 439  
 Curzio, E..... 198, 378  
 Cyriac, A..... 107  
 Czechowicz, A..... 50, 51, 454

## D

D'Abreu, J..... 268, 417  
 da Costa, L..... 428, 429  
 Daehn, G..... 196, 255, 379, 427  
 Daei, F..... 52  
 Daglilar, S..... 165, 225, 367  
 Dahle, A..... 367  
 Dahlman, A..... 365  
 Dahmen, U..... 239, 245  
 Dai, C..... 254  
 Dai, J..... 206, 458  
 Dai, L..... 61, 117  
 Dai, X..... 411, 413  
 Dai, Y..... 190, 333, 472, 490  
 Dalal, V..... 289  
 Dal Martello, E..... 55  
 Daloz, W..... 408  
 Daly, S..... 18  
 Dames, C..... 312, 477, 515  
 Damoah, L..... 112, 461  
 D'Amours, G..... 482  
 Danaie, M..... 88  
 Dando, N..... 123, 180  
 Daniels, E..... 112  
 Daniels, J..... 185  
 Daniil, M..... 230, 264  
 Dan, L..... 518, 521  
 Dannenberg, A..... 277  
 Danoix, F..... 124  
 Dantzig, J..... 316  
 Dao, M..... 109  
 Daowu, Y..... 12  
 Daoxin, W..... 517, 518  
 Daphalapurkar, N..... 248  
 Daqiang, C..... 470  
 Darbandi, P..... 274, 501  
 Darling, K..... 232, 492  
 Darmstadt, H..... 256  
 Darsell, J..... 81  
 Das, D..... 241  
 Dasgupta, A..... 201, 246  
 da Silva, A..... 130, 438  
 da Silva, I..... 427, 429  
 da Silva, M..... 429  
 Das, R..... 151  
 Das, S..... 64, 108, 121, 149,  
 ..... 178, 236, 298, 358, 466  
 Dastjerd, H..... 515  
 Dauskardt, R..... 372, 393  
 Daveau, G..... 272, 342  
 Davies, B..... 34  
 Davies, R..... 33  
 Davis, B..... 36, 37, 39, 132, 206, 273, 388  
 Davis, J..... 245  
 Davis, T..... 200  
 Davydov, V..... 163  
 Dawson, K..... 183

# TMS2011

## 140th Annual Meeting & Exhibition

|                         |                              |                           |                              |                           |                                   |
|-------------------------|------------------------------|---------------------------|------------------------------|---------------------------|-----------------------------------|
| Dawson, P.....          | 163, 374, 383                | De Silva, K.....          | 520                          | Dogan, Ö.....             | 28, 392                           |
| Daymond, M.....         | 52, 105, 163, 222,           | DesJardins, J.....        | 241                          | Doherty, R.....           | 389                               |
| .....                   | 278, 342, 371, 401, 430, 454 | Desquines, J.....         | 430                          | Dohi, K.....              | 270                               |
| de Alcantara, N.....    | 438                          | Deuerling, J.....         | 305, 361                     | Do, K.....                | 481, 505                          |
| De Angelis, R.....      | 321                          | Deutchman, H.....         | 290                          | Dolan, M.....             | 423                               |
| Dean, M.....            | 303                          | Deutsch, T.....           | 431                          | Domack, M.....            | 200, 201                          |
| de Avillez, R.....      | 72                           | De Valle, S.....          | 460                          | Domain, C.....            | 42, 94, 215, 216, 271             |
| De-backer, A.....       | 215                          | Devanathan, R.....        | 154                          | Dombrowski, D.....        | 430                               |
| De Backer, A.....       | 216                          | Devaraj, A.....           | 66, 239                      | Dominguez Almaraz, G..... | 257                               |
| deBakker, J.....        | 132                          | De Vincentis, N.....      | 23                           | Dominique, G.....         | 391                               |
| deBarbadillo, J.....    | 345                          | Devincere, B.....         | 231, 272, 342                | Donaldson, D.....         | 357                               |
| Décamps, B.....         | 158, 270                     | DeWald, A.....            | 200, 431                     | Donati, D.....            | 53                                |
| De Carlo, F.....        | 433                          | Dewen, H.....             | 507, 508                     | Donati, L.....            | 122                               |
| De Cicco, M.....        | 202, 439, 440                | Dey, G.....               | 128, 188, 469                | Dong, A.....              | 461                               |
| Decker, R.....          | 37, 150                      | De Young, D.....          | 129                          | Dongare, A.....           | 322                               |
| Dedyukhin, A.....       | 466                          | Dharmendra, C.....        | 205                          | Dong, C.....              | 39, 70                            |
| Deepan, D.....          | 12                           | Dhedra, S.....            | 18                           | Dong, G.....              | 21, 357                           |
| DeFouw, J.....          | 107                          | Dheeradhada, V.....       | 312                          | Dong, H.....              | 479                               |
| De Graef, M.....        | 51, 309                      | Diao, J.....              | 294                          | Dong, L.....              | 174                               |
| Dehm, G.....            | 372, 412                     | Diaz, F.....              | 500                          | Donlon, W.....            | 37, 317                           |
| Dehoff, R.....          | 463, 487                     | Díaz, F.....              | 433                          | Dopita, M.....            | 224, 246                          |
| DeHoff, R.....          | 75                           | Diaz, G.....              | 73                           | Dorantes Rosales, H.....  | 428                               |
| De Hossou, J.....       | 295, 311                     | Dibbern, J.....           | 386                          | Dorantes-Rosales, H.....  | 507                               |
| Deibler, L.....         | 468                          | Dib, G.....               | 502                          | Dorogin, L.....           | 356                               |
| de Jaeger, J.....       | 107                          | DiCarlo, D.....           | 453                          | Dorreen, M.....           | 180, 238                          |
| De la Garza, M.....     | 519                          | Dick, A.....              | 27, 74, 75, 76               | dos Santos, J.....        | 200, 258, 382, 438                |
| Delaire, O.....         | 191                          | Dickerson, C.....         | 496                          | Dos Santos, J.....        | 336                               |
| Delaleau, P.....        | 201                          | Dickerson, P.....         | 427, 464, 472                | Doude, H.....             | 383                               |
| Delannay, L.....        | 106                          | Dickerson, R.....         | 16, 472                      | Doutre, D.....            | 367                               |
| Delcorde, X.....        | 360                          | Dickson, J.....           | 203                          | Dou, Z.....               | 30                                |
| D'Elia, F.....          | 179                          | Dickson, R.....           | 298                          | Downey, J.....            | 60, 116, 174, 233, 293, 354, 417  |
| del Mastro, N.....      | 421                          | Diedrich, E.....          | 310                          | Dragon, A.....            | 373                               |
| DeLorme, R.....         | 34, 37, 39, 273, 388         | Diehl, M.....             | 454                          | Drake, D.....             | 341                               |
| Delplanque, J.....      | 27, 172                      | Dignonnet, H.....         | 55                           | Drautz, R.....            | 347                               |
| Del Prado, J.....       | 18                           | Dik, J.....               | 309                          | Dreizin, E.....           | 17                                |
| Delsante, S.....        | 451                          | Diliegros Godines, C..... | 71                           | Drelich, J.....           | 13, 60, 116, 173, 174, 233,       |
| Delshad Khatibi, P..... | 281                          | Di Lisa, D.....           | 138                          | .....                     | 241, 293, 295, 354, 369, 417, 506 |
| De Lucas, R.....        | 413                          | Diller, T.....            | 344                          | Drillet, J.....           | 124                               |
| DeLucas, R.....         | 413                          | Dillon, Jr., O.....       | 494                          | Driscoll, D.....          | 54                                |
| DeMarco, J.....         | 121                          | Di Maio, D.....           | 219                          | Drobosyuk, M.....         | 151                               |
| Demetriou, M.....       | 69, 70, 128, 243, 306, 422   | Dimiduk, D.....           | 77, 135, 209, 230,           | Droz, V.....              | 89                                |
| DeMint, A.....          | 154                          | .....                     | 231, 250, 280, 289, 355, 375 | Drumond, W.....           | 433                               |
| Demiray, Y.....         | 234                          | Dimitrov, N.....          | 398                          | Druschitz, A.....         | 348, 396, 410                     |
| Demirci, F.....         | 517                          | D'Incau, M.....           | 101                          | Druschitz, E.....         | 396                               |
| Demirci, G.....         | 190                          | Dinda, G.....             | 201, 246                     | Dryepondt, S.....         | 198, 346                          |
| Demirkesen, E.....      | 369                          | Ding, H.....              | 70                           | Dry, M.....               | 73                                |
| Demkowicz, M.....       | 75, 100                      | Ding, K.....              | 323                          | Duan, J.....              | 203, 227                          |
| Demopoulos, G.....      | 73, 132                      | Dingreville, R.....       | 247, 248, 314, 374, 434, 473 | Duan, Z.....              | 349                               |
| de Morais, V.....       | 488                          | Ding, T.....              | 21                           | Duarte, G.....            | 23                                |
| Dempsey, N.....         | 207                          | Ding, W.....              | 33, 205, 206, 242            | Dubé, D.....              | 475                               |
| Demuth, M.....          | 327                          | Ding, Y.....              | 372                          | Dubé, N.....              | 300                               |
| Deng, C.....            | 442                          | Dinwiddie, R.....         | 229                          | Dubois, J.....            | 299                               |
| Deng, J.....            | 186, 475                     | Dion, M.....              | 256                          | Dubois, S.....            | 107                               |
| Deng, L.....            | 471                          | Diop, M.....              | 479                          | Dubon, O.....             | 233                               |
| Dennis, A.....          | 85, 415                      | Dirras, G.....            | 395                          | Du, C.....                | 190                               |
| Dennis, K.....          | 390                          | Dispinar, D.....          | 245, 348, 410                | Duchesneau, L.....        | 256                               |
| Dennis-Koller, D.....   | 195, 196, 380, 381           | Divan, R.....             | 101                          | Duchesne, C.....          | 238, 322                          |
| Deo, C.....             | 445                          | Divinski, S.....          | 19, 127, 171, 262            | Dudamell, N.....          | 32, 35                            |
| Depan, D.....           | 68                           | Dixit, M.....             | 288                          | Duerig, T.....            | 452                               |
| Dere Ozdemir, O.....    | 406                          | Dixit, V.....             | 135, 309                     | Duffield, A.....          | 30                                |
| Derin, B.....           | 165, 268, 457                | Djorgbenoo, A.....        | 269                          | Duffie, N.....            | 384                               |
| D'Errico, F.....        | 92                           | Dmitrieva, O.....         | 124                          | Duffy, M.....             | 13                                |
| de Sá, A.....           | 499                          | Dmowski, W.....           | 184, 185                     | Dufour, G.....            | 299                               |
| Desai, S.....           | 251                          | Dobatkina, S.....         | 187                          | Dufresne, E.....          | 448                               |
| Desgardin, P.....       | 270                          | Dodbiba, G.....           | 111, 112                     | Dugne, O.....             | 476                               |
| Desgroseilliers, B..... | 360                          | Dogan, E.....             | 50                           | Duh, J.....               | 45, 47, 48, 68, 85, 339, 397      |
| Desilets, M.....        | 382, 459                     | Dogan, O.....             | 212, 284, 285,               | Du, J.....                | 15, 491, 494                      |
| Désilets, M.....        | 382, 459                     | .....                     | 346, 391, 407, 457, 500      | Duman, I.....             | 235, 293, 354, 404, 483, 510      |



$Q(\phi, \sigma)$

$kT_g = \frac{2(B)(V)(\epsilon_1)}{K_a}$

|                       |   |                     |                                       |                     |                                      |
|-----------------------|---|---------------------|---------------------------------------|---------------------|--------------------------------------|
| Duman, U              | 514   | Elder, K            | 260                                   | Evans, P            | 240                                  |
| Dumas-Bouchiat, F     | 207   | El-Desouky, A       | 54, 164, 213, 223, 224, 280, 343, 403 | Evcimen, N          | 335                                  |
| Dumitrache, F         | 415   | Elfimov, I          | 23                                    | Evis, Z             | 516                                  |
| Dunand, D             | 51, 194, 400                                    | Elhalawaty, S       | 85                                    | Ewh, A              | 203                                  |
| Dunn, D               | 95  | Elhami Khorasani, A | 25                                    | Eyckens, P          | 374                                  |
| Dunne, D              | 188   | Elisseeff, J        | 125, 126                              | Ezaz, T             | 104                                  |
| Dunne, F              | 474   | Eljach, C           | 241                                   | <b>F</b>            |                                      |
| Dupiano, P            | 17  | El-Kaddah, N        | 148                                   | Fabrichnaya, O      | 376                                  |
| Dupon, E              | 511   | El Kadiri, H        | 34, 76, 223, 330, 484                 | Fabritius, H        | 361                                  |
| Dupont, V             | 254   | El-Khodary, K       | 474                                   | Fabry, B            | 442                                  |
| Dupuis, C             | 307   | Elliott, R          | 277                                   | Facco, G            | 96                                   |
| Dupuis, M             | 419   | Elmer, J            | 310, 336                              | Fafard, M           | 30, 322, 323, 420, 482               |
| Dupuy, A              | 519   | Elmkhah, H          | 372                                   | Fager Franzén, S    | 487                                  |
| Duscher, G            | 110   | El-Refaie, A        | 264                                   | Fähler, S           | 221, 340                             |
| Dussoubs, B           | 30  | Elsamadiy, a        | 497                                   | Fahrman, M          | 119                                  |
| Dutdibi, C            | 404   | Elsayed, A          | 493                                   | Faierson, E         | 347                                  |
| Duterrail, Y          | 30  | El-Sayed, M         | 348                                   | Faivre, G           | 31, 143, 202                         |
| Dutra, R              | 416   | Elsener, A          | 247                                   | Falk, M             | 67, 153                              |
| Dutrizac, J           | 246   | Elstnerova, P       | 361                                   | Fan, C              | 133, 217                             |
| Dutta, B              | 246   | Eluri, R            | 13                                    | Faney, T            | 211                                  |
| Dutta, I              | 45, 102, 103, 159, 219, 274, 337, 338, 397, 449 | Emadi, R            | 15                                    | Fang, H             | 261                                  |
| Dutta, S              | 53  | Emamy, M            | 108, 179, 225, 226, 508, 509, 520     | Fang, J             | 399, 498                             |
| Dutton, R             | 205   | Emery, J            | 474                                   | Fang, X             | 173, 262                             |
| Dutu, E               | 14  | Emrich, M           | 234                                   | Fang, Z             | 145                                  |
| Duval, P              | 342   | EM, V               | 446                                   | Fan, H              | 418                                  |
| Duval, T              | 488   | Enayati, M          | 15, 16, 17                            | Fanisalek, H        | 414                                  |
| Dye, D                | 221, 223, 252, 290                              | Endo, M             | 140                                   | Fan, J              | 354, 417                             |
| Dymek, S              | 200   | Engh, T             | 244, 308                              | Fan, P              | 145                                  |
| Dziaszyk, S           | 310   | England, C          | 142                                   | Fan, X              | 61, 295, 355, 417                    |
| Dzieciol, K           | 310   | Engler, O           | 28                                    | Fan, Z              | 61                                   |
| <b>E</b>              |   | English, C          | 43                                    | Fare, S             | 92                                   |
| Eakins, D             | 254, 379  | Engström, A         | 203                                   | Farhi, N            | 18                                   |
| Eapen, J              | 333, 371  | Eno, D              | 97                                    | Faria Jr., R        | 500                                  |
| Earthman, J           | 303, 324, 486                                   | Enser, J            | 236                                   | Farias, P           | 416                                  |
| Eason, P              | 344   | Entel, P            | 277, 495                              | Farina, J           | 241                                  |
| Eastman, C            | 203   | Epicier, T          | 124                                   | Farkas, D           | 93, 94, 152, 194, 208, 209, 240, 247 |
| Easton, M             | 205, 456  | Epishin, A          | 449                                   | Farrington, S       | 346                                  |
| Ebin, B               | 505, 516, 518                                   | Erdegren, M         | 186                                   | Farzadfar, S        | 35, 387                              |
| Ebrahimi, F           | 153, 376  | Erdeniz, D          | 344                                   | Fast, T             | 90                                   |
| Echeverría, A         | 438   | Ergun, C            | 484                                   | Fateh, B            | 245                                  |
| Echeverri Restrepo, S | 248   | Ergüven, H          | 404                                   | Fathi, M            | 324                                  |
| Eckert, J             | 18, 127, 422, 468                               | Erhart, P           | 41                                    | Faure, M            | 181                                  |
| Eckert, S             | 409   | Ermolayev, V        | 354                                   | Fautrelle, Y        | 30, 201                              |
| Economy, R            | 168   | Ertorer, O          | 15, 37, 224                           | Feaugas, X          | 43                                   |
| Edalati, K            | 20, 193   | Escalera-Lozano, R  | 283                                   | Fecht, H            | 243                                  |
| Eden, T               | 344   | Escobedo, J         | 255, 321, 381                         | Fehrenbacher, A     | 384                                  |
| Edick, J              | 241   | Escoda, L           | 151                                   | Feichtenschlager, B | 363                                  |
| Edwards, D            | 270   | Esen, Z             | 492                                   | Fei, H              | 49, 314, 450                         |
| Edwards, L            | 197, 256  | Esezobor, D         | 214                                   | Feinberg, Z         | 384                                  |
| Edwards, P            | 141   | Eskin, D            | 186                                   | Fei-Shuo, H         | 514                                  |
| Efe, M                | 34, 292   | Esmacili, S         | 237                                   | Fei-Yi, H           | 38, 514                              |
| Efrem, V              | 137   | Espinosa, D         | 57, 171, 407, 441, 499                | Felberbaum, M       | 367                                  |
| Egami, T              | 184, 185, 272                                   | Espinoza, E         | 521                                   | Fellicelli, S       | 227, 348, 349                        |
| Eggeler, G            | 310, 340, 400                                   | Espinoza, F         | 125, 126                              | Fell, C             | 218                                  |
| Eiersebner, M         | 438   | Essadiqi, E         | 33, 35, 147                           | Fellner, P          | 360                                  |
| Eifler, D             | 114, 115, 140, 199, 253, 259                    | Es-Sadiqi, E        | 387                                   | Feng, C             | 344                                  |
| Eiken, J              | 143   | Etienne, A          | 41, 181, 211, 393                     | Feng, G             | 296                                  |
| Einarsrud, K          | 420   | Etter, T            | 63                                    | Feng, J             | 382                                  |
| Eisenlohr, P          | 135, 368, 374, 375, 402, 454                    | Eudy, J             | 199                                   | Feng, L             | 39                                   |
| Eisman, M             | 63  | Eufrazio, M         | 138                                   | Feng, N             | 30, 149, 381                         |
| Ekerim, A             | 335   | Euh, K              | 246                                   | Feng, Q             | 307, 487                             |
| Ekiz, E               | 66  | Eung-Ryul, B        | 481                                   | Feng, Y             | 420                                  |
| Elam, J               | 173   | Evanoff, K          | 464                                   | Feng, Z             | 383, 396, 431, 446                   |
| El-Awady, J           | 77, 135, 209, 230, 231, 355                     | Evans, A            | 63, 447                               | Fensin, S           | 79, 255                              |
| El-Azab, A            | 154, 216, 475                                   | Evans, C            | 223                                   | Fenton, G           | 196, 379                             |
|                       |   | Evans, J            | 346                                   | Ferek, P            | 325                                  |
|                       |   | Evans, N            | 23, 66, 124, 156, 181, 239, 282, 345  |                     |                                      |

INDEX

# TMS2011

## 140th Annual Meeting & Exhibition

|                       |                              |                       |   |                         |  |
|-----------------------|------------------------------|-----------------------|---|-------------------------|--|
| Fergus, J.....        | 267, 409                     | Foroozmehr, E.....    | 237   | Funkhouser, C.....      | 435  |
| Fergusson, L.....     | 235                          | Forrester, J.....     | 273   | Fu, P.....              | 205  |
| Ferreira, A.....      | 428                          | Forsmark, J.....      | 480, 482, 484   | Furar, I.....           | 311  |
| Ferreira, N.....      | 188, 458                     | Forsyth, R.....       | 430, 486  | Furlan Ferreira, F..... | 72   |
| Ferreira Neto, J..... | 461                          | Fortin, H.....        | 323   | Furrer, D.....          | 62, 90, 118, 176, 205  |
| Ferreira, P.....      | 418, 419                     | Foster, J.....        | 333   | Furuhara, T.....        | 124  |
| Ferrell, J.....       | 425                          | Fourty, A.....        | 455   | Furukawa, A.....        | 244  |
| Ferrier, N.....       | 384                          | Fox, K.....           | 266   | Furuta, T.....          | 193  |
| Ferris, K.....        | 146                          | Foy, P.....           | 169   | Fu, Y.....              | 131, 133, 491  |
| Ferry, M.....         | 310                          | França, S.....        | 177   |                         |  |
| Fersi, R.....         | 515                          | Franco, B.....        | 161   | <b>G</b>                |  |
| Fèvre, M.....         | 249                          | Franco, V.....        | 150, 207, 208, 263, 331, 332, 389, 443, 444, 495          | Gaal, S.....            | 55   |
| Feyerabend, F.....    | 92                           | Frandsen, C.....      | 184   | Gabb, T.....            | 119, 257   |
| Fezkaa, K.....        | 448                          | Franke, O.....        | 185   | Gadre, M.....           | 249  |
| Fiebig, J.....        | 19                           | Franklin, J.....      | 379   | Gadzuric, S.....        | 266  |
| Fiedler, T.....       | 113                          | Franklin, T.....      | 114   | Gaertner, H.....        | 180  |
| Field, D.....         | 278, 279, 310, 455, 474      | Franz, H.....         | 448   | Gagne, J.....           | 122  |
| Fielden, D.....       | 199                          | Frary, M.....         | 96, 347   | Gagnon, F.....          | 420  |
| Field, F.....         | 406                          | Fraser, H.....        | 17, 66, 135, 181, 182, 204, 239, 288, 309                 | Gaies, J.....           | 64   |
| Fielding, R.....      | 265                          | Fray, D.....          | 476, 504  | Gaines, L.....          | 301  |
| Field, K.....         | 158                          | Frear, D.....         | 45, 102, 159, 219, 274, 337, 397, 449                     | Gaines, M.....          | 350  |
| Field, R.....         | 104, 380, 430, 486           | Frechette, L.....     | 462   | Gajewski, G.....        | 250  |
| Fields, K.....        | 427                          | Fredericks, G.....    | 189   | Gallagher, M.....       | 489  |
| Fife, J.....          | 202                          | Freels, M.....        | 32  | Gallerneault, M.....    | 237  |
| Figueroa, I.....      | 185, 468                     | Free, M.....          | 298, 440, 476, 477, 491                                   | Gall, K.....            | 105, 161, 304  |
| Finch, J.....         | 311                          | Freeman, A.....       | 408   | Gallup, K.....          | 488  |
| Fine, M.....          | 320, 449                     | Freeman, C.....       | 366   | Gálvez, F.....          | 32, 35   |
| Finlayson, T.....     | 449                          | Freeman, J.....       | 201   | Gambone, M.....         | 119  |
| Fiory, A.....         | 432                          | Frei, A.....          | 469   | Gandhi, A.....          | 15   |
| Fiot, N.....          | 138                          | Fressengeas, C.....   | 290, 434  | Gandin, C.....          | 30, 31, 55   |
| Firrao, D.....        | 130, 188, 246, 493           | Freudenberger, J..... | 18  | Ganegoda, H.....        | 473  |
| Fischer, F.....       | 221                          | Freund, S.....        | 413   | Ganesan, K.....         | 490  |
| Fischer, T.....       | 336                          | Friak, M.....         | 194, 343, 361   | Ganesan, Y.....         | 228, 418   |
| Fischer, W.....       | 436                          | Frias Gomez, C.....   | 73  | Gangopadhyay, A.....    | 230, 467   |
| Fisher, I.....        | 101                          | Friedland, E.....     | 446   | Ganguli, S.....         | 107, 462   |
| Fivel, M.....         | 231                          | Friedman, L.....      | 116   | Gan, J.....             | 265, 496   |
| Fjaer, H.....         | 273                          | Friedman, P.....      | 389   | Gan, M.....             | 355, 417   |
| Fjeld, A.....         | 97                           | Frigola, P.....       | 280   | Gannon, P.....          | 334  |
| Flanagan, T.....      | 423                          | Frihart, C.....       | 421   | Gansert, R.....         | 311, 480   |
| Flandorfer, H.....    | 275, 339, 398, 451, 452, 497 | Frisbie, B.....       | 159   | Gantan, I.....          | 309  |
| Flater, P.....        | 321                          | Frishman, A.....      | 177   | Gao, B.....             | 87, 149, 190, 239  |
| Fleaca, C.....        | 415                          | Frizon, F.....        | 442   | Gao, C.....             | 387  |
| Fleck, C.....         | 361, 421                     | Frolov, T.....        | 83  | Gao, F.....             | 40, 99, 100, 154   |
| Fleckenstein, J.....  | 180                          | Fromm, B.....         | 319   | Gao, H.....             | 361  |
| Fleming, N.....       | 406                          | Fruchart, D.....      | 495   | Gao, J.....             | 127, 308   |
| Fletcher, M.....      | 150                          | Fu, C.....            | 44, 86, 181, 216, 249, 339                                | Gao, M.....             | 28, 47, 212, 376, 377, 392, 407, 457   |
| Flicker, J.....       | 116                          | Fuchs, G.....         | 490   | Gao, P.....             | 507  |
| Fliffet, A.....       | 344                          | Fu, E.....            | 43, 496   | Gao, S.....             | 328  |
| Florando, J.....      | 254, 320                     | Fuesz, P.....         | 100   | Gao, W.....             | 25, 130  |
| Florea, R.....        | 298                          | Fugetsu, B.....       | 167   | Gao, Y.....             | 22, 39, 69, 100, 123, 127, 150, 168, 180, 184, 242, 261, 305, 319, 364, 422, 424, 437, 447, 467, 520 |
| Flores, K.....        | 193, 242, 243, 306, 364, 421 | Fujda, M.....         | 187   | Garay, J.....           | 223, 312, 463, 477, 515, 516, 519  |
| Floyd, M.....         | 128                          | Fujii, H.....         | 82, 325   | Garbacz, H.....         | 19   |
| Fluss, M.....         | 393                          | Fujishiro, T.....     | 125   | Garces, G.....          | 92   |
| Foেকে, T.....         | 121                          | Fujita, K.....        | 69, 70  | Garcia, C.....          | 293  |
| Fogagnolo, J.....     | 20                           | Fujita, T.....        | 111, 112  | Garcia Cardona, C.....  | 156  |
| Foiles, S.....        | 74                           | Fuks, D.....          | 250   | Garcia, H.....          | 230  |
| Foley, D.....         | 33, 293                      | Fukusumi, M.....      | 82, 522   | García, J.....          | 151  |
| Foley, J.....         | 30, 94                       | Fuller, B.....        | 165, 403  | Garcia-Mateo, C.....    | 125  |
| Folkers, A.....       | 299                          | Fuller, T.....        | 464   | Garcia, R.....          | 506, 521   |
| Fong, H.....          | 68                           | Fullwood, D.....      | 72, 278, 310, 318, 319, 456                               | Garcia Rocha, J.....    | 428  |
| Fonseca, J.....       | 253                          | Fultz, B.....         | 44, 100, 133, 159, 182, 191, 192, 217, 271, 335, 394, 446 | Garcia-Sanchez, E.....  | 21   |
| Fontes, A.....        | 416                          | Fumagalli, L.....     | 400   | Gardiner, B.....        | 426  |
| Font, J.....          | 221                          | Fu, N.....            | 73  | Gardner, C.....         | 72   |
| Fontus, M.....        | 365                          | Funkenbusch, P.....   | 72  | Gardner, D.....         | 428  |
| Fook, M.....          | 500                          |                       |   | Garg, A.....            | 105, 161, 162, 341   |
| Forato, O.....        | 138                          |                       |   |                         |  |
| Forest, S.....        | 374                          |                       |   |                         |  |
| Fornell, J.....       | 468                          |                       |   |                         |  |

$Q(\varphi, \sigma)$

$kT_g = \frac{2(B)(V)(\epsilon_1)}{K_a}$

|                              |                                  |                        |                    |                         |   |
|------------------------------|----------------------------------|------------------------|--------------------|-------------------------|---|
| Gariépy, R.....              | 360                              | Gibson, J.....         | 149                | Gostovic, D.....        | 115   |
| Garkida, A.....              | 499                              | Gibson, M.....         | 205, 262           | Goswami, R.....         | 37, 230, 256, 264, 298                              |
| Garlea, E.....               | 32, 52, 273                      | Gierlotka, W.....      | 451, 497           | Gottstein, G.....       | 28, 65, 171   |
| Garlea, O.....               | 178                              | Giese, D.....          | 381                | Goudy, A.....           | 89  |
| Garmestani, H.....           | 18, 126, 230, 283, 304           | Gihleengen, B.....     | 406                | Gould, J.....           | 489   |
| Garpinger, O.....            | 141                              | Gilbert, M.....        | 180                | Govindarajan, M.....    | 139   |
| Garrano, A.....              | 302                              | Gilbon, D.....         | 43                 | Gower, L.....           | 68  |
| Garrett, G.....              | 128                              | Gill, A.....           | 245                | Goyeau, B.....          | 30  |
| Garrido, F.....              | 120, 130, 131                    | Gill, J.....           | 367                | Gracio, J.....          | 283, 401, 403                                       |
| Garriga, M.....              | 13                               | Gillner, A.....        | 187                | Gragg, D.....           | 333, 427  |
| Garrison, L.....             | 43                               | Gil, Y.....            | 54                 | Graham, J.....          | 126   |
| Garside, G.....              | 208, 251, 449                    | Jimenez Britos, P..... | 382                | Gramma, I.....          | 238   |
| Garza, M.....                | 284                              | Giovanni, S.....       | 374                | Granasy, L.....         | 260   |
| Gascoyne, S.....             | 258                              | Girard, J.....         | 447                | Gránásy, L.....         | 31  |
| Gassa, L.....                | 349                              | Girase, B.....         | 68                 | Grandfield, J.....      | 129, 186, 244, 273, 307, 366                        |
| Gastan, E.....               | 481                              | Girault, G.....        | 181                | Grano, A.....           | 169   |
| Gaston, D.....               | 154                              | Giri, U.....           | 178                | Grant, D.....           | 201, 311, 480                                       |
| Gaune-Escard, M.....         | 266                              | Girshick, S.....       | 228                | Grant, G.....           | 81, 258, 325, 438                                   |
| Gaur, M.....                 | 17                               | Gittard, S.....        | 351                | Grassini, S.....        | 493   |
| Gaustad, G.....              | 301                              | Givord, D.....         | 207                | Gratz, E.....           | 149   |
| Gautam, U.....               | 173                              | Givorm, R.....         | 383                | Graves, K.....          | 169   |
| Gauvin, G.....               | 323                              | Glass, R.....          | 250                | Gray, G.....            | 78, 79, 136, 195, 252, 253, 255, 320, 321, 379, 380 |
| Gavras, A.....               | 320                              | Gleeson, B.....        | 405                | Gray III, G.....        | 79, 246, 255  |
| Gavrila Florescu, L.....     | 14                               | Gnäupel-Herold, T..... | 402                | Gray-Weale, A.....      | 27  |
| Gawad, J.....                | 374                              | Goasguen, S.....       | 152                | Greenfield, S.....      | 195   |
| Gaydosh, D.....              | 105, 278                         | Gobin, D.....          | 30                 | Green, N.....           | 226   |
| Gaytan, S.....               | 71, 196, 480                     | Goddard, W.....        | 93                 | Greenwood, M.....       | 316   |
| Gbenebor, O.....             | 237                              | Goel, M.....           | 424, 469, 470      | Greer, J.....           | 56, 355, 356, 462, 465, 467                         |
| Geantil, P.....              | 272                              | Goenka, S.....         | 241                | Greger, M.....          | 237, 479  |
| Geathers, J.....             | 396                              | Goetz, R.....          | 205                | Gregori, F.....         | 254   |
| Ge, D.....                   | 470                              | Gokce, H.....          | 404                | Grennerat, F.....       | 342   |
| Geetha Priyadarshini, B..... | 312                              | Gökçe, H.....          | 404                | Greve, B.....           | 192   |
| Geier, G.....                | 507                              | Golberg, D.....        | 173                | Griesche, A.....        | 202   |
| Gelisio, L.....              | 218                              | Golden, P.....         | 176                | Griessacher, T.....     | 469, 517  |
| Gell, M.....                 | 170                              | Goldman, J.....        | 241                | Griffin, J.....         | 348   |
| Geltmacher, A.....           | 279, 315                         | Gold, S.....           | 344                | Griffin, R.....         | 501   |
| Gendre, M.....               | 138                              | Goljandin, D.....      | 111                | Griffiths, W.....       | 285, 348, 410                                       |
| Geng, S.....                 | 268                              | Golkar, F.....         | 390                | Groeber, M.....         | 72, 118, 280, 375                                   |
| Genis, A.....                | 102                              | Goller, G.....         | 515, 519           | Groebner, J.....        | 205   |
| Gentleman, M.....            | 71, 183                          | Golubov, S.....        | 99                 | Grolmund, D.....        | 394   |
| Geoffroy, D.....             | 314                              | Golumbfskie, W.....    | 64                 | Gronbech-Jensen, N..... | 191   |
| George, C.....               | 310                              | Gomes da Silva, M..... | 370                | Grosse, M.....          | 472   |
| George, E.....               | 76, 134, 192, 250, 317, 350, 377 | Gomes, J.....          | 72, 268, 476       | Gross, J.....           | 438   |
| George, J.....               | 85                               | Gómez, M.....          | 417                | Gross, T.....           | 238   |
| Georgeta, C.....             | 391                              | Gong, J.....           | 228                | Groves, J.....          | 356   |
| Gerberich, W.....            | 228, 295, 350                    | Gong, W.....           | 266                | Groza, J.....           | 27, 172   |
| Gerbeth, G.....              | 409                              | Gong, Y.....           | 480                | Gruner, M.....          | 277   |
| Gergaud, P.....              | 395                              | Goñi, A.....           | 13                 | Grupke, R.....          | 410   |
| Germann, H.....              | 140                              | Gonzalez, J.....       | 43                 | Grylls, R.....          | 459   |
| Germann, T.....              | 78, 113, 254, 255, 380, 423      | Goob, B.....           | 521                | Gschneider, Jr., K..... | 152, 495  |
| German, R.....               | 19, 164, 214, 223, 293           | Gooch, J.....          | 154                | Gschneider, K.....      | 95, 150, 444, 445, 495                              |
| Gerstenberger, R.....        | 336                              | Goodall, R.....        | 185                | Gstoehl, D.....         | 424   |
| Gesto, D.....                | 326                              | Good, B.....           | 445                | Guan, H.....            | 384   |
| Getty, H.....                | 241                              | Goodman, A.....        | 392                | Guan, Z.....            | 173, 359  |
| Geveci, A.....               | 354                              | Goods, S.....          | 271                | Gudbrandsen, H.....     | 300   |
| Gharghour, M.....            | 35                               | Goossens, D.....       | 217, 218, 273      | Gudmundsson, H.....     | 360   |
| Ghassemi, H.....             | 296                              | Gorbatov, O.....       | 387                | Guduru, R.....          | 405, 432, 478, 482, 498                             |
| Ghazavizadeh, A.....         | 230                              | Gordillo, M.....       | 479                | Guebels, C.....         | 27, 172   |
| Ghazisaefi, M.....           | 75                               | Gordillo, S.....       | 23                 | Gueijman, S.....        | 510   |
| Gheno, T.....                | 404                              | Gordon, A.....         | 121                | Guerrero, M.....        | 519   |
| Gholipour, J.....            | 294                              | Gorkaya, T.....        | 171                | Guglielmini, E.....     | 469   |
| Ghosh, G.....                | 449, 489                         | Gorman, B.....         | 471                | Guilin, L.....          | 22  |
| Ghosh, S.....                | 421                              | Gorman, T.....         | 119                | Guillen, D.....         | 413   |
| Ghosn, L.....                | 257                              | Gornostyrev, Y.....    | 387                | Guillot, M.....         | 323, 482  |
| Gianola, D.....              | 228, 296                         | Gorr, B.....           | 285, 408           | Guillou, F.....         | 332   |
| Gibala, R.....               | 74                               | Gorsse, S.....         | 332                | Gulsoy, G.....          | 210   |
| Gibbons, J.....              | 183                              | Gorti, S.....          | 164, 165, 336, 403 | Gumbsch, P.....         | 90, 172, 233, 287                                   |
| Gibilaro, M.....             | 461, 476                         | Gosau, S.....          | 197                |                         |   |

INDEX



# TMS2011

## 140th Annual Meeting & Exhibition

|                                     |   |                       |   |                         |  |
|-------------------------------------|---|-----------------------|---|-------------------------|--|
| Guney, O.....                       | 369   | Halary, J.....        | 362                                     | Ha, S.....              | 47, 192  |
| Gungormus, M.....                   | 68, 242   | Haldar, S.....        | 252                                     | Hasan, S.....           | 98   |
| Guo, F.....                         | 46, 160, 397  | Hale, C.....          | 199                                     | Hasegawa, M.....        | 42   |
| Guo, J.....                         | 286, 397  | Hales, S.....         | 200                                     | Hasegawa, R.....        | 444  |
| Guo, Q.....                         | 125   | Haller, E.....        | 233                                     | Hasegawa, T.....        | 125, 393                                       |
| Guo, S.....                         | 98, 118, 132, 175, 355                                      | Hallil, A.....        | 248                                     | Hashemi, B.....         | 513  |
| Guo, W.....                         | 184, 185, 272   | Hall, T.....          | 268                                     | Hashemi-Sadraei, L..... | 167  |
| Guo, X.....                         | 379   | Hamada, G.....        | 388                                     | Hashida, T.....         | 188  |
| Guo, Y.....                         | 174, 321, 354, 417, 518                                     | Hamaguchi, M.....     | 197                                     | Hashimoto, A.....       | 37, 388  |
| Guoyin, Z.....                      | 65, 283   | Ham, B.....           | 88, 144                                 | Hashimoto, K.....       | 384  |
| Guozhi, L.....                      | 120, 297  | Hamed, M.....         | 12                                      | Hashimoto, N.....       | 158  |
| Gupta, A.....                       | 388, 421  | Hamel, S.....         | 402                                     | Haskel, D.....          | 150  |
| Gupta, D.....                       | 482   | Hamid, S.....         | 481                                     | Hassan, H.....          | 300  |
| Gupta, M.....                       | 32, 188   | Hamilton, C.....      | 196, 200                                | Hassan, J.....          | 367  |
| Gupta, N.....                       | 169, 196, 287   | Hamilton, R.....      | 285                                     | Hatada, N.....          | 369  |
| Gupta, R.....                       | 320   | Hammerschmidt, T..... | 347                                     | Hatakeyama, M.....      | 271  |
| Gupta, S.....                       | 56  | Hammi, Y.....         | 34                                      | Hatkevich, S.....       | 312, 484                                       |
| Gurao, N.....                       | 223   | Hammon, D.....        | 232, 430                                | Hattar, K.....          | 271, 349, 350                                  |
| Gurevich, S.....                    | 147, 260  | Hammond, V.....       | 313                                     | Haugan, J.....          | 86   |
| Gurmen, S.....                      | 505, 516, 518   | Hamouda, A.....       | 32                                      | Haupt, T.....           | 90   |
| Guruprasad, P.....                  | 48, 412   | Hanan, J.....         | 107, 128                                | Hausler, A.....         | 288  |
| Guruswamy, S.....                   | 208, 251, 449   | Han, B.....           | 393                                     | Hausmann, J.....        | 374  |
| Gu, S.....                          | 235, 360  | Handyside, A.....     | 201, 259                                | Hautus, M.....          | 22   |
| Gusberti, V.....                    | 138   | Haney, E.....         | 41, 393                                 | Hawkins, T.....         | 169  |
| Gutfleisch, O.....                  | 150, 151, 207, 208, 263,<br>331, 389, 390, 443, 444, 495    | Han, G.....           | 295, 363                                | Hawk, J.....            | 119, 155, 212, 213,<br>267, 282, 284, 334, 391 |
| Guthikonda, V.....                  | 277   | Hang, W.....          | 466                                     | Hawreliak, J.....       | 78   |
| Güth, K.....                        | 390   | Han, H.....           | 36, 53, 239                             | Haxhijaj, A.....        | 295  |
| Guthrie, R.....                     | 367, 409  | Han, J.....           | 21, 450, 485, 506, 510                  | Hayashida, K.....       | 386  |
| Gutierrez, H.....                   | 295   | Hanken, B.....        | 191                                     | Haykin, R.....          | 165  |
| Gutierrez Ladron de Guevara, L..... | 71  | Hanlon, T.....        | 319                                     | Haynes, A.....          | 213  |
| Güven, G.....                       | 268   | Hanlunmyuang, Y.....  | 288                                     | Hay, R.....             | 54   |
| Guyer, J.....                       | 146, 289, 316   | Han, M.....           | 47, 120, 392                            | Hayslett, M.....        | 83   |
| Gu, Z.....                          | 103   | Hanna, M.....         | 226                                     | Hazeli, K.....          | 198  |
| Guzman, J.....                      | 233   | Hannart, B.....       | 129                                     | Headlam-Shaw, R.....    | 178  |
| <b>H</b>                            |   |                       |   |                         |  |
| Haakonsen, H.....                   | 299   | Hänninen, H.....      | 200                                     | Headrick, R.....        | 102  |
| Haarberg, G.....                    | 300   | Hannon, A.....        | 366                                     | Hearon, K.....          | 363  |
| Haataja, M.....                     | 27, 74, 133, 191, 249,<br>315, 316, 365, 373, 376, 435, 464 | Han, S.....           | 28, 246, 295, 296, 355, 356, 418, 464   | He, B.....              | 447  |
| Habe, D.....                        | 507   | Hansen, B.....        | 195, 196, 321, 381                      | Hebert, R.....          | 168, 243, 467                                  |
| Haberl, K.....                      | 286   | Hansen, H.....        | 250                                     | Hebesberger, T.....     | 402  |
| Habibi, M.....                      | 213, 324, 372   | Hansen, J.....        | 381                                     | He, C.....              | 175  |
| Habibi-parsa, M.....                | 19  | Han, W.....           | 139                                     | Hecht, U.....           | 143  |
| Habibi Parsa, M.....                | 315   | Han, Z.....           | 89, 203, 227                            | Hector Jr, L.....       | 88, 144  |
| Habib, K.....                       | 299   | Hao, B.....           | 470                                     | Hector, L.....          | 92, 251  |
| Hacini, L.....                      | 382   | Hao, H.....           | 160, 354, 479                           | Hedström, P.....        | 189, 317                                       |
| Hacioglu, T.....                    | 165   | Hao, X.....           | 164, 337                                | Heerdegen, A.....       | 217  |
| Hackenberg, R.....                  | 486   | Hapke, J.....         | 412                                     | He, H.....              | 46, 382, 397                                   |
| Hackett, M.....                     | 95, 154, 210, 265   | Haq, A.....           | 188                                     | Heidari, H.....         | 475  |
| Haddad, D.....                      | 38  | Hara, T.....          | 341                                     | Heidary, P.....         | 465  |
| Haddadi, F.....                     | 114   | Harcuba, P.....       | 24, 35, 49, 246, 487                    | Heidloff, A.....        | 280  |
| Hadjipanayis, G.....                | 207, 389  | Hardin, C.....        | 515                                     | Heil, J.....            | 456  |
| Haefner, D.....                     | 100   | Hardy, M.....         | 79, 80                                  | Heilmaier, M.....       | 292, 407, 427                                  |
| Hafley, R.....                      | 200   | Hardy, V.....         | 332                                     | Heim, A.....            | 446  |
| Hagglund, T.....                    | 141   | Harimkar, S.....      | 55, 91, 110, 169,<br>170, 229, 288, 350 | Heinimann, M.....       | 90   |
| Hagni, A.....                       | 131   | Harlow, D.....        | 257                                     | Heinz, N.....           | 239  |
| Hahm, M.....                        | 463   | Harmon, C.....        | 306                                     | Heinz, S.....           | 114  |
| Hahn, H.....                        | 44, 66, 344   | Harper, D.....        | 229                                     | Heisser, C.....         | 226  |
| Hai-ding, G.....                    | 198   | Harrigan, T.....      | 379                                     | Heitling, T.....        | 300  |
| Haidoux, A.....                     | 144   | Harrigan, W.....      | 313                                     | He, J.....              | 30   |
| Haik, Y.....                        | 416   | Harringa, J.....      | 219, 274                                | Hejazi, D.....          | 188  |
| Haines, C.....                      | 224, 293, 358   | Harris, A.....        | 42                                      | Helberg, L.....         | 132  |
| Haixia, T.....                      | 12  | Harris, V.....        | 230                                     | Helfen, L.....          | 309  |
| Haiyan, Y.....                      | 21, 22  | Hart, G.....          | 249                                     | Heller, L.....          | 400  |
| Hakonsen, A.....                    | 186, 366  | Hartley, C.....       | 231, 454, 455                           | Helm, D.....            | 90   |
|                                     |   | Hartl, M.....         | 98                                      | Hemker, K.....          | 134, 251, 320                                  |
|                                     |   | Hartmaier, A.....     | 474                                     | Hemphill, G.....        | 486  |
|                                     |   | Hartmann, C.....      | 187                                     | Hemphill, M.....        | 273  |
|                                     |   | Hartwig, K.....       | 33, 43, 293, 501                        | Hemrick, J.....         | 328  |

|                             |                            |                      |   |                   |  |
|-----------------------------|----------------------------|----------------------|---|-------------------|--|
| Henager Jr, C .....         | 40                         | Hoelscher, T.....    | 480   | Hou, M.....       | 215  |
| Henager Jr., C.....         | 99, 260                    | Hoelzer, D.....      | 41, 393   | Houng, B .....    | 127  |
| Henderson, H.....           | 143                        | Hoffman, D.....      | 369   | House, J.....     | 321  |
| Henein, H.....              | 281, 459, 460, 484         | Hoffman, E.....      | 160, 200, 333   | Hovanski, Y.....  | 81, 141, 142, 199,<br>258, 325, 382, 437, 438                                    |
| Henry, J.....               | 158                        | Hofman, G.....       | 40, 445   | Howard, B .....   | 392  |
| Henry, K.....               | 369                        | Hofmann, D.....      | 185, 305  | Howard, S.....    | 81, 357, 489   |
| Heo, T.....                 | 147, 315                   | Hofmann, M.....      | 139   | Howe, J.....      | 150  |
| He, Q.....                  | 244                        | Hogan, P.....        | 199   | Howell, R.....    | 34   |
| Herbani, Y.....             | 15, 416                    | Hogel, M.....        | 257   | Howe, S.....      | 347  |
| Herbert, J.....             | 245, 327                   | Hoglund, L.....      | 143   | Hoyt, J.....      | 27, 29, 30, 74, 82, 83, 133, 142, 191,<br>201, 239, 249, 260, 315, 376, 377, 435 |
| Herbig, M.....              | 80, 272                    | Höglund, L.....      | 203   | Hoyt, K.....      | 334  |
| Herbold, E.....             | 137                        | Holcomb, G.....      | 212   | Hrkac, G.....     | 207  |
| Heringer, M.....            | 81, 489                    | Holda, A.....        | 62  | Hryn, J.....      | 112  |
| Hériprié, E.....            | 314                        | Holden, T.....       | 163, 337, 431   | Hsiao, H.....     | 47, 339  |
| Hernandez, D.....           | 71, 280                    | Holdsworth, S.....   | 447   | Hsiao, Y.....     | 50   |
| Hernandez Hernandez, L..... | 428                        | Holland, L.....      | 229   | Hsieh, W.....     | 12   |
| Hernández, J.....           | 131, 491                   | Holland, T.....      | 486   | Hsiung, L.....    | 254, 393   |
| Hernandez, M.....           | 440                        | Holleis, B.....      | 327   | Hsu, C.....       | 452, 498   |
| Hernández, M.....           | 214                        | Holm, E.....         | 27, 446, 500  | Hsu, D.....       | 341  |
| Hernando, B.....            | 151                        | Holm, K.....         | 436   | Hsu, E.....       | 456  |
| Herrera, H.....             | 359                        | Holten, R.....       | 86  | Hsueh, S.....     | 498  |
| Hertzman, S.....            | 87                         | Holt, R.....         | 100, 101  | Hsu, F.....       | 227  |
| Herz, A.....                | 292                        | Holt, M.....         | 222, 430  | Hsu, H.....       | 49, 399  |
| Herzig, N.....              | 78                         | Holtz, R.....        | 256, 298  | Hsu, J.....       | 173  |
| Hesabi, Z.....              | 283                        | Homayonifar, M.....  | 330, 474  | Hsu, L.....       | 276  |
| Hetherly, J.....            | 216                        | Homer, E.....        | 153   | Hua, F.....       | 219  |
| Heuser, B.....              | 88                         | Homma, T.....        | 262   | Huang, B.....     | 77   |
| He, W.....                  | 424                        | Hongbin, L.....      | 189   | Huang, C.....     | 174  |
| Hewertson, R.....           | 326                        | Hong, H.....         | 217   | Huang, D.....     | 62   |
| He, X.....                  | 508, 509                   | Hong, J.....         | 502   | Huang, E.....     | 139, 198, 271, 272, 447  |
| He, Y.....                  | 77, 86                     | Hongliang, Z.....    | 297   | Huang, H.....     | 33, 99, 425  |
| Hial, S.....                | 357                        | Hong, S.....         | 56  | Huang, J.....     | 12, 14, 37, 109, 115, 127,<br>150, 228, 318, 353, 418, 509                       |
| Hickel, T.....              | 27, 75, 144, 251, 277, 361 | Hong, T.....         | 56  | Huang, K.....     | 22, 50, 190, 387, 391, 470, 477, 478   |
| Hideharu, N.....            | 194                        | Hong, W.....         | 338   | Huang, L.....     | 228, 307, 424, 467, 486  |
| Hiel, C.....                | 44, 344                    | Hongwei, G.....      | 498   | Huang, M.....     | 511  |
| Hierro, M.....              | 405                        | Hongxu, L.....       | 470   | Huangnian, Z..... | 508  |
| Higashida, K.....           | 318, 329                   | Hong, Y.....         | 139, 288  | Huang, Q.....     | 118, 234   |
| Higashi, K.....             | 511                        | Hong, Z.....         | 518   | Huang, R.....     | 61, 305, 306   |
| Higashi, M.....             | 515                        | Honjo, T.....        | 442, 478, 479   | Huang, S.....     | 85, 145, 317, 345, 449   |
| Higginbotham, A.....        | 78                         | Honkimäki, V.....    | 448   | Huang, T.....     | 340  |
| Highland, M.....            | 101                        | Hono, K.....         | 150, 169, 207, 208, 240,<br>262, 263, 331, 389, 390, 443, 444, 495                              | Huang, W.....     | 103  |
| Highsmith, A.....           | 56                         | Hooks, D.....        | 363   | Huang, X.....     | 62, 138, 162, 220, 271, 401, 499   |
| Hildeman, G.....            | 55, 460, 503               | Horbach, J.....      | 202   | Huang, Y.....     | 148, 295, 363, 399   |
| Hild, S.....                | 361                        | Horita, T.....       | 95, 155, 212, 267, 334, 391   | Huang, Z.....     | 15, 61, 89, 117, 175, 218, 338, 425  |
| Hilgert, J.....             | 258                        | Horita, Z.....       | 20, 193   | Huannian, Z.....  | 507  |
| Hill, M.....                | 95, 200, 431               | Horky, J.....        | 20  | Hu, B.....        | 61, 117  |
| Hillman, D.....             | 274                        | Hornbuckle, B.....   | 161, 222  | Hubbard, C.....   | 140, 179, 272, 396, 431  |
| Hill, R.....                | 502                        | Horne, M.....        | 453   | Hubbard, J.....   | 195  |
| Hiltmann, F.....            | 436                        | Horsfield, A.....    | 83  | Huber, D.....     | 199  |
| Hilty, R.....               | 160                        | Horstemeyer, M.....  | 34, 38, 39, 76, 100,<br>121, 149, 150, 209, 223, 253, 286,<br>319, 329, 330, 388, 484, 493, 514 | Huberman, S.....  | 237  |
| Hirano, S.....              | 81, 200                    | Horstemeyer, S.....  | 121   | Huber, N.....     | 258, 330, 336, 382   |
| Hiraoka, K.....             | 384                        | Horstermeyer, M..... | 479   | Huber, T.....     | 463  |
| Hirata, G.....              | 68, 69, 362                | Hort, N.....         | 92, 148, 205, 441   | Hu, C.....        | 180  |
| Hirata, T.....              | 511                        | Horton, D.....       | 306   | Hudak, N.....     | 115, 418   |
| Hiremath, S.....            | 485                        | Hosemann, P.....     | 41, 42, 82, 393, 394, 472   | Hudish, G.....    | 161  |
| Hirosawa, S.....            | 207, 389, 390              | Hosford, W.....      | 321   | Huebner, W.....   | 111  |
| Hirth, J.....               | 100, 279, 464              | Hoshino, A.....      | 112   | Hue, K.....       | 368  |
| Hiura, F.....               | 34                         | Hosler, B.....       | 360   | Huettner, W.....  | 480  |
| Hiveš, J.....               | 360                        | Hosoda, H.....       | 341   | Hufnagel, T.....  | 67, 184, 448   |
| Hjelm, R.....               | 472                        | Hosokawa, H.....     | 516, 522  | Hu, H.....        | 148, 493   |
| Hoagland, R.....            | 79, 100, 113, 380          | Hotchkiss, A.....    | 442   | Huh, J.....       | 398  |
| Ho, C.....                  | 46, 276, 339               | Houbart, I.....      | 519   | huilan, S.....    | 357  |
| Hochhalter, J.....          | 314                        | Hou, H.....          | 139   | Huilan, S.....    | 21   |
| Hochrainer, T.....          | 287                        | Hou, J.....          | 475, 477  | Huin, D.....      | 459  |
| Hock, S.....                | 132                        |                      |   | Hui, X.....       | 366  |
| Hoc, T.....                 | 272, 342                   |                      |   |                   |  |
| Hodge, A.....               | 20, 349, 422, 461          |                      |   |                   |  |
| Hoeche, D.....              | 494                        |                      |   |                   |  |

# TMS2011

## 140th Annual Meeting & Exhibition

|                          |  |                          |   |                          |  |
|--------------------------|--|--------------------------|---|--------------------------|--|
| Hu, J.....               | 462  | Inbar, M.....            | 301   | Jaouen, G.....           | 129  |
| Hu, L.....               | 121, 402, 417  | Inden, G.....            | 124   | Jaques, B.....           | 96, 224, 225, 266  |
| Hull, D.....             | 119  | Ingier-Stocka, E.....    | 266   | Jaradat, Y.....          | 338  |
| Humadi, H.....           | 83   | Ingole, S.....           | 56  | Jaramillo-Botero, A..... | 93   |
| Humphry-Baker, S.....    | 43, 181  | Ingraffea, A.....        | 314   | Jaramillo, L.....        | 214  |
| Hung, F.....             | 259, 372   | in het Panhuis, M.....   | 126   | Jardim, P.....           | 72   |
| Hung, W.....             | 284, 482   | Inoue, A.....            | 19, 69, 70, 91, 127,<br>184, 185, 307, 423, 424             | Jared, B.....            | 484  |
| Hunt, C.....             | 219  | Inoue, K.....            | 74, 112   | Jarmakani, H.....        | 196  |
| Hunter, J.....           | 473  | Inoue, T.....            | 206   | Jarry, P.....            | 187  |
| Hunter, L.....           | 315  | Inozemtsev, V.....       | 44  | jasthi, b.....           | 82   |
| Huo, D.....              | 359, 482   | Insepov, Z.....          | 40  | Jasthi, B.....           | 81, 82, 489  |
| Huo, L.....              | 203  | Instone, S.....          | 308   | Javaid, A.....           | 33   |
| Hu, P.....               | 117, 471   | Inui, H.....             | 76, 77, 134, 192, 250, 317, 377                             | Jawahir, I.....          | 494  |
| Hu, R.....               | 28, 212, 270, 392  | Ionescu, I.....          | 222, 375  | Jayakumar, B.....        | 128  |
| Hur, C.....              | 453  | Ipser, H.....            | 451, 452  | Jayaraj, J.....          | 263  |
| Hurley, M.....           | 266  | Iqbal, N.....            | 485   | Jayaraman, T.....        | 332, 443   |
| Hürrieh, C.....          | 51   | Irissou, E.....          | 214, 481, 509   | Jayaram, V.....          | 312  |
| Hu, S.....               | 40, 64, 99, 157, 215,<br>260, 270, 315, 393, 445, 496            | Irwin, G.....            | 72, 476   | Jayathilaka, P.....      | 208  |
| Huskins, E.....          | 380  | Isaac, A.....            | 245, 310  | Jee, K.....              | 510  |
| Husøy, A.....            | 86   | Isac, M.....             | 367, 409  | Jekl, J.....             | 147  |
| Hussain, R.....          | 24, 485  | Isakov, A.....           | 461   | Jeltsch, R.....          | 381  |
| Husseini, N.....         | 396  | Isheim, D.....           | 320, 352, 489   | Jena, U.....             | 241  |
| Hutchinson, C.....       | 88, 139, 262   | Ishida, K.....           | 81, 341, 451  | Jennerjohn, S.....       | 209, 343   |
| Hutchinson, N.....       | 243  | Ishikawa, S.....         | 192   | Jennings, A.....         | 56, 356  |
| Hütsch, L.....           | 382  | Ishimatsu, T.....        | 453   | Jensen, E.....           | 381  |
| Hu, W.....               | 149  | Islam, M.....            | 72, 476   | Jensen, T.....           | 297  |
| Hu, X.....               | 87, 149, 190   | Islam, Z.....            | 101, 335  | Jentoftsen, T.....       | 300  |
| Huxhold, S.....          | 115  | Islir, M.....            | 280   | Jeong, D.....            | 453  |
| Hu, Z.....               | 384  | Itoh, K.....             | 352   | Jeong, J.....            | 170, 491   |
| Hwang, I.....            | 38, 311  | Ito, K.....              | 453   | Jeong, K.....            | 353, 415   |
| Hwang, J.....            | 60, 62, 116, 117, 174, 182,<br>233, 242, 293, 309, 354, 417, 499 | Iung, T.....             | 124   | Jeong, M.....            | 46, 276  |
| Hwang, S.....            | 103, 385, 507, 519   | Ivancik, J.....          | 362   | Jeong, W.....            | 433  |
| Hyers, R.....            | 283, 502   | Ivanov, T.....           | 187   | Jeong, Y.....            | 401  |
| Hyland, M.....           | 123, 238, 308, 437   | Ivchenko, M.....         | 44  | Jeon, J.....             | 490  |
| Hyland, P.....           | 220  | Iwashita, T.....         | 185   | Jeon, S.....             | 452  |
| Hynes, R.....            | 413  | Iwata, S.....            | 207   | Jepson, P.....           | 106  |
| Hyun, S.....             | 452  | Iyengar, R.....          | 431   | Jerez, O.....            | 440  |
|                          |  | Izadbakhsh, A.....       | 223   | Jerred, N.....           | 96   |
| <b>I</b>                 |  |                          |   | Jetta, N.....            | 51   |
| Iadicola, M.....         | 121  | <b>J</b>                 |   | Jha, A.....              | 469  |
| Ibarra, A.....           | 105  | Jablonski, P.....        | 62, 87, 118, 156, 176,<br>212, 267, 281, 282, 345, 377, 404 | Jha, M.....              | 171, 424   |
| Ibrahim Mohammed, H..... | 432  | Jackson, J.....          | 413   | Jha, S.....              | 147, 176   |
| Ibrahim, R.....          | 449  | Jacob, A.....            | 27  | Jhon, M.....             | 75, 361  |
| Ice, G.....              | 100, 101, 135, 370, 402  | Jacobson, M.....         | 94  | Jia, H.....              | 128, 424   |
| Idrissi, H.....          | 108  | Jadhav, N.....           | 159, 160  | Jiang, B.....            | 387  |
| Iijima, S.....           | 327  | Jafari Nodooshan, H..... | 108, 225, 226   | Jiang, F.....            | 136, 137, 366, 503   |
| Ikeda, S.....            | 140  | Jahazi, M.....           | 294   | Jiang, H.....            | 49, 314, 450   |
| Ikeda, T.....            | 239, 453   | Jahed, H.....            | 39  | Jiang, J.....            | 422, 448   |
| Ikhmayies, S.....        | 55, 245, 368, 369, 460, 503                                      | Jain, V.....             | 33, 212   | Jiang, L.....            | 91, 119, 315, 319, 330, 337                                      |
| Ikponmwosa, E.....       | 385  | Jakes, J.....            | 242, 421, 468   | Jiang, T.....            | 60, 61, 116, 174, 175, 233,<br>235, 293, 295, 354, 355, 363, 417 |
| Ila, D.....              | 229  | Jakkali, V.....          | 315, 433  | Jian-guang, Y.....       | 510, 517   |
| ILA, D.....              | 497  | Jamaati, R.....          | 505   | Jiang, W.....            | 26   |
| Ilavsky, J.....          | 217  | Jame, S.....             | 268   | Jiang, Y.....            | 173, 193, 252, 318, 320, 494                                     |
| Ilbagi, A.....           | 281  | James, M.....            | 90  | Jianping, P.....         | 357, 381   |
| Imam, M.....             | 344  | James, R.....            | 220, 277  | Jiao, K.....             | 437  |
| Imanasa Azof, F.....     | 480  | Jana, S.....             | 258, 325  | Jiao, S.....             | 190, 478   |
| Imano, S.....            | 81   | Jandhyala, S.....        | 13, 17  | Jiao, Y.....             | 503  |
| Im, C.....               | 139  | Janecek, M.....          | 24, 35, 49, 246, 487  | Jiao, Z.....             | 42, 127, 154, 159, 270, 271                                      |
| Imhoff, S.....           | 112, 182   | Jang, D.....             | 243, 356, 467   | Jia, Q.....              | 496  |
| Im, J.....               | 198  | Jang, J.....             | 49, 127, 293, 318, 350, 394                                 | Jia, R.....              | 393  |
| Imura, M.....            | 173  | Jang, S.....             | 110, 415  | Jia, W.....              | 500  |
| Inacio, W.....           | 26   | Jang, W.....             | 510   | Jia, Z.....              | 16   |
| Inada, K.....            | 325  | Jan, K.....              | 514   | Jie, C.....              | 175  |
| Inal, K.....             | 223  | Janney, D.....           | 266, 517  | Jie, G.....              | 26   |
| Inamura, P.....          | 421  | Janssens, K.....         | 247, 314, 374, 434, 473                                     | Jie, L.....              | 30   |
|                          |  |                          |   | Jihong, D.....           | 476, 477   |
|                          |  |                          |   | Ji, J.....               | 385  |



$Q(\varphi, \sigma)$

$kT_g = \frac{2(B)(V)(\epsilon_1)}{K_g}$

|                      |                                      |                                     |                             |                            |   |
|----------------------|--------------------------------------|-------------------------------------|-----------------------------|----------------------------|---|
| Jimbo, I.....        | 183                                  | Jund, P.....                        | 249, 414                    | Kaneko, T.....             | 156   |
| Jing, L.....         | 311                                  | Jung, B.....                        | 506                         | Kaneno, Y.....             | 77  |
| Jing, T.....         | 32, 89                               | Jung, G.....                        | 518                         | Kang, B.....               | 71, 371   |
| Jing, Y.....         | 357                                  | Jung, H.....                        | 485                         | Kang, D.....               | 517   |
| Jin, H.....          | 23, 42, 237, 252, 293, 394, 497, 523 | Jung, I.....                        | 149, 387, 398               | Kang, H.....               | 35  |
| Jinhui, P.....       | 311                                  | Jung, J.....                        | 189, 490                    | Kang, J.....               | 330, 411  |
| Jin, J.....          | 491                                  | Jung, K.....                        | 156, 334                    | Kang, K.....               | 434   |
| Jin, L.....          | 388                                  | Jung, M.....                        | 353, 498                    | Kang, N.....               | 56  |
| Jin-long, Z.....     | 500                                  | Jung, S.....                        | 47                          | Kang, S.....               | 45, 53, 84, 102, 115, 159, 179, 219, 274, 293, 337, 352, 391, 394, 397, 415, 449, 450, 477, 497 |
| Jin, S.....          | 25, 60, 102, 183, 184, 241           | Jung, Y.....                        | 463                         | Kang, T.....               | 353, 516  |
| Jin, X.....          | 30, 365                              | Junkaew, A.....                     | 144                         | Kang, X.....               | 205   |
| Jinxia, N.....       | 407                                  | Jun, L.....                         | 381                         | Kan, H.....                | 360   |
| Jin, Y.....          | 27, 84, 315, 512                     | Jun, Z.....                         | 269                         | Kanjarla, A.....           | 53, 222   |
| Jin, Z.....          | 21                                   | Jurczyk, M.....                     | 89                          | Kanno, N.....              | 345   |
| Ji, X.....           | 503                                  | Jur, J.....                         | 174                         | Kano, K.....               | 197   |
| Ji, Z.....           | 73                                   | Juul Jensen, D.....                 | 252                         | Kanturk Figen, A.....      | 404   |
| Jody, B.....         | 112                                  | Juzeliunas, E.....                  | 504                         | Kao, C.....                | 45, 48, 219   |
| Joe, C.....          | 513                                  |                                     |                             | Kao, T.....                | 398   |
| Johansson, B.....    | 387                                  | <b>K</b>                            |                             | Kaoumi, D.....             | 211, 216  |
| Johansson, S.....    | 447                                  | Kabir, M.....                       | 106                         | Kao, W.....                | 232   |
| John, R.....         | 176, 205                             | Kabra, S.....                       | 139                         | Kapala, J.....             | 266   |
| Johnsen, L.....      | 256                                  | Kabulashvili, V.....                | 510                         | Kaplan, D.....             | 126   |
| Johnson, A.....      | 76, 202                              | Kad, B.....                         | 254                         | Kapoglou, A.....           | 128   |
| Johnson, D.....      | 226                                  | Kadiri, H.....                      | 329                         | Kapoor, A.....             | 323   |
| Johnson, E.....      | 272                                  | Kafari, Z.....                      | 140                         | Kapoor, D.....             | 166, 224, 293, 358  |
| Johnson, F.....      | 264, 444, 495                        | Kaftelen, H.....                    | 484                         | Kapoor, M.....             | 489   |
| Johnson, J.....      | 58, 196, 379                         | Kaga, S.....                        | 200                         | Karaca, H.....             | 105   |
| Johnson, M.....      | 410                                  | Kageyama, T.....                    | 503                         | Karacasu, O.....           | 373   |
| Johnson, N.....      | 13                                   | Kahleel, M.....                     | 154, 304, 362               | Karadeniz, O.....          | 367   |
| Johnson, R.....      | 94                                   | Kahofer, S.....                     | 20                          | Karakaya, I.....           | 190   |
| Johnson, T.....      | 189, 439                             | Kahraman, V.....                    | 518                         | Karaman, I.....            | 16, 33, 50, 51, 104, 161, 162, 220, 221, 277, 340, 341, 400, 401, 452, 453                      |
| Johnson, W.....      | 69, 70, 128, 243, 305, 306, 422      | Kainer, K.....                      | 92, 148, 205, 388, 492, 494 | Karamched, P.....          | 79  |
| Jo, J.....           | 275                                  | Kainuma, R.....                     | 340, 341, 451, 453          | Karamian, E.....           | 22, 224   |
| Jolly, M.....        | 226, 411, 413                        | Kain, V.....                        | 188                         | Karamouz, M.....           | 179, 225, 508, 509, 520   |
| Jo, M.....           | 485                                  | Kai-Ping, T.....                    | 394                         | Karamouz Ravari, M.....    | 520   |
| Jonas, J.....        | 330                                  | Kai, W.....                         | 117, 128, 129               | Karapetrova, E.....        | 102   |
| Jones, A.....        | 484                                  | Kajihara, M.....                    | 339                         | Karcher, C.....            | 98, 409   |
| Jones, D.....        | 146                                  | Kalaantari, H.....                  | 31, 341                     | Karewar, S.....            | 287   |
| Jones, J.....        | 37, 150, 191, 218, 262, 396          | Kalantar, D.....                    | 196                         | Karhausen, K.....          | 65, 66  |
| Jones, M.....        | 492                                  | Kalay, E.....                       | 242                         | Karimi Dehcheshmeh, A..... | 280   |
| Jones, N.....        | 221, 223, 252, 290                   | Kalay, I.....                       | 422                         | Karl, J.....               | 121   |
| Jones, R.....        | 93                                   | Kalay, Y.....                       | 422                         | Karlsson, J.....           | 487   |
| Jones, T.....        | 37, 442                              | Kalidass, S.....                    | 205                         | Karna, A.....              | 260   |
| Jonnet, J.....       | 40                                   | Kalidindi, N.....                   | 498                         | Karna, M.....              | 463   |
| Jonville, C.....     | 129, 138                             | Kalidindi, S.....                   | 90, 309, 343, 349, 375, 389 | Karna, S.....              | 60, 352, 463  |
| Joo, J.....          | 243                                  | Kalinina, E.....                    | 44                          | Karnesky, R.....           | 232   |
| Joo, Y.....          | 46, 103, 353                         | Kalisvaart, P.....                  | 88                          | Karpowicz, S.....          | 350   |
| Jordan, B.....       | 38, 319                              | Kaliya Perumal Veerapandian, S..... | 214                         | Kar, S.....                | 298   |
| Jordan, E.....       | 170                                  | Kalkan, K.....                      | 229, 288                    | Kasap, S.....              | 406   |
| Jordan, J.....       | 137                                  | Kaltenboeck, G.....                 | 69, 70, 243                 | Kaschner, G.....           | 223   |
| Jordon, B.....       | 298, 479                             | Kalyanaraman, R.....                | 230                         | Kasetty, R.....            | 515   |
| Jordon, J.....       | 39, 149, 150, 388, 438               | Kamado, S.....                      | 262                         | Kashyap, S.....            | 241   |
| Josell, D.....       | 289                                  | Kamali, R.....                      | 414                         | Kasprzak, W.....           | 178   |
| Jost, C.....         | 144                                  | Kameda, H.....                      | 267                         | Kassegne, S.....           | 213, 214, 224   |
| Jo, T.....           | 506                                  | Kameda, J.....                      | 158                         | Kassner, M.....            | 140, 272  |
| Jouet, J.....        | 136                                  | Kamfjord, N.....                    | 117                         | Katgerman, L.....          | 186   |
| Jouet-Pastré, L..... | 129                                  | Kaminieni, P.....                   | 205                         | Kato, C.....               | 180, 197, 466   |
| Joulain, A.....      | 107                                  | Kamisetty, V.....                   | 309                         | Kato, H.....               | 70, 74, 127, 389  |
| Jo, Y.....           | 398                                  | Kamkin, R.....                      | 62                          | Kato, K.....               | 516, 522  |
| Juan, D.....         | 120                                  | Kammers, A.....                     | 18                          | Katsman, A.....            | 263   |
| Juanri, J.....       | 344                                  | Kampe, S.....                       | 293, 294                    | Kattner, U.....            | 87, 146   |
| Juan, W.....         | 491                                  | Kamran, K.....                      | 366                         | Katz, J.....               | 430   |
| Juan, Y.....         | 13                                   | Kandasamy, K.....                   | 259                         | Kauffman, D.....           | 16  |
| Juárez, J.....       | 359                                  | Kandeil, A.....                     | 348                         | Kauffman, K.....           | 16, 392   |
| Jue, J.....          | 154, 430, 445, 473                   | Kander, L.....                      | 237                         | Kaufman, L.....            | 87, 143, 202, 261, 328, 376, 386  |
| Ju, H.....           | 88                                   | Kandev, N.....                      | 323                         |                            |   |
| Ju, J.....           | 373                                  | Kane, J.....                        | 43, 211                     |                            |   |
| Jun, C.....          | 507                                  |                                     |                             |                            |   |

INDEX

# TMS2011

## 140th Annual Meeting & Exhibition

|                      |                                  |                      |  |                      |   |
|----------------------|----------------------------------|----------------------|--|----------------------|---|
| Kaufman, M.....      | 161, 341, 344                    | Khomyakov, E.....    | 165  | Klarner, A.....      | 463   |
| Kaufmann, H.....     | 121                              | Khorujaya, V.....    | 376  | Klassen, R.....      | 150   |
| Kaur, J.....         | 433                              | Khoshnevis, D.....   | 177  | Klaumünzer, D.....   | 185   |
| Kawaguchi, K.....    | 441                              | Khosravani, A.....   | 318, 319   | Klein, R.....        | 409   |
| Kawakita, H.....     | 74, 112                          | Khunathai, K.....    | 74   | Klett, C.....        | 297   |
| Kawamura, K.....     | 334, 405                         | Kiang, J.....        | 422  | Klingbeil, N.....    | 508   |
| Kawamura, Y.....     | 262, 329, 352                    | Kiani-Rashid, A..... | 25, 513  | Klingensmith, D..... | 211, 333, 393, 395                            |
| Kawasaki, A.....     | 424                              | Kickelbick, G.....   | 363  | Klingensmith, R..... | 33  |
| Kayali, E.....       | 23, 481                          | Kida, K.....         | 384  | Klockow, H.....      | 413   |
| Kazimirov, A.....    | 395                              | Kiener, D.....       | 227, 394, 412  | Kloss, C.....        | 152   |
| Kealey, C.....       | 453                              | Kiggans, J.....      | 165, 403   | Klotz, U.....        | 247   |
| Keckses, L.....      | 33, 136, 232, 321, 347, 377, 492 | Kikuchi, K.....      | 225  | Klug, M.....         | 431   |
| KeeDo, W.....        | 213                              | Kikuchi, T.....      | 70   | Klut, P.....         | 511   |
| Keer, L.....         | 365                              | Kikugawa, T.....     | 135  | Knabl, W.....        | 501   |
| Keiser, B.....       | 357                              | Kildea, J.....       | 357  | Kneissl, C.....      | 286   |
| Keiser, D.....       | 154, 445                         | Kim, B.....          | 46, 54, 103, 170, 281, 465   | Knez, M.....         | 60  |
| Keiser, J.....       | 405                              | Kim, C.....          | 156, 166, 275, 311, 337, 371, 431, 432, 451  | Knigge, J.....       | 483   |
| Keiser, Jr., D.....  | 203                              | Kim, D.....          | 36, 37, 53, 70, 96, 110, 153, 162, 179, 186, 293, 415, 422, 506, 508   | Knio, O.....         | 67  |
| Keith, B.....        | 192                              | Kim, E.....          | 491  | Knipling, K.....     | 230, 264, 332                                 |
| Ke, J.....           | 45, 48                           | Kim, G.....          | 330, 412   | Knorvosky, G.....    | 484   |
| Keles, O.....        | 479                              | Kim, H.....          | 35, 36, 65, 104, 173, 198, 246, 302, 389, 392, 410, 512  | Kobayashi, K.....    | 85, 225, 343                                  |
| Keles, Ö.....        | 510                              | Kim, I.....          | 148  | Kobayashi, T.....    | 274   |
| Keller, F.....       | 138                              | Kiminami, C.....     | 20, 69, 468  | Kobbeltvedt, O.....  | 299   |
| Kellis, D.....       | 50                               | Kim, J.....          | 12, 13, 14, 17, 24, 36, 41, 46, 49, 50, 55, 56, 59, 67, 96, 102, 110, 115, 148, 149, 162, 169, 173, 179, 198, 229, 232, 262, 276, 279, 288, 292, 309, 350, 352, 353, 356, 415, 428, 462, 463, 465, 498, 505, 508, 510, 512, 513, 514, 515, 517, 520, 521 | Kobe, S.....         | 152   |
| Kelly, A.....        | 430, 486                         | Kim, K.....          | 49, 139, 275, 350, 397, 520  | Kobyashi, M.....     | 252   |
| Kelly, S.....        | 67, 136, 448                     | Kim, M.....          | 14, 49, 56, 149, 170, 352, 353, 491, 510, 519  | Ko, C.....           | 103   |
| Kelton, K.....       | 244, 467                         | Kim, N.....          | 36, 263  | Koch, C.....         | 17, 18, 20, 232, 415                          |
| Kendig, K.....       | 348                              | Kim, S.....          | 24, 36, 53, 54, 96, 148, 157, 189, 198, 199, 209, 213, 230, 246, 253, 281, 329, 334, 355, 385, 388, 410, 423, 446, 462, 508, 509, 517, 520   | Koch, H.....         | 187   |
| Kenesei, P.....      | 273                              | Kim, T.....          | 520  | Koch, T.....         | 363   |
| Ken-ichi, I.....     | 194                              | Kimura, H.....       | 72   | Kocich, R.....       | 479   |
| Kenik, E.....        | 35, 206, 446, 471                | Kimura, K.....       | 156  | Kockan, U.....       | 516   |
| Kennedy, J.....      | 203                              | Kimura, Y.....       | 192, 452   | Kockelmann, W.....   | 473   |
| Kennedy, M.....      | 98, 168, 240, 241, 308           | Kim, W.....          | 37, 149, 186, 422  | Koc, M.....          | 36  |
| Kennedy, R.....      | 266                              | Kim, Y.....          | 40, 51, 56, 96, 149, 199, 221, 350, 398, 410, 445, 487, 489, 506, 508, 513   | Kodentsov, A.....    | 398   |
| Keralavarma, S.....  | 287, 412                         | King, A.....         | 80, 164, 272   | Kodera, Y.....       | 477   |
| Kerber, M.....       | 415                              | King, S.....         | 432  | Koduri, S.....       | 135, 204, 309                                 |
| Kercher, A.....      | 338                              | Kink, I.....         | 356  | Kögler, R.....       | 41  |
| Kerr, M.....         | 95, 370, 430, 431, 472           | Kinoshita, H.....    | 158  | Köhler, H.....       | 268, 417                                      |
| Kers, J.....         | 56, 111, 170                     | Kipouros, G.....     | 493  | Kohl, J.....         | 191   |
| Kerti, I.....        | 165, 225, 367                    | Kirby, B.....        | 331  | Kohl, P.....         | 102   |
| Ke, S.....           | 133                              | Kirchain, R.....     | 301, 406   | Kohnert, A.....      | 211   |
| Kesarwani, P.....    | 23                               | Kirchheim, R.....    | 292  | Koh, S.....          | 12, 14, 59, 115, 173, 232, 292, 352, 415, 463 |
| Keselowsky, B.....   | 25, 441                          | Kirk, M.....         | 40, 99, 158, 216, 446  | Kohse, G.....        | 333   |
| Keshri, A.....       | 167, 351                         | Kirkpatrick, D.....  | 256  | Koide, J.....        | 197   |
| Keskinkilic, E.....  | 354                              | Kisailus, D.....     | 302, 361   | Koike, J.....        | 33  |
| Kessler, M.....      | 433                              | Kishimoto, H.....    | 267  | Koike, K.....        | 389   |
| Kestens, L.....      | 106                              | Kishore, R.....      | 128  | Koizumi, Y.....      | 76, 329, 385, 488                             |
| Ketabchi, M.....     | 237, 519                         | Kisner, R.....       | 31   | Kokabi, A.....       | 259   |
| Keul, E.....         | 59                               | Kiss, L.....         | 323, 466   | Kokawa, H.....       | 81  |
| Ke, X.....           | 387                              | Kitamura, K.....     | 401, 453   | Kolenda, Z.....      | 62  |
| Keyvani, M.....      | 34                               | Ki, W.....           | 48   | Kolesnikova, A.....  | 356   |
| Khabarova, I.....    | 130                              | Kiyota, H.....       | 515  | Kolesnikov, J.....   | 98  |
| Khachaturyan, A..... | 277                              | Kiziltas, A.....     | 428  | Kolesnikov, Y.....   | 409   |
| Khajeh, E.....       | 227                              | Klag, O.....         | 259  | Koleva, E.....       | 509   |
| Khaki, J.....        | 284                              |                      |  | Koller, D.....       | 321   |
| Khalaf Allam, N..... | 18                               |                      |  | Kolluri, K.....      | 74, 75  |
| Khaleel, M.....      | 40, 99, 100, 488                 |                      |  | Kolmskog, P.....     | 189   |
| Khaleghi, E.....     | 293, 294                         |                      |  | Komatsu, N.....      | 197   |
| Khalid, F.....       | 108                              |                      |  | Komazaki, S.....     | 188   |
| Khalil, S.....       | 446                              |                      |  | Komuro, M.....       | 390   |
| Khaliq, A.....       | 308                              |                      |  | Konchakova, N.....   | 253   |
| Khammas, R.....      | 258                              |                      |  | Konda, S.....        | 207   |
| Khan, M.....         | 24, 485                          |                      |  | Kondoh, K.....       | 167, 442, 479, 493                            |
| Khan, T.....         | 502                              |                      |  | Kong, C.....         | 52  |
| Kharicha, A.....     | 157, 178                         |                      |  | Kongoli, F.....      | 61  |
| Khatun, A.....       | 382                              |                      |  | Konishi, H.....      | 492   |
| Khazzan, S.....      | 443                              |                      |  |                      |   |
| Khodadad, R.....     | 316                              |                      |  |                      |   |

Konno, T.....487  
 Konstantinidis, A.....356  
 Konstantinovic, M.....271  
 Kontsevoi, O.....408  
 Kotsos, A.....139, 198  
 Koodakal, R.....349  
 Koo, H.....102  
 Koporulina, E.....130  
 Kords, C.....374  
 Körmann, F.....27  
 Korniyenko, K.....376  
 Korzekwa, D.....430  
 Korzhavyi, P.....387  
 Kosiba, E.....160  
 Koskelo, A.....195  
 Kos, L.....184  
 Kostorz, G.....217  
 Koten, M.....332  
 Kotomin, E.....250  
 Kotsis, I.....236  
 Kou, H.....19  
 Kou, S.....492  
 Kovacevic, R.....25, 27, 39, 268,  
 .....294, 345, 481, 483  
 Kovalev, A.....130  
 Kovarik, L.....161, 193, 427  
 Kowalczyk-Gajewska, K.....223  
 Kown, Y.....519  
 Ko, Y.....24, 38, 54, 311  
 Kozar, R.....251  
 Kozeschnik, E.....203  
 Kozlov, A.....205  
 Krabbe, R.....156  
 Kraft, O.....228, 296  
 Kraide, F.....421  
 Krajewski, P.....387, 389  
 Kral, M.....283, 346, 426  
 Král, R.....35  
 Kramer, M.....242, 390, 407,  
 .....408, 422, 443, 447, 470  
 Krause, A.....486  
 Kraus, L.....187  
 Krautz, M.....151  
 Krcmar, M.....249  
 Krebs, J.....462  
 Krempaszky, C.....402  
 Kreuger, J.....454  
 Kriegel, M.....376  
 Krishna, H.....230  
 Krishnamurthy, R.....373  
 Krishnan, K.....195, 266  
 Krishnan, M.....51  
 Krishnaswamy, S.....91  
 Kropf, J.....473  
 Krost, A.....102  
 Krueger, C.....107  
 Krüger, M.....407  
 Krug, M.....194  
 Krumdick, G.....56, 111, 170, 301, 311, 371, 431  
 Kruzic, J.....23, 67, 125, 183, 240,  
 .....285, 302, 305, 306, 361, 420  
 Krywopusk, N.....136  
 Krzywosinski, K.....183  
 Kshatriya, N.....22, 120, 235  
 K.S.R., R.....300  
 Kubin, L.....230, 342, 378, 434  
 Ku, C.....49  
 Cucuk, A.....370

Kugler, G.....97, 294  
 Kuji, T.....442, 478, 479, 515  
 Kukimoto, Y.....397  
 Kuksenko, V.....270  
 Kuksin, A.....40  
 Kulak, M.....90  
 Kulcinski, G.....43  
 Kulkarni, N.....32, 261  
 Kulovits, A.....31, 96, 368  
 Kulpe, J.....72  
 Ku, M.....259  
 Kumar, A.....30, 171, 180, 187, 381  
 Kumaran, S.....359  
 Kumar, C.....178  
 Kumar, D.....198, 210, 378  
 Kumar, G.....69, 185  
 Kumari, A.....112  
 Kumar Jha, M.....112  
 Kumar, K.....34, 170  
 Kumar, M.....216, 254, 320, 455  
 Kumar, N.....326  
 Kumar, P.....103, 104, 283, 338, 483, 484  
 Kumar, R.....12, 112  
 Kumar, S.....76, 159, 313, 317, 320  
 Kumar, T.....241  
 Kumar, V.....112, 171  
 Kuncser, V.....415  
 Kundu, A.....505  
 Kung, H.....140  
 Kunz, A.....56  
 Kunz, M.....103, 272, 462, 464  
 Kuo, C.....314, 456  
 Kuo, H.....494  
 Kuo, S.....46  
 Kuper, J.....203  
 Kupka, D.....378  
 Kuplin, S.....226  
 Kuramoto, A.....42  
 Kuramoto, S.....193, 412  
 Kurath, P.....290, 402  
 Kurdadze, L.....155  
 Kurosu, S.....76, 385, 488  
 Kurtz, R.....270  
 Kurumaddali, K.....338  
 Kury, S.....438  
 Kurzydowski, K.....19  
 Kushima, A.....418  
 Kusimov, S.....233  
 Kustov, M.....207  
 Kuykendall, K.....383  
 Kuzel, R.....487  
 Kužel, R.....163, 246  
 Kuzmin, A.....295  
 Kuznetsov, A.....62  
 Kuznetsova, N.....511  
 Kvithyld, A.....55, 244, 245, 308, 406, 460, 503  
 Kwak, B.....46  
 Kwak, C.....213, 506  
 Kwatara, M.....133  
 Kwon, B.....34  
 Kwong, K.....155, 156  
 Kwon, J.....42, 199, 497  
 Kwon, S.....428, 521  
 Kwon, Y.....37, 481, 505  
 Kyeong, J.....37

## L

Lacroix, M.....459  
 Ladam, Y.....238  
 Lados, D.....194, 320  
 Lagoudas, D.....104, 221, 277  
 LaGrange, T.....31, 216, 399, 455  
 Laha, T.....167  
 lahellec, N.....342  
 Lahiri, D.....167, 184, 351, 421  
 Lahiri, I.....17, 514  
 Lahlouh, B.....432  
 Lahrman, D.....309  
 Lai, B.....370  
 Lai, Q.....475  
 Laird, B.....82, 83  
 Lai, Y.....46, 85, 475  
 Lajnef, N.....502  
 Lakes, R.....492  
 Lakshmanan, V.....26, 73, 74, 132, 189  
 Lalpoor, M.....186  
 Lal, R.....303  
 LaMarre, J.....132  
 LaMattina, B.....322  
 Lambertin, D.....442  
 Lamberti, W.....146  
 Lambert, S.....39  
 Lamb, J.....88, 89, 423  
 Lam, P.....160  
 Lam, T.....155  
 Landa, A.....376, 506  
 Landi, G.....90  
 Lan, G.....48  
 Langbein, S.....50, 51, 401, 453, 454  
 Lange, F.....481  
 Langemeier, L.....332  
 Langer, K.....199, 290  
 Lang, G.....86, 328  
 Lang, X.....199  
 Lankarani, H.....201, 259  
 Lan Levengood, S.....67  
 Laplanche, G.....107  
 Laplante, F.....256  
 Laplume, F.....411  
 Lara-Curzio, E.....346  
 Laradji, M.....436  
 Larouche, D.....323  
 Larsen, J.....135, 147, 176  
 Larsen, R.....55  
 Larsen, S.....442  
 Larson, B.....168, 272, 335, 475  
 Larsson, H.....203  
 La Salvia, J.....253  
 LaSalvia, J.....380  
 La Saponara, V.....313, 314  
 Lass, E.....145, 331  
 Launey, M.....305, 306, 362  
 Laurent, V.....475  
 Lauridsen, E.....172, 202, 271  
 Laurita, N.....208  
 Laurmaa, V.....111  
 Lau, S.....315  
 Laux, B.....199  
 Lauzon-Gauthier, J.....322  
 Lavender, C.....33  
 Lavernia, E.....15, 19, 20, 37, 167, 224,  
 .....226, 232, 236, 244, 292,  
 .....293, 319, 321, 358, 403, 404



# TMS2011

## 140th Annual Meeting & Exhibition

|                    |   |                        |  |                      |   |
|--------------------|---|------------------------|--|----------------------|---|
| Lavoie, P.....     | 238, 436  | Lett, R.....           | 348, 349   | Lim, J.....          | 506   |
| Law, J.....        | 332   | Letzig, D.....         | 35, 388  | Lim, K.....          | 186   |
| Laws, K.....       | 467   | Leu, L.....            | 131  | Lim, S.....          | 36  |
| Leary, A.....      | 208   | Leung, A.....          | 285  | Li, N.....           | 109, 379  |
| LeBeau, S.....     | 37, 150   | Levendis, Y.....       | 368, 369, 456  | Lin, A.....          | 303   |
| lebensohn, r.....  | 455   | Levesque, M.....       | 216  | Lin, C.....          | 46, 276, 326, 339, 464  |
| Lebensohn, R.....  | 52, 53, 54, 105, 147,<br>163, 195, 222, 278, 321,<br>342, 375, 381, 401, 402, 454                             | Levi, C.....           | 210  | Lindberg, F.....     | 317   |
| Lebeuf, M.....     | 437   | Levi, D.....           | 453  | Linden, M.....       | 110   |
| Leblanc, D.....    | 503   | Levine, L.....         | 101, 195, 209, 217, 272, 343   | Lind, J.....         | 71  |
| Le Bourlot, C..... | 395, 448  | Levinson, A.....       | 389  | Lindley, T.....      | 223, 252  |
| LeBreux, M.....    | 459   | Levy, O.....           | 249  | Lindner, F.....      | 197   |
| Le Brun, P.....    | 244   | Levy, Y.....           | 213  | Lindsay, S.....      | 22, 122, 123, 179,<br>238, 298, 299, 360, 419, 466                                    |
| Lebyodkin, M.....  | 290   | Lewandowska, M.....    | 19   | Lin, F.....          | 282   |
| Ledonne, J.....    | 232   | Lewandowski, J.....    | 184, 185, 468  | Lingman, H.....      | 89  |
| Lee, A.....        | 274, 338, 398, 449, 450   | Lewellyn, M.....       | 236  | Ling, Z.....         | 521   |
| Lee, B.....        | 13, 17, 23, 38, 276, 385, 398   | Lewis, A.....          | 279, 315   | Lin, H.....          | 227, 340, 397   |
| Lee, C.....        | 13, 28, 45, 47, 48, 132,<br>173, 276, 305, 339, 510   | Lewis, B.....          | 220  | Lin, J.....          | 134, 399  |
| Lee, D.....        | 36, 410, 460, 489, 510, 519   | Lewis, D.....          | 30, 82, 142, 201, 260  | Lin, K.....          | 46  |
| Lee, E.....        | 246   | Lewis, W.....          | 158  | Link, T.....         | 449   |
| Lee, G.....        | 17, 149, 189, 462   | Lezama-Alvarez, S..... | 507  | Lin, P.....          | 128, 129  |
| Lee, H.....        | 49, 54, 115, 157, 181, 199, 276,<br>281, 302, 339, 353, 389, 392, 398,<br>399, 410, 451, 452, 498, 508, 521   | Li, A.....             | 281  | Lin Peng, R.....     | 447   |
| Lee, J.....        | 37, 47, 49, 54, 84, 112, 162, 170,<br>171, 275, 339, 353, 398, 425, 433,<br>447, 451, 491, 497, 498, 510, 518 | Liang, C.....          | 44, 516  | Lin, S.....          | 72, 276, 339, 376   |
| Lee, K.....        | 14, 24, 28, 46, 49, 54, 119, 139,<br>219, 275, 281, 311, 371, 465, 511, 512                                   | Liang, L.....          | 115  | Lin, T.....          | 452   |
| Lee, M.....        | 12, 14, 167, 279, 353   | Liang, X.....          | 180  | Lin, W.....          | 136   |
| Lee, P.....        | 31, 62, 63, 83, 285, 488, 521   | Liang, Y.....          | 45   | Lin, X.....          | 180   |
| Lee, R.....        | 136   | Liang, Z.....          | 128, 129, 512  | Lin, Y.....          | 76, 241, 276, 303, 339, 397, 399, 477   |
| Lee, S.....        | 19, 35, 36, 96, 140, 198,<br>256, 319, 353, 362, 385,<br>396, 447, 505, 509, 513, 519                         | Lian, L.....           | 281  | Liou, W.....         | 511   |
| Lee, T.....        | 45, 47, 64, 102, 103, 159,<br>219, 274, 275, 337, 397, 449, 451   | Liao, C.....           | 233, 452   | Li, P.....           | 79, 414   |
| Lee, W.....        | 396, 474  | Liao, L.....           | 237  | Lipkin, D.....       | 312   |
| Lee, Y.....        | 45, 110, 162, 249, 334, 398, 453, 505   | Liao, X.....           | 236, 293   | Lippold, J.....      | 82, 142, 239, 326, 385, 448   |
| Lefebvre, G.....   | 402   | Liao, Z.....           | 117  | Li, Q.....           | 26, 28, 175, 193, 252, 318, 320, 476, 491   |
| Leggett, P.....    | 481   | Liau, L.....           | 84   | Li, R.....           | 422   |
| Legoux, J.....     | 214, 481, 509   | Liaw, P.....           | 32, 44, 69, 79, 91, 100, 127, 128,<br>129, 139, 140, 159, 184, 185, 198,<br>199, 217, 242, 243, 256, 271, 272,<br>273, 305, 306, 307, 319, 321, 323,<br>335, 337, 345, 346, 364, 365, 366,<br>394, 396, 422, 424, 446, 447, 449, 467 | Lira, H.....         | 513   |
| Legros, M.....     | 228, 378  | Li, B.....             | 133, 135, 157, 190, 321,<br>330, 381, 449, 466, 480  | Li, S.....           | 189, 280, 471   |
| Lehar, M.....      | 413   | Libo, Z.....           | 311  | Liss, K.....         | 271, 336  |
| Lehmann, E.....    | 472, 473  | Li, C.....             | 45, 98, 191, 192   | Li, T.....           | 121, 269, 288, 403  |
| Lehmann, T.....    | 498   | Lichao, D.....         | 457  | Littlefair, G.....   | 259, 319  |
| Lei, L.....        | 61, 508   | Lichtenberger, H.....  | 48   | Littlewood, P.....   | 79  |
| Leitner, H.....    | 501   | Li, D.....             | 29, 126, 131, 154, 175,<br>304, 361, 362, 367, 421, 451, 514   | Littrell, K.....     | 185   |
| Lei, W.....        | 518   | Lienert, U.....        | 252, 273, 309  | Litzenberger, D..... | 456   |
| Lei, Y.....        | 98, 132, 355, 485   | Lifschitz, J.....      | 180  | Liu, B.....          | 62, 63, 89, 145, 147,<br>156, 203, 227, 385, 449                                      |
| Lekakh, S.....     | 97  | Li, G.....             | 61, 175, 235, 295, 363   | Liu, C.....          | 46, 50, 76, 77, 124,<br>128, 134, 192, 243, 250, 252,<br>276, 317, 340, 345, 377, 471 |
| Lemberg, J.....    | 408   | Li, H.....             | 458  | Liu, D.....          | 218, 358, 490, 520  |
| Lennon, A.....     | 379   | Li, J.....             | 27, 40, 64, 71, 84, 109, 113,<br>116, 188, 193, 227, 228, 235, 263,<br>269, 328, 359, 364, 365, 407, 408,<br>418, 427, 464, 475, 482, 490, 503   | Liu, F.....          | 360, 424  |
| Lenosky, T.....    | 113   | Li, K.....             | 518  | Liu, G.....          | 157, 318  |
| Leonard, C.....    | 410   | Li, L.....             | 167, 189, 264, 269, 319, 509   | Liu, H.....          | 38, 89, 271, 312, 338, 392, 426   |
| Leonardi, A.....   | 218   | Lillard, S.....        | 30   | Liu, J.....          | 118, 151, 239, 300,<br>408, 414, 443, 444, 486, 503                                   |
| Leonhardt, T.....  | 500, 501  | Lilleodden, E.....     | 44, 100, 108, 159, 167,<br>217, 227, 271, 286, 330, 335,<br>349, 378, 394, 411, 412, 446, 461  | Liu, K.....          | 45, 47, 274, 275,<br>337, 338, 449, 451, 475  |
| Leoni, M.....      | 101, 218  | Lilleoden, E.....      | 335  | Liu, L.....          | 118, 175, 264, 470, 477, 478, 509   |
| Leo, P.....        | 64, 237   | Li, M.....             | 89, 102, 146, 147, 190, 203,<br>269, 317, 365, 370, 430, 470, 472  | Liu, M.....          | 179   |
| Le, Q.....         | 33  | Lim, A.....            | 435  | Liu, P.....          | 397   |
| LeSar, R.....      | 434, 435  | Lim, C.....            | 302  | Liu, Q.....          | 25, 130, 131, 382   |
| Leser, P.....      | 453   | Limem, S.....          | 126  | Liu, R.....          | 410, 463  |
| Leser, W.....      | 453   | Lim, H.....            | 279  | Liu, S.....          | 174, 371  |
| Leslie, S.....     | 338   |                        |  | Liu, T.....          | 76  |
| Lestari, W.....    | 314   |                        |  | Liu, W.....          | 135, 272, 281, 369, 402, 476, 481   |
| Letourneau, S..... | 131   |                        |  | Liu, X.....          | 100, 144, 155, 198, 212,<br>267, 268, 281, 303, 334,<br>345, 391, 404, 413, 418, 447  |

Liu, Z..... 22, 28, 44, 87, 143, 148, 152,  
 ..... 155, 202, 212, 261, 267, 328,  
 ..... 334, 366, 377, 386, 391, 516  
 Livescu, V..... 255, 380  
 Livingston, J..... 82, 326  
 Li, W..... 19, 22, 38, 73, 109, 132, 156,  
 ..... 179, 181, 214, 222, 354, 355, 392  
 Li, X..... 22, 160, 174, 179, 201, 202, 258,  
 ..... 303, 355, 356, 439, 440, 470, 492  
 Li, Y..... 15, 19, 20, 37, 40, 70, 76, 86, 98,  
 ..... 99, 118, 132, 154, 167, 224, 226,  
 ..... 232, 281, 290, 293, 319, 321, 328, 355,  
 ..... 358, 385, 403, 404, 415, 449, 485, 488  
 Li-yuan, C..... 500  
 Li, Z..... 205, 236, 494, 507, 511  
 LLorca, J..... 287  
 Lloyd, D..... 237  
 Llubani, S..... 61  
 Lo, C..... 177  
 Löffler, J..... 185, 467  
 Logan, K..... 347  
 Logan, R..... 86, 328  
 Loh, K..... 91  
 Loiola, R..... 428  
 Lokesh, R..... 43  
 Lokshin, K..... 185  
 Lombardi, A..... 179  
 Long, F..... 430  
 Long, G..... 101, 217  
 Long, H..... 417  
 Longhurst, G..... 332, 333  
 Long, N..... 241  
 Longoria, L..... 491  
 Long, S..... 443  
 Long, Z..... 64, 79, 121, 139, 178,  
 ..... 198, 236, 256, 298, 323, 358  
 Lookman, T..... 277  
 Lopes, A..... 403  
 Lopes, F..... 25, 427, 428, 429  
 Lopez-Chipres, E..... 21  
 López-Echarri, A..... 105  
 Lopez-Ferreño, I..... 105  
 Lopez-Hirata, V..... 188, 507  
 López, L..... 71  
 Lopez, M..... 68, 79, 303, 361, 422  
 Lopez, V..... 18  
 Loppinet, N..... 26  
 Loprang, R..... 421  
 Lordi, V..... 266  
 Lorentsen, O..... 238  
 Lorich, A..... 501  
 Lossius, L..... 137, 256  
 Lotfi, B..... 17  
 Louca, D..... 307, 365  
 Lou, J..... 115, 190, 227, 228, 418  
 Lourie, O..... 419  
 Loutas, T..... 198  
 Loutzenhiser, P..... 424, 469  
 Louzguine, D..... 423  
 Lowe, M..... 245  
 Lowengrub, J..... 29  
 Loya, M..... 241  
 Loya, P..... 418  
 Loyola, B..... 91  
 Luan, B..... 179  
 Lubin, M..... 256  
 Lu, C..... 130, 205, 215, 254, 276  
 Lucas, M..... 182, 191, 192

Lucente, A..... 306  
 Lücke, M..... 483  
 Luculescu, C..... 14, 415  
 Lucy, J..... 288  
 Ludtka, G..... 31, 143  
 Ludwig, W..... 80, 164, 172, 271, 272, 374  
 Lue, S..... 12, 28  
 Lues, J..... 379  
 Lu, G..... 479  
 Lugan, D..... 311, 480  
 Luganov, V..... 354  
 Lugo, M..... 388  
 Lu, H..... 228, 269, 392, 458, 460  
 Lui, T..... 48, 259, 326, 372  
 Lu, J..... 19, 128, 145, 243  
 Lu, K..... 109, 334, 380  
 Lukáš, P..... 163  
 Lu, L..... 109  
 Lunking, D..... 136  
 Luo, A..... 85, 205, 262, 263, 439, 478  
 Luo, H..... 98, 118, 252, 359, 439, 440, 485  
 Luo, J..... 127, 261, 307, 418  
 Luong, Q..... 379  
 Luo, R..... 494  
 Luo, S..... 195  
 Luo, T..... 116  
 Luo, W..... 498  
 Luo, Z..... 50  
 Lu, S..... 153  
 Luscher, W..... 332, 333  
 Lu, W..... 169, 252  
 Lü, X..... 475  
 Lu, Y..... 228, 418  
 Lu, Z..... 21, 127, 366  
 Lv, D..... 300  
 Lv, G..... 30  
 L. Voigt, H..... 487  
 L'vov, V..... 105  
 Lv, X..... 61, 417  
 Lv, Z..... 359  
 Lygin, K..... 401, 453, 454  
 Lymperakis, L..... 361  
 Lynch, D..... 460, 503  
 Lynch, I..... 183  
 Lyubina, J..... 151, 390

**M**

Maass, R..... 185  
 Mabe, J..... 454  
 Ma, C..... 478  
 MacArthur, K..... 102  
 Macedo, E..... 469  
 Machado, B..... 71, 196  
 Machin, A..... 179  
 Machta, B..... 436  
 Mackay, G..... 122  
 Mackay, K..... 122  
 Mackay, R..... 179, 348  
 Mackiewicz Ludtka, G..... 31, 143  
 MacKinnon, R..... 252  
 MacLean Chichester, H..... 333  
 Macrander, A..... 102  
 Ma, D..... 185, 337, 343  
 Maddala, D..... 467  
 Maddock, T..... 333  
 Maddox, B..... 196, 254  
 Maddox Saylor, F..... 169

Madec, R..... 434  
 Madison, J..... 446  
 Madland, R..... 426  
 Madsen, K..... 392  
 Ma, E..... 228, 244, 364, 365, 366, 418, 419  
 Maeda, M..... 72, 503  
 Maerten, A..... 361  
 Magyar, R..... 94  
 Ma, H..... 274, 275, 337, 338, 451  
 Mahadevan, G..... 128  
 Mahadevapuram, R..... 289  
 Mahaffey, D..... 62  
 Mahajan, D..... 474  
 Mahajan, R..... 338  
 Mahboubi, F..... 372  
 Mahdipoor, M..... 324, 372  
 Mahendiran, R..... 152  
 Mahesh, S..... 52, 222  
 Mahieu, P..... 138  
 Mahmood, M..... 22, 122, 179,  
 ..... 238, 299, 360, 419, 466  
 Mahmudi, R..... 34  
 Mahoney, M..... 81, 141, 199, 200,  
 ..... 258, 325, 326, 382, 383, 437  
 Maier, H..... 16  
 Maier, J..... 250  
 Maijer, D..... 226, 227, 308  
 Maile, K..... 371  
 Maisano, A..... 379  
 Maiti, A..... 167  
 Maitland, D..... 363  
 Maitra, P..... 39  
 Maiwald, D..... 138  
 Maizono, M..... 515  
 Ma, J..... 401, 475  
 Maji, B..... 51  
 Majidi, C..... 464  
 Majta, J..... 455  
 Majumdar, B..... 20, 166, 374  
 Majumdar, S..... 470  
 Majzoub, E..... 88, 144, 145  
 Makas, A..... 252  
 Makhlof, M..... 367  
 Maki, A..... 67, 187  
 Makul, N..... 429  
 Ma, L..... 14, 209, 269, 313, 343, 491  
 Malecki, H..... 13  
 Malherbe, J..... 446  
 Mallick, G..... 352, 463  
 Maloney, C..... 366  
 Maloy, S..... 41, 42, 43, 158,  
 ..... 211, 394, 427, 472, 473  
 Maltais, B..... 307  
 Mamaev, A..... 62  
 Ma, N..... 146, 251, 329, 406  
 Manavbasi, A..... 482, 494  
 Manchiraju, S..... 134, 278, 341, 412  
 Mandal, D..... 241  
 Mangler, C..... 221  
 Manivasagam, G..... 24  
 Manley, M..... 133, 159  
 Mannava, S..... 199, 245, 290, 309  
 Manning, L..... 365  
 Mann, V..... 58  
 Mannweiler, U..... 436  
 Man, O..... 163  
 Manohar, P..... 230  
 Mantese, J..... 49

# TMS2011

## 140th Annual Meeting & Exhibition

|                            |                             |                    |   |                         |                                  |
|----------------------------|-----------------------------|--------------------|---|-------------------------|----------------------------------|
| Mantha, D.....             | 28                          | Masson, I.....     | 492   | McKenna, I.....         | 172                              |
| Manuel, M.....             | 25, 143, 153, 341, 441      | Massot, L.....     | 461, 476  | McKillip, R.....        | 453                              |
| Manygoats, R.....          | 460                         | Mastorakos, I..... | 15  | McKittrick, J.....      | 68, 69, 214, 303, 361, 362, 422  |
| Mao, J.....                | 180                         | Masuda, C.....     | 166   | McLarren, W.....        | 510                              |
| Mao, L.....                | 242                         | Matadi, R.....     | 363   | McMahon, C.....         | 310                              |
| Mao, P.....                | 148                         | Mathaudhu, S.....  | 12, 32, 33, 59, 92, 115, 147, 149, 173, 205, 232, 262, 292, 321, 329, 352, 387, 415, 441, 463, 492, 493 | McMillen, C.....        | 169                              |
| Mao, S.....                | 127, 418                    | Mathiesen, R.....  | 201   | McNaney, J.....         | 254                              |
| Mao, X.....                | 417                         | Mathis, A.....     | 307   | McNelley, T.....        | 141, 142                         |
| Ma, Q.....                 | 34, 330                     | Mathon, M.....     | 448   | McNerney, J.....        | 177                              |
| Mara, N.....               | 16, 162, 168, 232, 292, 496 | Mathur, A.....     | 515   | McPhie, M.....          | 474                              |
| Maranchi, J.....           | 126                         | Matin, P.....      | 315   | McQueeney, R.....       | 134                              |
| Marangoni, R.....          | 26                          | Mato, M.....       | 405   | McQueen, H.....         | 64, 236, 237, 290                |
| Marathe, G.....            | 168                         | Matranga, C.....   | 16, 288, 392  | McQueen, J.....         | 510                              |
| Marceau, D.....            | 323, 382                    | Matsukawa, Y.....  | 157, 271  | McWhinney, H.....       | 72, 111                          |
| Marcin, J.....             | 264                         | Matsuki, T.....    | 367   | Meador, M.....          | 373                              |
| Mardon, J.....             | 43                          | Matsumoto, A.....  | 516, 522  | Means, D.....           | 67                               |
| Mareau, C.....             | 455                         | Matsumoto, H.....  | 76, 385, 487, 488   | Medeiros, M.....        | 120, 130, 131                    |
| Margem, F.....             | 26                          | Matsumoto, N.....  | 73  | Medina, E.....          | 176                              |
| Mariam, F.....             | 473                         | Matsumoto, S.....  | 73  | Medina, F.....          | 71, 280, 491                     |
| Marian, J.....             | 41, 434                     | Matsunaga, H.....  | 386   | Medlin, D.....          | 239                              |
| Mariaux, A.....            | 142                         | Matsuno, K.....    | 386   | Medvedeva, E.....       | 44                               |
| Marichal, C.....           | 394                         | Matsuoka, H.....   | 390   | Medvedev, P.....        | 445, 473                         |
| Marin, E.....              | 34, 121                     | Matsuoka, H.....   | 390   | Megharaj, P.....        | 12                               |
| Marinica, M.....           | 44                          | Matsuo, S.....     | 111, 112  | Meher, S.....           | 22                               |
| Marinkovic, B.....         | 72                          | Matsushita, M..... | 423   | Mehmood, S.....         | 247                              |
| Marino, J.....             | 256                         | Matsuzaki, K.....  | 327, 493  | Mehra, P.....           | 213                              |
| Markenscoff, X.....        | 78                          | Matsuzaki, Y.....  | 267   | Meier, A.....           | 424                              |
| Markkula, S.....           | 13                          | Matteis, P.....    | 188, 246, 493   | Meier, G.....           | 156, 334                         |
| Markovskiy, N.....         | 191                         | Mattern, N.....    | 468   | Meier, H.....           | 50, 51, 454                      |
| Marks, J.....              | 179                         | Matthies, C.....   | 187   | Meier, M.....           | 138, 436                         |
| Marois, M.....             | 459                         | Mattlin, K.....    | 258   | Meijer, M.....          | 299                              |
| Marone, F.....             | 202                         | Mauger, L.....     | 182   | Meilong, H.....         | 476                              |
| Maroto, J.....             | 348                         | Maugis, P.....     | 124   | Meinel, D.....          | 421                              |
| Marquez, M.....            | 460                         | Mauldin, T.....    | 433   | Meister, S.....         | 399                              |
| Marquis, E.....            | 43, 181, 239, 270           | Mauro, N.....      | 467   | Mejias, A.....          | 73                               |
| Marra, J.....              | 266                         | Ma, X.....         | 189, 226  | Mekala, P.....          | 309                              |
| Marshall, D.....           | 108                         | Maxime, S.....     | 342   | Melgarejo, Z.....       | 242, 468                         |
| Marshall, P.....           | 408                         | Ma, Y.....         | 391   | Melnyk, C.....          | 311, 480                         |
| Marshman, J.....           | 119                         | Mayama, T.....     | 329   | Melo, D.....            | 123                              |
| Martin, D.....             | 73, 224, 293, 358           | Mayer, C.....      | 332   | Melo, T.....            | 513, 515, 522                    |
| Martinez, D.....           | 246                         | May, S.....        | 102   | Melzer, C.....          | 236                              |
| Martinez, E.....           | 71, 93, 196, 280            | Ma, Z.....         | 250   | Mendelev, M.....        | 83                               |
| Martinez Flores, E.....    | 428                         | Maziasz, P.....    | 156, 198, 282, 345  | Mendes, M.....          | 188, 458                         |
| Martinez, J.....           | 71, 280                     | Mazumder, J.....   | 23, 201, 246  | Mendes, V.....          | 116, 234                         |
| Martinez Saez, E.....      | 29, 216                     | McBow, I.....      | 61  | Mendez, P.....          | 514                              |
| Martinez Sanchez, R.....   | 428                         | McBride, J.....    | 110   | Mendis, C.....          | 240, 263                         |
| Martinez-Villafaña, A..... | 220                         | McCabe, R.....     | 16, 104, 222, 430   | Mendoza Jr., A.....     | 490                              |
| Martin, G.....             | 66, 231                     | McCallum, D.....   | 126   | Meng, S.....            | 115, 218                         |
| Martin, H.....             | 38, 493                     | McCallum, R.....   | 390, 443  | Meng, X.....            | 157                              |
| Martin, I.....             | 144                         | McCally, R.....    | 125, 126  | Menon, S.....           | 141, 142                         |
| Martin, J.....             | 141, 258                    | McCauley, J.....   | 380   | Meratian, M.....        | 34                               |
| Martin, L.....             | 357                         | McClary, K.....    | 62  | Mercado, V.....         | 257                              |
| Martin, M.....             | 323                         | McClellan, K.....  | 195, 266  | Mercier, S.....         | 106, 195                         |
| Martin, O.....             | 466                         | McCoppin, J.....   | 450   | Merkel, S.....          | 163, 396                         |
| Martin, S.....             | 116                         | McCoy, T.....      | 313   | Merkle, A.....          | 379                              |
| Martins, L.....            | 429                         | McCrabb, H.....    | 268   | Merzkirch, M.....       | 188                              |
| Martorano, M.....          | 461                         | McCulloch, R.....  | 300   | Mesarovic, S.....       | 484                              |
| Marus, L.....              | 181, 393                    | McCune, R.....     | 493, 494  | Meschter, S.....        | 160                              |
| Maruyama, K.....           | 192                         | McDonald, A.....   | 432   | Meskers, C.....         | 94                               |
| Maruyama, T.....           | 334, 405                    | McDowell, D.....   | 118, 140, 145, 146, 209, 210, 315, 479  | Meslin, E.....          | 158                              |
| Marxer, N.....             | 462                         | McEvily, A.....    | 140   | Mesquita, A.....        | 500                              |
| Ma, S.....                 | 381                         | McGrath, É.....    | 183   | Metelva-Fischer, Y..... | 461, 503                         |
| Maser, J.....              | 100, 101                    | McGuinness, P..... | 152   | Metson, J.....          | 21, 120, 123, 177, 235, 297, 357 |
| Mason, D.....              | 100                         | McHenry, M.....    | 208, 264  | Meydanoglu, O.....      | 481                              |
| Mason, P.....              | 89, 146, 203                | McIlwraith, W..... | 428   | Meyer, A.....           | 202                              |
| Mason, T.....              | 255                         | McJunkin, T.....   | 517   | Meyer, J.....           | 282                              |
| Massambi, S.....           | 181                         |                    |   | Meyer, L.....           | 78                               |
| Masset, P.....             | 27, 117, 174, 175, 489      |                    |   | Meyer, M.....           | 96, 154, 333                     |



|                       |  |                            |   |                         |  |
|-----------------------|--|----------------------------|---|-------------------------|--|
| Meyers, M .....       | 68, 78, 136, 137,                      | Mishra, H .....            | 355                                     | Montazeri, M .....      | 372                                    |
| .....                 | 195, 196, 241, 253, 254,               | Mishra, R .....            | 33, 34, 81, 141, 155, 199,              | Monteiro, A .....       | 357                                    |
| .....                 | 303, 320, 361, 379, 402, 422           | .....                      | 206, 223, 228, 258, 259, 325, 326,      | Monteiro, S .....       | 25, 26, 71, 130, 187, 245,             |
| M'Guil, S .....       | 106                                    | .....                      | 330, 382, 388, 389, 437, 438, 451       | .....                   | 309, 368, 427, 428, 429, 499           |
| Mhaede, M .....       | 198                                    | Mishra, S .....            | 126                                     | Montgomery, J .....     | 37                                     |
| Mhamdi, L .....       | 502                                    | Miskioglu, I .....         | 369                                     | Montoro, E .....        | 123                                    |
| Miao, J .....         | 80                                     | Misra, A .....             | 43, 100, 108, 109, 167, 168, 227,       | Montoya-Davila, M ..... | 283                                    |
| Miao, Y .....         | 99                                     | .....                      | 286, 342, 343, 349, 411, 423, 426, 427, | Montoya, J .....        | 214                                    |
| Michael, N .....      | 311, 371, 431, 432                     | .....                      | 448, 457, 461, 464, 480, 482, 484, 496  | Moody, K .....          | 130                                    |
| Micha, J .....        | 395, 448                               | Misra, C .....             | 297                                     | Moody, N .....          | 168                                    |
| Michalicka, J .....   | 42                                     | Misra, D .....             | 25, 68, 184, 363, 364                   | Mook, W .....           | 418                                    |
| Michalski, S .....    | 331                                    | Misra, R .....             | 16                                      | Moon, K .....           | 213, 214, 224                          |
| Michelic, S .....     | 98                                     | Missalla, M .....          | 297, 298                                | Moon, M .....           | 213, 506                               |
| Michel, M .....       | 304                                    | Misture, S .....           | 131                                     | Moore, G .....          | 473                                    |
| Michler, J .....      | 349, 418                               | Mitchell, N .....          | 241                                     | Moore, J .....          | 151                                    |
| Mickael, P .....      | 121                                    | Mitchell, R .....          | 80                                      | Moorthy Babu, S .....   | 12                                     |
| Middlemas, M .....    | 408                                    | Mithieux, J .....          | 402                                     | Moraes, E .....         | 357                                    |
| Middleton, J .....    | 502                                    | Mitlin, D .....            | 88                                      | Moraes, V .....         | 171                                    |
| Migchielsen, J .....  | 129                                    | Mitra, A .....             | 463, 511                                | Morais, A .....         | 499                                    |
| Mihaila, B .....      | 430                                    | Miura, S .....             | 341                                     | Morales, A .....        | 440                                    |
| Mikami, K .....       | 305                                    | Miura, T .....             | 154                                     | Morales, F .....        | 138                                    |
| Mikami, M .....       | 85                                     | Miwa, K .....              | 147, 367                                | Morales, J .....        | 312, 463                               |
| Mikli, V .....        | 111                                    | Miyake, M .....            | 81                                      | Moran, M .....          | 73                                     |
| Miko, C .....         | 462                                    | Miyamoto, G .....          | 124                                     | Moras, A .....          | 123                                    |
| Mikolajczak, P .....  | 511                                    | Miyamoto, H .....          | 507                                     | Moravsky, A .....       | 374                                    |
| Miksis, M .....       | 202                                    | Miyazaki, S .....          | 50, 104, 161, 220,                      | Mordehai, D .....       | 231, 248                               |
| Miles, M .....        | 142, 319                               | .....                      | 277, 340, 400, 452                      | Mordi, G .....          | 13, 17                                 |
| Milewski, J .....     | 310                                    | Mizuno, T .....            | 82                                      | MoreiraJorge, A .....   | 20                                     |
| Militzer, M .....     | 23, 75                                 | Mladenov, G .....          | 509                                     | Moreno, C .....         | 180                                    |
| Millán, J .....       | 124                                    | Mliki, N .....             | 443, 515                                | Moretto, C .....        | 459                                    |
| Miller, B .....       | 413                                    | Mnikoleiski, P .....       | 138                                     | Morey, E .....          | 503                                    |
| Miller, C .....       | 208, 331                               | Moats, M .....             | 491                                     | Morgan, B .....         | 444                                    |
| Miller, H .....       | 172, 204                               | Modarres Razavi, S .....   | 33                                      | Morgan, D .....         | 40, 99, 157, 159, 215, 249,            |
| Miller, J .....       | 62, 63, 491                            | Moelans, N .....           | 315, 316, 451                           | .....                   | 270, 376, 393, 445, 446, 496, 497      |
| Miller, M .....       | 124, 125, 181, 182,                    | Moffatt, J .....           | 236                                     | Morgan, E .....         | 421                                    |
| .....                 | 249, 273, 289, 345, 393, 395, 427      | Mogford, J .....           | 140                                     | Mori, G .....           | 257                                    |
| Miller, R .....       | 284, 450                               | Mogilevsky, P .....        | 176                                     | Morimitsu, M .....      | 441                                    |
| Miller, S .....       | 191, 344                               | Mohamadi Zahrani, E .....  | 22, 224                                 | Morisada, Y .....       | 82, 325, 522                           |
| Millett, J .....      | 255                                    | Mohamed, F .....           | 18                                      | Morishige, T .....      | 511                                    |
| Millett, P .....      | 99, 154, 216, 436                      | Mohamed, M .....           | 475                                     | Morishita, H .....      | 85                                     |
| Mills, M .....        | 53, 134, 161, 162,                     | Mohamed, W .....           | 333                                     | Morita, K .....         | 174, 461, 503                          |
| .....                 | 193, 251, 273, 290, 377, 412, 427      | Mohammadi, H .....         | 237                                     | Morita, M .....         | 385                                    |
| Mills, R .....        | 337                                    | Mohammadi Zahrani, M ..... | 34                                      | Morjan, I .....         | 14, 415                                |
| Milovantseva, N ..... | 171                                    | Mohammed, A .....          | 23, 24                                  | Mornaghini, F .....     | 462                                    |
| Milshstein, J .....   | 149                                    | Mohammed, F .....          | 19                                      | Moroka, S .....         | 385                                    |
| Mimna, R .....        | 357                                    | Mohanchandra, K .....      | 453                                     | Moromugi, S .....       | 453                                    |
| Minamoto, Y .....     | 329                                    | Mohan, R .....             | 233                                     | Moroydor Derun, E ..... | 485, 486                               |
| Mingchun, L .....     | 297                                    | Mohanty, P .....           | 405, 432, 478, 482, 498                 | Morral, J .....         | 261, 387                               |
| Mingliang, S .....    | 177                                    | Mohanty, R .....           | 329                                     | Morral, M .....         | 445                                    |
| Minich, R .....       | 196, 254                               | Mohapatra, B .....         | 235                                     | Morreale, B .....       | 392                                    |
| Miniño, P .....       | 326                                    | Mohapatra, S .....         | 186                                     | Morrell, J .....        | 32, 273                                |
| Minor, A .....        | 108, 167, 227, 228, 233, 245,          | Mohebbali, M .....         | 14                                      | Morris, C .....         | 473                                    |
| .....                 | 286, 349, 411, 412, 413, 418, 419, 461 | Mohles, V .....            | 28, 65                                  | Morris, D .....         | 209, 343                               |
| Minowa, T .....       | 207, 444                               | Mohri, M .....             | 52                                      | Morris, J .....         | 27, 74, 82, 133, 191, 193, 219, 249,   |
| Miotto, P .....       | 123                                    | Moitra, A .....            | 50, 194, 286, 330                       | .....                   | 288, 315, 350, 365, 376, 412, 413, 435 |
| Miracle, D .....      | 284, 307, 346, 364, 365, 366           | Mo, K .....                | 370                                     | Morris, R .....         | 214                                    |
| Miranda, J .....      | 123                                    | Molenaar, D .....          | 323                                     | Morris, S .....         | 169                                    |
| Mirihanage, W .....   | 286                                    | Molinari, A .....          | 105, 106, 195                           | Morrow, B .....         | 251                                    |
| Mirnezami, M .....    | 311                                    | Molodov, D .....           | 171                                     | Morsi, K .....          | 54, 164, 213, 214,                     |
| Mironov, S .....      | 206                                    | Momeni, K .....            | 296                                     | .....                   | 223, 224, 280, 343, 403                |
| Mirpuri, K .....      | 47                                     | Momprou, F .....           | 101, 228, 378                           | Morsi, Y .....          | 466                                    |
| Mirsepasi, A .....    | 19                                     | Mondal, D .....            | 108                                     | Mortarino, G .....      | 246                                    |
| Mirshahi, F .....     | 34                                     | Mönig, R .....             | 296                                     | Mortazavi, B .....      | 293                                    |
| Mirzazadeh, M .....   | 199                                    | Monk, J .....              | 94                                      | Mortensen, A .....      | 107, 462                               |
| Mishima, Y .....      | 452                                    | Monnet, G .....            | 94, 231, 291                            | Mortensen, D .....      | 273                                    |
| Mishin, Y .....       | 83                                     | Monroe, J .....            | 453                                     | Morusupalli, R .....    | 103                                    |
| Mishra, B .....       | 235, 324                               | Monshi, A .....            | 224                                     | Mosbah, S .....         | 30                                     |
| Mishra, C .....       | 235, 355                               | Montagnat, M .....         | 342                                     | Mosca, H .....          | 445                                    |

# TMS2011

## 140th Annual Meeting & Exhibition

|                         |                              |                          |   |                         |   |
|-------------------------|------------------------------|--------------------------|---|-------------------------|---|
| Moscicki, M.....        | 273                          | Mu, W.....               | 494   | Nazarov, R.....         | 144   |
| Moscoco, W.....         | 34, 292                      | Myneni, G.....           | 211   | Ncapayi, V.....         | 14  |
| Mosler, J.....          | 330, 474                     |                          |   | Neal, W.....            | 379   |
| Moss, W.....            | 224                          | <b>N</b>                 |   | Nebebe, M.....          | 330   |
| Mostafavi, S.....       | 14                           | Nabavi, A.....           | 284   | Necker, C.....          | 310, 430  |
| Mota, L.....            | 429                          | Nabei, A.....            | 234   | Neelameggham, N.....    | 32, 92, 147, 149, 189, 205,<br>262, 329, 387, 424, 441, 469, 492, 493 |
| Motta, A.....           | 158, 211, 216, 370, 371, 473 | Nadendla, H.....         | 85, 86, 178, 415                                      | Neilsen, M.....         | 322   |
| Moulinec, H.....        | 342                          | Nadgorny, E.....         | 77  | Neises, M.....          | 425   |
| Moura, E.....           | 421, 433                     | Nadler, J.....           | 72  | Neklyudov, I.....       | 467   |
| Mourer, D.....          | 193                          | Næss, M.....             | 117   | Nele, M.....            | 177   |
| Mousavi, S.....         | 167                          | Nagai, T.....            | 72, 503   | Nelson, A.....          | 41  |
| Moutanabbir, O.....     | 352                          | Nagai, Y.....            | 40, 42, 99, 157, 158,<br>215, 270, 271, 393, 445, 496 | Nelson, B.....          | 142, 174  |
| Movahedi, B.....        | 16                           | Nagaoka, T.....          | 82, 522   | Nelson, G.....          | 432   |
| Moxnes, B.....          | 466                          | Nagasako, N.....         | 193   | Nelson, T.....          | 81, 141, 258, 383   |
| Mrovec, M.....          | 172                          | Nagasekhar, A.....       | 456   | Nemati, N.....          | 225, 465  |
| Mubarok, A.....         | 243                          | Nagaumi, H.....          | 178   | Nemati, Z.....          | 14  |
| Mudryk, Y.....          | 495                          | Naghipour, P.....        | 374   | Nemir, D.....           | 413   |
| Mueller, R.....         | 253                          | Nag, S.....              | 17, 66, 182, 239                                      | Nemoto, M.....          | 361   |
| Mughrabi, H.....        | 378                          | Nagy, P.....             | 176   | Nemoto, N.....          | 275   |
| Muhaffel, F.....        | 23                           | Nainar, V.....           | 24  | Neogy, S.....           | 188, 469  |
| Muhlstein, C.....       | 295                          | Naixiang, F.....         | 357, 381  | Neple, S.....           | 138   |
| Mukai, T.....           | 93, 206, 263                 | Na, J.....               | 176, 422  | Nerikar, P.....         | 144   |
| Mukherjee, A.....       | 486                          | Najiba, S.....           | 89  | Neri, M.....            | 220   |
| Mukherjee, K.....       | 317                          | Nakagawa, K.....         | 305   | Nesterenko, V.....      | 136, 137  |
| Mukherjee, T.....       | 331                          | Nakagawa, N.....         | 176, 177  | Nestler, B.....         | 32  |
| Mukhlis, R.....         | 437                          | Nakagawa, T.....         | 275   | Neuchterlein, J.....    | 341   |
| Mula, S.....            | 17                           | Nakai, Y.....            | 305   | Neugebauer, J.....      | 27, 75, 76, 144,<br>194, 248, 251, 277, 343, 361                      |
| Mulay, R.....           | 336                          | Nakamura, H.....         | 318   | Neumann, S.....         | 66  |
| Mulder, A.....          | 299                          | Nakamura, T.....         | 15, 416   | Neu, R.....             | 375   |
| Mulford, R.....         | 317, 377                     | Nakanishi, N.....        | 479   | Neurohr, A.....         | 400   |
| Muller, C.....          | 496                          | Nakano, J.....           | 155, 156  | Neves Monteiro, S.....  | 499   |
| Müller, M.....          | 336                          | Nakashima, H.....        | 135   | Newaz, G.....           | 107, 166, 225, 283  |
| Muller, R.....          | 363                          | Nakawaki, S.....         | 262   | Newman, J.....          | 453   |
| Mullett, M.....         | 235                          | Nakayama, H.....         | 225   | Nezafati, M.....        | 423   |
| Mulligan, R.....        | 449                          | Nalwa, K.....            | 289   | Ngan, A.....            | 356, 411  |
| Müllner, P.....         | 50, 51, 220, 221             | Namboothiri, S.....      | 238   | Ngayam Happy, R.....    | 271   |
| Mulreany, D.....        | 125                          | Nambu, A.....            | 390   | Ng, K.....              | 411   |
| Mun, H.....             | 221                          | Nam, S.....              | 457   | Nguyen, J.....          | 19  |
| Munich, C.....          | 460                          | Nam, T.....              | 51, 162, 221, 278                                     | Nguyen, K.....          | 227   |
| Munirathnam, N.....     | 509                          | Nanda, S.....            | 186   | Nguyen, Q.....          | 32  |
| Munir, Z.....           | 487                          | Nandy.....               | 24  | Nibhanupudi, S.....     | 494   |
| Munoz, J.....           | 182, 191, 192                | Nanninga, N.....         | 213   | Nicholson, D.....       | 161   |
| Muñoz - Saldaña, J..... | 71                           | Nanpazi, A.....          | 487   | Nickolai, I.....        | 214   |
| Munroe, P.....          | 52                           | Nanstad, R.....          | 97, 211, 333  | Nicola, L.....          | 350   |
| Muntasell, J.....       | 221                          | Napolitano, R.....       | 202, 366, 422   | Niedermair, F.....      | 327   |
| Muntele, C.....         | 229, 497                     | Narasimhan, N.....       | 247   | Niehoff, T.....         | 326, 327  |
| Mura, A.....            | 478                          | Narayanan, S.....        | 109   | Nieh, T.....            | 318   |
| Murakami, Y.....        | 147                          | Narayan, R.....          | 185, 311, 351,<br>371, 384, 431, 486, 489             | Nie, J.....             | 205   |
| Murakoshi, Y.....       | 493                          | Nascimento, D.....       | 427   | Nielsen, J.....         | 333   |
| Muralidharan, G.....    | 12, 206, 336, 338            | Nascimento, J.....       | 517, 522  | Niewczas, M.....        | 34  |
| Muralidharan, S.....    | 316                          | Nascimento, M.....       | 433, 492  | Nie, Z.....             | 151, 218  |
| Murashkin, M.....       | 292                          | Nassyrov, D.....         | 13  | Niezgoda, S.....        | 90, 309   |
| Murch, G.....           | 113, 261                     | Nastac, L.....           | 411   | Nikles, D.....          | 12  |
| Murcia, S.....          | 508                          | Nastar, M.....           | 216   | Nikolov, S.....         | 361   |
| Murdock, H.....         | 285                          | Nastasi, M.....          | 43, 100, 168, 427, 496                                | Ni, L.....              | 78  |
| Murphy, R.....          | 177                          | Natarajarathinam, A..... | 56  | Nili-Ahmadabadi, M..... | 19, 52, 468, 490  |
| Murray, C.....          | 217                          | Natesan, K.....          | 470, 472  | Nimityongskul, S.....   | 492   |
| Murray, J.....          | 111                          | Nathalie, B.....         | 121   | Ningileri, S.....       | 236   |
| Murray, P.....          | 333, 415                     | Nath, R.....             | 410   | Ning, X.....            | 190   |
| Murr, L.....            | 71, 196, 280, 480, 491       | Nath, S.....             | 20  | Nino, J.....            | 189   |
| Murthy, A.....          | 97                           | Navid, A.....            | 20  | Nishida, K.....         | 270   |
| Murti, V.....           | 98                           | Nayak, S.....            | 91  | Nishihara, T.....       | 325   |
| Murty, B.....           | 292                          | Nayar, V.....            | 422   | Nishikawa, H.....       | 450   |
| Murty, K.....           | 96, 155, 333, 371            | Nayebi, A.....           | 506   | Nishimoto, H.....       | 503   |
| Musinski, W.....        | 140                          | Nayyeri, G.....          | 34  | Nishimura, T.....       | 166, 450  |
| Muszka, K.....          | 455                          |                          |   | Nishiuchi, T.....       | 390   |
| Muth, T.....            | 206                          |                          |   |                         |   |
| Muthur Srinatha, P..... | 449                          |                          |   |                         |   |

|                |   |
|----------------|---|
| Nishiyama, Y   | 158   |
| Nisr, C        | 396   |
| Nissley, N     | 146   |
| Niu, H         | 98, 485   |
| Niu, X         | 148   |
| Nixon, M       | 321   |
| Nix, W         | 296, 356  |
| Nochang, P     | 477   |
| Noebe, R       | 50, 104, 105, 161, 162, 220,<br>222, 277, 278, 340, 341, 400, 452 |
| Noecker, R     | 146   |
| Nogita, K      | 450   |
| Nogueira, B    | 433   |
| Nogués, J      | 468   |
| Noh, K         | 184   |
| Nolan, T       | 96  |
| Nó, M          | 105   |
| Nomoto, A      | 270   |
| Noor-A-Alam, M | 15  |
| Nora, D        | 391   |
| Nordmark, A    | 245, 348  |
| Norman, G      | 40  |
| Nortan, J      | 413   |
| Norton, G      | 460   |
| Nose, Y        | 369   |
| Nosov, K       | 352   |
| Novitskaya, E  | 68, 69, 361, 362  |
| Novitski, V    | 315   |
| Novotnak, D    | 463   |
| Nowak, M       | 86, 89, 178   |
| Noyan, I       | 163, 217  |
| Nozawa, Y      | 271   |
| Numula, A      | 214   |
| Nunn, S        | 164, 165, 403   |
| Nutt, S        | 20  |
| Nwankpa, A     | 243   |
| Nyberg, E      | 32, 33, 85, 329, 439, 478   |
| Nychka, J      | 126, 240, 241, 432  |

## O

|                |  |
|----------------|--|
| Oakes, J       | 327  |
| Oaks, A        | 40, 99   |
| Oasaimah, A    | 274  |
| O'Brien, D     | 207  |
| O'Brien, E     | 61   |
| O'Brien, J     | 321, 335   |
| Ocelik, V      | 311  |
| Oddershede, J  | 252  |
| Odette, G      | 41, 181, 210, 211, 215,<br>270, 333, 371, 393, 395, 427, 470 |
| Odette, R      | 393  |
| Odqvist, J     | 87, 317  |
| Oduor, J       | 82   |
| Oezelt, H      | 207  |
| Ofico, I       | 138  |
| Ofori-Opoku, N | 29   |
| Ogawa, F       | 166  |
| Ogden, D       | 333  |
| Ogunseitun, O  | 170  |
| Ogura, K       | 425  |
| O'Hagan, P     | 368  |
| Ohashi, T      | 329  |
| Oh, C          | 338  |
| Oh, I          | 512  |
| Oh-ishi, K     | 240, 262, 263  |
| Oh, J          | 213, 350, 419  |
| Oh, K          | 36, 53, 293  |

|               |  |
|---------------|--|
| Ohkubo, T     | 169, 207, 240, 263, 390                            |
| Oh, M         | 452  |
| Ohnuki, S     | 158  |
| Ohnuma, I     | 275, 339, 341, 398, 451, 497                       |
| Ohodnicki, P  | 16, 150, 207, 208, 263,<br>331, 389, 443, 444, 495 |
| Ohriner, E    | 284  |
| Oh, S         | 514  |
| Ohshima, Y    | 461  |
| Oh, T         | 509, 518   |
| Ohta, M       | 263  |
| Ohto, K       | 74, 112  |
| Oh, Y         | 513  |
| Ohyanagi, M   | 145  |
| Oinuma, S     | 135  |
| Ojebuoboh, F  | 94   |
| Okabe, T      | 174  |
| Oka, H        | 70, 158  |
| Okamoto, K    | 150, 206, 398                                      |
| Okasinski, J  | 473  |
| Okaya, K      | 111, 112   |
| O'Keefe, M    | 111  |
| Okelman, M    | 460  |
| Okuniewski, M | 329, 430, 445, 473                                 |
| Okuyama, N    | 197  |
| Oladoye, A    | 214  |
| Olander, D    | 265  |
| Olevsky, E    | 19, 156, 214, 224, 241, 293, 303                   |
| Olivas, E     | 394  |
| Olive, D      | 472, 473   |
| Oliveira, A   | 515  |
| Oliveira, T   | 461  |
| Oliver, G     | 391  |
| Oliveros, H   | 171  |
| Olivetti, E   | 301, 406   |
| Olivier, F    | 391  |
| Olney, K      | 137  |
| Olsen, U      | 252, 271   |
| Olson, D      | 324  |
| Olson, G      | 204, 240, 383, 386                                 |
| Oluwatobi, O  | 14   |
| Omori, T      | 81, 341, 451                                       |
| Omura, N      | 147  |
| Ong, M        | 168  |
| Onimus, F     | 43   |
| Onishi, T     | 369  |
| Onizawa, H    | 183  |
| Onizawa, K    | 158  |
| Ono, H        | 112  |
| Onose, M      | 200  |
| Ono, Y        | 385  |
| Onsoien, M    | 286  |
| Opalka, S     | 210  |
| Ophus, C      | 239  |
| Oppedal, A    | 223, 330   |
| Ordronneau, F | 138  |
| Ortiz, C      | 215, 416   |
| Ortiz, L      | 60, 425  |
| Osawa, Y      | 263  |
| Osborne, W    | 460  |
| Osborn, T     | 313  |
| Osenbach, J   | 45, 102, 159, 160,<br>219, 274, 337, 397, 449      |
| Osen, K       | 122, 180   |
| Osetskiy, Y   | 216  |
| Osetsky, Y    | 41, 99, 215  |
| Ossa, A       | 508  |
| Ostendorp, S  | 19   |

|               |  |
|---------------|--|
| Osterberg, D  | 266  |
| Oster, N      | 390  |
| Osting, B     | 217  |
| Ostrander, M  | 396  |
| Ostrem, O     | 436  |
| Otani, S      | 452  |
| Otaviano, M   | 268  |
| Otomo, T      | 76, 488                                      |
| Ott, R        | 447  |
| Ott, T        | 30   |
| Ouchi, M      | 329  |
| Ouyang, F     | 397  |
| Öveçoglu, L   | 484  |
| Öveçoglu, M   | 404  |
| Overfield, N  | 141  |
| Ovsianikov, A | 351  |
| Owusu, K      | 463  |
| Øye, H        | 256  |
| Øyen, G       | 406  |
| Ozaki, K      | 85, 343                                      |
| Ozaltun, H    | 473  |
| Ozdemir, N    | 51, 162                                      |
| Ozkal, B      | 404, 479                                     |
| Özkal, B      | 403, 507, 513                                |
| Ozkan, C      | 56, 173                                      |
| Ozolins, V    | 27, 74, 133, 145,<br>191, 249, 315, 376, 435 |

## P

|                       |                    |
|-----------------------|--------------------|
| Pabel, T              | 286, 507           |
| Pabisch, S            | 363                |
| Pacheco, M            | 315                |
| Packer, S             | 141                |
| Padap, A              | 20                 |
| Padhan, P             | 332                |
| Padhi, B              | 86                 |
| PadhiI, B             | 22                 |
| Padilla, R            | 234, 440           |
| Padilla, V            | 384                |
| Padiyar, J            | 502                |
| Padula II, S          | 452                |
| Padula, S             | 104, 105, 161, 400 |
| Paglieri, S           | 423                |
| Paidar, V             | 76                 |
| Paine, I              | 86                 |
| Paithankar, K         | 15                 |
| Paiva, A              | 73                 |
| Palacios, E           | 495                |
| Palaflox-Hernandez, J | 82                 |
| Palchoudhury, S       | 351, 352           |
| Palchowdhury, A       | 186                |
| Paliwal, B            | 416, 473           |
| Paliwal, M            | 149                |
| Palkowski, H          | 98, 313            |
| Palla, M              | 361                |
| Palla, V              | 268                |
| Pallavkar, S          | 72                 |
| Palmer, M             | 84, 477, 505       |
| Pal, N                | 423                |
| Palomar, M            | 359                |
| Pal, S                | 312                |
| Pal, U                | 149, 504           |
| Paluri, R             | 56                 |
| Panahi, D             | 88                 |
| Panat, R              | 449                |
| Panchal, J            | 255                |
| Pancoast, R           | 392                |



# TMS2011

## 140th Annual Meeting & Exhibition

|                       |  |                         |                                      |                        |  |
|-----------------------|--|-------------------------|--------------------------------------|------------------------|--|
| Panda, A.....         | 463, 511   | Patlazhan, S.....       | 304                                  | Peshwe, D.....         | 15                                     |
| Pande, C.....         | 318  | Patnaik, R.....         | 358                                  | Pete, D.....           | 162                                    |
| Pandey, A.....        | 241  | Patterson, B.....       | 75, 196, 381                         | Peterlechner, M.....   | 221, 467                               |
| Pandey, B.....        | 170, 491   | Patterson, T.....       | 166                                  | Peterlik, H.....       | 363                                    |
| Pandey, R.....        | 60   | Pattnaik, P.....        | 178                                  | Petersen, M.....       | 141                                    |
| Pandey, S.....        | 289  | Paudyal, D.....         | 495                                  | Peterson, J.....       | 141                                    |
| Pang, J.....          | 242  | Paul, B.....            | 13                                   | Peterson, M.....       | 428                                    |
| Pang, S.....          | 424  | Paul-Boncour, V.....    | 151                                  | Peter, W.....          | 164, 165, 206, 463, 487                |
| Paniagua, M.....      | 508  | Paul, G.....            | 400                                  | Pethe, N.....          | 459                                    |
| Panigrahi, S.....     | 34, 259  | Paul, R.....            | 473                                  | Petit, C.....          | 493                                    |
| Panishev, N.....      | 61   | Paulsen, K.....         | 299                                  | Petit, I.....          | 322                                    |
| Pan, J.....           | 114, 116, 175, 220,<br>233, 234, 354, 355, 437     | Paulus, R.....          | 437                                  | Petit, J.....          | 448                                    |
| Panov, A.....         | 511  | Paul, W.....            | 360                                  | Petkov, T.....         | 507                                    |
| Pan, T.....           | 114  | Pauly, S.....           | 468                                  | Petrenc, M.....        | 163                                    |
| Panteli, L.....       | 114  | Pavlyuchkov, D.....     | 376                                  | Petrolito, J.....      | 87                                     |
| Pantleon, K.....      | 273, 394   | Payán, S.....           | 68                                   | Petrov, M.....         | 361                                    |
| Pant, P.....          | 51   | Payton, E.....          | 310                                  | Petrus, B.....         | 459                                    |
| Pan, X.....           | 21, 445  | Pearson, J.....         | 101                                  | Petrusenko, Y.....     | 467                                    |
| Pan, Z.....           | 136, 321, 347                                      | Pearson, T.....         | 274                                  | Pettifor, D.....       | 347                                    |
| Pao, C.....           | 76, 250  | Peaslee, D.....         | 144                                  | Pettit, F.....         | 156, 334                               |
| Pao, P.....           | 256, 298   | Pecharsky, V.....       | 150, 152, 495                        | Pettit, R.....         | 194                                    |
| Papangelakis, V.....  | 132, 189   | Pech-Canul, M.....      | 107, 166, 225, 283                   | Pfefferkorn, F.....    | 384                                    |
| Papanikolaou, S.....  | 18, 520  | Pedrazas, N.....        | 500                                  | Pfennig, A.....        | 507                                    |
| Papin, P.....         | 430, 486   | Peek, E.....            | 132, 133                             | Phan, M.....           | 208, 331                               |
| Paradowska, A.....    | 63, 273, 449                                       | Peel, A.....            | 245, 327                             | Phanon, D.....         | 88, 89                                 |
| Páramo, V.....        | 519  | Peetsalu, P.....        | 111                                  | Pharr, M.....          | 397                                    |
| Paranjape, H.....     | 341  | Pei, F.....             | 159, 160                             | Phejar, M.....         | 151                                    |
| Paras, J.....         | 166, 358   | Peikrshvili, A.....     | 136                                  | Phillion, A.....       | 285                                    |
| Pardoen, T.....       | 108  | Pei, Y.....             | 295                                  | Phillips, C.....       | 94                                     |
| Pareige, C.....       | 270  | Peiyu, Z.....           | 28                                   | Phillips, E.....       | 357                                    |
| Pareige, P.....       | 270  | Pena, G.....            | 326                                  | Phillips, P.....       | 193, 290                               |
| Paretsky, V.....      | 62   | Peña, O.....            | 13                                   | Phillpot, S.....       | 99, 153                                |
| Parga, J.....         | 441  | Peng, C.....            | 228, 418                             | Philo, S.....          | 306                                    |
| Parish, C.....        | 158, 181, 487                                      | Peng, H.....            | 61                                   | Picard, D.....         | 30, 322                                |
| Parkar, A.....        | 121  | Peng, J.....            | 62, 98, 117, 118, 132, 175, 355, 485 | Pichler, A.....        | 402                                    |
| Park, B.....          | 28, 430, 473                                       | Peng, L.....            | 82, 205, 514                         | Picornell, C.....      | 221                                    |
| Park, C.....          | 24, 198, 296                                       | Peng, Q.....            | 508, 509                             | Pierre, L.....         | 121                                    |
| Park, D.....          | 481, 512, 519                                      | Peng, Z.....            | 62, 117                              | Pierre-Olivier, B..... | 121                                    |
| Park, E.....          | 37, 243, 514                                       | Penilla, E.....         | 516                                  | Pierret, S.....        | 63                                     |
| Park, G.....          | 505  | Penin, N.....           | 88, 89                               | Pierson, D.....        | 241                                    |
| Park, H.....          | 254  | Pennycook, S.....       | 110                                  | Pieta, G.....          | 438                                    |
| Park, J.....          | 36, 139, 149, 186, 276,<br>398, 446, 485, 497, 510 | Pennycook, T.....       | 110                                  | Pike, L.....           | 396                                    |
| Park, K.....          | 385  | Pentyala, N.....        | 478                                  | Pilchak, A.....        | 62, 63                                 |
| Park, M.....          | 46, 315  | Penumadu, D.....        | 52, 363                              | Pilch, J.....          | 400                                    |
| Park, N.....          | 78, 255  | Peralta, P.....         | 195, 252, 266                        | Pilkey, K.....         | 489                                    |
| Park, S.....          | 47, 81, 115, 162, 200, 497, 517                    | Perander, L.....        | 123, 297                             | Pilote, S.....         | 382                                    |
| Park, T.....          | 352  | Pereira, A.....         | 26                                   | Pineault, J.....       | 431                                    |
| Park, W.....          | 148  | Pereloma, E.....        | 124, 188                             | Ping, X.....           | 28, 215                                |
| Park, Y.....          | 46, 276  | Perepezko, J.....       | 112, 182, 202                        | Pint, B.....           | 198, 212, 213, 281, 345, 346, 404, 405 |
| Paromova, I.....      | 511  | Peres, M.....           | 20                                   | Piochaud, J.....       | 42                                     |
| Parsons, G.....       | 174  | Perez-Bergquist, A..... | 255                                  | Pipetz, A.....         | 38                                     |
| Parthasarathy, T..... | 54, 135, 176,<br>205, 209, 231, 375                | Perez-Bergquist, S..... | 79, 386, 473                         | Pirayesh, H.....       | 241                                    |
| Parvin, N.....        | 519  | Perez, E.....           | 203                                  | Pires, R.....          | 300                                    |
| Pasang, T.....        | 319  | Perez, J.....           | 453                                  | Pirogov, A.....        | 506                                    |
| Pasebani, S.....      | 224, 326   | Perez, M.....           | 153                                  | Pirowski, Z.....       | 282                                    |
| Patchan, M.....       | 126  | Pérez, M.....           | 131                                  | Pisano, J.....         | 122                                    |
| Patel, A.....         | 205  | Pérez Prado, M.....     | 19                                   | Piskin, M.....         | 485                                    |
| Patel, H.....         | 39   | Pérez-Prado, M.....     | 32, 35                               | Piskin, S.....         | 404, 406, 486                          |
| Patel, M.....         | 496  | Pérez-Trujillo, F.....  | 405                                  | Pitarresi, J.....      | 48                                     |
| Patel, P.....         | 380, 436   | Perez, V.....           | 349                                  | Pitman, S.....         | 332                                    |
| Pate, T.....          | 82   | Perkins, M.....         | 335                                  | Pivato, J.....         | 476                                    |
| Pathak, S.....        | 56, 343, 349, 415, 418                             | Perovic, D.....         | 160, 219                             | Plapp, M.....          | 32, 260                                |
| Pathania, R.....      | 154  | Perrett, J.....         | 39, 141                              | Pleitt, J.....         | 44                                     |
| Patiño, F.....        | 131  | Perron, A.....          | 466                                  | Plikas, T.....         | 419                                    |
| Patí, S.....          | 149, 504   | Perruchoud, R.....      | 436                                  | Plimpton, S.....       | 93                                     |
|                       |  | Perrut, M.....          | 202                                  | Pluchon, C.....        | 129                                    |
|                       |  | Persson, D.....         | 423                                  | Plummer, J.....        | 185, 468                               |
|                       |  | Persson, K.....         | 249                                  | Plumtree, A.....       | 199                                    |

|                  |   |
|------------------|---|
| Podmiljšak, B    | 152   |
| Poizeau, S       | 238   |
| Pokharel, R      | 71  |
| Polak, S         | 67  |
| Polat, D         | 479   |
| Polesak, F       | 388   |
| Poliak, E        | 459   |
| Pollack, L       | 301   |
| Pollock, T       | 37, 63, 77, 80, 119, 193, 199, 246, 262, 312, 317, 381, 386, 396, 488 |
| Polyakova, V     | 233   |
| Polyakov, P      | 58  |
| Pomerleau, L     | 138   |
| Pomrehn, G       | 27  |
| Pomykala, J      | 112, 406, 456, 499  |
| Pond, R          | 376   |
| Ponge, D         | 124   |
| Pons, J          | 221   |
| Pontes, L        | 517, 522  |
| Poole, K         | 169   |
| Poole, W         | 36  |
| Poon, S          | 202, 264  |
| Pooyan, P        | 126   |
| Pope, D          | 377   |
| Popovici, E      | 14  |
| Popovic, M       | 65  |
| Portela, T       | 428, 429  |
| Portillo, B      | 458   |
| Posazhennikov, A | 61  |
| Potesser, M      | 327   |
| Potirniche, G    | 209, 211, 375   |
| Pötschke, M      | 51  |
| Potter, A        | 239   |
| Pottlacher, G    | 247   |
| Poulsen, H       | 252, 271  |
| Poulsen, S       | 172, 202  |
| Pourboghrat, F   | 274, 501  |
| Pournaderi, S    | 354   |
| Pourroy, G       | 432   |
| Pouryazdan, M    | 66  |
| Powell, A        | 149   |
| Powell, C        | 155   |
| Powell, G        | 273   |
| Powers, M        | 220, 284, 482   |
| Pozuelo, M       | 232   |
| Prabhakaran, R   | 154, 155, 333   |
| Prabhakaran, S   | 264   |
| Prabhu, B        | 247   |
| Pradhan, R       | 178   |
| Prahl, U         | 317   |
| Prakash, T       | 509   |
| Pramanick, A     | 191   |
| Pranger, W       | 221   |
| Prangnell, P     | 114, 438  |
| Prasad, A        | 187   |
| Prasad, R        | 188, 283  |
| Prasad, Y        | 205   |
| Prellier, W      | 332   |
| Presser, V       | 21, 492   |
| Preuss, M        | 253, 430  |
| Price, J         | 449   |
| Prida, V         | 151, 331  |
| Prillhofer, R    | 236   |
| Primig, S        | 501   |
| Privat, K        | 52  |
| Procive, N       | 439   |
| Prokofyev, E     | 19  |
| Prolubnikova, T  | 352   |

|                |                       |
|----------------|-----------------------|
| Proudhon, H    | 80, 272, 374          |
| Proud, W       | 320, 379              |
| Provatas, N    | 29, 74, 147, 260, 316 |
| Provenzano, V  | 331                   |
| Proville, L    | 172                   |
| Prucz, J       | 226                   |
| Przybyla, C    | 147                   |
| Pucher, P      | 121                   |
| Puebla, K      | 480                   |
| Puhakka, B     | 285, 410              |
| Puleo, D       | 494                   |
| Pullum, B      | 30                    |
| Puncreobutr, C | 31                    |
| Punessen, W    | 148                   |
| Purcek, G      | 16                    |
| Purdy, G       | 87, 88                |
| Purgert, R     | 281, 282              |
| Purohit, Y     | 233                   |
| Pursche, F     | 78                    |
| Puskar, J      | 271                   |
| Pusztai, T     | 31, 260               |
| Puthoff, J     | 242, 468              |
| Putla, R       | 229                   |
| Putyera, K     | 503                   |
| Pu, Z          | 494                   |
| Pyczak, F      | 336                   |
| Pyle, J        | 317                   |
| Pyshkin, S     | 478                   |
| Pyun, Y        | 24, 198               |
| Pyzalla, A     | 273                   |

## Q

|                |               |
|----------------|---------------|
| Qasaimeh, A    | 338           |
| Qian, D        | 199, 290, 309 |
| Qiang, D       | 65, 283       |
| Qiang, Z       | 500           |
| Qian, J        | 239           |
| Qian, M        | 179, 478      |
| Qian, S        | 51, 372       |
| Qiao, J        | 424           |
| Qiao, L        | 257           |
| Qiao, Y        | 169, 381      |
| Qidwai, S      | 279, 315      |
| Qi, H          | 307           |
| Qi, L          | 418           |
| Qingge, X      | 106           |
| Qinghua, T     | 215           |
| Qingsheng, L   | 357, 407      |
| Qing, X        | 294           |
| Qin, H         | 180           |
| Qin, J         | 300, 359      |
| Qin, Q         | 414           |
| Qiu, G         | 61, 174, 417  |
| Qiu, S         | 70, 278       |
| Qiuyue, Z      | 297           |
| Qi, X          | 300           |
| Quackenbush, M | 480           |
| Quackenbush, T | 453           |
| Quadir, M      | 52, 310       |
| Quan, L        | 313           |
| Quatravaux, T  | 30            |
| Quek, S        | 27, 75        |
| Querin, J      | 382           |
| Quey, R        | 374           |
| Queyreau, S    | 434           |
| Quick, A       | 459           |
| Quiroga, G     | 180           |

|       |          |
|-------|----------|
| Qu, P | 245, 247 |
| Qu, R | 423      |
| Qu, S | 79       |
| Qu, W | 485      |

## R

|                       |   |
|-----------------------|---|
| Raabe, D              | 124, 194, 343, 361, 374                   |
| Raab, G               | 187, 292                                  |
| Raahauge, B           | 297                                       |
| Raanness, O           | 55  |
| Rabin, B              | 473                                       |
| Rabkin, E             | 248                                       |
| Race, C               | 100, 248                                  |
| Rack, H               | 487                                       |
| Raddad, B             | 483                                       |
| Radetic, T            | 65, 245                                   |
| Radhakrishnan, B      | 336                                       |
| Radhakrishnan, R      | 442                                       |
| Radin, M              | 249                                       |
| Radmilovic, V         | 239, 413                                  |
| Radovic, M            | 32  |
| Rady, M               | 30  |
| Rae, D                | 103                                       |
| Ragan, R              | 14, 111, 353                              |
| Raghavan, P           | 22, 120, 130, 235, 425                    |
| Rahbar, N             | 23, 67, 125, 183, 240, 302, 361, 420, 421 |
| Rahem, A              | 482                                       |
| Rahimipour, M         | 324                                       |
| Rahnemaye Rahsepar, S | 515                                       |
| Rainforth, M          | 36  |
| Rajagopalan, S        | 239, 251                                  |
| Rajamohan, D          | 452                                       |
| Rajan, K              | 146                                       |
| Raja, P               | 86  |
| Rajaprakash, B        | 299                                       |
| Rajaram, G            | 359                                       |
| Rajendaran, G         | 12  |
| Rajendran, A          | 322                                       |
| Rajesha, S            | 484                                       |
| Raj, S                | 50, 104, 161, 220, 277, 340, 400, 452     |
| Raj Singh Gautam, A   | 239                                       |
| Raju, T               | 486                                       |
| Ramachandran, M       | 229                                       |
| Ramachandran, V       | 73  |
| Ramamurty, U          | 185                                       |
| Raman, A              | 449                                       |
| Ramana, C             | 15, 498                                   |
| Ramanathan, M         | 208, 251                                  |
| Ramana, Y             | 358                                       |
| Ramanujan, R          | 332                                       |
| Ramesh, K             | 248, 320, 321, 380, 412, 478              |
| Ramesh, P             | 421                                       |
| Ramirez, A            | 162, 220, 401                             |
| Ramirez, D            | 71, 280                                   |
| Ramirez, F            | 502                                       |
| Ramirez, N            | 428                                       |
| Ramirez, N            | 71  |
| Ramos, G              | 440                                       |
| Rampton, T            | 318                                       |
| Ram, R                | 444                                       |
| Randall, C            | 328                                       |
| Randall, N            | 421                                       |
| Randman, D            | 206                                       |
| Rangajanardhan, G     | 98  |
| Ranganathan, S        | 469                                       |
| Ranjbar, H            | 506                                       |

# TMS2011

## 140th Annual Meeting & Exhibition

|                         |   |                                  |                         |                            |   |
|-------------------------|---|----------------------------------|-------------------------|----------------------------|---|
| Rao, A.....             | 110   | Reuther, H.....                  | 50                      | Rodriguez, R.....          | 26, 428, 429  |
| Rao, M.....             | 235   | Reuther, K.....                  | 29, 50                  | Rodriguez-Rivera, J.....   | 218   |
| Rao, R.....             | 311   | Rey Boero, J.....                | 138                     | Rødseth, J.....            | 327   |
| Rao, S.....             | 77, 135, 176, 209, 230, 231, 355                    | Rey, C.....                      | 107                     | Roeb, M.....               | 425   |
| Raoufi, M.....          | 372   | reyes, A.....                    | 18                      | Roeder, R.....             | 305, 361  |
| Rao, W.....             | 277, 316  | Reyes, M.....                    | 131                     | Rogers, J.....             | 283   |
| Raphael, J.....         | 199, 307, 365                                       | Reyngoud, B.....                 | 346                     | Rogers, S.....             | 319   |
| Rappaz, J.....          | 466   | Reynolds, A.....                 | 201, 325                | Roggeman, B.....           | 48  |
| Rappaz, M.....          | 142   | Reynolds, R.....                 | 199                     | Rogge, P.....              | 443   |
| Rashkeev, S.....        | 445   | Reynolds, T.....                 | 437, 505                | Rogge, R.....              | 140, 472  |
| Rasizadeh, J.....       | 508, 509, 520                                       | Rey, P.....                      | 326                     | Rohatgi, P.....            | 107, 166  |
| Raskin, J.....          | 108   | Rezaeean, H.....                 | 52                      | Rohrer, G.....             | 72, 171, 172, 204   |
| Rassizadehghani, J..... | 179, 225, 490, 520                                  | Rezaeian, A.....                 | 481                     | Rojas, J.....              | 145   |
| Rasty, J.....           | 513   | Rezaie, H.....                   | 13, 16                  | Rojo, A.....               | 428   |
| Rathbun, H.....         | 431   | Rhamdhani, M.....                | 245, 308, 437           | Roland, T.....             | 432   |
| Ratke, L.....           | 511   | Rhim, Y.....                     | 125                     | Rolle, J.....              | 255   |
| Ratvik, A.....          | 137, 180  | Ribarik, G.....                  | 396                     | Rollett, A.....            | 53, 54, 71, 72, 118, 121, 232, 292, 309, 375, 402, 454, 455 |
| Rauch, E.....           | 279, 403  | Ribeiro Alves Filho, J.....      | 177                     | Romanelli, J.....          | 411   |
| Ravindra, N.....        | 311, 371, 431, 432                                  | Ribeiro, F.....                  | 197, 430                | Roman, K.....              | 341   |
| Ravindran, R.....       | 179   | Ribeiro, J.....                  | 298                     | Romanksy, M.....           | 160   |
| Rawls, P.....           | 281   | Ribeiro, M.....                  | 499                     | Romanov, A.....            | 356   |
| Ray, P.....             | 407, 408  | Riccardo, R.....                 | 288                     | Romero, M.....             | 359   |
| Razaghian, A.....       | 225, 226  | Rice, R.....                     | 169                     | Romero, T.....             | 472, 473  |
| Razavizadeh, H.....     | 13, 16  | Richard, D.....                  | 419                     | Romhanji, E.....           | 65  |
| R. Daymond, M.....      | 455   | Richards, N.....                 | 58                      | Rong, C.....               | 443   |
| Read, C.....            | 22, 122, 179, 238, 299, 360, 419, 466               | Richards, V.....                 | 97                      | Rongxing, L.....           | 508   |
| Ready, J.....           | 83, 116, 140, 415                                   | Richeton, T.....                 | 434                     | Roohibakhsh, R.....        | 13  |
| Ready, W.....           | 464   | Richter, A.....                  | 41                      | Roos, A.....               | 314   |
| Rebak, R.....           | 95, 154, 210, 211, 265                              | Richter, G.....                  | 296                     | Roose, D.....              | 374   |
| Reck, J.....            | 494   | Rickman, J.....                  | 112                     | Root, J.....               | 35  |
| Redden, C.....          | 56  | Riddervold, H.....               | 406                     | Rørvik, S.....             | 137, 436  |
| Reddy, L.....           | 167   | Riddle, Y.....                   | 312                     | Rosa, N.....               | 429   |
| Reddy, R.....           | 28, 55, 110, 111, 169, 229, 288, 350, 424, 425, 469 | Ridges, C.....                   | 142                     | Rosa, W.....               | 151   |
| Redkin, A.....          | 466   | Riedel, R.....                   | 191                     | Rosc, J.....               | 507   |
| Reeb, B.....            | 297   | Riegner, D.....                  | 274                     | Rosefort, M.....           | 187   |
| Reece, M.....           | 271   | Rieiro, I.....                   | 290                     | Rosenkilde, C.....         | 180   |
| Reed, B.....            | 31, 216, 254, 399, 455                              | Rieken, J.....                   | 280, 282, 470           | Rosenthal, S.....          | 110   |
| Reed, R.....            | 62, 386, 387  | Rimkus, N.....                   | 148                     | Rose, S.....               | 383   |
| Reedy Jr., E.....       | 168   | Ringer, S.....                   | 263                     | Rose, V.....               | 100   |
| Reek, T.....            | 238   | Rink, K.....                     | 211, 375                | Rosin, H.....              | 341   |
| Reggiani, B.....        | 122   | Rios, F.....                     | 522                     | Rösner, H.....             | 19, 127   |
| Reglitz, G.....         | 127   | Rios, O.....                     | 31, 143, 487            | Rossell, M.....            | 239   |
| Reilly, C.....          | 226, 227, 308                                       | Rios, S.....                     | 51, 341                 | Rossetto, M.....           | 493   |
| Reimanis, I.....        | 471   | Ritchie, R.....                  | 108, 253, 305, 362, 408 | Rossinyol, E.....          | 468   |
| Reimers, W.....         | 252, 336  | Ritter, Y.....                   | 153                     | Ross, K.....               | 383   |
| Reischig, P.....        | 80, 164, 272, 309                                   | Rivera-Diaz-del-Castillo, P..... | 376                     | Roters, F.....             | 374, 454  |
| Reis, J.....            | 73  | Rivera, I.....                   | 131                     | Roth, R.....               | 406   |
| Reis, S.....            | 73  | Rivero, R.....                   | 432                     | Roth, S.....               | 51, 422   |
| Reitz, T.....           | 450   | Rizzi, F.....                    | 67                      | Rotjer, T.....             | 86  |
| Rellinghaus, B.....     | 51  | Rizzo, F.....                    | 72, 427                 | Rottler, J.....            | 316   |
| Remington, B.....       | 78, 253, 254  | Roan, A.....                     | 504                     | Rouleau, M.....            | 323   |
| Remond, Y.....          | 304   | Robach, O.....                   | 272, 342, 395, 448      | Rout, A.....               | 22  |
| Rémond, Y.....          | 230   | Roberson, L.....                 | 191                     | Rowan, M.....              | 483   |
| Renaudier, S.....       | 466   | Robertson, I.....                | 157, 318                | Rowenhorst, D.....         | 118, 279  |
| Renavikar, M.....       | 338   | Robertson, J.....                | 134                     | Rowland, R.....            | 166   |
| Ren, C.....             | 208, 251  | Roberts, S.....                  | 285                     | Roy, A.....                | 420   |
| Ren, F.....             | 431   | Robertsson, A.....               | 141                     | Roy, C.....                | 15  |
| Ren, Y.....             | 151, 184, 185, 217, 218, 309, 321, 335, 336, 472    | Robichaud, P.....                | 307                     | Roychowdhury, S.....       | 188   |
| Ren, Z.....             | 201, 324, 426, 490                                  | Robinson, A.....                 | 154, 445                | Roy, P.....                | 138   |
| Rest, J.....            | 40, 446   | Robinson, J.....                 | 200                     | Roy, R.....                | 73, 74, 463, 511  |
| Restrepo, O.....        | 171, 214, 240                                       | Rocha, A.....                    | 60                      | Rozak, G.....              | 346, 500  |
| Retamal, J.....         | 440   | Rodelas, J.....                  | 82, 142, 326, 385       | Rozmus-Górnikowska, M..... | 514   |
| Rettberg, L.....        | 150   | Rodney, D.....                   | 171, 172                | Ruan, F.....               | 175   |
| Rettenmayr, M.....      | 29, 50, 377   | Rodrigues, G.....                | 499                     | Ruano, O.....              | 290   |
| Reusch, F.....          | 308   | Rodrigues, M.....                | 441                     | Ruban, A.....              | 387   |
| Reuter, M.....          | 56, 111, 170  | Rodrigues-Schroer, A.....        | 328                     | Ruch, D.....               | 230, 293, 304   |
|                         |   | Rodrigues, W.....                | 469                     | Ruda, M.....               | 240   |
|                         |   | Rodriguez-Nieva, J.....          | 94                      |                            |   |



$Q(\varphi, \sigma)$

$kT_g = \frac{2(B)(V)(\epsilon_1)}{K_0}$

|                      |                                       |                             |                    |                          |  |
|----------------------|---------------------------------------|-----------------------------|--------------------|--------------------------|--|
| Rudland, D.....      | 431                                   | Salau, M.....               | 385                | Sarma, S.....            | 292  |
| Rudman, K.....       | 266                                   | Salazar-Villalpando, M..... | 424, 425, 469      | Sarntinoranont, M.....   | 25, 441                                    |
| Rudy, D.....         | 361                                   | Salce, A.....               | 503                | Sarosi, P.....           | 134  |
| Rueschhoff, L.....   | 116                                   | Salehinia, I.....           | 349                | Sarrafi, R.....          | 39, 259, 268, 483                          |
| Rugg, D.....         | 223                                   | Saleh, T.....               | 473                | Sarswat, P.....          | 477  |
| Ruimeng, S.....      | 476                                   | Salem, H.....               | 348, 474           | Sarvinis, J.....         | 413  |
| Ruiz, E.....         | 144                                   | Salgado, J.....             | 428                | Sasaki, M.....           | 150  |
| Ruiz-Larrea, I.....  | 105                                   | Salgado-Ordorica, M.....    | 148                | Sasaki, T.....           | 161, 222, 341                              |
| Ruiz, M.....         | 234, 440                              | Saliklis, E.....            | 304                | Sastry, S.....           | 283  |
| Rule, J.....         | 142, 326                              | Salinas, E.....             | 131, 491           | Satapathy, S.....        | 196  |
| Russier, V.....      | 443                                   | Salles, M.....              | 466                | Sato, E.....             | 451  |
| Russell, T.....      | 140                                   | Salman, F.....              | 56                 | Sato, K.....             | 44, 385, 487                               |
| Rutman, D.....       | 476                                   | Salomon, A.....             | 224                | SATO, M.....             | 442  |
| Rutter, J.....       | 160, 219                              | Salston, M.....             | 427                | Sato, N.....             | 111  |
| Ryan, P.....         | 102, 394                              | Samadi Khoshkhou, M.....    | 18                 | Sato, S.....             | 15, 416, 488                               |
| Ryan, T.....         | 432                                   | Samajdar, I.....            | 51                 | Satoshi, H.....          | 194  |
| Rycerz, L.....       | 266                                   | Samarov, V.....             | 63, 165            | Satou, K.....            | 401  |
| Rye, K.....          | 30, 137, 197, 255, 322, 381, 436, 475 | Sampaio, J.....             | 120, 130, 131      | Sato, Y.....             | 81, 141, 199, 206, 258, 325, 382, 436, 437 |
| Ryou, H.....         | 362                                   | Sams, B.....                | 333                | Satsu, Y.....            | 390  |
| Ryu, I.....          | 296                                   | Samson, H.....              | 32                 | Sattler, C.....          | 425  |
| Ryu, J.....          | 505                                   | Samuel, E.....              | 411                | Saucedo-Muñoz, M.....    | 188, 507                                   |
| Ryu, S.....          | 434                                   | Sanaty-Zadeh, A.....        | 166                | Saunders, A.....         | 473  |
| <b>S</b>             |                                       |                             |                    |                          |  |
| Saadi, B.....        | 201                                   | Sanchez, F.....             | 73                 | Savage, S.....           | 423  |
| Saarna, M.....       | 111                                   | Sanchez, J.....             | 405                | Savolainen, K.....       | 200  |
| Sabahi, A.....       | 465                                   | Sánchez-Saavedra, M.....    | 69                 | Sawada, K.....           | 156  |
| Sabau, A.....        | 164, 165, 229, 403                    | Sánchez, T.....             | 151                | Saxena, A.....           | 277, 377                                   |
| Sabbagh, E.....      | 177                                   | Sandala, R.....             | 253                | Sayler Maddox, F.....    | 110  |
| Sabbagh, H.....      | 177                                   | Sander, B.....              | 343                | Saylor, D.....           | 316  |
| Sabirianov, R.....   | 331                                   | Sanderson, S.....           | 81                 | Säynäjäkangas, J.....    | 386  |
| Sachan, R.....       | 230                                   | Sanders, T.....             | 313                | Scapin, M.....           | 421  |
| Sachdev, A.....      | 388                                   | Sandfeld, S.....            | 90, 287            | Scardi, P.....           | 101, 218                                   |
| Sadamatsu, S.....    | 318                                   | Sandlöbes, S.....           | 35                 | Scarisoreanu, M.....     | 14   |
| Sadawy, M.....       | 324                                   | Sandnes, E.....             | 420                | Scarlett, T.....         | 506  |
| Sadeghian, Z.....    | 17                                    | Sandoval, J.....            | 519                | Scattergood, R.....      | 17, 20, 415                                |
| Sadek, T.....        | 401, 453, 454                         | Sandschneider, N.....       | 144                | Scavino, G.....          | 188, 246, 493                              |
| Sadiq, M.....        | 98                                    | Sandy, A.....               | 217                | Schaefer, C.....         | 65   |
| Sadler, B.....       | 30, 137, 197, 255, 322, 381, 436, 475 | Sangid, M.....              | 80, 107, 209       | Schäfer, C.....          | 65   |
| Sadoway, D.....      | 60, 238, 425, 476                     | Sanjari, M.....             | 35, 52, 387        | Schäfer, J.....          | 287  |
| Sadrnezhaad, S.....  | 12, 14                                | San Jose, R.....            | 348                | Schatteman, G.....       | 83   |
| Saeidi, F.....       | 468                                   | San Juan, J.....            | 105                | Schattenkirchner, M..... | 257  |
| Saengdeejing, A..... | 377                                   | Sankaran, R.....            | 412, 413           | Scheck, C.....           | 298  |
| Sagapuram, D.....    | 34                                    | San Marchi, C.....          | 232, 510           | Scheck, R.....           | 371  |
| Saghaian, S.....     | 105                                   | Sano, N.....                | 125                | Scheid, M.....           | 201  |
| Sagin, A.....        | 165, 225, 367                         | Sano, T.....                | 388                | Schein, O.....           | 125, 126                                   |
| Saha, B.....         | 208, 251                              | Santafé, H.....             | 428                | Schestakow, I.....       | 35   |
| Saha, P.....         | 33, 205                               | Santala, M.....             | 399                | Scheuermann, T.....      | 442  |
| Saha, R.....         | 102, 178                              | Santamarta, R.....          | 221                | Schlosser, N.....        | 98   |
| Sahayam, U.....      | 460                                   | Santanilla, A.....          | 57                 | Schlutig, S.....         | 472  |
| Sahin, F.....        | 515                                   | Santella, M.....            | 114, 345, 378, 438 | Schmetterer, C.....      | 175, 275, 339, 398, 451, 452, 497          |
| Sahin, Y.....        | 358                                   | Santhanakrishnan, S.....    | 25, 27, 294, 345   | Schmid-Fetzer, R.....    | 205  |
| Sahoo, M.....        | 492                                   | Santharam, S.....           | 53, 162            | Schmidlin, J.....        | 272, 431                                   |
| Sahoo, S.....        | 371                                   | Santisteban, J.....         | 370, 473           | Schmidt, E.....          | 502  |
| Sahu, K.....         | 467                                   | Santo Domingo, A.....       | 154                | Schmidt, H.....          | 297, 298                                   |
| Saida, J.....        | 423                                   | Santos, B.....              | 416                | Schmidt, M.....          | 13   |
| Saidi, P.....        | 485                                   | Santos, H.....              | 123                | Schmidt, S.....          | 252, 271                                   |
| Saigal, A.....       | 384, 478, 485                         | Santos, J.....              | 123                | Schmidt, T.....          | 129  |
| Saje, B.....         | 152                                   | Santos, K.....              | 522                | Schneibel, J.....        | 262, 427                                   |
| Sajjad, M.....       | 363                                   | Santos, M.....              | 73                 | Schneider, A.....        | 419  |
| Sajja, U.....        | 227                                   | Santos, P.....              | 469                | Schneider, I.....        | 441  |
| Sakai, T.....        | 37, 388                               | Saphores, J.....            | 170, 171           | Schneider, J.....        | 68, 125, 382, 383, 384, 486, 489           |
| Sakuragi, K.....     | 442                                   | Sarac, B.....               | 185                | Schneider, R.....        | 220  |
| Sakurai, H.....      | 397                                   | Saray, O.....               | 16                 | Schoenfeld, B.....       | 217  |
| Salame, P.....       | 44                                    | Saremi, M.....              | 213                | Schoenung, J.....        | 20, 167, 226, 293, 358, 486                |
| Salas, A.....        | 519                                   | Saridede, M.....            | 407, 456           | Schonewille, R.....      | 133  |
|                      |                                       | Sarikaya, M.....            | 68, 126, 242       | Schoonover, J.....       | 293, 294                                   |
|                      |                                       | Sari Yilmaz, M.....         | 406                | Schramm, J.....          | 69, 70, 243                                |
|                      |                                       | Sarkar, P.....              | 463, 511           |                          |  |
|                      |                                       | Sarkar, S.....              | 113                |                          |  |

# TMS2011

## 140th Annual Meeting & Exhibition

|                            |  |                            |                                  |                        |  |
|----------------------------|--|----------------------------|----------------------------------|------------------------|--|
| Schrefl, T .....           | 207                                    | Senturk, B .....           | 49                               | Sherburne, M .....     | 288  |
| Schreyer, A .....          | 336                                    | Sen, W .....               | 490                              | Shet, S .....          | 431, 432                                   |
| Schroers, J .....          | 69, 70, 185                            | Seo, J .....               | 110, 465                         | Shi, B .....           | 102  |
| Schryvers, D .....         | 108, 221                               | Seo, M .....               | 189                              | Shibata, T .....       | 473  |
| Schuh, C .....             | 153, 185                               | Seong, B .....             | 395, 446, 506                    | Shield, J .....        | 85, 332, 390, 443                          |
| Schüler, P .....           | 421                                    | Seong, T .....             | 465                              | Shields, J .....       | 346  |
| Schulson, E .....          | 250, 317                               | Seo, S .....               | 339                              | Shieu, F .....         | 50   |
| Schulte, T .....           | 40                                     | Sepehrband, P .....        | 237                              | Shi, F .....           | 392  |
| Schultz, J .....           | 325                                    | Sepehri-Amin, H .....      | 390                              | Shiflet, G .....       | 202, 264                                   |
| Schultz, L .....           | 51, 390                                | Serefoglu, M .....         | 143                              | Shi, G .....           | 512  |
| Schulze, K .....           | 374                                    | Serizawa, A .....          | 124                              | Shigesato, G .....     | 125  |
| Schulze, V .....           | 188                                    | Serna, L .....             | 484                              | Shih, D .....          | 204  |
| Schulz, P .....            | 236                                    | Serp, J .....              | 26                               | Shi, J .....           | 252, 359, 439                              |
| Schulz, R .....            | 475                                    | Server, W .....            | 333                              | Shiju, L .....         | 13   |
| Schumacher, P .....        | 263, 285, 286, 366, 507                | Sethna, J .....            | 18                               | Shikama, T .....       | 497  |
| Schuman, T .....           | 56, 111, 112, 170                      | Setman, D .....            | 415                              | Shi, L .....           | 244  |
| Schuren, J .....           | 395                                    | Setyawan, A .....          | 423                              | Shima, T .....         | 390  |
| Schuster, B .....          | 458                                    | Setyawan, W .....          | 249                              | Shimizu, T .....       | 493  |
| Schütze, M .....           | 396, 489                               | Severo, D .....            | 138                              | Shim, M .....          | 36   |
| Schvezov, C .....          | 349, 510                               | Severs, K .....            | 407                              | Shimajima, K .....     | 516, 522                                   |
| Schwarz, M .....           | 117                                    | Seyed Ahmadi, M .....      | 367                              | Shimonosono, T .....   | 267  |
| Schwarz, P .....           | 420                                    | Seyedrezai, H .....        | 489                              | Shim, Y .....          | 507  |
| Schwen, D .....            | 66                                     | Shabadi, R .....           | 182                              | Shin, B .....          | 35   |
| Schwingenschloegl, U ..... | 83                                     | Shade, P .....             | 77, 147, 230, 280, 355, 375, 462 | Shin, C .....          | 42, 302, 497                               |
| Scott, J .....             | 319, 517                               | Shaeffer, M .....          | 166                              | Shin, D .....          | 24, 38, 311, 508                           |
| Scott, S .....             | 286                                    | Shaffer, J .....           | 375                              | Shin, E .....          | 415, 506                                   |
| Scudino, S .....           | 18                                     | Sha, G .....               | 263                              | Shingledecker, J ..... | 281, 345                                   |
| Scully, J .....            | 306                                    | Shahandeh, S .....         | 75                               | Shin, H .....          | 353  |
| Sczerzenie, F .....        | 400                                    | Shahbazian-Yassar, R ..... | 295, 296, 355, 418, 464          | Shin, J .....          | 166  |
| Seal, S .....              | 351                                    | Shah, D .....              | 192, 250                         | Shin, K .....          | 24, 34, 35, 509                            |
| Searson, P .....           | 351                                    | Shah, U .....              | 419                              | Shin, S .....          | 233, 489                                   |
| Sebastian, M .....         | 131                                    | Sha, L .....               | 215                              | Shin, Y .....          | 200, 467                                   |
| Sediako, A .....           | 262                                    | Shalchi, B .....           | 259                              | Shi, R .....           | 329  |
| Sediako, D .....           | 150, 178, 179, 262                     | Shamanian, M .....         | 324                              | Shirato, N .....       | 230  |
| Sedlmayr, A .....          | 228, 296                               | Shamsuzzoha, M .....       | 252, 378, 488                    | Shishvan, S .....      | 287  |
| Seelam, U .....            | 169                                    | Sham, T .....              | 426                              | Shiveley, A .....      | 17   |
| Segatori, A .....          | 122                                    | Shang, C .....             | 139, 256, 257                    | Shi, W .....           | 55, 110, 111, 189, 264, 351                |
| Segatz, M .....            | 238                                    | Shang, J .....             | 312, 338, 397, 484               | Shiwen, B .....        | 21, 22, 357                                |
| Segre, C .....             | 371                                    | Shankar, R .....           | 96, 176                          | Shi, X .....           | 131, 269, 313, 491                         |
| Seguin, D .....            | 298                                    | Shankar, V .....           | 42                               | Shi, Y .....           | 85, 131, 160, 258, 365, 372, 415           |
| Segurado, J .....          | 287                                    | Shan, L .....              | 26                               | Shi, Z .....           | 87, 149, 190, 425                          |
| Sehitoglu, H .....         | 80, 104, 107, 161, 209                 | Shanmugasandaram, P .....  | 247                              | Shofner, M .....       | 312, 373, 433                              |
| Seidler, S .....           | 363                                    | Shannon, C .....           | 46                               | Shokuhfar, A .....     | 14, 108, 464, 465                          |
| Seidman, D .....           | 23, 66, 124, 181, 194, 239, 352        | Shan, T .....              | 153                              | Sholl, D .....         | 391  |
| Seifert, H .....           | 224, 376, 489, 498                     | Shan, Y .....              | 471                              | Shook, S .....         | 262  |
| Seifert, S .....           | 371, 473                               | Shan, Z .....              | 228, 356, 419                    | Shore, S .....         | 89   |
| Seif, m .....              | 497                                    | Shaofeng, F .....          | 381                              | Shoukry, S .....       | 226  |
| Seif, M .....              | 229                                    | Shapiro, A .....           | 170                              | Shrader, D .....       | 446  |
| Seifoddini, A .....        | 468                                    | Sharaf, S .....            | 522                              | Shrestha, T .....      | 211, 375                                   |
| Seiser, B .....            | 347                                    | Sharma, A .....            | 86, 299, 482, 483, 484           | Shroads, A .....       | 460  |
| Sekiguchi, T .....         | 183                                    | Sharma, P .....            | 235                              | Shuchan, W .....       | 297  |
| Seki, Y .....              | 303                                    | Sharma, S .....            | 128                              | Shull, R .....         | 140, 331                                   |
| Sekunowo, O .....          | 237                                    | Sharma, V .....            | 351                              | Shute, C .....         | 109  |
| Seliverstov, D .....       | 63, 165                                | Shashok, A .....           | 44                               | Shutthanandan, S ..... | 393  |
| Sellmayr, D .....          | 162                                    | Sha, W .....               | 471                              | Shyam, A .....         | 150  |
| Sellmyer, D .....          | 331                                    | Shaw, J .....              | 400                              | Siavashi, K .....      | 410  |
| Semenova, I .....          | 233                                    | Shaw, M .....              | 115                              | Sickafus, K .....      | 266, 496                                   |
| Semiatiin, L .....         | 62                                     | Sheikholeslami, S .....    | 490                              | Siddiqui, A .....      | 386  |
| Semiatiin, S .....         | 63, 135                                | Shekhar, S .....           | 96                               | Sidhu, R .....         | 45, 102, 159, 219, 274, 337, 338, 397, 449 |
| Sen, A .....               | 351                                    | Shen, C .....              | 193, 319                         | Sidor, J .....         | 106  |
| Sencer, B .....            | 203                                    | Shenghui, G .....          | 311                              | Siegel, D .....        | 249  |
| Senger, J .....            | 287                                    | Sheng, X .....             | 433                              | Sietsma, J .....       | 124  |
| Sengupta, J .....          | 410                                    | Shen, H .....              | 156                              | Siewert, M .....       | 277  |
| Sen, I .....               | 185, 363                               | Shen, J .....              | 194, 328                         | Signorelli, J .....    | 455  |
| Senkova, S .....           | 348                                    | Shen, M .....              | 190                              | Siham, A .....         | 121  |
| Senkov, O .....            | 200, 284, 307, 346, 348, 364, 365, 366 | Shenoy, R .....            | 200, 201                         | Sikand, R .....        | 388  |
| Senor, D .....             | 332, 333                               | Shen, W .....              | 471, 494                         | Silk, J .....          | 220  |
|                            |  | Shen, Y .....              | 103, 167, 175, 447, 464          |                        |  |

|                         |   |                        |                                 |                        |                        |
|-------------------------|---|------------------------|---------------------------------|------------------------|------------------------|
| Sillekens, W.....       | 32, 92, 147, 149, 205, 262,<br>329, 387, 441, 442, 492, 493 | Soderholm, L.....      | 370                             | Spector, M.....        | 153                    |
| Silva, D.....           | 500   | Söderlind, P.....      | 376                             | Spencer, B.....        | 256                    |
| Silva, F.....           | 120   | Soderžnik, M.....      | 152                             | Spichkin, Y.....       | 495                    |
| Silva, J.....           | 416   | Sodesetti, V.....      | 82                              | Spolenak, R.....       | 101, 462               |
| Silvas, F.....          | 441   | Soffer, M.....         | 180                             | Spoljaric, D.....      | 327                    |
| Simard, A.....          | 411   | Sofie, S.....          | 54, 512                         | Spowart, J.....        | 107, 137, 373, 415     |
| Simard, C.....          | 360   | Sofou, S.....          | 436                             | Sprague, A.....        | 75                     |
| Simensen, C.....        | 85  | Sohatsky, A.....       | 44                              | Sprague, W.....        | 312                    |
| Simmons, J.....         | 62, 89, 118, 119, 146, 176, 203                             | Sohn, H.....           | 61                              | Sprenger, M.....       | 333                    |
| Simpson, J.....         | 440   | Sohn, Y.....           | 32, 166, 202, 203, 261, 329     | Springer, H.....       | 136, 137               |
| Simpson, M.....         | 357   | Soisson, F.....        | 66, 216                         | Squatrito, R.....      | 286                    |
| Sinclair, C.....        | 36, 401, 402  | Sokolova, O.....       | 313                             | Srba, O.....           | 246                    |
| Sindelar, R.....        | 333   | Sokolov, M.....        | 97, 212                         | Sreenivasan, R.....    | 344                    |
| Singaperumal, M.....    | 485   | Sokolovskiy, V.....    | 495                             | Sridharan, K.....      | 265, 333               |
| Singh, A.....           | 55, 93, 109, 170, 182, 206, 262, 263                        | Solanki, K.....        | 50, 88, 100, 194, 286, 298, 330 | Sridhar, R.....        | 73, 74                 |
| Singh, C.....           | 209, 373  | Solari, P.....         | 472                             | Sridhar, S.....        | 155, 156               |
| Singh, D.....           | 86  | Solas, D.....          | 107                             | Srikanth, H.....       | 208, 331               |
| Singh, J.....           | 210, 389  | Solheim, A.....        | 122, 180, 238, 300, 436         | Srinath, M.....        | 483                    |
| Singh, P.....           | 155, 185  | Solis, F.....          | 435                             | Srinivasan, A.....     | 151                    |
| Singh, R.....           | 19, 169, 262, 357   | Solli, L.....          | 86                              | Srinivasan, R.....     | 17                     |
| Singh, S.....           | 24, 463, 511  | Soltanie, M.....       | 372                             | Sriram, C.....         | 224                    |
| Singh, V.....           | 351, 415  | Somekawa, H.....       | 93, 206, 263                    | Srivastava, D.....     | 188                    |
| Singleton, V.....       | 475   | Somers, K.....         | 95                              | Srivastava, K.....     | 119, 172               |
| Sinha, V.....           | 107   | Sommerseth, C.....     | 122, 180                        | Srivastava, V.....     | 220                    |
| Sinnott, S.....         | 93, 152, 153, 208   | Son, D.....            | 17                              | Srivatsa, S.....       | 204                    |
| Sirén, M.....           | 386   | Soneda, N.....         | 270                             | Srivilliputhur, S..... | 196, 239, 286, 287     |
| Siriruk, A.....         | 52  | Song, B.....           | 359                             | Srolovitz, D.....      | 248, 435, 464          |
| Sisneros, T.....        | 53, 163, 220, 273, 431                                      | Song, C.....           | 480, 508, 509, 518              | Stafslien, S.....      | 351                    |
| Sisson, R.....          | 386, 387  | Songca, S.....         | 14                              | Staiger, M.....        | 441                    |
| Sitaud, B.....          | 472   | Song, G.....           | 38, 494                         | Stalheim, D.....       | 139                    |
| Sittner, P.....         | 340, 400  | Song, H.....           | 377, 458, 482                   | Stalick, J.....        | 101                    |
| Sivilotti, O.....       | 149   | Song, J.....           | 213, 275, 398, 464              | Stamatiou, A.....      | 424                    |
| Siyahjani, F.....       | 24  | Song, L.....           | 23                              | Stamatis, D.....       | 17                     |
| Sket, F.....            | 310, 371  | Song, S.....           | 494                             | Stam, M.....           | 123, 179, 299          |
| Skjellerudsveen, M..... | 423   | Song, W.....           | 317                             | Stampanoni, M.....     | 202                    |
| Skokov, K.....          | 151   | Song, Y.....           | 160, 220                        | Stanculescu, A.....    | 44                     |
| Skomski, R.....         | 331   | Songyun, D.....        | 30                              | Stanek, C.....         | 144, 191, 266, 513     |
| Skorpenske, H.....      | 191, 335, 337   | Son, H.....            | 103, 453                        | Stan, G.....           | 296                    |
| Skorvanek, I.....       | 264   | Son, K.....            | 179                             | Stanhope, C.....       | 258                    |
| Skuratov, V.....        | 44  | Sonmez, M.....         | 457                             | Stan, M.....           | 215, 430               |
| Skybakmoen, E.....      | 122, 180, 300, 436  | Sonobe, M.....         | 70                              | Stanton, K.....        | 183                    |
| Skyllas-Kazacos, M..... | 475   | Son, S.....            | 302                             | Starikov, S.....       | 40                     |
| Slade, S.....           | 92  | Son, Y.....            | 385                             | Stark, A.....          | 336                    |
| Slifka, A.....          | 213   | Sopori, B.....         | 431, 432                        | Starke, P.....         | 140                    |
| Sluiter, M.....         | 182, 376  | Sopu, D.....           | 153                             | Starke, P.....         | 322                    |
| Smardz, L.....          | 89  | Sorensen, C.....       | 81, 141, 142, 258, 382, 383     | Starnes, A.....        | 110                    |
| Smatt, J.....           | 110   | Sorhuus, A.....        | 123                             | Staron, P.....         | 336                    |
| Smialek, J.....         | 119   | Soriano Vargas, O..... | 507                             | Starosselsky, A.....   | 289                    |
| Smilauerova, J.....     | 487   | Sort, J.....           | 468                             | Stebner, A.....        | 277, 454               |
| Smith, C.....           | 20, 166, 229, 247,<br>266, 301, 313, 325, 326               | Sosa, J.....           | 243, 309                        | Steele, T.....         | 130                    |
| Smith, D.....           | 209, 375  | Sosale, G.....         | 462                             | Steel, R.....          | 141, 142               |
| Smith, E.....           | 86  | Soucy, G.....          | 437, 459                        | Steen, I.....          | 366                    |
| Smith, J.....           | 328   | Soulami, A.....        | 488                             | Stefani, F.....        | 409                    |
| Smith, K.....           | 210   | Sousa Junior, C.....   | 492                             | Stegailov, V.....      | 40                     |
| Smith, M.....           | 134, 317  | Souza, C.....          | 468                             | Steighner, M.....      | 295                    |
| Smith, N.....           | 82  | Souza, E.....          | 458                             | Steinbach, I.....      | 260, 328               |
| Smith, R.....           | 265, 480, 501   | Souza, J.....          | 469                             | Steiner, G.....        | 221                    |
| Snead, L.....           | 265, 501  | Souza, L.....          | 123                             | Steinfeld, A.....      | 424, 469               |
| Snell, R.....           | 36  | Souza, T.....          | 433                             | Steinlechner, S.....   | 517                    |
| Snigirev, A.....        | 271   | Souza, V.....          | 500                             | Steinmetz, A.....      | 274                    |
| Snugovsky, L.....       | 160, 219  | Soyler, A.....         | 403, 404, 513                   | Stenger, S.....        | 425                    |
| Snugovsky, P.....       | 160, 219, 397   | Söyler, A.....         | 507                             | Stephens, E.....       | 33                     |
| Snyder, G.....          | 27, 239   | Spangenberger, J.....  | 112, 456, 499                   | Stephenson, B.....     | 100                    |
| Soare, I.....           | 14, 415   | Sparks, C.....         | 347                             | Stephenson, G.....     | 101                    |
| Soboyejo, W.....        | 420   | Spathis, D.....        | 65                              | Stepp, D.....          | 140                    |
| Sobrinho, A.....        | 517, 522  | Spearot, D.....        | 304                             | Stergar, E.....        | 41, 181, 211, 393, 427 |
|                         |   | Specht, E.....         | 336                             | Steurer, W.....        | 217                    |
|                         |   |                        |                                 | Steuwer, A.....        | 430                    |



# TMS2011

## 140th Annual Meeting & Exhibition

|                     |   |                        |   |                        |   |
|---------------------|---|------------------------|---|------------------------|---|
| Stevens, D.....     | 244   | Summers, A.....        | 303   | Tahautdinov, R.....    | 61  |
| Stevens, K.....     | 90  | Sun, C.....            | 41, 43, 168   | Tahija, D.....         | 425   |
| Stevenson, J.....   | 334   | Sun, D.....            | 83  | Tai-Ho, K.....         | 481   |
| Steves, D.....      | 513   | Sundararajan, T.....   | 230   | Taillard, R.....       | 182   |
| Stewart, J.....     | 199   | Sundaraman, M.....     | 210   | Tailleart, N.....      | 306   |
| St-Georges, L.....  | 323   | Sundman, B.....        | 316   | Tajouri, A.....        | 512   |
| Stickler, R.....    | 501   | Sun, F.....            | 350   | Takagi, K.....         | 343   |
| Stiegert, J.....    | 197   | Sung, M.....           | 19  | Takahashi, K.....      | 111   |
| Stinson, J.....     | 241, 442  | Sung, S.....           | 226   | Takahashi, N.....      | 150   |
| Stoica, A.....      | 185, 191, 335, 337                                    | Sung, W.....           | 45  | Takaku, Y.....         | 451   |
| Stoica, G.....      | 336   | Sun, H.....            | 242   | Takasugi, T.....       | 77, 192   |
| Stoica, M.....      | 422   | Sun, J.....            | 228   | Takei, R.....          | 479   |
| Stolken, J.....     | 254, 455  | Sun, K.....            | 392   | Takemoto, T.....       | 450, 522  |
| Stollberg, D.....   | 12, 14, 59, 115, 173,<br>232, 292, 352, 415, 416, 463 | Sun, L.....            | 269, 516  | Takeuchi, I.....       | 443   |
| Stolle, J.....      | 74  | Sun, M.....            | 206, 476, 514   | Takeuchi, T.....       | 42, 158   |
| Stoller, R.....     | 41, 99, 216, 335                                      | Suñol, J.....          | 151   | Takeuchi, Y.....       | 401   |
| Stone, D.....       | 242, 421, 468   | Sun, P.....            | 293, 306, 319   | Takeyama, M.....       | 135, 192, 345, 405                                    |
| Stone, H.....       | 396, 457  | Sun, Q.....            | 508   | Taleff, E.....         | 500   |
| Stone, M.....       | 185, 191  | Sun, X.....            | 40, 86, 99, 100, 154, 167, 180,<br>252, 315, 359, 379, 384, 439, 447, 488 | Talekar, A.....        | 89, 309, 423  |
| Stone, P.....       | 233   | Sun, Y.....            | 89, 160, 289, 325,<br>336, 408, 490, 514, 516                             | Tall, K.....           | 111   |
| Storer, R.....      | 290, 402  | Sun, Z.....            | 75, 148, 295, 487   | Tallman, D.....        | 333   |
| Stormvinter, A..... | 29  | Suo, Z.....            | 397   | Tamerler, C.....       | 23, 67, 68, 125, 183,<br>240, 242, 302, 361, 420, 507 |
| Stoudt, M.....      | 195   | Suquet, P.....         | 342   | Tamimi, S.....         | 52, 403, 519  |
| Stover, A.....      | 136   | Suresha, C.....        | 299   | Tamura, N.....         | 103, 272, 462, 464                                    |
| Strader, J.....     | 230   | Suriñach, S.....       | 468   | Tamura, T.....         | 147, 367  |
| Strasky, J.....     | 487   | Suryanarayana, C.....  | 169   | Tanaka, H.....         | 244   |
| Stráský, J.....     | 24  | Suss, A.....           | 511   | Tanaka, I.....         | 264   |
| Strbik, O.....      | 313   | Suter, R.....          | 71  | Tanaka, M.....         | 318   |
| Strehin, I.....     | 126   | Sutliff, J.....        | 317   | Tanaka, S.....         | 267   |
| Streiffer, S.....   | 101   | Sutou, Y.....          | 33, 341   | Tanaka, Y.....         | 341   |
| Strong, D.....      | 114   | Sutton, A.....         | 100   | Tang, H.....           | 431   |
| Strunz, P.....      | 163, 449  | Suwas, S.....          | 53, 162, 223  | Tang, M.....           | 216, 266, 455, 496                                    |
| Stuart, S.....      | 152   | Su, X.....             | 21, 39  | Tang, N.....           | 63  |
| Stubbins, J.....    | 40, 99, 370, 446                                      | Su, Y.....             | 426   | Tangstad, M.....       | 55, 308   |
| Students, I.....    | 337   | Su, Z.....             | 295   | Tang, T.....           | 38, 209, 319, 388                                     |
| Studer, A.....      | 273   | Suzuki, A.....         | 77, 386   | Tang, W.....           | 325, 390, 443   |
| Stukowski, A.....   | 196, 247, 287   | Suzuki, H.....         | 390   | Tang, X.....           | 192   |
| Sturhahn, W.....    | 191   | Suzuki, S.....         | 76  | Tang, Y.....           | 78, 402   |
| Stutz, L.....       | 388   | Svec, P.....           | 264   | Taniguchi, S.....      | 125   |
| Suarez, C.....      | 21, 120, 177, 235, 297, 357                           | Swab, J.....           | 380   | Tan, L.....            | 212, 405, 471   |
| Suárez, O.....      | 440   | Swain, R.....          | 403   | Tan, M.....            | 242   |
| Subbarayan, G.....  | 274   | Swainson, I.....       | 178   | Tanna, V.....          | 433   |
| Subedi, S.....      | 278, 517  | Swaminathan, N.....    | 497   | Tannenbaum, J.....     | 71, 371   |
| Subodh, G.....      | 131   | Swartzentruber, P..... | 285   | Tannenbaum, R.....     | 126, 364  |
| Subramanian, A..... | 115, 418  | Sweatman, K.....       | 450   | Tan, P.....            | 39, 157, 270, 516, 519, 521                           |
| Subramanian, K..... | 274, 338, 398, 450                                    | Swenson, H.....        | 471   | Tan, X.....            | 71  |
| Subramanian, R..... | 352   | Switznier, N.....      | 510   | Tao, J.....            | 26, 491   |
| Su, C.....          | 46, 275   | Syahbuddin, S.....     | 52  | Tao, N.....            | 109, 380  |
| Sucharev, Y.....    | 352   | Syed Asif, S.....      | 419   | Tao, S.....            | 88  |
| Sudbrack, C.....    | 119   | Sylvain, L.....        | 180   | Tao, X.....            | 174, 414  |
| Sudibjo, A.....     | 304   | Symanski, R.....       | 439   | Taranenko, I.....      | 495   |
| Suganuma, K.....    | 49, 275, 397  | Syvertsen, F.....      | 348   | Tarbe, R.....          | 111   |
| Sugar, J.....       | 239   | Szajek, A.....         | 89  | Tarcy, G.....          | 58, 180, 238, 360                                     |
| Sugawara, A.....    | 390   | Szczepanski, C.....    | 135, 147  | Tardy, N.....          | 129   |
| Sugiyama, M.....    | 125   | Szlufarska, I.....     | 446, 497  | Tarigan, I.....        | 345   |
| Suharto, J.....     | 54  | Szymanski, R.....      | 438   | Tashtoush, T.....      | 338   |
| Suh, B.....         | 36  | <b>T</b>               |   | Taskaev, S.....        | 151, 495  |
| Suh, C.....         | 198   | Tabereaux, A.....      | 180   | Tauber, M.....         | 116   |
| Suh, J.....         | 128   | Taber, G.....          | 196, 255, 379   | Taupin, V.....         | 434   |
| Suh, M.....         | 103   | Tachi, Y.....          | 497   | Tavangarian, F.....    | 15  |
| Suh, S.....         | 59  | Tadano, Y.....         | 329   | Tavazza, F.....        | 209, 272  |
| Sui, M.....         | 186   | Tada, S.....           | 147   | Tavera, F.....         | 506   |
| Sui, Z.....         | 73  | Tafen, D.....          | 212   | Tavera Miranda, F..... | 521   |
| Su, J.....          | 33, 93  | Taghavi, G.....        | 16  | Taxil, P.....          | 461   |
| Sukhram, M.....     | 409   |                        |   | Tayabally, J.....      | 133   |
| Sulger, P.....      | 138   |                        |   | Taya, M.....           | 340   |
| Sullivan, J.....    | 115, 301, 418   |                        |   | Taylor, E.....         | 268   |

$Q(\phi, \sigma)$

$kT_g = \frac{2(B)(V)(\epsilon_1)}{K_d}$

|                        |  |                      |   |                       |                                       |
|------------------------|--|----------------------|---|-----------------------|---------------------------------------|
| Taylor, J.....         | 245  | Tin'ghaev, P.....    | 466   | Trujillo, C.....      | 79, 246, 255, 321                     |
| Taylor, K.....         | 235  | Tipton, W.....       | 444   | Trumble, K.....       | 34, 226, 292                          |
| Taylor, M.....         | 22, 59, 123, 180, 238, 299, 520                    | Tiryakioglu, M.....  | 226, 285, 348, 410                                      | Truong, T.....        | 336                                   |
| Tayon, W.....          | 200, 201, 402                                      | Tischler, J.....     | 168, 272, 335   | Tsai, C.....          | 49, 275                               |
| Tedenac, J.....        | 144  | Tiwari, A.....       | 477   | Tsai, J.....          | 522                                   |
| Tédenac, J.....        | 249, 414   | Tiwari, S.....       | 209, 210  | Tsai, M.....          | 45                                    |
| Tegze, G.....          | 31, 260  | Tjahjanto, D.....    | 374   | Tsai, T.....          | 127, 498                              |
| Teixeira, A.....       | 131  | Tjahyono, N.....     | 123   | Tsakiropoulos, P..... | 457, 458, 487                         |
| Tekkaya, A.....        | 122  | T.N., R.....         | 162   | Tsao, C.....          | 37, 244                               |
| Telesman, I.....       | 257  | Toader, O.....       | 43  | Tschopp, M.....       | 100, 194, 209, 330, 388               |
| Telles, V.....         | 407  | Toda, H.....         | 252   | Tseng, C.....         | 47                                    |
| Tello, K.....          | 341  | Toda, I.....         | 182   | Tsiros, J.....        | 65                                    |
| Templeton, J.....      | 93, 334  | Todaro, I.....       | 286   | Tso, C.....           | 314                                   |
| Teng, C.....           | 403, 479   | Todd, A.....         | 41  | Tsubaki, T.....       | 461                                   |
| Teng, Z.....           | 345, 449   | Todd, I.....         | 185, 366, 468   | Tsuboi, H.....        | 401                                   |
| Tenório, J.....        | 57, 171, 368, 369, 407, 441, 456, 499              | Tokunaga, H.....     | 69  | Tsui, T.....          | 462                                   |
| Teran, A.....          | 433  | Toll, T.....         | 307   | Tsujikawa, M.....     | 511                                   |
| TerBush, J.....        | 262  | Tome, C.....         | 52, 105, 164, 222, 342                                  | Tsukamoto, H.....     | 450                                   |
| Terceelj, M.....       | 97, 294  | Tomé, C.....         | 53, 104, 163, 164, 223, 330                             | Tsung-Cheng, C.....   | 488                                   |
| Terentyev, D.....      | 94   | Tomesani, L.....     | 122, 286  | Tucker, G.....        | 209, 315                              |
| Terrani, K.....        | 265  | Tominaga, N.....     | 200   | Tucker, J.....        | 80, 95, 96, 97                        |
| Terry, J.....          | 472, 473   | Tomlinson, P.....    | 36  | Tucker, M.....        | 252                                   |
| ter Weer, P.....       | 120  | Tomsett, A.....      | 30, 137, 197, 255, 322, 381, 436, 475                   | Tucker, T.....        | 30, 486                               |
| Tessier, J.....        | 238, 322   | Tomsia, A.....       | 67  | Tu, G.....            | 359                                   |
| Tewari, R.....         | 128, 188, 458, 469                                 | Tomus, D.....        | 179   | Tugrul, N.....        | 485, 486                              |
| Thadhani, N.....       | 78, 128, 136, 137, 195, 253, 254, 313, 320, 379    | Tong, H.....         | 29  | Tu, K.....            | 450                                   |
| Thangaraju, S.....     | 292  | Tong, J.....         | 33  | Tulk, E.....          | 430                                   |
| Thanh, P.....          | 27, 172  | Tong, P.....         | 307   | Tummala, R.....       | 432, 498                              |
| Thebault, J.....       | 107  | Tong, Z.....         | 281   | Tung, H.....          | 370                                   |
| Theiss, S.....         | 187  | Toniazzo, V.....     | 304   | Tupper, C.....        | 104                                   |
| Thekdi, A.....         | 413  | Tonks, D.....        | 195, 255, 321, 380, 381                                 | Turbini, L.....       | 45, 102, 159, 219, 274, 337, 397, 449 |
| Thess, A.....          | 98, 409  | Tonks, M.....        | 99, 154, 216  | Turchi, P.....        | 146, 266, 376, 506                    |
| Thiaudière, D.....     | 448  | Topbasi, C.....      | 158   | Turhan, S.....        | 358                                   |
| Thijsse, B.....        | 248  | Topkaya, Y.....      | 354   | Turner, J.....        | 431                                   |
| Thirumalai, N.....     | 146, 251   | Topping, C.....      | 410   | Turner, T.....        | 62                                    |
| Thoma, D.....          | 380  | Topping, T.....      | 19, 20, 37, 224, 226, 232, 236, 293, 319, 358, 403, 404 | Turng, L.....         | 202                                   |
| Thomas, A.....         | 83   | Toptan, F.....       | 165, 225, 367   | Turpain, C.....       | 360                                   |
| Thomas, B.....         | 409, 410, 459, 460, 502                            | Torabi, S.....       | 29  | Turski, M.....        | 273                                   |
| Thomas, H.....         | 156  | Torbet, C.....       | 396   | Tu, W.....            | 119                                   |
| Thomas, J.....         | 62   | Torikai, K.....      | 325   | Twidwell, L.....      | 440                                   |
| Thomas, S.....         | 131  | Toroghinejad, M..... | 505   |                       |                                       |
| Thomas, W.....         | 391  | Torraiva, B.....     | 381   |                       |                                       |
| Thompson, B.....       | 142  | Tortop, R.....       | 334   |                       |                                       |
| Thompson, C.....       | 101  | Tortorelli, P.....   | 281, 345, 404   |                       |                                       |
| Thompson, G.....       | 12, 67, 161, 173, 214, 222, 341, 369               | Toth, G.....         | 31, 260   |                       |                                       |
| Thompson, R.....       | 176, 288   | Tournadre, L.....    | 43  |                       |                                       |
| Thonstad, J.....       | 360  | Touret, D.....       | 31  |                       |                                       |
| Thornton, K.....       | 328, 381, 435                                      | Toyama, T.....       | 42, 158, 271  |                       |                                       |
| Thota, S.....          | 332  | Toyoura, K.....      | 369   |                       |                                       |
| Threrujirapong, T..... | 167  | Tracy, S.....        | 30, 192, 222  |                       |                                       |
| Thula, T.....          | 68   | Tran, D.....         | 72  |                       |                                       |
| Tian, L.....           | 475  | Tranell, G.....      | 55, 117, 174, 460, 503                                  |                       |                                       |
| Tian, S.....           | 316, 386   | Tran, K.....         | 298   |                       |                                       |
| Tian, Z.....           | 269  | Tran, S.....         | 324   |                       |                                       |
| Tiefenbach, P.....     | 436  | Tran, V.....         | 437   |                       |                                       |
| TIE, J.....            | 39   | Traykova, T.....     | 361   |                       |                                       |
| Tien, R.....           | 345  | Treglio, J.....      | 83  |                       |                                       |
| Tikare, V.....         | 75, 156, 446                                       | Trempe, O.....       | 323   |                       |                                       |
| Tikasz, L.....         | 300  | Tremsin, A.....      | 473   |                       |                                       |
| Tiley, J.....          | 17, 44, 62, 100, 159, 182, 217, 271, 335, 394, 446 | Trenikhina, Y.....   | 473   |                       |                                       |
| Timmel, K.....         | 409  | Trexler, M.....      | 125, 126, 128, 379, 458                                 |                       |                                       |
| Timokhina, I.....      | 124  | Trinh, M.....        | 410   |                       |                                       |
| Ting-an, Z.....        | 120, 297   | Trinkle, D.....      | 75, 88, 92, 144, 251                                    |                       |                                       |
| Tingaud, D.....        | 124  | Tripathi, G.....     | 421   |                       |                                       |
|                        |  | Troev, T.....        | 44  |                       |                                       |
|                        |  | Trowbridge, T.....   | 517   |                       |                                       |

INDEX

U

|                     |  |
|---------------------|--|
| Uberuaga, B.....    | 100, 144, 496, 513                                       |
| Ubic, R.....        | 43, 131, 211   |
| Uchic, M.....       | 53, 77, 134, 135, 209, 230, 231, 280, 290, 355, 375, 462 |
| Uda, T.....         | 369  |
| Uddin, S.....       | 311  |
| Udpa, L.....        | 502  |
| Udyansky, A.....    | 76   |
| Ueda, K.....        | 390  |
| Ueda, M.....        | 334, 405   |
| Uehara, T.....      | 267  |
| Ueshima, M.....     | 276  |
| Uggowitzter, P..... | 121  |
| Uglov, V.....       | 44   |
| Ukolkina, T.....    | 352  |
| Ullakko, K.....     | 50, 220  |
| Ullal, V.....       | 304  |
| Ulrich, G.....      | 284  |
| Ulrich, O.....      | 395, 448   |
| Ulrich, T.....      | 252  |
| Umeda, J.....       | 167, 479, 493  |
| Umezawa, O.....     | 385  |
| Unal, C.....        | 144  |
| Undisz, A.....      | 50   |

# TMS2011

## 140th Annual Meeting & Exhibition

Ungar, T.....396  
 Ungár, T.....35, 273, 395, 396, 448  
 Unger, L.....368  
 Ünlü, N.....484  
 Unocic, K.....405  
 Unocic, R.....193  
 Upadhyaya, S.....299  
 Upadhyaya, A.....165, 512  
 Upadhyay, P.....201  
 Upmanyu, M.....28, 67, 204, 463  
 Upton, M.....217  
 Urbaniak, R.....362  
 Urbano, M.....278, 400  
 Urciuoli, D.....444  
 Usta, B.....358  
 Utsunomiya, H.....37, 388  
 Uysal, O.....358

**V**

Vaden, D.....189  
 Vadiraja, S.....242  
 Vahed, N.....481  
 Vaidyanathan, R.....50, 104, 161, 218,  
 .....220, 277, 278, 340, 400, 452  
 Valavala, P.....153  
 Valdez, S.....323, 440, 513  
 Valente, A.....358, 386  
 Valentina, T.....214  
 Valenzuela, J.....441  
 Valiev, R.....19, 233, 244, 292, 319  
 Valiveti, D.....251  
 Valle, N.....124  
 Valone, S.....113, 380  
 Van Aken, D.....97  
 Van Bael, B.....106, 374  
 Van De Car, S.....431  
 van den Bergh, M.....20, 166  
 Van den Bosch, J.....472  
 Van Den Bosch, J.....473  
 van der Berg, N.....446  
 Van der Giessen, E.....287, 350  
 Van der Ven, A.....113  
 van der Zwaag, S.....261  
 Van De Voorde, M.....60  
 van de Walle, A.....27, 134  
 Van De Walle, A.....29  
 van Duin, A.....152  
 Van Dyck, S.....271  
 Vanfleet, R.....369  
 Van Houtte, P.....106, 374  
 van Lieshout, K.....442  
 Van Petegem, S.....247, 394, 447  
 Van Renterghem, W.....271  
 Van Sluytman, J.....246  
 Van Son, V.....180  
 Van Swygenhoven, H.....63, 163, 247, 394, 447  
 Van Tendeloo, G.....443  
 Vanvoren, C.....58  
 Varadaraajan, V.....405, 482  
 Varea, A.....468  
 Vargas, H.....429  
 Varma, S.....457, 458  
 Vasile, C.....496  
 Vasile, E.....14  
 Vasquez, J.....362  
 Vassileva, V.....509  
 Vasudevan, V.....199, 245, 290, 309, 426, 458

Vatanakul, M.....413  
 Vaughan, G.....271, 396, 422  
 Vaynman, S.....320, 489  
 Vazquez, M.....331  
 Veatch, S.....436  
 Vecchio, K.....136, 137  
 Vedamanickam, S.....162, 486  
 Vedantam, S.....277  
 Vega, V.....151, 331  
 Veilleux, M.....314  
 Vékony, K.....466  
 Velamati, M.....284  
 Velasco, E.....189  
 Velasco, M.....247  
 Veliz, M.....325  
 Venancio, L.....469  
 Vengallatore, S.....462  
 Venkatanarayan, A.....55  
 Venkatesan, D.....12  
 Venkateshan, A.....169  
 Venkitanarayanan, P.....52  
 Ventelon, L.....44, 172  
 Verbaan, N.....73  
 Verdera, D.....326  
 Vergani, G.....400  
 Verhulst, D.....26, 73, 132, 189  
 Verma, A.....210  
 Verma, N.....312  
 Verma, R.....33, 64, 81, 141, 199,  
 .....258, 325, 382, 437, 438  
 Verma, V.....17  
 Vernigora, A.....60, 62  
 Veron, M.....279  
 Verreault, J.....360  
 Vershnyia, A.....419  
 Vicente-Alvarez, M.....370  
 Viegas, L.....441  
 Vieira, C.....499  
 Viennois, R.....249, 414  
 Vijaykumar, M.....162  
 Villa, E.....105  
 Villalon, J.....257  
 Villa, R.....234  
 Villechaise, P.....488  
 Vilsaar, K.....111  
 Vincze, G.....403  
 Vinogradov, A.....139, 233  
 Vinogradov-Jabrov, O.....461  
 Vinson, D.....333  
 Vinuela, F.....453  
 Virtanen, S.....442  
 Vishwanadh, B.....128  
 Viswanathan, B.....135  
 Viswanathan, G.....17, 66, 182  
 Viswanathan, L.....482  
 Viswanathan, R.....281  
 Viswanathan, S.....33, 205, 409, 459, 502  
 Vitthus, B.....256  
 Vitek, V.....76  
 Vitorino, J.....499  
 Vitter, J.....305  
 Vivas, L.....331  
 Vivek, A.....379  
 Viyyuri, S.....327  
 Vizcaino, P.....370  
 Vogel, S.....16, 139, 164, 223, 262,  
 .....273, 330, 337, 430, 446, 473  
 Vogt, R.....20, 167, 226, 293

Voicu, I.....14  
 Voigt, H.....393  
 Voit, D.....132  
 Voit, W.....304, 313, 363  
 Volz, H.....486  
 Vo, N.....66, 240, 287, 292  
 von Kaenel, R.....420  
 von Krüger, P.....122  
 von Pezold, J.....76, 248, 251  
 Vontobel, P.....333, 472  
 Voorhees, P.....76, 172, 202  
 Voter, A.....113  
 Voyer, R.....326  
 Voyles, P.....182, 242, 468  
 Vrátná, J.....24, 35  
 Vroomen, U.....187  
 Vry, B.....197  
 Vu, Q.....342  
 Vural, L.....519  
 Vutova, K.....509

**W**

Wachs, D.....154  
 Wachs, G.....333  
 Wada, T.....70  
 Wagatsuma, K.....488  
 Wagner, F.....279, 455  
 Wagner, G.....93, 114, 115, 199, 259, 382  
 Wagner, L.....24, 198  
 Wagner, R.....209  
 Wagner, W.....333  
 Wagoner Johnson, A.....67  
 Wagoner, R.....278, 279  
 Wahl, A.....332  
 Wain, N.....164, 337  
 Waitz, T.....221, 400, 467  
 Wakeman, T.....459  
 Walker, J.....247  
 Walker, L.....338, 396  
 Wallace, G.....126  
 Wallace, J.....211  
 Wallace, R.....17  
 Wallace, T.....453  
 Wallert, A.....309  
 Walley, J.....53, 290  
 Wallis, R.....176  
 Walser, J.....258  
 Wanderka, N.....210, 407  
 Wang, A.....203  
 Wang, B.....67, 108, 261  
 Wang, C.....16, 167, 275, 288,  
 .....339, 398, 418, 451, 497  
 Wang, D.....86, 392, 439, 440  
 Wang, F.....157, 257, 268, 381  
 Wang, G.....69, 86, 91, 127, 139, 184,  
 .....199, 242, 305, 306, 307, 364,  
 .....365, 422, 424, 425, 434, 467  
 Wang, H.....28, 30, 61, 67, 109, 118, 164,  
 .....168, 189, 255, 265, 431, 463, 482  
 Wang, I.....48, 397  
 Wang, J.....31, 48, 83, 109, 113, 155, 167,  
 .....168, 222, 292, 317, 360, 380, 477  
 Wang, K.....363, 397  
 Wang, L.....12, 15, 42, 135, 227,  
 .....349, 359, 368, 402, 508, 509  
 Wang, M.....32  
 Wang, N.....190



|                        |   |
|------------------------|---|
| Wang, P.....           | 34, 38, 76, 121, 319, 388, 484, 493   |
| Wang, Q.....           | 150, 190, 243, 361  |
| Wang, R.....           | 407   |
| Wang, S.....           | 84, 137, 344  |
| Wang, T.....           | 366   |
| Wang, W.....           | 86, 382, 471  |
| Wang, X.....           | 14, 27, 44, 74, 100, 124, 133,<br>159, 165, 174, 181, 185, 191, 193, 217,<br>237, 249, 252, 271, 315, 318, 319, 321,<br>335, 336, 337, 360, 376, 394, 408, 425,<br>431, 435, 446, 447, 448, 471, 503, 516 |
| Wang, Y.....           | 39, 41, 42, 43, 44, 84,<br>100, 102, 113, 118, 149, 151,<br>159, 161, 193, 217, 218, 261, 271, 295,<br>305, 315, 316, 328, 329, 335, 366, 379,<br>387, 394, 436, 445, 446, 447, 494, 503                  |
| Wang, Z.....           | 78, 87, 149, 190, 338, 477, 478   |
| Wan, H.....            | 490   |
| Wanjara, P.....        | 294   |
| Warczok, P.....        | 203   |
| Ward, C.....           | 90  |
| Ward, D.....           | 209   |
| Ward, L.....           | 364   |
| Ware, B.....           | 313   |
| Ware, T.....           | 304, 363  |
| Warner, D.....         | 209   |
| Warnken, N.....        | 29, 387   |
| Warren, J.....         | 89, 146, 203, 316   |
| Warren, O.....         | 419   |
| Warsinski, K.....      | 201   |
| Was, G.....            | 40, 42, 99, 154, 157, 159, 210,<br>215, 270, 271, 393, 394, 402, 445, 496, 497  |
| Wass, J.....           | 189   |
| Watanabe, H.....       | 158   |
| Watanabe, M.....       | 233, 497  |
| Waterman, J.....       | 441   |
| Watkins, T.....        | 206, 272, 396   |
| Watson, A.....         | 451   |
| Watson, T.....         | 479   |
| Watt, D.....           | 25  |
| Wauthier, A.....       | 395   |
| Wayne Jones, J.....    | 80  |
| Wayne, L.....          | 195   |
| Waz, E.....            | 187   |
| Weaver, D.....         | 62, 63  |
| Weaver, M.....         | 148, 161, 169, 222  |
| Webb, J.....           | 177, 347  |
| Weber, J.....          | 442   |
| Weber, M.....          | 349   |
| Wedde, G.....          | 123   |
| Weden, B.....          | 361   |
| Weertman, J.....       | 109, 318  |
| Wehrli, J.....         | 235   |
| Wei, C.....            | 137, 196  |
| Wei, D.....            | 119, 193  |
| Weidenmann, K.....     | 188   |
| Weihls, T.....         | 67, 136, 448  |
| Wei, J.....            | 475   |
| Wei, L.....            | 311   |
| Weiland, J.....        | 422   |
| Weil, S.....           | 81  |
| Weinberg, D.....       | 301   |
| Weinberger, C.....     | 355   |
| Weinstein, B.....      | 311, 480  |
| Wei, Q.....            | 136, 168, 321, 347, 458   |
| Weisenstein, A.....    | 54, 512   |
| Weiss, D.....          | 464   |
| Weisser, M.....        | 247, 394, 447   |
| Weiwei, T.....         | 518   |
| Wejdemann, C.....      | 252   |
| Welberry, R.....       | 217   |
| Welberry, T.....       | 218   |
| Welch, B.....          | 58, 180, 308, 437, 475  |
| Wells, M.....          | 460   |
| Welsch, G.....         | 489   |
| Welshons, D.....       | 177   |
| Wendler, E.....        | 446   |
| Wen, H.....            | 15  |
| Wen, J.....            | 130   |
| Wenk, H.....           | 342   |
| Wentlent, L.....       | 274   |
| Wen, W.....            | 79, 80, 346   |
| Wen, X.....            | 236, 426  |
| Wenxin, H.....         | 357   |
| Wen, Y.....            | 213   |
| Wenzhong, C.....       | 518   |
| Werkhoven, R.....      | 442   |
| Werner, E.....         | 402   |
| Wesch, W.....          | 446   |
| Wessels, V.....        | 467   |
| West, E.....           | 402   |
| West, M.....           | 82, 201, 437, 439   |
| Westphal, B.....       | 189   |
| Weygand, D.....        | 90, 172   |
| Wharry, J.....         | 159   |
| Wheatley, C.....       | 64  |
| Wheeler, D.....        | 146   |
| Wheeler, M.....        | 67  |
| Wheeler, R.....        | 53, 107, 147, 280, 290, 462   |
| Wheeler, T.....        | 30  |
| White, B.....          | 137   |
| White, C.....          | 298   |
| White, D.....          | 326   |
| White, E.....          | 116   |
| White, H.....          | 282   |
| Whiteman, G.....       | 255   |
| White, P.....          | 334   |
| Whitfield, R.....      | 218, 273  |
| Whitley, B.....        | 56  |
| Whitted, L.....        | 199   |
| Wicker, R.....         | 71, 280, 480, 491   |
| Wickwire, A.....       | 379   |
| Widener, C.....        | 439   |
| Widom, M.....          | 212   |
| Wieser, H.....         | 257   |
| Wiezorek, J.....       | 31, 96, 368   |
| Wijayaratne, H.....    | 238   |
| Wilde, G.....          | 19, 127, 262, 467   |
| Wilde, J.....          | 477   |
| Wilgen, J.....         | 31  |
| Wilkerson, J.....      | 164   |
| Wilkerson, L.....      | 312, 484  |
| Wilkinson, A.....      | 79, 192, 228, 278   |
| Wilkinson, D.....      | 330   |
| Wilks, G.....          | 284, 346, 364, 365  |
| Wilks, T.....          | 273   |
| Willaime, F.....       | 44, 172   |
| Willard, M.....        | 230, 264, 332   |
| William, G.....        | 226   |
| Williams, A.....       | 36  |
| Williams, C.....       | 181   |
| Williams, D.....       | 331, 350  |
| Williams, F.....       | 297   |
| Williams, J.....       | 193, 257, 315, 433  |
| Williams, R.....       | 66, 239, 288  |
| Wilson, S.....         | 118, 244  |
| Wimroither, G.....     | 327   |
| Winarski, R.....       | 101   |
| Winarski, R.....       | 100   |
| Windl, W.....          | 240, 364  |
| Wind, S.....           | 297   |
| Winiarski, B.....      | 306, 467  |
| Winkelmann, C.....     | 314   |
| Winther, G.....        | 105, 106, 252   |
| Wiraseranee, C.....    | 174   |
| Wirth, B.....          | 159, 181, 211, 393, 395, 434, 487   |
| Wischniewski, R.....   | 298, 357  |
| Wiskel, J.....         | 460   |
| Withers, P.....        | 306, 467  |
| Witherspoon, C.....    | 51, 220   |
| Withey, E.....         | 412   |
| Witkin, D.....         | 274   |
| Witte, F.....          | 92  |
| Witthar, K.....        | 439   |
| Wohlmuether, M.....    | 333   |
| Wolf, A.....           | 197   |
| Wolf, D.....           | 99, 445, 487  |
| Wolf, J.....           | 309   |
| Wolk, J.....           | 141, 309  |
| Wollmershauser, J..... | 164   |
| Woloshyn, J.....       | 419   |
| Wolverton, C.....      | 23, 66, 74, 124, 181, 239, 250  |
| Wondrak, T.....        | 409   |
| Wong, C.....           | 64  |
| Wong, D.....           | 123, 180  |
| Wong, S.....           | 163   |
| Won Sik, H.....        | 477   |
| Woodcock, T.....       | 207   |
| Woods, K.....          | 272   |
| Wood, T.....           | 492   |
| Woodward, C.....       | 62, 77, 112, 118, 135, 171,<br>176, 209, 230, 231, 289, 355, 375  |
| Woodward, P.....       | 288   |
| Woo, K.....            | 165, 506, 517   |
| Wooten, J.....         | 491   |
| Woo, W.....            | 446   |
| Worthington, D.....    | 172, 500  |
| Wright, J.....         | 273   |
| Wright, R.....         | 426   |
| Wu, A.....             | 45, 46, 49, 102, 159,<br>219, 274, 275, 337, 397,<br>399, 449, 450, 451, 452, 477   |
| Wu, C.....             | 366, 367, 372   |
| Wu, D.....             | 27, 75, 162, 372  |
| Wu, F.....             | 423   |
| Wu, G.....             | 206, 242, 274, 379  |
| Wu, H.....             | 144, 296, 397, 452  |
| Wu, J.....             | 268, 328  |
| Wu, K.....             | 212, 285  |
| Wu, L.....             | 41  |
| Wu, M.....             | 297   |
| Wunderlich, R.....     | 243   |
| Wu, P.....             | 164, 523  |
| Wu, S.....             | 136, 507, 511   |
| Wuthrich, Z.....       | 211   |
| Wu, W.....             | 176, 199, 339   |
| Wu, X.....             | 109, 164, 173, 193, 232, 264, 337, 403  |
| Wu, Y.....             | 41, 64, 128, 129, 181, 211,<br>257, 266, 270, 297, 390, 393, 443  |
| Wyatt, J.....          | 411   |
| Wyborne, M.....        | 255   |
| Wynn, A.....           | 130   |
| Wynne, B.....          | 36  |
| Wynn, T.....           | 16, 232, 496  |

# TMS2011

## 140th Annual Meeting & Exhibition

Wypych, F..... 26

### X

Xenidis, A..... 236  
 Xia, G..... 61, 334  
 Xia, K..... 403  
 Xiang, Y..... 335, 391  
 Xiangyang, Z..... 13  
 Xianqing, L..... 178  
 Xiaobing, L..... 65, 283  
 Xiaobing, Y..... 177, 178  
 Xiaofang, C..... 28  
 Xiaohua, Y..... 22, 508  
 Xiao, J..... 239  
 Xiao, K..... 316  
 Xiaoping, Y..... 178  
 Xiao, X..... 131, 269, 433, 491  
 Xiaoxiao, W..... 120  
 Xiao, Y..... 354, 407  
 Xiao, Z..... 29, 131, 250, 372  
 Xia, Q..... 509  
 Xia, W..... 120  
 Xie, B..... 118, 234, 294  
 Xie, G..... 22, 508  
 Xie, H..... 47  
 Xie, J..... 336, 386  
 Xie, L..... 295  
 Xie, S..... 117  
 Xie, W..... 275  
 Xie, X..... 282, 467  
 Xinyu, L..... 364  
 Xiong, D..... 407  
 Xiong, Y..... 358, 486  
 Xiquan, Q..... 381  
 Xi, W..... 25  
 Xi, Z..... 476, 477, 494  
 Xu, B..... 61, 190, 490  
 Xu, C..... 394  
 Xu, D..... 253  
 Xue, J..... 39, 40, 269, 382, 437, 475  
 Xue, L..... 344  
 Xuwei, L..... 476  
 Xue, Y..... 121, 186, 378, 403, 479  
 Xueyi, G..... 215  
 Xuezheng, Z..... 21  
 Xu, G..... 46, 160, 372, 397  
 Xu, H..... 131, 269, 275, 424, 451, 491  
 Xu, J..... 167, 175, 229, 244, 460, 501  
 Xu, P..... 40, 333, 405  
 Xu, Q..... 44, 63, 89, 491  
 Xu, R..... 67, 217  
 Xu, T..... 173  
 Xu, W..... 403, 418  
 Xu, Y..... 346, 351, 352  
 Xuyang, L..... 476  
 Xu, Z..... 38, 80

### Y

Yablinsky, C..... 193  
 Yacout, A..... 40, 445, 446  
 Yadav, D..... 235  
 Yadav, V..... 229  
 Yakoubi, S..... 493  
 Yalisove, S..... 381  
 Yamabe-Mitarai, Y..... 341  
 Yamada, R..... 424

Yamada, T..... 275  
 Yamada, Y..... 257, 323  
 Yamaguchi, K..... 234  
 Yamaguchi, N..... 158  
 Yamaji, K..... 267  
 Yamamoto, T..... 181, 210, 211, 215, 270, 333, 371, 395  
 Yamamoto, Y..... 156, 164, 165, 345, 378, 403, 405  
 Yamamura, K..... 267, 325  
 Yamane, L..... 57  
 Yamanoglu, R..... 19  
 Yamasaki, N..... 145  
 Yamasaki, T..... 69, 70  
 Yamashita, M..... 405  
 Yamashita, S..... 267  
 Yan, A..... 390, 444  
 Yanar, N..... 334  
 Yanase, K..... 140, 373  
 Yan, D..... 319  
 Yang, B..... 48, 91, 190, 490  
 Yang, C..... 48, 337, 476, 477  
 Yang, D..... 324, 426, 490, 500  
 Yang, F..... 87, 149, 161, 190, 194, 288  
 Yang, H..... 89, 221, 250, 494  
 Yang, J..... 25, 41, 44, 118, 125, 130, 210, 232, 344, 372, 384, 498  
 Yang, K..... 399, 456, 471  
 Yang, L..... 269, 274, 335, 337  
 Yang, M..... 25, 84, 115, 387, 425  
 Yang, N..... 232  
 Yang, Q..... 206, 258  
 Yang, R..... 509  
 Yang, S..... 87, 149, 190, 278, 476, 494  
 Yang, T..... 48, 476  
 Yang, W..... 218, 227, 303, 466  
 Yang, X..... 131, 269, 491  
 Yang, Y..... 27, 28, 39, 41, 43, 83, 84, 128, 135, 243, 333, 368, 394, 402, 417, 461, 472, 496, 497, 503  
 Yang, Z..... 94, 155, 212, 267, 334, 391  
 Yanilkin, A..... 40  
 Yan, J..... 167  
 Yan, L..... 120, 297  
 Yan, P..... 252, 359, 439  
 Yanping, Q..... 297  
 Yanqing, L..... 30  
 Yan, S..... 273  
 Yan, W..... 471  
 Yan, X..... 437  
 Yan, Y..... 431  
 Yao, B..... 166, 203  
 Yao, C..... 130  
 Yao, G..... 15, 30, 98, 252, 312, 359, 439, 475  
 Yaohua, Y..... 28  
 Yao, K..... 70  
 Yao, L..... 308  
 Yao, W..... 486  
 Yaowu, W..... 357  
 Yao, Y..... 500  
 Yap, Y..... 13, 173, 296  
 Yashiki, H..... 264  
 Yasi, J..... 92, 251  
 Yasir, M..... 257  
 Yasuda, N..... 267  
 Yavari, A..... 69  
 Yazdaniyan, S..... 259  
 Yazdipour, N..... 188

Yazici, H..... 242  
 Yazici, S..... 457  
 Yazzie, K..... 49, 314, 450  
 Yeager, J..... 168, 363  
 Ye, B..... 40, 51, 99, 446  
 Yeddu, H..... 54  
 Yee, J..... 422  
 Yeh, C..... 399, 450  
 Ye, J..... 128, 243, 393  
 Yelle, D..... 421  
 Yen, H..... 125  
 Yen, Y..... 275, 276, 339, 398, 451, 497, 511  
 Ye, X..... 283  
 Yexiang, L..... 30  
 Yi, F..... 182  
 Yi, L..... 117  
 Yilmaz, G..... 507  
 Yim, T..... 498  
 Yin, D..... 150  
 Ying, A..... 217  
 Yingfu, T..... 466  
 Yingjun, G..... 28, 54  
 Ying, W..... 321  
 Yingwei, B..... 177  
 Yin, H..... 227  
 Yin, J..... 120, 417  
 Yin, L..... 274, 398  
 Yin, Z..... 480  
 Yi, S..... 35, 148  
 Yisgedu, T..... 89  
 Yodoshi, N..... 424  
 Yokogawa, T..... 73  
 Yokokawa, H..... 267  
 Yokoyama, Y..... 69, 91, 127, 184, 185, 305, 306, 307, 424  
 Yongqiang, W..... 496  
 Yoo, B..... 350  
 Yoo, K..... 457, 519  
 Yoo, M..... 506  
 Yoon, H..... 428  
 Yoon, J..... 47, 508  
 Yoon, S..... 230, 428, 465, 505, 510, 521  
 Yoon, U..... 149  
 Yoo, S..... 45, 47, 48, 276, 510  
 Yoo, Y..... 465  
 Yoshida, N..... 158  
 Yoshiie, T..... 42, 44  
 Yoshikawa, T..... 461  
 Yoshimi, K..... 192  
 Yoshimi, Y..... 453  
 Yoshimura, Y..... 200  
 Yoshizawa, Y..... 263  
 You, J..... 265, 391  
 Young, D..... 404  
 Young, E..... 96  
 Young, G..... 95, 96, 97, 265  
 Young, H..... 450  
 Young, S..... 363  
 Youngsman, J..... 347, 471  
 Youn, J..... 513  
 Younsi, K..... 443  
 Youssef, K..... 17, 232  
 Youssefpour, H..... 303  
 Yu, A..... 49  
 Yuan, C..... 233  
 Yuan, G..... 33, 205, 242  
 Yuan, K..... 379  
 Yuan, L..... 63, 295

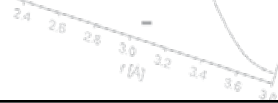
|                  |                             |                   |   |                      |                                       |
|------------------|-----------------------------|-------------------|---|----------------------|---------------------------------------|
| Yuan, Q.....     | 363, 364                    | Zhai, T.....      | 64, 79, 80, 121, 139, 178, 198,             | Zhong, Y.....        | 377                                   |
| Yuan, W.....     | 206, 438                    | .....             | 236, 256, 257, 298, 323, 358, 501           | Zhou, B.....         | 47, 274, 421, 449                     |
| Yuan, Y.....     | 12, 392                     | Zhai, X.....      | 133, 359                                    | Zhou, C.....         | 434, 435                              |
| Yubuta, K.....   | 70                          | Zhang, C.....     | 26, 242, 263, 269, 394, 468                 | Zhou, D.....         | 269                                   |
| Yu, C.....       | 45, 339, 397                | Zhang, D.....     | 295   | Zhou, F.....         | 145, 191, 249                         |
| Yucel, O.....    | 165, 515, 517, 518          | Zhang, F.....     | 56, 57, 119, 217, 302, 345, 515             | Zhou, H.....         | 102, 397                              |
| Yücel, O.....    | 234, 268                    | Zhang, G.....     | 167, 303                                    | Zhou, J.....         | 84, 305, 316                          |
| Yue, J.....      | 26, 269                     | Zhang, H.....     | 31, 152, 175,                               | Zhou, L.....         | 102, 148, 245, 247                    |
| Yuepeng, Z.....  | 391                         | .....             | 267, 268, 346, 384, 475                     | ZhouLan, Y.....      | 518                                   |
| Yue, S.....      | 35, 214, 294, 387, 481, 509 | Zhang, J.....     | 28, 175, 236, 320, 404, 507                 | Zhou, N.....         | 261, 329                              |
| Yuezhong, D..... | 357                         | Zhang, K.....     | 175, 313, 439, 451                          | Zhou, P.....         | 384                                   |
| Yu, H.....       | 175, 328                    | Zhang, L.....     | 12, 40, 56, 71, 98, 111, 112, 118,          | Zhou, Q.....         | 281, 369, 476, 481                    |
| Yu, J.....       | 50, 215, 388, 418           | .....             | 132, 170, 175, 269, 308, 355, 409,          | Zhou, S.....         | 516                                   |
| Yu, K.....       | 233                         | .....             | 418, 459, 461, 475, 479, 485, 502           | Zhou, X.....         | 355, 359, 459, 482                    |
| Yuksel, F.....   | 225                         | Zhang, M.....     | 12, 15, 359, 503                            | Zhou, Y.....         | 19, 37, 226, 244, 358, 403            |
| Yumakgil, K..... | 507                         | Zhang, N.....     | 360   | Zhu, A.....          | 202                                   |
| Yun, D.....      | 40, 99                      | Zhang, P.....     | 79  | Zhuang, F.....       | 408                                   |
| Yung, K.....     | 450                         | Zhang, Q.....     | 332, 493                                    | Zhu-Cheng, H.....    | 117                                   |
| Yun, J.....      | 54, 281                     | Zhang, R.....     | 292, 317, 397                               | Zhu, D.....          | 116, 175, 233, 234, 354, 355          |
| Yunnen, C.....   | 407, 457                    | Zhang, S.....     | 205, 240, 316, 381, 447                     | Zhu, F.....          | 190                                   |
| Yun, Y.....      | 513                         | Zhang, T.....     | 30, 128, 133, 359, 424, 460, 467            | Zhu, H.....          | 22, 117, 190, 387, 425, 470, 477, 478 |
| Yu, Q.....       | 190, 228, 320, 414          | Zhang, W.....     | 70, 123, 174, 180,                          | Zhu, J.....          | 39, 40, 56, 57, 269,                  |
| Yurko, J.....    | 409, 424, 459, 469, 502     | .....             | 284, 383, 431, 446                          | .....                | 286, 302, 305, 308, 312, 437          |
| Yu, S.....       | 73                          | Zhang, X.....     | 30, 41, 43, 51, 66,                         | Zhu, L.....          | 38, 392, 480, 518                     |
| Yushin, G.....   | 464                         | .....             | 88, 109, 114, 144, 168, 240,                | Zhuo, C.....         | 368, 369, 456                         |
| Yutaka, N.....   | 42                          | .....             | 242, 269, 293, 341, 381, 475, 479           | Zhuo, M.....         | 496                                   |
| Yu, W.....       | 233, 354                    | Zhang, Y.....     | 20, 61, 70, 80, 99, 117,                    | Zhu, P.....          | 482, 516                              |
| Yu, X.....       | 448                         | .....             | 139, 175, 207, 255, 295, 324,               | Zhu, Q.....          | 338                                   |
| Yu, Z.....       | 35, 383, 396, 417, 446      | .....             | 363, 380, 393, 443, 480, 490, 496           | Zhu, S.....          | 205                                   |
| Yvon, K.....     | 88, 89                      | Zhang, Z.....     | 15, 19, 20, 30, 33, 79, 124, 167,           | Zhu, T.....          | 109, 145, 205                         |
|                  |                             | .....             | 226, 232, 293, 323, 403, 423, 471, 475, 503 | Zhu, X.....          | 167, 203                              |
|                  |                             | Zhan, J.....      | 26, 269                                     | Zhu, Y.....          | 21, 109, 232, 236, 293                |
|                  |                             | Zhan, L.....      | 382   | Zhylliev, A.....     | 19                                    |
|                  |                             | Zhan, Q.....      | 404   | Zi, C.....           | 470                                   |
|                  |                             | Zhan, Y.....      | 115   | Ziegler, D.....      | 30, 197, 322, 323, 420                |
|                  |                             | Zhan, Z.....      | 267   | Zigler, A.....       | 361                                   |
|                  |                             | Zhao, A.....      | 139   | Zikry, M.....        | 322, 474                              |
|                  |                             | Zhao, C.....      | 519   | Zimmerman, J.....    | 93, 315                               |
|                  |                             | Zhao, H.....      | 46, 249, 359, 408                           | Zimmerman, M.....    | 384, 478, 485                         |
|                  |                             | Zhao, J.....      | 89, 145, 197, 203, 387, 423, 520            | Zimmermann, J.....   | 394                                   |
|                  |                             | Zhao, K.....      | 397   | Zimmermann, M.....   | 396                                   |
|                  |                             | Zhao, L.....      | 405   | Zimmerman, R.....    | 229                                   |
|                  |                             | Zhao, Q.....      | 30  | Zinck, A.....        | 91                                    |
|                  |                             | Zhao, W.....      | 405   | Zin, E.....          | 275, 432                              |
|                  |                             | Zhao, X.....      | 239, 335                                    | Zinkle, S.....       | 95                                    |
|                  |                             | Zhao, Y.....      | 15, 236, 267, 292, 293,                     | Zinn, M.....         | 384                                   |
|                  |                             | .....             | 309, 319, 321, 337, 404, 448                | Zirker, L.....       | 96                                    |
|                  |                             | Zheng, B.....     | 37, 244, 358                                | Zlotski, S.....      | 44                                    |
|                  |                             | Zheng, C.....     | 25, 411                                     | Zody, M.....         | 500                                   |
|                  |                             | Zheng, G.....     | 355   | Zografidis, C.....   | 236                                   |
|                  |                             | Zheng, H.....     | 130, 418, 480                               | Zolotoyabko, E.....  | 101                                   |
|                  |                             | Zheng, K.....     | 459   | Zolriasatein, A..... | 108, 225, 226, 465                    |
|                  |                             | Zheng, L.....     | 447   | Zou, J.....          | 439                                   |
|                  |                             | Zheng, M.....     | 206   | Zoul, L.....         | 46, 275                               |
|                  |                             | Zheng, P.....     | 51  | Zou, M.....          | 152                                   |
|                  |                             | Zheng, Q.....     | 384   | Zou, Y.....          | 214, 481, 509                         |
|                  |                             | Zheng, S.....     | 522   | Zou, Z.....          | 475                                   |
|                  |                             | Zheng, W.....     | 29, 188                                     | Zrnik, J.....        | 187, 368, 449                         |
|                  |                             | Zheng, X.....     | 387   | Zschau, H.....       | 396                                   |
|                  |                             | Zheng, Y.....     | 40, 239, 269, 441, 487                      | Zu, G.....           | 359                                   |
|                  |                             | Zhenawen, G.....  | 177   | Zuidema, J.....      | 241                                   |
|                  |                             | Zhen, X.....      | 234   | Zúñiga, C.....       | 440                                   |
|                  |                             | Zhernakov, V..... | 233   | Zuo, X.....          | 112                                   |
|                  |                             | Zhifeng, L.....   | 364   | Zupan, M.....        | 13, 141, 298, 309                     |
|                  |                             | Zhihe, D.....     | 120, 297                                    | Zurob, H.....        | 88                                    |
|                  |                             | Zhihui, W.....    | 357   | Zweiacker, K.....    | 368                                   |
|                  |                             | Zhong, L.....     | 418   |                      |                                       |
|                  |                             | Zhong, X.....     | 60, 152                                     |                      |                                       |

**Z**





$Q(\varphi, \sigma)$



$$kT_g = \frac{2(B)(V)(\epsilon_1)}{K_a}$$

0.000  
0.25

NOTES





### UPCOMING MEETINGS

When it comes to professional development and networking, there is nothing like a face-to-face connection with colleagues. TMS provides members with numerous opportunities for advancing research and collaboration on the latest technology through a series of diverse conferences. Take advantage of these engaging events for the materials science and technology community.



#### **Electronic Materials Conference 2011**

**June 22-24, 2011**

University of California  
Santa Barbara, CA



#### **1st World Congress on Integrated Computational Materials Engineering**

**July 10-14, 2011**

Seven Springs Mountain Resort  
Seven Springs, PA



#### **15th International Conference on Environmental Degradation of Materials in Nuclear Power Systems – Water Reactors**

**Water Reactors**

**August 7-11, 2011**

Cheyenne Mountain Resort  
Colorado Springs, CO



#### **Materials Science & Technology 2011 Conference & Exhibition**

**October 16-20, 2011**

Greater Columbus Convention Center  
Columbus, OH



#### **TMS 2012 Annual Meeting & Exhibition**

**March 11-15, 2012**

Walt Disney World  
Lake Buena Vista, FL

|    |    |    |    |    |    |    |    |    |    |    |    |    |    |    |    |    |    |
|----|----|----|----|----|----|----|----|----|----|----|----|----|----|----|----|----|----|
| H  | He |    |    |    |    |    |    |    |    |    |    |    |    |    |    |    |    |
| Li | Be | B  | C  | N  | O  | F  | Ne |    |    |    |    |    |    |    |    |    |    |
| Na | Mg | Al | Si | P  | S  | Cl | Ar |    |    |    |    |    |    |    |    |    |    |
| K  | Ca | Sc | Ti | V  | Cr | Mn | Fe | Co | Ni | Cu | Zn | Ga | Ge | As | Se | Br | Kr |
| Rb | Sr | Y  | Zr | Nb | Mo | Tc | Ru | Rh | Pd | Ag | Cd | In | Sn | Sb | Te | I  | Xe |
| Cs | Ba | La | Hf | Ta | W  | Re | Os | Ir | Pt | Au | Hg | Tl | Pb | Bi | Po | At | Rn |

|    |    |    |    |    |    |    |    |    |    |    |    |    |    |
|----|----|----|----|----|----|----|----|----|----|----|----|----|----|
| Ce | Pr | Nd | Pm | Sm | Eu | Gd | Tb | Dy | Ho | Er | Tm | Yb | Lu |
| Th | Pa | U  | Np | Pu | Am | Cm | Bk | Cf | Es | Fm | Md | No | Lr |

# Now Invent.™



**World's Leading Manufacturer of Engineered & Advanced Materials**

**catalog: americanelements.com**

© 2001-2011. American Elements is a U.S. Registered Trademark.